MODERN ELECTROPLATING

MODERN ELECTROPLATING

Fifth Edition

Edited by

MORDECHAY SCHLESINGER
University of Windsor, Windsor Ontario, Canada

MILAN PAUNOVIC
IBM T.J. Watson Research Center, Yorktown Heights, NY (Retired)

Sponsored by
THE ELECTROCHEMICAL SOCIETY, INC. ***Pennington, New Jersey***

WILEY
A JOHN WILEY & SONS, INC., PUBLICATION

Published by John Wiley & Sons, Inc., Hoboken, New Jersey
Published simultaneously in Canada

Library of Congress Cataloging-in-Publication Data:

Modern eletroplating / edited by Mordechay Schlesinger, Milan Paunovic. – 5th ed.
p. cm. – (The ECS series of texts and monographs ; 52)
Includes index.
Summary: ‘‘Electroplating is the coating of an electrically conductive object with a layer of metal using electrical current resulting in a thin, smooth, even coat of metal on the object. This text covers the methods and applications of electrochemical deposition of metals, alloys, semiconductors, and conductive polymers. It provides practical advice and some theortical background to those entering the field of electrodeposition. Like previous editions, the fifth edition will be the first stop referece for the electroplating conmmunity. This fully updated edition includes significant advances in the field, from emerging electrodepostion techniques to electroplating in medical and data storage industries’’ – Provided by publisher.
ISBN 978-0-470-16778-6 (hardback)
1. Electroplating. I. Schlesinger, Mordechay. II. Paunovic, Millan.
TS670.M554 2010
671.7’32–dc22

Printed in the United States of America

10 9 8 7 6 5 4 3 2 1

CONTENTS

PREFACE vii

PREFACE TO THE FOURTH EDITION ix

CONTRIBUTORS xi

CONVERSION FACTORS xiii

GRAPHICAL CONVERSIONS xv

THE ELECTROCHEMICAL SOCIETY SERIES xvii

1 Fundamental Considerations 1
Milan Paunovic, Mordechay Schlesinger, and Dexter D. Snyder

2 Electrodeposition of Copper 33
Jack W. Dini and Dexter D. Snyder

3 Electrodeposition of Nickel 79
George A. Di Bari

4 Electrodeposition of Gold 115
Paul A. Kohl

5 Electroless and Electrodeposition of Silver 131
Mordechay Schlesinger

6 Tin and Tin Alloys for Lead-Free Solder 139
Yun Zhang

7 Electrodeposition of Chromium 205
Nenad V. Mandich and Donald L. Snyder

8 Electrodeposition of Lead and Lead Alloys 249
Manfred Jordan

9 Electrodeposition of Tin–Lead Alloys 265
Manfred Jordan

10 Electrodeposition of Zinc and Zinc Alloys 285
René Winand

11 Electrodeposition of Iron and Iron Alloys **309**
Masanobu Izaki

12 Palladium Electroplating **327**
Joseph A. Abys

13 Electrochemical Deposition Process for ULSI Interconnection Devices **369**
Tetsuya Osaka and Masahiro Yoshino

14 Electrodeposition of Semiconductors **383**
T. E. Schlesinger, Krishnan Rajeshwar, and Norma R. De Tacconi

15 Deposition on Nonconductors **413**
Mordechay Schlesinger

16 Conductive Polymers: Electroplating of Organic Films **421**
Tetsuya Osaka, Shinichi Komaba, and Toshiyuki Momma

17 Electroless Deposition of Copper **433**
Milan Paunovic

18 Electroless Deposition of Nickel **447**
Mordechay Schlesinger

19 Electrochemical Synthesis of Metal Alloys for Magnetic Recording Systems **459**
Atsushi Sugiyama, Masahiro Yoshino, Takuma Hachisu, and Tetsuya Osaka

20 Electroless Deposition of Palladium and Platinum **477**
Izumi Ohno

21 Electroless Deposition of Gold **483**
Yutaka Okinaka and Masaru Kato

22 Electroless Deposition of Alloys **499**
Izumi Ohno

23 Preparation for Deposition **507**
Dexter D. Snyder

24 Manufacturing Tools **513**
Tom Ritzdorf

25 Monitoring and Control **527**
Tom Ritzdorf

26 Environmental Aspects of Electrodeposition **555**
Micha Tomkiewicz

27 Applications to Magnetic Recording and Microelectronic Technologies **573**
Stanko R. Brankovic, Natasa Vasiljevic, and Nikolay Dimitrov

28 Microelectromechanical Systems **617**
Giovanni Zangari

29 Analysis of Electroplated Films Using Dual-Beam FIB/SEM and TEM Techniques **637**
Xianying Meng-Burany

30 Ionic Liquid Treatments for Enhanced Corrosion Resistance of Magnesium-Based Substrates **665**
Robert Petro, Mordechay Schlesinger, and Guang-Ling Song

APPENDIX **687**

INDEX **701**

PREFACE

Ours is the information age. Consequently, the demand for high-performance, low-cost, and nonvolatile information storage systems is on a constant rise. There are a great variety of information storage systems, with varying degrees of development and commercialization. Those include, but are not limited to, magnetic tape drives, hard disc drives, magnetic floppy disc drives, magneto-optic (MO) disc drives, phase change optic disc drives, semiconductor flush memory, magnetic random-access memory (RAM), and holographic optical storage. Electrochemical deposition techniques are essential in the production of most of the above. This, among many others, is the raison d'être for the present (fifth) and the earlier (fourth) editions.

The fourth edition of *Modern Electroplating* appeared some 10 years ago. A great deal of progress has taken place in those years in the area of electrochemical plating and related fields. It is these developments that make this new edition both desirable and necessary. Those profound changes are reflected in the present edition in a number of different ways. Essentially, all chapters were rewritten, some by different authors, and/or updated. Unfortunately, two authors who contributed to the fourth edition (Drs. Rolf Wyle and Ned Mandich) have since passed on. Two chapters have been removed altogether and new ones are replacing them. The two new chapters are titled "Electrochemical Deposition Process for ULSI Interconnection Devices" by Osaka and Yoshino and "Electrochemical Synthesis of Metal Alloys for Magnetic Recording Systems" by Sugiyama, Yoshino, Hachisu, and Osaka. Four new chapters have been added: "Applications to Magnetic Recording and Microelectronic Technologies" by Brankovic, Vasiljevic, and Dimitrov; "Microelectromechanical Systems" by Zangari; "Analysis of Electroplated Films Using Dual-Beam FIB/SEM and TEM Techniques" by Meng-Burany; and "Ionic Liquid Treatments for Enhanced Corrosion Resistance of Magnesium-Based Substrates" by Petro, Schlesinger, and Song. These and most other changes, including the publication of the new second edition in 2006 of *Fundamentals of Electrochemical Deposition*, reflect the present tendency of the applications of electroplating more and more in the arena of nanoelectronics in particular and nanotechnology in general as alluded to above. Typically, it may be observed that whereas the fourth edition is comprised of 26 chapters on about 800 pages, the present edition contains 30 chapters and is about the same number of substantially enlarged pages. In this edition as in the previous the chapters are self-contained in that those may be read in any order that the reader finds useful. Thanks are due to the over 30 contributors/authors who made this edition possible.

MORDECHAY SCHLESINGER

Windsor Ontario, Canada

MILAN PAUNOVIC

Port Washington, New York

PREFACE TO THE FOURTH EDITION

In planning this new edition of *Modern Electroplating*, we have realized from the start that it would be impossible to include in one volume both the fundamental aspects and the technology itself. For this reason we have decided to publish the recent developments in the science of deposition in a separate volume titled *Fundamentals of Electrochemical Deposition*. That volume was published in November 1998. Therefore, the present volume includes only a brief summary of fundamental technological advancements, and this is presented in the first, introductory chapter.

Since the last edition of *Modern Electroplating* in 1975, electrochemical deposition has evolved from an ill-defined area, as the Preface to the previous edition calls it, into an exact science. This development is, in the first place, seen as responsible for the ever-increasing number and widening types of applications of this branch of practical science and engineering.

The most significant developments in any field of science or technology in general, and in electrochemistry in particular, are made by those who possess a good understanding of the fundamental aspects of the discipline, which in this case is electrochemical deposition. We, the editors, found it necessary and highly desirable to seek and present to the reader a companion volume that, for all intents and purposes, makes essentially a completely new contribution and not just a revised version of the earlier editions. Thus, for the sake of illustration, the present edition includes a chapter devoted to the electrodeposition of semiconductors. Another deals with environmental issues. Last, but not least, in this connection, neither of the editors nor the vast majority of the contributors were associated with any of the earlier editions.

Technological areas in which the possession of technical knowledge of electroplating is found to be essential include all aspects of electronics; macro-, micro-, and nano-optics; opto-etectronics; and sensors of most types. In addition, a number of key industries, such as the automotive industry, employ methods of electroplating. This is so even when other methods such as evaporation and sputtering CVD (chemical vapor deposition) are an option. Electroplating is therefore often used for reasons of economy and/or convenience.

This volume is divided into 26 chapters. After a three-part introductory chapter by Paunovic, Schlesinger, and Weil come 13 chapters dealing with the electrodeposition of copper (Dini), nickel (DiBari), gold (Kohl), silver (Schlesinger), tin (Abys et al.). chromium (Snyder et al.), lead and alloys (Jordan), tin-lead alloys (Jordan), zinc and alloys (Winand), iron and alloys (Izaki), palladium and alloys (Abys et al.), nickel and cobalt alloys (DiBari), and semiconductors (T. E. Schlesinger). Closing this series of chapters is one on deposition on nonconductors (Schlesinger), and conductive polymers (Osaka et al.). Next come 6 chapters dealing with electroless deposition of copper (Paunovic), nickel (Schlesinger), cobalt (Osaka), palladium and platinum (Ohno), gold (Okinaka), and electroless alloys (Ohno). Finally, 4 chapters close the book, and these are on preparation for deposition (Dexter Snyder), manufacturing technologies (Turner), manufacturing control (Turner), and environmental considerations (Tomkiewicz).

In the preface to *Fundamentals of Electrochemical Deposition* we stated that it may be considered a lucky coincidence that this volume is published close to the time that copper interconnection technology is introduced in the microelectronic industry. This is still the case. There has been a truly revolutionary change from physical to electrochemical techniques in the production of microconductors on silicon, and developments in electrochemical deposition are bound to generate and maintain in the twenty-first century an increased interest and urgent need for up-to-date information regarding

the technology. The present volume together with the *Fundamentals* volume should be of great help in understanding these advancements.

The chapters were written by different authors and so differences in style and approach will be evident. We the editors have tried to smooth those differences without changing the basic message present in each chapter. We also intend this volume to be a useful reference for practitioners of deposition as well as for individuals who are about to enter this modern ever-evolving field of practical knowledge. For this reason each chapter is complete and may be read and consulted separately, and certainly the book can be read in any order.

Our thanks and heartfelt gratitude go to many members of the Electrochemical Society and in particular to those of the Electrodeposition Division. Our thanks also go to our respective families for their patience and understanding during the hectic long hours we spent in preparing this volume.

MOROECHAY SCHLESINOER

Windsor Ontario. Canada

MILAN PAUNOVIC

Yorktown Heights. New York

CONTRIBUTORS

Joseph A. Abys Cookson Electronics–Enthone Inc., Orange, CT

Stanko R. Brankovic Cullen College of Engineering, University of Houston, Houston, TX

Jack W. Dini Lawrence Livermore National Laboratory, Livermore, CA (Retired)

George A. Di Bari INCO, Saddle Brook, NJ (Retired)

Norma R. de Tacconi University of Texas at Arlington, Arlington, TX

Nikolay Dimitrov Department of Chemistry, Binghamton University–SUNY, Binghamton, NY

Takuma Hachisu Waseda University, Tokyo, Japan

Masanobu Izaki Toyohashi University of Technology, Toyohashi, Japan

Manfred Jordan Dr. Ing. Max Schlotter, Geislingen/ Steige, Germany

Paul A. Kohl School of Chemical Engineering, Georgia Institute of Technology, Atlanta, GA

Sinichi Komaba Department of Applied Chemistry, Tokyo University of Science, Shinjuku-ku, Tokyo, Japan

Masaru Kato Kanto Chemical Co., Soka Saitama-ken, Japan

Nenend V. Mandich (Deceased)

Toshiyuki Momma Waseda University, Tokyo, Japan

Xianying Meng-Burany University of Windsor, Windsor, ON, Canada

Tetsuya Osaka Waseda University, Tokyo, Japan

Izumi Ohno Tokyo Institute of Technology, Tokyo, Japan (Retired)

Yutaka Okinaka Waseda University, Tokyo, Japan

Milan Paunovic IBM T J Watson Research Center, Yorktown Heights, NY

Robert Petro University of Windsor, Windsor, ON, Canada

Krishnan Rajeshwar University of Texas at Arlington, Arlington, TX

Tom Ritzdorf Semitool, Inc., Kalispell, MT

Mordechay Schlesinger University of Windsor, Windsor, ON, Canada

Dexter D. Snyder GM Research and Development Center, Warren, MI (Retired)

Donald L. Snyder ATO Tech, Cleveland, OH

T. E. Schlesinger Carnegie Mellon University, Pittsburgh, PA

Atsushi Sugiyama Waseda University, Tokyo, Japan

Guang-Ling Song GM Research and Development Center, Warren, MI

Micha Tomkiewicz Department of Physics, Brooklyn College–CUNY, Brooklyn, NY

Natasa Vasiljevic Physics Department, University of Bristol, Bristol, UK

René Winand University of Bruxelles, Bruxelle, Belgium (Retired)

Masahiro Yoshino Waseda University, Tokyo, Japan

Yun Zhang Cookson Electronics–Enthone Inc., Orange, CT

Giovanni Zangari University of Virginia, Charlottesville, VA

CONVERSION FACTORS

1 centimeter (cm) = 0.934 inch (in.)
1 millimeter (mm) = 0.0394 inch (in.)
1 micrometer (μm, micron) = 0.0394 mil = 39.37 microinch (μin.)
1 square decimeter (dm^2) = 15.5 square inch ($in.^2$) = 0.1076 square foot (ft^2)
1 square centimeter (cm^2) = 0.155 square inch ($in.^2$)
1 square millimeter (mm^2) = 0.00155 square inch ($in.^2$)
1 kilogram (kg) = 2.205 pound (lb)
1 gram (g) = 0.0353 ounce (oz) avoirdupois = 0.0321 ounce Troy
1 liter (L) = 0.264 gallon U.S. (gal) = 0.220 gallon British
1 ampere per square decimeter (A/dm^2) = 9.29 ampere per square foot (A/ft^2)—sec chart
1 gram per liter (g/L) = 0.133 ounce per gallon. U.S. (oz/gal)—see chart
1 kilogram per square millimeter (kg/mm^2) = 1.422 pounds per square inch $lb/in.^2$, psi)—see chart;
strictly, unit should be kilogram-force, or kgf/mm^2; in SI units, 1 $kgf/mm^2 = 9.806 \times l0^6$ newton/square meter (N/m^2) = 9.806 MN/m^2; 1 N/m^2 = 1 Pa (pascal)

Approximate Conversion Factors for Mental Calculation (accurate to 10% or better)

To convert from	To	Do this
A/dm^2	A/ft^2	Multiply by 10
A/dm^2	$A/in.^2$	Divide by 15 (multiply by 2, divide by 30)
Celsius (Centigrade)*	Fahrenheit, F	Multiply by 9/5 (1.8) and add 32
g/L	oz/gal	Divide by 7.5 (multiply by 4, divide by 30)
kg/mm^2	$lb/in.^2$(psi)	Multiply by 1500
mm	in.	Divide by 25 (multiply by 4, divide by 100)
micrometers (m)	mil	Divide by 25 (multiply by 4, divide by 100)

*Exact.

GRAPHICAL CONVERSIONS

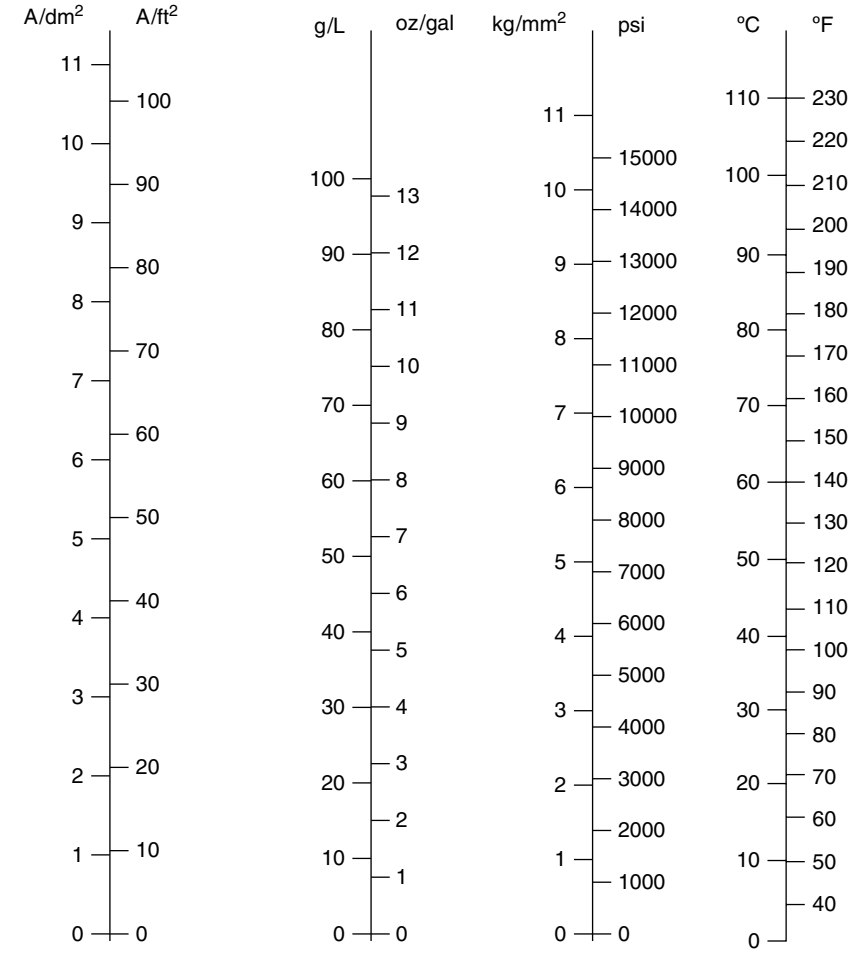

(1 A/dm^2 = 9.29 A/ft^2) (1g/L = 0.133 oz/gal) (1kg/mm^2 = 1422 psi)

THE ELECTROCHEMICAL SOCIETY SERIES

Corrosion Handbook
Edited by Herbert H. Uhlig

Modern Electroplating, Third Edition
Edited by Frederick A. Lowenheim

Modem Electroplating, Fourth Edition
Edited by Mordechay Schlesinger and Milan Paunovic

The Electron Microprobe
Edited by T. D. McKinley, K. F. J. Heinrich, and D. B. Wittry

Chemical Physics of Ionic Solutions
Edited by B. E. Conway and R. G. Barradas

High-Temperature Materials and Technology
Edited by Ivor E. Campbell and Edwin M. Sherwood

Alkaline Storage Batteries
S. Uno Falk and Alvin J. Salkind

The Primary Battery (*in Two Volumes*)
Volume I Edited by George W. Heise and N. Corey Cahoon
Volume II Edited by N. Corey Cahoon and George W. Heise

Zinc-Silver Oxide Batteries
Edited by Arthur Fleischer and J. J. Lander

Lead-Acid Batteries
Hans Bode
Translated by R. J. Brodd and Karl V. Kordesch

Thin Films-Interdiffusion and Reactions
Edited by J. M. Poate, M. N. Tu, and J. W. Mayer

Lithium Battery Technology
Edited by H. V. Venkatasetty

Quality and Reliability Methods for Primary Batteries
P. Bro and S. C. Levy

Techniques for Characterization of Electrodes and Electrochemical Processes
Edited by Ravi Varma and J. R. Selman

Electrochemical Oxygen Technology
Kim Kinoshita

Synthetic Diamond: Emerging CVD Science and Technology
Edited by Kari E. Spear and John P. Dismukes

Corrosion of Stainless Steels
A. John Sedriks

Fundamentals of Electrochemical Deposition
Milan Paunovic and Mordechay Schlesinger

Semiconductor Wafer Bonding: Science and Technology
Q.-Y. Tong and U. Göscle

Uhlig's Corrosion Handbook, Second Edition
Edited by R. Winston Revie

The Electrochemical Society
65 South Main Street
Pennington, NJ 08534-2839 USA
http://www.electrochem.org

1

FUNDAMENTAL CONSIDERATIONS

MILAN PAUNOVIC,[1] MORDECHAY SCHLESINGER,[2] AND DEXTER D. SNYDER[3]

1.1 INTRODUCTION

Already in the preparation of the fourth edition of *Modern Electroplating*, we realized that the first chapter in the third edition (1974) needed to be enlarged considerably in order to cover all the significant progress made since 1974. As the prospect of adding material to the chapter on fundamentals began to suggest an inbalance in the new edition, we chose to publish a separate volume titled *Fundamentals of Electrochemical Deposition (Fundamentals* in further text) that would treat the basic aspects of electrochemical deposition [1]. For this reason we provided in the fourth and now in the present fifth edition only a brief review of these fundamentals. The number of references in this chapter is also limited, and the reader is urged to consult the more extensive list of references given in both editions of *Fundamentals*.

This chapter is divided into three parts. Part A treats electrochemical aspects, part B treats physical aspects, and part C treats material science. For this presentation of the fundamentals our objective is to provide the basis for understanding only the electrochemical deposition processes treated in this volume. Information on a higher level is presented in the *Funamentals* volume.

PART A ELECTROCHEMICAL ASPECTS

In Part A we discuss (1) electrode potential, (2) kinetics and mechanism of electrodeposition, (3) growth mechanism, and (4) electroless and displacement depositions. All four topics are presented in a concise manner that emphasizes the most important points. Most concepts are clarified by solutions of numerical examples. These examples are useful for this chapter and for the chapters that follow.

1.2 ELECTRODE POTENTIAL

When a metal M is immersed in an aqueous solution containing ions of that metal, M^{z+} (e.g., salt MA), there will be an exchange of metal ions M^{z+} between two phases, the metal and the solution. Some M^{z+} ions from the crystal lattice enter the solution, and some ions from the solution enter the crystal lattice. Initially one of these reactions may occur

[1] Milan Paunovic, Part A.
[2] Mordechay Schlesinger, Part B.
[3] Dexter D. Synder, Part C.

Modern Electroplating, Fifth Edition Edited by Mordechay Schlesinger and Milan Paunovic

faster than the other. Let us assume that conditions are such that more M^{z+} ions leave than enter the crystal lattice. In this case there is an excess of electrons on the metal and the metal acquires negative charge, q_M^- (charge on the metal per unit area). In response to the charging of the metal side of the interphase, there is also a rearrangement of charges on the solution side of the interphase. The negative charge on the metal attracts positively charged M^{z+} ions from the solution and repels negatively charged A^{z-} ions. The result of this is an excess of positive M^{z+} ions in the solution in the vicinity of the metal interphase. Thus, in this case, the solution side of the interphase acquires opposite and equal charge, q_s^+ (the charge per unit area on the solution side of the interphase). This positive charge at the solution side of the interphase slows down the rate of M^{z+} ions leaving the crystal lattice (due to repulsion) and accelerates the rate of ions entering the crystal lattice. After a certain period of time a dynamic equilibrium between the metal M and its ions in the solution will result:

$$M^{z+} + ze \leftrightarrows M \tag{1.1a}$$

where z is the number of electrons involved in the reaction. Reaction from left to right consumes electrons and is called reduction. Reaction from right to left liberates electrons and is called oxidation. At the dynamic equilibrium the same number of M^{z+} ions enter, $\vec{n}$, and the same number of M^{z+} ions leave the crystal lattice, $\vec{n}$, (see Fig. 1.1):

$$\vec{n} = \overleftarrow{n} \tag{1.1b}$$

The interphase region is neutral at equilibrium:

$$q_M = -q_S \tag{1.1c}$$

The result of the charging of the interphase is the potential difference, $\Delta\phi$ (M, S), between the potentials of the metal, ϕ_M, and the solution, ϕ_S:

$$\Delta\phi(M, S) = \phi_M - \phi_S \tag{1.2}$$

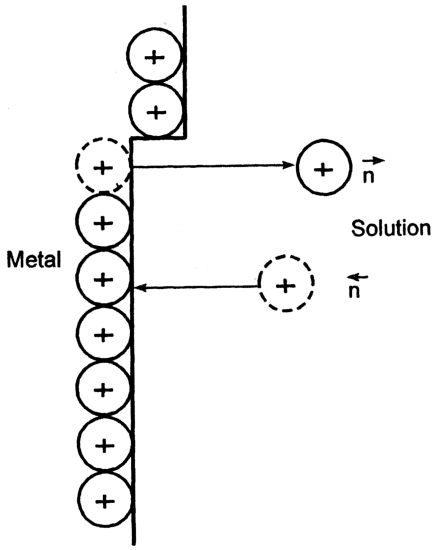

FIGURE 1.1 Formation of metal–solution interphase; equlibrium state: $\vec{n} = \overleftarrow{n}$.

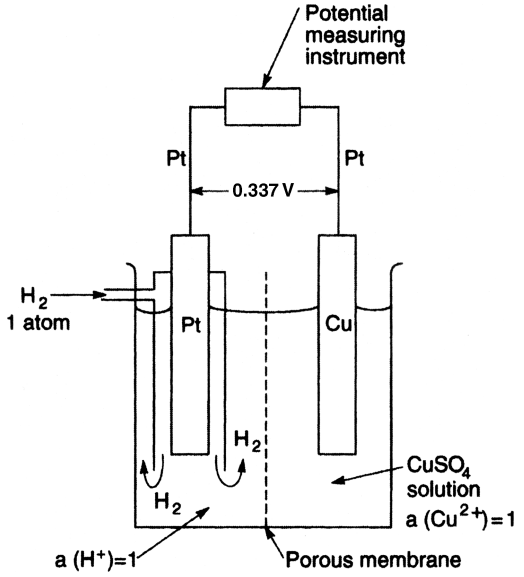

FIGURE 1.2 Relative standard electrode potential E^0 of a Cu/Cu^{2+} electrode.

In order to measure the potential difference of an interphase, one must connect it to another one and thus form an electrochemical cell. The potential difference across this electrochemical cell can be measured.

For example, consider the cell shown in Figure 2.2. This cell may be schematically represented in the following way:

$$Pt, H_2(p = 1)|H^+(a = 1)\|Cu^{2+}(a = 1)|Cu|Pt$$

where the left-hand electrode is the normal hydrogen reference electrode; a stands for activity and p for the pressure of H_2. When $p = 1$ atm and the activity of H^+ ions is 1, the hydrogen electrode is called the standard hydrogen electrode (SHE) and its potential is zero by convention. The measured value of the potential difference of this cell is $+0.337$ V at 250°C. This measured cell potential difference, $+0.337$ V, is called the relative standard electrode potential of Cu and is denoted E^0. The standard electrode potential of other electrodes is obtained in a similar way, by forming a cell consisting of the SHE and the electrode under investigation. Standard electrode potentials at 25°C are listed in Table 1.1.

The potential E of the M^{z+}/M electrode is a function of the activity [see Eq. (1.5)] of metal ions in the solution according to the Nernst equation,

$$E = E^0 + \frac{RT}{zF} \ln a(M^{z+}) \tag{1.3}$$

TABLE 1.1 Standard Electrode Potentials

Metal/Metal Ion Couple	Electrode Reaction	Standard Value (V)
Au/Au^{+}	$Au^{+} + e \Leftrightarrow Au$	1.692
Au/Au^{3+}	$Au^{3+} + 3e \Leftrightarrow Au$	1.498
Pd/Pd^{2+}	$Pd^{2+} + 2e \Leftrightarrow Pd$	0.951
Cu/Cu^{+}	$Cu^{+} + e \Leftrightarrow Cu$	0.521
Cu/Cu^{2+}	$Cu^{2+} + 2e \Leftrightarrow Cu$	0.3419
Fe/Fe^{3+}	$Fe^{3+} + 3e \Leftrightarrow Fe$	−0.037
Pb/Pb^{2+}	$Pb^{2+} + 2e \Leftrightarrow Pb$	−0.1262
Ni/Ni^{2+}	$Ni^{2+} + 2e \Leftrightarrow Ni$	−0.257
Co/Co^{2+}	$Co^{2+} + 2e \Leftrightarrow Co$	−0.28
Fe/Fe^{2+}	$Fe^{1+} + 2e \Leftrightarrow Fe$	−0.447
Zn/Zn^{2+}	$Zn^{2+} + 2e \Leftrightarrow Zn$	−0.7618
$A1/A1^{3+}$	$Al^{3+} + 3e \Leftrightarrow Al$	−1.662
Na/Na^{+}	$Na^{+} + e \Leftrightarrow Na$	−2.71

Source: G. Millazzo and S. Caroli, *Tables of Standard Electrode Potentials*, Wiley, New York, 1978.

or converting the natural logarithm into the decimal logarithm yields

$$E = E^0 + 2.303\frac{RT}{zF}\ln a(M^{z+}) \tag{1.4}$$

where R, T, z, and F are the gas constant, absolute temperature, number of electrons involved in reaction (1.1a), and Faraday's constant (96,500 C), respectively. The activity of the ion, $a(M^{z+})$, is defined by

$$a(M^{z+}) = \gamma c(M^{z+}) \tag{1.5}$$

where $c(M^{z+})$ is the concentration of M^{z+} in moles per liter and $\gamma(M^{z+})$ is the activity coefficient of M^{z+}; when the concentration of a solution is low, such as 0.001 M or lower, the activity may be replaced by concentration in moles per liter.

The activity coefficient γ is a dimensionless quantity which depends on the concentration of all ions present in the solution (ionic strength). The individual activity coefficients of the specific ionic species cannot be measured experimentally, but it can be calculated. The experimentally measurable quantity is the mean total ionic activity $\gamma_{\pm}$:

$$\gamma_{\pm} = \sqrt{\gamma_{+}\gamma_{-}} \tag{1.6}$$

which is the geometric mean (the square root of the product) of the activity coefficients of the individual ionic species [2].

When the activity of M^{z+} in the solution is equal to 1, $a(M^{z+}) = 1$, then by Eqs. (1.3) and (1.4), since $\ln 1 = 0$,

$$E = E^0 \tag{1.7}$$

where E^0 is the relative standard electrode potential of the M^{z+}/M electrode. The quantity RT/F has the dimension of voltage and at 298 K (25°C) has the value of 0.0257 V and 2.303 $(RT/F) = 0.0592$ V. With these values Eq. (1.4) reads

$$E = E^0 + \frac{0.0592}{z}\log a(M^{z+}) \tag{1.8}$$

The use of Eq. (1.8) is illustrated in Examples 1.1 and 1.2.

Example 1.1 Calculate the reversible electrode potential of a Cu electrode immersed in a $CuSO_4$ aqueous solution with concentrations 1.0, 0.1, 0.01, and 0.001 mol L^{-1} at 25°C. The standard electrode potential for a Cu/Cu^{2+} electrode is 0.337 V. Use concentrations in Eq. (1.8) instead of activities in an approximate calculation.

From Eq. (1.8), for $z = 2$, $E^0 = 0.337$, and the concentration 1.0 mol L^{-1} solution, we obtain $E = 0.337 + (0.0592/2)$ $\log 1 = 0.337$ V, since $\log 1 = 0$. For the 0.1 mol L^{-1} solution, we obtain $E = 0.337 + (0.0592/2)\log\ 0.1 = 0.37$ V, since log 0.1 is −1. Using the same procedure for 0.01 and 0.001 mol L^{-1} solutions, we find that $E = 0.278$ and 0.248 V, respectively.

Example 1.2 Now calculate the reversible electrode potential of a Cu electrode for the conditions given in the Example 1.1, but use activities in Eq. (1.8) instead of concentrations. The mean activity coefficients of the above solutions, 1.0, 0.1, 0.01, and 0.001 are 0.043, 0.158, 0.387, and 0.700, respectively. Activities of these solutions are calculated using Eq. (1.5). For the 1.0 mol L^{-1} solution and $\gamma = 0.043$, we find that the activity of this solution is $a_{1.00} = \gamma c(Cu^{2+}) = 0.043 \times 1 = 0.043$. Activities for solutions 0.1,0.01, and 0.001 mol L^{-1} are 1.58×10^{-2}, 3.87×10^{-3}, and 7.00×10^{-4}, respectively.

Using Eq. (1.8) for the 1.00 mol L^{-1} solution, the reversible electrode potential at 25°C is $E = 0.337 + (0.0592/2)$ $\log\ 0.043 = 0.337 - 0.0400 = 0.297$ V. For 0.1, 0.01, and 0.001 mol L^{-1} solutions, the reversible electrode potentials at 25°C are 0.284, 0.266, and 0.244 V, respectively.

Hence Examples 1.1 and 1.2 illustrate that the effect of considering the activity coefficient in calculating electrode potential values is not substantial, and its effect decreases with a decrease in concentration, as seen in column 5 Table 1.2.

TABLE 1.2 Reversible Electrode Potential E of a Cu Electrode Immersed in a $CuSO_4$ Aqueous Solution

$CuSO_4$ Concentration, c (mol L^{-1})	E, V Calculated Using c	Activity, a	E, V Calculated Using a	ΔE, V
1.0	0.337	4.3×10^{-2}	0.297	0.040
0.1	0.307	1.58×10^{-2}	0.284	0.023
0.01	0.278	3.87×10^{-3}	0.266	0.012
0.001	0.248	7.00×10^{-4}	0.244	0.004

Note: See Example 1.2.

The difference ΔE in Table 1.2 is due to ion–ion interactions in the solution (1.1). The ion–ion interactions include interactions of the hydrated Cu^{2+} ions with one another and with SO_4^{2-} anions. In using concentration in Eq. (1.8) instead of activity, one thus neglects the ion–ion interactions.

In deposition of alloys it is frequently necessary to complex metal ions, as will be shown in Part B of this chapter. In this case the concentration or activity of metal ions in solution and the reversible electrode potential are calculated using the stability constant of the complex.

1.3 KINETICS AND MECHANISM OF ELECTRODEPOSITTON

1.3.1 Relationship between Current and Potential

When an electrode is made a part of an electrochemical cell through which current is flowing, its potential will differ from the equilibrium potential. If the equilibrium potential of the electrode (potential in the absence of current) is E and the potential of the same electrode as a result of current flowing is $E(I)$, then the difference η between these two potentials,

$$\eta = E(I) - E \tag{1.9}$$

is called *overpotential*.

An example of an electrochemical cell of industrial importance is shown in Figure 1.3. This figure shows how the potential $E(I)$ of a copper cathode in the etectrodeposition of copper can be measured using the three-electrode cell. The potential $E(I)$ of a Cu cathode, the test electrode, is measured versus a reference electrode (e.g., saturated calomel electrode), a Lugin capillary, and a high-input-impedance device (voltmeter) so that a negligible current is drawn through the reference electrode.

For large negative values of overpotentials ($\eta \geq 100$ mV) the current density i ($i = I/S$, where S is the surface area of the electrode) increases exponentially with the overpotential η according to the equation

$$i = -i_0 e^{-\alpha z f \eta} \tag{1.10}$$

and for large positive values of overpotential (anodic processes) according to the equation

$$i = -i_0 e^{(1-\alpha) z f \eta} \tag{1.11}$$

where i_0 is the exchange current density ($i_0 = i$ when $\eta = 0$), α the transfer coefficient, F the Faraday constant, R the gas constant, T the absolute temperature, and

$$f = \frac{F}{RT} \tag{1.12}$$

From Eqs. (1.10) and (1.11) it follows that, for $\eta = 0$, $i = i_0$ Thus, when an electrode is at equilibrium, there is a constant exchange of charge carriers (electrons or ions) across the metal–solution interphase (Eq. 1.1b).

At 25°C,

$$f = \frac{96487\ \text{C mol}^{-1}}{8.3144\ \text{J K}^{-1}\ \text{mol}^{-1} \times 298\ \text{K}} = 38.94\ \text{V} \tag{1.13}$$

since the Faraday constant $F = 96{,}487.0\ \text{C mol}^{-1}$, the gas constant $R = 8.3144\ \text{J mol}^{-1}\ \text{deg K}^{-1}$, and joules = volts × coulombs. These exponential relationships show that even small changes in η produce large changes in the current density, as seen from Figure 1.4. Taking the logarithm of Eqs. (1.10) and (1.11) and solving the resulting equations for η, one obtains the Tafel equation:

$$\eta = a \pm b \log|i| \tag{1.14}$$

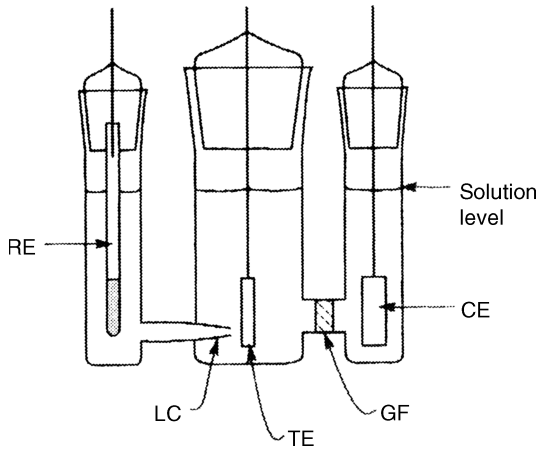

FIGURE 1.3 Three-component, three-electrode electrochemical cell: RE, reference electrode; LC, Lugin capilary; TE, test electrode; GF, glass frit; CE, counterelectrode.

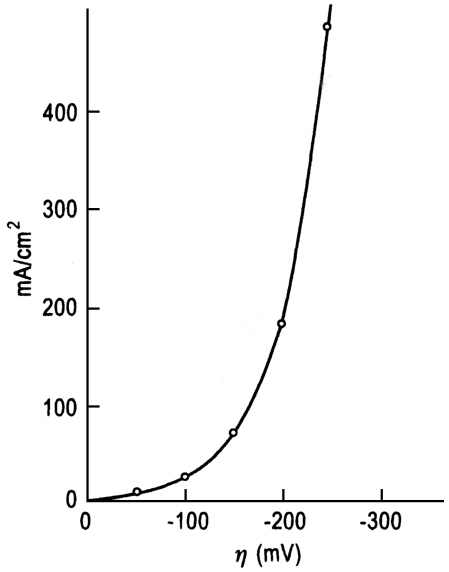

FIGURE 1.4 Exponential relationship between current density and overpotential for electrodeposition of copper from an aqueous solution of 0.15 N $CuSO_4$ and 1.0 N H_2SO_4.

where a and b are constants and $|i|$ is the absolute value of the current density. The $\pm$ sign holds for anodic and cathodic processes, respectively. The theoretical value of the constant a for the cathodic process (a_c), is

$$a_c = \frac{2.303RT}{\alpha zF} \log i_0 \tag{1.15}$$

and that of b_c is

$$b_c = \frac{2.303RT}{\alpha zF} \tag{1.16}$$

The use of Eqs. (1.10) and (1.14) is illustrated in Examples 1.3 and 1.4.

Example 1.3 Mattsson and Bockris [3] studied the electrodeposition of copper from the aqueous solution 0.15 N $CuSO_4$ and 1.0 N H_2SO_4 and determined that the exchange current density for this process is 3.7 mA cn^{-2} (3.7×10^{-3} A cm^{-2}). Using Eq. (1.10), we calculate the cathodic current densities i as a function of overpotential value of -50, -100, -150, -200, and -250 mV. For α we take the most frequent value, $\alpha = 0.5$, and for temperature, 25°C. Next we plot $i = f(\eta)$.

Using Eq. (1.10), we see that i (in A cm^{-2}) for $\eta = -50$ mV (-0.050 V) is

$$i = -i_0 e^{-\alpha f \eta} = (-3.7 \times 10^{-3}) e^{0.9737} = -9.80 \times 10^{-3}\,\text{A cm}^{-2}$$

since we have $-\alpha f \eta = -0.5 \times 38.94 \times (-0.050) = 0.9737$ and $e = 2.7183$. For $\eta = -100$ mV(0.100 V),

$$i = -i_0 e^{-\alpha f \eta} = (-3.7 \times 10^{-3}) e^{1.947} = -25.9 \times 10^{-3}\,\text{Acm}^{-2}$$

since we now have $-\alpha f \eta = -0.5 \times 38.94 \times (-0.100) = 1.947$.

In the same way we find i for the other η values. These are shown in Table 1.3.

The calculated values of η are used to plot the $i = f(\eta)$ function corresponding to this example Fig. 1.4. It again illustrates that even small increases in η result in large changes in the current density i.

TABLE 1.3 Current and Overpotential for Electrodeposition of Copper from Add Copper Sulfate Solution

Overpotential $-\eta$ (mV)	Current Density, i (mA cm^{-2})	log i
50	9.80	0.991
100	25.9	1.41
150	68.7	1.84
200	182	2.26

Note: See Example 1.3.

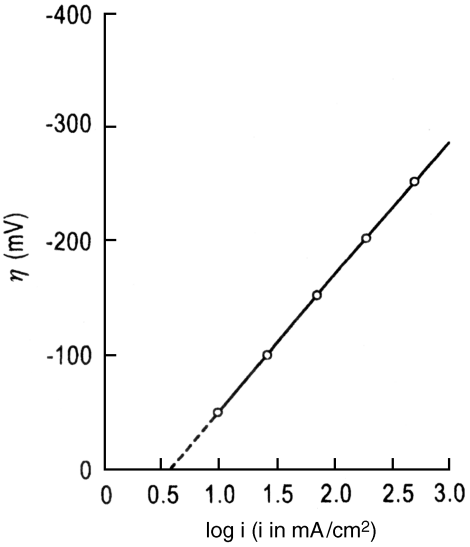

FIGURE 1.5 Tafel plot, $\eta = f(\log i)$, for electrodeposition of copper from the aqueous solution of 0.15 N $CuSO_4$ and 1.0 N H_2SO_4.

Example 1.4 Using the calculated values of i for the given values of η from Table 1.3 plot the corresponding Tafel equation, $\eta = f$ (log i).

The solution is given in Figure 1.5. It shows that for large values of $\eta (\eta \geq 100\,\text{mV})$ the function $\eta = f$ (log i) is a straight line. The experimentally determined cathodic and anodic Tafel lines for electrodeposition of copper in acid copper sulfate solution are shown in Figure 1.6. The figure shows that the transfer coefficients for the anodic and cathodic processes are different and that the extrapolated value of i at $\eta = 0$ gives the exchange currenty density. The transfer coefficient α_c for the cathodic process (deposition of Cu^{2+}) is obtained from the slope $d\eta/d(\log i)$ of the cathodic Tafel line. That for the anodic process, α_a, is obtained from the slope of the Tafel line for the anodic process.

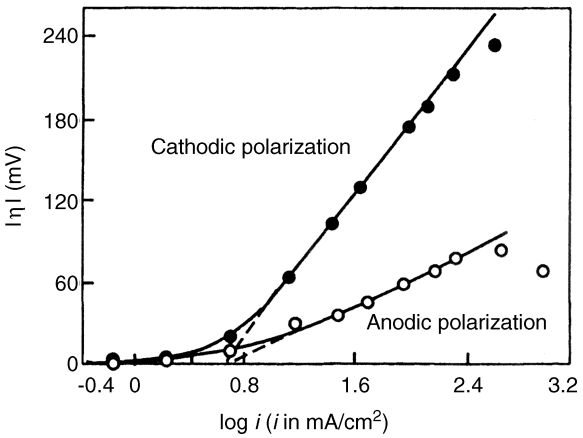

FIGURE 1.6 Current–potential relationship for the electrodeposition of copper from an acid $CuSO_4$ solution. (From J. O'M. Bockris, in *Transactions of the Symposium on Electrode Processes*, E. Yeager, Ed., Wiley, New York, 1961, with permission from the Electrochemical Society.)

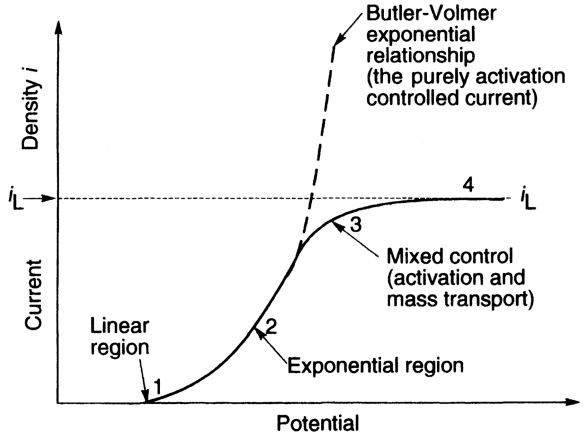

FIGURE 1.7 Four regions in the general current–overpotential relationship: 1, linear; 2, exponential; 3, mixed control; 4, limiting current density region.

1.3.2 Influence of Mass Transport on Electrode Kinetics

The current–potential relationship defined by Eqs. (1.10, 1.11) and (1.14) is valid for the case where the charge transfer, Eq. (1.1), is the slow process (rate-determining step). This relationship has a limit where the rate of deposition reaction is limited by transport of M^{z+} ions. A general current–potential relationship is shown in Figure 1.7. The limiting, or maximum, current density is given by [4]

$$i_L = \frac{nFD}{\delta} c_b \tag{1.17}$$

where D is the diffusion coefficient of the depositing species M^{z+}, c_b is the bulk concentration of M^{z+} ions in the solution, δ is the diffusion layer thickness, n the number of electrons involved in the reaction, and F the Faraday constant. The diffusion layer thickness δ is defined by the Nernst diffusion layer model illustrated in Figure 1.8. This model assumes that the concentration of M^{z+} ions has a bulk concentration c_b up to a distance δ from the electrode surface and then falls off linearly to $c_{x=0}$ at the electrode surface. In this model it is assumed that the liquid layer of thickness δ is practically stationary (quiescent). At a distance greater than δ from the surface, the concentration of the reactant M^{z+} is assumed to be equal to that in the bulk. At these distances, $x > \delta$, stirring is efficient. Ions M^{z+} must diffuse through the diffusion layer to reach the electrode surface.

At the values of the limiting (maximum) current density the species M^{z+} are reduced as soon as they reach the electrode. At these conditions the concentration of the reactant M^{z+} at the electrode is nil, and the rate of deposition reaction is controlled by the rate of transport of the reactant M^{z+} to the electrode. If an external current greater than the limiting current i_L is forced through the electrode, the double

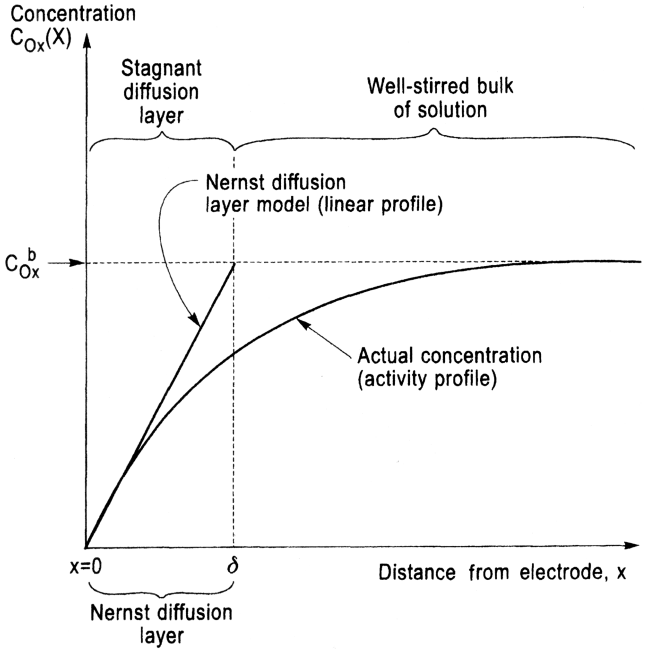

FIGURE 1.8 Variation of the concentration of the reactant during non-steady-state electrolysis; c_{Ox}^{b} is the concentration in the bulk; $c_{Ox}(x)$ is the concentration at the surface.

layer is further charged, and the potential of the electrode will change until some other process, other than reduction of M^{z+}, can occur. It will be shown later that the limiting current density is of great practical importance in metal deposition since the type and quality of metal deposits depend on the relative values of the deposition current and the limiting current. One extreme example is shown in Figure 1.9.

Example 1.5 Calculate the diffusion limiting current density i_L for the deposition of a metal ion M^{2+} at a cathode in a quiescent (unstirred) solution assuming the diffusion

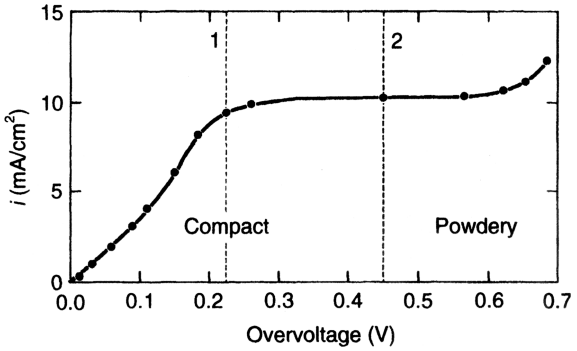

FIGURE 1.9 Overpotential characteristic of transition from compact to powdery deposit in electrodeposition of Cu from $CuSO_4$ (0.1 M) + H_2SO_4 (0.5 M) solution. (From N. Ibl, in *Advances in Electrochemistry and Electrochemical Engineering*, Vol. 2, C. W. Tobias, Ed., Wiley, New York, 1962, with permission from Wiley.)

layer thickness δ is 0.05 cm. The concentration of M^{2+} ions in the bulk (c_b) is 10^{-2} mol L^{-1} (10^{-5} mol cm^{-3}) and the diffusion coefficient D of M^{2+}, in the unstirred solution, is 2×10^{-5} cm^2 s^{-1}.

Using Eq. (1.17), we calculate that the limiting diffusion current density for this case is

$$i_L = \frac{nFD}{\delta} c_b = \frac{2 \times 96487 \times 2 \times 10^{-5} \times 10^{-5}}{0.05}$$
$$= 7.72 \times 10^{-4} \text{ A cm}^{-2} = 0.72 \text{ mA cm}^{-2}$$

In the same way we find that, for $c_b = 10^{-1}$ mol L^{-1} (10^{-4} mol cm^{-3}), $i_L = 7.20$ mA cm^{-2}.

In the stirred electrolyte solution the diffusion layer thickness δ and the limiting current density i_L depend on the nature of stirring.

For a rotating electrode the diffusion layer thickness depends on the angular speed of rotation ω according to

$$\delta = \frac{1.61 D^{1/6} \nu^{1/6}}{\sqrt{\omega}} \tag{1.18}$$

and the limiting current density depends on ω according to

$$i_L = \frac{0.62 nFaD^{2/3} c}{\nu^{1/6}} \sqrt{\omega} \tag{1.19}$$

where D is the diffusion coefficient, ν the kinematic viscosity (the coefficient of viscosity/density of the liquid), ω the rotation angular speed (in radians per second), c the concentration of the solution, and a the disc surface area [4]. We use these equations in the next two examples.

Example 1.6 Determine the diffusion layer thickness for a rotating electrode at 60, 240, and 360 rpm. For kinematic viscosity ν use 10^{-2} cm^2 s^{-1} and for the diffusion coefficient D use 10^{-5} cm^2 s^{-1}.

For the above given values for ν and D, Eq. (1.18) becomes

$$\delta = \frac{1.61 \times 10^{-2}}{\sqrt{\omega}} = \frac{1.61 \times 10^{-2}}{\sqrt{2\pi N}}$$

In the above equation the rotation speed w in radians per second is replaced by $\omega = 2\pi N$, where N is the number of rotations per second, rps.

Applying the above equation for $N = 1$ rps (60 rpm), one gets $\delta = 64$ μm. For $N = 4$ rps (240 rpm), $\delta = 32$ μm, and for $N = 6$ rps (360 rpm), $\delta = 26$ μm.

Example 1.7 Calculate the limiting current density i_L for the deposition of a metal ion M^{2+} at a rotating disc cathode with a surface area $a = 1$ cm^2 and the rotating speed 300 rpm (5 rps) using Eq. (1.19) assuming that the concentration of M^{2+} is 10^{-5} mol cm^{-3} (10^{-2} mol L^{-1}). The diffusion coefficient D of M^{2+} is 2×10^{-5} cm^2, $\nu = 10^{-5}$ cm^2 s^{-1}.

Substitution of the above given values for a, D, and ν into Eq. (1.19) yields

$$i_L = (1.91 \times 10^2) c \sqrt{\omega}$$

For $c = 10^{-2}$ mol $L^{-1} = 10^{-5}$ mol cm^{-3} and $\omega = 2\pi N = 31.41$

$$i_L = 1.07 \times 10^{-2} \text{ A cm}^{-2} = 10.7 \text{ mA cm}^{-2}$$

This value should be compared with the i_L value for a quiescent (unstirred) solution in Example 1.5.

1.3.3 Faraday's Law

Faraday's law states that the amount of electrochemical reaction that occurs at an electrode is proportional to the quantity of electric charge Q passed through an electrochemical cell. Thus, if the weight of a product of electrolysis is w, then Faraday's law states that

$$w = ZQ \tag{1.20}$$

where Z is *the electrochemical equivalent*, the constant of proportionality. Since Q is the product of the current I in amperes and the elapsed time t in seconds,

$$Q = It \tag{1.21}$$

$$w = ZIt \tag{1.22}$$

According to Faraday's law the production of one gram equivalent of a product at the electrode, W_{eq}, in a cell requires 96,487 C. The constant 96,487 is termed the Faraday *constant F*. The coulomb (C) is the quantity of electricity transported by the flow of one ampere for one second.

The Faraday constant represents one mole of electrons and its value can be calculated from

$$F = N_A e \tag{1.23}$$

where N_A is Avogadro's number (6.0225×10^{23} molecules mol^{-1}) and e is the charge of a single electron (1.6021×10^{-19} C):

$$F = (6.0225 \times 10^{23})(1.6021 \times 10^{-19}) = 96,487 \text{ C mol}^{-1} \tag{1.24}$$

One equivalent, w_{eq}, is that fraction of a molar (atomic) unit of reaction that corresponds to the transfer of one electron. For example, w_{eq} for silver is the gram atomic

weight of silver, since the reduction of Ag^+ requires one electron. The deposition of copper from a Cu^{2+} salt involves two electrons, and the w_{eq} for Cu is (gram atomic weight of Cu)/2. In general,

$$w_{eq} = \frac{A_{wt}}{n} \tag{1.25}$$

where A_{wt} is the atomic weight of metal deposited on the cathode and n the number of electrons involved in the deposition reaction.

From Eqs. (1.20) and (1.22) it follows that when $Q = 1$ C, or $Q = 1$ A s, then

$$w_{Q=1} = Z \tag{1.26}$$

Thus the electrochemical equivalent of a metal M, Z(M), is the weight in grams produced, or consumed, by one coulomb (one ampere second). The combination of Eqs. (1.20) and (1.26) yields

$$w = w_{Q=1}Q \tag{1.27}$$

The value of Z, or $w_{Q=1}$, can be evaluated in the following way. Since 96,487 C is required for the deposition of an equivalent of a metal, w_{eq}, from Eq. (1.20) it follows that

$$w_{eq} = 96,487Z \tag{1.28}$$

and

$$Z = w_{Q=1} = \frac{w_{eq}}{96,487} = \frac{w_{eq}}{F} \tag{1.29}$$

Since $w_{eq} = A_{wt}/n$ [Eq. (1.25)],

$$Z = \frac{A_{wt}}{nF} \tag{1.30}$$

Finally, from Eqs. (1.20) and (1.30)

$$w = ZQ = \frac{A_{wt}}{nF}Q \tag{1.31}$$

Example 1.8 Determine the electrochemical equivalent of Cu for the case of electrodeposition of Cu from Cu^{2+} solutions. The atomic weight of Cu is 63.55.

From Eq. (1.29),

$$Z(Cu^{2+}) = \frac{A_{wt}Cu}{nF} = \frac{63.55}{2 \times 96,487} = 3.293 \times 10^{-4}\ gC^{-1}$$

Example 1.9 A current of 300 mA was passed for 20 min through an electrochemical cell containing copper electrodes in H_2SO_4 acidified $CuSO_4$ aqueous solution. Calculate the amount of copper deposited at the cathode. The gram atomic weight of Cu is 63.55.

In order to calculate w using Eq. (1.31), we find first the number of coulombs Q, the quantity of electricity passed during the electrolysis,

$$Q = It = 0.300A \times 1200\ s = 360\ As = 360\ C$$

The number of electrons n involved in the Cu deposition reaction

$$Cu^{2+} + 2e = Cu$$

is 2. Substituting these values into Eq. (1.31), we get the amount of Cu deposited at the electrode,

$$w = \frac{63.55 \times 360}{2 \times 96,487} = 0.118g$$

Alternatively, using the value of the electrochemical equivalent for Cu, $Z(Cu^{2+}) = 3.293 \times 10^{-4}$ g C^{-1}, and Eq. (1.31), we get

$$w = ZQ = 3.293 \times 10^{-4} \times 0.300 \times 1200 = 0.118g$$

1.3.4 Current Efficiency

When two or more reactions occur simultaneously at an electrode, the number of coulombs of electricity passed corresponds to the sum of the number of equivalents of each reaction. For example, during deposition of Cu from a solution of cupric nitrate in dilute nitric acid, three cathodic reactions occur: the deposition of Cu (the reduction of cupric ions) and the reduction of both nitrate and hydrogen ions.

The current efficiency CE of the jth process, namely of any one of the simultaneous reactions, is defined as the number of coulombs required for that reaction, Q_j, divided by the total number of coulombs passed, Q_{total}:

$$CE = \frac{Q_j}{Q_{total}} \tag{1.32}$$

An alternative equation defining current efficiency is

$$CE = \frac{w_j}{w_{total}} \tag{1.33}$$

where w_j is the weight of metal j actually deposited and w_{total} is that which would have been deposited if all the current had been used for depositing metal j.

Thus, in general, at a current efficiency under 100%, the remainder of the current is used in side processes, such as the reduction of hydrogen and nitrate ions in the example above.

Example 1.10 When a current of 3 A flows for 8 min through a cell composed of two Pt electrodes in a solution of $Cu(NO_3)_2$ in dilute HNO_3 acid, 0.36 g of Cu is deposited on the cathode. Calculate the current efficiency for the deposition of copper.

The number of coulombs required for deposition of 0.36 g of Cu is obtained from Eq. (1.31):

$$Q_j = \frac{wn \times 96,487}{A_{wt}} = \frac{0.36 \times 2 \times 96,487}{63.55} = 1093$$

$$Q_{total} = It = 3 \times 480 = 1440$$

and

$$\text{CE} = \frac{Q_j}{Q_{total}} = \frac{1093}{1440} = 0.759 \text{ or CE} = 75.9\%$$

1.3.5 Deposit Thickness

The deposit thickness may be evaluated by considering the volume of the deposit. Since the volume of the deposit V is the product of the plated surface area a and the thickness (height) h, it follows that $h = V/a$. The volume of the deposit is related to the weight of the deposit w and the density of the deposit d by the relationship defining the density, $d = w/V$. Thus

$$h = \frac{V}{a} = \frac{w}{ad} \tag{1.34}$$

In the case where it is necessary to calculate the time t (in seconds) required to obtain the desired deposit thickness h at a given current density, we introduce Faraday's law [Eq. (1.31)], into Eq. (1.34) and obtain

$$h = \frac{w}{ad} = \frac{ZQ}{ad} = \frac{ZIt}{ad} \text{ cm} \tag{1.35}$$

$$t = \frac{had}{ZI} \text{ s} \tag{1.36}$$

Example 1.11 The weight of a Co deposit is 0.00208 g on a substrate with surface area of 7.5 cm^2. What is the thickness of the Co deposit. Remember that the density of Co is 8.71 g cm^{-3}.

Using Eq. (1.34), we have that

$$h = \frac{0.00208}{7.5 \times 8.71} = 3.184 \times 10^{-5} \text{ cm} = 3184\text{Å}$$

Example 1.12 Determine the time required to obtain a Cu deposit of thickness 1 μm (10^{-4}cm) when electrodeposition is done at 4 and 6 A. The surface area a of the substrate is 314 cm^2.

From Eq. (1.36), for $I = 4$A,

$$t = \frac{had}{ZI} = \frac{10^{-4} \times 314 \times 8.93}{3.29 \times 10^{-4} \times 4} = 213 \text{ s} = 3 \text{ min}, 33 \text{ s}$$

for $I = 6$A, in the same way, one obtains that $t = 142$ s = 2 min, 22 s.

1.3.6 Atomistic Aspects of Electrodeposition

In the electrodeposition of metals, generally a metal ion M^{z+} is transferred from the solution into the ionic metal lattice. A simplified atomistic representation of this process is

$$M^{z+}(\text{solution}) \rightarrow M^{z+}(\text{lattice}) \tag{1.37}$$

This reaction is accompanied by the transfer of z electrons from an external electron source (e.g., power supply) to the electron gas in the metal M.

Before discussing the individual atomistic processes that make up the overall electrodeposition process, [Eq. (1.37)], it is necessary to consider the basic characteristics of the bulk and the surface structures of metals [1]. A metal may be considered to be a fixed lattice of positive ions permeated by a gas of free electrons. Positive ions are the atomic cores, while the negative charges are the valence electrons. For example, the copper atom has a configuration (electronic structure) $1s^2 2s^2 2p^6 3s^2 3p^6 3d^{10} 4s^1$ (the superscripts indicate the number of electrons in the orbitconfiguration) with a single valence electron (4s). The atomic core of Cu^+ has the set of configurations given above less the one valence electron $4s^1$. The free electrons form what is known as the *electron gas* in the metal, and they move nearly freely through the volume of the metal. Each metal atom thus contributes its single valence electron to the electron gas in the metal. Interactions between the free electrons and the metal ions are largely responsible for the metallic bond.

Surfaces may be divided into ideal and real. Ideal surfaces exhibit no surface lattice defects (vacancies, impurities, grain boundaries, dislocations, etc.). Real surfaces have a variety of defects. For example, the density of metal surface atoms is about $10^{15} cm^{-2}$, while the density of dislocations is of the order of $10^8 cm^{-2}$. The structure of real surfaces differs from those of ideal surfaces by surface roughness. While an ideal surface is atomically smooth, a real surface may have defects, steps, kinks, vacancies, and clusters of adatoms (Fig. 1.10).

The atomic processes that make up the electrodeposition process [Eq. (1.37)] can be viewed considering the structure of the initial, M^{z+} (solution), and the final state, M^{z+} (lattice). Since metal ions in an aqueous solution are hydrated, the structure of the initial state in Eq. (1.37) should be

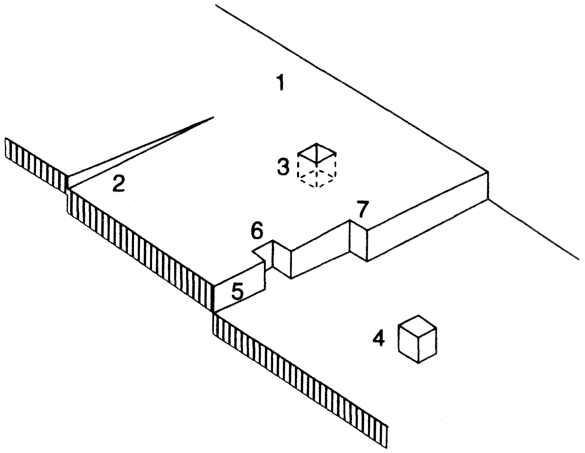

FIGURE 1.10 Some simple defects found on a low-index crystal face: 1, perfect flat face, terrace; 2, an emerging screw dislocation; 3, a vacancy in the terrace; 4, an adatom on the terrace; 5, a monatomic step in the surface, a ledge; 6, a vacancy in the ledge; 7, a kink, a step in the ledge.

represented by $[M(H_2O)_x]^{z+}$. The structure of the final state is an M adion (adatom; adsorbed ion, atom) at a kink site (Fig. 1.11), since it is generally assumed that atoms (ions) are attached to a crystal via a kink site [1]. Thus the final step of the overall reaction [Eq. (1.37)] is the incorporation of the M^{z+} adion into the kink site. Because of surface inhomogeneity, the transition from the initial state $[M(H_2O_x)]^{z-}$ (solution) to the final state M^{z+} (kink),

$$[M(H_2O)_x]^{z+}\,(\text{solution}) \rightarrow M^{z+}\,(\text{kink}) \qquad (1.38)$$

may proceed via either of the two mechanisms: (1) step-edge site ion transfer or (2) terrace site ion transfer.

Step-Edge Ion-Transfer Mechanism The step-edge site ion transfer, or direct transfer mechanism, is illustrated in Figure 1.12. As the figure shows, this mechanism ion transfer from the solution takes place on a kink site of a step edge or on any other site on the step edge. In both cases the result of

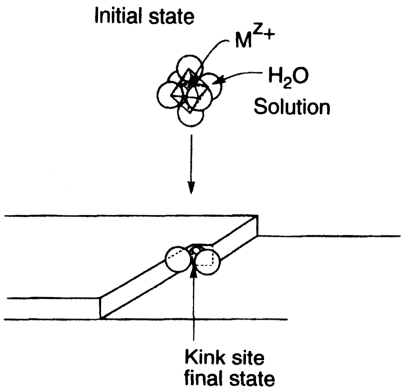

FIGURE 1.11 Initial and final states in metal deposition.

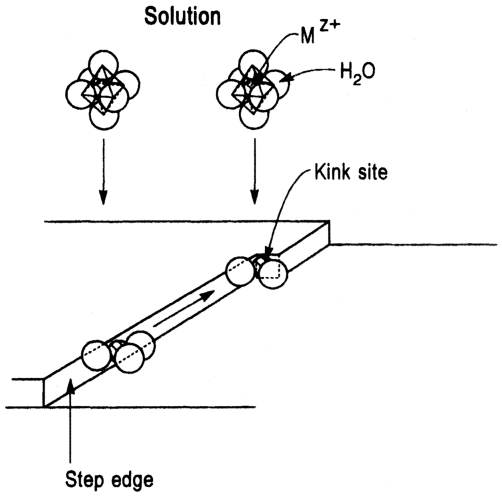

FIGURE 1.12 Step-edge ion-transfer mechanism.

the ion transfer is an M adion in the metal crystal lattice. In the first case of a direct transfer to the kink site, the M adion is in the half-crystal position, where it is bonded to the crystal lattice with one-half of the bonding energy of the bulk ion. Thus the M adion belongs to the bulk crystal. However, it still has some water of hydration (Fig. 1.12). In the second case of a direct transfer to the step-edge site other than a kink, the transferred metal ion diffuses along the step edge until it finds a kink site (Fig. 1.12). Thus, in a step-edge site transfer mechanism, there are two possible paths: direct transfer to a kink site and the step-edge diffusion path.

Terrace Ion-Transfer Mechanism In the terrace site transfer mechanism a metal ion is transferred from the solution to the flat face of the terrace region (Fig. 1.13). At this position the metal ion is in the adion (adsorbedlike) state having most of the water of hydration. It is weakly bound to the crystal lattice. From this position it diffuses on the surface, seeking a position of lower energy. The final position is a kink site.

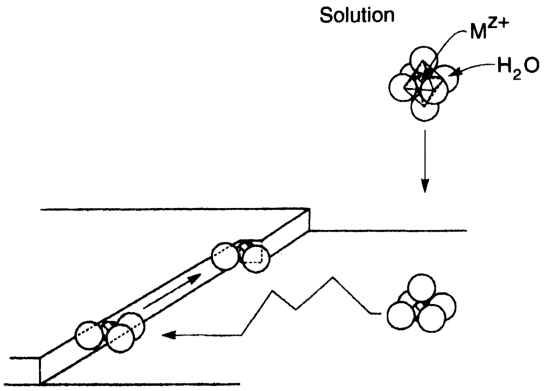

FIGURE 1.13 Ion transfer to a terrace site, surface diffusion, and incorporation at kink site.

In view of these two mechanisms—the step edge and terrace ion transfer—the overall current density i is considered to be composed of two components:

$$i = i_{se} + i_{te} \tag{1.39}$$

where i_{se} and i_{te} are the step-edge and terrace site current density components, respectively.

The initial theoretical treatment of these mechanisms of deposition was given by Lorenz [5–8], The initial experimental studies on surface diffusion were published by Mehl and Bockris [9, 10]. Conway and Bockris [11, 12] calculated the activation energies for the ion-transfer process at various surface sites, Simulation of crystal growth via surface diffusion was discussed by Gilmer and Bennema [13].

1.3.7 Pulse Deposition Techniques

One important effect in pulse deposition techniques is a modification of the diffusion layer [14]. The Nernst diffusion layer model is illustrated in Figure 1.8 and described in Section 1.3.2. Under pulse deposition conditions the Nernst diffusion layer is split into two diffusion layers, as is schematically shown in Figure 1.14. In the pulsating diffusion layer, which is in the immediate vicinity of the cathode, the metal ion concentration pulsates with the frequency of the pulsating current [14]. Pulse deposition techniques are used mostly to improve the distribution of the deposit (current distribution), the leveling, and the brightness of the deposit [15].

The four major waveforms that are used in pulse deposition techniques are shown in Figure 1.15. In the *rectangular-pulse deposition* technique the waveform consists of pulses of a current or potential of a rectangular shape separated by intervals of zero current or potential. The shape of this waveform is shown in Figure 1.15*a*. where I or E is

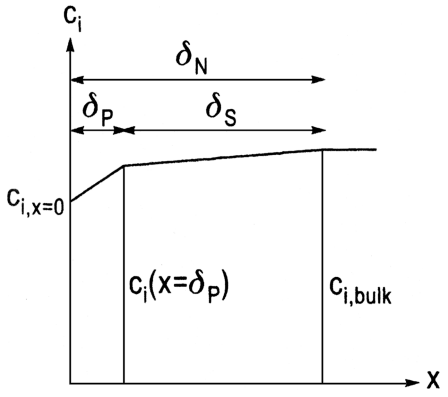

FIGURE 1.14 Schematic concentration profile at the cathode for pulse plating conditions: δ_p, pulsating diffusion layer thickness; δ_s, stationary diffusion layer thickness; δ_N, Nernst diffusion layer thickness.

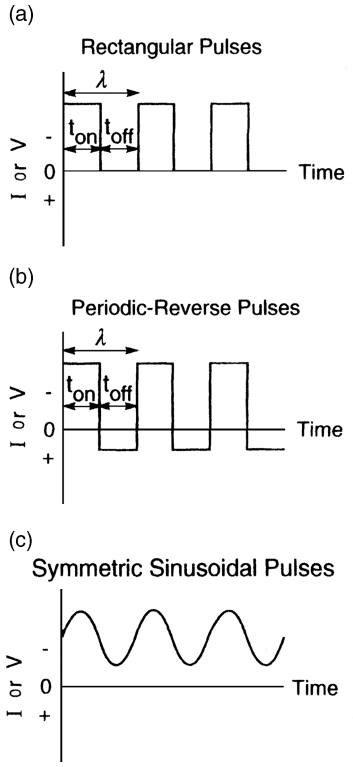

FIGURE 1.15 Three major waveforms used in pulse deposition: t_{on}, the on period of a pulse; t_{off}, the off period; λ, the cycle time; t_c, the cathodic pulse period; t_a, the anodic pulse period.

the maguitude of the applied current or potential, t_{on} is the on period of a pulse, t_{off} is the off period, and λ is the cycle time. The waveform of *periodic reverse deposition* is shown in Figure 1.15*b*. It is seen that in this technique the applied current or potential is periodically switched from cathodic to anodic polarization; t_c is the cathodic pulse period, t_a the anodic pulse period, and λ the cycle time.

A *superimposed sinusoidal deposition* waveform is shown in Figure 1.15*c*. This waveform is the sum of a sinusoidal alternating (ac) wave, current or potential, and a direct cathodic current (dc). If the amplitude of the sine wave is greater than the dc offset, then the waveform consists of both a cathodic and an anodic portion.

There is now increased interest in pulse deposition techniques because of recently published data on the beneficial use of pulse plating in the fabrication process of integrated circuits [16].

1.4 GROWTH MECHANISM

There are two basic mechanisms for formation of a coherent deposit [1, 17]: layer growth and three-dimensional (3D) crystallite growth (or nucleation–coalescence growth). A schematic illustration of these two mechanisms is given in Figure 1.16.

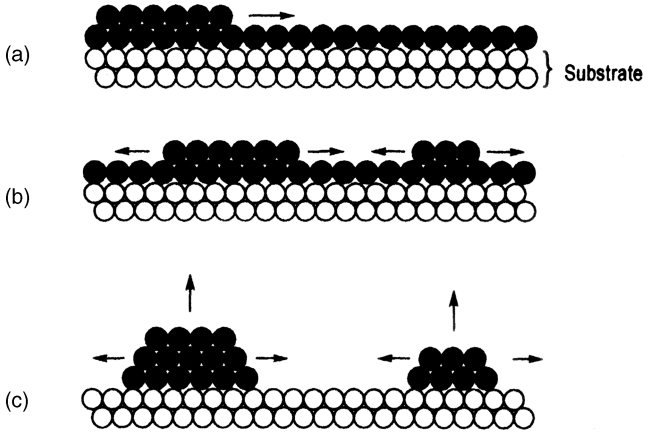

FIGURE 1.16 Schematic representation of layer growth (*a, b*) and the nucleation–coalescence mechanism (*c*).

In the layer growth mechanism a crystal enlarges by a spreading of discrete layers (steps), one after another across the surface. In this case a growth layer, a step, is a structure component of a coherent deposit. Steps, or growth layers, are the structural components for the construction of a variety of growth forms in the electro-deposition of metals (e.g., columnar crystals, whiskers, and fiber texture). We can distinguish among monoatomic steps, polyatomic microsteps, and polyatomic macrosteps. In general, there is a tendency for a large number of thin steps to bunch into a system of a few thick steps. Many monoatomic steps can unite (bunch, coalesce) to form a polyatomic step.

In the 3D crystallite growth mechanism the structural components are 3D crystallites, and a coherent deposit is built up as a result of coalescence (joining) of these crystallites. The growth sequence of electrodeposition via nucleation–coalescence consists of four stages: (1) formation of isolated nuclei and their growth to TDC (three dimensional crystallites), (2) coalescence of TDC, (3) formation of linked network, and (4) formation of a continuous deposit.

Development of Columnar Microstructure The columnar microstructure is perpendicular to the substrate surface, as shown schematically in Figure 1.17. This microstructure is composed of relatively fine grains near the substrate but then changes to a columnar microstructure with much coarser grains at greater distances from the substrate. The development of the columnar microstructure may be interpreted as the result of growth competition among adjacent grains. The low-surface-energy grains grow faster than the high-energy ones. This rapid growth of the low-surface-energy grains at the expense of the high-energy grains results in an increase in mean grain size with increased thickness of deposit and the transition from a fine grain size near the substrate to a coarse, columnar grain size [1, 18].

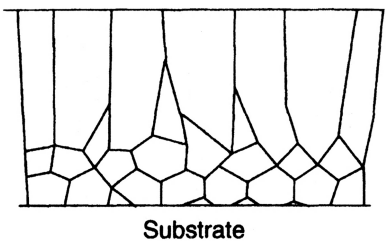

FIGURE 1.17 Schematic cross section (perpendicular to the substrate) of the columnar deposit.

Overpotential Dependence of Growth Forms The development of growth forms on overpotentials stems from the potential dependence of the nucleation and growth processes. Competition between nucleation and growth processes is strongly influenced by the potential of the cathode [1, 19].

1.4.1 Effect of Additives

Additives affect deposition and crystal-building processes as adsorbates (adsorbed substances) at the surface of the cathode. There are two basic types of adsorption: chemisorption (an abreviation of *chemical adsorption*) and physisorption (an abreviation of *physical adsorption*). In chemisorption the chemical attractive forces of adsorption act between the surface and the absorbate (usually these are covalent bonds). Thus there is a chemical combination between the substrate and the adsorbate where electrons are shared and/or transferred. New electronic configurations may be formed through this sharing of electrons. In physisorption the physical forces of adsorption, van der Waals or electrostatic forces, act between the surface and the adsorbate; there is no electron transfer and no electron sharing.

The adsorption energy for chemisorbed species is greater than that for physisorbed species. Typical values for chemisorption are in the range of 20–100 kcal mol^{-1} and for physisorption, around 5 kcal mol^{-1}.

1.4.2 Effect of Additives on Nudeation and Growth

Adsorbed additives affect the kinetics of electrodeposition and the growth mechanism by changing the concentration of growth sites on a surface, the concentration of adions on the surface, the diffusion coefficient D, and the activation energy of surface diffusion of adions. In the presence of adsorbed additives the mean free path for lateral diffusion of adions is diminished, which is equivalent to a decrease in the diffusion coefficient D (diffusivity) of adions. This decrease in D may result in an increase in adion concentration at steady state and thus an increase in the frequency of the two-dimensional nucleation between diffusing adions.

Additives can also influence the propagation of microsteps and cause bunching and the formation of macrosteps.

The type of deposit obtained at constant current density may depend on the surface coverage of additives.

1.4.3 Leveling

Leveling is defined as the progressive reduction of the surface roughness during deposition. Surface roughness may be the result of mechanical polishing. In this case scratches on the cathode represent the initial roughness and the result of cathodic leveling is a smooth (flat) deposit or a deposit of reduced roughness. During this type of leveling more metal is deposited in recessed areas than on peaks (bumps). This leveling is of great value in the metal-finishing industry. Leveling can be achieved in solutions either in the absence of addition agents or in the presence of leveling agents. Thus there are two types of leveling processes: (1) geometric leveling corresponding to leveling in the absence of specific agents and (2) true or electrochemical leveling corresponding to leveling in the presence of leveling agents.

Dukovic and Tobias [20] and Madore and Landolt [21] developed theoretical models of leveling during electrodeposition in both the absence and presence of additives. Both models indicate that a significant leveling of semicircular and triangular grooves by uniform current distribution (geometric leveling) is achieved when the thickness of deposit is at least equal to to the depth of the groove. Leveling in the presence of leveling agents (true leveling) is achieved at much lower deposit thickness.

Theories of leveling by additives are based on (1) the correlation between an increase in the polarization produced by the leveling agents [22] and (2) preferential adsorption of a leveling agent on the high point (peaks of the substrate or flat surfaces) and by this inhibition (slowing down) of deposition at these points [1, 23].

1.4.4 Brightening

The brightness of a surface is defined as the optical reflecting power of the surface. It is measured by the amount of light specularly reflected (Fig. 1.18). Weil and Paquin [24] showed a linear relationship between the logarithm of the amount of light specularly reflected by a surface and the fraction of the surface having roughness of less than 1500 Å. Kardos and Foulke [23] distinguish three possible mechanisms for bright deposition: (1) diffusion-controlled leveling, (2) grain refining, and (3) randomization of crystal growth. Some fundamental aspects of brightening and leveling are reviewed by Oniciu and Muresan [25].

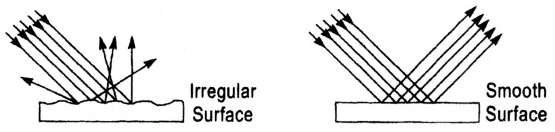

FIGURE 1.18 Diffuse and specular reflection. The surface of the object that has irregularities diverges out an initially parallel beam of light in all directions to produce diffusion reflection (*a*). A smooth, bright surface specularly reflects a parralel beam of light in one direction only (*b*).

1.4.5 Consumption of Additives

An additive can be consumed at the cathode by incorporation into the deposit and/or by the electrochemical reaction at the cathode or anode. Consumption of coumarin in the deposition of nickel from the Watts-type solution was studied extensively. For example, Rogers and Taylor [26] found that the coumarin concentration decreases linearly with time and that the rate of coumarin consumption is a function of concentration. The rate of consumption increases with increase in the bulk concentration of the coumarin. Thus, in the electrodeposition of nickel from a Watts-type solution, the total current density is the sum of the current densities for nickel deposition, hydrogen evolution, and additive reduction.

In general, the control of an electrodeposition solution involves monitoring the concentration of additives and by-products of the reaction of additives at the electrodes.

1.5 ELECTROLESS AND DISPLACEMENT DEPOSITION

Electroless and displacement depositions have one basic characteristic in common: No power supply is necessary to drive the deposition reaction

$$M^{z+}_{solution} + ze \xrightarrow{\text{electrode}} M_{lattice} \tag{1.40}$$

In the electroless deposition process z electrons are supplied by a reducing agent, Red, present in the solution. The electron-donating species Red donates electrons to the catalytic surface. In the displacement deposition process z electrons are supplied by the substrate; the substrate S is the electron-donating species.

In general, an electrode with lower electrode potential in Table 1.1 will reduce ions of an electrode with higher electrode potential (Fig. 1.19).

1.5.1 Electroless Deposition

The overall reaction of electroless metal deposition is

$$M^{z+}_{solution} + Red_{solution} \xrightarrow{\text{catalytic surface}} M_{lattic} + OX_{solution} \tag{1.41}$$

where Ox is the oxidation product of the reducing agent Red. The catalytic surface may be the substrate S itself or catalytic

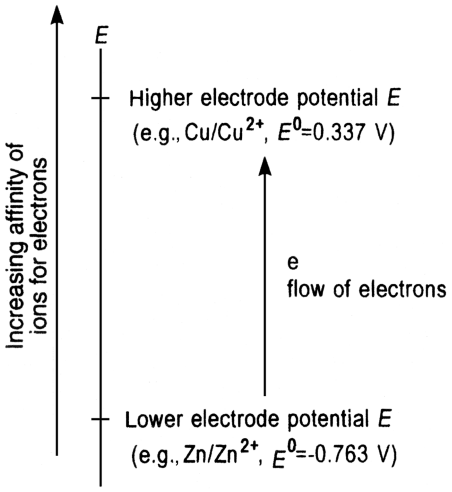

FIGURE 1.19 An electrode with lower electrode potential will reduce ions of an electrode with higher electrode potential.

nuclei of the metal M dispersed on a noncatalytic substrate surface. The reaction represented by Eq. (1.41) must be conducted in a way such that a homogeneous reaction between M^{z+} and Red, in the bulk of the solution, is suppressed.

According to the mixed-potential theory of electroless deposition [27–29] the overall reaction given by Eq. (1.41) can be decomposed into one reduction reaction, *the cathodic partial reaction*

$$M^{z+}_{solution} + ze \xrightarrow{\text{catalytic surface}} M_{lattice} \qquad (1.42)$$

and one oxidation reaction, *the anodic partial reaction*

$$Red_{solution} \xrightarrow{\text{catalytic surface}} Ox_{solution} + me \qquad (1.43)$$

Thus the overall reaction, [Eq. (1.41)] is the result of the combination of two different partial reactions, Eqs. (1.42) and (1.43). These two partial reactions, however, occur at one and the same electrode, the same metal–solution interphase. In order that the overall electroless deposition reaction may proceed, the equilibrium (rest) potential of the reducing agent, $E_{eq,Red}$ [Eq. (1.43)], must be more negative than that of the metal electrode, $E_{eq,M}$ [Eq. (1.42)], so that the reducing agent Red can function as an electron donor and M^{2+} as an electron acceptor. This is in accord with the discussion in Section 1.5.1.

Evans Diagram According to the mixed-potential theory, the overall reaction of the electroless deposition can be described electrochemically in terms of two current–potential *(i–E)* curves, as shown schematically in Figure 1.20. This figure shows a general Evans diagram with current–potential functions $i = f(E)$ for the individual electrode processes [Eqs. (1.42) and (1.43)]. In this the sign of the current density is supressed. According to this presentation of the mixed-potential theory, the current–potential curves for the individual processes $i_{cathodic} = i_M = f(E)$ and $i_{anodic} = i_{Red} = f(E)$ intersect. The coordinates of this intersection have the following meaning: (1) the abscisa, the current density of the intersection, is the deposition current density i_{dep} (i.e., log i_{dep}), that is, the rate of electroless deposition in terms of milliamperes per centimeter squared, and (2) the ordinate, the potential of the intersection, is the mixed potential, E_{mp}.

Mixed Potential, E_{mp} When a catalytic surface S is introduced into an aqueous solution containing M^{z+} ions and a reducing agent, the partial reaction of reduction [Eq. (1.42)] and the partial reaction of oxidation [Eq. (1.43)] occur simultaneously. Each of these partial reactions strives to establish its own equilibrium potential, E_{eq}. The result of this "competition" is the creation of a steady state with the compromised potential called the *steady-state mixed potential,* E_{mp}. The result of this mixed potential is that the potential of the redox couple Red/Ox [Eq. (1.43)] is raised anodically from the reversible value $E_{eq,Red}$ (Fig. 1.20), and the potential of the metal electrode M/M^{z+} Eq. (1.42) is depressed cathodically from its reversible value $E_{eq,M}$. down to the mixed potential E_{mp} (Fig. 1.20).

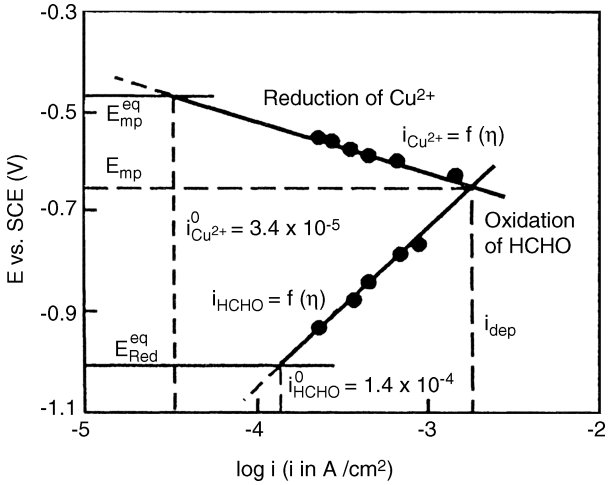

FIGURE 1.20 Current–potential curves for reduction of Cu^{2+} ions and for oxidation of reducing agent Red, formaldehyde, combined into one graph (Evans diagram). Solution for the Tafel line for the reduction of Cu^{2+} ions: 0.1 *M* $CuSO_4$, 0.175 *M* ethylenediaminetetraacetic acid (EDTA), pH 12.50, E_{eq}, $(Cu/Cu^{2+}) =$ 0.47 V versus saturated calomel electrode (SCE); for the oxidation of formaldehyde: 0.05 *M* HCHO and 0.075 *M* EDTA, pH 12.50, E_{eq} (HCHO) = 1.0 V versus SCE; temperature 25°C (±0.5°C). (From M. Paunovic, *Plating,* **55**, 1161 (1968), with permission from American Electroplaters and Metal Finishers Society.)

Mixed-potential theory was tested experimentally and verified extensivelly for the case of electroless deposition of Cu, Au, and Ni [1]. Its significance is in the fact that the kinetics and mechanism of clectroless deposition can be studied and interpreted by examining partial electrode processes [29].

1.5.2 Displacement Deposition

Section 1.5.1 mentioned that in the displacement deposition process z electrons in the deposition reaction [Eq. (1.40)], are supplied by the substrate. The substrate is the electron-donating species. We describe here an example of the displacement deposition of Cu on Zn which occurs when a strip of Zn is placed in a solution of $CuSO_4$. In order to find out what reactions will occur in this system, is necessary to consider standard electrode potentials (Table 1.1). The standard electrode potential E^0 of Cu/Cu^{2+} is 0.337 V and that for Zn/Zn^{2+} is -0.763 V. Since Zn/Zn^{2+} has a lower electrode potential than the Cu/Cu^{2+} system, Zn will reduce Cu^{2+} ions in the solution. Thus there are two partial reactions in this system, as in an electroless deposition system (Fig. 1.21). In displacement deposition of Cu on Zn, electrons are supplied in the oxidation reaction of Zn,

$$Zn \rightarrow Zn^{2+} + 2e \tag{1.44}$$

where Zn from the substrate dissolves into the solution and thus supplies electrons necessary for the reduction–deposition reaction

$$Cu^{2+} + 2e \rightarrow Cu \tag{1.45}$$

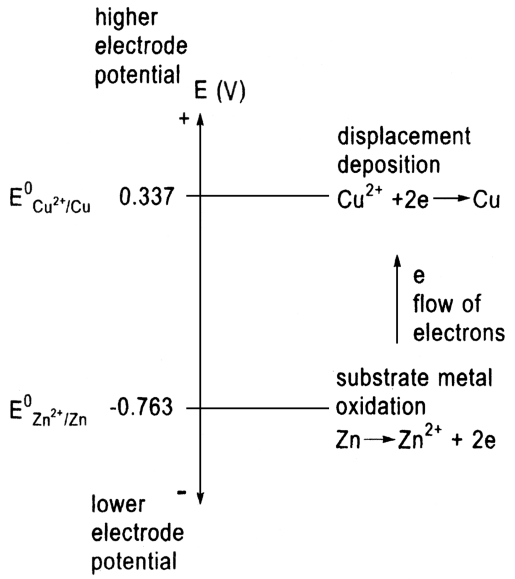

FIGURE 1.21 Relationship between partial reactions in displacement deposition of Cu on Zn, $Zn + Cu^{2+} = Zn^{2+} + Cu$.

The overall displacement deposition reaction is

$$Zn + Cu^{2+} \rightarrow Zn^{2+} + Cu \tag{1.46}$$

It is obtained by combination of the two partial reactions, oxidation and reduction, (1.44) and (1.45), respectively.

In general, Ox/Red (M^{z+}/M) couples with high standard electrode potentials are reduced by Ox/Red (M^{z+}/M) couples with low standard electrode potentials. In other words, low-potential couples reduce high-potential couples (see Table 1.1 and Fig. 1.19). The thickness of the deposited metal in this case is self-limiting since the displacement deposition process needs an exposed (free) substrate surface in order to proceed.

1.6 ELECTROLESS DIFFUSION BARRIER

Copper has been replacing Al in the fabrication of interconnects in chips due to the low-bulk electrical resistivity and superior electromigration resistance. The electrical resistance of pure Al and Cu are 2.9 and 1.7 mΩ-cm, respectively. Activation energies for electromigration are 0.81 (± 0.03) and 1.1 (± 0.03) for Al and Cu, respectively.

Copper introduces new problems, however, in the fabrication of interconnects on chips, the most important of which is possible diffusion of Cu into Si, Si dioxide, and the reaction of Cu with Si-forming silicides.

Thus, diffusion barrier layers are an integral part of the fabrication of Cu interconnects. Barrier layers can be represented schematically as

Si, Si dioxide–barrier layer–Cu

Yoshino et al. [29a] proposed an electroless NiB layer as the diffusion barrier layer.

In this process the reaction of electroless NiB deposition is activated by a self-assembled monolayer (SAM) containing Pd. Yoshino et al. found that this novel fabrication process yields high-quality film with high adhesion and satisfactory Cu barrier properties on low-k substrate. A low-k material is one with a small dielectric constant relative to silicon dioxide. In physics the symbol used for the dielectric constant is the Greek letter κ (kappa) while in semiconductor manufacturing the later-k is used.

It has been demonstrated that an electroless NiB film is effective as a barrier layer at a thickness as small as 20 nm.

1.7 PEG AND PPG AS SUPPRESSORS IN COPPER ELECTRODEPOSITION

The copper electrodeposition bath is typically a solution of cupric sulfate and sulfuric acid, containing a small concen-

tration of chloride ions. As explained in Section 1.6 the electrodeposition of copper is currently the method of choice for on-chip production of interconnects in microelectronics. Copper is electrodeposited in submicrometer trenches and vias. In order to get copper of high quality, a deposition suppressor is used.

Polyethylene glycol (PEG) and polypropylene glycol (PPG) or a combination of the two is used as suppressor. The original paper [29b] treats PEG, PPG, and their triblock copolymers, but here we are limited to PEG and PPG. The suppressor increases the overpotential for copper ion reduction by a surface adsorption interaction with chloride ions. Polypropylene glycal is causing great suppression in the copper deposition current, but using a mixture of PEG and PPG indicates that PEG dominates when both suppressors are present. Competitive adsorption is capable of explaining the mechanism of suppression.

In the absence of adsorption reduction the reaction of Cu ions is given by

$$i = i(0)\exp\left(\frac{-\eta}{b}\right) \tag{1.47}$$

where i (0) is the exchange current density, η is the electrode overpotential, and b is the Tafel slope (Section 1.3.1).

When competitive adsorption is present, the reduction current for Cu is given by

$$i(\text{ads}) = i(0)[1-\theta(\text{eff})]\exp\left(\frac{-\eta}{b}\right) \tag{1.48}$$

where θ(eff) is the effective surface coverage. Dividing Eq. (1.48) by Eq. (1.47) results in

$$\theta(\text{SS}) = 1-\left(\frac{i(\text{ads})}{i}\right) \tag{1.49}$$

where θ(SS) is the effective steady-state coverage. The available surface sites are given by $1 - \theta$(SS).

1.8 INFLUENCE OF ADDITIVES AND THE EFFECT OF AGING IN ELECTRODEPOSITED COPPER

In Section 1.4.1 we described the effect of additives on the deposition and crystal-building process as adsorbates (adsorbed substances) at the surface of the cathode.

In this section we describe the influence of additives and the effect of aging in modifying surface topography of electrodeposited copper [29c]. As a result of room temperature aging there is a change in the grain size and the microstructure of the copper deposit.

The X-ray diffraction patterns of the copper deposit exhibits a prominent (111) orientation in addition to (200), (220), and (311) planes. However, during room temperature aging copper deposit has a prominent (200) plane orientation.

The authors used scanning electron microscopy (SEM) and atomic force microscopy (AFM) in order to follow the influence of additives and the effect of aging.

On analysis SEM showed that the deposits have round or globular features and there is a change in grain size related to a particular additive. Additives used are PEG (Section 1.7), chloride ion, and PEG and chloride ion.

Atomic force microscopy showed that the average grain size strongly depends on the deposition rate and the type of additive. Additives used are the same as studied with SEM. It was found that there is a change in the grain size and the morphology of the copper deposit due to the room temperature aging.

PART B PHYSICAL CONSIDERATIONS

1.9 ELECTRODEPOSITION OF ALLOYS

1.9.1 General

Alloy deposition is as old an art and science as the electrodeposition of individual metals (e.g., brass, which is an alloy of copper and zinc, deposition was invented circa 1840). As can be expected, alloy deposition is subject to the same principles as single-metal plating. Indeed progress in both types of plating has depended on similar advances in electrodeposition science and/or technology. The subject of alloy electroplating is being dealt with by an ever-increasing number of scientific and technical publications. The reason for this is the vastness of the number of possible alloy combinations and the concomitant possible practical applications.

Properties of alloy deposits superior to those of single-metal electroplates are commonplace and are widely described in the literature. In other words, it is recognized that alloy deposition often provides deposits with properties not obtained by employing electrodeposition of single metals. It is further the case that, relative to the single-component metals involved, alloy deposits can have different properties in certain composition ranges. They can be denser, harder, more corrosion resistant, more protective of the underlying basis metal, tougher and stronger, more wear resistant, different (better) in magnetic properties, more suitable for subsequent electroplate overlays and conversion chemical treatments, and superior in antifriction applications.

Electrodeposited binary alloys may or may not be the same in phase structure as those formed metallurgically. By way of illustration, we note that in the case of brass (Cu–Zn alloy), X-ray examination reveals that, apart from the superstructure of β-brass, virtually the same phases occur in the alloys deposited electrolyticalty as those formed in the melt. Phase limits of electrodeposited alloys closely agree with those in the bulk form. Somewhat opposite is the case of the Ag–Pb alloy. In the cast alloy form it contains "large" silver crystals with lead present in the grain boundaries as dendrites. In the electrodeposited form the alloy contains exceedingly fine grains exhibiting no segregation of lead.

By choosing specific metal combinations, electrodeposited alloys can be made to exhibit hardening as a result of heat treatment subsequent to deposition. Such treatment, it should be noted, causes solid precipitation. When alloys (e.g., Cu–Ag, Cu–Pb, and Cu–Ni) are coelectrodeposited within the limits of diffusion currents, equilibrium solutions or supersaturated solid solutions are in evidence, as is observed by X-ray analysis. The actual type of deposit can, for instance, be determined by the work value of nucleus formation under the overpotential conditions of the more electronegative metal. When the metals are codeposited at low polarization values, the formation of solid solutions or of supersaturated solid solutions results. This is so even when the metals are not mutually soluble in the solid state according to the corresponding phase diagram. As a rule, codeposition at high polarization values, on the other hand, results in two phase alloys even with systems capable of forming continuous series of solid solutions.

1.9.2 Principles

The electrodeposition of an alloy requires, by definition, the codeposition of two or more metals. In other words, their ions must be present in an electrolyte that provides a "cathode film" where the individual deposition potentials can be made to be close or even the same,

Three main stages in the cathodic deposition of alloys (or single metals) are to be recognized:

1. *Ionic Migration* The hydrated ion(s) in the electrolyte migrate(s) toward the cathode under the influence of the applied potential as well as through diffusion and/or convection.
2. *Electron Transfer* At the cathode surface area, the hydrated metal ion(s) enter the diffusion double layer where the water molecules of the hydrated ion are aligned by the field present in this layer. Subsequently the metal ion(s) enter(s) the fixed double layer where, because of the higher field present, the hydrated shell is lost. Then on the cathode surface the individual ion may be neutralized and is adsorbed.
3. *Incorporation* The adsorbed atom wanders to a growth point on the cathode and is incorporated in the growing lattice.

1.9.3 Deposition

Now the deposition potential, which is the potential at which deposition occurs for a given metal, is determined by two major quantities, as was discussed in the first part of this chapter [see Eqs. (1.3) and (1.4)]. Specifically, one quantity is the standard electrode potential, E° (it is defined as the potential that exists when the metal is immersed in a solution of its ions at unit activity) which is a characteristic of the metal in question. The other quantity is a function of the ion's activity value in the electrolyte. This value is in turn proportional to the ionic concentration as long as the latter is of moderate value; otherwise, it is a complicated function of all the units in the solution. For two metals to be codeposited and thus produce an alloy, they must both be present in the electrolyte, and their individual deposition potential should be the same or nearly the same. It is clear that for two metals whose standard electrode potentials differ by a great amount, the only way to achieve these deposition potentials is by controlling the value of the activity, that is, changing the respective concentrations. The deposition potentials can thus be brought into harmony. Detailed calculations (see *Fundamentals*), for instance, indicate that copper ion concentration can be brought into harmony with zinc ion concentration in certain solutions and thus can be used in Zn–Cu alloy plating.

Using an example, we wish to stress the point that in a solution containing "simple" salts of zinc and copper where ion concentration, and so the activity, values are close together, an alloy deposition is virtually impossible. That is due to the large difference between the standard electrode potentials E^0 for copper (-0.345 at 25°C) and that for zinc (-0.762 at 25°C).

In a mixed copper–zinc solution of complex cyanide, however, the Cu^+ ion concentration can be reduced to the order of 10^{-18} mol L^{-1} and the concentration ratio (zinc ion)/(copper ion) will be made very large. This will compensate for the large difference in their standard electrode potentials. A detailed treatment for this case shows that copper cyanide complex is of the form $Cu(CN)_4^{2-}$ for which the dissociation constant value is known. The dissociation constant for the zinc cyanide complex $Zn(CN)_4^{2-}$ is also well known. Calculations using these values make it clear that their respective deposition electrode potentials can be brought close enough together.

To express the above in a different, more specific way, we state that codeposition of two or more metals is possible under suitable conditions of potential and polarization. The necessary condition for the simultaneous deposition of two or more metals is that the cathode potential–current density curves (polarization curves) be similar and close together.

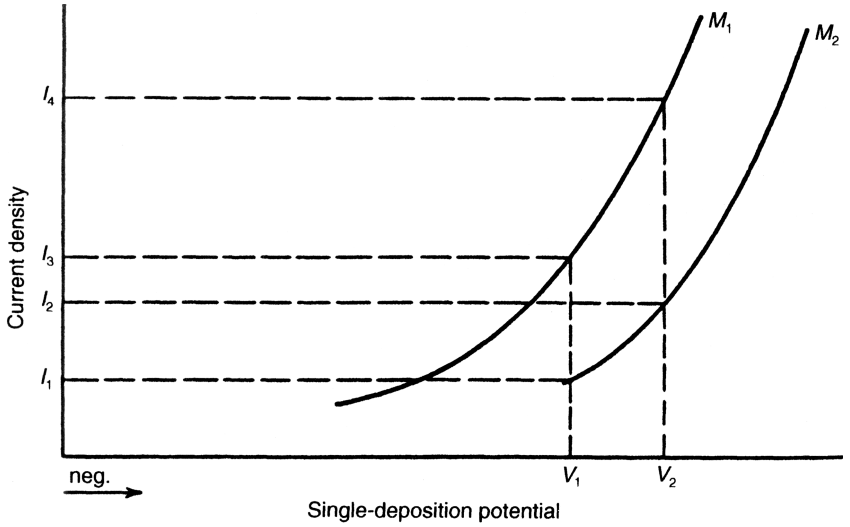

FIGURE 1.22 Single-electrode potentials of metals M_1, and M_2 versus current density in the same type of bath.

Figure 1.22 depicts a typical deposition potential plotted against current density for two different individual metals. The curves indicate that in a bath containing both metals, M_1 and M_2, may codeposit at, say, potential V_2 in the ratio I_4/I_2.

It should be understood that the plating bath may be depleted of one metal ion faster than of another. In order to keep deposition conditions under control, (uniform), metal ions must be replenished in direct proportion to their rates of deposition dictated by the specific alloy. Clearly, the ideal case is where the polarization curves of the component metals being codeposited are identical. In practice, however, it is next to impossible to realize this condition.

Electrochemically viewed, even when a single-metal deposition is accompanied by hydrogen evolution, it may well be said that one deals with alloy plating in which hydrogen is the codepositing element. This is equally so when hydrogen is discharged as gas, since the conditions for codeposition are met. Alloy plating of metals makes it into a process of production of hydrogen and the two or more metals that are being alloyed.

Another path to alloy deposition is that via interdiffusion in electrodeposited bilayers or multilayers. In this case different coatings are deposited alternately using two different plating baths or even one bath where the deposition potential is varied periodically and then heat treatment is applied to promote mutual diffusion, thus ending up with an alloy. For example, an alloy of 80% Ni and 20% Cr can be produced by the deposition of alternating layers of 19-μm-thick Ni and 6-μm-thick Cr. Subsequent heating to 1000°C for 4–5 h produces completely diffused alloys of rather high quality in terms of their corrosion properties. Brass can also be produced by interdiffusion of Cu and Zn under suitable conditions.

1.10 STRUCTURE AND PROPERTIES OF DEPOSITS

1.10.1 General

In their solid state, atoms (ions) are arranged in a regular pattern that may be described by the three-dimensional repetition of a certain pattern unit. The structure therefore is said to be periodic. When the periodicity of the pattern extends throughout a piece of the material, we refer to it as a *single crystal.* In polycrystalline material the periodicity is interrupted at so-called grain boundaries. The size of grains through which the structure is periodic varies markedly, as discussed below. When the size of the grains or crystallites becomes comparable to the size of the pattern unit, the substance is called *amorphous.*

Grains are understood here to be individual crystallites in a polycrystalline body of material. This definition, however, is not common to all authors. Thus some authors refer to clumps of crystallites as "grains" while others call such clumps "islands."

Crystalline material, as stated above (whether single-crystal, polycrystalline, or even nanocrystalline amorphous), is made such that its component (constituent-based) ions. atoms, or molecules are arranged on a three-dimensional regular, repetitive pattern called a *lattice.* In metals the constituent bases are singly or multiply ionized metal atoms. The commonest form among (plated) metals is the face-centered-cubic (fcc) lattice, which is the lattice structure of Ag, Al, Au, Cu, Ni, and others. Here fcc refers to a lattice arrangement of metal ions at each of the corners of a cube plus one atom each in the center of every cube face.

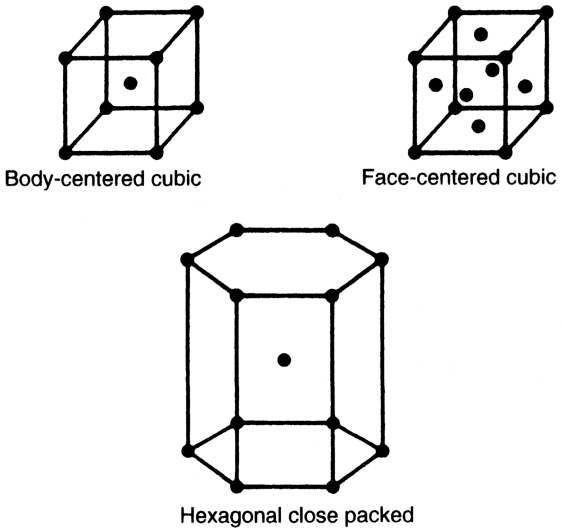

FIGURE 1.23 Unit cells of the three most important lattices. (From C. Kittel, *Introduction to Solid State Physics*, 6th ed., Wiley, 1986. Reproduced with permission.)

Next in frequency is the hexagonal close-packed (hcp) lattice, which is assumed by Co, Zn, and some others. Here hcp refers to an arrangement of metal ions with planes of ions placed at the corners of hexagons which are separated by planes of ions grouped in sets of three between hexagons in the adjacent planes. This way one of the two close-packing arrangements of hard spheres is realized. The other way of close packing of hard spheres is realized by the fee arrangement. That arrangement is therefore sometimes referred to as *cubic close packed.*

The body-centered-cubic (bcc) is the lattice symmetry of Fe, for instance. Here bcc refers to a crystal arrangement of ions at the corners of a cube and one ion in the center of the cube equidistant from each face. Figure 1.23 depicts the unit cells corresponding to the above-mentioned structures. In the last analysis, the crystalline structure exhibited as a product of electrodeposition depends on a "competition" between rates of new crystallite formation and existing crystal growth.

It ought to be stressed that actually a large number of variables in the plating process have bearing on structure. Among these are metal ion concentration, additives, current density, temperature, agitation, and polarization. It is outside the scope of this chapter to discuss these effects in more detail.

1.10.2 Substrate and Environment

Another factor that has substantial influence on electrodeposits, their structure, and their properties is the nature of the substrate upon which the plating occurs. Two phenomena are important in this context: *epitaxy* and *pseudomorphism.* Epitaxy refers to the systematic structural kinship between the atomic lattices of the substrate and the deposit at or near the interface. In other words, it concerns the induced continuation of the morphology and/or structure of the substrate material into a coating applied on to it. An important parameter of epitaxial growth is the substrate's temperature. For a given material being deposited on a substrate, all other conditions being fixed, there exists an *epitaxial temperature.* That is a temperature above which epitaxial growth is possible; below this temperature no epitaxial growth can occur. For example, for silver evaporated on NaCl, the temperature is 150°C, Pseudomorphism is the continuation of grain boundaries and similar geometric features of the substrate into the deposit. An alternative definition states that deposits that are stressed to fit upon a substrate are said to be pseudomorphic. A working rule is that pseudomorphism persists deeper (up to 10 nm) into the deposit than epitaxy.

Prior cleaning, or the cleanliness state of the substrate, also greatly influences the structure and adhesion of the deposit. In general, both mechanical and chemical cleaning methods may be required.

Metal surfaces exposed to certain types of gas will generally undergo transformation, and their transformation can be accompanied by significant changes in their properties. The rate and the extent of change are dependent on the metal, the gases, and the new phase/product that will form at the interface between the two original phases. We mention here the case of Si oxidizing to form SiO_2 which undergoes expansion, thus creating strong (compressive) stress on the interfacial surface.

An example of high practical significance is the copper deposits used in microelectronics, mirrors, and other optical applications. These deposits have been observed to soften over time even when stored at room temperature for as short as four to six weeks. The surfaces of mirrors and other precision objects made of copper will deform after a few months. This kind of degradation can be counterweighed by a suitable metal overcoating. Another, though not always practical, way is to subject the object to heat treatment at about 300°C. These degradation phenomena are the direct results of microstructural instabilities, often referred to as *recrystallization* in the copper. It is worth stressing that recrystallization is not limited to copper. "As-deposited" electroless Ni–P is subject to a similar process.

Crystals grown via electroplating may be oriented every which way. That is to say, the direction axes of individual crystallites may be randomly distributed. The case, however, where one axis is oriented or fixed in *nearly* one direction is said to be a single texture. Where two axes are fixed or oriented, it is said to be double texture. Monocrystalline orientation refers to the case where there are three such nearly oriented axes. This includes, for instance, epitaxial films. Orientation is viewed with respect to any fixed (in space) frame of reference.

Electrochemical parameters, and not substrate properties, are the main deciding factors in the texture of deposits. This is particularly evident if the deposit's thickness is 1 μm or more. In deposits of lesser thickness, the substrate plays an important role as well (see above). Another nonelectrochemical factor may be the codeposition of particulate matter with some metal deposits. To summarize, we note that texture is mostly influenced by deposition current density, itself being a function of bath parameters. Not surprising, then, is the fact that in the case of physical vapor deposition (PVD) the deposition rate, which serves as the effective current density, is the determining factor in setting the texture of the coating.

1.10.3 Properties

The functional relationship between structure and property is complex. To be precise, there are different microscopic and macroscopic interactions involved in materials. There are both quantum-mechanical interactions between constituent atoms or molecules and classical-type interactions between grains and groups of grains. Electrodeposition adds some measure of complication since it is inherently a nonequilibrium process. The product films thus exhibit many imperfections that vary in number and nature from grain to grain. In this connection it is also important to remember that the most basic imperfection of a crystal lattice is the surface itself where the periodicity, the hallmark of bulk material, is cut off.

For illustration of the complexity discussed above, we note the following few practical cases:

1. Gold, when electrodeposited with about 0.5% cobalt, has a hardness of about four to five times that of annealed electrodeposited gold. This degree of hardness cannot be achieved using any of the known metallurgical methods. It is widely believed that grain sizes of 20–30 nm in this material are responsible for this high degree of hardness. Cobalt-hardened gold films have found a large number of applications in electronics and other areas.
2. Texture has a marked influence on the properties of a given deposit. Seemingly unrelated parameters (properties) such as corrosion resistance, hardness, magnetic properties, porosity, and contact resistance are all texture dependent. The specific texture of a copper substrate upon which a nanomultilayer system such as Cu–Ni layer pairs are deposited has direct bearing on the deposit's texture and consequently magnetic characteristics.
3. Different nickel deposits show a great variety of contact resistance values. This is particularly so after the deposits have been exposed to the atmosphere for extended periods of time. The differences in these values may be best explained in terms of variations in plated texture. Nickel electrodeposits with polycrystalline nature have been observed to behave as single crystals if their grains are oriented such that the (100) planes are parallel to the surface. Not surprisingly the oxidation rate in (100) oriented single crystals is self-limiting at ambient temperature.
4. The optical properties of some thin-film light polarizers owe their ability to polarize light to the specific texture of their structure.

1.10.4 Impurities

Electroplated films almost always contain various types of inclusions or impurities. These additives may be from one or more of the following origins:

1. Added chemicals (levelers, brighteners, etc.)
2. Added particles (for composite coating)
3. Cathodic products (complex metal ions)
4. Hydroxides (of the depositing metals)
5. Bubbles (e.g., hydrogen gas)

In general, it may be stated that deposits produced using low current densities possess higher impurity content than deposits produced using high current densities (see *Fundamentals*).

Small amounts (in ppm) of impurities can also influence material strength. For example, as noted earlier, a small amount of cobalt in electrodeposited gold enhances its hardness. Sulfur impurities can, on the other hand, be detrimental to nickel deposits. An increase in sulfur content is known to reduce the fracture resistance of electroformed nickel. If no other impurities are present in the electrodeposited nickel, hardness alone can be used as an indicator of sulfur impurity content.

From the foregoing discussion it should be clear that in practice it is virtually impossible to obtain and maintain electrodepositing baths free from impurities. This is a big consideration in the research laboratory. In research work on electrode kinetics, for example, careful and often complex purification procedures are followed in order to remove some key contaminants. Otherwise, no reproducible or reliable results can be obtained. The plating shop worker, on the other hand, deals with highly contaminated (from the point of view of the researcher) solutions from a variety and by and large unknown sources. It is for this reason that technical practice must and does rely on empirical observations.

In some deposits, notably those of nickel, electrical resistance follows current density at low temperatures in the sense that films deposited at a low current density (e.g., 10 mA cm^{-2}) show lower resistance than those deposited at higher density.

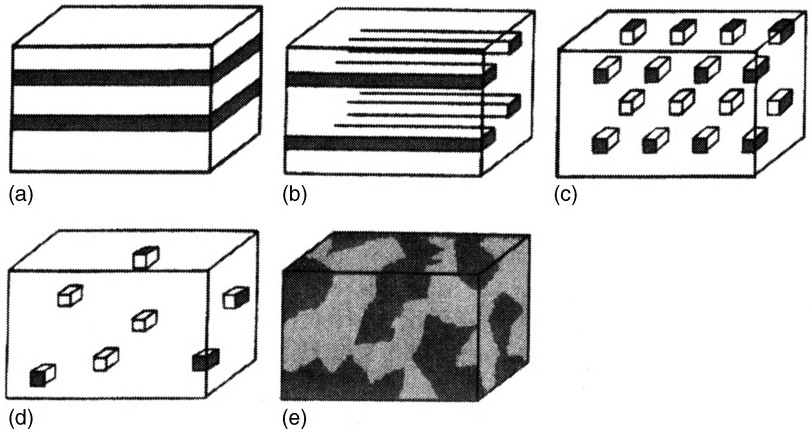

FIGURE 1.24 (a) Quantum wells, multilayers; (b) quantum wires; (c) ordered dots; (d) random dots; (e) nanometer-sized dots.

This effect of low resistance occurs in the low-temperature range of 4–40 K but disappears at closer to room temperature.

A special type of impurity is hydrogen. Hydrogen is codeposited with most metals. Because of its low atomic number, it can be expected to be readily adsorbed by the basis metal. The source of the hydrogen may vary from the associated preparatory processes such as electrocleaning to the specific chemical reactions associated with the plating process itself. Regardless of its origin the presence of hydrogen may result in embrittlement, which means a substantial reduction in ductility. Hydrogen embrittlement (HE) is an expression used to describe a large variety of fracture phenomena having in common the presence of hydrogen in the metal or alloy as a solute.

Many types of mechanisms have been suggested in the attempts to explain HE in different systems. No consensus has been reached to date as to the validity of these. The absorbed hydrogen in steel, for instance, makes it most susceptible to embrittlement. At least in part, this is due to the hydrogen interfering with the normal flow or slip of the lattice planes under stress. If, as often is the case, a deposit contains voids on the microscopic scale, hydrogen may accumulate in molecular form possibly developing pressures exceeding the tensile strength of the basis metal leading to the development of blisters.

Finally, in physical vapor-deposited as well as sputter-deposited films, incorporated gases can increase stress and raise annealing temperatures. Similar effects are present in electron-beam-evaporated films.

1.11 MULTILAYERED AND COMPOSITE FILMS

1.11.1 General

With the introduction of many different reliable ways, including electrodeposition, to produce systems with nanometer- scale structural and composition variations, there has come the ability for greater control of material properties, which has led to the design of new materials.

Nanostructural materials are divided into three main types: one-dimensional (commonly known as multilayered) structures made of alternate thin layers of different composition; two-dimensional structures (commonly known as wire-type elements suspended within a three-dimensional matrix); and three-dimensional constructs which may be made of a distribution of fine particles suspended within a matrix (either in periodic or random fashion) or an aggregate of two or more phases with a nanometer grain size. Figure 1.24 depicts the above-mentioned constructs.

The semiconductor community has made band gap engineering a reality by exploiting the ability to produce multiple quantum well material. Here the quantum well refers to a potential well with dimensions such that quantum-mechanical effects are taken into account. In other words, one thinks of electrons/holes as being trapped in the well, having distinct energy levels rather than a continuum. The progress from one-dimensional nanostructural materials to two- and three-dimensional ones (i.e., to quantum wires and quantum dots; see Fig. 1.24) has provided enhanced carrier (electrons and/or holes) confinement by their presence, which permits more control of the energy band structure.

Accurate control of a microstructure on the nanometer scale makes it possible to control magnetic and mechanical properties to a hitherto unattainable degree. In particular, magnetic nanostructures have recently become the subject of an increasing number of experimental and theoretical studies. The materials are made of alternating layers, around 10 Å thick, of magnetic (e.g., cobalt) and nonmagnetic metals (e.g., copper).

The magnetic layers are exchange coupled to one another with a sign that oscillates with the thickness of the spacer (nonmagnetic) layer. This arrangement can be understood if one considers the multilayer systems as magnetic layers separated by nonmagnetic layers. The number of free conduction electrons is dependent on the number of nonmagnetic

atoms, that is, the thickness of the nonmagnetic layer. As this number increases, subsequent orbitals in the magnetic atoms will experience alternating electron surpluses and deficits, causing a sinusoidal variation in the average magneton number per atom. Thus the magnitude of the exchange interaction varies not only in the usual fashion, inversely with the square of the distance between magnetic layers, but also in a sinusoidal manner. These results were known recently for sputtered, evaporated, and molecular beam epitaxy (MBE) grown samples.

Electrodeposition of composition-modulated films was first performed by Brenner in 1939 [30], who employed two separate baths for the two components and a "periodic" immersion of the deposit in the two baths. This method proved too cumbersome to be adopted in practice, however. Deposition from a single bath with the presence of salts of the two components of the multilayer is what has evolved.

A serious problem was found in the deposition of two metals from one bath. Specifically, while a layer of the more noble member could be deposited by choosing the potential to be between the reduction potentials of the two metals, the potential had to be set to a value appropriate for the reduction of the less noble member so that both would be deposited and result in an alloy layer rather than a pure metal.

1.11.2 Electrodeposition of Nanostructures

In 1986 Yahalom and Zadok [31] pointed to methods to produce composition-modulated alloys by electrodeposition, initially for the Cu–Ni couple. Modulation was obtained to thicknesses down to 8 Å. The principle of their method follows.

Traces of metal A ions are introduced into a concentrated solution of metal B, assuming that metal A is nobler than B. At a low enough polarization potential the rate of reduction of metal B is high because it is determined by its activation polarization. The rate of reduction of metal A is slow and controlled by diffusion. At a predetermined considerably less negative polarization potential only metal A is reduced. The potential is simply switched between these two potential values, forming a modulated structure composed of pure A layers and layers of B with traces of A in the B layers. The actual deposition of the multilayered composite can be carried out by either current or potential control.

The method is suitable for a considerable number of metal couples. The main caveat, however, is that both metals can be deposited from similar baths. Another is that they differ sufficiently in their degree of nobility.

The method was first tried using the Cu–Ni system, which is still the most-studied system by far when it comes to electrochemically produced layered structures. The reasons for this are quite compelling. There is a sufficient difference in reduction potentials of the two metals. There is the similarity in crystal structure (fcc) and proximity of lattice parameters, ensuring a good coherency between the layers. Further considerable data exist on the magnetic, mechanical, and other properties of the Cu–Ni system deposited by other than electrodeposition, enabling comparison of the modulated layers produced by the chemical method.

1.11.3 Analysis of the Deposit

A standard method for confirming the coherence of the layers is via X-ray diffraction spectra. If the layers are coherent and there are a sufficient number of them to provide a relatively strong Bragg diffraction pattern, then satellites due to superlattice formation should appear on each side of the Bragg diffraction peak (superlattice refers here to the periodicity of the layered structure).

The mathematical expression for the difference between the sine values of the two satellites is

$$\sin\theta_s^+ - \sin\theta_s^- = \frac{\lambda}{\Lambda}$$

where λ is the X-ray wavelength and Λ is the superlattice repetitive period. The expression is a consequence of an analogous formula for light diffraction by optical grating.

In general, one can expect systems like these to have properties different from the bulk. In bulk materials, most ions are in a crystalline environment; that is, they do not "see" the surface. In a crystalline superlattice most atoms "know" they are near an interface, that is, in a noncrystalline/nonperiodic environment. For an extended treatment of the mechanical, magnetic, and other properties of muitilayered thin-film systems, the reader should consult *Fundamentals* (Chapter 17).

1.11.4 Conclusion

All the possible methods of deposition have inherent advantages and disadvantages with regard to the quality of the multilayers they create and the ease of their production. However, electrodeposition seems best to fulfill imposed financial and temporal restrictions. Specifically, vapor deposition is expensive, creates quasiamorphous interfaces, and is time consuming in terms of controlling the alternation of deposition material. Electroless deposition may suffer from the same drawback with regard to mechanical switching between solutions for alternating layer materials. Finally, sputtering requires an expensive vacuum system and cannot easily be extended to industrial usage. For these reasons electrodeposition is now the production method of choice for most practical needs.

The constructs thus obtained provide a useful paradigm for fundamental studies as well as for a plethora of applica-

tions. Some applications are in magnetically operated read/write heads, others in sensors, but these are just a precious few. Recently (January 1998) IBM became the first company to market giant magnetoresistance (GMR)–based multilayer read/write heads in a family of disc drive products designated Deskstar 16 GP. The use of such technology allows the reading and writing of extremely small magnetic bits of information that facilitates high-density storage. This provides for the ability to store 3.2 gigabytes of data on a 95-mm-diameter disc.

We must again emphasize that electrodeposition presents, in principle, several advantages for the investigation and production of layered alloys. Among these characteristics are the tendency of electrodeposited materials to grow epitaxial and thus to form materials with a texture influenced by the substrate. Electrodeposition thus can be used in systems that do not lend themselves to vacuum deposition. The electrodeposition process is inexpensive, and it can be scaled up with relative ease for use on large parts; further it is a room temperature technology. This last point is important for systems in which undesirable interdiffusion between the adjacent layers may readily occur.

The studies so far of electrodeposited multilayer materials clearly show that electrodeposition is a viable technique for the production of thin muitilayered materials in systems that, from the electrochemical standpoint, are adaptable to the pulsed deposition technique.

Recent results have been able to demonstrate that the coatings produced by electrodeposition display the same coherency and layer thickness uniformity as those composition-modulated alloys produced by vacuum evaporation or sputter deposition. Demonstration of the capability of electrodeposition to produce materials with predesignable, variable, and controllable composition down to practically the atomic scale constitutes an important step toward the realization of custom-tailored materials. On the theoretical side, the lack, at the time of writing, of a single satisfactory theory for the possible explanation of the ever-growing amount of empirical results is still somewhat disappointing and surprising.

1.12 INTERDIFFUSION IN THIN FILMS

1.12.1 General

Modern integrated circuits are made of layered thin-film structures which are subject to interdiffusion during the thermal processing stage in fabrication. Diffusion, in general and not only in the case of thin films, is a thermodynamically irreversible self-driven process. It is best defined in simple terms such as the tendency of two different gases to mix when separated by a porous partition. It drives toward an equilibrium, maximum-entropy state of a system. It does so by eliminating concentration gradients of, for instance, impurity atoms or vacancies in a solid or between physically connected thin films. In case of two gases separated by a porous partition, it leads to the eventual perfect mixing of the two.

In equilibrium in a solid, the impurities or vacancies will be distributed uniformly. Similarly, in the case of two gases, as above, once a thorough mixture has been formed on both sides of the partition, the diffusion process is complete. As well at that stage, the entropy of the system has reached its maximum value by virtue of the fact that the *information* regarding the whereabouts of the two gases has been minimized. In general, it ought to be remembered that entropy of a system is a measure of the information available about the system. Thus the constant increase of entropy in the universe, it is argued, should lead eventually to an absolute chaotic state where no information is available at all.

The diffusion process in general may be viewed as the model for specific, well-defined transport problems. In particle diffusion, one is concerned with the transport of particles through systems of particles in a direction perpendicular to surfaces of constant concentration. In a viscous fluid flow, one is concerned with the transport of momentum by particles in a direction perpendicular to the flow. In electrical conductivity it is with the transport of charges by particles in a direction perpendicular to equal potential surfaces. In solids, for instance, the chemical potential is identified with the Fermi energy level. When two solids or thin films are brought into contact, such as in the case of a *p–n* junction, charged particles will undergo interdiffusion such that the chemical potentials or Fermi levels will be balanced, that is, reach the same level.

Let us assume now that particle diffusion occurs as a result of the difference in concentrations, as is the case in a deposition bath. Then a relation known as *Fick's law* is in effect, and it is written as

$$\text{Particle flux} = (\text{diffusion coefficient}) \times (\text{driving force})$$

or using the language of mathematics,

$$J_n = -D \operatorname{grad} c \tag{1.50}$$

where c is the concentration of the diffusing species (ions or particles). The concentration gradient is acting as the driving force.

The term *flux* here refers to the amount of the diffusing substance passing through a cross section of unit area in unit time. The term *gradient* refers to the change in substance concentration as a function of distance. Both quantities, since they have directionality in addition to a numeric value, are viewed as vector quantities. It has been found experimentally that the diffusion constant/coefficient, D in Eq. (1.50), depends on temperature according to an exponential-type

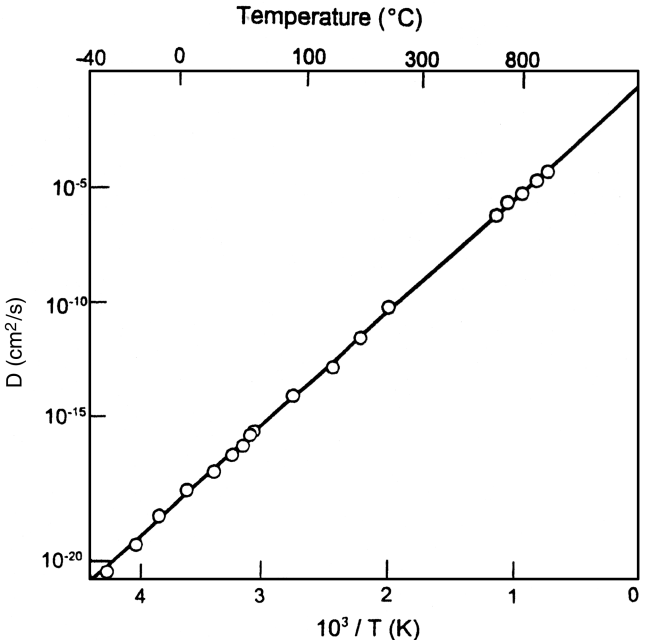

FIGURE 1.25 Diffusion coefficient of carbon in alpha iron. (From C. Kittel, *Introduction to Solid State Physics*, Vol. 7, Wiley, New York, with permission from John Wiley & Sons.)

expression (see Fig. 1.25), This type of temperature dependency is indeed typical of activation energy driven processes, in general.

To actually diffuse, an atom ion must overcome a potential energy barrier due to neighbors. If, as above, the potential energy barrier height is E, then the statistical mechanical considerations indicate that the atom will have sufficient thermal energy to pass over the barrier a fraction $\exp(-E/kT)$ of the time. Here T stands for the absolute (Kelvin) temperature while k is Boltzmann's constant. If f is a characteristic atomic vibrational frequency, then the probability p that during unit time the atom will pass the potential energy barrier is given by

$$p \cong f \exp\left(\frac{-E}{kT}\right) \tag{1.51}$$

In other words, in unit time the atom makes f (of the order of $10^{14}\,s^{-1}$) attempts to surmount the barrier with the probability each time of the exponent. Thus the quantity p is also known as *jump frequency*.

1.12.2 Diffusion in Electrodeposits

Diffusion is liable to corrupt the properties of a deposit and defeat the purpose for which the electrodeposition was performed in the first place. This may particularly be so at the basis metal–film interface. Thus, for instance, in deposits for decorative purposes, diffusion of the coated underlayer (metal) to the surface will debase the intended appearance. Another example is gold plating of electronic contacts, which is often practiced in order to avoid corrosion of the contact areas. In gold plating the underlayer is often copper. The copper can diffuse to the surface of the gold. As a result of the copper oxidation the contact resistance will be altered and markedly for the worse. As a practical fact we note here that a 3-μm-thick gold film deposit will be covered with the oxide of its underlying copper if exposed to 300°C within one month. If exposed to 500°C a gold layer of 30 μm thickness will be diffused through in four to five days.

In some instances, to improve solder ability, tin is deposited on nickel surfaces. In a short time, however, interdiffusion of the two metals results in the growth of an intermetallic $NiSn_3$ compound that is much less amenable to soldering. In the case of tin electrolessly deposited over nickel surfaces, the interdiffusion results in pores in both films. Pores are to be avoided, of course, if conductivity or contact resistance is an issue.

Earlier in this chapter mention was made of hydrogen embrittlement. It was indicated that the presence of hydrogen in, say, steel will result in the same effect. That predicament concerns an interstitial solid solution. The solute atoms (hydrogen in this case) may move along the interstices between the solvent atoms (iron in this case) without having to displace them. This state of affairs is facilitated by the hydrogen atoms being much smaller than the interionic space in the lattice of the solvent.

Diffusion must not, however, always be viewed as a harmful phenomenon. In some cases it is desirable, if not essential, as in welding, where diffusion ensures joining of the welded parts. Steel is often coated with tin to protect it from corrosion. In this case the formation, via interdiffusion, of the intermetallic $FeSn_2$ is the key for effective protection.

Yet another positive aspect of the diffusion phenomenon is the creation of alloys by first depositing alternate layers of different coatings, and then an alloy is created by heating to promote interdiffusion to produce an alloy. Specifically brass deposits can be produced by first depositing copper and zinc layers alternately. Subsequent heating produces the required brass. This type of approach obviates the undesired direct method of brass deposition via a cyanide process.

In the case of jet engine parts which are routinely subject to temperatures close to 500°C, diffusion-alloyed nickel–cadmium is found to serve as an effective corrosion protective agent.

1.12.3 Void Formation

Whenever the interdiffusion of two metals is uneven, it can create vacancies or voids. The uneven diffusion is the result of unequal mobilities between a metal couple. The voids

occur individually near the common interface. Voids like bubbles coalesce, resulting in porosity and loss of strength. Many thin-film couples exhibit this phenomenon, which is referred to as *Kirkendall void creation*. A few examples are Al–Au, Cu–Pt, and Cu–Au. To be specific, it has been found, for instance, that in Au–Ni about five times more Ni atoms diffuse into Au than Au atoms diffuse into Ni.

Kirkendall void formation can, however, be prevented from occurring by choosing the "right" metal species. For instance, while platinum coating upon copper is subject to the Kirkendall void creation process, the same coating upon electrodeposited nickel is free of it, even if the surface is heated to as high as 600°C for many hours (more than 10 h).

Again, the effect has useful aspects as well. It can help in controlling porosity, say, of an electroformed object requiring cooling. Indeed, this is a consideration in a number of electronics applications.

1.12.4 Diffusion Barriers

Diffusion barriers are coatings that serve to protect against undesirable diffusion. One of the best examples is that of a 100-μm-thick electrodeposited copper layer. That serves as an effective barrier against the diffusion of carbon. Another example is nickel and nickel alloys (notably electrolessly deposited Ni–P) that block diffusion of copper into and through gold over plate. This is achieved by the deposition of a relatively thin Ni–P layer (less than 1 μm) between the copper and its overlayer. Naturally the effectiveness of the diffusion barrier increases with its thickness. Another factor in the effectiveness of a diffusion barrier is its crystallographic properties such as grain size and preferred crystalline orientation.

In electronic applications it is usual to deposit copper and/or copper alloy and tin in sequence. With a nickel diffusion barrier layer 0.5 um thick between the layers present, no failure occurs. Without the nickel layers between bronze, copper, or tin layers, for instance, intermetallic brittle layer(s) and Kirkendall voids are formed, leading eventually to separation of the coated system and substrate.

Also, when tin-containing solder connections are made to copper, intermetallic materials are formed. These materials keep growing to render weak surfaces. Again, a nickel layer between substrate and solder provides a solution to the problem.

1.12.5 Diffusion Welding

Here one utilizes diffusion to bring about joints of high quality. In other words, here, again, we have practical and useful aspects of thin-film interdiffusion. In practice, clean (very clean) cleaved or otherwise smoothened metal surfaces must be made for these to be in a firm mechanical contact while using a strong force that is still insufficient to cause macroscopic deformation even at an elevated temperature. This contact is usually done in vacuum or at least in an inert atmosphere. The problems of hard-to-reach joints and objectionable thermal conditions and the resultant undesired microstructures such as Kirkendall voids are minimized if not eliminated all together. Thus there can be achieved good-quality, distortion-free joints that require no additional machining or other posttreatment.

Often before welding can be performed, a special layer must be applied in the form of a thin-film coating or a thin foil in order to promote joining. Such coating can be applied by electroless or electrodeposition methods.

Five essential process variables common to all diffusion bonding techniques are to be considered: (1) temperature, (2) pressure, (3) time, (4) surface condition, and (5) process atmosphere.

Process temperature is usually one-half to three-fourths of the melting point of the lower melting point metal in the intended weld or bond. The purpose of attaining an elevated temperature is to promote or accelerate the interdiffusion of atoms at the joint interface and also to provide some metal softening, which in turn aids in surface deformation. The pressure application establishes a firm and robust mechanical contact of the surfaces and further breaks up surface oxides (hence the frequent use of silver). As a result, the surface is clean for bonding. The period of time at which the elevated temperature is maintained depends on metallurgical and other considerations.

1.12.6 Electromigration

In an electrical cord or wire, electricity is conducted without transport of atoms in the conductor. The common, free-electron model of electric conductivity makes a basic assumption that electrons are free to move in and through a metal lattice constrained only by scattering events. Scattering is the cause of electrical resistance and what is termed Joule heating. Scattening, however, does not cause displacement of atoms or ions as long as the current density is moderate. At high current densities (of about $10^4\,\mathrm{A\,cm^{-2}}$) the current can displace ions and thus cause transport of mass. The mass transport caused by the electric field and the charge carriers is known as *electromigration.* It is present in interconnecting lines in microelectronic devices, since in these lines the current density values are high. By way of example, a current of 2 mA applied to a 1-μm-wide aluminum line of 0.2 μm thickness, represents a current density value of $10^5\,\mathrm{A\,cm^{-2}}$; this current density will cause mass transport in the line even at room temperature. It constitutes a reliability failure endemic to thin-film circuits. As modern electronic circuitry becomes smaller and smaller, the current densities will become larger and the probability of circuit failure due to electromigration will be more of a problem. Both voids and extrusions can result. A line of aluminum that is subject to

an electric field and current density of sufficient magnitude can cause electromigration. The line can be expected to undergo morphological change such that depletion occurs at the negative (cathode) end while extrusion is present at the positive (anode) side. This means that the material migration is in the direction of the movement of the charge-carrying electrons. The driving force behind electromigration consists of two parts. The first is the direct action of the electrostatic field on the diffusing atoms. The second is the momentum exchange of the moving charge carriers with the diffusing atoms. These forces are referred to as the *direct* force and the *electron wind* force, respectively. The electron wind force is usually far greater than the direct force. There have been attempts to quantitatively, using quantum-mechanical methods, explain and estimate the electron wind force. None is widely accepted, and the common practice is to adhere to semiclassical treatments. Remedies include lowering the operating temperature or using other metals (than Al) that have a higher activation energy for diffusion where electromigration is less of a problem.

PART C MATERIALS SCIENCE OF ELECTRODEPOSITS

Electrodeposition has become a science capable of producing materials atom by atom with sophisticated, controllable structures and properties [32]. Historically, the structures formed have been characterized by the forms they take, such as grains, layers, needles, or a combination. Key aspects of electrodeposited materials that are relevant to the functional properties are grain dimension, preferred orientation, atomic density gradients, and composition. A high fraction of atoms in a granular electrodeposit are in interfacial zones. When grain size is in the 10–20-nm range, half the atoms are associated with grain boundaries or interfacial zones. These are high-energy regions, and since there is normally a large fraction of this material, the driving force for grain growth can be high.

Recently, electrodeposition has become a major nanotechnology enabler and benefits from application of modern analysis and processing methods [33, 34]. As an example, nanosized grains are produced in copper that is pulse plated or electrodeposited with direct current from baths containing complexing agents [35]. High-technology applications now include ultra-large-scale integration (ULSI) and microelectromechanical system (MEMS) packaging [36], thermoelectrics [37, 38], magnetics [39], and solar energy conversion [40, 41]. The improving nanotechnology theories and processes are combining with electrodeposition capabilities to give innovations such as stress-controlled structures [42], catalysts, and phase change materials [43].

1.13 STRUCTURE AND COMPOSITION

Electrodeposition yields a range of nano- and microstructures, depending on the material and the condition of deposition. In the majority of electrodeposited materials, the atoms are arranged in a uniform, three-dimensional array. The volume over which this arrangement extends uniformly is called a crystal. Most electrodeposits exist in one of three crystal habits: fcc, bcc, or hcp (see Part B).

When many crystals combine to form a solid material, they are called grains. If the array of atoms is random, the material is amorphous. However, in materials considered to be amorphous, there are generally still very small groups of atoms that possess the same arrangement as crystals [44].

Grain shape and size are determined by the plating conditions and the composition of the solution. If the grains are not randomly oriented, the condition is called a texture. In the case of electrodeposits the texture is a fiber axis because just as in a wire drawn through a die the directions perpendicular to the preferred orientation are randomly oriented. When electrodeposits are annealed, they generally recrystallize; that is, new grains form. When deposits recrystallize, the texture often changes. Simple plating solutions, such as acidified copper sulfate, produce large, columnar grains that generally exhibit a fiber axis. Solutions based on complex compounds, such as copper cyanide, or solutions containing active addition agents tend to yield fine-grained deposits that usually do not exhibit a texture.

There are defects in the crystalline arrangement. At the boundaries of grains there has to be a departure from the regular crystalline arrangement to accommodate different orientations or different crystal structures. Other defects in electrodeposits are primarily dislocations, twins, and codeposited foreign atoms or molecular groups. A dislocation is a line defect that can be thought of as being the boundary between a portion of a crystal plane that has been displaced by an applied force (i.e., slipped) and the portion that has not. However, dislocations can originate due to factors other than slip.

The density of dislocations in electrodeposits often approaches that of heavily, plastically deformed metals. Twins are a special type of grain that possesses two boundaries; the crystal arrangement on one side is the mirror image of that on the other side. Codeposited foreign atoms or molecular groups originate from intentional additions to the plating solutions or impurities in it.

Some deposits such as bright nickel show the so-called banded structure [45]. It manifests itself by a series of closely spaced, parallel lines seen in the cross section. It is caused by periodic variations of the overpotential. When the magnitude of the overpotential reaches its maximum value, growth is interrupted. This growth interruption appears as a line in the cross section. The periodicity of the interruptions results in the banded structure.

The substrate can affect the structure of the electrodeposit. If the interatomic distance in a particular crystal plane of the substrate closely matches that of a crystal plane of the deposit, the structure of the former may be continued into the latter (*epitaxy*). Oxides and other films on the substrate surface and distortions due to plastic flow from mechanical polishing hinder the development of epitaxy. Plating conditions that result in high overvoltages such as high current densities or certain additions to the plating solution are favorable to the formation of three-dimensional nuclei, that is, new grains. Then the relationship between the substrate and the deposit tends to be lost. On the other hand, elevated plating temperatures and low current densities favor epitaxial growth by allowing migration of atoms to sites where they can be incorporated into the existing structure.

There is a second way that substrate morphology can affect electrodeposit structure. Despite being cathodic, the substrate surface may dissolve in the plating solution and then redeposit with the plated metal as an alloy. Such is the case in some trivalent chromium plating solutions [46]. Etched substrate surfaces have been observed [47] to cause twins to form in the deposit.

Determining the structure and properties of electrodeposited materials entered a new phase with the emergence of nanotechnology as a field. Many electrodeposits are nanocrystalline or amorphous at the time of formation. Certain electrodeposit properties such as hardness, wear resistance, and electrical resistivity are strongly affected by grain size. Properties such as thermal expansion, Young's modulus, and saturation magnetization show little grain size dependence. Potential applications range from corrosion- and wear-resistant coatings to soft magnetic materials for magnetic recording.

1.13.1 Characterization

Microscopy and diffractometry are the main tools for determining the structure of electrodeposits. The transmission electron microscope permits measurement of structures on the nanoscale and is used to determine grain size. The scanning electron microscope is most widely used for monitoring deposit structures and chemical composition using X-ray fluorescence. X-ray diffraction (XRD) provides detailed structure information with less sample processing than is required for transmission electron microscopy (TEM). Scanning probe microscopes give the additional option for following electrodeposit growth in situ.

The transmission electron microscope has better resolution than the scanning electron microscope, with the capability to obtain electron diffraction patterns. By special techniques it is possible to obtain atomic resolution in TEM. The main disadvantage of TEM is that only very thin specimens can be examined. Thus extensive specimen preparation is required for most deposits.

With the transmission electron microscope, it is possible to determine the grain size unambiguously by placing the field-limiting aperature around an area believed to be a grain. Care must be taken that surrounding areas are not included by the aperature. An electron diffraction pattern is then obtained from the defined area. If the pattern is that of a single crystal, the area is a grain. The orientation of the grain as well as the direction in it can be determined from the diffraction pattern.

The scanning electron microscope is most frequently used for revealing the structure of electrodeposits. Its advantage over the optical microscope is a greater depth of field allowing a rough topography to be completely in focus. Surfaces that are electrically conducting can be examined with essentially no preparation. The scanning electron microscope also has better resolution than the optical one. The main disadvantage of SEM is that is is not possible to produce electron diffraction patterns. Thus the crystal structure and orientation of grains cannot be determined. Great care has to be taken when SEM is used to determine the grain size.

Most scanning electron microscopes have an attachment for chemical analysis by X-ray fluorescence. Because the electron beam can be focused on a small area, individual structural components can be chemically analyzed. Characteristic X rays can also be imaged so that the distribution of a particular chemical element can be seen.

When secondary electrons are used for imaging, nodules consisting of many crystallites can have the appearance of grains and be easily mistaken for them. It is possible to use backscattered electrons to image differences in orientation in the specimen and thus between grains. However, if there is a texture, which is frequently the case in electrodeposits, such a determination of grain size is difficult. The scanning electron microscope can also be operated to detect shorts in electrical circuits.

Recently a new class of scanning tunneling microscopes with resolution comparable to TEM has come into use for the study of the structure of electrodeposits. Their main advantage for the study of electrodeposits is that they can operate in liquids and can be used for in situ studies [48]. However, scanning tunneling microscopy (STM) cannot be used to observe continually changing processes because it takes a relatively long time to form an image. The tip is embedded in a cantilever beam. A laser measures the deflection of the beam and thereby the movement of the tip. The tunneling current controls the distance between the tip and the specimen surface in STM. A precisely controlled feedback system keeps the distance between the tip and the specimen surface constant, allowing it to follow the surface topography. Scanning tunneling microscopy has two disadvantages for studying electrodeposits. The tunneling current can affect the structure of an electrodeposit and all studied materials have to be electrical conductors.

The fiber axis is generally determined by XRD. The crystal direction perpendicular to the planes that result in

the highest intensity diffraction lines is usually taken as the fiber axis. Care must be taken to ensure that the preferred orientation is not a direction perpendicular to crystal planes that do not diffract, as, for example, the {211} planes of fcc metals.

Other methods used to characterize electrodeposits include:

- Differential Scanning Calorimetry (DSC) Phase transitions are detected using controlled measurement of temperature as heat is added or removed from a material.
- Scanning Electrochemical Microscopy (SECM) Chemical reactivity of a surface is mapped and monitored with a scanned probe. This is useful to evaluate materials for applications such as corrosion resistance.

1.14 PROPERTIES

1.14.1 Mechanical

The relevant mechanical properties are the modulus of elasticity; the yield, tensile, and fatigue strengths; and the ductility. The slope in the elastic portion is the modulus of elasticity. Yield strength is the stress to produce a small amount of plastic deformation called the *offset*. Tensile strength is the maximum stress. Ductility is the strain to fracture. Fatigue strength cannot be determined from a stress–strain curve. The mechanical properties are of particular importance for electroforms and printed circuits.

The two methods for determining the mechanical properties are the tensile and bulge tests. Tensile testing consists of applying a load continuously to a so-called dog-bone-shaped specimen until it fractures. The normally used tensile specimens are unsuitable for most electrodeposits. The 2-in.-wide reduced section of the standard tensile specimen has a width-to-thickness ratio that results in a nonuniform strain and therefore low values of the ductility [49].

Using a width-to-thickness ratio typical of the wiring of printed circuits and then scaling the other dimensions result in a tiny tensile specimen. Several machines to test such small specimens are in use [50]. The bulge test consists of clamping a foil over an orifice and introducing a fluid to cause a hemispherical bulge. A stress–strain curve can be constructed using measurements of the fluid pressure and the bulge height. The wiring of printed circuits, which are thermally cycled, can fail due to stresses that develop because of differences in the coefficients of thermal expansion between deposit and substrate. Thermal-cycling tests are used to test for such failures.

Sandia has developed a suite of mechanical properties measurements to measure stress–strain and fatigue properties of thin films used in MEMS fabrication. One documented example is Ni electrodeposited on metallized Si [51].

The moduli of elasticity of electrodeposits are generally smaller than those of the same metal formed in other ways. Possible reasons are the difficulty of obtaining accurate values and the possibility that deposits do not behave elastically.

The primary sources of strength are impediments to the movement of dislocations. In electrodeposits the main impediments are grain boundaries. Addition agents strengthen deposits primarily by refining the grains. Codeposited foreign substances can also increase the dislocation density. Dislocations can hinder the movement of others and thus strengthen materials.

Ductility is the amount of plastic deformation that can occur prior to fracture. Some deposits are inherently brittle because they contain cracks that readily lead to fracture. The cracks can be caused by the internal stresses, which will be subsequently discussed, and by stress corrosion.

Fine-grained deposits tend to be brittle because plastic deformation that occurs primarily by dislocation motion is impeded by the grain boundaries. Some deposits appear to be brittle but are really quite ductile. The reason for this behavior is a phenomenom called *necking*. Here the plastic deformation prior to fracture occurs in a very small volume. The overall plastic deformation is then quite small and thus indicative of poor ductility. However, the ductility, as indicated by the reduction in the cross-sectional area prior to fracture, may be quite good. When the deposit adheres well to the substrate, necking is essentially prevented.

Annealing of electrodeposits is mostly a low-temperature heat treatment to remove hydrogen, which can be a source of embrittlement. Electroforms may be heat treated so as to cause recrystallization. The recrystallization temperature of electrodeposits is generally lower than that of the same wrought metals. Some fine-grained copper electrodeposits have been observed by the author to recrystallize at ambient temperatures.

Precipitation hardening is possible for some supersaturated solid solution. Electroless nickel is an example of such an alloy that can be heat treated to cause the precipitation of Ni_3P or Ni_3B and thereby substantially increase the hardness and wear resistance [52].

Electrodeposition is well suited for the production of composites. The incorporation of hard material such as diamonds or ceramic particles can markedly improve the wear resistance. Composites consisting of thin alternate layers of two different materials can possess better strength properties than those of the individual ones. Composites have been produced consisting of alternate layers of two different metals such as nickel and copper, layers of alloys of different composition, or layers of different phases such as alpha and beta brass. These composites have been produced in one solution by alternately changing the plating conditions rather than by plating in two different solutions, which is impractical.

1.14.2 Magnetic

Allongue et al. [39] have demonstrated that electrodeposition can provide high-quality, epitaxial, ultrathin, magnetic layers with perpendicular magnetic anisotropy. This allows control of magnetism on a nanometer scale. The Allongue group also found that Co electrodeposited on Au(111) shows enhanced perpendicular magnetization anisotropy which is of interest for magnetic data storage [53].

Magnetic materials are classified as hard or soft depending on the value of the coercive force. Materials with coercive forces exceeding 200 Oe are considered magnetically hard. They are used, for example, in disc elements for information storage. Electroless cobalt–phosphorus alloys are magnetically hard materials. When it is desired that relatively low fields are capable of switching from cine remanence state to another, for example, as in plated-wire memory elements, magnetically soft materials are used. Examples of magnetically soft materials are iron–nickel alloys. A high remanence and a square hysteresis loop are desirable for both types of materials.

The principal structural element in magnetism is the domain. It is a small region that has a spontaneous magnetization. The sizes of domains vary greatly. For information storage, the domains should be as small as possible; their size is then limited by the width of their walls, which is less than 1 μm. At the other extreme, a whole magnet can be one domain. If the magnetization directions of all domains are randomly oriented, there is no net bulk magnetization. The effect of an imposed field is to align domains along its direction.

Domains already aligned grow at the expense of less favorably oriented ones by moving their walls. At the saturation magnetization, the only existing domains are those oriented in the proper direction. Since domains do not completely revert to the random orientation when the field is removed, there is remenance. The coercive force is that required to cause a random orientation of the magnetization directions of the various domains. A ferromagnetic element used for storing information is in either the positive or the negative remenence state, which constitutes its memory. The magnitude of the magnetization decreases drastically when the material is heated to the Curie temperature.

The microstructure of electrodeposited materials affects the magnetic properties in several ways. The previously discussed defects, namely dislocations, grain and twin boundaries, and some codeposited materials, make it more difficult for domain walls to move, and this results in higher coercive forces. The ease of moving domains also depends on the crystallographic orientations. Since each magnetic material possesses a particular orientation in which it is most easily magnetized, the texture is in this case of practical importance.

When a material is magnetized, its shape and volume change. The change, which is called *magnetostriction*, is due to a strain resulting from the magnetization. Magnetostriction can also be a change in the magnetization due to strains. When deposition occurs in a magnetic field, the structure, texture, and throwing power of both magnetic and nonmagnetic materials can be affected.

1.14.3 Internal Stress

Electrodeposits are often laid down in a state of stress termed either internal or residual because all or part of it remains in the deposit. Electroplaters are familiar with macrostress, as it manifests itself in the bending of parts plated on one side. If one end of a strip is clamped and the other one bends toward where the anode was located, the macrostress is tensile. If the strip bends in the opposite way, the macrostress is compressive. Macrostresses can cause distortions, cracking of the deposit, loss of adhesion to the substrate, and increased corrosion. Tensile macrostresses can also deteriorate the fatigue properties. The other type of stress—microstress—manifests itself primarily in an increase in the hardness.

The most commonly commercially used macrostress-measuring device is the spiral contractometer. The problem with devices such as the contractometer in which the specimen is allowed to deform is that some of the stress is relieved. There are devices used in research in which an opposing force is applied so as not to allow the specimen to deform. Microstresses can be determined only from the broadening of XRD lines. X-ray diffraction can also be used to measure macrostresses. However, it usually does not yield accurate values for electrodeposits because of the broadening of the diffraction lines due to microstresses and their symmetry due to twinning.

The structural causes of internal macrostresses are not fully understood. There is evidence that the coalescence of grains or parts of them growing laterally from different nucleation centers is a cause. The stress fields around oriented arrays of dislocation produced by coalescence or other growth processes can add in such a way as to result in macrostresses. The sign of the macrostress depends on the orientation of the array. The codeposition of hydrogen has been identified as a cause of macrostress.

If hydrogen diffuses out of a layer of the deposit allowing it to shrink, a tensile macrostress can develop. A tensile macrostress can also develop if hydrogen diffuses onto the substrate or previously laid-down layers causing them to expand. If micropores form during deposition and hydrogen then diffuses into them, causing them to expand, a compressive macrostress can be caused.

Polycrystalline thin films develop intrinsic stress, which can impede applications. As an example, the Sandia group determined that stress level tends to stabilize within the first 200 nm of film growth [54].

1.14.4 Hardness

The most frequently conducted test of the properties of electrodeposits that may be indicative of the strength and ductility is that of hardness. Hardness readings are of value when they have been experimentally related to the strength or ductility of a specific material. They can also be useful as an indication of wear resistance.

For electrodeposits, even the qualitative relationships commonly observed among hardness, tensile strength, and ductility do not always prevail. For example, it would be expected that hardness increases with tensile strength and decreases with ductility. However, the reverse effect is common among electrodeposits. It is particularly important, therefore, in dealing with deposits to be sure of the significance of the hardness values.

The most commonly performed hardness test is the indention test. It consists of pushing an indentor into the material via an applied load. The diameter or diagonal of the indent is measured with a microscope having a filar eyepiece. The indention is generally made on the cross section because the thickness of the coating has to be at east 14 times greater than the depth of the indent. Failing this requirement, the substrate affects the hardness value by what is commonly called the anvil effect.

The largest indent on the cross section for the greatest accuracy is obtained with the Knoop indentor, which is a symmetric, pyramidal, diamond point. It produces an indent whose length is about 7 times its width and 30 times its depth. The length of the indent should be, of course, parallel to the substrate–deposit interface. The Vickers indentor, which produces an indent whose length and width are equal, is also used for deposits. The nanohardness tester produces such a small indent that it can be used on the surface without causing the anvil effect. Since the hardness depends on the applied load, it should always be specified.

The useful Hall–Petch correlation tends to break for extremely small grain size. In one study of electrodeposited Ni and Co, the materials appear to strain harden and have reduced tensile strength when nanocrystal size decreases to the 5–20-nm range [55].

1.14.5 Adhesion

Adhesion can be regarded as the degree to which a bond has been developed from place to place at the coating–substrate interface. The strength of such a bond should equal or exceed the cohesive strength of the weaker of the two materials involved. Adhesion of metallic substrates is generally better than is required for normal service. Plating on plastics can present a serious adhesion problem.

There are several accepted methods for evaluating adhesion of electrodeposited coatings [32], Generally, the coating is pulled off mechanically, and tests should be performed with production items rather than test specimens where possible.

The Ollard test for bonding consists of plating a metal cylinder to a thickness of about 2.5 mm and then machining the deposit so as to leave a shoulder that is supported by a die. A load is applied to separate the deposit from the substrate and is indicative of the bond strength. Roehl [56] refined Ollard's method and extensively studied nickel on steel. His work and other investigations indicated that the bond strength equals or exceeds the cohesive strength of the weaker of the two involved metals.

Fracture rarely occurs at the interface if a good plating technique was employed. If the load is applied perpendicular to the deposit–substrate interface, the value of the bond strength is more quantitative. To apply the load in this way, a nodule shaped by an electroforming technique is deposited on the substrate and subsequently pulled off. The bond strength is then the load needed to pull off the nodule divided by its area.

The main factor that is detrimental to adhesion is a brittle layer which can form by diffusion between the deposit and substrate. Brittle layers form especially if annealing is involved. An example is copper plated on zinc die castings, which forms blisters during the baking of enamels applied over the coating.

1.15 APPLICATIONS

Electrodeposited thin films are playing a major role in the development of new magnetic materials. Allongue and his group [39] are developing a picture of epitaxial growth and magnetism for ultrathin magnetic layers, such as Ni, Co, and Fe on Au(111). Their research supports development of both bit-patterned storage media where each nanostructure will bear one bit of information and magnetic random-access memory.

Thermoelectric devices are another emerging technology that uses electrodeposited materials [38]. Nanostructured deposits of the alloys of bismuth, antimony, tellurium, and select other elements have useful thermoelectric properties. One successful fabrication technique is to electrodeposit the materials into nanoscale pores [37]. Thermoelectrics are an important energy conservation enabler for turning waste heat into useful electricity.

Electrodeposition of materials that can change phase on heating or cooling is opening up new application opportunities. In one example, SbTe is deposited in the amorphous state at room temperature. On heating, the film crystallizes to Sb_2Te_3 at 120°C. This switching between amorphous and crystalline forms is potentially useful for rewritable optical storage and solid-state memory [43].

Electrolytic deposition is uniquely suited to produce the wiring of printed circuits and the interconnections of multilayer microchips. By the use of photoresist, the areas to be plated can be precisely defined. Autocatalytics, known as electroless plating, permit a conducting layer to be deposited on insulating materials. Thin layers of solder can be deposited for making connections. Some unique materials for use in electronic applications have been developed. Of special importance are materials having structures on the nanometer scale [36].

REFERENCES

1. M. Paunovic and M. Schlesinger, *Fundamentals of Electrochemical Deposition*, Wiley, New York, 1998 and 2006.
2. J. O'M. Bockris and A. K. N. Reddy, *Modern Electrochemistry*, Vol. 1, Plenum, New York, 1998.
3. E. Mattsson and J. O'M. Bockris, *Trans. Faraday Soc*, **55**, 1586 (1959).
4. A. J. Bard and L. R. Faulkner, *Electrochemical Methods*, Wiley, New York, 1980.
5. W. Lorenz, *Z. Phys. Chem.*, **202B**, 275 (1953).
6. W. Lorenz, *Z. Elektrochem.*, **57**, 382 (1953).
7. W. Lorenz, *Naturwissenschaften*, **40**, 576 (1953).
8. W. J. Lorenz, *Z. Naturforsch*, **9a**, 716 (1954).
9. W. Mehl and J. O'M. Bockris, *J. Chem. Phys.*, **27**, 817 (1957).
10. W. Mehl and J. O'M. Bockris, *Can. J. Chem.*, **37**, 190 (1959).
11. B. E. Conway and J. O'M. Bockris, *Proc. Roy. Soc. London*, **A248**, 394 (1958).
12. B. E. Conway and J. O'M. Bockris, *Electrochim. Acta*, **3**, 340 (1961).
13. G. H. Gilmer and P. Bennema, *J. Appl. Phys.*, **43**, 1347 (1972).
14. N. Ibl, *Surf. Technol.*, **10**, 81 (1980).
15. A. M. Pesco and H. Y. Cheh, in *Modern Aspects of Electrochemistry*, No. 19, B. E. Conway, J. O'M. Bockris, and R. E. White, Eds., Plenum, New York, 1989.
16. C. H. Ting, V. Dubin, and R. Cheung, in *Fundamental Aspects of Electrochemical Deposition and Dissolution Including Modeling*, M. Paunovic, M. Datta, M. Matlosz, T. Osaka, and J. B. Talbot, Eds., *Proceedings,* Vol. 97-27, Electrochemical Society, Pennington, NJ, 1997, p. 321.
17. E. Budevski, G. Staikov, and W. J. Lorenz, *Electrochemical Phase Formation and Growth*, VCH Publishers, New York, 1996.
18. D. J. Srolovitz, A. Mazor, and G. G. Bukiet, *J. Vac. Sci. Technol.*, **A6**, 2371 (1988).
19. A. Damjanovic, M. Paunovic, and J. O'M. Bockris, *J. Electroanal. Chem.*, **9**, 93 (1965).
20. J. O. Dukovic and C. Tobias, *J. Electrochem. Soc.*, **137**, 3748 (1990).
21. C. Madore and D. Landolt, *J. Electrochem. Soc.*, **143**, 3936 (1996).
22. H. Leidheiser Jr., *Z. Elektrochemie*, **59**, 756 (1955).
23. O. Kardos and D. G. Foulke, in *Advances in Electrochemistry and Electrochemical Engineering*, Vol. 2, C. W. Tobia, Ed., Wiley-Interscience, New York, 1962.
24. R. Weil and R. Paquin, *J. Electrochem. Soc.*, **107**, 87 (1960).
25. L. Oniciu and J. Muresan, *J. Appl. Electrochem.*, **21**, 565 (1991).
26. G. T. Rogers and K. J. Taylor, *Electrochim. Acta*, **8**, 887 (1963); **11**, 1685 (1966); **13**, 109 (1968).
27. M. Paunovic, *Plating*, **55**, 1161 (1968).
28. M. Satto, *J. Met. Fin. Soc. Jpn.*, **17**, 14 (1966).
29. M. Paunovic, in *Electrochemistry in Transition*, O. J. Murphy, S. Srinivasan, and B. E. Conway, Eds., Plenum, New York, 1992, p. 479. [29a] M. Yoshino, T. Masuda, T. Yokoshima, J. Sasono, Y. Shacham-Diamand, I. Matsuda, T. Osaka, Y. Hagiwara, and I. Sato, *J. Electrochem. Soc.*, **154** (3), D122 (2007). [29b] J. W. Gallaway and A. C. West, *J. Electrochem. Soc.*, **155**, D632 (2008). [29c] R. Manu and S. Jayakrishnan, *J. Electrochem. Soc.*, **156** (7), D215 (2009).
30. A. Brenner, Ph.D. Thesis, University of Maryland, 1939.
31. J. Yahalom and O. Zadok, *J. Mater. Sci.*, **22**, 499 (1987).
32. W. Dini, *Electrodeposition: The Materials Science of Coatings and Substrates*, Noyes, New York, 1993.
33. I. Gurrappa and L. Ginder, *Sci. Technol. Adv. Mater.*, **9**, 043001 (2008).
34. S. C. Tjong and H. Chen, *Mater. Sci. Eng.*, **R45**, 1 (2004).
35. L. P. Bicelli et al., *Int. J. Electrochem. Sci.*, **3**, 356 (2008).
36. M. Datta and D. Landolt, *Electrochim. Acta*, **45**, 2535 (2000).
37. E. Kouiharenko et al., *J. Micromech. Microeng.*, **18**, 104015 (2008).
38. F. Xiao et al., *Electrochim. Acta*, **53**, 8103 (2008).
39. P. Allongue et al., *Surf. Sci.*, **603**, 1831 (2009).
40. K. Kajeshwar, N. R. de Tacconi and C. R. Chenthamarakshan, *Curr. Opin. Solid State Mater. Sci.*, **8**, 173 (2005).
41. I. M. Dharmadasa and J. Haigh, *J. Electrochem. Soc.*, **153** (1), G47 (2006).
42. C. C. Koch, *J. Phys. Conf. Ser.*, **l44**, 012081 (2009).
43. Q. Huang, A. J. Kellock, and S. Ranoux, *J. Electrochem. Soc.*, **155** (2), D104 (2008).
44. R. Weil and K. Parker, in *Elctroless Plating*, G. O. Mallory and J. B. Hajdu, Eds., American Electroplaters and Surface Finishers Society, Orlando, FL, 1990, pp. 111–138.
45. C. C. Nee and R. Weil, *Surf. Technol.*, **25**, 7 (1985).
46. C. Sheu and R. Weil, *J. Electrochem. Soc.*, **137**, 2052 (1990).
47. E. C. Felder, S. Nakahara, and R. Weil, *Thin Solid Films*, **84**, 197 (1981).
48. C. J. Weber, H. W. Pickering, and K. G. Weil, *J. Electrochem. Soc.*, **144**, 2364 (1997).
49. K. Lin, I. Kim, and R. J. Weil, *Plating Surf. Finish.*, **75**, 52 (1988).

50. Kim and R. Weil, in *Testing of Metallic and Inorganic Coatings*, ASTM **STP** 947, W. B. Harding and G. DiBari, Eds., American Society for Testing and Materials, Philadelphia, PA, 1987, pp. 11–18.
51. S. J. Hearne et al., Report SAND 2005-7067, Sandia National Laboratories, Albuquerque, NM, 2005.
52. R. J. Weil and K. Parker, in *Electroless Plating*, G. O. Mallory and J. B. Hajdu, Eds., American Electroplaters and Surface Finishers Society, Orlando, FL, 1990, p. 111.
53. P. Prudhomme et al., Abstract 293, Presented at the 207th ECS Meeting, 2005.
54. A. Bhandari, B. W. Sheldon, and S. J. Hearne, *J. Appl. Phys.*, **101** (3), 033528 (2007).
55. L. Brooks et al., *Mater. Sci. Eng.*, **A491**, 412 (2008).
56. E. J. Roehl, *Iron Age*, **146** (13), 17 (1940); **146** (14), 30 (1940).

2

ELECTRODEPOSITION OF COPPER

JACK W. DINI AND DEXTER D. SNYDER[1]

Copper is the most common metal plated, exclusive of continuous strip plating and nickel [1]. The major uses of electroplated copper are plating on plastics, printed wiring boards, zinc die castings, automotive bumpers, rotogravure rolls, electrorefining, and electroforming [2]. Electroplated copper is playing a major role in the change from aluminum to copper in semiconductor interconnect technology. This materials change was heralded as a "major breakthrough" in *The New York Times* (September 22, 1997) and a "dazzling technical advance" by *Time* magazine (October 10, 1997) [2a]. It signals one of the most important changes in materials that the semiconductor industry has experienced since its creation [2b]. Copper is electrodeposited for numerous engineering and decorative applications requiring a wide range of mechanical and physical properties. The range extends from properties superior to full-hard wrought copper to properties equivalent to annealed pure copper [3].

Copper is an excellent choice for an underplate, since it often covers minor imperfections in the base metal. It is relatively inert in most plating solutions of other common metals; it has a very high plating efficiency, resulting in excellent coverage even on difficult-to-plate parts; and lastly, it is highly conductive, making it an excellent coating for printed wiring boards or as a coating on steel wire used to conduct electricity [1].

Copper deposits also act as thermal expansion barriers by absorbing the stress produced when metals with different thermal expansion coefficients undergo temperature changes, and this is particularly helpful with plastic substrates. The leveling and brightness properties of copper deposits can be further enhanced by buffing, and since copper is much softer than steel or nickel, it is easy and relatively inexpensive to buff [4].

Of the plating systems that have been studied, only relatively few have revealed a stage of commercial importance for electrodeposition of copper. These are the alkaline cyanide and pyrophosphate complex ion systems and the acid sulfate and fluoborate simple ion systems. Other types of solutions have been too unstable or lacking in good deposit characteristics over sufficiently wide current density ranges [5]. In recent years some alkaline noncyanide systems have been developed for replacing cyanide.

The areas of application of the various copper plating solutions overlap somewhat, but each has its fairly well-defined area of usefulness. Clearly, the most heavily used are the acid copper sulfate solutions. Open literature publications and patents for sulfate solutions since the 1974 edition of this book in [6] far outnumber those of all the other solutions combined. Deposits produced in cyanide solutions are typically thin ($<12.5\,\mu m$) and are used as an undercoating for nickel and chromium, as a heat treatment slop-off for selective hardening of ferrous parts, or as an intermediate step prior to additional plating. For example, a copper cyanide deposit is typically a key part of the activation cycle for preparing aluminum, beryllium, and zinc die castings for plating.

Copper deposits from cyanide solutions are not generally suitable for deposition of relatively thick deposits for electroforming and similar applications. Cyanide solutions are finding less and less favor because of their toxicity and waste treatment problems and are being replaced by noncyanide solutions. Pyrophosphate solutions, once used heavily for plating through holes on printed wiring boards, have been almost completely replaced by high-throw acid sulfate solutions. Fluoborate solutions have been advertised for many years as having the capability to deposit copper at very high

[1] Dexter D. Snyder, Part F.

Modern Electroplating, Fifth Edition Edited by Mordechay Schlesinger and Milan Paunovic

current densities. However, present commercial usage of this type of solution is minimal simply because other solutions such as those with sulfate ions can do the same job and are less expensive, easier to control, and less susceptible to impurities. The chemical cost of acid fluoborate electrolyte is approximately twice that of acid sulfate per gallon, which is one strong reason why fluoborate copper has not gained a significant share of the through-hole plating market [7]. Continuous copper plating from fluoborate solutions on electroless coated plastic circuits has been reported [8].

PART A ACID COPPER*

2.1 HISTORY AND DEVELOPMENT

Acid copper deposition was referred to as early as 1810 [9]. In 1831 Bessemer [10] copper plated steel castings of frogs, insects, and plants by immersion in copper sulfate solution on a zinc tray. In 1836 the Daniel cell was first used for electrodepositing copper [11] and a technical report was published by De la Rue [12]. In 1839 Jacobi made Russian bank notes using copper-plated electrotypes, and in 1840 he received the first patent for making electrotypes [13]. Smee discussed commercial copper plating processes in 1843 [9]. During the next 70 years, progress was directed principally toward developing specific applications for acid copper electrodeposition. Most of the efforts dealt with Cu^{2+} sulfate–sulfuric acid solutions, but oxalate [14], nitrate [15], acetate [15], fluosilicate [16, 17], and Cu^{1+} chloride [16] solutions were also investigated.

In more recent times the following solutions have been evaluated: sulfate–oxalate–boric acid [18], sulfate–oxalate [19, 20], Cu^{1+} chloride [21], Cu^{1+} chloride–sodium thiosulfate [22], benzene disulfonic acid [23], Cu^{1+} iodide and bromide [24], iodide and chloride [25], fluoborate [26, 27], alkane sulfonic acid [28, 29], sulfamic acid [30, 31], Cu^{2+} formate with ammonium salts [32], phosphate–sulfate [33], fluosilicate [34], fluosilicate–silicic acid [35], Cu^{2+} glycolate, lactate, malate, and tartrate [36].

At the present time only the sulfate and fluoborate solutions are commercially used. Passal reviewed the first 50 years of AES (American Electroplaters' Society) copper plating history in 1959 [5] and Van Tilburg covered the 75-year history in 1984 [11]. Other reviews of acid copper plating can be found in the literature [6, 37–41].

2.2 APPLICATIONS

Electrodeposition of copper from acid solutions is extensively used for electroforming, electrorefining, and electroplating. Refiners and electroformers, in particular, employ acid solutions because costs of chemicals and power are low and because the solutions are simple and easy to control. In the electrowinning and electrorefining industries, acid solutions are employed exclusively. More than 80% of the domestic production of primary copper is refined electrolytically.

Acid copper sulfate solutions are widely used for plating of printed wiring boards and for semiconductor interconnect technology. Electroformed copper articles include band instruments, heat exchangers, reflectors, and a variety of articles for military and aerospace applications. All three main types of printing processes (electrotyping, rotogravure work, and lithography) use copper and sometimes nickel and chromium [42].

Acid copper solutions containing organic brightening and leveling agents are used extensively to deposit smooth copper on rough steel and etched plastics. Zinc die castings are plated with approximately 15 μm of leveling acid copper [43, 44], before nickel and chromium plating, to eliminate buffing before plating. Because of the excellent microthrowing power of the acid copper, pits, pores, or crevices in either steel or zinc surfaces are well filled with copper, and this improves resistance to corrosion or blistering [45–47]. Acid copper deposits are one part of the sequence for decorative plating of aluminum wheels for automotive applications. In some cases the copper is buffed to add luster to the low-current-density areas of the wheel and to flow some of the copper over small pits and voids [48]. Coatings on plastics need to be bright and ductile and have the capability to expand and contract with the thermal expansion of the plastic without cracking, blistering, or peeling. Bright decorative acid copper deposits meet these requirements [4, 49].

One of the most important steps in the production of plated wire for memory use is copper plating in acid sulfate solution [50]. Many kilometers of steel wire are given a copper cyanide strike and plated with copper in acid solutions to produce a high-strength electrical cable. Thick deposits (200 μm) of copper are applied to steel rolls and then engraved for use in printing and marking papers and textiles. Stainless steel cooking vessels are copper plated in acid solutions to improve the heat diffusion characteristics of outer surfaces and avoid local hot spots. Copper plating for stopping off carburizing on selected areas is accomplished by striking in a cyanide solution followed by plating in acid solutions. Acid copper plating is sometimes used for building up worn or overmachined parts, especially when copper surfaces are desired for protection against fretting corrosion. Optical surfaces can be produced on parts by single-point diamond turning specific acid copper deposits [51–54].

Metal powders produced by deposition in acid solutions are used for making sintered compacts and pigments. The powder is deposited from dilute solutions at high temperatures, brushed off the cathodes, filtered, washed, ground into fine particles, screened, and blended for use in manufacturing

* Revision of section by W. H. Safranek in the 1974 edition.

powder compacts [55, 56]. Copper sulfate solutions have also been recommended for plating "low-density" powder compacts to fill porosity near the surface [57].

2.3 PRINCIPLES

The Cu^{2+} salts in either the sulfate or the fluoborate solution are highly ionized except for small amounts of less ionized complex salts formed with certain addition agents. The addition of sulfuric acid to the sulfate solution, or fluoboric acid to the fluoborate solution, is necessary for obtaining acceptable deposits. Because of the high conductivity of commercial solutions and because anode and cathode polarizations are small, voltages required for depositing copper are less for acid than for alkaline solutions. Electrorefining plants employ the copper sulfate solution largely for this reason. Tank voltages for refining copper are frequently as low as 0.2 V for a cathode and anode current density of 1.6–2.2 A dm^{-2}.

Anode and cathode polarizations are nearly negligible in purified solutions used at low current densities. Even at the high cathode current density of 21.5 A dm^{-2}, a 6-V current source is ample when the solution is efficiently agitated. Excessive polarization of the anodes in the sulfate solution may occur when the anode current density exceeds about 5 A dm^{-2}. With the fluoborate solution, the anode current density can be at least 40 A dm^{-2} without encountering excessive anode polarization. Anode and cathode efficiencies are nearly 100% at all practical current densities. The rate of deposition obtainable depends chiefly on the efficiency of agitation in preventing excessive polarization. Acceptable deposits were reported at a current density as high as 260 A dm^{-2}, equivalent to 3.63 mm h^{-1} [58], with violent agitation.

The first stages of the formation of a copper deposit depend on the deposition rate, the substrate surface nature, and the deposition technique [59]. The final stage in the growth involves an equilibrium of copper electrochemically dissolving and precipitating [60]. The character of copper deposits is influenced by the concentrations of copper salts, additives, free acid, temperature, cathode current density, and the nature and degree of agitation. At potentials between −60 and −30 mV, the growth of bulk copper proceeds in cycles of nucleation, agglomeration, and crystallization.

The concentration profile of copper in an acid electrolyte has been measured in an attempt to understand the effects of the supporting electrolyte on the rate of mass transfer of Cu^{2+} ion toward the cathode surface [61]. Overpotential relaxation experiments have shown that calculated mass-transfer boundary layer thicknesses increased with increasing electrode length and solution viscosity and decreased with increasing current density [62]. Impedance behavior of a copper cathode in an acid copper electrolyte has also been studied [63].

2.4 FUNCTIONS OF SOLUTION CONSTITUENTS

2.4.1 Copper and Sulfuric Acid

Cu^{2+} sulfate ($CuSO_4 \cdot 5H_2O$) and sulfuric acid, or Cu^{2+} fluoborate [$Cu(BF_4)_2$] and fluoboric acid, are the primary constituents of the sulfate and fluoborate solutions, respectively. The copper salts furnish the metal ions in solutions such as those given in Table 2.1, which contains formulations for conventional and high-throw solutions. The latter are used for plating printed wiring boards and are discussed in detail in a subsequent section. Copper can be deposited at very low cathode current densities from the acid-free aqueous solutions of the salts [64, 65], but at higher current densities the deposits from the sulfate solution are spongy and contain occluded salts. Plate characteristics are improved, solution conductivity is increased, and anode and cathode polarizations are greatly reduced when free acid is added to either solution [26, 66]. The acid also prevents the precipitation of basic salts.

The concentration of copper sulfate is not particularly critical, although the resistivity of the solution is greater when the concentration is increased [67]. Cathode polarization increases slightly at copper sulfate concentrations above 1*M* (250 g L^{-1}) [68]. A concentration of less than 60 g L^{-1} copper sulfate results in a decreased cathode efficiency [69]. Changes in the concentration of copper sulfate have little

TABLE 2.1 Formulations of Acid Copper Solutions

Copper Sulfate Solutions	Conventional Solutions	High-Throw Solutions
Copper sulfate, $CuSO_4 \cdot 5H_2O$, g L^{-1}	200–250	60–100
Sulfuric acid, H_2SO_4, g L^{-1}	45–90	180–270
Chloride, mg L^{-1}	—	50–100
Copper Fluoborate Solutions	**Low-Concentration Solutions**	**High-Concentration Solutions**
Copper fluoborate, $Cu(BF_4)_2$, g L^{-1}	225	450
Fluoboric acid, HBF_4, g L^{-1}	15	30
Boric acid, H_3BO_3, g L^{-1}	15	30

effect on grain size, but some grain refinement occurs as a result of increasing the sulfuric acid concentration to 1.5 N (72 g L^{-1}) [70]. When very high cathode current densities are used, a high concentration of copper sulfate, within the limits given in Table 2.1, is recommended. The solubility of copper sulfate is decreased when the sulfuric acid concentration is increased [66].

Changes in sulfuric acid concentration have more influence than changes in copper sulfate concentration on anode and cathode polarization and on solution conductivity. Cathode polarization decreases when a small amount of sulfuric acid is added to a solution of copper sulfate, reaches a minimum at about 0.4 M (38 g L^{-1}), and increases with a further increase in sulfuric acid concentration [68]. Throwing power increases dramatically in low-copper (15 g L^{-1}), high-sulfuric-acid solutions [71]. Excess sulfuric acid drastically increases the cathodic overpotential and introduces a smaller ratio of level plane of electrodeposits resulting in nodular precipitates [72]. It also drastically changes the X-ray diffraction pattern by increasing the surface overpotential and inducing three-dimensional nucleation at the higher overpotential [73]. Specific conductivity is nearly doubled when the concentration of sulfuric acid is raised from 50 to 100 g L^{-1} [74]. An additional increase in free-acid concentration to 200 g L^{-1}, which is the level widely used in electrorefining, reduces the resistivity from 4.2–4.3 to 1.6–1.9 μΩ-cm [75].

2.4.2 Chloride

The chloride ion, in bright and high-throw acid sulfate solutions, reduces anode polarization [76] and eliminates striated deposits in high-current-density areas [40]. It is important to control the chloride ion at 60–80 ppm. Below 30 ppm, deposits will be dull, striated, coarse, and step plated. Above 120 ppm, deposits will be coarse grained and dull, and the anodes will polarize, causing plating to stop [41]. The chloride ion affects the surface appearance, structure, microhardness, crystallographic orientation, and internal stress of the deposits [77–79]. A minimal amount of chloride was essential to the ductility of deposits from two different proprietary copper plating solutions. The elongation in each case was found to rise dramatically for chloride additions in the 10-mg L^{-1} range [80].

Among the halides, Cl^- is the most effective over a wide range of concentrations (40–150 mg L^{-1}) in keeping stress to a null value, and this is particularly important considering the synergistic effect of Cl^- over some brightening additives normally used [81]. The presence of about 50 mg L^{-1} chloride is optimum for permitting an increase in microhardness without raising internal stress [82]. The chloride ion exerts no influence on throwing power [82, 83].

In the presence of Cl^- and additives, such as thiourea or a commercial proprietary brightener, it is suggested that in addition to CuCl surface films adsorbed Cu(I) or Cu(I) complex–Cl bridge films inhibit surface diffusion of adsorbed Cu atoms, and this becomes the rate-determining step in the deposition mechanism [84–86]. With solutions containing polyethylene glycols (PEGs), the absence or reduced quantities of chloride alters the suppression effect of PEG, adversely affecting deposit morphology. In the presence of chloride, PEG fractions inhibited currents much more strongly than in the presence of PEG alone [87].

Small amounts of chloride ion are known to have an accelerating effect on the deposition of copper. This supports the hypothesis that chloride ions act as binding sites for surfactants such as PEG to the electrode surface [88–90]. Excess chloride can produce insoluble copper chlorides at the anode surface, hindering the deposition process [91]. Although chloride ion is adsorbed on depositing copper, up to 10^{-3} M chloride ion has little effect on the current–voltage curve for acid sulfate solutions containing no brighteners or additives [92].

2.4.3 Fluoborate

Copper fluoborate is more soluble than copper sulfate. Metal ion concentration can be more than double in the fluoborate solution in comparison with a copper sulfate solution containing 50–75 g L^{-1} of sulfuric acid. If the acid concentration in the fluoborate solution is too low (pH more than 1.7), deposits are dull, dark, and brittle. Boric acid is added to stabilize the solution and prevent decomposition of copper fluoborate; this increases resistivity slightly. In a solution with a concentration of more than 15 g L^{-1} fluoboric acid or 220 g L^{-1} copper fluoborate, an increase in the concentration of either the salt or the acid lowers the resistivity.

2.5 ADDITION AGENTS

Addition agents for brightening, hardening, grain refining, surface smoothing, increasing the limiting current density, and reducing trees are frequently added to acid copper sulfate solutions. An extensive list of additives used in acid copper plating prior to 1959 can be found in the literature [5] and in the acid copper chapter in a previous edition of this book [6]. Additives covered in patents granted in recent years are listed in Table 2.2. Materials that have been reported in recent technical literature publications include benzotriazole [84, 85, 93, 94], cadmium [95], casein [96], cobalt [97], dextrin [96], dimethylamino derivatives [98], disulfides [98, 99], 1,8-disulfonic acid [93], disodic 3,3-dithiobispropanesulfonate [100], 4,5-dithiaoctane-l,8 disulfonic acid [93], dithiothreitol [101], ethylene oxide [100], gelatin [102], glue [76, 96], gulac [76], lactose benzoylhydrazone [103], 2-mercaptoethanol [104], molasses [96], sulfonated petroleum [76], *o*-phenanthroline [95, 105], polyethoxy

TABLE 2.2 Additives That Have Been Patented for Copper Plating

Patent Reference	Date of Issue	Investigator	Additives
		Acid Copper Sulfate	
U.S.5,433,840	7/18/95	Dahms et al.	Polyalkylene glycol
U.S.5,431,803	7/11/95	DiFranco et al.	Animal glue
U.S.5,417,841	5/23/95	Frisby	Alkoxythio and sulfonated compounds
U.S.5,403,465	4/4/95	Apperson et al.	Animal glue and an impurity
U.S.5,328,589	7/12/94	Martin	Polymers comprising ether groups
U.S.5,252,196	10/12/93	Sonnenberg et al.	Numerous additives
U.S.5,215,645	6/1/93	DiFranco et al.	High-protein polymers of amino acids
U.S.5,174,886	12/29/92	King et al.	Polyalkylene glycols
U.S.5,151,170	8/29/92	Montgomery et al.	Peroxide oxidation; product of a dialkylaminothioxomethylthioalkane sulfonic acid
U.S.5,145,572	8/8/92	Hupe et al.	Hydroquinone or ethoxylated alkylphenols
U.S.5,068,013	11/26/91	Bernards et al.	Polyethylene oxides
U.S.5,051,154	9/24/91	Bernards et al.	Polyethylene oxides, glycols, and amines
U.S.5,024,736	6/18/91	Clauss et al.	Disubstituted ethane sulfonic compounds
U.S.4,990,224	2/5/91	Mahmoud	Urea, sodium lauryl sulfate, and tosyl or mesyl sulfonic acid
U.S.4,975,159	12/4/90	Dahms	Alkoxylated lactam amides
U.S.4,954,226	9/4/90	Mahmoud	Urea and glycerin
U.S.4,948,474	8/14/90	Miljkovic	Alkylarylene
U.S.4,897,165	1/30/90	Bernards et al.	Copper/sulfuric acid ratios
U.S.4,781,801	11/1/88	Frisby	Polyether surfactants + sulfurized benzene + grain refiner
U.S.4,673,467	6/16/87	Nee	Polyethers + mercaptoimidazole + sulfurized benzene
U.S.4,555,315	11/26/85	Barbieri et al.	Polyethers + organic divalent sulfur compound + tertiary alkyl amine with polyepichlorohydrin
U.S.4,551,212	11/5/85	Rao et al.	Phenazine dyestuffs
U.S.4,540,473	11/22/83	Bindra et al.	S-containing anions other than SO_4
U.S.4,521,282	7/11/84	Tremmel	Sulfamic acid
U.S.4,490,220	12/25/84	Houman	Nitrogen–carbon–sulfur compound
U.S.4,430,173	2/7/84	Boudot et al.	Sodium salt of *W*-sulfo-*n*-propyl *N*,*N*-diethyldithiocarbamate, PEG, and crystal violet
U.S.4,376,685	6/24/81	Watson	Alkylated polyalkyleneimine
U.S.4,347,108	8/31/82	Willis	Nitrogen- and sulfur-containing compounds
U.S.4,336,114	6/22/82	Mayer et al.	Phthalocyanine, tertiary alkyl amine with polyepichloro hydrin, polyethyleneimine
U.S.4,334,966	12/2/81	Beach et al.	Polyether, mercaptoimidazole, sulfurized benzene
U.S.4,310,392	1/12/82	Kohl	Phenolphthalein
U.S.4,272,335	2/19/80	Combs	Substituted phthalocyanine radical
U.S.4,242,181	12/30/80	Malak	Regular coffee
U.S.4,134,803	1/16/79	Eckles et al.	Disulfides, sulfonic acids, and aliphatic aldehyde
U.S.4,110,176	8/29/78	Creutz et al.	Alkoxylated polyalkyleneimine
U.S.4,038,161	7/26/77	Eckles et al.	Epihalohydrins
U.S.4,036,710	7/19/77	Kardos et al.	Di- or triaminotriphenylmethane dyes and sulfoalkylsulfides
U.S.4,014,760	3/29/77	Kardos et al.	Aryl and sulfoalkyl sulfide compounds
U.S.4,009,087	2/22/77	Kardos et al.	Heteroaromatic, sulfoalkylsulfide and sulfoarylsulfide compounds
U.S.3,966,565	6/29/76	Kardos et al.	Aryl amine and sulfoalkyl sulfide compounds
U.S.3,956,120	5/11/76	Kardos et al.	Amines and sulfoalkyl sulfide compounds
U.S.3,956,084	11/21/74	Kardos et al.	Aryl amine and sulfoalkyl sulfide compounds
U.S.3,956,078	5/11/76	Kardos et al.	Amines and sulfoalkyl sulfide compounds
U.S.3,956,079	5/11/76	Kardos et al.	Aryl amine and sulfoalkyl sulfide compounds
U.S.3,940,320	2/24/76	Kardos et al.	Aryl *N*-heteroaromatic and sulfoalkyl sulfide compounds
U.S.3,923,613	8/27/74	Immel	Urea
U.S.3,841,979	10/15/74	Arcilesi	Polyethers
U.S.3,804,729	4/16/74	Kardos et al.	Polysulfides, heterocyclic sulfur and polyether compounds
U.S.3,798,138	3/19/74	Ostrow et al.	2-thia- or 2-imidazolidinethiones, aldehydes, and carbon sulfur groups
U.S.3,778,354	12/11/73	Toledo	cobalt

(*continued*)

TABLE 2.2 (*Continued*)

Patent Reference	Date of Issue	Investigator	Additives
U.S.3,775,265	8/25/70	Bharucha	Amine for plating on Al
U.S.3,775,264	3/9/72	Bharucha	Amine and ammonia for plating on aluminum
U.S.3,770,598	11/6/73	Creutz	Polyethyleneimine
U.S.3,770,597	3/16/71	Tixier	Formaldehyde and thiourea
U.S.3,769,179	1/19/72	DuRose	High-acid, low-copper + grain refiners
U.S.3,715,289	2/8/71	Pope Jr.	Ethylene oxide adduct + 2-mercaptopyridine
U.S.3,682,788	8/8/72	Kardos et al.	Polysulfides, thiourea, and polyethers
U.S.3,767,539	10/23/73	Clauss et al.	Selenium compounds
U.S.3,751,289	8/7/73	Arcilesi	Polyethers
U.S.3,743,584	7/3/73	Clauss et al.	Polymeric phenazonium compounds
U.S.3,732,151	5/8/73	Abbott	Triarylmethane and sulfurized sulfonated aromatics
U.S.3,725,220	4/3/73	Kessler et al.	Sulfonium compounds
		Pyrophosphate Copper	
U.S.5,100,517	3/31/92	Starinshak et al.	Plating of wire with insoluble anodes
U.S.3,928,148	12/23/75	Lerner	Pyro + cyanide
U.S.3,784,454	1/8/74	Lyde	Mercaptothiadiazoles, aliphatic dicarboxylic acids, and hydroxyethyl cellulose
U.S.3,729,393	4/24/73	Lyde	Mercaptothiazoles, thiazoles, or pyrimidines + alkaryl-sulfonic acids
U.S.3,775,268	12/30/71	Fino et al.	Lead
U.S.3,674,660	7/4/72	Lyde	Iminodiacetic, cinammic, aliphatic, carboxylic acids, and hydroxyethylcellulose
		Cyanide Copper	
U.S.3,790,451	2/5/74	Weisenberger et al.	Acetylenic alcohol + complexing agent + hydroxy acid
		Cyanide-Free Copper	
U.S.4,933,051	6/12/90	Kline	Organophosphonates
U.S.4,521,282	6/4/85	Tremmel	Sulfamic acid
U.S.4,469,569	9/4/84	Tomaszewski et al.	pH 7.5–10.5 + a Cu-soluble anode and a ferrite-insoluble anode
U.S.4,462,874	7/31/84	Tomaszewski et al.	pH 6–10.5 + a Cu-soluble anode and a Ni–Fe alloy–insoluble anode
U.S.4,389,286	8/28/82	McCoy	Copper, tin, lead, and glucoheptonic acid
U.S.3,928,147	10/9/73	Kowalski	Phosphonates for zinc die castings
U.S.3,833,486	3/26/73	Nobel et al.	Phosphonates
U.S.3,706,635	11/15/71	Kowalski	Phosphonates
U.S.3,706,634	11/15/71	Kowalski	Phosphonates
U,S.3,475,293	10/28/69	Haynes et al.	Phosphonates

ether [106], polyethylene glycol [87, 107, 108], polyethylene imine [107], poly *N*,*N*′-diethylsaphranin [100], polypropylene ether [109, 110], propylene oxide [100], sugar [96], thiocarbamoyl-thio-alkane sulfonates [111], and thiourea [76, 81, 84, 85, 96, 112–114]. Chloride, which can also be considered an additive, is discussed in Section 2.4.2.

Many of the present-day, commercially available additives contain three components designated as carrier, leveler, and brightener. Reid [115] reports that "Carriers are typically polyalkylene glycol type polymers with a molecular weight around 2000, levelers are typically alkane surfactants containing sulfonic acids and amine or amide functionalities, and brighteners are typically propane sulfonic acids which are derivatized with surface active groups containing pendant sulfur atoms."

The use of a particular additive must be evaluated for each application because undesirable characteristics can then be avoided. For example, many of the addition agents proposed result in embrittlement of the plate. Deposition potentials are generally higher when addition agents are added. Cathode polarization is greatly increased by adding gelatin ($0.2\ g\ L^{-1}$) [70, 116] or glue [68, 117]. These additions result in grain refinement, but this is chiefly unidirectional because the structure remains columnar and becomes more fibrous [70]. Gelatin additions to the sulfate solution introduce porosity, organic inclusions [64, 118], or both.

Phenolsulfonic acid is used in the electrotyping industry, but results with it depend on the sulfonation and purification procedures [119]. Deposits become harder and smoother after a solution has been electrolyzed or dummied for a short

time following an addition of phenol or phenolsulfonic acid [120].

The smoothing and grain-refining tendencies of addition agents are sometimes associated with the formation of complex ions with copper or of colloids at or near the cathode interface. Gelatin or glycine, for example, forms complex ions with copper [121–123] and also exists in colloidal form [124]. Particles of colloids arising from additions of selenious and arsenic oxides have been observed by ultramicroscopic examination to concentrate at the cathode [125].

Nodulation prevention in refineries is of high priority, and it is the major concern in overall cathode quality [114]. Nodulation is suppressed by proper selection of solution operating conditions but, most important, by proper choice of addition agents. In most refineries operating presently, addition agents consist of animal glue, thiourea, chloride ion, and sometimes a sulfonated hydrocarbon. It has recently been shown that thiourea, which is added to give a smooth copper surface, can initiate nodulation, and this effect is always associated with a large increase in overpotential, >100 mV [114].

2.6 OPERATING CONDITIONS

2.6.1 Temperature

Temperatures may vary from 18 to 60°C; however, a temperature between 32 and 43°C is common, since it can be maintained economically with little or no heating or cooling. An increase in the temperature results in a higher conductivity and reduced anode and cathode polarization [70]. A temperature below 30°C is recommended for plating bright copper in acid solutions to maintain good leveling power. These solutions are customarily agitated with air.

2.6.2 Current Density/Agitation

An increase in current density in either the sulfate or the fluoborate solution results in increased cathode polarization (but not to the extent noted for many other solutions). Cathode films become more depleted in Cu(II) ion and more concentrated in sulfate ion when the current density is increased [126]. Clear evidence has been reported of grain refinement produced by increasing the current density [127–130]. For example, an increase in current density from 1 to 7 A dm^{-2} reduced grain size by about one-third [130].

Current density and agitation must be balanced in order to obtain deposits having the desired properties. For producing electrotypes, cathode current densities of 16–22 A dm^{-2} are generally employed when using the sulfate solution agitated with air. Fast-moving, endless wire can be plated at 50 A dm^{-2} [131]. Still higher current densities are used when sufficient agitation can be supplied. When movement of the work is impractical or when air agitation fails to provide good mixing at all significant surfaces, the current density is usually kept at 3.7–5.4 A dm^{-2}. It is claimed that higher current densities are practical with the fluoborate solution when agitation is the same as for the sulfate solution [26, 27].

2.6.3 Ultrasonic Agitation

Although results with ultrasonic agitation have shown some improvements, practical applications are still limited to surface cleaning processes [132, 133]. Researchers have shown that ultrasonic agitation can result in an increase in limiting current density and current efficiency and a decrease in concentration polarization in acid sulfate solutions [134, 135] as well as pyrophosphate [134] and ethylenediaminetetraacetic acid (EDTA) solutions [136]. It can also increase the hardness of deposits. This change is believed to be due to a substantial reduction in porosity and to work hardening caused by the repeated impacts of electrolyte jets on the surface of the deposit during the collapse of cavities at high intensities of 13 kHz [137, 138]. Ultrasonic agitation is dependent on the location of the transducer in the plating tank.

2.6.4 Other Forms of Agitation

A reciprocating paddle cell has been used to deposit coatings of uniform thickness on large surface areas [139]. The paddle is a pair of confronting, separated triangular blocks aligned parallel to the cathode and was designed in this manner to provide uniform laminar flow. Mass-transfer characteristics of the paddle cell, which induces a nearly periodic flow, have been evaluated for acid copper solutions. Of importance are the paddle length scales and spatial location of the cathode relative to the paddle stroke boundary [140]. Also the paddle height above the cathode significantly affects deposition uniformity [141].

2.6.5 Filtration and Purification

Filtration requirements depend on the dirt load of air, any dirt brought in by the work, and the amount of detached anode sludge particles. If the cathodes are steel and if they are incompletely protected with a copper or nickel strike, particles that become detached from immersion deposits will also contribute to the filtration requirements. Although it is possible to maintain acceptably smooth deposits with only occasional batch filtration, continuous filtration is usually preferred. Cellulosic filter aids are satisfactory, but siliceous filter aids should be avoided when the fluoborate solution is filtered; filter papers are satisfactory.

Potassium permanganate is often added to solutions used for plating of printed wiring boards to oxidize contaminants to species that are more easily removed by carbon treatment. Manganese, which accumulates in the solutions as a result of

this procedure, exerts a detrimental effect on deposit tensile properties and interferes with cyclic voltammetric stripping analysis for the additive. Use of hydrogen peroxide at slightly elevated temperatures produces comparable purification results without the disadvantages associated with the use of permanganate [142].

Up to the early to mid-1980s many of the bright leveling acid copper processes contained some hazardous organic additives. By contrast, acid copper processes available today can produce the same leveling and fine-grained amorphous deposits as older processes, but without the concern for the safety of workers and the environment due to the additives. Waste treatment is easily accomplished by increasing the pH to about 9 to precipitate the copper. Once the precipitated copper is filtered out, the remaining solution does not contain any controlled material [4].

2.6.6 Equipment

Steel tanks with rubber or plastic are preferred for large acid copper solutions, but glass fiber-reinforced plastic tanks are used for small volumes of solution. Lining materials that are generally suitable for either the sulfate or the fluoborate solution are properly formulated natural hard rubber, neoprene rubber, polyethylene, or plasticized vinyl chloride polymers. Air lines can be made of hard rubber or polymerized vinylidine chloride. Special grades of carbon pipe and tubing make efficient heat exchangers or cooling coils. Lead is, however, satisfactory in the sulfate solution and is less expensive. Rubber or rubber-lined filters are used for continuous filtration, but stainless steel is satisfactory for short periods.

Graphite is recommended for use as a heat exchanger for copper fluoborate solutions [143]. For further details, see [144].

2.6.7 Anodes

Rolled and cast bars and electrolytic copper sheets have been employed as anodes in sulfate and fluoborate solutions. Another choice is high-purity, oxygen-free anodes, which are commercially available in several shapes and sizes. The benefit of oxygen-free anodes is that anode sludge is decreased [145]. On the other hand, the tenacity of the anode film is improved, and the number of particles that become detached from anode surfaces in air-agitated solutions is decreased by adding 0.02–0.04% phosphorus to cast copper [146, 147]. The films on phosphorized copper anodes are responsible for the slight polarization of about 0.5 V [145]. Rolled copper anodes containing at least 0.004% phosphorus are customarily recommended by the vendors of brighteners for plating bright copper in copper sulfate solutions. Chunks of polarized copper are frequently used in titanium anode baskets. Bagged copper anodes of phosphorized copper are frequently used in acid copper plating of printed wiring boards to minimize sludge formation and to produce better anode corrosion. The black film formed on copper anodes containing phosphorus contains Cu^+, chlorine and phosphorus and is envisioned to be a porouslike CuCl-like matrix that is laden with aqueous copper sulfate solution. The beneficial effect of phosphorus in copper anodes is to inhibit disproportionation of Cu^+ [148].

Anode film particles often become detached from the anodes. Air agitation promotes the detachment, causing some particles to be dissolved by the free acid. If the work is racked so that cathode shelves lie in a horizontal plane, particles will settle out on these areas and roughen the plate. In such cases the anode sludge can sometimes be decreased and the deposits made smoother by raising the solution temperature or increasing the acid concentration. Fine copper particles can be prevented from reaching the cathode by bagging anodes with woven Dynel or polypropylene. To allow good mixing of the solution adjacent to the anodes, bags can be made in the form of envelopes, enclosing several anodes placed edgewise to the cathodes.

To avoid excessive polarization at any anode in the copper sulfate solution, the anode current density should not be more than about 5 A dm^{-2} in unagitated solutions. With vigorous agitation, the limiting anode current density is more than 17 A dm^{-2}. The anode current density in an unagitated fluoborate solution can be as high as 40 A dm^{-2}, and with air agitation, it can be increased to 55 A dm^{-2}.

Small amounts of silver, sulfur, lead, tin, nickel, and other elements are common impurities in rolled, cast, and electrolytic copper [145]. Silver as an impurity in the anodes employed in sulfate and fluoborate solutions is of much less consequence than it is in cyanide solutions. Oxygen-free high-conductivity and electrolytic copper were found to have a lower impurity content than rolled or ordinary cast anodes. Two batches of high-purity anodes with average grain sizes of 10 and 0.01 mm performed similarly [145]. The anodic behavior of copper anodes containing arsenic or antimony as impurities has been investigated for electrorefining operations [149]. Lead containing 3% tin and 3% antimony has been proposed as an insoluble anode for facilitating the plating of printing rolls [150]. An insoluble anode that has been used in copper electrowinning was made of an alloy of copper, silicon, iron, and lead [69]. Graphite is the only electrically conductive material known to be insoluble as an anode in the fluoborate solution. When used as an anode, graphite produces a sludge of finely divided carbon particles. Recent reviews on anode reactions can be found in [151–154].

2.6.8 Specifications

Information on standards, specifications, and recommended uses for copper plating can be found in [39, 155].

2.7 EFFECTS OF IMPURITIES IN PLATING SOLUTIONS

Acid copper solutions are more tolerant of ionic impurities than many other plating solutions. Many metallic ions introduced regularly by carryover with the work, by dissolution of impurities in the anode, or by dissolution of the basis metal (e.g., iron, nickel, or zinc) can be expected to accumulate in the solution because conditions are usually not satisfied for effecting codeposition of such metallic impurities (nickel, cobalt, zinc, iron) with copper. For example, less than 2 ppm nickel was codeposited with copper in a sulfate solution containing $15\,g\,L^{-1}$ nickel [156].

Nickel and iron reduce the conductivity of the sulfate solution to the same degree as an equivalent increase in copper. The deposition potentials of arsenic and antimony are apparently near that of copper in the sulfate solution, since codeposition was reported to occur [157]. Arsenic and antimony in concentrations of $10–80\,g\,L^{-1}$ and $0.02–0.1\,g\,L^{-1}$, respectively, embrittled deposits and roughened surfaces. Addition of gelatin or tannin, however, effectively inhibited codeposition of these impurities and prevented roughness and embrittlement caused by them. Antimony readily codeposits with copper, but only small amounts of arsenic could be detected [158]. Bismuth, like arsenic and antimony, caused granular deposits [159]. Antimony and bismuth are believed to form insoluble complex compounds with arsenate [160].

Small concentrations of alkali metal and alkaline earth salts were found to smooth copper deposits [16]. Tin salts were also reported to smooth deposits and were, at one time, purposely added to the sulfate solution for this reason [15]. Lead is completely precipitated as partly sulfate and partly silver. If silver is a contaminant, a small amount will be codeposited with copper. A high current density favors the codeposition of silver [156]. Silver chloride caused pitting in semibright copper plate [161].

Nitrates are reduced to ammonia at the cathode in copper sulfate solutions [162]. A reduction product of the sulfate ion, which is said to have a grain-coarsening effect, can be removed by heating the solution and adding an oxidizing agent [163], but oxidizing agents such as hydrogen peroxide or potassium permanganate are said to reduce throwing power [161].

In the fluoborate solution, lead is the only metallic impurity known to interfere with the deposition of ductile plates; it can be precipitated by adding sulfuric acid. Besides lead, metals like silver, gold, arsenic, and antimony might be codeposited with copper, but the effects of such impurities are not known.

Organic impurities originating from decomposition of addition agents or leaching of elastomeric tank linings sometimes embrittle deposits, but they can be removed by treating the solution with an appropriate activated carbon followed by filtration. Treatment with activated carbon is desirable when a new solution is being prepared—especially the fluoborate solution, which may be contaminated with impurities leached from rubber shipping drums.

2.8 ANALYTICAL METHODS

The concentration of copper sulfate or copper fluoborate can be approximated by specific gravity measurements, but the contribution of sulfuric acid to the specific gravity of the sulfate solution must be taken into account [164]. The acid concentration of fluoborate solutions is controlled by measuring pH using colorimetric pH papers. Analytical methods for determining copper and sulfate concentration are described by Langford [165], who also presents procedures for determining copper and fluoboric acid concentration. Methods for determining trace amounts of lead [166], nickel [167], chromium [168], and chloride [77, 169] have been reported.

The concentration of addition agents is controlled by many techniques: empirical methods, such as evaluating the appearance of deposits on special bent or sloping cathodes immersed in beaker samples of the plating solution, Hull cell tests [170–172], and a variety of sophisticated analytical procedures.

Tench and Ogden and their colleagues pioneered in the use of cyclic voltammetry stripping (CVS) [173–177]. They were also instrumental in using CVS with copper pyrophosphate solutions; this is covered later in this chapter. Others who have used CVS with acid copper solutions can be found in [111, 112, 178–183]. One difficulty with CVS stems from the tendency of most acid copper solutions to "age" during operation by forming additive by-products [183]. Therefore a standard curve of stripping charge versus additive concentration for a fresh solution cannot be used for an aged one. Tench and White [184] modified the technique to step the electrode potential over a range to include plating, stripping, cleaning, and equilibration and called this technique cyclic pulse voltammetric stripping (CPVS). These researchers and others reported that CPVS was highly effective in mitigating the effects of additive breakdown products and other contaminants [181, 183–185].

Other methods that have been used with acid copper solutions include chromatography [102, 186], ion chromatography [180], high-performance liquid chromatography [180, 187–190], differential pulse polarography [191], and spectrophotometry [192–194]. Kanazawa et al. [195] used a quartz crystal microbalance to measure efficiency of an acid copper solution, and Mansfeld [196] developed a copper plating solution unit that operates by monitoring the polarization of a copper cathode at a constant applied direct current (dc). This unit is used to detect the presence of excess amounts of organic contaminant in the solutions, and it has worked well in production situations. Another technique for

testing the influence of additives is a modified rotating-cone electrode, which is recommended because of reproducible and controlled mass-transfer performance at fixed rotation speeds [197]. Troubleshooting has been covered by Mohler [198] and Rudolph [199].

2.9 PROPERTIES AND STRUCTURE

Copper is electrodeposited for numerous engineering and decorative applications requiring a wide range of mechanical and physical properties. This range extends from properties superior to full-hard wrought copper to properties equivalent of annealed pure copper and is summarized in Table 2.3. This subject is extremely broad, and no attempt will be made to provide comprehensive coverage on the matter since there already exists a number of excellent reviews on the topic. The best source is Safranek's book on the properties of electrodeposits [3]. An extensive research project sponsored by the American Electroplaters and Surface Finishers Society showed that the mechanical properties of electroplated copper varied widely depending on factors such as solution composition, current density, temperature, impurities, and addition agents [200–202].

The grain structures of copper deposits usually correspond to one of four types, shown in Figure 2.1. Deposits from the sulfate solutions containing no addition agents are columnar (Fig. 2.1*a*). Additions of gelatin, phenolsulfonic acid, and many other agents cause the fibrous structure shown in Figure 2.1*b*. Such copper usually is 15–20% harder than columnar copper. The fine-grained deposit in Figure 2.1*c* is characteristic of copper deposited in copper cyanide solutions at high temperatures (70–80°C), copper pyrophosphate solutions, copper sulfate solutions containing tri-isopropanolamine or other amines, and copper sulfate solutions containing popularly used brighteners. The banded copper in Figure 2.1*d* is characteristic of copper deposited with periodic current reversal from cyanide solutions containing brighteners. Copper is deposited from the sulfate solution as face-centered-cubic (fcc) crystals that are randomly oriented [203] unless deposited at less than 1.5 A dm^{-2}, when the basis metal can exert an influence on the structure so that crystals in the basis metal and plate are oriented similarly [204].

Grain continuity from the basis metal into sulfate copper deposits has been detected by many investigators [129, 205, 206]. Thus the structure of the deposit is often influenced by that of the basis metal. The basis metal structure was reproduced in the copper plate when the copper substrate was cleaned and immersed in an acid solution before plating [207, 208] but was not reproduced when the basis metal was cleaned but not dipped in acid solution before plating [208]. The grain size of the substrate appeared to influence the reproduction of the basis metal structure in the copper deposit [208]. The structure of copper, electrodeposited from sulfate solutions, was not influenced by dislocations such as etch pits in the substrate surface, unless the etch pits contained oxides or sulfides [209]. Oxide and sulfide particles in the surface layer of the substrate behaved as nucleation sites.

Tensile strength, in general, is inversely proportional to the square root of the grain diameter, as shown in Figure 2.2 for a variety of copper deposits and wrought copper [210]. Loss of tensile properties such as reduced elongation and tensile strength of electrodeposited copper has been noted by many researchers. It affects copper in a number of applications: printed wiring boards that exhibit cracking in deposits as a result of soldering operations, optics parts for physics experiments that require high-temperature stability of the copper to maintain precise stability during usage, and shaped charge parts which undergo deformation at very high strain rates. It is postulated that segregation at grain boundaries is driven by a reduction in grain boundary interfacial energy which, in turn, leads to a reduction in the grain boundary cohesive strength [211–213].

TABLE 2.3 Ranges of Properties of Copper Electrodeposits

Outstanding Characteristic	Tensile Strength		Elongation, % (2 in.)	Internal Stress[a]		Hardness (VHN_{200}), kg mm^{-2}	Electrical Resistivity, μΩ-cm
	kg mm^{-2}	kpsi		kg mm^{-2}	psi		
High strength	45–63	64–90	4–18	−4.2 or 3.6 to 5.5	−6000 or 5000 to 7800	131–159	1.75–2.02
Hardness	3.5–55	5–79	0–10	−4.2 or 3.5	−6000–5000	193–350	1.96–4.60
Low electrical resistivity	18–27	26–38	15–41	−0.5–1.6	−700–2200	48–64	1.70–1.73
Near-zero stress	14–23	20–33	8–24	−0.08–0.06	−110–80	56–57	1.71–1.72
Good leveling	36	51	14–19	2.0	2900	128–137	1.82
Thermal stability[b]	22.5–30	32–43	26–39	0.5–2.9	700–4100	55–106	1.73–1.76

Source: From Safranek [3]. Reprinted with permission of the American Electroplaters and Surface Finishers Society, Orlando, FL.

[a] Negative values indicate a comprcssive stress.

[b] Deposits that changed <0.02% in length after heating to 400°C.

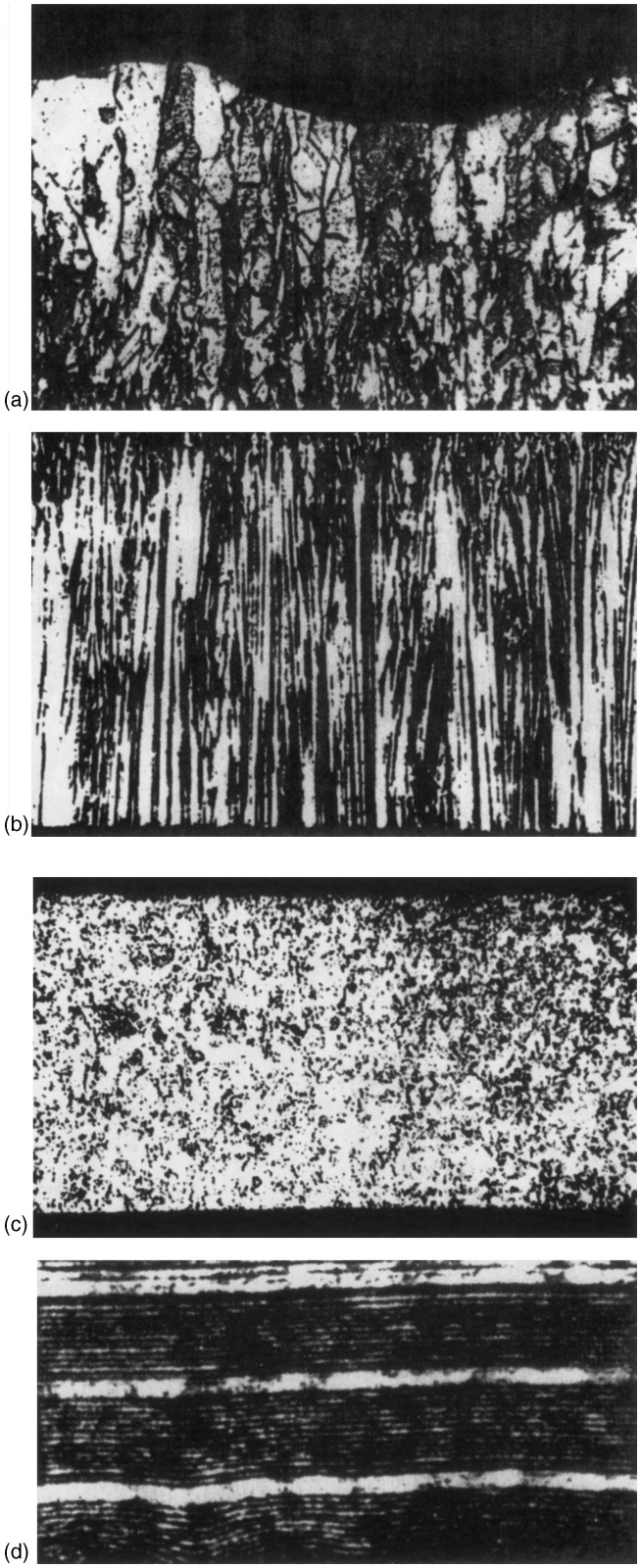

FIGURE 2.1 Structure of copper deposits; cross-sectional views (∼500×) after etching with ferric chloride reagent: (*a*) columnar; (*b*) fibrous; (*c*) fine grained; (*d*) banded. (From Lowenheim [6]. Reprinted with permission of John Wiley & Sons, Inc.)

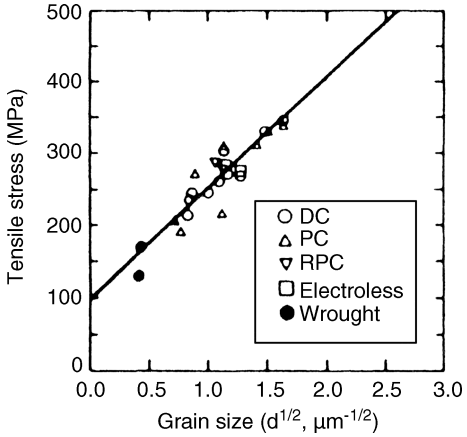

FIGURE 2.2 Plot of tensile strength versus inverse square root of grain size. (From Woodman [210]. Reproduced by permission of the Electrochemical Society, Inc.)

Zakraysek [214–217] observed a thermally induced ductile–brittle transition in electrodeposited copper with embrittlement occurring as a result of fracture along grain boundaries. Lin and Sheppard [218] noted an embrittlement effect when electroplated copper having a columnar grain structure was tensile tested at temperatures between 150 and 300°C. The effect was also strain rate dependent at the lower temperature. This was not noted for deposits annealed without straining at the same temperatures and then tested at room temperature. The behavior is believed to be associated with inhibition of grain growth and grain boundary weakening, possibly as the result of vacancy effects at the grain boundaries resulting from chloride in the deposit [218].

The surface mobilities of vacancies in copper can be increased by as much as four orders of magnitude by the presence of monolayers of adsorbed halides [219]; chloride surface contamination can induce cracking in copper by the vacancy mechanism at temperatures as tow as 200°C [220]. Since small quantities of chloride are used in acid copper sulfate solutions, some chloride can be incorporated in the deposit [218]. Thin copper chloride crystals have been epitaxially absorbed onto copper single crystals from a sulfate solution containing only 7 ppm chloride [221].

Others noted poor performance of electrodeposited copper in shaped-charge applications [211, 222]. In these cases, strain rates were very high (10^4 and higher) compared to rates around 10^{-3} for typical tensile tests. Despite the radical difference in deformation history, Lassila [211] postulates that the fundamental material characteristic of high-temperature embrittlement is the primary cause of the poor performance. The presence of segregated impurities is believed to be the primary cause of brittle fracture and participation. Support of this hypothesis was provided by Sole and Szendrei [223], who electroformed shaped-charge liners that exhibited good performance by using additive-free acid

sulfate solutions with pulse plating. In a similar vein, Woodman et al. [210] suggested that use of pulse plating can provide high strengths without additives, thereby avoiding embrittlement.

Merchant [224, 225] characterized thermal response of electrodeposited copper by monitoring changes in microstructure, tensile strength, elongation, and microhardness following 30 min isothermal annealing at temperatures between 23 and 400°C. By judicious control of additives to the electrolyte, considerable enhancements of strength and hardness were obtained. The annealing gradually removed embrittlement with the removal rate dependent on the time/temperature parameters of the thermal exposure [225]. Embrittlement at 180°C with increasing deposit thickness was attributed to developing low-density regions in the morphological boundaries [226]. Others who have investigated thermal response of acid copper coatings can be found in [227, 228].

2.10 CURRENT MODULATION TECHNIQUES

Current modulation techniques such as periodic reverse, pulse plating, and asymmetric alternating current plating have been used to improve deposit properties. For overviews of these techniques, see [229–235].

With periodic reverse (PR) plating, parts are plated in a conventional manner for a selected time and are then deplated for a shorter period by reversing the current. Malone [236] used PR plating to enhance the uniformity and grain structure regardless of deposit thickness. A current density of about 5 A dm^{-2} and a PR cycle with a cathodic-to-anodic ratio of 2:1 in a solution containing no additives provided consistent mechanical properties and excellent thermal stability. Wan [237] observed that the hardness of deposits increased when PR or pulse plating were used instead of dc.

Pulsed-current techniques involve application of a forward current for a certain time interval with a short, high-energy reverse pulse periodically interposed. The main difference between dc and pulsed current is that with dc plating only voltage (or current) can be controlled, while with pulse plating three parameters—on-time, off-time, and peak current density—can be varied independently [238]. These variables are believed by many to create a mass transport situation, an electrocrystallization condition, and adsorption and desorption phenomena which are not otherwise possible [229, 238, 239].

In acid copper deposition, pulsed current has been used for improvement of mechanical and physical properties of deposits [210, 234, 240]. Benefits include finer grain structure [210, 241–245], increased hardness [237, 246, 247], reduced stress [248], reduced surface roughness [238, 249, 250], reduced porosity [246], and improved leveling [251, 252] and throwing power [253]. Use of pulsed reversed current in acid copper sulfate solutions containing a combination of polyethers, sulfopropyl sulfides, and chloride ions can provide enhanced throwing power because of a change in the polarization characteristics of the electrolyte [239, 254]. Enhanced throwing power was not obtained when single additives were present. Best results were obtained with an anodic–cathodic ratio of 3:1 and a cathodic–anodic ratio of 20:1 [254]. Macrothrowing power was poor for pulse plating [251].

Benefits claimed for printed wiring board plating include improving the through-hole distribution of solutions used for plating printed wiring boards [238, 254–259], a reduction in average plating time by 30–50% [259], a reduction in average track height of 50% [259], and a finer grained, more ductile deposit with less stress [248]. Holmbom and Jacobsson [260] observed that by pulse plating at high frequencies (above 1 kHz) through-hole plating uniformity was improved compared with that of dc deposits. At lower current frequencies, the uniformity was worse than that of dc plating. Deposits prepared by periodic reverse plating exhibited a similar uniformity to pulse-plated deposits. However, appearance was completely dull due to loss of brighteners which were desorbed during the reversal part of the plating cycle. In addition, chlorine evolution occurred at the cathodes during the reversed pulses. A computer model that predicts the effect of pulse plating copper in small holes was developed by Ng et al. [253]. Leisner et al. [261] investigated throwing power under pulsed-current conditions in an attempt to optimize through-hole plating. However, as subsequently mentioned in the section on printed wiring boards [262], although many claims have been made for pulse plating, no manufacturing process based on this technology other than that described by Engelhaupt [258] has been reported.

Deposits produced by using pulse plating to selectively deposit copper (spot plating) were brighter and contained larger crystallites than those applied by using direct current [263]. Puippe and Ibl [245] noted that an increase in off time was accompanied by an increase in grain size, similar to the way this system reacts with dc. For optics applications, a dendritic crystal structure is deposited using a bipolar pulse plating technique. This surface is then oxidized to provide a highly antireflective surface [264]. Wan et al. [265] reported that pulse time exerted the greatest effect on current efficiency, and Popov et al. [266] showed that the effective current density is dependent not only on values of the effective overpotential but also on the ratio of pulse-to-pause duration and on the frequency of the input pulsating potential. Rudder [267] compared pulse plating of acid copper against cyanide copper and found that the leveling and thickness performance of the pulse-plated cyanide copper was better than that of acid copper.

Reverse pulse plating was investigated by a number of researchers. White and Galasco [268] obtained surface

distributions on variably spaced, 50-μm-wide lines and deposit properties typical for dc by employing reverse pulsed current in additive-free solutions. Current efficiency for reverse pulse plating was lower than that for pulse plating or for dc plating [269]. Mann [270] noted that, when using high reversal frequencies, plating speed, throwing power, and surface quality were improved in comparison with dc plating. By combining pulse current and pulse reverse current, Zhou et al. [271] developed an additive-free solution that produced deposits comparable to commercial additive solutions. A benefit claimed for this approach is that waste disposal cost can be greatly reduced compared to the current process due to the possible in-process recycling of rinse water and plating solution in the additive-free solution.

Morphological changes in copper deposits caused by use of superimposed alternating current (ac) were correlated with reduction in grain size and smooth deposits. Hexagonal pyramidal growth obtained with dc on the [111] copper plane transformed to layers, triangular pyramids, and polycrystalline deposits under the influence of superimposed ac [272].

Additional information on pulse plating with acid copper solutions can be found in the literature [273–276]. Pulsed-current techniques have been used by researchers at Battelle; this is discussed in more detail in Section 2.15.

2.11 PLATING ON STEEL, ZINC, PLASTICS, AND ALUMINUM

Historically, buffed acid copper deposits have been widely used as an undercoat for nickel–chromium deposits. The development of reliable processes capable of producing fully bright, ductile, high leveling deposits that did not require buffing served to promote even wider use of acid copper solutions [277].

The fact that copper is much cheaper than nickel suggests that it might be considered an economical replacement for a large proportion of the total thickness of electroplated coatings. However, an equal thickness of copper undercoat is not comparable with nickel. It has been proved fairly conclusively that inferior corrosion resistance results when part of the bright nickel layer in a bright nickel plus decorative chromium coating is replaced by an equal thickness of copper [278].

In terms of corrosion performance, copper underlayers are generally not detrimental when there is adequate thicknesses of double-layer nickel. Under microdiscontinuous chromium and double-layer nickel, copper layers are neither detrimental nor beneficial. In essence, the nickel and chromium layers are so protective that parts are obsolete before the copper would even start to corrode [279]. These general characteristics have been confirmed in panel exposure programs involving steel, zinc, plastics, and aluminium [280–281]. Jonkind [282] compared various processes for Cu–Ni–Cr plating of aluminum bumper bar stock (Alloy X-7046) with Ni–Cr-plated steel bumpers. The aluminum-plated parts showed at least equal corrosion test results with the steel-plated parts in CASS, neutral salt spray, and atmospheric tests.

Acid copper deposits are used over a cyanide copper strike for plating zinc die castings [283]. The ductility of copper deposits is one of the most important parameters in the coating of plastics [284]. It is suggested that elongation should be at least 15% [285]. Typical bright copper solutions for plating on plastics contain around $60\,g\,L^{-1}$ copper and $60\,g\,L^{-1}$ sulfuric acid. Lower copper concentrations ($10–20\,g\,L^{-1}$) and higher contents of sulfuric acid ($200\,g\,L^{-1}$) are also used because of their excellent leveling capability and throwing power [284]. A high-throw acid copper strike is very effective in improving quality by increasing the copper thickness in low-current-density areas while also reducing cost and waste treatment requirements when compared to a nickel or pyrophosphate copper strike [49].

2.12 PLATING OF PRINTED WIRING BOARDS

When printed conductors are used on both sides of a printed wiring board, electrical connections between the two sides of the board are most reliably made via plated through holes in the board. Because copper is widely used as the base conductor metal in a printed circuit, it is natural that copper also be used for plating the through holes. A historical summary of the evolution of acid sulfate copper-plating processes and their benefits as they relate to printed wiring board market needs is presented in Table 2.4.

The precise technical requirements of electronic products and the demands of environmental safety compliance have been the driving forces exerting major influence on plating practices [41]. The preferred plating process is acid copper sulfate with organic additives. Copper pyrophosphate deposits, once the standard of the industry, have been almost entirely replaced by acid copper, except for some military and special applications [41, 262].

The success of the acid copper sulfate solutions is attributed to their good throwing power, ease of control, good mechanical and physical properties, and favorable properties regarding waste disposal and treatment compared to pyrophosphate and cyanide solutions. The major factors that affect throwing power, the ability of a plating solution to produce a relatively uniform distribution of metal upon a cathode of irregular shape, are cathode polarization, cathode efficiency, and solution conductivity. Rothschild [71] compared throwing power for a variety of copper plating solutions by using a Haring cell [286]. This work, summarized in Table 2.5, clearly shows the benefit obtained with the low

TABLE 2.4 Historical Summary of Acid Copper Evolution Related to Printed Wiring Plating

Year	Innovation	Benefits
1970	Original high-throw process	Improved throwing power when compared to conventionally used pyrophosphate copper
1973	Ductile high-throw process	Improved ductility agents to consistently pass thermal shock testing
1976	Process for high-aspect-ratio MLB	Improved ductility for MLBs with high aspect ratios
1979	High temperature and high throw	Improved distribution without need for chillers
1983	Increased current density with high throw (4.3–6.5 A dm^{-2})	Improved productivity and lower operational cost
1984	Process control/additive analysis	Elimination of subjective readings and lower operational costs
1984	High current density and high throw (10.8 A dm^{-2})	Improved productivity and lower operational cost

Source: From Mayer and Barbieri [178].

copper–high acid formulations which have become the standard of the industry for plating printed wiring boards. Some chloride is also essential in these solutions; this is discussed in Section 2.4.2. Turner [287] and Walker and Cook [82] obtained results similar to those of Rothschild [71], namely through-hole plating ability improved with decreasing copper concentration and increasing acid content. A noncyanide formulation provided even better throwing power than the low copper–high acid formulation.

TABLE 2.5 Values of Throwing Power (Haring Cell 11:1 Ratio)

Solution	Throwing Power
Conventional acid sulfate copper[a]	14
Conventional acid fluoborate copper[b]	14
Cyanide copper	50
Low copper–high fluoboric acid copper[c]	58
Pyrophosphate copper	62
Low copper–high sulfuric acid copper[d]	87
Alkaline noncyanide copper[e]	95

Sources: From Rothschild [71]. Ratio from (H. E. Haring and W. Blum, *Trans. Am. Electrochem. Soc.*, **44**, 313 (1923).

[a] Copper, 48 g L^{-1}; sulfuric acid, 75 g L^{-1}.
[b] Copper, 120 g L^{-1}; fluoboric acid, 30 g L^{-1}.
[c] Copper, 15 g L^{-1}; fluoboric acid, 340 g L^{-1}.
[d] Copper, 15 g L^{-1}; sulfuric acid, 210 g L^{-1}; 30 mg L^{-1} chloride.
[e] From L. C. Tomaszewski and R. A. Tremmel, Proc. AESF SUR/FIN 85, Session D, Detroit, MI (1985).

Fundamental studies on through-hole electroplating [288] and a thorough review of plating into through holes and blind holes were published by Yung et al. [262]. A mathematical model for through-hole plating was developed by Hazlebeck and Talbot [289]. Kessler and Alkire outlined procedures for investigating complex electrochemical phenomena appearing during plating of printed wiring boards [290] and developed a model for predicting copper thickness distribution on multilayer printed wiring board through holes [291]. References [292–295] provide additional information on plating high-aspect-ratio holes.

Innovative agitation schemes such as jet plating for high-speed plating (>10 A dm^{-2}) of printed wiring boards have been implemented in production lines [262, 288, 296, 297]. Other techniques that have been used include high-speed additives [41], vibratory agitation [298], and forced solution flooding [299]. Deposit distribution on a printed wiring board was not improved when ultrasonic agitation was compared with mechanical agitation [300]. Hewlett-Packard utilized a conveyorized impingement-agitated plating system where copper plating was done at 7.5 A dm^{-2}, which is at least twice the current density usually used for plating printed wiring boards. The significant agitation in the process was accomplished by use of hydraulic injection. Agitation via panel motion or entrained air bubbles was insignificant [301].

Most additive systems for acid copper sulfate solutions used for plating printed wiring boards are based on some combination of a polymer surfactant of a high molecular weight such as PEG, which apparently inhibits copper deposition by forming an adsorbed film on the cathode that mediates transport of species from the solution, and a sulfur-containing and/or nitrogen-containing organic species such as disulfide or organic sulfonate, which induces leveling [80]. Some single-blend additives can be comprised of three components: (1) carrier agent, (2) leveling agent, and (3) ductility agent. Carrier agents are the primary grain refiners and impart brightness to the deposit. Leveling agents level out drilling imperfections in plated through holes and also prevent fault planes and foldovers in multilayer board plating. Ductility agents create the equiaxed grain structure that is best suited to withstand thermal shocks [178, 302].

In a study of eight commercial acid copper solutions, all yielded sufficiently ductile deposits for multilayer circuit board applications, but some of the solutions exhibited a relatively strong dependence on solution agitation [303]. In one production situation, a 40% annual savings was realized by operating a solution with additives at 6.4 A dm^{-2} versus 3.2 A dm^{-2} [178]. In additive-free solutions, increased levels of agitation improved deposit quality dramatically up to the point of eliminating ion concentration gradients causing mass transport–limited plating conditions. With additives, the plating solutions were considerably less sensitive to changes in plating parameters such as the current density

and level of agitation [304]. Byle and Bratin [305] also studied the effects of additives.

Yung et al. [288] utilized a gap cell, which provided accurate nondestructive profile measurements without tedious cross sectioning to show that agitation, which is necessary inside the holes to replenish the plating solution, is also necessary to provide a certain amount of agitation on the surface of the board.

Pulsed-current techniques (discussed in detail in Section 1.10 on current modulation techniques) are claimed to offer benefits for plating of printed wiring boards. However, aside from Engelhaupt [258], no other manufacturing process based on this technology has been reported [262].

Nonuniform copper plating on printed wiring boards may be attributed to nonuniform anode currents due to high contact resistances between anode hooks and anode rods. Turner [306] developed an anode hook design to make a stable low-resistance contact by clamping the hook to the anode rod. Use of titanium for the hook and rod resulted in a low-maintenance-contact system.

Optimizing the performance of a plating process does not need to involve extensive, tedious testing. The traditional approach of examining one variable at a time while holding all others constant not only requires repeated tedious experiments but also allows bias error in each measurement [307]. Use of factorial, screening, response-surface designs, or Taguchi techniques allows for accurate solutions from a minimum of test runs [308]. Any of these approaches in studying the effects of many variables is highly recommended for both research and production activities.

Barringer and Carano [309] used the Taguchi technique to optimize the leveling of an acid copper plating solution for printed wiring boards. The effects of temperature, leveler (one component included in the addition agent), and ratio of sulfuric acid to copper metal were investigated. The best leveling was obtained at the low temperature, increasing the ratio of sulfuric acid to copper resulted in some slight improvement of leveling, and additions of leveler produced no improvements. Taguchi techniques were applied by Wan and McCaskie [307] to elucidate the relative importance of various process parameters on dendrite formation in an acid copper system. Chloride and arsenic concentrations were two critical factors that affected dendritic growth, while lead and temperature exerted little effect. Elbs and Rasmussen [310] utilized Taguchi techniques for optimizing the current efficiency of a cyanide copper solution.

An important requirement of copper deposits is that they have sufficient strength to withstand subsequent soldering of the circuits. During this operation, high forces are generated by differential expansion of the board material (usually epoxy glass) and the copper. Therefore the copper must be either strong enough to contain and deform the epoxy glass or have sufficient elongation to be stretched without fracture [311]. With the proper additives, fine-grained deposits with tensile strengths around 345 MPa and a minimum elongation of 10% are routinely produced [41].

Most of the studies on the ductility of copper deposits for printed circuit boards (PCBs) have been done under a uniaxial stress state. However, the stress state of electrodeposited copper in through holes of a PCB is definitely biaxial. Therefore Ye et al. [312] correlated cathodic overpotential, solution composition, and aging with characteristics such as crystallographic texture, roughness, and ductility. Copper foils with a low [220] preferred crystallographic orientation and a smooth surface were obtained when deposition was done at 87–113 mV cathodic overpotential from solutions with a low chloride content (<40 ppm). Highest ductilities were achieved under these plating conditions,

Kang et al. [313] studied surface morphologies of foils with different textures. Increasing solution temperature and decreasing current density changed the texture from $\langle 111 \rangle$ to $\langle 110 \rangle$. The mechanical properties at elevated temperature of a proprietary formulation for multilayer board plating were evaluated in detail by Fox [314]. The deposit was found to exhibit adequate localized ductility, although, as is generally the case for electroplated copper, its final elongation after fracture was lower than that for wrought, annealed copper. Merchant reported on the defect structure, isothermal anneal kinetics, and thermal response of electrodeposited copper [224, 225, 315, 316].

2.13 PATTERNED ELECTRODEPQSITION FOR MICROELECTRONICS

Computers, microprocessors, and other microelectronic devices could not exist without the technology of depositing thin metal or alloy films with fine lithographic patterns [317]. Romankiw et al. [318–321] have demonstrated the capabilities of resist patterned electroplating for the past two decades. Dukovic [317] suggests that there are three trends that appear to be propelling patterned electrodeposition into a phase of major expansion. First, high-speed machines require the high conductivity of copper, and acid copper plating is simple and capable of reaching high rates. Second, the pattern replication powers of electrodeposition are ideally suited to the level of miniaturization required for wiring structures. Third, demands for cost reduction have increased the importance of reducing the capital and operating expenses associated with metal deposition processes, and it is therefore likely that electroplated copper thin film, which is important today, will continue to play a central role in the future.

IBM researchers have successfully implemented copper electroplating technology for the fabrication of chip interconnect structures [2a, 2b, 321a]. The process, termed *damascene copper electroplating*, meets the challenges of filling trenches and vias with copper without creating a void or

seam. Under proper conditions, electroplating inside trenches occurs preferentially in the bottom, leading to void-free deposits, a phenomenon referred to as *superfilling*. Proprietary additives are used in the plating solution to produce the superfilling properties.

Electrodeposited bonding bumps are indispensable microconnectors for high-density interconnection in recent microelectronics applications. The bumps generally have mushroom shape and are deposited onto dot-shaped cavities of several 10–200 μm in diameter formed by photoresist. Kondo et al. [322] discussed the shape evolution of copper bumps, and Dukovic [323] developed a two-dimensional numerical computation of tertiary current distribution.

High-speed selective jet electrodeposition has also been used to produce deposits in a selective manner without the need for masking [324]. The principle is that a nonsubmersed, free-standing electrolyte jet impinges onto a substrate and deposition occurs within the impingement region, with little or no deposition occurring in the surrounding areas. Booking [324] determined the effects of temperature, velocity, and concentration during high-speed selective jet plating in an acid copper sulfate solution without additives.

The development of laser-enhanced electroplating processes offers a promising technique for high-speed and mask less selective plating and/or as a repair and engineering design change scheme for microcircuits [300, 325–328]. For this, temperature is used to modify the position of the equilibrium potential in a localized region so that electrodeposition is driven by the potential difference between this region and the nonirradiated regions. Use of a focused argon laser beam (488 nm) in an acid copper solution provided plating rates as high as $25\,\mu m\,s^{-1}$ [300]. Bindra et al. [327, 328] discussed the mechanism of laser-enhanced acid copper plating and Paatsch et al. [329] reported on laser-induced deposition of copper on *p*-type silicon. It was demonstrated that the increase in the plating rate under laser illumination results principally from photoinduced heating of the electrode surface [328].

2.14 ELECTROFORMING

Copper finds extensive use in electroforming [330, 331]. Acid sulfate with periodic reversal of current [236, 332], acid sulfate with oxygen reduction additive, and pyrophosphate solutions provide excellent properties for aerospace applications [236]. However, although acceptable properties are attainable via pyrophosphate deposition, very little electroforming is done with these solutions. Electroforming with acid copper or nickel is used as one of the primary methods of fabricating the outer shells of regeneratively cooled thrust chambers for advanced design rockets and other applications.

Typically the process involves filling machined (or etched) channels with wax, making the wax conductive with silver powder, plating thick copper to seal over the channels, and then removing the wax. Some thrust chamber requirements for copper require that the deposits retain useful mechanical properties and metallurgical structure at temperatures up to 400°C. The electroformed copper deposits often contain some oxygen, and this can be deleterious at high temperatures because hydrogen can combine with the oxygen and produce water.

With the high temperatures involved, steam pressure generated by the reaction often exceeds the strength of the copper and causes plastic deformation and/or tearing, frequently manifesting itself by grain boundary cracking or cavities [333, 334]. This problem is avoided by using an oxygen control additive such as sugar [335, 336] or potassium aluminum sulfate [337].

All of the pentoses are suitable for use in the copper sulfate solution, such as xylose, arabinose, ribose, and lyxose. These materials act as oxygen scavengers in the solution by picking up oxygen and thereby preventing the anodes from being oxidized [172]. Table 2.6 includes the gas and carbon content of a variety of copper deposits and clearly shows the high purity attainable with an oxygen control additive such as *d*-xylose [338].

Farmer et al. [339], in evaluating copper for a physics accelerator application, noted that copper deposited from acid sulfate solution containing one set of proprietary additives was unstable during heat treatment and exhibited void formation around 450°C. By contrast, another acid copper solution with different proprietary additives formed no voids when heated at 1000°C. Deposits from a cyanide solution and an acid copper solution containing *d*-xylose also showed no void formation after heating at 1000°C, giving further proof that deposits with low carbon and gas contents (Table 2.6) are stable at high temperatures.

Electroformed targets for a 14-MeV neutron source facility did not require the high-temperature stability just discussed. However, they did require a deposit elongation around 20% because of a forming operation after plating. This was

TABLE 2.6 Carbon and Gas Contents of Various Copper Electrodeposits and OFHC[a] Copper

	Content (wt. ppm)			
Plating Solution	C	H	O	N
Low copper–high acid proprietary	50	11	50	5
d-Xylose[b]	12	1	11	2
Pyrophosphate proprietary	21	6	140	17
High copper–low acid proprietary	190	14	50	9
Cyanide	NA	3	53	6
OFHC (wrought)	90	4	50	<10

Source: From Dini [338].

[a] Trademark: American Metal Climax, Inc.

[b] Oxygen control additive.

obtained by using a medium-copper (150 g L^{-1} copper sulfate), high-acid (188 g L^{-1} sulfuric acid) formulation [340].

Copper deposits usually contain small amounts of other impurities besides oxygen, and these can affect properties such as electrical resistivity [3]. Hydrogen is present in different bound states in the deposits and the total amount of hydrogen is often five to six orders of magnitude larger than the equilibrium solubility of hydrogen at room temperature [341]. It is most likely that the hydrogen is bound to crystal lattice defects such as vacancies and dislocations or adsorbed at the grain boundaries or present in microvoids. Deposits obtained at low current densities contain a larger amount of hydrogen than those obtained at high current densities.

Hydrogen is evolved from the deposits as a function of temperature with the major amount being eliminated at temperatures around 450°C [341]. Sulfate (0.071–0.099 wt %) and sulfide (0.040–0.069 wt %) have been found in deposits from acid copper solutions. These impurities decreased with the increase in plating temperature, with the increase in acidity of the plating solution, and with the addition of 0.1 g L^{-1} gelatin [342].

Strongly enhanced ductility (up to 40%) and reflectivity were achieved in the presence of dimethylamino derivatives [98]. The ductility of the coatings in contrast to the tensile strength appeared to be correlated to the amounts of codeposited carbon and sulfur. An elongation of 15% and low stress were obtained from solutions containing polypropylene ether. These deposits were essentially sulfur free, with carbon and nitrogen contents of about 0.015 to 0.003 and 0.001 wt % [110]. A high-throw acid copper solution has been used with glue and phenol sulfonic acid for electroforming of bellows [343].

Although not electroforming, very thick deposits (around 5000 μm) were produced on the outer surface rotor of a 300-MVA superconducting generator. This was done in acid sulfate solution with a proprietary brightener. Deposit properties were yield strength around 210 MPa, elongation 15%, and high electrical conductivity at cryogenic temperatures [344]. Radio-frequency quadrapole accelerator components up to 4 m long were plated with 250 μm copper in an acid sulfate solution containing a brightener system [345].

2.15 HIGH-SPEED ELECTROPLATING

A current density of 300 A dm^{-2} or more is practical for depositing most metals if the solution flow rate is in the range of 1.0–1.2 m s^{-1}, depending on the topography of the surface, the solution viscosity, and other factors [346]. High current densities for achieving fast rates have been used in both copper sulfate and copper fluoborate solutions. Large variations in the copper and sulfuric acid concentrations had no significant effect on the appearance of deposits from the sulfate solution. The tensile strength of copper deposited with turbulent flow in a sulfate solution increased from 350 to 450 MPa as the current density was raised from 100 to 300 A dm^{-2}, which increased the deposition rate from 25 to 75 μm min^{-1}. High-speed copper deposited in a fluoborate solution exhibited a lower tensile strength, 280 to 350 MPa over the range of 100–300 A dm^{-2}. However, all of these values are higher than those reported for copper deposited at conventional rates.

High-speed copper plating has been developed for commercial applications such as electroforming of flexible printed circuits [347], in-mold plating of polymeric materials [348], and plating of round bars [349]. A process for electroforming copper circuit paths on a reusable metal substrate and transferring the circuitry to a flexible polymeric surface coated with adhesive has been advanced to production. The copper circuit paths are electroformed at rates up to 50 μm min^{-1} using fast-rate electrodeposition technology. The process does not generate spent etching solutions or plating rinse water and costs can be 70–80% of those associated with the conventional etched-circuit process for high-volume production. Another benefit is that high-speed deposition conserves equipment and floor space [348].

A combination of high-speed plating with pulsed current (fast-rate, interrupted current, FRIC) allows for deposition of copper with different structures at rates of 50 μm min^{-1} or higher [350]. By controlling the frequency and/or duty cycle with the high-speed deposition rate, it is possible to tailor the deposit structure to suit the application. For example, with applications that need structural strength particularly at corners, the FRIC technique at high frequency would be used to promote growth of mainly polycrystalline copper which would be equally strong in all directions. By contrast, for applications such as wire coatings that require maximum electrical conductivity, columnar structures produced at moderate frequency are preferred [350].

For agitation of the electrolyte, forced circulation across the cathode by pumping electrolyte is most commonly used, although ultrasonic agitation and gas sparging have also been investigated [351]. When plating wire and strip using direct current, the deposition rate can be increased by intensifying the electrolyte flow, by optimizing the gap between the cathode and anode, and by the use of high-performance electrical contacts [352].

2.16 DIAMOND TURNING

Diamond-turning surface finishing uses single-point diamond tools on a precision lathe under precisely controlled machine and environmental conditions. Diamond tools are used when it is necessary to machine the smoothest possible surface texture. When the surface to be cut is one of the preferred diamond-turnable materials such as copper,

electroless nickel, or aluminum, surface textures as smooth as 1 nm can be obtained. Coatings offer significant advantages for diamond-turning applications inasmuch as they can be applied to lightweight substrates such as aluminum or beryllium, and copper coatings produced in acid sulfate solutions have been used in many applications. A number of 1.3-m-diameter molybdenum parts required form accuracy of approximately 250 Å, and this was obtained by coating the parts with 0.3–0.45 mm of copper prior to diamond turning [52]. A physical vapor deposition process was used to provide an initial, thin (6-μm) adherent copper layer, and this was followed by thick plating in an acid copper solution containing proprietary additives. An important requirement for these parts, as well as for many other diamond-turning applications, is long-term microstructural stability. If the deposit undergoes recrystallization after machining, the precise surface finish is degraded. Copper deposits have been shown to markedly soften after storage at room temperature for 30 days [353]. For example, copper mirror surfaces for the Antares laser system changed over a six-month period due to recrystallization [51]. The problem was eliminated by employing a low-temperature heat treatment (1 h at 250°C). This same treatment provided stability for the proprietary copper used for the 1.3-m-diameter molybdenum parts mentioned earlier [52].

Rao and Trager [354] reported that copper for diamond turning should have a grain size from about 200 to 500 Å and a hardness from about 250 to 320 Knoop (15-g load). An additive comprising a mixture of phenazine dyestuffs in the combination from about 30 to 40% by weight of a Janus Green B–type dyestuff and from about 70 to 60% by weight of Safranine T provided these properties.

By judicious choice of plating operating conditions, such as current density, pH, solution composition, and additive concentration, it is possible to deposit coatings that are in a stress-free state. A plot of current density versus stress was used to define conditions for depositing 1-mm-thick copper with zero stress on glass substrates and on pyrex optics. This deposit was capable of withstanding single-point diamond turning to provide an optical surface and was able to withstand heating at 250°C for 4 h without degradation of the metal–glass bond [53].

Occasionally, a phenomenon referred to as *black spots* has been obtained. These are small, localized defects noted on electroplated copper after single-point diamond turning. Analysis of these spots has revealed oxides, sulfates, and chlorides, materials which are components of the plating solution [355, 356]. It is speculated that the most likely cause of these defects is a void or pit exposed by the diamond-cutting tool. In an effort to eliminate these minuscule pits Dini et al. [356] evaluated plating under reduced pressure (around 100 torr). Copper deposits produced under these conditions exhibited finer and denser grain structure and a reduced surface roughness.

2.17 MISCELLANEOUS

2.17.1 Magnetics

Effects of magnetic fields on electroplating of copper were investigated by Takeo et al. [357], who noted a reduction in energy required for deposition with increasing magnetic field as a consequence of reduced concentration overpotential. Changes in structure and hardness were also noted as the applied magnetic field strength was increased. Ismail and Fahidy [358] studied the effect of uniform magnetic fields on the morphological properties of fine-mesh metal screen deposits. Popov et al. [359] provided some correlation between dendritic growth and copper powder formation.

2.17.2 Striations

Occasionally spiral patterns (striations) that follow the streamlines of the fluid are obtained during electrodeposition of copper, zinc, and silver [360]. This is accompanied by small or negative polarization resistance and is typically observed only below a certain current density. The range of current density depends on the electrolyte and its concentration. Studies with rotating hemispherical electrodes (RHEs) revealed no striations in the deposition of copper from sulfate solution unless a certain amount of gelatin was added. With increasing additions of gelatin (10–20 ppm), the polarization curve became progressively steeper, vertical, and finally S shaped while shifting to a more negative potential [360]. Spiral patterns were also observed in acid copper sulfate solutions containing PEGs and chloride [89].

2.17.3 Underpotential Deposition

Underpotential deposition (UPD) involves formation of up to a monolayer of atoms on foreign substrates at potentials that are more positive than the potential of the reversible deposition in the same solution, that is, before bulk deposition can occur. The fact that UPD exists means that the chemical potential of adatoms deposited at the underpotentials is different from that of the corresponding bulk metal. The adatoms are more strongly bound to the surface of the foreign substrate than to the surface of its own species [361, 362].

The likelihood that UPD plays an important role in electroplating processes has long been recognized [363]. An example wherein UPD plays an important role is in the electroplating of gold where ions of metal (or semimetal) serve as brightening agents for gold plated from cyanide and noncyanide solutions. Gold deposition proceeds in the region of UPD of the foreign metals, which are incorporated only at trace levels in the deposit. These foreign metals act as brighteners because of their strong influence on the nucleation process [363]. With copper, it has been demonstrated that the UPD of Pb or Sn on copper can be used to produce electroplated Cu–Pb and Cu–Sn alloys, with small amounts

of alloyed Pb and Sn. This is done in acid solutions that do not contain complexants. These alloys are of interest as possible on-chip wiring for very large scale integration where the content of alloying agent must be kept small in order to maintain a low resistivity [363]. Some other studies on UPD include Cu on Au [364] and Cu and Ag on Pt [365].

PART B
CYANIDE COPPER*

2.18 HISTORY AND DEVELOPMENT

Before 1915 copper cyanide solutions were invariably prepared by dissolving copper carbonate in alkali cyanide. The use of tartrates is mentioned in early references [366, 367], but their value apparently was not fully recognized. An exception was the combination cleaning and plating solution described by Watts [368] in 1915. Deposits from these early solutions were relatively thin and were used largely as bases for oxidized and other decorative types of finishes.

The first commercially successful high-efficiency solution was introduced in 1938. It was used extensively throughout the automotive industry in subsequent years for plating zinc die castings as well as steel parts. High rates of deposition were achieved by operating at temperatures around 80°C. Alkali was added to improve anode corrosion and to increase the conductivity of the solution [369]. Alkali thiocyanate was used by Wernlund [370] in 1941 to brighten the deposits. Successful commercialization of the process required the use of specific surface-active agents to sequester organic contaminants and prevent pitting [371]. This solution permitted deposition of smooth, bright deposits in the thickness range of 25–50 μm. The basic formulations of the proprietary high-efficiency solutions now in commercial operation are similar to these, except that thiocyanate and other active sulfur-containing constituents are not recommended in the new processes.

The next major advance in high-efficiency cyanide copper solutions was achieved by employing periodic reverse plating cycles [372]. Other current manipulation techniques such as interrupted current are occasionally used to modify the properties of the coatings. A wide variety of addition agents have been developed; this is covered in Section 2.22. Reviews of cyanide copper plating can be found in [373–379].

2.19 APPLICATIONS

Cyanide copper plating is used throughout the metal-finishing industry for many applications, although not as extensively today as in the 1970s because of environmental issues. Horner [380] estimates that present usage is less than 50% of that in the 1970s. Possible site contamination, worker safety considerations, and high waste treatment and reporting costs are some drawbacks [381].

Applications include as an undercoat for other deposits to protect basis metal or promote adhesion; for surface improvement in buffing, soldering, lubricity, rotogravure, printing rolls, and decorative plating of zinc die castings [382–385]; in plating of steel parts with copper before nickel and chromium plating [384, 385]; as a stopoff to prevent case hardening on selected areas of ferrous metal surfaces; and in plating of coinage [386, 387]. A high-speed cyanide copper plating process is used to produce heavy coatings of copper on steel wire for electrical use. For noncorrosive environments, aluminum is often plated with copper cyanide after zincating. This is followed by a decorative nickel–chromium coating [388].

2.20 FUNCTIONS OF MAJOR SOLUTION CONSTITUENTS

2.20.1 Copper Cyanide

Typical formulations for cyanide solutions are give in Table 2.7. Copper cyanide is insoluble in water but dissolves in aqueous solutions containing alkali metal cyanides to form four stable soluble complexes and free species in water: $CuCN_{aq}$, $[Cu(CN)_2]^-$, $[Cu(CN)_3]^{2-}$, $[Cu(CN)_4]^{3-}$, and Cu^+ and CN^-. In all four oxidation complexes, the oxidation number of copper is $+1$. A model of copper discharge from cyanide electrolyte was developed by Dudek and Fedkiw [389].

Deposition occurs from the $Cu(CN)_2^-$ and $Cu(Cn)_3^{2-}$ complexes [390]. Cuprous cyanide complexes shift the copper deposition potential to more negative values which avoid displacement deposition on less noble substrates. The predominant copper cyanide species discharged in copper strike plating is proposed to be $Cu(CN)_3^{2-}$; although $Cu(CN)_4^{3-}$ is at a higher concentration, it is not as electroactive. These kinetics give rise to the inherent good "macroscopic throwing power" observed in the cyanide solution [391]. Additional information on kinetics can be found in [392].

The Taguchi method was used to evaluate a number of parameters in a copper cyanide solution. An increase in copper concentration and a decrease in potassium cyanide resulted in good current efficiency over a wide current density range. Hydroxide and carbonate concentration were of secondary importance [393].

2.20.2 Free Cyanide

The alkali cyanide in excess of the tricomplex salt $Na_2[Cu(CN)_3]$ is termed *free cyanide.* The ratio of the free

* Revision of section by R. R. Bair and A. K. Graham in the 1974 edition.

TABLE 2.7 Copper Cyanide Solution Formulations

	Strike ($g\,L^{-1}$)		Rochelle ($g\,L^{-1}$)		High Efficiency ($g\,L^{-1}$)	
Constituent	Typical	Limits	Typical	Limits	Typical	Limits
CuCN	22	15–30	26	19–45	75	49–127
NaCN	33	23–48	35	26–68	102	62–154
or						
KCN	43	31–64	—		136	76–178
Na_2CO_3	15	0–15	30	15–16		
NaOH	—	—	—		15	22–37
or						
KOH	—	—	—		15	31–52
Rochelle salt ($KNaC_4H_4O_6 \cdot 4H_2O$)	15	15	45	30–60	—	—
			By Analysis			
Copper	16	11–21	18	13–32	55	34–89
Free cyanide	9	6–11	6	4–9	19	10–20

cyanide to the copper metal content in the strike and Rochelle solutions is somewhat higher than in the high-efficiency solutions. This accounts, in part, for the lower cathode efficiency. Hydrogen is simultaneously liberated at the cathode in the strike and Rochelle solutions, and this hydrogen evolution provides additional cleaning. Strike and Rochelle solutions are also operated at a relatively high free cyanide–metal ratio in order to produce the desired type of deposit. The excellent adhesion of strike deposits can be attributed largely to the high free cyanide combined with low metal, which minimizes any tendency to form nonadherent immersion deposits. Free cyanide is essential in all cyanide copper plating solutions in order to obtain good corrosion of the copper anodes. If it is too low, the anodes polarize and become coated with an insulating film. Free cyanide contributes to conductivity in strike and Rochelle solutions, but not significantly in high-efficiency solutions that contain alkali and higher concentrations of the complex copper ions. The concentration of the free cyanide increases at higher temperatures, since lower complexes are formed and free cyanide is thereby liberated [390]. Free cyanide is normally determined by titrating a sample of the solution with silver nitrate at or below room temperature using potassium iodide as an indicator.

2.20.3 Sodium or Potassium Hydroxide

Sodium or potassium hydroxide is added to high-efficiency solutions primarily to provide good electrical conductivity and to improve throwing power. Alkali is also essential in these solutions for good anode corrosion. The brightness of the deposits from high-efficiency solutions is also influenced by the alkali metal hydroxide. Usually only small amounts of caustic are added to strike or Rochelle solutions for adjusting or maintaining the pH within the proper range. Many users of high-efficiency cyanide copper solutions base their formulations on sodium cyanide to complex the cyanide copper and add potassium hydroxide as a means of introducing the potassium ion.

2.21 COMPARISON OF SODIUM AND POTASSIUM FORMULATIONS

The complex salts formed with sodium or potassium cyanide are similar in composition, but the potassium salts are more soluble. Horner [394] compared the throwing power and efficiencies of sodium and potassium formulations and the effects of free cyanide, carbonate content, and other factors. He concluded that potassium salts offered no advantage for cathode efficiency over sodium salts but did show improved throwing power. Hatherley et al. [387] reported that sodium and potassium formulations each possess various advantages and disadvantages. Conductivity is higher in potassium solutions, especially at high concentrations of carbonate. Cathode polarization curves also favor potassium formulations over sodium. By contrast, sodium solutions exhibit less of a risk of anode passivation. Juhos et al. [395] also found that sodium formulations favored the anode reactions. Hatherley et al. [387] suggest that commercial considerations might be used to specify optimum carbonate level where the advantage of high conductivity has to be set against reduced cathode efficiency.

2.21.1 Carbonate

Carbonate exerts a strong buffer action at a pH of 10.8–11.5 in strike and Rochelle solutions [396, 397] and facilitates pH control. It also reduces anode polarization in these solutions.

No beneficial effects of carbonate have been observed in high-efficiency solutions that contain substantial amounts of caustic. Commercial high-efficiency cyanide copper solutions contain an average of about $50\,g\,L^{-1}$ sodium carbonate. It is formed by oxidation of the cyanide radical at the surface of polarized anodes or insoluble anodic metal surfaces. Absorption of carbon dioxide from the air by the caustic alkali in the solution and hydrolysis of the cyanide are other sources of carbonates formed in the high-efficiency solutions.

The oxidation of cyanide should be avoided because it increases the cyanide consumption, causes a rapid buildup of carbonates, and complicates control of free cyanide. Concentrations up to about $90\,g\,L^{-1}$ sodium carbonate or $120\,g\,L^{-1}$ potassium carbonate have no significant effect in reducing the plating speed of high-efficiency solutions. If maximum plating speed is required, however, the concentrations should be controlled below these levels.

2.21.2 Tartrates

Tartrates are used primarily in the low-efficiency solutions. It is believed that the potassium–sodium tartrate or Rochelle salt ($KNaC_4H_4O_6 \cdot 4H_2O$) forms temporary complexes with copper by reacting with products of electrolysis produced in the anode film. Solutions containing tartrates may be operated with lower free cyanide and at higher current densities and efficiencies without impairing anode corrosion [396, 398]. Obtaining better quality deposits by the use of Rochelle salt is associated in part with the formation of complex salts which are probably present in the cathode film. Solutions are normally operated with about $45\,g\,L^{-1}$ Rochelle salt. Wagner and Beckwith [398] claimed that the optimum concentration was about $22.5\,g\,L^{-1}$, with somewhat lower efficiencies being obtained at higher values. The substitution of sodium–potassium citrate for Rochelle salt [399] has been investigated and several other proprietary compounds of a similar type are claimed to offer advantages.

2.22 ADDITION AGENTS

Additives for cyanide copper systems include compounds having active sulfur groups and/or containing metalloids such as selenium or tellurium. Other agents that have worked are organic amines or their reaction products with active sulfur-containing compounds; inorganic compounds containing metals such as selenium, tellurium, lead, thallium, antimony, and arsenic; nitrogen and sulfur heterocyclic compounds; and unsaturated alcohols, saccharin, and PEG. An extensive listing of additives used in acid and cyanide copper prior to 1959 can be found in [374] and more recent information in [400–411]. Of interest are data from Table 2.2 in the section on acid copper plating which lists only one U.S. patent for cyanide copper plating since the mid-1970s compared to over 60 for acid copper.

2.23 SOLUTION TYPES: STRIKE AND ROCHELLE SOLUTIONS

Copper cyanide solutions may be classified in three categories: strike, Rochelle, and high efficiency. Strike solutions are used extensively to apply relatively thin coatings of copper as an undercoating for other metals. Rochelle solutions, in general, are not as sensitive to contamination as the high-efficiency solutions and are used in applications where an intermediate thickness of copper is applied. Deposits from these solutions vary from dull to semibright; the brightness or luster is not of major importance for most applications.

Copper strike solutions are used for applying a thin coating of copper on aluminum and zinc die castings before plating with other metals [384]. The adherent copper coating prevents chemical attack when these substrates are subsequently plated with heavier coatings from other solutions. The thickness of strike deposits normally varies from about 0.5 to 1 μm, although it may sometimes be as high as 2.5 μm. The heavier strike deposits must be used when the subsequent plating operation is from an acid electrolyte. For instance, the copper strike deposit on zinc die castings must be three to five times as heavy for subsequent acid copper plating as compared with cyanide copper plating.

The bond strength between electroless nickel and a variety of aluminum alloys is higher when a copper strike is used [412]. Besides showing good adhesion of subsequent electrodeposits, the copper strike from cyanide solutions is an additional cleaning operation. Furthermore a thin copper strike (1.3 μm) under lead coatings over steel has shown improved protective value in atmospheric exposure tests compared to lead coatings alone [413, 414]. Aluminum parts can be plated in a barrel if the free cyanide in the copper strike is high enough ($15–20\,g\,L^{-1}$) to prevent displacement of copper on zinc [415]. A good review of copper cyanide striking is provided by Mohler [416].

2.24 OPERATING CONDITIONS AND SOLUTION CHARACTERISTICS

The operating conditions of strike and Rochelle solutions are given in Table 2.8. Strike solutions are usually operated in the temperature range of 40–60° C. The cathode efficiencies are relatively low (10–60%) in the normal plating range of $1.0–3.2\,A\,dm^{-2}$. The solution composition and operating characteristics vary widely in actual commercial practice. Many users prefer to add $15–30\,g\,L^{-1}$ sodium carbonate. When steel parts are plated, $15–30\,g\,L^{-1}$ sodium hydroxide may be added to improve the conductivity. Rochelle salt, or its equivalent, is sometimes used to improve anode and cathode characteristics.

Because of the higher cathode efficiency, heavier deposits can be more practically produced from Rochelle solutions

TABLE 2.8 Operating Conditions for Typical Cyanide Solutions

Conditions	Strike	Rochelle	High Efficiency
Temperature (°C)	40–60	55–75	60–80
Cathode current density ($A\,dm^{-2}$)	0.5–4	1.5–6.5	1–11
Anode current density($A\,dm^{-2}$)	0.5–1	0.8–3.3	1.5–5
Efficiency range			
Cathode (%)	10–60	30–90	70–99 +
Anode (%)	95–100	50–70	—
Ratio of anode to cathode area	3:1	2:1	3:2
Agitation			
Cathode rod	Optional	Preferred	Either or both
Air			
Solution voltage (V)	6	6	0.75–4
Limiting thickness (μm)	2.5	13	>25

than from strike solutions. These plating characteristics are achieved by operating at higher temperatures, controlled pH, and higher metal concentration and adding substantial amounts of Rochelle salt to the solution. The average cathode efficiency is approximately 50% higher than that obtained from strike solutions. The anode and cathode efficiencies vary with the temperature and degree of agitation [396]. Rochelle solutions are normally operated without metal-containing addition agents, but lead had been used as a grain refining and brightening agent [417].

Polarization phenomena in copper cyanide solutions have been extensively investigated [387, 390, 396, 418, 419]. Hatherley and co-workers [387] reported that potassium- and sodium-based solutions may both be operated at close to 100% cathode efficiencies but potassium solutions can sustain efficient copper deposition to a higher maximum current than can sodium. They also noted that increasing free cyanide diminishes the limited current density that can be sustained at maximum efficiency, and this relationship is linear for both sodium and potassium solutions. An increase in the carbonate or hydroxide content is also associated with a reduction in the maximum current for efficient copper deposition. Last, the efficiency of solutions cannot be restored by precipitation of carbonate with lime, nor by any of the other chemical agents that have been proposed in the past [387, 390].

Graham and Read [396, 418, 419] defined the limiting current density beyond which excessive polarization occurs for a given set of solution variables. Excessive polarization causes insulation of the anodes and usually necessitates their removal for cleaning. Variations in metal content and free cyanide have little effect on the limiting current density. If the carbonate content is too high, the copper may act as an insoluble anode without exhibiting excessive polarization. Reducing the pH from 12.8 to as low as 10.3 does not greatly alter the limiting current density. The presence of tartrates does not overcome the tendency of the anodes to polarize excessively, but the allowable current density is raised when both carbonate and tartrate are present. If insoluble iron anodes are used along with copper anodes, higher anode current densities may be used because the iron anodes depolarize the copper.

The throwing power of Rochelle solutions is superior to that of high-efficiency cyanide solutions. Most of the published data on throwing power are limited to current densities below $1.0\,A\,dm^{-2}$. The factors influencing the throwing power of Rochelle solutions when operated at more practical current densities and temperatures may be quite different. The greatest single factor contributing to good throwing power and metal distribution appears to be associated with a decrease in cathode efficiency with increasing current density. High efficiencies, in general, contribute to poor throwing power, but there are also other factors, as discussed later.

2.25 MAINTENANCE AND CONTROL

Copper strike solutions in commercial use vary in metal content but are usually maintained at a copper metal concentration of about 10–16 $g\,L^{-1}$. The metal content increases during operation because the copper anode efficiency is higher than the cathode efficiency. It is common practice to use a combination of steel and copper anodes in the strike solutions to obtain an overall anode efficiency equal to the average cathode efficiency. The control of the critical free sodium cyanide is simplified, and a more stable solution composition is thereby attained. The free sodium cyanide should be controlled within the range of 6–11 $g\,L^{-1}$.

Continuous filtration of the strike solutions through activated carbon is recommended for the best results. This prevents particle roughness on the shelf areas of the plated parts and minimizes drag in of organic contamination into subsequent plating solutions.

Control of the pH of Rochelle solutions is important for obtaining the best performance. Operation within the pH range of 12.2–12.8 is recommended [396]. The range 12.5–12.8 is preferred because the solution is buffered in this range by the carbonate. Operation at a pH in excess of 12.9 should be avoided, owing to decreased anode efficiencies and chemical attack of the solution on zinc die castings.

The pH of Rochelle copper solutions can be determined by a pH meter, by colorimetric methods, or by titrating with hydrochloric or sulfuric acid. The first two methods are rapid and simple; the titration method, however, has the advantage of indicating directly the approximate excess of caustic above the sulfo-orange sodium carbonate endpoint. The pH at the sodium carbonate buffer point is approximately 11.5; it can be raised to 12.7 by the addition of 0.75 $g\,L^{-1}$ caustic soda.

Controlling the free-cyanide concentration of Rochelle solutions within the range of 4–9 g L^{-1} is also important. Excessive anode polarization is encountered at very low free cyanide and the quality of the deposits is also adversely affected. Operating with a significantly higher free-cyanide concentration than recommended results in lower cathode efficiencies and in the production of dull deposits that are difficult to buff.

2.26 HIGH-EFFICIENCY CYANIDE COPPER SOLUTIONS

Solutions that are formulated and operated under conditions that give essentially 100% anode and cathode efficiencies are classified in this category. The rates of deposition are appreciably higher than can be obtained from strike or Rochelle solutions.

Many of the high-efficiency cyanide copper solutions are used for plating of automotive bright trim parts. As pointed out earlier, Rochelle solutions may be used for plating zinc die castings. Most installations, however, use high-efficiency solutions in order to obtain the required thickness relatively quickly. The brightness of deposits from the high-efficiency solutions is also an important factor.

Copper is also plated from high-efficiency solutions on selected surfaces of ferrous metal parts to prevent carbon penetration during case hardening. Thickness requirements vary from 13 to 25 μm, depending on the type of carburizing medium used, time of treatment in the carburizing solution, and type of surface finish on the steel. Another use of high-efficiency solutions is the plating of steel wire with a heavy coating of copper [420–422]. Part-to-part spread in deposit thickness for barrel plating is considerably less for alkaline solutions (cyanide, pyrophosphate, and amine) than for acid solutions (sulfate and fluoborate) [423].

2.27 OPERATING CONDITIONS AND SOLUTION CHARACTERISTICS

High-efficiency cyanide solutions are normally operated in the temperature range of 60–80°C (see Table 2.8), with the higher temperature preferred for maximum plating speed. Many of the high-efficiency electrolytes are operated at temperatures as low as 60°C to fit specific needs and equipment. It is emphasized that a reduction in solution temperature can restrict the width of bright plating range and maximum usable current densities. The cathode current density range in commercial practice varies from about 1 to 11 A dm^{-2}, depending on the contour of the parts being plated. Automotive parts are generally plated at current densities in the range of 2–5.5 A dm^{-2}, whereas wire is plated from high-metal solutions at current densities as high as 11 A dm^{-1}. Maximum plating speeds are achieved with potassium formulated solutions containing high metal and operated with vigorous solution circulation. The solutions must be operated at substantially 100% cathode efficiency in order to produce good-quality deposits and to avoid hydrogen evolution at the cathode, which produces dull, burned deposits.

These high-efficiency solutions would normally be expected to have poor throwing power. However, metal distribution on plated parts is better than would be predicted from the efficiency factor alone. One reason for this is that the high concentration of salts, particularly alkali, and high operating temperatures greatly improve the conductivity and reduce the difference in current density on protruding and recessed areas. Rochelle salt solutions have good throwing power because the cathode efficiency decreases with increase in current density.

The anode current densities may vary from 1.5 to 5 A dm^{-2}. The anode efficiency under these conditions is essentially 100%. At very low anode current densities (0.2–0.6 A dm^{-2}), particles of copper may be formed or generated at the anode surface through intercrystalline corrosion. The particles settle on shelf areas of the parts and produce serious roughness. Certain types of proprietary organic addition agents are claimed to play an important role in improving anode corrosion [424]. They apparently form a thin organic film over the anode surface and thereby promote smooth anode corrosion and minimize any tendency to generate copper particles.

Solution circulation or movement of the electrolyte is also important in obtaining performance. In addition to increasing the plating rate, vigorous circulation is effective in minimizing pitting caused by hydrogen bubbles clinging to the surface of parts being plated. Circulation is accomplished commercially by pumping the electrolyte or by air agitation.

The plating characteristics of some of the high-efficiency solutions can be improved by utilizing current manipulation techniques (discussed in more detail in Section 2.10). Parts are plated in the conventional manner for a selected lime and are then deplated for a shorter period by reversing the current. This technique is referred to as PR current plating. Direct plating cycles of 2–40 s with 0.5–10 s reverse (deplating) cycles were described by Jernstedt [372]. Longer cycles, in excess of 60 s direct with reverse cycles in excess of 12 s, were disclosed by Wernlund [425]. Ismail [426] reported that surface roughness increased with frequency and amplitude of the PR current used. Increasing the solution temperature led to brighter surfaces up to 50°C, and a PR ratio of 2 gave the best surface brightness. The PR plate was brighter and had a higher corrosion resistance than the corresponding dc plated deposits. A number of production applications utilizing PR plating are discussed in [427].

Current interruption cycles are also used. For example, zinc die castings are frequently plated using a 10-s plating cycle followed by interrupting the current for 1 s and then repeating the cycle. This approach can provide excellent

deposit brightness from bright plating solutions which are contaminated sufficiently that acceptable deposits cannot be produced by use of continuous direct current.

One of the advantages gained by employing periodic current reversal or interrupted cycles is leveling. The degree of leveling obtained is greatest with PR, particularly with relatively long reversal cycles. Deposits so plated show a laminar structure, whereas those plated with conventional direct current are columnar. The leveling obtained with current interruption is less than with current reversal, but it is adequate for covering minor surface marks such as buffing wheel lap marks on zinc die castings. The uniformity of distribution of the copper on irregularly shaped parts is also improved when current reversal is used. It prevents excessive buildup of metal on high-current-density areas and yields significant savings in anode consumption.

The choice between periodic current reversal and current interruption greatly favors the latter. Periodic reversal has a low net rate of deposition because on the reversal the copper is being depleted. As an example, a 60/20 PR cycle has only a 50% net deposition rate if the current applied is the same for the plate and deplete cycles. The use of PR plating has not had broad acceptance because of this factor. Rudder [428] compared pulse plating of cyanide copper versus acid copper and found that the leveling and thickness performance of the pulse-plated cyanide copper was better than that of the acid copper.

2.28 MAINTENANCE AND CONTROL

High-quality copper deposits can be produced consistently from the high-efficiency solutions by following good plating practice. Analytical methods are available for determining the concentrations of the normal solution components [429–433]. Methods are also available for determining contaminants such as carbonates, ferrocyanide, and zinc. The Hull cell is used extensively for detecting organic contamination, controlling addition agents, and determining the effectiveness of various purification treatments [434–436].

The composition of the solutions in commercial operations varies widely. The copper metal content of the average solution is maintained at about 45–55 g L^{-1}. Solutions used for plating steel wire or rod, however, are usually maintained at a metal concentration of 60–90 g L^{-1}. The free-sodium cyanide is normally maintained in the range 10–20 g L^{-1}. The free cyanide can be lower when the metal content is low. Solutions containing high metal usually require a slight increase in free cyanide for optimum plating performance. An interesting exception to the usual composition and operating conditions for so-called stable copper cyanide plating solutions has been described by Dingley [437], who operated solutions under conditions to give high current efficiencies. Anode-to-cathode areas had to be greater than 4:1 to maintain solution stability.

Good cleaning and thorough rinsing of the parts before plating are very important, since high-efficiency solutions are sensitive to organic contamination, which produces dull deposits and sometimes pitting. Continuous carbon treatment of the copper strike is recommended as a precaution in minimizing drag-in of organic contaminants. The high-efficiency solutions are normally purified continuously by passing them through a filter packed with activated carbon. A periodic batch treatment with activated carbon may be required if excessive amounts of contaminants are present. The effectiveness of the purification can, in some cases, be improved by adding about 1 mL L^{-1} of 30% hydrogen peroxide to the solution before adding the carbon. The peroxide can be added safely by first diluting it with 15 parts of water. Its effectiveness is attributed largely to its ability to convert some types of organic contaminants to a less soluble form by oxidation.

Excessive carbonate in high-efficiency solutions reduces the bright current density range and produces grainy deposits. Carbonate should be removed if the concentration exceeds about 90 g L^{-1} sodium carbonate or 118 g L^{-1} potassium carbonate. It can be precipitated by adding calcium hydroxide (hydrated lime). Excess sodium carbonate may also be crystallized out of sodium formulated plating solutions by cooling the solutions to about $-30°C$. This procedure is unsuitable for solutions maintained solely with potassium salts because of the greater solubility of potassium carbonate at all temperatures. Crain and others [438] discuss the causes of carbonate buildup in cyanide copper plating solutions and control procedures, including a patented method applicable to both sodium and potassium solutions.

Chromate is harmful in the high-efficiency solutions even when present in very low concentrations (5–10 ppm). Its action is similar to that observed in other cyanide copper-plating solutions in that it produces dull, nonuniform deposits. In low concentrations it produces blotchy deposits at low current densities and this condition is extended to higher current densities as the concentration of chromate increases. Adverse effects of chromate can be eliminated by adding a chelating agent of the EDTA type. Although chelating agents of this type do not function as reducing agents, the chromate is probably reduced to a Cr^{3+} compound by the Cu^{1+} ion in the presence of the chelating agent. Reducing agents such as sugar derivatives and sodium stannite are also used [439]. In the absence of Rochelle salt, the reduced chromium will gradually precipitate and is removed by filtration.

Hexavalent chromium in just a few ppm can cause dullness, blistering, skip plating, and reduced cathode efficiency. It also gives rise to a reduced bond strength between the copper deposit and steel substrate [440]. Proprietary compounds are available that reduce the hexavalent chromium to the trivalent state without any side effects.

Zinc, which contributes to step plating in low-current-density areas, codeposits with the copper to form brass deposits which are somewhat brittle. The brassy appearance

of the deposits can be detected when zinc concentrations are as low as 1.5–2.25 g L^{-1}. Excessive buildup of zinc in high-efficiency solutions can be avoided by removing die castings that fall off racks into the plating solution and by applying an adequate thickness of copper in the strike before the higher speed copper plating. If the zinc builds up to an objectionable concentration, the excess can be removed by dummy electrolysis using an average cathode current density of 0.3–0.5 A dm^{-2}. Small amounts of sodium thiocyanate are effective in sequestering excessive zinc.

Iron contamination comes from salts, water, drag-in, and attack of steel in the cyanide solution. The iron can be complexed into a stable ferrocyanide salt that does not codeposit but does accumulate in the solution. If the iron level gets too high, the anode efficiency is lowered, thus causing carbonate buildup.

For a discussion of impurities in copper cyanide plating solutions, including their effects on the deposits and methods for their removal, see [382, 441, 442]. Horner [382] is an excellent source on troubleshooting of copper cyanide solutions.

2.29 ANODES

Cast ball, cast elliptical, or electrolytic copper sheet anodes are generally used with strike solutions. Steel anodes are sometimes used in conjunction with copper in a low-efficiency solution such as a strike to safeguard against excessive anode polarization and as a means of controlling the metal content [396, 418]. Copper compounds formed at the anode are soluble in these solutions when the anodes are operated below the critical current density [418]. Excessive current densities usually cause polarization of the anodes by formation of an insulating film. Cast, rolled, or oxygen-free high-purity copper anodes are preferred for Rochelle and high-efficiency solutions.

Copper anodes for high-efficiency solutions should be substantially free of oxide inclusions. Copper oxide particles produce serious roughness on the plated parts because copper oxide is readily reduced to particles of copper at the cathode. Electrolytic sheet copper contains substantial amounts of oxide and other occlusions; it is therefore not recommended for high-efficiency solutions. Crystal structure of the copper is also an important factor in anode corrosion. A large grain structure, in general, is preferred. Several types of good-quality copper anodes produced by melting, extrusion, or casting under an inert atmosphere are available.

2.30 MATERIALS OF CONSTRUCTION

Rubber or polyvinylchloride (PVC)–lined steel plating tanks are more satisfactory than plain steel for high-efficiency cyanide copper plating solutions. Polypropylene tanks with adequate reinforcing may also be used, provided that the operating temperature is not excessive [378]. Leaching should be done on any new tanks or equipment coming in contact with the plating solution. This removes any material that may leach into the plating solution and cause poor-quality deposits.

Unlined steel tanks are also widely used. However, under certain adverse conditions the steel may become susceptible to corrosion from the electrolyte. Increasing the alkalinity of the solution by adding hydroxide and raising the free-cyanide content serve to protect the steel and prevent its dissolution [382, 443].

The most satisfactory method of heating the electrolyte is to circulate it through an external heat exchanger and return it to the plating tank through a filter. Particles that may be generated in the heat exchanger are thereby removed. Brass or bronze fittings of any type are not recommended, since they are chemically attacked by the electrolyte. Lead-containing equipment parts must also be avoided, since lead can contaminate some types of high-efficiency processes.

2.31 ENVIRONMENTAL

Copper cyanide processes are relatively easy to operate and produce excellent deposits; however, they use extremely dangerous solutions and therefore must be monitored carefully because of the potential of poisoning the workers and the environment. Accidental spills of acid into the cyanide tank or cyanide spilled into a sewer system can result in a very dangerous condition. Cyanide's waste treatment must also be very carefully conducted in a separate tank under closely controlled conditions [444]. Cyanide-bearing solutions require oxidation of the cyanide with an oxidizing agent such as chlorine or hypochlorite, followed by precipitation of the heavy metals [378]. While it is unlikely to happen on a frequent basis, if the cyanide copper solution ever requires disposal, the cost is prohibitive compared to alkaline non-cyanide copper [445].

2.32 STRUCTURE AND PROPERTIES

The best source for property data is Safranek's [446] treatise on properties of electrodeposits. Another comprehensive reference is that of Lamb et al. [447, 448], who provide data on Young's modulus, fatigue strength, effects of cold rolling and annealing on mechanical properties, tensile and elongation data for temperatures from −78 to 325°C, thermal expansivity, texture analysis, and gas content for solutions containing no addition agents. The following paragraph summarizes information that appeared in Safranek's book; very little has appeared on properties of cyanide deposits since publication of his book [446]:

Copper deposited in low concentration cyanide solutions at low temperatures (40°C) was coarse grained. Fibrous structure, which is typical of cyanide deposited at 60°C was changed to a fine-grained, equiaxed structure by adding Rochelle salts or increasing the copper cyanide concentration to 75 g l^{-1} and the temperature to 80°C. Strong and hard deposits with a tensile strength of at least 43 MPa were deposited with periodically reversed current in solutions at 80°C containing 75 g l^{-1} copper cyanide.

Copper plated from cyanide solutions is highly embrittling to high-strength steel substrates because of the inefficiency of the solutions and the fact that cyanide solutions are highly conducive to hydrogen entry into steel [449]. For waveguide applications, copper deposited from a cyanide solution formed no voids during heat treatment to 1000°C [450].

PART C ALKALINE NONCYANIDE COPPER

Alkaline noncyanide copper plating solutions have found increasing popularity since the mid-1980s because of environmental issues. The cost of using and disposing of cyanides and associated environmental concerns have led to efforts to replace cyanides. Besides the obvious plus of elimination of cyanide from the wastewater stream, these new solutions are safe to work with and are easily waste treated with lime in the same treatment process used for nickel, acid copper, and acids [451]. Other benefits include faster barrel plating speed, lower sludge volume generation because of lower metal concentrations, simplified wastewater treatment, no trouble with carbonate buildup, and lower Occupational Safety and Health Administration (OSHA) safety concerns. Disadvantages include higher operating costs, difficulty in using the process on zinc die castings, greater sensitivity to impurities, and a chemistry more difficult to control [451]. Copper concentration limits and operating conditions for alkaline noncyanide solutions are summarized in Table 2.9.

Typically the throwing power of the noncyanide solutions is very good, as can be seen from Table 2.5. An alkaline noncyanide solution provided even better throwing power than the high-throw acid copper formulation used for plating printed wiring boards. Since the noncyanide processes use cupric copper ions while the cyanide processes contain monovalent copper, the latter provide for faster plating at the same current density. However, the noncyanide processes can operate at higher current densities, thus yielding faster plating overall [452]. Most noncyanide processes use air agitation, while at least one (phosphonate) uses a purification cell, with proprietary anodes to prevent buildup of too much cuprous copper [453]. The noncyanide processes require excellent cleaning prior to plating and are not as tolerant of poor cleaning practices as cyanide processes. However, adhesion can be as good as that obtained with cyanide. For example, excellent results have been reported for aluminum prepared for plating by substituting a pyrophosphate strike for cyanide [454, 455]. Similar good results were obtained with 1018 steel and cast iron. The deposits have good mechanical properties, including higher ductility than cyanide deposits, as well as outstanding metal distribution and very good tolerance to common impurities [456]. Safranek and Miller [457, 458] reported that a cyanide strike can be replaced with a pyrophosphate strike if ultrasonic agitation is used during the striking process. Applications where the copper deposit is used as a heat treat masking barrier prior to carburizing, nitriding, or through hardening have proved successful [459, 460]. A number of proprietary formulations are available and these are based on a variety of chelating ligands, most commonly carboxylic acids, amines, and phosphonates [460–463]. Table 2.2 on acid copper plating lists a number of U.S. patents. Nonproprietary formulations that have been evaluated include solutions containing amine–ammonia [464], chloride [465], citrate [465, 466], EDTA [467, 468], glycerolate [469], phosphate [470], pyrophosphate [454, 455, 471], tartrate [472, 473], and triethanolamine [474].

TABLE 2.9 Concentration Limits and Operating Conditions of Alkaline Noncyanide Copper Plating Solutions

Constituent or Condition	Range
Copper metal (g L^{-1})	5–14
PH	9–10.5
Temperature (°C)	38–65
Cathode current density (A dm^{-2})	0.5–3.0
Tank voltage	2–12
Anode–cathode ratio	1.5:1
Copper anodes	OFHC or EFT 110 copper

PART D PYROPHOSPHATE COPPER*

2.33 HISTORY AND DEVELOPMENT

The earliest published reference to copper pyrophosphate deposition was by Roseleur in 1847 [475]. In 1883 Gutensohn [476] was granted a patent for copper pyrophosphate plating on a number of substrates. Others associated with the early state of the art included Brand [477], Delval [478],

* Revision of Section by J. W. Dini in the 1974 edition.

Royer [479], and Regelsberger [480]. Pioneering work by Stareck [481, 482] led to the development of a commercial copper pyrophosphate in 1941. The same year Coyle [483] described the main aspects of the process. Reviews of copper pyrophosphate plating can be found in [484–490].

2.34 APPLICATIONS

Pyrophosphate copper is used in the production of electroformed objects such as waveguides, paint spray masks [491], helical antennae [492], heat exchangers [493], molds for making toys [491, 494], and hard, high-strength [495], wear-resistant [496] deposits. Pyrophosphate deposits are also used on steel [491, 497, 498] and aluminum parts [499–504], and in some cases, they serve as a replacement for cyanide deposits [505, 506]. Other applications include plating zinc die castings [507, 508] before bright nickel and chromium plating, as a lubricant for wire deep drawing operations [485, 491], as a stopoff on steel for selective hardening operations such as nitriding and carburizing [485, 509–512], in roll plating [485], in minimizing hydrogen embrittlement [513, 514], and in the manufacture of plated steel cord for radial tires and high-pressure plastic pipes [515, 516]. Pyrophosphate solutions are also used for plating through holes on printed wiring boards, although in most cases this application has been replaced by high-throw acid copper sulfate formulations [490, 517–519]. Use of pyrophosphate processes for automotive decorative plating has been completely eliminated for many years [520]. Pyrophosphate solutions have been used for plating on plastics; however, these solutions are considerably more expensive to make up than high-throw acid copper formulations [521].

2.35 BASIC CHEMISTRY

The copper pyrophosphate plating solution contains copper pyrophosphate ($Cu_2P_2O_7 \cdot 3H_2O$), either potassium pyrophosphate ($K_4P_2O_7$) or the corresponding sodium salt ($Na_4P_2O_7$), nitrate (NO_3), and ammonia (NH_3). The pyrophosphate salts react in aqueous solution to form alkaline complex anions, the major complex $Cu(P_2O_7)_2^{6-}$ and also $(Cu_2P_2O_7)^{2-}$. The solution is of intermediate stability [522]. Between pH values of 7 and 11, the stability of the complex anion is evidenced by the slow but sure hydrolysis of $(P_2O_7)^{4-}$ to $(PO_4)^{3-}$. At pH values above 11, $Cu(OH)_2$ precipitates; at pH values noticeably below 7 either $CuH_2P_2O_7$ or $Cu_2P_2O_7$ precipitates. Acidification below pH 7 converts the $(P_2O_7)^{4-}$ to either $(H_2P_2O_7)^{2-}$ or $(HPO_4)^{2-}$ and thus destroys the complex anion [523]. Additional information on the chemistry of copper pyrophosphate complexes may be found in [486–488, 524–534].

TABLE 2.10 Optimum Range of Solution Constituents

Analytical Constitutent	Composition ($g\,L^{-1}$)
Copper, Cu^{2+}	22–38
Pyrophosphate, $(P_2O_7)^{4-}$	150–250
Nitrate, NO_3^-	5–10
Ammonia, NH_3	1–3
Orthophosphate, $(HPO_4)^{2-}$	No greater than 113
Organic additives	As required

2.36 CONSTITUENTS

2.36.1 Copper and Pyrophosphate

Typical formulations are included in Table 2.10. The copper and pyrophosphate contents of the plating solution are critical in terms of the ratio of one to the other. To promote anode corrosion and to increase electrical conductivity, the solution must contain excess complexing compound. Although either may be used, potassium pyrophosphate is preferred over the sodium salt because it is more soluble, and a potassium solution has a higher electrical conductivity because of the higher mobility of potassium ions.

2.36.2 Nitrate

The presence of a nitrate results in a higher maximum current density because, especially at current densities above $3.2\,A\,dm^2$, the nitrate ion reduces cathode polarization by acting as a hydrogen acceptor according to the equation [485]

$$NO_3^- + 10H^+ + 8e = NH_4^+ + 3H_2O$$

As the solution is used extensively, reduction of the nitrate ion also leads to a buildup of nitrite [535].

2.36.3 Ammonia

A small amount of ammonia is used to produce more uniform and lustrous deposits and to improve anode corrosion. Excess ammonia can cause cuprous oxide to form and this can hinder adhesion [522].

Because ammonia evaporates from the plating solution, it is usually added daily in quantities either dependent on the size of the tank, for example, 140 g of ammonium hydroxide per square meter of exposed surface per day [536], or as determined by chemical analysis of the solution. In some installations, gaseous ammonia is used [537]. Kojima [538] disclosed that ammonia consumption increased with increasing temperature, pH, agitation, and ammonia content in the solution, while current had little effect on consumption.

2.36.4 Orthophosphate

Orthophosphate formed by the hydrolysis of pyrophosphate is beneficial in that it promotes anode corrosion and acts as

a buffer. At all concentrations it affects the properties of the plating solutions and deposits. Increasing orthophosphate concentration decreases the throwing power and efficiency of the solution and causes a reduction in the ductility of deposits [539].

Low pH (less than 7), increasing P_2O_7 concentration, high P_2O_7–Cu ratio, high temperatures (greater than 60°C) in the plating solution or heat exchanger, or local overheating will cause orthophosphate to build up. Orthophosphate cannot be removed chemically from a pyrophosphate solution. The concentration can be reduced only by either discarding the solution altogether or by diluting and rebuilding it.

2.36.5 Additives

Additives have more of an influence on deposit properties than any other plating variable, as will be shown in the section on properties and structure. When used at controlled, limited concentrations, organic additives refine the grain structure, provide desired tensile and ductility properties, impart leveling characteristics to the plating solution, and act as brighteners. However, decomposition products from an excessive additive concentration can cause brittle copper deposits. Thus, for optimum quality deposits, no more additive should be added to a solution than is necessary to replace losses by consumption.

Organic additives covered in the patent literature as brighteners include mercaptothiadiazoles [540–550], mercaptothiazoles [551–556], mercaptobenzimidazole [557], and pyrimidines [555, 558, 559]. Other organic and inorganic materials, such as glycerol [560, 561], triethanolamine [560, 561], trioxyglutaric acid [525, 562], diphenylamine sulfonic acid [561], naphthalene disulfonic acid [563], gelatin, bakers yeast, casein, glycocoll [564], hydroxyethylcellulose [565], sodium selenite [525, 559], sodium sulfite [560, 561], Rochelle salt, sodium thiosulfate, potassium bromide [561], and the chlorides of As, Bi, Fe, Cr, Sn, Zn, Cd, Pb [482, 563], and alkali metals have been used as brighteners. Additions of small amounts of lead are reported to improve plating properties [566, 567]. Organic acids such as oxalic, lactic, tartaric, malic, and citric or their ammonium or alkali salts also produce some brightening [482].

2.36.6 Operating Conditions

A copper pyrophosphate plating solution may be operated over a relatively wide range of conditions. The optimum range, similar to that given by Couch and Stareck [568], is shown in Table 2.11.

TABLE 2.11 Optimum Operating Conditions

P_2O_7–Cu ratio	7.0:1–8.0:1
pH	8.0–8.8
Temperature, °C	50–60
Cathode current density, A dm^{-2}	1–8
Anode and cathode efficiency, %	100
Anode–cathode ratio	1:1–2:1
Agitation	1–1.5 m^3/(min) (m^{-2}) of surface

2.36.7 Pyrophosphate–Copper Ratio

The copper pyrophosphate solution is analyzed for both copper and pyrophosphate, and it is therefore convenient to describe the solution in terms of the ratio between these constituents. For optimum plating, the weight ratio of pyrophosphate to copper should be kept in the range 7:1–8:1. Ratios of 8.5:1 or higher promote formation of orthophosphate and thereby decrease the bright plating range. Operation with a ratio of less than 7:1 tends to produce a rough-surfaced plate and renders the solution unstable.

2.36.8 pH

The optimum solution pH is in the range of 8–9. As discussed earlier, a pH outside this range results in hydrolysis of pyrophosphate to orthophosphate or the formation of precipitates. Also, if the pH is too high, both anode corrosion and operating current density range decrease. Radin [569] states that a pyrophosphate solution will operate acceptably even at pH values as high as 9.3 provided the copper concentration exceeds 26 g L^{-1}. When a solution is operated at this high pH, the tendency toward roughness can be eliminated by increasing the P_2O_7–Cu ratio. In practice, a pH of 7–9 is easily maintained because at this pH both anode and cathode efficiencies are virtually 100%. Clearly, there is no chemical breakdown of the constituents, and the solution is highly buffered. When adjustments must be made, pyrophosphoric acid is used for lowering pH and potassium hydroxide for raising it.

2.36.9 Temperature

The solution is usually operated between 50 and 60°C. Temperatures greater than 60°C can lead to rapid formation of orthophosphate.

2.36.10 Current Density

Cathode current density is a function of the temperature and agitation of the plating solution. However, under standard operating conditions, a current density of 1–9 A dm^{-2} is appropriate. The anode current density is fairly critical, and it should be kept between 2 and 4 A dm^{-2}. At too high an anode current density, an insoluble oxide tends to form. The operating current density range may be increased by

ultrasonics, by current interruption or reversal, and by increased metal concentration.

2.36.11 Agitation

Copper pyrophosphate solutions are among those that must be most vigorously agitated. Without sufficient agitation, a brownish deposit is obtained, and the operating current density range is drastically lowered. A solution can be continuously agitated by either one or a combination of three methods: air, mechanical movement of the cathode, or ultrasonics. When air agitation is used, the air should be supplied by a low-pressure blower because compressed air can contain oil.

Gurylev et al. [570] claimed that ultrasonic agitation reduces anode and cathode polarization and permits a 4–4.5 times increase in the deposition rate over that obtained with intensive mechanical agitation. The combination of ultrasonics and periodic reverse current increased current efficiency and allowable anode current density. Rutter et al. [571] reported that the use of ultrasonics resulted in improved adhesion and a denser deposit. Safranek and Miller [507, 508] and others who have plated over zinc die castings showed that ultrasonic agitation of copper pyrophosphate solutions displaced air or hydrogen from blind pockets and resulted in more uniform deposits than could be obtained with copper cyanide strikes. Uspenskii and Schluger [572] investigated pH variations in an ultrasonic field and Trofinov and Galushko [573] polarization characteristics. Trofinov [574] concluded that metal distribution from a copper pyrophosphate electrolyte could not be influenced much by an ultrasonic field. Vasudevan et al, [575] reported an improvement in both anodic and cathodic current efficiencies under ultrasonic agitation but no change in hardness of the deposit.

2.36.12 Equipment

The equipment—a tank, heater, and filter—is similar to that used for bright nickel plating. A steel tank coated with rubber, Koroseal (Trademark: B. F. Goodrich Co.), PVC, or a plastisol is suitable, although rubber linings should be leached before use with a dilute solution of potassium hydroxide to remove all alkali soluble matter that can contaminate the plating solution. For heating the solution, either steam heating coils or electric immersion heaters made of stainless steel or Duriron may be used. Continuous filtration helps prevent rough deposits. The filter should be constructed of stainless steel, rubber, or PVC-lined steel or cast iron.

2.36.13 Anodes

OFHC anodes are the best available; however, electrolytic sheet and rolled electrolytic copper anodes are also satisfactory. Cast anodes of good purity can also be used, but they should be free of impurities such as lead, nickel, silver, and tin because these tend to promote deposit roughness. Anode bags are not usually used; they are not needed and can restrict circulation of the plating solution around the anode and cause polarization. Anodes can be left in the solution when it is not being used since they do not dissolve in the absence of applied current.

2.37 MAINTENANCE AND CONTROL

2.37.1 Analysis

For the analytical determination of copper, pyrophosphate, and orthophosphate, the simplest procedure is that of Konishi [576], where all three constituents are determined by titration with EDTA. Copper can also be determined electrolytically [577] or by titration by the iodine–thiosulfate method [577–579], pyrophosphate by titration with standard alkali [577–579], and orthophosphate gravimetrically [578, 579] or colorimetrically [580]. Ammonia is analyzed by distillation and adsorption in standard acid [577, 579] or by cyclic voltammetric stripping (CVS) [581]. Tench and Ogden and their circle of researchers have pioneered in the use of CVS, particularly for controlling additives and contaminants in copper plating solutions for printed wiring board production. Their work with pyrophosphate solutions is covered in references [542–549] and reviewed in detail in [582]. Tam and co-workers [534, 535] also used CVS to study the effects of all constituents on cathodic and anodic reactions.

2.37.2 Impurities and Purification

Cyanide, oil, lead, decomposition products of the organic additives, residues from photoresists and solvents used in circuit development, epoxy laminate residues, excess orthophosphate, and substances leached from plating tanks are the impurities most often encountered in a copper pyrophosphate plating solution. These impurities cause streaked, dull deposits and also lower the effective current density range. Precautionary methods will prevent these materials from entering the solution. Thorough rinsing, when copper cyanide striking is used, will prevent cyanide contamination; a clean air line for solution agitation will prevent oil contamination; and avoiding the use of lead coils, lining, fittings, or filters will prevent lead contamination.

Cyanide, which can be detected by a copper benzidine test [583], can be removed by treatment with either 1.25 mL L^{-1} of 30% H_2O_2 or 0.1–0.2 g L^{-1} potassium permanganate followed by treatment with activated carbon. The tendency toward streaked, nonuniform pyrophosphate deposits due to residual traces of cyanide left on the surface after copper cyanide striking can be minimized by brief cathodic treatment in a solution of potassium pyrophosphate before it is placed

in the plating solution. Oil can be removed by treating the solution with 2.5–6 g L^{-1} of activated carbon at 55°C for 4–8 h. Low-current-density electrolysis will remove lead.

Copper pyrophosphate solutions are quite tolerant of metallic contamination because many metals besides copper form complexes with the pyrophosphate ion and remain in solution. For example, no harmful effects have been reported from zinc which may be introduced when the solution is used to plate zinc die castings. It has been recommended, however, that a high P_2O_7/Cu ratio (preferably 7.5: 1) be maintained under this circumstance so as to allow some excess pyrophosphate for complexing with the contaminant. Phosphorus included in the deposit was reported to influence external appearance, microhardness, and microstructure [584]. Iron and lead can alter deposit morphology and concentrations below 200 and 1000 ppm, respectively, are recommended [516]. Chloride ion, which is known to affect anode reactions, can be tolerated at concentrations lower than 0.1 *M* with vigorous agitation of the solution [515].

Organic contaminants, besides reducing deposit ductility and strength, can also cause loss of throwing power and irregular deposition. The contamination can come from decomposition products from organic additives, air agitation, leaching of photoresists, and the carbon used for removing contaminants. Rothschild et al. [585] provide an excellent review on carbon treating of pyrophosphate solutions for keeping them free of organic contaminants and recommend the use of Hull cell tests to determine the effectiveness of treatment. In some cases an activated carbon treatment alone is not sufficient purification. To ensure removal of the decomposition products, it is best to carbon treat the solution, H_2O_2 treat, and then carbon treat again. The carbon should be plating grade and sulfur free.

Cyclic voltammetric stripping analysis is an excellent means for detecting a wide range of contaminants in addition to organic additives in pyrophosphate solutions. Excellent correlation has been obtained between the measured contaminant level and plating problems normally attributed to solution contamination such as poor solder adhesion and low deposit ductility [542, 544, 545, 548].

Waste pyrophosphate solutions are difficult to treat because of ammonia in the solutions and also the complexes that are formed [586]. Wastes require low-pH hydrolysis to orthophosphate followed by precipitation of the heavy metals [488].

2.38 STRUCTURE AND PROPERTIES

The best source for property data is Safranek's treatise on properties of electrodeposits [587]. Another comprehensive reference is that of Lamb et al. [588], who provide data on Young's modulus, fatigue strength, effects of cold rolling and annealing on mechanical properties, tensile and elongation data for temperatures from −78 to 325°C, thermal expansion, texture analysis, and gas content for solutions containing no addition agents.

Copper pyrophosphate deposits show tensile strength variations from 27 to 70 kg mm^{-2}, yield strengths from 14 to 36 kg mm^{-2}, hardness from 83 to 250 kg mm^{-2}, and elongations from 1 to 39%. Several investigators have related these variables to solution content and operating variables with additive concentration being the most important variable [495, 547, 589–595].

Optimum ductility has been obtained by using solutions free of organic additives [588]. In some cases, continuous filtration is also used [589, 596]. High-purity, high-quality deposits have been produced on internal walls of colliders in beam tubes by using multistage purification and pulsed reverse current in solutions with no additives [597, 598].

A comparison of recrystallization temperature for electrodeposited pyrophosphate copper and wrought copper with various degrees of cold work suggests that the electrodeposited copper exhibits behavior expected of 100% cold-worked material [592]. Malone [599] reported that pyrophosphate copper electrolytes were capable of producing deposits with excellent mechanical properties. However, he cautioned that the pyrophosphate electrolyte is very difficult to control and maintain in comparison with the acid sulfate solution, and producing deposits consistently within a specific range may prove difficult unless the electroplater has considerable experience with the pyrophosphate solution and the many pecularities associated with it. The influence of pH, temperature, agitation, and current density on throwing power and efficiency can be found in [600].

2.39 PLATING OF PRINTED WIRING BOARDS

The 1974 edition of this book [484] devoted a section to this topic in the chapter on copper pyrophosphate. Around the time of publication of that volume, high-throwing-power acid copper sulfate solutions were developed [601]. Today these solutions are used instead of pyrophosphate for most printed wiring board applications, except in some military and special applications [490]. It is estimated that greater than 95% of all printed wiring boards today are plated in acid copper sulfate solutions [518]; this is discussed in more detail in Section 2.12. A good review of present practice with pyrophosphate plating of printed wiring boards can be found in [490].

PART E COPPER COMPOSITES

Present-day structural materials have two major shortcomings: loss of strength at elevated temperatures and relatively

low elastic moduli [602]. One way to solve these problems is in strengthening materials by incorporating high-strength and high-modulus particles, fibers, or continuous filaments in a metal matrix. The major disadvantages of present methods (internal oxidation, powder metallurgy, high-pressure bonding, and infiltration) in producing dispersion-strengthened and fiber-reinforced composites are the high process temperatures and pressures required. Degradation of the fibers due to handling and difficulties encountered in machining the finished composite structure are also concerns.

A less common method of producing these composites is electrodeposition. There is no requirement in electrodeposition for high temperatures that can damage the fibers. The strengthening of electrodeposits can be accomplished by the encapsulation of inert particles, fibers (whiskers), or filaments during plating to produce high-performance coatings [602–604]. Two terms commonly used to refer to use of electrodeposition to produce composite materials are *composite plating* and *electrocomposites.* Electrodeposition of Copper and nickel are the two plating processes most commonly used to produce composites; copper will be covered in this section. Reviews on composite plating can be found in [602–610].

Copper composite materials have typically been produced in sulfate solutions, although acid fluoborate and alkaline cyanide solutions have also been used. Particles that have been codeposited with copper include alumina, barium sulfate, borides, carbides, carborundum, corundum, graphite, molybdenum disulfide, polystyrene, phosphorus, polytetrafluoroethylene (PTFE), quartz, titania, tungsten disulfide, and zirconium oxide. Mechanical or ultrasonic agitation was required to uniformly disperse the particles, which ranged from 50 to 200 g L^{-1}, in the solution.

A variety of techniques can be used for codeposition of particles. Namely occlusion plating particles are allowed to codeposit on the cathode surface while some intermittent vigorous mechanical stirring of the plating solution is applied [609], sediment codeposition particles are allowed to sediment on a flat cathode as electrolysis proceeds and are only occasionally agitated [611–614], and composite plating particles are deposited on a vertical cathode [609]. Particles are kept in suspension by either mechanical or chemical means. Suspension by mechanical means is accomplished by use of a vibrating perforated bottom plate or by the use of air agitation. Suspension by chemical means typically requires the addition of appropriate surfactants to the plating solution.

The optimum conditions for preparing particle suspensions and codepositing a designated volume fraction of uniformly dispersed inert particles have not been firmly established. Most of the literature data have been derived empirically. Particle diameters have ranged from 0.02 to 100 μm. Quantities dispersed in solution have varied from 50 to 200 g L^{-1} [604]. Wetting agents, monovalent cations and aliphatic amines absorbed on particle surfaces, promoted encapsulation and improved dispersion [609, 615, 616]. Particle encapsulation was less during operation of a copper sulfate solution, in comparison with the amounts reported for code position in cyanide solutions [604, 609, 615–617].

2.40 ALUMINA

The copper–alumina system has been investigated by many researchers [604, 605, 607, 618–641]. Both α-alumina (0.3–1.0 μm) and rutile titania (0.3 μm) were readily codeposited with copper in an acid solution, but γ-alumina (0.2 μm) and anatase titania were not. Calcining (20 h at 1125°C) promoted the codeposition of γ-alumina particles in copper [618]. This effectively transformed the surface of γ particles into an α structure, as verified by X-ray studies. Lakshminarayanan et al. [619–621] concluded that α- and γ-alumina could be codeposited provided that the plating solution was free of chloride. By contrast, Roos et al. [622] reported that both γ- and α-alumina could be codeposhed in an acid sulfate solution with or without the presence of chloride ions in the solution. However, under identical conditions, much smaller quantities of γ-alumina were codeposited as compared with α-alumina.

With pulsed or periodically reversed current, increasing the current density increased the alumina content of copper [623, 624]. Ultrasonic agitation reduced agglomeration, improved particle distribution, and improved the strength retention of copper–alumina composites [625].

2.41 PROPERTIES

Lakshminarayanan et al. [620] reported that codeposition of 1.2%, by volume, of 0.03 μm γ-alumina increased the yield and ultimate tensile strengths of copper from 97 and 197 MPa to 128 and 246 MPa, respectively, while elongation was reduced from 32 to 20%. An increase in the alumina content to 2.4% increased the yield and tensile strengths to 217 and 345, respectively, while the elongation was 15% [620]. A fairly high yield strength of 50 MPa was retained after the copper–alumina composites were annealed at 420°C. Stankovic and Gojo [641] noted that tensile strength increased to about 290 MPa with increasing alumina particle content. Further increases in the particle content did not affect the tensile strength significantly. As regards electrical resistivity, a 2.2% alumina composite exhibited a moderate increase over pure copper (1.86 vs. 1.72 μΩ-cm) [620].

Abrasive wear was reduced 83–85% by codepositing 5.5 or 7.3% of carborundum particles [642]. Based on friction measurements, copper–graphite composites appeared to be the best self-lubricating coating when compared with composites containing molybdenum disulfide or PTFE particles [643]. Silicon carbide codeposited particles provided

a high hardness which was retained up to 900°C. Abrasion and oxidation resistance also improved as a result of inclusion of silicon carbide [605]. A summary on property data can be found in reference [606].

2.42 MECHANISM

A two-step mechanism was proposed by Guglielmi [644] in which the combined effect of adsorption and electrophoretic attraction is held responsible for the encapsulation of participate matter in a growing electrodeposited layer. The validity of Guglielmi's model has been verified for different codeposition systems, including copper with alumina from acidic sulfate solutions, with and without the addition of thallium. However, Guglielmi's model does not allow prediction of the manner in which process parameters such as size, type, and pretreatment of the particles, composition, temperature, and pH of the plating solution affect the electrolytic codeposition [609].

Foster and Kariapper [627] proposed a mathematical model in 1974 that could describe the effect of hydrodynamics on codeposition, but only a limited amount of quantitative work has been done to prove its validity. Snaith and Groves [645–647] also reported on mechanisms.

In 1987 Celis et al. [639] proposed a model that contains measurable parameters so that the prediction of the amount of codeposited particles for a given system becomes feasible. As described, "This mathematical model is developed on the basis of two fundamental postulates related to the mechanism of codeposition, namely: 1—an adsorbed layer of ionic species is created around particles at the time these particles are added to the plating solution or pretreated in ionic solutions and 2—the reduction of some of these adsorbed ionic species is required for the incorporation of particles in the metallic matrix" [639].

Figure 2.3 shows that the particle has to proceed through five stages: (1) the adsorption of ionic species upon the particle, (2) the movement of the particle by convection toward the hydrodynamic boundary layer at the cathode, (3) the diffusion of the particle through the diffusion double layer, (4) the adsorption of the particle with its adsorbed ionic cloud at the cathode surface, and (5) the reduction of some adsorbed ionic species by which the particle becomes irreversibly incorporated in the metal matrix. The model has been demonstrated to be valid for the codeposition of alumina particles with copper from acid copper sulfate plating solutions [609, 639].

2.43 CONTINUOUS FIBER-REINFORCED COMPOSITES

Acid copper solutions have been used in fabricating fiber-reinforcing metal composites. In these processes, simple salt solutions work satisfactorily, whereas highly complexed solutions such as cyanide do not [648]. Continuous, unidirectional filament-reinforced electrocomposites that have been produced include 25 μm tungsten in copper and 100 μm boron in copper [604]. A composite containing 40% volume of tungsten filaments, produced by continuously winding tungsten wire on the cathode during copper deposition, exhibited a tensile strength of 1325 MPa [649].

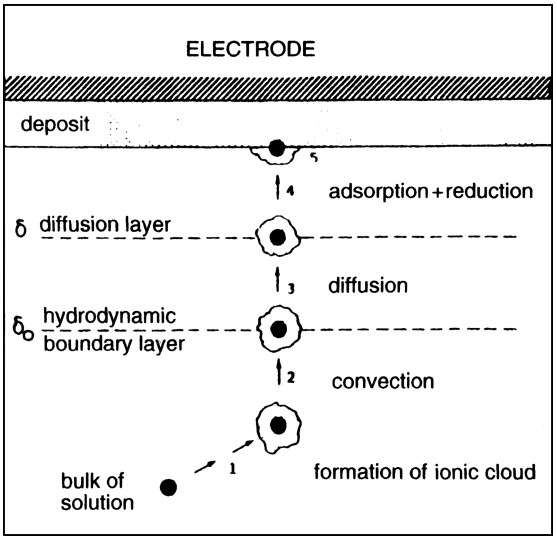

FIGURE 2.3 The five stages in the codeposition of a particle. (From Celis et al. [639]. Reproduced by permission of the Electrochemical Society, Inc.)

Graphite–copper composite panels have been fabricated by weaving copper-coated graphite fibers into a fabric and then consolidating by hot pressing. This offers a potential technique for low-cost processing of metal matrix composite electronic heat sinks [650]. Carbon fibers are continuously coated with copper in a pyrophosphate–HEDP (hydroxyethylidene diphosphonic acid) electrolyte [651].

PART F
COPPER PLATING IN MICROELECTRONICS

New applications are opening up for copper conductors in microelectronics, microelectromechanical systems (MEMSs), and nanotechnology [652]. Incorporating material into three-dimensional geometries is a strength of electrodeposition. A major success has been the replacement of aluminum and its alloys by copper for ultra-large-scale integration (ULSI) interconnects [653]. The deep reservoir of copper plating knowledge has enabled a natural and rapid emergence of process technology. Implementation of copper

results in a 40% lower wire resistance, 20–30% anticipated boost in chip performance, improvements in wire reliability, and 10–15% lower chip cost.

Moore's law for microelectronics states that the density of elements on integrated circuits will increase steadily as predictable process improvements are implemented. As stated today, the number of transistors that can be placed on an integrated circuit with commercial processes doubles approximately every three years. As feature size reached submicrometer level, the drawbacks of aluminum interconnects became apparent, notably the high electrical resistance. The microelectronics industry identified copper as a likely interconnect replacement material and began to incorporate this change in plans such as the SEMATECH Roadmap [653].

SEMATECH creates its Roadmap with targets such as the required half-pitch of dynamic random-access memory (DRAM) designs. As feature size on ULSI devices decreases, this minimum size requirement decreases. The industry is currently operating at the 45-nm SEMATECH Roadmap node. When a new feature size node becomes the norm, major changes and investment are required for new microfabrication facilities. Programs are in progress to prepare for the coming shift to the 32-nm node. And a further shift to the 22-nm minimum-size node is projected within six to eight years.

In 1998, IBM announced its successful development of copper electroplating technology for fabrication of chip interconnect structures [654, 655]. The challenge was to fill trenches and vias within the silicon chip without creating voids or seams and without degrading the circuit materials and patterns. IBM found that it could fill submicrometer-size features completely, that is, without voids, if the plating solution contained an appropriate mixture of additives. They termed this phenomenon "superfilling" and named the process "damascene copper," after the classic art form of metal inlay. The silicon substrate is first configured with its trenches and vias. Then an insulating coating is applied followed by a seed layer of copper. At this point, copper metal is added by electrodeposition to fill the trenches and the vias, completing the interconnect pattern. Finally, excess over plated copper is removed from the wafer surface. Filling of trenches only is termed single damascene, and simultaneous filling of trenches and vias is termed dual damascene.

It was understood that success with superconformal feature filling depended heavily on the additive mix, and their relative diffusion/adsorption characteristics, in the plating solution. Copper electrodeposition had been well studied, so there was a solid base from which to build and refine the process. Other tools were also available, such as controlled agitation and pulse reversal deposition. Projections based only on today's technology for depositing seed layers and for damascene filling indicate that copper superconformal filling will be the preferred practice down to at least the 22-nm node on the SEMATECH Roadmap [656].

Understanding of the phenomena operating was incomplete during the early development of the copper damascene process [657]. A National Institute for Standards and Technology (NIST) group determined that the superconformal filling of trenches and vias by electrodeposited copper involved competitive interaction between additive species that accelerate and inhibit deposition. The accelerator adsorbs on the cavity wall and, as electrodeposition proceeds, the feature diameter generally decreases. Current understanding suggests that the surface density of accelerator increases with decreasing feature diameter, leading to an increase in deposition. This occurs as the base of trenches and vias, becoming the basis for bottom-up filling. Normally, in the absence of additives, a cavity in a surface would be capped with overgrowing deposit, trapping a microcavity—a situation that must be avoided with ULSI fabrication.

Additives and basic ingredients of acidic copper plating solutions fall into one of the following categories:

- Copper sulfate provides the source of copper ions.
- Sulfuric acid gives conductivity and induces soluble anode corrosion.
- Chloride is synergistic with organic additives in the brightening and leveling.
- The brightener, or accelerator, typically contains low-molecular-weight sulfur and a second atom of high polarity and/or ionic character. Its function is to refine the grain structure in normal copper electrodeposition. Typical brighteners include thiourea, disulfides, thiocarbamates, and thiocarboxylic acid amides.
- Inhibitors convert an unevenly distributed stationary cathode diffusion layer into a more evenly distributed layer and reduce the variation in copper deposit thickness across the surface. Examples include high-molecular-weight polyether compounds, surfactants, and polyoxyalkylene glycols.
- The polar leveler slows down the charge transfer of copper ions to copper metal, thus slowing the plating rate in those areas considered high current density.

NIST developed a quantitative process model on this basis—curvature-enhanced accelerator coverage (CEAC)—that has guided development [658]. The basic idea is that (a) the growth velocity of the infilling copper is proportional to the local accelerator, or catalyst, coverage, and (b) the catalyst remains segregated at the metal–electrolyte interface during metal deposition. This leads to catalyst enrichment on advancing concave surfaces and catalyst dilution on advancing convex surfaces. The result is the desired bottom-up filling of submicrometer features in the integrated circuit. The NIST group validated the CEAC model with an archetypical additive package of chloride, PEG, and a sulfide such as 3-mercapto-1-propanesulfonate (MPSA) or

$[Na_2(SO_3(CH_2)_3S)_2]$ (SPS). In acidified copper sulfate solution, inhibition is provided by interaction between PEG–C1 and the copper surface. Acceleration is associated with the competitive adsorption of the sulfide or its derivatives.

Damascene copper has the tendency to form bumps above filled features, termed overshoot. The NIST group recently reported on using a cationic surfactant additive to inhibit this undesirable copper overplate [659]. The surfactant is included at a level that permits the desired SPS-derived bottom-up filling but quenches the SPS mechanism as filling is completed. NIST has published an extensive coverage of the nature and modeling of superconformal film growth [660].

As damascene processing is used for ULSI designs with ever-smaller features, the copper grain size becomes a factor. Pulse current and periodic pulse reverse current tend to give improved distribution of copper on high-aspect-ratio surfaces when compared to direct current plating. And copper grain size tends to decrease with increasing pulse frequency [661].

Vereecken and IBM colleagues have shed more light on the mechanism by which damascene additives interact with the cuprous and cupric ions to create the balance of acceleration and inhibition [662]. Kim and NIST colleagues also applied electroanalytical methods to probe the mechanism [663]. They conclude that inhibiting additives limit access of cupric ions to the copper surface. They further determined that cationic surfactant additives deactivate SPS (sulfur-containing) accelerator additive by tying up the anionic group. The combined process can be optimized to enable superfilling to be sustained while simultaneously attenuating overfill bump formation.

As of 2004, over 200 damascene electroplating systems were in use in semiconductor fabrication worldwide [664]. Wafers are typically held face down in the electrolyte and rotated during electrodeposition. Superconformal filling of via holes and trenches and production of void-free vias and lines is largely dependent on the action of organic additives in solution. The organic additive concentrations must be kept within a process window. IBM accomplishes this with a combination of monitoring and makeup of solution. They consider analysis by cyclic voltammetry analysis to be one option for tracking bath composition [665]. Organic additives added to copper electroplating baths typically include suppressor (polymers such as PEGs), accelerators (sulfur-containing compounds), and levelers (secondary suppressors). Organic components are consumed during the actual damoscene processing step. Innovators continue to identify chemistries and added surface treatments to suppress void formation and reduce stress in the filled features and vias [666, 667].

The IBM announcement [654, 655] included an initial model to guide future process development and control. NIST developed further insights on bump suppressions using its CEAC model [668]. And the Alkire University of Illinois group has contributed a series of improvements to the algorithms and computation methods [669–673].

Electrochemical phenomena such as copper damascene are embraced as a challenge of current nanotechnology research because their behavior results from linked interactions spanning many length scales. At one extreme is the molecular scale of adsorbed additives and copper nanostructures. At the other extreme is the macroscale of the silicon wafer and its features. Multiscale simulation has become a priority for all fields of science and engineering [668, 669]. As a result of increased investment and sharing, computing power and algorithms are becoming ever more powerful. The improvement in scientific understanding and modeling capability will continue. Computing is no longer an issue. The research focus is on developing improved models and algorithms, which can come from related fields as well as electrochemical science and engineering.

REFERENCES

1. L. W. Flott, *Metal Finish.*, **94**, 55 (Mar. 1996).
2. R. Sard, in *Encyclopedia of Materials Science and Engineering*, Vol. 2, M. B. Bever, Ed., Wiley, New York, 1986.

2a. P. C. Andricacos, *Interface*, **7**, 23 (Spring 1998).

2b. P. C. Andricacos, *Interface*, **8**, 32 (Spring 1998).

3. W. H. Safranek, *The Properties of Electrodeposited Metals and Alloys*, 2nd ed., American Electroplaters and Surface Finishers Soc., Orlando, FL, 1986.
4. D. L. Snyder, *Met. Finish.*, **89**, 37 (Apr. 1991).
5. F. Passal, *Plating*, **46**, 628 (1959).
6. F. A. Lowenheim, *Modern Electroplating*, 3rd ed., Wiley, New York, 1974.
7. M. Carano, *Electronics*, **32** (3), 29 (Mar. 1986).
8. J. F. D'Amico and M. A. De Angelo, *J. Electrochem. Soc.*, **123**, 478 (1976).
9. A. Smee, *Elements of Electrometallurgy*, 2nd ed., Longmans, Green, London, 1843.
10. G. R. Strickland, *Prod. Finish. (London)*, **24**, 24 (Sept. 1971).
11. G. C. Van Tilburg, *Plating Surf. Finish.*, **71**, 78, (Apr. 1984).
12. W. De la Rue, *London Edinborough Philos. Mag.*, **9**, 484 (1836).
13. W. H. Safranek, F. B. Dahle, and C. L. Faust, *Plating*, **35**, 39 (1948).
14. Langbein, *Electrochem. Metall.*, **3**, 310 (1903).
15. Beadle, *Electrochem. Metall.*, **1**, 163 (1901).
16. E. F. Kern, *Trans. Am. Electrochem. Soc.*, **15**, 441 (1909).
17. E. F. Kern, U.S. Patent 946,903 (1910).
18. C. G. Fink and C. Y. Wong, *Trans. Electrochem. Soc.*, **63**, 65 (1933).
19. A. I. Levin, S. M. Scherbakov, F. A. Zorin, V. M. Svitskii, and R. A. Gokhina, *J. Appl. Chem. (USSR)*, **13**, 686 (1940); *Chem. Abstr.*, **35**, 3536.
20. A. I. Levin, *J. Appl. Chem. (USSR)*, **14**, 78; 1941; *Chem. Abstr.*, **36**, 972.

21. N. P. Diev and A. J. Loshkarev, *J. Appl. Chem. (USSR)*, **12**, 585 (1939); *Chem. Abstr.*, **33**, 8504.
22. D. C. Gernes, G. A. Lorenz, and G. H. Montillon, *Trans. Electrochem. Soc.*, **77**, 177 (1940).
23. J. R. Stack, U.S. Patent 2,294,053 (1942)
24. M. Schlotter, J. Korpiun, and W. Nurmeister, *Z. Metall.*, **25**, 107 (1933).
25. D. Thomas and J. C. Silva, *J. Electrochem. Soc.*, **143**, 458 (1996).
26. C. Struyk and A. E. Carlson, *Mon. Rev. Am. Electroplat. Soc.*, **33**, 923 (1946).
27. K. S. Willson, A. H. DuRose, and D. G. Ellis, *Plating*, **35**, 252, 304 (1948).
28. C. L. Faust, B. Agruss, E. L. Combs, and W. A. Pruell, *Mon. Rev. Am. Electroplat. Soc.*, **34**, 541, 709 (1947).
29. W. A. Proell, U. S. Patent 2,525,943 (1950).
30. L. Cambi and R. Piontelli, *Rend. 1st. Lombardo Sci. Lett.*, **72** (1), 128 (1939); *Chem Abstr.*, **34**, 4995 (1940).
31. S. Venkatachalam and T. L. Rama Char, *Electroplat. Met. Finish.*, **14**, 3 (1961).
32. J. E. Stareck and F. Passal, U. S. Patent 2,383,895 1945.
33. C. B. F. Young, *Met. Finish.*, **47**, 56 (Nov. 1949).
34. D. Uceda, T. O'Keefe, and E. Cole, *J. Electrochem. Soc.*, **137**, 1397 (1990).
35. I. Hoshino and T. Fumoto, Japanese Patent 5306 (1955).
36. K. Hosokawa and T. Inui, *Kinzoku Hyomen Gijutsu*, **17** (4), 138 (1966); *Chem Abstr.*, **67**, 70009.
37. F. A. Lowenheim, *Electroplating*, McGraw-Hill, New York, 1978.
38. L. M. Weisenberger, "Copper Plating," in *Metals Handbook*, 9th ed., Vol. 5, *Surface Cleaning, Finishing and Coating*, American Society for Metals, 1982.
39. L. M. Weisenberger and B. J. Durkin, "Copper Plating," in *ASM Handbook*, Vol. 5, *Surface Engineering*, ASM International, 1994.
40. A. Sato and R. Barauskas, *Metal Finishing, 64th Guidebook and Directory Issue*, **94** (1A), 214 (1996).
41. E. F. Duffek, "Plating," in *Printed Circuits Handbook*, 4th ed., C. F. Coombs, Jr. Ed., McGraw-Hill, New York, 1996.
42. G. F. Bidmead, *Trans. Inst. Met. Finish.*, **59**, 129 (1981).
43. W. H. Safranek and H. R. Miller, *Plating*, **55**, 233 (1968); **56**, 11 (1969).
44. W. H. Safranek and J. G. Beach, *Technical Report on Electroplating Bright, Leveling and Ductile Copper*, Copper Development Assoc., Inc., New York (Oct. 1968).
45. D. R. Millage, *Precision Metal Molding*, **23**, 38 (Feb. 1965).
46. H. G. Creutz, *Proc. Am. Electroplat. Soc.*, **51**, 82 (1964).
47. W. H. Safranek, Tech. Paper 105, Society of Die Casting Engineers, Wheeling, IL (1966)
48. L. Harrison, N. Martyak, J. McCaskie, M. McNeil, R. Schultz, and H. Smith, *Met. Finish.*, **92**, 11 (Dec. 1994).
49. D. J. Combs, in *Proc. AESF SUR/FIN 80*, Session B, Boston, June 1981; *Plating Surf. Finish.*, **68**, 58 (July 1981).
50. R. L. Barauskas and A. E. Guttensohn, *Plating*, **60**, 355 (1973).
51. B. M. Hogan, in *Proc. AESF SUR/FIN 84*, Session H, New York, July 1984.
52. T. G. Beat, W. K. Kelley, and J. W. Dini, *Plating Surf. Finish.*, **75**, 7 (Feb. 1988).
53. W. C. Cowden, T. G. Beat, T. A. Wash and J. W. Dini, in *Metallized Plastics*, Vol. 1, *Fundamental and Applied Aspects*, K. L. Mittal and J. R. Susko, Eds., Plenum, New York, 1989, p. 93.
54. J. W. Dini, *Plating Surf. Finish.*, **79**, 121 (May 1992).
55. F. Wills and E. J. Clugston, *J. Electrochem. Soc.*, **106**, 362 (1959).
56. H. J. Modi and G. S. Tendolkar, *J. Sci. Ind. Res.*, **12B**, 431 (1953).
57. W. H. Safranek and M. Wirth, *Mater. Methods*, **44** (5), 104 (1956).
58. C. W. Bennett, *Trans. Am. Electrochem. Soc.*, **21**, 253 (1912).
59. P. Vanden Brande and R. Winand, *J. Appl. Electrochem.*, **23**, 1089 (1993).
60. J. E. T. Anderson, G. Bech-Nielson and P. Moller, *Surf. Coatings Technol.*, **70**, 87 (1994).
61. Y. Fukunaka, K. Denpo, M. Iwata, K. Maruoka, and Y. Kondo, *J. Electrochem. Soc.*, **130**, 2492 (1983).
62. V. Anantharaman and P. N. Pintauro, *J. Electrochem. Soc.*, **136**, 1727 (1989).
63. J. D. Reid and A. P. David, *J. Electrochem. Soc.*, **134**, 1389 (1987).
64. R. Taft and H. E. Messmore, *J. Phys. Chem.*, **35**, 2585 (1931).
65. R. Taft and O. R. Bingham, *J. Phys. Chem.*, **36**, 2338 (1932).
66. H. M. Goodwin and W. H. Horsch, *Chem. Metall. Eng.*, **21**, 181 (1919).
67. E. F. Kern and M. Y. Chang, *Trans. Am. Electrochem. Soc.*, **41**, 181 (1922).
68. G. M. Kimber, D. H. Napier, and D. H. Smith, *J. Appl. Chem.*, **17**, 29 (1967).
69. C. W. Eichrodt, *Trans. Am. Electrochem. Soc.*, **45**, 381 (1924).
70. A. K. Graham, *Trans. Am. Electrochem. Soc.*, **52**, 157 (1927).
71. B. F. Rothschild, *Plating Surf. Finish.*, **66**, 70 (May 1979).
72. Y. Fukunaka, H. Doi, Y. Nakamura, and Y. Kondo, in *Electrochemical Technology in Electronics*, Vol. 88-23, L T. Romankiw and T. Osaka, Eds., Electrochemical Society, Pennington, NJ, 1988, p. 83.
73. Y. Fukunaka, H. Doi, and Y. Kondo, *J. Electrochem. Soc.*, **137**, 88 (1990).
74. H. K. Richardson and F. D. Taylor, *Trans. Am. Electrochem. Soc.*, **20**, 179 (1911).
75. S. Skowronski and E. A. Reinsoso, *Trans. Am. Electrochem. Soc.*, **52**, 205 (1927).
76. G. Fabricius and G. Sundholm, *J. Appl. Electrochem.*, **15**, 797 (1985).
77. A. Suresh, *Plating Surf. Finish.*, **71**, 108 (May 1984).
78. N. Pradhan, P. G. Krishna, and S. C. Das, *Plating Surf. Finish.*, **83**, 56 (Mar. 1996).

79. J. W. Chang and R. Weil, in *Proc. AESF SUR/FIN 86*, Session G, Philadelphia, NASF, Washington, DC, 1986.
80. D. Anderson, R. Haak, C. Ogden, D. Tench, and J. White, *J. Appl. Electrochem.*, **15**, 631 (1985).
81. R. E. Gana, M. G. Figueroa, and R. J. Larrain, *J. Appl. Electrochem.*, **9**, 465 (1979).
82. R. Walker and S. D. Cook, *Surf. Technol.*, **11**, 189 (1980).
83. W. A. Fairweather, *Trans. Inst. Met. Finish.*, **62**, 5 (1984).
84. S. Yoon, M. Schwartz, and K. Nobe, *Plating Surf. Finish.*, **81**, 65 (Dec. 1994).
85. S. Yoon, M. Schwartz, and K. Nobe, *Plating Surf. Finish.*, **82**, 64 (Feb. 1995).
86. Z. Nagy, J. P. Blaudeau, N. C. Hung, L. A. Curtiss and D. J. Zurawski, *J. Electrochem. Soc.*, **142**, L87 (June 1995).
87. J. D. Reid and A. P. David, *Plating Surf. Finish.*, **74**, 66 (Jan. 1987).
88. L. S. Melnicki, in *Proceedings of Electrochemical Technology in Electronics*, Vol. 88-23, L T. Romankiw and T. Osaka, Eds., Electrochemical Society, Pennington, NJ, 1988, p. 95.
89. M. Hill and G. T. Rogers, *J. Electroanal. Chem.*, **86**, 179 (1978).
90. M. Yokoi, S. Konishi, and T. Hayashi, *Denki Kagaku*, **51**, 460 (1933).
91. M. Goodenough and K. J. Whitlaw, *Trans. Inst. Met. Finish.*, **67**, 57 (1989).
92. M. R. H. Hill and G. T. Rogers, *J. Electroanal Chem.*, **68**, 149 (1976).
93. E. E. Farndon, F. C. Walsh, and S. A. Campbell, *J. Appl. Electrochem.*, **25**, 574 (1995).
94. M. J. Armstrong and R. H. Muller, *J. Electrochem. Soc.*, **138**, 2303 (1991).
95. R. Weil and J.-W. Chang, *Plating Surf. Finish.*, **75**, 60, (Nov. 1988).
96. J. B. Mohler, *Met. Finish.*, **85**, 121 (June 1987).
97. J. E. Breen, E. Toledo, and V. White, Paper 710793, Society of Automotive Engineers, Los Angeles, CA (Sept. 1971).
98. D. Stoychev, I. Vitanova, R. Buyukliev, N. Petkova, I. Popova, and I. Pojarliev, *J. Appl. Electrochem.*, **22**, 987 (1992).
99. D. Stoychev, I. Vitanova, R. Buyukliev, N. Petkova, I. Popova, and I. Pojarliev, *J. Appl. Electrochem.*, **22**, 978 (1992).
100. R. Rashkov and C. Nanev, *J. Appl. Electrochem.*, **25**, 603 (1995).
101. Y. N. Sadana and S. Nageswar, *J. Appl. Electrochem.*, **14**, 489 (1984).
102. N. Koura, A. Tsutsumi, and K. Watanabe, *Plating Surf. Finish.*, **77**, 58 (Sept. 1990).
103. G. H. Awad, F. M. Abdel Halim, and M. I. El-Diehey, *Met. Finish.*, **78**, 65 (Sept. 1980).
104. R. Lakshmana Sarma and S. Nageswar, *J. Appl. Electrochem.*, **12**, 329 (1982).
105. J. W. Chang and R. Weil, in *Proc. AESF SUR/FIN 85*, Session F, Detroit, NASF, Washington, DC, 1985.
106. K. S. Rajam and I. Rajagopal, *Met. Finish.*, **77**, 17 (Apr. 1979).
107. G. A. Hope, G. M. Brown, D. P. Schweinsberg, K. Shimizu, and K. Kobayashi, *J. Appl. Electrochem.*, **25**, 890 (1995).
108. D. Stoychev and C. Tsvetanov, *J. Appl. Electrochem.*, **26**, 741 (1996).
109. E. Knaak, J. Hupe, and W. Metzger, in *Proc. 12th World Congress on Surface Finishing*, Paris, Oct. 1988, p. 347.
110. W. Metzger, E. Knaak, and J. Hupe, *Plating Surf. Finish.*, **75**, 64 (July 1988).
111. M. Grall, G. Durand, and J. M. Couret, *Plating Surf. Finish.*, **72**, 72 (Dec. 1985).
112. H. M. Wu, M. L. Lay, and C. H. Huang, *Plating Surf. Finish.*, **79**, 66 (Sept. 1992).
113. P. Malathy and B. A. Shenoi, *Met. Finish.*, **75**, 56 (Mar. 1977).
114. D. F. Suarez and F. A. Olson, *J. Appl. Electrochem.*, **22**, 1002 (1992).
115. J. Reid, *PC Fab*, **10**, 65 (Nov. 1987).
116. C. G. Fink and, C. A. Philippi, *Trans. Am. Electrochem. Soc.*, **50**, 267 (1926).
117. E. F. Kern and R. W. Rowen, *Trans. Am. Electrochem. Soc.*, **41**, 379 (1929).
118. C. Marie and P. Jacquet *J. Chim. Phys.*, **26**, 189 (1929); *Chem Abstr.*, **23**, 5091 (1929).
119. E. I. Peters, *Electrotypers and Stereotypers Mag.*, **44**, 48 (1958).
120. R. O. Hull and W. Blum, *J. Res. Natl. Bur. Stand.*, **5**, 767 (1930).
121. G. Fuseya and K. Murata, *Trans. Am. Electrochem. Soc.*, **50**, 235 (1926).
122. G. Fuseya and K. Murata, *Trans. Am. Electrochem. Soc.*, **52**, 249 (1927).
123. T. J. Barker, *Chem. News*, **97**, 37, 51 (1908).
124. P. K. Frolich, *Trans. Am. Electrochem. Soc.*, **46**, 67 (1924).
125. M. N. Polukarov, *J. Gen. Chem. (USSR)*, **18**, 1249 (1948).
126. A. Brenner, *Proc. Am. Electroplat. Soc.*, **28**, 1941.
127. V. DeNora, *Met. Ital.*, **31**, 607 (1939); *Chem. Abstr.*, **35**, 5797 (1940)
128. L. L. Shreir and J. W. Smith, *J. Electrochem. Soc.*, **99**, 64 (1952).
129. L. L. Shreir and J. W. Smith, *J. Electrochem. Soc.*, **99**, 450 (1952).
130. A. Butts and V. DeNora, *Trans. Electrochem. Soc.*, **79**, 163 (1941).
131. O. E. Adler and M. J. Krinowitz, U. S. Patent 2,317,350 (1943).
132. M. C. Hsiao and C. C. Wan, *Plating Surf. Finish.*, **76**, 46 (Mar. 1989).
133. M. C. Hsiao and C. C. Wan, in *Proc. AESF SUR/FIN 89*, Session J-2, Cleveland, NASF, Washington, DC, 1989.
134. R. Vasudevan, R. Devanathan, and K. G. Chidambaram, *Met. Finish.*, **90**, 23 (Oct. 1992).
135. W. R. Wolfe, H. Chessin, E. Yeager, and F. Hovorka, *J. Electrochem. Soc.*, **101**, 590 (1954).
136. A. Chiba and W. C. Wu, *Plating Surf. Finish.*, **79**, 62 (Dec. 1992).

137. R. Walker and C. T. Walker, *Nature*, **250**, 410 (Aug. 2, 1974).
138. C. T. Walker and R. Walker, *J. Electrochem. Soc.*, **124**, 661 (1977).
139. J. V. Powers and L. T. Romankiw, U. S. Patent 3,652,442 (1972).
140. D. T. Schwartz, B. G. Higgins, P. Stroeve, and D. Borowski, *J. Electrochem. Soc.*, **134**, 1639 (1987).
141. D. E. Rice, D. Sundstrom, M. F. McEachern, L. A. Klumb, and J. B. Talbot, *J. Electrochem. Soc.*, **135**, 2777 (1988).
142. D. Anderson, M. Hanna, C. Ogden, and D. Tench, *Plating Surf. Finish.*, **70**, 70 (Dec. 1983).
143. A. E. Carlson and C. Struyk, *Metal Finishing Guidebook-Directory*, Metals and Plastics Publications, Westwood, NJ, 1970, p. 276.
144. L. J. Durney, Ed., *Electroplating Engineering Handbook*, 4th ed., Van Nostrand Reinhold, New York, 1984.
145. W. H. Safranek and C. L. Faust, *Plating*, **42**, 1541 (1955).
146. R. P. Nevers, R. L. Hungerford, and E. W. Palmer, *Plating*, **41**, 1301 (1954).
147. R. P. Nevers, R. L. Hungerford, and E. W. Palmer, *Iron Age*, **174**, 114 (Aug. 12, 1954).
148. G. S. Frankel, A. G. Schrott, H. S. Isaacs, J. Horkans, and P. C. Andricacos, *J. Electrochem Soc.*, **140**, 961 (1993).
149. J. C. Minotas, H. Djellab, and E. Ghali, *J. Appl. Electrochem.*, **19**, 777 (1989).
150. E. H. Mundell, U. S. Patent 2,852,450 (1958).
151. C. T. Walker, *Met. Finish.*, **86**, 37 (Apr. 1988).
152. W. C. Walker, *Plating Surf. Finish.*, **77**, 16 (Oct. 1990).
153. D. R. Gabe, in *Oxides and Oxide Films*, Vol. 6, A K. Vijh, Ed., Marcel Dekker, New York, 1981.
154. J. Aromaa, O. Forsen, J. Kukkonen, M. Tavi, and Y. Leppanen, in *Proc. 12th World Congress on Surface Finishing*, Paris, Oct. 1988, p. 487.
155. A. C. Hamilton, Jr., *AESF Shop Guide*, 9th ed., **79**, (1991).
156. S. J. Wallden, S. T. Henriksson, P. J. Arbstedt, and T. Mioen, *J. Met.*, **11** (8), 528 (1959).
157. C. Yu Wen and E. F. Kern, *Trans. Am. Electrochem. Soc.*, **20**, 121 (1911).
158. V. Hospadaruk and C. A. Winkler, *Trans. Am. Inst. Min. Met. Eng.*, **197**, 1375 (1953).
159. H. Bovet, *Pro-metal*, **7** (43), 452 (1955); Translation 3738, H. Butcher, Altadena, CA.
160. M. A. Mosher, *J. Electrochem. Soc.*, **107**, 7C. 1960.
161. M. R. Marshall, *Met. Finish. J.*, **3**, 457 (1957).
162. R. Taft, *Trans. Am. Electrochem. Soc.*, **63**, 75 (1933).
163. L. L. Shreir and J. W. Smith, *Trans. Faraday Soc.*, **50**, 393 (1954).
164. J. B. Mohler, *Met. Finish.*, **85**, 47 (July 1987).
165. K. E. Langford, *Analysis of Electroplating and Related Solutions*, 4th ed., Robert Draper, Teddington, Middlesex, England, 1971.
166. E. J. Serfass, W. S. Levine, and M. H. Perry, *Plating*, **37**, 166 (1950).
167. E. J. Serfass, W. S. Levine, P. J. Prong, M. H. Perry, and R. B. Freeman, *Plating*, **37**, 495 (1950).
168. E. J. Serfass, M. H. Perry, and S. Sen, *Plating*, **37**, 389 (1950).
169. E. J. Serfass and M. H. Perry, *Plating*, **37**, 62 (1950).
170. R. O. Hull, U. S. Patent 2,149,344 (1939).
171. M. K. Sanicky, *Plating Surf. Finish.*, **72**, 20 (Oct. 1985).
172. J. W. Dini, *Electrodeposition: The Materials Science of Coatings and Substrates*, Noyes, Park Ridge, NJ, 1993.
173. C. Ogden and D. Tench, in *Proc. AES Second Design and Finishing of Printed Wiring and Hybrid Circuits Symp.*, San Francisco, CA, AESF, Kissimmee, FL, Jan. 1980.
174. R. Haak, C. Ogden, and D. Tench, *Plating Surf. Finish.*, **68**, 52 (Apr. 1981).
175. R. Haak, C. Ogden and D. Tench, *Plating Surf. Finish.*, **69**, 62 (Mar. 1982).
176. W. O. Freitag, C. Ogden, D. Tench, and J. White, *Plating Surf. Finish.*, **70**, 55, (Oct. 1983).
177. C. Ogden and D. Tench, in *Application of Polarization Measurements in the Control of Metal Deposition*, I. H. Warren, Ed., Elsevier, New York, 1984.
178. L. J. Mayer and S. C. Barbieri, in *Proc. AES 12th Plating in the Electronics Industry Symp*., AESF, Kissimmee, FL, 1985.
179. R. Gluzman, *Trans. Inst. Met. Finish.*, **63**, 134 (1985).
180. J. E. McCaskie, in *Proc. AESF SVR/FIN 87*, Session M-3, Chicago, AESF, Kissimmee, FL, July 1987.
181. G. L. Fisher and P. J. Pellegrino, in *Proc. AESF SUR/FIN 87*, Session M-7, Chicago, July 1987.
182. S. Yamato and M. Tadakoshi, *Met. Finish.*, **85**, 67 (Oct. 1987).
183. G. L. Fisher and P. J. Pellegrino, *Plating Surf. Finish.*, **75**, 88 (June 1988).
184. D. Tench and J. White, *J. Electrochem. Soc.*, **132**, 831 (1985).
185. D. Tench et al., Final Report, *Manufacturing Technology for Printed Wiring Board Electrodeposition Processes*, AFWAL Contract No. F33615-81-C-5108 (1985).
186. A. Gemmler, T. Bolch, R. De Donker, and J. Vanhumbeeck, in *Proc. AESFSUR/FIN 87*, Session O-6, Chicago, AESF, Kissimmee, FL, July 1987.
187. B. Bressel, *Galvanotechnik.*, **75**, 1488 (1984).
188. B. Bressel, *Galvanotechnik*, **76**, 1970 (1985).
189. J. D. Reid, *Plating Surf. Finish.*, **75**, 108 (May 1988).
190. J. D. Reid, in *Proc. AESF SVR/FIN 90*, Session H, Boston, AESF, Kissimmee, FL, July 1990.
191. D. Engelhaupt and J. Canright, in *Proc. AESF SUR/FIN 84*, Session J, New York, AESF, Kissimmee, FL, July 1984.
192. T. R. Mattoon, P. McSwiggen, and S. A. George, *Met. Finish.*, **83**, 83 (Feb. 1985).
193. S. A. George and T. R. Mattoon, *Met. Finish.*, **83**, 23 (Mar. 1985).
194. S. A. George and T. R. Mattoon, *Met. Finish.*, **83**, 29 (Apr. 1985).

195. K. K. Kanazawa, G. L. Borges, S. Doss, and C. Hildebrand, in *Proc. AESF SUR/FIN 95*, Session B, Baltimore, AESF, Kissimmee, FL, June 1995.
196. F. Mansfeld, *Plating Surf. Finish.*, **65**, 60 (May 1978).
197. D. Reichenbach, *Plating Surf. Finish.*, **81**, 106 (May 1994).
198. J. B. Mohler, *Met. Finish.*, **85**, 49 (Aug. 1987).
199. T. Rudolph, *Plating Surf. Finish.*, **64**, 34 (Dec. 1977).
200. V. A. Lamb and D. R. Valentine, *Plating*, **52**, 1289 (1965).
201. V. A. Lamb and D. R. Valentine, *Plating*, **53**, 86 (1966).
202. V. A. Lamb, C. E. Johnson, and D. R. Valentine, *J. Electrochem. Soc.*, **117**, 291C, 341C, 381C (1970).
203. J. W. Cuthbertson, *Trans. Electrochem. Soc.*, **77**, 157 (1940).
204. W. A. Wood, *Proc. Phys. Soc. (London)*, **43**, 138 (1931).
205. A. K. Huntington, *Trans. Faraday Soc.*, **1**, 324 (1905).
206. A. W. Hothersall, *Trans. Faraday Soc.*, **31**, 1242 (1935).
207. W. Blum and H. S. Rawdon, *Trans. Am. Electrochem. Soc.*, **44**, 305 (1923).
208. A. K. Graham, *Trans. Am. Electrochem. Soc.*, **44**, 427 (1923).
209. T. B. Vaughan and H. J. Pick, *Electrochim. Acta*, **2**, 179 (1960).
210. A. S. Woodman et al., in *Proc 2nd International Symp. on Electrochemical Technology Applications in Electronics*, L. T. Romankiw, M. Datta, T. Osaka, and Y. Yamazaki, Eds., Electrochemical Society, Pennington, NJ, 1993, p. 86.
211. D. H. Lassila, in *Shock Wave and High Strain Rate Phenomena in Materials*, M. A. Meyers, L. E. Murr, and K. P. Staudhammer, Eds., Marcel Dekker, New York, 1992, p. 543.
212. D. McLean and H. R. Tipler, *Met. Set. J.*, **4**, 103 (1970).
213. D. L. Wood, *Trans. TMS-AIME,* **209**, 209 (1957).
214. L. Zakraysek, in *Fractography and Material Science*, ASTM STP 733, L. N. Gilbertson and R. D. Zipp, Eds., ASTM, Philadelphia, PA, 1981, p. 428.
215. L. Zakraysek, *Circuits Manuf.*, **23**, 38 (Dec. 1983).
216. L. Zakraysek, *Met. Finish.*, **85**, 29 (Apr. 1987).
217. L. Zakraysek, *Circuit World*, **15** (4), 9 (1989).
218. K. Lin and K. G. Sheppard, *Plating Surf. Finish.*, **80**, 40 (Aug. 1993).
219. F. Delamare and G. E. Rhead, *Surf. Sci.*, **28**, 267 (1971).
220. C. L. Bianchi and J. R. Galvele, *Corrosion Set.*, **27**, 631 (1987).
221. J. W. Chang, Ph.D. Thesis, Stevens Institute of Technology, Hoboken, NJ (1988).
222. J. W. Dini and W. H. Gourdin, *Plating Surf. Finish.*, **77**, 54 (Aug. 1990).
223. M. J. Sole and T. Szendrei, in *Proc. AESF SUR/FIN 91*, Session H, Toronto, 423, AESF, Kissimmee, FL, 1991.
224. H. D. Merchant, in *Defect Structure, Morphology and Properties of Deposits*, H. D. Merchant, Ed., Minerals, Metals and Materials Soc., Warrendale, PA, 1995, p. 301.
225. H. D. Merchant, *J. Electron. Mater.*, **22**, 631 (1993).
226. R. J. De Angelis, D. B. Knorr, and H. D. Merchant, in *Defect Structure, Morphology and Properties of Deposits*, H. D. Merchant, Ed., Minerals, Metals and Materials Society, Warrendale, PA, 1995, p. 87.
227. D. S. Stoychev, I. V. Tomov, and I. B. Vitanova, *J. Appl. Electrochem.*, **15**, 879 (1985).
228. Sv. Surnev and I. Tomov, *J. Appl. Electrochem.*, **19**, 752 (1989).
229. J. Cl. Puippe, F. Leaman, Eds., *Theory and Practice of Pulse Plating*, AESF, Kissimmee, FL, 1986.
230. *Proc. AESF 1st Intl. Pulse Plating Symp*., Boston MA, (Apr. 1979).
231. *Proc. AESF 2nd Intl. Pulse Plating Symp*., Rosemont IL, (Oct. 1981).
232. *Proc. AESF 3rd Intl. Pulse Plating Symp*., Washington DC, (Oct. 1986).
233. C. C. Wan, H. Y. Cheh, and H. B. Linford, *Plating*, **61**, 559 (1974).
234. G. Devaraj and S. Guruviah, *Mater. Chem. Phys.*, **25**, 439 (1990).
235. J. W. Dini, *Met. Finish.*, **61**, 52 (July 1963).
236. G. A. Malone, "Investigation of Electrofonning Techniques," NASA-CR-134776 (Apr. 1975) and NASA-CR-134959 (Dec. 1975).
237. C. C. Wan, in *Proc. AESF 1st Intl. Pulse Plating Symp*., AESF, Kissimmee, FL, 1979.
238. M. R. Kalantary and D. R. Gabe, *J. Mater. Sci.*, **30**, 4515 (1995).
239. T. Pearson and J. K. Dennis, *J. Appl. Electrochem.*, **20**, 196 (1990).
240. A. J. Avila and M. J. Brown, *Plating*, **57**, 70 (1970).
241. A. Hickling and H. P. Rothbaum, *Trans. Inst. Met. Finish*., **34**, 199 (1957).
242. N. Ibl, J. Cl. Puippe, and H. Angerer, *Surf. Tech.*, **6**, 287 (1978).
243. Y. M. Polukarov et al., *Electrokhim.*, **18**, 1224 (1982).
244. M. Yokoi and T. Hayashi, *Denki Kagaku*, **46**, 195 (1978).
245. J. Cl. Puippe and N. Ibl, *Plating Surf. Finish.*, **67**, 68 (June 1980).
246. G. Devaraj and S. K. Seshadri, *Plating Surf. Finish.*, **79**, 72 (Aug. 1992).
247. D. S. Stoychev and M. S. Aroyo, in *Proc. SUR/FIN 96*, Session U, Cleveland, AESF, Kissimmee, FL, 1996, p. 851.
248. W. F. Hall and A. R. Chaudhuri, in *Proc. AESF 10th Symp. on Plating in the Electronics Industry*, San Francisco, 1983.
249. A. R. Despic and K. I. Popov, *J. Appl. Electrochem.*, **1**, 275 (1971).
250. K. I. Popov, M. D. Maksimovic, and D. C. Totovski, *Surf. Technol.*, **17**, 125 (1982).
251. H. Y. Cheh, H. B. Linford, and C. C. Warr, Project 35, American Electroplaters Society Research, AESF, Kissimmee, FL (1977).
252. K. I. Popov, D. C. Totovski, and M. D. Maksimovic, *Surf. Technol.*, **19**, 181 (1983).
253. H. K. Ng, A. C. C. Tseung, and D. B. Hibbart, *J. Electrochem. Soc.*, **127**, 1034 (1980).

254. T. Pearson, J. K. Dennis, J. F. Houlston, and M. Dorey, *Trans. Inst. Met. Finish.*, **69**, 9 (1991).
255. T. Pearson and J. K. Dennis, *Trans. Inst. Met. Finish.*, **69**, 75 (1991).
256. A. Montgomery, *Circuit World*, **15**, 33 (Jan. 1989).
257. M. R. Kalantary, D. R. Gabe, and M. Goodenough, *Met. Finish.*, **89**, 21 (Apr. 1991).
258. D. Engelhaupt,"Pulse Plating of Copper for Printed Wiring Boards," Report OR 18, 258, Martin Marietta Orlando Aerospace, Lockheed Martin, Bethesda, MD (March 1985).
259. S. Coughlan, *Trans. Inst. Met. Finish.*, **73**, 54 (1995).
260. G. Holmbom and B. E. Jacobsson, *Surf. Coatings Technol.*, **35**, 333 (1988).
261. P. Leisner, G. Bech-Nielsen, and P. Moller, in *Proc. AESF SUR/FIN 92*, Session S, Atlanta, AESF, Kissimmee, FL, 1992, p. 1011.
262. E. K. Yung, L. T. Romankiw, and R. C. Alkire, in *Electrodeposition Technology, Theory and Practice*, L. T. Romankiw and D. R. Turner, Eds., Electrochemical Society, Pennington, NJ, 1987, p. 75; *J. Electrochem. Soc.*, **136**, 206 (1989).
263. N. R. K. Vilambi and D.-T. Chin, *Plating Surf. Finish.*, **75**, 67 (Jan. 1988).
264. D. E. Engelhaupt, U. S. Patent 5,326,454 (July 5 1994).
265. C. C. Wan, H. Y. Cheh and H. B. Linford, *J. Appl. Electrochem.*, **9**, 29 (1979).
266. K. I. Popov, M. V. Vojnovic, L. J. M. Vracar and B. J. Lazarevic, *J. Appl. Electrochem.*, **4**, 267 (1974).
267. D. R. Rudder, in *Proc. AESF SUR/FIN85*, Session F, Detroit, AESF, Kissimmee, FL, 1985.
268. J. R. White and R. T. Galasco, *Plating Surf. Finish.*, **75**, 122 (May 1988).
269. J. R. White, *J. Appl. Electrochem.*, **17**, 977 (1987).
270. J. Mann, *Trans. Inst. Metal Finish.*, **56**, 70 (1978).
271. C. D. Zhou, R. P. Renz, E. J. Taylor, E. C. Stortz, and B. Grant, in *Proc. AESF SUR/FIN 96*, Cleveland, AESF, Kissimmee, FL, 1996 p. 517.
272. B. S. Sheshadi, *Plating Surf. Finish.*, **65**, 43 (July 1978).
273. N. Ibl, in *Proc. 2nd Int. Pulse Plating Symp*., Rosemont IL, AESF, Kissimmee, FL, Oct. 1981.
274. C. C. Wan, in *Proc. 2nd Int. Pulse Plating Symp*., Rosemont, IL, AESF, Kissimmee, FL, 1981.
275. D.-T. Chin, *J. Electrochem. Soc.*, **130**, 1657 (1983).
276. C. W. Yeow and D. B. Hibbert, *J. Electrochem. Soc.*, **130**, 786 (1983).
277. R. J. Clauss and N. C. Adamowicz, *Plating Surf. Finish.*, **57**, 236 (Mar. 1970).
278. J. K. Dennis and T. E. Such, *Nickel and Chromium Plating*, 3rd ed., Woodhead Publ., Cambridge, England, 1993.
279. G. A. DiBari, private communication, Sept. 1996.
280. G. A. DiBari, *Met. Finish.*, **75**, 17 (June 1977); **75**, 17 (July 1977).
281. G. A. DiBari, *Plating Surf. Finish.*, **64**, 68 (May 1977).
282. J. C. Jongkind, *Plating Surf. Finish.*, **62**, 1135 (1975).
283. S. K. Jalota, *Electroplating of Zinc Die Castings*, Bath Press, Bath, Avon, 1987.
284. R. Suchentrunk, in *Metallizing of Plastics—A Handbook of Theory and Practice*, R. Suchentrunk, Ed., Finishing Publications, Orlando, FL, 1993.
285. W. Meyer, *Metalloberflache*, **34**, 489 (1980).
286. H. E. Haring and W. Blum, *Trans. Am. Electrochem. Soc.*, **44**, 313 (1923).
287. D. R. Turner, *Plating Surf. Finish.*, **66**, 32 (July 1979).
288. E. K. Yung and L. T. Romankiw, in *Electrodeposition Technology, Theory and Practice*, L. T. Romankiw and D. R. Turner, Eds., Electrochemical Society, Pennington, NJ, 1987, p. 607; *J. Electrochem. Soc.*, **136**, 756 (1989).
289. D. A. Hazlebeck and J. B. Talbot, in *Proc. Electrochemical Technology in Electronics*, Vol. 88-23, L. T. Romankiw and T. Osaka, Eds., Electrochemical Society, Pennington, NJ, 1988, p. 143.
290. T. Kessler and R. Alkire, *Plating Surf Finish.*, **63**, 22 (Sept. 1976).
291. T. Kessler and R. Alkire, *J. Electrochem. Soc.*, **123**, 990 (1976).
292. L. Mayer and S. Barbieri, *Plating Surf Finish.*, **68**, 46 (Mar. 1981).
293. S. Barbieri, L. Mayer and J.-H. Shyu, *Trans. Inst. Met. Finish.*, **62**, 25 (1984).
294. G. L. Fisher, W. Sonnenberg, J. Bladon and R. Bernards, *Trans. Inst. Met. Finish.*, **68**, 50 (1990).
295. S. Yamato, C. Kan and A. Ohharada, in *Proc. AESF SUR/FIN 92*, Session L, Atlanta, AESF, Kissimmee, FL, 1992, p. 679.
296. P. Davidson, in *Proc. AESF SUR/FIN 86*, Session I, Philadelphia, AESF, Kissimmee, FL, 1986, p. 27.
297. M. Carano, in *Proc. 13th AESF Symp. on Plating in the Electronics and Printed Circuit Industry*, AESF, Kissimmee, FL, 1986, p. 14.
298. S. A. Amadi, D. R. Gabe, and M. R. Goodenough, *Met. Finish.*, **91**, 23 (May 1993).
299. E. J. Glantz, *PC Fab.*, **12**, 60 (Feb. 1989).
300. M. C. Hsiao and C. C. Wan, *J. Electrochem. Soc.*, **138**, 2273 (1991).
301. D. P. Davidson, *Circuits Manufacturing*, **27**, 36 (Aug. 1987).
302. L. J. Mayer and S. C. Barbieri, *Plating Surf. Finish.*, **68**, 46 (1981).
303. R. Haak, C. Ogden, and D. Tench, *Plating Surf. Finish.*, **68**, 59 (Oct. 1981).
304. W. Engelmaier and T. Kessler, *J. Electrochem. Soc.*, **125**, 36 (1978).
305. F. Byle and P. Bratin, in *Proc. AESF SUR/FIN 90*, Session H, Boston, AESF, Kissimmee, FL, 1990.
306. D. R. Turner, *Plating Surf. Finish.*, **63**, 41 (Jan. 1976).
307. H. H. Wan and J. E. McCaskie, *Plating Surf. Finish.*, **78**, 80 (Nov. 1991).
308. J. W. Dini, *Plating Surf. Finish.*, **76**, 64 (Sept. 1989).
309. T. Barringer and M. Carano, *Plating Surf. Finish.*, **73**, 36 (Mar. 1986).

310. A. Elbs and J. Rasmussen, *Galvanotechnik*, **85**, 3998 (1994).
311. D. A. Luke, *Trans. Inst. Met. Finish.*, **51**, 113 (1973).
312. X. Ye, M. DeBonte, J. P. Celis, and J. R. Roos, *J. Electrochem. Soc.*, **139**, 1592 (1992).
313. S. Kang, J.-S. Yang, and D. N. Lee, *Plating Surf. Finish.*, **82**, 67 (Oct. 1995).
314. A. Fox, *J. Test. Eval.*, **4** (1), 74 (Jan. 1976).
315. H. D. Merchant, *J. Electron. Mater.*, **24**, 919 (1995).
316. H. D. Merchant, in *Defect Structure, Morphology and Properties of Deposits*, H. D. Merchant, Ed., Minerals, Metals and Materials Soc., Warrendale, PA, 1995, p. 1.
317. J. O. Dukovic, in *Advances in Electrochemical Science and Engineering*, H. Gerischer and C. W. Tobias, Eds., VCH, Germany, 1994, p. 117.
318. L. T. Romankiw, "A Review of Plating through Polymeric Resist Masks," in *Extended Abstracts of the Electrochemical Society*, 79-2, Abstract No. 462, Electrochemical Society, Pennington, NJ, 1979, pp. 1165–1166.
319. L. T. Romankiw, *Oberflache-Surface*, **25**, 238 (1984).
320. L. T. Romankiw and T. A. Palumbo, in *Electrodeposition Technology, Theory and Practice*, L. T. Romankiw and D. R. Turner, Eds., Electrochemical Society, Pennington, NJ, 1987, p. 13.
321. L. T. Romankiw, "Electrochemical Technology in the Electronics Industry and Its Future," in *New Materials and New Processes*, JEC Press, Cleveland, OH, 1988, pp. 3, 39.

321a. P. C. Andricacos, C. Uzoh, J. O. Dukovic, J. Horkans, and H. Deligianni, *IBM J. Res. Develop.*, **42**, 567 (1998).

322. K. Kondo, K. Fukui, K. Uno, and K. Shinohara, *J. Electrochem. Soc.*, **143**, 1880 (1996).
323. J. O. Dukovic, *IBM J. Res. Develop.*, **37**, 125 (Mar. 1993).
324. C. Booking, *Trans. Inst. Met. Finish.*, **69**, 119 (1991).
325. R. J. von Gutfeld, R. E. Acosta, and L. T. Romankiw, *IBM J. Res. Develop.*, **26**, 136 (Mar. 1982).
326. J. Cl. Puippe, R. E. Acosta, and R. J. von Gutfeld, *J. Electrochem. Soc.*, **128**, 2539 (1981).
327. P. Bindra, G. V. Arbach and U. Slimming, *J. Electrochem. Soc.*, **134**, 2893 (1987).
328. P. Bindra, D. Light, G. V. Arbach, and U. Stimming, in *Proc. Electrochemical Technology in Electronics*, Vol. 88-23, L. T. Romankiw and T. Osaka, Eds., Electrochemical Society, Pennington, NJ, 1988, p. 341.
329. W. Paatsch, W. Kautck and N. Sorg, in *Proc. AESF SUR/FIN 90*, Session I, Boston, AESF, Kissimmee, FL, 1990.
330. M. J. Sole, *J. Metals*, **46**, 29 (June 1994).
331. R. Suchentrunk, *Trans. Inst. Met. Finish.*, **64**, 19 (1986).
332. G. A. Malone, in *Proc. AESF SUR/FIN 79*, Session H, Atlanta, AESF, Kissimmee, FL, 1979.
333. M. R. Louthan, Jr., "The Effect of Hydrogen on Metals," in *Corrosion Mechanisms*, F. Mansfeld, Ed., Marcel Dekker, New York, 1987.
334. M. Koiwa, A. Yamanaka, M. Arita, and H. Numakura, *J. Inst. Met.*, **30**, 991 (1989).
335. J. R. Denchfield, U. S. Patent 3,616,330 (1971).
336. F. T. Schuler and F. Mansfeld, *J. Vac. Sci. Technol.*, **12**, 758 (July–Aug. 1975).
337. D. Engelhaupt, private communication, July 1996.
338. J. W. Dini, *Thin Solid Films*, **95**, 123 (1982).
339. J. C. Farmer, et al. *Plating Surf. Finish.*, **75**, 48 (Mar. 1988).
340. W. K. Kelley, J. W. Dini, C. M. Logan, *Plating Surf. Finish.*, **69**, 54 (Mar. 1982).
341. V. V. Gubin, L. T. Zhuravlev, B. M. Platonov and Yu. M. Polukarov, *Soviet Electrochem.*, **20** (5), 671 (1984).
342. R. D. Srivastava and S. Kumar, *Trans. Inst. Met. Finish.*, **50**, 102 (1972).
343. N. V. Shanmugam and S. J. Pr. Thangavelu, *Trans. Met. Finish. Assoc. India*, **3** (3), **27**, (July–Sept. 1994).
344. L. A. Doggrell and G. D. Hooper, in *Proc. AES Int. Symp. on Electroformingj Deposition Techniques*, Los Angeles, CA, AESF, Kissimmee, FL, 1983.
345. A. Mayer, J. L. Uher, and W. A. Wright, *Plating Surf. Finish.*, **70**, 29 (Oct. 1983).
346. W. H. Safranek, *Plating Surf. Finish.*, **69**, 48 (Apr. 1982).
347. G. R. Schaer and T. Wada, *Plating Surf. Finish.*, **68**, 52 (July 1981).
348. G. R. Schaer and J. R. Preston, U. S. Patent 4,597,836 (1986).
349. L. J. J. Janssen, *J. Appl. Electrochem.*, **18**, 339 (1988).
350. M. F. El-Shazly, J. L. White, and E. W. Brooman, in *Proc. AESF 3rd Int. Pulse Plating Symp*., AESF, Kissimmee, FL, 1986.
351. D. A. Uceda and T. J. O'Keefe, *J. Appl. Electrochem.*, **20**, 327 (1990).
352. P. Kutzschbach, W. Rempt, K.-D. Baum, and H. Liebscher, *Wire*, **45** (6), 336 (1995).
353. H. J. Wiesner and W. J. Frey, *Plating Surf. Finish.*, **66**, 51 (Feb. 1979).
354. S. T. Rao and L. Trager, U. S. Patent 4,551,212 (Nov. 1985).
355. M. S. Abrahams, S. T. Rao, C. J. Buiocchi, and L. Trager, *J. Electrochem. Soc.*, **133**, 1786 (1986).
356. J. W. Dini, T. G. Beat, W. C. Cowden, L. E. Ryan, and W. B. Hewitt, in *Proc. SUR/FIN 92*, Session R, Atlanta, AESF, Kissimmee, FL, 1992.
357. H. Takeo, C. Tarn, and J. Dash, "Magnetic Effects on Electroplating of Copper," in *Proc. AES 11th Plating in the Electronics Industry Symp*., Orlando, FL, AESF, Kissimmee, FL, 1984.
358. M. I. Ismail and T. Z. Fahidy, *J. Appl. Electrochem.*, **11**, 543 (1981).
359. K. I. Popov, L. J. M. Djukic, M. G. Pavlovic, and M. D. Maksimovic, *J. Appl. Electrochem.*, **9**, 527 (1979).
360. J. Jorne and M. G. Lee, *J. Electrochem. Soc.*, **143**, 865 (1996).
361. R. R. Adzic, in *Advances in Electrochemistry and Electrochemical Engineering*, Vol. 13, H. Gerischer, Ed., Wiley, New York, 1984, p. 159.
362. D. M. Kolb, in *Advances in Electrochemistry and Electrochemical Engineering*, Vol. 11, H. Gerischer and C. Tobias, Eds., Wiley, New York, 1978, p. 125.

363. J. Horkans, I.-C. H. Chang, P. C. Andricacos, and H. Deligianni, *J. Electrochem. Soc.*, **142**, 2244 (1995).
364. J. C. Farmer, *J. Electrochem. Soc.*, **132**, 2640 (1985).
365. J. S. Hammond and N. Winograd, *J. Electrochem. Soc.*, **124**, 826 (1977).
366. Walenn, British Patent 1540 (1857).
367. A. Watt and A. Philip, *Electro-Plating and Electro-Refining of Metals*, 2nd ed., Van Nostrand, New York, 1911, p. 156.
368. O. P. Watts, *Trans. Am. Electrochem. Soc.*, **27**, 141 (1915).
369. C. J. Wernlund, H. L. Benner, and R. R. Bair, U. S. Patent 2,287,654 (1942).
370. C. J. Wernlund, U. S. Patent 2,347,448 (1944).
371. D. A. Holt, U. S. Patent 2,255,057 (1941).
372. G. W. Jernstedt, U. S. Patents 2,451,340; 2,451,341 (1948).
373. F. A. Lowenheim, *Modern Electroplating*, 3rd ed., Wiley, New York, 1974.
374. F. Passal, *Plating*, **46**, 628 (1959).
375. G. C. Van Tilburg, *Plating Surf. Finish.*, **71**, 78 (Apr. 1984).
376. F. A. Lowenheim, *Electroplating*, McGraw-Hill, New York, 1978.
377. L. M. Weisenberger, "Copper Plating," in *Metals Handbook*, 9th ed., Vol. 5, *Surface Cleaning, Finishing and Coating*, ASM International, Cleveland, OH, 1982.
378. L. M. Weisenberger and B. J. Durkin, "Copper Plating," in *ASM Handbook*, Vol. 5, *Surface Engineering*, ASM International, Cleveland, OH, 1994.
379. A. Sato and R. Barauskas, *Metal Finishing, 64th Guidebook and Directory Issue*, **94** (1A), 214 (1996).
380. J. Horner, private communication, May 1996.
381. B. A. Smith, W. S. Rapacki, and T. S. Davidson, *Plating Surf. Finish.*, **79**, 11 (Aug. 1992).
382. J. Horner, *Plating Surf. Finish.*, **74**, 34 (Mar. 1987).
383. S. K. Jalota, *Electroplating of Zinc Die Castings*, Bath Press, Bath, Avon, 1987.
384. J. K. Dennis and T. E. Such, *Nickel and Chromium Plating*, 3rd ed., Woodhead Publ., Cambridge, England, 1993.
385. G. A. DiBari, *Met. Finish.*, **75**, 17 (June 1977); **75**, 17 (July 1977).
386. Staff Report, *Plating Surf. Finish.*, **68**, 36 (July 1981).
387. P. G. Hatherley, K. G. Watkins, and M. McMahon, *Trans. Inst. Met. Finish.*, **70**, 177 (1992).
388. D. S. Lashmore, *Plating Surf. Finish.*, **67**, 36 (Jan. 1980).
389. D. A. Dudek and P. S. Fedkiw, *Proc. AESF SUR/FIN 96,* Session T, Cleveland, AESF, Kissimmee, FL, 1996.
390. P. G. Hatherley and P. J. Carpenter, *Trans. Inst. Met. Finish.*, **73**, 85 (1995).
391. D. Chu and P. S. Fedkiw, *J. Electronanal. Chem.*, **345**, 107 (1993).
392. R. E. Sinitski, V. Srinivasan and R. Haynes, *J. Electrochem. Soc.*, **127**, 47 (1980).
393. A. Elbs and J. Rasmussen, *Galvanotechnik*, **85**, 3998 (1994).
394. J. Horner, *Proc. Am. Electroplaters' Soc.*, **51**, 71 (1964).
395. Cs. Juhos, Sf. Gheorghe, E. Gruenwald, and Cs. Varhely, *Galvanotechnik*, **81**, 857 (1990).
396. A. K. Graham and H. J. Read, *Met. Ind. (NY)*, **35**, 559, 617 (1937); **36**, 15, 77, 120, 169 (1938).
397. A. K. Graham, *Met. Ind. (NY)*, **36**, 279 (1938).
398. R. M. Wagner and M. M. Beckwith, *Proc. Am. Electroplat. Soc.*, **25**, 147 (1938).
399. C. W. Smith and C. B. Munton, *Met. Finish.*, **39**, 415 (1941).
400. B. Ostrow and F. Nobel, U. S. Patent 3,021,266 (1962).
401. F. Passal, U. S. Patent 3,030,282 (1962).
402. F. Passal, U. S. Patent 3,111,465 (1963).
403. P. Leenders and H. Creutz, U. S. Patent 3,084,112 (1963).
404. E. Hadley, U. S. Patent 3,179,577 (1965).
405. P. Leenders, U. S. Patent 3,219,560 (1965),
406. A. Debo, U. S. Patent 3,216,913 (1965).
407. A. H. DuRose, U. S. Patent 3,269,925 (1966).
408. B. D. Ostrow and F. I. Nobel, U. S. Patent 3,309,292 (1967).
409. J. R. Grain, U. S. Patent 3,296,101 (1967).
410. L. M. Weisenberger et al., U. S. Patent 3,790,451 (Feb. 1974).
411. M. Pushpavanam, *Met. Finish.*, **84**, 53 (Apr. 1986).
412. J. W. Dini and H. R. Johnson, in *Proc. Electroless Nickel Conf. III, Products Finishing Magazine*, Gardner, Cincinnati OH, Mar. 1983.
413. A. H. DuRose, *ASTM Special Tech. Publ.* **197** (1956).
414. International Lead-Zinc Research Organization, Project LE-36, Report 28, ILZRO, Durham, NC (Dec. 1968).
415. G. Schaer, *Plating Surf. Finish.*, **68**, 51 (Mar. 1981).
416. J. B. Mohler, *Met. Finish.*, **82**, 41 (May 1984).
417. H. L. Benner and C. J. Wernlund, *Trans. Electrochem. Soc.*, **80**, 355 (1941).
418. H. J. Read and A. K. Graham, *Trans. Electrochem. Soc.*, **74**, 411 (1938).
419. A. K. Graham, *Plating and Metal Finishing Guidebook, Met. Ind. (NY)*, **26** (1940).
420. *Iron Age*, **184** (2), 98 (1959).
421. H. Kenmore and Manson, U. S. Patent 2,680,710 (1954).
422. E. D. Boelter, U. S. Patent 2,854,389 (1948).
423. S. E. CraigJr., R. E. Harr, and S. Y. Wu, *Plating*, **60**, 1239 (1973).
424. C. J. Wernlund, U. S. Patent 2,774,728 (1956).
425. C. J. Wernlund, U. S. Patent 2,701,234 (1955).
426. M. I. Ismail, *J. Appl. Electrochem.*, **9**, 407 (1979).
427. J. W. Dini, *Met. Finish.*, **61**, 52 (July 1963).
428. D. R. Rudder, *Proc. AESF SUR/FIN 85*, Session L, Detroit, MI (1985).
429. K. E. Langford, *Analysis of Electroplating and Related Solutions*, 4th ed., Robert Draper, Teddington, Middlesex, England, 1971.
430. S. Sriveeraraghaven and S. R. Natarajan, *Met. Finish.*, **73**, 37 (Aug. 1975).
431. J. D. Kostura, *Plating Surf. Finish.*, **70**, 70 (June 1983).
432. L. J. Durney, Ed., *Electroplating Engineering Handbook*, 4th ed., Van Nostrand Reinhold, New York, 1984.

433. J.-Y. Hwang, Y.-Y. Wang, and C.-C. Wan, *Plating Surf Finish.*, **74**, 56 (Apr. 1987).
434. R. O. Hull, U. S. Patent 2,149,344 (1939).
435. M. K. Sanicky, *Plating Surf. Finish.*, **72**, 20 (Oct. 1985).
436. J. W. Dini, *Electrodeposition: The Materials Science of Coatings and Substrates*, Noyes, Park Ridge, NJ, 1993.
437. W. Dingley, J. Bednar and R. R. Rogers, *Plating*, **53**, 602 (1966); Discussion, **54**, 397 (1967).
438. J. R. Crain, *Plating*, **51**, 31 (1964); W. L. Bohman and M. Ceresa, U. S. Patent 2,858,257 (1958); M. Ceresa and J. Crain, U. S. Patent 2,861,927 (1958); W. L. Bohman and M. Ceresa, U. S. Patent 2,861,928 (1958).
439. H. G. McLeod and D. A. Swalheim, U. S. Patent 2,885,331 (1959).
440. N. W. Phasey, *Trans. Inst. Met. Finish.*, **51**, 77 (1973).
441. F. I. Nobel and B. D. Ostrow, *Plating*, **50**, 823 (1963).
442. D. A. Swalheim, *Plating Surf. Finish.*, **64**, 36 (Apr 1977).
443. K. G. Watkins, P. J. Carpenter and P. G. Hatherley, *Trans. Inst. Metal. Finish.*, **71**, 85 (1993).
444. D. L. Snyder, *Met. Finish.*, **89**, 37 (Apr. 1991).
445. F. Altmayer, *Plating Surf. Finish.*, **80**, 42 (Feb. 1993).
446. W. H. Safranek, *The Properties of Electrodeposited Metals and Alloys*, 2nd ed., American Electroplaters and Surface Finishers Society, Orlando, FL, 1986.
447. V. A. Lamb and D. R. Valentine, *Plating*, **52**, 1289 (1965) **53**, 86 (1966).
448. V. A. Lamb C. E. Johnson, and D. R. Valentine, *J. Electrochem. Soc.*, **117**, 291C, 341C, 381C 1970.
449. N. V. Parthasaradhy, *Met. Finish.*, **72**, 36 (Aug. 1974).
450. J. C. Farmer, H. R. Johnson, H. A. Johnsen, J. W. Dini, D. Hopkins, and C. P. Steffani, *Plating Surf. Finish.*, **75**, 48 (Mar. 1988).
451. D. L. Snyder, *Met. Finish.*, **89**, 37 (Apr. 1991).
452. F. Altmayer, *Plating Surf. Finish.*, **80**, 40 (Feb. 1993).
453. T. W. Bleeks and T. S. Davidson, "An Alternative to Cyanide Copper," in *Proc. 13th AESF/EPA Conf. on Environmental Control for the Surface Finishing Industry*, Orlando, FL, AESF, Kissimmee, FL, 1992, p. 179.
454. H. R. Johnson, W. D. Bonivert, and J. Hachman,"Alternatives for Cyanide Copper Plating," Spring Meeting, Materials Research Society (MRS), Symposium W, Environmentally Conscious Materials Processing (May 1991).
455. C. P. Steffani and J. W. Dini, *Int. J. Environmentally Conscious Design Manuf.*, **3** (2), 43 (1994).
456. L. C. Tomaszewski and R. A. Tremmel, in *Proc. AESF SUR/FIN 85*, Session D, Detroit, MI, AESF, Kissimmee, FL, 1985.
457. W. H. Safranek and H. R. Miller, *Plating*, **55**, 233 (1968).
458. W. H. Safranek, *Plating*, **56**, 11 (1969).
459. B. A. Smith, S. Papacki, and T. S. Davidson, *Plating Surf. Finish.*, **79**, 11 (Aug. 1992).
460. L. M. Weisenberger and B. J. Durkin, "Copper Plating," in *ASM Handbook*, Vol. 5, *Surface Engineering*, ASM International, Cleveland, OH, 1994.
461. R. T. Haynes, R. R. Irani, and R. P. Langguth, U. S. Patent 3,475,293 (1969).
462. J. Szotek, in *Proc. AESF SUR/FIN 93*, Session F, Anaheim, CA, 1993.
463. D. F. Maule and B. Srinivasan, in *Proc. AESF SUR/FIN 93*, Session F, Anaheim, CA, AESF, Kissimmee, FL, 1993.
464. M. B. I. Janjua, J. Yernaux, P. J. Nicoll, and N. R. Bharucha, *Plating*, **60**, 1124 (1973).
465. G. Carneval and J. Bebczuk de Cusminsky, *J. Electrochem. Soc.*, **128**, 1215 (1981).
466. E. Chassaing, K. Vu Quang, and R. Wiart, *J. Appl. Electrochem.*, **16**, 591 (1986).
467. A. Chiba and W. C. Wu, *Plating Surf Finish.*, **79**, 62 (Dec. 1992).
468. R. M. Krishnan, M. Kanagasabapathy, S. Jayakrishnan, S. Sriveeraraghavan, R. Anantharam and S. R. Natarajan, *Plating Surf. Finish.*, **82**, 56 (July 1995).
469. O. Trost and B. Pihlar, *Met. Finish.*, **90**, 125 (June 1992).
470. F. M. Al-Kharaft and Y. A. El-Tantawy, *J. Electrochem. Soc.*, **128**, 2073 (1981).
471. Y. Gan, *Plating Surf. Finish.*, **79**, 81 (June 1992).
472. P. L. Cavallotti, D. Colombo, E. Galbiati, A. Piotti, and F. Kruger, *Plating Surf. Finish.*, **75**, 78 (Apr. 1988).
473. S. Bharathi, S. Rajendran, V. N. Loganathan, C. Krishna, and K. R. Ananndakumarannair, in *Proc. AESF SUR/FIN 96*, Session G, Cleveland, OH, AESF, Kissimmee, FL, 1996.
474. S. M. Mayanna and B. N. Maruthi, *Met. Finish.*, **94**, 42 (Mar. 1996).
475. A. Roseleur, *Manipulations Hydroplastiques—Guide Practique du Doreur, de L'Argenteur et de Galvanoplaste*, 1st ed., Roseleur, Paris, 1855.
476. A. Gutensohn, British Patent 4784 (1893).
477. A. Brand, *Z. Anal. Chem.*, **28**, 581 (1888).
478. E. Delvai, in *Manipulations Hydroplastiques — Guide Practique du Doreur de L'argenteur et du Galvanoplaste*, A. Roseleur, Ed., W.H. Wahl, 1892.
479. L. F. Royer, French Patent 381,475 (1908).
480. F. Regelsberger, *Elektrochem. Z.*, **19**, 181 (1912).
481. J. E. Stareck, U. S. Patent 2,081,121 (1937).
482. J. E. Stareck, U. S. Patent 2,250,556 (1941).
483. T. G. Coyle, *Proc. Am. Electroplat. Soc.*, **28**, 113 (1941).
484. F. A. Lowenheim, *Modern Electroplating*, 3rd ed., Wiley, New York, 1974.
485. F. Passal, *Plating*, **46**, 628 (1959). (a) G. C. Van Tilburg, *Plating Surf. Finish.*, **71**, 78 (Apr. 1984).
486. F. A. Lowenheim, *Electroplating*, McGraw-Hill, New York, 1978.
487. L. M. Weisenberger, "Copper Plating," in *Metals Handbook*, 9th ed., Vol. 5, *Surface Cleaning, Finishing and Coating*, American Society for Metals, Cleveland, OH, 1982.
488. L. M. Weisenberger and B. J. Durkin, "Copper Plating," in *ASM Handbook*, 10th ed., Vol. 5, *Surface Engineering*, ASM International, Cleveland, OH, 1994.

489. A. Sato and R. Barauskas, *Metal Finishing, 64th Guidebook and Directory Issue*, **94** (1A), 214 (1996).
490. E. F. Duffek, "Plating," in *Printed Circuits Handbook*, 4th ed., C. F. Coombs Jr., Ed., McGraw-Hill, New York, 1996.
491. D. M. Lyde, *Met. Ind. (London)*, **101**, 82 (Aug. 1962).
492. L. Missel and M. E. Shaheen, *Met. Finish.*, **62**, 61 (Sept. 1964).
493. H. F. Maddocks, French Patent 2,020,754 (1969).
494. H. Wolfson and B. Thomson, British Patent 600,873 (1948).
495. H. J. Wiesner and W. P. Frey, *Plating Surf. Finish.*, **66**, 51 (Feb.) 1979.
496. Y. T. Chen, J. R. DePew and H. D. McCabe, *J. Vac. Sci. Technol*, **11**, 777 (1974).
497. A. I. Levin and V. V. Gulylev, *Draht*, **14** (1), 18 (1963) *Met. Finish. Abstr*, **5**, 51 (1963).
498. A. A. Voronko, S. P. Pilite, and A. M. Molchadskiy, Russian Patent 159,368 (1962); *Met. Finish. Abstr.*, **6**, 52, (1964).
499. J. T. N. Atkinson, U. S. Patent 2,871,171 (1959).
500. R. D. Potlushnewa, *Galvanotechnik*, **54** (3), 142 (1963); *Met. Finish. Abstr.*, **5**, 91, (1963).
501. Pernix, Enthone, French Patent 1,448,839 (1965); *Met. Finish. Abstr.*, **8**, 249, (1966).
502. Yu. Ya. Lukomskiy, L. N. Zapatrina, and A. N. Aleksandrova, Russian Patent 191,983 (1963); *Met. Finish. Abstr.*, **9**, 204, (1967).
503. B. E. Bunce, *Met. Finish.*, **52**, 70 (Jan. 1954).
504. S. Wernick and R. Pinner, Eds., *Surface Treatment of Aluminum*, 3rd ed., Robert Draper, Teddington, Middlesex, England, 1964.
505. H. R. Johnson, W. D. Bonivert, and J. Hachman,"Alternatives for Cyanide Copper Plating," Spring Meeting, Materials Research Society (MRS), Symposium W, Environmentally Conscious Materials Processing (May 1991).
506. C. P. Steffani and J. W. Dini, *Int. J. Environmentally Conscious Design Manuf.*, **3** (2), 43 (1994).
507. W. H. Safranek and H. R. Miller, *Plating*, **55**, 233 (1968).
508. W. H. Safranek, *Plating*, **56**, 11 (1969).
509. J. E. Stareck, *Mon. Rev. Am. Electroplat. Soc.*, **30**, 25 (1943).
510. W. V. Sternberger and E. R. Fahy, *Met. Prog.*, **47**, 278 (1945); **48**, 1311 (1945).
511. C. J. Miller, *Met. Prog.*, **49**, 783 (1946).
512. N. Solowjow, *Met. Finish. Abstr.*, **55**, 71 (Sept. 1957).
513. H. Fischer and H. Baermann, *Korros. Metallschutz*, **16**, 405 (1940).
514. E. E. Dougherty, *Plating*, **51**, 415 (1964).
515. D. DeFilippo, A. Rossi, and M. A. Spezziga, *J. Appl. Electrochem.*, **16**, 463 (1986).
516. D. DeFilippo, L. Dessi, and A. Rossi, *J. Appl. Electrochem.*, **19**, 37 (1989).
517. E. K. Yung, L. T. Romankiw, and R. C. Alkire, in *Electrodeposition Technology, Theory and Practice*, L. T. Romankiw and D. R. Turner, Eds., Electrochemical Society, Pennington, NJ, 1987, p. 75; *J. Electrochem. Soc.*, **136**, 206 (1989).
518. J. P. Langan, private communication, May 1996.
519. L. Lourch, private communication, May 1996.
520. D. L. Snyder, *Met. Finish.*, **89**, 37 (Apr. 1991).
521. D. J. Combs, in *Proc. AESF SUR/FIN 80*, Session B, Milwaukee, WI, AESF, Kissimmee, FL, 1980.
522. S. Senderoff, *Met. Finish.*, **48**, 59 (July 1950).
523. I. M. Kolthoff, *Pharm. Weekbl.*, **57**, 474 (1920).
524. B. C. Halder, *Sci. Cult. (India)*, **14**, 340 (1949); *Chem. Abstr.*, **43**, 6103 (1949).
525. *Theory and Practice of Bright Electroplating*, transl. from Russian, U. S. Department of Commerce, TT 65-50000 Clearinghouse for Federal Scientific and Technical Information, Springfield, VA, B. A. Purin and E. A. Ozola, pp. 146–163; V. I. Lainer, pp. 181–185 (1962).
526. R. N. Bell, *Ind. Eng. Chem.*, **39**, 136 (1947).
527. H. Bassett, W. L. Bedwell, and J. B. Hutchinson, *J. Chem. Soc. (London)*, 1412 (1936).
528. J. I. Walters and A. Aaron, *J. Am. Chem. Soc.*, **76**, 611 (1953).
529. J.1. Watters, E. D. Loughran, and S. M. Lambert, *J. Am. Chan. Soc.*, **78**, 4855 (1956).
530. J. R. Van Wazer and C. F. Callis, *Chem. Rev.*, **58**, 1011 (1958).
531. N. T. Kudryavtsev and B. M. Dikova, *Prot. Met. (USSR)*, **5**, 147 (1969).
532. H. Konno and M. Nagayama, *Electrochim. Acta*, **22**, 353 (1977).
533. H. Konno and M. Nagayama, *Electrochim. Acta*, **23**, 1001 (1978).
534. T. M. Tam and R. Taylor, *J. Electrochem. Soc.*, **133**, 1101 (1986).
535. T. M. Tam and G. A. Fung, *J. Electrochem. Soc.*, **130**, 874 (1983).
536. T. A. Dickinson, *Met. Finish. J.*, **1**, 343 (1955).
537. T. H. Irvine, *Plating*, **54**, 1251 (1967).
538. T. Kojima, *J. Met. Finish. Soc. Japan*, **21** (4), **166**, 1970; *Met. Abstr.*, **3**, 1521 (Nov. 1970).
539. B. R. Rothschild, *Met. Finish.*, **76**, 49 (Jan. 1978).
540. F. H. Wells and D. M. Lyde, British Patent 939,997 (1963).
541. F. H. Wells and D. M. Lyde, U. S. Patent 3,161,575 (1964).
542. D. Tench and C. Ogden, *J. Electrochem. Soc.*, **125**, 194 (1978).
543. D. Tench and C. Ogden, *J. Electrochem. Soc.*, **125**, 1218 (1978).
544. C. Ogden and D. Tench, *Plating Surf. Finish.*, **66**, 30 (Sept. 1979).
545. C. Ogden and D. Tench, *Plating Surf. Finish.*, **66**, 45 (Dec. 1979).
546. C. Ogden and D. Tench, *J. Electrochem. Soc.*, **128**, 539 (1981).
547. C. Ogden, D. Tench and J. White, *J. Appl. Electrochem.*, **12**, 619 (1982).
548. B. Lowry, C. Ogden, D. Tench, and R. Young, *Plating Surf. Finish.*, **70**, 70 (Sept. 1983).
549. M. Jawitz, C. Ogden, D. Tench, and R. Thompson, *Plating Surf. Finish.*, **71**, 58 (Jan. 1984).
550. D. M. Lyde, U. S. Patent 3,784,454 (1974).

551. F. H. Wells and D. M. Lyde, British Patent 940,282 (1963).
552. F. H. Wells and D. M. Lyde, U. S. Patent 3,157,586 (1964).
553. Albright & Wilson Ltd. and Wilmot Breeden, Ltd., French Patent 1,329,175 (1962); *Met. Finish. Abstr.*, **5**, 148 (1963).
554. Kamimura Chobei Co., Ltd., Japanese Patent 20,805/66 (1966); *Met. Finish. Abstr.*, **9**, 144 (1967).
555. Albright & Wilson Ltd., Belgian Patent 714,454 (1968); *Met. Finish. Abstr.*, **11**, 13 (1969).
556. D. M. Lyde, U. S. Patent 3,729,393 (1973).
557. Metal and Thermit Corp., British Patent 774,424 (1957).
558. W. Canning & Company, Ltd., British Patent 1,051,150 (1966).
559. Okuno Seiyaku Kogyo, Ltd., Japanese Patent 24,285/68 (1968); *Met. Finish. Abstr.*, **11**, 14 (1969).
560. T. L. Rama Char, *Electroplating*, **10**, 347 (1957).
561. S. K. Panikkar and T. L. Rama Char, *J. Sci. Ind. Res. (India)*, **19A** (June 1960).
562. B. A. Purin and E. A. Ozola, Russian Patent 351,764 (1961).
563. L. Serota, *Met. Finish.*, **58**, 76 (Apr. 1960).
564. I. Hampel, G. Stumpf, and H. Zeng, *Elektrie*, **17** (8), 269 (1963); *Met. Finish. Abstr.*, **5**, 181 (1963).
565. D. M. Lyde, U. S. Patent 3,674,660 (1972).
566. E. Toledo, *Circ. Manuf.*, **11** (1), 46 (1971).
567. E. Fino et al., U. S. Patent 3,775,268 (1971).
568. D. E. Couch and J. E. Stareck, in *Modern Electroplating*, 2nd ed., F. A. Lowenheim, Ed. Wiley, New York, 1963.
569. A. Radin, *Prod. Finish.*, **31**, 62 (July 1967).
570. V. V. Gurylev, A. I. Levin, and M. Nasakina, *J. Appl. Chem., (USSR)*, **37**, 1055 (1964); *Met. Finish*, **67**, 59 (Apr. 1969).
571. E. G. Rutter et al., Russian Patent 121,002 (1958); *Met. Finish. Abstr.*, **1**, 228 (1959).
572. S. I. Uspenskii and M. A. Schluger, *Sov. Electrochem.*, **2**, 226, (1966); *Met. Finish.*, **68**, 40 (July 1970).
573. A. N. Trofinov and A. P. Galushko, *Sov. Electrochem.*, **1**, 877 (1965).
574. A. N. Trofinov, *Sov. Electrochem.*, **1**, 1029 (1965).
575. R. Vasudevan, R. Devanathan, and K. G. Chidambaram, *Met. Finish.*, **90**, 23 (Oct. 1992).
576. S. Konishi, *Met. Finish.*, **63**, 58 (Mar. 1965).
577. K. E. Langford, *Analysis of Electroplating and Related Solutions*, 4th ed., Robert Draper, Teddington, Middlesex, England, 1971.
578. D. Foulke and F. Crane, *Electroplater's Process Control Handbook*, Reinhold, New York, 1953.
579. L. J. Durney, Ed., *Electroplating Engineering Handbook*, Van Nostrand Reinhold, New York, 1984.
580. C. H. Fiske and Y. Subborow, *J. Biol. Chem.*, **66**, 375 (1925).
581. T. M. Tam and J. S. Zevely, *J. Electrochem. Soc.*, **131**, 109 (1984).
582. J. W. Dini, *Etectrodeposition: The Materials Science of Coatings and Substrates*, Noyes Publications, Park Ridge, NJ, 1993.
583. F. Feigl, *Spot Tests in Inorganic Chemistry*, 5th ed., Elsevier, Amsterdam, 1958, p. 276.
584. G. N. Sorkin, Yu. G. Lavrent'ev, and R. Yu. Bek, *J. Appl. Chem. (USSR)*, **44**, 679 (1971).
585. B. F. Rothschild, J. E. Semar, and H. K. Omata, *Plating Surf. Finish.*, **64**, 53 (Nov. 1977).
586. F. Altmayer, private communication, Apr. 1996.
587. W. H. Safranek, *The Properties of Electrodeposited Metals and Alloys*, 2nd ed., American Electroplaters and Surface Finishers Society, Orlando, FL, 1986.
588. V. A. Lamb, C. E. Johnson, and D. R. Valentine, *J. Electrochem. Soc.*, **117**, 281C, 341C, 381C (1970).
589. M. H. Smith,"Failure Analysis of Plated Through-Holes in Multilayer Printed Wiring," McDonnell Douglas Astronautics Co., Paper WD 1023, Jan. 1970, presented to IPC, Washington, DC, Apr. 15, (1969).
590. C. Schmitz, *Insul./Circ*, **16** (11), 35 (1970).
591. P. E. Hinton,"Structure Modifications Produced in Electrodeposited Copper by an Organic Compound in the Electrolyte," M. S. Thesis, University of Arizona, Tucson, Arizona (1968).
592. D. E. Sherlin and L. K. Bjelland, *Circuit World*, **4**, 22 (Oct. 1977).
593. W. T. Hollar, *Prod. Finish.*, **31**, 58 (Mar. 1967); 62 (July 1967).
594. NASA Tech Brief 67-10358, "Steel Test Panel Helps Control Additives in Pyrophosphate Copper Plating," Clearinghouse for Federal Scientific and Information, Springfield, VA.
595. C. J. Owen, *Plating*, **57**, 1012 (1970).
596. C. J. Owen, H. Jackson, and E. R. York, *Plating*, **54**, 821 (1967).
597. J. Cl. Puippe and W. Fluhmann, in *Supercollider* Vol. 4, J. Nonte, Ed., Plenum, New York, 1992, p. 381.
598. W. Fluhmann and W. Saxer, *Plating*, **59**, 1140 (1972); U. S. Patent 3,660,251 (1972).
599. G. A. Malone,"Investigation of Electroforming Techniques," NASA CR 134959 (Dec. 1975).
600. J. W. Dini, H. R. Johnson, and J. R. Helms, *Plating*, **54**, 1337 (1967).
601. B. F. Rothschild, *Plating Surf. Finish.*, **66**, 70 (May 1979).
602. V. P. Greco, "Electrocomposites: The Strengthening of Metals with Particles or Fibers by Electrodeposition Techniques and Other Methods," Course Notes, American Electroplaters and Surface Finishers Soc., Orlando, FL (Feb. 1987).
603. V. P. Greco, *Plating Surf. Finish.*, **76**, 62 (July 1989).
604. V. P. Greco, *Plating Surf. Finish.*, **76**, 68 (Oct. 1989).
605. R. Narayan and B. H. Narayana, *Rev. Coatings Corrosion*, **4** (2), 113 (1981).
606. W. H. Safranek, *The Properties of Electrodeposited Metals and Alloys*, 2nd ed., American Electroplaters and Surface Finishers Soc., Orlando, FL, 1986.
607. I. Rajagopal, "Composite Coatings," in *Surface Modification Technologies*, T. S. Sudarshan, Ed., Marcel Dekker, New York, 1989.

608. C. E. Johnson and M. Browning, in *Proc. AESF SUR/FIN 90*, Session T, Boston, MA, AESF, Kissimmee, FL, 1990.
609. J. R. Roos, J. P. Celis, and M. De Bonte, in *Materials Science and Technology: A Comprehensive Treatment*, R. W. Cahn, P. Haasen, and E. J. Kramer, Eds., VCH, New York, Vol. 15, *Processing of Metals and Alloys*, R. W. Cahn, Eds., 1991, p. 481.
610. L. C. Archibald and P. R. Ebdon, *Met. Finish.*, **90**, 23 (Feb. 1992).
611. M. Viswanathan and K. S. G. Doss, *Met. Finish.*, **70**, 83 (Feb. 1972).
612. M. Ghouse, M. Viswanathan, and E. G. Ramachandran, *Met. Finish.*, **78**, 31 (Mar. 1980).
613. M. Ghouse, M. Viswanathan, and E. G. Ramachandran, *Met. Finish.*, **78**, 55 (Nov. 1980).
614. M. Ghouse and E. G. Ramachandran, *Met. Finish.*, **79**, 85 (June 1981).
615. J. E. Hoffman and C. L. Mantell, *Trans. AIME*, **236**, 1015 (1966).
616. T. W. Tomaszewski, L. C. Tomaszewski, and H. Brown, *Plating*, **56**, 1234 (1969).
617. E. A. Brandes and D. Goldthorpe, *Metallurgica*, **195** (Nov. 1967).
618. E. S. Chen, G. R. Lakshminarayanan and F. K. Sautter, *Met. Trans.*, **2**, 937 (1971).
619. G. R. Lakshminarayanan, E. S. Chen, and F. K. Sautter, *Plating Surf Finish.*, **63**, 38 (Apr. 1976).
620. G. R. Lakshminarayanan, E. S. Chen, and F. K. Sautter, *Plating Surf Finish.*, **63**, 35 (May 1976).
621. G. R. Lakshminarayanan,"Codeposition of Alumina with Copper," Manufacturing Technology Note NTN-78/0746, U. S. Army Materiel Development and Readiness Command, Alexandria, VA (Oct. 1978).
622. J. R. Roos, J. P. Celis, and J. A. Helsen, *Trans. Inst. Met. Finish.*, **55**, 113 (1977).
623. V. V. Grinina and Y. M. Polukarov,"Effect of Periodic Current on the Incorporation of Foreign Particles in Electrolytic Copper Deposits," Institute of Physical Chemistry, Academy of Sciences of the USSR, Moscow, Russia (Nov. 1985).
624. M. M. Davliev, G. P. Petrov, I. A. Abdullin, V. A. Golovin, and P. A. Norden, *Elektronnaya Obrabotka Materialov*, No. (3), 26 (1986).
625. E. S. Chen and F. K. Sautter, *Plating Surf. Finish.*, **63**, 28 (Sept. 1976).
626. J. Hoashi, *J. Met. Finish., Soc. Jpn.*, **15** (7), 258 (1964).
627. J. Foster and A. M. J. Kariapper, *Trans. Inst. Met. Finish.*, **51**, 27 (1973).
628. A. M. J. Kariapper and J. Foster, *Trans. Inst Met. Finish.*, **52**, 87 (1974).
629. J. M. Sykes and D. J. Alner, *Trans. Inst. Met. Finish.*, **52**, 28 (1974).
630. J. P. Celis and J. R. Roos, *J. Electrochem. Soc.*, **124**, 1508 (1977).
631. J. R. Roos, J. P. Celis, and H. Kelchtermans, *Thin Solid Films*, **54**, 173 (1978).
632. J. P. Celis, H. Kelchtermans, and J. R. Roos, *Trans. Inst. Met. Finish.*, **56**, 41 (1978).
633. C. White and J. Foster, *Trans. Inst. Met. Finish.*, **56**, 92 (1978).
634. J. R. Roos, J. R. Celis, H. Kelchtermans, M. Van Camp, and C. Buelens, in *Proc. of Interfinish 80*, Kyoto, Japan, Int. Union Suface Finishers, Kissimmee, FL, 1980, p. 203.
635. C. White and J. Foster, *Trans. Inst. Met. Finish.*, **59**, 8 (1981).
636. C. Buelens, J. P. Celis, and J. R. Roos, *J. Appl. Electrochem.*, **13**, 541 (1983).
637. C. C. Lee and C. C. Wan, *J. Electrochem. Soc.*, **135**, 1930 (1988).
638. H. Hayashi, S. Izumi, and I. Tari, *J. Electrochem. Soc.*, **140**, 362 (1993).
639. J. P. Celis, J. R. Roos, and C. Buelens, *J. Electrochem. Soc.*, **134**, 1402 (1987).
640. M. H. Fawzy, M. M. Ashour, and A. M. Abd El-Halim, *Trans. Inst. Met. Finish.*, **73**, 132 (1995).
641. V. D. Stankovic and M. Gojo, *Surf. Coatings Technol.*, **81**, 225 (1996).
642. R. S. Saifullen and L. N. Akulova, *Prot. Metals*, **8**, 74 (1972).
643. V. Bhalla, C. Ramasamy, N. Singh, and M. Pushpavanam, *Plating Surf. Finish.*, **82**, 58 (Nov. 1995).
644. N. Guglielmi, *J. Electrochem. Soc.*, **119**, 1009 (1972).
645. D. W. Snaith and P. D. Groves, *Trans. Inst. Met. Finish.*, **50**, 95 (1972).
646. D. W. Snaith and P. D. Groves, *Trans. Inst. Met. Finish.*, **55**, 136 (1977).
647. D. W. Snaith and P. D. Groves, *Trans. Inst. Met. Finish.*, **56**, 9 (1978).
648. A. A. Baker, M. B. P. Allery, and S. J. Harris, *J. Mater. Sci.*, **4**, 242 (1969).
649. J. C. Withers and E. F. Abrams, *Plating*, **55**, 605 (1968).
650. D. A. Foster, *SAMPE Quarterly*, **21**, 58 (Oct. 1989).
651. Y. Gan, *Plating Surf. Finish.*, **79**, 81 (June 1992).
652. W. Swarzacher, *Electrochem. Soc. Interface*, **15** (1), 32 (2006).
653. SEMETECH Roadmap, available: www.itrs.net.
654. P. Andriacacos, *Electrochem. Soc. Interface*, **8** (1), 32 (1999).
655. P. C. Andriacacos, C. Uzoh, J. O. Dukovic, J. Horkans, and H. Deligianni, *IBM J. Res. Develop.*, **42** (5), 567 (1998).
656. R. Haveman, "Cu/Low k Interconnect Technologies for 32 nm and Beyond," Novellus Systems, www.novellus.com (2008).
657. T. P. Moffat, D. Wheeler, W. H. Huber, and D. Josell, *Electrochem. and Solid-State Lett*, **4** (4), C26 2001.
658. T. P. Moffat, D. Wheeler, and D. Josell, *Electrochem. Soc. Interface*, **13** (4), 46 (2004).
659. T. P. Moffat, D. Wheeler, S.-K. Kim, and D. Josell, *Electrochim. Acta*, **53**, 145 (2007).
660. T. P. Moffat, D. Wheeler, and D. Josell, "Superconformal Film Growth," in *Electrochemical Surface Modification*, R. M. Alkire, D. M. Kolb, J. Lipkowski, and P. N. Ross, Eds., Wiley, Hoboken, NJ, 2008.
661. M. Trzaska and Z. W. Trsaska, 2008 American Control Conference, Seattle, 978-1-4244-2079-7/08 (2008).

662. P. M. Vereecken, R. A. Binstead, H. Deligniannni, and P. C. Andricacos, *IBM J. Res. Develop.*, **49** (1), 2005.

663. S.-K. Kim, D. Josell, and T. P. Moffat, *J. Electrochem. Soc.*, **153** (12), C826 (2006).

664. C. L. Beaudry and J. O. Dukovic, *Electrochem. Soc. Interface*, **13** (4), 40 (2004).

665. IBM Microelectronics and ECI Technology communication, Semiconductor, available: ecitechnology.com/articles/ClosedLoop.pdf (2004).

666. Altera Corp., U.S. Patent 7,235,884 (June 26, 2007).

667. Enthone, U. S. Patent Applications 2007/0289875 (Dec. 20, 2007).

668. S.-K. Kim, D. Josell, and T. P. Moffat, *J. Electrochem. Soc.*, **153** (9), C616 (2006).

669. R. D. Braatz, E. G. Seebauer, and R. C. Alkire, "Multiscale Modeling and Design of Electrochemical Systems," in *Advances Electrochemical Science Engineering*, Vol. 10, R. C. Alkire, D. M. Kolb, J. Lipkowski, and P. N. Ross, Eds., Wiley, Hoboken, NJ, 2008.

670. R. C. Alkire and R. D. Braattz, *AIChE J.*, **50** (9), 2000 (2004).

671. E. Rusli, F. Xue, T. O. Drews, P. M. Vereecken, P. Andriacacos, H. Deligianni, R. D. Braatz, and R. C. Alkire, *J. Electrochem. Soc.*, **154** (11), D584 (2007).

672. Y. Qin, X. Li, F. Xue, P. M. Vereeken, P. Andricacos, H. Deligianni, R. D. Braatz, and R. C. Alkire, *J. Electrochem. Soc.*, **155** (3), D223 (2008).

673. Z. Zheng, R. M. Stephens, R. D. Braatz, R. C. Alkire, and L. P. Petzold, *J. Comp. Phys.*, **227**, 5185 (2008).

3

ELECTRODEPOSITION OF NICKEL

GEORGE A. DI BARI

Nickel electroplating is a commercially important and versatile surface-finishing process. Its commercial importance may be judged from the amount of nickel in the form of metal and salts consumed annually for electroplating, now roughly 100,000 metric tons worldwide, as well as its versatility from its many current applications [1]. The applications of nickel electroplating fall into three main categories: decorative, functional, and electroforming.

In decorative applications, electroplated nickel is most often applied in combination with electrodeposited chromium. The thin layer of chromium was first specified to prevent the nickel from tarnishing. It was originally deposited on top of a relatively thick, single layer of nickel that had been polished and buffed to a mirror-bright finish. Today decorative nickel coatings are mirror bright *as deposited* and do not require polishing prior to chromium plating. Multilayered nickel coatings outperform single-layer ones of equal thickness and are widely specified to protect materials exposed to severely corrosive conditions. The corrosion performance of decorative, electroplated nickel plus chromium coatings has been further improved by the development of processes by which the porosity of chromium can be varied and controlled on a microscopic scale (microdiscontinuous chromium). Modern multilayered nickel coatings in combination with microdiscontinuous chromium are capable of protecting steel, zinc, copper, aluminum, and many other materials from corrosion for extended periods of time. The complexity of modern-day nickel plus chromium coatings is more than offset by the greatly improved corrosion resistance that has been achieved without significantly increasing coating thickness and costs.

There are many functional applications where decoration is not the issue. Instead, nickel and nickel alloys with matte or dull finishes are deposited on surfaces to improve corrosion and wear resistance or modify magnetic and other properties. The properties of nickel electrodeposits produced under different conditions of operation are of particular interest in this connection.

Electroforming is electroplating applied to the fabrication of products of various kinds. Nickel is deposited onto a mandrel and then removed from it to create a part made entirely of nickel. A variation of this is electrofabrication where the deposit is not separated from the substrate and where fabrication may involve electrodeposition through masks rather than the use of traditional mandrels.

The many current applications of nickel electroplating are the result of developments and improvements that have been made almost since the day the process was discovered. This is evident in the following retrospective on the development of nickel electroplating solutions as well as in subsequent sections that deal with basics, decorative electroplating, functional applications and deposit properties, nickel electroforming, nickel anode materials, quality control, and pollution prevention.

3.1 RETROSPECTIVE ON NICKEL ELECTROPLATING SOLUTIONS

Bottger developed the first practical formulation for nickel plating, an aqueous solution of nickel and ammonium sulfates in 1843, but earlier references to nickel plating can be found. Bird apparently deposited nickel on a platinum electrode in 1837 from a solution of nickel chloride or sulfate, and Shore patented a nickel nitrate solution in 1840 [2, 3]. The solution developed by Bottger remained in commercial use for 70 years, however, and he is acknowledged to be the originator of nickel plating [4].

Modern Electroplating, Fifth Edition Edited by Mordechay Schlesinger and Milan Paunovic

Dr. Isaac Adams, Jr., a medical doctor educated at Harvard University and at the École de Médicine in Paris, was one of the first to commercialize nickel plating in the United States, and his patented process gave his company a virtual monopoly in commercial nickel plating from 1869 to 1886. His patent covered the use of pure nickel ammonium sulfate. Although Adams's solution was similar to Bottger's, his emphasis on operating the bath at neutral pH was undoubtedly vital for controlling the quality of the nickel deposited, since excessive amounts of ammonia would tend to lower cathode efficiency and embrittle the deposit. Largely as a result of the publicity generated by Adams, nickel plating became known worldwide, and by 1886, the annual consumption of nickel for plating had grown to about 135 metric tons [5, 6].

Remington, an American residing in Boston, attempted to market a nickel ammonium chloride electroplating solution in 1868, but perhaps of greater significance, in view of subsequent developments, were his attempts to use small pieces of electrolytic nickel as an anode material in a platinum anode basket [7]. Weston introduced the use of boric acid and Bancroft was one of the first to realize that chlorides were essential to ensure efficient dissolution of nickel anode materials [8, 9].

Professor Oliver P. Watts at the University of Wisconsin, aware of most of these developments, formulated an electrolyte in 1916 that combined nickel sulfate, nickel chloride, and boric acid and optimized the composition of the nickel electroplating solution [10]. The advantages of his hot, high-speed formula became recognized and eventually led to the elimination of nickel ammonium sulfate and other proprietary solutions. Today the Watts solution is widely applied, and its impact on the development of modern nickel electroplating technology cannot be overstated.

Decorative nickel plating solutions are variations of the original Watts formulation, the main difference being the presence in solution of organic and certain metallic compounds to brighten and level the nickel deposit. Because of his use of organic additives like benzene and naphthalene di- and trisulfonic acids, Schlotter's decision to market a bright nickel plating solution in 1934 is a milestone in the commercial development of decorative nickel plating [11],

The introduction of coumarin-containing, semibright nickel plating solutions by DuRose in 1945 was a major contribution because it subsequently led to the development of double- and triple-layer nickel coatings with greatly improved corrosion resistance [12]. His introduction of semibright nickel processes came at a critical time in the history of decorative nickel electroplating, when confidence in the ability of single-layer, bright nickel coatings to prevent corrosion of automotive components was at a relatively low point.

The dominant position of Watts solutions has been challenged from time to time, but the only ones that have been adopted on a substantial scale are nickel sulfamate solutions [13]. The Watts solution is the basis for most decorative nickel plating solutions, although considerable variation in the chloride content of different proprietary decorative processes may be specified by the suppliers of those processes. Sulfamate solutions are rarely, if ever, used for decorative plating. Watts and nickel sulfamate solutions are used for functional plating and for electroforming, but sulfamate is more popular for the latter.

3.2 BASICS

Nickel electroplating is similar to other electrodeposition processes that employ soluble metal anodes; that is, direct current is made to flow between two electrodes immersed in a conductive, aqueous solution of nickel salts. The flow of direct current causes one of the electrodes (the anode) to dissolve and the other electrode (the cathode) to become covered with nickel. The nickel in solution is present in the form of divalent, positively charged ions (Ni^{2+}). When current flows, the positive ions react with two electrons ($2e^-$) and are converted to metallic nickel (Ni^0) at the cathode surface. The reverse occurs at the anode where metallic nickel is dissolved to form divalent, positively charged ions which enter the solution. The nickel ions discharged at the cathode are thus replenished by those formed at the anode.

3.2.1 Application of Faraday's Laws to Nickel

The amount of nickel deposited at the cathode and the amount dissolved at the anode are directly proportional to the product of the current and time and may be calculated from the expression

$$m = 1.095 \times aIt \tag{3.1}$$

where m is the amount of nickel deposited at the cathode (or dissolved at the anode) in grams, I is the current that flows through the plating tank in amperes, t is the time that the current flows in hours, and a is the current efficiency ratio (see Chapter 1 for the definition of current efficiency). The proportionality constant (1.095) in grams per ampere hour equals M/nF, where M is the atomic weight of nickel (58.69), n is the number of electrons in the electrochemical reaction (2), and F is Faraday's constant, equal to 26.799 A-h (more commonly given as 96,500 C).

The proportionality constant must be multiplied by the actual electrode efficiency ratio if precise values are required. The anode efficiency for nickel dissolution is almost always 100% under practical electroplating conditions; that is, $a = 1$ when estimating anode weight loss. If the pH of the solution is too high and/or the chloride ion concentration too low, hydroxyl ions may be discharged in preference to the

dissolution of nickel, and oxygen will be evolved. Under those unusual conditions the nickel anode becomes passive, and the efficiency of anode dissolution is close to zero.

The cathode efficiency of different nickel plating solutions may vary from 90 to 97% and, accordingly, a will vary from 0.90 to 0.97. A small percentage of the current is consumed in the discharge of hydrogen ions from water. That reduces the cathode efficiency for nickel deposition from 100% to approximately 96% in an additive-free nickel electroplating solution. The discharged hydrogen atoms form bubbles of hydrogen gas at the cathode surface. Cathode efficiencies as low as 90% are characteristic of some bright nickel plating solutions that are formulated to give highly leveled, mirrorlike deposits rapidly, that is, at thicknesses below 12 μm [14]. An average cathode efficiency of 95.5% is commonly used to make estimates when precise values are not essential.

Because the anode and cathode efficiencies are not exactly equal, the nickel ion concentration and the pH of the solution will slowly increase as plating proceeds. The rate of increase in nickel ion concentration depends on the difference between cathode and anode efficiencies. Because cathode efficiencies may vary from 90 to 97%, whereas anode efficiency is almost always 100%, the rate of increase in nickel ion concentration depends on the cathode efficiency and the nature of the plating solution, not on the type of soluble nickel anode material that is used. The use of a special insoluble anode in combination with soluble anodes has been developed to help control the rate of increase of the nickel ion concentration [15].

3.2.2 Average Coating Thickness

An expression for calculating nickel thickness, s in micrometers, can be derived by dividing Eq. (3.1) by the product of the density of nickel, d (8.907 g cm^{-3}), and the surface area to be electroplated, A, and multiplying by 100 to obtain the thickness in micrometers:

$$s = \frac{m \times 100}{dA} = \frac{109.5 \times aIt}{8.097A} = \frac{12.294 \times aIt}{A} \qquad (3.2)$$

The ratio I/A is the current density and thus the above expression shows that the coating thickness depends on the *current density* and time, whereas the amount or mass of nickel deposited, Eq. (3.1), depends on the *current* and time. Equation (3.2) is the basis for the electrodeposition data compiled in Table 3.1, which gives the time *in minutes* required to deposit a nickel coating of specified thickness at different values of current density. The expression above and Table 3.1 provide a means of estimating the *average* coating thickness.

3.2.3 Current and Metal Distribution

The *actual* thickness at any point on the surface of a shaped article is dependent on the current density at that point. The current density at any point is determined by how the current is apportioned over the surface of the article being electroplated. In nickel plating, the current distribution is largely determined by geometric factors, that is, by the shape of the part, the relative placement of the part with respect to the anode, how the parts are placed on plating racks, and the dimensions of the system. Because almost all except the simplest shapes to be electroplated have prominent surfaces that are nearer to the anode than recessed areas, a uniformly thick nickel coating is difficult to produce. The current density at prominences is greater due to the shorter anode-to-cathode distance and the lower resistance to current flow that implies. Conversely, recessed areas, being further away from the anode, will have a lower current density because of increased resistance to current flow. This inevitably means

TABLE 3.1 Nickel Electrodeposition Data

Deposit Thickness (μm)	Weight per Unit Area (g dm^{-2})	Ampere Hours per Unit (Ah dm^{-2})	Time (min) to Obtain Deposit at Various Current Densities (A dm^{-2})									
			0.5	1	1.5	2	3	4	5	6	8	10
2	0.18	0.17	20	10	6.8	5.1	3.4	2.6	2.0	1.7	1.3	1
4	0.36	0.34	41	20	14	10	6.8	5.1	4.1	3.4	2.6	2
6	0.53	0.51	61	31	20	15	10	7.7	6.1	5.1	3.8	3.1
8	0.71	0.68	82	41	27	20	13	10	8.2	6.8	5.1	4.1
10	0.89	0.85	100	51	34	26	17	13	10	8.5	6.4	S.I
12	1.1	1.0	120	61	41	31	20	15	12	10	7.7	6.1
14	1.2	1.2	140	71	48	36	24	18	14	12	8.9	7.1
16	1.4	1.4	160	82	54	41	27	20	16	14	10	8.2
18	1.6	1.5	180	92	61	46	31	23	18	15	11	*9.2*
20	1.8	1.7	200	100	68	51	34	26	20	17	13	10
40	3.6	3.4	410	200	140	100	68	51	41	34	26	20

Note: Based on 95.5% cathode efficiency.

that prominent areas will have thicker coatings than recessed ones.

Because geometric factors exert the greatest influence on current density at localized areas in the case of nickel plating, current distribution is virtually the same as metal distribution. Thus shields and auxiliary anodes can be used effectively to obtain acceptable thickness uniformity. Shields are made of nonconductive materials, and they may be placed on the anode, on the cathode, or between electrodes to block or control current flow. Auxiliary anodes may be either soluble or insoluble, and are placed closer to the cathode than principal anodes so as to direct the current to a recessed or relatively small area on the cathode. The analysis of geometric effects by computer modeling has received attention [16].

3.2.4 Throwing Power

In addition to the geometric factors, metal distribution is influenced by cathode polarization, the cathode efficiency–current density relationship, and the electrical conductivity of the solution [17]. The complex relationship between the factors that influence current distribution and hence metal distribution is called *throwing power*. A solution with a high throwing power is capable of depositing almost equal thicknesses on both recessed and prominent areas. For example, in copper cyanide solutions, high cathode polarization and the favorable cathode efficiency–current density relationship (cathode efficiency is lower at high than at low current densities) result in a solution with excellent throwing power. As already implied, cathode polarization and current efficiency do not significantly affect the throwing power of acid nickel plating solutions formulated with simple salts. The cathode polarization is low and the cathode efficiency is high and relatively constant above 1 A dm^{-2}.

Throwing power can be measured to give relative values [18]. Measurements indicate that the throwing power of nickel electroplating solutions can be somewhat improved by lowering the current density, increasing the electrical conductivity of the solution, increasing the distance between anode and cathode, and raising the pH and the temperature. Table 3.2 compares the throwing power of various plating solutions; it is based on the work of Watson, who applied a Hull cell to make the measurements. The nickel plating solution with the best throwing power contained a high concentration of anhydrous sodium sulfate; its composition is given in Table 3.3, which also indicates that throwing power decreases as the current density is increased [19].

3.2.5 Internal Stress

Internal stress refers to forces created within the deposit as a result of the electrocrystallization process and/or the codeposition of impurities such as hydrogen, sulfur, and other elements [20]. Internal stress is either tensile (contractile) or compressive (expansive) in nature. In tensively stressed deposits, the average distance between nickel atoms in the lattice is greater than the equilibrium value, creating a force that tends to drive the atoms closer together. When a tensively stressed deposit is detached from its substrate, it contracts. In addition, if a thin cathode strip is electroplated on one side only (by painting the back and placing the bare side facing the anode), a deposit stressed in tension will cause the strip to bend or curl toward the anode. In compressively stressed deposits, the atoms are closer together and the force tends to drive them further apart. When detached from the substrate,

TABLE 3.2 Throwing Power of Various Electroplating Solutions

	Average Current Density		Throwing Power (%) at Primary Current Density Ratios		
Solution	A dm^{-2}	A ft^{-2}	5 : 1	12 : 1	25 : 1
Watts nickel	4.3	40	8	7	14
Sulfamate nickel	4.3	40	11	13	19
All-chloride nickel	4.3	40	18	18	27
Na/high sulfate	4.3	40	23	31	40
Mg/high sulfate	4.3	40	16	18	32
Proprietary bright nickel A	4.3	40	1	−12	−6
Proprietary bright nickel B	4.3	40	3	−12	−6
Acid copper	4.3	40	0	−29	−61
Rochelle copper	4.3	40	86	91	93
Conventional chromium	16	150	−42	−48	−100

Source: Watson [19].
Note: The 100% represents a uniform thickness over the cathode surface; −100 indicates the opposite extreme, where recessed areas are thinly plated and prominent areas are thickly plated.

TABLE 3.3 Composition and Throwing Power at Various Current Densities of a High-Sulfate Solution

Average Current Density		Throwing Power (%) at Primary Current Density Ratios		
A dm^{-2}	A ft^{-2}	5 : 1	12 : 1	25 : 1
0.2	2	63	76	85
1.0	10	38	50	64
4.3	40	23	31	40

Source: Watson [19].
Note: Nickel sulfate, 30 g L^{-1}; nickel chloride, 38 g L^{-1}; boric acid, 25 g L^{-1}; sodium sulfate (anhydrous), 180 g L^{-1}. The 100% represents a uniform thickness over the cathode surface; −100 indicates the opposite extreme where recessed areas are thinly plated and prominent areas are thickly plated.

TABLE 3.4 Nickel Electroplating Solutions

	Electrolyte Composition[a] ($g\,L^{-1}$)		
	Watts Nickel	Nickel Sulfamate	Basic Semibright Bath[b]
Nickel sulfate, $NiSO_4 \cdot 6H_2O$	225–400		300
Nickel sulfamate, $Ni(SO_3NH_2)_2$		30–45	
Nickel chloride, $NiCl_2 \cdot 6H_2O$	30–60	300–450	35
Boric acid, H_3BO_3	30–45	0–30	45
		Operating Conditions	
Temperature (°C)	44–66	32–60	54
Agitation	Air or mechanical	Air or mechanical	Air or mechanical
Cathode current density ($A\,dm^{-2}$)	3–11	0.5–30	3–10
Anodes	Nickel	Nickel	Nickel
pH	2–4.5	3.5–5.0	3.5–4.5
		Mechanical Properties	
Tensile strength (MPa)	345–435	415–610	—
Elongation (%)	10–30	5–30	8–20
Vickers hardness (100 g load)	130–200	170–230	300–400
Internal stress (MPa)	125–185 (tensile)	0–55 (tensile)	35–150 (tensile)

[a] Antipitting agents formulated for nickel plating are added to control pitting.
[b] Organic additives available from plating supply houses are required for semibright nickel plating.
Note: Some typical properties of *fully-bright* nickel deposits are as follows: Elongation percentage, 2–5; Vickers hardness, 100 g load, 600–800; internal stress (MPa), 12–25 compressive.

compressively stressed deposits expand and a thin strip plated on one side only, as described, will bend away from the anode. Dislocation theory provides a logical explanation of the origins of internal stress in etectrodeposits [21, 22].

Stress in electrodeposited nickel can vary over a wide range depending on solution composition and operating conditions. In general, nickel electrodeposited from additive-free Watts solutions exhibits a tensile stress that is 125–185 MPa for the conditions given in Table 3.4. Deposits from sulfamate solutions display lower tensile stress within the range of 0–55 MPa. Compressively stressed nickel deposits are obtained from solutions that contain sulfur-containing organic additives similar to the carriers that are added to bright nickel plating solutions (discussed below). As far as is known, compressively stressed nickel deposits are almost always associated with the codeposition of sulfur. High deposit stress can be especially troublesome in electroforming where the adhesion between the electrodeposit and the mandrel is deliberately kept as low as possible to facilitate separation.

3.2.6 Adhesion

With the exception of electroforming, a high degree of adhesion between the deposit and the substrate is critical in all applications. Under favorable conditions, the crystal lattice of the substrate extends into the deposit (epitaxy). Epitaxial growth rarely occurs in commercial electroplating, however, where adhesion is due to cohesive forces between metal atoms. Atoms of the electrodeposited metal align themselves in opposition to atoms of the substrate and are held to the surface by interatomic forces that result in the formation of metallic, covalent, ionic, polar, or other types of bonds. *Perfect* adhesion in electoplating is achieved when the bond strength is greater than the tensile strength of the weaker component; that is, in measuring adhesion by means of a quantitative test, failure occurs not at the interface but either within the deposit or within the substrate. In commercial electroplating, good adhesion is achieved by means of standard preparation methods that are described in American Society for Testing and Materials (ASTM) standards and elsewhere [23, 24].

3.2.7 Leveling and Microthrowing Power

The ability of an electroplating solution to fill in defects and scratches on the surface *preferentially* is called leveling. The deposit fills defects and tiny scratches, eventually covering them, and as a result the surface becomes smoother as the deposit increases in thickness. The semibright and bright nickel electroplating solutions described in the next section have excellent leveling properties. Organic additives in those solutions are adsorbed preferentially at micropeaks; the resulting increase in the local resistance to current flow increases the current density in microgrooves, thereby promoting leveling [25].

Microthrowing power refers to the ability of an electroplating solution to fill tiny crevices with deposits that follow

the contour of a defect or scratch without any leveling action whatsoever [26]. Additive-free nickel plating solutions have excellent microthrowing power but little leveling ability. In the absence of specifically adsorbed organic additives, the current density in micropeaks and microgrooves is uniform because of the low polarization and high cathode efficiency of most nickel electroplating solutions.

3.3 DECORATIVE ELECTROPLATING

The technology of decorative nickel electroplating has been improved continually over the years due to the development of bright and semibright nickel plating solutions, multilayer nickel coatings, and microdiscontinuous chromium. The major effect has been an increase in the corrosion resistance of decorative, electroplated nickel plus chromium coatings. In addition new and improved techniques for plating on plastics, aluminum alloys, and stainless steel have broadened the scope of decorative applications.

3.3.1 Bright Nickel Solutions

Modem bright nickel electroplating solutions employ combinations of additives carefully formulated to produce bright deposits over a wide range of current density. The deposits have excellent leveling or scratch-filling characteristics, fair ductility, and low internal stress. Modern processes produce bright deposits in areas of low current density, permit use of high average current densities and bath temperatures, are less sensitive to metallic contaminants than some of the solutions first commercialized, permit continuous purification of the plating solution by filtering through activated carbon, and produce breakdown products that can also be removed by activated carbon treatment and are not overly sensitive to anode effects. Bright nickel electroplating solutions have similar compositions as the Watts nickel electrolyte included in Table 3.4. Because the exact formulations of commercial processes are proprietary, the recommendations of the suppliers of decorative nickel plating processes should be followed.

The additives for bright nickel electroplating fall roughly into three categories: carriers, brighteners, and auxiliary brighteners. Those are the terms preferred by electroplaters, but the terminology is not standardized. To avoid confusion, alternative terms mentioned in the literature are shown in parentheses [6, pp. 96–103; 27].

Carriers (Brighteners of the First Class, Secondary Brighteners, Control Agents) These are usually aromatic organic compounds. Examples are benzene sulfonic acid, 1,3,6-naphthalene sulfonic acid (sodium salt), *p*-toluene sufonamide, saccharin (*o*-benzoic sulfonimide), thiophen-2-sulfonic acid, benzene sulfinic acid, and allyl sulfonic acid. Carriers are the principal source of the sulfur codeposited with the nickel. Their main function is to refine grain size and provide deposits with increased luster compared with matte or dull deposits from baths without additives. When used by themselves, carriers do not produce mirror-bright deposits. Carriers are used in concentrations of about 1–25 g L^{-1}, the exact concentration depending on the specific compound. Carriers are not consumed rapidly by electrolysis, and consumption is primarily by dragout and by losses during activated carbon treatments. The stress-reducing property of carriers is increased if they contain amido or imido nitrogen. For example, saccharin is a most effective stress reducer and often helps to decrease or eliminate hazes.

Brighteners (Brigkteners of the Second Class, Primary Brighteners, Leveling Agents) In combination with carriers and auxiliary brighteners, brighteners produce brilliant deposits having good ductility and leveling characteristics over a wide range of current densities. Some of these compounds include formaldehyde chloral hydrate, *o*-sulfobenzaldehyde, allyl sulfonic acid, coumarin; *o*-hydroxy cinnamic acid, diethyl maleate, 2-butyne-l,4-diol; 2-butyne-l,4-disulfonic acid; ethyl cyanohydrin, *p*-amino azo benzene, thiourea, and allyl thiourea and polyethylene glycols of various kinds. The best-known example in this class may be coumarin (1,2-benzopyrone), the leveling agent introduced by DuRose for producing semibright nickel deposits. Because they increase the internal stress and promote brittleness of nickel deposits, brightener concentrations are kept low and carefully controlled. Concentrations of 0.005–0.2 g L^{-1} are generally used. The rates of consumption of these materials may vary within wide limits.

Auxiliary Brighteners Auxiliary brighteners augment the luster attainable with carriers and brighteners and increase the rate of brightening and leveling. Some examples are sodium allyl sulfonate; zinc, cobalt, cadmium; and 1,4-butyne 2-diol. The concentration of these additives may vary from about 0.1 to 4 g L^{-1} Sulfobetaines, such as pyridinium propyl sulfonate, are especially active sulfur-containing organic compounds that have a powerful effect on leveling in nickel deposits. However, because they introduce sulfur into the deposit, they cannot be used for semibright nickel plating [6, pp. 96–103]. They can be especially effective when added to bright nickel plating solutions in low, carefully controlled concentrations. The inorganic metallic ions—zinc cobalt, cadmium—are not often used anymore as auxiliary brighteners.

3.3.2 Electrocrystallization

The mechanism of nickel electrodeposition involves surface adsorption of species formed in the cathode film accompanied

by inhibition of growth of certain crystal faces. In the absence of organic additives, species like H_2, H_{ads}, and $Ni(OH)_2$, which form as a result of the reduction of hydrogen ions, determine most of the microstructural features of the nickel deposit [28, 29].

The mechanism by which *unsaturated* organic additives modify the electrocrystallization process to yield mirror-bright surfaces also involves adsorption, hydrogenation, and desorption. The organic molecule is adsorbed on the surface via the unsaturated bond, blocking certain sites on the nickel lattice and thus altering the growth rates of different crystal faces. The unsaturated bond reacts with hydrogen in the cathode film and the resulting reduction products are desorbed from the surface and/or incorporated into the deposit. The rates of those processes are influenced by the degree of unsaturation, the size and shape of the organic molecule, the functional groups present, aromatic rings, and other stereochemical factors.

That general mechanism has been confirmed and clarified by studying the effects of individual additives [30]. For example, the active group in a carrier like sodium benzene sulfonate is $=C-S$. Hydrogenolysis of the $=C-S$ bonds results in the formation of sulfur anions that are adsorbed on the (110) crystallization direction causing the [100] texture to predominate. The sulfur is incorporated into the deposit as the sulfide. Below 25 A dm^{-2} the active groups in saccharin, $=C-S$ and $S=O$, react with hydrogen to form sulfur anions that are also codeposited and suppress growth in the (110) direction, promoting the formation of the [100] texture and extending the [100] planes in the surface of the deposits, but above that current density, hydrogenation of adsorbed $C=C$ and $C\equiv C$ bonds also takes place. This promotes reduction of hydrogen ions and increases the pH in the cathode film with the consequent formation of a colloidal suspension of nickel hydroxide. The selective adsorption of colloidal nickel hydroxide inhibits growth in the (100) direction, favoring formation of [211], [211] + [111], and [111] textures. The active groups in sulfur-free brighteners include $C=C$, $C\equiv C$, $C\equiv N$, and others, and the mechanism by which these modify crystal growth also involves hydrogenation, increased alkalinity in the cathode film, and precipitation and inhibition of crystal growth by colloidal nickel hydroxide causing [211] and [111] textures to dominate crystallographic features. The two mechanisms by which sulfur-containing and sulfur-free organic addition agents influence crystal growth are thus distinctly different, and complex sulfur-containing compounds like saccharin apparently display features of both. The effect of pulsed reversed current in the presence of organic additives has also been studied [31].

Brightness is attained if the microstructural components of the surface form a plane from which they do not vary by distances greater than the wavelength of light [32]. The criterion for brightness is thus not simply the production of fine-grained deposits but the creation of *flat* crystals. Exactly how a complex mixture of carriers, brighteners, and auxiliary brighteners act in concert to meet those criteria may need further elucidation, but the synergistic effects first described in the classical work of Edwards are probably involved [33].

3.3.3 Effects of Codeposited Sulfur

The incorporation of sulfur has several important effects. Sulfur increases the electrochemical reactivity of bright nickel compared to sulfur-free nickel, and that effect is applied in multilayer coatings to improve corrosion performance. Codeposition of sulfur changes the intrinsic internal stress of electrodeposited nickel from tensile (contractile) to compressive (expansive) and the incorporation of sulfide, an anion considerably larger than the nickel atom, must compress the nickel atoms in the crystal lattice. Carriers are thus useful for controlling internal stress. In addition, sulfur increases the hardness and lowers the elongation percentage of electrodeposited nickel (Table 3.4).

3.3.4 Semibright Nickel

Semibright nickel solutions contain nickel sulfate, nickel chloride, boric acid, and leveling agents. A typical composition is included in Table 3.4. Coumarin has, for the most part, been superseded by other organic compounds [34], notably the acetylenics that are now widely employed. Although the ability of coumarin to level nickel deposits is excellent, the acetylenics form reduction products that have little or no effect on the properties of the semibright nickel deposit, whereas the melilotic acid formed by the cathodic reduction of coumarin is incorporated in the deposit, lowering its ductility and raising its hardness, The effect of melilotic acid must be controlled by frequent treatments with activated carbon. Coumarin-free semibright nickel solutions need to be carbon treated less frequently, may be easier and more economical to maintain, and may produce deposits with consistent properties.

Semibright nickel plating processes yield smooth, sulfur-free deposits that are semilustrous with columnar structures similar to Watts nickel deposits, in contrast to full-bright nickel deposits that have banded (laminar) structures as a result of the periodicity of sulfur codeposition. The highly leveled surface is easy to polish and buff to a mirror finish. The good ductility of semibright nickel deposits is important in those applications where multilayer coatings are stressed in service. Semibright nickel deposits are an essential part of multilayer nickel coatings.

3.3.5 Multilayer Nickel Coatings

Single-layer bright nickel plus chromium coatings proved to be less resistant to corrosion than the polished Watts

nickel plus chromium coatings that they replaced. The lower resistance to corrosion was attributed to the activating effect of the sulfur incorporated in bright nickel electrodeposits. The search for coatings with improved corrosion resistance led, first, to the development of semibright nickel coatings. Semibright nickel deposits, being sulfur free, are equivalent in corrosion resistance to polished Watts nickel deposits and for a while (1945–1950) were applied as single-layer coatings in the production of automobile bumpers to obtain improved corrosion performance despite the disadvantage of having to polish the coatings after electroplating to achieve full brightness.

The idea of combining layers of bright and semibright nickel was conceived later as a means of eliminating the costly polishing operation [35]. The fact that decorative double-layer nickel coatings are much more resistant to corrosion than equivalent thicknesses of single-layer bright nickel was discovered as a result of studies conducted after the double-layer coatings were applied commercially. The introduction of triple-layer coatings occurred later [36]. Today single-layer bright nickel coatings are only specified for mild corrosion service with nickel thickness commonly in the range of 5–12 μm. For severe and very severe corrosion service, thicker, multilayered coatings are specified.

Double-layer nickel coatings have an undercoat of highly leveled, sulfur-free, semibright nickel covered with sufficient bright nickel to give a mirror finish without having to polish the coating. The excellent leveling characteristics of the semibright nickel layer also helps minimize the requirement for expensive mechanical finishing of the substrate. Because the undercoat of sulfur-free, semibright nickel is electrochemically more noble than bright nickel, corrosive attack, when it does occur, is preferentially directed toward the bright nickel and a flat-based pit is formed (Fig. 3.1). This effectively retards the pitting attack because, before the pit can penetrate the coating further, a considerable portion of the bright nickel layer must be removed. As a result double-layer coatings show a marked improvement in corrosion performance over single-layer coatings.

The electrochemical basis for the improved corrosion performance observed with double-layer coatings was provided by Flint and Melbourne, DuRose, Safranek, and others [37–39]. Petrocelli, Hospadaruk, and DiBari [40] constructed Evans-type corrosion diagrams from which the galvanic relationships between nickel and chromium in various test electrolytes were deduced. They showed that galvanically coupling semibright nickel to bright nickel caused the semibright nickel to become cathodically polarized, lowering its rate of corrosion, whereas the bright nickel became anodically polarized, increasing its rate of corrosion. When bright nickel, semibright nickel, and chromium were galvanically coupled in the same solution, chromium was cathodic to both the bright and the semibright nickel, and as a result coupling to chromium increased the rate of corrosion of both types of nickel.

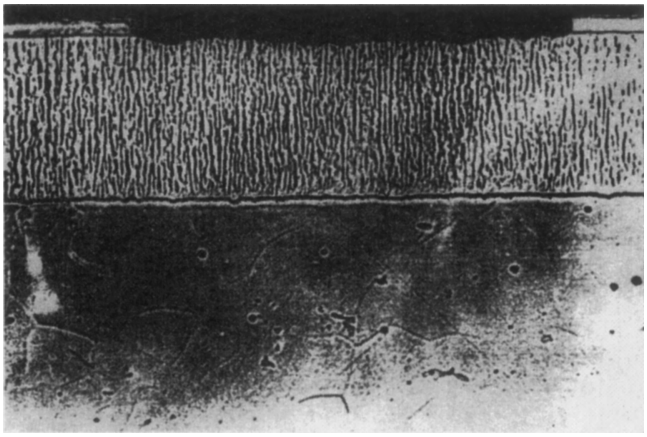

FIGURE 3.1 In double-layer nickel coatings, corrosion is initially confined to the top, full-bright nickel layer and penetration through the underlying semibright nickel layer is delayed (after 30 months exposure outdoors in an industrial atmoshpere).

During electrochemical studies of the behavior of various types of nickel deposits, it became clear that there were basically two types of proprietary bright nickel processes commercially available, one with a significantly higher reactivity than the other [41]. When equal areas of semibright nickel were coupled to each type, the highly reactive bright nickel provided greater protection of the semibright nickel than the low-reactivity type. The relative merits of using high-reactivity bright nickel in combination with semibright nickel was confirmed in outdoor stationary and mobile exposure programs performed with contoured panels [42]. Contoured panels have raised and recessed areas, and the thickness of the coating is greater on the relatively flat portion of the panel than in the recessed areas where the average thickness of the coating is 45% of the nominal value. The fact that recessed areas performed better with the high-reactivity bright nickel not only confirmed the observations made in the laboratory but also showed that the improvement in corrosion performance due to double-layer nickel coatings becomes more important as coating thickness is decreased. Snyder [43] refers to the two types as high- and low-potential bright nickel and states that the low-potential types may give better performance as single-layer coatings.

In triple-layer coatings, semibright and bright nickel layers are separated by a thin, highly active nickel layer containing about 0.15% sulfur deposited from a special solution [34, 44], The thickness of the very active nickel layer is of the order of 1.2–2.5 μm. The corrosion mechanism is similar to that of double-layer nickel coatings; once a corrosion pit reaches the very active nickel layer, corrosion proceeds laterally, the top layer of bright nickel becomes

cathodically polarized, and its rate of corrosion is decreased. Whether or not triple-layer nickel coatings give significantly better corrosion performance compared to double-layer nickel coatings of equal thickness over extended periods of time is still not completely settled, but certainly the appearance in the initial stages of corrosion is improved because much of the corrosion takes place beneath the top layer of bright nickel and is difficult to see. Double- and triple-layer nickel coatings delay penetration of corrosion to the substrate and are effective in improving corrosion performance of nickel plus chromium coatings.

3.3.6 Microdiscontinuous Chromium

On surfaces that are electroplated with nickel plus conventional chromium, corrosion of the nickel begins at a pore in the chromium coating. Because conventional electrodeposited chromium has relatively few discontinuities, any pore or crack is surrounded by a large cathodic area of chromium that draws current from a relatively small area of nickel, and as a result the rate of pit penetration through the nickel can be quite rapid. Corrosion may be under anodic control during the initial stages, but as the exposed nickel anode area increases, the rate of corrosion becomes cathodically controlled.

These observations led some investigators to conclude that a pore-free, electrodeposited chromium coating would lead to significant improvement in the corrosion performance of nickel plus chromium coatings. Crack-free chromium electroplating processes were introduced in the 1960s but quickly disappeared when it became apparent that crack-free chromium develops porosity in service, similar to the porosity of conventional chromium. (Crack-free chromium has a predominantly hexagonal close-packed structure, unlike conventional chromium, which is body-centered cubic. The very high wear rate of crack-free chromium was attributed to its different crystal structure [22].)

Saur was one of the first to establish that an inverse relationship exists between the number of pores in the chromium and the degree of substrate corrosion [45]. Based on his evaluation of test panels and parts that had been in service for up to 21 years, he concluded that "an increase in chromium discontinuities increases the area of nickel corrosion, the increase in exposed nickel is associated with an increase in basis metal protection, and a minimum chromium imperfection density is beneficial for corrosion protection of the substrate." Saur and his co-workers [46] at the General Motors Research Laboratory also developed the test described in ASTM Standard B 627 [23], Electrolytic Corrosion Testing (EC Test), which applies potentiostatic and galvanostatic polarization in a specified sequence to simulate anodic and cathodic corrosion control and permits a quantitative evaluation of the protectiveness of nickel plus chromium coatings to be made. Use of an interference microscope made it possible to examine specimens subjected to that test; measure pit densities, radii, and depths; and correlate that data to basis metal protection and appearance in nickel chromium coating systems [47]. Saur's work and that of others led to the development of commercial processes for increasing the number of discontinuities in electrodeposited chromium [48].

Commercial processes for producing microdiscontinuous chromium result either in the creation of micropores that are essentially circular in shape or in microcracks that form a fine, invisible, continuous network of cracks over the entire surface. One of the most popular processes for producing microporous chromium requires the deposition of a thin layer of bright nickel, prior to chromium plating, from a solution that contains insoluble, extremely fine, nonmetallic particles dispersed throughout the tank. The resulting chromium deposit is completely microporous when applied over the special nickel layer. Methods that involve mild impingement with fine particles after the deposition of chromium are effective in producing microporous chromium [49].

The development of microcracked chromium began with dual chromium which had the requisite crack pattern [50] and the work of Safranek and others [51] who added selenium to conventional chromium plating solutions to induce microcracking; those methods are no longer in commercial use. Still in limited use is a method that requires the deposition of a thin, highly stressed nickel deposit from an all-chloride nickel plating solution, prior to chromium plating, which gives the desired crack pattern after plating with chromium. One difficulty with the latter process is controlling the crack pattern in low-current-density areas. The most popular processes for producing microdiscontinuous chromium then are those based on deposition of special nickel strikes *prior* to chromium plating or on particle impingement *after* electroplating with chromium.

The use of microdiscontinuous chromium in combination with decorative multilayer nickel coatings, with or without copper underlayers, has resulted in great improvement in outdoor corrosion performance under severely corrosive conditions. The effect of the microdiscontinuities is to distribute the corrosion current over many tiny cells. The current available at any cell or pit is small, and the rate at which a pit proceeds through the bright nickel layer is correspondingly small. As the defect area increases, the area of exposed nickel (the anode) increases while the area of chromium (the cathode) decreases. Because the corrosion reaction is under cathodic control, reducing the size of the cathode surrounding each pit reduces the rate of nickel corrosion. The mechanism is consistent with the principles of galvanic corrosion. The area of exposed nickel was estimated by assuming that pits are cylindrically shaped, with pit radii and densities described in the literature; at very high chromium defect densities, the exposed nickel area is

approximately 3.5% [42]. The rate of pitting of double-layer nickel coatings 40 μm thick electroplated with microdiscontinuous chromium appeared to be approximately 2 μm per year, and steel panels plated with those coatings did not rust in a moderately severe, outdoor marine exposure under static conditions for more than 15 years [52]. Similar results have been obtained in programs conducted by members of ASTM Committee B 8 and others [53–55].

3.3.7 The STEP Test

The focus on electrochemical aspects of corrosion culminated in the development of the STEP test by Harbulak [56]. The test made it possible to measure potential differences between various layers in a multilayer nickel coating on actual electroplated parts rather than on deposits detached from the substrate. STEP is an acronym for simultaneous thickness and electrode potential measurement. In the test, which is a simple but brilliant modification of the well-known coulometric method of thickness testing, the electrode potential is monitored continuously as the coating is dissolved anodically. This is made possible by placing a reference electrode in the form of a silver or platinum wire in the coulometric cell used for stripping the coating. (Silver is preferred because the silver–silver chloride electrode has a constant potential whereas the potential exhibited by platinum is sensitive to the exact surface state of the platinum.) By recording the changes in potential with time, the potential differences, as well as the thicknesses, of the individual nickel layers can be measured. Unpublished work on the precision of the STEP test by ASTM Committee B 8 members indicate that potential differences and thicknesses can be measured with a standard deviation of less than 5% on standard reference materials. The STEP test is described in ASTM Standard B 764 [23].

Although there are no universally accepted values for the optimum potential differences between nickel layers, ASTM Standard B 456 [23] provides the following guidelines: (1) The STEP potential difference between the semibright and bright nickel layer generally falls within the range of 100–200 mV and in all combinations the semibright nickel layer is more noble (more positive) than the bright nickel layer; (2) the STEP potential difference between the high-activity layer and the bright nickel layer in triple-layer coatings has a potential range of 15–35 mV, and the high-activity layer is more active (anodic) than the bright nickel layer; and (3) the STEP potential difference between the bright nickel and any thin layer applied just prior to chromium plating for producing microporous or microcracked chromium has a potential range of 0–30 mV, and the bright nickel layer is more active. The importance of the latter in minimizing the deterioration in surface appearance that may occur in severe outdoor conditions or during accelerated corrosion testing has been stressed by Tremmel [57].

3.3.8 Electroplating Plastics, Aluminum, and Stainless Steel

Electroplating on plastics, aluminum, and stainless steel has broadened the scope of decorative nickel plating.

Plastics The discovery that ABS plastics can be chemically etched and rendered electrically conductive made it possible to deposit *decorative* nickel/chromium coatings onto injection-molded plastic parts with a level of adhesion not previously attainable [58]*. ABS is a terpolymer of acrylonitrile, butadiene, and styrene. When parts made of that material are immersed in strong chromic or chromic plus sulfuric acid solutions, the relatively soft, tiny butadiene rubber particles dispersed in the acrylonitrile–styrene matrix are chemically etched. The effectiveness of etching depends on how uniformly the butadiene particles are dispersed throughout the part and other factors related to injection-molding parameters. The physical bond achieved by the *keying* of the deposit into microscopic etch pits on the surface no doubt plays an important role in achieving adhesion, but the observation that the hexavalent chromium in the etching solution is reduced to trivalent chromium and must be periodically replenished led to speculation that the bonding might be chemical in nature [59]. Regardless of the exact mechanism, the adhesion (perhaps, 50–120 g mm^{-1} peel strength) is sufficient to prevent coatings from blistering at elevated temperatures on parts that are properly processed.

The traditional preparation sequence includes conditioning, etching, neutralizing, catalyzing, and autocatalytic deposition. Conditioning prior to etching can eliminate certain types of adhesion problems and may be done in a chromic/sulfuric acid solution or in an organic solvent (2,4-pentadione* and other ketones are sometimes used). The organic solvent softens and swells the plastic surface, making it more receptive to subsequent processing steps. Etchants are either chromic, chromic/sulfuric, or chromic/sulfuric/phosphoric acid types. The purpose of the neutralization step that follows etching is to remove all residual chromic acid from the surface of the parts, and this is accomplished by immersing them in acid or alkaline solutions that may contain complexing or reducing agents. After neutralization, catalyzing is commonly accomplished by immersing in a solution containing colloidal stannous/palladium chloride [60] and an excess of hydrochloric acid. Tiny amounts of palladium are deposited on the surface; the palladium acts as a catalyst for the autocatalytic (electroless) deposition of either copper or nickel. To pass thermal cycle tests, substantial thicknesses of ductile acid copper must be electroplated on top of the autocatalytically deposited metal, and it is expedient to use electroless copper rather than electroless nickel to avoid

*See [6], Chapter 12, pp. 330–341 and 360–362 for bibliography on electroplating onto plastics.

*The use of 2, 4-pentadione is patented.

processing problems, such as immersion deposition of copper and bipolar effects [61]. In addition electroless nickel can sometimes corrode preferentially at the metal–plastic interface, causing blistering and lifting of the coating [62, 63]. (That is most likely due to low phosphorus in the electroless nickel. Small amounts of phosphorus activate nickel [64]; large amounts tend to passivate it [65].) Electroless copper followed by electroplating with bright acid copper is now common practice, although electroless nickel is also used successfully. This basic method for preparing plastics for electroplating is discussed in ASTM Standard B 727 and elsewhere [23, 66].

Efforts to simplify the traditional method have been made, including gas etching with sulfur dioxide and the use of permanganates to replace chromates [67] The activation of plastic surfaces by plasma and ozone etching are other ways to prepare plastics for electroplating [68].

Decorative nickel plus chromium coatings can be deposited on top of electroplated bright acid copper by established procedures. ASTM Standard B 604 [23] specifies the use of multilayer nickel coatings for the most severe corrosion conditions on the basis of the comprehensive corrosion performance program conducted in the 1970s by members of ASTM and the American Society for Electroplated Plastics (ASEP) that showed that copper underlayers corroded during mobile, static, and accelerated corrosion tests if the nickel deposit was too thin [69, 70], The coatings specified in the standard are intended to protect the underlying copper layer from corrosion for extended periods of time. The chromium layer should be either microcracked or microporous for severe and very severe corrosion service.

The original applications for electroplated plastics were established with ABS, but many polymers can be successfully electroplated, including polypropylene, polysulfone, polyphenylene oxide, polycarbonate, polyester, nylon, and others [6, pp. 341–344, 360]. In general, catalysis with palladium is common to most preparation sequences, but different etching solutions and etching times are required to process different plastics. Automotive applications for decorative electroplated plastics appear to be growing [71].

Aluminum Immersion deposition is the most widely used technique for preparing aluminum and its alloys for electroplating. Immersion deposition processes are either alkaline zincate or alkaline stannate solutions that strip the oxide film from the aluminum and deposit a thin film of zinc or tin, respectively, on the surface before the oxide film can re-form. Although immersion deposition films are generally nonadherent, their adhesion on aluminum and its alloys can be excellent; the bond strength can equal or exceed the tensile strength of the aluminum or aluminum alloy [72]. Traditionally, treatment in zincate would be followed by electroplating in a tartrate-type copper cyanide solution, but methods for direct nickel deposition on the zinc surface have been introduced employing nickel glycolate [73] or autocatalytic (electroless) nickel strike [74]. A proprietary tin immersion/bronze strike is reportedly less susceptible to undercutting and blistering in corrosive environments than the zinc immersion/copper cyanide strike [75]. The preparation of aluminum for electroplating is discussed in detail in ASTM standard B 253 [23].

The performance of decorative, electroplated nickel plus chromium coatings on aluminum alloys was studied in connection with the development of lightweight automobile bumpers in the mid-1970s [76]. The effects on corrosion performance of various preparation methods, alloy type, nickel thickness, and type of chromium coatings were evaluated [77]. In reviewing the results, it was concluded that the use of microdiscontinuous chromium was probably the most important factor contributing to the improved corrosion performance of electroplated aluminum [78]. The experience gained during the development program has led to increased use of plated aluminum on truck bumpers and on styled aluminum wheels for trucks and passenger cars.

Stainless Steel Decorative nickel plus chromium plating of stainless steel is primarily applied in automotive applications and only to a limited extent. The justification for electroplating stainless steel is the cost and difficulty of achieving a mirror finish on the material by mechanical means and the need to color match bumper inserts and other components placed in proximity to nickel/chromium plated ones. The methods of preparing stainless steel for electroplating described in ASTM Standard B 254 [23] are suitable for decorative plating.

3.3.9 Standards and Coating Requirements

ASTM Standard B 456 [23] provides information on specific requirements for decorative nickel plus chromium coatings to achieve acceptable performance under different conditions of service. The standard classifies various coating systems according to their resistance to corrosion and recommends specific coatings for different service conditions. The thicknesses that are specified in most cases have been verified by corrosion performance studies conducted by members of the committee.

The requirements for double- and triple-layer nickel coatings included in the standard are summarized in Table 3.5. The sulfur contents are specified to identify the type of nickel and to control the electrochemical potentials between individual nickel layers. Coating classification numbers appropriate for each service condition are given in Table 3.6 for steel. The classification numbers for aluminum alloys given in Table 3.7 are adapted from the International Organization for Standardization (ISO) standard 1456 [79]. The ones for plastics in Table 3.8 are from ASTM Standard B 604 [23].

TABLE 3.5 Requirements for Double- and Triple-Layer Nickel Coatings

Layer (Type of Nickel Coating)	Specific Elongation (%)	Sulfur Content (%, mm^{-1})	Thickness Percentage of Total Nickel Thickness	
			Double Layer	Triple Layer
Bottom (s)	> 8	< 0.005	> 60 (but at least 75 for steel)	> 50 (but not more than 70)
Middle (b)	—	> 0.15	—	10 max
Top (b)	—	0.04–0.15	> 10 but < 40	≥ 30

Source: Adapted from ASTM Standard B 456.
Note: s designates the semibright nickel layer applied prior to bright nickel; b designates full-bright nickel that contains the amount of sulfur specified.

The service condition numbers grade the severity of corrosion environments in service as follows:

- *Service Condition No. SC 5 (Extended Very Severe)* Service conditions that include likely damage from denting, scratching, and abrasive wear in addition to corrosive environments where *long-time protection* of the substrate is required, for example, conditions encountered by some exterior components of automobiles.
- *Service Condition No. SC 4 (Very Severe)* Service conditions that include likely damage from denting, scratching, and abrasive wear in addition to exposure to corrosive environments, for example, conditions encountered by exterior components of automobiles and by boat fittings in salt water service.
- *Service Condition No. SC 3 (Severe)* Exposure that is likely to include frequent or occasional wetting by rain or dew or possibly strong cleaners and saline solutions, for example, conditions encountered by porch and lawn furniture, bicycle and perambulator parts, and hospital furniture and fixtures.
- *Service Condition No. SC 2 (Moderate)* Exposure indoors in places where condensation of moisture may occur, for example, in kitchens and bathrooms.
- *Service Condition No. SC 1 (Mild)* Exposure indoors in normally warm, dry atmospheres with coating subject to minimum wear or abrasion.

TABLE 3.6 Decorative Nickel Plus Chromium Coatings on Steel

Service Condition Number	Classification Number	Minimum Nickel Thickness (μm)
SC 5: extended very severe	Fe/Ni35d Cr mc	35
	Fe/Ni35d Cr mp	35
SC 4: very severe	Fe/Ni40d Cr r	40
	Fe/Ni30d Cr mp	30
	Fe/Ni30d Cr mc	30
SC 3: severe	Fe/Ni30d Cr r	30
	Fe/Ni25d Cr mp	25
	Fe/Ni25d Cr mc	25
	Fe/Ni40p Cr r	40
	Fe/Ni30p Cr mp	30
	Fe/Ni30p Cr mc	30
SC 2: moderate service	Fe/Ni20b Cr r	20
	Fe/Ni15b Cr mp	15
	Fe/Ni15b Cr mc	15
SC 1: mild	Fe/Ni10b Cr r	10

Source. Adapted from ASTM Standard B 456.

TABLE 3.7 Decorative Nickel Plus Chromium Coatings on Aluminum

Service Condition Number	Classification Number	Minimum Nickel Thickness (μrn)
SC 4: very severe	Al/Ni50d Cr r	50
	Al/Ni35d Cr mp	35
	Al/Ni35d Cr mc	35
SC 3: severe	Al/Ni30d Cr r	30
	Al/Ni25d Cr mp	25
	AI/Ni25d Cr mc	25
	Al/Ni35p Cr r	35
	Al/Ni30p Cr mp	30
	Al/Ni30p Cr mc	30
SC 2: moderate	AI/Ni20b Cr r	20
SC 1: mild	Al/Ni10b Cr r	10

Source: Adapted from ISO standard 1456.

TABLE 3.8 Decorative Nickel Plus Chromium Coatings on Plastics

Service Condition Number	Classification Number	Minimum Nickel Thickness (μm)
SC 5: extended very severe	Pl/Cul5a Ni30d Cr mc	30
	Pl/Cul5a Ni30d Cr mp	30
SC 4: very severe	PI/Cul5a Ni30d Cr r	30
	PI/Cul5a Ni25d Cr mp	25
	Pl/Cul5a Ni25d Cr mc	25
SC 3: severe	Pl/Cul5a Ni25d Cr r	25
	Pl/Cul5a Ni20d Cr mp	20
	Pl/Cul5a Ni20d Cr mc	20
SC 2: moderate service	Pl/Cul5a Ni15b Cr r	15
	Pl/Cul5a Ni10b Cr mp	10
	Pl/Cul5a Ni10b Cr mc	10
SC 1: mild	Pl/Cul5a Ni7b Cr r	7

Source: Adapted from ASTM Standard B 604.

The classification numbers are a way to specify the coatings that are appropriate for each service condition; for example, the classification number

Fe/Ni30d Cr mp

indicates that the coating is applied to steel (Fe), consists of 30 μm of double-layer nickel (d) with a top-layer of microporous chromium (mp) 0.3 μm thick. (The thickness of chromium is not included in the classification number unless it differs from 0.3 μm. If different, the number would appear immediately next to the symbol for chromium.)

The type of nickel is designated in the tables by the following symbols: b for electrodeposited bright nickel (single layer); d for double- or triple-layer nickel coatings; p for dull, satin, or semibright nickel that is not polished; s for polished dull or semibright nickel. The symbol a is used to designate ductile copper deposited from bright acid-type baths. The type of chromium is designated by the following symbols: r for regular or conventional chromium; mp for microporous chromium having a minimum of 10,000 pores cm^{-2}; mc for microcracked chromium having more than 300 cracks cm^{-1} in any direction over the entire surface.

ASTM standard B 456 [23] provides test methods for measuring coating requirements. It is a comprehensive guide to controlling the quality of decorative, electroplated nickel plus chromium coatings.

3.3.10 Decorative Applications and Market Size

Decorative applications may be placed into two categories: automotive and nonautomotive. The decline in decorative plating for automotive applications noted in the 1980s has abated as a result of the popularity and increased production of light trucks and recreational vehicles that have retained brightwork, the development of nickel chromium–plated steel and aluminum-styled wheels, and an increase in the number of automotive applications for plated plastics [1]. Nonautomotive decorative applications comprise a large number of consumer products, including furniture and building hardware, plumbing fixtures, housewares, hand tools, major appliances, wire goods, bicycles, mopeds, motorcycles, and others. These continue to expand with the growth of the global economy. Approximately 80% of the nickel consumed for electroplating annually is for decorative purposes. The balance, 20%, is consumed for functional electroplating and electroforming.

3.4 FUNCTIONAL ELECTROPLATING AND DEPOSIT PROPERTIES

Electrodeposited nickel coatings are applied in functional applications to modify or improve corrosion resistance, hardness, wear, magnetic, and other properties. Although the appearance of the coating is important and the plated surface should be defect free, the lustrous mirrorlike deposits described in the previous section are not required.

Typical formulations for Watts and sulfamate solutions, the two most popular ones for functional applications, have been included in Table 3.4 along with recommended operating conditions and representative mechanical properties of deposits from each solution. Although the table indicates that the maximum current density for depositing nickel from a Watts solution is 11 A dm^{-2}, higher deposition rates can be achieved with increased agitation and solution flowrates. Other nickel electroplating solutions (Table 3.9) have been applied in functional applications, and deposits from those solutions have useful properties.

3.4.1 Deposit Properties

The main constituents in Watts solutions affect the properties of electrodeposited nickel. Nickel sulfate improves conductivity and metal distribution and determines the limiting cathode current density for producing sound nickel deposits. Nickel chloride improves anode corrosion but also increases conductivity, throwing power, and uniformity of coating thickness distribution. In addition chlorides increase the internal stress of the deposits, and they tend to refine grain size and minimize formation of nodules and trees. Boric acid is added for buffering purposes and affects the appearance of the deposits. Deposits may be cracked and burnt at low boric acid concentrations. Anionic wetting agents or surfactants that lower the surface tension of the plating solution so that air and hydrogen bubbles do not cling to the parts being plated are almost always added to control pitting and, by eliminating porosity, have an indirect effect on corrosion performance.

Operating conditions, such as pH, temperature, current density and chloride content, affect the properties of deposits from Watts solutions [80]. In a Watts solution, hardness, tensile strength, and internal stress increase above pH 5.0 while the elongation percentage decreases (Fig. 3.2), The hardness increases rapidly at low values of current density (Fig. 3.3). Increasing the temperature of the plating solution causes hardness and tensile strength to reach minimum values at about 55°C, while the elongation percentage is a maximum at that temperature (Fig. 3.4). Increasing the chloride ion concentration affects the properties of deposits from Watts solutions; for example, the elongation percentage is at a maximum, and hardness and tensile strength are at minimum values when the solution contains 25% by weight nickel chloride (Fig. 3.5). In general, conditions that increase the hardness of a nickel deposit will increase its tensile strength and lower its ductility. Close control of the main constituents and the operating conditions is thus required to produce nickel electrodeposits with consistent and known properties.

TABLE 3.9 Other Nickel Plating Solutions and Some Properties of Deposits

Type	Composition[a] ($g\,L^{-1}$)	pH	Temperature (°C)	Cathode Current Density ($A\,dm^{-2}$)	Vickers Hardness, (100 g load)	Tensile Strength (MPa)	Elongation (%)	Internal Stress (MPa)
Fluborate	Nickel fluoborate, 225–300 Nickel chloride, 0–15 Boric acid, 15–30	2.5–4	38–70	3–30	125–300	380–600	5–30	90–200
Hard nickel	Nickel sulfate, 180 Ammonium chloride, 25 Boric acid, 30	5.6–5.9	43–60	2–10	350–500	990–1100	5–8	300
All chloride	Nickel chloride, 225–300 Boric acid, 30–35	1–4	50–70	2.5–10	230–260	620–930	4–20	275–340
All sulfate	Nickel sufate, 225–410 Boric acid, 30–45	1.5–4	38–70	1–10	180–275	410–480	20	120
Sulfate/chloride	Nickel sulfate, 150–225 Nickel chloride, 150–225 Boric acid, 30–45	1.5–2.5	43–52	2.5–15	150–280	480–720	5–25	210–280
High sulfate	Nickel sulfate, 75–110 Soidum sulfate, 75–110 Ammonium chloride, 15–35 Boric acid, 15	5.3–5.8	20–32	0.5–2.5				
Black nickel (sulfate bath)	Nickel sulfate, 75 Zinc sulfate, 30 Ammonium sulfate, 35 Sodium thiocyanate, 15	5.6	24–32	0.15				
Black nickel (chloride bath)	Nickel chloride, 75 Zinc chloride, 30 Ammonium chloride, 30 Sodium thiocyanate, 15	5.0	24–32	0.15–0.6				
Nickel phosphorus	Nickel sulfate, 170 or 330 Nickel chloride, 35–55 Boric acid, 0 or 4 Phosphoric acid, 50 or 0 Phosphorus acid, 2–40	0.5–3.0	60–95	2–5				

[a] The formulas of the compounds in the table are as follows: nickel fluoborate, $Ni(BF_4)_2$; nickel sulfate, $NiSO_4 \cdot 6H_2O$; nickel chloride, $NiCl_2 \cdot 6H_2O$; boric acid, H_3BO_3; ammonium chloride, NH_4CI; ammonium sulfate, $(NH_4)_2SO_4$; sodium sulfate, Na_2SO_4; phosphoric aicd, H_3PO_4; phosphorus acid, H_3PO_3; zinc sulfate, $ZnSO_4 \cdot 7H_2O$; zinc chloride, $ZnCl_2$; sodium thiocyanate, NaSCN.

The properties of deposits from Watts and sulfamate solutions are affected in different ways by changes in operating conditions, as illustrated qualitatively in Figure 3.6 [81], For example, internal stress is not significantly affected by increasing the temperature of a Watts bath, whereas increasing the temperature in a sulfamate solution reduces internal stress significantly. Cathode current density has a relatively small effect on the tensile strength of deposits from a Watts solution, but increasing current density reduces the tensile strength of deposits from a sulfamate solution.

The mechanical properties measured at temperatures from −195 to 870°C of nickel electrodeposited from Watts, sulfamate, and all-chloride solutions were determined and compared to the properties of wrought nickel by Knapp and Sample [82] (Fig. 3.7). At −195°C, chloride and sulfamate nickel had ultimate tensile strength in excess of 100 kg mm^{-2} compared to a value of 56 kg mm^{-2} for Watts and annealed wrought nickel. The reduction in the elongation percentage above 450°C for the three types of electrodeposited nickel was attributed to the presence of small amounts of sulfur in the electrodeposited nickel. Although wrought nickel has comparable levels of sulfur, it also contains small amounts of manganese that prevent sulfur from migrating to grain boundaries at elevated temperatures where it forms nickel sulfide, which reduces high-temperature ductility. The codeposition of small amounts of manganese with nickel has since been shown to improve high-temperature ductility [83]. Considerable information on the physical and mechanical properties of electrodeposited nickel, nickel alloys, and nickel composite coatings is available [84, 85].

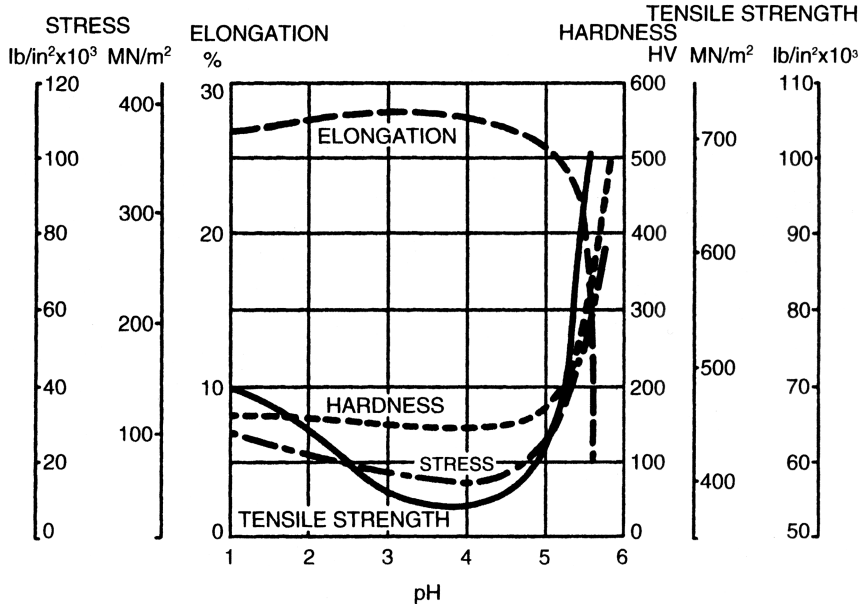

FIGURE 3.2 Influence of pH on the internal stress, tensile strength, ductility, and hardness of nickel electrodeposited from a Watts solution at 55°C and 5 A dm^{-2} [80].

3.4.2 Coating Requirements in Functional Applications

Corrosion performance in functional applications depends on nickel thickness and other factors, including the condition of the surface prior to plating. The thickness that should be applied depends on the specific application. For example, nickel thickness in optical and electronic applications where nickel is applied as an undercoat prior to electroplating with other metals may be 5 μm. To protect product purity, thickness may be 7 μm thick on processing equipment, such as ferrous containers. For drying cylinders and rolls for paper processing, for condenser and calender rolls for the textile industry, and for externally and internally plated pipe, fittings, and other components for chemical and nuclear plants, nickel coating thicknesses of 125 μm have been specified. Nickel coatings on automotive components, such as hydraulic rams, cylinder liners, and shock absorbers, may be 125 μm thick to provide corrosion and wear resistance. Coatings to prevent fretting corrosion and to enhance wear resistance are generally greater than 125 μm thick and have been used in the automotive and mining industries to coat pistons, cylinder

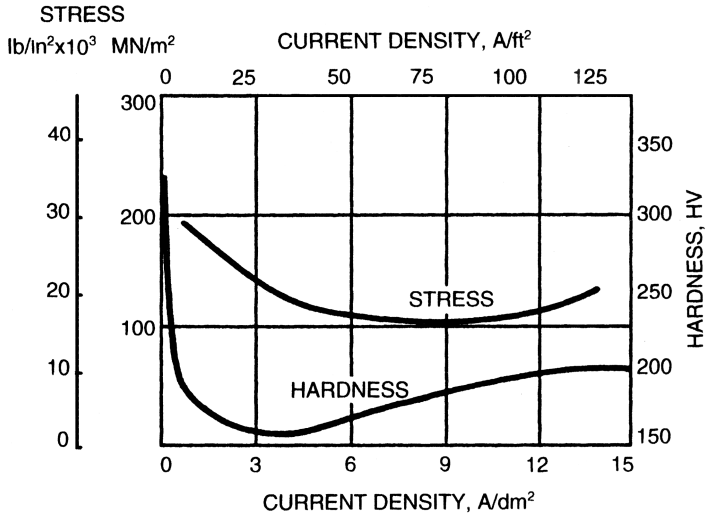

FIGURE 3.3 Influence of current density on the internal stress and hardness of nickel electrodeposited from a Watts solution at 55°C and pH 3.0 [80].

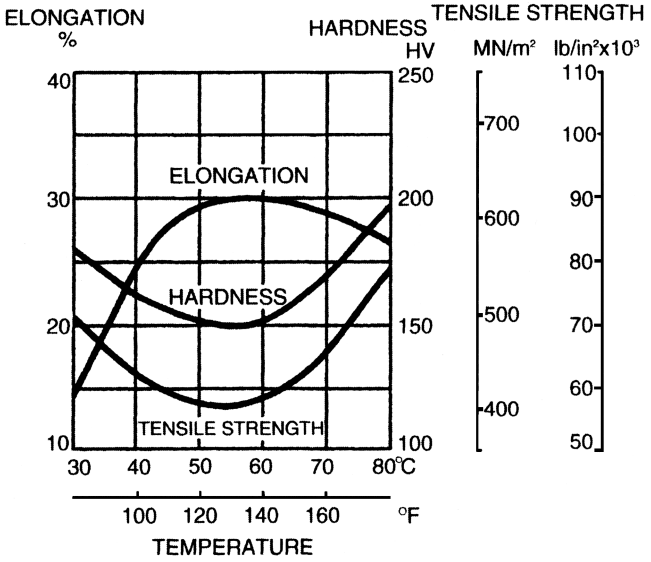

FIGURE 3.4 Influence of temperature on the elongation, tensile strength, and hardness of nickel electrodeposited from a Watts solution at pH 3.0 and 5 A dm^{-2} [80].

walls, rotary engine housings, gear shafts, drive shafts, pump rods, and hydraulic pistons. When nickel is applied to salvage worn or mismachined components, thickness is determined by the extent of the repair required. Other requirements for functional nickel coatings are discussed in ASTM Standard B 689 [23]. Nickel coatings used as diffusion barriers beneath precious metal deposits in electronic applications, nickel electroplating of strip and hardware in the production of batteries, and nickel-electroplated steel coin blanks are a few examples of functional applications that have grown in importance.

3.4.3 Other Solutions

Other nickel plating solutions for functional applications are listed in Table 3.9, along with typical mechanical properties of the deposits. Many of these solutions were developed to meet specific engineering requirements; all are used to a lesser extent than Watts and nickel sulfamate solutions.

Fluoborate The fluoborate solution can be operated over a wide range of nickel concentrations, temperature, and current density and is relatively simple to control [86]. The fluoborate anion is corrosive, however, and some materials that contact the solution are chemically attacked. The mechanical and physical properties of deposits from a fluoborate bath are similar to those from Watts solutions. The major advantage is that electrodeposition from a nickel fluoborate solution can be performed at high current density.

Hard Nickel Developed especially for functional applications, this solution is applied where controlled hardness, improved abrasion resistance, greater tensile strength, and good ductility are required without using sulfur-containing organic addition agents [87]. Close control of pH, temperature, and current density is necessary for this bath

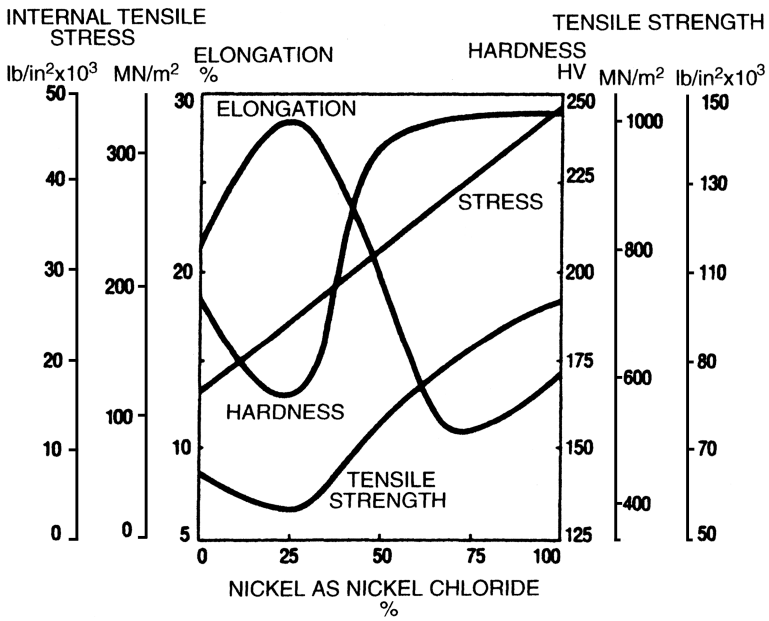

FIGURE 3.5 Influence of chloride concentration on the elongation, internal stress, hardness, and tensile strength of nickel electrodeposited from Watts-type solutions at pH 3.0, 55°C, and 5 A dm^{-2} [80].

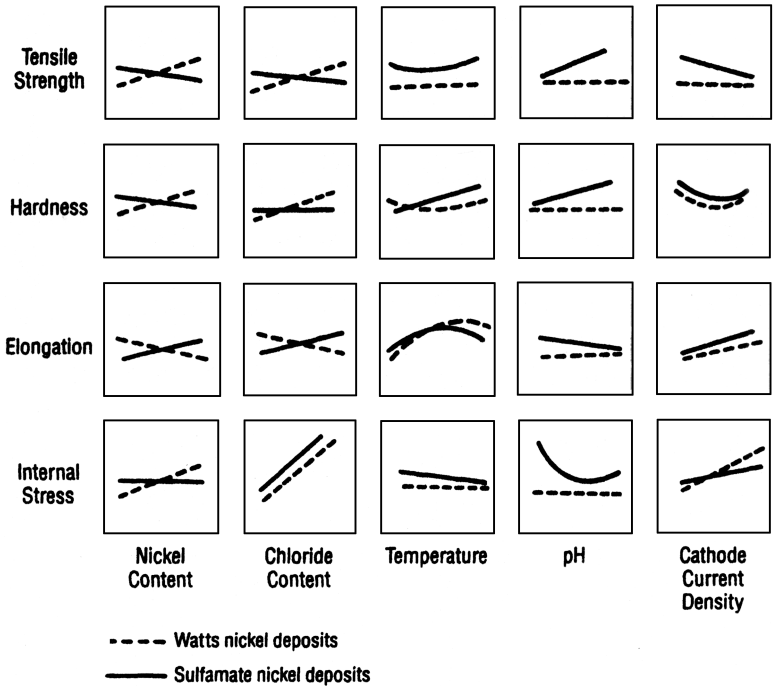

FIGURE 3.6 Qualitative effects of operating conditions on the properties of nickel electrodeposited from Watts and sulfamate solutions.

to give reproducible results. The internal stress is slightly higher than in deposits from Watts solutions. The disadvantages of the hard-nickel bath are its tendency to form nodules on edges and the low annealing temperature (230°C) of its deposits. Hard-nickel deposits are used primarily for buildup or salvage purposes. For optimum results, the ammonium ion concentration should be maintained at $8\,g\,L^{-1}$. In applications where the part being plated is not going to be exposed to elevated temperatures in service, it is easier to add organic compounds such as saccharin, *p*-toluene sulfonamide, and *p*-benzene sulfonamide to Watts or sulfamate solutions to achieve hardness without increased internal stress. Since these additives introduce 0.03% sulfur (or more), this approach must not be used for parts to be exposed to high temperatures where sulfur severely embrittles the nickel deposit. Leveling agents (brighteners) are effective in increasing the hardness of electrodeposited nickel without introducing sulfur, but they tend to raise internal stress [88].

All Chloride The principal advantage of the all-chloride solution is its ability to operate effectively at high cathode current densities. Other advantages include its high conductivity, its slightly better throwing power, and a reduced tendency to form nodular growths on edges [89]. Deposits from this electrolyte are smoother, finer grained, harder, and stronger than those from Watts solutions and more highly stressed. Because of the partial solubility of lead chloride, lead cannot be used in contact with the all-chloride solution, and mists from this solution are corrosive to the superstructure, vents, and other plant equipment if not well protected. The solution has been used for salvaging undersize or worn shafts and gears.

All Sulfate This solution has been applied for electrodepositing nickel where the principal or auxiliary anodes are insoluble [90]. For example, insoluble auxiliary or conforming anodes may be required to plate the insides of steel pipes and fittings. Oxygen is evolved at insoluble anodes, and as a result the nickel concentration and pH decrease during plating. The pH is controlled and the nickel ion concentration is maintained by adding nickel carbonate. Another procedure that has been used in low-pH solutions replenishes the nickel electrolytically by employing a separate replenishment tank with nickel anodes; the current in the replenishment tank is periodically reversed to keep the nickel nodes actively dissolving in the absence of chlorides [90]. The insoluble anodes in all-sulfate solutions may be lead, carbon, graphite, or platinum. If a small anode area is required, solid platinum (in the form of wire) may be used. For large anode areas, platinum-plated or platinum-clad titanium is recommended; iridium-coated titanium is now in commercial use. In some forms, carbon and graphite are too fragile; lead has the disadvantage of forming loose oxide layers, especially if it is immersed in other solutions in the course of a plating cycle. In chloride-free solution, pure nickel is *almost* insoluble and may function as an internal anode if properly bagged.

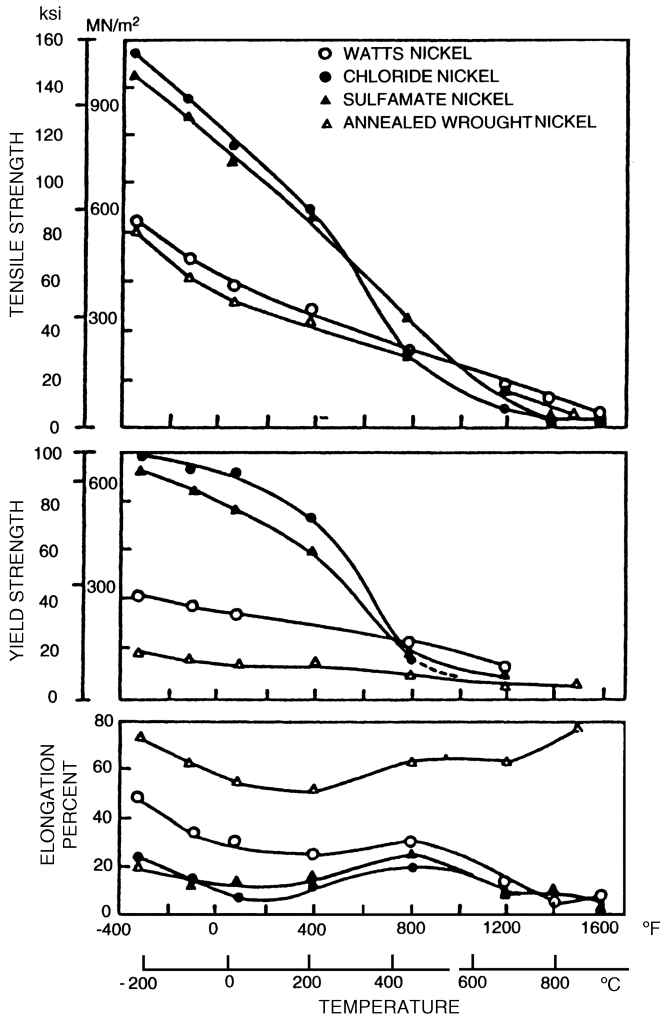

FIGURE 3.7 Effect of temperature on the tensile strength, yield strength, and elongation of dectrodeposited nickel.

Sulfate–Choride The sulfate–chloride solution included in Table 3.9 has roughly equivalent amounts of nickel sulfate and nickel chloride and was developed to overcome some of the disadvantages of the all-chloride solution [91]. It has high conductivity and can be operated at high current densities. Although the internal stress of the deposits is higher than in deposits from Watts solutions, the stress is lower than in the all-chloride solution. The other properties are about midway between those for deposits from Watts and all-chloride solutions. Lead may not be used for equipment in contact with this solution because of the high chloride content.

High Sulfate The high-sulfate bath was developed for plating nickel directly on zinc-based die casting [92]. It has been used to plate nickel on aluminum that has been given a zincate or comparable surface preparation treatment. The high-sulfate and low-nickel contents, together with the high pH, provide good throwing power with little attack of the zinc. The deposits are less ductile and more highly stressed than nickel deposited from a Watts bath. In general, the deposition of copper from a cyanide solution directly on zinc-based die castings prior to the deposition of nickel is simpler and more reliable. Nickel glycolate and autocatalytic nickel solutions, as mentioned above, are preferred for depositing nickel directly on aluminum that has been given a zincate treatment.

Black Nickel There are at least two formulations for producing black nickel deposits; these incorporate zinc (Zn) and thiocyanate (CNS–) ions. Table 3.9 gives the [93] composition and operating conditions for sulfate and chloride black nickel plating baths [93]. The process was developed for decorative reasons: color matching and blending. The black nickel deposit has little wear or corrosion resistance and is usually deposited over a layer of nickel deposited from a bright or dull nickel plating solution. Black nickel deposit is still in commercial use, and the deposit is often protected with a clear lacquer coating.

Nickel–Phosphorus These solutions result in the electrodeposition of nickel–phosphorus alloys that are analogous to those deposited autocatalytically using sodium hypophosphite as the reducing agent [94]. The hardness of the electrolytic deposits can be increased by heat treatment in the same way that autocatalytic nickel deposits can with maximum hardness occurring at 400°C. The phosphorus content of the deposits is controlled by frequent additions of phosphite or phosphorus acid. The electrodeposition of nickel phosphorus alloys is receiving increased attention because deposits with greater than 10% phosphorus are amorphous and therefore have enhanced resistance to corrosion [95].

3.4.4 Fatigue Strength

Thick nickel deposits applied to steel substrates may cause significant reductions in composite fatigue strength when subjected to cyclical stress loading. The reduction in fatigue strength is influenced by the internal stress and thickness of the coating and by the hardness and tensile strength of the steel. The fatigue limit of nickel-plated steel is reduced almost proportionally to the amount of residual tensile stress in the nickel. Compressively stressed deposits have less of an effect on fatigue, and as a result, steel crankshafts have been nickel electroplated for resistance to wear and corrosion with low-stressed deposits from nickel sulfamate solutions. Specifying the thinnest coating consistent with design requirements is also beneficial for minimizing the effect on fatigue life. In some cases, specifying a steel with increased hardness and tensile strength may be necessary. Shot peening the steel prior to electroplating minimizes the reduction in fatigue strength; see ASTM Standard B 851 for details of the shot

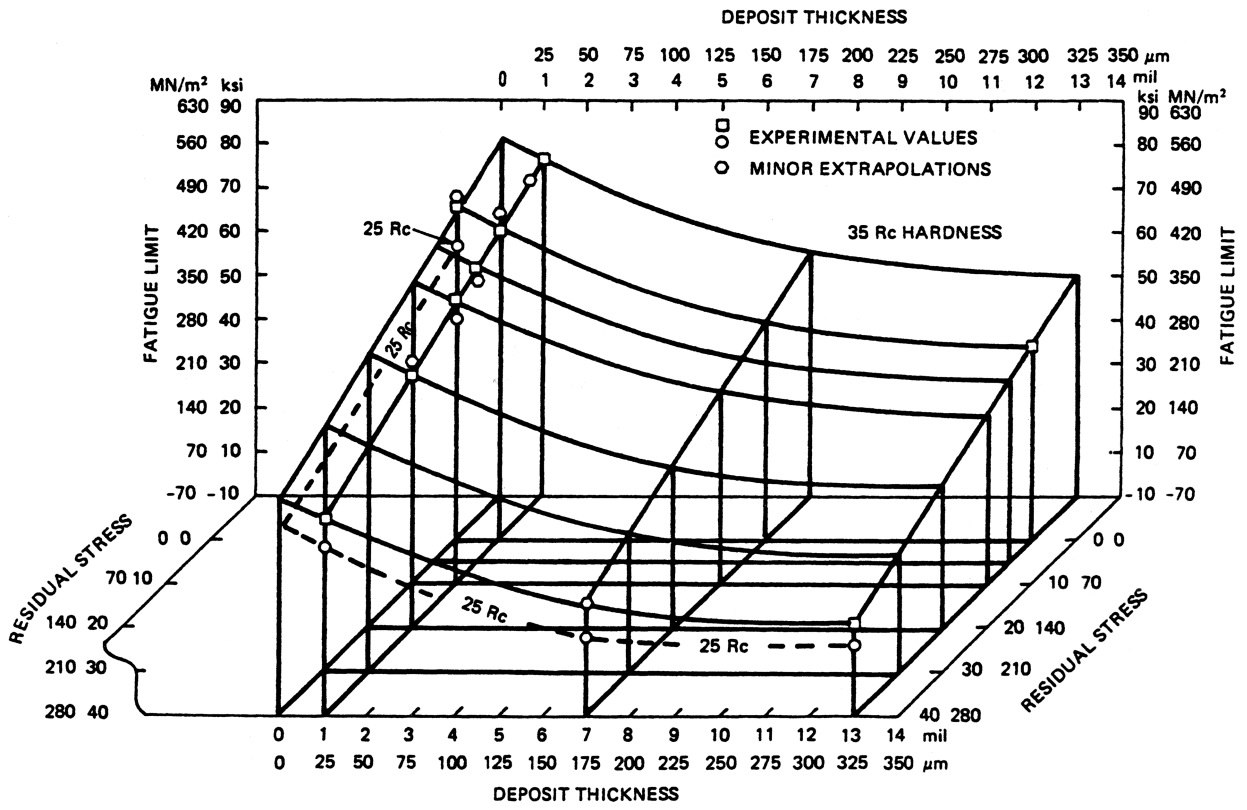

FIGURE 3.8 Effect of deposit thickness and internal stress on the 100 million cycle fatigue life of nickel-electroplated American Iron and Steel Institute (AISI) 4340 steel.

peening strength, process [23]. The effect of these variables on the fatigue limit of a nickel-plated high-strength steel is shown in Figure 3.8 [96].

3.4.5 Hydrogen Embrittlement

Highly stressed, high-strength steels are susceptible to hydrogen embrittlement during normal plating operations. Although nickel plating per se may not be the cause of embrittlement, the preparation of steels for electroplating involves exposures to acids and alkalis that are capable of introducing hydrogen into the steel. In general, parts made from steel with tensile strengths that are equal or greater than 1000 MPa should be heat treated after electroplating to avoid hydrogen embrittlement; depending on the state of the steel, stress relief prior to electroplating may be required to minimize hydrogen embrittlement susceptibility. Recommended treatments are given in ASTM Standards B 849 and B 850 [23].

3.5 NICKEL ELECTROFORMING

Electroforming with copper was conceived in 1838 by Jacobi of the Academy of Sciences, St. Peterburg, Russia [97]. Bottger reportedly electroformed nickel in 1843. Today nickel is utilized in the largest number of applications because it is strong, tough, and resistant to corrosion, erosion, and wear and because its mechanical properties can be varied and controlled by changing solution composition and operating conditions, by alloying, and by incorporating particles and fibers within the electrodeposited nickel matrix [98],

3.5.1 Electroforming and Electrofabrication

Electroforming is electroplating applied to the production of parts. In decorative and functional applications, good adhesion of the coating to its substrate is critical to its function. In electroforming, metal is deliberately electrodeposited nonadherently so that it can be separated from the substrate. The substrate in electroforming is a *mandrel or mold*, and the nickel that is separated from the mandrel becomes the final product. The mandrel is usually a negative or reverse replica of the product to be fabricated and is often recovered and reused. Electrofabrication also describes processes that result in the production of components and parts but that do not involve the use of traditional mandrels. In electrofabrication, the substrate often becomes an integral part of the component, and electrodeposition takes place selectively through masks or by means of specially designed cells [99, 100]. The

distinction between electroforming and electrofabrication lies in the nature of the mandrel and the role of the substrate.

3.5.2 Capabilities of Nickel Electroforming

Nickel electroforming processes can reproduce fine surfaces with great accuracy due to the excellent microthrowing power of nickel plating solutions. In the production of stampers for pressing compact audio and video discs, the accuracy of reproduction is within a fraction of a micrometer. An extension of this property is in the reproduction of complex surface finishes; for example, bright and semibright surfaces can be reproduced without the need for machining or polishing individual parts. The combination of electroforming and modern photolithographic techniques for generating patterns makes it possible to produce parts with extreme precision and fineness of detail on a microscopic scale. Parts can be reproduced in quantity with a high degree of dimensional accuracy. The mechanical and physical properties of nickel can be closely controlled by selecting the appropriate solution and the operating conditions. There is virtually no limitation to the size and thickness of the parts that can be electroformed. Shapes can be made that are impossible or too expensive to make any other way.

3.5.3 Mandrels

The ability to produce an electroformed part depends on the design and fabrication of the mandrel. A key consideration is to facilitate separation of the electroform. Rounding exterior angles, tapering the mandrel where possible, eliminating reentrant angles, controlling the mandrel's surface finish, and designing a fixture to assist in parting the electroform from the mandrel should be considered at the design stage. Mandrels may be manufactured by casting, machining, electroforming, and conventional pattern-making techniques, and they may be conductors or nonconductors of electricity and expendable or permanent. The nature of the material will determine how the mandrel is prepared for electroforming; in some cases there is a need to passivate the surface of the mandrel to prevent adhesion. Some of these details are discussed in ASTM standard B 832 [23].

3.5.4 Nickel Electroforming Solutions

Nickel sulfamate solutions (Table 3.4) are popular for electroforming because of the low internal stress of the deposits, the high rates of deposition possible, and the improved throwing power. Watts nickel solutions are utilized in a number of applications, but often with the addition of stress-reducing agents.

Nickel sulfamate is similar to nickel sulfate except that one of the hydroxyl groups is replaced by an amido group. The formula of the normal crystallized form of nickel sulfamate may be written, $Ni(SO_3NH_2)_2 \cdot 4H_2O$. Crystallized forms are not readily available in the United States where prepurified concentrated liquid solutions are preferred. Nickel sulfamate can be prepared by reacting high-purity nickel powder or high-purity nickel carbonate with sulfamic acid under controlled conditions. Because of the high solubility of nickel sulfamate, higher nickel metal concentration is possible than in other nickel electrolytes, permitting higher plating rates. A small amount of nickel chloride is usually added to nickel sulfamate solutions to minimize anode passivity, especially at high current densities. If nickel chloride is not added, sulfur-containing nickel anode materials are required to avoid anodic oxidation of sulfamate anions (discussed below). Prolonged use of sulfamate solutions at temperatures above 70°C or at a pH of less than 3.0 can hydrolyze the nickel sulfamate to the less soluble form of nickel ammonium sulfate. Ammonium and sulfate ions increase the internal tensile stress and hardness of the deposits [101]. As far as is known, there is no *simple* way to remove ammonium ions from sulfamate solutions.

3.5.5 Anodic Oxidation of Sulfamate Anions and the Ni-Speed Process

A phenomenon that apparently occurs only in sulfamate solutions is anodic oxidation of sulfamate anions to form species that diffuse to the cathode where they can affect the internal stress and the composition of the deposit. This occurs at insoluble anodes operating at high potentials. At an insoluble platinum anode, a stress reducer forms which was identified as an azodisulfonate [102]; it reacts at the cathode, introduces sulfur into the deposit, especially at low current density, and lowers internal stress. The stress can be less than zero (compressive) depending on the amount of current flowing through the small insoluble platinum anode. A small auxiliary platinum anode that drew 1–2% of the total current passing through the electroplating cell was effective in controlling stress at compressive levels but resulted in the codeposition of small amounts of sulfur with the nickel [103], The codeposited sulfur affected the ductility and other mechanical properties of the deposit, and its tendency to become embrittled at elevated temperatures [104].

The concentrated nickel sulfamate process, *Ni-Speed*, was developed for electroforming at high current densities and low internal stress [105]. Because low- to zero-stress conditions can be achieved without organic addition agents, there is no incorporation of sulfur and the deposits do not become embrittled when heated above 200°C. The solution contains about 500–650 g L^{-1} of nickel sulfamate; 5–15g L^{-1} of nickel chloride hexahydrate, and 30–45 g L^{-1} boric acid. After purification with carbon and permanganate to remove all organic impurities, the solution is conditioned

electrolytically with a nonactivated anode material. When properly conditioned, a deposit prepared at 5 A dm^{-2} and at 60°C will be semilustrous and have a compressive stress. During operation, the solution is circulated through a separate conditioning tank where it is continuously electrolyzed at low current density; the conditioning tank has 10–20% of the capacity of the main tank and is operated with a nonactivated, sulfur-free anode material. The main electroforming tank is operated with an activated sulfur-containing anode material. Controlling the stress at or very close to zero depends on maintaining the solution temperature and current density at specified, *coupled* values; for example, internal stress is approximately zero at 50°C and 8 A dm^{-2}, at 60°C and 18 A dm^{-2}, or at 70°C and 32 A dm^{-2}.

The reaction that occurs at an insoluble platinum anode is apparently different from the reaction that occurs at the anode in the conditioning tank. The potential of a platinum anode in the nickel sulfamate solution is approximately + 1 V versus the saturated calomel electrode (SCE). The potential of the nonactivated nickel anode material in the conditioning tank will be approximately + 0.2 to + 0.4 V versus SCE because of the presence of chlorides, whereas the activated anode in the electroforming tank will dissolve at −0.2 V versus SCE. It has been postulated that the oxidation reaction that occurs at the high potential is different from the reaction that occurs at intermediate potentials [106]. At an active anode dissolving at −0.2 V versus SCE, anodic oxidation of sulfamate anions does not occur. The existence of several oxidation species in sulfamate solutions has been reported [107]. The Ni-Speed process has been operated successfully in Europe where it has been used to electroform electrolytic nickel foil at low internal stress continuously on rotating drums at current densities as high as 40 A dm^{-2}. It has not been used to any great extent in North America where it is considered difficult to control and where its reproducibility has been questioned.

Zero stress can reportedly be maintained in conventional nickel sulfamate solutions by eliminating nickel chloride entirely using a sulfur-activated nickel anode material and continuously purifying the solution by means of an auxiliary tank similar to the conditioning tank described above.

3.5.6 Leveling Agents for Electroforming

The use of a leveling agent, for example, 2-butyne 1,4-diol, can improve metal distribution on the mandrel by suppressing the growth of nodules and by preventing the formation of planes of weakness when electroforming into comers [108]. Leveling agents increase internal stress, but the increase may be tolerable when the initial stress is at or close to zero. The breakdown products formed by butyne diol can be removed by continuous filtration of the solution through carbon and this helps control the effect on internal stress.

3.5.7 Postelectroforming Operations

After electrodeposition is complete operations such as machining and finishing, parting and separating from the mandrel, and backing the electroform are usually required [109].

3.5.8 Nickel Electroforming Applications

Products made by nickel electroforming include stampers for the production of phonograph records, compact discs, videodiscs, holograms, and information storage discs; textile printing screens; a wide assortment of molds and dies for processing plastics; abrasion strips for helicopter blades; seamless belts for photocopiers and facsimile machines; and porous nickel foam for making battery electrodes [110]. The electrofabrication of thin-film heads for magnetic recording, thin-film chip carriers, micromovable parts, and cooling channels in rocket thrust chambers involves the deposition of one or more layers of metal onto a substrate that becomes an integral part of the final product [111–113].

3.6 NICKEL ANODE MATERIALS

Most nickel plating processes are operated with soluble nickel anode materials. Nickel from the anode is converted into ions which enter the plating solution to replace those discharged at the cathode. In addition, the anode distributes current to the parts being electroplated and influences metal distribution. Commercially available nickel anode materials made to strict chemical specifications do not introduce impurities into the electroplating solution and influence quality only to the extent that they affect current and metal distribution.

The simplest way to satisfy anode requirements is to suspend an electrolytic nickel strip from hooks placed on an anode bar so that the nickel, not the hook, is immersed in the plating solution. Although significant quantities of the electrolytic nickel strip are still consumed for that purpose, it is the least satisfactory way to satisfy anode requirements. The electrolytic nickel strip dissolves preferentially at its bottom and its sides, which results in an ever-changing anode area accompanied by a corresponding increase in anode current density. The strip dissolves nonuniformly, becoming fragile and spongy and, as a result, tends to break and disintegrate before it is completely consumed, creating scrap that has to be discarded or recycled. Replacement of the electrolytic nickel strip usually requires interruption of the plating process and yields anode spears or stubs that have to be disposed of. The fact that the nickel strip is available in limited lengths is perhaps its greatest disadvantage. These limitations led to the development of wrought (rolled) products that dominated the market for many years and later to the development of improved primary forms of electrolytic nickel for titanium anode baskets.

3.6.1 Wrought Nickel Anode Materials

The first anode material developed intentionally to obtain improved performance was wrought depolarized nickel (ca. 1929). That material contains greater than 99% nickel, about 0.5% nickel oxide, and a minute amount of sulfur. In discussing the uniform dissolution and enhanced activity of wrought depolarized nickel, Wesley considered the effect of nickel oxide on sulfur distribution to be the key factor [114]; nickel oxide may prevent or interfere with the formation of nickel sulfide at grain boundaries where it would lead to nonuniform anode dissolution in wrought materials. Wrought depolarized nickel anodes form a brown film and metallic particles during dissolution, and they must be encased in anode bags to prevent those residues from entering the solution and causing roughness at the cathode. Although this anode material dissolves smoothly, it still has some of the disadvantages of the electrolytic nickel strip; that is, anode area and current density change during electroplating and operations usually have to be interrupted to replace anodes and anode bags. But because this material is made by hot rolling, there is no size limitation, and lengths suitable for large-scale electroplating in deep tanks are commercially available.

The wrought carbon anodes introduced in 1938 contain about 0.25% carbon and about 0.25% silicon. During dissolution, silicon is oxidized to silicic acid which, in combination with carbon, forms a thick, highly retentive, black film on the surface which keeps tiny metallic particles in contact with the anode long enough for them to dissolve [115]. Increased acidity of the anolyte due to the silicic acid is believed to promote uniform dissolution of this material. Rolled carbon anodes form little, if any, metallic residue, but they are nevertheless used with anode bags to keep carbon plus silicon residues out of solution. Because the silicon is oxidized, anode efficiency depends on the silicon content of the anode material, which is less than 100%. Work to develop an improved auxiliary anode material for use without anode bags indicated that lowering the carbon to 0.15% and increasing the silicon content to 1% or more was beneficial in eliminating roughness-producing metallic particles [116].

3.6.2 Anodic Behavior of Primary Nickel

The limitations of primary electrolytic nickel are related to its tendency to become passive when dissolved anodically. In nickel sulfate solutions, the anodic polarization curve for nickel obtained potentiostatically under *quasi-equilibrium* conditions exhibits distinct active, passive, and transpassive regions [117]. The departure of the active portion of the curve from linearity as E_{pp} is approached, as illustrated in Figure 3.9, is the point where an oxide film begins to form on the anode surface, where E_{pp} is the critical or principal passivation potential. The Flade potential, E_p, is the point

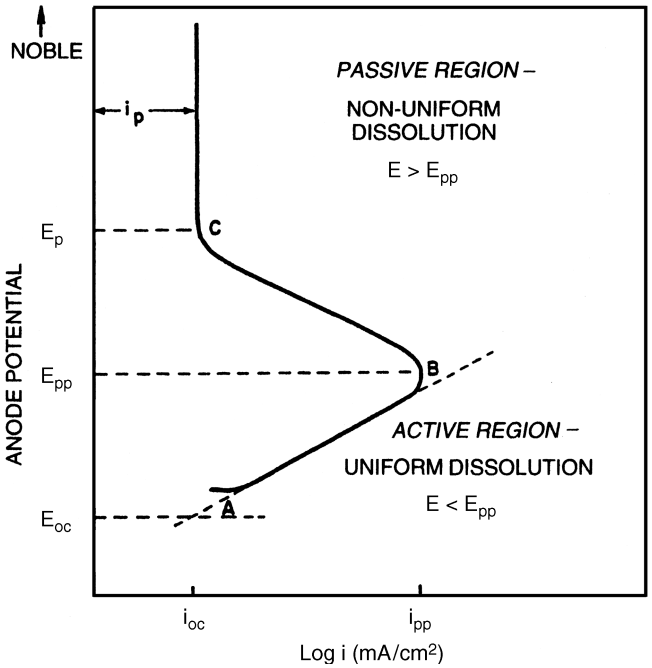

FIGURE 3.9 Idealized anodic polarization curve obtained potentiostatically for pure nickel in chloride-free nickel sulfate solutions [120]: E_{oc}, open-circuit potential; E_{pp}, principal or critical passivation potential; E_p, passivation potential; i_{oc}, corrosion current density; i_{pp}, principal passivation current density; i_p, current density in passive region. *AB* is the active region, *BC* the active-to-passive transition region, and *C* the beginning of the passive region.

where film formation is complete; that is, where an oxide film completely covers the surface and conducts electricity electronically rather than ionically. In the passive region, the nickel oxide film increases in thickness. In the transpassive region, the current density increases rapidly as a result of the oxidation of hydroxyl ions and the generation of oxygen. Because the value of the current density at E_{pp} is very low, pure electrolytic nickel cannot be used to replenish nickel ions in a nickel sulfate electroplating solution that does not contain chloride ions.

When *E–I* curves are measured *potentiodynamically*, the shapes of the curves are affected by the sweep rate and two peaks corresponding to the formation of NiO and NiO_2 appear at low and high potentials, respectively, as reported by Hart and by Chatfield and Shreir [118, 119]. Whether the higher oxides of nickel are formed under actual electroplating conditions is not known.

When nickel chloride (Fig. 3.10) is added to nickel sulfate solutions, the active-to-passive transition region is still observed, but at an applied potential of about $+0.2$ V versus SCE, the current on the anode rises rapidly [120]. Hart and co-workers confirmed that the transition from active to passive dissolution occurs even at very high chloride

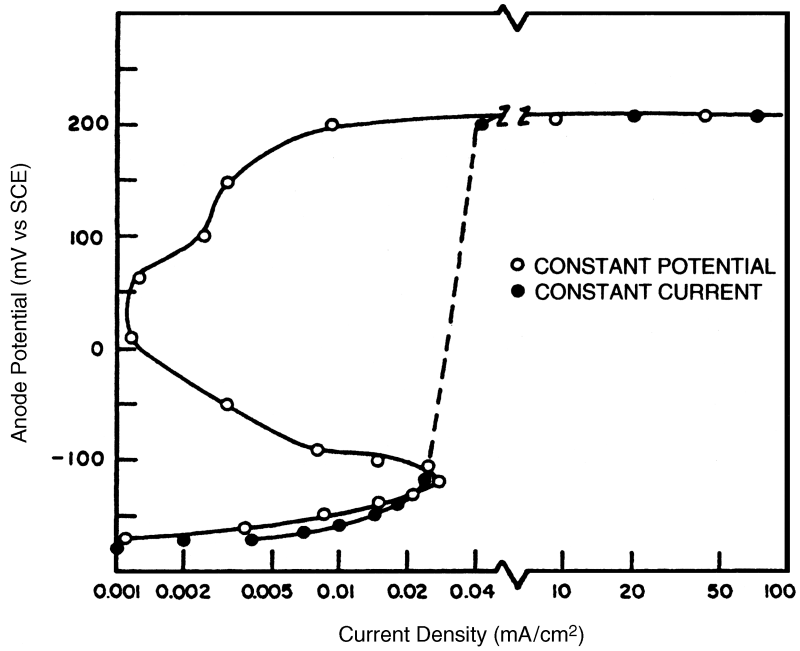

FIGURE 3.10 Anodic polarization of pure nickel in a Watts solution containing $14\,g\,L^{-1}$ of chloride at pH 4, 55°C, obtained potentiostatically (constant potential) and galvanostatically (constant current) from [120].

concentrations [121]. The persistence of the active-to-passive transition region suggests that an oxide film forms in the presence of chlorides but does not increase in thickness. Under practical plating conditions, pure electrolytic nickel dissolves at a constant potential, $+0.2$ V versus SCE, over a wide range of current density when chlorides are present, and the rate of dissolution is virtually independent of the anode potential [120].

The nonuniform dissolution of electrolytic nickel observed in most commercial nickel electroplating solutions, that is, its tendency to dissolve through pits on the surface and to become spongy at advanced stages of dissolution, is due to the oxide film on its surface, and a correlation between the electrochemical and the *physical* dissolution characteristics exists. That is, nickel dissolves nonuniformly when its dissolution potential exceeds the peak potential, E_{pp}, and uniformly below that potential [120].

It is unlikely that the reaction taking place in the active region is simply $Ni \rightarrow Ni^{2+} + 2e^-$. Active dissolution of nickel in a chloride-free nickel sulfate solution involves adsorbed hydroxyl ions and may proceed in three consecutive steps as follows [122].

1. $Ni + OH \rightarrow NiOH_{adsorbed} + e^-$
2. $NiOH_{adsorbed} \rightarrow NiOH^+ + e^-$
3. $NiOH^+ \rightarrow Ni^{2+} + OH^-$

The reactions responsible for the transition from active-to-passive behavior may be written

4. $NiOH_{adsorbed} + OH^- \rightarrow Ni(OH)_{2\downarrow} + e^-$
5. $Ni(OH)_{2\downarrow} \rightarrow NiO_{\downarrow} + H_2O$

The anodic polarization characteristics of nickel are the result of the competition among these reactions. The rate-determining step changes (from 3 to 2 to 1) as overvoltage is increased. At potentials where reactions 4 and 5 are possible, the percentage of the surface area covered with an oxide film increases, and accordingly, the current density gradually decreases in the transition region. In the presence of chlorides, species like $NiCl_{adsorbed}$ and $NiCl^+$ interfere with the formation of nickel hydroxide and thickening of the oxide film. This *chloride-assisted* dissolution increases anode efficiency to 100%, but dissolution is localized and occurs beneath or through the oxide film.

3.6.3 Titanium Anode Basket and Primary Forms of Nickel

The introduction of titanium anode baskets [123] transformed nickel anode practices and led to the development of special forms of primary nickel for electroplating.

Titanium Anode Baskets Baskets for nickel electroplating are made of titanium mesh strengthened by solid strips of titanium at tops, bottoms, and edges. The baskets are encased in cloth anode bags, suspended on the anode bar by hooks that are an integral part of the baskets, and loaded with small

pieces of nickel. The mesh facilitates the free flow of plating solution. Baskets that incorporate hoppers at the tops facilitate basket loading and help prevent pieces of nickel from falling into the tank.

Titanium anode baskets were quickly accepted because of their many advantages [124]. The basket anode is large and unchanging, assuring that a uniform anode area gives constant current distribution and consistent thickness for repeat batches of the same work. Anode maintenance can be done without interfering with electroplating, and it involves topping up the load to keep the baskets filled. Conforming baskets are possible in virtually any size and shape. The anode-to-cathode distance is constant, contributing to good current distribution. Lowest cost, primary forms of nickel can be used to fill the baskets. Baskets can be semiautomatically or automatically filled with nickel, and that practice is growing in progressive electroplating shops. Anode bags last longer with anode baskets, and if the bags are tight fitting, less metallic residues are formed by electrolytic nickel anode materials.

Titanium can corrode in nickel plating solutions if it is not in contact with nickel metal (titanium is protected by the nickel), or if excessively large, solid areas of titanium are used to fabricate the baskets. Titanium cannot be used in concentrated fluoborate solutions or in solutions containing fluoride ions; small amounts of fluoride in solution activate titanium, causing it to corrode [125].

Sulfur-Containing Electrolytic Nickel Work to develop an improved primary form of nickel for use in baskets focused on finding additives that would increase the activity of the metal in electroplating solutions. Sulfur, selenium, tellurium, phosphorus, carbon, and silicon were studied. The most effective additive proved to be sulfur [117, 120]. Sulfur lowers the dissolution potential by at least 0.4 V compared to pure electrolytic nickel and transforms the mode of dissolution from nonuniform to uniform. Sulfur-containing electrolytic nickel is the most active anode material commercially available, as indicated by the data in Figure 3.11. A black nickel sulfide film forms on the

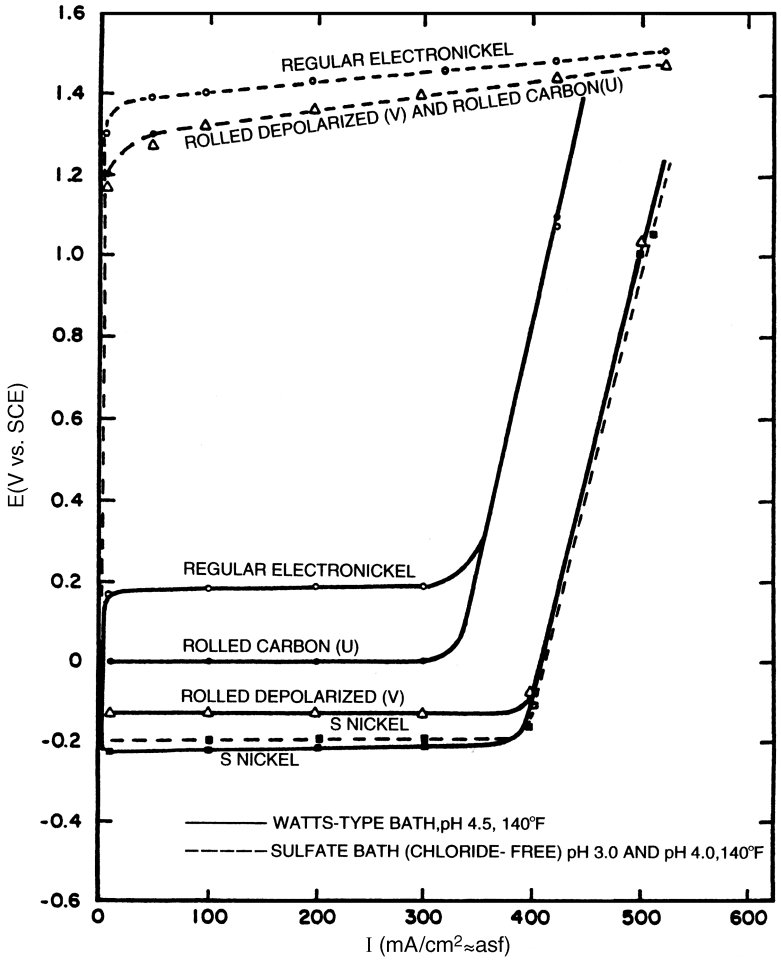

FIGURE 3.11 Anodic polarization under galvanostatic conditions of various nickel anode materials in a Watts and a chloride-free nickel sulfate solution.

surface as sulfur-activated nickel anode materials are dissolved. Because nickel sulfide is highly insoluble, sulfur in the anode material does not enter the solution but is retained in the anode bag as part of the residue. The amount of residue is less than 0.1% of the metal dissolved; that is, more than 99.9% of the nickel goes into solution. The lowering of the dissolution potential conserves energy and reduces power costs, as confirmed by tests conducted in the laboratory and in plating shops [126]. Sulfur-containing electrolytic nickel dissolves at 100% efficiency even in the absence of chloride ions, and this makes it possible to control deposit stress by eliminating chlorides from solution.

The mechanism by which sulfur depolarizes or activates electrolytic nickel has not been fully defined. Because the sulfur is present in the anode material as a sulfide and is electronegative, it may lower the effective concentration of hydroxyl ions in the anode film so that the nickel oxide film can only form at high anodic overvoltage *in the absence of chlorides*. Sulfur-containing electrolytic nickel does not appear to form an oxide film when chlorides are present in solution. DiBari and Petrocelli first suggested that adsorbed sulfur-containing anions might be responsible for the activation [117]; Morris and Fisher proposed that a tiny amount of the sulfur in the anode material is oxidized to form an anion, perhaps thiosulfate, that prevents oxide film formation by specific adsorption [127].

Electrolytic nickel containing a small amount of sulfur first became available in the form of sheared squares in 1963 [128]. Two forms of sulfur-containing nickel were introduced in 1972: a button-shaped material made by electro winning and a spherical form made by the decomposition of nickel carbonyl. Electroplaters quickly converted to the round and spherical forms because of their better settling characteristics compared to the electrolytic nickel squares that bridge and hang up at their corners.

Other Primary Forms of Nickel for Baskets Available forms of primary nickel for baskets include nonactivated, high-purity electrolytic nickel in buttonlike shapes [129] and screened nickel pellet made by the decomposition of nickel carbonyl. Electrolytic nickel squares about 25×25 mm and, to a less extent, squares that are 100×100 mm are used to fill baskets, but that practice is becoming obsolete except in some rapidly developing economies.

3.7 QUALITY CONTROL

Process quality control involves maintaining the concentrations of the main constituents within specified limits; controlling pH, temperature, and current density; and maintaining the purity of nickel electroplating solutions. Product quality control includes eliminating coating defects, properly preparing substrates prior to electroplating, as well as conducting tests to verify that specified product requirements have been met. The basic nickel electroplating facts in Table 3.10 and the conversion factors in Table 3.11 are often required for calculations related to quality control.

TABLE 3.10 Nickel Electroplating Facts

Symbol	Ni	
Atomic weight	58.69	
Valency	2	
Specific gravity	8.90	
Plating rate, at 100% cathode efficiency	1.095 g Am-h^{-1} (0.039 oz Am-h^{-1})	
Nickel sulfate	$NiSO_4 \cdot 6H_2O$	Contains 22.3% nickel
Nickel chloride	$NiCl_2 \cdot 6H_2O$	Contains 24.7% nickel
Nickel sulfamate	$Ni(NH_2SO_3)_2$	Contains 23.2% nickel
Nickel carbonate	$NiCO_3$	Contains about 46% nickel

3.7.1 Process Control

Controlling the composition of the plating bath is one of the most important factors contributing to the quality of electrodeposited nickel. At the outset, the bath must be prepared to the specified composition, adjusted to the proper pH, and purified before use. Thereafter the composition and pH of the solution must be controlled within specified limits, and contamination by metallic, organic, and gaseous substances must be prevented.

Main Constituents The basic constituents of nickel electroplating solutions that are regularly controlled are the nickel metal content, the chloride concentration, the boric acid level, and the concentration of all addition agents. Nickel metal concentration is maintained between 60 and 80 g L^{-1} in most commercial applications. It is desirable to have a minimum of 25 g L^{-1} nickel chloride in the solution to promote anode corrosion except when sulfur-activated electrolytic nickel anode materials are used. Boric acid is the most commonly used buffering agent for nickel plating baths. Boric acid is effective in stabilizing the pH in the cathode film within the ranges normally required for best plating performance. It is available in a purified form and is inexpensive. Organic addition agents must be controlled within the limits specified by the suppliers of proprietary processes, and they must be replenished due to losses from drag-out, electrolytic consumption, and the effects of carbon filtration (or batch treatment).

Traditional procedures for chemical analysis of nickel, chloride, boric acid, and organic addition agents in nickel electroplating solutions exist that are based on titration, precipitation, and other wet chemical techniques, but these procedures have been supplanted in many cases by

TABLE 3.11 Units and Conversion Factors for Electroplating

Quantity	Traditional Unit (A)	SI Unit[a] (B)	To Convert from A to B Multiply by	To Convert from B to A Multiply by
Coating thickness	mil	μm	25.4	0.0394
	in.	mm	25.4	0.0394
Coating mass (weight)	mg in.$^{-2}$	g m^{-2}	1.55	0.645
	mg in.$^{-2}$	mg cm^{-2}	0.155	6.45
	oz in.$^{-2}$	kg m^{-2}	43.9	0.0228
	oz ft^{-2}	kg m^{-2}	0.305	3.28
Current density	A ft^{-2}	A m^{-2}	10.76	0.0929
	A ft^{-2}	A dm^{-2}	0.1076	9.29
	A in.$^{-2}$	A m^{-2}	1550	6.45×10^{-4}
	A in.$^{-2}$	A cm^{-2}	0.155	6.45
Plating rate	A-h ft^{-2} -mil	A-s m^{-2} -mm	1530	6.55×10^{-4}
Volume	gal	m^3	0.00379	264
	gal	L	3.79	0.264
	fl oz	mL	29.6	0.0338
Mass concentration	oz gal^{-1}	g L^{-1}	7.49	0.134
		kg m^{-3}	7.49	0.134
Volume concentration	fl oz gal^{-1}	M L^{-1}	7.81	0.128
		cm^3 L^{-1}	7.81	0.128
Force (internal stress)	1000 psi	MPa (Mn m^{-2})	6.89	0.145

instrumental techniques that are rapid and accurate. Suppliers of decorative nickel electroplating solutions usually provide methods for analyzing and controlling the specific organic additives in their processes. Liquid chromatography has become popular for controlling organic additives, and electroanalytical methods, like polarography, have been applied to the control of electroplating solutions [130, 131].

Controlling pH, Temperature, Current Density, and Water Quality The pH of the nickel plating solution will rise during normal operation of the bath, necessitating regular additions of acid to maintain the pH within the prescribed limits. (A decrease in pH accompanied by a decrease in nickel ion concentration indicates that the process is not functioning properly.) In Watts solutions, sulfuric acid is added for pH adjustment; sulfamic acid is added to control the pH of nickel sulfamate solutions. The pH of nickel plating solutions should be measured frequently, and it is most often done by an electrometric method employing a glass electrode and a saturated calomel reference electrode.

The operating temperature has a significant effect on the properties of the deposits and should be maintained within specified limits (±2°C) of the recommended value. In general, most commercial nickel plating baths are operated between 40 and 60°C.

The nickel plating process should be controlled by estimating the surface area of the parts to be electroplated and the ampere-hours required to deposit a specified thickness of nickel at a specified current density. The practice of operating the process at a fixed voltage is not recommended. Controlling cathode current density is important for meeting minimum coating thickness requirements and for producing deposits with consistent and predictable properties.

Since current density determines the rate of deposition, it must be as uniform as possible to achieve uniformly thick nickel deposits. Current distribution is controlled by proper rack design and proper placement of components on racks, by the use of nonconducting shields and baffles, and by the use of auxiliary anodes, when necessary. With care, relatively good thickness distribution can be achieved.

The quality of the water used in making up the bath and in replacing water lost by evaporation is important. Demineralized water should be used, especially if the local tap water has a high calcium content, greater than 200 ppm. Filtering the water before it is added to the plating tank is a useful precaution to eliminate particles that can cause rough deposits.

Controlling Impurities Inorganic, organic, and gaseous impurities may be introduced into nickel plating solutions during normal operations. Continuing efforts to eliminate the sources of these impurities from the plating shop can improve the quality of the deposits as well as productivity and profitability. Inorganic contaminants arise from numerous sources, including nickel salts of technical grade, hard water, carry-over from acid dip tanks, airborne dust, bipolar attack of metallic immersion heaters, corrosion of the tank material through cracks in the lining, corrosion of anode bars, dirt

TABLE 3.12 Maximum Concentrations for Contaminants in Nickel Plating Solutions

Contaminant	Maximum Concentration (ppm)
Aluminum	60
Chromium	10
Copper	30
Iron	50
Lead	2
Zinc	20
Calcium	[a]

Note: The limits are different when several contaminants are present at the same time when complexing agents are part of the solution formulation.

[a] Calcium will precipitate at the saturation point, about $0.5\,g\,L^{-1}$, but the exact saturation point is dependent on solution pH.

from structures above the tank, and parts that fall into the solution and are not removed.

Table 3.12 lists maximum limits for inorganic, metallic impurities in nickel plating baths. The degree of contamination by many inorganic materials may be controlled by continuous filtration and low-current-density electrolysis at 0.2–0.5 A dm^{-2}. This may be accomplished on a batch basis or continuously by installing a compartment and overflow dam at one end of the electroplating tank. Solution from the filter is pumped into the bottom of the compartment, up past corrugated cathode sheets, over the dam, into the electroplating section of the tank, out through a bottom outlet at the far end of the tank, and back to the filter. Solid particles and soluble metallic impurities (e.g., copper, zinc, and lead) are removed simultaneously by this procedure. The effects of chromium, copper, iron, zinc, and lead impurities on some properties of nickel deposits were evaluated many years ago, and that information is still useful [132].

Organic contaminants may arise from many sources, including buffing compounds, lubricating oil dropped from overhead equipment, sizing from anode bags, waving lubricants on plastic anode bags, uncured rack coatings or stop-off lacquers, adhesives on certain types of masking tape, decomposition products from wetting agents, organic stabilizers in hydrogen peroxide, paint spray, and new or patched rubber tank linings.

Many organic contaminants can be effectively removed from nickel plating solutions by adsorption on activated carbon on either a batch or a continuous basis. On a batch basis, the solution is transferred to a spare tank, heated to 60–71°C, stirred for several hours with a slurry of $6\,g\,L^{-1}$ minimum of activated carbon, permitted to settle, and then filtered back into the plating tank. It is usually necessary to do a complete chemical analysis and adjust the composition of the solution after this type of treatment.

For solutions in which organic contamination is a recurring problem, continuous circulation of the solution through a filter, coated at frequent intervals with small amounts of fresh activated carbon, is recommended. When continuous carbon filtration is used, the wetting agent in the solution must be replenished and controlled more carefully to prevent pitting of the nickel deposits. In cases of severe organic contamination, it may be necessary to treat the solution with potassium permanganate prior to treating with carbon [133]. This should be used only as a last resort because of the difficulty of removing manganese dioxide and other precipitated solids; in the case of a proprietary solution, the supplier of the process should first be consulted.

Gaseous contamination of nickel plating solutions usually consists of dissolved air or carbon dioxide. Dissolved air in small amounts may lead to a type of pitting characterized by a teardrop pattern. Dissolved air in the plating solution usually can be traced to entrainment of air in the pumping system when the solution is circulated. If this occurs, circulating pump and valves should be checked and modified, if necessary. Nickel plating solutions can be purged of dissolved air by heating to a temperature at least 6°C higher than the normal operating temperature for several hours. The solution is cooled to the operating temperature before plating is resumed. Dissolved carbon dioxide in a nickel plating solution is usually found after nickel carbonate has been added to raise the pH and is liberated from warm nickel plating solutions after several hours. If solutions containing carbon dioxide are scheduled for immediate use, they should be purged by a combination of heating and air agitation for approximately 1 h at 6°C or more above the normal plating temperature.

Effects of Impurities on Bright Nickel Plating Metallic and organic contaminants affect bright nickel electrodeposition in the following ways [134]:

- Aluminum and silicon produce hazes, generally in areas of medium-to-high current density, and they may also cause a fine roughness called salt and pepper, or stardust.
- Iron may produce roughness, particularly at high pH.
- Calcium contributes to needletike roughness as a result of the precipitation of calcium sulfate when calcium in solution exceeds the saturation point of $0.5\,g\,L^{-1}$ at 60°C.
- Chromium as chromate causes dark streaks, high-current-density gassing, and peeling. After reduction to the trivalent form by reaction with organic materials in the solution or at the cathode, chromium may produce hazing and roughness effects similar to those produced by iron, silicon, and aluminum.
- Copper, zinc, cadmium, and lead affect areas of low current density, producing hazes and dark-to-black deposits.

- Organic contaminants may also produce hazes or cloudiness on a bright deposit or result in a degradation of mechanical properties. Haze defects may occur over a broad or narrow current density range.
- Mechanical defects producing hairline cracks, called macrocracking, may be encountered if the coating is sufficiently stressed as a result of solution contamination. These cracks usually appear in areas of heavier plating thickness, but they are not necessarily confined to those areas.

Contamination by zinc, aluminum, and copper is most often caused by the dissolution of zinc-based die castings that have fallen from racks into the plating tank and been permitted to remain there. Inadequate rinsing before nickel plating increases the drag-in of metallics. The presence of cadmium and lead may be attributed to a number of sources, including lead-lined equipment and tanks, impure salts, and drag-in of other plating solutions on poorly rinsed racks. Chromium is almost always carried into the nickel solution on rack tips that have not been chromium stripped or on poorly maintained racks that have been used in the chromium tank and have trapped chromium plating solution in holes, pockets, and tears in the rack coating.

Purification Techniques and Starting Up a New Bath The following procedures can be used singly or in combination to purify nickel electroplating solutions:

- The high-pH treatment consists of adding nickel carbonate to the hot solution until a pH of 5.0–5.5 is obtained. This precipitates the hydroxides of metals such as iron, aluminum, and silicon, which in turn frequently absorb other impurities. Addition of hydrogen peroxide oxidizes iron to the ferric state, making it more easily precipitated at high pH, and frequently destroys organic impurities.
- Treatment with activated carbon removes organic impurities.
- Electrolytic purification removes many harmful metallic and organic impurities.

A complete purification procedure for a freshly prepared solution consists of the following steps:

1. Use a separate treatment tank (not the plating tank) to dissolve the nickel sulfate and nickel chloride in hot water at 38–49°C to about 80% of desired volume.
2. Add 1–2 $M\,L^{-1}$ of 30% hydrogen peroxide; agitate briefly and allow to settle for 1 h.
3. Add 1.2–2.5 $g\,L^{-1}$ activated carbon and agitate thoroughly.
4. Heat to 66°C, then add 1.2–2.5 g L^{-1} of nickel carbonate to the solution, with agitation to adjust the pH to 5.2–5.5. More nickel carbonate may be required and the mixture should be stirred to assist the dissolution of the carbonate. Allow to settle 8–16 h.
5. Filter into the plating tank.
6. Add and dissolve boric acid; add water to bring bath up to its desired volume.
7. Electrolytically purify by using a large area of nickel-plated corrugated steel sheets as cathodes. The average cathode current density should be 0.5 A dm^{-2} and treatment should continue until 0.5–1.5 Ah L^{-1} has passed through the solution. The solution should be agitated and the temperature held at 49–60°C. Prepare deposits at normal current densities at some point to check appearance, stress, and sulfur content; if not acceptable, continue the electrolytic purification until the properties are acceptable.
8. Remove the dummy cathodes and adjust the pH of the solution to the desired value.

3.7.2 Product Control

The nature of coating defects in parts that have been unsuccessfully electroplated may indicate the source of quality problems. Other aspects of product quality control include preparation of metals prior to electroplating and testing nickel electrodeposits.

Coating Defects Common defects include roughness, pitting, blistering, high stress and low ductility, discoloration, burning at high current density areas, and failure to meet thickness specifications [133].

- Roughness is usually caused by the incorporation of insoluble particles in the deposit. In bright nickel baths, chlorine generated at an auxiliary anode that is close to the cathode can react with organic additives to form insoluble particles. Insoluble particles may arise from incomplete polishing of the basis metal so that silvers of metal protrude from the surface, incomplete cleaning of the surface so that soil particles remain on the surface, detached flakes of deposit from improperly cleaned racks, dust carried into the tank from metal-polishing operations and other activities, insoluble salts, and metallic residues from the anode material.
- Roughness from incomplete polishing, cleaning, and inadequate rack maintenance is avoided by good housekeeping and regular inspection and control. Roughness caused by dust can be controlled by isolating surface preparation and metal-polishing operations from the plating area, by providing a supply of clean air, and by removing dirt from areas near and above the tanks.

Roughness caused by the precipitation of calcium sulfate can be avoided by using de-mineralized water. Continuous filtration of the plating solution so as to turn over the solution at least once an hour is important for minimizing roughness problems. Anode residues must be retained within anode bags, and care should be taken not to damage the bags or allow the solution level to rise above the tops of the bags.

- Pitting is caused by many factors, including adhesion of air or hydrogen bubbles to the parts being plated. Air should be expelled, as already mentioned. Pitting from adherent hydrogen bubbles can result from a solution that is chemically out of balance, at too low a pH, or is inadequately agitated. Incorrect racking of complicated components, too low a concentration of wetting or antipitting agents, use of incompatible wetting agents, the presence of organic contaminants, the presence of copper ions and other inorganic impurities, incomplete cleaning of the basis material, incomplete dissolution of organic additives that may form oily globules can all result in pitting. Pitting is therefore avoided by maintaining the composition of the plating solution within specified limits, by controlling the pH and temperature, and by preventing impurities of all kinds from entering the solution.
- Blistering is generally due to poor adhesion as a result of poor or incorrect surface preparation prior to plating (see next section). Blistering may also be related to incomplete removal of grease, dirt, or oxides; formation of metal soaps from polishing compounds; or silica films from cleaning solutions. In the case of zinc-based die castings or aluminum castings, blistering during or immediately after plating may be due to surface porosity and imperfections that trap plating solution under the coating.
- High stress and low ductility usually occur when organic addition agents are out of balance and also because of the presence of impurities.
- Discoloration in low-current-density areas is most likely the consequence of metallic contamination of the plating solution. The effects can be evaluated systematically by plating over a reproducible range of current densities on a Hull cell cathode. Hull cells are available from plating supply houses and are shaped so that nickel can be deposited onto a standard panel over a predictable range of current densities. The variation in current density over the face of the panel is achieved by placing the panel at a specified angle to the anode. Bent panels that are L shaped and that are plated with the recessed area facing the anode can also be used to assess discoloration at low-current-density areas, and they may provide information on roughness problems.
- Burning at high current densities can be caused by applying the full load on the rectifier to the lowest parts on a rack as it is lowered into the tank. This can be controlled by applying a reduced load or ramping the current during immersion of the rack. Burning is sometimes related to the presence of phosphates in solution introduced via contaminated activated carbon. Incorrect levels of organic additives can cause burning.
- Failure to meet thickness specifications is most frequently due to the application of too low a current and/or too short a plating time. This can be avoided by measuring the area of the parts to be plated, then calculating the total current required for a specified current density, and plating for the appropriate time. Another major cause of failure to meet thickness requirements is nonuniform distribution of current leading to insufficient deposit in low-current-density areas. Poor electrical contacts and stray currents can also cause thin deposits. Anode and cathode bars, hooks, and contacts should be kept clean.

Preparation Prior to Plating Nickel can be deposited adherently on most metals and alloys, plastics, and other materials by following standard methods of preparation and activation, including proper use of intermediate deposits such as cyanide copper, acid copper, and acid (Wood's) nickel chloride strikes. Standard procedures for the preparation of materials prior to electroplating can be found in handbooks and in ASTM standards [23, 24].

Controlling and Testing Deposits Properties The requirements for testing electrodeposited nickel coatings vary depending on the application. In decorative applications the appearance and the thickness of the deposit should be controlled and monitored on a regular basis. The plated surface must be free of defects such as blisters, roughness, pits, cracks, discoloration, stains, and unplated areas. It must also have the required finish: bright, satin, or semibright. In the case of decorative multilayered coatings, the sulfur contents of the deposits, the relative thicknesses of individual layers, the ductility of the semibright nickel layer, and the differences in electrochemical potentials between individual layers should be controlled. Requirements for corrosion performance and adhesion may also be specified and may require additional testing. In functional and electroforming applications, it may be necessary to monitor hardness, ductility, and internal stress in addition to thickness and appearance. Some test methods are briefly reviewed below:

- *Thickness* The coulometric method described in ISO Standard 2177 [79] and ASTM Standard B 504 [23] can be used to measure the chromium and nickel

thicknesses as well as the thickness of copper undercoats, if present. The coulometric method measures the quantity of electrical energy required to deplate a small, carefully defined area of the component under test. A cell is sealed to the test surface and filled with the appropriate electrolyte; then a cathode is inserted. The component is made the anode, and the circuit is connected to the power supply via an electronic coulometer. By integrating time in seconds with the current passing, the electronic coulometer provides a direct reading in coulombs; modern instruments provide a direct reading of thickness. The completion of the deplating is shown by a marked change in the applied voltage. For routine control of production, it is convenient to monitor nickel thickness nondestructively by means of a magnetic gauge, calibrating the gauge at intervals with standard samples. Instruments for measuring thickness by beta backscatter, X-ray spectrometry, and eddy current techniques are also available. The traditional method of measuring thickness by microscopic examination of a metallographically prepared cross section of the plated part is still employed, but it is time consuming, expensive, and destructive. ASTM Standard B 659 [23] is a general guide to the measurement of thickness of electrodeposited coatings on different substrates.

- *STEP Test* This test was developed to measure potential differences between individual layers of nickel in decorative nickel coatings on production parts. It is similar to the coulometric method just described. By including a reference electrode in the circuit, however, it is possible to measure the potential of the material being dissolved at the same time that the thickness of the individual layers is being measured. With a double-layer nickel coating, a relatively large change in potential occurs when the bright nickel layer has dissolved and the semibright nickel layer begins to be attacked. The potential difference is related to overall corrosion resistance and should be greater than 100 mV. Details can be found in ASTM Standard Test Method B-764 [23].
- *Corrosion Testing* When corrosion performance is specified, the electroplater may be required to perform accelerated corrosion tests on a specified number of production parts. Three accelerated corrosion tests are recognized internationally. They are the copper-accelerated acetic acid salt spray (CASS), the Corrodkote, and the acetic acid salt spray tests. The CASS and Corrodkote tests were developed when conventional chromium was the only type of chromium available; when used to evaluate microdiscontinuous chromium coatings, the surface appearance deteriorates more rapidly than in real-world environments. Details of these three tests can be found in ISO Standard 1456 [79] as well as in ASTM Standards B 368 (CASS) and B 380 {Corrodkote) [23]. CASS and other corrosion test requirements are specified in ASTM Standard Specification B 456 [23] for nickel-plus-chromium coatings applied to steel, zinc alloys, or copper alloys. Similar information for nickel-plus-chromium coatings on plastics is given in ASTM Standard Specification B 604 [23].
- *Thermal Cycle Testing* Thermal cycle testing is specified for controlling the quality of decorative nickel/chromium-electroplated plastics and involves exposure of electroplated parts to low and high temperatures under controlled conditions. Thermal cycle testing may be combined with accelerated corrosion testing. Test procedures are described in ASTM Standard B 604 [23].
- *Ductility* The ductility of the semibright nickel layer in a multilayered nickel coating is specified to control the properties of the deposit and to check that the solution is in good working condition. The simple test described in ISO Standard 1456 [79] and in ASTM B 489 [23] is based on bending a test strip of the deposit over a mandrel of specified diameter until the two ends of the strip are parallel. A semibright nickel deposit that meets the requirements of the bend test has an elongation percentage greater than 8. Other tests based on hydraulic or mechanical bulge testing are available [135]. The elongation percentage can also be determined by machining a test sample from relatively thick electroformed nickel and subjecting it to the conventional tensile test. Difficulties with conventional tensile testing as applied to electrodeposited coatings and films have been discussed, and improved techniques have been described [136]. Since ductility is affected by the thickness of the coating, ductility should be measured at the actual thickness specified in a specific end use [80,104, 136].
- *Adhesion* Qualitative tests for adhesion are frequently used in the electroplating shop because quantitative tests are considered costly and time consuming. The tests described in ASTM B 571 [23] include bend, burnish, chisel, file, and others that are qualitative in nature. The method for determining the peel strength of metal-electroplated plastics (ASTM Standard B 533 [23]) is quantitative and provides an average value of the bond strength when a universal tensile test machine is used in making the measurements; a less rigorous variation of the test is often applied for process control. Quantitative results can also be obtained by conical head and ring shear tensile testing and by ultrasonic, centrifuge, and flyer plate methods, which have been described in the literature [137].
- *Internal Stress Measurements* There are many ways that the internal stress of electrodeposits can be

measured, but the one most frequently applied in production is the spiral contractometer method (ASTM standard B 636 [23]). The method is based on electrodepositing nickel on the outside of a helix formed by winding a strip of metal around a cylinder followed by annealing. During the measurement of stress, one end of the helix is fixed in the contractometer and the free end is attached to an indicating needle that moves as stress develops. Internal stress can be calculated from the degree of needle deflection on the circular dial. Contractometers and precoated helices to prevent internal electroplating are commercially available. Modifications of the contractometer method, including measuring the needle deflection electronically, have been made [138]. Rigid and flexible strip methods are alternative techniques that give reliable results [139] (see also [21, 37]). The strain gage method permits stress to be monitored and controlled throughout the electrodeposition process, and the method has been applied in the production of electroformed optical parts having dimensional accuracies of 0.15 μm [140]. The dilatometer method also allows stress to be monitored continuously [141].

- *Microhardness Testing* The hardness of electrodeposited coatings can be determined by the methods described in ASTM Standard B 578 [23] and E 384. Measurements are made on the cross section of a deposit of specified thickness using a specified load on the Knoop indenter.

3.8 POLLUTION PREVENTION

Regulations to prevent pollution and to protect health and safety in the workplace have affected nickel and chromium electroplating technically and commercially. Technically, a great deal of the research effort over the past 25 years has been devoted to finding substitutes for hazardous materials and making process changes to comply with government regulations. For example, trivalent chromium to replace hexavalent chromium, zinc–nickel alloy deposits to replace cadmium, substitution of permanganates for chromates in the preparation of plastics, elimination of coumarin from nickel electroplating processes, and development of alkaline cyanide-free copper electrolytes have been driven by pollution prevention considerations to a great extent. Commercially, pollution control has increased electroplating costs and some shops that were only marginally profitable have gone out of business. The number of nickel plating shops has declined in the United States and Europe, but continues to increase in China, India, and Southeast Asia.

Although there was great resistance to plating pollution prevention and control in the early 1970s, most electroplaters in the United States and many other parts of the world are complying with existing regulations. In some cases the recycling and recovery of salts and metals coupled with the conservation of water and energy have led to economies that partially offset the cost of compliance. Efforts to minimize waste generation in an electroplating plant require good housekeeping and operating practices that tend to improve overall quality.

Strict environmental regulations have been imposed on the electroplating industry to prevent nickel and other metallic ions from entering the environment via plant effluents. Conventional processes for wastewater treatment include precipitation of nickel and other metals as hydroxides (or sulfides). If hexavalent chromium is present, it must first be reduced to the trivalent form before being precipitated. Cyanides are commonly removed by alkaline chlorination using sodium hypochlorite, but ozonation and electrochemical, thermal, and precipitation methods are known. The solid wastes generated in conventional processes for wastewater treatment are then disposed of in landfills. Because disposal of the solid waste is expensive and wasteful, the recovery of metal values by reverse osmosis, ion exchange, electrowinning, and other methods is becoming important and economically feasible [142]. Nickel producers accept nickel-containing sludges for recycling through smelters or special plants, and companies that collect and recycle electroplating wastes have grown in number.

The adoption and enforcement of strict environmental regulations arise from concern with the possible effects of metal contaminants on human health. Although the general perception is that these health effects are completely understood, the reality is that our knowledge is extremely limited. It is only when metals are present in high concentrations and in very specific forms that they may be toxic.

In a nickel electroplating shop, three types of exposure are possible: nickel and its compounds may be inadvertently ingested, nickel-containing solutions may be allowed to remain on the skin for long periods of time, and nickel and its compounds may be taken into the body by breathing [143]. Nickel and its inorganic compounds are not highly toxic substances and exposure to small amounts does not present serious health risks. Nevertheless, it is advisable to avoid ingesting even small amounts of these substances by taking some simple precautions in the workplace—wearing work gloves, washing one's hands before eating, and not eating in the workplace. Only one compound, gaseous nickel carbonyl, is known to be acutely toxic. This compound forms under special conditions in the few nickel refineries that produce high-purity nickel using nickel carbonyl as a process intermediate. It is not present or formed in the electroplating shop.

People who have become skin sensitized should avoid contact with nickel and its compounds. To avoid *becoming* sensitized, one must limit contact with nickel and its compounds. In electroplating, this may mean wearing work gloves and washing one's hands immediately after coming

in contact with nickel electroplating solutions. The risk of cancer appears to be limited to the inhalation of high concentrations of dusts containing nickel subsulfides and oxides under conditions previously existing in certain nickel refineries. Similar health problems have not been observed in electroplating and other workplaces where nickel is found. Airborne nickel in the workplace should be kept below regulatory or other acceptable exposure limits.

REFERENCES

1. G. A. DiBari, "Nickel Electroplating Applications and Trends," *Plating Surf. Finish.*, **83** (10), 10 (1996); G. A. DiBari and S. A. Watson, "A Review of Recent Trends in Nickel Electroplating Technology in North America and Europe," *NiDI Reprint Series*, No. 14024, Nickel Development Institute, Toronto, Ontario, Canada (Nov. 1992); G. A. DiBari, "Plenary Paper—Survey of New Applications in Surface Finishing Technology," *Proc. 4th Int. Congress on Surface Technology, Berlin '87*, published by AMK Berlin, Berlin.
2. G. Bird, *Philos. Trans.*, **127**, 37 (1837).
3. J. Shore, U.K.. Patent 8407 (1840).
4. R. Bottger, "Investigation of Nickel Plating on Metals," *Erdmann's J. Praktische Chemie*, **30**, 267 (1843).
5. G. Dubpernell, 'The Story of Nickel Plating," *Plating*, **46**, 599 (1959).
6. J. K. Dennis and T. E. Such, *Nickel and Chromium Plating*, 3rd ed., Woodhead Publ., Cambridge, England, 1993.
7. W. H. Remington, U.S. Patent 82,877 (1868).
8. E. Weston, U.S. Patent 211,071 (1878).
9. W. D. Bancroft, *Trans. Am. Electrochem. Soc*, **9**, 218 (1906).
10. O. P. Watts, *Trans. Am. Electrochem. Soc.*, **29**, 395 (1916).
11. M: Schlotter, U.S. Patent 1,972,693 (1934).
12. A. S. DuRose, U.S. Patent 2,635,076 (1953).
13. L. Cambi and R. Piontelli, Italian Patent 368,824 (1939).
14. P. C. Crouch and H. V. Hendricksen, *Trans. Inst. Metal Finish.*, **61**, 133 (1983).
15. G. A. DiBari and R. A. Covert, "Nickel Buildup in Plating Baths," *Products Finishing*, Nov. 1989, p. 70. See summary of presentation at AESF Sur/Fin '89 by Craig Brown, Exec. VP, Eco-Tech Ltd., Pickering, Ontario, Canada, included in that paper.
16. U. Landau, "Morphology and Thickness Distribution of Electrodeposits," in *Proc. Symp. on Electrodeposition Technology, Theory and Practice*, L. T. Romankiw and D. R. Turner, Eds., Electrochemical Society, Pennington, NJ, 1987, p. 589; G. E. Giles, "Electroforming Cell Design Tool Development," in *Proc. AESF Electroforming Symposium*, Mar. 27–29, 1996, p. 75.
17. J. Kronsbein, *Plating*, **37**, 851 (1950).
18. H. E. Haring and W. Blum, *Trans. Am. Electrochem. Soc.*, **44**, 313 (1923).
19. S. A. Watson, *Trans. Inst. Met. Finish.*, **37**, 28 (1950).
20. M. Ya. Popereka, *Internal Stresses in Electrolytically Deposited Metals*, transl, from Russian, Indian National Scientific Documentation Center, New Delhi, National Bureau of Standards and the National Science Foundation, Washington, DC, 1970.
21. R. Weil, "The Origins of Stress in Electrodeposits," *Plating*, **57**, 1231 (1970); **58**, 137 (1971).
22. J. W. Dini, *Electrodeposition—The Materials Science of Coatings and Substrates*, Noyes, Park Ridge, NJ, 1993, Ch. 9, p. 279; Ch. 11, p. 331.
23. *Annual Book of ASTM Standards*, Vol. 02.05, American Society for Testing and Materials, West Conshohocken, PA, 1996.
24. "1996 Metal Finishing Guidebook and Directory," *Met. Finish.*, **94** (1a), 105 (1996); D. L. Snyder and J. K. Long, "Typical Processing and Operating Sequences," in *Electroplating Engineering Handbook*, L. J. Durney, Ed., Van Nostrand Reinhold, New York, 1984, p. 174; J. B. Hadju and G. Krulik, "Plastics," *Electroplating and Engineering Handbook*, L. J. Durney, Ed., Van Nostrand Reinhold, New York, 1984, p. 202.
25. S. A. Watson and J. Edwards, *Trans. Inst. Met. Finish.*, **34**, 167 (1957).
26. O. Kardos, *Proc. Am, Electroplates Soc*, **43**, 181 (1956).
27. G. A. DiBari, "Nickel Plating," in *ASM Handbook-Surface Engineering*, Vol. 5, S. Lapman, Ed., ASM International, Materials Park, OH, 1994, p. 204.
28. R. Weil, "Epitaxial Electrocrystallization under Inhibited Growth Conditions," in *Proc. Symp. on Electrocrystallization*, R. Weil, Ed., Electrochemical Society, Pennington, NJ, 1981, p. 134.
29. M. Jousellin and R. Wiart, "Anion Dependence of Nickel Electrodeposition in Acidic Electrolytes," in *Proc. Symp. on Electrocrystallization*, R. Weil, Ed., Electrochemical Society, Pennington, NJ, 1981, p. 111; K. Raghunathan and R. Weil, *Surf. Technol.*, **10**, 1472, (1973); M. Froment and J. Thevenin, *Metaus, Corrosion, Industrie*, **59** (4), 1 (1975); J. Ambard, M. Froment, and N. Spyrellis, *Surf. Technol.*, **5**, 205 (1977); J. Amblard, I. Epelboin, M. Froment, and G. Maurin, *J. Appl. Electrochem.*, **9**, 233 (1979).
30. J. Macheras, D. Vouros, C. Kollia, and N. Spyrellis, "Nickel Electrocrystallization: Influence of Unsaturated Organic Additives on the Mechanism of Oriented Crystal Growth," *Trans. Inst. Met. Finish.*, **74** (2), 55 (1996).
31. C. Kollia and N. Spyrellis, "Crystal Growth Inhibition in Nickel Electrodeposition under Pulse Reversed Current Conditions," *Trans. Inst. Met. Finish.*, **72** (3), 124 (1994); F. Kotzia, C. Kollia, and N. Spyrellis, "Influence of Butyne-2-diol 1,4 in Nickel Electrocrystallization under Pulse Reversed Current Regime," *Trans. Inst. Met. Finish.*, **71** (1), 34 (1993).
32. R. Weil and R. Paquin, *J. Electrochem. Soc.*, **107**, 87 (1960); H. J. Read and R. Weil, *Plating*, **37**, 1257 (1950).
33. J. Edwards, "Aspects of Addition Agent Behavior," *Trans. Inst. Met. Finish.*, **41**, 169 (1964); **39**, 33, 45, 52 (1962); **41**, 140, 147, 157 (1964); **45**, 12 (1967). Several of these papers were coauthored by Margaret J. Levett.
34. D. L. Snyder, "Electroplating in the Nineties," in *Asia Pacific Interfinish 90 Proc*, Nov. 19–22, 1990, Singapore, Australian

Institute of Metal Finishing and the Singapore Metal Finishing Society, pp. 21–16.

35. J. F. Vogt and R. J. Herbert, U.S. Patent 2,635,075 (1953); C. N. Isackson, British Patent 684,434 (1952).
36. H. Brown, *Metalloberflache*, **11**, 333 (1962).
37. G. N. Flint and S. H. Melbourne, *Trans. Inst. Met. Finish.*, **39**, 85 (1960).
38. A. H. DuRose, in *Proc. AES 47th Annual Conference*, 1960, p. 83; A. H. DuRose and W. J. Pierce, *Met. Finish.*, **57**, 44 (1959).
39. W. H. Safranek, R. W. Hardy, and H. R. Miller, in *Proc. AES 48th Annual Conf.*, AESF, Orlando, FL, 1961, p. 156.
40. J. V. Petrocelli, V. Hospadaruk, and G. DiBari, "The Electrochemistry of Copper, Nickel and Chromium in the Corrodkote and CASS Test Electrolytes," *Plating*, **49**, 1 (1962).
41. G. A. DiBari, A. J. Dill, and B. B. Knapp, in *Proc. 1st AES Decorative Plating Symp.,* Dearborn, MI, 1973, p. 93.
42. G. A. DiBari, "Corrosion of Decorative Electroplated Nickel Chromium Coatings on Steel, Zinc, Aluminum and Plastics," *Met. Finish.*, **75**, 17–20 (June 1977); **75**, 17–24 (July 1977).
43. D. L. Snyder, "Quality Decorative Plating," *Prod. Finish.*, **61** (3), 40 (Dec. 1996).
44. B. B. Knapp and H. Brown, in *Modern Electroplating*, 3rd ed., F. A. Lowenheim, Ed., Wiley, New York, 1974, p. 308.
45. R. L. Saw, "Toward Protective Decorative Chromium Plating," *Plating*, **48**, 1310 (1961); R. L. Saur, "Influence of Pit Density on the Dimensions of Corrosion Pits in Decorative Plating Systems," *Pating*, **58**, 1075 (1971).
46. R. L. Saur and R. P. Basco, "An Accelerated Electrolytic Corrosion Test and a Corrosion Analysis Procedure for the Nickel-Chromium Plating System. Part I," *Plating*, **53**, 35 (1966).
47. R. L. Saur, "New Interference Microscope Techniques for Microphotographic Measurements in the Electroplating Laboratory," *Plating*, **52**, 663 (1965).
48. H. Brown and T. W. Tomaszewski, in *Proc. International Conf., Surfaces'66 (Basel)*, Forster Verlag A. G., Zurich, 1967, p. 88;U.S. Patents 3,152,971 (1964) and 3,152,973 (1964).
49. T. Malak, D. Snyder, and A. H. DuRose, "Physical Method for Creating Microporosity in Chromium," *Plating*, **59**, 659 (1972); T. G. Kubach, W. H. R. Pritsch, and W. Bolay, U.S. Patent 3,625,039 (1971).
50. W. E. Lovell, E. H. Shotwell, and J. Boyd, *Proc. Am. Electroplaters Soc*, **47**, 215 (1960); J. H. Lindsay, D. W. Hardesty, and W. E. Lovell, *Proc. Am. Electroplaters Soc.*, **48**, 165 (1961); E. J. Seyb, *Proc. Am. Electroplaters Soc.*, **47**, 209 (1960).
51. W. H. Safranek, H. R. Miller, and C. L. Faust, *Plating*, **49**, 607 (1962); W. H. Safranek and C. L. Faust, *Trans. Inst. Met. Finish.*, **42**, 41 (1964).
52. G. A. DiBari and F. X. Carlin, "Decorative Nickel Chromium Electrodeposits on Steel—15 Years of Corrosion Performance Data," *Plating*, **72** (5), 1 (1985).
53. D. L. Snyder, "Fifteen Years of Outdoor Corrosion of Trivalent and Hexavalent Chromium Deposits," *Met. Finish.*, **90**, 113 (1992); "Electroplating in the Nineties," Asia Pacific Proceedings, Metal Finishing Institute of Australia and Singapore Metal Finishing Society, Singapore, 1990, pp. 12–14.
54. Unpublished results of ASTM Corrosion Performance Programs, nos. 8–12.
55. R. J. Clauss and R. W. Klein, in *Proc. 7th International Met. Finish. Conf. Interfinish 68,* Deutsche Gesellschaft für Galvanotechnik e. V., Dusseldorf, May 1968, p. 124; E. J. Seyb, *Proc. Am. Electroptat. Soc.*, **50**, 175 (1963); W. H. Safranek and H. R. Miller, *Plating*, **55**, 233 (1968); V. E. Carter, *Trans. Inst. Met. Finish.*, **48**, 16, 19 (1970).
56. E. P. Harbulak, "Simultaneous Thickness and Electrochemical Potential Determination of Individual Layers in Multilayer Nickel Deposits," *Plating Surf. Finish.*, **67** (2), 49 (1980).
57. R. A. Tremmel, "Methods to Improve the Corrosion Performance of Microporous Nickel Deposits," *Plating Surf. Finish.*, **83** (10), 24 (1996).
58. E. B. Saubestre, L. J. Durney, J. Hajdu, and E. Bastenbeck, "The Adhesion of Electrodeposits to Plastic," *Plating*, **52**, 982 (1965); W. P. Innes, J. J. Grunwald, E. D. D'Ottavio, W. H. Toller, and C. Carmichael, "Chromium-Plated ABS and Polypropylene Plastics: Performance in Typical Tests," *Plating*, **56** (1), 51 (1969).
59. A. Rantell, *Trans. Inst. Met. Finish.*, **47**, 197 (1969); E. B. Saubestre and R. P. Khera, *Plating*, **58**, 464 (1971).
60. U.S. Patents 3,011,920; 3,874,772; 3,904,792; 3,672,923; 3,672,938; 3,682,671; 3,960,573; 3,961,109.
61. R. L. Coombes, "Electroless Copper Preplating on ABS Plastics," *Plating*, **57**, 675 (1970).
62. R. R. Wiggle, V. Hospadaruk, and D. R. Fitchmun, "The Mechanism of Adhesion Failure of Plated Plastics in Corrosive Environments," *J. Electrochem. Soc.*, **118** (1), 158 (1971).
63. R. G. Wedel, *Plating*, **62**, **40**, 235 (1975).
64. G. A. DiBari and J. V. Petrocelli, *J. Electrochem. Soc.*, **112**, 99 (1965).
65. G. A. DiBari, "Marine Corrosion Performance of Electroless Nickel Coatings on Steel—Final Report of ASTM Program 14," in *Proc. EN Conf. '91*, Orlando, FL, Gardner Publ., Cincinnati, OH, 1991.
66. J. L. Adcock, "Electroplating Plastics—An AESF Illustrated Lecture," American Electroplaters and Surface Finishers Society, Orlando, FL, 1978.
67. J. E. McCaskie, "Electroless Plating (Sulfur Dioxide Etching) of Plastic Enclosures for EMI/RFI Shielding," in *Proc. AESF Second Electroless Plating Symp.*, American Electroplaters and Surface Finishers Society (Feb. 1984).
68. J. M. Jobbins and P. Sopchak, "Chromic Acid-Free Etching (Ozone Etching)," *Met. Finish.*, **83**, 15 (1985); J. H. Lindsay and V. LaSala, "Vacuum Preplate Process (Plasma Etching) for Plating on Acrylonitrile-Butadiene-Styrene (ABS)," *Plating Surf. Finish.*, **72**, 54 (1985).
69. "Performance of Decorative Electrodeposited Copper-Nickel Chromium Coatings on Plastics," final report on programs conducted by ASEP and ASTM, on file at ASTM Headquarters, Report Number RR B-8-1003.

70. P. C. Crouch, "The Effect of Nickel Thickness and Copper Undercoats on the Performance of Plated Plastics," *Trans. Inst. Met. Finish.*, **49**, 141 (1971).
71. A. C. Hart, "Decorative Electroplating of Plastics," *Materials World*, May 1996, p. 265.
72. B. B. Knapp, *Met. Finish.*, **47** (12), 42 (1949).
73. L. Missel, *Plating Surf. Finish.*, **64** (7), 32 (1977).
74. D. W. Baudrand, "Electroless Nickel Plating of Aluminum," *Aluminum Finishing Seminar—Technical Papers*, Vol. II, Seminar held Mar 30–April 1, 1982, St. Louis, MO, Aluminum Association, Washington, DC, p. 595. (Proprietary solutions are available from plating supply houses.)
75. J. C. Jongkind and E. J. Seyb, "Pretreatment for Plating on Aluminum Using the Stannate Process," *Aluminum Finishing Seminar—Technical Papers*, Vol. II, Seminar held Mar 30–April 1, 1982, St. Louis, MO, Aluminum Association, Washington, DC, p. 539.
76. J. C. Jongkind, *Plating Surf. Finish.*, **62**, 1136 (1975); G. A. DiBari, Presentation before AESF Golden West Regional Meeting, San Diego, CA, Mar. 1981.
77. G. A. DiBari, "Plating on Aluminum—Pretreatments and Corrosion Performance," *Plating Surf. Finish.*, **64**, 68 (1977).
78. G. A. DiBari, "Decorative Electroplated Aluminum—Applications and Performance," *Aluminum Finishing Seminar—Technical Papers*, Vol. II, Seminar held Mar 30–April 1, 1982, St. Louis, MO, Aluminum Association, Washington, DC, p. 577.
79. ISO International Standard 1456, International Standards Organization, Geneva, Switzerland (1987).
80. P. Zentner, A. Brenner, and C. W. Jennings, *Plating*, **39**, 365, 1229 (1952).
81. C. B. Sanborn, "Electroforming Applications—Why They Exist," *Symp. Electrodeposited Metals as Materials for Selected Applications. Metals and Ceramics Information Center*, Battelle Columbus Laboratories, Columbus, OH, MCIC Report/Jan. 1972, p. 65.
82. B. B. Knapp and C. H. Sample, "Physical and Mechanical Properties of Electroformed Nickel at Elevated and Sub-Zero Temperatures," *Symp. on Electroforming—Applications, Uses and Properties of Electroformed Metals*, ASTM Special Technical Publication No. 318, 32–43 (1962).
83. J. W. Dini, H. R. Johnson, and L. A. West, "On the High Temperature Ductility Properties of Electrodeposited Nickel," *Plating Surf. Finish.*, **65** (2), 36 (1978); W. R. Wearmouth and K. C. Belt, "Electroforming with Heat-Resistant Sulfur-Hardened Nickel," *Plating Surf. Finish.*, **66** (10), 53 (1979).
84. W. H. Safranek, *The Properties of Electrodeposited Metals and Alloys*, 2nd ed., American Electroplaters and Surface Finishers Society, Orlando, FL, 1986.
85. J. W. Dini, *Electrodeposition—The Materials Science of Coatings and Substrates*, Noyes, Park Ridge, NJ, 1993, Ch. 5.
86. W. A. Wesley and E. J. Roehl, *Plating*, **37**, 142 (1950); C. Struyk and A. E. Carlson, *Plating*, **37**, 1242 (1950).
87. W. A. Wesley, U.S. Patent 2,331,751 (1943); W. A. Wesley and E. J. Roehl, *Trans. Electrochem. Soc.*, **82**, 37 (1942).
88. A. J. Dill, "Sulfur-Free Hardening Agents for Electrodeposited Nickel," *Plating Surf. Finish.*, **62**, 770 (1975).
89. W. A. Wesley and J. W. Carey, *Trans. Electrochem. Soc.*, **75**, 209 (1939).
90. W. A. Wesley, D. S. Carr, and E. J. Roehl, "Nickel Plating with Insoluble Anodes," *Plating*, **38**, 1243 (1951).
91. W. L. Pinner and R. B. Kinnaman, *Mon. Rev. Am. Electroplaters Soc*, **32**, 227 (1945).
92. M. R. Thompson, *Trans. Am. Electrochem. Soc*, **47**, 163 (1925).
93. *Sulfate solution:* J. G. Poor, *Met. Finish.*, **4** (11), 694 (1943). *Chloride solution:* W. A. Wesley and B. B. Knapp, U.S. Patent 2,844,530 (1958).
94. A. Brenner, D. E. Couch, and E. K. Williams, "Electrodeposition of Alloys of Phosphorus and Nickel or Cobalt," *Plating*, **37** (1), 36, (1950); **37** (2), 161 (1950).
95. D. S. Lashmore, R. Oberle, and M. P. Dariel, "Electrodeposition of Artificially Layered Materials," in *Proc. AESF 3rd Int. Pulse Plating Symposium*, American Electroplaters and Surface Finishers Society, 1986; D. S. Lashmore and J. P. Weinroth, "Pulsed Electrodeposition of Nickel-Phosphorus Metallic Glass Alloys," *Plating Surf. Finish.*, **69** (8), 72 (1982).
96. C. B. Sanborn and F. X. Carlin, 'influence of Nickel Plating on the Fatigue Life of Hardened Steel," *Symp. on Electrodeposited Metals for Selected Applications*, Battelle Columbus Laboratories, Columbus, OH, Nov. 1973.
97. O. I. Pavlova, *Electrodeposition of Metals—An Historical Survey*, U.S. Department of Commerce, Springfield, VA; C. A. Smith, "Early Electroplating, Part 2, Commencement of Industrial Applications (1836–1852)," *Finish. Ind.*, **1** (3), 24 (1978).
98. E. Gnass, "Electroforming with Dispersed Particles," *Eight Ulmer Gesprach-Galvanoformung*, Eugen G. Leuze, Saulgau, 1986, p. 75 (in German); G. Malone, "Electrodeposition of Dispersion Stengthened Alloys," *Symp. on Electrodeposited Metals for Selected Applications*, Battelle Columbus Laboratories, Columbus, OH, Nov. 1973; S. J. Harris, A. A. Baker, A. F. Hall, and R. J. Bache, "Electroforming Filament Winding Process—Method of Producing Metal Matrix Composites," *Trans. Inst. Met. Finish.*, **49** (5), 205 (1971).
99. L. T. Romankiw, "Electroforming of Electronic Devices," *Plating*, **84** (1), 10 (1997); L. T. Romankiw, "Evolution of Plating through Lithographic Mask Technology," in *Proc, ECS Symp. on Magnetic Materials, Processes and Devices IV, Applications to Storage and Microelectromechanical Systems (MEMS)*, L. T. Romankiw and D. A. Herman Jr., Eds., Electrochemical Society, Pennington, NJ, 1995.
100. E. W. Becker, W. Ehrfeld, P. Hagman, A. Mauer, and D. Muchmayer, "Fabrication of Microstructure with High Aspect Ratios and Great Structural Heights by Synchrotron Radiation Lithography, Galvanoforming and Plastic Molding," *Microelectron. Eng.*, **4**, 34 (1986).
101. J. L. Marti, "Effect of Some Variables upon Internal Stress of Nickel Deposited from Sulfamate Solutions," *Plating*, **53** (1), 61 (1966).

102. A. F. Greene, *Plating*, **55**, 594 (1968); O. J. Klingenmaier, *Plating*, **52**, 1138 (1965).
103. B. B. Knapp, "Notes on Nickel Plating From Sulfamate Solutions," *Plating*, **58**, 1187 (1971).
104. G. A. DiBari, "Evaluation of a Simple, Thin Film Ductility Tester and Review of the Ductility of Nickel Sulfamate Deposits," *Plating*, **79**, 63 (1992).
105. R. J. Kendrick, "High-Speed Nickel Plating from Sulfamate Solutions," *Proc. 6th Int. Conf, on Electrodeposition, Trans. Ins I. Met. Finish.*, **41**, 235 (1964).
106. R. J. Kendrick and S. A. Watson, in *Proc. Symp. on Sulfamic Acid,* Milan, May 1966, p. 197.
107. Z. Hai-Yan and Z. Liang-Yu, in *Proc. AESF Annual Conf.,* Session O, Chicago, 1987.
108. J. M. Notley, "Corner Weakness in Nickel Electroforms," *Trans. Inst. Met. Finish.*, **50** (1), 6 (1972).
109. G. A. DiBari, "Electroforming," in *Electroplating Engineering Handbook*, 4th ed., L. J. Durney, Ed., Van Nostrand Reinhold, New York, 1984, p. 474; *Nickel Electroforming*, International Nickel, Saddle Brook, NJ, 1991; booklet available on request.
110. S. A. Watson, "Electroforming Today," *Asia Pacific Interfinish '90 Proc.*, Australian Institute of Metal Finishing and Singapore Metal Finishing Society, Singapore, 1990, p. 5–1.
111. L. T. Romankiw and T. A. Palumbo, "Electrodeposition in the Electronics Industry," in *Proc. Symp. on Electrodeposition Technology, Theory and Practice*, L. T. Romankiw and D. R. Turner, Eds., Electrochemical Society, Pennington, NJ, 1987.
112. I. M. Croll and L. T. Romankiw, "Iron, Cobalt and Nickel Plating for Electronics," in *Proc. Symp. on Electrodeposition Technology*, L. T. Romankiew and D. R. Turner, Eds., Electrochemical Society, Pennington, NJ, 1987, p. 285.
113. S. Harsch, D. Muchmayer, and H. Reinecke, "Electroforming of Movable Microdevices Manufactured by the LIGA-Process," in *Proc. Electroforming Session (Toronto)*, American Electroplaters and Surface Finishers Society, Orlando, FL, 1991.
114. W. A. Wesley, "Nickel Atoms, Ions and Electrons," *Trans. Inst. Met. Finish.*, **33**, 452 (1956).
115. B. Wenderott, "The Solubility of Carbonised Nickel Anodes," *Metalloberflache*, **17** (6), 169 (1963).
116. G. A. DiBari, B. B. Knapp, and C. H. Sample, U.S. Patent 3,449,224 (1969).
117. G. A. DiBari and J. V. Petrocelli, "Effect of Composition and Structure on the Electrochemical Reactivity of Nickel," *J. Electrochem. Soc.*, **112** (1), 99 (1965).
118. A. C. Hart, "The Anodic Behavior of Nickel in Electroplating Solutions," *Proc. 9th Int. Metal Finishing Congress*, VOM, Amsterdam, 1976; *Metalloberflache*, **31**, 334 (1977); *Galvanotechnik*, **68** (7), 232 (1977).
119. C. J. Chatfield and L. L. Shreir, "Effect of Sweep Rate on the Active-Passive Transitions of the Ni/H_2SO_4 Systems," *Corrosion Sci.*, **12**, 563 (1972).
120. G. A. DiBari, "Notes on Nickel Anode Materials," *Plating Surf. Finish.*, **66**, 76 (1979); "The Effect of Sulfur, Phosphorus and Silicon Additives on Activity and Type of Corrosion of Nickel Anodes," *Plating*, **53** (12), 1440 (1966).
121. A. C. Hart, W. R. Wearmouth, and A. C. Warner, *Trans. Inst. Met. Finish.*, **54**, 56 (1976); A. C. Hart and S. A. Watson, *Met. Finish. J.*, **19**, 332 (1973).
122. G. Okamoto and N. Sato, *J. Electrochem. Soc*, **110**, 605 (1963).
123. A. G, Sleeker and V. J. Cassidy, *Plating*, **49**, 597 (1962).
124. P. Berger, "Experiences with Primary Nickel and Titanium Baskets," *Electroplating Met. Finish.*, **16** (7), 227, 253 (1963); T. J. Callaghan, "Nickel Plating with Raw Nickel," *Galvanotechnik*, **15** (8), 432 (1963).
125. F. X. Carlin and W. A. Sellers, "The Anodic Behavior of Nickel in Electroplating," *Plating*, **52** (3), 215 (1965).
126. G. L. Fisher, "Power Savings Using Sulfur-Activated Nickel Anode Materials," *Plating Surf. Finish.*, **65**, 46 (1978).
127. G. L. Fisher and P. E. Morris, *Trans. Inst. Met. Finish.*, **53**, 145 (1975).
128. G. A. DiBari, B. B. Knapp, F. X. Carlin, and L. S. Renzoni, U.S. Patent 3,437,571 (1969).
129. W. G. Borner, A. J. Dill, and G. L. Fisher, U.S. Patent 4,147,597 (1979).
130. C. Rosenstein and S. Hirsch, "Chemical Analysis of Plating Solutions," in *Metal Finishing Guidebook and Directory Issue*, Elsevier Science, New York, 1996, p. 479.
131. J. W. Dini, *Electrodeposition—The Materials Science of Coatings and Substrates*, Noyes, Park Ridge, NJ, 1993, Ch. 7, pp. 195–248.
132. "Reports of American Electroplaters' Society Research Project Number 5," *Plating*, **40**, 1391 (1953); **37**, 1157 (1950); **39**, 1343 (1952); **39**, 1033 (1952); **41**, 1307 (1954); G. J. Greenall and C. M. Whittington, "Metallic Impurities in Nickel Plating Solutions," *Plating*, **53**, 217 (1966).
133. *Inco Guide to Nickel Plating*, International Nickel, Saddle Brook, NJ, 1996.
134. L. Gianelos, 'Troubleshooting of Nickel Plating Solutions," *Plating Surf. Finish.*, **64** (8), 32 (1977); **64** (9), 32 (1977); **64** (10), 22 (1977).
135. S. Nakahara, Y. Okinaka, and H. K. Strashil, "Ductility of Plated Films: Its Measurement and Relationship to Microstructure," in *Testing of Metallic and Inorganic Coatings*, ASTM STP 947, W. B. Harding and G. A. DiBari, Eds., American Society for Testing and Materials (ASTM), West Conshohocken, PA, 1987, pp. 32–51; R. Rolff, "Significance or Ductility and New Methods of Measuring the Same," in *Testing of Metallic and Inorganic Coatings*, ASTM STP 947, W. B. Harding and G. A. DiBari, Eds., ASTM, West Conshohocken, PA, 1987, pp. 19–31.
136. I. Kim and R. Weil, 'Tension Testing of Very Thin Electrodeposits," in *Testing of Metallic and Inorganic Coatings*, ASTM STP 947, W. B. Harding and G. A. DiBari, Eds., ASTM, West Conshohocken, PA, 1987, pp. 11–18; T. D. Dudderar and F. B. Koch, "Mechanical Property Measurements

on Electrodeposited Metal Foils," in *Properties of Electrodeposits, Their Measurement and Significance*, R. Sard, H. Leidheiser, Jr., and F. Ogburn, Eds., The Electrochemical Society, Pennington, NJ, 1975.

137. J. W. Dini, *Electrodeposition—The Materials Science of Coatings and Substrates*, Noyes, Park Ridge, NJ, 1993, Ch. 3, pp. 46–89.
138. R. Weil, "The Measurement of Internal Stress in Electrodeposits," in *Properties of Electrodeposits, Their Measurement and Significance*, R. Sard, H. Leidheiser, Jr., and F. Ogburn, Eds., The Electrochemical Society, Pennington, NJ, 1975, p. 319.
139. B. Stein, "A Practical Guide to Understanding, Measuring and Controlling Stress in Electroformed Metals," in *Proc. AESF Electroforming Symp., Mar. 27–29,1996*, American Electroplaters and Surface Finishers Society, Orlando, FL, 1996, p. 49; L. Borchert, "Investigation of Methods for the Measurement of Stress in Electrodeposits," in *Proc. 50th Annual Conf.*, American Electroplaters Society, Orlando, FL, 1963.
140. R. W. George et al., "Apparatus and Method for Controlling Plating Induced Stress in Electroforming and Electroplating Processes," U.S. Patent 4,648,944 (1987).
141. W. H. Cleghorn, K. S. A. Gnanasekaran, and D. J. Hall, "Measurement of Internal Stress in Electrodeposits by a Dilatometric Method," *Met. Finish. J.*, **18** (4), 92 (1972).
142. G. C. Cushnie, *Pollution Prevention and Control Technology for Plating Operations*, National Center for Manufacturing Sciences, Ann Arbor, MI, 1994.
143. *Facts about Nickel and Health*, Inco Limited, Toronto, ON, 1996, pamphlet available on request. *Safe Use of Nickel in the Workplace-Health Guide; Safe Use of Nickel in the Workplace-Summary; and Safe Use of Nickel in the Workplace-Health Brochure*, Nickel Development Institute, Toronto, Ontario, Canada.

4

ELECTRODEPOSITION OF GOLD

PAUL A. KOHL

While all that glitters may not be gold, it is the most beautiful of all the elements in their pure form. The name *gold* comes from the Old English Anglo-Saxon word for *geolo* meaning "yellow" while the symbol, *Au*, comes from the Latin word *aurum*, meaning "glowing dawn." Historically gold was one of the first metals known. Gold has been valuable throughout the ages chiefly because of its physical properties of softness, ductility, corrosion resistance, density, and scarcity. The first gold coin dates back to about 560 BC. Gold cups and jewelry predating 3500 BC have been found in Iraq. The ancient Egyptians knew how to hammer gold into leaf as thin as 66 nm. The importance of gold as a form of currency was at a high point in the 1900s when most countries were on the gold standard. The bullion price of gold over the past 21 years is shown in Figure 4.1.

There have been about 160 metric kilotons of gold mined since it was first discovered, and it occupies about 0.005 ppm of the earth's crust. The world demand for gold in 2007 was approximately 80,000,000 troy ounces. Figure 4.2 shows the breakdown of the gold usage by industry. Jewelry comprises the largest fraction of the usage; however, much of that is not electroplated. For jewelry applications, gold is commonly alloyed with group IB or IIB metals, particularly copper, silver, platinum, and palladium, principally to improve its strength and wear resistance.

The electrodeposition of gold is a relatively new process; it has been traced to the early work of Brugnatelli in 1805 [1]. The motives behind the use of electroplated gold changed dramatically in the mid-twentieth century when the emerging electronics industry required special-purpose electrical connections. The electronics industry consumed 5,330,000 troy ounces in 1994. Figure 4.3 shows the growth in the use of gold in the electronics industry by year. The use of electroplated gold in a variety of different functions in the electronics industry has led to (1) many advances in our fundamental understanding of the electrodeposition process and (2) new electroplating technologies over the past 25 years.

Electrochemically deposited gold has satisfied many of the demands of the electronics industry. Gold has the third best electrical and thermal conductivity of all metals at room temperature. Also it has high ductility and excellent wear resistance, which are important for electrical contacts. The inertness of gold prevents the formation of insulating surface oxides (as compared to metals like aluminum). Group IIB metals (e.g., gold) are not good catalysts for other reactions, thus avoiding certain problems. For example, group IB metals (particularly platinum and palladium) can catalyze the polymerization of organic molecules forming insulating layers. In addition, gold is an excellent metal for wire bonding integrated circuits (ICs). Gold wires can be bonded to pure, soft gold pads by thermocompression bonding (300–400°C at high pressure to form a weld) or thermosonic bonding (150–200°C with ultrasonic energy to form a weld). Aluminum wires can be attached by ultrasonic bonding (ambient temperature with ultrasonic energy). These benefits have justified the high cost of gold in the packaging and interconnection of ICs.

A geographical breakdown of the use of gold in the electronics industry is also shown in Figure 4.3. Japan is the largest consumer of gold for electronic applications, followed by North America, Western Europe, and the Pacific rim (excluding Japan). Although the use of gold for electronic interconnections has maintained steady growth over the past two decades, its use has not kept pace with the more rapid growth in the microelectronics industry, primarily because of gold's high cost. The microelectronics industry has increased speed, performance, and packing density (number of transistors per unit area) while maintaining

Modern Electroplating, Fifth Edition Edited by Mordechay Schlesinger and Milan Paunovic

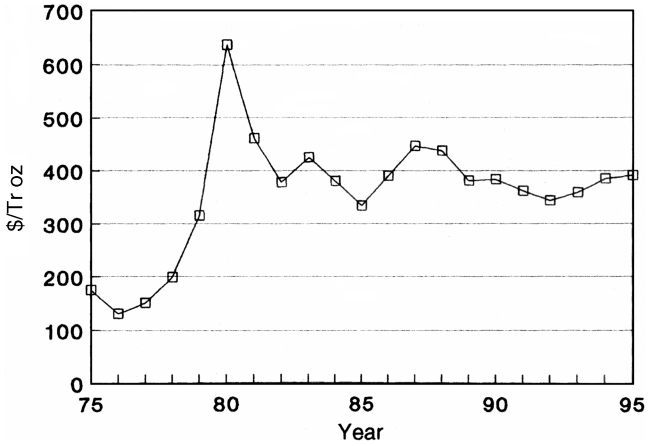

FIGURE 4.1 Gold bullion price of gold in U.S. dollars per troy ounce during the period from 1975 to 1995.

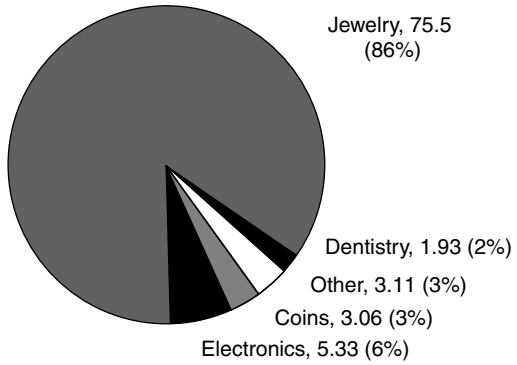

FIGURE 4.2 World gold demand in millions of troy ounces and percentage of market share by industry in 1994.

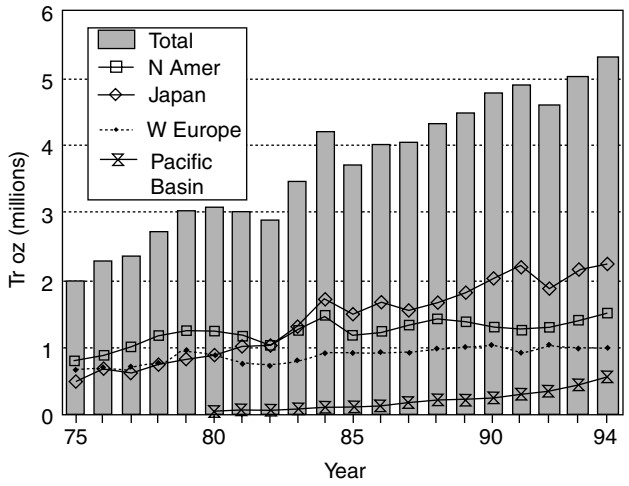

FIGURE 4.3 Gold demand in the electronics industry for Japan, North America, Western Europe, and the Pacific Basin (not Japan).

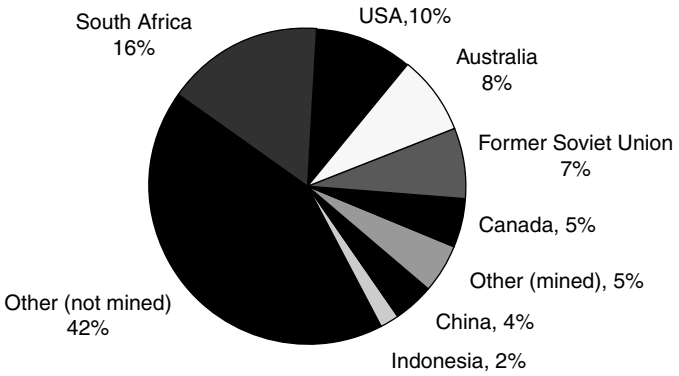

FIGURE 4.4 Gold supply in 1995 by percent. The total supply in 1995 was 98 million troy ounces.

nearly a constant cost per unit area for ICs. This has been achieved in part by reducing the consumption of expensive materials (e.g., gold), by closely controlling the amount of material needed for specific functions (thickness and area), and finding less expensive replacements for some functions. Palladium and palladium alloys have replaced gold in some electrical contact applications without a significant drop in performance.

The worldwide demand for gold has been met by recycling existing gold supplies and through the mining of metal reserves, as shown in Figure 4.4. The leading producer of mined gold is the Republic of South Africa followed by the United States and Australia.

Gold exists primarily in the $+1$ and $+3$ oxidation states. The standard potential versus the normal hydrogen electrode (NH.E) for a variety of Au(I) and Au(III) complexes is given in Table 4.1 [2, 3]. The most important ion for electrodeposition is $[Au(CN)_2]^-$. The stability of the Au(I) cyanide complex is reflected in the shift of the reduction potential for Au(I) from 1.71 V (aquo complex) to -0.611 V (cyanide complex). The stability constant for $[Au(CN)_2]^-$ is 10^{39} [4]. Two other gold complexes are of interest for electrodeposition, gold sulfite ($K = 10^{10}$) and gold thiosulfate ($K = 10^{28}$) [5]:

$$Au^+ + 2CN^- \rightarrow [Au(CN)_2]^- \qquad K = 10^{39} \qquad (4.1)$$

$$Au^+ + 2S_2O_3^{2-} \rightarrow [Au(S_2O_3)_2]^{3-} \qquad K = 10^{28} \qquad (4.2)$$

$$Au^+ + 2SO_3^{2-} \rightarrow [Au(SO_3)_2]^{3-} \qquad K = 10^{10} \qquad (4.3)$$

The potentials for the reduction of Au(III) to Au and Au(III) to Au(I), as shown in Table 4.1, are important because Au(III) can also be used as the source of gold in baths in place of Au(I), and Au(III) can also be formed at the anode during plating through the oxidation of Au(I).

In the next section, the chemical formulation of gold plating baths will be presented followed by comments on

TABLE 4.1 Standard Reduction Potentials for Gold Ions (V vs. NHE)

Half Reactions	Potential
$Au(I) \rightarrow Au$	
$Au^+ + e^- \rightarrow Au$	1.71–1.85
$AuCl_2^- + e^- \rightarrow Au + 2Cl^-$	1.15
$AuBr_2^- + e^- \rightarrow Au + 2Br^-$	0.96
$AuI_2^- + e^- \rightarrow Au + 2I^-$	0.58
$[Au(SCN)_2]^- + e^- \rightarrow Au + 2SCN^-$	0.66
$[Au(S_2O_3)_2]^{3-} + e^- \rightarrow Au + 2S_2O_3^{2-}$	0.15
$[Au(CN)_2]^- + e^- \rightarrow Au + 2CN^-$	−0.61
$Au(III) \rightarrow Au$	
$Au^{3+} + 3e^- \rightarrow Au$	1.71–1.85
$AuCl_4^- + 3e^- \rightarrow Au + 4Cl^-$	1.0
$AuBr_4^- + 3e^- \rightarrow Au + 4Br^-$	0.85
$[AuI_4]^- + 3e^- \rightarrow Au + 4I^-$	0.56
$[Au(SCN)_4]^- + 3e^- \rightarrow Au + 4SCN^-$	0.64
$Au(III) \rightarrow Au(I)$	
$Au^{3+} + 2e^- \rightarrow Au^+$	1.40
$[AuCl_4]^- + 2e^- \rightarrow [AuCl_2]^- + 2Cl^-$	0.92
$[AuBr_4]^- + 2e^- \rightarrow [AuBr_2]^- + 2Br^-$	0.80
$[AuI_4]^- + 2e^- \rightarrow [AuI_2]^- + 2I^-$	0.55
$[Au(SCN)_4]^- + 3e^- \rightarrow [Au(SCN)_2]^- + 2SCN^-$	0.62

the mechanism of gold deposition and other issues concerning the deposition process.

4.1 TYPICAL DIRECT CURRENT (DC) PLATING BATHS

Numerous proprietary gold plating baths and additives are used industrially. In this section the composition and operating parameters of representative baths are presented. The cyanide-based baths are divided into three classifications in Table 4.2: (1) the alkaline gold cyanide bath (pH > 8.5), (2) acidic, buffered baths (pH between 1.8 and 6), and (3) the neutral, buffered gold cyanide bath (pH between 6 and 8.5). The fourth group of baths, (4) noncyanide plating baths, are discussed after the three groups of cyanide baths. High-purity potassium gold cyanide, 68% metal (weight percent), can be obtained from commercial vendors in high purity.

Gold readily forms alloys with other metals during the deposition process or by diffusion with the gold substrate onto which it was plated. Gold deposits can be hard or soft, dull or bright, depending on the impurities and deposition conditions.

The potassium form of each salt is preferred over the sodium analogue because the solubility is higher. In cases where solubility is not a concern, sodium salts are sometimes used. Excessively high concentrations of gold in the baths are sometimes avoided due to the cost of the gold lost during drag-out of the salts.

The pH range between 8 and 10 is a critical region because the pK_a of hydrogen cyanide is 9.46. The equilibrium constant for HCN(aq) going to HCN(g) is $10^{1.4}$, making the pK_a for HCN(g) 8.06 [6]:

$$HCN(g) \rightarrow H^+ + CN^- \qquad pK_a = 8.06 \qquad (4.4)$$

Thus, at pH > 10, the equilibrium in Eq. (4.4) is shifted to the right, and free cyanide is stable in the bath. At pH < 8, the predominate form of cyanide is HCN(g), which evolves as a gaseous product. HCN gas is highly toxic, and its evolution from plating baths is a health concern. Appropriate ventilation is required for all cyanide baths. The presence of significant concentrations of free cyanide in the bath, such as in the case of alkaline baths, is also a health risk because accidental cyanide ingestion or injection can occur.

The presence of free cyanide in the bath is a major consideration in the selection of the anode and metal ion replenishment method. In the presence of free cyanide, gold metal can be used as a consumable anode because it can be electrochemically oxidized forming the gold cyanide complex. In the absence of free cyanide, gold is not oxidized to any appreciable extent, so it acts like an inert electrode. The ramifications of this will be included for each bath.

TABLE 4.2 Typical Cyanide-Based Plating Baths (Concentrations in g L^{-1})

Bath	Alkaline Cyanide		Buffered Citrate		Buffered Phosphate	
Operation	Rack	Barrel	Rack	Barrel	Rack	Barrel
$KAu(CN)_2$	12	6	20	20	20	20
KCN	20	30				
K_2HPO_4	20	30	—	—	40	40
KH_2PO_4					10	10
K_2CO_3	20	30	—	—		
K_2H citrate			50	50		
T (°C)	50–60	50–65	60–70	60–70	60–70	60–70
I (mA cm^{-2})	1–5	1–5	1–2	4–6	0.7–2	4–6
pH	11–11.5	11–11.5	4–5.8[a]	4–5.8[a]	6–8	6–8

[a] pH may drift during use. Citric acid or KOH can be used to adjust pH.

4.1.1 Alkaline Cyanide Baths

Alkaline cyanide baths operate at high pH and with an excess of free cyanide. The potassium gold cyanide concentrations used in the low-current-density baths shown in Table 4.2 range from 2 to 12 g L^{-1}, with 6 g L^{-1} often used. Higher gold concentrations will support higher current densities.

Potassium cyanide is often used as the source of the free cyanide in these baths. Since there is appreciable free cyanide present, the cyanide released during the deposition reaction does not significantly alter the cyanide concentration in the bath. Thus the Nernstian shifts in the reduction potential of Au(I) cyanide due to accumulation of free cyanide (even in the vicinity of the electrode surface) do not occur. In lower pH baths, large shifts in the free-cyanide concentration at the electrode surface have many ramifications, including a shift in the reduction potential during deposition. The excess cyanide permits the use of gold anodes for the replenishment of the metal plated from the bath:

$$\text{Cathode:}\quad [Au(CN)_2]^- + e^- \rightarrow Au + 2CN^- \tag{4.5}$$

$$\text{Anode:}\quad Au + 2CN^- \rightarrow [Au(CN)_2]^- + e^- \tag{4.6}$$

$$\text{Full cell:}\quad \text{No change to plating solution} \tag{4.7}$$

The main changes that occur in the bath are due to oxidation or reduction side reactions, drag-out of plating salts, and drag-in of water or impurities. The free cyanide promotes the corrosion of the gold anode (forming $[Au(CN)_2]^-$), increases the throwing power, and improves the conductivity. Free cyanide also retards the codeposition of some metals because the stability of their cyanide complexes shifts their reduction potential to values more negative than those used during deposition. The absorption of atmospheric carbon dioxide increases the concentration of carbonate in the solution as a result of the reaction between cyanide and CO_2. The carbonate can help to stabilize the pH and improve throwing power slightly.

Nonsoluble, dimensionally stable anodes, like platinized titanium or stainless steel, are sometimes used. Oxygen gas and hydrogen ions are the dominant products at the insoluble, dimensionally stable anodes, as shown in Eq. (4.9):

$$\text{Cathode:}\quad 4[Au(CN)_2]^- + 4e^- \rightarrow 4Au + 8CN^- \tag{4.8}$$

$$\text{Anode:}\quad 2H_2O \rightarrow 4H^+ + O_2 + 4e^- \tag{4.9}$$

$$\text{Full cell:}\quad 4[Au(CN)_2]^- + 2H_2O \rightarrow 4Au + 8CN^- + 4H^+ + O_2 \tag{4.10}$$

The hydrogen ions produced in Eq. (4.9) and shown in Eq. (4.10) for the full cell can either be neutralized by hydroxide (lowering the pH of the solution) or form HCN (g) and evolve from the bath as a gas depending on the operating pH, as shown previously in Eq. (4.4). Thus the pH and the gold cyanide ion concentration of the bath in Eq. (4.10) will drop as current is passed, as shown by the two half reactions. Both these effects must be reversed through the addition of plating salts and KOH. The addition of KOH and $KAu(CN)_2$ as a replenishment for the right-hand side of Eq. (4.10) will result in the accumulation of KCN (in the form of K^+ and CN^- until the KCN solubility product is reached) in the bath. The buildup of KCN is somewhat mitigated by drag-out. An insoluble anode is convenient because the cathode current distribution is reproducible and consistent over long periods of time. Also the anode docs not have to be replaced as it corrodes. Thus, anode maintenance is replaced by bath maintenance [KOH and $KAu(CN)_2$ additions].

The cathodic current efficiency for the deposition of the metal from alkaline baths can be as high as 90–100% with adequate gold content in the bath and sufficient agitation [7, 8]. For example, 100% efficiency has been obtained at 10 mA cm^{-2} and 12 g L^{-1} $KAu(CN)_2$ under mild agitation, whereas the current efficiency was only about 50% at 4 g L^{-1} $KAu(CN)_2$ (otherwise similar conditions) [7].

The preferred operating temperature of the baths is 50–60°F. The codeposition of impurities (e.g., antimony) will increase the hardness and brightness of the deposits [9]. The codeposition of silver, nickel, copper, and cobalt has been used to alter the color of the deposit. This effect is used mostly for decorative purposes.

Alkaline bath formulations are generally not compatible with many polymers used in the microelectronics industry. The high-pH and high-cyanide concentration degrades photoresist and organic laminates. Thus there has been considerable work on developing neutral pH formulations. The alkaline, soft gold deposits are not acceptable for sliding electronic contacts in telephones where wear resistance is critical. The parts will gall and fail quickly.

4.1.2 Acid Cyanide Baths

The nonalkaline, cyanide-based baths which contain other metals normally use a citrate buffer and operate around pH 4. Low-pH buffered baths were originally developed for the jewelry trade but now find wide application throughout the electronics industry for contact surfaces, corrosion protection, bonding surfaces, and special electroforming. The pH of the baths allows the use of photoresist and other polymers. Typical formulations are given in Table 4.2. Anodes in these baths are usually platinized titanium, gold, or gold-plated platinized titanium. The gold-plated electrodes are found not to dissolve readily at low current densities because of the low free-cyanide concentration. This, however, is not the case at high current densities and low solution volume where

appreciable transient concentrations of free cyanide can build up and lead to the oxidation and dissolution of a pure gold anode. Stainless steel and carbon anodes are found to introduce contamination, and their use is discouraged. The use of insoluble anodes requires that plating salts be added to the bath to replenish the gold content [e.g., $KAu(CN)_2$] and maintain pH control. Although K^+ removal and pH control can be accomplished by an ion exchange method, drag-out and salt addition are the usual method of bath maintenance [10].

The codeposition of other metals with gold is easily accomplished in acid cyanide baths, resulting in marked changes in the physical properties (especially hardness) of the deposits. Hard gold is of great importance to electronic components where low contact resistance, pore-free deposits, wear resistance, and chemical inertness are functional requirements. Such applications include the multiple-insertion electrical contacts found on printed wiring board contacts or spring contacts.

Bright, hard deposits can be produced from alkaline and acid cyanide baths containing cobalt, nickel, indium, silver, arsenic, or cadmium. However, the most reliable connector finish is from acid cyanide baths with nickel or cobalt salts as the brightener [11–13]. A typical range of concentrations is given below [14]:

$KAu(CN)_2$	12–15 g L^{-1}
Citric acid	90–115 g L^{-1}
Cobalt (added as acetate or sulfate)	0.07–0.1 g L^{-1}
pH (adjust with KOH)	3.6–4.7
Temperature	40–65°C

To establish the proper pH, KOH is added to the bath. A concentration of 50 g L^{-1} KOH will produce a bath of about pH 4.0 [14]. Baths that produce pure gold deposits often operate at close to 100% current efficiency [15]. A yellow color that develops in the bath has been attributed to the formation of the $[Co(CN)_6]^{3-}$ complex [14]. The typical grain size of cobalt-hardened gold is 225–275 Å [16].

The high current density used in high-speed baths can produce a temporary buildup of free cyanide in the bath that may lead to the corrosion of a gold anode or even the slow oxidation of a platinum anode. It has also been found that $[Au(CN)_4]^-$ can be formed at the anode, especially under high current and high cobalt concentrations at a platinum anode [17]. The buildup of Au(III) results in lower current efficiencies at the cathode for the production of gold metal because it takes 3 eq mol^{-1} to reduce $[Au(CN)_4]^-$ to Au whereas it only takes 1 eq mol^{-1} to reduce $[Au(CN)_2]^-$ to Au.

One of the limiting factors for the current density is the rise in pH in the vicinity of the electrode during the reduction process, through either gold deposition or hydrogen gas production. For example, at pH 3.5 and 15 g L^{-1} $KAu(CN)_2$, the current efficiency is 20–30% for current densities less than 50 mA cm^{-2} [13]. Hydrogen gas is the main side product of the cathodic reaction. The reduction of the gold cyanide complex is inhibited by the cobalt ion, as seen by the Tafel slopes (see Section 4.2 on deposition mechanisms), significantly dropping the current efficiently [13, 18]. The cobalt content of the pH 3.5 bath is a complex function of current density and mass transport [13]. The typical range of the incorporated cobalt is around 0.05% of the gold at high current density (>50 mA cm^{-2}) and low agitation [Reynolds number (Re) < 3000] to 0.6% of the gold at low current (25 mA cm^{-2}) and high agitation (Re > 13,000).

At higher pH or higher temperature, the cobalt and carbon contents of the deposit decrease [19]. An increase in pH above 5.5 virtually eliminates the cobalt from the deposit, which demonstrates the ability of acid cyanide baths to codeposit metals with gold. Lower current densities (smaller rate of consumption of protons at the cathode) or higher mass transport (higher rate of delivery of protons from the solution) will mitigate the rise in pH in the electrode boundary layer during deposition. Thus the higher the solution agitation, the greater is the allowable current density. The cobalt or nickel ions are known to codeposit in the gold in at least two different forms, the cyano complex and as a substitutional alloy [20–22]. The increase in hardness is due to the grain-refining effect of the codeposited cyano complex [23].

The porosity of the deposited gold also decreases with higher mass transport and lower current density [13]. The lowest porosity cobalt-hardened gold deposits were obtained at 2 mA cm^{-2} and Re > 9000.

Although cobalt salts are the most common hardening agents for acid cyanide baths, the addition of nickel acetate ($\sim$ 1 g L^{-1} nickel) to the citrate bath also results in the hardening of the deposit and a drop in the current efficiency [12]. The wear properties of high-speed gold deposits were studied as a function of nickel or cobalt concentration, the form of the cobalt complex in solution (strongly chelating vs. weakly chelating), and current density using commercial baths [24]. The stronger chelating agent was shown to prevent the formation of cyanide complexes. Strongly chelating nickel was found to have the widest operating window. Cobalt concentrations from 1.0 to 2.0 g L^{-1} and current densities from 100 to 500 mA cm^{-2} were acceptable. As stated above, the weakly chelating cobalt complex required only 0.1 g L^{-1}. Most deposits showing good wear characteristics were bright; however, all bright deposits were not wear resistant. Although specific ranges for cobalt or nickel were studied, no fundamental basis for the wear properties was established. Generally speaking, empirical relationships for the bath parameters are used to optimize wear properties.

The addition of iron salts to the plating bath will harden the gold deposit, just as cobalt and nickel do. However, iron-hardened gold is much more brittle than cobalt- or nickel-hardened gold, which is unacceptable in many applications

where ductility is critical, such as in electrical contacts. The accidental contamination of baths with iron is a concern whenever iron or steel parts are used in bath construction, piping, or pretreatment equipment.

Liljestrand et al. studied the effect of nickel concentration and other plating parameters on wear for nickel-hardened gold at 60°C, 16 g L^{-1} gold concentration, and pH 3.8–4.8 [25]. The nickel concentration in the bath was varied and the resulting content in the deposit ranged from 0.2 to 2.5 wt %. In the higher current density range from 10 to 40 mA cm^{-2}, the wear changed from severe to mild and then to brittle upon increasing the nickel content. However, in the current density range from 1 to 16 mA cm^{-2}, the wear changed from severe to adhesive brittle and then to mild with increasing nickel content. The terms *severe*, *adhesive brittle*, and *mild* refer to the physical, conditions of the surface. The severe wear at low nickel content was characterized by cold welding between the spring and pin used in the test. During the first wear cycles, the gold was smeared from one part to the other followed by early failure (less than 200 wear cycles). At high nickel content, plated at low current density, brittle wear occurred characterized by cracks reaching down to the nickel underplate. This clearly shows the need for tight control over bath and plating parameters with metal-hardened gold. X-ray diffraction was used to show an increase in the lattice contraction strain with increasing nickel content. Since the solubility of nickel in gold is about 5%, it was concluded that most of the nickel is in a solid solution and that the hardness is due to lattice strain caused by the soluted nickel atoms.

The codeposition of an insulating film from cobalt- or nickel-hardened acid gold baths has caused significant problems for electrical contacts. High electrical resistivity can be observed upon thermal aging (e.g., 150°C), especially in films plated at high speeds with high cobalt concentration [26]. The subject has received considerable attention since the late 1960s when high contact resistance on telephone spring contacts was correlated with an orange-brown film on gold-plated contacts. Munier was the first to isolate the transparent film on the cobalt-hardened gold and presumed it to be an organic polymer [27]. The indiscriminate use of the word "polymer" to refer to either the electrodeposited inclusion or the extract from the plated metal is not correct. Nevertheless, most of the literature published on the identification and elimination of the material refers to it as an insulating codeposited polymer.

Microchemical determination of the carbon content of the gold deposited from cobalt- or nickel-hardened baths based on citrate-buffered gold cyanide provides a clear link between a carbonaceous impurity and the insulating film, as shown in Table 4.3 [27]. In the absence of cobalt or nickel or at high pH (i.e., pH > 10 using a phosphate buffer and potassium gold cyanide) in the presence of cobalt salts which are not codeposited, no carbon is detected in the deposit.

TABLE 4.3 Determination of Carbon in Gold Deposits[a]

Gold Bath	Hardener	Carbon in Gold (%)
Potassium gold cyanide, 13 g L^{-1}	None	0.01–0.04
Potassium hydroxide, 15 g L^{-1}	Cobalt	0.20–0.30
Citric acid, 90 g L^{-1}	Nickel	0.19–0.43
Cobalt or nickel citrate, 0.3 g L^{-1}		

Note: pH range 3.6–4.5.

Carbon-14 labeled complexes were used to quantity the carbon content in the deposits at levels in excess of 1% [28]. Electron microscopy studies showed the deposits to exist in discrete pockets usually 1000 Å and smaller in size with a few as large as 25,000 Å [29]. A study of gold deposited from pure potassium gold cyanide as a function of temperature, of current density, and with anode isolation (in a separate compartment) led to the conclusions that (1) the carbonaceous contamination was minimized at temperatures above 65°C, (2) deposits plated at lower temperature (~ 25°C) had more carbon and were much harder and brittle, and (3) the carbon was the result of a cathodic process only and not the re-reduction of an oxidized species released from the anode [30]. However, it led the authors to the inaccurate speculation of the origin of the carbon as potassium cyanide, Au(I) cyanide, potassium cyanoaurate, or hydrogen cyanide. Mossbauer spectroscopy was later used to show that no AuCN, $KAu(CN)_2$, or $KAu(CN)_4$ were in the deposit [31].

A detailed study of the gold appearance and carbon and cobalt contents as a function of pH clearly showed the drop in codeposited cobalt and carbon as the pH was increased to 6 [19]. The slow change in the cobalt-containing hard gold solution from reddish-pink, the color of Co^{2+} citrate, to yellow, the color of $[Co(CN)_6]^{3-}$, was noted. This occurred as free cyanide was released from the reduction of $[Au(CN)_2]^-$.

A study by Okinaka et al. [14] clarified many issues. It was shown that the carbon-containing deposits obtained from dissolving cobalt-hardened gold in aqua regia were not an organic material but the cobalt complex $Co_3^{II}[Co^{III}(CN)_6]_2 \cdot xH_2O$. When dissolved in mercury, $K_3Co^{III}(CN)_6$ was found. It was concluded that there is an additional source of both cobalt and carbon in the gold deposit apart from the cobalt cyanide complex. Substitutional metallic cobalt is the additional source of cobalt.

4.1.3 Neutral Cyanide Baths

Nonalkaline baths exhibit a wider range of physical and chemical properties than possible at higher pH. In the previous section on acid baths, it was related that the codeposition of other metals from the bath provided metallurgical hardening of the deposit. The hardness is the result of a reduction in the grain size of the gold caused by the codeposit

increasing the rate of grain nucleation. It was also noted that the amount of codeposited metal (e.g., cobalt or nickel) decreased to nearly zero at pH > 5.5. Although the metals used to harden gold are not readily codeposited from neutral pH baths, it has been found that hard gold (as well as soft gold) can be formed in neutral baths by the careful selection of the plating parameters without the use of additives. In the neutral baths the gold salt used is the same as in alkaline and acid baths, $KAu(CN)_2$. The neutral pH and absence of free cyanide make these formulations the preferred ones for use with photoresist and other polymeric materials.

The neutral baths shown in Table 4.2 produce pure, soft gold at relatively low current densities, typically 2–5 mA cm^{-2} and 60–70°C. The phosphate salts serve only as the supporting electrolyte and pH control, so that strict control of their concentration is not critical. The phosphate buffer can be used for acid, neutral, or basic conditions with pH adjustment carried out by the addition of KOH or H_3PO_4. Control of pH, temperature, and gold concentration is critical.

Additive-free hard gold (AFHG) can be produced from neutral baths using phosphate as the buffer, as shown in Table 4.4 [32]. Although the "low-speed" column is under acid conditions, it is included here for completeness because of its similarities with the high-speed AFHG bath. The advantages of AFHG baths over metal hardened baths are (1) no need to control additive concentration, (2) high current efficiency, (3) greater tolerance for heavy metal impurities due to the insolubility of many metal phosphates, and (4) high ductility and thermally stable contact resistance for electronic components.

However, AFHG baths are highly susceptible to bath contamination. Small amounts of impurities, such as nickel, cobalt, or iron ions, can cause large changes to the physical properties deposited from the bath. It can be difficult to purge the plating bath of the unwanted impurities.

AFGH plating was first observed in 1974 [33]. It was shown that the grain size of the deposits from the AFGH bath was 250–750 Å, which is slightly larger than those from the cobalt-hardened bath (225–275 Å) but much smaller than the grains from soft gold (1–2 μm) [16]. AuCN is codeposited in AFHG and accounts for about 50–70% of the carbon content in the deposit. The deposited AuCN forms a polymeric structure and hardens the gold by promoting the nucleation of grains or by inhibiting the growth of the existing gold grains, in a role analogous to cobalt hardening of acid gold baths mentioned in the previous section [34]. Thus the conventional bath (Table 4.2) that produces soft gold at 70°C will produce hard gold at 25°C. The population density of the AuCN in AFHG gold plated from a bath containing $KAu(CN)_2 = 44\,g\,L^{-1}$, $KH_2PO_4 = 100\,g\,L^{-1}$, $KOH = 28\,g\,L^{-1}$, and pH 7.0 was $10^{17}\,cm^{-3}$ with a volume ratio of 1.3–1.9% [34].

Data on the plating efficiency and deposit appearance of an additive-free, neutral bath is shown in Table 4.5 [32]. At low current density, the hardness was found to be independent of temperature in the range of 10–45°C (~ 160 KHN_{25}), whereas the hardness decreased to 104 KHN_{25} at 70°C. At higher plating speeds, 86–252 mA cm^{-2} and 30–43°C, the hardness was about 180 KHN_{25}. Wear tests using lubricated sliding contacts showed severe galling for the soft gold plated at 70°C (104 KHN_{25}), whereas the harder deposits formed at lower temperatures (22–45°C) showed excellent wear. The AFHG bath was shown to have superior tensile strength, total elongation (high ductility), and more stable contact resistance than comparable deposits from a cobalt-hardened acid bath. However, a small increase in contact resistance was found when the deposit was heated to >100°C due to the surface segregation of AuCN [34].

The effect of gold cyanide concentration on current efficiency and the appearance of the finish for the high-speed bath are shown in Table 4.5 [32, 35]. The conditions were the same as the "high-speed" portion of Table 4.4 except for the gold cyanide concentration. At $KAu(CN)_2$ concentrations below $23\,g\,L^{-1}$, a matte finish was obtained with cathodic current efficiencies of 80–85%. At $KAu(CN)_2$ concentrations from 23–44 $g\,L^{-1}$, a bright finish was obtained and the current efficiency was 90–95%.

Certain metallic additives can be used as a grain refiner in the baths, such as thallium or arsenic, to increase the

TABLE 4.4 Bath Composition and Plating Conditions for Additive-Free, Neutral Gold Plating Bath

	Low Speed	High Speed
$KAu(CN)_2$	$40\,g\,L^{-1}$	$44–59\,g\,L^{-1}$
KH_2PO_4	$100\,g\,L^{-1}$	$100\,g\,L^{-1}$
pH (KOH of H_3PO_4)	4.3–4.5	6.5–7.5
Temperature	25 ± 2°C	40 ± 2°C
Agitation	Mild	Vigorous
Current density	10–20 mA cm^{-2}	200–300 mA cm^{-2}

TABLE 4.5 Appearance and Plating Efficiency of High-Speed Additive-Free Hard Gold

Temperature (°C)	Current Density (mA cm^{-2})	Appearance	Plating Efficiency (%)	Hardness
20	121	0	78	
25	198	0	72	
25	155	2	81	
25	138	3	81	
25	121	4	86	
30	155	2	83	193
30	138	4	85	
43	259	2	87	
43	172	5	85	188
61	172	0	91	
61	86	0	82	

Note: Visual appearance defined as 0 = burned appearance to 5 = completely bright.

brightness/smoothness range of the deposit. The military specification for bondable gold (MIL-G-45204B) requires that chromium, copper, tin, lead, silver, cadmium, or zinc not be present in the deposit at a concentration greater than 0.1%.

The residual stress of gold films deposited on silicon wafers is important for microsystems and microelectromechanical systems (MEMSs). Gold is an excellent structural and contact material for MEMSs because it is difficult to oxidize. The residual stress of gold films annealed at different temperatures plated from a neutral-pH cyanide bath was measured [36]. Recrystallization of the gold occurs at high temperature, which relieves the stress due to mismatch of the coefficient of thermal expansion (CTE) between the gold and the silicon substrate. Normally, the gold achieves a stress-neutral point at the highest temperature. The CTE mismatch between the metal and the substrate caused tensile stress in the gold during cooldown. Stresses on the order of 50, 200, and 350 MPa were observed at anneal temperatures of 100, 250, and 400°C [36].

Residual stress is a particular problem for free-standing gold structures where flatness is desired, such as in X-ray lithography masks. The stress films deposited from a neutral-pH cyanide bath was found to be 50 MPa tensile whereas the addition of 25 ppm arsenic changes the stress to 30 MPa compressive. Pulsed current reduced the stress to <5 MPa compressive [37]. In other applications, the stress gradient in gold films deposited at different conditions was used to build precise-curvature cantilever beams for microswitches [38].

Anodes in these baths are normally platinized titanium, gold, or gold-plated platinized titanium. Stainless steel and carbon anodes are not recommended because of contamination. Gold or gold-plated anodes do not dissolve readily because the concentration of free cyanide is very low. However, at high current density and small solution volumes (or close anode-to-cathode spacings), the transient concentration of free cyanide can become significant and promote the oxidation and dissolution of a gold anode. High-current-density baths, especially those with high gold cyanide concentrations, are susceptible to the formation and buildup of Au(III) as $[Au(CN)_4]^-$ [17]. The presence of $[Au(CN)_4]^-$ will result in a lower apparent current efficiency at the cathode because it requires 3 eq mol^{-1} to deposit Au from Au(III) as opposed to 1 eq mol^{-1} for Au(I). This is different from the acid gold plating case where hydrogen gas was the side product responsible for lowering the plating efficiency. This creates a process control problem. As the Au(III) concentration builds up in the bath, the plating time, or current (coulombs per square centimeters) will have to be increased to achieve the same deposit thickness. Figure 4.5 shows the current efficiency and percent Au(III) in the bath as a function of weight of gold plated or number of bath turnovers for three different anodes [17]. The cathodic current density was 230–300 mA cm^{-2}, the anodic current density was 150–200 mA cm^{-2}, and the bath was the same as

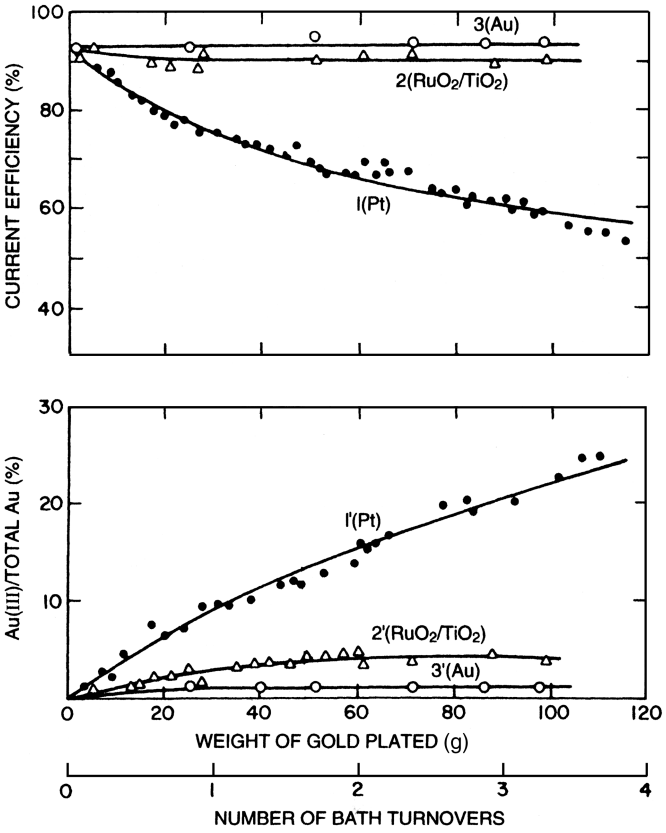

FIGURE 4.5 Variation in plating efficiency and Au(III) content with bath age (AFHG bath). (Curves 1, 1′: Pt anode; curves 2, 2′: RuO_2/TiO_2 anode, curves 3, 3′: Au anode.) (From Okinaka and Wolowodiuk [17].)

in Table 4.4 (high-speed bath). The gold anode did not result in a significant buildup of Au(III) because it was oxidized resulting in dissolution caused by the high transient concentration of free cyanide. The use of a gold anode is usually an unacceptable solution to the Au(III) problem because of the anode maintenance and changing cathodic current distribution as the anode corrodes and changes shape. The buildup of Au(III) is somewhat mitigated by the dilution effects due to drag-out. Other possible solutions to the Au(III) problem are to use a RuO_2/TiO_2 (often called dimensionally stable anode, DSA), adjust the current density to correct for the lower current efficiency, or chemically treat the Au(III) by reduction (e.g., hydrazine) or removal (activated carbon) [17].

4.1.4 Noncyanide Baths

The Au(I) cyanide complex is by far the most important for electrodeposition. However, there are several shortcomings to the use of $[Au(CN)_2]^-$ which have stimulated the investigation and commercialization of other gold complexes in plating baths [39]. The stability of the gold cyanide complex causes the reduction potential to occur at very negative potentials, resulting in the coreduction of hydrogen ions,

which lowers the plating efficiency and makes the development of electroless plating baths difficult [40]. The release of free cyanide during the reduction of $[Au(CN)_2]^-$ can be incompatible with positive photoresists used in the microelectronics industry [41, 42]. It has also been found that the residual stress of the plated gold can be controlled in noncyanide baths [43, 44]. Low-stress deposits are of particular interest for X-ray lithography masks because they must be thin, flat, and made from high-atomic-number elements. Lastly, the health and safety of workers and the environmental impact of the wide-scale use of cyanide are a concern.

The operating parameters of commercial gold sulfite baths have been presented with special attention given to the effect of plating temperature and current density on residual stress in the deposited metal [43, 44]. For example, Figure 4.6 shows the stress change from compressive to tensile as the temperature or current is raised. Thallium was used as the stress-reducing agent at concentrations up to 80 ppm, a value that can be more easily maintained than the low-thallium-concentration baths [43]. Alkaline sulfite baths can also be used without the use of thallium, which itself is a health hazard [44].

Although Au(I) sulfite has been used in commercial baths, the complex is susceptible to disproportionation, forming Au(III) and metallic gold. This spontaneous decomposition of the bath has led commercial baths to use proprietary stabilizing additives. Gold (I) sulfite ($pK_a\ 10^{10}$) is particularly troublesome at $pH < 7$ where sulfite protonates, forming bisulfite [45–48]. Gold (I) thiosulfate has a stability constant ($pK_a\ 10^{28}$) which is between that of Au(I) sulfite and Au(I) cyanide ($pK_a\ 10^{39}$). The Au(I) thiosulfate complex is stable in weakly acidic solutions because of the low pK_a for thiosulfate.

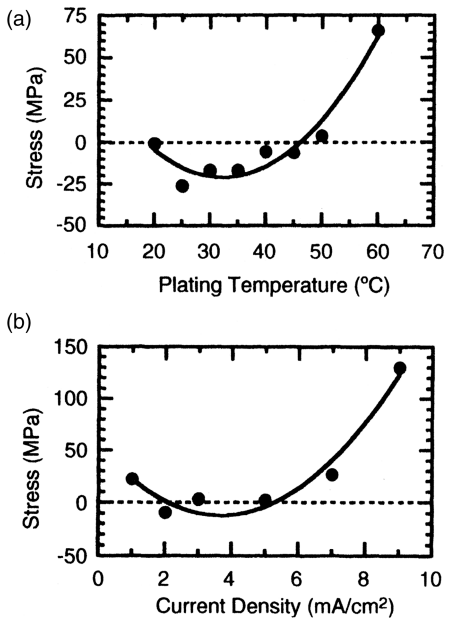

FIGURE 4.6 (*a*) Stress versus plating temperature for samples plated at 3 mA cm^{-2} form a bath containing 75 ppm thallium. (*b*) Stress versus current denisty for samples plated at 50°C from a bath containing 75 ppm thallium. (From Dauksher et al. [43].

The dominant species in mixed-complex baths, $S_2O_3^{2-}$ and $S_2O_3^{2-}$, at neutral or basic conditions have been reported to be $Au(S_2O_3)(SO_3)^{3-}$ [49]. The thiosulfate-only complex is dominant at low pH. The existence of the mixed ion complex was suggested in previous studies based on the deposition potential. It was also reported that the results from the sulfide-only bath are consistent with a higher stability constant (10^{27}), rather than the commonly assumed value of 10^{10} [49].

$$H_2S_2O_3 \rightarrow H^+ + HS_2O_3^- \qquad pK_{a1} = 0.3 \tag{4.11}$$

$$HS_2O_3^- \rightarrow H^+ + S_2O_3^{2-} \qquad pK_{a2} = 1.7 \tag{4.12}$$

The reduction of Au(I) thiosulfate was shown to have an overall reaction producing thiosulfate and gold [50]:

$$[Au(S_2O_3)_2]^{3-} + e^- \rightarrow Au + 2S_2O_3^{2-} \tag{4.13}$$

The standard heterogeneous rate constant for the reduction was found to be 1.6×10^{-3} cm s^{-1}, a transfer coefficient α of 0.23, and a diffusion coefficient of 7×10^{-6} cm^2 s^{-1} [40]. The effect of mixed thiosulfate–sulfite electrolytes has been studied shown to produce soft gold deposits suitable for forming gold "bumps" on ICs and in electronic interconnections [41]. The Vickers hardness of the electrodeposited gold was 80 kg mm^{-2} in the as-deposited state and 50 kg mm^{-2} after annealing. The optimum bath with thallium was composed of the following formulation:

$NaAuCl_4 \cdot 2H_2O$	0.06 *M*
Na_2SO_3	0.42 *M*
$Na_2S_2O_3 \cdot 5H_2O$	0.42 *M*
Na_2HPO_4	0.03 *M*
Tl^+ (added as Tl_2SO_4)	0.03 *M*
pH	6
Temperature	60°C
Current density	5 mA cm^{-2}

The mixed sulfide–thiosulfate plating bath was used to produce soft gold deposits for gold bumps and wire-bonding applications [51]. Bright gold deposits were obtained at a cathodic deposition efficiency (current efficiency) of greater than 99%. The purity of the gold deposits was greater than 99.99% and had a hardness between 60 and 80 Knoop. The bath composition is as follows:

Gold as metal	10 g L^{-1}
Sulfide	70 g L^{-1}
Thiosulfate	70 g L^{-1}
Additives	10 g L^{-1}
pH	5
Temperature	50°C

The deposition of gold from the iodide–thiosulfate bath was also studied [42]. It was suggested that the chemical reaction preceding the electron transfer step is the dissociation of the $[Au(S_2O_3)_2]^{3-}$ to form $[Au(S_2O_3)_2]^-$ and $S_2O_3^{2-}$

In each of the studies involving a mixed-thiosulfate bath (sulfite–thiosulfate and iodide–thiosulfate), it was observed that the mixed-salt gold complex is more stable and harder to reduce than either of the single-salt complexes [39–42]. That is, the Au(I) sulfite–thiosulfate complex is reduced at potentials more negative than either the Au(I) sulfite or Au(I) thiosulfate complex.

4.1.5 Gold Alloy Plating

The deposition of specific gold alloys has become important for specific industrial applications. Gold–tin alloys are useful as solders for electronic and optoelectronic die attachment. A weakly acidic, noncyanide electroplating solution based on gold and tin chloride salts with ammonium citrate as a buffer has been developed [52]. Tin contents from 27 to 42% were obtained:

Ammonium citrate	$200\,g\,L^{-1}$
$KAuCl_4$	$20\,g\,L^{-1}$
$SnCl_2 * 2H_2O$	$14\,g\,L^{-1}$
L-ascorbic acid	$30\,g\,L^{-1}$
$NiCl_2$	$1\,g\,L^{-1}$
Peptone	$5\,g\,L^{-1}$

Pulse plating was used with a similar chloride bath to produce alloys with a gold composition from 50 to 85% [53, 54]. It was shown that the microstructure produced under the pulsed-current conditions depended on the current density. At low current the grain growth occurred while at high current grain initiation was favored [55]:

Ammonium citrate	Buffer
$KAuCL_4$	$5\,g\,L^{-1}$
$SnCl_2 * 2H_2O$	$2–5\,g\,L^{-1}$
L-ascorbic acid	Tin stablizer
Ethylenediamine	$0.01–0.135$ moles L^{-1}
Sodium sulfite	Gold stablizer

A more traditional bath using $Au(CN)_2^-$ was used to obtain Au–Sn deposits [56]. The eutectic alloy is 71% atomic (or 80% by weight) gold. Alloys ranging from 75 to 98% gold were obtained by changing the bath composition and current density.

A variety of other gold alloys include gold–cobalt alloys deposited from a cyanide bath with an oxalate–citrate buffer and organic additives [57]. Gold–palladium alloys were deposited from an ionic liquid in the Lewis base form [58], and gold–silver was deposited from a cyanide bath by use of pulse plating [59].

4.2 MECHANISM OF DEPOSITION

Electrodeposition from the $[Au(CN)_2]^-$ complex is by far the most common and well studied. Two distinct mechanisms for gold deposition have been proposed [60–62]. The cathodic deposition of gold under activation control can be described by Butler–Volmer kinetics. At lower currents or less negative potentials the first step is the chemical adsorption of the $[Au(CN)_2]^-$ complex

$$[Au(CN)_2]^- \rightarrow (AuCN)_{ad} + CN^- \tag{4.14}$$

The electron transfer step is the rate-limiting one:

$$(AuCN)_{ad} + e \rightarrow (Au^0CN)_{ad}^- \tag{4.15}$$

$$(Au^0CN)_{ad}^- \Leftrightarrow Au_{lattice} + CN^- \tag{4.16}$$

The chemical desorption and crystallization make up the final step, as shown in Eq. (4.16) [61, 62]. The equilibria depend on the crystal orientation of the substrate and presence of impurities such as nickel or cobalt that can affect the nucleation rate and hardness of the gold. The Tafel slope at pH 4.4 for additive-free soft gold and nickel-hardened gold were found to be -0.35 and -0.47 V decade^{-1} respectively, as determined by chronopotentiometry and chronoamperometry [60]. The Tafel slope found for soft gold by linear sweep voltammetry was slightly smaller, -0.39 V decade^{-1}. The smaller Tafel slope for nickel-hardened gold shows the strong inhibiting influence of nickel ions on the deposition process. It was found that at low current density ($0.25\,mA\,cm^{-2}$) a hexagonal crystalline structure was observed. The hexagonal structure dominates the deposit at short deposition times and is stabilized by metal ions in the bath, which led to underpotential deposition, such as Cu^{2+} and Tl^+ [63].

At more negative potentials, a second Tafel slope was obtained indicating a different mechanism for deposition, where the direct electroreduction of the gold cyanide ion takes place. Steeper Tafel slopes (more negative slopes) at higher currents were observed for soft gold (-0.154 V decade^{-1}) and nickel-hardened gold (-0.186 V decade^{-1}), as measured by chronopotentiometry and chronoamperometry. The two Tafel slopes were not observed by linear sweep voltammetry because nucleation begins gradually at less negative potentials and then the rate of crystal growth and nucleation increases, whereas the rates of nucleation and crystal growth are initially high for constant-potential or constant-current methods.

Surface-enhanced Raman spectroscopy (SERS) was used to examine the chemical moieties on the gold surface during deposition as a function of potential [64]. At high cathodic potentials and high current density ($1\,mA\,cm^{-2}$) the direct reduction of gold cyanide dominates. A SERS peak corre-

sponding to CN^- stretching of the absorbed species is observed. At more positive potentials and lower current density, ($100\ \mu A\ cm^{-2}$), the mechanism shown in Eqs. (4.14), (4.15) and (4.16) dominates. The SERS peak broadening is consistent with this model. Similar methods were used to analyze the intermediates from deposition from $Au(CN^-)_4$ [65]. The results suggest that Au(III) also undergoes reduction via two different intermediates. The transition between the two mechanisms occurred at about the same potential for both Au(I) and Au(III). SERS was also used to show that the amount of hydrogen incorporation in the deposited gold could be reduced by using benzyldimethylphenylammonium chloride [66]. A peak at -0.7 V versus Ag/AgCl was linked to the conversion of the cyano group of the cyano-aurate complex into dyanide bonded to the metallic gold surface. A second peak at -1.05 V versus Ag/AgCl has been associated with the Au^0–CN to Au^0–NC reorientation.

In weakly acidic oxalate–phosphate baths, two Tafel regions were also found (-0.315 and $-0.110\ V\ decade^{-1}$) for soft gold. Only one Tafel region was reported for hard gold ($-0.200\ V\ decade^{-1}$); however, the nickel concentration was two orders of magnitude lower than that used in [60]. The linear sweep voltammograms show a strange dependence on the mass transport rate of the solution. In addition to the expected supply of reactants to the electrode surface, CN^- or HCN produced at the electrode surface can inhibit the reactions. Higher mass transport rates will reduce the concentration of these inhibitors at the surface.

The structure of electrodeposited soft gold is referred to as columnar because etched cross sections show long crystallites whose length axis coincides with the growth direction of the deposit. The nucleation rate of soft gold is low, and the tendency toward preferred growth on existing grains is high. In contrast, hard gold deposits have a high nucleation rate and submicrometer grain size, as noted earlier. Thus the principal difference between hard and soft gold is the grain size, which is derived from the rates of nucleation. That is, the effect of both impurities, current density, and other plating parameters on the mechanical properties of the deposit can be understood in terms of the nucleation and growth rate.

The surface roughness of gold deposits from a commercial gold cyanide solution was examined by scanning tunneling microscopy using smooth (111) gold surfaces [67]. It was found that the surface of the gold was roughened by simple immersion into the plating bath, an effect of the exchange current (the zero-applied-current) condition. The result of 100 Å of electrodeposited gold was "rolling hills" of gold 200 Å wide and 30 Å high.

4.3 PULSE PLATING

Pulse plating usually yields finer grain deposits than dc baths because of the high pulse current density and resulting high nucleation rate. Low porosity has been observed with pulse-plated gold due to grain refinement [68]. The growth of gold on crystalline copper is initially dependent on the structure of the substrate under pulse or dc plating. When the deposit reaches 50–100 nm in thickness, the growth gradually changes from substrate controlled to transport controlled [69]. In studies on orientated copper substrates, single-crystal growth was observed for [001] and [011] gold grains. The nuclei forming these grains coalesce when they come in contact with each other, which leads to single-crystal grain growth. For larger nuclei, the growing grains obtain equal orientation. These observations for pulse-plated gold are probably due to desorption of impurities during the relaxation time between successive pulses. Coalescence is more likely to occur if the growing surfaces are clean; if not, impurities are pushed into the film from the growing surface and prevent adjacent grains from coalescing, resulting in the formation of a grain boundary. Although the nucleation rate is high in pulse plating, the grain refinement is due to the different surface diffusion conditions. During pulse plating, the diffusion paths are blocked due to a high adion concentration, resulting in decreased surface mobility, and the structure becomes columnar. In dc plating, the adion mobility is high and a crystalline structure is developed [69]. The ductility, tensile strength, and yield strength were found to be improved in alternating current electrolysis; however, higher contact resistance was also reported [68]. The current distribution for selective pulse plating was quantitatively described as a function of peak current and anode-to-cathode ratio [70]. The current distribution is generally less uniform at small Wagner numbers. One problem common to all pulse plating strategies is the availability and cost of power supplies. The formation of high current pulses is expensive, and the rarity of users limits the benefits of mass production.

4.4 SUBSTRATE PREPARATION

Gold plating is often the last step in a long series of processing steps, making it immediately suspect when difficulties are encountered. However, in many cases the problems that appear at the gold plating step are due to the cleaning and preparation processes preceding gold deposition. Poor, incomplete, or inappropriate cleaning can result in inadequate gold deposits. While problems do occur in the gold plating process, only a good engineering evaluation of the defective deposits can elucidate the failure mechanism.

4.4.1 Cleaning and Surface Preparation

Copper, brass, and silver parts are easily plated once cleaned. The normal practice may require degreasing in an alkaline spray or soak or by a solvent vapor degreaser. A copper part may require a bright dip (10% sulfuric acid in water) to

remove the native oxide. Beryllium copper spring material or castings should be carefully cleaned by a 15-min soak in boiling NaCN and NaOH solution (38 g NaCN, 38 g NaOH, and 1 L H_2O) followed by a water rinse and bright dip and final rinse. Other procedures use a dip in 60% by volume H_2SO_4 at 50°C for 30 s followed by a water rinse.

Nickel parts must be activated before gold plating or the plate may peel. Activation can be accomplished by a dip in warm 1 : 1 HCl in water. It is very important not to allow the nickel parts to dry after activation before gold plating. Nickel alloys like Kovar can be cleaned by soaking for many minutes in hot 18% HCl. The oxide-free surface is prepared for plating by bright dipping for several seconds in 1 : 3 nitric acid–acetic acid with 15 mL HCl per liter of solution at 70°C. Kovar can be first plated with Woods or Watts nickel before gold plating or to gold strike the nickel alloy directly at high current in a low-gold-content bath followed by normal gold plating.

Gold plating onto aluminum and aluminum alloys has become more common, particularly for electronics and space applications. The surface is first degreased, such as in trichloroethylene vapors, followed by alkaline cleaning in trisodium orthophosphate (Na_3PO_4, 12 g L^{-1}; H_2O, 25 g L^{-1}; and Na_2CO_3, 20 g L^{-1}) at 60°C for 2–3 min. After water rinsing, the aluminum surface is cleaned in a mixed-acid solution (sulfuric acid, 10 mL L^{-1}; hydrofluoric acid (40%), 12.5 mL L^{-1}, and nitric acid, 25 mL L^{-1}) for 2–3 min. A zinc displacement deposition process can precede the electroless nickel underlayer (nickel sulfate, 30 g L^{-1}; zinc sulfate, 40 g L^{-1}; sodium hydroxide, 106 g L^{-1}; potassium cyanide, 10 g L^{-1}; potassium bitartrate, 40 g L^{-1}; copper sulfate, 5 g L^{-1}; and ferric chloride, 2 g L^{-1}) for 1 min. The first zinc layer is stripped in 50% nitric acid followed by a second zinc layer by immersion for 30 s [71]. Extreme caution should be practiced when handling hydrofluoric acid and potassium cyanide, especially when the cyanide is in the same vicinity as acids.

Gold films are widely used in MEMS applications because of its excellent physicochemical stability, low resistivity, and high reflectivity for infrared radiation. However, adhesion onto silicon has been problematic. A two-step electrodeposition process was found to give growth directly onto a silicon surface [72]. After stripping the surface oxide from the silicon, gold is plated and annealed and then a final coating of gold is plated. The current density of the initial gold plate is critical.

The adhesion of gold directly to glass is very difficult. An ion beam mixing process has been used to produce gold films directly bonded to glass [73]. An Au–C bilayer film was deposited on glass followed by ion beam "mixing" caused by the Xe^+ ion implantation. The ion implantation process provides for atomic mixing of the thin layer with the glass. A thicker film of gold could then be deposited. Excellent adhesion of the gold film on glass was obtained.

Thin electroplated gold wires were bonded to hydrogen silsesquioxane glass by a transfer process using imprint lithography [74]. The transfer process first produced thin gold wires on silicon from $AuCN_4^-$ immersion plating onto silicon. Silicon serves as the reducing agent for gold deposition. The plating bath contained free fluoride to dissolve the oxidized silicon. The lack of adhesion of the gold wire onto the silicon surface allows easy release and transfer onto the glass.

The direct thermocompression bonding of plated gold surfaces was used to achieve MEMS packaging [75]. Two silicon wafers were bonded together at a pressure of 2.5 MPa and temperature of 320°C. The gold film produced on the side walls of via holes was used for bonding to two parts together, providing a hermetic seal for the MEMS package.

4.4.2 Barrier Metals

Service requirements may need an underplate between the base metal and the gold electroplate. Specifications for gold-plated copper parts exposed to temperatures > 60°C often require an intervening nickel-plated barrier to prevent copper–gold interdiffusion and subsequent copper bleed through to the surface. The barrier may be 5–10 μm of low-stress nickel, like that plated from a sulfamate bath. Gold plating on zinc-based alloys should have at least 8 μm of nickel over 8 μm of copper. Tin or lead should have 8 μm of nickel over 2 μm of copper.

4.4.3 Gold Strike

The use of a gold strike is common before the deposition of a thick gold plate. The thickness of a gold strike may be 0.02–0.25 μm, depending on the thickness and requirements of the full gold thickness. A gold strike bath is usually a dilute version of a normal gold plating bath. A high current density is used to overcome activation control of the plating process. A large fraction of the gold cyanide ions at the electrode surface are reduced to gold at a high nucleation rate. Thus a uniform deposit is formed over the electrode surface compensating for inhomogeneities across it, which may have created problems under normal gold plating conditions. The gold strike surface has increased adhesion and porosity, and less contamination is dragged into the main plating bath. A typical strike bath would have 0.8 g L^{-1} gold versus 8 g L^{-1} and current densities 2–10 times higher than the conventional bath.

4.4.4 High-Speed Strip Plating

There has been extensive use of high-speed plating as well as selective plating in the semiconductor industry since around 1970. In particular, reducing cost and materials in the reel-to-reel electroplating of electrical connectors has led to many

innovations in high-speed plating. Reel-to-reel plating of connectors includes facilities for cleaning and preparation of parts, strike plating, and transport of parts and chemicals. The sequence of the processes is similar to those in batch plating; however, size, space, and time limitations have stimulated a fine tuning of the processes, which makes their review worthwhile. The strip plating process for electrical connectors is composed of the following processes: (1) ultrasonic clean, (2) electropolish, (3) acid dip, (4) nickel plate, (5) gold strike, (6) hard gold plate, (7) hot rinse, and (8) dry [76]. Cleaning is limited to nonfoaming solutions because of the need for rapid recirculation of the liquid from a reservoir tank. Ultrasonic agitation speeds up the cleaning process by dislodging the contaminants from the surface through cavitation. Electropolishing is an anodic process where metal dissolves (cleaning and deburring) in proportion to the anode current density. Copper alloys used for electrical connectors electropolish well in 1 : 1 phosphoric acid in water. Current densities as high as 4000 mA cm^{-2} can be used to accommodate high-speed processing with small electroplating cells. A major problem in electropolishing is the deposition of copper powder at the cathode, which must be removed periodically to avoid cell shorting. While it is desirable to have the electrodes in close proximity to reduce solution heating and voltage, wider spacing (e.g., 1.5 cm) is necessary to mitigate cell shorting from powdery copper loosely adherent to the cathode. The copper phosphate residue can be removed by a hot-water rinse followed by a rinse in 10% sulfuric acid (by volume) at 60°C. The nickel underplate (∼0.14 μm) can be from a nickel sulfate or nickel sulfamate bath. The AFHG baths used in reel-to-reel gold strike are shown below:

	Gold Strike	High-Speed Bath
$KAu(CN)_2$	4 g L^{-1}	44 g L^{-1}
K_2HPO_4	120 g L^{-1}	—
KH_2PO_4	30 g L^{-1}	100 g L^{-1}
KOH	—	28 g L^{-1}
Temperature	65°C	40°C
pH	7.0	7.0

The current density for the gold strike is 30 mA cm^{-2}. The hardness of the final deposit is achieved by producing small grains, which is the result of high current density at low temperature. The hardness of the gold plated from the high-speed bath given above is 180 KHN_{25} for current densities between 150 and 250 mA cm^{-2}. The hardness drops off at lower current densities, to 150 KHN_{25} for 100 mA cm^{-2}, and 125 KHN_{25} at 50 mA cm^{-2} [76]. Others have used even higher current densities (800–2000 mA cm^{-2}), although the conditions are different [77]. A final hot rinse and drying complete the strip plating process. The plating process can be accomplished in relatively short-length plating cells (∼18 in. long) with insoluble anodes that allow precise placement of the hardware in an attempt to selectively plate the gold only on the functional area of the connectors. Although a majority of the gold can be deposited on the contact area of connectors, it is extremely difficult to prevent some plating on nonfunctional areas immersed in the plating bath. Laser-assisted plating has been shown to assist in the selective plating process. Laser processes have been developed to improve the selectivity of the deposition process. The direct irradiation by a pulsed laser has been shown to cause extremely rapid surface heating, increasing the agitation and deposition rate. It also increases the interdiffusion of the deposited atoms [78, 79]. Lasers have also been used in a patterning technique where the whole component was coated with an insulator, such as glycol phthalate, paraffin wax, or photoresist, and an yttrium–aluminum–garnet (YAG) laser was used to burn off the material in small areas which were then plated [79]. One problem is the precise alignment of the laser to the part either in a moving or a step-and-repeat process.

4.5 STAINS

Staining of precious metal–plated surfaces is a critical concern, especially since chlorofluorocarbon (CFC) usage is discouraged. The CFC displacement method did not dry the plated metal surface; it displaced the water from the plated surface. The plating stains are often caused by potassium cyanide or other plating salts precipitating on the surface as the water evaporates. Stains are often seen as irregularly shaped "hollow" blemishes where the stained area is smaller than the original water drop size, and the center of the stain is not very discolored. Droplets form on the wetted areas as the plated parts are removed from the rinse water. The rinsing water simply dilutes the plating salts, leaving a low concentration of salt. As the rinse water dries from the surface, the volume of the original water droplet is reduced through evaporation. The concentration of the salt in the droplet increases as the volume decreases. When the concentration of the salts exceeds their solubility, they precipitate onto the surface. The "hollow" center is formed because the salts continue to precipitate onto the existing deposit. The oxidation of the gold surface is not an issue as it would be with less noble metals. There are many things which can be done to reduce the staining of electroplated gold parts: (1) use high-quality rinse water, (2) countercurrent rinsing techniques are desirable, (3) removing the final rinse water from the surface by CFC displacement, and (4) removal of rinse water by hot air knives, centrifugal dryers, or alcohol absorption. Isopropyl alcohol is often preferred, especially over methanol because the rate of evaporation is slower. Rapid evaporation can result in cooling of the surface below the ambient dew point, resulting in condensation of water and nucleation of spots.

4.6 TEST METHODS

The physical properties of significance for the gold deposits are appearance, wear resistance, hardness, brittleness, residual stress, porosity, thickness, density, and deposit uniformity. The chemical properties of importance include the chemical composition of the deposits and solutions, segregation of impurities, and inertness to oxidation. Each of the physical and chemical properties can be tested.

4.6.1 Physical Properties

Appearance tests are often subjective and reflect only the surface texture and color of the deposit. Color match and uniformity are critical for decorative plating. The appearance is best controlled through strict control of the plating variables. Changes in the deposit are often the result of unintentional codeposition of unwanted metals. Lead from solder baths and iron from plating fixtures are common problems. Burned deposits can be the result of a depleted bath, excessively high current density, or non uniform current distribution such as would occur from defective or misshaped anodes.

Wear resistance is an important attribute for gold finishes in high-wear situations, such as sliding contacts. An abrasive test applicable to jewelry applications has been described [80]. Wear tests applicable to electrical parts have been described [24, 25, 80, 81]. The purpose of the tests is to determine how fast a deposit fails under laboratory-imposed mechanical loads, with commercial testers providing a convenient method for comparison. The variables include shape of the parts exposed to wear, cleaning, lubrication, and load.

Deposit hardness can be determined by mechanical deformation of test specimens. Commercial instrumentation and scales of hardness exist [82]. Two of the most common instruments use pyramidal diamond indenters with equal (Vickers) or unequal (Knoop) diagonals. The use of these for gold parts has been discussed [83]. Hardness is usually determined using cross sections of suitable thickness. Indenting normal to the surface often leads to erroneous results because surface roughness can lead to nonuniform loads and thin samples give hardness representative of the base substrate and not the plated gold. Electroplated soft gold has a Knoop hardness of about 60 under a 25-g load. Hard gold can have Knoop values near 200.

Brittleness is the result of the presence of some particular phase or compound in the gold, such as can occur by the alloying of gold, either intentional or unintentional. Nickel and cobalt are intentionally added to improve hardness, whereas tin can cause brittle solder joints [84]. When all the gold does not dissolve in the solder, brittle failure can occur. Identification of brittle failures can be performed through metallographic examination. Gold hardened by codepositon of iron at the 0.1% level leads to stressed deposits that are brittle and that fail under mechanical loads milder than acceptable for printed wiring boards and connectors. Iron contamination is a particular concern because of the ease of contamination of gold baths from steel components. The degree of brittleness can be quantified in a flex test of the deposit, such as bending mandrill tests. Other tests include uniaxial tensile tests and diamond scribe tests [32].

Pure gold is electrodeposited in virtually a zero-stress state. The gold can be brought to a low-stress state if it is deposited onto a substrate whose coefficient of thermal expansion is different from gold and the deposition occurs at other than room temperature. During cooling from the deposition temperature, the different rate of contraction of the gold and its substrate produces residual stress. Temperature cycling of plated gold onto a substrate can result in significant stress, depending on the temperature excursion. At sufficiently high temperatures ($\sim$150°C), gold can recrystallize, reducing the stress at high temperature via grain growth. Upon cooling, the process is not reversible. That is, the coefficient of thermal expansion mismatch will produce a high-stress state in the gold.

There are several common test methods for porosity [85]. Chemical tests are used to determine the area of the exposed base metal by visual examination of the quantity of accumulated corrosion products. The base metal is oxidized by anodic dissolution or by chemical attack. This class of tests are easy to perform. Common forms of the test use polysulfide solutions [86] or atmospheres containing moist sulfur dioxide [87, 88] or nitric acid [85, 89]. The electrooxidation of the gold-plated part using a moist paper or a gel as a support for the electrolyte containing a dye or complexing agent can be used to quantify the porosity of the gold [90]. In the test, the complexed gold forms a colored species that can easily be identified and counted. Specific tests have been developed for copper and nickel.

The electromigration resistance of gold was measured using a four-terminal Kelvin line structure using a stress current of $2.0\,\mathrm{MA\,cm^{-2}}$ at temperatures between 325 and 375°C [91]. The activation energy for electromigration was 0.59 ± 0.09 eV. A diffusion mechanism for void formation was suggested. The Young's modulus, residual stress, and stress gradient in electroplated films were measured using surface micromachined beam structures [92]. The Young's modulus was calculated to be from 35.2 to 43.9 GPa using a value of Poisson's ratio of 0.42 for gold.

4.6.2 Chemical Analysis

Atomic absorption (AA) spectrophotometry is a rapid and easy method for analyzing gold films. The gold deposit can be separated from the base metal by immersing the part in an etchant that oxidizes and dissolves the base metal without oxidizing the gold or leaching out its impurities. The gold is then dissolved and the solution is analyzed by AA using the

appropriate standards. Such tests are needed in meeting specifications such as military specification MIL-G-45204B for pure, bondable gold where metallic impurities such as chromium, copper, tin, lead, silver, cadmium, or zinc should not be present in the deposit at a concentration greater than 0.1 %. Polarography can be used to analyzed solutions for various impurities and well as the gold baths themselves. The concentration of Au(III) has been quantified by polarography [17]. More exotic techniques can be used for specific analysis. For example, Mossbauer spectroscopy of Fe^{57} was used to uncover the form of the cobalt in gold deposits [22]. Radioactive Co^{57} was added to the common Co^{59} additive in the cobalt-hardened bath. The Co^{57} decayed to Fe^{57}, which could be studied by Mossbauer spectroscopy. Another example of a specific analytical method is the analysis of carbon. The carbon content of the deposits has been determined by combustion, converting it to CO_2, which could be measured by coulometric titration [93].

Surface analytical techniques, such as Auger electron spectroscopy and X-ray photoelectron spectroscopy, are often used to determine the elemental analysis of the gold surface as well as thin surface films when combined with sputter etching. Rutherford backscattering (α-particle backscattering) is a powerful technique for identifying impurities and the distribution of impurities with depth in a rapid and nondestructive test. The thickness of thin films of gold can also be determined [94]. β-ray scattering can also be used for thickness measurements, and the apparatus is quite simple. X-ray fluorescence can also be used for thickness and impurity analysis; however, standards and tight control of analysis geometry are essential for accurate results. Structural aspects of gold deposits, such as grain size, are best determined by transmission electron microscopy. While sample preparation can require considerable effort, the results are irreplaceable [34, 43]. A technique known as through-focus imaging was used to observe organic and gaseous inclusions in gold, which cannot be done by conventional imaging techniques [34]. The availability of scanning probe techniques has provided new tools for examining growth and nucleation of deposits [67]. Last, surface contamination of electrical parts has created a need for evaluating and monitoring the contact resistance of electrical parts. Typical values of about 1 mΩ are obtained for electrical contacts. The contact force and area of the contact need to be controlled. Contact resistance increases of 2- to 50-fold have been observed for aged cobalt-hardened gold [32].

REFERENCES

1. G. Langbein and W. T. Brannt, *Electroplating of Metal*, 4th ed., Henry Carey Baird and Co., Philadelphia, PA, 1902, p. 3.
2. M. Pourbaix, *Atlas of Electrochemical Equilibra in Aqueous Solutions*, Pergamon, New York, 1966.
3. W. M. Latimer, *The Oxidation States of the Elements and Their Properties in Aqueous Solutions*, Prentice-Hall, Englewood Cliffs, NJ, 1985.
4. G. M. Schmid and M. E. Curly-Florino, in *Encyclopedia of Electrochemistry of the Element*, Vol. 4, A. J. Bard, Ed., Marcel Dekker, New York, 1978.
5. R. Puddephatt,in *Comprehensive Inorganic Chemistry*, Vol. 4, J. C. Bailar Jr., H. J. Emeleus, R. Nyholm, and A. F. Trotman-Dickenson, Eds., Pergamon, Elmsford, NY, 1973.
6. G. H. Kelsall, *J. Electrochem. Soc.*, **138**, 108 (1991).
7. W. T. Lee, *Corrosion Technol.*, **39** (Apr. 1963).
8. E. D. Winters, *Plating*, **59**, 213 (1972).
9. S. A. Losi, F. L. Zuntini, and A. R. Meyer, *Electrodeposition Surf. Treatment*, **1**, 3 (1972).
10. L. Silverman, B. Bernauer, and F. Pettinger, *Met. Finish.*, **68**, 48 (Aug. 1970).
11. W. A. Fairweather, *Met. Finish.*, **64**, 15 (May 1986).
12. J. M. Leeds and M. Clarke, *Trans. Inst. Met. Finish.*, **47**, 163 (1969).
13. H. Angerer and N. Ibl, *J. Appl. Electrochem.*, **9**, 219 (1979).
14. Y. Okinaka, F. B. Koch, C. Wolowodiuk, and D. R. Blessington, *J. Electrochem. Soc.*, **125**, 1745 (1978).
15. E. D. Winters, *Plating*, **59**, 213 (1972).
16. Y. Okinaka and S. Nakahara, *J. Electrochem. Soc.*, **123**, 1284 (1976).
17. Y. Okinaka and C. Wolowodiuk, *J. Electrochem. Soc.*, **128**, 288 (1981).
18. A. Knodler, *Metalloberflache*, **28**, 465 (1974).
19. C. J. Raub, A. Knodler, and J. Lendvay, *Plating*, **63**, 35 (1976).
20. Y. Okinaka, F. B. Koch, C. Wolowodiuk, and D. R. Blessington, *J. Electrochem. Soc.*, **125**, 1745 (1978).
21. H. Leideiser, Jr., A. Vertes, M. L. Varsanyi, and I. Czako-Nagy, *J. Electrochem. Soc.*, **126**, 391 (1979).
22. R. L. Cohen, F. B. Koch, L. N. Schoenberg, and K. W. West, *J. Electrochem. Soc.*, **126**, 1608 (1979).
23. C. C. Lo, J. A. Angis, and M. R. Pinnel, *J. Appl Phys.*, **50**, 6887 (1979).
24. K. J. Whitlaw, J. W. Souter, I. S. Wright, and M. C. Nottingham, *IEEE Trans. CHMT*, **8**, 46 (1985).
25. L.-G. Liljestrand, L. Sjohren, L. B. Revay, and B. Asthner, *IEEE Trans. CHMT*, **8**, 123 (1985).
26. J. H. Thomas III and S. P. Sharma, *J. Electrochem. Soc.*, **126**, 445 (1979).
27. G. B. Munier, *Plating*, **56**, 1151 (1969).
28. L. Holt, R. J. Ellis, and J. Stanyer, *Plating*, **60**, 910 (1973).
29. M. Antler, *Plating*, **60**, 468 (1973).
30. H. A. Reinheimer, *J. Electrochem. Soc.*, **121**, 490 (1974).
31. R. L. Cohen, K. W. West, and M. Antler, *J. Electrochem. Soc.*, **124**, 342 (1977).
32. F. B. Koch, Y. Okinaka, C. Wolowodiuk, and D. R. Blessington, *Plating*, **67**, 50 (1980).
33. H. A. Reinheimer, *J. Electrochem, Soc.*, **121**, 490 (1974).
34. S. Nakahara and Y. Okinaka, *J. Electrochem. Soc.*, **128**, 284 (1981).

35. F. B. Koch, Y. Okinaka, C. Wolowodiuk, and D. R. Blessington, *Plating*, **67**, 43 (1980).
36. S. Kal, A. Bagolini, B. Margesin, and M. Zen, *Microelectron. J.*, **37**, 1329 (2006).
37. J. J. Kelly, N. Yang, T. Headley, and J. Hachman, *J. Electrochem. Soc.*, **150**, C445 (2003).
38. A. Chinthakindi, D. Bhusari, B. Dusch, J. Musolf, B. Willemsend, E. Prophet, M. Roberson, and P. A. Kohl, *J. Electrochem. Soc.*, **149**, HI39 (2002).
39. M. Paunovic and C. Sambucetti, in *Electrochemically Deposited Thin Films, Proc.*, Vol. 94–31, M. Paunovic, Ed., Electrochemical Society, Pennington, NJ, 1995, pp. 34–44.
40. A. M. Sullivan and P. A. Kohl, *J. Electrochem. Soc.*, **144**, 1686 (1997).
41. T. Osaka, A. Kodera, T. Misato, T. Homma, Y. Okinaka, and O. Yoshioka, *J. Electrochem. Soc.*, **144** (1997).
42. X. Wang, N. Issaev, and J. G. Osteryoung, *J. Electrochem. Soc.*, **144** (1997).
43. W. J. Dauksher, D. J. Resnick, W. A. Johnson, and A. W. Yanof, *Microelectron. Eng.*, **23**, 235 (1994).
44. W. Chu, M. L. Schattenburg, and H. I. Smith, *Microelectron. Eng.*, **17**, 223 (1992).
45. H. Homma and Y. Kagaya, *J. Electrochem. Soc.*, **140**, L135 (1993).
46. T. Inoue, S. Ando, H. Okudaira, J. Ushio, A. Tomizawa, H. Takehara, T. Shimazaki, H. Yamamoto, and H. Yokono,in *Proc. 45th Electronic Components and Technology Conf.*, IEEE, New York, 1995, p. 1059.
47. M. Kato, K. Nikura, S. Hoshino, and I. Ohono, *J. Surf. Finish. Soc. Jpn.*, **42**, 69 (1991).
48. Y. Okinaka and T. Osaka,in *Advances in Electrochemical Science and Engineering*, Vol. 3, H. Gerischer and C. Tobias, Eds., VCH Publishing, New York, 1994, p. 55.
49. T. A. Green and S. Roy, *J. Electrochem. Soc.*, **153**, C157 (2006).
50. A. M. Sullivan and P. A. Kohl, *J. Electrochem. Soc.*, **142**, 2250 (1995).
51. K. Wang, R. Beica, and N. Brown, *29th International Manufacturing Technology Symposium,* IEEE/SEMI, 2004, pp. 242– 246.
52. W. Sun and D. Ivey, *Mat. Sci. Eng.*, **B65**, 111 (1999).
53. J. Doesberg and D. Ivey, *Plating Surf. Finish*, **88**, 78 (Apr. 2001).
54. A. He, B. Djurfors, S. Aldhlaghi, and D. Ivey, *Plating Surf. Fin.*, **89**, 48 (Nov. 2002).
55. J. Doesberg and D. Ivey, *Mater. Sci. Eng.*, **B78**, 44 (2000).
56. G Hoimbom, J. Abys, H. Straschil, and M Svensson, *Plating Surf. Finish*, (Apr. 1998).
57. L. Chalumeau, M. Wery, H. Ayedi, M. Chabouni, and C. Leclere, *Surf. Coating Tech.*, **201**, 1363 (2006).
58. F. Su, J. Huang, and I. Sun, *J. Electrochem. Soc.*, **151**, C811 (2004).
59. H. Sanchez, P. Ozil, E. Chainet, B. Nguyen, and Y. Meas, *J. Electrochem. Soc.*, **144**, 2004 (1997).
60. W. Chirzanowski, Y. G. Li, and A. Lasia, *J. Appl. Electrochem.*, **26**, 385 (1996).
61. E. T. Eisenmann, *J. Electrochem. Soc.*, **125**, 717 (1978).
62. G. Holmbom and B. E. Jacobson, *J. Electrochem. Soc.*, **135**, 787 (1988).
63. B. Bozzini, G., Giovannelli, S. Natali, A. Fanigliulo, and P. Cavallotti, *J. Mater. Sci.*, **37**, 3903 (2002).
64. B. Bozzini, C. Mele, and V. Romanello, *J. Electroanal. Chem.*, **592**, 25 (2006).
65. B. Bozzini, B. Busson, G. De Gaudenzi, L. D'Urzo, C. Mele, and A. Tadjeddine, *J. Electroanal. Chem.*, **602**, 61 (2007).
66. A. Fanigliulo and B. Bozzini, *J. Electroanal. Chem.*, **530**, 53 (2002).
67. J. Schneir, V. Elings, and P. K. Hansma, *J. Electrochem. Soc.*, **135**, 2774 (1988).
68. G. Decaraj and S. Gurrviah, *Mater. Chem. Phys.*, **25**, 439 (1990).
69. G. Holmbom and B. E. Jacobson, *J. Electrochem. Soc.*, **135**, 2720 (1988).
70. D. T. Chin, N. R. K. Vilambi, and M. K. Sunkara, *Plating*, **76**, 74 (1989).
71. A. K. Sharma, *Trans. Inst. Met. Finish.*, **67**, 87 (Aug. 1989).
72. T. Fujita, S. Nakamichi, S. Iodu, K. Maenaka, and Y. Takayama, *Sensors Actuators A*, **135**, 50 (2007).
73. L. Guzman, A. Miotello, R. Checchetto, and M. Adami, *Surf. Coating Tech.*, **158**, 558 (2002).
74. J. Chen. J. Liu, Y Hsu, J. Syu, and S. Huang, *Nanotechnology*, **16**, 2913 (2005).
75. G. Park, Y. Kim, K. Paek, J. Kim, J. Lee, and B. Ju, *Electrochem. Solid-State Lett.*, **8**, G330 (2005).
76. D. R. Turner, *Met. Finish.*, **63**, 41 (Nov. 1987).
77. D. W. Endicott and G. J. Casey, Jr., *Plating*, **67**, 58 (1980).
78. R. J. von Gutfeld, M. H. Gelchins, and L. T. Romankiw, *J. Electrochem. Soc.*, **130**, 1840 (1983).
79. I. R. Christie, *Trans. Inst. Met. Finish.*, **64**, 47 (1986).
80. R. Duva and D. G. Foulke, *Plating*, **55**, 1056 (1968).
81. A. J. Solomon and M. Antler, *Plating*, **57**, 812 (1970).
82. V. E. Lysaght, *Indentation Hardness Testing*, Reingold, New York, 1948.
83. R. G. Baker and T. R. Palumbo, *Plating*, **58**, 791 (1971).
84. F. G. Foster, *ASTM Spec. Tech. Pub.*, **319**, 3113 (1963).
85. A. A. Khan, *Plating*, **56**, 1374 (1969).
86. F. I. Nobel, B. D. Ostrow, and D. W. Thomson, *Plating*, **52**, 1001 (1965).
87. R. W. Beattie, G. Forshow, and E. N. Loney, *Proc. IEE (London)*, **B-109** (suppl. 21), 109 (1962).
88. M. Clarke and J. M. Leeds, *Trans. Inst. Met. Finish.*, **46**, 81 (1968).
89. F. Knoop, C. G. Peters, and W. E. J. Emerson, *J. Res. Natl. Bur. Stand.*, **23**, RP 1220 (1939).
90. F. V. Bedette and R. V. Chiarinzelli, *Plating*, **53**, 305 (1956).
91. S. Kilgore, C. Gaw, H. Henry, D. Hill, and D. Schroder, *Mater. Res. Soc. Symp. Proc*, **863**, B8.30.1 (2005).
92. C. Baek, Y. Kim, Y. Ahn, and Y. Kim, *Sensors Actuators A*, **117**, 17 (2005).
93. E. N. Wiese, P. W. Gilles, and C. A. Reynolds, *Anal Chem.*, **25**, 1344 (1953).
94. J. Zahavi, *Met. Finish.*, **83**, 61 (July 1985).

5

ELECTROLESS AND ELECTRODEPOSITION OF SILVER

MORDECHAY SCHLESINGER

Silver metal has been known since ancient times. It is mentioned in Exodus and Genesis. There exist strong indication that man was able to separate silver from lead as early as 3000 BC. Silver may be found native and in ores. Lead, lead zinc, copper, and other ores are principal sources. Silver may also be recovered during electrolytic refining of copper. Pure silver has the highest electrical and thermal conductivity of all metals. It retains that property in the form of electroplated thin film as well. This makes electroplated silver an important component of many printed circuit systems.

There is indication that silver was plated as far back as the beginning of the nineteenth century. If correct, it must have been done in connection with producing mirrors. The earliest patent for silver plating, however, was not granted until 1840 [1]. That may be viewed as signifying the start of the electroplating industry. That bath is still one of the more used ones to this day, and it is the double-silver cyanide complex [$KAg(CN)_2$] with excess free cyanide. Over the years many other baths have been proposed [2], such as the ones involving nitrate, iodide, thiourea, thiocyanate, sulfamate, and thiosulfate. The usages of silver plating are many. Those include mirrors and deposits for tableware due to its decorative effect as well as resistance to corrosion in its contact with foods. There are a number of industrial uses as well. Those include, but are not limited to, electronic component applications, bearings, hot-gas seals, to name but a few. Silver may be plated using either electrodeposition methods or electroless methods. We discuss here both methods, starting with the latter.

5.1 ELECTROLESS DEPOSITION

It is often necessary to silver coat insulators such as glass or ceramics. While a number of methods may be employed for this purpose (e.g., chemical vapor deposition, ion sputtering), chemical methods, and in particular the methods of electroless deposition, offer an effective, easy to operate path. In general, electrochemical methods may be classified into two types. One is galvanic exchange. Here the potential difference between metals is used to replace one metal layer with another (e.g., in "zincation"). The other is electroless plating where reducing agents are used. Electroless plating is the main focus in this presentation. As mentioned in a number of other chapters in this book, the electroless methods are effective because of the simplicity of the apparatus used, and they can be done on complex substrates; last, but not least, the methods are suitable for mass production.

5.1.1 Pretreatment

The substrate pretreatment for electroless silver plating involves, besides cleaning and degreasing, immersion in $SnCl_2$ solution and subsequent rinse in water. If, for instance, the substrate is glass, then the next step is immersion in the silver metallizing bath. Fine silver particles that are positively charged in solution will adhere to the glass surface, and the Sn^{2+} species will reduce the silver ions to metallic silver by being oxidized themselves to the Sn^{4+} state. Since silver is autocatalytic for the electrodeposition of itself, plating will continue as long as the substrate is immersed in the bath. For substrates other than glass, there will be the need to add the step of immersion in $PdCl_2$ before proceeding to the metallizing stage.

5.1.2 Metallizing Baths Compositions

In practice, the metallizing bath is made by combining two separate baths. One is a silver ion solution, while the other is

Modern Electroplating, Fifth Edition Edited by Mordechay Schlesinger and Milan Paunovic

a reducing agent solution. In what follows we will denote them as A an B, respectively.

1. Rochelle salt based [3] (most often used)
   A: Silver nitrate 450 g, saturated ammonia solution 350 mL water 5.5 L
   B: Rochelle salt 1600g Epsom salt, 110 g water 3.6 L
2. Glucose method [4]
   A: Silver nitrate 3.5 g, ammonia solution as required, water 60 mL, sodium hydroxide solution 2.5 g $100\,mL^{-1}$
   B: Glucose 45 g, tartaric acid 4g, water 1 L, ethyl alcohol 100 mL
3. Hydrazine method [3] (used for spray method, see below)
   A: Silver nitrate 100 g, ammonia solution (as required) 230 mL
   B: Hydrazine sulfate 43 g, ammonia solution 45 mL

In case 3, the A and B are diluted to 4.5 L and then mixed to the ratio 1 : 1.

5.1.3 Bath Properties

Electroless silver plating baths are very unstable and so short lived. It is desirable to stabilize the baths for electroless deposition of nickel and copper. In the case of silver this becomes imperative. Indeed, if the bath can be made more stable, it will be that much more useful. It has been found [5] that a small amount of 3-iodotyrosine or 3,5-diiodotyrosine added to a bath (referred to as DIT bath) can work as stabilizer.

There seems to be a strong indication that the electroless plating reaction progresses with a combination of a cathodic reaction of a cation, that is, $M^{n+} + ne \rightarrow M$, and an anodic oxidation of the reducing agent $R \rightarrow O + ne$. Here it is assumed that a metal ion is cathodically reduced to metal on the surface that is activated by a catalyst. This state of affairs is valid for silver as well as for other metals on which autocatalytic reaction will occur. A number of examples with representative reducing agents are given above. In all silver oxide precipitation is avoided because the electroless silver plating is carried out in a basic solution. The complexing agent is added to the solution.

Not at all surprising is the fact that bath stability and plating rate are markedly affected by the pH of the bath. Consequently the parameters affecting the bath pH were investigated [5], It was found, for instance, that the pH changes with the addition of silver nitrate. The change is most noted when the pH values are below 10.5. The complex formation between silver ion and ethylene diamine (en) is most likely as follows:

$$Ag^+ + 2H_2O + 2en \leftrightarrow [Ag(OH)_2en_2]^- + 2H^+$$

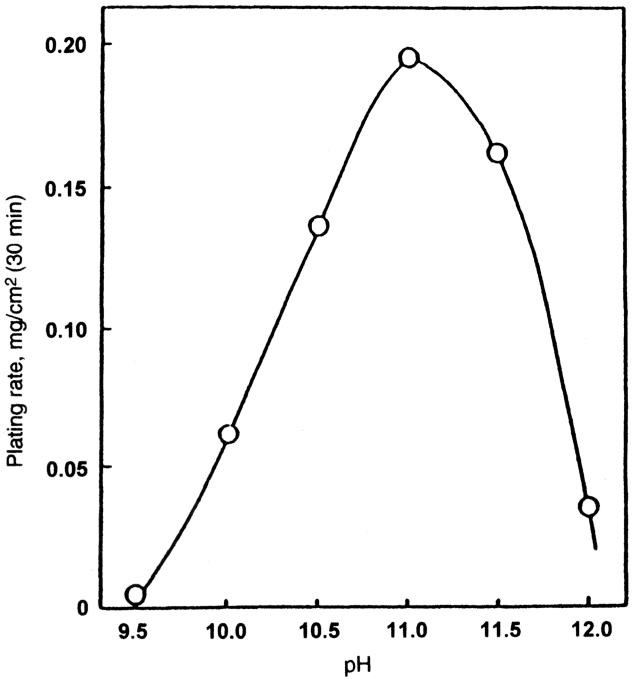

FIGURE 5.1 Electroless plating rate of silver as a function of bath pH: Silver nitrate $2.9 \times 10^{-3}M$, ethylenediamine $1.8 \times 10^{-2}M$, Rochelle salt $3.5 \times 10^{-2}M$, 3,5-diiodotyrosine $4 \times 10^{-5}M$, 35°C. Reproduced with permission of American Electroplaters and Surface Finishers, Inc. [3].

Equilibrium consideration of the reaction indicates that the bath pH changes with concentrations of Ag^+ and en. Even in the case of a stabilized bath (using 3,5-diiodotyrosine), the plating reaction all but stopped after 24 h and the pH of the bath dropped. To clarify the foregoing, we present in Figure 5.1 the electroless plating rate of silver as a function of bath pH. From the figure it is evident that a slight drop in pH value may drastically reduce the plating rate.

Other stabilizers have been reported in the literature. They include metal ions (Co^{2+}, Ni^{2+}, Co^{2+}) [6], Na-2-3-mercaptopropane sulfonate ($NaBH_4$, N_2H_4, CN^- system bath) [7], and a number more.

5.1.4 Polarization

The specific effects of pretreatment and the mechanism of silver plating can be inferred from the partial anodic and cathodic polarization curves [5]. Both the partial cathodic polarization curve for a solution without Rochelle salt as the reducing agent and the partial anodic curve for a solution without silver nitrate are given in Figure 5.2. In these the stabilized DIT bath was used. The result for the (electrode) surface pretreated with a $SnCl_2$ solution is shown by a solid line, while that for a nontreated one is shown by a dotted line. The difference between the partial cathodic polarization curves in Figure 5.2 is minimal. This is not so with the

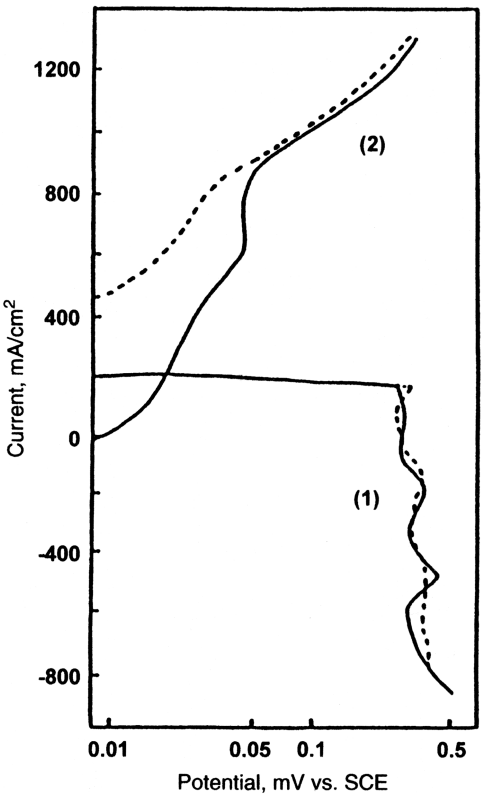

FIGURE 5.2 Partial polarization curves for various electrodes: (1) partial cathodic polarization curve of electroless silver plating solution without Rochelle salt—$AgNO_3$ (0.88 *M*), ethylenediamine (0.054 M), DIT (4×10^{-5}*M*), 3S°C, pH 10.0; (2) partial anodic polarization curve for electroless silver plating solution without silver nitrate—ethylenediamine (0.054 *M*), Rochelle salt (0.035 *M*), DIT ($4^{-5} \times 10^{-5}$*M*), 35°C, pH 10.0. (*Solid line*) Pt electrode sensitized with $SnCI_2$ solution; (*dotted line*) Pt electrode, not sensitized. Reproduced with permission of American Electroplaters and Surface Finishers, Inc. [5].

difference between the anodic polarization curves of the treated and the untreated electrodes being plainly evident. In the case of the treated electrode, an anodic current appears also in the range of 100–600 mV versus the saturated calomel electrode (SCE). At the same time the rest potential of the untreated electrode becomes 25 mV versus SCE while that of the treated becomes −81 mV versus SCE. The difference in the rest potential may be attributed to the adsorption of Sn^{2+} ions on the electrode. In other words, it is assumed that the anodic current due to oxidation of Sn^{2+} flows at potentials of 100–600 mV versus SCE. When the anodic and cathodic polarization curves for the treated electrodes are combined, a point of intersection appears at 0.02 mA cm^{-2} of current density. When this value of current density is converted to plating rate, it is found to be equivalent to 0.04 mg cm^{-2} over 30 min. This value is found to be close to the actual plating rate as determined experimentally. In the case of the untreated electrode, the current density at the intersection is extremely small. Thus, at least in the case of the DIT bath, it may be assumed that the electroless silver plating reaction proceeds only on the nucleation centers established by the $SnCl_2$ surface treatment and does not occur on the untreated surface.

5.1.5 Deposition in Practice

In the practical silvering operation the silver ion solution and the reducing agent solution are prepared separately. They are combined just before plating. Upon addition of the ammonia solution to the silver nitrate solution, a dark black-brown precipitate begins to form. The ammonia solution should be added until the precipitate all but dissolves. The solution ends up dark brown and clear.

In the spray method a number of different, specially designed guns [8] are used. One such gun has two tubes. The two solutions are sprayed separately and mixed on the substrate. There are a number of different final baths [5, 9–15] suggested in the literature, given at the end of this chapter.

Displacement methods [16] can be used in electroless silver plating on metal. For instance, the bath composition for silver plating on copper alloy is made of silver nitrate 7.5 g L^{-1}, sodium thiosulfate 100 g L^{-1}, and ammonia 75 g L^{-1}. There are many other formulations [17] given in the literature.

The applications of electroless silver deposits are many, but they may be divided into two categories:

1. Decorations and optical uses
2. Electrical conductivity and undercoating prior to other plating
3. Over coating in the process of manufacturing printed circuit boards

Mirrors [18] are an example of the first type, and undercoating for electroless gold plating or for silver plating on ceramics is an example of the second application type. One other important application is the plating of silver on ceramics for the purposes of SEM (scanning electron microscopy) measurements of surface properties [19]. Still other applications include quantitative analysis for trace amounts of arsenic [20], for the determination of pore diameter of a membrane [21], and for the recovery of mercury.

In connection with 3 above, it should be noted that the commercial process for depositing electroless silver uses an aqueous $AgNO_3$ solution in the presence of HNO_3 [22]. The manufacturers of printed circuit boards employ the electroless deposition of silver metal to prevent the degradation of exposed copper conduction tracks prior to the final assembly procedure of the devices (which can sometimes be up to several months). Of course, silver is much more susceptible to aerobic oxidation than copper; however, silver

oxide and sulfide, along with underlying silver metal, are very soluble in the tin- and tin/lead-based molten solders that are used to bond the circuit components to the copper tracks of the circuit board.

The conventional processes use strong inorganic agents, such as HNO_3, that can etch the copper substrate, but as component sizes keep shrinking, the etching of the copper tracks during silver plating is becoming a serious problem for the electronics industry. More specifically, component failures can occur due to copper etching by the electroless bath before the surfaces have been silver plated. The work in [22] demonstrated that a sustained galvanic coating of silver can be deposited onto copper substrates from a solution of Ag^+ ions in an ionic liquid (IL) based on a choline chloride (ChCl) eutectic. The sustained, electroless but not autocatalytic growth of the silver deposit is facilitated by the porous nature of the film. This was proven using acoustic impedance spectroscopy on a quartz crystal microbalance (QCM). The silver and copper surfaces were characterized using atomic force microscopy (AFM) and scanning electron microscopy (SEM/EDX). In comparison, it should be stressed that in the commercial process of dip coating of silver from ions from aqueous media, deposition does not continue once surface coverage has been arrived at without the use of catalysts. The process referred to in this discussion using ionic liquids [23] produces silver deposits of several micrometers by dip coating without the use of catalysts or strong inorganic acids [24].

This section may not be considered complete without accurate general definition of the concept of ionic liquid. That is particularly true as the last decade or so has witnessed a growing interest in the field of ionic liquids. Ionic liquids are essentially low-temperature molten salts and as such are responsible for a wealth of intellectual and technological challenges as well as opportunities for the production of new chemical processes, fuel cells, batteries, and new composite materials (see, Chapter 30 in this volume and [25]).

5.2 ELECTRODEPOSITION

5.2.1 Bath Composition

The specific composition of silver (cyanide) plating baths has to fit the required silver plate. For instance, silver plate for decorative purposes is best achieved from baths with a lower silver content than those used for engineering purposes where thicker deposits are needed. Higher silver concentrations make higher current densities possible, and as a consequence more economic plating speeds can be employed.

It is worth noting out here that many present-day silver plating baths are similar to that described in the first patent over 150 years ago. Table 5.1 gives the silver deposition bath compositions that are in common use to date. Indeed, even a typical bath composition offered recently [26] in the literature for silver electroplating is made as follows:

TABLE 5.1 Typical Bath Composition ($g\,L^{-1}$)

	Bright Silver (Conventional)	High Speed (Thick Deposit)
Silver (metal)	20–45	35–120
Silver cyanide	31–55	45–150
Potassium cyanide (total)	50–80	70–230
Potassium cyanide (free)	35–50	45–160
Potassium carbonate	15–90	15–90
Potassium nitrate	—	40–60
Potassium hydroxide	—	4–30
Current density ($A\,dm^{-1}$)	0.5–1.5	0.5–10.0
Temperature (°C)	20–28	35–50

Note: Brighteners are added as required.

AgCN	0.0185 *M*
$K_4P_2O_7$	0.3027 *M*
KCN	0.1228 *M*

Such a bath may be operated at pH 10.8 with a value of −100 mV (vs. Ag) polarization.

A number of attempts have been made to replace AgCN and thus the cyanoargentite ions by different silver electrolytes based on nitrate (see Section 5.1 on electroless deposition), thiourea, and other compounds. These solutions, however, exhibit instability, and the resulting deposits are of low quality in terms of adhesion and the like. So cyanide solutions are used at the present time despite their toxicity. The only way to minimize the cyanide concentration is to employ a lower amount as the formulation in [26] suggests. This approach requires sophisticated deposition methods such as pulse plating.

5.2.2 About Bath Constituents

It is evident from the discussion above that alkaline silver cyanide provides the silver for deposition on the cathode. From a practical point of view low silver content and high free cyanide yields improved throwing power. On the other hand, higher silver concentrations allow the use of higher current densities. Thus for this reason baths low in silver content are used for deposits of thickness between 2 and 5 μm. The alkali cyanide increases the conductivity, and the cathode polarization provides good anode corrosion, not to mention its function in forming the silver complex ion. Also KCN and not NaCN is used because it induces higher solution conductivity, higher solubility of the resultant potassium carbonate buildup, and higher limiting current densities. Potassium carbonate too increases the conductivity of the bath and also the anode and cathode polarizations, which improves throwing power. The concentration of the

carbonate rises with the decomposition of the cyanide. Thus initially the concentration added to the bath is kept to the recommended minimum.

Silver cyanide forms a complex $KAg(CN)_2$. One gram of AgCN requires about 0.5 g KCN in addition to the free cyanide indicated in Table 5.1. Over the years we have found that the most convenient way to prepare a tank full of silver plating bath is as follows: Dissolve the bath constituents other than the potassium silver cyanide and dissolve the possible brighteners in a separate container of water equal to about half of the bath volume. Heat the solution to about 70°C; the solution can be heated with the presence of activated carbon (1.5 g L^{-1}). Stir until the constituents dissolve (about 40–45 min) and then filter it into the operating tank. Fill the tank almost to the full volume and then add the $KAg(CN)_2$ to the tank while stirring. This way no silver will be removed with the carbon. At this stage brighteners can be added and the tank filled up to the right volume. Now, at the risk of repeating what has already been stated above, we offer the following advice: Silver deposition is a well-studied technology in the area of metal deposition. While electron transfer to silver ion should be rapid, ideal silver surfaces may have slow nucleation, as shown by Budevski et al. [27]. For a majority of substrates and simple silver solutions, dendritic silver is produced through nucleation and three-dimensional (3D) growth of individual metal grains with little or no tendency to merge and compact. Thus, to obtain smooth deposits of silver, plating from cyanide complexes is practiced in most cases.

5.2.3 Anodes and Anodic Reactions

Cyanide silver plating baths are fairly stable and easy to maintain. Cathode and anode current efficiencies are close to 100%, and the solution can be kept in balance for long periods of operation. For this reason the use of high-quality silver anodes (purity of 99.98% or better) is recommended.

It may be useful at this point to elucidate the process of silver dissolution in cyanide solutions. Cyanide leaching, first introduced in 1887 [28], remains to this day the common means to recover gold and silver from ores. The reaction was recognized by early workers to be electrochemical in nature [29]. The kinetics of silver cyanidation has been widely studied, but very little has been said about the reaction mechanism. Vielstich and Gerischer [30], using the potential step method, verified the Butler–Volmer equation (see *Fundamentals*, Chapter 6, Eq. 6.45) with transfer coefficient α values of 0.5 and 0.44 for $[CN^-] > 0.2\,M$ and $< 0.1\,M$, respectively. The predominant complex ion of silver was assumed in their study to be $[Ag(CN)_3^{2-}]$, and it did not depend on cyanide concentration. Nachaev and Beck [31], on the other hand, studied the discharging of silver in cyanide solutions measuring the Faraday impedance. They found that through all potential values more negative than -0.45 V silver was deposited through the discharging of $[Ag(CN)_2^-]$ ions independent of the composition of the bath and the conditions of electrolysis.

It was found [32, 33] that a surface-enhanced Raman scattering (SERS) spectrum may be obtained from cyanide adsorbed on a silver electrode. As a result silver has been reaffirmed as an electrode of much interest. Lately a number of studies have concentrated on the method and efforts to correlate SERS with electrochemical methods prevail. For instance, voltammograms for the silver cyanide system with the corresponding SERS spectra of adsorbed silver cyanide were presented by Benner and co-workers [34]. Fleischman and co-workers [35] obtained SERS spectra of $^{12}CN^-$ and $^{13}CN^-$ adsorbed on silver electrodes. These spectra were shown to arise from a complex species whose coordination number did not change with the electrode potential. The species were proposed to be $[Ag(CN)_2^-]$. Blondeau and co-workers [36], using radiochemical means, found that after several dissolution redeposition cycles the quantity of cyanide adsorbed remained constant and the silver cyanide reaction was reversible. New information from SERS spectra prompted Baltruschat and Vielstich [37] to study the system again via potentiostatic pulse methods. Using the exact methods of mathematics rather than extrapolating, they obtained better accuracy for exchange current densities. Their results indicated that neither the anodic dissolution of silver in cyanide solution nor its reverse process involved simple charge transfer reactions: that is, (1) the reaction orders are not integers, (2) the apparent transfer coefficient is dependent on concentration or potential, and (3) the rate-determining step is not purely charge-transfer controlled. They also showed that pH has no influence on the process. A more recent work by Zhu and co-workers [38] is also of some interest. They point out that up to the early 1990s (1) research had focused on concentrated cyanide solutions (above 0.1 *M*), (2) the mechanisms require further clarification, (3) the combined effect of intrinsic kinetics and physical processes (e.g., diffusion) are yet to be measured, and (4) the adsorption of cyanide ions on silver surfaces is a steady-state phenomenon. Their work, in which electrochemical techniques were used to examine the kinetics of silver cyanidation in oxygen-free alkaline solutions, drew the following conclusions: The reaction between silver and cyanide may be separated into the two elementary steps: a charge-transfer reaction followed by a chemical reaction. Since the charge-transfer step, which includes the diffusion of cyanide ions from the bulk solution to the silver surface, is rate limiting, the rate of dissolution is calculated using the combined Butler–Volmer and Levich equations.

From the electrochemical measurements the diffusion coefficient of cyanide ions in 0.5*M* KNO_3 solutions (pH 11; $[Ag] = 5 \times 10^{-5}\,M$ and $[CN] = 5 \times 10^{-4}$–$1 \times 10^{-2} M$) is found to be $1.6 \times 10^{-5}\,cm^2\,s^{-1}$ at 24°C and the activation energy 13.7 kJ. The apparent exchange current density in the

solutions has been concluded to have an activation energy of 21.1 kJ mol^{-1}. The transfer coefficient has been found to be close to 0.5, but it changes somewhat with temperature (between 0.56 and 0.43).

5.2.4 Deposition on Metals

The pretreatment of the metal surfaces that will be silver plated includes the standard steps of cleaning and etching to which is added a silver strike. The explanation for this additional treatment is that most basic metals are less noble than silver (as is even gold in the cyanide system). Consequently they will precipitate silver by immersion, from the regular silver plating baths, and cause the silver deposits to poorly adhere. The strike baths should contain low silver metal and high free-cyanide concentrations. In this way the tendency for electrochemical displacement by the base metal is greatly lowered. Besides, the process involves low-efficiency hydrogen activation. The procedure for steel surfaces is to use a double strike: the first in a solution containing low silver content with some copper cyanide and the second in a regular strike solution. The latter may be used as the first strike solution for copper, its alloys, nickel, and nickel silver. Solution compositions are given in Tables 5.2 and 5.3. The strike can also be used for surfaces made of more than one metal or with soldered parts. The recommended immersion times range from 10 to 25 s for decorative silver plating, while for thicker deposits it can range from 15 to 40 s. It is also recommended that the object to be plated be made cathodic before immersion in either the strike or the plating bath.

5.2.5 Additives

In general, small quantities of certain substances, mostly organic, can markedly affect the form or structure of the deposits. Since it can be assumed that adsorption takes place at the cathode surface during electrolysis, one added molecule affects many thousand metal ions. Often the added effects are undesirable. If, however, the result is a bright or level surface or if internal stress is reduced, the added substance is not considered a contaminant. A decrease in the activation overpotential is observed, for instance, for carbon disulfide in the cyanide silver bath. (The effect is the opposite in other metal's bath.) The subject of additives and their nature is discussed in detail in Chapter 10 of *Fundamentals*. For this reason we will only make a few general practical observations and leave it to the reader to consult that text.

The susceptibility of the different metals to the inhibition of electrodeposition by many additives is nearly parallel to their melting point, hardness, and strength, increasing in this order: Pb, Sn, Ag, Cd, Zn, Cu, Fe, Ni. This sequence also fits the order of the increasing tendency of their ions to form complexes. The sequence further fits the order of increasing activation polarization in electrodeposition from their aquated ions.

The additives are generally consumed in the deposition process. They may be decomposed, and the products in parts incorporated into the deposit, or released back into the electrolyte. As a rule we note that they will affect the internal stresses in the deposits positively or negatively.

Carbon disulfide and thiosulfate have been widely used as additives (brighteners) in silver plating baths. A host of other materials have been used as well. Some are gums, sugars, unsaturated alcohols, sulfonated aliphatic acids, turkey red oil, rhodamine red, and compounds of antimony and bismuth. The majority are sulfur-bearing organic compounds or else reaction products of sulfur and organic compounds. There exist a good number of effective proprietary additives that yield highly desirable deposits in terms of mirror brightness. Such products, when available, obviate the need for buffing the final plate, which not only saves precious metal but also assures a more uniform thickness.

TABLE 5.2 First Strike Bath for Steel

Silver cyanide	1.5–2.5 g L^{-1}
Copper cyanide	10–15 g L^{-1}
Potassium cyanide	75–90 g L^{-1}
Temperature	22–30°C
Current density	1.5–3.0 A dm^{-2}
Volts	4–6

TABLE 5.3 Strike for Nickel and Nonferrous Metals and Second Bath for Steel

Silver cyanide	1.5–5 g L^{-1}
Potassium cyanide	75–90 g L^{-1}
Temperature	22–30°C
Current density	1.5–3.0 A dm^{-2}

5.2.6 Physical Properties

One of the underlying concepts of thin-film science is that of surface energy (SE). This is the energy required to create a surface. Interestingly metals, as a rule, have a high SE, while oxides have a low SE. The relative values of SE determine whether one material wets another and thus forms a uniform adherent layer as required in the case of electroplated metal. Material with low SE will tend to wet a material of high SE. Conversely, if the deposited material has a higher SE, it will tend to form clusters; that is, it will "ball up" on the low-SE substrate. Water proofing is a way of manipulating surface energies. Organic materials tend to have low SE; thus a car waxed with an organic substrate will

TABLE 5.4 Relationship between Surface Energy and Latent Heat

Metal	Surface Energy (erg cm^{-2})	Latent Heat Evaporation (kcal mol^{-1})	Ratio SE/LH	Interatomic Potential (eV atom^{-1})	Cohesive Energy (kcal mol^{-1})
Copper	1700	73.3	0.22	0.58	80.4
Silver	1200	82	0.15	0.65	68
Gold	1400	60	0.24	0.47	87.96

cause water droplets to form on its wet surface. As stated above, SE is defined as the energy spent to create a surface. It is a positive quantity, since energy is added to the system. A liquid balls up to reduce its surface area, and crystals will facet in order to expose their lowest energy surfaces. When one breaks a solid, two new surfaces are created and bonds are broken. It should thus be clear that SE is related to bond energy and to the number of broken bonds creating surfaces. This dynamic in turn is related to the binding energy of the material.

The binding energy is defined as the energy needed to transform one mole of solid or liquid into gas at a low pressure. That is nearly the same as the energy of sublimation (transforming solid to gas) or the energy of evaporation (transforming liquid to gas), except that the gas is measured at the pressure of one atmosphere rather than at low pressure. These energies are related to the interatomic potential energy between atoms.

Using "nearest-neighbor-only interaction" approximation, we are able to relate the heat energy of sublimation, evaporation, melting, and crystallization to surface energies. The binding energy per mole of a substance is expressed as

$$E_b = \tfrac{1}{2} n_c N_A \varepsilon_b$$

where n_c = coordination number, which is the number of nearest neighbors
A_A = Avogadro's number
ε_b = binding energy per single bond

The factor of $\frac{1}{2}$ comes as a result of having counted bonds twice.

To evaluate surface energy from the point of view of nearest-neighbor bonds, we first define N_S to be the number of atoms per unit area and E_S/A to be the surface energy per unit area. Across any atomic plane each atom has an average $n_c/2$ nearest neighbors, so the number of bonds to be broken per unit area of cleavage along the plane is $1/2 n_c N_S$. Now, since we create two surfaces in cleaving, the surface energy per unit area is $n_c N_S \varepsilon_B$. Finally, the ratio of SE per atom to binding energy per atom, $1/4 n_c \varepsilon$, is given by

$$\frac{E_S/AN_S}{E_B/N_A} = \frac{1/4 n_c \varepsilon_b}{1/2 n_c \varepsilon_b} = \frac{1}{2}$$

From measured values shown in Table 5.4, we can calculate the ratio of surface energy per atom to bond (or latent heat, LH) per atom. Indeed, from the table we can infer whether it is easier to deposit silver on copper or whether it is easier to deposit copper on silver.

Silver metal is noted for its extremely high electrical conductivity, $0.0162\,\Omega\text{-cm}^2\,\text{m}^{-1}$. It is somewhat unique in that even in its thin-film form it exhibits nearly the same property, $0.017–0.024\,\Omega\text{-cm}^2\,\text{m}^{-1}$, depending on deposition conditions and additives. For instance, sulfur and selenium containing electrolytes yield deposits with conductivities of up to 90% that of bulk silver metal.

Another physical property of importance in the case of electrodeposits is microstructural instabilities due to creep (relief) of stress with ensuing time. An optically flat mirror made of silver deposit will deform in a matter of a few months. This is due to room temperature relief of stress in the silver electroplate. Brass mirrors made optically flat and subsequently silver plated show deformation as a result of stress in the silver plate. Removing the silver by machining will restore the original flatness of the brass. Heat treating the silver-plated part at 150°C for 1 h seems to eliminate the problem.

5.2.7 Fractals

In general, electrodeposits made using baths containing no additives are dendritic or treelike. These types of deposits are of no practical value. In recent years these types of deposits contributed to the study of fractals. A fractal is an object with a pattern that under magnification exhibits repetitive levels of structures; a similar structure exists on all levels. In other words, a fractal looks the same whether it is viewed on the scale of a meter, a millimeter, or a micrometer. In the human body, for instance, fractallike structures make up the blood vessels, nerves, and so on. In nature, coastlines and tree branching are the obvious examples. In the material sciences, the importance of fractals is that it leads the way to the study and quantitative analysis of the microstructure of metals in fashion hitherto thought impossible. Kahanda and Tomkiewicz [39], for instance, undertook the issue of fractality in regard to the impedance of electrochemically grown silver deposits. (See references

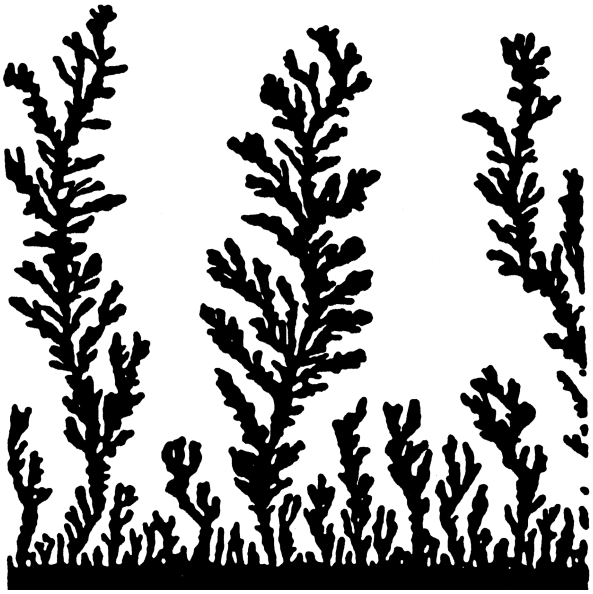

FIGURE 5.3 Electrodeposited clusters (about 0.5 cm in length) photographed 15 minutes after start of growth. Reproduced with permission of The Electrochemical Society [39].

in [39] regarding fractals in general.) To illustrate the fractal nature of some electrodeposits, we present in Figure 5.3 a photograph of metal clusters obtained after 15 min in a bath with no additives.

REFERENCES

1. G. Elkington and H. Elkington, British Patent 8447 (1840).
2. S. R. Natarajan and K. Krishman, *Met. Finish.*, **50** (2), 51 (1971).
3. S. K. Gupata, *Cent. Glass. Ceram. Res. Int. Bull.*, **14**, 18 (1967).
4. T. Ishibashi, *Less Met. Finish.*, **9**, 42 (1968).
5. A, Kubota and N. Koura, *J. Met. Finish. Soc. Jpn.*, **37**, 131, 694 (1986).
6. T. Hata and T. Hanada, U.S. Patent 3,337,350 (1967).
7. A. Vaskelis and O. Diemontaite, *TSR Mokslu Akad. Darb.*, **B4**, 23 (1975).
8. I. Cross, *Met. Finish*, **48**, 77 (1950).
9. S. Noguchi, Japan Patent 7,593,234 (1975).
10. S. Horst, German Patent 2,063,334 (1972).
11. T. Mukaiyama, Japan Patent 7,216,819 (1972).
12. S. Werner, German Patent 2,639,287 (1978).
13. Max Ernes, German Patent 950,230 (1956).
14. D. J. Hood, U.S. Patent 2,120,203 (1938).
15. Y. Mori, Japan Patent 7,606,135 (1976).
16. T. Kanabe and M. Ise, *Ind. Met. Sur.*, **7**, 64 (1979).
17. B. A. Bochkarev and E. Z. Napukh, *Elktrokhimia*, **18**, 6, 843 (1982).
18. G. Maurice, German Patent 2,153,837 (1971).
19. V. J. Pakolenko, *Zanod. Lab.*, **48**, 10, 89 (1982).
20. L. V. Markova, *Z. Anal, Khim.*, **25**, 8, 1620 (1970).
21. K. Wekua and B. Hoffman, *Furbe u. Lack*, **58**, 250 (1952).
22. A. P. Abbot, J. Griffith, S. Nandhra, C. O'Connor, S. Postlethwaite, K. S. Ryder, and E. L. Smith, *Surface Coating Technol.*, **202**, 2033 (2008).
23. K. J. McKenzie and A. P. Abbot, *Phys. Chem., Chem. Phys.*, **8**, 4265 (2006)
24. A. P. Abbot, G. Capper, D. Davies, and R. K. Rashid, *Inorg. Chem.*, **43**, 3447 (2004)
25. K. E. Johnson, *Electrochem. Soc. Interface*, **16**, 38 (Spring 2007).
26. H. Sanches, E. Chainet, B. Nguyen, P. Ozil, and Y. Meas, *J. Electrochem. Soc*, **143**, 2799 (1996).
27. E. Budevski, W. Bostanoff, T. Vitanoff, Z. Soinov, A. Kotzen, and R. Kaischev, *Phys. Status Solidi.*, **13**, 577 (1966).
28. J. V. N. Dorr, *Cyanidation and Concentration of Gold and Silver Ores*, McGraw-Hill, New York, 1936, Ch. 1.
29. V. Kudryk and H. H. Kellog, *J. Metals*, **6**, 541 (1954).
30. W. Vielstich and H. Gerischer, *Z. Phys. Chem.* (new series), **4**, 10 (1955).
31. E. A. Nachaev and R. Yu. Beck, *Electrokhimia*, **2**, 150 (1966).
32. A. Otto, *Surf. Sci*, **75**, L392 (1978).
33. J. Billman, G. Kovacs, and A. Otto, *Surf. Sci.*, **92**, 153 (1980).
34. R. E. Benner, R. Dornhouse, R, K. Cheng and B. L. Laube, *Surf. Sci.*, **101**, 341 (1980).
35. M. Fleischman, I. R. Hill, and M. E. Plembe, *J. Electroanal. Chem.*, **136**, 361 (1982).
36. G. Blondeau, J. Zerbino, and N. Jaffrezic-Renault, *J. Electroanal. Chem.*, **112**, 127 (1980).
37. H. Baltruschat and W. Vielstich, *J. Electroanal. Chem.*, **154**, 141 (1983).
38. X. Zhu, J. Li, D. M. Bodily, and M. E. Wadsworth, *J. Electrochem Soc.*, **140**, 1927 (1996).
39. G. L. M. K. S. Kahanda and M. Tomkiewicz, *J. Electrochem Soc.*, **137**, 3423 (1990).

6

TIN AND TIN ALLOYS FOR LEAD-FREE SOLDER

YUN ZHANG

6.1 INTRODUCTION

6.1.1 A Brief History of Solders

Soldering is technically defined as the joining of two base materials through the use of a third "filler" metal with a melting temperature well below those of the substrates and typically less than 450°C. Solder alloys are categorized as either soft or hard. Soft solders typically contain tin and lead, although indium, cadmium, and bismuth are also found in soft solders. Hard solders contain metals such as gold, zinc, aluminum, and silicon. A more rigorous classification is based on the melting temperature where soft solders melt below approximately 350 °C while hard solders melt above 350 °C.

The historical use of solders is illustrated by the timeline in Figure 6.1, which extends from approximately 4000 BC, through the Bronze and Iron Ages, and into the present "Silicon Age." The earliest archeological evidence of soldering dates back to 4000 BC, when gold-based, hard solders were developed by artisans in Mesopotamia and soon spread into Egypt (3600 BC), Ur (3400 BC), Greece (2600 BC), and other Mediterranean regions. The Etruscans clearly refined hard soldering techniques during the Bronze Age (∼ 2500 BC). A gold pendant illustrated their mastery of the "step-joining" technique in which three different melting temperatures were formed over a distance of 5 mm. There is also evidence of high-quality, gold-based hard solder joints being used by the La Tolita Indians of South America in AD 20.

Tin–lead soft solder compositions and their uses in ancient cultures are obscure, largely because the reduction of the tin component to stannic acid makes solder identification quite difficult. Furthermore, written descriptions of soldering technique are very limited since this craft was performed by artisan-slaves. Such endeavors were deemed unimportant by the upper ruling class and were not well documented. Some well-preserved soft-soldered artifacts were discovered in King Tut's tomb, which dates to 1350 BC The pieces were of crude construction, suggesting that soft soldering was not as well developed as hard soldering techniques in the Mediterranean cultures. Historians now believe that soft soldering was also developed in Northern and Central Europe by Celts and Gauls in ca. 1900 BC. The high quality of the Celtic artifacts constructed with tin–lead soft soldering was noted by the first Romans to enter the region. Access to rich tin ores in Northern Europe is cited as the reason for their exceptional soft soldering practices; in contrast, tin was not readily available to the Mediterranean cultures.

In ancient times, tin–lead solders were used primarily for the manufacture and repair of cooking utensils and metal tools. In 350 BC, the Greeks sealed their bronze-based water pumps, air pumps, and organs with tin–lead alloys. The Romans used tin–lead solders extensively in the construction of aqueducts. The lead sheets that lined the interior of the water passages were joined together by soft soldering. As is the case today, the higher cost of tin relative to lead provided the Roman engineers with the economic incentives to use the less expensive tin–lead alloys.

Very little changed in soldering from the Iron Age to the Middle Ages. The technique was used primarily by artisans in the fabrication of jewelry and other crafts. Tin–lead solders were used to make joints in objects comprised of copper and brass.

The Industrial Revolution greatly expanded the use of soldering technology. For example, the development of portable heat sources such as the oxy-gas torch and electricity (the soldering iron) facilitated the use of soft soldering in applications such as plumbing (first lead and then copper pipes and tubing), the sealing of food and water containers,

Modern Electroplating, Fifth Edition Edited by Mordechay Schlesinger and Milan Paunovic

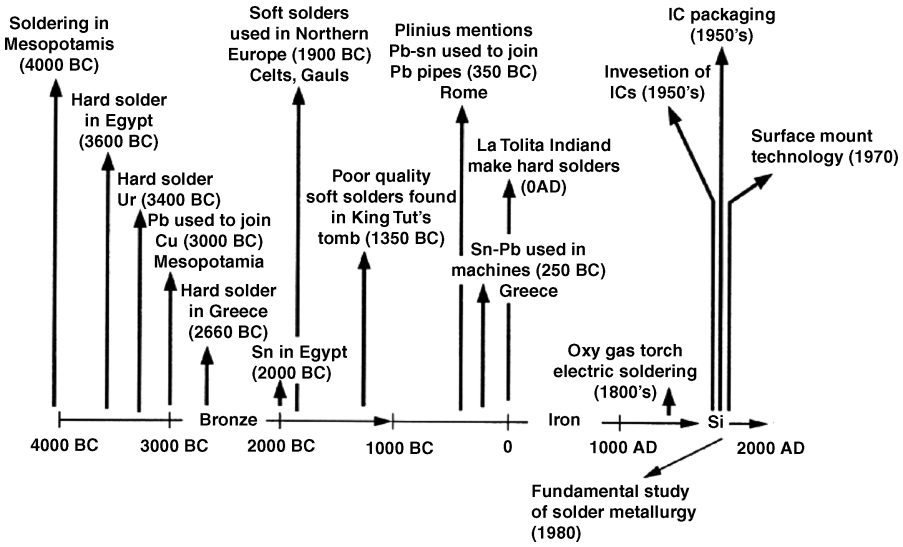

FIGURE 6.1 Time line illustrating use of solders as determined by archeological evidence. (Reprinted with permission from P. T. Vianco et al., July 1993, *Journal of Materials*, pp. 14–19).

and later the fabrication of larger structures (e.g., automobile radiators). It was in the early twentieth century that soldering entered the electronics industry as a reliable means of connecting copper wires for power and signal transmission. In those early applications, the solder joint served primarily to ensure electrical continuity.

With the advent of silicon chip technology, the electronics revolution has fostered further miniaturization and increased functionality of devices. Soft soldering has been adapted to microchip packaging and higher level system assembly. However, the reduction of package-sized requirements and demand for solder joints to be a mechanical and an electrical connection have challenged the strength as well as the creep and fatigue resistance of tin–lead solders. The advent of surface-mount technology clearly illustrated the limitations of tin–lead solder technology. Reliability losses in many electronic systems were identified with failure of the solder joints rather than device malfunctions. These presented opportunities for the materials community to search for new solders with better mechanical strength and reliabilities. It is important to point out though that the driving forces for developing lead-free solders mainly were not technological but because of environmental, health, and commercial considerations.

6.1.2 Driving Forces of Lead-Free Solder Development

The selection of materials and processes in modern manufacturing no longer will be driven solely by product performance, reliability, and cost but will be profoundly influenced by environmental and health considerations. Tin–lead solders have been the most prominent material for the interconnection and packaging of electronic components, primarily due to the low cost and convenient material properties. However, in view of increasing environmental and health concerns, the time has come for the materials science community to seriously consider developing new alternatives. In order to successfully replace lead from tin–lead solders, understanding its role in solders is essential.

6.1.3 Roles of Lead in Solders

The role of lead in solders can be understood by examining its effects on the material properties of its alloys with tin. Melting temperature, electrical and thermal conductivity, coefficient of thermal expansion, fluidity, surface tension, mechanical properties, microstructure, and metallurgical reactions are some of the most important properties of interest. For example, lead lowers the melting temperatures for tin-rich solders, as shown in the tin–lead phase diagram in Figure 6.2. When its content increases in tin–lead solders, both electrical and thermal conductivity decrease, as shown in Figure 6.3 [1], whereas the density and coefficient of thermal expansion of tin–lead solders increase, as shown in Figure 6.4 [1]. The viscosity of the tin–lead solders is significantly reduced when lead content goes up [2], but the surface tension is lowered relative to pure tin, improving the wetting of solder into gaps and holes. Sometimes "spreading" is discussed in the context of solder evaluation. Wetting and spreading are related in the sense that both depend on the surface tension of a solder. However, the latter is also associated with the fluidity (or viscosity) of the solder. One of the most important aspects of lead in tin–lead solders is its impact on the mechanical strength, usually represented by tensile and shear strength. The effect of lead on tensile and shear strength in tin–lead solders is illustrated in Figures 6.5 [3] and 6.6 [1]. Materials

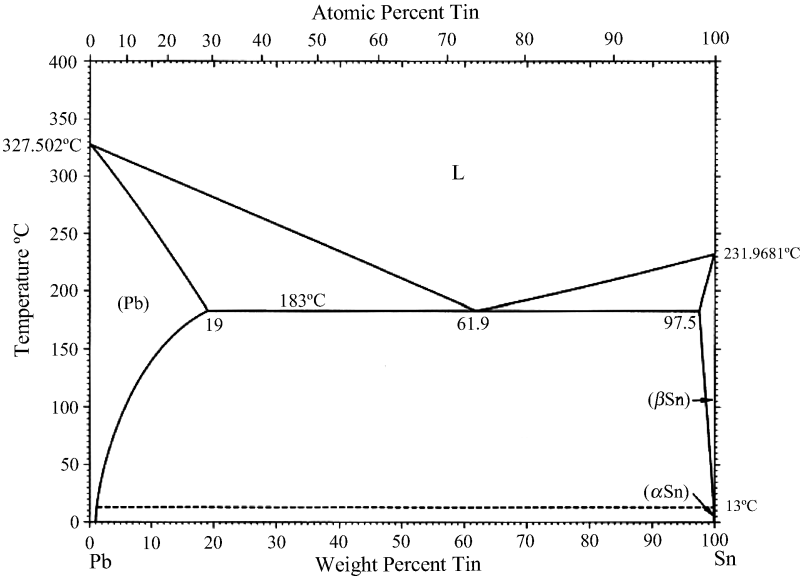

FIGURE 6.2 Phase diagram of tin–lead binary solder [1]. Sn melting point 231.968°C, Pb melting point 327.562°C.

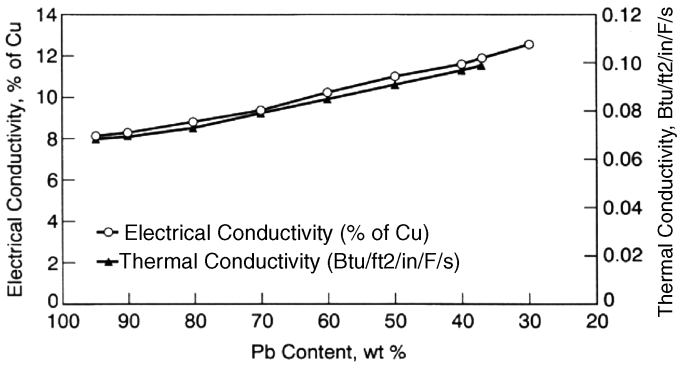

FIGURE 6.3 Electrical and thermal conductivities of tin–lead solders [1].

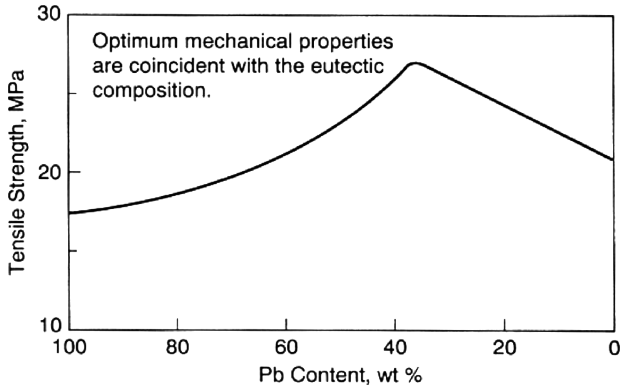

FIGURE 6.5 Tensile strength of cast bars of tin–lead alloys [3]. Eutectic solder, 63% Sn, 37% Pb.

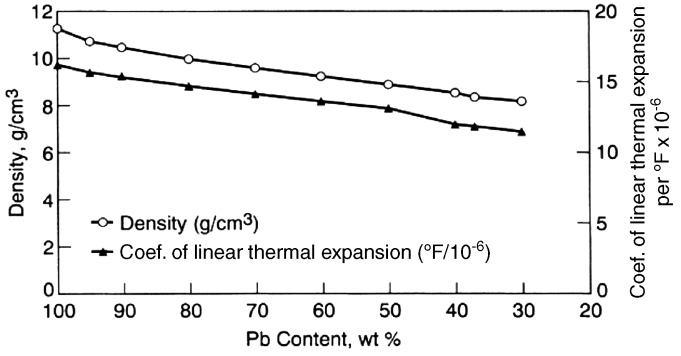

FIGURE 6.4 Density and expansion properties of tin–lead solders [1].

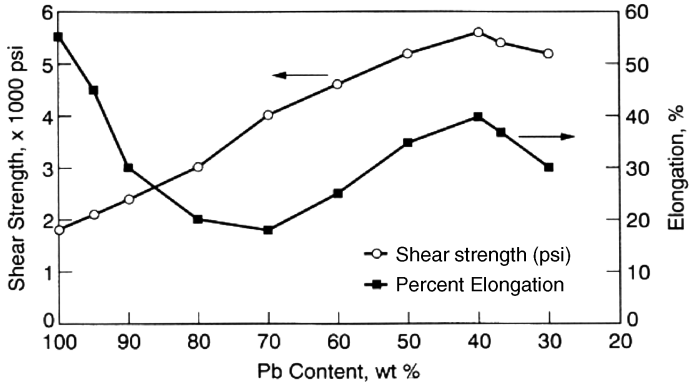

FIGURE 6.6 Shear strength of Cu joints soldered with tin–lead solders [1]. Eutectic solder, 63% Sn, 37% Pb.

TABLE 6.1 Material Properties of Tin, Lead, and Eutectic Solder

Materials Properties	100Sn	63Sn37Pb	100Pb
Melting point, °C	232	183	328
Electrical conductivity, $\Omega^{-1}\,cm^{-1}$	9.1	6.9	4.8
Thermal conductivity, $W\,m^{-1}\cdot K^{-1}$	66	50.9	35
Coefficient of thermal expansion, 10^{-6}/°C	22	24.1	28.9
Surface tension, $dyn\,cm^{-1}$	545	490	439
Shear strength, psi	4000	3450	2000
Tensile strength, MPa	21.5	27.5	17.3
Percent elongation	<0.82	40	55

properties of tin, lead, and eutectic solders are summarized in Table 6.1.

In failure mode analysis of tin–lead solders in electronics, it is often observed that a decrease in solder joint strength is closely related to microstructure changes. Upon solidification of eutectic solder 63Sn37Pb, a two-phase microstructure is developed, the morphology of which is dependent upon the rate of solidification [4]. The microstructure changes at room temperature, and it includes precipitation of tin colonies within the lead-rich phase as well as an overall coarsening of lead-rich particles contained within the tin-rich matrix. A decrease in the strength of the solder is observed with these microstructural changes [5], thereby counteracting improvements in the mechanical strength realized through the finer morphology generated by faster cooling rates.

Metallurgically, lead is relatively "inert" compared to tin. For example, when tin–lead solders are deposited on copper, lead itself does not react with copper, but it affects the solid-state growth kinetics of the tin–copper intermetallics. While comparing pure tin and eutectic tin–lead solders, even though the total intermetallic compound thickness ($Cu_6Sn_5 + Cu_3Sn$) is quite similar, the percentage of Cu_3Sn, the bad actor in solderability because it is brittle and nonsolderable, differs significantly [4]. In tin–lead coatings, tin segregates strongly to the surface because of its higher affinity for oxygen, forming tin oxide, which is one of the culprits in solderability degradation. Lead oxides, on the other hand, improve the corrosion resistance of tin–lead solders [6].

6.1.4 Environmental, Health, and Safety Concerns of Lead-Bearing Solders

Lead in the electronic industry today accounts for approximately 1% of total consumption. The largest use is in storage batteries, which accounts for 80% of the total consumption (Fig. 6.7). Other major uses include ammunition, paints, cable sheathing, and sheet lead [7].

Lead and its compounds are one of the top 17 chemicals that impose the greatest threat to human health [8–10], including disorder of nervous and reproductive systems, delayed neurological and physical development, reduced production of hemoglobin, anemia, and hypertension [8]. Lead poisoning is particularly damaging to the neurological development of young children [11].

Lead is heavily regulated in the plumbing, paint, and gasoline industries. Lead-bearing solders, on the other hand, have been used extensively in the electronics industry since the early 1950s. The first radio Philips mass produced was hand soldered on a printed wiring board in 1954, containing 136 solder joints. Today, a typical cell phone has thousands of solder joints made by either surface-mount soldering or flip-chip wafer bumping. Yet, the size of today's cell phone is only a fraction of the first radio mentioned above. In the last 50 years, we have witnessed tremendous technology advances in the electronics industry. This technology advance has improved our standard of living and changed the way we live, work, and entertain. As consumers, we are constantly looking for products that provide better features but take up less space and cost less. We dispose of television, computers, and cell phones, not because they do not work anymore but because there are products with better functionality on the market that are easily accessible and affordable. This did (and still does) pose significant challenges in countries such as Japan because of its small land area, decreasing landfill capacity, and limited natural resources.

Therefore, in Japan, waste disposal has been an important matter of national concern. Throughout the 1990s, the Japanese government has taken a very active role in environmental issues largely in response to heightened public awareness. It encouraged companies to recycle, reuse, and produce "green products." Reducing the use of lead at the manufacturing stage would enable electronics companies to better comply with product end-of-life recycling requirements. In

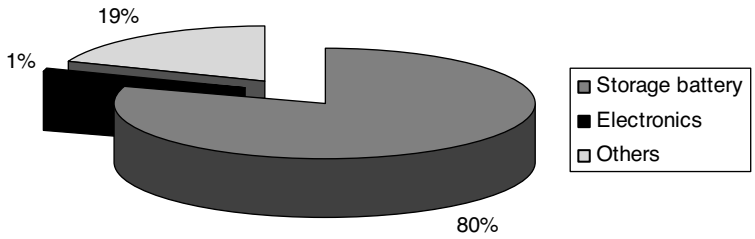

FIGURE 6.7 Lead consumption [12].

addition, companies that produced first lead-free products enjoyed significant increase in market share. For instance, Matsushita's market share increased up to 15% when it introduced the first lead-free portable mini-disc player; Sony's market share soared more than 20% when it introduced the first lead-free compact stereo system. Obviously, to stay competitive, other Japanese electronics companies followed the lead. As a whole, Japan has been leading the world in the lead-free transition.

The second in line is the European Union, which comprises many small countries. In late 2002, the European Parliament approved two directives related to the reduction of electrical and electronic waste. As part of the legislation, the use of lead in most electrical and electronic components would be banned or severely restricted. The Waste Electrical and Electronic Equipment (WEEE) and Restriction of Hazardous Substances (RoHS) directives call for the elimination of lead from most electronic equipment starting July 1, 2006. In addition to these two directives, the European Community (EC) has also passed a Directive on End-of-Life Vehicles (ELV) which targets lead used in automotive applications. To respond to the legislation pressure as well as the potential penalty for not having lead-free products, many European electronics companies began taking action during the early 2000s.

The United States lagged behind Japan and Europe even though it was the first to introduce legislation to reduce the use of lead. For instance, the Lead Exposure Reduction Act (S. 729) was introduced in April 1993 and passed on the Senate floor on May 25, 1994, but it failed to pass in the House. The Lead Tax Act (HR 2479) introduced in June 1993 would impose a $0.45 per pound tax on all lead smelted in the United States and on all imported lead-containing products. Obviously, it did not become a law. Many U.S. companies held a look-and-see attitude toward lead-free products, and some lobbyed to stop the WEEE and RoHS directives and lead-free implementation.

As of December 2008, it is estimated that 90% of the electronics products covered by the RoHS directive was already lead free. However, there are still debates among technologists as to whether lead-free products are really a good thing. History has shown that it can be done and lead-free products are possible.

There are three primary sources of lead in electrical and electronic assemblies: the solder alloy, the printed wiring board (PWB) finish, and the component finish. In a typical solder joint, the solder alloy accounts for the largest lead contribution from the total amount. The PWB finish and the component finish contribute significantly less lead to the assembly. As a result, the initial focus of the industry has been to eliminate lead from the solder alloy. The following section briefly recounts challenges the industry encountered in finding the right lead-free solder alloys for the electronics industry.

6.1.5 Material Properties Considerations for Lead-free Solder Candidates

Leaded solders are used primarily as mechanical, electrical, and thermal interconnections and as surface coatings for corrosion protection and solderability. Modern technology demands improved solders that prosess enhanced mechanical and metallurgical properties. This provides opportunities to develop materials that (1) have solidous/liquidus temperature equivalent or close to that of tin–lead eutectic solders (183°C) to be comparable with existing processing technologies, (2) equal or better mechanical properties in terms of shear and tensile strength, (3) equal or better physical properties in terms of electrical/thermal conductivity, thermal expansion coefficient and wettability, and (4) improved shelf life and microstructure stability, and (5) equal or better corrosion resistance, ductility, and solderability. See Tables 6.2 and 6.3 for a comparison of material properties of tin–lead and lead-free alloys.

TABLE 6.2 Binary Lead-Free Solder Candidates Compared with 63Sn37Pb

Materials Properties	63Sn37Pb	58Sn42Bi	96.5Sn3.5Ag
Melting point,°C	183	138	221
Electrical resistivity, $\mu\Omega \cdot$ cm	14.6	36.4	12.3
Thermal conductivity, $W\,m^{-1} \cdot K^{-1}$	50.9	19	55.3
Coefficient of thermal expansion, 10^{-6}/°C	24.1	14	23
Surface tension, $dyn\,cm^{-1}$	490	300	460
Wetting, contact angle (time, s)	17° (3.8)	43° (3.3)	36° (2.0)
Shear strength, MPa	42	63	55
Ultimate tensile strength, $MN\,m^{-2}$	19–56	54–73	20–56
Creep resistance	Poor	Excellent	Good

Source: Reference [13–16].

TABLE 6.3 Ternary and Quaternary Lead-Free Solder Candidates

System	Known Composition	Melting Temperature,°C
SnBiAg	83.5Sn/14Bi/2.5Ag	142–218
	91.8Sn/4.8Bi/3.4Ag (E)	142–218
SnInAg	77.2Sn/20In/2.5Ag	178
	>90Sn/<8In/Ag	195
SnBiAgCu	95.9Sn/1Bi/0.1Ag/3Cu	206–223
	90Sn/7.5Bi/2Ag/0.5Cu	207–212
SnAgCu	Sn4Ag0.5Cu	217
	Sn3.8Ag0.7Cu	217–219

Source: Reference [17–20].

6.1.6 Rules of Selection and Lead-Free Solders Adopted by the Electronics Industry

As can be surmised from the above discussion, any alternative to lead-bearing solder must meet certain criteria to be considered a serious contender. Furthermore, any element that will replace lead has to be nontoxic or significantly less toxic, relatively abundant in supply, and not significantly more costly than lead. In addition to the materials properties consideration mentioned above, the lead-free solders should be compatible with existing flux systems. Finally, the reliability of lead-free solder joints would have to be tested under various environmental conditions, for example, thermal cycling from −55 to 180°C. Models and test methods would have to be established to predict long-term reliability. An extensive review of these issues can be found elsewhere [12].

After taking into considerationd all the criteria, there are only a handful of lead-free solder alternatives that could be considered. For binary alloys, SnBi, SnCu, and SnAg appear to be the choices. In the right soldering temperature range, there are some ternary and quaternary lead-free alloy alternatives, such as SnBiAg, SnAgIn, SnAgCu, SnBiAgCu, and SnAgSbBi.

Results of numerous investigations by consortia, industry alliances, and individual companies during the late 1990s and early 2000s have led the industry to converge on the tin-silver–copper (SnAgCu) family of alloys as the primary replacement for the lead-bearing solder. For reflow applications, a SnAgCu alloy composition close to the eutectic is the most popular choice. For wave solder applications, on the other hand, eutectic SnCu is the most commonly chosen alloy.

While the soldering alloy was selected, the electronics industry focused its collective effort on finding the right PWB surface finishes and component finishes. It is important to point out that though they contribute significantly less lead in weight percentage in a solder joint, they can have a asignificant impact on solder joint reliability. It took the industry a few years through trial and error to finalize on PWB surface finishes and component lead finishes.

Currenty, the most popular lead-free PWB surface finishes are OSP (organic solder preservative) and lead-free HASL (hot-air solder leveling) followed by immersion silver, immersion tin, electroplated Ni/Au, and electroless Ni/immersion Au (ENIG), shown in Figure 6.8.

For component finishes, there are two schools: (1) tin, tin–bismuth, and tin–silver and (2) palladium and palladium alloys with or without a gold flash. For consumer or noncritical applications, tin, tin–bismuth, and tin–silver (2–3%) are the most common component finishes; for military, aerospace and critical medical applications, one often finds nickel–palladium with a gold flash on a component lead. We will discuss this in more detail in Section 6.6.

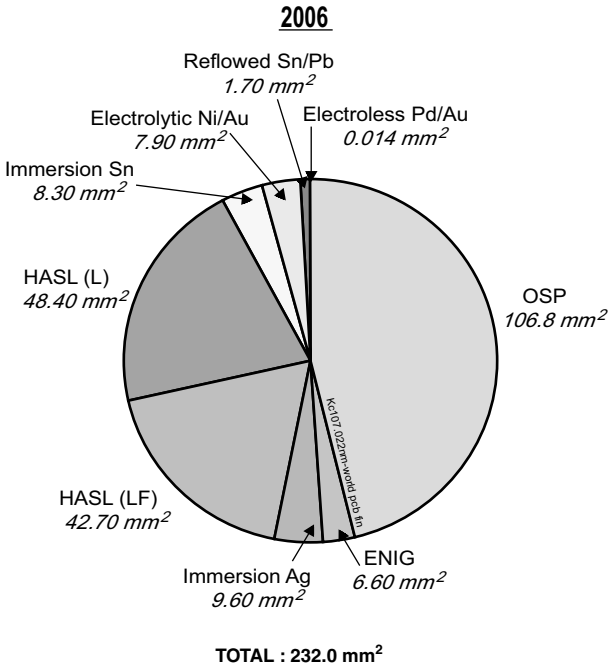

FIGURE 6.8 PWB surface finish lead-free status in 2006. (From Prismark PWB report.)

An understanding of the electrodeposition of tin is a prerequisite to understand the of electrodeposition of tin alloys. In the next section, a detailed account is given of the chemical and physical properties of tin and basic principles of tin plating as well as common tin electroplating electrolytes.

6.2 ELECTRODEPOSITION OF TIN

6.2.1 Physical Properties of Tin

Tin metal is silver white, soft, ductile, and nontoxic, with excellent corrosion resistance in air, lubricity, and ability to form many useful alloys. With its low melting point and high boiling point, tin has a liquidus range exceeded by few metals. It readily alloys with many metals and forms several intermetallic compounds of commercial importance. Copper, nickel, silver, gold, and palladium are soluble in liquid tin. Molten tin wets and adheres readily to clean iron, steel, copper, and copper-based alloys, which is why tin is an excellent solder by itself.

There are two allotropic forms of tin: white (β) and gray (α). White, or ordinary, tin is the familiar form, processing properties that make it useful; it crystallizes in the body-centered tetragonal system. Gray tin has a diamond lattice; it is considerably less dense than β-tin and is nonmetallic in appearance and properties. It is a semiconductor. The allotropic transformation occurs at 13°C and is extremely

slow. In fact, the existence of gray tin was not even discovered until the mid-nineteenth century, when some tin organ pipes in Moscow were found to have disintegrated during an exceptionally cold winter. The allotropic change is known as "tin pest," probably because it appears to spread from the center of "infection." The transformation is inhibited or prevented by the incorporation into the tin of a few tenths of a percent of antimony, lead, or bismuth.

Tin whiskers were first reported in 1947 [21]. They are single crystals of tin filaments usually having diameters of 0.5–5 μm and lengths of 1–2 mm. They can be straight or kinked, and during their growth, which occurs by extrusion from the tin electrodeposits, their orientation with respect to the substrate may vary. Tin whisker growth rate has been reported in numerous studies in the range of 0.03–9 mm/year. This phenomenon has been observed from a few hours to a few years after electrodeposition. They are not easily detached from the substrate and can carry currents as large as 25 mA before they burn out. They can therefore sustain potential drops to a few tenths of a volt per millimeter. There are some remedies for the tin whiskers. Reflowing the deposit by heating it is one method. Others include HASL, hot-dipped tin, and alloying tin with a small percentage of lead or other metals. However, as we shall discuss in detail in Section 6.5, there is no complete cure of the whisker problem today.

6.2.2 Chemical Properties of Tin

Tin has atomic number 50, and its atomic weight is 118.69. It has the electronic configuration of $4d^{10}5s^25p^2$. Thus there are four electrons available for bonding. Accordingly tin is tetravalent in many of its compounds. As with its homologies germanium and lead, however, the 5s electrons may act as an "inert pair," and tin is also divalent. In this respect tin is intermediate between germanium and lead; with the former, bivalency is uncommon, and lead exhibits tetravalency only in its organic compounds. For tin, the two valence states are almost equally stable and readily interconvertible. In theory, solutions of stannic tin or Sn(IV) should be readily reduced to stannous tin or Sn(II) by many reducing agents, especially metals such as antimony and nickel. In practice, Sn(IV) does not exist in simple ion form; instead, it most likely forms hydroxyl compounds such as $Sn(OH)_6^{2-}$, which eventually becomes insoluble SnO_2 and drops out from the solution because of gravity. We will discuss this point in more detail in Section 6.2.6. Tin(II) is readily oxidized to Sn(IV) by common oxidants including dissolved oxygen from air.

Tin is amphoteric: It reacts with acids and bases and is relatively resistant to neutral solutions. This is evident from Figure 6.9. The overpotential of hydrogen on the tin surface is quite high, about 0.75 V, so that attack by acids and bases is slow unless an oxidizing agent is present to depolarize the evolution of hydrogen. Distilled water has no effect on tin,

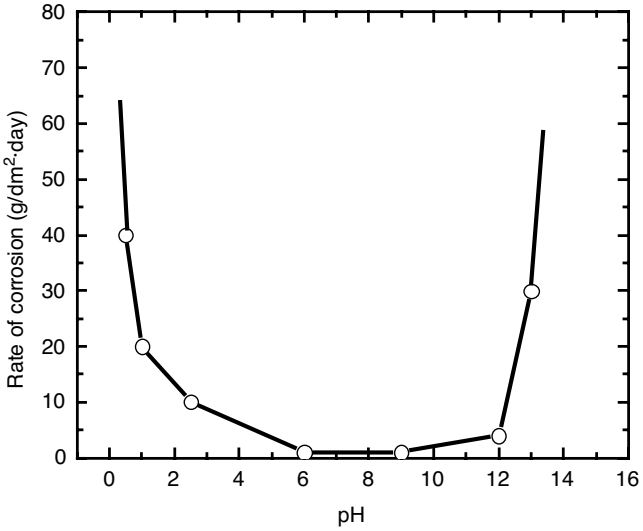

FIGURE 6.9 Tin corrosion behavior in aqueous media.

which has been the preferred medium for preparing and storing it.

In acidic solutions, Sn(II) compounds probably exist in the form of Sn^{2+} aquo ion, but Sn^{4+} probably does not exist as such. It is either hydrolyzed or complexed, as in $SnCl_6^{2-}$ and $Sn(OH)_6^{2-}$.

In alkaline media, Sn(IV) is the most stable; alkaline stannite or stannate(II) solutions disproportionate according to

$$2[Sn(OH)_4]^{2-} \rightarrow [Sn(OH)_6]^{2-} + Sn + 2OH^-$$

This reaction is important in plating from alkaline stannate solutions, as will be shown in Section 6.2.8. All tin compounds tend to hydrolyze in aqueous solution: Alkaline solutions must be stabilized by the presence of excess alkali, acid solutions of excess acid.

6.2.3 Thermodynamic Treatment of Tin and Lead

One of the most thorough and complete thermodynamic considerations of the electrochemistry of tin and lead can be found in Chapter 8 [22]. At room temperature, the standard potentials for the deposition of tin and lead are -0.136 and -0.125 V, respectively. Lead is the more noble metal. The reduction potentials of the two are very close together; therefore tin–lead alloy is one of the easiest to be codeposited.

The half reactions for Sn^{2+} and Pb^{2+} under standard conditions (i.e., $[M^{2+}] = 1\,M$, temperature 298 K, 1 atm pressure) are

$$Sn^{2+} + 2e^- \rightarrow Sn \qquad E^0 = -0.136\text{ V}$$
$$Pb^{2+} + 2e^- \rightarrow Pb \qquad E^0 = -0.125\text{ V}$$

In noncomplexing acidic media, in order to maintain simple Sn^{2+} and Pb^{2+} ions in solution, the pH of the solution needs to be less than 1.

Different oxidation states of tin and lead and their interconversions are displayed in the potential diagram below. Data are only available in acidic solutions:

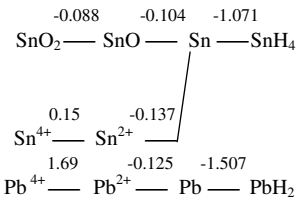

Normal electrodeposition conditions deviate significantly from the standard condition, or the equilibrium condition. The reduction potential of tin or lead at any given temperature and concentration can be expressed by the following equation:

$$E = E^0 + \left(\frac{RT}{nF}\right) \ln a + C$$

where

E = reduction potential, V
R = gas constant = 8.31441 J mol^{-1} K^{-1}
T = temperature, K
n = number of electrons involved in electrodeposition process
F = Faraday constant = 96485 C mol^{-1}
a = concentration or activity of metal ion, in this case, tin or lead
C = term that includes all other factors that contribute to polarization electrodeposition process

As one can see, changing the temperature or the concentration of tin or lead or using a complexant, which contributes to the C term, will affect the reduction potential. The electrodeposition of tin alloys will be discussed in more detail in Section 6.3.

6.2.4 Reduction Potentials of Tin and Lead in Different Acidic Media

Listed in Table 6.4 are onset reduction potentials (onset potential is the potential at which an electrochemical process initiates) for tin, lead, and tin–lead obtained by cyclic voltammertry in sulfate [23], fluoborate [24, 25], and methane sulfonic acid (MSA) solutions [26]. It is important to point out that the potentials reported in the table were not the half-wave or peak potentials but the onset potentials. In order to obtain direct correlation with an actual plating bath, high metal concentrations were utilized in the electrochemical experiments. This can have a distortion effect on the redox waves caused by a combination of factors such as large solution resistance or *IR* drop and complicated chemical and electrochemical reaction kinetics, which makes it difficult to obtain a clear-cut peak potential or a half-wave potential. Therefore, onset potentials are more useful. A discussion of this phenomenon is beyond the scope of this work and can be found in standard electrochemical textbooks [27–30].

Nonetheless, the data shown in Table 6.4 have practical implications and are useful for comparative analysis. For instance, in MSA, the presence of "additives" which contain organic compounds such as quaternary ammonium surfactants and aromatic aldehydes makes tin and lead deposition more negative when these two metals are deposited separately. However, when tin–lead alloys are deposited, the presence of "additives" makes it more positive. More can be learned if one examines the work of Kohl [24] and Igor [26]. Kohl used cyclic voltammetry to evaluate the effect of Triton X-100 and phenolphthalein in fluoborate solutions shown in Figure 6.10. As can be discerned from the figure, both Triton X-100 and phenolphthalein significantly suppress the deposition of tin and lead. The effect becomes more pronounced when both additives are used. Another example is given in Figure 6.11. In this case, the additives significantly suppress the electrodeposition of tin and lead. In addition, the onset potential for tin–lead was shifted to more positive values, which means that the tin–lead alloy could be plated out at lower current densities compared to the situation when additives were absent. The redox waves were

TABLE 6.4 Onset Reduction Potentials (V) of Tin, Lead, and Tin–Lead in Various Acidic Media

	Sulfate[a]		Fluoborate[b]		MSA[a]	
Half Reaction	No BA	BA	No TX/Ph	TX/Ph	No Additives	Additives
$Sn^{2+} \rightarrow Sn$	−0.53	−0.55	0.07	—	−0.38	−0.50
$Pb^{2+} \rightarrow Pb$	—	—	0.08	—	−0.40	−0.60
$M^{2+} \rightarrow M$, M = Sn, Pb	—	—	0.07	0.0	−0.39	−0.33

Note: Solution compositions (1) sulfate/sulfuric solution 0.01 *M* Sn^{2+} + 0.56 *M* H_2SO_4; (2) fluoborate solution, 0.14 *M* Sn^{2+} + 0.05 *M* Pb^{2+} + 5 *M* HBF_4; (3) methane sulfonic acid solution, 0.21 *M* Sn^{2+} + 0.058 *M* Pb^{2+} + 1 *M* MSA. BA: benzaldehyde; TX/Ph: Triton X-100 and phenolphthalein; starter: organic additives.

[a] Reference electrode, saturated calomel electrode (SCE).
[b] Reference electrode, $Pb/PbSO_4$, −0.65 V vs. SCE.

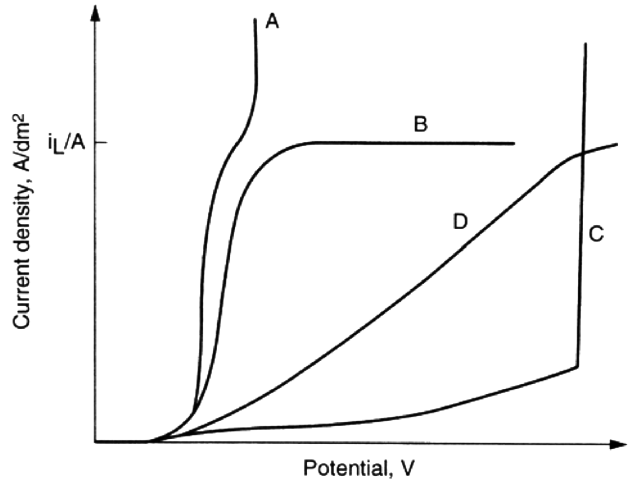

FIGURE 6.10 Current–voltage behavior of Sn electrode in solder baths with (*A*) no additives, (*B*) Triton X-100, (*C*) phenolphthalein, and (*D*) Triton X-100 and phenolphthalein. (Reprinted with permission from P. A. Kohl, *P&SF*, August 1981, p. 45.)

much better defined and it was correlated with a bright, smooth tin–lead surface.

6.2.5 Important Electrode Reactions in Tin Electrodeposition

In electrodeposition, tin ions are reduced at the cathode via the following reactions:

$$\text{pH} < 1: \quad Sn^{2+} + 2e^- \rightarrow Sn$$
$$\text{pH} > 13: \quad [Sn(OH)_6]^{2-} + 4e^- \rightarrow Sn + 6OH^-$$

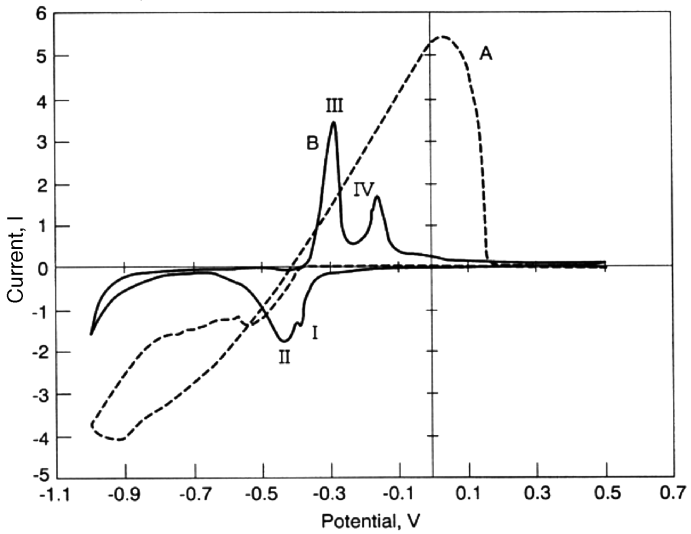

FIGURE 6.11 Cyclic voltammograms of Sn electrode in solder solution (*a*) with no starter additive and (b) with starter additive. Wave I: $Sn^{4+} \rightarrow Sn^{2+}$; wave II: $Sn^{2+} \rightarrow Sn$; wave III: $Sn \rightarrow Sn^{2+}$; wave IV: $Sn^{2+} \rightarrow Sn^{4+}$. Current scale: for *A*, $10\,mAV^{-1}$; for *B*, $1\,mAV^{-1}$.

Under ideal conditions, these should be the only cathodic reactions and the current efficiency should be 100%. In practice, other side reactions have to be taken into consideration. For instance, discharge of hydrogen occurs at current densities close to or exceeding the limiting current density of the deposited metal, especially in acidic media. Decomposition of some organic additives is another possible side reaction. Therefore, it is very rare that the cathode current efficiency is 100%.

At the anode, one of the following oxidation reactions can occur depending on the type of anodes. If a soluble anode is used, the anodic oxidation reactions are

$$\text{pH} < 1: \quad Sn \rightarrow Sn^{2+} + 2e^-$$
$$\text{pH} > 13: \quad Sn + 4OH^- \rightarrow [Sn(OH)_4]^{2-} + 2e^-$$

The stannite ion so formed is not stable in alkaline solution and most likely will disproportionate into Sn and $Sn(OH)_6^{2-}$ via the following reaction:

$$[2Sn(OH)_4]^{2-} \rightarrow [Sn(OH)_6]^{2-} + Sn + 2OH^-$$

The thus formed tin is loose and sponge like. Undesirable deposit may be obtained if it gets incorporated in the tin. This is why an insoluble anode is usually preferred in alkaline tin plating.

If an insoluble anode is used, then the anodic oxidation reactions are

$$\text{pH} < 1: \quad 2H_2O \rightarrow O_2\uparrow + 4H^+ + 4e^-$$
$$\text{pH} > 13: \quad 4OH^- \rightarrow O_2\uparrow + 2H_2O + 4e^-$$

The overall reactions are

$$\text{pH} < 1: \quad 2Sn^{2+} + 2H_2O \rightarrow O_2\uparrow + 2Sn + 4H^+$$
$$\text{pH} > 13: \quad [Sn(OH)_6]^{2-} \rightarrow Sn + O_2\uparrow + 2OH^- + 2H_2O$$

Disregarding the pH of a solution, that is, acidic or basic, oxygen will form at the anode when an insoluble anode is used. As will be discussed later, in acidic solutions, this will cause excessive Sn(IV) formation. Therefore, whenever possible, a soluble anode should be used. By contrast, in alkaline media, the oxidation of Sn(II) to Sn(IV) is beneficial because Sn(II) is not desirable.

It is equally true that side reactions will occur at the anode. For example, the oxidation of organic compounds which are used as wetting agents, grain refiners, and brighteners is especially susceptible if an insoluble anode is used. Generally speaking, breakdown products from the organic additives are often generated from anodic reactions rather than cathodic reactions.

Once the electrodeposition takes place, the deposition rate is governed by the Faraday law, expressed as

$$Q = I\,t = \frac{nFW}{M}$$

where

Q = Coulombs
I = current, A
t = time, s
n = number of electrons involved in electrodeposition process
F = Faraday constant 96,485 C mol^{-1}
W = weight of deposit, g
M = atomic weight of deposited metal

As one can see, the same amount of metal can be deposited by either increasing the current while shortening the plating time or reducing the current but increasing the plating time. Of course, in production, the first option is a better choice. However, this is not always possible to implement since it is sometimes limited by the plating processes. Examples will be given in Section 6.2 when specific plating processes are discussed. Furthermore, it is shown that in order to deposit a fixed amount of metal, it requires twice as much energy when the number of electrons involved is 4 (as in alkaline tin plating bath) compared to 2 (as in acid tin plating baths). This is why acid tin plating chemistries are more efficient than alkaline tin plating chemistries and are most preferred to deposit tin or tin–lead.

6.2.6 General Consideration in Tin Plating

Equipment Depending on whether the electroplating process is acidic or alkaline, requirements on the plating equipment are different. In acidic media it matters whether the acid is fluoborate or sulfuric or methane sulfonic acid. A fluoborate-based system mandates the use of the most acid resistant materials. Sulfuric acid and MSA-based systems, although corrosive by definition, are much less severe on equipment. Polypropylene or rubber-lined steel can be used to construct plating tanks. Heaters made from porcelain or quartz with polypropylene guard can be used in sulfuric acid and MSA-media. For alkaline plating processes, a plain welded steel tank is generally employed, the tank being fitted with the necessary anode and cathode rods and provided with a means of solution heating, for example, a plain steel steam coil or steel cased electric immersion heaters.

There are three general types of plating, and therefore three different types of plating equipment, when it comes to tin and tin alloy plating: barrel, rack, and reel-to-reel plating.

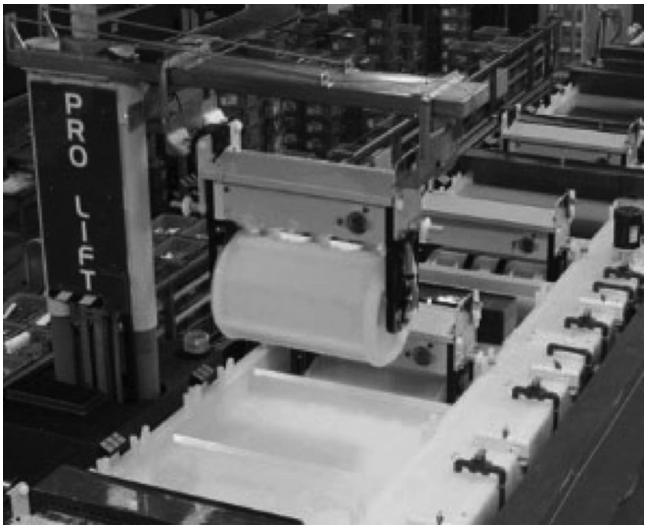

FIGURE 6.12 Example of automatic barrel plating line.

By its name, in barrel plating, parts are tumbled in a barrel while current passes through the plating solution (Fig. 6.12). It is used mostly to plate loose parts such as contacts, bolts and nuts, washers, and passive components such as inductors, resistors and capacitors. The size of the barrel varies a great deal; it could hold a few liters to a few hundred liters of solution.

In rack plating, by definition, plating parts are hung on racks that are immersed into the plating solution (Fig. 6.13). The racks serve as cathodes, and they move back and forth to provide solution agitation. Rack plating is used to plate

FIGURE 6.13 Example of manual rack plating line. The balls floating on top of the tank reduce solution evaporation.

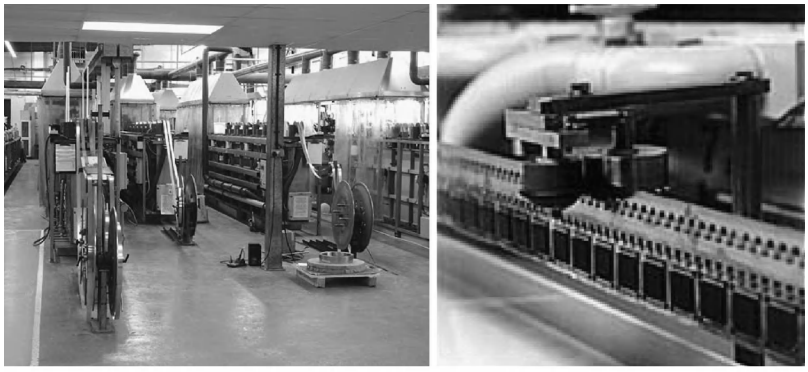

(a) (b)

FIGURE 6.14 Examples of (*a*) an automatic connector reel-to-reel plating line and (*b*) an automatic leadframe cut strip plating line.

irregular-shaped parts (in some cases huge parts) and parts that have complicated geometries that could not be processed in a barrel.

Barrel plating and rack plating are considered low speed because the current density is typically lower than 50 ASF (amps per square foot) or 5 ASD (amps per square decimeter).

In a reel-to-reel plating line, parts are prewrapped on a wheel so the pretreatment, plating, and postplating treatment can be a continuous operation. At the end of the line, there is a wheel to receive the coil and wrap it tightly around the axial. Reel-to-reel plating is commonly found in connector and leadframe plating (Fig. 6.14). It is often considered high speed because the current density can be as high as 800 ASF or 80 ASD.

Lastly, this section would not be complete if wafer plating equipment were not mentioned. There are in general two types of wafer plating tools: paddle and fountain type. Figure 6.15 shows (a) paddle-type and (b) fountain-type tools. Even though both are capable of producing excellent plating results, there are significant differences in process capability, throughput, and cost.

Anodes In tin plating, both insoluble and soluble anodes are used. Soluble anodes are usually used in acidic solutions while insoluble anodes find their use in alkaline solutions. Depending on the type of anodes used, the anodic reactions are different.

At insoluble anode, oxygen is generated. In acidic solutions, this leads to a pH decrease and a buildup of free acid, which may cause anode passivation, as in the case of sulfuric/sulfate chemistry. This is because when free sulfuric acid is present in large excess, the conductivity of the solution is reduced significantly. Because of the common ion effect, the solubility of stannous sulfate is also substantially reduced. As a result, the stannous sulfate will "salt out" at the anode, thus causing anode passivation. When anode is passivated, the cell voltage "jumps" and prevents plating operation to continue unless the problem is corrected. This phenomenon is best explained in Figure 6.16. In alkaline solutions, electrodeposition of tin leads to a pH increase as shown by the overall reaction in Section 6.2 and subsequently causes substantial reduction in cathodic current efficiency, which will be discussed in Section 6.2. Therefore, it is important to monitor the acid or the base concentration closely if an insoluble anode is used.

Different types of insoluble anodes are used in electrodeposition of tin. In alkylsulfonic acid media, platinized titanium is usually used. This type of anode should not be

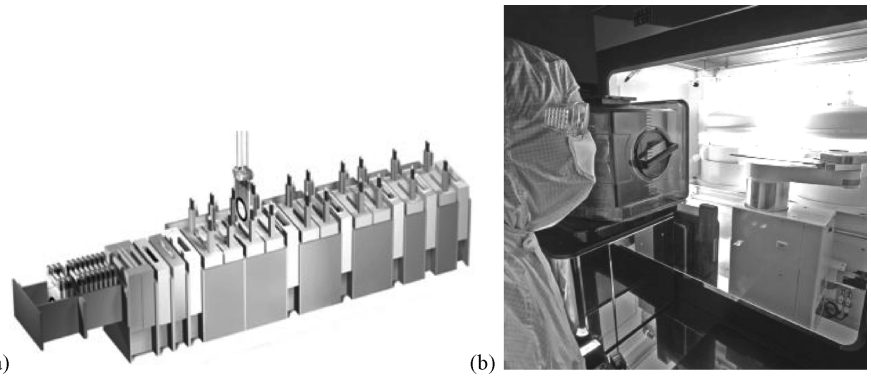

(a) (b)

FIGURE 6.15 Examples of (*a*) paddle cell (courtesy of NEXX systems) and (b) fountain cup plater (courtesy of Semitool, Inc.).

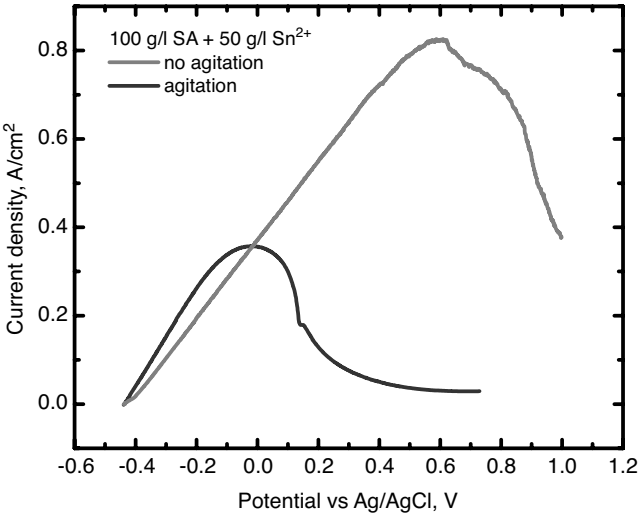

FIGURE 6.16 Anode passivation from a sulfate and sulfuric acid tin electrolyte is shown by the gray curve. A large cell potential jump at the anode is indicative of an anode passivation.

used in sulfate-based chemistry because sulfuric acid will attack the material. In sulfuric acid, tantalum and niobium are the recommended materials.

The purity of tin anodes is the subject of standards in many countries. The most likely impurities are Sb, As, Bi, Cu, Fe, Pb, Al, Cd, and Zn. The tin content should not be less than 99.9%. Impurity levels permitted by typical standards are as follows:

Impurity	Sb	As	Bi	Cu	Fe	Pb	Al + Cd + Zn
Maximum percent	0.03	0.03	0.01	0.02	0.01	0.04	0.002

In the case of wafer bumping, it is critical that low α-tin anodes are utilized in addition to satisfying the above impurity requirements.

Metal Distribution Metal distribution or throwing power and covering power are very important in applications of tin plating. Throwing power is a term associated with the entire spectrum of the current density, and it is a measure of deposit thickness uniformity across a plated part. Covering power specifically reveals whether the deposition will occur at low-current-density areas of a plated part.

There are theoretical treatments on the throwing power [31, 32] in addition to empirical treatments such as Haring–Blum [33], Heathley [34], and Field [35] equations. Although it is arguable that the theoretical model given by Tan [31, 32] allows good correlation to the observables, the experimental procedures are tedious and require computer simulation to obtain the final throwing power number. Alternatively, the Haring–Blum cell is more popular for its simplicity. However, it does have some severe limitations, as pointed out by Maisano and co-workers [36]. Recently, Kohl [25] used an empirical equation and based the ratio of electrode resistance and solution resistance, R_e/R_s, to represent the throwing power of a high-speed electroplating solder solution. The concept is simple and experiments are relatively easy to carry out. Since the measured properties have direct correlation with solution characteristics such as conductivity and metal and additive concentrations, it is much easier to interpret the data.

Ideally, one would like to obtain the exact target thickness throughout the entire plated part with tin or tin alloy plating because this ensures good corrosion resistance and solderability of the entire part. In reality, we always obtain a thickness range, not a single value. This is because the electric field across the part is never exactly the same. If the part has a complicated geometry such as a tube, it is close to impossible to achieve the same electric field everywhere in the tube. If no special consideration is given to balance the electric field inside and outside the tube, the electric field will be stronger outside the tube than inside. Consequently, one would obtain a thicker coating outside the tube than inside the tube.

It is outside the scope of this chapter to discuss the electrochemical cell and plating equipment design in detail. However, excellent treaties can be found in many electrochemical engineering textbooks.

Additives The generic term "additive" covers a wide variety of chemicals which affect plating processes and deposits characteristics. The additives can be organic or metallic and ionic or nonionic and are adsorbed on the plated surface and often incorporated in the deposits. The use of additives in aqueous electroplating solutions is extremely important owing mainly to the interesting and important effects produced on the growth and structure of deposits. The potential benefits of additives include brightening the deposit, reducing grain size, reducing the tendency to form dendritic growth, increasing the current density range, promoting leveling, changing mechanical and physical properties, reducing stress, and reducing pitting. However, it is equally important to point out that when wrong additives are used or additives are out of control, the opposite of all of the above can happen. The striking effects on the electrocrystallization of small concentrations of addition agents, ranging from a few milligrams per liter to a few percent but generally in the concentration range of 10^{-4}–$10^{-2}\,M$, point to their adsorption on high-energy surfaces producing a poisoning or inhibiting effect on the most active growth sites [37]. The results obtained with additives seem to be out of proportion to their concentrations in solution; one added molecule may affect many thousands of metal ions. Their function and mechanism of interaction are not yet clearly understood and their investigation so far has been mostly empirical.

Owing to the advent of spectroelectrochemistry, we now have tools available which allow direct in situ detection and study of the competitive adsorption/desorption and interfacial reactions among various additives in a plating solution. Spectroelectrochemistry is a methodology that *simultaneously* applies electrochemical and optical spectroscopic techniques to investigate a phenomenon. An excellent treaty can be found in [37a]. Another comprehensive review can be found in [37b]. Contributors include world-renowned scientists such as Arthur T. Hubbard, William R. Heinemana, Allan J. Bard, Fred C. Anson, John O'M. Bockris, Michael J. Weaver, and Dieter M. Kolb. Though spectroelectrochemistry has been firmly established as a powerful methodology since early 1990, research in this area has been mostly limited in academia, and the chemical and electrochemical reactions studied are simple, pseudoideal inorganic or organic systems [38–41]. While at Lucent Technology Bell Labs, the author and her team applied spectroelectrochemistry in studying a commercial tin plating chemistry. Detailed account of this study will be given in Section 6.5.3 in the discussion on tin layers.

Plating additives are extremely important and establishing the proper agents most often determines the success or failure of a given plating process [42]. Among the additives that are used in plating chemistries, the ones in nickel plating are the most studied [43, 44]. There are much fewer studies on tin and tin alloys [26, 45, 46].

Additives act as surfactants, grain refiners, and brighteners because of their effects on (1) electrode kinetics and (2) the structure of the electrical double layer at the electrode–electrolyte interface. Modern analytical and electroanalytical methods make it possible to understand these phenomena at a molecular level [47–49]. Numerous mechanisms have been suggested to explain the behavior of additives, such as (1) surface modification by blocking, (2) modification of Helmholtz potential, (3) surface complex formation including adsorption and ion bridging, (4) changes in surface work function and film formation of the electrode, (5) hydrogen adsorption and evolution, and (6) the effect of intermediates. These are discussed in detail in a comprehensive review by Frankin [50]. Additional excellent coverage on mechanisms of additives can be found in more recent papers by Oniciu and Muresan [51] and in Section 6.5.3 in the discussion of tin layers.

Regardless of the mechanism by which additives function, their effects can be found in (1) the influence of mechanical properties such as tensile strength and elongation [52], (2) appearance and surface structure [53], (3) purity, (4) hardness [54, 55], and (5) solderability of the deposits [56, 57]. More will be discussed in Section 6.4.

Lack of control of the constituents of a plating solution is a major problem which leads to reduced reliability and increased costs for plated parts. One reason is the difficulty in performing quantitative analysis on additives which are often a mixture of two or more compounds (not to mention the numerous additive breakdown products that accumulate with time) in the parts-per-million (ppm) and parts-per-billion (ppb) ranges in the presence of high concentrations of electrolytes. Techniques such as wet chemical analysis, ultraviolet (UV)–visible spectroscopy, and high-performance liquid chromatography (HPLC) have been commonly used and there are companies that specialize in developing analytical methods, software, and hardware for plating applications. Other practical tools such as the Hull cell or hydrodynamically controlled Hull cell (HCHC) [58, 59] are also useful in monitoring and controlling additive concentrations. However, interpretation of Hull cell results are usually not straightforward; hence it is better when coupled with chemical analysis. It is possible to quantitatively analyze the additives and their breakdown products in an acid tin plating chemistry [60]. An example will be given when MSA chemistry is discussed.

Oxidation of Sn(II) to Sn(IV) In acidic solutions, Sn(II) and Sn(IV) are equally stable and Sn(II) can be easily oxidized to Sn(IV) by atmospheric and anodic oxidation. The loss of stannous tin, if not corrected, causes loss in the deposition rate and productivity. Furthermore, Sn(IV) forms fine colloidal particulates which may be incorporated in the deposits causing surface roughness and degradation of solderability. The oxidants could be atmospheric oxygen or any metal ions that have reduction potential more noble than Sn(II) in acidic electrolytes. The known culprits are Cu^{2+}, Ag^{+}, Bi^{3+}, and Fe^{3+}; these reactions will be discussed in more detail in Section 6.3. However, it is important to point out that, while iron is typically not present as an alloy metal with tin, it is often an impurity in the tin plating bath by dissolution of iron from the steel substrate. The ion Fe^{2+} is easily oxidized to Fe^{3+} due to atomospheric oxygen, and the latter oxidizes Sn(II) to Sn(IV), causing the so-called sludge formation.

Most of the proprietary tin plating processes contain antioxidants to minimize the oxidation of the divalent tin by atmospheric oxygen. Theoretically, another way to minimize Sn(IV) formation is to add a piece of pure tin in the plating tank according to the reaction:

$$\mathrm{Sn(IV)} + \mathrm{Sn} \rightarrow 2\mathrm{Sn(II)}$$

However, the author has not met one customer who is successful with such an approach in practice.

The mechanisms [61] of inhibition for Sn(IV) formation by antioxidants can be summarized by one of the following: (1) the additives form stable complexes with Sn(II); (2) the additives reduce oxygen solubility in the plating solution, thereby reducing the rate of oxidation; and (3) the additives "tie up" the soluble oxygen in the solution and thereby lower the oxidation rate [62]. Though it is difficult to separate which

Antioxidant	Sn^{2+} Concentration (Initial 50 g/L)
None	20
Catechol	48
Hydroquinone	48
Catechol + actic acid	48
Gluconic acid	27
Citric acid	27
Phenol sulfonic acid	40
Glycolic acid	32
Lactic acid	29

FIGURE 6.17 Effectiveness of various antioxidants in MSA tin plating electrolyte.

mechanism is operative in a plating bath or which one is dominant, the effectiveness of catechol, a known antioxidant in tin and tin alloy plating, is clearly seen in Figure 6.17.

Bath Maintenance and Process Control Any high-quality electrodeposition process demands good-quality control. Unfortunately, this is not a reality for many plating shops where only tin and electrolyte concentrations are monitored regularly. It is common knowledge that in many cases process performance deteriorates because the organic additives are out of control or due to the presence of harmful breakdown products or excessive Sn(IV) formation. Therefore more attention should be directed toward monitoring and controlling the organics in a plating bath. Tin and tin alloy plating shops should analyze the additives in their plating baths at least once a week to ensure that the additives are within the normal operating range. A practical and relative fast way to do so is by cyclic voltametric stripping (CVS) or HPLC. A number of companies offer both bench-top and online units to do this.

6.2.7 Major Acid Electroplating Tin Chemistries

The most commonly encountered acidic electroplating tin chemistries are based on one of the following acids: fluoboric acid, sulfuric acid, phenolsulfonic acid (PSA), hydrochloric/hydrofloric acid, and MSA. The PSA-based method is the most widely used based on volume since it is used in the production of tin plate in the Ferrostan process [63]. Some 70% of the 130–140 continuous tin-plate lines around the world use this process. Sulfuric acid–based chemistry is mainly found in bright tin plating. In this section, a brief description of the advantages and disadvantages of each chemistry will be presented.

Fluoborate Chemistry One of the oldest electroplating acid tin chemistries, fluoborate is usually used in high-speed plating. Tin tetrafluobarate, $Sn(BF_4)_2$, is very soluble; therefore, it permits the use of high current densities. Organic additives most commonly used in fluobarate chemistry are peptone, gelatin, β-naphthol, catechol, and hydroquinone, the last two generally used as antioxidants. With the aforementioned organic additives, smooth, fine-grained deposits are usually obtained. In the last decade or so, there has been some development in proprietary additive formulation for this chemistry. Typical bath compositions from this electrolyte are summarized in Tables 6.5.

TABLE 6.5 Typical Bath Composition and Operating Parameters of a Fluoborate Chemistry

Parameters	Rack and Barrel	Reel to Reel
$Sn(BF_4)_2$, $g\,L^{-1}$	75–113	225–300
Sn, $g\,L^{-1}$	30–45	45–60
HBF_4, $g\,L^{-1}$	188–263	225–300
H_3BO_3, $g\,L^{-1}$	22.5–37.5	22.5–37.5
Anode current density, ASF	20–25	Do not exceed 25
Cathode current density, ASF	1–80	Up to 300
Temperature, °C	30–55	30–55

Note: Typical additives: peptone, β-naphthol, hydroquinone.
Anode: pure tin, bagged with Dynel or polypropylene.
Agitation: mild, mechanical.
Filtration: Constant filtration using a nonsilicated filter aid is desirable, although not necessary; such treatment keeps the solution clean and affords agitation.
Source: Reference [64].

Fluoborate ion undergoes some hydrolysis in solution:

$$BF_4^- + H_2O \rightarrow [HO\text{–}BF_3]^- + HF$$

Formation of fluoride ion can be reduced by adding boric acid:

$$H_3BO_3 + 4HF \rightarrow HBF_4 + 3H_2O$$

This is especially important in the case of tin–lead deposition because of the precipitation of PbF_2.

The advantages of fluoborate chemistry are its ability to operate at high current densities and its high throwing power and high current efficiencies at both anode and cathode. The major disadvantages of fluoborate are the environmental concerns for the fluoride and the boric ions and hence the high cost of the waste treatments. It is also the most corrosive of all acidic tin electroplating solutions.

Sulfate/Sulfuric Acid Electrolyte The characteristics of this chemistry are its high cathode (100%) and anode current efficiencies under normal operating conditions, that is, current densities < 30 ASF, although 100–150 ASF has been achieved in a few selected reel-to-reel applications where line speed is extremely fast. It is a low-initial-cost

TABLE 6.6 Typical Bath Composition and Operating Parameters for a Sulfate/Sulfuric Acid–Based Electroplating Chemistry

Parameters	Range
$SnSO_4$, $g\,L^{-1}$	15–45
Sn, $g\,L^{-1}$	7.5–22.5
Sulfuric acid, $g\,L^{-1}$	135–210
Additives [62]	Alkylphenol, imidazoline, heterocyclic aldehydes
Anodes	Pure tin
Anode current density, ASF	25 max
Cathode current density, ASF	1–25
Temperature	Room temperature
Agitation	Mechanical, cathode rod

Source: Reference [65].

chemistry and is relatively easy to maintain and control because of the following reaction:

$$SnSO_4 + H_2O \rightarrow [Sn(OH)]^+ + HSO_4^-$$

A sulfuric acid concentration which provides pH near zero or less than zero should be maintained. It is important to avoid adding too much sulfuric acid since concentrations exceeding $400\,g\,L^{-1}$ decrease the conductivity of the solution drastically [61]. This suppresses the solubility of the tin complex assessible current density range and also leads to anode passivation. Typical tin sulfate bath formulation and operating conditions are found in Table 6.6.

The most advantageous feature of a sulfate/sulfuric acid system is the low initial cost and its relatively high throwing power. Deposits ranging from matte, semibright, to bright can be obtained from sulfate chemistry by using additives such as phenol- or cresol-sulfonic acid, gelatin, β-naphthol, and resorcinol. Proprietary additives from electroplating chemical suppliers are also available. The major disadvantages of sulfate chemistry are anode passivation at high current densities (CD > 30 ASF), oxidation of Sn(II) to Sn(IV), and corrosivity of the solution to the plating equipment. Furthermore, its use is restricted to pure tin plating because of very limited solubility of $PbSO_4$. Unlike fluoride-containing baths, where Sn(IV) compounds exist as the hexafluostannate ion, SnF_6^{2-}, no such complex can form in sulfate chemistry. Therefore turbidity, which is caused by fine colloids of SnO_2, is expected.

In bright tin plating, it is essential that chloride ion concentration be kept as low as possible. The $SnSO_4$ should not contain chloride higher than 0.1%. The 100 ppm Cl^- causes a marked decrease in brightness of the deposits [65].

Phenolsulfonic Acid Electrolyte/Halogen Electrolyte These two chemistries are mostly used to plate pure tin in the continuous steel strip plating industry. Typical bath formulations and operating conditions of the two chemistries can be found in Tables 6.7 and 6.8.

TABLE 6.7 Typical Bath Composition and Operating Conditions of a Phenolsulfonic Acid–Based Chemistry

Parameters	Range
Sn, $g\,L^{-1}$	20–35 $g\,L^{-1}$
Phenolsulfonic acid, $g\,L^{-1}$	40–80 $g\,L^{-1}$
Additives [66, 67]	Ethoylated β-naphtholsulfonic acid
Antioxidant[a]	—
Current density, ASF	200–500
Temperature, °C	30–40

Source: References [66, 67].

[a] Phenolsulfonic acid acts as an antioxidant

An attractive feature of these two processes is their ability to operate at very high current densities, which is very important in the steel industry. The PSA process uses a vertical cell design with either a soluble or insoluble anode whereas the halogen process utilizes a horizontal cell design with a soluble anode. The two processes are not interchangeable without major plant reconstruction. The PSA process usually runs at pH <1, whereas the halogen process runs at pH around 3.4.

Sludge formation is a major problem in halogen chemistry where typically more than 20% of tin goes to sludge. Another problem is related to the waste treatment of the sludge because of ferro–ferric cyanide hazardous waste. Because of the steel strip and the horizontal cell design, the halogen bath is always contaminated with ferrous ions. The ferrous ions react with oxygen to form ferric ions and they oxidize the stannous to stannic ions, thus reducing ferric ions to ferrous ions whereby the cycle repeats. The result is that even at a low concentration of iron there is a large loss of stannous ions and a loss of plating efficiency and quality of deposit. It is

TABLE 6.8 Typical Bath Composition and Operating Parameters of a Halogen Chemistry

Parameters	Concentration or Condition
NaF, $g\,L^{-1}$	30
$NaHF_2$, $g\,L^{-1}$	31
SnF_2, $g\,L^{-1}$	19
$SnCl_2 \cdot 5H_2O$, $g\,L^{-1}$	22
$Na_4Fe(CN)_6 \cdot 10H_2O$,[a] $g\,L^{-1}$	2–4
Additives [65]	Naphtholsulfonic acid and polyalkylene oxides
Antioxidant [67]	p-$NH_2C_6H_4NHCOMe$
pH	3–4
Current density, ASF	200–500
Temperature, °C	55–65

Source: Reference [68].

[a] $Na_4Fe(CN)_6 \cdot 10H_2O$: a reagent to precipitate ferric ions.

desirable to keep the concentration of iron in the electrolyte in the range of 5–7 g L^{-1}. Usually, sodium ferricyanide is used in the halogen bath to precipitate ferric ions. The reaction products, ferro–ferric cyanide solids, which are highly toxic, are part of the sludge. Therefore sludge removal for halogen chemistry is quite costly.

Compared with the halogen process, sludge formation is much less severe for the PSA process. This is because PSA, which is the main electrolyte, also acts as an antioxidant. A drawback of the PSA process is the toxicity of the phenol group which is released during the electrodeposition process.

In the last decade, MSA-based chemistry has been considered an alternative for PSA and halogen chemistry because it is environmentally more benign. MSA is twice as conductive as PSA chemistry, and hence lower tin concentration needs to be used, which reduces significantly the loss of tin due to drag-out. Although in theory MSA and PSA chemistries can be interchanged without any major plant reconstruction, the initial *chemical* cost for MSA chemistry is significantly higher than for PSA. To convert halogen chemistry to MSA chemistry requires some major plant modification, partly because MSA chemistry (pH $\sim$ 0) is more corrosive than the halogen chemistry (pH $\sim$ 3). Even though the MSA process can be operated with a horizontal plating line, the construction materials need to be polypropylene type; concrete and steel cannot be used unless they are coated with acid-resistant materials. The chemical cost of a halogen chemistry is again less than that of MSA.

Methane Sulfonic Acid Electrolyte In the 1940s, Proell [69] recognized the utility of alkane sulfonic acids for electroplating applications. Alkane sulfonic acids, having between one and five carbon atoms in the alkyl group, form water-soluble salts of various metals (mesylates). The alkane sulfonates do not undergo any appreciable hydrolysis, regardless of the process temperatures. Additionally, the alkane sulfonates are stable in acidic, neutral, or alkaline solutions. Proell indicated that it is possible to plate many metals from alkane sulfonate baths, including cadmium, lead, nickel, silver, and zinc.

Although the usefulness of the alkane sulfonic acid system was known for several decades, it only gained commercial acceptability during the early 1980s and became a desirable electrolyte for tin, lead, and tin–lead plating. Various plating baths and additives have been formulated for MSA electroplating systems and many patents have been granted [70–74]. Obata [69] described tin, lead, and tin–lead plating baths that remained stable over a broad pH range (2.0–9.0) and were used over a wide current density range.

MSA chemistry shows clear advantages over fluoborate, sulfate, halogen, and phenolsulfonic acid chemistries. It is less corrosive than fluoborate and sulfate chemistries, Sn(II) to Sn(IV) conversion is less a problem, and it is less costly than fluoborate, PSA, and halogen chemistries for effluent treatment and disposal. Thus, it is environmentally more friendly.

An additional attractive feature of MSA chemistry is its ability to access very high current densities. The throwing power and covering power of this chemistry are adequate to applications such as PWB and connectors with restricted areas [74]. Insoluble anodes can be used in MSA chemistry.

Table 6.9 summarizes three typical bath compositions and operating parameters for PWB, high-speed reel-to-reel, and wire applications utilizing a satin bright MSA chemistry.

Bright deposits are not desirable for PWB and wire applications; instead, matte or semibright finishes are preferred because of ductility, solderability, and corrosion resistance requirements. However, for some applications, appearance is the most critical consideration and a bright tin chemistry needs to be considered.

For a bright tin chemistry, the most important aspects to take into account other than throwing/covering power of the bath are (1) foaming, especially in controlled depth cell applications; (2) Sn(IV) formation; and (3) brightener control.

Foaming can be generated from one of the following: (1) high surfactant/brightener concentration and (2) anodic or cathodic gas formation. Foaming can be corrected if lower additive concentrations may be used. When that is not possible, an antifoaming agent is used. Alcohols may act as antifoaming agents, but care has to be taken since they can be fire hazards. In addition, their effects may be short lived since high agitation or anodic and cathodic gas formation may accelerate their dispersion from solution. Another well-known class of antifoaming agents is silicon-based surfactants. They are not stable in MSA-based chemistry because the operating pH is normally less than 1, which is too acidic for this class of materials.

When anodic or cathodic gas formation becomes the predominant source of foam usually consisting of tiny bubbles instead of large bubbles as generated by mechanical agitation, simply adding antifoaming agents will not solve the problem. Organic additives that will selectively suppress

TABLE 6.9 Typical Bath Compositions and Operating Conditions of a Satin Bright MSA-Based Tin Chemistry for Various Applications

Parameters	PWB	Reel to Reel	Wire
Sn, g L^{-1}	15–25	30–50	50–70
MSA, mL L^{-1}	225–275	175–225	175–225
Surfactant [60], mL L^{-1}	20–30	30–45	30–45
Grain refiner [60], mL L^{-1}	10–20	20–30	20–30
Antioxidants [60], g L^{-1}	—	—	0.75
Current density, ASF	<100	25–250	50–700
Temperature, °C	30–60	30–60	30–60

the gas formation at the electrodes are required. This usually requires an understanding of the overall plating chemistry and the effects of the organic foam suppressors on deposit properties.

Another concern in high-speed reel-to-reel application is the Sn(IV) formation, especially in flood cell. Conversion of Sn(II) to Sn(IV) may be severe due to constant and extensive exposure of the plating solution to air. A common remedy is to use antioxidants. In MSA-based chemistries, hydroquinone and its derivatives have been used extensively for this purpose. Because of the active nature of this type of compound and its potential adverse effects on deposit properties, care has to be taken to maintain optimum concentrations.

Because of the difficulties in controlling the brightener levels in the plating bath, it is challenging to control the amount of included organic matters in the deposits in a high-volume manufacturing environment. This could cause a number of problems such as inconsistent appearance or color, brittle coating, and poor solderability. It is therefore sensible to use a satin bright or semibright tin chemistry when those properties are of concern.

The most significant difference between a satin or semibright tin chemistry and a bright chemistry is in the organic compounds used as additives. In a satin or semibright tin chemistry only wetting agents and grain refiners are utilized. Of course, depending on the number and chemical nature of the organic compounds used as wetting agents and grain refiners, one may find that some satin or semibright chemistries are rather complicated as well.

The appearance of connectors plated from the satin bright chemistry summarized in Table 6.8 is shown in Figure 6.18. Ductility and solderability are good and consistent. Figure 6.19 displays the control of the additives by HPLC. Among the two additives, only the grain refiner was consumed during the electrodeposition, and there was very little consumption of the surfactant. The slight decrease of surfactant concentration was mainly caused by drag-out. The HPLC data were also useful in determining the concentration of breakdown products [60].

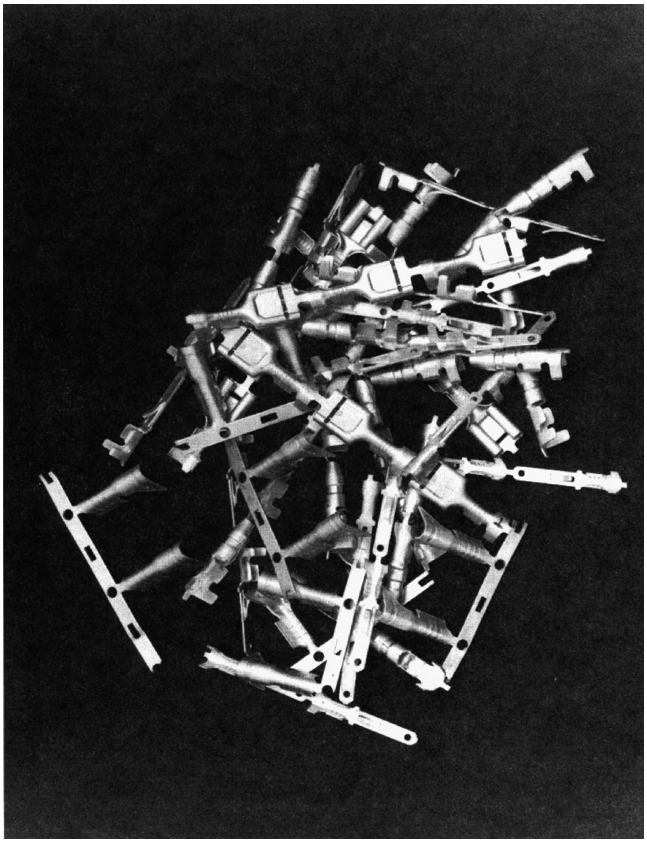

FIGURE 6.18 Connectors obtained from satin bright tin chemistry. (Photo courtesy of Electroplating Chemicals and Services, Lucent Technologies Bell Labs.)

Alkaline Tin Plating Chemistries and Processes There are essentially two types of alkaline tin plating chemistries based on either potassium or sodium stannate [65, 75, 76]. Typical bath formulations and operating parameters can be found in Tables 6.10 and 6.11. Of the two types, the potassium stannate formulation is superior. Potassium stannate is more soluble than sodium stannate, and it allows operation at higher current densities with higher current efficiency. The choice between them depends on a balancing of the superior operating properties of the potassium bath against the lower chemical cost of the sodium.

In general, these processes are simple and can operate without additives. According to Haring and Blum [33], the throwing power of an alkaline tin plating bath is among the highest. These baths are usually operated at high temperatures, which allows higher cathodic current density and faster anodic dissolution of tin. Usually a minimum temperature of 60°C is maintained.

Nonetheless, there are some concerns in operating alkaline baths. In order to maintain reasonable cathode current efficiency, the free alkaline concentration has to be under tight control for the following reasons: If the alkalinity is too low, hydrolysis of Sn(IV) occurs because of the following reaction:

$$[Sn(OH)_6]^{2-} \leftrightarrow SnO_2 + 2OH^- + 2H_2O$$

On the other hand, if the alkalinity is too high, the reduction potential for $Sn(OH)_6^{2-}$ will be pushed to a more negative value according to the following:

$$[Sn(OH)_6]^{2-} + 4e^- \rightarrow Sn + 6OH^-$$

$$E = E_0 - 3\frac{RT}{2F}\ln\left(\frac{[OH^-]}{[Sn(OH)_6]^{2-}}\right) \qquad [OH^-] > [Sn(OH)_6]^{2-}$$

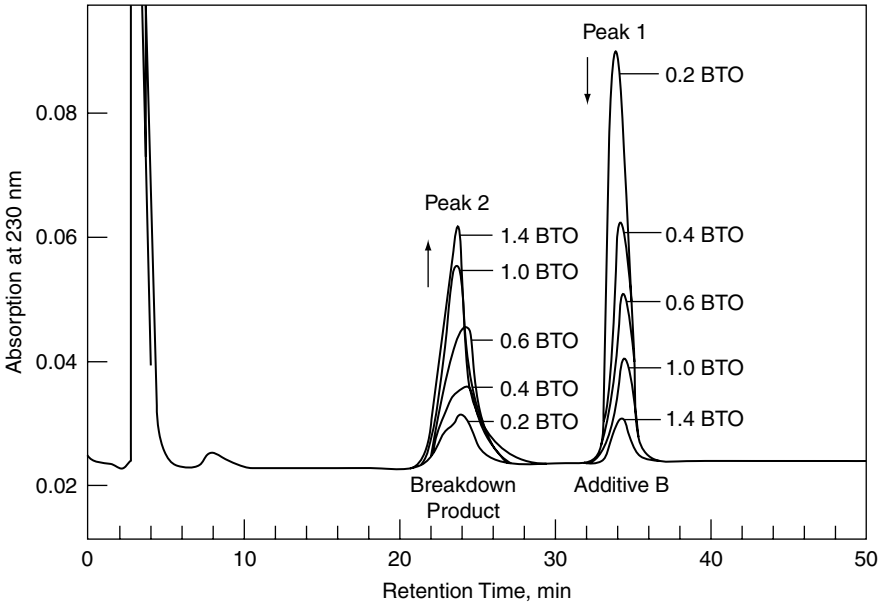

FIGURE 6.19 HPLC monitoring of additives and breakdown products in satin bright tin electroplating chemistry as function of bath turnovers (BTOs) [60].

Consequently, the codeposition of hydrogen becomes relatively more important, thereby reducing the cathode current efficiency for the electrodeposition of tin.

As discussed under Anodes in Section 6.2.6, if an insoluble anode is used, it is inevitable that the pH will increase and the excess OH^- has to be neutralized. Acetic acid is commonly employed for this purpose. Accompanying the increase in alkalinity, the stannate concentration decreases as a result of electrodeposition, and potassium or sodium stannate has to be replenished. The resulting salt buildup decreases stannate solubility and current efficiency and at some point the bath cannot be rejuvenated.

When a soluble anode is used, it has to be "filmed" first. Lack of the proper film will cause tin to dissolve as Sn(II), which is the main cause of unsatisfactory deposits. In order to film tin anode, a higher-than-normal current density—a "surge"—must be applied for a few seconds to a minute; the current is then reduced to its operating value. If this process is carried out properly, a yellowish film will form and will be maintained as long as current flows. The film dissolves fairly quickly on shutdowns and must be re-formed on start-up. If the current density is too high for the operating conditions, the film will thicken and turn black; the tin is now covered with an impervious film of oxides and is essentially inert and insoluble. If the current is too low, the film will be lost and Sn(II) will form in the bath. Ninety percent of the problems encountered in operating alkaline bath are attributed to anode reactions [76].

Compared with acid tin electroplating chemistries, alkaline tin chemistries are not as widely used, mostly because the current densities are limited.

6.3 ELECTRODEPOSITION OF TIN ALLOYS

The development of lead-free solder plating chemistries has not been easy because of the inherent difficulties in plating these alloys that (1) meet melting temperature requirements and (2) have material properties that yield good solderability and ductility and are compatible with the materials and

TABLE 6.10 Typical Bath Formulations and Operating Conditions of Potassium Stannate Baths

Parameters	Barrel	Rack
$K_2Sn(OH)_6$, g L^{-1}	95–110	390–450
KOH, g L^{-1}	13–19	15–30
Cathode current density, ASF	3–10	Up to 40
Temperature, °C	65–90	80–90

Source: Reference [76].

TABLE 6.11 Typical Bath Formulation and Operating Conditions of a Sodium Stannate Bath

Parameters	Range
$Na_2Sn(OH)_6$, g L^{-1}	95–110
NaOH, g L^{-1}	7.5–11.5
Cathode current densities, ASF	0.5–3
Temperature, °C	60–85

Source: Reference [76].

TABLE 6.12 Materials Properties of Binary Lead-Free Tin Alloys

Alloy	Composition	Melting Temperature, °C	Properties
Sn–Bi	98Sn2Bi	226	Good strength and thermal fatigue, best whisker resistance
Sn–Cu	99.3Sn0.7Cu	227	Good creep and thermal fatigue, susceptible to whiskers
Sn–Ag	96.5Sn3.5Ag	221	Good wetting and shear strength, whisker resistance

process technologies during downstream device packaging and final product assembly. Last but not least, they need to be cost comparable with tin–lead finishes with the same performance and reliability.

The majority of the tin–lead solder utilized in the electronic industry is eutectic tin–lead or near eutectic tin–lead; therefore the most urgent need was to find a "drop-in" lead-free solder for eutectic tin–lead.

As described previously, the most suitable lead-free soldering material is SnAgCu, or the SAC alloy. To electroplate a ternary alloy is not impossible; however, it would be cost prohibitive to run it in a manufacturing environment. The plating industry looked to develop binary alloy plating processes such as tin–bismuth, tin–copper, or tin–silver based on their desirable materials properties to replace eutectic tin–lead (Table 6.12).

It is appropriate to take a look at the phase diagrams of tin–bismuth, tin–copper, and tin–silver and redox potentials of these binary systems to fully understand the difficult tasks at hand and to recognize the necessary trade-offs in both lead-free solder plating development and implementation.

6.3.1 Phase Diagrams of Tin–Bismuth, Tin–Copper, and Tin–Silver

Figures 6.20–6.22 [77] display the phase diagrams of tin–bismuth, tin–copper, and tin–silver, respectively.

The bismuth–tin binary system is favored when low soldering temperatures are required. The eutectic forms at around 57 wt % Bi and with a eutectic temperature of approximately 139°C. In some ways, the phase diagram and microstructure of tin–bismuth are fairly similar to that of tin–lead; however, the mechanical properties are significantly different. Bismuth itself has several unusual properties that translate into the properties of the eutectic due to the relatively high content of the metal; for instance, the element is brittle, and the eutectic can therefore suffer from lack of ductility, particularly under conditions of impact and rapid stressing. In addition, tin–bismuth–lead forms a ternary eutectic at even lower temperature (95°C), which can lead to associated process problems during soldering (such as fillet lifting). To reduce brittleness, increase ductility, and avoid the harmful ternary eutectic, the electronic industry has selected a tin–3 wt % Bi alloy through trial and error during the late 1990s and early 2000s. In the next sections, we will focus only on tin–bismuth alloys that contain between 2 and 3 wt % Bi, which has a melting point of 226°C.

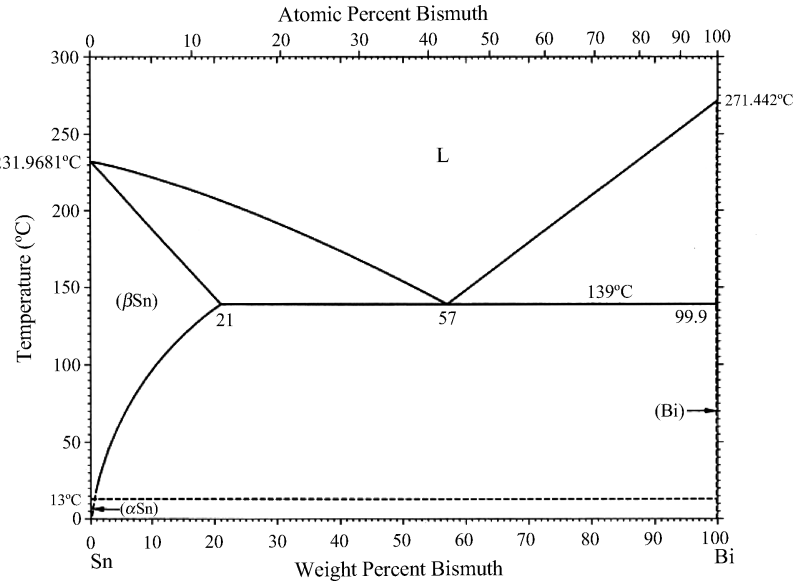

FIGURE 6.20 Phase diagram of tin–bismuth [77].

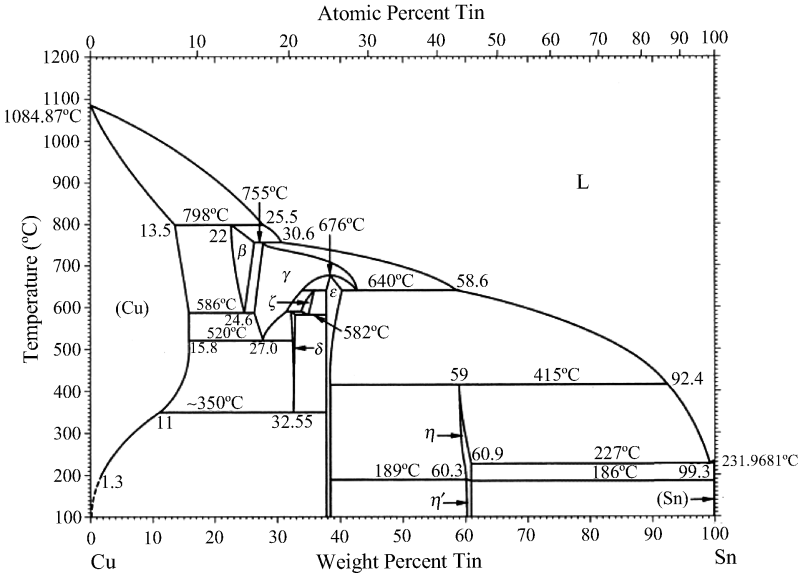

FIGURE 6.21 Phase diagram of tin–copper [77].

The tin–copper binary system is favored in low-cost applications within electronics assembly. The tin–copper binary eutectic forms at round 0.7 wt % Cu and with a eutectic temperature of approximately 227°C. It should be noted that the liquidus rises steeply to high temperatures if the copper level is increased above 0.7 wt %. For instance, the Sn–3Cu solder melts between 227 and 325°C. This would result in insufficient melting or nonmelting if the peak reflow or wave soldering temperature is at 260°C, thus adversely affecting solder joint reliability.

Over many years, the tin–silver eutectic has been used in many applications not mainly because of its lead-free properties but because it provides good fatigue resistance and was found to be particularly suited to some of the most demanding applications. The binary eutectic exists at around 3.5 wt % silver and a temperature of approximately 221°C. The microstructure is a eutectic of a tin-rich phase with very low levels of silver in solid solution and fine Ag_3Sn intermetallics that tend to form as thin platelets. With compositions of higher silver content than the eutectic alloy there is a very steep rise in liquidus temperature, for example, to around 250°C at 5% Ag.

Therefore, the target binary lead-free tin–bismuth, tin–copper, and tin–silver alloys should contain bismuth and silver less than 3 wt % and copper as close as possible to 0.7 wt %.

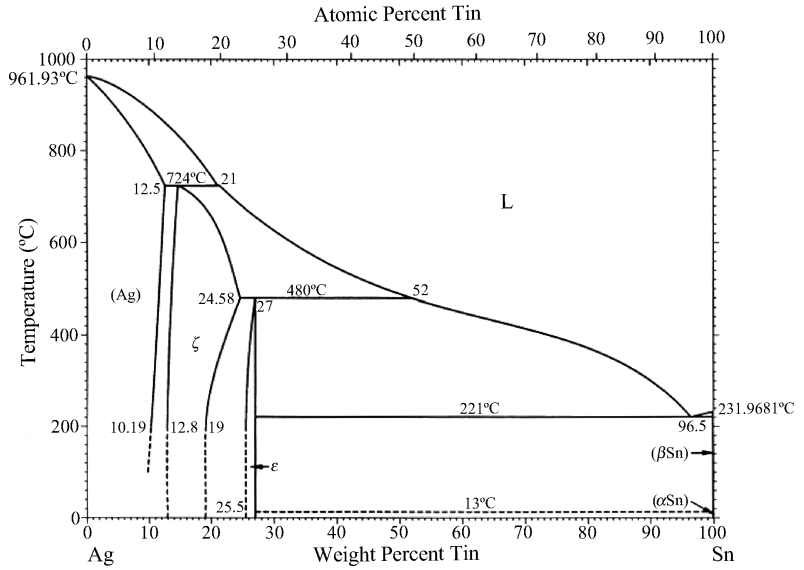

FIGURE 6.22 Phase diagram of tin–silver [77].

TABLE 6.13 Standard Potentials in Aqueous Acidic Solutions

Half Reaction	E^0 (V)
$In^{3+} + 3e^- \rightarrow In$	−0.338
$Sn^{2+} + 2e^- \rightarrow Sn$	−0.137
$Pb^{2+} + 2e^- \rightarrow Pb$	−0.125
$Sn^{4+} + 2e^- \rightarrow Sn^{2+}$	0.150
$SbO^+ + 2H^+ + 3e^- \rightarrow Sb + H_2O$	0.204
$Bi^{3+} + 3e^- \rightarrow Bi$	0.317
$Cu^{2+} + 2e^- \rightarrow Cu$	0.340
$Ag^+ + e^- \rightarrow Ag$	0.799

6.3.2 Redox Potentials

Tin–lead solders are among the easiest to be plated from various electrolytes compared to other tin alloys. The fundamental reason is that the redox potentials of tin and lead in aqueous solutions are very close, allowing for efficient codeposition. For instance, in a 1 *M* solution of acidic electrolyte, there is only 12 mV difference in deposition potentials between the two. Table 6.13 lists the standard potentials of various metals in aqueous acidic solution [22].

6.3.3 Thermodynamic and Kinetic Considerations

For electrodeposition of an alloy the respective metals should have similar reduction potentials, preferably within 200 mV. When looking at the standard potentials of stannous ion and bismuth ion, one realizes that in a noncomplexing aqueous solution, bismuth will preferentially plate out, because the standard deposition potential of Bi^{3+} is much more positive than that of Sn^{2+} (see Table 6.13). Since the difference in deposition potentials is 454 mV, one may not be able to obtain an alloy at all. However, certain approaches may be taken to narrow the potential difference between the metal components. For instance, one may choose the following to modify the deposition potentials of each metal:

1. Adjust the concentration of one metal component. In other words, making the concentration of the more noble metal diffusion limited so that the less noble metal can plate out before the complete depletion of the more noble metal. This would be difficult for tin/bismuth, but it may be possible for tin/silver.
2. Use complexants.
3. Use organic additives to poison or block the electrodeposition of the more noble metal.

According to the modified Nernst equation, the potential of a metal ion in solution is given by the sum of its Standard potential and a term expressing its activity (a), shown below:

$$E = E^0 + \left(\frac{RT}{nF}\right)\ln a + C$$

where C includes all the factors which contribute to the polarization in the electrodeposition process. In the case where two metals are simultaneously deposited, the two equations for the two species can be expressed as follows:

$$E_1 = {E_1}^0 + \left(\frac{RT}{nF}\right)\ln a_1 + C_1$$

$$E_2 = {E_2}^0 + \left(\frac{RT}{nF}\right)\ln a_2 + C_2$$

The difference in potential between the two metals involved can be expressed by

$$\Delta E = E_1 - E_2 = {E_1}^0 - {E_2}^0 + \left(\frac{RT}{nF}\right)\ln\left(\frac{a_1}{a_2}\right) + (C_1 - C_2)$$

For successful alloy deposition, ΔE must be minimized. The codeposition condition can be met either when the two values ${E_1}^0$ and ${E_2}^0$ are similar, such as in the cases for Sn and Pb, or by adjusting the concentration of one species in solution, so altering its activity, or by arranging a suitable difference in the term C, which can be achieved by introducing complexants. The most commonly used method for modifying the deposition potentials is to use complexants, especially when the difference between the standard potentials is large. The activity term is log dependent and therefore difficult to alter potentials significantly. The complexant may react with both metal ions or only react selectively with one or the other. No matter what is the case, the end result should be that ΔE be minimized.

If all of the above fail, one may consider using organic additives to preferentially inhibit the deposition of the more noble metal. Caution, however, has to be taken when this approach is considered. As discussed throughout this chapter, organic additives can have detrimental effects on deposit properties such as ductility and solderability. Furthermore, there are no generic recipes for choosing organic additives or "poisons." And in most cases, a "trial-and-error" approach is used because of the lack of fundamental understanding of the role of individual additives at a molecular level during the electrodeposition process.

Even though thermodynamics determines whether an electrodeposition process can take place, it is the kinetics that determines how fast the deposition takes place and what kind of deposit one will obtain. In order to simplify the following discussion, we now consider the electrodeposition of one metal.

For any electrodeposition to take place, a current has to flow through an electrochemical cell. This may be limited by any of three factors:

1. Conductance of the bulk solution
2. Transport of reactants to the electrode or products away from the electrode

3. Rate of electron transfer and/or chemical reactions coupled to the electron transfer step

When a net current flows through the cell, the cell is not at equilibrium. The cathodic potential can be expressed by

$$E_{ca} = E_e + \eta$$

where η is the overpotential and E_e is the equilibrium potential at which no current flows through the cell or there is no electrodeposition. The overpotential η is contributed by all the factors that make the cathode deviate from its equilibrium condition. For instance, it is influenced by solution and interfacial processes that are involved in the three major parameters outlined above and also by the external electrical field that is applied in an electrodeposition process. In order to get a physical meaning for the significance of the overpotential, it is helpful to say that small η generally means slow electron transfer reactions whereas large η yields fast electron transfer reactions.

The conductance or conductivity of the bulk solution is important because it is a measure of the rate of charge transport through the solution under the influence of an electric potential gradient. Typically, this parameter is controllable and one can obtain sufficient conductivity of the solution by adding electrolytes that contain ions for electrolytic conductance. Under normal circumstances, step 2 is usually the rate-limiting step. The electron transfer rates (step 3) for the reduction of simple metal ions are usually much faster than step 2. In electrodeposition, it is generally not desirable to have step 2 be the rate-limiting step. Dendritic deposits will result from the lack of metal ions transported to the electrode interface to support further cathodic reduction. Under such circumstances, the incipient fine crystals recrystallize and grow larger to lower the total energy of the system. At the electrode interface, the dimension that has more degrees of freedom is the direction perpendicular to the electrode surface. This is normally how dendrites are formed. In order to avoid dendritic growth, it is necessary to make the electron transfer process (step 3) the rate-limiting step. Common practice includes plating at lower current density, that is, providing small η or using organic molecules to inhibit or slow down the electron transfer process by blocking the high-energy sites of the electrode surface, thus increasing the activation energy for step 3. The latter approach is used widely in the surface-finishing industry to obtain smooth, dendrite-free deposits. With the help of organic additives, sometimes it is possible to electrodeposit a metal close to its limiting current, which is desirable in view of the productivity of a plating operation.

Obviously, the above considerations are further complicated when binary or ternary alloys are concerned. As discussed previously, one must consider the relative reduction potentials of each respective metal and provide an electrolyte/complexant which allows significant overlap of the reduction potentials, thus ensuring codeposition. Additionally, one wants to prevent plating at or close to the limiting current of each metal to avoid dendrite formation or undesirable alloy composition by utilizing organic additives. Needless to say, the processes must be environmentally friendly and robust enough to be used in a manufacturing operation.

6.3.4 Practical Considerations

In a typical tin alloy plating bath, one would find a tin salt, a bismuth, copper, or silver salt, an electrolyte (typically an acid), a chelating agent, a surfactant, a grain refiner, and/or a brightener. Depending on the tin alloy, one may or may not utilize a chelating agent. Depending on whether a bright or matte finish is desirable, one may or may not utilize a brightener. We will first focus on the inorganic part of the bath composition.

In the case of tin–bismuth, tin–copper, and tin–silver plating, if no chelating agents are present and the electrolyte is methanesulfonic acid, all the metal ions are more or less dissociated in the solution. These systems are not thermodynamically stable because of the large electrochemical potential differences between the metals, and a "displacement reaction" or "immersion plating" reaction would take place during idle (i.e., no current) flow if a soluble tin anode is exposed to the solution. These displacement reactions can be written as

$$2Bi^{3+} + 3Sn(\text{anode}) \rightarrow 2Bi\downarrow(\text{black, powdery film}) + 3Sn^{2+}$$

$$Cu^{2+} + Sn(\text{anode}) \rightarrow Cu\downarrow(\text{black, powdery film}) + Sn^{2+}$$

$$2Ag^{+} + Sn(\text{anode}) \rightarrow 2Ag\downarrow(\text{black, powdery film}) + Sn^{2+}$$

There are a few problems with the displacement reactions. First, the powdery film may dislodge into the solution, getting stirred up and codeposited into the deposit causing surface roughness. Second, the bismuth, copper, or silver concentration in the bath will be out of balance, which in turn would result in the wrong alloy composition in the deposit. Third, the anode could become passivated if the black film is excessive.

To avoid immersion plating, one could elect to use an insoluble or a dimensional stable anode. However, as discussed previously, this would result in oxygen generation at the anode and consequently would cause significant Sn(II)-to-Sn(IV) formation, which is not desirable. In addition, running the lead-free tin alloy bath using insoluble anode is much more expensive than using a soluble anode because replenishing tin with tin salts is more expensive than with tin anodes.

The trade-off typically is to introduce one or more chelating agents which typically form a stronger complex with

bismuth (or copper, or silver) than with tin. This helps to push the reduction potential of bismuth (or copper or silver) closer to tin, thus reducing the tendency for immersion plating. The challenge is to find the right chelating agents for the right alloy bath.

There has been significant innovation in tin and tin alloy deposition [78–111] since the early 1960s, although most of the breakthrough took place during the last decade [89–111]. The author strongly refers the readers to the references [78–111] to gain detailed and in-depth knowledge of the various plating chemistries. Owing to its acceptance and importance in leadframe (tin–bismuth) and wafer bumping (tin–silver) applications, we will look at the deposition and material properties of electroplated tin–bismuth and tin–silver. Very few electronics applications use eutectic tin–copper because of whisker propensity and the difficult-to-control tin–copper plating process. Therefore additional details will not be provided for tin–copper plating.

6.3.5 Electrodeposition and Material Properties of Electrodeposited Tin–Bismuth

There are very few reported studies on the electrodeposition of eutectic tin–bismuth alloy [78–80], although the codeposition of $<1\%$ bismuth with tin has been documented for more than two decades [81–84]. The small amount of bismuth in the latter case was aimed at stopping the harmful phase transformation of pure tin from the α phase to the β phase at temperatures below 13°C, sometimes referred to as tin pest. Plating baths of this type are largely sulfuric acid–based systems.

The challenges of depositing eutectic tin–bismuth can be attributed to the following: (1) The difference between the reduction potentials of the two is too large and (2) Displacement of tin by bismuth according to the following replacement reaction:

$$2Bi^{3+} + 3Sn(\text{anode}) \rightarrow 2Bi\downarrow + 3Sn^{2+}$$

The first difficulty can be lessened by using complexant, as explained earlier. Ethylenediaminetetraacetic acid (EDTA) [82] and diethylenetriaminepentaacetic acid (DPTA) [79] have been used to plate eutectic tin–bismuth. Even though Cavallotti [79] and co-workers obtained encouraging results for the eutectic tin–bismuth coatings by using DPTA as complexant, the plating process was difficult to control. At low current densities, bismuth plated out preferentially. On the other hand, at high current densities, tin plated out preferentially. The alloy composition was also very sensitive to the plating temperature. If a pure tin anode is used, bismuth ion in the solution will replace tin from the anode. If care is not taken, a black slime will form at the anode, causing anode passivation. One remedy to this problem is to use tin anode doped with a small percentage of bismuth [85]. At the same time, it is important to not leave plated pieces immersed in the solution when deposition is done because the deposit will become gray/black due to the displacement reaction.

Recently, Katayama and Okuno [86] reported another approach to obtain eutectic tin–bismuth; that is, they plated bismuth and tin layers separately, and the total thickness was around 10 μm. Then the double-layer deposit was reflowed at 195°C. The reflowed coating had comparable adhesive strength as that of eutectic tin–lead coatings on copper. The thickness ratio of bismuth–tin was a critical parameter in order to obtain crack-free reflowed eutectic tin–bismuth. A similar approach was used in [87, 88], but not successfully due to a relatively weaker bond between the sandwich and the copper substrate.

When bismuth is added into tin, the phase diagram of tin–bismuth indicates that the solubility of bismuth is reduced sharply from 21 wt % at the melting point (139°C) to about 4 wt % at 20°C. As mentioned earlier, eutectic tin–bismuth is too brittle and not suited as a component finish; a tin–bismuth alloy with 2–3 wt % bismuth is preferred. The reason that we need to keep the bismuth content below 3 wt % is because tin–bismuth plating typically takes place at room temperature whereby the soluble bismuth content is about 4 wt %. To obtain a true tin–bismuth alloy, it is good practice to keep the bismuth content in electrodeposited tin–bismuth at less than 3 wt %. Otherwise bismuth will precipitate out of the tin-rich phase resulting in bismuth "needles" that will not melt at lead-free reflow temperatures.

During the last decade, a number of commercial viable tin–bismuth plating processes have been developed by plating chemical suppliers and/or large vertically integrated semiconductor companies [89–93]

Just as one example, the plated 97.5Sn2.5Bi starts to melt at 226°C and has a fairly good pasty range (Fig. 6.23). In addition, the elongation of this alloy in the practical thickness range is about 36% (eutectic tin–lead is 40%) and with a

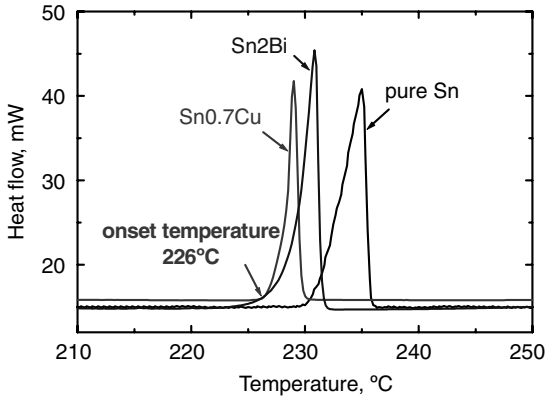

FIGURE 6.23 DSC curve of tin–bismuth; also shown are those of tin–copper and pure tin [91].

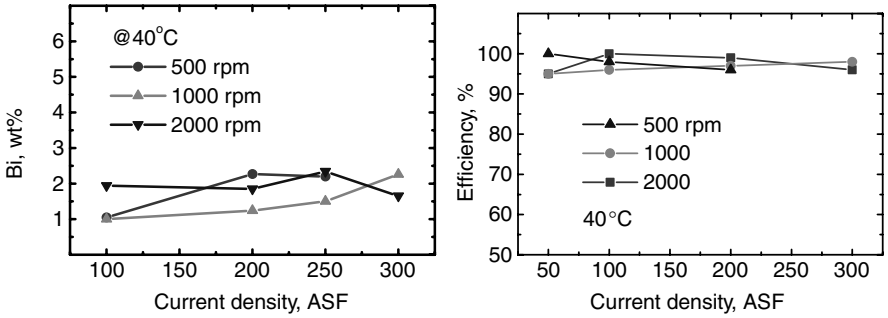

FIGURE 6.24 Process window for tin–bismuth plating process [91].

hardness of 10 KHN_{5g}, also similar to eutectic tin–lead. It is important to point out that this tin–bismuth process has a wide operating window for current density and solution agitation (Fig. 6.24) in addition to low carbon content (less than 50 ppm) under these plating conditions. Alloy composition, current efficiency, and carbon content remain stable during bath aging (Fig. 6.25). Furthermore, this alloy has excellent solderability evident from the wetting balance test results (Fig. 6.26). This coupled with high elongation and low whisker propensity makes it a good candidate as a lead-free leadframe finish [94–96].

6.3.6 Electrodeposition and Material Properties of Electrodeposited Tin–Silver

Little was published on the electrodeposition of tin–silver alloys in 2000. Because of the large difference in their deposition potential (0.94 V, see Table 6.12), the alloys cannot be obtained from simple ion solutions. Since silver is the more noble metal, it is desirable to use complexant to bring its reduction potential closer to that of tin. Silver readily forms complexes with simple anionic species such as CN^-, SCN^-, $S_2O_3^{2-}$, and $S_2O_8^{2-}$. The reduction potentials of these silver complexes are in the range of 0.21 V to −0.31 V versus the normal hydrogen electrode (NHE). Taking into consideration the chemical nature (i.e., reactivity) of these anionic species in acidic medium, the best are SCN^- and $S_2O_8^{2-}$. An early attempt to electrodeposit tin–silver from a MSA-based chemistry was not successful due to the reaction between $Sn(MSA)^{2+}$ and the silver complexes of SCN^- and $S_2O_8^{2-}$. Therefore, the option now seems to be limited to alkaline medium using CN^-.

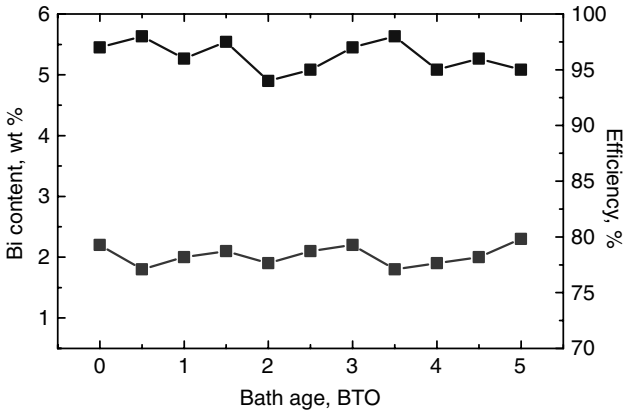

FIGURE 6.25 Aging study of tin–bismuth plating process [91].

Electroplating baths which contain cyanide for tin–silver electrodeposition have been reported [97, 98]. Tin was introduced as tin sulfate ($SnSO_4$) or tin pyrophosphate ($Sn_2P_2O_7$) and silver as potassium silver cyanide. In these cases, the pH of the solutions were around 9, and alloys contained from 10 to 16% silver. As shown in the phase diagram of tin–silver, such high silver content would render it not useful in applications that require solder reflow.

Eutectic tin–silver has comparable elongation and shear strength compared with eutectic tin–lead. It has superior room temperature isothermal fatigue behavior compared with eutectic tin–lead. Its higher melting temperature and superior thermal fatigue property make it a good candidate for automotive and flip-chip applications. This realization motivated researchers in industrial laboratories as well as academia to develop a number of commercially viable tin–silver plating processes [92, 93, 99–107].

Tin–silver suffers worse immersion plating than tin–bismuth to the extent that soluble anodes are rarely used for this alloy plating, and they have never been used in wafer bumping.

Due to the large potential difference, complexants are used in eutectic tin–silver baths in addition to surfactant, grain refiners, and antioxidant. Depending on the nature of the complexant and additives utilized, the operating process window (i.e, current density, solution flow, etc.) can be significantly different. We show two examples: one low speed (Fig. 6.27 [99]) and one high speed (Fig. 6.28 [100]). In addition to a stable alloy composition over a wide current density range, it is important that the plated bumps do not exhibit voids after reflow. When examined by X-ray tomography, there should be no voids which show as white dots in the X-ray maps. Kiumi et al. [108] showed that excessive complexant, too high or too low current densities, as well as improper reflow profile and/or flux could all contribute to

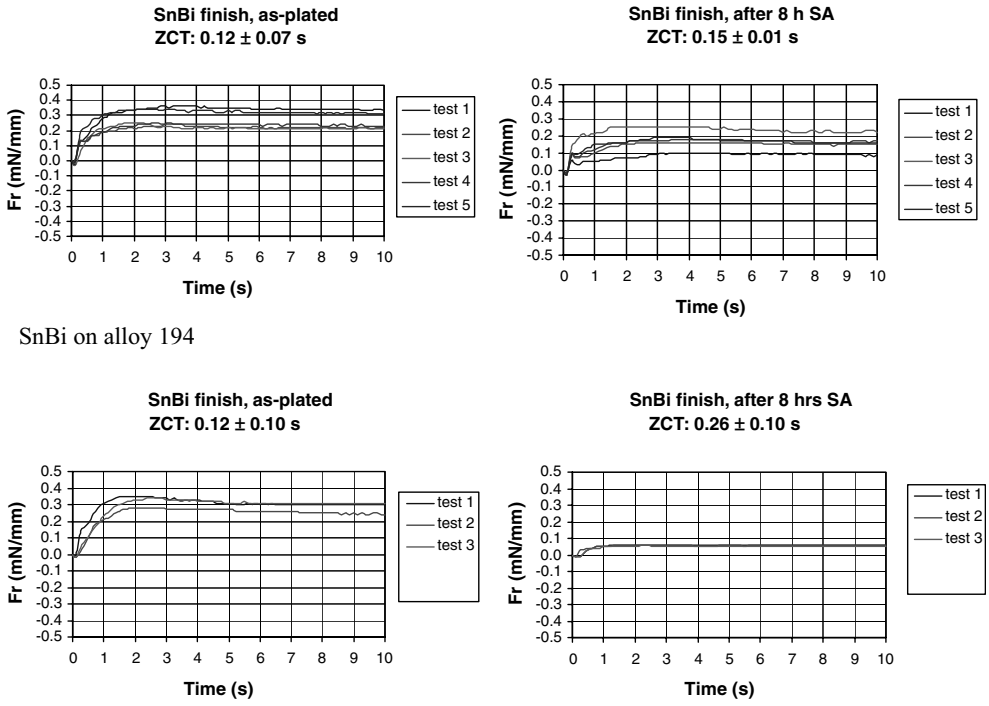

FIGURE 6.26 Wetting balance tests of tin–bismuth plated on Cu (top) and alloy 42 (bottom) leadframes.

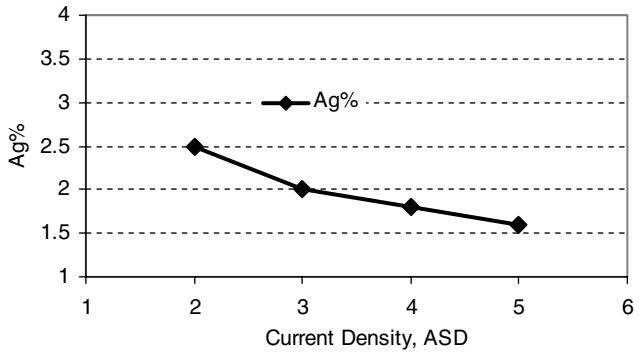

FIGURE 6.27 Current density range of low-speed tin–silver plating process [99].

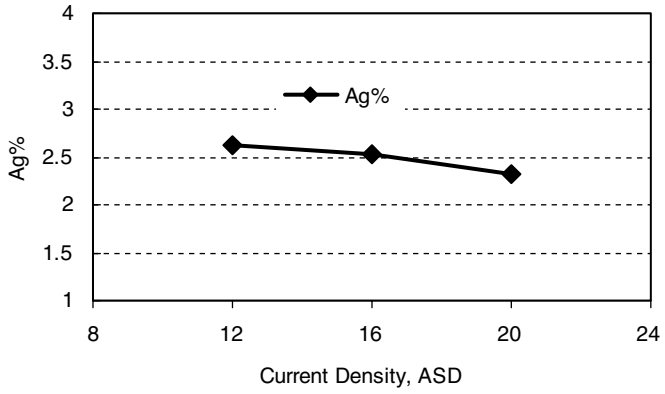

FIGURE 6.28 Current density range of high-speed tin–silver plating process [100].

void formation. Their main conclusion was that finding the right complexant for tin–silver plating was the key to void-free bumps.

The electroplated tin–silver bumps exhibit excellent bump shape and morphology as plated and after reflow (Fig. 6.29). Its microstructure suggests it is a true alloy as plated and after reflow there is minimum amount of Ag_3Sn intermetallic compound formation because of the absence of typical platelets (Fig. 6.30).

6.3.7 Considerations of Electrodeposition of Ternary and Quaternary Tin Alloys

From the discussion above we can surmise that the potential difficulties of plating ternary and quaternary lead-free solders are significantly more challenging than those of binary alloys. Take ternary SnBiAg, for example: The standard potentials are −0.137, 0.317, and 0.799 V for tin, bismuth, and silver, respectively. The smallest ΔE is 0.454 V and the largest ΔE is 0.94 V. According to the discussion in Section 6.4.3, the difference is too large for codeposition to take place without a complexant or some kinetic maneuvers. If using a complexant is the method of choice, considering the alloy composition 83.5Sn14Bi2.5Ag, what is needed is a complexant that would bind to silver the strongest and to tin the weakest so that the reduction potentials could be pushed closer together. Or to maneuver the kinetics of the electrodeposition process, one wants to force silver ion reduction under transport limiting rate while tin is deposited under

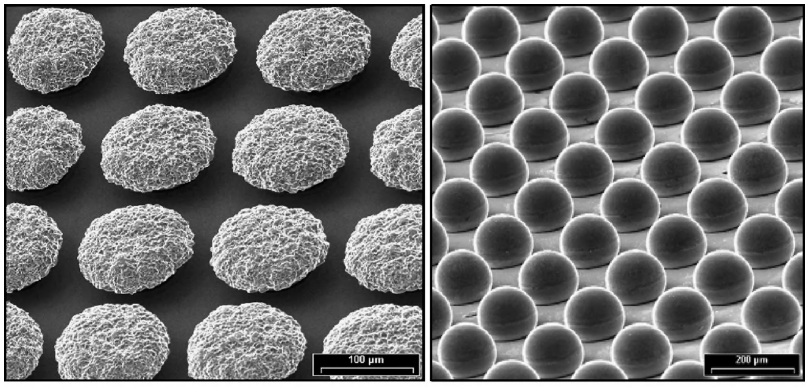

(a) (b)

FIGURE 6.29 Tin–silver bumps: (*a*) as plated; (*b*) after reflow [100].

kinetic control. (In another word, using organic additives to suppress tin deposition). This type of deposition is sensitive to the concentration of the respective metal ions, solution agitation, and the surface features of the parts. Therefore it may not be practical in many applications.

Nonetheless, it is possible to electrodeposit ternary and quaternary tin alloys. Currently, there have been a number of successful demonstrations of electroplating a near-eutectic tin–silver–copper alloy [109–111] for wafer bumping applications. Due to the intrinsic difficulties and challenges to maintain and control the alloy composition in a production environment, this alloy plating process has not been qualified or implemented in manufacturing.

6.4 MATERIAL PROPERTIES AND APPLICATIONS OF ELECTROPLATED TIN AND TIN ALLOYS

Any discussion on electrodeposition will not be complete if the material properties of the deposits are not discussed. In this section, an effort will be made to correlate materials properties such as appearance, surface morphology, ductility, purity, and hardness of electrodeposited tin and tin alloys to the electroplating chemistries and process parameters.

6.4.1 Appearance

Appearance is a generic term used to describe the overall quality of a deposit when examined visually or with the help of some quantitative instrument such as a glossmeter [112]. It is one of the most important properties of a deposit, and it is critical to many applications. For instance, it is a primary indicator of the deposit quality and the long-term performance of the chemistry. Despite its importance, very little work has been done to establish a system that will quantitatively evaluate the appearance of a surface and/or rank various surface finishes for their brightness. In the electroplating industry, people loosely use terms such as *dull*, *matte*, *satin bright*, *semibright*, and *bright* finishes. There exist a lot of inconsistencies. This is especially true for electroplating using tin chemistries.

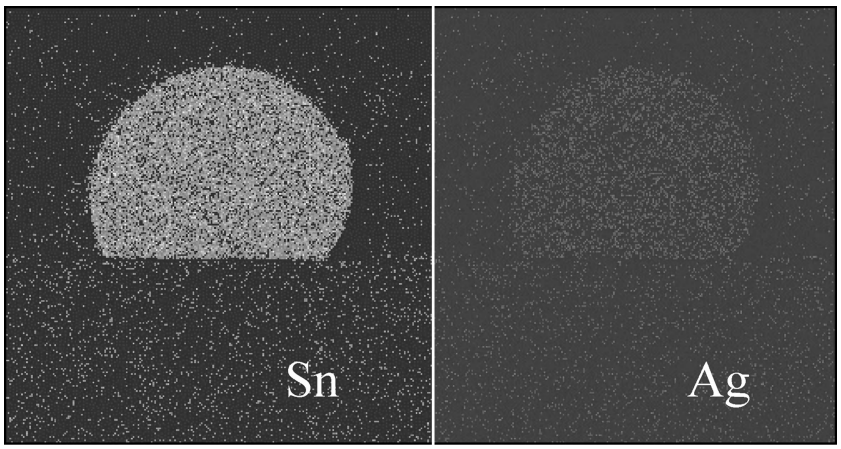

FIGURE 6.30 X-ray elemental mapping of cross section of tin–silver bump after reflow [100].

A glossmeter appears to be a simple, quantitative tool to evaluate appearance. It is based on the measurement of the specular component of the reflected light. The measurement values are related to a highly polished, black glass standard. The black glass standard has an assigned specular gloss value of 100 (calibration). The specular component of the reflected light is mostly associated with the brightness of a surface. By measuring the percentage of specular reflectance of high-, semi-, or low-gloss surfaces, equivalent to bright, semibright, or matte surfaces, a quantitative relationship can be established between the glossmeter reading and the brightness scale [113].

In tin electroplating, brighteners usually have the most profound effect on appearance, though metal and acid concentrations also exert some effects but not with the same magnitude. In terms of plating parameters, for a nonbright chemistry, changing current densities can make a deposit look matte to semibright. For example, of the MSA-based chemistries, the one illustrated in Section 6.2.7 yields brighter deposits with higher current densities until the limiting current is reached. Pulsed current also has a significant effect on appearance. Principles and applications of pulse plating can be found elsewhere [114]. Although there are extensive publications on the use of pulse plating in the electroplating industry, most of the work is done with gold, silver, copper, and nickel chemistries. Little has been published on tin and tin–lead chemistries. As will be shown in the next section, the pulse current modifies the surface morphology substantially, which is reflected by the change in the appearance of the deposit.

6.4.2 Surface Morphology and Texture

As discussed by Dini [115], the properties of all materials are determined by their structures. Even minor structural differences often have profound effects on the properties of electrodeposited metals [116]. Therefore it is important to obtain structural information of deposits at a microscopic level. Scanning tunneling microscopy is commonly used to study surface morphologies. Besides grain size and shape, which can be obtained from surface morphological studies, texture of deposits (defined as preferred distribution of grains having a particular crystallographic orientation with respect to a fixed reference frame) is also important. Texture is usually studied by X-ray diffraction.

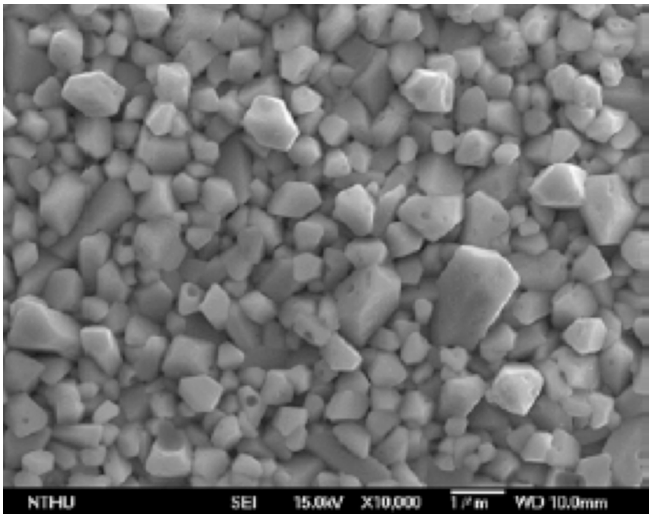

FIGURE 6.31 Typical columnar type of structure of electrodeposited matte tin coating.

The three most often encountered structures of electrodeposited tin are (1) columnar, (2) polygonized, large grained, and (3) fine grained. Columnar structures are characteristic of deposits from simple ion acidic solutions containing no or low additives such as tin from sulfate, fluoborate, or MSA solutions operated at elevated temperature or low current density. An example of this type of structure is shown in Figure 6.31, which was obtained from a MSA matte tin chemistry.

Well-polygonized, large-grained tin deposits have been reported from a satin bright tin chemistry [60] and a bright tin chemistry [117] under different deposition conditions. Figure 6.32*a* shows an example of this structure where

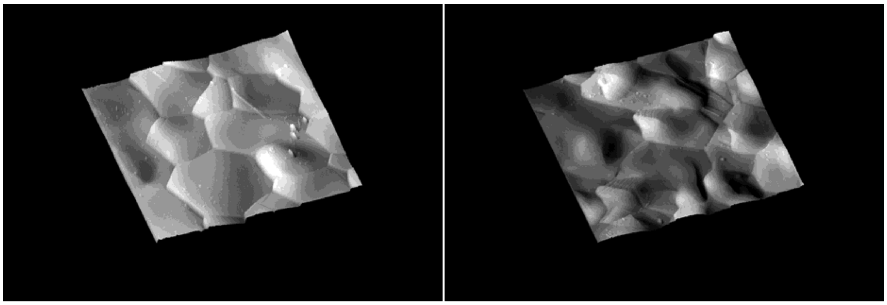

(a) (b)

FIGURE 6.32 Electrodeposited tin coatings obtained from satin bright tin chemistry obtained by (*a*) pulsed-current plating and (*b*) direct current plating [60].

the main features are well-polygonized grains in the range of roughly 1–8 μm. As can be discerned in Figure 6.32*a*, pulse current changes the surface morphology significantly from a columnar-type structure (Fig. 6.32*b*) to a well-polygonized, large-grained structure. As demonstrated by Kakeshita et al. [117], this type of structure is instrumental in preventing whisker growth and this will be discussed in Section 6.5.

Fine-grained structures are normally obtained from complex ion solutions such as cyanide copper solution or with the presence of brighteners in the case of tin plating. Fine-grained deposits usually are bright, and grain sizes normally fall below 0.15 μm. They are less pure, harder, and more brittle, exhibiting higher electrical resistance due to organic inclusions. The biggest problem with bright deposits is solderability degradation caused by high organic inclusions, intermetallic compound formation, and surface oxidation. They should not be used in applications that require reflow.

It is well known that organic inclusions have profound effects on deposit properties such as ductility and hardness. Texture or preferred orientation plays an important role as well on these properties. The latter is not fully recognized and less studied. Tin deposited from alkaline stannate solutions was reported to have a preferred orientation with (100) crystal planes whereas a (110) orientation was observed from an acid tin solution [118]. Zhang et al. [119] also observed by X-ray measurement that the substrate texture could influence the texture of tin on top.

Nonetheless, surface morphology and texture of a deposit are influenced by plating parameters. The effect of metal ion concentration, additives, current density, temperature, agitation, and polarization on surface morphology is illustrated in Figure 6.33 [115]. The effect of the same plating parameters on texture is more complex and less studied, so it is difficult to show even pictorially how individual plating variables influence texture.

6.4.3 Purity

The purity of electrodeposited metals is mostly affected by the specific electroplating chemistries and anode materials. The conventional methods for purity analysis of electrodeposited tin coatings are (1) elemental and (2) differential thermal analysis. Organic contents such as carbon, sulfur, and hydrogen are usually reported in weight percent (C, S) or in parts per million (H) in the elemental analysis. Differential scanning calorimetry has been employed to measure the purity of a satin bright tin deposit [60] and to determine solder alloy composition and liquidus temperature [120, 121]. The accurate assessment of liquidus temperature, at which a metal or an alloy totally melts, is very important in setting up reflow profiles.

Typically, organic inclusions from a nonbright tin chemistry are less than those from a bright tin chemistry. It was reported [60] that the carbon content in a satin bright tin deposit was $<0.004\%$. Carbon contents in bright coatings are usually $>0.1\%$ and are typically much higher. High organic inclusions are usually associated with poor ductility, higher hardness, and poor solderability and reflow characteristics. On the contrary, the satin bright tin deposit mentioned earlier has excellent ductility ($\%E > 26\%$), excellent solderability, and reflows without dewetting.

Although most of the impurity problems are related to organic inclusions, metallic and inorganic impurities can be just as harmful. Common metallic impurities in electroplating pure tin are copper, iron, zinc, and nickel. In acidic tin plating solutions, copper, zinc, and iron usually come from substrates. Nickel is usually a result of drag-in from the nickel plating tank. These contaminants can have profound effects on the brightness of tin deposits as demonstrated by Zhang and co-workers [122]. Among inorganic species, it is known that the ppm level of Cl^- has a dramatic effect on the appearance of either satin bright [122] or bright tin coatings [65]. It also reduces covering power of a pure tin bath [122].

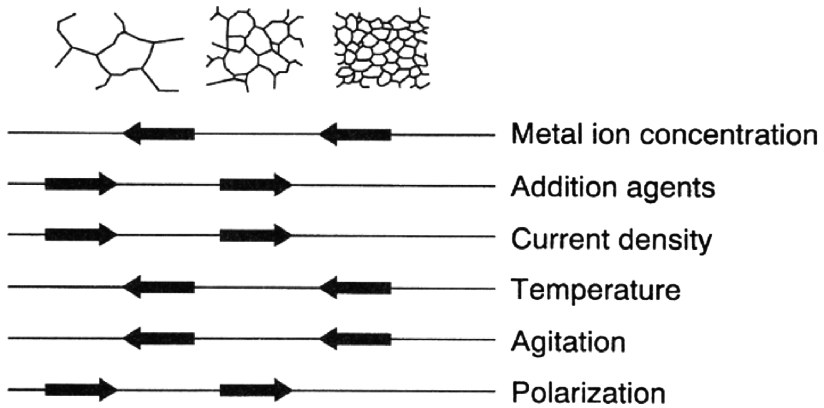

FIGURE 6.33 Relation of structure of electrodeposits to operating conditions of solutions [115, p. 147].

6.4.4 Solderability

Solderability is defined as the ability of a base metal surface to be wetted by molten solder under specified conditions of time, temperature, and environmental exposure. Four factors must be considered during a soldering operation:

1. *Thermal Demand* The thermal characteristics of the component must allow heating of the solder joint area to the desired temperature within the time available for the soldering operation.
2. *Wettability* The surface must allow wetting by molten solder within the time available for the soldering operation and without subsequent dewetting. Wettability is generally measured by the degree of coverage of a surface, that is, lack of dewetting, or by some measure of the wetting angle, time, or force.
3. *Resistance to Soldering Heat* The temperature of the solder and the associated thermal stresses must not affect the function of the component.
4. *Resistance of Metallization* This issue revolves around the dissolution of the surface finish, which can lead to the exposure of an underlying nonsolderable surface.

For tin–lead coated components solderability evaluation, 2 and 4 are especially important.

The major solderability tests for components are dip-and-look test, wetting balance test, and sequential electrochemical reduction analysis (SERA) [123]. Of the three, the dip-and-look test is still the most popular, but the wetting balance test is the most quantitative and informative.

The dip-and-look test is the oldest, simplest, cheapest, and most widely used solderability test. The specimen is fluxed and then dipped vertically into a molten solder bath. Both the rate of immersion and withdrawal must be controlled as well as the dwell time and temperature of the solder. The test is frequently performed manually but can be automated. The measured value is percent coverage of the surface. The evaluation is normally done by the naked eye. The subjectivity of this measurement is the principal drawback.

The wetting balance was invented by Duis in 1967, and acceptance and use of this methodology was initially much better in Europe than in the United States or the Pacific Rim. In this method, the specimen is suspended from a very sensitive balance over a solder pot. Subsequently, the pot is raised at a controlled speed and the specimen is immersed to a specified depth in the molten solder. After a specified dwell time the pot is lowered. The output of the test is a curve of the measured weight change of the specimen during the test. Wetting force and speed can be obtained from the wetting curve, which can be correlated to solderability. The principal issues are one of repeatability both for individual machines and from site to site and pass–fail criteria. Interpretation of the results can be arguable, and because of these issues, the American National Standards Institute (ANSI) states that the wetting balance is a test "without established accept/reject criteria" and leaves it to the suppliers and users to determine the acceptance criteria.

Solderability is one of the most important properties of tin–lead solders for obvious reasons. The single most important parameter for unacceptable solderability is organic inclusions in the deposits. Although the mechanisms proposed on the effects of organic content on solderability remain a matter of debate, the simple fact is that bright finishes have worse solderability than matte or satin/semibright finishes, especially after storage under ambient conditions. Therefore, when solderability is of critical concern, a satin bright or semibright finish should be sought.

Another matter to take into account is the use of underlayer as a means to preserve solderability. For instance, for electronics applications, the following thickness specification is not uncommon: 4 μm Sn or SnPb over 1.5 μm Ni on a copper alloy substrate. The purpose of a nickel underplate is to reduce the rate of Sn–Cu intermetallic compound formation. Nickel forms intermetallic compounds with tin under a much slower rate [124]. Over 4 μm tin or tin–lead thickness ensures that the intermetallic compounds and/or substrate will not be exposed to air because of pores generated in the deposit during plating or complete depletion of tin in the deposit due to the formation of intermetallics.

The most commonly encountered solderability failures in the dip-and-look test are nonwetting and dewetting, which are often attributed to the formation of surface oxides, organic occlusions, and intermetallic compounds. Of the three, organic content is largely dependent on the type of chemistry one chooses. The formation of surface oxides and intermetallic compounds is time and temperature dependent. In their recent work [125], Zhang and co-workers demonstrated that the extent of surface oxide formation is comparable for a bright and a semibright 90/10 tin–lead deposit. Specifically, the same surface species (SnO_2) and thickness of the oxide were identified after 48 h steam aging by Auger depth profiles for both finishes. However, the intermetallic compound layer was three times thicker in the case of the bright 90/10 tin–lead deposit. In both cases, there was no evidence of the substrate and intermetallic compounds at the surface. The solderability failure, which was nonwetting, was therefore attributed mostly to the surface oxide formation.

The detrimental effect of organic inclusions was illustrated in a controlled study with a bright 90/10 tin–lead finish and a semibright 90/10 tin–lead finish [125]. After plating, done under identical conditions, both types of finishes were subjected to a thermal bake test for 4 min; the resulting surfaces were then examined visually and by scanning electron microscopy (SEM). It was shown that the bright finish had gross dewetting whereas the semibright finish had excellent wetting characteristics.

In summary, it is important to know not only how to perform and interpret solderability tests but also how to choose the proper plating processes and control plating parameters to ensure good solderability. Specific examples will be given when we discuss applications of electroplated tin and tin alloys in Section 6.6.

6.4.5 Ductility

Ductility, as evidenced by percent elongation, is a measure of plastic deformation of a thin coating prior to fracture. Tin and tin–lead coatings are usually known for their high ductility or elongation up to 40%. This property is highly dependent on the specific chemistry and the plating parameters. In general, it is true that bright tin and tin alloy deposits have lower ductility [126] than matte or satin bright deposits.

Other than the plating chemistry, ductility of a thin coating is also influenced by the substrate and the thickness of the coating. For instance, ductility is usually higher when the deposit is attached to its substrate on which it has been plated. Lower ductilities of the foils tested without their substrate are probably caused by the more severe local plastic deformation in the region where fracture subsequently occurs. Murphy [127] has shown that the percent elongation of electrodeposited copper increased significantly as the thickness of the deposit increased.

6.4.6 Hardness

Tin and lead coatings are known to be soft [128]; lead is softer than tin, as shown in Figure 6.34. As far as tin–lead coatings are concerned, matte finishes usually have lower hardness values ($\sim$ 8–10 kg mm^{-2}) than those of bright finishes ($\sim$ 15–20 kg mm^{-2}) [65]. Bright deposits often result in cracking when they are bent, exposing the substrate so that both solderability and corrosion resistance suffer. In general, the hardness of an electrodeposited metal is proportional to

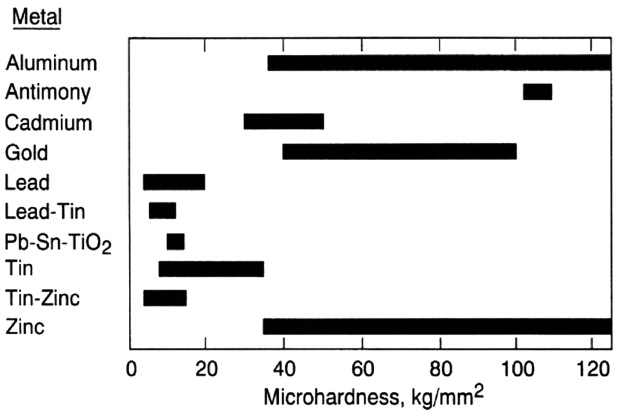

FIGURE 6.34 Microhardness ranges for relatively soft electrodeposited metals and alloys [128].

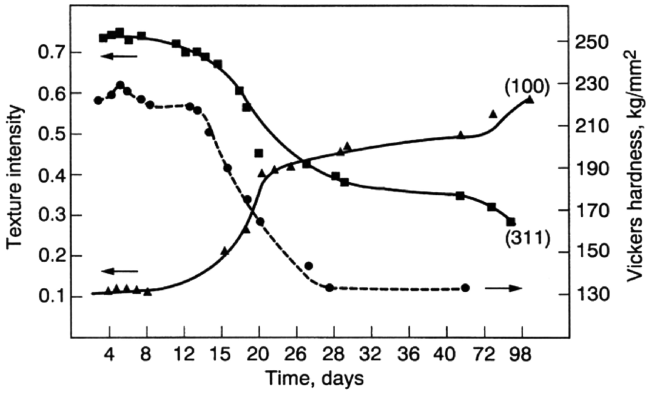

FIGURE 6.35 Relationship between texture and hardness of electrodeposited copper [129, p. 167].

the amount of organic content in the deposit. However, texture or preferred orientation of the crystal growth sometimes plays a more important role. It has been shown that, by changing the preferred orientation, which can be accomplished by manipulating the electroplating conditions, the hardness of a copper foil changed drastically [129] (Fig. 6.35). Therefore, it is possible for a deposit containing higher organics to have lower hardness value, depending on the texture. This phenomenon has been observed in laboratories working on bright tin–lead deposits [130].

6.4.7 Stress

Stress in tin became important when the electronics industry began to look to pure tin as a replacement for tin–lead. As it will be demonstrated clearly in the next section, compressive stress in the tin coating could contribute to eventual whisker growth in the coating or in the final product.

In general, the residue stress in a tin deposit is very low. Typically it is less than 10 MPa. This is because tin is a soft and giving material. Because of such low stress level, it is difficult to measure it precisely with conventional stress measurement techniques such as stress tab and X-ray diffraction.

Stress tab is a simple in situ stress measurement method which can yield fast, qualitative information regarding stress magnitude and direction. The simplest form of such measurement consists of two tabs. One is completely insolated on both sides so no plating can take place; the other tab is insulated on one side but conductive on the other side. Depending on which direction the tab is bending upon tin deposition with regard to the reference tab, one can tell whether the tin layer is compressive or tensile stressed. Depending on the distance it bends away from the reference tab, one can calculate roughly the stress value. This method is fast and simple, but it is not reliable when measuring stress in tin and tin alloy coatings because intrinsically it is so low.

The preferred way is to use X-ray diffraction. The tradeoff is that one cannot measure stress in situ. The stress measurement must be carried out after the plating is finished. In addition, special care would have to be taken in setting up the measurements and in the calculation. More detailed discussions can be found in the next section.

6.5 TIN WHISKERS

According to the second edition of the *American Heritage Dictionary*, the chemistry definition of a whisker is an extremely fine filamentary crystal that can be grown from supersaturated solutions of certain minerals and metals and that possesses extraordinary shear strength and unusual electrical and surface properties. Though tin whisker possesses some of the unique physical and materials characteristics, its growth phenomenon is entirely different from what was described above. In this section, we will specifically discuss *spontaneous* whisker growth from electroplated tin and tin alloy coatings. This growth process is a solid-state phenomenon.

In 1947, Hunsicker and Kenspf [21] first discovered tin whiskers at Aluminum Research Laboratories of Aluminum Co. of America when they were working on improving casting properties of aluminum alloys for engine-bearing applications. The following is the excerpt regarding tin whiskers from their original manuscript in *Transactions Quarterly* of the SAE:

> An unexplained phenomenon which occurs in the solid state has been observed repeatedly in aluminum alloys containing tin. Microscopic examination of metallographic samples a day or more after preparation of the *polished* surface has revealed thin metallic filaments extending outward from the prepared surface. These filaments appear much like minute extrusions with a thickness or diameter in the range of 1 to 4 microns and a length which varies with the time and temperature during their preparation.
>
> The filamentary material was found to be attached in all cases to a particle of tin-aluminum eutectic. However, it was observed that each small filament protrudes from only a portion of the area of an individual tin-rich particle, that more than one filament might be associated with a single particle, and that only a relatively small percentage of the tin-rich particles were so affected, at least in the early stages. The most remarkable example of this phenomenon is illustrated of an aluminum alloy-bearing insert containing 25% tin which had been stored at room temperature for four years subsequent to *machining*. A myriad of the filaments formed a deep pile projecting about 0.080 inch from the initial *machined* surfaces. A considerable quantity of this material was removed, and chemical and X-ray diffraction analyses revealed it to be principally elemental tetragonal β-tin. The specific cause of this phenomenon remains an enigma.

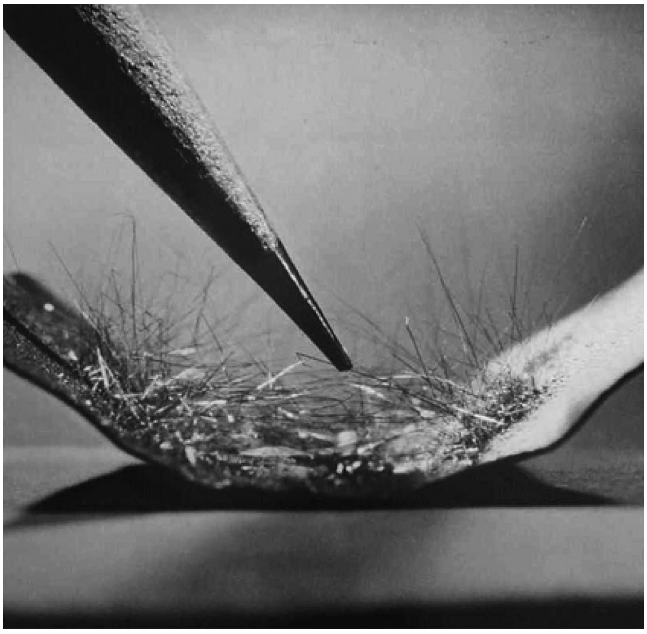

FIGURE 6.36 Filament tin whiskers observed on bright tin plated contact from faulty telephone. (Courtesy of AT&T Bell Labs Archives, photo taken in 1950).

This phenomenon did not receive much attention until 1952 when Herring and Galt [131] from Western Electric Bell Laboratories discovered that the mechanical strength of a tin whisker approached the theoretical value. Further interest in whisker arose when it was discovered that the spontaneous growth of tin whiskers in electronic equipment was causing short circuits and equipment failures [132–135]. Figure 6.36 shows the hairlike whiskers that were found on a *compressively bent* contact surface from a faulty telephone [131]. The risk of electric shorts becomes a greater issue today as a result of continued miniaturization in electronic device sizes and dimensions (Fig. 6.37) [136]. Therefore, interest in tin whiskers has continued as their properties have been studied [137]. Figure 6.38 clearly reflects the increased activities in this regard. During the 1960s, studies by S. M. Arnold from Bell Laboratories led to the discovery that whisker growth could be substantially suppressed by small alloy additions to the finish [138]. As a result, a tin–lead solder finish has been adopted for use throughout the Bell System and much of the electronic industry. This was also reflected by the decline of research activities on tin whiskers throughout the 1980s and during early 1990s (Fig. 6.38).

6.5.1 Tin Whisker Definition

As mentioned earlier, the dictionary definition of whisker does not apply to the phenomenon described herein. As the name implies, tin whiskers are hairlike single crystalline structures of tin that grow outward from electroplated films.

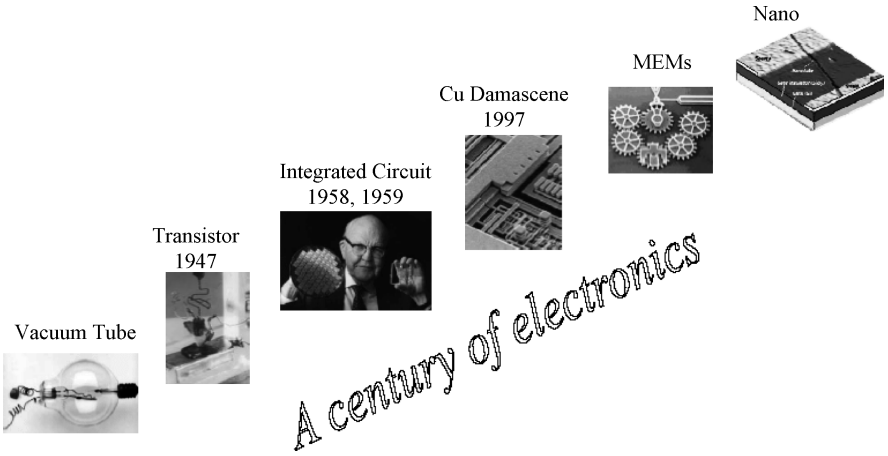

FIGURE 6.37 Technology breakthroughs during last century result in continued miniaturization. (From Y. Zhang, "Challenges and Opportunities in Advanced Packaging," invited talk, ECS Meeting, Cancun, Mexico, November 2006.)

This definition of whisker, or a slight variation of it, has been utilized since its discovery. As we shall see later, this definition is too narrow.

Before we introduce the new definition of whisker, it helps to rule out the cases that are not tin whiskers. These include tin dendrites, tin needles, and tin pest.

Tin Dendrites Tin dendrites are tin crystallizing in a branching or treelike manner. Figure 6.39 illustrates how tin dendrites look. Unlike tin whiskers, they are not single crystals but polycrystals. They form during, not after, electrodeposition. A few factors contribute to their formation, namely, lack of surfactant or wetting agent, improper metal concentration, and plating current density. When tin dendrites occur, they are usually the result of one or a combination of the aforementioned factors. The most significant factor is the surfactant concentrations. Tin dendrites can be eliminated readily by either adjusting surfactant and/or metal concentration and/or by adjusting the plating current density.

Tin Needles These plating defects can be easily confused with tin whiskers because they look like needles (Fig. 6.40). In the literature, whiskers are very often described as needles, which is incorrect. As its name implies, the needle is bigger at one end and has a sharp point at the other end whereas the single-crystal diameter of a tin whisker remains the same throughout its length. This criterion can be used as a rule of thumb to distinguish a tin whisker from a tin needle. Tin needles form during electrodeposition, not after. A few factors contribute to needle formation, namely, metal

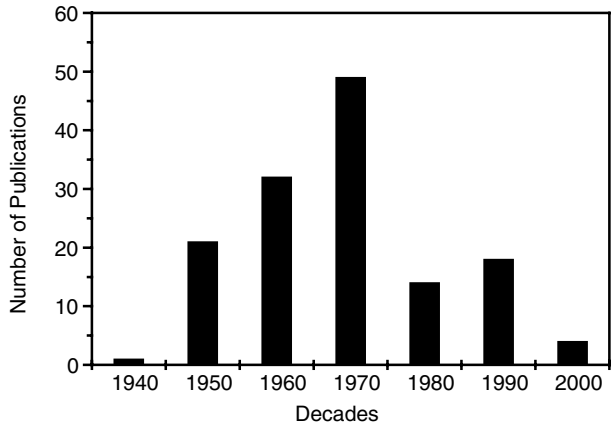

FIGURE 6.38 Number of publications on tin whiskers, 1947–2000. (From *Chemical Abstracts*.)

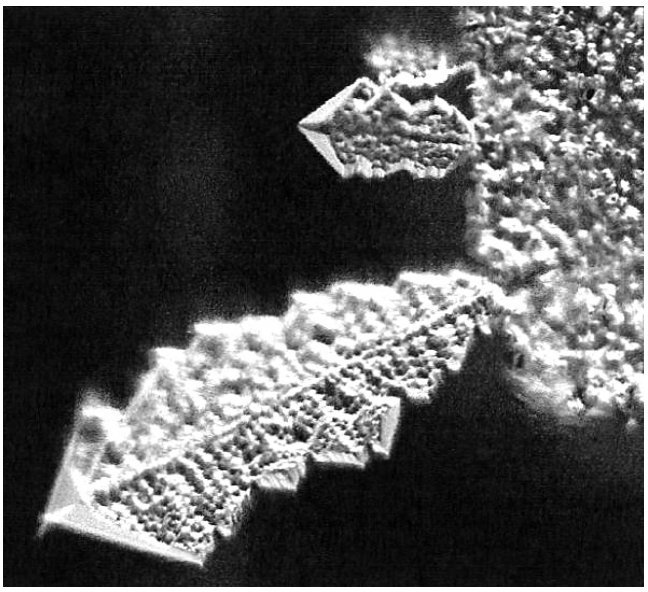

FIGURE 6.39 Tin dendrite resulting from high-current-density area (edge of leadframe).

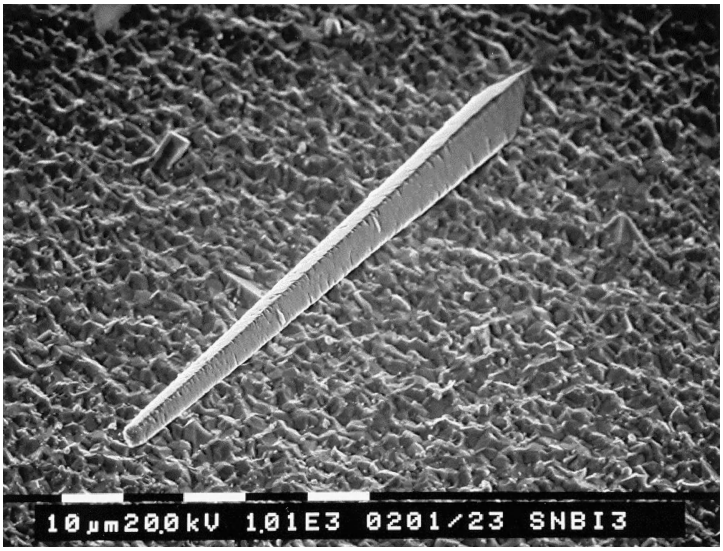

FIGURE 6.40 Picture of tin needle resulting from Bi contamination. (Photo courtesy of Pascal Oberndorff from Philips Semiconductors.)

impurities, inadequate grain refiner, and/or improper metal concentrations. As we explained earlier, if Bi content is higher than 4 wt %, elemental Bi will precipitate out in the form of a needle. Tin needles can be eliminated by removing the metal impurities and/or by adjusting the grain refiner and/or the metal concentration.

Figure 6.41 shows another example of tin needles. This needle resulted from improper substrate descaling process. During the plating process, tin plated over the protruding substrate and formed a tin needle.

Tin Pest There are two allotropic forms of tin: white (β) and gray (α). The gray tin is also known as tin pest. While white tin crystallizes in the body-centered tetragonal system, gray tin has a diamond lattice. It is considerably less dense than white tin and is nonmetallic in appearance and properties. It is a semiconductor. The allotropic transformation occurs at 13°C and is extremely slow. In fact, the existence of gray tin was not discovered until the mid-nineteenth century, when some tin organ pipes in Moscow were found to have disintegrated during an

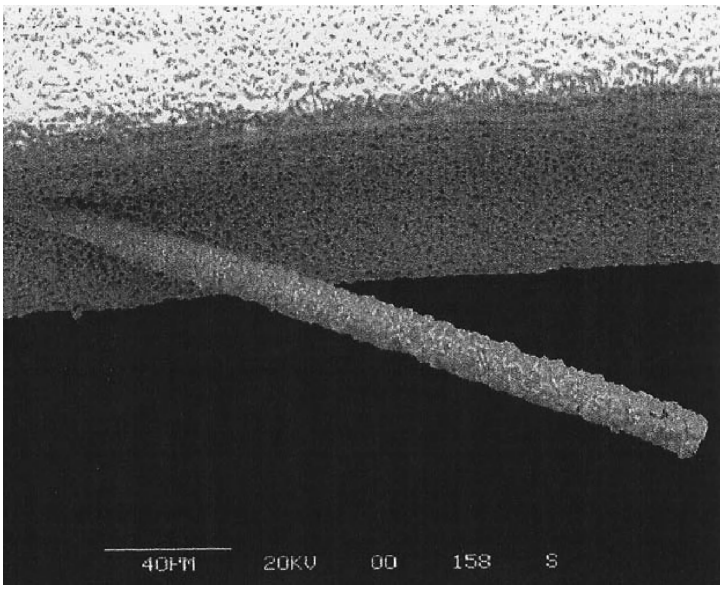

FIGURE 6.41 Substrate defect that looks like a needle resulting from improper pretreatment of substrate. During the subsequent tin plating process, tin plated over the protruding needle and formed a tin needle.

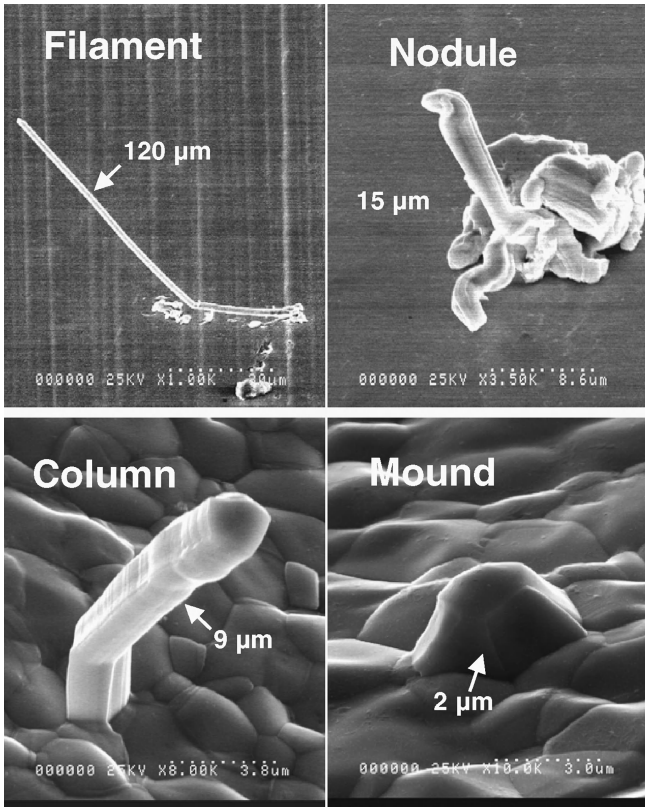

FIGURE 6.42 Different shapes of commonly observed whiskers.

exceptionally cold winter. This transformation is inhibited or prevented by incorporating a few tenths of a percent of antimony, lead, or bismuth into tin. Because tin pest can also be suppressed by addition of small amounts of other metals, it is sometimes mistaken as tin whiskers.

Tin Whiskers We are now ready for a definition of tin whiskers. Tin whiskers are tin and tin alloy materials that extrude from the electroplated thin tin films after plating when the compressive stress in the tin layer exceeds a certain threshold. They can exhibit different forms. Figure 6.42 illustrates four most commonly observed whiskers in the author's laboratories [139–150]. Type 1 is called a filament. It is mostly associated with the bright finishes. They can grow up to a few millimeters. Type 2 is called a nodule. It is also mostly associated with bright finishes, but normally appears as precursors to filament whiskers. The filament whiskers grow from or on top of nodular whiskers. The shape and size of nodular whiskers vary greatly. Type 3 is called a column whisker. It is mostly associated with matte finishes. Its diameter is normally between 2 and 4 μm, and the length varies from a few micrometers to hundreds of micrometers. From a practical prospective, filament and column whiskers can be considered the same; however, they do differ in shape and diameter and in the type of finishes from which they grow. The diameter of a column whisker is about the average grain size of a matte finish, whereas the diameter of a filament is about the average grain size of a bright finish, which is less than 0.4 μm. In addition, the column whisker sometimes is a multicrystal, whereas a filament whisker is a true single crystal. Type 4 is called a mound. It is mostly associated with satin bright finishes. Its diameter is slightly larger than the column whisker ($\sim$ 3–6 μm); its length normally is limited to $\sim$ 10 μm.

Unlike the tin dendrites and tin needles, tin whiskers form after plating. The incubation time varies from a few days to a few years. Deceivingly, whisker growth does not appear to require environmental stimuli; therefore, it is often referred to as *spontaneous* whisker growth. As we shall discuss in Section 6.5.3, environmental stimuli are always there; it is a matter of whether we recognize them or not.

As one can clearly see in Figure 6.42, the filament whisker is only one of four types of tin whiskers, which is why the old definition is too narrow.

6.5.2 Tin Whisker Properties

Chemical Composition It has been the assumption since its discovery that tin whiskers consist of pure tin because they originate from a pure tin layer. Today, we know that some whiskers consist of 100% tin while others show various amounts of copper, zinc, and oxygen, though they all grow from electroplated pure tin coatings [142, 151]. Figure 6.43 displays two cases. The filament whisker in Figure 6.43*b* was observed on a bright tin coating; a focused ion beam (FIB) cross section and Auger elemental mapping showed that it consisted of 100% tin. The column whisker in Figure 6.43*a* was observed on a matte tin finish. As shown by the Auger elemental mapping, it consisted of a tin–copper alloy. Given the current understanding of whisker growth mechanisms, it is not surprising that the chemical composition of a tin whisker may not be 100% tin. Pure tin whiskers have the crystallographic structure of white (β) tin.

Physical Appearance, Shapes, and Sizes We have shown the physical shapes of four types of whiskers in Figure 6.42. As one can surmise, the most detrimental types are the filament and column whiskers. Even though their diameters hardly exceed 4 μm, their lengths can reach a few millimeters. The next most dangerous type is the nodule whisker, especially when its base or "diameter" extends tens of micrometers across the surface. The mound-type whiskers do not represent any real concerns regarding bridging because they do not grow to tens of micrometers. Their maximum length is typically less than 10 μm. In modern microelectronics applications, the column whiskers are the most common. Of these four types, filaments, columns, and mounds are single crystals whereas nodules are typically polycrystals.

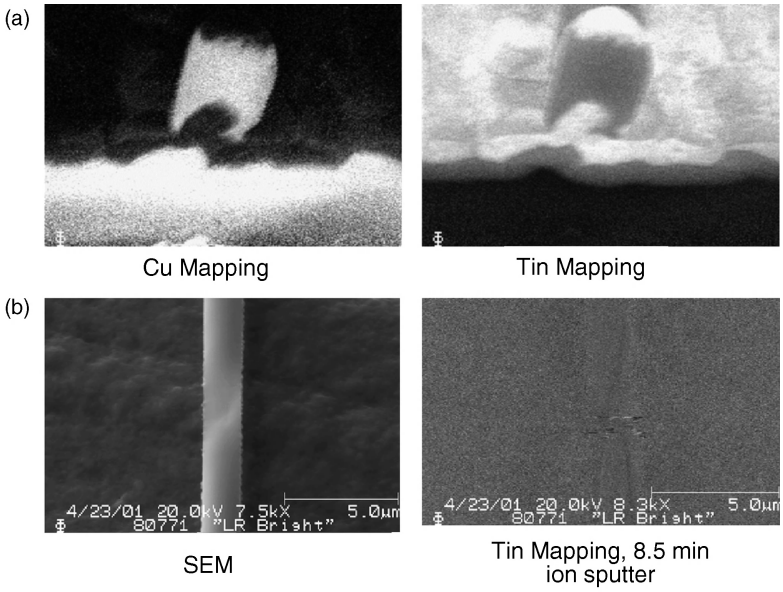

FIGURE 6.43 Chemical composition of whiskers: (a) column whisker that contains significant amount of copper; (b) filament whisker that contains 100% pure tin.

Close examination of filament, column, and mound whiskers reveal that they are striated (grooved) along lines parallel to their growth direction giving the appearance of having been "extruded." Though nodule whiskers can also exhibit striations along their growth directions, their diameters are much less regular. It ranges from a few micrometers to 100 μm. These nodule whiskers sometimes are called "flowers" [152] and "Hershey kiss eruptions" by some investigators [153].

With the advent of FIB technology, it becomes possible to make cross sections of tin whiskers. It has been confirmed by numerous researchers that whiskers are solid, not hollow [142, 151, 154–157]. It is important to point out here that FIB cross sections of tin whiskers reveal that whiskers originate from inside the tin coatings, not at the tin surface, as suggested in reference [158].

Physical Properties The physical properties of tin whiskers depend on their microstructures. As mentioned earlier, tin whiskers can be polycrystals as well as single crystals. The physical properties of polycrystalline tin whiskers are the same as those of polycrystalline white tin whereas those of single-crystal whiskers are rather distinct and different.

Single-crystal tin whiskers are 1000 times stronger than ordinary tin single crystals and this strength is approaching the theoretical value. This discovery helped to resolve a problem that has confounded researchers for almost half a century: the discrepancy between the actual and the theoretical strength of solids. Most solids exhibit only a fraction of their ideal strength. This is because their single crystals are never perfect. They possess crystal defects such as dislocations, vacancies, and so on. Crystals of copper, tin, and aluminum deform at stresses 100–1000 times less than those suggested by theory. The large and apparently unbridgeable gap between the real and the ideal seemed to indicate that the theoretical strengths were too high. Investigators began to ask whether the theoretical estimates might be wrong. The answer, provided by the whiskers of tin, was definitely no. The small dimensions of these whiskers apparently allow little room for the defects that weaken larger crystals, and their strength closely approximates the prediction of theory. The growing of tin whiskers and the study of the process by which these nearly ideal crystals grow have led to a deeper understanding of the relationship between crystal structure and many of the gross properties of solids, including their magnetic and mechanical behavior.

In addition to their strength, these tiny whiskers also exhibit exceptional electric properties. The current-carrying capacity of a tin whisker at a given baseplate temperature approaches its maximum value as whisker approaches its melting point. Assuming cooling along the length of the whisker by conduction only, this relationship has been shown to be [159]:

$$I_{\text{melt}} = 0.076 \times \frac{A}{L}\ \text{mA}$$

where A is the cross-sectional area of the whisker in micrometers squared and L is the whisker length in centimeters. For a whisker whose diameter is 2.8 μm and length is 0.8 mm, this value is 5.85 mA. The actual measured capacity of a whisker with these dimensions was 22 mA [160]. The discrepancy between the predicted and actual value is due to idealization in the predictor equation and the fact that area measurements of whiskers are complicated by their fluted cross sections.

Based upon their cross-sectional area and length, whiskers which create short circuits fall into three categories: those which sustain current flow indefinitely, those which burn out within seconds or microseconds, and those which burn out instantly. A statistically significant, empirical mapping between whisker dimensions and these three categories does not exist; however, hard failures due to shorting tend to occur in high-impedance, low-current applications, while transient failures tend to occur in medium-power circuits drawing between 1 and 60 mA of current [161]. At ambient pressures of 0.5 torr and below, electric fields around the sharp tip of a whisker can accelerate electrons in the surrounding gas, resulting in a discharge capable of melting the whisker tip. When this blunt whisker makes contact with an opposing surface, a transient conducting path with a current-carrying capacity of several hundred amperes may occur. This phenomenon has been termed *vacuum metal arcing*. Experiments have shown that vacuum metal arcs will not appear when there is less than 12 V of potential across the whisker, but they may appear when the potential exceeds 18 V. Current levels of 15 A and above have sustained vacuum metal arcs across 30 V [161]. The arcs persist until available tin has been consumed or until no additional current is available.

Though it was studied extensively during the 1960s and 1970s, it is not widely known that tin whiskers are also "one-dimensional" superconductors [162–164].

6.5.3 Whisker Growth Phenomenon: Key Factors Affecting Whisker Growth

Whisker growth is associated with many pure metals, including tin, cadmium, zinc, antimony, and indium, and less frequently with lead, iron, silver, gold, nickel, and palladium. It is a phenomenon most known to electroplated coatings, but it also occurs with thin tin coatings ($<1\,\mu m$) resulting from electroless processes. In this section, we will concentrate on the whisker growth phenomenon from electrodeposited tin coatings.

While there is general agreement on the attributes of whiskers, especially tin whiskers, considerable controversy exists concerning the conditions and reasons for growth. Indeed, much conflicting evidence has been reported in the last 30 years [159]. Controversy stems from the fact that the precise cause of whisker growth is not understood; consequently, potentially crucial variables have not been controlled during experimentation [165]. Aggravating the situation is the fact that spontaneous whisker growth has occurred as late as 20 years after the plating operation was performed, forcing meaningful experiments to span for decades.

Though the mechanisms by which whisker grows are not well understood, some key factors that influence the whisker growth have been identified and confirmed over the last 50 years. There still exist some inconsistencies among the reported body of work. However, owing to an emerging consensus of a standard whisker test method, there is less debate on some of the key issues. In this section, a detailed account of various factors that contribute to whisker growth will be presented and attempts will be made in terms of ranking their relative importance.

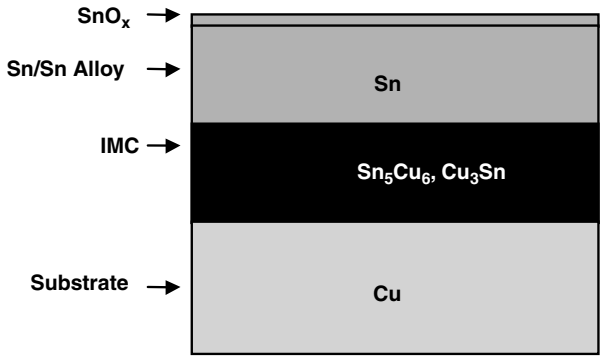

FIGURE 6.44 Schematic diagram of relationships among various factors that are key to whisker formation. These factors include surface oxide layer, tin layer, intermetallic layer, and substrate layer.

Before we introduce the various factors, it is important to give the reader an overview of what these factors are, their relationships in real physical space, and their interactions as chemical and metallurgical reactions and the consequences of these interactions.

Figure 6.44 schematically displays the relationships of these factors, which include, from top to the bottom, *surface oxide layer*, *tin layer, intermetallic compound layer*, and *substrate layer*. Each of these factors influences whisker formation from the tin layer, as will become evident later.

Surface Oxide Layer Owing to the affinity of tin toward oxygen, a thin film of surface oxide layer forms immediately after electrodeposition. Since the free energies of formation for the various Sn(II) and Sn(IV) oxide/hydroxide species are very close in value (e.g., $-515.0\,kJ\,mol^{-1}$ for SnO vs. $-515.8\,kJ\,mol^{-1}$ for SnO_2), the surface oxide formed is likely a mixture. The ratio of the two types is governed primarily by kinetics. Applying low-energy electron loss spectroscopy (LEELS), Bevolo et al. [166] showed that the oxide formed on both polycrystalline and single-crystal tin from room temperature to nearly the melting temperature is continuous after one monolayer of coverage and is sharply enriched in SnO_2 at the outer surface. For tin exposed to an ambient environment, the same group found that the outer surface was completely covered with the SnO_2 layer.

The amount of oxide formed on tin has generally been found to increase with the square root of time [167, 168] or logarithm of time [167, 169]. The activation energy would be expected to depend on the type of tin finish and its surface morphology, the oxidizing atmosphere, and the temperature

range. A systematic study of these factors has yet to be performed.

From an understanding of its role in whisker formation, we know that surface oxidation under ambient conditions is of primary concern because most of the electroplated components will be stored under ambient conditions before final assembly. In their work, Britton and Bright [169] applied coulometric electrochemical reduction to show that oxides formed on tin and tin plates at room temperature for periods of up to 5 years are generally less than 5 nm (50 Å) thick. They observed that about 1.5 nm of oxide forms within a few minutes and grows rapidly to about 2 nm within a week and then much more slowly to a maximum thickness of 7 nm after as long as 20 years. Britton and Bright also found that the oxides on tin grow 50% thicker when the relative humidity is very high (80%).

It has been proposed that the surface oxide layer is a necessary condition for whisker formation [170]. In addition, it is beneficial for whisker reduction because it acts as a physical barrier to prevent whiskers from protruding through. In this regard, theoretically, if a perfect surface oxide layer exists, there would be no whisker formation. In reality, the surface oxide layer is never perfect. There will always be defects such as pores and pinholes and surface corrosion products. These defect sites serve as the "weakest link" for whisker formation.

To summarize, after plating, a continuous thin film of tin oxide on the order of a few nanometers forms. The chemical composition of the outer layer is mostly SnO_2. With increased temperature and humidity, a thicker oxide layer forms. These results support the observation; that is, while everything else is the same, the whisker growth propensity is higher at room temperature than at room temperature but with high humidity.

Tin Layer The tin layer is the focal point in this section. As plated, the tin electrodeposits can have the appearance of bright, satin bright, and matte. The atomic force microscopy (AFM) images in Figure 6.45 illustrate how they look three dimensionally. As shown, the bright deposit is much smoother compared with the matte and satin bright finishes. This point is further illustrated in Figure 6.46, a plot of gloss reflectance measured at 60° versus surface roughness (via AFM). Of particular interest in the AFM view is the distinct presence of the well-polygonized and relatively smooth surface of the satin bright finish. Another way to describe the different types of finishes is to look at grain size, shape, and codeposited carbon. Table 6.14 summarizes typical grain sizes and carbon contents of various tin deposits.

As expected the bright finish has the smallest grain size and highest carbon content, whereas it is not apparent that a satin bright finish would have the largest grain size and lowest carbon content.

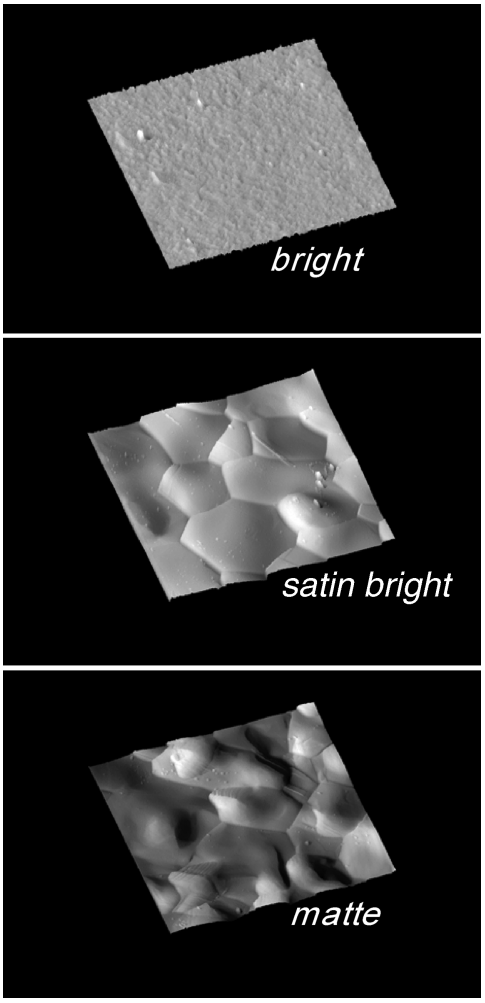

FIGURE 6.45 AFM Images of (*a*) bright, (*b*) satin bright, and (*c*) matte tin deposit.

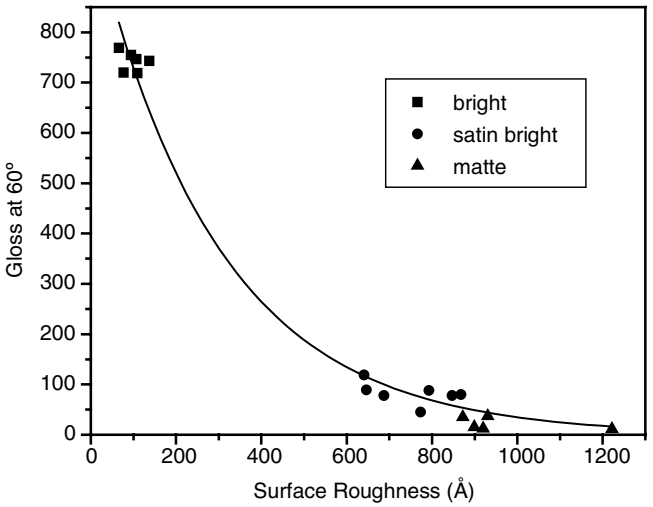

FIGURE 6.46 Gloss reflectance measured at 60° versus surface roughness.

TABLE 6.14 Material Properties of Electroplated Tin Deposits

Finish	Grain Size, μm	Carbon Content, wt %
Bright	<0.2	0.2
Satin bright	~8	0.004
Matte	~2–8	0.01

Later the whisker growth behavior observed on these different finishes will be discussed in detail. Here, let us examine what makes a deposit bright or matte and what chemical and process parameters determine their corresponding material properties (e.g., grain size and carbon content) in relation to whisker growth behavior.

In a typical electroplating bath for tin and tin alloys, besides a basic electrolyte, a metal salt, organic compounds such as surfactants, grain refiners, and brighterners are intentionally added. As their names imply, surfactants are organic molecules that serve to clean and wet the substrate surface before plating. In addition, because of the specific adsorption of these normally large molecules on the surface, they significantly "block" the high-energy surface sites, thus slowing down the electrodeposition (or electroreduction) process. Their presence in adequate amounts dictates that dendritic growth does not take place. Grain refiners are classes of organic molecules that make a deposited metal surface more uniform and smooth. They are normally smaller molecules than surfactants and often have aromatic moieties as part of the molecule. They are also called levelers. The balance of its strength with the surfactants in a plating bath is critical. Otherwise, their effects will not be fully realized and a rough deposit or a deposit with small needles will result. Without exception only surfactants and grain refiners are required to produce the matte or the satin bright finish. In order to obtain a bright finish, a brightener is employed. As its name implies, a brightener is an organic molecule that makes the deposit bright. Brighteners are small organic molecules that usually have aromatic rings in addition to other electron-rich functional groups such as a C=C or C=O bond.

Nobody knows exactly how these organic molecules work on a molecular level. However, empirical experience tells us that these organic molecules have a drastic impact on electrodeposition mechanisms. To understand this, it is useful to review the existing theories on electrodeposition mechanism. Figure 6.47 illustrates three most popular models: three-dimensional (3D) island growth, 3D island growth on top of predeposited monolayers, and 2D layer-by-layer growth. Obviously, the 2D layer-by-layer growth is the most desirable.

As is clearly depicted in Figure 6.47*a*, when the interaction between the metal and the substrate is much weaker than the metal-and-metal interaction, 3D island growth becomes the dominant mechanism.

Three-dimensional island growth is usually a result of not employing surfactants or inadequate amounts of surfactants.

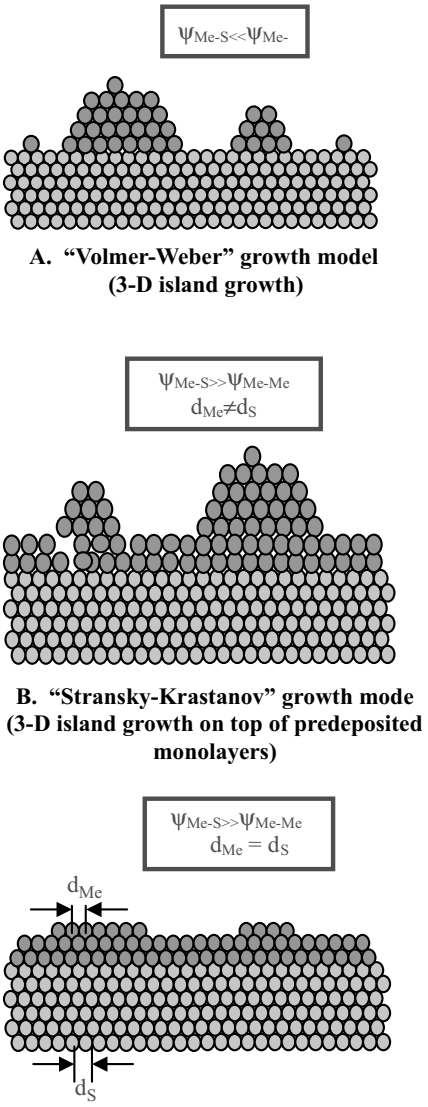

FIGURE 6.47 Model of growth mechanisms.

It is believed that nucleation initiates from defect sites such as steps and kinks, and the nuclei grow in such a rapid rate that "islands" will form, as illustrated by model 1. In practical electroplating terms, dendritic growth described previously will result from such a plating bath. The deposited layer is nonadhesive and coarse due to the weak metal–substrate interaction and therefore renders it useless in practice. Accompanying the dendrites, a portion of the surface may be exposed in severe cases, as suggested in the 3D island growth model.

To improve the deposit quality, surfactants are added in the plating bath. It significantly slows down the electrodeposition rate, as suggested by Figure 6.47*b*. It is believed that surfactants preferentially adsorb on the defect sites such as atomic steps and kinks of the substrates, and they force metal

ions to discharge in the atomic planes rather than steps and kinks. Since atomic planes constitute the majority of the substrate surface, there will be more nucleation sites and the initial growth will be much slower. This scenario fits model 2, which is the 3D island growth on top of the predeposited monolayers. In this case, there is a much stronger interaction between the metal and the substrate, resulting in an adhesive layer. Also inferred in model 2 is that the first few monolayers of growth are epitaxial; that is, the deposited metal lattice matches that of the substrate. However, because of the atomic size difference between the deposited metal and the substrate, as the layer builds up, the grain size of the deposited metal increases. As a result, the surface of the finish is still relatively rough.

The deposits that result from model 2 are not suitable for microelectronics applications. To improve surface smoothness, grain refiners are added in the plating bath. When properly instituted, grain refiners can impart a much smoother surface due to overall grain size reduction. However, this level of smoothness may still not be satisfactory for some customers who prefer a mirror-bright surface because it is cosmetically more pleasing. To obtain such optical property, it is necessary to have grain sizes that are significantly smaller than the wavelengths of visible light (0.4–0.7 μm), so that light is not scattered or absorbed but is reflected from the plated surface.

As we have shown previously, the grain size can be further reduced by introducing a brightener. The ideal case when carrying out this action is to obtain a completely smooth surface, illustrated by the 2D layer-by-layer growth model (Fig. 6.47*c*). In this case, in addition to a strong interaction between the metal and the substrate, the grain size of the deposited metal is similar to that of the substrate. Furthermore, the kinetics is so slow due to the strong inhibition of the brightener that the nuclei grow preferentially laminar rather than columnar.

Though these models are invaluable in helping formulators and electrochemists to understand electrodeposition at an empirical level, there is a need to obtain a molecular-level understanding on how these additives work. This is especially true when we attempt to successfully electroplate tin–copper, tin–bismuth, and tin–silver alloys. While at Lucent Technologies EC&S, the author and her team made the first attempt toward the molecular-level understanding of how these organic molecules work using a commercial pure tin electroplating chemistry [26, 60, 74]. We studied the chemical nature of adsorbed species by in situ surface-enhanced Raman spectroscopy (in situ SERS). In SERS experiments, only the Raman bands associated with functional groups that adsorb on the surface are enhanced. We attempted to answer the following questions: How does an organic additive adsorb on the substrate surface? What is its adsorption strength and orientation? What part of the molecule, that is, the functional group, is in contact with the substrate surface? Is there a difference in adsorption before and during electrodeposition? How does this impact (1) the initial stage of the grain growth, (2) subsequent layer buildup, and (3) materials properties of the finished layer? Is there a quantitative difference in adsorption strength among surfactant, grain refiner, and brightener? The growth mechanism was studied by in situ scanning tunneling microscopy (STM). We attempted to find answers for the following questions: Where does the nucleation originate—steps and kinks or atomic planes? How do the various organic molecules (surfactant, grain refiner, and brightener) affect the initial nucleation and subsequent growth? How do the grain refiner and brightener work at a molecular level?

Description of these experiments and results were given elsewhere [26]. A concise summary will be provided here to demonstrate the importance of why plating bath maintenance and proper plating parameters are important in whisker reduction and prevention and, most importantly, why matte or satin bright tin is preferred over bright tin.

In tin and tin/lead plating, the most commonly used surfactants are polyethylene glycols with different numbers of ethylene oxide (EO) groups. Sometimes other surfactants are also used. In this work the surfactant Triton X-100, shown in Figure 6.48, was used. It not only has ethylene oxide, which is hydrophilic, but also contains a substituted benzene ring, which is hydrophobic. Using surface-enhanced Raman spectroscopy, we found that at open-circuit potential (OCP) and potential equivalent to low current densities (0.2 V vs. Ag/AgCl), no Raman shift of the EO groups could be detected, suggesting that the EO groups are tilted away from the substrate surface. From the Raman spectra, it was deduced that the benzene ring and the alkyl group are in direct contact with the substrate surface. At −0.5 V, equivalent to >10 ASD in current density, the Raman bands of both the substituted benzene ring and the EO groups could be discerned. Based on these observations, the model shown in Figure 6.49 was proposed. The direct consequence of the specific adsorption of the organic molecules on the electrode is increase of the surface resistance, which can be measured by the double-layer capacitance. The surface resistance increase results in reduced current density at the same applied potential. This is further illustrated by Figure 6.50. As can be surmised, the surfactant adsorption is beneficial in reducing the electrodeposition rate, resulting in a smooth surface 5 s into the deposition—Figure 6.51*b* (with surfactant) compared with Figure 6.51*a* (without surfactant). The latter develops into dendrites if longer plating time is permitted.

However, the surface obtained from this system, when it is sufficiently thick (>3 μm), is not smooth. This is because as the layer grows, the grain size of the tin deposit grows as well. This is illustrated in Table 6.15. Results obtained from two surfactant systems are tabulated.

As one can see, the deposit grain size grows into the micrometer range during the first 20 s. To further refine the

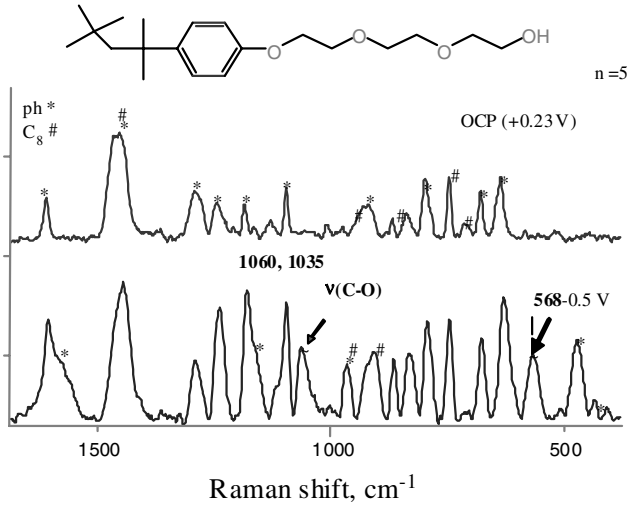

FIGURE 6.48 Raman spectra of Triton X-100 in tin plating bath obtained at various potentials. The molecular structure of Triton X-100 is shown on top.

surface, we introduced a grain refiner, phenolphthalein, into the system. In the surface-enhanced Raman spectroscopic experiments, we found that most of the bands associated with Triton X-100 decreased in intensity and bands assignable to phenolphthalein became relatively much stronger, indicating that there is a competitive adsorption between Triton X-100 and phenolphthalein. The latter adsorbs stronger than the former. Of most importance are the bands associated with the two phenol groups from phenolphthalein. We observed them at OCP and –0.5 V. The suggested adsorption mode of phenolphthalein shown in Figure 6.52 agrees with the Raman data.

It is important to point out that phenolphthalein is not soluble in water, and it does not adsorb on the surface by itself. Most likely it is "wrapped" in micelles of Triton X-100, which serves as a "carrier." The surface obtained in the presence of both Triton X-100 and phenolphthalein is much smoother than with Triton X-100 alone, and it has a satin bright appearance. Why? Exactly how does the grain refiner work? And how is it different from the surfactant? In situ STM studies illustrated that the difference lies in the first few seconds during the deposition. As shown in Figure 6.53, instead of forming small (~ 0.15 μm), irregular grains, as in the case of surfactant alone, in the presence of the grain refiner, the tin grains are regular (disclike) and relatively larger (~ 0.5 μm) at the very beginning. Most important, these grains appear to be very flat, and disc size remains unchanged during the first 10 s. This behavior is very different from that of the surfactant. As pointed out previously, with Triton X-100 alone, grains grow significantly larger in the first 5–10 s.

The significance of this finding is the following: The grain refiners regulate the size of the grains from the beginning to

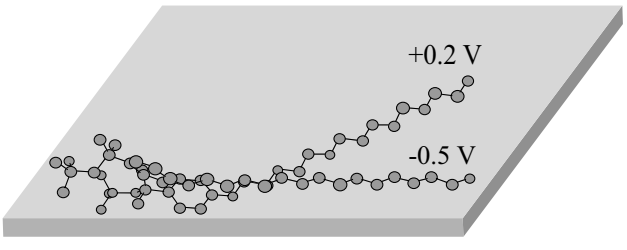

FIGURE 6.49 Model describing adsorption behavior of Triton X-100 at various potentials. Larger dots are carbon atoms, smaller dots are oxygen atoms.

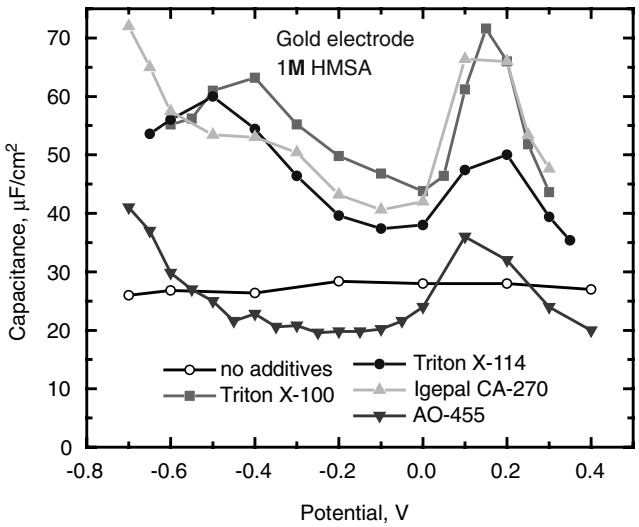

FIGURE 6.50 Impedance measurements of Triton X-100 among other surfactants.

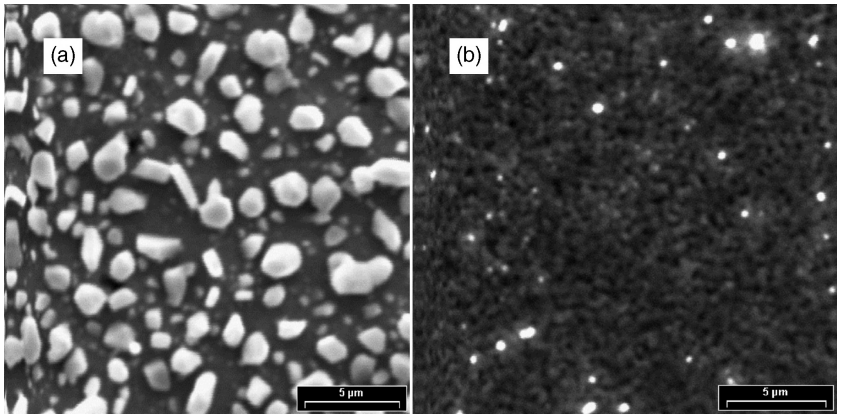

FIGURE 6.51 Surface morphology of electrodeposited thin films of tin obtained 5 s after onset of electrodeposition: (*a*) without surfactant; (*b*) with surfactant Triton X-100.

the end of the deposition. Since the grains are flat discs, when they grow layer by layer, it results in a smooth surface. The 0.5-μm grain size dictates that it is not bright. It is reasonable to speculate that the brightener behaves the same way except that the grain size is smaller ($\leq$0.4 μm).

TABLE 6.15 Grain Growth and Roughness of Tin Electrodeposits as Function of Time: First 40 s

Time, s	Polyethylene Glycol		Triton X-100	
	Grain Size, μm	Roughness, μm	Grain Size, μm	Roughness, μm
5	0.5–1.1	0.1–0.2	0.1–0.2	0.01–0.02
20	0.75–1.5	0.2–0.4	1.0–1.5	0.1–0.2
40	1.2–2.0	0.3–0.6	2.0–7.5	0.3–0.6

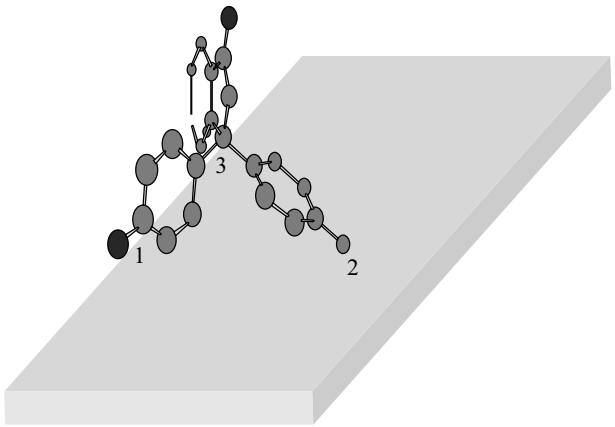

FIGURE 6.52 Model simulating adsorption behavior of grain refiner, phenolphthalein, on substrate surface at different potentials. Atoms marked 1 and 2 are oxygen. This model agrees well with the in situ SERS data.

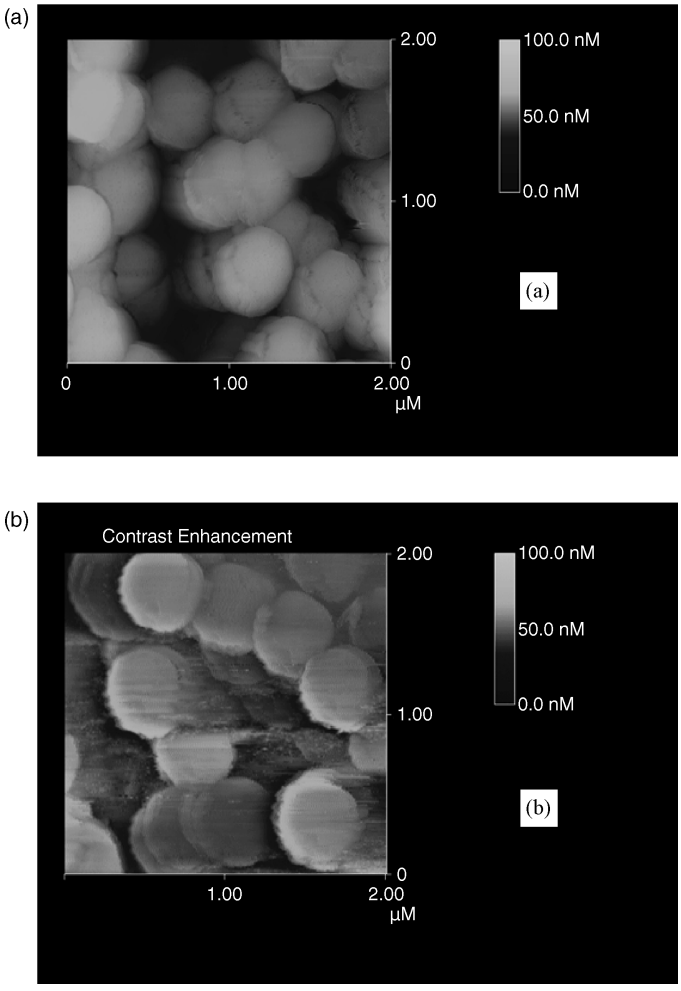

FIGURE 6.53 Scanning tunneling microscopic images of grain size of tin in presence of both Triton X-100 and phenolphthalein: (*a*) after 5 s; (*b*) after 20 s.

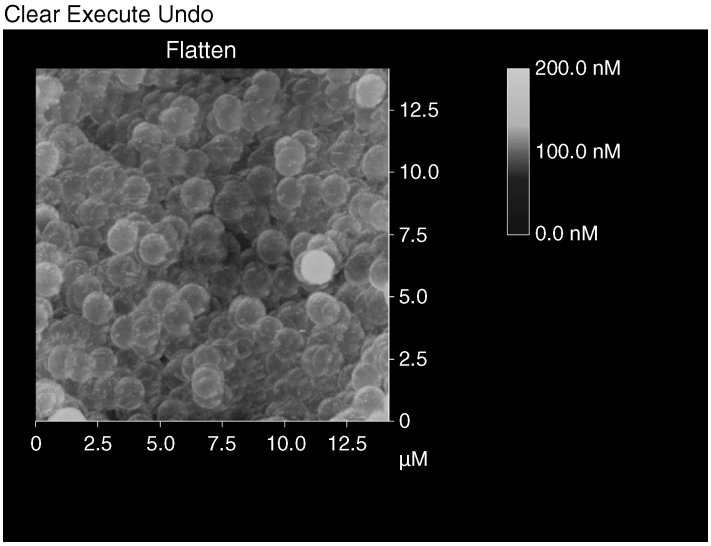

FIGURE 6.54 Scanning tunneling microscopic image of grain size of tin in presence of polyethylene glycol and cinimonaldehyde.

We introduced a known commercial brightener, cinimonaldehyde, in the tin bath. Preliminary results shown in Figure 6.54 suggest that the aforementioned hypothesis holds true. However, since a different surfactant was utilized in this experiment, we cannot compare directly the results between the grain refiner, phenolphthalein, and the brightener, cinimonaldehyde. It is important to point out that the Raman intensity of cinimonaldehyde is about a magnitude higher than that of phenolphthalein, confirming the common belief that brighteners adsorb strongly on the substrate.

Another aspect of brighteners warrants a brief discussion. The brightener molecule is much smaller than both the surfactant and the grain refiner. Combined with much stronger adsorption, it can be trapped in the "gaps" among large molecules. As a result, it is codeposited with tin, resulting in high organic content in the tin coating. Without exception, bright finishes contain much higher included carbon ($\sim$ 0.05–0.4 wt %) when compared with matte and satin bright finishes ($\sim$ 0.001–0.05 wt %).

Grain Size and Shape and Carbon Content Based on the discussion above, plating chemistries utilizing different organic molecules result in deposit with different appearances and properties. They can be bright, matte, or satin bright. Microscopically, there is a difference in included carbon, grain size, and grain shapes. Bright finishes have grain sizes ranging from 0.05 to 0.25 μm. The satin bright and the matte finishes, on the other hand, have grain sizes ranging from submicrometers to several micrometers. Conventional wisdom predicts that a matte finish would have a larger grain size than a satin bright finish. We found that this is not the case. As shown in Figure 6.55, the matte finish has smaller grain sizes than the satin bright finish.

Nonetheless, how do these finishes differ with regard to whisker formation? In a systematic study utilizing these three finishes, we found a direct correlation between whisker growth propensity and deposit grain size and shape and carbon content. Specifically, the bright finish showed the worst growth behavior, as expected; the matte finish

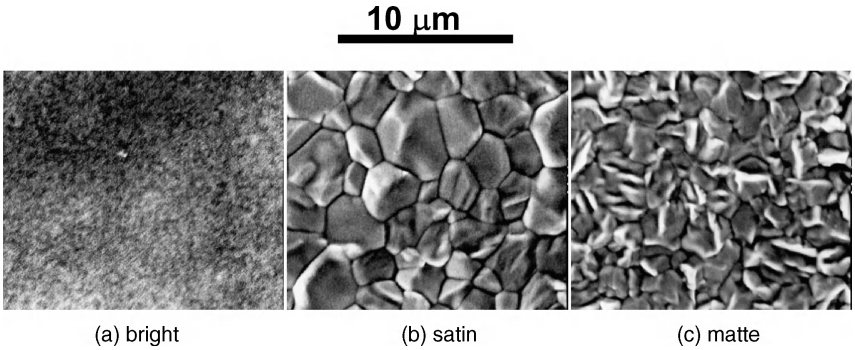

FIGURE 6.55 SEM photos of three different finishes: (*a*) bright, (*b*) satin bright, and (*c*) matte. Note that the grain size of satin bright is larger than that of matte.

showed better growth; and the satin bright finish performed the best [141].

It is important to point out that in this study an oxygen-free annealed copper substrate was utilized to minimize the substrate effect so the observations made with regard to whisker growth pertain mainly to the differences in the deposit properties and subsequent interfacial reactions.

In addition to the grain size and shape and codeposited carbon, the crystallographic orientation of the tin deposits has been observed as an important factor.

Crystallographic Orientation To date, the most studied whiskers by X-ray diffraction are the filaments. Crystallographic investigations have indicated that the growth direction of the filament whiskers are of the low-index faces such as ⟨111⟩, ⟨101⟩, and ⟨100⟩ [171–174], and the growth direction of the whiskers is different from the preferred orientation of the tin deposit. Though much work needs to be carried out to systematically investigate the relationship between preferred orientations of tin deposit and whisker growth direction, it has been generally observed that tin coatings with a strong preferred orientation of ⟨220⟩ have a reduced whisker propensity [175, 176].

Fundamentally, it is of great interest to understand what affects the preferred orientations of the tin deposits. Is it current density, the nature of the organic additives, the substrate, or a combination of all of these?

It suffices to say that substrate material and its stress and orientation all influence the stress and orientation of the tin layer. In addition, the pretreatment process plays a significant role in determining the stress and orientation of the tin deposits. Current density has been shown to influence not only the preferred orientation but also the stress of the tin layer. We can speculate that the nature of the organic additives also plays a role.

Plating Bath Conditions and Range Plating chemistry plays a very important role in whisker growth propensity. In general, bright chemistries are prohibited in electronics applications because bright finishes have higher whisker growth propensity compared with matte finishes. Many large semiconductor manufacturers have chosen matte tin in their microelectronics application. Most notable among them is the E4 group, a partnership formed by Infineon, Freescale, ST Microelectronics, and Philips.

In a matte tin plating bath, besides tin salts, there are surfactants and grain refiners. As was described earlier, it is important that these components be within the working range, often referred by chemical suppliers as operating window. For instance, if surfactant concentration is too low in the bath, one may experience dendrite growth. If grain refiner concentration is too low, the plated surface may be too rough. This may lead to more than normal surface oxide formation, which may be beneficial in reducing the whisker propensity but may be less desirable for long-term solderability. On the other hand, if the grain refiner concentration becomes too high, one may experience the formation of tin needles, which can be easily confused with tin whiskers.

In addition, it has been reported introducing impurities such as copper and iron into the plating bath, that significantly increases whisker growth propensity [153, 156]. Therefore, care needs to be taken to not introduce impurities such as copper, nickel, iron, and lead into the plating bath. If these elements are present in the pure tin bath and are in the amount in excess of 50 ppm, corrective action such as dummy plating should be taken to remove them before plating.

Plating Parameters Plating parameters refer to all the factors which complete the task of plating other than bath components. They include parameters such as current density, solution agitation, parts movements, bath temperature, and cell voltage. It has been shown that when tin deposition was carried out outside of the limiting current density where hydrogen evolution occurs, whisker growth propensity is greatly increased. It has been speculated that the included hydrogen caused high internal stress in the deposit and is responsible for the increased whisker propensity. In addition, varying current density could also result in deposit microstructure (i.e., grain size, shape, and texture or preferred orientation) changes, which as we have shown earlier has direct implications with regard to whisker formation.

It is important to note that plating chemistries supplied by various chemical suppliers may differ significantly in terms of the window of operation. Sometimes the term *robustness* is used to refer to a chemistry that is not sensitive to typical plating parameter fluctuations.

Intermetallic Compound Layer The word interface refers to a surface that forms a common boundary between adjacent regions. In this case, we are referring to the interface between the tin layer and the substrate. This interface forms as a result of interfacial diffusion due to the difference in chemical energy between the two metals [177]. There are two main pathways for interfacial diffusion: diffusion through bulk and diffusion through grain boundaries. The diffusion process takes place in both directions. It has been established previously that predominantly copper diffused into tin for this diffusion couple. Tin diffusion into copper is minimal.

The interfacial diffusion between tin and copper happens readily at normal soldering temperature, resulting in a duplex Cu–Sn intermetallic layer, comprised of Cu_6Sn_5 (η-phase) in contact with tin and Cu_3Sn (ε-phase) in contact with copper substrate. After a rapid initial reaction, the thickness increases as the square root of time at a given temperature [178–180]. Cu_6Sn_5 forms first [180, 181] and the copper-rich Cu_3Sn phase results from tin depletion at the reaction site. As tin is depleted, the copper rich phase, Cu_3Sn,

increases in thickness at the expense of the Cu_6Sn_5 phase. This Cu_3Sn phase grows at a temperature above 80°C [182]. It has been reported that both tin and copper are mobile in the intermetallic phase.

Intermetallic growth rate increases exponentially with temperature [178, 180, 183]. The rate also depends on the microstructure of the substrate metal and whether the tin electrodeposit is bright, matte, or reflowed [180] At temperatures below 170°C, the growth rate is faster on hard copper than on soft copper substrate, and it is faster with a bright finish than a matte finish. As might be expected, the presence of steam has no effect on intermetallic growth rate [182]. This point is important when considering an accelerated whisker test method.

Although the tin–copper interface has been studied extensively, there is a lack of detailed understanding with regard to the following questions: (1) Does the interfacial diffusion take place faster at the grain boundaries or through the bulk? How does this phenomenon depend on the temperature? (2) What is (are) the morphology of the intermetallic phases? Does the morphology change with temperature? (3) Is there a grain growth accompanying the intermetallic layer thickness growth at normal annealing and soldering temperatures?

Recently Lee [184] and Tu [185] reported their investigation of the diffusion process between a copper substrate and an electroplated matte tin finish. At room temperature, Tu reported an irregular intermetallic layer of Cu_6Sn_5 between copper and tin. Similar observations were made in the author's laboratories [143, 148, 150] (Fig. 6.56). In addition, we found that at room temperature and 50°C the intermetallic compound (IMC) growth takes place predominantly at tin grain boundaries (Fig. 6.57). Direct stress measurements in the tin layer by X-ray diffraction immediately after plating and three months later showed zero stress and a compressive stress of $\sim$ 10 MPa, respectively. Apparently this stress increases during storage at these temperatures and is responsible for whisker growth a few months after plating.

At elevated temperatures, the growth behavior of the IMC is different. The growth mechanism appears to be taken over by bulk diffusion. Consequently, a relatively dense and regular intermetallic layer is formed (Fig. 6.58). Accompanying the IMC thickness increase, there is significant grain growth at these temperatures. Figure 6.59 shows the grain growth of Cu_6Sn_5 at 175°C at various time intervals. As one can see, the average grain size of Cu_6Sn_5 has grown to 1 and 4 μm after 5 and 60 min, respectively. Simultaneously the tin grains have grown to an average of 10 and 30 μm judging by the "residue" tin grain boundaries.

In addition, direct stress measurements on reflowed samples showed that a compressive stress of $\sim$ 7 MPa in the tin deposit measured before reflow was completely removed after reflow owing to grain growths (both Cu_6Sn_5 and Sn). Furthermore, these samples have been stress free 18 months after reflow, suggesting the dense and regular intermetallic layer formed during reflow process serves as a barrier to effectively stop the additional interfacial diffusion between tin and copper. The stress generation source has been essentially removed.

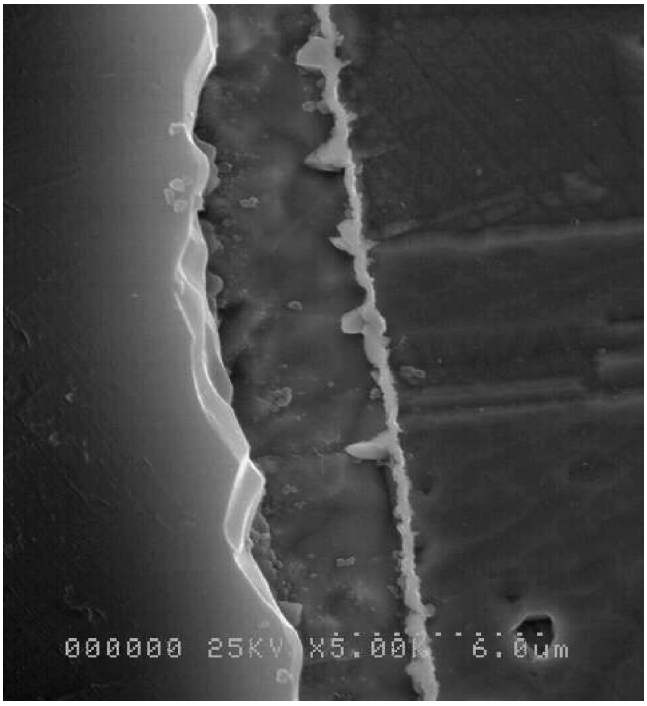

FIGURE 6.56 Cross-sectional view of irregular IMC formation at 50°C.

In summary, irregular IMC formation results in compressive stress in tin. The irregular growth behavior is associated with diffusion through tin grain boundaries, which is dominant at ambient temperatures (room temperature and 50°C). At elevated temperatures such as 150 and 175°C, the intermetallic growth behavior is governed by bulk diffusion, which results in a dense, regular IMC layer. At these temperatures, the stress relaxation due to grain growth largely removes any residue stress in the tin layer and therefore effectively eliminates the danger of whiskering. No or little compressive stress will build up again because the dense and regular intermetallic layer effectively acts as a barrier layer.

To elaborate further, the key to achieving whisker freedom is to remove any compressive stress source. One effective way to do this is to introduce a barrier layer such as a nickel layer between copper and tin. Studies have shown that a nickel layer from 0.2 to 1.5 μm is effective in eliminating whisker formation, though there are contradictory reports.

Substrate Layer The most common substrates for tin and tin alloy plating are copper and copper alloys. Examples include Olin 194, 151, and 7025, phosphor bronze, brass, and pure copper. Noncopper substrates such as alloy 42 (a nickel–iron alloy) and steel are also utilized.

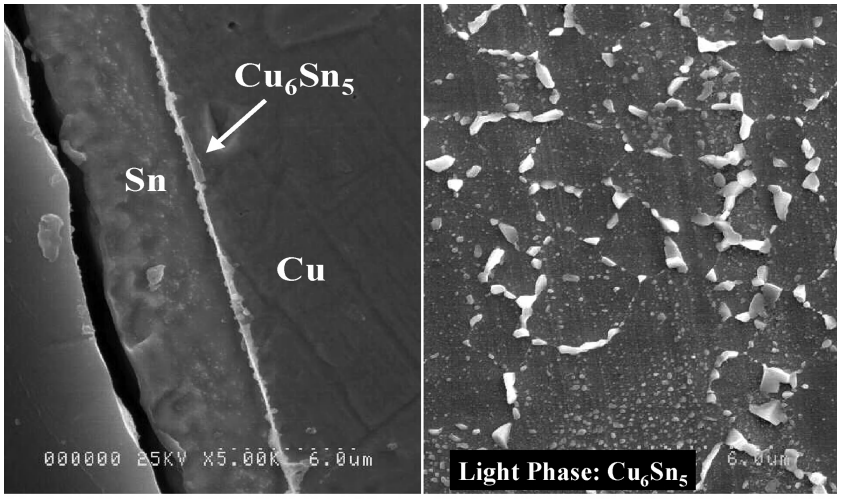

(a) (b)

FIGURE 6.57 SEM photo of Cu_6Sn_5 phase: (*a*) cross sectional view; (*b*) top view.

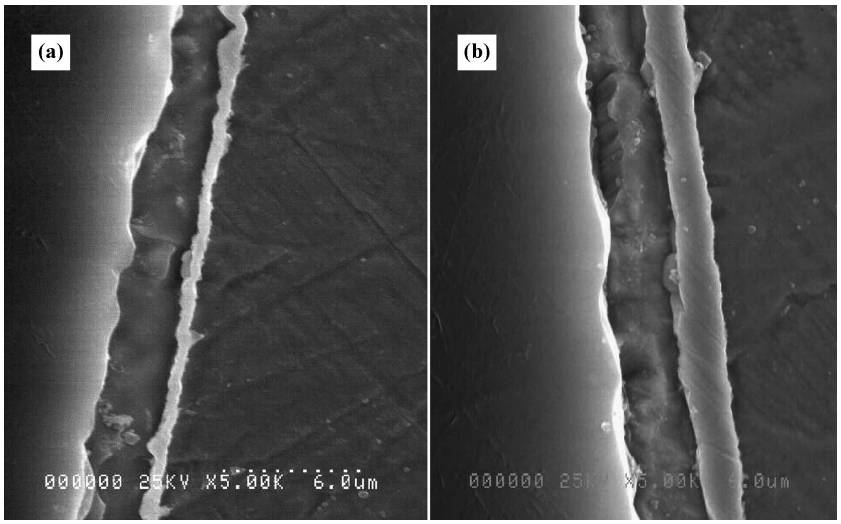

FIGURE 6.58 Cross-sectional views of regular and dense IMC formation at: (*a*) 120°C, 60 min; (*b*) 175°C, 60 min.

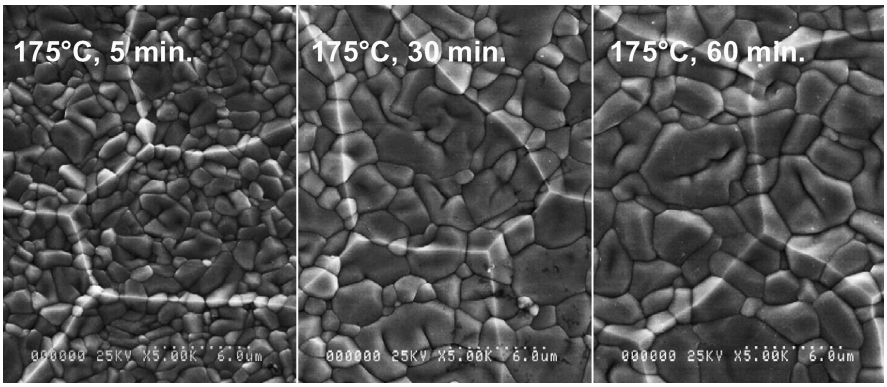

FIGURE 6.59 IMC and tin grain growth at 175°C.

The nature of the substrate has long been recognized as having a profound effect on whiskering. It is generally observed and agreed upon that, among the most common substrate materials, brass has the worst effect followed by phosphor bronze. Copper and copper alloy, nickel, and iron are comparatively much better. In particular, it has been reported that, of the common leadframe substrates, tin plated on alloy 42 is more whisker resistant than on Olin 194, 151, and 7025. It has also been observed that there is a significant difference in whisker growth behavior when the leadframe material is stamped versus etched.

Recently, it has been shown that the stress and crystal orientation of the substrate materials have significant influence on tin electrodeposite stress and orientation [186]. In addition, orientations such as ⟨220⟩ in the tin layer appear to be more whisker resistant than others. At the same time, orientations such as ⟨321⟩ appears to be associated with the visual defects of the deposits right after plating and increased whisker propensity [187, 188] during storage.

These recent observations and studies raise the following questions:

1. Is the stress in the tin layer influenced by the substrate residue stress? How?
2. Which has bigger impact on the tin deposit stress, organic additives used in the plating bath or substrate residue stress?
3. How does the pretreatment of the leadframe materials influence the substrate stress and orientation?
4. Is orientation and stress related?

Zhang and Schetty [187] carried out a study to systematically investigate the stress and preferred orientation of the substrate material before and after pretreatment, a step before the tin plating operation. They found that the common leadframe and connector substrates all possess compressive stress before the plating step. Table 6.16 summarizes the residue stress values measured by X-ray diffraction (XRD). As one can see, the substrate follows the order below in terms of decreased compressive stress: brass > Olin 7025 > Phos Bronze > Olin 194 > Olin 151.

TABLE 6.16 Stress Measurements of Substrates by XRD Before and After Pretreatments

Substrate	Before Pretreatment, MPa	After Pretreatment, MPa
Olin 151	-8 ± 2	-16 ± 2
Olin 194	-10 ± 2	10 ± 2
Phos Bronze	-15 ± 2	-22 ± 2
Olin 7025	-56 ± 2	-32 ± 2
Brass	-73 ± 2	-62 ± 2

TABLE 6.17 Preferred Orientation and Stress of Matte Tin Plating on Olin 151 Substrate with Two Different Pretreatment Methods

Pretreatment Method	Preferred Orientation(s)	Stress, MPa
Mild	⟨220⟩	5
Aggressive	⟨220⟩,⟨321⟩,⟨211⟩	−4

However, when these substrate materials go through a pretreatment procedure such as descale (for leadframe plating) or cathodic clean (for connector plating), their stress states are altered. It is very important to recognize that the pretreatment process is able to introduce stress so significantly that it can become one of the most important sources for initial deposit stress. In addition, the same substrate possesses different stress level when a different pretreatment process is employed. Zhang and Schetty [187] found that when Olin 151 was treated with a more aggressive descale process, its stress changed from -8 ± 2 MPa to -42 ± 2 MPa, whereas with a mild pretreatment process, its stress changed only to -16 ± 2 MPa, as shown in Table 6.16.

It is interesting to note that the preferred orientation of these copper alloy materials does not change regardless of the pretreatment process. The preferred orientation remained as ⟨220⟩. However, different pretreatment methods do affect the preferred orientation as well as stress in the tin layer, as suggested in Table 6.17. This finding is significant because it means that even though chemistry can characteristically produce tensile-stressed tin coatings on a substrate material with the proper pretreatment method, if attention is not paid to the pretreatment process, under certain conditions, the same chemistry could yield a compressively stressed tin layer.

Nonetheless, it should be noted that very limited work has been done on this subject; more systematic investigations are needed and are strongly recommended by the author.

External Mechanical Stress During electronic assembly processes, there are many sources of mechanical stress exerted on the electroplated deposits. Some are intentional, and they are integral parts of the manufacturing processes. For example, after tin plating, the leadframes go through "trim and form." This step entails that the leads are trimmed from the carrier strips and then are formed with either a J or a gullwing bend. This bending angle is approximately 90° (Fig. 6.60). As a result of the trim and form, part of the lead will be tensile stressed, and part of the same lead will be compressive stressed. On the other hand, there are unintentionally introduced mechanical stresses. For instance, improper sample handling could result in physical damages such as scratches and indentations on the plated parts.

Experimentally, mechanically applied stresses are frequently observed to result in whisker growth [141, 143, 160, 165, 189]. Common examples include growths adjacent

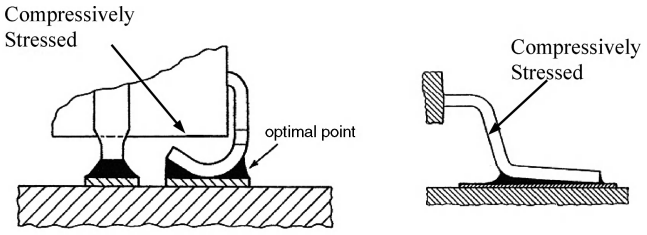

FIGURE 6.60 Schematic illustrating J and gullwing bend.

to load-bearing connections (e.g., bolts) or at the cut edge of stampings. In Hunsicker and Kenspf's case [21], the tin–aluminum surface was polished, which resulted in localized whisker growth days after the sample preparation. Physical damage to coatings, such as scratches or indentations, can also result in localized whisker growth. It must be said that not all investigators reported the same observations when similar experiments were performed. For instance, Dunn did not report any increase in whisker formation after application of compressive stresses to tin-coated brass C-rings [165]. However, it is important to point out that in Dunn's experiment a bright tin finish was utilized. The plated samples showed gross whisker formation days after plating even without any mechanical compressive stress, indicating that the residue stress in the tin layer alone was high enough to induce whisker growth readily.

In summary, in addition to the surface oxide layer, tin layer, intermetallic compound layer, and substrate, the external mechanical stress is one of the key factors that contribute to tin whisker formation.

Thermal Stress Thermal stress originates from the thermal expansion or contraction of materials when they are mechanically constrained. Integrated circuit (IC) fabrication generally involves bi- or multilayers of different materials. The simplest structure is a bilayer structure which consists of a surface film and a substrate. Internal stress will develop at the film and substrate interface because of thermal mismatch between the film and substrate at the film formation and device service temperatures. During the lifetime of an electronic device, it experiences temperature fluctuations responding to the changes in its service environment. In some cases, the temperature gradient could be large, and the resulting thermal stress could be substantial and should not be ignored. Since temperature fluctuation is a real-life situation, a thermal cycling test was developed to understand the thermal fatigue behavior of solder joints.

In passive component manufacturing, materials with vastly different thermal expansion coefficients are utilized in making the chip capacitors, resistors, and inductors. Among them are ceramics and glasses. The manufacturing process consists of many steps and is beyond the scope of this chapter. Readers interested in this subject should refer to [190].

In today's passive component manufacturing, the last step is electroplating. Specifically, a matte tin coating with a thickness of 5–10 μm is plated over a Ni barrier layer. The Ni barrier layer is typically ∼5 μm thick and is also electroplated.

At the end of the manufacturing steps, the passive components could contain many layers of materials (ceramics, glass, silver, nickel, and tin). Their relationship is illustrated in Figure 6.61. These different materials have rather different thermal expansion coefficients. These components are subjected to temperature cycling where temperature is varied from extremely cold (as low as −55°C) to extremely warm (as high as 125°C). Because of the thermal mismatches among these layers of materials, thermal stress develops at various interfaces. After a number of cycles from low to high temperatures, the thermal stress generated can be substantial enough to induce whisker formation. Brusse [191] demonstrated profuse whisker formation of tin-plated capacitors after thermal cycling the parts for 500 cycles from − 40°C to + 90°C (Fig. 6.62).

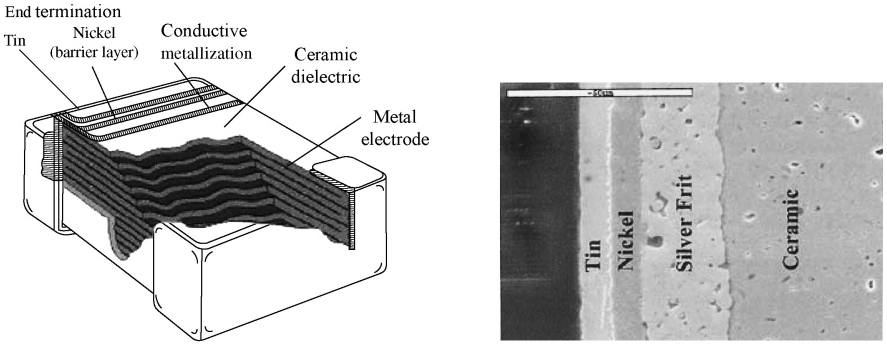

FIGURE 6.61 (*a*) Cutaway view of tin-plated multilayer ceramic chip capacitor (Kemet Electronics Corp. data sheet); (*b*) cross-sectional view of sequence of materials at metal termination. Tin finish is the final finish. (Photo courtesy of Jay Brusse, NASA.)

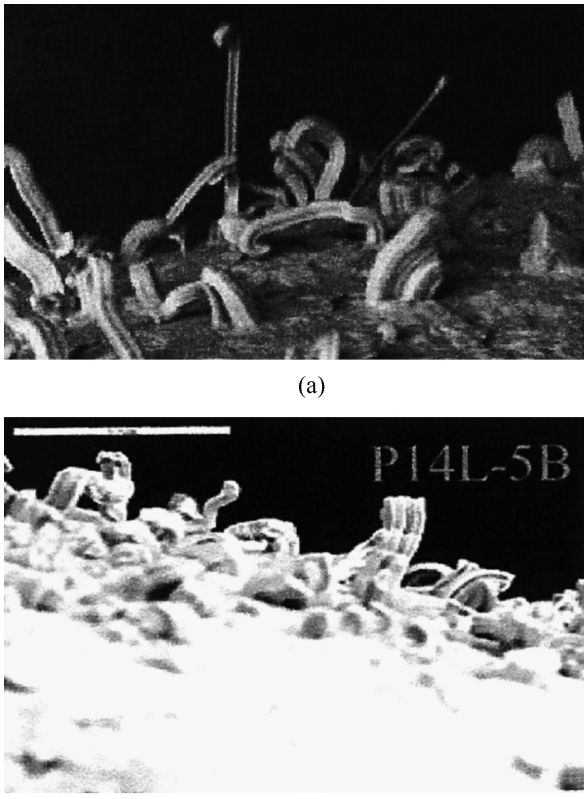

(a)

(b)

FIGURE 6.62 Examples of whiskers found on ceramic chip capacitors after thermal cycling from −40 to +90°C.

It is important to point out that until recently the effect of thermal stress on whisker growth was not recognized by the electronic industry. The awareness was largely brought out by NASA and companies such as Chippac, Motorola, and the National Electronics Manufacturing Initiative (NEMI) whisker testing task group.

Though whisker growth induced by thermal stress is demonstrated with chip capacitors, we also find its place in IC fabrications such as leadframe manufacturing. It has long been recognized that the whisker propensity is significantly lower on alloy 42 (a Ni/Fe alloy) than on copper-based leadframe materials such as alloy 194, alloy 151, and alloy 7025 while employing normal whisker test conditions. These conditions include room and elevated temperature storage with low and high humidity. Recently, it was reported that under temperature cycling conditions [148, 150, 192, 193] whisker propensity is significantly higher on alloy 42 substrate and whiskers appear quicker than from copper leadframe materials. It is believed that in this case [148] whisker growth is induced by thermal stress due to coefficient of thermal expansion (CTE) mismatch rather than the irregular intermetallic compound formation such as in the tin–copper interface (Fig. 6.63).

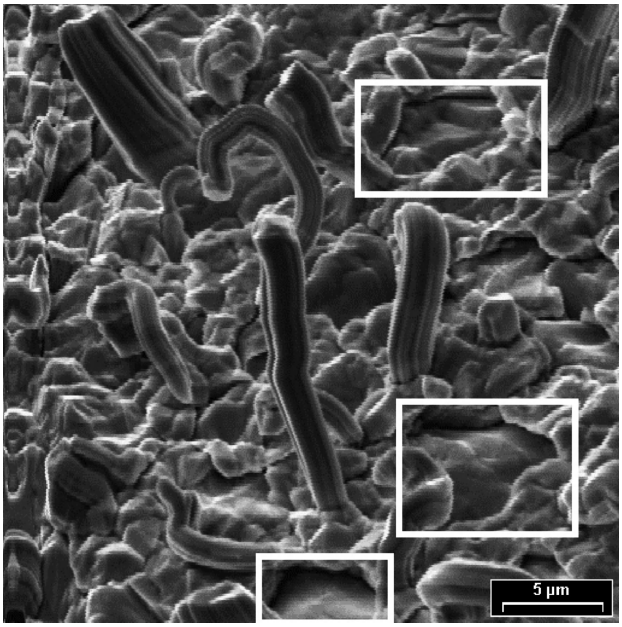

FIGURE 6.63 Example of tin whisker growth on alloy 42 after thermal cycling from −55 to +85°C.

The most popular thermal cycling profiles are −55–85°C and −35–125°C for 2000 cycles. However, recently [194], Texas Instruments concluded from internal studies that a longer cycle time up to 4000 cycles may be needed to ensure confidence of parts reliability.

Overall, there are many new findings on the subject of whisker formation in terms of external mechanical stress and thermal stress. Collectively, we have gained a better understanding of these effects. However, conflicting results still exist. Different and inconsistent whisker storage and test conditions and whisker examination methodology are the main sources of the confusion. Therefore, before discussing the whisker growth mechanism in detail it is necessary to examine the whisker investigation methodology.

6.5.4 Whisker Test Conditions and Observation Methodology

As demonstrated in previous sections, the whisker growth phenomenon is very complex. It involves many interrelated factors. In order to investigate such a complicated phenomenon, it is critical to establish a systematic and careful sample handling and examination plan. A systematic approach calls for handling samples the same way throughout the life span of the whisker study. All samples need to be handled with care to ensure that physical damages such as scratch and bending do not occur unless they are part of the whisker test matrix. Samples should be stored in an environment where there is no persistent vibration. Temperature and humidity should be well controlled.

In addition to sample handling, frequent and consistent examination of whiskers is equally important. An examination plan entails the followings:

1. *Examination Area* It should be large enough so the results are representative.
2. *Data Points in Observation Area* Sufficient data points need to be taken so the results have statistical significance.
3. *Examination Method* Optical or SEM or both? Samples are best tilted by an angle (45° often used) for SEM examinations.
4. *Examination Frequency* Time zero data are essential. Afterward, twice a month is sufficient.

After whiskers are found, they should be classified into categories for easy data interpretation and analysis. Whisker frequency, length, and diameter are to be estimated. The author and co-workers [141, 150] went a step further: A concept called "whisker index" was introduced to quantitatively characterize and measure the whisker growth propensity by taking into consideration all physical dimensions as well as frequencies of whiskers. An empirical equation was developed to calculate the whisker index [141]. A slightly different version of the whisker index was reported by Whitlaw and Crosby a year later [195].

Although a systematic sample handling and examination plan is critical in obtaining meaningful results, the most critical part of the whisker growth investigation is choosing the right whisker test method. Specifically, it means choosing a set of environmental conditions under which the electroplated tin parts are stored. Furthermore, it is implied that under such conditions whiskers will grow most quickly. The determination of this set of conditions requires an understanding of the whisker growth mechanism and the relative importance of the key factors that contribute to whisker formation.

To date, there is no established standard whisker test method. The fundamental reason is a lack of complete understanding of the whisker growth mechanism.

Historically, the following environmental storage conditions have been utilized: room temperature; room temperature/85% relative humidity (RH), 50°C, 50°C/85% RH, and 85°C/85% RH. In addition, thermal bake at various temperatures such as 125, 155, and 175°C with different durations has been utilized. Recently, various original equipment manufacturers (OEMs) as well as NEMI's whisker testing group have considered temperature cycling as the accelerating factor. The most common program was to cycle the plated parts between -35 and 125°C for 500 cycles. Although temperature cycling appears to produce whiskers on tin-plated parts more readily than some other test conditions, questions remain as whether it is most representative of real-world situations. In addition, a correlation between the whisker test and device reliability needs to be established.

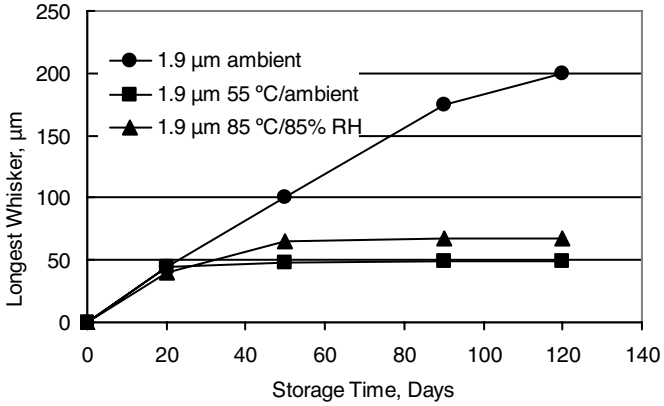

FIGURE 6.64 Maximum length of tin whiskers found on tin finishes stored at different conditions as function of time. Note that ambient condition produced the longest whisker. (Courtesy of M. Dittes, Infineon.)

Recently, the E3 group has come up with not only a whisker specification but also a whisker test method which has shown to grow whiskers more readily at ambient temperatures than at other accelerated conditions such as elevated temperature and high-temperature and high-humidity storage (Fig. 6.64).

Their test method calls for using alloy K75 (a copper alloy, similar to alloy 151 in composition) as substrate; plating 2 µm pure tin without the use of a Ni barrier layer; storing the plated leadframes at room temperature; and observing whiskers at time zero, week 1, week 2, and so on, up to week 8. If there is no whisker longer than 50 µm during this eight-week period, this tin finish meets the specification regarding whisker reliability. This test method was derived from extensive internal studies on the part of the E3 group, Figurs 6.65 and 6.66 explain the basis why the E3 group chose K75 as the substrate material and why 2 µm was the tin thickness chosen for the whisker test. Figure 6.67 explains why eight weeks was chosen as the test duration. The author believes that this is a more realistic whisker test. It is relatively quick; therefore it is practical for companies to carry out their own internal whisker tests.

Parallel to finding a standard whisker test method, efforts have been made to characterize quantitatively the stress and microstructure of various tin deposits. In this regard, some recently developed analytical tools have been utilized to characterize the physical structure and morphology of tin whiskers. In the following sections, we will discuss the stress and orientation measurements and cross sectional studies of whiskers by FIB.

Stress Measurements Reports of stress in electrodeposits date from the middle of the nineteenth century. Gore [196]

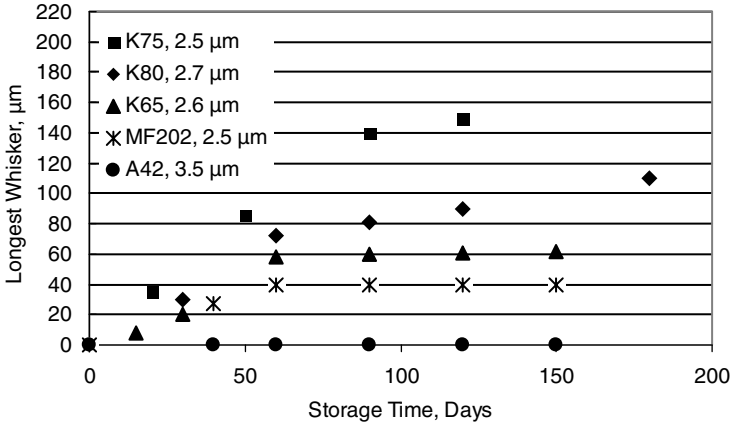

FIGURE 6.65 Maximum length of tin whiskers found on tin finishes on different substrate materials. Note that the whisker growth rate on K75 appears to be the fastest. (Courtesy of M. Dittes, Infineon.)

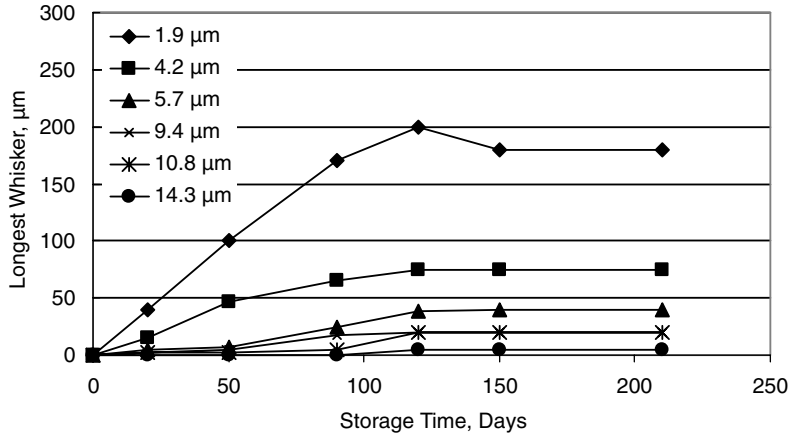

FIGURE 6.66 Maximum length of tin whiskers found on tin finishes plated on K75 substrate with different thicknesses, varying from ~2 µm to ~15 µm. Note that the 2-µm finish showed the fastest growth rate. (Courtesy of M. Dittes from Infineon.)

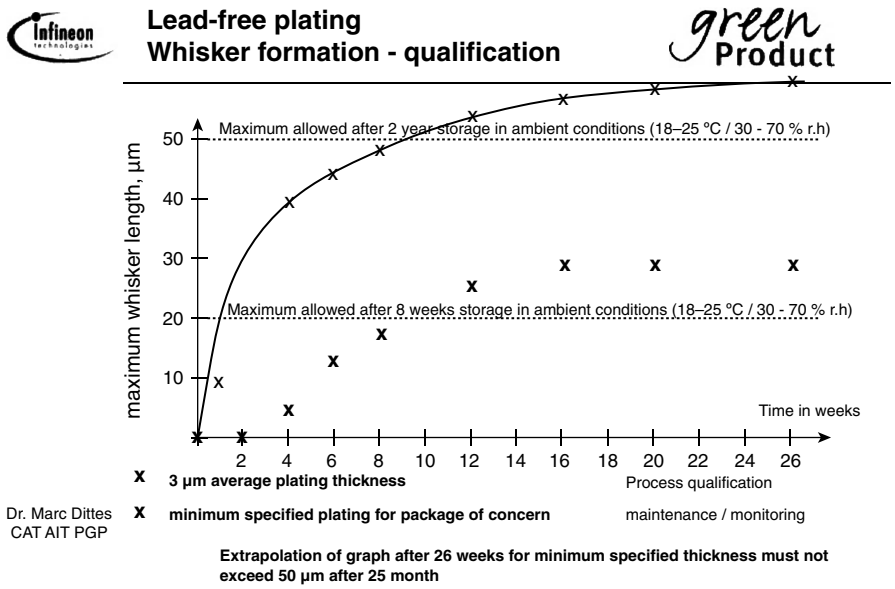

FIGURE 6.67 Diagram explaining justifications: for (1) whisker test method, (2) whisker specification, and (3) pass-or-fail criterion.

reported in 1858 that the inner and outer surfaces of electrodeposited antimony were in a state of unequal cohesive tension. Mills [197] made the first measurement of stress in 1877 by observing the rise or fall of mercury in a thermometer bulb, which was initially chemically coated with silver. When subsequently plating copper, nickel, and iron, a rise in "temperature" (tensile stress) was observed. Plating cadmium and zinc resulted in a temperature drop (compressive stress). Bouty [198] confirmed Mills's results and developed a formula for converting the temperature rise to stress. Since those early days, there have been many experiments dealing with the phenomenon of stress in electrodeposits.

Before we talk about stress measurements, it is important that we know what stress we are measuring. The stress mentioned here specifically referred to the deposit residue stress, which is defined as the stress that developed in the tin coating. It can be further classified as intrinsic and extrinsic. Intrinsic stresses are said to develop independently of the substrate, whereas the extrinsic type is due to the interaction of the substrate and the deposit.

There are two ways of measuring stress in electroplated coatings: mechanical and X-ray diffraction. As its name infers, the first method means that the stress is measured mechanically. The simplest and still most widely used mechanical means of measuring deposit stress is the flexible cathode. It consists of a metal strip insulated on one side which deflects upon being coated on the other side with a stressed deposit. There are a number of different versions of this stress-measuring device that differ mainly in the way deflection is measured. An excellent treatment of mechanical stress methods can be found in Weil's AES Research Project 32 review in 1970 [199]. The advantage of the mechanical method lies in the fact that stress can be measured in situ, that is, when electrodeposition takes place. This would allow quick and direct assessment of deposit stress resulting from a particular chemistry. The stress measured mechanically is the average deposit stress or macrostress.

It is important to recognize that though it is normally not an issue to measure stress in electrodeposits such as Ni, Zn, and Rh, it remains a challenge to measure stress in tin coating since the stress intrinsically is very low for tin finishes. However, recently, due to significant improvements in the mechanical sensor system with the deflection method or flexible cathode method, accurate results have been obtained with tin deposits [143]. Figures 6.68 and 6.69 demonstrate the hardware of such a device and results from it.

X-ray diffraction is widely used as a nondestructive method for stress measurement. In essence, this method is based on the changes in spacing between crystal planes induced by stress. If the spacing of the planes is known in the unstressed condition, the stress can be readily calculated. However, because of the codeposition of foreign materials, it is incorrect to assume that the interplanar spacings of an electrodeposited metal are the same as the published values for wrought or cast material. The "two-angle" method does not require knowledge about the spacing between planes in the unstressed condition. By determining the interplanar spacing perpendicular to the surface at an inclined angle ψ, the unknown quantity (spacing in the unstressed condition) can be mathematically eliminated. The stresses in the two directions are assumed to be related by the conventional elasticity equations, which assume isotropic elastic constants. The following equation is used to calculate the stress from the Bragg angles.

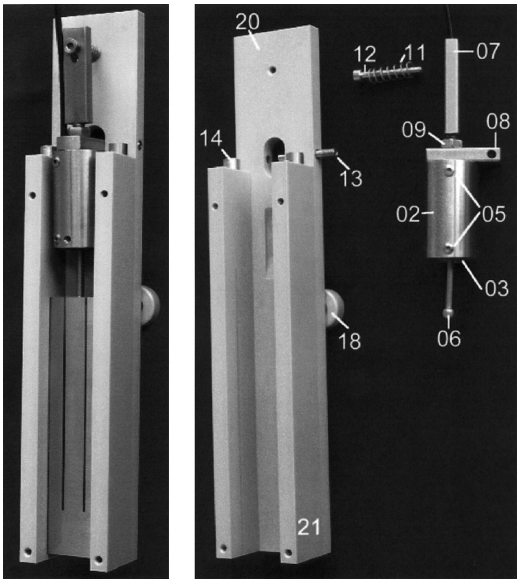

FIGURE 6.68 Pictures illustrating mechanics of hardware to measure stress in tin layer during deposition.

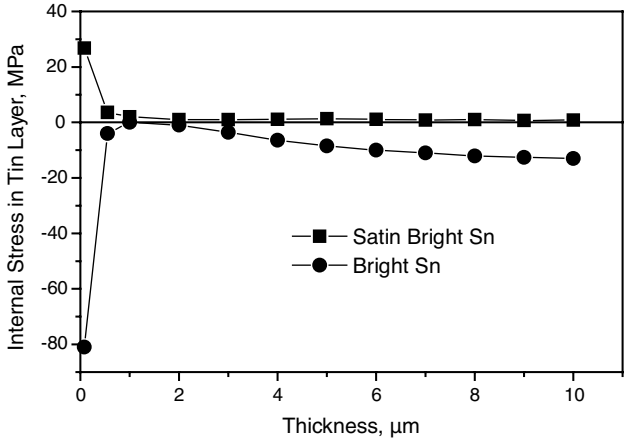

FIGURE 6.69 In situ stress measurement of bright and satin bright tin coating during plating. Note that the satin bright finish is stress free regardless of thickness, while the bright tin becomes more and more compressive stressed as the layer grows.

$$\sigma = \frac{E \cot\theta(2\theta_{\perp} - 2\theta_{\psi})}{2(1+\nu)\sin^2\psi}$$

where

E = modulus of elasticity of substrate
σ = average deposit stress
θ = Bragg angle
$\theta_{\perp}$ = Bragg angle when specimen surface normal bisects angle between incident and diffracted beams
θ_{ψ} = Bragg angle when specimen surface normal is inclined by angle ψ
ν = Poisson's ratio

It can be seen that the above equation involves a small difference between the two angles $(2\theta_{\perp} - 2\theta_{\psi})$. An angular difference on the order of 0.01° corresponds to a stress of 1 kg/mm^{-2} or 10 MPa. It is difficult to determine the two Bragg angles with sufficient accuracy because of the grain size and the anisotropic nature of the deposit. In addition, if the deposit is textured or highly oriented, the intensity of some diffraction lines may become so weak as the specimen is rotated to the inclined angle that it becomes almost impossible to make sufficiently precise determination of the Bragg angle. This is why we expect relatively large experimental errors in determining the absolute values of the stress for tin finishes.

Having said that, there are things one can do to improve the accuracy as well as precision of the measurements. First instead of using the standard Cu Kα radiation, one can use either a Co or a Cr radiation source as they are higher energy beams and give deeper penetration depths. Second, using a solid-state two-dimensional detector will significantly reduce the dark current and increase the signal-to-noise ratio.

In addition, during a specific experiment, using a diffraction line at the highest possible angle will improve the precision of the measurements. Furthermore, in the $\sin^2\psi$ test, it is desirable to include as many ψ angles as possible in both the negative and positive directrions.

With the sophisticated state-of-art X-ray diffractometers available today, it has been shown that stress in tin electrodeposits can be measured with much improved precision utilizing the two-angle method. However, care has to be taken to calibrate the equipment with samples with known stresses and with both high- and low-stress standards. For measuring stress in tin finishes, calibrating the equipment with a stress-free sample is strongly recommended.

It is important to point out that the X-ray method measures not only the macrostress but also the microstress. The latter involves using an X-ray synchrotron source capable of delivering a white X-ray beam focused to 1 μm. The size of the beam is smaller than the grain size of the deposit so the single-grain white-beam Laue pattern can be obtained for each individual grain. In such an experiment, Tu et al. revealed that the growth direction of the whisker is ⟨001⟩ whereas the tin grains in the deposits have a strong texture of ⟨321⟩. In addition, in the same investigation, they found that the overall deposit stress was compressive when whiskers were observed, but the stress level just below the whisker was slightly less compressive than areas that were farther away from the whisker. This is because the stress near the whisker is somewhat relieved by the whisker growth.

Whisker Cross Sections by FIB The FIB is an analytical tool developed in the last decade by the semiconductor industry. It is used primarily to obtain cross sections of microvias embedded in semiconductor wafers. It has two unique features. First FIB technology resembles SEM. However, instead of using electron beams, as in SEM, gallium ions generated in a liquid metal ion source are employed as the imaging beam. In the optical column these ions are electrostatically focused into a fine beam that scans the specimen surface, releasing secondary electrons for fine structural imaging. Second, the high-energy (10–25 keV) Ga beam is like a milling machine. It precisely cuts small trenches in fine circuitries with nanometer accuracy. By simply reducing the intensity of the ion beam, one can effectively "polish" or smooth out the cross sections so that detailed microstructural information such as individual grains and grain boundaries can be revealed. Figure 6.70 gives examples of FIB cross sections of whiskers from a matte tin finish, a satin bright finish, and a bright finish [142].

From these photos, it is clear that whiskers grow outward from electroplated tin coatings. They are "pushed" out of the tin layer by the need to relieve the compressive stress in the tin layer.

It is also shown from these photos that IMC formation at ambient temperature is rather irregular, and its growth is faster at grain boundaries than through the bulk tin layer. This difference in growth rate generates compressive stress at or near tin grain boundaries. In turn a whisker is "pushed" out at the weakest grain boundary when the compressive stress reaches the threshold.

Both the matte and satin bright tin deposits were 3 μm thick, and were aged at room temperature for 18 months. The FIB photos suggest that the IMC grows faster in a matte finish than in a satin bright finish. Furthermore, the average grain size is about 2 μm for matte tin and about 5 μm for satin bright. This result proves that IMC growth is faster with a smaller grained deposit.

In addition, as is clearly shown in Figure 6.70*a* and 6.70*b*, whiskers are "sitting" on top of the IMC compound. This explains why in these cases whiskers contain significant amounts of copper.

It is worth mentioning that FIB technology was also utilized to understand the whisker growth phenomenon with

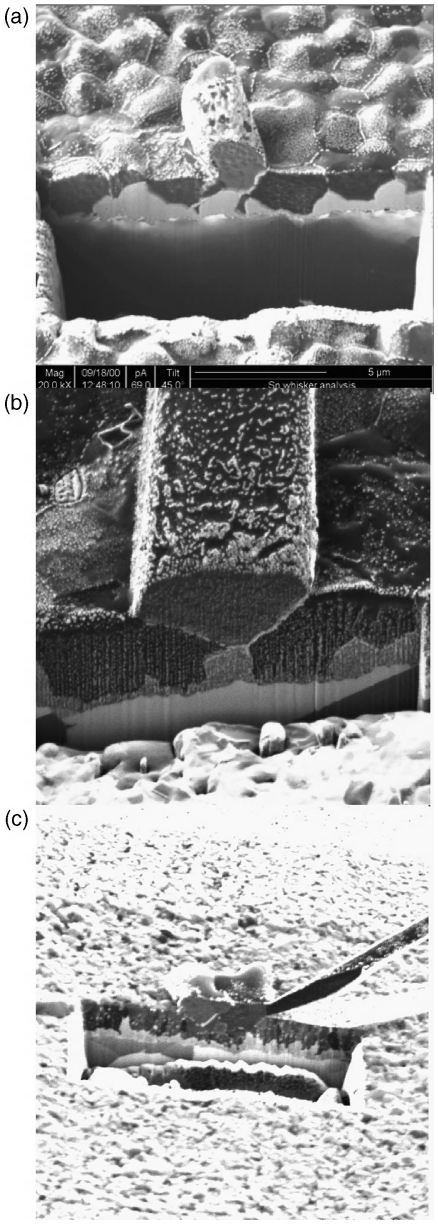

FIGURE 6.70 Images of whiskers cross sectioned by FIB: (*a*) matte finish; (*b*) satin bright finish; (*c*) bright finish. Tin thickness was 3 µm. All samples were stored at room temperature for 18 months before the FIB experiments.

tin/copper finishes [157, 200]. Similar observations were made with regard to the driving force for whisker formation.

6.5.5 Whisker Growth Mechanism

In seeking the whisker growth mechanism, we are setting out to find the steps in whisker growth to find the automatic and consistent response of whisker growth to various stimuli (factors), and to define and determine the *fundamental* physical, material, and mechanical principles that govern whisker growth.

We will first examine the steps of whisker development. Regardless of the type tin finish utilized and type of whiskers forms, the process of whisker development consists of three steps: (1) incubation or nucleation period, (2) period of growth, and (3) reduction and termination of growth.

The incubation period varies greatly from one case to another. What is the determining factor that defines the incubation time? The author believes that it is a combination of the thermodynamic driving force and the growth kinetics. Specifically, compressive stress is the driving force for whisker formation. If a tin deposit is tensile stressed throughout its life, one should not expect to observe whiskers because thermodynamically it is not possible. A threshold of the compressive stress has to be reached before whisker growth becomes thermodynamically favorable.

The incubation time and nucleation period are determined from the time that it takes for the compressive stress to reach the threshold and the kinetics for whisker nucleation and growth.

What factors govern the kinetics of whisker nucleation and growth? Is it grain size, grain shape, preferred orientation, and/or crystal defects such as dislocations?

As expected, electroplated pure tin coatings are far from perfect. The number of dislocations in an as-plated tin layer is likely to be high. The presence of a high concentration of dislocations within the tin layer presents an unstable microstructure with local sites of high-energy content [200]. Any additional stress can produce a change or recrystallization at or around dislocation sites; this lowers the total free energy of the plated layer according to the laws of thermodynamics [201, 202]

It is most likely that whisker grows as a result of recrystallizations of tin grains at dislocation sites. Therefore, to reduce whisker growth propensity, one needs to reduce the number of dislocations or increase the activation energy of recrystallization. When tin grains have very strong texture, it is usually true that there are fewer dislocation sites. In addition, we know from experience that it is harder for large-grained deposits to recrystallize than for small-grained deposits. Therefore, we can deduce that a large, well-polygonized, highly textured tin deposit has fewer defects such as dislocations, and it is beneficial in whisker reduction when everything else is equal.

All the work reported to date supports the above statement. However, the question now becomes "is there a specific texture that is beneficial?" "How large a grain is large?" Examining finishes that are known to be whisker resistant, Schetty [175] found that these finishes all have a common orientation, $\langle 220 \rangle$. In a separate and unrelated study, Zhang et al. [60, 74] observed the minimum whisker formation from a tin finish that showed only the $\langle 220 \rangle$ and $\langle 440 \rangle$ diffraction lines in the 2θ scan. This tin finish also displayed large,

well-polygonized grains. The average grain size determined by TEM was about 5 μm. Incidentally, in his work "A Laboratory Study of Tin Whisker Growth," Dunn [165] observed that the recrystallization rate of tin was dependent on the crystallographic orientation of the grains and the growth direction. Specifically, he observed that whisker growth directions were of the ⟨101⟩, ⟨100⟩, and ⟨111⟩ orientations. (Note that ⟨110⟩ was missing in his and other studies cited previously.)

Once the whisker nucleation begins, the growth period most likely is determined by the sustained compressive stress in the tin layer, and the availability of the tin atoms that diffuse towards the nucleation site. When tin grain size is small, there are a lot of grain boundaries; therefore there are many paths for tin atoms to diffuse to the nucleation site.

Once the whisker forms, the compressive stress in its vicinity is reduced or partially released This point is demonstrated by Tu's group [203]where the researchers utilized the synchrotron X-ray source to measure microstress within the tin layer. They were able to measure the stress on the whisker and next to the whisker. They found that the compressive stress is lower in the vicinity of the growing whisker. It is important to point out that Tu's work also demonstrates that there is a threshold of the compressive stress. When the stress level is higher than this value, whisker growth becomes inevitable. However, once the compressive stress is reduced to below this level, no additional whiskers grow until additional compressive stress builds up again in the tin layer.

The above description of the whisker growth mechanism is preliminary. To obtain a complete understanding of the whisker growth mechanism, we need to bear in mind that the compressive stress can be generated chemically (e.g., IMC), thermally (e. g., CTE mismatch), and mechanically (e.g., bending and scratching). Therefore we should focus on understanding better these origins of compressive stress. We should also focus on better understanding where the whisker nucleation site is and how this nucleation site is influenced by pretreatment, plating chemistries and process parameters, deposit properties, and environmental stimuli after plating.

6.5.6 Whisker Prevention

To prevent whisker formation, we need to develop and maintain a tensile stress in the tin deposit. Therefore, it is beneficial to have plating chemistries that can yield tensile-stressed tin deposit.

In addition, we could use a barrier layer such as nickel to stop or reduce IMC formation at the tin and the substrate interface, we could anneal the parts at temperatures above 100°C or reflow the parts to relieve the residue stress, we could rethink and redesign the materials used in making chip capacitors, transistors, and inductors to reduce the CTE mismatch, and we could be more stringent with our process control parameters during substrate pretreatment and tin plating. With these precautions, we should be able to significantly minimize the whisker growth propensity.

6.5.7 Whisker Applications

Although whiskers can have a detrimental effect in electronic devices by shorting the circuits, a few examples are given below of their benifits in out daily lives.

In a recent documentary by the BBC [203], scientists have discovered that a seal uses its whiskers to detect the watery trail of a swimming fish. The work, carried out by a German team, used a miniature submarine to simulate the trail made by a swimming fish. Two captive seals were able to locate the vessel in the dark: "We found that a seal was able to follow a hydrodynamic trail using its whiskers," co-researcher Bjorn Mauck of the University of Bonn, Germany, told BBC News Online. "This is the first time that an animal has been shown to do this." It is interesting to note that when the seal's whiskers were covered with stocking, it failed to locate the submarine.

In the technology world, it is not difficult to find unique applications of various kinds of whiskers. For instance, SiC whisker-reinforced ceramic composites [204] were innovations that came into prominence for potential structural applications because of the significant improvements in the mechanical properties these materials offered as compared to the monolithic materials. The incorporation of SiC whiskers into alumina ceramics resulted in increases in strength, fracture toughness, thermal conductivity, thermal shock resistance, and high-temperature creep resistance.

SiC whiskers used for reinforcement are discontinuous, rod- or needle-shaped fibers ranging in size from 0.1 to 1 μm in diameter and from 5 to 100 μm in length. Because they are nearly perfect single crystals, the whiskers typically have very high tensile strengths (up to 7 GPa) and elastic modulus (up to 550 GPa). SiC whisker–reinforced ceramics were introduced commercially for cutting tool applications in 1985 by Greenleaf Corporation. In one reported case history, changing from a conventional tool to a SiC whisker alumina one reduced a 5-h machining operation of inconel to 20 min [205].

In another application [206] by Containerless Research, Inc., precision, single-crystal microwhiskers have been grown epitaxially from ⟨111⟩ silicon wafers (Fig. 6.71) or ⟨111⟩ silicon posts (Fig. 6.72), with finely controlled microscopic dimensions. Whiskers covering an area of 1, 2, 3, or 5 mm diameter on 10 mm square substrate with an array spacing of 15, 30, and 60 μm can be precisely controlled (Fig. 6.73). The whiskers 3, 4, and 5 μm in diameter and 30–100 μm high. In addition, the whisker tips can be sharpened to radii less than 10 nm, which makes them ideal for scanning tunneling microscopy (STM) tips.

Nanometallic whiskers have been produced by ion track technology developed at GSI Materials Research [207]. Scientists were able to produce stochastic arrays of monocrystalline metal whiskers at the nanoscale for magnetic

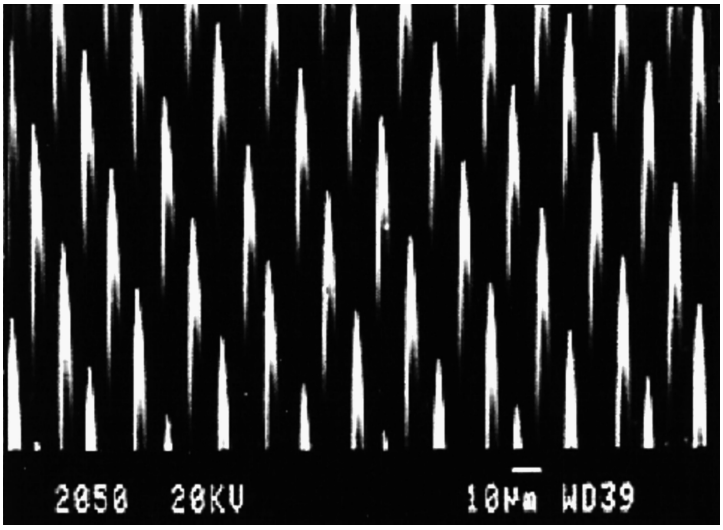

FIGURE 6.71 Whiskers grown epitaxially from ⟨111⟩ silicon wafers with finely controlled microscopic dimensions. The whiskers are fabricated in precise arrays with uniform diameter and length by the vapor–liquid–solid (VLS) process. (Photo courtesy of Containerless Research, Inc.)

sensors, flat screen, and trace-impurity sensors applications. Figure 6.74 illustrates a free-standing array of the metal whiskers.

The most important property employed in the above applications regarding whiskers is their mechanic strength and small dimensions. Needless to say, there are many other applications of whiskers in the micro- and nanotechnology world that are not included in this section.

6.6 APPLICATIONS OF ELECTROPLATED TIN AND TIN ALLOYS IN ELECTRONICS

Tin and tin alloys have been widely used in the electronics industry as a component finish because of their ideal chemical, physical, and material properties, as discussed throughout this chapter. This section will give examples of using electroplated lead-free tin and tin alloys in connectors, leadframes, passives, and wafer bumping applications.

6.6.1 Connectors

A connector is a device (more precisely, a mating pair of devices, often a plug and a socket) for connecting together two wires, cables, or a PWB board, allowing electricity to flow but also allowing easy disconnection and reconnection when necessary. There are many kinds of connectors manufactured by large corporations such as Tyco Electronics, Molex, FCI, and Hua Mei. Figure 6.75 shows a few examples.

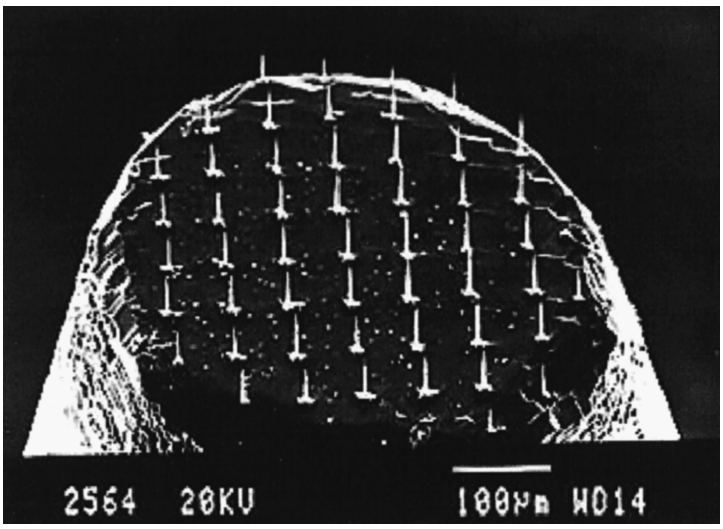

FIGURE 6.72 Single-crystal whiskers grown expitaxially from ⟨111⟩ silicon posts with finely controlled microscopic dimensions. The whiskers are fabricated in precise arrays with uniform diameter and length by VLS process. (Photo courtesy of Containerless Research, Inc.)

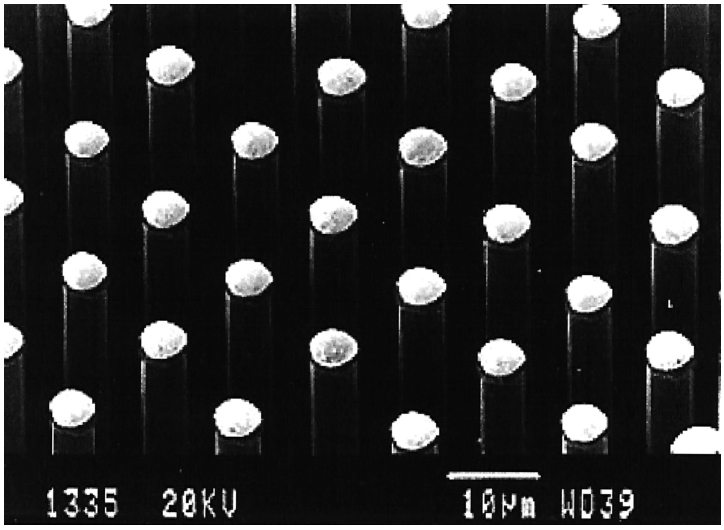

FIGURE 6.73 Note that the whisker tips were gold coated. The array spacing is ~15 µm. (Photo courtesy of Containerless Research, Inc.)

A connector is often a part of a solder joint which is formed when the connector is soldered onto a PWB board. In this case, the connector needs to be solderable. The majority of the base materials for connectors are copper and copper alloys. They corrode easily even in an ambient environment without surface protection. Electroplated tin and tin alloys offer excellent corrosion protection and solderability. This is why tin–lead has been a good connector finish for many decades.

The connector industry has gone through the same learning curve during the last decade in searching for the lead-free replacement for tin–lead. Today, almost 100% of the connectors are lead free. Roughly 95% of the connectors worldwide are tin plated and the rest are tin–bismuth plated.

The connector industry chose pure tin over tin alloys because pure tin provides excellent corrosion resistance, solderability, ductility, and manufacturability [207]. In addition, when combined with a nickel barrier layer, it offers as good whisker resistance as tin alloys [145, 208]. Tin plating is simpler than tin alloy plating and is easier to control and manage in high-volume production environments. And in most cases, one can plate pure tin at higher current densities than tin alloys and therefore increase throughput or productivity.

Determining whether bright tin is better than matte tin or vise versa comes from understanding the connector application requirements. If it is an application that requires multiple insertions and there is no requirement for reflow, thermal anneal, or stamping, then bright tin is the better choice. This is because a bright tin finish is typically harder and has lower friction coefficient and thus better wear resistance than matte tin. In addition, with a nickel barrier

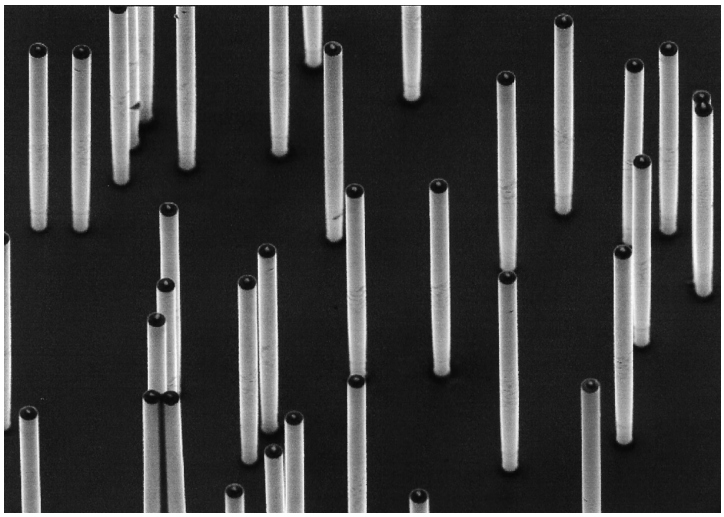

FIGURE 6.74 Free-standing metallic whiskers. (Photo courtesy of GSI Materials and Research.)

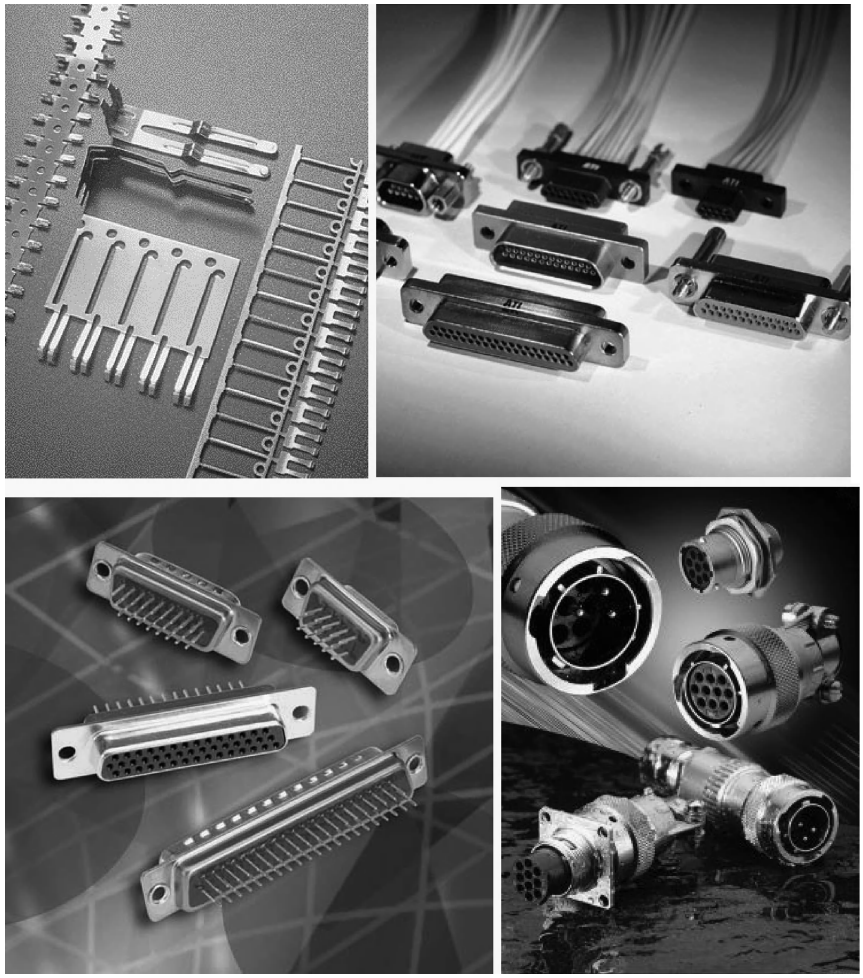

FIGURE 6.75 Examples of connectors.

layer, it has as good whisker resistance as nonbright tin finish (Fig, 6.76) [145]. On the other hand, if reflow, thermal anneal, or stamping is required, matte tin is the better choice. This is because owing to its low organic inclusions, slower rate of IMC formation, and higher ductility, a matte tin finish yields better solderability performance and discoloration resistance.

In summary, both bright tin and matte tin are used in connector applications. Readers are referred to the references and websites of the various connector manufacturers for more updated information.

6.6.2 Leadframes

A leadframe is the metal frame that semiconductors are attached to during the package assembly process. Typically a leadframe is a long metal frame with positions for multiple chips. After the chips are attached to the leadframe tiny wires are used to connect the chip bond pads to the frame and then the positions on the frame where chips are located are

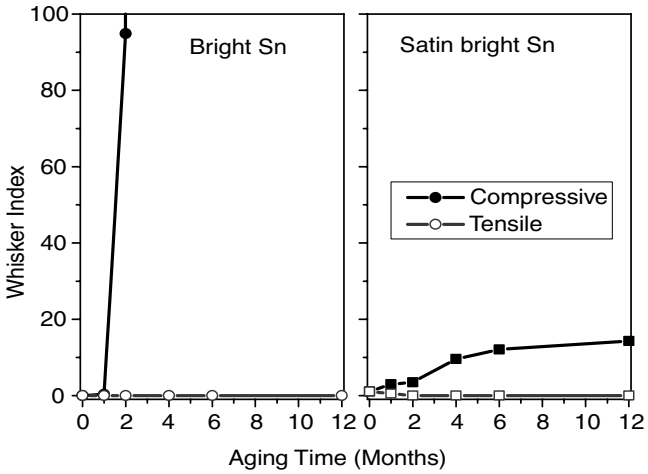

FIGURE 6.76 Whisker index of bright and satin bright tin deposits with (tensile stress in tin layer) and without Ni underlayer (compressive stress in tin layer). Note that with a Ni underlayer both tin coatings have whisker index of zero.

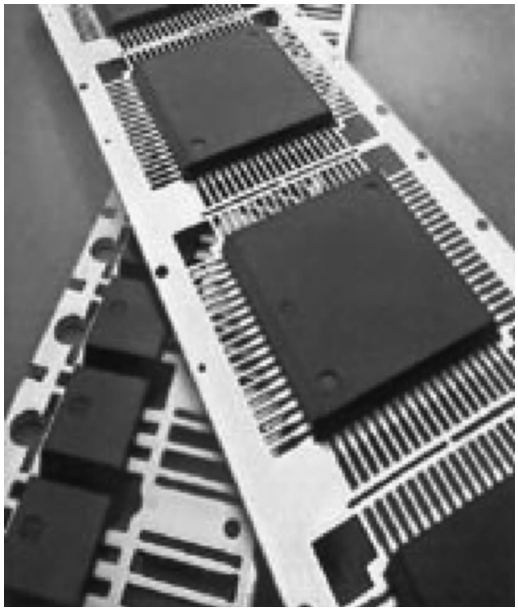

FIGURE 6.77 Example of metal frame with encapsulated packages.

encapsulated in epoxy (shown in Fig. 6.77). At this point, the leadframe package goes through a solder plating process whereby the meal frame with the leads are plated with a tin–lead or lead-free tin or tin alloy finish. After the plating step, the metal frame goes through a trim-and-form process whereby leads are separated from the frame and each package is diced, separated, and made ready for assembly (Fig. 6.78. During the assembly process, each package is picked up by a pick-and-place machine and placed where an interconnection needs to be made between the package and the PWB by melting the solder (reflow), then letting it solidify to make a solder joint. Two key factors are worth pointing out. First the leads need to be ductile after plating so during trim and form the protective surface does not crack to expose the base material. Second, the leads need to be solderable during the reflow operation.

Commonly encountered leadframe base materials are alloy 194, alloy 7025, alloy 151, and alloy 42. The first three are copper alloys, whereas alloy 42 is a nickel–iron alloy. As in the case of connectors, without surface protection, these base materials get corroded easily and are unfit for subsequent reflow operation during assembly. With the advent of reflow soldering, electroplated tin–lead has been used successfully as a lead finish. Electroplated tin–lead is perfect when sufficiently thick; it provides excellent corrosion resistance, retards Cu_3Sn IMC formation, and is very ductile.

Given what we have learned so far about tin and tin alloys, it is easy to reach the conclusion that a matte tin would be the most desirable leadframe finish. Indeed, matte tin has been chosen as the lead-free leadframe finish by large semiconductor companies such as Intel, Freescale, Micron, AMD, Phillips, STMicro, and Infineon [209–211]. However, it needs to be pointed out that most large Japanese companies, such as Toshiba, Sony, Sharp, Fujitsu, and Renesas Technology, preferred tin–bismuth over pure tin based on reportedly lower whisker propensity [96]*. Samsung and TI[212], on the other hand, stayed away from tin and tin alloys and chose NiPdAu as the lead-free lead finish.

As we mentioned earlier, two types of base materials are used in leadframe manufacturing: copper alloys and alloy 42. Historically, 10–15 μm of tin–lead is plated directly on these substrates. Whiskers were not a concern because everyone thought that adding 2–3% of lead would eliminate tin whisker formation. As tin and tin–bismuth is replacing tin–lead as the leadframe finish, its effectiveness in whisker resistance has been examined in great detail and by many companies. To summarize briefly, on alloy 194, 151, and 7025, whisker propensity is greatly reduced when a tin or tin–bismuth layer is sufficiently thick, that is, $>10\,\mu m$. On alloy 42, whisker growth is actually worse with a thicker tin layer. Instead, the only remedy appears to be a thin tin layer ($<3\,\mu m$) with a nickel barrier layer (0.5–1.5 μm) on alloy 42 [150]. This is because the sandwich structure develops a relatively large *tensile stress* in the tin layer as measured by XRD (Fig. 6.79). This tensile stress cancels out the compressive stress generated in the tin layer during the heating cycle, preventing whisker formation [148, 150]. In addition, the tin finish is perfectly solderable after being exposed to severe environmental test conditions [150].

6.6.3 Passive Components

Passive components are electronic components that do not amplify or switch signals. Examples are capacitors, resistors, transformers, and inductors (Fig. 6.80). While their constructions and base materials vary, the surface protection methodology is the same for all passive components. Typically, a nickel barrier is applied by electroplating on the base material before the tin and tin alloy plating. Again, matte tin is chosen as the preferred lead-free finish over tin–bismuth, tin-copper, and tin–silver [213].

6.6.4 Wafer Bumping

Wafer bumping is the process by which contact points on a wafer are heightened above the wafer surface by adding conducting material. These contact bumps are bonded or fused to make all required electrical connections to tape, packages, or other interconnect substrates in a single process step. Bumps may be provided on the die edges or distributed over the surface of the die in an area array (Fig. 6.81). This

*Toshiba chose SnBi for leadframe lead-free finish.

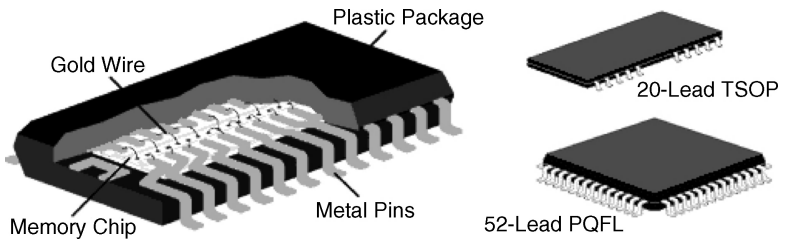

FIGURE 6.78 Example of package that has gone through "trim and form" and singulation.

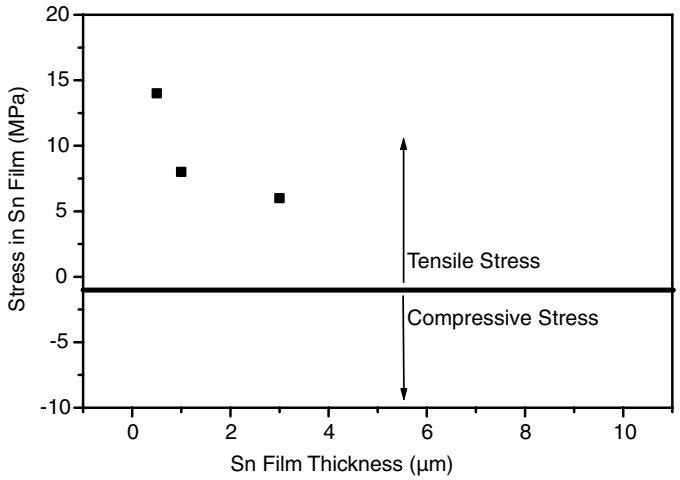

3 um matte Sn on 1.5 um Ni after room temperature aging for 30 days

FIGURE 6.79 Stress measurements of matte tin coating (3 μm) with a nickel underlayer (1.5 μm) on alloy 194 aged at room temperature for 30 days.

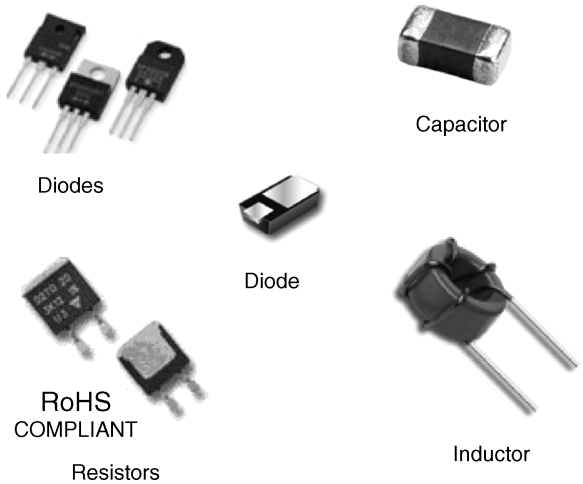

FIGURE 6.80 Examples of passive components.

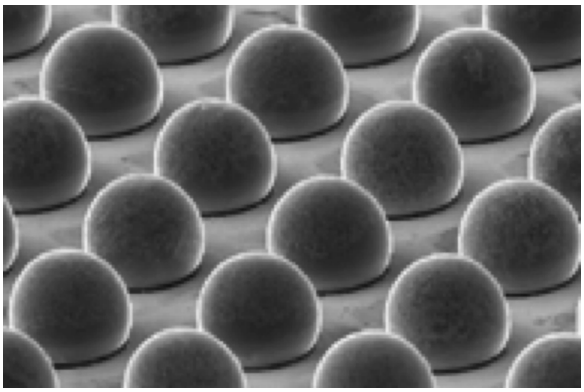

FIGURE 6.81 Example of reflowed solder bump arrays.

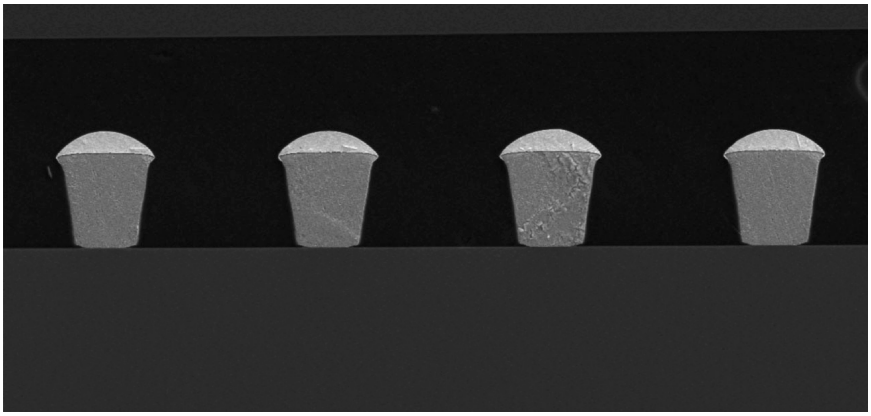

FIGURE 6.82 Example of copper pillar with a tin–silver cap.

process is also referred to as C4 (controlled collapse chip connection), a term coined by IBM during the early 1960s. Bumping material or metallurgy was either eutectic tin–lead (63Sn37Pb) or high-lead (97Pb3Sn) solders. Initially IBM used vacuum deposition to make these bumps. The equipment is expensive and maintenance is high though a variety of alloys can be produced by sequential deposition of two or more metals. During the 1990s, IBM began to use electroplating methods to make these C4 bumps. Although it is not the lowest cost process, electroplating allows extremely good control with regard to within-die and within-wafer uniformity and therefore promises to be the preferred method for high I/O fine pitch.

IBM is not the only semiconductor company that has wafer bumping expertise and capability. Intel, the largest semiconductor chip maker, utilized electroplated high-lead bumps inside the MPU chips since the early 1990s. Others, such as Freescale, Amkor, ASE, StatChipPac, offered eutectic tin–lead solder bumping as a service internally and externally. Even though lead used in wafer bumping is exempt per the RoHS directive until December 31, 2014, many of the companies mentioned above have been working toward a lead-free solution for many years and some already have lead-free solutions. For instance, Intel has replaced the high-lead bumps with copper pillars in its current and future microprocessors; Amkor, ASE, and others have reportedly developed lead-free SnAg bumps to replace eutectic tin–lead.

Copper pillar was chosen as a high-lead bump replacement due to its excellent electrical and thermal conductivity, better electron migration resistance, and high stand-off, which is beneficial for high I/O fine pitch [214]. Copper will not melt during typical solder reflow; therefore a tin–silver cap or tin cap is often found on top of the copper pillar (Fig. 6.82). During reflow operation, the solderable cap melts and connects with another package or substrate.

Owing to its superior material properties, near-eutectic tin–silver becomes the best lead-free alternative to replace tin–lead bumps (Fig. 6.29). It also has the advantage of being close to the SAC (tin–silver-copper) alloy composition; therefore reflow soldering is relatively more straightforward compared to other tin alloys such as tin–bismuth. It is chosen over pure tin for the same reason. However, since 2008, there are more and more companies looking into pure tin as both the replacement for eutectic solder bumps and the lead-free solder cap on top of the copper pillar.

One of the drawbacks of the tin–silver bumping process is it is difficult to control alloy composition. This could result in reliability issues if the silver content is higher than 3 wt %. In that case, during or after reflow, excessive Ag_3Sn intermetallic compound, a platelet, would form at the copper and tin–silver interface (Fig. 6.83). This could lead to premature

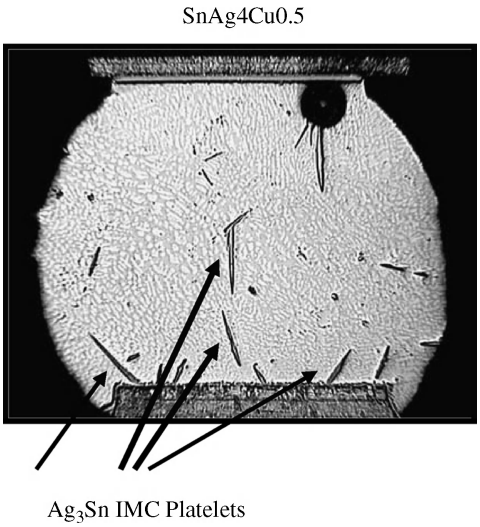

FIGURE 6.83 Excessive Ag_3Sn formation during reflow because of high silver content. Silver content is 4 wt %.

electromigration failure and/or solder bump shear because of a weaker interface.

6.6.5 Future for Electroplated Tin and Tin Alloys

The electronics industry will continue its march toward smaller, cheaper devices with more features and functionality. Accompanying this is continued miniturization. At the board and chip level, I/O pitch will continue to shrink, which would render certain interconnect technology obsolete. Electroplating, on the other hand, becomes more and more attractive as component pitch size becomes smaller and smaller. Looking back in the history of soldering and interconnects, tin and tin alloys have been the interconnect materials throughout the centuries owing to their unique chemical and material properties. The author believes that their use in the electronic industry will continue into the next centuries. In this regard, electroplated tin and tin alloys will continue to be used in the electronics industry. It is certain that new challenges in plating will emerge as the electronics industry forges ahead. However, armed with theoretical as well as practical understanding of tin and tin alloy plating and the availability of sophisticated electrochemical tools, the author is certain that scientists and engineers will overcome the challenges along the way.

ACKNOWLEDGMENT

The author would like to thank Joe Abys for offering her the opportunity at AT&T Bell Labs to develop lead-free solder plating chemistries in the early 1990s, for inspiring her to develop a career in plating, for many insightful discussions on this and other matters, and above all for being a true friend.

REFERENCES

1. *Soldering Manual*, 2nd ed., American Welding Society, Miami, FL, 1977.
2. H. J. Fisher and A. Phillips, "Viscosity and Density of Liquid Lead-Tin and Antimony-Cadmium Alloys," *J. Inst. Met.*, **11**, 1060 (1954).
3. H. Inoue, Y. Kurthara, and H. Hachino, "Pb-Sn Solder for Die Bonding of Silicon Chips," *IEEE Trans. Components, Hybrids Manuf. Technol.*, **9**, 190 (1986).
4. P. T. Vianco and D. R. Frear, "Issues in the Replacement of Lead-Bearing Solders," *Journal of Materials*, pp. 14–18 (July 1993).
5. R. J. Klein Wassink, *Soldering in Electronics*, 2nd ed., Electrochemical Publications Ltd, Scotland, 1989, pp. 141–147.
6. H. H. Manko, *Solders and Soldering*, 3rd ed., McGraw-Hill, New York, 1992.
7. W. D. Woodbury, *Lead*, U.S. Department of the Interior, Bureau of Mines, Washington, DC, Apr. 1992, p. 22.
8. U.S. Environmental Protection Agengy (EPA), Washington, DC.
9. N. Irving Sax, *Dangerous Properties of Industrial Materials*, 6th ed., Van Nostrand Reinhold, New York, 1984.
10. H. H. Manko, "Lead Poison, Solder and Safety in the Workplace," *EP&P*, **92** (1992).
11. S. Waldman,"Lead and Your Kids," *Newsweek*, July 15, 1991, p. 42.
12. L. C. Lee, "Lead-Free Soldering," paper presented at SMI Workshop, San Jose, CA, Sept. 1995.
13. J. Glazer, "Metallurgy of Low Temperature Lead-Free Solders for Electronic Assembly," *Int. Mater. Rev.*, **40**, 65 (1995).
14. L. E. Felton, C. H. Raeder, and D. B. Knorr, "The Properties of Tin-Bismuth Alloy Solders," *Journal of Materials*, **28** (1993).
15. G. Humpston and D. M. Jacobson, *Principles of Soldering and Brazing*, ASM International, Materials Park, OH, 1993.
16. P. T. Vianco, F. M. Hoskings, and D. R. Frear, "Lead-free Solders for Electronics Applications—Wetting Analysis," Paper presented at the Conference: Materials Developments in Microelectronics Packaging: Performance and Reliability, Montreal, Quebec, Canada, 1991, p. 373.
17. I. Artaki, A. M. Jackson, and P. T. Vianco, "Evaluation of Lead-free Solder Joints in Electronic Assemblies," *J. Electron. Mater.*, **23**, 757 (1994).
18. U. R. Kattner, and W. J. Boettinger, "On the Sn-Bi-Ag Ternary Phase Diagram," *J. Electron. Mater.*, **23**, 603 (1994).
19. J. A. Slattery, and C. E. T. White,"Lead-Free Alloy Containing Tin, Silver, and Indium," Patent EP0568952A1 (Nov. 10, 1993).
20. S. Tulman,"Tin Base Lead-Free Solder Composition Containing Bismuth, Silver and Antimony," U.S. Patent 4,806,309 (Jan. 5, 1988).
21. H. Y. Hunsicker and L. W. Kenspf, "Growth of Whiskers on Tin-Aluminum Bearings," *Quart. Trans. SAE*, **1**, 6 (1947).
22. A. J. Bard, R. Parsons, and J. Jordan, Eds., *Standard Potentials in Aqueous Solution*, Marcel Dekker, New York, 1985.
23. G. S. Tzeng, "Effects of Additive Agents on the Kinetics of Tin Electrodeposition from an Acidic Solution of Tin (II) Sulfate," *Plating and Surface Finishing*, 67 (Nov. 1995).
24. P. A. Kohl, "The High Speed Electrodeposition of Sn/Pb Alloys," *J. Electrochem. Soc.*, **129**, 1196 (1982).
25. P. A. Kohl, "High-Speed Solder Plating Baths," *Plating and Surface Finishing*, 45 (Aug. 1981).
26. I. Zavarine, O. Khaselev, and Y. Zhang, "Spectroelectrochemical Study of the Effect of Organic Additives on the Electrodeposition of Tin," *J. Electrochemic. Soc.*, **150**(4), c202 (2003).
27. J. O'M. Bockris and A. Reddy, *Modern Electrochemistry*, Plenum, New York, 1970.
28. P. H. Reiger, *Electrochemistry*, 2nd ed., Chapman and Hall, New York, 1993.

29. A. J. Bard and L. R. Faulkner, *Electrochemical Methods*, Wiley, New York, 1980.
30. J. O'M. Bockris and S. U. M. Khan, *Surface Electrochemistry—A Molecular Level Approach*, Plenum, New York, 1993.
31. T. C. Tan, "Model for Calculating Metal Distribution and Throwing Power of Plating Baths," *Plating and Surface Finishing*, **67** (July 1987).
32. T. C. Tan, "A Novel Experimental Cell for the Determination of the Throwing Power of an Electroplating System," *J. Electrochem. Soc.*, **44**, 3011 (1987).
33. H. Haring and W. Blum, *Trans. Electrochem. Soc.*, **44**, 313 (1923).
34. A. H. Heathley, *Trans. Electrochem. Soc.*, **44**, 283 (1923).
35. S. Field, *J. Electrodepos. Tech. Soc.*, **7**, 83 (1932)
36. J. J. Maisano, I. Kadija, and J. A. Abys, "A Rotating Cylinder Throwing Power Electrode," in *Proc. Annual Conference, American Electroplaters & Surface Finishers Society*, pp. 703–718 (June 1992).
37. M. Schwartz, "Deposition from Aqueous Solutions: An Overview," in *Deposition Technologies for Films and Coatings*, R. F. Bunshah, Ed., Noyes, Park Ridge, NJ, 1982, Ch. 10.

37a. W. Kaim and A. Klein, Eds., *Spectroelectrochemistry*, RSC Publishing, 2008.

37b. J. Leddy, V. Birss, and P. Wanysek, *Historical Perspectives on the Evolution of Electrochemical Tools*, 2002.

38. R. J. Witting and C. P. Kubiak, "IR Spectroelectrochemical Studies of the Metal Carbonyl Dimers ($Mn_2(CO)_{10}$ and $[CpM(CO)_5]_2$ (M = Mn, Mo). Cross Coupling and Liquid Substitution Reactions of Electrochemical Generated Organometallic Radicals," *J. Electrochem. Soc.*, **393** (1–2), 75–86 (1995).
39. R. S. Czermuszewicz and K. A. Macor, "A Low-Temperature Bulk Electrolysis Cell for In-Situ Resonance Raman Spectroelectrochemistry: Observation of the Fe^{IV} = O Stretching Frequency for Electrogenerated Ferry Tetramesitylporphyrin," *J. Raman Spectrosc.*, **19**(8), 553 (2005).
40. J. R. Kirchhoff, "Luminescence Spectroelectrochemistry," *Current Separations*, **16**, 1 (1997).
41. R. J. Gale, *Spectroelectrochemistry: Theory and Practice*, Springer, 1988.
42. U. Landau, "Plating—New Prospects for an Old Art," in *Electrochemistry in Industry, New Directions*, U. Landau, E. Yeager, and D. Kortan, Eds., Plenum, New York, 1982.
43. J. W. Dini, "Electrodeposition—The Materials Science of Coatings and Substrates," in *Additives*, Noyes, Park Ridge, NJ, 1993, Ch. 7.
44. H. Brown, "Addition Agents, Anions, and Inclusions in Bright Nickel Plating," 9th William Blum Lecture, *Plating*, **55**, 1047 (1968).
45. A. H. DuRose, in *Modern Electroplating*, 2nd ed., F. A. Lowerheim, Ed., Wiley, New York, 1963, p. 377.
46. A. K. Graham and H., L. Pinkerton, "Properties and Comparative Performance of Electrodeposited Terne Alloys," *Plating*, **54** (1967).
47. Y. Zhang and M. J. Weaver, "Application of Surface Enhanced Roman Spectroscopy to Organic Electrocatalytic Systems: Decomposition and Electrooxidation of Methanol and Formic Acid on Gold and Platinum-Film Electrodes," *Langmuir*, **9**, 1397 (1993).
48. X. Gao, Y. Zhang, and M. J. Weaver, "Observing Redox-Induced Surface Molecular Transformations by Atomic-Resolution Scanning Tunneling Microscopy: Sulfide Electrooxidation on Au(111) in Aqueous Solutions," *J. Phys. Chem.*, **28**, 4156 (1992).
49. N. Batina, T. Will, and D. M. Kolb, "Study of Initial Stages of Copper Deposition by In-Situ Scanning Tunneling Microscopy," *Faraday Discuss.*, **94**, 93 (1992).
50. T. C. Frankin, "Some Mechanisms of Action of Additives in Electrodeposition Processes," *Surface Coatings Technol.*, **30**, 415 (1987).
51. L. Oniciu and L. Muresan, "Some Fundamental Aspects of Leveling and Brightening in Metal Electrodeposition," *J. Appl. Electrochem.*, **21**, 565 (1991).
52. C. Ogden, D. Trench, and J. White, "Tensile Properties and Morphologies of Pyrophosphate Copper Deposits," *J. Appl. Electrochem.*, **12**, 619 (1982).
53. R. Weil and R. Paquin, "The Relationship between Brightness and Structure in Electrodeposited Nickel," *J. Electrochem. Soc.*, **107**, 87 (1960).
54. Y. Zhang et al., U.S. Patents, 6,267,863 (2001); 6,730,209 (2004).
55. M. Jordan, *Electrodeposition of Tin and Its Alloys*, Eugen G. Leuze, Saulgau/Wurtt, Germany, 1995, p. 64.
56. D. A. Vermilyea, "Additives and Grain Refinement," *J. Electrochem. Soc.*, **106**, 66 (1959).
57. C. C. Roth and H. Leidheiser, Jr., "The Interaction of Organic Compounds with the Surface During the Electrodeposition of Nickel," *J. Electrochem. Soc.*, **100**, 553 (1953).
58. I. Kadija, J. A. Abys, V. Chinchankar, and H. K. Strashil, *Plating and Surface Finishing*, **78**, 60 (1991).
59. J. A. Abys and I. Kadija, U.S. Patent 5,413,692 (1995).
60. Y. Zhang and J. A. Abys, "An alternative Surface Finish for SnPb Solders: Pure Tin," in *Proc. Annual Conference American Electroplaters & Surface Finishers Society,* Cleveland, OH, June 1996.
61. R. Moshohoritou, I. Tsangaraki, and C. Kotira, *Plating and Surface Finishing*, 53 (Feb. 1994).
62. S. Meibuhr and P. R. Carter., *Electrochem. Tech.*, **2**, 267 (1964).
63. M. Carano, "Tin Plating," *Plating and Surface Finishing*, **72** (1995).
64. S. Hirsch, "Tin-Lead, Lead and Tin Plating," in *Metal Finishing, Guidebook and Directory Issue for 1994*, p. 282.
65. M. Jordan, *Electrodeposition of Tin and Its Alloys*, Eugen G. Leuze, Saulgau/Wurtt, Germany, 1995, p. 54.
66. DOS1,956,144.
67. W. R. Johnson, *Stahl and Eisen*, **95**, 301 (1975).
68. R. N. Steinbicker,U.S. Patent 4,073,701 (1978).

69. W. A. Procell,U.S. Patent 2,525,942 (1950).
70. K. Obata et. al., U.S. Patent 4,459,185 (1984).
71. F. I. Nobel et al., U.S. Patent 4,565,609 (1986).
72. F. I. Nobel et al., U.S. Patent 4,7174,60 (1988).
73. G. Karustis et al., U.S. Patent 3,850,765 (1994).
74. Y. Zhang,U.S. Patent 5,750,017 (1998).
75. J. C. Jongkind, *Plating*, 901 (Sept. 1970).
76. F. A. Lowenheim, "Alkaline Tin Plating," in *Modern Electroplating*, F. A. Lowenheim, Ed., McGraw-Hill, New York, 1978, p. 310.
77. G. Humpston and D. M. Jacobson, Eds., *Principles of Soldering*, ASM International, Materials Park, OH, 2004.
78. B. I. Skirstymonskaya, "Electrodeposition of Alloys," *Russian Chemical Review*, **33**(3), 220–233 (1964).
79. P. L. Cavallotti, L. Nobili, G. Zangari, and V. Sirtori, "Tin and Bismuth Substitutes for Electrodeposited Lead," in *Proc. of SURFIN'94*, Indianapolis, IN, 1994, p. 499.
80. V. V. Kuznetsov, T. N. Kuzovkova, *Chem. Abstr.*, **88**, 43103 (1975).
81. A. V. Kasyanov, *Tekhnol. Organ. Proizvod.*, **60** (1970).
82. G. I. Medvedev and G. S. Solovev, *Zh. Prikl. Khim.*, **51**, 2734 (1978).
83. J. C. Jongkind, *Plating*, **722** (July 1968).
84. V. V. Orekhova and L. V. Trubnikova, *Khim. Khim. Teknol.*, **25**, 734 (1982).
85. A. V. Kasyanov, *Teknol. Organ. Proizvod.*, **58** (1973).
86. J. Katayama and K. Okuno, "Solderability of Bismuth-Tin Double Layer Deposits," *Met. Finish.*, **12** (Jan. 1996).
87. T. Murphy, "Tin-Bismuth Alloy Plating, a Fusible Low Temperature Etch for High Aspect Ratio PC Boards," *IPC Tech. Rev.* (Apr. 1992).
88. Z. Mei and J. W. Morris, Jr., "Characterization of Eutectic Tin-Bismuth Solder Joints," *J. Electron. Mat.*, **21**, 599 (1992).
89. S. Arai, U.S. Patent 5,948,235 (1999).
90. M. Kaneko et al., U.S. Patent 6,416,571 (2002).
91. Y. Zhang et al., U.S. Patents 6,726,827 (2004); 6,808,614 (2004); and 6,982,030 (2006).
92. W. M. Cheung et al., European Patent 1,148,548.
93. R. Kiumi et al., "Electroplating Process for Lead-free Bumping in Flip Chip Packaging," paper presented at Advanced Metallization Conference 2003 (AMC2003), Montreal, Canada.
94. R. Shetty, "Pb-Free External Lead Finishes for Electronic Components: Tin-Bismuth and Tin-Silver," paper presented at IEMT/IMC Symposium, April 15–17, 1998, pp. 380–385.
95. S. K. Kang, S. Cuchwalter, and C. Tsang, "Characterization of Electroplating Bismuth-Tin Alloys for Electrically Conducting Materials." *J. Electron. Mater.*, **29**(10), 1278–1283 (2000).
96. "Misconceptions Regarding the Use of Tin-Bismuth Plating in Component Packages," No. PKG-WK-435d, Internal Technical Document, Renesas, Apr. 6, 2005.
97. N. Kubota, T. Horikoshi, and E. Sato, *Metal Finishing*, **53** (Mar. 1984).
98. J. C. Puippe and W. Fluehmann, *Plating and Surface Finishing*, **46** (Jan. 1983).
99. SnAg Technical Data Sheet, Ishihara, 2005.
100. SnAg Technical Data Sheet, Enthone, 2005.
101. Y. Zhang, I. Zavarine, O. Steinius, M. Kleinfeld, C. Rietman, and T. Richardson, "Lead Free Bumping and Its Challenges," in *Proceedings of IWLPC*, San Jose, CA, Oct. 2004.
102. R. Kiumiet al, "Process, Properties and Reliability of Electroplated Lead-Free Solder Bumps," paper presented at the IEEE/ITherm Symposium, 2002, pp. 909–914.
103. R. Beica, K. Wang, and N. Brown, "Tin-Silver Electroplating for Pb-Free Wafer Bumps," paper presented at the Peaks and Plating Symposium, Kalispell, MT, 2003.
104. J. Y. Kim, J. Yu, J. H. Lee, and T. Y. Lee, "The Effects of Electroplating Parameters on the Composition and Morphology of Sn-Ag Solder," *J. Electron. Mater.*, **33**(12), 1459–1469 (2004).
105. B. Kim and T. Ritzdorf, "Electrodeposition of Near-Eutectic SnAg Solders for Wafer-Level Packaging," *J. Electrochem. Soc.*, **150** (9), c577 (2003).
106. B. Ebersberger, R. Bauer, and L. Alexa, "Qualification of SnAg Bumps for Lead-free Filp-Chip Applications", in *Proceedings in ECTC 2004*, pp. 683–691.
107. C. J. Berry and E. Kung, "Electroplated SnAg Wafer Bumping and Assembly Considerations," in *Presentation*, July 15, 2004.
108. R. Kiumi et al., "Void-Free Bumping Process for Lead-Free Solder," paper presented at the Peaks and Packaging Conference, Kalispell, MT, 2006.
109. R. Beica and D. Lau, "Tin-Sivler-Copper Electrodeposition of Lead-Free Wafer Bumps," paper presented at IMAPS 2004, Long Beach, CA.
110. R. Beica, E. Chiu, N. Brese, and A. Chirafisi, "Production Feasibility of Tin-Silver-Copper Electrodeposition for Wafer Bump Applications, Part I," paper presented at IMAPS 2006, Scottsdale, AZ.
111. R. Beica, E. Chiu, N. Brese, and A. Chirafisi, "Production Feasibility of Tin-Silver-Copper Electrodeposition for Wafer Bump Applications, Part II," paper presented at IMAPS 2006, San Diego, CA.
112. G. K. Boeckler, "Measurement of Gloss and Reflection Properties of Surfaces," *Metal Finishing*, 28 (May 1995).
113. C. Xu, Y. Zhang, C. Fan, P. Chiu, and J. A. Abys, "Morphology, Appearance and Tribology of Electroplated Tin Films," *Plating and Surface Finishing* (Sept. 2000).
114. N. M. Osero, "An Overview of Pulse Plating," *Plating and Surface Finishing*, **73**, 20 (1986).
115. J. W. Dini, "Deposit Structure," *Plating and Surface Finishing*, **75**, 11 (1988).
116. W. H. Safranek, *The Properties of Electrodeposited Metals and Alloys*, 2nd ed., American Electroplaters and Surface Finishers Society, Orlando, FL, 1986.
117. T. Kakeshita, K. Shimizu, R. Kawanaka, and T. Hasegawa, "Grain Size Effect of Electroplated Tin Coatings on Whisker Growth," *J. Mater. Sci.*, **17**, 2560 (1982).

118. T. Sonosa, H. Nawafune, and S. Mizumoto, "Properties of Bright Tin-Lead Alloy Deposits from Neutral Gluconate Baths," *P&SF*, **66** (Mar. 1995).
119. Y. Zhang and R. Shetty, "Whisker Growth: The Substrate Effect and Beyond," in *Proceedings of IPC/JEDEC International Conference on Lead-Free Electronics and Assembly*, Dec. 2002.
120. V. J. Kuck, "Analysis of Tin/Lead Solders Using Differential Thermal Analysis," in *Proc. of the North American Thermal Analysis Society Conference*, Sept. 23–36, 1984, p. 306.
121. V. J. Kuck, "Determination of the Liquidus Temperature and Composition of Tin/Lead Solders Using Differential Thermal Analysis," *Thermochim. Acta*, **99**, 233 (1986).
122. Y. Zhang, K. Murski, F. Humiec, and J. A. Abys, "Throwing and Covering Power Evaluations of a Pure Tin Chemistry by Hydrodynamically Controlled Rotating Cylinder Throwing Power Electrode and Hull Cell Studies," presented at *SUR/FIN 97*, Detroit, MI, June 23–26, 1997.
123. MIL-STD 202F, method 208 and J-STD-002 and J-STD-003.
124. J. Haimovich, "Intermetallic Compound Growth in Tin and Tin/Lead Plating over Nickel and Its Effects on Solderability," *Weld. Res. Suppl.*, **102**, 102–111 (Mar. 1989).
125. Y. Zhang, K. Murski, G. F. Breck, J. Maisano, and J. A. Abys, "A Unique Electroplating Solder Chemistry," in *Proc. of IICIT*, Boston, Sept. 1996, p. 255.
126. R. R. Vandervoort, E. L. Raymond, H. J. Wiesner, and W. P. Frey, "Strengthening of Electrodeposited Lead and Lead Alloys, II—Mechanical Properties," *Plating*, **57**, 362 (1970).
127. T. I. Murphy, "The Structure and Properties of Electrodeposited Copper Foil," *Finishing Highlights*, **71** (1978).
128. W. H. Safranek, *The Properties of Electrodeposited Metals and Alloys*, 2nd ed., American Electroplaters and Surface Finishers, 1986.
129. T. F. Battey, N. Nelson, and P. A. Martens, "Etching Electropolished Copper Foil," *PC Fab*, **10**, 60 (1987).
130. Y. Zhang et al., U.S. Patents 6,267,863 (2001); 6,808,614 (2004).
131. C. Herring and J. K. Galt, *Phys. Rev.*, **85**, 1060 (1952).
132. Food and Drug Administration, "ITG #42: Tin Whiskers—Problems, Causes and Solutions," available: http://www.fda.gove/inspect_ref/itg/itg42.htm, Mar. 1, 1986.
133. K. Heutel and R. Vetter, "Problem Notification: Tin Whisker Growth in Electronic Assemblies," Internal Memo, US Missile Program, NASA, Feb. 19, 1988.
134. B. Nordell, "Air Force Links Radar Problems to Growth of Tin Whiskers," *Aviat. Week Space Technol.*, June 20, 1986, pp. 65–70.
135. J. Richardson, and B. Lasley, "Tin Whisker Initiated Vacuum Metal Arcing in Spacecraft Electronics," *Proc. 1992 Government Microcircuit Appl. Conf.*, **18**, 119 (Nov. 10–12 1992).
136. M. Ohring, *Reliability and Failure of Electronic Materials and Devices*, Academic, San Diego, 1998.
137. D.T. Hawkins,"Metal Whiskers, 1945–1975," Internal Document, comprehensive collection of 886 references on metal whiskers, Bell Labs.
138. S. M. Arnold, "Repressing the Growth of Tin Whiskers," *Plating*, **53**, 96 (Jan. 1966).
139. Y. Zhang, G. Breck, F. Humiec, K. Murski, and J. A. Abys, "An Alternative Surface Finish for Tin-Lead Solders: Pure Tin," in *Proceedings of SMI'96*, San Jose, CA, Sept. 1996, pp. 641–649.
140. Y. Zhang and J. A. Abys, "A Unique Electroplating Tin Chemistry," *Circuit World*, **25** (1), 35 (1998).
141. Y. Zhang, C. Xu, C. Fan, and J. A. Abys, "Whisker Growth and Prevention," *J. Surface Mount Technol.*, **13**(4), 1 (2000).
142. Y. Zhang, C. Xu, C. Fan, and J. Abys, "Electroplated Tin and the Whisker Phenomenon," in *Proceedings of UIM Conference*, UIM, Germany, May 2000.
143. Y. Zhang, C. Xu, J. Abys, C. Fan, and A. Vysotskaya, "Understanding Whisker Phenomenon, Part I—Whisker Index and Tin/Copper, Tin/Nickel Interface," in *Proceedings of APEX Expo*, San Diego, CA, Jan. 24–28, 2002, pp. 506-1-1 to 506-1-10.
144. C. Xu, Y. Zhang, C. Fan, and J. Abys, "Understanding Whisker Phenomenon—Part II—Competitive Mechanisms," in *Proceedings of the APEX Expo*, San Diego, CA, Jan. 24–28, 2002.
145. C. Xu, Y. Zhang, C. Fan, and J. A. Abys, "Whisker Prevention," *CircuiTree*, pp. 10–21, May, 2002.
146. Y. Zhang, "Understanding Whisker Growth Phenomenon," in *Proceedings of CALCE Meeting*, University of Maryland, Oct. 10, 2002.
147. C. Xu, Y, Zhang, F. Fan, and J. A. Abys, "Driving Force for the Formation of Sn Whiskers: Compressive Stress-Pathways for its Generation and Remedies for its Elimination and Minimization," *IEEE Transactions in Electronics Packaging Manufacturing*, Tin Whisker Workshop, Las Vegas, NV, **28**, 31–35 (2005).
148. Y. Zhang, C. Fan, C. Xu, O. Khaselev, and J. A. Abys, "Tin Whisker Growth—Substrate Effect. Understanding CTE Mismatch and IMC Formation," in Proceedings of the APEX Expo, 2004.
149. Y. Zhang, C. Fan, C. Xu, O. Khaselev, and J. Abys "Whisker Growth—Substrate Effect," *CircuiTree*, June, 2004.
150. C. Xu, Y. Zhang, C. Fan, and J. A. Abys, "Thin Tin Over Ni—One Strategy for Whisker Minimization," *CircuiTree*, July 2005.
151. P. Harris, *The Growth of Tin Whiskers*, Publication No. 734, International Tin Research Institute, 1994.
152. NEMI Whisker Test Group Definition, NEMI, July 2001.
153. M. E. Williams, C. E. Johnson, K. W. Moon, G. R. Stanford, C. A. handwerker, and W. J. Boettinger, "Whisker Formation on Electroplated Sn-Cu," in *Proceedings of SUR/FIN'2002*, Chicago, IL, pp. 19–30, 2002.
154. U. S. Welzel,"Diffraction Analysis of Residual Stress: Modeling Elastic Grain Interaction," Ph.D. Thesis, University Stuttgart (May 2002).
155. E4 (Infineon, Freescale, ST, and Philips), "Whisker Formation on Tin Plated Cu Leadframes—Results and Conclusions," presentation to NEMI Whisker Test Group, NEMI, Herndon, VA, Oct. 29, 2004.
156. C. A. Handwerker, C. E. Johnson, G. R. Stafford, K. W. Moon, M. E. Williams, W. J. Boettinger, and L. A. Bendersky,

"Investigation of the Mechanism of Sn Whisker Formation on Sn and Sn Alloy Electrodeposits," presentation at NEMI Tin Whisker Workshop, ECTC, Las Vegas, NV, 2004.

157. G. T. Galyon, *IEEE Trans. Electron. Packag. Manuf.*, **28**, 94 (2005).
158. G. W. Stupian,"Tin Whiskers in Electronic Circuits," Aerospace Technical Report No. 92, 1992, pp. 2925–2917.
159. S. C. Britton, "Spontaneous Growth of Whisker on Tin Coatings: 20 Years of Observation," *Trans. Inst. Met. Finish.*, **52**, 95 (1974).
160. M. E. McDowell, *Product/Process Problem Alert Bulletin 9202*, Aerospace Corporation, May 14, 1992.
161. J. H. Davis, M. J. Skove, and E. P. Stillwell, "Superconducting Transition Temperature and Resistivity of Tin Whiskers as a Function of Uniaxial Tension," *Solid State Commun.*, **4** (11), 597 (1966).
162. W. W. Webb, "Stage Steps in the Resistive Transitions of Superconducting Microcrystals," *Sci. Tech. Aerosp. Rep.*, **7** (3), 557 (1969).
163. T. E. Lukens, R. J. Warburton, and W. W. Webb, "Onset of Quantized Thermal Fluctuations in 'One-Dimensional' Superconductors," *Phys. Rev. Lett.*, **25** (17), 1180 (1970).
164. N. A. J. Sabbagh and H. J. McQueen, "Tin Whiskers: Causes and Remedies," *Metal Finishing* (Mar. 1975).
165. B. D. Dunn,"A Laboratory Study of Tin Whisker Growth," Report No. STR-223, European Space Agency, Noordwijk, The Netherlands, Sept. 1987.
166. A. J. Bevolo, J. D. Verhoeven, and M. Noack, *Surf. Sci.*, **134**, 499 (1983).
167. R. A. Konetzki, Y. A. Chang, and V. C. Marcotte, *J. Mater. Res.*, **4**, 1421 (1989).
168. R. G. Miller, and C. Q. Bowles, *Oxid. Met.*, **33**, 95 (1990).
169. S. C. Britton, and K. Bright, *Metallurgia*, **56**, 163 (1957).
170. K. N. Tu, "Irreversible Processes of Spontaneous Growth Mechanism of Tin Whiskers," *Phys. Rev. B*, **49** (3), 2030 (1994).
171. W. J. Choi, T. Y. lee, K. N. Tu, N. Tamura, R. S. Celestre, A. A. MacDowell, Y. Y. Bong, L. Nguyen, and G. T. T. Sheng, "Structure and Kinetics of Sn Whisker Growth on Pb-Free Solder Finish," in *52 Electronic Component & Technology Conference Proceedings*, IEEE Catalog No. 02CH3734-5, San Diego, CA, 2002, pp. 628–633.
172. B. D. Dunn, *E.S.A. Sci. Tech. Rev.*, **2**, 1 (1976).
173. S. M. Arnold, *Electrical Manufacturing*, 110–114, Nov. 1954.
174. S. M. Arnold, *Plating*, **53**, 96 (1966).
175. R. Schetty, "Tin Whisker Growth and the Metallurgical Properties of Electrodeposited Tin," in *Proceedings of the JPC/JEDEC International Conference on Pb-free Electronic Assemblies*, San Jose, CA, May 1–2, 2002, pp. 92–94.
176. NEMI Whisker Test Group Communication, NEMI, Meating Minutes, Herndon, VA, Oct. 2002.
177. K. N. Tu, "Interdiffusion and Reaction in Bimetallic Cu-Sn Thin Films," *Acta. Metall.*, **21** (94), 347 (1973).
178. Klein-Wassink, *Soldering in Electronics*, Electrochemical Publications, LLT, Scotland, 1989.
179. B. G. LeFevre and R. A. Barczykowski, *Wire J. Int.*, **18**, 66 (1985).
180. C. A. Mackay, *Welding Materials Febrication*, 53 (Jan/Feb 1979).
181. V. Simic, and Z. Marinkovic, *J. Less Common Met.*, **72**, 133 (1980).
182. H. A. H. Steen and A. Bengston, *Brazing and Soldering*, **13**, 28 (1987).
183. D. A. Unsworth and C. A. Mackay, *Trans Inst. Met. Finish.*, **51**, 85 (1973).
184. B. Z. Lee and D. N. Lee, "Spontaneous Growth Mechanism of Tin Whiskers," *Acta Mater.*, **46** (10), 3703 (1998).
185. K. N. Tu, "Cu/Sn Interfacial Reactions: Tin Film Case Versus Bulk Case," *Mater. Chem. Phys.*, **46**, 217 (1994).
186. A. Ugli, in *Proceedings of IPC Annual Meeting*, New Orleans, LA, Nov. 2002.
187. Y. Zhang and R. Schetty, "Whisker Growth: The Substrate Effect and Beyond," in *Proceedings of IPC/JEDEC Meeting*, Taipei, Taiwan, Dec. 2002.
188. R. Shetty, "Sn Whisker Growth and the Metallurgical Properties of Electrodeposited Sn," in *Proceedings of IPC/JEDEC International Conference on Pb-Free Assemblies*, San Jose, CA, 2002, pp. 92–94.
189. K. Kujiwara and R. Kawanaka, "Observation of the Sn Whisker by Micro-Auger Electron Spectroscopy," *J. Appl. Phys.*, **51** (2), 6231 (1980).
190. P.-U. Fägerholt *Handbook on Passive Components*, rev. ed., CLR Konsult, 2002.
191. J. Brusse, "Tin Whisker Observations on Pure Tin-Plated Ceramic Chip Capacitors," in *Proceedings of SUR/FIN'2002*, Chicago, IL, June 2002.
192. M. Dittes, P. Oberndorff, P. Crema, and V. Schroeder, "The Effect of Temperature Cycling on Tin Whisker Formation," in Proceedings of IEEE- ECTC, 2003.
193. J. W. Shin and E. Chason, "Stress Behavior of Electroplated Sn Films During Thermal Cycling," *J. Mater. Res.*, **24**, 1522 (2009).
194. NEMI whisker testing group meeting minutes, Texas Instruments, Sept. 12, 2002.
195. K. Whitlaw and J. Crosby, "An Empirical Study into Whisker Growth of Tin and Tin Ally Electrodeposits," in *Proceedings of SUR/FIN'2002*, Chicago, IL, June 2002.
196. G. Gore, "On the Properties of Electrodeposited Antimony," *Trans. Roy. Soc. (London)*, **158** (Part I) (1858).
197. E. J. Millis, "On Electrostriction," *Proc. Roy Soc.*, **26**, 504 (1877).
198. M. Bouty, "Pressures Caused by Electrodeposits," *Compt. Rend.*, **88**, 714 (1879).
199. R. Weil, "The Origins of Stress Measurements," AES Research Project 32, *Plating*, 1231. (Dec. 1970).
200. G. T. Sheng, C. F. Hu, W. J. Choi, K. N. Tu, Y. Y. Bong, and L. Ngugen, "Sn Whiskers Studies by Focused Ion Beam Imaging and Transimission Electron Microscopy," *J. Appl Phys*, **92**, 64 (2002).
201. W. J. Choi, T. Y. Lee, K. N. Tu, N. Tamura, R. S. Celestre, A. A. McDowell, Y. Y. Bong, and L. Ngugen, "Tin Whiskers Studied

by Synchrotron Radiation Scanning X-Ray Micro-Diffraction," *Acta Meterialia*, **51** (20), 6253 (Nov. 2003).

202. E. Chason, N. Jadhav, W. L. Chan, L. Reinbold, and K. S. Kumar, "Whisker Formation in Sn and Pb-Sn Costings: Role of Intermetallic Growth, Stress Evolution and Plastic Deformation Process," *Appl. Phys. Lett.*, **92**, 171901 (2008).
203. "Seals Use Whiskers to Track Prey," *BBC News Online*, July 6, 2001.
204. "SiC Whisker-Reinforced Ceramic Composites," available: http://www.ornl.gov/MC-CPS/sic.htm, Dec. 4, 2002.
205. "Precision, Single Crystal Silicon Micro-Whiskers," Containerless Research, Inc., available: http://www.containerless.com/whisker.htm, Dec. 4, 2002.
206. "Nano Whiskers," GSI Materials Research, available: http://www-wnt.gsi.de/mr/nano_whiskers.htm, Dec. 4, 2002.
207. P. Elmgren,"Lead-Free Connectors—An Overview," Internal Document, Molex, www.Molex.com Aug. 15, 2003.
208. B. Hilty,"Tin Plating at Tyco Electronics," Internal Technical Paper, Tyco, www.Tyco.com June 30, 2006.
209. M. Dittes, "Lead-Free Post-Mold Plating for Semiconductor Devices," in *EFIP2003*, T2-10, Cologne, 2002.
210. "Control of Whisker Growth in Tin Alloy Coatings," Internal Document, STMicroelectronics, www.st.com Apr. 2006.
211. P. Su, S. Bai, M. Ding, and S. Chopin, "The Effects of Plating Parameters on the Microstructure and Whsiker Growth Propensity of Pure Sn Finish."
212. D. Romm,"Selecting the Right RoHS Compliant Finish," Internal Document, Texas Instruments, www. TI.com 2005.
213. Http://www.vishay.com/how/leadfree; http://www.kemet/web/homepage/kechome.nsf/weben/green%20product%20roadmap.
214. A. Yeoh, M. Chang, C. Pelto, T. L. Huang, S. Balakrishnan, G. Leatherman, S. Agraharam, G. Wang, Z. Wang, D. Chiang, P. Stover, and P. Brandenburger, "Copper Die Bumps (First Level Interconnect) an Low–K Dielectrics in 65 nm High Volume Manufacturing," in Proceedings of IEEE-ECTC, San Diego, 2006, pp. 1611–1615.

7

ELECTRODEPOSITION OF CHROMIUM

NENAD V. MANDICH AND DONALD L. SNYDER

Electroplated chromium deposits rank among the most important plated metals and are used almost exclusively as the final deposit on parts. Without the physical properties offered by electroplated chromium deposits, the service life of most parts would be much shorter due to wear, corrosion, and the like. Parts would have to be replaced or repaired more frequently, or they would have to be made from more expensive materials, thus wasting valuable resources.

The thickness of electroplated chromium deposits falls into two classifications: decorative and functional. Decorative deposits are usually under 0.80 μm in thickness. They offer a pleasing, reflective appearance while also providing corrosion resistance, lubricity, and durability. Decorative chromium deposits are typically plated over nickel but are occasionally plated directly over the substrate of the part.

Functional ''hard chrome'' deposits have a thickness customarily greater than 0.80 μm and are used for industrial, not decorative, applications. In contrast to decorative deposits, functional chromium is usually plated directly on the substrate and only occasionally over other electrodeposits, such as nickel. Industrial coatings take advantage of the special properties of chromium, including resistance to heat, hardness, wear, corrosion, and erosion, and a low coefficient of friction. Even though it has nothing to do with performance, many users want their functional chromium deposits also to be decorative in appearance. Functional deposits are also used on parts such as cutting tools and strip steel and are even thinner than decorative deposits.

The most common and oldest commercial type of chromium process utilizes hexavalent chromium (Cr^{6+}) in an aqueous solution containing one or more catalysts. The commercial process of hexavalent chromium plating resulted principally from the work in 1923 and 1924 of Dubpernell [1] and Fink [2]. Liebreich [3] made similar discoveries more or less simultaneously, but his work was masked by an overemphasis of the importance of the trivalent chromium ion.

Early in the 1970s aqueous decorative trivalent chromium (Cr^{3+}) processes started to attain commercial success. It took to the early 2000s for functional (thick deposits) trivalent processes to become available. Most functional trivalent chromium deposits are not crystalline like those produced from hexavalent chromium processes resulting in reduced physical properties.

Noteworthy improvements in hexavalent chromium plating came with the introduction of double- and organic-catalyzed systems. Double-catalyzed (mixed-catalyst) systems introduced in 1949 generally contain sulfate and silicofluoride in forms that are either self-regulating [4] or operator regulated. In comparison to the initial commercial processes that were only sulfate catalyzed, double-catalyzed processes offer higher plating speeds and help activate the part prior to plating by mildly etching the substrate. Fluoride compounds with limited solubility supply the free-fluoride catalyst in self-regulating processes. Undissolved fluoride compounds stayed in the bath until they dissolved to increase the concentration of free fluoride. Operator-regulated baths depend upon the proper additions of free fluoride from outside the tank.

Organic-catalyzed processes have increased plating speeds and improved deposit physical properties, and they do not etch iron substrates. Proprietary organic additives are added from outside the tank to maintain the proper

Modern Electroplating, Fifth Edition Edited by Mordechay Schlesinger and Milan Paunovic

concentration. This process is well suited for functional applications.

For more details on the history of chromium plating, see [1, 5–7]. Blum and Hogaboom [7] emphasize the effect of the introduction of chromium plating on other electroplating processes.

7.1 PRINCIPLES

Unlike most other platable metals, chromium cannot be deposited from an aqueous solution containing the metal ions only. Chromium processes must contain one or more acid radicals that act as catalysts (for hexchromium) or complexers (for trichromium) to bring about or aid in the cathodic deposition of chromium metal. The catalysts most commonly used for double- (mixed-) catalyzed, hexchromium processes are sulfate and fluoride. The fluoride is generally in the form of a complex such as silicofluoride (SiF_6^{2-}) [8], since simple fluorides are effective in such small quantities that process control becomes difficult. For successful continuous operation, the ratio (by weight) of chromic acid to total catalyst acid radicals must be maintained within definite limits: preferably about 100 : 1 in the case of sulfate [2, 3].

Proprietary organic additives introduced in the mid-1980s are used in conjunction with sulfate for organic-catalyzed, high-speed hexavalent chromium processes. Since fluoride is not used, these processes do not etch steel, which could contribute to a buildup of iron contaminate. Concentrations of hexavalent chrome, sulfate, and organic acids must be controlled within range to operate. These processes can also operate at higher temperatures than other hexavalent chromium processes, permitting the use of higher current densities to obtain faster plating speeds.

The conductivity and density of pure chromic acid solutions are shown in Figure 7.1. They are based on measurements made at the National Institute for Standards and Technology (NIST) [9] (originally named the National Bureau of Standards, NBS). Small amounts of Cr(III) (Cr^{3+}, trivalent chromium) and other cations decrease the conductivity. The maximum conductivity is not achieved until a concentration of 400–500 g L^{-1} chromic acid is reached. Commercial chromium plating processes generally use baths containing 200–400 g L^{-1} chromic acid in order to obtain the best conductivity possible, along with acceptable current efficiency, satisfactory deposits, and stable, easy-to-maintain solution composition. In practice, chromic acid concentrations are increased to overcome the effect of contaminates that decrease bath conductivity. Higher chromic acid concentrations increase solution losses due to higher drag-out, resulting in an increased requirement for solution recovery or waste treatment. The specific gravity of the baths provides a rough measure of the concentration of chromic acid, especially if due allowance is made for other salts known to be present.

Sulfate is ordinarily present in all hexavalent chromium plating baths, because even the best commercial grades of chromium trioxide (CrO_3) contain sulfate as an impurity. Chromium trioxide, also called chromium anhydride, is the most common source of hexavalent chromium ions. Even though chemically incorrect, chromium trioxide is usually referred to as chromic acid. The acid is actually formed in aqueous solution.

Sulfuric acid and sodium sulfate are the most common sources of additional sulfate; fluorosilicic acid and silicofluorides [8] are the most common sources of fluoride. References to the amount of catalytic agent or acid radical in a bath usually mean the total quantity of sulfate and fluoride ions, although the method of determining those may vary among the processes and needs to be well understood when using a particular process.

Although the current efficiency in hexavalent chromium plating baths is low (generally between 10 and 25%, depending on the process), a fairly high rate of bright plate is obtained when relatively high current densities are used. Figure 7.2 shows deposits offering the best physical properties. In this figure the semidashed lines *A* and *B* circumscribe bright plate areas of low and high concentrations of chromium trioxide, respectively. The complete bright plating area is circumscribed by line *X*.

The voltages required are higher than in most other electroplating processes, generally 4–12 V depending on operating conditions. Also the high current and voltage must be applied with very low ripple [the percentage of alternating current (ac) superimposed on the direct current (dc)]. Consequently rectifiers used must have a lower ripple and higher capacity for chromium plating than is required for most other metal plating, but this disadvantage has not seriously hindered the widespread and increasing use of this process.

The throwing power (coating distribution over the part's current density range) of hexavalent chromium plating is relatively poor compared to most other platable metals such as nickel. Trivalent chromium processes have much greater throwing power and closely approximate that of Watts-based nickel processes. However, usable coverage is obtainable with hexavalent chromium processes even in the plating of irregular shaped articles if the optimum bath conditions are carefully maintained. Special auxiliary anodes, masks, and shields are sometimes used in order to cover deep hollows or recessed portions and especially used to obtain more uniform thickness. These techniques are similar to those used with other plating processes but must be designed in

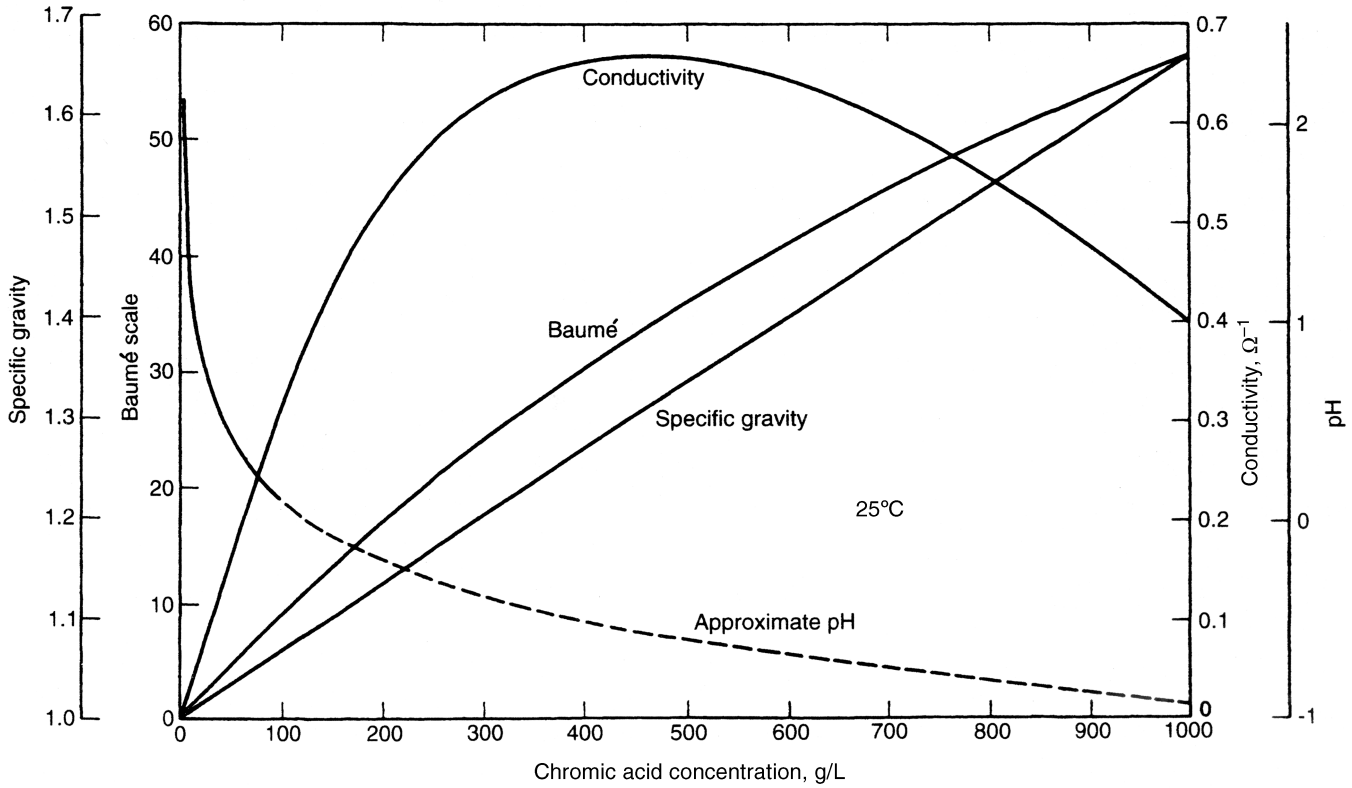

FIGURE 7.1 Some physical properties of chromium plate.

accord with established principles of ample size for current-carrying requirements and proper spacing for uniform current distribution.

Proprietary complexers in the form of organic acid radicals stabilize the trivalent chromium ions in an aqueous, pH 2–4, solution [10, 11]. Sulfates and chlorides, in varying amounts, are used to increase bath conductivity. Commercial trivalent chromium formulations are much more complex than hexavalent chromium formulations and, at present, are all proprietary. Trivalent processes plate between two and three times faster than hexavalent chromium processes at much lower current densities.

The current altering techniques used in hexavalent chromium processes are not typically necessary with trivalent chromium processes, since both the throwing and covering (ability to plate in low current density) powers are better than those of hexavalent chromium processes. Since they are already present, sulfate and chloride ion concentrations do not have to be tightly controlled in trivalent chromium processes as is required in hexavalent chromium processes. Hexavalent chromium processes, on the other hand, are less sensitive to metallic contamination than trivalent processes, but metallic contaminates are easily removed from trivalent processes by continuous bath circulation through ion exchange resins. Organic contamination can usually be removed by carbon filtration. Bath operation and maintenance for trivalent chromium processes are much closer to what is required for nickel processes than for hexavalent chromium processes. Very little process information has been published for trivalent chromium processes because it is still kept proprietary, much new, and several different chemistries are commercially available.

7.2 THEORY OF CHROMIUM ELECTRODEPOSITION

A typical transition element, chromium forms many compounds that are colored and paramagnetic. Chromium has oxidation states as follows: -2, -1, 0, $+1$, $+2$, $+3$, $+4$, $+5$, $+6$; the highest oxidation state, $+6$, corresponds to the sum of the numbers of 3d and 4s electrons. The lowest, -2, -1,0, and $+1$, are formal oxidation states displayed by chromium in compounds such as carbonyls, nitrosyls, and organometallic complexes.

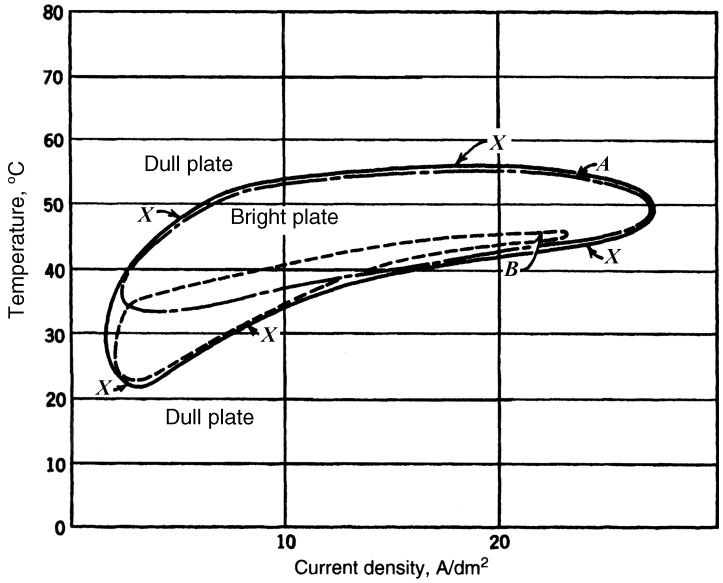

FIGURE 7.2 Bright plating range.

Divalent chromium in the oxidation state $+2$ was not considered in the past to be of particular interest for etectrodeposition mechanisms. It does play a role, however, in the passivation of chromium. Recently it has been recognized that, probably, it plays a role in the deposition and dissolution mechanisms. The outstanding characteristic of the Cr^{2+} ion (sky blue in aqueous solution) is its strength as a reducing agent $Cr^{3+} + e \leftrightarrow Cr^{2+}$, $E_0 = 0.41$ V. Because it is easily oxidized by oxygen, preservation of the solution requires exclusion of air. Even under such conditions the Cr^{2+} ion is oxidized by water with the formation of hydrogen. The rate of oxidation depends on several factors, including the acidity and anions present.

It has been known for some time [12] that pure chromium (usually obtained electrolytically) dissolves in acids to form Cr^{2+} with no (or very little) Cr^{3+} if the solution is protected from air; impurities apparently catalyze formation of Cr^{3+}. Chromium $(+2)$ solutions may also be obtained [13, 14] by electrolytic reduction of Cr^{3+} chromium $(+3)$.

Chromium $(+3)$ is the most stable and most important oxidation state of the element. The E_0 values [15] show that both the oxidation of Cr^{2+} to Cr^{3+} and the reduction of Cr^{6+} to Cr^{3+} are favored in acidic aqueous solutions. The preparation of Cr^{3+} compounds from either state presents few difficulties and does not require special conditions [16].

The chemistry of Cr^{3+} in aqueous solutions is coordination chemistry. It is demonstrated by the formation of kinetically inert outer orbital octahedral complexes. The bonding can be explained by $d^2 sp^3$ hybridization; a great number of complexes have been prepared. The kinetic inertness results from the $3d^3$ electric configuration of Cr^{3+} ion [17]. The type of orbital charge distribution makes liquid displacement and substitution reactions very slow and allows separation, persistence, and/or isolation or Cr^{3+} species under thermodynamically unstable conditions.

Chromium $(+3)$ is characterized by a marked tendency to form polynuclear complexes. Literally thousands of Cr^{3+} complexes have been isolated and characterized and, with a few exceptions, are all hexacoordinate. The principal characteristic of these complexes in aqueous solution is their relative kinetic inertness. Ligand displacement reactions of Cr^{3+} complexes have half-times in the range of several hours. It is largely because of this kinetic inertness that so many complex species can be isolated as solids and that they persist for relatively long periods in solution, even under conditions of marked thermodynamic instability.

The hexaaqua ion $[Cr(H_2O)_6]^{3+}$, which is a regular octahedral, occurs in numerous salts, such as the violet hydrate $[Cr(H_2O)_6]Cl_3$, and in an extensive series of alums, $MCr(SO_4)_2 \cdot 12H_2O$, where M usually is NH_4^+ or K^+ ion. The aqua ion is acidic ($pK = 4$), and the hydroxo ion condenses to give dimeric hydroxo bridged species.

On further addition of base, a precipitate is formed that consists of H-bonded layers of $Cr(OH)_3(H_2O)_3$, which readily redissolves in acid. Within 1 min, however, this precipitate begins ''aging'' to an oligomeric or polymeric structure that is much less soluble [18–20].

The Cr^{3+} ion may also polymerize, as a result of hydrolysis and associated reactions, to form bridged complexes with a certain composition whose existence is indicated by indirect but substantial evidence. Complexes of this type range from dimers through polymers of colloidal dimensions to precipitated Cr^{3+} hydroxide. Except under special circumstances, such reactions are inevitable in neutral and basic solutions and highly probable in slightly acid solutions,

What makes the chemistry of Cr^{3+} complexes interesting and often difficult for researchers is the large number of steps and mechanisms possible. The processes include aquation, hydrolysis, olation, polymerization, oxolation and anion penetration.

7.2.1 Aquation

Chromium salts (chloride, sulfate, nitrate, etc.) are aqua complexes characterized by ions such as $[Cr(H_2O)_6]^{3+}$, $[Cr(H_2O)_5Cl]^{2+}$, and $[Cr(H_2O)_4Cl_2]^{+1}$. In aqueous solutions the replacement of coordinated groups by water molecules (aquation) is a common reaction: $[CrA_5X]^{2+} + H_2O \leftrightarrow [CrA_5H_2O]^{3+}$, where A is a singly coordinated neutral molecule and X is a singly charge coordinated negative ion (e.g., Cl, CN, CNS).

The extent of aquation depends on several factors, including the relative coordinating tendencies of H_2O and X and the concentration of X. Accordingly every aqueous solution of Cr^{3+} is potentially a solution of aqua complexes. The Cr^{2+} ion (whose complexes are labile) catalyzes such reactions, which are usually quite slow otherwise. Electron-transfer reactions between Cr^{2+} and $[Cr(H_2O)_5]^{+}$ proceed predominantly through bridged intermediates $\{[CT–X–Cr]^{4+}\}$. Ligand transfer accompanies electron transfer. In the investigations establishing these conclusions, the reaction conditions have generally been characterized by relatively low $[Cr^{2+}]$ and relatively high $[H^+]$. With relatively high $[Cr^{2+}]$ and relatively low $[H^+]$, another pathway is available [21] with the rate determining reaction involving a hydroxy bridged complex: $[(H_2O)_4–X–CrOHCr_6]^{3+}$.

The role of Cr^{2+} is very important, however, in industrial ''hard'' chromium applications when plating thick layers of chromium or Cr–Ni and/or Cr–Ni–Fe alloys from trivalent chromium solutions, as an alternative for Cr(+6)-based solutions. Failure to control the transient levels of Cr^{2+} is recognized as the reason for Cr(+3)-based solutions not to sustain heavy deposition with an appreciable deposition rate. The problem is recognized as massive olation, catalyzed by a buildup of Cr^{2+} in the high-pH region in the vicinity of the cathode. Although the bulk of the electrolyte can be about pH 2, the diffusion layer can reach pH 4. At this pH and with Cr^{2+} promoted catalysis, oligomeric species are released into the bulk of the electrolyte, where they can build up and reduce the level of active species and, consequently, the deposition rate [22–25].

7.2.2 Hydrolysis

The behavior of aqua complexes as acids leads to far-reaching consequences. The acidity of such solutions arises because of the $[Cr(H_2O)]^{3+} \leftrightarrow [Cr(H_2O)]^{2+} + H^+$ reaction. The equilibrium can be displaced to the right by heating and, of course, by the addition of base. The order of magnitude of the first hydrolysis constant is $K = 10^{-4}$. As the pH of the Cr^{3+} solution is raised, the equilibrium is shifted, and more of the coordinated water molecules are converted to OH groups, which brings into the picture a new process called *olation*.

7.2.3 Olation

Olated compounds are complexes in which the metal atoms are linked through bridging with OH groups. Such a group is designated as an *ol* group to distinguish it from the *hydroxo* group (i.e., a coordinated OH linked to only one metal atom). The process of formation of ol compounds from hydroxo compounds is called olation. Olation results from the formation of polynuclear complexes consisting of chains or rings of Cr^{3+} ions connected by bridging OH groups. The first step of this process may be as follows [26]:

$$[Cr(H_2O)_6]^{+3} + [Cr(H_2O)_5OH]^{+2} \rightarrow [(H_2O)_5Cr\ \ Cr(H_2O)_5]^{+5} + H_2O \quad (7.1)$$

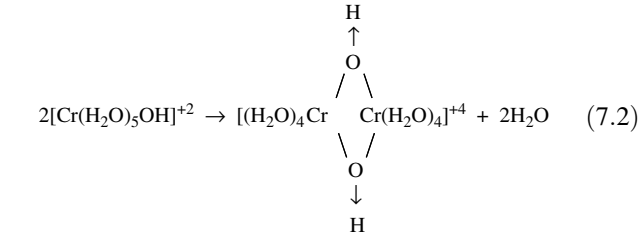

$$2[Cr(H_2O)_5OH]^{+2} \rightarrow [(H_2O)_4Cr\ \ Cr(H_2O)_4]^{+4} + 2H_2O \quad (7.2)$$

Because the *diol* produced by reaction (7.2) is stabilized by the four-member ring, there is a driving force tending to convert the singly bridged to a doubly bridged complex. This diol is produced by polymerization of $[Cr(H_2O)_5OH]^{2+}$, oxidation of Cr^{2+} by molecular oxygen, warming an equimolar mixture of Cr^{3+} and NaOH, and boiling an aqueous solution of $[Cr(H_2O)_6]^{3+}$.

The diol and any other polynuclear products containing water molecules (or a group that can be displaced by, water molecules) can still act as acids, releasing hydrogen ions and leaving coordinated OH groups.

7.2.4 Polymerization

Instead of reaching a definite termination, reaction (7.2) may continue, with the formation of larger and larger molecules, the polymers, as a continued process of olation. This will occur if the product of each successive step contains aqua or hydroxo groups. The ultimate consequence is precipitation of chromium hydroxide, $Cr(OH)_3 \times H_2O$, a tridimensional olated complex [27]. Olation reactions are pH and time dependent. At moderate acidity they are quite slow. It can take days for higher oligomers to be formed after addition of the base to aqueous Cr^{3+} solution, but they will subsequently decay, contributing to pH stabilization after a few weeks [28].

The continued process of olation starts with the hydrolysis of salts of such metals as Al or Cr. The acidity of solution of such salts results from conversion of aqua to hydroxo groups: $[Cr(H_2O)_6]^{3+} \leftrightarrow [Cr(H_2O)_6OH]^{2+} + H^+$. The degree of hydrolysis increases as the temperature is raised, and this relationship depends on the nature of the anion, and especially on the pH of the solution. If alkali is added to a warm solution of hydrolyzed chromium salt, but not enough for complete neutralization, polymerization occurs instead of precipitation of the basic salt or hydroxide.

Because of the octahedral configuration of complexes of metals such as chromium, the bonds of a given metal occur in pairs, each of which lies in a plane perpendicular to the planes of the other two pairs. Accordingly such cross-linked polymers are three dimensional.

The process of olation is favored by an increase in concentration, temperature, and basicity. The process reverses slowly when the solution of olated complexes is diluted or when the solution is cooled (i.e., olation decreases the reactivity of coordinated OH groups).

7.2.5 Oxolation

Oxolation may accompany or follow olation, particularly if the reaction mixture is heated. This reaction converts bridging OH^- groups to O^- groups. Olation and oxolation account for changes in reactivity of chromium hydroxide as it ages. Freshly precipitated chromium hydroxide usually dissolves quite rapidly in mineral acids, but after standing some hours, it becomes difficult to dissolve. Presumably olation continues in the precipitate; because bridged OH^- groups react more slowly with acids than singly coordinated OH^- groups, the reactivity of the precipitated hydroxide progressively diminishes. If the hydrate is heated, there is a drastic decrease in reactivity as a result of oxotation, a process even more difficult to reverse than olation. While olation and oxolation are both reversible, the long times required for the acidity of solutions, which have been heated and then cooled, to return to the original values lead to the conclusion that deoxolation is extremely slow. In general, ol groups are more readily depolymerized than oxo compounds because protons react more rapidly with oxo groups.

7.2.6 Anion Penetration

It is well known that the addition of neutral salts to a solution of basic sulfate changes the hydrogen ion concentration. Coordinated water molecules, OH^- groups, OH bridges, or other ligands are replaced by anions in the solution. The extent to which anion penetration occurs with ol complexes is determined by the relative coordination tendencies of the entering anions and the groups that they replace and the length of time that the solutions are allowed to stand [29]. Anions that can enter the coordinated sphere easily and displace OH groups can effectively prevent olation. Penetration by anions into basic chromium complexes decreases in the following order [30]:

Oxalate > glycinate > tartarate citrate > glucolate > acetate > monochloracetate > formate > sulfate > chloride > nitrate > perchlorate

Consequently, if a solution of $[Cr(H_2O)]^{3+}$ is required, the only anion that should be weakly coordinated is nitrate or perchlorate because anions of greater coordinating tendency will displace one or more of the coordinated molecules. In a stock solution of basic chromium sulfate, Serfas et al. [29] found ionic species having molecular weights of 68,000.

7.2.7 Reaction Rates

In a system containing Cr^{3+} complexes, after a parameter is changed, the corresponding change in composition of the complexes generally occurs only slowly. Heating a solution (or dispersion) of such complexes promotes olation and oxolation, both of which reverse at a low rate when the system is cooled. Reversal of oxolation is much slower than reversal of olation. If the pH of a solution containing olated complexes is reduced to a value at which normally only monometric Cr^{3+} complexes would exist, it may take a long time for the state of aggregation corresponding to the new pH to be attained.

7.3 HEXAVALENT CHROMIUM

The mechanisms of the electroreduction of chromic acid are of great interest, not only from a theoretical point of view but also for their application in industry. The vast majority of decorative, and almost all hard, chromium plating is carried out using CrO_3 as the electrolyte. The fact that chromium can be deposited from Cr^{6+} solutions but not from simple aqueous solutions of lower valency salts is a disadvantage for the following reasons:

1. Because the electrochemical equivalent of Cr in a CrO_3 solution is $0.3234\ g\ h^{-1}$ and cathode current efficiency is typically 10–20%, the passage of current of 1 Ah yields only 0.032–0.064 g of metal. This is 15–30 times

less than for nickel, 18–36 times less than for copper from acid solution, and 63–126 times less than for silver. The only way to offset this is to increase the working current density via increase in mass transport and temperature and/or plating time.

2. The minimum current density at which electrodeposition takes place is two to three orders of magnitude larger than in the case of other metals (Zn, Ni, Sn, Ag, Au, etc.).
3. The electrodeposition of chromium is more sensitive to operating conditions (temperature and current density) than any other deposition process.
4. In contrast to other processes, the cathodic current efficiency varies inversely with temperature but is proportional to current density (which causes low throwing power).
5. Chromium will plate only in the presence of a catalyst (e.g., H_2SO_4), whose concentration influences the plating rate.
6. On the positive side, hexavalent chromium electrolytes are relatively less sensitive to the presence of impurities, and the anode material is lead or lead alloys, which can easily be made to conform to any shape.

Despite its paramount technological importance and with all the advances of modern science and instrumentation, the exact mechanisms of chromium electrodeposition are still open to considerable conjecture. The main difficulty is the necessary formation and presence of a cathodic film on the surface of the metal being plated. The argument of whether the reduction of Cr^{6+} ions to chromium is direct or indirect developed during the last decade into a discussion of whether or not the cathodic film is useful (and in what way it should be modified to improve the process, inasmuch as the existence of this film is no longer in question).

Because of the absence of complete understanding of the deposition mechanism, it is important to understand the chemistry of chromium with all its intricacies of condensation, polymerization, number of different valence states, ability to make anion/cation compounds [e.g., $Cr_2(Cr_2O_7)_3$], existence of a number of double salts (alums), isomers, oxyhydrates, and so on. Virtually all Cr^{3+} compounds contain a Cr–O unit.

7.3.1 Chromic Acid

The primary Cr–O bonded species is chromium (+ 6) oxide, CrO_3, which is better known as chromic acid, the commercial and common name. This compound is also known as chromic oxide and chromic acid anhydride. Chromium (+ 6) forms a large number and considerable variety of oxygen compounds, most of which may be regarded as derived from Cr^{6+} oxide. These include the oxy-halogen complexes and chromyl compounds, chromates, dichromates, trichromates, tetrachromates, and basic chromates. All these Cr^{3+} compounds are quite potent oxidizing agents, although kinetically they cover a wide range.

Chromic trioxide has a molecular weight of 100.01 and forms dark red prismatic crystals belonging to the orthorhombic system, the bipyramidal subclass. The density of the solid is $2.79\,g\,cm^{-3}$. It melts with some decomposition at 197°C. CrO_3 is very hygroscopic. Its solubility in water varies from 61.7% at 0°C to 67.5% at 100°C. Oxidation potentials of CrO_3 and chromate solutions are augmented by increasing the acidity of the solution. Chromic acid, H_2CrO_4, is not known except in solution, where it shows a marked tendency to form polyacids by elimination of water [31].

The change from $H_2Cr_2O_4$ to $H_2Cr_2O_7$ is rapid, but further polymerization takes measurable time. The color of CrO_3 indicates that it is itself highly polymerized, for it is redder than the di- or trichromates and is approached in color by the tetrachromates. De-polymerization of CrO_3 solution in water is very rapid. It also seems to depolymerize on heating.

7.3.2 Chromates and Dichromates

Chromates are salts of the hypothetical chromic acid H_2CrO_4. Salts of the hypothetical polybasic chromic acids, $H_2Cr_2O_7$, $H_2Cr_3O_{10}$, $H_2Cr_4O_{13}$, are known as dichromates, trichromates, tetrachromates, and so on.

The chromate ion and most of the normal solid chromates are yellow, but upon acidifying, the solutions change colors through orange to red. The dichromates are red in the solid state and in solution. The higher polychromates are even of deeper red than the dichromate in the solid state. Although the various ions, CrO_4^-, $Cr_2O_7^{2-}$, $Cr_3O_{10}^{2-}$, $Cr_4O_{13}^{2-}$, and so on, exist together in equilibrium in solution, the ions higher than dichromate exist only in the most concentrated solutions. Water is easily added to the higher polychromate ions, causing them to revert to the dichromate. On further dilution, even the dichromate ion adds water, forming the chromates. The $HCrO_4^-$ ion exists in quantity only in dilute solution, according to Udy [32], but more recently Raman spectroscopy proved nonexistence of $HCrO_4^-$ ions in dilute and concentrated solutions [33–36].

7.3.3 Polychromates

Potychromate ions are of particular interest because of their role in chromium plating from hexavalent solutions. It is recognized and accepted that chromium cannot be electrodeposited from Cr^{6+} solutions without the addition of a catalyst, usually in the form of the sulfate. Because the strength of commercial solutions is customarily 1–3 M, at this concentration, considering the low pH and taking into account the dark red color of the solution, at least the tri- and possibly the tetrachromate ions are present. It should be noted

that in the absence of electric current, the pH of the chromium plating solution is subject to considerable variation, depending on the initial concentration of chromic and sulfuric acids. If the amount of CrO_3 is increased from 10 to 300 g L^{-1} (0.1–3 *M*), the pH changes from 1.4 to 0.08. Martens and Carpeni [37] using radioactive chromium measured the autodiffusion coefficients of isopolychromates at 25°C in aqueous solution as a function of concentration. They found that in the plating operating ranges ($1.5 < CrO_3 < 3.5$ mol L^{-1}), the predominant species are di- and trichromate ions.

The dominant role of trichromates in chromium deposition is advanced by Hoare [38]. According to his model, in the absence of the bisulfate ion (or sulfate, which at low pH dissociates to bisulfate) the trichromate ion will in successive steps (of electron transfer and loss of oxygen and reaction with H_3O^+ ion) decompose to chromous hydroxide and dichromates, which in turn may undergo condensation with other chromates to regenerate trichromates. The process then includes an intermediate step of formation of chromic ($+3$), then chromous ($+2$) dichromates, finally discharging at the cathode as black chromium at very low current efficiency. In the presence of sulfates, the next step of the reduction mechanism is the formation of a complex between the Cr^{2+} hydroxide and the bisulfate through hydrogen bonding:

$$Cr(OH)_2 \Leftrightarrow Cr = O + H_2O \tag{7.3}$$

$$Cr = O + HSO_4^- \Leftrightarrow {}^{+\delta}Cr{-}OH \ldots O{-}SO_3^- \tag{7.4}$$

where the ellipses represent the hydrogen bond and $^{+}\delta$ represents a dipole generated on the chromium end (left side) of the complex. Now, the positively charged complex may be specifically adsorbed on the cathode, two electrons transferred to this end on configuration with formation of metallic Cr and regeneration of HSO_4^-:

$${}^{+\delta}Cr{-}OH \ldots O{-}SO_3^- \xrightarrow{2e^-,2H^+} Cr^0 + HSO_4^- + H_2O \tag{7.5}$$

According to this model, the chromic–dichromate complex is necessary to protect the Cr^{3-} from forming stable Cr (3^+) aquocomplexes. As a refinement of this model, the HSO_4^- ion has a dual role—it also ''blocks'' other chromium atoms in trichromate ions from being reduced (leading to Cr^{3+} aquocomplex formation). The ideally protected trichromate ion would be

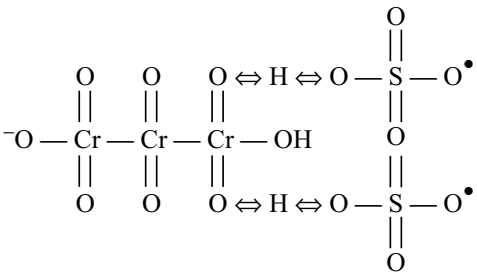

(7.6)

This would leave one end [the right side of (7.6)] protected, preventing formation of unwanted dichromatic chromate complex, decomposition of which would lead to unwanted $[Cr(H_2O)_6]^{3+}$ formation. This also explains the narrow range ($CrO_3 : HSO_4^- = 100 : 1$) of bisulfate concentration in the chromium plating solution. Too little HSO_4^- will cause insufficient protection of the Cr at the right end of the trichromate ion (undercatalization); too much will block the left-end Cr, which is necessary for reactions (7.3)–(7.6) and Cr deposition (overcatalization).

According to Hoare [39, 40] for fluoride-catalyzed CrO_3-based plating systems, almost the identical mechanism is proposed in which F^- plays the role of blocking agent and catalyst. Although not complete, this mechanism is the most accepted to date. The incompleteness of his remarkable theory is that it treated the chromium deposition mechanism without reference to the structure and influence of the liquid layer adjacent to the cathode (L-film), which is formed at the beginning of the cathodic process and is continuously forming and re-forming in the steady-state condition.

Research originating in Russia is extensive on the L-film formation and reactions that occur in the film. They recognized quite early its decisive importance for the deposition mechanism in general and for current efficiency in particular. On the other hand, it is a well-known fact that halide ions (X) such as Cl^- and F^- have a marked improving effect on the cathode current efficiency of chromium electro deposition as recently reported [41].

Because the hydration of halide anions is incomplete, they can penetrate the hydrogen layer and be absorbed onto the metal surface. X-ray photoelectron spectroscopy (XPS) results [41] show that F^- and Cl^- ions, which are stable in the chromic acid bath, may participate in the film formation. The probable activation steps of halides are the absorbed halide first penetrates the hydrogen layer at the chromium surface and then forms a bridged transition surface complex. The electrons on the cathode are transferred to Cr^{3+} through halides, and Cr^{3+} is reduced to metallic chromium. By the formation of the transition complex, the activation energy of the reduction of Cr^{3+} to Cr^0 is decreased. The overpotential of chromium deposition apparently is decreased, which facilitates chromium electrodeposition. The rate of reaction follows a first-order rate equation [42]. In case of a rotating cylinder, the specific reaction rate constant was found to increase with increasing rotation speed up to a limiting value which is reached with further increase in the rotation speed. A study of the reaction mechanisms has shown that at a relatively low rotation speed the reduction of chromium is partially controlled by diffusion; at higher speeds the reaction becomes kinetically controlled. Agitation (cylinder rotation) increases the rate of chromium reduction by decreasing the degree of cathode coverage by hydrogen bubbles, consequently increasing the effective cathode area [43, 44]. In this sense it seems that nonstationary currents can be of great

advantage, since the current interruptions and/or current reversal can promote hydrogen liberation [45]. In addition the use of current pulses interrupts the nucleation and resulting crystal growth. Each pulse enables a fresh renucleation with the net effect of refining the structure and size of grains. Grain consolidation appears to interfere with the accumulation of internal stresses and to act as an inhibitor of crack formation, as noted in earlier studies [46].

As reported in a recent paper [35], an X-ray diffraction study was done to identify the predominant species in an industrial CrO_3–H_2O system. Structural analysis showed that dichromate ions may have maximum likelihood, but that linear trichromate ions may also exist in significant concentrations. This study also concluded that formation of a complex shown in (7.6) can be hardly assumed because of steric hindrance and that it is more realistic that one HSO_4^- ion reacts with polychromate.

A recent paper [47] studied the existence of various chromium complexes in CrO_3/H_2SO_4 plating solutions for different $X = CrO_3/H_2SO_4$ ratios. They concluded that although five different chromium complexes exist, the reduction to metal proceeds only from the following type of complexes $[HSO_4]_n^- \cdot [Cr_2O_7]_m^{2-}$, where $n = 1$, $m = 1$, and $25 < X < 150$–200. They concluded that those complexes are characterized by a single hydrogen bond between two ions in the complex.

In another recent paper on chromium mechanisms [48], potentiodynamic and impedance measurements are used to further corroborate their mechanism of deposition, based on formation of a cathode film (with solid and liquid phases) consisting of oxide–hydroxide Cr^{3+} compounds. It is felt that an in situ method is needed to study the deposition mechanisms under both transient and steady-state conditions.

Pressure from environmentalists is leading to research regarding the issue of replacing Cr^{6+} solutions by the less toxic Cr^{3+}. At the same time it becomes obvious that mechanisms of deposition from trivalent and hexavalent solutions are rather intertwined and that in both cases chromium coordination chemistry is heavily involved.

Despite the flurry of research on chromium deposition mechanisms in the 1950s, 1960s, and 1970s, the flow of papers on chromium was later reduced to a trickle. The reason is the complexity of the problem and the difficulties involved in the highly colored, highly concentrated solutions of chromium salts, the number of different valence states involved, and general lack of in-depth information regarding chromium coordination chemistry.

What further complicated the matter is that at the onset of the deposition process one set of reactions occurs—formation of a compact film independent of the anions present with a rather thin profiles, $5\ mg\ m^{-2}$. Some Russian workers use the term ''product of partial reduction of $Cr^{6+} \rightarrow Cr^{3+}$,'' and this film forms in the first branch of the chromium polarization curve, at potentials up to about 700 mV. Once this film is formed (the C-film, short for compact film), another cathodic film (layer) is formed on the surface of the C-film and closer to the bulk of the solution—the L-film (short for liquid film).

Yoshida et al. [49] studied the behavior and composition of a cathode film with the help of radioactive tracers in the form of ^{35}S radioactive-labeled sulfuric acid and over-the-counter, high-grade CrO_3 treated with radiation to obtain ^{51}Cr as a tracer. A special, rather simple plating cell was constructed with a rapid rinsing station. In essence, a steel cathode was plated for a short time, so that the C- and/or L-films were formed and could be analyzed. Because the L-film is liquid and soluble in either hot plating solution or hot alkali, by dissolution or simple brushing, its formation and influence on the deposition of metallic chromium was studied. By initially forming the C- and L-films with radioactive-labeled Cr or H_2SO_4 and plating in pure (unlabeled) solution, and vice versa, they came to these important conclusions:

1. The cathode film is composed of two layers with different forming properties in terms of thickness and composition. The outer layer, referred to as the L-film, and the inner layer, the C-film, differ in that the L-film contains sulfate ions and dissolves easily in the electrolyte and is about 10 times thicker than the C-film.
2. The C-film has a mass of about $5\ mg\ m^{-2}$, contains very few sulfate ions, and does not dissolve easily in the electrolyte.
3. The cathode film itself is not reduced to metallic chromium, which is deposited from a separate chromium complex compound that passes through the cathode films (C and L) from the bulk of the solution.
4. In the electrolyte, the L-film vigorously repeats the dissolving and forming cycles, while the C-film remains constant, once formed.
5. The cathode film may be a chromium hydroxy *aquo* complex or primarily an oxolated version of this compound. Assuming that the cathode film is formed from such chromium complexes, the authors suggest that the L-film is a compound with lower molecular Weight, while the C-film is a large complex with a high degree of polymerization.

Kimura and Hayashi [50] also used sulfates labeled with radioactive ^{35}S to overcome the difficulties of determining the amount of sulfate in the cathode film. They used standard analytical methods (because of the relatively small content) to study sulfate content in the cathodic film which is formed during potentiostatic polarization of 0.4, 1.5, and 2.5 M CrO_3 baths on Fe, Au, and Pt cathodes. They found that the sulfate content is directly related to the potential in the region of

−0.6 to −1.0 V, which in turn is controlling the state of the cathode surface (L-film formations) and the accompanying electrochemical reactions. In the region of −0.2 to −0.8 V, where current is increasing (C-film), sulfate content was negligible for Pt, Au, and Fe cathodes. In the region > −0.8 V, where current starts to decrease and L-film starts to form, sulfate concentration increases sharply. In the potential regions between −1.0 and −1.1 V (beginning of Cr deposit region), the sulfate concentration in the film drops as a result of liberation of sulfates from the complexes, At potentials more than −1.1 V, the sulfate concentration increases slightly again because of inclusion in the cracks and imperfections in metallic chromium deposits. They also found that as sulfate concentration in a 0.4 *M* CrO_3 bath is increased from 0.002 *M* (200 : 1) to 0.008 *M* (50 : 1), sulfate content in the L-film tends to increase. A temperature increase has a similar effect, while an increase in CrO_3 concentration at constant ratio has the opposite effect. At any given CrO_3 concentration, the maximum amount of sulfates in the L-film is predictably in a 100 : 1 ratio of sulfuric acid. The authors also investigated the influence of other anions in addition to H_2SO_4. Specifically, HCl or KBr (0.01 *M*) added to 1.5 *M* CrO_3 + 0.01 *M* H_2SO_4 solution considerably increased the sulfate content of the L-film, while 0.01 *M* Na_2SiF_6 addition had the opposite effect, demonstrating the substantial film dissolution effect of Na_2SiF_6. The effects of HCl, KBr, and Na_2SiF_6 on the film were also proportional to increases in their respective concentrations.

Nagayama and Izumitani [51] studied the coordination chemistry of chromium complexes as related to deposition mechanisms. They started with the observations made by Levitan [52] that during galvanostatic ($I = 75\,\text{mA cm}^{-2}$) chromium deposition from a sulfate-catalyzed bath, a chromic acid dimer is formed together with a polymer of unknown structure as well as mononuclear $[Cr(H_2O)_6]^{3+}$, the stable aquocomplex. Rather than use the galvanostatic method, where current is kept constant and potential changes, they chose to keep potential fixed at −0.75 V [vs. the saturated calomel electrode (SCE)]. Here only $Cr^{6+} \rightarrow Cr^{3+}$ and $2H^+ \rightarrow H_2$ reactions are in progress (for the $Cr^{6+} \rightarrow Cr^{3+}$ reaction to happen, this potential is too positive). During electrolysis (0–60 min) they took samples at different time intervals, and with the use of anion and cation exchange chromatography, they separated the mononuclear, binuclear, and polynuclear Cr^{3+} complexes. They found that the complex formation rate for mononuclear complexes increases linearly with time, while for the other two complexes the rate increase is more gradual. They concluded that each complex is forming at its own constant rate.

They repeated the experiment at −1.10 V (Cr^0 formation region) and obtained similar results. The authors concluded that the cathode layer, made of the dense film of various Cr^{3+} complexes, is a necessary condition for the deposition reaction $Cr^{6+} \rightarrow Cr^{3+} \rightarrow Cr^{2+} \rightarrow Cr^0$ to happen. The catalyst (e.g., H_2SO_4) promotes formation and dissolution of binuclear and polynuclear soluble Cr^{3+} complexes, thus maintaining a film of constant thickness where deposition proceeds via intermediate Cr^{3+} (inner orbital) complex rather than through the extremely stable $[Cr(H_2O)_6]^{3+}$ (outer orbital) complex.

Okada [53] holds that SO_4^{2-} ions will penetrate an olated compound to form a complex and that from this complex metallic chromium is deposited. According to Okada, reduced solubility of the L-film causes the OH cross-linking level to rise together with the increase in pH.

Yoshida et al. [54] used electron spectroscopy for chemical analysis (ESCA) to further elaborate their previous research, in which they noted that there are two layers, the L- and C-films, within the cathode film. They obtained a depth profile of these films and demonstrated that the C-film is a highly polymerized complex, with very few anions present, if any. The L-film appears to be mostly in the Cr^{3+} state, but the exact valence could not be established, suggesting the possibility of two- and four valence states, as well.

They suggested that Cr^{3+} complexes are the main constituents of L-film and that metallic chromium does not deposit from this cathode film but from the Cr^{6+} state. That contributes to the formation of the cathode film and also forms olated complexes, hydroxy aquocomplexes, and polymers of higher molecular weight. These olated complexes will penetrate the cathode film from the bulk of the solution before being reduced to metallic chromium [55].

7.4 METHODS OF OPERATIONS OF CHROMIUM PLATING SOLUTIONS

7.4.1 Constituents of Chromium Baths and Their Actions

The chromium plating bath, used for decorative and hard chromium baths, is still mostly of the type originally investigated by Sargent. It is the simplest plating bath to make up, and it consists of two essential ingredients: (1) a water-soluble salt of chromium and (2) a small but critical amount of an anion, which for want of a better name is called the catalyst. The catalyst is supplied in the form of sulfuric acid alone or in combination with another acid radical, or anion(s), usually fluoride or fluoroborate or a mixture of them. Relatively recently an organic acid radical in the form of alkene-sulfonic acid [e.g., methane disulfonic acid, $CH_2(SO_3H)_2$, or one of its alkali metal salts] has been successfully included in the high-efficiency etch-free, (HEEF®) formulation introduced by Atotech, Inc. (USA) [56].

Because chromium metal will not serve satisfactorily as an anode, owing to its close to 100% anodic dissolution efficiency, insoluble anodes are used generally as a lead alloy. The source for the chromium trioxide, CrO_3 (chromic anhydride), is commonly referred to as chromic acid. It is a deep

red to reddish-brown crystal that volatilizes at 110°C. It is highly soluble in water (165 g/100 g at 0°C and 206 g/100 g at 100°C), producing a solution containing a mixture of $H_2Cr_2O_7$ and polychromic acids. Many manufacturers are now aware of the effect of even small amounts of catalyst acid radicals, and they furnish a pure grade of chromic acid especially suited for chromium plating. This chromic acid is made to meet specifications that require it to contain not more than a small fraction of a percent of sulfate that is free from other catalysts such as chloride.

A most popular solution containing $250\,g\,L^{-1}$ chromic acid contains about 50%, or $125\,g\,L^{-1}$, chromium metal. With complete current utilization, which is never the case, and no losses, 200 g of chromium would be sufficient to cover an about $110\,m^2$ surface with a deposit 0.156 μm thick.

The conversion of a pure chromic acid into a chromium plating bath requires the addition of a sulfate catalyst. With a given set of conditions of bath temperature, current density, and chromic acid concentration, too low amounts of catalyst will result in either no current flow, at first, or no plate or in an iridescent to brown oxide stain. Too high a catalyst content will result in an adverse effect: either partial plating with poor throwing power or, with great excess, no plate at all. The latter effect is due to depolarization action or easy formation of Cr(III) at the cathode. By increasing the current density and temperature to a sufficiently high value, plating can be accomplished with a very low ratio (up to 10 : 1). The essential criterion of bath composition for chromium plating from the congenital chromic acid–sulfate solution is the ratio, by weight, of chromic acid to sulfate. This ratio should be kept within the limits of 50 : 1 to 250 : 1 and preferably at about 100 : 1. A ratio of 90 : 1 is common; ratios of 70 : 1–80 : 1 are common in hard chromium baths, especially at higher temperatures.

A typical formula for chromium plating using a sulfate as the catalyst acid radical is presented in Table 7.1.

Although concentrations of chromic acid from about $50\,g\,L^{-1}$ up to saturation (about $900\,g\,L^{-1}$) can be used, most commercial baths are operated between 150 and 400 $g\,L^{-1}$. Still higher concentration gives very low current efficiencies. The important requirement is the proper ratio already mentioned.

Baths containing $200\,g\,L^{-1}$ chromic acid have a slightly higher current efficiency than more concentrated solutions. They also have a lower conductivity and therefore require a higher voltage for a given current density. The more dilute baths are also more sensitive to the changes of catalyst acid radicals from drag-in and drag-out. Hence they require more frequent and more careful adjustment for maintenance. Usually the more concentrated solutions are favored for decorative applications and the more dilute baths for heavy hard chromium plating.

Silicofluoride has had wide use as a catalyst in chromic acid baths since Fink and McLeese first proposed it in 1932 [8]. Such solutions were difficult to analyze and maintain. Yet those baths have definite advantages compared to sulfate-only catalyzed baths. They have inherently higher current efficiency, can be operated at higher deposition rates, and produce somewhat harder and brighter deposits. Fluorides or rare earth metals give better throwing and covering power. On the other hand, there are some important disadvantages. These metals are sensitive to changes in composition and to impurities such as iron and aluminum, and consequently more careful attention to bath purification, frequent analytical control, and housekeeping are required. Also analytical control of simple or complex fluorides are relatively more complicated, and finally, those solutions will attack or etch the base metal at low current density as well as unmasked areas such as blind holes. If masking is less than optimum, which sometimes cannot be avoided, proper attention must be paid to the possible etching effect. The solutions are aggressive toward plating equipment such as tank liners and heating/cooling coils.

7.4.2 High-Efficiency Chromium Plating Baths

The extra efficiency available from fluoride-containing baths still resulted in chromium deposition rates which, in relation to the high current densities employed, were much lower than for most other plating baths. However, in 1986, proprietary plating solutions were introduced that had higher cathodic efficiencies than obtainable from the fluoride-containing bath and these baths were established as viable industrial processes. They are based on chromic acid solutions which do not contain any fluorides or other halogens. Their chromic acid content is between 250 and $300\,g\,L^{-1}$. The only other constituent of these solutions which is known is the primary catalyst, which is a sulfate ion, within the ratio of 100 : 1, and

TABLE 7.1 Basic Chromium Plating Baths

	Dilute Bath		Standard Bath		Concentrated Bath	
	$g\,L^{-1}$	Molarity	$g\,L^{-1}$	Molarity	$g\,L^{-1}$	Molarity
Chromic acid, CrO_3	100	1.0	250	2.5	400	4.0
Sulfate, SO_4^{2-}	1.0	0.001	2.5	0.026	4	0.042

Note: Ratio $CrO_3/SO_4 = 100$.

1–3% of alkene sulfonic acid as secondary catalyst. These proprietary solutions provide extra high cathodic efficiencies of up to 25%. These constituent catalysts have either been patented [56–59] or been kept secret. The properties of the deposits have been documented [60, 61], together with optimum operating parameters of these plating processes. The solutions are usually operated at temperatures between 55 and 60°C and typical cathodic current densities are 30–75 A dm^{-2}. Even at these high current densities, deposit distribution is superior to that obtained from conventional baths, with less edge buildup. The deposits have good hardness (1000–1150 KHN_{100}) and retain it better than conventional chromium when heated. The chromium plate always microcracked, having 200–700 cracks per centimeter.

One of the greatest benefits of these fluoride-free plating solutions is that they do not attack steel on those portions of the cathodes where the current density is too low for chromium to be deposited. This low-current-density etching is especially detrimental when complex shaped steel objects are hard chromium plated for a long period of time in fluoride-containing baths. The fluoride ion dissolves the protective oxide film off those portions of the substrate steel exposed to low current densities and thus the acid solution can then dissolve it with consequent iron buildup. This etching attack has been a limiting factor in the use of those baths for hard chromium deposit. Consequently many decorative and hard chromium platers prefer to use either conventional or nonfluoride high-speed chromium solutions despite their lower cathodic efficiency or the HEEF® bath. The ability to plate at higher current efficiencies without this detrimental attack at low-current-density areas has been the major feature of the HEEF® bath, which has resulted in these processes gaining a significant role in the hard chromium plating field.

In practice, relatively high concentrations of chromic acid are used, for example, from 250 to 400 g L^{-1} (33 and 53 oz gal^{-1}) of CrO_3. This increase in concentration increases the conductivity up to a maximum but decreases the cathode efficiency. In some cases these two factors, concentration and conductivity, may offset each other at the higher current density obtainable at a given voltage in a more concentrated chromic acid bath and may not yield a greater weight of deposited chromium.

Bright Plating Range The wide use of decorative chromium coatings depends largely on the fact that under appropriate conditions it is possible to obtain bright smooth deposits at a fair range of current densities. The conditions under which bright deposits are obtainable are often defined as the plating range for bright chromium. This dependence of the appearance on the conditions of deposition makes it necessary in chromium plating to hold the temperature nearly constant. For example, if a decorative bath is operated at 45°C (113°F), this temperature should be kept, preferably by automatic control, between 44 and 46°C (111 and 115°F).

It is also desirable to keep the current density as nearly uniform as practicable. On flat sheet cylinder rods, or nearly symmetrical articles, there is no difficulty in obtaining a nearly uniform cathode current density. However, on irregular shapes the ratio of the maximum to the minimum current density is usually at least 2, and it may be 5 or larger. The bright range for chromium deposits seldom covers a current density greater than about 3 to 1. Hence with more irregularly shaped articles, it is not possible to produce bright deposits or, in some cases, any deposit in the areas with low current densities without obtaining burnt deposits on the more exposed areas. In all such cases efforts must be made to make the primary current distribution more nearly uniform by (1) conforming anodes, (2) intermediate or bipolar anodes, (3) thieves to detract current from points or edges, or (4) shields to obstruct current to more exposed areas. Much of the success in chromium plating has resulted from ingenious applications of these methods. The acidity of chromium plating baths is very high; it is not ordinary controlled or measured. The measurements that have been made (with glass electrode) indicate values for acidity off the usual pH scale and in the range of small negative values of pH [62].

7.5 MIXED CATALYSTS AND SELF-REGULATING BATHS

If a fluoride, silicofluoride, or fluoroborate anion is added (mixed) into the sulfate-catalyzed bath, a *mixed-catalyst* bath is obtained. Although higher speed and other beneficial effects are obtained, the difficulty of controlling these baths, due to their reactivity analytical problems, speaks against their wider commercial use. Self-regulating high-speed, or simply SRHS, baths, developed by United Chromium, Inc. (now, Atotech), is an attempt to simplify the handling of the catalyst by automatically controlling the CrO_3/catalyst ratio by virtue of the solubility characteristics of the chemicals used. The advantages and results to be obtained were described by Stareck, Passal, and Mahlstedt [4, 63, 64]. The influence of cryolite [65], fluoroborate [66], magnesium [67], calcium [68], and ammonium fluoride [69] is presented in the literature. Little is available in the literature regarding the theoretical aspects of the role of the fluorides in electrochemical reactions related to the deposition mechanism [70, 71].

The main advantage of SRHS baths is their higher current efficiency. In addition they are less sensitive to current interruptions, less subject to chemical control, have a wider plating range, yield brighter and slightly harder deposits, and exhibit better ability to activate passive nickel surfaces.

Moderate disturbances of the bath balance, as by drag-in or contamination, are minimized by the nature of the system.

If a fresh catalyst is needed, a reservoir is normally present on the bottom of the tank in the form of undissolved salts, which can be readily dissolved, as desired, by heating and stirring.

When a bath gives low-catalyst results such as good coverage but a dull or rough deposit and it is desired to increase the catalyst concentration, it is only necessary to dilute a little and then stir to reestablish saturation. This yields a slightly higher catalyst concentration, which together with the lower chromic acid concentration gives the desired adjustment.

Similarly, if a bath gives poor coverage and is overcatalyzed, it can be adjusted by increasing the concentration a little and stirring to establish equilibrium. This will lower the catalyst and increase the chromic acid concentration,

Increasing the temperature of a self-regulating bath has two simultaneous effects: (1) The warmer solution has a wider bright range and less tendency to burning, as with ordinary baths, and (2) the increased solubility of catalyst gives a pronounced decrease in ratio. In general, these effects are of about the same magnitude or the latter may be greater. If it is desired to operate at a higher temperature, it may be necessary to maintain a higher concentration so as to balance the increased catalyst content. Conversely, when operating at a lower temperature, some dilution of the bath may be in order.

The first self-regulating bath to be introduced [63] was a simple combination of chromic acid with an excess of low-solubility catalysts, which gave bath systems with a proper catalyst concentration in the range of about 350–400 g L^{-1} CrO_3. In order to produce bath systems with good catalyst balance in lower concentration ranges as 200 to 250 g L^{-1} CrO_3, the solubility of the catalyst salts was suppressed by means of the common-ion effect [64]. Thus, if the sulfate was furnished by saturating the bath with strontium sulfate, the solubility was suppressed by adding strontium chromate or strontium carbonate. Similarly, if silicofluoride was furnished by saturating with potassium silicofluoride, the solubility was suppressed by addition of potassium dichromate. Postins and Longland [72] have briefly discussed the operation of self-regulating solutions containing suppressants.

While formulas are sometimes given in the literature for self-regulating solutions, it should be realized that these are not simple formulations where all the constituents are completely soluble. Generally, the formulas include an excess quantity of catalyst which only partially dissolves.

Romanowski and Brown [73] have patented the use of fluorides and complex fluorides of lanthanum, neodymium, and praseodymium and their mixtures. These rare earth fluorides, especially the silicofluorides, are only slightly soluble in the chromic acid baths and therefore are self-regulating with respect to the complex fluoride ion. The ratio of CrO_3 to SO_4 generally used with these fluorides is about 160 : 1.

A self-regulating bath system was adapted to the production of crack-free chromium deposits by Dow and Stareck in 1953 [74]. This process involves the use of rather high temperature (65°C) and gives smooth, satiny deposits that can be buffed to a higher luster. They are used where a combination of corrosion and wear resistance is required, as on washing machine shafts [75], high-temperature-resistant coatings [76, 77], gun barrels [78], and gas turbine buckets [79]. They have been employed for the decorative plating of zinc die-cast parts without undercoating [80], and two-tone, brushed finishes may be obtained by buffing part of the surface through a mask.

Seyb et al. [81] have developed a self-regulating bath for thicker decorative coatings for bright crack-free chromium plating up to a thickness of 1.3–2.5 μm, compared to the maximum of about 0.5 um which had been used previously. This process was of interest in the search for more corrosion-resistant decorative coatings and had the added advantage of better throwing or covering power than had been obtained previously [82]. Similar procedures were advocated with sulfate-catalyzed baths [83]. Similar procedures were found by Safranek and Faust [84] to give substantially improved corrosion resistance to decorative deposits on zinc die castings when the bright crack-free chromium deposits were 2 μm thick. Wiener [85] confirmed the improvement obtained with bright crack-free chromium.

Complex fluoride catalysts have the advantage of giving higher current efficiencies at higher temperature of operation, whereas sulfate-catalyzed baths decrease markedly in efficiency at higher temperature [86–89].

Bilfinger [90] and Hood [91] discussed the operating characteristics of mixed catalyst baths. Bilfinger's curves of the current efficiency due to sulfate, fluoride, and silicofluoride catalysts are given in Figure 7.3. The best bright plate range is indicated by featherlike markings on each curve.

It should be noted that simple fluoride is a much "stronger" catalyst than sulfate and silicofluoride is much "weaker," thus making its effect easier to control because of the larger quantities required [92, 93].

Fluoride is not only a very powerful catalyst; it is also a very reactive one. The hydrofluoric acid, which it generates in the strongly acid chromic acid bath, is unstable as a catalyst. It will etch glass and dissolve silica in any form, thus converting to the weaker silicofluoride. It combines readily with boric acid, which may be dragged in from nickel baths, and the list of other "complexing agents" is long. A method of determining the relative strength of complex fluoride catalysts by means of the rate of solution of aluminum has been patented [94].

An unexpected behavior of solutions catalyzed largely with fluoride or silicofluoride is that the current efficiency increases with increasing chromic acid concentration in the usual commercial range, whereas in sulfate-catalyzed baths the reverse is true. This behavior is portrayed in Figure 7.4. The main disadvantages of the SRHS solution are its corrosive nature, which shortens the life of the plating equipment

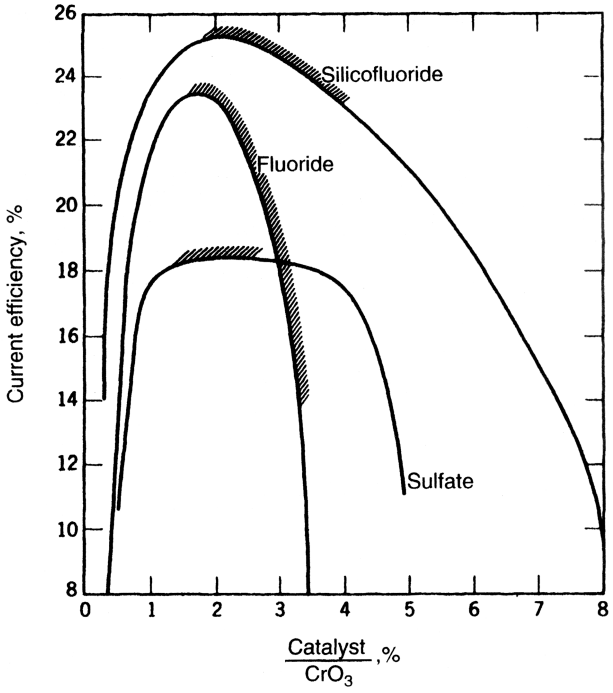

FIGURE 7.3 Chromium plating speed in 250 g L^{-1} 100 : 1 solution (25 μm = 1 mil).

(e.g., heating/cooling coils), and its sensitivity to the iron, aluminum, boric acid, and chloride contaminations.

7.6 CHROMIC ACID BATHS: OPERATING CONDITIONS

In general, bright plate is obtained by keeping temperature and current density within definite limits, taking into account the chromic acid concentration of the bath and the catalyst ratio. A convenient chart [2] showing the conditions for bright plating is given in Figure 7.2. In that figure the semidashed line *A* circumscribes the bright plate area for solutions containing about 250 g L^{-1} CrO_3, and the dashed line *B* circumscribed by the line *X* is typical of the behavior of most chromium plating baths. Thus, to produce bright deposits from a solution containing 250 g L^{-1} chromic acid and

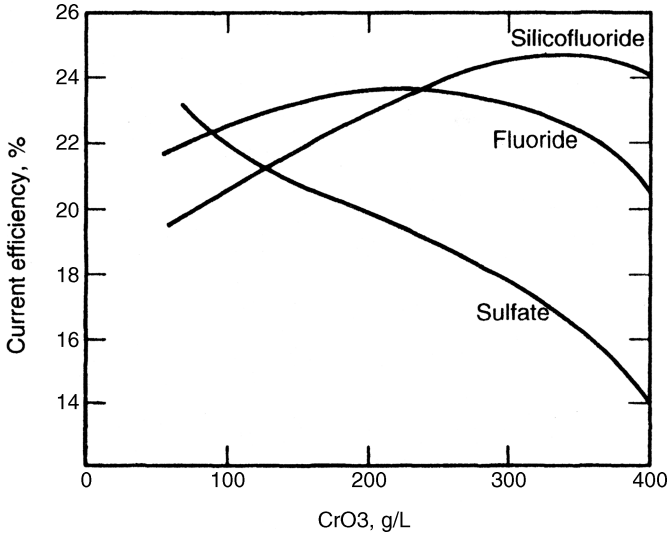

FIGURE 7.4 Chromium plating speed in 400 g L^{-1} 100 : 1 solution (25 μm = 1 mil).

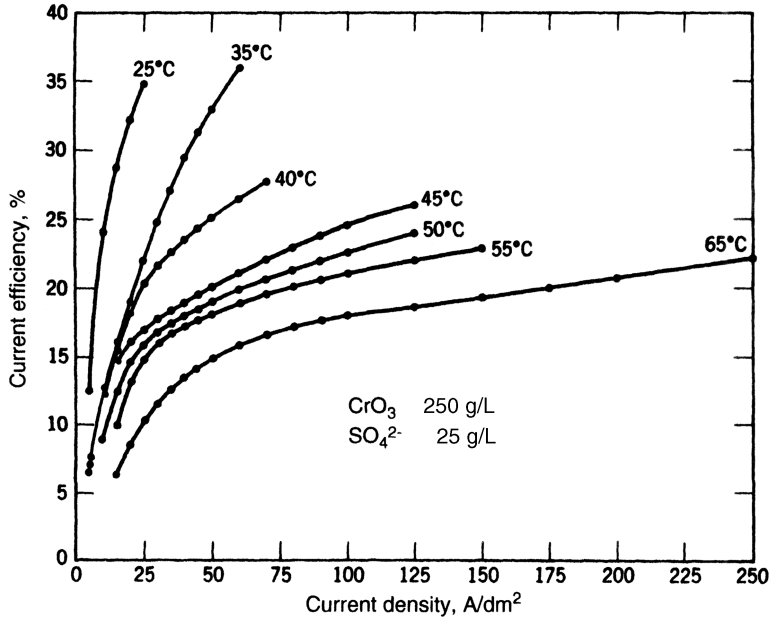

FIGURE 7.5 Current efficiency in 250 g L^{-1} CrO_3 bath with sulfate, fluoride, and silicofluoride catalysts.

2.5 g L^{-1} sulfate at a temperature of 40°C, cathode current densities between 3 and 16 A dm^{-2} must be used; at 45°C the current densities must be 50% higher.

If faster plating is desired and sufficient dc power is available, the temperature is often increased to about 55°C and the current density to about 30 A dm^{-2}. These conditions, when used with the 250 g L^{-1} solution for building up a heavy plate for industrial purposes, result in a plating speed of almost 25 μm of chromium per hour. Higher plating speeds can be obtained at higher current densities at 80 : 1 ratio, but the deposits are prone to become slightly rough and nodular, which presents no problem if the parts are going to be ground.

Figures 7.5–7.8 [95] show the current efficiencies and plating speeds of two chromium plating solutions as determined in the laboratory. Actual speeds in production plating will not conform with these exactly because shop conditions never exactly duplicate laboratory conditions. Other current efficiency data were published by Griffin [96].

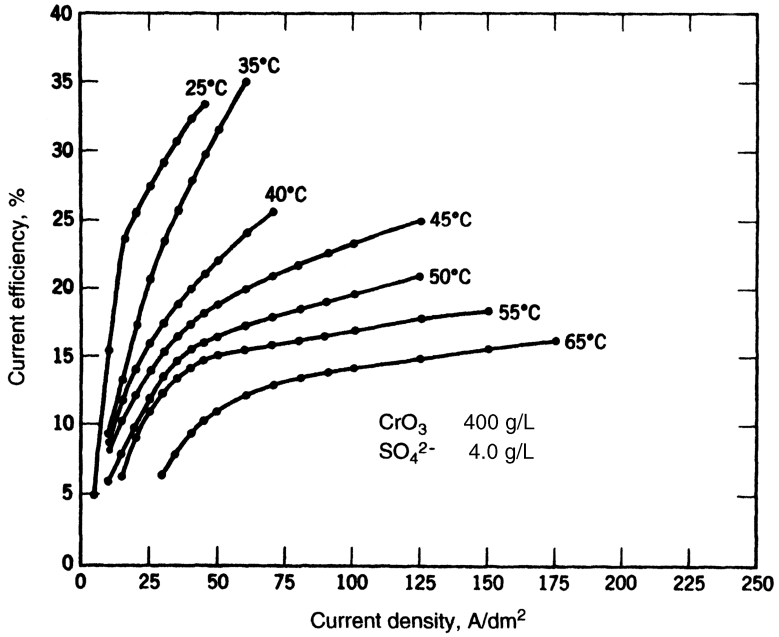

FIGURE 7.6 Current efficiency versus CrO_3 concentration.

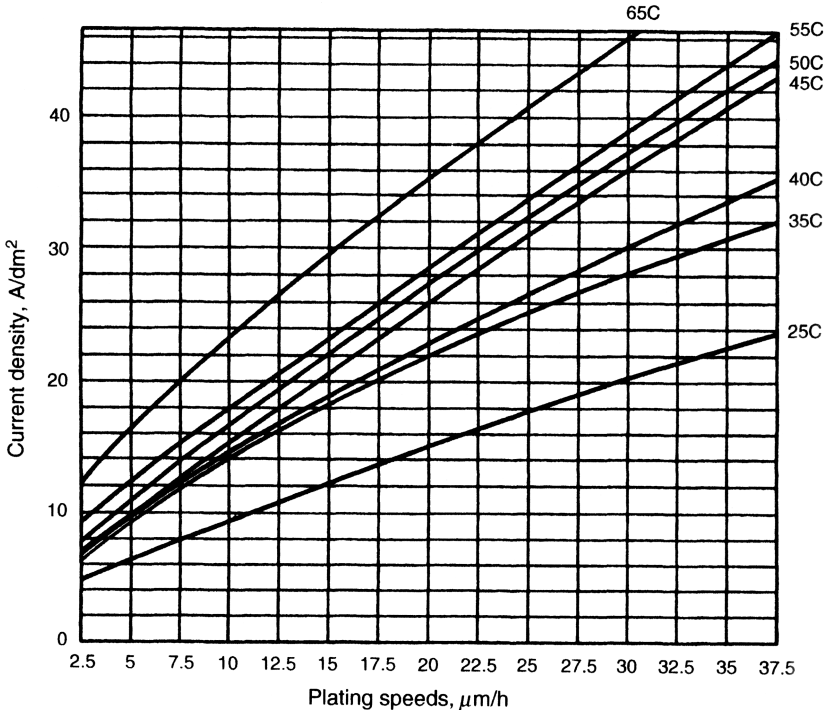

FIGURE 7.7 Current efficiency in 250 g L^{-1} CrO_3 bath.

The current efficiency increases regularly as the concentration of CrO_3 decreases down to 75 g L^{-1}. The average increase in efficiency on diluting the solution, with a 100 : 1 ratio, 55°C, and current density 30 A dm^{-2}, was about 0.25% per 10 g L^{-1} decrease in concentration of chromic acid [97]. These figures are useful in calculating the plating speed variation with small changes in chromic acid concentration.

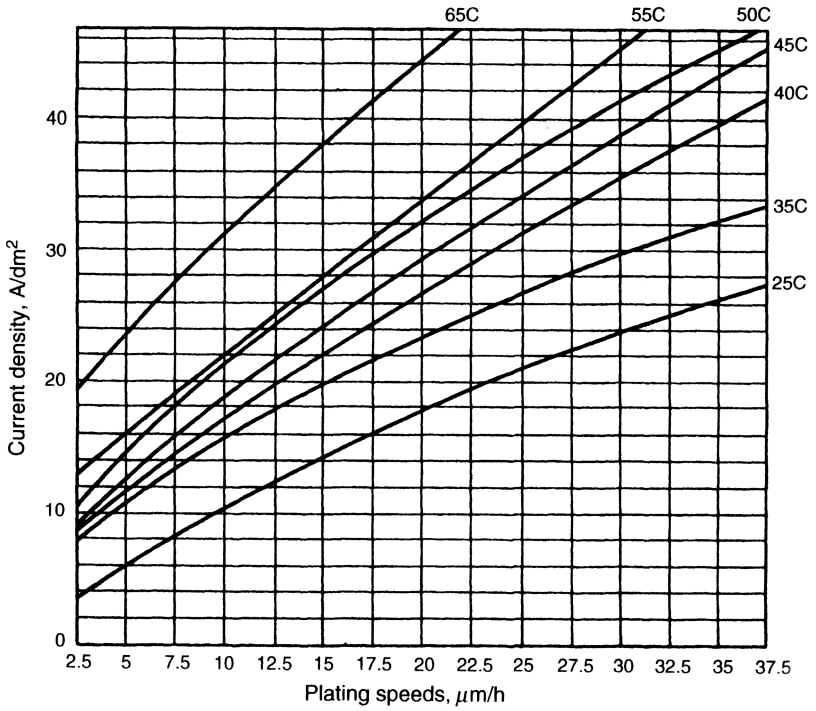

FIGURE 7.8 Current efficiency in 400 g L^{-1} CrO_3 bath.

The acidity of chromium plating baths is very high; it is not ordinary controlled or measured. Those measurements that have been made (with glass electrode) indicate values for acidity off the usual pH scale and in the range of small negative values of PH [98]. (See Fig. 7.1.)

7.7 THROWING POWER

The poor throwing power of chromic acid plating solutions frequently refers to three different but related phenomena: (1) covering power, (2) throwing power, and (3) bright plating range, previously discussed. By virtue of their effectual interrelation, the terms ''covering'' and ''throwing'' power are at times erroneously used synonymously, perhaps because plating baths with poor throwing power generally exhibit poor covering power and vice versa.

7.7.1 Covering Power

The covering power (CP) of chromium plating solutions refers to the ability to initiate deposition over the entire cathode surface at varying current densities (CDs). While other plating baths may permit metal deposition at very low current densities, chromium will not generally deposit below 1 A dm^{-2} (10 A ft^{-2}), depending of course on specific plating conditions. Below the critical density, a manyhued nonmetallic deposit is sometimes formed. It has the appearance of a rainbow—a pleasant name for a troublesome phenomenon. According to Pan [99], angle cathodes with different angles and various side lengths, slotted cathodes, and slit cells are normally used to determine the covering power.

The covering power depends on the electrolysis conditions and on its nature, any pretreatment, and the surface condition of the base metal. CP improves with increasing CD, and this fact is used particularly for chromium plating. Thus for a short time the plating is carried out at higher than normal CD (''strike'' or ''covering'' current). Then plating is continued at normal CD, as soon as the part has been completely covered with a thin chromium layer. The CP of the chromium bath is less on aluminum and aluminum alloys, for example, than on copper or iron, although it can be improved by the use of an appropriate intermediate layer. On iron, it is better than on copper or nickel.

7.7.2 Throwing Power

The ability of a plating bath to uniformly deposit metal on the cathode surface is a measure of its throwing power (TP). The major factors influencing TP in a chromium plating bath are the primary current distribution, polarization, secondary current distribution, and cathode efficiency. The primary current distribution is a function of the geometrical properties of the system, that is, the shape and distance of the anode to the cathode. The electrochemical properties of the system transform the primary current distribution into the secondary current distribution, which is determined by all the factors that influence the polarization during chromium deposition. Polarization is the change in potential on the cathode, which is mainly due to concentration gradients and the rates of electrochemical reactions, and in the case of chromium it is fairly constant. In general, polarization increases with an increase in CD. As the polarization becomes greater at the projected (higher CD) areas, the net result is a more uniform secondary current distribution. Unfortunately, in chromium plating, the cathode efficiency increases with the CD, and its effect on metal distribution can counteract any benefit of polarization. In the operation of a chromium plating bath the TP is generally improved by increasing the bath temperature and plating CD. As opposed to covering power, higher ratio baths have a tendency to improve TP. Increasing the anode-to-cathode gap is helpful, but this usually requires higher operating voltages; an initial high strike current may be necessary in order to obtain adequate coverage. On irregular cathodes, the CD varies widely, being highest on corners, edges, and areas closest to the anode; it is lowest in recesses, reentrant angles, concavities, and areas farthest from the anode. It is then evident that cathode efficiencies being highest at the high-CD areas result in heavier deposition, whereas the low-CD areas have thinner deposits.

Consequently the major variables connected with throwing power in bright chromium plating are the current efficiency and the bright plating range. If a certain set of conditions gives the widest possible bright plate range, and the plating is done at an average cathode current density near the upper limit of current density for this bright plate range, optimum throwing power will be attained.

In the conventional throwing power cell, cyanide copper plating baths with good throwing power generally have a rating of around 20–40%, whereas most nickel plating and acid copper plating baths have a rating near zero. The throwing power in chromium plating has been found to vary from around −13% under the best conditions to −100% and even lower [7, 97, 100]. The relative throwing power of chromium plating baths is often estimated by an empirical test as the Hull cell test, described in the next section.

7.8 METALLIC IMPURITIES

They are two general classes of impurities in a chromium bath: (1) inorganic impurities such as chlorides, excess of sulfates or fluorides, boric acid, and organic matter and (2) metallic impurities. The former are most common in the form of detrimental impurities such as iron, copper, and zinc. These metals enter the solution from parts accidentally dropped into the bath and not recovered, attack of the solution on racks and fixtures, attack on anode or cathode bars, and corrosion of plating tanks through pinholes in the tank

linings. The maximum acceptable concentrations of these metals will depend somewhat on the overall bath composition and the type of work being processed. However, approximate limits are $15\,g\,L^{-1}$ for iron and $0.2\,g\,L^{-1}$ for copper. At or near these concentrations, copper and iron will restrict bright coverage in low-CD areas. It should be noted that harm done by metallic impurities is very much synergetic; while one impurity alone even at high concentrations is not necessarily highly damaging, a combination of impurities even with less total concentration certainly is.

Other cations that may commonly be present in chromium plating baths include Cr(III), which usually results when baths are operated with too large a cathodic area and too small an anode area or when organic matter is introduced. The Cr (III) content can be kept down by increasing the area of the lead anodes used relative to the cathode area or, where this is not practical, by electrolyzing the solution for a time with a relatively large anode area and a small cathode area.

Of all the impurities that can be present, Cr(III) is particularly detrimental, although contrary statements have been made [101]. The tradition has emerged that a small amount of Cr(III) is beneficial when added to a new bath. This is due to making such additions in the early days in the form of chromic sulfate or chromium hydroxide precipitated from chromic sulfate and containing some sulfate, thus affecting the catalyst content of the bath. A number of investigations have failed to indicate any improvement in new baths with the addition of small amounts of Cr(III), and there is no need to electrolyze a properly made up new bath for this purpose.

Buildup of metallic impurities can be corrected only by two procedures: discarding a portion of the bath (only as a last resort) and sending it to the authorized landfill or purification through a properly selected method [102]. The rapidly growing problem of chromium waste disposal has both helped and aggravated the problem of metallic contamination. Extensive use of drag-out tanks or the use of closed-loop systems accumulates and concentrates the impurities in the bath that might otherwise reduce itself in normal drag-out. On the other hand, the incentive for the plater to install chromium recovery and reclamation units has given many plants the facilities for electrolytic, selective membrane, or ion exchange treatment of contaminated baths.

Periodic checks with a magnet and, if nonferrous parts are processed, periodically pumping out the bath should be performed on any chromium installation to determine and remove fallen or broken anodes, processed parts, racks, tools, sludge, and the like.

7.9 MAINTENANCE AND CONTROL

Chromium plating baths are very stable in use, and their composition can be readily maintained by physical analysis or by more accurate chemical or instrumental analysis. If the bath is meant to be operated faultlessly, continuous correction in the control of bath composition is inevitable. Since chromium deposition is sensitive and controlled by such small amounts of catalyst, it was recognized even in the early times that maintaining the proper catalyst ratio is of utmost importance.

Analysis of the catalyst concentrations in such small range, while routine to the fully equipped analytical laboratory, are complicated and of debatable accuracy for the average electroplating plant setting. Even if this were not the case, the validity of such tests is often subject to questions, in view of the fact that a bath's operating characteristics depend on the effect of the concentrations of the total catalyst content in the bath. Analysis for sulfate alone may neglect traces of chlorides, fluorides, and so on, which mole for mole have a much more marked effect on the bright electroplating characteristics from a similar bath using high-chloride-content tap water.

Analysis for sulfate content can be a complicated procedure. The simplest procedure is to use the centrifuge method. This method is adequate for routine control and, if desired, may be checked occasionally by the classic but more elaborate gravimetric method given in the literature [103–106]. Since gravimetric methods require equipment that may not be available in the average electroplating plant laboratory, the straightforward titrimetric method may be of value [107]. It requires no special equipment and it is relatively fast. The most accurate is the ion chromatographic (IC) method [108, 109].

Analytical testing methods for radicals other than sulfate are quite complicated, which is one of the drawbacks of these solutions. Data on these testing methods can be found in the literature or in the process manuals of a particular solution supplier. Organic catalyst determinations, as in the case of HEEF®-25, need an accurate, reliable, and rather specialized equipment, which is the ion chromatograph. This elegant instrumental technique can simultaneously determine many common ions. The attractive feature of the IC method is for process control, where in a matter of a fraction of an hour, CrO_3, sulfates, fluorides, silicofluorides, and chloride anions can be determined in a single experiment [110]. The separation mechanism is based on differential absorbency and affinities toward the material used in the anion-separating column. Concentration of each anion is determined with highly selective conductivity detector. Trivalent chromium is determined in the cation separation column using an ultraviolet detector. For determination of alkenesulfonic acids, which are constituents of modern high-speed baths, this is the only practical method. These analyses are usually performed by the supplier.

Chemical analysis for the chromic acid content is not an excessively complicated procedure, and typical methods can be found in the literature. Hydrometer readings based on the

density of the solution are a common and quite accurate method of chromic acid determination in new and relatively pure baths. A wide difference in hydrometer compared with analysis readings is not inevitable. Unfortunately, this is the case in most baths which, with age, build up in trivalent chromium, metallic, and organic impurities. Thus daily or at least weekly hydrometer checks, coupled with a periodic analytical determination, will form an acceptable and reliable control procedure for a chromium bath if done frequently enough. The standard hydrometer, calibrated to read solution density or, better, to read directly in ounces per gallon of chromic acid at the normal bath operating temperatures, is an essential tool and can be placed directly in the bath. The specific gravity is a good indication of the chromic acid content with new baths, but it may show considerable deviation as the bath is used and accumulates metallic impurities. Sulfate is often determined centrifugally, but this method is not always reliable. Excess sulfate is commonly precipitated by the addition of barium carbonate, but it can also be counterbalanced by the addition of chromic acid, if convenient.

In the absence of silicofluoride-containing chromium, plating baths were found difficult to analyze and control. Many methods were proposed, but they were not generally dependable for the total fluorine content. There is considerable confusion and inaccuracy in the literature about fluoride- and silicofluoride-containing chromium baths. Despite the difficulties, present-day silicofluoride-containing baths with or without self-regulating features still have more than compensating advantages. The estimation of fluorine can be done in a comparatively simple method with the aid of a fluoride-sensitive electrode [62].

Probably in no other electroplating solution, except perhaps that of bright nickel, is the value of electroplating tests greater than in chromium baths. In most electroplating baths, control tests (e.g., the Hull cell) are important additions to chemical analysis. In chromium baths, when properly employed, control tests can supersede and often eliminate some of the routine chemical analysis. The reason for this is the extreme sensitivity of the bath to relatively minute changes in catalyst content. A standard bath with of 2.5 g L^{-1} of sulfates will exhibit detectable narrowing or widening of the bright electroplating range when this concentration is altered 10% (0.25 g L^{-1}) or a mere 250 ppm. The interpretation of the Hull cell or other electroplating cell panels requires only a moderate amount of experience and average amount of skill. It is an invaluable toot for day-to-day solution control, especially for troubleshooting.

Hull cell electroplating tests are fast, effective, and rather simple [111–114], On the other hand, the chromium electroplating operations that thrive on excellence should also employ advanced versions of electroplating cell tests like hanging Hull cell, jiggle cell, and rotating cathode cell [16–20]. The ultimate testing cell accomplice is the hanging Hull cell, which eliminates the major drawbacks of the regular Hull cell, namely a lack of correlation with actual bath agitation, preplating cycle, and possible rectifier ripple, bipolar effects, and stray currents. Since the hanging Hull cell operates directly in the electroplating solution, a much closer picture of the actual electroplating range present in the bath is obtained from these test panels than from the laboratory-type Hull cells.

Some of the chromic acid is reduced to Cr(III) concentration at a relatively low figure under usual operating conditions, especially if the area of the lead anodes is sufficient [115]. If iron or other nonlead anodes are used for special purposes, they do not reoxidize the Cr(III) to chromic acid as well as do lead anodes, and a higher equilibrium concentration of Cr(III) is reached after the bath has been used for some time. Furthermore these other anodes, unless highly insoluble as lead, introduce contaminating metals such as iron into the solution and therefore should generally be avoided. A rise of Cr(III) content can be seen by darkening of the color of the solution.

Wetting agents are frequently used to suppress the mist of solution carried into the atmosphere by the hydrogen evolution at the cathode, rather than to prevent pitting as in other plating baths. A great variety of wetting agents have been developed to minimize the fumes evolved during plating; the prospective user of such compounds should satisfy himself about their stability under his or her particular conditions. If they are used, surface tension measurements may become desirable for control, although visual observation of the fume suppression or amount of foaming may be sufficient.

Due to the high oxidizing power of chromic acid, plating baths are seldom filtered, although filtering has been recommended [116, 117]. If some clarification is desired, it can be accomplished by settling overnight and decanting. If desired, a chromium solution may be filtered through a pad of glass or through a fiber glass filter cloth. Filtering cloths of Vinylite (Vinyon) and Saran are also available and have substantially complete resistance to chromic acid.

7.9.1 Anodes

While it is possible to use anodes made of solid chromium, there are four serious objections; (1) Chromium anodes are much more expensive than chromium purchased in the form of chromic acid. (2) Chromium metal dissolves with much higher anodic efficiency (85–100%) than the prevailing cathode current efficiency (12–24%) and hence rapidly increase the chromium content in the bath. (3) Unlike lead anodes, there may be reoxidation of Cr(III) to Cr(VI), an unfortunate reaction that proceeds in parallel with the main, chromium deposition reaction. (4) No metal can match ease of lead for forming and joining together (‘‘burning’’) when making conforming anodes.

While many anode materials such as iron, steel, stainless steel, nickel, and titanium can be used for special purposes, as auxiliary or conforming anodes, they are unsatisfactory for extended use, since they dissolve and contaminate the solution and also increase the Cr(III) content. Although pure lead can be used for its ease for conforming, platers generally prefer more corrosion-resistive anode material, such as lead alloyed with silver, tin, or antimony. Many anode materials other than lead alloys have been tried, but nothing better has been found [119]. Recently, it was revealed that bismuth-doped lead anodes can triple the anodic reoxidation of Cr(III) [120]. Pure iron, such as Armco or electrolytic iron, dissolves less when used as an anode than steel, nickel, stainless steel, or similar alloys. Iron anodes have occasionally been used, particularly in industrial chromium plating, in special instances where greater strength and rigidity than are obtainable with lead are desired. Their continued use, however, leads to the accumulation of iron and Cr(III) in the bath. Small platinum wire anodes can be used for special purposes, such as plating the insides of very small openings, such as those of wire-drawing dies. Antimonial lead anodes are preferable to chemical lead due to the greater corrosion resistance and strength, but they do not eliminate the formation of copious amount of lead chromate sludge. Lead–tin alloys have higher corrosion resistance but less rigidity than antimonial lead anodes, and these are widely used. A good compromise is achieved by using Pb–Sb–Sn ternary alloy. The best are silver containing lead and lead alloys [121], but they are more expensive. Those anodes not only have the advantage of increased durability but also give quick or immediate startup after downtime without special reactivation.

Lead and lead alloys serve two key functions in the chromic acid plating bath: (1) They provide effective current distribution and (2) reoxidize Cr(III) to Cr(VI). Lead peroxide film, which forms on these anodes during use, causes continuous reoxidization of the Cr(III), forming chromic acid and thereby keeping its concentration at a low, acceptable value [122].

Lead and lead alloy anodes of varying shapes and cross sections have been proposed and used from time to time. They have to be thick enough to conduct the high currents required. Anodes that are too thin will overheat in use and will corrode and warp excessively. This difficulty can be avoided by the use of solid round copper core in the center of lead anodes. The copper core aids in rigidity and securing good current distribution because considerable current can come from the back as well as the front.

Auxiliary conforming anodes are sometimes used in hard chromium plating or through the complete cycles of decorative plating. Improved coverage is obtained on difficult shapes, and more uniform plate distribution is achieved on large surfaces where a minimum plate thickness is required, as for the production of microcracked chromium. Pure nickel anodes are perhaps the best for this service, and cast nickel is sometimes used to produce a number of anodes of a special shape. Platinized titanium anodes are also used for this service, but they have the disadvantage of a limited life and insufficient indication of when they are becoming inoperative, except for increasing rejects. Nickel dissolves slowly in use and can be replaced when visibly worn away.

Lead anodes used in chromium plating cannot have too heavy or irregular a coating of lead dioxide on them or the current distribution may be affected. It is beneficial to clean the anodes regularly, especially those used in heavy hard chromium plating that conform closely to the article being plated. The cleaning is done by acid dips and scratch brushing, but the process is difficult and time consuming; frequently not all the semi-insulating coating is removed. Hyner [123] developed the method of electrolytic reduction of the coating to metallic lead by cathodic treatment in an alkaline pyrophosphate solution. Lead anodes coated with lead dioxide tend to become somewhat passive after standing idle for some time. Some platers would electrolyze the bath with full tank voltage from several minutes to an hour for reactivation in order to reestablish the original conductivity. However, other platers found it unnecessary to do this. This passivation tendency, investigated by Hardesty [124], is presumably due to the insulating effects of insoluble lead compounds such as lead chromate and lead fluoride. The only way found to avoid this effect, aside from recleaning as described, is to remove the anodes from the tank promptly after use and to permit the solution to dry on them rather than rinsing it off. This gives good results but is not always practical. Platinized titanium anodes with thermally deposited indium dioxide are proposed [125]. Titanium anodes coated with PtO_2 are recently recommended for chromium plating [126]. Practical experience with platinum-plated titanium anodes in chromium plating solution is described [127].

7.9.2 Materials of Construction

Most tanks for chromium plating are made from steel and lined with some kind of acid-resistant material. In the past, chromium plating tanks were made of lead or antimonial lead-lined steel. Acid-proof brick linings have also proved very satisfactory for chromium plating tanks made of steel [128], although they are seldom used any more. The type of lining now used, which gives satisfactory service, consists of flexible synthetic resin sheets (plasticized polyvinyl chloride, PVC) cemented to the steel tank and welded at seams and corners. This type of lining saves space compared to a brick lining but is generally not recommended for temperatures above 60°C. Special insulating materials of the vinyl type (Corroseal) haw; been developed [129] to withstand the action of hot chromium plating solutions and thus have good mechanical properties. These insulators are used in sheet, rod, tube, tape, and other solid forms in the construction of composite racks and in liquid

form for coating ordinary racks or for stop-offs. The use of insulated racks results in a saving of power and chemicals and gives much better plating. Microcrystalline, high-melting paraffin wax and still higher melting chlorinated naphthalene wax compounds are also used for stopping off in industrial chromium plating.

Tanks can be heated and cooled by lead alloy coils submerged in the solution. Titanium, columbium, tantalum, Teflon, or Teflon-coated stainless steel coils and heat exchangers have come to be used extensively for their extremely long life and efficient operation. More durable than titanium, tantalum is probably the most suitable material. Its high initial cost can be justified by a long period of trouble-free operations. Titanium coils are not the best choice for fluoride-based solutions.

Owing to the relatively high current densities used in chromium plating, it is necessary for all compounds of the circuit to be of sufficient size to carry the amperage required without overheating or excessive voltage drop. The plating tanks have to be of such a size that the parts can be positioned 10–25 cm (4–10 in.) from the sides and the bottom of the lank as well as from the surface. When designing the tank and the rectifier's capacity, consideration should be given to an ideal current loading of l–1.5 AL^{-1} of the tank volume. This will save energy required for heating and cooling in improperly designed tanks.

7.9.3 Safety and Health Considerations

The chromium metal and trivalenl chromium compounds are nontoxic in comparison with the much more hazardous sixvalent compounds. The chromic acid is sharply irritating and corrosive to the mucous membranes of the nose and throat. This spray therefore requires removal or suppression to protect the workers and equipment, and adequate exhaust facilities must be provided for the purpose. Carcinogenic factors are also suspected. Skin contact can cause ulcers and dermatitis; different persons may react differently to dermatitis effects. Chromium plating solutions emit mist as they are used. The mist contains, in addition to hydrogen and oxygen gas, basically the same ingredients as the plating solution and therefore presents a health hazard to the workers and the community. The mist must therefore be captured and removed from the air and the tank to protect the workers and equipment, and adequate exhaust facilities must be provided for the purpose. The U.S. Environmental Protection Agency (EPA) regulates the amount of chromium that may remain in the air discharged from hard chromium plating facilities with different levels for large new facilities and for small facilities.

Many measures have been proposed to replace or supplement the necessary exhaust hoods and to prevent some of the chromic acid and heal losses these entail. The proposed use of a layer of floating plastic beads [130, 131] or of stable wetting agents may in some cases offer a partial solution to the problem, but they may not make it possible to dispense with an adequate exhaust system. The development of completely stable perfluorinated sulfonate wetting agents [132, 133] made an important difference. They are effective in reducing the emission between 93 and 98% depending on the operating conditions and the type of foaming/wetting agent used. These wetting agents would not induce but may accentuate basis metal pitting in thick, hard chromium plating deposits [117, 134–137]. Their use is quite widespread in decorative baths and permit economies in chromic acid and heat losses, among other advantages. Floating balls pose the problem of traveling from tank to tank and also can become stuck in the crevices of the parts.

Studies of industrial dermatitis arising in workers exposed to chromates or chromic acid have been published [138, 139]. The remedies suggested include avoidance of contact with the irritating chemicals, cleanliness, thorough washing, use of protective and healing salves and ointments, and visits to a physician when necessary.

The disposal of wastewaters containing chromic acid is a problem of increasing importance [140, 141]. Chromic acid-based plating solution also presents a fire hazard when in contact with organic matter such as paper.

7.9.4 Bulk Chromium Plating

Chromium plating barrels of both the batch and continuous types have been described [142–145] and are operating successfully in a number of plants. The barrel plating time, for decorative purposes, is about 5–10 min, but heavy hard chromium plates can also be reduced in the barrel by using longer plating times [146]. Deposition from trivalent baths has been recently described [147]. Round or cylindrical articles, which roll easily, that are not too light lend themselves best for barrel plating. The lower limit is about 3 g, although the most important aspect is the ratio between area and weight. The preferred solution is sulfate-free chromic acid baths containing silicofluorides as a catalyst. This solution has the lowest threshold current density requirement (as low as 0.6 A dm^{-2}), has relatively the best activating properties, and can withstand short current interruptions, which occur repeatedly when plating in a barrel. Small parts such as screws, nuts, bolts, and rivets can be chromium plated in wire mesh baskets or by stringing them on wires. Stringing on wires or racking is convenient for articles of moderate size, perhaps 25 mm long or longer. For basket plating, horizontal copper wire mesh trays are generally used with a rim about 13 mm high soldered to a frame for suspension from the cathode rod. The small parts should be spread in a thin layer on a tray so that they do not cover each other. They are typically plated, at as high a current density as possible without burning, for 5–10 min. Generally the entire basket is shaken or jarred a little a few times during plating or even rotated to cause the parts to shift position and avoid contact

marks. Flat articles, which fit closely on top of one another, do not lend themselves readily to basket plating.

7.9.5 Preparation of Basis Metals

In order to ensure the satisfactory adhesion of chromium deposits, the parts must be almost perfectly clean and free of any grease. If parts are transferred from nickel or other baths to the chromium bath without unmerited delay, only an acid dip and a water rinse may be enough. On the other hand, if the nickel is buffed or the parts are handled or stored for a time, further treatment may be necessary before chromium plating.

The cleaning of work to be chromium plated for bright or decorative finish (as distinguished from work for thick deposits or for industrial applications) may be divided into tree general classifications—solution cleaning, dry cleaning, and vapor degreasing. Typical solution-cleaning procedures are detailed in the chapter on preparation for plating. Dry cleaning consists of wiping the work on a buff wheel or by hand with pumice powder without dipping it in solutions of any type.

Where solution cleaning is feasible, it generally gives better results than dry cleaning. It helps to remove any oxide or tarnish on a nickel surface, whether visible or invisible, and results in ''activating'' the nickel or making it easier for chromium plate. Nickel surfaces are considered ''passive'' if they are oxidized and difficult to cover with bright chromium plate. Cathodic alkaline cleaning is quite effective in removing this condition if it is not too severe. Acid dipping is even more effective. Typical acid immersion procedures for maximum nickel activation are as follows:

1. Chemical activation in 30–50% (volume) HCl for 30–60s
2. Chemical activation in 5–20% (volume) H_2SO_4 for about 2–5 min
3. Cathodic activation in 5% (volume) H_2SO_4 at 4–6 V for about 15 s

Where wet cleaning is not feasible, the plater must sometimes resort to dry cleaning. Success of this procedure depends on the fact that the chromium plating solution itself serves to some extent as both cleaner and acid dip. The vigorous evolution of gas during plating, together with the strong cleansing action of the hot chromic acid, tends to remove light soil films. If the dirt, grease, and oxide are excessive, the cleansing action of the plating solution is overtaxed, with the result that the chromium plate is defective.

The importance of a satisfactory wet cleaning procedure for nickel surfaces has been confirmed by Tucker and Flint [148]. They reviewed some of the previous work in the field. Cathodic electrolytic cleaning is also helpful, and special solutions and procedures are sometimes used [149]. Mandich recently discussed the practical and theoretical aspects of nickel and chromium activation as well as chromium reverse etching [150]. Anodic cleaning in the usual alkaline cleaners must be scrupulously avoided, since it tends to oxidize nickel surfaces and make them impossible to chromium plate.

Plating over stainless steel also requires wet cleaning and activation. The surface should be freshly buffed and not be permitted to stand from one day to another. Often it can be placed after a short dwell time, particularly if a silicofluoride-type solution is used under conditions of higher than normal catalyst concentration or low ratio and high temperature. Heavy chromium deposits used in industrial or hard chromium plating usually require extraordinary good adhesion to the basis metal because the plated articles are often subject to severe stress in service. A high degree of adhesion of chromium to steel is the normal result of plating in a hot chromic acid bath, but adhesion tendencies can best be treated using electrolytic cleaning or etching of the steel surface before chromium plating. A satisfactory etch for steel parts is obtained by setting the anode at 6 V for about 1 min in chromic acid solution or in the plating bath. Anodic etching in sulfuric acid (sp. 1.53g) at about 25°C for about 1 min gives the highest adhesion. Similar results are obtained by electropolishing [151]. Additional details for the preparation of steel for heavy chromium plating are given in a recommended practice of the American Society for Testing and Materials (ASTM) [152], Greenwood [153], Morisset [154], Guffie [155], Peger [156], and Mandich [150]. Levy [157] and Johnson Dini [158] give procedures for plating on some special alloys.

Zmihorski [159] has investigated the adhesion of heavy chromium deposits on steel by means of a shear test; he found that an adhesion of about 40 to 45 kg mm^{-2} is obtained by the usual hard chromium plating procedures. He also found that etching in sulfuric acid gives somewhat better adhesion than etching in chromic acid, that a low current density gives somewhat better adhesion than high current densities, that thin deposits are better than thick, that deposits from pure solutions containing no iron and Cr(III) are better than those from contaminated solutions, that silicofluoride solutions are better than sulfate solutions, and that heat treatment appears to have no effect on adhesion.

The adhesion of thick chromium deposits is difficult to measure because it is commonly greater than the tensile strength of the coating, which will fail before it can be pulled off the base metal. Williams and Hammond [160] made direct measurements on the range of 16–32 kg mm^{-2}. Beams [161] used a centrifugal force method. Chessin and Poor [162] first used an indentation method for adhesion and later [163, 164] developed a ''push-out'' test in which a 6-mm-diameter hole was pushed out of the basis metal from underneath the coating, and the nature of the fracture around the hole was examined. Dini and Johnson [165] described a

''flyer plate'' test for measuring the adhesion under dynamic conditions. Methods for measuring adhesion have been critically reviewed by Davies and Whittaker [166] and Ploog [167].

High-carbon cast irons and steels may be difficult to chromium plate directly if acid pickled before plating. Pickling apparently develops a low-overvoltage surface which makes it easy to deposit hydrogen and difficult to plate chromium. It is therefore recommended that acid pickling be avoided in such cases and that sandblasting or other methods of cleaning be used.

Zinc and zinc-based die castings are commonly chromium plated for decorative purposes after previous copper and nickel plating. If the castings are satisfactorily nickel plated, the chromium plating is the same as for any other nickel-plated basis metals. If the nickel plate, directly applied on a zinc-based article, does not completely cover it or is too thin, it will be difficult or impossible to deposit chromium at or near the bare or thin points. A remedy for such a difficulty is to plate a substantial thickness of copper under the nickel. There is a certain amount of chromium plating directly on zinc die castings, generally for wear purposes.

7.9.6 Hard Chromium Plating

Dubpernell's book treates the behavior of the sulfate- and fluoride-type catalysts [168]. Morriset [6, 169], and Weiner and Walmsley [170] have published some general books on the subject. Practical plant manuals have been published by Greenwood [171, 172], Guffie [155], and Peger [156]. Dennis and Such [174] covered both nickel and chromium plating in their book. Racking for hard chromium plating is well elaborated by Logozzo [175] and Peger [156]. Mandich treated practical problems in hard chromium plating in a series of papers [176].

The success of the chromium plate in industrial applications may be attributed to its unique combination of properties not possessed by any other single material available commercially. The most important of these are hardness, adhesion, corrosion resistance, nongalling and nonwetting qualities, low coefficient of friction, and high melting point. These properties make hard chromium invaluable for industrial and engineering purposes. The hardness alone, although approaching that of diamond, would not be sufficient to secure widespread use, because a number of other hard materials or hardening processes are available. It is the combination of very high degree of hardness with extremely good corrosion resistance (equal or even superior under most conditions to that of gold or platinum) and very low coefficient of friction or unique surface qualities which has given remarkable results in many applications of the chromium plate. To these should also be added the relative ease of application and control, which ensures maintenance of fixed standards of quality and durability, together with moderate cost. There is also the ease of stripping and replanting for repeated salvage in cases where the plate wears beyond suitable limits.

The benefit of the harness of chromium deposits is not efficiently obtained unless the coating is deposited on a sufficiently hard basis metal and to satisfactory thickness. Generally, hardened steel is used for the basis metal. Even a relatively heavy deposit of chromium may be crushed or indented if applied over a soft basis metal such as copper. The best possible adhesion is also important in many uses where the surface may be subjected to severe stress or shock and any chipping of the deposit would be injurious.

The low coefficient of friction and desirable surface properties of chromium are realized for the most part only on relatively smooth surfaces, although the advantages of certain types of interrupted surfaces are also described in Section 7.12.4. Frequently chromium deposits are ground or lapped to size. The deposits are easily ground but are sensitive to the heat generated and usually need to be ground with very light cuts [177, 178].

Sometimes a bright deposit is applied to a smooth surface and used without further mechanical treatment. By means of careful operation it is possible to plate to size within very close limits. Worn machine parts are salvaged by chromium plating oversize and grinding back to size.

Some outstanding applications of the industrial chromium plate include gages, tools, and machine parts generally, both new and worn parts, which are plated or replated for salvage purposes. Taps, reamers, drills, saws, milling cutters, burnishing tools, and so on, have all been successfully plated. Molds for plastics and rubber are plated to reduce wear and sticking and to improve appearance. Drawing dies and mandrels, coinage dies, rolls for cold-rolling metals to high luster, calendar rolls for various materials, and printing and engraving dies are other examples of common uses. Oswald [179] reported an increased life of over 4 times for rolls used for the cold rolling of steel and 8–10 times for printing cylinders. Wilson [180] mentions sometimes getting 3,000,000 copies from rotogravure cylinders without apparent wear.

Gun barrels are frequently plated for the maintenance of accuracy over a long period of use [181–186]. It is reported that the life of machine gun barrels is increased 30 times by chromium plating [187]. Oil drilling rods, pump shafts, and the cylinders of internal combustion engines have been plated with good results. The list of special uses could be greatly extended [128],

In each application the most desirable thickness of chromium and hardness of the basis metal have to be determined empirically with the aid of previous experience. If high corrosion resistance is desired in addition to wear resistance, as with rotary dryers for corrosive chemicals and paper mill machinery, relatively thick deposits are required. Sometimes

substantial undercoats of nickel or copper are used in such applications.

A hard chromium plate has been found useful on basis metals of widely varying hardness, although the basis metal should generally be as hard as possible. Thus, on one end of the scale, good results have been obtained by chromium plating cutting tools tipped with tungsten carbide [188]. On the other hand, zinc alloy dies for autostamping have been chromium plated for longer life [189, 190], and the hard chromium plating of aluminum has been developed [191–193], especially in connection with small internal combustion engine cylinders [191, 194, 195].

Additional information on hard chromium plating is given in other sections of this chapter.

7.9.7 Etch Prevention in Hard Chromium Plating

The biggest disadvantage that self-regulating baths have in common with all baths containing fluorides or complex fluorides is a tendency to etch the areas where cathodic current density is low or areas not covered with chromium. Because of this risk, fluoride-containing baths are often discouraged. This tendency to etching is especially noted on steel; conversely, the ordinary baths with sulfate catalyst have a strong tendency to etch copper, bronze, and brass. This etching tendency is especially marked in overcatalyzed baths and can be overcome to a considerable extent by keeping the bath in proper balance or operating at as low a catalyst concentration as possible. In addition this tendency results in the increase of the iron content of the bath, which when it reaches a certain level may slow down the plating rate, produce roughness, and if not checked make the bath unusable. Stareck and Dow [196] overcame etching by prefilming the surface to be plated as a cathode in a plain chromic acid solution. This procedure is effective only in higher ratio baths.

Etching and pitting of the basis metal are sometimes encountered in hard chromium plating even when using only sulfate catalyzed processes. If stray current is permitted to leave nonplating areas such as the exterior of cast iron diesel cylinder liners, it will plate only on the inside. This can be prevented by greater care in maintaining full insulation on racks and fixtures or by insulating the protected surface [150, 197, 198].

Bedi [199] found that immersion deposits of noble metals such as platinum and palladium on steel would prevent the etching that occurs in low-current-density recesses, particularly in baths containing fluoride catalysts. Such immersion deposits of noble metals create a low-overvoltage condition on the steel surface, which favors hydrogen evolution and tends to prevent other reactions. They may even prevent chromium deposition at higher current densities, and Bedi and Dubpernell [200] demonstrated the possible use for stopping-off purposes.

7.9.8 Black Chromium Deposits

Black chromium plating now has reached the stage where it is a completely practical plating operation that can be conducted in any existing plating plant. This process received the proper amount of attention in the last few decades. Black chromium selective surfaces have held the promise of being the most suitable coating for a wide range of low- to medium-temperature applications as solar selective coatings because of their excellent optical properties and apparent high degree of stability under diverse operating conditions. Mcdonald [201] reported that black chrome is not susceptible to degradation in humid atmospheres and possesses excellent selectivity. Mattox [202] reported excellent selectivity and thermal stability in air and in vacuum up to 350°C, and these authors have reported similar characteristics for black chrome.

The ideal selective absorber will have a high absorbency to incident solar radiation with wavelengths below 3000 nm and a low emittance beyond 3000 nm; this means that it will absorb solar radiation but simultaneously will emit little long-wave thermal radiation. Black chromium comes close to this ideal and will retain more heat energy than other types of black coatings.

The coating has good thermal stability. At temperatures below 480°C (900°F) there is no effect by the coating; at temperatures up to 590°C (1100°F) there is a slight graying of the deposit but the color reverts to black on cooling. The use of black chromium is not recommended on components subject to temperatures in excess of 700°C (1300°F).

Black chromium deposits have a high degree of microporosity, and this produces a corrosion resistance that is better than standard bright chromium. The same porosity gives it the ability to absorb and retain oil and paint films, which make it useful for the machine tool and electronic industries, and these properties are retained even after such operations as stamping, forming, drawing, and welding. An early ''black'' deposit was produced by using high current density in a cold bath principally containing chromic and acetic acids [203–205].

Modifications of this process for black chromium plating were proposed [206–211]. Current interruption [212] and nitrate, borate, and fluorosilicate [213] sulfate-free acid with a fluoride or complex fluoride catalyst [214] have been used. Mechanisms and structure of black chromium were studied [215–217]. There is some controversy among authors in the area of surface structure and composition, with the only real agreement being that black chromium is a homogeneous deposit of chromium metal and its compounds. The coating is generally believed to consist of particular chromium metal and chromium oxides and compounds. Baths based on trivalent chromium [218] and tetrachromates have been proposed [219, 220].

7.9.9 Postplating Treatments

Postplating treatments are not commonly used on chromium plate, since the great passivity and tarnish resistance of the metal usually make them unnecessary for most commercial parts. The normal ''air passivity'' of the metal, however, can be increased considerably by treatment with an oxidizing agent such as nitric acid, where this is practical. Flasch [221] treated thick chromium deposits with hot nitric acid, chromic acid, or permanganate solutions for many hours. He found that the passive chromium would no longer dissolve in hydrochloric acid and was nobler than platinum. Except for nitric acid, such treatments tend to discolor the chromium surface.

Willson [222] found that electrodeposited chromium foils 250 μm or more thick (produced by stripping the brass basis metal from them in concentrated nitric acid and then baking overnight at 165°C) resisted corrosion for 2 h in concentrated hydrochloric acid. It should be noted, however, that this is a metastable condition, and any slight disturbance or handling may result in a sudden violent attack of the chromium by the hydrochloric acid with the evolution of hydrogen gas.

Although treatment in a sodium hydroxide–sodium nitrite solution has been recommended for improving the corrosion resistance of thick chromium deposits on steel, other workers have disputed the efficacy of this procedure. Electrolytic polishing of the steel before chromium plating was effective in giving hard chromium deposits greater corrosion resistance [223].

Giesker and Britton [224] improved the corrosion resistance of chromium-plated steel surfaces by treating them cathodically in 50 g L^{-1} sodium dichromate solution of pH 4.5 at about 95°C and 0.3–0.5 A dm^{-2} for 1–2 min. Similar results were obtained by simple immersion in the same solution for about 2 h [225].

Safranek and co-workers [226] improved the corrosion resistance of chromium-plated parts with supplementary surface films applied by cathodic treatment for about 1 min in a solution of 50 g L^{-1} sodium dichromate and 1 g L^{-1} chromic sulfate at 85–95°C and pH 2.0–2.5 using 0.32–0.64 A dm^{-2}. The extent and permanence of the improved corrosion resistance are not certain. There are indications that the effect tends to be lost after a year or two of outdoor exposure. Occasionally chromium plate is used as an undercoat [227, 228]; for example, chromium is about the only undercoat that readily bonds to molybdenum [229]. In such cases, or whenever it is desired to deposit another metal over chromium, special precautions are necessary, owing to chromium's passive surface condition. This can be readily overcome by dipping in strong hydrochloric or other strong acid until the chromium starts to etch and hydrogen is briskly evolved. Quick rinsing and plating will then result in an adherent electrodeposit of almost any metal.

This etching procedure has the disadvantage of removing more chromium than is permissible or results in greater dulling and roughening of the surface than is desired. In such cases the chromium can be activated without etching by cathodic cleaning in alkali and followed by a short dip in mild acid such as dilute sulfuric at about 25°C or else by cathodic treatment in weak acid. One may follow with a strongly acid nickel strike [227, 228], and no difficulty should be experienced in obtaining a good bond to the chromium. A strongly acid copper chloride strike was used to obtain adherent copper coatings on chromium many years ago [230].

If the current is interrupted even briefly during hexavalent chromium plating, the subsequent layer of chromium may peel from the first due to the intervening passivity. The subsequent layer of chromium is also likely to be dull. This difficulty of plating one layer of chromium on another can be decreased by using a high catalyst or low ratio composition of the chromium bath, silicofluoride along with the sulfate catalyst, and high bath temperatures. If a current interruption occurs, chromium can be plated on the first layer of chromium by permitting it to come up to the temperature of the bath while submerged without current in the bath. The current can then be applied slowly in increments over a period of 1–2 min, starting with less than the plating current [231]. The hot, strong chromic acid solution has considerable activating action that only needs to be assisted by gentle gassing at just below the current density for the beginning of chromium deposition.

Current interruptions during trivalent chromium electroplating will not passivate the chromium deposit. Removing the part from the plating solution, rinsing, inspecting, and then returning it to the tank and continuing with the plating process can be done. Thus activating the surface before plating is not typically required. There will also be no loss of appearance. Trivalent chromium processes typically plate over passive deposits much easier than hexavalent chromium processes. The activation steps developed for plating hexavalent chromium deposits might not be necessary when trivalent chromium processes are used.

Occasionally organic coatings need to be applied over chromium, and once again obtaining good adhesion is of major concern. In general, organic coatings baked at a high temperature will adhere to chromium, whereas air-dried coatings will not. A detailed investigation of the adhesion of organic coatings to chromium plate was published by Safranek and Milter [232]. Practical experience is reported by a number of workers [234], One requirement appears to be to apply the organic coating to the fresh clean chromium surface before it can become contaminated with grease, dirt, or other foreign matter. Waiting even a few hours after chromium plating to apply organic coatings increases the degree of difficulty of application. Additional experience with the application of lacquer to chromium-plated surfaces can be found in the section on tin-free steel (TFS).

7.9.10 Stripping

Every chromium plater is eventually faced with the necessity of stripping chromium plate. Chemical, electrochemical, and mechanical methods are used to remove chromium plate.

In view of its passivity and usefulness, chromium is remarkable for ease of stripping. The metal dissolves readily as an anode in almost any aqueous solution to form chromic acid (Cr^{6+}) with close to 100% efficiency. It is only necessary to select a solution in which the basis metal suffers little attack from anodic action or in which the action is not too injurious for the purpose at hand. The most common strip is a dilute alkaline solution, such as an alkaline cleaner used with reverse (anodic) current. The cleaner becomes contaminated with chromate, and it is therefore best to use separate solutions for cleaning and stripping. A solution containing 70–100 g L^{-1} of sodium carbonate or 50–100 g L^{-1} of caustic soda can be used. It is important that the solution is free of chloride to prevent attack on the basis metal. For chromium thicknesses above 0.010 in. (250 μm) is more economical to grind the chromium deposit rather than to use any stripping method. A soft grinding wheel with a lot of coolant is required.

Chromium deposits from trivalent chromium processes containing metallic contamination might not strip completely in alkaline solutions. Activating the deposit in hydrochloric acid prior to the anodic alkaline strip is effective if dissolving it completely in hydrochloric acid is not desirable.

Simple immersion in hydrochloric acid from 10% (vol) to the concentrated acid of about 1.18 specific gravity, at 25°C, will dissolve a thin decorative chromium coating with hydrogen gas evolution in a few seconds and will generally leave the underlying nickel in condition for immediate replating. Care must be taken to rinse thoroughly to avoid contaminating the hexavalent chromium solution with chloride. Stareck [235] developed an alkaline pyrophosphate strip for chromium and other metals. This has the merit of leaving the steel, cast iron, or other basis metal clean and ready for further finishing operations. An alkaline strip tends to oxidize or passivate the underlying nickel and to make it difficult or impossible to replate with chromium. If, however, the strip is used cold at low concentration, low current density, and for the shortest possible time, replating is sometimes possible.

Thick chromium deposits are sometimes stripped in hydrochloric acid, but the action tends to slow down or stop where the deposit is thickest and to be too corrosive to the basis metal. Reverse current in a plain chromic acid solution of about 100–400 g L^{-1} is a better and safer stripping method for heavy chromium deposits on steel.

Another useful thickness test for thin decorative coatings is the anodic solution method [236].

7.10 TESTS OF DEPOSITS

7.10.1 Porosity and Cracking

Dubpernell [168] reported that acid copper plating over chromium up to about 25 μm thick could detect pores and cracks. Under the conditions of the test, acid copper does not deposit on chromium, owing to the passivity of the surface, and the copper deposits only in pores or cracks of sufficient magnitude to permit the solution to penetrate them to the basis metal. This makes the pores and cracks visible to the naked eye and easy to study at low magnifications.

Baker and Pinner [237] used this test to study the porosity and cracking of decorative chromium coatings. An important precaution is to apply it only to articles completely covered with chromium or to insulate all areas not chromium plated. Otherwise, all the copper will deposit on the areas not covered by chromium, and none will plate on the pores or cracks in the chromium plate. Another way of treating this difficulty is to increase the voltage during the acid copper plating step until some copper is deposited on the chromium-plated areas. However, too much voltage will plate copper directly on the chromium, thus hiding the pores and cracks. Masking off the unplated areas is preferred over increasing the voltage.

Another important precaution is to rinse the chromium plate in hot water to establish the equilibrium amount of cracking for the particular plate being tested. If this is not done, the deposit may appear relatively crack free and yet develop cracks with time, and the test will fail to give reproducible results. A certain amount of low-temperature heat treatment is necessary to stabilize the crack structure. Chessin and Seyb [238] used a 2-min immersion in boiling water. Some inconsistencies in the literature may possibly be due to the use of a hot-water rinse by some workers and the drying of specimens after a cold-water rinse under laboratory conditions by others.

Additional studies of the porosity and cracking of chromium plate were reported [5]. The cracks in thicker deposits were made evident by Gebauer [239] by anodic etching in 10% caustic soda solution followed by microscopic examination. Anodic treatment in chromic acid solution has been used by Dubpernell as a test for cracks in heavy chromium deposits. Almost any brief treatment is sufficient, a typical one being 60 A dm^{-2} for 15 s. These tests are of much shorter duration than the anodic treatment described below for the production of porous chromium deposits. A very fast method usable on some deposits, involves covering the surface with the ink from a solvent-based, dark felt pen, wiping off the excess surface ink, and examining the ink retained in the cracks under low magnification (100–150×).

Wyllie [240] used the copper plating test to show the cracks in chromium deposits after tensile testing. Cohen [241] studied the film of chromium compounds found

in the crack network of heavy chromium deposits, particularly after heat treatment of the metal.

7.10.2 Corrosion Resistance

The need in recent years for more durable decorative chromium deposits has led to something of a revolution in the specification and testing of such deposits. This in turn has led to several new developments to help meet the new requirements with thicker bright copper, nickel, and chromium coatings.

Until about 1960 decorative chromium deposits were generally confined to thicknesses of 0.5 μm or less since macrocracking would begin at this thickness. Under normal service conditions, macrocracks in thick deposits would contribute to a reduction in corrosion resistance [237]. Since the development of bright macrocrack-free chromium plating [242, 243], it has been demonstrated that if the undercoating of nickel or copper and nickel is of adequate thickness (generally more than 25 μm), a thicker decorative chromium plate adds substantially to the corrosion resistance. This is evidenced by accelerated corrosion and outdoor exposure tests. This development was foreshadowed as early as 1934 [244, 246], but it remained for the development of better accelerated tests and intensive testing to demonstrate the usefulness of thicker chromium coatings.

An electrolytic corrosion (EC) test was developed by Saur and Basco [247]. This test is highly accelerated and permits the examination of decorative chromium-plated parts in a few minutes as compared with many hours in other tests such as CASS (copper-accelerated acetic acid-salt spray (FOG) testing). Even though this test is fast, it has not received wide acceptance.

Seyb and Rowan [248] showed the improvement that could be obtained by means of thicker decorative chromium deposits, whether cracked or crack free. This demonstration was followed by the recommendation of duplex chromium coatings [249–252] for greater corrosion protection of both steel and zinc die castings. Because of the color change and the difficulty of plating decorative duplex chromium, this approach lost importance for extended corrosion resistance. The use of decorative microporous chromium over two or more layers of nickel is now preferred.

7.10.3 Microcracked and Microporous Deposits

A substantial improvement in the corrosion resistance afforded by thicker decorative chromium deposits was made with the introduction of ''duplex'' or ''dual'' chromium plating procedures in 1959 [249]. By first plating with ''crack-free'' chromium with good throwing or covering power and then with a second layer of highly cracked or microcracked chromium, a convenient means was found for applying heavier decorative coatings with good corrosion resistance. Seyb [250] has explained the corrosion resistance of duplex chromium coatings as depending on many small electrochemical cells with a relatively low rate of corrosion of the nickel undercoat and decreased tendency to basis metal corrosion. Lovell and co-workers [251], who detailed the same explanation, also report their experience with dual chromium systems and emphasize the need for a substantial copper layer under the nickel and chromium for best results.

The duplex chromium plate provides a convenient means of increasing the thickness and obtaining a microcracked plate with existing equipment, as well as combining the properties of different types of coatings. The most commonly used duplex system is a first plate of bright crack-free chromium with good coverage and adequate thickness in recesses followed with an ordinary cracked or microcracked chromium plate. The total thickness of the two deposits generally ranges from 0.75 to 2.5 μm. Specifications usually call for a minimum of 0.8 μm [252, 253].

Even with the improvements in duplex chromium plating, this system was difficult to consistently produce. Crack-free chromium deposits quickly develop cracks in service, thus reducing their corrosion resistance. It was also found in practice that it was difficult to plate two layers of chromium and that the color of the deposits changed because of the two layers of chromium. This approach has almost been completely replaced by 0.25 μm thick of microdiscontinuous chromium over two or more layers of nickel [254–257]. Another development is the use of an undercoat of chromium [228, 258, 259].

The need for a minimum thickness, about 0.75 μm, to obtain microcracking brings with it a need for good plate distribution into recesses in order to avoid unduly prolonged plating times. This need was lessened by Chessin and Seyb [238], who produced low-current-density microcracking by programming the current density during plating.

Microcracking of chromium in conventional thickness (0.25–0.75 μm) was obtained by several workers using a thin substrate of highly stressed nickel over the bright nickel layer before chromium plating [260, 261]. Du Rose et al. [260] also used hot-water treatment and the addition of selenium compounds to the chromium bath to increase microcracking in thinner chromium deposits.

The use of thin microporous chromium plate to improve corrosion resistance originated through the work of Brown and Tomaszewski [262]. They produced decorative, satin-finished nickel–chromium coatings by means of particle inclusion in the bright nickel undercoat. Chromium did not plate where the inclusions were on the nickel surface. Odekerken [263] and Chessin [264] have described other methods for producing microporous and thin microcracked chromium deposits. Improvement in the corrosion resistance of microporous chromium plate can also be effected by a low impact impingement of fine hard particles onto the brittle chromium-plated surface [265, 266].

Du Rose [267], Ogburn and Schlissel [268], and Willson [269] reported that chromium may be anodic or cathodic to the nickel depending on exposure conditions. Willson further suggested that residual stresses in the chromium–nickel system may be a factor in determining the type of corrosion that occurs.

The large number of papers that have appeared dealing with the general subject of improved corrosion resistance indicates the intense interest in these developments. The copper undercoat, the nature and thickness of the nickel, and the nature and thickness of the chromium as well as the galvanic effects between the dissimilar metals have all been discussed, and it appears that all play a part in the final result [261]. These improved decorative chromium deposits are being used more widely on a commercial scale and are included in recent specifications [220, 221]. Beacom [271] points out that the same kinds of systems that are used on die castings and steel are also desirable for plating over plastics.

The importance of the potential difference between adjacent nickel layers has been demonstrated in actual service. Microdiscontinuous chromium is now required by most decorative exterior automotive specifications, with microporous chromium being preferred. Harbulack developed an easy-to-use STEP test that simultaneously measures nickel thickness and adjacent electrode potential on completed parts [272]. ASTM Standard B764 details the operating conditions of the test [273].

7.10.4 Structure of Deposits

Chromium deposits are somewhat unique among the commercially used electroplated metals due to the deposit structure's influence on its performance. Many variations in structure and physical properties can be obtained by proper adjustment of the plating conditions and postplating treatments.

Chromium deposits 0.5 μm or less thick are normally crack free but porous, whereas thicker deposits are generally cracked after rinsing in hot water or after time in service. Up to a certain thickness, which varies depending on the plating conditions, the surface of the deposit is usually smooth and bright appearing to the unaided eye. When viewed under the microscope, however, the surface is revealed as having numerous domelike projections. Figure 7.9 shows a typical hard chromium surface. These projections become more prominent as the thickness increases, up to the point that they become visible to the unaided eye.

Figure 7.10 shows ordinary bright chromium deposit built up over the usually decorative thickness. The crack pattern is clearly shown, along with vestiges of "plated-over" cracks. All conventional bright plates more than 0.5 μm thick are cracked in this fashion. Figure 7.11 shows a crack-free, slightly "milky" type of plate such as is produced by the Mahlstedt process [274], plating at high temperature and low current density. Such deposits crack readily when heat treated, however.

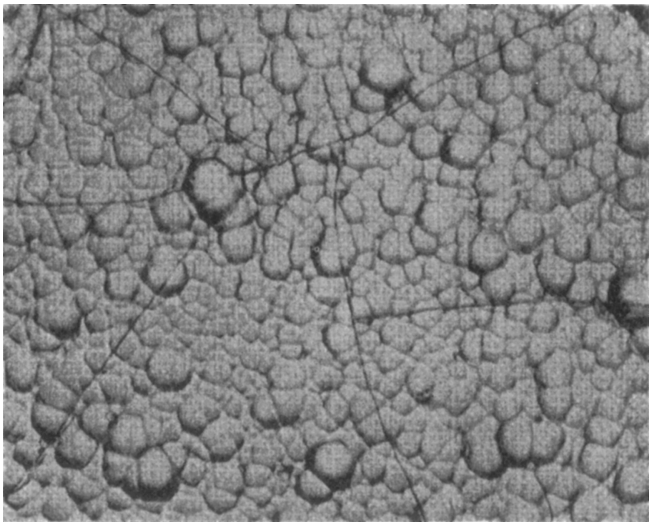

FIGURE 7.9 Semibright hard chromium plate, 100×.

Although other causes have been suggested, the basic cause of the cracks in deposits was believed by Snavely [275] to be related to the formation of unstable chromium hydrides of variable composition during the plating operation. Hydrides can be electrodeposited in either the hexagonal crystal form (formula Cr_2H to CrH) or the face-centered-cubic (fcc) crystal form (from CrH to CrH_2). The hexagonal hydride is most likely the one formed under normal plating conditions. It decomposes to body-centered-cubic (bcc) chromium and free hydrogen, even at 25°C. Some of the hydrogen escapes during the deposition process; the remainder is included in the deposit.

Data on the structure of the chromium hydrides were reported by Snavely and Vaughn [276]. The normal structure

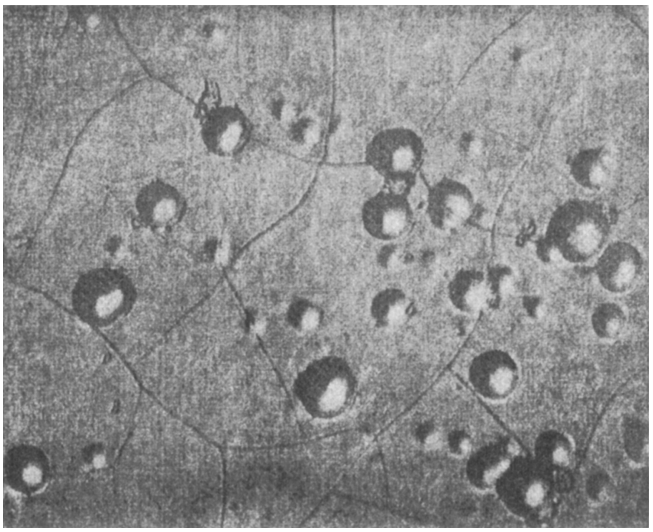

FIGURE 7.10 Thick bright chromium plate, 100×.

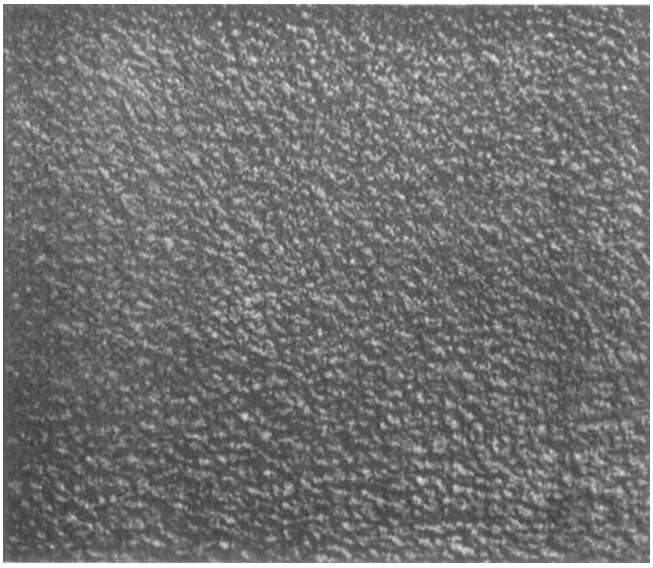

FIGURE 7.11 Crack-free ''milky'' low current density chromium plate, 100×.

of hexavalent chromium electrodeposits is bcc and is typically formed through deposition from warm solutions. Trivalent chromium electrodeposits are microporous under 0.8 μm and microcracked over this thickness. The structure is amorphous as plated but becomes bcc if heated. The amount of heating required is time and temperature dependent, but 1 h at 200°C is sufficient.

The decomposition of either hexagonal or fcc chromium hydrides to bcc chromium may involve a volume shrinkage of over 15%. Because the deposit is restrained in the plane of the basis metal, surface cracks form normal to that surface. The chemical constituents making up the cathode film are drawn into these cracks and may be bridged over by newly deposited chromium. These crack-filling constituents are the inclusion films studied by Cohen [241].

In addition to the oxide film inclusions in the cracks, which are readily detectable by metallographic examination of as-deposited chromium, experimental evidence indicates that there may be additional quantities of oxide or oxide-forming compounds finely dispersed through the plate. This dispersed oxide appears to be agglomerated on heating and then may be detected by the microscope [86, 277, 278].

Wood [279] measured the grain size of various chromium deposits by X-ray diffraction and arrived at a figure of 14×10^{-6} mm for bright plate made at 50°C. As a comparison, the smallest grains producible by cold-working metals are about 10^{-3} mm in average diameter. The extremely fine grains in chromium plate have been explained as resulting from the hydride decomposition [275].

Hardesty [280] reviewed cases of epitaxial chromium deposition in crystalline form. By working at over 80°C in a solution containing 250 g L^{-1} CrO_3 and 5 g L^{-1} fluoride ions with 500–700 mA cm^{-2}, he demonstrated the continued growth of the crystals of an electropolished nickel basis metal in the cross section of a thick chromium deposit.

Structural changes taking place on beading chromium plate are those normal for a highly stressed, fine-grained metal [277, 281]. Recrystallization takes place on prolonged heating in the temperature range 300–500°C or on shorter exposure at higher temperatures. The new grains are elongated normal to the basis metal. On prolonged exposure at temperatures of about 1100°C, large equiaxed grains are formed. During this heating the inclusion films remain in their original positions, although they are agglomerated into lines of spheroidal particles.

Brittain and Smith [282] examined the grain size of annealed chromium plate under the electron microscope and concluded that it increased to about 10^{-4} mm at 450°C in 1 h and to about 2×10^{-3} mm in the same time at 1000°C.

Bright hexavalent chromium plate is strongly grain oriented, with the (111) plane parallel to the basis metal [283]. This preferred orientation persists even after recrystallization [281]. The initial layer of plate is unoriented, and the preferred orientation is achieved as plating continues. Chromium plates on polished brass or electropolished steel attain the preferred orientation rapidly, whereas plates on a machine-ground basis metal receive a relatively thick layer of unoriented plate before the preferred orientation appears.

The laminations or striations in chromium deposits parallel to the basis metal [281] were found [284] to have an important connection with the crack structure; many cracks start and stop in the striations. Cracking occurred periodically, corresponding to the striations in deposits [285].

X-ray and other work on the structure of hexavalent chromium deposits were reviewed in 1967 [286]. Chromium generally has a bcc structure (α-chromium). Hexagonal chromium (β-chromium) was shown [266] to be an unstable chromium hydride rather than an allotropic modification. These hydrides decompose into the normal bcc chromium at 25°C in three to eight weeks, but decomposition is complete in 1 h at 150°C. Snavely [275] gives the best conditions for plating the hexagonal close-packed (hcp) hydride in dull gray form as 600 g L^{-1} chromic acid, 3 g L^{-1} sulfate, and 10 g L^{-1} sugar to reduce some chromic acid to Cr(III). The temperature was maintained below 12°C and current densities were 4.6–9.3 A dm^{-2}. These were essentially the conditions reported earlier by Wood [287].

''Cold'' chromium plate, deposited from solutions of widely varying composition at 25°C or less, has a distinctive, velvet-smooth, mouse-gray appearance and is obtained at current efficiencies up to about 35–40%. Such cold chromium plate is generally crack free and has an entirely different aspect from ordinary bright plate from warm solutions. Nevertheless, both cold chromium and bright plate were said to be entirely of the normal bcc structure [275]. Cold chromium plates significantly slower than regular chromium

processes. One would think that cold chromium plate would be formed by the decomposition of the hexagonal hydride, and the results of a number of workers [288, 289] have confirmed chromium plate to consist primarily of it.

Shluger and Kazakov [290] reported a thick cathode film on deposits of the hexagonal type made at 20°C but a thin film on cubic deposits made at higher temperatures. Okada and Ishida [291] found mixed crystals of hexagonal and cubic chromium in black chromium deposits. Matsunaga [292] obtained hexagonal chromium from Wood's solution at lower temperatures and higher current densities and cubic chromium under other conditions. He observed the oxide film on all of his deposits on X-ray examination, unless they were first etched with hydrochloric acid.

Cold chromium plate has the disadvantage of poor adhesion, in addition to being relatively soft and expensive to buff to a high luster. The poor adhesion can be partially overcome by special care in the preparation of the basis metal, as by electro polishing [293].

Cold chromium has been used to a limited extent commercially, particularly in Europe and North America. A common method is the Bornhauser process [294, 295], often called the tetrachromate or D-chromium bath (direct chromium plating).

Snavely [275, 296] also found some fcc chromium hydride in his hexagonal hydride deposits. By using a bath containing $1020\,g\,L^{-1}$ chromic acid, 300; 1 ratio of chromic acid to sulfate, and $20\,g\,L^{-1}$ sugar, at 0–4°C and $12.4\,A\,dm^{-2}$, Snavely produced a black plate which was the fcc hydride. This deposit was stable for about a week before X-ray tests showed appreciable decomposition. Dubpernell [119] studied such black deposits in 1942 but found the current efficiency to be extremely low, and thick deposits were difficult to produce by prolonged plating. The hardness was about 600 Brinell.

The dull deposits produced with interrupted current from single-phase rectification were partly hexagonal [297]. X-ray results [298] showed that dull deposits from interrupted current and from periodic reverse current were cubic but the current from a half-wave rectifier gave a mixture of cubic and hexagonal chromium.

Metallographic investigation of deposits of different structures showed that the hexagonal or β modification could be identified in the unetched cross section by means of polarized light [291]. Some deposits were found to be partly hexagonal and partly cubic. It was necessary to increase the Cr(III) content of Wood's [279] bath by adding $32.4\,g\,L^{-1}$ sugar instead of $10\,g\,L^{-1}$ in order to get completely hexagonal chromium [300]. The hydrogen overvoltage was considerably lower on hexagonal than on cubic chromium, although the same source later reported the opposite [301, 302]. Stress measurements [289] indicated that cubic chromium absorbs hydrogen and converts to hexagonal at least partly when treated as a cathode in $71\,g\,L^{-1}$ Na_2SO_4.

7.11 PHYSICAL PROPERTIES OF CHROMIUM PLATE

A number of convenient summaries of the physical and chemical properties of hexavalent chromium and of chromium deposits are available [286, 303–305].

7.11.1 Hardness and Wear Resistance

The hardness and wear resistance of chromium deposits are generally quite good in service, regardless of moderate variations in the conditions of plating. This is true as long as a satisfactory thickness is applied for the intended use. There also has to be good coordination between the hardness of the basis metal and the pressures encountered [306]. Frequently service is at elevated temperatures, and some of the as-plated hardness is lost. On the other hand, relatively soft deposits produced from hot solutions have often given especially good service, possibly owing to freedom from cracks or to greater strength and cohesion of this type of plate. Trivalent chromium deposits become harder when heated. Chrome carbides are thought to form by a reaction between the chromium and the codeposited carbon.

Hardness measurements are difficult to make and not very rewarding, since so many other factors are involved in service life. Unfortunately, hardness is not a simple elementary property; it depends on other properties in a little-known manner [307]. For these reasons the hardness measurement is not often used in chromium plate specifications.

Generally, the hardness of bright hexavalent chromium deposits is given as about $900–1000\,kg\,mm^{-2}$. Approximately the same values are obtained whether on the Brinell, Knoop, Vickers, or diamond pyramid scale [6]. Organic-catalyzed hexavalent chromium deposits can reach 1100 Knoop or Vickers with a 50–100-g load. As-plated trivalent chromium deposits fall into the same hardness range. After heat treatment the hardness can reach 1500 Knoop or Vickers (50–100-g loads).

The microhardness number depends to some extent on the test load used, and the deposit must be thick enough to withstand it or be conducted on a thick enough cross section. On a soft basis metal, a thin chromium deposit will show only the hardness of the basis metal; it would have to be extremely thick to indicate its full hardness. Chromium deposits 25 μm or more on a hardened steel base are thick enough for satisfactory measurement of the hardened metal with 50–100-g loads. It is recommended that the plate thickness should be at least 14 times the depth of penetration of the indenter [308]. Low loads often result in a considerable increase in the hardness number. Tests are sometimes made on the cross section of the deposit if it is thick enough and well supported [281]. If the deposit cracks around the indention, a smaller load should be used.

Brenner et al. [86] reported Knoop hardnesses for as-deposited chromium ranging from 300 to 1000, the softest deposits being from boiling solutions. Hosdowich [309] converted scratch hardnesses to the Brinell scale and reported figures from 640 to 1165 Brinell. The softest deposits were dull plates obtained at 15°C, and the hardest were burnt nodules. The hardness of the deposits was closely correlated with the appearance. All the bright deposits had a hardness of about 1000 Brinell.

Eilender and co-workers [310, 311] also made an extensive investigation. Wahl and Gebauer [312] determined Vickers hardnesses of 390–1280 with a 50-g load on deposits from 250 g L^{-1} solutions at 20–80°C and 10–200 A dm^2.

In tests with fluoride-catalyzed baths at 85°C Brenner et al. [86] found that the deposits were harder than corresponding ones from sulfate-catalyzed baths. Wahl and Gebauer [312] found slightly higher hardnesses for deposits from solutions containing silicofluoride catalyst. In general, deposits from solutions containing fluoride or complex fluoride catalysts seem to be about 100–200 units harder than corresponding deposits from solutions containing only sulfate catalyst. There also seems to be definite evidence of better retention of hardness by such deposits when exposed to heat.

The wear resistance is perhaps even more difficult to measure than the hardness. Two types of measurement have been used: abrasive wear with relatively light load similar to grinding [309, 312] and rubbing or frictional wear under higher pressures against a harder material such as a tungsten carbide wheel. There is considerable evidence that the hardest deposits do not necessarily give the greatest wear resistance. Thus Hosdowich [309] found the bright or slightly frosty deposits around 1000 Brinell to have the greatest wear resistance, and the burnt deposits up to about 1165 Brinell had somewhat less, perhaps because of brittleness. Likewise deposits of medium hardness around 750–800 Vickers were found to have the best frictional wear resistance, whether obtained as deposited or by moderate heat treatment of still harder deposits [310, 311].

Radioactive chromium plate is used to follow the wear of chromium-plated piston rings and to check the chromium transferred to the cylinder walls [313] or the lubricating oil [314, 315]. See Section 7.3 on porous chromium plating.

7.11.2 Coefficient of Friction

The low coefficient of friction of chromium plate against other metals is an important factor in its use on shafting, piston rings, internal-combustion engine cylinders, and similar applications. Table 7.2 illustrates the superiority of chromium in terms of this property.

Bright chromium plate against cast iron gave a lower coefficient of friction than mat or burned plates [318]. The coefficient of friction of chromium plate against steel or cast iron increases rapidly with temperature [319]. The increase may be avoided by final polishing after heat treating.

TABLE 7.2 Coefficient of Friction for Various Metal Combinations

Metal	Static Coefficient	Sliding Coefficient
Reference [316]		
Chromium-plated steel on chromium-plated steel	0.14	0.12
Chromium-plated steel on babbitt	0.15	0.13
Chromium-plated steel on steel	0.17	0.16
Steel on babbitt	0.25	0.20
Babbitt on babbitt	0.54	0.19
Steel on steel	0.30	0.20
Reference [317]		
Bright chromium plate on cast iron		0.06
Bright chromium plate on bronze		0.05
Bright chromium plate on babbitt		0.08
Hardened steel on cast iron		0.22
Hardened steel on bronze		0.11
Hardened steel on babbitt		0.19

7.11.3 Coefficient of Expansion

Hindent [320] found an average coefficient of expansion of 6.8×10^{-6} °C^{-1} for annealed electrolytic hexavalent chromium in the temperature range of 20–100°C. The coefficient of expansion at any temperature t between -75 and $+650$°C was shown to be expressed by the formula $a_t = (5.88 + 0.01584t - 0.00001163t^2) \times 10^{-6}$. Within the temperature range -100–700°C, the length of a chromium plate specimen is expressed by the formula $L_t = L_{0a}\ [l + 5.88t + 0.00774t^2 - 0.00000388t^3) \times 10^{-6}]$. Hindent also noted a linear shrinkage of approximately 1.1% during heating the deposits to 500°C for the first time. During subsequent heating and cooling cycles, the expansion and contraction were normal. Snavely [275] ascribed the initial shrinkage to relief of internal stress and closing up of voids between crystallites. These voids are a result of the decomposition of chromium hydrides.

Because of this unusual behavior, there is little hope that a basis metal can be found that will match the expansion and contraction characteristics of the chromium plate from chromic acid baths during heating cycles.

7.11.4 Melting Point

Sully and Brandies [286] tabulate measurements ranging from 1560 to 1920°C. Udy [303] selects the high value of 1930 ± 10°C based on results in [321] and [322]. Currently the American Society for Metals [304] has adopted the value of 1875°C after work at the National Bureau of

Standards [305]. Sully and Brandies [286] discuss much of the work in this area and state that it is not possible to come to any final conclusion but that a value close to $1878 \pm 22°C$ seems to be the most likely.

7.11.5 Density

The density of chromium plate varies according to the amount of inclusions in the plate, the number and size of cracks, and the magnitude of internal strain. Brenner and co-workers [86] reported a systematic study of the density of chromium deposited under various conditions. Values from 6.90 to 7.21 $g\,cm^{-3}$ were obtained. The oxide content decreased as the density increased. After annealing at 1200°C the density of the deposits increased to within the range 7.09–7.22 $g\,cm^{-3}$. The density of pure chromium is 7.20 $g\,cm^{-3}$, as calculated from its lattice parameter. Therefore the reported values over 7.20 can be considered anomalies related to the precision of the measurements. Hindent [320] reported a density of 6.93 $g\,cm^{-3}$ for as-deposited chromium, and this value is considered representative of most commercially deposited chromium.

Knoedler [288] reported a density of 6.143 for cold chromium or hexagonal hydride as deposited at 12–15°C, compared to 7.017 for as-deposited cubic chromium and 7.148 after annealing 2 h at 900°C.

7.11.6 Reflecting Power

Coblentz and Stair [323] studied the reflectivity of hexavalent chromium plate over a light range from ultraviolet to infrared. For the visible range of light, 4000–7000 Å in wavelength, they obtained reflectivity values between 62 and 72%. For ultraviolet light, the reflectivity ranged from 55 to 70%, and for infrared from 62% at 7000 Å to 88% at 40,000 Å. These high reflectivity values are usually retained over prolonged periods of exposure of chromium plate because of its corrosion and tarnish resistance. The reflectivity may be seriously reduced when the plate is exposed to highly corrosive atmospheres.

7.11.7 Electrical Resistivity

Electrical resistivity, like density, is a measure of the continuity, purity, and general soundness of a metal. The number, distribution, and size of the inclusion-filled cracks in chromium are related to the plating conditions. Therefore the electrical resistivity varies according to these conditions. Brenner and co-workers [86] reported electrical resistivity values for a wide range of deposition conditions. They showed that a resistivity of about 50–60 μΩ-cm at 28°C may be expected for conventional chromium plate, with much lower values down to 14 μΩ-cm for deposits from hot solutions. After annealing at 1200°C, the oxide film inclusions are spheroidized, and the cracks in which they originated are no longer continuous. As a result the resistivity of annealed electrolytic chromium approaches a common value of 13 μΩ-cm at 28°C, regardless of conditions of deposition [119].

7.11.8 Internal Stress

According to the theory of chromium hydride formation and decomposition during chromium plating [275], the cracks in the plate result from internal stresses that exceed the cohesive strength of the metal. Cracking relieves these stresses to the point where they are no longer of sufficient magnitude to extend the cracks. Most thick plates are cracked and contain residual internal stress. Thin plates may contain even higher stress because they are restrained from cracking by the basis metal and transfer their stress to it.

Brenner et al. [86] reported stress values as high as 56 $kg\,mm^{-2}$ for very thin chromium deposits which were not cracked. Conventional plating practices produced thicker cracked plates having internal stress of about 12 $kg\,mm^{-2}$. Plates from a dilute bath at 85°C were crack free but contained stresses of 45 $kg\,mm^{-2}$.

Stareck et al. [324] investigated deposits up to 100 μm thick and found that the stress in highly cracked deposits might become negative or compressive with increasing thickness. Compressive stress as high as $-12\,kg\,mm^{-2}$ was found. This was explained as due to a wedge effect of chromium plated into previously formed cracks. Williams and Hammond [325] confirmed the presence of moderate compressive stress in some thick chromium deposits in the as-plated condition.

Nishihara et al. [289] showed that the stress was lower in the hexagonal hydride but that cathodic treatment of ordinary bcc deposits in 71 $g\,L^{-1}$ Na_2SO_4 at 40°C and 1 $A\,dm^{-2}$ decreased the stress in less than 1 h to less than that of the cold chromium (hexagonal hydride). Additional work on stress in chromium deposits has been reviewed [326, 327].

7.11.9 Effect on Fatigue Strength of Basis Metal

The stress in various hexavalent chromium deposits was correlated with the crack structure and thickness [324], and it was found that because of a wedge effect of chromium deposited in previously formed cracks the stress frequently decreased with thickness, and heavy deposits even developed compressive stress. This was in turn correlated with the effect of the deposits on the fatigue strength of steel [328]. Two types of deposits that had a minimum effect on the reduction of fatigue strength were found: highly cracked deposits with low stress as plated and deposits from high-concentration baths that could cause stress damage as plated but could be heat treated with good results.

Chromium plate generally reduces the fatigue strength of steel markedly [329–331]. Stareck et al. [324, 328, 330] found that the decrease in strength was due to the stress in the deposits that weakened the basis metal. They found several ways to overcome or minimize the effect, such as by producing deposits of low or compressive stress or by heating to high temperatures to eliminate the stresses as far as possible. These results were confirmed and extended by Williams and Hammond [332].

Shot peening [333], roller burnishing [334], and grit blasting [335] of the basis metal have also been shown to be helpful. In this way there is introduced into the surface before plating a compressive stress which tends to counterbalance any tensile stresses in the deposit.

Continuing investigations of these matters are quite extensive. German work has been reviewed [336–339]. Effects of surface finishes in gun barrel manufacture were investigated by Greco and Penned [340]. The detrimental effect of chromium plate on other basis metals and methods of overcoming it have also been investigated for aluminum [341–344] and titanium [345].

7.11.10 Ductility

No ductility was found in chromium deposits from aqueous solutions by Wyllie [240] or Brenner et al. [86], although the latter found tensile strengths of 6–56 kg mm^{-2}. Deposits from fused salt baths have, however, been found to be ductile [304].

Klopp [346] reviews progress in improving the ductility and strength of chromium and chromium base alloys. Brandes and Whittaker [347] reported a tensile strength of 20 kg mm^{-2} and an elongation of 17% on electrolytic chromium at room temperature after annealing in hydrogen at 1600°C.

7.12 CHEMICAL PROPERTIES

7.12.1 Oxidation and Tarnish Resistance

Chromium plate normally has a very thin oxide film on its surface. This film is so stable, tenacious, refractory, and self-healing that it protects the metal underneath from further oxidation. The plate remains bright at temperatures up to 260°C. On prolonged heating of chromium plate to temperatures of about 315°C in air, the oxide film thickens and darkens. At higher temperatures, temper colors are produced, and a black or green-black oxide layer is finally formed. At temperatures around 1000°C, an oxide layer forms on the surface and an extremely hard chromium nitride layer forms between the oxide and the chemically unaffected portion of the plate [281]. Pure trivalent chromium deposits undergo similar color changes due to heating. Deposits containing metallic codeposits such as iron and copper darken faster and to a greater degree.

The thin oxide film on chromium plate forms quickly when plating is completed or is present during plating, so tarnishing of the plate is not likely to be encountered. The chromium oxide is a satisfactory protection against sulfides, which cause serious tarnishing of silver, copper, or nickel.

7.12.2 Chemical Resistance

The chemical resistance of chromium plate is not so great as might be supposed from its performance in the atmosphere. Chromium is readily attacked by mineral acids and by reducing solutions in general. It is resistant to nitric acid, which heals the protective oxide film, and nitric acid may be used to dissolve other metals such as copper or nickel away from chromium plate. Smith and Dubpernell [348] found it possible to improve the acid resistance by anodizing.

Christov and Pangarov [300] found their cold chromium plate (β or hexagonal chromium) to be more passive and corrosion resistant than bright α cubic chromium plate deposited at 45°C. Thus a pH of about 1 was required to dissolve hexagonal chromium, while cubic chromium dissolved at pH 2; cubic chromium stopped dissolving when the pH was increased to about 2.6, while hexagonal chromium stopped dissolving around pH 1.7–1.8.

The chemical resistance of chromium plate may be used to the best advantage only if the underlying metal is completely covered [349]. For that reason hard or industrial chromium plates for corrosive service should be at least 25–50 μm thick to ensure that the cracks are not continuous to the basis metal. Otherwise, a crack-free type of deposit should be used. Many trivalent chromium deposits tend to have more substrate exposed than hexavalent chromium deposits. Many thin (under 0.8 μm) trivalent chromium deposits are microporous as plated. Over 0.80 μm the deposits are microcracked. Over about 2 μm the deposits tend to develop macrocracks, many of which extend to the substrate.

In general, hexavalent chromium plate may be used in the same types of corrosion-resistant service as the high-chromium stainless steels at ordinary temperatures, depending on the physical properties required of the basis metal. Even though trivalent chromium deposits contain the same type of oxide film, these deposits may not have the same chemical resistance. Codeposited metals with chromium from trivalent chromium can have a significant influence on chemical resistance.

Resistance to corrosion and wear in high-purity water at high temperatures in atomic reactors is a field where hexavalent chromium plate appears to have some utility, but many special application problems are involved [340]. Suss [351] found contradictory results on chromium-plated stainless steel, probably because of electrochemical effects. The general behavior of chromium exposed to corrosion in aqueous media at 25°C has been comprehensively outlined

on a thermodynamic basis by means of potential pH diagrams [352, 353].

A considerable number of specific corrosion tests on chromium and chromium plates were made [8, 245, 329]. These tests included a wide variety of acid and salt solutions, and organic compounds and acids as well, at 12 and 58°C.

7.12.3 Chromium-Plated Strip Steel–Tin-Free Steel

Chromium-plated strip steel for the production of ''tin cans'' originated commercially in Japan in 1962, as described by Uchida and co-workers of the Fuji Iron and Steel Company [354–356]. The process originally consisted in chromium plating for 10 s to get a thickness of 0.05 Å followed by a chemical dip treatment in 1% chromic acid or 2–3% sodium bichromate to improve the corrosion resistance and finally lacquering with a high-temperature baking lacquer.

Some further developments in the United States as well as in Japan have been reviewed [357–362]. Commercial production began in the United States in 1967. The resultant tin-free steel (TFS) has been used for the manufacture of beverage cans, a large proportion of which is now made from this material. The tin-free steel lacks the easy solderability of tin plate for high-speed can production and has necessitated the use of processes for cementing or welding the seams of cans. The resulting cans are more readily recyclable because they contain no tin.

In newer procedures the chromium thickness has been cut down to 0.005–0.0075 Å (35–54 mg m^{-2}) [363] but is sufficient to prevent filiform or underfilm rusting in the corrosion tests used [359] when combined with the oxide coating produced in a final cathodic posttreatment solution compatible with the plating bath [359]. The latter oxide is about five times the thickness of the natural oxide film present on most chromium plate, which is about 3.75 mg m^{-2} [357, 359, 365] in terms of weight of chromium in the oxide. Not much more than 16 mg m^{-2} of chromium as oxide can be applied without getting a colored coating instead of a transparent one.

In plating the steel strip moving at 300–550 mm mm^{-1}, Seyb and co-workers [366] found it necessary to use fluoride or complex fluoride containing electrolytes, and they formulated the first practical baths for this application, which have become the standard in commercial use. Current efficiencies of about 25% are obtained in practice. Typically the moving strip passes between four pairs of 38-cm-long sections of anode placed vertically, or six pairs counting the somewhat longer cathodic posttreatment. This gives a plating time of about 0.05 s in front of each pair of anodes, or a total plating time of about 0.30 s to produce the finished product, which is then rinsed, dried, oiled, and lacquered.

The reception of this product has been good, and its use has grown rapidly, resulting in the saving of substantial quantities of tin for other purposes. Tin-free steel is less expensive than comparable tin plate [362].

7.12.4 Porous Chromium Plate

This name has been given to modified chromium deposits with oil-retaining properties used on internal-combustion engine cylinders and piston rings. Such deposits were used especially on aircraft and diesel engine to make the engines last longer. Today most parts plated with hard chromium benefit from the cracks.

Three main types of ''porous'' chromium plate have come into common use. The first is the ''mechanical'' type produced by grit blasting the basis metal, chromium plating, and finally finishing to size by grinding, honing, or polishing [367]. The second and third types of plate are those with ''pitted'' and ''channel'' porosity. Both of these are obtained by treating the chromium deposit in an etching solution. The type of porosity obtained depends on careful control and regulation of the conditions of deposition. Numerous publications and patents describe the production of all these types of porous chromium plate and the results obtained with them [368–376].

Another variation is to etch pits into the surface of the deposit through a plastic mask [371] or a photoresist [372]. Etching by ion bombardment through a screen [372] and with alternating current [379] is proposed. Raymond [380] plates at extremely high current densities from 232 to 1160 A dm^{-2} at 30–55°C to produce a porous deposit directly. Still another variation is to impregnate the porosity with Teflon to provide the possibility of dry lubrication [381], but this does not seem to have become important commercially. Patents were issued to Forestek [382] and Letendre [383]. Zubrisky [384] patented the final grit blasting of polished or honed porous chromium surfaces to provide better breaking in qualities.

The ''pit'' type of porous chromium may be produced, for example, by plating under ordinary hard chromium plating conditions. Baths containing 250 g L^{-1} chromic acid and 2.5 g L^{-1} sulfate at 50°C are used. Plating took place at 46–54 A dm^{-2} for a minimum of 2–3 h to get a deposit at least 100 Å thick. They were then treated as an anode or cathode in a suitable etching solution or by simple immersion in acid. A typical anodic treatment [365] is about 150 A-min dm^{-2}, but this may be prolonged or repeated if it is desired to remove more metal or to obtain deeper porosity. After the deposit has been heavily attacked, numerous cracks are found to be eaten away, and a surface crust of undermined metal remains. When this crust is ground, honed, or polished away to the extent of 25–50 Å, numerous pits remain in the chromium plate.

Good conditions for producing the ''channel'' type of porous chromium plate are 60°C and a ratio of chromic acid to sulfate of 115 : 1. The usual current densities of 46–62 A dm^{-2} are employed for a deposit thickness of at least 100 or 125 μm. After treatment in the etching solution, the deposit does not have a loose surface crust but only a

network of fissures so that grinding, polishing, or honing off about 25 μm leaves channels, with dense chromium '' plateaus'' or ''lands'' between. This type of porous chromium has been largely used for aircraft engine cylinders, whereas the pit type has been more extensively employed in diesel engines and on piston rings.

Several specifications have been issued on porous chromium plating [385]. It is a well-established procedure conducted on a large scale in a limited number of plants. The merits of the product are confirmed by carefully controlled tests. Thus Kishi et al. [386] with radiotracer techniques determined that the wear on porous chromium and ordinary hard chromium was about equal under low loads. The ordinary hard chromium showed a rapidly increasing weight loss; the porous chromium showed very little wear.

7.13 TRIVALENT CHROMIUM BATHS

7.13.1 Trivalent Chromium Processes

Historically trivalent chromium baths have always been the first and favorite approach to chromium plating because of the increased safety and health properties [387]. It was not until the mid-1970s [388] that a commercial process was available and increased productivity became more important than health and safety in choosing this process.

The U.S. Bureau of Mines developed a process for electrowinning of pure chromium metal from the ore or from ferrochromium using a mixed bivalent and trivalent chromium sulfate solution [389–391], but the process has not been adapted successfully for plating purposes. A two-compartment cell has been used at the Union Carbide Corporation, Marietta, Ohio, plant. Continuous operation on a large scale seems necessary for good results [392]. In another review of the operation [392a], Bacon mentions that low efficiencies always prevail during the startup of a cell.

Success was very limited in efforts to use such baths for plating [393–403]. A chromium ammonium chloride solution was used for brush plating [399, 400]. Better results in brush plating were obtained with Gregory's salt, ammonium chromium oxalate [406–409].

More recent efforts were made to commercialize the use of chromium chloride solutions in, or containing, organic solvents. Bharucha and Ward [410] of the British Non-Ferrous Metals Research Association obtained several patents and published several articles [411, 412]. Diamond Shamrock Chemical Company has offered a similar process [413]. The deposits are darker than those from chromic acid solutions and some chlorine gas is generally evolved at the anode. Levy and Momyer of Lockheed [414] reported tests with chromium thiocyanate and chromium format dissolved in organic solvents. Brown and Tomaszewski also give a brief report of their work with trivalent baths [262].

In recent years, there has been many references on trivalent chromium research [415–419]. Snyder [420] reviewed the deposit's physical properties of one commercial formulation. Corrosion, a concern with decorative deposits, has also been extensively studied. The same author [421, 422] published corrosion data showing that, except for thin nickel applications, trivalent chromium deposits have equal or better corrosion resistance than hexavalent chromium deposits. Trivalent chromium processes do not contain hexavalent chromium ions that can react with unplated metal and offer short term corrosion protection. This makes trivalent chromium less corrosion resistant over thin nickel or bare steel. Carter and co-worker [423] also reviewed trivalent chromium corrosion studies using a different formulation to produce the deposits. One major advantage of some trivalent chromium formulations is that metallic impurities can be easily removed by directly passing the plating solution through an ion exchange [424].

7.13.2 Chromium Alloy Plating

One major advantage of trivalent chromium chemistry versus hexavalent chromium chemistry is the ability to easily produce chromium alloys. Chrome iron [425, 426] and chrome nickel–iron [427, 428] are the most typical alloys produced.

Chromium alloy plating can be considered a subheading under trivalent baths; there is almost no alloy plating possible from hexavalent solutions. There has been a great deal of work, and some reviews are available [429–431], but nothing of commercial importance seems to have been developed. Now that trivalent chromium processes are commercial, it is expected that there will be more research of chromium alloys. It is very easy to alloy metals such as nickel, iron, copper, and zinc from a trivalent chromium electrolyte.

One exception to the rule of no alloy plating from chromic acid baths is the work of Vagramyan and his collaborators [430]. Alloys of up to 37% selenium, 15% manganese, 2% molybdenum, and 1% rhenium were obtained with cold chromium deposits at about 20°C. These alloys are, on the whole, no longer obtained as the temperature is raised, so presumably they are alloys produced with the dull hexagonal hydride at low temperatures and not with the bcc deposits which form ordinary bright plate.

Snavely and co-workers [432] reported the physical data for chromium alloys containing iron, molybdenum, nickel, phosphorus, or tungsten from trivalent chromium baths. Alloys containing 6–10% iron were harder after heating to 800°C than hexavalent chromium from conventional baths. However, they were softer than conventional deposits prior to heating. Alloys containing 6% iron retained their hardness of 600–700 kg mm^{-2} after heating to 600°C [433]. Alloys with 15% iron exhibited a hardness of 1000–1025 kg mm^{-2} prior to heating [434]. Chromium alloys with up to 60% iron

exhibited stress of 36,000–38,000 psi [435], even though they had many cracks. Coefficients of expansion for chromium alloys containing 6–18% iron were slightly higher than those for conventional chromium [436].

Much work has been done, mainly in France, to investigate claims of improved wear resistance of chromium–molybdenum alloys produced from chromic acid solutions [437, 438]. It appears that bright deposits generally contain less than 1% molybdenum, and this could possibly result from solution contamination of the deposit instead of alloying. Hard chromium plating baths are frequently deficient in catalyst due to too strict adherence to the 100 : 1 ratio of chromic acid to sulfate. The improved wear resistance of deposits from solutions containing molybdenum compounds might in fact be due to the catalytic imbalance.

Chromic acid plating baths containing molybdenum salts have been employed for obtaining deposits requiring high abrasion resistance and wear [439–442]. Abrasion resistance was improved 200–300% over conventional deposits with the inclusion of molybdenum. A deposit containing 3% molybdenum had a reported hardness of 1000–1300 kg cm^{-2}. The hardness increased as the concentration of molybdate increased to 100 g L^{-1} [434]. X-ray diffraction studies showed the presence of molybdenum trioxide indicating a dispersion [439].

Chromium–ammonium sulfate solutions containing sodium hypophosphite produced deposits with increasing hardness as the phosphorous content increased up to 15% [444]. Hassion and co-workers studied formulations containing magnesium oxide, zirconia, and thoria and found that dispersions were produced [445]. The hardness of the deposits increased in every case. Additions of sodium tungstate or magnesium oxide [446] increased hardness. The same was reported for the addition of titanium oxide [447].

7.14 OTHER SPECIAL TYPES OF CHROMIUM PLATE

A ''frosty'' or satin-finish plate in between cold chromium and bright plate was found desirable for press plates [448]. Such smooth-bubbly or natural rounded nodular plate has been found useful for handling textile materials. Trist [449] used a special cold chromium plate produced in refrigerated electrolytes for printing plates.

Carveth [450] obtained a black color on chromium deposits by immersion in molten cyanide. The carburizing of chromium deposits for greater hardness has also been frequently attempted [451–453]. Although the plate is first softened by the heat, it does appear possible to obtain very hard chromium carbide coatings.

Bohlman [454] was successful in spot plating with a jet of ordinary chromic acid solution and achieved extremely high local rates of deposition. Chessin and Walker [455] developed a bath with organic additions to give a uniformly iridescent chromium plate, and Chessin and Gempel [456] obtained similar results with additions of molybdenum compounds.

7.15 REGULATIONS

In many developed nations, plating is one of the most regulated industries with hexavalent chromium plating one of the most regulated processes. Hexavalent chromium is a suspected or confirmed carcinogenic agent depending upon the regulator. It is also a strong oxidizer. Even the classical wetting agent used in hexavalent chromium electroplating, PFOS (perfluoro-octanesulfonic acid), which was almost universally used to improve the safety of the process by reducing the misting generated during plating, is being banned in many countries because it is extremely stable and does not break down. This stability is what is required to exist in a hexavalent chromium solution but is bad for the environment.

The plater must contend with regulations controlling the amount of hexavalent chromium ions inside the workplace, the amount discharged in the air outside of the plant, and the potential residual presence in the discharged waste. There are even tight controls on the disposal of precipitated trivalent chromium produced in the waste treatment process. Even the European Union's End-of-Life Directive, which was developed to regulate passivates for zinc and zinc alloy, impacts hexavalent chromium platers. Although the chromium metal on the plated part is not regulated, insufficient rinsing after hexavalent chromium plating leaves enough hexavalent chromium ions on the part to fail the End-of-Life leaching test. However, using good plating practices and the correct control mechanisms, most hexavalent chromium platers can meet the regulations, but in some locations only trivalent chromium plating is permitted.

Trivalent chromium processes are much less regulated because trivalent chromium ions are not strong oxidizers and are not even suspected carcinogenic agents. Under most regulations, if a wetting agent is used, trivalent processers are regulated similarly to nickel electroplating processes. Since in most trivalent chromium processes the wetting agent is also a required additive for producing bright decorative deposits, wetting agents are used. Trivalent chromium wetting agents are not in the PFOS family and remain unregulated.

Because regulations can be very different in different countries, different states/regions, and even different local communities, chromium platers must be very diligent in understanding and following the regulations that their operation must meet. Regulations also have a tendency to change because of the evolving understanding of the effects that chromium ions have on our environment/health/safety. This means platers must investigate their individual requirements and not solely use general literature cited values. Also, as in

the case where insufficient rinsing puts hexavalent chromium plating under the End-of-Life directive, all regulations should at least be considered even if they do not appear to be relevant.

REFERENCES

1. G. Dubpernell, *Plating*, **47**, 35 (1960).
2. C. G. Fink,U.S. Patents 1,581,188 (1926); 1,802,463 (1931).
3. Elektro-Chrom-G.m.b.H. (assignee of E. Leibreich), German Patent 448,526 (1927); British Patent 237,288 (1925); French Patent 601,059 (1926); Swiss Patent 118,632 (1927).
4. J. Stareck, F. Passal, and H. Mahlstedt, *Proc. Am. Electroplat. Soc.*, **37**, 31 (1950).
5. G. Dubpernell, in *Modern Electroplating*, 2nd ed., F. A. Lowenheim, Ed., Wiley, New York, 1963, pp. 80–140.
6. P. Morisset, J. W, Oswald, C. R. Draper, and R. Pinner, *Chromium Plating*, Robert Draper, Teddington, Middlesex, England, 1954.
7. W. Blum and G. B. Hogaboom, *Principles of Electroplating and Electroforming*, 3rd ed., McGraw-Hill, New York, 1949, p. 344.
8. C. G. Fink and H. D. McLeese(to United Chromium, Inc.), U.S. Patent 1,844,751 (1932).
9. H. R. Moore and W. Blum, *Natt. Bur. Stand. Res. Papers*, **198**, 255 (1930).
10. U.S. Patents: 3,954,574 (1976); 4.038,160 (1977); 4,053,374; 4,093,521; and 4,054,494 (1980).
11. D. L. Snyder, *AESF Chromium Colloquium*, NASF, Washington, DC, 1987.
12. J. Koppel, *Z. Anorg. u. Aligem. Chem.*, **45**, 359 (1905).
13. F. Hein and S. Herzog, in *Handbook of Preparative Inorganic Chemistry*, 2nd ed., Vol. 2, Georg Brauer, Ed., Academic, New York, 1965, pp. 1361–1370.
14. *Inorganic Synthesis*, Vol. 10, David G. Holah and John P. Fackler, Jr., Eds. McGraw-Hill, New York, 1967, p. 26.
15. F. A. Cotton and G., Wilkinson, *Advanced Inorganic Chemistry*, 5th ed., Wiley, New York, 1985, pp. 679–697.
16. *Kirk-Othmer Encyclopedia of Chemical Technology*, 4th ed., Vol. 6, Wiley, New York, p. 267.
17. F. Basal and R. G. Pearson, *Mechanisms of Inorganic Reactions*, Wiley, New York, 1967, pp. 141–145.
18. L. Spicia, H. Stoeckli-Evans, H. Marty, and R. Giovanoli, *Inorg. Chem.*, **26**, 474 (1987).
19. L. Spicia and W. Marty, *Inorg. Chem.*, **25**, 266 (1986).
20. D. Rai et al., *Inorg. Chem.*, **26**, 474 (1987).
21. D. E. Pennington and A. Haim, *Inorg. Chem.*, **5**, 1887 (1966).
22. M. R. El-Sharif, S. Ma, and C. U. Chisholm, *Trans. Inst. Met. Finish.*, **73** (1), 19 (1995).
23. M. R. El-Sharif, A. Watson, and C. U. Chisholm, *Trans. Inst. Met. Finish.*, **66**, 34 (1988).
24. A. Smith, A. Watson, and D. Waughan, *Trans. Inst. Met. Finish.*, **71** (3), 106 (1993).
25. M. R. El-Sharif, S. Ma, C. U. Chisholm, and A. Watson, *Proc. AESF SUR/FIN'93*, NASF, Washington, DC.
26. J. C. Blair, *Comprehensive Inorganic Chemistry*, Vol. 3, Pergamon, New York, 1970.
27. J. E. Earley and R. D. Cannon, *Aqueous Chemistry of Chromium (III) in Transition Metal Chemistry*, Vol. 1, Marcel Decker, New York, 1966, p. 64.
28. H. Stunzi, L. Spicia, F. P. Rotzinger, and W. Marty, *Inorg. Chem.*, **28**, 66 (1989).
29. E. Serfas, E. Theis, and T. Thovensen, *J. Am. Leather Chem. Assoc.*, **43**, 132 (1948).
30. E. Serfas, G. Wilson, and E. Theis, *J. Am. Leather Chem. Assoc.*, **44**, 647 (1949).
31. J. W. Mellor, *A Comprehensive Treatise on Inorganic and Theoretical Chemistry*, Vol. II, Longmans, London, 1931.
32. M. J. Udy, *Chromium*, Vol. 1, Reinhold, New York, 1956.
33. G. Michel and R. Cahay, *J. Raman Spectrosc.*, **17**, 76 (1986).
34. G. Michel and R. Machiroux, *J. Raman Spectrosc.*, **14**, 22 (1983).
35. T. Radnai and C. Dorgai, *Electrochim. Acta*, **37** (7), 1239 (1992).
36. N. V. Mandich and N. V. Vyazovikina, Extend. Abstracts, paper presented at 49th Meeting of Int. Soc. Electrochem., Kitakyushu, Japan, 1998.
37. A. Martens and G. Carpeni, *J. Chim. Phys.*, **60**, 534 (1963).
38. J. P. Hoare, *Plating Surf. Finish.*, **76**, 46 (1989); *J. Electrochem. Soc*, **126** (2), 190 (1979).
39. J. P. Hoare, *Plating Surf. Finish.*, **76** (9), 46 (1989); *J. Electrochem. Soc.*, **126** (2), 190 (1979).
40. J. P. Hoare and M. A. La Boda, *J. Electrochem. Soc.*, **132** (4), 798 (1985).
41. J.-L. Fang, N.-J. Wu, and Z.-W. Wang, *J. Appl. Electrochem.*, **23** (5), 495 (1993).
42. A. Radwan, A. El-Kiar, H. Farag, and G. Sedahmed, *J. Appl. Electrochem.*, **22** (12), 1161 (1922).
43. D. Landolt, R. Acosta, R. H. Mullar, and C. W. Tobias, *J. Electrochem. Soc.*, **117**, 839 (1970).
44. H. Voght, *Electrochim. Acta*, **3**, 633 (1987).
45. N. V. Mandich, Ph.D. Thesis, Aston University, Birmingham, Great Britain (1996).
46. T. C. Saiddington and G. R. Hoey, *J. Electrochem. Soc.*, **120**, 1475 (1973).
47. V. Guro, M. Schluger, O. Khodzhaev, and Sh. Ganiev, *Electrokhimiya*, **30** (2), 251 (1994).
48. Z. A. Soloveva, Yu. V. Kondashov, and S. V. Vashenko, *Elektrokhimiya*, **30** (2), 228 (1994).
49. K. Yoshida, A. Suzuki, K. Doi, and K. Arai, *Kinzoku Hyomen Gijutsu*, **30**, 338 (1979).
50. H. Kimura and T. Hayashi, *Denki Kagaku*, **37**, 5 (1969).
51. M. Nagayama and T. Izumitani, *Kinzoku Hyomen Gijutsu*, **21**, 505 (1970).
52. J. Levitan, *J. Electrochem. Soc.*, **111** (3), 286 (1964).

53. H. Okada, *Kinzoku Hyomen Gijutsu*, **11**, 623 (1960); *Kinzoku Kagaku*, **4**, 1 (1967).
54. K. Yoshida, Y. Tsukahara, and K. Koyama, *Kinzoku Hyomen Gijutsu*, **30** (9), 457 (1979).
55. N. V. Mandich, *Plating Surf. Finish.*: (a) **84** (6), 97 (1997);(b) **84** (5), 108 (1997).
56. H.Chessin and K. Newby, U.S. Patent 4,588.481 (1986).
57. N. Martyak, U.S. Patent 4,810.336 (1989).
58. W. Korbach and W. McMullen, U.S. Patent 4,828.650 (1989).
59. W. Korbach, U.S. Patent 4,790.674 (1989).
60. A. R. Jones and A. Neidgrer, *Proc. 2nd AESF Chromium Colloquium*, Miami, NASF, Washington, DC, 1990.
61. K. Newby, *Proc. AESF Sur/Fin* 1999.
62. M. S. Frant, *Plating Surf. Finish.*, **54**, 102 (1967).
63. F. Passal(to United Chromium, Inc.), U.S. Patent 2,640,021 (1953).
64. J. E. Stareck (to United Chromium, Inc.), U.S. Patent 2,640,022 (1953).
65. R. Chellapa and N. V. Pathasaradhy, *Met. Finish.*, **75** (2), 93 (1981).
66. S. R. Natarjan, *Met. Finish.*, **79** (5), 93 (1981).
67. R. Krishnan, *Met. Finish.*, **84** (11), 31 (1981).
68. S. Sriveraraghavan, *Met. Finish.*, **94** (2), 68 (1946).
69. R. M. Krishnan and N. V. Pathasaradhy, *Met. Finish.*, **69** (9), 59 (1971).
70. J. P. Hoare and M. A. La Boda, *J. Electrochem. Soc.*, **132** (4), 798 (1985).
71. Z. A. Soloveva and A. E. Lapshina, *Soviet Electrochem.*, **1** (8), 840 (1965).
72. C. C. Postins and J. E. Longland, *Prod. Finish.*, **22**, 51 (1969).
73. E. A. Romanowski and H. Brown, U.S. Patent 3,334,033 (1967).
74. R. Dow and J. E. Stareck, *Proc. Am. Electroplat. Soc*, **40**, 53 (1953); *Plating*, **40**, 987 (1953); J. E. Stareck and R. Dow, U.S. Patents 2,686,756 (1954); 2,787,588; 2,787,589 (1957).
75. Maytag Company, *Steel*, **136**, 122 (1955); *Iron Age*, **175**, 140 (1955).
76. W. H. Safranek and G. R. Schaer, *Proc. Am. Electroplat. Soc.*, **43**, 105 (1956).
77. S. Zirinsky and D. S. Carr, *Proc. Am. Electroplat. Soc*, **45**, 97 (1958).
78. V. A. Lamb and J. P. Young,"Experimental Plating of Gun Bores to Retard Erosion," PB Rep. 151,405, Natl. Bur. Stand. Tech, Note 46, Office of Technical Services, Washington, DC, 1960.
79. W. M. Spurgeon and O. Isaacs, *Proc. Am. Electroplat, Soc*, **45**, 145 (1958).
80. T. P. McFarlane, *Iron Age*, **176**, 103 (1955).
81. E. J. Seyb, A. A. Johnson, and A. C. Tulumello, *Proc. Am. Electroplat. Soc*, **44**, 29 (1957); see also J. E. Stareck, E. J. Seyb, A. A. Johnson, and W. H. Rowan, U.S. Patents 2,916,424 (1959); 2,952,590 (1960).
82. H. Mahlstedt, *Automot. Ind.*, **118** (10), 48 (1958).
83. H. Brown, M. Weinberg, and R. J. Clauss, *Plating*, **45**, 144 (1958).
84. W. H. Safranek and C. L. Faust, *Plating*, **45**, 1027 (1958).
85. D. E. Weimer, *Met. Finish. J.*, **5**, 89 (1959).
86. A. Brenner, P. Burkhead, and C. Jennings, *Proc. Am. Electroplat. Soc*, **34**, 32 (1947); Res. Natl. Bur. Stand., **40**, 31 (1948); Res. Paper 1854.
87. N. E. Ryan, F. Henderson, S. T. M. Johnstone, and H. L. Wain, *Nature*, **180**, 1406 (1957); N. E. Ryanand, E. J. Lumley, *J. Electrochem. Soc.*, **106**, 388 (1959); N. E. Ryan, *J. Electrochem. Soc.*, **107**, 397 (1960).
88. P. C. Good, D. H. Yee, and F. E. Block,"High Purity Chromium by Electrolysis," U.S. Bur. Mines Rep. Invest. 5589, 1960.
89. M. J. Ferrante, P. C. Good, F. E. Block, and D. H. Yee, *J. Met.*, **12**, 861 (1960).
90. R. Bilfinger, *Das Hartverchromungs—Verfahren*, Herm. Beyer Verlag, Leipzig, 1939, p. 84; 2nd ed. (1942), pp. 39, 134–135; republished by Edwards Bros., Ann Arbor, MI, 1946.
91. T. A. Hood, *Plating Notes (Aust.)*, **4**, 31 (1952); *Met. Finish.*, **50**, 103 (1952).
92. E. J. Seyb, Jr., R. E. Woehrle, and J. G. Neitzel, U.S. Patent 3,498,892 (1970).
93. E. M. Baker and P. J, Merkus, *Trans. Electrochem. Soc*, **61**, 327 (1932).
94. A. A. Johnson and P. G. Kenedi, U.S. Patent 3,393,980 (1968).
95. T. H, Webersinn and J. M. Hosdowich, Research Report No. 128, United Chromium, New York, 1932.
96. J. L. Griffin, *Plating*, **53**, 196 (1966).
97. W. L. Grube and F. L. Clifton, *Mon. Rev. Am. Electroplat. Soc*, **34**, 140, 471 (1947).
98. W. H. Hartford, *Ind. Eng. Chem. (Anal. Ed.)*, **14**, 174 (1942); *Ind. Eng. Chem.*, **41**, 1993 (1949).
99. L. C. Pan, *Trans. Electrochem. Soc.*, **58**, 423 (1930); *Met. Ind. (NY)*, **28**, 271 (1963).
100. H. L. Farber and W. Blum, *Natl. Bur. Stand. Res. Papers*, **131**, 27 (1930).
101. E. A. Ollard and E. B. Smith, *Sheet Met. Ind.*, **23**, 1129 (1946).
102. N. V. Mandich, J. R. Selman, and C.-C. Lee, *Plating Surf. Finish.*, **84** (12), 82 (1997).
103. K. E. Langford, *Analysis of Electroplating and Related Solutions*, Electrodeposition and Metal Finishing, Teddington, U.K., 1951.
104. D. G. Foulke and F. E. Crane, *Electroplaters Process Control Handbook*, Van Nostrand, New York, 1963.
105. A. F. Bogenschutz and U. George, *Analysis and Testing*, Finishing Publications, Teddington, U.K., 1985.
106. K. R. Newby, "Chromium," in *Metal Finishing Guidebook*, Vol. 95, no. 1A, Reginald E. Tucker, Ed., Elsevier, New York, 1998.
107. W. W. White and M. C. Henry, *Plating Surf. Finish.*, **59** (5), 429 (1972).
108. M. Traficante, "Analytical Methods For Hexavalent Chromium Electroplating Solutions," *Proc. AESF Chromium Colloquium*, Orlando, FL, NASF, Washington, DC, Jan. 1994.

109. S. S. Heberling, D. Campbell, and S. Carson, ''Analysts of Chromium Electroplating Solutions and Wastewaters by Ion Chromatography,'' *Proc. 2nd Chromium Colloqium*, AESF, Miami, FL, Feb. 1990.
110. Technical Note 24, ''Determination of Chromium'' (1987), Dionex Corporation, Sunnyvale, CA.
111. R. O. Hull, U.S. Patent 2,149.344 (1935).
112. W. Nohse, *The Hull Cell*, Robert Draper, Teddington, U.K., 1966.
113. R. O. Hull and J. B. Winters, *Proc. AES 38th Annual Conf*., 1951, p. 133.
114. A. K. Graham and H. L. Pinkerton, *Proc. AES 50th Annual Conf*., 1963, p. 13.
115. R. Seegmiller and V. A. Lamb, *Proc. Am. Electroplat. Soc.*, **35**, 125 (1948).
116. R. F. Ledford and L. O. Gilbert, *Proc. Am. Electroplat. Soc*, **42**, 33 (1955).
117. V. Massuet Grau, *Met. Finish. J.*, **4**, 467 (1958).
118. N. V. Mandich, *Proc. AESF Tech. Conf. SUR/FIN' 96*.
119. G. Dubpernell, *Trans. Electrochem. Soc.*, **80**, 589 (1941).
120. K. Mondal, N. V. Mandich, and S. Lalvani, *J. Appl. Electrochem.*, **31**, 165 (2001).
121. J. B. Niles, U.S. Patent 2,398,110 (1946); W. Cibulskis, M. Shaeat, and H. Mahlstedt, U.S. Patent 2,840,523 (1958).
122. F. I. Danilov and A. B. Velichenko, *Electrochim. Acta*, **28**, 437 (1993).
123. J. Hyner, U.S. Patent 2,456,281 (1948).
124. D. W. Hardesty, *Plating*, **56**, 705 (1969).
125. F. Hine, K. Takayasu, and N. Koyagani, *J. Electrochem. Soc.*, **133** (2), 346 (1986).
126. M. Veda, *Electrochim. Acta*, **40**, 817 (1995).
127. R. M. Krishan et al., *Met. Finish.*, **93** (9), 46 (1995).
128. J. M. Hosdowich, in *Chromium*, Vol. 2, M. J. Udy, Ed., Reinhold, New York, 1956, pp. 65–92; see also K. G. LeFevre, *Proc. Am. Electroplat. Soc*, **43**, 34 (1956).
129. C. F. Corfe, *Electroplating*, **13** (5), 48 (1960).
130. J. E. Molos, *Ind. Med.*, **16**, 404 (1947);*Proc. Am. Electroplat. Soc*, **34**, 270 (1947).
131. A. C. Stern, L. P. Benjamin, and H. Goldberg, *J. Electrochem. Soc.*, **93**, 67 (1948); *Plating*, **35**, 565, 958 (1948).
132. H. Brown, U.S. Patent 2,750,334 (1956); see also U.S. Patents 2,750,335; 2,750,336; 2,750,337 (1956); 2,846,380; 2,857,295 (1958); 2,913,377 (1959).
133. G. Hama, W. Frederick, D. Millage, and H. Brown, *Am. Ind. Hyg. Assoc. Q.*, **15**, 211 (1954).
134. D. E. Weimer, *Met. Finish.*, **5**, 89 (1959).
135. P. J. Ramsden, *Electroplat. Met. Finish..*, **10**, 152 (1957).
136. D. Millage and W. Hague, *Proc. Am. Electroplat. Soc.*, **45**, 118 (1958).
137. A. L. Jones, ''Sources of Nodules and Pits in Hard Chromium Plating,'' paper presented at the AESF Hard Chromium Workshop, NASF, Washington, DC, 1992.
138. L. Schwartz, *U.S. Public Health Service Bull.*, **229** (1936);**249** (1939).
139. A. R. Wilkerson, *J. Am. Leather Chem. Assoc.*, **39**, 90 (1944).
140. C. L. Faust, in Reference 135, pp. 108–126.
141. ''Recommended Practice for Chromium Plating on Steel for Engineering Use,'' ASTM designation B177–68, 1968.
142. G. Dubpernell and S. M. Martin U.S. Patent 2,624,728 (1953).
143. R. G. Bikales, U.S. Patent 2,868,709 (1959).
144. L. F. Howard, U.S. Patent 2,898,293 (1959).
145. Fuji Plant Industrial Co., U.S. Patent, 3,425.926 (1969), U.K. Patent 1,062.360 (1967).
146. J. Hyner, *Met. Finish. Guidebook*, **40**, 263 (1972).
147. G. E. Shahin, *Plating Surf. Finish.*, **79** (8), 19 (1992).
148. W. M. Tucker and R. L. Flint, *Trans. Electrochem. Soc*, **88**, 335 (1945).
149. E. M. Relitz,Canadian Patent 378,303 (1938).
150. N. V. Mandich, *Plating Surf. Finish.*, **85** (12), 91 (1998).
151. C. L. Faust, in Reference 135, pp. 108–126.
152. ''Recommended Practice for Chromium Plating on Steel for Engineering Use,'' ASTM Designation B177–68, 1968.
153. J. D. Greenwood, *Hard Chromium Electroplating*, 3rd ed., Robert Draper, Teddington, U.K., 1984.
154. R. Morisset, *Chromium Electroplating*, Robert Draper, Teddington, U.K., 1954.
155. R. K. Guffie, *The Handbook of Hard Chromium Electroplating*, Gardener Publ., Cincinnati, OH, 1986.
156. C. H. Peger, *Chrome Electroplating Simplified*, 4th ed., Hard Chrome Plating Consultants, Cleveland, OH, 1981.
157. C. Levy, *Proc. Am. Electroplat. Soc.*, **43**, 219 (1956).
158. J. W. Dini and H. R. Johnson, *Plat. Surf. Finish.*, **68** (10), 64 (1981).
159. E. Zmihorski, *J. Electrodeposhors' Tech. Soc.*, **23**, 203 (1948).
160. C. Williams and R. A. F. Hammond, *Trans. Inst. Met. Finish.*, **31**, 124 (1954).
161. J. W. Beams, *Proc. Am. Electroplat. Soc*, **43**, 211 (1956).
162. H. Chessin and J. G. Poor, *Plating*, **43**, 913 (1956).
163. H. Chessin and J. G. Poor, *Plating*, **46**, 1037 (1959).
164. J. G. Poor, H. Chessin, and C. L. Alderuccio, *Plating*, **47**, 811 (1960).
165. J. W. Dini and H. R. Johnson, *Met. Finish.*, **54** (4), 48 (1977).
166. D. Davies and F. A. Whittaker, *Met. Mater.*, **1** (2), (1967).
167. H. Ploog, *Galvanotechnik*, **61**, 155 (1970).
168. G. Dubpernell, *Electrodeposition of Chromium from Chromic Acid Solution*, Pergamon, New York, 1977.
169. P. Morisset, *Chromage, Dur et Decoratif* (Chromium Plating-Hard and Decorative), Centre d'Information du Chrome Dur, Paris, 1961.
170. R. Weiner and A. Walmsley, *Chromium Electroplating*, Finishing Publ., Teddington, U.K., 1980.

171. J. D. Greenwood, *Hard Chromium Plating*, 2nd ed., Robert Draper, Teddington, Middlesex, England, 1971.
172. J. D. Greenwood, *Heavy Deposition*, Robert Draper, Teddington, Middlesex, England, 1970.
173. C. H. Peger, *Hard Chromium Fixtures*, Hard Chromium Consultants, Cleveland, OH, 1982.
174. J. K. Dennis and A. Such, *Nickel and Chromium Electroplating*, 3rd ed., Woodhead Publ., Cambridge, U.K., 1993.
175. A. W. Logozzo, *Plating*, **56**, 1019 (1969).
176. N. V. Mandich, *Met. Finish.*, **97** (6) 100; **97** (7), 42; **97** (8), 42 (1999); **97** (9), 72; **97** (10), 30 (1999).
177. H. J. Wills, *Am. Mach.*, **81**, 247 (1937).
178. F. J. Benn, *Grits and Grinds*, **37** (5), 8 (1946).
179. J. W. Oswald, *Trans. Inst. Met. Finish.*, **48**, 169 (1870).
180. H. T. Wilson, *Plating*, **58**, 345 (1971).
181. W. Blum, *33rd Com. Am. Electroplat. Soc*, 1946, p. 16; *Trans. Electrochem. Soc*, **90**, 85 (1946); *Metal. Finish.*, **45**, 66 (1947).
182. J. L. Vaughan and I. A. Usher, *Can. Met.*, **7**, 20, 53 (1944).
183. A. L. Fry, *Met. Finish.*, **44**, 467, 478 (1946).
184. V. A. Lamb and J. P. Young, *Proc. Am. Electroplat. Soc*, **43**, 260 (1956);"PB 151," 405, *Nad. Bur. Stand. Tech. Note No. 46* (1960); *Ordnance*, **45**, 725 (1961).
185. R. A. F. Hammond, *Trans. Inst. Met. Finish.*, **34**, 83 (1957).
186. R. J. Girard and E. F. Koetsch, Jr., *Proc. Am. Electroplat. Soc*, **47**, 199 (1960).
187. F. O'Neill, *Plating*, **58**, 19 (1971).
188. A. W. Ehlers, *Tool and Die J.*, **98**, 120 (1945).
189. S. Menton, *Steel*, **120**, 124 (1947).
190. W. G. Patton, *Iron Age*, **161**, 78 (1948).
191. P. Csokan, *Metalloberflache*, **13**, 81, 113 (1959).
192. S. Wernick and R. Pinner, *The Surface Treatment and Finishing of Aluminum and Its Alloys*, 2nd ed., Robert Draper, Teddington, Middlesex, England, 1959.
193. E. Herrmann, *Galvanotechnik*, **51**, 336 (1960).
194. *Automob. Eng.*, **35**, 508 (1945); **38**, 236 (1948).
195. A. W. Mall, *Mach. Des.,* **20**, 136 (1948); *Iron Age*, **164** (22), 86 (1949).
196. J. E. Stareck and R. Dow, U.S. Patent 2,812,297 (1957).
197. V. E. Guersney, *Plating Surf. Finish.*, **63** (2), 38 (1976).
198. V. E. Guersney, *Plating Surf. Finish.*, **63** (3), 44 (1976).
199. R. D. Bedi, *Plating*, **55**, 238, 365 (1968).
200. R. D. Bedi and G. Dubpernell, *Plating*, **55**, 246 (1968).
201. G. E. Mcdonald, *Solar Energy*, **17**, 119 (1975).
202. D. M. Mattox, *Plating Surf. Finish.*, **63**, 55 (1976).
203. Siemens and Halske A. G.,German Patents 607,420 (1929); 611,200 (1931); 612,255 (1933); French Patent 754,360 (1933); British Patent 408,097 (1934).
204. A. Ungelunk, J. Fischer, and H. Endrass, U.S. Patent 1,975,239 (1934).
205. E. A. Ollard, *J. Electrodepositors Tech. Soc*, **12**, 33 (1936).
206. L. O. Gilbert and C. C. Buhman, U.S. Patent 2,623,847 (1952).
207. M. F. Quaely, *Plating*, **40**, 982 (1953);*Proc. Am. Electroplat. Soc*, **40**, 48 (1953); U.S. Patents 2,739,108-9 (1956); 2,772,227 (1956); 2,824,829 (1958).
208. G. E. Oleson and R. M. Woods (to Corilliurn Corp.), U. S. Patent 3,414,492 (1968);R. M. Woods and D. R. Moul, U.S. Patents: 3,418,221 (1968); 3,442,777 (1969); 3,454,474 (1969).
209. K. S. Willson, U.S. Patent 3,620,935 (1971).
210. J. P. Branciaroti and P. G. Stutzman, *Plating*, **56**, 37 (1969).
211. J. P. Branciaroli, *Trans. Inst. Met. Finish.*, **48**, 172 (1970).
212. J. H. Hunter and L. K. Kosowsky, U.S. Patent 2,826,538 (1958).
213. V. Grips, S. Rajagopalan, and I. Rajagopal, U.S. Patent 5,019.223 (1991).
214. A. K. Graham, *Proc. Am. Electroplat. Soc*, **46**, 61 (1959).
215. B. N. Popov, R. E. White, D. Slavkov, and Z. Koneska, *J. Electrochem. Soc*, **139** (1), 91 (1992).
216. M. Driver, *Solar Energy Mat.*, **4**, 179 (1981).
217. F. J. Monteio, F. Oliveira, R. Reis, and O. Pavia, *Plating Surf. Finish.*, **79** (1), 46 (1992).
218. M. Selvam, *Met. Finish.*, **80** (5), 107 (1982).
219. K. J. Kathro, *Met. Finish.*, **76** (10), 57 (1978).
220. L. Sivaswamy, S. Gowri, and B. S. Shenoi, *Met. Finish.*, **78**, 48 (1974).
221. H. Flasch, German Patent 722,364 (1942).
222. K. S. Willson, *Plating*, **54**, 49 (1967).
223. W. Eilender, H. Arend, and F. Sadrizil, *Metalloberflache*, **3**, 32 (1949).
224. W. C. Giesker and R. K. Britton, U.S. Patent 2,746,915 (1956).
225. W. C. Giesker and R. K. Britton, U.S. Patent 2,788,292 (1957).
226. W. H. Safranek, H. R. Miller, and C. L. Faust, *Plating*, **50**, 507 (1963).
227. B. B. Knapp, *Trans. Inst. Met. Finish.*, **35**, 139 (1958).
228. H. Brown and M. Weinberg, *Proc. Am. Electroplat. Soc*, **46**, 128 (1959); see also M. Weinberg and H. S Brown, U.S. Patent 2,871,550 (1959).
229. A. Korbelak, *Plating*, **40**, 1126 (1953); *Proc. Am. Electroplat. Soc.*, **40**, 90 (1953).
230. D. Gray and B. K. Northrop, U.S. Patent 1,892,051 (1932).
231. C. G. Fink and C. H. Eldridge,U.S. Patent 1,942,356 (1934).
232. W. H. Safranek and H. R. Miller,"Adherence of Paint on Chromium-Plated Zinc Die Castings," Reprint No, 668C, Society of Automotive Engineers, New York (Mar. 1963); *Prod. Finish.*, **27**, 38 (1963).
233. B. K. Dent, *Plating*, **50**, 1100 (1963).
234. W. S. Garwood, *Plating*, **53**, 1323 (1966); **54**, 403 (1967).
235. J. E. Stareck, Canadian Patent 434,632 (1946).
236. C. F. Waite, *Proc. Am. Electroplat. Soc*, **40**, 113 (1953); *Plating*, **40**, 1245 (1953).
237. E. M. Baker and W. L. Pinner, *J. Soc. Aut. Eng.*, **22**, 331 (1928); Discussion, **23**, 50 (1928).
238. H. Chessin and E. J. Seyb, *Plating*, **55**, 821 (1968).

239. K. Gebauer, *Korros. Metalischutz*, **16**, 297, Table 1 (1940); *Oberflhchentech.*, **18**, 2, 11, 19, 31 (1941); *Metallwirtschaft*, **21**, 468 (1942).
240. M. R. J. Wyllie, *Trans. Electrochem. Soc*, **92**, 519 (1947).
241. J. B. Cohen, *Trans. Electrochem. Soc*, **86**, 441 (1944).
242. E. J. Seyb, A. A. Johnson, and A. C. Tulumello, *Proc. Am. Electroplat. Soc*, **44**, 29 (1957); see also J. E. Stareck, E. J. Seyb, A. A. Johnson, and W. H. Rowan, U.S. Patents 2,916,424 (1959); 2,952,590 (1960).
243. H. Brown, M. Weinberg, and R. J. Clauss, *Plating*, **45**, 144 (1958).
244. W. Blum, P. W. C. Strausser, and A. Brenner, *J. Res. Nat. Bur. Stand.*, **13**, 331 (1934), Res. Paper 712.
245. W. A. Wesley, in *Corrosion Handbook*, H. H. Uhlig, Ed., Wiley, New York, 1948, p. 817.
246. J. Chadwick, *Electropl. Met. Finish.*, **6**, 451 (1953).
247. R. L. Saur and R. P. Basco, *Plating*, **53**, 35, 320, 981, U 24 (1966).
248. E. J. Seyb and W. H. Rowan, *Plating*, **46**, 144 (1959).
249. E. J. Seyb, *Prod. Finish.*, **23**, 64 (1959); *Plating*, **46**, 852 (1959); *Metal. Prog.*, **76**, 113 (1959); see also D. E. Weimer, *Electroplat. Met. Finish.*, **12**, 340 (1959).
250. E. J. Seyb, *Proc. Am. Electroplat. Soc*, **47**, 209 (1960).
251. W. E. Lovell, E. H. Shotwell, and J. Boyd, *Proc. Am. Electroplat. Soc*, **47**, 215 (1960).
252. *ASTM Designation B4S6-7I, Book of Standards*, American Society for Testing and Materials, West Conshohocken, PA, 1971, p. 7, 718.
253. British Standard 1224, (1970), *Specification for Electroplated Coatings of Nickel and Chromium*, British Standards Institution, London, 1970.
254. M. M. Beckwith, *Plating*, **47**, 402 (1960); see also M. N. Beckwith, Canadian Patent 558,991 (1958).
255. M. R. Caldwell, *Met. Prog.*, **75**, 78 (1959);*Precision Met. Molding*, **17**, 47 (1959); *Inco Nickel Topics*, **12** (7), 6 (1959).
256. D. M. Bigge, *Plating*, **47**, 1263 (1960).
257. H. Brown, *Electroplating*, **15**, 398 (1962); H. Brown, U.S. Patent 3,090,733 (1963).
258. H. Brown and D. Millage, *Trans. Inst. Met. Finish.*, **37**, 21 (1960).
259. D. Millage, E. Romanowski, and H. Brown, Paper No. 24, First National Die Casting Exposition and Congress, Detroit, MI., Nov. 8–11, 1960.
260. A. H. DuRose, K. S. Willson, and G. C. Tejada, U.S. Patent 3,563,864 (1971).
261. O. D. DeCastelet, U.S. Patent 3,620,936 (1971).
262. H. Brown and T. W. Tomaszewski, *Proc. Int. Conf. Surfaces 66* (Basel), Nov. 1966, Forster-Verlag AG, Zurich, 1967, p. 88; U.S. Patents 3,152,971–3 (1964); see also T. W. Tomaszewski, R. J. Clauss, and H. Brown, *Proc. Am. Electroplat. Soc.*, **50**, 169, 201 (1963).
263. J. M. Odekerken, *Electroplat. Met. Finish.*, **17**, 2 (1964).
264. H. Chessin, U.S. Patents 3,574,068 (1971); 3,595,762 (1971).
265. T. G. Kubach, W. H. R. Pritsch, and W. Bolay, U.S. Patent 3,625,039 (1971).
266. T. Malak, D. Snyder, and A. H. DuRose, *Plating*, **59**, 659 (1972).
267. A. H. DuRose, *Proc. Am. Electroplat. Soc*, **48**, 83 (1960).
268. F. Ogburn and M. Schlissel, *Plating*, **54**, 54 (1967).
269. K. S. Willson, *Plating*, **59**, 226 (1972).
270. W. Blum, *Plating*, **48**, 613 (1961).
271. S. E. Beacom, *Prod. Finish.*, **33**, 130 (June 1969).
272. E. P. Harbulak, *Plating Surf. Finish.*, **67**, 49 (1980); U.S. Patent 4,310,389 (1980).
273. ASTM B 764, American Society for Testing and Metals, West Conshohocken, PA.
274. H. Mahlstedt, U.S. Patent 1,967,716 (1934).
275. C. A. Snavely, *Trans. Electrochem. Soc*, **92**, 537 (1947).
276. C. A. Snavely and D. A. Vaughan, *J. Am. Chem. Soc.*, **71**, 313 (1949).
277. J. J. Dale, *Proc. 3rd Int. Electrodeposition Conf.,* Electrodepositors' Tech. Soc, London, NASF, Washington, DC, 1947, p. 185.
278. J. J. Dale, A. Brenner, C. A. Snavely, and C. L. Faust, Discussion, *J. Electrochem. Soc*, **97**, 466 (1950).
279. W. A. Wood, *Trans. Faraday Soc*, **31**, 1248 (1935).
280. D. W. Hardesty, *J. Electrochem. Soc*, **116**, 1194 (1969).
281. C. A. Snavely and C. L. Faust, *J. Electrochem. Soc*, **97**, 99 (1950).
282. C. P. Brittain and G. C. Smith, *Trans. Inst. Met. Finish.*, **31**, 146 (1954).
283. W. Hutne-Rothery and M. J. R. Wyllie, *Proc Roy. Soc. (London)*, **A181**, 331 (1943); **AIS2**, 415 (1943).
284. H. Fry, *Trans. Inst. Met. Finish.*, **32**, 107 (1955).
285. C. P. Brittain and G. C. Smith, *Trans. Inst. Met. Finish.*, **33**, 289 (1956).
286. A. H. Sully and E. A. Brandes, *Chromium*, 2nd ed., Plenum, New York, 1967.
287. W. A. Wood, *Phil. Mag.*, **24**, 511, 772 (1937).
288. A. Knoedler, *Metailoberflache*, **17**, 161, 331 (1963).
289. K. Nishihara, M. Kurachi, Y. Sakamoto, and M. Nishihara Jr., *Interfinish,* Deutsche Gesellschaft fur Galvanotechnik, Dusseldorf, 1968, pp. 118–123.
290. M. A. Shluger and V. A. Kazakov, *Zh. Priki. Khim.*, **33**, 644 (1960);*Chem. Abstr.*, **54**, 18126 (1960).
291. H. Okada and T. Isbida, *Nature*, **187**, 496 (1960); *Met. Finish. Abstr.*, **2**, 168 (1960).
292. M. Matsunaga, *Set. Pap. Inst. Phys. Chem. Res. (Tokyo)*, **54**, 177 (1960); *Chem. Abstr.*, **55**, 5188 (1961).
293. A. J. Steiger, *Met. Finish.*, **56**, 56 (1958).
294. O. Bomhauser, U.S. Patent 1,985,308 (1934).
295. F. Taylor, *Electropl. Met. Finish.*, **5**, 109 (1952).
296. C. A. Snavely, U.S. Patent 2,635,993 (1953).
297. M. E. Beckman and F. Maass-Graefe, *Metalloberflache*, **5**, 161A (1951).

298. V. G. Kakovkina and A. N. Sysoev, *Trudy Kharkovsk. Politekh. Inst., Ser. Khim. Tekhnol.*, **18** (5), 107 (1958);*Chem. Abstr.*, **54**, 24001 (1960).

299. L. Koch and G. Hein, *Metalloberflache*, **7**, 145A (1953).

300. S. G. Christov and N. A. Pangarov, *Z. Elektrochem.*, **61**, 113 (1957);see also *Izv. Khim. Inst. Bulgar. Akad. Nauk*, **7**, 237, 257 (1960);*Chem. Abstr.*, **55**, 2309 (1961).

301. S. G. Christov, I. P. Nenov, and R. G. Raichev, in *Proc. 3rd Int. Congr. on Metallic Corrosion*, Vol. 1, Moscow, NASF, Washington, DC, 1969, pp. 389–395.

302. I. P. Nenov, S. G. Christov, R. Raicev, and Z. Georgiev, *Electrochim. Acta*, **12**, 1537 (1967).

303. M. C. Udy, in *Chromium*, Vol. 2, M. J. Udy, Ed., Reinhold, New York 1956, p. 101.

304. F. Henderson, S.T.M. Johanstone, and H.L. Wein, *Ductile Chromium*, American Society for Metals, Cleveland, OH, 1957.

305. F. E. Bacon, *ASM Metals Handbook*, Vol. 1, American Society for Metals, Metals Park, OH, 1961, p. 1200.

306. T. G. Coyle, *Proc. ASTM*, **43**, 556 (1943).

307. A. Kutzelnigg, *Testing Metallic Coatings*, Robert Draper, Teddington, Middlesex, England, 1963.

308. C. G. Peters and F. Knoop, *Met. Alloys*, **12**, 292 (1940).

309. J. M. Hosdowich, *Proc. Am. Electroplat. Soc.*, **36**, 103 (1949).

310. W. Eilender, H. Arend, and E. Schmidtmann, *Metalloberflache*, **2**, 49 (1948).

311. W. Eilender, H. Arend, and E. Schmidtmann, *Metalloberflache*, **3**, 57 (1949).

312. H. Wahl and K. Gebauer, *Metalloberflache*, **2**, 25, (1948).

313. J. T. Burwell and S. F. Murray, *Nucleonics*, **6** (1), 34 (1950).

314. R. G. Abowd, Jr. and C. E. Alsterberg, paper presented at the Symposium on Applications of Radioactivity at Traceflabs, Inc., Boston, MA, 1956.

315. R. G. Abowd Jr.,Preprint No. 57LC-3, Meeting Am. Soc. Lubrication Engineers, Toronto, Canada, Oct. 7, 1957; also Preprint No. 171, Nuclear Eng. and Sci. Conf., Chicago, IL, Mar. 17–21, 1958; and Paper No. 8U, S.A.E. Annual Meeting, Detroit, MI, Jan. 12–16, 1959.

316. Worthington Pump and Machinery Corp., ''Industrial Chromium Plating,'' Bull. S-2001-A (1931);F. E. Allen,*Worthington News* (Worthington Pump and Machinery Corp. house organ), **2** (6), 2 (Oct. 1930); **2** (7), 1 (Nov. 1930); **2** (8), 1 (Dec. 1930); **2** (9), 1 (Jan. 1931); **2** (10), 2 (Feb. 1931); **2** (11), 1 (Mar. 1931).

317. V. I. Arkharov, A. M. Tagrubskii, and S. A. Nemnonov, *Vestn. Metalloprom.*, **20**, 13 (1940).

318. M. Kontorovich and V. L. Arkharov, *Vestn. Metalloprom.*, **20**, 10 (1940).

319. R. Graham, K. R. Williams, and R. W. Wilson, *Engineering*, **167**, 241 (1940); 265 (1940).

320. P. Hindent, *J. Res. Nat. Bur. Stand.*, **26**, 81 (1941).

321. D. S. Bloom and N. J. Grant, *Trans. Am. Inst. Met. Eng.*, **188**, 4 (1950);**191**, 1009 (1951).

322. R. M. Parke and F. P. Bens, *Symposium on Materials for Gas Turbines*, ASTM Spec. Publ., American Society for Testing and Materials, Philadelphia, PA, 1946, p. 80.

323. W. W. Coblentz and R. Stair, *J. Res. Nail. Bur. Stand.*, **2**, 343 (1929).

324. J. E. Stareck, E. J. Seyb, and A. C. Tulumello, *Plating*, **41**, 1171 (1954); *Proc. Am. Electroplat. Soc*, **41**, 209 (1954).

325. C. Williams and R. A. F. Hammond, *Trans. Inst. Met. Finish.*, **32**, 85 (1955).

326. R. Walker, *Internal Stress in Electrodeposited Metallic Coatings*, published by Metal Finishing Journal, London, 1968.

327. M. Ya. Popereka, *Internal Stresses in Electrolytcally Deposited Metals*, TT68-50634, Clearinghouse for Federal Scientific and Technical Information, Springfield, VA, 1970.

328. J. E. Stareck, E. J. Seyb, and A. C. Tulumello, *Plating*, **42**, 1935 (1955); *Proc. Am. Electroplat. Soc*, **42**, 129 (1955).

329. M. Kolodney,''Chromium Plating,'' Information Release No. 4, War Metallurgy Comm., Nat. Acad. Sci., Res. Council, 1943; American Documentation Institute, Washington, DC, Document No. 1806.

330. J. E. Stareck et al., U.S. Patents 2, 800, 436–7–8; 2,800,443 (1957).

331. R. A. F. Hammond and C. Williams, *Metal. Rev.*, **5** (18), 165 (1960).

332. C. Williams and R. A. F. Hammond, *Trans. Inst. Met. Finish.*, **32**, 85 (1955); **34**, 317 (1957);*Proc. Am. Electroplat. Soc*, **46**, 195 (1959).

333. B. Cohen, *Proc. Am. Electroplat. Soc*, **45**, 33 (1958).

334. G. P. Kotlyarevskii, *Metalloved. i Obrab, Metal.*, No. 7, 52 (1958).

335. R. Brunetaud, R. Chevalier, and P. Lessop, *Chrome Dur 1959–1960*, Centre d'Information du Chrome Dur, Paris, 1959, pp. 3–14.

336. H, Wiegand and U. H. Furstenberg, *Hartverchromung-Eigenschaften and Auswirkungen auf den Grundwerkstoff* (Hard Chromium Plate-Properties and Effects on the Basis Metal), Maschinenbau-Verlag GmbH, Frankfurt, 1968.

337. H. Speckhardt, *Metalloberflache*, **23**, 272 (1969).

338. A. Buch, *Metalloberflache*, **24**, 124 (1970).

339. H. Wiegand and U. H. Furstenberg, *Metalloberflache*, **25**, 123 (1971).

340. V. P. Greco and B. L. Pennell, *Plating*, **58**, 35 (1971).

341. H. Wiegand, *Metallwirtschaft*, **20**, 165 (1941).

342. A. Beerwald, *Laftfahit-Forsch.*, **18**, 368 (1941);Translations: *Eng. Digest*, **3**, 252 (1942); *Sheet Met. Ind.*, **16**, 1889 (1942); **17**, 68 (1943).

343. E. Raub, *Metallforschung*, **2**, 121 (1947).

344. C. J. Morgan and F. E. Brine, *Trans. Inst. Met. Finish.*, **47**, 77 (1969).

345. C. J. Morgan and W. A. Marshall, *Trans. Inst. Met. Finish.*, **46**, 144 (1968).

346. W. D. Klopp, *J. Met.*, **21** (11), 23 (1969).

347. E. A. Brandes and J. A. Whittaker, *Engineer*, **220**, 929 (1965).

348. P. J. Smith and G. Dubpernell, Canadian Patent 791,698 (1968).
349. H. Silman, *Met. Ind. (London)*, **78** (17), 327 (1951).
350. D. J. De Paul, *Corrosion*, **13**, 91 (1957).
351. H. Suss, *Corrosion*, **16**, 105 (1960).
352. M. Pourbaix, *Atlas of Electrochemical Equilibria*, Pergamon, New York, 1966.
353. E. Deltombe, N. de Zoubov, and M. Pourbaix, "Electrochemical Behavior of Chromium-Potential-pH Equilibrium Diagram of the System Chromium-Water at 25°C" (in French), Tech. Rep. No. 41, Centre Beige d'Etude de la Corrosion, 1956.
354. H. Uchida and A. Horiguchi, *Met. Prog.*, **83**, 113 (1963).
355. H. Uchida, O. Yanabu, A. Horiguchi, and H. Sato, *Trans. Inst. Met. Finish.*, **40**, 212 (1963);**42**, 138 (1964).
356. H. Uchida and O. Yanabu, U.S. Patent 3,113,845 (1963).
357. E. J. Smith, *Iron Steel Eng.*, **44**, 125 (1967).
358. G. W. Ward and S. E. Rauch, Jr., *Blast Furnace and Steel Plant*, **56**, 229 (1968).
359. G. G. Kamm, A. R. Willey, and N. J. Linde, *J. Electrochem. Soc*, **116**, 1299 (1969).
360. J. E. Allen, *Iron Steel Eng.*, **47**, 88 (1970).
361. M. W. Dippold, *Iron Steel Eng.*, **48**, 62 (1971).
362. H. Uchida, *J. Met. Finish. Soc. Jpn.*, **21**, 341 (1970).
363. E. J. Smith, L. C. Beale, Jr., and L. W. Austin, U.S. Patent 3,526,486 (1970).
364. C. E. Roberts and G. W. Ward, U.S. Patent 3,574,069 (1971).
365. O. Yanabu, T. Saito, K. Doi, T. Enari, K. Miyakawa, and H. Kawasaki, *Interfinish 1968*, Conference Report, Deutsche Ges. fur Galvanotechnik, pp. 312–320.
366. E. J. Seyb, Jr., R. E. Woebrle, and J. G. Neitzel, U.S. Patent 3,498,892 (1970).
367. R. E. Cleveland, U.S. Patent 2,114,072 (1938); E. R. Granger and R. E. Cleveland, U.S. Patent 2,248,530 (1941).
368. H. van der Horst, *Proc. Am. Electroplat. Soc*, **31**, 56 (1943).
369. T. G. Coyle, *Proc. Am. Electroplat. Soc*, **32**, 20 (1944).
370. R. Pyles, *Proc. Am. Electroplat. Soc*, **32**, 136 (1944).
371. H. van der Horst, U.S. Patents 2,314,604 (1943); 2,412,698 (1946); British Patent 518,694 (1940); Dutch Patent 57,383 (1946).
372. T. H. Webersinn and J. Hyne, Forestek, U.S. Patent 3,279,936 (1966).
373. T. C. Jarrett and R. D. Guerke (to Koppers Co., Inc.), U.S. Patent 2,433,457 (1947).
374. F. Passal, U.S. Patent 2,450,296 (1948).
375. W. S. Bohlman and D. S. Bruce, U.S. Patent 2,453,404 (1948).
376. United Chromium, British Patents 600,818; 600,850; 601,065 (1948).
377. S. C. Wilsdon, U.S. Patent 2,620,296 (1952); British Patent 561,788 (1943).
378. H. M. Bendler, C. E. Bleil, T. W. Hertzog, M. A. LaBoda, and M. Ben, U.S. Patent 2,968,555 (1961).
379. J. A. Andrisek and T. R. Gill, U.S. Patent 2,947,674 (1960); Canadian Patent 593,405 (1960); British Patent 835,821 (1960).
380. L. W, Raymond, U.S. Patent 2,830,015 (1958).
381. Van der Horst Corp. of America, *Steel*, **152**, 52 (1963).
382. C. W. Forestek, U.S. Patent, 3,279.936 (1966).
383. C. O. Letendre, U.S. Patent, 3,341,348 (1967).
384. W. J. Zubrisky, U.S. Patent 3,063,763 (1962), U.S. Patent 2,430,750 (1947).
385. "Army Air Force Specif. 20031A" (1944); "Bureau of Ships, Navy Dept.," (MIL-P-20218C, Dec. 29, 1959); *Society of Automotive Engineers Specif. AMS 2407A* (1951).
386. S. Kishi, Ti Furusawa, H. Yamaguchi, and H. Sugano, *Bull. Doc. Cent. Inform. Chrome Dur*, pp. 1–10 (1971).
387. A. K. Sidney and H. Salem, *J. Appl. Toxicol.*, **13** (3), 1992.
388. J. C. Crowther and S. Renton, *Electroplat. Met. Finish.*, **28** (5), 6 (1975).
389. R. S. Dean, *U.S. Bur. Mines Rep. Invest. 3547* (1941);*Rep. Invest. 3600* (1941).
390. R. R. Lloyd et al., *Trans. Electrochem. Soc*, **89**, 443 (1946); *Eng. Mm. J.*, **148** (7), 95 (1947); *J. Electrochem. Soc.*, **94**, 122 (1948); **97**, 227 (1950); U.S. Patents 2,507,475–6 (1950).
391. J. B. Rosenbaum, R. R. Lloyd, and C. C. Merrill, *U.S. Bur. Mines Rep. Invest. 5322* (1957).
392. F. E. Bacon, "Chromium Electrowining," in *Encyclopedia of Electrochemistry*, C. A. Hampel, Ed., Reinhold, New York, 1964, pp. 198–201.
392a. F. E. Bacon, "Chromium and Chromium Alloys," in *Kirk-Othmer Encyclopedia of Chemical Technology*, 2nd ed., Vol. 5, Wiley-Interscience, New York, 1964, p. 451.
393. C. A. Snavely, C. L. Faust, and J. E. Bride, U.S. Patent 2,693,444 (1954).
394. W. H. Safranek, U.S. Patent 2,822,326 (1958).
395. G. R. Schaer, U.S. Patent 2,927,066 (1960).
396. L. D. McGraw, J. A. Gurklis, C. L. Faust, and J. E. Bride, *J. Electrochem. Soc*, **106**, 302 (1959).
397. T. Yoshida and R. Yoshida, *J. Chem. Soc. Japan, Ind., Chem. Sect.*, **58**, 89 (1955); *Chem. Abstr.*, **49**, 14540 (1955); U.S. Patents 2,704,273 (1955); 2,766,196 (1956).
398. M. R. Zell, *Met. Finish.*, **55**, (1) 57 (1957); U.S. Patent 2,801,214 (1957).
399. H. Nitto, U.S. Patent 2,938,842 (1960).
400. J. A. Bodrov and N. T. Kudryavtsev, *Plating*, **46**, 157 (1959) (Abstract only).
401. K. Firoyu, *Bull. Inst. Politekh. Bucuresti*, **20** (1), 53 (1958) (in Russian); *Bull. Cent. Inform. Chrome Dur*, pp. 1–13 (Dec. 1960) (in French); *Chem. Abstr.*, **54**, 5290 (1960).
402. W. Machu and M. F. M. El-Ghandour, *Werkst. Karros.*, **10**, 556 (1959);**11**, 274, 420, 481 (1960).
403. G. R. Sherwood, M. R. Holmes, and F. Bergishagen, *J. Electrochem. Soc*, **106**, 204C (1959) (Abstract only).
404. Warner Electric Company, *Business Week*, No. 757, 81 (1944).

405. L. W. Skala (to M. M. Warner and H. Blech), U.S. Patent 2,470,378 (1949).
406. J. G. Icxi, U.S. Patent 2,748,069 (1956); French Patent 1,007,691 (1952); German Patent 933,720 (1955); British Patent 697,225 (1948); Canadian Patent 493,784 (1953).
407. M. Rubinstein, *Mater. Methods*, **40** (12), 98 (1954);*Proc. Am. Electroplat. Soc*, **43**, 246 (1956).
408. H. D. Hughes, *Trans. Inst. Met. Finish.*, **33**, 424 (1956).
409. W. Machu, *Galvanotechnik*, **49**, 467 (1958).
410. N. R. Bharucha and J. J. B. Ward,British Patents 1,144,913 (1969); 1,213,556 (1970).
411. N. R. Bharucha and J. J. B. Ward, *Prod. Finish.*, **33**, 64 (1969).
412. J. J. B. Ward, I. R. A. Christie, and V. E. Carter, *Trans. Inst. Met. Finish.*, **49**, 97, 148, 172 (1971).
413. J. E. Bride, *Plating*, **59**, 1027 (1972); U.S. Patents 3,706,636–43 (1972).
414. D. J. Levy and W. R. Momyer, *Plating*, **57**, 1125 (1970); *J. Electrochem. Soc*, **118**, 1563 (1971).
415. C. Barnes, J. Ward, and J. R. House, *Trans. Inst. Met. Finish.*, **55** (2), 73 (1977).
416. L. Gianelos, *Plating Surf. Finish.*, **66** (5) 56 (1979).
417. J. E. Bride, *Plating Met. Finish.*, **59** (11), 1027 (1972).
418. A. K. Hsieh, T. H. Ee, and K. N. Chen, *Met. Finish.*, **91** (4) (1993).
419. A. Watson, A. M. H. Anderson, M. R. el-Sharif, and C. U. Chisholm, *IMF Ann. Tech. Conf.*, York, UK, 1990, 26.
420. D. L. Snyder, *Proceed. AESF 2nd Chromium Colloquium,* Miami, FL, NASF, Washington, DC, 1990.
421. D. L., Snyder, *Plating Surf. Finish.*, **66** (6), 60 (1979).
422. D. L. Snyder, *Prod. Finish.*, **53** (3), 56 (1988);**54**(8), 61 (1989); **55**(12), 42 (1990).
423. V. E. Carter and I. R. A. Christie, *Trans. IMF*, **51** (1973), 41.
424. V. Opaskar and D. Crawford, *Mel. Finish.*, **89**, 49 (1991).
425. G. Shahin, *Plating Surf. Finish.*, **79**, 19 (1992).
426. G. Shahin, U.S. Patent 5,294,326 (1994).
427. H. Tadao and A. Ishihama, *Plating Surf. Finish.*, **66** (9), 36 (1979).
428. A. Ishihama and T. Hayashi, *Proc. of Interfinish 80*, Kyoto, Japan (1980).
429. A. T. Vagramyan and N. T. Kudryavtsev, Eds., *Theory and Practice of Chromium Electroplating*, TT65-. 50001, Clearinghouse for Federal Scientific and Technical Information, Springfield, VA, 1965.
430. A. T. Vagramyan,in *Electrodeposition of Alloys*, V. A. Averkin, Ed., OTS64-11015, Office of Technical Services, U.S. Department of Commerce, Washington, DC, 1964, pp. 182–189.
431. A. Brenner, *Electrodeposition of Alloys*, Vol. 2, Academic, New York, 1963, pp. 110–136.
432. C. A. Snavely, C. L. Faust, and J. E. Bride, U.S. Patent 2,693,444 (1954).
433. C. A. Snavely and G. R. Shear, U.S. Patent 2,693.444 (1954).
434. L. D. McGraw, J. A. Gurklis, C. L. Faust, and J. E. Bride, *J. Electrochem. Soc*, **106** (4) 301 (1951).
435. P. L. Elsie, S. Govri, and B. Shenoi, *Met. Finish.*, **68** (11), 52 (1970).
436. W. H. Safranek and G. R. Schaer, *Proc. Am. Electroplat. Soc*, **34**, 32–73 (1947).
437. C. Fridmann and J. Royon, *Bull. Doc. Cent. Inform. Chrome Dur*, pp. 1–46 (June 1970).
438. A. Kaichinger, *Bull. Doc. Cent. Inform. Chrome Dur*, pp. 25–38 (July-Aug. 1970).
439. K. Aotani and K. Nishimoto, *Kinzoku Hyomen Gijutsu (Japan)*, **21** (7), 356 (1970).
440. P. A. Jacquet and P. Lepetit, *Bull. Doc, Centre Inform. Chrome Dur*, pp. 1–26 (Sept. 4–Oct. 1965).
441. P. A. Jacquet, J. J. Galbrun, and A. Popoff, *Chrome Dur*, **46** (1959–1960).
442. N. V. Korovin, *Electropl. Metal Finish.*, **17** (6), 188 (1964).
443. B. A. Shenoi and K. S. Indira, *Met. Finish.*, **63** (5), 56; (6), 94 (1965).
444. V. V. Bondar and I. I. Potapov, *Zashchita Metallov*, **5** (3), 346 (1969).
445. F. X. Hassion and J. Szanto, Springfield Armory, U.S. Dept. Comm., AD-621 920, 1965, p. 43.
446. Yu. N. Petrov, L. I. Dekhtyar, and A. E. Beznosov, ''Effect on Microhardness of Alloying of Electrodeposited Chromium with Tungsten and Magnesium,'' *Izv. Akad. Nauk. Mold. SSR*, **6**, 74–78 (1967).
447. V. P. Greco and W. Baldauf, ''Electrodeposition of Ni–$AliO_3$, Ni–TiO_2 and Cr–TiO_2 Dispersion-Hardened Alloys,'' *Plating*, **55** (3), 250–257 (1968).
448. W. H. Mason,U.S. Patent 1,844,921 (1932).
449. A. R. Trist,British Patents 475,902 (1937); 491,530 (1938); U.S. Patent 2,203,849 (1940).
450. H. R. Carveth, U.S. Patent 1,937,629 (1933).
451. C. A. Marlies and G. E. White, U.S. Patent 2,048,276 (1936).
452. V. I. Arkharov and S. A. Nemnonov, *Bull. Acad. Sci. URSS Classe Sci. Tech. (9110)*, 32 (1943); also V. I. Arkharov and V. N. Konev, *Vestn. Mashinostr.*, **35** (11), 55 (1955).
453. A. F. Gerds and M. W. Mallett, *Treats. Am. Soc. Met.*, **52**, 1027 (1960).
454. W. S. Bohlman (to Chromium Corp. of Am.), U.S. Patent 1,809,826 (1931).
455. H. Chessin and P. D. Walker (to M&T Chemicals, Inc.), German Patent Publ. DOS 2,025,751 (1970).
456. H. Chessin and R. F. Gempel (to M&T Chemicals, Inc.), German Patent Publ. DOS 2,005,254 (1970).

8

ELECTRODEPOSITION OF LEAD AND LEAD ALLOYS

MANFRED JORDAN

The standard potential for lead in aqueous solutions is −0.12 V. This metal has a high hydrogen overpotential, which means that it is easily deposited electrolytically from strongly acidic solutions with a cathodic efficiency approaching 100%. The values for the hydrogen overpotential are dependent on the surface and structure of the electrode and are given in the literature as varying between 0.84 V for 99.8% pure Pb [1] to about 1.2 V for electrolytically deposited coatings [2].

The electrochemical equivalent for the reaction

$$Pb^{2+} + 2e \rightarrow Pb \qquad (8.1)$$

is 3.865 g Ah^{-1}. The lead deposition can be used for coulometric determinations because of the high cathodic current efficiency.

Electrolytic deposition of lead has been investigated using several different processes. Important prerequisites for such a process are a high solubility of the lead salts to be used and stability of the anion against hydrolysis in the electrolyte. Table 8.1 lists some data on the solubility of the most relevant lead salts.

In the past the two most commonly used lead electrolytes were the fluoroborate- and fluorosilicate-based processes. In more recent years (since the 1980s) electrolytes based on methanesulfonic acid are becoming the prefered systems, particularly for electrodeposition of tin–lead alloys.

Electrolytes based on nitric acid are not recommended for the electrodeposition of metals because the nitrate anion undergoes cathodic reduction, which leads to the occurrence of unfavorable side reactions. Nitrate contamination can also be very detrimental to other lead electrolytes, leading to a reduction of the cathodic efficiency and poor coverage in the low-current-density areas [3].

The sections that follow give a brief description of some processes that are used for the electrodeposition of lead.

8.1 ELECTROLYTE TYPES

8.1.1 Perchlorate Electrolytes

Perchloric acid electrolytes are very suitable for electrodeposition of lead because of the high solubility of lead in such electrolytes and the high electrical conductivity of the solution. However, such electrolytes are not widely used in practice, partly because of the high price of the acid and also the acid's hazardous nature, which can lead to the risk of explosion. There are varying descriptions of this hazardous nature in the literature [4, 5]. More recent reports in the literature [6] describe fatal accidents where perchloric acid has penetrated through cracks in stone or concrete floors and reacted with wood in the underlying construction to form cellulose perchlorates, which are very shock sensitive. Since many plating shops frequently have catwalks supported by wooden frameworks, such hazards would be virtually unavoidable at some point in time. For these reasons the use of perchloric-based electrolytes is not generally recommended.

8.1.2 Amidosulfonate Electrolytes

There are several articles in the literature which refer to electrodeposition of lead from amidosulfonic acid–based electrolytes [7–11]. The use of such electrolytes for electrolytic refining of raw lead which is contaminated with high levels of antimony and bismuth is also described [12, 13]. One problem that can occur in this particular application of such electrolytes is the tendency for the sulfamate anion to be

Modern Electroplating, Fifth Edition Edited by Mordechay Schlesinger and Milan Paunovic

TABLE 8.1 Solubility of Lead Salts

Lead Salt	Solubility (g in 100 mL solution)
Lead nitrate, $Pb(NO_3)_2$	36
Lead perchlorate, $Pb(ClO_4)_2$	226
Lead fluoroborate, $Pb(BF_4)_2$	No data available in literature; commercial
Lead fluorosilicate, $PbSiP_6$	68.9
Lead acetate, $Pb(CH_3COO)_2$	30.7
Lead chloride, $PbCl_2$	0.97
Lead sulfate, $PbSO_4$	0.004
Lead methanesulfonate, $Pb(CH_3SO_3)_2$	54
Lead amidosulfonate, $Pb(NH_2SO_3)_2$	70.9

hydrolyzed into ammonia and sulfate. This reaction causes the precipitation of lead sulfate and thus a high formation of sludge and a loss of lead in the electroraffination [12].

The rate of hydrolysis of amidosulfonic acid in aqueous solutions increases rapidly once the temperature exceeds 60°C and the pH of the solution is less than 1 [14].

8.1.3 Hexafluorosilicate Electrolytes

The hexafluorosilicate electrolyte was developed for electrolytic refining of lead by a process known as the Betts process [15, 16]. This process is suitable for the purification of raw lead that is contaminated with high levels of As, Sb, Cu, Ag, and Au. The hexafluorosilicate electrolyte is considered to be more stable (and hence more economical) than the sulfamate electrolyte [13]. These electrolytes are not however used for electrodeposition of lead. Typical parameters of such an electrolyte for electrolytic refining of lead are given in Table 8.2 [17].

In the recent literature no papers were published dealing with the use of hexafluorosilicate electrolytes for electroplating of lead. As general information in Table 8.3, the electrolyte and process parameters are given as they were published by Wiesner [31].

8.1.4 Tetrafluoroborate Electrolytes

The tetrafluoroborate electrolyte is the most common process for the electrolytic deposition of lead. Lead tetraflouroborate is a stable lead salt that is very soluble in water. Tetrafluoroboric acid is formed in the reaction between hydrofluoric acid and boric acid according to the reaction

$$4\,HF + H_3BO_3 \rightarrow HBF_4 + 3\,H_2O \qquad (8.2)$$

It is possible that in the reverse reaction the tetrafluoroborate anion can be hydrolyzed into free fluoride and boric acid, which could lead to the possibility of the formation and precipitation of lead fluoride, PbF_2. The hydrolysis of

TABLE 8.2 Parameters of a Lead Electrorefining Plant

Electrolyte composition	
H_2SiF_6	70–120 g L^{-1}
Pb	60–100 g L^{-1}
Additives	Aloe extract Lignin sulfonate
Current density	1.3–2.2 A dm^{-2}
Voltage	0.3–0.5 V
Temperature	35–42°C
Anode composition (wt %)	
Sb	1.0–1.2%
As	0.3–0.6%
Cu	0.04–0.07%
Bi	0.1–0.2%
Ag	0.1–0.6%
Anode sludge (wt %)	
Sb	40–50%
As	20–30%
Pb	10–20%
Bi	5–15%
Ag	5–15%
Electrorefining cells	800, each 2700 L
Production capacity	120,000 tons/year

tetrafluoroboric acid occurs through the following sequence of reactions:

$$HBF_4 + H_2O \rightarrow HBF_3(OH) + HF \qquad (8.3)$$

$$HBF_3(OH) + H_2O \rightarrow HBF_2(OH)_2 + HF \qquad (8.4)$$

$$HBF_2(OH)_2 + H_2O \rightarrow HBF(OH)_3 + HF \qquad (8.5)$$

$$HBF(OH)_3 + H_2O \rightarrow [HB(OH)_4] + HF \qquad (8.6)$$

The tendency for this hydrolysis to occur can be reduced by the addition of boric acid. For this reason lead or lead alloy electrolytes based on tetrafluoroboric acid usually contain

TABLE 8.3 Compositions of Hexafluorosilicate Electrolytes

	Electrolyte 1	Electrolyte 2
Lead	75 g L^{-1}	180 g L^{-1}
Total fluorosilicate	150 g L^{-1}	140 g L^{-1}
Glue	0.2 g L^{-1}	5.4 g L^{-1}
Temperature	35–40°C	
Cathodic current density	0.5–8 A dm^{-2}	
Anodic current density	0.5–3 A dm^{-2}	
Voltage at 1A dm^{-2}	0.1–0.2 V	
Cathodic current efficiency	100%	
Anodic current efficiency	100%	

TABLE 8.4 Composition of a Methanesulfonate Lead Electrolyte

	Deposition of Thin Layers (<50 μm)	Deposition of Thick Layers (up to 200 μm)
Methanesulfonic acid	100 g L^{-1}	100 g L^{-1}
Lead	50 g L^{-1}	200 g L^{-1}
Organic additives	Proprietary	
Electrolyte temperature	20–30°C	
Cathodic current density	< 1.5 A dm^{-2}	3–6 A dm^{-2}
Deposition rate	0.85 μm min^{-1} at 1.5 A dm^{-2}	1.7 μm min^{-1} at 3 A dm^{-2}

20–30 g L^{-1} boric acid, which shifts the equilibrium in the reactions in (8.3)–(8.6) toward the left-hand side.

8.1.5 Methanesulfonate Electrolytes

Electrolytes based on short-chained alkylsulfonic acids (in particular methanesulfonic acid), Table 8.4, are gaining increasing popularity since about 1980. The use of methanesulfonic acid (MSA) for deposition of lead was first mentioned in a patent by Proell in 1950 [18], but there was not practical application of the process at that time.

Fluoride-free processes were initially developed for environmental reasons because they offer less hazardous alternatives to the fluoroborate systems and produce waste streams that are more easily dealt with. Since their introduction to the marketplace, these processes have proved to be more stable and easier to operate and in some applications technically superior, which explains the rapid growth in their popularity.

8.1.6 Other Electrolytes

Several other electrolytes have been investigated for deposition of lead. A detailed discussion on all would go beyond the scope of this chapter. The only electrolytes that have reached any significant importance for industrial applications are those already mentioned. A detailed survey of all possible lead electrolytes is given in *Gmelin's Handbook of Inorganic Chemistry* [33].

Alkaline Electrolytes The two most usual alkaline electrolytes used for the deposition of lead are the pyrophosphate and plumbite processes.

Pyrophosphate Electrolytes As an example for the deposition from alkaline solutions, Table 8.5 gives the parameters for the pyrophosphate process. The pyrophosphate electrolytes are renowned for having particularly good throwing power.

Plumbite Electrolytes Electrodeposition of lead from alkaline plumbite(II) electrolytes is possible. But opposite to the tin deposition, where the alkaline stannate processes still have some technical importance, the alkaline plumbite processes do not find technical applications. In the alkaline solution the lead ion is present in a complexed form. The electrodeposition has therefore a higher overpotential compared to the acidic solution, where the lead ion is uncomplexed. For this reason alkaline solutions can be operated without inhibitors and show normally a high throwing power. Additionally alkaline solutions are less corrosive to plants and equipment. The main disadvantages are process engineering problems. The cathodic current densities that can be reached from alkaline solutions are low, even at high temperatures up to 90°C, and do not normally exceed 2 A dm^{-2}. A smooth dissolution of the anodes is only possible at low anodic current densities. Above 1 or 2 A dm^{-2} there is a steep increase of the potential, and lead dioxide, PbO_2, is formed on the anode surface [38]. One example for an alkaline lead electrolyte is given in Table 8.6 [39].

8.2 GENERAL INFORMATION ON THE ELECTRODEPOSITION OF LEAD

The softness and dull finish of lead deposits limit their use commercially. They are not suitable for decorative purposes. As a coating material for corrosion protection, lead can only be used with some limitations. The standard potential of lead

TABLE 8.5 Lead Pyrophosphate Electrolyte

Lead (g L^{-1})	Pyrophosphate (g L^{-1})	Cation	Additive	Temperature (°C)	Current density (A dm^{-2})	References
20.7	79.2	Na	Glue	50–60	≤5	34
20.3	78	Na		60	≤4.2	35
20.3	78	K	Glue	60	≤3.5	35
41.4	87	K	Phenols	20–40	0.5–2	36
20.7	65	K	Dicyandiamide/formaldehyde/ hexamethylenete tramine reaction product	60	0.5–5	37

TABLE 8.6 Composition of Alkaline Plumbite Electrolyte

Pb	$40\,g\,L^{-1}$
NaOH	$200\,g\,L^{-1}$
Na acetate	$23.4\,g\,L^{-1}$
Na tartrate	$26.2\,g\,L^{-1}$
Temperature	60–90°C
Cathodic current density	$1–2\,A\,dm^{-2}$
Additive	$6\,g\,L^{-1}$ colophony

is more noble than steel, and the base material therefore cannot be protected anodically. An effective corrosion protection is only given when the coating can be deposited in a pore-free form. The main use of lead as a coating material is for applications where lead coming into contact with those aggressive media forms insoluble, tightly adhering layers. The preferred application of lead coatings is therefore in corrosion protection against sulfuric acid–containing media. The surface of the lead coating is covered by a tightly adhering layer of lead sulfate, which protects the underlying metal against any further attack by the sulfuric acid. For such applications coatings with a thickness up to 200 μm are normally used. This has to be considered when making up the electrolytes. Some details on the makeup and operating parameters of the more important lead electrolytes are given in the sections that follow.

8.2.1 Additives

Lead is one of a group of metals that can be deposited with a low overpotential from aqueous solutions. In additive-free acidic electrolytes, lead will be deposited in a dendritic form, as seen in Figure 8.1. Large isolated lead crystals are formed especially around the edges of the cathode. Deposition of dense pore-free coatings is therefore possible only when the electrolyte contains special inhibitors in a sufficient quantity. Table 8.7 lists some organic chemicals that can be used as grain refiners in lead electrolytes. This table lists compounds published in technical literature or in patents. It can be assumed that there are several other chemicals not mentioned in publications that are used in proprietary additives. In the patent literature, in particular that relating to MSA electrolytes, there are many additives listed for use for the deposition of lead, tin, and tin–lead. In most of the patent applications the effect of the additives is described with reference to the tin–lead deposition.

Extensive experimentation was carried out by Graham and Pinkerton [19, 20] to select suitable additives for the lead deposition. Their findings are included in Table 8.7.

8.2.2 Anodes

Insoluble anodes cannot be used in lead plating electrolytes as lead dioxide, PbO_2, will form on the surface of the anodes. The purity of the soluble lead anodes used determines the extent to which a film forms on the surface of the anodes. These layers are caused by the metallic impurities in the anodes, which are more noble than lead and are therefore not dissolved anodically. The typical contaminants found in lead anodes are bismuth, copper, antimony, silver, arsenic, and tin. If the level of these contaminants in the lead anodes is not too high, anode passivation is not problematic in the more common lead electrolytes (fluoroborate-, fluorosilicate-, and MSA-based electrolytes).

Lead can also be dissolved by chemical dissolution in acidic electrolytes, which results in an equivalent current

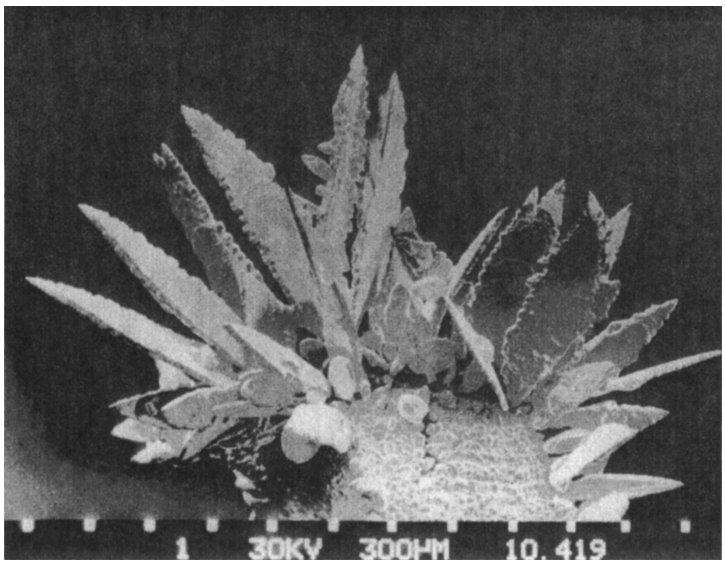

FIGURE 8.1 Lead deposition from an acidic, additive-free electrolyte. The electrodeposition occurs under this condition in a typical dendritic form. (SEM picture courtesy of Heinz Brennenstuhl, Esslingen.)

TABLE 8.7 Additives for Lead Deposition in Acidic Electrolytes

Compound	Electrolyte Type	Concentration ($g\,L^{-1}$)	References
Quinone	HBF_4	10	19
Quinhydrone	HBF_4	10	19
1,4-Naphthoquinone	HBF_4	<1	19
Hydroquinone	HBF_4	10	19
1,2-Naphthoquinone	HBF_4	10	19
Eugenole	HBF_4	1	19
Ligninsulfonic acid	HBF_4	1	19
6-amino-1-naphlhol-3-sulfonic acid	HBF_4	2	19
1,4-naphthoisulfonic acid	HBF_4	1	19
Coumarin + ligninsulfonic acid	HBF_4	2 + 1	19
Glue	HBF_4	1	21
Resorcinol + peptone	HBF_4	Each 0.23	22
Dibenzenesulfoneamide	HBF_4	0.5–5	23
Gelatine	HBF_4; MSA	0,2	24, 27
Ethoxilated alkylphenols	HBF_4	0.1-10	25, 26
Hydroxylated cellulose	MSA	2	27
Polyethyleneglycol	MSA	0.25	27
Peptone	HBF_4	1–10	28
Cetytrimethylammoniumbromide	$H_2N–SO_3H$	2–15	29
Phenol, cresol	H_2SiF_6	No exact data given	30

efficiency of greater than 100%. However, because of the high hydrogen overpotential, such dissolution occurs only when oxygen is available. The lead anodes are therefore immersed completely in the electrolyte to prevent dissolution. If any part of the anode is not covered by the electrolyte, chemical dissolution of the lead will occur at the interface between the electrolyte and air.

8.2.3 Temperature

Increasing the electrolyte temperature will increase the limiting current density and thus allow the electrolyte to be operated with a higher current density [40]. The electrolyte temperature for the electrodeposition of lead is usually between 20 and 40°C. In most common lead electrolytes an increase in the electrolyte temperature leads to a coarser grain structure [41] to a greater or less extent, depending on the grain refiner used in the electrolyte.

8.2.4 Electrolyte Agitation

Electrolyte agitation influences the maximum cathodic current density at which smooth dendrite-free deposition is possible. Graham and Pinkerton [42] investigated the influence of cathode rotation on the limiting current density. During their experiments they noted that at constant rotation speed of the cathode the limiting current density can also be affected by the type of inhibitor used.

Agitation of the electrolyte is also important to keep the lead concentration in the electrolyte constant. Without agitation, the lead which is dissolved from the anode can build up at the bottom of the plating cell because of the higher density of this solution.

8.2.5 Troubleshooting

The electrodeposition of lead is mainly used where corrosion-resistant coatings are required. In such applications the coatings have to be dense and pore free. The most frequent failures that occur in lead plating are defects in the deposits such as nodules, "growths," or treeing. The main cause for such failures and suitable countermeasures are described in the following paragraphs.

Treeing The formation of treeing is normally seen on edges of the cathode. It can happen when there is a lack of additives in the electrolyte. A typical example of treeing is shown in Figure 8.1 for lead deposited from an additive-free electrolyte. Such defects can be corrected by addition of additive according to the instructions given for the electrolyte system.

Nodules or "Growths" During the deposition of thick lead coatings (up to 200 µm) formation of nodules or growths can occur, as seen in Figure 8.2 of a lead deposit from a methanesulfonate electrolyte. In this electrolyte the additive system consisted of a mixture of nonionic surfactants and hydroquinone as grain refiner.

This failure does not generally occur with a freshly made-up solution, and when it does occur, it can in most cases be

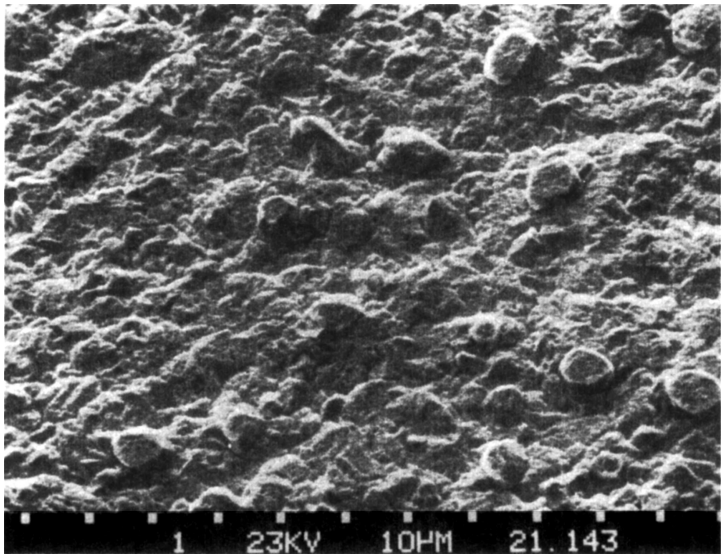

FIGURE 8.2 Lead deposition from a methanesulfonate-based electrolyte with hydroquinone as additive. The formation of dendrites and nodules can be seen. Especially when plating thick layers ($< 200\,\mu m$) from such systems, the formation of nodules can be severe.

rectified by purification of the electrolyte with activated carbon. The cause for the problem is therefore probably the contamination of the electrolyte by breakdown products of the organic additives.

In practice, such failures had been seen together with a rapid decrease of the lead concentration in the electrolyte. The drop of the lead concentration from 200 to 135 g L^{-1} was parallel to a dark discoloration of the electrolyte. The anodic current efficiency was reduced, which caused the drop in lead content in the bath. By passivation of the anode, lead dioxide was formed on the anode surface, which caused partial oxidation of the organic additives.

This failure mechanism can be confirmed by using insoluble anodes. On the anode surface a layer of lead dioxide forms that leads either to anodic oxidation of the organic additives on the anode surface during operation of the electrolyte or during idle periods by chemical oxidation of the organic additives by the lead dioxide [43].

In contrast to the problem of treeing, this formation of dendrites and growths can normally not be corrected by more additives, since it is caused not by a lack of additives but by contamination with breakdown products in the electrolyte. The only remedy for such problems is purification of the electrolyte by a carbon treatment.

Streaking or Step Plating Dini and Helms [44] and Wiesner and co-workers [45] referred to defects in lead plating in the form of step plating that sometimes followed the flow pattern of the solution across the plated surface. In both papers fluoroborate electrolytes were investigated in which resorcinol and peptone or hydroquinone were used as inhibitors. The experiments confirmed that the problem of streaking or step plating is caused by oxidation of the resorcinol or hydroquinone. Dini and Helms observed that the failure only occurred after the electrolyte had been operated for several ampere-hours and could be corrected by a carbon treatment. The use of organic additives, which can be modified by either anodic oxidation or contact with the oxygen from the air, is therefore not recommended for the electrodeposition of lead. Wiesner et al. [45] recommend a mixture of ligninsulfonic acid and coumarin.

Figure 8.3 shows the morphology of the lead surface deposited from an electrolyte based on MSA. The additive system is a proprietary mixture, and it does not contain compounds like resorcinol or hydroquinone [46]. In comparison to Figure 8.2, which shows the surface of a lead layer plated from an MSA-based electrolyte containing hydroquinone, Figure 8.3 shows very little sign of dendritic deposition.

Figure 8.4 shows the surface of a lead layer that was deposited from a commercial fluoroborate electrolyte. Although no nodules or dendrites are seen, the comparison with Figure 8.3 clearly shows that a finer grained deposit can be obtained from MSA electrolytes with suitable additive systems.

Pores (Voids) Lead is electropositive relative to iron, which means that lead cannot offer sacrificial anodic corrosion protection to steel. Therefore lead coatings used to protect steel from corrosion must be completely pore (void) free.

The number of pores in an electrodeposited layer of lead depends on the additive system and the thickness of the layer. The formation of pores can also be caused by contamination in the electrolyte, which will reduce the throwing power of

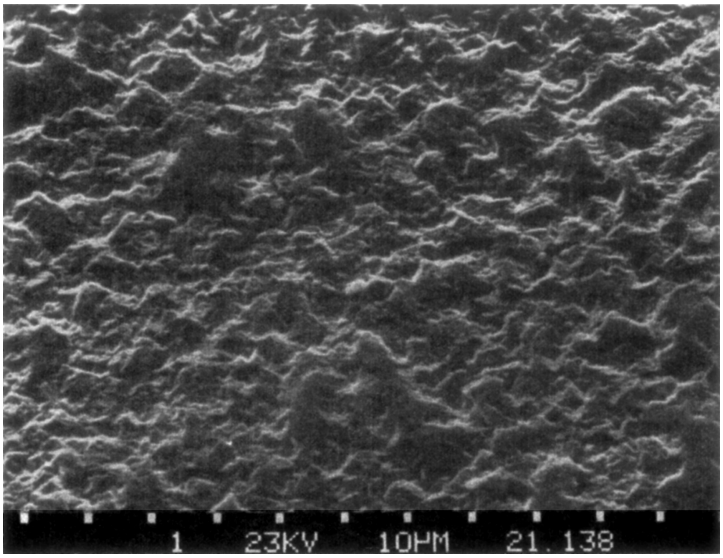

FIGURE 8.3 Lead deposition from a methanesulfonate-based electrolyte. Opposite to the sample shown in Figure 8.2, the additive system did not contain hydroquinone or similar chemicals, which can be oxidized during bath aging and thus cause the formation of a nodular deposition.

the electrolyte. Such failures can be caused by contamination of nitrates or halide ions. Because nitrate is reduced at the cathode, an increase in the level of nitrate contamination leads to a reduction of the cathodic current efficiency of the lead deposition, which can eventually lead to the situation where there is no lead deposition in the low current density at all [3, 47].

Contamination with chloride ions can lead to a severe reduction of coverage and widespread formation of pores. In a sulfamate electrolyte contamination with 300–500 mg L^{-1} chloride causes dendritic plating [48].

In one particular application, where cable shoes manufactured from steel were being plated with lead using an MSA-based electrolyte, the deposit appeared very porous, which led to corrosion in the form of red rust after only several hours [43]. The pores were caused by chloride contamination in the electrolyte on the order of 300 mg L^{-1} which was caused by drag-over of a hydrochloric acid pickling solution from pretreatment of the steel parts. Such a problem would not occur if the same pretreatment sequence were used in conjunction with a tetrafluoroborate electrolyte. This is because addition of chloride to a tetrafluoroborate-based

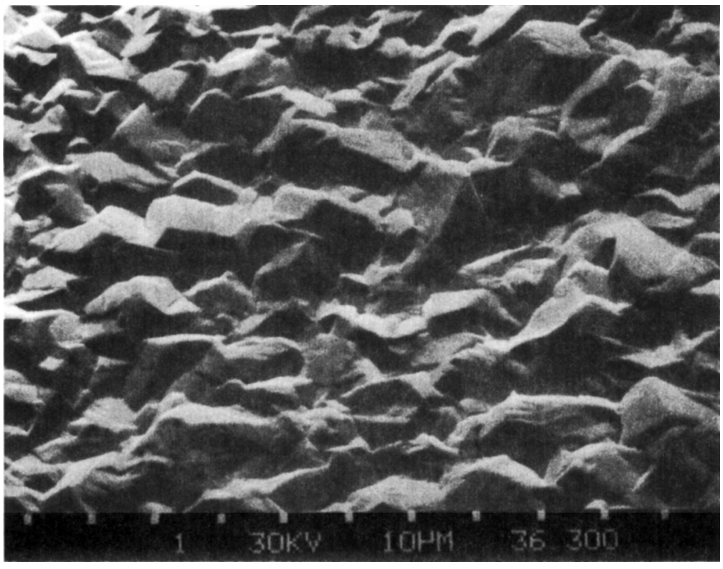

FIGURE 8.4 Lead deposition from a fluoroborate-based electrolyte. The big-shaped crystal shows that under this plating condition an additive system with insufficient grain refining was used.

lead electrolyte leads to precipitation of the white, crystalline compound PbClF. In the fluoride-free MSA electrolyte such precipitation of chloride cannot occur, so there is no "self-curing" mechanism for chloride contamination. Precipitation of chloride from an MSA-based electrolyte is possible by the addition of sodium fluoride to the electrolyte. Figure 8.5 shows the reduction of chloride in an MSA-based lead electrolyte in relation to the addition of sodium fluoride.

Discoloration Lead deposits are generally not used for decorative applications. The color and appearance of the coatings are therefore of little importance as long as the deposit meets the specified technical requirements.

Copper contamination can, however, lead to unacceptable discoloration of the deposit. Copper that is present in the electrolyte will be codeposited with the lead during electrolysis, but this codeposition will not cause discoloration of the deposit. Discoloration of the lead deposit to a brown or black color occurs due to deposition of copper onto the lead surface by a displacement reaction that can happen in the electrolyte if the current is left switched off while the parts are still immersed or in the rinses if they are heavily contaminated with copper.

If the plating parameters and rinsing conditions are properly controlled, lead electrolytes will seldom show copper contamination in excess of $50\,mg\,L^{-1}$, even when copper parts are plated.

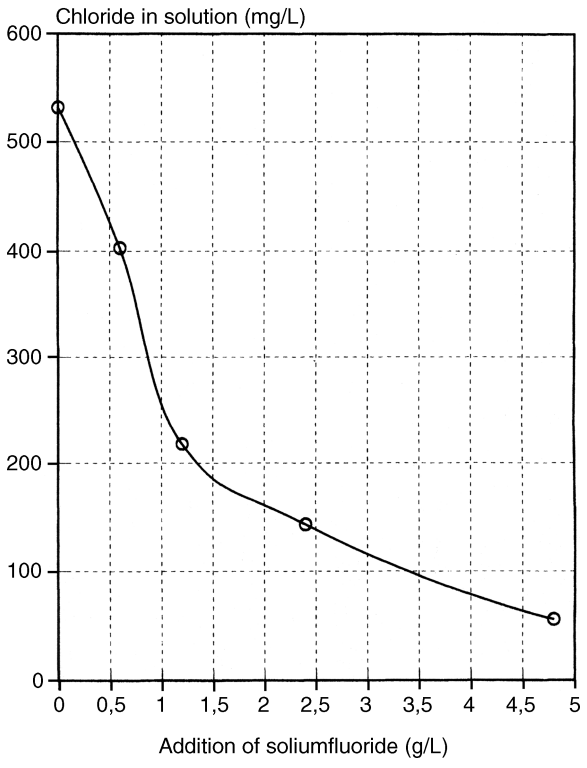

FIGURE 8.5 Removal of chloride ions from a methanesulfonate-based lead electrolyte by addition of sodium fluoride. Chloride is precipitated as PbClF.

8.3 PROPERTIES OF ELECTRODEPOSITED LEAD COATINGS

8.3.1 Hardness

The data for the hardness of electrodeposited lead layers given in the literature differ considerably. Because of the creep behavior of lead, it is not easy to compare all the results. They depend on the load and the measuring time. Typical values for the Knoop hardness with a load of 25 g are in the range of 4 [49]. For a load of 5 g, the hardness is given as 7–8 [44].

8.3.2 Elongation

The elongation of electrodeposited lead coatings with a thickness of 750 μm is 50–52%. The elongation was calculated by measuring the change of length of the sample in a section of 1 in. around the fracture in the measurement of tensile strength [44].

8.3.3 Tensile Strength

The tensile strength of electrodeposited lead layers is about $14–16\,kg\,mm^{-2}$ and is thus comparable with that of a sample produced from the molten metal [44].

8.3.4 Density

The density of conventionally electrodeposited lead layers is not different from that from a molten sample; a value of $11.34\,g\,cm^{-3}$ is given. Under high-speed conditions deposited layers showed a slightly lower density of $11.22–11.34\,g\,cm^{-3}$ [50].

8.3.5 Electrical Resistivity

The electrical resistivity of electrodeposited lead layers is 20–22.9 μΩ·cm, and thus it is slightly higher than that of a sample prepared from molten lead (20.6 μΩ·cm) [50].

8.3.6 Corrosion Resistance

The corrosion resistance of electrodeposited lead coatings was investigated by Graham and Pinkerton [49] in atmospheric exposure tests in severe industrial, rural, and maritime climates. Coatings with thicknesses of 25 and 50 μm on steel panels did not show base material corrosion after three years.

To have a better comparison of the behavior of lead in the different test climates, the thickness was reduced to 6.4 μm. Even with such a thin deposit less than 20% base material corrosion was observed after 8 months in the maritime,

16 months in the industrial, and 24 months in the rural climate. The influence of the additive system on the corrosion resistance of the lead deposit was shown by using glue instead of hydroquinone as the inhibitor. The corrosion resistance of the same thickness of deposit in this case was reduced to 4, 9, and 16 months, respectively.

Deposition of thin layers of tin or iron prior to lead plating reduced the corrosion resistance compared to those samples with the lead coating directly plated on the steel. But the deposition of a thin copper layer (1.3 μm) prior to lead plating improved the corrosion resistance considerably.

8.4 DISPERSION PLATING

The codeposition of suspended solid particles in etectrodeposited lead coatings was investigated by Pini and Weber [51], Vandervoort and co-workers [52], and Wiesner and co-workers [45]. Fluoroborate electrolytes were used for lead deposition with hydroquinone [51] or ligninsulfonic acid and coumarin [45] as the inhibitors.

Pini and Weber investigated the dispersion plating of boron carbide or titanium carbide. The particle sizes of the suspended solids were 3.3–18 and 20–50 μm for boron carbide and 20–60 μm for titanium carbide. With 150 g L^{-1} each suspended material a rate of codeposition of about 20% was reached. The codeposition of the carbides doubled the hardness of the deposit. The corrosion resistance was slightly improved by the codeposition of the small boron carbide particles, but the codeposition of the bigger particles caused a significant reduction of the corrosion resistance.

Wiesner and co-workers investigated the codeposition of PbO, PbO_2, Pb_3O_4, $A1_2O_3$, TiO_2, and $BaSO_4$ particles. The lead oxides and the alumina agglomerated in the electrolyte. The codeposition of $BaSO_4$ and TiO_2 was possible at rates of codeposition of 0.49% for TiO_2 and 2.7% for $BaSO_4$. Codeposition of TiO_2, especially when codeposition of about 0.1% tin was also included in the deposit, improved the mechanical properties of the deposited layer considerably.

8.5 LEAD ALLOYS

The most important electroplated lead alloy is the tin–lead alloy. This will therefore be treated in a separate section. All the other lead alloys described in the paragraphs that follow have limited applications.

8.5.1 Lead–Antimony

Deposition of lead–antimony alloys was investigated from fluoroborate electrolytes with pepton and resorcinol as additives [53]. This electrolyte differed from the known fluoroborate electrolytes for the deposition of lead or lead alloys in that the electrolyte for the deposition of lead–antimony alloys contained free fluoroboric acid and also free hydrofluoric acid. Codeposition of antimony at a concentration of between 0 and 15% increases the hardness from 8 to 21.5 and increases the tensile strength from 15 to 65 kg mm^{-2}, but the ductility severely reduced. The electrolyte composition for a lead–antimony deposition is shown in Table 8.8.

TABLE 8.8 Composition of Lead–Antimony Electrolyte

Pb	62 g L^{-1}
Sb	11.5 g L^{-1}
HBF_4	74 g L^{-1}
Boric acid	20.6 g L^{-1}
Pepton	0.25 g L^{-1}
Resorcinol	0.25 g L^{-1}

A tetrafluroboric acid–based electrolyte with diethanolamine and tartaric acid [96] was used to investigate the improvement that could be achieved in the corrosion resistance of lead deposits against sulfuric acid by codeposition of antimony. It was established that an antimony content of 10% gave the maximum of corrosion resistance [54].

8.5.2 Lead–Bismuth

Brenner [55] makes only one reference to deposition of lead–bismuth deposition. There is only one other reference in recent literature [56] to such an electrolyte. Codeposition of bismuth was investigated to improve the corrosion resistance, and it was confirmed that the optimum alloy was found to contain 17% bismuth. The electrolyte used was the HBF_4 electrolyte with additions of Trilon B and glue.

8.5.3 Lead–Thallium

Thallium was investigated as a possible coating for metal bearings [57]. Attention then turned to the possibility of using lead–thallium for such applications using a sulfamate electrolyte with pepton and gelatine as additives. With a ratio of 3 : 1 lead–thallium in the electrolyte at a current density of 0.5–1 A dm^{-2}, deposits with 2–35% Tl could be achieved.

However, because the alloy composition in the deposit has a high dependency on the applied current density, such an electrolyte will only find use in applications where the geometry of the anode to cathode can be precisely controlled to ensure uniform distribution of current density. This requirement can normally be met in bearings.

8.5.4 Lead–Cadmium

Investigations into the deposition of lead–cadmium alloys were made with the aim of a possible application for bearings. Lead–indium alloys are a good bearing alloy because of the high fatigue strength and corrosion resistance against

oxidation products of the lubricating oils, but there is still demand for alternatives because of the high price of indium.

This led to the development of lead–cadmium alloys with a cadmium content up to 30%. Because the standard potentials of Pb (−0.126 V) and Cd (−0.403 V) are relatively close, codeposition from uncomplexed solutions should be possible [58–60]. Investigations were made into solutions based on fluorosilicates [58], fluoroborates [59], sulfamates, and a citrate–acetate electrolyte [60]. The electrochemical measurements were made using polarographic techniques and the alloy composition was measured using atomic absorption spectroscopy after dissolving the deposits in HNO_3–HCl mixtures.

No further evaluations on the suitability of those layers as bearing metals were described in the cited papers. In the fluorosilicate electrolyte with an electrolyte composition of 220 g L^{-1} Cd, 50 g L^{-1} Pb, and 6 g L^{-1} resorcinol alloys with 10–20% Cd were plated at a current density of 2–5 A dm^{-2}. It was noted that the alloy composition is very sensitive to variations in the plating parameters.

In the fluoroborate system an electrolyte composition with 220 g L^{-1} Cd and 50 to at most 75 g L^{-1} Pb deposited alloys with a maximum of 30% Cd. Resorcinol, pepton, and polyethyleneglycol were tested as possible additives in this system. The temperature was kept at 30–60°C, and the deposition was made under potential-controlled conditions at −600 mV against SCE (saturated calomel electrode, corresponding to a cathodic current density of about 10 A dm^{-2}). The properties of the electrolyte changed within several days, probably because of the formation of oxidation products of the resorcinol.

The experiments using the sulfamate electrolyte, in which resorcinol at a concentration of 6 g L^{-1} was also used, gave essentially the same results. Deposition of alloys with up to 20% Cd is possible, but the alloy composition is very dependent on the plating parameters. No codeposition of cadmium was possible from the electrolyte based on citrates and acetates.

8.5.5 Lead–Silver

The deposition of lead–silver alloys was investigated as a possible option for coating metal bearings. Small additions of silver (1–2%) increases the stability of lead anodes in their use in sulfate-based electrolytes.

Deposition of the lead–silver alloy is made from electrolytes containing cyanides. Brenner [55] has compiled a list of lead-silver electrolytes that have been investigated. The cyanide ion is a selective complexing agent for silver, so an increase in the cyanide concentration will lead to a stronger inhibition of the silver deposition. Lead is complexed in such electrolytes by tartrate.

The electrolyte formulations discussed in the literature yield deposits of approximately 10% lead. The lead content in the alloy increases with increasing current density, especially when the electrolyte contains a high concentration of free cyanide. Codeposition of lead in silver causes a considerable increase of the hardness from about 70–100 kg mm^{-2} to values of about 200 kg mm^{-2}. The maximum hardness is achieved by codeposition of about 2% Pb. Table 8.9 shows the composition of an electrolyte for the deposition of a lead–silver alloy [61].

TABLE 8.9 Composition of Lead–Silver Electrolyte

Ag (as $KAg(CN)_2$)	8–16 g L^{-1}
Pb (as $Pb(NO_3)_2$)	4–16g L^{-1}
KSCN	120 g L^{-1}
K-Na-tartrate ($KNaC_4H_4O_6{\cdot}4H_2O$)	240 g L^{-1}
NaOH	To adjust pH 9

While silver–lead alloys with a lead content up to 10% were investigated mainly for their possible application as a coating for metal bearings, recent publications refer to lead–silver alloys with up to 10% silver for the production of lead dioxide. Such coatings can be deposited from cyanide-based electrolytes that use glycerol as a complexing agent for lead. In comparison to the electrolytes using tartrate as the complexing agent that were mentioned earlier, the glycerol-based electrolytes exhibit higher cathodic current efficiencies [62]. The typical composition for such electrolytes is about 4 mol L^{-1} potassium hydroxide, 0.31–0.36 mL L^{-1} lead, 0.031–0.063 mol L^{-1} silver, 0.62–0.73 mol L^{-1} free cyanide, and about 60 mL L^{-1} glycerol. A modified electrolyte formulation for the deposition of alloys with about 2.5% Ag is claimed by the same authors in a Japanese patent application [63].

Lead anodes with a silver content of about 1% are used in the electrolytic production of zinc. To save silver it is suggested that a lead–silver alloy with about 0.45–1% Ag and a thickness of 100–200 μm as the active anode surface on a lead anode will suffice [64].

Deposition of lead–silver alloys from cyanide-free electrolytes was also investigated. Electrolytes using potassium hexacyanoferrate(II), $K_4Fe(CN)_6$, and polyethylenepolyamines as complexing agents were tested [65, 66].

8.5.6 Zinc–Lead Alloys

Deposition of zinc–lead alloys with codeposition of about 10% lead was investigated with the aim of improving corrosion resistance in comparison to pure zinc coatings [67]. The authors investigated the deposition from alkaline zincate, plumbite, pyrophosphate electrolytes and acidic perchlorate, fluoroborate, and acetate electrolytes.

Deposits from the alkaline electrolytes tended to be porous and spongy when operated at the usual working temperatures (30–80°C). The deposits from the perchlorate

electrolyte were dark and rough, and codeposition of zinc only occurred in traces. The optimum parameters for the acetate electrolyte are quoted in the literature as pH 3–3.5 and electrolyte temperature 30°C. With a ratio of 0.5 *M* Zn and 3.10^{-4} *M* Pb in the electrolyte, codeposition of 16% Pb can be achieved. Lead is present in the acetate solution in an uncomplexed form, and it is preferentially deposited as the more noble element.

The optimum parameters for the fluoroborate electrolyte are a pH 3–3.5 and temperatures 30–40°C. With similar molar ratios of Zn and Pb as given above, alloy codeposition of 1.9% Pb can be achieved with this electrolyte. The best results are achieved from a pyrophosphate electrolyte at a temperature of 30–60°C. Lead is also the more noble element in this electrolyte. To achieve the desired alloy composition of about 10% Pb, the Zn–Pb ratio has to be about 100.

The corrosion resistances of the coatings with the different Pb contents were tested using salt-spray tests and atmospheric exposure tests. Deposits with 9.1% Pb were inferior in all tests to pure zinc coatings. An improvement of the corrosion resistance was found for alloys with a lead content between 2.5 and 4.75%. The corrosion resistance was tested on samples without any posttreatment.

Deposition of zinc–lead deposits with up to 5.6% Pb from weakly acidic electrolyte systems (chloride, fluoroborate, or fluorosilicate electrolytes) is referred to in the literature with the use of ethoxilated or mixed ethoxilated–propoxilated alkylsubstituted phenols as additives [68]. There is one reference in the literature [68] to the use of zinc–lead alloys for coating bearings that claims an improved wear resistance when this coating is applied.

8.5.7 Lead–Copper

The deposition of copper–lead alloys had been investigated also as a possible coating to improve wear resistance on metal bearings. Electrodeposition of this alloy also offers the possibility to produce lead–copper alloys that cannot be produced by melting the individual metals because of limited solubility. A comprehensive list of lead–copper electrolytes has been compiled by Brenner [55].

Because of the large difference in the standard potentials between copper and lead, complexing agents are necessary in the electrolyte to bring the standard potentials closer to one other. Cyanide is a suitable complexant for such electrolytes, which reacts selectively with copper to form the complex anion $[Cu(CN)_3]^{2-}$. Lead can be complexed by hydroxycarbonic acids or pyrophosphate. Alloys with up to 60% lead can be deposited from such systems, its composition being very dependent on the operating parameters of the electrolyte. Because such systems have not found any commercial applications, they will not be discussed in any detail in this text. For further information, refer to the literature by Brenner [55].

In the recent literature further investigation into the deposition on lead–copper alloys is described. All papers are concentrated essentially on investigation of the deposition of copper–lead alloys from cyanide-free systems. The deposition of a copper-lead alloy with a lead content up to 6% is possible in an electrolyte based on sulfamate/citrate/tartrate at pH 9–12 [69]. The use of ethylenediamine as a complexing agent for copper was first mentioned by Brockman and Mote [70] or perhaps Roszkowski and coworkers [71], and it has been further investigated in recent years [72–74]. Deposits with a lead content up to 40% can be deposited from such electrolytes. Deposits with a lead content up to 20% are red to yellow in color, and those with a higher lead content have a dark, matte appearance [74].

Acidic electrolytes which contain the metals in an uncomplexed form were also investigated for the deposition of copper–lead alloys (Brenner [55] also makes reference to these electrolytes). However, deposition of lead–copper alloys from acidic solutions is difficult because of the large difference in the standard potentials of the two metals. In analytical chemistry this difference is used for the quantitative separation of copper and lead. In solutions containing free nitric acid, the copper can be deposited at the cathode, while lead is deposited as lead dioxide at the anode. During the production of lead dioxide anodes, copper is very often added to the solution to prevent the dendritic deposition of lead at the cathode [75]. By additions of cetyltrimethyl ammonium bromide, Udupa et al. [75] were successful in plating a copper–lead alloy as long as the copper–lead ratio in the electrolyte was not too high.

In the recent literature only a few papers have been published [76–78]. There were no technically important applications found in these systems.

Electrodeposited copper–lead layers with lead contents up to 6% have a microhardness of 250–350 kg mm^{-2}. They are thus much harder than the corresponding alloys produced by melting the two metals together, which show a hardness of about 40 kg mm^{-2}. References have been made in the literature with regard to the superconductivity of supersaturated alloys of copper and lead [79, 80].

8.5.8 Lead–Indium

Lead–indium alloys have some importance as a material for coating bearings. The inclusion of up to 10% indium into a lead deposit will improve the corrosion resistance. The usual way to produce a lead–indium alloy is to plate separate layers of lead and indium and then form the alloy by heating the sample to 150°C. Layers produced by this diffusion mechanism show a gradient of the indium concentration from the outside to the inner side.

For this reason electrolyte formulations for the electrodeposition of homogeneous alloys were examined. The standard potentials for lead and indium differ by only about

0.2 V. Acidic electrolytes based on tetrafluoroboric acid, sulfamic acid, and perchloric acid as well as solutions containing complexing agents and weakly acidic and alkaline electrolytes were all investigated. Brenner describes a number of electrolyte formulations [55]. There are some further references to such electrolytes given in more recent literature, including those electrolytes that use complexing agents such as tartrates [81], diethylenetriamine pentaacetate/gluconate [82], diethylenetriamine–pentaacetate [83], and polyethylenepolyamine [84].

Eastham compared the properties of lead–indium and the ternary lead–tin–copper alloys as wear-resistant coatings for bearings [85]. He found that the lead–indium layer has a higher fatigue strength but a lower wear resistance compared with the ternary alloy.

There is still some production of lead–indium alloys for steel-backed silver–lead or lead–bronze bearings. In such applications the lead–indium layer is still produced by plating the two individual layers and diffusing [86].

8.5.9 Lead–Cobalt and Lead–Nickel

A U.S. patent [87] refers to the deposition of a cobalt–nickel–lead alloy onto aluminum. The function of this deposit is to enable the aluminum parts to be welded with each other or with other metals. The electrolyte used for such deposition is a citrate-based electrolyte at pH 10.5.

Investigations into the magnetic properties and the structure of cobalt–lead alloys with 20–70% Co were described by Surzhko and Korolinko [88]. A pyrophosphate electrolyte with tartrate and citrate as complexing agents operated at pH 9.7–10 and 60°C was used to deposit the alloy.

The influence of thiocyanate ions on the deposition of nickel–lead or cobalt–lead alloys was investigated by Franklin and co-workers [89]. The thiocyanate ion catalyzes the deposition of the transition metals with a corresponding higher rate of codeposition in the alloy.

8.6 ELECTRODEPOSITION OF LEAD DIOXIDE

Electrodeposition of lead dioxide is of commercial importance because it is the method used for the production of lead dioxide anodes. PbO_2 has a high electrical conductivity ($0.5 \times 10^4\ \Omega^{-1}$) and a high overpotential for the production of oxygen. Such anodes are therefore used in many technical applications (production of zinc by electrolysis from electrolytes containing sulfates, persulfate production, etc.).

Lead can be used as anode material. During anodic polarization the lead surface passivates and forms lead dioxide. The lead for the reaction comes from the underlying layers of lead. If lead anodes, which contain 1% silver, are used as the starting material, the lead dioxide anodes subsequently produced will be extremely stable.

TABLE 8.10 Electrolyte Composition and Working Parameters for the Lead Dioxide Deposition

Lead nitrate, $Pb(NO_3)_2$	$350\ g\ L^{-1}$
Copper nitrate, $Cu(NO_3)_2{\cdot}3H_2O$	$20\ g\ L^{-1}$
Substrate for the anode	Titanium
Cathode	Copper
Electrolyte temperature	60°C
Current density	$4–8\ A\ dm^{-2}$

For other applications, deposition of lead dioxide can be made on suitable substrates, especially titanium [90] or graphite [91]. The valve function of titanium during anodic polarization is prevented either by deposition of thin layers of platinum or palladium or by addition of fluoride [90] to the electrolyte. The electrolyte is normally a solution of lead nitrate and copper nitrate. The addition of copper is made to prevent unwanted cathodic deposition of lead. Table 8.10 shows a typical electrolyte composition and the working parameters for the deposition of lead dioxide [92].

The combination of the cathode and anode reaction leads to a liberation of nitric acid. In order to keep the metals in the solution and the pH constant, the addition of lead oxide, PbO, and copper metal is recommended [92]. Investigation into the formation of stresses in electrolytically deposited lead dioxide layers were reported by Gnanasekaram and co-workers [93]. The existence of internal stresses can lead to cracks in the anodes and thus can have an adverse effect on the stability and the shelf-life of the anodes. The operating parameters of the electrolyte must therefore be carefully controlled.

8.7 DEPOSITION FROM NONAQUEOUS SOLUTIONS

Investigations into the deposition of lead alloys from nonaqueous solutions were made for those metals that cannot be plated from aqueous solutions because of their negative standard potential.

8.7.1 Depositions from Aprotic Solvents

Deposition of a wide range of lead–aluminum alloys from organic solvents is described in many papers. Alloys with a lead content of 32.6–99.3% have been plated from an electrolyte based on ethylbenzene/toluene with $AlBr_3$ ($3\ mol\ L^{-1}$), tetraethyl ammonium bromide ($0.5\ mol\ L^{-1}$) and lead in the form of lead tartrate. The molar ratio between aluminum and lead has to be greater than 100 [94].

In an earlier publication the same authors investigated the deposition of aluminum–lead alloys from benzene, toluene, or ethylbenzene electrolytes with $AlBr_3$, $PbBr_2$, and tetraethyl ammonium bromide or KBr as conducting salts. Lead deposition is favored (90–95%). To achieve alloys with a

higher aluminum content, the lead concentration has to be limited to a maximum of $0.005\,\text{mol}\,L^{-1}$ when the Al concentration is 2–3 $\text{mol}\,L^{-1}$. It is also possible to complex the lead by addition of tartrate [95].

The anodic dissolution of aluminum–lead alloys in electrolytes based on $AlBr_3$, $PbBr_2$, and KBr was investigated using cyclic voltammetry [96]. Investigation into the cathodic deposition by cyclic voltammetry shows that the potential difference between lead and aluminum in ethylbenzene electrolytes is only about 300 mV, compared to 1.5 V in aqueous solutions [97].

It is not possible to plate aluminum–lead alloys from electrolytes based on $A1C1_3$ and $LiAlH_4$ in tetrahydrofuran or diethylether, which are the electrolytes used for deposition of aluminum [95], Capuano [98] gives a review on the electrolytic deposition of Al alloys with specific reference to the use of plating technologies such as pulse plating and barrel plating.

8.7.2 Depositions from Molten Salts

Deposition of lead–calcium alloys from molten salts based on mixtures of $CaCl_2$–CaF_2–$PbCl_2$ has been described in the literature. Deposition of calcium is favored from such mixtures, since the concentration of lead in the mixture is limited to 3–5% by weight [99].

Production of a lead–calcium alloy by using molten lead as the cathode and depositing calcium on this from a molten salt mixture of $CaCl_2$–CaF_2–CaO at 750°C is referenced in a Japanese patent [100]. A similar reaction for the deposition of a lead–zinc alloy that involves the deposition of zinc from a mixture of LiCl–KCl–$ZnCl_2$ at 400°C has also been described in the literature [101].

Ternary alloys of lead such as K–Na–Pb, Mg–Na–Pb, or K–Mg–Pb can be deposited from molten salt mixtures of Na_2CO_3, KCl and NaCl [102], NaCl/$MgCl_2$, or KCl/$MgCl_2$ using liquid lead as a cathode. The current efficiency of such deposition of sodium or potassium can be reduced by sulfate ions, probably by a reaction of the alkali metals with sulfate to form alkali oxides and sulfides [103]:

$$8\,Na_{(liq)} + Na_2SO_4 \rightarrow 4\,Na_2O + Na_2S \qquad (8.7)$$

8.8 UNDERPOTENTIAL DEPOSITION

The study of the literature under the keywords "electrodeposition" and "electroplating" of lead shows a lot of references to underpotential deposition (UPD) of lead. Underpotential deposition is the deposition of a metal ion on the surface of a metal that is electropositive in relation to that metal. The deposition occurs at potentials that are considerably more anodic than the theoretical thermodynamic value. The energy for this process is given by a high energy of adsorption of the metal ion onto the surface of the base metal. Investigation into the UPD of lead has been made on silver or gold substrates. Besides theoretical investigations to study the phenomenon itself, experiments were carried out in an attempt to modify the catalytic properties of gold electrodes by the adsorption of lead layers for electrochemical reductions [104, 105].

The UPD of lead onto stainless steel was examined [106, 107]. It was discovered that the evolution of hydrogen on the cathode and thus the adsorption in the steel (known as hydrogen embrittlement) could be considerably reduced.

Underpotential deposition is a process which is different from the objectives of the lead deposition in the conventional meaning of electroplating. A detailed discussion of this process is beyond the scope of this text.

8.9 APPLICATIONS OF ELECTRODEPOSITED LEAD

The main applications of electrodeposited lead are a result of corrosion-resistant properties against such corrosive chemicals as sulfuric acid, chromic acid, or phosphorics acid. In the atmosphere several corrosion products, mainly carbonates and alkaline carbonates, form protective layers that prevent the underlying metal against further attack.

A huge field of application of electroplated lead is in the production of lead accumulators. All the parts that come into contact with sulfuric acid are plated with 200 μm lead. The base material is most usually copper, but there is also reference made to the use of aluminum because of the weight reduction of the components [108].

Lead is a superconducting metal with a jump temperature of 7.2 K. The use of electrodeposited lead layers for applications in the field of superconductivity is described in the literature [109–111].

REFERENCES

1. J. O. M. Bockris, *Trans. Faraday Soc.*, **43**, 417 (1947).
2. G. Milazzo, *Electrochemistry*, Elsevier, New York, 1963, p. 230.
3. N. Marinkov and J. Zagorov, *Mashinostroene (Sofia)*, **17**, 113 (1968); CA 69:32425.
4. E. R. Thews, *Chem. Tech.*, **18**, 41 (1945).
5. T. Richards, *Met. Finish.*, **51** (2), 59 (1953).
6. W. Hasenpusch, *Galvanotechnik*, **86**, 64 (1995).
7. F. Mathers and F. Forney, *Trans. Electrochem. Soc.*, **76**, 371 (1939).
8. E. Schweikher, *Proc. Am. Electroplate. Soc.*, 90 (1942).
9. R. Piontelli, *J. Electrochem. Soc.*, **94**, 106 (1948).
10. K. S. Indira and H. V. K. Udupa, *Met. Finish.*, 94 (1971).
11. L. Domnikov, *Met. Finish.*, 67 (1968).

12. G. Tremolada and L. Abduini, in *Proc. Symp. on Sulfamic Acid and Its Electrometallurgical Applications*, Editio dalla Associazione Italiana di Metallurgia, Milan, 1966, p. 353.
13. E. R. Freni, in *Proc. Symp. on Sulfamic Acid and Its Electrometallurgical Applications*, Editio dalla Associazione Italiana di Metallurgia, Milan, 1966, p. 367.
14. C. H. Huang, *Plating Surf. Finish.*, **11**(9), 64 (1964).
15. A. Betts, U.S. Patent 679,824 (1901).
16. A. Betts, U.S. Patent 713,277 (1902).
17. D. L. Thomas, C. J. Krauss, and R. C. Kerby, TMS Paper Selection A81-8, AIME, 1981.
18. W. A. Proell, U.S. Patent 2,525,942 (1950).
19. A. K. Graham and H. L. Pinkerton, *Proc. Am. Electroplat. Soc.*, **50**, 139 (1963).
20. A. K. Graham and H. L. Pinkerton, *Proc. Am. Electroplat. Soc.*, **50**, 135 (1963).
21. H. J. Wiesner, W. P. Frey, R. R. Vandervoort, and E. L. Raymond, *Plating*, **57**, 358 (1970).
22. J. W. Dini and J. R. Helms, *Met. Finish.*, **67**, 53 (1969).
23. Harshaw Chemical Co., U.S. Patent 2,773,819.
24. A. F. Orlov and N. B. Pleteneva, *Tsvetn. Met.*, **23**, 24 (1950).
25. I. Rajagopal and K. S. Rajam, *Met. Finish.*, 51 (1978).
26. F. Elser and E. Raub, *Metalloberfläche*, **31**, 171 (1977).
27. M. Goodenough and K. J. Whitlaw, *Trans. Inst. Met. Finish.*, **67**, 44 (1989).
28. T. M. Tam, *J. Electrochem. Soc.*, **133**, 9 (1986).
29. K. S. Indira and H. V. K. Udupa, *Met. Finish.*, **69**(1) 94 (1971).
30. T. Richards, *Met. Finish.*, **51**(2), 59 (1953).
31. H. J. Wiesner, in *Modern Electroplating*, 3rd ed., F. A. Lowenheim, Wiley, New York, 1974, p. 272.
32. M. Jordan, *Galvano-Trommel* (company journal, Max Schlötter, Ed.), **36**, 12 1984.
33. *Gmelin's Handbook of Inorganic Chemistry*, **47**, B2.
34. T. L. Rama Char, *Electroplat. Met. Finish.*, **10**, 347 (1957).
35. V. Sree, *J. Sci. Ind. Res. (India)*, **A18**, 478 (1959).
36. M. A. Loshkarev and T. F. Dýachenko, *J. Appt. Chem. USSR*, **37**, 79 (1964).
37. N. V. Gudovich and O. K. Kudra, *Ukr. Khim. Zh.*, **27**, 121 (1961).
38. N. P. Fedotév, B. P. Artamonov, and N. I. Rasmerova, *J. Electrodepositors' Tech. Soc.*, **13**, Paper No. 11, 6 (1937).
39. F. C. Mathers, *Metal Finishing Guidebook-Directory*, 27th ed., Westwood, NJ, 1959, p. 353.
40. A. K. Graham and H. L. Pinkerton, *Plating*, **49**, 1071 (1962).
41. T. Richards, *Met. Finish.*, **51**(2), 59 (1953).
42. A. K. Graham and H. L. Pinkerton, *Trans. Inst. Met. Finish.*, **40**, 249 (1963).
43. Max Schlötter, Geislingen, unpublished investigations.
44. J. W. Dini and J. R. Helms, *Met. Finish*, **67**(8), 53 (1969).
45. H. J. Wiesner, W. P. Frey, R. R. Vandervoort, and E. L. Raymond, *Plating*, **57**, 358 (1970).
46. Max Schlötter, Geislinger, Lead Bath MSN-10.
47. F. A. Lowenheim, *Electroplating*, McGraw-Hill, New York, 1978, p. 325.
48. N. B. Pleteneva and T. V. Globa, *Tsvetn. Met.*, **27**, 53 (1954).
49. A. K. Graham and H. L. Pinkerton, *Plating*, **54**, 367 (1967).
50. W. H. Safranek and C. H. Layer, *Trans. Inst. Met. Finish.*, **53**, 121 (1975).
51. G. C. Pini and J. Weber, *Oberfläche-Surf*, **19**, 54, (1978); 9th World Congress on Metal Finishing Abstracts, Amsterdam, 1976.
52. R. R. Vandervoort, E. L. Raymond, H. J. Wiesner and W. P. Frey, *Plating*, 362 (1970).
53. J. W. Dini and J. R. Helms, *J. Electrochem. Soc.*, **117**, 269 (1970).
54. V. V. Bogoslovskii, K. M. Tyutina, and L. T. Kudryavtsev, *Zash. Met.*, **11**, 499 (1975).
55. A. Brenner, *Electrodeposition of Alloys*, Academic, New York, 1963.
56. K. M. Tyutina and G. G. Svirshchevskaya, *Tr. Mosk. Khim.-Tekhnol. Inst.*, **81**, 130 (1974).
57. C. P. S. Johal, D. R. Gabe, and D. R. Eastham, *Surf. Technol.*, **35**, 181 (1988).
58. D. Eyre, D. R. Gabe, and D. R. Eastham, *Trans. Inst. Met. Finish.*, **62**, 113 (1984).
59. D. Eyre, D. R. Gabe, and D. R. Eastham, *Plating Surf. Finish.*, **72**(4), 74 (1985).
60. D. Eyre, D. R. Gabe, and D. R. Eastham, *Trans. Inst. Met. Finish.*, **63**, 22 (1985).
61. I. Krastev, M. E. Baumgärtner, and C. J. Raub, *Galvanotechnik*, **86**, 731 (1995).
62. M. Ueba and A. Watanabe, *Kagaku Gijutsu Kenkyusho Hokoku*, **86**, 177 (1991); CAN 116:64568.
63. M. Ueba and A. Watanabe, JP 61, 12890; CAN 105:10515.
64. G. Haberstroh, European Patent EP 194321.
65. A. M. Kolomoets and P. 1. Kukoz, USSR 386032; CAN 80: 221641.
66. F. I. Kukoz, A. M. Kolomoets, and V. P. Kolomoets, *Elektrokhim. Osazhdenic. Primen. Pokrytii. Dragotsennymi Redk. Met.*, 33 (1972); CAN 80:115373.
67. J. P. G. Fair and S. V. Kulkarni, *Electrodeposition Surf. Treat.*, **3**, 307 (1975).
68. N. Doi, K. Obata, and T. Sonoda, JP 60 152693; CAN 104:138265.
69. R. Pionteili, P. Cavalotti, and L. Giuliani, in *Proc. Symp. on Sulfamic Acid and Its Electrometallurgical Applications*, Editio dalla Associazione Italiana di Metallurgia, Milan, 1966, p. 329.
70. C. J. Brockman and J. H. Mote, *Trans. Electrochem. Soc.*, **73**, 371 (1938).
71. E. S. Roszkowski, H. R. Hanley, W. T. Schrenk, and C. Y. Clayton, *Trans. Electrochem. Soc.*, **80**, 235 (1941).
72. J. Gala, A. Budniok, and P. Rehlich, *Rudy Met. Niezelaz.*, **24**, 525 (1979).
73. J. Gala and R. Kopiec, *Metall.*, **35**, 882 (1981).

74. J. Gala, A. Budniok, and P. Rehlich, PL 115265; CAN 99:79041.
75. H. V. K. Udupa, K. C. Narasimham, and P. S. Gomathi, *Plating Surf. Finish.*, **62**, 1150 (1975).
76. Y. M. Polukarov and V. V. Grinina, *Primen. Elektrokhim. Pokrytii. Splavami Kompoz, Mater. Prom-sti. Mater. Semin.*, 1981, 50; CAN 99:29938.
77. V. M. San'kov, A. N. Latyshov, and V. A. Evgrafov,USSR 503941; CAN 84:128070.
78. V. V. Kuznetsov, V. P. Grigorév, O. A. Osipov, and S. P. Shpan'ko, USSR 490869; CAN 84:51524.
79. Ch. J. Raub and E. Raub, *Z. Physik*, **186**, 310 (1965).
80. E. M. Savitskii, J. V. Jefimov, Ch. J. Raub, H. R. Khan, T. M. Frolova, and G. T. Omarova, *J. Less Common Metals*, (1982).
81. Y. P. Perelygin, *Sashch. Met.*, **26**, 683 (1990).
82. W. J. Waterman, U.K. Patent Appl. 2039298; CAN 94:92622.
83. W. J. Waterman and B. J. Woolford, Ger. Offen. 2415653; CAN 84:51510.
84. A. V. Ryabchenkov, A. A. Gerasimenko, and M. P. Krivoruchko, USSR 305205; CAN 75:104543.
85. D. R. Eastham, *J. Eng. Gas Turbines Power*, **115**, 706 (1993).
86. Indium Corporation of Europe, private communication.
87. K. F. Dockus,U.S. Patent 4,028,200; CAN 87:45974.
88. O. A. Surzhko and V. A. Korolenko, *Tr. Novocherk. Politekh. Inst.*, **322**, 52 (1976).
89. T. C. Franklin, J. Chappel, R. Fierro, A. I. Aktan, and R. Wickham, *Surf. Coat. Technol.*, **34**, 515 (1988).
90. GB 1189183 (BASF, 1966).
91. F. D. Gibson,U.S. Patent 2,945,791 (1958).
92. P. Krishnaswamy, E. G. Usha Bhai, and Y. Koteswara Rao, *Plating Surf. Finish.*, **72**(9), 70 (1985).
93. K. S. A. Gnanasekaram, K. C. Narasimham, and H. V. K. Udupa, *Electrochim. Acta*, **15**, 1615 (1970).
94. M. Galova, L. Lux, and K. Zupcanova, *Zb. Ved. Pr. Vys. Sk. Tech. Kosiciach*, 199 (1988).
95. M. Galova, K. Zupcanova, and L. Lux, *Hutn. Listy*, **39**, 340 (1984).
96. M. Galova and L. Lux, *Chem. Pap.*, **42**, 457 (1988).
97. M. Galova, L. Lux, and K. Zupcanova, *Chem. Pap.*, **42**, 281 (1988).
98. G. A. Capuano, *J. Electrochem. Soc.*, **138**, 484 (1991).
99. J. P. Millet, H. Pham, G. Pourcelly, and M. Rolin, *Ext. Abstr., Meet.—Int. Soc. Electrochem.*, **30**, 228 (1979).
100. J. Tsuruki and Y. Yoshida, JP 79,162619; CAN 92:219622.
101. M. Kamaludeen, K. Balakrishnan, G. Singh, and N. S. Rawat, *Bull. Electrochem.*, **4**, 491 (1988).
102. S. A. Zaretskii, V. Busse-Macukas, F. I. L'vovich, and A. G. Morachevskii, *Ref. Zh., Khim.*, 1971, Abstr. No. 14L331; CAN 77:55619.
103. F. I. L'vovich, V. Busse-Macukas, A. G. Morachevskii, and V. I. Markin, *Zh. Prikl. Khim.*, **47**, 1654 (1974); CAN 81:130168.
104. G. Kokkinidis, A. Papoutsis, and G. Papanastasiou, *J. Electroanal, Chem.*, **359**, 253 (1993).
105. A. Papoutsis and G. Kokkinidis, *J. Electroanal. Chem.*, **371**, 231 (1994).
106. B. N. Popov, G. Zheng, and R. E. White, *Proc. AESF Annu. Tech. Conf.*, **80**, 809 (1993).
107. G. Zheng, B. N. Popov, and R. E. White, *J. Electrochem. Soc.*, **140**, 3153 (1993).
108. R. L. Seth, *Electroplat. Met. Finish.*, **25**(2), 5 (1972).
109. E. Lüders, *Abstracts of 3. Ulmer Gespräch*, German Society for Surface Technology, 1989, p. 79.
110. R. A. Alvaret, D. Birx, D. Byrne, M. Mindonca, and R. M. Johnson, *IEEE Trans. Magnetics*, **17**, 935 (1981).
111. J. R. Delayen, G. J. Dick, and J. E. Mercereau, *IEEE Trans. Magnetics*, **17**, 939 (1981).

9

ELECTRODEPOSITION OF TIN–LEAD ALLOYS

MANFRED JORDAN

The deposition of tin–lead alloys has the most technical importance among all tin or lead alloys. Processes for the electrolytical deposition of tin–lead alloys are known since 1921 and were first developed for the coating of naval torpedos [1, 2]. A second field of application evaluated was the deposition of tin–lead alloys for bearings [3–5]. Intensive research in the field of tin–lead plating has been stimulated by the different requirements in the production of electronic components such as PCB (printed circuit board), semiconductors, connectors, and the like. A further impulse has come since about 1980 with the development of fluoride-free tin–lead electrolytes.

The standard potentials for tin and lead are very close together (Pb: −0.126 V; Sn: −0.136 V). Alloy deposition is therefore possible in all alloy compositions. Both metals have a high hydrogen overvoltage, so deposition of tin–lead alloys is possible from strong acid solutions without complexing agents with high current efficiencies. The current efficiency can be reduced by adding a range of different types of organic additives to such electrolytes as brightener systems.

9.1 ELECTROLYTE SYSTEMS

Electrolyte systems based on tetrafluoroboric or methanesulfonic acid (MSA) are mainly used for the deposition of tin–lead alloys. For special applications weakly acidic systems with special complexing agents are also on the market. Electrolytes can also be divided into those for the deposition of matte tin–lead coatings and for the deposition of bright deposits. A further division can then be made into processes for conventional plating such as rack-and-barrel plating and those for high-speed applications such as wire plating, reel-to-reel processes for connectors, and continuous processes for IC leadframe finishing.

9.2 ALLOY COMPOSITIONS

Although tin–lead alloys can form over the entire compositional range, they tend to fall into three classes in terms of technical applications:

- High-lead alloys
- Eutectic or near-eutectic alloys
- Alloys with 5–15% Pb

In the first category are alloys with around 93% Pb and 7% Sn that are used as coatings for fuel tanks and on various bearings. For bearing applications there is also usually a codeposition of about 2% copper. The deposition is in a form of a matte coating. In this category fluoroborate electrolytes are still the most frequently used systems.

Eutectic alloys are those that possess the lowest melting point, which makes them suitable for solderable coatings. The eutectic alloy contains 63% tin. A considerable field of application has been the production of PCBs using the metal-resist technique. When the electrodeposited tin–lead layer is used as a reflowed coating, which remains on the board, an alloy composition very close to the eutectic composition is important so that the boards are reflowed with the lowest possible temperature. The main function of the reflow process is to eliminate the overhangs of tin–lead, which are caused by underetching during the copper etching. By reflowing the electroplated tin–lead layer this is completely converted into a liquid form. The overhangs are thus removed.

Modern Electroplating, Fifth Edition Edited by Mordechay Schlesinger and Milan Paunovic

In the liquid state the tin–lead is covering the side walls of the tracks and thus provides an additional corrosion protection.

The reflow process can be made by immersing the boards into a heat bath of synthetic or natural oils above the melting point of the tin–lead alloy or by heating the boards by infrared (IR) radiation.

The process causes a high thermal stress to the boards. Because of this and other disadvantages this process has been substituted by other techniques. A detailed description is given in [6].

The importance of the reflow process has diminished in recent years. When tin–lead is used as a metal resist, the alloy composition is no longer so important. For reflow processes matte-depositing electrolytes are used because, in general, bright coatings cannot be reflowed as the codeposited organic additives will cause dewetting. Eutectic bright tin–lead coatings are used in some applications for electronic components. The lower melting point of the coating can be beneficial for reflow soldering processes.

Alloys in the third category, with 5–15% Pb, are mainly used for coating electrical or electronic assemblies. In the past many of these components had been plated with pure tin. Because of the risk of formation of whiskers, the codeposition of some percent of lead became almost a standard for such applications. Electrolytes to deposit low-lead-containing alloys are now the most widely used tin–lead electrolytes. Because of growing environmental and health concerns, in the future the use of lead will be reduced to a minimum, and the application of low-lead-containing alloys will further increase. Both matte and bright plating systems are available for the deposition of low-lead-containing alloys. The decision on which deposit to use depends on technical requirements, specification limitations, and the properties of the coatings.

The decade after the publication *Modern Electroplating, Fourth Edition*, brought a decisive turning point in the use of lead in many technical applications. In the European Union directive 2002/95/EC restricting the use of certain hazardous substances in electrical and electronics equipment (ROHS) and directive 2002/96/EC on waste electrical and electronic equipment have been enacted. The use of tin–lead alloys for the manufacturing of components for those applications is therefore no longer allowed. The limit of lead in any homogeneous material is 0.1 wt%. Although due to the globalization of the markets all manufacturers of electronic components worldwide follow these regulations.

The main advantage of co-deposition of lead in tin coatings is the prevention of the formation of tin whiskers in the coating. New lead-free systems have therefore been developed, The mainstream of production is now done in new developed tin electrolytes, mainly for matt deposition. Together with additional measures, like plating of an undercoat of nickel or heat-treatment of tin coatings an copper substrate (e.g., 1 h at 150 °C) directly after tinplating the risk of whisker formation can be reduced to a minimum. Alternative tin alloy electrolytes for deposition of tin–bismuth alloys (about 2–4% Bi) or tin–silver alloys (about 2–5% Ag) have been developed and are in use in production of electronic components.

9.3 BATH COMPOSITIONS

Because their deposition potentials are so close to one another, the ratio of metal ions in the electrolyte can, to a first approximation, be taken as the same as the ratio of the two metals in the electrodeposited alloy. The proportion of either metal in the electrolyte is thus expressed as

$$\%\mathrm{Sn} = \frac{\mathrm{Sn}(\mathrm{gL}^{-1})}{[\mathrm{Pb} + \mathrm{Sn}](\mathrm{gL}^{-1})} \times 100 \qquad (9.1)$$

The slightly more positive electrodeposition potential of lead favors deposition of this metal, especially at low current densities. The deposition potential difference between the two metals can be increased somewhat by the use of certain organic additives. Under certain circumstances the order of deposition potentials can even be reversed, making tin the more noble metal. By means of such manipulations, Pb/Sn alloys of the same composition can be deposited from baths with quite different Pb and Sn ionic ratios, and a change in the type of organic additive used can be reflected in the composition of the electrodeposited alloy [7].

The total metal ion concentration ranges from 10 g L^{-1} for barrel plating systems up to 100 g L^{-1} for high-rate deposition processes. Electrolytes for deposition of thick deposits of 93% Pb–7% Sn may contain up to 150 g L^{-1} total metals. These levels may appear high compared with, say, nickel or copper plating solutions. However, the atomic weights of tin (118.7) and lead (207) are very high in comparison to copper (63.5) and nickel (58.7) and comparisons on a molar basis would be more valid.

9.3.1 Tetrafluoroboric Acid Electrolytes

Until about 1980 tetrafluoroboric acid baths were the most widely used for tin–lead alloy deposition. The basic components, tetrafluoroboric acid, tin, and lead fluoborate salts, are not known in their pure form and are commercially available as aqueous solutions. These are usually 50 wt % for the free acid, 27 wt % for the lead salt, and 20 wt % for the tin fluoroborate. Typical specifications for these are shown in Table 9.1 [8].

Tetrafluoroboric acid for use in tin–lead plating can be treated with a lead salt to remove any sulfate present by precipitation as the lead sulfate. This may give rise to a slight excess of lead ions in the acid. Although this is not a

TABLE 9.1 Typical Compositions of Fluoroborates

	Colorless Clear Liquids			
Appearance	HBF_4, Technical Grade	HBF_4, Special Grade	$Pb(BF_4)_2$	$Sn(BF_4)_2$
Density, D_{20}	1.40	1.40	1.78	1.65
Composition (min)	49.5%	49.5%	27.2% (as Pb), 470 g L^{-1} Pb	20.3% (as Sn), 335 g L^{-1} Sn
Boric acid	max 2.5%	max 2.5%	max 2.5%	max 2.5%
Fe	≤0.01%	≤0.005%	≤0.005%	≤0.001%
Cu		≤0.001%	≤0.002%	≤0.001%
Ni		≤0.001%	≤0.002%	≤0.001%
Zn		≤0.001%	≤0.002%	≤0.001%
Chloride		≤0.005%	≤0.005%	≤0.005%

problem when operating a tin–lead plating bath, it may be a problem if the acid is to be used for deposition of other metals.

As a rule, fluoroborate tin–lead plating bath are operated with addition of 10–25 g L^{-1} boric acid (H_3BO_3). The fluoroboric acid has the tendency to hydrolyze, releasing free HF:

$$HBF_4 + H_2O \rightarrow HBF_3OH + HF \tag{9.2}$$

Boric acid reacts with the so-formed free HF to regenerate the fluoroboric acid:

$$4HF + H_3BO_3 \rightarrow HBF_4 + 3H_2O \tag{9.3}$$

This reaction prevents the precipitation of the sparingly soluble lead fluoride. However, fluoride ions can also serve to retain tin in solution in the form of its Sn(IV) hexafluorostannate ion:

$$Sn^{4+} + 6F^- \rightarrow [SnF_6]^{2-} \tag{9.4}$$

Thus fluoroborate electrolytes containing boric acid close to its solubility limit are more prone to form sludges based on Sn (IV) species than solutions with a lower boric acid concentration, which then split off fluoride ions to complex fourvalent tin.

In the third edition of *Modern Electroplating* Wiesner [9] provides solution compositions for various tin–lead alloys. Compositions are given here for high-lead-containing alloys with a maximum tin content of 60%. Additives recommended include gelatine or glue and resorcinol or peptone.

Table 9.2 lists typical bath formulations for deposition of various Sn–Pb alloy compositions, including high-tin-containing alloys that have been published in the recent literature. The two versions for tin–lead electrolytes with high throwing power show the influence of the additives on the throwing power. With conventional peptone a very high acid concentration is necessary to achieve good results. The second bath uses a proprietary additive system based on nonionic wetting agents, and this electrolyte can be used with much lower acid concentration.

9.3.2 Alkylsulfonic Acid Electrolytes

Electrolyte systems based on alkylsulfonic acids for the deposition of tin–lead alloys have been developed since about 1980. In principle, a number of alkylsulfonic acids are suitable for tin–lead electrolytes, such as MSA, alkylsulfonic acids with more than one carbon atom in the chain (ethane-, propane-, butanesulfonic acid), β-hydroxysubstituted derivatives like hydroxyethane-, 2-hydroxypropanesulfonic acid, or alkyldisulfonic acids such as methanedisulfonic acid. Of all these possible derivatives, MSA is by far the

TABLE 9.2 Solution Compactions for Tin–Lead Fluoroborate Electrolytes

Alloy Composition	HBF_4(g L^{-1})	Sn (g L^{-1})	Pb (g L^{-1})	Temperature (°C)	Current Density (A dm^{-2})	References
93/7 Pb/Sn rack and barrel	15–30	10–20	195–239	21–38	2–7	10
60/40 Sn/Pb rack and barrel	100–150	53–60	23–30	21–29	2.5–3.5	10
60/40 Sn/Pb high throw	350–500	12–20	8–14	21–38	1.5–2.5	10
60/40 Sn/Pb high throw	50–100	20–30	9–14	20–60	0.5–2	11
90/10 Sn/Pb rack and barrel	150–200	70–80	8–12	21–38	0.1–8	10

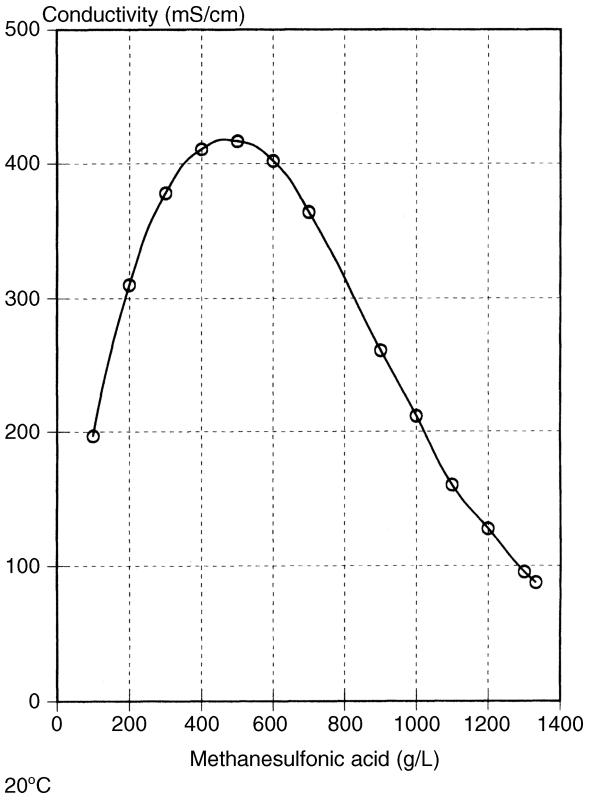

FIGURE 9.1 Electrical conductivity of MSA solutions.

most commonly used. Tin and lead methanesulfonates are highly soluble in water. For subsequent effluent treatment, the alkyl side chain should be as short as possible to keep the COD (chemical oxygen demand) value of the solution to a minimum. Obviously MSA best matches this criterion. Methanedisulfonic acid would give even lower COD values, but this type of acid is not commercially available in sufficient quantities. Alkylsulfonic acids are strong acids, comparable with sulfuric acid, and they provide electrolyte solutions with very high conductivity. Conductivity of MSA is plotted in Figure 9.1 [6]. As with sulfuric acid, conductivity increases sharply with concentration, reaches a maximum, and then falls more slowly, which reflects a supression of dissociation at the high concentrations. From Figure 9.1 it can be seen that a concentration of up to 400 g L^{-1} MSA could be used in electrolyte applications, but for economic reasons one will seldom go higher than 200 g L^{-1} (calculated as 100% MSA).

Likewise, as for fluoroborate-based electrolytes, the ratio of the metal ions in the methanesulfonate solutions can, as a first approximation, be taken as the same as the ratio of the two metals in the electrodeposited alloy. Typical electrolyte formulations for methanesulfonate electrolytes are given in Table 9.3.

9.3.3 Tin–Lead Deposition from Moderate pH Solutions

Apart from strongly acidic solutions there are some applications of electrolytes for tin–lead deposition which are operated in a moderate pH range, mainly 4–9. At these pH values tin is only soluble in the presence of complexants. Commonly used complexing agents are the different types of hydroxycarbonic acids, such as gluconic, citric, and tartaric acids or diphosphates.

Compared with acid-type baths, these near-neutral electrolytes show no significant advantages. Because they contain complexing agents, wastewater treatment is more critical. The electrical conductivity of these solutions is also lower than that of acid types, which increases the energy required for the deposition. In general, because of the lower conductivity, such systems can only be operated at lower current densities compared with acidic electrolytes.

In certain cases, the neutral solutions can have advantages, especially when plating electronic components incorporating ceramics or special types of glass. These can be sensitive to acid or alkali chemical attack, which may result in acidic or alkaline media. Table 9.4 gives some bath compositions with their operating data for the tin–lead deposition from moderate-pH electrolytes.

9.4 ADDITIVES

In general, the same organic additives can be used for fluoroborate or methanesulfonate electrolytes, but it can be seen in many cases that the same type of additive is more effective in the methanesulfonate systems and requires a lower dosage.

TABLE 9.3 Solution Compositions of Tin–Lead Methanesulfonate Electrolytes

Alloy Composition	MSA (g L^{-1})	Sn(g L^{-1})	Pb (g L^{-1})	Temperature (°C)	Current Density (A dmT^{-2})	References
90/10 SnPb rack and barrel	200–250	17–25	2–4	20–50	0.1–25	10
90/10 Sn/Pb high speed	100–200	35–70	3–7	20–60	5–25	10
60/40 Sn/Pb rack and barrel	200–250	12–20	6–10	21–29	0.1–25	10
60/40 Sn/Pb high speed	100–200	35–70	12–25	20–60	5–25	11
93/7 Pb/Sn rack and barrel	30–50	4–5	56–72	21–29	0.1–4	10

TABLE 9.4 Parameters of Tin–Lead Electrolytes Operating at Moderate pH Values

Complexing Agent	pH Range	Temperature (°C)	Current Density (A dm^{-2})	References
Citric acid; ammonium tartrate	6			12
Aliphatic or aromatic sulfocarboxylic acids	3–8.5	20–30	0.5–3	13
Gluconate, citrate, malate, tartrate, malonate	1.5–5.5	25	0.5–1	14
Gluconate				15

For the deposition of matte finish surfaces from fluoroborate baths, the earliest addition agents to be described were combinations of bone glue and resorcinol [16], bone glue, gelatine and resorcinol [17], or peptone as a single additive [18] (peptone remains widely used to this day). These additives are not used in methanesulfonate electrolytes. In 1988 Bulwith [19] reported defects associated with incorporation of peptone. Peptone is a protein and, as such, not very stable in acid solutions, so the peptide linkages can become split in this medium. The breakdown products build up in solution, and periodic treatment with activated carbon is necessary. Since some of these breakdown products are quite malodorous, conditions for operating staff can become unpleasant. Hobson [20] has examined this topic in detail. Possible alternatives to peptone are the nonionic surfactants used in conjunction with Janus green or phenolphthalein [21].

In recent patents, mainly those dealing with modern methanesulfonate systems, additive combinations consisting of different types of nonionic and cationic surface-active components together with different types of grain refiners are mentioned. The nonionic surface-active compounds are mostly ethoxilated derivatives of linear or branched aliphatic alcohols, alkylsubstituted phenols, or ethoxilated naphthols.

For deposition of fully bright deposits, special brighteners are necessary. These systems also normally contain different types of nonionic wetting agents. In these systems they have a double function: They inhibit the formation of nodules, and they also act as a solubilizer for the brighteners, which in most cases are not soluble in water. Typical brighteners for tin–lead depositions are aromatic aldehydes or aromatic ketones, which are insoluble in water if they do not have a functional group, such as a sulfo group, in their molecule, which provides water solubility. The water-insoluble brighteners are emulsified by the nonionic wetting agents.

All modern electrolytes are based on proprietary additive systems. It is therefore not possible to give recommendations for the maintenance. This can be made only as per instruction of the supply houses. Some general information on troubleshooting is given in Table 9.5.

Besides these grain refiners and brighteners tin–lead electrolytes contain in most cases antioxidants to prevent the formation of stannic tin in the electrolyte. Although this formation of stannic tin is normally not harmful for tin–lead deposition, it is an unwanted reaction because it causes a loss of tin from the bath as the Sn(IV) precipitates in the form of stannic oxide; therefore the formation of stannic tin must be prevented in the plating reaction.

In acidic tin electrolytes based on phenolsulfonic acids prevention of the oxidation of tin is well known [22]. The actual antioxidants are phenolic compounds, which are present as by-products in technical grades of phenolsulfonic acid. It is therefore obvious that phenolic compounds themselves are also used as antioxidants [23]. Besides their function as antioxidants, such compounds are also active as grain refiners; they are also often used in pure lead electrolytes.

Chi Pong Ho [24] describes a new system of prevention of the oxidation of Sn(II) to Sn(IV). It depends on the use of reducing agents based on vanadium pentoxide in divalent tin sulfate–sulfuric acid solutions to limit the sludge formation. This reaction mechanism was also investigated in MSA-based solutions to prevent the formation of tin sludge, especially in the presence of high contaminations of iron [25].

9.5 ANODES

9.5.1 Soluble Anodes

Normal practice is to use anodes with the same composition as that which is desired for the deposit. These anodes dissolve anodically in fluoroborate and methanesulfonate electrolytes even at high current densities in a uniform manner without passivation. In the electrolyte, a modest rate of oxidation of Sn (II) must always be assumed. This loss of tin in its depositable form can, to some extent, be countered by using anodes with a slightly higher tin content than what actually is required in the deposit. However, increase in lead concentrations in solution should be avoided as much as possible, and it is often necessary to add tin salts to maintain the correct balance. Depending on the bath formulation used, around 2–10 g L^{-1} of tin (in salt form) should be added for each excess grams per liter of Pb. While such measures maintain the correct Pb–Sn ratio in solution, the total metal content will increase, and metal distribution (throwing power) may suffer.

It is possible to operate continously using pure tin anodes, with additions of lead salts to the solution as required. However, since the anodic dissolution of tin is 100% efficient while its deposition efficiency at the cathode is lower (since part of the current is used to deposit lead ions), a progressive buildup of tin in solution may occur. This method of operation is only realistic for alloys with up to 5% Pb because

TABLE 9.5 Troubleshooting for Lead–Tin Electrolytes

Defect	Possible Cause	Remedy
Dendritic treelike growth	Deficiency of organic additives, especially surfactants	Addition of additives
	Limiting current density exceeded by	
Rough dark deposits in high-current-density region ("burning")	Too high cathodic current density	Reduce current density
	Too low metal content	Increase metal content
	Bath temperature too low	Increase temperature
	Insufficient agitation	Increase work movement or bath circulation
Rough deposits over the entire current density range	Additive concentration too low	Increase additive concentration stepwise
	Suspendend matter in the bath (e.g., anode slimes or lead sulfate)	Check filtration, anode bags; locate source of sulfate contamination
	Organic impurities	Activated carbon treatment necessary
	Insufficient coverage power due to	
No deposition at low-current-density region	Chloride impurities	Locate source of chloride ions; precipitation of chlorides is difficult; bath dilution may be the only answer
	High bath temperature	Cool the bath, perhaps reduce bath loading
	High metal content	Dilute electrolyte, perhaps use insoluble anodes
	Low concentration of additives	Increase additive concentration stepwise
	Contamination by nitric acid	Remove nitric acid–containing pretreatment; nitrate can partly be removed by dummying the bath
Poor metal distribution	High metal concentration	Dilute electrolyte or use insoluble anodes where possible
	Low acid concentration	Add acid
	Low additive concentration	Increase additive concentration
Gassing at cathode (in some electrolytes this can be a normal reaction when additives cause a reduced cathodic efficiency)	Exceeding limiting current density, see second entry	See second entry
	Excess brightener concentration	Add surface-active compounds; dummy bath where possible
	Anode passivation (in lead–tin electrolytes unusual)	
Gassing at anode	Anode bag clogged	Check anode bags
	Copper contamination in the anode	Check anode quality; prevent copper contamination in the bath, which can lead to chemial deposition of copper on the lead–tin anodes
	Anode current density too high	Monitor anode surface area
Uneven, patchy plating; blistering of deposit	Insufficient pretreatment of the base material	Check degreasing and activating, solutions
Step plating, especially at regions of high electrolyte flow	Overdosing of brightener	Check brightener concentration, reduce brightener by dummy plating; add surfactants
Brown stains on bright lead–tin coatings in low-current-density region	Copper contamination	Remove by plating out at low current density; locate source of copper contamination
Flaking of deposits (normally only with bright deposits)	Overdosing of brightener	Add surfactants

drag-out losses and Sn(II) oxidation serve to keep the tin in solution more or less constant.

Under normal operating conditions a black slime will form on the anodes. This is caused by the metallic impurities in the anode material. Most commonly found impurities such as Sb, Bi, Cu, and As are not dissolved anodically, as they are more noble than Pb or Sn. Above a certain impurity concentration, especially for antimony, a dark spongelike coating forms on the anode surface. Should this impurity pass into the electrolyte, the result will be rough deposit on the cathode. Use of anode bags made of an acid-resistant material is thus strongly recommended. Table 9.6 lists the tolerable metallic contaminations for tin–lead anodes recommended for use in tin–lead electrolytes.

TABLE 9.6 Tolerable Metallic Contaminations in Anodes

Metallic Contaminant	Maximum Permissible Contamination (%)
Antimony	0.03
Arsenic	0.03
Bismuth	0.01
Copper	0.02
Iron	0.01
Aluminum + cadmium + zinc	0.002

Anodes are used in forms of rectangular or oval shapes. The anode hooks must be made of acid-resistant material. For fluoroborate systems normally polymer-coated hooks are used. One of several advantages of methanesulfonate electrolytes is the stability of titanium in those systems, which can therefore be used as the material for anode hooks. It is also possible to use titanium baskets filled with Pb/Sn balls or chunks. This form is normally used in high-speed installations because it allows easy maintenance and anode control. The stability of titanium as an anode hook or basket is very sensitive to traces of fluorides, which attack the passive layer of titanium oxides. Any contamination should therefore be avoided. When, for example, an MSA-based electrolyte is installed in a line that previously contained a fluoroborate, it is very difficult to remove all traces of fluoride from the tank and equipment.

9.5.2 Insoluble Anodes

The use of insoluble anodes is not very common in tin–lead plating. In this case in the anodic reaction oxygen is formed by the reaction

$$2H_2O - 4e \rightarrow O_2 + 4H^+ \qquad (9.5)$$

The first prerequisite to enable insoluble anodes to be used is a very effective antioxidant to prevent the formation of stannic tin by the anodically produced oxygen; the second is a stability of the additives themselves against anodic oxidation.

When using insoluble anodes the free-acid concentration increases in the electrolyte, Eq. (9.5). To compensate for this increase, Sn^{2+} is either replenished by stannous oxide or in an electrolytic cell with separate anode and cathode compartments. In both reactions the hydrogen ions, produced in the anodic reaction (9.5), are consumed by the following reactions:

- Replenishing Sn^{2+} by SnO:

$$SnO + 2H^+ \rightarrow Sn^{2+} + H_2O \qquad (9.6)$$

- Electrolytical replenishing:

$$\text{Anodic reaction:} \quad Sn - 2e \rightarrow Sn^{2+} \qquad (9.7)$$

$$\text{Cathodic reaction:} \quad 2H^+ + 2e \rightarrow H_2 \qquad (9.8)$$

Insoluble anodes are used for tin–lead plating in special plants under jet-plating conditions or to balance the metal concentration in an electrolyte when it increases in the bath due to a reduced cathodic current efficiency. In this case both soluble and insoluble anodes are used in the same systems. Because the formation of oxygen on the insoluble anodes occurs at higher voltage than the dissolution of Sn and Pb, insoluble and soluble anodes cannot be installed in one circuit; separate rectifiers have to be used. Standard material for insoluble anodes is platinum-coated titanium or niobium.

9.6 MAINTENANCE AND CONTROL

9.6.1 Electrolyte Composition

Metal Concentration The metal concentration in a tin–lead electrolyte has to be controlled in terms of the total metal content and the ratio between Sn and Pb. While the total metal content has influence on the limiting cathodic current density and the throwing power of the electrolyte, the ratio will of course influence the alloy composition of the coating. In bright systems a high metal content will cause problems with dullness in low-current-density areas.

If the electrolyte is working with a high cathodic current efficiency, there will be a balance between the anodically dissolved and cathodically deposited metals. In general, there will be a steady loss of metals in the bath due to drag-out. This has to be replenished accordingly by the metal salts in the form of their liquid concentrates. The ratio between tin and lead in the bath is kept by using the appropriate alloy composition in the anodes. Since in the electrolyte there will always be some loss of tin by formation of tin oxides, a slightly higher Sn content in the anodes will compensate for this loss (e.g., anode composition 70/30 Sn/Pb when the desired alloy composition is 65/35 Sn/Pb). Corrections in the Sn/Pb ratio in the electrolyte can also be made by using a part of the total anodes in the form of either 100% Sn or 100% Pb anodes. These measures do not correct the deposited alloy composition immediately; this only happens when the required Sn/Pb ratio in the electrolyte is achieved.

When the organic additive system causes a reduced cathodic current efficiency, the metal content in the bath will increase correspondingly. To keep the total metal content in the specified range, either dilutions have to be made

or the surplus of metal is worked out by using insoluble anodes.

Acid Concentration The acid concentration in the tin–lead electrolyte is important for the throwing power and especially in high-speed electrolytes for the conductivity of the solution. Similar to the metal concentration there will be a loss of free acid by drag-out when anode and cathode efficiencies are both 100%. If the cathodic efficiency is lower, there will be a loss of free acid by the cathodic side reaction according to

$$2H^+ + 2e \rightarrow H_2 \qquad (9.9)$$

9.6.2 Electrolyte Temperature

Tin–lead electrolytes for rack-and-barrel plating are used normally at temperatures between 15 and 30°C. The low temperatures are especially recommended for bright electrolytes. With the lower temperature consumption of additives can be reduced considerably. This improves the solderability of the deposited coatings. Such electrolytes need efficient cooling systems. Stainless steel with thin polyethylene coatings is suitable as cooling coils. Bare stainless steel can be used as long as the electrolyte is not contaminated by chloride ions and the temperature does not go above 50°C. Fluoropolymer heat exchangers can be used, but since the thermal conductivity of this material is low, specially designed coils have to be used for effective cooling.

Matte-depositing electrolytes are less sensitive to higher temperature; such systems are often operated at temperatures between 40 and 60°C in high-speed plating [26]. The higher temperature increases the limiting current density. But, since the temperature can influence the alloy composition, the maximum usable temperature also depends on the additive system.

9.6.3 Agitation

Electrolyte agitation is a very important parameter in tin–lead plating. As in any electrolyte, increasing agitation improves the maximum permissible cathodic current density. Intensive flow rates are therefore essential for all high-speed plating processes. Table 9.7 gives some data on the thickness of the diffusion layer and thus the limiting current density in relation to the electrolyte agitation [27].

The flow rate can influence the alloy composition. How sensitive this can be depends also on the type of additive system and the temperature. Some data on the alloy composition in relation to the current density at different rotation speeds are shown in Figure 9.2.

TABLE 9.7 Limiting Current Densities and Diffusion Layer Thicknesses

Hydrodynamic Regime	Limiting Current Density ($A\,dm^{-2}$)	Diffusion Layer Thickness (μm)
Natural convection to vertical electrode	1.44	200
Natural convection to horizontal electrode	3.65	80
Electrolyte flow along the plane of the electrode ($v = 25\,cm\,s^{-1}$; laminar)	3	100
Force flow cell (25 m s^{-1}, turbulent flow	365	0.8
Rotating cylinder (180 rpm, peripheral velocity, 94 $cm\,s^{-1}$)	8.1	36
Gas-evolving electrode		
13 cm^3 gas $cm^{-2} \cdot min$	72	4
1 cm^3 gas $cm^{-2} \cdot min$	19.4	15
Gas feed through frit		
65 μm pore size, 0.1 L gas min^{-1}	2.76	100
65 μm pore size, 17 L gas min^{-1}	13.2	20
Ultrasound (7 W cm^{-2})	50	6

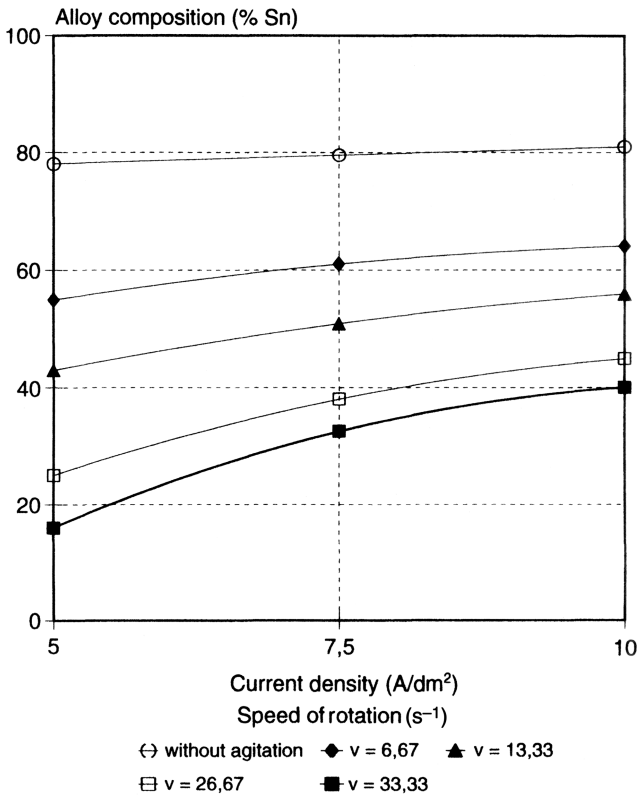

FIGURE 9.2 Effect of rotation rate using a rotating disc electrode on composition of Pb–Sn alloy from a fluoroborate bath. (Data after Madry [28].)

9.6.4 Contaminants

The most common sources of contaminants in tin–lead plating solutions are as follows:

- Impurities in bath chemicals
- Drag-in of pretreatment solutions
- Contaminants from the work to be plated
- Breakdown products of organic additives
- Impurities from anode reactions

Supply houses aim to provide the basic bath chemicals with a guaranteed purity level more than sufficient for use in plating systems. When using commodity chemicals, the buyer must make sure that their purity is high enough, either by having analyses done or by obtaining specifications from the supplier. Impurities may be present in a dissolved form or as insoluble particles. Thus it may be useful to filter a solution before using it in the plating bath.

Dragged-in impurities can come from cleaner or activating solutions or from other plating baths in cases where an intermediate layer is deposited. Since chloride ions can lead to problems in most tin–lead electrolytes, acid pickling bath based on HCl should not be used. Chloride ions are harmful to the throwing power of such baths, and in the case of matte-plating solutions, they promote dendritic growth.

Drag-in of sulfates can also cause problems resulting in roughness due to inclusions of insoluble lead sulfate particles. If tin–lead coatings with such inclusions are reflow melted, dewetting can take place. Thorough filtration is the only means of avoiding such problems. Eliminating chloride ions is much more difficult since the solubility of lead chloride is too high to allow precipitation as a means for their removal. Though silver ions can be used to form the insoluble AgCl, the cost of such treatment is usually prohibitive.

Metallic Contaminants Nickel and copper are the most commonly found contaminants, since this metals are widely used to form interlayers in the substrate. Drag-in from activating solutions has also been mentioned and these can introduce zinc or iron into the bath. Especially in the case of barrel plating, bipolarity effects at the commencement of each tin–lead plating operation can result in anodic dissolution of the substrate metal and thus provides a further source of contaminant.

Because of its more positive deposition potential, copper will be codeposited in any tin–lead plating bath. In the case of matte deposits, up to 100 mg L^{-1} can be tolerated without ill effects. With bright deposit baths, copper can lead to darkening or staining, especially at low current densities. In the case of matte tin–lead deposits, copper can act to give a finer grain structure. In the case of peptone-containing baths, copper contamination can lead to increased levels of organic inclusions that are harmful if the deposit is then reflowed [19]. In the molten state, copper reacts with tin to form an intermetallic phase, which then crystallizes out during cooling, giving a rough appearance. Typical incorporation rates of copper as a function of Cu^{2+} concentration in solution are plotted in Figure 9.3 for a fluoroborate bath with peptone addition and for a methanesulfonate bath with synthetic additives.

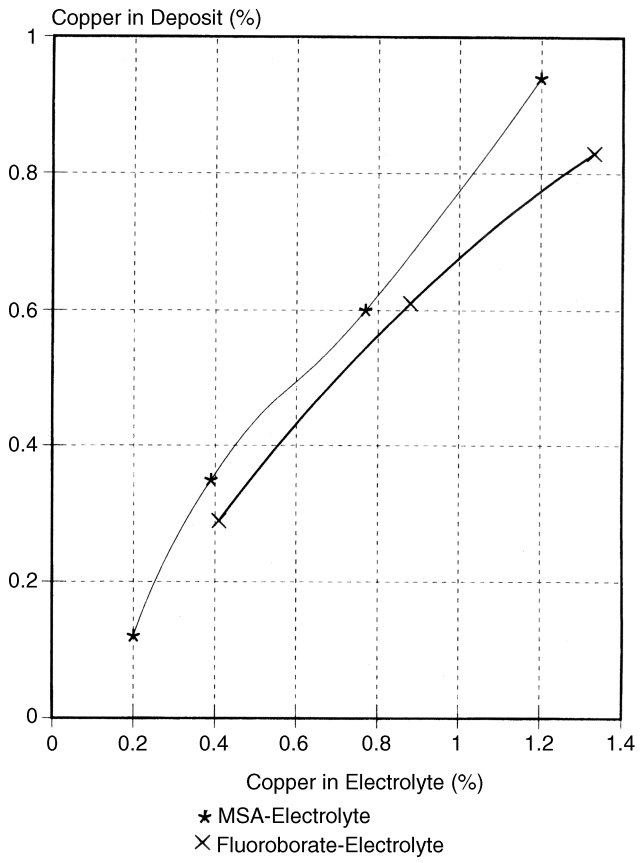

FIGURE 9.3 Codeposition of copper from tin–lead alloy plating baths based on MSA or tetrafluoroboric acid.

Nickel contamination stems from drag-in from nickel-plating baths that are specified immediately prior to the tin–lead plating stage to form an interlayer. Since nickel is not deposited from strongly acid type bath, the presence of nickel ions is not usually a problem here. However, most nickel plating baths contain chloride ions to improve anode solubility. In the case of the widely used Watts nickel bath, this is present at 10–15 g L^{-1} chloride. Problems associated with chloride have been previously discussed, and drag-in from nickel plating baths is a source of problems mainly only as far as chloride ions are involved.

Iron can enter the system by being dragged in or by dissolution of the substrate metal. A common problem is small parts falling off the racks to the bottom of the tank, where they slowly dissolve. Iron, nickel, and zinc as possible

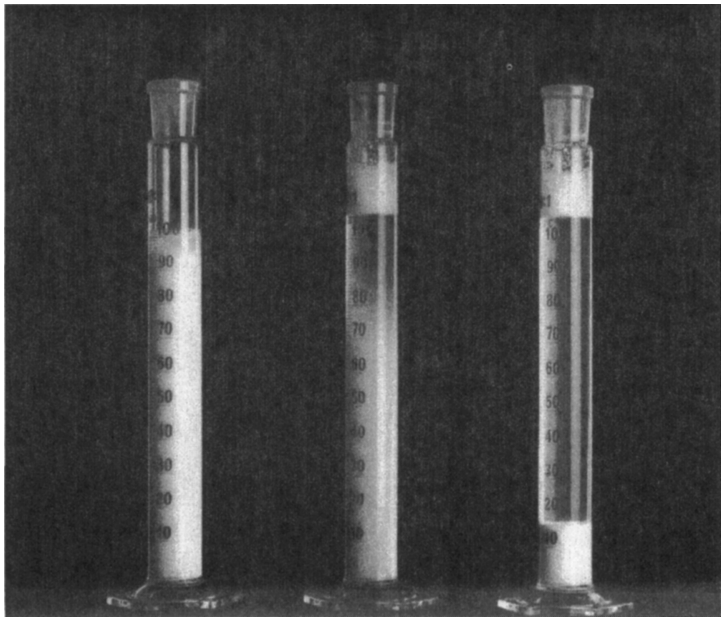

FIGURE 9.4 Precipitation of Sn(IV) compounds from an acid tin–lead plating solution. *Left*: original sample; *center*: commencement of precipitation after addition of precipitating agent; *right*: after completion of precipitation.

contaminations in lead plating solutions are not codeposited, even when their concentration is as high as $10\,g\,L^{-1}$. Indirect problems can be caused by incorrect analysis results, when the presence of lead is established in the solution by a complexometric titration. During the analysis any nickel contaminants will also be complexed, giving incorrect results. Because of the large difference in the atomic weights of lead and the contaminants, a contamination with $1\,g\,L^{-1}$ Ni will simulate $3.5\,g\,L^{-1}$ Pb.

High contaminations of iron can cause an increased rate of formation of stannic tin. Iron will enter the solution in its divalent form, which is easily oxidized to Fe(III) by air. This Fe(III) reacts with Sn(II) to form stannic tin according to

$$2Fe(III) + Sn(II) \rightarrow 2Fe(II) + Sn(IV) \qquad (9.10)$$

It follows that iron as a contaminant should be held as low as possible.

Tin(IV) Concentration Depending on the stabilizer system used, a given concentration of Sn(IV) will be found in the solution. In the case of fluoroborate baths, Sn(IV) is soluble up to around $20\,g\,L^{-1}$. In the case of MSA baths, Sn(IV) is partially soluble, and if the cathode efficiency of the tin–lead deposition is less than 100%, some of this will be reduced to Sn(II). Tin(IV) will precipitate from the fluoroborate bath when insufficient free fluoride ion is present to complex it. In methanesulfonate baths, Sn(IV) exists in a form of metastannic acid. Splitting off water and aging, in general, convert this to tin dioxide, SnO_2. Both of these mentioned species can exist in a colloidal form which has a very high specific surface area. They can adsorb the organic additives used in solution and so cause problems because their effective concentration in solution is thereby decreased [29]. If necessary, the stannic tin can be precipitated by means of special flocculating agents, as demonstrated in Figure 9.4. They are proprietary chemicals available from supply houses.

Decomposition Products of Organic Additives The properties of electrodeposited tin–lead alloys can be affected as a result of changes in the original composition of the organic additives added to the solution. These changes can arise from chemical reactions within solution components or as a result of electrochemical reactions of additives at the anode or cathode. For example, peptone, widely used as an additive in fluoroborate baths, can be hydrolytically split. Peptone breakdown products may be incorporated into a deposit to a greater extent than peptone. This can result in dewetting on the surface during reflowing operations. To prevent the deposition of such breakdown products from peptone-type baths, a regular activated carbon treatment on a three-month cycle is recommended [30].

The additives in recently developed electrolytes are chemically more stable and, in the case of matte deposit baths, activated carbon treatment is only necessary if organic impurities are dragged in from external sources.

In bright deposits a variety of by-products can form depending on the additives used, particularly in the solutions

that use formaldehyde. As concentrations of these extraneous organic species increase in solution, the extent to which they become incorporated into the deposit will increase, so solderability may suffer.

Impurities Resulting from Anodic Reactions Tin–lead anodes over the entire compositional range dissolve readily in fluoroborate or methanesulfonate baths. On the anode surface a black slime will form which is caused by the metallic impurities in the tin–lead anode, which are more electropositive (Sb, Bi, Cu, As, Ag). These metals exist in the anode as intermetallic compounds with tin; consequently, the volume of their slimes is higher than one would predict on the basis of their volumes as pure metals. Should this slime contamine the electrolyte, it will cause rough deposits to form. Antimony is specially prone to form such sludges so its concentration in the anode should be as low as possible.

Where soluble anodes are used, anodic oxidation of organic additives in solution is not usually significant. However, where insoluble anodes are used, a range of side reactions is possible by either direct anodic oxidation or chemical reaction with the dissolved oxygen formed as oxygen gas evolves at the anode.

9.7 ELECTROCHEMICAL DEPOSITION EQUIVALENT FOR TIN–LEAD ALLOYS

The electrochemical deposition equivalent for any tin–lead alloy may be calculated using the formula [31]

$$\text{Tin–lead deposition equivalent} = \frac{3.861 \times 2.214}{f_1 \times 3.861 + f_2 \times 2.214}$$

where $3.861 =$ deposition equivalent for lead (g Ah^{-1})
$2.214 =$ deposition equivalent for tin (g Ah^{-1})
$f_1 =$ weight fraction of tin in alloy
$f_2 =$ weight fraction of lead in alloy
$f_1 + f_2 = 1$

The data for the electrochemical deposition equivalents for the entire range of the tin–lead system are given in Table 9.8 together with the densities and the deposition rates.

9.8 DENSITY OF TIN–LEAD ALLOYS

For the density of a deposited alloy to be determined, a foil of the alloy is formed by deposition on a highly polished and passivated stainless steel cathode. The foil is stripped from the cathode, washed, dried, and weighed. It is then introduced into a pycnometer filled with water thermostatically controlled at 20°C. The density of the alloy is then given by the expression

$$d_{\text{Alloy}} = \frac{m}{(M+m)-M'} d'$$

where $m =$ weight of foil
$M =$ weight of water-filled pycnometer
$M' =$ weight of water-filled pycnometer + foil
$d' =$ density of water at 20°C

The density of a tin–lead alloy can be calculated as

$$\frac{1}{d_{\text{Alloy}}} = \frac{f_1}{d_1} + \frac{f_2}{d_2}$$

where $d_{\text{Alloy}} =$ density of alloy
$d_1 =$ density of component 1
$d_2 =$ density of component 2
$f_1, f_2 =$ weight fractions of components 1 and 2, respectively
$f_1 + f_2 = 1$

This expression may be used for the calculation of any tin–lead alloy because a study of the determination of the

TABLE 9.8 Data on Electrochemical Deposition Equivalent, Density, and Deposition Rate for Tin–Lead Allays

Alloy Composition (% Pb)	Density (g cm^{-3})	Electrochemical Deposition Equivalent (g Ah^{-1})	Deposition Rate ($\mu\text{m min}^{-1}$)
0	7.28	2.214	0.507
5	7.41	2.262	0.509
10	7.55	2.312	0.51
15	7.69	2.365	0.512
20	7.84	2.421	0.515
25	8.00	2.478	0.516
30	8.16	2.539	0.518
35	8.33	2.6	0.520
40	8.50	2.669	0.523
45	8.68	2.74	0.526
50	8.87	2.814	0.529
55	9.07	2.893	0.532
60	9.28	2.975	0.534
65	9.50	3.063	0.537
70	9.72	3.156	0.541
75	9.96	3.256	0.545
80	10.21	3.361	0.549
85	10.47	3.473	0.553
90	10.75	3.594	0.557
95	11.05	3.723	0.562
100	11.36	3.861	0.566

density of samples produced by mixing the molten metals showed only a low volume shrinkage [32].

9.9 DEPOSITION RATE

The theoretical deposition rate for tin–lead alloys can be calculated from the mass of metal plated per unit surface, the plating time, and the calculated density. The data are shown in Table 9.8. The values range from 0.505 μm min^{-1} for 100% Sn to 0.57 μm min^{-1} for 100% Pb at 1 A dm^{-2} assuming 100% cathodic efficiency. It can be seen that for practical purposes one can consider deposition rate of about 0.5 μm min^{-1} for low-lead-containing tin–lead alloys.

9.10 PROPERTIES OF ELECTROPLATED TIN–LEAD FILMS

9.10.1 Long-Term Corrosion Tests

The long-term corrosion resistance of tin–lead alloys in atmospheric exposure tests was studied by Jostan et al. [33]. The aim of these investigations was to test the behavior of tin–lead coatings in electronic component applications. The corrosion resistance was therefore mainly judged by its effects on contact resistance. The coatings perform well in aggressive and moderately severe industrial environments, with electrical contact resistance increasing slowly. In a marine environment, tin–lead surfaces are rapidly attacked; the contact resistance reaches values in the kilohm range after relatively short exposure.

9.10.2 Short- Term Corrosion Tests

Short-term corrosion tests were conducted by the same authors using environmental chambers with artificial atmospheres. As with the atmospheric tests, the most damaging conditions are those where chlorine is present, such as HCl.

9.10.3 Oxide Formation

The formation of oxides on tin–lead surfaces affects their solderability. On initial contact with air a freshly electroplated tin–lead layer forms an oxide layer of about 1.5 nm [34]. These oxide layers are very stable and further growth is extremely slow. After one year, it will typically be around 3 nm.

If the metal is stored at higher temperatures, say 200°C, an oxide layer around 30 nm thick will form in 24 h. The oxidation rate under these conditions is twice as fast as at 100°C. In humid atmospheres, the growth rate is accelerated. Figure 9.5 shows the oxide formation as a function of time over boiling water [34].

The oxides on a tin–lead surface, which are formed during heating in normal atmosphere, consist mainly of tin oxides, as it is shown by the Auger spectrum in Figure 9.6 of a 90/10 Sn/Pb alloy heated to 175°C for 24 h.

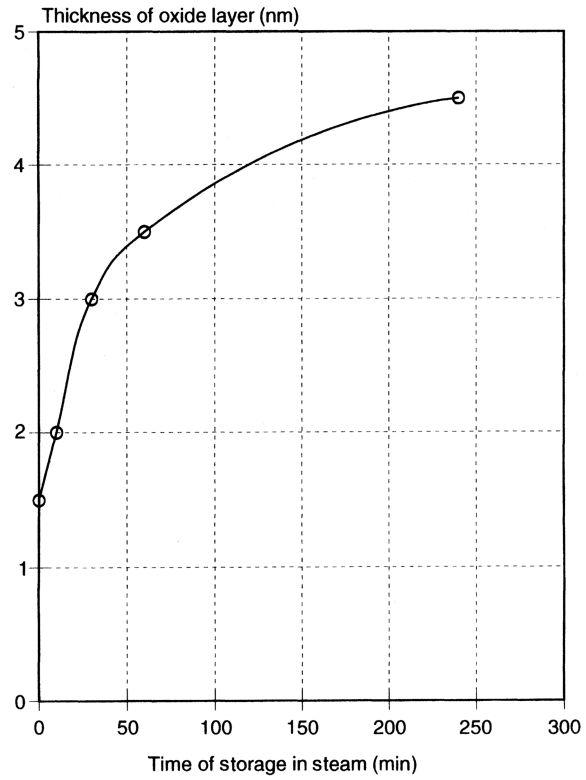

FIGURE 9.5 Oxide formation on lead–tin alloy surfaces during exposure over boiling water.

9.11 SOLDERABILITY

As mentioned above, there is a close correlation between the formation of oxides and the solderability of tin–lead coatings. It is therefore now standard practice to test solderability after accelerated aging tests, which simulate some reactions which can occur on the surface of tin–lead coatings during storage. Aging tests also show the influence on solderability of the formation of intermetallic layers. Standard aging tests are as follows:

- Dry heat aging at 155 or 175°C for 4, 8, 16 h
- Steam aging up to 8 h
- Storage in moist heat [40°C, 93% relative humidity (RH)] for 4, 10, 21, or 56 days
- Storage in a distilled water cyclic test sequence (24-h cycle; from 25 to 55°C in 3 h, 9 h at 55°C, then cooling to 25°C at 95% RH)

9.11.1 Carbon Content of Tin–Lead Deposits

Because all acid tin–lead electrolytes use organic additives as grain refiners or brighteners, there is always some codeposition of these organics with the tin–lead coating. These organics can cause a deterioriation of the solderability, and

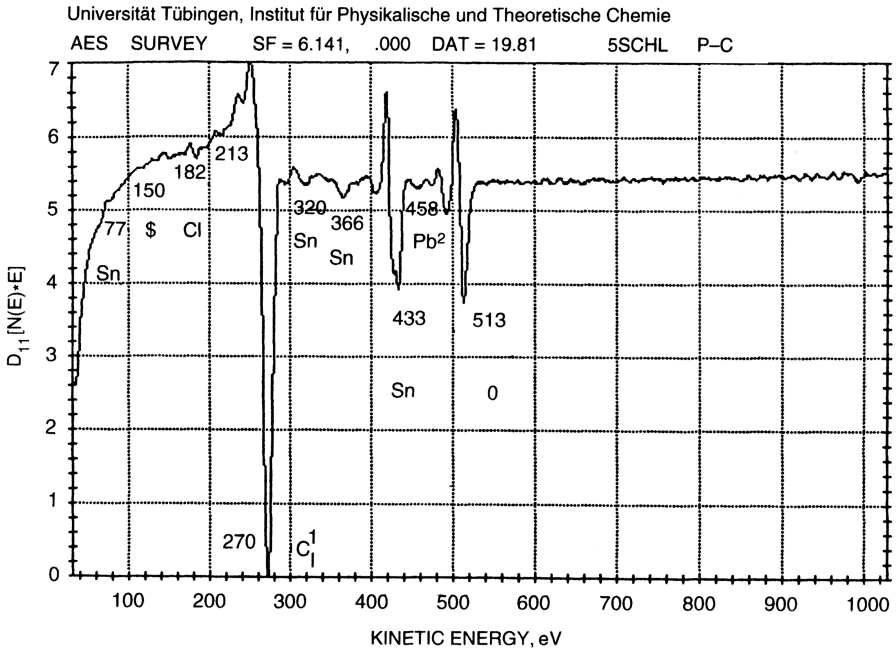

FIGURE 9.6 Auger spectrum of a bright lead–tin surface after 24 h heat treatment at 175°C. The enrichment of carbon compounds at the surface can be seen.

the amount of codeposition permitted is therefore limited to 0.05%, calculated as carbon [35]. Matte tin–lead deposits have usually much lower carbon contents; typical values are 0.005% [26, 36]. Bright coatings show generally higher codepositions, which are sometimes higher than the 0.05% value. Levels as high as 0.35% have been reported in the literature [37]. In bright electrolytes there is in addition often a problem that in the solution a buildup of breakdown products of the organic brighteners can occur, which leads to a further increase of codeposition of organics. Bright tin–lead coatings are therefore not allowed for applications required to comply to MIL-STD-81728A. This specification calls for the use of matte or reflowed coatings.

9.11.2 Solderability Test

Solderability is tested either by the dip-and-look test (MIL-STD-202; DIN 32506 part 3) or by the wetting-balance method (MIL-STD 883; DIN 32506, part 4). The standard test conditions are

Solder bath	60/40 Sn/Pb
Temperature	235°C
Flux	Nonactivated; R-type (pure colophony in isopropanol)
Immersion time	5 s

The criterion for acceptance is a wetting of not less than 95% of the immersed surface.

9.12 ELECTRICAL CONTACT RESISTANCE

Changes in electrical contact resistance of electrodeposited coatings used to form protective coatings in electronics were studied by Jostan et al. [33]. Exposed to H_2S- or SO_2-containing atmospheres, tin–lead surfaces show good performance with only slight increase in contact resistance. In chloride-containing atmospheres, tin–lead behaves better than tin, possibly because formation of lead chloride layers inhibits further attack. Tin–lead surfaces perform very well when exposed to NO_2- or NH_3-containing atmospheres. Figure 9.7 shows the change in electrical contact resistance after exposure to various test gas mixtures.

Storage in air at 120°C changes the electrical contact resistance very little. For bright tin–lead coatings the authors observed an increase of the electrical contact resistance during storage at 120°C; it reached a maximum in the first 10 h, after which the values fell slowly and then increased again. The behavior is shown in Figure 9.8.

A possible explanation given by the authors is that by grain boundary diffusion the incorporated organics migrate to the surface with a resulting increase of electrical contact resistance. This is followed by their evaporation or oxidative destruction which is reflected in the fall in resistance values. Finally, progressive oxide growth causes resistance to increase again. The Auger spectrum in Figure 9.6 shows how carbon-containing compounds build up at the surface.

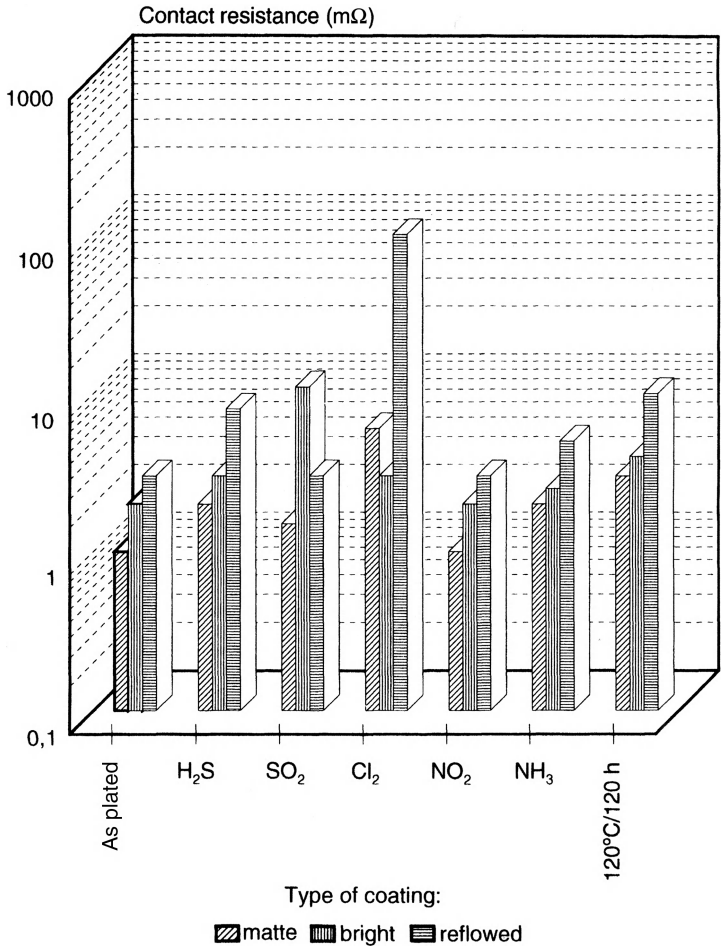

FIGURE 9.7 Change in electrical contact resistance of lead–tin alloy surfaces after exposure to various gas mixtures. (Data after Jostan and co-workers [33]).

9.13 HARDNESS

Hardness values for electrodeposited tin–lead alloys are low. In the case of matte deposits, the value is largely independent of alloy composition, typically being 8–10 Vickers hardness with a 15-g load. According to Raub and Blum [29], addition of tin results in an increased hardness compared with pure lead with a maximum reached at about 10% Sn.

Bright tin–lead coatings show significantly higher hardness values. They depend strongly on alloy composition and the brightener used. Up to 10% lead, Vickers hardness values HV_{15} are between 15 and 20. By using increased concentrations of additives hardness can be raised to 25 HV. With increasing lead content hardness decreases markedly, though not linearly. In several systems a sudden decrease in hardness was found at around 15–20% Pb alloy values. At this point hardness values drop from 15 to 5–6 (HV_{15}).

The hardness of tin–lead alloys can be increased by codeposition of small amounts of copper, antimony, or bismuth. The use of the first two is well known in the bearing industry, whereas the role of bismuth is mainly considered as a side effect when this metal is used to improve brightness in bright deposit electrolytes [38].

The move from matte to bright alloy deposits is accompanied by a doubling in hardness. At the same time, the crystal structure is seen to change. Matt Pb/Sn deposits exhibit a predominantly nonorientated growth. In the case of bright Pb/Sn with hardness values around 20 HV_{15}, definite field-orientated columnar crystal growth can be seen.

Since the harder deposits are also more brittle, these changes in crystal structure can lead to problems if the plated components are to be subjected to any kind of mechanical deformation. So much cracking can take place that the base metal can be exposed, and oxidation within these cracks results in poor solderability. In surface-mounted (SMT) electronic components the cracking would occur close to the soldered connections [39]. For these applications the use of matte tin–lead deposits is preferred. Figure 9.9 shows cracking in a bright tin–lead deposit. Note that the cracking extends right down to the substrate.

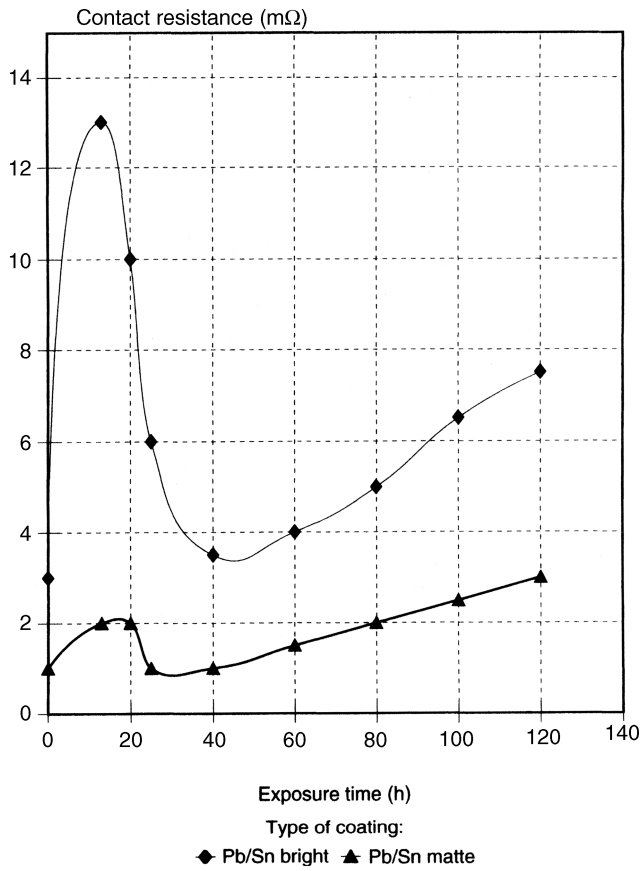

FIGURE 9.8 Change in electrical contact resistance of a lead–tin alloy surface after storing at elevated temperature. (Data after Jostan and co-workers [33]).

9.14 APPLICATIONS OF TIN–LEAD COATINGS

9.14.1 Terne Plate

Steel sheet coated with tin–lead of composition 93% Pb, 7% Sn is known as a terne plate. The main consumer of this product is the automotive industry where it is used for fuel tanks, filter casings, sump pans, and radiator components. Global production is around 600,000 tons [40], and up to 1973, hot dipping was the only method of production. This was when an electroplated equivalent was developed. In 1983 a second plant started production [41]. As with tin plates, the newer method offered better control of coating thickness. It also enabled the production of single-side coated sheet.

The electrolytes developed were based on fluoroborate and used hydroquinone as an inhibitor, according to suggestions by Graham and Pinkerton [42].

9.14.2 Bearing Alloys

Alloys of about the same composition are used for running surfaces on bearing shells. The shell itself is of steel, and the bearing alloy is cast onto it. Various alloy compositions are used, with aluminum bronzes among the most favored. The shell is mechanically finished and a nickel interlayer laid down. The bearing alloy is Pb/Sn or Pb/Sn/Cu and is typically 25 μm thick. One particular composition is 88% Pb, 10% Sn, and 2% Cu and is specially effective as an antiseize coating [43].

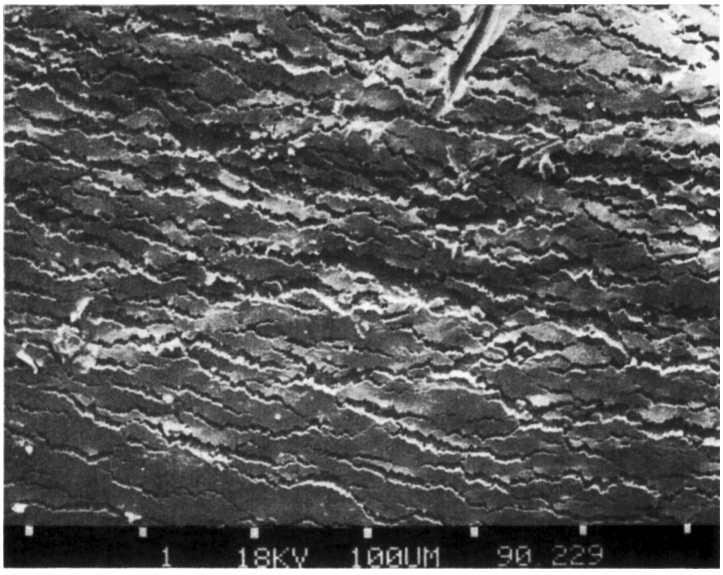

FIGURE 9.9 Formation of cracks in a bright tin–lead coating during a bending process of leads of electronic components. By this crack formation the base material surface can be exposed, and the solderability can be detoriated, when these cracks are formed in the area, where the solder joint has to be formed, for example at the tip of a J-formed lead of a SMT device. Bright tin–lead coatings are therefore not recommended when a mechanical bending process follows after plating.

9.14.3 Anodes for Chromium Plating Bath

Tin–lead alloys with 7% Sn are used as insoluble anodes for chromium plating from chromic acid solutions. In most cases, the anodes are made by melting the solid metals in their correct proportions. However, in certain cases such as auxiliary anodes for plating internal surfaces, there are advantages in the use of shaped anodes that are plated with tin–lead [44]. Using a total metal concentration in solution of 150–200 $g\,L^{-1}$ and using suitable inhibitors, pore-free deposits of up to several millimeters can be formed.

9.14.4 Eutectic Alloys

Tin–lead coatings with the eutectic composition 63% Sn, 37% Pb are used in the production of printed circuits and as a solderable coating for electronic components. Flip-chip technology, a new application, requires the deposition of Sn/Pb bumps of either 95Pb–5Sn or 65Sn–35Pb composition on the Si wafer for the connection of unpackaged chips directly to PCBs [45].

In the PCB production, eutectic tin–lead coatings have been used as metallic etch resists; after copper etching the tin–lead coating was reflowed. While tin–lead is still used widely today as an etch resist, the quantity of boards with reflowed coatings is now very small. In the newer technologies the tin–lead coating is only used as a protective coating in the copper-etching process. After this step it is removed by special tin–lead strippers. The PCB is then coated with a solder resist, which leaves only those parts uncovered where the assembling process solder connections have to be formed. To preserve the solderability of those areas, the PCB is selectively coated with tin–lead by dipping into molten solder. By this hot-air-leveling (HAL) process only the unprotected copper can react with the molten solder. The solder resist, which is an organic resin, is not wetted by the molten solder. Consequently there is almost no real need for tin–lead deposits for metal-resist applications, and it has been substituted by pure tin deposits in many cases [46]. But for special applications the specifications still demand the use of reflowed tin–lead on PCBs.

A problem with coatings that are normally produced from reflow tin–lead processes is a very uneven thickness distribution after reflow. On the corner or knee of the plated through holes the thickness of tin–lead is less than 1 μm. This causes solderability problems [47], especially if a solder mask that needs high-temperature curing is also required, for example, 2 h at 160°C. The low tin–lead coating on the corner will be converted to an intermetallic Cu/Sn layer that is no longer solderable with nonactivated or mildly activated fluxes. To overcome this problem, a special sequence for reflowing has been developed. It consists of preheating the boards at 185°C for 45 s and the actual reflow then takes place in a second bath at 205°C with a short dip time of about 5 s [48].

Another approach that guarantees a minimum thickness of 1 μm after reflow as specified by the European Space Agency (ESA) specification PSS-50 QRM-17E is two-stage plating of a pure lead layer of about 2 μm followed by an 8–10-μm-thick tin–lead layer (70% Sn) (SLOTOLON Process [49, 50]). This combination of deposits is reflowed using any of the normal processes. The result is a Pb/Sn coating which, at the edge of the through-hole, is at least 2 μm thick. During reflowing, an alloying of the tin into the lead layer takes place and a copper–tin diffusion layer forms, as in conventional reflowing. The improved coating thickness around the hole edge is presumably due to increased viscosity due to the lead layer, which prevents the molten layer from flowing down from the edge. An increase in temperature will again result in a retreat of the coating from the hole edge.

9.14.5 Tin–Lead Deposits for Electronic Components

A major application for electroplated tin–lead coatings is in the production of electronic components. Tin–lead coatings are a prerequisite for reliable soldering when making interconnections on PCBs.

In terms of the type of connections, components can be grouped under four headings:

1. Wire-lead components with axial connections
2. Components with radial connectors for insertion mounting (DIL, dual-in-line, or DIP, dual in-line package components)
3. Components with radial connections suitable for surface mounting
4. Leadless connections

Within the first group are the traditional components that feature connecting leads for through-hole insertion. These leads or wires are normally made from preplated wire, although in some cases plating is carried out on the completed components. In the second group there are the DIP- or DIL-type components. These have two rows of pins that are inserted in plated through holes on the PCB. In the third group are mainly packaging types similiar to those in the second group except that the connector pins are mechanically formed for surface-mount application into a "gull-wing" if they are turned out or in a J-format beneath the package. Leadless components are either square-shaped or cylindrical components such as chip resistors and MELF (metal electrode face) components. Their mating surfaces are metallized and serve as solder faces for solder connections.

All components require a coating if solderability is to be assured. The type of coating depends on various factors, but the following coating types are mainly used:

- Matte tin–lead, approx. 5–20% Pb
- Matte tin–lead, approx. 35% Pb
- Bright tin–lead, approx. 5–20% Pb
- Bright tin–lead, approx. 35% Pb

Various factors govern the choice from this range, and consideration must be given to the mechanical processing of components, solderability, and long-term storage. In the past pure tin coatings have been used for such applications. While these are still being used to a considerable extent, tin–lead deposits have been introduced primarily to avoid whisker formation, and the most common electrolytes give matte deposits with approximately 15% Pb. Bright tin–lead coatings suffer from the problem of cracking during bending and are not recommended therefore for applications where any trim-and-form steps follow after plating. Bright solutions are best used only where no mechanical deformation of the components is involved. A major application here is in the finishing of leadless components.

Matte tin–lead deposits have a rougher surface than their bright counterparts. The typical morphologies of a matte and a bright electroplated tin–lead surface are shown in Figures 9.10 and 9.11. The rougher surface of matte coatings, together with their lower hardness, results in a degree of metal loss in the trim-and-form process. In addition the relative softness of tin–lead coatings results in the formation of solder peeling and scratches in the trim-and-form process. This problem cannot be overcome by modifications to the deposit characteristics alone but only in combination adjustments to the bending process. Figure 9.12 shows typical scratches in the surface of the tin–lead layer after trim and form. This abrasion of tin–lead metal causes problems by contaminating the trim-and-form tools. This foreign material can be pressed into areas during trim and form. Solderability can also be affected when cracking occurs, during the bending process, in the area where the pin comes into contact with the solder on the solder pad, for example, the shoulder of a J-formed lead.

The formation of cracks after bending of a bright tin–lead coating is shown in Figure 9.9. It can easily be seen that in the cracks the base material is exposed, and therefore oxidation of the base material can occur here. Reliable solderability cannot be assured in such cases. The formation of cracks in the bending of bright tin–lead coatings is caused by their rather brittle, field-orientated structure. Figure 9.13 shows the structure of such a layer after cooling in liquid nitrogen and bending. Unlike this field-orientated structure, matte tin–lead coatings are deposited in an unorientated dispersion type (UD) structure. They do not form cracks under normal trim-and-form conditions. Here again the coating was made brittle by cooling in liquid nitrogen to demonstrate the orientation of crystallization during electrodeposition, as shown in Figure 9.14.

Coating Thickness For electronic component terminations, the thickness of electrodeposited tin–lead coatings should not be less than 5 μm and the required value depends on the subsequent processing of the component. The upper limit is about 20 μm. Too high a thickness can enhance problems in the trim-and-form process due to increased solder shedding. In their deposited state and without any posttreatment, coatings as thin as 2 μm are normally pore free and have sufficient solderability under normal storage conditions for

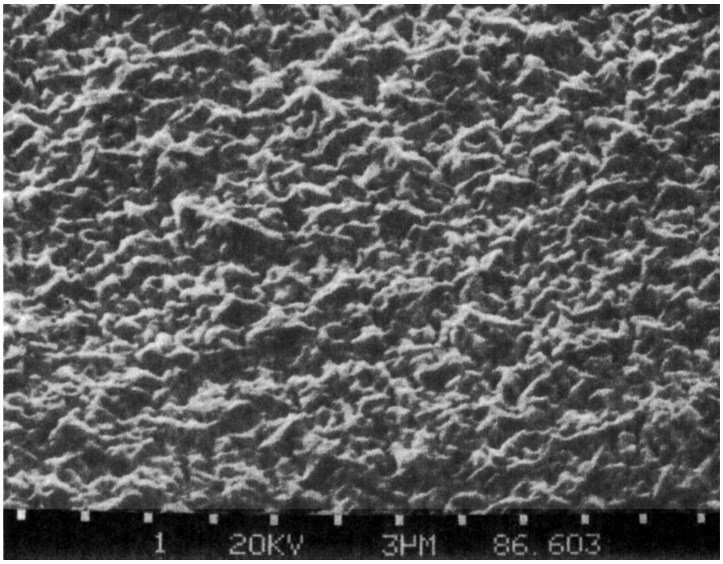

FIGURE 9.10 Morphology of a matte lead–tin alloy electrodeposit from an alkylsulfonic electrolyte.

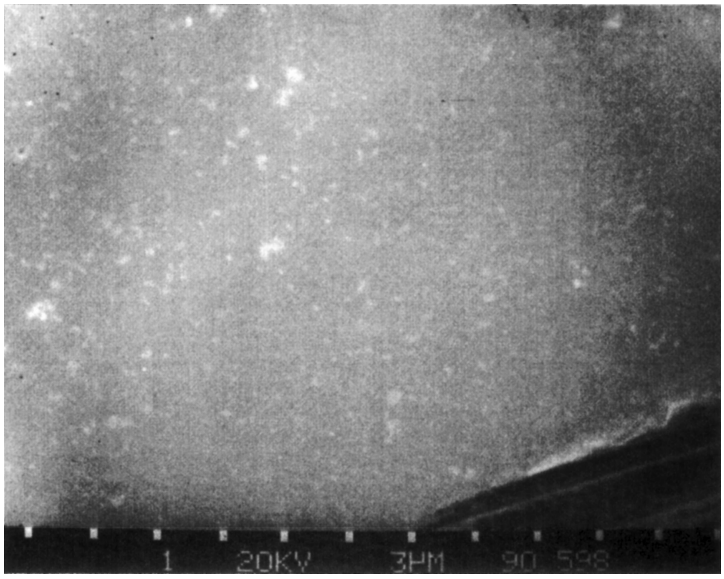

FIGURE 9.11 Morphology of a bright lead–tin alloy electrodeposit from an alkylsulfonic electrolyte.

up to three months. But since most coatings undergo processes involving exposure to heat after plating, such as applying identifaction markings and burn-in tests for high-reliabilty components, such thin coatings will normally not be used.

9.14.6 Interlayers

Interlayers have to be plated on brass. If this is not done, there will be a rapid diffusion of zinc from the brass into the tin–lead surface, causing severe detoriation of its solderability. Interlayers of copper or nickel can be used. The minimum thickness is 2 μm for nickel and 3–5 μm for copper [51]. Copper is plated using either cyanide or acid electrolytes or nickel using an additive-free system such as sulfamate nickel or Watts nickel. Interlayers of copper are sometimes also recommended for special copper alloys used as base materials when they are difficult to activate or contain alloying elements, which can interfere with the subsequent tin–lead plating (types of bronze with different tin content, beryllium–copper alloys, copper alloys containing traces of zirconium, silicon, nickel, etc.).

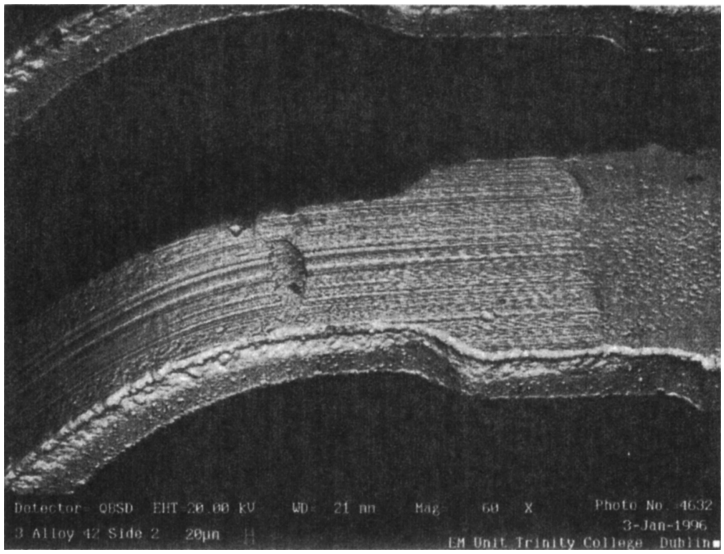

FIGURE 9.12 Scratches in an electroplated lead–tin deposit formed during the trim-and-form process of leads. The solderability is normally not detoriated by these scratches, but the material removed from the surfaces can cause problems by contaminations of the bending tools. Lead–tin particles can thus be transferred to following components and can cause short circuits between the leads.

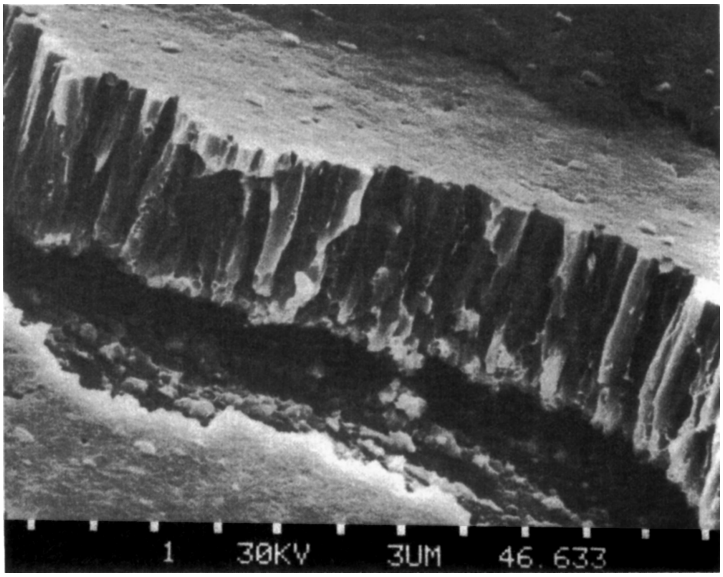

FIGURE 9.13 Fracture surface of a bright electroplated lead–tin deposit. The layer shows typical field-orientated growth (fibrous structure). This type of structure is very sensitive to form cracks during bending, as shown in Figure 9.9.

9.14.7 Tin–Lead Coatings for Plug Connectors

Tin–lead alloys under atmospheric conditions form thin oxide layers that lead to increased contact resistance. However, since these oxides are very soft, the oxide layer is readily fractured and metal-to-metal contact is restored. Tin–lead coatings are only suitable for plug connectors when the insertion force is high enough to break these oxide layers and to make a reliable contact. Because of its low hardness values and the need for a somewhat higher insertion force than with other contact materials, a degree of wear does take place. Therefore tin–lead coated contacts are only suitable for applications where a modest number of total insertions and withdrawals are foreseen. The tribological aspects of tin coatings were reported by Hamman and Schedin with $CuSn_4$ (bronze) as a substrate [52]. Use of a suitable lubricant can reduce the wear behavior and the insertion force required [53]. Use of composite coatings in which graphite particles are dispersed in a tin matrix also gives lubricant action [54].

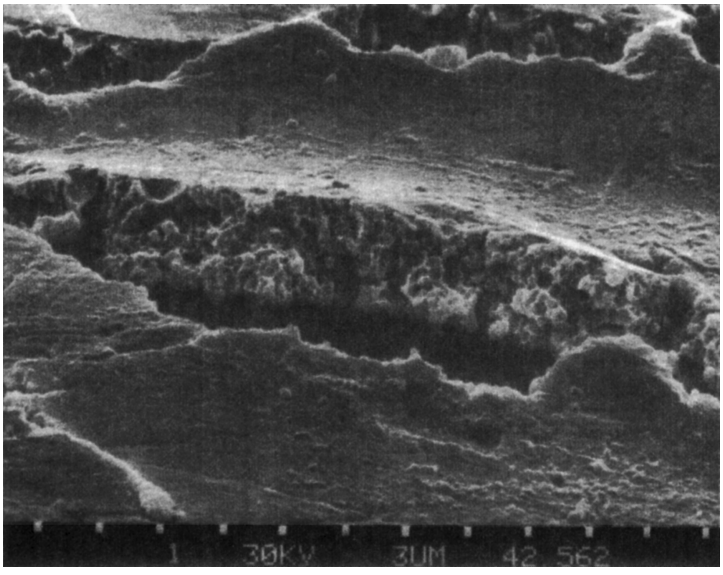

FIGURE 9.14 Fracture surface of a matte-electroplated lead–tin deposit. The layer shows a growth in the form of an unorientated structure (UD-type, unorientated dispersion type). Such coatings are very ductile and do not form cracks during bending. For the preparation of this fracture the sample was cooled in liquid nitrogen.

Tin–lead coated plug connectors can also suffer from wear corrosion. Where a contact is capable of oscillation or other movement in operation, the oxides formed are repeatedly broken up. The pure metal exposed on the surface then becomes oxidized. This process continues until an oxide layer has formed that is so thick that it cannot be broken by the contact force of the mating contact. The result is a contact resistance so high that failure occurs. Studies by Ireland et al. [55] suggest that in the case of relative movement of 75 μm at a 50 Hz frequency, failure will occur after some 50,000 cycles, and under current flow conditions, this may reduce to 30,000 cycles with temperature increases also occuring. As a criterion for failure, an increase in contact resistance from the original value of 0.5–200 mΩ has been established.

REFERENCES

1. J. F. Groff, U.S. Patent 1,364,051 (1920).
2. C. H. Chandler, U.S. Patent 1,373,488 (1921).
3. R. Schaefer and J. B. Mohler, U.S. Patent 2,461,350 (1949).
4. D. L. Cox, *Plating*, **51**, 976 (1964).
5. R. Putman and E. Roser, *Plating*, **42**, 1133 (1955).
6. M. Jordan, *The Electrodeposition of Tin and its Alloys*, Eugen G. Leuze Verlag, Saulgau, Germany, 1995, p. 103.
7. C. Rosenstein, *Met. Finish.*, **88**(1), 17 (1990).
8. H. Benninghoff, *Oberfläche* (Berlin), **8**(1), 10 (1970).
9. F. A. Lowenheim, Ed., *Modern Electroplating*, 3rd ed., Wiley, New York, 1974.
10. S. Hirsch and C. Rosenstein, *Metal. Finish. Guidebook and Directory*, **94**, 289 (1996).
11. G. Strube, *Galvanotechnik*, **73**, 1330 (1982).
12. Japanese Patent 89.152295.
13. European Patent 0192273.
14. U.S. Patent 4,691,670.
15. T. Sonoda, H. Nawafune, and S. Mizumoto, *Plating Surf. Finish.*, **82**, 66 (1995).
16. A. H. DuRose and D. M. Hutchinson, *Plating*, **40**, 470 (1953).
17. J. B. Mohler, *Met. Finish.*, **69**(12), 45 (1971).
18. B. T. Rothschild, US Patent 3,554,878.
19. R. A. Bulwith, *PC Fab.*, 46 (1988).
20. W. T. Hobson, *Plat. Electron. Ind. Symp.*, 4th (1973), p. 161.
21. P. A. Kohl, *Oberfläche-Surf.*, **23**, 190 (1982).
22. J. A. McCarthy, *Plating*, **47**, 805 (1960).
23. Lea-Ronal, U.S. Patent 4,717,460 (1987).
24. C. -P. Ho, *Materials Protect.*, **24**, 20 (1991).
25. Lea-Ronal, U.S. Patent 5,378,347 (1993).
26. R. Schetty, *Electron. Packaging Prod.*, 114 (Feb. 1994).
27. N. Ibl, *Oberfläche-Surface*, **14**, 367 (1973).
28. K. Madry, *Oberfläche-Surface*, **27** (10), 9 (1986).
29. E. Raub and W. Blum, *Metalloberfläche*, (part A), **9**, 54 (1955).
30. G. Cavanaugh and J. P. Langan, *Plating* **57**, 369 (1970).
31. A. G. Gray, Ed., *Modern Electroplating*, Wiley, New York, 1953, p. 92.
32. J. Goebel, *Z. Metallkunde*, **14**, 357, 388, 425, 499 (1922).
33. J. L. Jostan, W. Mussinger, and A. F. Bogenschütz, *Korrosionsschutz in der Elektronik*, Eugen G. Leuze Verlag, Saulgau, Germany, 1986.
34. U. R. Evans, *The Corrosion and Oxidation of Metals*, Arnold, London, 1960, Suppl. 1968.
35. Military Standard MIL-STD-38510 H.
36. M. Jordan, *Galvanotechnik*, **78**, 480 (1987).
37. B. F. Rothschild, *Met. Finish.*, **78**(5), 35 (1980).
38. F. L. Nobel and B. D. Oshow, U.S. Patent 4,701,244.
39. J. Schütt and R. Schmid, *Galvanotechnik*, **81**, 255 (1990).
40. B. Meuthen, *Metall.*, **36**, 958 (1982).
41. Rasselstein, company brochure, 1990.
42. A. Graham and H. L. Pinkerton, *Plating*, **52**, 309 (1965).
43. D. R. Eastham and C. S. Crooks, *Trans. Inst. Met. Finish.*, **60**, 9 (1982).
44. R. Subramanan and S. Ramachandran, *Met. Finish.*, **64**(4), 53 (1966).
45. H. Richter, K. Ruess, A. Gemmler, and W. Leonhard, *83rd AESF Annual Technical Conf. SUR/FIN'96, Proc*, 247.
46. M. Jordan, *Galvanotechnik*, **79**, 3053 (1988).
47. R. W. Woodgate, *PC Fabrication*, 56 (1991).
48. B. D. Dunn, *Trans. Inst. Met. Finish.*, **58**, 26 (1980).
49. German Patent DE 3440668, Schlötter.
50. G. Strube, *Galvanotechnik*, **76**, 417 (1985).
51. German Standard DIN 50965 or American National Standard ASTM B 545–85.
52. T. Hamman and E. Schedin, in *Proc. 6th Nordic Symp. on Tribology, NORDTRIB '94,* Uppsala, June 1994.
53. S. Karpel, *Tin and Its Use*, **146**, 1 (1985).
54. European Patent EP 195995, Siemens AG.
55. T. P. Ireland, N. A. Stennett, and D. S. Campbels, *Trans. Inst. Met. Finish.*, **67**, 127 (1989).
56. M. Jordan, *Galvanotechnik*, **84**, 797 (1993).

10

ELECTRODEPOSITION OF ZINC AND ZINC ALLOYS

RENÉ WINAND

Zinc has a standard reversible potential [−0.76 V/standard hydrogen electrode (SHE)] that is more negative than that of iron (Fe/Fe^{2+}—0.44V/SHE). For this reason zinc is used for sacrificial cathodic protection of steel against corrosion.

According to Fischer [1], in metal electrodeposition, zinc can be considered as an intermediate metal, giving rise to medium values of overpotentials due to secondary inhibition resulting from adsorbed hydrolized species.

In acid sulfate solutions without an organic additive, BR metallographic cross-sectional structures are obtained (BR: basis reproduction; coherent deposits with coarse crystals whose diameter increases with the deposit thickness; see Fig. 10.1). In chloride electrolytes, even coarser grains are observed, because of the more activating character of chloride ions against sulfate ions [2] and despite the complex formation in solution [3, p. 464]. In cyanide baths, on the other hand, much finer grains are obtained, and the deposits pertain to the FT (field-oriented texture: coherent deposits, with elongated crystals perpendicular to the substrate, with almost constant diameter throughout the deposit thickness) or UD types (UD: unoriented dispersion type; coherent deposit, with small crystals showing three-dimensional nucleation to occur all the time during electrodeposition).

Figure 10.2 shows a deposit obtained in a cyanide solution without an organic additive: the structure is initially FT, but it becomes progressively bad. Going from a cyanide bath to a noncyanide alkaline bath should result in still worse deposits because electrolyte complexation decreases [3] and exchange current density increases [4, pp. 528–543].

Accordingly, when rather thick deposits are needed and/or if a bright surface is required, organic additives are always present at high concentration (1 g L^{-1} or more). This always occurs in barrel-and-rack plating of small pieces of equipment, because the local current densities will vary over a wide range. For continuous plating on steel sheets or wires, constant current density and rather good hydrodynamic control may be achieved over the whole cathodic surface, and organic additives are not so much in use.

Whatever the pH, zinc is always more negative than hydrogen [5]. In electrolytes where zinc is complexed, its standard reversible potential is still more negative; for instance, for cyanide baths, the reversible potential for reaction

$$[Zn(CN)_4]^{2-} + 2e \leftrightarrow Zn + 4CN^-$$

in alkaline solution is −1.26 V/SHE [6]. Consequently hydrogen evolution occurs at the cathode as a competitor to zinc deposition, resulting in a decrease of current efficiency and eventually in some atomic hydrogen diffusion into the substrate.

Finally, in industrial processes electrolytic plating is an alternative to hot-dip galvanizing. Both processes have advantages and disadvantages. Continual technological improvements make it difficult to conclude in favor of one process over the other. However, hot dip always includes some surface alloying by diffusion, and the deposit thickness is less easily controlled than in electroplating.

In this chapter, barrel-and-rack plating will be discussed separately from continuous plating on sheets and wires. The reason is that the electrolytes and required properties of the deposits are different. Of course some overlap is inevitable.

Since the third edition of *Modern Electroplating* [7], the main trends in zinc and zinc alloy plating are as follows:

- Replacement of cyanide baths in barrel-and-rack plating by noncyanide alkaline baths or by acid baths

Modern Electroplating, Fifth Edition Edited by Mordechay Schlesinger and Milan Paunovic

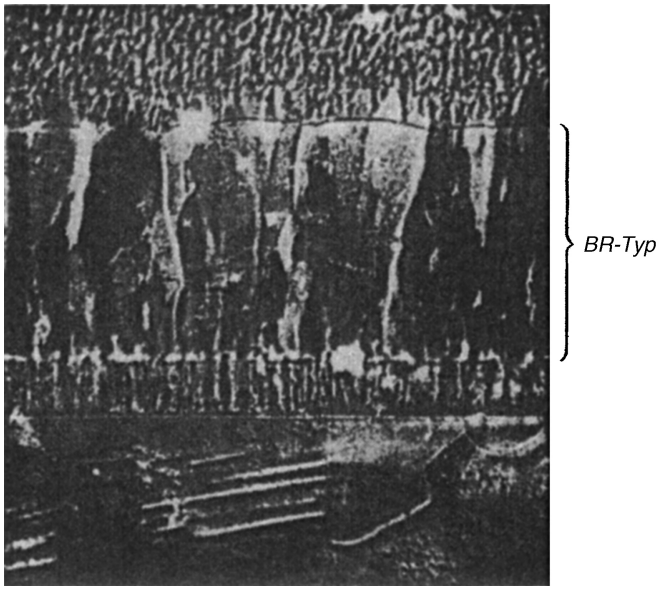

FIGURE 10.1 Zinc electrodeposited from a sulfate electrolyte (×400). After [1], p. 619—BR deposit.

- Large development of high-current-density plating of zinc and zinc alloys on continuous steel sheets or wires with a very active competition against hot dip
- Enforcement of environmental constraints

It should be emphasized that approximately half of the world's consumption of zinc is used to coat steel by various processes. This is a huge business, representing each year about 4 million tons of zinc and, in the case of sheets, more than 40 million tons of steel. Electroplating of steel sheets covers between 25 and 30% of zinc production [8, 9].

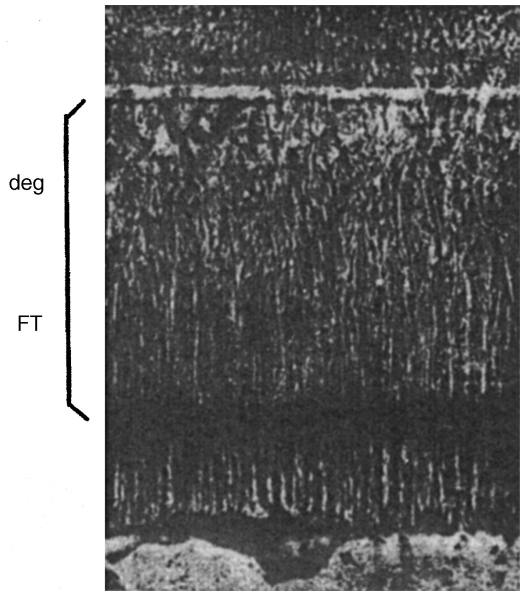

FIGURE 10.2 Zinc deposited from a cyanide electrolyte without organic additive (×400). After [1], p. 476—Initial FT deposit progressively degenerated.

10.1 BARREL-AND-RACK PLATING [7, 10–13]

Zinc is often used for coating iron and steel parts when protection from either atmospheric or indoor corrosion is the primary objective. Without subsequent treatment, electroplated zinc becomes dull gray after exposure to air, so that bright zinc is always given a chromate conversion coating or a coating of a clear lacquer (or both) if a decorative finish is required.

Commercial zinc plating is accomplished in cyanide baths, alkaline noncyanide baths, and acid chloride baths. In the 1970s most commercial zinc plating was done in conventional cyanide baths, but the strong international effort to lower pollution emissions has led to the development of other processes. Today alkaline noncyanide and acid chloride baths comprise most of the production.

10.1.1 Cyanide Zinc Baths

Bright cyanide zinc baths can be divided into four broad classifications based on their cyanide content:

- Regular cyanide zinc baths
- Midcyanide baths
- Low-cyanide baths
- Microcyanide baths

Table 10.1 summarizes the various compositions of cyanide zinc baths [10].

Normally temperature ranges from 20 to 40°C. In barrel plating, the average current density is 0.6 A dm^{-2} with 12–25 V. In rack plating, the current density is between 2 and 5 A dm^{-2} with 3–6 V.

As can be seen in the table, most cyanide baths are prepared from zinc cyanide, sodium cyanide, and sodium hydroxide, with sodium polysulfide acting as a bath purifier and thus precipitating heavy metals such as lead and

TABLE 10.1 Composition of Cyanide Zinc Baths (g L^{-1})

Constituent	Regular	Mid	Low	Micro
$Zn(CN)_2$	60	30	10	—[a]
NaCN	40	20	8	1
NaOH	80	75	65	75
Na_2CO_3	15	15	15	—
Na_xS_y	2	2	—	—
Brightener	1–4	1–4	1–4	1–5

[a]Zinc anodes are dissolved to the desired concentration of zinc metal in solution, that is, 7.5 g L^{-1}.

cadmium that enter the bath as soluble anode impurities. In looking at the chemistry of these baths, it should be emphasized that zinc cyanide is practically insoluble in water. Nevertheless, when added to sodium cyanide, the zinc cyanide dissolves to produce a complex salt, sodium zinc cyanide, as follows:

$$Zn(CN)_2 + 2NaCN \rightarrow Na_2Zn(CN)_4$$

On the other hand, when used with sodium hydroxide, zinc cyanide yields sodium zincate and sodium cyanide:

$$Zn(CN)_2 + 4NaOH \rightarrow Na_2Zn(OH)_4 + 2NaCN$$

Clearly, an equilibrium exists in solution between the cyanide zinc complex and the zincate ion according to

$$Na_2Zn(CN)_4 + 4NaOH \leftrightarrow Na_2Zn(OH)_4 + 4NaCN$$

or

$$Zn(CN)_4^{2-} + 4OH^- \leftrightarrow Zn(OH)_4^{2-} + 4CN^-$$

Thus the addition of sodium hydroxide reduces the amount of cyanide zinc complex and increases the zincate ion concentration. Accordingly the cyanide baths may be considered mixtures of two different solutions: pure cyanide and pure zincate. The dissolution constant of $Zn(CN)_4^{2-}$ is very low (in the range of 10^{-9}–10^{-20}; see [1, p. 174]), and the concentration of free Zn^{2+} ions in solution is very low. In zincate solutions at high pH, if some dissociation of $Zn(OH)_3^-$ and $Zn(OH)_2$ is observed, the concentration of free Zn^{2+} ions in solution is also very low, as shown in Figure 10.3 [3, p. 464].

An investigation of the cathode reaction mechanism at a mercury electrode has shown that in cyanide and in alkaline noncyanide baths the reacting species at the surface of the electrode remains the same. Therefore the reaction mechanism was suggested to be as follows [4, pp. 536, 539]:

For cyanide baths,

$$Zn(CN)_4^{2-} + 2OH^- \leftrightarrow Zn(OH)_2 + 4CN^-$$
$$Zn(OH)_2 + 2e \rightarrow Zn + 2OH^-$$

For noncyanide alkaline baths,

$$[Zn(OH)_4]^{2-} \leftrightarrow Zn(OH)_2 + 2OH^-$$
$$Zn(OH)_2 + 2e \rightarrow Zn + 2OH^-$$

A more detailed examination of the cathode mechanism revealed that in the reaction ZnOH is adsorbed [3, pp. 477,480].

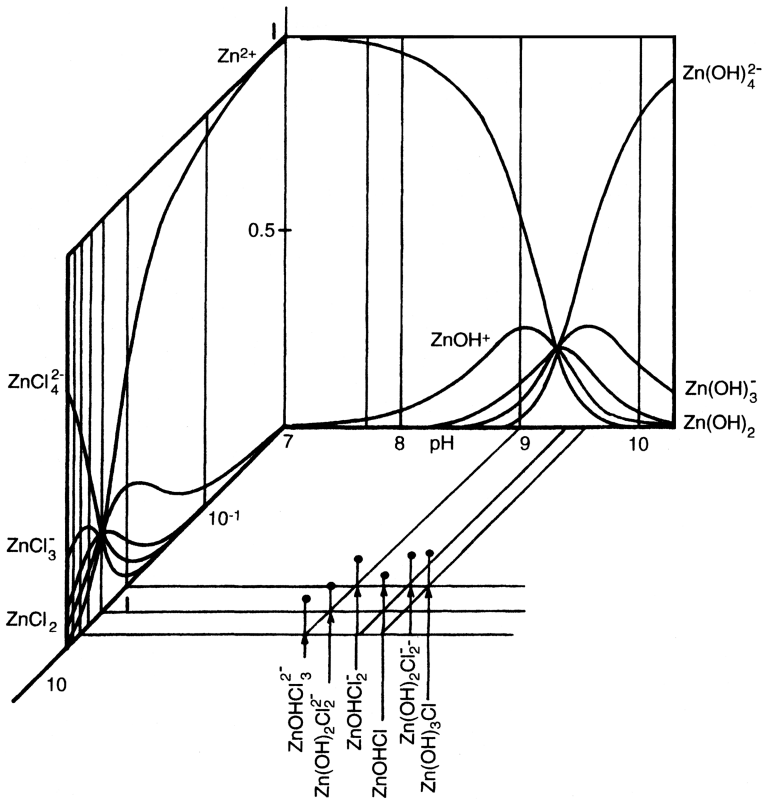

FIGURE 10.3 Relative concentrations of basic zinc and zinc chloride species in aqueous solution as a function of pH.

Therefore the second reaction in each above-mentioned formula is replaced by

$$\mathrm{Zn(OH)_2 + e \rightarrow [Zn(OH)_2]^-}$$
$$\mathrm{[Zn(OH)_2]^- \leftrightarrow ZnOH + OH^-}$$
$$\mathrm{Zn(OH) + e \rightarrow Zn + OH^-}$$

In this last row of reactions at low current density (or overpotential) the chemical reaction is the rate-determining step, whereas at high current density (or overpotential), the last electrochemical reaction is rate determining.

From a practical point of view, passing from regular to low-cyanide zinc baths is a continuous process without drastic changes in bath behavior. In every case the current efficiency drops from about 90% at $1\,\mathrm{A\,dm^{-2}}$ to less than 60% at $6\,\mathrm{A\,dm^{-2}}$. This achieves very good throwing and covering power. Microcyanide baths represent essentially a retrogression from alkaline noncyanide baths; cyanide acts as an additive that can be replaced by organic ones.

Zinc plating bath brighteners are almost exclusively proprietary mixtures of organic additives, usually combinations of polyproxyamine reaction products, polyvinyl alcohols, aromatic aldehydes, and quaternary nicotinates. Quaternary pyridinium compounds are also used as brighteners [14]. All additives are formulated at high concentrations in order to achieve brightness at both low- and high-current-density areas and to maintain stability at elevated temperatures.

10.1.2 Alkaline Noncyanide Zinc Baths

These baths are a logical development in the effort to produce a nontoxic cyanide-free zinc electrolyte. Initially these baths were considered as able only to give spongy or powdery deposits, which were of interest mainly for electrochemical power sources. The same type of electrolyte was used to investigate the dendritic electrocrystallization of zinc [15] with exchange current densities in the range of $10\,\mathrm{A\,dm^{-2}}$. From a more practical point of view, it was shown in a flow-through channel cell that various types of deposits (flat, bulbous, or dendritic) could be obtained as a function of current density and Reynolds number [16]. Further research on the subject concentrated on the deposit morphology [15–23], with the aim to improve the control of surfaces with powdery deposits, and also on the quality of dense deposits made, first, by pulsated current or by superimposing alternating current (ac) on direct current (dc) and, second, with organic additives or on the electrode mechanism [24–32]. To summarize, because of the high value of the exchange current density (see [30, p. 2657]; values in the literature are between 2 and $31\,\mathrm{A\,dm^{-2}}$), surface diffusion should not be rate determining; diffusion in solution is more likely to play this role [18]. A very important role is played by good hydrodynamic control, and it is also important to concentrate on brighteners that are necessary in industrial practice. A drawback is that some contamination of the zinc deposits is possible, and these may be up to 0.3 and 0.5% carbon originating from the additives. This is 10 times the amount of carbon found in deposits using the cyanide system.

TABLE 10.2 Composition Characteristics or Alkaline Noncyanide Zinc Baths ($\mathrm{g\,L^{-1}}$)

Constituent	LC	HC
Zn	6–9	13.5–22.5
NaOH	75–105	120–150
Proprietary additives	(as specified, 1–3%)	

Table 10.2 summarizes the composition characteristics of alkaline noncyanide zinc baths. They pertain to two different ranges of concentrations, called low chemistry (LC) and high chemistry (HC) [11]. Operating temperatures are between 15 and 45°C (optimum 25–30°C; see [3, pp. 477–480]). For barrel plating, cathode current density ranges from 2 to $4\,\mathrm{A\,dm^{-2}}$ with cell voltage 12–18 V. For rack plating, cathode current density is around $0.6\,\mathrm{A\,dm^{-2}}$ with 3–6 V.

In comparison with cyanide systems, noncyanide alkaline zinc baths have a narrower range of optimum operating zinc concentration. For instance, if the zinc metal content is around $7.5\,\mathrm{g\,L^{-1}}$ (LC) at $3\,\mathrm{A\,dm^{-2}}$, a bright deposit is obtained at 80% current efficiency. However, at $5.3\,\mathrm{g\,L^{-1}}$ zinc, at the same current density, the current efficiency is already lower than 60%. Still, raising the zinc content above $17\,\mathrm{g\,L^{-1}}$ will result in dull gray deposits. Also increasing sodium hydroxide concentration increases current efficiency but causes metal buildup on sharp-cornered edges [10, p. 246]. Accordingly, for the adopted two types of composition—low chemistry and high chemistry—the zinc and sodium hydroxide concentrations are increased at the same time.

Of course additives are essential [14, pp. 33–35]. In the first commercial alkaline noncyanide zinc baths, it was necessary to replace the complexing effect of cyanide ions by other complexing agents like ethylenediamine tetraacetic acid (EDTA), gluconate, tartrate, and triethanolamine. However, this created new effluent problems (e.g., EDTA can prevent precipitation of zinc following pH adjustement and can also delay precipitation of other metals in mixed effluents). This approach has fallen out of use, and the alkaline noncyanide zinc baths may now be considered zincate baths. The deposition of zinc from such an electrolyte follows a four-step mechanism [36]:

$$\mathrm{[Zn(OH)_4]^{2-} \leftrightarrow [Zn(OH)_3]^- + OH^-}$$
$$\mathrm{[Zn(OH)_3]^- + e \rightarrow [Zn(OH)_2] + OH^-}$$
$$\mathrm{[Zn(OH)_2]^- \leftrightarrow Zn(OH) + OH^-}$$
$$\mathrm{ZnOH + e \rightarrow Zn + OH^-}$$

The second step is the rate-determining step, and it reduces the rate of the reaction to give zinc time to form a dense deposit instead of powdery nonadherent deposits.

Organic additives fall in two categories: carriers and brighteners. The most commonly used carrier is poly vinyl alcohol (PVA). Owing to the polarity of the carbon–oxygen bond, it is possible for this material to be present in significant amounts in the cathode film, forming a weak physical barrier that hinders zinc deposition. More efficient carriers are polyaliphatic amines, aliphatic polyamines containing tertiary or quaternary nitrogen atoms, and heterocyclic amines (imidazole, pyrazole with epichlorohydrin, etc.). When tertiary and particularly quaternary nitrogen atoms are introduced into the polymer chain, extreme brilliance is obtained, even at high current densities. Less effort has been put toward studying brighteners, and hence aromatic aldehydes are still in use.

At the start of the 1980s, zincate plating had not proved to be as reliable as plating from cyanide baths. Four main problems remained to be solved;

- Intermittent deposit blistering (due to initial considerable hydrogen evolution and adsorption into the steel base). This was solved by efficient pretreatment and activation of the substrate, higher solution temperature, higher NaOH/Zn ratio, and avoiding additives with excessive cationic character leading to high carbon content in the deposits that are highly stressed.
- Burning or pitting. This was solved by solution agitation and higher solution temperature.
- Zinc anode passivation [37, 38] due to saturation of the surface by $Zn(OH)_4^{2-}$ and $Zn(OH)_3^-$ forming a solid film progressively converted to $ZnO_{1-x}(OH)_{2x}$, OH^- doped ZnO, and finally Zn-doped ZnO. This can be solved by solution agitation and by choosing not too high a value for the anode current density.
- Chromating problems. This was solved by a very efficient rinse of the plated parts to eliminate any residual zincate plating solution.

Today zincate plating is a highly successful process. In 1970, only 4% of zinc electroplating was achieved by this method, and in 1990, 30%. During the two decades cyanide plating decreased from 97 to 20%; the large percentage is now covered by acid plating, mainly from chloride solutions [39]. Other comments in this direction can be found in [40–43].

10.1.3 Acid Chloride Zinc Baths

This type of bath radically changed the technology of zinc plating since the early 1970s and constitutes about 50% of all zinc baths for rack-and-barrel plating in most developed nations.

Despite zinc complexation in solution shown in Figure 10.3 [44], it was recognized rather early that the exchange current density was high in concentrated solutions: at $2\,g\,L^{-1}Zn^{II}$, $J_0 = 0.7a_{Zn^{II}}$ in A cm^{-2}, resulting in $J_0 = 70$ A dm^{-2} if $a_{Zn^{II}}$ is unity (in [45] values ranging from 5 to 10 A dm^{-2} were found at pH 2–3.5, after converting from 10^{-2} to 1 mol L^{-1} Zn^{II}). Concerning the cathode reaction mechanism, it was considered [46] that a fraction of the electrode is covered by adsorbed atomic hydrogen, partially consumed during hydrogen evolution:

$$H^+ + e \rightarrow H_{ads}$$
$$H^+ + H_{ads} + e \rightarrow H_2$$

For zinc electrocrystallization, Zn^I_{ads} adions weakly bound to the metal and able to diffuse along the electrode surface were considered, undergoing the following reactions:

$$Zn^{II} + Zn^I_{ads} + e \leftrightarrow 2Zn^I_{ads}$$
$$Zn^{II} + e \rightarrow Zn^I_{ads}$$
$$Zn^I_{ads} + H_{ads} \rightarrow Zn + H^+$$
$$Zn^I_{ads} + e \rightarrow Zn$$

The last two reactions led to the growth of the deposit. Other growth sites were also considered, but this is beyond the scope of this chapter.

Because of the high values of the exchange current density, noncoherent deposits (dendritic or powdery) are expected if organic additives and/or close hydrodynamic control are not in use [47–50]. In fact, this type of electrolyte was used to study the growth of zinc dendrites [51]. Even for electrowinning, the need of organic additives was recognized [52–55], also at high current density (up to 31 A dm^{-2}; see [56]). However, while for electrowinning rather low concentrations of organics are enough (less than $0.1\,g\,L^{-1}$), such is not the case in plating if bright deposits are required.

Table 10.3 gives the composition and operating characteristics of acid chloride zinc plating baths [10, p. 251; 11, pp. 330–335]. These are the electrolytes used at temperatures ranging from 15 to 55°C; the pH values are between 5 and 6. In barrel plating, at current densities between 0.3 and 1 A dm^{-2}, the cell voltage is between 4 and 12 V, while in rack plating, at current densities between 2 and 5 A dm^{-2}, the cell voltage lies between 1 and 5 V.

Although organic additives are proprietary, brighteners are again subdivided into two categories [57–61]: carriers (polyalcohol, polyamine, fatty alcohols, polyglycolether, and quaternary nitrogen bonds) and primary brighteners (aliphatic, aromatic, and heterocyclic carbonyl bonds). Carriers, acting as wetting agents, are often necessary to solubilize the primary brighteners.

Bright chloride acid zinc baths have a number of intrinsic advantages:

- Waste disposal is minimized (neutralization at pH 8.5–9).

TABLE 10.3 Composition and Operating Characteristics of Acid Chloride Zinc Plating Baths ($g\,L^{-1}$)

Constituent	All Ammonium Chloride	Low Ammonium		No Ammonium, Potassium Chloride
		Potassium Chloride	Sodium Chloride	
Zn	15–30	15–30	15–30	22–38
NH_4Cl	120–180	30–45	30–45	—
KC1	—	120–150	—	185–225
NaCl	—	—	120	—
H_3BO_3	—	—	—	22–38
Carrier brightener	4 vol %	4 vol %	4 vol %	4 vol %
Primary brightener	0.25%	0.25%	0.25%	0.25%

- Current efficiencies are high, even at high current densities.
- In the presence of organic additives, leveling ability is obtained, resulting in superb out-of-bath brightness.
- Cast iron, malleable iron, and carbonitrided parts, almost impossible to plate in cyanide and zincate baths, are readily plated in acid zinc baths.
- Electrical conductivity is much higher, resulting in substantial energy savings.
- Hydrogen embrittlement is reduced.

There are however a few drawbacks:

- Acid chloride electrolyte is very corrosive.
- Eventual bleed-out of entrapped solution in the deposit will ruin the part so that special care should be taken when plating complex assemblies.

As can be seen in Table 10.3, acid chloride baths are principally of two types: with ammonium chloride or with potassium chloride. Ammonium-based baths were developed first. They can be operated at high current density, but ammonium ions act as complexing agents for nickel and copper in waste streams and can require expensive chlorination for disposal. This is the main reason for the development of the potassium chloride baths.

Other acid baths were developed: sulfate [10, p. 253; 58,59,62], fluoborate [10, p. 253], sulfamate, acetate [63], perchlorate [64], and even very low melting point molten salts [65–67], They are not much in use in barrel-and-rack plating, except for the sulfate bath for specific applications (e.g., complex assemblies).

10.1.4 Some Further Considerations Concerning Zinc Barrel-and-Rack Plating

The main characteristics of the various processes used for zinc barrel-and-rack plating can be compared: cyanide, zincate, and acid chloride baths. Figure 10.4 [42, 68] shows that acid electrolytes (including the sulfate high-acid one) have high current efficiencies (above 95%) over a wide range of current densities, while cyanide electrolytes, especially the zincate electrolytes, show a sharp decrease in current efficiency at increasing current density. The throwing power, especially for bright deposit, can be estimated by penetration inside a tube [42, 68]. Table 10.4 [42] gives some properties of the bright zinc deposits. Further readings on the subject are in [69, 70]. Internal stresses were studied in [71, 72].

Pulsated or periodically reversed currents were assumed to decrease the grain size and increase brightness, eventually without additives [73–77]. Interestingly, the multilayers of zinc are obtained both by pulse plating [77] and by self-oscillations of current at constant cathode potential [78]. Ultrasonic agitation was considered to smooth the surface [79, 80]. The influence of impurities and additives in

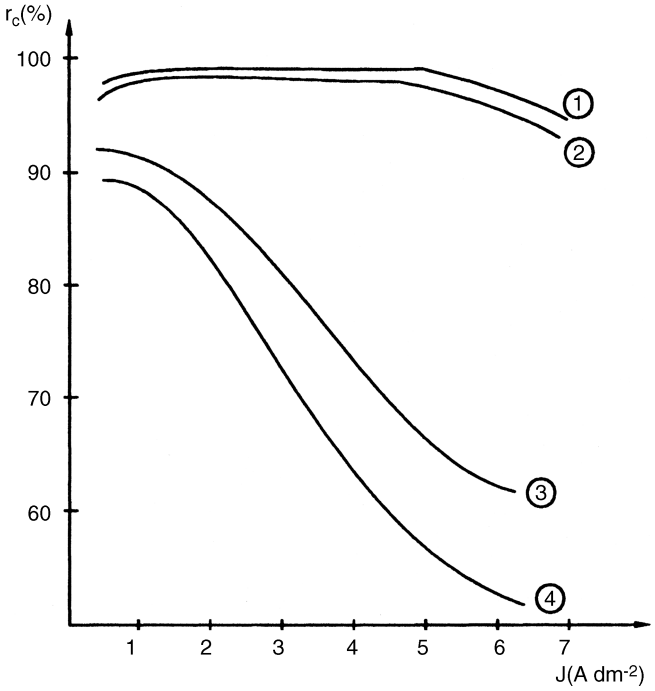

FIGURE 10.4 Current efficiency as a function of current density for various electrolytes used in zinc barrel-and-rack plating. 1: acid chloride; 2: acid sulfate; 3: cyanide; 4: noncyanide (zincate).

TABLE 10.4 Properties of Bright Zinc Deposits

Parameter or Property	Dimension	Acid Chloride	Bright Deposit from Noncyanide	
			Alkaline	Cyanide
Crystal structure	—	Hex	Hex	Hex
Deposit structure	—	UD	FT-UD	FT-UD
Crystal diameter	nm	70 ± 30	90 ± 40	130 ± 50
Microinternal stress	$N\,mm^2$	80	120	150
Macrointernal stress	$N\,mm^2$	-40	$+$ 80	-40
Micro–Vickers hardness	—	100 ± 30	130 ± 3 0	140 ± 40
Ductility	%	0.5–7.5	1–5.5	0.2–3.2

Source: Paatsch [42, p. 2635].

solution was studied especially in acid sulfate solutions, where electroplating conditions are not very far from electrowinning [81–101]. From a more technical point of view, special care must be taken in plating tank construction, especially for acid chloride baths. Tanks may not be constructed of unlined steel in this case, whereas steel is suitable for alkaline noncyanide and for cyanide baths [11, p. 328].

10.1.5 Zinc Alloy Plating

In barrel-and-rack plating, pure zinc remains the principal coating material for steel [12; 10, p. 285, and 39]. However, during the last three decades alloys were introduced to meet demands for higher quality finishes and longer lasting finishes. The push came mainly from the automotive industry and from the aerospace field in its demand for fastener and electrical components. Today, there is talk to replace cadmium because of its toxic nature [102].

Zinc alloy plating will be discussed further in the continuous plating section. In this section, only the characteristics and properties specific to barrel-and-rack plating will be considered.

Zinc–nickel alloys can be plated from acid or alkaline noncyanide solutions. The acid bath yields a higher nickel content than an alkaline bath (10–14% vs. 6–9%). Corrosion protection of steel increases with increasing nickel content up to approximately 15%. Beyond that level, the deposit becomes more noble than the substrate, losing its sacrificial properties. Also above 10% the deposit becomes more passive and accordingly less receptive to form a good chromate conversion coating. Finally, the deposit from the acid bath has a poor thickness distribution, and significant alloy variation is observed from low- to high-current-density areas. On the other hand, the plating rate is lower with the alkaline bath. Finally, the columnar structure of the alkaline bath is preferred to the laminar structure of the acid bath, especially when the part must be mechanically formed after plating. Table 10.5 summarizes bath parameters for both types.

Zinc–cobalt alloys are plated from conventional low-ammonium or ammonium-free acid chloride baths, with the addition of a small amount of cobalt. The alloy contains generally up to 1% cobalt. The current efficiency is high and so is the plating rate. There is reduced hydrogen embrittlement compared with alkaline systems, but the thickness distribution varies with the current density. An alkaline bath is also available. Zinc–cobalt alloys accept blue, bright yellow iridescent, and nonsilver black chromate conversion coatings. Table 10.6 summarizes bath parameters for both types of baths.

Zinc–iron alloys are mainly used for their ability to produce a nonsilver black chromate. At iron concentrations between 0.3 and 0.9%, they proved to have a very good resistance to the new methanol fuel blend [39]. They are mostly deposited from alkaline baths. Table 10.7 gives the bath parameters.

Tin–zinc alloys [12] are deposited from acid, alkaline, and neutral baths. In general, alloys range from 70 to 75% tin and

TABLE 10.5 Bath Parameters for Zinc–Nickel Barrel-and-Rack Plating ($g\,L^{-1}$)

Parameter	Acid Baths		Alkaline Bath
	Rack	Barrel	
Zinc chloride	130	120	—
Zinc metal	—	—	8
Nickel chloride	130	110	—
Nickel metal	—	—	1.6
Potassium chloride	230	—	—
Sodium hydroxide	—	—	130
PH	5–6	5–6	
Temperature (°C)	24–30	35–40	23–26
Cathode current Density ($A\,dm^2$)	0.1–4	0.5–3	2–10
Anodes	Zinc and nickel separately, eventually with separate rectifiers		Mix: nickel-plated steel 70%–zinc 30%

Source: Budman and Sizelove [12].

TABLE 10.6 Bath Parameters for Zinc–Cobalt Barrel-and-Rack Plating ($g\,L^{-1}$)

Parameter	Acid Baths		Alkaline Bath
	Rack	Barrel	
Zinc metal	30	30	6–9
Potassium chloride	180	225	—
Ammonium chloride	45	—	—
Caustic soda	—	—	75–105
Cobalt metal	1.9–3.8	1.9–3.8	0.03–0.05
Boric acid	15–25	15–25	—
PH	5–6	5–6	
Temperature (°C)	21–38	21–38	21–32
Cathode current Density ($A\,dm^{-2}$)	0.1–5.0	1–50	2–4
Anodes	Pure zinc	Pure zinc	Steel (passivated)

Source: Budman and Sizelove [12].

TABLE 10.7 Alkaline Bath Parameters for Zinc–Iron Alloy Barrel-and-Rack Plating ($g\,L^{-1}$)

Parameter	Value
Zinc metal	20–25
Iron metal	0.25–0.50
Caustic soda	120–140
Temperature (°C)	18–23
Cathodic current Density ($A\,dm^{-2}$)	1.5–3.0
Anodes	Steel (passivated)

Source: Budman and Sizelove [12].

are accordingly more on the tin side. They have excellent resistance to SO_2 atmospheres, frictional properties, and ductility allowing forming after plating. However, they are very soft and so are susceptible to mechanical damage. They have low electrical contact resistance and do not undergo bimetallic corrosion. As a result they are used for steel fasteners for aluminum alloy panels.

Brass (zinc–copper alloy) [10, p. 285] can be plated from pure zinc to pure copper. It is used in many applications:

- For bright decorative finishes on wire goods, picture frames, cosmetic items, builders' hardware as a thin layer on bright nickel or on other bright plates
- For antique or other dark finishes, in heavier thicknesses on items that are then burnished, brushed, or buffed
- For engineering applications as a good drawing lubricant on steel sheet and to provide good adherence of rubber to steel (e.g., steel tire cord wire)

Commercial brass plating solutions are cyanide based. Noncyanide solutions usually suffer from a lack of stability, resulting in difficulties with alloy control on wide ranges of current density. It should be remembered that the reversible standard potentials of the two metals differ by more than 1 V. Some sodium carbonate may be added to the cyanide bath to achieve some buffering action and thus keep the color of the alloy constant.

The critical factor is the ratio of cyanide to zinc. The copper content is usually between 15 and $30\,g\,L^{-1}$ and the zinc content between 4 and $10\,g\,L^{-1}$. Current density ranges from near 0 to $16\,A\,dm^{-2}$ at temperatures between 30 and 80°C (according to the bath composition) at pH 10. Proprietary additives arc available, but if plated on a bright base metal, brass deposits are fully bright up to a thickness of

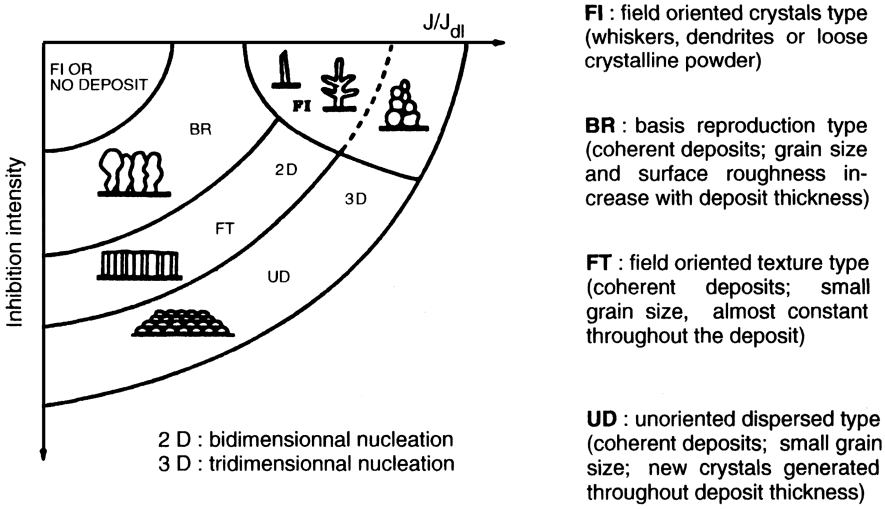

FIGURE 10.5 Fields of stability of the main deposit metallographic structures.

2.5 μm. Alkaline tartrates [103, 104] and glucoheptonates [105, 106] have been evaluated to replace the cyanides.

10.2 CONTINUOUS PLATING

Considerable interest has developed over the last 30 years in high-current-density continuous plating of zinc on steel sheets. Current densities ranging from 90 to 150 A dm^{-2} are currently used, and values up to 300 A dm^{-2} were successfully used at large pilot scale for 5–15 μm thick deposits [47–49, 107, 108], while 450 A dm^{-2} was reported for lower thicknesses, around 1 μm [47]. These processes, used now at large industrial scale, are mainly for protecting car bodies against corrosion, and they require close control of current density and hydrodynamic conditions at the surface of the continuous plate. For this reason equipment design and process control become essential.

Electrocrystallization studies have shown that in simple acid baths with no organic additive, the zinc deposit metallographic structure remains the same up to very high current densities, provided that the ratio of the cathode current density to the diffusion limiting current density is kept constant. In Figure 10.5 the fields of stability of the main zinc deposit structures are a function of this ratio, and if the inhibition intensity stays at the same position while the current density and agitation are increased simultaneously, the point characterizing the electrodeposition conditions stays at the same position [109, 110]. Further studies on hydrodynamics related to high-current-density plating can be found in the literature [111–117].

Many electrolytic cells were designed, respecting more or less the above-mentioned condition on the whole surface of the cathode. Some of them are shown in Figures 10.6–10.17. There are four main types of cells:

- Those where the steel sheet is pressed against a rotating conducting cylinder feeding the current directly inside the electrolytic cell (radial cell [112], carosel cell [112], and Kawasaki KC cell [118]: Figs. 10.6, 10.7, and 10.8).

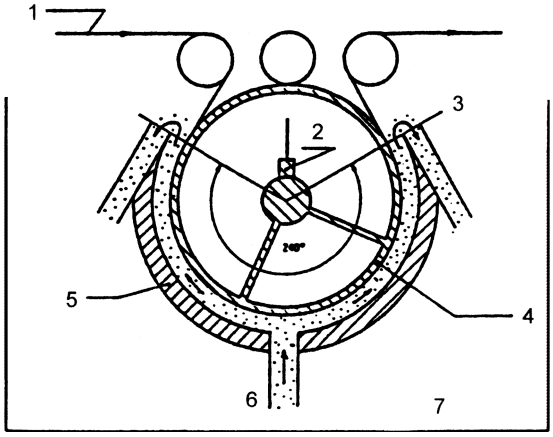

FIGURE 10.6 Radial cell (U.S. Steel) [112]. The electrolyte is injected in the middle and flows in directions co- or countercurrent to the steel sheet: 1, steel sheet; 2, electrical brushes; 3, electrolyte outlet; 4, cathode conducting cylinder; 5, anodes; 6, electrolyte inlet; 7, electrolyte tank.

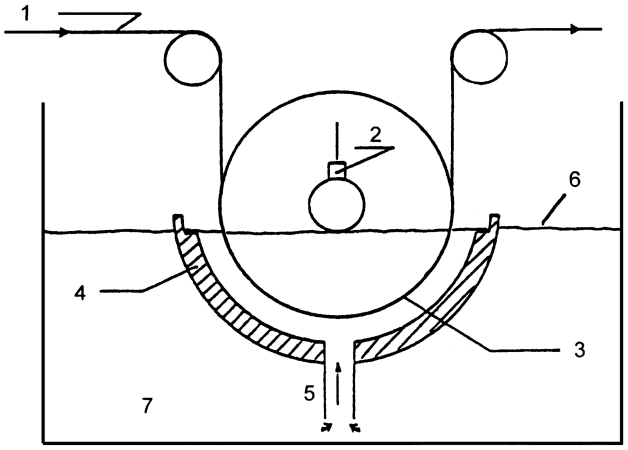

FIGURE 10.7 Carosel cell (U.S. Steel) [112]. The electrolyte is also injected in the middle and flows in directions co- or countercurrent to the steel sheet but overflows directly in the electrolyte tank: 1, steel sheet; 2, electrical brushes; 3, cathode conducting cylinder; 4, anodes; 5, electrolyte inlet; 6, electrolyte level; 7, electrolyte tank.

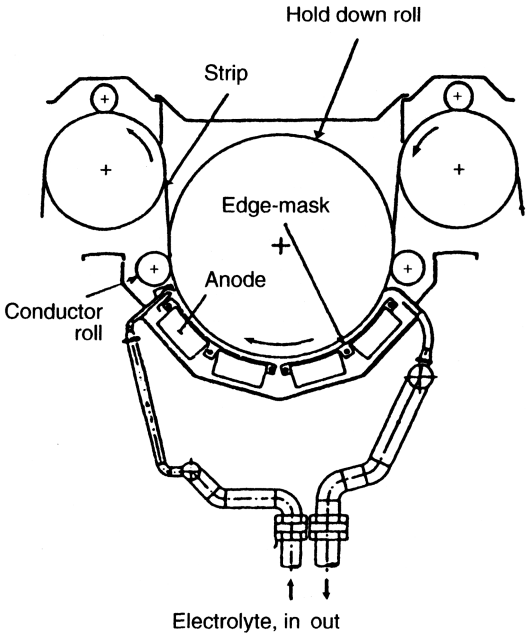

FIGURE 10.8 Kawasaki KC cell [118]. The electrolyte is injected on one side in countercurrent to the steel sheet.

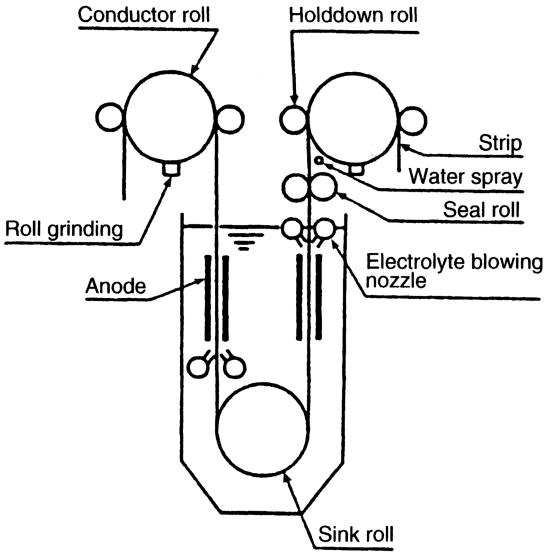

FIGURE 10.9 Sumitomo vertical cell [119].

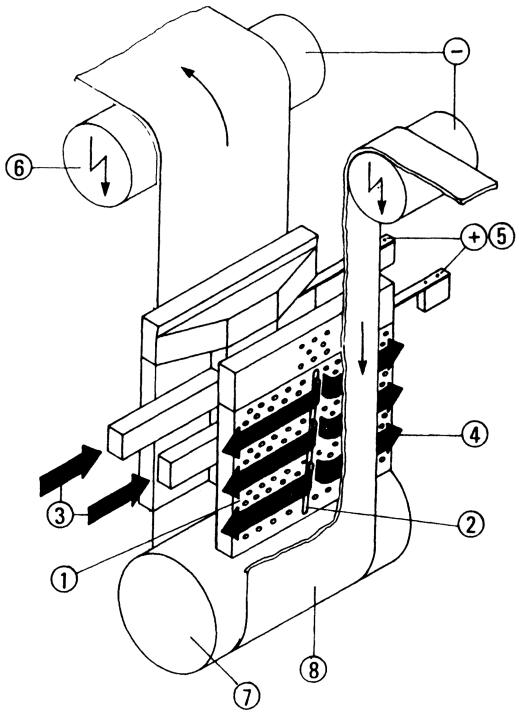

FIGURE 10.11 Rasselstein VHC cell [121]. 1: Titanium anode basket, containing eventually granulated zinc and nickel if operated in the soluble anode mode; if not, the basket is provided with a perforated insoluble anode; 2: nozzle in anode basket through which the electrolyte is injected between the steel sheet and the anode; 3: electrolyte inlet; 4: electrolyte in anode/cathode gap; 5: anode current supply; 6: cathode conductor rolls; 7: deflector roll; 8: steel sheet.

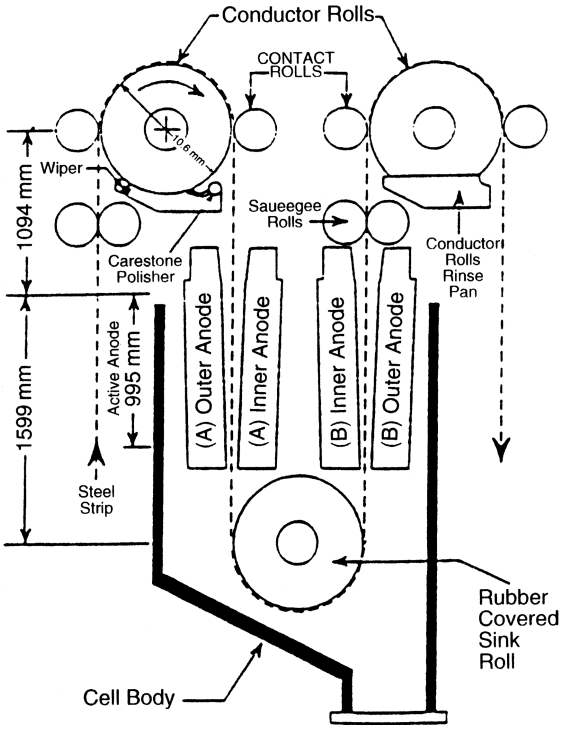

FIGURE 10.10 Andritz-Ruthner Gravitel cell [120] with hollow anode boxes through which the electrolyte is fed by overflow on the upper side of the channels between the steel sheet and the catalytic anodes. The electrolyte flows by gravity in these channels.

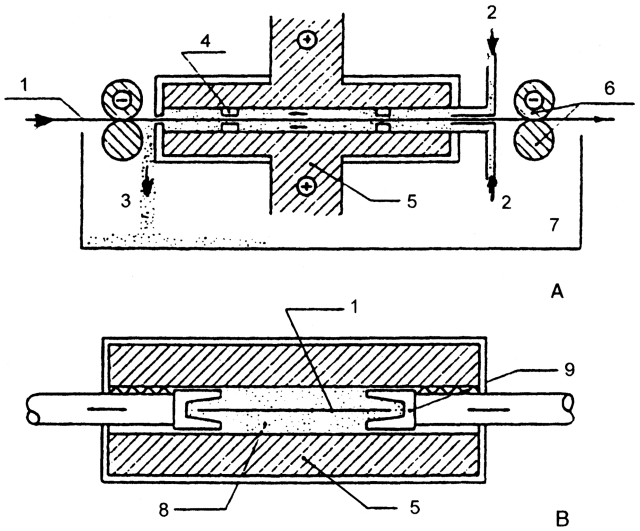

FIGURE 10.12 Nippon steel jet cell [112]. A: Lateral view; B: transverse section. 1: Steel sheet; 2: electrolyte inlet. 3: electrolyte outlet; 4: insulators; 5: anodes; 6: cathode conducting rolls; 7: electrolyte tank; 8: electrolyte; 9: side masks.

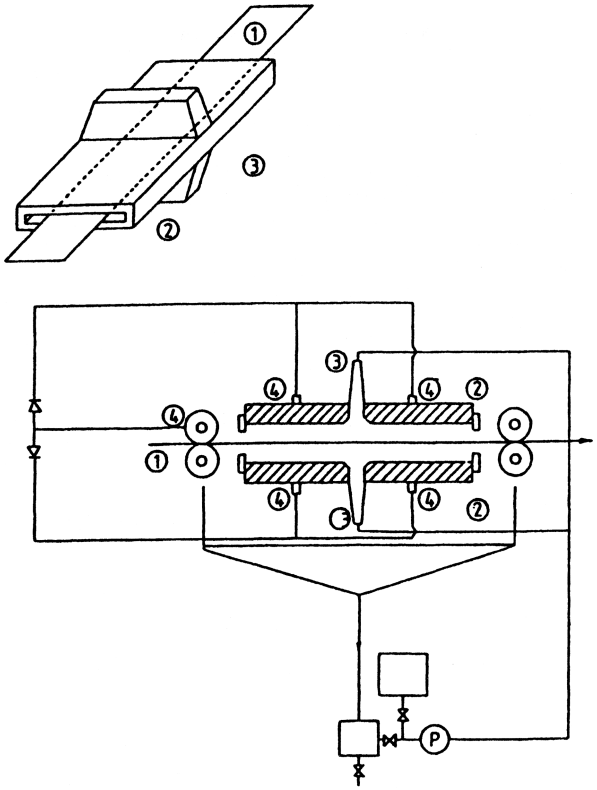

FIGURE 10.13 Nippon steel liquid cushion cell [112, 122, 123]: 1, steel sheet; 2, anodes; 3, electrolyte injectors (the electrolyte flows in co- or countercurrent to the steel sheet); 4, cathode and anode feeders.

- Those where the steel sheet moves vertically between anodes, the current feeder rolls being outside the electrolytic cell (Sumitomo vertical cell [119], Andritz–Ruthner Gravitel cell [120], and Rasselstein vertical hydrojet cell [121]: Figs. 10.9–10.11).
- Those where the steel sheet moves horizontally between the anodes, the current feeder rolls being outside the electrolytic cell (Nippon steel jet cell [112], Nippon steel liquid cushion cell [112, 122, 123], Sumitomo horizontal cell and its modified version [124], Cockerill-Sambre flash cell [47]: Figs. 10.12–10.16).
- Those where the steel sheet moves horizontally, pressed against a cathode feeder facing the anode directly in the electrolytic cell (Cockerill-Sambre belt cell [47]: Fig. 10.17)

Most electrolytic cells are able to deposit zinc only on one side of the steel sheet. This has proved to be an advantage for spot welding [125–129].

Electrolytes are acid, chloride, or sulfate, usually without organic additive. Solutions can be either highly acidic (pH lower than 1: eventually $130\,g\,L^{-1}$ H_2SO_4) or slightly acidic (pH around 3.5). In the latter case, salts of aluminum, sodium, or ammonium are added to increase conductivity. Chloride electrolytes have higher electrical conductivity, but they have the drawback, unlike sulfate baths, that they cannot operate with the insoluble anodes because chlorine evolves. Owing to high electrolyte agitation (Reynolds numbers between 15,000 and 60,000 are currently achieved), diffusion-limiting current densities are very high (from 210 to more than $900\,A\,dm^{-2}$). At the same time, due to the high hydrogen overpotential on pure zinc, cathodic current efficiencies higher than 95% are obtained, as shown in Figure 10.18 [107, 110], despite rather high temperatures (50°C). Figure 10.19 [47, 108] shows very dearly how a surface structure of 10-μm-thick zinc deposits is improved at high current density compared with low-current-density plating in the same electrolyte without the organic additive. It should be emphasized that bright deposits are not required. A good phosphate conversion posttreatment is always applied for good paint adhesion.

It is important to remember that electroplated steel sheets are rarely used in that form. In most applications (automobile, construction, household, electricity, etc.) they undergo

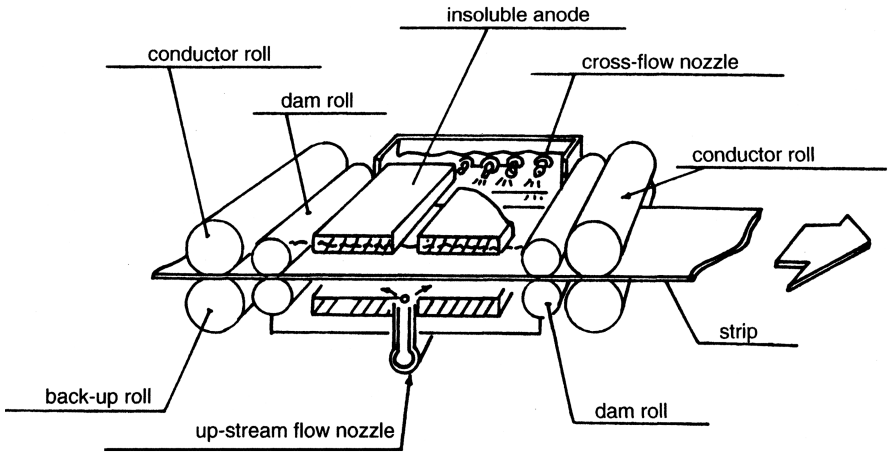

FIGURE 10.14 Sumitomo horizontal celL [124]. Initial design with central upstream flow nozzle and lateral cross-flow nozzles.

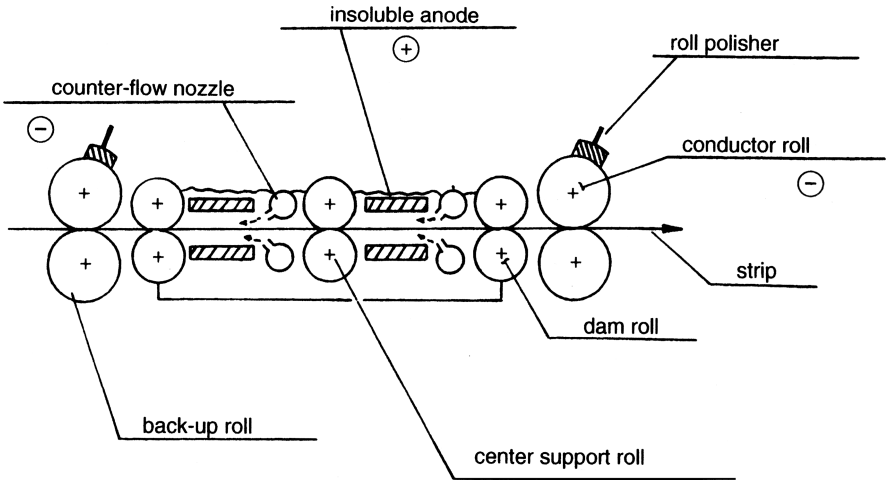

FIGURE 10.15 Sumitomo horizontal cell [124]. improved design with central support roll to avoid oscillations of the steel sheet and counterflow nozzle for injection of the electrolyte.

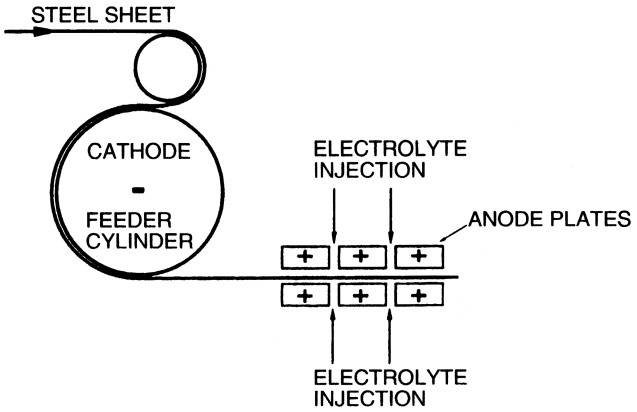

FIGURE 10.16 Cockerill-Sambre flash cell [47] designed for very high current density fully covering thin films.

surface conversion (phosphatation, chromatation) and are painted. To evaluate the characteristics of an electroplating process, the properties of the electroplated sheets must be checked according to the manufacturing system creating the final product and according to the market requirements for this final product [130]. For instance, Figure 10.20 shows a picture of a generalized multilayer coating system for automotive body panels. The steel sheets are stamped or deep drawed after electroplating prior to surface conversion, and the surface morphology of zinc influences the forming accuracy. The zinc deposit surface consists of a collection of discrete hexagonal-shaped grains (Fig. 10.19), and their size and orientation influence the friction coefficient with the tooling.

The grain size usually decreases with increasing current density, all other factors being fixed. The crystal orientation in sulfate electrolytes is strongly influenced by pH [131] and by electrolyte flow rate [115, 132]. The surface microroughness is influenced also by zinc ion supply (agitation) and current density [133]. Studies were made of the die-sheet metal friction for zinc deposits whose grains are oriented with basal planes parallel or approaching normal to the substrate surface. Using a light mill oil lubricant a higher friction coefficient (0.19) was measured with the basal planes parallel to the substrate (0.13 in the other case). The more efficient lubricant reduced the difference. Other authors observed similar results and noted the higher degree of surface galling associated with the parallel basal orientation [134, 135]. The characterization of the surface of the

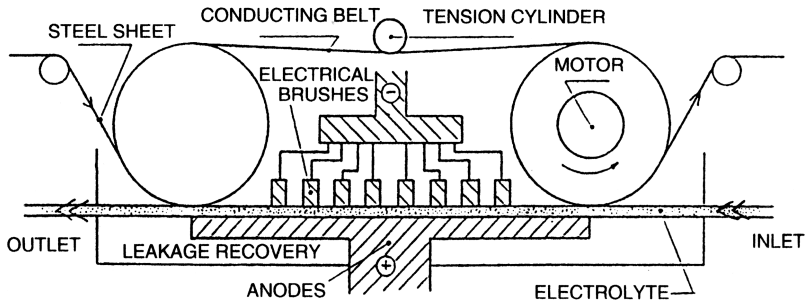

FIGURE 10.17 Cockerill-Sambre belt cell [47] reproducing a rectangular flat flow-through channel cell with perfect control of the ratio of the current density to the diffusion-limiting current density.

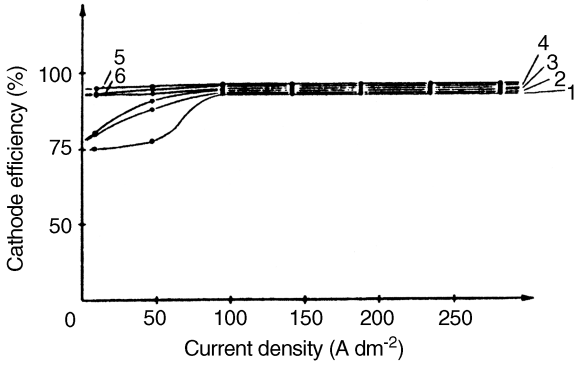

FIGURE 10.18 Cathode current efficiency as a function of current density for zinc plating for $80\,g\,L^{-1}$ Zn^{2+}; $135\,g\,L^{-1}$ H_2SO_4, channel cell all at 50°C and electrolyte speed at $4\,m\,s^{-1}$. Theoretical deposit thickness: (1) 5 μm; (2) 10 μm; (3) 25 μm; (4) 50 μm; (5) 100 μm; (6) 200 μm.

electroplated sheet is therefore very important [136]. It is beyond the scope of this chapter to discuss in detail all the other factors that must be considered in terms of deposit integrity after forming and problems connected to spot welding (especially electrode life), phosphatation [phosphophyllite $ZnFe_2(PO_4)_2 \cdot 4H_2O$ is preferred to hopeite $Zn_3(PO_4)_2 \cdot 4H_2O$, and commercial attack solutions now contain the nickel, iron, and/or manganese ions to regulate crystal nucleation and growth; the results are independent of the zinc crystal size and orientation], and painting (priming by electrophoresis generates crating if a threshold voltage of about 250 V is exceeded on zinc-coated substrates instead of 400–450 V for cold-rolled steel; interaction of the curing of the base and top coats can occur in the phosphate layer and/or the electrodeposit). Corrosion studies are also beyond the scope of this chapter.

A number of alloys were electroplated [137], and research in the field is still very active, with the aim to improve the general behavior of the plate in connection with customer requirements, mainly deformability, weldability, paintability, and corrosion resistance after surface conversion and painting.

Zinc–nickel alloys were at first investigated at low current densities (up to $5\,A\,dm^{-2}$). A complete study of the system in sulfate solutions was performed [138–144]. It was shown that in a large field of composition (relative zinc concentration between 0.1 and 0.8) the cathode deposits have a complex structure corresponding to the so-called γ phase. A flat and rather bright surface was obtained that had a silvery white appearance. This γ phase behaves like a monometallic electrode, has a higher hydrogen overpotential than pure zinc, is electronegative versus iron, and has compressive internal stress. This alloy was considered as a possible substitute to cadmium [102, 145, 146]. More recently

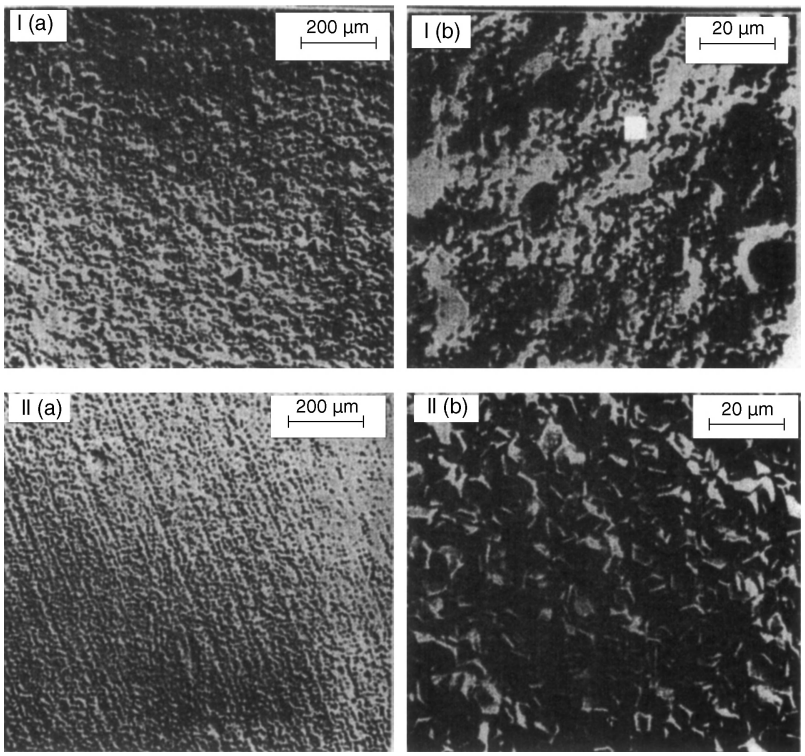

FIGURE 10.19 Surface of 10 μm-thick zinc deposit on steel. Pure sulfate solution: $80\,g\,L^{-1}$ Zn^{2+}, $135\,g\,L^{-1}$ H_2SO_4, 50°C. Electrolyte flow rate: $3\,m\,s^{-1}$. I: $10\,A\,dm^{-2}$ (*a*) ×100; (*b*) ×1000. II: $200\,A\,dm^{-2}$ (*a*) ×100; (*b*) ×1000.

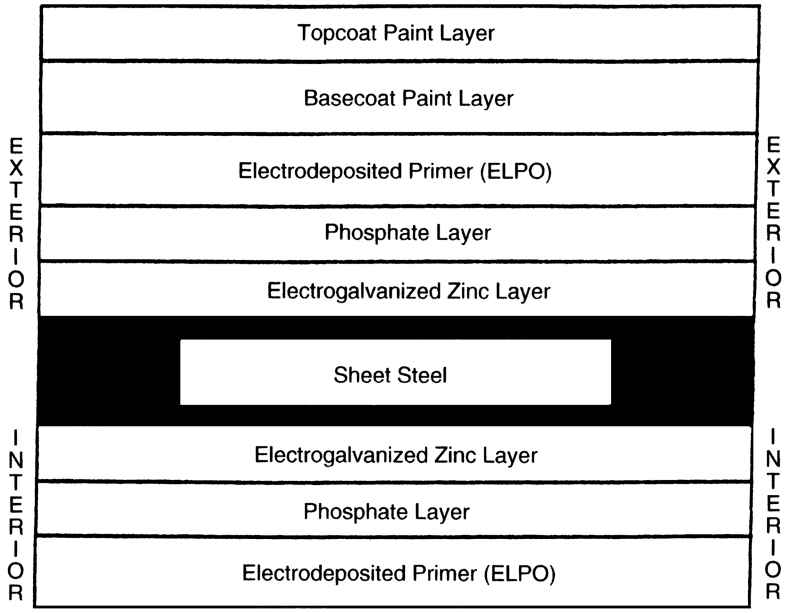

FIGURE 10.20 Generalized multilayer coating system for automotive body panels [130].

the same alloy was prepared at high current densities from various electrolytes: sulfates at medium pH 121, [147–150] (Ni^{2+}: 50–70 g L^{-1}; Zn^{2+}: 15–30 g L^{-1}; Na^{+}: 20–30 g L^{-1}; pH 1–3), at low pH [151, 152] (Ni^{2+}: 30–40 g L^{-1}; Zn^{2+}: 40–50 g L^{-1}; H_2SO_4: 35–50 g L^{-1}), or chloride [153–156]. Again, a zinc–nickel alloy pertaining to the γ phase at about 13% nickel was found to show the best corrosion resistance among the nickel–zinc alloys and was said to be four times better than pure zinc. Moreover coating adhesion and weldability were excellent [157]. However, current efficiencies were lower than for zinc deposition due to hydrogen evolution, 75–90%. Phosphatability and paintability were somewhat poorer. It was easy to obtain almost constant composition of the alloy over a wide range of electrodeposition conditions.

Though more difficult to plate than zinc–nickel, zinc–iron alloys were also studied, mainly with the idea of improving phosphatability and paintability, the two weaknesses of zinc–nickel alloys. Again, various electrolytes are possible: sulfates at moderate pH [150, 158–164] ($FeSO_4 \cdot 7H_2O$: 300 g L^{-1}; $ZnSO_4 \cdot 7H_2O$: 200 g L^{-1}; Na_2SO_4: 30 g L^{-1}; $CH_3COONa \cdot 3H_2O$: 12 g L^{-1}; pH 1–3; 50 A dm^{-2}; 50°C; flow rate of electrolyte: 0.7–3 m s^{-1}), at low pH [109, 110, 151, 152, 165–167].

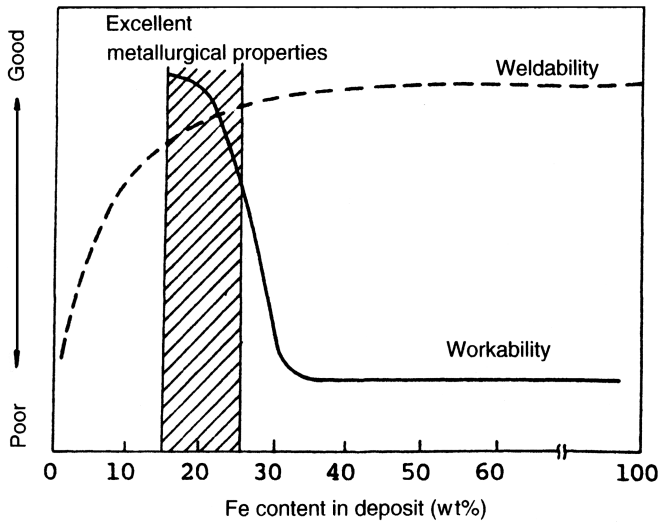

FIGURE 10.21 Metallurgical properties of zinc–iron alloys versus their iron content [174].

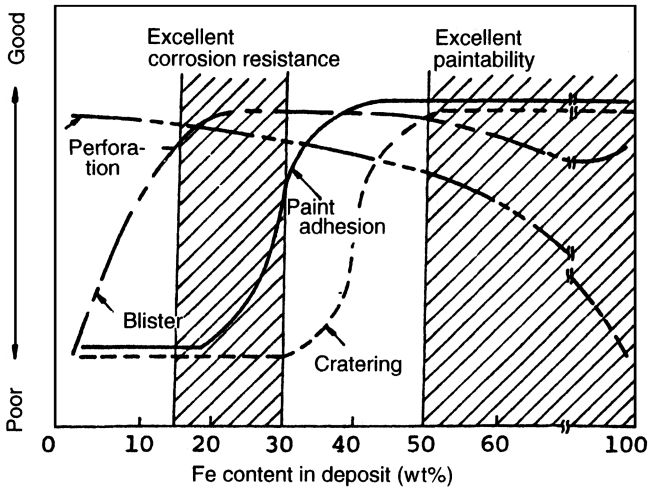

FIGURE 10.22 Performance after painting of zinc–iron alloys versus their iron content [174].

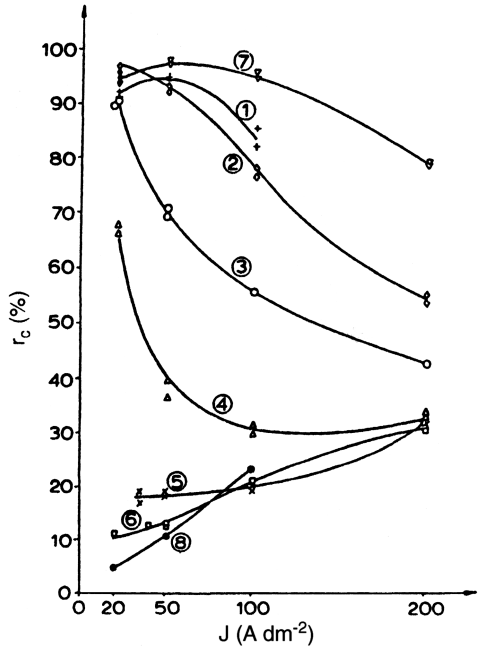

FIGURE 10.23 Cathode current efficiency as a function of current density for zinc–iron alloy plating. Channel cell. Deposit thickness 5–10 μm. Electrolyte velocity: 2 m s^{-1} for 0.2 M H_2SO_4. $T = 50°C$ [110].

(Zn^{2+}: 15–35 g L^{-1}; Fe^{2+}: 40–60 g L^{-1}; H_2SO_4: 3 5–60 g L^{-1}; Fe^{3+}: <4 g L^{-1}), or chlorides [168, 169]. Without going into the details [159, 164, 170–172], Figures 10.21 and 10.22 show that if excellent workability and corrosion resistance are achieved in the range of iron content between 15 and 25%, good paintability is obtained when the iron content is higher than 50% [173, 174]. Accordingly dual-layer iron–zinc alloys were considered: a first layer at about 18% iron and a top layer at more than 50% iron; and eventually a first layer of nickel–zinc alloy and a top layer of the iron-rich zinc alloy [137, 175, 176]. Close control of the hydrodynamic conditions was found to be essential in order to achieve alloy composition homogeneity on the steel strip [177]. Figure 10.23 shows the difficulties associated with zinc–iron alloy electroplating. Current efficiency is very sensitive to current density and electrolyte composition at constant electrolyte flow rate. Figures 10.24 and 10.25 illustrate metallographic structures and Figure 10.26 their field of stability. Their surface microscopic structure is given in Figure 10.27 [110].

Zinc–cobalt alloys were also investigated, at first at low current density (lower than 7.5 A dm^{-2}) and in two ranges of cobalt concentrations in the alloy (higher than 1.5% [178] and lower than 0.9% [179]). Alloys at low cobalt concentration, around 0.3%, show already interesting properties, and they have been considered for high-current-density plating in a ternary zinc–nickel–cobalt alloy [180]. On further research performed in the field, see [181–192].

More fundamentally all the zinc alloys with a metal from the iron group (nickel, iron, cobalt) are obtained under so-called anomalous codeposition [193], that is, with preferential deposition of the less noble zinc. Recent investigations on the mechanism of the reaction [149, 165, 167, 194–208] show that this phenomenon is linked to a local rise in pH at the surface of the cathode, due to hydrogen evolution, resulting in some zinc hydroxide adsorbed species through which the discharge of the iron metal is slowed down. Moreover, these

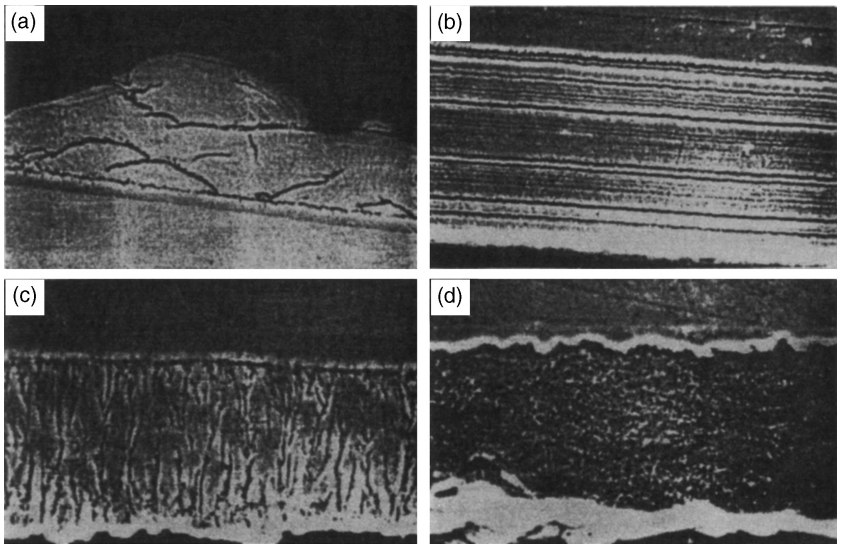

FIGURE 10.24 Various metallographic structures observed in the system Fe–Zn: N, RL, FT, and pseudo U (later shown as BR) structures are observed: (*a*) nodular (N); (*b*) rhythmic lamellar (RL); (*c*) field-oriented texture (FT); (*d*) unoriented dispersed (UD) [110].

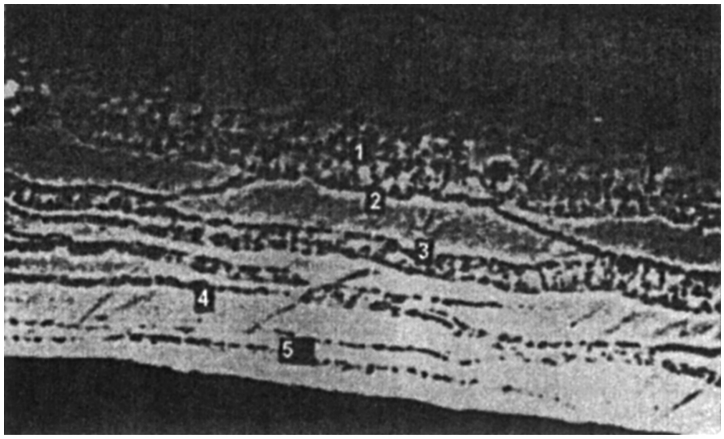

FIGURE 10.25 Detail of a metallographic structure obtained for a multiphase Fe–Zn deposit at 35% Fe [110].

alloys show large discrepancies of crystal structure with thermal equilibrium ones, as shown in Figure 10.28 [196] and Figure 10.29 [110].

Zinc–manganese alloys have recently received attention for their extremely high corrosion resistance without the aid of painting, for the formation of dense corrosion product of γ-phase Mn_2O_3, for their excellent corrosion resistance after painting with thin alloy coating layers, and for their excellent paintability properties allowing them to meet the requirements for both interior and exterior surfaces of autobody panels [209]. Electroplating needs complexation because zinc and manganese have reversible potentials different by more than 0.4 V and the system Zn–Mn does not show anomalous deposition. Citrate is usually used as the complexant in solutions of sulfates [210–215]. The difficulties arising from low cathode efficiency and poor bath stability seem to explain why no commercial applications have appeared so far.

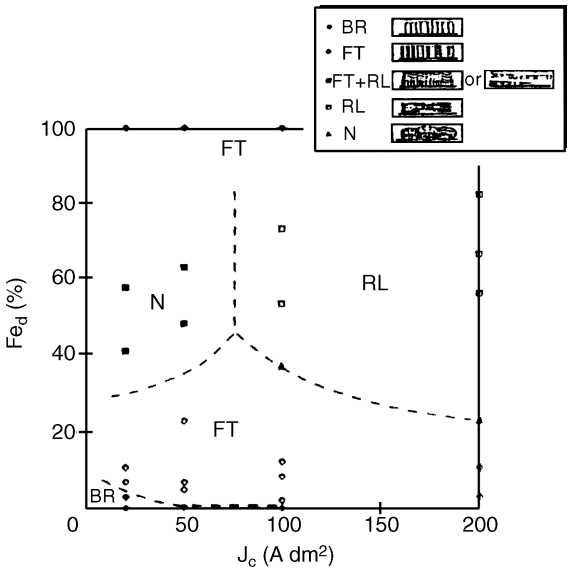

FIGURE 10.26 Cross section of metallographic structures of zinc–iron alloy deposits as a function of current density and composition. Channel cell: 0.2 *M* H_2SO_4 with Fe^{2+} and Zn^{2+} as sulfates at 50°C. Electrolyte speed: 2 m s^{-1} [110].

In the field of multilayer electrogalvanized steel sheet, zinc–chromium oxide (so-called Zn–Cr–CrO_x or zincrox) is worth mention [216–218]. This coating is made of a first layer of sacrificial zinc (99% of the coating weight); a second layer of a metal capable of protecting zinc from too early sacrificial corrosion, from acid atmosphere, and from contact with the welding electrodes and consisting of chromium (0.9% of the coating weight); and a final layer of a very effective paint bonder, consisting of chromium oxide (0.1% of the total coating weight). All layers are obtained by the continuous electrolytic process. It should be added that the zinc thickness is in the usual range of about 3–11 μm (18–80 g m^{-2}), the chromium layer (0.5 g m^{-2}) is only 70 nm thick, while the chromium oxide is in the range of 5–10 nm thick as in stainless steel.

So-called composite layers are also mentioned in recent literature. The objective is to improve the mechanical properties of the electroplated zinc or zinc alloy to facilitate forming and also to obtain better temporary protection before phosphatation. This can be achieved by two different methods:

- Include in the zinc or zinc alloy deposits tiny particles of oxides, chromates, carbides [219–227], or even polystyrene [228].
- (Or more easily) Place a thin layer of some organic composite on top of the zinc or zinc alloy deposit [137, 229–232].

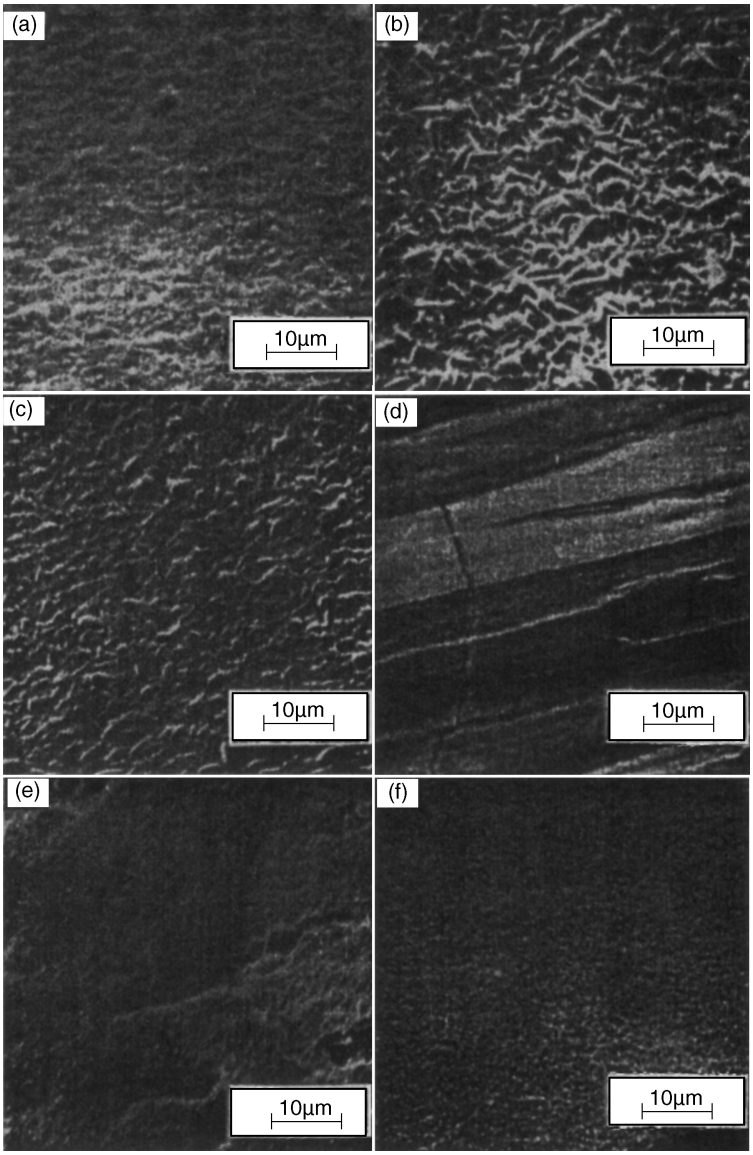

FIGURE 10.27 Surface microscope examination of various Zn–Fe deposits. Channel cell: 0.2 M H_2SO_4 with Fe^{2+} and Zn^{2+} as sulfates at 50°C. Electrolyte velocity 2 m s^{-1}. Current density 100 A dm^{-2}. (*a*) $Fe_d = 1\%$; (*b*) $Fe_d = 10\%$; (*c*) $Fe_d = 13\%$; (*d*) $Fe_d = 36\%$; (*e*) $Fe_d = 54\%$; and (*f*) $Fe_d = 100\%$.

Zinc–nickel and zinc–cobalt alloys have been electrodeposited on steel wires to replace the current brass coating [233, 234]. Zinc–manganese coating has been used as reported [235].

Hydrogen embrittlement of the steel substrates, especially for high-strength low-alloyed steel, is a matter of concern. However, it was shown that the substrates are mainly contaminated by atomic hydrogen during the period when full coverage by the first layers of zinc (or zinc alloy) is not achieved. Zinc and zinc alloys constitute a good diffusion barrier to hydrogen. If full coverage is readily achieved, this is an advantage. It can be a drawback, however, if the substrate is charged with atomic hydrogen. As the hydrogen is removed by heat treatment, blistering occurs [236–251]. Acid baths and high-current-density plating aid in decreasing the hydrogen embrittlement risk.

Insoluble lead-based anodes have been replaced by catalytic dimensionally stable anodes for oxygen evolution. IrO_2-based catalytic layers appear to be favored on titanium substrates [252–256]. They might be challenged by Magnéli phase titanium oxides [257].

Finally, some effort has been devoted to zinc plating on aluminum substrate. The objective is to allow phosphatation of car bodies made partly of steel and partly of aluminum. Surface conditioning is a critical step [258, 259],

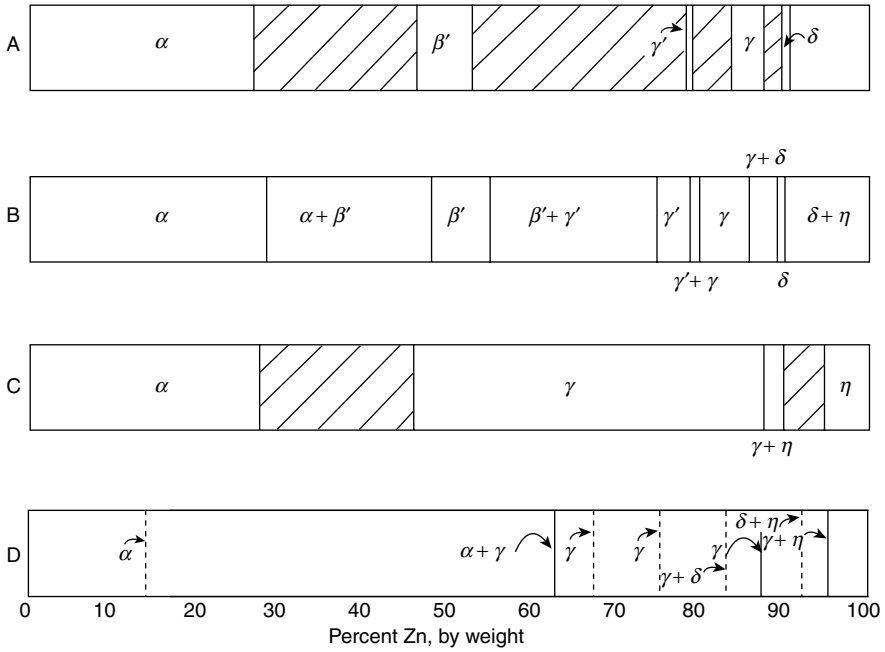

FIGURE 10.28 (*a*, *b*) Phase versus composition diagrams for pyrometallurgically and (*c*, *d*) electrochemically prepared Zn–Ni alloys (no phase determination reported in hatched regions) [196].

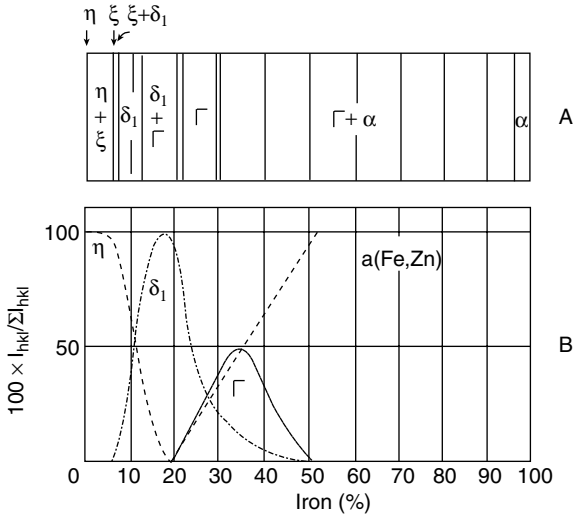

FIGURE 10.29 Comparison of (*b*) electrodeposited phases with (*a*) thermal equilibrium for iron–zinc alloys [110].

10.3 RECENT RESEARCH ADVANCES

During the last decade, research remained very active in the field. Among the large number of papers, some are of special interest because they illustrate general trends: pulse plating is studied in order to generate nanocrystalline zinc deposits [260–263]; organic additives are studied in order to control the morphology and the properties of the deposits, eventually in combination with pulse plating [264–275]; texture and surface morphology of zinc and zinc alloys deposited on low carbon steel substrate were further investigated [276–278].

REFERENCES

1. H. Fischer, *Elektrolytische Abscheidung und Elektrokristallisation von Metallen*, Springer Verlag, Berlin, 1954, pp. 618–623.
2. A. T. Vagramyan and M. A. Zhamagortsyants,"Electrodeposition of Metals and Inhibiting Adsorption," translation from Russian, U.S. Dept. of Commerce, NTIS, Springfield, VA, Contract NSF C-466, 1974, pp. 40–54.
3. A. Despic, in *Comprehensive Treatise of Electrochemistry*, Vol. 7, B. E. Conway, J. O'M. Bockris, E. Yeager, S. U. M. Khan, and R. E. White, Eds., Plenum, New York, 1983, Ch. 7.
4. K. J. Vetter, *Elektrockemische Kinetik*, Springer Verlag, Berlin, 1961.
5. M. Pourbaix, *Atlas d'équilibres électrochimiques*, Gauthier-Villars, Paris, 1963, p. 409.
6. R. Parsons, *Handbook of Electrochemical Constants*, Butterworths Scientific, London, 1959.
7. F. A. Lowenheim, Ed., *Modern Electroplating*, 3rd ed., Wiley, New York, 1974.
8. T. Asamura, in *Proc. 4th Int. Conf. on Zinc and Zinc Alloy Coated Steel Sheet* (Galvatech, 98), 1998, Chiba, Japan, The Iron and Steel Institute of Japan, pp. 14–21.
9. F. E. Goodwin, in *Proc. 4th Int. Conf. on Zinc and Zinc Alloy Coated Steel Sheet* (Galvatech, 98), 1998, Chiba, Japan, The Iron and Steel Institute of Japan, pp. 31–39.

10. H. Geduld, in *Metals Handbook*, 9th ed., Vol. 5, American Society for Metals, 1982, pp. 244–255.
11. Cl. Biddulph and M. Marzano, in *99 Guide and Directory Issue of Metal Finishing*, New York, 1999, pp. 328–337.
12. E. Budman and R. R. Sizelove, in *99 Guide and Directory Issue of Metal Finishing*, New York, 1999, pp. 338–345.
13. R. Winand, in *Electrodeposition Technology, Theory and Practice*, Vol. 17, L. T. Romankiw and D. Turner, Eds., Electrochemical Sociey, Pennington, NJ, 1987, pp. 207–232.
14. B. S. James and W. R. McWhinnie, *Trans. Inst. Met. Finish*, **58**, 72 (1980).
15. J. Diggle, A. Despic, and J. O'M. Bockris, *J. Electrochem. Soc.*, **116**, 1503 (1969).
16. R. Naybour, *J. Electrochem. Soc.*, **116**, 520 (1969).
17. I. Justnijanovic and A. Despic, *Electrochim. Acta*, **18**, 709 (1973).
18. D. Drazic, S. Jordanov, and Z. Nagy, *Croatica Chem. Acta*, **45**, 199 (1973).
19. M. Froment and G. Maurin, *Electrodep. Surf. Treat.*, **3**, 245 (1975).
20. J. Jovicevic, D. Drazic, and A. Despic, *Electrochim. Acta*, **22**, 589 (1977).
21. R. Walker and N. S. Holt, *Plating Surf. Finish.*, **68**, 44 (1981).
22. D. T. Chin, R. Sethi and J. McBreen, *J. Electrochem. Soc.*, **129**, 2677 (1982).
23. K. Popov and N. Krstajic, *J. Appl. Electrochem.*, **13**, 775 (1983).
24. I. Epelboin, M. Ksouri, and R. Wiart, *J. Electrochem. Soc.*, **122**, 1206 (1975).
25. A. Despic, D. Jovanovic, and T. Rakic, *Electrochim. Acta*, **21**, 63 (1976).
26. J. Jovicevic, D. Drazic, and A. Despic, *Electrochim. Acta*, **22**, 589 (1977).
27. J. Bressan, and R. Wiart, *J. Appl. Electrochem.*, **9**, 43 (1979).
28. J. Bressan and R. Wiart, *J. Appl. Electrochem.*, **9**, 615 (1979).
29. C. Cachet, U. Stroder, and R. Wiart, *J. Appl. Electrochem.*, **11**, 613 (1981).
30. M. Abyaneh, J. Hendrikx, W. Visscher and E. Barendrecht, *J. Electrochem. Soc.*, **129**, 2654 (1982).
31. C. Cachet, U. Stroder, and R. Wiart, *Electrochim. Acta*, **27**, 903 (1982).
32. J. Hendrikx, A. van der Putten, W. Visscher, and E. Barendrecht, *Electrochim. Acta*, **29**, 81 (1984).
33. J. Darken, *Trans. Inst. Met. Finish.*, **57**, 145 (1979).
34. L. Oniciu and L. Muresan, *J. Appl. Electrochem.*, **21**, 565 (1991).
35. F. Galvani and I. A. Carlos, *Met. Finish.*, **95**, 70 (1970).
36. J. O'M. Bockris, Z. Nagy, and A. Damjanovic, *J. Electrochem. Soc.*, **119**, 285 (1972).
37. P. L. Cabot, M. Cortes, F. Centellas, and E. Perez, *J. Appl. Electrochem.*, **23**, 371 (1993).
38. M. Cai and S. M. Park, *J. Electrochem. Soc.*, **143**, 2125 (1996).
39. Th. Natorski, *Met. Finish.*, **90**, 15 (1992).
40. W. Mandel and V. van der Putten, *J. Oberflächentech.*, **33**, 48 (1993).
41. G. D. Wilcox and P. J. Mitchell, *Trans. Inst. Met. Finish.*, **65**, 76 (1987).
42. W. Paatsch, *Galvanotechnik*, **83**, 2633 (1992).
43. S. J. Wake and T. Pearson, *Proc. AESF Ann. Tech. Conf.*, **83**, 157 (1996).
44. R. Winand, *Hydrometall.*, **27**, 285 (1991).
45. H. Sierra Alcazar and J. Harrison, *Electrochim. Acta*, **22**, 627 (1977).
46. J. Bressan and R. Wiart, *J. Appt. Electrochem.*, **9**, 43 (1979).
47. R. Winand, *Hydrometall.*, **29**, 567 (1992).
48. R. Winand, *Electrochim. Acta*, **39**, 1091 (1994).
49. R. Winand, *Electrochim. Acta*, **43**, 2925 (1998).
50. R. Winand, in *Parker Int. Symp. on Surf. Technologies*, Nihon Parkerizing, Tokyo, 1998, pp. 85–92.
51. Y. Oren and U. Landau, *Electrochim. Acta*, **27**, 739 (1982).
52. D. J. Mackinnon, J. Brannen, and V. Lakshmanan, *J. Appl. Electrochem.*, **9**, 603 (1979).
53. D. J. Mackinnon, J. Brannen, and V. Lakshmanan, *J. Appl. Electrochem.*, **10**, 321 (1980).
54. D. J. Mackinnon, J. Brannen, and R. Morrison, *J. Appl. Electrochem.*, **12**, 39 (1982).
55. D. Mackinnon and J. Brannen, *J. Appl. Electrochem.*, **12**, 21 (1982).
56. B. Thomas and D. Fray, *J. Appl. Electrochem.*, **11**, 677 (1981).
57. G. K. Schwartz, *Galvanotechnik*, **68**, 874 (1977).
58. M. Pushpavanam and B. A. Shenoi, *Met. Finish.*, **75**, 29 (1977).
59. M. Harsanyi, J. Harsanyi, E. Grunwald, and C. Varhelyi, *Galvanotechnik*, **72**, 123 (1981).
60. E. Jeannier, *Oberflächen Werkst*, **34**, 14 (1993).
61. Th. C. Franklin, T. Williams, T. S. N. Sankara Narayanan, R. Guhl, and G. Hair, *J. Electrochem. Soc.*, **144**, 3064 (1997).
62. S. Morisaki, T. Mori, and S. Tajima, *Plating Surf. Finish.*, **68**, 55 (1981).
63. S. S. Abd el Rehim, S. M. Abd el Wahaab, E. E. Fouad, and H. H. Hassan, *J. Appl. Electrochem.*, **24**, 350 (1994).
64. S. Sreeveeraraghavan, R. M. Krishnan, S. R. Natarajan, and B. Balakrishnan, *Trans. SAEST*, **31**, 41 (1996).
65. W. R. Pitner and Ch. L. Hussey, *J. Electrochem. Soc.*, **144**, 3095 (1997).
66. Y. F. Lin and I. W. Sun, *J. Electrochem. Soc.*, **146**, 1054 (1999).
67. Y. F. Lin and I. W. Sun, *Electrochim. Acta*, **44**, 2771 (1999).
68. W. Paatsch, *Galvanotechnik*, **68**, 392 (1977).
69. H. Benninghoff, *Metalloberflache*, **34**, 445 (1980).
70. G. Strube, *Galvanotechnik*, **77**, 1318 (1986).
71. S. A. Armyanov and G. S. Sotirova, *Surf. Tech.*, **79**, 311 (1979).
72. S. A. Armyanov and G. S. Sotirova, *Surf. Tech.,* **79**, 325 (1979).
73. A. R. Despic and K. I. Popov *J. Appl. Electrochem.*, **1**, 275 (1971).
74. H. D. Hedrich, W. Gunther, and Ch. J. Raub, *Metalloberflache*, **34**, 462 (1980).

75. W. Paatch, *Metalloberflache*, **41**, 39 (1987).
76. Y. Plin and J. R. Selman, *J. Electrochem. Soc.*, **138**, 3525 (1991).
77. V. A. Zabludovsky, N. V. Fedotova, and E. F. Shtapenko, *Trans. IMF*, **74**, 106 (1996).
78. H. Yan, J. Dowries, P. J. Boden, and S. J. Harris, *J. Electrochem. Soc.*, **143**, 1577 (1996).
79. R. Walker and N. S. Holt, *Plating Surf. Finish.*, **67**, 92 (1980).
80. R. Walker and N. S. Holt, *Plating Surf. Finish.*, **68**, 44 (1981).
81. D. J. Mackinnon and J. M. Brannen, *J. Appl. Electrochem.*, **7**, 451 (1977).
82. D. J. Mackinnon, J. M. Brannen and R. C. Kerby, *J. Appl. Electrochem.*, **9**, 55 (1979).
83. D. J. Mackinnon, J. M. Brannen and R. C. Kerby, *J. Appl. Electrochem.*, **9**, 71 (1979).
84. M. Saloma, J. Avila-Mendoza, G. Alonso-Viveros, and A. Ramirez-Delgado, *Hydrometall.*, **20**, 121 (1988).
85. V. Srinivasan, J. S. Cuzmar, and Th. O'Keefe, *Metall. Trans. B*, **21B**, 81 (1990).
86. S. Rashkov, M. Petrova, and C. Bozhkov, *J. Appl. Electrochem.*, **20**, 11 (1990).
87. C. Bozhkov, M. Petrova, and S. Rashkov, *J. Appl. Electrochem.*, **20**, 17 (1990).
88. R. Wiart, C. Cachet, C. Bozhkov, and S. Rashkov, *J. Appl. Electrochem.*, **20**, 381 (1990).
89. C. Bozhkov, I. Ivanov, and S. Rashkov, *J. Appl. Electrochem.*, **20**, 447 (1990).
90. N. Masse and D. Piron, *J. Appl. Electrochem.*, **20**, 630 (1990).
91. D. J. Mackinnon, R. M. Morrison, J. E. Mouland, and P. E. Warren, *J. Appl. Electrochem.*, **20**, 728 (1990).
92. D. J. Mackinnon, R. M. Morrison, J. E. Mouland, and P. E. Warren, *J. Appl. Electrochem.*, **20**, 955 (1990).
93. C. Cachet, and R. Wiart, *J. Appl. Electrochem.*, **20**, 1009 (1990).
94. C. Bozhkov, M. Petrova, and S. Rashkov, *J. Appl. Electrochem.*, **22**, 73 (1992).
95. C. Cachet and R. Wiart, *J. Electrochem. Soc.*, **141**, 131 (1994).
96. J. C. Lin and S. L. Tsai, *J. Appl. Electrochem.*, **24**, 1044 (1994).
97. R. Ichino, C. Cachet, and R. Wiart, *J. Appl. Electrochem.*, **25**, 556 (1995).
98. B. C. Tripathy, S. C. Das, G. T. Hefter, and P. Singh, *J. Appl. Electrochem.*, **27**, 673 (1997).
99. S. C. Das, P. Singh, and G. T. Hefter, *J. Appl. Electrochem.*, **27**, 738 (1997).
100. B. C. Tripathy, S. C. Das, G. T. Hefter, and P. Singh, *J. Appl. Electrochem.*, **28**, 915 (1998).
101. T. Dobrev, C. Cachet, and R. Wiart, *J. Appl. Electrochem.*, **28**, 1195 (1998).
102. M. D. Thomson, *Trans. IMF (Bull)*, **74** (3), 3 (1996).
103. S. S. Abd el Rehim and M. E. el Ayashy, *J. Appl. Electrochem.*, **8**, 33 (1978).
104. S. S. Abd el Rehim, *J. Appl. Electrochem.*, **8**, 569 (1978).
105. Y. Fujiwara and H. Enomoto, *Surf. Coatings Technol.*, **35**, 101 (1988).
106. Y. Fujiwara and H. Enomoto, *Surf. Coatings Technol.*, **35**, 113 (1988).
107. A. Weymeersch, R. Winand, and L. Renard, *Plating Surf. Finish.*, **68**, 56 (1981).
108. A. Weymeersch, R. Winand, and L. Renard, *Plating Surf. Finish.*, **68**, 118 (1981).
109. R. Winand, in *Proc. Int. Conf. on Zinc and Zinc Alloy Coated Steel Sheet* (Galvatech'89), Iron and Steel Inst. of Japan, Tokyo, 1989, pp. 27–36.
110. R. Winand, *J. Appl. Electrochem.*, **21**, 377 (1991).
111. B. Meuthen and D. Wolfhard, *Metalloberflache*, **36**, 70 (1982).
112. R. Winand, *Oberfläche-Surface*, **25** (11), 369 (1984).
113. M. Kawabe, M. Sagiyama, A. Tonouchi, Y. Okubo, T. Adaniya, and T. Hara, *Trans. ISIJ*, **25**, B-260 (1985).
114. R. Winand, *Interfinish*, **88**, Paris (Oct. 1988), Vol. I, pp. 189–202.
115. J. M. Ting, D. Duffy, R. Y. Lin, F. H. Guzzetta, and T. R. Roberts, in *Proc. Int. Conf. on Zinc and Zinc Alloys Coated Steel Sheet* (Galvatech'89), Iron and Steel Inst. of Japan, Tokyo, 1989, pp. 179–185.
116. H. M. Wang, S. F. Chen, T. J. O'Keefe, M. Degrez, and R. Winand, *J. Appl. Electrochem.*, **19**, 174 (1989).
117. L. Van Hee, J. C. Monnier, R. Winand, and M. Stanislas, *J. Appl. Electrochem.*, **24**, 303 (1994).
118. A. Komoda, A. Kibata, S. Murakami, H. Kimura, K. Mochizuki, and R. Muko, in *Proc. Int. Conf. on Zinc and Zinc Alloy Coated Steel Sheets* (Galvatech'89), Iron and Steel Inst. of Japan, Tokyo, 1989, pp. 170–177.
119. H. Onishi, T. Shiohara, T. Hattori, and T. Motoyama, paper presented at AESF Continuous Steel Strip Plating Symp., Dearborn, MI, May 1993, pp. 23–29.
120. M. S. Blaser and E. T. Nowak, paper presented at AESF Continuous Steel Strip Plating Symp., Dearborn, MI, May 1993, pp. 31–39.
121. K. H. Killian, K. Taffner, F. Weber, and H. U. Weigel, paper presented at AESF, 5th Continuous Steel Strip Plating Symp., Dearborn, MI, May 1987, p. T1-22.
122. K. Sakai, H. Nitto, M. Kamada, and R. Yoshihara, paper presented at AESF 4th Continuous Steel Strip Plating Symp., Chicago, 1984, p. J1–25.
123. K. Sakai, H. Nitto, R. Yoshihara, and M. Kitayama, *Iron Steel Eng.*, **62** (8), 49 (1985).
124. T. Nonaka, H. Oishi, H. Nagasaki, S. Shoda, A. Shibuya, and T. Hattori, paper presented at AESF 5th Continuous Steel Strip Plating Symp., Dearborn, May 1987, p. D1-20.
125. A. Matthews, Eurozinc 1979, Report on seminar Zinc in Europe, London, Apr. 1979, pp. 39–41.
126. E. Gorl and B. Meuthen, *Stahl und Eisen*, **103** (17), 790 (1983).
127. G. J. Harvey and P. N. Richards, *Mel. Forum*, **6** (4), 234 (1983).
128. S. Dinda and R. J. Traficante, *Automotive Eng.*, **92** (12), 38 (1984).

129. B. Meuthen and J. H. Meyer zu Bexten, *Iron Steel Eng.*, **62** (6), 26 (1985).
130. J. H. Lindsay, *Proc. 78th AESF Ann. Tech. Conf.*, 25–43 (1991).
131. J. H. Lindsay, R. F. Paluch, H. D. Nine, U. R. Miller, and T. J. O'Keefe, *Plating Surf. Finish.*, **76** (3), 62 (1989).
132. S. Alota, N. Azzeri, R. Bruno, M. Memmi, and S. Ramundo, *Metall, Ital.*, **79** (3), 217–224 (1987).
133. T. R. Roberts, F. H. Guzzetta, and R. Y. Lin, in *Proc. AESF 5th Continuous Strip Plating Symp*., Dearborn, MI, May 1987, pp. J1–22.
134. S. J. Shaffer, A. M. Philip, and J. W. Morris Jr., in *Proc. Int. Conf. on Zinc and Zinc Alloy Coated Steel Sheet* (Galvatech'89), Iron and Steel Inst. of Japan, Tokyo, 1989, pp. 338–344.
135. S. F. Shaffer, W. E. Nojima, P. N. Skarpelos, and J. W. Morris, Jr., in *Zinc-Based Steel Coating Systems: Metallurgy and Performance*, G. Krauss and D. K. Matlock, Eds., The Metals Society, Warrendale, PA, 1990, pp. 251–262.
136. V. Leroy, in *Proc. Int. Conf. on Zinc and Zinc Alloy Coated Steel Sheet* (Galvatech'89), Iron and Steel Inst. of Japan, Tokyo, 1989, pp. 399–409.
137. R. Winand, *Surf. Coatings Technol.*, **37**, 65 (1989).
138. M. Kurachi, K. Fujiwara, *Denki Kagaku*, **38**, 600 (1970).
139. Y. Imai and M. Kurachi, *Denki Kagaku*, **45**, 728 (1977).
140. Y. Imai, Sh. Ohsumi, and M. Kurachi, *Denki Kagaku*, **46**, 264 (1978).
141. Y. Imai, T. Watanabe, and M. Kurachi, *Denki Kagaku*, **46**, 202 (1978).
142. Y. Imai and M. Kurachi, *Denki Kagaku*, **47**, 89 (1979).
143. M. Kurachi and K. Fujiwara, *Trans. J. I. M.*, **11**, 311 (1970).
144. M. Kurachi, K. Fujiwara, and T. Tanaka, in *Proc. 8th Congress of the Int. Union for Electrodep. and Surf. Finish*, 1973, pp. 152–157.
145. J. Dini and H. Johnson, *Met. Finish.*, **77** (8), 31 (1979).
146. J. Dini and H. Johnson, *Met. Finish.*, **77** (9), 53 (1979).
147. R. Noumi, H. Nagasaki, Y. Foboh, and A. Shibuya, SAE Technical Paper Series 820332, Detroit, Feb. 1982, pp. 22–26.
148. S. G. Fountoulakis, R. N. Steinbicker, and T. W. Fisher, paper presented at the AES 4th Continuous Strip Plating Symp., Chicago, May 1984, pp. F1–21.
149. H. Fukushima, T. Akiyama, K. Higashi, R. Kammel, and M. Karimkani, *Metallwissenschaft Technik*, **42** (3), 242 1988.
150. T. Akiyama, H. Fukushima, K. Higashi, M. Karimkhani, and R. Kammel, in *Proc. Int. Conf. on Zinc and Zinc Alloy Coated Steel Sheet* (Galvatech'89), Iron and Steel Inst. of Japan, Tokyo, 1989, pp. 45–50.
151. A. Weymeersch, L. Renard, J. J. Conreur, R. Winand, M. Jordan, and C. Pellet, in *Proc. 4th AES Continuous Strip Plating Symp*., Chicago, May 1984, pp. Bl–20.
152. A. Weymeersch, L. Renard, J. J. Conreur, R. Winand, M. Jordan, and C. Pellet, *Plating Surf. Finish.*, **73**, 68–73 (1986).
153. J. Beers, Bethlehem Steel Research Department Report, Apr. 15, 1983.
154. A. Matsuda, T. Yoshihara, K. Miyachi, A. Komoda, and S. Kikuchi, *Trans. ISIJ*, **24**, B267 (1984).
155. A. Komoda, A. Matsuda, T. Yoshihara, and K. Kimura, in *Proc. 4th AES Continuous Strip Plating Symp*., Chicago, May 1984, pp. C1–29.
156. J. Keller, G. Colin, P. Seurin, and E. Millon, in *Proc. Int. Conf. on Zinc and Zinc Alloy Coated Steel Sheet* (Galvatech'89), Tokyo, 1989, pp. 161–177.
157. A. Shibuya, T. Kurimoto, Y. Hoboh, and N. Usiki, *Trans. ISIJ*, **23**, 923 (1983).
158. T. Watanabe, M. Ohmura, T. Honma, and T. Adaniya, *SAE*, **90** (3), 30, (1982).
159. T. Hara, T. Adaniya, M. Sagiyama, T. Honma, A. Tonouchi, T. Watanabe, and H. Ohmura, *Trans. ISIJ*, **23**, 954 (1983).
160. T. Tsuda, K. Asano, and A. Shibuya, *Trans. ISIJ*, **26** (1), **53**, (1986).
161. K. Kondo, S. Hinotani, and Y. Ohmori, *J. Appl. Electrochem.*, **18**, 154 (1988).
162. K. Kondo, *ISIJ Int.*, **30**, 464–468 (1990).
163. A. van Cauter, J. Dilewijns, B. C. de Cooman, and A. de Boeck, in *Proc. Int. Conf. on Zinc and Zinc Alloy Coated Steel Sheet* (Galvatech'95), Chicago, 1995, pp. 393–398.
164. K. de Wit, J. Dilewijns, A. de Boeck, and B. C, de Cooman, in *Proc. Int. Conf. on Zinc and Zinc Alloy Coated Steel Sheet* (Galvatech'95), Chicago, 1995, pp. 399–406.
165. A. Rodriguez Fajardo, R. Winand, A. Weymeersch, and L. Renard, in *Proc. 5th AES Continuous Strip Plating Symp*., Dearborn, May 1987, pp. S1–28.
166. A. A. Rodriguez Fajardo, M. Degrez, and R. Winand, *Oberfläche-Surf.*, **30** (8), 20 (1989).
167. M. Degrez, A. A. Rodriguez Fajardo, and R. Winand, *Oberfläche-Surf.*, **30** (9), 14, (1989).
168. A. Matsuda, T. Yoshihara, K. Miyachi, A. Komoda, K. Kyono, and K. Yamato, *Trans. ISIJ*, **24**, B266 (1984).
169. T. Irie, K. Kyono, H. Kimura, T. Honjo, K. Yamata, T. Yoshihara, and A. Matsuda, in *Proc. 4th AES Continuous Strip Plating Symp,* Chicago, May 1984, pp. G1–24.
170. T. Irie, K. Kyono, H. Kimura, T. Honjo, and K. Yamato, Research Rep. Kawasaki Steel Co., Mar. 1984, p. 31.
171. T. Hada, T. Kanamaru, M. Nakayama, K. Arai, T. Fujiwara, Y. Suemitsu, M. Sato, and Y. Ogawa, Nippon Steel Tech. Rep. no. 25, Apr. 1985, pp. 11–18.
172. T. Adaniya, M. Sagiyama, and T. Honma, Nippon Kokan Tech. Rep. Overseas, no. 43, 1985, pp. 33–39.
173. T. Adaniya, T. Hara, M. Sagiyama, T. Honma, and T. Watanabe, *Plating Surf. Finish.*, **72**, 52–56 (1985).
174. T. Adaniya, T. Hara, M. Sagiyama, T. Honma, and T. Watanabe, in *Proc. 4th AES Continuous Strip Plating Symp*., Chicago, May 1984, pp. H1–15.
175. N. Miura, T. Saito, T. Kanamura, Y. Shindo, and Y. Kitazawa, *Trans. ISIJ*, **23**, 913 (1983).
176. S. Nomura, H. Sakai, H. Nishimoto, T. Uegaki, M. Sakaguchi, M. Iwai, and I. Kobuko, *Trans. ISIJ*, **23**, 930 (1983).
177. T. Tsuda, K. Asano, and A. Shibuya, *Trans. ISIJ*, **26**, 53 (1986).

178. R. Srivastava, O. Gupta, and Ja. La Luddin, *Metalloberfläche*, **34**, 76 (1980).
179. W. Verberne, *Trans. Inst. Met. Finish.*, **64**, 30 (1986).
180. T. Saito, R. Wake, J. Oka, and M. Kitayama, Nippon Steel Technical Report No. 25, Apr. 1985, pp. 1–10.
181. W. Siegert, *Metalloberfläche*, **41** (6), 259, (1987).
182. Ch. Karwas, T. Hepel, *J. Electrochem. Soc.*, **136**, 1672 (1989).
183. Th. E. Sharpies, in *Proc. 78th AESF Ann. Tech. Conf.*, 1991, pp. 73–86.
184. T. Zhen-Mi, Z. Jing-Shuang, L. Wennliang, Y. Zhe-Long, and A. Maozhong, *Trans. IMF*, **73** (2), 48 (1995).
185. R. Fratesi, G. Roventi, G. Giulani, and C. R. Tomachuk, *J. Appl. Electrochem.*, **27**, 1088 (1997).
186. I. Kirilova, I. Ivanov, and S. Rashkov, *J. Appl. Electrochem.*, **27**, 1380 (1997).
187. A. Stankeviciute, K. Leinartas, G. Bikulcius, D. Virbalyte, A. Sudavicius, and E. Juzeliunas, *J. Appl. Electrochem.*, **28**, 89 (1998).
188. E. O. S. Carpenter, and J. P. G. Farr, *Trans. IMF*, **76** (4), 135 (1998).
189. I. Kirilova, I. Ivanov, and S. Rashkov, *J. Appl. Electrochem.*, **28**, 637 (1998).
190. I. Kirilova, I. Ivanov, and S. Rashkov, *J. Appl. Electrochem.*, **28**, 1359 (1998).
191. V. Narasimhamurthy and B. S. Sheshadri, *Trans. IMF*, **77** (1), **29**, (1999).
192. S. S. Abd el Rehim, M. A. M. Ibrahim, S. M. Abd el Wahaab, and M. Dankeria, *Trans. IMF*, **77** (1), 31 (1999).
193. A. Brenner, *Electrodeposition of Alloys*, Vol. 2, Academic, New York, 1963, pp. 194–228.
194. K. Higashi, H. Fukushima, T. Urakawa, T. Adaniya, and K. Matsudo, *J. Electrochem. Soc.*, **128**, 2081 (1981).
195. H. Fukushima, T. Adaniya, and K. Higashi, *J. Jpn. Met. Finish. Soc.*, **34** (9), 446 (1983).
196. D. E. Hall, *Plating Surf. Finish.*, **70**, (11), 59 (1983).
197. S. Swathirajan, *J. Electroanal. Chem. Interfacial Electrochem.*, **221** (1–2), 211 (1987).
198. Ch. Karwas and T. Hepel, *J. Electrochem. Soc.*, **135**, 839 (1988).
199. H. Fukushima, in *Proc. Int. Conf. on Zinc and Zinc Alloy Coated Steel Sheet* (Galvatech'89), Iron and Steel Inst. of Japan, Tokyo, 1989, pp. 19–26.
200. H. Fukushima, T. Akiyama, K. Higashi, R. Kammel, and M. Karimkhani, *Metall.*, **44** (8), 754 (1990).
201. K. Kondo, *ISIJ Int.*, **30** (6), 464 (1990).
202. E. Chassaing and R. Wiart, *Electrochim. Acta*, **37**, 545 (1992).
203. H. M. Wang and T. J. O'Keefe, *J. Appl. Electrochem.*, **24**, 900 (1994).
204. A. M. Alfanlazi, J. Page, and U. Erb, *J. Appl. Electrochem.*, **26**, 1225 (1996).
205. V. G. Roev and N. V. Gudin, *Trans. IMF*, **74**(5), 153 (1996).
206. F. J. Fabri Miranda, O. E. Barcia, O. R. Mattos, and R. Wiart, *J. Electrochem. Soc.*, **144**, 3441 (1997).
207. F. J. Fabri Miranda, O. E. Barcia, O. R. Mattos, and R. Wiart, *J. Electrochem. Soc.*, 144, 3449 (1997).
208. F. Elkhatabi, M. Benbella, M. Sarret, and C. Muller, *Electrochim. Acta*, **44**, 1645 (1999).
209. T. Hara, M. Sagiyama, and T. Urakawa, Nippon Kokan Tech. Rep. Overseas, 48, 29, Feb. 1987.
210. M. Sagiyama, T. Urakawa, T. Adaniya, T. Hara, and Y. Fukuda, in *Proc. 5th AES Continuous Strip Plating Symp.*, Dearborn, May 1987, pp. V1–16.
211. M. Sagiyama, T. Urakawa, T. Adaniya, T. Hara, and Y. Fukuda, *Plating Surf. Finish.*, **74** (11), 77 (1987).
212. T. Urakawa, Y. Sugimoto, M. Sagiyama, and T. Watanabe, in *Proc. Int. Conf. on Zinc and Zinc Alloys Coated Steel Sheet* (Galvatech'89), Iron and Steel Inst. of Japan, Tokyo, 1989, pp. 51–58.
213. H. Yoshikawa, H. Iwata, T. Urukawa, and M. Sagiyama, in *Proc. Int. Conf. on Zinc and Zinc Alloys Coated Steel Sheet* (Galvatech'89), Iron and Steel Inst. of Japan, Tokyo, 1989, pp. 59–65.
214. G. D. Wilcox and B. Petersen, *Trans. IMF*, **74** (4), 115 (1996).
215. B. Bozzini, F. Pavan, G. Bollini, and P. L. Cavalotti, *Trans. IMF*, **75** (5), 175 (1997).
216. A. Catanzano and M. Palladino,TEKSID Technical Note No. 2 (1983) and United Nations Economic Commission for Europe, Steel Seminar 8/R35, Apr. 1982.
217. A. Catanzano, S. Borsari, V. Matullo, G. Santunione, and N. Zagni, in *Proc. 4th AES Continuous Strip Plating Symp.*, Chicago, May 1984, pp. 11–21.
218. V. Ferrari, L. Pacelli, E. Severini, and M. Campioni, in *Proc. 2nd Int. Conf. on Zinc and Zinc Alloy Coated Steel Sheet* (Galvatech'92), CRM, Amsterdam, 1992, pp. 511–517.
219. K. Mori, H. Ishii, T. Miyawaki, and Y. Matsushima, in *Proc. Int. Conf. on Zinc and Zinc Alloy Coated Steel Sheet* (Galvatech'89), Iron and Steel Inst. of Japan, Tokyo, 1989, pp. 66–72.
220. S. Umino, C. Kato, T. Komori, A. Yasuda, and K. Yamato, in *Proc. Int. Conf. on Zinc and Zinc Alloy Coated Steel Sheet* (Galvatech'89), Iron and Steel Inst. of Japan, Tokyo, 1989, pp. 73–79.
221. J. P. Celis, J. R. Roos, C. Buelens, and J. Fransaer, in *Proc. 2nd Int. Conf. on Zinc and Zinc Alloy Coated Steel Sheet* (Galvatech'92), CRM, Amsterdam, 1992, pp. 506–510.
222. M. Yoshida and T. Izaki, in *Proc. AESF Continuous Steel Strip Plating Symp.*, Dearborn, MI, May 1993, pp. 111–122.
223. V. John, in *Proc. 3rd Int. Conf. on Zinc and Zinc Alloy Coaled Steel Sheet* (Galvatech'95), ISS, Chicago, Sept. 1995, pp. 249–262.
224. D. Aslanidis, J. Fransaer, and J. P. Celis, *J. Electrochem. Soc.*, **144**, 2352 (1997).
225. A. Sachian, M. Blidariu, E. Roman, and C. Raducanu, *Trans. IMF*, **75** (6), 213 (1997).
226. D. Aslanidis, J. Fransaer, J. P. Celis, U. Meers, and L. Renard, in *Proc. 4th Int. Conf. on Zinc and Zinc Alloys Coated Steel Sheet* (Galvatech'98), Iron and Steel Inst. of Japan, Chiba, 1998, pp. 515–520.

227. H. Nakakoji and K. Mochizuki, in *Proc. 4th Int. Conf. on Zinc and Zinc Alloys Coated Steel Sheet* (Galvatech'98), Iron and Steel Inst. of Japan, Chiba, 1998, pp. 570–574.
228. A. Hovestad, R. J. C. H. Heesen, and L. J. J. Janssen, *J. Appl. Electrochem.*, **29**, 331 (1999).
229. F. M. Androsch, K. Kosters, and W. Schiefermuller, in *Proc. AESF Continuous Steel Strip Plating Symp*., Dearborn, May 1993, pp. 69–79.
230. T. Ichida, in *Proc. 4th Int. Conf. on Zinc and Zinc Alloy Coated Steel Sheet* (Galvatech'98), Iron and Steel Inst. of Japan, Chiba, 1998, pp. 272–279.
231. L. Conde Moragues, in *Proc. 4th Int. Conf. on Zinc and Zinc Alloy Coated Steel Sheet* (Galvatech'98), Iron and Steel Inst. of Japan, Chiba, 1998, pp. 280–283.
232. T. Kubota, K. Sasaki, Y. Sugimoto, M. Yamashita, and M. Sagiyama, in *Proc. 4th Int. Conf. on Zinc and Zinc Alloy Coated Steel Sheet* (Galvatech'98), Iron and Steel Inst. of Japan, Chiba, 1998, pp. 284–289.
233. J. Giridhar and W. J. van Ooij, *Surf. Coatings Technol.*, **52**, 17 (1992).
234. H. Yan, J. Downes, P. J. Boden and S. J. Harris, *Trans. IMF*, **77** (2), 71 (1999).
235. B. Bozzini, F. Pavan and P. L. Cavallotti, *Trans. IMF*, **76** (5), 171 (1998).
236. J. A. Zehnder, J. Hadju and J. Nagy, *Plating Surf. Finish.*, **62** (9), 862 (1975).
237. H. Zeilmaker, L. C. van den Boogaard and E. Barendrecht, *Metalloberfläche*, **31** (8), 342 (1977).
238. W. Paatsch, *Galvanotechnik*, **70** (8), 706–710 (1979).
239. W. Paatsch, *Metalloberfläche*, **34** (4), 174 (1980).
240. K. N. Srinivasan, M. Selvam, and S. Venkata Krishna Iyer, *J. Appl. Electrochem.*, **23**, 358 (1993).
241. J. H. Payer, S. L. Amey, and G. M. Michal, *Proc. AESF Continuous Steel Strip Plating Symp*., Dearborn, May 1993, pp. 259–264.
242. M. J. Carr and M. J. Robinson, *Trans. IMF*, **73** (2), 58 (1995).
243. L. Mirkova, C. Tsvetkova, I. Krastev, M. Monev, and S. Rashkov, *Trans. IMF*, **73** (2), 44 (1995).
244. D. H. Coleman, G. Zheng, B. N. Popov, and R. E. White, *J. Electrochem. Soc.*, **143** (6), (1871) 1996.
245. M. Pushpavanam and K. Balakrishnan, *Trans. IMF*, **74** (1), 33 (1996).
246. W. Paatsch, *Plating Surf. Finish.*, **83** (9), 70 (1996).
247. W. Paatsch, W. Kautek, and M. Sahre, *Trans. IMF*, **75** (6), 216 (1997).
248. M. Monev, L. Mirkova, I. Krastev, H. Tsvetkova, S. Rashkov, and W. Richtering, *J. Appl. Electrochem.*, **28**, 1107 (1998).
249. D. H. Coleman, B. N. Popov, and R. E. White, *J. Appl. Electrochem.*, **28**, 889 (1998).
250. M. Ramasubramanian, B. N. Popov, and R. E. White, *J. Electrochem. Soc.*, **145**, 1907 (1998).
251. F. Yuse and T. Nakayama, in *Proc. 4th Int. Conf. on Zinc and Zinc Alloy Coated Steel Sheet* (Galvatech'98), Iron and Steel Inst. of Japan, Chiba, 1998, pp. 553–557.
252. K. L. Hardee, L. K. Mitchell, and E. J. Rudd, *Plating Surf. Finish.*, **76** (4), 68 (1989).
253. R. H. Newnham, *J. Appl. Electrochem.*, **22**, 116 (1992).
254. K. L. Hardee, L. M. Ernes, C. W. Brown, and T. E. Moore, in *Proc. AESF Continuous Steel Strip Plating Symp*., Dearborn, May 1993, pp. 239–252.
255. S. Kulandaisamy, J. Prabhakar Rethinaraj, S. C. Chockalingam, S. Visvanathan, K. V. Venkateswaran, P. Ramachandran, and V. Nandakumar, *J. Appl. Electrochem.*, **27**, 579 (1997).
256. R. Otagawa, K. Soda, S. Yamauchi, M. Morimitsu, and M. Matsunaga, in *Proc. 4th Int. Conf. on Zinc and Zinc Alloy Coated Steel Sheet* (Galvatech'98), Iron and Steel Inst. of Japan, Chiba, 1998, pp. 768–771.
257. J. R. Smith, F. C. Walsh, and R. Clarke, *J. Appl. Electrochem.*, **28**, 1021 (1998).
258. M. Turner and J. K. Dennis, *Trans. IMF*, **64**, 94 (1986).
259. T. Xue, W. C. Cooper, R. Pascual, and S. Saimoto, *J. Appl. Electrochem.*, **21**, 231 (1991).
260. K. Saber, C. C. Koch, and P. S. Fedkiw, *Mat. Sci. and Eng. A*, **341**, 174 (2003).
261. K. M. Youssef, C. C. Koch, and P. S. Fedkiw, *Etectrochim., Acta*, **54**, 677 (2008).
262. D. L. Wang, Y. Q. Whu, X. Y. Zong, W. Q. Zhang, M. C. Li, and J. N. Shen, *Russ. J. Electrochem.*, **45**, 291 (2009).
263. M. S. Chandrasekar, Sh. Srinivasan, and M. Pushparanam, *J. Mat. Sci.*, **45**, 1160 (2010).
264. A. Gomes and M. I. da Silva Pereira, *Electrochim., Acta*, **51**, 1342 (2006).
265. M. Mouanga, L. Ricq, G. Douglade, J. Douglade, and P. Berçot, *Surf. Coatings Technol.*, **201**, 762 (2006).
266. J. C. Ballestros, P. Diaz-Arista, Y. Meas, R. Ortega, and G. Trejo, *Electrochim. Acta*, **52**, 3686 (2007).
267. M. Ch. Li, L L. Jiang, W. Q. Zhang, Y. H. Qian, S. Z. Luo, and J. N. Shen. *J. Solid State Electrochem.*, **11**, 549 (2007).
268. M. Mouanga, L, Ricq, L. Ismaili, B. Refouvelet, and P. Berçot, *Surf. Coatings Technol.*, **201**, 7143 (2007).
269. M. Li, S. Luo, Y. Qian, W. Zhang, L. Jiang, and J. Shen, *J. Electrochem. Soc.*, **154**, D567 (2007).
270. M. Mouango, L. Ricq, and P. Berçot, *Surf. Coatings Technol.*, **202**, 1645 (2008).
271. Q. Zhang and Y. Hua, *J. Appl. Electrochem.*, **39**, 261 (2009).
272. Q. Zhang and Y. Hua, *J. Appl. Electrochem.*, **39**, 1185 (2009).
273. Q. Zhang, Y. Hua, T. Dong, and D. Zhou, *J. Appl. Electrochem.*, **39**, 1207 (2009).
274. Q. Zhang, Y. Hua, Y. Lei, and Q. Pei, *J. Appl. Electrochem.*, **39**, 2329 (2009).
275. K. O. Nayana and T. V. Venkatesha, *Synthesis and Reactivity in Inorg., Metal-Org. and Nano-Metal Chem.*, **40**, 170 (2010).
276. K. Raeissi, A. Tufani, A. Saatchi, M.A. Golozar, and J.A. Szpunar, *J. Electrochem. Soc.*, **155**, D783 (2008).
277. D. Vasilakopoulos, M. Bouroushia, and N. Spyrellis, *Electrochim. Acta.* **54**, 2509 (2009).
278. H, Nakano, *Trans. Non Ferrous Met. Soc. China*, **19**, 835 (2009).

11

ELECTRODEPOSITION OF IRON AND IRON ALLOYS

MASANOBU IZAKI

Iron plating is the principal material used for numerous applications due to the desirable physical properties of iron and its low cost. The early literature on iron deposition, which was concerned with both commercial applications and electrorefining, has been comprehensively surveyed in a monograph [1]. The production of electrotypes in Russia [2] and of driving bands for shells in Germany during World War I, the electroforming of iron sheets and tubes [3], and the rebuilding of worn parts [4, 5] were among the early applications of electrodeposited iron. The good magnetic properties which may be obtained with electrolytic iron led to its use by the Western Electric Company [6] in the cores of Pupin induction coils prior to the development of nickel–iron alloys with even better magnetic properties.

Another application is a process reported in 1930 [7] in which intaglio plates for printing government currency and bonds were made by depositing a nickel face backed by a heavy deposit of electrolytic iron from a hot chloride bath.

In order to conserve nickel and copper, iron plating was used during World War II to make electrotypes and to coat stereotypes [8, 9]. During the same period, the United States Rubber Company electroformed iron molds for rubber, glass, and plastics [10]. Soldering tips are plated with iron commercially, and undoubtedly there are many other small-scale applications. The electrodeposition of iron as a means of producing iron powder for powder metallurgy is an application that continues to be used [11].

Interest in iron plating persists despite the fact that many of its applications have been short-lived. This is attested by several publications on, for example, the production of iron strips [12, 13], electrowinning [14, 15], the electroforming of phonograph record stampers [16, 17], rolls and molds [18], and the use of iron for restoring worn parts [19]. Continuous iron strips produced by iron plating have been used for composite roofing materials, low-wattage resistance heating elements, and several magnetic products such as laminated cores for coils, magnetic display boards, and magnetic shielding [20–22]. Hard iron plating was employed on aluminum pistons to enhance wear resistance, to eliminate the need for iron or steel sleeves, and to allow the use of die casting methods [23]. Over five million pistons were plated with hard iron deposits at General Motors Corporation [24]. A 1973 patent mentioned the effectiveness of intermediate thin iron deposits with low stress to obtain thick and highly stressed iron deposits on a soft material without any peeling or spalling of the iron deposits [25].

There are several reasons for this persistent interest in iron plating. Iron is cheap and abundant. It can be deposited as a hard and brittle metal which, by heat treatment, can be rendered soft and malleable, or as a soft and ductile metal to which surface hardness can be imparted by carburizing, cyaniding, and nitriding. The fatigue strength of surfaces prepared by case hardening electrodeposited iron has been reported to be equal to the best commercial rolling-element bearing materials [26]. Electrodeposited iron can be welded readily, other metals can be easily plated on it, and in the soft state it has superior drawing properties [27]. Electrodeposited iron is relatively resistant to corrosion, as would be expected from its high purity; the contrary opinion, which has been quoted in the literature [28], probably arose due to a failure to rinse deposits completely free of electrolyte traces. The throwing power of iron baths is comparable to that of nickel baths.

The production of several types of iron alloy plating has been one of the most important developments of the last two decades in the metal finishing industry. Iron–nickel alloy plating has been widely used for decorative coating [29], for the surface coating of continuous casting molds in the steel

Modern Electroplating, Fifth Edition Edited by Mordechay Schlesinger and Milan Paunovic

making industry [30], and for magnetic devices [31–37]. Iron–zinc alloy plating has been used in the steel industry for the corrosion protection of iron-based materials [38] in rack-or-barrel operation [39] and continuous plating operation [40]. There have been developments in the production of iron oxides in the last decade, and some applications have been found in medical and electronics industries.

A significant problem with iron and iron alloy plating that has limited its usage to specialized or high-volume applications is that, despite usually lower costs for anodes and solutions, the expenditure for capital equipment and maintenance may be higher for an iron plating bath than for other more commonly used plating baths. Special high-temperature or corrosion-resistant equipment may be required to heat, agitate, filter, or ventilate the iron plating bath. Also, unless used regularly, the solution will oxidize gradually. The time and effort required to restore the electrolyte to an operable condition may outweigh the economic benefit of depositing a lower cost metal.

11.1 PRINCIPLES

Practically all iron is plated from acidic solutions of Fe(II) (ferrous) salts. The presence of iron in the Fe(III) (ferric) state in these baths, in an appreciable concentration, is undesirable because it lowers the cathode efficiency for depositing the metal and it may cause deposits to be brittle, stressed, and pitted. In practice, it is not difficult to maintain the concentration of Fe(III) ion at harmless levels.

Until recently, practically all iron was plated from baths containing Fe(II) sulfate, Fe(II) chloride, or a mixture of the two. Iron(II) fluoborate and Fe(II) sulfamate baths have been used to some extent. Research on plating from solutions of other iron salts has not been neglected. In 1887, Watt [41] investigated deposition from solutions of a large number of iron salts and concluded incorrectly that only sulfate baths were practical. Baths based on the iron salts of several fluorine-substituted phosphoric acids and fatty acids were investigated but did not yield satisfactory deposits [42]. Selected baths of other types are described in a later section of this chapter.

The most frequent addition to both the sulfate and chloride bath is conducting salts, such as a corresponding alkali and alkaline earth salts. Many other salts, such as those of various organic acids, have been recommended. Oxycarboxylic and dicarboxylic acids such as citric, malic, malonic, tartaric, and ascorbic have been used to prevent the formation of ferric hydroxide precipitation [43]. These acids may give codeposition of an impurity element which affects the properties of an iron deposit and may be justified in special circumstances. The simple bath combinations described next should fill most requirements and have been used generally for the production of an iron strip.

11.2 FERROUS SULFATE BATH

The Fe(II) (ferrous) sulfate bath produces deposits that are smooth and normally light gray in color. There is little tendency toward pitting, and thick deposits can be produced. Disadvantages of the bath are that it yields brittle deposits, the deposition rate is slow, and the current density at which burning occurs is about one-half that of a hot chloride bath. An advantage is that it can be operated at room temperature (about 25°C), in contrast with the ferrous chloride–calcium chloride bath.

The most common sulfate bath is the one containing the double salt, ferrous ammonium sulfate. It has been used principally for building up undersized machine parts [4, 5] and also to apply a hard facing to stereotype [8].

Iron(II) sulfate may also be used alone, or other salts such as sodium, magnesium, or aluminum sulfate may be added [1, 44]. Addition of a small amount of ammonium fluoborate to the high-pH sulfate bath is claimed to make the slimy Fe(III) hydroxide precipitate that accumulates in it more easily filterable [45].

The different added salts probably have minor specific effects on the properties of the deposits, but no data are available. The presence of ammonium ion appears to reduce the rate of air oxidation of Fe(II) ion and the internal stress.

It will be noted in Table 11.1 that the two ranges of pH are shown for the sulfate bath at 25°C. The two distinct ranges result from the fact that Fe(III) hydroxide precipitates at a pH of about 3.5, whereas Fe(II) hydroxide precipitates at a pH of about 6. In the low–pH range, even in a well-reduced bath, some Fe(III) ion is present because of air oxidation; therefore, operation at a pH too close to 3.5 results in dark-colored, excessively stressed deposits, probably caused by inclusion of basic Fe(III) salts in the deposits. Operation at a pH below the recommended minimum for the low pH–range results in lower cathode efficiency and increased deposit stress.

In the high-pH range a very low concentration of Fe(III) ion is automatically maintained [equal to the solubility of Fe (III) hydroxide], because the pH is above that at which Fe(III) hydroxide precipitates. The bath in this pH range therefore tends to be "sludgy." The sludge does not cause significant roughness of deposits up to a few tens of micrometers in thickness, but if heavy deposits are to be produced, filtration may be required. The high-pH sulfate bath has better covering power and yields deposits that are less stressed than those from the low-pH bath. Deposits with minimum stress are obtained at pH value in the range 4.0–5.0. The internal stress of the deposit generally increases with the increase in current density.

At the higher operating temperatures, sludging due to air oxidation is rapid at high pH. Therefore only the lower pH range is recommended for operation at elevated temperatures. The advantage of an elevated temperature is the higher permissible current density. The disadvantages of operating

at temperature higher than about 60°C probably outweigh any gain in permissible current density. Deposits from the sulfate bath do not become significantly ductile even if the bath is operated at the boiling point.

11.3 FERROUS CHLORIDE BATH

The important and distinctive characteristics of the chloride baths is that they permit high current density or fast deposition rates and yield ductile deposits when operated at temperatures higher than about 85°C. The most commonly used bath is a solution of Fe(II) and calcium chlorides, which has been referred to as the Fischer–Langbein solution [46]. This bath yields dark-colored, hard, highly stressed deposits at 25°C. At increasingly higher temperatures, the deposits gradually become lighter colored.

The composition of the Fischer–Langbein solution as modified by Thomas and Blum [7] and that modified in industrial use [47] are shown in Table 11.1. The lower concentrations introduced by Thomas and Blum permit the use of moderate current densities and do not lead to crystallization of the salts when the bath is cooled. The presence of calcium chloride in the hot-chloride bath leads to increases in bath conductivity and cathode efficiency and does not appear to have significant effects on the structure and physical properties of deposits [48]. The importance of the hygroscopic character of calcium chloride in reducing evaporation of water from this type of bath and in raising boiling point seems overstressed in the literature [46]. Elimination of calcium chloride from the bath permits the use of higher ferrous chloride concentrations with resultant higher operable current densities. For rapid deposition at current density as high as 40 $A dm^{-2}$, a solution of ferrous chloride alone has been used at concentration from 120 to 150 $g L^{-1}$ as Fe^{2+} [22]. For lower stressed deposits, concentrations as high as 725 $g L^{-1}$ $FeCl_2 \cdot 4H_2O$ have been used [49].

Numerous modifications of the hot–chloride bath have been described in which calcium chloride has been replaced by other alkaline earth chlorides [1, 50]. The presence of a low concentration of Mn(II) chloride has been claimed to result in deposits of finer grain size [51], and a bath containing a large amount of this salt has been recommended for plating machine parts [52]. The presence of $AlCl_3$, $BeCl_2$, or $CrCl_2$ in low concentration has been reported to render deposit that is softer and more ductile [53]. The presence of 20–100 $g L^{-1}$ $AlCl_3$ has been claimed to produce better stability [54]. The maintenance of a small concentration of Fe(III), up to about 0.5 $g L^{-1}$, has been stated to result in better throwing power [55] and in the elimination of pitting [16]. The presence of Fe(III), however, causes deposits to be harder, less ductile, and more highly stressed than those from well-reduced baths. From the bath with concentration ratio of Fe(III) to Fe(II) below 0.09, a deposit with good quality is produced [21]. The internal stress increases with the increase in the current density or with the decrease in the

TABLE 11.1 Composition and Operating Conditions for Iron Plating Baths

Type of Solution	Composition	Operating Conditions
Sulfate	$FeSO_4 \cdot (NH_4)_2SO_4 \cdot 6H_2O$: 250–300 $g L^{-1}$ $FeSO_4 \cdot 7H_2O$: 250 $g L^{-1}$ $(NH_4)_2SO_4$: 120 $g L^{-1}$	Low pH 2.8–3.4 or high pH 4.0–5.5, 2 $A dm^{-2}$, 25°C pH 2.1–2.4, 4–10 $A dm^{-2}$, 60°C
For production of strip	$FeSO_4 \cdot 7H_2O$: 600 $g L^{-1}$	pH 1.4, 6.7 $A dm^{-2}$, 47°C
Chloride (Fischer–Langbein)	$FeCl_2 \cdot 4H_2O$: 300 $g L^{-1}$ $CaCl_2$: 335 $g L^{-1}$ $FeCl_2 \cdot 4H_2O$: 300–450 $g L^{-1}$ $CaCl_2$:150–190 $g L^{-1}$	pH 0.8–1.5, 6.5 $A dm^{-2}$, 90°C pH 0.2–1.8, 2–9 $A dm^{-2}$, 88–99°C
For electrotype	$FeCl_2 \cdot 4H_2O$: 240 $g L^{-1}$ KCl: 180 $g L^{-1}$	pH 5–5.5, 2–5 $A dm^{-2}$, 25–40°C
For production of strip	Ferrous chloride: 120–150 $g L^{-1}$ as Fe^{2+}	pH 0.5–4.7, 33–40 $A dm^{-2}$, 98–106°C
Sulfate–chloride, for electrotype	$FeSO_4 \cdot 7H_2O$: 250 $g L^{-1}$ $FeCl_2 \cdot 4H_2O$: 42 $g L^{-1}$ NH_4Cl: 20 $g L^{-1}$	pH 3.5–5.5, 5–10Adm^{-2}, 40–43°C
For production of strip	$FeSO_4 \cdot 7H_2O$: 500 $g L^{-1}$ NaCl: 50 $g L^{-1}$	pH 2.5, 3–27.5 $A dm^{-2}$, 80°C
Sulfamate	Iron(II) sulfamate: 250 $g L^{-1}$ Ammonium sulfamate: 30 $g L^{-1}$	pH 3.2–15 $A dm^{-2}$, 50–70°C
Fluoborate	$Fe(BF_4)_2$: 226 $g L^{-1}$ NaCl: 10 $g L^{-1}$	pH 2–3, 2–10 $A dm^{-2}$, 55–60°C

bath temperature. The deposit with excellent ductility is obtained at higher temperature, lower pH, and high current density.

11.3.1 Fluoborate Bath

Iron plating from fluoborate solution is not new, but since a variety of fluoborate salts became commercially available, interest in their use in plating was stimulated, and several Fe (II) fluoborate baths have been described [56–60]. The composition shown in Table 11.1 has been recommended for plating stereotypes [56] and is probably satisfactory for general-purpose baths. A bath prepared from the commercially available concentrated solution will contain a small excess of fluoboric and boric acids, which are present in the concentrate. The boric acid probably has a desirable buffering action. In the iron fluoborate bath described by Kudryavtsev and Mel'nikova [59] the recommended concentration of boric acid is $18\,g\,L^{-1}$. Fluoboric acid may be used to adjust the pH.

The fluoborate bath has good stability, high conductivity, and high tolerance to metallic impurities. The disadvantage of the bath is that it is more expensive than chloride or sulfate bath. The fluoborate bath yields deposits similar in brittleness and in most other properties to those from the sulfate bath.

11.3.2 Other Baths

Solution Used for Iron Electrotypes The two baths listed in Table 11.1 were developed for making iron electrotypes [8, 9]. Although the ferrous chloride–potassium chloride bath appears to be similar to the Fischer–Langbein type, it differs from the latter in performance in yielding light-gray, stress-free deposits at 25°C. The deposits are, however, brittle. This difference in performance appears to be caused specifically by the potassium ion. The sulfate–chloride bath yields brittle deposits that are under moderate stress. It has somewhat better " covering power," which is improved by the presence of ammonium ion, as is also the case with nickel electrotyping solutions. Both iron plating solutions operate satisfactorily at higher temperatures than are shown in the table. The upper limits of temperature were imposed because of the low softening points of wax or plastic electrotype molding media.

Solution Used for Production of Iron Strip The three baths of simple sulfate [61], chloride [22, 62], and sulfate–chloride bath [63] listed in Table 11.1 have been developed for production of continuous iron strip. These baths contained ferrous salts at higher concentration than those for rack operation and generally operated at higher current density, higher bath temperature, and higher flow rate of the solutions by using a special electrolytic cell which will be mentioned later in this chapter. Chloride bath is favorable for this purpose because of the allowance of higher current density as high as $100\,A\,dm^{-2}$ at which satisfactory deposit was obtained. A mixed fluoborate–sulfamate Fe(II) electrolyte has been used by Levy and Hutton for the deposition of high–strength iron strips [64].

Other Special-Purpose and Less Common Baths Many iron plating baths based on unusual salts or special formulations for specific purposes have been described.

Good performance was claimed by Piontelli [65], Barrett [66], Ueno [67], and Lowrie [47] for Fe(II) sulfamate baths. Current densities up to $10\,A\,dm^{-2}$ and cathode efficiency up to 96% were described by Misra and Rama Char [68] in a bath containing Fe(II) sulfamate and ammonium sulfamate. The effectiveness of saccharin addition to decrease internal stress was mentioned in sulfamate–ammonium fluoride acidic bath [67]. Iron sulfamate in the concentrated solution is available commercially.

An iron bath of a mixed chloride–sulfate type containing boric acid and sodium formate has been recommended for depositing a starting plate on active basis metals such as aluminum, beryllium, or uranium [69] and for applying an intermediate layer of iron between steel and electrodeposited antimony deposit [70].

Two types of alkaline iron plating baths have been described. In one, Fe(III) is complexed with triethanolamine and ethylenediaminetetraacetic acid [71, 72]. In the other, the main constituent of the bath is Fe(III) pyophosphate [73]. Only thin deposits have been reported from these baths. Both suffer from the disadvantage that iron does not dissolve in them anodically. Other baths based on complexes of Fe(III), such as oxalate or citrate, have been described [74]; this type of bath, however, is useful primarily for electroanalysis rather than for electroplating.

Iron powder obtained by electrodeposition is used commercially. Conditions for depositing iron in powder form have been defined by several authors [75–78]. The bath described in [76] is unusual in that it consists of an aqueous solution of Fe(III) oxide and sodium hydroxide, in which the iron is probably present as sodium ferrate. Procedures for producing iron powders by crushing brittle deposits were reviewed by Shafer and Harr [11], who report that sintered parts made from electrolytic iron powder have higher density and better physical properties than those made from nonelectrolytic powders.

The electrodeposition of binary and ternary iron alloys has been reviewed in several articles [79–82]. Twenty-two elements, including carbon, have been electrodeposited with iron. Electrochemical investigations of anomalous deposition behavior in iron alloy systems have been discussed in many papers [83–86]. The bath composition and operating conditions for the production of iron alloy deposits are presented in Table 11.2.

TABLE 11.2 Bath Composition and Operating Conditions of Iron Alloy Plating

Alloy	Purpose and Reference	Bath Composition	Operating Conditions	Characteristics
Iron–nickel	Decorative [88]	$NiSO_4 \cdot 6H_2O$: 150 g L^{-1} $NiCl_2 \cdot 6H_2O$: 90 g L^{-1} $FeSO_4 \cdot 7H_2O$:20 g L^{-1} H_3BO_3: 45 g L^{-1} Stabilizer and brightener	60°C, pH 3.5, 4 A dm^{-2}	Fe–50%Ni, hardness: 508 Knoop
	Magnetic [37]	Nickel sulfate: 16 g L^{-1} Nickel chloride: 40 g L^{-1} Ferrous sulfate:1 g L^{-1} Boric acid: 25 g L^{-1} Sodium saccharin: 0.375–3 g L^{-1} Sodium lauryl sulfate: 0.2 g L^{-1}	26°C, pH 2.5, 1.5 A dm^{-2}	Fe–80%Ni (705 nm thick), Hc: 0.25 Oe
	Invar [97]	Nickel sulfamate: 0.75 mol L^{-1} Ferrous chloride: 0.25 mol L^{-1} Boric acid: 0.5 mol L^{-1} Sodium dodecyl sulfate: 0.5 g L^{-1} Ascorbic acid: 1 g L^{-1} Saccharin: 2 g L^{-1}	50°C, pH 2.5, 10 A dm^{-2}	Fe–39%Ni: thermal expansion coefficient of 8.1 × 10^{-6}/°C, 4–5 × 10^{-6}/°C (after annealing at 680°C)
	Invar [99]	$NiSO_4 \cdot 6H_2O$: 0.95 mol L^{-1} $NiCl_2 \cdot 6H_2O$: 0.17 mol L^{-1} $FeSO_4 \cdot 7H_2O$: 0–0.35 mol L^{-1} H_3BO_3: 0.49 mol L^{-1} Saccharin: 8 mmol L^{-1} Malonic acid: 0.05 mol L^{-1}	50°C, pH 2.5, 4 A dm^{-2}	Fe–42%Ni: thermal expansion coefficient of 6.6 × 10^{-6}/°C, 6.1 × 10^{-6}/°C (after annealing at 680°C)
Iron–zinc	Corrosion protection [40]	$FeSO_4 \cdot 7H_2O + ZnSO_4 \cdot 7H_2O$:500 g L^{-1} Na_2SO_4: 30 g L^{-1} $CH_3COONa \cdot 3H_2O$: 20 g L^{-1} $C_6H_8O_7$: 5 g L^{-1}	50°C, pH 2.5, 3 A dm^{-2}	
	Corrosion protection [121]	Ferrous chloride: 0.8 mol L^{-1} Zinc chloride: 0.8 mol L^{-1} Ammonium chloride: 100 g L^{-1}	50°C, pH 2.5, ~4 A dm^{-2}	
	Corrosion protection [122]	ZnO: 0.15–0.4 mol L^{-1} Ferrous gluconate: 0.05–0.075 mol L^{-1} KOH: 6.6 mol L^{-1}	25°C, pH>14, 50–800 mA cm^{-2}	

(*continued*)

TABLE 11.2 (*Continued*)

Alloy	Purpose and Reference	Bath Composition	Operating Conditions	Characteristics
Iron–platinum	Magnetic [120]	$FeCl_2$: 0.11 mol L^{-1} $PtCl_2$:0.3–30 mmol L^{-1} NaCl: 0.5 mol L^{-1}	20°C, pH 2.5, −0.4 to −0.8 V (SCE)	$L1_0$–FePt
Iron–cobalt	Antifriction [115]	$FeCl_2$: 227 g L^{-1} $CoCl_2{\cdot}6H_2O$: 8 g L^{-1} H_3BO_3: 10 g L^{-1} NH_4Cl: 75 g L^{-1} NaCl: 75 g L^{-1} NH_4BF_4: 10 g L^{-1}	50°C, pH 1, 5–40 A dm^{-2}	Fe–6%Co, hardness: 640 Vickers
	Magnetic [106]	$CoSO_47H_2O$: 0.10 mol dm^{-3} $CoCl_2{\cdot}6H_2O$:0.10 mol dm^{-3} $FeSO_47H_2O$: 0.02 mol dm^{-3} H_3BO_3: 0.50 mol dm^{-3} NH_4Cl: 0.50 mol dm^{-3}	40°C, pH 2.9, 1.5 A dm^{-2}	Heating under 2 kOe $Co_{95}Fe_{5.5}$, Bs:1.6 T, Hc: 0.5 Oe
Iron–cobalt–nickel	Magnetic [115]	Ferrous sulfate: 0.005–0.045 mol dm^{-3} Cobalt sulfate: 0.03–0.0875 mol dm^{-3} Nickel sulfate: 0.2 mol dm^{-3} Ammonium chloride: 0.28 mol dm^{-3} Boric acid: 0.4 mol dm^{-3} Sodium lauryl sulfate: 0.01 mol dm^{-3}	20°C, pH 2.5–3.0, 3–20 mA cm^{-2}	$Co_{65}Ni_{12}Fe_{23}$, Bs: 2.1 T, Hc: 1.2 Oe, permeability: 600 at 1 MHz, ρ: 21 μΩ-cm
	Magnetic [116]	$CoSO_4{\cdot}7H_2O$: 0.01–0.05 mol L^{-1} $NiSO_4{\cdot}6H_2O$: 0.2 mol L^{-1} $FeSO_4{\cdot}7H_2O$:0.01–0.05 mol L^{-1} H_3BO_3: 0.4 mol L^{-1}	25°C, pH2–3.5, 5–50 mA cm^{-2}	Electrodeposition under 600 Oe, Bs: 2.15 T, Hc: 1 Oe, permeability: 200 at 1 GHz, fr: 1.85 GHz, ρ: 50 μΩ-cm
Iron–cobalt–vanadium	Magnetic [118]	Iron(II) sulfamate: 0.5 mol L^{-1} Cobalt(II) sulfamate: 0.5–0.75 mol L^{-1} Ammonium metavanadate: 0.4 mol L^{-1} Boric acid: 0.4 mol L^{-1} Sodium borate: 0.25 mol L^{-1} L-ascorbic acid: 0.025 mol L^{-1} Saccharin: 1 g L^{-1} Surfactant: 0.5 vol %	45–55°C, P H3.0, 40 mA cm^{-2}	Fe52.3Co46.5V1.2, Bs: 2.2 T, Hc: 6Oe
Iron–chromium–nickel	Corrosion protection [142]	$K_2Cr_2(SO_4)_4{\cdot}25H_2O$: 326 g L^{-1} Nickel sulfate: 84 g L^{-1} Ferrous sulfate: 56 g L^{-1} Glycine: 150 g L^{-1}	20°C, pH 2–2.2, 8.5 A dm^{-2}	9.8–11%Cr, 7.3–6%Ni

Iron–phosphorus	Corrosion protection [123]	Fe $Cl_2{\cdot}4H_2O$: 240 g L^{-1} KCl: 180 g L^{-1} Hypophosphorus acid	40°C, pH 2, 40 A dm^{-2}	Fe–0.4%P
	Magnetic [124]	$FeSO_4{\cdot}7H_2O$: 1.0 mol L^{-1} $(NH_4)_2SO_4$: 0.1 mol L^{-1} $C_6H_7O_6$: 0.1 mol L^{-1} $NaH_2PO_2H_2O$: 0.01 mol L^{-1}	25°C, pH 2.5, 1 A dm^{-2}	Fe–6%P, Hc: 2Oe
Iron–boron	Magnetic [126]	$FeSO_4{\cdot}7H_2O$: 0.07 mol L^{-1} KBH_4: 0.3 mol L^{-1} $KNaC_4H_4O_6{\cdot}4H_2O$: 0.6 mol L^{-1} $(NH_4)_2SO_4$: 0.08 mol L^{-1} NaOH: 0.4 mol L^{-1}	30°C, pH 12.5, 1 A dm^{-2}	Fe–8%B, Hc: 3.6O e, saturation magnetostriction: 27×10^{-6}
Iron–carbon	Antifriction [132]	$FeSO_4{\cdot}7H_2O$: 40 g L^{-1} L-ascorbic acid: 3.0 g L^{-1} Citric acid: 1.2 g L^{-1}	50°C, pH 2.5, 3 A dm^{-2}	Fe–1%C, hardness: 800 Vickers
Iron–carbon–boron	Antifriction [134]	Fe $Cl_2{\cdot}4H_2O$: 1.0 mol L^{-1} Malic acid: 5 mmol L^{-1} Boric acid: 0.65 mol L^{-1} Dimethylamineborane: 50 mmol L^{-1}	50°C, pH 3.5, 5 A dm^{-2}	Fe–0.2%C–0.11%B, hardness: 700 Vickers, KIc: 1400 N $mm^{-3/2}$
Iron–carbon–phosphorus	Antifriction [135]	Iron(II) chloride: 0.15 mol L^{-1} Citric acid: 6.2 mmol L^{-1} L-ascorbic acid: 1.7 mmol L^{-1} Phosphinic acid: 0.15 mol L^{-1}	50°C, pH 3.5, 30 mA cm^{-2}	Fe–1.1%C–7%P, Hardness: 6700 Vickers, KIc: 400 kg $mm^{-3/2}$

Note: Bs: magnetic flux density, Ms: saturation magnetization, Hc: coercive force.

The greatest interest in iron binary alloys in recent years, as indicated by the number of publications, has been in iron–nickel alloy plating. Iron–nickel alloy deposit is favorable to decorative and protective deposit as undercoats of thin chromium deposit, because the operating costs can be reduced to a level lower than that required for nickel plating [87, 88]. The alloy deposits are used for appliance hardware, tubular furniture, plumbing goods, jewelry, and wire products. Most baths used for decorative nickel–iron alloy plating contain nickel sulfate, nickel chloride, ferrous sulfate, boric acid, and a brightener as well as a hydroxycarboxylic acid stabilizer, such as citric acid, to prevent the oxidation of ferrous ions. Saccharin or specific aromatic sulfonamides are used as primary brighteners and give codeposition of sulfur in the deposits. Heterocyclic amine, nitrils, and secondary acetylenic alcohol have been used as secondary brighteners. These brighteners tend to increase the stress and hardness. A nickel content ranging from 10 to 45% has no detrimental effect on brittleness, leveling characteristics, or subsequent chromium plating. Bath temperature, ferric ion concentration, and the buffering ability of the added stabilizer affect the leveling and cathode efficiency. Alloy deposits have been used as replacements for bright nickel in mild or moderate service conditions since the corrosion protection of the alloy deposits is equivalent to that of comparable nickel/chromium deposits [88, 89].

Iron (4–10%)–nickel alloy deposits have been used for the inner surface coatings of continuous casting molds to prolong mold life, to improve product quality, and to reduce the running cost. The same is true of other coatings of chromium plating, thick and tapered nickel coating, and multiple-layer coatings of nickel/nickel–phosphorus/chromium plating [90]. Alloy deposits have twice the hardness and half the elongation of nickel plating and the same thermal expansion coefficient as the copper mold base. One paper mentioned that iron–nickel alloy deposits prolong mold life to about 1.2–1.7 times that attained with nickel plating or multiple-layer coating [91].

Iron (20%)–nickel alloy (Permalloy) deposits have been the subject of considerable interest for their use in magnetic devices such as thin-film recording heads, magnetic yokes in printer heads, bubble memories, shielding, logic devices, and magnetic cores in microsolenoids because of their magnetic flux density of 1.6 T [92, 93]. When employed for discrete elements, they are frequently deposited as a full film and the magnetic pattern is then defined with an etch resist [94]. One paper mentioned a micromachining technique for producing a microcantilever, three-dimensional microcoil with an integrated magnetic core, a magnetically driven microvalve, and a microturbine using an electroforming technique of iron–nickel alloy deposits [95]. The bath compositions and operating conditions for the production of magnetic iron–nickel alloy plating were surveyed in literature [96] and are presented in Table 11.2. The deposition of an iron–39% nickel alloy with a low expansion coefficient (Invar) was achieved from a sulfamate bath [97] and has been discussed for use of waveguides [98]. The linear expansion coefficient depends on the Fe content and heating conditions after electrodeposition. Coefficients close to that of the bulk material have been reported for iron–42% nickel alloy deposits heated at 600°C [99]. An active area of research in iron–nickel alloy deposits centers on the improvement of magnetic properties by codeposition of a third element such as phosphorous [100], arsenic [101], sulfur [102], molybdenum [103], copper [104], cobalt [105–108], chromium [109], or indium [110]. Another active area centers on developing techniques to control the composition so that it stays within a tighter range. Most baths used for this purpose contain saccharin, which results in a decrease in grain size and coercive force [96]. Permalloy deposits with a coercive force below 1 Oe [37], which is lower than that of iron deposits, is obtained. The effects of current waveforms, such as a pulsating current, a reversing current, or a sinusoidal alternating current superimposed on a direct current, on the cathode efficiency, composition, or phase structure of the alloy deposits have been mentioned in the literature [111–114].

Iron–cobalt–nickel alloy electrodeposits have attracted increasing attention for their use in magnetic applications, such as magnetic recording heads, micro–magnetic actuators, and thin–film inductors, because of their magnetic characteristics. A systematic study on the relationships between the composition, phase structure, and magnetic characteristics of coercive force for iron–cobalt–nickel ternary alloy electrodeposits was carried out in 1998 [115], and the alloy composition and plating conditions required to get the magnetic and electrical characteristics appropriate for a magnetic recording head application have been found. High magnetic flux density of 2.1 T, low coercive force of 1.2 Oe, permeability of 600 at a frequency of 1 MHz, and resistivity of 21 μΩ-cm were obtained for a $Co_{65}Ni_{12}Fe_{23}$ alloy electrodeposited from an electrolyte containing an organic compound but without any sulfur-containing additives. Body-centered cubic (bcc) and face-centered cubic (fcc) lattices and mixtures of the two are formed in this alloy system. It was pointed out that the relationships between the composition, phase structure, and magnetic characteristics of coercive force strongly depend on the content of sulfur originating from the sulfur-containing additives in the electrolyte. Great success in using iron–cobalt–nickel alloy electrodeposits as magnetic recording heads in magnetic storage systems has been achieved in Japan. An iron–cobalt–nickel alloy electrodeposited from an electrolyte not containing any organic compounds, including sulfur-containing additives, showed a high magnetic flux density of 2.15 T, a low coercive force of around 1 Oe, a resonance frequency of 1.8 GHz, a real permeability of around 1000, and a resistivity of 50 μΩ–cm [116]. A giant magnetoresistance (GMR) of about 4.5% has been reported for iron–cobalt–nickel/copper multi layered electrodeposits [117].

Iron–cobalt–vanadium alloy electrodeposits with a magnetic flux density of 2.2 T and a coercive force of 6 Oe have been reported, and research on this alloy system has been seen in the last decade [118, 119]. The plating of iron–platinum alloys with an $L1_0$ ordered structure has attracted increasing attention for its use in high-density perpendicular recording media as well as cobalt–platinum alloy [120].

The production of iron–zinc alloy deposits was one of the most important developments for the corrosion protection of iron-based materials [38,121, 122]. Iron(0.2–0.5%)–zinc alloy plating is conducted by rack-and-barrel operations [39]. Single-layer deposits of iron (15–25%)–zinc alloys have been used commercially in Japan for the inside surfaces of fenders, doors, trunk lids, and other unexposed automotive body parts because of their good weldability, formability, and corrosion resistance after painting [40]. Iron–rich iron-zinc alloy deposits with an iron concentration exceeding 40% have been used for upper layers on zinc-rich iron (20%)–zinc or zinc-nickel alloy deposits to give good corrosion resistance since the deposits have good paint adhesion and compatibility with cationic electropainting [40].

For several years, iron–0.4% phosphorus alloy plating has been used for upper layers on zinc–iron or zinc–nickel alloy deposits to enhance the paintability and phosphatability of steel strips used for automotive body parts in Japan [123]. Amorphous iron–phosphorus alloy plating with a phosphorus concentration exceeding 6% is under industrial evaluation for use in soft magnetic materials because of its low coercive force and high magnetic flux density [124, 125]. Details on a bath formulation procedure used to obtain an amorphous iron–8% boron alloy were published in 1998 [126]. Iron–boron alloy plating is under industrial evaluation for use in strain sensors and microcantilevers because of its very large magnetomechanical coupling factor, large magnetostriction, and high permeability [127].

A 1983 patent mentioned the electrodeposition of low-stress, hard iron–6% cobalt alloy deposits produced from a chloride bath with a high cathode efficiency of 96% [128].

Attempts to produce steel by co–depositing carbon in iron deposits and then performing heat treating were reported even in the early literature on iron plating. A bath reportedly used for this purpose consists of a hot ferrous chloride solution containing a relatively high concentration of glycerol, sugar, or starch [129]. Deposits are described that contain 0.7% carbon and have a hardness of 477 Brinell after heat treatment. Details on a bath formulation procedure used to obtain hard iron–1% carbon alloy deposits at a high current efficiency of above 70% were published in 1989 [130]. The bath was a ferrous sulfate solution containing small amounts of carboxylic acids as a carbon source and L-ascorbic acid to prevent the oxidation of ferrous ions in the solution. Deposits with carbon contents of 0.13, 0.56, 0.6, and 1% were obtained with oxalic, succinic, malic, and citric acids, respectively [131]. The cathode efficiency varied in the range 70–90% according to the added carboxylic acids. The iron–carbon alloy deposits with a carbon concentration exceeding 1% had a black and bright appearance and exhibited a high hardness of above 800 Vickers [132, 133]. Oxygen incorporated in iron–carbon alloy deposits adversely affected the mechanical properties, especially toughness. The oxygen content depended on the plating conditions and the added carboxylic acid. The addition of reducing agents such as dimethylamineborane (DMAB) [134] and hypophosphorus acid [135] is effective for decreasing the oxygen content to a harmless level. Iron–carbon–boron and iron–carbon–phosphorus alloy electrodeposits prepared under optimized conditions exhibited a high hardness of HV 800 and improved toughness as estimated from the stress intensity factor. Iron–carbon alloy deposits have been under industrial evaluation for use as hard coating or alternatives to thermal surface hardening materials such as carburizing or nitriding steels because of their comparable hardness and lower levels of thermal distortion [136, 137].

One area of activity centers on attempts to electrodeposit iron–nickel–chromium alloys; electrolytes for producing stainless steel deposits for decorative or corrosion-resistant coating [138–142] are described. The alloy deposits obtained contain chromium and nickel at concentrations that vary in the ranges 2.9–29% and 8–54%, respectively, according to the type of bath and operating conditions. In general, the deposits are highly stressed and are limited to a thickness of less than 30 μm. Cathode efficiency is generally low (18–35%) [142]. Cathode efficiency rapidly drops and deposit quality deteriorates with the passage of deposition time. A paper mentioned that iron–18% chromium–8% nickel alloy deposits with a high current efficiency of 60% exhibited ferro magnetic characteristics and poor corrosion resistance [143], which differs from thermally prepared stainless steel. Amorphous iron–chromium–nickel–phosphorus–carbon alloy deposits with good corrosion resistance have been described in the literature [144]. Most baths used for iron–chromium–nickel alloy plating contain glycine, which acts not only as a pH buffer but also as a complexing agent and prevents the codeposition of basic salts.

11.4 IRON OXIDES

There has been much activity in the development of iron oxide plating for magnetic and electronic applications in the last decade. The bath composition, operating conditions, and characteristics for iron oxide deposits are presented in Table 11.3. Several types of plating processes have been developed to form iron oxides of magnetite (Fe_3O_4) and hematite (α-Fe_2O_3). In 1984, a ferrite plating process used to form magnetite with ferromagnetic features was reported in Japan [145] and was expanded to ferrite ($M_xFe_{3-x}O_4$, M: nickel, zinc, cobalt, manganese) [146] and garnet

TABLE 11.3 Bath Composition and Operating Conditions of Iron Oxide Plating

Oxide	Purpose References	Bath composition	Operating conditions	Characteristics
Magnetite (Fe_3O_4)	Magnetic [145]	$FeCl_2$: 1–2 mmol L^{-1} Air bubbling	70°C, pH 7.4	Hc: 200 Oe
	Magnetic [151]	Iron(III) nitrate: 0.01 mol L^{-1} Dimethylamineborane: 0.03 mol L^{-1}	60°C, pH 2.5, −0.6 to −1.4 V (Ag/AgCl)	Ms: 320 emu/cc, Hc: 80 Oe
	Magnetic [150]	K(CH3COO): 0.04 mol L^{-1} $Fe(NH_4)_2(SO_4)_26H_2O$:0.01 mol L^{-1}	90 °C, pH 6.5, −0.4 V (Ag/AgCl)	[110]Fe_3O_4//[110] Au
Hematite (αFe_2O_3)	Semiconductor [154]	$FeCl_3$: 5 mmol L^{-1} KF: 5 mmol L^{-1} H_2O_2: 1 mol L^{-1} KCl: 0.1 mol L^{-1}	50°C, pH 2.5, −0.9–0 V (SMSE)	Bandgap: 2.2 eV (after heating at 500°C)
Zn–Fe–O	Magnetic [157]	Zinc sulfate: 1 mmol L^{-1} Ferrous sulfate: 10 mmol L^{-1}	27°C, pH 4.3–4.8, −0.9 V	αFe-ZnO, Hc: 25 Oe (300 K)
Fe–Ce–O	Magnetic [158]	$FeSO_4$: 10–40 mmol L^{-1} $CoCl_3$: 4 mmol L^{-1} L-ascorbic acid: 1.1–4.5 mmol L^{-1} NH_4SO_4: 4 mmol L^{-1} $(NH_4)_2SO_4$: 10 mmol L^{-1}	60°C, −4 mA cm^{-2}	Ms: 160 emu/cc, Hc: 50 Oe

($Y_3Fe_5O_{12}$) [147]. A nickel–zinc ferrite layer prepared with the ferrite plating process is under evaluation for use in an electromagnetic noise suppressor for printed circuit boards [148] because of its high permeability of 40 at a frequency of 1 GHz and resonance frequency of 1.2 GHz [149]. The ferrite plating process consists of the oxidation of Fe(II) ions adsorbed on substrates. The electroplating of magnetite is classified into two different processes of anodic and cathodic depositions in electrolytes containing Fe(II) ions. The ferrite plating process is classified as anodic deposition, where the magnetite is synthesized by the oxidation of Fe(II) ions adsorbed on the conductive substrate, as represented by the potential–pH diagram [150]:

$$3Fe^{2+} + 4H_2O \rightarrow Fe_3O_4 + 8H^+ + 2e^-$$

An alternative method is cathodic deposition in an electrolyte containing Fe(II) and nitrate ions [151]. Oxygen sources such as nitrate ions and molecular oxygen are indispensable for forming oxides. The deposition reaction with the nitrate ions is believed to be as follows [152]:

$$NO_3^- + H_2O + 2e^- \rightarrow NO_2^- + 2OH^-$$

$$Fe^{2+} + 2Fe^{3+} + 8OH^- \rightarrow Fe_3O_4 + 4H_2O$$

The magnetite layer deposited by cathodic deposition exhibits a saturation magnetization of 0.61 T and a coercive force of 11.9 kA m^{-1}. A magnetite layer with almost the same magnetic characteristics can be obtained from the same solution without any external power supply, that is, by chemical deposition [152].

A plating of hematite (α-Fe_2O_3) has been developed, but heating at around 500°C is needed to form the crystalline oxide [153, 154]. Platings of zinc–iron oxide (zinc-doped magnetite and iron-doped zinc oxide) and iron–cerium oxide have been reported in the last decade [155–157] Zinc-doped magnetite ($Zn_{0.16}Fe_{2.84}O_4$) exhibits excellent high-frequency characteristics, with a resonance frequency of 600 MHz and a permeability of 400 [158]. Iron-doped zinc oxide is a transparent semiconductor with room temperature ferromagnetic features, and the heated oxide layer exhibits a magnetoresistance of 0.4% at room temperature [159].

11.5 PREPARATION, MAINTENANCE, AND CONTROL

Commercial Fe(II) salts, and even reagent-grade salts, are likely to contain a significant amount of Fe(III). Therefore, it is usually necessary to reduce the Fe(III) ion before using a freshly prepared bath. This is done by adding degreased iron turnings or steel wool to the bath together with sufficient acid to lower pH to about 0.5 (sulfuric or hydrochloric acid for the sulfate or chloride bath). The reduction treatment requires 24–48 h, during which further addition of acid may be required to maintain a low pH. Alternatively, the iron(III) may be reduced by dummying the bath at a low pH. Completion of a reduction treatment is indicated by the color of the solution, which should be a clear green, free from any yellow tint.

An operating bath, if used steadily, remains fully reduced as a result of cathodic reduction of Fe(III). If a bath is idle,

maintenance of a small excess of acid helps to prevent oxidation. Since excess acid is rapidly depleted by reaction with anodes, the anodes should be removed from a bath that will be idle more than a day or so. Cubes of gum rubber floating on the surface of the bath reduce oxidation, conserve heat, and limit evolution of spray [160]. Expanded polyethylene chips or hollow balls of polypropylene serve the same purpose and are most useful for hot plating baths. For several applications such as production of iron or iron alloy plated steel strips and electroplating of magnetic iron–nickel alloy (Pearmalloy) deposit, an anion exchange membrane [161] or regeneration tank [162] has been employed to keep ferric ion concentration below desirable level.

11.5.1 Impurities

Iron baths are similar to nickel baths in that small amounts of metallic and organic impurities may cause deposits to be brittle, stressed, or pitted. Therefore, a freshly prepared bath requires purification, which is best performed after the mentioned reduction treatment. Organic impurities are removed by adsorption on activated carbon, and the carbon is removed by filtration. If the pH of the solution during treatment with carbon is adjusted to 5.0–5.5, contaminant metals that precipitate as hydroxide in this pH range are also removed. The pH may be adjusted by adding sodium, potassium, or ammonium hydroxide or by suspending Fe(II) carbonate in the bath. High-pH treatment is not recommended for the more concentrated chloride and fluoborate baths in that rapid oxidation of Fe(II) occurs with subsequent precipitation of Fe(III) hydroxide. Metallic impurities such as copper, lead, and nickel are removed by dummying the bath at an average cathode current density of 0.5 A dm^{-2} with a corrugated cathode. Details of these procedures are similar to those described for purifying nickel baths, with the notable exception that hydrogen peroxide or other oxidizing agents often added to nickel baths during treatment with activated carbon must not be added to an Fe(II) solution.

Not much is known concerning effects of specific impurities. It was found that more than 0.2 g L^{-1} zinc in the Fe(II) chloride–potassium chloride electrotyping bath causes no harm in the hot-chloride bath [51], and iron–zinc alloy can be produced from sulfate baths [163, 164]. Low tolerance limits have been reported for copper lead, arsenic, tin, and molybdenum in the hot-chloride bath [51]. Copper at a concentration of 0.2 g L^{-1} in the hot-chloride bath has been reported to cause spongy roughness in areas where the current density is high and to decrease ductility [17]. Experience with the hot-chloride bath indicates that copper or lead concentrations above 0.1 g L^{-1} and nickel or cobalt concentrations above 0.2 g L^{-1} may result in roughness and poor throwing power in low-current-density areas ($<$2.5 A dm^{-2}). In a sulfamate-ammonium fluoride bath, zinc ($>$0.1 g L^{-1}), stannous (0.1 g L^{-1}), and manganese ($>$0.5 g L^{-1}) increase the internal stress and chromium and copper($>$1 g L^{-1}) gave black deposit with rough surface [67]. In general, continuously worked baths tend to remain free of impurities in harmful amounts but occasionally may require treatment for reduction or purification, as already described.

11.5.2 pH

As indicated in the discussion of the various baths, control of pH is essential. The pH can be measured most conveniently with a glass electrode. When operated at pH below 3.5, the acid content of the bath is slowly depleted, because the anode efficiency is higher than the cathode efficiency: 100% and 80–99%, respectively. It is therefore necessary to add the appropriate acid to maintain the pH.

In the high-pH range, both anode and cathode efficiencies are close to 100%. Air oxidation of Fe(II), however, followed by precipitation of Fe(III) hydroxide results in a decrease in pH; it may be maintained by adding the appropriate hydroxide (KOH or NH_4OH). Iron(II) carbonate suspended in the bath has been used to control the pH in this range.

11.5.3 Surfactants

Although a highly purified and well-worked iron bath does not usually yield pitted deposits, pitting is sometimes encountered. Use of a wetting agent tends to increase deposit stress, but it may be helpful if used judiciously. Sodium lauryl sulfate has been reported by several authors to be a suitable wetting agent and seems to be compatible with all types of iron and iron–nickel plating solutions. The addition of 1 g L^{-1} of a condensate of sodium naphthalene sulfonate and formaldehyde to the Fe(II) chloride bath is reported to eliminate pitting regardless of Fe(III) content [23]. Reference has already been made to the control of pitting by maintaining a small concentration of Fe(III) in the hot-chloride bath [17]. Stirring of the solution or mechanical agitation of the cathode may also reduce pitting. A "bumping" type of motion is most effective. Air agitation should not be used because it results in excessive oxidation of Fe(II).

11.5.4 Analytical Technique

The approximate concentration of iron is determined by measurement of the specific gravity. Only an occasional analysis for iron is necessary. Standard analytical procedures are used to determine Fe(II), chloride, and sulfate [165]. The quantitative analysis of iron may be performed by titrimetry or spectrophotometry [166].

11.6 EQUIPMENT

All the iron plating solutions described, except the alkaline baths, require acid-proof material for tanks and auxiliary

equipment. Equipment similar to that used for acid pickling is satisfactory. For most rubber-coated steel tanks are adequate; they may be further lined with acid-proof brick for heavy service. Steel tanks with vinyl resin or fiber-reinforced plastic (FRP) linings are satisfactory at temperatures up to 60°C. Glass and glass-lined equipment is resistant to corrosion in sulfate or chloride electrolytes, but it is hardly rugged enough for commercial use unless precautions are taken to protect the cell surface from thermal and mechanical shock. Rubber-lined pumps and pumps constructed of impregnated carbon, Teflon, or titanium parts have given satisfactory service with the hot-chloride bath. Vinyl plastisols are satisfactory as rack coatings and stopoffs, even in the hot-chloride bath.

When the heat that developed from the passage of the plating current through the bath is sufficient or nearly so to maintain the proper working temperature, it has been found practical to inject live steam directly into the solution as the simplest means of initial heating. If there is too much condensate, heat exchangers of tantalum, titanium, zirconium, or Teflon may be used. Quartz immersion heaters can be used in all solutions and carbon immersion heaters can be used in fluoborate or fluoride solutions. If the nature of the work permits, mechanical agitation of the bath makes possible the use of higher current densities and facilitates the formation of a more even deposit.

For iron plating on large-volume articles as molds and rolls, a deep tank with a depth above 4 m is used to settle the ferric hydroxide precipitation on the bottom. A 1977 patent mentioned the process for exchanging a surface layer of a moving steel strip with iron deposit in an iron plating solution [167]. Special plating cells such as a paddle cell and rotating cathode cell have been employed for production of magnetic devices such as thin-film Permalloy (iron–nickel alloy) heads to maximize thickness uniformity. Several types of continuous plating cell [168] have been employed for production of iron strip and iron alloy plated steel strips in industrial fields. A paper mentioned the usage of rotating-strippable-drum system for production of an iron strip and the allowance of high current density as high as 40 A dm^{-2} [22]. The thickness of the deposit is determined by the rotating rate of drums and deposition rate. In the drum system, a bare or chromium-plated stainless steel drum was used as cathode and iron and steel scraps were used as anode. Iron alloy plating on a steel strip have been carried out at high flow rate ranging from 0.1 to 0.4 m/s and narrow strip–electrode distance ranging from 9 to 50 mm [169, 170] by using insoluble anode. When an insoluble anode is used, an anion exchange membrane is effective in preventing the oxidation of ferrous ion in the bath if it is used for separating the plating cell into two compartments of catholyte and anolyte. A regeneration reactor [133] filled with iron scraps has been used for rapid reduction of ferric ion by circulating the used anolyte solution.

11.7 ANODES

Iron anodes of high purity, such as ingot iron, wrought iron, or Swedish iron, are preferred, but anodes of steel or cast iron have been used. High-purity iron anode is necessary to obtain ductile deposits, since a hot-chloride bath is easily contaminated by impurities contained in the anode materials. All of these dissolve with high efficiency but produce some insoluble sludge residue that may cause rough deposits. It is therefore usually desirable to bag the anodes. Glass cloth, although fragile, can be used and has been reported to be quite satisfactory when coated with phenolic resin [51]. Porous stoneware diaphragms have been used, but they are rather cumbersome and have a relatively high electrical resistance. The synthetic fabrics Orlon and Dynel are satisfactory bag materials. These fabrics are more durable when used as a cover on a frame, rather than as loose bags. Polypropylene cloth has excellent chemical resistance and durability in all iron plating baths and is commonly used in the hot-chloride electrolyte. The necessity for bagging may be obviated by continuous filtration. Passivity of iron anodes has not been reported, even in high-pH sulfate baths. For the production of iron strip and iron alloy-plated steel strips, insoluble materials such as platinum-plated titanium sheets or graphite sheets have been used as anode.

11.8 CHARACTERISTICS OF DEPOSITS

The data available in 1935 on the physical properties of electrolytic iron, including mechanical, magnetic, and electrical properties, was summarized by Cleaves and Thompson [1]. The data on mechanical and physical properties of iron and iron alloy deposits have been comprehensively surveyed in a monograph [171]. A representative selection of data on physical and mechanical properties is given in Table 11.4. In general, an iron deposit is an aggregate of columnar grains with a bcc lattice which corresponds to that of the equilibrium state at ambient temperature. In general, the hardness, tensile strength, and internal stress decrease and the elongation increases with an increase in bath temperature or a decrease in current density. Hardness ranging from 120 to 350 Vickers is obtained from a simple chloride or sulfate bath. A high hardness of 450 Vickers is obtained at a low bath temperature and high current density in a hot-chloride bath. The influence of current density and boric acid addition on the oxygen content was reported for a chloride bath [172]. Codeposited oxygen in the form of iron oxide deteriorates the hardness and ductility of iron–carbon alloy deposits [132]. Adding small amounts of hypophosphorus acid or dimethylamineborane to the iron–carbon alloy plating bath reduces the oxygen content to a harmless level, which results in the enhancement of ductility [134, 135]. The sulfur and carbon contents in iron–nickel alloy

TABLE 11.4 Properties of Iron Deposits

	Bath Composition and References	pH	Temperature (°C)	Current Density (A dm^{-2})	Tensile Strength (kg mm^{-2})	Elongation (%)	Hardness	Coercive Force
Iron	Sulfate bath, $Fe(NH_4)_2(SO_4)_2$ [177]	3.4	20	0.5			263	
		3.4	20	2.0			354	
		4.4	19	0.5			182	
		4.4	41	2.0			240 (Brinell)	
	Chloride bath, $FeCl_2$ (120–150 g L^{-1} as Fe^{2+}) [22]	3.5–4.7	100–106	400	50–56	5–15		9.5–11.0 (Oe)
	Chloride bath, $FeCl_2{\cdot}4H_2O$: 400 g L^{-1}	0-3	86	20	45	2.1		19.5
	$CaCl_2$: 80 g L^{-1}		96	10	42	3.33		18
	wetting agent: 2 mL L^{-1} [21]		96	20	43	4.67		17.5
			96	30	43	5.54		225
			108	20	36	2.67		17.5 (Am^{-1})
	Chloride bath, $FeCl_2{\cdot}4H_2O$:465 g L^{-1}, H_3BO_3: 38 g L^{-1} [24]	0.2–0.4	70	15			450	
				5			300	
				2.5			170	
			95	15			150	
				5			150	
				2.5			120 (Vickers)	
	Chloride bath, $FeCl_2{\cdot}4H_2O$: 1.57 mol dm^{-3}, $CaCl_2$: 2.04 mol dm^{-3} [175]	0	60	2.0			280	
		1		2.0			250	
		2		2.0			200 (Vickers)	

(*continued*)

TABLE 11.4 (*Continued*)

	Bath Composition and References	pH	Temperature (°C)	Current Density (A dm^{-2})	Tensile Strength (kg mm^{-2})	Elongation (%)	Hardness	Coercive Force
	Sulfate–chloride bath, $FeSO_4 \cdot 7H_2O$:500 g L^{-1} NaCl:50 g L^{-1} [63]	2.5	80	8	46	4.3		
				15	56	5.3		
				27	64	2.7		
	Deposits from either sulfate or chloride baths annealed at 900°C [1]					40	70–90 (Brinell)	
Iron–carbon	$FeSO_4 \cdot 7H_2O$: 40 g L^{-1}, L-ascorbic acid: 3.0 g L^{-1}, Citric acid: 1.2 g L^{-1} [117]	2.5	50	3			800 (1%C)	
	$FeSO_4 \cdot 7H_2O$: 0.14 mol L^{-1} Organic acid: 5.4 mmol L^{-1}	2.5	50	1				
	Oxalic acid						280 (0.15%C)	
	Malonic acid						460 (0.2%C)	
	Acetic acid						500 (0.2%C)	
	Adipic acid						700 (0.6%C)	
	Succinic acid [131]						850 (1.3%C)	

deposits were quantitatively determined for a sulfate–chloride bath containing saccharin [173]. The data in Table 11.4 show that annealing electrolytic iron at 900°C results in properties approaching those of thermally prepared iron ingot. Heating the deposits at 200–300°C has no significant effect on their properties. A high hardness of 800 Vickers has been obtained for iron–carbon alloy deposits with a carbon concentration exceeding 1% which had a martensitic phase with a body-centered tetragonal lattice. With annealing at 350°C, iron–carbon alloy deposits attained a high hardness of 1200 Vickers [174]. Iron–nickel alloy deposits have the phase structure of α-iron with bcc lattice or a γ-nickel structure with an fee lattice or a mixture of the two, depending on the alloy composition [97, 176]. The phase structure of iron–nickel, iron–cobalt, and iron–cobalt–nickel alloy systems is slightly different than the equilibrium state of cast material, and the difference depends on the solution formulation, plating conditions, and impurities incorporated into the deposits originating from additives in the solutions. The phase structure is transformed to the equilibrium state by heating, resulting in a change in the mechanical and physical characteristics. Iron and iron–nickel alloy deposits have attracted increasing attention as components in spintronics with a semiconductor such as gallium–arsenide (GaAs), where the quality, including preferred orientation and lattice mismatch to the semiconductor is important. [178, 179]

REFERENCES

1. H. E. Cleaves and J. G. Thompson, *The Metal-Iron, Alloys of Iron Research Monograph Series*, McGraw-Hill, New York, 1935.
2. M. Klein, *Chem. News*, **18**, 133 (1868).
3. D. Belcher, *Trans. Am. Electrochem. Soc.*, **45**, 455 (1924).
4. W. A. MacFadyen, *Trans. Faraday Soc.*, **15** (3), 98 (1920).
5. D. R. Kellog, *Min. Metall.*, **3**, 61 (1922).
6. G. F. McMahon, *Chem. Metall. Eng.*, **26**, 639 (1922).
7. C. T. Thomas and W. Blum, *Trans. Am. Electrochem. Soc.*, **57**, 59 (1930).
8. V. A. Lamb and W. Blum, *Proc. Am. Electroplat. Soc.* 106 (1942).
9. R. M. Shaffert and B. W. Gonser, *Trans. Electrochem. Soc.*, **84**, 319 (1943).
10. A. W. Bull, J. W. Bishop, M. H. Orbaugh and E. H. Wallace, *Met. Ind. (N.Y.)* **37**, 461 (1939).
11. W. M. Shafer and C. R. Harr, *J. Electrochem. Soc.*, **105**, 413 (1958).
12. Montau Union, Handelsgesellshaft m. b. H., German Patent 1,018, 286 (1957).
13. H. Silman, *Met. Finish. (Westwood)*, **62** (12), 36 (1969); *Met. Finish. Abstr.*, **12** (2), 65 (1970).
14. E. H. Konrad and W. E. C. Eustis (to Sulfide Ore Process Co.), U.S. Patent 2,587, 630 (1952).
15. P. D. Vasudeva Rao, H. V. K. Udupa, and B. B. Dey, Symp. Electrodeposition Metal Finish., Bangalore, India Sect., *Electrochem. Soc., Indian Inst. Sci.* 77 (1960).
16. L. K. Kosowsky, (to Columbia Records. Inc.), U.S. Patent 2,758, 961 (1956).
17. A. M. Max and G. R. Van Houten, *Proc. Am. Electroplat. Soc.,* 136 (1956).
18. Technical Catalogue "Purealone", Fuso Company, Ltd., Hyogo, Japan.
19. M. M. Lekhikoinen, *Dokl. Akad. Nauk Tadzhik SSR*, No. (20), 86 (1957).
20. J. A. James, (to British Thompson-Houston Co., Ltd.), U.S. Patent 2,792,340 (1957).
21. S. F. Harty, J. A. McGeough, and R. M. Tulloch, *Surf. Tech.*, **12**, 39 (1981).
22. P. K. Subramanyan and W. M. King, *Plating Surf. Finish.*, **69**, (2), 48 (1982).
23. O. J. Kllingenmaier, (to General Motors Corp.), U.S. Patent 3,404,074 (1968).
24. O. J. Kllingenmaier, *Plating*, **61**, 741 (1974).
25. O. J. Kllingenmaier, (to General Motors Corporation), U.S. Patent, 3,753,664 (1973).
26. R. K. Kepple, E. R. Mantel, R. L. Mattson, and O. J. Kllingenmaier, *ASME Spring Symposium* Paper No. 70-Lub.S-20, 1970.
27. G. P. Fuller, *Trans. Am. Electrochem. Soc.*, **50**, 371 (1926).
28. W. E. Hughes, *Chem. Metall. Eng.*, **29**, 536 (1923).
29. Technical Catalogue "NIRON", Udylite Co., Tokyo, Japan.
30. Technical Catalogue "Tough Alloy-I", Nomura Plating Co., Osaka, Japan.
31. I. W. Wolf and W. P. McConell, *Proc. Am. Electroplat.Soc.*, **43**, 215 (1956).
32. R. S. Smith, L. E. Godycki, and J. C. Lloyd, *J. Electrochem. Soc.*, **108**, 996 (1961).
33. W. O. Freitag and J. J. Mathias, *Electroplat. Met. Finish.*, **17** (2), 42 (1964).
34. A. F. Bogenshutz and J. L. Josten, *Galvanotechnik (Saulgau)*, **61** (4), 279; **61**(5), 362 (1970) *Met. Finish. Abst.*, **12** (4), 183 (1970).
35. H. V. Vekatasetti, *J. Electrochem. Soc.*, **117**, 403 (1970).
36. S. H. Liao and S. E. Anderson, *J. Electrochem. Soc.*, **140**, 208 (1993).
37. P. Duke, T. Montelbono, and L. Missel, *Plating Surf. Finish.*, **69** (9), 61 (1982).
38. R. Sard, *Plating Surf. Finish.*, **74**, No (2), 30 (1987).
39. G. W. Loar, K. R. Romer, and T. J. Aoe, *Plating and Surf. Finish.*, **78** (3), 74 (1991).
40. T. Adaniya, T. Hara, M. Sagiyama, T. Homma and T. Watanabe, *Plating Surf. Finish.*, **72** (8), 52 (1985).
41. A. Watt, *Electrician*, **20**, 6 (1887–1888).
42. H. Conner and V. A. Lamb, *Plating*, **48**, 388 (1961).
43. A. Ohwada, *Japan Kokai Tokkyo Koho, JPN* **78**, 103, 935 (1978).

44. N. T. Kudryavtsev and L. A. Yakovleva, *Tr. Mosk. Khim-Tekhol. Inst.*, No. 22, 135 (1956) *Chem. Abstr.*, **51**, 16142a (1957).
45. R. E. Harr (to Western Electric Co., Inc.) U.S. Patent 2,710,832 (1955).
46. F. Fischer, *Z. Electrochem.*, **15**, 595 (1909); German Patent 212,994 (1908); U. S. Patent 992,951 (1911).
47. C. F. Lowrie, *Metal Finishing Magazine*, Hackensack, NJ, 1996, p. 247.
48. C. Kasper, *J. Res. Natl. Bur. Stand.*, **18**, 535 (1937).
49. J. D. Thomas, O. J. Kllingenmaier, and D. W. Hardesty, *Trans. Inst. Met. Fin.*, **47**, 209 (1969).
50. M. P. Melkov, *Vestn. Mashinostr.*, **33** (3), 50 (1953); *Chem. Abstr;* **47**, 10375 (1953)
51. W. B. Stoddard, Jr., *Trans. Electrochem. Soc.*, **84**, 305 (1943).
52. V. P. Revyakin and P. D. Myaniskov, *Vestn. Mashostr.*, **37** (4), 64 (1957), *Chem. Abstr.*, **51**, 11887b (1957).
53. Fr. Muller, E. Heuer, and O Witnes, *Z. Electrochem.*, **47**, 135 (1941).
54. M. P. Melkov and B. V. Namakonov, (Moskow Motering Inst.), Russian Patent 238,981 (1968); *Metal Finish. Abstr.*, **11** (4), 159 (1969).
55. E. H. Wallace and R. K. Iler,U.S. Patent 2,306,917 (1943).
56. S. Okada,Japanese Patent 329 (1950).
57. K. L. Kossler and R. R. Sloan, *Electrotyp. Stereotyp. Mag.*, **38** (7), 7 (1952).
58. J. Poor (to Van der Horst Corp. of Am.), U.S. Patent 2,745,800 (1956).
59. N. T. Kudryavtsev and M. M. Mel'nikov, *Nauchn. Dokl. Vyssh. Shk. Khim. i Khim. Tecknol.*, No. 1, 173 (1958);*Chem. Abstr.*, **53**, 913c (1959).
60. M. E. Farmer, D. C. West, and C. D. Darlington, *Plating*, **56**, 699 (1969).
61. Y. Kondo and K. Koike, *J. Surf. Finish. Soc. Jpn.*, **25**, 62 (1974).
62. S. Matsubara, N. Nakamura, K. Takagi, T. Omi, and K. Miyanami, *J. Iron Steel Inst. Jpn.*, **76**, 2167 (1990).
63. K. V. Gow, S. P. Iyer, H. H. Wu, K. M. Castelliz, and G. J. Hutton, *Surf. Tech.*, **8**, 333 (1979).
64. E. M. Levy and G. J. Hutton, *Plating*, **55**, 138 (1968).
65. R. Piontelli, *Korros. Metallschutz*, **19**, 110 (1943).
66. R. C. Barret, *Proc. Am. Electroplat. Soc.* **47**, 170 (1960).
67. H. Ueno, H. Hayashi, S. Takagi, S. Miwa and T. Hayashi, *J. Sur. Finish. Soc. Jpn.*, **23**, 72, 186, 252, 316, (1972).
68. S. S. Misra and T. L. Rama Char, *J. Sci. Indai Res.*, **20D** (1), 43 (1961).
69. J. G. Beach, *Plating*, **43**, 616 (1956).
70. G. R. Schaer, U.S. Patent 2,918,415 (1959).
71. E. F. Foley, Jr. H. B. Linford, and W. R. Mayer, *Plating*, **40**, 887 (1953).
72. A. Nakagawa, *J. Met. Finish. Soc. Jpn*, **11** (5), 85 (1960) *Met. Finish. Abstr.*, **2** (4), 130 (1960).
73. V. Sree and T. L. Rama Char, *Bull. India Sect. Electrochem. Soc.*, **9**, 59 (1960).
74. M. Deutsch, J. R. Downing, L. G. Elliott, J. W. Irvine, Jr., and A. Roberts, *Phys. Rev.*, **62**, 3 (1942).
75. *Metal Bulletin*, 34 (Sept. 14, 1973).
76. G. Wranglen, *J. Electrochem. Soc.*, **97**, 353 (1950).
77. A. I. Levin and S. A. Pushkareva, *J. Appl. Chem. (USSR)* **29**, 1323 (1956) (in English); *Chem. Abstr.*, **51**, 8551e; 13613h (1957).
78. J. A. M. LeDuc, R. E. Loftfield, and L. E. Vaaler, *J. Electrochem. Soc.*, **106**, 659 1959.
79. S. S. Misra and T. L. Rama Char, *Bull. India Sect. Electrochem. Soc.*, **11**, 64 1962.
80. M. Sarojamma and T. L. Rama Char, *Electroplat. Met. Finish.*, **18** (2), 51 1965.
81. R. Sevakuma and T. L. Rama Char, *Electroplat. Met. Finish.*, **24** (1), 14 1971.
82. A. Krohn and C. W. Bohn, *Plating*, **58** (3), 237 1971.
83. J. O'M. Bockris, D. Drazic, and A. R. Despic, *Electrochim., Acta*, **4**, 325 1961.
84. H. Dahms and I. M. Croll, *J. Electrochem. Soc.*, **112**, 771 1965.
85. J. Horkans, *J. Electrochem. Soc.*, **128**, 45 (1981).
86. K. Y. Sasaki and J. B. Talbot, *J. Electrochem. Soc.*, **142**, 775 1995.
87. R. J. Clauss, R. A. Tremmel, and R. W. Klein, *Trans. Inst. Met. Finish.*, **53**, 22 1975.
88. R. A. Tremmel, *Plating. Surf. Finish.*, **68** (1), 22 1981.
89. M. Pushpavanam, S. Jayakrishnan, S. R. Natarajan, and R. Subramanian, *Metal Finish.*, **84** (1), 32 1986.
90. T. Nakashima, M. Kawamoto, M. Kouzuma, K. Sekine, and S. Kurihara, *Technical Report of Sumitomo Metal Industries*, **43** (2), 77 1991.
91. H. Kanayama, A. Ichihara, Y. Watanabe, G. Hattori, and K. Suzuki, *Kawasaki Steel GIHO*, **14** (4), 12 1982.
92. R. L. White, *Plating Surf. Finish.*, **75** (4), 70 1988.
93. K. Komaki, *J. Electrochem. Soc.*, **140**, 529 1993.
94. S. Herrera, *Trans. Inst. Met. Finish.*, **73** (1), 12 1995.
95. B. Lochel and A. Maciossek, *J. Electrochem. Soc.*, **143**, 3343 1996.
96. S. N. Srimathi, S. M. Mayanna, and B. S. Sheshaeri, *Surf. Tech.*, **16**, 277 1982.
97. D. L. Grimmett, M. Schwartz, and K. Nobe, *J. Electrochem. Soc.*, **140**, 973 1993.
98. A. F. Bogenshutz, J. L. Jostan, and W. Hemmrich, *Oberflache (Berlin)* No. (12), 506 (1970)*, Met. Finish. Abstr.*, **13** (2), 84 (1971)
99. T. Nagayama, Y. Mizutani, T. Nakamura, N. Shinohara, and Hyoumen Gizyutsu, *J. Surf. Fin. Soc. Jpn*, **57**, 733 (2006).
100. K. Mukasa, M. Sato, and M. Maeda, *J. Electrochem. Soc.*, **117**, 22 (1970).
101. W. O. Freitag, G. V. DiGuilio, and J. S. Mathias, *J. Electrochem.Soc.*, **113**, 64 (1970).

102. F. E. Luborsky, *IEEE, Trans. Magn.*, **4**, 19 (1968).
103. W. O. Freitag and J. S. Mathias, *J. Electrochem. Soc.*, **112**, 64 (1965).
104. J. P. Leekstin, *IEEE Trans. Magn.*, **1**, 246 (1965); IBM Corp., British Patent 1,055,452 (1967).
105. E. Toledo and R. Mo, *Plating*, **57**, 43 (1970).
106. O. Shinoura, A. Kamijima, and H. Glzyutsu, *J. Surf. Fin. Soc. Jpn.*, **44**, 1114 (1993).
107. S. H. Liao, *IEEE Trans. Magn.* **MAG-23**, 2981 (1987).
108. S. Kelcher, D. Y. Park, B. Y. Yoo, and N. V. Myung, *Plating Surf. Finish.*, **92**, 24 Jan. (2005).
109. T. M. Harris, G. M. Whitney, and I. M. Croll, *J. Electrochem. Soc.*, **142**, 1031 (1995).
110. H. V. Venkatasetty, *J. Electrochem. Soc.*, **120**, 618 (1973).
111. M. D. Maksimovic, *Surf. Tech.*, **31**, 325 (1987); **35**, 21 (1988).
112. D. L. Grimmett, M. Schwartz, and K. Nobe, *J. Electrochem. Soc.*, **137**, 3414 (1990).
113. D. L. Grimmett, M. Schwartz, and K. Nobe, *Plating Surf. Finish.*, **75** (6), 94 (1988).
114. N. Phan, M. Schwartz and K. Nobe, *Plating Surf. Finish.*, **75** (8), 46 (1988).
115. T. Osaka, M. Takai, K. Hayashi, K. Ohashi, M. Saito, and K. Yamada, *Nature*, **392**, 796 (1998).
116. X. Liu, G. Zangari and M. Shamsuzzoha, *J. Electrochem. Soc.*, **150**, C159 (2003).
117. D. M. Davis, M. Moldovan, D. P. Young, M. Henk, X. Xie, and E. J. Podlaha, *Electrochem. Solid State Lett.*, **9**, C153 (2006).
118. I. Shao, P. M. Vereecken, C. L. Chien, R. C. Cammarata, and P. C. Shearson, *J. Electrochem. Soc.*, **150**, C184 (2003).
119. M. Shwartz, C. Arcos and K. Nobe, *Plating Surf. Finish.*, **90**, 46 (June 2003).
120. J. J. Mallett, E. B. Svedberg, S. Sayan, A. J. Shapiro, L. Wielunski, T. E. Madey, W. E. Egelhoff, Jr., and T. P. Moffat, *Electrochem. Solid State Lett.*, **7**, C121 (2004).
121. Y. Liao, D. R. Gaba and G. D. Wilcox, *Plating Surf. Finish.*, **85**, 60 (Mar. 1998).
122. C. J. Lan, W. Y. Liu, and T. S. Chin, *J. Electrochem. Soc.*, **154**, D30 (2007).
123. T. Honjo, K. Kyono, K. Yamato, T. Ichida, and T. Irie, *J. Iron steel Inst. Jpn.*, **72**, 976 (1986).
124. T. Osaka, M. Takai, A. Nakamura, and F. Aso, *Denki Kagaku*, **62**, 453 (1994).
125. A. Miko, Hempelmann, M. Lakatos-Versanyl, and E. Kalman, *Electrochem. Solid State Lett.*, **9**, C126 (2006).
126. N. Fujita, M. Inoue, K.-I. Arai, P. B. Lim, and T. Fujii, *J. Appl. Phys.*, **83**, 7294 (1998).
127. N. Fujita, M. Inoue, K. -I. Arai, M. Izaki, and T. Fujii, *J. Appl. Phys.*, **85**, 4503 (1999).
128. O. J. Kllingenmaier (to General Motors Corporation), U.S. Patent, 4,388,379 (1983).
129. Yu. Petrov, *Avtomob.*, **29** (2), 31 (1951); *Dokl. Akad. Nauk Tadzh. SSR*, No 20, 67 (1957); *Chem. Abstr.*, **53**, 8879d, 8880b (1959).
130. M. Izaki, H. Enomoto, and T. Omi, *J. Surf. Finish. Soc. Jpn.*, **40**, 1304 (1989).
131. Y. Fujiwara, T. Nagayama, A. Nakae, M. Izaki, H. Enomoto, and E. Yamauchi, *J. Electrochem. Soc.*, **143**, 2584 (1996).
132. M. Izaki and T. Omi, *Met. Mater. Trans. A*, **27A**, 483 (1996).
133. Y. Fujiwara, M. Izaki, H. Enomoto, T. Nagayama, E. Yamauchi, and A. Nakae, *J. Appl. Electrochem.*, **28**, 855 (1998).
134. M. Izaki, N. Miyamato, A. Akae, T. Hasegawa, S. Watase, M. Chigane, Y. Fujiwara, M. Ishikawa, and H. Nomoto, *J. Electrochem. Soc.*, **149**, C370 (2002).
135. N. Miyamoto, K. Yoshida, M. Matsuoka, and J. Tamai, *J. Electrochem. Soc.*, **151**, C645 (2004).
136. M. Izaki, Y. Fujiwara, H. Enomoto, A. Nakae, and N. Miyamoto, *Kokai Tokkyo Koho*, JPN 9-202991 (1997).
137. Technical Catalogue "Carboplus®," Fuso Chemical Company, Osaka, Japan.
138. A. L. Rotinyan, L. A. Aytner, and N. P. Fedot'ev, *Zh. Prikl. Khim.*, **41** (10), 2201 (1968); *Metal Finish. Abstr.*, **11** (1), 8 (1969)
139. I. M. Katser, O. A. Pterova, and A. I. Vitkin, *Zh. Prikl. Khim.*, **41** (10), 2300 (1968); *Metal Finish. Abstr.*, **11** (1), 8 (1969)
140. W. H. Cleghorn, S. Gowrie, P. L. Elsie, and B. A. Shenoi, *Met. Finish.*, **67** (8), 65 (1969).
141. L. Domnikov, *Met. Finish. (Westwood)* **68** (2), 57 (1970);**68** (4), 56 (1970); **68** (5), 56 (1970); *Met. Finish. Abstr.*, **12** (3), 119 (1970);**12** (4),181 (1970).
142. C. U. Chisholm and R. J. G. Carnegie, *Plating*, **59** (1), (1972).
143. M. Matsuoka, R. Kammel and U. Landau, *Plating Surf. Finish.*, **74** (10), 56 (1987).
144. J.-C. Kang and S. B. Lalvani, *J. Appl. Electrochem.*, **25**, 376 (1995).
145. M. Abe and Y. Tamaura, *J. Appl. Hys.*, **55**, 2614 (1984).
146. T. Ito, S. Hori, M. Abe and Y. Tamaura, *J. Appl. Phys.*, **69**, 5911 (1991).
147. Q. Zhang, T. Itoh, M. Abe, and M. J. Zhang, *J. Appl. Phys.*, **75**, 6094 (1994).
148. K. Kondo, T. Chiba, H. Ono, S. Yoshida, and M. Abe, *NEC Tokin Tech Rev.*, **30**, 48 (2003), in Japanese.
149. N. Matsushita, C. P. Chong, T. Mizutani, and M. Abe, *J. Appl. Phys.*, **91**, 7376 (2002).
150. T. A. Sorenson, S. A. Morton, G. D. Waddilli, and J. A. Switzer, *J. Am. Chem. Soc.*, **124**, 7604 (2002).
151. M. Izaki and O. Shinoura, Japanese Patent 2001-329381 (2001).
152. M. Izaki and O. Shinoura, *Adv. Mater.*, **13**, 142 (2001).
153. R. Schrebler, K. Bello, F. Vera, P. Cury, E. Munoz, R. Del Rio, H. G. Meier, R. Cordova, and E. A. Dalchiele, *Electrochem. Solid State Lett.*, **9**, C110 (2006).
154. M. Wu, R. -H. Lee, J. -J. Jow, W.-D. Yang, C.-Y. Hsieh, and B. -J. Weng, *Electrochem. Solid State Lett.*, **12**, A1 (2009).
155. M. Izaki, A. Takino, T. Shinagawa, and A. Tasaka, *Trans. Mater. Res. Soc.*, **28**, 337 (2003).

156. B. B. Lipinski, D. H. Mosca, N. Mottoso, W. H. Schreiner, and A. J. A. de Oliveira, *Electrochem. Solid State Lett.*, **7**, C115 (2004).

157. N. Fujita, M. Izaki and M. Inoue, *J. Mag. Magn. Mater.*, **300**, e350 2006.

158. M. Izaki, A. Takino, N. Fujita, T. Shinagawa, M. Chigane, S. Ikeda, M. Yamaguchi, K.-I. Arai, and A. Tasaka, *J. Electrochem. Soc.*, **151**, C519 (2004).

159. T. Shinagawa, M. Izaki, H. Inui, K. Murase, and Y. Awakura, *J. Electrochem. Soc.*, **152**, G736 (2005), C. T. Thomas, *Mon. Rev. Am. Electroplat. Soc.*, **30**, 720 (1943).

160. C. T. Thomas, *Mon. Rev. Am. Electroplat. Soc.*, **30**, 720 (1943).

161. N. Suzuki, A. Shibuya, T. Tsuda, T. Izuo, and Y. Terada, *J. Iron Steel Inst. Jpn.*, **72**, 932 (1986).

162. Y. Miwa, S. Matsubara, K. Takagi, T. Omi, and K. Miyanami, *Powder Technol.*, **64**, 168 (1991).

163. S. Jepson, S. Meecham, and F. W. Salt, *Trans. Inst. Met. Finish.*, **32**, 160 (1955).

164. W. H. Safranek (to Rockwell Spring and Axle Co.), U.S. Patents 2,809,156 (1957); 2,832,729 (1958).

165. "Guide Book Directory 1987," *Metal Finish*., 562 (1987).

166. J. Bassett, R. C. Denney, G. H. Jeffery, and J. Mendham, *Vogel's Textbook of Quantitative Inorganic Analysis*, 4th ed., Longman Scientific & Technical, England, 1986.

167. O. J. Kllingenmaier, (to General Motors Corporation), U.S. Patent 4,050,996 (1977).

168. K. Sakai and R. Yoshihara, *J. Iron Steel Jpn.*, **72**, 940 (1986).

169. K. Matsuzuka, *J. Iron Steel of Jpn.*, **72**, 891 (1986).

170. A. Weymeersh, L. Renard, J. J. Conreur, R. Winand, M. Jorda, and C. Pettet, *Plating Surf. Finish.*, **73** (7), 68 (1986).

171. W. H. Safranek, *The Properties of Electrodeposited Metals and Alloys*, American Electroplaters and Surface Finishers Society, Orlando, FL,1986, p. 195.

172. S. Gadad and T. M. Harris, *J. Electrochem. Soc.*, **145**, 3699 (1998).

173. M. Kounchenova, G. Raichevski, and St. Vitkova, *Surf. Tech.*, **31**, 137 (1987).

174. M. Izaki, H. Enomoto, A. Nakae, S. Terada, E. Yamauchi, and T. Omi, *J. Surf. Finish. Soc. Jpn.*, **45**, 1302 (1994).

175. S. Yoshimura, S. Yoshihara, T. Shirakashi, and E. Sato, *Trans. Inst. Met. Finish.*, **73** (1), 31 (1995).

176. K. Nakamura, M. Umetani, and T. Hayashi, *Surf. Tech.*, **25**, 111 (1985).

177. D. J. Macnaughton, *J. Iron Steel Inst. (London)* **109**, 409 (1924).

178. E. B. Svedberg, J. J. Mallett, L. A. Bendersky, A. G. Roy, W. F. Wegelhoff, and T. P. Moffat, *J. Electrochem. Soc.*, **153**, C807 (2006).

179. Z. L. Bao, S. Majumder, A. A. Talin, A. S. Arrott, and K. L. Kavanagh, *J. Electrochem. Soc.*, **155**, H841 (2008).

12

PALLADIUM ELECTROPLATING

JOSEPH A. ABYS

Palladium (Pd) metal was discovered and named by the English medical doctor W. H. Wollaston in 1803 while he was conducting experiments on the isolation and purification of platinum. Dr. Wollaston, a renowned scientist and astronomer, initially named his discovery "ceresium" after the newly discovered asteroid Ceres; however, he quickly changed his mind and named the metal in honor of the then newly discovered asteroid Pallas.

"Pallas" has its roots in Greek mythology and relates to the "gift by Zeus" of the statue of Pallas Athena that stood at the gates of Troy to "safeguard" the city. Mythology tells us that during the Trojan Wars, Odysseus and Diomedes stole the statue and carried it to the Greek camp, after which Troy was conquered. Pallas is most likely derived from the Greek *pallo*, meaning "to brandish a spear."

In Roman legend, Pallas Athena was obtained by Aenes during the sacking of Troy and taken to Italy where it was installed in the Temple of Vesta in Rome. The Romans venerated the statue and believed it would ensure the existence of the Empire. Thus, the word palladium became synonymous with "safeguard" and more specifically the "safeguard of liberty" [1, 2]. An excellent review [3] of the discovery and history of palladium was written by Ian E. Cottington of Johnson Matthey.

12.1 GEOLOGICAL OCCURRENCE [4–6]

Unlike other metals, the platinum group metals (PGMs) exist in the earth's crust mostly as metallic alloys, especially of nickel and iron, and only a few mineral compounds are known. Their natural abundance in the earth's crust is very low with palladium being the most abundant [5] (see Table 12.1). Interestingly enough, PGMs exist in relatively high concentrations in meteorites rich in iron and nickel as opposed to the "stony" or rock-type meteors. This has led geochemists to the supposition that on earth a similar metallurgy took place, and PGMs concentrated during the earth's formation mainly in the iron–nickel core. This accounts for their relatively low abundance in the lithosphere. An interesting phenomenon is the presence of unusually high concentrations of iridium in layers of rock dating to the time of the disappearance of the dinosaurs. This fact supports the scientific postulate that the extinction of the dinosaurs was caused by the impact of a large meteor on the Yucatan peninsula in Mexico.

12.2 SUPPLY, DEMAND, AND USES OF PALLADIUM

The economically significant sources of PGMs are Russia, South Africa, and North America. PGMs from these countries are primary deposits usually associated with platinum, copper, and nickel mining. Table 12.2 provides the estimated concentration of PGMs for each geographic region [7]. The Russian sources of Pd are the most abundant, and indeed Russia is the largest supplier of Pd today. However, the Stillwater mine in southern Montana (United States) contains the richest Pd deposits in the world and output has grown rapidly since the late 1990s. Figure 12.1 is a history of the Pd supply [7] from 1995 to 2008 which reached a peak of $\sim 8.6 \times 10^6$ troy ounces (TrOz)* in 2004. Palladium shipments averaged $\sim 8 \times 10^6$ TrOz over the last five years with Russia and South Africa supplying the majority of the yearly demand.

*One troy ounce equals 31.1 g

Modern Electroplating, Fifth Edition Edited by Mordechay Schlesinger and Milan Paunovic

TABLE 12.1 Concentration of Platinum Group Metals in Earth's Crust

Metal	Concentration in Crust (ppm)
Palladium	0.01
Platinum	0.005
Rhodium	0.001
Iridium	0.001
Ruthenium	0.001
Osmium	0.001

TABLE 12.2 Concentration of Platinum Group Metals: Geographic Distribution (wt %)

	Percentage by Weight		
Metal	Canada	Russia	South Africa
Platinum	43.4	30	64.02
Palladium	42.9	60	25.61
Iridium	2.2	2	0.64
Rhodium	3.0	2	3.20
Ruthenium	8.5	6	6.40
Approximate ratio Pt : Pd	1:1	1:2	2.5 : 1

Figure 12.2 exhibits the demand by geographic region from 1995 to 2008 and clearly demonstrates the globalization of manufacturing and its shift from the industrialized world (North America, Japan, and Europe) to China and other parts of Asia. It is interesting to note the convergence of demand in 2008 as Asia rapidly industrialized. Demand hit a low of $\sim 4.9 \times 10^6$ TrOz in 2002 following the burst of the "dot-com" bubble and the ensuing economic recession. Since then, demand has increased $\sim$45% reaching $\sim 7.2 \times 10^6$ TrOz in 2005. China's demand grew rapidly, surpassing Japan in 2008 with a consumption of 1.445×10^6 TrOz. The increases in North America and Europe were spurred by auto catalysts, and it is noteworthy that recycling programs increased supply from $\sim$100,000 TrOz in 1995, or $\sim$2% of total demand, to $\sim 1.2 \times 10^6$ TrOz in 2008, or $\sim$15% of total demand. Supply–demand charts shown in Figure 12.3 indicate that cumulatively from 1995 to 2008 more than 6×10^6 TrOz is in surplus not including the supply from recycling of auto catalysts.

Consumption of Pd by individual applications [7] is seen in Figure 12.4. Electronics was the largest consumer, accounting for $\sim$42% of total demand in 1995; however, by 2008 the automotive sector accounted for 54% of demand and electronics at $\sim$17%. If recycling of auto catalysts is included, the automotive sector accounts for $\sim$61% of demand with electronics as the second largest consumer at $\sim$15%.

Palladium is extensively used in electronic devices from basic consumer products to complex military hardware. Although each component contains relatively small quantities of metal, they are produced in the billions accounting for the substantial demand of $\sim 1.3 \times 10^6$ TrOz in 2008. "Pastes" in multilayered ceramic capacitors represent the largest demand with smaller amounts used in sputtering and plating operations.

The dental industry accounted for 21% of Pd consumption in 1995 but only 8% by 2008. This drop in demand is attributed to "speculative" increase in the price of Pd from 1999 to 2001 (Fig. 12.6). Dental, jewelry (nonplated), and in recent years investments accounted for the remaining 29% of consumption. It is interesting to note the increase in jewelry applications is driven by the rapid economic rise of China and a significant increase in investment stocks in North America.

12.3 BRIEF HISTORY OF ELECTROPLATED PALLADIUM

The earliest known example of plated Pd is in the Percy collection at the Science Museum of London. It is a thin sheet of copper coated with Pd prepared by T. H. Henry circa 1855 [35]. Henry's initial formulation used a nitrate electrolyte from Smee [35], and in a later formulation an ammoniacal solution of "ammonia-muriate." Interestingly enough, today the most utilized processes for Pd and Pd alloy electrodeposition are based on ammoniacal electrolytes. An excellent historical review including numerous recipes for plating Pd was written by Atkinson and Raper in 1933 [35].

Electroplating accounts for $\sim$4–8% of worldwide Pd consumption. Figure 12.5 is a chronological overview of major applications and demonstrates that in the mid-1970s plating Pd became technologically significant. Palladium is utilized in interconnection products especially for telecommunication, computer, and automotive connectors; semiconductor packaging and recently in the printed circuit industry; integrated circuit (IC) packaging substrates; land grid arrays; IC wafer probe cards; and a variety of nanotechnology applications. Furthermore, since the emergence of legislation in Europe banning nickel due to nickel dermatitis, Pd found wide acceptance in the decorative industry.

The use of thick electroplated gold (Au) films for electronic applications was common until the mid-1970s. The relatively low cost of gold and the availability and reliability of existing gold electrodeposition technologies precluded the use of any alternate material. However, the deregulation of gold in the early 1970s coupled with the political and economic events of that era brought about an astronomical

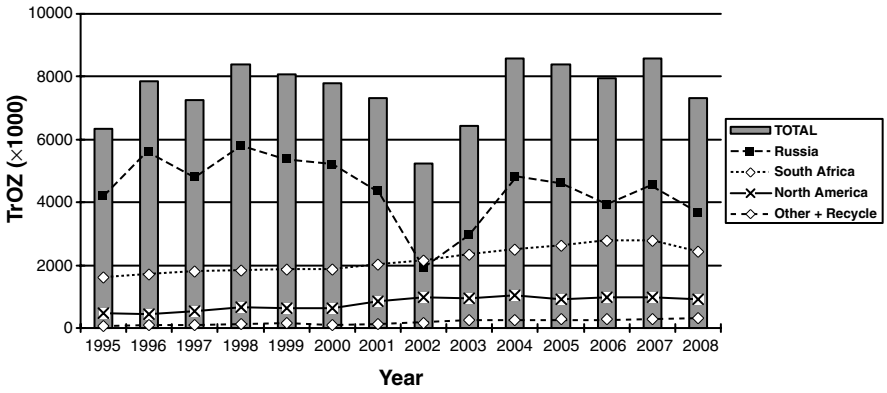

FIGURE 12.1 World Pd supply by geographic region, 1995–2008, in troy ounces.

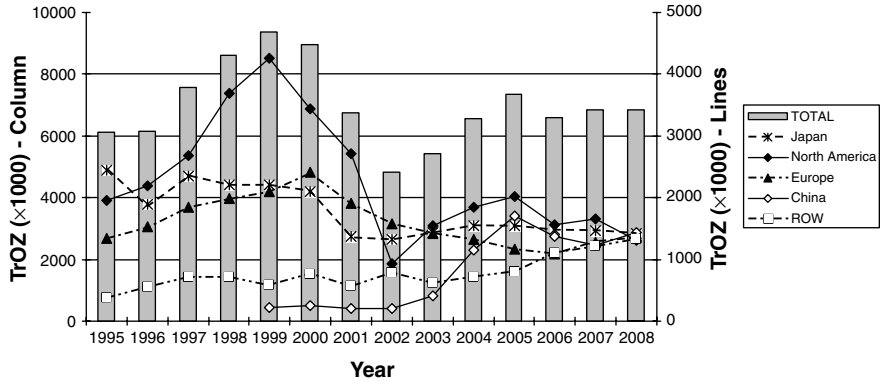

FIGURE 12.2 World Pd demand by geographic region, 1995–2008, in troy ounces.

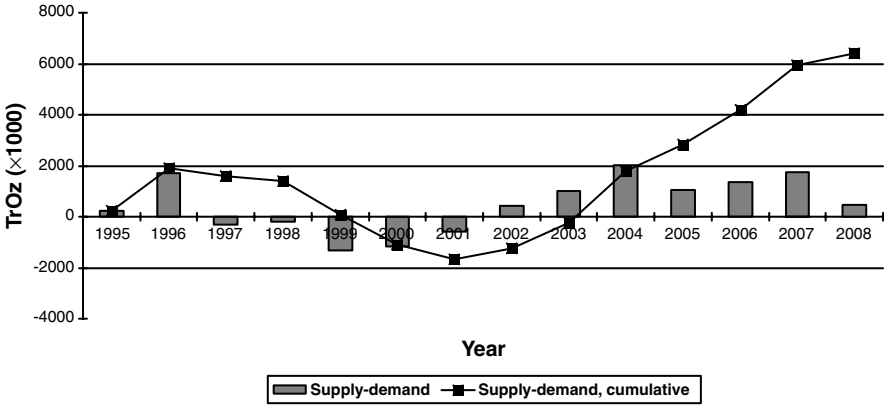

FIGURE 12.3 World Pd supply–demand, 1995–2008, in troy ounces.

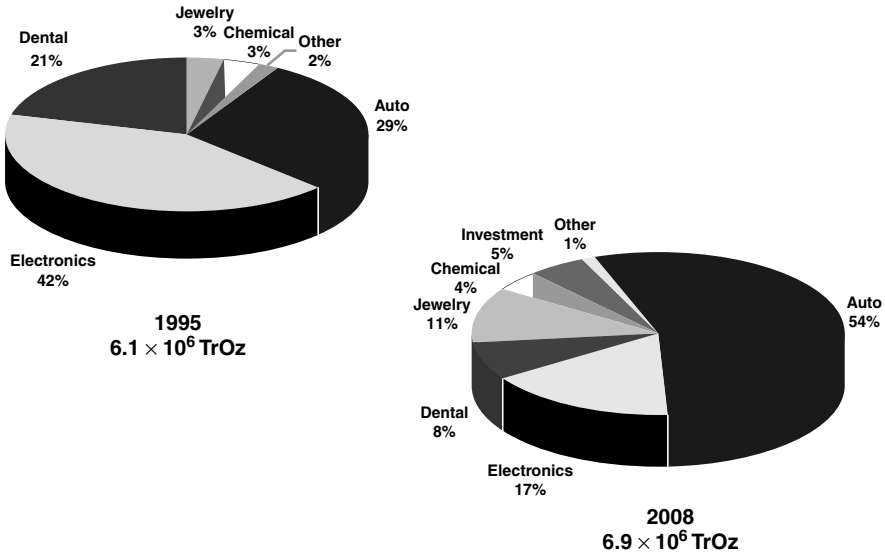

FIGURE 12.4 World Pd demand by industry, 1995 and 2008, in troy ounces.

increase in its price in the late 1970s and early 1980s (Fig. 12.6). From 1981 to 2002, gold traded in the range of \$320–\$440 $TrOz^{-1}$; since 2002, gold has again seen a meteoric rise in its price to greater than \$900 $TrOz^{-1}$. Thus, the major impetus for substituting gold has been and remains economic. The rise in the price of gold spurred significant research in the reduction of gold usage [19, 20] and in the search for a suitable, more economic alternative [8–34].

Palladium is viewed as a suitable alternative. Figure 12.6 compares the relative price of Pd to Au and demonstrates Pd's historical lower price with the exception of a four-year period from 1999 to 2002. Disruptions of supplies from Russia, lower output from South Africa, the increased usage of Pd for automotive catalysts, and speculative activities in Pd stocks conspired to increase its price [7]. However, increased production and active recycling programs resulted

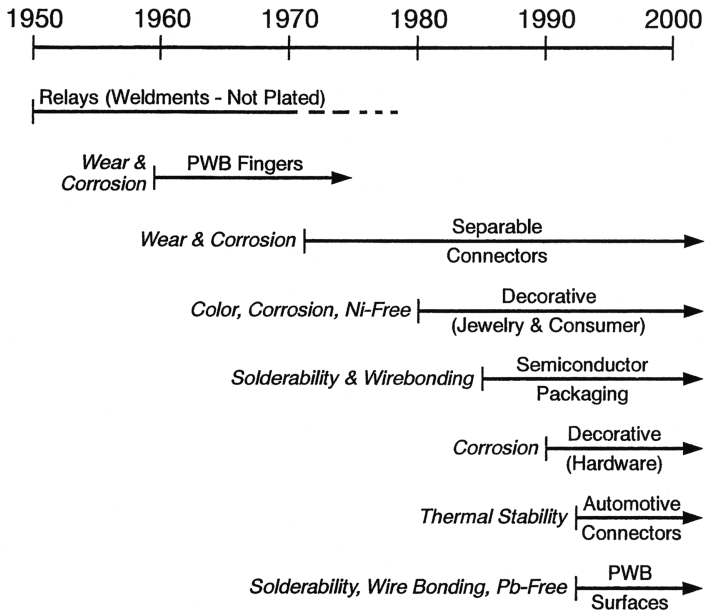

FIGURE 12.5 History of Pd electroplating by application from about 1960 to 2000.

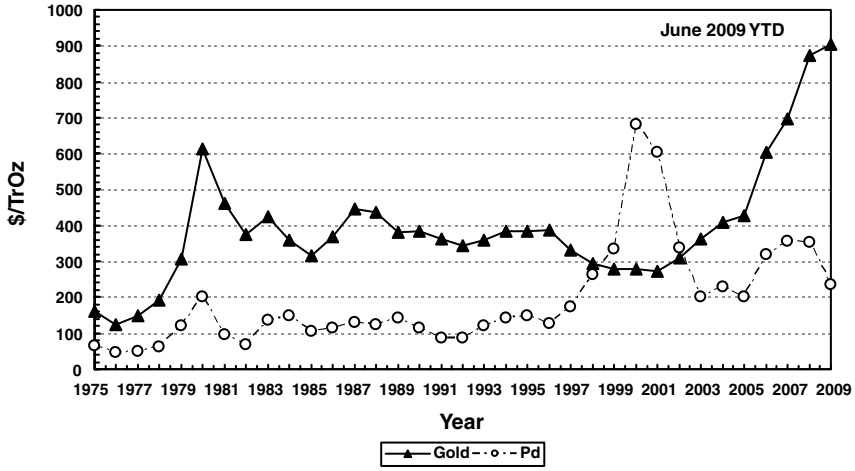

FIGURE 12.6 Gold and Pd bullion prices in dollars per troy ounce, 1975–2009.

in an "excess" supply (Fig. 12.3) and correspondingly lower prices.

The price of Pd coupled with its lower density (Table 12.3) implies considerable cost savings in replacing gold or other metals such as platinum. Today not only the economic but also the technological advantages of substituting Pd or Pd-alloys for gold are generally recognized [8–27]. The material properties (e.g., hardness, ductility, thermal stability) of Pd are in many instances superior to hard gold. For example, higher hardness is beneficial for wear resistance, which can be further enhanced by a thin coating of electroplated gold as a solid lubricant [16]. The lower porosity of electroplated Pd alloys (e.g., PdNi) enhances the corrosion resistance of plated articles [29].

Electroplated Pd, first plated by Henry circa 1855 [35], found numerous technological uses only during the last two

TABLE 12.3 Physical Properties of Palladium, Platinum, and Gold

Properties	Palladium	Platinum	Gold
Atomic structure	Kr-$4d^{10}5s^0$	Xe-$4f^{14}5d^96s^1$	Xe-$4f^{14}5d^{10}6s^1$
Atomic number	46	78	79
Atomic weight	106.4	195.09	196.967
Crystal structure	fcc	fcc	fcc
Atomic radius, Å	1.37	1.39	1.46
Covalent radius, Å	1.28	1.30	1.34
Ionic radius, Å	0.896 (+2)	0.96 (+2)	1.37 (+1)
Density, $gFcm^{-3}$	12.16	21.4	19.3
Hardness (DPN)			
Annealed	37	37	
Electrodeposited (KHN_{50})	250–400	400–500	140–200[a]
Ultimate tensile strength (annealed), lb $in.^{-2}$	25,000	18,000	
Young's modulus, lb $in.^{-2} \times 10^6$	16	25	
Coefficient of linear thermal expansion, 20°C, μ in.°C	11.8	8.9	14.2
Thermal conductivity (0–100°C), $J\,cm^{-1}$, $cm^{-2}\,°Cs^{-1}$	0.76	0.73	
Electrical resistivity, μΩ-cm	10.8 (20°C)	9.83 (0°C)	2.19 (0°C)
Reflectivity (average over visible spectrum), %	62	67	
Electronegativity	2.2	2.2	2.4
First ionization potential, k cal, $g\text{-}mol^{-1}$	192	207	213
Common oxidation states	+2, +4	+2, +4	+1, +3
Melting point, °C	1552	1769	1063
Boiling point, °C	3980	4530	2970

[a] Ni/Co-hardened gold; DPN is the hardness in older SI system.

decades. Demand was low due to the relative difficulty of plating Pd with satisfactory material properties. Several critical reviews on this subject were published in the 1960s and 1970s [35–40]. Since then, Pd electrodeposition technology evolved slowly [35–40], and in the 1980s processes suitable for large-scale manufacturing became available [8, 14–20]. This was especially true for high-speed ($>50\,mA\,cm^{-2}$) plating operations [8].

12.4 PHYSICAL AND CHEMICAL PROPERTIES OF PALLADIUM

12.4.1 Physical Properties of Palladium, Platinum, and Gold [41–43]

Table 12.3 describes the significant physical properties of Pd and compares them to platinum, the most widely recognized PGM, and gold, the "target metal" that Pd has been substituting. The properties cited are descriptive only insofar as possible to obtain the purest available specimens since they are greatly affected by the presence of impurities. Furthermore, since PGMs have a marked tendency to absorb gases such as hydrogen, it is understandable that obtaining accurate quantitative data on their properties is problematic. Nonetheless, Table 12.3 provides needed information utilized in practical applications. For additional information on the properties of other PGMs see [41–49].

Properties such as melting point, boiling point, hardness, or mechanical strength can be understood by examining the electronic structure of these elements and other PGMs: iridium, osmium, rhodium, and ruthenium. This analysis reveals a progressive decrease in coherence or bond strength among atoms in each of the periodic groups (Ru, Rh, and Pd vs. Os, Ir, and Pt where Au is associated with the latter group). For example, the melting points of Os, Ir, Pt, and Au are 3050, 2443, 1768, and 1063°C, respectively, and correlate with progressive decrease in the number of electrons available for bonding in the solid state that occupy hybridized orbitals from s, p, and d states. The amount of "d character" hybridization is presumed to decrease as electrons become paired in atomic d orbitals and thereby prevent them from contributing to metallic bonds. This tendency continues to the corresponding members of groups I and IIB [44]. Thus, it is the electronic structure that dictates the physical and chemical properties of Pd and other PGMs.

Palladium is silvery white, malleable, and ductile with a face-centered cubic (fcc) crystal structure. It Pd, has the electronic structure $(Kr)4d^{10}5s^{0}$, element number 46 with atomic weight of $106.4\,g\,mol^{-1}$, a density of $12.16\,g\,cm^{-3}$, and a melting point of 1555°C. Table 12.3 compares the material properties of Pd with two other precious metals, gold and platinum [41–43]. Palladium is known to form alloys with other metals of groups VIII and IB that display distinct advantages over the pure metals [45]. In general, the alloying elements tend to increase resistivity, hardness, and tensile strength of Pd. Copper, nickel, gold, iridium, rhodium, and ruthenium have been used to manufacture Pd alloys for many practical applications. For example, an alloy of silver (60/40 weight percent Pd/Ag) is commonly used in electric relay contacts.

12.4.2 Chemical Properties of Palladium

General Reactivity PGMs are relatively inert with respect to chemical attack by oxygen or many acids, and this is one of the properties that make them of practical value. The formation and decomposition of the oxides of PGMs are summarized in Table 12.4 [43]. Osmium forms a considerably volatile oxide at room temperature, and to a lesser extent Pd forms an oxide when heated in air to ~350°C; however, the other PGMs require temperatures exceeding 700°C to form oxides. This provides some understanding of their chemical inertness. However, it must be emphasized that the chemical reactivity of the PGMs is greatly affected by the state of the subdivision of the metal or the particle size (i.e., surface area). Thus, Pd "sponge" is more readily attacked than the compact metal and is readily used in the synthesis of Pd compounds. Also, if alloyed with other metals, namely lead or silver, it is more reactive. Palladium finely dispersed on supporting media such as silica gel is still more reactive and displays remarkable catalytic properties.

TABLE 12.4 Reaction of Platinum Group Metals with Oxygen

Metal	Extent of Oxide Formation (25°C)	Oxide Formed	Formation Temperature (°C)	Decomposition Temperature (°C)
Platinum	Negligible	Platinum (IV) oxide, PtO_2	<1000	
Palladium	Superficial	Palladium (II) oxide, PdO	>350	>870
Rhodium	Superficial	Rhodium (III) oxide, Rh_2O_3	~700	1100
Iridium	Superficial	Iridium (IV) oxide, IrO_2	~700	1140
Osmium	Considerable	Osmium (VIII) oxide, OsO_4	200	
Ruthenium	Superficial	Ruthenium (IV) oxide, RuO_2	700	

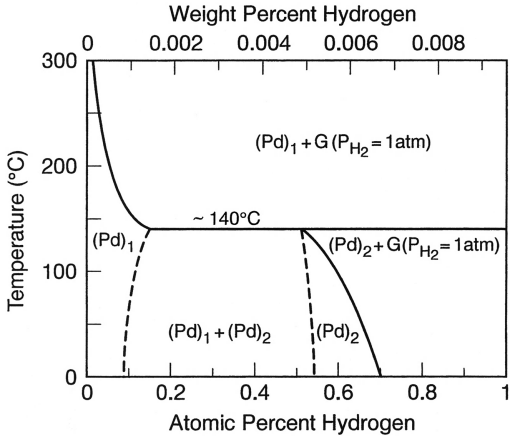

FIGURE 12.7 Binary alloy phase diagram of palladium–hydrogen system.

The "inertness" of PGMs stems from their strong atomic bonds in the solid state. The increase in reactivity exhibited by samples with high surface area, compared to the bulk, is attributed to an increase in the number of atoms with higher energy associated with surface sites, or "dangling bonds." This becomes especially significant in electroplated Pd where the grain size can be on the order of 50–250 Å, and thus the reactivity at the grain boundaries can be significantly higher than the bulk metal by the argument presented above.

Palladium, of all the PGMs, has the highest capacity to absorb hydrogen [47]—as much as 900 times its own volume. The uptake of hydrogen corresponds roughly to the composition Pd_2H, but modern studies appear to have largely ruled out the formation of such discrete substance (Fig. 12.7). Instead it is inferred that below 300°C there are two phases, each consisting of a solid solution, whereas above this critical temperature there is only a single solution phase. In each phase, hydrogen atoms are held interstitially in such a way as to involve actual chemical bonding, as deduced from changes in electric conductance and magnetic susceptibility. To a smaller degree, platinum and rhodium exhibit similar absorption characteristics.

The ability of Pd to absorb hydrogen poses a significant problem for electrodeposition from aqueous solution. This issue—the hydrogen embrittlement problem—will be discussed in some detail in Section 12.5.2.

Table 12.5 summarizes the reaction of acids on PGMs [43] where resistance to attack is shown in increasing order. Palladium is more reactive and dissolves in nitric acid, giving $Pd^{IV}(NO_3)_2(OH)_2$; in bulk form attack is slow but is accelerated by oxygen and oxides of nitrogen. As a sponge, Pd dissolves in HCl in the presence of chlorine or oxygen. The action of aqua regia on Pd yields chloropalladic acid, H_2PdCl_6; however, on evaporation of this solution the polymeric dichloride, $(PdCl_2)_x$, is formed. Thus $PdCl_2$ is a significant starting material for the synthesis of most electrolytes used for the electrodeposition of Pd.

TABLE 12.5 Attack of Platinum Group Metals by Mineral Acids

Metal	Form	Nature of Attack
Palladium	Compact	Attacked by hot concentrated nitric acid and boiling sulfuric acid; Dissolved by aqua regia
	Sponge	Dissolved by all the above acids
Platinum	Compact or sponge	Not attacked by single mineral acids; dissolved by aqua regia
Rhodium	Compact	Attacked by boiling sulfuric acid or hydrobromic acid
		Not dissolved by aqua regia
Iridium	Compact	Practically Insoluble in mineral acids or aqua regia
	Sponge	Dissolved in Carius tube by hot hydrochloric acid plus an oxidizing agent (nitric acid or sodium chlorate) [4]
Ruthenium	Any	Virtually Insoluble in hot mineral acids or aqua regia
Osmium	Any	Virtually Insoluble in hot mineral acids or aqua regia

Oxidation States and Coordination Chemistry The principal oxidation state of Pd is $+2$, although less common there exists a rich chemistry for Pd^{4+}. There is also some important chemistry in the monovalent state, where metal–metal bonds are involved, and in the zerovalent state for certain tertiary phosphine, CO, or other π-acid organometallic compounds [48–50].

The coordination chemistry of Pt and Pd has attracted considerable attention because of the large numbers of compounds of great intrinsic value. For example, use of these metals as catalysts and more recently as anticancer agents has spurred significant technological interest. Furthermore, the square-planar geometry of the bivalent oxidation state made possible the study of cis and trans isomerism which is of great academic interest [51, 52]. Coordination chemistry of Pd(II) is of importance since electrodeposition from aqueous solution is basically the chemistry of the bivalent state. Therefore, the rest of this discussion will be restricted to the Pd(II) oxidation state.

Palladium $+2$ is the most common oxidation state and possesses a d^8 electronic structure [49]. Most Pd(II) complexes have a coordination number of 4 and form stable 16-electron complexes. The tendency of transition metals to form complexes in which the metal has an "effective number" corresponding to the next higher inert gas has long been recognized [53]. Therefore, the group VIII elements form well-characterized stable compounds with either 16 or 18 valence electrons [54, 55]. Furthermore, the structure of tetracoordinated Pd is square planar rather than tetrahedral, since ligand field stabilization energy is relatively more

important than valence shell electron pair repulsion, which would dictate a tetrahedral structure. A detailed discourse on the chemistry and structure of Pd compounds can be found in [43, 48] and references within.

12.5 ELECTROCHEMISTRY OF PALLADIUM

12.5.1 General Electrochemistry: Thermodynamics

One of the most complete thermodynamic considerations of the electrochemistry of Pd can be found in Chapter 12 of the handbook *Standard Potentials in Aqueous Solutions* [56]. Under standard conditions, in solutions of zero ionic strength, the standard potentials for the electroreduction of Pd^{2+} were reported by various investigators to occur between 0.915 and 0.979 V.

The half-cell potential of the Pd^{2+}/Pd couple in HClO4 solutions at zero ionic strength was reported by Izatt et al. [57] as follows:

$$Pd^{2+}(aq) + 2e^- \rightarrow Pd(s) \quad E^0 = 0.915 \pm 0.005\ V \quad (12.1)$$

However, Templeton [58, 59] reported a value of $E^0 = 0.987$ V from an $HClO_4$ solution at ionic strength $I = 4\ mol\ L^{-1}$ which, when adjusted to zero ionic strength [59], yields $E^0 = 0.945$ V. Other measurements by various investigators [60] have yielded $E^0 = 0.978\ V \pm 0.0005$ V while polarographic [61] measurements confirmed the value of Izatt et al.

Pourboix [62] used thermodynamic data to calculate the formal potential of the formation of palladium from palladium hydroxide:

$$Pd(OH)_2(s) + 2H^+ + 2e^- \rightarrow Pd(s) + 2H_2O \quad E^0 = 0.897\ V \quad (12.2)$$

Table 12.6 provides available thermodynamic data for various aqueous complexes of Pd(II) along with either the measured or calculated E^0. For example, the electroreduction of Pd from $PdCl_4^{2-}$ in HCl(aq) media was reported by several authors [58, 63] to be

$$PdCl_4^{2-}(aq) + 2e^- \rightarrow Pd(s) + 4Cl^-(aq) \quad E^0 = 0.62\ V \quad (12.3)$$

and $E^0 = 0.60$ V for $1\,M$ KCl. These values were confirmed [64] for $1\,M$ HCl, $E^0 = 0.59$ V, and by the study of the equilibrium constants for the stepwise dissociation [65]

$$Pd^{2+}(aq) + 4Cl^-(aq) \rightarrow PdCl_4^{-2}(aq) \quad \log \beta 4 = 12.2 \quad (12.4)$$

For the amine complex, which is very important for the electrodeposition of Pd, the following potential has been calculated:

$$Pd(NH_3)_4^{2+}(aq) + 2e^- \rightarrow Pd(s) + 4NH_3 \quad E^0 = 0.0\ V \quad (12.5)$$

on the basis of the stability constants ($\log\ \beta 4 = 30.5$) measured for the equilibrium in ammonia solutions at $I = 1\ mol\ L^{-1}$.

For Pd(IV), one of the potentials for the half reaction is

$$PdO_2(s) + 2H^+(aq) + 2e^- \rightarrow PdO(s) + H_2O \quad E^0 = 1.263\ V \quad (12.6)$$

This was calculated by Pourboix [62] from thermodynamic data. Furthermore, for Pd^{4+} in the important ethylenediamine systems the following potentials were obtained from electromotive force (emf) determinations [66] at 25°C and 10^{-5}–$10^{-6}\ mol\ L^{-1}$ nitrate solutions:

$$PdCl_2(en)_2^{2+}(aq) + 2e^- \rightarrow Pd(en)_2^{2+}(aq) + 2Cl^-(aq) \quad E^0 = 1.15\ V \quad (12.7)$$

TABLE 12.6 Thermodynamic and Electrochemical Data on Palladium (II)

Formula (Aqueous)	ΔH° (kJ mol^{-1})	ΔG° (kJ mol^{-1})	S° (J mol^{-1} K^{-1})	log β_x	E^0 (V)
Pd^{2+}	149.0	176.5	−184	<3	0.915
$Pd(SO_4)^{2-}$				3.16	0.82
$PdCl_4^{2-}$ (1*M* HCl)	−550.2	−417.1	16.7	12.2	0.62
$PdBr_4^{-2}$	−384.9	−318.0	247	15	0.49
$PdI4_4^{-2}$		−159.0	—	25	0.18
$Pd(NO_2)_4^{+2}$		−68	—	—	0.34
$Pd(OH)_2$					0.07
$Pd(en)_2^{+2}$				26.9	−0.79
$Pd(NH_3)_4^{+2}$		−75	—	30.5	0.0
$Pd(CNS)_4^{-2}$		410.5			
$Pd(CN)_4^{-2}$		628	—	51.6	−1.52

For Pd(VI), from data on the anodic formation of PdO_3 in alkaline solutions, Pourboix [62] found the following:

$$PdO_3(s) + 2H^+(aq) + 2e^- \rightarrow PdO_2(s) + H_2O \quad E^0 = 2.030\,V \tag{12.8}$$

Thus, the overall potential diagram for the electroreduction of Pd is as follows:

$$Pd^{6+} \xrightarrow{2.03} Pd^{4+} \xrightarrow{1.263} Pd^{2+} \xrightarrow{0.915} Pd^0$$

However, normal electrodeposition conditions deviate significantly from the standard, or equilibrium, condition. The reduction potential at any given temperature and concentration for a simple ion reaction can be expressed by the following equation:

$$E = E^0 + \left(\frac{RT}{nF}\right) \ln a + C \tag{12.9}$$

It can be seen that in addition to the standard or formal potential, the reduction potential for Pd or any other species (e.g., H_3O+) can be affected by temperature and concentration of the species at the electrode surface and any other factors that contribute to the C term, such as complexing ligands for metals, and organic additives that may affect the overvoltages for the metal deposition.

Finally, the deposition of Pd from aqueous solutions is usually accompanied by the codeposition of hydrogen and the formation of palladium hydrides, PdH_x. As will be seen in Section 12.5.2, the successful electrodeposition of Pd and its alloys is highly dependent on the avoidance of codeposited hydrogen. In this regard, we will attempt to understand this phenomenon and how to control it by treating the electrode surface as the scene of more than one electrochemical reaction; see Section 12.5.3.

12.5.2 Hydrogen Embrittlement Problem

So-called hydrogen embrittlement is a generic term used to describe a variety of fracture phenomena having a common relationship to the presence of hydrogen in a metal or alloy as a solute element [67]. The ramifications of hydrogen-embrittled metals and alloys can be very serious and in some cases, such as aircraft parts or nuclear reactor components, even life threatening.

It appears that most materials can become embrittled if hydrogen is introduced under "pressure" by means such as electrodepostion and this state remains unchanged until hydrogen escapes [69]. The failure can be abrupt and forceful as to become almost explosive [70]. It has been said that "one of the most spectacular and memorable sounds associated with zinc plating is standing in a quiet storage room next to drums of freshly zinc plated steel springs and listening to the metallic shriek as the springs slowly destroy themselves in order to release occluded hydrogen" [68–71]. Likewise, the author personally plated palladium with such large amounts of occluded hydrogen that immediately after electrodeposition the plated coupons violently twisted into a cylindrical shape and released enough heat from the exothermic release of hydrogen to turn the coupons "red hot" and burn his fingers.

The phase diagram of Pd and hydrogen is seen in Figure 12.7. This system has been well studied [47], and in the 1980s renewed interest was triggered by the speculative phenomena of "cold fusion" [72–74]. Classical fundamental work on this system was carried out by Lacher [75] and Gillepsie and co-workers [76, 77] from 1935 to 1939. They determined that palladium hydride exists as a fcc α phase up to an atomic concentration of [H]/[Pd] = 0.03, which is thermodynamically stable. Simons and Flanagan [78] found that the lattice of α-PdH_x increases slightly from pure Pd, which is 3.889–3.893 Å due to hydrogen absorption. However, the pure β phase prevails at a minimum atomic ratio of [H]/[Pd] = 0.57. This phase, also fcc, has a larger lattice constant of 4.04 Å. Furthermore, the β phase is dependent on the temperature of the system and on the hydrogen pressure and is thermodynamically unstable under ambient conditions. For example, Frumkin and Aladjalowa [79] state that an atomic ratio of [H]/[Pd] = 0.68 is obtained from 1 atm of hydrogen pressure; furthermore, Hoan and Arrowsmith [80] state that this ratio equals 0.61 between 20 and 30°C. In the concentration range of ratios from 0.03 to 0.57 [H]/[Pd], the two phases are at heterogeneous equilibrium.

The hydrogen embrittlement problem stems from the thermodynamic instability of β-PdH_x. Immediately after deposition, β-PdH_x spontaneously decomposes evolving H_2 gas and is transformed to the thermodynamically stable α-PdH_x. This transformation is accompanied by corresponding lattice contractions and changes in the mechanical properties of the Pd films (Fig. 12.8). During the contraction, the deposits become highly stressed, and as the tensile components of this stress exceed the yield point, the stress is relieved by cracking. The effects of such a phenomenon are seen in Figure 12.9.

The electrodeposition and material properties of Pd are thus greatly affected by the chemistry and deposition parameters (e.g., temperature and pH) since they determine the amount of codeposited hydrogen. The electrochemistry and mechanisms of hydrogen inclusion during Pd electrodeposition are discussed elsewhere [72–74, 81–87]. This phenomenon and the electrochemical parameters that affect it must be understood if one is to successfully electroplate Pd with the desired material properties.

12.5.3 Electrochemistry of Simultaneous Reactions: Electrokinetics

The hydrogen embrittlement of electrodeposited Pd is a matter of great concern when one attempts to deposit Pd

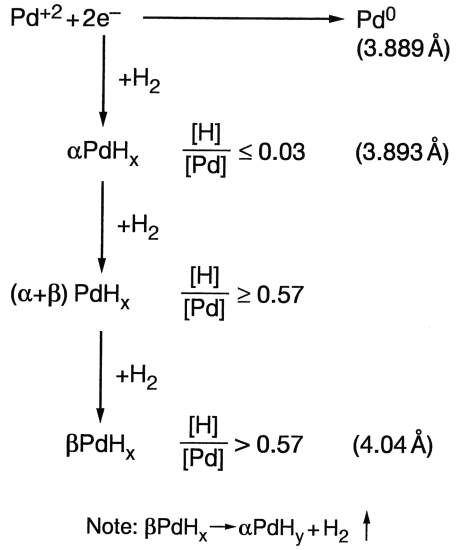

FIGURE 12.8 Schematic of palladium–hydrogen embrittlement phenomenon.

films of technological use. Obviously these films must possess mechanical integrity and thus be crack free and of low stress. Therefore, it is important to eliminate or inhibit the codeposition of hydrogen with Pd. Alternatively, the electrodeposition of Pd alloys such as PdNi, PdCo, and PdAg where the alloying metals are in the range of 10–50% are of significant technological interest. Thus, there exists the situation where in the latter case a high degree of codeposition for alloy formation is desired and in the former case codeposition is undesirable. Identical electrochemical considerations can be utilized to understand both phenomena in which the interface is the scene of more than one electrochemical reaction.

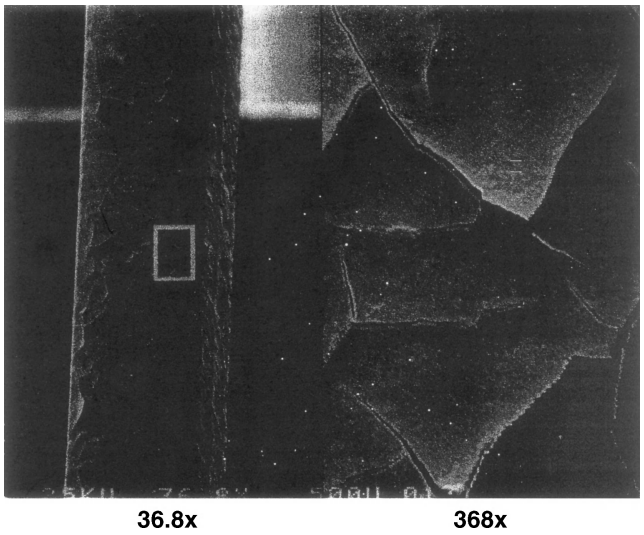

FIGURE 12.9 Scanning electron micrograph of hydrogen-embattled Pd film.

The treatment of simultaneous reactions at an electrode interface [88, 89] is based on an important fact: Although the current densities of $i_1, i_2 \ldots, i_n$ may be different for each reaction, they are produced by the same absolute Galvani potential difference $\Delta\text{Ø}$ at the interface. In the case of two simultaneous reactions, the following equation will determine the relative current densities for each electroreduction:

$$\frac{i_1}{i_2} = \left[\frac{i_{0,1}}{i_{0,2}}\exp\left(\frac{F}{RT}\right)\left[(\boldsymbol{\alpha}_1\,\Delta\phi_{e,1} - \boldsymbol{\alpha}_2\phi\,\Delta\phi_{e,2}\right]\right] \times \exp\left(\frac{F}{RT}\right)(\boldsymbol{\alpha}_1 - \boldsymbol{\alpha}_2)\,\Delta\phi \tag{12.10}$$

Thus, the value of the current density ratio and the degree of "codeposition" depend not only upon the exchange current densities$(i_{0,i})$, the transfer coefficients(α_i), and the equilibrium potentials $(\Delta\phi_{e,1}, \Delta\phi_{e,2})$, but also, in an exponential way, upon the potential difference across the interface $(\Delta\phi)$. Thus, even if the deposition of a second species (i_2) is inhibited by lower exchange current density (i.e., $i_{0,2} < i_{0,1}$) and more negative equilibrium potentials (i.e., $\Delta\phi_{e,2} < \Delta\phi_{e,1}$), it can have a higher deposition–current density if its transfer coefficient $\boldsymbol{\alpha}_2$ is greater than that of the other, $\boldsymbol{\alpha}_1$.

Another situation in which a species with a more negative equilibrium potential can be deposited to a greater extent occurs when the deposition of the second species is limited by mass transport. Under such conditions

$$i_1 = i_{\text{L}} = \frac{DnFC_1^0}{\delta} \tag{12.11}$$

where D = diffusion coefficient
n = number of electrons
F = Faraday's constant
δ = diffusion layer thickness
C_1^0 = concentration in the bulk

If i_2 is not transport limited, then i_2 can, most likely, be greater than i_1.

Electrokinetics of Hydrogen Evolution The arguments in Section 12.5.3 are equally valid for a situation where metal deposition occurs with any other cathodic reduction such as the formation of hydrogen [88, 89]. From a technological point of view, in most cases, one seeks to electrodeposit a metal at high current efficiencies (i.e., limit hydrogen formation). The reasons are obvious since hydrogen embrittlement, as discussed in Section 12.5.2, can be problematic. Furthermore, a high current efficiency implies that the desired reaction occurs at a faster rate and less time is utilized to deposit the desired amount of metal at a given total current density. Technologically speaking, this is

of great importance since it "speeds up" the process and increases manufacturing throughput.

In order to achieve this objective, it becomes important to understand the current density ratio i_H/i_M or the percentage of current efficiency $\left[i_M/(i_M + i_H)\right] \times 100$ which is attributed to metal deposition. The intent is to utilize the current only for metal deposition, that is, metal deposition current efficiency equals 100%.

The basic factors determining current efficiency are revealed by considering i_1 as the hydrogen evolution current and i_2 as the metal deposition current in Eqs. (12.10) and (12.11). Thus, the same principles apply, that is, the current going toward hydrogen evolution depends upon the ratio of the exchange current densities, the equilibrium potentials, and the relative transfer coefficients of hydrogen evolution and metal deposition reactions. In general, the deposition of metal is favored by a more positive equilibrium potential with respect to hydrogen, a higher exchange current density, and a lower value of the transfer coefficient. Even if these parameters are unfavorable for the deposition of a metal, it may be possible to obtain high current efficiencies by ensuring that i_H is transport limited. Utilizing Eq. (12.11) for i_L it becomes clear that limiting $C^0_{H^+}$ can be accomplished by manipulating the pH of the reaction. However, if one exceeds i_L for metal deposition (there is always a limit), hydrogen evolution will occur. In aqueous solutions, hydrogen evolution will always occur if the total deposition current is made sufficiently high and exceeds the limiting current of the metal in question; the hydrogen may come not only from H_3O^+ but, if limited at high pH, from water itself.

The effects of hydrogen codeposition on the crystallography of metal deposition are rather complicated and beyond the scope of this chapter. However, several ramifications of hydrogen evolution must be noted. As discussed in Section 12.5.2, hydrogen may codeposit with a metal and change its structural and mechanical properties. It may also adsorb more efficiently on certain crystal planes "blocking" them from further deposition so that the metal grows preferentially on others. If hydrogen gas evolution is significant, a "curtain" of gas may inhibit the transport of certain species to the electrode surface and thus impair any intended reaction. Finally removal of H_3O^+ from the diffusion layer may significantly increase the pH, which may alter the intended chemical and electrochemical reactions at the interface. If the solution at the interface becomes sufficiently alkaline, it may cause the solubility product of a hydroxide of the metal ion present to be exceeded, which may cause inclusion of such a species in the deposit. This can be problematic in terms of deposit properties or mechanical properties such as stress and ductility. Alternatively, it could cause the formation of relatively thick $(10^2 - 10^3$ Å) films on plated parts, thus "passivating" the cathode surface.

In summary, hydrogen codeposition usually leads to many undesirable effects in metal deposition. Therefore, selective control over the rate of hydrogen evolution is vital—hence the need to understand the reaction. Electrode kinetics, as discussed above, is important in determining i_H/i_M and the factors that affect it; however; the "hydrogen overvoltage" is also an important phenomenon that determines the parameters under which a metal can be deposited.

Hydrogen Overvoltage An operating electrolytic cell that has net current flowing through it is not at equilibrium [88]. The potential will differ from equilibrium as follows:

$$\eta = E_i - E_q \tag{12.12}$$

Where E_i is the potential when current is flowing and E_q is the potential at equilibrium. The overpotential or overvoltage, η, is impacted by several factors. For example, concentration polarization at the electrode surface caused by depletion of reactants is described by the Nernst equation:

$$\eta_{conc} = \frac{RT}{nF} \ln\left(\frac{a_e}{a_0}\right) \tag{12.13}$$

This is referred to as concentration overpotential, where a_e is the activity of the depositing ion at the electrode surface and a_o that of the bulk solution. In the case of hydrogen evolution, concentration overpotential occurs when surface hydrogen concentration changes (i.e., is depleted) with surface pH changes. Alternatively, overpotential may be required to overcome various kinetic barriers to a reaction; this is referred to as activation overpotential [88]. This is the minimum energy or potential barrier that must be overcome for the reaction to proceed, and for the hydrogen evolution reaction occurring on specific metals, it is referred to as the "hydrogen overvoltage."

If it were not for hydrogen overvoltage, many metals could not be deposited from aqueous solutions. For example, at pH 4, which is a common pH for nickel plating, E^0 for hydrogen evolution is about –0.236 V; in alkaline solutions with pH 10, it is –0.59 V. These potentials are significantly more positive than the reduction potentials of many metals plated from these solutions. Activation overvoltage is extremely high in the evolution of hydrogen, and it enables metal deposition or inhibits hydrogen evolution.

The hydrogen overvoltage is dependent on the nature (i.e., electronic structure) and structure (morphology) of the electrode surface. For example, at cathodes of tin, zinc, or lead, it can be more than 1 V negative than its equilibrium potential, and this is why these metals can be deposited from very acidic solutions, $pH < 1$, where the concentrations of H_3O^+ is very high. Alternatively, it is extremely low for metals such as Pt or Pd. On platinum black it is negligible, which is why it is used in "setting up" the hydrogen electrode. Therefore, it is a challenge to plate Pd from aqueous solution without the interference of hydrogen, and one cannot rely on the

hydrogen overvoltage to avoid codeposition. Thus, most chemical formulations used to deposit Pd are neutral to alkaline in order to reduce or inhibit the evolution of hydrogen.

An additional factor that can suppress hydrogen formation is the use of additives or "poisons" that adsorb on an electrode surface but are essentially electrochemically inactive. Such impurities adsorbed on the cathode surface may increase hydrogen overvoltage. Furthermore, such impurities often include addition agents that poison selected sites and are useful for leveling or brightening the deposit. A detailed discussion of the mechanisms of hydrogen formation is beyond the scope of this chapter and can be found in [88].

Minimization of Hydrogen Codeposition So far this section has demonstrated, in a theoretical sense, what is required to either minimize or maximize the current ratio, i_1/i_2, of two simultaneous reactions occurring at an electrode interface. It now becomes important to understand what factors, chemical, physical, and/or electrochemical, can be utilized to achieve the end objective, which in the case of Pd plating is to minimize i_1 and maximize i_2. It is stated by the arguments Section 12.5.3 that the following parameters must be considered:

1. Exchange current densities, i_0
2. Transfer coefficients, α
3. Equilibrium potentials, ΔE_e
4. Potential difference, ΔE, across interface
5. $i_{L,1}$ versus. $i_{L,2}$, limiting current
6. Hydrogen overvoltage modifiers
   - Metallic (e.g., Ni for PdNi alloy)
   - Organic (surfactants, brighteners, etc.)

The exchange current densities, the transfer coefficients, and the equilibrium potentials are, for the most part, determined by the nature of species 1 and 2, in this case palladium and hydrogen, and the nature of the electrode material, which in this case will be palladium. These are constants at a given temperature and cannot be manipulated. In this situation only the relative concentration of species 1 and 2 at the electrode surface and the temperature can be altered significantly. However, what can be modified by changing the chemical system and the plating conditions (e.g., solution agitation) are the relative reduction potentials of each species, the concentration of each at the electrode surface, and potentially the overvoltage of hydrogen and/or metal deposition at a "modified" palladium surface through the use of metallic or organic additives.

As stated in Section 12.5.1, the reduction potential of an element at any given temperature and concentration is described by the sum of its standard potential and a term expressing its activity (a) as shown below:

$$E_1 = E_1^0 + \frac{nF}{RT}\ln(a_1) + C_1 \tag{12.14}$$

$$E_2 = E_2^0 + \frac{nF}{RT}\ln(a_2) + C_2 \tag{12.15}$$

The difference in potential between the two elements involved can be expressed as

$$\Delta E = E_1 - E_2 \tag{12.16}$$

For successful alloy deposition, ΔE must be minimized. The condition can be met when the two values $E_1^o$and E_2^o are similar or by adjusting the concentration of one species in solution, so altering its activity, or by arranging a suitable difference in the C term, which can be achieved by introducing complexants. The latter is the most common manipulation, especially when the difference between the standard potentials is large.

Alternatively, to avoid or inhibit hydrogen codeposition one must maximize ΔE. That is, the reduction potential for Pd must be as positive as possible while the hydrogen reduction potential must be as negative as possible. In this regard, we will utilize cyclic voltammetry to examine the reduction characteristics (peak potentials, E_p) of various chemical systems and demonstrate how to achieve the above objective.

For a totally irreversible system, the expression for the peak potential E_p is [90]

$$E_p = E^{o'} - \frac{RT}{\alpha nF}\left[0.78 + \ln\left(\frac{D_0{}^{1/2}}{k^0}\right) + \ln\left(\frac{\alpha nFv}{RT}\right)^{1/2}\right] \tag{12.17}$$

where $E^{o'}$ is the formal potential [see Eq. (12.27)], α is the transfer coefficient, n is the number of electrons, F is Faraday's constant, D_0 is the diffusion coefficient, k^0 is the standard heterogeneous rate constant, and v is the linear potential scan rate. The objective is to obtain maximum separation of $E_p(\mathrm{Pd})$ and $E_p(\mathrm{H_2})$ as shown below:

$$\Delta E_p = E_p(\mathrm{Pd}) - E_p(\mathrm{H_2}) \tag{12.18}$$

Examination of the expression for E_p [Eq. (12.17)] indicates that the formal potential of each species and to some extent temperature, transfer coefficients, diffusion coefficients, and standard rate constants for each reaction will dictate the reduction potential of each species in question. The reduction potential E is described through the Nernst equations below:

$$E(\mathrm{Pd}) = E_{\mathrm{Pd}}^o + \frac{0.0591}{2}\log\left[\mathrm{Pd}^{2+}\right]_0 \tag{12.19}$$

$$E(\mathrm{H_2}) = E_{\mathrm{H_2}}^o + 0.0591\log[\mathrm{H}^+]_0 \tag{12.20}$$

where E^0 are formal potentials and $[Pd^{2+}]_0$, $[H^+]_0$ are the concentrations at the electrode surface.

Formal potentials, of course, are dependent on the standard potential [Eq. (12.27)] and the relative concentration of each species at the electrode surface, which in turn is dependent on the equilibrium constants for specific Pd chemistries (Table 12.6) and the pH for the hydronium ion concentration. In Section 12.6, we will examine how to manipulate these factors to maximize ΔE_p. However, prior to this discussion, we must examine the equilibrium constants of various Pd complexes and other factors that are important in these considerations.

Theoretical and Practical Considerations for Palladium Plating The standard potential E^0 of Pd^{2+}/Pd^0 as described in Section 12.5.1 ranges from $+0.915$ to $+0.979$ V. This highly positive value, as would be expected for a noble metal, implies facile reduction of Pd (II) to Pd(0) metal from an aqueous solution of its simple salts, namely noncomplexed ion. For example, for the $[Pd(SO)_4]^{-2}$ system in Table 12.6, $\log \beta_4 = 3.16$ indicates that this aquo species is of low stability. As a matter of fact, tetra-aquo Pd(II), present in acidic media, can be reduced by less noble metals (e.g., Cu) as a result of charge exchange or "displacement" plating. In this case, even though the H_3O^+ concentration is high, it can be plated with 100% efficiency and thus avoid hydrogen codeposition. However, Pd films produced as a product of electrodeposition coupled with displacement plating are powdery and nonadherent [37]. Furthermore, electrodeposition from solutions of $pH < 1$ is problematic in a practical sense.

On the other hand, reduction from aqueous solution of highly stable complexes such as $[Pd(CN)_4]^{2-}$ is impractical. The stability constant β_4 of tetracyanopalladate is

$$\beta_4 = \frac{[Pd(CN)_4^{2-}]}{[Pd^{2+}][CN^-]^4} = 10^{51.6} \qquad (12.21)$$

which indicates this complex is much too stable with a reduction potential more negative than the onset of hydrogen evolution, and thus hydrogen is preferentially discharged. It has been reported [35] that only traces of Pd can be deposited from this complex even if the electrolyte is strongly alkaline and a metal with a high hydrogen overvoltage is employed as the cathode. In 1919 Smee made use of this fact to separate Au from Pd by electrolysis of a solution containing the complex cyanides of both metals [34]; he found that Pd was not deposited from such a solution until the cyanide species had been decomposed. The relationship between β_x and E^0 can be seen in Table 12.6.

Complexes with nitrogen-containing ligands, such as ammonia, are well suited for Pd deposition; they are stable enough to prevent immersion plating and yet amenable to cathodic reduction. For example, Pd tetra-ammine complex has the following stability constant:

$$\beta_4 = \frac{[Pd(NH_3)_4^{2+}]}{[Pd^{2+}][NH_3]^4} = 10^{30.5} \qquad (12.22)$$

which is more than 20 orders of magnitude lower than the cyano complex. Likewise, monoamines such as CH_3–NH_2, and multidentate ligands such as diamines (e.g., 1,3-diaminopropane) can be used to electrodeposit Pd. Thus Pd complexes within an intermediate range of stability are very useful in practical electroplating processes.

Hydrogen embrittlement is the most prominent but not the only challenge that needs to be considered when developing a Pd plating process. In summary, the factors that must be considered are as follows:

Hydrogen embrittlement: all factors that affect hydrogen evolution and incorporation

Stability of the chemical system
- Pd complex electrolyte (also solubility)
- Ligands for Pd complex (chemical and electrochemical stability)
- Replenishment system (ligand buildup)
- Counterion effects (e.g., salt buildup)
- Conducting electrolyte effects
- Additives and their decomposition products: brighteners, levelers, stress-reducing agents

Buffer system
- Ability to maintain pH at cathode and anode
- Stability at cathode and anode

Chemical attack on non–noble metal substrates
- Cu and Cu alloys (e.g., parts being plated)
- Steel (e.g., parts for the plating machine)
- Platinized anodes

Environmental considerations
- Toxicity of chemicals
- Waste disposal
- Vapor discharge (e.g., NH_3)

Cost of process
- Cost of chemicals
- Speed of deposition
- Efficiency of deposition
- Analysis and maintenance procedures
- Precious metal recovery

In the following section, we will discuss electrodeposition chemistries for alkaline, neutral, and acid electrolytes. We will begin with the examination of a highly alkaline ($pH \sim 12$), additive "free" chemistry which utilizes 1,3-diaminopropane as the ligand of choice. This analysis will demonstrate how to manipulate the chemical and physical properties of the

process in order to avoid hydrogen embrittlement and deposit "smooth," "crack-free" Pd films.

12.6 ELECTRODEPOSITION OF PALLADIUM

Palladium has been plated from a wide variety of electrolytes which are far too numerous to include in this chapter. This work will summarize what the author believes to be the most important processes, and in an attempt to organize this information, the processes will be broadly classified as alkaline (pH 9–13), neutral (pH 5–9), and acidic (pH < 1–5).

12.6.1 Alkaline Electrolytes (pH 9–13)

In the presence of ammonia or amines, Pd ions exhibit a very strong tendency to form stable complexes. As shown in Table 12.6, log $\beta_4$and log β_2 for ammonia and ethylenediamine are 30.5 and 26.9, respectively. While certainly not as stable as the cyano complex, they are nonetheless more stable than the aquo or halide complexes and are not susceptible to displacement plating.

The amine complexes are readily formed in palladium chloride solutions by the general equation:

$$PdX_2 + xNH_2 - R \rightarrow Pd(NH_2R)_x^{2+} + 2X^- \qquad (12.23)$$

where X = halides (Cl^-, Br^-, I^-); NO_3^-; SO_4^{-2}
R = H; CH_3; $C_yH_{2y}-CH_3$; $C_yH_{2y}-NH_2$
$x = 2, 4$ (depending on whether it is a diamine or a monoamine)
$y = 1, 2, \ldots$

Table 12.7 is a summary of various alkaline processes that have been found in the literature.

In this pH range (>9), only the diamine processes can be considered of practical use. While ammonia systems certainly can plate Pd with respectable properties, additives and wetting agents are essential if one requires smooth, bright to semibright deposits. In the absence of additives, the deposits are nodular, of dull appearance, and susceptible to "fingerprinting" or easily stained [37, 40]. Furthermore, at pH > 8, the presence of high concentrations of ammonia, especially at elevated temperatures, becomes problematic due to its excessive outgassing from solution, which in many cases is being subjected to aggressive solution movement or agitation. This makes it difficult to control pH, requires extensive replenishment with ammonium hydroxide, and poses an obvious environmental challenge. Thus, the only real contenders in this pH range are the "ammonia-free" systems. The remainder of this section will be restricted to the diamine processes (C, Table 12.7), which are an excellent example to demonstrate the hydrogen embrittlement issues discussed above [8, 99].

1,3-Diaminopropane Electrolyte [8, 99] The ligand of choice in the formulation of bath C is 1,3-diaminopropane (pn), whose formula is $NH_2C_3H_6NH_2$. It is a bidentate nitrogen-containing ligand that forms a classical 16-electron, square planar coordination complex, $[Pd(pn)_2]^{2+}$.

The choice of 1,3-diaminopropane was based on the analysis of numerous possibilities. Other ligands considered were additional aliphatic diamines (e.g., 1,4-diaminobutane), aliphatic triamines (e.g., diethylenetriamine), substituted diamine and triamine species (e.g., 2-hydroxypropanediamine), numerous substituted and unsubstituted monoamines (e.g., triethanolamine), and pyridines and numerous substituted and unsubstituted aromatic amines (e.g., diphenylamine). 1,3-Diaminopropane was chosen based on an exhaustive diagnostic analysis which took into account the requirements of performance, cost, and environmental considerations.

Counterion Effects Equation (12.23) describes the synthesis of an amine Pd complex where the counterion can be Cl^-, Br^-, NO_3^-, and SO_4^{2-}. Cyclic voltammograms of these systems are shown in Figure 12.10. The Pd^{2+} reduction peak potential [−0.91 V vs. the saturated calomel electrode (SCE)] is essentially unaffected by the change in anion, and it is concluded that the counterion has little or no effect on the electrochemical reduction of Pd. This phenomenon was also studied in an ammonia system by LePenven et al. [100] for Br^-, Cl^- and NO_2^- electrolytes.

However, there are other factors which must be considered in choosing the counter ion. For example NO_3^- is not electrochemically stable. This is also true for the nitrite systems where ammonium nitrate is subsequently formed by electrolysis but is itself unstable [101]. The SO_4^{2-} ion is electrochemically stable, but due to the difficulty of preparing $PdSO_4$, the cost becomes prohibitive, although within the last decade a number of sulfate systems have been formulated which can provide advantages over the chloride systems at a reasonable cost differential [126, 160, 162, 163]. The Br^- ion is easily oxidized at an insoluble anode, and one would like to avoid the formation of Br_2.

The most reasonable choice from a technical and cost perspective is chloride. It is "relatively" electrochemically stable at a Pt anode, very soluble, and easily transported across anion-permeable membranes [36].* Furthermore, the starting chemical, $PdCl_2$, is readily available and the least expensive of the Pd salts. The remainder of this discussion will deal solely with the $Pd(pn)_2Cl_2$ system.

Temperature and pH Effects Figure 12.11 shows a cyclic voltammogram of the $Pd(pn)_2Cl_2$ system at a gold rotating-disk electrode (RDE, 0.49 cm^2; $w = 0$) at 25°C. At pH 11.5,

*This property becomes important when removal of excess anion is necessary.

TABLE 12.7 Palladium Electroplating Alkaline Electrolytes (pH 9–13)

Parameter	Bath Type						
	A[71,37,35,98]	B[92]	C [8,99]	D[81,40,96]	E[93,94]	F[97]	G[98]
Source of Pd	$PdCl_2$	$PdCl_2$	$PdCl_2$	$Pd(NH_3)_2(NO_2)_2$	$Pd(NH_3)_2Br_2$	$Pd(NH_3)_2(NO_2)_2$	$Pd(OOOC(H_xNH_2)_2$
Pd metal (g/L)	10-20	28	1-40	4-25	25-35	4-18	1-50
Ligand*	NH_3	en^+	pn^+	NH_3	NH_3	NH_3	$OOCCH^2NH^2$
Amino acetic acid (g/L)						20	1–150
Ammonium bromide (g/L)					45		
Ammonium chloride (g/L)	60–90						
Ammonium hydroxide (g/L)			25–75	Adjust pH	Adjust pH		
Ammonium sulfate (g/L)							
Ammonium sulfamate (g/L)							
Ammonium nitrate (g/L)				90–100			
Tetrapotassium pyrophosphate (g/L)						5–300	
Potassium chloride (g/L)							
Potassium hydroxide (g/L)						Adjust to pH	Adjust to pH
Potassium phosphate (g/L)			50–100				
Potassium hydroxide (g/L)			Adjust to pH				
EDTA (g/L)							5
Sodium sulfate (g/L)		140					
Sodium nitrate (g/L)				9–12			
Hydrochloric acid (g/L)			Adjust pH				
Additives	See appropriate data in the literature	None	See appropriate data in the literature	See appropriate data in the literature	See appropriate data in the literature	See appropriate data in the literature	See appropriate data in the literature
pH	9–10	11–12	10–13	9–10	9–9.5	8.5–11	7–12
Temperature (°C)	25–50	25	40–70	25–55	25–55	35–45	60
Current density mA/cm^2	0.1–2.5	20	1–500	1–300	2.5–100	2–50	1–100

*Ligand is used in approximately stoichiometric (e.g.$PdNH_3$ 4:1) or slight excess of stoichimetry ~0.2–0.3 molar. + en = 1,2 ethylenediamine pn = 1,3 diaminopropane

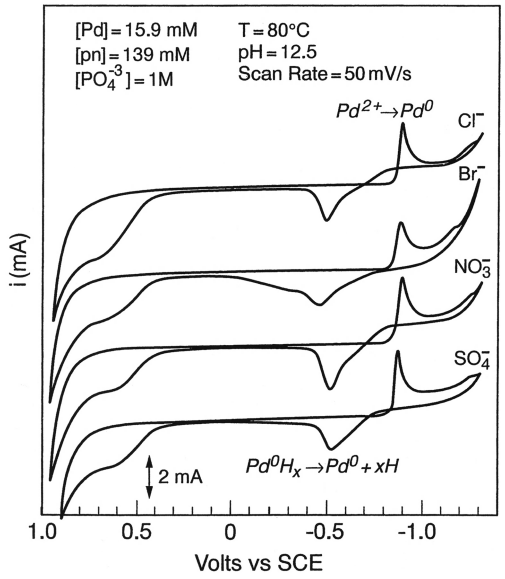

FIGURE 12.10 Cyclic voltammograms: palladium–diaminopropane with chloride, bromide, nitrate, and sulfate counterions.

the Pd reduction peak potential (-1.04 V vs. SCE) and the H^+ reduction peak potential (-1.10 V vs. SCE) are separated by only ~60 mV. Formation of PdH_x is evident by both the reduction peak (labeled PdH_x) and the hydrogen oxidation peak at -0.32 V observed on the reverse waves.

As the pH is varied from 11.5 to 12.5, the hydrogen reduction peak is shifted to more negative potentials. This shift (~0.059 V/pH) decreases the overlap with Pd reduction peak and reduces the formation of PdH_x, as evident by the relative decrease in the height of the PdH_x peak and the corresponding decrease in the hydrogen oxidation peak. Thus ΔE_p [see Eq. (12.18)] is increased and an overall reduction in hydrogen incorporation is accomplished by controlling the C^0_{H+}, as was discussed in Section 12.5.3.

A further increase in the value of ΔE_p is achieved by thermal destabilization of the Pd chelate complex which

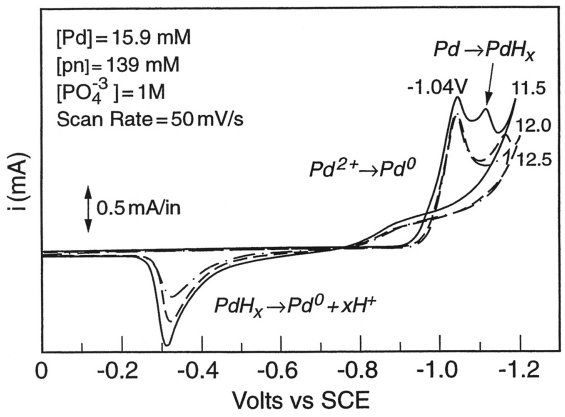

FIGURE 12.11 Cyclic voltammograms: palladium–diaminopropane system; variation of pH 11.5–12.5.

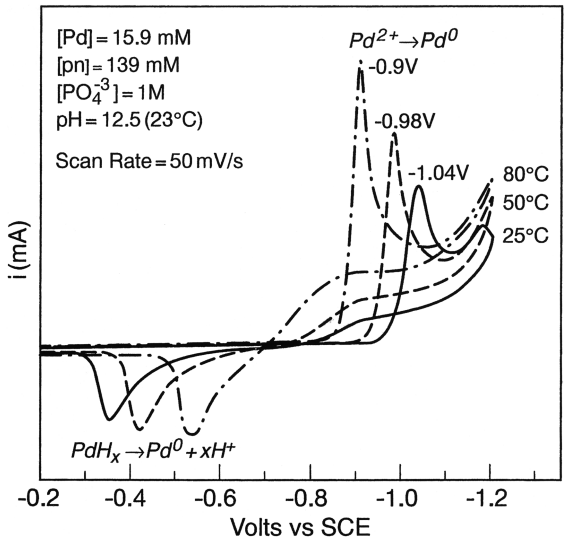

FIGURE 12.12 Cyclic voltammograms: palladium–diaminopropane system; variation of temperature, 25–80°C.

shifts Pd reduction to more positive potentials and away from the hydrogen reduction, as illustrated in Figure 12.12. Temperature variation from 25 to 80°C shifts the peak potential E_p from -1.04 to -0.91 V, or approximately 130 mV. A corresponding increase in i_p is realized due to an increase in the diffusivity of ions.

The shift in $E_p$with temperature is mostly due to the thermodynamic destabilization of the Pd chelate complex, which changes $E^{o'}$, and to a lesser extent changes in RT and k^0, which affect $E^{o'}$ and E_p, as predicted by Eq. (12.17).

The pH dependence at elevated temperature is dramatically demonstrated in Figure 12.13. Voltammograms taken at

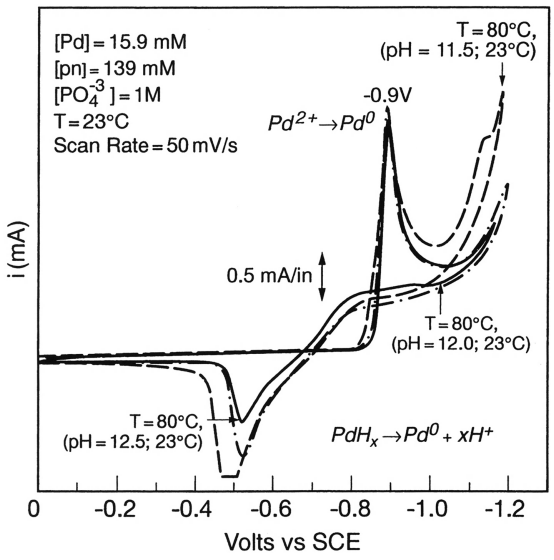

FIGURE 12.13 Cyclic voltammograms: palladium–diaminopropane system; variation of pH 11.5–12.5 at 80°C.

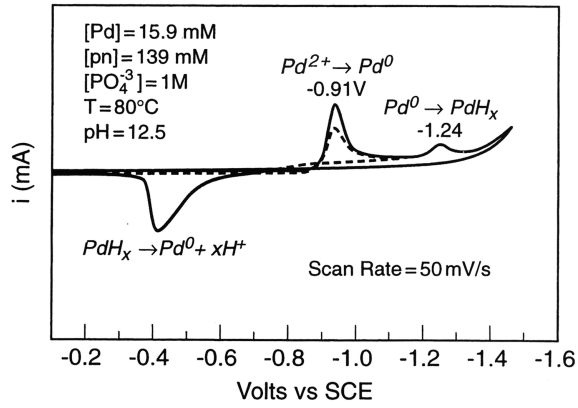

FIGURE 12.14 Cyclic voltammograms: palladium–diaminopropane system.

80°C and various pH show a decrease in the formation of PdH_x and the corresponding hydrogen oxidation peak with decreasing $[H^+]$. Therefore, through the use of $Pd(pn)_2^{2+}$ as the complex electrolyte, the exclusion of additives which cause strong kinetic inhibition of the Pd reduction, and the manipulation of temperature and pH, one can separate the Pd^{2+} reduction peak from the hydrogen reduction peak and obtain a ΔE_p of approximately 330 mV. Figure 12.14 demonstrates that one can reach the limiting current and avoid hydrogen incorporation as evident by the absence of a hydrogen oxidation peak.

Ligand Concentration Effects and Replenishment Schemes The overall reaction for Pd electrodeposition using a nonconsumable anode is

$$Pd(pn)_2Cl_2 + H_2O \longrightarrow Pd^0(s) + 2H^+ + 2Cl^- + 2pn + \tfrac{1}{2}O_2 \tag{12.24}$$

This indicates that for every Pd^{2+} reduced 2pn molecules and $2Cl^{-1}$ ions remain in solution, and $2H^+$ are generated lowering the pH of the solution.

Figure 12.15 shows voltammograms of $[Pd(pn)_2]^{2+}$ as the pn concentration is varied from stoichiometry to 100X excess. The Pd^{2+} reduction peak shifts to more negative potentials and thus closer to the hydrogen regime. This phenomenon can be predicted through use of the Nernst relationship [see Eq. (12.19)] and stability constants.

Also, the formation of the Pd diamine complex is represented by the following equilibrium:

$$Pd^{2+} + 2pn \Leftrightarrow Pd(pn)_2^{2+} \tag{12.25}$$

for which the formation constant is

$$K_f = \frac{[Pd(pn)_2^{2+}]}{[Pd^{2+}][pn]^2} \tag{12.26}$$

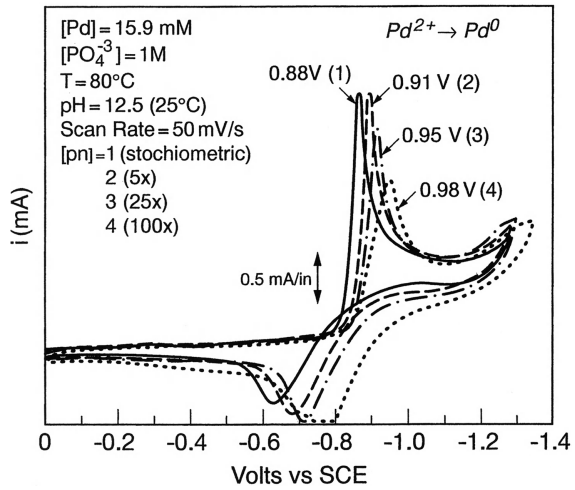

FIGURE 12.15 Cyclic voltammograms: palladium–diaminopropane system; ligand concentration effects.

Combining Eqs. (12.19) and (12.26) yields the following at $T = 25°C$:

$$E^{o'} = E^o - \frac{0.0591}{2}\log\beta_2 - \frac{0.0591}{2}\log[pn]^2 + \frac{0.0591}{2}\log\left[Pd(pn)_2^{2+}\right] \tag{12.27}$$

This equation predicts a negative shift in $E^{o'}$ as the pn concentration increases. This, of course, shifts E_p in a similar direction [see Eq. (10.17)] as is experimentally observed in Figure 12.15.

In order to avoid this situation, $PdCl_2$ is used as the starting and replenishment chemical. The overall reactions are shown below:

$$\begin{array}{l} PdCl_2 + y(pn) \longrightarrow Pd(pn)_2\,Cl_2 + (y-2)\,pn \\ \qquad\qquad\nwarrow \\ \qquad\qquad\quad PdCl_2 \updownarrow 2e \\ \qquad\qquad\swarrow \\ \qquad\qquad y(pn) + Pd(s) + 2\,Cl^- \end{array} \tag{12.28}$$

For this chemical system, it is optimum to maintain the [pn] in excess of stoichiometry (y varies from 3 to 5 excess) which is useful in the dissolution of $PdCl_2$; however, the pn concentration remains relatively constant and the problem of the Pd^{2+} reduction shifting closer to the hydrogen is eliminated. As can be seen, the Cl^- buildup and pH control remain potential problem areas.

The pH is controlled through use of a buffer system and periodic additions of KOH. While large amounts of Cl^- (KCl) do not seem to adversely affect the process, eventually salts may precipitate, necessitating filtration of the system. In this regard, a soluble form of $PdO \cdot xH_2O$ as the starting material and replenishment salt solves both problems and is preferred [102–104]. Equation (12.29) describes the system if a soluble form of $PdO \cdot xH_2O$ could be utilized:

$$\mathrm{PdO}\cdot x\,\mathrm{H_2O} + y(\mathrm{pn}) \xrightarrow[\Delta]{\mathrm{H_2O}} \mathrm{Pd(pn)_2(OH)_2} + (y-2)\,\mathrm{pn}$$

$$\uparrow \qquad \downarrow +2\,\mathrm{e}$$

$$\mathrm{Pd^0(s)} + y(\mathrm{pn}) + \tfrac{1}{2}\mathrm{O_2} + 2(\mathrm{OH})^- + 2\,\mathrm{H}^+ \quad (12.29)$$

Buffer System and Supporting Electrolyte The buffer of choice is K_2HPO_4/K_3PO_4 since the pH range desired is from 10.5 to 12.5. It is fortuitous that the phosphate system is also desirable from a stability perspective. It is electrochemically and thermally stable and does not significantly affect the morphology of the deposit. In this case the buffer salts also act as the supporting electrolyte.

Limiting Currents i_L The concentration and mobility of metal ions and the degree of solution agitation dictate the limiting current. Figure 12.16 shows current–voltage profiles of the Pd reduction process and demonstrates how i_L varies with rotation speed (ω) at a RDE. The Levich equation

$$i_L = nFAC_TD^{2/3}\omega^{1/2}v^{-1/6} \quad (12.30)$$

where i_L is the limiting current, n is the number of electrons, F is Faraday's constant, A is the area of the electrode, C_T is the total bulk concentration of Pd^{2+}, D is the diffusion coefficient, ω is the rotation speed, and v is the kinematic viscosity implies that a process is mass transfer controlled when a linear relationship exists between i_L and $\omega^{1/2}$, where ω is the only changing variable. Figure 12.16*b* shows that this reduction process is mass-transfer controlled. Furthermore, the relatively "flat" current plateau implies that all metal ions reaching the surface are reduced, that no other reaction is taking place, and that the surface of the deposit is macroscopically smooth.

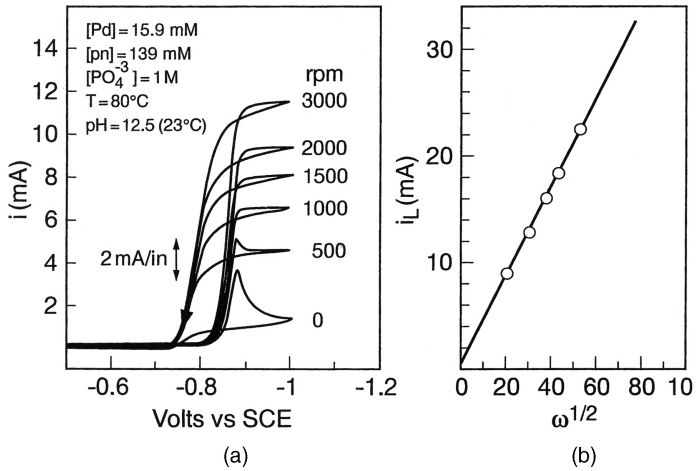

FIGURE 12.16 (*a*) Cyclic voltammograms, palladium–diaminopropane system, i_L versus rotation speed ω; (*b*) plot of m_L (mA) versus $\omega^{1/2}$.

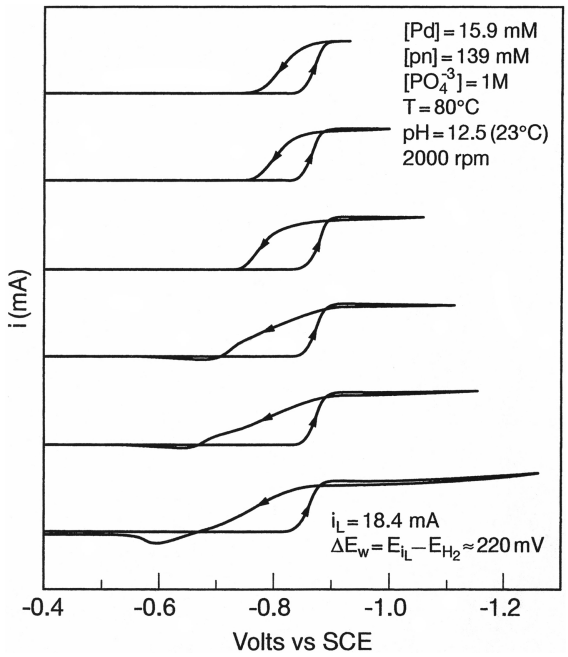

FIGURE 12.17 Cyclic voltammograms: palladium–diaminopropane system; determination of ΔE_ω.

Quantitative Hydrogen Analysis Figure 12.17 demonstrates qualitatively how the pn process behaves regarding hydrogen incorporation. The limiting current is reached with little or no incorporation of H_2, as is evident by the smooth plateaus and the absence of a hydrogen oxidation peak until the termination potential of the cathodic scan reaches approximately −1.1 V. An operating window (ΔE_w), which is described as the difference in potential between $E_{i_L}(\mathrm{Pd})$ and $E_{\mathrm{onset}}(\mathrm{H_2})$, is given as

$$\Delta E_{iL}(\mathrm{Pd}^{2+}) \text{ and } E_{\mathrm{onset}}(\mathrm{H_2}) \quad (12.31)$$

where ΔE_w of approximately 220 mV (compare to $\Delta E_p \sim 330$ mV) is realized. Thus to a first approximation, ΔE_p and ΔE_w yield information regarding the probability of a system to avoid hydrogen incorporation. Maximization of ΔE_p and ΔE_w is desired.

However, a quantitative, albeit more time-consuming, analysis is obtained via the coulometric anodic stripping of hydrogen described elsewhere [8, 86, 102]. Figure 12.18 is a plot of $\%H_2$ versus i/i_L at pH 12.5 (25°C)*. The increase in temperature (25–70°C) substantially reduces the amount of hydrogen incorporated in the Pd films. It must be kept in mind that the [Pd] is 15.9 *mM* and that operating at higher Pd concentrations and greater solution agitation allows much

* The parameter i/i_L is more informative than merely i(mA) for it takes into account the operating parameters of ω, [Pd], and T. It is believed that morphology and material properties vary with this parameter and not simply i(mA).

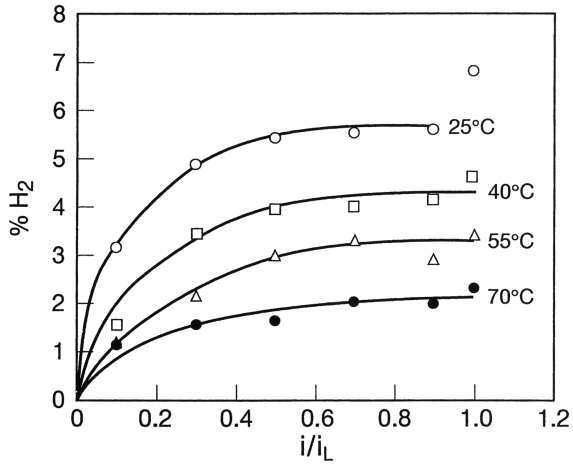

FIGURE 12.18 Percentage of hydrogen versus i/i_L *at* various temperatures.

higher limiting currents, making high rates of deposition possible with reduced hydrogen content (see arguments in Section 12.5.3). Note also that the Pd films deposited under these conditions were bright to semibright, adherent, and crack free up to thicknesses exceeding 2.5 μm. Figures 12.19 and 12.20 are scanning electron micrographs of Pd deposited at high speeds. As can be seen, the deposits are smooth, uniform, and crack free at current densities of 500 mA cm^{-2}.

Material Properties [8, 102] Deposits plated from the diaminopropane system have been found to exhibit excellent properties for technological applications. The deposits are smooth and the brightness can be controlled by the bath temperature, pH, and operating current density. In general, the brightness, hardness, and internal stress are increased by operating at lower temperatures (25°C) and lower pH (10.5) and higher current densities (i.e., $i/i_L > 0.6$).

The deposit hardness ranges from 250 to 350 KHN_{50} (Knoop hardness), where the values increase as i/i_L increases. Ductility, measured by the method of Nakahara et al. [105], is in the range of 3–7% elongation for films of 1.25 μm thickness. In general, the films are harder and more ductile than hard gold.

Transmission electron microscopy indicates that the grain growth is not epitaxial and that grain size varies with the operation current ratio, i/i_L. Preliminary results show that for $i/i_L = 0.1$ the grain size ranges from 150 to 800 Å, while for $i/i_L = 0.9$ the grain size ranges from 30 to 50 Å. Thus, as the operating i/i_L increases, one obtains smaller grain, smoother deposits. Comparably hard gold grain size ranges from 150 to 350 Å.

Mass spectrographic evolved gas analysis performed on Pd films electroplated at various i/i_L indicates that the amount of occluded impurities is independent of the operating current ratio. A total weight loss ranging from about 0.8 to 1.7% occurred when the films were treated at 260–270°C; all other gases evolved above 1000°C. Overall the Pd films are substantially cleaner than electrodeposited gold films [113].

Environmental and standard wear tests [27] and fretting wear tests [16] have demonstrated that this process produces deposits which can be utilized for connector and other applications.

12.6.2 Acid Electrolytes (pH < 1–5)

Table 12.8 provides the formulas for a number of acid electrolyte processes.

Acid Chlorides (pH < 1) The simplest bath to prepare is an acid chloride system (A, Table 12.8) according to the following equation:

$$Pd^{2+} + 4Cl^- + 2H^+ \Leftrightarrow H_2PdCl_4 \qquad (12.32)$$

In these systems [37] of high acid and chloride content, the equilibrium constant is

$$\beta_4 = \frac{[H_2PdCl_4]}{[Pd^{2+}][Cl^-]^4[H^+]} = 10^{12.2} \qquad (12.33)$$

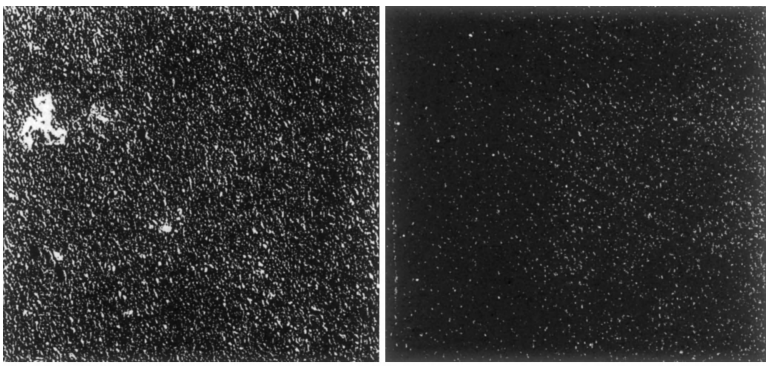

FIGURE 12.19 Scanning electron micrograph: palladium plated at 500 mA cm^{-2} and 2.5 μm in thickness.

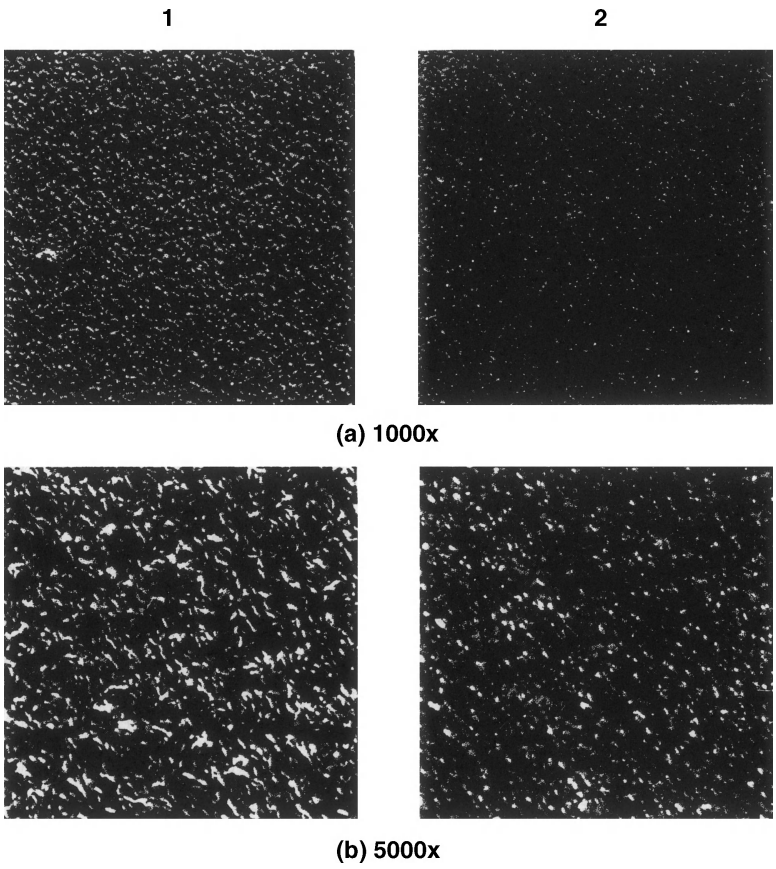

FIGURE 12.20 Scanning electron micrograph: palladium plated at i/i_L value of 0.1, 0.3, and 2.5 μm in thickness.

TABLE 12.8 Palladium Electroplating Acid Electrolytes pH (<1 to 5)

	Bath Type				
Parameter	H[35,37,39,109]	I[35]	J[39,110]	K[35]	L[111]
Source of Pd	$PdCl_2$	H_2PdCl_4	$Pd(NO_3)_2$	$Na_2Pd(NO_2)_4$	$PdCl_2$
Pd metal (g/L)	5–50	5	2–15	5–10	0.1–3.0
Pd sulfite (g/L)			0.2–2		
Ligand	H_2O	Cl^-	H_2O	NO^2	Organic diamines
Ammonium chloride (g/L)	20–50				
Sodium nitrite (g/L)		14			
Sodium chloride (g/L)		40		10–40	10–60
Sodium sulfite (g/L)					
Phosphoric acid (g/L)	As needed				
Boric acid (g/L)	As needed	10–30			
Oxalic acid (g/L)	As needed				
Hydrochloric acid (g/L)		As needed			
Sulfuric acid (g/L)			98		
Additives				See appropriate data in the literature	See appropriate data in the literature
pH	0–0.5	4.5–6	0	4.9–8	2–6
Temperature (°C)	25–60	50	20–35	40–50	25–45
Current density mA/cm^2	10	4–10	5–80	~1	5–50

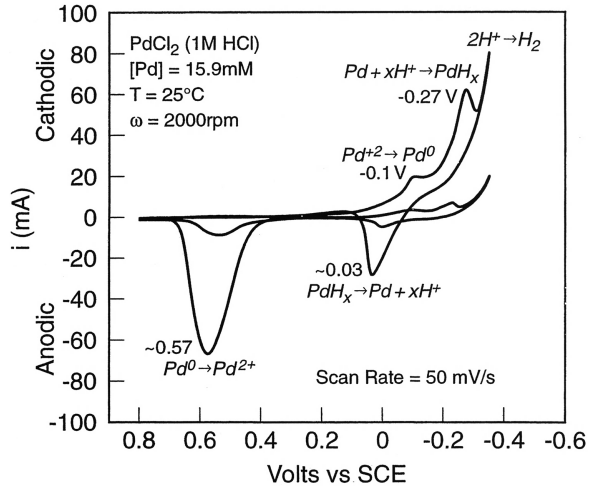

FIGURE 12.21 Cyclic voltammograms: $PdCl_{2l}$, in HCl, 0 and 2000 rpm.

This relatively weak Pd complex implies that immersion plating on a non–noble metal would occur quite readily.

A cyclic voltammogram of $PdCl_2$ in 1 *M* HCl electrolyte is seen in Figure 12.21 [114]. The E_p (Pd^{2+}) is about 0.1 V relative to SCE, and the PdH_x peak potential is at about 0.27 V before bulk hydrogen evolution. On the return scan, the hydrogen is anodically stripped [8, 102] from Pd hydride [E_p (oxidation) $+0.03$ V). Finally, Pd is dissolved at about 0.57 V.

Palladium deposition from acid electrolytes is typically 97–100% efficient. Compact, dense crack-free films have been reported even at thicknesses of 10 μm (Table 12.8). The deposits generally have a satin finish extending to full bright and gray. Depending on deposition conditions, they have a microhardness of 250–350 HV (HV = Vickers hardness) [37].

According to Hedrich and Raub [37], in the current density of 1–100 mA cm^2 at temperatures of 10–50°C, Pd is deposited at $+0.1$ to $+0.5$ V relative to the normal hydrogen electrode (NHE). The temperature dependence of the cathodic overpotential can be easily observed in Figure 12.22.

Palladium deposited from an electrolyte with lower chloride content exhibits a lower cathodic overvoltage for reduction (see Fig. 12.23). This occurs because the Pd free-ion concentration remains higher since the lower chloride and hydrogen concentrations reduce the stability of the Pd(II) chloro complex; see Eqs. (12.32) and (12.33) and arguments in Section 12.5.3.

For this system, low hydrogen codeposition has been reported at potentials of $+0.5$ to $+0.1$ V. Hydrogen discharge complies with Nernst's law at an equilibrium potential; see Eq. (12.20). Thus, even in strong chloride solutions with 10 N hydrogen ion concentration, the H_2 evolution starts only at an equilibrium of $+0.059$ V.

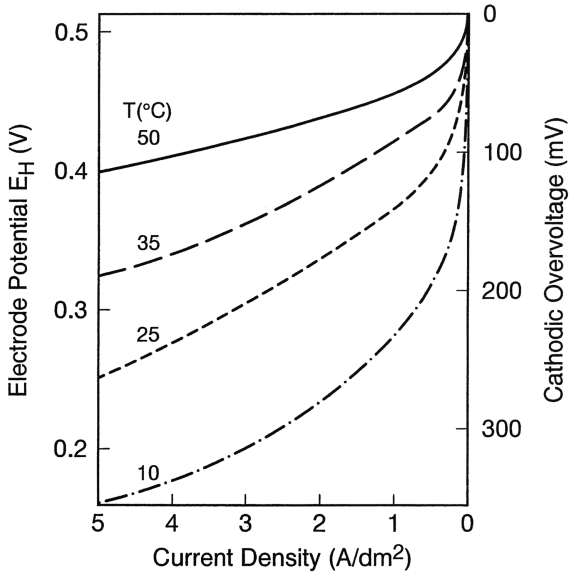

FIGURE 12.22 Current voltage curves: 0.1 *M* $PdCI_2$, in 5 *M* HCl, $di/dt = 0.2$ A $dm^{-2} \cdot$ s at various temperatures.

At current densities between 1 and 5 A dm^{-2} it is below 3 N ml H_2/gPd, which makes the [H]/[Pd] < 0.03. This implies that deposited films are in the range of the α phase.

X-ray analysis of Pd films deposited from 0.1 M $PdCl_2$ solution at 5 N HCl concentration at current densities of 1–3 A/dm^{-2} shows a slight expansion of the α-Pd lattice to 3.895 Å compared to 3.890 Å for pure Pd. These films are finely crystalline and irregularly oriented with no preferential

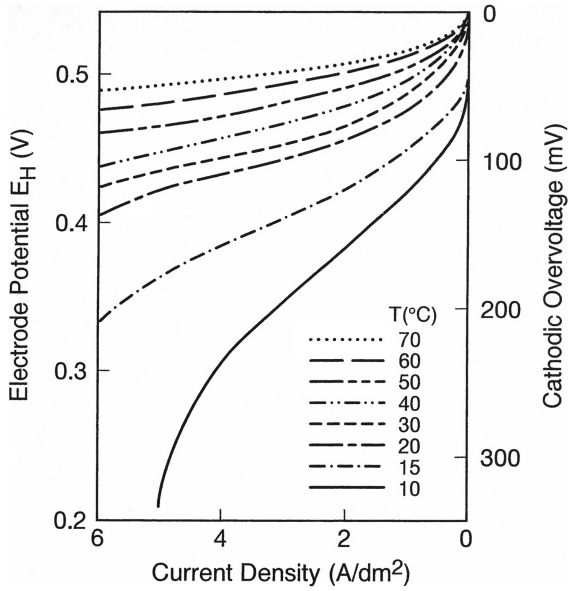

FIGURE 12.23 Current-voltage curves: 0.1 *M* $PdCl_2$ in 0.5 *M* HCl, pH 5.0, for $di/dt = 0.2$ A $dm^{-2} \cdot$ s.

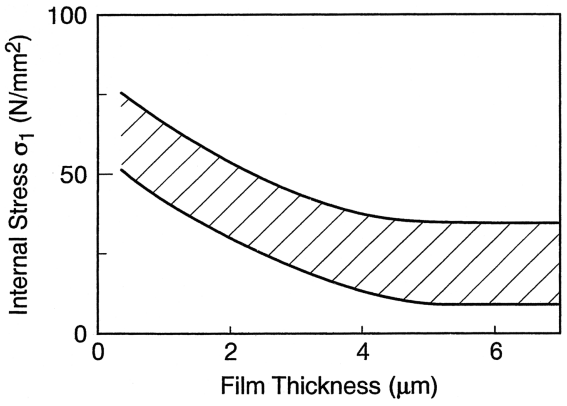

FIGURE 12.24 Internal stress versus film thickness, 0.1 *M* $PdCl_2$ in 5 *M* HCl at 1 and 3 A dm^{-2}.

orientation. They exhibit very low internal stress which decreases with increasing film thickness (Fig. 12.24).

Hedrich and Raub [37] stated that acid Pd chloride electrolytes are well suited for depositing thick Pd films of low internal stress at about 100% current efficiency. The disadvantages of these systems is their attack on non–noble base metals used for substrates which cannot be directly plated and their attack of metals used in plating equipment. An excellent analysis of this system, including the measurement of exchange current densities and the determination of an activation energy for charge transfer reaction of Pd^{2+}/Pd, is found in [37].

Acid Sulfates (pH < 1) Sulfuric acid electrolytes that used a Pd nitrate salt (bath J, Table 12.8) were investigated by Hedrich and Raub [39] and Simon and Zilske [110], who reported that the drawbacks of the Cl^- baths are eliminated. A solution of Pd nitrate in sulfuric acid produces black, spongy, loosely adhering Pd films. Alternatively, smooth, lustrous Pd precipitates can be obtained only after adding 5–20% Pd sulfite. The formation of a Pd sulfite complex ($[Pd(SO_3)_2]^{2-}$) decreases the Pd free-ion concentration and shifts its reduction potential to a more negative point. The increased cathodic overvoltage for metal deposition has a positive effect on the film properties.

Smooth, lustrous, low-stress films that contain relatively little hydrogen with a hardness of 350 HVare obtained [39]. Sulfite is reduced to sulfide during deposition of the Pd and adsorbed on the cathode. Palladium sulfide inhibits Pd deposition and is incorporated during crystallization. The sulfur content increases with electrolyte sulfite content and cathodic current density. The properties of these films are largely determined by the sulfur content and in general are fine grain sized, relatively hard, and have a pronounced ⟨100⟩ orientation.

The disadvantages of this process are the necessity of a noble metal strike (e.g., gold) to prevent attack of non–noble metal surfaces and the necessity for continuous filtration to reduce the tendency for the reduction of Pd ions to metal according to the following equation [39]:

$$Pd^{2+} + SO_3^{2-} + H_2O \longrightarrow Pd + H_2SO_4 \qquad (12.34)$$

Acid Strikes (pH 3–4) An acidic Pd "strike" process was developed by Straschil et al. [111, 112] (bath L, Table 12.8). This process uses organic diamines to stabilize a complex in the pH range of 3–4. Unlike the highly acidic baths with $pH \leq 1$, this chemistry does not undergo "displacement" plating or attack on non–noble metal substrates. However, it promotes the removal of surface oxides, especially on nickel, which makes it ideal as a strike process. This process also reduces the porosity of subsequent noble metal layers by increasing the nucleation and "coverage" of substrate surfaces. It exhibits good chemical and electrochemical stability along with stable pH due to the high buffer capacity. The limitations of this process are the inability to plate greater than 0.2 μm without the formation of cracks due to hydrogen embrittlement [112]. However, for a strike process only thin layers are required.

Dullaghan et al. [176] reported a very low pH Pd strike with unique capabilities that combines the "activating" power of a very low pH (<1) with the advantage of room temperature operation. Bright Pd is deposited on various substrates with surprisingly high cathode efficiencies. The system leads to improved adhesion on easily passivated surfaces (e.g., nickel) and reduces the porosity of subsequent Pd and Pd alloy or other precious metal deposits.

The chemistry is robust and can withstand relatively high levels of foreign metal contamination, for example, copper and nickel. The components are claimed to be compatible with chloride- and sulfate-based Pd plating electrolytes. One other important advantage over prior art is the ability to plate relatively thick deposits with a high degree of leveling, as seen in Figure 12.25.

12.6.3 Neutral Electrolytes (pH 5–9)

Numerous chemical systems have been investigated in this pH range, including oxalates and sulfamates. While in many cases these systems possessed the proper current–voltage profiles to deposit Pd and avoid hydrogen codeposition and the initial deposits from a "nonaged" electrolyte could provide films of excellent hardness, ductility, and surface appearance, these systems did not stand up during extensive aging or bath use.

Hydrogen embrittlement is not the only challenge when developing a plating process for commercial use. The chemical and electrochemical stability of the ligand system poses concern. Furthermore, simple replenishing systems were difficult to devise due to slow attack of these ligands on salts such as $PdCl_2$. Furthermore, the decomposition and buildup of ligands in solution lead to an aggravation of the hydrogen

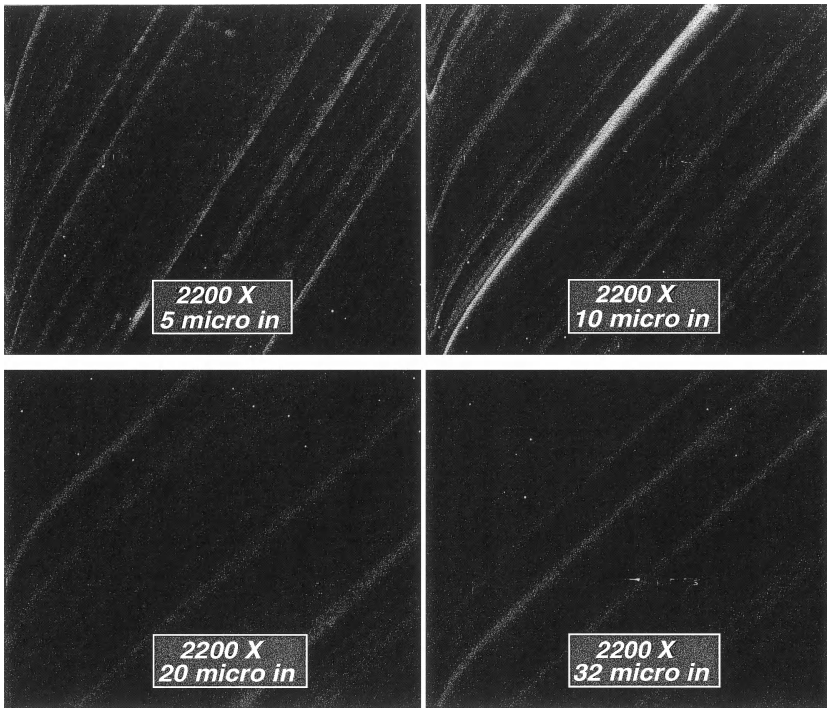

FIGURE 12.25 Scanning electron micrographs: palladium acid strike at 5, 10, 20, and 32 μm.

problem and microcracking. However, Pd electrolytes based on ammonia ligand have proved to be viable and are used almost exclusively in the pH range of 5–9.

Hedrich and Raub [37, 39, 40] studied "nonadditive" ammonia systems extensively and found them "well suited to deposit palladium films for technological applications" (baths N and O, Table 12.9). The reduction takes place at essentially less noble potentials than in acid systems (see Fig. 12.26). For example, the Pd potential E_H in 0.1 m $PdCl_2$ solution is $+0.55$ V, whereas the Pd tetramine complex of the same concentration is $+0.22$ V. In Pd diamino dinitro electrolyte, P-Salt, reduction takes place in approximately the same potential range as the ammonia system.

Tetramine Electrolytes: "Nonadditive" Systems Amine complexes form in Pd chloride solutions in the presence of ammonia at pH values above 4.5 and are completely transformed into the square planar complex at pH 7.5. Upon acidification with hydrochloric acid, the complex is transformed step by step into Pd diamino complex, which is stable in the acid range. Starting from pH 6, yellow $Pd(NH_3)_2Cl_2$ is precipitated in cold $0.1\,M$ solution; the precipitation process is complete at pH 4.

The following composition was chosen as the standard electrolyte for electrodeposition experiments:

$$0.1\,M\,PdCl_2 + 1.0\,M\,NH_4Cl + x\,M(NH_3H_2O) \quad (12.35)$$

The pH value was set between 8 and 10 with NH_4OH.

Palladium is deposited from the tetramine complex at current densities from 1 to 5 A dm^2 at an overpotential of 300 and 600 mV (Fig. 12.27). The current–voltage characteristics exhibit a strong temperature dependence since the stability of the $[Pd(NH_3)_4]^{2+}$ decreases with increasing temperature. The current efficiency is below 100% so that the cathode always represents a double electrode. Current efficiency measurements in agitated electrolytes indicate that hydrogen evolution is strongly dependent on the current density and electrolyte temperature (Fig. 12.28). The current yield increases with increasing cathodic current density and at high higher electrolyte temperatures [37]. The Pd tetramine complex stability increases with increasing pH values, so the cathodic overpotential required for Pd deposition increases distinctly (Fig. 12.29).

The hardness of these Pd deposits varies according to the deposition conditions (usually measured at ~25-μm-thick films). Palladium deposited at electrolyte temperatures between 15 and 25°C and at current densities from 1 to 2 A dm^{-2} have hardness values between 270 and 320 HV directly after deposition, which is significantly reduced to between 150 and 180 HV when deposited at 60°C.

The deposits exhibit tensile stresses (Fig. 12.30) that decrease with increasing electrolyte deposition temperature and increasing film thickness. Hydrogen codeposited is associated with this phenomenon, which results in considerable stress in the lattice as revealed by X-ray analysis.

Quantitative hydrogen analysis via anodic stripping indicates the hydrogen content is strongly affected by current

TABLE 12.9 Palladium Electroplating Neutral Electrolytes (pH 5–9)

	Bath Type						
Parameter	M[35,37,35,40,98]	N[36,40]	O[36,40]	P[40,81,96]	Q[93,94,106]	R[97,107]	S[98,108]
Pd source	$Pd(NH_3)_4(NO_3)_2$	$PdNH_3)_2(NO_2)_2$	$Pd(NH_3)_2Cl_2$	$Pd(NH_3)_4Cl_2$	$Pd(NH_3)_2Cl_2$	$Pd(NH_3)_2Cl_2$	$Pd(NH3)_4Cl_2$
Pd metal (g/L)	10	4	20	10–20	20–30	10	5–25
Ligand	NH_3	NH_3	NH_3	NH_3	NH_3	NH_3	NH_3
EDTA (g/L)						20	
Ammonium nitrate (g/L)	90–100						
Ammonium chloride (g/L)			10	60–90	30–60		90
Ammonium sulfate (g/L)			20				
Ammonium carbonate (g/L)			10				
Sodium nitrate (g/L)		10–11					
Ammonium sulfamate (g/L)					30–40		
Ammonium hydroxide (g/L)	Adjust pH	Adjust pH	Adjust pH	Adjust pH			Adjust pH
Ammonium phosphate (g/L)							90
Sodium sulfite (g/L)					1–1000 ppm	28	
Potassium phosphate (g/L)						80	Adjust to pH
Hydrochloric acid (g/L)							Adjust to pH
Additives			Proprietary (see data in the literature)	Proprietary (see data in the literature)	Proprietary (see data in the literature)	Proprietary (see data in the literature)	Proprietary (see data in the literature)
pH	9.1	7.5–10	7.5–9	8.0–9.5	~9	8.5–9	7–8
Temperature (°C)	60–80	40–55	20–40	25–50	25–40	35	30–50
Current density mA/cm^2	5–20	1–40	5–15	1–25	15–25	50	1–>250

*Diaphragm proccess.

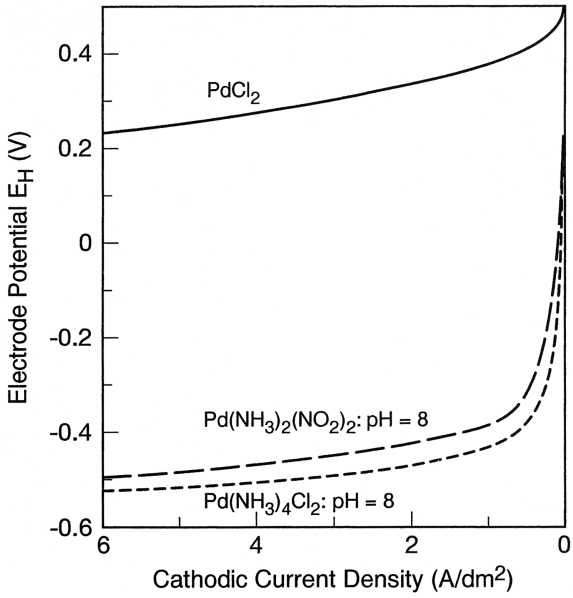

FIGURE 12.26 Current–voltage curves: acid Pd versus ammoniacal Pd chemistries, $di/dt = 0.2$ A dm^{-2} · s.

density and deposition temperature (Fig. 12.31). At low deposition temperatures, <40°C, the hydrogen content increases rapidly with current densities, whereas at temperatures greater than 40°C, the increase in hydrogen content is much lower.

Hedrich and Raub [37] found that Pd films with a hydrogen content below $10N$ ML H_2/g Pd or atomic H/Pd ratios below 0.1 have a metallic brilliance and are suited for decorative and technological applications. For higher H/Pd ratios, the Pd deposits become dull and dark, and at H/Pd ratios ≥0.8 they are black and powdery, that is, the so-called burned deposits.

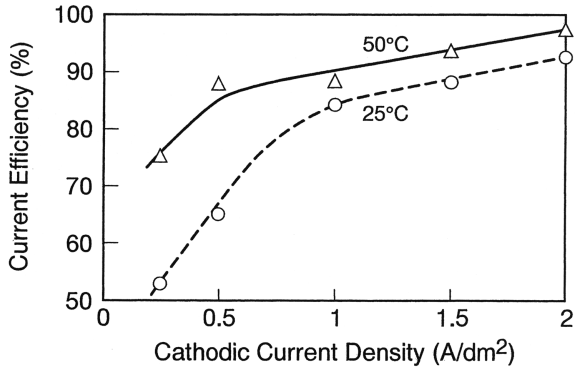

FIGURE 12.28 Current efficiency versus current density: $Pd(NH_3)_4CI_2$ at 25 and 50°C.

Palladium deposits from tetramine electrolytes without additives are dull and gray in appearance. Viewed under a scanning electron microscope, the deposit surface is "budded" and nodular [40]. These deposits are very sensitive to "finger prints" and other contaminants since "oils" readily adhere to microrough surfaces.

In terms of processing technology, electrolytes high in ammonia content are difficult to operate and control at pH > 7.5 and temperature >35°C. Ammonia vaporization losses are significant and require the pH be monitored and controlled. In the presence of halides, significant attack on metals such as copper, brass, and stainless steel (in plating equipment) occurs. Furthermore, the resulting metallic impurities degrade the appearance and the mechanical properties and decrease the partial current density and the covering power of Pd deposition.

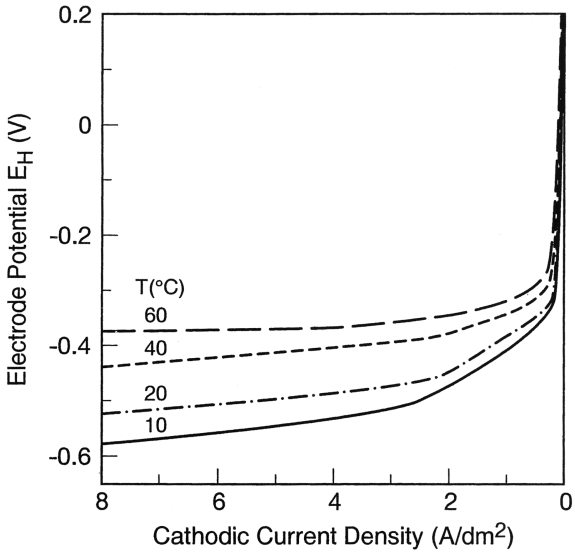

FIGURE 12.27 Current–voltage curves: $Pd(NH_3)_4Cl_2$ at various temperatues, $di/dt = 0.2$ A dm^{-2} · s.

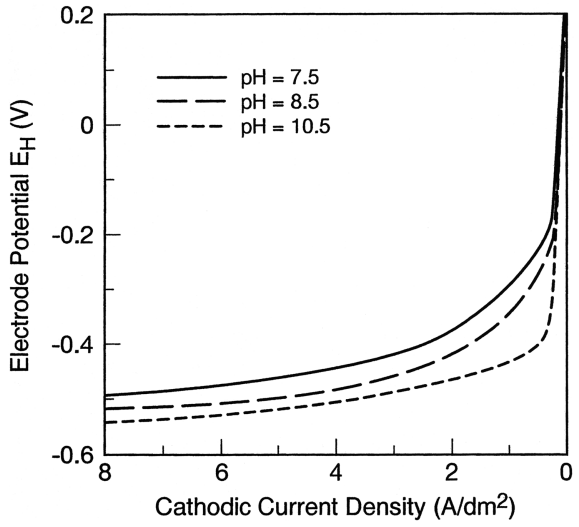

FIGURE 12.29 Current–voltage curves: $Pd(NH_3)_4Cl_2$ at various pH, $di/dt = 0.2$ A dm^{-2} · s.

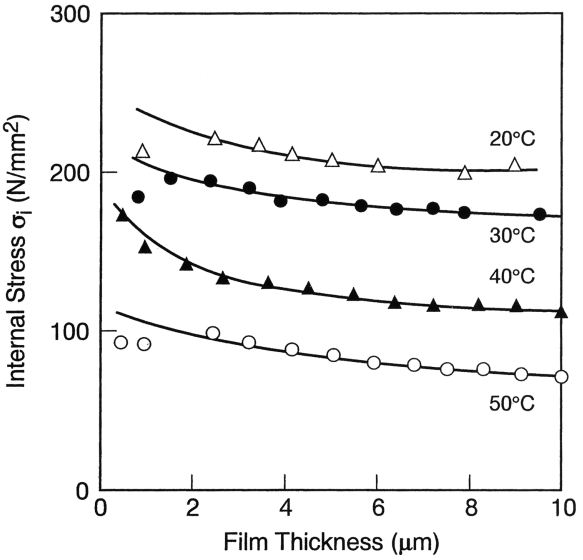

FIGURE 12.30 Internal stress versus film thickness: $Pd(NH_3)_4Cl_2$; pH 9: at 2 A dm^{-2}.

Hedrich and Raub [115] also studied the effects of "additives" in these systems to improve the surface appearance and reduce the "roughness" of the deposits. They studied the effects of citrates, benzoates and salicylate, nicotinic acid, and nicotinamide. In general, these additives displace the reduction potential to more negative values closer to the hydrogen regime and increase the hydrogen content of the films.

Aliphatic citrates produce an irregular crystallization, whereas benzoates and salicylates produce a ⟨110⟩ preferred orientation; however, they also increase the hydrogen content and tensile stress in the plated films resulting in microcracked deposits. The electrodeposition of smooth, full-bright, adherent, crack-free films from tetramine systems requires the use of additives. In the next section, we will discuss some of these systems.

Tetramine Chloride Electrolytes with Additives There exists numerous patents on the use of additives in palladium–ammonia electrolytes whose function is to deposit dense, full-bright Pd films of low porosity without microcracks at thicknesses in excess of 25 μm.

For example, Deuber [107] patented a process (bath R, Table 12.9) using an alkylene diamine phosphonate derivative of the following formula:

$$[(MO)_2{-}OP{-}R]_2{-}N{-}R{-}N[R' - OP(OM)_2]_2 \quad (12.36)$$

where R is an alkylene group of two to six carbon atoms, each R′ is an alkylene group of one to four carbon atoms, and each M is a nondeleterious cationic moiety which does not interfere with the plating process, such as hydrogen, alkali metals, and ammonium moiety. This phosphonic compound is believed to act as a buffering compound, a conducting salt, and a complexing agent for contaminant metal ions which are not desired to plate out. The concentration of the phosphonic compound should be from 5 up to 100 g L^{-1}. Dequest 2041 is ethylene diamine tetramethylphosphonic acid which contains approximately 10% water and is one of the preferred phosphonates.

The pH of the electroplating solution should be maintained at a value of from 4.5 to 12 in order to avoid stability problems. Values from 4.5 to 7.0 are preferred for strike plating. For ordinary electroplating, a pH value from 7 to 10 is preferred. The bath parameters are as follows:

Component	Concentration (g L^{-1})
Ethylene diamine tetramethylphosphonic acid	45
$Pd(NH_3)_2Cl_2$	1–10 (metal)
Sulfamic acid	40
Ammonium chloride	50–150
Ammonium monohydrogen phosphate	25–75
Ammonium hydroxide	pH 6.5–10

The bath may be employed to plate Pd or its alloys. Deuber makes use of class I and class II organic brighteners with this palladium–amine system.

The Pd is supplied as any electrodepositable form (e.g., $[Pd(NH_3)_4]^{2+}$). The stability is by employing ligands such as urea or an amine complex with the following counterions: chloride, bromide, nitrite, and sulfite. The Pd concentration is in the range of 0.1–50 g L^{-1}.

Class I brighteners are generally unsaturated sulfonic compounds with the general formula

$$A{-}SO_3{-}B$$

where A is an aryl or alkylene group, substituted or unsubstituted; B is OH, OR, OM, $NH_{2'}$, NH, H, R; M being an alkali metal, or else ammonium, and R being an alkyl group of not more than six carbon atoms.

Class II brighteners are generally unsaturated or carbonyl organic compounds. Examples are compounds containing >C=O; >C=C<;C≡N; >C=N; C≡C; N=N. Concentration of the individual brighteners may range from 0.001 to 25 g L^{-1}. Some compounds may fall within the description of both class I and class II. Such compounds may be employed alone, but particularly improved results are obtained when a second different compound of either class is also employed.

The temperature of the Pd bath should be maintained between room temperature and approximately 50°C. Current densities from 0.1 to 50 mA cm^{-2} are suitable. For rack plating, a current density from 5 to 15 mA cm^{-2} may be employed. For barrel plating, the preferred range is from 0.5 to 3 mA cm^{-2}.

An example of such a bath is as follows:

Component	Concentration ($g\,L^{-1}$)
Ethylenediaminetetraacetic acid EDTA	20
$(NH_4)_2HPO_4$	80
Na_2SO_3	28
Pd as $Pd(NH_3)_2Cl_2$	10
Class I brightener	0.005–2
Class II brightener	0.005–2

The pH is maintained between 8.5 and 9 and plating performed at a temperature of 40°C and current density of $5\,mA\,cm^{-2}$.

When neither brightener was present, only hazy deposits were obtained. The class I brightener employed was methylenebisnaphthalene sodium sulfonate, and the class II was benzaldehyde-*o*-sodium sulfonate. The class I brightener was added first and was ineffective at concentrations up to $2\,g\,L^{-1}$. The class II brightener resulted in a semibright deposit at $0.02\,g\,L^{-1}$ and bright deposits from 0.37 to $2.0\,g\,L^{-1}$. Similar results were obtained when 2-butene-1,4-diol was employed as the class II brightener. Please note that unlike the work of Hedrich and Raub [115] with extensive electrochemical and material properties data, no such information was found in regard to these systems. Furthermore, in neither Hedrich and Raub's [115] nor Deuber's [107] work is there any information on the aging of such systems.

Abys et al. [12, 108] developed a process to electroplate full-bright pure Pd to thicknesses of $>25\,\mu m$ with low porosity and high hardness. This chemistry employs a tetrammonium chloride complex in a buffered electrolyte system containing a combination of two additives. Low- and high-speed formulations are shown below:

Chemical Constituent	Low Speed	High Speed
Pd (as metal)	$2–10\,g\,L^{-1}$	$15–40\,g\,L^{-1}$
NH_4Cl	$50–100\,g\,L^{-1}$	$50–200\,g\,L^{-1}$
K_2HPO_4	$80–100\,g\,L^{-1}$	$80–100\,g\,L^{-1}$
Surfactant	$2–25\,mL\,L^{-1}$	$2–50\,mL\,L^{-1}$
Brightener	$0.1–20\,mL\,L^{-1}$	$0.2–20\,mL\,L^{-1}$
Specific gravity	1.05–1.15	1.10–1.25

The surfactant improves wettability and acts as a carrier for the brightener which imparts luster and leveling to the deposit. Potassium phosphate and ammonium chloride are used as buffering agents and supporting electrolytes for conductivity. This chemistry was developed to operate under generally mild conditions of low temperature (~35°C) and a neutral to slightly alkaline pH. Operating parameters for low- and high-speed plating baths are shown below:

	Low Speed	
Operating Parameter	Typical	Range
Temperature	35°C	30–40°C
pH	7.5	7.0–8.0
Current density	$5\,mA\,cm^{-2}$	$2–10\,mA\,cm^{-2}$
Agitation	$5\,cm\,s^{-1}$	$5–50\,cm\,s^{-1}$
Cathode efficiency	87%	75–98%
Plating rate	$0.12\,\mu m\,min^{-1}$	$0.04–0.25\,\mu m\,min^{-1}$
Anode/cathode area	2 : 1	1 : 1–5 : 1

	High Speed	
Operating Parameter	Typical	Range
Temperature	35°C	30–40°C
pH	7.5	7.0–8.0
Current density	$100\,mA\,cm^{-2}$	40 to $\geq$500 $mA\,cm^{-2}$
Agitation	$100\,cm\,s^{-1}$	50 to $\geq$200 $cm\,s^{-1}$
Cathode efficiency	87%	75–98%
Plating rate	$2.2\,\mu m\,min^{-1}$	$0.75–12.4\,\mu m\,min^{-1}$
Anode/cathode area	2 : 1	1 : 1–5 : 1

The current density can be varied from <5 to $>500\,mA\,cm^{-2}$ with the appropriate selection of metal content, additive balance, and agitation conditions. It can be used for barrel, rack, and reel-to-reel applications [12, 108].

An important aspect of any electrodeposition technology is to determine the physical characteristics of plated films. Below is a discussion of the material properties deposited from the above-described formulation.

1. *Grain Size* Transmission electron microscopy studies show that the grain size depends on the presence or absence of additives (Fig. 12.32). The additive-free deposits exhibit grain size ranging from 500 to 5000 A°, in contrast to the additive system where the size decreases to 50 and 200 A°. This change in crystallinity contributes to the brightness and hardness of the deposit.
2. *Surface Appearance* Deposit brightness varies with plating conditions and is often a measure of the surface microroughness. Reflectivity measurements were made using a bifurcated fiber system with a green light-emitting diode (LED) source ($\lambda_{max} \sim 560\,nm$, λ range $\sim 535-625\,nm$). Both specular and diffuse reflectivities were measured, in contrast to the reflectivity of a highly polished bulk Pd metal standard set at 100% reflectance. Figure 12.33 shows the relative reflectivity of Pd films as a function of bath aging, which is constant at about 98%, indicating that this specular surface does not degrade with bath aging.

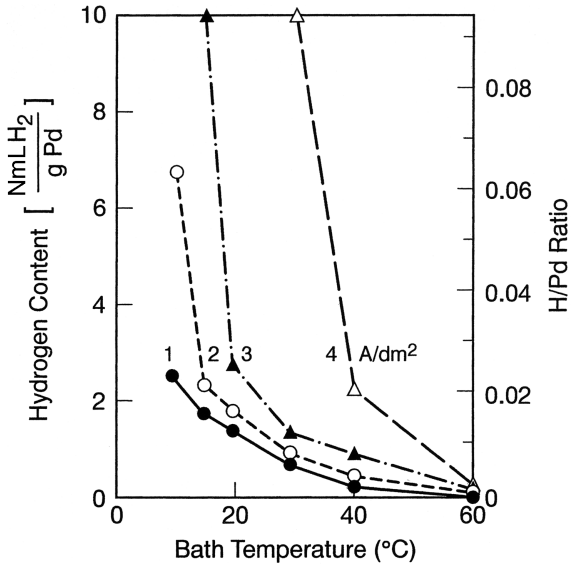

FIGURE 12.31 Hydrogen content versus bath temperature at various current densities: $Pd(NH_3)_4Cl_2$, 1 min after termination of electrolysis.

3. *Leveling Effect* Figure 12.34 exhibits the leveling capability of this process under high-speed plating conditions. Scanning electron micrography (SEM) of a 5-μm-thick deposit clearly shows the rolling marks of the copper substrate at 0 μm of Pd which disappears as the thickness of Pd increases to 25 μm.
4. *Density* The density of the plated deposit was measured via pycnometry and is approximately 11.75 g cm^{-3}, that is, 98% of the theoretical value. Values for low- and high-speed deposited films are shown below:

	Density of Deposits	
Bath Type	Plated Density (g cm^{-3})	Theoretical Density (g cm^{-3})
High speed (~250 mA cm^{-2})	11.79	12.02
Low speed (~5 mA cm^{-2})	11.71	12.02

5. *Density Purity and Thermal Stability* Thermogravimetric and differential scanning calorimetry were performed on Pd films electroplated at current density of 100 mA cm^{-2}. The films were plated at 0, 1.0, and 3.5 metal turnovers. The films were heated from 30–950°C at the rate of 20°C/min under an atmosphere of nitrogen. As can be seen from the data below, essentially no weight loss was observed:

Pd Samples (Metal Turnover (MTO))	Thermogrammetric Analysis (TGA)(%W)	Weight Loss (%)
0	99.79	0.21
1.0	99.68	0.32
3.5	99.89	0.11

The purity of the deposits are high (>99%), and the contaminant inclusion is low (<1%) and remains low throughout the lifetime of the bath. Differential scanning calorimetry was carried out from 25 to 450°C at a scan rate of 10°C min^{-1}. No thermal reaction was detected in Pd deposits, which implies good bulk thermal stability up to 450°C.

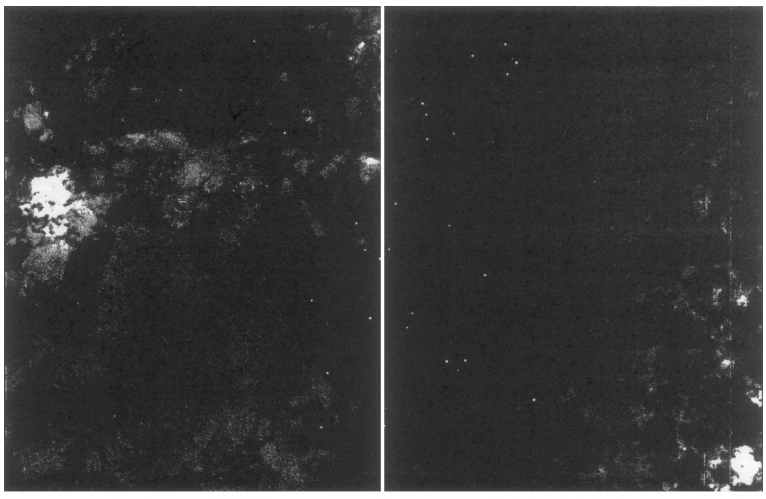

FIGURE 12.32 Transmission electron micrographs at 100,000×: $Pd(NH_3)_4Cl_2$ electrolyte effect of additive.

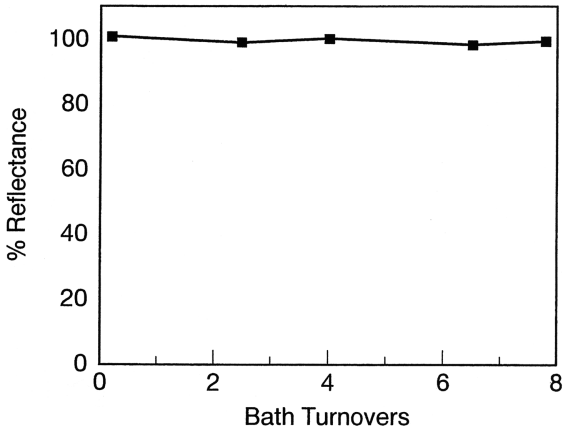

FIGURE 12.33 Percentage of reflectance versus bath turnovers: $Pd(NH_3)_4Cl_2$ electrolyte.

6. *Solderability* Solderability was determined by the IPC method TM-650-2.414.1, which entails immersion in molten solder. Palladium deposits were exposed to 90% humidity at 90°C for 8 and 36 h to simulate "shelf life." The results below of Pd solderability test solder coverage (IPC-TM-650) indicate that both 0.75- and 0.15-μm-thick deposits provide excellent solderability:

Sample Preparation	% Coverage		
Cu Substrate	As Is	8 h	36 h
0.75 μm Ni	0	0	0
0.75 μm Ni/0.075 μm Pd	99	99	98
0.75 μm Ni/0.15 μm Pd	99	99	99
1.5 μm Ni/0.15 μm Pd	99	99	97

7. *Ductility* Ductility was measured by the American Society for Testing and Materials (ASTM) B-489-85 method, which entails plating Pd on a thin Cu substrate and bending through a series of angles over mandrils of various diameters. Inspection for cracks is conducted at 10× magnification. The angle of bend was 180°, and the diameter of the mandrils varied from 3.3 to 0.5 mm. A more rigorous inspection was carried out at 1000× magnification.

   Five-micrometer-thick deposits from a low-speed bath were bent over 0.5 mm diameter while the high-speed samples were bent over 1.25 mm diameter (Fig. 12.35). In both instances, the deposit elongation was greater than 9% and is comparable to soft gold and far superior to cobalt-hardened gold.

8. *Hardness* The Knoop hardness was measured by a Tukon hardness tester using a diamond indenter at 50 g load. Figure 12.36 shows the effect of brightener concentration on hardness, which is in the range of 100–150 KHN_{50} for the additive-free bath. The hardness increases to 400–500 KHN_{50} at 1 mL L^{-1} of brightener and remains unchanged at higher additive concentrations.

Overall, this process is reported to produce adherent, mechanically stable, specular Pd films at rates ranging from <5 to >500 mA cm^{-2}. The deposits are smooth and crack free.

12.7 PALLADIUM ALLOYS

Palladium is known to form alloys with other metals of group VIII and IB that display distinct advantages over the pure metals [45]. The alloys tend to exhibit higher hardness, tensile strength, and ductility. They can be plated with a smaller grain size and are brighter than Pd even in the absence of additives. Furthermore, and of great importance, is the ability of the alloying element, in some cases, to increase the hydrogen overpotential and thus decrease the amount of codeposited hydrogen.

The arguments for the technological use of Pd could thus be more valid for Pd alloys. Accordingly alloys such as PdNi (80/20 wt %) have been extensively studied [8–33]. This alloy

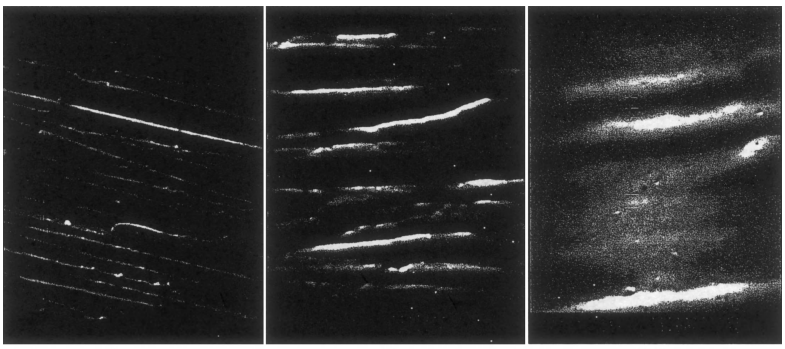

FIGURE 12.34 Scanning electron micrographs at 1000×: levelling effect at 0, 5, and 25 μm film thickness; $Pd(NH_3)_4Cl_2$ electrolyte.

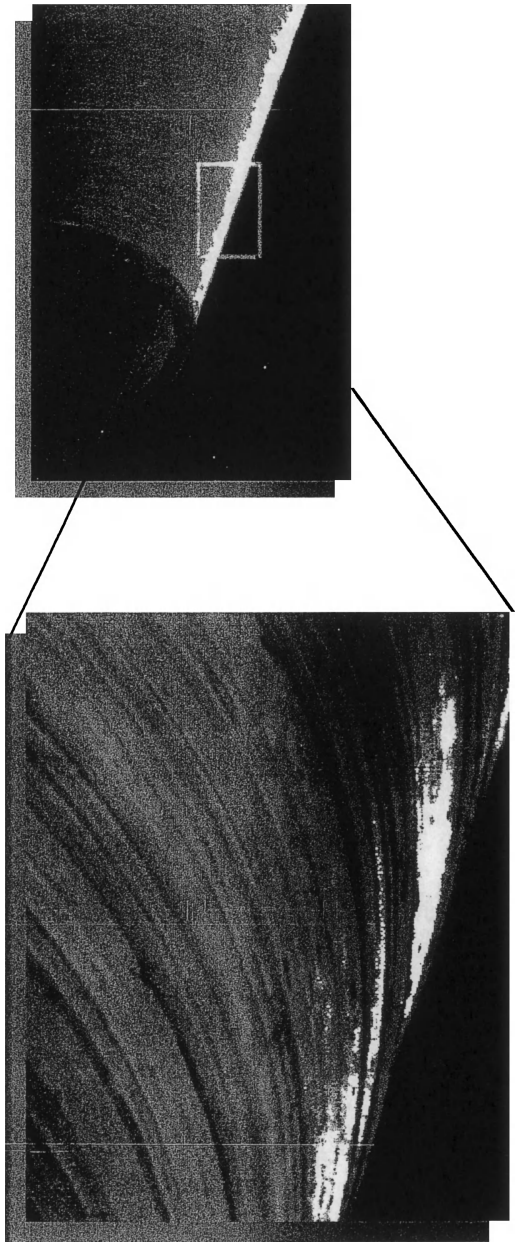

FIGURE 12.35 Scanning electron micrographs of bent 5-μm deposit: $Pd(NH_3)_4Cl_2$ electrolyte.

is much less susceptible to hydrogen embrittlement, exhibits a brighter appearance, forms harder and more ductile deposit, and has lower porosity and better wear characteristics than either pure Pd or Au. Overall, the general material properties of Pd–Ni suggest that it is an excellent contact material, and indeed it is in significant commercial use for connector applications worldwide. Likewise metallurgically prepared PdAg (60/40 wt %) exhibits excellent material properties but has not been successfully plated in commercial applications [116–118]. The reasons of course lie in the fundamental differences among the chemistry of Pd, Ni, and Ag.

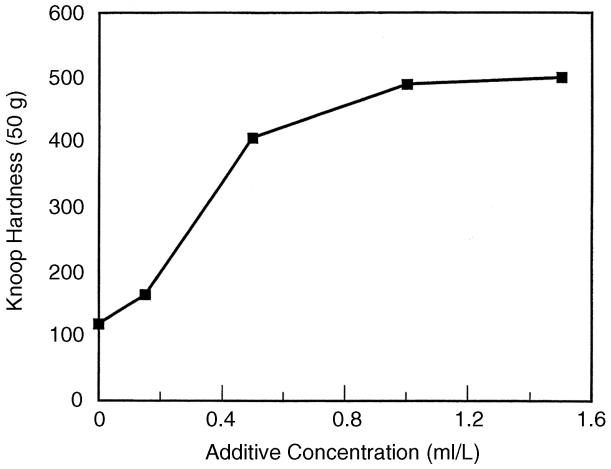

FIGURE 12.36 Hardness versus additive concentration: $Pd(NH_3)_4Cl_2$ electrolyte.

The development of electrodeposition processes for plating Pd alloys requires considerations of phase diagrams, coordination chemistry in the aqueous phase, understanding of redox potentials, thermodynamics, and kinetics. For the electrodeposition of an alloy, as discussed in Section 12.5.3, the ΔE [Eq. (12.16)] must be minimized in order to successfully control the alloy composition. In general, the respective metals should have similar reduction potentials, preferably less than 200 mV apart. As previously discussed, this is highly dependent on the specific metal(s) and the chemical system employed.

Table 12.10 exhibits standard reduction potentials for various metals in aqueous media and demonstrates that the relative standard potential for Pd and the desired alloying metals are significantly different. This requires manipulation of the complexing ligand and of the additive systems in order to codeposit a stable alloy composition. In this section, we describe the chemical systems that have been reported for Pd alloys and pay specific attention to Pd–Ni because of its technological importance while briefly describing other alloy systems.

12.7.1 PdNi (80/20 wt %)

While acidic Pd–Ni electroplating baths have been proposed [119], most processes appear to be ammoniacal solutions in the pH range from 7 to 9. Recommended metal sources for Pd are complexes with ammonia or organic amines; for Ni, the chloride, sulfate, hydroxide, and sulfamate complexes. A Pd–Ni plating bath reported by Morrisey [91] contains 6 g L^{-1} $Pd(NH_3)_2(NO_2)_2$, 3 g L^{-1} nickel sulfamate, 90 g L^{-1} ammonium sulfamate, and ammonium hydroxide to pH 8–9. This bath operates at 20–40 °C at current densities between 5 and 10 mA cm^{-2}, and it is suitable for plating an alloy of about 25% Ni. Other chemistries use

TABLE 12.10 PdNi Alloy Plating

Parameter	Bath Type			
	^{120}T	$^{121-123}U$	^{124}V	^{125}W
Pd Source	$Pd(NH_3)_2C1_2$	$Pd(NH_3)_4C1_2$	$Pd(NH_3)_4C1_2$	Pd sulfamate
Pd metal (g Li^{-1})	25	20	20	10.6
Ni source	$Ni(NH_3)_4SO_4$	$Ni(NH_3)_6SO_4$	$Ni(NH_3)_4SO_4$	Ni sulfamate
$(NH_4)_2$ SO_4(g Li^{-1})	50	10	9	5.9
NH_4Cl (g Li^{-1})	—	50	10	
NH_4OH (mL Li^{-1})	100	To pH	To pH	
Ligand (other) additives				
3-Pyridine sulfonic acid (g Li^{-1})	—	—	—	en 80 g Li^{-1}
	5	See appropriate data in the literature	See appropriate data in the literature	
pH	7.74	8.5	8	4.5 – 6.0
Temperature (°C)	60	30	25	20–60
Current density (mA/cm^2)	3–250	10	10	10–30

plating temperatures up to 60°C in the pH range 7–9, metal concentrations of up to 25 g L^{-1} Pd and 30 g L^{-1} Ni, and up to four different proprietary additives.

Such processes exhibit a number of disadvantages in their operation, most notably lack of pH stability, which results in undesirable fluctuations in alloy composition and material properties. Another concern is the environmental and occupational hazards associated with ammonia vapors during plating. This is particularly true in high-speed operations where the pH, temperature, and solution agitation tend to be high, thus favoring the release of ammonia. Additionally the loss of deposit brightness with bath aging can shorten its useful life. Last, but not least, highly stressed and cracked deposits are frequently encountered, especially in high-speed operations.

Chemistries and Material Properties of PdNi Figure 12.37 is the phase diagram of PdNi demonstrating that it forms a solid solution across all compositions. This implies the possibility to plate PdNi of any composition; however, the 80/20 PdNi alloy is preferred, although in some cases a 90/10 alloy is utilized commercially.

Table 12.10 exhibits four PdNi bath compositions, and in general, they utilize a Pd diamine or tetramine chloride salt and a nickel hexamine sulfate salt. The supporting electrolytes are either ammonium sulfate or ammonium chloride, and ammonium hydroxide is used to adjust pH in the range of 6–8.5. The temperature is in the range of 25–60°C and the maximum current density [120] reported is 250 mA cm^{-2}. Organic surfactants, brighteners, levelers, and stress reducers are commonly added to the bath composition, but in most situations they are proprietary and are either patented or kept as a trade secret.

The only nonammonia system extensively studied was reported by Walz and Raub [125]; it is based on ethylene diamine. It was reported that bright Pd–Ni deposits up to 40% nickel could be obtained over a wide current density range, Figure 12.38. This system does not suffer from evaporation of ammonia and subsequently has a stable pH. There is less attack on substrate metals such as copper and brass and thus less chance of contaminating the plating solution. However, in general, this system suffers from high tensile stress.

Abys et al. reported a highly stable process that was widely commercialized in the 1990s [13]. Boguslavsky et al. [126] further developed this process to overcome many deficiencies as noted above. The deposits from this chemistry exhibit excellent alloy stability ($+2$ wt %) over a wide current density range (~50–800 mA cm^{-2}) (Fig. 12.39) and are full bright in appearance, of high hardness (~550 KHN_{50}), and of good ductility. This process is reported to be less corrosive than previous processes and environmentally benign. The chemistry, material properties, and contact reliability of this technology are detailed by Abys et al. [159–161, 163].

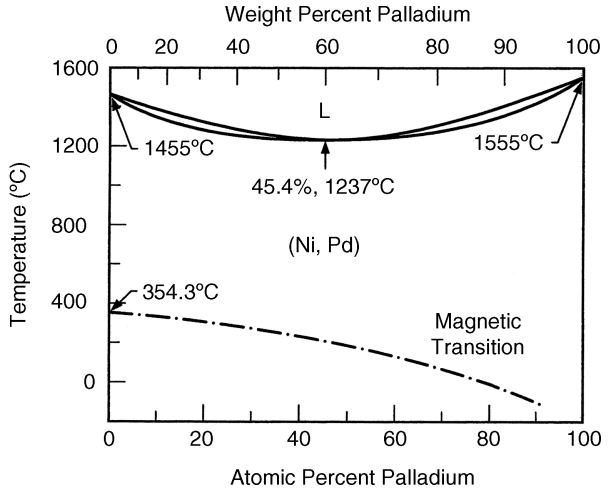

FIGURE 12.37 Binary alloy phase diagram of Pd–Ni system.

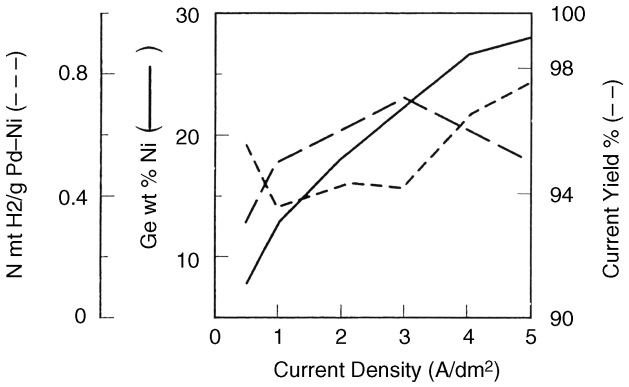

FIGURE 12.38 Hydrogen content versus current density at various wt % Ni content: $Pd(en)_2Cl_2$ + Ni sulfamate system at 50°C, pH 4.5.

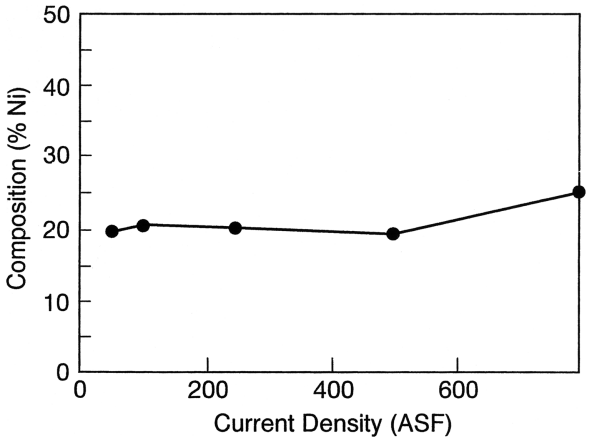

FIGURE 12.39 Percentage by weight of nickel versus current density: Pd–Ni system from ammoniacal electrolyte.

12.7.2 Palladium–Cobalt

Palladium–cobalt, like Pd–Ni, forms a solid solution over the entire composition range and exhibits similar materials properties. Unlike Ni, Co has a +2 and +3 aqueous chemistry, and the standard potentials for Co reduction are significantly more negative than Pd (see Table 12.11). However, the stability of Co complexes with various ammonia electrolytes at relatively neutral pH indicates that its reduction potential could be nobler than Pd in the same electrolyte. This becomes problematic when attempting to plate a consistent alloy composition over a wide range of operating parameters.

Kume [127] reports on the electrochemical behavior and effect of plating parameters on the alloy composition of PdCo from an ammoniacal electrolyte. The basic bath composition is as follows:

Parameter	Concentration
$Pd(NH_3)_2Cl_2$	0.1 *M*
$CoSO_4 \cdot 7H_2O$	0.03 *M*
$(NH_4)_2SO_4$	0.4 *M*
NH_4OH	pH 7–10

Kume states that the standard potentials for Pd and Co are, respectively +0.987 V and −0.250 V, the difference being 1.23 V. However, in ammoniacal plating baths, the potential difference is much smaller, for example, 0.27 V at current densities of 10 mA cm^{-2}. Figure 12.40 shows polarization curves for the deposition of Pd, Co, and Pd–Co alloys. Figure 12.41 is a graph of alloy composition as a function of current density and shows that Co varies between 20 and 30% by weight when plated between 5 and 20 mA cm^{-2} and clearly demonstrates that a higher Co content is deposited at lower current densities. This seems in conflict with Kume's assertion that the Co deposition is either at the same or more negative potential than Pd. When one considers that Pd concentrations are three times greater than Co, once again the conclusion must be that the electrochemistry needs to be reexamined. Cavallotti et al. plated Pd–Co from electrolytes based on Co amino-citrates and Pd amino-nitrite complexes [147]. However, none of these technologies appeared to have been commercially developed.

TABLE 12.11 Standard Potentials in Aqueous Media

Half Reaction	Acid	Neutral/Basic
$Pd^{2+} + 2e^- \rightarrow Pd(s)$	0.915	0
$Ag^+ + 2e^- \rightarrow Ag(s)$	0.799	0.342
$Cu^{2+} + 1e^- \rightarrow Cu(s)$	0.340	−0.100
$Bi^{3+} + 3e^- \rightarrow Bi(s)$	0.317	0.072
$Sn^{2+} + 2e^- \rightarrow Sn(s)$	−0.137	−0.631
$Ni^{2+} + 2e^- \rightarrow Ni(s)$	−0.257	−0.49
$Co^{2+} + 2e^- \rightarrow Co(s)$	−0.277	−0.733
$Fe^{2+} + 2e^- \rightarrow Fe(s)$	+0.44	−0.8

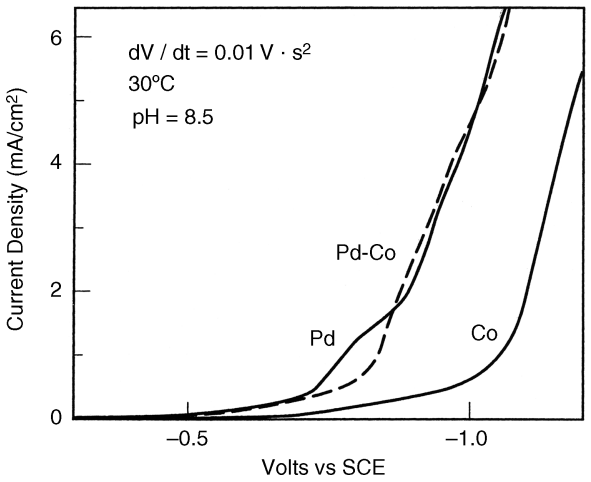

FIGURE 12.40 Current–potential curves: palladium, cobalt, and palladium–cobalt from ammoniacal electrolyte.

TABLE 12.12 80/20 PdCo Alloy Plating Chemistry

Component	Typical
Pd as metal (g Li^{-1})	40
Co as metal (g Li^{-1})	8
Conducting Salt (g Li^{-1})	40
Additives (mL Li^{-1})	20
Ligand (mL Li^{-1})	150

Chemistry and Material Properties of PdCo The development of a controllable and stable plating chemistry capable of depositing an 80/20 alloy of Pd–Co was reported in 1996 [180]. Additional publications detailing the chemistry and more importantly its deposit properties and new applications have appeared in the literature [157–163, 181, 184]. An attempt will be made here to summarize and identify the key features of PdCo as compared to hard gold.

With respect to bath chemistry, Table 12.12 provides a snapshot of the key chemical components and their respective concentrations. A key innovation was the choice of the appropriate ligands and buffer systems which controlled the relative reduction potentials of Pd and Co and minimized ΔE, as discussed in Section 12.5.3 [159, 163]. The PdCo alloy composition is also highly dependent on metal concentration, pH, current density, temperature, and solution agitation. This system allows excellent control of PdCo alloy composition and provides deposits that are bright, hard, and of very low porosity. For a detailed discussion on how the alloy composition varies as a function of any of the aforementioned variables, the reader is referred to [159, 160, 163].

Following is a summary of important material properties for both gold-flashed palladium cobalt (GFPdCo) and hard gold in Table 12.13 [160]:

1. *Density* The density of plated hard gold is 17.3 g cm^{-3} compared to 80/20 PdCo, which is ~10.8 g cm^{-3}. Thus, for an equivalent surface area and thickness an immediate material "mass" reduction of ~40% can be realized. Figure 12.42 compares the cost savings in dollars per troy ounce of gold substituted with either GFPdNi or GFPdCo based on relative density and price differences (Fig. 12.6). For example, in 2009 the average price per troy ounce for Au was approximately $905, in contrast to the price of Pd, which averaged $235 per troy ounce. Figure 12.41 demonstrates that a greater than 85% dollar savings could be achieved in 2009 by replacing gold with an equivalent thickness of GFPdNi or GFPdCo. The following hardness and porosity summaries support further cost savings through a reduction in deposit thickness due to the superior material properties of Pd alloys compared to hard gold.
2. *Hardness* A Knoop hardness value in the range of 590–640 for PdCo can be obtained using the plating chemistry described by Abys et al. [160] compared to "hard" gold, which is ~150 Knoop. The higher hardness of Pd alloys should increase wear resistance, inhibit wear through to the base metals (i.e., exposed nickel or copper alloys), and thus result in lower contact resistance change. To test this hypothesis, a sliding wear test (the conditions and experimental details are given elsewhere [160]) was conducted. The results, summarized in Figure 12.43, clearly demonstrate that gold-flashed PdCo exhibits higher wear resistance when compared to hard gold (or even gold-flashed PdNi). These results make an argument for utilizing the lower thickness of Pd alloys to obtain equivalent performance to gold (see Fig. 12.42).

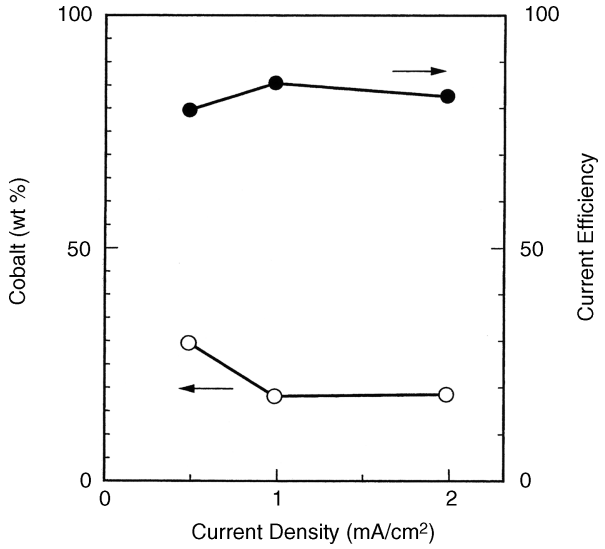

FIGURE 12.41 Percentage by weight of cobalt versus current density: Pd–Co system from ammoniacal electrolyte.

TABLE 12.13 Comparative Material Properties

Material Properties	Hard Au	GFPdCo
Density (g cm^{-3})	17.3	10.8
Thermal stability (°C)	150	395
Hardness (KHN_{25})	140–200	590–640
Ductility (%E at 2.5 μm)	<3	3–9
Porosity index		
Connector pins (1.5 μm/2.5 μm Ni)	0.70	0.02
Wear properties (load 100 g)		
Cycles to failure (×1000)	20	>80
Coefficient of friction at 10,000 cycles	0.60	0.43

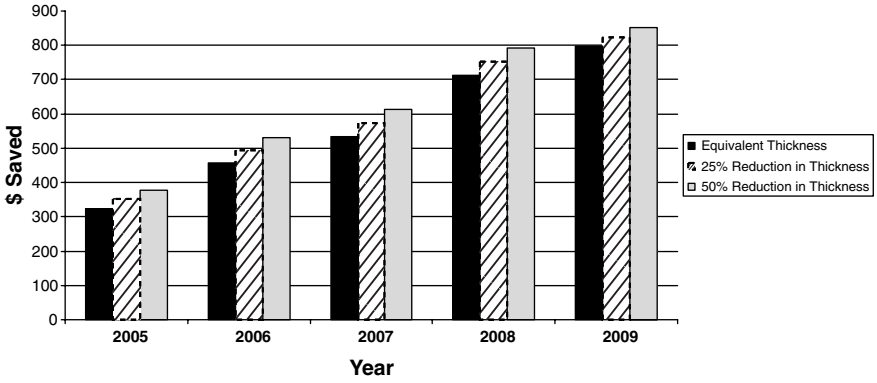

FIGURE 12.42 Cost savings per ounce—80/20 Pd alloy versus hard gold from 2005 to 2009 for an equivalent thickness and 25 and 50% reduction in Pd alloy thickness.

3. *Porosity* One of the most common failure mechanisms, which for electronic connectors are typically a change in contact resistance greater than 10 mΩ, is pore corrosion [164]. The creep of corrosion salts through pores—especially copper salts on precious metals—results in high contact resistance. Thus, a porosity test (ASTM B799-88) is typically utilized for many qualification programs. This entails exposure to SO_2 followed by ammonium sulfide for fixed periods of time. A porosity index scale, described elsewhere by Kudrak [112, 160, 165], can be used for comparative purposes. GFPdCo possesses the lowest intrinsic porosity and is unequivocally superior to hard gold in its overall ability to inhibit corrosion and provide excellent wear; see Figures 12.43 and 12.44.

In summary, PdCo is a fine-grain, single-phase alloy with high hardness, low porosity, and high thermal stability that outperforms hard gold and in many instances pure Pd and PdNi for high-wear applications such as connectors and printed wiring boards (PWBs) in circuit testing (ICT) pin probes [160].

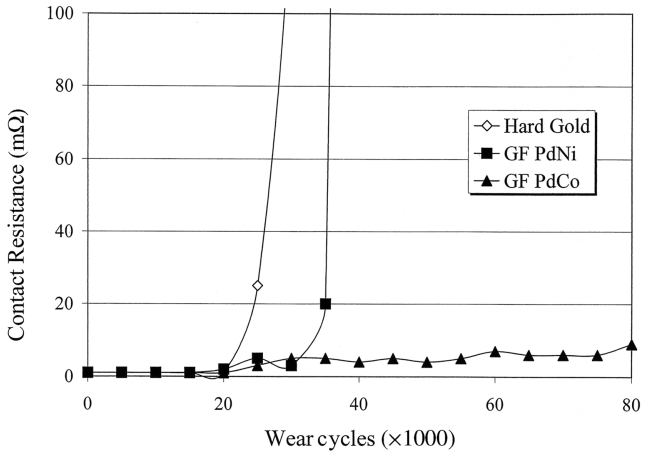

FIGURE 12.43 Sliding wear–contact resistance (100 g load).

12.7.3 Palladium–Iron

The Pd–Fe alloys prepared metallurgically are known to be hard magnetic materials [1]. These alloys can also be used as CO sensors in catalytic combustion chambers [129].

The galvanic deposition of Pd–Fe alloys is reported by Juzkis et al. [130] from an ammoniacal electrolyte containing a complexing agent for Fe(III). The electrolyte composition and operating temperature are as follows:

Parameter	Concentration/Operating Conditions
$PdCl_2$	0.05–0.2 *M* (as Pd)
$Fe_2(SO_4)_3$	0.1–0.3 *M* (as Fe)
Sulfosalicylic acid	0.2–0.6 *M*
NH_4OH	0.3 *M*
Temperature	25–50°C
Current density	5–300 mA cm^{-2}

Palladium–iron alloys deposited from the above electrolytes produce a light gray satin finish. Figure 12.45 shows the dependency of Pd content on the current density as the Fe content is kept constant. Thus a 0.1 *M* Pd–0.15 *M* Fe bath composition results in a Pd content of approximately 80 ± 5%. Utilizing direct-current plating at 50°C, the current efficiency is about 75%, and a significant amount of hydrogen is codeposited. The H/Pd + Fe ratio is about 0.15 and results in brittle deposits which are cracked. However, with pulsed electrolysis, the deposits contain less hydrogen and they are brighter in appearance and can be plated to 10 μm crack free.

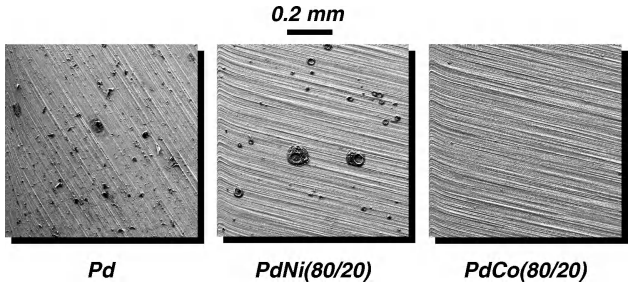

FIGURE 12.44 Scanning electron micrographs: porosity tested Pd, PdNi, and PdCo deposited films; Cu substrate without Ni under layer.

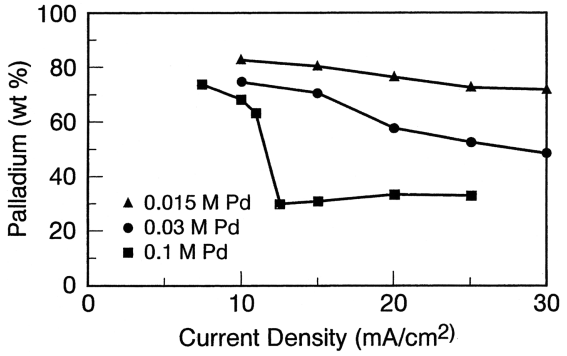

FIGURE 12.45 Percentage by weight of Pd versus current density at various [Pd]: Pd–Fe system from ammoniacal electrolyte.

Two noteworthy publications on the deposition of PdFe alloys were written by Baugartner and Gabe [177].

12.7.4 Palladium–Gold

A slightly alkaline gold plating solution, free of cyanide and phosphates, containing a sodium gold sulfite complex and a palladosamine chloride complex is used to plate a palladium–gold alloy [131]. A typical electroplating formulation is as follows:

Parameter	Concentration/Operating Conditions
$Pd(NH_3)_2\ Cl_2$	$1.8\,g\,L^{-1}$
$NaAu(SO_3)_2$	$10\,g\,L^{-1}$
$(NH_4)_2SO_3$	$15\,g\,L^{-1}$
$CuSO_4$	$0.095\,g\,L^{-1}$
$Na_2As_20_3$	$0.03\,g\,L^{-1}$
pH	8.2
Temperature	58 °C

At $5\,mA\,cm^{-2}$ a plating rate of $100\,mg\ A\ min^{-1}$ can be achieved which yields a fully bright, gold "flesh-toned" deposit.

12.7.5 Palladium–Indium

Interest in Pd–In goes back to the late 1970s and early 1980s [132–137]. According to these studies, Pd–In alloy crystallizes at 1285°C in a simple cubic structure of the CsCl type with a lattice parameter of 3.22 Å. This alloy belongs to compounds of the colored β-brass group and, depending on the In content, has a yellow, golden, or rose-lilac color. An article by Reshetnikova and Pedan [138] describes Pd in various properties, including coefficients of friction, resistivity, and contact resistance. A summary of their results is shown in Table 12.14. Another study by Dzhandubaeva et al. [139] provides the following recipes:

Parameter	Concentration/Operating Conditions
Palladium	$20\,g\,L^{-1}$
Indium	$20\,g\,L^{-1}$
Trilon β	$60\,g\,L^{-1}$
pH	$25\,g\,L^{-1}$
NH_4Cl	~8.5
Temperature	20°C

Film thicknesses of 10 μm could be deposited utilizing direct and pulsed electrolysis.

TABLE 12.14 Palladium–Indium Materials Properties

Coating Type	Indium Content (mass %)	Resistivity (μΩ–cm) At 20°C	Microhardness (kg/mm^{-2})	Constant Resistance (Ω) 10 mA Current Under Load (g)		Mass Loss Wear Resistance Rest (mg)	Coefficient of Friction Versus Steel	Internal Stress (log/cm^2)	Spreading Area POS-61 Lead–Tin Solder (mm^2)
				50 g	100 g				
Solid solution	3–6	59	290	0.0035	0.0023	20.9	0.18 – 0.19	3200	56–79
Intermetallic	45–55	88	450	0.0240	0.0740	2.7	0.12–013	8700	5–6
Palladium	0	20	260	0.0020	0.0015	28.3	0.2	3600	44–77

Additional formulations and material properties data can be found in publications by Su et al. [185].

12.7.6 Palladium–Silver

The properties of Pd–Ag alloys are known to be suitable for contact materials [140–144]. In particular, savings in material costs and comparable corrosion behavior to either Au or Pd have led a number of researchers to investigate the electrochemistry of Pd–Ag.

The PdAg forms homogeneous solid solutions over the entire composition range. The mechanical and electrical properties therefore will not be susceptible to precipitation of a second phase, as in a multiphase alloy, and will not exhibit erratic, abrupt, or irreproducible changes. Small changes in alloy composition have only a minor effect on such properties since, in a homogenous phase, properties, in general, vary gradually with composition. Cohen et al. [142–145] chose to utilize a concentrated lithium chloride bath which contains simple ions and no additives, as shown below:

Parameter	Concentration/Operating Conditions
$PdCl_2$	$3\ g\ L^{-1}$
AgCl	$12\ g\ L^{-1}$
LiCl	$500\ g\ L^{-1}$
HCl	$20\ mL\ L^{-1}$
Current density	$0.5–20\ mA\ cm^{-2}$

From this electrolyte it was possible to plate dense, uniform, single-phase alloys with Ag content of 40–70% at about 100% current efficiency. The Ag–Pd alloy properties appear to be favorable for contact applications processing a microhardness of about 200 $KHN_{25,}$ very low compressive internal stress, $1\ kg\ mm^{-2}$, and similar wear, friction, and corrosion properties to hard gold. However, this electrolyte composition is extremely corrosive and undergoes displacement plating with non–noble metal substrates.

Nobel et al. [145, 146] claimed to have developed a proprietary process for electroplating PdAg over a wide range of current densities. Deposits from this proprietary alloy are said to be "pore free" and comparable to hard gold in terms of excellent wear and fretting resistance, contact resistance, and corrosion resistance.

Kume and Tadeo [148] report plating a Pd–Ag alloy from ammoniacal alkaline solutions. Silver deposition takes place under mass transport controlled conditions. Their conclusion is that Pd–Ag is a useful substitute for hard gold in contact applications. However, they not discuss the possibility of the formation of silver fulminates (from ammonia-type systems), which could potentially be explosive. The author of this chapter is not aware of plated PdAg being used in any commercial application, and plating Pd–Ag with the desired composition remains a challenge today.

12.7.7 Other Palladium Alloys

Numerous Pd binary and ternary alloys have been reported in the literature or in patents; however, it is beyond the scope of this chapter to discuss them all. Two publications by Baumgartner and Gabe on PdFe contains a review of other "significant" Pd alloys (i.e., PdNi, PdAg, PdCo, PdFe), many useful formulations, and a long list of references [177]. Another notable alloy of Pd is a PdRe alloy [149] plated from ammoniacal solutions with Trilon as an additive. The Re content is about ∼24% and current efficiency 63–90%. The PdSn alloys plated from pyrophosphate baths contain diethylenetriamine pentaacetic acid [150]. Palladium–antimony alloy deposition was reported in a patent [153] where a Pd salt was dissolved in Trilon β at 60–70°C and pH 4. The plating of PdZn alloy and its comparison to Pd and PdNi are reported in [178, 179] and that of PdCu alloys in [182], the latter providing formulations, fundamental electrochemistry, and material properties. Alloys of PdTl and PdTe were reported by Nowsky et al. [183]. Palladium–arsenic alloy processes were patented by Abys and Straschil [151] in 1991 and Wang [152] in 1994. This alloy, usually 20 wt % arsenic, is extremely ductile and can be electroformed into various shapes, such as bellows, which can be "flexed" without cracking.

All novel Pd alloy developments focused on improving the materials properties of Pd for technological applications such as contact material or enabling new applications.

12.8 RECENT TECHNICAL ADVANCES AND EMERGING APPLICATIONS

12.8.1 Use of Palladium for PWB Applications

A detailed discussion of the uses of Pd, with particular reference to PWB-type applications is beyond the scope of this chapter. The PWB industry has been under severe stress to meet the demands of miniaturization and environmental legislation (i.e., Restriction on Hazardous Substance (ROHS)) that bans the use of lead and other typically used materials in electronic applications [166]. Certain original equipment manufacturers (OEMs) have self-imposed environmental programs which are even more aggressive than current legislation in their efforts to embrace the "green" movement. Lead is currently one of the principal components of soldering systems and ROHS legislation banned its use for many electronic applications.

This legislation had a dramatic effect in many sectors of the electronic markets, most notably "final finishes" for PWB applications. Furthermore, surface-mount technology dictated that the following must be taken into consideration in

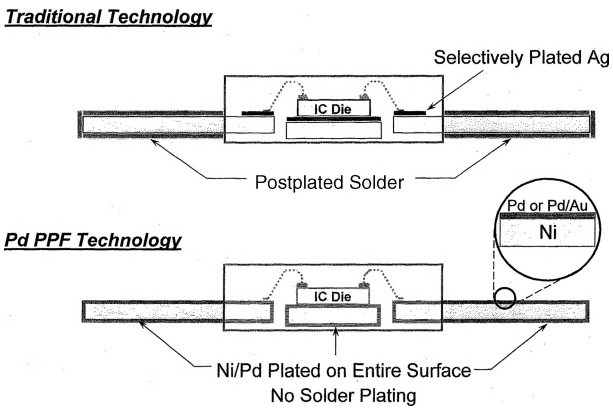

FIGURE 12.46 Schematic cross sections of leadframes plated with silver/solder or nickel/palladium after die attachment, wirebonding, and encapsulation and before trimming and forming.

order to meet the key current and future requirements of this industry:

- Enhanced uniform thickness distribution
- Solderability that meets lead-free requirements
- Wirebondability
- Use of lead-free materials
- Environmental acceptability
- Favorable economics

The idea of using Pd in PWB assembly was proposed as early as 1984 by Wilkinson and O'Hara [167] but was dismissed as the technology for plating pure Pd at the time was not as advanced as it is today; that is, deposits suffered from microcracking and low ductility. However, developments in Pd plating technology and its current use in large-scale leadframe applications (see Section 12.8.4) imply that it should be considered once again for PWB finishes. Thin Pd and Au-flashed Pd deposits, that is, <0.5 μm in thickness, could be used as an etch-resist, final finish for solderability and a contact surface for PWBs.

Literature exists to support this claim [168–174]. The benefits are (1) elimination of lead, (2) improved processing times (reduction in cycle times), (3) higher yields, and (4) ionically cleaner substrate. The benefits of using Pd as a final finish are (5) good solderability, (6) good wire and die bondability, (7) excellent diffusion/migration barrier properties, (8) thermally stable surfaces, (9) component coplanarity, (10) compatibility with active devices, and (11) compatibility with lead-free solders [170].

12.8.2 Palladium Preplated Leadframes

Palladium preplated leadframes (PPFs) were advanced in the mid-1980s [171–174]. This technology utilizes high-speed Ni and Pd plating over the entire leadframe surface, as opposed to selective Ag plating for die attachment and wirebonding, and solder plating for external leads. Schematically the two very different technologies are illustrated in Figure 12.46. There are four distinct areas where Pd PPF technology offers significant advantages [168, 175]:

1. *Plating Process Improvements* Whereby the need for costly selective plating is removed, yields and throughput are increased, and all wet processes are completed prior to package assembly.
2. *Quality Improvements* Enhanced coplanarity and the elimination of solder bridging with no possibility for silver migration.
3. *Environmental Improvements* Cyanide and lead are eliminated from the plating process.
4. *Overall Packaging Cost Reduction* Simplification of the plating process, the elimination of postassembly processing, reductions in waste treatment, and extension of the lead frame shelf life.

This technology has gained significant market share over the standard silver spot technology over the last decade.

12.8.3 Codeposited Palladium with Nanoparticles

The emergence of nanotechnology with its promises of enhanced functionality provided the impetus for Abys and Kudrak [186] to codeposit nano-Teflon particles in Pd in an attempt to further reduce its coefficient of friction and improve its wear resistance. Figure 12.47 is a scanning electron micrograph of a cross section of electroplated Pd with 200–80-nm Teflon spheres occluded in electroplated palladium [186].

12.9 CURRENT ECONOMIC CONCERNS

Early in 1998, the bullion prices of Au and Pd converged and consequently diverged, as depicted in Figure 12.6. Simple

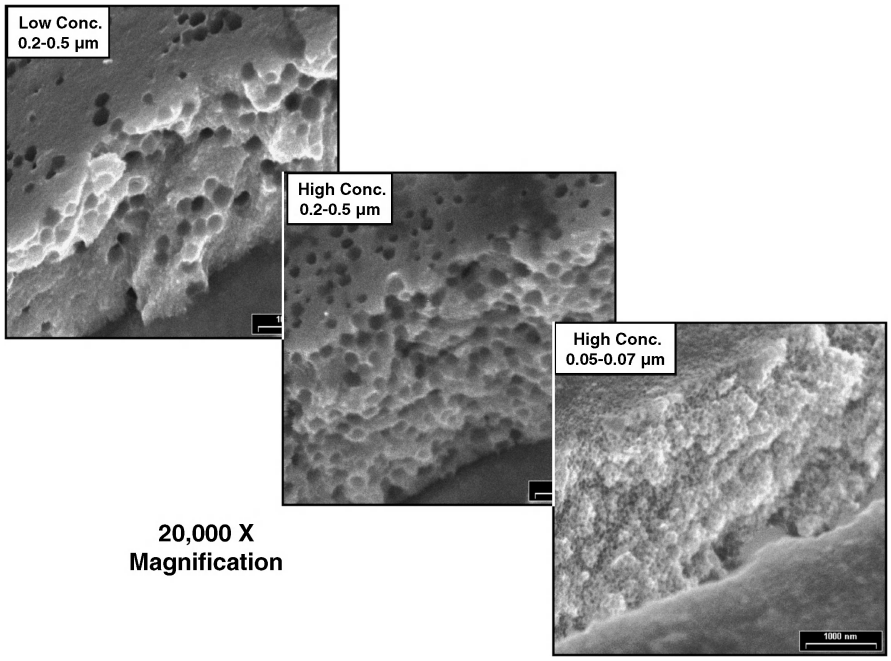

FIGURE 12.47 Scanning electron micrographs: cross section of Pd codeposited with Teflon particles of 50–500 nm; cross section coupon bent 180°.

economic principles of supply and demand rationalize this inversion of metal prices with significant increases for Pd. With respect to demand, there had been a strong trend toward increased use of Pd in automotive catalysts; for example, in 1996 auto catalyst demand was approximately 2.4×10^6 TrOz and in 1998 this figure almost doubled, to 4.5×10^6 TrOz [154]. Notwithstanding the increased demand from the automotive industry, there was increased demand from the electronics sector [154], as traditionally Au-plated components switched to Pd and its alloys. Relatively speaking, Au prices remained steady, trading in a low narrow range of $270–$300 per troy ounce from 1998 to 2001.

Supply nuances and speculation played a key role in the increase of Pd bullion prices from 1999 to 2001. As stated earlier (Section 12.2), almost two-thirds of the world's supply of Pd originated in Russia. In the 1990s lack of investments in mining infrastructure coupled with political and labor instability resulted in interruptions of Pd shipments. South African supplies were also reduced due to lower Pt production, which lowered Pd output. Furthermore, speculative activity from hedge funds played a role in artificially increasing the bullion price of Pd [156]. There has however never been a problem in delivering Pd-containing products to the consumer.

The outlook for a sharp downward correction in the price of Pd was predicted and occurred starting in 2001. There are abundant deposits of Pd in the world. Current *U.S. Geological Survey* reports [155] indicate that there is a total of 100×10^6 kg PGMs in reserves (metal in the ground at current mine sites) and in the reserve base (metal in the ground but having no current mining operation).

In contrast to the falling price of Pd, the price of Au has increase dramatically since 2002 and in 2009 averaged >$900 per troy ounce (Fig. 12.6). Once again, the significant difference in price, density, and material properties dictate that Pd should be utilized to replace Au for many applications. Figure 12.42 provides the cost reduction per troy ounce of Au metal in replacing Au with Pd at equivalent thickness and also at 25–50% thickness reduction. As can be seen, significant cost reductions with equivalent performance can be obtained.

12.10 CONCLUSIONS

The electrodeposition of Pd was first reported by Henry around 1855; however, it took well over one hundred years for this technology to mature. Knowledge of the electrochemistry of Pd and the effects of hydrogen codeposition were essential in devising robust chemical systems that plate Pd under a variety of conditions in a manufacturing environment. Furthermore, extensive material and reliability data on the use of Pd as a technologically useful finish was instrumental in its adaption for electronic components and other applications.

Palladium and its alloys have thus emerged as competitive substitutes for Au in electronic applications, and for Rh and Ni in the decorative industry, and enable new technical application in their own right. The electrodeposition of Pd

alloys, including Ni, have overcome many technical challenges and alloys with controllable composition and material properties under a variety of plating conditions are now commonplace [159–163].

ACKNOWLEDGMENTS

The author wishes to thank E. J. Kudrak, the late Dr. H. Strachil, Dr. C. Fan, Dr. C. Xu, Dr. I. Kadija, Dr. Y. Okinaka, and the R&D staff of Lucent Technologies Electroplating Chemicals & Services, who contributed much of the development work cited in this chapter and for many helpful discussions and recommendations. The author also wishes to extend a special note of appreciation to Dr. CH Raub for much of the seminal work on the electrochemistry and electrodeposition of palladium. A special note of gratitude to M. Klein of Cookson-Enthone and M. Lake, formerly of Lucent Technologies, for the long hours spent in the preparation of this chapter.

REFERENCES

1. Encyclopedia Americana, International Edition, Grolier Education, Danbury, CT, 1829–present.
2. *Compton's Interactive Encyclopedia*, 1993; 94 Compton's News Media, Inc.
3. I. E. Cottington, *Platinum Met. Rev.*, **35** (3), 141–151 (1991).
4. J. H. Crockett, "Platinum," in *Handbook of Geochemistry*, Vol. 2, H. H. Wedepohl, Ed., Springer-Veiloy, New York, 1969, Sections B–G, K, M, 0.
5. T. L. Wright and M. Fleischer, "Geochemistry of the Platinum Metals," in *Geological Survey Bulletin*, 1214-A, U.S. Government Printing Office, Washington, DC, 1965, p. 24.
6. B. Mason, *Principles of Geochemistry*, 2nd ed., Wiley, New York, 1951, p. 310.
7. *Platinum*, Johnson Matthey, 1996–2009.
8. J. A. Abys, "A Unique Palladium Electrochemistry—Characteristics and Film Properties," paper presented at Second American Electroplaters Society Symposium on Economic Use of and Substitution for Precious Metals in the Electronics Industry, Danvers, MA, Sept. 1980.
9. H. K. Straschil, I. Kadija, J. J. Maisano, and J. A. Abys, *PCIF Circuit World*, **17** (2), 9–15, (1991).
10. E. J. Kudrak, J. A. Abys, I. Kadija, and J. J. Maisano, "Wear Reliability of GFPd vs. Hard Gold on a High Speed Digital Connector System," in *Proc. 4th Annual Conf. American Electroplaters and Surfacee Finishers Society*, Vol. II, Boston, MA, July 1990, p. 739.
11. H. K. Straschil, I. Kadija, J. J. Maisano, and J. A. Abys, "Electroplating of Thick and Ductile Palladium Nickel Alloys," in *Proc. 4th Annual Conf. American Electroplaters and Surface Finishers Society*, Vol. II, Boston, MA, July 1990, p. 1003.
12. I. Kadija, J. A. Abys, V. Chinchankar, and H. K. Straschil, "Electroplating of Thick and Ductile Palladium: A New Electroplating Technology," in *Proc. 4th Annual Conf. American Electroplaters and Surface Finishers Society* Vol. II, Boston, MA, July 1990, p. 759.
13. J. A. Abys, H. K. Straschil, I. Kadija, E. J. Kudrak, and J. Blee, *Met. Finish.*, **89**, 43 (1991).
14. J. Stevenson and L. Mayer, paper presented at IICIT Annual Symp., Philadelphia, PA, 1989.
15. J. A. Abys, J. J. Masisano, C. Wolowodiuk, and H. K. Straschil, "Palladium Nickel Alloy Electroplating," *Proc. Connectors '89 Conf.*, Coventry, England, The Institute of Metal Finishing, March 1989, p. 19.
16. M. Antler, *Platinum Met. Rev.*, **31** (1), 13–19 (1987).
17. W. A. Fairweather, *Trans. Inst. Met. Finish.*, **64** (3), 1 (1986).
18. A. Graham and S. Updegraff, "Properties of Palladium-Nickel Alloy and Pure Palladium for Connector Applications," in *Proc. NEPCON Conf.*, Anaheim, CA, 1984.
19. American Electroplaters Society Symp. on Economic Use of and Substitution for Precious Metals in the Electronics Industry, Danvers, MA, 1982.
20. American Electroplaters Society Symp. on Substitution for Gold, Milwaukee, WI, 1980.
21. D. Gravitz, *Electronic Packaging Prod.* (Feb. 1982).
22. I. H. Brockman et al., in *Proc. Holm Conf.*, 1988, pp. 73–83.
23. H. Grossman et al., in *Proc. Holm Conf.*, 1984, pp. 551–560.
24. D. Ruhlicke et al., in *Proc. Holm Conf.*, 1984, pp. 83–88.
25. S. W. Updegraff, in *Proc. ICEC*, 1986, pp. 399–403.
26. A. H. Graham, in *Proc. Holm Conf.*, 1984, pp. 61–67.
27. G. J. Russ, *IEEE Trans. Component Hybrid Manuf. Tech.*, **CHMT 6** (4), 389–395 (Dec. 1983).
28. E. J. Kudrak, J. A. Abys, I. Kadija, and J. J. Maisano, in *Proc. Annual Conf. American Electroplaters and Surface Finishers Society*, Boston, MA, July 1990.
29. E. J. Kudrak et al., in *Proc. of the 78th Annual Conference of the American Electroplaters and Surface Finishing Society*, July 1991; H. K. Straschil et al., *Metal Finish*. (Jan. 1992); E. J. Kudrak et al., *Plating Surf. Finish.* (Feb. 1992).
30. T. Sato et al., in *Proc. 26th Annual Holm Conf. on Electrical Contacts*, 1980, pp. 41–47.
31. A. H. Graham, in *Proc. 30th Annual Holm Conf. on Electrical Contacts*, 1980, pp. 61–67.
32. T. Sato, *Plating Surf. Finish.*, **74**, 55–59 (1987).
33. M. Antler, *ASLE Trans.*, **26** (3), 376–380 (1983).
34. W. O. Freitag, in *Proc. of Holm Seminar on Electrical Contacts*, Chicago, 1975, pp. 17–23.
35. R. H. Atkinson and A. R. Raper, *J. Electrodep. Tech. Soc.*, **8** (10), 1 (1933).
36. F. H. Reid, *Plating*, **52**, 531 (1965).
37. H. D. Hedrich and C. J. Raub, *Metalloberflache*, **311** (11), 512–520 (1977).
38. R. Weil, *Plating*, **60**, 1231 (1970); **61**, 50, 127 (1971).

39. H. D. Hedrich and C. J. Raub, *Gaivanotechnik*, **70** (10), 934–939 (1979).
40. H. D. Hedrich and C. J. Raub, *Surface Technol.*, **8**, 347–362 (1979).
41. F. H. Reid, *Metall. Rev.*, **8** (30), 167–211 (1963).
42. Periodic Table of the Elements, Sargent-Welsh Scientific Company, Skokie, IL.
43. *Platinum Group Metals*, Printing and Publishing Office, National Academy of Science, Washington, DC.
44. A. R. Powell, "The Platinum Metals in the Periodic System: A Comparative Study of the Transition Metals," *Platinum Met. Rev.*, **4**, 144–149 (1960).
45. E. M. Wise, *Palladium Recovery, Projection and Use*, Academic, New York, 1968, p. 187.
46. W. Hume-Rothery, "The Platinum Metals and Their Alloys: A Review of Their Electronic Structure and Constitution," *Platinum Met. Rev.*, **10**, 94–100 (1966).
47. F. A. Lewis, *The Palladium-Hydrogen System*, Academic, New York, 1967, p. 178.
48. F. A. Cotton and G. Wilkinson, *Advanced Inorganic Chemistry*, 4th ed., Wiley, New York, 1980.
49. F. R. Hartley, *The Chemistry of Platinum and Palladium*, Wiley, New York, 1973, p. 544.
50. S. Otsuka, S. Y. Tatsuno, and K. Ataka, "Univalent Palladium Complexes," *J. Am. Chem. Soc.*, **93**, 6705–6706 (1971).
51. R. A. Reinhardt and W. W. Monk, *Inorg. Chem.*, **9**, 2026–2030 (1970).
52. F. Bosolo and R. G. Pearson, *Proc. Inorg. Chem.*, **4**, 381–453 (1962).
53. N. V. Sidgwick, *The Electronic Theory of Valency*, Oxford University Press, London, 1929, p. 163.
54. F. Basolo and R. O. Pearson, *Mechanisms of Inorganic Reactions*, Wiley, New York, 1967, p. 526.
55. G. E. Coates, M. L. H. Green, and K. Wade, *Organometallic Compounds*, Vol. 2, *The Transition Elements*, Methuen, London, 1968, p. 6.
56. A. F. Bard, R. Parsons, and J. Jordan, Eds., *Standard Potentials in Aqueous Solutions*, Marcel Dekker, New York, 1988.
57. R. M. Izatt, R. Eatough, and J. J. Christensen, *J. Chem. Soc. A*, 1301 (1967).
58. D. H. Templeton, G. W. Watt, and C. S. Garner, *J. Am. Chem. Soc.*, **65**, 1608 (1943).
59. R. N. Goldberg and L. H. Hepler, *Chem. Rev.*, **68**, 229 (1968).
60. R. M. Izatt et al., *J. Chem. Soc. A*, 2514 (1970).
61. E. Jackson and D. A. Pantony, *J. Appl. Electrochem.*, **1**, 283 (1971).
62. M. Pourboix, Ed., *Atlas Dequilibres Electrochimiques* @ 25'C, Gothier-Villars, Paris, 1963, p. 359.
63. A. B. Fasman, G. G. Kutyyukov, and D. V. Sokalski, *Zh. Neorg. Khim.*, **10**, 1338 (1965).
64. V. L. Kravstov and M. I. Zelenski, *Elektrokimiya*, **2**, 1138 (1966).
65. T. Ryhl, *Acta. Chem. Scand.*, **26**, 2961 (1972).
66. A. V. Babaeva and E. Y. Khananova, *Zh. Neorg. Khim.*, **10**, 2579 (1965).
67. H. K. Birnbaum, "Hydrogen Embrittlement," in *Encyclopedia of Material Science and Engineering*, M. B. Bever, Ed., Pergamon, New York, 1986.
68. J. W. Dini, *Electrodeposits, The Material Science of Coatings and Substrates*, Noyes Publication 367, Noyes, Park Ridge, NJ, 1993.
69. S. Nakahara and Y. Okinaka, "Microstructure and Ductility of Electroless Copper Deposits," *Acta Metall.*, **31**, 713 (1983).
70. L. J. Durney, "Hydrogen Embrittlement: Baking Prevents Breaking," *Prod. Finish.*, **49**, 90 (1995).
71. H. Geduld, *Zinc Plating*, ASM International, Columbus, OH, 1988, p. 203.
72. M. Fleischmann, S. Pons, and M. Hawkins, *J. Electroanal. Chem.*, **261**, 301 (1989).
73. S. E. Jones et al., *Nature*, **338**, 737 (1989).
74. J. M. Rosamilia, J. A. Abys, and B. Miller, *Electrochimica Acta*, **36** (7), 1203–1208 (1991).
75. J. R. Lacher, *Proc. Roy. Soc.*, **A161**, 525 (1937).
76. L. J. Gillespie and L. S. Galstoun, *J. Am. Chem. Soc.*, **58**, 2565 (1935).
77. L. J. Gillespie and W. R. Downs, *J. Am. Chem. Soc.*, **61**, 2496 (1939).
78. J. W. Simons and T. B. Flanagan, *J. Phys. Chem.*, **69**, 3581, 3773 (1965).
79. A. N. Frumkin and N. Aladjalowa, *Acta Physiochem. USSR*, **19**, I (1944).
80. T. P. Hoan and D. F. Arrowsmith, *Electroplat. Met. Finish.*, **10**, 5, 1 (1957).
81. M. Baidouf and D. M. Kolb, *Electrochim. Acta*, **38** (15), 2145–2153 (1994).
82. V. D. Jovic et al., *J. Serb. Chem. Soc.*, **57** (12), 951–962 (1993).
83. M. Enyo and P. C. Biswas, *J. Electroanal. Chem.*, **335** (1–2), 309–319 (1993).
84. L. J. Vracar and M. Stojanovic, *J. Serb. Chem. Soc.*, **61** (7), 567–575 (1996).
85. B. I. Podlovchenko, E. A. Kolyadko, and S. Lu, *J. Electroanal. Chem.*, **399** (1–2), 21–27 (1995).
86. I.-Y. Wei and J. Brewer, in *Proc. Annual Technical Conf. on American Electroplaters and Surface Finishers Society*, 1995, pp. 321–332.
87. A. V. Smolin, Y. M. Maksimov, and B. F. Podlovchenko, *Russ. J. Electrochem*, **31** (6), 520–525 (1995).
88. J. O. M. Bockris and A. K. N. Reddy, *Modern Electrochemistry*, Plenum, New York, 1970, pp. 1223, 1227, 1053.
89. P. H. Rieger, *Electrochemistry*, 2nd ed., Chapman and Hall, London, 1984, pp. 183–194.
90. A. J. Bard and L. R. Faulkner, *Electrochemical Methods*, Wiley, New York, 1980.
91. R. J. Morrisey, *Metal Finishing Guidebook-Directory 97*, p. 288.
92. USSR Patent 519,497 (June 30, 1976).

93. F. A. Lowenheim, *Electroplating*, McGraw-Hill, New York, 1978, p. 299.
94. J. M. Stevens, *Trans. Inst. Met. Fin.*, **46**, 26 (1968).
95. H. L. Grube, *Metalloberflache*, **B5** (4), 61 (1953).
96. W. Keitel and H. Zschiegner, *Trans. Electrochem. Soc.*, **59**, 273 (1931).
97. T. F. Davis, U.S. Patent 4,092,225 (May 30, 1978).
98. H. J. Schuster and K. D. Heppner, U.S. Patent 4,144,141 (Mar. 3, 1979).
99. J. A. Abys, U.S. Patent 4,486,274 (Dec. 4, 1984).
100. R. LePenven, W. Levanson, and W. Pletcher, *J. Appl. Electrochem.*, **22** (51), 421–424 (1992).
101. L. A. Heathcote, *Platinum Met. Rev.*, **9** (3), 80–82 (1965).
102. J. A. Abys, *The Electrodeposition of Pure Palladium with a Palladium Hydroxide Replenishment System*, American Electroplaters Society Symposium, AESF Week, Orlando, FL, 1991.
103. J. A. Abys and Y. Okinaka, U.S. Patent 4,468,296 (Aug. 28, 1984).
104. J. A. Abys and Y. Okinaka, U.S. Patent 5,135,622 (Aug. 4, 1992).
105. S. Nakhara et al., *J. Testing Eval.*, **5**, 178 (1977).
106. J. J. Caricchio and E. R. York, U.S. Patent 4,076,599 (Feb. 28, 1978).
107. J. M. Deuber, U.S. Patent 4,098,656 (July 4, 1978).
108. J. A. Abys, V. Chinchankar, V. T. Eckert, I. Kadija, E. J. Kudrak, J. J. Maisano, and H. K. Straschil, U.S. Patent 4,911,799 (Mar. 27, 1990).
109. U.S. Patent 2,457,021 (1948).
110. F. Simon and W. Zilske, *Plating Surf. Finish.*, **69**, 86 (1982).
111. J. A. Abys and H. K. Straschil, U.S. Patent 5,178,745 (Jan. 12, 1993).
112. H. K. Straschil, J. A. Abys, E. J. Kudrak, J. J. Maisano, and S. Nakahara, "New Palladium Strike Improves Adhesion and Porosity," *Met. Finish.*, **90**, 42–47 (1992).
113. P. K. Gallagher, *Thermochimica Acta*, **41**, 323–327 (1980).
114. J. A. Abys, unpublished data.
115. H. P. Hedrich and Ch. J. Raub, *Metalloberflache*, **33** (8), 308–315 (1979).
116. F. I. Nobel et al., *Plating Surf. Finish.*, **73** (6), 88–93 (1986).
117. U. Cohen and R. Sard, U.S. Patent 4,269,671 (May 26, 1981).
118. U. Cohen, F. Kohn, and R. Sard, *J. Electrochem. Soc.*, **130**, 1987 (1983).
119. D. Walz and Ch. J. Raub, *Metalloberflache*, **40**, 162–166, 199–203 (1986).
120. T. Hirano and M. Tsukemato, U.S. Patent 5,342,504 (Aug. 30, 1994).
121. K. S. Berge, U.K. Patent Application 2,115,440A (Sept. 22, 1982).
122. K. S. Berge, U.S. Patent 4,416,740 (Nov. 22, 1983).
123. K. S. Berge, U.S. Patent 4,430,172 (Feb. 7, 1984).
124. P. Wilkinson, U.K. Patent Application 2,115,440A (Sept. 7, 1983).
125. D. Walz and Ch. J. Raub, *Metalloberflache*, **40** (6), 239–241 (1986).
126. I. Boguslavsky, J. A. Abys, H. K. Straschil, M. Tsuruta, J. J. Maisano, and V. T. Eckert, in *Proc. Annual Conference American Electroplaters and Surface Finishers Society*, Detroit, MI, June 1997.
127. M. Kume, paper presented at 76th Technical Conf. of the Metal Finishing Society of Japan, Paper 3OC-7, 1987.
128. G. T. Rado and H. Suhl, *Magnetism*, Vol. 5, Academic, New York, 1973.
129. *Platinum Met. Rev.*, **37** (2), 120 (1993).
130. P. Juzkis, M. U. Kittel, and Ch. J. Raub, private communication, Research Institute for Precious Metals.
131. P. Stevens, U.S. Patent 4,048,023 (Sept. 13, 1977).
132. S. N. Vinogradow and P. Yu, *Perelygin, Zashch. Met.*, **16** (4), 507 (1980).
133. A. A. Tikhonov, P. M. Vyacheslavov, G. K. Burkat, and V. P. Bursin, *Modern Methods of Deposition of Electrolytic and Chemical Coatings* (in Russian), lzd. Mosk. Doma Nauchn.-Tekhn. Propagandy Im. F. E. Dzerzhinskogo, 1979, p. 79.
134. E. M. Savitskii et al., *Metallic Single Crystals* (in Russian), lzd. Nauka, Moscow, 1976, p. 127.
135. E. M. Savitskii et al., *Alloys of Noble Metals* (in Russian), lzd. Nauka, Moscow, 1977, p. 224.
136. L. M. Nomerovannaya et al., *Dokl. Akad. Nauk SSSR*, **246** (3), 585 (1979).
137. A. M. Meretskii et al., *Metally*, **5**, 193 (1976).
138. N. F. Reshetnikova and K. S. Pedan, *Zh. Prikladoni Khimii*, **55** (9), 1966–1999 (1982).
139. F. M. Dzhandubaeva, P. M. Vyacheslavov, and G. K. Burkat, *Zashchita Metallov*, **18** (3), 427–430 (1982).
140. R. Long and K. F. Bradform, in *Proc. 8th International Conf. on Electrical Contact Phenomena*, Tokyo, Japan, 1970.
141. W. A. Crossland and E. Knight, in *Proc. Seminar on Electrical Contacts*, Chicago, 1973, p. 247.
142. U. Cohen and R. Sard, U.S. Patent 4,269,671 (May 26, 1981).
143. U. Cohen, F. Kohn, and R. Sard, *J. Electrochem. Soc.*, **130**, 1987 (1983).
144. U. Cohen, K. R. Walton, and R. Sard, *J. Electrochem. Soc.*, **131** (11), 2489 (1988).
145. F. I. Nobel, *IEEE Trans. Components, Hybrids Manuf. Technol.*, **9** (1), (1985).
146. F. I. Nobel et al., *Plating Surf. Finish.*, **73**, 88 (1986).
147. P. L. Cavallotti et al., *Proc. Electrochem. Soc.*, **6**, 261–276 (1994).
148. M. Kume and U. Tadeo, *Hyomen Gijutsu*, **46** (17), 663–666 (1995).
149. S. N. Vinogradov and S. V. Plokohov, *Gai'venotekh Obrab. Poverkhn*, **1** (1–2), 32–34 (1992).
150. M. Noro et al., *Kagaku to Kogoyo*, **69** (3), 89–94 (1995).
151. J. A. Abys and H. K. Straschil, U.S. Patent 5,024,733 (June 18, 1991).

152. L. Wang, *Cailiao Baohu*, **27** (5), 24–25 (1994).
153. Soviet Union Patent 535,378 (Nov. 26, 1976).
154. *Platinum 1998*, Johnson Matthey.
155. *U.S. Geological Survey*, Mineral Commodity Summaries, Jan. 1999.
156. M. Lovatt, *Bridge News,* Feb. 16, 2000.
157. C. Fan et al., in *Proc. Annual Conference American Electroplaters and Surface Finishers Society*, Chicago, IL, June 2000.
158. E. J. Kudrak et al., *Proc. 32nd IICIT Connector and Interconnection Technology Symposium*, Anaheim, CA, Sept. 1999.
159. J. A. Abys et al., *Trans. Inst. Metal Finish.*, (July 1999).
160. J. A. Abys et al., *Connector Specifier*, Feb. 1999, p. 12.
161. J. Abys, paper presented at Fleck Materials Conf., Indian Wells, CA, Sept. 1998.
162. I. Boguslavsky et al., in *Proc. Annual Conference American Electroplaters and Surface Finishers Society*, Session L, Minneapolis, MN, June 1998.
163. J. A. Abys et al., *Plating Surf. Finish.*, **86**, 108 (Jan. 1999).
164. M. Clarke, in *"Properties of Electrodeposits,"* R. Sard, H. Leidheiser, and F. Ogburn, Eds., The Electrochemical Society, Princeton, NJ, 1975, p. 122.
165. Standard 17000, Sect. 1275, Western Electric Manufacturing, 1982, based on ASTM B-799.
166. G. C. Munie et al., *J. SMT*, Jan. 2000, p. 15.
167. P. Wilkinson and B. O'Hara, *IPC PC World Convention*, May 1984.
168. L. J. Mayer et al., in *Proc. IPC—Fall Session*, Sept. 1986.
169. I. Kadija et al., in *Proc. Annual Conference American Electroplaters and Surface Finishers Society*, June 1993.
170. I. Kadija et al., *Plating Surf. Finish.*, **82** (2), 56 (Feb. 1995).
171. T. Mc Guiggan and E. E. Benedetto, "Impact of Palladium Leadframes on PCA Manufacturing,"*Circuits Assembly*, Nov. 1997, pp. 32–36.
172. C. Fan et al., in *Proc. Symposium on Environmental Aspects of Electrochemical Technology: Applications in Electronics*, M. Datta, J. M. Fenton, and E. W. Brooman, Eds., PV 96-21, The Electrochemical Society, Pennington, NJ, 1997, p. 188.
173. European Patent Application 87305080.1 by Texas Instruments (1987).
174. European Patent Application 89302939.7 by Texas Instruments (1989).
175. D. C. Abbott et al., *IEEE Trans. Components Hybrids Manufacturing Technol.*, **14** (3), 567 (Sept. 1991).
176. C. A. Dullaghan et al., in *Proc. Annual Conference American Electroplaters and Surface Finishers Society*, Session 1, Chicago, IL, June 2000.
177. M. E. Baugartner and D. R. Gabe, *Trans. IMF*, **78** (1), 11; **78** (2), 79 (2000).
178. E. Von Gunther et al., *Galvanotechnik*, **1**, 206 (2007).
179. S. V. Kabanov et al., *Russian J. Appl. Chem.*, **74** (11), 1895 (2001).
180. I. Bougslavsky and J. A. Abys, in *Proc. 29th Annual Conference and Interconnection Symposium*, Oct. 1996.
181. M. Zhong, L. He, K. Xia and Z. Z. Chen, *J. Mater. Protection (Chinese)*, **39** (6), 26 (June 2006).
182. S. N. Vinogradov et al., *Russian Electrochem.*, **37** (7), 838–840 (2001).
183. H. H. Nowsky et al., *Russian J. of Electrochem.*, **42** (3), 264–271 (2006).
184. I. Gadschov and R. Mantcheva, *Galvanotechnik*, **97** (8), 1850–1854 (2006).
185. F. Y. Su, I. W. Sun, and C. C. Tai, Meeting Abstracts, presented at 207th Electrochemistry Society Meeting, Quebec, Canada, Mar. 2005.
186. J. A. Abys, in *Proceeding of the Symposium on Surface Engineering For Electronics, Singapore, Dec. 2006; Proceedings of EUROMAT*, Nuremberg, Germany, Sept. 2007.

13

ELECTROCHEMICAL DEPOSITION PROCESS FOR ULSI INTERCONNECTION DEVICES

TETSUYA OSAKA AND MASAHIRO YOSHINO

13.1 INTRODUCTION

13.1.1 Background

An integrated circuit (IC) consists of thousands or even millions of interconnected semiconductor devices, mainly transistors, as well as passive components such as resistors [1–7]. In the second half of the twentieth century, advancements in the fabrication of semiconductor devices and related experimental discoveries led to the advancement of IC technology. The integration of large numbers of small transistors onto a chip enormously improved the complexity and performance of electric systems. The properties of the ICs, such as small size, reliability, fast switching speeds, low power consumption, mass production capability, and ease of adding complexity, made them a dominant technology of today [8–10]. Computers, cellular phones, and other electronic devices are now critical to the makeup of our society, which is based on information technology. Indeed, many people hold that the digital revolution brought about by ICs was one of the most significant occurrences in the history of mankind. Integrated circuits require interconnection technology, which is the field that this chapter belongs to. In the next section we will review the Cu interconnection technology, which recently became an important technology of ultra large scale integrated (ULSI) circuits.

Large-scale integration (LSI) is the process of creating ICs by combining thousands of transistor-based circuits onto a single chip. LSI began in the 1970s with the achievement of complex semiconductor-based microelectronics [11]. Increasing demand for high-performance electronic devices is the main force driving the need for rapid advances in ULSI fabrication technology. In the semiconductor industry, developments in transistor and wiring technology continue to progress exponentially, as represented by Moore's law, which say that the number of transistors on a chip doubles every about two years [12, 13]. The law also states that the number of interconnections is increasing exponentially with time while their dimensions are decreasing exponentially with time.

For a long time Al was used as the wiring material in LSI devices [14–16]. In microelectronic ICs, when feature size shrank, the *RC* delay increased and significantly hindered further increases in a chip's operation frequency [17]. This increased *RC* delay can be reduced by replacing Al conducting wire with Cu, thus reducing resistance. Copper has several other advantages, such as high electrical conductivity and resistance to electromigration [18]. However, Cu interconnections can deteriorate by the diffusion of Cu atoms into the insulator layer and substrate. Copper ULSI technology has been developed through implementation of the damascene process developed by IBM [19, 20], which is illustrated in Figure 13.1. The process, whose name comes from a metal-working process used by swordmakers in ancient Damascus to produce beautiful inlay patterns on their blades and other works of art, has become the semiconductor interconnection process at the turn of the twenty-first century. There are a number of different approaches to the damascene process, but they all share certain basic essentials. The first step is putting down a blanket dielectric layer, such as one of the modern "low-*k*" materials, using either chemical vapor deposition (CVD) or a process in which a liquid is applied to the wafer while it is spinning, causing the liquid to flow evenly across the wafer surface, thereby creating a uniform layer [21, 22]. A lithography step and etch step are used to

Modern Electroplating, Fifth Edition Edited by Mordechay Schlesinger and Milan Paunovic

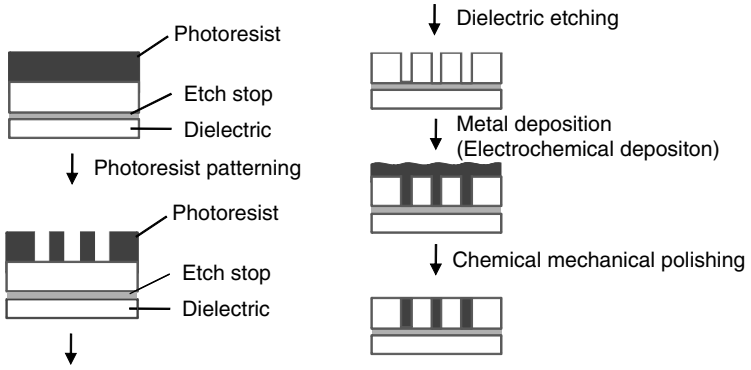

FIGURE 13.1 Illustration of the damascene process.

fabricate via holes to the next lower level of insulation and wiring and also fabricate trenches that will be filled in by the Cu [23–26]. As mentioned earlier, Cu has an undesirable tendency to diffuse after it is deposited, so the next step is to place a thin, strong barrier layer to prevent this diffusion [27] from happening. Next, in the physical vapor deposition (PVD) process, a thin layer of metal is laid down that will serve as a "seed layer" for the next step, electroplating. In this process, the wafer is immersed in a solution containing Cu ions, and an electrical current is applied, attracting the Cu ions to the seed layer on the wafer, where they are reduced to metallic Cu. Then the Cu is deposited, filling the via holes and trenches and forming the metal interconnections [28, 29]. The final step is the chemical mechanical polishing (CMP) process, in which the entire wafer is polished using a pad with acidic and abrasive liquid slurry [30]. This process ensures that the wafer's top surface is flat and ready for the next layer of metal to be deposited. The CMP process planarizes the surface of the deposit; that is, it fully removes Cu from the high shoulders of the trenches and via holes, while keeping Cu only in the trenches and in the via holes. Planarization is also essential for high-resolution lithography, which is fully compatible with the sub-90-nm interconnections in the damascene process.

13.1.2 Interconnection Material

Various Cu deposition processes have been investigated recently, such as PVD, CVD, and electrochemical deposition, and various researchers have developed electrodeposition and electroless deposition of Cu to fill submicrometer trenches and via holes with a very high aspect ratio [23–26, 31, 32]. Electrochemical Cu deposition techniques, including electrodeposition and electroless deposition, offer many advantages, such as high-quality Cu deposited trench and via hole-filling capability, high throughput, and good cost performance. Electrodeposition, in comparison with electroless deposition, can provide a higher deposition rate. Electrodeposition solutions are more stable and easier to control than those for electroless plating. On the other hand, electroless deposition provides high conformality and a very high intrinsic selective deposition.

The Cu electroplating process has been used extensively for a long time in the electronics industry for the fabrication of printed circuit boards and chip packages; however, its wide use in ULSI fabrication is very recent. The first mention of a electrodeposition process being used in the ULSI fabrication process was included in a 1995 report from IBM on the electromigration reliability study of Cu metallization [33]. In the electrodeposition process, the electrons are supplied from an external power supply. This process is easier to control than the electroless deposition process because the capability to control the current flow is well developed. The most important reason for using the Cu electrodeposition process with chemical additives in ULSI fabrication is super gap-filling capability. The process results in much better step coverage, better filling inside the trenches, and greater thickness in the field region than the process without chemical additives.

As mentioned above, the Cu electroless deposition process already has been demonstrated for ULSI fabrication [31, 32]. Also, as mentioned before, this process, which is relatively simple, can be used to deposit film selectively. The composition of a typical electroless deposition solution consists of $CuSO_4$ $5H_2O$, EDTA (ethylenediaminetetraacedic acid) as a complex agent, HCHO (formaldehyde) or glyoxylic acid as a reducing agent, KOH or TMAH (tetramethylammonium hydroxide), and a small amount of additives.

13.1.3 Diffusion Barrier Layer

To realize good Cu interconnections, it is essential to fabricate effective barrier and capping layers because Cu diffuses rapidly into the interlevel dielectric (ILD) such as SiO_2 and is oxidized easily, both of which degrade circuit performance. Today, in most microelectronics processes, the diffusion barrier layer is formed by a dry process, that is, PVD or CVD. Recently, atomic layer deposition (ALD) also has been investigated as a suitable process. Although PVD methods

such as sputtering yield high-quality layers, they simply cannot produce conformal coatings with high aspect ratio via holes and trenches narrower than 100 nm. On the other hand, CVD and ALD yield excellent conformal layers, but they require special precursors and multichambered equipment.

An alternative to such dry processes is a wet deposition process, such as electrochemical deposition. A wet process, which is simple, offers a good step coverage on substrates with nanoscale trenches and via holes and usually leads to a lower cost per wafer. Recently, another fabrication process, barrier layer by electroless deposition, has been proposed [34–37].

In this process, the barrier material must be thermally stable, remaining unchanged at normal Cu damascene processing temperatures of 300–425°C, to prevent outgassing of the barrier or ILD layer during barrier (Ta or TaN) or Cu seed deposition, which will ruin the conductivity and integrity of the metals. Also, the dielectric barrier material must adhere well to the metals to withstand the stresses caused by the expansion coefficient mismatch between the conductors and insulators during the heating and cooling cycles.

13.2 COPPER DEPOSITION FOR INTERCONNECTION BY ELECTROCHEMICAL TECHNIQUES

13.2.1 Copper Trench Filling by Electrodeposition

Effects of Additives on Copper Trench Filling The most important requirement for success of this process is its ability to fill trenches and via holes completely without producing voids and seams, which are undesirable because they lead to an increase in resistivity and an enhancement of electromigration. Furthermore, trapped electrolyte in voids corrodes Cu. Trenches and via holes can be filled without defect by using several bath additives in combination. In ordinary deposition, which does not use additives, voids or seams appeared, particularly in narrow and small trenches and via holes because the deposition rate at the trench openings tends to be higher than at other portions of trenches. The formation of voids and seams is caused by the current distribution that occurred on trenches, in which current density is concentrated at the opening of trenches for the geometrical reason [38].

Additives are known to adsorb on the cathode surface and affect both the rate of Cu deposition and the microstructure and morphology of deposits. Based on their function, these additives can be categorized into three types: deposition accelerator, inhibitor, and leveler [39–41].

The accelerator is essentially an organic sulfur-containing compound, while the inhibitor is a glycol, which decreases the deposition rate, especially in the presence of chloride ions. The leveler is generally a kind of an azo dye compound, which also acts as an inhibitor.

Conventional additives used for "superfilling" are chloride ions (Cl^-), polyethylene glycol (PEG), bis(3-sulfopropyl)disulfide (SPS) or 3-mercapto-1-propanesulfonate (MPS), and Janus Green B (JGB). Figure 13.2 shows typical conventional additives used in the process of trench filling by electrodeposition: PEG, SPS, MPS, and JGB.

The addition of chloride ions, which catalyze the rate-determining Cu^{2+}/Cu^{+} reaction, is known to accelerate Cu deposition [42–46]. However, it is also known to interact with PEG [42, 47] and SPS when they are present together. PEG, which is a kind of surfactant, is usually added to a damascene plating bath as a deposition inhibitor. PEG by itself is a weak inhibitor, but it is known to inhibit Cu deposition significantly in the presence of chloride ions. This compound adsorb on the metal surface and forms a polymeric PEG–Cl^- adlayer [42, 45, 47]. This PEG–Cl^- adlayer is considered to act as a blocking layer and strongly inhibit Cu deposition. Recent studies have suggested that this adlayer also contains cuprous ions. For instance, Yokoi et al. [42] suggested that this blocking layer might consist of a complex of cuprous ion

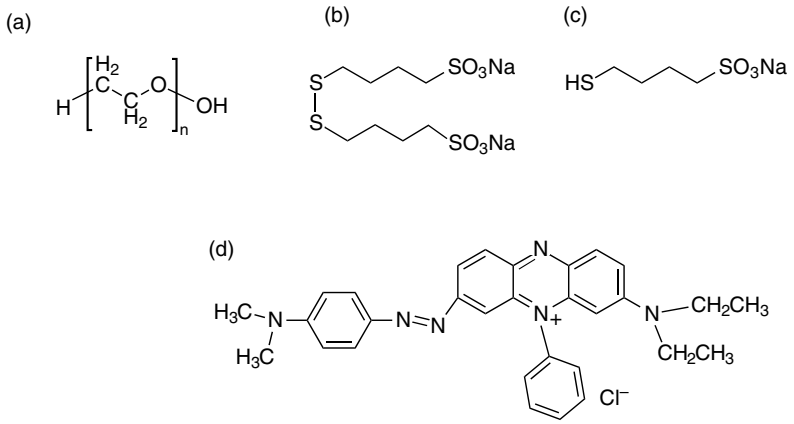

FIGURE 13.2 Conventional additives used in the process of trench filling by electrodeposition: (*a*) PEG, (*b*) SPS (*c*) MPS, and (*d*) JGB.

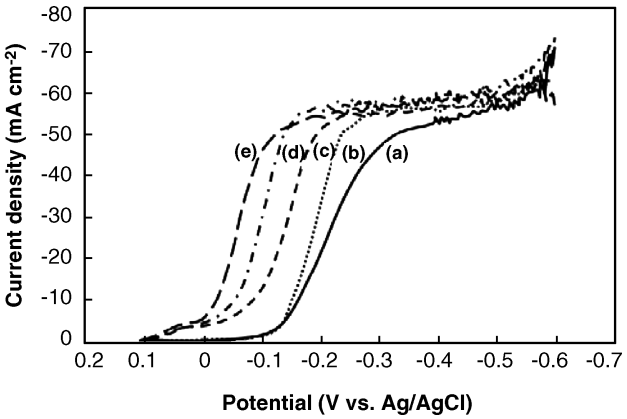

FIGURE 13.3 Effect of SPS concentration on polarization characteristics for Cu electrodeposition from Cl–PEG–SPS baths containing different amounts of SPS: (*a*) 0, (*b*) 1, (*c*) 10, (*d*) 100, and (*e*) 1000 ppm. (Reproduced by permission of The Electrochemical Society [48].)

and PEG formed on specifically adsorbed chloride ions. Figure 13.3 shows cathodic polarization curves for the Cl–PEG–SPS bath. The acceleration effect of SPS can be clearly seen in the polarization curves. The effect of suppressors is well known, but the mechanism of accelerators such as SPS or its monomeric compound, MPS, is unclear. Each of them is reported to act as a strong accelerator in the presence of Cl^- [49].

SPS and MPS similarly affect the bottom-up growth of Cu in trenches [50]. Thus, it is assumed that the disulfide linkage in SPS is cleaved under the conditions in which Cu electrodeposition takes place. It also is assumed that cuprous ions and SPS form an adsorbed species and that the complex formed by this reaction stabilizes the cuprous ions [51]. Because the reduction of Cu^{2+} to Cu^+ is the rate-limiting step of Cu electrodeposition, the stabilization of cuprous ions increases the number of cuprous ions near the surface of Cu, which results in an increased rate of Cu deposition. Another model for the catalytic effect of the accelerator is that SPS displaces the PEG–Cl^- layer, which inhibits Cu electrodeposition, and that this competitive adsorption between an accelerator and an inhibitor increases the Cu deposition rate [29]. However, the detailed reactions of these additives still remain unclear because of their complex interactions.

JGB is regarded as a leveling agent [40, 48, 52, 53]. It increases the overpotential of the Cu deposition; that is, it inhibits deposition. It also is consumed easily at the Cu surface during the electrodeposition. Polarization curves for the Cl–PEG–SPS–JGB bath containing various concentrations of JGB are shown in Figure 13.4. The addition of JGB to the Cl–PEG–SPS bath resulted in a negative shift of the potential in which the current density began to increase, which is opposite to the effect of the addition of SPS to the Cl–PEG bath. The degree of shift of the potential was greater when JGB concentrations were higher than 10 ppm. For the Cl–PEG–SPS–JGB bath, the current density in the mass-transfer-limited region fluctuated; nevertheless, it tended to be lower than that for the Cl–PEG–SPS bath. The shift of potential in the polarization curves is attributable to the inhibition of Cu deposition by JGB.

For the application to submicrometer interconnections, it has been reported that there is "bottom-up" growth, in which the deposition from trench bottoms is accelerated relative to that trench openings, in the bath containing Cl^-, PEG, and SPS or MPS, in combination. Figure 13.5 shows scanning electron microscopy (SEM) images of Cu electrodeposited in trenches for filling sequences from different baths. The Cu deposition at the bottom is significantly accelerated by the addition of SPS to the Cl–PEG bath (see Fig. 13.5*c*). On the other hand, both subconformal deposition and conformal

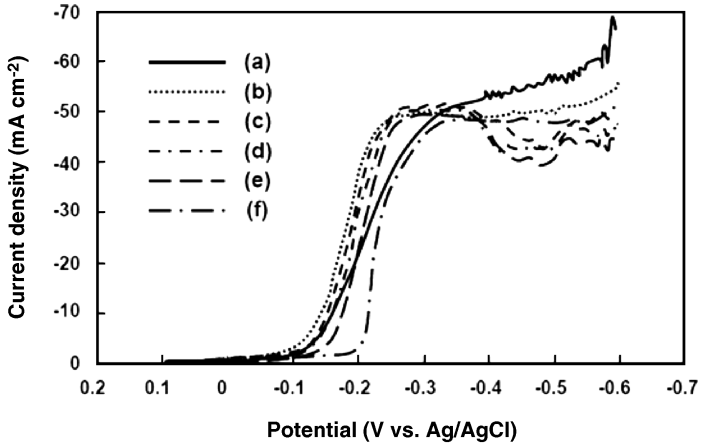

FIGURE 13.4 Effect on polarization characteristics for Cu electrodeposition from Cl–PEG–SPS–JGB baths containing different amounts of JGB: (*c*) 1, (*d*) 5, (*e*) 10, and (*f*) 50 ppm of JGB. SPS concentration was 5 ppm. Data for two baths not containing JGB are included for comparison: (*a*) Cl–PEG and (*b*) Cl–PEG–SPS. (Reproduced by permission of The Electrochemical Society [48].)

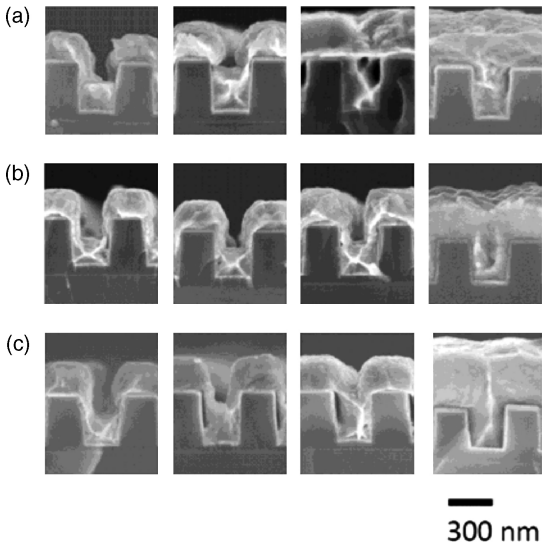

FIGURE 13.5 Cross-sectional SEM images of Cu electrodeposited in trenches for filling sequences from different baths: (*a*) additive-free; (*b*) Cl–PEG; (*c*) Cl–PEG–SPS. Deposition time (left to right): 15, 30, 60, and 90 s.

deposition were observed in the images of the specimens obtained from the additive-free bath (Fig. 13.5*a*) and the Cl–PEG bath (Fig. 13.5*b*). It has been suggested that the competitive adsorption between the accelerator and the inhibitor results in this bottom-up effect [29], which results in the superfilling of Cu in trenches and also the "overfill" phenomenon, in which Cu bumps are formed above the Cu-filled trenches.

Effects of Additives on Physical and Mechanical Properties of Copper Electrodeposits The effects of additives such as Cl^-, PEG, SPS, and JGB on the properties of Cu deposits are also of great interest for interconnection applications, because the properties of Cu are very important for maintaining the performance and reliability of interconnections [54–58]. These additives are very important for maintaining the properties of Cu deposited in trenches because it leads to significant change in the grain structure and resistivity. Several factors, inducing self-annealing, have been presented, including strain energy caused by residual stress [54, 57, 59–61], high internal strain energy originated from incorporated impurities [59–62], defect energy originated from dislocation [58], and grain boundary energy associated with fine grains [63]. Indeed, during self-annealing, the grain size increases by an order of magnitude [54, 64–66], and the resistivity decreases nearly to bulk value [29]. Although much research has been done on self-annealing, detailed knowledge, especially of the role of additives, is still lacking.

As is discussed in the previous section, additives have different effects when they are present together. Therefore, the effect of various combinations of additives is also considered to be important for the self-annealing mechanism. We investigated the effect of various combinations of additives based on the measurements of resistivity, the analysis of crystallographic structure, the microscopic observation of film structure, and the microanalysis of deposits.

Figure 13.6 compares the variations with time of the resistivity of Cu deposits obtained from four different baths. For each specimen, the first measurement was made 30 min after the electrodeposition current was turned off. The annealing effect was measured periodically at room temperature for seven days. The resistivity values of Cu deposits from the Cl–PEG–SPS and Cl–PEG–SPS–JGB baths decreased with time after deposition, while those of the deposits from the additive-free and Cl–PEG baths remained constant over the seven-day period. The value of resistivity of Cu from the Cl–PEG–SPS bath, which was initially higher than that for the deposit obtained from the additive-free and Cl–PEG baths, decreased continuously with time over the seven-day period after the deposition. For the deposits from the Cl–PEG–SPS–JGB bath, the resistivity also decreased with time. This result indicates that self-annealing occurred in the deposits from the Cl–PEG–SPS–JGB bath. However, the resistivity value of the deposits from this bath was higher than that for the Cl–PEG–SPS bath, and even seven days after deposition, it was the highest among all of the deposits from the baths examined in this study.

The annealing behavior was found to depend strongly on the concentration of SPS. The resistivity value also decreased with time when SPS was added at concentrations of 10 ppm or less, although the rate and extent of self-annealing did not depend on time. Because self-annealing occurred in the presence of SPS, it is clear that SPS plays a factor for inducing self-annealing. However, a decrease in resistivity

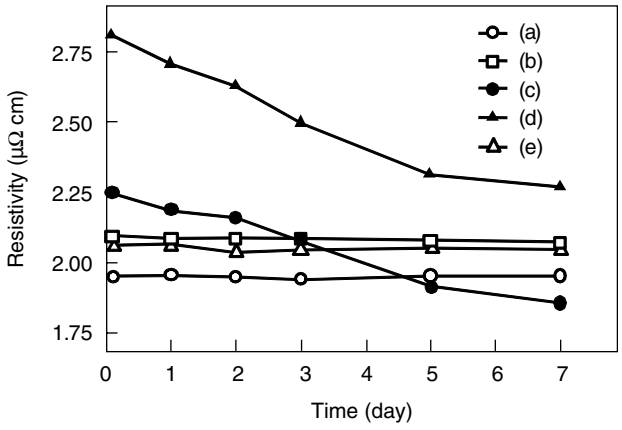

FIGURE 13.6 Changes in resistivity with time at room temperature of Cu deposits obtained from different baths: (*a*) additive free; (*b*) Cl–PEG; (*c*, *e*) Cl–PEG–SPS; and (*d*) Cl–PEG–SPS–JGB. SPS concentrations: (*c*, *d*) 10 and (*e*) 100 ppm.

was not observed with the addition of 100 ppm of SPS (Fig. 13.6*e*). Although SPS is essential for self-annealing, this result showed that excessive SPS suppresses self-annealing. In short, the surface morphology of the Cu deposit seemed to be dependent on the concentration of SPS. The deposit produced in the Cl–PEG–SPS (100 ppm) bath was dull, while that from the Cl–PEG–SPS bath containing 10 ppm of SPS was bright. This suggests that the microstructure such as grain size could be changed based on the concentration of SPS used in the bath.

Crystallographic Analysis of Copper Electrodeposits

Changes in X-ray diffraction (XRD) profiles with time agreed well with the results of the resistivity measurements. Figure 13.7 shows the XRD profiles recorded over the period of seven days after deposition. The crystallographic structure of the deposit obtained from the Cl–PEG–SPS bath (Fig. 13.7*c*) changed significantly with time after the deposition, while there were no changes in the deposits from the additive-free (Fig. 13.7*a*) and Cl–PEG (Fig. 13.7*b*) baths. The deposits from the Cl–PEG–SPS–JGB bath (Fig. 13.7*d*) clearly showed a change with time in the crystallographic structure. For the deposits from the Cl–PEG–SPS (Fig. 13.7*c*) and Cl–PEG–SPS–JGB (Fig. 13.7*d*) baths, the intensities of (111) and (200) diffraction peaks increased over the seven days after electrodeposition. The intensity of (111) for the Cl–PEG–SPS and Cl–PEG–SPS–JGB baths continuously increased over the seven-day period. On the other hand, the intensities of the other baths did not continuously increase. It was found that the changes in the peak intensity, I_{111}, corresponded well to the results of the resistivity measurements shown in Figure 13.6.

Figure 13.8 shows the variation with time at room temperature of relative intensity of (200) with respect to (111), I_{200}/I_{111}, obtained from the XRD profiles of Cu deposits. The values of I_{200}/I_{111} for the deposits from the Cl–PEG–SPS (plot *c*) and Cl–PEG–SPS–JGB (plot *d*) baths increased with time, while the values of I_{200}/I_{111} were essentially the same for the deposits from the additive-free (plot *a*) and Cl–PEG (plot *b*) baths. A similar finding also has been reported by Lee et al. [54]. The change in the value of I_{200}/I_{111} suggests that the anisotropic grain grew, which led to the change in preferred crystallographic orientation upon self-annealing. It has been suggested that this significant increase in (200) preferred orientation results from the anisotropy of the elastic constant of the Cu crystal [54]. Different elastic constants for different crystallographic orientations result in a difference in strain energy for crystals with different film orientations. Because the strain energy was the lowest for the (200)

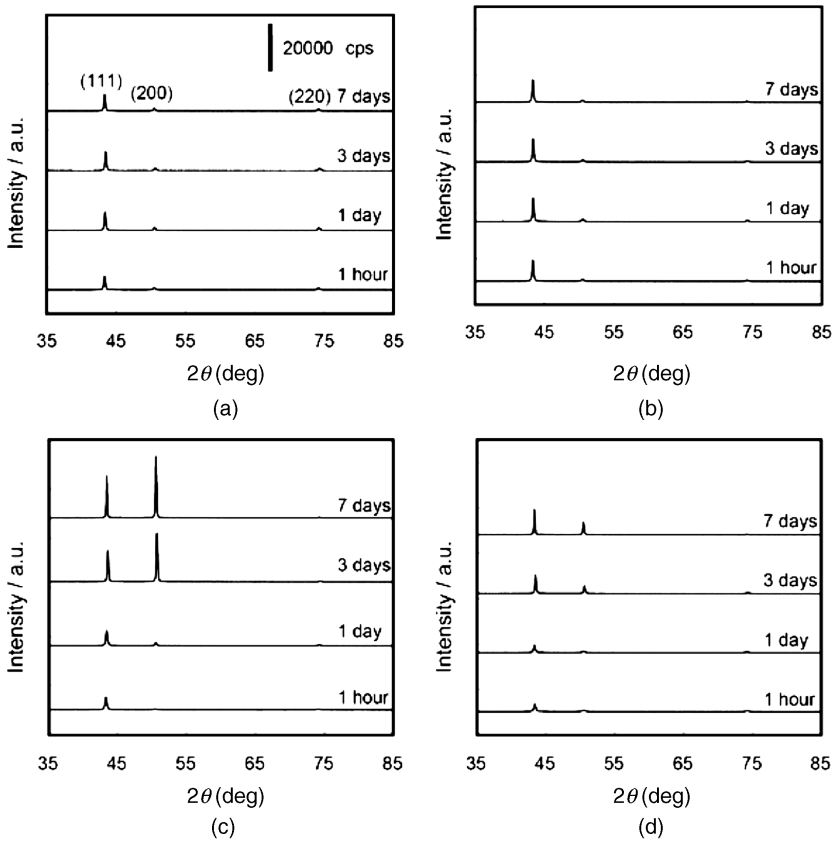

FIGURE 13.7 Changes in XRD profiles with time at room temperature of Cu deposits obtained from different baths: (*a*) additive free; (*b*) Cl–PEG; (*c*) Cl–PEG–SPS; (*d*) Cl–PEG–SPS–JGB.

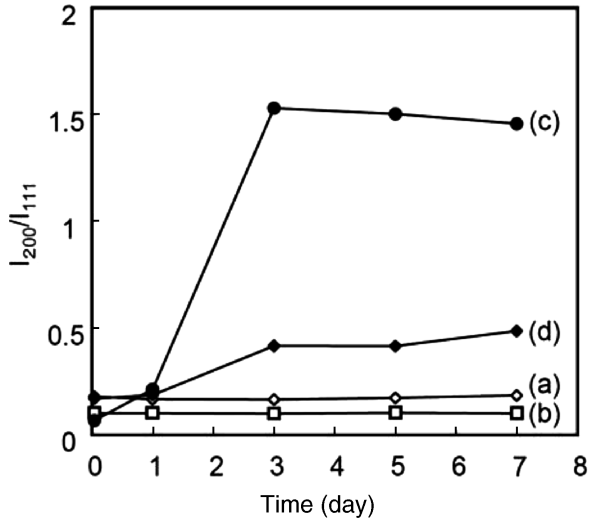

FIGURE 13.8 Changes in I_{200}/I_{111} in XRD profiles with time at room temperature of Cu deposits obtained from different baths: (*a*) additive free; (*b*) Cl–PEG; (*c*) Cl–PEG–SPS; (*d*) Cl–PEG–SPS–JGB.

orientation, the (200)-oriented grains grew preferentially during self-annealing.

Microstructure Analysis of Copper Electrodeposits As described above, a combination of additives was found to affect self-annealing significantly. To consider the effects of additives, we used a focused ion beam–scanning ion microscopy (FIB–SIM) system to investigate the microstructure of the deposits. Figure 13.9 shows cross-sectional FIB–SIM images of Cu deposits obtained from different baths. The images were obtained periodically over a one-month period after electrodeposition. The first measurements for the deposits from the various baths were carried out one day after deposition. The images of the deposits from the Cl–PEG–SPS (Fig. 13.9*c*) and Cl–PEG–SPS–JGB (Fig. 13.9*d*) baths changed with time after deposition. It is clear that the size of the grains in these two deposits observed one day after deposition was uniform and very small: The average grain size measured in the horizontal direction from the SIM image was 50 nm. It also is clear that the size of grains in these two samples increased within two days after deposition: The average grain size (not shown in the figure) was 1.5 μm, which was identical to those in the one-month-old deposits. On the other hand, no such grain growth was observed in the deposits obtained from either the additive-free bath or the Cl–PEG bath, even after one month. Comparison of the images obtained one day after deposition clearly shows that cross-sectional structures were different for the deposits obtained from the different baths. According to Fischer's classification [67], the deposit from the Cl–PEG–SPS bath (Fig. 13.9*c*) is regarded as an "unoriented dispersion (UD)"–type deposit. This structure indicates that three-dimensional nucleation occurred during electrodeposition [68, 69]. The grain structures of the specimens from the additive-free bath (Fig. 13.9*a*) and the Cl–PEG bath (Fig. 13.9*b*) were different from that of the specimen from the Cl–PEG–SPS bath (Fig. 13.9*c*). For the deposits from the former two baths, the grains were not uniform in size and shape; the grains distributed near the surface of the films were rough and large grains, while those distributed near the substrate were quite small. The size of the grains near the surface of both the deposits ranged from 200 nm to 1 μm, while the size of the grains near the substrate was consistent, at approximately 48 nm. This kind of structure is the intermediate type between the "basis reproduction (BR)" and the "field oriented (FT)", which may form when two-dimensional nucleation occurs [68, 69]. The observed difference in cross-sectional structures of the one-day-old deposits may result from the difference in the mode of film growth, which, in turn, is attributed to the difference in self-annealing behavior.

Generally, grain growth is considered to be driven by several different kinds of energies, such as interface/surface energy, grain boundary energy, strain energy, and defect

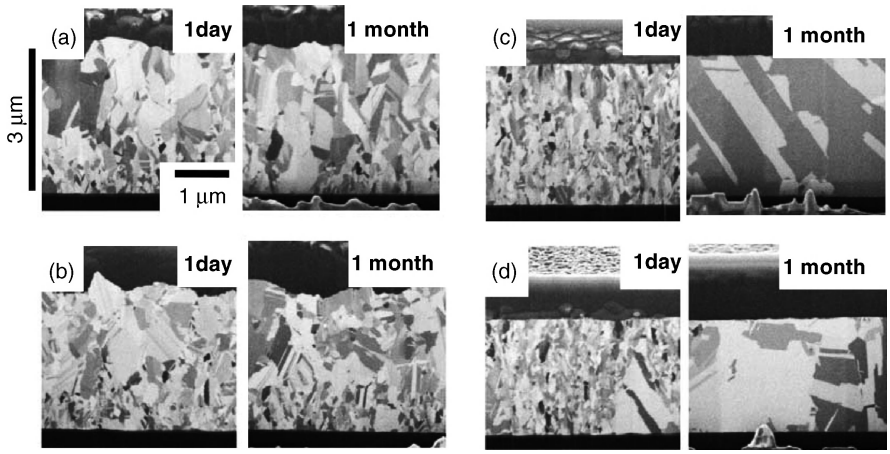

FIGURE 13.9 Cross-sectional FIB–SIM images showing changes with time at room temperature in cross-sectional microstucture of Cu deposits obtained from different baths: (*a*) additive free, (*b*) Cl–PEG; (*c*) Cl–PEG–SPS; (*d*) Cl–PEG–SPS–JGB.

energy [61, 70]. In the present case, it seems that grain growth during self-annealing was mainly driven by the grain boundary energy and local strain energy that originated from the additives incorporated in the deposits.

Grain growth also occurred in the deposit from the Cl–PEG–SPS–JGB bath (Fig. 13.9*d*). The image of the deposit from this bath recorded one day after deposition was similar to that of the deposition from the Cl–PEG–SPS bath (Fig. 13.9*c*), although the former deposit contained some large grains near the substrate. The reason for the formation of these large grains is not understood, it appears that they are related to the decrease in the rate and degree of self-annealing caused by JGB, which was observed in the XRD studies. After self-annealing, the grain size measured in the image for the Cl–PEG–SPS–JGB bath (Fig. 13.9*d*) was identical to that for the Cl–PEG–SPS bath (Fig. 13.9*c*). The time period in which grain size was observed by FIB–SIM corresponded to that in which anisotropic grain growth was observed in the XRD measurements. Thus, it is suggested that grain boundary diffusion occurs during anisotropic grain growth.

It is clear that SPS exerts the most significant effect on self-annealing. However, this additive also is known to interact with Cl^- and PEG. To gain insight into the effect of additive interaction on self-annealing, the microstructure of the deposits from the bath containing various combinations of Cl^-, SPS, and PEG were investigated. The deposits from the Cl^-, SPS, Cl–SPS, and PEG–SPS baths were observed by FIB–SIM. These images reveal that self-annealing did not occur in the deposits from all baths. The microstructure of the one-day-old deposits from these baths was almost identical to that of the deposits from the additive-free and Cl–PEG baths (see Fig. 13.9). These results support our assumption that initial grain size is a major factor to induce self-annealing. In more precise terms, the size and shape of grains in the area of the upper portion of the deposits depended on the combination of additives, although grains near the substrate were equally small in all one-day-old deposits, as can be seen in Figure 13.10.

Carbon Microanalysis of Copper Electrodeposits Strain energy originating from incorporated additives also should be considered as a factor of self-annealing. Lee and Park [61] calculated the strain energy caused by PEG incorporation by assuming that PEG is segregated at the grain boundary, and they concluded that the stress exerted by incorporated PEG on Cu atoms in the deposit is a significant factor of self-annealing. However, as discussed in the previous section, they did not evaluate the amount of incorporated PEG. To further investigate the effect of incorporation of additives on self-annealing, carbon microanalysis of the Cu electrodeposits was performed with the combustion-infrared absorption method. Table 13.1 lists the carbon contents of the Cu deposits produced in the baths containing various combinations of additives. As can be seen in the table, of the two self-annealing Cu deposits, the carbon content from the Cl–PEG–SPS bath was very low. It is interesting to note that the carbon content of the Cu deposit was decreased by adding SPS to the Cl–PEG bath. In addition, carbon was not detected in the deposit from the additive-free bath. The value of carbon content was increased to 0.046 wt % by adding Cl^- and PEG. Further addition of SPS decreased the carbon content of the deposit and the value of carbon content of the deposit from this bath was only 0.003 wt %, which was smaller than the reliable detection limits of 0.01 wt %. Furthermore, the addition of JGB to the Cl–PEG–SPS bath increased the carbon content of the deposit. This result corresponds to the finding reported by Haba et al. [71] that JGB is consumed during electrodepositon. As mentioned earlier, self-annealing is suppressed by adding JGB to the Cl–PEG–SPS bath. This result suggests that the suppression of self-annealing results from the pinning of grain growth by the incorporated JGB molecules. For the Cl, SPS, Cl–SPS, and PEG–SPS baths, the carbon contents were very low, which indicates that the additives in these baths were not incorporated in the deposits. The results of carbon microanalysis suggest that the incorporation of additives suppressed grain growth. The results also indicate that the

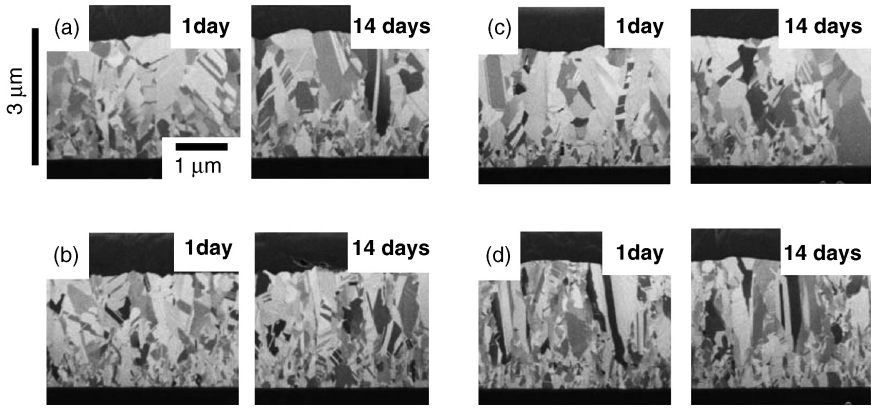

FIGURE 13.10 FIB-SIM images showing changes with time at room temperature in cross-sectional microstucture of Cu deposits obtained from different baths: (*a*) Cl^-; (*b*) SPS; (*c*) Cl–SPS; (*d*) PEG–SPS.

TABLE 13.1 Carbon Content in Cu Electrodeposits

Cu Deposits	Carbon Content (wt %)
Additive free	Not detected
Cl–PEG	0.046
Cl–PEG–SPS	0.003
Cl–PEG–SPS–JGB	0.016
Cl	0.002
SPS	0.003
Cl–SPS	0.002
PEG–SPS	0.003

strain originating from trapped additives is not an important factor to induce self-annealing.

Self-annealing occurs in Cu deposits obtained from the bath containing Cl^-, PEG, and SPS in combination: the Cl–PEG–SPS and Cl–PEG–SPS–JGB baths. The grain size of the deposits before self-annealing was very small. The large grain boundary energy associated with the small grains is considered to be a cause of self-annealing. The addition of JGB to the Cl–PEG–SPS bath was found to inhibit self-annealing. Furthermore, it was found that the behavior of self-annealing strongly depended on the concentration of SPS used in the bath. Significant self-annealing occurred in the deposits from the bath containing an appropriate amount of SPS, while it was suppressed completely with an excess SPS.

13.2.2 Copper Trench Filling by Electroless Deposition

Before the electrodeposition process can produce superfilling, some critical issues, such as the need for the deposition of a uniform seed layer of sputtered Cu and the problem of uneven current distribution on the wafer, still need to be addressed.

The filling of trenches and via holes by electroless Cu deposition is expected to be an effective alternative for dealing with these issues, because electroless deposition is, in principle, capable of forming a uniform thin film on large substrates with superior step coverage. Furthermore, electroless deposition is advantageous because it does not require a Cu seed layer. It already has been demonstrated that superfilling can be realized in an electroless Cu plating bath containing small amounts of those additives that are used in the electrodeposition bath. Various researchers have reported that they have achieved superfilling by using SPS as an inhibiting additive [72–74] or by using baths containing SPS, although the SPS accelerated Cu deposition at very low concentrations [75, 76].

In this section, we introduce the Cu filling process by electroless deposition using an electroless plating bath containing $0.04\,mol\,L^{-1}$ $CuSO_4$, $0.08\,mol\,L^{-1}$ glyoxylic acid, $0.08\,mol\,L^{-1}$ tetrasodium ethylenediamine tetraacetic acid, and a very small amount of PEG with an average molecular weight of 4000 as an inhibiting additive [77]. The bath was operated at 70°C without forced agitation.

Figure 13.11*a* shows the evolution with time of the trench filling with the bath containing 1 ppm of PEG. It is clear in the figure that deposition was very slow at trench openings, while it was much faster at trench bottoms. To estimate the difference between the deposition rate at the trench opening ($T_{opening}$) and that at the trench bottom (T_{bottom}), the thickness of the Cu deposit at both places was measured from the cross sections shown in Figure 13.11*a*, and the results were plotted against deposition time, as shown in Figure 13.11*b*. It is interesting to note that the thickness of Cu in the area of the trench openings remained almost constant during the period of trench filling (0.5–5 min), while that at the bottoms increased significantly with time. The deposition rates at the bottoms, estimated from Figure 13.11*b*, were more than $10\,\mu m\,h^{-1}$ during the filling process (0.5–1 min). After the trenches were filled with Cu (5–10 min), the thickness at the openings began to increase. In this period, the rate of the increase in film thickness at the openings was essentially identical to that at the bottom; both rates were approximately equal to $1\,\mu m\,h^{-1}$. These results clearly show that a significant bottom-up growth occurred in this bath at the early stages of the deposition. This filling behavior clearly is a demonstration of superfilling by electroless deposition. It is particularly interesting to note that the difference in the deposition behavior at the bottom and at the opening of the trenches is assumed to be caused by the difference in the concentration of PEG at these different places.

13.3 ELECTROLESS PROCESS FOR ULSI INTERCONNECT FABRICATION PROCESS

13.3.1 Background

In this section, we introduce a new process of fabricating a diffusion barrier layer by the electrochemical deposition technique.

We already have developed a new, low-cost process of fabricating both the diffusion barrier layer and the Cu wiring by an "all-wet process" (see Figure 13.12), in which an electroless NiB layer formed on an organosilane layer of APTES (3-aminopropyltriethoxy silane) serves as an effective barrier layer when its thickness is greater than 20 nm [78–82] at a thickness less than 20 nm, the NiB layer was found to become porous and discontinuous. Since, the ongoing miniaturization of ULSI devices, requires a process that can produce a barrier layer that is both thin and uniform, we had to find a substitute for APTES. In the present work we replaced APTES with a different organosilane compound of TAS (3-[2-(2-aminoethylamino)ethylamino] propylmethoxysilane), which produced a uniform and highly efficient electroless NiB barrier layer as thin as 6 nm. There is a larger number of amino groups in the TAS molecule than in the

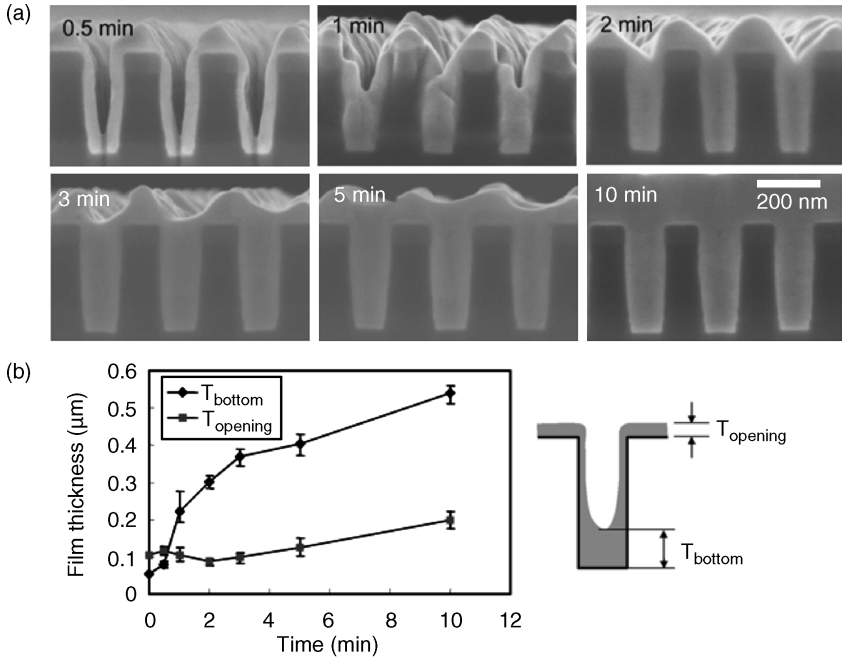

FIGURE 13.11 Different perspectives of Cu deposits in a trench-patterned substrate. (*a*) SEM images showing changes with time in cross-sectional characteristics of Cu deposited in trenches from a PEG bath. Concentration of PEG was 1 ppm. (*b*) Changes with time of the thickness of Cu deposits at bottom (T_{bottom}) and opening ($T_{opening}$) of trenches.Data were obtained from an analysis of the SEM images shown in (*a*).

APTES molecule, which allows the formation of a higher density of immobilized catalytic Pd atoms, which in turn results in the formation of a thinner and also more uniform and continuous NiB layer. This updated version of our all-wet process is highly significant for advancing the further miniaturization of ULSI devices.

13.3.2 Surface Modification of Insulator

The thicknesses of the organosilane layers were measured by ellipsometry to be 1.0 nm for APTES and 2.2 nm for TAS. These values approximately agree with the theoretical lengths of corresponding organosilane molecules, 0.6 nm for APTES and 1.6 nm for TAS, indicating that both molecules formed either a full- or sub-monolayer. The chemical constituents of the modified surfaces of the insulator were characterized by X-ray photoelectron spectroscopy (XPS). Figure 13.13 shows nitrogen (1s) peaks of the XPS spectra of the modified surfaces. The spectrum of the APTES-modified surface consists of two components, one at 398.7 eV and the other at 400.5 eV, which can be assigned to $–NH_2$ and $–NH_3$, respectively [83, 84]. The spectrum of the TAS-modified surface consists of three components, at 398.9, 399.9, and 400.9 eV, which can be assigned to $–NH_2$, –NH–C–C–NH–, and NH^{3+}, respectively.

Wafer surfaces, both before and after modification with the organic molecules, were observed by tapping-mode atomic force microscopy (AFM) (scan size: 500 nm × 500 nm, *z*-range: 5 nm). Radium values of the surfaces were 0.13 nm (SiO_2), 0.13 nm (APTES), and 0.11 nm (TAS). The modified surfaces are seen to be flat and homogeneous. It was ascertained by these AFM observations that both organosilane molecules formed uniformly. Furthermore, it was found that similar organosilane layers were formed on

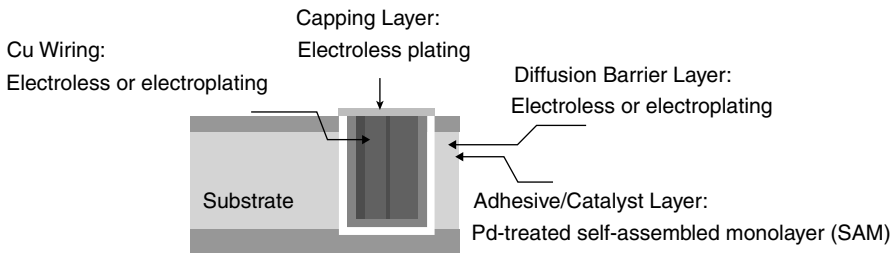

FIGURE 13.12 Illustration of our proposed wet fabrication process for ULSI interconnections.

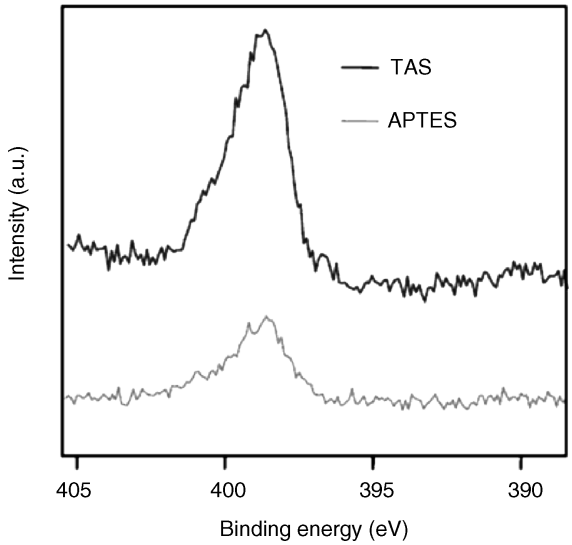

FIGURE 13.13 XPS spectra for nitrogen (1s) peaks recorded with TAS- and APTES- modified surfaces.

SiOC, which is a material known to have a low dielectric constant (low k) [85].

Conditions of the catalyst strongly affect properties of the electroless deposit produced, because the initial reaction of electroless deposition occurs on the catalyst surface. Figures 13.14*a* and *b* show plan-view transmission electron microscopy (TEM) bright-field images of Pd catalyst immobilized on the TAS- and APTES-treated surfaces. The specimens were treated with a solution containing DMAB to reduce the Pd ions before observation by TEM. The lattice parameters of the dark spots in the TEM images correspond to the face-centered-cubic (fcc) structure of Pd. The average diameter of the Pd particles that formed on the TAS layer was 2.5 nm, while on the APTES layer the average diameter was 4 nm. Figures 13.14*a* and *b* show that the Pd catalyst particles are similar in size on the two modified surfaces but that they are more uniformly distributed on the TAS-modified surface than on the APTES-modified surface. Chemical properties of the modified surfaces after Pd catalyzation were characterized by XPS. The spectra of both the APTES- and TAS-modified surfaces consist of two components, one at 335.6 eV and the other at 334.9 eV, which are assigned to PdO and Pd^0, respectively. These results show that the Pd catalyst particles that formed on both the APTES- and TAS-modified layers were composed of PdO and Pd^0. The amount of Pd catalyst, calculated from the area of the XPS spectrum, was approximately 6 times larger on the TAS surface than on the APTES surface. Also, the TEM images show that a higher density of Pd catalyst particles was formed on the TAS-modified surface than on the APTES-modified surface. The reason for this is that the TAS layer strongly immobilizes Pd ions, because each Pd ion becomes coordinated with three amino groups in an individual TAS molecule, and also because Pd ions easily adsorb electrostatically on the TAS-modified surface.

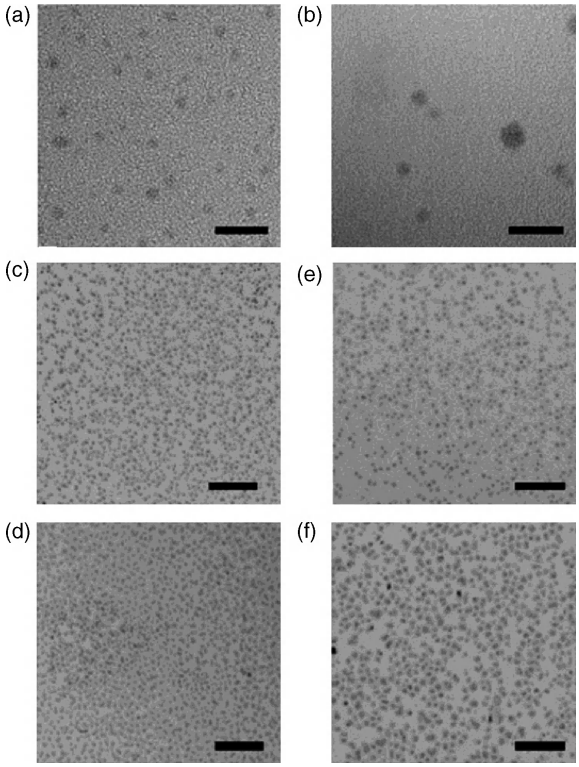

FIGURE 13.14 High-resolution plan-view TEM images: (*a*) Pd catalyst immobilized on TAS-modified surface; (*b*) Pd catalyst immobilized on APTES-modified surface; (*c*, *d*) NiB deposits produced on TAS-modified surface; (*e*, *f*) NiB deposits produced on APTES-modified surface. Specimens for TEM images in (*c*) and (*e*) were immersed in NiB solution for 5 s while those for (*d*) and (*f*) were immersed for 10 s. Scale bars: (*a*, *b*)10 nm, (*c*–*f*) 50 nm.

13.3.3 Electroless Deposition of Ni Alloys on Insulator

Initial stages of the electroless deposition of NiB were studied on two different surfaces: one modified with TAS and the other modified with APTES. The two specimens were immersed into an electroless NiB bath for either 5 or 10 s. The NiB deposits were formed on the Pd catalyst in the first 5 s, and they grew larger during the next 5 s. Figures 13.14*c*–*f* show plan-view TEM bright-field images of NiB deposits produced on those surfaces. Finer NiB nuclei were formed uniformly on the TAS-modified surface than on the APTES-modified surface. The initial electroless deposition was strongly affected by the conditions of the catalyzed surface, such as the number density of Pd particles. A higher Ni nucleation density, which enables the formation of thinner continuous layer, was evident on the TAS-modified surface.

Figure 13.15*a* shows a cross-sectional TEM image of the electroless NiB barrier layer with a thickness of 6 nm that was deposited on a TAS-modified, trench-patterned substrate. The width and the aspect ratio of the trench were 100 nm and 2.5, respectively. It is clear from the image that a thin and uniform electroless NiB layer formed on the trench-patterned

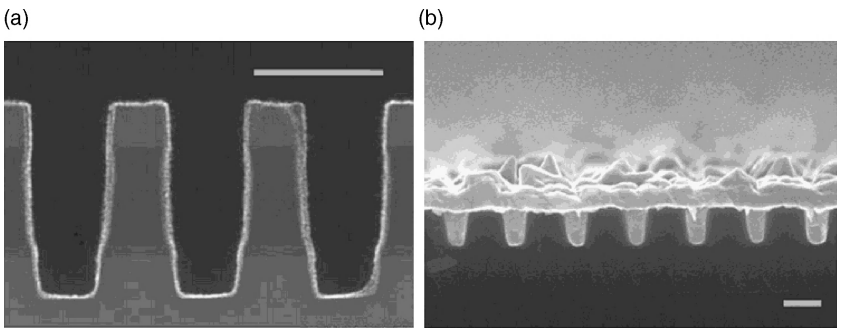

FIGURE 13.15 Cross-sectional SEM images of metal films formed by electroless deposition on trench walls: (*a*) electroless NiB barrier layer deposited on TAS-modified, trench-patterned substrate; (*b*) electroless Cu film deposited on electroless NiB barrier layer. Scale bar: 200 nm.

substrate. In terms of step coverage and uniformity of film thickness, the electroless NiB layer was superior to the layers deposited by sputtering.

13.3.4 Properties of Deposits on Insulator

Adhesion tests were performed for the NiB layer by following the specifications of JIS8504 and using Scotch tape (3M Corp.) [86, 87]. The layers showed a good adhesion property even after annealing at 400°C for 30 min. The thermal stability of the barrier property against Cu diffusion was evaluated by measuring the change in sheet resistance at various annealing temperatures. An increase in sheet resistance was assumed to indicate that Cu diffused into the barrier layer and/or the substrate. The sheet resistance of a specimen with a 6-nm-thick NiB barrier layer formed on TAS as well as that of a 20-nm-thick NiB layer formed on APTES remained nearly constant up to 400°C for 30 min. This result shows that the electroless NiB layer effectively prevented Cu atoms from diffusing into the substrate. In addition, after 400°C annealing, the effectiveness of the 6-nm-thick NiB layer formed on TAS as a barrier layer was identical to that of the 20-nm-thick NiB formed on APTES. Figure 13.15*b* shows that the electroless Cu deposited [88] on the electroless NiB barrier layer filled the trenches completely without voids or seams. In one of our previous studies [79], Cu was filled on an electroless barrier layer by an electrodeposition method. Thus, overall we have demonstrated that the NiB barrier layer can be used in combination with either the electroless or the electrodeposition Cu process.

It has been demonstrated that the electroless NiB layer formed on a TAS-modified dielectric surface in our updated all-wet process of fabricating ULSI interconnections is superior in barrier properties to that formed on an APTES-modified surface. The uniform and nonporous NiB layer can be much thinner on the TAS-modified surface than it can be on APTES-modified surface. The other advantage of using TAS instead of APTES as the olganosilane layer is that TAS provides a more uniform distribution of Pd catalyst particles on which to deposit the electroless NiB layer.

13.4 SUMMARY

Electrochemical metal deposition techniques are essential in several research fields and industrial applications. We reviewed our recent developments on electrochemical deposition technique applications to ULSI interconnection fabrication process. In short, our all-wet process, which contains both the Cu filling and the barrier layer deposition, is highly significant for advancing the further miniaturization of ULSI devices. It is believed that the electrochemical deposition process will become an essential part of electronic device fabrication process.

13.5 ACKNOWLEDGMENT

The authors wish to thank Professor Robert DiGiovanni for his many useful recommendations.

REFERENCES

1. M. Hepher, *J. Photo. Sci.*, **12**, 181 (1964).
2. J. S. Kilby, *IEEE Trans. Electron Devices*, **ED-23**, 648 (1976).
3. R. N. Noyce, U.S. Patent 2,981,877 (1961).
4. R. M. Dennard, U.S. Patent 3,387,286 (1968).
5. R. E. Kerwin, D. L. Klen, and J. C. Sarace, U.S. Patent 3,475,234 (1969).
6. R. Rung, H. Momose, and Y. Nagakubo, *Tech. Dig. IEEE Int. Electron Devices Meet.*, 237 (1982).
7. J. Bardeen and W. H. Brattain, *Phys. Rev.*, **71**, 230 (1948).
8. W. Shockley, *Bell Syst. Tech. J.*, **28**, 435 (1949).
9. J. J. Ebers, *Proc. IRE*, **40**, 1361 (1952).
10. H. Kroemer, *Proc. IRE*, **45**, 1535 (1957).
11. C. Y. Chang and S. M. Sze, in *ULSI Technology*, C. Y. Lin and W. Y. Lee, Eds., McGraw-Hill, New York, 1996.
12. *The International Technology Roadmap for Semiconductor*, Semiconductor Ind. Assoc., San Jose, CA, 1999.
13. F. Masuoka, *Proc. Int. Electron Devices Mater. Symp.*, 83 (1996).

14. M. Eizwnberg, *J. Vac. Sci. Technol.*, **A13**, 590 (1995).
15. T. Harada, *Conf. Proc. ULSI XIV*, Materials Research Soc., 1999, p. 329.
16. T. Ohba, M. Shirasaki, N. Misawa, T. Suzuki, T. Hara, and Y. Furumura, *VLSI Multilevel Interconnection Conference, Proc. Seventh Int. IEEE*, **12**, 226 (1990).
17. T. Homma, *Mater. Sci. Eng.*, **23**, 243 (1998).
18. J. Paraszczak, *Tech. Dig. IEEE Int. Electron Devices Meet.*, 261 (1993).
19. P. C. Andricacos, C. Uzoh, J. O. Dukovic, J. Horkans, and H. Deligianni, *IBM J. Res. Devel.*, **42**, 567 (1998).
20. P. C. Andricacos, *Interface*, **8**, 32 (1999).
21. S. M. Sze, in *Dielectric and Polysilicon Film Deposition*, A. C. Adams, Ed., McGraw-Hill, New York, 1983.
22. K. Eujino, *J. Electrochem. Soc.*, **138**, 3019 (1991).
23. S. M. Sze, *Semiconductor Devices: Physical and Technology*, 2nd ed., N. IIzuka, Ed., Sangyo-Tosho Co., Tokyo, 2004.
24. S. M. Sze, in *VSLI Technology*, D. A. McGillis, Ed., McGraw-Hill, New York, 1983.
25. N. G. Einspruch, in *VLSI Electronics*, Vol. 1, M. C. King, Ed., Academic, New York, 1981.
26. L. F. Thompson and C. G. Willson, in *Lithography and Dry Etching*, J. A. Mucha and D. W. Hess, Eds., American Chemical Society, Washington, DC, 1984.
27. N. J. Bae, K. I. Na, H. I. Cho, K. Y. Park, S. E. Boo, J. H. Ba, and J. H. Lee, *J. Appl. Phys. Jpn.*, **45**, 12, 9072 (2006).
28. J. J. Kelly and A. C. West, *Electrochem. Solid-State Lett.*, **2**, 561 (1999).
29. T. P. Moffat, J. E. Bonevich, W. H. Huber, A. Stanishevsky, D. R. Kelly, G. R. Stafford, and D. Josell, *J. Electrochem. Soc.*, **147**, 4524 (2000).
30. L. M. Cook, *Semicond. Int.*, **11**, 141 (1995).
31. Z. Wang, O. Yaegashi, H. Sakaue, T. Takahagi, and S. Shingubara, *J. Electrochem. Soc.*, **151**, 12, C781 (2004).
32. Z. Wang, T. Ida, H. Sakaue, S. Shingubara, and T. Takahagi, *Electrochem. Solid-State Lett.*, **6**, 3, C38 (2003).
33. C. K. Hu, B. Luther, F. B. Kaufman, J. Hummel, C. Uzoh, and D. J. Pearson, *Thin Solid Films*, **262**, 84 (1995).
34. Y. Shacham-Diamand and S. Lopatin, *Microelectron. Eng.*, **37/38**, 77 (1997).
35. Y. Shacham-Diamand and S. Lopatin, *Electrochim. Acta*, **44**, 3639 (1999).
36. Y. Shacham-Diamand and Y. Sverdlow, *Microelectron. Eng.*, **50**, 525 (2000).
37. E. J. O'Sullivan, A. G. Schrott, M. Paunovic, C. J. Sambucetti, J. R. Marino, P. J. Bailey, S. Kaja, and K. W. Semkow, *IBM J. Res. Devel.*, **42**, 607 (1998).
38. S. Soukane S. Sen, T. Cale, and S. Feature, *J. Electrochem. Soc.*, **149**, C74 (2002).
39. J. Reid, *Jpn. J. Appl. Phys. PART 1*, **40**, 2650 (2001).
40. J. J. Kelly and A. C. West, *Electrochem. Solid-State Lett.*, **2**, 561 (1999).
41. L. Mirkova, S. Rashkov, and C. Nanev, *Surf. Tech.*, **15**, 181 (1982).
42. M. Yokoi, S. Konishi, and T. Hayashi, *Denki Kagaku*, **52**, 218 (1984).
43. J. J. Kelly and A. C. West, *J. Electrochem. Soc.*, **145**, 3472 (1998).
44. J. J. Kelly and A. C. West, *J. Electrochem. Soc.*, **145**, 3477 (1998).
45. D. Stoychev and C. Tsvetanov, *J. Appl. Electrochem.*, **26**, 741 (1996).
46. T. P. Moffat, D. Wheeler, and D. Josell, *J. Electrochem. Soc.*, **151**, C262 (2004).
47. J. P. Healy, D. Pletcher, and M. Goodenough, *J. Electroanal. Chem.*, **338**, 155 (1992).
48. M. Hasegawa, Y. Negishi, T. Nakanishi, and T. Osaka, *J. Electrochem. Soc.*, **152**, C221 (2005).
49. M. Kang, M. Gross, and A. A. Gewirth, *J. Electrochem. Soc.*, **150**, C292 (2003).
50. T. P. Moffat, D. Wheeler, M. D. Edelstein, and D. Josell, *IBM J. Res. Dev.*, **49**, 19 (2005).
51. P. M. Vereecken, R. A. Binstead, H. Deligianni, and P. C. Andricacos, *IBM J. Res. Dev.*, **49**, 3 (2005).
52. S. Miura, F. Oyamada, Y. Takada, and H. Honma, *Electrochemistry*, **69**, 773 (2001).
53. P. Taephaisitphongse, Y. Cao, and A. C. West, *J. Electrochem. Soc.*, **148**, C492 (2001).
54. H. Lee, S. S. Wong, and S. D. Lopatin, *J. Appl. Phys.*, **93**, 3796 (2003).
55. S. H. Brongersma, E. Kerr, I. Vervoort, A. Saerens, and K. Maex, *J. Mater. Res.*, **17**, 582 (2002).
56. M. Hasegawa and Y. Hirai, *J. Appl. Phys.*, **90**, 2792 (2001).
57. C. Lingk and M. E. Gross, *J. Appl. Phys.*, **84**, 5547 (1998).
58. Q. T. Jiang, M. E. Gross, G. Bersuker, B. Foran, R. Mikkola, B. Carpenter, and J. Oemando, *Mat. Res. Soc. Symp. Proc.*, **564**, 429 (1999).
59. S. Lagrange, S. H. Brongersma, M. Judelewicz, A. Saerens, I. Vervoort, E. Richard, R. Palmans, and K. Maex, *Microelectron. Eng.*, **50**, 449 (2000).
60. S. H. Brongersma, E. Richard, I. Vervoort, H. Bender, W. Vandervorst, S. Lagrange, G. Beyer, and K. Maex, *J. Appl. Phys.*, **86**, 3642 (1999).
61. C. H. Lee and C. O. Park, *Jpn. J. Appl. Phys. 1 Reg. Pap. Short Notes*, **42**, 4484 (2003).
62. M. Stangl, J. Acker, V. Dittel, W. Gruner, V. Hoffmann, and K. Wetzig, *Microelectron. Eng.*, **82**, 189 (2005).
63. K. Ueno, T. Ritzdorf, and S. Grace, *J. Appl. Phys.*, **86**, 4930 (1999).
64. H. Lee, W. D. Nix, and S. S. Wong, *J. Vac. Sci. Technol. B*, **22**, 2369 (2004).
65. V. A. Vas'ko, I. Tabakovic, S. C. Riemer, and M. T. Kief, *Microelectron. Eng.*, **75**, 71 (2004).
66. V. A. Vas'ko, I. Tabakovic, and S. C. Riemer, *Electrochem. Solid-State Lett.*, **6**, C100 (2003).
67. H. Fischer, *Electrochim. Acta*, **2**, 50 (1960).
68. R. Winand, P. VanHam, R. Colin, and D. Milojevic, *J. Electrochem. Soc.*, **144**, 428 (1997).

69. R. Winand, *Hydrometallurgy*, **29**, 567 (1992).
70. C. V. Thompson, *Annu. Rev. Mat. Sci.*, **30**, 159 (2000).
71. T. Haba, T. Itabashi, H. Akahoshi, A. Sano, K. Kobayashi, and H. Miyazaki, *Mater. Trans.*, **43**, 1593 (2002).
72. S. Shingubara, Z. Wang, O. Yaegashi, R. Obata, H. Sakaue, and T. Takahagi, *Electrochem. Solid-State Lett.*, **7**, C78 (2004).
73. Z. Wang, O. Yaegashi, H. Sakaue, T. Takahagi, and S. Shingubara, *J. Electrochem. Soc.*, **151**, C781 (2004).
74. Z. Wang, O. Yaegashi, H. Sakaue, T. Takahagi, and S. Shingubara, *Jpn. J. Appl. Phys.*, **43**, 7000 (2004).
75. C. H. Lee, S. C. Lee, and J. J. Kim, *Electrochim. Acta*, **50**, 3563 (2005).
76. C. H. Lee, S. C. Lee, and J. J. Kim, *Electrochem. Solid-State Lett.*, **8** (C110), 30 (2005).
77. M. Hasegawa, N. Yamachika, Y. Schanham-Diamand, Y. Okinaka, and T. Osaka, *J. Appl. Phys. Lett.*, **90**, 101916 (2007).
78. M. Yoshino, Y. Nonaka, J. Sasano, I. Matsuda, Y. Shacham-Diamand, and T. Osaka, *Electrochim. Acta*, **51**, 916 (2005).
79. T. Osaka and M. Yoshino, *Electrochim. Acta*, **53**, 271 (2007).
80. M. Yoshino, T. Masuda, T. Yokoshima, J. Sasano, Y. Shacham-Diamand, I. Matsuda, T. Osaka, A. Hashimoto, Y. Hagiwara, and I. Isao, *J. Electrochem. Soc.*, **154**, D122 (2007).
81. J. Uhm and H. Jeon, *Jpn. J. Appl. Phys.*, **40**, 4657 (2001).
82. H. Kim, C. Detavenier, O. van der Straten, S. M. Rossnagel, and A. J. Robust Kellock, *J. Appl. Phys.*, **98**, 014308 (2005).
83. F. Zhang and M. P. Srinivasan, *Langmuir*, **20**, 2309 (2004).
84. D. Kowalczyk, S. Slomkowski, M. M. Chehimi, and M. Delamar, *Int. J. Adhesion Adhs.*, **16**, 227 (1993).
85. K. Maex, M. R. Baklanow, D. Shamiyan, and F. Lacopi, *J. Appl. Phys.*, **93**, 8793 (2003).
86. H. Wada, K. Takahashi, and T. Nishizaka, *J. Mater. Sci. Lett.*, **9**, 810 (1990).
87. T. Fujita, S. Nakamichi, S. Ioku, K. Maenaka, K. Maenaka, and Y. Takayama, *Sens. Actuators A*, **135**, 50 (2007).
88. M. Hasegawa, N. Yamachika, Y. Okinaka, Y. Shacham-Diamand, and T. Osaka, *Electrochemistry*, **75**, 349 (2007).

14

ELECTRODEPOSITION OF SEMICONDUCTORS

T. E. Schlesinger, Krishnan Rajeshwar, and Norma R. de Tacconi

14.1 INTRODUCTION

The electrodeposition of semiconductors has been investigated in detail and demonstrated by a large number of workers over many years. This effort is primarily motivated by the fact that electrodeposition is a relatively simple and inexpensive deposition technology that may be scaled up easily. In general, the films deposited by this method do not possess the crystalline perfection or low levels of electrically active impurities of single-crystal epitaxial films deposited by techniques such as molecular beam epitaxy or chemical vapor deposition. Nonetheless, in applications where large areas of semiconductors are required, such as photovoltaic power generation or corrosion protection as opposed to integrated circuit fabrication, the low cost and comparatively low material demands make this deposition technology attractive in terms of ultimate commercialization. In addition, for application in solar cells electrodeposition allows one to easily alter both the bandgap and lattice constant by composition modulation through the control of growth parameters such as applied potential, pH, and temperature of the bath. Thus, it is at least in principle possible to easily grow large areas of tandem cells designed for the most efficient conversion of the solar spectrum.

Typical arrangements for electrolytic cells as well as the fundamental electrochemistry and thermodynamics associated with the deposition process are discussed in detail by Paunovic and Schlesinger [1]. Since a large number of semiconductors have been electrodeposited with varying degrees of success, this chapter will focus on the historical development of what has been accomplished in the area of the deposition of semiconductor layers. An attempt is made to indicate the state of the art in each instance. Short summaries as well as the particulars of some of the methods used and an extensive list of references to the literature are provided.

14.2 SILICON (Si)

The electrodeposition of silicon must employ a nonaqeous medium because of its very large reduction potential and the high reactivity of most of its compounds to water. A great deal of effort has been reported on the electrodeposition of silicon. Many workers have employed either silica or fluorosilicates as the solutes [2–7] and obtained either amorphous silicon or metal silicides. Cohen and Huggins [8] were the first to prepare both mono and polycrystalline silicon by electrolysis of the alkaline fluorosilicates in a LiF–KF eutectic. A review of the deposition of continuous films of silicon from LiF–KF–NaF–K_2SiF_6 melts is provided by Elwell and Rao [9]. Deposition of silicon also includes attempts to deposit silicon electrochemically from silicates at temperatures above its melting point [10] and the work of Monnier [11] on melts containing silicon dioxide. Some effort has also been focused on the deposition of silicon powders, for example, the work of Andriiko and co-workers [12], as there are applications where a source of pure Silicon powder is required. Agrawal and Austin [13] deposited amorphous silicon from nonaqueous baths using $SiHCl_3$ as the silicon source in a bath of 1.0 *M* $SiHCl_3$ in propylene carbonate containing 0.1 *M* tetrabutyl ammonium chloride as the supporting electrolyte. Deposits were made potentiostatically at −2.5 V versus a platinum reference electrode with a vitreous carbon counter electrode at temperatures of 35–145°C and on a variety of materials as substrates including Pt, Ti, Si, and others. With increasing solute concentration and increasing temperature thicker deposits were

Modern Electroplating, Fifth Edition Edited by Mordechay Schlesinger and Milan Paunovic

obtained. Postdeposition anneals at 470°C drove off bonded hydrogen in these films. These amorphous silicon layers were developed as a possible inexpensive material for solar cell applications. Takeda and co-workers [14] deposited amorphous silicon on a nickel substrate by the electrolysis of a solution of tetraethylorthosilicate in acetic acid. Lee and Kröger [15] deposited amorphous silicon containing fluorine and carbon (and doped with boron or phosphorus) cathodically from solutions of K_2SiF_6 in acetone with HF. Boen and Bouteillon [16] deposited silicon using alkali fluorosilicates as the solute and succeeded in depositing layers of up to 1 mm thickness on silver electrodes and on graphite using a pulsed-current technique. These films were polycrystalline with preferred orientations $\langle 111\rangle$, $\langle 311\rangle$, and $\langle 220\rangle$.

Gobet and Tannenberger [17] investigated the electroplating of silicon from solutions of $SiHCl_3$, $SiCl_4$, $SiBr_4$, $Si(Ch_2CH_3)_4$, $Si(OCH_2CH_3)_4$, $Si(OOCCH_3)_4$, and $Si[N(CH_3)_2]_4$ in tetrahydrofuran and $LiClO_4$ (0.3 *M*), tetrabutylammonium perchlorate (TBAP) (0.3 *M*), or tetrabutylammonium bromide(TBAB) (0.2 *M*) as supporting electrolyte. Depositions were carried out at room temperature in a three-electrode cell. Platinum was used as the counter electrode while the cathode was a polished disk of platinum, gold, or other material. The reference electrode was $Ag/AgClO_4$. Though the Si–O, Si–C, and Si–N bonds are apparently too stable to be reduced, Silicon films deposited from $SiHCl_3$ and $SiCl_4$ were smooth up to thicknesses of 0.25 and 0.12 μm, respectively. These films were amorphous as determined by *x*-ray diffraction and their thickness probably not uniform. Bulk concentrations of Si ∼ 82 at %, O ∼ 8 at %, C ∼ 8 at %, and Cl ∼ 1.5 at % were measured by sputter Auger spectroscopy and a Si: H ratio of 1 : 0.9 determined by proton scattering.

The electrolysis of alkali metal fluorosilicates has also been investigated as a method to produce pure silicon suitable for photovoltaic applications [18]. The following reduction mechanism of K_2SiF_6 in a LiF–KF eutectic mixture at 750°C has been suggested by these authors:

$$\begin{aligned} \mathrm{Si(IV)} + 2\mathrm{e} \quad &\rightarrow \quad \mathrm{Si(II)} + 2\mathrm{e} \rightarrow \mathrm{Si} \\ \mathrm{S(IV)} + \mathrm{Si} \quad &\overset{k_b}{\longleftrightarrow} \quad 2\mathrm{S(II)} \end{aligned} \tag{14.1}$$

Metal silicide formation is avoided by using a potential step as small negative as possible with pulsed currents producing the best structure of the deposit as well as the best fit between the electrolysis conditions and the proposed mechanism. Growth rates of several micrometers per hour have been achieved with a total thickness of 3 μm demonstrated. Neutron activation shows these films to contain impurities such as Fe, Cr, Mb, and alkali metals below the parts-per-million (ppm) range.

Frolenko and co-workers [19] investigated the structure of silicon films deposited with the use of mixed chloride–fluoride melts. This work showed that both polycrystalline and single-crystal silicon layers can be obtained with the substrate and temperature being key factors in determining the structure of the deposit. For this melt and process a (110) texture is typical.

Silicon is the one semiconductor material that can be grown in very high quality and in large quantities at relatively low cost by a huge industrial infrastructure. It therefore remains a significant challenge for electrodeposition to compete in terms of supplying material for most applications.

14.3 GROUPS III–V (13–15) COMPOUNDS

14.3.1 Gallium Arsenide (GaAs)

As with other semiconductor materials electrodeposition of GaAs offers the potential advantages of the ease of control of film thickness, morphology, and composition by the control of voltage and current density. The inexpensive equipment that can be used, the use of ambient temperature and pressure, and an aqueous solution reduce operating costs while at the same time eliminating the need for the use of volatile and dangerous materials such as AsH_3 and $AsCl_3$, as is often used in other growth techniques.

The electrode reactions and the corresponding potentials are [20].

$$\mathrm{Ga}^{3+} + 3\mathrm{e} \leftrightarrow \mathrm{Ga(s)}$$

$$E = E^0_{Ga} + \frac{RT}{3F}\ln\left(\frac{a_{\mathrm{Ga}^{3+}}}{a_{Ga}}\right) = -0.529 + 0.0197\log(a_{\mathrm{Ga}^{3+}})$$

$$\mathrm{HAsO}_3^{2-} + 3\mathrm{H}^+ + 3\mathrm{e} \leftrightarrow \mathrm{As(s)} + 2\mathrm{H_2O} \qquad (-1 > \mathrm{pH} > 8)$$

$$\begin{aligned} E &= E^o_{\mathrm{As}} + \frac{RT}{3F}\ln\left(\frac{a_{\mathrm{HAsO_3}}}{a_{\mathrm{As}}}\right) + \frac{RT}{F}\ln(C_{\mathrm{H}^+}) \\ &= 0.248 + 0.0197\log(a_{\mathrm{HAsO_3}}) - 0.0591\mathrm{pH} \end{aligned} \tag{14.2}$$

where E is the electrode potential with respect to the normal hydrogen electrode, T is the temperature, R is the universal gas constant, F is Faraday's constant, E^0 is the standard reduction potential, and $a_{Ga^{3+}}$, $a_{\mathrm{HAsO_3}}$ are the activities of the ions in the solution while a_{Ga}, a_{As} are the activities of the atoms in the electrodeposits.

DeMattei and co-workers [21] deposited GaAs from a molten salt containing 67.4% B_2O_3, 20.3% NaF, 4.2% Ga_2O_3, and 8.1% $NaAsO_2$ by weight at 720–760°C. Deposition at 300°C from $GaCl_3$–KCl melt has also been reported [22], and it was shown that under potentiostatic conditions only As was formed while GaAs was formed in this work under galvanostatic conditions. Room temperature deposition of GaAs using $AlCl_3$–1-butylpyridinium chloride or $AlCl_3$–1-methyl-3-ethylimidazolium chloride has also been reported [23]. A room temperature melt of $GaCl_3$ and 1-methyl-3-ethylimidazolium cholride and an $AsCl_3$ solute has also been used [24, 25]. Electrodeposition from aqueous

solutions of $Ga_2(SO_4)_3$, As_2O_3, and H_2SO_4 has been reported [26] and Murali and co-workers [27] electrodeposited gallium on copper foil from sodium galate solution and arsenic from arsenite solution followed by an anneal at 250–530°C.

Gallium arsenide has been deposited from both alkaline and acid aqueous electrolytes by Yang et al [28]. In this last work, a typical three-electrode setup was used using a titanium rod as the working electrode, a platinum counter electrode, and one of three reference electrodes: Ag/AgCl in saturated KCl [0.197 V vs. a normal hydrogen electrode (NHE)], Hg/HgO in 0.1 *M* NaOH (0.157 vs. NHE), or saturated calomel (0.241 V vs. NHE). The acidic electrolyte employed was 1 *M* As_2O_3 solution in concentrated HCl in deionized water with reagent-grade amoniumhydroxide or KOH solution used to adjust pH to less than 3. The alkaline electrolyte employed was As_2O_3 in Ga_2O_3 solution with the pH adjusted by the addition of KOH solution to greater than 12. For films deposited in alkaline solutions the composition depended greatly on the potential with more negative potentials resulting in more Ga-rich deposits. For potentials between −1.65 and −1.73 V (vs. Hg/HgO) the deposit was about 64% Ga. Room temperature resulted in constant composition of the deposit with higher temperatures resulting in nonuniform deposits. The substrate also had a major effect on the deposition with Ti being the preferred substrate for its low reactivity with Ga and its high hydrogen overpotential. The as-depostied film was amorphous and was therefore annealed in nitrogen atmosphere at 300°C for 12 h. X-ray diffraction analysis did reveal peaks associated with GaAs after anneal. In acidic solutions, pH 2.5–3.0, the Ga content was found to be about 65% for potentials between −1.5 and −1.6 V (vs. Ag/AgCl) and 50% Ga could be obtained at lower pH, 0.7, with higher current density (350 mA/cm^2) or very negative potentials. An anneal at 260°C for 8 h resulted in films that did display GaAs peaks in X-ray diffraction spectra. Auger electron spectroscopy indicated that the films were about 3200 Å thick.

Villegas and Stickney [29] have investigated the use of electrochemical atomic layer epitaxy for the deposition of GaAs. As in the case of the deposition of CdTe this technique relies on the use of successive underpotential depositions of atomic layers of the different elements. They obtained low-coverage ordered layers of As by underpotential deposition from $HAsO_2$ and by oxidative underpotential depositions from AsH_3 solutions on (100) and (110) surfaces of Au. They also achieved Ga reductive underpotential deposition on the low-index surfaces of Au as well as ordered structures on Au (100) and (110) surfaces by the successive underpotential deposition of atomic layers of As and Ga. This technique, which is described in more detail in Section 14.4.3 on CdTe is most promising for producing high-quality films.

14.3.2 Gallium Phosphide (GaP)

Gallium phosphide has been electrodeposited at 800–900°C in a melt containing sodium metaphosphate, sodium fluoride, and gallium oxide [30].

14.3.3 Indium Compounds (InP, InAs, InSb)

The first discussion of the deposition of indium antimony alloys was made by Smart [31] and was subsequently studied by a number of workers. Sadana and Singh [32] provide a good discussion of the deposition of this alloy system up to 1985 along with a number of key references. Okubo and Landau [33] electrodeposited InSb from and aqueous solution of $InCl_3$, $SbCl_3$, citric acid ($H_3C_6H_5O_7$), and sodium citrate ($Na_3C_6H_5O_7$). Ortega and Herrero [34] investigated the deposition of InX (X = P, As, Sb) by electrodeposition. In their work they showed that both InSb and InAs can be grown by direct electroplating, that as-deposited InSb films are crystalline but that InAs layers have poor crystallinity even after anneal at 400°C, and that InP layers may be produced by phosphorization of an electroplated In layer in a phosphorous atmosphere. These latter films were shown, by X-ray diffraction, to be in the sphalerite phase and of good crystallinity. They employed, for InSb deposition, a bath of 0.3 *M* citric acid, 0.033 *M* $InCl_3$, and 0.047 *M* $SbCl_3$ at cathode potentials more positive than −0.6 V [vs. saturated calomel electrode (SCE)] for best results. For InAs they used 0.04 *M* $AsCl_3$ and 0.3 *M* citric acid.

The electrode reactions and the corresponding potentials for In and Sb given by Pourbaix [20] are

$$\mathrm{In}^{3+} + 3\mathrm{e} \leftrightarrow \mathrm{In(s)}$$

$$E = E^o_{\mathrm{In}} + \frac{RT}{3F}\ln\left(\frac{a_{\mathrm{In}^{3+}}}{a_{\mathrm{In}}}\right) = -0.342 + 0.0197\log(a_{\mathrm{In}^{3+}})$$

$$\mathrm{HSbO_2} + 3\mathrm{H}^+ + 3\mathrm{e} \leftrightarrow \mathrm{Sb(s)} + 2\mathrm{H_2O}$$

$$E = E^o_{\mathrm{Sb}} + \frac{RT}{3F}\ln\left(\frac{a_{\mathrm{HSbO_2}}}{a_{\mathrm{Sb}}}\right) + \frac{RT}{F}\ln(C_{\mathrm{H}^+}) \qquad (14.3)$$

$$= 0.23 + 0.0197\log(a_{\mathrm{HSbO_2}}) - 0.0591\mathrm{pH}$$

14.4 CHALCOGENIDE SEMICONDUCTORS

14.4.1 Indium Sulfide (In_2S_3)

Indium sulfide has been produced by the chalcogenization of electroplated metallic indium films on titanium substrates in flowing H_2S [35]. The metallic indium was plated from baths that contained 0.05 *M* $In_2(SO_4)_3$ and 0.4 *M* citric acid under potentiostatic conditions at −1.4 V/SCE with an indium

anode. Films were deposited between 3 and 5 μm in thickness. Chalcogenization was accomplished in flowing H_2S at 130°C for 3 h and then the films were heated in the same atmosphere for about 1 h at 350–400°C. X-ray diffraction spectra of these films showed that good quality β-In_2S_3 was produced.

14.4.2 Lead Sulfide (PbS)

Lead sulfide is an attractive material for a wide variety of applications, including infrared detectors and Pb ion sensors. It was deposited electrochemically by Scharifker and co-workers [36] and more recently on Ti by Takahashi and co-workers [37]. These latter workers used an aqueous solution of $Na_2S_2O_3$ (1 m*M*), $Pb(NO_3)_2$, and HNO_3 (pH 2.93) and observed a cathodic current to flow at potentials more negative than −0.2 V (vs. Ag/AgCl) with the reduction of $Na_2S_2O_3$ occurring in the presence of Pb^{2+}. They conclude that the formation of the PbS is due mainly to the following:

$$\begin{aligned} {S_2O_3}^{2-} + 2H^+ &\rightarrow (S) + SO_2 + H_2O \\ Pb^{2+} + (S) + 2e &\rightarrow PbS \end{aligned} \qquad (14.4)$$

Sharon and co-workers [38] deposited PbS in a similar manner to Takahashi et al. [37] and obtained similar results.

14.4.3 Cadmium Telluride (CdTe)

Cadmium telluride thin films are currently employed in a broad range of optoelectronic devices, including solar cells, infrared detectors, and X-ray and gamma-ray detectors [39–41]. This material is one of the more extensively studied semiconductor in terms of deposition by electrochemical means. Cadmium telluride can be deposited by pulse, potentiostatic, and galvanostatic electrodeposition techniques. The CdTe deposition details are described by Panicker and co-workers [42], Fulop and co-workers [43], Gerritsen [44], and Sella and co-workers [45]. Verbrugge and Tobbias [46] provide a good overview of the deposition details associated with this material as well as an extensive list of references. Most CdTe electrodeposition makes use of an aqueous cadmium sulfate, tellurium dioxide, and sulfuric acid electrolyte and either cathodic of anodic methods may be employed. Cathodic methods make use of the codeposition of higher valent metal and chalcogenide ions while anodic methods are based on the corrosion of the metal in a chalcogenide environement. A good review of the deposition of a number of II–VI semiconductor alloys is provided by Rajeshwar [47].

The basis for all research on cathodic electrodeposition of CdTe from aqueous solution is based on the work of Panicker and co-workers [42] in which they showed that Cd and Te can be reduced simultaneously from aqueous solution (1 *M* $CdSO_4$, 0.01–1 m*M* TeO_2, pH 2.5–3.0 adjusted with H_2SO_4) to grow CdTe according to the overall reaction

$$Cd^{2+} + HTeO_2^+ + 3H^+ + 6e \rightarrow CdTe + 2H_2O \qquad (14.5)$$

with the following electrode reactions and corresponding potentials [20]:

$$Cd^{2+} + 2e \leftrightarrow Cd(s)$$

$$E = E^o_{Cd} + \frac{RT}{2F}\ln\left(\frac{a_{Cd^{2+}}}{a_{Cd}}\right) = -0.403 + 0.0295\log(a_{Cd^{2+}})$$

$$Te^{2-} - 2e \leftrightarrow Te(s) \qquad (pH > 11)$$

$$E = E^o_{Te} + \frac{RT}{2F}\ln\left(\frac{a_{Te^{2-}}}{a_{Te}}\right) = -0.94 + 0.0295\log(a_{Te^{2-}})$$

$$Te^{4+} + 4e \leftrightarrow Te(s) \qquad (pH < -0.5) \qquad (14.6)$$

$$E = E^o_{Te} + \frac{RT}{4F}\ln\left(\frac{a_{Te^{4+}}}{a_{Te}}\right) = 0.568 + 0.0148\log(a_{Te^{4+}})$$

$$HTeO_2^+ + 3H^+ + 4e \leftrightarrow Te(s) + 2H_2O \qquad (0 < pH < 5)$$

$$E = E^o_{Te} + \frac{RT}{4F}\ln\left(\frac{a_{HTeO_2^+}}{a_{Te}}\right) + \frac{3RT}{4F}\ln(C_{H^+})$$

$$= 0.551 + 0.0148\log(a_{HTeO_2^+}) - 0.443pH$$

Cadmium telluride deposition occurs at a more positive potential than for Cd alone because of the negative free energy of formation of CdTe of $-92\,kJ\,mol^{-1}$.

It is the choice of Cd and Te concentrations and the deposition potential which permits the growth of near-stoichiometric CdTe. At the same time the substrate plays a crucial role in determining the quality of the grown film in terms of adhesion, crystallinity, and the like. Cadmium telluride has been electrodeposited on Ti and Nesatron glass substrates and characterized using X-ray diffraction, scanning electron microscopy, energy dispersive X-ray analysis, and optical transmission measurements [48]. These workers used a slightly modified bath compared to that used by Panicker and co-workers [42] where they speciated the TeO_2 with NaOH (pH 9–10) and then brought the solution into the acidic range. This approach allows for higher TeO_2 concentrations in the bath for growth of *p*-type films. Stoichiometric CdTe with strong preferred orientation has been grown on tin oxide–coated glass [49], CdS-covered tin oxide–coated glass [50, 51], GaAs [52], Si [53], and other semiconductors [54]. Indium- and copper-doped CdTe has been prepared by potentiostatic co-electrodeposition [42, 54].

Energy-dispersive analysis of X rays (EDAX) and X ray diffraction (XRD) measurements indicate that CdTe films deposited by pulse techniques have reduced porosity and improved conductivity [55]. The best quality films were

produced when the deposition took place at frequencies of 40–100 Hz. In these films a more intense ⟨111⟩ XRD peak is observed in films produced by galvanostatic or potentiostatic methods, implying more preferentially oriented films; however, in all films Te and Cd reflections are observed. In addition EDAX indicates that these films are also more stoichiometric [56]. Guo and Deng [57] deposited CdTe on nickel substrates, and those films deposited at a potential more positive than that for Cd electrodeposition were *p*-type while those deposited at a more negative potential were *n*-type. The use of a nonaqeous bath [58, 59] of anhydrous ethylene glycol 1 *M* $CdCl_2$, 0.01 *M* $TeCl_4$, and 0.33 *M* KI at 160°C for CdTe deposition has been explored. The aim was to eliminate hydrogen discharge, which can cause pinholes, and to allow for use of Te sources with reasonably high solubilities. KI was used to improve adhesion and to hinder ion complexation. Surimoto and Peter [60] investigated the effects of illumination on the electrodeposition process of CdTe. These workers used a standard three-electrode cell with a platinum secondary electrode, saturated calomel reference electrode, and a silicon substrate, from a solution containing 2 m*M* dm^{-3} TeO_2, 0.5 mol dm^{-3} $CdSO_4$, 0.5 mol dm^{-3} H_2SO_4, and 0.5 mol dm^{-3} NH_4F (pH 0.5), at a potential of −0.65 V, and with HeNe laser illumination to excite photocurrents during the CdTe deposition. These workers observed a dramatic effect in the growth morphology due to illumination with the nonilluminated areas being featureless while the illuminated areas were much rougher with features associated with elemental Te observed by energy dispersive X-ray spectroscopy. These workers conclude that, while the illumination intensities they use are quite high, some attention should nonetheless be paid to illumination conditions during film deposition.

Kampmann and co-workers [51] suggest the following mechanism for the electrodeposition of CdTe where surface sites "s" are involved:

$$\begin{aligned} HTeO_2^+ + s + 3H^+ + 4e &\rightarrow Te, s + 2H_2O \\ Te, s + Cd^{2+} + 2e &\rightarrow CdTe + s \end{aligned} \qquad (14.7)$$

They point out that if the second reaction above is not fast enough the Te on the surface site can be incorporated as a Te interstitial and that for applied potentials more negative than the cadmium deposition potential (−0.4 V vs. SHE) elemental Cd is deposited.

Cadmium telluride has also been deposited on Si using the method of continuous cycling of the potential [61]. This work used a solution of 0.1 *M* $CdSO_4$, 2×10^{-4} *M* TeO_2, and 0.5 *M* K_2SO_4 adjusted to a pH of 1.5 ± 0.2 by the addition of H_2SO_4. A conventional three-electrode setup was employed with a saturated (KCl) calomel reference electrode and a platinum gauze as a secondary electrode. The deposition was accomplished by setting the potential at −0.2 V (to minimize the formation of a Te layer) and cycling between this value and −0.66 V. By carrying out the deposition in the dark the formation of the Te layer is virtually eliminated. These films were annealed in an inert atmosphere at 400°C for 15 min, but some evidence of crystallinity was found in the as-grown CdTe layer. Each cycle contributes about 50–60 Å to the thickness. Meulenkamp and Peter [62] provide a good discussion of the kinetics of the electrodeposition of CdTe. In their work they used solutions of TeO_2, $CdSO_4$, and Na_2SO_4 at 85°C or at room temperature. A standard three-electrode configuration was used with a Pt or Cd counter electrode. The reference electrode was Cd wire immersed in 1.0 mol dm^{-3} $CdSO_4$ or Ag/AgCl. They conclude that at metallic substrates at which the current is diffusion limited poor-quality material is obtained. At substrates at which the current is or can be kinetically limited (including glassy carbon and silicon) poor-quality material is also obtained. At other semiconductor substrates at which the current is kinetically limited good-quality material is obtained.

Cadmium telluride has been deposited on indium tin oxide–coated glass plates from an acidic aqueous bath of sulfuric acid containing 0.2 *M* $CdSO_4$ and 1 m*M* $HTeO_2^+$ [63]. In this work the counter electrode, reference electrode, and substrate were a platinum sheet, saturated calomel electrode, and indium tin oxide (ITO)–coated glass, respectively. A potential between −0.35 and −0.64 V was found to be best for the deposition of CdTe. Films deposited at an electrolyte bath temperature of 18°C were not crystalline, but higher deposition temperatures (80°C) resulted in XRD spectra showing peaks corresponding to cubic CdTe. Higher current densities resulted in films with a rough surface and which could be easily removed mechanically from the substrate while films deposited at a lower current density were smooth and adhered well to the substrate.

The goal of achieving epitaxial films with long-range order is extremely important for many devices to be fabricated using these semiconductor layers. A technique has been demonstrated for the deposition of CdTe via electrochemical atomic-layer epitaxy (ECALE) [64–66]. This technique relies on the alternate deposition of the constitutent elements by electrochemical reduction or oxidation in the liquid phase to form the semiconductor compound. Surface-limited electrochemical reactions, also referred to as underpotential depositions, are exploited to produce single monolayers of the desired material in sequence. These workers have used this technique to deposit CdTe, CdSe, and CdS. The apparatus and details of this system are described in Gregory and Stickney [64], Huang et al. [67], and Colletti et al. [66]. For the deposition of CdTe, 0.5 *M* Na_2SO_4 was used, while perchlorate (0.5 *M* $NaClO_4$) was used for both CdS and CdSe depositions in water. A 0.5 m*M* $HTeO_2^+$ solution was prepared with TeO_2 and 10 m*M* borate buffer (pH 9.2). A 5.0 m*M* $HSeO_3^-$ solution was prepared with SeO_2 and 5 m*M* acetic acid (pH 4.5) and an S^{2-} solution was made with 1 m*M*

$Na_2S.9H_20$ (pH 10.5). Substrates were silicon coated with Au (with a thin intervening layer of Ti or Cr). This technique also allows for the decomposition of the deposition process into a series of individual steps with each step being independently optimized. Huang and co-workers [67] showed that thick films of CdTe (beyond 10 monolayers) can be deposited with this technique; however, they stated that film morphology suffers above 100 cycles. This technology relies on a thorough understanding of the fundamental mechanisms for the deposition of the constituent elements in atomic monolayers, and this was investigated by this group [68–70] and useful experimental data are provided in these references. This has also been investigated in detail for Te by Hayden and Nandhakumar [71], who investigated the structure of well-ordered Te layers by scanning tunneling microscopy through the deposition cycle and for Cd by Niece and Gewirth [72]. Smooth films of CdTe semiconductors have been deposited with predominantly (111) orientation, although these films appear to contain more particulates or crystallites as film thickness is increased. More recently Villegas and Napolitano [73] demonstrated a computer-controlled continuous-flow systems for electrochemical atomic-layer epitaxy for CdTe. Depositon rates of $30\,\text{nm}\,\text{h}^{-1}$ have been demonstrated with good uniformity and composition and with CdTe ordered at the 10–100-nm range with preferred (111) orientation. The development of ECALE may be particularly important for the realization of films of the quality required for more demanding applications.

14.4.4 Cadmium Selenide (CdSe)

In both single-crystal and thin-film forms CdSe has been investigated for its application in solar cells, photoconductors, thin-film transistors, and gamma-ray detectors. The growth of this material via electrodeposition would benefit the production of low-cost large-area devices such as solar cells. There is a fair amount of experience in the electrodeposition of CdSe films [74, 75]. These films have been deposited on Ti and Ni from an aqueous solution of HCl, $CdCl_2$, and SeO_2 [76]. The CdSe thin films have been electrodeposited for some time from selenosulfate solutions [77] and a Cd/Se ratio close to 1 was demonstrated [78]. The CdSe films electrodeposited on titanium substrates were characterized using a number of techniques, including photoluminescence, Raman scattering, and XRD [79].

While a number of competing reactions are discussed in the literature, the deposition of CdSe proceeds via the net reaction [80]

$$H_2SeO_3 + Cd^{2+} + 6e + 4H^+ \rightarrow CdSe + 3H_2O \qquad (14.8)$$

This competes with reactions producing excess Se, such as that suggested by [81, 82]:

$$\begin{aligned} H_2SeO_3 + 6H^+ + 6e &\rightarrow H_2Se + 3H_2O \\ 2H_2Se + H_2SeO_3 &\rightarrow 3Se + 3H_2O \end{aligned} \qquad (14.9)$$

Skyllas-Kazacos and Miller [82] suggested a process to avoid the reaction of H_2SeO_3 and H_2Se by the reduction of $SeSO_3^{2-}$. Using 5 m*M* Na_2SeSO_3 solutions were prepared by introducing 0.1 *M* Na_2SO_3 in 1 *M* NH_3/N H_4^+ buffer until the Se dissolved. At a pH 10 one has

$$Se + HSO_3^- \leftrightarrow SeSO_3^{2-} + H^+ \qquad (14.10)$$

The $SeSO_3^{2-}$ and SO_3^{2-} ions do not oxidize Se^{2-} and thus Se contamination of the CdSe is not expected.

To avoid the deposition of excess Se, a sequential monolayer electrodeposition process has been employed [83]. In this work sequential layers of CdSe are deposited by sweeping the potential of Ti or Ni substrates continuously between −0.4 and −0.8 V (vs. SCE). A conventional three-electrode setup was used using a Pt counter electrode, Ti or Ni working electrode, and saturated calomel reference electrode. A typical plating solution contained 0.1 *M* $CdCl_2$, 0.5 *M* HCl, and 0.3 m*M* SeO_2 or 0.3 *M* $CdSO_4$, 0.25 *M* H_2SO_4, and 0.3 m*M* SeO_2. At a scan rate of $10\,\text{Vs}^{-1}$ a submonolayer of CdSe (and far less Se) is deposited in the time it takes to reach the deposition potential for bulk Cd. During the anodic half of the scan excess Cd is stripped back off leaving behind a small amount of CdSe. This process is then repeated. Films produced in this manner were shiny in appearance and adhered well to the Ni but were easily removed from the Ti substrates (though on unpolished Ti the films adhered better). The films were stoichiometric as determined by electron microprobe analysis. These films were annealed at 650°C after which the XRD spectrum contained sharp lines consistent with the hexagonal wurzite structure of CdSe, as had been previously observed in conventionally (potentiostatic or galvanostatic) electrodeposited CdSe [79, 84]. Gutierrez and Ortega [85] studied the corrosion properties of electrodeposited CdSe and found that the selenium layer obtained by photoetching on polycrystalline *n*-CdSe prevents photocorrosion.

Murali and co-workers [86] and Subramanian and co-workers [87] used a pulsed deposition technique to obtain CdSe at room temperature on SiO_2 and Ti substrates using a bath of 0.5 *M* $CdSO_4$ and 0.1 *M* SeO_2. Wyands and Cocivera [88] electrodeposited doped CdSe films and showed that it could be doped via diffusion of Se, Cd, or In during the postdeposition anneal. The Se, Cd, or In was prepared as a layer on the indium tin oxide substrate prior to deposition. The CdSe was deposited from an aqueous solution containing 0.0211 *M* $CdCl_2$, 0.03 *M* trisodium nitrilotriacetic acid, 0.0368 *M* Na_2SeSO_3, and 0.54 *M* Na_2SO_3. Typical conditions used by these workers included a deposition for 40 min (1 μm film thickness) at a potential of −1.0 V (vs. a saturated calomel electrode) followed by an anneal at 500°C in a

nitrogen atmosphere. In these studies carrier concentrations ranged from 10^{19} to $10^{9}\,cm^{-3}$ with mobilites from 1 to $50\,cm^2\,Vs^{-1}$.

Golan et al. [89] showed that it is possible to obtain epitaxial films of CdSe onto gold films from a nonaqueous electrolyte. Epitaxial CdSe films have been electrodeposited onto (111) InP substrates with the CdSe films being nearly stoichiometric [90]. In this latter work, the CdSe was cathodically deposited in a three-electrode cell from an acidic solution containing $0.2\,M$ $CdSO_4$ to which various amounts of selenious acid (0.125–5 mM [Se]) were added. The pH was adjusted to 2.2 and the temperature maintained at 85°C. The CdSe layer was 30–250 nm thick and the ideal conditions for epitaxial growth ([Se] = 0.5 mM and deposition potential equal to the beginning of the diffusion plateau region of the *IV* curve −0.95 V vs. SSE—saturated sulfate electrode) were determined from a systematic reflection high-energy electron diffraction (RHEED) study. Pole figures showed six peaks rather than three corresponding to the (220) reflections, indicating that the films were twinned and their full width at half maximum (FWHM) was 4°. Transmission electron microscopy (TEM) images of the CdSe/InP interface revealed the presence of planar defects but the interface was nonetheless quite good and good epitaxy was achieved in spite of the large (3.6%) lattice mismatch between CdSe and InP.

14.4.5 Zinc Chalcogenides [Zinc Selenide (ZnSe) and Zinc Telluride (ZnTe)]

Zinc selenide has been studied because of its potential for use in a number of semiconductor devices and as a window material for solar cells since it has a bandgap of 2.7 eV. Pramanik and Biswas [91] investigated the deposition of ZnSe including Tl-doped ZnSe in a chemical bath. Singh and Rai [92–94] deposited polycrystalline ZnSe films from solutions containing selenium dioxide and zinc sulfate and using limiting currents. Mishra and Rajeshwar [80] investigated the deposition of CdX and ZnX (X = Se or Te) and some of their results have been discussed in this chapter in the context of the deposition of some of these other materials. In the case of ZnTe and ZnSe they employed a standard three-electrode cell with a platinum counter electrode and a Ag/AgCl/1.0 M KCl reference electrode. For ZnSe the supporting electrolyte was $0.5\,M$ H_2SO_4 with 2 mM H_2SeO_3 and 10 mM $ZnSO_4$. A cathodic wave observed at −0.8 V was assigned by these workers to

$$Zn^{2+} + H_2SeO_3 + 4H^+ + 6e \rightarrow ZnSe + 3H_2O \quad (14.11)$$

For ZnTe the conditions employed were the same but the electrolyte contained 1 mM $HTeO_2$ and 1 mM $ZnSO_4$. The primary contribution of this work was to elucidate the unifying features of the CdSe, CdTe, ZnSe, and ZnTe deposition mechanisms. Natarajan and co-workers [95] deposited ZnSe from an aqueous bath using a potentiostatic method and concluded that to get a Zn/Se ratio close to 1 the bath should contain a higher concentration of Zn^{2+} and a low concentration of H_2SeO_3. They employed a bath containing $<0.2\,M$ $ZnSO_4$ and 0.1–3 mM H_2SeO_3 at a pH of 2–2.5 and at a temperature of 65°C. Stainless steel was the preferred substrate. A potential between −0.6 and −1.0 V was used and under these conditions the XRD spectra reveals peaks associated exclusively with cubic ZnSe. A number of unwanted side reactions can compete with that of Eq. (14.11). At sufficiently negative potentials H_2Se formed via Eq. (14.12) can react with zinc ions leading to the precipitation of ZnSe but H_2Se may also react with selenous acid to form elemental Se:

$$\begin{aligned} Se + 2e + 2H^+ &\rightarrow H_2Se(aq) \\ Zn^{2+} + H_2Se &\rightarrow ZnSe + 2H^+ \\ 2H_2Se + H_2SeO_3 &\rightarrow 3Se + 3H_2O \end{aligned} \quad (14.12)$$

This latter reaction can lead to additional Se precipitates in the film and reduction of the Zn/Se ratio.

14.4.6 Mixed Zinc–Cadmium Compounds

Zinc Cadmium Selenide ($Zn_{1-x}Cd_xSe$) $Zn_{1-x}Cd_xSe$ (ZCS) is a potential alternative to CdS as a window material for solar cells. Cubic ZCS has been deposited from an acidic solution containing H_2SeO_3 as Se precursor, and it was observed that excess Cd and Se incorporation into the film was unavoidable even with very low concentrations of their precursors in the bath [95]. An acidic plating bath was used in this work consisting of $0.2\,M$ $ZnSO_4$ and 1.2 mM H_2SeO_3 with various $CdSO_4$ concentrations and the pH adjusted using $0.1\,M$ sulfuric acid. The bath temperature was maintained at 65–70°C. Here the reaction proceeds according to

$$\begin{aligned} H_2SeO_3 + 4H^+ + 4e &\rightarrow Se + 3H_2O \\ (1-x)Zn^{2+} + xCd^{2+} + Se + 2e &\rightarrow Zn_{1-x}Cd_xSe \end{aligned} \quad (14.13)$$

ZCS has also been deposited from alkaline solutions by the electrodeposition of CdSe from aqueous solutions containing seleno sulfite ions as a selenium precursor [96]. Natarajan et al. [95] have also demonstrated the electrodeposition of ZCS from basic aqueous selenosulfite solutions on stainless steel and titanium substrates. In this process the reduction of Cd selenocomplex leads to CdSe nucleation followed by Se^{2-} formation from the reduction of $SeSO_3^{2-}$, and its subsequent reaction with metal ions results in the metal selenide formation. These authors used a cyclic photovoltametry process (cyclic voltametry under chopped illumination) and concluded that CdSe semiconductor formation begins at a

potential of −1.1 V vs. SCE via

$$Cd^{2+} + xSeSO_3^{2-} \leftrightarrow Cd(SeSO_3)_x^{2-2x}(aq) \qquad (14.14)$$

The Cd–selenosulfite complex is then reduced either directly to CdSe or to Cd:

$$\begin{aligned} Cd(SeSO_3)_x^{2-2x} + 2e &\rightarrow CdSe + (x-1)SeSO_3^{2-} + SO_3^{2-} \\ Cd(SeSO_3)_x^{2-2x} + 2e &\rightarrow Cd + xSeSO_3^{2-} \end{aligned} \qquad (14.15)$$

The Cd thus formed may react to form CdSe:

$$Cd + SeSO_3^{2-} \rightarrow CdSe + SO_3^{2-} \qquad (14.16)$$

At this potential the cubic phase was dominant while the hexagonal phase increased with an increase in the cathodic deposition potential and was predominant over the cubic phase at −1.4 V. The as-deposited films were amorphous and became polycrystalline after 30 min sintering at 600°C.

A second reduction peak at −1.25 V was attributed to the formation of Se^{2-} via

$$SeSO_3^{2-} + 2e \rightarrow Se^{2-} + SO_3^{2-} \qquad (14.17)$$

This will also lead to the formation of CdSe via

$$Cd^{2+} + Se^{2-} \rightarrow CdSe \qquad (14.18)$$

Here Zn^{2+} also forms a complex with $SeSO_3^{2-}$ and undergoes a reduction at −1.35 V leading to the formation of Zn with a very thin film of ZnSe via

$$\begin{aligned} Zn(SeSO_3^{2-})_x^{2-2x} + 2e &\rightarrow Zn + SeSO_3^{2-} \\ Zn + SeSO_3^{2-} &\rightarrow ZnSe + SO_3^{2-} \end{aligned} \qquad (14.19)$$

However, Zn reacts very weakly with $SeSO_3^{2-}$ and therefore the Zn is not converted efficiently to ZnSe. In the case of ZCS the initial reaction is the reduction of the Cd-seleno complex with the subsequent formation of Se^{2-} leading to the formation of ZCS via

$$Se^{2-} + xCd^{2+} + (1-x)Zn^{2+} \rightarrow Zn_{(1-x)}Cd_xSe \qquad (14.20)$$

CdS_xSe_{1-x} and $Zn_xCd_{1-x}S$ have also been electrodeposited [97]. These films were deposited onto ITO glass substrates in dimethylsulfoxide electrolyte solution. For CdS, these workers used $CdCl_2$ (0.055 *M*) and saturated sulfur (0.19 M): for CdS_xSe_{1-x} they used $CdCl_2$ (0.055 *M*) and saturated selenium (0.01 *M*) with varying concentration of sulfur between 0.05 and 0.19 *M*; and for $Zn_xCd_{1-x}S$, they used saturated sulfur (0.019 *M*), $CdCl_2$, and $ZnCl_2$, where the concentration of $ZnCl_2$ + $CdCl_2$ remained 0.055 *M* and the [Zn]/[Cd] ratio in the solution varied between around 10/1 and 1/10. The deposition was carried out at 120°C, and the resulting films had a hexagonal structure with the *c* axis predominantly perpendicular to the substrate. These workers were also able to determine that the films had a direct bandgap and that their dark resistivities were higher than that of pure CdS and increased with increasing Zn or Se concentration.

Cadmium Zinc Telluride ($Cd_{1-x}Zn_xTe$) A two-stage process has been employed for the deposition of $Cd_{1-x}Zn_xTe$ in a manner similar to that employed for CdTe, $CuInSe_2$, and ZnTe. In this process thin layers of Cd, Zn, and Te are sequentially deposited and then annealed in a furnace under a controlled atmosphere [98]. Tellurium was carried out in this work in an acidic solution containing $HTeO_2^+$ (TeO_2 dissolved into a 1 *M* H_2SO_4 solution) as follows:

$$HTeO_2^+ + 3H^+ + 4e \rightarrow Te + 2H_2O \qquad (14.21)$$

Cadmium was electrodeposited using acidic $CdSO_4$ electrolytes, but the authors of this work [98] do not give details of the the Zn baths employed. Anneals at 550°C for 1 h of films 0.6–1.0 μm thick resulted in $Cd_{1-x}Zn_xTe$ alloys, as seen by XRD spectra.

14.4.7 Cadmium Sulfide (CdS)

Cadmium sulfide is widely used in solar cells in a CdS/Cu_2S heterojunction cell. A concise review of CdS solar cells, their history, and some of the methods used for the deposition of this material and the fabrication of junctions for this application is given by Hill [99]. If deposited on ITO it also has potential for use as a window material and for light meters. Cadmium sulfide has been formed from the anodization of the metal in alkaline sulfide solution [100] and in buffered sulfide solution [101, 102]. It has been deposited cathodically from a solution containing cadmium and thiosulfate ions [103, 104]. Lowering the pH by the addition of dilute H_2SO_4 was shown to cause the decomposition of the $S_2O_3^{2-}$ to form colloidal sulfur and improve the deposition by elimination of the anodic stripping peak in the cyclic voltammogram compared to that observed with thiosulfate at its natural pH of 6.7. The overall electrode reaction is

$$Cd^{2+} + S_2O_3^{2-} + 2e \leftrightarrow CdS + SO_3^{2-} \qquad (14.22)$$

The CdS films have been deposited on Pt, Mo, and Al with the best results reported on Al. The electrode material has a significant influence on the formation of the CdS films in terms of both thickness and stoichiometry, although all films tend to contain sulfur-rich regions as well as regions of cadmium-rich CdS. Pulsed electrodeposition has also been used to deposit CdS from solutions of cadmium chloride and sodium thiosulfate at 90°C [105] on glass/ITO substrates. Good results were obtained and the details of this

method are reported in this reference. While pulsed electrodeposition has been demonstrated by these workers, it does not appear from the literature that is is the preferred electrodeposition method. Edamura and Muto [97] deposited Cu-doped CdS onto ITO galvanostatically at a current density of 1.4 mA cm^{-2} using dimethylsulfoxide solutions at 120°C containing $CdCl_2$ (0.055 *M*), elemental sulfur (0.19 *M*), and $CuCl_2$ (up to 1 m*M*). These workers obtained films of hexagonal crystallites with preferred *c*-axis orientation and with decreasing grain size as Cu content increased. Increasing the Cu content also caused the films to become porous and to adhere poorly to the substrate. Dennison [106] used both potentiostatic and galvanostatic techniques to deposit CdS and to study the reasons for the degradation in performance of the CdS electrodeposition process and to determine the mechanism of CdS formation. They suggested that along with Eq. (14.22) a second overall reaction should be considered, namely

$$2Cd^{2+} + S_2O_3{}^{2-} + 6H^+ + 8e \rightarrow 2CdS + 3H_2O \quad (14.23)$$

Das and Morris [107] prepared CdS/CdTe solar cells by periodic pulse electrodeposition. For CdS deposition they employed a bath of 0.2 *M* Cd^{2+} (from $CdCl_2$) and 0.01 *M* $Se_2O_3{}^{2-}$ from sodium thiosulfate at a pH of 2 by adding HCl. For CdTe deposition they employed a bath of 2.5 *M* Cd^{2+} from cadmium sulfate, $HTeO_2^+$ introduced from a spectroscopic-grade tellurium rod in a solution of pH 2 using H_2SO_4. The deposited layers were annealed at 400°C and XRD spectra showed good CdS and CdTe peaks. The final solar cell efficiency was 10% indicating good-quality layers and junctions. Demir and Shannon [108–110] investigated the deposition of CdS on Au via underpotential deposition and found that hexagonal CdS is preferred on both the (111) and (100) low-index planes of Au. Shirai and co-workers [111] showed that Raman scattering could be used to characterize the quality of electrodeposited CdS films and Boone and Shannon [112] employed resonance Raman and photoluminescence to characterize ultrathin films of CdS deposited via ECALE. They conclude, based on their work and on scanning probe microscopy, that layer-by-layer growth is the growth mechanism in operation in ECALE, and they suggest that this growth technique may be particularly useful for the growth of samples needed for a variety of materials investigations. For films deposited using a bath similar to that of Fatas and co-workers [103], they observed an longitudinal optical (LO) phonon Raman peak whose FWHM decreased from 18.2 cm^{-1} for as-deposited films to 12.7 cm^{-1} for films annealed at 500°C, though this is still larger than the 6.5 cm^{-1} expected for single-crystal CdS. It was suggested that Raman scattering might be useful as an in situ method for monitoring film quality during deposition.

Cadmium sulfide has also been deposited on ITO-coated glass using the potentiostatic method [113]. In this work an aqueous solution of 0.2 *M* $CdCl_2 \cdot 2H_2O$ and 0.01 *M* $Na_2S_2O_3$ adjusted to a pH in the range of 2–3 using HCl was used with a bath temperature of 90°C. For pH > 3 the solution produced precipitates of cadmium hydroxide and, for pH < 2, CdS precipitates were produced. Cadmium sulfide was deposited via a codeposition process obeying the overall reaction of Eq. (14.23). Between −0.5 and −0.6 V versus SCE the resulting films were yellow in color, indicating stoichiometric CdS. Films were annealed at 350°C in a hydrogen atmosphere for 30 min. For more negative potentials the films became Cd rich and then essentially metallic. Bath temperature was also found to affect growth significantly with increasing bath temperature resulting in higher growth rates and smoothness and adhesion of the films enhanced. X-ray diffraction analysis of these films showed reflections associated with the hexagonal wurzite α-CdS phase. Cadmium sulfide has also been deposited from a nonaqueous bath using 0.5 *M* $Na_2S_2O_3$, 0.05 *M* $CdSO_4$, 0.1 *M* EDTA (ethylenediaminetetraacetic acid tetrasodium salt) in ethylene glycol on stainless steel, titanium, and ITO-coated glass [114]. Good-quality CdS was obtained with a graphite anode at 90°C and a pH of 8. Polycrystalline CdS was obtained as determined by XRD and no postdeposition anneal was employed by these workers.

Goto and co-workers [114] used a bath of 2 m*M* $CdSO_4$ and 100 m*M* $Na_2S_2O_3$ at a pH of 2.5 adjusted with H_2SO_4 to deposit CdS films. They studied the effect of the annealing atmosphere (O_2, air, or N_2) using photoluminescence spectroscopy. Annealing in nitrogen resulted in an increasing concentration of native defects as the anneal temperature was raised, while annealing in oxygen resulted in little native defect formation with the oxygen expected to fill any sulfur vacancies formed since it is isoelectronic to S. Annealing in air was similar to annealing in oxygen; however, the photoluminescence linewidths were broader, indicating poorer quality material.

Other materials have also been electrodeposited though information on these is not as extensive as some of the other materials covered so far. Among these is SnS [115, 116].

14.4.8 Copper Sulfide (Cu_2S)

The formation of junctions suitable for use as solar cells can be accomplished by replacing the Cd ions of CdS by two cuprous ions. This usually involves the substitution

$$CdS + 2CuCl_2^- \rightarrow Cu_2S + CdCl_3^- + Cl^- \quad (14.24)$$

by dipping cadmium sulfide into a solution of cuprous chloride. A variant of the above suggested by Nakayama [117] is a cathodic reduction of cupric ions in solution:

$$2Cu^{2+} + 2e + CdS \rightarrow Cu_2S + Cd^{2+} \quad (14.25)$$

But this reaction is disturbed by the deposition of Cu and the formation of cupric sulfide according to

$$Cu^{2+} + CdS \rightarrow Cd^{2+} + CuS \qquad (14.26)$$

Vedel and co-workers [118, 119] improved on this electrolytic method by using 0.1 *M* sodium acetate, 1 m*M* cupric perchlorate, and 0.7 m*M* triethylenetetramine. They minimized Eq. (14.26) by use of the triethylenetetramine masking agent, which reacts with Cu(II) and Cd(II). Al-Dhafiri and coworkers [120] showed that the phase of the Cu_xS layers formed on CdS by dipping in a solution containing Cu ions can be controlled by applying a potential to the CdS substrate and that the most efficient photovoltaic cells made using this technique were produced when the CdS was biased in a narrow range between 0.01 and 0.02 V. It has been suggested that the applied bias affects the exchange of the Cd^{2+} and Cu^{+} ions involved in the formation of the Cu_xS by causing the formation of a Cd-rich layer at the Cu_xS/CdS interface and preventing the diffusion of Cu^{+} ions deeper into the CdS [120–122]. In their earlier work Al-Dhafiri and coworkers [121] suggested that both substrate and postdeposition anneal play an important role in determining the stability of the CdS–Cu_2S photovoltaic devices as well.

14.4.9 Indium Selenide (In_2Se_3)

Indium selenide forms a pseudobinary system with Cu_2Se with the formula $(Cu_2Se)_{1-x}(In_2Se_3)_x$ which for $x = 0.5$ becomes $CuInSe_2$. The In_2Se_3 has been electrodeposited by alternate deposition of selenium and indium from separate baths onto titanium substrates and thermal annealing [123]. The titanium was pretreated with concentrated HNO_3–HCl (1 : 1) and NaOH 10% by weight in water. The selenium was deposited potentiostatically from an aqueous bath of 1 m*M* SeO_2, 0.25 *M* citric acid, and 0.15 *M* sodium citrate at a pH of 4 with a plating potential of −0.8 V/SCE at 80°C. Indium was electrodeposited from 1 m*M* $InCl_3$, 0.8 % of ethanolamine, and 0.4% of NH_3 with a pH of 2 by the addition of HCl at −1.1 V/SCE. After deposition of In/Se in the ratio 2 : 3 anneals were carried out under Ar at 150–600°C. Films annealed at 500°C displayed XRD spectra with the best β-hexagonal crystalline structure. Anneals at 600°C resulted in δ-In_2Se_3.

14.4.10 Copper Indium Diselenide ($CuInSe_2$)

Copper indium diselenide electrodeposition techniques can be divided into two categories: those in which the metals are delivered separately from the Se and those where the Se is incorporated with the metals during material deposition. An example of the first method includes the work of Dongcheng and co-workers [124] in which the authors electroplated Cu and In onto Mo- or Ti-coated glass substrates followed by high-temperature anneal in H_2S at 400°C. Electrodeposition within the second category has been demonstrated by a number of workers [92, 125–129]. Bhattacharya [125] used an SeO_2-based bath containing $InCl_3$ and $CuCl_2$ complexed by triethanolamine and ammonia. The deposits obtained were amorphous and an anneal was required to improve the crystallinity. Noufi and co-workers [130] and Hodes and Cahen [131] attempted plating Cu–In–Se from aqueous electrolytes containing SeO_2, $InCl_3$, and $CuCl_2$ without a complexing agent, but this resulted in Cu–Se deposits containing no In. Lokhande [132] employed a pulse plating technique to deposit stoichiometric $CuInSe_2$ films from an acidic bath. Ueno and co-workers [133] reported the deposition of $CuInSe_2$ from a sulfate-containing bath and no complexing agent but the films were microdendritic and required a postdeposition anneal to improve their solar conversion efficiency. Pottier and Maurin [134] pointed out that one of the difficulties associated with the direct deposition of the ternary compound is that the conditions which are favorable for the deposition of one metal differs from those necessary for the other constituent elements. For example, a difficulty arises from the very different equilibrium potentials. The electrochemical deposition reactions of the three metals are

$$Cu^{2+} + 2e \leftrightarrow Cu(s)$$

$$E = E^0_{Cu} + \frac{RT}{2F}\ln\left(\frac{a_{Cu^{2+}}}{a_{Cu}}\right) = -0.2998 + 0.0295\log(a_{Cu^{2+}})$$

$$In^{3+} + 3e \leftrightarrow In(s)$$

$$E = E^o_{In} + \frac{RT}{3F}\ln\left(\frac{a_{In^{3+}}}{a_{In}}\right) = -0.9800 + 0.0197\log(a_{In^{3+}})$$

$$HSeO_2^+ + 4H^+ + 4e + OH^- \leftrightarrow H_2SeO_3 + 4H^+ + 4e \leftrightarrow Se(s) + 3H_2O$$

$$E = E^o_{Se} + \frac{RT}{4F}\ln\left(\frac{a_{HSeO_2^+}}{a_{Se}}\right) + \frac{3RT}{4F}\ln(C_{H^+})$$

$$= 0.10 + 0.0148\log(a_{HSeO_2^+}) - 0.043pH \qquad (14.27)$$

where E is the electrode potential with respect to a SSE [Hg/$HgSO_4$,K_2SO_4 (sat)] and $a_{Cu^{2+}}$, $a_{In^{3+}}$, $a_{HSeO_2^+}$ are the activities of the ions in the solution while a_{Cu}, a_{In}, a_{Se} are the activities of the atoms in the electrodeposits. Pottier and Maurin [134] found optimal conditions for the deposition of $CuInSe_2$ by finding the potential range corresponding to a weak or negative slope of the I–*V* curve using an acidic (pH 1.5–4.5) aqueous solution of $CuSO_4$ (5–10 m*M*), $In_2(SO_4)_3$ (10–20 m*M*), SeO_2 (10 m*M*), and K_2SO_4 (60–80 m*M*) containing 0–80 m*M* sodium citrate. They suggested that the formation of smooth layers is correlated with a

slow surface process. In a somewhat similar manner Sahu et al. [135] deposited $CuInSe_2$ using a solution of $CuCl_2$ (0.37 m*M*), $InCl_3$ (5.27 m*M*), and SeO_2 (0.9 m*M*) in distilled water. This solution was chosen so as to obtain a concentration of the ions and a pH that makes the potentials of the three elements coincident. They obtained $CuInSe_2$ films; however, due to the differing nobilities of the ions, the composition was not uniform. Annealing at 350°C did improve the stoichiometry and crystallinity of the films. These authors suggested that the compound formation proceed according to

$$\begin{aligned} CuCl &\rightarrow Cu^+ + Cl^- \\ InCl_3 &\rightarrow In^{3+} + 3Cl^- \\ SeO_2 + H_2O &\rightarrow HSeO_2^+ + OH^- \end{aligned} \tag{14.28}$$

In the initial stages of the deposition either of the following reactions is possible:

$$\begin{aligned} Cu^+ + HSeO_2^+ + 3H^+ + 5e &\rightarrow CuSe + 2H_2O \\ Cu^+ + 2HSeO_2^+ + 6H^+ + 9e &\rightarrow CuSe_2 + 4H_2O \end{aligned} \tag{14.29}$$

Later, when In begins to deposit, a possible reaction is either of the following:

$$\begin{aligned} 2In^{3+} + 3HSeO_2^+ + 9H^+ + 18e &\rightarrow In_2Se_3 + 6H_2O \\ In^{3+} + HSeO_2^+ + 3H^+ + 7e &\rightarrow InSe + 2H_2O \end{aligned} \tag{14.30}$$

When the three constituents deposit together, a possible reaction is

$$Cu^+ + In^{3+} + 2HSeO_2^+ + 6H^+ + 12e \rightarrow CuInSe_2 + 4H_2O \tag{14.31}$$

Mishra and Rajeshwar [136] proposed a mechanism in which $CuInSe_2$ is formed by the reduction of nonstoichiometric cuprous selenide into copper and H_2Se which then reacts with In(III) in the solution and some nonreduced Cu_2Se to form $CuInSe_2$. Khare and co-workers [137] employed a similar electrolyte—$CuCl_2$ (3.7 m*M*), $InCl_3$ (22 m*M*), and SeO_2 (3.6 m*M*)—in water at a pH of 1.5. At a potential of −0.8 V (vs. SCE) these authors deposited films of 1.5 μm thickness with grain sizes up to 400 Å after anneal of 400°C in a nitrogen/oxygen atmosphere for 20 min. Pern and co-workers [138] conducted a similar study in which they investigated the effects of annealing conditions on the structure of $CuInSe_2$. They showed that annealing and chemical treatments can determine whether the films are copper-rich chalcopyrites or indium-rich spalerites and that the presence of oxygen during anneal is detrimental to the films in that this results in the formation of indium oxides, loss of selenium, and a large increase in film conductivity. Guillen and co-workers [139] deposited $CuInSe_2$ using a bath containing $CuSO_4.5H_20$, $In_2(SO_4)_3$, and SeO_2 in acqueous citrate solution at a pH 1.7 (adjusted using H_2SO_4 and NaOH) on titanium substrates at −0.6 V (vs. SCE). The $CuInSe_2$ was *p*-type and the chalcopyrite phase was observed by XRD with the best crystallinity obtained after 400°C anneal for 15 min. Gomez et al. [140] reported similar results. Kumar and co-workers [141] investigated the use of a rapid thermal annealing technique to prepare $CuInSe_2$ films from stacked Cu–In/Se layers. In this work the Cu–In film was prepared in a nonaqueous bath and the Se was deposited by thermal evaporation with the rapid thermal anneal taking place in the vacuum deposition system at temperatures of 300–500°C with the best results in terms of crystallinity and stoichiometry obtained at 400°C. Thouin and co-workers [142] studied the deposition of copper indium diselenide in the presence of excess In(III) and showed that the presence of the In(III) in the solution favors the reduction of Se(IV) to Se(II) via the formation of $CuInSe_2$. Edamura and Muto [143] employed a pulse plating technique to deposit $CuInSe_2$ on ITO substrates. They used and aqueous solution of 2 m*M* SeO_2, 2 m*M* $CuSO_4$, and 20 m*M* $InCl_3$ at a pH of 1.5 at room temperature using an ITO–glass substrate as the working electrode, platinum counter electrode, and saturated calomel reference electrode. When annealed above 300°C in air for 1 h these films displayed a chalcopyrite structure *n*-type conductivity with a direct bandgap of 0.99 eV. These films were smooth and uniform in appearance and had a compact columnar structure when viewed in cross section.

More recently Fernandez and co-workers [129] demonstrated co-electrodeposition of the three elements and a layer-by-layer electrodeposition process of the precursor materials In_2Se_3 and Cu_2Se using both the potensiostatic technique and a conventional three-electrode cell on Mo substrates. For codeposition they used different chemical baths with bath temperature maintained at 22°C and an applied potential −0.5 V versus SCE. For In, a plating bath of 50 m*M* $InCl_3$ with pH 1.5 adjusted with 10% HCl and an applied voltage of −1.0 V versus SCE was used. In the layer-by-layer case the precursor materials were deposited using two different chemical baths: 25 m*M* $InCl_3$ with 25 m*M* H_2SeO_3 and 25 m*M* $Cu(SO_4)_2$ with 25 m*M* H_2SeO_3. These workers found that the Cu/In ratio can be adjusted in the codeposition case by controlling the $InCl_3$ concentration. In the co-electrodeposited case they observed that a 500-Å Cu layer on the Mo substrate reacts with the In–Se layer to form an indium-rich layer upon which another Cu–Se layer can be electrodeposited. After an anneal in Ar at 500°C for 10 min the major phase observed via XRD is the tetragonal $CuInSe_2$. If the In–Se layer on the Cu/Mo substrate is annealed at 450°C in Ar and then the Cu–Se layer is electrodeposited and annealed again in Ar at 500°C for 10 min, stoichiometric $CuInSe_2$ is

obtained. The layer-by-layer method results in device quality films more easily than co-electrodeposited films. However, the morphology of the co-electrodeposited films appears better with more dense grains of larger size. A good discussion of both multistep and single-step processes for the deposition of $CuInSe_2$ is given by Vedel [144].

14.4.11 Mercury Cadmium Telluride ($Hg_{1-x}Cd_xTe$)

Mercury cadmium telluride (MCT) is well established as an important material for infrared detectors and imagers and in solar cells where multilayer tandem cells are fabricated for optimal performance. Basol and co-workers [145] deposited MCT in a CdS/MCT thin-film solar cell.

MCT has also been deposited onto ITO-coated glass [146]. A bath is maintained at 95°C in a three-compartment cell with a Cd metal counter electrode and a Ag/AgCl reference electrode. A constant potential of −0.99 V was applied to maintain a current density between 30 and $-50\,\mu A\,cm^{-2}$. The electrolyte contained 98.9 mM tri-*n*-butylphosphine telluride, 0.7 m*M* HgI_2 and 7.1 m*M* $Cd(ClO_4)_2$ in propylene carbonate. Ethylenediamine (7.8 m*M*) was used to complex the Hg^{2+} and Cd^{2+} and prevent the precipitation of tellurium induced by these ions. As-deposited films were quite smooth and were annealed for 1 h at 200°C in an argon atmosphere or for 20 min at 300°C in air with the latter resulting in larger grain sizes: 220 versus 75 Å. Temperatures above these resulted in significant Hg loss from the films. In this study also the Hg–Te ratio in the deposited films depended linearly on the ratio of Hg^{2+} and Cd^{2+} in the electrolyte. The bath temperature and potential affected the composition with the [Hg] varying from 0.14 to 0.07 when the temperature was varied from 80 to 94°C (with a potential of −1.08 V) or the voltage was varied from −1.08 to −0.98 V (with the temperature at 94°C). A direct optical bandgap was observed.

MCT has also been electrodeposited using a standard three-electrode cell [147]. A saturated calomel electrode was used as a reference electrode with a large platinum sheet as the counter electrode and the working electrode was titanium or SnO_2 glass. Films were grown at a constant potential in an aqueous solution of 0.5 *M* $CdSO_4$, 1 m*M* TeO_2 and concentrations of $HgCl_2$ from 0.05 to 0.2 m*M*. The pH was adjusted to 1.6 with H_2SO_4 and the temperature maintained at 90°C for titanium substrates and 70°C for SnO_2. Current densities observed were between 2 and $4\,mA\,cm^{-2}$ for the titanium substrate and 0.2–0.4 $mA\,cm^{-2}$ for the SnO_2. Adhesion was observed to be better for the titanium. Films of 1 μm thickness were produced and the mercury content controlled by either fixing the potential (−0.65 V) but using different values of $[Hg^{2+}]$ or fixing the $[Hg^{2+}]$ and varying the potential with more negative potentials resulting in more mercury in the films. Metallic Cd appears in all films but is decreased when mercury in solution is increased. X-ray diffraction spectra do show peaks associated with MCT and these authors do not report any postdeposition anneal process.

14.5 ELECTRODEPOSITION OF OXIDE SEMICONDUCTORS

14.5.1 Introduction

Anodically formed ("native") oxide films play a key role in the stability of metals such as titanium in a variety of corrosive environments [148]. Such films, which range in thickness from molecular dimensions (subnanometers) to micrometers, however, are not of interest when the application requires a large surface area such as solar energy conversion and environmental remediation or sensing. Thus many of the early studies on anodically formed oxide layers [e.g., 149–151] involve ultrathin, compact films and are not further addressed herein. *Deliberately deposited* metal oxide films by electrochemical growth have a much more recent history [152]. The driver for the study of such oxide films (of much higher surface area) mainly stems from their charge storage capability, electrochromic activity, electrocatalytic property, and photoelectrochemical activity. These are the oxide materials which are addressed below. Other than the present work, reviews also exist on the electrochemical synthesis of metal oxides and hydroxides [153], electrochemical and photoelectrochemical processing for oxide films [154], and a general review on the electrodeposition of semiconductors, including specific data on one oxide semiconductor, namely, zinc oxide (ZnO) [155]. Two of the present authors (Rajeshwar and de Tacconi) have reviewed the use of templates for the electrosynthesis of semiconductors, including oxides [156]. Every attempt is made in avoiding overlap of the material below with these earlier reviews. As with the rest of this chapter, the literature cited is representative rather than exhaustive.

The pioneering work of Tench and Warren [152], cited above, involves either the anodic oxidation of a metal or a (dissolved) transition metal cation to a higher valent state followed by its chemical reaction with water (to form an oxide layer) or the cathodic reduction of a dissolved metal ion followed by dehydration of the initially deposited hydroxide. The anodic approach was demonstrated for the oxides of Ni, Cu, Fe, and Mn while the cathodic approach was demonstrated for Cu [152].

Base electrogeneration is a versatile cathodic approach for the electrodeposition of oxide films. Any electrochemical reaction which consumes H^+ (such as hydrogen generation) or which generates OH^- species (such as electroreduction of nitrate anion) at the electrode–electrolyte interface will invariably result in the precipitation of the corresponding hydroxide (due to the low-solubility product value) when the metal cation is simultaneously present in solution [153]. As discussed below, this cathodic electrodeposition strategy has

been successfully applied for the preparation of ZnO films. On the other hand, the mechanistic aspects of the cathodic electrosynthesis of TiO_2 and WO_3 (starting from the corresponding metal oxy salt precursors) are much less clear-cut and require more directed studies.

Finally, inspired by a pioneering study by Zwilling and coworkers [157] which showed that *nanoporous* oxide could be electrochemically generated by anodization of titanium in fluorinated electrolytes, a corpus of studies are emerging on the growth of nanotubular arrays of a variety of oxides as reviewed below. It is worth noting that these anodically formed oxide nanotubes (of very high surface area) stand in stark contrast to the *compact* anodic oxide layers discussed earlier in this introduction.

14.5.2 Titanium Dioxide (TiO_2)

This is perhaps the "mother" of all oxides, especially in view of applicability in diverse technological sectors. Historically, this is the material which really sparked interest in the solar photoelectrolysis of water and hydrogen generation. Another driver for the study of TiO_2 stems from its use for environmental remediation of water and air. This oxide is a staple in the paint/pigment industry and in cosmetic and skin care formulations and is widely used as an active material in sensors and as a support for heterogeneous metal-based catalysts. In spite of this very broad range of applications, it is interesting that electrodeposition of TiO_2 films has a relatively new and sparse history. Cathodic approaches are reviewed first followed by anodic electrosynthesis routes.

The first report on the cathodic electrosynthesis of TiO_2 thin films dates back to 1996 [158]. These authors point out that the base electrogeneration method as conventionally applied to nitrate-containing aqueous media (see above) does not work as the Ti^{4+} ion undergoes very rapid hydrolysis in aqueous solutions of $pH > 1$. On the other hand, the titanyl ion (TiO^{2+}) can be generated [159, 160] which can be precipitated as the oxyhydroxide gel when the pH is increased. Subsequent heat treatment of the gel at temperatures in the 300–400°C range results in gel dehydration and formation of TiO_2. This method was developed by Natarajan and Nogami [158] and subsequently applied by two other groups [161–163] for preparing TiO_2 films for use in dye-sensitized solar cell devices. Another variant of the above cathodic approach relies on the base-assisted hydrolysis of the initial complex formed between Ti^{4+} species and H_2O_2 and subsequent decomposition of this complex to yield the oxide [164]. The base was electrogenerated via water electrolysis (see above).

Other than the classical anodization studies discussed at the onset of Section 14.5.1, the use of fluoride deposition baths and the formation of $[TiF_6]^{2-}$ complexes represents the predecessor approach to the anodic preparation of TiO_2 nanotube arrays (NTAs) discussed below. Thus the $[TiF_6]^{2-}$ anionic species migrate toward the cathode where they dissociate into Ti^{4+} cationic species. These in turn undergo oxidation by the anodically generated $OH^{\bullet}$ radicals to form TiO_2 [165]. We will elaborate on this approach within the context of TiO_2 NTAs later in this section.

Other anodic electrodeposition variants have been described for TiO_2. Thus anodic oxidative hydrolysis of acidic aqueous $TiCl_3$ solutions affords a route to preparation of TiO_2 films which have been deposited on transparent conducting oxide (TCO) [166], metal [166], or B-doped diamond [167] surfaces. Micro- and nanostructured TiO_2 *thick* films were prepared in H_2SO_4–H_2O_2–H_3PO_4–HF solution by anodization at low voltages (10–50 V range) by varying the anodization time [168]. Titanium dioxide thin films were electrodeposited from a basic aqueous solution of titanate stabilized by $(CH_3)_4N^+$ cation and containing hydroquinone [169]. Proton formation by oxidation of hydroquinone to benzoquinone promoted precipitation of Ti(IV) species at the anode [169]. Finally, a dispersion of Degussa P-25 particles in 2-methoxyethanol was used to deposit porous thin layers of nanocolloidal TiO_2 films on TCO substrate [170]. Unlike the cathodic or anodic approaches discussed earlier, a constant-current *electrophoretic* method was used in this study.

As with their cathodically electrosynthesized counterparts, the anodic films have been used for application in dye-sensitized solar cells [166–170] or for the photoelectrocatalytic oxidation of compounds such as ethanol [167] or bisphenol A [168].

Controlling morphology of materials on a nanoscopic-size scale and examining their subsequent properties has both fundamental and practical relevance and this is no different with electrodeposited oxide films. In fact, this is a recurrent theme also with other oxides such as WO_3, Cu_2O, and ZnO, as discussed below. Highly ordered vertically oriented TiO_2 NTAs prepared by anodization of Ti substrates constitutes an architecture that offers a large internal surface area without a concomitant decrease in geometric area and structural order. The highly oriented nature of these NTAs makes them eminently attractive electron percolation pathways for vectorial charge transfer between interfaces. It is no surprise then that this area of research on TiO_2 has literally exploded after initial reports appeared from two laboratories [171–175].

As in the predecessor cases described earlier [157, 165], anodization of Ti foil is performed in fluoride-based media [176, 177]. Electrolyte composition and pH play a critical role in NTA growth and additives play an as-yet incompletely understood key role in the microscopic aspects of NTA self-assembly and growth. Both potentiostatic and constant-current anodizations have been performed and the merits of a pulse anodization approach have been exposed [178, 179]. The interested reader is referred to these original articles and the review papers for further details [171–182].

From a materials development standpoint, another development in the anodic NTA preparation strategy has been to incorporate dopant species (both metal and nonmetal) into the host oxide matrix during or (post-) nanotube growth [183–188]. The driver for this is the rather large optical bandgap of TiO_2 (~3.0–3.2 eV) which makes its response confined only to the UV region of the solar spectrum. Incorporation of dopants shifts the TiO_2 response toward visible light wavelengths, thus enhancing the applicability of this material for use in photovoltaic and photocatalytic solar cell devices (see below).

The TiO_2 NTAs anodically prepared as discussed above have been deployed for hydrogen sensing [189–194], solar or UV-assisted water photoelectrolysis [187, 195–199], electrocatalytic methanol oxidation [200], dye-sensitized solar photovoltaic cells [197, 201–206], and heterogeneous photocatalytic remediation of environmental pollutants [207].

14.5.3 Zinc Oxide

Zinc oxide is an important material for many applications, including varistors, transistors, piezoelectric devices, solar cell windows, and UV and blue light-emitting. The fact that ZnO is both a semiconductor and is piezoelectric material lends itself naturally for microfabrication of electromechanically coupled sensors and transducers. It is also relatively biosafe and biocompatible and can be deployed for biomedical applications with little worry of toxicity. Finally, ZnO exhibits the most diverse array of nanostructures known so far, such as nanorods, nanowires, nanobelts, nanosprings, and nanohelices.

The fist reports of the cathodic electrodeposition of ZnO films came simultaneously in 1996 from two different laboratories [208, 209]. While Izaki and Omi [208] relied on the base electrogeneration route (using nitrate electroreduction, see above), Peulon and Lincot [209] used the reduction of O_2 in the presence of Zn^{2+} ions [155]:

$$Zn^{2+} + 0.5O_2 + 2e^- \rightarrow ZnO \qquad (14.32)$$

They showed that ZnO films of "remarkable" structural quality could be prepared by this method with different morphologies ranging from arrays of single-crystal microcolumns to continuous films depending on substrate activation, solution composition, and deposition time [209].

Subsequent work by Izaki and Omi has sought to optimize the electrolyte composition [210] and to characterize the transparent ZnO films deposited by a variety of techniques [211]. This nitrate-based bath approach was also extended by other researchers [162, 212–214]. On the other hand, follow-up work by Lincot and co-workers has addressed the mechanistic aspects of cathodic electrodeposition in oxygenated aqueous zinc chloride solutions [215] and temperature effects on ZnO electrodeposition [216]. Another innovation from this group is the use of H_2O_2 as an oxygen precursor [217, 218]. Epitaxial growth of ZnO on GaN by the cathodic electrosynthesis route using oxygen reduction [Eq. (14.32)] has been reported [219].

In the above films, the ZnO films are spontaneously self-doped (*n*-type) by oxygen deficiency, although chloride doping was also claimed by Peulon and Lincot [215]. Deliberate doping has been reported by adding either aluminum chloride [220] or dimethylaminoborane [221] to secure Al or B doping, respectively. Similarly In-doped ZnO thin films were cathodically electrosynthesized from aqueous nitrate media using $InCl_3$ as a dopant precursor [222].

Nonaqueous electrolyte baths have also been effectively employed for ZnO electrodeposition. Thus either $ZnCl_2$ or $Zn(ClO_4)_2$ along with oxygenated LiCl of $LiClO_4$ supporting electrolyte were used in a dimethylsulfoxide (DMSO) medium [223, 224]. Another similar study from a different group uses $ZnCl_2$ with KCl as supporting electrolyte to deposit the oxide film on Si substrates from a DMSO bath [225].

As with the TiO_2 case discussed in the preceding section, control of morphology at the nanoscale level during electrodeposition has been a recent area of activity in ZnO electrodeposition. Thus Xu et al. [226] obtained a variety of ZnO morphologies by the electroreduction of nitrate ions in Zn^{2+}-containing KCl aqueous solutions. They speculated that preferential adsorption of Cl^- ions on (0001) ZnO particle surfaces leads to the plateletlike morphology observed [226]. The role of chloride ions on the cathodic electrodeposition of ZnO nanowire arrays was further elucidated by Tena-Zaera and co-workers [227].

Subsequent studies by Elias and co-workers show that the $ZnCl_2$ concentration is a major parameter to control the dimensions of ZnO nanowires [228]. Mean nanowire diameters from 25 to 80 nm were obtained by only modifying the $ZnCl_2$ concentration. A hybrid electrochemical–chemical etch in KCl was used to convert ZnO nanowires into nanotubes with tailored dimensions [229].

Colloidal ZnO suspensions have been used to electrophoretically deposit the oxide particles either on a SnO_2-coated glass slide [230] or a Pd sheet [231] substrate. No chemical additives were used in the first study [230] while a cationic polyelectrolyte (polyethylenimide) was used to modify the ZnO nanoparticle surfaces in the second case [231]. These studies include an examination of the deposition kinetics [230] and the rheology of ZnO suspensions [231].

Finally, applications of electrodeposited ZnO films are noted. The one-step electrodeposition of ZnO in baths also containing organic molecules (dyes) offers a route to preparation of hybrid inorganic oxide—organic functionalized frameworks for a variety of applications [232–234]. Strong specific chemical interactions between the ZnO surfaces and the organic functionalities are implicated in the growth of these hybrid architectures. One possible application is dye-sensitized solar cells [234]. Electrodeposition of *p*-type

CuSCN onto a dye-modified, electrodeposited *n*-type ZnO has been used to fabricate a *p–n* heterojunction solid-state solar cell [235]. A CdSe-sensitized variation of this device has been described [236].

The extremely thin absorber (ETA) solar cell is a new photovoltaic device design using an extra thin absorber layer sandwiched between two strongly interpenetrating transparent (wide-bandgap) semiconductors. It consists of a nanostructured *n*-type window layer, an absorber conformably deposited on this layer, and a void-filling *p*-type back contact to complete the structure. The ZnO/CdSe/CuSCN solar cell configuration mentioned above [236] falls into this category.

Thus a CdTe/ZnO composite film prepared by vapor-phase epitaxy of the absorber CdSe layer on an electrodeposited ZnO window layer has been characterized for ETA solar cell applications [237]. Another device architecture comprising of ZnO/CdTe/CuSCN has also been described by the same group [238]. ZnO nanowire arrays were electrodeposited on an electrodeposited ZnO buffer layer for photovoltaic applications [239]. Increased nanowire density (by a factor of 6 times) was observed (relative to the "naked" substrate case) in the presence of the buffer layer.

Electrodeposited ZnO layers have also been evaluated for optoelectronic applications. These include, for example, epitaxial ZnO film on GaN layers for photoluminescent emission [240, 241], hybrid layers of ZnO/lanthanide complexes [242], ZnO/lanthanide hybrids sensitized with eosyn Y dye for red/green luminescence [243], and hybrid ZnO and different tetrasulfonated metallophthalocyanines with multicolored electrochromic properties [244].

Given the importance of the electroreduction of O_2 (e.g., in fuel cells, metal–air batteries, corrosion, or biology), this reaction has been investigated on electrodeposited ZnO surfaces compared to the behavior on platinum [245]. Relative to the noble metal, the voltammogram wave shifted toward more negative potentials on ZnO, reflecting slower kinetics for the multielectron transfer process. Finally, mesoporous ZnO thin films were used as photocatalysts for the degradation of methylene blue dye chosen as a model organic water pollutant [246].

14.5.4 Tungsten Trioxide (WO_3)

Tungsten trioxide is an oxide semiconductor of interest from a variety of application perspectives. First and foremost, it is both electrochromic and photochromic and so is applicable to architectural glazings, automobile and building sun-roofs, electrochromic rear-view mirrors in automobiles, smart windows, and display panels. Tungsten trioxide is also an attractive material for semiconductor gas sensors. Various devices using WO_3 have been developed or proposed for detecting NO_x, NH_3, H_2S, and son on. Finally, this material is also attractive for solar photoelectrochemical water-splitting and environmental remediation applications.

The cathodic electrodeposition of WO_3 from a peroxytungstate precursor bath was first developed by Yamanaka et al. in 1986 [247, 248]. This method was further refined by Shin and co-workers [249, 250]. In the original variant [249, 250], the precursor solution was prepared by mixing colloidal tungstic acid and H_2O_2. The acid was prepared by treating an aqueous solution of potassium tungstate with an ion exchange resin in the strong-acid form. The most generally utilized approach for preparing the peroxytungstate precursor involves dissolving W metal in concentrated H_2O_2 solution [251, 252]. The excess peroxide is decomposed with a Pt black catalyst. The solution chemistry is complex and is further complicated by chemical stability of the oligomeric peroxo species formed in the initial reaction. Attempts have been made to identify the key precursor species, including polytungstate and peroxytungstate ions [251–253].

A simplified procedure for a "stable" precursor solution for cathodic WO_3 electrodeposition has been reported [254]. Stability here was defined in terms of the solution remaining transparent and with no visible turbidity after storage at room temperature for periods up to one week. Other innovations in the cathodic approach include adding dopant species (nickel or cobalt) in the precursor medium [249]. The doping was done to minimize the electrical resistivity and overpotential for proton reduction, thereby improving the response time and power consumption for electrochromic device applications of the resultant WO_3 films [249]. Composite films containing WO_3 and an electronically conducting polymer (polyaniline) have also been electrochemically deposited using a double-pulse plating technique [255]. The resultant films have an electrochromic window between the anodic coloration of polyaniline and the cathodic coloration of WO_3, making them amenable for multicolor display devices.

Exactly as in the case of TiO_2, the early work on anodic compact WO_3 films (mainly for electrochromic applications) has given way to nanoporous film counterparts for solar applications. Thus nanoporous WO_3 films were obtained by galvanostatic anodization of tungsten in oxalic acid electrolyte [256]. Tsuchiga et al. prepared self-organized porous WO_3 from a NaF electrolyte medium [257] and these architectures showed higher photocurrent efficiency relative to a compact layer [258]. Nanoporous WO_3 films were anodically grown from a variety of aqueous electrolytes containing also organic additives such as glycerol in some cases [259]. Finally, such self-assembled nanoporous WO_3 layers, with preferential orientation of (002) planes, were used for the photocatalytic degradation of pentachlorophenol [260]. These materials showed better performance than compact WO_3 film or TiO_2 NTAs [260]. In another study [261] anodically grown nanoporous WO_3 films on W substrates showed better photocatalytic activity for the oxidation of methylene blue and reduction of Cr(VI) relative to a cathodically electrosynthesized WO_3 film counterpart.

Finally, in terms of other practical applications of electrodeposited WO_3 (both anodically and cathodically derived), mention may be made of studies oriented toward electrochromism [262–265], photoelectrochemistry [262], photocatalysis [265], and wastewater treatment [266].

14.5.5 Copper Oxide (Cu_2O)

Of all the oxide semiconductors prepared by electrochemical methods, copper oxide by far has received the most attention. There are several factors underlying this interest. First, the component elements are relatively plentiful and nontoxic. Second, Cu(I) oxide (Cu_2O) occurs as both *p*- and *n*-type semiconductors. It is also a textbook example of a Wannier–Mott excitonic solid [267]. The physics community is interested in the excitonic properties of Cu_2O since there evidence that Bose–Einstein condensation of excitons can occur in this material [268]. Aside from its fundamental properties, Cu_2O has also seen applications in solid-state photovoltaic cells, as a rectifier device component, and as a photocatalyst for solar water splitting. It is interesting to note that an early study of *p*-Cu_2O was pessimistic about the prospect of this material for solar photoelectrochemical applications [269] although the plethora of subsequent studies appears to refute this notion.

The corresponding Cu(II) oxide (CuO) is also a *p*-type semiconductor [270] and has been much less studied. This oxide can be anodically prepared on copper substrates in alkaline media [271]. More recently, Cu(II)–tartrate complexes in alkaline media (pH > 13) have been used as a precursor to CuO film formation on Pt substrates [272]. Given the paucity of studies on this copper oxide, attention will focus below on Cu_2O, which, as mentioned earlier, has been extensively studied from an electrodeposition perspective.

An earlier report on the cathodic electrodeposition of Cu_2O appeared in 1983 [152]. A copper acetate bath of near-neutral pH and a constant potential growth mode was used in this pioneering study. Citations of even earlier works dating back to 1958 may be found in a review by Rakhshani [273], who also cites early studies on the *anodic* oxidation of copper to Cu_2O. We will focus mainly on the cathodic approach in what follows.

In general, any Cu(II) salt can be utilized in a complexing medium. Lactic acid has been used as the complexing agent in the vast majority of cases, although other ligands such as amino acids [274, 275] have also been deployed. Additives such as ethylene glycol have been used with its role being speculated as being both an electrolyte modifier and a chelating agent [276]. It must be noted that in some instances no other intentionally added species other than the Cu(II) salt was present in an aqueous medium [277, 278], and one of these studies [278] invokes a base electrogeneration mechanism (see above) for Cu_2O formation.

The bath pH plays a key role in dictating the morphology and grain orientation of the electrosynthesized Cu_2O films. In an early report [279], the films derived from an ∼pH 9 bath were found to be highly oriented along the (100) plane regardless of the deposition history and the type of substrate. Subsequent work by the same group [280] revealed that at bath pH values higher than ∼9.5, a (111) preferred orientation was observed. Switzer et al. [281, 282] report a transition of the preferred grain orientation from (100) to (111) to occur around pH 12. A more recent study [283] in which the bath pH was varied from ∼7.5 to ∼12 reports a third preferred orientation, (110), to occur in a narrow pH range from ∼9.4 to ∼9.9. A computer simulation–based model for crystal growth was developed by the Switzer group [281], although a detailed mechanistic picture is as yet lacking for this interesting phenomenon. We shall return to a discussion of the morphological aspects later in this section.

Potential oscillations have been observed during the cathodic eletrodeposition of Cu/Cu_2O layered nanostructures from alkaline solutions of Cu(II) lactate [284, 285]. Subsequent studies of the same group using in situ electrochemical quartz crystal microgravimetry (EQCM) afforded measurements of the layer thicknesses and overall modulation wavelength of these films [286]. Based on these studies, the authors propose that Cu_2O is deposited during the positive spikes in electrode potential while a composite of Cu and Cu_2O is deposited during the more negative plateau region of the oscillation. These Cu/Cu_2O layered structures also exhibited the phenomenon of negative differential resistance at room temperature [287]. The authors suggest that thin space-charge regions at each Cu/Cu_2O interface produce double tunnel junctions and that tunneling occurs from the Cu-rich layers into hole states in Cu_2O through these space-charge regions.

Epitaxial growth of Cu_2O layers has been achieved by cathodic electrosynthesis on a variety of surfaces, including Pt [278], Au [288], Si [289], and InP [289]. Copper(II) lactate solutions were used by Switzer et al. [288, 289] while Lee and Tak used a weak *acidic* solution of Cu(II) nitrate for this purpose [278]. In the case of the single-crystal Au substrate, ordered nanostructures of Cu_2O were formed after a transition from a thermodynamically controlled orientation to a kinetically preferred orientation [288]. Other aspects of the cathodic electrodeposition of Cu_2O layers, including the use of nonaqueous baths, are contained in [290–297]. These electrodeposited films have been examined in terms of their optical and photoelectrochemical properties [293–296] and from the point of view of their applicability in Li ion batteries [297].

The applicability of electrodeposited Cu_2O films for solar water splitting has been explored. Direct photoelectrochemical water splitting on *p*-Cu_2O is precluded by the unfavorable alignment of its valence band edge relative to the redox level for oxidation of water (to O_2). Consistent

with this picture, two recent studies [294, 298] have reported negative results. In the presence of *sacrificial* electron donors, however, photoelectrochemical evolution of H_2 could be observed in a twin-compartment cell [298] attesting to the promise of this approach in *indirect* solar hydrogen evolution schemes. The sacrificial electron donor could even be a dye pollutant, thus combining environmental remediation and solar H_2 generation and adding value to the latter. The attractiveness of such a "hybrid" approach is enhanced by the fact that the component elements of Cu_2O are nontoxic and electrodeposition is a potentially low-cost preparation scheme for the oxide semiconductor active material.

Cathodically electrodeposited Cu_2O semiconductor films are *p*-type in the vast majority of the cases. However, recall that *n*-type photoconductivity was observed even in an early study (in 1986) on cathodically electrosynthesized Cu_2O [277]. Recognizing that oxygen vacancies contribute to *p*-type semiconductor behavior in Cu_2O, more recent studies by Tao and co-workers [299, 300] have prepared *p–n* homojunctions from Cu_2O by controlling solution pH during cathodic film growth. A subsequent study by the same group reports *n*-type doping of Cu_2O by adding a chlorine precursor ($CuCl_2$) to the deposition bath [301]. Another group also uses solution pH as a tool to prepare *n*-type Cu_2O electrodes [302].

This last study also reports photocurrent enhancement by controlling dendritic branching growth of *n*-Cu_2O during electrosynthesis [302]. Shape control of inorganic materials via electrodeposition is a research theme within the Choi group [303]. For example, without additives, Cu_2O electrodeposits as cubic crystals with the growth rate being slowest along the $\langle 100 \rangle$ direction. However, when sodium dodecyl sulfate is added to the medium, the surfactant preferentially adsorbs on $\{111\}$ planes rendering growth along the $\langle 111 \rangle$ direction significantly slower than along the $\langle 100 \rangle$ direction. As a result, *octahedral* Cu_2O crystals are electrochemically formed [304]. Other examples of the effect of the electrochemical growth mode (potentiostatic vs. galvanostatic), temperature, and additives on the growth and stability of Cu_2O surfaces may be found in [305, 306] from the same group. As a final example of control of crystal habit and branching during electrosynthesis, the role of overpotential and solution pH was demonstrated during cathodic growth of Cu_2O crystals [307].

14.5.6 Other Miscellaneous Oxides

The anodic growth of α-PbO_2 on Pt [308] and TCO [309] substrates from a buffered lead acetate medium was monitored in situ using laser interferometry, X-ray diffraction, and photoelectrochemical measurements. Analysis of the photocurrent spectra indicated that the photoactive species was the tetragonal PbO phase formed in situ as the potential was swept into the reduction regime of the originally deposited oxide. The anodic growth of HgO on Hg has also been studied by the same group using photocurrent spectroscopy [310]. The bandgap of the HgO film thus formed in situ on Hg in $NaHCO_3$ electrolyte was found to be 1.9 eV. A hybrid electrochemical–thermal method was used for forming *n*-CdO thin films [311]. Thus metallic Cd was first electrodeposited on Ti substrate (from an aqueous Cd^{2+}-loaded medium) followed by thermal oxidation in air to convert Cd to CdO [311].

Cadmium oxide films were electrodeposited on SnO_2-coated glass slides from a nonaqueous, DMSO bath containing dissolved oxygen and Cd^{2+} ions [224]. The basic electrogeneration strategy (see above) was used to cathodically electrodeposit *n*-CdO thin films on F-doped SnO_2 substrates from an oxygenated KCl medium containing $CdCl_2$ [312]. Like ZnO, CdO is an attractive window material for heterojunction solar cells because of the combination of high transparency in the visible range of the electromagnetic spectrum and high electronic conductivity.

Tin oxide is another material which combines transparency with good electronic conductivity upon doping (e.g., with F or Sb). It is also applicable as a gas sensor and as anode in secondary lithium batteries. Cathodic electrodeposition of nanostructured SnO_2 films from aqueous medium has been reported [313]. The as-deposited films at 85°C were amorphous but could be converted to nanocrystalline form by subsequent heat treatment at 400°C in vacuum.

Finally, γ-Fe_2O_3 films have been prepared by cathodic electrosynthesis on Pt disk substrate from a mixed ethanol–water medium [314]. The electrodeposited films were evaluated for possible applicability in electrochemical capacitor devices.

14.5.7 Mixed Oxides and Metal/Oxide Nanocomposites

Occlusion electrosynthesis is a versatile method for preparing both mixed oxides and metal–oxide nanocomposites. Thus the electrodeposition bath is dosed with nanosized particles (akin to the electrophoretic deposition case, see above) which are then occluded within an electrodeposited film matrix. This approach has been reviewed by two of the authors of this chapter [315]. Examples include the electrosynthesis of TiO_2/Ni [316], WO_3/Ni [316], TiO_2–WO_3/Ni [316], TiO_2/WO_3 [317], TiO_2/TiO_2 [318], TiO_2/Cu [319], and TiO_2/Ag [319]. In each of these examples the second component listed serves as the matrix or "glue" to bind the occluded particles to the underlying substrate and in all cases the matrix was *cathodically* electrodeposited. The photoelectrochemical and photocatalytic behavior of the resultant nanocomposite films was characterized in these studies [316–319]. The ability of these films to decompose organic pollutants under UV excitation was also probed in one of the studies [319].

Other examples of metal–oxide nanocomposites include the preparation of quantum-confined Cu/Cu_2O films prepared from a lactate bath containing Cu(II) species [267]. Nanocolumnar junctions of metal oxide and metal nanowires, that is, Cu_2O/Ni and ZnO/Ni, were prepared by a single electrodeposition technique [320]. In addition, the two metal oxides were combined into an integrated structure wherein the sequence was inverted, that is, Cu_2O/ZnO/Ni and ZnO/Cu_2O/Ni [320]. Since ZnO and Cu_2O are *n*-type and *p*-type, respectively (at least *nominally* prepared), these represent *p–n* or *n–p* heterojunctions grown on Ni. The mixed–oxide systems were prepared by a two-step process using electrochemical and chemical methods [320].

Cathodic electrodeposition is a relatively unexplored route for the synthesis of mixed oxides [321]. The major requirements for mixed thin-film formation were described and illustrated for two cases: ZnO/$Eu(OH)_x$ and TiO_2/WO_3 [321]. Pulsed electrodeposition was used to prepare thin films of WO_3/TiO_2 over a wide compositional range [322, 323]. Composite films containing comparable amounts of WO_3 and TiO_2 showed superior anodic photocurrents in aqueous Na_2SO_4 medium relative to the two component oxides separately present [322]. This behavior was rationalized on the basis of minimized electron–hole recombination in the mixed-oxide case because of vectorial electron and hole transfer. A subsequent study describes the morphology of these mixed-oxide films as probed by scanning tunneling microscopy and also their electrochromic behavior [323].

Other examples of mixed (or layered) oxide films involve *p*-Cu_2O as one component [324–327]. Thus *p*-Cu_2O was photochemically deposited on a chemically prepared *n*-ZnO/quartz substrate [324]. The rectifying properties of this *p–n* junction were then probed by the authors. In another study on *p*-Cu_2O/*n*-ZnO, ZnO was first prepared on SnO_2-coated glass by potentiostatic eletrodeposition followed by galvanostatic deposition of a Cu_2O layer to form *p*-Cu_2O/*n*-ZnO heterojunction solar cells [325]. A similar *p*-Cu_2O/*n*-TiO_2 heterojunction thin-film cathode was prepared for photoelectrocatalysis [326]. The Cu_2O layer was first cathodically electrodeposited on Ti substrates via a procedure earlier described by one of the authors of this study [327]. The heterojunction was formed by electron beam evaporation of a 100-nm-thick *n*-TiO_2 film on top of the underlying Cu_2O layer. In the last example [328], vertically oriented *p*-type Cu–Ti–O nanotube array films were grown by anodization of copper-rich Ti metal films cosputtered onto F-doped SnO_2 glass substrates. NTAs were then used as photoelectrochemical diodes for hydrogen generation [328].

A book chapter contains many examples of mixed-oxide superlattices and multilayers prepared by electrodeposition [329]. Not all the oxides featured in this chapter, however, are semiconductors; the interested reader may consult this review for further details.

Finally, whether a mixed-oxide film or an alloy (wherein the component elements are mixed on an atomic level) is obtained depends on the deposition potential as illustrated for the Zn–Cd–O ternary system [330]. Both types of behavior, that is, ZnO/CdO or $Zn_xCd_{1-x}O$ alloy could be electrogenerated as diagnosed by distinctly different X-ray diffraction signatures.

14.6 CONCLUDING REMARKS

There has clearly been a great deal of progress in the understanding of how one may deposit a wide variety of semiconductors by electrochemical means. Detailed understanding of the chemistry of the reactions that may be expected and the effects of pH, current density, potential, temperature, and annealing conditions have been investigated by many workers. Of particular note is the improved ability to control the deposition process on an atomic scale and the demonstration of epitaxial or nearly epitaxial growth in a limited number of cases. The driving force behind this field continues to be its relative simplicity, low cost, and scalability. Improved material quality is still required for this semiconductor layer to be widely used in all the applications for which they are intended.

The versatility of electrodeposition as a candidate for preparing semiconductors is illustrated by the wide range and scope of materials that can be generated, as reviewed in this chapter. These range from elemental semiconductors to compounds with a rich array of chemistries. Oxides offer a particularly promising avenue for controlling morphology and properties at the nanoscale. The resultant architectures may show enhanced performance for existing device application but equally important may lead to entirely *new* and hitherto unanticipated practical possibilities. The future is indeed bright for the semiconductor electrodeposition community.

REFERENCES

1. M. Paunovic and M. Schlesinger, *Fundamentals of Electrochemical Deposition*, Wiley, Hoboken, NJ, 2006.
2. R. Monnier and D. Barakat, "Contribution a L'etude du Comportement de la Silice Dans les Bains de Cryo Lithe Fondue," *Helv. Chem. Acta*, **40**, 2041 (1957).
3. K. Grojtheim, K. Matiasovsky, P. Fellner, and A. Silny, "Electrolytic Deposition of Silicon and Silicon Alloys, Part I: Physiochemical Properties of the Na_3AlF_6-Al_2O_3-SiO_2 Mixtures," *Canad. Met. Quart.*, **10**, 79 (1971).
4. Yu. K. Delimarskii, R. V. Chernov, and I. G. Kovzum, "Phase Diagrams of the System, Potassium Fluorosilicate Potassium and Sodium Halides," *Ukrain. Khim. Zhur.*, **33**, 675 (1967).

5. Yu. K. Delimarskii, N. N. Storchak, and R. V. Chernov, "Electrodeposition of Silicon on Solid Electrodes," *Electtokhimiya*, **9**, 1443 (1973).
6. Yu. K. Delimarskii, R. V. Chernov, and A. P. Nizov, *Ukrain. Khim. Zhur.*, **37**, 422 (1971).
7. A. J. Gay and J. Quarkernaat, "A Study of Electroless Siliconizing of Nickel," *J. Less Common Met.*, **40**, 21 (1975).
8. U. Cohen and R. A. Huggins, "Silicon Epitaxial Growth by Electrodeposition from Molten Fluorides," *J. Electrochem. Soc.*, **123**, 381 (1976).
9. D. Elwell and G. M. Rao, "Electrolytic Production of Silicon," *J. Appl. Electrochem.*, **18**, 15 (1988).
10. R. C. DeMattei, D. Elwell, and R. S. Feigelson, "Electrodeposition of Silicon at Temperatures above Its Melting Point," *J. Electrochem. Soc.*, **128**, 1712 (1981).
11. R. Monnier, "L'obtention et le Raffinage du Silicium par Voie Electrochimique," *Chimia*, **37**, 109 (1983).
12. A. A. Andriiko, E. V. Panov, O. I. Boiko, B. V. Yakovlev, and O. Ya Borovik, "Dependence of the K_2SiF_6 Content in the Cathodic Deposit on the Melt Composition During Electrodeposition of Powder-like Silicon from the KCl-KF-K_2SiF_6 Melt Containing Silicon Dioxide," *Russian J. Electrochem.*, **33**, 1343 (1997).
13. K. Agrawal and A. E. Austin, "Electrodeposition of Silicon from Solutions of Silicon Halides in Aprotic Solvents," *J. Electrochem. Soc.*, **128**, 2292 (1981).
14. Y. Takeda, R. Kanno, O. Yamamoto, T. R. Rama Mohan, C.-H. Lee, and F. A. Kröger, "Cathodic Deposition of Amorphous Silicon from Tetraethylorthosilicate in Organic Solvents," *J. Electrochem. Soc.*, **128**, 1221 (1981).
15. C. H. Lee and F. A. Kröger, "Cathodic Deposition of Amorphous Alloys of Silicon, Carbon, and Fluorine," *J. Electrochem. Soc.*, **129**, 936 (1982).
16. R. Boen, and J. Bouteillon, "The Electrodeposition of Silicon in Fluoride Melts," *J. Appl. Electrochem.*, **13**, 277 (1983).
17. J. Gobet and H. Tannenberger, "Electrodeposition of Silicon from a Nonaqueous Solvent," *J. Electrochem. Soc.*, **135**, 109 (1988).
18. J. DeLepinay, J. Bouteillon, S. Traore, D. Renaud, and M. J. Barbier, "Electroplating Silicon and Titanium in Molten Fluoride Media," *J. Appl. Electrochem.*, **17**, 294 (1987).
19. D. B. Frolenko, Z. S. Martem'yanova, Z. I. Valeev, and A. N. Baraboshkin, "Structure of Silicon Deposits Obtained by Electrolyzing Mixed Choloride-Fluoride Melts," *Sov. Electochem.*, **28**, 1427 (1993).
20. M. Pourbaix, *Atlas d'Equilibres Electrochimiques*, Gauthiers-Villars et Cie, Paris, 1963.
21. R. C. DeMattei, D. Elwell, and R. S. Feigelson, "The Synthesis of GaAs by Molten Salt Electrolysis," *J. Crystal Growth*, **43**, 643 (1978).
22. I. G. Dioum, J. Vedel, and B. Tremillon, "Properties of Arsenic in Molten Potassium Tetrachlorogallate at 300 C Formation of Gallium Arsenide," *J. Electroanal. Chem.*, **139**, 329 (1982).
23. S. P. Wicelinski and R. J. Gale, Abstract 1495, p. 2040, *The Electrochemical Society Extended Abstracts*, **Vol. 87-2** Honolulu, HI, Oct 18–23, 1987.
24. M. K. Carpenter and M. W. Verbrugge, Abstract 257, p. 3678, *The Elechrochemical Society Extended Abstracts*, **Vol. 89-2**, Hollywood, FL, Oct 15–20, 1989.
25. M. K. Carpenter and M. W. Verbrugge, "Electrochemical Codeposition of Gallium and Arsenic from a Room Temperature Chlorogallate Melt," *J. Electrochem. Soc.*, **137**, 123 (1990).
26. L. Astier, R. Michelis-Quiriconi, and M.-L. Astier, Fr. Demande FR 2,529,713 (Jan. 6, 1984). Appl. 82/11,797 (July 2, 1982).
27. K. R. Murali, M. Jayachandran, and N. Rangarajan, "Review of Techniques on Growth of GaAs and Related Compounds," *Bull. Electrochem.*, **3**, 261 (1987).
28. M.-C. Yang, U. Landau, and J. C. Angus, "Electrodeposition of GaAs from Aqueous Electrolytes," *J. Electrochem. Soc.*, **139**, 3480 (1992).
29. I. Villegas and J. L. Stickney, "Preliminary Studies of GaAs Deposition on Au(100), (110), and (111) Surfaces by Electrochemical Atomic Layer Epitaxy," *J. Electrochem. Soc.*, **139**, 686 (1992).
30. J. J. Cuomo and R. J. Gambino, "The Synthesis and Epitaxial Growth of GaP by Fused Salt Electrolysis," *J. Electrochem. Soc.*, **115**, 755 (1968).
31. C. F. Smart,U.S. Patent 2,755,537 (1956) and German patent 929,103 (1955).
32. Y. N. Sadana and J. P. Singh, "Electrodeposition and X-ray Structure of Antimony-Indium Alloys," *Plating Surf. Finish.*, **72**, 64 (1985).
33. T. Okubo and U. Landau, "Electrodeposition of Indium Antimonide Semiconductor from Aqueous Electrolyte," *Electrochem. Soc. Abs*., **88-2**, Chicago, IL, October 9–14, 1988.
34. J. Ortega and J. Herrero, "Preparation of InX (X = P, As, Sb) Thin Films by Electrochemical Methods," *J. Electrochem. Soc.*, **136**, 3388 (1989).
35. J. Herrero, and J. Ortega, "n-Type In_2S_3 Thin Films Prepared by Gas Chalcogenization of Metallic Electroplated Indium: Photoelectrochemical Characterizaton," *Solar Energy Mat.*, **17**, 357 (1988).
36. B. Scharifker, Z. Ferreira, and J. Mozota, "Electrodeposition of Lead Sulphide," *Electrochim. Acta*, **30**, 677 (1985).
37. M. Takahashi, Y. Ohshima, K. Nagata, and S. Furuta, "Electrodeposition of PbS Films from Acidic Solution," *J. Electroanal. Chem.*, **359**, 281 (1993).
38. M. Sharon, K. S. Ramaiah, M. Kumar, M. Neumann-Spallart, and C. Levy-Clement, "Electrodeposition of Lead Sulphide in Acidic Medium," *J. Electroanal. Chem.*, **436**, 49 (1997).
39. S. A. Ringel, A. W. Smith, M. H. MacDougal, and A. Rohatgi, "The Effects of $CdCl_2$ on the Electronic Properties of Molecular-Beam Epitaxially Grown CdTe/CdS Heterojunction Solar Cells," *J. Appl. Phys.*, **70**, 881 (1991).
40. C. K. Ard, *Properties of Narrow Gap Cd-based Compounds*, P. Capper, Ed., Inspec, London, UK, 1994, p. 598, and the references therein.

41. C. L. Johnson, E. E. Eissler, S. E. Cameron, Y. Kong, S. Fan, and K. G. Lynn, "Crystallographic and Metallurgical Characterization of Radiation Detector Grade Cadmium Telluride Materials," in *Semiconductors for Room Temperature Radiation Detector Applications*, R. B. James, T. E. Schlesinger, P. Siffert, and L. Franks, Eds. *Mater. Res. Soc*. 477 (1993).
42. M. P. R. Panicker, M. Knaster, and F. A. Kröger, "Cathodic Deposition of CdTe from Aqeous Electrolyte," *J. Electrochem. Soc.*, **52**, 566 (1978).
43. G. Fulop, M. Doty, P. Meyers, and C. H. Liu, "High-Efficiency Electrodeposited Cadmium Telluride Solar Cells," *Appl. Phys. Lett.*, **40**, 327 (1982).
44. H. J. Gerritsen, "Electrochemical Deposition of Photosensitive CdTe and ZnTe on Tellurium," *J. Electrochem. Soc.*, **131**, 136 (1984).
45. C. Sella, P. Boncorps, and J. Vedel, "The Electrodeposition Mechanism of CdTe from Acidic Aqueous Solutions," *J. Electrochem. Soc.*, **133**, 2043 (1986).
46. M. W. Verbrugg and C. W. Tobbias, "The Periodic Electrochemical Codeposition of Cadmium Telluride," *AlChE J.*, **33**, 628 (1987).
47. K. Rajeshwar, "Electrosynthesized Thin Films of Group II-VI Compound Semiconductors, Alloys, and Superstructures," *Adv. Mater.*, **4**, 23 (1992) and the references therein.
48. R. N. Bhattacharya and K. Rajeshwar, "Electrodepostion of CdTe Thin Films," *J. Electrochem. Soc.*, **131**, 2032 (1984).
49. P. Cowache, D. Lincot, and J. Vedel, "Cathodic Codepostion of Cadmium Telluride on Conducting Glass," *J. Electrochem. Soc.*, **136**, 1646 (1989).
50. A. Kampmann, P. Cowache, B. Mokili, D. Lincot, and J. Vedel, "Characterization of ⟨111⟩ Cadmium Telluride Electrodeposited on Cadmium Sulphide," *J. Crystal Growth*, **146**, 256 (1995).
51. A. Kampmann, P. Cowache, J. Vedel, and D. Lincot, "Investigation of the Influence of the Electrodeposition Potential on the Optical, Photoelectrochemical and Structural Properties of As-deposited CdTe," *J. Electroanal. Chem.*, **387**, 53 (1995).
52. P. Sircar, "Growth of CdTe on GaAs by Electrodeposition from an Aqueous Electrolyte," *Appl. Phys. Lett.*, **53**, 1184 (1988).
53. J. M. Fisher, L. E. A. Berlouis, L. J. M. Sawers, S. M. MacDonald, S. Affrossman, D. J. Diskett, and M. G. Astles, "Growth and Characterization of Electrodeposited Films of Cadmium Telluride on Silicon," *J. Crystal Growth*, **138**, 86 (1994).
54. J. A. VonWindheim and M. Cocivera, "Variation of Resistivity of Copper-Doped Cadmium Telluride Prepared by Electrodeposition," *J. Phys. D.*, **23**, 581 (1990).
55. S. M. Babu, R. Dehanasekaran, and P. Ramasamy, "Electrodeposition of CdTe by Potentiostatic and Pulse Technique," *Thin Solid Films*, **202**, 67 (1991).
56. P. D. Paulson, V. Dutta, and C. Sing, "A Comparative Study of Compositional and Structural Properties of CdTe Thin Films Prepared by Different Electroplating Techniques," in *Proceedings of First World Conference of Photovoltaic Energy Conversion,* **1**, 331 (1994).
57. Y. Guo and X. Deng, "Electrodeposition of CdTe Thin Films and Their Photoelectrochemical Behavior," *Solar Energy Mater. Solar Cells*, **29**, 115 (1993).
58. R. B. Gore, R. K. Pandey, and S. K. Kulkarni, "Investigation of Deposition Parameters for the Nonaqueous Electroplating of CdTe Films and Application in Electrochemical Photovoltaic Cells," *Sol. Energy Mater.*, **18**, 159 (1989).
59. R. K. Pandey, S. Maffi, and L. P. Bicelli, "Study of CdTe Electrodeposition from Nonaqueous Bath," *Mater. Chem. Phys.*, **35**, 15 (1993).
60. Y. Sugimoto and L. M. Peter, "Photoeffects During Cathodic Electrodeposition of CdTe," *J. Electroanal. Chem.*, **386**, 183 (1995).
61. F. Jackson, L. E. A. Berlouis, and P. Rocabois, "Layer-by-layer Electrodeposition of Cadmium Telluride onto Silicon," *J. Crystal Growth*, **159**, 200 (1996).
62. E. A. Meulenkamp and L. M. Peter, "MechanisticAspects of the Electrodeposition of Stoichiometric CdTe on Semiconductor Substrates," *J. Chem. Soc. Faraday, Trans.*, **92**, 4077 (1996).
63. M. Rami, E. Benamar, M. Fahoume, F. Chraibi, and A. Ennaoui, "Formation of CdTe by Electrodeposition: Thermodynamic Aspect," *Ann. Chim. Sci. Mat.*, **23**, 365 (1998).
64. B. W. Gregory and J. L. Stickney, "Electrochemical Atomic Layer Epitaxy (ECALE)," *J. Electroanal. Chem.*, **300**, 543 (1991).
65. B. W. Gregory, D. W. Suggs, and J. L. Stickney, "Conditions for the Deposition of CdTe by Electrochemical Atomic Layer Epitaxy," *J. Electrochem. Soc.*, **138**, 1279 (1991).
66. L. P. Colletti, B. H. Flowers Jr., and J. L. Stickney, "Formation of Thin Films of CdTe, CdSe, and CdS by Electrochemical Atomic Layer Epitaxy," *J. Electrochem. Soc.*, **145**, 1442 (1998).
67. B. M. Huang, L. P. Colletti, B. W. Gregory, J. L. Anderson, and J. L. Stickney, "Preliminary Studies of the Use of an Automated Flow-Cell Electrodeposition System for the Formation of CdTe Thin Films by Electrochemical Atomic Layer Epitaxy," *J. Electrochem. Soc.*, **142**, 3007 (1995).
68. B. W. Gregory, M. L. Norton, and J. L. Stickney, "Thin-Layer Electrochemical Studies of the Underpotential Deposition of Cadmium and Tellurium on Polycrystallline Au, Pt, and Cu Electrodes," *J. Electroanal. Chem.*, **293**, 85 (1990).
69. L. P. Colletti, D. Teklay, and J. L. Stickney, "Thin-Layer Electrochemical Studies of the Oxidative Underpotential Deposition of Sulphur and Its Application to the Electrochemical Atomic Layer Epitaxy Deposition of CdS," *J. Electroanal. Chem.*, **369**, 145 (1994).
70. L. P. Colletti, S. Thomas, E. M. Wilmer, and J. L. Stickney, "Thin Layer Electrochemical Studies of ZnS, ZnSe, and ZnTe Formation by Electrochemical Atomic Layer Epitaxy (ECALE)," *Mat. Res. Soc. Symp. Proc.*, **451**, 235 (1996).
71. B. E. Hayden and I. S. Nandhakumar, "In-Situ STM Study of Te UPD Layers on Low Index Planes of Gold," *J. Phys. Chem. B.*, **101**, 7751 (1997).
72. B. K. Niece and A. A. Gewirth, "Potential-Step Chronocoulometric and Quartz Crystal Microbalance Investigation of

Coadsorbed Cadmium and Sulphate on Au (111) Electrodes," *Langmuir*, **13**, 6302 (1997).

73. I. Villegas and P. Napolitano, "Development of a Continuous-Flow System for the Growth of Compound Semiconductor Thin Films via Electrochemical Atomic Layer Epitaxy," *J. Electrochem. Soc.*, **146**, 117 (1999).
74. Y. Avigal, D. Cahen, J. Manassen, and G. Hodes, "Solar Energy Conversion and Storage by a Photoelectrochemical Storage Cell," *Proc. 1977 Photovoltaic Solar Energy Conf.* (Reidel, Boston), 1302 (1977).
75. S. Chandra and R. K. Pandey, "Photoelectrochemical Cell for Solar Energy Conversion Using Electrocodeposited CdSe Films," *Phys. Stat. Sol.*, **59**, 787 (1980).
76. D. J. Miller and D. Haneman, "Preparation of Stable Efficient CdSe Films for Solar PEC Cells," *Solar Energy Mat.*, **4**, 223 (1981).
77. J. P. Szabo and M. Cocivera, "Effect of Annealing Atmosphere on the Properties of Thin-film CdSe," *J. Appl. Phys.*, **61**, 4820 (1987).
78. J. P. Szabo and M. Cocivera, "Composition and Performance of Thin Film CdSe Electrodeposited from Selenosulfite Solution," *J. Electrochem. Soc.*, **133**, 1247 (1986).
79. F. Cerdiera, I. Torriani, P. Motisuke, V. Lemos, and F. Decker, "Optical and Structural Properties of Polycrystalline CdSe Deposited on Titanium Substrates," *Appl. Phys. A.*, **46**, 107 (1988).
80. K. K. Mishra and K. J. Rajeshwar, "A Re-examination of the Mechanisms of Electrodeposition of CdX and ZnX (X=Se, Te) Semiconductors by the Cyclic Photovoltammetric Technique," *J. Electroanal. Chem.*, **273**, 169 (1989).
81. M. Skyllas-Kazacos and B. Miller, "Studies in Selenious Acid Reduction and CdSe Film Deposition," *J. Electrochem. Soc.*, **127**, 869 (1980).
82. M. Skyllas-Kazacos and B. Miller, "Electrodeposition of CdSe Films from Selenosulfite Solution," *J. Electrochem. Soc.*, **127**, 2378 (1980).
83. A. M. Kressin, V. V. Doan, J. D Klein, and M. J. Sailor, "Synthesis of Stoichiometric Cadmium Selenide Films via Sequential Monolayer Electrodeposition," *Chem. Mater.*, **3**, 1015 (1991).
84. M. Abramovich, M. J. P. Brasil, F. Decker, J. R. Moro, P. Motisuke, N. Muller-St., and P. Salvador, "Crystal Structure, Luminescence, and Photoelectrochemistry of Thin Electroplated Cd-chalcogenide Layers," *J. Solid State Chem.*, **59**, 1 (1985).
85. M. T. Gutierrez and J. Ortega, "Photoelectrochemical Study of Electrodeposited Polycrystalline CdSe in Ferro-Ferricyanide System," *J. Electrochem. Soc.*, **136**, 2316 (1989).
86. K. R. Murali, V. Subramanian, N. Rangarajan, A. S. Lakshmanan, and S. K. Rangarajan, "Preparation and Characterization of Pulse Plated CdSe Films," *SPIE Proc.*, **1523**, 121 (1992).
87. V. Subramanian, K. R. Murali, N. Rangarajan, and A. S. Lakshmanan, "Succesively Pulse Plated Cadmium Selenide Films and Their Photoelectrochemical Behaviour," *Bull. Mater. Sci.*, **17**, 10489 (1994).
88. H. Wyands and M. Cocivera, "Hall Effect and Resistivity Characterization of Doped Electrodeposited CdSe," *J. Electrochem. Soc.*, **139**, 2052 (1992).
89. Y. Golan, L. Margulis, G. Hodes, I. Rubinstein, and J. L. Hutchinson, "Electrodeposited Quantum Dots; High Resolution Electron Microscopy of Epitaxial CdSe Nanocrystals on (111) Gold," *Surf. Sci.*, **L633**, 311 (1994).
90. H. Cachet, R. Cortes, M. Froment, and G. Maurin, "Epitaxial Electrodeposition of Cadmium Selenide Thin Films on Indium Phosphide Single Crystals," *J. Solid State Electrochem.*, **1**, 100 (1997).
91. P. Pramamik and S. Biswas, "Deposition of Zinc Selenide Thin Films by Solution Growth Technique," *J. Electrochem. Soc.*, **133**, 350 (1986).
92. K. Singh and J. P. Rai, "Electrosynthesis of Polycrystalline Photoelectroactive p-zinc Selenide," *J. Mater. Sci. Lett.*, **4**, 1401 (1985).
93. K. Singh and J. P. Rai, "Electrosynthesis and Photoelectroactivity of Polycrystalline p-Zinc Selenide," *Phys. Stat. Sol. (a)*, **99**, 257 (1987).
94. K. Singh and J. P. Rai, "Electrosynthesis and Photoelectroactivity of Thallium Doped Polycrystalline Zinc Selenide," *B. Electrochem.*, **5**, 876 (1989).
95. C. Natarajan, H. Matsumoto, and G. Nogami, "Mechanism of Electrodeposition of MSe(M=Cd &Zn) Films from Selenosulfite Solution," *Bull. Electrochem.*, **13**, 123 (1997); C. Natarajan, G. Nogami, and M. Sharon, "Electrodeposition and Photovoltaic Properties of Zinc Cadmium Selenide Thin Films," *Bull. Electrochem.* **12**, 136 (1996); C. Natarajan, G. Nogami, and M. Sharon, "Electrodeposition of $Zn_{1-x}Cd_xSe$ (x=0–1) Thin Films," *Thin Solid Films*, **261**, 44 (1995).
96. A. Darkowski and A. Grabowski, "Electrodeposition of Cd-Zn-Se Thin Films from Selenosulphite Solutions," *Solar Energy Mater.*, **23**, 75 (1991).
97. T. Edamura and Muto, "Preparation and Properties of Electrodeposited Ternary CdS_xSe_{1-x} and $Zn_xCd_{1-x}S$ Films," *Thin Solid Films*, **226**, 135 (1993).
98. B. M. Basol, V. K. Kapur, and M. L. Ferris, "Low Cost Technique for Preparing $Cd_{1-x}Zn_xTe$ Films for Solar Cells," *J. Appl. Phys.,* **66**, 1816 (1989).
99. R. Hill, "Cadmium-Sulphide/Copper-Sulphide Thin-Film Solar Cells: Review of Methods of Producing the CdS and Cu_2S Layers," *Solid-State Electron. Dev.*, **2**, S49 (1978).
100. B. Miller, S. Menezes, and A. Heller, "Anodic Formation of Semiconductive Sulfide Films at Cadmium and Bismuth Rotating Ring-Disk Electrode Studies," *J. Electroanal. Chem.*, **94**, 85 (1978).
101. L. M. Peter, "The Electrocrystallisation of Cadmium Sulphide Films on Cadmium," *Electrochim. Acta*, **23**, 165 (1978).
102. L. M. Peter, "The Photoelectrochemical Properties of Anodic Cadmium Sulphide Films," *Electrochim. Acta*, **23**, 1073 (1978).
103. E. Fatas, R. Duo, P. Herrasti, F. Arjona, and E. Garcia-Camarero, "Electrochemical Deposition of CdS Thin Films on Mo and Al Substrates," *J. Electrochem. Soc.*, **131**, 2243 (1984).

104. G. P. Power, D. R. Peggs, and A. J. Parker, "The Cathodic Formation of Photoactive Cadmium Sulfide Films from Thiosulfate Solutions," *Electrochim. Acta*, **26**, 681 (1981).

105. G. C. Morris and R. Vanderveen, "Cadmium Sulphide Films Prepared by Pulsed Electrodeposition," *Solar Energy Mat.*, **27**, 305 (1992).

106. S. Dennison, "Studies of the Cathodic Electrodeposition of CdS from Aqueous Solution," *Electrochim. Acta*, **38**, 2395 (1993).

107. S. K. Das and G. C. Morris, "Preparation and Properties of CdS/CdTe Thin Film Solar Cell Produced by Periodic Pulse Electrodeposition Technique," *Solar Energy Mat. Solar Cells*, **30**, 107 (1993).

108. U. Demir and C. Shannon, "A Scanning Tunneling Microscopy Study of Electrochemicallly Grown Cadmium Sulphide Monolayers on Au (111)," *Langmuir*, **10**, 2794 (1994).

109. U. Demir and C. Shannon, "Reconstruction of Cadmium Sulfide Monolayers on Au (100)," *Langmuir*, **12**, 594 (1996).

110. U. Demir and C. Shannon, "Electrochemistry of Cd at $(\sqrt{3} \times \sqrt{3})$R30o-S/Au(111): Kinetics of Structural Changes in CdS Monolayers," *Langmuir*, **12**, 6091 (1996).

111. K. Shirai, Y. Moriguchi, M. Ichimura, A. Usami, and M. Saji, "Relationship Between Raman Spectra and Crystallinity of CdS Films Grown by Cathodic Electrodeposition," *Jpn. J. Appl. Phys.*, **35**, 2057 (1996).

112. B. E. Boone and C. Shannon, "Optical Properties of Ultrathin Electrodeposited CdS Films Probed by Resonance Raman Spectroscopy and Photoluminescence," *J. Phys. Chem.*, **100**, 9480 (1996).

113. G. Sasikala, R. Dhanasekaran, and C. Subramanian, "Electrodeposition and Optical Characterisation of CdS Thin Films on ITO-coated Glass," *Thin Solid Films*, **302**, 71 (1997).

114. F. Goto, K. Shirai, and M. Ichimura, "Defect Reduction in Electrochemically Deposited CdS Thin Films by Annealing in O_2," *Solar Energy Mat. Solar Cells*, **50**, 147 (1998).

115. Z. Zainal, M. Z. Hussein, A. Kassim, and A. Ghasali, "Electrodeposited SnS Thin-Films from Aqueous-Solution," *J. Mater. Sci. Lett.*, **16**, 1446 (1997).

116. Z. Zainal, M. Z. Hussein, and A. Ghasali, "Cathodic Electrodeposition of SnS Thin-Films from Aqueous-Solution," *Solar Energy Mater. Solar Cells*, **40**, 347 (1996).

117. N. Nakayama, "Ceramic CdS Solar Cell," *Jap. J. Appl. Phys.*, **8**, 450 (1969).

118. J. Vedel, P. Cowache, and D. Lincot, "Electrochemical Preparation and Conditioning of Cu_2S for Cu_2S-CdS Solar Cells," Proceedings of Fourth European Communities Photovolatic Solar Energy Conference, Stresa, Italy, May 10–14, 1982.

119. J. Vedel, P. Cowache, and M. Soubeyrand, "Electroplating of Cu_xS on CdS," *Solar Energy Mat.*, **10**, 25 (1984).

120. A. M. Al-Dhafiri, G. J. Russell, and J. Woods, "Electrochemical Control of the Cu_xS phase in Cu_xS-CdS Photovoltaic Cells," *Semicond. Sci. Technol.*, **6**, 983 (1991).

121. A. M. Al-Dhafiri, P. C. Pande, G. J. Russell, and J. Woods, "Electroplated Cu_xS-CdS Photovoltaic Cells," *J. Crystal. Growth*, **86**, 900 (1988).

122. A. C. Rastogi and S. Salkalachen, "Improvements in Stoichiometry and Stability of p-Cu_xS Thin-Film Solar Cells," *J. Appl. Phys.*, **58**, 4442 (1985).

123. J. Herrero and J. Ortega, "Electrochemical Synthesis of Photoactive In_2Se_3 Thin Films," *Solar Energy Mat.*, **16**, 477 (1987).

124. W. Dongcheng, L. Tao, L. Hua, and L. Zuming, "Electrochemical Depositing $CuInSe_2$ Thin Films," in *Proceedings of the 1989 Congress of the International Solar Energy Society*, Kobe City, Japan, 4–8, September 1989, **1**, 232 (1990).

125. R. N. Bhattacharya, "Solution Growth and Electrodeposited $CuInSe_2$ Thin Films," *J. Electrochem. Soc.*, **130**, 2040 (1983).

126. R. N. Bhattacharya and K. Rajeshwar, "Electrodeposition of CuInX (X=Se,Te) Thin Films," *Solar Cells*, **16**, 237 (1986).

127. V. K. Kapur, B. M. Basol, and E. S. Tseng, "Low Cost Methods for the Production of Semiconductor Films for $CuInSe_2$/CdS Solar Cells," *Solar Cells*, **21**, 65 (1987).

128. C. Guillen and J. Herrero, "Optical Properties of Electrochemically Deposited $CuInSe_2$ Thin Films," *Solar Energy Mat.*, **25**, 31 (1991).

129. A. M. Fernandez, P. J. Sebastain, A. M. Hermann, R. N. Bhattacharya, R. N. Noufi, and M. A. Contreras, "Electrodeposition of $CuInSe_2$ Thin Films for Photovoltaic Application," *World Renewable Energy Congress*, A. A. M. Sayigh,Ed., 8, 396 (1996).

130. R. Noufi, R. Powell, R. Axton, Y. Chen, and T. Datta,1984 Annual Report Solid State Photovoltaic Research Branch, SERI/PR-212-2601 DE85008812, April 1985.

131. G. Hodes and D. Cahen, "Electrodeposition of $CuInSe_2$ and $CuInS_2$ Films," *Solar Cells*, **16**, 245 (1986).

132. C. D. Lokhande, "Pulse Plated Electrodeposition of $CuInSe_2$ Films," *J. Electrochem. Soc.*, **134**, 1727 (1987).

133. Y. Ueno, H. Kawai, T. Sugiura, and H. Minoura, "Electrodeposition of $CuInSe_2$ Films from Sulphate Bath," *Thin Solid Films*, **157**, 159 (1988).

134. D. Pottier and G. Maurin, "Preparation of Polycrystalline Thin Films of $CuInSe_2$ by Electrodeposition," *J. Appl. Electrochem.*, **19**, 361 (1989).

135. S. N. Sahu, R. D. L. Kristensen, and D. Haneman, "Electrodeposition of $CuInSe_2$ Thin Films from Aqueous Solutions," *Solar Energy Mat.*, **18**, 385 (1989).

136. K. K. Mishra and K. Rajeshwar, "A Voltammetric Study of the Electrodeposition Chemistry in the Cu + In + Se System," *J. Electroanal. Chem.*, **271**, 279 (1989).

137. N. Khare, G. Razzini, and L. P. Bicelli, "Electrodeposition and Heat Treatment of CuInSe2 Films," *Thin Solid Films*, **186**, 113 (1990).

138. F. J. Pern, R. Noufi, A. Mason, and A. Franz, "Characterizations of Electrodeposited $CuInSe_2$ Thin Films: Structure, Deposition, and Formation Mechanism," *Thin Solid Films*, **202**, 299 (1991).

139. C. Guillen, E. Galiano, and J. Herrero, "Cathodic Electrodeposition of $CuInSe_2$ Thin Films," *Thin Solid Films*, **195**, 137 (1991).

140. H. Gomez, R. Schrebler, L. Basaez, and E. A. Dalchiele, "Electrochemical Growth and Characterization of Polycrystalline $CuInSe_2$ Thin Films," *J. Phys. Condens. Matt.*, **5**, A349 (1993).

141. S. R. Kumar, R. B. Gore, and R. K. Pandey, "Properties of $CuInSe_2$ Films Prepared by the Rapid Thermal Annealing Technique," *Thin Solid Films*, **223**, 109 (1993).

142. L. Thouin, S. Massaccesi, S. Sanchez, and J. Vedel, "Formation of Copper Indium Selenide by Electrodeposition," *J. Electroanal. Chem.*, **374**, 81 (1994).

143. T. Edamura and J. Muto, "Preparation and Characterization of Pulse-Plating Electrodeposited $CuInSe_2$ Thin Films," *J. Mater. Sci: Mater. Electron.*, **5**, 275 (1994).

144. J. Vedel, "An Electrochemical Route for the Preparation of Chalcopyrite Semiconductors," Inst. Phys. Conf. Set. No. 152: Section B: Thin Film Growth and Characterization. Presented at 11th Int. Conf. on Ternary and Multilayer Compounds, Salford, September 8–12, 1998), p. 261.

145. B. M. Basol, O. M. Stafsudd, and A. Bindal, "Thin Films of Mercury Cadmium Telluride for Solar Cell Applications," *Solar Cells*, **15**, 279 (1985).

146. C. L. Colyer and M. Cocivera, "Thin-Film Cadmium Mercury Telluride Prepared by Nonaqueous Electrodeposition," *J. Electrochem. Soc.*, **139**, 406 (1992).

147. J. Ramiro and A. Garcia Camarero, "Influence of Deposition Potential and Electrolyte Composition on the Structural and Photoelectrochemical Properties of Electrodeposited Mercury Cadmium Telluride," *J. Mat. Sci.*, **31**, 2047 (1996).

148. J. W. Diggle, Ed., *Oxides and Oxide Films*, Marcel Dekker, New York, 1972.

149. A. Eftekhari, Ed., *Nanostructured Materials in Electrochemistry*, Wiley-VCH, Weinheim, 2008.

150. D. J. Blackwood and L. M. Peter, "The Influence of Growth Rate on the Properties of Anodic Oxide Films on Titanium," *Electrochim. Acta*, **34**, 1505 (1989).

151. D. J. Blackwood and L. M. Peter, "Potential Modulated Reflectance Spectroscopy of Anodic Oxide Films on Titanium," *Electrochim. Acta*, **35**, 1073 (1990).

152. D. Tench and L. F. Warren, "Electrodeposition of Conducting Transition Metal Oxide/Hydroxide Films from Aqueous Solution," *J. Electrochem. Soc.*, **130**, 869 (1983).

153. G. H. A. Therese and P. V. Kamath, "Electrochemical Synthesis of Metal Oxides and Hydroxides," *Chem. Mater.*, **12**, 1195 (2000).

154. Y. Matsumoto, "Electrochemical and Photoelectrochemical Processing for Oxide Films," *MRS Bull.*, September, p. 47 (2000).

155. D. Lincot, "Electrodeposition of Semiconductors," *Thin Solid Films*, **487**, 40 (2005).

156. K. Rajeshwar, N. R. de Tacconi, and C. R. Chenthamarakshan, "Spatially Directed Electrosynthesis of Semiconductors for Photoelectrochemical Applications," *Curr. Opinion Solid-State Mater. Sci.*, **8**, 173 (2004).

157. V. Zwilling, M. Aucouturier, and E. Darque-Ceretti, "Anodic Oxidation of Titanium and TA6V Alloy in Chromic Media. An Electrochemical Approach," *Electrochim. Acta*, **45**, 921 (1991).

158. C. Natarajan and G. Nogami, "Cathodic Electrodeposition of Nanocrystalline Titanium Dioxide Thin Films," *J. Electrochem. Soc.*, **143**, 1547 (1996).

159. D. Schwarzenback, "The Structure of a Chelated Dinuclear Peroxytitanium (IV)," *Inorg. Chem.*, **9**, 2391 (1970).

160. P. Comba and A. Merbach, "The Titanyl Question Revisited," *Inorg. Chem.*, **26**, 1315 (1987).

161. S. Karuppuchamy, D. P. Amalnerkar, K. Yamaguchi, T. Yoshida, T. Sugiura, and H. Minoura, "Cathodic Electrodeposition of TiO_2 Thin Films for Dye-Sensitized Photoelectrochemical Applications," *Chem. Lett.*, 78 (2001).

162. S. Karuppuchamy, K. Nonomura, T. Yoshida, T. Sugiura, and H. Minoura, "Cathodic Electrodeposition of Oxide Semiconductor Thin Films and Their Application to Dye-Sensitized Solar Cells," *Solid State Ionics*, **151**, 19 (2002).

163. J. Yamamoto, A. Tan, R. Shiratsuchi, S. Hayase, C.R. Chenthamarakshan, and K. Rajeshwar, "A 4% Efficient Dye-Sensitized Solar Cell Fabricated from Cathodically Electrosynthesized Composite Titania Films," *Adv. Mater.*, **15**, 1823 (2003).

164. I. Zhitomirsky, "Cathodic Electrosynthesis of Titania Films and Powders," *Nanostructured Mater.*, **8**, 521 (1997).

165. L. H. Madkour and A. S. Fouda, "Electrodeposition of Titanium and Its Dioxide from Ilmenite," *J. Electronal. Chem.*, **199**, 207 (1986).

166. L. Kavan, B. O'Regan, A. Kay, and M. Grätzel, "Preparation of TiO_2 (Anatase) Films on Electrodes by Anodic Oxidative Hydrolysis of $TiCl_3$," *J. Electronal. Chem.*, **346**, 291 (1993).

167. A Manivannan, N. Spataru, K. Arihora, and A. Fujishima, "Electrochemical Deposition of Tatanium Oxide on Boron-Doped Diamond Electrodes," *Electrochem. Solid-State Lett.*, **8**, C138 (2005).

168. Y. B. Xie and X. Z. Li, "Preparation and Characterization of TiO_2/Ti Film Electrodes by Anodization of Low Voltage for Photoelectrocatalytic Applications," *J. Appl. Electrochem.*, **36**, 663 (2006).

169. S. Sawatani, T. Yoshida, T. Ohya, T. Ban, Y. Takahashi, and H. Minoura, "Electrodeposition of TiO_2 Thin Films by Anodic Formation of Titanate/Benzoquinone Hybrid," *Electrochem. Solid-State Lett.*, **8**, C69 (2005).

170. D. Matthews, A. Kay, and M. Grätzel, "Electrophoretically Deposited Titanium Dioxide Thin Films for Photovoltaic Cells," *Aust. J. Chem.*, **47**, 1869 (1994).

171. D. Gong, C. A. Grimes, O. K. Varghese, W. Hu, R. S. Singh, Z. Chen, and E. C. Dickey, "Titanium Oxide Nanotube Arrays Prepared by Anodic Oxidation," *J. Mater. Res.*, **16**, 3331 (2001).

172. M. Paulose, K. Shankar, S. Yoriya, H. E. Prakasam, O. K. Varghese, G. K. Mor, T. A. Latempa, A. Fitzgerald, and C. A.

Grimes, "Anodic Growth of Highly Ordered TiO_2 Nanotube Arrays to 134 μm in Length," *J. Phys. Chem. B*, **110**, 16179 (2006).

173. J. M. Macak, H. Tsuchiya, and P. Schmuki, "High-Aspect-Ratio TiO_2 Nanotubes by Anodization of Titanium," *Angew. Chem. Int. Ed.*, **44**, 2100 (2005).
174. J. M. Macak, H. Tsuchiya, L. Taveira, S. Aldabergerova, and P. Schmuki, "Smooth Anodic TiO_2 Nanotubes," *Angew. Chem. Int. Ed.*, **44**, 7463 (2005).
175. A. Ghicov, H. Tsuchiya, J. M. Macak, and P. Schmuki, "Titanium Oxide Nanotubes Prepared in Phosphate Electrolytes," *Electrochem. Commun.*, **7**, 505 (2005).
176. G. K. Mor, O. K. Varghese, M. Paulose, K. Shankar, and C. A. Grimes, "A Review on Highly Ordered, Vertically Oriented TiO_2 Nanotube Arrays: Fabrication, Material Properties, and Solar Energy Applications," [review], *Solar Energy Mater. Solar Cells*, **90**, 2011 (2006).
177. C. A. Grimes, "Synthesis and Application of Highly Ordered Arrays of TiO_2 Nanotubes," *J. Mater. Chem.*, **17**, 1451 (2007).
178. W. Chanmanee, A. Watcharenwong, C. R. Chenthamarakshan, P. Kajitvichyanukul, N. R. de Tacconi, and K. Rajeshwar, "Titania Nanotubes from Pulse Anodization of Titanium Foils," *Electrochem. Commun.*, **9**, 2145 (2007).
179. W. Chanmanee, A. Watcharenwong, C. R. Chenthamarakshan, P. Kajitvichyanukul, N. R. de Tacconi, and K. Rajeshwar, "Formation and Characterization of Self-Organized TiO_2 Nanotube Arrays by Pulse Anodization," *J. Am. Chem. Soc.*, **130**, 965 (2008).
180. K. S. Raja, M. Misra, and K. Paramgum, "Formation of Self-Ordered Nano-Tubular Structure of Anodic Oxide layer on Titanium," *Electrochim. Acta*, **51**, 154 (2005).
181. K. S. Raja, T. Gandhi, and M. Misra, "Effect of Water Content of Ethylene Glycol as Electrolyte for Synthesis of Ordered Titania Nanotubes," *Electrochem. Commun.*, **9**, 1069 (2007).
182. S. Kaneco, Y. Chen, P. Westerhoff, and J. C. Crittenden, "Fabrication of Uniform Size Titanium Oxide Nanotubes: Impact of Current Density and Solution Conditions," *Scripta Mater.*, **56**, 373 (2007).
183. A. Ghicov, J. M. Macak, H. Tsuchiya, J. Kunze, V. Haeublein, S. Kleber, and P. Schmuki, "TiO_2 Nanotube Layers: Dose Effects During Nitrogen Doping by Ion Implantation," *Chem. Phys. Lett.*, **419**, 426 (2006).
184. A. Ghicov, H. Tsuchiya, R. Hahn, J. M. Macak, A. G. Muñoz, and P. Schmuki, "TiO_2 Nanotubes: H^+ Insertion and Strong Electrochromic Effects," *Electrochem. Commun.*, **8**, 528 (2006).
185. R. P. Vitiello, J. M. Macak, A. Ghicov, H. Tsuchiya, L. E. P. Dick, and P. Schmuki, "N-Doping of Anodic TiO_2 Nanotubes Using Heat Treatment in Ammonia," *Electrochem. Commun.*, **8**, 544 (2006).
186. J. M. Macak, A. Ghicov, R. Hahn, H. Tsuchiya, and P. Schmuki, "Photoelectrochemical Properties of N-Doped Self-Organized Titania Nanotube Layers with Different Thicknesses," *J. Mater. Sci.*, **21**, 2824 (2006).
187. J. H. Park, S. Kim, and A. J. Bard, "Novel Carbon-Doped TiO_2 Nanotube Arrays with High Aspect Ratios for Efficient Solar Water Splitting," *Nano Lett.*, **6**, 24 (2006).
188. K. Shankar, M. Paulose, G. K. Mor, O. K. Varghese, and C. A. Grimes, "A Study on the Spectral Photoresponse and Photoelectrochemical Properties of Flame-Annealed Titania Nanotube-Arrays," *J. Phys. D: Appl. Phys.*, **38**, 3543 (2005).
189. G. K. Mor, O. K. Varghese, M. Paulose, and C. A. Grimes, "A Self-Cleaning, Room-Temperature Titania Nanotube Hydrogen Gas Sensor," *Sensor Lett.*, **1**, 42 (2003).
190. O. K. Varghese and C. A. Grimes, "Metal Oxide Nanoarchitectures for Environmental Sensing," *J. Nanosci. Nanotech.*, **3**, 277 (2003).
191. O. K. Varghese, D. Gong, M. Paulose, K. G. Ong, and C. A. Grimes, "Hydrogen Sensing Using Titania Nanotubes," *Sensors Actuators, B* **93**, 338 (2003).
192. O. K. Varghese, D. Gong, M. Paulose, K. G. Ong, and C. A. Grimes, "Extreme Changes in the Electrical Resistance of Titania Nanotubes with Hydrogen Exposure," *Adv. Mater.*, **15**, 624 (2003).
193. G. K. Mor, M. A. Carvalho, O. K. Varghese, M. V. Pishko, and C. A. Grimes, "A Room-Temperature TiO_2-Nanotube Hydrogen Sensor Able to Self-Clean Photoactively from Environmental Contamination," *J. Mater. Res.*, **19**, 628 (2004).
194. O. K. Varghese, G. K. Mor, C. A. Grimes, M. Paulose, and N. Mukherjee, "A Titania Nanotube-Array Room-Temperature Sensor for Selective Detection of Hydrogen at Low Concentrations," *J. Nanosci. Nanotech.*, **4**, 733 (2004).
195. G. K. Mor, K. Shankar, M. Paulose, O. K. Varghese, and C. A. Grimes, "Enhanced Photocleavage of Water Using Titania Nanotube Arrays," *Nano Lett.*, **5**, 191 (2005).
196. O. K. Varghese, M. Paulose, K. Shankar, G. K. Mor, and C. A. Grimes, "Water-Photolysis Properties of Micron-Length Highly-Ordered Titania Nanotube-Arrays," *J. Nanosci. Nanotech.*, **5**, 1158 (2005).
197. K. Shankar, G. K. Mor, H. E. Prakasam, S. Yoriya, M. Paulose, O. K. Varghese, and C. A. Grimes, "Highly-Ordered TiO_2 Nanotube Arrays up to 220 μm in Length: Use in Water Photoelectrolysis and Dye-Sensitized Solar Cells," *Nanotechnology*, **18**, 065707/1 (2007).
198. S. K. Mohapatra, M. Misra, V. K. Mahajan, and K. S. Raja, "Design of a Highly Efficient Photoelectrolytic Cell for Hydrogen Generation by Water Splitting: Application of $TiO_{2-x}C_x$ Nanotubes as a Photoanode and Pt/TiO_2 Nanotubes as a Cathode," *J. Phys. Chem. C*, **111**, 8677 (2007).
199. S. K. Mohapatra and M. Misra, "Enhanced Photoelectrochemical Generation of Hydrogen from Water by 2,6-Dihydroxyanthraquinone-Funtionalized Titanium Dioxide Nanotubes," *J. Phys. Chem. C*, **111**, 11506 (2007).
200. J. M. Macak, P. J. Barczuk, H. Tsuchiya, M. Z. Nawakowska, A Ghicov, M. Chojak, S. Bauer, S. Virtanen, P. J. Kulesza, and P. Schmuki, "Self-Organized Nanotubular TiO_2 Matrix as Support for Dispersed Pt/Ru Nanoparticles: Enhancement of the Electrocatalytic Oxidation of Methanol," *Electrochem. Commun.*, **7**, 1417 (2005).

201. J. M. Macak, H. Tsuchiya, A Ghicov, and P. Schmuki, "Dye-Sensitized Anodic TiO_2 Nanotubes," *Electrochem. Commun.*, **7**, 1133 (2005).
202. M. Paulose, K. Shankar, O. K. Varghese, G. K. Mor, and C. A. Grimes, "Application of Highly-Ordered TiO_2 Nanotube-Arrays in Heterojunction Dye-Sensitized Solar Cells," *J. Phys. D: Appl. Phys.*, **39**, 2498 (2006).
203. G. K. Mor, K. Shankar, M. Paulose, O. K. Varghese, and C. A. Grimes, "Use of Highly-ordered TiO_2 Nanotube Arrays in Dye-Sensitized Solar Cells," *Nano Lett.*, **6**, 215 (2006).
204. K. Zhu, N. R. Neale, A. Miedaner, and A. J. Frank, "Enhanced Charge-Collection Efficiencies and Light Scattering in Dye-Sensitized Solar Cells Using Oriented TiO_2 Nanotubes Arrays," *Nano Lett.*, **7**, 69 (2007).
205. D. Kuang, J. Brillet, P. Chen, M. Takata, S. Uchida, H. Miura, K. Sumioka, S. M. Zakeeruddin, and M. Grätzel, "Application of Highly Ordered TiO_2 Nanotube Arrays in Flexible Dye-Sensitized Solar Cells," *ACS Nano*, **2**, 1113 (2008).
206. N. R. de Tacconi, W. Chanmanee, K. Rajeshwar, J. Rochford, and E. Galoppini, "Photoelectrochemical Behavior of Polychelate Porphyrin Chromophores and Titanium Dioxide Nanotube Arrays in Dye-Sensitized Solar Cells," *J. Phys. Chem. C*, **113**, 2996 (2009).
207. X. Quan, S. Yang, X. Ruan, and H. Zhao, "Preparation of Titania Nanotubes and Their Environmental Applications as Electrode," *Environ. Sci. Technol.*, **39**, 3770 (2005).
208. M. Izaki and T. Omi, "Transparent Zinc Oxide Films Prepared by Electrochemical Reaction," *Appl. Phys. Lett.*, **68**, 2439 (1996).
209. S. Peulon and D. Lincot, "Cathodic Electrodeposition from Aqueous Solution of Dense or Open-Structured Zinc Oxide Films," *Adv. Mater.*, **8**, 166 (1996).
210. M. Izaki and T. Omi, "Electrolyte Optimization for Cathodic Growth of Zinc Oxide Films," *J. Electrochem. Soc.*, **143**, L53 (1996).
211. M. Izaki and T. Omi, "Characterization of Transparent Zinc Oxide Films Prepared by Electrochemical Reaction," *J. Electrochem. Soc.*, **144**, 1949 (1997).
212. T. Yoshino, S. Takanezawa, T. Ohmori, and H. Masuda, "Preparation of ZnO/Au Nanocomposite Thin Films by Electrodeposition," *J. Appl. Phys.*, **35**, L1512 (1996).
213. Z. H. Gu, T. Z. Fahidy, and R. Hornsey, "A Study of the Electrochemical Synthesis of ZnO Thin Films," *Can. J. Chem.*, **75**, 1439 (1997).
214. Z. H. Gu and T. Z. Fahidy, "Electrochemical Deposition of ZnO Thin Films on Tin-Coated Glasses," *J. Electrochem. Soc.*, **146**, 156 (1999).
215. S. Peulon and D. Lincot, "Mechanistic Study of Cathodic Electrodeposition of Zinc Oxide and Zinc Hydroxychloride Films from Oxygenated Aqueous Zinc Chloride Solutions," *J. Electrochem. Soc.*, **145**, 864 (1998).
216. A. Goux, T. Pauporté, J. Chivot, and D. Lincot, "Temperature Effects on ZnO Electrodeposition," *Electrochim. Acta*, **50**, 2239 (2005).
217. T. Pauporté and D. Lincot, "A New System for Fast Electrodeposition of Zinc Oxide Based on Hydrogen Peroxide Oxygen Precursor," *J. Electrochem. Soc.*, **148**, C310 (2001).
218. T. Pauporté and D. Lincot, "Hydrogen Peroxide Oxygen Precursor for Zinc Oxide Electrodeposition II—Mechanistic Aspects," *J. Electroanal. Chem.*, **517**, 54 (2001).
219. T. Pauporté and D. Lincot, "Heteroepitaxial Electrodeposition of Zinc Oxide Films on Gallium Nitride," *Appl. Phys. Lett.*, **75**, 3817 (1999).
220. R. Konenkamp, K. Boedecker, M. C. Lux-Steiner, M. Poschenrieder, F. Zenia, C. Lévy-Clément, and S. Warner, "Thin-Film Semiconductor Deposition on Free-Standing ZnO Columns," *Appl. Phys. Lett.*, **77**, 2575 (2000).
221. H. Ishizaki, M. Izaki, and T. Ito, "Influence of $(CH_3)_2NHBH_3$ Concentration on Electrical Properties of Electrochemically Grown ZnO Films," *J. Electrochem. Soc.*, **148**, C540 (2001).
222. G. Machado, D. N. Guerra, D. Leinen, J. R. Ramos-Borrado, R. E. Marotti, and E. A. Dalchiele, "Indium-Doped Zinc Oxide Thin Film Obtained by Electrodeposition," *Thin Solid Films*, **490**, 124 (2005). See also references therein.
223. D. Gal, G. Hodes, D. Lincot, and H.-W. Schock, "Electrochemical Deposition of Zinc Oxide Films from Non-Aqueous Solution: A New Buffer/Window Process for Thin Film Solar Cells," *Thin Solid Films*, **361**, 79 (2000).
224. J. Jayakrishnan and G. Hodes, "Non-Aqueous Electrodeposition of ZnO and CdO Films," *Thin Solid Films*, **440**, 19 (2003).
225. Y. L. Liu, Y. C. Liu, Y. X. Liu, D. Z. Shen, Y. M. Lu, J. Y. Zhang, and X. W. Fan, "Structural and Optical Properties of Nanocrystalline ZnO Films Grown by Cathodic Electrodeposition on Si Substrates," *Physica B*, **322**, 31 (2002).
226. L. Xu, Y. Guo, Q. Liao, J. Zhang, and D. Xu, "Morphological Control of ZnO Nanostructures by Electrodeposition," *J. Phys. Chem. B*, **109**, 13519 (2005).
227. R. Tena-Zaera, J. Elias, G. Wang, and C. Lévy-Clément, "Role of Chloride Ions on Electrochemical Deposition of ZnO Nanowire Arrays from O_2 Reduction," *J. Phys. Chem. C*, **111**, 16706 (2007).
228. J. Elias, R. Tena-Zaera, and C. Lévy-Clément, "Electrochemical Deposition of ZnO Nanowire Arrays with Tailored Dimensions," *J. Electroanal. Chem.*, **621**, 171 (2008).
229. J. Elias, R. Tena-Zaera, G.-Y. Wang, and C Lévy-Clément, "Corrosion of ZnO Nanowires into Nanotubes with Tailored Dimensions," *Chem. Mater.*, **20**, 6633 (2008).
230. E. M. Wong and P. C. Searson, "Kinetics of Electrophoretic Deposition of Zinc Oxide Quantum Particle Thin Films," *Chem. Mater.*, **11**, 1959 (1999).
231. F. Tang, T. Uchikashi, and Y. Sakkai, "Electrophoretic Deposition Behavior of Aqueous Nanosized Zinc Oxide Suspensions," *J. Am. Ceram. Soc.*, **85**, 2161 (2002).
232. T. Yoshida, K. Terada, D. Schlettwein, T. Oekermann, T. Sugiura, and H. Minoura, "Electrochemical Self-Assembly of Nanoporous ZnO/Eosin Y Thin Films and Their Sensitized Photoelectrochemical Performance," *Adv. Mater.*, **12**, 1214 (2000).

233. T. Pauporté, T. Yoshida, A. Goux, and D. Lincot, "One-Step Electrodeposition of ZnO/Eosin Y Hybrid Films from a Hydrogen Peroxide Oxygen Precursor," *J. Electroanal. Chem.*, **534**, 55 (2002).

234. T. Yoshida and H. Minoura, "Electrochemical Self-Assembly of Dye-Modified Zinc Oxide Thin Films," *Adv. Mater.*, **12**, 1219 (2000).

235. B. O'Regan, D. T. Schwartz, S. M. Zakeeruddin, and M. Grätzel, "Electrodeposited Nanocomposite n-p Heterojunction for Solid-State Dye-Sensitized Photovoltaics," *Adv. Mater.*, **12**, 1263 (2000).

236. C. Lévy-Clément, R. Tena-Zaera, M. A. Ryan, A. Katty, and G. Hodes, "CdSe-Sensitized p-CuSCN/Nanowire n-ZnO Heterojunctions," *Adv. Mater.*, **17**, 1512 (2005).

237. C. Lévy-Clément, A. Katty, S. Bastide, F. Zenia, I. Mora, and V. Muñoz-Sanjosé, "A New CdTe/ZnO Columnar Composire Film for ETA Solar Cells," *Physica E*, **14**, 229 (2004).

238. R. Tena-Zaera, A. Katty, S. Bastide, C. Lévy-Clément, B. O'Reagan, and V. Muñoz-Sanjosé, "ZnO/CdTe/CuSCN, A Promising Heterostructure to Act as Inorganic ETA-Solar Cell," *Thin Solid Films*, **483**, 372 (2005).

239. J. Elias, R. Tena-Zaera, and C. Lévy-Clément, "Electrodeposition of ZnO Nanowires with Controlled Dimensions for Photovoltaic Applications: Role of Buffer Layer," *Thin Solid Films*, **515**, 8553 (2007).

240. T. Pauporté and D. Lincot, "Electrodeposition of Semiconductors for Optoelectronic Devices: Results on Zinc Oxide," *Electrochim. Acta*, **45**, 3345 (2000).

241. T. Pauporté, D. Lincot, B. Viana, and F. Pellé, "Toward Laser Emission of Epitaxial Nanorod Arrays of ZnO Grown by Electrodeposition," *Appl. Phys. Lett.*, **89**, 233112 (2006).

242. T. Pauporté and T. Yoshida, "Hybrid Layers of ZnO/Lanthanide Complexes with High Visible Luminescence," *J. Mater. Chem.*, **16**, 4529 (2006).

243. T. Pauporté, T. Yoshida, D. Kamatsu, and H. Minoura, "Highly Porous Electrodeposited Zinc Oxide Films Functionalized for Red/Green Luminescence," *Electrochem. Solid-State Lett.*, **9**, H16 (2006).

244. T. Pauporté, F. Bedioni, and D. Lincot, "Nanostructured Zinc Oxide— Chromophore Hybrid Films with Multicolored Electrochromic Properties," *J. Mater. Chem.*, **15**, 1552 (2005).

245. A. Goux, T. Pauporté, and D. Lincot, "Oxygen Reduction Reaction on Electrodeposited Zinc Oxide in KCl Solution at 70°C," *Electrochim. Acta*, **51**, 3168 (2006).

246. T. Pauporté and J. Rathousky, "Electrodeposited Mesoporous ZnO as Efficient Photocatalysts for the Degradation of Dye Pollutants," *J. Phys. Chem. C*, **111**, 7629 (2007).

247. K. Yamanaka, H. Oakamoto, H. Kidou, and T. Kudo, "Peroxotungstic Acid Coated Films for Electrochromic Display Devices," *Jpn. J. Appl. Phys., Part I*, **25**, 1420 (1986).

248. K. Yamanaka, "Electrodeposited Films from Aqueous Tungstic Acid-Hydrogen Peroxide Solutions for Electrochromic Display Devices," *Jpn. J. Appl. Phys., Part I*, **26**, 1884 (1987).

249. P. K. Shin, J. Syed-Bokhari, and A. C. C. Tseung, "The Performance of Electrochromic Tungsten Trioxide Films Doped with Cobalt or Nickel," *J. Electrochem. Soc.*, **138**, 2778 (1991).

250. P. K. Shin and A. C. C. Tseung, "Study of Electrodeposited Tungsten Trioxide Thin Films," *J. Mater. Chem.*, **2**, 1141 (1992). See also references therein

251. T. Kudo, H. Okamoto, K. Matsumoto, and Y. Sasaki, "Peroxopolytungstic Acids Synthesized by Direct Reaction of Tungsten or Tungsten Carbide with Hydrogen Peroxide," *Inorg. Chim. Acta*, **111**, L27 (1986).

252. T. Nanba, S. Takano, I. Yasui, and T. Kudo, "Structural Study of Peroxopoly-Tungstic Acid Prepared from Metallic Tungsten and Hydrogen Peroxide," *J. Solid-State Chem.*, **90**, 47 (1991).

253. E. A. Meulenkamp, "Mechanism of WO_3 Electrodeposition from Peroxy-Tungstate Solutions," *J. Electrochem. Soc.*, **144**, 1664 (1997).

254. T. Pauporté, "A Simplified Method for WO_3 Electrodeposition," *J. Electrochem. Soc.*, **149**, C539 (2002).

255. P. K. Shin, H. T. Huang, and A. C. C. Tseung, "A Study of Tungsten Trioxide and Polyaniline Composite Films," *J. Electrochem. Soc.*, **139**, 1840 (1992).

256. N. Mukherjee, M. Paulose, O. K. Varghese, G. K. Mor, and C. A. Grimes, "Fabrication of Nanoporous Tungsten Oxide by Galvanostatic Anodization," *J. Mater. Res.*, **18**, 2296 (2003).

257. H. Tsuchiya, J. M. Macak, I. Sieber, L. Taveira, A. Ghicov, K. Sirotna, and P. Schmuki, "Self-Organized Porous WO_3 Formed in NaF Electrolytes," *Electrochem. Commun.*, **7**, 215 (2005).

258. S. Berger, H. Tsuchiya, A. Ghicov, and P. Schmuki, "High Photocurrent Conversion Efficiency in Self-Organized Porous WO_3," *Appl. Phys. Lett.*, **88**, 203119 (2006).

259. N. R. de Tacconi, C. R. Chenthamarakshan, G. Yogeeswaran, A. Watcharenwong, R. S. de Zoysa, N. A. Basit, and K. Rajeshwar, "Nanoporous TiO_2 and WO_3 Films by Anodization of Titanium and Tungsten Substrates: Influence of Process Variables on Morphology, and Photoelectrochemical Performance," *J. Phys. Chem. B*, **110**, 25347 (2006).

260. Y. Cuo, X. Quan, N. Lu, H. Zhao, and S. Chen, "High Photocatalytic Capability of Self-Assembled Nanoporous WO_3 with Preferential Orientations of (002) Planes," *Environ. Sci. Technol.*, **41**, 4422 (2007).

261. A. Watcharenwong, W. Chanmanee, N. R. de Tacconi, C. R. Chenthamarakshan, P. Kajitvichyanukul, and K. Rajeshwar, "Anodic Growth of Nanoporous WO_3 Films: Morphology, Photoelectrochemical response and Photocatalytic Activity for Methylene Blue and Hexavalent Chrome Conversion," *J. Electroanal. Chem.*, **612**, 112 (2008).

262. B. Reichman and A. J. Bard, "Semiconductor Electrodes. XXII. Electrochromism and Photoelectrochemistry of WO_3 Layers Prepared by Thermal and Anodic Oxidation of W," *J. Electrochem. Soc.*, **126**, 2133 (1979).

263. J. N. Yao, P. Chen, and A. Fujishima, "Electrochromic Behavior of Electrodeposited Tungsten Oxide Thin Films," *J. Electroanal. Chem.*, **406**, 223 (1996).

264. I. Shiyanovskaya, M. Hepel, and E. Tewksburry, "Electrochromism in Electrodeposited Nanocrystalline WO_3 Films. I. Electrochemical and Optical Properties," *J. New Mater. Electrochem. Syst.*, **3**, 241 (2000).
265. S.-H. Baeck, K.-S Choi, T. F. Jaramillo, G. D. Stucky, and E. W. McFarland, "Enhancement of Photocatalytic and Electrochromic Properties of Electrochemically Fabricated Mesoporous WO_3 Thin Films," *Adv. Mater.*, **15**, 1269 (2003).
266. H. Habazaki, Y. Hayashi, and H. Kanno, "Characterization of Electrodeposited WO_3 Films and Its Application to Electrochemical Wastewater Treatment," *Electrochim. Acta*, **47**, 4181 (2002).
267. J. A. Switzer, C.-J. Hung, E. W. Bohannan, M. G. Shumsky, T. D. Golden, and D. C. Van Aken, "Electrodeposition of Quantum-Confined Metal/Semiconductor Nanocomposites," *Adv. Mater.*, **9**, 334 (1997).
268. For example: J. L. Ling and J. P. Wolfe, "Bose-Einstein Condensation of Paraexcitons in Stressed Cu_2O," *Phys. Rev. Lett.*, **71**, 1222 (1993).
269. G. Nagasubramanian, A. S. Gioda, and A. J. Bard, "Semiconductor Electrodes. XXXVII. Photoelectrochemical Behavior of p-Type Cu_2O in Acetonitrile Solutions," *J. Electrochem. Soc.*, **128**, 2158 (1981).
270. F. P. Koffyberg and F. A. Benko, "A Photoelectrochemical Determination of the Position of the Conduction and Valence Band Edges of p-Type CuO," *J. Appl. Phys.*, **53**, 1173 (1982).
271. G. M. Brisard, J. D. Rudnicki, F. Mclarnon, and E. J. Cairns, "Application of Probe Beam Deflection to Study the Electrooxidation of Copper in Alkaline Media," *Electrochim. Acta*, **40**, 857 (1995).
272. P. Poizot, C.-J. Hung, M. P. Nikiforov, E. W. Bohannan, and J. A. Switzer, "An Electrochemical Method for CuO Thin Film Deposition from Aqueous Solutions," *Electrochem. Solid-State Lett.*, **6**, C21 (2003).
273. A. E. Rakhshani, "Preparation, Characteristics and Photovoltaic Properties of Cuprous Oxide—A Review," *Solid-State Electron.*, **29**, 7 (1986).
274. K. Nakaoka and K. Ogura, "Electrochemical Preparation of p-Type Cupric and Curpous Oxides on Platinum and Gold Substrates from Copper (II) Solutions with Various Amino Acids," *J. Electrochem. Soc.*, **149**, C579 (2002).
275. K. Nakaoka, J. Ueyama, and K. Ogura, "Photoelectrochemical behavior of Electrodeposited CuO and Cu_2O Thin Films on Conducting Substrates," *J. Electrochem. Soc.*, **151**, C661 (2004).
276. R. N. Briskman, "A Study of Electrodeposited Cuprous Oxide Photovoltaic Cells," *Solar Energy Mater. Solar Cells*, **27**, 361 (1992).
277. W. Siripala and J. R. P. Jayakody, "Observation of n-Type Photoconductivity in Electrodeposited Copper Oxide Film Electrodes in a Photoelectrochemical Cell," *Solar Energy Mater.*, **14**, 23 (1986).
278. J. Lee and Y. Tak, "Epitaxial Growth of Cu_2O (111) by Electrodeposition," *Electrochem. Solid-State Lett.*, **2**, 559 (1999).
279. A. E. Rakhshani, A. A. Al-Jassar, and J. Varghese, "Electrodeposition and Characterization of Cuprous Oxide," *Thin Solid Films*, **148**, 191 (1987).
280. A. E. Rakhshani and J. Varghese, "Surface Texture in Electrodeposited Films of Cuprous Oxide," *J. Mater. Sci.*, **23**, 3847 (1988).
281. Y. Zhou and J. A. Switzer, "Electrochemical Deposition and Microstructure of Copper (I) Oxide Films," *Scr. Mater.*, **38**, 1731 (1998).
282. T. D. Golden, M. G. Shumsky, Y. Zhou, R. A. VanderWerf, R. A. Van Leeuwen, and J. A. Switzer, "Electrochemical Deposition of Copper (I) Oxide Films," *Chem. Mater.*, **8**, 2499 (1996).
283. L. C. Wang, N. R. de Tacconi, C. R. Chenthamarakshan, K. Rajeshwar, and M. Tao, "Electrodeposited Copper Oxide Films: Effect of Bath pH on Grain Orientation and Orientation-Dependent Interfacial Behavior," *Thin Solid Films*, **515**, 3090 (2007).
284. J. A. Switzer, C.-J. Hung, L.-Y. Huang, E. R. Switzer, D. R. Kamnler, T. D. Golden, and E. W. Bohannan, "Electrochemical Self-Assembly of Copper/Cuprous Oxide Layered Nanostructures," *J. Am. Chem. Soc.*, **120**, 3530 (1998).
285. J. A. Switzer, C.-J. Hung, L.-Y. Huang, F. S. Miller, Y. Zhou, E. R. Raub, M. G. Shumsky, and E. W. Bohannan, "Potential Oscillations During the Electrochemical Self-Assembly of Copper/Cuprous Oxide Layered Nanostructures," *J. Mater. Res.*, **13**, 909 (1998).
286. E. W. Bohannan, L.-Y. Huang, F. S. Miller, M. G. Shumsky, and J. A. Switzer, "In Situ Electrochemical Quartz Crystal Microbalance Study of Potential Oscillations During the Electrodeposition of Cu/Cu_2O Layered Nanostructures," *Langmuir*, **15**, 813 (1999).
287. J. A. Switzer, B. M. Maune, E. R. Raub, and E. W. Bohannan, "Negative Differential Resistance in Electrochemically Self-Assembled Layered Nanostructures," *J. Phys. Chem. B*, **103**, 395 (1999).
288. J. A. Switzer, H. M. Kothari, and E. W. Bohannan, "Thermodynamic to Kinetic Transition in Epitaxial Electrodeposition," *J. Phys. Chem. B*, **106**, 4027 (2002).
289. F. Oba, F. Ernst, Y. Yu, R. Liu, H. M. Kothari, and J. A. Switzer, "Epitaxial Growth of Cuprous Oxide Electrodeposited onto Semiconductor and metal Substrates," *J. Am. Ceram. Soc.*, **88**, 253 (2005).
290. A. K. Mukhopadhyay, A. K. Chakraborty, A. P. Chatterjee, and S. K. Lahiri, "Galvanostatic Deposition and Electrical Characterization of Cuprous Oxide Thin Films," *Thin Solid Films*, **209**, 92 (1992).
291. V. Georgiev and M. Ristov, "Electrodeposited Cuprous Oxide on Indium Tin Oxide for Solar Applications," *Solar Energy Mater. Solar Cells*, **73**, 67 (2002).
292. K. Mizuno, M. Izaki, K. Murase, T. Shinagun, M. Chigane, M. Inaba, A. Tasaka, and Y. Awakura, "Structural and Electrical Characterization of Electrodeposited p-Type Semiconductor Films," *J. Electrochem. Soc.*, **152**, C179 (2005).
293. K. E. R. Brown and K.-S. Choi, "Electrochemical Synthesis and Characterization of Transparent Cu_2O Films and Their Conversion to CuO Films," *Electrochem. Commun.*, **8**, 3311 (2006).

294. P. E. de Jongh, D. Vanmaekelbergh, and J. J. Kelly, "Cu_2O: A Catalyst for the Photoelectrochemical Decomposition of Water?" *Chem. Commun.*, 1069 (1999).

295. P. E. de Jongh, D. Vanmaekelbergh, and J. J. Kelly, "Cu_2O: Electrodeposition and Characterization," *Chem. Mater.*, **11**, 3512 (1999).

296. P. E. de Jongh, D. Vanmaekelbergh, and J. J. Kelly, "Photoelectrochemistry of Electrodeposited Cu_2O," *J. Electrochem. Soc.*, **147**, 486 (2000).

297. J. Morales, L. Sánchez, S. Bijani, L. Martínez, M. Gabás, and J. R. Ramos-Barrado, "Electrodeposition of Cu_2O: An Excellent Method for Obtaining Films of Controlled Morphology and Good Performance in Li-Ion Batteries," *Electrochem. Solid-State Lett.*, **8**, A 159 (2005).

298. S. Somasundaram, C. R. Chenthamarakshan, N. R. de Tacconi, and K. Rajeshwar, "Photocatalytic Production of Hydrogen from Electrodeposited p-Cu_2O Film and Sacrificial Electron Donors," *Int. J. Hydrogen Energy*, **32**, 4661 (2007).

299. L. Wang and M. Tao, "Fabrication and Characterization of p-n Heterojunction in Cuprous Oxide by Electrochemical Deposition," *Electrochem. Solid-State Lett.*, **10**, H 248 (2007).

300. K. Han and M. Tao, "Electrochemically Deposited p-n Heterojunction Cuprous Oxide Solar Cells," *Solar Energy Mater. Solar Cells*, **93**, 153 (2009).

301. X. Han, K. Han, and M. Tao, "n-Type Cu_2O by Electrochemical Doping with Cl^-," *Electrochem. Solid-State Lett.*, **12**, H 89 (2009).

302. C. M. McShane and K.-S. Choi, "Photocurrent Enhancement of n-Type Cu_2O Electrodes Achieved by Controlling Dendritic Branching Growth," *J. Am. Chem. Soc.*, **131**, 2561 (2009).

303. K.-S. Choi, "Shape Control of Inorganic Materials via Electrodeposition," *Dalton Trans.*, 5432 (2008).

304. M. J. Siegfried and K.-S. Choi, "Electrochemical Crystallization of Cuprous Oxide with Systematic Shape Evolution," *Adv. Mater.*, **16**, 1743 (2004).

305. M. J. Siegfried and K.-S. Choi, "Directing the Architecture of Cuprous Oxide Crystals During Electrochemical Growth," *Angew. Chem. Int. Ed.*, **44**, 3218 (2005).

306. M. J. Siegfried and K.-S. Choi, "Elucidating the Effect of Additives on the Growth and Stability of Cu_2O Surfaces via Shape Transformation of Pre-Grown Crystals," *J. Am. Chem. Soc.*, **128**, 10356 (2006).

307. M. J. Siegfried and K.-S. Choi, "Elucidation of an Overpotential Limited Branching Phenomenon Observed During the Electrocrystallization of Cuprous Oxide," *Angew. Chem. Int. Ed.*, **47**, 368 (2008).

308. S. A. Campbell and L. M. Peter, "A Study of the Effect of Deposition Current Density on the Structure of Electrodeposited α-PbO_2," *Electrochim. Acta*, **34**, 943 (1989).

309. S. A. Campbell and L. M. Peter, "A Photoelectrochemical Study of the Reduction of Electrodeposited α-PbO_2 in Ethanoate Solution," *J. Electroanal. Chem.*, **309**, 213 (1991).

310. M. I. Da Silva Pereira and L. M. Peter, "Photocurrent Spectroscopy of Semiconducting Anodic Films on Mercury," *J. Electroanal. Chem.*, **131**, 167 (1982).

311. I. J. Ferrer, "Characterization of CdO Thin Films by EER and Photoelectrochemical Measurements," *Electrochim. Acta*, **38**, 2199 (1993).

312. A. Seshadri, N. R. de Tacconi, C. R. Chenthamarakshan, and K. Rajeshwar, "Cathodic Electrodeposition of CdO Thin Films from Oxygenated Aqueous Solutions," *Electrochem. Solid-State Lett.*, **9**, C1 (2006).

313. S. T. Chang, I. C. Leu, and M. H. Hon, "Preparation and Characterization of Nanostructured Tin Oxide Films by Electrochemical Deposition," *Electrochem. Solid-State Lett.*, **5**, C71 (2002).

314. N. Nagarajan and I. Zhitomirsky, "Cathodic Electrosynthesis of Iron Oxide Films for Electrochemical Supercapacitors," *J. Appl. Electrochem.*, **36**, 1399 (2006).

315. K. Rajeshwar and N. R. de Tacconi, in *Interfacial Electrochemistry*, A. Wieckowski, Ed., Marcel Dekker, New York and Basel, 1999; Ch. 40, pp. 721–736. See also references therein.

316. C. R. Chenthamarakshan, N. R. de Tacconi, R. Shiratsuchi, and K. Rajeshwar, "Tungsten Trioxide-Titanium Dioxide Composite Films Prepared by Occlusion Electrosynthesis in a Nickel Matrix," *J. Electroanal. Chem.*, **553**, 77 (2003).

317. S. Somasundaram, N. Tacconi, C. R. Chenthamarakshan, K. Rajeshwar, and N. R. de Tacconi, "Photoelectrochemical Behavior of Composite Metal Oxide Semiconductor Film with a WO_3 Matrix and Occluded Degussa P25 TiO_2 Particles, *J. Electroanal. Chem.*, **577**, 167 (2005).

318. C. R. Chenthamarakshan, N. R. de Tacconi, K. Rajeshwar, and R. Shiratsuchi, "Immobilizing Semiconductor Particles by Occlusion Electrosynthesis in an Oxide Film Matrix: The Titania Model Case," *Electrochem. Commun.*, **4**, 871 (2002).

319. K. Ui, T. Fujita, N. Koura, and F. Yamaguchi, "Development of Ag-TiO_2 (Anatase) Particle Composite Coating Film for Photocatalyst and Effect of the Matrix Metal," *J. Electrochem. Soc.*, **153**, C449 (2006).

320. J. Oh, T. Tak, and J. Lee, "Electrochemically Deposited NanoColumnar Junctions of Cu_2O on Ni Nanowires," *Electrochem. Solid-State Lett.*, **8**, C81 (2005).

321. T. Pauporté, A. Goux, A. Kahn-Harari, N. de Tacconi, C. R. Chenthamarakshan, K. Rajeshwar, and D. Lincot, "Cathodic Electrodeposition of Mixed Oxide Thin Films, " *J. Phys. Chem. Solids*, **64**, 1737 (2003).

322. N. R. de Tacconi, C. R. Chenthamarakshan, K. Rajeshwar, T. Pauporté, and D. Lincot, "Pulsed Electrodeposition of WO_3-TiO_2 Composite Films," *Electrochem. Commun.*, **5**, 220 (2003).

323. N. R. de Tacconi, C. R. Chenthamarakshan, K. L. Wouters, F. M. MacDonnell, and K. Rajeshwar, "Composite WO_3-TiO_2 Films Prepared by Pulsed Electrodeposition: Morphological Aspects and Electrochromic Behavior," *J. Electroanal. Chem.*, **566**, 249 (2004).

324. M. Izaki, K. Mizuno, T. Shinagawa, M. Inaba, and A. Tasaka, "Photochemical Construction of Photovoltaic Device Composed of p-Copper (I) Oxide and n-Zinc Oxide," *J. Electrochem. Soc.*, **153**, C668 (2000).

325. J. Katayama, K. Ito, M. Matsuoka, and J. Tamaki, "Performance of Cu_2O/ZnO Solar Cell Prepared by Two-Step Electrodeposition," *J. Appl. Electrochem.*, **34**, 687 (2004).

326. W. Siripala, A. Ivanovskaya, T. F. Jaramillo, S-H. Baeck, and E. W. McFarland, "A Cu_2O/TiO_2 Heterojunction Thin Film Cathode for Photoelectrocatalysis," *Solar Energy Mater. Solar Cells*, **77**, 229 (2003).

327. W. Siripala, L. D. R. D. Perara, K. T. L. De Silva, J. K. D. S. Jayanetti, and I. M. Dharmadasa, "Study of Annealing Effects of Cuprous Oxide Grown by Electrodeposition Technique," *Solar Energy Mater. Solar Cells*, **44**, 251 (1996).

328. G. K. Mor, O. K. Varghese, R. H. T. Wilke, S. Shama, K.-S Choi, and C. A. Grimes, "p-type Cu-Ti-O Nanotube Arrays and Their Use in Self-Biased Heterojunction Photoelectrochemical Diodes for Hydrogen Generation," *Nano Lett.*, **8**, 1906 (2008).

329. J. A. Switzer, in *Electrochemistry of Nanomaterials*, G. Hodes, Ed., Wiley-VCH, Weinheim, 2001, Ch. 3, pp. 67–101.

330. G. Yogeeswaran, C. R. Chenthamarakshan, A. Seshadri, N. R. de Tacconi, and K. Rajeshwar, "Cathodic Electrodeposition in the Ternary Zn-Cd-O System: Mixed $(ZnO)_x(CdO)_{1-x}$ Film Formation versus Cd-Doping of ZnO Films," *Thin Solid Films*, **487**, 40 (2005).

15

DEPOSITION ON NONCONDUCTORS

MORDECHAY SCHLESINGER

At about the same time that electroplating of silver was first being practiced (circa 1840), plating on nonconductors was developed for the purpose of electroforming and for making copper-engraving plates. Nearly a century ago the art entered into its artistic phase, producing metallic artistic elements on glass, wood, and the like. The one surviving remnant of this phase is the gold- or copper-plated baby shoe. Earlier in this century the art was put to use in the service of more practical applications. Those include graphic arts, toys, buttons, records, and the like.

In most of these applications a number of stages in the plating process were required. Typically the first of these was a roughening process. That was done mostly mechanically and sometimes chemically. As an example of the former we mention sandblasting, while as an example of the latter etching of glass with hydrofluoric acid comes to mind. The second stage is that of sealing, if required, such as in the case of wooden objects. The third and most important stage is the application of the conductive layer which then will make eventual electroplating possible. Here a number of methods were available to the plater:

- *Bronzing* Metallic powder mixed in varnish is applied with a brush. A silver immersion dip coating, to improve conductivity, follows.
- *Graphiting* Graphite powder with or without a lacquer binder is applied with a brush.
- *Metallic Painting* Fused metallic paint, silver base, is dispersed in a flux, applied, and subsequently fired to above 500°C
- *Metallizing* Metallic coating is directly produced by electrochemical (other than electroless) methods such as a $SnCl_2$ immersion followed by immersion in a silvering bath (consisting of silver nitrate and ammonium hydroxide). That bath is not autocatalytic.

The next stage was electroplating. Since the initial conductivity is, as a rule, marginal, a copper strike solution was used to deposit the first 8–12 μm and a standard electroplating solution for the rest. (A typical strike solution was made of 75 g L^{-1} $CuSO_4 \cdot H_2O$ as well as 2 mL L^{-1} H_2SO_4, resulting in a solution pH value of 2–2.5.) The final stage was that of polishing the finished product for appearance. Care had to be exercised not to overheat and thus damage the coating during polishing.

15.1 RECENT DEVELOPMENTS

In the corresponding chapter by E. B. Saubestre in the third edition of *Modern Electroplating*, 1960 is stated as the watershed year. The reason is the number of important developments that took place then and changed the practice of plating on nonconductors from an art to a practical science along the following lines:

1. *Plateable Plastics* It became evident to resin (particularly ABS, a terpolymer of acrylonitrile, butadiene, and styrene) producers that the composition of the copolymer and the molding conditions could be adapted to facilitate the subsequent exposure to electrolytes used in the preparation of surfaces for electroplating.
2. *Chemical Conditioners* It was found that variants of older etchants for plastics could be used on plastics (e.g., plateable ABS) properly molded to create

Modern Electroplating, Fifth Edition Edited by Mordechay Schlesinger and Milan Paunovic

enough mechanical and bonding sites to obviate the need for mechanical roughening processes. In addition there became less need or no need at all for a thick copper layer for encapsulation.

3. *Electroless Plating* It is customary to state that electroless (autocatalytic) plating was invented by Abner Brener in the 1940s, but it was not until about 1960 that improved copper baths showed up on the market (proprietary mostly). Their hallmark was their relative stability against decomposition, and they could be replenished a good number of times. That development made semiautomatic plating on nonconductors a matter of course. In the following few years electroless nickel plating baths followed. Their availability reduced considerably the need for rack plating. It eventually permitted the use of fully automated plating methods.
4. *Bright Acid Copper Electroplating* Decorative bright acid electroplating baths for the deposition of copper possessing brilliance and good leveling properties became available. This all but obviated the need for encapsulation and with it the required coating thicknesses of earlier times.

These developments led to the introduction of other advanced techniques for plating on nonconductors. As a result we have the present state of affairs where there exist a large number of ways to plate nonconductors by a variety of metals and upon a number of nonconductor types.

15.2 METALIZATION

15.2.1 Polyimide Metalization

Over the past 20 years or so, significant amount of work has been reported on the electrochemistry of polymers in general. Polyimides being a class of same, in particular, are used in the electronics industry as thin dielectric coating and as thick-film substrate for flexible circuitry.

In this context, for instance, macromolecules with known electrochemistry are obtained from organic or metal centered charge transfer. In the electrochemical charge transfer reaction between commercial Kapton^R film and highly reducing cluster anions of the main group metals, the anions are some times referred to as Zintl anions. This type of redox reaction leads to the formation of thin films of many of the main group metals on the polymer film surface. The basic electrochemistry of polyimides has now been studied sufficiently so that different techniques for the preparation of metal films on polyimides based upon the electrochemistry of the substrate is now available [1, 2] via nonaqueous or aqueous solutions. By way of illustration we delineate the procedure for metalizing a Kapton^R film. It is done through the following steps: First, electrochemical charge is injected onto/into the film. Second, the film is oxidized in, say, copper oxalate solution. Third, a thick copper film is formed by immersion in an electroless copper solution. More specifically now, a piece of Kapton^R film may be immersed in a solution of ethylenediamine tetraacetate (EDTA) for about 2 min, and after a rinse the (now greenish) radical anion film is immersed in a solution of cupric oxalate for about 3–4 min. This step results in a thin coating of copper metal. After a subsequent rinse the film goes into an electroless solution for the buildup of a film of the desired thickness.

15.2.2 Metalization of Plastics

As stated above, polyimides are a class of polymers. They, as well as many types of plastics, satisfy just about all the requirements for electronics applications. Plastics, in general, possess very good thermal chemical and mechanical properties. This is partly due to the inert nature of the surfaces of plastics/polyimides. For this reason it is somewhat difficult to obtain adhesive film bonds to the surfaces of this class of materials. If, as is the case, the bulk characteristics of the materials are to be conserved, then the answer to the problem of adhesion is surface modification. The modifications may consist in the application of any one or more of ion beams, particle beams, sputtering, plasmas, photo grafting (photolithography), chemical methods, and gamma-ray irradiation. In general, however, the science and engineering of surface-modified polymers could use some higher understanding. In particular, there remain questions of the optimum thickness and extent of modifications, extent of cross-linking, and structure and orientation of functional groups on the surface. Modern methods of surface characterization (e.g., X-ray photoelectron spectroscopy, XPS) have provided a great deal of information but much more must be resolved. We will consider the different methods that presently exist for the effective metallic coating of plastic surfaces.

Photolithography A good illustration is the practical procedure involving photolitographically controlled deposition of copper on a Mylar surface. First, the Mylar sheet is rinsed in acetone and distilled water. The clean sheet is next placed onto a watch glass carrier filled with H_2PtCl_6 alcohol solution. A laser beam or filtered mercury light source is used to illuminate the Mylar sheet for about 20 min (by a focused beam). The possible photochemistry of $[PtCl_6]^{2-}$ in alcohols is discussed in [3]. The reaction, it is stated, gives rise to a spatially well defined, albeit discontinuous, deposit of platinum metal upon the illuminated areas of the substrate. Finally, the sheet is placed into an electroless copper plating bath for a few minutes. The latter contains formaldehyde and formaldehydrate at 65°C and pH 11.4.

The ever-increasing present-day push toward fabrication of ultrasmall features on integrated chips drives much of

modern nanotechnology. A prerequisite for nanolithography is the ability to expose and develop photoresist on the scale of a few tens of nanometers. The advent of single optical nanoantennas [1–9] provides a method for producing ultrasmall features in resists. Optical nanoantennas are specifically engineered to produce greatly enhanced fields at visible and near-infrared (NIR) wavelengths and to confine them to regions ~20 nm in size, significantly defeating conventional diffraction limits. It is possible to fabricate ultrasmall photoresist nanodots using two-photon polymerization enabled by the huge localized enhancement in the vicinity of lithographically produced Au bowtie nanoantennas. Record-low voxel diameters <30 nm are generated at record low incident infrared average powers of 27 μW (30 kW cm^{-2}). While sub-diffraction-limited (SDL) resolution has been the goal of near-field optics for some time [10], nanoantennas comprised of plasmonically coupled metallic nanoparticles offer appreciable advantages over other near-field probes, most notably aperture-based and apertureless near-field scanning optical microscopes (NSOM and ANSOM, respectively).

Two-photon polymerization (TPP) of a photoresist, where a two-photon absorption event initiates a cross-linking chain reaction, is an established method for fabricating two- and three-dimensional (3D) structures with SDL resolution. Due to the nonlinear dependence of the polymerization on electromagnetic field intensity, exposure occurs only where field strength is greatest, and the fabrication of SDL objects has been demonstrated by both conventional [11] and tip-enhanced microscopy [12]. Much of the TPP work in the literature has concentrated on the commercially available epoxy-based photoresist SU-8, which has been optimized for high-aspect-ratio structure fabrication and is well-suited for 3D lithography [11]. Recently, minimum feature sizes of ~70 and ~30 nm have been demonstrated for ANSOM [12] and confocal-scanning excitation [13] techniques, respectively, the latter for a specialized structure. We note that while the absorption of wavelengths near 800 nm in SU-8 has traditionally been described as a two-photon process, it is possible that exposure is partially due to a higher order process [14–16].

Ion Beam Techniques Ion beam techniques traditionally were useful in semiconductor processes. They are now used in many different applications. Chief among them is the metalization of insulators. The metalization can be achieved in three ways: The first is ion implantation. Using the appropriate vacuum setup, an ion beam is directed to strike the material. The ions penetrate to a depth that depends on the beam's energy and other physical parameters. The ions then interact with the target's polymer molecules, resulting in an expulsion of volatile molecular fractions on the one hand and a carbon-rich surface layer on the other. The surface layer will show enhanced (though not metallic) conductivity. The enhancement enables a subsequent electrodeposition of a metallic layer. The second method is ion beam mixing. By this means, a degree of metallic conductivity can be achieved. The thin metallic layer is deposited by evaporation. The layer is bombarded by fast ions that have to be made able to penetrate the metal/polymer interface. There they cause collisions and/or electronic excitations which cause a broadening of the interface as well as metal/polymer chemical interactions. This promotes adhesion of the metal film. The third method is ion beam-assisted deposition. Here the metal deposition and ion bombardment are done simultaneously. At a given stage of film thickness the ions cannot reach the metal/polymer interface. The ion beam now affects the growth of the metallic thin film relieving possible stress, for instance.

The different ion beam methods have their advantages as well as disadvantages. The combination of almost any metal with any surface is made possible, giving rise to good adhesion. The process is also suitable for chemical deposition. As to the disadvantages, relatively complicated vacuum techniques are involved and the ''line-of-sight'' process excludes substrates of complex geometric features.

Focused ion beam (FIB) techniques have been implemented in recent years for many applications, including creation of electrical contacts to metallic nanowires with localized Pt deposition. The FIB technique is powerful both for patterning and deposition of materials and for rapid prototyping with resolution in the range of a few tens of nanometers. The basic principle is scanning the sample surface with a FIB that sputters the material of the exposed area. Introducing an organometallic compound in the beam path, secondary electrons generated in the sample by the ion beam decompose the precursor and part of the compound will be deposited on the sample surface (ion-assisted deposition) while volatile components are removed by the vacuum system. The dual-beam or cross-beam FIB is a combination of both scanning electron microscopy (SEM) and FIB with both beams focused on the same spot (shown in Fig. 15.1). With such type of instrument both electron beam–assisted deposition (EBAD) and ion beam–assisted deposition (IBAD) can be performed in a single instrument.

Typically, for instance, Pt ion– and electron beam-assisted deposition in a system may involve the decomposition of trimethyl-methylcyclopentadienyl-platinum ($C_9H_{16}Pt$) gas molecules. This will result in local deposition of Pt material on the sample, in the area where the ion beam is scanned in a predefined pattern. While it is the case that the mechanism for electron- and ion beam–assisted depositions are very similar, the deposition efficiency for the IBAD process is much higher than that for EBAD.

Electrochemical-Autocatalytic Methods Autocatalytic deposition (AD) places metal directly on objects immersed in a process solution, with no external electric current required. The metallic coating is deposited by a controlled electrochemical reduction that is catalyzed by the metal or alloy

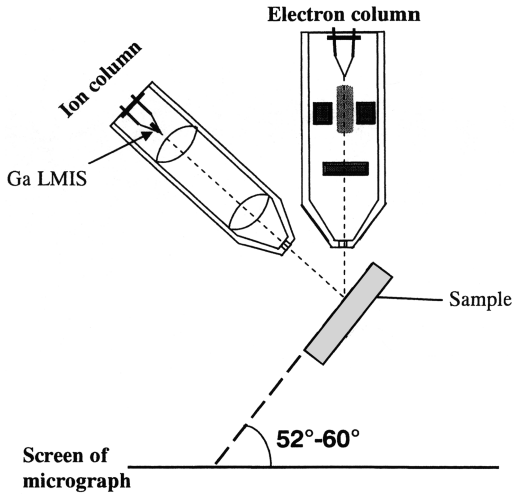

FIGURE 15.1 Schematic illustrating geometry of dual-beam arrangement for ion column, electron column, and sample stage tilted to 52°–60° in a FIB/SEM chamber.

being deposited. An electrochemical reduction agent in solution provides the electrons, and the process takes place only on catalytic surfaces rather than throughout the entire solution. AD is also referred to as "electroless plating." It possesses several characteristics not shared by other techniques. The process is an integral and necessary step in plating on nonconductors such as plastics and printed circuit boards. Some electroless deposits, it should be noted, have unusual or even unique magnetic properties. AD yields deposits of nickel, cobalt, palladium, platinum, copper, gold, silver, and alloys containing these metals plus phosphorus or boron. This commercially important technology has many desirable attributes for flexible circuit manufacture:

- AD coats objects uniformly.
- With surface catalyzation (activation), AD coats nonconductors.
- With ultraviolet patterning of a catalysed surface, AD reproduces patterns of micrometer dimensions with high resolution.

For more details, the reader should consult [17–19], as well as the relevant chapters in this volume. The preparatory steps for electroless deposition are discussed in some detail in Section 15.4.

Plasma-Induced Deposition In this technique a thin film of copper formate or copper chloride is coated on a substrate (polymeric dielectric substrates, including polystyrene, Kapton, and similar materials, are treated using these methods [20, 21]). Next this precursor layer is reduced to metallic copper in a hydrogen RF plasma. The reduction process is carried out at a low substrate temperature. Temperature-sensitive plastics can be metalized via this methodology. The subsequent annealing is another matter. In general, when large areas must be coated by a thin metallic layer, this method is suitable. Once deposited, a subsequent electroless deposited additional metal layer is always an option.

Sputtering Plastic specimens need proper pretreatment before the coating process so as to avoid surface contaminants which may cause undesired characteristics such as poor adhesion. Coatings are deposited on the high-power sputtering principle. To deposit TiN (which is an important diffusion barrier material), a Ti target is sputtered in a nitrogen reactive gas and argon inert gas atmosphere. The direct-current (dc) mode is the method of choice. Coating thickness is proportional to the coating time. Typically 200 nm is achieved in a matter of 5 min, while 10 times the thickness will require about 1 h. For more details on this method, the reader is advised to consult articles in [22].

15.3 DEPOSIT CHARACTERIZATION—ADHESION

Once a metal coating has been applied to a surface, it is critical to determine the adhesion properties of the deposit. Of the many and varied properties of thin films, adhesion to the substrate stands out as the most important and the most difficult one to measure in a quantitative fashion. Further, while in most applications good film adhesion between film and substrate is what is required, in some cases weak adhesion is desired so that the film can be removed from the substrate. These two different types of requirements almost never are present in one and the same application.

From a microscopic point of view, adhesion is a measure of the force between the constituent atoms-molecules of the thin film and those of the substrate at the interface. From macroscopic and practical points of view adhesion is simply a measure of the energy required for the removal of a thin film from the substrate. These two properties do often differ for a number of reasons. Stress or strain, which develop during film growth, can reduce the required energy for film removal. Structural imperfections in either the film or the substrate can reduce adhesion as well. Some types of growth methods result in porous films. The pores allow gas and/or water vapor to reach the interface and decrease the adhesion for practical purposes. These and many other complications prevent accurate measures of adhesion to be made, so the many different tests in practice are simply variants of two rather simple visual tests, the tape and the scratch tests. The first involves, in its fundamental form, the application of an adhesive tape to the film. If upon peeling it off no film material has been removed, it is said that the film has passed

TABLE 15.1 Silver Evaporated onto PET from Different Manufacturers (at ~43 nm s^{-1} to a thickness of ~650 nm)

Source of PET	Threshold Laser Energy Density (mJ cm^{-1})	Tape Test Amount Removed (%)
Dopont 700D	13	90
Kodak Estar	43	40
Hostaphan	47	60
Melinex	54	10

Note: PET = ployethyleneterephthalate.

the test. The second involves, in its fundamental form, the rubbing of an eraser across the film. The number of strokes needed to expose the substrate is a measure of the film's degree of adhesion. As stated, a number of refined variations of these tests are widely practiced. In case of the peel test, the use of a tensile tester to measure the force necessary to remove a film off a substrate is rather commonplace. In case of the scratch test, a common refinement is the use of a stylus loaded with a known weight, which then is pulled across the film. The weight necessary in order to scratch through the film is a measure of the degree of film adhesion. The size and past usage of the stylus affect the test results, making it difficult to compare results obtained in two different plating shops. Also, in the tape test, the thickness and elasticity of tape, film, and substrate all influence the results, as do the angle of removal and the rate of pulling the tape. Both tests are in common use despite these kinds of limitations. A number of other methods, however, have been proposed. One, suitable for flexible substrates, involves stretching the substrate in a tensile tester with the onset of film cracks being observed. Another is a laser test. In this, pulses of different energy densities are aimed at different sites on the sample. At the threshold energy of damage visible cracks appear, and the corresponding energy density is a quantitative measure of the film's adhesion.

Table 15.1 gives a summary of laser-type measurement results by Lindberg et al. [23]. Interestingly they felt it necessary to compare their numbers to those obtained using the tape test method as benchmark. It should be noted that the threshold energy densities for the development of cracks correlate very well with the tape test results.

15.4 SENSITIZAT1ON—CATALYSIS (PRIOR TO ELECTROLESS DEPOSITION)

The expression ''electroless deposition'' is not quite accurate. While there are no external electrodes, there is electric charge transfer involved. In place of an anode there is metal provided by the metal salt in solution; replenishment can be had either by adding salt or by an external loop with an anode that has a higher efficiency than the cathode. In place of a cathode there is a substrate, while the electrons are provided by a reducing agent in solution. The electroless deposition process is autocatalytic, and it is first initiated by active metals upon immersion in an electroless bath.

Since practically every substrate requires a different approach, depositing active metal on the surface of a nonconductor is an art. Such deposition requires one or more of the following steps: cleaning, surface modification (e.g., etching), sensitization, and subsequent catalyzing or catalyzing and activating. Rinsing between steps is usually a must. Figure 15.2 provides the schematics of the electroless deposition process.

Sensitization and catalysis here mean the absorbing of agents from a solution of Sn^{2+} and/or Sn^{4+}. Other sensitizing agents are $AgNO_3$, $AuCl_3$, and metallic Na (in a naphthalene solutions). A simplified model of sensitization and catalysis process is that the ''sensitizing'' ion reduces the ''active'' metal from the catalyst solution, which most often is $PdCl_2$ (again, Au, Pt, Rh, Os, and Ag solutions can also be used). Thus

$$Sn^{2+} + Pd^{2+} \rightarrow Sn^{4+} + Pd^{0}$$

If, as sometimes is the case, a given metal can be reduced by the sensitizing ion, then the substrate is immersed in the electroless bath right after sensitizing and rinsing. Such can be the case when electrolessly depositing Cu or Ag using Sn^{2+}-based sensitizer.

The other path, that of catalyzing and activating, consists of the use of a mixed colloidal catalyst. The colloid consists of reduced Pd stabilized by Sn^{2+} and Sn^{4+} tons. The activation step is the removal of the layer formed by the stabilizing agent using HCl, NaOH, or similar. In some instances the activation step may be omitted, but the plating solution becomes contaminated. In practical applications the mixed colloidal technology seems to be preferred. The reasons for this are as follows:

- The technology is more reproducible than the separate Sn–Pd technology.
- An object after removing from the mixed colloidal solution is covered by a Pd layer which is clearly visible. Not so in case of the Sn–Pd process.
- Mixed colloidal solutions are stable and do not exhibit aging effects as do the Sn solutions.
- Mixed colloidal solutions are rather resistant to impurities.
- Surface preparation is far less critical than in the case of Sn-based solutions.

Besides having to be clean, surfaces must be hydrophilic in order to be efficiently wetted by sensitizing solutions. Some workers feel that a rough surface is required, since bonding takes place through mechanical entrapment, and

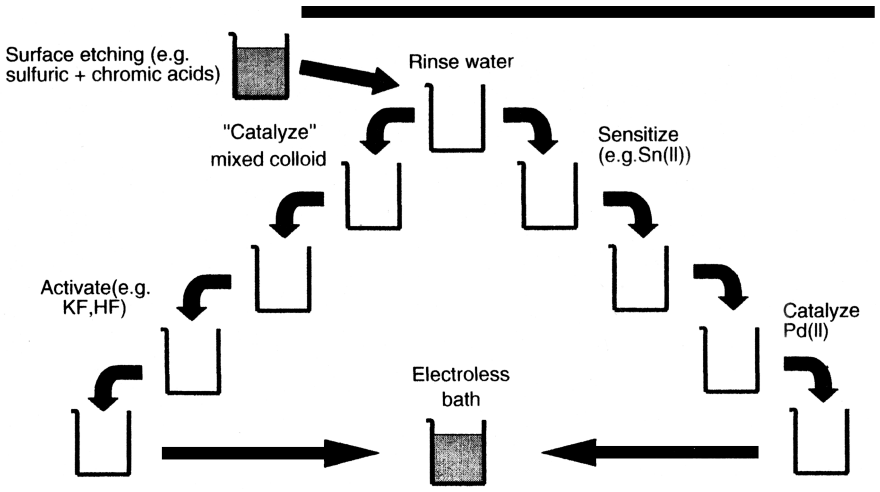

FIGURE 15.2 Schematic representation of the electroless deposition process.

there are many instances of efficient sensitization on very smooth surfaces such as glass slides. Clearly, the surface functional groups are an important, if not the dominant, factor in promoting adhesion on many surfaces.

Despite the above-mentioned advantages of the mixed colloidal technology over the Sn–Pd process, the initial nucleation site density achieved by the latter method is up to an order of magnitude greater than that obtained by using the former. This means that a continuous film can be obtained at smaller thickness [24]. In practical terms this translates into the following advantages:

- Less metal is needed if the only purpose is to render the surface conductive.
- Better adhesion due to higher density of fastening sites.
- Potential in the development of products where very thin coatings are required.

No discussion regarding sensitization and the like can be considered complete without reference to ultraviolet (UV) assisted patterning or selective electroless metal deposition. Schlesinger and co-workers [25] showed that it is possible to obtain patterned or selective deposition of, say, electroless copper by UV irradiation of a substrate through a quartz mask at different stages prior to immersion in an electroless bath. Deposition may be made to take place on the nonirradiated areas only (positive mask image) or on the irradiated areas only (negative mask image). Figure 15.3 presents the processing steps for the negative-type patterning of electroless copper deposit using a two-stage metalizing procedure.

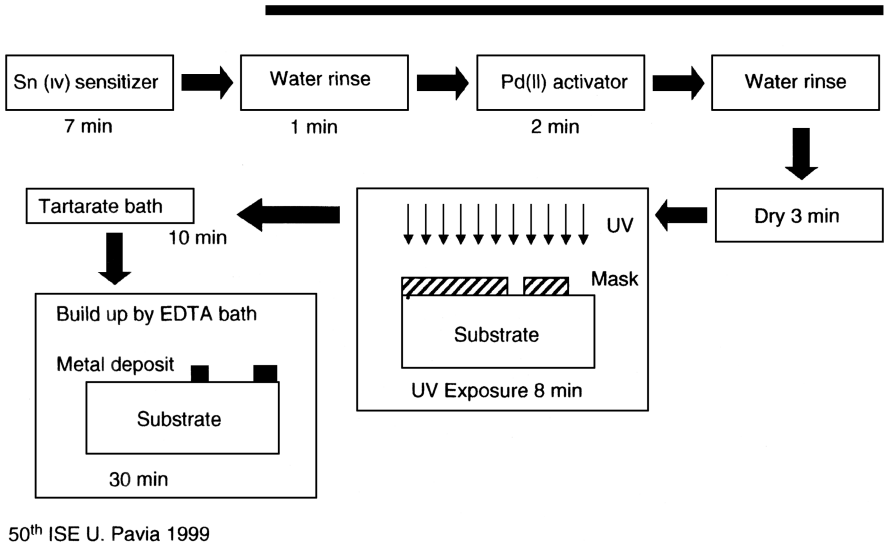

FIGURE 15.3 Processing steps involved in (negative) patterning of electroless copper.

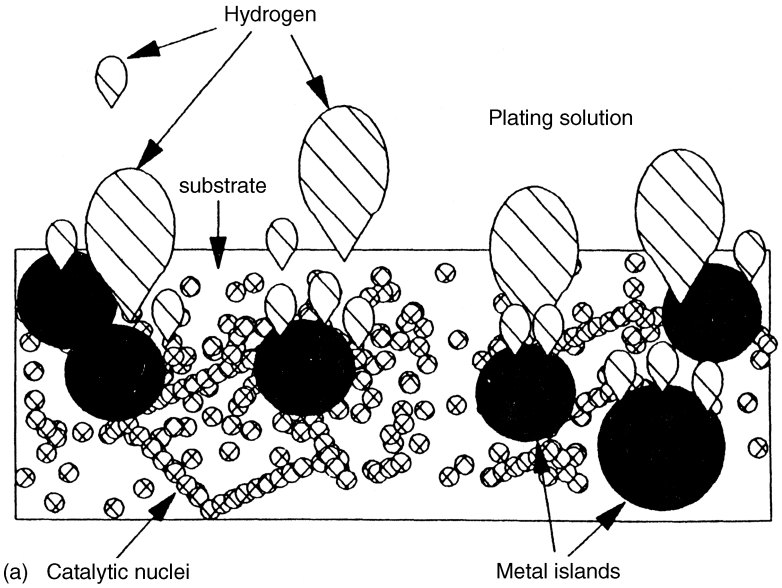

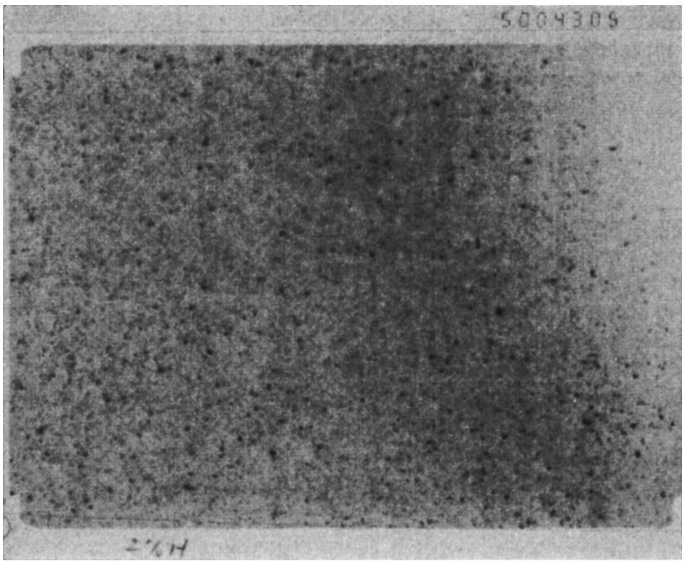

(b)

FIGURE 15.4 Schematic representation of the deposit propagation along nonconductive substrates: (*a*) substrate preseeded by conductive sites; (*b*) conventional electroplating with nonseeded substrate (1 in. = 1000 Å).

15.5 CONCLUSION

The metalization of nonconducting substrates is essential in a large number of industrial applications such as in the fabrication of printed circuits for microelectronics or in the coating of panels for many other uses. There is now mature technology and many practical methods of electroless plating. These, however, are not always acceptable due to a number of factors, such as slow deposition rates and adhesion quality. There are therefore a number of alternative methods based on direct electroplating on pretreated nonconducting substrates. Specifically, the surface is seeded with a small amount of conductive material such as palladium, carbon, or a thin layer of conductive polymer. Conventional electroplating follows the initial seeding stage with the cathodic lead connected to a metallized region on the substrate.

In practice, it is often observed [26], as depicted in Figure 15.4, that a thin electrodeposited layer builds up at the edge of the polarized metallic region, and it rapidly propagates along the seeded surface rather than producing buildup on the contact strip, as desired. For a treatment of the issue from a theoretical point of view, the reader is referred to [1].

REFERENCES

1. S. Mazur and S. Reich, *J. Phys. Chem.*, **90**, 1365 (1986).
2. L. J. Krause and J. A. Rider, U.S. Patents 4,775,556 (1988) and 4,710,403 (1987).
3. M. Zhou, R. Cameron, and F. J. Schwab,in *Metalized Plastics*, Vol. 2, K. L. Mittal, Ed., Plenum, New York, 1991, p. 57.
4. D. P. Fromm, A. Sundaramurthy, P. J. Schuck, G. S. Kino, and W. E. Moerner, *Nano Lett.*, **4**, 957–961 (2004).
5. P. J. Schuck, D. P. Fromm, A. Sundaramurthy, G. S. Kino, and W. E. Moerner, *Phys. Rev. Lett.*, **94**, 17402 (2005).
6. A. Sundaramurthy, K. B. Crozier, G. S. Kino, D. P. Fromm, P. J. Schuck, and W. E. Moerner, *Phys. Rev. B.*, **72**, 165409 (2005).
7. P. Muhlschlegel, H.-J. Eisler, O. J. F. Martin, B. Hecht, and D. W. Pohl, *Science*, 308 1607–1609 (2005).
8. E. Hao and G. C. Schatz, *Chem. Phys.*, **120**, 357–366 (2004).
9. J. P. Kottmann, O. J. F. Martin, D. R. Smith, and S. Schultz, *J. Microsc.*, **202**, 60–65 (2001).
10. D. A. Genov, A. K. Sarychev, V. M. Shalaev, and A. Wei, *Nano Lett.*, **4**, 153–158 (2003).
11. J. B. Jackson, S. L. Westcott, L. R. Hirsch, J. L. West, and N. J. Halas, *Appl. Phys. Lett.*, **82**, 257–259 (2003).
12. R. A. Farrer, F. L. Butterfield, V. W. Chen, and J. T. Fourkas, *Nano Lett.*, **5**, 1139–1142 (2005).
13. M. A. Paesler and P. J. Moyer, *Near-Field Optics Theory, Instrumentation, and Applications*, Wiley, New York, 1996.
14. W. H. Teh, U. Durig, U. Drechsler, C. G. Smith, and H.-J. Guntherodt, *J. Appl. Phys.*, **97**, 54907 (2005).
15. X. Yin, N. Fang, X. Zhang, I. B. Martini, and B. J. Schwartz, *Appl. Phys. Lett.*, **81**, 3663–3665 (2002).
16. S. Juodkazis, V. Mizeikis, K. K. Seet, M. Miwa, and H. Misawa, *Nanotechnology*, **16**, 846–849 (2005).
17. I. Kiflawi and Schlesinger, *J. Electrochem. Soc.*, **130**, 872 (1983); and references therein.
18. B. K. W. Baylis, C.-C. Huang, and M. Schlesinger, *J. Electrochem. Soc.*, **126**, 394 (1979).
19. B. K. W. Baylis, A. Busutil, N. E. Hedgecock, and M. Schlesinger, *J. Electrochem. Soc.*, **124**, 346 (1977); and references therein.
20. M. Ritz, S. V. Babu, V. Srinivasan, and R. C. Patel, in *Photon. Beam and Plasma Stimulated Processes at Surfaces*, Vol. 75, V. M. Donelly, I. Herman, and M. Hirose, Eds., Materials Research Society, Orlando, FL 1987, p. 433.
21. A. L. Gupta and R. Jagannathan, *Appl. Phys. Lett.*, **51**, 2254 (1989).
22. R. F Bunsha, Ed., *Deposition Technologies for Films and Coatings*, Noyes Publ, Park Ridge, NJ, (1982.).
23. W.-C. Lee, V. W. Lindberg, P. H. Wojciechowski, and F. J. Duarte, in Metalized Plastics, Vol. 2, K. L. Mittal, Ed., Plenum, New York, 1991.
24. J. P. Marton and M. Schlesinger, *J. Electrochem. Soc.*, **115**, 16 (1968).
25. M. Schlesinger et al., *J. Electrochem. Soc.*, **119**, 1013 (1972); **126**, 394 (1979); **136**, 872 (1983).
26. D. Weng and U. Landau, *J. Electrochem. Soc.*, **142**, 2598 (1995).

16

CONDUCTIVE POLYMERS: ELECTROPLATING OF ORGANIC FILMS

TETSUYA OSAKA, SHINICHI KOMABA, AND TOSHIYUKI MOMMA

16.1 ELECTROPOLYMERIZATION: ELECTROCHEMICAL SYNTHESIS OF CONDUCTING POLYMERS

Electron-conductive polymers were first reported in 1971 by Shirakawa and co-workers [1]. They synthesized conducting polyacetylene and found that it had a considerably high conductivity relative to other organic compounds, $10^3\,S\,cm^{-1}$ [1–3]. Since 1971, various conducting polymers and their synthesis mechanisms have been studied actively by many researchers [4]. The conductivities of these polymers are shown in Figure 16.1, compared with those of various inorganic and organic compounds and materials. Generally speaking, because conducting polymers have electrons that are delocalized in π-conjugated systems along the whole polymer chain, their electron conductivity is much higher than that of other polymers that do not have a π-conjugated system, as shown in Figure 16.1.

Furthermore, in 1979, Diaz and co-workers [5, 6] synthesized conductive polypyrrole film by electropolymerization (see Fig. 16.2). Electropolymerization is similar to electroplating of metal films. Its polymerization reactions occur electrochemically; that is, electrons go through the electrode–electrolyte interface when a potential is applied to an electrode, as shown in Figure 16.2. In the case of an insoluble polymer generated on the electrode, a film of conducting polymer is thus obtained easily. Essentially, regarding electron transfer, all electrochemical reactions are classifiable into oxidative or reductive reactions. Electrochemical polymerizations can be classified in a similar way. In almost all cases, electropolymerized polymers have been synthesized by electrooxidation. It seems, however, that films obtained by this method contain branching or cross-linking defects [7–9]. On the other hand, electroreductive polymerization performed by using a zero-valent nickel complex is sensitive to the halogen atom in the monomer, and therefore it yields polymers with well-defined linkages among the monomer units [10–13].

In the past four decades, many types of organic devices with conducting polymer films have been studied. Among the processes used to form these films, electropolymerization is one of the most interesting methods of preparing thin functional polymer films. Electropolymerized films directly deposited on various electrodes, for example, metals and semiconductors, have various functionalities and applications, as shown in Table 16.1. Also, it has been determined that electroinactive nonconducting polymer films are formed by electropolymerization [14]. When the electropolymerization solution contains nucleophilic reagents, such as, NaOH, $NaHCO_3$, or Na_2CO_3 with monomer reagents, polymerization occurs first, and then film propagation automatically stops, resulting in a changing nonconductive state caused by a nucleophilic attack reaction. Since the electrode of the film made by the process described above responds to the pH value, it can be applied to micro–pH sensors [15] and also to biosensors with a pH change enzymatic reaction [16–18].

This chapter introduces the functional design of electropolymerized films and their applications for polymer batteries, electric devices, and chemical sensors.

Modern Electroplating, Fifth Edition Edited by Mordechay Schlesinger and Milan Paunovic

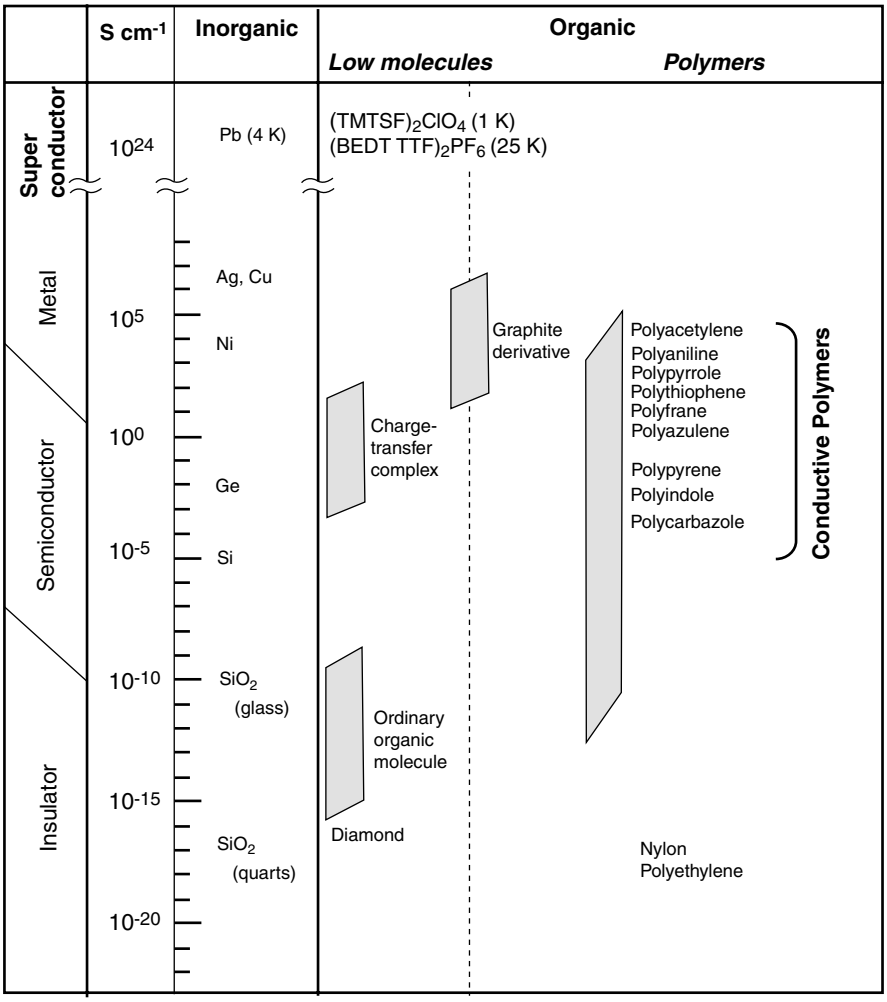

FIGURE 16.1 Conductivity of various inorganic and organic compounds and materials.

16.2 POLYMER BATTERIES

16.2.1 Introduction

Electropolymerization is one of the rather interesting methods used in the fabrication of electrodes for rechargeable batteries [19], since several characteristics of electropolymerized polymer films, such as electroactivity, conductivity, and film morphology, can be controlled by the conditions of film formation [20]. Among these polymers, polyaniline, polypyrrole, and polyazulene all show high electroactivity with good reversibility and chemical stability, as shown in Figure 16.3. When the neutral electroactive polymers are oxidized by applying an anodic potential/current, the electrons in a π-conjugated system are extracted and the polymer

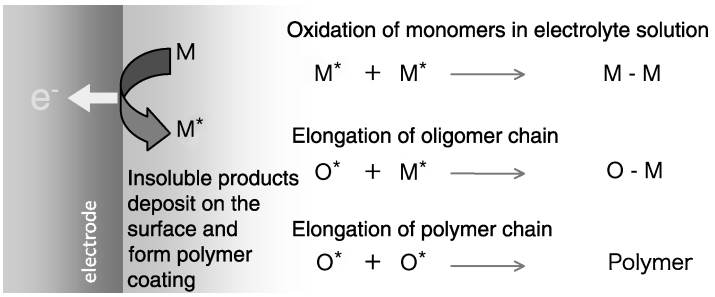

FIGURE 16.2 Illustration of electropolymerization.

TABLE 16.1 Functionality and Possible Applications of Electropolymerized Polymers

Functionality	Application
Electroactivity	Secondary battery Corrosion protection/prevention Ionic sensing
Semiconducting	Solar battery Optical device Electroluminescence device
Conductivity	Binder for electroactive powder Conductor sheet Electrification prevention Electromagnetic shield Diode Transistor Chemical sensor Physical sensor
Electrochromism	Display device Smart window
Ion exchange ability	Ion exchange memebrane Chemical sensor
Electrochemical catalysis	Electrode catalyst material

becomes conductive. The oxidized π-conjugated system will be reduced reversibly to a neutral insulating/semiconducting state. When the polymer is applied as a battery cathode, the battery is expected to exhibit both a high energy density and mechanical flexibility [21–23].

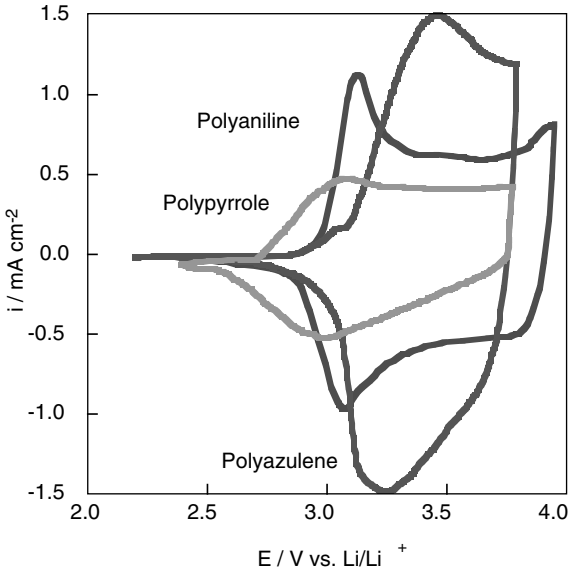

FIGURE 16.3 Cyclic voltammograms of polyaniline, polypyrrole, and polyazulene prepared by electrooxidative polymerization in propylene carbonate (PC) solutions. The voltammograms were obtained by the potential cycling of polymer-coated electrodes in 1.0 M $LiClO_4$/PC solutions with Li electrodes as reference/counter electrodes.

In the following section, we describe two typical methods to enhance characteristics of conducting polymers that have promise for battery applications, that is, the method to convert the *p*-type polymer to the *n*-type polymer for use in the rocking-chair battery and the method that adds ionic conducting materials to the polymer.

16.2.2 Polymer Cathode for Li Battery

Among a large number of electropolymerizaed polymers, polyaniline (PAn) and polypyrrole (PPy) are two of the promising candidates for cathode materials in rechargeable lithium battery systems [24]. Most candidates for electropolymerized polymer cathodes for Li batteries still are *p*-type polymers whose oxidation and reduction required anion incorporation and expulsion to compensate for the charge of the polymer film. A lithium battery constructed with a *p*-type cathode causes the electrolyte concentration to change during charge and discharge. Since a decrease in concentration of the electrolyte during charge causes the cell resistance to increase, the cell requires a large source of electrolyte solution. However, a cell using a lithium ion–compensated cathode (e.g., *n*-type cathode, manganese, cobalt, and nickel oxides) does not change the concentration of the electrolyte solution during cell operations, and thus it can be operated with a smaller amount of electrolyte solution and it enables the energy density of the battery to be increased.

Many researchers have directed their attention to PAn as a cathode material in lithium batteries, because of its high energy density, chemical stability, and high reversibility of the doping–undoping process. Recently, a disulfide compound with PAn also has attracted researchers because of its possible use as a high-energy density cathode material [25, 26]. In our research work, we have focused on PPy as a cathode for PPy/Li metal batteries because such batteries have high-cycle ability [20]. We have also developed a Li/gel electrolyte/PPy battery with more than 4000 cycles [27].

Some researchers have examined composite films of conducting polymers and other materials formed by electropolymerization [28–32]. Among these composite films, the one that consists of a polyanion with a *p*-type conducting polymer has many anionic groups that are neutralized by the many cations of the electrolyte. The charge of the film is compensated by cations during the oxidation and reduction of the polymer as a result of the presence of localized anion groups incorporated into the polymer chain [32]. By using a composite of a *p*-type polymer and a polyanion, Shimidzu and other researchers proposed and developed a rocking-chair-type rechargeable battery system, although the system used either an aqueous or nonaqueous electrolyte that is not applicable to a lithium battery system [33, 34]. Also, Shimizu and co-workers suggested using an electroactive composite film of polypyrrole and polystyrenesulfonate (PPy/PSS) in a propylene carbonate (PC) electrolyte, which is a typical

electrolyte for Li batteries, in combination with a carbon fiber electrode having an enormous surface area [35]. Here, we describe the electrochemical properties of a PPy/PSS composite cathode on a flat electrode surface for a rocking-chair-type rechargeable Li battery system [36, 37]. PPy/PSS composite film is formed by electropolymerization on Pt with the coexistence of PSS as a supporting electrolyte in an aqueous solution containing pyrrole. However, without further treatment, it shows no electroactivity in a typical electrolyte solution, such as $LiClO_4$–PC, for a Li battery. During cycling of the potential of the PPy/PSS film in a $LiClO_4$–dimethylsulfoxide (DMSO) electrolyte solution, the faradic current caused by the reversible redox of the PPy molecule gradually increases, as shown in Figure 16.4. By investigating the optimum preparation conditions for a rechargeable battery system, we found that PPy/PSS composite film showed a high redox charge and a good reproducibility in combination with the $LiClO_4$–DMSO electrolyte [37].

A battery was constructed that incorporated a lithium anode, a $LiClO_4$–PC electrolyte, and a PPy/PSS composite film, and the cathode performance of the film was evaluated [37]. The cell exhibited rechargeability with an output voltage of 3.9–2.8 V. The energy density of this cell is shown in Table 16.2 as the value per unit cathode. The energy density per unit volume of PPy/PSS film is superior to that of PPy/ClO_4 film, which is a typical *p*-type polymer for the cathode. It was confirmed that the Li^+ ions compensate mainly for the charge of the film generated in the PPy/PSS cathode during operation. The difference between the performances of the cells using the PPy/PSS film or the PPy/$LiClO_4$ film is small, but the cathode morphology is quite different, that is, the PPy/ClO_4 film is porous and thick while the PPy/PSS film is dense and thin.

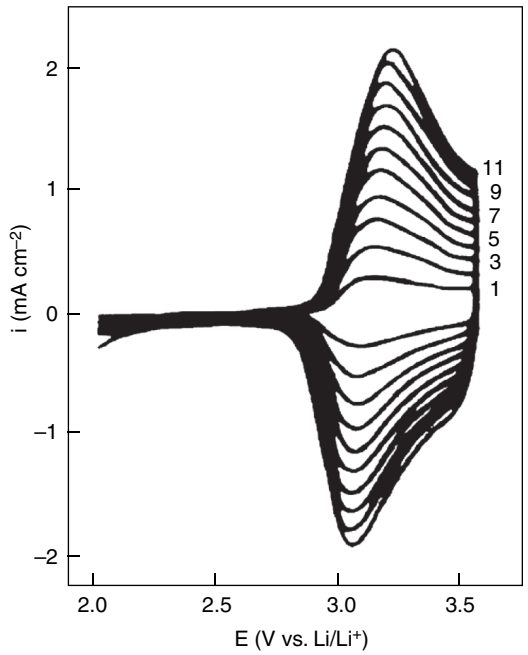

FIGURE 16.4 Continuous cyclic voltammograms of PPy/PSS film obtained in a 1.0 mol dm^{-3} $LiClO_4$–DMSO electrolyte solution at 20 mV s^{-1}. Current gradually increased with potential cycling until the voltammogram reached a steady state. Cycle numbers are shown in the figure. [Reproduced from *J. Electrochem. Soc.*, **141**, 2328 (1994). Copyright 1994 by The Electrochemical Society.]

TABLE 16.2 Specific Energy Densities per Unit Cathode Material in Lithium Battery Using PPy/PSS Film and Rougher PPy/ClO_4 Film with Different Film Formation Charges

Film	Film Formation Charge (C cm^{-2})	Specific Energy Density (Wh L^{-1})
PPy/PSS	8	220
PPy/ClO_4	8	142
PPy/PSS	0.5	230
PPy/ClO_4	0.5	51.2

Source: Form [37].

The results of the charge–discharge tests using PPy/PSS or PPy/ClO_4 cathodes showed that the *n*-type PPy/PSS composite film has high potential as a cathode material for a rocking-chair-type rechargeable battery with a high energy density.

16.2.3 Polymer Cathode in a Solid Polymer Electrolyte

The application of solid polymer electrolytes to electrochemical devices is expected to make these devices flexible, thin, and lightweight. Liquid-free devices also have the advantage of long-term reliability. Therefore, some researchers have made efforts to improve the interface between PPy and a solid polymer electrolyte [38]. The electrochemical properties of PPy films using different kinds of electrolytes—aqueous, organic liquid, and recently solid polymer—have been investigated [38–41]. It has been found that the performance of a PPy is strongly influenced by the kinetics of the doping/undoping process of the ions in the PPy films. For example, ionic movement has been improved by making PPy/anion composite films that accelerate the moving ion through the film [38, 42].

We have found that a porous PPy film shows much better redox properties in poly(ethylene oxide) [(PEO)–$LiClO_4$] than a dense PPy film [40]. Arbizzani and co-workers have reported that, in a solid polymer electrolyte, poly-*N*-(oxyalkyl)pyrrole film shows much better redox properties than PPy film [43]. We also should mention the introduction of the Nafion molecule, which supports ionic conduction, into the PPy electrode for enhancement of ionic diffusion [44, 45].

PPy/Nafion composite film is formed by electropolymerization of pyrrole from an aqueous solution containing

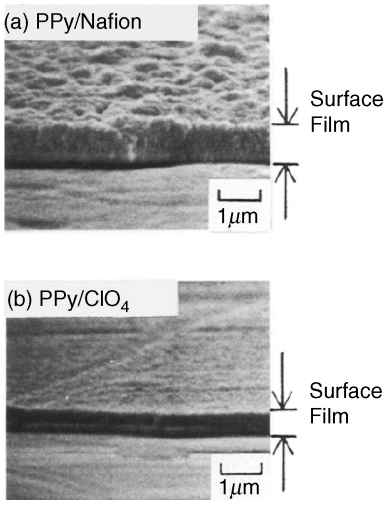

FIGURE 16.5 Cross-sectional SEM images: (*a*) PPy/Nafion film; (*b*) PPy/ClO_4 film prepared by electropolymerization. The charge for the film formation was 100 mC cm^{-2} in both films. [Reproduced from *J. Electrochem. Soc.*, **142**, 1766 (1995). Copyright 1995 by The Electrochemical Society.]

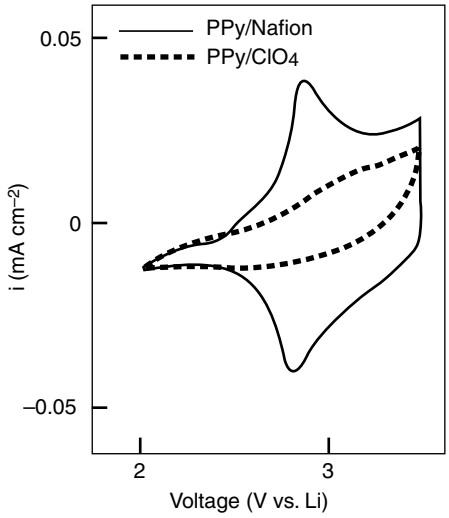

FIGURE 16.6 Cyclic voltammograms of PPy/Nafion and PPy/ClO_4 at 2 mV s^{-1} in PEO_8–$LiClO_4$ at 80°C. [Reproduced from *J. Electrochem. Soc.*, **142**, 1767 (1995). Copyright 1995 by The Electrochemical Society.]

a pyrrole monomer and a Nafion solution (Aldrich) as the supporting electrolyte. PPy/Nafion composite film was examined for its compatibility with a polymer solid electrolyte with PEO_8–$LiClO_4$ (PEO_n–$LiClO_4$; n is the ratio of ethylene oxide units of PEO to Li ions, i.e., $n = [EO]/[Li]$) as the electrolyte and Li metal as anode [44]. By the electropolymerization of pyrrole in the presence of Nafion, a Nafion molecule was introduced into a PPy matrix. The redox performance of the PPy/Nafion electrode in a PEO_8–$LiClO_4$ solid electrolyte system was investigated. A rough interface between the polymer cathode and the polymer electrolyte is usually needed for an all-solid battery; however, the PPy/Nafion cathode works well regardless of the surface texture of the PPy/Nafion film. When compared to PPy film doped with ClO_4^- anions with a similar morphology (see Fig. 16.5), PPy/Nafion film demonstrates much better redox performance in a solid polymer electrolyte, as shown in Figure 16.6. The results of alternating current (ac) impedance spectroscopy and potential-step chronoamperometry confirmed that the improvement in the redox reaction of PPy/Nafion film results from the enhancement of the ion diffusion rate in the film. The diffusion coefficients of the PPy/Nafion composite and the PPy/ClO_4 films were 2.78×10^{-11} and 1.63×10^{-14} $cm^2\,s^{-1}$, respectively. Judging from the change of electrolyte conductivity indicated by the ac impedance measurements, the ClO_4^- anion moves mainly through the PPy/Nafion film to neutralize the generated charge, and thus the PPy/Nafion film showed the redox reaction as a *p*-type polymer. Additionally, because the ion diffusion speed is slow, PPy/PSS composite film has poor redox performance in PEO_8–$LiClO_4$, although it has good redox performance in a liquid electrolyte, as mentioned above. The conclusion is that the incorporation of Nafion improves the diffusion rate of PPy film because the Nafion molecule promotes ionic movement.

This improvement increases the performance of the Li/PEO_8–$LiClO_4$/(PPy/Nafion) battery, which showed a coulombic efficiency exceeding 95% up to a 0.1 mA cm^{-2} discharge current density.

16.3 ELECTRONIC DEVICES

16.3.1 Introduction

Conjugated polymers are useful as semiconductors because they have such interesting electric properties, such as their delocalized π-electrons [46], as mentioned in the first section. These materials can be regarded as organic semiconductors with energy gaps corresponding to the UV–visible region. Among the various methods of preparing these polymer films, electropolymerization has many advantages: good processability, easy forming of thin films, and control of the films' electrical and optical properties. Some attempts have been made to utilize electropolymerized polymers as high-functionality films for electronic devices.

The key function of electropolymerized polymers is electroactivity, which is produced with the formation of a polaron, bipolaron, and soliton resulting from the process of doping counterions into the polymer matrix—the formation of polaron and bipolaron levels in the band structure is revealed in the UV–visible absorption spectra [47]. Hence, they can be applied to electrochromic devices [48, 49]. Moreover, very low conducting PPy films ($\sim 10^{-12}$ S cm^{-1})

formed by electrodeposition can be applied to metal–insulator–metal (MIM) switching devices for large-scale flat-panel liquid crystal displays (LCDs) [50, 51].

In 1991, it was reported that π-conjugated polymers could be applied as an active layer of a light-emitting diode (LED), that is, of electroluminescence (EL) devices [52]. In recent years, much attention has been paid to this possibility. Various methods have been used to produce active layers of EL devices: vacuum deposition, spin casting, and dip coating [53–60]. We have investigated electropolymerized poly(3-substituted thiophen) film as the light emission layer and the hole-transporting layer. Here, the application of electropolymerized polymers to polymer LEDs is introduced.

16.3.2 Electroluminescence Device

Light Emission Layer [61, 62] In the past several years, as mentioned above, EL devices with π-conjugated polymers have been reported. Since semiconducting luminescent polymers should be prepared as uniform thin films for EL devices, they can be mechanically formed through spin casting or dip coating after the polymerization process. "Electropolymerization" is one of the most important methods for both forming film and synthesizing π-conjugated polymer, because the optical characteristics of the films can be varied easily by the electrodeposition conditions. There is currently considerable interest in the use of such polymer films in electronic devices. Furthermore, it is expected that the electrochemical process will simplify the fabrication of EL devices because it reduces the number of fabrication steps. There have been some attempts to apply electropolymerized polymers to the light-emitting layer and the hole-transporting layer [61–63]. In this section, introduction of electropolymerized poly(3-substituted thiophen) composite film to EL devices is discussed.

By using various monomers such as 3-alkylthiophen (alkyl chain length: $n = 1, 4, 6, 7, 8, 9, 12$) and 3-phenylthiophen that are soluble in AN, polymer films can be deposited on bare indium tin oxide (ITO) glasses by electropolymerization. The deposition of poly(3-phenylthiophen) (PPhT), poly(3-hexylthiophen) (PAT6), and poly(3-octylthiophen) (PAT8) films became relatively uniform. Although these polymers were applied to a sandwich-type device, the current between the ITO and the indium was leaked because of the roughness of the polymer films. In this case, no light emission from the device was observed.

Using an ITO glass coated with nitrile butadiene rubber (NBR) thin film, the poly(3-substituted thiophen)/NBR composite film was prepared using the technique reported in [64]. By application of this composite to an EL device, current leakage was prevented because of significant improvement in the uniformity of the deposited film. Figure 16.7 shows the current–bias and bias–luminance characteristics of a device when PPhT/NBR composite film is used as an emission layer. The device has a rectified characteristic, and forward bias was obtained when the ITO was the positive and the In was grounded. As positive bias increases, an orange-red light is emitted at about 10 V, as shown in Figure 16.7, and becomes visible under ordinary dim light. PAT6/NBR and PAT8/NBR are other composite films that show similar characteristics. Since the insulating NBR film is nonfluorescent, it is confirmed that these poly(thiophen derivative)s act as light emitters.

The EL spectra of the devices utilizing various poly (thiophen derivative)/NBR composite films are shown in Figure 16.8. There is a little difference in EL emission peaks: the emission peak of the device with the PPhT/NBR composite film is around 650 nm, while those of the PAT6/NBR and PAT8/NBR composite films are around 610 and 590 nm, respectively. This peak shift suggests that the EL spectra depend on the substitute in the 3-position of the thiophen. Ohmori et al. reported a polymer LED prepared with PAT

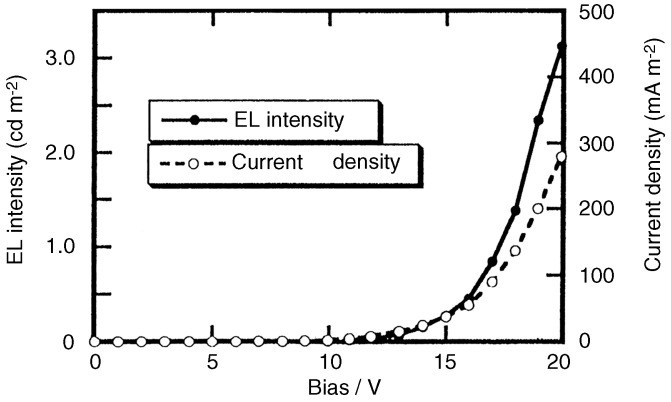

FIGURE 16.7 Dependence of EL intensity and current density on bias voltage for device using PPhT/NBR composite film. [Reproduced from *J. Electrochem. Soc.*, **144**, 745(1997). Copyright 1997 by The Electrochemical Society.]

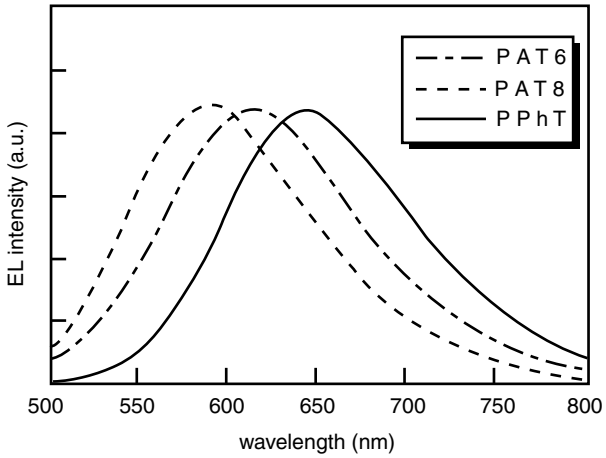

FIGURE 16.8 EL spectra of composite films of various poly (thiophen derivative)s with NBR. [Reproduced from *J. Electrochem. Soc.*, **144**, 745 (1997). Copyright 1997 by The Electrochemical Society.]

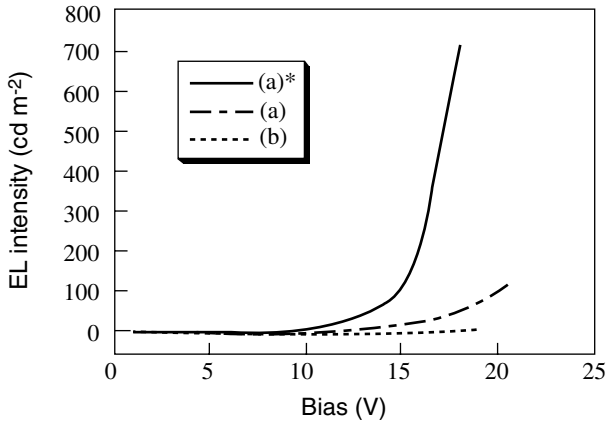

FIGURE 16.9 EL intensity as function of bias for different EL devices using: (*a*) PAT8 and dip-coated emitting layers, (*a*)* dried PAT8 and dip-coated emitting layers, and (*b*) dip-coated film only as active layer. The thicknesses of PAT8 and PVCz layers were 20 nm (1 min deposition) and 60 nm, respectively.

($n = 12$) spin-coated films polymerized by an oxidizing reagent [65]. In our system, however, the emission wavelength is shorter, owing to the difference of the degree of the polymerization and/or the conformation of the polymer chain. It seems that there is a possibility to enhance EL characteristics by controlling the electrolysis conditions and the selection of emitting materials in the electropolymerization process.

Hole-Transporting Layer [62, 63] Although a hole-transporting layer with a double-layer construction can be used to enhance the performance of an organic EL device, there have been reports that EL devices using a hole-transporting organic layer exhibited enhanced emission efficiency and durability [66, 67]. Yamamoto et al. [68] used a vacuum-deposited polythiophen film as a hole-transporting layer, and Hayashi et al. [69] attempted to use an electropolymerized poly(3-methyl-thiophen) film. Here, the possibility that an EL device can be fabricated with electropolymerized poly(thiophen derivative) film as a hole-transporting layer is discussed.

PAT8 film is electrochemically deposited, as mentioned above. The EL emission layer, a poly(*N*-vinylcarbazole) (PVCz) film dispersed with 2,5-bis(1-naphthyl)-1,3,4-oxadiazole (BND) and 3-(2′-benzothiazolyl)-7-diethyl-aminocoumarin (coumarin 6), is formed by a dip-coating method [63, 70]. An aluminum electrode for rectifying contact is deposited by vacuum evaporation onto the emitting layer. The film thicknesses of the dip coated emission layer and the electropolymerized PAT8 hole-transporting layer should be 50–60 nm and ∼20 nm, respectively. In a device without a PAT8 layer, light emission turns on at 13 V, and the maximum intensity is about 10 cd m^{-2}. A device with a PAT8 layer has a brighter emission starting at 8 V and a higher maximum intensity of ∼100 cd m^{-2}. So, adding a PAT8 layer reduces the turn-on bias by 5 V and increases the EL intensity 10-fold. Furthermore, the drying process of the PAT8 extremely improves the EL characteristics, as is seen in Figures 16.9*a* and *a**. The light emission starts at 8 V, which is lower than that of the device shown in Figure 16.9*b*, and the intensity reaches 700 cd m^{-2}, which is about 70 times higher than the device shown in Figure 16.9*b*. Since the PAT8 film does not affect emission color, the spectrum of an EL device using the film is identical to that of the PL of coumarin 6. This result shows that the PAT8 layer acts as a transparent hole-transporting layer. In summary, the device using a PVCz/PAT8 double layer shows high brightness and low turn-on bias, because the PAT8 layer acts as a highly effective hole-transporting layer.

16.4 CHEMICAL SENSORS

16.4.1 Introduction

Electropolymerization has advantages in that new film properties can be easily obtained by use of various supporting electrolytes or monomers and film thickness can be easily controlled by regulating the amount of charge passed. Additional advantages are that functional molecules are entrapped in one step during electropolymerization and the polymer film uniformly covers the surface of the substrate electrode regardless of its shape or size. Because of such advantages, the electropolymerization procedure is suitable for making micro–chemical sensors. Specifically, electropolymerized films are often utilized for the fabrication of functional electrodes having molecular selectivity [71], such as ion sensors [72–78], bionsensors [79–87], and gas sensors [88–91].

In this section, we introduce our previous attempts to fabricate a cation sensor with a PPy/PSS composite and a urea biosensor with an electroinactive PPy film electrode.

16.4.2 Cation-Sensitive Electrode

When an anodic potential is applied to an electrode inserted in a solution containing both a monomer and a polyanion, polymerization takes place, and the resulting PPy film is doped with polyanion. When PPy film is put into an electrolyte, the oxidation (cation undoping) and reduction (cation doping) states can be controlled, even in lithium secondary battery systems. Previously, we reported selective potential responses of the PPy/PSS electrode to cationic activities in test solutions [92]. Here, we describe our attempt to create a highly selective and highly stable response to concentration of K^+ by using a double layer of the PPy/PSS electrode covered with a plasticized poly(vinyl chloride) (PVC) membrane containing valinomycin.

The PPy/PSS composite film was electrochemically deposited on a 1-mm-diameter Pt disk. The PVC film was prepared on a bare Pt or PPy/PSS electrode surface by casting from a cocktail solution containing valinomycin, which is a famous ionophore for potassium ion [93]. The responses of the electrodes to ionic activities of chloride salts were measured at room temperature in the following cell: Ag/AgCl, KCl(sat.)–0.1 mol dm^{-3} NH_4NO_3–test solution–polymer film on Pt surface

By casting the plasticized PVC layer containing valinomycin as a K^+ ion carrier onto the two electrode, we prepared two types of all solid-state potassium ion–selective electrodes, that is, a single layer of PVC/Pt and a double layer of PVC/(PPy/PSS)/Pt. The response of the double-layer film electrode to each monovalent cation was investigated for selectivity, as shown in Figure 16.10. The double-layer electrode of PVC/(PPy/PSS)/Pt selectively responds to the concentration of the K^+ ion in the test solution (even when contaminated by the Na^+ ion), better than the single-layer electrode of PVC/Pt used as a coated-wire-type electrode (CWE). Furthermore, the PVC/(PPy/PSS)/Pt indicates a more stable response and a lower potential drift than the Pt/PVC [94, 95]. Figure 16.11 shows the mechanism of yielding potential for the CWE and Pt/(PPy/PSS)/PVC electrodes. In the CWE, the interface of the PVC and the Pt surface is electrochemically unstable and completely blocked electrically [96], as shown in Figure 16.11*a*. As can be seen in this figure, however, the Pt surface contacts electrochemically and electrically with the electroactive and conductive PPy/PSS film. It is expected that the potential of the internal electrode indicates a stable value resulting from a high redox capacity. This stability is caused by the formation of a concentration cell with a two-sided PVC membrane because of the cation exchange ability of the PPy/PSS [94]. The PVC/(PPy/PSS)/Pt electrode therefore acts as both an internal electrolyte solution and an internal reference electrode, like an internal Ag/AgCl reference electrode with a KCl solution in conventional ion-selective electrodes. Furthermore, we proved and analyzed the long-term stability of the all-solid-state potassium-selective electrode with the PPy/PSS [95]. There appears to be a high possibility that monovalent cation sensors can be fabricated using PPy/PSS composite film. In particular, the double-layer system using an *n*-type active and conductive polymer is also expected to allow the miniaturization of other important ion-selective electrodes.

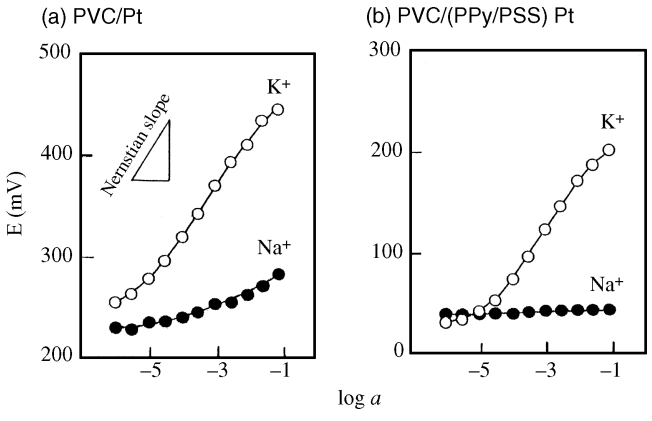

FIGURE 16.10 Potential responses to concentration of potassium sodium ions of (*a*) PVC/Pt and (*b*) PVC/(PPy/PSS)/Pt electrodes.

16.4.3 Potentiometric Biosensor for Urea

The idea of incorporating enzyme, such as glucose oxidase, into conducting polymers by electropolymerization has been reported [79, 97]. These biosensors, which were developed with electropolymerized conducting polymers, are amperometric sensors that measure the electrochemical current generated by oxygen or hydrogen peroxide [97]. However, these biosensors have a disadvantage: The conductivity of their films is decreased by degradation of the polymers [98]. So, we focused on the application of pH-sensitive nonconducting PPy to a potentiometric biosensor for urea.

Urea is often monitored in the blood to obtain information on kidney disease. The monitoring procedure for urea usually involves a catalytic reaction by enzyme. To make this monitoring procedure easier, many biosensors using urease (Urs)-immobilized electrodes have been studied [99–101]. Many urea sensors, such as an ion-selective membrane electrode [102, 103], a gas sensor [104], and an ion-sensitive field effect transistor (ISFET) [105], are structured such that an enzyme layer is formed directly on the active surface of a potentiometric transducer. The fabrication of a urea sensor using electropolymerized conducting PPy film containing Urs has been reported; however, its sensitivity was insuffi-

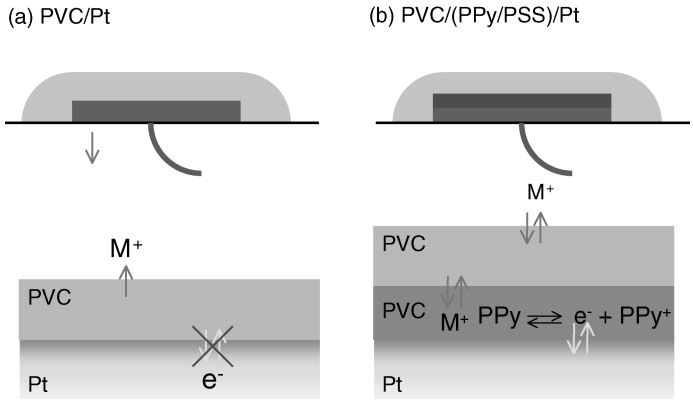

FIGURE 16.11 Potential response mechanism for (*a*) PVC/Pt and (*b*) PVC/(PPy/PSS)/Pt electrodes.

cient because the Nernstian slope was relatively low [106–108].

When pyrrole is electropolymerized in a solution containing a nucleophilic reagent as a supporting electrolyte, an electroinactive and low-conducting PPy-coated electrode is obtained [14, 50, 98]. A Pt electrode coated with this PPy film exhibits a good Nernstian response to pH value. By using this electrode, we attempted to fabricate an amperometric micro–pH sensor [15] Moreover, the film can be applied to a potentiometric biosensor for urea, since the pH changes according to the urea hydrolysis catalyzed by Urs proceed as follows:

$$NH_2CONH_2 + 2H_2O + H^+ \rightarrow 2NH_4^+ + HCO_3^-$$

The strategy to immobilize the enzyme is shown in Figure 16.12. In phase 1 of Figure 16.12, Urs is entrapped in the insulating PPy film by the addition of both Urs and nucleophilic electrolyte to the polymerizing solution, and the Urs-immobilized, electroinactive PPy- coated electrode is fabricated [16]. This electrode could be used as a urea sensor that shows a potential response with a slope of 31.8 mV decade^{-1}. Since it is considered that Urs is physically entrapped in the PPy film during its electrodeposition, this type of sensor can be fabricated by one electrochemical step. In this case, the PPy film acts as both pH detector and entrapment matrix. This process, however, seems to be unsuitable for immobilizing a large amount of enzyme molecules; since enzyme is an expensive material, a major problem for mass production is that most of the Urs dissolved in the polymerizing electrolyte is not trapped in the PPy and, therefore, is wasted. It is also considered that an increase in the amount of immobilized Urs in electroinactive PPy film might increase the sensitivity of the film. Thus, in an attempt to improve the design of the device, we developed a new one that utilizes a composite film consisting of electroinactive PPy and Urs modified with poly(acrylic acid) (PAA) by peptide bonding, as shown in phase 2 of Figure 16.12 [17]. In this type of sensor Urs is chemically wired with PAA by the condensation reaction of water-soluble carbodiimide, and subsequently, pyrrole is electropolymerized. This type of urea sensor demonstrates a potential response with a slope of 53 mV decade^{-1}, which is higher than that of phase 1 described above. It is considered that this higher sensitivity is attributable to both the increase in the loading amount of Urs and the covalent peptide bonding of the residual amino group of Urs and the carboxyl groups of PAA. However, since water-soluble PAA is employed in this system, it also is suggested that some amount of Urs, combined with PAA, is scattered and lost in the aqueous solution of pyrrole prior to electropolymerization. The conclusion is that the sensitivity of this type of sensor could be further improved by using water-insoluble material for the immobilization.

From this viewpoint, we fabricated a more sensitive urea sensor based on a composite film consisting of electroinactive PPy and a polyion complex, as shown in phase 3 of Figure 16.12. Mizutani et al. have reported various amperometric biosensors in which enzyme molecules were incorporated into a water-insoluble polyion complex formed with polycation and polyanion [109, 110]. Thus, we employed such a polyion complex as the material for immobilizing Urs [18]. After the polyion complex was coated, pyrrole was electropolymerized, and the composite film of PPy and polyion complex was obtained. This type of sensor demonstrates the fast potential response to urea by the same detection mechanism mentioned above. By using this system, the highest urea response with a slope of 110 mV decade^{-1} was obtained. Such a high sensitivity is considered attributable to the effective immobilization of a large amount of Urs by electropolymerization on the electrode precoated with a polyion complex.

16.5 FURTHER RESEARCH AND DEVELOPMENT OF ELECTROPOLYMERIZED COATINGS

In recent decades, there has been research on various applications for conducting polymers, such as photovoltaic

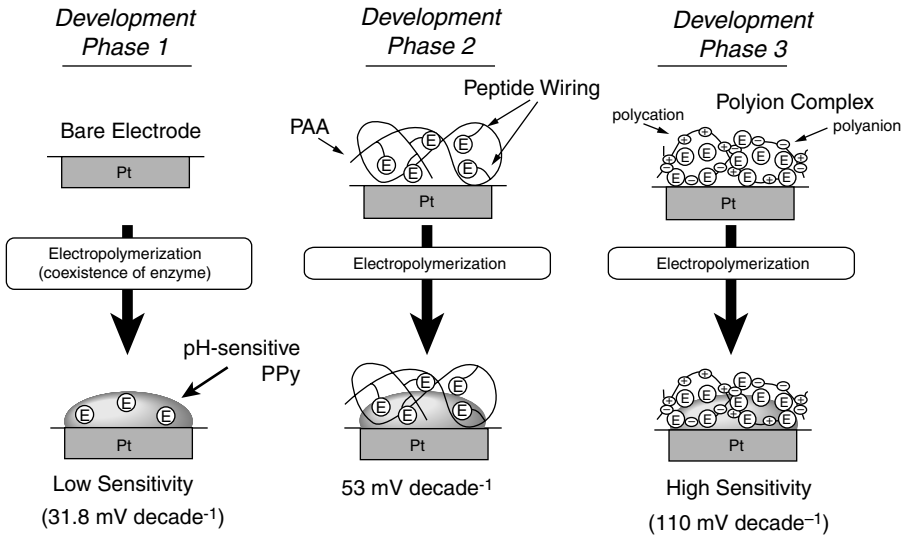

FIGURE 16.12 Illustration showing development of urea biosensor.

cells [111, 112], sensors [113, 114], and the creation of nanosized structure-controlled materials and functional composite membranes. In addition, the biocompatible features of electropolymerized polymer films also have attracted researchers. Serra-Moreno et al. have reported that a composite film of polypyrrole and polysaccharide was obtained by electropolymerization of pyrrole with polysaccharide as the supporting anion [115]. The biocompatibility of this composite film was demonstrated by the fact that human cells attached to the film survived.

Also, the application of electropolymerized polymer coatings for new functions has been reported. For example, a conducting electroactive polymer with cationic exchange properties has been formed by electropolymerization of aniline derivative with a substituted anionic group. A very thin layer of such a polymer can be applied for the surface treatment of the carbon particles in the catalyst layer of fuel cells to enhance the proton transportation around the particles. This enhancement is the result of oxidation of the *m*-aminobenzenesulfonic acid at the surface of the carbon [116].

REFERENCES

1. H. Shirakawa, T. Ito, and S. Ikeda, *Polym. J.*, **2**, 231 (1971).
2. T. Ito, H. Shirakawa, and S. Ikeda, *J. Polym. Sci., Polym. Chem. Ed.*, **12**, 11 (1974).
3. T. Ito, H. Shirakawa, and S. Ikeda, *J. Polym. Sci., Polym. Chem. Ed.*, **13**, 1943 (1975).
4. T. A. Skotheim, Ed. *Handbook of Conducting Polymers*, Vols. 1 and 2, Marcel Dekker, New York, 1986.
5. A. F. Diaz and K. K. Kanazawa, *J. Chem. Soc. Chem. Commun.*, 635 (1979).
6. K. K. Kanazawa, A. F. Diaz, R. H. Geiss, W. D. Gill, J. F. Kwak, J. A. Logan, J. F. Rabolt, and G. B. Street, *J. Chem. Soc. Chem. Commun.*, 854 (1979).
7. G. Tourillon and F. Garnier, *J. Electroanal. Chem.*, **135**, 173 (1982).
8. T. Yamamoto, Z. Zhou, I. Ando, and M. Kikuchi, *Makromol. Chem. Rapid Commun.*, **14**, 833 (1993).
9. L. M. Goldenberg and P. C. Lacaze, *Synth. Met.*, **58**, 271 (1993).
10. G. Schiavon, G. Zotti, and G. Bontempelli, *J. Electroanal. Chem.*, **194**, 327 (1985).
11. G. Zotti, G. Schiavon, N. Comisso, A. Berlin, and G. Pagani, *Synth. Met.*, **36**, 337 (1990).
12. G. Zotti and G. Schiavon, *J. Electroanal. Chem.*, **163**, 385 (1984).
13. G. Schiavon, G. Zotti, and G. Bontempelli, *J. Electroanal. Chem.*, **161**, 323 (1984).
14. T. Osaka, T. Momma, and H. Kanagawa, *Chem. Lett.*, **649**, (1993).
15. T. Osaka, T. Fukuda, H. Kanagawa, T. Momma, and S. Yamauchi, *Sensors Actuators B*, **13–14**, 205 (1993).
16. S. Komaba, M. Seyama, T. Momma, and T. Osaka, *Electrochim. Acta*, **42**, 383 (1997).
17. S. Komaba, M. Seyama, K. Tanabe, and T. Osaka, *Denki Kagaku*, **64**, 1228 (1996).
18. T. Osaka, S. Komaba, M. Seyama, and K. Tanabe, *Sensors and Actuators B*, **36**, 463 (1997).
19. R. J. Waltman, A. F. Diaz, and J. Bargon, *J. Electrochem. Soc.*, **131**, 740 (1984).
20. T. Osaka, K. Naoi, and S. Ogano, *J. Electrochem. Soc.*, **135**, 1071 (1988).
21. T. Osaka, K. Naoi, S. Ogano, and S. Nakamura, *J. Electrochem. Soc.*, **134**, 2096 (1987).
22. F. Croce, S. Panero, P. Prosperi, and B. Scrosati, *Solid State Ionics*, **28–30**, 895 (1988).

23. T. Osaka, T. Nakajima, K. Shiota, and B. B. Owens, in *Rechargeable Lithium Batteries/1989*, S. Subbarao, V. R. Koch, B. B. Owens, and W. H. Smyrl, Eds., PV 90–5, Electrochemical Society Pennington, NJ, 1990, p. 170.
24. T. Osaka, and K. Ueyama, *Kagaku-Kogyo* (*Chemical Industry*), 31 (Mar. 1989).
25. T. Sotomura, H. Uemachi, K. Takeyama, K. Naoi, and N. Oyama, *Electrochim. Acta*, **37**, 1851 (1993).
26. N. Oyama, T. Tatsuma, T. Sato, and T. Sotomura, *Nature*, **373**, 598 (1995).
27. T. Osaka, T. Momma, H. Ito, and B. Scrosati, *J. Power Sources*, **68**, 393 (1997).
28. M. D. Paoli, R. J. Waltman, A. F. Diaz, and J. Bargon, *J. Polym. Sci. Polym. Chem. Ed.*, **23**, 1067 (1985).
29. B. Kaye and A. E. Underhill, *Synth. Met.*, **28**, C97 (1989).
30. H. Yoneyama, Y. Li, and S. Kuwabata, *J. Electrochem. Soc.*, **139**, 28 (1992).
31. A. Boyle, E. Genies, and M. Fouletier, *J. Electroanal. Chem.*, **279**, 179 (1988).
32. L. L. Miller and Q. X. Zhou, *Macromolecules*, **20**, 1594 (1987).
33. T. Shimidzu, A. Ohtani, and K. Honda, *J. Electroanal. Chem.*, **251**, 323 (1988).
34. C. M. Elliott, A. B. Kopelove, W. J. Alberty, and Z. Chen, *J. Phys. Chem.*, **95**, 1743 (1991).
35. A. Shimizu, K. Yamanaka, and M. Kohno, *Bull. Chem. Soc. Jpn.*, **61**, 4401 (1988).
36. T. Osaka, T. Momma, and K. Nishimura, *Chem. Lett.*, 1787 (1992).
37. T. Momma, K. Nishimura, T. Osaka, N. Kondo, and S. Nakamura, *J. Electrochem. Soc.*, **141**, 2326 (1994).
38. X. Ren and P. G. Pickup, *J. Phys. Chem.*, **97**, 5356 (1993).
39. K. West, M. A. Careem, and S. Skaarup, *Solid State Ionics*, **60**, 153 (1993).
40. T. Osaka, T. Momma, K. Nishimura, S. Kakuda, and T. Ishii, *J. Electrochem. Soc.*, **141**, 1994 (1994).
41. K. Naoi and T. Osaka, *J. Electrochem. Soc.*, **134**, 2479 (1987).
42. K. Naoi, M. Asada, Y. Hayashi, and Y. Inoue, in *Proceedings of the Symposium on New Sealed Rechargeable Batteries and Supercapacitors*, B. M. Barnett, E. Dowgiallo, G. Halpert, Y. Matsuda, and Z. Takehara, Eds., PV 93–23, Electrochemical Society, Pennington, NJ, 1993, p. 86.
43. C. Arbizzani, A. M. Marinangeli, M. Mastragostino, L. Meneghello, T. Hamaide, and A. Guyot, *J. Power Sources*, **43–44**, 453 (1993).
44. T. Momma, S. Kakuda, H. Yarimizu, and T. Osaka, *J. Electrochem. Soc.*, **142**, 1766 (1995).
45. H. Yoneyama, T. Hirai, S. Kuwabata, and O. Ikeda, *Chem. Lett.*, 1243 (1986).
46. C. K. Chiang, S. C. Gau, C. R. Fincher, Jr., Y. W. Park, A. G. MacDiarmid, and A. J. Heeger, 33, 18 (1978).
47. J. L. Bredas and G. B. Street, *Acc. Chem. Res.*, **18**, 309 (1985).
48. A. Kitani, J. Yano, and K. Sasaki, *J. Electrochem. Soc.*, **209**, 227 (1986).
49. H. T. Chiu, J. S. Lin, and J. N. Shiau, *J. Appl. Electrochem.*, **22**, 522 (1992).
50. T. Osaka, T. Fukuda, K. Ouchi, and T. Nakajima, *Denki Kagaku*, **12**, 1019 (1991);T. Nakajima, F. Matsushima, T. Fukuda, and T. Osaka, *Denki Kagaku*, **12**, 1074 (1991).
51. T. Osaka, T. Fukuda, K. Ouchi, and T. Momma, *Thin Solid Films*, **215**, 200 (1992).
52. J. H. Burroughes, D. D. C. Bradley, A. R. Brown, R. N. Marks, K. Mackay, R. H. Friend, P. L. Burns, and A. B. Holmes, *Nature*, **347**, 539 (1990).
53. C. W. Tang and S. A. VanSlyke, *Appl. Phys. Lett.*, **51**, 913 (1987).
54. G. Grem, G. Leditzky, B. Ullrich, and G. Leising, *Adv. Mater.*, **4**, 36 (1992).
55. D. Brown and A. J. Heeger, *Appl. Phys. Lett.*, **58**, 1982 (1991).
56. M. Berggren, G. Gustafsson, O. Ingan, M. R. Andersson, O. Wennerstr, and T. Hjertberg, *Adv. Mater.*, **6**, 488 (1994).
57. M. Uchida, Y. Ohmori, T. Noguchi, T. Ohnishi, and K. Yoshino, *Jpn. J. Appl. Phys.*, **32**, L921 (1993).
58. G. Grem and G. Leising, *Synth. Metals*, **55–57**, 4105 (1993).
59. Y. Ohmori, M. Uchida, K. Muro, and K. Yoshino, *Solid State Commun.*, **80**, 605 (1991).
60. D. Brown, G. Gustafsson, D. McBranch, and A. J. Heeger, *J. Appl. Phys.*, **72**, 564 (1992).
61. S. Komaba, K. Fujihana, N. Kaneko, and T. Osaka, *Chem. Lett.*, 923 (1995).
62. T. Osaka, S. Komaba, K. Fujihana, N. Okamoto, T. Momma, and N. Kaneko, *J. Electrochem. Soc.*, **144**, 742 (1997).
63. T. Osaka, S. Komaba, K. Fujihana, N. Okamoto, and N. Kaneko, *Chem. Lett.*, 1023 (1995).
64. K. Naoi and T. Osaka, *J. Electrochem. Soc.*, **134**, 2479 (1987).
65. Y. Ohmori, M. Uchida, K. Muro, and K. Yoshino, *Jpn. J. Appl. Phys.*, **30**, L1938 (1991).
66. Y. Shirota, Y. Kuwabara, H. Inada, T. Wakimoto, H. Nakada, Y. Yonemoto, S. Kawami, and K. Imai, *Appl. Phys. Lett.*, **65**, 807 (1994).
67. G. Gustafsson, Y. Cao, G. M. Treacy, F. Klavetter, N. Colaneri, and A. J. Heeger, *Nature*, **357**, 477 (1992).
68. T. Yamamoto, T. Inoue, and T. Kanbara, *Jpn. J. Appl. Phys.*, **33**, L250 (1994).
69. S. Hayashi, H. Etoh, and S. Saito, *Jpn. J. Appl. Phys.*, **25**, L773 (1986).
70. Y. Mori, H. Endo, and Y. Hayashi, *Ouyoubutsuri*, **61**, 1044 (1991) (in Japanese).
71. S. Komaba, M. Seyama, and T. Osaka, *Chemical Sensors*, **12**, 97 (1996) (in Japanese).
72. W. R. Heineman, H. J. Wieck, and A. M. Yachnych, *Anal. Chem.*, **52**, 345 (1980).
73. S. Dong, Z. Sun, and Z. Lu, *Analyst*, **113**, 1525 (1988).
74. Q. Pei and R. Qian, *Synth. Met.*, **45**, 35 (1991).
75. S. Daunert, S. Wallace, A. Floride, and L. Bachas, *Anal. Chem.*, **63**, 1676 (1991).

76. T. Okada, H. Hayashi, K. Hiratani, H. Sugihara, and N. Koshizaki, *Analyst*, **116**, 923 (1991).
77. T. Okada, K. Hiratani, H. Sugihara, and N. Koshizaki, *Anal. Chim. Acta*, **272**, 89 (1992).
78. T. Okada, K. Hiratani, H. Sugihara, and N. Koshizaki, *Sensors Actuators B*, **13–14**, 563 (1993).
79. N. C. Foulds and C. R. Lowe, *J. Chem. Soc. Faraday Trans.*, **1**, **82**, 1259 (1986).
80. A. Begum, H. Tsushima, T. Suzawa, H. Shinohara, Y. Ikariyama, and M. Aizawa, *Sensors Actuators B*, **13–14**, 576 (1993).
81. P. N. Bartlett and P. R. Birkin, *Synth. Met.*, **61**, 15 (1993).
82. P. N. Bartlett and J. M. Cooper, *J. Electroanal. Chem.*, **371**, 1 (1993).
83. G. F. Khan, E. Kobatake, Y. Ikariyama, and M. Aizawa, *Anal. Chim. Acta*, **281**, 527 (1993).
84. F. Pslmisano, D. Centonze, and P. G. Zambonin, *Biosensens. Bioelectron.*, **9**, 471 (1994).
85. B. F. Y. Yon Hin and C. R. Lowe, *J. Electroanal. Chem.*, **374**, 167 (1994).
86. M. Aizawa, T. Haruyama, G. F. Kahn, E. Kobatake, and Y. Ikariyama, *Bionsens. Bioelectron.*, **9**, 601 (1994).
87. W. Schhmann, *Biosens. Bioelectron.*, **10**, 181 (1995).
88. J. J. Miasik, A. Hopper, and B. C. Tofield, *J. Chem. Soc. Faraday Trans.*, **1**, 82, 1117 (1986).
89. T. Hanawa, S. Kuwabata, and H. Yoneyama, *J. Chem. Soc. Faraday Trans.*, **1**, 84, 1587 (1988).
90. T. Hanawa and H. Yoneyama, *Bull. Chem. Soc. Jpn.*, **62**, 1710 (1989).
91. H. Nagase, K. Wakabayashi, and T. Imanaka, *Sensors Actuators B*, **13–14**, 596 (1993).
92. T. Momma, S. Komaba, T. Osaka, S. Nakamura, and Y. Takemura, *Bull. Chem. Soc. Jpn.*, **68**, 1297 (1995).
93. W. Simon and D. Stefanac, *Chimia*, **20**, 436 (1966).
94. T. Momma, S. Komaba, M. Yamamoto, T. Osaka, and S. Yamauchi, *Sensors Actuators B*, **25**, 724 (1995).
95. T. Momma, M. Yamamoto, S. Komaba, and T. Osaka, *J. Electroanal. Chem.*, **407**, 91 (1996).
96. B. P. Nikolskii and E. A. MAterova, *Ion Select. Electrode Rev.*, **7**, 3 (1985).
97. W. Schuhmann, *Mikrochim. Acta*, **121**, 1 (1995).
98. T. Osaka, T. Momma, S. Komaba, H. Kanagawa, and S. Nakamura, *J. Electroanal. Chem.*, **372**, 201 (1994).
99. M. Mascini and G. Guilbault, *Anal. Chem.*, **49**, 795 (1977).
100. M. Pryzgyt and H. Sugier, *Anal. Chim. Acta*, **237**, 399 (1990).
101. A. M. Nyamsi Hendji, N. Jaffrezic-Renault, C. Martelet, A. A. Shul'ga, S. V. Dzydevich, A. P. Soldatkin, and A. V. El'skaya, *Sensors Actuators B*, **21**, 123 (1994).
102. R. Koncki, P. Leszcynski, A. Hulanicki, and S. Glab, *Anal. Chim. Acta*, **257**, 67 (1992).
103. D. Martorell, E. Martinez-Fabregas, J. Bartoli, S. Alegret, and C. Tran-Minh, *Sensors Actuators B*, **15–16**, 448 (1993).
104. Y. J. Wang, C. H. Chen, G. H. Hsiue, and B. C. Yu, *Biotechnol. Bioeng.*, **40**, 44 (1992).
105. S. Alegret, J. Bartroli, C. Jimenez, E. Martinez-Fabregas, D. Martorell, and F. Valdes Perezgasga, *Sensors Actuators B*, **15–16**, **453**, (1993).
106. S. B. Adeloju, S. J. Shaw, and G. G. Wallace, *Anal. Chim. Acta*, **281**, 611 (1993).
107. S. B. Adeloju, S. J. Shaw, and G. G. Wallace, *Anal. Chim. Acta*, **281**, 621 (1993).
108. E. C. Hernandez, A. Witkowski, S. Daunert, and L. G. Bachas, *Mikrochim. Acta*, **121**, 63 (1995).
109. F. Mizutani, S. Yabuki, and Y. Hirata, *Denki Kagaku*, **63**, 1100 (1995).
110. F. Mizutani, S. Yabuki, and Y. Hirata, *Anal. Chim. Acta*, **314**, 233 (1995).
111. S. Y. Kim, K. H. Lee, B. D. Chin, and J.- W. Yu, *Solar Energy Mater. Solar Cells*, **93**, 129–135 (2009).
112. D. L. Wakeharn, S. W. Donne, W. J. Belcher, and P. C. Dastoor, *Synthetic Metals*, **158**, 661–669 (2008).
113. F. R. R. Teles and L. R. Foseca, *Mater. Sci. Eng. C-Biomimet. Supramol. Syst.*, **28**, 1530–1543 (2008).
114. A. Lu and C. M. Li, *Biosensors Bioelectron.*, **24**, 767–772 (2008).
115. J. Serra-Moreno, S. Panero, S. Materazzi, A. Martinelli, M. Giovanna-Sabbieti, D. Agas, and G. Materazzi, *J. Biomed. Mater. Res. Part A*, **88A**, 832–840 (2009).
116. S. Tominaka, K. Goto, T. Momma, and T. Osaka, *J. Power Sources*, **192**, 316 (2009).

17

ELECTROLESS DEPOSITION OF COPPER

MILAN PAUNOVIC

In Chapter 1 (Part A), we discuss the overall reaction and the mixed-potential theory of electroless metal deposition in general. In this chapter we discuss the specific case of copper: the overall reaction, fundamental, and technological aspects of its electroless deposition.

The overall reaction for electroless copper deposition, with formaldehyde (HCHO) as the reducing agent, is

$$Cu^{2+} + 2HCHO + 4OH^- \rightarrow Cu + 2HCOO^- + 2H_2O + H_2 \quad (17.1)$$

where $HCOO^-$ (formic acid) is the oxidation product of the reducing agent. The fundamental aspects of this reaction are presented in the following five sections: (17.1) electrochemical model, (17.2) anodic partial reaction, (17.3) cathodic partial reaction, (17.4) kinetics of deposition, and (17.5) modeling. Some special cases of electroless copper deposition solutions are given in an Appendix to this chapter.

17.1 ELECTROCHEMICAL MODEL

17.1.1 Mixed-Potential Theory

The mixed-potential theory was developed by Wagner and Traud [1] for the purpose of interpreting metal corrosion processes. Paunovic [2] and Saito [3] applied the theory to the interpretation of electroless deposition of copper.

According to the mixed-potential theory, the overall reaction, given by Eq. (17.1), can be decomposed into a simple reduction reaction, the cathodic partial reaction

$$Cu^{2+}_{solution} + 2e \xrightarrow{\text{catalytic surface}} Cu_{lattice} \quad (17.2)$$

and one oxidation reaction, the anodic partial reaction

$$HCHO + 2OH^- \rightarrow HCOO^- + H_2O + \tfrac{1}{2}H_2O + e \quad (17.3)$$

Thus the overall reaction (17.1) is the result of the combination of two different partial reactions, Eqs. (17.2) and (17.3). These two partial reactions, however, occur at one and the same electrode, namely the metal–solution interphase. Each of these reactions strives to establish its own equilibrium potential, E_{eq}. The result of this process is the creation of a steady state with the compromised potential called the *steady-state mixed potential,* E_{mp}.

17.1.2 Evans Diagram

According to the mixed-potential theory the overall reaction of the electroless copper deposition can be described electrochemically in terms of two current–potential (*i–E)* curves, as shown in Figure 17.1. Figure 17.1 was constructed in the following way: First, the current–potential curve of the reduction of cupric ions in the solution containing H_2O, 0.1 *M* $CuSO_4$, 0.175 *M* EDTA (ethylenediaminetetraacetic acid) and NaOH to pH 12.50 (no CH_2O present) at 24°C (±0.5) is determined using a galvanostatic technique. At this electrode only one reaction occurs, the reduction of Cu^{2+}. An electrode with only one electrode process is called a *single electrode*. The result is shown as $i(cu^{2+}) = f(E)$ in Figure 17.1. The current–potential curve was recorded starting from the equilibrium potential, $E_{eq}(Cu/Cu^{2+}) = -0.47$ V versus SCE. Second, the current–potential curve for the oxidation of formaldehyde at the single electrode was determined using the galvanostatic technique. The solution in this case contained H_2O, 0.05 *M* CH_2O, 0.075 *M* EDTA (excess of EDTA used in the solution for the single cathodic reaction), and NaOH to pH 12.50 (no $CuSO_4$ was present in this solution). The temperature was 24°C (±0.5). The result

Modern Electroplating, Fifth Edition Edited by Mordechay Schlesinger and Milan Paunovic

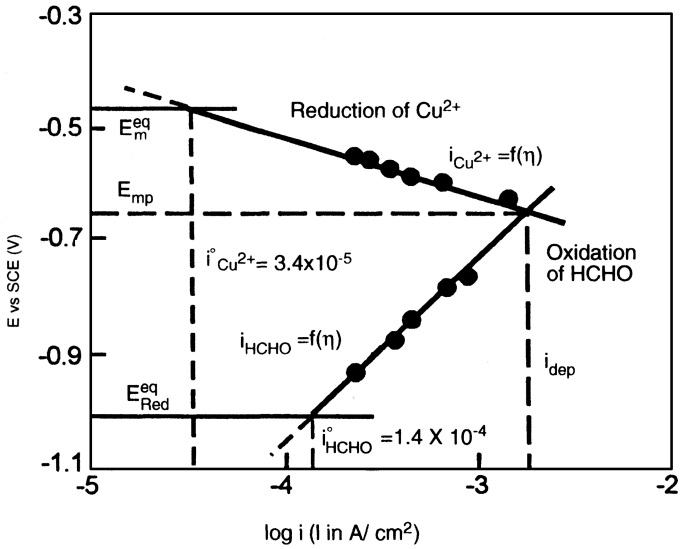

FIGURE 17.1 Current–potential curves for reduction of Cu^{2+} ions and for oxidation of reducing agent Red, formaldehyde, combined into one graph (Evans diagram). Solution for the Tafel line for the reduction of Cu^{2+} ions: 0.1 *M* $CuSO_4$, 0.175 *M* EDTA, pH 12.50, E_{eq} $(Cu/Cu^{2+}) = -0.47$ V versus a saturated calomel electrode (SCE); for the oxidation of formaldehyde: 0.05 *M* HCHO and 0.075 *M* EDTA, pH 12.50, E_{eq} (HCHO) $= -1.0$ V versus SCE; temperature 25°C (±0.50°C). (From Paunovic [2] with permission from the American Electroplaters and Surface Finishers Society.)

is shown as $i(CH_2O) = f(E)$ in Figure 17.1. The current–potential curve was recorded starting from the equilibrium potential, $E_{eq}(CH_2O) = -1.0$ V versus SCE. It is seen from Figure 17.1 that these two polarization curves, $i(Cu^{2+}) = f(E)$ and $i(CH_2O) = f(E)$, intersect. The coordinates of intersection are (1) abscisa, $i = 1.9 \times 10^{-3}$ A cm^{-2} and (2) ordinate, $E = -0.65$ V versus SCE. According to the mixed-potential theory, current density $i = 1.9 \times 10^{-3}$ A cm^{-2} is the rate of the electroless deposition of copper expressed in terms of amperes per square centimeter. The potential $E = -0.65$ V versus SCE is the mixed potential (E_{mp}) of the electroless copper system under study. The rate of deposition expressed in milligrams per hour per square centimeter is calculated on the basis of Faraday's law using the equation

$$w = i \times 1.18 \text{ mg h}^{-1}\text{cm}^{-2}$$

where i is given in milliamperes per square centimeter. For $i = 1.9 \times 10^{-3}$ A cm^{-2} it is 2.2 mg h^{-1} cm^{-1}.

The experimentally determined rate of electroless Cu deposition under the conditions above, using the weight gain method, is 1.8 mg h^{-1} cm^{-2}. This rate is obtained when the time of deposition is counted from the instant of immersion of the copper plate (substrate) into the solution. If the time of deposition is counted from the instant the mixed potential is reached (about 4 min after immersion of the Cu substrate), the deposition rate is 1.9 mg h^{-1} cm^{-2}. The experimentally determined mixed potential E_{mp} for the same conditions is −0.65 V versus SCE.

Examination of Figure 17.1 and the results of direct experimental measurements show that there is a relatively good agreement between the direct experimental and the theoretical values (Evans diagram). Thus we can conclude that the mixed-potential theory is essentially verified for this case of electroless copper deposition. These conclusions are confirmed by Donahue [4], Molenaar et al. [5], and El-Raghy and Abo-Salama [6]. The significance of this conclusion is that on the basis of the mixed-potential theory one can use the kinetic parameters for the partial anodic and cathodic reactions to deduce a variety of predictions and characteristics of the overall reaction of electroless copper deposition. For example, the effect of additives on the overall reaction can be resolved into separate effects on the partial reactions and use these results to select the best conditions for electroless deposition.

17.1.3 Interaction between Partial Reaction

The original mixed-potential theory assumes that the two partial reactions are independent of each other [1, 2]. In some cases this is a valid assumption. However, it was shown later that the partial reactions are not always independent of each other [7, 8]. For example, Schoenberg [9] has shown that the methylene glycol anion (the formaldehyde in an alkaline solution), the reducing agent in electroless copper deposition, enters the first coordination sphere of the copper tartrate complex and thus influences the rate of the cathodic partial reaction. Ohno and Haruyama [10] showed the presence of interference in partial reactions in terms of current–potential curves.

17.1.4 Presence of Interfering Reactions

In the presence of interfering (or side) reactions, partial reactions i_a and/or i_c may be composed of two or more components. One example is the electroless deposition of copper from solutions containing oxygen [11, 12]. In this case the interfering reaction is the reduction of the oxygen, and the cathodic partial current density i_c is the sum of two components,

$$i_c = i_c(Cu^{2+}) + i_c(O_2)$$

where $i_c(Cu^{2+})$ is the cathodic partial current density for reduction of copper ions Cu^{2+} and $i_c(O_2)$ is that for reduction of the oxygen.

17.2 ANODIC PARTIAL REACTION

17.2.1 Overall Reaction

Most electroless copper solutions employ formaldehyde as the reducing agent. The overall reaction of the electrochemical

oxidation of formaldehyde at the Cu electrode in an alkaline solution proceeds according to Eq. (17.3).

17.2.2 Mechanism

The overall anodic partial reaction (17.3) proceeds in at least two elementary steps:

1. Formation of electroactive species
2. Charge transfer from electroactive species to the catalytic surface (electron injection)

Formation of electroactive species proceeds in three steps:

1. Hydrolysis of H_2CO,

$$H_2CO + H_2O \rightarrow H_2C(OH)_2 \quad \text{(methylene glycol)} \tag{17.4}$$

2. Dissociation of methylene glycol,

$$H_2C(OH)_2 + OH^- \rightarrow H_2C(OH)O^- + H_2O \tag{17.5}$$

3. Dissociative adsorption of the intermediate $H_2C(OH)O^-$ involving breaking of C–H bond,

$$H_2C(OH)O^- \rightarrow [HC(OH)O^-]_{ads} + H_{ads} \tag{17.6}$$

where the subscript ads denotes adsorption of species and $[HC(OH)O^-]_{ads}$ is electroactive species.

Charge transfer, the electrochemical oxidation (desorption) of electroactive species, proceeds according to the reaction

$$[HC(OH)O^-]_{ads} + OH^- \rightarrow HCOO^- + H_2O + e \tag{17.7}$$

where $HCOO^-$ (formic acid) is the oxidation product.

The adsorbed hydrogen, H_{ads}, may be desorbed in the chemical reaction

$$H_{ads} \rightarrow \tfrac{1}{2}H_2 \tag{17.8}$$

or in the electrochemical reaction

$$H_{ads} \rightarrow H^+ + e \tag{17.9}$$

In electroless deposition of copper, when the reducing agent is formaldehyde and the substrate is Cu, H_{ads} desorbs in the chemical reaction (17.8). If the substrate is Pd or Pt, hydrogen desorbes according to the electrochemical reaction (17.9).

17.2.3 Cannizzaro Reaction

One important side reaction in electroless copper deposition is disproportionation of formaldehyde (Cannizzaro reaction):

$$2HCHO + OH^- \rightarrow HCOO^- + CH_3OH \tag{17.10}$$

In this reaction, between two molecules of formaldehyde, one molecule is oxidized into formic acid and the other is reduced into methanol. The rate of this reaction increases with increasing pH and temperature [13].

17.2.4 Kinetics

The major factors determining the rate of the anodic partial reaction are pH and additives. Since OH^- ions are reactants in the charge-transfer step, Eq. (17.7), the effect of pH is direct and significant [14, 15].

The reduction potential (the rest potential) of formaldehyde increases linearly with pH according to Nernst's equation

$$E = E^0_{csp} - 0.118\,\text{pH} \tag{17.11}$$

where E^0_{csp} combines the standard electrode potential E^0 and the concentration term in Nernst's equation [14]. The rest potential of a copper single electrode (absence of copper ions) in the solution of formaldehyde as a function of pH is shown in Figure 17.2. The average slope $\partial E/\partial(\text{pH})$ of experimental functions in Figure 17.2 is -0.096 V decade^{-1}. A

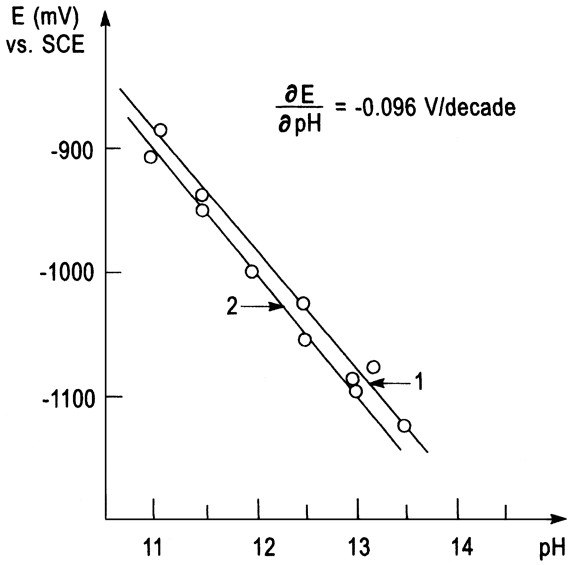

FIGURE 17.2 Rest potential of a copper electrode in 0.13 *M* formaldehyde and 1.0 *M* KCl as a function of pH. Curve 1: the absence of ligand; curve 2: the presence of 0.05 *M* EDTP (ethylenedinitrilo-tetra-2-propanol).

detailed discussion of the pH effect on the partial anodic reaction is given by Duffy et al. [14],

17.3 CATHODIC PARTIAL REACTION

17.3.1 Kinetic Scheme

Examination of the pH dependence of the reduction potential and the rate of oxidation of formaldehyde shows that the pH of the electroless copper solution should be above 11.0 in order to have practical rates of copper deposition [14]. This pH restriction imposes the use of complexed copper ions in the electroless solution in order to prevent precipitation of Cu (II) hydroxide. $Cu(OH)_2$·EDTA, EDTP, and tartaric acid are the most commonly used ligands for copper ions [16].

Thus the electroactive species in the partial cathodic reaction may be complexed or noncomplexed copper ions. In the first case the kinetic scheme of the cathodic partial reaction is one of the simple charge transfer

$$Cu^{2+} + e \xrightarrow{RDS} Cu^{+} \tag{17.12}$$

$$Cu^{+} + e \rightarrow Cu \tag{17.13}$$

where RDS stands for rate-determining step (slow step). In the second case the kinetic scheme is of the charge transfer preceded by the dissociation of the complex [16]. The mechanism of the second case involves a sequence of at least two basic elementary steps:

1. Formation of the electroactive species
2. Charge transfer from the catalytic surface to the electroactive species

Electroactive species Cu^{2+} are formed in the first step by dissociation of the complex $[CuL_x]^{2+xp}$:

$$[CuL_x]^{2+xp} \rightarrow Cu^{2+} + xL^{p} \tag{17.14}$$

where p is the charge state of the ligand L and $2 + xp$ is the charge of the complexed copper ion. The charge transfer

$$Cu^{2+} + 2e \rightarrow Cu_{lattice} \tag{17.15}$$

proceeds in steps, usually with the first charge transfer (one electron transfer), Eq. (17.12), serving as the rate-determining step [17].

Thus, from the kinetic aspects, the cathodic partial reaction is an electrochemical reaction, Eq. (17.15), that is preceded by a chemical reaction, Eq. (17.14).

Paunovic [16] has shown that in the electroless deposition of copper from the Cu(II)EDTA complex the reduction of the complex is preceded by dissociation of the same. A correlation has been established between the rate of dissociation of the complex and the rate of copper deposition [16].

17.3.2 Kinetics

The major factors determining the rate of the partial cathodic reaction are the concentration of the copper ions and the ligands, pH of the solution, and the type and the concentration of additives. These factors determine the kinetics of the partial cathodic reaction in a general way, as given by the fundamental electrochemical kinetic equations discussed in Chapter 1.

17.3.3 pH Effect

The rest potential of the copper electrode in an alkaline solution of cupric ions complexed with EDTP shows a linear pH dependence with a slope $\partial E/\partial(\text{pH}) = -0.066\,\text{V}$ decade^{-1} [14],

$$E = E^{0} - 0.066\,\text{pH} \tag{17.16}$$

This slope is in conformity with the reaction

$$Cu + H_2L' \rightarrow CuL' + 2H^{+} + 2e \tag{17.17}$$

where L = EDTP, L′ = EDTP $- 2H^{+}$ [14,18, 19]. The experimentally observed slope of -0.066 V decade^{-1} [14] is in good agreement with the theoretical slope of -0.059 V decade^{-1} [17].

In contrast to the anodic partial reaction, the rate of the cathodic partial reaction does not depend significantly on pH, since OH^{-} ion is not a reactant in the cathodic reaction. Moreover the large concentration of OH^{-} ions in the metal–solution interphase (the double layer) can hinder the process of reduction of complexed copper ions (CuL), especially if CuL is negatively charged, such as when L is EDTA or tartrate [3].

17.3.4 Effect of Additives

Schoenberg [9, 20] as well as Paunovic and Arndt [21] have shown that additives may have two opposing effects: acceleration and inhibition. For example, guanine and adenine show the accelerating effect on the cathodic reduction of Cu^{2+} ions in the electroless copper solution. The same additives show an increase in the rate of the electroless copper deposition. The accelerating and the inhibiting effects of dipyridyls were examined by Duda [22] as well as by Oita et al. [23]. In another example, the addition of NaCN to the electroless copper solution results in the inhibing effect for reduction of Cu^{2+} ions in an electroless solution. This inhibition increases with an increasing amount of NaCN in solution [24, 25].

17.4 KINETICS OF ELECTROLESS Cu DEPOSITION

Steady-state electroless copper deposition at mixed potential E_{mp} is preceded by a non-steady-state period, called the *induction period.*

17.4.1 Induction Period

The induction period is defined as the time necessary to reach the mixed potential E_{mp} at which the steady-state metal deposition starts to occur. It is determined in a simple experiment in which a piece of metal is immersed in a solution for electroless deposition of a metal and the potential of the metal recorded from the time of immersion (or the time of addition of the reducing agent), that is, time zero, until the steady-state mixed potential is established. A typical recorded curve for the electroless deposition of copper on copper substrate is shown in Figure 17.3. The curve has been recorded for the system in an argon atmosphere. For a system in air atmosphere and in the presence of additives in the solution, the duration of the induction period can be considerably longer [16].

The problem of the induction period for the overall process can be resolved into problems of the open-circuit potentials (OCPs) of the oxidation and reduction partial reactions, that is, the individual induction period for each process. Paunovic [16] found that the OCP for the Cu/Cn^{2+} system is reached instantaneously. A typical curve representing the change of the OCP with time for the reducing agent is presented in Figure 17.4. By comparing these OCP values, we can conclude that the setting of the OCP of the reducing agent, CH_2O, is the rate-determining partial reaction in the setting of the steady-state mixed potential in this example of electroless copper deposition.

The major factors that determine the time required to reach the rest potential of the reducing agent are the type and the concentration of the ligand present and the pH of the solution [16].

17.4.2 Steady-State Kinetics

There are three electrochemical methods for the determination of the steady-state rate of the electroless deposition of copper at mixed potential. Paunovic and Vitkavage [26, 27] used polarization data in the vicinity of the mixed potential to determine the rate of deposition [26, 27]. Ohno used alternating-current (ac) polarization measurements [28]. The third electrochemical method is the use of the Evans diagram, as described in Section 17.1. Ricco and Martin used an acoustic wave device for in situ determination and monitoring of the rate of deposition [29]. Various empirical rate equations were determined for electroless deposition of copper [4, 6].

17.4.3 Effect of pH on the Rate of Deposition

Electroless copper deposition is affected by the pH in two distinct ways. First, OH^- ions are reactants in the overall reaction (17.1) and the partial anodic reaction (17.7) and thus influence these reactions in a direct way (primary pH effects). Second, pH affects various phenomena associated with the structure and composition of the metal–solution interphase [14]. Those phenomena include (1) adsorption, (2) the structure of the double layer, (3) the structure of the copper species in the solution, and (4) the ionic strength of the solution. All these phenomena modulate the rate of electroless copper deposition in an indirect way (secondary pH effects).

The primary pH effect is expressed in terms of the reaction order with respect to OH^- ions and graphically as rate against pH. Plots of the experimentally observed plating rates against pH show an initial increase, a maximum value, and then a decrease of the rate with increasing pH. An example of the

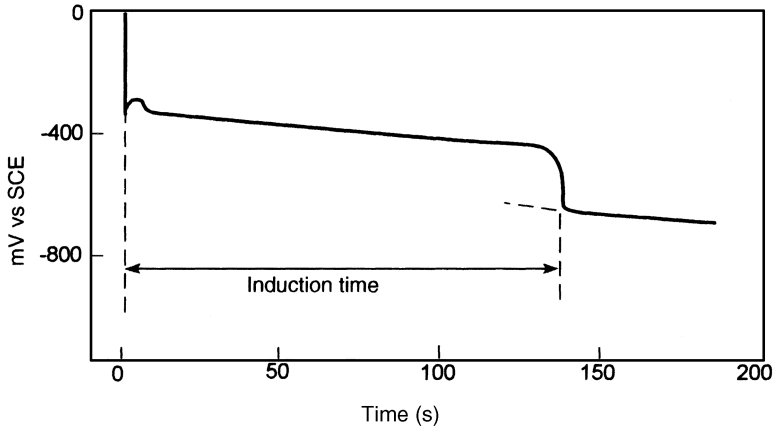

FIGURE 17.3 Induction period for the solution 0.3 *M* EDTA, 0.05 *M* $CuSO_4$, pH 12.50, 2.5 g L^{-1} paraformaldehyde, Cu electrode, 2.2cm^2, 25°C, SCE reference electrode, argon atmosphere. (From Paunovic [16], with permission from the Electrochemical Society.)

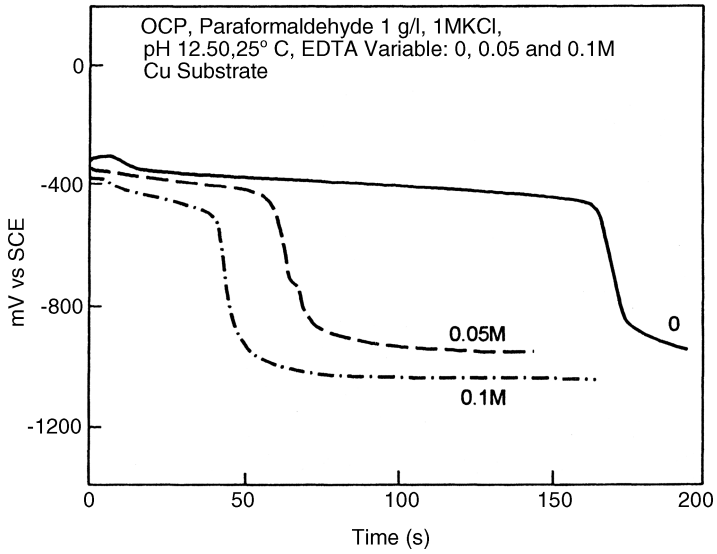

FIGURE 17.4 Open-circuit potential for the solution 1 g L^{-1} paraformaldehyde, pH 12.50, Cu electrode, SCE reference electrode, EDTA variable. (From Paunovic [16], with permission from the Electrochemical Society.)

rate of electroless copper deposition as a function of pH is shown in Figure 17.5. It can be seen from Figure 17.5 that the maximum rate of deposition, in this specific case (EDTP solution), is obtained at a pH value of 12.5. The initial increase of the rate is due to the primary pH effect. The maximum and decrease of the rate at high pH values were interpreted in terms of secondary pH effects. The maximum rate of deposition for the tartrate solution is at pH 12.8 [9]. Two secondary effects were suggested so far: (1) change of the relative concentration of the methylene glycol and the hydroxide ions with pH due to the dissociation of methylene glycol [20] and (2) variation of the transfer coefficient for the oxidation of formaldehyde with pH [15].

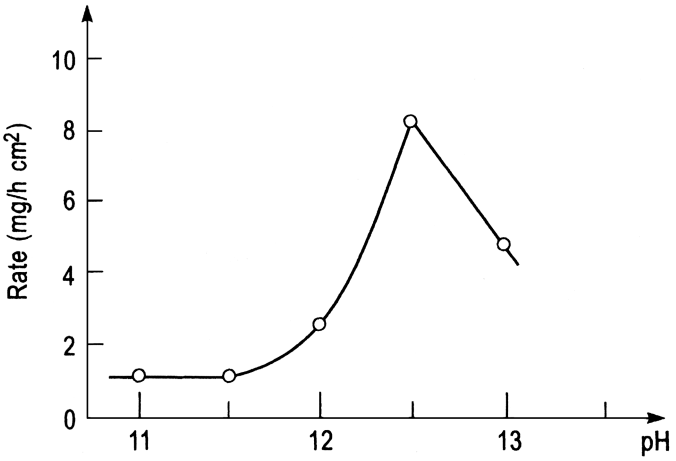

FIGURE 17.5 Rate of electroless copper deposition as a function of pH. The electroless copper solution contained 0.05 *M* $CuSO_4$, 0.15 *M* EDTP, 0.07 *M* paraformaldehyde, and NaOH to give a desired pH. Oxygen was removed by bubbling argon through the solution. (From Duffy et al. [14], with permission from the Electrochemical Society.)

Interpretation of the pH effect in terms of mathematical models was given by Paunovic [15]. From these it was concluded that the maximum and the falling off of the rate at high pH values are caused by the pH dependence of the kinetic parameters α_{Red} (the transfer coefficient for the oxidation of the reducing agent; Chapter 1, Part A) and i^0_{Red} (the exchange current density for the oxidation of the reducing agent; Chapter 1, Part A). Dissociation of methylene glycol, as proposed earlier, is an important factor in the electroless deposition of copper, but it is not sufficient to explain the pH effect.

17.4.4 Catalysis Phenomena

Catalysis in electroless deposition of copper was studied by Haruyama and Ohno [30] and by Wiese and Weil [31]. Haruyama and Ohno have shown that the catalytic activity of metals for the oxidation of the reducing agent in electroless deposition is mostly determined by the rate constants of the two reaction steps, that is, the oxidative adsorption and desorption of an anion radical (see Section 1.3). Wiese and Weil have shown that copper deposition from EDTA-containing solutions is catalyzed by chemisorbed methane–diolatc anion.

17.5 GROWTH MECHANISM

Mechanistically, electroless copper deposition proceeds in two steps: (1) the thin-film stage (up to 3 μm) and (2) the bulk stage.

17.5.1 Thin-Film Stage

The mechanism of the thin-film formation is characterized by three simultaneous crystal-building processes [32–34]: nucleation (formation), growth, and coalescence of three-dimensional crystallites (TDCs).

In the initial stages of electroless copper deposition on *a copper single-crystal substrate, (100) plane,* the average density of TDCs increases with time of deposition; in this stage the nucleation is the predominant process [32, 34]. Later the average density of TDCs reaches a maximum and then decreases with time. In the stage of decreasing density of TDCs, the coalescence is the predominant crystal-building process [34]. A continuous electroless film is formed by lateral growth and coalescence of TDCs. The process of coalescence deserves special attention, since many physical properties of deposit depend on the type of coalescence. There are two types of coalescence of TDCs. Coalescence without the proper filling of the space between TDCs results in incorporation of impurities or additives, generation of stress, voids, and dislocations (Fig. 17.6*b*). Coalescence with filling the space between TDCs, favorably joined crystallites (Fig. 17.6*a*), results in copper of better quality than in the first type of coalescence [35, 36]. The process (type) of coalescence depends to a great extent on the type and concentration of additives in the solution [34]. The initial stages of electroless copper deposition on *Pd-activated nonmetallic (nonconducting) substrates* were described by Sard [33] and Rantell [37].

17.5.2 Bulk Stage

After the formation of the continuous thin film, the deposition of a thick (1–15-μm) film proceeds, in most cases, through the following processes [27, 38–41]: (1) preferential growth of favorably oriented grains, (2) restriction (inhibition) of vertical growth of nonfavorably oriented grains, (3) lateral joining of preferentially growing grains, (4) cessation of growth of initial grains, and (5) nucleation and growth of a new layer of grains.

In the process of vertical and lateral growth, a preferentially growing grain (TDC) increases its width and subsequently joins laterally with other preferentially growing grains. Eventually the width of these grains becomes constant, and during further vertical growth, they develop a columnar shape, Figure 17.7 [38–41]. Then, at a certain stage, columnar grains no longer grow vertically. This cessation of growth of individual grains is followed by the nucleation and growth of a new layer of grains. Cessation of growth perpendicular to the substrate is influenced by the overpotential and degree of inhibition. This is one of the fundamental relationships in the correlation between (1) structure and variables in the plating solution and (2) structure and electrochemical kinetic parameters of processes composing electroless copper deposition.

The different growth rates on different single-crystal substrate orientations were observed experimentally. This experimental observation indicates that certain crystallographic surfaces are more favorable for growth than others [40, 42]. A shift in the preferred direction of the growth was observed depending on the solution composition and concentration of additives [40].

17.6 STRUCTURE

We discuss two different structures: thin-film (up to 1 μm) and thick-film (1–25 μm) structure. We also discuss microporosity in electroless copper films.

17.6.1 Thin-Film Structure

Nakahara and Okinaka [38] and Paunovic and Zeblisky [39] have shown that thin films of electroless Cu (up to 1 μm) are characterized by small, nearly equiaxial grains. The average grain diameter appears to be about 0.2 μm.

17.6.2 Thick-Film Structure

As mentioned in Section 17.5, a thick film (1–25 μm) of electroless copper has a columnar structure. Paunovic and Zeblisky [39] have shown that electroless copper deposited from EDTA solution containing NaCN, a wetting agent, formaldehyde, and NaOH exhibits a pH value between 10.8 and 12.5 and that it has a columnar structure with an average grain diameter, in a plane parallel to the substrate, between 0.3 and 0.7 μm and an average grain size (height), and in a plane perpendicular to the substrate, between 6 and 7 μm.

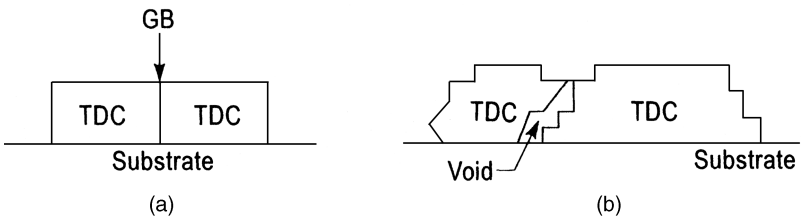

FIGURE 17.6 Two types of coalescence of the TDCs: (a) favorably joined TDC: copper of good quality; (b) improperly joined crystallites: results in incorporation of impurities or additives, generation of stress, voids, and dislocations.

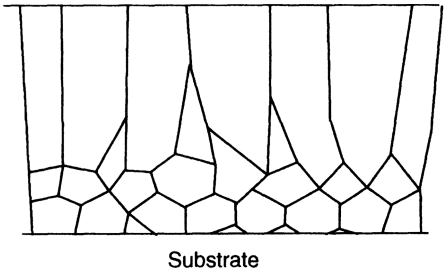

FIGURE 17.7 Schematic cross section (perpendicular to the substrate) of the columnar deposit.

17.6.3 Microporosity

Nakahara [35, 36], using transmission electron microscopy (TEM), has shown that both crystalline and noncystalline films prepared by evaporation, sputtering, electrodeposition, and electroless deposition contain a large number of microscopic voids (pores). The presence of vacancies (voids) in thin films implies that the films contain locally unfilled regions inside the lattice. Studies of the early stages of film formation have shown that most microvoids are generated at the boundaries between faceted TDCs (Section 17.5) during their coalescence. The mechanism by which these voids are formed is called ''coalescence-induced void formation.'' The proposed mechanism is based on the assumption that there is a geometrical misfit large enough to be left uncovered during the coalescence of TDCs (e.g., Fig. 17.6*b*). Voids inside grains could be generated during growth of multiple-atomic steps.

Voids are important lattice defects that influence the physical properties of a film, as is shown in the next section. In one example the number of voids per unit volume was 10^{15}–$10^{16}\,\text{cm}^{-3}$ and the average void size was 25 Å [45].

17.6.4 Hydrogen Incorporation

According to Eq. (17.1) the deposition of 1 mol of Cu is accompanied by the evolution of one equivalent mole of H_2. This results in the incorporation of H_2 gas bubbles into the deposit. As shown in Eqs. (17.6) and (17.8), hydrogen atoms in H_2 originate from the splitting of the C–H bond in the formaldehyde molecule during dissociative adsorption. Nakahara and Okinaka [38, 43–45] studied extensively the incorporation of hydrogen into copper deposit and the effect of hydrogen bubbles on deposit properties. The content of hydrogen in electroless copper can be as high as 930 ppm [43]. Nakahara [45] found, using TEM, that small (20–300-Å) gas bubbles are incorporated uniformly throughout the copper films (25–30 μm), whereas large (∼2000-Å) bubbles are trapped at the grain boundaries. Nakahara and Okinaka determined that the population distribution is broad [38]. The size distribution is shown in Figure 17.8. Thus the density of electroless copper is lower than that of bulk copper due to the presence of incorporated hydrogen.

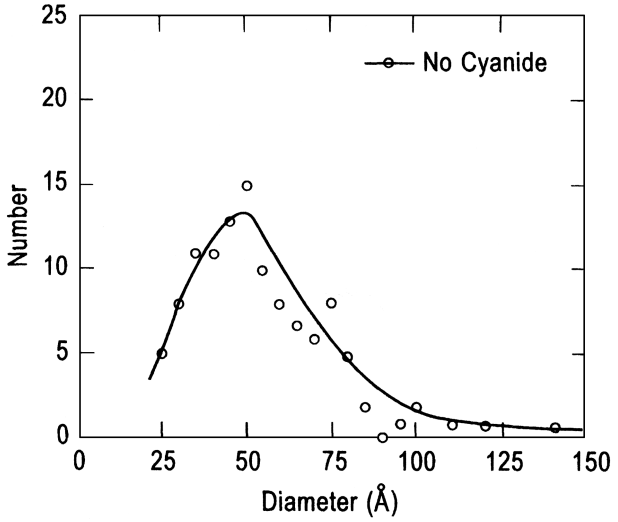

FIGURE 17.8 Population distribution of hydrogen gas bubbles as a function of bubble size.

Grunwald et al. [46] determined that the density of electroless Cu films is in the range from 8.56 to 8.76 g cm^{-3}. The density of bulk copper is 8.9331 (±0.0037) g cm^{-3}.

17.7 PROPERTIES

17.7.1 Film Ductility

Okinaka and Nakahara [47] showed that the formation of small voids and small gas bubbles containing hydrogen are major factors determining the ductility of electroless copper. Nakahara and Okinaka [38] showed that brittle films contain a large number of small as well as large gas bubbles. They also showed that ductility promoters, such as cyanide ions, and higher temperatures of deposition facilitate desorption of hydrogen gas generated in the reaction given by Eq. (17.1). Some ductility-promoting additives, for example, 2,2′-dipyridyl and $K_2Ni(CN)_4$, inhibit both the inclusion of hydrogen and the formation of voids [44]. Table 17.1 shows an example of the difference in properties between Cu deposited from a solution in the absence of ductility promoters (solution A) and a deposit from the solution containing NaCN as a

TABLE 17.1 Properties of Electroless Cu Deposit: Plexiglas Substrate

	Solution A (Absence of NaCN)	Solution B (Presence of NaCN)
Ductility (elongation %)		
As-deposited Cu	1.2	3.6
After 6 months	4.8	4.8
Grain size (μm)	0.5–1.0	0.5–1.0
Gas bubble density[a]	9×10^{15}	9×10^{14}

[a] $N\ \text{cm}^{-3}$, N = number of gas bubbles.

ductility promoter (solution B). It may be seen from Table 17.1 that the difference in ductility of as-deposited Cu and in gas bubble density is significant. The table also shows that there is ductility recovery during room temperature storage. In this example the ductility of the brittle copper recovered to a value comparable to that of the ductile copper. The hydrogen content of the brittle films, obtained from solution A, is in the range from 100 to 200 ppm.

17.7.2 Ductility Recovery during Room Temperature Storage

The ductility (percent elongation) of electroless copper generally increases during low-temperature (100–200°C) annealing. Two mechanisms were proposed to interpret this ductility recovery process.

According to the first mechanism, proposed by Nakahara et al. [48], the ductility improvement observed is attributed to the outdiffusion of hydrogen from the copper lattice. During electroless copper deposition hydrogen can be codeposited in atomic (H) as well as molecular (H_2) form. Most of the hydrogen codeposited in electroless copper is molecular. At room temperature or at low temperature (100–200°C) annealing the molecular hydrogen diffuses out of copper, interstitially, via a dissociative reaction

$$H_2(\text{in the gas-filled void in copper}) \rightarrow 2H(\text{in copper lattice}) \tag{17.18}$$

The annealing removes all the diffusible hydrogen, leaving in copper-only residual (nondiffussible) hydrogen. Nakahara et al. [48] distinguish four types of hydrogen incorporated in electroless copper deposit. Details may be found in the original literature.

According to the second mechanism, proposed by Honma and Mizushima [49], ductility improvement is due to structural changes involving recrystallization and grain growth in electroless copper deposit. They point out that the low-temperature recrystallization and grain growth are commonly observed in copper films prepared by other growth techniques such as vapor deposition [50], sputtering [51], and electrodeposition [52, 53]. The amount of ductility recovered in electroless copper deposition as a result of low-temperature annealing, either by the outdiffusion or the recrystallization mechanism, is determined also by impurity content [44, 54].

17.7.3 Crack-Free Electroless Copper

The printed circuit (PC) industry requires electroless copper with properties that allow the copper elements comprising the PC boards (PCBs) to maintain their integrity during processing and use. One critical step in processing PCBs with plated through-holes is by mounting or exchanging components by soldering. In this process the plated copper is subjected to thermal stress. During soldering, the plated copper in the through-holes usually expands less than the substrate. The difference (mismatch) in the thermal expansion depends on the type of substrate and temperature. In the case of the epoxy-glass substrate the difference at the soldering temperature (260°C) is large and the electroless copper in this case must be of high quality in order to maintain its integrity (continuity) during soldering [55].

Depending on the properties of the plating, the copper in the holes either cracks or resists the stress imposed without cracking during soldering. Paunovic and Zeblisjy [39] have shown that when EDTA-based electroless copper solutions containing NaCN are used the elongation (ductility) of the 25-μm-thick, crack-free copper ranges from 3 to 11%; the tensile strength of this copper is from 200 to 600 MPa (30,000 to 87,000 psi). These wide ranges may be subdivided into two smaller ones: class 1 with a high tensile strength and class 2 with a high elongation. A grain diameter in the plane parallel to the substrate is 0.1–1 μm, and the grain size in the plane perpendicular to the substrate is 4–10 μm, for the case Studied of crack-free electroless copper deposit.

17.7.4 Electrical Resistivity

Patterson et al. determined that an electroless Cu layer of thickness 5000 Å deposited on titanium nitride has a resistivity of 2.0–2.7 μΩ-cm depending on the solution used [56]. Lopatin et al. [57] reported that the electrical resistivity decreases with the increase of the deposition solution temperature (Fig. 17.9). Dubin et al. reported that the resistivity decreases down to 1.8–1.9 μΩ-cm after annealing at 200°C for 2 h in a H_2 ambient [58]. Electrical resistivity of the bulk copper is 1.7 μΩ-cm.

17.7.5 Electromigration Resistance

The free-electron theory of metals assumes that the valence electrons (the conduction electrons) are virtually free to move everywhere in the metal [59, 60]. In an electric field the electrons drift toward the positive direction of the field, producing an electric current in the metal. The high electronic conductivity of metals is explained in terms of the ease with which the free electrons move [61]. According to modern quantum electronic theory, the electrical resistivity of a metal results from the scattering of electrons by the lattice [61–64]. The scattering does not cause large displacement of the ions in the metal lattice when the current density is low. However, at a high current density (above 10^4 A cm^{-2}) the transport of electrons (current) can displace metal ions in crystal lattice and cause the transport of mass (positive ions) in the same direction as the electrons (Fig. 17.10). This mass transport is called *electromigration*. It occurs in interconnecting conductors (metallic fine lines) in integrated circuits where the current density is very high [65, 66]. For example,

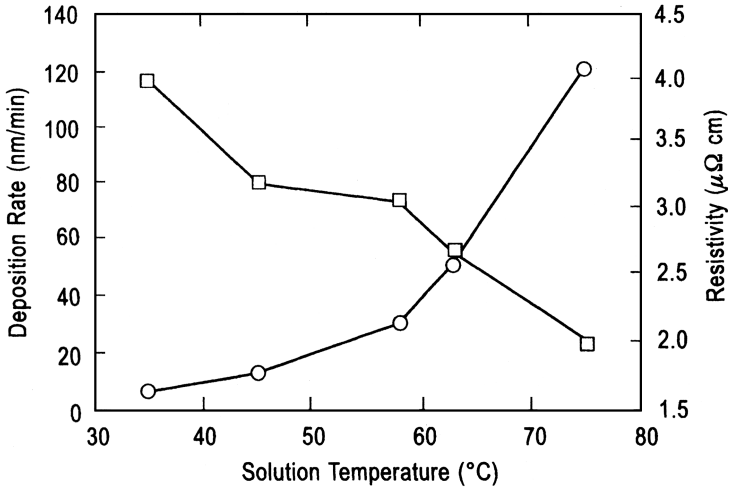

FIGURE 17.9 Electroless Cu deposition rate (○) and resistivity (□) versus solution temperature.

when a 1.0-μm-wide Al (or Cu) line of 0.2 μm thickness is subjected to a current I of 1 mA, the current density i is 5×10^5 A cm^{-2} (line cross-sectional area A in this case is $0.2 \times 10^{-4} \times 1 \times 10^{-4} = 0.2 \times 10^{-8}$ cm^2; current density $i = (I/A) = 1 \times 10^{-3}$ A/0.2×10^{-8}cm$^2 = 5 \times 10^5$ A cm^{-2}). Thus in microelectronic devices the transport of electrons (current) can cause the transport of metal ions (mass) in a metal lattice.

At high current densities ($i > 10^4$ A cm^{-2}) sufficient electron momentum is transferred to metal ions in the metal lattice to physically displace them toward the anode; hence a net mass transport occurs, as shown in Figure 17.10. This mass transport, electromigration, results in defect formation in conductors in microelectronics. Conductor lines undergo morphological changes due to electromigration where mass depletion (voids) occurs at the cathode and extrusion (hillocks) occurs at the anode.

Aluminum-based alloys (Al–Cu, Al–Si) are most widely used as interconnection materials in integrated circuits (ICs). One of the problems of the Al alloys is their poor resistance to electromigration (EM)–induced failures. One way to express resistance to electromigration is in terms of time to failure. *Time to failure* is defined as the point at which a 50% increase of the resistance due to the electromigration stressing has occurred. The direct-current (dc) and pulse-dc lifetime of electroless Cu is found to be about two orders of magnitude longer than that of Al–2% Si at 275°C and about four orders of magnitude longer than that of Al–2% Si when extrapolated to room temperature [67, 68].

Another way of expressing resistance to electromigration is in terms of the activation energy for electrotransport. The activation energy is about 0.81 eV for electroless Cu, which is much larger than the typical 0.4–0.5 eV for Al alloys [67]. Thus Cu lines in ICs are expected to have a larger lifetime than the Al–Si or Al–Cu alloy. For this reason, and because of the higher conductivity of Cu, electroless Cu and electrodeposited Cu are considered for application as conductors in IC fabrication [69–72].

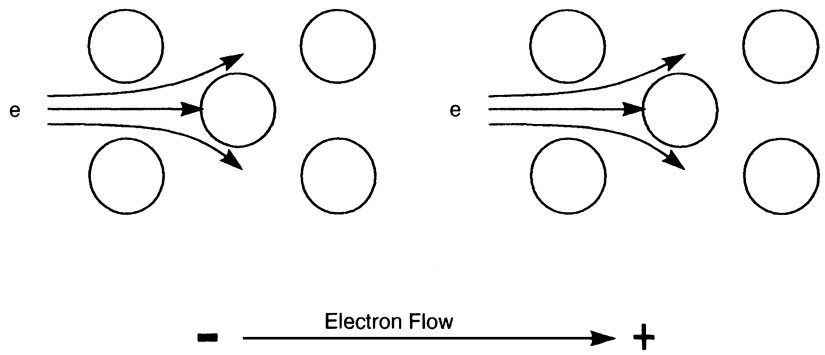

FIGURE 17.10 Atomic model of electromigration involving electron momentum transfer to metal ions in the metal lattice during a high-current-density flow ($i > 10^4$ A cm^{-2}).

17.8 DEPOSITION OF ELECTROLESS COPPER FOR IC ABRICATION

The feasibility of using electroless copper deposition for IC fabrication has been demonstrated by Ting and co-workers [73–75]. A selective electroless metal deposition process is a very attractive alternative to the conventional IC fabrication process. At the time of writing, there is renewed intrest in activity in this area.

Electroless deposition of copper for IC fabrication may be done on (a) noncatalytic and (b) catalytic surfaces.

17.8.1 Activation of Noncatalytic Surfaces

Two major types of processes have been used to produce catalytic metallic surfaces: (c) electrochemical and (d) photochemical.

Electrochemical Activation The catalytic metallic nuclei of metal M on the noncatalytic surface S can be generated in an electrochemical oxidation–reduction reaction,

$$M^{n+} + \text{Red} \rightarrow M + \text{Ox} \qquad (17.19)$$

where M^{n+} is the metallic ion and M is the metal catalyst. In many cases the preferred reducing agent Red is Sn. The preferred nucleating agent M^{n+} is Pd. The palladium catalytic sites on the activated surface are dispersed on the surface of a substrate in an island-type network [33, 76, 77].

Photochemical Activation Catalytic metallic nuclei of Pd, Pt, Au, and Cu can be generated in an intramolecular-type electron transfer resulting from absorption of photon. For example, catalytic palladium can be formed in the photochemical reaction

$$\text{PdAc} \rightarrow \text{Pd} + \text{Ox} \qquad (17.20)$$

where Ox is the oxidation product of acetate ion, Ac [78]. Other photochemical methods were, for instance, reviewed by Paunovic [78].

17.8.2 Diffusion Barriers

Fabrication of interconnects on chips made of copper introduces new problems, the most important of which is the diffusion of Cu into Si, SiO_2, and other dielectrics [79] and the reaction of Cu with Si, forming silicides. Diffusion of Cu through Si results in poisoning of devices (transistors) and diffusion through SiO_2 leads to degradation of dielectrics. Thus, diffusion barrier layers are an integral part of the fabrication of copper interconnects. Barrier films isolate (encapsulate) Cu interconnects from adjacent dielectric material. Diffusion barrier layer is usually formed by physical vapor deposition (PVD) or chemical vapor deposition (CVD). However, thin electroless Co or Ni diffusion barriers were demonstrated by Yoshino et al. [80].

17.8.3 Electroless Deposition of Copper on Catalytic, Activated Surfaces, and Diffusion Barriers

It is possible to directly deposit electroless Cu on tungsten (W) barrier layer, as shown by Kim et al. [81]. They used glyoxylic acid as a reducing agent as proposed by Sacham-Diamand [82]. The use of glyoxylic acid was proposed as a nontoxic, environmentally friendly alternative to formaldehyde.

Since barrier metals have relatively high electrical resistivity (e.g., Ta is 12.4 μΩ-cm), it is necessary to cover the barrier layer with a conductive metal layer. This conductive metal layer may be a Cu seed layer deposited using PVD or CVD. When the electroless Cu deposition on a bilayer of barrier/Cu seed layer is completed, vias and trenches may be, filled with electroless Cu. The excess Cu is removed using chemical–mechanical polishing [83].

An activated surface of TiN barrier layer was used for electroless Cu deposition [84]. The TiN was activated in a CuSO4–HF solution. For activation, Pd was used, itself deposited on the barrier layer either by (a) chemical reaction in solution or by (b) PVD. The Pd catalytic layer can be formed by an ionized cluster beam (ICB). Electroless Cu film was successfully deposited on a TaN barrier over a Pd catalytic layer [85, 86].

17.9 FORMATION OF Cu NANOPARTICLES BY ELECTROLESS DEPOSITION OF Cu

Copper nanoparticles are of great interest in microprinting technology in electronics. Understanding the mechanism of Cu nanoparticle formation and control of particle size is very important for this application. Yagi et al. [87] formed Cu nanoparticles electrochemically (electroless deposition) using a hydrazine aqueous solution and dispersed CuO particles.

The deposition rate of Cu nanoparticle formation was examined in situ by an electrochemical quartz crystal microbalance (QCM). Hydrazine acts as a reducing agent:

$$N_2H_4 + 4OH^- \rightarrow N_2 + 4H_2O + 4e \qquad (17.21)$$

$$N_2H_4 + OH^- \rightarrow \tfrac{1}{2}N_2 + NH_3 + H_2O + e \qquad (17.22)$$

The reduction of Cu^{2+} ions by hydrazine proceeds through the reactions

$$2Cu^{2+} + N_2H_4 + 4OH^- \rightarrow 2Cu + N_2 + 4H_2O \qquad (17.23)$$

$$Cu^{2+} + 2N_2H_4 + 2OH^- \rightarrow Cu + N_2 + 2NH_3 + 2H_2O \qquad (17.24)$$

Fabrication of Cu nanoparticles was done in the following steps. First, a CuO colloidal aqueous suspension was prepared by dispersing CuO powder in distilled water. Next, aqueous solution of gelatin was added as a dispersing agent. Hydrazine solution was then added to the CuO aqueous suspension as a reducing agent to deposit Cu nanoparticles.

17.10 ELECTROCHEMICAL CONTROL SYSTEM FOR ELECTROLESS COPPER DEPOSITION

Electroless deposition of Cu for IC fabrication demands the computerized in situ monitoring and control of the deposition process. An automatic analyzer for the analysis of the composition and performance of the production of electroless Cu [88–91] is described here. The duration of the electrochemical analysis is in the range of milliseconds, or seconds, at most.

This work describes the applications of chronopotentiometry and voltametry in the study and control of electroless Cu deposition. An EDTA-type electroless Cu solution was used for these studies, and CH_2O (formaldehyde) was the reducing agent. The anodic partial reaction is described in the Section 17.2.

17.10.1 Chronopotentiometry

The potential–time curves were recorded on a Tetronix storage oscilloscope. Oscilloscope traces were photographed with a Polaroid camera. Chropotentiograms can be used for determination of cupric ions and formaldehyde. However, in this application this is not necessary. It is sufficient to detect the transition time only. This can be done automatically by introducing a time interval counter into the electrolysis circuit [89].

The effect of additives can be determined by recording potential time curves in the millisecond or microsecond range [90].

17.10.2 Voltammetry

The voltammograms were obtained with a PAR (Princeton Applied Research) polarographic analyzer, and the current–voltage was recorded on an X–Y recorder. Voltammetry, or cyclic voltammetry [91], can be used for determination of formaldehyde, cupric ions, additives, and impurities.

APPENDIX

TABLE 17.A1 Electroless Copper Deposition Solution and Plating Conditions from an Alkali-Free Solution

$CuSO_4 \cdot 5H_2O$	0.05–0.1 *M*
$N(C_2H_5)_4OH$	0.5–l.0 *M*
EDTA	0.1 *M*
CH_2O	0.01 *M*
$N(CH_3)_4CN$	0.01 *M*
GAF RE–610	0.5–2%
Temperature	45–55°C
pH, adjusted with $N(C_2H_5)_4OH$, tetraethylammonium hydroxide	11.9–12.3

Source: Shacham-Diamand [92, p. 136].

TABLE 17.A2 Solution Composition and Plating Condition for Electroless Cu Deposition Using Glyoxylic Acid as Reducing Agent

$CuSO_4 \cdot 5H_2O$	0.03 *M*
EDTA	0.24 *M*
CHOCOOH (glyoxylic acid)	0.20 *M*
2,2′-Bipyridine	10 ppm
Temperature	60°C
pH (adjusted with NaOH), air agitation, continuous	12.5

Source: Honma and Kobayashi [93] and Burke, Bruton, and Collins [94].

TABLE 17.A3 Solution Composition and Plating Conditions for Electroless Cu Deposition Using Hypophosphite as Reducing Agent

$CuSO_4$	0.024 *M*
$NiSO_4$	0.002 *M*
H_3BO_3	0.5 *M*
NaH_2PO_2	0.27 *M*
$Na_3C_6H_5O_7$ (sodium citrate)	0.052 *M*
EDTA	0.026 *M*
pH	9.2

Sources: Hung and Chen [95] and Saubestre [96].

TABLE 17.A4 Solution Composition and Plating Conditions for Electroless Cu Deposition Using Tartrate as Complexing Agent and Formaldehyde Reducing Agent

	Solution A	Solution B
$CuSO_4 \cdot 5H_2O$,g L^{-1}	5	13
$KNaC_4H_4O_6 \cdot 4H_2O$, g L^{-1} (sodium potassium tartrate)	25	66
NaOH, g L^{-1}	7	19.3
MBT, g L^{-1} (mercaptobenzothiazole[a])	—	0.013
HCOOH (37%), (formaldehyde)[b] mL L^{-1}	10	38
Temperature, °C	20	25

Sources: Solution A: Goldie [97]; Solution B: Pearlstein [98].

[a]Added as solution of 10 g L^{-1} MBT in 0.2 *M* NaOH.

[b]Formaldehyde solution with 12.5% methanol as preservative.

REFERENCES

1. C. Wagner and W. Traud, *Z. Electrochem.*, **44**, 391 (1938).
2. M. Paunovic, *Plating*, **55**, 1161 (1968).
3. M. Saito, *J. Met. Finish. Soc. Jpn.*, **17**, 14 (1966).
4. F. M. Donahue, *Oberflache-Surf.*, **13** (12), *301* (1972).
5. A. Molenaar, M. F. E. Holdrinet, and L. K. H. van Beek, *Plating*, **61**, 238 (1974).
6. S. M. El-Raghy and A. A. Abo-Salama, *J. Electrochem. Soc.*, **126**, 171 (1979).

7. P. Bindra and J. Tweedie, *J. Electrochem. Soc.*, **130**, 1112 (1983).
8. A. Vashkialis and I. lachiayskene, *Electrochemistry* (Academy of Sciences USSR), **17**, 1816 (1981).
9. L. N. Schoenberg, *J. Electrochem. Soc.*, **118**, 1571 (1971).
10. I. Ohno, S. Haruyama, *Surf. Technol.*, **13**, 1 (1981).
11. T. Hayashi, *Met. Finish.*, **85** (6), 85 (1985).
12. J. W. Jacobs and J. M. G. Rikken, in *Electroless Deposition of Metals and Alloys*, M. Paunovic and I. Ohno, Eds., *Proceedings*, Vol. 12, Electrochemical Society, Pennington, NJ, 1988, p. 75.
13. J. W. Walker, *Formaldehyde*, Reinhold, New York, 1964.
14. J. Duffy, L. Pearson, and M. Paunovic, *J. Electrochem. Soc.*, **130**, 876 (1983).
15. M. Paunovic, *J. Electrochem. Soc.*, **125**, 173 (1978).
16. M. Paunovic, *J. Electrochem. Soc.*, **124**, 349 (1977).
17. E. Mattson and J. O'M. Bockris, *Trans. Faraday Soc.*, **55**, 1586 (1959).
18. J. L. Hall, R. F. Jones, C. E. Delchamp, C. W. McWillams, *J. Am. Chem. Soc.*, **79**, 3361 (1957).
19. D. A. Keyworth, *Talanta*, **2**, 383 (1959).
20. N. Schoenberg, *J. Electrochem. Soc.*, **119**, 1491 (1972).
21. M. Paunovic and R. Arndt, *J. Electrochem. Soc.*, **130**, 794 (1983).
22. L. L. Duda, *Plating Surf. Finish.*, **85** (7), 60 (1998).
23. M. Oita, M. Matsuoka, and C. Iwakura, *Electrochim. Acta*, **42**, 1435 (1997).
24. D. Vitkavage and M. Paunovic, *Plating Surf. Finish.*, **70** (4), 48 (1983).
25. M. Paunovic, *J. Electrochem. Soc.*, **132**, 1155 (1985).
26. M. Paunovic and D. Vitkavage, *J. Electrochem. Soc.*, **126**, 2282 (1979).
27. M. Paunovic, in *Electrodeposition Technology, Theory and Practice*, L. T. Romankiw and D. R. Turner, Eds., *Proceedings*, Vol. 17, Electrochemical Society, Pennington, NJ, 1987, p. 349.
28. I. Ohno, in *Electroless Deposition of Metals and Alloys*, M. Paunovic and I. Ohno, Eds., *Proceedings*, Vol. 12, Electrochemical Society, Pennington, NJ, 1988, p. 129.
29. A. J. Ricco and S. J. Martin, in *Electroless Deposition of Metals and Alloys*, M. Paunovic and I. Ohno, Eds., *Proceedings*, Vol. 12, Electrochemical Society, Pennington, NJ, 1988, p. 142.
30. S. Haruyama and I. Ohno, in *Electroless Deposition of Metals and Alloys*, M. Paunovic and I. Ohno, Eds., *Proceedings*, Vol. 12, Electrochemical Society, Pennington, NJ, 1988, p. 20.
31. H. Wiese and K. G. Weil, in *Electroless Deposition of Metals and Alloys*, M. Paunovic and I. Ohno, Eds., *Proceedings*, Vol. 12, Electrochemical Society, Pennington, NJ, 1988, p. 53.
32. M. Paunovic and C. H. Ting, in *Electroless Deposition of Metals and Alloys*, M. Paunovic and I. Ohno, Eds., *Proceedings*, Vol. 12, Electrochemical Society, Pennington, NJ, 1988, p. 170.
33. R. Sard, *J. Electrochem. Soc.*, **117**, 864 (1970).
34. M. Paunovic and C. Stack, in *Electrocrystallization*, R. Weil and R, G. Baradas, Eds., *Proceedings*, Vol. 6, Electrochemical Society, Pennington, NJ, 1981, p. 205.
35. S. Nakahara, *Thin Solid Films*, **45**, 421 (1977).
36. S. Nakahara, *Thin Solid Films*, **64**, 149 (1979).
37. A. Rantell, *Treats. Inst. Met. Finish.*, **48**, 191 (1970).
38. S. Nakahara and Y. Okinaka, *Ada Metall.*, **31**, 713 (1983).
39. M. Paunovic and R. Zeblisky, *Plating Surf. Finish.*, **72** (2), 52 (1985).
40. J. Kim, S. H. Wess, D. Y. Jung, and R. W. Johnson, *IBM J. Res. Develop.*, **8**, 697 (1984).
41. H. J. Choi, R. Weil, *Plating Surf. Finish.*, **68**, (5), 110 (1981).
42. A. Danjanovic, M. Paunovic, T.H.V. Setty, and J. O'M. Bockris, *Acta Metall.*, **13**, 1092 (1965).
43. J. E. Graebner, Y. Okinaka, *J. Appl. Phys.*, **60** (1), 36 (1986).
44. Y. Okinaka, and H. K. Straschil, *J. Electrochem. Soc.*, **133**, 2608 (1986).
45. S. Nakahara, *Acta Metall.*, **36** (7), 1669 (1988).
46. J. J. Grunwald, L. Slominski, and A. Landau, *Plating*, **60**, 1022 (1973).
47. Y. Okinaka, and S. Nakahara, *J. Electrochem. Soc.*, **123**, 475 (1976).
48. S. Nakahara, C. Y. Mak, and Y. Okinaka, *J. Electrochem. Soc.*, **138**, 1421 (1991).
49. H. Honma and S. Mizushima, *J. Met. Finish. Soc. Jpn.*, **34**, 290 (1983).
50. M. Yoshida, S. Nakahara, and H. Suto, *J. Jpn. Inst. Met.*, **39**, 414 (1975).
51. J. W. Patten, E. G. McClanahan, and J. W. Johnston, *J. Appl. Phys.*, **42**, 4371 (1971).
52. D. S. Stoychev, I. V. Tomov, and I. B. Vitanova, *J. Appl. Electrochem.*, **15**, 879 (1985).
53. I. V. Tomov, D. S. Stoychev, and I. B. Vitanova, *J. Appl. Electrochem.*, **15**, 887 (1985).
54. S. Nakahara, Y. Okinaka, and H. K. Straschil, *J. Electrochem. Soc.*, **136**, 1120 (1989).
55. M. Paunovic, *Plating Surf. Finish.*, **70** (2), 62 (1983).
56. J. C. Patterson, M. O'Reilly, G. M. Crean, and J. Barrett, *Microelectron. Eng.*, **33**, 65 (1997).
57. S. Lopatin, Y. Shacham-Diamand, V. M. Dubin, P. K. Vasudev, B. Zhao, and J. Pellerin, in *Electrochemically Deposited Thin Films*, M. Paunovic and D. A. Scherson, Eds., *Proceedings*, Vol. 19, Electrochemical Society, Pennington, NJ, 1997, p. 271.
58. V. M. Dubin, Y. Shacham-Diamand, B. Zhao, P. K. Vasudev, and C. H. Ting, *J. Electrochem. Soc.*, **144**, 898 (1997).
59. H.-K. Kang, J. S. H. Cho, I. Asano, and S. S. Wong, *VMIV Conf.*, June 9–10, 1992.
60. J. Tao, N. W. Cheung, C. Hu, H. -K. Kang, and S. S. Wong, *IEEE Electron Device Lett.*, **13**, 433 (1992).
61. M. Paunovic and M. Schlesinger, *Fundamentals of Electrochemical Deposition*, Wiley, New York, 1998, Ch. 3.
62. J. Bardeen, *J. Appl. Phys.*, **11**, 88 (1940).
63. P. L. Rossiter, *The Electrical Resistivity of Metals and Alloys*, Cambridge University Press, Cambridge, 1987.
64. M. Paunovic, L. A. Clevenger, J. Gupta, C. Cabral, Jr., and M. E. Harper, *J. Electrochem. Soc.*, **140**, 2690 (1993).

65. K.-N. Tu, J. W. Mayer, and L. C. Feldman, *Electronic Thin Film Science*, Macmillan, New York, 1992.
66. M. Ohring, *The Materials Science of Thin Films*, Academic, New York, 1992.
67. 'H.-K. Kang, J. S. H. Cho, I. Asano, and S. S.Wong, *Proc. VLSI Multilevel Interconnection Conf. (VMIC)*, June 9–10, 1992, p. 337.
68. J. Tao, N. W. Cheung, C. Hu, H. K. Kang, and S. S. Wong, *IEEE Electron Device Lett.*, **13**(8), 433 (1992).
69. P. Pai, W. G. Oldham, C. H. Ting, and M. Paunovic, Abstract 481, Electrochemical Society Fall Meeting, Oct. 18–23, 1987.
70. Y. Shacham-Diamand, in *Electrochemically Deposited Thin Films II*, M. Paunovic, Ed., *Proceedings*, Vol. 31, Electrochemical Society, Pennington, NJ, 1995, p. 293.
71. P. C. Andricacos, *Interface*, **8**, 32 (1999).
72. P. C. Andricacos, C. Uzoh, J. O. Dukovic, J. Horkans, and H. Deligianni, *IBM J. Res. Develop.*, **42**, 567 (1998).
73. C. H. Ting and M. Paunovic, *J. Electrochem. Soc.*, **136**, 456 (1989).
74. C. H. Ting, M. Paunovic, P. Pai, and G. Chiu, *Electrochem. Soc.*, **136**, 462 (1989).
75. C. H. Ting and M. Paunovic, U.S. Patent 5,169,680 (1992).
76. J. P. Marton and M. Schlesinger, *J. Electrochem. Soc.*, **115**, 16 (1968).
77. C.H. deMinjer and P.F.G. v. d. Boom, *J. Electrochem. Soc.*, **120**, 1644 (1973).
78. M. Paunovic, *J. Electrochem. Soc.*, **127**, 441C (1980).
79. D. S. Gardner, J. Omuki, K. Kudoo, Y. Misawa, and Q. T. Vu, *Thin Solid Films*, **262**, 104 (1955).
80. M. Yoshino, et al., *J. Electrochem. Soc.*, **154**(3) D122 (2007).
81. Youg-Soon Kim et al., *J. Electrochem. Soc.*, **152**(2) C89 (2005).
82. Y. Y. Sacham-Diamand, *Solid-State Lett.*, **3**, 279 (2000).
83. M. Paunovic and M. Schlesinger, *Fundamentals of Electrochemical Deposition*, 2nd ed., Wiley, Hoboken, NJ, 2006.
84. S. Zhong, et al., *J. Electrochem. Soc.*, **152** (7) C446 (2005).
85. Z. Wang, et al., *J. Electrochem. Soc.*, **152** (10) C684 (2005).
86. Z. Wang et al., *J. Electrochem. Soc.*, **151** (12) C781 (2004).
87. S. Yagi, et al., *J. Electrochem. Soc.*, **155** (6) D474 (2008).
88. M. Paunovic, *J. Electrochem. Soc.*, **127** (2) 365 (1980).
89. M. Paunovic, *J. Electrochem. Soc.*, **114**, 472 (1967).
90. M. Paunovic and R. Oechslin, *Plating*, **58**, 602 (1971).
91. S. R. Morrison, *Electrochemistry at Semiconductor and Oxidized Metal Electrodes*, Plenum, New York, 1980.
92. Y. Shacham-Diamand, B.-X. Sun, V. Yip, and R. Bielski,in *Electrochemically Deposited Thin Films II*, M. Paunovic, Ed., *Proceedings*, Vol. 31, Electrochemical Society, Pennington, NJ, 1995, p. 136.
93. H. Honma and T. Kobayashi, in *Electrochemically Deposited Thin Films*, M. Paunovic, I. Ohno, and Y. Miyoshi, Eds., *Proceedings*, Vol. 26, Electrochemical Society, Pennyngton, NJ, 1993, p. 344.
94. L. D. Burke, G. M. Bruton, and J. A. Collins, *Electrochim. Acta*, **44**, 1467 (1998),
95. A. Hung, K. -M. Chen, *J. Electrochem. Soc.*, **136**, 72 (1987).
96. E. B. Saubestre, *Proc. Am. Electropl. Soc.*, **46**, 264 (1959).
97. W. Goldie, *Plating*, **51**, 1069 (1964).
98. F. Pearlstein,U.S. Patent 3,222,195 (1965).

18

ELECTROLESS DEPOSITION OF NICKEL

MORDECHAY SCHLESINGER

Electroless (autocatalytic) plating involves the presence of a chemical reducing agent in solution to reduce metallic ions to the metal state. The name *electroless* is somewhat misleading, however. There are no external electrodes present, but there is electric current (charge transfer) involved. Instead of an anode, the metal is supplied by the metal salt; replenishment is achieved by adding either salt or an external loop with an anode of the corresponding metal that has higher efficiency than the cathode. There is therefore, instead of a cathode to reduce the metal, a substrate serving as the cathode, while the electrons are provided by a reducing agent. The process takes place only on catalytic surfaces rather than throughout the solution (if the process is not properly controlled, the reduction can take place throughout the solution, possibly on particles of dust or of catalytic metals, with undesirable results).

Brenner and Riddell [1] invented electroless Ni plating in 1946 rather accidentally when they observed that the additive NaH_2PO_2 caused apparent cathode efficiencies of more than 100% in a nickel electroplating bath. This led them to the correct conclusion that some chemical reduction was involved. Further research resulted in the development of the original process that the inventors named *electrodeless* plating. The name soon lost the *de,* and later the name *autocatalytic* was formally adopted, although *electroless* is still widely used. The words are synonymous.

Autocatalytic plating is defined as the deposition of a metallic coating by a controlled chemical reduction that is catalyzed by the metal or alloy being deposited. Such plating has been used to yield deposits of Ni, Co, Pd, Cu, Au, and Ag as well as some alloys containing these metals plus P or B. Electroless Cr deposition has also been claimed. Chemical reducing agents have included NaH_2PO_2 (the one originally used by the inventors for Ni and Cu deposition and still the most important and widely investigated), formaldehyde—especially for Cu—hydrazine, borohydrides, amine boranes, and some of their derivatives.

Electroless plating possesses several characteristics not shared by other techniques, and that accounts for its ever-growing popularity. Its throwing power is essentially perfect, at least on any surface to which the solution has access, with no excessive buildup on edges and projections. Deposits may be less porous than electroplates and hence have better corrosion resistance. Power supplies, electrical contacts, and the other apparatus necessary for electroplating are not required. The process is usually an integral and necessary step in plating on nonconductors such as plastics (see Chapter 15 of this volume). The process is particularly important in the printed circuit industry. Some electroless deposits have unusual or even unique magnetic properties.

Experience shows that each substrate requires its own specific techniques; depositing active metal onto the surface of a non(semi)conductor is still somewhat of an art. The surface preparation (i.e., cleaning process) requires very careful selection and application. It must be stressed that cleaning may affect the porosity of the metal deposit. Residues from cleaners and deoxidizers may create inactive spots that will not initiate electroless deposition. This may result in the necessity to have a thicker deposit before continuity is achieved. In extreme cases continuity is never reached.

In general, deposition requires one or more of the following steps (see Fig. 18.1): (1) cleaning, (2) surface modification, (3) sensitization, (4) catalyzing or (3′) catalyzing, and (4) activation (acceleration). Rinsing is required between the steps. We refer to the steps 3 and 4 (shown in Fig. 18.1) as *sensitization and catalyzing.* By these terms we mean

Modern Electroplating, Fifth Edition Edited by Mordechay Schlesinger and Milan Paunovic

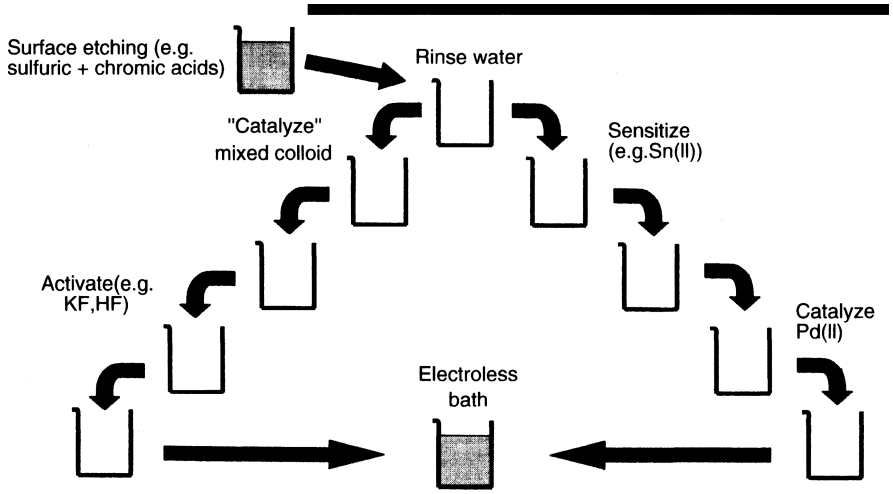

FIGURE 18.1 Schematic representation of the electroless deposition process.

absorbing ions or molecules from a solution such as acidic Sn(II) and/or Sn(IV). Other much less frequently used sensitizing agents are, for example, [2], $AgNO_3$, $AuCl_3$, and metallic Na (in naphtalene solution). An oversimplified model assumes that the sensitizing ion can reduce the active metal from the catalyst solution, usually $PdCl_2$ (Au, Pt, Rh, Os, and Ag solutions have also been used), for example,

$$Pd^{2+} + Sn^{2+} \rightarrow Sn^{4+} + Pd^{0}$$

If the metal to be deposited electrolessly can be reduced by the sensitizing ion, then it is not necessary to reduce the active metal first. Instead, the substrate is immersed in the electroless bath immediately after sensitizing and rinsing [e.g., electroless copper or silver when using Sn(II)-based sensitization].

The alternate method of *catalyzing and activating* makes use of a mixed colloidal catalyst bath. The colloid is reduced Pd stabilized by Sn(II) and Sn(IV) ions. The activation (acceleration) step is the removal of the layer formed by the stabilizing agent with KF, HF, or other chemicals such as HCl or NaOH. In some cases the activation (acceleration) step can be omitted, but then the plating solution may get contaminated. There are also a good number of proprietary and patented processes reported.

18.1 NUCLEATION

In the process of electroless thin-metal-film deposition, the density of nucleation sites on the catalyzed substrate determines the adhesion properties of the end-product films. Film thickness at which continuity is reached and to some extent packing rearrangement after heat treatment are also affected by this parameter. Now the growth initiation upon the catalytic sites is a probabilistic process by nature; hence metal island density and island size distribution are time-dependent functions during the immersion period in the metallizing bath.

In order to evaluate the sensitizer and the subsequent catalyst deposition process, the density of sites capable of nucleation should be determined prior to the metallizing step. If one is to study the final product's physical properties, then the density of nucleation sites at the time when the film reaches continuity is of interest.

Immediately following the catalytic process, before immersion in the metallizing bath, the amount of material present on the surface makes it difficult to obtain reliable data. In addition, in that stage the ultrathin supporting substrate (formvar) and the deposit are virtually nonconductors; they quickly become charged by the electron microscope's electron beam. As a result they usually disintegrate before an electromicrograph can be taken.

The direct determination of nucleation site density at the time when film continuity is reached is also all but impossible. The reason is clear: By definition, by the time continuity is reached there are no islands to speak of.

In light of these problems the following procedure has to be applied [2]: Using a variety of sensitizing solutions (listed in Table 18.1) and the catalytic solution (listed in Table 18.2), a metal (nickel) is deposited electrolessly on the sensitized catalyzed surface by immersion in the metallizing bath for fixed amounts of time. The sensitizers chosen represent a wide range of adsorption properties. The island's size and the

TABLE 18.1 Sensitizers

Sensitizer	0.1 $SnCl_2 \cdot 2H_2O$ + 0.1 *M* HCl plus	Aging (h)
1	—	0
2	10 mg L^{-1} hydroquinone	3
3	10 mg L^{-1} hydroquinone	48
4	0.05% Triton X-100 (weight)	0
5	—	48
6	10 mg L^{-1} thiourea	72
7	—	288
8	—	96
9	—	144
10	10 mg L^{-1} thiourea	24
11	0.05% Triton X-100 (weight)	240

TABLE 18.2 Catalyst Solution

$PdCl_2$	0.1 g L^{-1}
HCl(12 *M*)	0.1 ml L^{-1}
H_2O	Balance to 1 L, temperature 23 °C

TABLE 18.3 Average Island Diameters

Sensitizer	Time in Plating Bath (s)	Diameter Average (nm)	Standard Deviation (nm)
1	60	140.6	—
2	10	6.4	1.1
2	60	80.6	7.6
3	10	4.9	1.4
3	60	39.7	14.6
4	10	17.7	2.3
4	60	95.3	17.8
5	10	6.3	<1
5	60	29.7	4.3
6	10	2.1	1.2
6	60	17.2	4.5
7	10	1.5	—
7	60	8.1	2.6
8	10	1.7	—
8	60	11.2	2.8
9	10	<1	—
9	60	4.5	3.9
10	60	7.6	5.3
11	10	<1	—
11	60	4.9	1.1

density value of the island's distribution are then determined. In Table 18.3 we report the number of the average metal (nickel) island diameter for two (10- and 60-s) immersion times in the metallizing bath. Note that the listing order of sensitizers in Tables 18.1 and 18.3 are identical, that is, in the order of increasing material adsorption values. A close inspection of Table 18.3 shows that for a given sensitizer, as it changes its adsorption properties with time (sensitizers 1, 5, 7, 8, 9), the tendency is for the higher nucleation site density to correspond to the smaller average island size. This is particularly evident for the 60-s immersion time. Sensitizers corresponding to higher levels of adsorption yield not only smaller averaged-sized islands but also less broadening of the size distribution with the same time spent in the metallizing bath.

At this point we need to explain that in recent years mixed colloidal technology has been favored by most practitioners. The main reason given is that only a single step is necessary for implementation. This is not quite the case. The procedure, in fact, often requires two steps, since the activator (accelerator) is made of a separate bath. It is, however, more reproducible than the separate Sn–Pd technology, and that is a good enough reason for it being more popular. In Chapter 15 we compare a number of observations on the two technologies.

To complete the discussion we present in Table 18.4 a typical combined Sn–Pd activating bath composition. In Table 18.5 a practical suggested scheme is given, which naturally can be modified as needed. Despite the number of disadvantages in using the separate Sn–Pd process, sometimes the initial nucleation density achieved is up to an

TABLE 18.4 Typical Combined Sn/Pd Catalyzing Bath

$SnCl_2$	2 g L^{-1}
$PdCl_2$	0.2 g L^{-1}
HCl	10 mL L^{-1}

TABLE 18.5 Suggested Practical Schemes

Sensitizer Solution	
Stock	
Stannous chloride, $SnCl2 \cdot H_2O$	10 g
Hydrochloric acid, HCl	10 mL
Working Solution	
0.5 mL stock solution in 160 mL H_2O	
Activator Solution	
Stock	
Palladium chloride, $PdCl_2$	10 g
Hydrochloric acid, HCl	10 mL
Working Solution	
1 mL stock solution in 200 mL H_2O	

Solution	Time
Deposition Process	
Sensitizer	1–2 min
Rinse	30 s
Activator	1–2 min
Rinse	30 s
Metallizing	Temperature pH dependent

order of magnitude greater than what can be expected using the mixed colloidal technology. Thus a continuous film is obtained at a smaller thickness. This translates into the following:

- An economical advantage, since less metal is needed when the only purpose is to render the surface conductive
- Better adhesion due to higher density of fastening sites
- Potential for the development of special products where very thin coatings are needed

Before closing this section it is worth mentioning, in passing, that in electroless nickel deposition on silicon a presensitization step is required. That involves immersion in dilute HF solution. Perhaps more practical is the addition of 450 mL L^{-1} HF (48%) and 1 mL L^{-1} HCl to 1 g L^{-1} $PdCl_2$. Thus an activator solution for the deposition of electroless nickel on silicon obviates the need for an extra step in the predeposition stage.

18.2 METALLIZING PRINCIPLES

Chapter 8 in *Fundamentals* deals with the subject of electroless metal deposition. In what follows we will attempt not to duplicate the material presented there. We may begin our discussion here by stating that interest in electroless thin-metal deposition, in general, and that in electroless deposition of nickel, in particular, has been steadily growing since its invention. This very special process involves a continuous buildup of metal coating on a substrate by the mere immersion in a suitable aqueous solution. A chemical reducing agent in solution supplies the electrons for converting metal ions to the metal form,

$$M^{2+} + 2e \text{ (supplied by reducing agent)} \xrightarrow[\text{Surface}]{\text{Catalytic}} M^0$$

The important point is that the catalytic surface is the only place where this simplified reaction occurs. Once the deposition starts on a surface, the deposited metal must also be catalytic for the deposition to continue. The progress of electroless deposition is linear in time. This means, as has been demonstrated by Marton and Schlesinger [3], that the deposition of, say, Ni–P on a sensitized-activated surface starts at specific activation sites on the surface and continues on these points only. As deposition progresses, islands are formed around these nucleation sites. The islands grow in size until they merge and a continuous film results. Those early observations helped establish the fact that the surface of a Sn–Pd-treated dielectric substrate is not completely activated. The activation produces small catalytic sites dispersed on the surface serving as the nuclei for electroless nickel deposition. It was also established [3] that the film mass thickness growth rate in electroless deposition is linear in time once film continuity has been reached. The mass thickness of a deposit is the deposited film's volume per unit area. This thickness factor refers to the total material deposited as a continuous film of even thickness, and it is compared to electrodeposition under conditions of constant current density.

As stated above, Chapter 8 in *Fundamentals* deals with the subject of electroless deposition. Consequently we offer here a short discussion of the electrochemical path leading to the reduction of, nickel.

According to Van Den Meerakker [4] electroless deposition processes may be viewed and understood by what is referred to as a universal electrochemical mechanism regardless of the nature of the many possible reducing agents R. Each process can be viewed as made up of a series of elementary anodic and cathodic reactions. The first anodic stage is the dehydrogenation of the reductant. Thus the following four anodic stages are recognized in the case of alkaline media:

1. Dehydrogenation, $RH \rightarrow R + H$
2. Oxidation, $R + OH^- \rightarrow ROH + e$
3. Recombination, $H + H \rightarrow H_2$
4. Oxidation, $H + OH^- \rightarrow H_2O + e$

In the case of alkaline media the following two cathodic stages are recognized:

5. Metal deposition, $M^{+n} + ne \rightarrow M^0$
6. Hydrogen evolution, $2H_2O + 2e \rightarrow H_2O + 2OH^-$

In acid media stages 4 and 6 are to be written as follows:

4′. Oxidation, $H \rightarrow H^+ + e$

6′. Hydrogen evolution, $2H^+ + 2e \rightarrow H_2$

Thus an electroless deposition reaction can be considered to be the combined result of two independent electrode reactions:

- Cathodic partial reactions such as stage 5 above
- Anodic partial reaction such as stage 2 or 4′ above

Mixed-potential theory, advocated by Paunovic [5] in 1968, holds that electroless deposition processes can be predicted from the polarization curves of the partial anodic and cathodic processes. In *Fundamentals* the verifications of the mixed potential theory for a wide number of cases of electroless systems is delineated. Historically deMinjer [6] was the first to test the validity of the mixed-potential theory in electroless nickel deposited using hypophosphite as reducing agent.

18.3 ELECTROLESS NICKEL PLATING BATHS

18.3.1 Basic Baths

The literature abounds in the number of possible bath formulations for the electroless deposition of nickel using many different reducing agents and under widely different plating conditions. For this reason the reader is advised to consult [3, 7, 8] and the many references therein. We present here some representative formulations. Table 18.6 gives a summary of possible bath formulations for the electroless deposition of nickel where no additives are suggested (except for baths 3 and 5 where the often-used additive Pb^{2+} is included) and with sodium hypophosphite as reducing agent. It is evident from the table that a wide range of baths with pH values from about 4 to about 11 are possible. It is expected that many of the end product deposit's properties will depend on this important parameter value. Indeed, at low bath (acidic) pH values the resulting film will have an increased phosphorous content, up to 25 at % at pH 4. At pH values in the alkaline range less than 1% phosphorous content is rather common place. Electroless deposited films do develop stress. Films produced in acidic baths tend to show tensile stress, while those from alkaline baths "shift" their stress in the compressive direction. Another pH-dependent property is the fact that films grown using acidic baths exhibit good adhesion characteristics to steel, and this is likely why those film types are more common in industry. In addition it is observed that raising a bath's pH value has a marked effect on the deposition rate. Alkaline baths tend to have a higher deposition rate with the concomitant result of decreased stability and, as a further result, possible "plate-out." It should be clear that for reliable and repeatable results it is essential that a constant-solution pH be maintained during the entire deposition process.

Another important parameter is that of bath temperature. The deposition rate (everything else being equal) increases exponentially with increased temperature. Indeed, all practical baths will require operating temperatures of 60°C and above. However, bath temperature should rarely, if ever, be above that of 90°C since solution "plate-out" or bath decomposition then becomes a real possibility. From the foregoing it is not difficult to see why alkaline plating solutions are of relatively little use, say, in the automotive industry. Their use seems to be specific to applications where plating is to be done at relatively low temperatures (no higher than 70°C) such as on polymeric substrates and other applications where a low phosphorous content is a requirement.

In addition to hypophosphite, which is useful as a reducing agent for the electroless deposition of nickel containing phosphorus (Ni–P), there are three others:

1. Sodium borohydride, $NaBH_4$—in the bath pH range of 12–14
2. Dimethylamine borane, (DMAB) $(CH_3)_2NHBH_3$—in the pH range of 6–10
3. Hydrazine, $N_2H_4{\cdot}H_2O$—in the pH range of 8–11

The first and second, when acting as reducing agents in a nickel metallizing bath, yield electroless nickel films containing boron (Ni–B). The third yields nitrogen-containing (Ni–N) films.

With respect to type 1 above, in Table 18.7 we list three different compositions of sodium borohydride electroless nickel plating solutions. The properties such as hardness of

TABLE 18.6 Bath Compositions for Electroless Nickel Deposition Using Hypophosphite Reducing Agent

	Acid Baths				Alkaline Baths			
Bath Constituents ($g\,L^{-1}$)	1	2	3	4	5	6	7	8
Nickel chloride, $NiCl_2{\cdot}6H_2O$	30	30	—	21	26	30	20	—
Nickel sulfate, $NiSO_4{\cdot}6H_2O$	—	—	25	—	—	—	—	25
Sodium hypophosphate, $NaH_2PO_3{\cdot}H_2O$	10	10	23	24	24	10	20	25
Hydroxyacetic acid, $HOCH_2COOH$	35	—	—	—	—	—	—	—
Sodium citrate, $Na_3C_6H_5O_7{\cdot}H_2O$	—	12.6	—	—	—	84	10	—
Sodium acetate, $NaC_2H_3O_2$	—	5	9	—	—	—	—	—
Succinic acid, $C_4H_6O_4$	—	—	—	7	—	—	—	—
Sodium fluoride, NaF	—	—	—	5	—	—	—	—
Lactic acid, $C_3H_6O_3$	—	—	—	—	27	—	—	—
Propionic acid, $C_3H_6O_2$	—	—	—	—	2.2	—	—	—
Ammonium chloride, NH_4Cl	—	—	—	—	—	50	35	—
Sodium pyrophosphate, $Na_4P_2O_7$	—	—	—	—	—	—	—	50
Lead ion, Pb^{2+}	—	—	0.001	—	0.002	—	—	—
pH	4–6	4–6	4–8	6	4–6	8–10	9–10	10–11
Temperature (°C)	100	100	85	100	100	95	85	70

Source: DeMinjer [7].

TABLE 18.7 Composition of Sodium Borohydride Electroless Nickel Plating Solutions

Component	Bath 1	Bath 2	Bath 3
Ni^{2+}	2.5	5	6
EDTA disodium salt	35	—	—
Sodium potassium tartarate	—	65	—
Ammonium hydroxide (28%)	—	—	120 mL L^{-1}
Sodium hydroxide	40	40	—
Sodium borohydride	0.5	0.75	0.4
$TINO_2$ (mg L^{-1})	50	—	—
$Pb(NO_3)_2$ (mg L^{-1})	—	10	—
2-MBT (mg L^{-1})	—	—	20
Temperature (°C)	95	92	60
pH	14	13	12

Source: Mallory and Hajdu [8].
Note: Concentrations in grams per liter.

the Ni–B films, in particular, bath 1 in the table, which contains thallium, have become of considerable interest due to their use in a number of applications. The baths themselves have, however, some important disadvantages. For example, there is the need to maintain pH values above 12 in order to suppress the possibility of nickel boride precipitation. As a consequence only substrates that can withstand the high alkalinity can benefit from these solutions. The inclusion of thallium in bath 1 as a stabilizer (see below) enables the deposition process to take place at a lower practical temperature with a relatively high deposition rate. Note here the dramatic effect that stabilizers can have on the properties of the metallizing baths. Stabilizers and their effects are discussed in the next section. As a final point, environmental considerations seem to dictate the type and ultimate compositions of plating baths used in practical industrial settings. For instance, often the use of thallium results in thallium being codeposited in the Ni–B films (up to 6% for some baths).

With respect to type 2 above, it should be noted that replacing hypophosphite as a reducing agent in a plating bath by amine boranes also results in a "workable" solution for the plating of electroless nickel. The formulations of both acid and alkaline plating baths are available in the literature.

With respect to type 3 above we observe that electroless deposition can be likewise achieved using hydrazine-based baths [7, 9, 10]. The baths consist of a nickel salt complexing agent such as tartrate, malonate, or ethylenediaminetetraacetic acid (EDTA) and the reducing agent hydrazine. The pH is adjusted to the level desired with sodium hydroxide. The electroless nickel deposits produced from hydrazine solutions contain up to 99% nickel, with oxygen and nitrogen present to the tune of tenths of a percent. One good example is a bath containing 4.8 g L^{-1} nickel chloride hexahydrate, 32 g L^{-1} hydrazine, and 4.6 g L^{-1} sodium tartrate dihydrate at pH 10 and deposition temperature of 95°C. The magnetic properties of such films compare well with those of electrodeposited counterparts.

18.3.2 Bath Additives

Over the decades of practicing electroless nickel deposition a number of workers have developed special additives to the plating bath that make the bath more practical in various ways. Among these are bath stability, deposition rate, product film grain structure, and surface smoothness and brightness.

One family of additives is referred to as complexing agents. These are usually organic acids or their salts, with some notable exceptions. One is the ammonium ion that is added for pH control. Another, which is used in alkaline baths, is the pyrophosphate ion. In Table 18.8 we list a number of practical complexing agents. These additives play three roles:

1. Help maintain stable pH level
2. Help prevent precipitation of nickel salts such as phosphites
3. Reduce the concentration of free nickel ions

A few words on the concept of complexing are in order here. When nickel ions are in aqueous solution, they are bound to a well-defined number of water molecules. That is the coordination number. In the case of Ni^{2+} ions, the number is 4 or 6. In a situation where water molecules which are coordinated to the hydrated (free, simple) nickel ion are replaced by another ion or molecule, we speak of a nickel complex, and the combining ion or molecular group is the complexing agent. Clearly, the chemical properties of the nickel ions are expected to change as a result of complexation. More specifically, the rate of nickel deposition is proportional to the rate at which the nickel complex dissociates to form free nickel ion. Thus the plating rate is inversely proportional to the complexing ion's stability constant (see Table 18.8).

Yet another family of additives are the stabilizers. As every practitioner of electroless plating knows, plating baths can be used for long periods of time without stabilizers. A bath can, however, decompose suddenly without signs of

TABLE 18.8 Complexing Agents Commonly Used in Electroless Nickel Baths

Anion	Acid	Stability, $pK = -\log K$
Acetate	CH_3COOH	1.5
Succinate	$HOOCCH_2CH_2COOH$	2.2
Aminoacetate	NH_2CH_2COOH	6.1
Malonate	$HOOCHCH_2COOH$	4.2
Pyrophosphate	$H_2O_3POPO_3H_2$	5.3
Malate	$HOOCCH_2(OH)COOH$	3.4
Citrate	$HOOCCH_2(OH)C(COOH)_2$	6.9

warning. Actually an increase in the volume of the evolving hydrogen gas is followed by the precipitation of fine black particles before the solution caves in completely. The particles that precipitate are nickel phosphide or nickel boride, depending on the reducing agent used. Fortunately, a number of compounds, referred to as stabilizers, exist which can render an electroless deposition bath stable or at the least retard precipitation. Besides providing stability, some of them accelerate the rate of plating. In general, there are four "classes" or types of stabilizers in common use:

1. Compounds of group IV elements (Se, Te, etc.)
2. Unsaturated organic acids (maleic, etc.)
3. Heavy metal cations (Sn^{+2}, Pb^{+2}, etc.)
4. Oxygen-containing compounds (AsO_2^-, MoO_4^{2-}, etc.)

The stabilizer's concentration in a bath is a crucial parameter. For instance, stabilizers of types 1 and 4 are effective at concentrations as low as 0.1 ppm. At concentrations of about 3 ppm, plating is stopped altogether. On the other hand, certain stabilizers of type 1 such as thiourea in the proper concentration range can enhance deposition rates to a considerable degree. Stabilizers of types 3 and 2 are used in concentration ranges of 10^{-3}–10^{-6} and 10^{-1}–10^{-3} molar concentration ranges, respectively. In the last analysis, the stabilizers alter the activity of the catalytic substrate—hence their marked influence at even low concentrations.

In addition to the above, air agitation of the metallizing bath will result in improved bath stability. Specifically, it was observed [11] that when pure oxygen is bubbled through a nonstabilized solution the mixed potential shifted from about −620 to −550 mV [vs. saturated calomel electrode (SCE)]. That is to say, the oxygen-agitated solution is markedly more stable than its quiescent counterpart. A number of methods are available to the practitioner in order to determine solution stability or stabilizer efficiency. One of the best is as follows: Add a couple of milliliters of a 100-ppm palladium chloride solution to a sample of the warm plating solution. The bath is considered stable if no visible black precipitate is in evidence within the first 60 s.

Still another family of additives is known as buffers. Buffers are substances or combination of substances that are capable of neutralizing both acid and base alike without changing the pH of the solution by much. A measure of the buffer's efficiency is the amount of, say, acid required to change the solution's pH. Clearly, the greater that amount, the better the buffer. Titration methods may be used to determine that amount and so the buffer's quality. In Table 18.9 we list a few acids used as buffer for electroless nickel solutions. The maintenance of the pH value in a deposition bath is as crucial as the deposition rate, and the composition of the end-product film is strongly dependent on it. Figure 18.2 [12] depicts the effect of pH value on the deposition rate of an electroless nickel bath which employs sodium hypophosphite as the reducing agent. The effect of bath pH on the phosphorous content of the end-product film is shown in Figure 18.3. In practice it has been observed that 3 mol of H^+ is produced for every mole of Ni^{2+} deposited. This means that without any type of buffering, as deposition progresses, the pH value in a bath is expected to become lower. This is reflected in a gradual lowering of the deposition rate as well (see Fig. 18.2). In addition the film composition will change (see Fig. 18.3). Whether, in practice, these changes are harmful or undesired depends on the type of application for which the film is required. For instance, if corrosion resistance (low porosity) or a nonmagnetic state in the freshly as-deposited state is the desired property, then lowering the pH value is an asset rather than a hindrance. If, on the other hand, the phosphorous content must remain stable, then a change in the pH value is to be avoided. As is the case with all rules, there are exceptions. Electroless nickel plating using dimethylaminoborane (DMAB) as reducing agent is accompanied by the evolution of hydrogen ion,

TABLE 18.9 Acids Commonly Used as Buffer in Electroless Plating Baths

Acetic
Propionic
Glutaric
Succinic
Adipic

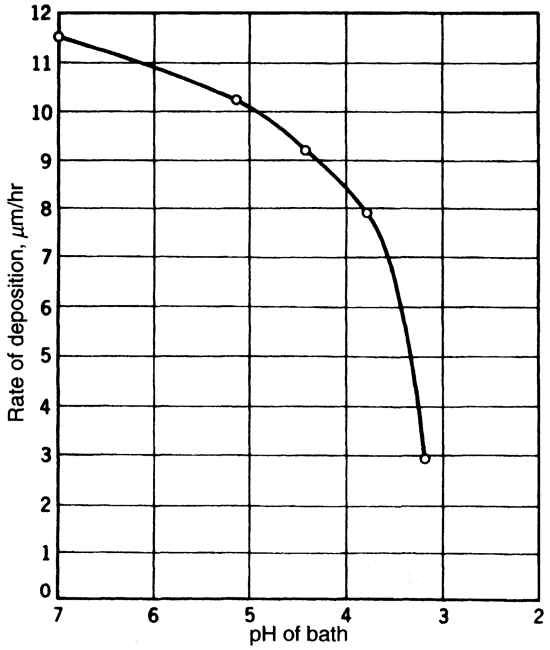

FIGURE 18.2 Effect of pH on electroless nickel deposition rate. Bath: $NiCl_2 \cdot 6H_2O$, 30 g L^{-1}; $NaH_2PO_2 \cdot H_2O$, 10 g L^{-1}; sodium glycolate, 10 g L^{-1} [12].

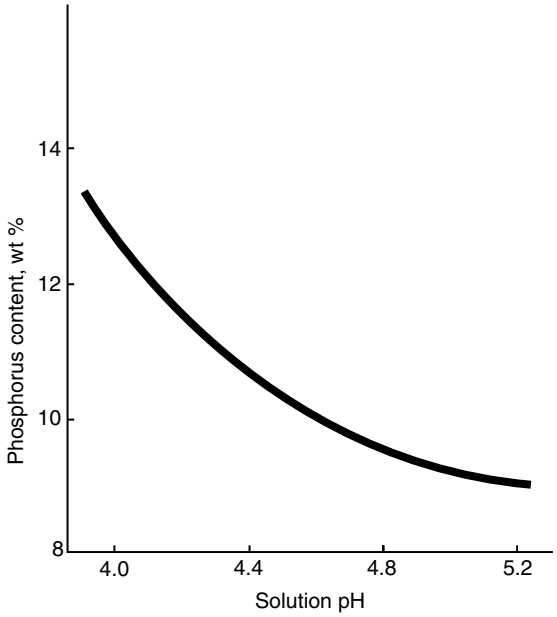

FIGURE 18.3 Effect of pH on phosphorous content. (Reproduced with permission of the American Electroplaters and Surface Finishers Society [8].)

hydrogen gas, and the creation of boric acid and dimethylamine. Boric acid and its salts, together with the amine, serve as buffering agents, decreasing the effect of the evolution of hydrogen ions. In some plating baths the pH values were observed to increase slightly. As an aside, but an important practical observation, it ought to be noted that electroless nickel baths using DMAB have a very long operating life. This may be due to the plating reaction by-product being soluble in the bath.

18.4 FILM PROPERTIES

18.4.1 Structure

Electroless deposits in general and electroless nickel in particular have a wide number of industrial applications. This is due to their unique properties of corrosion and wear resistance. These and other important properties are a direct result of the structure and chemical makeup of the end-product thin films. The properties in turn depend on the deposition bath makeup and deposition parameters such as temperature and agitation. Yet another important practical advantage offered by electroless deposition is their uniform deposition even on objects of arbitrary shape. For these reasons a discussion of film properties is included here together with a list of relevant references.

Electroless nickel deposits come in two groups, depending on the specific reducing agent used in the deposition process. The first are the nickel–phosphorus alloys, Ni–P; the others are the nickel–boron alloys, Ni–B.

As-deposited electroless nickel is a metastable supersaturated alloy [13]. The structure of electroless nickel grown in acidic bath using hypophosphate as the reducing agent is said to be amorphous or liquidlike [3]. Heat treatment to about 330°C was found ([3, 13]; see also *Fundamentals,* Chapter 16) to result in semicrystalline, face-centered-cubic (fcc) nickel interspersed with intermetallics such as Ni_3P and Ni_3B. Those intermetallics cannot form during plating, so in the as-deposited state, phosphorus is trapped between nickel atoms in a random fashion. The amount of phosphorus in a Ni–P film is bath pH dependent, as discussed above (see Fig. 18.3). In general, it may be stated that the higher the bath pH value, the lower is the phosphorous content of the film and the higher is the degree of crystallinity of the nickel. That is to say, the lower the phosphorous content, the higher, on average, are the sizes of the component nickel crystallites making up the film. Therefore phosphorus is thought to act as an inhibitor of crystal formation. This may be understood in simple terms as follows: When the phosphorous atoms are trapped between the nickel atoms, their presence reduces the possibility of contact among nickel atoms such as might form extended nickel crystallites. During deposition and the concomitant hydrogen evolution, the pH value close to the growing film will become higher while subsequent stirring action lowers that value. This periodic change results in the phosphorous content varying as a function of film layer thickness. This behavior had already been observed by a number of workers in the 1950s [14], Another phosphorous content-dependent property is that of material density. As Figure 18.4 shows, the material density of films

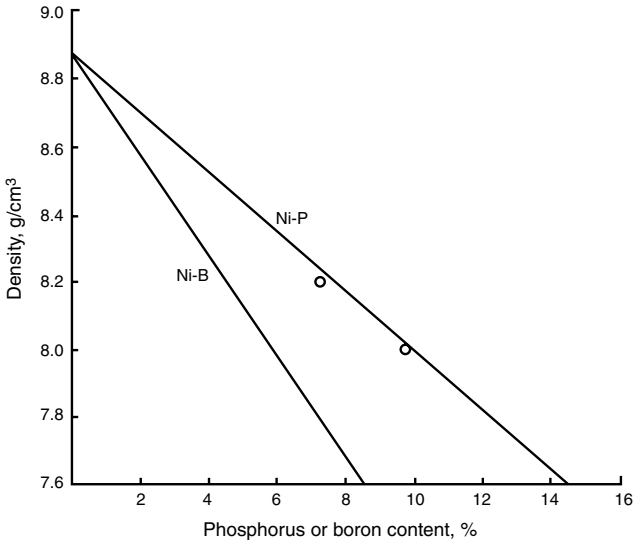

FIGURE 18.4 Effects of alloy composition on density for Ni–P and Ni–B deposits. (Reproduced with permission of the American Electroplaters and Surface Finishers Society [8].)

tends to their bulk value at the zero concentration value of phosphorus [15].

18.4.2 Hardness

Hardness is defined as the reluctance of a material to permanently deform, or indent. This is an easy quantity to measure, and for that reason hardness has been frequently the subject of analysis. Hardness has no direct connection to material strength, but it is a reliable indicator of the degree of abrasive-wear resistance. The hardness of as-deposited Ni–P films is close to 550 $kg\,mm^{-2}$, as determined by the Knoop or Vickers indenter using a 100-g load. With increasing phosphorous content a gradual decrease in hardness is observed. As plated, Ni–B films have higher hardness—about 700 $kg\,mm^{-2}$. In contrast to Ni–P films, the hardness of Ni–B films is not dependent on composition. Hardness, in general, is affected by heat treatment. The exact functional dependency, however, of hardness versus heat treatment temperature and duration is rather complex, so it will not be discussed here in detail. In general, as-deposited Ni–P films can have their hardness raised from about 550 to nearly 1000 $kg\,mm^{-2}$ by heating them to 300°C for about 10 min. If kept heated longer, the hardness will fall back to the lower value. Similarly at higher temperatures the film loses hardness if kept heated for even shorter periods. In other words, hardness values peak and then decline with increasing heat treatment, and this is likely due to the formation of intermetallics.

The addition of a third element affects hardness as well. Thus it has been noted by many that the addition of molybdenum will markedly increase the hardness of Ni–B films.

18.4.3 Corrosion and Wear Resistance

It has been observed that electroless nickel generally provides a coating that has lower porosity and more uniform thickness than the equivalent electroplated nickel alloy, such as Ni(P) or Ni(B). This makes the film an effective corrosion-protecting agent. When it comes to actual application of the electroless film as an anticorrosion layer, the substrate pretreatment and the actual plating assure good adhesion and continuity of the coating.

The effectivity of an anticorrosion layer is measured by a neutral 5% salt spray as well as outdoor exposure. Thus it has been observed that Ni–P layers with about 9% by weight phosphorous content provide longer corrosion protection than an electroplated nickel alloy.

The difference in electrochemical potential between electroless nickel and the substrate is thought to determine what happens in the presence of voids or pores in the coating. That difference is actually dependent on the nature of the corrosive agent. For instance, in an electrolytic cell, the electroless nickel will constitute the cathode against aluminum or steel in most environments. Now, if an area of the substrate (which is the anode) is exposed due to pores in the coat, then the current density (i.e., corrosion rate) will be high there. More specifically a 300-mV difference will maintain the corrosion of an aluminum or steel substrate if the electroless coating does not provide complete coverage. In cases where the electroless nickel is the anode, the coating is said to corrode sacrificially. The anode area is large and consequently the current density (i.e., corrosion rates) are rather low. The inclusion of zinc in proper quantities in electroless nickel may tip the balance such that it may become an effective corrosion-protecting agent even for steel.

By way of summary, in engineering applications electroless nickel is used to render protection for metal surfaces exposed to corrosion and/or wear. The factors that set the conditions for the corrosion resistance of electroless nickel may be listed as follows:

1. Surface properties and finish
2. Surface pretreatment
3. Deposit thickness
4. Deposit properties
5. Plating posttreatment
6. Nature of the corrosive medium

Heat treatment to about 350°C, in a view to rendering the coating extra hardness, lowers the corrosion resistance of electroless nickel. This is perhaps due to microcracking. On the other hand, heat treatment up to 650°C improves corrosion resistance, since there is improved bonding to, say, steel. Finally, so many different parameters affect the properties of electroless nickel coating that it is difficult to accurately predict, a priori, their corrosion resistance. Field performance is likewise difficult to base on laboratory observed test results, thus adding to the complexity of the issue at hand.

As indicated above, electroless nickel is used not only for corrosion protection but also for wear protection. If properly applied, electroless nickel is considered to enhance the useful life of pumps, valves, shaft, connector pins, and rotor blades, to name just a few example applications.

Wear is the gradual mechanical deterioration of surfaces in contact. Generally, two types of wear are recognized: adhesive and abrasive. The first is the welding of the two surfaces. The other is the result of the lateral movement shearing the welds. If that does not occur at the original weld, material from one surface can still adhere to another. The resulting weight loss is known as abrasive wear.

Wear, in general, is related to the hardness of the surfaces in contact. Lubrication too reduces friction and wear by reducing the intimate contact between surfaces. When hard particles such as diamond [16] are included in electroless nickel, they form the principal areas of contact with another surface. The result is reduced adhesive wear. If, however,

they are pulled out of the matrix, abrasive wear will result from the mutual surface motion.

Again, it should be clear that wear is a complex process. Among the many factors that affect wear and make it difficult to predict and control are finish and surface hardness, the contact area and its shape, the type of motion and its duration and speed, the temperature and environment, and the type of lubrication. Laboratory tests provide only clues; the actual working conditions under service are the only reliable indicators of how a surface will wear. The following is a summary of the general conditions for wear applications of electroless nickel:

1. Coating should be heat treated to increase hardness.
2. Hardness of coat should be greater on rotating parts than the mating surface.
3. Phosphorous content has to be greater than 10%.
4. Contacting surfaces should be smooth and lubricated.
5. Electroless nickel is not fit to be used under high-shear and high-load conditions.

18.4.4 Electric and Magnetic Properties

As-deposited electroless nickel films from acidic baths possess an amorphous structure, as noted above. The structural changes that occur as a result of heat treatment can be illustrated by observing the changes of film resistivity as heat treatment proceeds. This is seen in Figure 18.5 [17]. In the figure the resistivity changes over time as heat treatment proceeds are given for acid bath (pH 5.4) grown films of different thicknesses. From the figure it is evident that as the films change from a solid solution of phosphorus in amorphous nickel to a mixture of polycrystalline nickel metal and the intermetallics Ni_3P, the resistivity decreases. Thermal conductivity usually is in direct relation (proportional) to electric conductivity, so Figure 18.5 can be viewed as representing that parameter's characteristics too. Heat treatment changes the nature of the amorphous films from nonmagnetic to weakly ferromagnetic due to the nickel crystallization. The magnetic coercivities of low phosphorus to microcrystalline films increase as well after heat treatment. The reason may be that the paramagnetic intermetallic Ni_3P impedes the movement of domain walls. In Table 18.10 we list some physical properties of electroless nickel films grown in baths with different phosphorous contents.

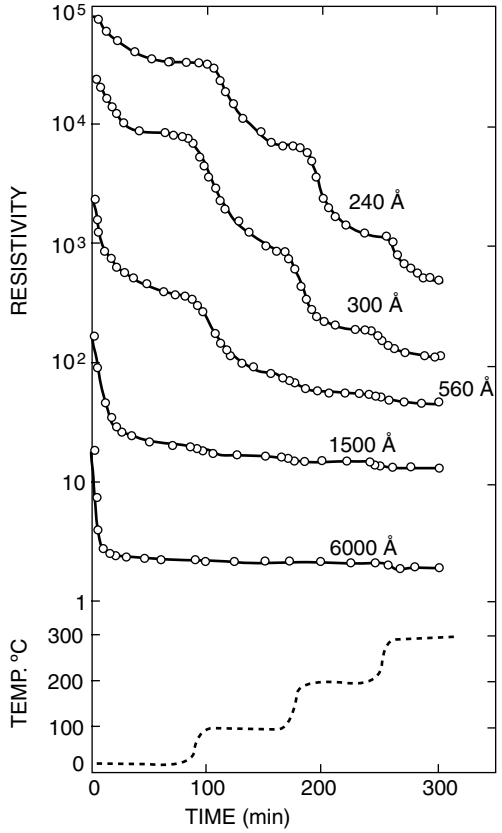

FIGURE 18.5 Upper curves: the resistivity (in ohms per square) changes over time of Ni–P films during heating. Film thicknesses as indicated. Bottom (dashed) curve: heat treatment temperature as a function of time [17].

TABLE 18.10 Some Properties of Electroless Nickel Films

Solid Solution (%)	Density (g cm^{-3})	Resistivity (μΩ-cm)
1–3 P	8.6	30
1–2 B		6–12
5–7 P	8.3	50–70
4–5 B	8.5	
8–9 P	8.1	70–100
5 B	8.3	100
>10 P	8	<120
7 B	7.8	200

18.5 COMPOSITES

18.5.1 Composite Electroless Coatings

Abdel Hamid et al. [18], Gay et al. [19], and Sheela and Pushpavanam [20] incorporated abrasives such as oxides, diamonds, and carbides, respectively, in electroless Ni–P and thus markedly improved microhardness and the wear resistance.

In general, diamond powder–incorporated cladding of various tools has resulted in important industrial materials, enhancing productivity in metalworking, materials production, grinding and finishing, precision cutting, and machining. Specifically, diamond coatings have entered into commercial markets via tool inserts, audio speakers, X-ray windows, and heat sinks and directly interface with the heavy automotive and high-technology areas as well as the stone processing industries for cutting, slicing, polishing, and

finishing. It has been learned through practice that hard coatings applied to cutting tools increases tool life by 2–10 times that of uncoated tools.

Diamond particles incorporated into a metal matrix are usually designed for at least one of several purposes such as grinding or abrasive applications, wear resistance or surface protection properties, controlled surface topography involving specific ranges of roughness or surface friction qualities, antigalling or lubricating uses, and corrosion resistance. By codepositing nickel with very fine particles or polycrystalline diamond, composite coatings with high wear resistance have been produced, adopting both electrolytic and electroless techniques. The wear properties of these coatings will depend on how firmly the particles are anchored in the matrix [21, 22]. Electroless nickel solutions are found to be suitable for composite coatings resulting in consistent, homogeneous concentration of the particulate material in the composite.

The electroless nickel plating technique is well known for its simplification of electroplating in avoiding problems of current distribution, throwing power, and anode–cathode orientation within the bath. Its inherent problem in the present context is that stability is aggravated by the inclusion of particulate matter in the bath. Despite this, the process is a practical as well as a commercial reality [23, 24].

Diamond powders are available in several forms. Broadly, there are two types: monocrystalline and polycrystalline. Single crystals of diamond fracture along cleavage planes and result in sharply defined edges and points. Natural diamond and certain types of synthetic diamond belong in this category. Shock-synthesized diamond, on the other hand, is polycrystalline. The choice of the type of powder that can be used for making composites depends upon the end use of the composite [25, 26].

18.5.2 Production of Composite Coatings (Ni–P)

A most recent work [27] suggests that, before coating, a diamond powder of typically $\sim$80 μm size should be subjected to a three-step activation procedure as follows:

1. Wash in nitric acid (1% HNO_3) for 1 min.
2. Rinse in distilled water.
3. Immerse for 2 min in a stannous chloride ($2\,g\,L^{-1}$)–HCl ($5\,mL\,L^{-1}$) solution.

The plating bath constituents and operating conditions typically are as follows:

Nickel chloride $30\,g\,L^{-1}$
Sodium hypophoshite $40\,g\,L^{-1}$
Sodium citrate $25\,g\,L^{-1}$
Ammonium chloride $50\,g\,L^{-1}$
Temperature of plating bath 86 ($\pm$1°C);
pH of bath 9–10

The pH may be maintained within the above range by addition of appropriate amounts of concentrated ammonia solution.

The heat treatment temperatures used in the case of electroless Ni–P/diamond deposits were 350 and 500°C selected after an iterative optimization. In all cases the as-coated sample was taken as the standard against which the properties of the heat-treated samples were compared [20].

It is good to remember that the hardness values of codeposits, estimated using conventional microhardness testers, provide only an average value for the hardness of the composite due to the dispersion of particles within the Ni–P matrix.

REFERENCES

1. A. Brenner and G. Riddell, *J. Res. Nat. Bur. Std.*, **37**, 31 (1946).
2. J. Kisel, Ph.D. Thesis, University of Windsor (1988); M. Schlesinger and J. Kisel, *J. Electrochem. Soc*, **136**, 1658 (1989).
3. J. P. Marton and M. Schlesinger, *J. Electrochem. Soc.*, **115**, 16 (1968).
4. J. E. A. M. Van den Meerakker, *J. Appl. Electrochem.*, **11**, 395 (1981).
5. M. Paunovic, *Plating*, **55**, 1161 (1968).
6. C. H. de Minjer, *Electrodeposition Surf. Treat.*, **3**, 261 (1975).
7. F. Pearlstein,in *Modern Electroplating*, 3rd ed., F. A. Lowenheim, Ed., Wiley, New York, 1974.
8. G. O. Mallory and Juan B. Hajdu, Eds., *Electroless Plating—Fundamentals and Applications*, American Electroplaters and Surface Finishers Society, Chs. 1–11, and references therein.
9. D. J. Levy, *Electrochem. Technol.*, **1**, 38 (1963).
10. J. W. Dini and P. R. Coronado, *Plating*, **54**, 385 (1967).
11. G. Gabrielly and F. Raulin, *J. Appl. Electrochem.*, **1**, 167 (1971).
12. K. M. Gorbunova and A. A. Nikiforawa, *J. Phys. Chem. USSR*, **28**, 883 (1954).
13. M. Schlesinger and J. P. Marton, *J. Phys. Chem. Solids*, **29**, 188 (1968); *J. Appl. Phys.*, **40**, 507 (1969); also S. L. Chow, N. E. Hedgecock, M. Schlesinger, and J. Rezek, *J. Electrochem. Soc*, **119**, 1614 (1972).
14. A. W. Goldenstein, W. Rostoker, F. Schlossberger, and G. Gutzeit, *J. Electrochem. Soc.*, **104**, 104 (1957); see also F. Ogburn and C. E. Johnson, *Plating*, **60**, 1043 (1973).
15. T. Schmidt et al., *Nucl. Instr. and Methods*, **199**, 359 (1982); see also reference 17.
16. K. Parker, *Plating*, **61**, 834 (1974).
17. M. Schlesinger and J. P. Marton, *J. Appl. Phys.*, **40**, 507 (1969).
18. Z. Abdel Hamid, S. A. El Badry, and A. Abdel Aal, "Electroless Deposition and Characterization of Ni–P–WC Composite Alloys," *Surf. Coat. Technol.*, **201**, 5948–5953 (2007).

19. P. A. Gay, J. M. Limat, P. A., Steinmann, and J. Pagetti, "Characterisation and Mechanical Properties of Electroless NiP–ZrO2 Coatings. *Surf. Coat. Technol.*, **202**, 1167–1171 (2007).
20. G. Sheela and M. Pushpavanam, "Diamond-Dispersed Electroless Nickel Coatings" *Met. Finish.*, **100**, 45–47 (2002).
21. W. Feldstein and T. Lancsek, *Products Finish.*, **61**, 35 (1983).
22. W. Riedel, *Electroless Nickel Plating*, Finishing Publications, London, UK; 1991.
23. K. Parker, Proc. 8th Congress International Union Electrodeposition & Surface Finishing Interfinish, 1972.
24. N. Feldstein, *Met. Finish.*, **61** (8), 35 (1983)
25. J. Lukschandel, *Trans. Inst. Met. Finish.*, **56**, 118 (1978).
26. T. Sudharshan, *Surface Modification Technologies*, Marcel Dekker, New York, 1989.
27. J. T. Winowlin Jappes, B. Ramamoorty, and P. Kesavan Nair, *J. Mat. Proc. Tech.* **209**, 1004–1010 (2009).

19

ELECTROCHEMICAL SYNTHESIS OF METAL ALLOYS FOR MAGNETIC RECORDING SYSTEMS

ATSUSHI SUGIYAMA, MASAHIRO YOSHINO, TAKUMA HACHISU, AND TETSUYA OSAKA

19.1 INTRODUCTION

19.1.1 Magnetic Recording Systems

Magnetic recording devices that store a mass of electronic data and offer high-speed random access to the data are one of the most important keys to the advancement of information technology since its invention more than 100 years ago by Valdemar Poulsen [1]. The major magnetic recording and storage devices are video tapes, floppy disks, and hard disk drives (HDDs). In particular, HDDs with increased recording density are installed as external storage devices in highly functional electrical and electronic products.

19.1.2 Estimation of Increase in HDD Areal Density and Technology Development

In 1956, IBM introduced the first HDD, the IBM 350 Disk File, which was the storage unit of the IBM RAMAC 305 computer [2]. It was composed of aluminum disks coated with iron oxide paint. It provided an areal density of $0.002\,\text{Mbit} \cdot \text{in.}^{-2}$; since then, the density has been increasing at a rapid rate for half a century.

Figure 19.1 shows the estimated increase of HDD areal density and related technology development from 1985 to 2020.

Such a rapid progress of HDD areal density was attained through epochal developments of magnetic thin-film materials [3]. One of the most significant innovations from the viewpoint of material improvement is the electrodeposition of permalloy ($Ni_{80}Fe_{20}$), which was introduced by IBM in 1979 as the core material of a thin-film inductive head [4]. After the introduction by IBM in 1991 of the magnetoresistive element as a read head, the areal density of HDDs jumped from 30% per year to 60% per year [5]. Following these developments, the replacement of the magnetoresistive element by a giant magnetoresistive element in the read component has led to a jump in the HDD areal density growth rate of over 100% per year since 1999, which is very impressive progress. At the beginning of 2004, the areal density of commercial HDDs approached $100\,\text{Gbits} \cdot \text{in.}^{-2}$ [6], and demonstration of $170\,\text{Gbits} \cdot \text{in.}^{-2}$ [7] was reported. However, there has been an apparent slowdown in this increase of density. The perpendicular magnetic recording system that was advocated by Professor Iwasaki in 1977 [8] was recently introduced to the market by Toshiba [9]. This system is a critical innovation for developing high-performance HDD systems with a high recording density. The design of the magnetic recording head also was changed because of the change in the recording system. For example, a longitudinal recording media system with a ring-type head and recording layer exhibiting in-plane anisotropy has been applied to the conventional HDD. For a perpendicular medium, the sputter deposition of CoCr alloy film, which was first reported by Iwasaki and Ouchi [10], and the control of grain orientation, grain size, and magnetic properties of film also have contributed to the progress in areal density [9–12]. To meet the strong demand for high-performance write heads to be used for high-density magnetic recording, soft magnetic materials with high saturation magnetic flux density, B_s, are being developed. Although the sputtering technique has become paramount, the electrochemical technique also has played an important role in the development of magnetic recording systems [13]. The electrochemical approach has

Modern Electroplating, Fifth Edition Edited by Mordechay Schlesinger and Milan Paunovic

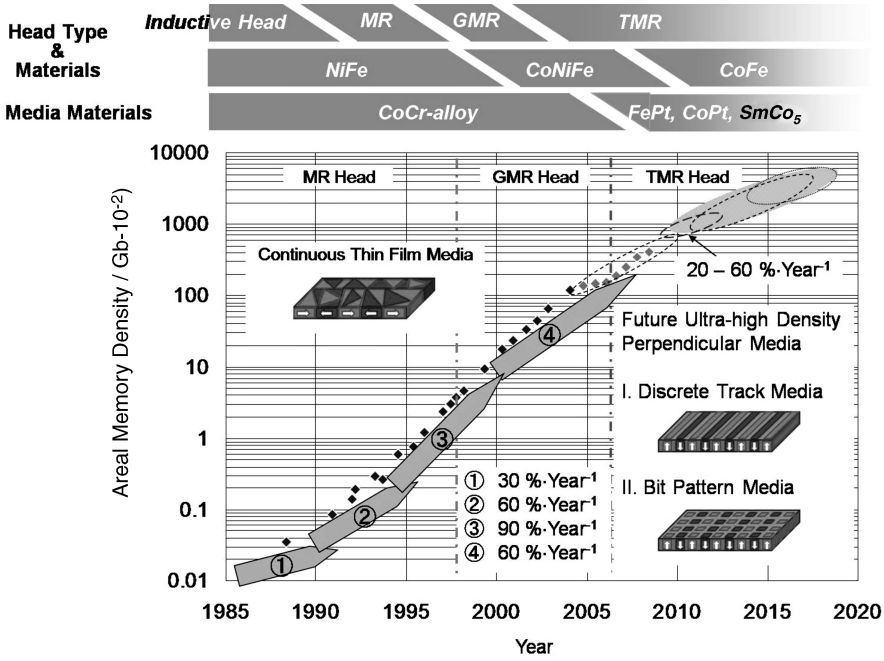

FIGURE 19.1 Estimated increase of areal density and technology development. MR: magnetoresistive, GMR: giant magnetoresistive, TMR: tunnel magnetoresistive, DTR: discrete track recording media, TAMR: thermal assist magnetic recording media, BPR: bit-patterned media [3–9].

spawned a new interdisciplinary study: electrochemical nanotechnology, specifically, the degree to which nanostructure control becomes possible by material functional processing. This new interdisciplinary study of electrochemical nanotechnology also has been enhancing the development of magnetic materials.

The following sections describe the various electrochemical techniques that have been developed to create high-performance magnetic thin films. First, we present the preparation of thin films with a highlight on the key for obtaining a high B_s by electroplating and electroless plating techniques. Next, we discuss the preparation of effective underlayers by displacement plating for the sputter-deposited [Co/Pd] multilayered films. In addition to these electrochemical processes, we introduce chemically produced FePt nanoparticles, which have potential as magnetic recording medium with high, uniaxial, magnetocrystalline anisotropy.

19.2 PREPARATION OF HIGH-B_s SOFT MAGNETIC FILM USING ELECTRODEPOSITION TECHNIQUES

19.2.1 Introduction

A magnetic recording head with soft magnetic thin films as the core materials is a key device for achieving high-density magnetic recording. A $Ni_{80}Fe_{20}$ permalloy has been used as the main core material for thin-film inductive heads since 1979 [4]. As the coercivity H_c of magnetic recording media increased, soft magnetic thin films with a high B_s were desired for writing magnetic signals on the media.

Bozorth [14] presented a well-known diagram showing the relation between film compositions and B_s values for the bulk materials of CoNiFe ternary alloy (see Fig. 19.2). According to the diagram, the B_s values greatly depend on the composition of the ferromagnetism metal. The CoNiFe alloys in the regions of Co-rich and/or Fe-rich compositions show relatively high B_s values. Many high B_s films have been reported: CoFe with B_s values of 1.8–1.9 T [15–18] and CoNiFe with B_s of 1.6–1.8 T [19–21]. A high-performance head requires high B_s and low H_c values as the core material. It is difficult to use conventional electrodeposited films as the core material for magnetic heads, however, since the H_c value of the films increases with an increased B_s value.

For a low H_c value, the grain size should be small; in fact, the grain diameter of CoNiFe alloy must be smaller than 20 nm [22]. Moreover, these fine grains with uniform crystalline structure should be homogeneously distributed in the amorphous phase. For the formation of CoNiFe soft magnetic films with such a nanocrystalline structure, electrochemical deposition is suitable and normally preferred over sputtering.

Electrodeposition of CoNiFeB with conventional baths provided films with a B_s greater than 1.6 T and a H_c larger than 5 Oe [23]. In addition, transmission electron microscopy (TEM) images revealed that films with B_s greater than 1.6 T consist of homogeneous grains with a diameter higher than

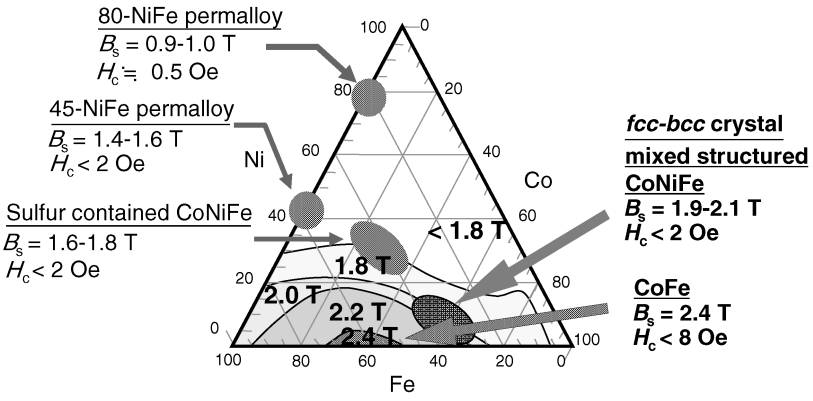

FIGURE 19.2 Phase diagram of CoNiFe ternary alloys indicating relation between film compositions and B_s values.

$\sim$ 20 nm [24]. It is known that grain growth in films fabricated with conventional baths could be suppressed by inclusion of impurities in the baths. CoNiFe films, for instance, contained sulfur 0.3 at %, coming from saccharin used as an additive to reduce film stress [25]. However, sulfur of 0.3 at% was not enough to decrease H_c values [25, 26]. To decrease the crystal grain size of films, other additives were put into the electrodeposition bath. For example, the addition of thiourea effectively reduced H_c [27, 28]. CoNiFe films electrodeposited from the thiourea bath showed, as can be seen in the phase diagram of Figure 19.2, a lower H_c value, less than 2 Oe, in the high-B_s region of 1.6–1.8 T, because the characteristic boundary showing low H_c shifted into the high-B_s region. This behavior was attributed to an inclusion of sulfur as high as 0.9 at % in the CoNiFe film, causing a decrease in crystal grain size [24, 27]. Thus, the selection of proper additives for the electrodepopsition process is an important factor for the production of films with good soft magnetic properties.

Various methods to fabricate soft magnetic films have been thoroughly investigated. CoNiFe films with an extremely low value of H_c (0.06 Oe) have been electrodeposited that contained very fine crystallites; these films can be placed in the region near the face-centered-cubic–body-centered-cubic (fcc–bcc) phase boundary in Figure 19.2. Furthermore, increasing the sulfur content shifted the phase boundary from the high-B_s region to the low-B_s region [29]. We used sulfur as an additive, but we decided not to use saccharin or thiourea, and we succeeded in obtaining $Co_{65}Ni_{12}Fe_{23}$ with B_s as high as 2.0 T and H_c as small as 1.2 Oe [29]. Figure 19.3 shows TEM bright-field images of bcc single phase, fcc–bcc mixed phase, and fcc single phase of the high-B_s CoNiFe films. With the fcc–bcc mixed phase, a low H_c value was obtained. From these images, it is clear that the fcc–bcc mixed phase is formed with fine crystal grains, compared with those of the bcc or fcc single phases. It is thus likely that the newly developed soft magnetic film can be prepared only by electrodeposition [30, 31]. The mixed-phase lines are

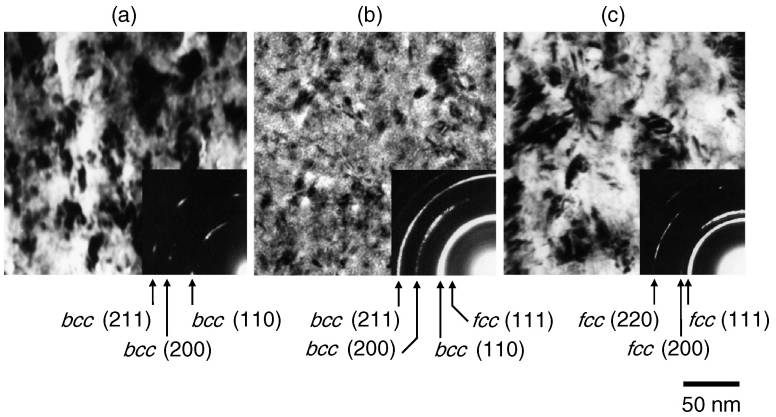

FIGURE 19.3 TEM bright-field images of CoNiFe thin films electrodeposited from no-SCA bath with various crystalline structures: (a) bcc structure; (b) bcc–fcc mixed structure; (c) fcc structure. SAED patterns are also shown [32].

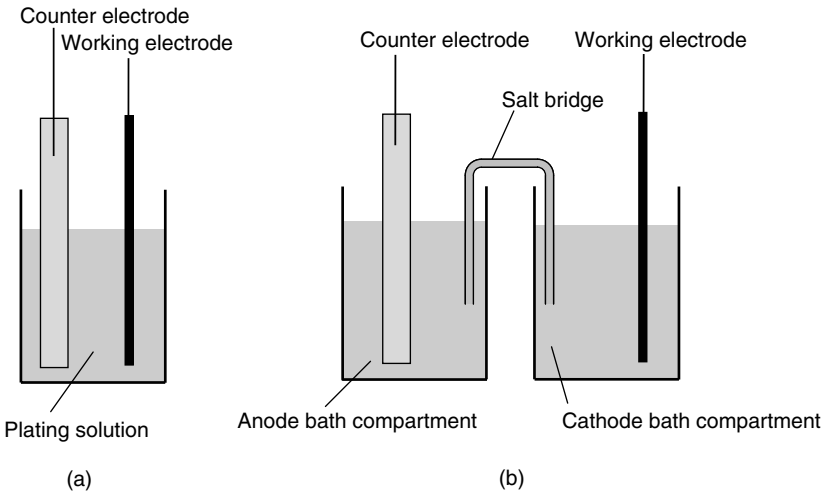

FIGURE 19.4 Schematic representation of two cell systems: (a) single-cell system; (b) dual-cell system consisting of anode and cathode compartments.

clearly dependent on the trace amount of sulfur inclusion. The film electrodeposited with no- sulfur-containing additive (SCA) exhibited the fcc–bcc mixed-phase line in the highest B_s region.

19.2.2 Highest B_s CoFe Soft Magnetic Thin Films

The Co–Fe binary alloy is known as a material with high saturation magnetic flux density. The Co_{40}–Fe_{60} alloy has a B_s value of about 2.4 T, which is close to the limiting value achievable with ferromagnetic alloys, as shown in Figure 19.2. The B_s value of the Co–Fe films prepared with an alloy with a high Fe content that is electrodeposited using the conventional electrolytic cell of the single-bath type (shown in Figure 19.4*a*) is usually lower than that of the bulk alloys [14].

To clarify the reason for the low B_s value of the electrodeposited Co–Fe films, we analyzed the state of Fe ions in the plating baths. The concentration ratios of [Fe^{3+} ion] to [Fe^{2+} and Fe^{3+} ions] in the various plating baths before and after electrodeposition are shown in Figure 19.5.

The production of Fe^{3+} in the baths before electrodeposition is caused by the oxidization of Fe^{2+} by oxygen dissolved in the baths. The concentration ratio in the conventional single bath increased dramatically after electrodeposition (see Fig. 19.4*a*), because Fe^{2+} could be electrooxidized to Fe^{3+} at the anode during electrodeposition [33]. Thus, it was suggested that Fe^{3+} was produced by the anodic reaction. Moreover, the solubility product constant K_{sp} of $Fe(OH)_3$ had the very low value of 3.16×10^{-38} [34]; therefore, Fe^{3+} must have formed $Fe(OH)_3$ at the anode surface during electrodeposition because the pH near the anode surface during electrodeposition decreased from 3.5 to a little more than 2.3. Thus, $Fe(OH)_3$ was assumed to be present in the outer shell of the deposit, and it was suggested that the adsorbed $Fe(OH)_3$ was included in the film and this inclusion caused the decrease in the B_s value.

Confirmation of the production of Fe^{3+} is important for understanding the electrodeposition of Fe and Fe alloy films. In the bath containing over 0.5% of Fe^{3+}, $Fe(OH)_3$ could form at a pH greater than 2.5; therefore, the bath should be operated at a pH lower than 2.5. On the other hand, a pH lower than 2.3 is unsuitable; since the current efficiency for the alloy deposition is too low to form good films, a brittle film was fabricated as the result of a parallel cathode reaction of H_2 evolution. Therefore, a pH value of exactly 2.3 was required.

On the basis of the results obtained with the conventional bath, attempts were made to suppress the oxidation of Fe^{2+} in the plating bath. First, a $Co_{35}Fe_{65}$ film was electrodeposited from a bath containing trimethylamineborane (TMAB),

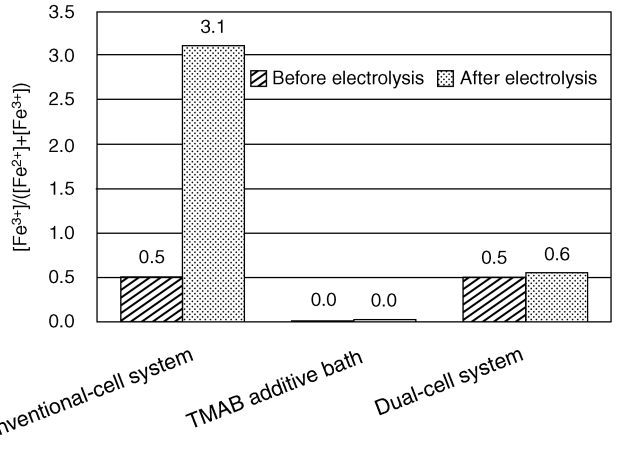

FIGURE 19.5 Concentration ratio of $[Fe^{3+}]/([Fe^{2+}] + [Fe^{3+}])$ in various baths used for electrodeposition of high-moment Co–Fe thin films.

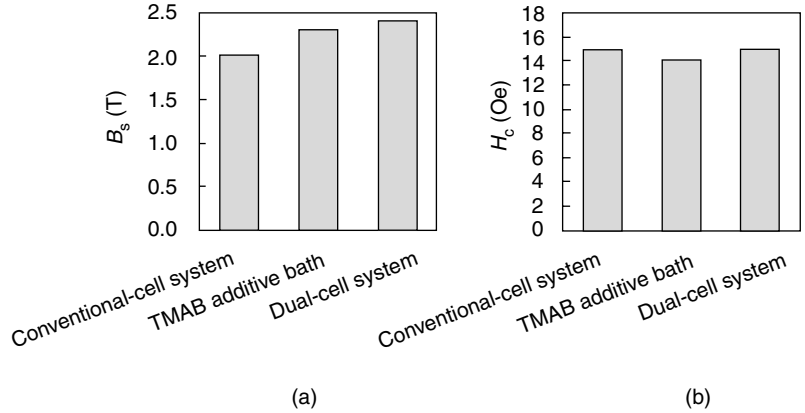

FIGURE 19.6 Values of Co–Fe thin films deposited from various plating baths: (a) B_s values; (b) H_c values.

which inhibited the Fe^{2+} oxidation at pH 2.3. From Figure 19.6, it is seen that the addition of TMAB completely suppressed the production of Fe^{3+} in the bath before and after electrodeposition. As shown in Figure 19.6*a*, the $Co_{35}Fe_{65}$ thin film deposited from the TMAB bath exhibited a B_s value of 2.3 T, which was higher than that of the film deposited from the conventional bath. It was suggested that $Fe(OH)_3$ inclusion was suppressed with the decrease in Fe^{3+} concentration. However, the B_s value of this film was still lower than 2.4 T. This result was attributed to the presence about 0.3 at % of boron in the film [35]. In addition, the H_c value could be decreased to a value around 10 Oe by annealing in a vacuum at an appropriate temperature (350–400°C).

Second, an improved electrodeposition cell system was investigated for suppressing the oxidization of Fe^{2+}. A separated compartment dual-cell system was used, as shown in the schematic of Figure 19.4*b*, in which the anode and cathode cells were physically separated from each other but electrochemically connected by a salt bridge.

Figure 19.7 shows the relation between the Fe content and the B_s value of Co–Fe thin films electrodeposited using the conventional cell system and the dual-cell system. In the case of the dual-cell system, the B_s value of the film increased gradually with the increase in Fe content of up to around 65 at %, and it decreased gradually with an increase over 65 at %. These values were as same as those reported for bulk alloys [14]. In the case of the conventional cell system, the value of the films with Fe content of over 10 at % was lower than that of the film deposited using the dual-cell system. In addition, the films with 30–80 at % did not show a value of over 2.1 T. It has been reported that the inclusion of Fe(OH) decreases the B_s value of electrodeposited Co–Fe films and that a B_s value as high as that of bulk alloys can be obtained using the dual-cell system, because formation of the Fe ion is suppressed by a side reaction at the anode [36]. Therefore, suppressing the formation of the Fe ion is important for preparing electrodeposited thin films with a high-B_s Co–Fe alloy. In short, Co–Fe thin films with a B_s value as high as that of bulk alloys can be fabricated using the dual-cell system.

In addition, to decrease the H_c of the electrodeposited Co–Fe thin films, we annealed the film at various temperatures in a vacuum. Figure 19.8 shows the effect of annealing temperature on the H_c value of electrodeposited Co–Fe thin films. A decrease in H_c value to less than 10 Oe was achieved at 350–400°C, while, as is well known, the B_s value remained constant at about 2.4 T. Thus, we succeeded in preparing electrodeposited Co–Fe soft magnetic thin films with B_s as high as 2.4 T and H_c as low as 8 Oe.

To clarify the reason for these changes in the H_c value, we observed the crystalline structure of the films with different Fe content. Figure 19.9 shows X-ray diffraction (XRD) patterns of the electrodeposited Co–Fe thin films before and after annealing at a temperature of 400°C. For all of the films

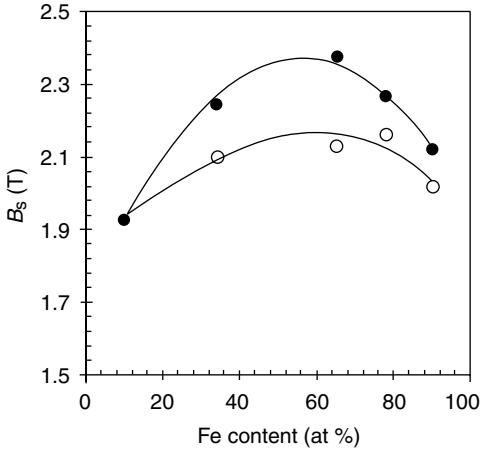

FIGURE 19.7 Saturation magnetic flux density of electrodeposited Co–Fe thin films as a function of Fe content. Solid circles: Co–Fe films deposited using dual-cell system; open circles: Co–Fe films deposited using conventional cell. Curves are not theoretical; they indicate the results of two-dimensional, least mean square approximation from experimental data.

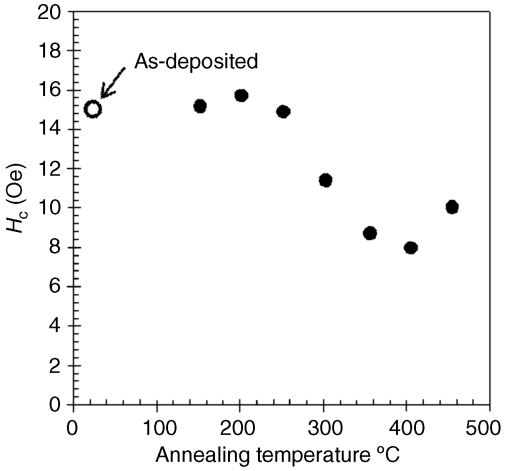

FIGURE 19.8 Change in H_c value of electrodeposited high moment Co–Fe thin films as function of annealing temperature. Films were annealed for 1 h in a vacuum with 500 Oe magnetic field applied.

before and after annealing, the peak at 2θ between 44.5° and 45.25° can be assigned to bcc (110). The intensity of the films increased after annealing, and the intensity peaks sharpened. Moreover, the peak angle decreased. It was suggested that the lattice constant was increased by annealing. The lattice constant of the film after annealing approached the reported value of the quenched alloys [37] and the value calculated by using a reported equation [38]. It has been suggested that a decrease in the H_c value of the films with annealing is caused by the relaxation of lattice distortion [39]. Also, the sharper peak after annealing indicates that the grain size of the films may be increased by annealing. In fact, increasing grain size usually means an increase in the H_c value [40]. However, it is reported that Co–Fe film has a large grain size and that the value of this film mainly depends on lattice distortion [41]. Therefore, indications are that

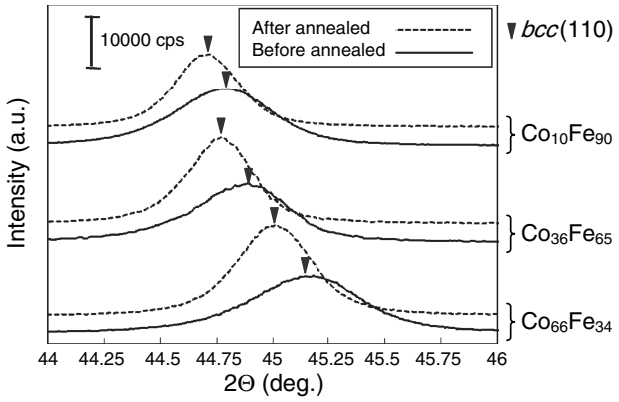

FIGURE 19.9 X-ray diffraction patterns of electrodeposited Co–Fe thin films before and after annealing at 400°C.

the relaxation of lattice distortion is more effective for decreasing the H_c value of Co–Fe films with 50–65 at % Fe. In the case of Co–Fe film, annealing was not effective for decreasing the H_c value. As a result, it is suggested that the H_c value of Co–Fe film does not mainly depend on lattice distortion, because Co–Fe film has a low B_s value. So, it is indicated that a high H_c value is the result of large crystalline magnetic anisotropy [42].

19.3 PREPARATION OF HIGH-MAGNETIC-FLUX-DENSITY CoNiFeB FILM BY ELECTROLESS DEPOSITION

19.3.1 Introduction

A soft magnetic thin film with a high B_s value is a critical material to achieve high recording density in magnetic recording devices. For magnetic heads, a soft magnetic thin film with both a high B_s and a low H_c is required. By using sputtering, several researchers have developed soft magnetic thin films with a high B_s value, such as CoFeB [21], CoNiFe [23, 27, 43–46], and Fe-based nanocrystalline alloy systems, for example, FeNAlO [47] or FeCoN [29]. The electrodeposited soft magnetic CoNiFe thin film with a high B_s value of 2.0–2.1 T [25, 48] shows superior overwrite performance [49, 50]. In regard to producing microsized head cores, electroless deposition has advantages over the conventional electrodeposition method. Specifically, electroless deposition has a high potential to form a uniform film selectively on complicated shapes and isolated parts and also to form a thick film on a large surface.

A high B_s value, which depends on the composition of the film, is the most important property of head core materials. CoNiFeB ternary alloys with a range of 50–70 wt % Fe and a low content of Ni exhibit a high B_s value at room temperature. However, it is difficult for electroless deposition to co-deposit a large amount of Fe, because the Fe itself cannot act as a catalyst to bring about the reductive reaction of a reducing agent such as dimethylamino borane (DMAB). In our previous work, a film with a high B_s value was successfully deposited by increasing the $FeSO_4$ concentration in the plating solution. However, a high concentration of Fe ions leads to the destabilization of the solution [51]. In the following section we introduce a new development: an electroless deposition process that yields a magnetic thin film with both high B_s and low H_c values.

19.3.2 Enhancement of Magnetic Properties

Concentration of Fe Source Table 19.1 summarizes the electroless solution composition and plating conditions of our film preparation. The metal composition in the film can be controlled by changing the concentration ratio of the three

TABLE 19.1 Electroless Solution Composition

Chemicals	Composition ($mol\,dm^{-3}$)
DMAB,$(CH_3)_2HNBH_3$	0.15
$C_3H_4(OH)(COONa)_3$	0.015–0.05
$C_2H_2(OH)(COONa)_2$	0.15–0.35
$(NH_4)SO_4$	0.20
H_3PO_3	0.06
$FeSO_4 \cdot 7H_2O$	0.01–0.06
$NiSO_4 \cdot 6H_2O$	0.004
$CoSO_4 \cdot 7H_2O$	0.036

Note: Plating conditions were bath pH 9.0 and bath temperature of 70°C.

metal ions, Co, Ni, and Fe. An increase in Fe content in the film improves the B_s value. In our work, the Fe content of the film gradually increased with increased $FeSO_4$ concentration, reaching a maximum of 46 at % at $0.06\,mol\,dm^{-3}$. On the other hand, the Co content gradually decreased with increased $FeSO_4$ concentration. The Ni content was almost constant under all conditions. Furthermore, the deposition rate gradually decreased with increased $FeSO_4$ concentration. In this solution, the concentrations of citric acid and tartaric acid were adjusted to 0.023 and $0.35\,mol\,dm^{-3}$, respectively.

The film $Co_{38}Ni_{15}Fe_{46}B_1$ with the highest B_s value (2.0 T) was obtained from a solution containing $0.06\,mol\,dm^{-3}$ $FeSO_4$. In addition, the H_c value increased drastically with increased $FeSO_4$ concentration—in fact, the H_c value of the $Co_{38}Ni_{15}Fe_{46}B_1$ films was higher than 20 Oe.

It is known that, at high $FeSO_4$ concentrations, a hydroxide oligomer forms in the solution. The formation of this hydroxide oligomer probably has an adverse effect on both the magnetic properties and the stability of the electroless solution. In solutions containing Fe ions, it is likely that the rate of complex formation between the Fe ions and the complexing agents is very slow. The Fe^{2+} ions in high-pH solution are easily oxidized to Fe^{3+}, forming a hexa-aquo ferrate ($[Fe(H_2O)_6]^{3+}$) complex. This hexa-aquo ferrate complex reacts competitively with the complexing agent and H_2O according to Eq. (19.1) and (19.2), respectively:

$$[Fe(H_2O)_6]^{3+} + L \leftrightarrow [Fe(H_2O)_{6-n}L]^{3+} + nH_2O \quad (19.1)$$

$$[Fe(H_2O)_6]^{3+} + H_2O \leftrightarrow H_3O^+ + [Fe(OH)(H_2O)_5]^{2+} \quad (19.2)$$

where L is a ligand and n is the coordination number.

The hexa-aquo ferrate ($[Fe(OH)(H_2O)_5]^{2+}$) complex subsequently transforms into hydroxide polymers. It is suggested that the two kinds of reactions shown below form the hydroxide polymers:

$$2[Fe(OH)(H_2O)_5]^{2+} \leftrightarrow [(H_2O)_5Fe(-OH)Fe(H_2O)_5]^{5+} + OH^- \quad (19.3)$$

$$2[Fe(OH)(H_2O)_5]^{2+} \leftrightarrow [(H_2O)_4Fe(-OH)_2Fe(H_2O)_4]^{4+} + 2H_2O \quad (19.4)$$

In a solution with a high concentration of OH^-, two reactions simultaneously occur: one by which the coordinated water is replaced by OH^- [see Eq. (19.5)] and the other by which the polynuclear complexes are formed [see Eq. (19.6)]. The terminal form of the polynuclear complex results in precipitation:

$$[Fe(OH)_n(H_2O)_{6-n}]^{(3-n)+} + nOH^- \leftrightarrow [Fe(OH)_{n+1}(H_2O)_{5-n}]^{(2-n)+} + nH_2O \quad \text{at } n < 1 \quad (19.5)$$

$$[(H_2O)_4Fe(-OH)_2Fe(H_2O)_4]^{4+} + OH^- \leftrightarrow [(H_2O)_4Fe(-OH)_2Fe(OH)(H_2O)_3]^{3+} + H_2O \leftrightarrow [(H_2O)_4Fe(-OH)_3Fe(H_2O)_3]^{3+} + H_2O \quad (19.6)$$

The directions in which these reactions proceed are controlled by the OH^- concentration of the solution. According to the thermodynamic equilibrium, pK_1 and pK_2 of Fe^{3+} are 2.5 and 3.3, respectively. Therefore, the hydroxide formation can be suppressed by keeping the pH value lower than 2.5. On the other hand, the complex formation is also suppressed at a low pH because both tartaric acid and citric acid have a pK_a of about 2.9. Therefore, since rapid change of the pH value from 2.5 to 2.9 causes the reaction of Equation (19.2) to occur exponentially, both slow pH adjustment and retention time are required.

Concentration of Complex Agents Effects of the concentration of citric acid and tartaric acid on film properties are as follows. The H_c value decreases with a decreased concentration of citric acid; it goes down to 11 Oe at a citric acid concentration of $0.015\,mol\,dm^{-3}$, where the concentrations of tartaric acid and $FeSO_4$ were 0.35 and $0.06\,mol\,dm^{-3}$, respectively. When the concentration of citric acid was lower than $0.01\,mol\,dm^{-3}$, the solution became unstable, and the H_c value of the deposit drastically increased. The concentrations of tartaric acid were varied between 0.15 and $0.35\,mol\,dm^{-3}$, while the concentrations of citric acid ($0.015\,mol\,dm^{-3}$) and $FeSO_4$ ($0.06\,mol\,dm^{-3}$) were kept constant. The solution became unstable when the concentration of tartaric acid was less than $0.15\,mol\,dm^{-3}$. On the other hand, it was difficult to dissolve

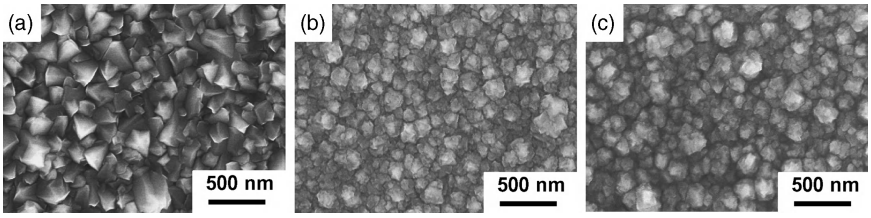

FIGURE 19.10 SEM images showing surface morphologies of CoNiFeB films obtained from solutions containing various amounts of tartaric acid; (*a*) 0.35 mol dm^{-3}; (*b*) 0.25 mol dm^{-3}; (*c*) 0.15 mol dm^{-3}. All three solutions contained 0.015 mol dm^{-3} of citric acid and 0.06 mol dm^{-3} of $FeSO_4$.

the reagents when the concentration of tartaric acid exceeded 0.35 mol dm^{-3}. The deposition rate slightly increased with a decreased concentration of tartaric acid. It was seen that the Fe content of the deposit decreased with a decreasing concentration of tartaric acid in the solution, and the Fe content went down to 33 at % at a tartaric acid concentration of 0.15 mol dm^{-3}. In contrast, the Ni content increased with a decreased concentration of tartaric acid. This phenomenon was probably caused by the difference in the stability constant between the cobalt–tartaric acid complex and the nickel–tartaric acid complex. The H_c value decreased with a decreasing concentration of tartaric acid, and it reached 6 Oe at a tartaric acid concentration of 0.15 mol dm^{-3}. In addition, the B_s value slightly decreased to 1.8 T with a decreasing concentration of tartaric acid. This slight decrease in the B_s value occurred because of the decreased Fe content of the deposit.

Figure 19.10 presents SEM images that show the surface morphologies of the CoNiFeB films obtained in the presence of 0.35, 0.25, and 0.15 mol dm^{-3} of tartaric acid. It is clear from the images that the surface morphology significantly changed with the change in tartaric acid concentration.

19.3.3 Summary

A CoNiFeB soft magnetic thin film with a high B_s prepared by electroless deposition was developed as a material for the core of a magnetic recording head. The B_s was increased to 2.0 T by increasing the concentration of $FeSO_4$. It was confirmed that controlling the pH during preparation of the plating solution was effective for stabilizing the solution. Furthermore, the magnetic properties of the CoNiFeB film were significantly influenced by the tartaric acid concentration in the plating solution. The H_c value of the CoNiFeB film with a high B_s decreased with a decreased concentration of tartaric acid in the solution, and it reached a low H_c value of 6 Oe. Moreover, adding an excessive amount of complex agent stabilized the solution for electroless deposition. An optimized concentration of complex agent improved both the magnetic properties of the films and the stability of the solution.

19.4 PREPARATION OF MAGNETIC SEED LAYER OF Pd NANOCLUSTER BY DISPLACEMENT PLATING

19.4.1 Formation of Pd Seeds from $PdCl_2$ Solution

Cobalt–palladium multilayered film [52–65] is a potential material for a perpendicular magnetic recording layer since it has a perpendicular squareness ratio of unity because of its high perpendicular magnetic anisotropy [53]. The suppression of intergranular exchange coupling is significant for improving the read–write (R/W) characteristics of a Co/Pd multilayered medium with a soft magnetic underlayer (SUL). It has been reported that ultrathin Pd-based seed layers such as Pd–SiN [66], PtB/Pd/MgO [67], and Pd/Si [64] conventionally deposited on SULs using a sputtering method have successfully reduced the intergranular exchange coupling of Co/Pd multilayered films. Figure 19.11 shows cross-sectional TEM images of various films. Various aspects of these films, which are labeled Media I, II, III, and IV, are shown in Table 19.2, and Figure 19.12 is a schematic representation of Co/Pd multilayer, double-layered medium with a Pd/Si dual seed layer prepared in different ways.

Nitrogen gas is useful for decreasing the Pd grain size of $[Co(0.2\,nm)/Pd(0.8\,nm)]_{20}$ film. Diffusion of Si into the Co/Pd upper seed layer can be observed in Figure 19.11. In the images of media III and IV, the region between the two white bands clearly separates the $[Co/Pd]_n$ film and Co/Pd upper seed layer. This region is considered to represent amorphous Si compounds that diffuse because of postannealing through the Pd upper seed layer.

In addition, we also focused on the fabrication of metallic seeds on the SUL using an electrochemical displacement plating. We deposited Pd metal seeds on a CoZrNb SUL surface by utilizing an electrochemical that resulted from the difference in redox potential among Co, Zr, Nb, and Pd [68]. By using this process, semispherical Pd clusters with a diameter of less than 10 nm were densely formed only by immersing the SUL into the $PdCl_2$ solution, and the Co/Pd multilayered film sputter deposited on the SUL exhibited fine magnetic clusters [69].

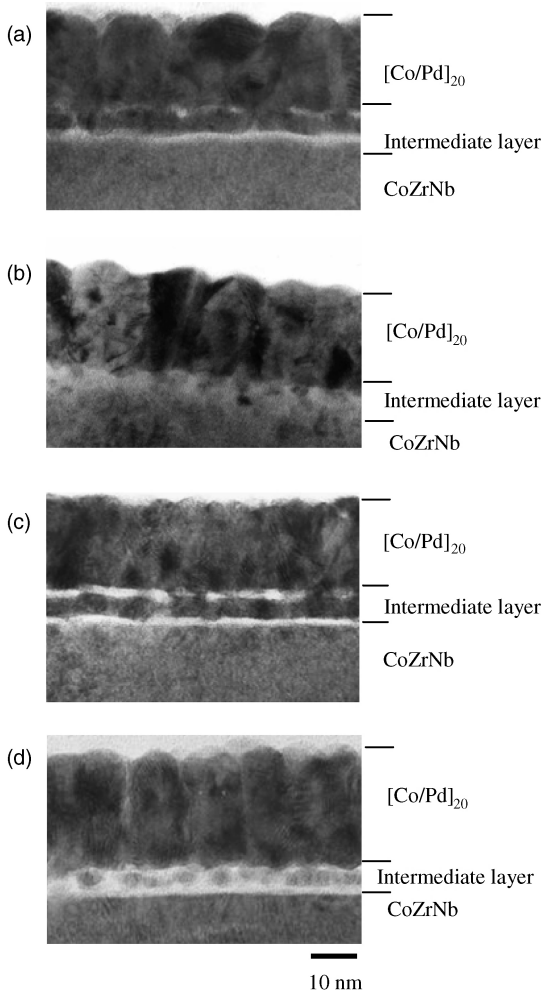

FIGURE 19.11 Cross-sectional TEM images of various media: (*a*) medium I;. (*b*) medium II; (*c*) medium III; (*d*) medium IV. Acceleration voltage for micrographs (*a*)–(*c*) was 300 kV and that for micrograph (*d*) was 200 kV.

Figure 19.13 shows high-resolution SEM images of two CoZrNb SUL surfaces, one treated with the $PdCl_2$ solution and one not treated. A $Co_{91}Zr_5Nb_4$ (300-nm-thick) SUL was sputter deposited on a glass substrate. After being cleaned with 1 mol dm^{-3} H_2SO_4 solution and rinsed with ultrapure water, the SUL was immersed into a 0.1 g dm^{-3} $PdCl_2$ solution for 40s. Then, a $[Co(0.2\,nm)/Pd(0.8\,nm)]_{20}$ film was deposited on the treated SUL using a direct-current (dc) magnetron sputtering method. A semispherical deposit with an average diameter of ~ 9 nm was formed on the CoZrNb SUL; the deposit had a high density, in which the average distance between adjacent clusters was ~ 18 nm, as shown in Figure 19.13*a*. From X-ray photoelectron spectroscopy (XPS) and XRD analyses, the semispherical deposits were identified as the metal Pd with an fcc structure [69], which hereafter will be called "Pd cluster seeds."

Figure 19.14 shows MFM images at alternating-current (ac)–demagnetized states of $[Co(0.2\,nm)/Pd(0.8\,nm)]_{20}$ film with different intermediate layers.

The mazelike patterns with large magnetic clusters were observed for medium II of the sputter-deposited Pd medium, while smaller magnetic clusters with a diameter of $\sim$100 nm were observed for medium I, the electrochemically deposited Pd medium. These results confirmed that the Pd cluster seeds formed by an electrochemical method were quite effective in suppressing the magnetic intergranular exchange coupling, which in turn reduced both the α value, defined as $4\pi[dM/dH]$ at $H = H_c$, and the magnetic cluster size of the Co/Pd multilayered film. Furthermore, the increment of H_c in medium I was considered to result from the change in magnetization reversal mode from magnetic domain wall displacement to magnetization rotation, which was caused by the reduction of intergranular exchange coupling.

Figure 19.15 shows the dependence of normalized medium noise (N/S_0) on linear recording density, where S_0 represents the reproduced voltage at the recording density of 2 kFCI.

TABLE 19.2 Film Composition, Preparation Condition, and Magnetic Properties for Sputter-Deposited $[Co/Pd]_n$ Media

Parameter	Medium I	Medium II	Medium III	Medium IV
Film composition				
Thickness of $[Co(0.2\,nm)/Pd(0.8\,nm)]_{20}$, t (nm)	20	20	20	20
Magnetic cluster size, d (nm)	235	145	174	128
Preparation condition				
N_2 partial pressure in Pd sputtering deposition, ρ (mTorr)	0	5	0	5
Temperature in postannealing, T (°C)	—	—	400	400
Magnetic properties				
Perpendicular coercivity, H_c (kOe)	2.9	4.7	3.6	5.7
Magnetic anisotropy filed, H_k (kOe)	28	20	25	20
H_c/H_k	0.10	0.24	0.14	0.29
Saturation magnetization, M_s (emu · cm^{-3})	340	320	360	330
M–H slope parameter, α $(=4\pi[dM/dH]_{H=H_c})$	11.0	6.2	10.0	1.9

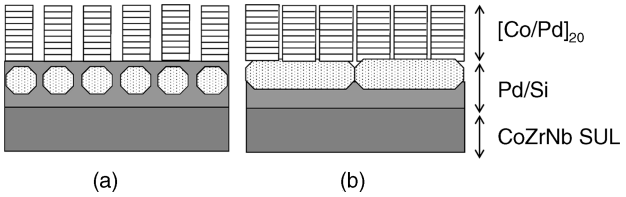

FIGURE 19.12 Schematic representation of Co/Pd multilayer, double-layered medium with Pd/Si dual seed layer prepared in different ways: (*a*) with the addition of N_2 gas and postannealing; (*b*) without the addition of N_2 gas and postannealing. Representations are based on the cross-sectional TEM images shown in Figure 19.11.

As can be seen in the figure, medium I, with the electrochemically deposited Pd cluster seeds, exhibited low N/S_0 values compared with medium II, with the sputter-deposited Pd seed layer.

Moreover, the increasing ratio of N/S_0 values of medium I with an increase in recording density was smaller than that of medium II, which suggested that the transition noise caused by the fluctuation of boundaries between recorded bits were suppressed by applying the Pd cluster seeds to the Co/Pd multilayered media.

Figure 19.16 shows cross-sectional TEM bright images of media I and II. The Co/Pd multilayered film in the electrochemically deposited medium I (Fig. 19.16*a*) evidently possessed a band structure compared with that in the sputter-deposited medium II (Fig. 19.16*b*). The total thickness of the Co/Pd multilayer and Pd layer was ∼30 nm in medium II, which is consistent with the film composition described above. On the other hand, the total thickness of the Co/Pd multilayer and Pd cluster seeds was ∼27 nm in medium I. Based on this result, we estimated the height of the Pd cluster seeds to be ∼7 nm, which is compatible with the average diameter of the Pd clusters shown in Figure 19.13*a*. In Figure 19.16*a*, an amorphous region was observed in the uppermost layer of CoZrNb; it is likely that this region represents the oxidization layer of the CoZrNb film. However, the origin of oxidization layer has not been revealed.

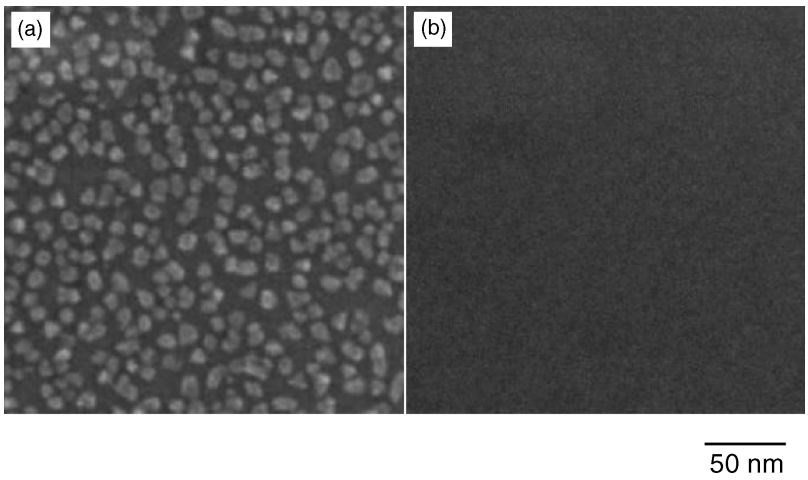

FIGURE 19.13 High-resolution SEM images of different CoZrNb SUL surfaces:(*a*) surface treated with $PdCl_2$ solution; (*b*) surface not treated.

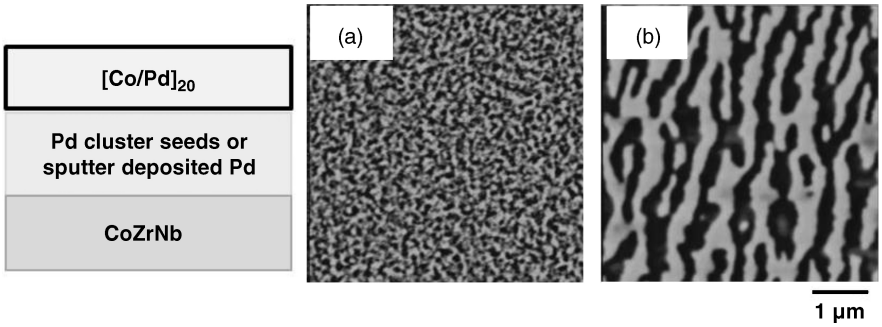

FIGURE 19.14 MFM images at ac-demagnetized states of $[Co(0.2\,nm)/Pd(0.8\,nm)]_{20}$ film with different intermediate layers: (*a*) layer of electrochemically deposited Pd of medium I; (*b*) layer of sputter-deposited Pd of medium-II.

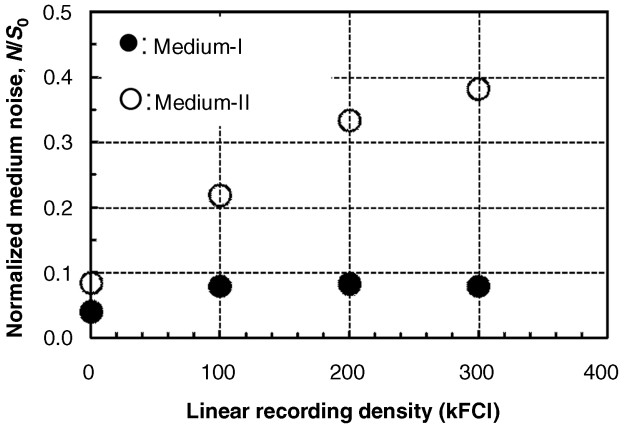

FIGURE 19.15 Dependence of normalized medium noise N/S_0 on linear recording density (S_0 is the reproduced voltage at a recording density of 2 kFCI). Solid circles: medium I; open circles: medium II.

Figure 19.17 shows plane-view TEM bright-field images of media I and II, while Figure 19.18 shows the electron diffraction patterns corresponding to these images.

Clear grain boundaries were observed in medium I (Fig. 19.17*a*), revealing Co/Pd grains with an average diameter of 15.8 nm, whereas grain boundaries were hardly seen in medium II (Fig. 19.17*b*). As can be seen in Figure 19.18, electron diffraction rings attributable to fcc-Co/Pd {111}, {200}, {220}, and {311} planes were observed for medium II. Among these rings, that of fcc {220} was found to be the strongest. Some planes equivalent to fcc {2 0 0}, such as (2 −2 0) and (−2 2 0), are vertical to the fcc (111). This result indicates that fcc Co/Pd (111) for medium II preferably orients in the direction perpendicular to the film surface. On the contrary, the diffraction ring of fcc {220} was not seen in medium I, which confirmed that the orientation of fcc Co/Pd ⟨111⟩ was widely distributed in medium I. Maesaka et al. reported that perpendicular anisotropy was attained more effectively by preparing the Co/Pd multilayer with fcc ⟨111⟩ orientation perpendicular to the film surface rather than that with fcc ⟨100⟩ or fcc ⟨110⟩ orientation [70]. Therefore, it seems that the distribution of fcc ⟨111⟩ orientation, which resulted from the application of the Pd cluster seeds, decreased the perpendicular magnetic anisotropy of medium I.

As shown in Figure 19.17, high-resolution SEM images showed that the surface roughness of CoZrNb SUL was increased by the formation of semispherical Pd seed clusters on it and the value of arithmetic average roughness (R_a) of medium I was 1.3 nm, which was larger than that of medium II (0.78 nm). This difference in the surface roughness is also seen in the plane-view TEM bright-field image shown in Figure 19.17. It is suggested that the surface morphology of

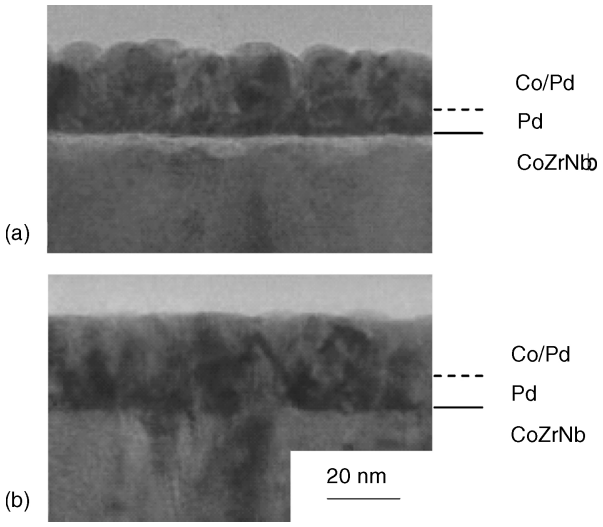

FIGURE 19.16 Cross-sectional TEM bright-field images of media I and II with different Pd layers: (*a*) Electrochemically deposited Pd of medium I; (*b*) sputter-deposited Pd of medium II.

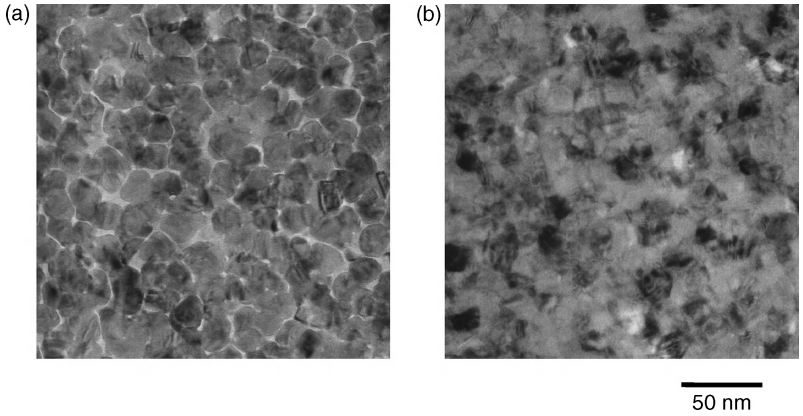

FIGURE 19.17 Plane-view TEM bright-field images of (*a*) medium I and (*b*) medium II.

the SUL affected the crystalline orientation of the film. Therefore, to improve the preferred orientation of the Co/Pd multilayer, the surface roughness of the treated SUL should be decreased by modifying the conditions of the electrochemical treatment.

19.4.2 Formation of Pd Seeds from $SnCl_2$ Solution

We made two attempts to suppress the increase in the surface roughness of SULs: (1) increasing the $PdCl_2$ concentration (process A) and (2) applying a $SnCl_2$ pretreatment [71] (process B). A CoNiFeB film electroless deposited onto a Si (100) disk substrate [72] was used as the SUL of the $[Co/Pd]_n$ medium. Based on a measurement of open-circuit potential [73], the potential of the CoNiFeB film in the $PdCl_2$ solution was more negative than that of CoZrNb film, indicating that the CoNiFeB film was more likely to be dissolved into the solution. Excessive dissolving seemed to make the CoNiFeB film surface rough ($R_a = 1.5$ nm) [74].

In process A, it was expected that the high $PdCl_2$ concentration promoted the Pd nucleation process, and thereby the treatment duration for forming a sufficient amount of Pd seeds decreased. As a result, the high $PdCl_2$ concentration suppressed the dissolution of the CoNiFeB film. On the other hand, in process B, the Sn^{2+} ions are likely to be adsorbed into the CoNiFeB film surface and release their electrons during immersion into the $PdCl_2$ solution [73], according to

$$Sn^{2+} + Pd^{2+} \leftrightarrow Sn^{4+} + Pd \tag{19.7}$$

In process A, electrons for the Pd deposition were provided only by the electrochemical dissolution of the CoNiFeB film. On the contrary, in process B, the adsorbed Sn^{2+} ions also worked as a reducing agent for the Pd deposition. Thus, it was expected that the excessive dissolution of CoNiFeB film would be suppressed by using process B. Figure 19.19 shows high-resolution SEM images of the CoNiFeB SUL surfaces treated with processes A and B.

In Figure 19.19*a*, the fine Pd deposits are clearly seen, owing to the enhancement of the nucleation of the Pd seeds by the high $PdCl_2$ concentration. However, some Pd deposits aggregated to form large clusters. As can be seen in Figure 19.19*b*, this aggregation was successfully prevented by using the $SnCl_2$ pretreatment in process B, where fine and well-distributed Pd seeds as small as 5 nm were formed. The effect of $SnCl_2$ pretreatment on the morphology of Pd deposits is described in detail elsewhere [71, 75]. It already has been reported that decreasing the size of Pd seeds reduces

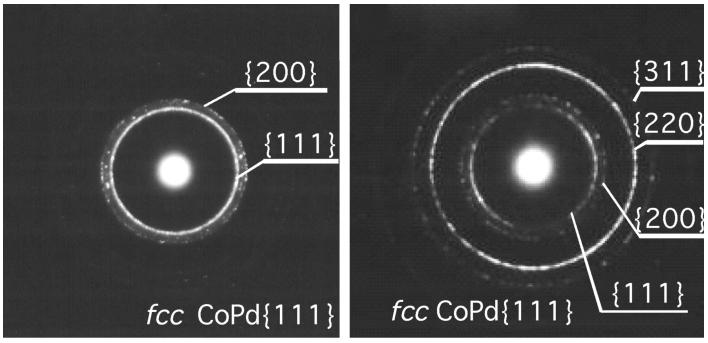

FIGURE 19.18 Electron diffraction rings corresponding to images in Figure 10.17: (*a*) medium I; (*b*) medium II.

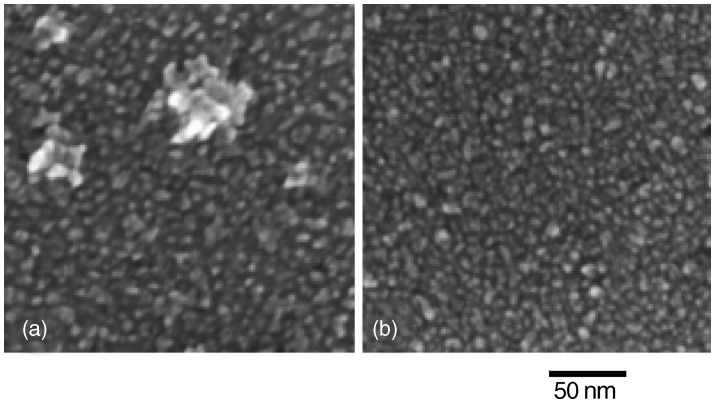

FIGURE 19.19 High-resolution SEM images of Pd seed clusters formed on CoNiFeB SULs prepared by different processes: (*a*) by process A; (*b*) by process B.

the average $[Co/Pd]_n$ grain diameter [71] so a similar effect was expected in this study. Figure 19.20 shows a Kerr hysteresis loop and an MFM image for the $[Co/Pd]_{20}$ film deposited by using sputter on the Pd seeds formed with Process-B. In Figure 19.20*a*, the film showed a high H_c of 7.8 kOe. From the Kerr hysteresis loop, the loop slope parameter α was obtained using the equation

$$\alpha = 4\pi\left(\frac{dM}{dH}\right)_{H=H_c} = 4\pi\left(\frac{d\theta_k}{dH}\right)_{H=H_c} \times \left(\frac{M_s}{\theta_{k,\max}}\right) \quad (19.8)$$

where θ_k and $\theta_{k,max}$ are the Kerr rotation angle and its maximum values, respectively. The saturation magnetization M_s was assumed to be the same as that of $[Co/Pd]_n$ film without SUL.

Furthermore, magnetic domain size was 69 nm (Fig. 19.20*b*), which is as small as that of the $[Co/Pd]_n$ medium with a sputter-deposited seed layer reported by another research group [51].

The R_a value of the $[Co/Pd]_{20}$ film prepared with a hybrid process of $PdCl_2$ and $SnCl_2$ treatment was ~ 0.8 nm, almost half the size of that prepared with the $PdCl_2$ treatment alone. It is likely that this was the result of the suppression of the excessive dissolution of CoNiFeB film by Sn^{2+} ions and the decrease in the size of Pd seeds, as shown in Figure 19.19*b*. These results indicated that a relatively smooth CoNiFeB film surface with fine Pd seeds was obtained by adjusting the electrochemical treatment conditions and the obtained Pd seeds worked as an effective intermediate layer for the $[Co/Pd]_n$ recording medium exhibiting small magnetic domains. The R_a value of $[Co/Pd]_{20}$ film is still larger than that of the untreated CoNiFeB SUL ($R_a < 0.5$ nm); this value would be further decreased by optimizing the treatment conditions.

19.5 CHEMICAL SYNTHESIS OF FePt NANOPARTICLES FOR HIGH-DENSITY MAGNETIC RECORDING MEDIA

19.5.1 Chemical Synthesis of Magnetic Nanoparticles

FePt alloy particles with the $L1_0$ structure have a very high uniaxial magnetic anisotropy. As a result, superparamagnetic

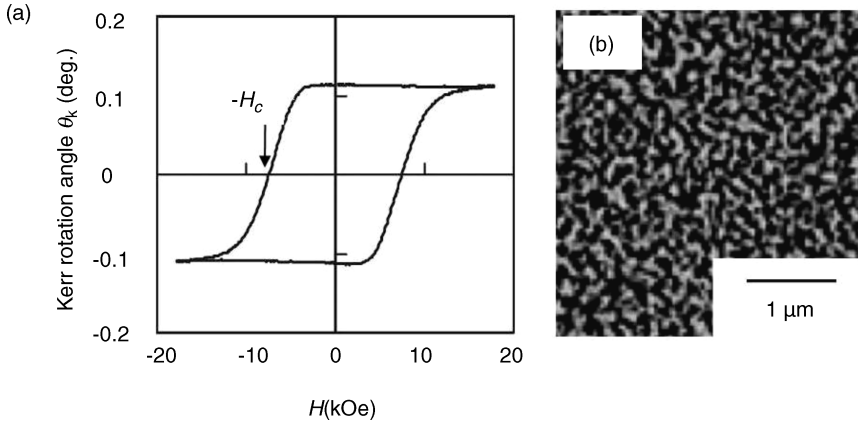

FIGURE 19.20 Different representations of $[Co/Pd]_{20}$ film deposited by using sputter on the Pd seeds formed with process B: (*a*) Kerr hysteresis loop; (*b*) MFM image at ac-demagnetized state.

fluctuation of room temperature magnetization can be suppressed even for particles 2.7–3.0 nm in diameter, making an appropriate array of these nanoparticles a promising candidate for a future ultrahigh density magnetic recording medium of >10 Tbits $\cdot$ in^{-2} [76–79]. Since the preparation of FePt nanoparticles by Sun et al. [80–82], many researchers have paid attention to such nanoparticles [83–97].

19.5.2 Effect of Growth Temperature on Shape and Crystallinity of Chemically Produced FePt Nanoparticles

First, we aimed at chemically producing $L1_0$–FePt nanoparticles with a controlled shape, grain size, and composition. To control these parameters, we focused our attention on the crystal growth temperature, the temperature at which the atomic diffusion between the Pt-rich and Fe-rich phases leads to the formation of uniform $L1_0$–FePt nanoparticles, and we evaluated the effect of the growth temperature on the magnetic properties obtained after annealing.

Iron–platinum nanoparticles were chemically produced by mixing oleic acid and $Fe(CO)_5$ with a benzyl ether/1-octadecene solution of $Pt(acac)_2$ and heating the mixture to the "mixing temperature" of 120°C for about 5 min before oleylamine was added. Platinum-rich nuclei were formed from the reduction of $Pt(acac)_2$ that took place simultaneously with a partial decomposition of $Fe(CO)_5$ at temperatures lower than 185°C. This process allowed the existing Pt-rich nuclei to be coated with additional Fe atoms, thus forming larger clusters at a higher temperature. Heating the clusters by refluxing at the growth temperature led to atomic diffusion and the formation of fcc-structured FePt nanoparticles. In the presence of an excess of $Fe(CO)_5$, the extra Fe atoms continued to coat the fcc nanoparticles, leading to the core/shell structure of FePt/Fe, while at the same time the top layer was oxidized to form a FePt/Fe oxide. The mixture was heated at a growth temperature between 195 and 275°C for up to 2 h. A black product was precipitated by adding ethanol to the mixture, which was then cooled to room temperature, separated by centrifugation, and redispersed in hexane.

The shape and composition of chemically produced FePt nanoparticles depended on the growth temperature, whereas no such temperature dependence was observed for their size. The FePt nanoparticles obtained at a growth temperature lower than 215°C and higher than 255°C had a spherical shape with an estimated average size diameter of 5.6 ± 0.5 nm, while those obtained at a growth temperature between 215 and 255°C had a cubic shape with an estimated average diameter of 5.5 ± 0.5 nm. In addition, in previous reports [80, 81] it was suggested that treatment at a growth temperature of 215–255°C is suitable for the preparation of cubic nanoparticles. On the other hand, the composition of chemically produced FePt nanoparticles is almost constant at $Fe_{53}Pt_{47}$ irrespective of the growth temperature. Figure 19.21

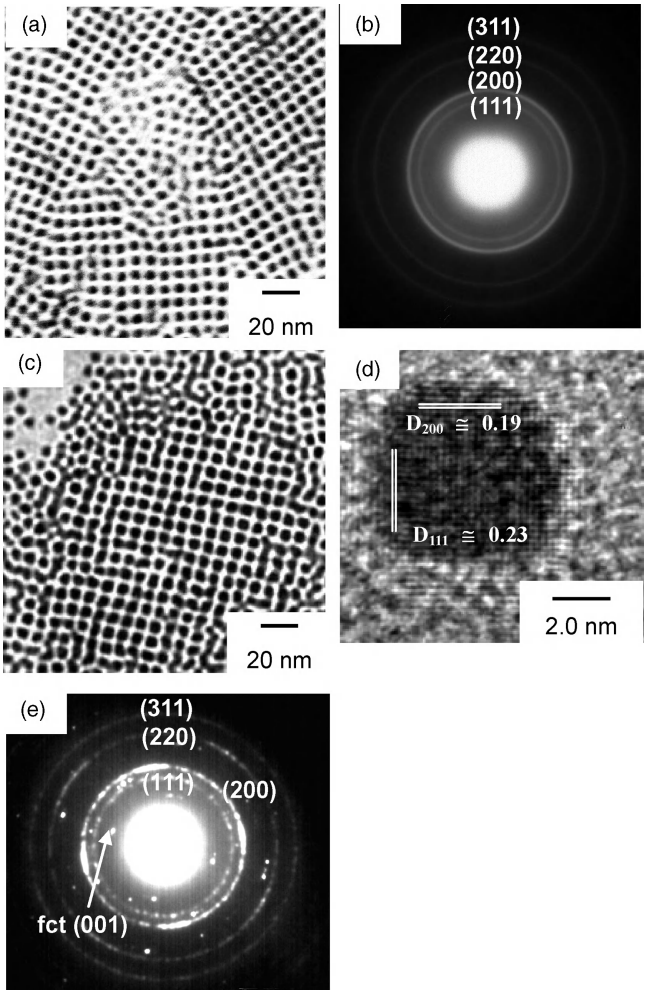

FIGURE 19.21 Various images of FePt nanoparticles chemically produced at different growth temperatures: (*a*) TEM image at 225°C; (*b*) SAED image at 225°C in which (111), (200), (220), and (311) indicate the four rings of the nanoparticle structure; (*c*), (*d*) TEM images at 245°C; (*e*) SAED image at 245°C in which (111), (200), (220), and (311) indicate the four major orientations and fct(001) the four spots of the nanoparticle structure.

presents various images of chemically produced FePt nanoparticles at different growth temperatures. The TEM image in Figure 19.21*a* shows a uniform arrangement of nanoparticles at 225°C. The selected area electron deflection (SAED) image in Figure 19.21*b* shows a ring pattern of nanoparticles at 225°C; the rings indicate that the crystal structure of the nanoparticles is that of the formatted fcc phase. The TEM images in Figures 19.21*c* show a uniform arrangement of nanoparticles at 245°C: Figure 19.21*d* shows a small portion of the image shown in Figure 19.21*c* that has been highly magnified. The suggested shape of the chemically produced nanoparticles at a growth temperature of 245°C was cubic, and the lattice constants of the nanoparticles were found to be

$d_{200} = 0.19$ nm and $d_{111} = 0.23$ nm. Therefore, it is suggested that the crystallinity of the nanoparticles is essentially that of the fcc phase. Finally, the SAED image in Figure 19.21*e* also shows a ring pattern of nanoparticles at 245°C; the image exhibits four bright reflections [all in the (200) ring] linked by a fourfold symmetry, making the diffraction intensity strong for the (200) ring. The image also shows that the (111) ring has no bright reflections, making its diffraction intensity very weak. These results indicate that the arrangement of FePt nanoparticles in Figure 19.21*c* is (100) textured. Based on previous reports [80, 81] it is expected that the (100) textured nanoparticles would exhibit a cubical shape. Additionally, it was confirmed that the fourfold symmetry resulted from face-centered tetragonal (fct)–FePt(0 0 1). Although there is only a small amount of the fct phase contained in the nanoparticles, it can be detected not only in the XRD profile but also in the TEM image, showing that the crystallinity of the nanocubes at a growth temperature of 245°C has not only the fcc phase structure but partially also the fct phase structure. Thus, we succeeded in controlling both the shape and crystallinity of partial $L1_0$–$Fe_{52}Pt_{48}$ cubic nanoparticles with monodispersion.

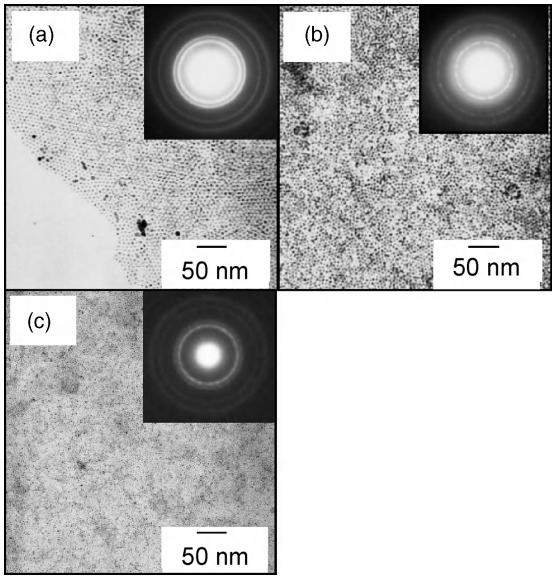

FIGURE 19.22 TEM images with inset SAED images of FePt nanoparticles chemically produced in various solutions: (*a*) in DOE; (*b*) in EMI-BF_4; (*c*) in BMP-TF.

19.5.3 Preparation of FePt Nanoparticles with Narrow Size Distribution in Ionic Liquids

We focused our attention on the use of ionic liquid (IL) not only as a solvent but also as a dispersant for the preparation of FePt nanoparticles. Since the preparation of monodispersed Ir, Ag, Pt, and CoPt nanoparticles in ILs already has been reported [98], IL is considered to be a feasible solvent for preparing a dispersed solution of FePt nanoparticles with a controlled size and size distribution. The technique of producing monodispersed FePt nanoparticles without using centrifugation is expected to simplify the fabrication process and also reduce the loss of materials. In this study we examined the size and composition of FePt nanoparticles prepared using ILs instead of dioctyl ether (DOE).

In the preparation of FePt nanoparticles, 1-ethyl-3-methylimidazilium tetrafluoroborate (EMI-BF_4) or 1-butyl-1-methylpyrrolidinium trifluoromethane-sulfonate (BMP-TF) was used as a solvent. These ILs were synthesized by Toyo Gosei Co.. First, $Pt(acac)_2$ (98.5 mg, 0.25 mmol), 1,2-hexadecanediol (198 mg, 0.75 mmol), and IL (20 mL) or DOE (10 mL) were mixed and stirred in a flask under an Ar gas atmosphere. After the resulting solution was heated to 100°C, $Fe(CO)_5$ (0.07 mL, 0.5 mmol) was added. This mixture was then heated to 190°C and kept at that temperature for 30 min. After particles were produced, the reaction mixture was allowed to cool to room temperature. Finally, the particles produced in the ILs were washed three times with acetone and then collected in hexane. Essentially the same procedure was employed for the preparation of FePt nanoparticles in DOE, except that oleic acid (0.08 mL) and oleylamine (0.08 mL) were added as surfactants, the reaction temperature was set at 230°C, and the ILs were washed once with ethanol and twice with acetone.

The TEM and SAED images were taken of the nanoparticles produced in DOE and ILs, and the images were examined for nanoparticle size and morphology (see Fig. 19.22). The particles produced in both ILs (Figs. 19.22*b*, *c*) were well dispersed, like the particles produced in DOE (Fig. 19.22*a*)) with the addition of oleic acid and oleylamine. The fact that the particles produced in both ILs were well dispersed suggested that there would be a high redispersibility of the nanoparticles in hexane. Because no surfactants were added during the preparation in the ILs, it was suggested that IL serves not only as a solvent but also as a stabilizer. The four rings observed in the SAED patterns were assigned to (111), (200), (220), and (311) reflections of the fcc structure of the FePt alloy. The XRD patterns (not shown) also indicated the formation of fcc FePt.

Figure 19.23 shows the particle size distribution of FePt nanoparticles chemically produced in various solutions. The values of standard deviation for the particles made in EMI-BF_4, BMP-TF, and DOE were 0.55, 0.63, and 1.16 nm, respectively.

The particles formed in both ILs (Figs. 19.23*b*,*c*) showed a size distribution narrower than that of the particles formed in DOE. This result indicated that the ionic species of ILs interact with the surface of growing FePt nanoparticles more strongly than oleic acid and oleylamine do, because the IL stabilizers are known to control the growth of FePt nanoparticles [99, 100]. Based on the fact that IL behaves both as solvent and as stabilizer in the present case, it was assumed

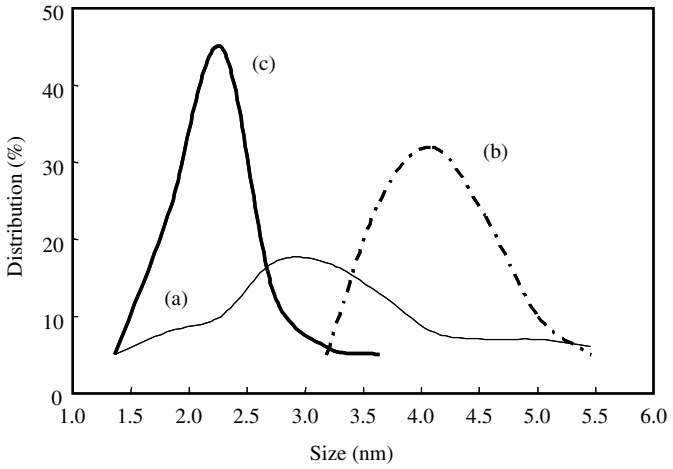

FIGURE 19.23 Particle size distribution curves of FePt nanoparticles chemically produced in various solutions. (a) In DOE. (b) In EMI-BF_4. (c) In BMP-TF.

that interionic interactions of ILs narrowed down the size distribution of grown particles. Our results showed that the use of IL as a solvent resulted in a narrow size distribution of particles without depending on a size-selection process involving centrifugation. Thus, this new method simplifies the preparation procedure of FePt nanoparticles, and it results in $\sim$ 70% fabrication yield, much higher than the average yield of $\sim$ 50%. The mean diameters of the particles made in EMI-BF_4, BMP-TF, and DOE estimated from TEM micrographs were 4.3, 2.4, and 3.2 nm, respectively. This solvent dependency also was confirmed by the XRD profile. Although the preparations in EMI-BF_4 and BMP-TF were carried out at the same temperature (190°C), the sizes of the nanoparticles produced in the two different ILs were different. Some properties of ILs, such as viscosity, heat capacity, conductivity, and dependence on temperature [101–103], are considered to influence the particle formation mechanism proposed by Sun et al. [80, 99], in which the reduction of $Pt(acac)_2$ to Pt leads to the formation of Pt-rich nuclei, and Fe atoms from thermally decomposed $Fe(CO)_5$ contribute to the particle growth. Thus, the size of FePt nanoparticles prepared in ILs can be controlled by combining the anion and cation of ILs. The compositions of the particles formed in EMI-BF_4 and BMP-TF were $Fe_{30}Pt_{70}$ and $Fe_{50}Pt_{50}$, respectively. When a cloud of smoke caused by the thermal decomposition of $Fe(CO)_5$ appeared in the flask during the reaction in EMI-BF_4, we assumed that the coating of Pt-rich nuclei by Fe atoms in the growth process of FePt nanoparticles [99] did not proceed efficiently. Since the thermal decomposition of $Fe(CO)_5$ occurs in the gas phase, it is thought that the difference in efficiency of Fe coating originates from the differences in gas solubility, viscosity, or density, depending on the kind of IL employed [101]. Furthermore, smaller Pt nuclei may become richer in Fe compared to larger Pt nuclei because the smaller Pt nuclei have a larger surface area per Pt atom [103]. By using the BMP-TF preparation, we obtained particles with the Fe–Pt composition of nearly 50:50, which is desirable for conversion to the fct structure.

19.6 SUMMARY

The results presented in this chapter demonstrate that we have successfully produced FePt nanoparticles with a controlled shape and a uniform size distribution and the crystallinity of the nanoparticles improved as the growth temperature was increased. Furthermore, it is suggested that the magnetic properties of annealed, chemically produced FePt nanoparticles are dependent on their shape and crystallinity before annealing. Our study demonstrated that the shape and crystallinity of FePt nanoparticles can be controlled by controlling the growth temperature. Additionally, FePt nanoparticles with a narrow size distribution were successfully prepared in ILs of EMI-BF_4 and BMP-TF without using centrifugation. And the nanoparticles prepared by this method were redispersed in hexane without adding surfactants. The application of other ILs to the preparation of FePt nanoparticles is now being explored.

REFERENCES

1. D. D. Eric, M. C. Denis, and H. C. Mark, Ed. *Magnetic Recording: The First 100 Years*, IEEE Press, New York, 1998.
2. T. Noyes and W. E. Dickson, *IBM J Res Devel.*, **1**, 72–75 (1957).
3. P. C. Andricacos and N. Robertson, *IBM J. Res. Devel.*, **42**, 671 (1998).
4. R. E. Jones, Jr. *IBM Disk Storage Tech.*, **3**, 6 (1990).
5. C. Tsang, M. M. Chon, T. Yogi, and K. Ju, *IEEE Trans. Magn.*, **MAG-26**, 1689 (1990).
6. J. Hong, J. Kane, J. Hashimoto, M. Yamagishi, K. Noma, and H. Kanai, *IEEE Trans. Magn.*, **38**, 15 (2002).
7. M. H. Kryderand and R. Gustafson, *J. Magn. Magn. Mater.*, **287**, 449 (2005).
8. S. Iwasaki and Y. Nakamura, *IEEE Trans. Magn.*, **MAG-13**, 1272–1277 (1977).
9. Y. Tanaka, *J. Magn. Magn. Mater.*, **287**, 468 (2005).
10. S. Iwasaki and K. Ouchi, *IEEE Trans. Magn.*, **MAG-14**, 849 (1978).
11. A. Ajan, B. R. Acharya, E. N. Abrra, and I. Okamoto, *IEEE Trans. Magn.*, **37**, 1508 (2001).
12. E. N. Abrra, H. Sato, M. Suzuki, and I. Okamoto, *IEEE Trans. Magn.*, **36**, 2450 (2000).
13. T. Osaka, and J. Kawaji, "Electrochemical Technology," in *Electrochemical Technology, Innovation and New Development*, N. Masuko, T. Osaka, and Y. Ito, Eds., Kodansha, Tokyo (1996).

14. R. M. Bozorth, *Ferromagnetism*, vol. 5, D. Van Nostrand, New York, 1951, p. 160.
15. S. H. Liao, *IEEE Trans. Magn.*, **MAG-23**, 2981 (1987).
16. J. W. Chang, P. C. Andricacos, B. Petek, and L. T. Romankiw, *Electrochem. Soc. Proc.*, **PV92–10**, 275 (1992).
17. O. Shinoura and A. Kamijima, *J. Surf. Finish. Soc. Jpn.*, **44**, 1114 (1993).
18. Y. Hoshi and M. Naoe, *J. Magn. Soc. Jpn.*, **10**, 315 (1986).
19. N. C. Anderson and R. B. Chesnutt (IBM), U.S. Patent 4,661,216 (1987).
20. Y. Omata, S. Mitani, T. Taniguchi, and S. Nakagawa, *J. Magn. Soc. Jpn.*, **14**, 111 (1990).
21. O. Shinoura, A. Kamijima, and Y. Narumiya, *J. Magn. Soc. Jpn.*, **18**, 277 (1994).
22. T. Osaka, *Electrochim. Acta*, **47**, 23 (2001).
23. A. Nakamura, M. Takai, K. Hayashi, and T. Osaka, *J. Surf. Finsh. Soc. Jpn.*, **47**, 934 (1996).
24. H. S. Nam, T. Yokoshima, T. Nakanishi, T. Osaka, Y. Yamazaki, and D. N. Lee, *Thin Solid Films*, **384**, 288 (2001).
25. T. Osaka, M. Takai, K. Hayashi, Y. Sogawa, K. Ohashi, Y. Yasue, M. Saito, and K. Yamada, *IEEE Trans. Magn.*, **34**, 1632 (1998).
26. T. Osaka, T. Sawaguchi, F. Mizutani, T. Yokoshima, M. Takai, and Y. Okinaka, *J. Electrochem. Soc.*, **146**, 3295 (1999).
27. M. Takai, K. Hayashi, M. Aoyagi, and T. Osaka, *J. Electrochem. Soc.*, **144**, L203 (1997).
28. M. Takai, K. Hayashi, M. Aoyagi, and T. Osaka, *J. Magn. Soc. Jpn.*, **21**, 443 (1997).
29. T. Osaka, M. Takai, K. Hayashi, K. Ohashi, M. Saito, and K. Yamada, *Nature*, **387**, 796 (1998).
30. T. Osaka, M. Takai, Y. Sogawa, T. Momma, K. Ohashi, M. Saito, and K. Yamada, *J. Electrochem. Soc.*, **146**, 2092 (1999).
31. M. Takai, F. Mera, A. Kondo, M. Kaseda, and T. Osaka, *J. Surf. Finsh. Soc. Jpn.*, **49**, 292 (1997).
32. M. Takai, F. Mera, M. Kaseda, and T. Osaka, *J. Magn. Soc. Jpn.*, **22**, 629 (1998).
33. G. Milazzo and S. Caroli, *Tables of Standard Electrode Potentials*, Wiley, New York, 1978, p. 320.
34. *Chemical Handbook—Basic Volume*, 3rd ed., Chemical Society of Japan, Maruzen, Tokyo, 1984, p. 11.
35. T. Osaka, T. Homma, K. Kageyama, and Y. Matsunae, *Denki Kagaku (Electrochemistry)*, **62**, 987 (1994).
36. T. Osaka, T. Yokoshima, D. Shiga, K. Imai, and K. Takashima, *Electrochem. Solid-State Lett.*, **6**, C53 (2003).
37. H. Asano, Y. Bando, N. Nakanishi, and S. Kachi, *J. Jpn. Inst. Metals*, **30**, 684 (1966).
38. M. Shiga, *AIP Conf. Proc.*, **18**, 463 (1974).
39. T. Shimatsu, H. Katada, I. Watanabe, H. Muraoka, and Y. Nakamura, *IEEE Trans. Magn.*, **39**, 2365 (2003).
40. G. Herzer, *IEEE Trans. Magn.*, **26**, 1397 (1990).
41. T. Shimatsu, H. Uwazumi, M. Takahashi, and T. Wakiyama, *J. Magn. Soc. Jpn.*, **15**, 375 (1991).
42. T. Yokoshima, K. Imai, T. Hiraiwa, and T. Osaka, *IEEE Trans. Magn.,* **40**, 2332 (2004).
43. T. Osaka, *Electrochim. Acta*, **44**, 3885 (1999).
44. I. Tabakovic, S. Riemer, V. Inturi, P. Jallen, and A. Thayer, *J. Electrochem. Soc.*, **147**, 219 (2000).
45. X. Liu, P. Evans, and G. Zangari, *IEEE Trans. Magn.*, **36**, 3479 (2000).
46. S. Ikeda, Y. Uehara, I. Tagawa, N. Takeguchi, and M. Kakehi, *IEEE Trans. Magn.*, **36**, 3470 (2000).
47. N. X. Sun and S. X. Wang, *IEEE Trans. Magn.*, **36**, 2506 (2000).
48. K. Ohashi, Y. Yasue, M. Saito, K. Yamada, T. Osaka, M. Takai, and K. Hayashi, *IEEE Trans. Magn.*, **34**, 1432 (1998).
49. K. Ohashi, N. Morita, T. Tsuda, and Y. Nonaka, *IEEE Trans. Magn.*, **35**, 2538 (1999).
50. T. Osaka, T. Yokoshima, and T. Nakanishi, *IEEE Trans. Magn.*, **37**, 1761 (2001).
51. N. J. Speetzen and B. J. H. Stadler, *J. Appl. Phys.*, **97**, 10N118 (2005).
52. B. M. Lairson, J. Perez, and C. Baldwin, *IEEE Trans. Magn.*, **30**, 4014 (1994).
53. P. F. Carcia, A. D. Meinhaldt, and A. Suna, *Appl. Phys. Lett.*, **47**, 178 (1985).
54. L. Wu, S. Yanese, N. Honda, and K. Ouchi, *IEEE Trans. Magn.*, **33**, 3094 (1997).
55. L. Wu, N. Honda, and K. Ouchi, *IEEE Trans. Magn.*, **35**, 2775 (1999).
56. G. Chen, *J. Appl. Phys.*, **87**, 6887 (2000).
57. H. Ohmori and A. Maesaka, *J. Magn. Magn. Mater.*, **235**, 45 (2001).
58. W. Peng, R. H. Victoria, J. H. Judy, K. Gao, and J. M. Sovertsen, *J. Appl. Phys.*, **87**, 6358 (2000).
59. N. Honda, K. Ouchi, and S. Iwasaki, *IEEE Trans. Magn.*, **38**, 1615 (2002).
60. J. Kawaji, T. Asahi, T. Onoue, J. Sayama, J. Hokkyo, and T. Osaka, *J. Magn. Magn. Mater.*, **251**, 220 (2002).
61. J. Sayama, J. Kawaji, T. Asahi, J. Hokkyo, and T. Osaka, *IEEE Trans. Magn.*, **39**, 1059 (2003).
62. J. Sayama, J. Kawaji, M. Tanaka, T. Asahi, S. Matsunuma, and T. Osaka, *Trans. Magn. Soc. Jpn.*, **3**, 8 (2003).
63. J. Kawaji, T. Asahi, H. Hashimoto, T. Osaka, and K. Asami, *Trans. Magn. Soc. Jpn.*, **3**, 1 (2003).
64. J. Kawaji, T. Asahi, H. Hashimoto, J. Hokkyo, T. Osaka, S. Matsunuma, G. Sáfrán, J. Ariake, and K. Ouchi, *J. Appl. Phys.*, **95**, 8023 (2004).
65. M. Schlesinger and M. Paunovic, *Modern Electroplating*, 4th ed., Wiley, New York, p. 24.
66. S. Matsunuma, A. Yano, E. Fujita, T. Onuma, T. Takayama, and N. Ota, *J. Appl. Phys.*, **91**, 8073 (2002).
67. H. Nakagawa, I. Takekuma, H. Nemoto, Y. Takahashi, Y. Hirayama, Y. Nishida, and Y. Hosoe, *IEEE Trans. Magn.*, **39**, 2311 (2003).
68. R. C. Weast, *Handbook of Chemistry and Physics*, 67th ed., CRC Press, Boca Raton, FL, 1999, p. D151,
69. J. Kawaji, M. Tanaka, K. Kimura, T. Asahi, T. Homma, and T. Osaka, *IEEE Trans. Magn.*, **40**, 2473 (2004).

70. A. Maesaka and H. Ohmori, *IEEE Trans. Magn.*, **38**, 2676 (2002).
71. M. Tanaka, J. Kawaji, K. Kimura, T. Asahi, T. Homma, S. Matsunuma, and T. Osaka, *J. Magn. Magn. Mater*., **287**, 188 (2005).
72. T. Osaka, T. Asahi, T. Yokoshima, and J. Kawaji, *J. Magn. Magn. Mater.*, **287**, 292 (2005).
73. M. Chemla, T. Homma, V. Bertagna, R. Erre, N. Kubo, and T. Osaka, *J. Electroanal. Chem.*, **559**, 111 (2003).
74. J. Kawaji, K. Kimura, T. Asahi, T. Homma, and T. Osaka, *J. Magn. Magn. Mater.*, **303**, e128 (2006).
75. S. Y. Chang, C. J. Hsu, R. H. Fang, and S. J. Lin, *J. Electrochem. Soc.*, **150**, C603 (2003).
76. H. N. Bertram, H. Zhou, and R. Gustafson, *IEEE Trans. Magn.*, **34**, 1845 (1998).
77. S. H. Charap, P.-L. Lu, and Y. He, *IEEE Trans. Magn.*, **33**, 978 (1997).
78. D. Weller and A. Moser, *IEEE Trans. Magn.*, **35**, 4423 (1999).
79. D. Weller, A. Moser, L. Folks, M. E. Best, W. Lee, M. F. Toney, M. Schwickert, J. Thiele, and M. F. Doerner, *IEEE Trans. Magn.*, **36**, 10 (2000).
80. S. Sun, C. B. Murray, D. Weller, L. Folks, and A. Moser, *Science*, **287**, 1989 (2000).
81. M. Chen, J. Kim, J. P. Liu, H. Fan, and S. Sun, *J. Am. Chem. Soc.*, **128**, 7132 (2006).
82. S. Sun, *Adv. Mater.*, **18**, 393 (2006).
83. A. Ulman, *Adv. Mater.*, **2**, 573 (1990).
84. G. M. Whitesides, J. P. Mathias, and C. T. Seto, *Science*, **254**, 1312 (1991).
85. M. D. Bendnarski, T. E. Wilson, and M. S. Mastandra, U.S. Patent 5,510,481 (1996).
86. S. I. Stupp, V. LeBonheur, K. Walker, L. S. Li, K. E. Huggins, M. Keser, and A. Amstuz, *Science*, **276**, 384 (1997).
87. N. C. Seeman, *Acc. Chem. Res.*, **30**, 357 (1997).
88. G. Schmid, *Chem. Rev.*, **92**, 1709 (1992).
89. V. Blisnyuk, B. Ruhstaller, P. J. Brock, U. Scherf, and S. A. Carter, *Adv. Mater.*, **11**, 1257 (1999).
90. E. Kumacheva, O. Kalimima, and L. Lilge, *Adv. Mater.*, **11**, 231 (1999).
91. A. P. Alivisatos, *Science*, **271**, 933 (1996).
92. D. L. Klein, R. Roth, A. K. L. Lim, A. P. Alivisatos, and P. L. McEuen, *Nature*, **389**, 699 (1997).
93. R. P. Andres, *Science*, **272**, 1323 (1996).
94. M. Mizuno, Y. Sasaki, A. C. C. Yu, and M. Inoue, *Langmuir*, **20**, 11305 (2004).
95. M. S. Wellons, W. H. Morris, Z. Gai, J. Shen, J. Bentley, J. E. Wittig, and C. M. Lukehart, *Chem. Mater.*, **19**, 2483 (2007).
96. I. Zafiropoulou, E. Devlin, N. Boukos, D. Niarchos, D. Petridis, and V. Tzitzios, *Chem. Mater.*, **19**, 1898 (2007).
97. S. Kang, Z. Jia, S. Shi, D. E. Nikles, and J. W. Harrell, *Appl. Phys. Lett.*, **86**, 062503 (2005).
98. L. Cammarata, S. G. Kazarian, P. A. Salter, and T. Welton, *Phys. Chem. Chem. Phys.*, **3**, 5192 (2001).
99. M. Chen, J. P. Liu, and S. Sun, *J. Am. Chem. Soc.*, **126**, 8394 (2004).
100. H. L. Nguyen, L. E. M. Howard, G. W. Stinton, S. R. Giblin, B. K. Tanner, I. Terry, A. K. Hughes, I. M. Ross, A. Serres, and J. S. O. Evans, *Chem. Mater.*, **18**, 6414 (2006).
101. B. G. Trewyn, C. M. Whitman, and V. S. Y. Lin, *Nano Lett.*, **4**, 2139 (2004).
102. C. P. Fredlake, J. M. Crosthwaite, D. G. Hert, S. N. V. K. Aki, and J. F. Brennecke, *J. Chem. Eng. Data*, **49**, 954 (2004).
103. H. G. Bagaria, D. T. Johnson, C. Srivastava, G. B. Thompson, M. Shamsuzzoha, D. E. Nikles, *J. Appl. Phys.*, **101**, 104313 (2007).

20

ELECTROLESS DEPOSITION OF PALLADIUM AND PLATINUM

IZUMI OHNO

Much effort has been invested in the development of methods for electroless plating of palladium and platinum alongside the rapid technological growth in the electronics industry. In particular, it is the communication industry that requires electroless palladium plating, since it yields uniform deposits on minute integrated circuitry made of intricate design and provides stable contact surfaces for conductors which operate at elevated temperatures. Palladium coating is useful as a substitute for gold coating and also as diffusion barrier layers between gold coating and copper or silver substrate in the electronics industry. The utility of palladium coating is attributable to its good corrosion resistance, low contact resistance, and last but not least relatively lower price. It was recognized by Brenner [1] that electroless deposition of palladium is possible but also that the progress toward homogeneous deposition of palladium results in a high degree of instability of the deposition bath. Fortunately, today the instability of electroless palladium baths can be controlled by a proper selection of additives.

On the other hand, there are only a small number of reports available about the electroless plating of platinum as compared to electroless palladium plating at least up to the 1990s. Since that time there has been significant progress in the field of fuel cell technology (particularly during the late 1990s); many studies have been reported regarding the electroless deposition of nanoscale particles of platinum or platinum alloys on special materials, for example, carbon powder, carbon paper, carbon nanotubes, and Nafion (perfluorosulfonic acid polymer), as well as the deposition of palladium on porous electrodes of fuel cells. Recently Rao and Trivedi [2] reviewed past studies of the electroless and electrochemical deposition of platinum group metals and their applications. In this chapter, electroless palladium and platinum plating baths and the materials used as substrate are briefly reviewed.

20.1 ELECTROLESS PLATING OF PALLADIUM

20.1.1 Electroless Plating Bath for Palladium

Electroless palladium plating baths may be classified through the nature of the reducing agent. The typical baths of two different reducing agents are summarized in Table 20.1.

Hydrazine Baths Rhoda [3–5] developed several electroless palladium plating baths using hydrazine as reducing agent. Palladium tetrammine complex used in the baths was prepared by a careful addition of ammonium hydroxide to a palladium chloride solution. The solution was then heated to dissolve possible precipitates. Ethylenediaminetetraacetic acid (EDTA) was found to be an effective stabilizer against spontaneous decomposition of the solution. Bath 1 in Table 20.1 was recommended also for barrel plating [3]. The hardness of the deposits ranged from 150 to 350 Knoop (25-g load), where softer deposits were formed at higher deposition rates. The deposits consisted of a minimum of 99.4% palladium and exhibited a density of 11.96 g cm^{-3}.

A disadvantage of the hydrazine baths is that the deposition rate decreases drastically after several hours of use, before any significant consumption of the bath constituents has taken place. Several modified electroless palladium solutions have been presented [6–8] to prevent this problem.

The electrochemical aspect of electroless palladium deposition of baths 3 and 5 in Table 20.1 has been studied

Modern Electroplating, Fifth Edition Edited by Mordechay Schlesinger and Milan Paunovic

TABLE 20.1 Composition of Electroless Palladium Plating Bath

	Hydrazine Type			Hypophosphite Type	
Baths	1	2	3	4	5
Palladium (as ammine complex), $[Pd(NH_3)_4]^{2+}$ ($g\,L^{-1}$)	5.4	7.5			
Palladium chloride, $PdCl_2$	—	—	0.023 *M*	2 $g\,L^{-1}$	0.023 *M*
Hydrochloric acid, HCl (38%)	—	—	2–8 $mL\,L^{-1}$	4 $mL\,L^{-1}$	2–8 $mL\,L^{-1}$
Ammonium hydroxide, NH_4OH ($g\,L^{-1}$)	350	280	300 $mL\,L^{-1}$	160 $mL\,L^{-1}$	160 $mL\,L^{-1}$
EDTA (disodium salt), Na_2EDTA ($g\,L^{-1}$)	33.6	8	0.1 *M*		
Ammonium chloride, NH_4Cl	—	—	—	27 $g\,L^{-1}$	0.485 *M*
Hydrazine, $N_2H_4{\cdot}H_2O$ ($g\,L^{-1}$)	0.3	—	0.005 M		
Hydrazine (1 *M* solution)	—	8 ml/l			
Sodium hypophosphite, $NaH_2PO_2{\cdot}2H_2O$	—	—	—	10 $g\,L^{-1}$	0.094 *M*
Temperature (°C)	80	35	60	55	40
Deposition rate ($\mu m\,h^{-1}$)	2.5	0.9	2.5	2.5	0.9
References	3	3, 4	6	10	6

by Paunovic and Ting [6]. They reported that the exchange current density for oxidation of hydrazine (7.8×10^{-5} A cm^{-2}) is higher than that of hypophosphite (2.6×10^{-5} A cm^{-2}). Shu and co-workers [9] have studied an autocatalytic effect during electroless palladium deposition in an alkaline bath containing palladium–ammine complex, EDTA, and hydrazine using electrochemical polarization measurements. Tetravalent palladium species in the bath may be stabilized through interaction with coexisting tin oxide on a palladium–tin activated substrate.

Hypophosphite Baths In most practical electroless palladium plating baths, palladium–ammine complex is employed, together with ammonium chloride and hypophosphite as stabilizer and reducing agent, respectively [6, 10–14]. A representative makeup of this type of bath presented by Pearlstein and Weightman [10] is shown as bath 4 in Table 20.1. The palladium deposits in this bath contained about 1.5% phosphorus and approximately 3 g of sodium hypophosphite monohydrate was consumed to producing 1 g of the electroless palladium deposit [10]. Sergienko developed a stable electroless palladium plating bath containing EDTA and hypophosphite [15].

Other Reducing Agent Baths Stremsdoerfer et al. [16] proposed a new type of electroless deposition of palladium and gold–palladium alloys on a bare *n*-GaAs surface using hydroxylamine as reducing agent. The plating bath is composed of two solutions, as shown in Table 20.2.

Hydrofluoride and potassium chloride in solutions A and B, respectively, act as stabilizers. The autoctalytic bath for electroless palladium plating on bare *n*-GaAs as substrate is prepared by adding a small quantity of solution A to 40 mL of solution B.

The bath exhibited a deposition rate of 0.5 $\mu m\,h^{-1}$ in acidic media at 20°C. The deposits obtained from this bath were well structured and adherent. In addition Stremsdoerfer et al. have also reported that palladium deposited using this bath formed a good metal–semiconductor junction (Pd/*n*-GaAs junction) by subsequent annealing up to 550°C [17]. Nawafune et al. [18] have reported electroless plating of pure palladium from palladium–ethylenediamine complex baths using formic acid as reducing agent. Electroless pure palladium was deposited using the following basic bath composition: 0.01 *M* palladium chloride, 0.08 *M* ethylenediamine, 0.2 *M* formic acid, and pH 6 at 60°. When phosphite or trimethylamine borane was used as reducing agent, the content of phosphorus in the deposit was reduced [19].

TABLE 20.2 Electroless Palladium Plating Bath Using Hydroxylamine

Solution A for 900 mL	
0.3 g $PdCl_2$ dissolved in 9 mL HCl	
5 mL deionized (DI) water	
864 mL glacial acetic acid	
22 mL HF (48%)	
Solution B for 100 mL	
$NH_2OH{\cdot}HCl$	0.416 g (0.06 *M*)
KHF_2	0.937 g (0.12 *M*)
KCl	14.912 g (2.0 *M*)
Citric acid ($C_6H_8O_7{\cdot}H_2O$)	2.101 g (0.1 *M*)
DI water	

Source: From [16].

20.1.2 Electroless Plating of Palladium Alloy

Electroless palladium-based ternary alloys have been produced by adding different metal salts to the electroless palladium bath (bath 4 in Table 20.1) [10]. For example, a palladium–nickel–phosphorus alloy of hardness over 600 Knoop was produced using a hypophosphite bath containing 29.6 g L^{-1} nickel sulfate hexahydrate. This alloy deposit contained up to 6% nickel. By replacing nickel sulfate hexahydrate with the same amount of cobalt sulfate in the bath, less than 10% cobalt was codeposited with the palladium. When 36 g L^{-1} of zinc sulfate was added to the electroless palladium bath (bath 4 in Table 20.1), 36% zinc–palladim alloy was deposited. Electroless palladium–silver [7], palladium–gold [16, 20], and palladium–nickel [10, 21] alloys have been reported as well.

20.1.3 Electroless Palladium Plating on Specific Substrates

Since palladium is a noble metal and has a catalytic activity for anodic oxidation of several reducing agents used in electroless plating [22], electroless palladium is spontaneously deposited at an appreciable rate on many less noble metals and alloys, such as copper, brass, steel, and electroless nickel. Electroless palladium deposits of good quality have been produced on aluminum, chromium, cobalt, gold, iron, molybdenum, nickel, palladium, platinum, rhodium, ruthenium, silver, steel, tin, and tungsten [10]. Electroless palladium has also been deposited on various special substrates such as single-crystal (100) GaAs [16, 17], sputtered aluminum [15, 23, 24], and zirconium thin films [8]. Alloys, such as stainless steel [9], kovar, and brass [25], can also be used as the substrates for electroless palladium. Nonconductors, such as glass or plastics, activated by immersing the stannous chloride and then palladium chloride solutions are also readily plated with electroless palladium [26]. Baylis and co-workers [27] reported in detail the effect of ultraviolet (UV) irradiation on the rate of electroless palladium deposition on palladium–tin activated substrates. The effect of laser irradiation on the rate of electroless palladium plating on nickel substrate has also been reported [28]. There is a particular investigation regarding electroless palladium plating on a polyaniline film [29] and a modified Nafion (perfluorosulfonic acid polymer) as the substrate [30].

20.2 ELECTROLESS PLATING OF PLATINUM

20.2.1 Electroless Plating Bath for Platinum

Several reports on basic electroless platinum plating can be seen in old technical papers and patents. There are two types of electroless platinum plating baths, essentially alkaline and acidic baths. Rhoda and Vines [31] reported an alkaline electroless platinum plating bath containing complex alkaline tetravalent platinum hydroxide and hydrazine, as shown in Table 20.3. Walter and Leaman [32, 33] reported an acidic electroless platinum plating bath that contains platinum hydroxide and hydrazine, as shown in Table 20.4.

TABLE 20.3 Alkaline Electroless Platinum Plating Bath

Disodiumhexahydroxy platinate, $Na_2Pt(OH)_6$	10 g L^{-1}
Sodium hydroxide, NaOH	5 g L^{-1}
Ethylenediamine, $C_2H_8N_2$	10 g L^{-1}
Hydrazine monohydrate, $N_2H_4{\cdot}H_2O$	1 g L^{-1}
Temperature	35°C
pH	10
Deposition rate	12.7 μm h^{-1}

Source: From [31].

The other baths presented utilize dinitrodiammine platinate, $Pt(NO_2)_2(NH_3)_2$, or potassium tetranitroplatinate, $K_2Pt(NO_2)_4$, as the source of metal. The patent of Kozlov et al. [34] shows that electroless platinum may be deposited in an acidic bath on an alloys such as Co superalloy, Inconel, pure Al, Al–Ti alloy, and graphite. The bath composition is presented in Table 20.5.

Further, Rao et al. [35] have also reported that platinum can be deposited on titanium panels, titanium powder, and polyethylene therephthalate (PET) in an acidic bath, which is

TABLE 20.4 Acidic Electroless Platinum Plating Bath Using Chloroplatinate Complex

Dipotassium hexachloroplatinate, K_2PtCl_2	1.0 g L^{-1}
$H_2N_4{\cdot}H_2O$	3.7 g L^{-1}
HCl	33.0 g L^{-1}
Sulfosalicylic acid	1.0 g L^{-1}
Benzenesulfonic acid	0.5 g L^{-1}
2,7-Naphthalene disulfonic acid disodium salt	0.1 g L^{-1}
pH	0.5–1.0
Temperature	60–70°C

Source: From [33].

TABLE 20.5 Acidic Electroless Platinum Plating Bath Using Dinitrodiammine Platinate

Dinitrodiammine platinate, $Pt(NH_3)_2(NO_2)_2$	2 g L^{-1}
Hydrazine hydrate $N_2H_4{\cdot}H_2O$	3.0 g L^{-1}
Acetic acid (CH_3COOH) adjusted to pH 3	
Temperature	50°C
Deposition rate	0.1–2.0 μm h^{-1}

Source: From [34].

an improvement over that presented by Leaman [33]. They reported that a dispersed platinum coating on titanium powder was successfully obtained using another modified bath which contains 1 g L^{-1} of platinum metal and three types of additives such as 3,6-naphthalene-trisulfonic acid trisodium salt, benzene-*m*-disulfonic acid, and sulfosalicylic acid. There is a report in the literature that carbon-supported platinum nanocatalysts can be prepared by the polyol process using ethylene glycol [36]. The authors reported that platinum particles of 39.5 wt % in 2.8 nm size were deposited on Ketjen black (polyfluorene covering a carbon black) by intricated procedure. There exists a patented method for depositing platinum particle from a colloidal state by a reducing agent which is claimed to be applicable to electrocatalyst for fuel cells [37].

20.2.2 Electroless Plating of Platinum Alloy

Several baths have been developed for the electroless plating of platinum alloys with rhodium, iridium, ruthenium, and palladium. Electroless platinum alloy plating baths were patented first in 1969 by Rhoda and Vines [31]. In this patent, the electroless baths for platinum alloys with rhodium, iridium, and ruthenium were prepared adding soluble salts of the respective metals into the platinum plating bath. Suitable salts for this purpose are $[(NH_4)_3RhCl_6]$, $[(NH_4)_3IrCl_6]$, $[(NH_4)_3RuCl_6]$, $[Rh(NO_3)_3]$, $[(NH_4)_3NaRhCl_6]$, and $[(NH_4)_3Rh(NO_2)_6]$. The patent also indicated that the maximum amount of rhodium added to the bath was about 20 wt % platinum, while that of iridium and ruthenium were about 10 wt %. Hydrazine may be added to the bath as the solution of hydrate or sulfate or chloride with sodium or potassium hydroxide. An example of the electroless Pt–Rh plating bath is shown in Table 20.6.

Another electroless Pt–Rh alloy plating bath was patented by Kozlov et al. in 2004 [38]. This patent claims that the bath is applicable to the deposition of a Pt–Rh alloy on virtually any material of any geometrical shape including fiber and powder. Pt–Rh alloy films are useful also for corrosion protection and catalysis.

TABLE 20.6 Electroless Pt–Rh Alloy Plating Bath: Chloroplatinate and Rhodium Chloride

Pt (as sodium platinum hydroxide), $[Na_2Pt(OH)_6]$	10–20 g L^{-1}
Rh (as ammonium rhodium chloride), $[(NH_4)_3RhCl_6]$	1–2 g L^{-1}
NaOH adjusted to pH 10	
Hydrazine	0.5–1.0 g L^{-1}
Ethylamine	2–45 g L^{-1}
Temperature	25–35°C
10% Rh in deposit	

Source: From [31].

TABLE 20.7 Electroless Pt–Rh Alloy Plating Bath: Dinitro Diammonium Platinate and Rhodium Nitrite

Dinitro diammonium platinate, $Pt(NH_3)_2(NO_2)_2$	1.6 g L^{-1}
Ammonium Rh(III) nitrate, $(NH_4)_2Na[Rh(NO_2)_6]$	0.4 g L^{-1}
Ammonium hydroxide, NH_4OH	200 mL
Hydrazine hydrate $N_2H_4{\cdot}H_2O$	1.0 g L^{-1}
Temperature	75°C
Deposition rate	0.8 μm (45 min) 5.7 wt % Rh in the alloy

Source: From [38].

The bath composition is shown in Table 20.7. The outstanding feature of this bath is that the composition of the end product Pt–Rh alloy deposit may be regulated through adding diamminebis(nitrito-*N*,*N*)pt(II) and triamminetri(nitrito-*N*,*N*,*N*)Rh(III) [38]. The Pt–Pd alloy plating bath that contains two reducing agents is shown in Table 20.8.

The bath preparation consists of dissolving the two metal salts in ammonium hydroxide solution while heating and then adding the extra solution B that contains hydroxylamine and hydrazine.

20.2.3 Electroless Platinum Plating on Specific Substrates

In recent years, applications of electroless platinum and platinum-based alloy plating have been extended to the field of electrocatalysts for fuel cells. For this purpose, various forms of carbon such as carbon fiber, carbon paper, carbon powder, or carbon nanotubes are used as substrate for electroless platinum plating [2, 40–42]. These specific materials need special pretreatments to serve as the substrate of electroless plating. Also nanoparticle deposits of platinum or palladium and other platinum group metals are widely studied as an electrocatalyst for the electrodes of fuel cells. There is a report that platinum nanoparticles 1–5 nm

TABLE 20.8 Electroless Pt–Pd Alloy Plating Bath with Two Reducing Agents: Hydroxylamine and Hydrazine

Solution A	
Potassium tetranitroplatinate, $K_2Pt(NO_2)_4$	0.05 g
Potassium tetranitropalladium, $K_2Pd(NO_2)_4$	0.05 g
Ammonium hydroxide, $NH_4OH(28\%NH_3)$	5 mg
Water, H_2O	50 mL
Solution B	
Hydroxylamine hydrochlorate, $NH_2OH.HCl$ (50%)	0.1 g
Hydrazine monohydrate, $N_2H_4.H_2O$ (30%)	1.5 mL
Water, H_2O	total 40 mL
pH	11.7
Temperature	60°C

Source: From [39].

in diameter were successfully deposited on the carbon nanotubes (CNTs) by electroless plating after the two-step sensitization–activation pretreatment [40]. The results showed that the Pt/CNT electrocatalysts for fuel cell contained 67.3% of Pt(0) and 32.7% of Pt(IV). Kokkinidis et al. [43] studied the catalytic activity of electrolessly deposited platinum on titanium for a hydrogen evolution reaction using electrochemical measurements. The hydrogen evolution reaction was used as a probe reaction for testing both the catalytic activity and deposition conditions. They were able to clarify and show that the catalytic activity of electroless platinum for a hydrogen evolution reaction increased with decreasing grain size. This is not surprising as smaller grain sizes represent more surface area. Diaz et al. [44] studied electroless deposition of platinum for the metallization of intrapore spaces of porous gallium nitride, which is of interest in the field of optoelectronics. Rao et al. [45] reported a new process for electroless platinum plating on PET in acidic bath, where the sensitizing process of the substrate was eliminated. This process involves dipping an etched PET film in a $PdCl_2$–dimethylsulfoxide (DMSO) complex solution followed by immersing in a hydrazine solution.

20.3 SUMMARY

The discussion of the utilization of electroless plating of palladium, platinum, and their alloys were extended as a result of recent technological advance. Attention now is focused on their application in various fields of material research, such as superconductivity, optoelectronics, and electrocatalysis. Particularly, due to the significant progress in the field of fuel cell technology, advanced and intricate materials have been utilized as substrates upon which metallic palladium and platinum particles in nanoscale dimensions are dispersed as the catalyst. Thus, the required compositions of the baths for electroless palladium and platinum plating are becoming more and more complicated, which in turn requires suitable stabilizers. Most of the studies in these fields, however, still remain at the laboratory level for the present. Further research is required for the practical application of electroless palladium and platinum plating in the new and emerging fields.

REFERENCES

1. A. Brenner, *Met. Finish.*, **52** (11), 68; **52** (12), 61 (1954).
2. C. R. K. Rao and D. C. Trivedi, *Coord. Chem. Rev.*, **249**, 613 (2005).
3. R. N. Rhoda, *Trans. Inst. Met. Finish.*, **36**, 82 (1959).
4. R. N. Rhoda, *J. Electrochem. Soc.*, **108**, 707 (1961).
5. R. N. Rhoda, *Plating*, **50**, 307 (1963).
6. M. Paunovic and C. H. Ting, in *Proc. Symp. on Electroless Deposition of Metals and Alloys*, Vol. 12, M. Paunovic and I. Ohno, Eds., Electrochemical Society, Pennington, NJ, 1988, p. 170.
7. J. Shu, B. P. A. Grandjean, E. Ghali, and S. Kaliaguine, *J. Membr. Sci.*, **77**, 181 (1993).
8. C. Hsu and R. Buxbaum, *J. Electrochem. Soc.*, **132**, 2419 (1985).
9. J. Shu, B. P. A. Grandjean, E. Ghali, and S. Kaliaguine, *J. Electrochem. Soc.*, **140**, 3175 (1993).
10. F. Pearlstein and F. Weightman, *Plating*, **56**, 1158 (1969).
11. J. P. Abys and N. J. Brindgewater, U.S. Patent, 4,424,241 (Sept. 27, 1982).
12. S. Mizumoto, H. Nawafune, E. Uchida, and M. Haga, *J. Surf. Finish. Soc. Jpn.*, **40**, 477 (1989).
13. S. S. Djokic, *Plating Surf. Finish.*, **86**, 104 (1999).
14. F. Pearlstein,in *Modern Electroplating*, F.A. Lowenheim, Ed., Wiley-Interscience, New York, 1974, p. 739.
15. A. Sergienko,U.S. Patent 3,418,143 (Dec. 24, 1968).
16. G. Stremsdoerfer, H. Perrot, J. R. Martin, and P. Clechet, *J. Electrochem. Soc.*, **135**, 2881 (1988).
17. G. Stremsdoerfer, D. Nguyen, N. J. Renault, J. R. Martin, and P. Clechet, *J. Electrochem. Soc.*, **140**, 519 (1993).
18. H. Nawafune, S. Nakano, S. Mizumoto, E. Uchida, and T. Okada, *J. Surf. Finish. Soc. Jpn.*, **48**, 474 (1997).
19. H. Nawafune, S. Mizumoto, M. Haga, and E. Uchida, *Trans. Inst. Metal Finish*, **74**, 21 (1996).
20. D. Lamouche, P. Clechet, J. R. Martin, E. Haroutiounian, and J. P. Sandino, *Solid-State Electron.*, **29**, 625 (1985).
21. M. Haga, K. Tsuji, H. Nawafune, S. Mizumoto, and E. Uchida, U.S. Patent 4,804,410 (1989).
22. I. Ohno, O. Wakabayashi, and S. Haruyama, *J. Electrochem. Soc.*, **132**, 2323 (1985).
23. C. H. Ting, in *Proc. Symp. on Electroless Deposition of Metals and Alloys*, Vol. 12, M. Paunovic and I. Ohno, Eds., Electrochemical Society, Pennington, NJ, 1988, p. 223.
24. C. H. Ting and M. Paunovic, in *Proc. Symp. on Electroless Deposition of Metals and Alloys*, Vol. 12, M. Paunovic and I. Ohno, Eds., Electrochemical Society, Pennington, NJ, 1988, p. 252.
25. W. Hawk, *Met. Finish.*, **84** (3), 11 (1986).
26. F. Pearlstein, *Met. Finish.*, **53** (8), 59 (1955).
27. B. K. W. Baylis, C. C. Huang, and M. Schlesinger, *J. Electrochem. Soc.*, **126**, 394 (1979).
28. Y. Sato, M. Yanase, A. Yoshida, T. Nishiyama, K. Kobayakawa, and K. Tennichi, *J. Surf. Finish. Soc. Jpn.*, **46**, 375 (1995).
29. Z. H. Ma, K. L. Tan, and E. T. Kang, *Synthetic Mater.*, **114**, 17 (2000).
30. H. Sun, G. Sun, S. Wang, J. Liu, X. Zhao, G. Wang, H. Xu, S. Hou, and Q. Xin, *J. Memb. Sci.*, **259**, 27 (2005).
31. R. N. Rhoda and R. F. Vines, U.S. Patent 3,486,928 (1969).
32. C. W. Walter and F. H. Leaman,U.S. Patent 3,562,911 (1971).
33. F. H. Leaman, *Plating*, **59**, 440 (1972).

34. A. S. Kozlov, T. Palanisamy, and D. Narasimham,U.S. Patent 6,391,477B1 (2002).
35. C. R. K. Rao and M. Pushpavanan, *Mater. Chem. Phys.*, **68**, 62 (2001).
36. H. S. Oh, J. G. Oh, Y. G. Hong, and H. Kim, *Electrochim. Acta.*, **52**, 7278 (2007).
37. E. Kawasumi, Kokai Tokkyo Koho, Japanese Patent, DP2006-175365A (2006).
38. A. S. Kozlov, T. Palanisamy, and D. Narasimham,U.S. Patent 6,706,420B1 (2004).
39. E. Torigai, K. Takenaka, and Y. Kawami,Japanese Patent 84-80764 (1984).
40. Z. Liu, X. Lin, J. Y. Lee, W. Zhang, M. Han, and L. M. Gan, *Langmuir*, **18**, 4054 (2002).
41. W. Li, C. Liang, W. Zhou, J. Qui, Z. Zhou, G. Sun, and Q. Xin, *J. Phys. Chem. B*, **107**, 6292 (2003).
42. J. W. Guo, T. S. Zhao, J. Prabhuram, and C. W. Wong, *Electrochim. Acta*, **50**, 1973 (2005).
43. G. Kokkinidis, A. Papoutsis, D. Stoychev, and A. Milchev, *J.Electroanal. Chem.*, **486**, 48 (2000).
44. D. J. Diaz, T. L. Williamson, X. Guo, A. Sood, and P. W. Bohn, *Thin Solid Films*, **514**, 120 (2006).
45. Z. Rao, E. K. Chong, N. L. Anderson, M. G. Stevens, R. Driver, and K. V. Paulose, *J. Mater. Sci. Lett.*, **17**, 303 (1998).

21

ELECTROLESS DEPOSITION OF GOLD

YUTAKA OKINAKA AND MASARU KATO

The term *electroless plating* was originally used by Brenner and Riddell [1], inventors of the well-known *autocatalytic* nickel and cobalt plating processes using hypophosphite as the reducing agent. A literature survey indicates, however, that this term is currently being used to describe three mechanistically different, nonelectrolytic processes for depositing metals and alloys: (1) galvanic displacement plating (also called *immersion plating* or *cementation*), (2) substrate-catalyzed plating, and (3) autocatalytic plating. In this chapter only autocatalytic gold plating processes are reviewed.

The first autocatalytic, electroless gold plating bath was developed in 1970 at Bell Laboratories [1a] to plate thick, pure soft gold on semiconductors and circuit boards without employing an external source of electric current. The bath contained potassium cyanoaurate (I), $KAu(CN)_2$, as the source of gold, potassium borohydride, KBH_4, or dimethylamine borane, $(CH_3)_2NH{\cdot}BH_3$, as the reducing agent, potassium cyanide, and potassium hydroxide. Typical bath compositions are given in Table 21.1. The original baths did not contain stabilizing additives, and they were sensitive to minute amounts of impurities, which tended to lead to spontaneous decomposition. Nevertheless, those baths were employed successfully with sufficient stability under carefully controlled conditions [2–5], yielding highly pure, soft gold useful for the purpose of bonding semiconductor devices [6]. Other successful applications documented in the open literature include (1) metallization of GaAs microwave field-effect transistors [7], (2) formation of ohmic contacts consisting of Pd/Sn/Au films on *n*-GaAs [8], (3) metallization of polyvinylidene fluoride (PVDF) films used for making piezoelectric devices [9], (4) deposition of a conducting layer on the interior surface of waveguide tubes made of an aluminum alloy [10], and (5) deposition of a gold layer on tungsten-metallized ceramics for packaging semiconductor devices [11].

More recently the accelerating trend of miniaturization and the need for greater reliability of electronic components have resulted in the development of new technologies for mounting devices on circuit boards, which in turn created new requirements for compatibility of the plating process with substrate materials and also for properties of gold films to be deposited on semiconductors and circuit boards. Quite generally, the method of electroplating has inherent advantages over that of electroless plating in terms of the ease of maintaining the bath and controlling the film thickness and properties. On the other hand, electroless plating has, in principle, a distinct advantage over electroplating in its capability of minimizing the number of processing steps when gold is needed in areas which are electrically isolated from each other. Under these circumstances, efforts have been made to improve the original borohydride and dimethylamine borane (DMAB) baths, especially in their stability and plating rate, and such improved baths are now commercially available. However, those baths have certain properties that are inherently incompatible with the requirements of the current technology. Thus baths with entirely different compositions have been developed in recent years to overcome those problems.

In this chapter the characteristics and problems of the conventional borohydride and DMAB baths will be summarized first, followed by a brief description of the improvements made to those baths. Then, the current status of development of new noncyanide baths will be reviewed.

Modern Electroplating, Fifth Edition Edited by Mordechay Schlesinger and Milan Paunovic

TABLE 21.1 Examples of Original Borohydride and DMAB Baths Containing No Additives

	Borohydride Bath	DMAB Bath
$KAu(CN)_2$	0.02 *M*	0.02 *M*
KCN	0.2	0.02
KOH	0.2	0.8
KBH_4	0.4	—
DMAB	—	0.4
Temperature	75°C	85°C
Plating rate	0.7 μm h^{-1}	0.4 μm h^{-1}

Source: Okinaka [1a].

21.1 CHARACTERISTICS OF BOROHYDRIDE AND DMAB BATHS

The reactions involved in the borohydride process were studied in detail by means of electrochemical techniques [4]. In the original study it was shown that the species that reduces $[Au(CN)_2]^-$ to Au is BH_3OH^-, which is an intermediate produced during the hydrolysis of borohydride ion, BH_4^-, rather than the latter ion itself:

$$BH_4^- + H_2O \rightarrow BH_3OH^- + H_2 \tag{21.1}$$

$$BH_3OH^- + H_2O \rightarrow BO_2^- + 3H_2 \tag{21.2}$$

$$BH_3OH^- + 3OH^- \rightarrow BO_2^- + \left(\frac{3}{2}\right)H_2 + 2H_2O + 3e^- \tag{21.3}$$

$$[Au(CN)_2]^- + e^- \rightarrow Au + 2CN^- \tag{21.4}$$

The overall reaction (21.5) is obtained by combining the two partial reactions (21.3) and (21.4):

$$BH_3OH^- + 3[Au(CN)_2]^- + 3OH^- \rightarrow BO_2^- + \left(\frac{3}{2}\right)H_2 + 2H_2O + 3Au + 6CN^- \tag{21.5}$$

The anodic partial reaction (21.3) was written here under the assumption that this reaction, which was originally derived from a polarographic study at the dropping mercury electrode [12], is also operative on gold. Later Efimov et al. [13, 14] reported that another hydrolysis intermediate, $BH_2(OH)_2^-$, is also involved in the electroless plating process and that all hydrogen gas produced during the plating results from the hydrolysis reactions and the plating reaction per se does not produce hydrogen. Thus these authors proposed the following reactions instead of reaction (21.5) to describe the overall plating process:

$$6[Au(CN)_2]^- + BH_3OH^- + 6OH^- \rightarrow 6Au + BO_2^- + 12CN^- + 5H_2O \tag{21.6}$$

$$4[Au(CN)_2]^- + BH_2(OH)_2^- + 4OH^- \rightarrow 4Au + BO_2^- + 8CN^- + 4H_2O \tag{21.7}$$

Irrespective of the mechanisms of the actual plating reaction, a polarographic analysis of the kinetics of the hydrolysis reactions (21.1) and (21.2) has shown that the rate of reaction (21.2) is almost 500 times faster than that of reaction (21.1) under the conditions of electroless gold plating. Thus the utilization efficiency of borohydride as the reducing agent is very low, and most of the borohydride is lost by hydrolysis. The utilization efficiency obtained under typical plating conditions amounts to only 2–3%.

The hydrolysis reactions above are known to be acid catalyzed, and therefore they proceed more rapidly at lower pH. Accordingly, the electroless deposition rate of gold increases with decreasing KOH concentration. However, to prevent spontaneous decomposition, the KOH concentration of the bath must be kept greater than 0.1 *M*. The dependence of the plating rate on KOH concentration is illustrated in Figure 21.1.

If DMAB is used in place of borohydride, an opposite dependence is found; that is, the plating rate increases with KOH concentration (Fig. 21.2). The difference in the effect of KOH concentration on the plating rate between the two baths has been explained by assuming that the actual reducing species in the DMAB bath is also BH_3OH^- and that this species is produced by the direct reaction of DMAB and OH^- ions:

$$(CH_3)_2NH \cdot BH_3 + OH^- \rightarrow (CH_3)_2NH + BH_3OH^- \tag{21.8}$$

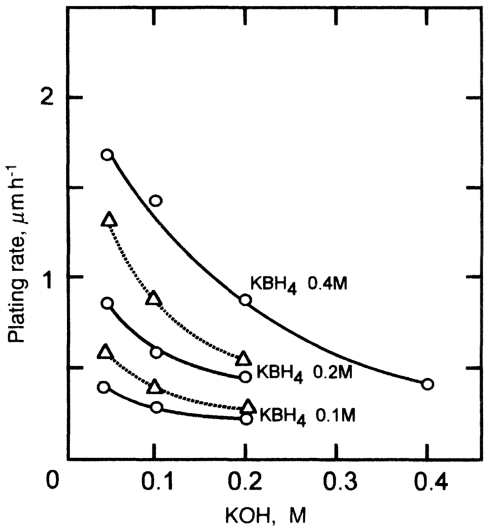

FIGURE 21.1 Effect of KOH concentration on plating rate of borohydride bath: 0.02 *M* $KAu(CN)_2$, 0.2 *M* KCN (solid line), 0.1 *M* KCN (broken line), 80°C [1a].

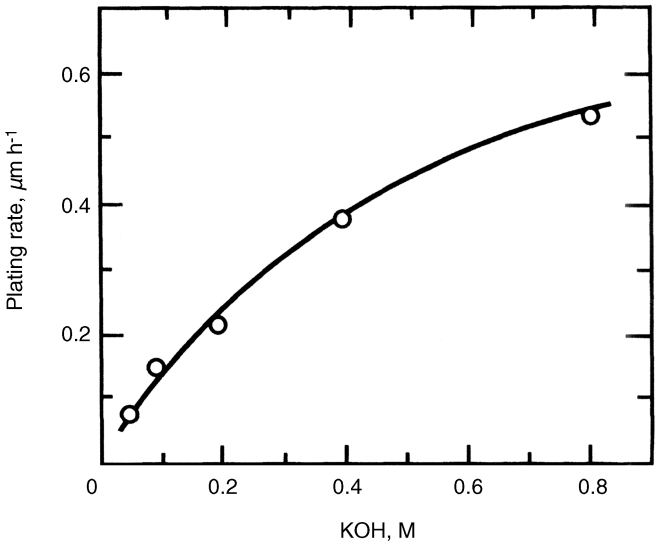

FIGURE 21.2 Effect of KOH concentration on plating rate of DMAB bath: 0.02 *M* $KAu(CN)_2$, 0.02 *M* KCN, 0.4 *M* DMAB, 75°C [1a].

Sargent et al. [14a] studied the nature of reactive intermediates formed from DMAB. They report that the assumption that BH_3OH^- is the electroactive intermediate in the electroless gold plating process is not supported by their experimental results. However, Sadik et al. [14b] continued their mechanistic study and concluded that the actual reducing species in the DMAB bath can be either BH_3OH^-, $BH_2(OH)_2^-$, or $BH(OH)_3^-$, depending on the potential where gold deposition takes place.

Another unique feature of the borohydride system is found in the dependence of plating rate on the concentration of $[Au(CN)_2]^-$; that is, the plot of plating rate against gold concentration exhibits a maximum at approximately 0.003 *M*. This unusual dependence is attributed to competitive adsorption of BH_3OH^- and a gold-containing species for the same site on the gold surface. Namely the gold species is apparently more strongly adsorbed on gold than the reducing species, BH_3OH^-, thereby acting as a catalytic poison for the oxidation of BH_3OH^-. The adsorbed gold species is actually believed to be AuCN, which has been proposed as an intermediate formed during the reduction of $[Au(CN)_2]^-$ [15, 16]:

$$[Au(CN)_2]^- \rightarrow AuCN_{ads} + CN^- \qquad (21.9)$$

$$AuCN_{ads} + e^- \rightarrow Au + CN^- \qquad (21.10)$$

The adsorbed AuCN has recently been positively identified on a single crystal of Au(111) and the structure of the adsorbed layer investigated using low-energy electron diffraction (LEED), Auger electron spectroscopy (AES), and in situ electrochemical scanning tunneling microscopy (ESTM) [17].

The electroless gold deposition from the borohydride and DMAB systems takes place on noble metals such as Pd, Rh, Ag, and Au itself as well as on base metals such as Cu, Ni, Co, Fe, and their alloys. On noble metals the reaction is catalytic from the very beginning. On the other hand, the gold deposition on the base metals is initiated by galvanic displacement, which results in accumulation of ions of those base metals in the bath. No adverse effect occurs with copper, whereas the introduction of ions of Ni, Co, and Fe into the solution is highly detrimental. Further details of such impurity effects will be described in the subsequent section.

21.2 PRACTICAL PROBLEMS ASSOCIATED WITH ORIGINAL BOROHYDRIDE AND DMAB BATHS

From the standpoint of practical applications, these basic baths have the following problems:

1. The plating rate is low.
2. The bath stability is insufficient.
3. The baths are sensitive to contamination with minute amounts of nickel ions.
4. A high pH is required.
5. The baths contain free cyanide.

Much effort has been expended by many investigators to improve on items 1–3. On the other hand, items 4 and 5 are inherent to the baths, and they cannot be changed. Both the high alkalinity and the use of cyanide make the baths incompatible with positive photoresists commonly used to delineate patterns on semiconductor devices and circuit boards.

21.3 IMPROVED BOROHYDRIDE AND DMAB BATHS

21.3.1 Methods of Increasing the Plating Rate

To obtain a plating rate as large as possible simply by adjusting basic bath compositions and operating conditions without resorting to the special methods described below, the following approaches are useful: (1) increase the agitation speed of the bath; (2) raise the bath temperature; (3) lower the free-cyanide concentration; (4) decrease the free-alkali-hydroxide concentration for the borohydride bath or increase it for the DMAB bath; and (5) increase the reducing agent concentration. However, an attempt to obtain a plating rate greater than $2\,\mu m\,h^{-1}$ by these simple approaches will be futile, because it will lead to spontaneous bath decomposition.

The following methods are known to be useful for formulating high-speed baths.

Adding a Depolarizer It is well known that the addition of a small amount of Pb^{2+} or Tl^{+} depolarizes the gold electrode in the electrolytic soft gold plating bath [18]; namely these ions shift the gold deposition potential in the positive direction. These ions are known to undergo the so-called underpotential deposition (UPD) on gold, in which the strongly adsorbed metal atoms form on gold at potentials considerably less negative than corresponding equilibrium potentials. The depolarization effect of these UPD ions has been explained by assuming that the adsorbed metal atoms formed by the UPD mechanism chemically react with $Au(CN)_2^-$ by galvanic displacement, which regenerates the original metal ions. Thus the UPD ions act as a catalyst for the reduction of the gold species:

$$M^{n+} + ne^- \longrightarrow M^0_{UPD} \tag{21.11}$$

$$M^0_{UPD} + n[Au(CN)_2]^- \longrightarrow M^{n+} + nAu + 2nCN^- \tag{21.12}$$

with the overall reaction being

$$[Au(CN)_2]^- + e^- \rightarrow Au + 2CN^- \tag{21.13}$$

When ions of such UPD metals are added to the borohydride or DMAB bath, the reduction potential of $[Au(CN)_2]^-$ shifts in the positive direction, and therefore the plating rate increases.

Matsuoka et al. [19] added $PbCl_2$ or T1C1 to a borohydride bath containing $KAu^{III}(CN)_4$ instead of $KAu^{I}(CN)_2$, and they obtained a plating rate 8–9 times faster than that obtained in the absence of the additives. Since the $[Au(CN)_4]^-$ ion in this bath is reduced by the borohydride to $[Au(CN)_2]^-$ ion, the plating reaction is basically the same as that of the conventional borohydride bath. However, because the reduction of $[Au(CN)_4]^-$ to $[Au(CN)_2]^-$ produces free CN^- ions, there is no need to add CN^- at the time of bath makeup, which is claimed to be a practical advantage of this system. The composition of the bath proposed by the above authors is given in Table 21.2. The depolarizing effect of Pb^{2+} on the reduction of $[Au(CN)_2]^-$ is demonstrated in Figure 21.3, and the remarkable accelerating effects of Pb^{2+} and Tl^{+} are shown in Figure 21.4.

TABLE 21.2 Borohydride Bath with Cyanoaurate(III) Instead of Cyanoaurate(I)

$KAu(CN)_4$	$3\,g\,L^{-1}$
KOH	11.2
KBH_4	3
$PbCl_2$	$0.5\,mg\,L^{-1}$
Temperature	70°C

Source: Matsuoka et al. [19].

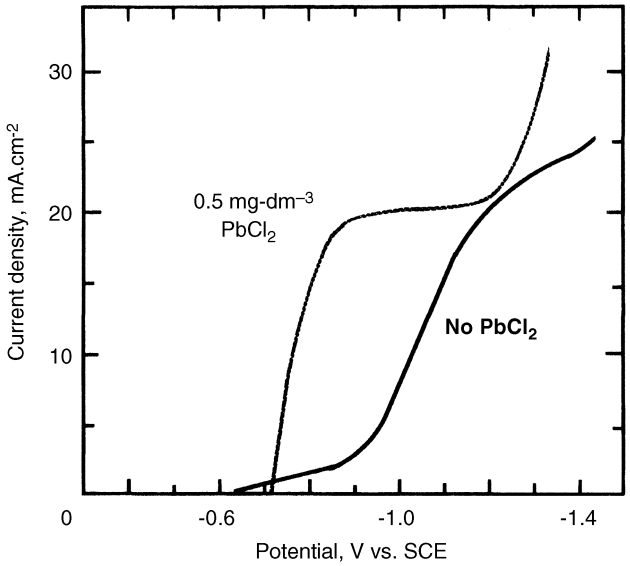

FIGURE 21.3 Effect of $PbCl_2$ addition on polarization curve for the reduction of $Au(CN)_2^-$. (Matsuoka et at. [19]).

Adding a Stabilizer Some attempts have been made in the past to increase the plating rate by adding an organic compound which poisons the catalytic activity of gold while raising the plating temperature or increasing the

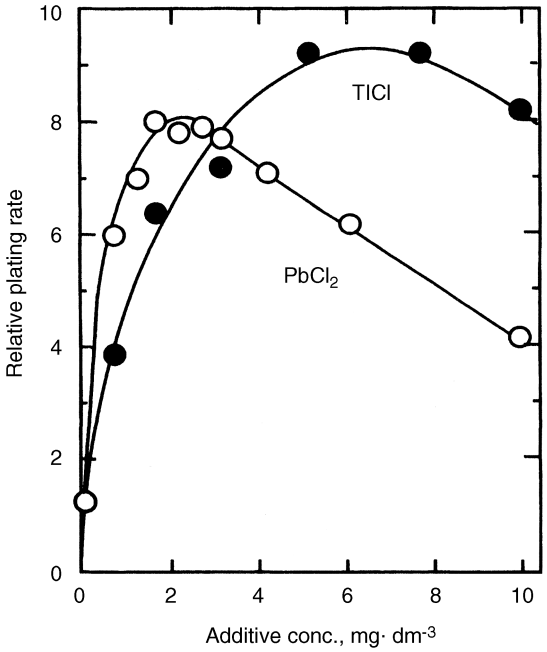

FIGURE 21.4 Effect of $PbCl_2$ and TlCl concentrations on plating rate of borohydride bath. (Matsuoka et al. [19]).

concentration of the reducing agent to compensate for the loss of plating rate caused by the poisoning effect. For example, a bath stabilized in this manner was operated at a temperature as high as 90°C to obtain 12–23 $\mu m\, h^{-1}$ [20]. However, it should be realized that at such a high temperature the hydrolysis reaction of the reducing agent is greatly accelerated to make the control of bath composition difficult. Thus, for all practical purposes this approach cannot be recommended.

On the other hand, Homma [21] successfully increased the plating rate to 5 $\mu m\, h^{-1}$ without causing bath instability by adding a trace of *p*-dimethylaminobenzylidene rhodanine as a stabilizer while doubling the borohydride concentration. Ott [22] also found that compounds such as ethylene glycol monoethylether, diethyleneglycol monoethylether, and polyethyleneimine also serve as effective stabilizers for the same purpose.

Using Cyanoaurate(III) instead of Cyanoaurate(I) Besides the cyanoaurate(III) bath of Matsuoka et al. mentioned above, El-Shazley and Baker [23] also developed a bath containing $KAu^{III}(CN)_4$ as the source of gold and achieved a plating rate ranging from 2 to 8 $\mu m\, h^{-1}$ without any additives. A distinct advantage of using the Au(III) compound is that it allows the use of $KAuO_2$ or $KAu(OH)_4$ instead of the cyanide compound for the replenishment of gold, preventing the accumulation of free CN^-, which is known to lower the plating rate. Corresponding Au(I) compounds do not exist in a stable form. Thus the Au(III) bath should be advantageous for maintaining the plating rate at a constant level for an extended period of bath usage.

Ohtsuka et al. [24] made a detailed investigation of their DMAB bath containing cyanoaurate(III) as the source of gold. They showed that the Au(III) species is reduced immediately by borohydride to Au(I) at the plating temperature of 70–75°C, and therefore the ordinary Au(I) cyanide salt, $KAu(CN)_2$, can be used for initial bath makeup while a solution prepared by dissolving $Au^{III}(OH)_3$ in dilute KOH is used for replenishment.

Simon [25] described the use of an "accelerator" to suppress the deleterious effect of the accumulation of free CN^- in the DMAB bath. The chemical composition of the accelerator has not been disclosed, however.

Adding an Accelerator for Anodic Oxidation of the Reducing Agent If the anodic oxidation of the reducing agent can be accelerated by adding a suitable catalyst in the bath, then the potential for this reaction should shift in the negative direction. From the general principle of autocatalytic metal deposition, it follows that the negative shift of the potential for the oxidation of reducing agent should increase the plating rate. Iacovangelo [26] found that carbonate ions and triethanolamine accelerate the oxidation of DMAB. The mechanism of the accelerating effect has not been clarified to the author's knowledge.

21.3.2 Methods of Improving Bath Stability

Quite generally, conditions favoring an increase in plating rate decrease bath stability in all autocatalytic systems, except when the rate increase under mass transport limiting conditions is brought about by raising the degree of bath agitation or the speed of substrate movement. The bath instability resulting from the use of conditions providing an excessive activity of the bath may be brought under control by adding a stabilizer such as one of the compounds mentioned in Section 21.3.1.

On the other hand, it should be realized that bath instability can be triggered by the introduction of certain impurities. As briefly touched upon in Section 21.1, the borohydride and DMAB baths are extremely sensitive to contamination with Ni^{2+}, Co^{2+}, or Fe^{2+}, while they are unaffected by Cu^{2+}. Figure 21.5 compares the effect of the addition of Ni^{2+} on the plating rate with that of Cu^{2+}, where the plating rate in the absence of the contaminating ions was the same as the constant rate obtained at the various concentrations of Cu^{2+}. It is seen that the presence of only $10^{-5}M$ of Ni^{2+} causes the plating rate to decline, and bath decomposition sets in at $10^{-3}M$. Ions of Co^{2+} and Fe^{2+} exert similar effects. An electrochemical study of the effect of Ni^{2+} showed that the anodic oxidation of the reducing species, BH_3OH^-, is greatly inhibited by the preferential adsorption of $[Ni(CN)_4]^{2-}$ on the surface of gold [4]. As a method of preventing bath decomposition resulting from the presence of ions of the transition metals, Ali and Christie [27] added ethylenediaminetetraacetic acid (EDTA) and ethanolamine, which form highly stable complex ions with the metals and suppress their reactions with the reducing agent (Table 21.3).

Decomposition of the borohydride and DMAB baths can also occur when they are contaminated with certain organics

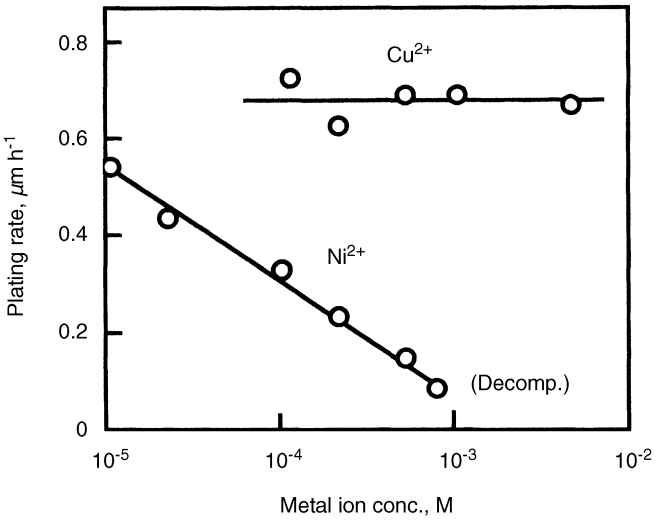

FIGURE 21.5 Effect of bath contamination with Ni^{2+} and Cu^{2+} ions on plating rate of borohydride bath [5].

TABLE 21.3 Borohydride Bath with EDTA and Ethanolamine

$KAu(CN)_2$	0.005 *M*
KCN	0.17
KOH	0.2
KBH_4	0.2
Na_2EDTA	5 g L^{-1}
Monoethanolamine	50 cm^3 L^{-1}
Temperature	72°C
Plating rate	1.5 μm h^{-1}

Source: Ali and Christie [27].

such as polyethylene [5]. One should be aware of possibilities of contamination with trace amounts of organic materials from storage bottles and vessels as well as from the water used to prepare the solutions.

21.3.3 Methods of Plating on Nickel Substrates

For the reasons described above, the borohydride or DMAB bath is not suitable for plating gold directly on nickel metal. It is a general practice to coat the nickel substrate with a thin layer of immersion (galvanic displacement) gold prior to plating electroless gold. However, because a complete coverage of the nickel substrate with immersion gold is virtually impossible, and because the bath is highly sensitive to an extremely small amount of dissolved nickel ions, the above approach cannot be expected to provide completely satisfactory solution to the nickel contamination problem.

More recently Iacovangelo [26] proposed a new method of plating electroless gold on nickel without using displacement gold. The bath used in this method contains two different reducing agents: DMAB and hydrazine. The bath composition is given in Table 21.4. Lead acetate and potassium carbonate are added to accelerate partial cathodic and partial anodic reactions, respectively, leading to an increased plating rate. Upon immersion of a metallic nickel substrate in this bath, the initial deposition of gold takes place via the catalytic oxidation of hydrazine on the nickel coupled with the reduction of Au(I) to Au. After the nickel is completely covered with gold, DMAB serves as the sole reducing agent to deposit gold continuously on gold via the autocatalytic mechanism. In this method the dissolution of nickel by galvanic displacement can be virtually eliminated by selecting a proper bath composition. From the anodic polarization curves for the oxidation of hydrazine and DMAB on Ni and Au electrodes, Iacovangelo showed that in the potential range of interest hydrazine is oxidized on Ni but not on Au (see Fig. 21.6), whereas DMAB is oxidized nearly 100 times faster on Au than on Ni (Fig. 21.7). The idea used in formulating this bath is based on the clever utilization of the difference in catalytic activity between Ni and Au for the oxidation of the two reducing agents. This concept should be of general virtue when substrate metal needs to be protected from its galvanic displacement reaction with a bath component.

TABLE 21.4 Bath with Two Reducing Agents (DMAB and Hydrazine)

$KAu(CN)_2$	0.005 *M*
KCN	0.035
KOH	0.8
K_2CO_3	0.45
Pb acetate	15 ppm
DMAB	0.05 *M*
N_2H_4	0.25
Temperature	80°C
Plating rate	
Initial (on Ni)	2.6 μm h^{-1}
On Au	7.8 μm h^{-1}

Source: Iacovangelo [26].

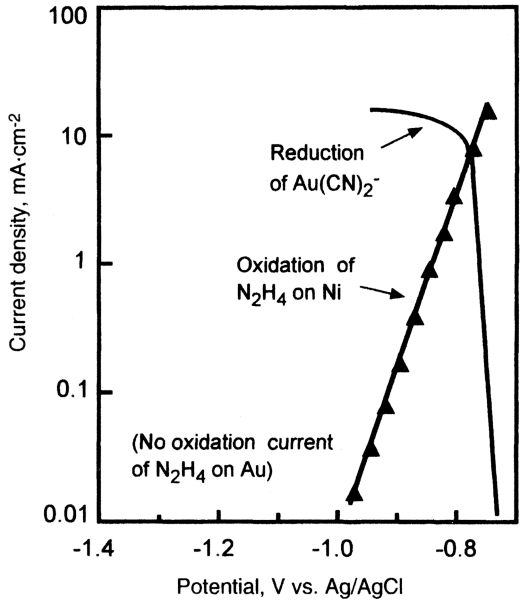

FIGURE 21.6 Polarization curves for the reduction of $Au(CN)_2^-$ and for the oxidation of hydrazine on nickel electrode: 0.8 *M* KOH, 0.035 *M* KCN, 0.05 *M* N_2H_4, 80°C [126].

In another development Iacovangelo and Zarnoch [28] found that the substrate-catalyzed deposition of gold on nickel with hydrazine as the sole reducing agent can be made to proceed to obtain a gold layer which is sufficiently thick for the purpose of bonding electronic devices and components. They demonstrated that the maximum thickness of gold obtained by the substrate-catalyzed reaction depends on the concentration of free CN^- ions in their bath (Fig. 21.8). Thus the maximum thickness of gold obtained from this bath is determined by the free CN^- concentration rather than the plating time as in conventional autocatalytic processes.

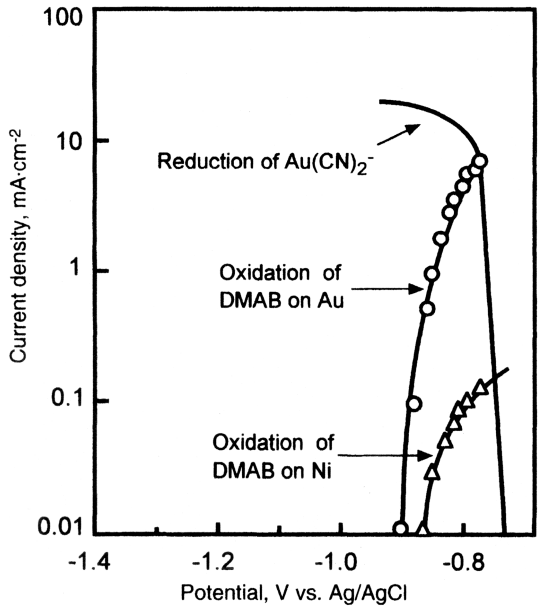

FIGURE 21.7 Polarization curves for the reduction of $Au(CN)_2^-$ and for the oxidation of DMAB on nickel and gold electrodes [20].

21.4 CYANIDE BATHS WITH OTHER REDUCING AGENTS

There are many descriptions, mostly in the patent literature, of cyanide-based electroless gold plating baths containing reducing agents other than borohydride or DMAB. One of the present authors already published extensive reviews of such baths [29, 30], and they will not be described in detail in this chapter. Table 21.5 lists those baths only with reducing agents used, pH, temperature, and references. It should be noted that the list includes baths operated at low pH values [e.g., those with hydroxylamine, Ti(III) trichloride, or thiourea] and those which do not generate gaseous hydrogen [e.g., the bath with Ti(III) trichloride]. Because of such unusual features, those baths may find applications with special requirements. It should be cautioned, however, that some baths included in the list have been shown to be nonautocatalytic, and hence the maximum gold thickness that can be obtained with those baths is rather limited.

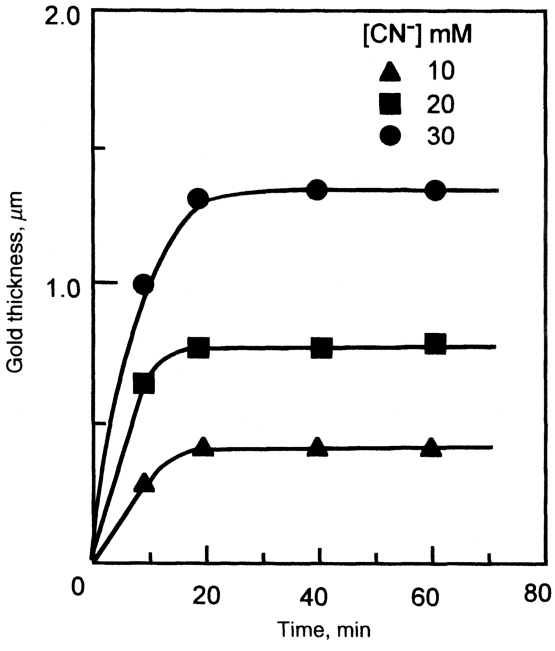

FIGURE 21.8 Gold plating thickness-vs.-time curves at various cyanide concentrations for substrate-catalyzed plating with hydrazine as reducing agent. [28].

TABLE 21.5 Cyanide Baths with Reducing Agents Other Than Borohydride or DMAB

Reducing Agent	PH	Temperature (°C)	References
Hypophosphite	7–7.5	93	31
	7.5–13.5	96	32
	3–4	70–80	33
Hydrazine	7–7.5	92–95	34
	5.8–5.9	95	35, 36
	11.7	95	137
Hydroxylamine	2.3–2.8	70–85	38
Cyanoborohydride	3.5	90	39
Hydrazinoborane	>13	60	40
Thiourea	6.5–7.0	83–90	41
	4.2	80–85	42
Ascorbic acid	8	63	43
Titanium trichloride	5	75	44

21.5 NONCYANIDE BATHS

The use of cyanide is undesirable for a few reasons other than its toxicity. In applications requiring gold deposition on a substrate with a circuit pattern delineated with a conventional positive photoresist, cyanide ions are known to attack the interface between the photoresist and the substrate, lifting the photoresist and causing extraneous gold deposition under the photoresist. The high alkalinity of the cyanide-based baths is also incompatible with the positive photoresist. In the borohydride or DMAB bath, the accumulation of cyanide ions with bath usage lowers the plating rate. For these reasons noncyanide baths are currently in demand.

Gold salts other than cyanide complexes used for formulating electroless gold baths include chloroaurate(III), Au(I)–sulfite complex, Au(I)–thiosulfate complex, and Au(I)–thiomalate. The noncyanide electroless gold baths developed prior to 1980 have been reviewed by Mathe [45] and Ganu and Mahapatra [46]; the reader is referred to these works. More recently a large number of patents and papers have appeared on electroless gold baths based on

Au(I)–sulfite and/or Au(I)–thiosulfate complex and operated at near-neutral pH. Those baths have been studied in detail for the reaction mechanism, process control methodology with replenishment of bath constituents, and deposit characteristics. Here only the noncyanide baths developed and investigated after 1980 will be reviewed.

21.5.1 Baths with Au(I)–Sulfite Complex

Gold(I)–sulfite complex has been in use for many years as the source of gold in commercial noncyanide, *electrolytic* gold plating baths. Those baths contain proprietary stabilizing agent(s) because Au(I)–sulfite complex undergoes a disproportionation reaction in aqueous solution and decomposes spontaneously on standing to produce Au(III) and metallic Au(0).

For electroless gold plating, Richter et al. and Gesemann et al. [47–50] developed baths containing 1,2-diaminoethane and KBr as stabilizers in combination with hypophosphite, formaldehyde, hydrazine, borohydride, or DMAB as the reducing agent. Also described by Richter et al. [51] is a sulfite-based bath containing ethylenediamine or EDTA as the stabilizing agent, formaldehyde or hydrazine derivatives as the reducing agent, and an arsenic compound, which is reported to yield hard gold deposits.

Sato et al. [52], using Au(I)–sulfite-ethylenediamine complex as the source of gold, investigated the possibility of employing thiourea or its derivatives as the reducing agent. They found that the performance of the bath with methyl thiourea or acetyl thiourea was strongly pH dependent and that the deposit obtained from the former bath was porous, whereas good deposits were obtained from the bath containing both thiourea and methyl thiourea at the concentration ratio of 3.

Ohtani et al. [52a] investigated the possibility of using polyphenol as the reducing agent in an Au(l)–sulfite bath. Among the three polyphenol compounds tested (catechol, pyrogallol, and gallic acid), catechol was found to be most suitable in terms of bath stability and deposit appearance. The composition and operating conditions of this bath are tabulated in Table 21.6.

Shindo and Honma [53] found that the stability of the sulfite bath can be improved by adding triethanolamine, nitrilo-triacetic acid, or sodium thiosulfate. Using ascorbic acid as the reducing agent, Kato et al. [54, 55] had previously shown that Au(I)–sulfite complex can be reduced to gold metal autocatalytically, but the deposition rate is very low. They found that the deposition rate can be increased greatly by adding thiosulfatc as the second complexing agent. The mixed-ligand system will be described further in Section 21.5.3. Baths containing thiosulfate as the sole ligand will be described first in the following section.

A sulfite-based plating solution containing formaldehyde as the reducing agent was used by Delvaux et al. [55a] for the fabrication of gold nanotube arrays within the pores of a polycarbonate membrane to be used as an enzyme biosensor. Their plating solution had the following composition: $7.9 \times 10^{-3}\,M$ $Na_3Au(SO_3)_2$, $0.127\,M$ Na_2SO_3, and $0.625\,M$ HCHO. The plating was carried out at 4°C.

A commercial sulfite–formaldehyde electroless gold plating solution was used exclusively in recent nanotechnological applications, which will be reviewed briefly in Section 21.6.

21.5.2 Baths with Au(I)–Thiosulfate Complex

The Au(I)–thiosulfate complex, $[Au(S_2O_3)_2]^{3-}$, has been known since the 1910s. This complex ion has a large stability constant, 10^{26} [56], ranking next to that of $[Au(CN)_2]^-$, which is 10^{39}. For comparison, the stability constant of the sulfite complex, $[Au(SO_3)_2]^{3-}$, is only $I0^{10}$ [57]. It is thus natural that the use of the thiosulfate complex had been proposed for formulating electrolytic gold plating baths [58]. In contrast, the use of the thiosulfate complex for electroless gold plating is only a recent development. Sullivan et al. [59] made an extensive cyclic voltammetric study of the cathodic reduction of $[Au(S_2O_3)_2]^{3-}$ and the anodic oxidation of various reducing agents. They showed that among a number of reducing agents investigated, ascorbic acid is the only compound that is electro-catalytically oxidized at a reasonable rate within the potential range of the reduction of $[Au(S_2O_3)_2]^{3-}$ at a pH between 6.4 and 9.2 and at room temperature. They thus formulated the electroless gold plating bath with the composition listed in Table 21.7. An interesting observation made by the above authors is that the gold deposition rate is greater in air than in nitrogen atmosphere. This effect is attributed to the formation of H_2O_2

TABLE 21.6 Au(l)–Sulfite–Catechol Bath

$Na_3Au(SO_3)_2$	$0.01\,M$
EDTA·2Na	0.3
KH_2PO_4	0.04
Catechol	0.1
PH	7.0
Temperature	65°C
Plating rate	$0.25\,\mu m\,h^{-1}$

Source: Ohtani et al. [52a].

TABLE 21.7 Au(I) Thiosulfate–Ascorbic Add Bath

$Na_3\ Au(S_2O_3)_2$	$0.03\,M$
Na L-ascorbate	0.05
Citric acid	0.4
pH (KOH)	6.4
Temperature	30°C
Plating rate	$0.76\,\mu rn\,h^{-1}$

Source: Sullivan et al. [59].

as a by-product of air oxidation of ascorbic acid, which reacts with excess free $S_2O_3^{2-}$ produced as a result of the reduction of the Au(I)–thiosulfate complex. The accumulation of free $S_2O_3^{2-}$ ions has been shown to decelerate the gold deposition. It has also been shown that the air oxidation of ascorbic acid is catalyzed by the presence of $[Au(S_2O_3)_2]^{3-}$ ions. Sullivan and Kohl [60] extended the above study further to obtain an understanding of the reactions involved in this plating system by using a rotating-ring disk electrode. They showed that hydrogen peroxide does not significantly react with the Au(I)–thiosulfate complex or ascorbic acid but reacts with free $S_2O_3^{2-}$ ions to form trithionate $(S_3O_6^{2-})$ and sulfate (SO_4^{2-}) ions. Utilizing the latter reaction to suppress the accumulation of free thiosulfate ions during the plating, they recommend periodic addition of H_2O_2 into the bath to maintain a constant plating rate. It should be noted that because this bath does not contain any stabilizing additive, the bath life is relatively short (<2 h), which needs to be improved for practical purposes.

21.5.3 Baths Containing Both Sulfite and Thiosulfate

The noncyanide baths described above containing either sulfite or thiosulfate as a sole complexing agent appear to be of limited use because of insufficient stability of the systems. Baths containing both sulfite and thiosulfate are more stable, and those containing thiourea, ascorbic acid, hypophosphite, hydrazine, erythorbic acid, or polyphenol as the reducing agent have been developed. More recently baths containing both sulfite and thiosulfate but no additional reducing agent have been patented. Below, those baths will be described separately.

Thiourea Bath The thiourea bath was developed and subsequently improved by a group of investigators at Hitachi [61–73]. An improved version of the bath composition and operating conditions is shown in Table 21.8 [69]. It is seen that the bath is operated under a set of mild conditions. In this system thiourea has been shown to undergo complex chemical reactions through the formation of a radical intermediate, $(NH)(NH_2)CS\cdot$, to form final products including urea, a major product, and dicyandiamide [69]. This radical intermediate is believed to react with dissolved oxygen in the bath to form formamidine sulfinic acid, $(NH_2)_2CSO_2$, which appears to be responsible for bath instability. Hydroquinone appearing in Table 21.8 as an additional component of the bath reacts quickly with the radical intermediate before it produces the undesirable compound. It is also significant that the reaction between hydroquinone and the radical intermediate regenerates thiourea [72]. Thus hydroquinone acts as a stabilizer as well as a recycling agent for thiourea.

Ascorbic Acid Bath One of the present authors (M.K.) and his co-workers developed the ascorbic acid bath, which is operated at a near-neutral pH and at a mildly elevated temperature. The reason why ascorbic acid was chosen among a large number of reducing agents tested was explained based on the comparison of anodic polarization curves at a gold electrode. A similar approach was used by Sullivan et al. [59] in selecting ascorbic acid as the reducing agent for their room temperature, pure thiosulfate bath described in the preceding section. The original bath [54, 55] has since been improved considerably in terms of bath stability, plating rate, and substrate compatibility [74–77], and a comprehensive review of the improvements has been presented recently [76]. An example of the improved bath composition and operating conditions is given in Table 21.9.

The improvements made were primarily in bath stability, selectivity in plating patterned substrates, and plating rate. The addition of a minute amount of a heterocyclic mercapto compound such as 2-mercaptobenzothiazole (MBT), 2-mercaptobenzoimidazole (MBI), and 6-ethoxy-2-mercaptobenzothiazole (EMBT) stabilizes the bath considerably while maintaining the plating rate at an acceptable level. The bath life of only 3 h in the absence of stabilizers can be increased to more than 35 h by the addition of a suitable amount of these stabilizers [76]. It has also been shown that increasing the sulfite concentration improves bath stability and the addition of excess sulfite helps prevent extraneous gold deposition from occurring on the surface of ceramic substrates with a circuit pattern delineated by using a conventional technique.

The plating rate of the improved bath containing a stabilizer such as MBT is of the order of 1 $\mu m\,h^{-1}$. It has been

TABLE 21.8 Sulfite–Thiosulfate–Thiourea Bath

$NaAuCl_4$	0.005–0.025 *M*
Na_2SO_3	0.04–0.2
$Na_2S_2O_3$	0.2–0.6
$Na_2B_4O_7$	0.066–0.13
Thiourea	0.0013–0.013
Hydroquinone	0.0018–0.018
pH	7.5–8.5
Temperature	60–90°C

Source: Inoue et al. [69].

TABLE 21.9 Sulfite–Thiosulfate-Ascorbic Add Bath

$NaAuCl_4$	0.01 *M*
Na_2SO_3	0.08–0.32
$Na_2S_2O_3$	0.08–032
Na_2HPO_4	0.05–0.20
Na L-ascorbate	0.05–0.20
2-Mercaptobenzothiazol	Trace
pH	7.5
Temperature	60°C

Source: Kato et al. [76].

shown that certain additives increase the plating rate significantly. For example, the addition of 0.005 *M* of ethylenediamine increases the rate by a factor of 3. The thallous ion is also an effective accelerator. The addition of 1 ppm of Tl^+ doubles the rate. The acceleration effect of Tl^+ has been shown to be due to its depolarization effect on the partial cathodic reaction brought about by the UPD of Tl on gold. The effect is similar to what is known for the cyanide system with borohydride as the reducing agent.

More recently Honma and co-workers [78, 79] investigated the ascorbic acid bath containing both sulfite and thiosulfate as complexing agents. They found that the addition of nitrilotriacetic acid (NTA) improves the stability of the Au(I)–sulfite complex through the formation of a complex which is more stable with respect to the disproportionation of Au^+. However, the bath stability was still insuficient, and effects of other additives were examined. They reported that $K_4Fe(CN)_6$, $K_2Ni(CN)_4$, 2,2′-bipyridyl, and cupferron were effective in the concentration range of 0.1–100 ppm. It was found that the bond strength between gold wire and the deposit was much greater when the bath with $K_2Ni(CN)_4$ or cupferron was used than that with 2,2′-bipyridyl. This difference was attributed, not to impurity content or deposit surface morphology, but to crystal orientation. Namely the deposits with good bondability had (220) and (311) preferred orientations. The above authors also found that aeration helps to stabilize the bath by suppressing the disproportionation reaction of Au^+. However, it should be noted that dissolved oxygen will react with free sulfite ions to form sulfate ions, which must be taken into consideration in controlling the concentrations of bath constituents. Another significant finding reported is that the addition of hydrazine as a second reducing agent increases the plating rate by a factor of up to 2. Plating rates up to approximately 1.7 μm h^{-1} were achieved at pH 6 and 60°C. (See the section below for hydrazine bath.)

Hypophosphite Bath Paunovic and Sambucetti [80] made an extensive investigation of noncyanide electroless gold plating systems on the basis of polarization measurements. The results of their study using sulfite alone, thiosulfate atone, their mixture, phosphate, and pyrophosphate as complexing agents and hypophosphite, formaldehyde, DMAB, and TMAB (trimethylamine borane) as reducing agents showed that the sulfite–thiosulfale mixed-ligand system combined with hypophosphite gives the most satisfactoty performance in terms of bath stability and plating rate. Their baths were prepared by mixing equal parts of two solutions, A and B, followed by the addition of a reducing agent. The compositions of the two solutions were as follows: solution A consisting of 0.005 *M* $NaAuCl_4$, 0.16 *M* boric acid, NaOH to adjust pH, and solution B consisting of 0.1 *M* each of Na_2SO_3 and $Na_2S_2O_3$, 0.16 *M* boric acid, and NaOH to adjust pH. The concentration of Na_2HPO_2 in the bath was 0.075 *M*. The above authors found that the addition of citrate at the concentration of 0.5 *M* increases the plating rate con siderably. They state that citrate appears to act as an additional reducing agent. The plating rate achieved at pH 7.5 and 70°C was 0.9 μm h^{-1}. The bath stability was about 10 h, but the authors state that it can be extended for much longer periods of time by the addition of a stabilizer such as SCN^-. The RBS and Auger spectrometric analyses of the gold deposit showed that sulfur is not incorporated in the deposit. Microprobe analysis showed none or less than 200 ppm of sulfur. Good bondability of gold wire to the deposit was confirmed.

Hydrazine Bath Shiokawa et al. [81] used hydrazine as the reducing agent in their sulfite–thiosulfate bath. An Au(I)–sulfite complex salt was used as the source of gold. They found that the presence of both sulfite and thiosulfate is necessary for bath stability. The following compounds were also incorporated for the reasons stated: EDTA or a similar strong complexing agent to mask metallic impurities such as Cu^{2+} and Ni^{2+}; an amine such as triethanolamine, ethylenediamine, or dimethylamine to suppress the formation of "gas pits"; a quinoline derivative such as 2-chloroquinoline or 2-chloromethylquinoline to prevent extraneous deposition on substrates patterned with photoresist; a salt of hydroxy polycarboxylic acid such as sodium or potassium citrate or tartrate which helps to stabilize the bath; and a minute amount of As^{3+}, Tl^+, or Pb^{2+} to improve plating uniformity. The bath is operated at pH 6–7 and 50–75°C, and it yields a plating rate in the range of 0.4–1.5 μm h^{-1}. The bath was operated successfully with replenishment up to five turnovers. An example of bath composition and operating conditions given in the patent disclosure is as follows: $(NH_4)_3Au(SO_3)_2$ 4 g L^{-1}, Na_2EDTA 100 g L^{-1}, dimethylamine 3 g L^{-1}, $Na_2S_2O_3$ 10 g L^{-1}, 2-chloromethylquinoline 10 mg L^{-1}, K-tartrate 30 g L^{-1}, Tl_2SO_4 3 mg L^{-1}, hydrazine monohydrochloride 25 g L^{-1}; pH 6.5; and temperature 60°C. This bath plated 0.93 μm in 1 h.

In a later investigation by the same inventors, it was found that when the hydrazine bath was used to plate gold on copper-clad printed circuit boards with fine circuit patterns, the copper-tended to dissolve into the bath, causing abnormal gold deposition in the areas where copper was attacked. The accumulation of dissolved copper also caused the bath to decompose. To prevent these phenomena from occurring, the addition of benzotriazole (BTA), a well-known corrosion inhibitor for copper metal, at a concentration in the range of 3–10 g L^{-1} was found to be effective [82].

Erythorbic Acid Bath Kurashima et al. [82a] developed a sulfite–thiosulfate mixed bath with erythorbic acid as the reducing agent. The bath composition and operating conditions are listed in Table 21.10. On a sheet of copper coated with a 5-μm-thick electroless Ni–P film and a 0.047-μm-thick galvanic displacement gold layer, the gold deposition

TABLE 21.10 Sulfite–Thiosulfate–Erythorbic Acid Bath

$Na_3Au(SO_3)_2$	0.015 *M*
$Na_2S_2O_3$	0.1
Na_2SO_3	0.4
Na–erythorbate	0.05
KNa–tartrate	0.18
Additives	
BTA	0.0075 *M*
EDTA	0.067
en	?
pH	7.3
Temperature	65°C
Plating rate (without additives)	0.72 μm h^{-1}

Source: Kurashima et al. [82a].

proceeded partly by a galvanic displacement reaction with Ni and partly by the autocatalytic reaction. The ratio of the two participating reactions was studied under various conditions. The deposition rates by both reactions were found to increase with increasing erythorbic acid concentration. It was found that the displacement reaction is almost completely suppressed, and the autocatalytic gold deposition is promoted, by the addition of BTA, EDTA, and ethylenediamine.

Reaction Mechanisms To prepare the baths described above, either a salt of Au(I)–sulfite complex or sodium chloroaurate(III) can be used as the source of gold. When a solution of the latter compound is mixed with that containing sulfite and/or thiosulfate, Au(III) is reduced to form Au(I) complexes. Two Au(I) complex species can form according to the following reactions:

$$\begin{aligned} &Au(III) + SO_3^{2-} + 2S_2O_3^{2-} + H_2O \\ &\quad \Leftrightarrow [Au(S_2O_3)_2]^{3-} + SO_4^{2-} + 2H^+ \end{aligned} \tag{21.14}$$

$$Au(III) + 3SO_3^{2-} + H_2O \Leftrightarrow [Au(SO_3)_2]^{3-} + SO_4^{2-} + 2H^+ \tag{21.15}$$

Thus both Au(I) complex species can be present in the bath.

Kato et al. [55] determined cathodic polarization curves for the deposition of gold in solutions containing, respectively, sulfite alone, thiosulfate alone, and both sulfite and thiosulfate to obtain information as to which Au(I) complex is reduced from the mixed-ligand system. The polarization curves obtained with equal concentrations of sulfite and thiosulfate (0.1 or 0.4 *M*) are shown in Figure 21.9. It is seen that the addition of thiosulfate ions to the solution of Au(I) containing sulfite alone shifts the polarization curve for the reduction of the Au(I)–sulfite complex to the potential range where the reduction of the Au(I)–thiosulfate complex takes

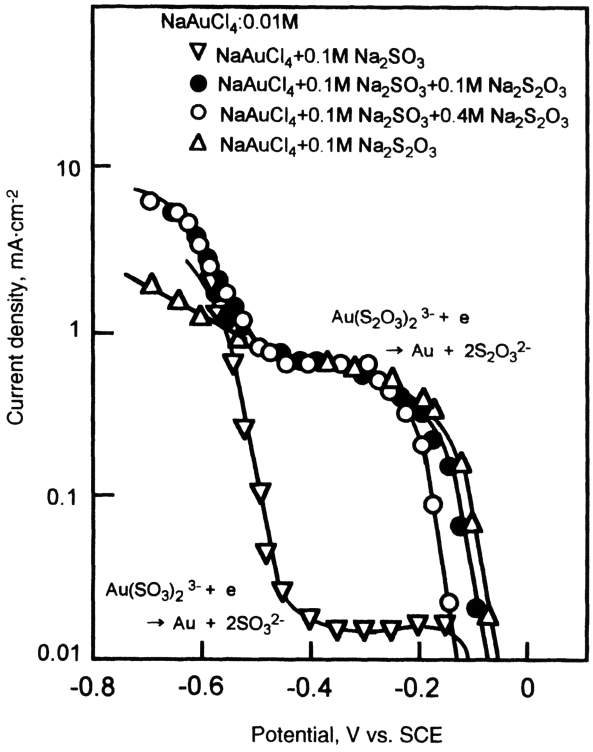

FIGURE 21.9 Polarization curves for gold deposition from various mixtures of $NaAuCl_4$, Na_2SO_3, and $Na_2S_2O_3$. Concentrations of SO_3^{2-} and $S_2O_3^{2-}$ were equal to each other in mixtures containing both anions [55].

place. This result indicates that the gold deposition takes place from the Au(I)–thiosulfate complex. This conclusion seemed reasonable in view of the fact that $[Au(S_2O_3)_2]^{3-}$ is much more stable than $[Au(SO_3)]_2^{3-}$ as indicated by their stability constants mentioned in the preceding section. In a later study [76], however, it was found that when sulfite was added in large excess over thiosulfale, such as 0.32 *M* of SO_3^{2-} and 0.08 *M* of $S_2O_3^{2-}$ the situation was completely different. Namely the polarization curve for the solution containing both sulfite and thiosulfate was closer to that for the solution containing sulfite alone rather than thiosulfate alone, as shown in Figure 21.10. Apparently, in the presence of a large excess of sulfite, the gold deposition does not take place from $Au(S_2O_3)_2^{3-}$ as it does in the solution containing 0.1 *M* each of sulfite and thiosulfate. Okudaira and Takehara [73] made an ion chromatographic study of gold complexes formed in the sulfite–thiosulfate system and concluded that the mixed-ligand complex, $[Au(SO_3)(S_2O_3)]^{3-}$, can also form depending on the concentration ratio of the components.

In conjunction with the generally known anodic oxidation reactions of thiourea, ascorbic acid, hypophosphite, and hydrazine, major cathodic and anodic partial reactions comprising the overall electroless gold deposition reaction from

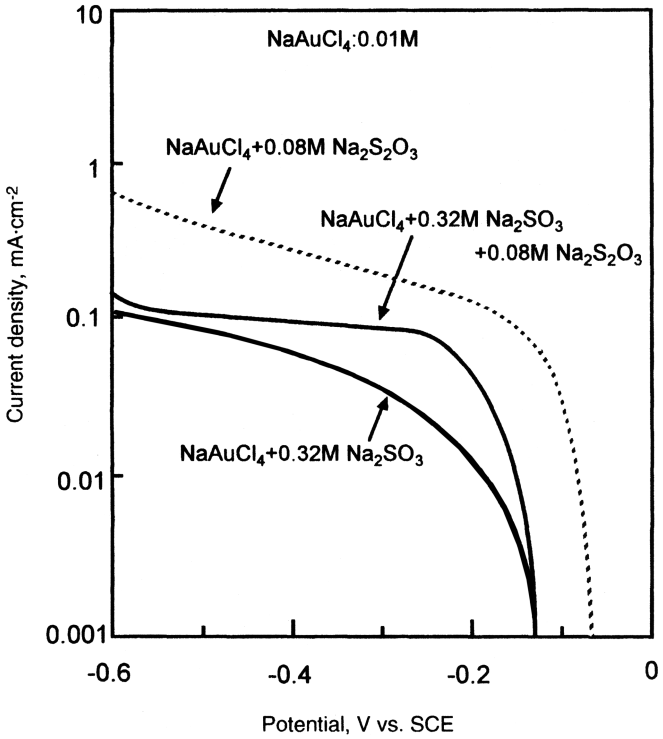

FIGURE 21.10 Polarization curves for gold deposition from various mixtures of $NaAuCl_4$, Na_2SO_3, and $Na_2S_2O_3$ with large excess of SO_3^{2-} over $S_2O_3^{2-}$ [76].

sulfite–thiosulfate mixtures can be written as follows:

Cathodic partial reactions:

$$[Au(SO_3)_2]^{3-} + e^- \rightarrow Au + 2SO_3^{2-} \quad (21.16)$$

$$[Au(S_2O_3)_2]^{3-} + e^- \rightarrow Au + 2S_2O_3^{2-} \quad (21.17)$$

$$[Au(SO_3)(S_2O_3)_2]^{3-} + e^- \rightarrow Au + SO_3^{2-} + S_2O_3^{2-} \quad (21.18)$$

Anodic partial reactions:

- Thiourea bath,

$$\underset{\text{(urea)}}{CS(NH_2)_2} + 5H_2O \rightarrow CO(NH_2)_2 + H_2SO_4 + 8H^+ + 8e^- \quad (21.19)$$

- Ascorbic acid bath,

$$C_6H_8O_6 \rightarrow \underset{\left(\begin{array}{c}\text{dehydro-}\\ \text{ascorbic acid}\end{array}\right)}{C_6H_6O_6} + 2H^+ + 2e^- \quad (21.20)$$

- Hypophosphite bath,

$$2H_2PO_2^- + 2OH^- \rightarrow 2H_2PO_3^- + H_2 + 2e^- \quad (21.21)$$

- Hydrazine bath,

$$N_2H_4 + 4OH^- \rightarrow N_2 + 4H_2O + 4e^- \quad (21.22)$$

Anodic partial reactions for the catechol bath and the erythorbic acid bath are not described in the corresponding references [52a, 82a].

Baths Containing No Additional Reducing Agent Recently, Krulik and Mandich [83] discovered that the Au(I) sulfite–thiosulfate system functions as an autocatalytic gold plating bath without adding any conventional reducing agent. Such a bath was found to plate 0.03–0.3 μm of gold in 15min at pH 6.5–9.0 and 55–75°C directly on electroless nickel deposited on copper-clad epoxy glass laminated printed circuit board. The gold deposition was confirmed to occur on a layer of immersion (galvanic displacement) gold deposited on the electroless nickel, indicating the autocatalytic nature of the gold deposition process. The inventors believe that the sulfite–thiosulfate mixture itself is a reducing agent system and that especially sulfite functions as the main reducing agent in this bath. Because sulfite is oxidized by air and the oxidation catalyzed by impurities such as Cu^{2+} and Ni^{2+} ions, the addition of a strong complexing agent such as EDTA and NTA is recommended to reduce the effect of such contaminants. The bath is said to be completely stable for more than 10 replenishment cycles over the period of many months.

In another patent the same inventors [84] describe that the plating rate of the above system can be increased by adding an amino acid such as glycine, alanine, glutamine, leucine, lysine, and valine. They obtained 0.39–1.0 μm of gold in 10 min using baths containing one of the amino acids or mixtures of two or more of those compounds.

21.5.4 Bath Containing Sulfite and Thiocyanate

Kawashima and Nakao [85] developed a bath containing sulfite and thiocyanate in place of thiosulfate as mixed ligands. Ascorbic acid was used as the reducing agent. The bath contained 0.01 *M* $HAuCl_4$, 0.1 *M* Na_2SO_3, 0.1 *M* KSCN, and 0.1 *M* ascorbic acid, and it was operated at pH 6.0 and 60°C. The plating rate was approximately 0.5 μm h^{-1} on a copper or brass plate with successive layers of electroless nickel and displacement gold. The plating rate decreased with increasing concentration of Na_2SO_3 and increased with increasing KSCN concentration. The bath exhibited good stability during two to three temperature cycles consisting

of heating at 60°C for 6 h and room temperature stand for 18 h, including the period for natural cooling. Good wire bondability is reported on a 0.5-μm-thick film plated in this bath.

21.5.5 Bath with Au(III)–Phosphate Complex

Based on polarization measurements for the reduction of chloroaurate(III) in solutions of various complexing agents (phosphate, pyrophosphate, and glycine) combined with those for the oxidatin of various reducing agents (hydrazine, borohydride, and DMAB), Ohno and co-workers [86] selected a combination of phosphate and DMAB. Their typical bath composition is as follows: 0.005 *M* $NaAuCl_4$, 0.2 *M* Na_2HPO_4, 0.01 *M* DMAB, and 0.5×10^{-5}–1.0×10^{-5} *M* MBT. The bath is operated at pH 11.0 and 60°C. The system is of interest because of the simplicity in bath composition. However, the plating rate reported is only 0.16 μm h^{-1}, which is too low for most applications. A further study is necessary to make the bath more practical.

Paunovic and Sambucetti [80] also evaluated an Au(IU) phosphate bath using formaldehyde as the reducing agent. They found that the bath was stable for only 2–3 h with a plating rate of 0.9–1.5 μm h^{-1}. It was stated that stabilizer addition must be investigated to improve this system.

21.5.6 Bath with Au(I)–Mercaptosuccinate

Takeuchi et al. [87] report that the electroless gold plating bath they developed with mercaptosuccinic acid as the complexing agent for Au(l) and L-cysteine as reducing agent is highly stable and deposits gold autocatalytically at neutral pH of 7.0. Unlike the cyanide-based bath using borohydride or DMAB as the reducing agent, the mercaptosuccinate bath is not sensitive to contamination of the bath with nickel ions. However, this bath was found to be highly sensitive to copper contamination even at the copper concentration as low as 2 ppm, resulting in bath decomposition. Thus, when a copper substrate is to be plated with gold in this bath, the inventors recommend that the substrate be coated with a 2-μm-thick layer of electroless Ni–P deposit to prevent the dissolution of the copper. The bath composition and operating conditions are shown in Table 21.11.

TABLE 21.11 Mercaptosuccinate–L-Cysteine Bath

Au(l)–mercaptosuccinate	0.01 *M*
Mercaptosuccinic acid	0.27
L-Cysteine	0.08
KH_2PO_4	0.15
pH	7.0
Temperature	80°C
Plating rate	0.4 μm h^{-1}

Source: Takeuchi et al. [87].

21.5.7 Bath Prepared by Mixing Au(lll)–Iodide Complex with Ascorbic Acid

Yasutake et al. [88] recently prepared a unique electroless gold plating bath by dissolving thin gold films in a commercially available medical liquid known as iodine tincture and adding ascorbic acid as the reducing agent. Iodine tincture is a mixture of I_2 and Kl in ethanol and contains I_3^-, which reacts with the gold film to form $[AuI_4]^-$. The addition of ascorbic acid reduces excess I_3^- to I^- and the Au(lll) complex to Au on the gold surface. This plating solution was utilized for fabricating nanogap gold electrodes on SiO_2/Si substrates. (See Section 21.6.)

21.6 RECENT APPLICATIONS

This section briefly describes several recent applications of electroless gold reported in the open literature.

1. Electroless gold is used in high-density semiconductor packages in which semiconductor chips are connected to gold-plated terminals on package substrates by gold wire bonding performed at an elevated temperature and with ultrasonic irradiation. The package substrates are mounted on a printed wiring board using solder balls, which are formed also at an elevated temperature on gold-plated pads. When electroless gold is plated directly on the layer of nickel on the pads, the elevated temperature involved in the wire bonding operation causes the nickel to diffuse to the gold surface, which deteriorates the reliability of bond strength. The soldering causes the formation of a corrosion layer between gold and nickel, resulting in a decrease in the strength of solder ball joints. Hasegawa et al. [89] found that the deposition of a layer of electroless (immersion) palladium on the nickel helped alleviate these problems.
2. As was mentioned in Section 21.5.1, Delvaux and Demoustier-Champagne [55a] prepared arrays of nanoscopic gold tubes within the perfectly cylindrical pores of 15–1000 nm in diameter in polycarbonate track-etched membranes (called PTM) by electroless deposition in a sulfite-based solution containing formaldehyde as the reducing agent. The gold-plated nanoporous PTM was shown to be useful as a highly sensitive glucose biosensor. In this application glucose oxidase was immobilized on self-assembled monolayers (SAMs) of mercaptoethylamine or mercaptopropionic acid on the surface of electroless gold nanotubes.
3. Yasutake et al. [88], utilizing the electroless gold deposition process from the Au(lll)–iodide/ascorbic acid bath (see Section 21.5.7), developed a method of

simultaneous fabrication of multiple nanogap electrodes on SiO_2/Si substrate with the electrode pattern delineated by electron beam lithography on the thin Au(15 nm)/Cr(5 nm) metallization layer. The separation distance of less than 5 nm between the nanogap electrodes was achieved with a high yield. The nanogap electrodes are useful for fabricating single-electron and single-molecule devices.

4. It is known that gold is a desirable stationary phase support material for an electrochemically modulated liquid chromatography apparatus for protein separation. For reasons of the high cost of gold and its softness, deformability, and possibility of cold sintering, resulting in high pressure drop occurring in the chromatography column, Lam et al. [90] proposed to use instead 316L stainless steel beads coated with electroless gold. The thiosulfate–ascorbic acid bath [59] was used for this purpose. Complete removal of the passive oxide layer on the stainless steel beads was critically important for successful electroless gold deposition. It was noted that the first gold layer was formed by the galvanic displacement reaction between metallic iron and gold ions in the solution. The average gold deposition rate obtained was reported to be about $0.15\,\mu m\,h^{-1}$ and the gold thickness used was about 80 nm.
5. Ishikawa et al. [91] used a cyanide-based electroless gold plating solution with hydrazine as the reducing agent to coat poly(*p*-phenylene benzobisoxazole) (PBO) fibers (known as Zylon) with gold for both functional and decorative applications. Prior to the electroless gold deposition, the fibers were coated with electroless copper and electroless nickel. Because of the light weight, high modulus, and high strength of the fiber combined with high electrical conductivity and high corrosion resistance of the gold layer, the electroless gold-coated PBO is expected to find functional applications in the field of aircraft and aerospace manufacturing in addition to decorative applications.
6. It is noteworthy that the technique of electroless gold deposition has been utilized extensively in recent years for preparing various nanostructured materials and devices [92–99]. In addition to the fabrication of multiple nanogap gold electrodes described in example 3 above [88], the following applications are noted:
   - Fabrication of gold nanotubular membrane for chemical and biological separations [95, 96].
   - Preparation of gold nanotubes and nanowires supported by polycarbonate fiber with cylindrical nanopores for the fabrication of nanoelectrode ensembles, molecular filters, and chemical switches [97, 98].
   - Synthesis of gold nanoparticles measuring 5–9 nm by depositing electroless gold in a mesoporous material (SBA-15) with ordered pore structure [99].

For further information on these interesting applications, the reader is referred to the original articles.

21.7 CONCLUSION

An extensive literature survey conducted to update this chapter indicates that much effort has been devoted to the development, mechanistic understanding, and characterization of new electroless gold plating processes, especially noncyanide systems. It is hoped that no major contributions published in the open literature were missed in this revision. New applications of electroless gold plating, particularly in the area of nanotechnology, are noteworthy.

Although only autocatalytic processes are reviewed in this chapter, it should be remembered that the other two mechanistically different "electroless" processes, that is, galvanic displacement (immersion) and substrate-catalyzed processes, are also useful, particularly when requirements for the thickness and porosity of the gold film are not stringent. Those non-autocatalytic plating baths are inherently more stable than autocatalytic baths, the latter being thermodynamically unstable and hence requiring much more careful maintenance of solution composition and operating conditions. The importance of understanding the reaction mechanism and the limitation of each process cannot be overemphasized for its successful practical application.

In view of the recent, significant applications to nanotechnology briefly introduced in this revision, it is anticipated that "electroless" gold plating, including all three mechanistically different processes, will find an increasing number of novel applications in the near future.

REFERENCES

1. A. Brenner and G. Riddell, *J. Res. Natl. Bur. Std.*, **37**, 31 (1946); **39**, 385 (1947). (a) Y. Okinaka, *Plating*, **57**, 914 (1970).
2. Y. Okinaka and C. Wolowodiuk, *Plating*, **58**, 1080 (1971).
3. R. Sard, Y. Okinaka, and J. R. Rushton, *Plating*, **58**, 893 (1971).
4. Y. Okinaka, *J. Electrochem. Soc.*, **120**, 739 (1973).
5. Y. Okinaka, R. Sard, C. Wolowodiuk, W. H. Craft, and T. F. Retajczyk, *J. Electrochem. Soc.*, **121**, 56 (1974).
6. R. Sard, Y. Okinaka, and H. A. Waggener, *J. Electrochem. Soc.*, **121**, 62 (1974).
7. L. A. D'Asaro, S. Nakahara, and Y. Okinaka, *J. Electrochem. Soc.*, **127**, 1935 (1980).
8. D. Lamouche, P. Clechet, J. R. Martin, G. Haroutionian, and J. P. Sandino, *Surf. Sci.*, **161**, L554 (1985).

9. L. M. Schiavone, *J. Electrochem. Soc.*, **125**, 851 (1978).
10. Y. Takakura, *Jitsumu Hyomen Gijutsu* (Metal Finishing Practice), **27** (1), 31 (1980).
11. Y. Takakura, Kokai Tokkyo Koho (Japanese Patent Disclosure), 269 (1981).
12. J. A. Gardiner and J. W. Collat, *J. Am. Chem. Soc*, **86**, 3165 (1964); **87**, 1692 (1965); *Inorg. Chem.*, **4**, 1208 (1965).
13. E. A. Efimov, T. V. Gerish, and I. G. Erusalimchik, *Zaschita Metallov.*, **11** (3), 383 (1975).
14. E. A. Efimov, T. V. Gerish, and J. G. Erusalimchik, *Zaschita Metalloy*, **12** (6), 724 (1976). (a) A. Sargent, O. A. Sadik, and L. J. Matienzo, *J. Electrochem. Soc*, **148** (4), C257 (2001). (b) O. A. Sadik, H. Xu, and A. Sargent, *J. Electroanal. Chem.*, **583**, 167 (2005).
15. D. M. MacArthur, *J. Electrochem. Soc*, **119**, 672 (1972).
16. J. A. Harrison and J. Thompson, *J. Etectroanal. Chem.*, **40**, 113 (1972).
17. T. Sawaguchi, T. Yamada, Y. Okinaka, and K. Itaya, *J. Phys. Chem.*, **99**, 14149 (1995).
18. J. D. E. McIntyre and W. F. Peck, *J. Electrochem. Soc*, **123**, 1800 (1976).
19. M. Matsuoka, S. Imanishi, M. Sahara, and T. Hayashi, *Plating Surf. Finish.*, **75** (5), 102 (1988).
20. S. Sasaki, Kokai Tokkyo Koho (Japanese Patent Disclosure), 59-124428, (1984.).
21. N. Honma, Kokai Tokkyo Koho (Japanese Patent Disclosure), 59-229478 (1984).
22. W. Ott, European Patent Application, EP 281804 (1988).
23. M. F. El-Shazley and K. D. Baker, U.S. Patent 4,337,091 (1982).
24. K. Ohtsuka, K. Okuno, N. Hattori, and E. Torikai, paper presented at the Printed Circuit World Convention, Paper No. C 1/2, Scotland, 1980.
25. F. Simon, *Gold Bull.*, **26** (1), 14 (1993).
26. C. D. Iacovangelo, *J. Electrochem. Soc*, **138**, 976 (1991).
27. H. O. Ali and I. R. A. Christie, *Gold Bull*, **17** (4), 118, (1984).
28. C. D. Iacovangelo and K. P. Zarnoch, *J. Electrochem. Soc*, **138**, 983 (1991).
29. Y. Okinaka, in *Gold Plating Technology*, F. H. Reid and W. Goldie, Eds., Electrochemical Publications, Ayr, Scotland, 1974, Ch. 11.
30. Y. Okinaka, in *Electroless Plating: Fundamentals and Applications*, G. O. Mallory and J. B. Haydu, Eds., American Electroplaters and Surface Finishers Society, Orlando, FL, 1990, Ch. 15.
31. S. D. Swan and E. L. Gostin, *Met. Finish.*, 59 (4), 52 (1961).
32. R. R. Brookshire, U.S. Patent 2,976,181 (1961).
33. T. Ezawa and H. Ito, Kokai Tokkyo Koho (Japanese Patent Disclosure), 40-1081 (1962).
34. E. L. Gostin and S. D. Swan, U.S. Patent 3,032,436 (1962).
35. A. N. Moskvichev, G. A. Kurnoskin, and V. N. Flerov, *Zhur. Prikl. Khim.*, **54** (9), 2150 (1981).
36. A. N. Moskvichev, G. A. Kurnoskin, V. N. Flerov, and Z. P. Gerasimova, *Izv. Vyssh. Vchebn. Zaved. Khim. Tekhnol.*, **25** (9), 1104 (1982).
37. K. Wundt, B. Mankau, J. Schaad, and H. Meyer, German Patent DE 3614090 (1987); *Gold Patent Digest*, **5** (3), 14 (1987).
38. M. Dettke and L. Stein, German Patent DE 3029785 (1982); *Gold Patent Digest*, Pilot issue, **8** (1982).
39. H. E. Bellis, U.S. Patent 3,697,296 (1972).
40. H. A. Efimov and T. V. Gerish, *Zaschita Metallov.*, **15** (2), **240** (1979).
41. T. Oda and K. Hayashi, U.S. Patent 3,506,462 (1970).
42. R. Gesemann, J. Spindler, A. Eysert, R. Broulik, U.Heinzig, and H.-U. Galgon, German Patent DD 263307;*Gold Bull.*, **22 (3)**, 75 (1989).
43. E. Andrascek, H. Hadersbeck, and F. Wollenhorst, German Patent DE 3237394 (1984).
44. Y. Nishiyama, S. Wakabayashi, and N. Wakabayashi, Kokai Tokkyo Koho (Japanese Patent Disclosure) 60-125379 (1985).
45. Z. Mathe, *Met. Finish.*, **90** (1), 33 (1992).
46. G. M. Ganu and S. Mahapatra, *J. Sci. Ind. Res.*, **46** (4), 154 (1987).
47. F. Richter, R. Gesemann, L. Gierth, and E. Hoyer, German Patent DD 150762 (1981).
48. R. Gesemann, F. Richter, L. Gierth, U. Bechtloff, and E. Hoyer, German Patent, 160283 (1983).
49. R. Gesemann, F. Richter, L. Gierth, E. Hoyer, and J. Hartung, German Patent, 160284 (1983).
50. F. Richter, R. Gesemann, L. Gierth, and E. Hoyer, German Patent, 240915 (1986).
51. F. Richter, R.Gesemann, L. Gierth, and E. Hoyer, German Patent, 268484 (1989).
52. Y. Sato, T. Osawa, K. Kaieda, and K. Kobayakawa, *Plating Surf. Finish.*, **81** (9), 74 (1994). (a) Y. Ohtani, A. Horiuchi, A. Yamaguchi, K. Oyaizu, and M. Yuasa, *J. Electrochem. Soc*, **153** (1), C63 (2006).
53. H. Shindo and H. Honma, *Proc. 84th Conf Surface Finish. Soc. Jpn.*, 163 (1991).
54. M. Kato, S. Hoshino, and I. Ohno, Kokai Tokkyo Koho (Japanese Patent Disclosure), 1-191782 (1989).
55. M. Kato, K. Niikura, S. Hoshino, and I. Ohno, *Proc. 82nd Conf. Surface Finish. Soc. Japan,* 109 (1990); *Hyomen Gijutsu (J. Surf. Finish. Soc. Japan)*, **42**, 729 (1991). (a) M. Delvaux and S. Demoustier-Champagne, *Biosensors Bioelectron.*, **18**, 943 (2003).
56. J. Pouradier and M. C. Gadet, *J. Chim. Phys.*, **66**, 109, 1969.
57. P. Wilkinson, *Gold Bull*, **19** (3), 21 (1986).
58. W. S. Rapson and T. Groenewald, *Gold Usage*, Academic, London, 1978, Ch. 10.
59. A. Sullivan, A. Patel, and P. A. Kohl, in *Proc. 81st AESF Technical Conf.,* American Eteciroplaters and Surface Finishers Society, Indianapolis, IN, 1994, p. 595.
60. A. Sullivan and P. A. Kohl, *J. Electrochem. Soc*, **142**, 2250 (1995).
61. J. Ushio, O. Miyazawa, A. Tomizawa, A. Matsuura, and H. Yokono, Kokai Tokkyo Koho (Japanese Patent Disclosure), 87-247081 (1987).
62. J. Ushio, O. Miyazawa, H. Yokono, and A. Tomizawa, Kokai Tokkyo Koho (Japanese Patent Disclosure) 87-86171 (1987).

63. O. Miyazawa, J. Ushio, A. Tomizawa, N. Matsuura, and H. Yokono, Kokai Tokkyo Koho (Japanese Patent Disclosure) 88-79976 (1988).
64. J. Ushio, O, Miyazawa, A. Tomizawa, H. Yokono, N. Kanda, N. Matsuura, S. Ando, H. Okudaira, and K. Mori, Kokai Tokkyo Koho (Japanese Patent Disclosure), 89-268876 (1989).
65. J. Ushio, O. Miyazawa, H. Yokono, and A. Tomizawa, U.S. Patent 4,804,559 (1989).
66. J. Ushio, O. Miyazawa, H. Yokono, and A. Tomizawa, U.S. Patent, 4,880,464 (1989).
67. J. Ushio, O. Miyazawa, A. Tomizawa, H. Yokono, N. Kanda, N. Matsuura, S. Ando, and H. Okudaira, U.S. Patent, 4,963,974 (1990).
68. H. Takehara, U.S. Patent, 94-73554 (1994).
69. T. Inoue, S. Ando, H. Okudaira, J. Ushio, A. Tomizawa, H. Takehara, T. Shimazaki, H. Yamamoto, and H. Yokono, *Proc. 45th IEEE Electronic Components Technol. Conf.*, 1059 (1995).
70. S. Ando, T. Inoue, J. Ushio, H. Okudaira, A. Tomizawa, H. Takehara, T. Shimazaki, H. Yamamoto, and H. Yokono, *Proc. '95 Asian Conf. Electrochem*., 408 (1995).
71. H. Okudaira, S. Ando, T. Inoue, J. Ushio, H. Takehara, A. Tomizawa, and H. Yokono, *Proc. 89th Conf. Surf ace Finish. Soc. Japan*, 29 (1994).
72. H. Okudaira, T. Inoue, S. Ando, T. Shimazaki, H. Yamamoto, and H. Yokono, *Proc. 89th Conf. Surface Finish. Soc. Japan*, 32 (1994).
73. H. Okudaira and H. Takehara, *Proc. 89th Conf. Surface Finish. Soc. Japan*, 30 (1994).
74. M. Kato, Y. Yazawa, and Y. Okinaka, *Proc. 90th Conf. Surface Finish. Soc. Japan*, 146 (1994).
75. M. Kato, Y. Yazawa, and Y. Okinaka, *Proc. 90th Conf. Finish. Soc. Japan*, 148 (1994).
76. M. Kato, Y. Yazawa, and Y. Okinaka, in *Proc. AESF Technical Conf.,* SUR/FIN '95, American Electroplaters and Surface Finishers Society, Baltimore, MD, 1995, pp. 805–813.
77. M. Kato, Y. Yazawa, and S. Hoshino, U.S. Patent 5,470,381 (1995).
78. H, Honma, A. Hasegawa, S. Hotta, and K. Hagiwara, *Plating Surf. Finish.*, **82** (4), 89 (1995).
79. Y. Nishiwaki, H. Honma, and K. Hagiwara, in *Proc. 9th JIPC Conf.,* Japan Institute of Printed Circuits, 1995, p. 45.
80. M. Paunovic and C. Sambucetti, in *Proc. Symp. on Electrochemically Deposited Thin Films,* Vol. 31, M. Paunovic, Ed., Electrochemical Society, Pennington, NJ, 1994, p. 34.
81. K. Shiokawa, T. Kudo, and N. Asaoka, Kokai Tokkyo Koho (Japanese Patent Disclosure), 3-215677 (1991).
82. K. Shiokawa, T. Kudo, and N. Asaoka, Kokai Tokkyo Koho (Japanese Patent Disclosure), 4-314871 (1992). (a) T. Kurashima, H. Nishinakayama, N. Kaneko, N. Shinohara, and H. Nawafune, *Electrochemistry*, **74** (6), 479, (2006).
83. G. A. Krulik and N. V. Mandich, U.S. Patent 5,232,492 (1993).
84. G. A. Krulik and N. V. Mandich, U.S. Patent, 5,318,621 (1994).
85. S. Kawashima and H. Nakao, in *Proc. 10th JIPC Conf.,* Japan Institute of Printed Circuits, Tokyo, 1996, p. 45.
86. I. Ohno, H. Yajima, and H. Numata, in *Proc. Symp. on Electrochemically Deposited Thin Films,* Vol. 26, Electrochemical Society, Pennington, NJ, 1993, p. 130.
87. T. Takeuchi, Y. Kohashi, D.-H. Kim, H. Nawafune, M. Tanikubo, and S. Mizumoto, *Plating Surf. Finish.*, **90** (4), 56 (2003).
88. Y. Yasutake, K. Kono, M. Kanehara, T. Teranishi, M. R. Buitelaar, C. G. Smith, and Y. Majima, *Appl. Phys. Lett.*, **91**, 203107 (2007).
89. K. Hasegawa, A. Takahashi, and A. Nakaso, in *1997 IEMT/IMC Proceedings*, Saitama, Japan, 1997, pp. 230–233.
90. P. Lam, K. Kumar, G. E. Wnek, and T. M. Przybycien, *J. Electrochem. Soc*, **146** (7), 2517 (1999).
91. H. lshikawa, Q. Chen, Y. Bin, K. Komatsu, and M. Matsuo, *J. Mater. Sci.*, **42**, 7772 (2007).
92. K. B. Jirage, J. C. Hulteen, and C. R. Martin, *Science*, **278**, 655 (1997).
93. J. C. Hulteen, K. B. Jirage, and C. R. Martin, *J. Am. Chem. Soc*, **120**, 6603 (1998).
94. K. B. Jirage, J. C. Hulteen, and C. R. Martin, *Anal. Chem.*, **71**, 4913 (1999).
95. S. B. Lee and C. R. Martin, *Anal. Chem.*, **73**, 768 (2001).
96. C. C. Harrell, S. B. Lee, and C. R. Martin, *Anal. Chem.*, **75**, 6861 (2003).
97. M. Wirtz and C. R. Martin, *Adv. Mater.*, **15** (5), 455 (2003).
98. J.-Y. Jung, Y.-S. Kim, H.-S. Shim, and W.-B. Kim, *Solid State Phenom.*, **124–126**, 1729 (2007).
99. T. Asefa and R. B. Lennox, *Chem. Mater*, **17** (10), 2481 (2005).

22

ELECTROLESS DEPOSITION OF ALLOYS

IZUMI OHNO

Electroless metal deposits are mostly a binary alloy containing a metalloid such as phosphorous or boron which itself is a component of the reducing agent. Brenner and Riddel were the first to develop the process of electroless deposition of nickel–cobalt–phosphorus ternary alloy in 1946 [1]. At present, electroless alloy deposition is a practical and effective method for controlling the physicochemical properties of nickel– and cobalt–phosphorus deposits, thereby extending the range of application of electroless deposition. The recent tendency in this field is toward applications in the electronics industry. Despite an increasing number of publications concerning electroless alloy deposition, the details of its mechanisms are not clear yet.

Electroless alloy deposition consists of several electrochemical partial reactions, such as cathodic deposition of the respective alloy components and the anodic oxidation of the reducing agent, although these partial reactions are not always independent of each another. Electroless metal deposition occurs under the condition that the oxidation potential of the reducing agent is less noble than the deposition potential of the metal. In case of alloy deposition, however, the deposition potential E_M^* of a constituent metal M in the alloy M–N shifts to a nobler potential by virtue of the negative Gibbs energy of the alloy formation ΔG_M; thus

$$\Delta E_M = E_M^* - E_M = -\frac{\Delta G_M}{mF} > 0 \qquad (22.1)$$

where ΔE_M is the potential shift, E_M the normal deposition potential of M, m the number of electrons, and F the Faraday constant. The potential shift ΔE_M is of the order of 10^{-2} V at most for solid–solution alloys, but sometimes it reaches up to 1 V in case of compound alloys. Therefore, it is possible to codeposit a metal that cannot be deposited otherwise as a pure metal [2]. Another requirement in electroless deposition is that the metal being deposited requires to have a catalytic activity for the anodic oxidation of the reducing agent [3]. In case of electroless alloy deposition, however, the catalytic activity depends in the last analysis on the composition of the depositing alloy. As shown in Figure 22.1, the rate of electroless nickel–iron alloy deposition using DMAB (dimethylamine borane) decreases with the increase of the iron content in the deposits. This behavior is attributable to the decrease in catalytic activity of the deposits for the anodic oxidation of DMAB, since iron is less active for this reaction than nickel [4, 5].

22.1 ELECTROLESS ALLOY PLATING BATHS

22.1.1 Nickel-Based Alloys

Electroless nickel-based alloys have been produced by adding cations or anionic complexes of the alloying elements into the normal electroless nickel bath [6]. Thus, electroless nickel–phosphorus alloys containing iron [7–12], rhenium [13–20], molybdenum [21–26], tungsten [27–32], zinc [14, 33], tin [14, 23, 34], and copper [35–37] have been produced. Typical bath compositions for electroless nickel-based alloys are summarized in Table 22.1. Electroless nickel–cobalt alloys will be described in Section 22.1.2.

Nickel–Iron Alloys Electroless nickel–iron–phosphorus alloys that contain up to 30%Fe and approximately only 1% P have been reported [8]. Specifically, replacing the reducing agent hypophosphite with DMAB in the bath resulted in Ni–Fe–B alloys [9]. Sodium potassium tartrate in the Ni–Fe–P bath of Table 22.1 may be replaced by the other complexing agents, such as tartrate–glycine [11] or

Modern Electroplating, Fifth Edition Edited by Mordechay Schlesinger and Milan Paunovic

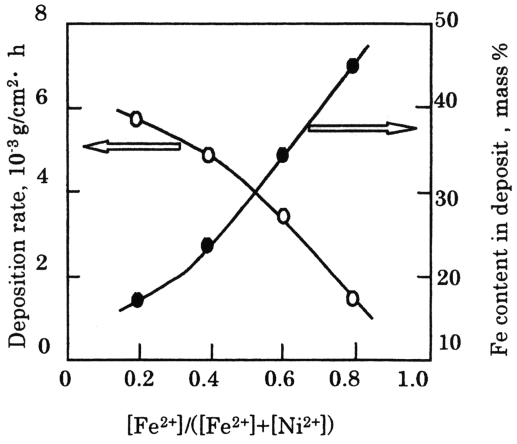

FIGURE 22.1 Effect of bath composition on rate ○ (open circle) and deposited iron mass ● (solid circle) in electroless Ni–Fe deposition. Bath composition: (0.05-x)M $NiSO_4$, 0.0025 M DMAB, 0.1 M Na citrate, xM $Fe(NH_4)_2(SO_4)_2 \cdot 6H_2O$.

tartrate–citrate [12]. Some other electroless Ni–Fe–P and Ni–Fe–B plating baths have been studied employing electrochemical polarization measurements [4, 5]. As a specific example, the polarization curve in a bath which consists of nickel sulfate, ferrous ammonium sulfate, sodium citrate, and DMAB is shown in Figure 22.2. The polarization curves in the absence of the metal sulfates or DMAB are shown as broken and dotted lines respectively in the figure. It is noteworthy that from Figure 22.2 the rate of alloy deposition may be determined by weight gain measurements. Furthermore this value is in good agreement with the estimated value as obtained from the intersection point of the simulated partial anodic and cathodic polarization curves based on the mixed-potential theory. It was also shown that iron as a constituent of the alloy starts to deposit at a nobler potential than that of pure iron [5]. There are some reports dealing with the composition, structure, and corrosion characteristics of Ni–Fe–P and Ni–Fe–P–B alloys [35, 36].

Nickel–Rhenium Alloys Electroless nickel–rhenium–phosphorus alloys have been reported by several workers [13–20]. The alloys deposited contain a large amount of rhenium. Several electroless ternary alloys (Ni–Re–P, Ni–W–P, Ni–Zn–P, Ni–Sn–P) and quaternary alloys (Ni–Re–P–Zn, Ni–Re–P–Sn, Ni–Re–P–W) were reported by Pearlstein and Weightman [14]. Electroless Ni–Re alloy baths reported later are based on those reports [14]. An acidic electroless Ni–Re–P bath presented by Mencer is shown in Table 22.2 [37]. Alloys deposited from this bath contain 0–3.5 at % Re.

Mechanistic study of the reduction of perrhenate ion during electroless Ni–P–Re deposition was performed by Genutiene et al. [38] based on the mass spectrometric analysis of gas that evolved from the deuterium-labeled electroleas plating baths and X-ray photoelectron spectroscopy (XPS) analysis of the electroless Ni–P–Re deposits.

Nickel–Molybdenum Alloys Electroless nickel-based alloys containing molybdenum, tungsten, or zinc can be

TABLE 22.1 Composition of Baths for Electroless Nickel-Based Alloys

Ni-Based Alloys	Ni–Fe–P	Ni–Re–P	Ni–Mo–P	Ni–W–P	Ni–Zn–P
Nickel sulfate, $NiSO_4 \cdot 6H_2O$	56 mM L^{-1}	3.5 g L^{-1}	0.10 M	7 g L^{-1}	—
Nickel chloride, $NiCl_2 \cdot 6H_2O$	—	—	—	—	7.5 g L^{-1}
Sodium potassium tartrate, $KNaC_4H_4O_6 \cdot 4H_2O$	100-350 mM L^{-1}	—	—	—	—
Sodium citrate, $Na_3C_6H_5O_7 \cdot 2H_2O$	—	8.5 g L^{-1}	—	40 g L^{-1}	—
Citric acid, $H_3C_6H_5O_7 \cdot H_2O$	—	—	—	—	19.8 g L^{-1}
Hydroxy acetic acid, $CH_2(OH)COOH$	—	—	0.30 M	—	—
Sodium hypophosphite, $NaH_2PO_2 \cdot 2H_2O$	10 g L^{-1}	10 g L^{-1}	0.28 M	10 g L^{-1}	3.5 g L^{-1}
Ammonium hydroxide, NH_4OH	3.6 mL L^{-1}	50 mL L^{-1}	—	50 mL L^{-1}	—
Ferrous ammonium sulfate, $Fe(NH_4)_2(SO_4)_2 \cdot 6H_2O$	20 g L^{-1}	—	—	—	—
Potassium perrhenate, $KReO_4$	—	0.2 g L^{-1}	—	—	—
Sodium molybdate, $NaMoO_4 \cdot 2H_2O$ (as oxy anionic complex)	—	—	0.05 M	—	—
Sodium tungstate, $NaWO_4 \cdot 2H_2O$	—	—	—	3.5 g L^{-1}	—
Zinc chloride, $ZnCl_2 \cdot 7H_2O$	—	—	—	—	5 g L^{-1}
pH	11.2	8.8–9.2	9	8.2	6-2
Temperature, °C	75	98	87	90	75
Deposits, wt %	25% Fe, 1–0.5% P	46% Re	7.0% Mo, 1.8% P	20% W, 10% P	4–12 at % Zn, 2–26% P
Reference	8	14	23	14	33

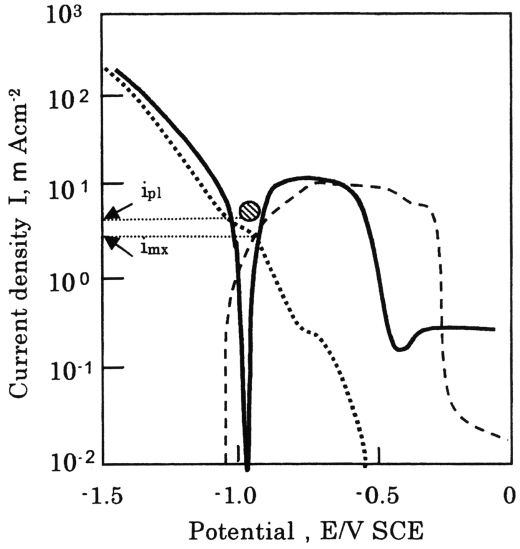

FIGURE 22.2 Polarization curves in electroless Ni–Fe alloy baths. Bath composition: 0.035 *M* $NiSO_4$, 0.015 *M* $Fe(NH_4)_2(SO_4)_2 \cdot 6H_2O$, 0.1 *M* Na citrate, 0.0025 *M* DEAB, ▨: plating rate by weight gain (i_p1).

deposited from the nickel baths containing oxy-anionic complexes of molybdenum, tungsten, and zinc, respectively, using hypophosphite [21–26]. By replacing the hypophosphite with DMAB in the baths, nickel–molybdenum–boron alloys are obtained [21, 22]. The nickel–molybdenum alloys obtained were Ni–7.0% Mo–1.8% P and Ni–31.0% Mo-3.2% B, respectively [22].

Nickel–Tungsten Alloys Electroless deposition of ternary nickel–tungsten–phosphorus alloy was reported first by Pearlstein et al. [27] in 1963. The electroless plating baths are similar to those for electroless nickel–tungsten and nickel–molybdenum alloys, which contain citrate. There have been many publications dealing with electroless nickel—tungsten alloys containing either phosphorus or boron [14, 23, 27–32]. The efficiency of DMAB in electroless deposition of nickel–tungsten–boron is about twice that reported in binary nickel–boron alloys.

TABLE 22.2 Composition of Electroless Ni–Re–P Plating Bath

Nickel sulfate, $NiSO_4 \cdot 7\ H_2O$	0.10 *M*
Potasium perrhenate, $KReO_4$	0–0.007 *M*
Sodium hypophosphite, $NaH_2PO_2 \cdot H_2O$	0.20 *M*
Succinic acid, $C_4H_6O_4$	0.20 *M*
Sodium succinate, $Na_2C_4H_4O_4 \cdot 6H_2O$	0.20 *M*
pH	4.5
Temperature	90–95°C

TABLE 22.3 Composition of Ni–W–B Plating Bath

Bath A		Bath B	
Nickel acetate	7.5–15.0 g L^{-1}	Nickel sulfate	5.6 g L^{-1}
Sodium tungstate	33 g L^{-1}	Sodium tungstate	56 g L^{-1}
DMAB	1.2–2.5 g L^{-1}	DMAB	3.5 g L^{-1}
Malic acid	27 g L^{-1}	Sodium gluconate	37 g L^{-1}
pH	5.0	Thiodiglycolic acid	0.1 g L^{-1}
Temperature	70°C	Sulfosalicylic acid	5 g L^{-1}
		pH	6.0
		Temperature	75°C

Drovosekov et al. [39] studied in detail the composition and structure as well as the chemical states of the elements in electroless Ni–W–B alloy deposits using X-ray structure analysis and XPS. The two types of baths that were used in the study are shown in Table 22.3. Electroless quaternary Ni–W–Cu–P alloy deposition was studied by Balaraju et al. [40, 41].

Nickel–Zinc Alloys Electroless Ni–42 at % Zn–26 at % P alloys [33] were produced by modifying an electroless Co–Zn–P bath [42, 43].

Nickel–Tin Alloys Electroless nickel–tin–phosphorus alloys containing up to 3% Sn and 10% P were deposited from a hydroxyl acetate bath using sodium hypophosphite as reducing agent. By replacing hypophosphite with DMAB in the bath, nickel–tin–boron alloys containing up to 44% Sn and 3.4% B were deposited [21]. Addition of cupric salt to this bath results in quaternary Ni–Sn–Cu–P alloy [23].

Nickel–Copper Alloys Amorphous Nr–(1–4)% Cu–(1–16)% P alloys were produced by Schwartz and Mallory [23], and the thermal stability of the alloys was reported by other workers [44, 45]. Copper–nickel alloys with a wide range of compositions were deposited in electroless nickel baths containing copper sulfate, hypophosphite, and boric acid. Addition of ferrous sulfate to the bath results in a ternary Cu–(6–10) %Ni–(2–4)% Fe [46]. Electroless nickel–palladium [47], nickel–vanadium [48], nickel–platinum [49], nickel–chromium [50], and nickel–boron–phosphorus alloys [51–53] have also been reported.

22.1.2 Cobalt-Based Alloys

The magnetic properties of electroless cobalt alloy films for magnetic recording devices are reviewed in Chapter 19. Similar to electroless nickel-based alloys, it is possible to produce electroless cobalt–phosphorus and cobalt–boron alloys containing one or more additional metals such as nickel [54–65], iron [66–69], rhenium [60], tungsten [60], zinc [42, 43], or silver [70].

Cobalt–Nickel Alloys It is possible to deposit nickel–cobalt–phosphorus alloys with a complete range of nickel–cobalt compositions from alkaline baths since each component metal is capable of electroless deposition independently. The alloy deposits containing cobalt are, however, not deposited from acidic baths containing hypophosphite. Typical electroless plating baths for cobalt–nickel–phosphorus alloys are listed in Table 22.4.

Addition of sodium tungstate dihydrate or potassium perrhenate instead of nickel sulfate hexahydrate in bath 3 in Table 22.4 results in cobalt–phosphorus deposits containing about 9% W or 30% Re, respectively [60]. Bath 5 in Table 22.4 has been developed especially for selective deposition of Co–Ni alloy used for electric contact of complementary metal–oxide–silicon (CMOS) devices [65].

Cobalt–Iron Alloys Electroless cobalt deposits containing up to 45% Fe [66] or 4% Zn [42, 43] have also been produced. Some of the alloys exhibited an improved resistance to tarnishing in salty environments [60] or a superior magnetic property [55–60, 66]. Further, an intentional gradient control of the magnetic properties of an electroless Co–Ni–P alloy deposit was studied by Homma et al. [71, 72].

22.1.3 Other Alloys

There have been several reports on electroless alloys, such as gold-based alloys [73–77], copper-based alloys [15, 28, 78, 79], zinc–arsenic [80], silver–tungsten [81–83], indium–antimony [84], and iron–tin alloy [85].

Gold–Copper Alloys There is a report by Molenaar [73] that electroless gold–copper alloys with a wide range of compositions were deposited from alkaline baths containing copper sulfate, tetrasodium salt of ethylenediaminetetraacetic acid, potassium cyanoaurate, and formaldehyde. Electrochemical polarization measurements of electroless gold–copper plating baths were also performed by the same author [74]. It was suggested that the competitive adsorption of formaldehyde and cyanide on the alloy surface determined the catalytic properties for electroless Au–Cu alloy deposition. The rate of oxidation of formaldehyde on gold–copper alloys was lower than that on gold-rich alloys in cyanide baths.

Copper–Selenium Alloys Copper–selenium alloy has been formed by electroless deposition from a selenium bath containing copper sulfate and indium sulfate. Subsequently indium was incorporated into the film by cathodic polarization [78, 79]. Several quaternary alloys were obtained by addition of cations or anionic complexes of different alloying elements to the plating baths of ternary alloys [76, 86–89].

Copper–Nickel Alloys An acidic bath for electroless deposition of copper-rich Cu–Ni–P alloys was reported by Touir et al. [90]. They reported that the presence of a small amount of nickel ions in the bath make it possible to deposit

TABLE 22.4 Composition of Baths for Electroless Cobalt–Nickel–Phosphorus Alloys

Co–Ni–P Alloys	1	2	3	4	5
Cobalt chloride, $CoCl \cdot H_2O$	$30\,g\,L^{-1}$	—	$30\,g\,L^{-1}$	—	—
Cobalt sulfate, $CoSO_4 \cdot 7H_2O$	—	$10\,g\,L^{-1}$	—	$30\,g\,L^{-1}$	$60\,g\,L^{-1}$
Nickel chloride, $NiCl_2 \cdot 6H_2O$	$15\,g\,L^{-1}$	—	—	—	—
Nickel sulfate, $NiSO_4 \cdot 6H_2O$	—	$15\,g\,L^{-1}$	$30\,g\,L^{-1}$	$30\,g\,L^{-1}$	$2\,g\,L^{-1}$
Sodium citrate, $Na_3C_6H_5O_7 \cdot 2H_2O$	$100\,g\,L^{-1}$	$84\,g\,L^{-1}$	$84.5\,g\,L^{-1}$	—	—
Ammonium citrate, $(NH_4)_2HC_6H_5O_7 \cdot 2H_2O$	—	—	—	—	$55\,g\,L^{-1}$
Sodium potassium tartrate, $KNaC_4H_4O_6 \cdot 4H_2O$	—	—	—	$200\,g\,L^{-1}$	—
Ammonium chloride, NH_4Cl	$50\,g\,L^{-1}$	—	$50\,g\,L^{-1}$	—	—
Ammonium sulfate, $(NH_4)_2SO_4$	—	$42\,g\,L^{-1}$	—	$3\,0\,g\,L^{-1}$	$40\,g\,L^{-1}$
Ammonium hypophosphite, $NH_4H_2PO_2 \cdot 2H_2O$	$20\,g\,L^{-1}$	—	—	—	—
Sodium hypophosphite, $NaH_2PO_2 \cdot 2H_2O$	—	—	—	$20\,g\,L^{-1}$	—
Hypophosphorous acid, H_3PO_2	—	$8\,mL\,L^{-1}$	—	—	$8\,mL\,L^{-1}$
Ammonium hydroxide, NH_4OH	—	$13.2\,mL\,L^{-1}$	—	—	—
pH	9.5	8.5	8.9	8–11	8.5
Temperature, °C	95	90	98	85	90
Deposits, wt %	57–70% Ni, 5.5–6.9% P, 23–37% Co	50% Ni, 5% P	30–75% Ni, 6% P	65% Ni	2 at % Ni, 3 at % P
Reference	54	55	60	63	65

TABLE 22.5 Composition of Electroless Cu–Ni–P Plating Bath

Copper sulfate, $CuSO_4 \cdot 5H_2O$	0.4×10^{-3} $1.6 \times 10^{-3} M$
Nickel sulfate, $NiSO_4 \cdot 7\ H_2O$	0.10–0.085 *M*
Trisodium citrate, $Na_3C_6H_5O_7$	0.20–0.30 *M*
Ammonium acetate, $NH_4CH_3CO_2$	0.50–1.0 *M*
Hypophosphite, $NaH_2PO_2 \cdot H_2O$	0.28 *M*
Ph	5.0
Temperature	78°C

copper-rich alloy. The phosphorous content of the deposits decreases from 13 to 1% with increasing copper content. The composition of the acidic bath is shown in Table 22.5. Copper-based alloys with Ni, Co, Zn, or Sn can be deposited in alkaline electroless baths by combinations of the alloying metal salts [81]. The bath components are copper sulfate, nickel chloride, cobalt sulfide, zinc chloride, and tin chloride and the complexing agent is Rochelle salt or ethylenediaminetetracetic acid (EDTA) or ammonium hydroxide, and the reducing agent is formaldehyde or sodium borohydride. The bath is operated at pH 12–13 and 21–65°C.

Silver–Tungsten Alloys Electroless deposition of silver–tungsten alloys was studied for application in microelectronics and micromechanical system (MEMS) technology by Diamand et al. [81–83]. Both the ammonia acetate and benzoate silver complex baths for alloying are shown in Table 22.6. The tungsten content of the alloy deposits reached up to 3.1 at %. The resistivity of silver–tungsten alloy layers thicker than 200 nm was about 2 μΩ-cm. The Ag–W films showed better corrosion resistance than pure Ag film. These workers have shown in their subsequent publication that the rate of deposition of the alloy was controlled by the anodic charge-transfer reaction in ammonia acetate bath and by the diffusion of reduced silver ions to the substrate in benzoate complex bath [83].

TABLE 22.6 Composition of Electroless Ag–W Plating Bath

Ammonia Acetate Bath		Benzoate Bath	
$AgNO_3$	0.03 *M*	$AgNO_3$	0.03 *M*
Na_2WO_4	0.03 *M*	Na_2WO_4	0.015 *M*
Ammonia	1.0 *M*	Benzoic acid	0.33 *M*
Acetic acid	0.5 *M*	Hydrazine hydrate	0.09 *M*
Hydrazine hydrate	0.03 *M*	Ammonium acetate	0.26 *M*
Additional complexing agent, EDTA $Na_2 \cdot 2H_2O$	0.017 *M*		
Additives:			
Sodium saccharin	0.004 *M*		
Sodium dodecyl sulfate	0.001 *M*		
Polyethyleneglycol	$6 \times 10^{-6} M$		
pH	11.1–11.4		

Source: From [81].

TABLE 22.7 Composition of Electroless In–Sb Plating Bath

Indium trichloride, $InCl_3$	0.08 *M*
Antimony trichloride, $SbCl_3$	0.0002 *M*
Trisodium citrate, $C_6H_5O_7Na_3 \cdot 2H_2O$	0.34 *M*
Trisodium nitrilotriacetate, $N(CH_2COONa)_3$	0.14 *M*
Titanium trichloride, $TiCl_3$(HCl soln.)	0.04 *M*
pH (adjusted with 20% $NaCO_3$)	7.8
Temperature	60°C

Indium–Antimony Alloy Electroless plating of indium–antimony alloys on an alumina substrate was achieved with the bath given in Table 22.7 using titanium trichloride as the reducing agent [84].

22.2 PHYSICAL PROPERTIES OF ELECTROLESS ALLOY DEPOSITS

Electroless alloy films have been used as conductors, contacts, resistors, magnetic memory devices, and underlayers in floppy disks in the electronics industry.

Magnetic Properties Initially the magnetic properties of electroless alloys of iron group metals were of considerable interest. Electroless alloy films exhibit soft or hard magnetic property depending on the nickel content in nickel–cobalt and nickel–iron alloys. It was reported [54] that electroless cobalt–nickel alloys deposited from acid alkaline baths have different magnetic properties. Electroless nickel–iron films have magnetic characteristics useful as computer memory [55]. The magnetic properties of nickel–molybdenum–phosphorus alloys were found to be dependent on the molybdenum content and heat treatment. In addition Ni–17% Mo–0.2% P did not exhibit any sign of ferromagnetism even after aging up to 400°C [22]. The magnetic properties of cobalt–phosphorus films, which were deposited from bath 1 in Table 22.2, were $H_c = 0.14$–4.5 Oe, $B_r = 300$–3000 G, and $B_m = 3000$–6000 G, slightly depending on the concentration of nickel chloride in the plating bath. Many workers have reported the possible application of electroless cobalt–nickel–phosphorus films for rapid memory devices. Heritage and Walker [55] reported that an electroless cobalt–nickel–5%phosphorus film exhibited a well-defined anisotropy ($H_c = 2$ Oe, $H_k = 6$ Oe) and switching constant of 1.5 μs. It was also reported [56] that superimposition of a magnetic field during electroless deposition had an appreciable effect on the anisotropy of the deposited film.

Electroless alloy films were further applied to a perpendicular magnetic recording device [86–88]. Electroless multicomponent alloys (Co–Ni–Mn–P, Co–Ni–Re–Mn–P) for fabricating perpendicular recording devices have been reviewed by Osaka [91].

Thermal Stabilities Thermal stabilities of electroless nickel-based alloys are enhanced by codeposition of refractory metals, such as rhenium [19, 20], molybdenum [24–26], and tungsten [28–31]. Electroless Ni–44 at % Re–P can be used for thin-film resistors with high thermal stability [19]. The Ni–Mo–P alloy film was developed for a film resistor with a low temperature coefficient and high thermal stability [24]. Electroless Ni–W–P alloy films have been applied to thermal heads for a heating resistor [31]. Its deposition on the nickel–tungsten–phosphorus underlayer enhances crystallinity and smoothness of the surface of cobalt alloy films and hence increases the recording density [30].

Structure Nucleation and growth of electroless cobalt–65% nickel–phosphorus alloy were discussed by Chow et al. [63], where it was claimed that codeposited phosphorus acts as inhibitor for the growth of cobalt and nickel nuclei. The morphology and structure of a multilayer component nickel–molybdenum–phosphorus/tin oxide/titanium (Ni–Mo–P/SnO_2/Ti) were analyzed by Lo and Hwang [26]. The structure and properties of electroless cobalt–iron–boron film deposited on an amorphous nickel-based alloy ribbon have been studied as a candidate for perpendicular magnetic recording medium. Residual compressive stress in the deposited film was expected to enhance the perpendicular magnetic anisotropy during annealing [69]. Electroless nickel–boron–phosphorus films are used for an undercoat of magnetic films in many memory devices [51–53].

22.3 SUMMARY

Electroless alloy plating has many potential applications, especially in the electronics industry. In this chapter, the recent progresses in electroless alloy plating were briefly reviewed mainly as far as the electroless alloy systems and the plating baths compositions are concerned. Currently, electroless alloy deposits are extended as various functional materials in the field of micro and nanotechnologies. However, there is scarcely systematic study on the process control of electroless alloy deposition since there are too many interdependent factors affecting the composition and properties of the alloy. It is also not possible at the present time to establish a relationship among the specific properties, the alloy composition, and the structure of electroless alloy. It seems that further basic studies are needed to develop the application of electroless deposited alloys.

REFERENCES

1. A. Brenner and G. Riddell, *J. Res. Natl. Bur. Standards*, **37**, 31 (1946).
2. I. Ohno and S. Haruyama, *Bull. Jpn. Inst. Met.*, **30**, 735 (1991).
3. I. Ohno, O. Wakabayashi, and S. Haruyama, *J. Electrochem. Soc.*, **132**, 2323 (1985).
4. I. Ohno, in *Proc. Symp. on Fundamental Aspects of Electrochemical Deposition and Dissolution Including Modeling*, Vol. 97-27, M. Paunovic, M. Datta, M. Matosz, T. Osaka, and J. B. Talbot, Eds., Electrochemical Society, Pennington, NJ, 1998, p. 255.
5. H. Yajima, H. Numata, and I. Ohno, *J. Surf. Finish. Soc. Jpn*, **48**, 62 (1997).
6. I. Ohno, in *Modern Electroplating*, M. Schlesinger and M. Paunovic, Ed., Wiley, New York, 2000, p. 729.
7. P. H. Eisenberg, U.S. Patent 2,827,399 (1958).
8. A. F. Schmeckenbecher, *J. Electrochem. Soc.*, **113**, 778 (1966).
9. A. F. Schmeckenbecher, *Plating*, **58**, 905 (1971).
10. H. Matsubara, H. Mizutani, S. Mitamura, and T. Osaka, *Trans. IEEE Magn.*, **26** (3), 1210 (1990).
11. M. Matsuoka and T. Hayashi, *Plating Surf. Finish.*, **69** (12), 53 (1982).
12. D. Kim, H. Matsuda, K. Aoki, and O. Takano, *Plating Surf. Finish.*, **83** (2), 78 (1996).
13. K. M. Gorbunova, A. A. Nikiforova, and G. A. Sadakov, "Modern Problems of Metal Depsition by Reductin with Hypophosphite," in *Electrochemistry*, M. M. Melikova, Ed., Soviet Academy NAUK, Moscow, 1966, p. 41.
14. F. Pearlstein and R. F. Weightman, *Electrochem. Technol.*, **6**, 427 (1968).
15. F. Pearlstein, U.S. Patent 3,485,597 (1969).
16. International Business Machines, British Patent 1,314,745 (1970).
17. F. Pearlstein and R. F. Weightman, U.S. Patent 3,754,939 (1973).
18. M. Gulla, U. S. Patent 3,764,352 (1973).
19. T. Osaka, T. Homma, M. Fukawa, H. Iwamoto, and J. Kawaguchi, *Denki Kagaku*, **59**, 723 (1991).
20. T. Osaka, M. Fukawa, and J. Kawaguchi, *Denki Kagaku*, **60** (6), 523 (1992).
21. G. O. Mallory and T. R. Horhn, *Plating Surf. Finish.*, **66** (4), 40 523 (1979).
22. G. Mallory, *Plating Surf. Finish.*, **63** (6), 34 (1976).
23. M. Schwartz and G. O. Mallory, *J. Electrochem. Soc.*, **123**, 606 (1976).
24. I. Koiwa, M. Usuda, K. Yamada, and T. Osaka, *J. Electrochem. Soc.*, **135**, 718 (1988).
25. T. Osaka, H. Yamazaki, and I. Saito, *J. Electrochem. Soc.*, **136**, 3418 (1989).
26. Y. L. Lo and B. J. Hwang, *J. Electrochem. Soc.*, **43**, 2158 (1996).

27. F. Pearlstein, R. F. Weightman, and R. Wick, *Met Finish.*, **61**, (11), 77 (1963).
28. K. Aoki and O. Takano, *Plating Surf Finish.*, **73** (5), 136 (1986).
29. K. Aoki and O. Takano, *Plating Surf. Finish.*, **77** (3), 48 (1990).
30. I. Koiwa, M. Usuda, and T. Osaka, *J. Electrochem. Soc.*, **135**, 1222 (1988).
31. H. Sawai, T. Kanamori, I. Koiwa, S. Shibata, and K. Nihei, *J.Electrochem.Soc.*, **137**, 3653 (1990).
32. J. L. X. Hu and D. Wang, *Plating Surf. Finsh.*, **83** (8), 62 (1996).
33. M. Schlesinger and X. Meng, *J. Electrochem. Soc.*, **138**, 406 (1991).
34. H. Shimauchi, S. Ozawa, K. Tamura, and T. Osaka, *J. Electrochem. Soc.*, **141**, 1471 (1994).
35. L. Wang, L. Guifang, X. Yuan, B. Zhang, and J. Zhang, *Surf. Coat. Technol.*, **126**, 272 (2000).
36. S.-L Wang, *Surface Coating Technol.*, **186**, 372 (2004).
37. D. Mencer, *J. Alloys Comp.*, **306**, 158 (2000).
38. I. Genutiene, J. Lenkaitien, Z. Jusys, and A. Luneckas, *J. Appl. Electrochem.*, **26**, 118 (1996).
39. A. B. Drovosekov, M. V. Ivanov, V. M. Krutskikh, E. N. Lubnin, and Yu. M. Polukarov, *Protection of Metals*, **4**, 55 (2005).
40. J. N. Balaraju, C. Anandan, and K. S. Rajam, *Surface Coating Technol.*, **200**, (12–13), 3675 (2006).
41. J. N. Balaraju, S. M.Jahan, C. Anandan, and K. S. Rajam, *Surface Coating Technol.*, **200** (16–17), 4885 (2006).
42. R. D. Fisher, *IEEE Trans. Magn.*, **2**, 681 (1966).
43. M. Soraya, *Plating*, **54**, 549 (1967).
44. A. M. Lunyatskas, *Zaschhita Metallov*, **4** (3), 315 (1968).
45. N. Krasteva, V. Fotty, and S. Armyanov, *J. Electrochem. Soc.*, **141**, 2864 (1994).
46. A. Hung, P. C. Hung, and I. Ohno, *Plating Surf. Finish.*, **76** (12), 60 (1989).
47. F. Pearlstein and R. F. Weightman, *Plating*, **56**, 1158 (1969).
48. P. H. Eisenberg and D. O. Raleigh, U.S. Patent 2,828,227 (1958).
49. K. Aoki, O. Takano, and D.-H. Kim, *J. Surf Finish. Soc. Jpn*, **46**, 79 (1995).
50. K. Iwamatsu, in *Proc. 4th AESFAnn. Tech. Conf.*, B4-1, 1987.
51. D. W. Baudrand, *Plating Surf. Finish.*, **66** (11), 18 (1979).
52. G. O. Mallory, "Recent Advances in Electroless Nickel Plating of Aluminum Connectors," paper presented at the 17th Annual Connectors and Interconnection Technology Symp., Anaheim, CA, Sept. 19–21, 1984.
53. D. W. Baudrand and M. Malik, *Met. Finish.*, **84** (3), 15 (1986).
54. K. M. Gorbunova and A. A. Nikiforova, *Fiziko-khimicheskie osnovy protsessa khimicheskogo nikelirovaniya* (Physico-chemical Principles of Chemical Nickel Plating), Moskva, AN SSSR. 1960 (RZhKhim, No.21: 85470, 1960).
55. R. J. Heritage and M. T. Walker, *J. Electron. Control*, **7**, 542 (1960).
56. J. Ragrowski and M. Lauriente, *J. Electrochem. Soc.*, **109**, 987 (1962).
57. J. C. Hendy, H. D. Richards, and A. W. Simpson, *J. Mater. Sci.*, **1**, 127 (1966).
58. T. Yokoshima, D. Kaneko, T. Osaka, S. Takefusa, and M. Oshiki, *J. Magn. Soc. Jpn*., **23**, 1397 (1999).
59. G. W. Lawless and R. D. Fisher, *Plating*, **54**, 709 (1967).
60. F. Pearlstein and R. F. Weightman, *Plating*, **54**, 714 (1967).
61. R. D. Fisher and W. H. Chilton, *Plating*, **54**, 537 (1967).
62. J. H. Kefalas, *Plating*, **54**, 543 (1967).
63. S. L. Chow, N. E. Hedgecock, M. Schlesinger, and J. Rezek, *J. Electrochem. Soc.*, **119**, 1614 (1972).
64. T. Homma, K. Inoue, H. Asai, K. Ohrui, and T. Osaka, *IEEE Trans. Magn.*, **27**, 4909 (1991).
65. G. E. Georgiou, F. A. Baiocchi, H. S. Luftman, T. T. Sheng, M. J. Vasile, and R. V. Knoell, *J. Electrochem. Soc.*, **138**, 2061 (1991).
66. J. R. DePew and D. E. Speliotis, *Plating*, **54**, 705 (1967).
67. T. Osaka, N. Kasai, I. Koiwa, F. Goto, and Y. Sugiyama, *J. Electrochem. Soc.*, **130**, 568 (1983).
68. T. Osaka, T. Homma, K. Saito, A. Takekoshi, Y. Yamazaki, and T. Namikawa, *J. Electrochem. Soc.*, **139**, 1311 (1992).
69. K. Maruyama, T. Sato, I. Ohno, and H. Numata, in *Proc. Int. Conf. on Microstructures and Functions of Material*, ICMFM 96, N. Igata, Y. Hiki, I. Yoshida, and S. Sato, Eds., Science University of Tokyo, 1996, p. 185.
70. T. Miyabayashi, H. Wakayama, M. Miyata, and K. Kobayashi, in *Proc. Symp. on Electroless Deposition of Metals and Alloys*, Vol. 12, M. Paunovic and I. Ohno, Eds., Electrochemical Society, Penington, NJ, 1988, p. 196.
71. T. Homma, Y. Kita, and T. Osaka, *J. Electrochem. Soc.*, **147**, 160 (2000).
72. T. Homma, M. Suzuki, and T. Osaka, *J. Electrochem. Soc.*, **145**, 134 (1998).
73. A. Molenaar, *J. Electrochem. Soc.*, **129**, 1917 (1982).
74. A. Molenaar, and B. C. M. Meenderick, *J. Electrochem. Soc.*, **132**, 574 (1985).
75. G. Tomkyavichyus et al., *Zaschita Metallov.*, **24**, 849 (1988).
76. D. Lamouche, P. Clechet, J. R. Martin, E. Horoutiounian, and J. P. Sandino, *J. Electrochem. Soc.,* **134**, 692 (1987).
77. G. Stremsdoerfer, H. Perrt, J. R. Martin, and P. Clechet, *J. Electochem. Soc.*, **135**, 2881 (1988).
78. R. N. O'Brien and K. S. V. Santhanam, *J. Electroanal. Chem.*, **260**, 231 (1989).
79. R. N. O'Brien and K. S. V. Santhanam, *J. Electrochem. Soc.*, **139**, 434 (1992).
80. H. J. West, *Met. Finish.*, **55** (1), 56 (1957).
81. Y. S.-Diamand, A. Inberg, Y. Sverdlov, V. Bogush, N. Croitoru, H. Moscovich, and F. Freeman, *Electrochim. Acta*, **48**, 2987 (2003).
82. Y. S.-Diamand, A. Inberg, Y. Sverdlov, and N. Croitoru, *J. Electrochem. Soc.*, **147**, 3345 (2000).
83. A. Inberg, V. Bogush, N. Croitoru, and Y. S.-Diamand, *J. Electrochem. Soc.*, **154** (1), D1–D4, (2007).

84. A. Senda, Y. Takano, Y. Kanbayashi, and K. Morita, *J. Surf. Finish. Soc. Jpn.*, **45**, 923 (1994).

85. L. Wang, L. Zhao, B. Zhang, W. Hu, X. Shu, X. Sheng, and Z. Fang, *J. Alloys Comp.*, **287**, 234 (1999).

86. I. Koiwa, M. Toda, and T. Osaka, *J. Electrochemf. Soc.*, **133**, 597 (1986).

87. T. Osaka, T. Homma, K. Noda, T. Watanabe, and F. Goto, *IEEE Trans. Magn.*, **27**, 4963 (1991).

88. T. Osaka, N. Kasai, I. Koiwa, F. Goto, and Y. Sugiyama, *J. Electrochem. Soc.*, **130**, 568 (1983).

89. D. H. Kim, K. Aoki, and O. Takano, *J. Surf. Finish. Soc. Jpn.*, **46**, 79 (1995).

90. R.Touir, H. Larhzil, M. Ebntouhami, M. Cherkaoui, and E. Chassaing, *J. Appl. Electrochem*., **36**, 69 (2006).

91. T. Osaka, *Electrochim. Acta*, **37**, 989 (1992).

23

PREPARATION FOR DEPOSITION

DEXTER D. SNYDER

23.1 PRINCIPLES

The success of electroplating or surface conversion depends on removing contaminants and films from the substrate. Organic and nonmetallic films interfere with bonding to cause poor adhesion and even prevent deposition. This surface contamination can be extrinsic, comprised of organic debris and mineral dust from the environment or preceding processes. It can also be intrinsic, one example being a native oxide layer. Cleaning methods are designed to minimize substrate damage while removing the film or debris. If a metal's surface chemistry and processing history are known, one can anticipate cleaning needs and strategies.

Extrinsic organic and inorganic soils originate with processing of the substrate before plating as well as from the general environment. Specific residues include lubricants, phosphate coatings, quenching oils, rust-proofing oils, drawing compounds, and stamping lubricants. The mixture of potential contaminants to which a part is exposed is typically complex.

All metals form oxide and inorganic films with environmental gases and chemicals to a degree. Some of these films are protective against continuing attack, such as the hydrous aluminum oxide formed on aluminum alloys. Some are nonprotective such as ferrous/ferric oxides on steel. Some of these films can even be plated directly, with nickel on aluminum oxide over aluminum being an example. The cleaning and activation steps must account for the fact that surface oxide re-forms at different rates on the different metals. For iron and nickel, the oxide re-forms slowly enough that the parts can be transferred from a cleaning solution to a plating bath at a normal rate. For aluminum and magnesium, the oxide re-forms extremely fast, so special processing steps are necessary to preserve the metal surface during transit into electroplating.

Porous substrates, such as cast iron, are a major challenge. Organic and inorganic residues penetrate the pores and must be removed to avoid their interfering with subsequent operations. Left in the pores, these residues decompose or vaporize during electroplating or when the component is used, causing blisters. To remove residues, the cleaner must penetrate the pores, dissolve the residue, then itself be removed.

Metals react with atmospheric constituents, such as water and oxygen, to form intrinsic films, which also must be removed through cleaning before plating. Pourbaix diagrams [1, 2], which are graphical renderings of metal–reactant equilibria, help one understand how to remove these films. Iron has a relatively large passivation range and shows immunity to corrosion at moderate cathodic potential [3], as shown in Figure 23.1. Copper, by contrast, is attacked at both high and low pH [3], as seen in Figure 23.2, so cleaners are designed for this window of passivation. The *E*–pH diagrams are available for all common materials and plating systems [1]. Diagrams useful to evaluate cleaning approaches can be constructed for systems containing complexing agents and other constituents.

Cleaning processes are based on two approaches. In physical cleaning, kinetic energy is introduced to release both extrinsic and intrinsic contaminants from the metal surface. Examples are glass bead peening, ultrasonic agitation, and brush abrasion. In chemical cleaning, contaminant films are removed by active materials dissolved or emulsified in the cleaning solution. Extrinsic contaminants are removed with surface-active chemicals, and the chemical energies involved are modest. Intrinsic films are removed with aggressive chemicals that dissolve the contaminant and often react with the metal itself, and the energies involved are significant.

Modern Electroplating, Fifth Edition Edited by Mordechay Schlesinger and Milan Paunovic

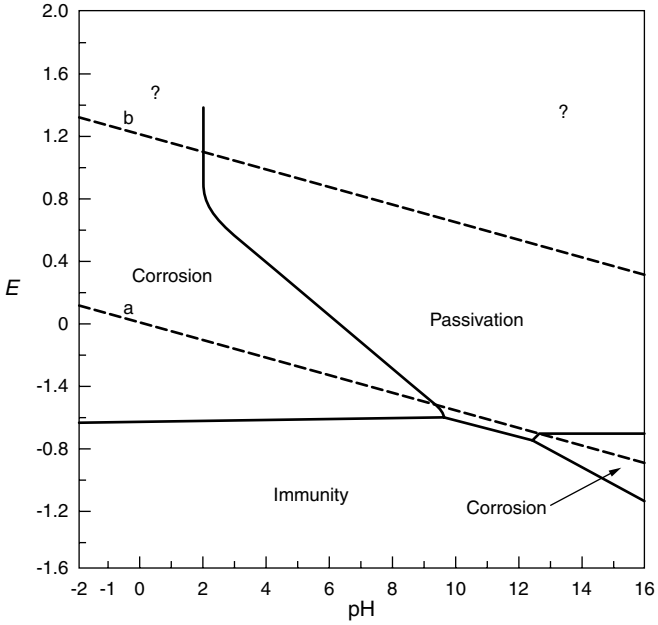

FIGURE 23.1 Simplified Pourbaix diagram for iron.

The substrate metal properties must be considered in balancing cleaning power with aggressiveness. Ferrous alloys are attacked by acids, withstand very alkaline cleaners, and have a nonprotective oxide [4–6]. It is important to protect iron alloys from oxidizing between plating steps. Iron oxide is nonprotective and must be dissolved by mixtures of acid and iron salts. Normal alkaline cleaners will not remove this film.

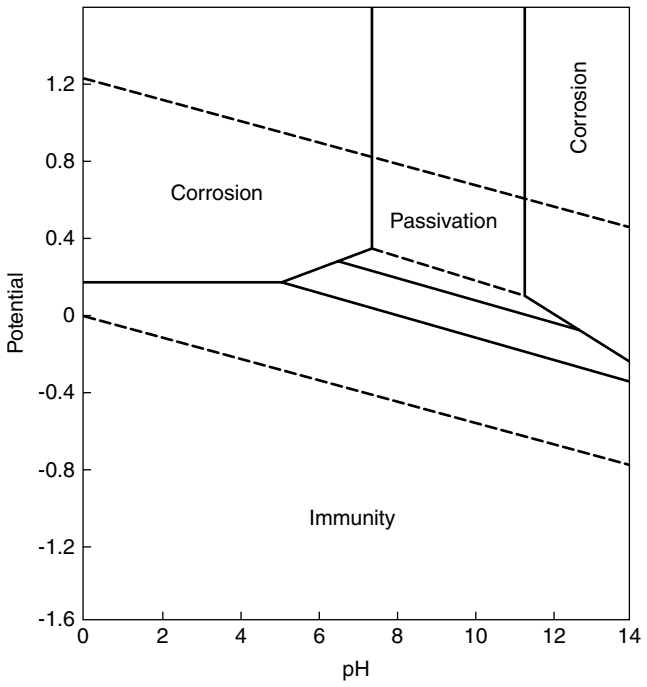

FIGURE 23.2 Simplified Pourbaix diagram for copper.

In air, aluminum and its alloys are coated with a thin native oxide only a few monolayers thick which forms very quickly on the metal [7]. Fortunately, this film is protective in many environments, and one effective protective technology for aluminum alloys is to anodize or purposely thicken the native oxide layer to micrometer thickness. Aluminum oxide layers can be dissolved in alkalis. Both strong acids and strong alkalis attack aluminum alloys.

Copper and its alloys require a milder cleaner than many other metals [8]. They are attacked by oxidizing acids, such as nitric, but they withstand alkalis. A copper cleaner can be built on a reducing acid, with complexing and wetting agents and a corrosion inhibitor. Zinc is more active than copper, it is attacked by acids and alkalis at pH $>$ 10 [9], and it requires a mild alkaline cleaner.

Cleaning of plastics and polymers before plating involves removing extrinsic organics and also etching the surface to provide for mechanical interlocking, where possible. The polymers most commonly electroplated include fluorocarbons, polycarbonates, and acrylonitrilebutadienes.

The literature of metal cleaning for electroplating is extensive [10–13]. Change continues in several areas:

- Search for efficient cleaning processes having no adverse environmental impact
- Databases to identify best cleaning alternatives for a given substrate, surface condition, and subsequent plating requirements
- Increasingly smaller and more complex elements to be plated
- Search for methods to monitor degree of surface cleanliness

While principles of cleaning are well known, the key is selecting workable combinations of metals and processes for specific situations.

Mechanical blast cleaning works for nonprecision parts that are capable of withstanding the friction and force from the cleaning media. While one avoids the need to deal with solvents, there is a requirement for high capital costs and large facilities. Mechanical surface preparation is expected to increase in use over traditional chemical surface preparation.

For extrinsic contaminants, solvents are preferred cleaners because they evaporate quickly and leave little to no residue on the metallic object. The cleaning ability of an organic solvent depends strongly on its normal boiling temperature. This follows due to the large dependence of the contaminant's viscosity on temperature. Solvent cleaners have long been a mainstay for vapor degreasing, and common chemicals have been tri- and tetrachloroethylene. However, solvents are being actively replaced wherever possible with environmentally benign alternatives [14, 15]. One should select a solvent-based cleaner at this time only if there is no

technical alternative. In that case the process must be designed for compliance with environmental and worksite regulations, and the added cost can be significant.

Aqueous cleaning is a function of the chemistry, temperature, agitation, and processing time [16]. The goal to maintaining the process is to remove oil and suspended solids from the medium that can be recycled. Aqueous systems tend to emulsify the oil, which then becomes part of the cleaner and eventually degrades its performance. In working out the optimum balance, one should team with the cleaner chemical suppliers to have all wisdom and alternatives available. One trend is to choose a cleaner that does not build a stable emulsion with the waste oil but rather holds it loosely in suspension, then ejects it as a floating layer. This makes possible a steady-state performance of the cleaning system. Alkaline systems are effective in removing soils and tend not to attack the substrate except at high pH. Acidic systems normally do attack the substrate, so this type of cleaning (called also pickling or activation in different applications) must be carefully controlled by concentration and exposure time.

For special cases, no cleaning is required before electrodeposition. For example, in the electrodeposition of copper conductors in integrated circuit (IC) fabrication, no cleaning is necessary when copper is electrodeposited on a PVD (physical vapor deposited) copper seed layer.

23.2 CONVENTIONAL PROCESSES

23.2.1 Organic Solvent Cleaners

While 1,1,1-trichloroethane has been banned for its role as an atmospheric ozone depleter, solvent cleaning is still possible within the current environmental and safety/health regulations [15, 17]. Three replacements without ozone depletion capability are methylene chloride, perchloroethylene, and trichloroethylene. Hydrofluoroethers are also available as alternatives to CFCs (chlorofluorohydrocarbons). These solvents must still be kept out of liquid waste disposal systems and below predetermined thresholds in the workplace. All solvent-based cleaning must now be closed loop and zero discharge. Solvents must be kept relatively clean for both vapor degreasing and soak degreasing. When the solvent is dirty, the contaminants can be redeposited on the part.

23.2.2 Aqueous Cleaners

Aqueous cleaners normally contain surfactants, builders—such as alkali for neutralizing acid—to assist in cleaning, binders to hold the ingredients together, and buffers to help neutralize the surface activity of the parts [16]. Surfactants work by having the hydrophobic tail seek the oil. The negatively charged metal repels the negatively charged end, and the oil is gradually lifted from the surface. Sodium ions enhance the function of a surfactant.

Alkaline cleaners are largely intended to neutralize acidic species and soften the water to prevent formation of insoluble calcium and magnesium soaps. Sodium hydroxide is the most important alkali in cleaners, but sodium carbonate is also used. Phosphates are used primarily for the water softening. Pyrophosphates are used for sequestering and chelating of zinc, copper, and magnesium, but they are not effective for calcium. The most effective all-around version is sodium pyrophosphate. Silicates are good buffers, and they are included in many alkaline cleaners.

Acid cleaners attack the metal substrate to remove the intrinsic films, and they also can facilitate removal of extrinsic soils. More care must be taken with acid cleaning, however, to avoid damaging the substrates. Oxide scale is removed from ferrous alloys using inorganic acids or acid salts with combinations of inhibitors, solvents, and surfactants. Organic acids and acid salts have the added advantage of sequestering some contaminant species, after chemical reaction, to remove them from the surface. For electrolytic cleaning, sulfuric acid is the main choice. Acid treatment is used for aluminum alloys mainly to desmut, and exposure is normally a few minutes only. Copper cleaners are normally a mixture of acid, such as sulfuric, with an oxidizing agent, such as nitric acid. Aluminum is active in nonoxidizing acids but inactive in oxidizing solutions. Zinc can be deoxidized with cold, dilute nitric acid containing an oxidizer.

In aqueous cleaning, problems still exist in the areas of rinsing and drying [17]. Rinsing is best addressed in closed-loop systems where the contaminant level can be monitored and controlled. Drying technology offers considerable advantages, and the contributors are to be found with air blow-offs and vacuum drying. Another major area for improving cleaning is to design products to be easy to clean. It is better to reduce the problem as much as possible, for example, by avoiding blind holes and screw configurations.

Parts washers are often used with the aqueous systems used to replace solvent cleaners. Here, one uses a cleaning cabinet with high-pressure streams applied to the parts. These are basically industrial dishwashing machines. The detergent used is typically biodegradable.

In ultrasonic cleaning [18], sound waves dissipate energy which evaporates water into small vapor bubbles. Most of this energy dissipation occurs at nucleation sites on the metal surface and when the bubbles collapse. When the bubbles collapse, the implosion tends to dislodge the oil. Ultrasonic energy is generally added at 20–40 kHz. Higher frequencies produce smaller bubbles. There is some thought that large bubbles are preferred because the larger bubbles generate more energy when they implode. Another school of thought says smaller bubbles are desired because they penetrate more easily into crevices and pores. There is no definitive evidence to decide this matter.

Electrocleaning is used as the final step, for such tasks as plating precision steel parts [10]. The actual cleaning comes from generation of tiny bubbles that lift and remove soils. Anodic cleaning, called *reverse*, involves production of oxygen bubbles. Cathodic cleaning, called *direct*, involves production of hydrogen bubbles.

23.2.3 Semiaqueous Cleaners

Semiaqueous cleaners are an alternative to solvent cleaning [11], These cleaners are made of synthetic organic solvents, surfactants, corrosion inhibitors, and other additives. Water is used in some portion. For water-immiscible cleaners, the active ingredients are held as an emulsion. For water-miscible cleaners, the water is actually filler to reduce volatile organic compound emissions. This class of cleaners still has some potential for volatile organics, aquatic toxicity, flammability, and human health effects.

23.2.4 Rinsing

Cleaning solutions can be inactivated by carryover from previous steps. This requires they be dumped prematurely. It can periodically reduce their cleaning effectiveness and the extra dumping increases disposal costs. Furthermore, contaminated cleaners can be carried over to degrade the plating solutions, compounding the cost. Effective rinsing is an integral part of cost-effective plating systems.

Rinsing system design is well covered in several texts [10]. Water requirements are reduced dramatically with multiple-stage rinsing, including countercurrent flow where feasible. Water use efficiency is increased with such mixing tools as pressure spray, heating, mechanical agitation, and ultrasonic irradiation. With the trend to closed-loop operation, used rinse water can be reclaimed with combinations of filtration, evaporation, and ion exchange. In any event, maintaining a predetermined rinse water quality is critical to ensuring consistent rinsing results.

23.3 EMERGING TECHNOLOGY

There will be a steady increase in the number of environmentally alternatives to conventional solvent and water-based metal cleaning. As an example, carbon dioxide is being considered as a cleaning medium because it removes the threat of pollution.

Cold–jet CO_2 (dry ice) blasting, commercialized in the 1980s, has potential to be used more in electroplating cleaning [14b]. Carbon dioxide granules are produced and blasted onto the workplace with special nozzles, similar to blasting with sand, plastic beads, or soda. However, the particles sublimate on impact to yield a rapidly expanding gas and to release energy that creates microshocks to aid with the cleaning. CO_2 particles are nonabrasive, but one must tailor the process to avoid damage to the substrate. Dry ice blasting removes particular and light hydrocarbons from metals, although it tends to lose effectiveness with porous surfaces. Use of dry ice formed from carbon dioxide that would otherwise be released to the atmosphere is favored since this is a greenhouse gas.

Supercritical fluids (SCFs) have proven effective for cleaning metal surfaces [14a]. This medium possesses liquid-like density and solvency combined with gaslike viscosity and diffusivity. SCF carbon dioxide has a lower surface tension than liquid carbon dioxide, and it spreads more easily over a surface than does the liquid. This means SCF can penetrate substrates and interstices to dislodge and remove contaminants, then be easily and completely removed. This is a closed-loop, batch process operating at moderate temperatures and pressures on the order of 2000 psig. Cleaning times are 10–30 min, and the surface contaminants are the sole waste. Operating costs are low, but capital costs are high. This process does require pressure vessels and high-pressure controls. SCF cleaning is presently an alternative only for high-value-added components.

23.4 MEASURING DEGREE OF CLEANLINESS

Increasingly surface analysis and characterization are accompanying cleaning decisions so one can detect when a cleanliness goal is reached [14c]. The objective is to present to the metallizing process a surface free of foreign matter or films which interfere with adhesion. In the past the proof of cleaning success was in the plated part performing as required. This approach works as long as the substrate condition, the surface contaminants, and the cleaning baths do not vary. Many failures occur only after extended use as product. With affordable, modern surface and solution analysis systems, the situation has changed. Unwanted surface species can be linked with future failure issues, then monitored during manufacturing.

The final condition of a surface is the product of cleaning. Therefore surface analysis to monitor cleaning adds value by enabling one to find and maintain the optimum trade-off among several factors:

- Substrate being used
- Contaminants being removed in cleaning
- Sensitivity of plating/surface conversion to state of cleanliness
- Cost of plating/surface conversion per part
- Budget

The surface condition before and after cleaning can be linked to requirements for subsequent surface conversion and plating steps. In some cases a cleaned surface can be validated before a particularly sensitive plating or surface

conversion step in a high-value-added product. Where simple, inexpensive monitors are not yet available, one can still define the required cleanliness with laboratory analysis systems and then check the substrate cleanliness periodically as parts exit cleaning.

The University of Massachusetts TURI Laboratory builds its program on the following set of surface cleanliness measurement techniques (14c):

- *Fluorescence* Many organic contaminants, such as lubricants, have naturally fluorescing ingredients that can be monitored under black light.
- *Fourier Transform Infrared (FTIR) Spectroscopy* Instrumentation is relatively expensive, but FTIR is useful when the origins of contamination are unknown.
- *Goniometry* Contact angle measurement is relatively simple and usable in the plant.
- *Gravimetric Analysis* This simple weight loss determination is the least expensive member of this group and usable in the plant.
- *Microscopy* Both scanning electron and stereooptical microscopes are commonly used, with computer software packages that calculate soil load.
- *Optically Stimulated Electron Emission* (*OSEE*) This simple technique is based on the emission of electrons from a metal surface under UV illumination. It is best suited to revealing the degree of contamination for thin films such as oil.

Other approaches, used more for product development and research, include:

- Energy-dispersive electron analysis (EDAX)
- Auger spectroscopy
- Laser ablation spectroscopy
- Raman spectroscopy
- Total organic carbon analysis
- Ion chromatography
- Electron spectroscopy (ESCA)
- Atomic tunneling microscopy (AFM)
- Scanning tunneling microscopy (STM)
- Cyclic voltammetry (CV)
- Electrochemical impedance spectroscopy (EIS)

23.5 STRATEGIES FOR CLEANING

Cleaning processes are designed to have maximum possible life, minimal maintenance, low environmental impact, and the ability to recycle fluids. This design for the environmental approach is a major shift from the past when cleaning performance was the only criterion. The extrinsic dirt can be dealt with through physical and chemical methods, and the part often must be shielded from the atmosphere between cleaning and metallization. Intrinsic residues more often involve intimate bonding with the substrate, so chemical cleaning is dictated. Important in this step is to document all prior processing for the metal part up to plating. This identifies compounds and surface modifications to which the metal has been subjected and points to likely cleaning needs.

Cleaning technology has been traditionally the product of cut-and-try experience, and suppliers have closely held the knowledge. Therefore it is prudent to work in partnership with the effective suppliers—those with a track record of success—to find robust cleaners and pretreatment processes with a company having the knowledge to maintain them. With the Internet and computer databases, one can tap into the accumulated knowledge of commercial cleaning processes. Two resources are:

- Cleantool, a European Union sponsored online database for Optimization of Metal Cleaning, cleantool.org/en/index.php (19)
- CleanerSolutions Database, maintained by Toxic Use Reduction Institute (TURI), University of Massachusetts, cfeanersolutions.org (20)

Electroplaters will be increasingly able to identify and work with the cleaning suppliers having the most relevant products and experience.

The choice and control of a cleaning process requires optimization of the several factors governing the plating outcome:

- Cost, including waste/recycle
- Substrates that can be handled
- Toxics
- Contaminants that can be handled
- Safety
- Maintenance (life, contamination)
- Analyses and control
- What specific contaminants must be removed
- To what level must specific contaminants be reduced

REFERENCES

1. M. Pourbaix, *Atlas of Electrochemical Equilibria in Aqueous Solutions*, Pergamon, Oxford, 1966.
2. M. Pourbaix, *Lectures on Electrochemical Corrosion*, Plenum, New York, 1973.
3. U. Evans, *An Introduction to Metallic Corrosion*, Edward Arnold and American Society for Metals, London UK, 1981.

4. American Society for Testing and Materials (ASTM), "Preparation of Low-Carbon Steel for Electroplating," ASTM, B-l83, ASTM, West Conshohocken, PA, 2009
5. American Society for Testing and Materials (ASTM), "Preparation of High-Carbon Steel for Electroplating," ASTM B-242, ASTM, West Conshohocken, PA, 2009.
6. American Society for Testing and Materials (ASTM), "Preparation of and Electroplating on Stainless Steel," ASTM B-254, ASTM, West Conshohocken, PA, 2009.
7. American Society for Testing and Materials (ASTM), "Preparation of Aluminum Alloys for Electroplating," ASTM B-253, ASTM, West Conshohocken, PA, 2005.
8. American Society for Testing and Materials (ASTM), "Preparation of Copper and Copper Alloys for Electroplating and Conversion Coating," ASTM B-281, ASTM, West Conshohocken, PA, 2008.
9. American Society for Testing and Materials (ASTM), "Preparation of Zinc Alloy Die Castings for Electroplating and Conversion Coatings," ASTM B-252, ASTM, West Conshohocken, PA, 2009.
10. D. R. Gabe, *Principles of Metal Surface Treatment and Protection*, Pergamon, Oxford, 1978.
11. *ASM Handbook Volume*, Vol. 5, ASM International, Metals Park, OH, 2007.
12. *Metal Finishing Guidebook*, R. Tucker, Ed., Metal Finishing, New York, 2010.
13. *The Aqueous Cleaning Handbook*, Alconox, White Plains, NY, 2008.
14. B. Konesberg and E. Konegsberg, *Handbook of Critical Cleaning*, CRC, Boca Raton, FL, 2000: (a) W. M. Nelson, Ch. 2.13, "Dense-Phase CO_2 as a Cleaning Solvent," (b) F. Cano, Ch. 2.14, "Carbon Dioxide Dry Ice Snow Cleaning," (c) C. LeBlanc, Ch. 5.2, "Cleaning Metals: Strategies for the New Millennium."
15. "Bio-Based Alternative Solvents," a TURI Research Initiative, available: turi.org/laboratory/cleaning_research_projects/bio_based_alternative_solvents
16. Products Finishing On-line, "Second Generation Aqueous Cleaning-An Update in Conventional Wisdom," pfonline.com/past.html Aug. 1997.
17. Products Finishing On-line, "Solvent Cleaning is Alive and Well," pfonline.com/past.html Nov. 1998.
18. R. Walker, "Ultrasonic Agitation in Metal Finishing," in *Advances in Sonochemistry*, Vol. 3, T. J. Mason, Ed., JAI Press, Greenwich, CT, 1993, pp. 125–144.
19. Cleantool Database, available: cleantool.org/en/index.php.
20. Cleaner Solutions Database, available: turi.org.

24

MANUFACTURING TOOLS

TOM RITZDORF

Commercial electroplating began almost two centuries ago. The manufacturing technology for a long time consisted of what we consider the minimum elements needed to deposit metal: open tanks, simple solutions for cleaning, rinsing, and electrodeposition, soluble or insoluble anodes, and a power source. There was virtually no ventilation or proper waste disposal. The entire operation was manual. Electroplating quality depended greatly on the experience and skill of the operator. Certain physical properties of deposits were improved after plating by heat treating or buffing [1]. Over the years the industry grew as an art. Improved processes and techniques were discovered along the way and many were kept secret until others heard about them or stumbled on the technology themselves. Eventually platers began filing patents to protect their rights to discoveries. About the same time entrepreneurs emerged to make a business of developing and selling new ideas for better plating solutions, techniques, and machinery.

Following Edison's success with his research laboratory, many industrial companies established their own research and development laboratories, which included electroplating sections supporting manufacturing operations. Electroplating manufacturing technology was developed as needed: (1) to solve production problems, (2) to reduce cost, (3) to increase production rates, (4) to improve quality of the product, and (5) to meet new standards set by product designers and waste disposal regulations. Modern electroplating technologies developed for manufacturing include solutions with the best chemistry available, machines that automatically transport the product through all stages of processing, computerized monitoring, and control systems that also store and process data, online and offline inspection facility, rapid chemical analysis systems, and an efficient waste treatment system. Many developments have resulted from attempts to reduce manufacturing costs, such as increasing production rates with the same equipment, utilizing cheaper materials, or eliminating unnecessary process steps or equipment. Also new technologies originally developed in non-electroplating industries have been adopted for use in advanced electroplating. Software for machine automation, data logging, and data processing are good examples. Equipment designed specifically for electroplating semiconductor wafers and related microelectronic components have brought together all of the advanced control concepts and have led to great improvements in understanding the nature of the electroplating chemistries and processes that have been utilized in these applications.

Fully automatic electroplating equipment can be justified only when large volumes of the same or similar product are processed. Modern automatic tools can be operated with fewer operators, but these people often must be more skilled and knowledgeable about instrumentation, sensors, and computers as well as electroplating.

24.1 ELECTROPLATING EQUIPMENT

Automated plating machines were invented to do more cost-effective plating through increased worker productivity, improved quality and reproducibility, and higher plating speeds. Equipment design and development improved as time progressed. Better materials, especially special plastics, minimized solution contamination from the machine. Stronger and more corrosion-resistant construction materials extended machine life while allowing operation at higher

Modern Electroplating, Fifth Edition Edited by Mordechay Schlesinger and Milan Paunovic

production rates. Modern electronics and sensor technology have made possible more fully automatic plating machines.

Equipment for electroplating should be designed with the plating processes in mind. In this regard, care should be taken to provide mass transfer through solution (or part) agitation, replenishment of the plating chemistry, and appropriate distribution of the current density among the parts to be plated. Additionally, the temperature of the chemistry and parts and the solution concentrations should be well controlled to provide repeatable results. This may mean paying close attention to solution drag-in and drag-out, depending on the type of equipment being considered. It is also important to pay close attention to how electrical contact is made to the parts to be processed in order to ensure reliable and repeatable performance.

Much of the development that has gone into providing efficient automated electroplating of various parts has been to increase the deposition speed of the electrolytic processes to improve equipment throughput. This is important in order to get the best return on the money spent to buy the automated processing equipment. Since the maximum deposition rate that is reasonable in a manufacturing process is usually related to the limiting current density, this effort essentially consists of boosting the limiting current density for a particular process. Of course, increasing the limiting current density usually involves one or more of the following three changes to the process:

1. Increase the metal concentration in the bath
2. Increase the deposition temperature
3. Increase the agitation rate at the workpiece (decrease the diffusion boundary layer thickness)

While the metal concentration depends more on the chemistry than the hardware, the equipment may need to be adapted in order to deal with the high metal concentration by reducing salt crystal formation or to be compatible with modified base electrolyte chemistry. An increase in deposition temperature may also require equipment changes to minimize evaporation or control hazardous fumes or to handle increased corrosive effects of the plating chemistry. Typically, increasing the agitation rate near the cathode in a plating process involves increasing solution flow rates and/or adding agitation through mechanical means or gas bubblers. While the cathode surface is usually the focus in order to increase the flux of metal ions to the surface to enable faster plating rates, the anodic reactions and adequate supply of reactants and removal of reaction products may also be important to avoid limiting the deposition rate due to anode polarization.

Modern electroplating manufacturing technology is concerned with mass production, automation, quality, and flexibility. Mass production is important for low-cost manufacturing. It requires machines that will process parts at a high rate while meeting all the specified requirements [2]. Automation helps to minimize labor costs and produce a uniform product. Quality is required to meet market acceptability and product life. Flexibility provides the ability of plating machines to process a variety of parts without extensive machine modification. It can significantly reduce the capital cost of accommodating multiple part types. It is important, at the same time, to consider the type of parts being plated and their particular requirements in order to use equipment that is optimally designed for those parts. Plating machine types include barrel, vibratory, rack, edge board, strip and wire platers, and wafer platers.

24.2 BARREL PLATERS

Barrel plating began in the post–Civil War years. Barrels were the first plating device to dramatically increase productivity [3]. There is no racking and unracking of parts, and the operation corresponds well with other bulk treatment operations such as barrel polishing, burnishing, deburring, phosphating, and oxide coating. Barrel plating machines usually require less space, and they are easily automated, minimizing operator attention.

Plating barrels come in many sizes and designs, but there are two basic types: horizontal and oblique. Horizontal barrels are usually hexagonal with perforated cylinder walls and have a removable panel through which parts are loaded and unloaded (Fig. 24.1). They may be partially or entirely immersed and rotated via plastic gears. Oblique, or 45°, barrels may have solid walls, open at the top, and contain plating solution, anodes, and the parts being plated or they may have perforated walls and be partially or totally immersed in a tank with outside anodes. A cross section of an automatic barrel plating machine is shown in Figure 24.2.

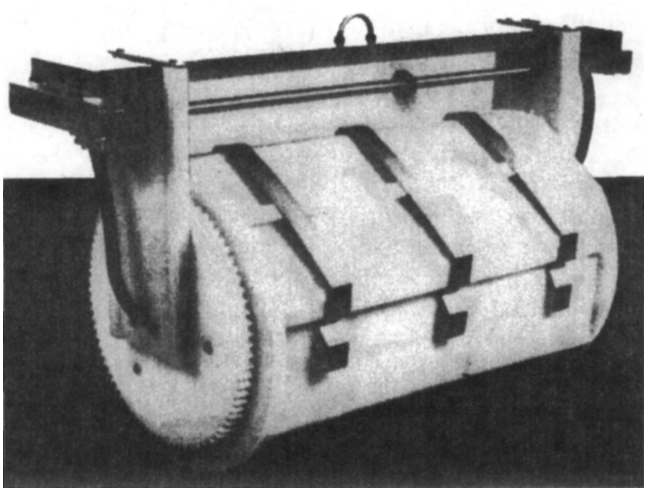

FIGURE 24.1 Rotating plating barrel fixture.

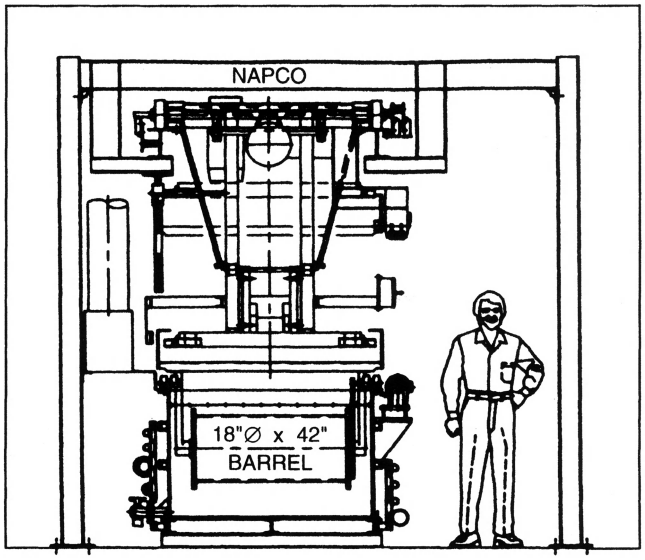

FIGURE 24.2 Cross section of automated barrel plating machine.

Considerable work has gone into plating barrel design and evaluation of construction materials [3]. Construction of a typical barrel plating machine is concerned with (1) the barrel which is rotated so that parts inside are tumbled to expose different areas to plating, (2) a tank that holds the plating solution, anodes, support for the barrel assembly, and means for connecting the barrel to a current source, (3) a gearing system to transfer motor power to barrel rotation, and (4) a means of making electrical contact to parts with flexible probes called *danglers* fed in through the rotating bearings or with metal studs fastened to the inside barrel walls. To achieve the optimum in barrel plating performance in plating speed and deposit distribution, careful consideration must be given to part size, weight, shape, and type of plating to be applied [4]. Deposit thickness is made more uniform by the following processes:

1. Decreasing the deposit thickness
2. Increasing the plating time
3. Increasing the rotation speed of the barrel
4. Increasing the amount of barrel periphery open to plating solution
5. Decreasing the size of the load
6. Decreasing the size of the barrel

Plating current densities are usually low-l0 to 20 mA cm^{-2} [or 1–2 amperes per square foot (ASF)]. Since the number of piece parts plated in a barrel is very large, the productivity of plating is high even though the plating rate is slow. Barrel plating machines are automated using lift arm or elevator-type barrel carriers. They are operated by indexing or stop-and-go movement. In more recent developments of automatic barrels, the cylinder and superstructure assembly is mounted in a carriage, permitting up-and-down movement and a motor drive to rotate and elevate the cylinder. The carriage moves from tank to tank along rails either overhead or on the tanks.

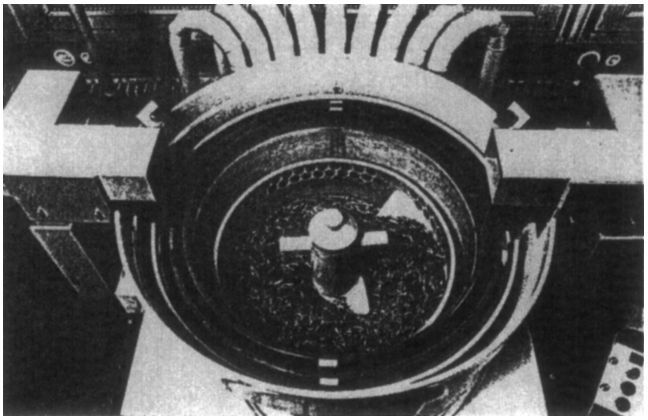

FIGURE 24.3 Vibratory plating unit where all processing is done in one place moving solutions in and out using different anodes.

24.3 VIBRATORY PLATERS

Vibratory plating is one of the newer developments in plating machines. It is used to plate small parts in bulklike barrel plating, but instead of rotating, it relies on vibrational energy applied to the bottom of the processing cell to move parts about [5]. More uniform deposits are claimed for the vibratory plater compared to barrel plating. The technique is able to handle fragile parts without distortion or damage. At present there are two types of vibratory platers: (1) where all processing is done in one place with solutions moved in an out for the plating sequence (Fig. 24.3) and (2) where the processing moves a basket with a vibrator attached from tank to tank in a sequence like a conventional barrel line [6, 7]. Both vibration frequency and amplitude are adjustable. This is necessary to compensate for process solution viscosity differences to achieve optimum agitation conditions.

24.4 RACK PLATERS

Rack plating consists of attaching parts to an insulated frame and either manually or automatically moving the racks of parts through all plating and rinsing steps [8]. Figure 24.4 is a cross section of a typical rack plating hoist assembly for printed circuit boards.

Good rack design and construction are important to successful rack plating. The following factors must be considered:

1. Size and shape of parts to be plated
2. Size and shape of rack based on tank size and other equipment

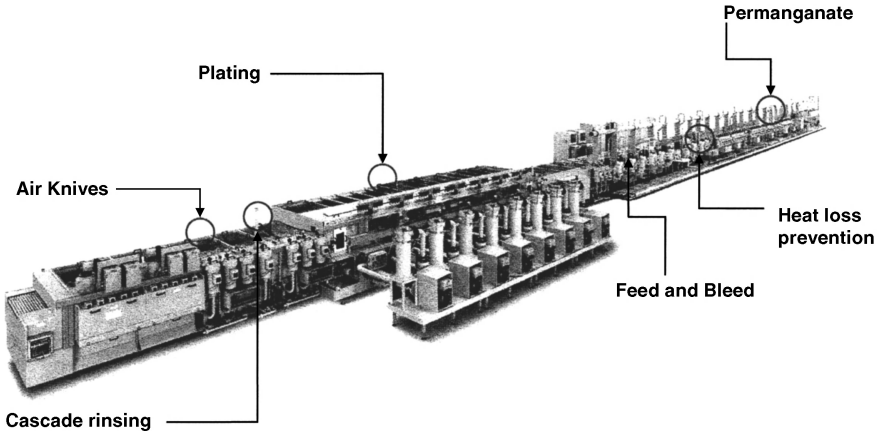

FIGURE 24.4 Cross section of a typical rack plating hoist assembly for printed circuit boards.

3. Method of supporting and making electrical contact to parts
4. Insulation of metal parts of rack other than contacts
5. Dielectric shielding to control plating distribution on parts

Rack plating machines are of two types: straight line or return. Straight-line machines may be loaded at one end and unloaded at the other, or the process controller can be programmed to bring the rack carrier to the starting point where the same operator can unload and reload the carrier. Return machines are designed to have the carriers always move in the same direction and the tanks are laid out so that racks circle back and the unload station is next to, or the same as, the load position.

Rack carrier movement through the machine can be step-and-repeat or continuous. Step-and-repeat machines move carriers a fixed distance on a preset time cycle. When racks are moved from one tank to another, they are raised before carrier movement, then lowered. If racks are in a long plating tank, they are not raised until they reach the end of the tank. Plating thickness is determined by cathode current density and dwell time in the tank. Machines with continuous rack movement automatically raise and lower racks to move from tank to tank. As with step and repeat, dwell time at each process step is controlled by line speed.

Electroplating equipment is designed to deposit metal uniformly on the parts to be plated. Current distribution within plating tanks is usually controlled by incorporating dielectric baffles as current shields and by proper design of anode size and placement within the tank. In some cases, bipolar electrodes may be used to improve current distribution. Solution agitation in rack plating equipment may be accomplished in one or more of several methods. The most common methods of solution agitation include mechanical agitators, bubble agitation (usually air), or forced-solution eductors (jet pumps) that mix the solution and direct the flow within the tank across the cathodes to be plated. Ultrasonic agitation has also been used in some cases to provide agitation at the electrode surfaces.

Electroless plating is typically a slow deposition process but can deposit uniform films and can deposit on nonconductive substrates. Electroless plating solutions rely on a reducing agent to supply the electrons. The choice of pH, temperature, reducing agent, metal ion, and their concentrations determines the electroless deposition rate. The slow plating rate can be compensated by plating many parts at one time. Plating equipment for electroless plating is similar to that for electroplating but different in several important respects. There is no power supply. This provides advantages in that the equipment is simpler, with no electrical connections. The operating cost may be increased due to higher bath temperatures, though. Dwell time in the plating tank is usually long, often 24 hours for a "full build" of copper on printed circuit boards (PCBs). Continuous solution filtration is essential to remove particulates that could cause spontaneous metal deposition which depletes metal ions from solution and potentially "crashes" the bath. Also, an additional tank containing an acidic stripping solution may be necessary for periodic removal of metal that has plated out on the equipment. The manufacture of PCBs using fully electroless copper is a viable technology to produce fine-line conductors and high-aspect-ratio through holes [9]. Other electroless processes that are in industrial use include nickel for decorative coating of plastics or wear-resistant coatings and electroless nickel/immersion gold (ENIG) for pad finishing of microelectronic components. Many of the pad finishing processes that have historically been used also contained palladium as a barrier between the nickel and gold, and increasingly only nickel and gold are being used.

24.5 STRIP PLATERS

Most strip platers can be divided into two groups: (1) electrotinning and electrogalvanizing mill steel platers and (2)

strip platers for electronic parts. Both types of strip platers are usually operated reel to reel continuously with splicing "on the fly."

24.5.1 Electrotinning

Prior to 1937 all commercial tin plate was manufactured by the hot-dipping process. Electrolytic tin plate on steel became more economical than the hot-dipping process when continuous cold reduction mills came into operation in the early 1930s [10, 11]. By 1935 small experimental plating machines were designed and built that were capable of electroplating tin on steel strip at high speeds. Electrolytic tin plate became a commercial item in 1937. Electrotinning could produce a thinner, more uniform tin coating than the hot-dipping process [12–14].

Three plating processes were developed: (1) alkaline stannate, (2) ferrostan [registered trademark of US Steel] (polysulfonate), and (3) Halogen (fluoride and chloride).

Plating baths for electrotinning are designed for very high speed tin deposition. Most commercial tin plating lines in the world use the ferrostan process, which is based on a sulfonic acid electrolyte. Figure 24.5 shows schematic arrangements of three types of handling and processing machines. These are big machines designed for high-speed strip travel at over 11 m s^{-1} (2000 ft min^{-1}). The entry end "pays off" strip into a looping tower that stores a large amount of strip. When the payoff strip approaches its end, it is stopped and quickly spliced by welding to a new roll of strip. While the payoff speed is below normal line speed, strip in the looping tower keeps it going until the payoff strip catches up and restores the volume of strip in the looping tower. A steady tension is put on the strip after the looping tower.

Figure 24.6 shows the entry end of an electrolytic tinning line. The steel is cleaned and acid pickled before entering the plating section. Tin anodes need to be replaced often. The procedure is illustrated in Figure 24.7. Note the size of the bus bars that carry current to the cathode contact cylinders. High-speed strip travel requires very high currents to deposit the required tin. The typical electrical power capacity for a ferrostan line is 100,000 A at 24 V.

Solution drag-out control is important since it can amount to 30 gal h^{-1}. After rinsing, the tin-plated strip passes a reflow tower that heats the strip above the melting point of tin. This gives the tin a brilliant luster typical of hot dipping. The fused and quenched tin is given a chemical treatment, rinsed, and dried. Finally, a lubricant oil film such as dioctyl sebacate is applied to improve its handling properties in succeeding operations. This is usually an electrostatic process using a high potential between the strip and a fixed electrode while a mist of the oil is produced in between the surfaces.

The strip next enters the unit which supplies traction power to pull it through the machine. A tachometer generator is attached to the drive motor which produces the signals to regulate the plating and melting currents in relation to strip speed.

24.5.2 Electrogalvanizing

Electrogalvanizing strip plating machines were developed after electrotinning machines [10]. They are similar in design, as shown in the schematic arrangement of a line at

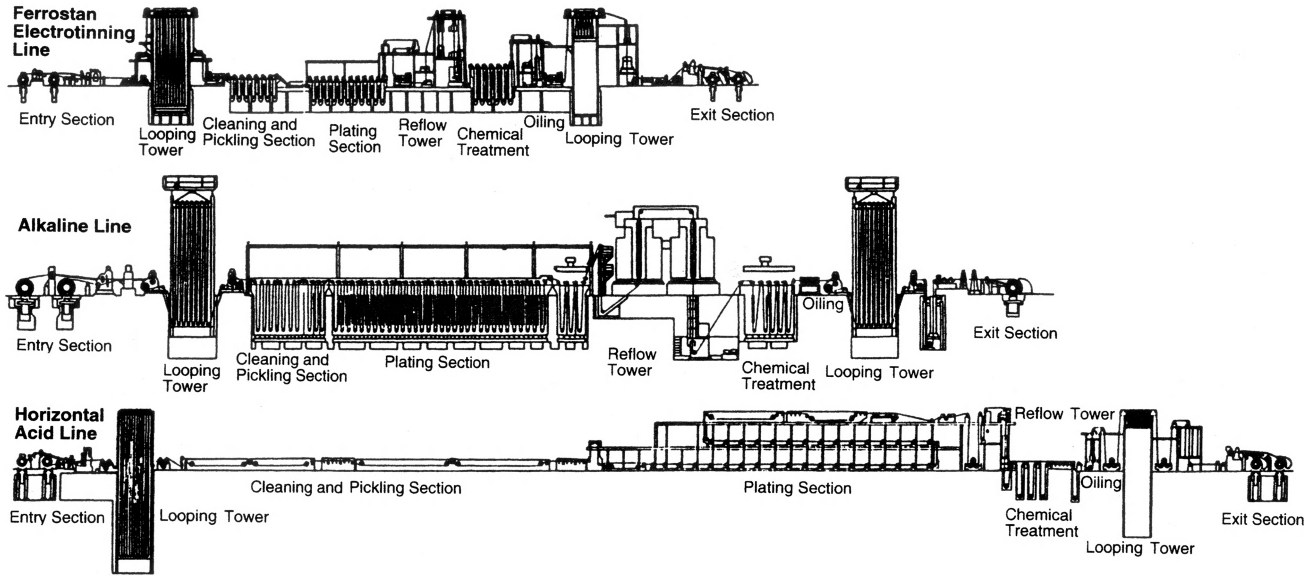

FIGURE 24.5 Schematic arrangement of handling and processing units of three types of electrotinning lines.

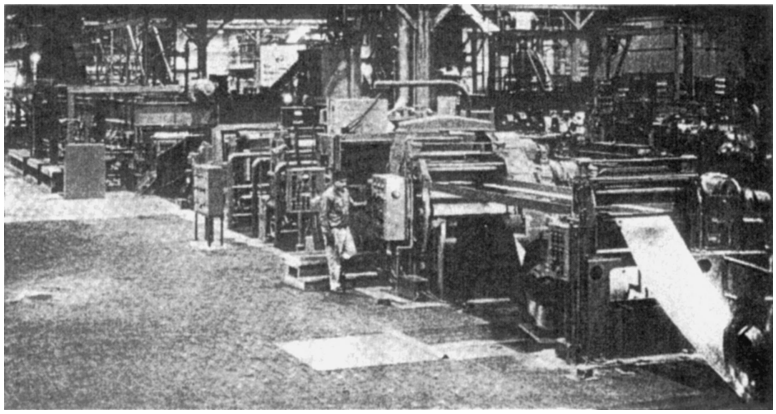

FIGURE 24.6 Entry end of electrotinning line with one coil being paid off and another in reserve position—splice by wleding.

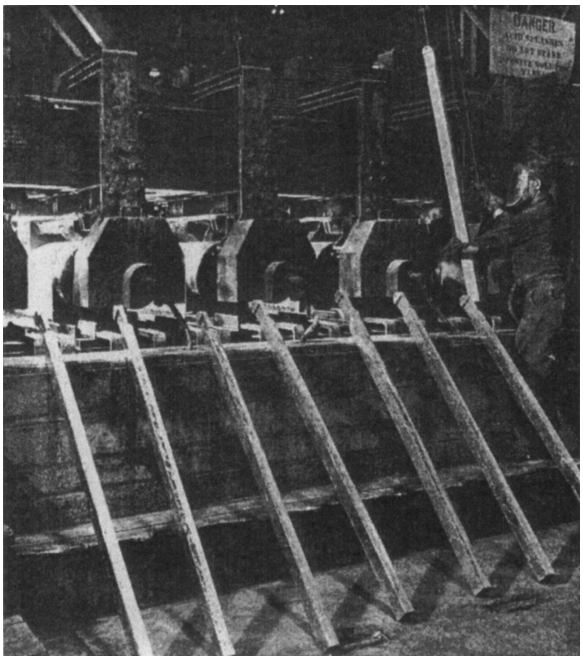

FIGURE 24.7 Tin anodes being placed in tank. Note the size of the bus barscarrying current to cells.

United States Steel (Fig. 24.8). A looping unit is employed at both ends to enable splicing while the machine is running at full speed. Machines for plating on both sides use vertical cells like those used for electrotinning with either soluble or insoluble anodes and a zinc sulfate electrolyte.

The auto industry requires one-sided zinc-coated steel. United States Steel developed the radial cell system for single-side zinc deposition illustrated in Figure 24.9. The design achieves efficient plating power usage by reducing the distance between anodes and strip. The conductor rolls are 2.4 m (8 ft) in diameter. The total plating pass length is about 67 m (220 ft) for all 18 cells. The zinc for electrolytic replenishment is provided from cast zinc anodes supported on conducting bridges.

The anodes are moved across the bridges at a rate determined by the line control computer. Approximately one-half of the anode is consumed as it moves across the bridge. It is then removed and remelted for casting into new anodes. The plating current at each cell is 28,000 A for the 18 cells. The maximum plating voltage is 12 V. Strip widths on the line range from 91.4 to166.4 cm (36 to 65.5 in.). Line speed is computer controlled to maximize production with the available current. Maximum line speed is 183 m min^{-1} (600 ft min^{-1}).

After leaving the plating section, the strip is rinsed, dried, and moved to the main pulling station. An X-ray coating gauge continuously monitors the coating thickness and provides a feedback signal to the computer for line speed adjustments to maintain the specified zinc thickness.

Electrogalvanizing one side of strip up to 6 ft in width at 600 ft min^{-1} is a commercial process. Machines for doing this generally operate 24 h a day seven days a week and stop only for maintenance. Splices are made by welding "on the fly," and the plating thickness is continuously monitored by X ray with the output signal fed to a plating current controller to

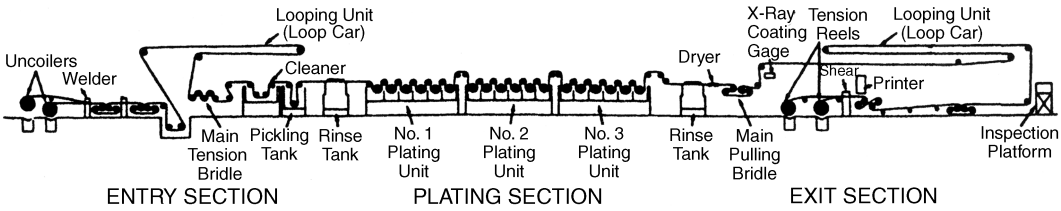

FIGURE 24.8 Schematic arrangement of one-sided electrogalvanizing line.

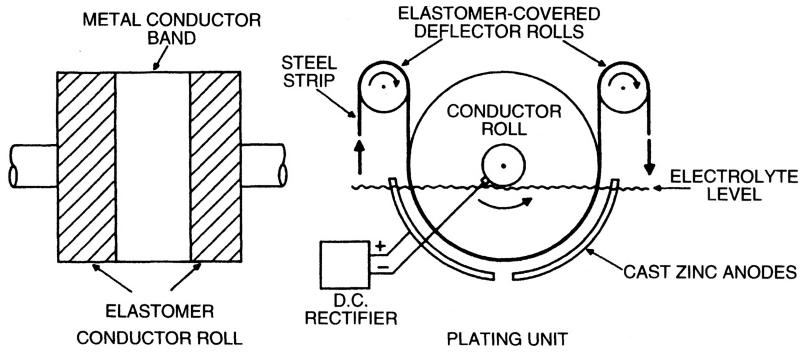

FIGURE 24.9 Schematic arrangement of conductor roll and plating unit CAROSEL for one-sided electrogalvanizing.

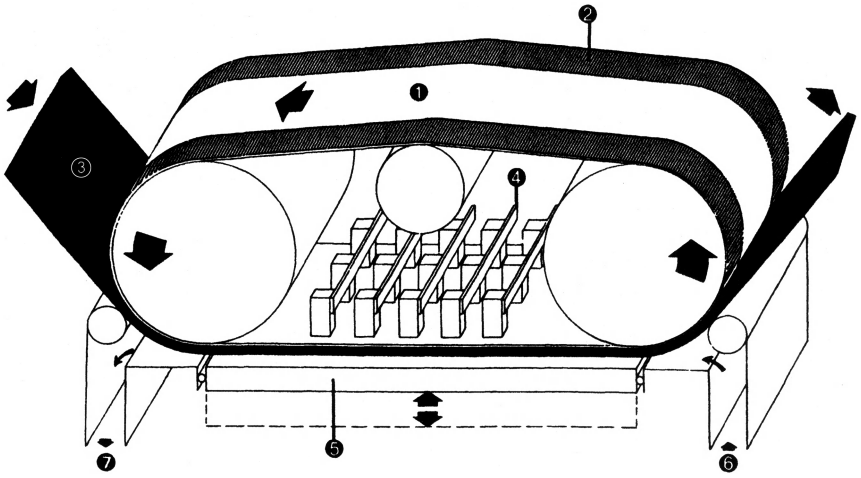

FIGURE 24.10 Schematic of belt cell for one-sided electrogalvanizing steel strip: (1) metal belt, (2) rubber bonded to top of metal belt, (3) continuous moving steel strip, (4) electrical contact to metal belt, (5) insoluble anode, (6) solution into cell, and (7) solution exit.

maintain a constant deposit thickness. The large expense of these machines can only be justified if there is a large volume of product to be plated over several years.

Another commercial electrogalvanizing plating cell design developed for depositing zinc on only one side of sheet steel is shown schematically in Figure 24.10 [11, 15]. The "belt cell" uses solution flow between an insoluble anode and a cathode 6 mm apart at $4\,m\,s^{-1}$ to achieve turbulent flow. Steel strip moves through the cell in the opposite direction to solution flow at speeds up to $200\,m^{-1}$. Dense, coherent zinc deposits are obtained from sulfate solutions at high current densities up to 350 ASD [16, 17]. Cathode efficiencies are as high as 95%, which is attributed to the high solution flow rate.

24.5.3 Strip Plating for Electronics

The explosive growth of the electronics industry began about 40 years ago, and it continues today. It led to a tremendous demand for contacts, lead frames, wire leads, chip carriers, and many other components requiring electroplating of tin, solder, nickel, silver, gold, palladium, or palladium–nickel. The huge number of components required makes it necessary to develop electroplating technology capable of high speed and sometimes selective processing. Loose parts such as pins can be plated in high volume in barrels and vibratory machines. Gold and other precious metals often must be deposited selectively for economic reasons and strip platers are best suited to the job. These are usually reel-to-reel plating machines designed to process one or more part shapes. Modern technology has provided strip plating machine designers with a vast array of chemically stable materials, electrical and electronic devices, and subsystems. High-speed reel-to-reel platers can be divided into four segments: (1) strip transport system, (2) a table with small plating cells and larger solution reservoirs, (3) electrical power sources and controls, and (4) a display of plating conditions. An example of such a machine is shown in Figure 24.11. The machine was designed to electropolish, nickel plate, and gold plate telephone modular cord plug blades. All cells and reservoir tanks were covered to minimize contamination from the environment and make fume exhaust more efficient. It has four separate plating lines each

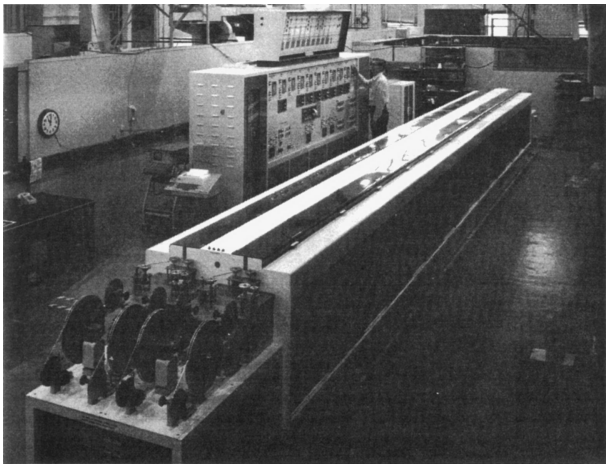

FIGURE 24.11 Four-line automatic strip plater for telephone modular cord blade plugs.

running at 12 ft min^{-1}. Figure 24.12 is a schematic of the strip plater.

Since the blade being processed in the equipment shown in Figure 24.11 was formed by punching, the contact area had a shear/break surface and needed considerable electropolishing. Dwell time in the electropolishing cells required electropolishing selectively at a current density of about 4000 A ft^{-2} to achieve the desired finish. A high current to a strip can lead to several problems: (1) electrical arcing at the contacts can eventually cause a poor contact, (2) excessive heating of the strip, and (3) excessive heating of the solution. The arcing problem was solved by using tungsten/silver alloy contacting material.

Electropolishing quality degrades with solution heating. Strip heating is minimized by keeping the cell short and electrically contacting strip at both ends to minimize resistive heating. Solution heating is also controlled by keeping anode–cathode spacing as close as possible and cooling the phosphoric acid electropolishing solution in the tank. Another problem occurs when electropolishing copper alloy strip. The solution becomes saturated with copper and eventually starts depositing a powder at the cathode. The copper powder bridges the cell, causing an electrical short so electropolishing stops. The powder is easily removed manually, but an automatic method is more economical. Two methods can be used: (1) a rotating cylindrical cathode with a scraper to remove the powder or (2) periodically vacuuming off the solution with powder next to the cathode. The solution is returned to the tank after the powder is separated out.

Good rinsing between chemical and electrochemical steps is very important in all electroplating systems. Spray rinsing is very effective. Nickel plating cells use small titanium baskets with bags and nickel pellets inside. The entire strip receives a gold strike followed by a selective hard gold plate just at the contact edge. Sensors detect when a payoff reel empties or a take-up reel becomes full. That particular line automatically stops until the operator changes reels and restarts the line.

Narrow strip platers are used mainly to process parts for electronic applications. These are reel-to-reel platers and often deposit metal selectively. Considerable development has gone into these machines in recent years [18]. They are highly automated, plate at high speeds, and deposit metal with excellent precision. Typical applications are connector terminals and semiconductor lead frames. Gold was often used in these applications, but recently palladium and palladium–nickel alloy with a gold flash has replaced most of the gold [18]. Specially designed selective plating systems have been developed to minimize the usage of precious metals [19].

Strip may be punched or unpunched. Plating unpunched strip is referred to as *stripe on strip*, with punching done afterward. Most connector terminal plating is done on punched strip with terminals held together with tie bars which are removed during connector assembly.

Development of high-speed strip platers began just at the time small low-cost microprocessors became available for machine control. This led to programmable logic controllers (PLCs) being used for overall process and machine control of strip platers. More recently, small computers such as PCs

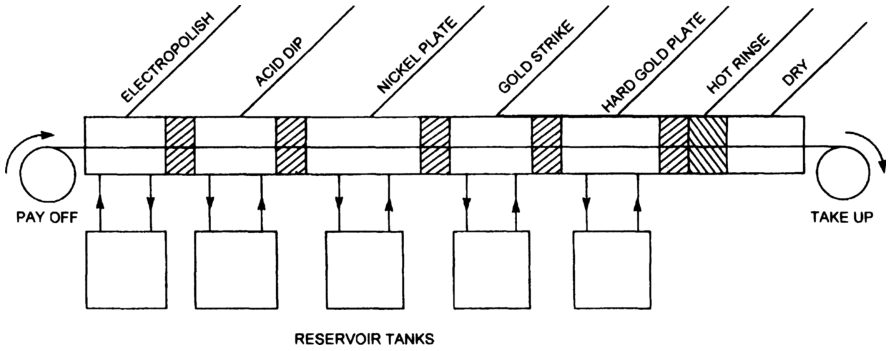

FIGURE 24.12 Schematic of strip plating facility. Each cell is a miniature chemical processing tank.

have been used but not in direct machine control. PCs are very good for operator interface and reporting functions. PLCs are better for direct control [20, 21]. Often both electronic devices are used in combination for plating machine monitoring and control [22]. A main plant computer can be programmed to watch over plating operations and alert engineers of problems as they occur. The machine shown in Figure 24.12 utilizes a PLC for process monitoring and control with an interface PC for data logging and analysis. Customers often request data on the processes used to electroplate their product and will pay extra for the information. A central console and process display panel (Fig. 24.13) allows the operator to quickly see the status of machine operation. Each process segment of the machine is designed to run in either the manual or automatic mode. This is desirable when a segment may not be functioning properly in the automatic mode.

Another type of strip plater is used in the printed circuit board industry to electroform a thin continuous sheet of copper which is bonded to a plastic dielectric. Copper is plated on the outside of a large rotating polished stainless steel drum. The drum is treated so the copper is removed easily in a continuous sheet. The outside surface of the sheet is purposely plated with a slightly rough copper surface to improve adhesion when it is bonded to a plastic dielectric. This is called *vendor* copper and may be applied to one or both sides of a flexible or rigid dielectric.

FIGURE 24.13 Central console and process display panel.

A third type of strip plater manufactures flexible printed circuits. All chemical and electrochemical processing is done on wide roll-to-roll strip plating machines. A thin copper sheet is bonded to one or both sides of a flexible dielectric material such as mylar. A plating mask is applied to one or both sides. Rolls of strip, or *web* as it is called, then are passed through the plating machine to produce a printed circuit copper much thicker than the initial copper. Tin–lead solder may be plated over the copper for solderability and/or as an etching mask for definition of electrical circuits after the plating mask is removed. The web moves over wide rollers on top and down into each tank in the processing line. The end of each roll is spliced to the next, so the machine sees a continuous web.

Bandoleer Plating Bandoleer plating involves attaching individual parts such as connector terminals to a carrier belt that moves through all processing steps like a strip plater. Parts that otherwise would be plated all over in a barrel or vibratory plater can be selectively plated on a bandoleer machine. A vibrator parts handler orients and moves the parts to the carrier belt where they are attached. At the end of the line, parts are detached and the belt circles back to the front of the machine.

Edge Board Platers Edge board or tab platers are designed to plate precious metal contacts on printed circuit boards. These are relatively new machines in the plating industry and were developed to serve a specific need for rapid selective plating of gold on contact fingers. Boards are loaded automatically into the continuous motion transport system by indexing the board carrier at the proper time so that moving belts can grasp the board and start it through all processing steps similar to plating nickel and gold on connector contacts in a strip plater. Rubber belts also serve as plating masks for selective plating to eliminate taping. Transport and plating belts are specially designed to firmly contact boards with compliant rubber that will not wear excessively and not stretch. These properties can only be achieved with a compound belt made up of several layers. The belt may also incorporate metal inserts for electrical contact to the contact fingers.

Good solution agitation around the cathode is essential for high-speed plating which is necessary for rapid movement of boards through the machine. Plating cell length is another factor that can determine machine speed. If line speed is limited by plating rate in a particular cell, any increase in that cell length can increase line speed. Improving solution agitation around the cathode area may also allow higher line speeds.

Good rinsing between chemical treatments is important. Belts also must be rinsed thoroughly before the belts return and contact new boards coming into the plating line.

Drying is done with a blast of hot air directed at the wet areas. Unloading is automatic with boards pushed into board carriers that are indexed to receive each board as it comes off the plating line. Most edge board platers are single lines to avoid being too complicated, especially when belt transport and masking are used.

Some tab platers do not use belts. Masking is done with tape that can be done by machine, but this operation is more costly. In such machines contact to the fingers is made via a tie bar around the outer edge of the board which is cut off later. Electric current is brought to the tie bar at either the side or top. Board transport is by moving belts or an overhead trolley with fasteners holding boards.

24.5.4 Wire Platers

Wire platers were the first high-speed platers, with plating current densities up to 2000 ASF [10]. These high current densities are made possible by moving the wire at high speeds through plating solution causing rapid wire motion relative to solution, not only parallel to the pull direction but also perpendicular as the result of wire vibration as it travels through the plating cell. Wire is an ideal cathode, usually being round in cross section and continuously uniform in shape throughout the plating operation. Wire also lends itself to multiple line platers, which is important in achieving high-volume production of plated wire needed in a variety of applications. Tin and tin–lead alloys are plated on copper for electrical wire. Gold or palladium–gold is plated on copper wire for connector jacks, copper on steel wire for communication systems, and zinc on steel for fencing and other outdoor applications.

Classification of various cell designs is done on the basis of the direction of forced fluid flow which may be axial, normal/radial, or tangential. These are modified somewhat in practical cells [23–25]. Conditions which produce turbulent flow are favored for high-speed plating.

24.6 DECORATIVE AND ENGINEERING PLATING

At one time a thin bright chromium deposit over bright nickel plating was used extensively on automobile and appliance parts. In recent times, a combination of product styling changes and increased cost of the Ni–Cr finish due to tougher environmental regulations has reduced its use mainly to just trim. A significant improvement in the cost of hexavalent chromium disposal or recovery would help bring greater use of the attractive bright Ni–Cr electroplated finish.

Engineering electroplating technology generally involves improving mechanical wear or corrosion protection by applying metal with special physical properties on very small or very large objects [26]. Outdoor objects such as statues and building domes are usually made decorative by plating but the process of doing the plating involves many engineering factors. The technique of brush plating is used extensively for applications where the part to be plated is too large or in a fixed position away from a plating shop. Special plating fixtures and solutions for substrate cleaning and depositing a variety of metals have been developed [27]. The technique is also used to repair worn or poorly machined parts. Electroforming of metal shapes can be another type of engineering plating [28]. Complicated forms impossible to machine are examples of ideal applications of electroforming. These can be very large objects or extremely tiny forms such as inertial elements in MEMS (microelectromechanical systems) gyroscopes and acceleration sensors or the copper coils and magnetic yokes used in computer memory disk drive and tape read–write heads [29, 30]. Another example is the manufacture of compact discs (CDs) where electroplated nickel stampers are electroformed with the precise image of the master audio or video recording [31]. Where these small devices are plated on silicon wafers or similar substrates, the equipment used will be wafer plating equipment, as described in the next section.

24.7 WAFER PLATING EQUIPMENT

Electroplating of wafers used in semiconductor or microelectronic manufacturing has matured dramatically over the last two decades [32–34]. As electroplating has moved from the thin-film recording head and GaAs semiconductor device manufacturing areas to mainstream silicon semiconductors and the manufacturing of numerous MEMS devices, the understanding of the chemistry, process, and equipment interactions has grown dramatically. In addition to advances in chemistry formulations specifically designed to provide superconformal deposition profiles ($>100\%$ step coverage) or relatively high deposition rates, several advances have been made to electroplating equipment that is used in the microelectronics industry. These advances include such things as current shielding and virtual anode designs [35, 36], multiple anodes for current distribution control, independently controlled current thieving, and membrane solution separation systems. Many advances have also been made in automated analysis and replenishment systems that are integrated into or support the plating equipment, as will be described in the next chapter.

The considerations that are usually the most important in microelectronics plating include process robustness and repeatability. Plating processes usually occur late in the manufacture of microelectronics components, where their value is greatest, and the batch processing nature of microelectronics manufacturing means that between hundreds and hundreds of thousands of devices may be at risk on a single wafer if it is misprocessed. Wafer-to-wafer repeatability is very important in order to ensure uniform product

characteristics, and within-die or within-feature thickness or alloy composition uniformity may also be critical factors. Some of these considerations mean that the microscale pattern density of the substrate may be important in terms of determining the results on the wafer or substrate [37–39].

Generally, semiconductor wafers and similar microelectronic substrates are plated in machines that are automated. The automation required in a manufacturing environment for leading-edge semiconductor devices typically involves completely automatic unloading of the wafers from the holder (cassette or FOUP—front opening unified pod), automatic transfer and processing of the wafers through each of the process steps, and loading the wafers back into the correct holder after they are rinsed and dried. Complete data logging of all the process parameters and response data is also typical, as well as sending these data files to a host computer system over a network connection automatically to facilitate data archiving. Most of these aspects are accomplished according to industry standard specifications for equipment automation, ergonomics, data handling, and general semiconductor equipment guidelines [40–44]. There are also special regulations that apply to equipment that will be used in the European Union [45]. All of these special requirements and specifications, coupled with the understanding that the value of the product being processed may be much more than the equipment itself, results in processing equipment that is relatively complex and costs multiple millions of dollars to purchase (see Fig. 24.13). Also, wafer plating systems have sophisticated error recovery schemes in order to minimize the chance of scrapping wafers when a processing fault occurs. Sometimes semiautomated versions of the equipment are used for research and development or for troubleshooting process and integration problems in a manufacturing line. In these cases, an evaluation of which of the standard semiconductor equipment guidelines must be met should be completed prior to manufacturing of the equipment.

Laboratory facilities are also important to help solve production problems when the plating process does not perform as expected. Experimental runs on a small scale can be set up to determine the cause of a problem and also how it may be corrected on the production line. Laboratories are also set up to do routine chemical analysis and plating tests such as the Hull cell or the hydrodynamically controlled Hull cell, which can provide insight to manufacturing problems [46].

Microelectronic plating is done in several types of plating chamber designs. Cell designs based on paddle agitation were some of the first configurations used in microelectronic plating processes. Most often, a fountain plating cell is used for semiconductor plating applications. Rack plating systems can also be configured to handle microelectronic substrates. These plating cells may be configured with the wafer oriented vertically or horizontally, with different advantages and disadvantages for each particular design and configuration.

24.7.1 Paddle Cells

Electroplating manufacturing technologies are often developed first in a laboratory. An example is the reciprocating paddle plating cell which was developed by IBM for uniform and rapid deposition of NiFe, Cu, and Au on micrometer-scale features for electronic and magnetic devices [47–49]. These cells were designed to provide cathode agitation and reproducible alloy composition uniformity on substrates that could not easily be rotated during the deposition of magnetic films deposited in the presence of an aligning magnetic field. Cells based on this original design have been used in the magnetic recording head industry for the last 30–40 years (see Fig. 24.14). More recently, the reciprocating paddle design has been updated to provide more uniform agitation at the cathode surface along with better control of the current distribution across the face of the substrate and compatibility with automated microelectronic processing systems, as described above [50, 51].

24.7.2 Fountain Cells

Most electrochemical deposition on semiconductor wafers or similar substrates occurs in fountain electroplating cells. These are cells, or electrochemical reactors, where the solution flow is generally from the bottom to the top of the chamber and where the solution exits the main processing area by flowing over a weir near the edge of the wafer. Figure 24.15 shows two examples of common fountain plating cells used in semiconductor processing. Fountain

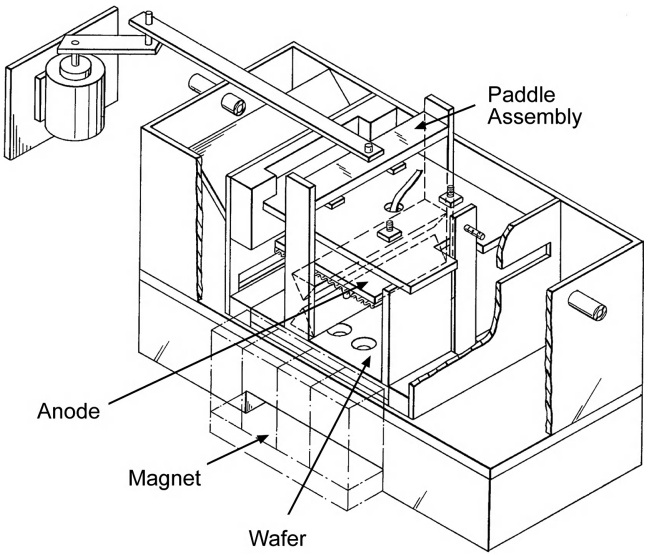

FIGURE 24.14 Deposition cell designed to provide cathode agitation.

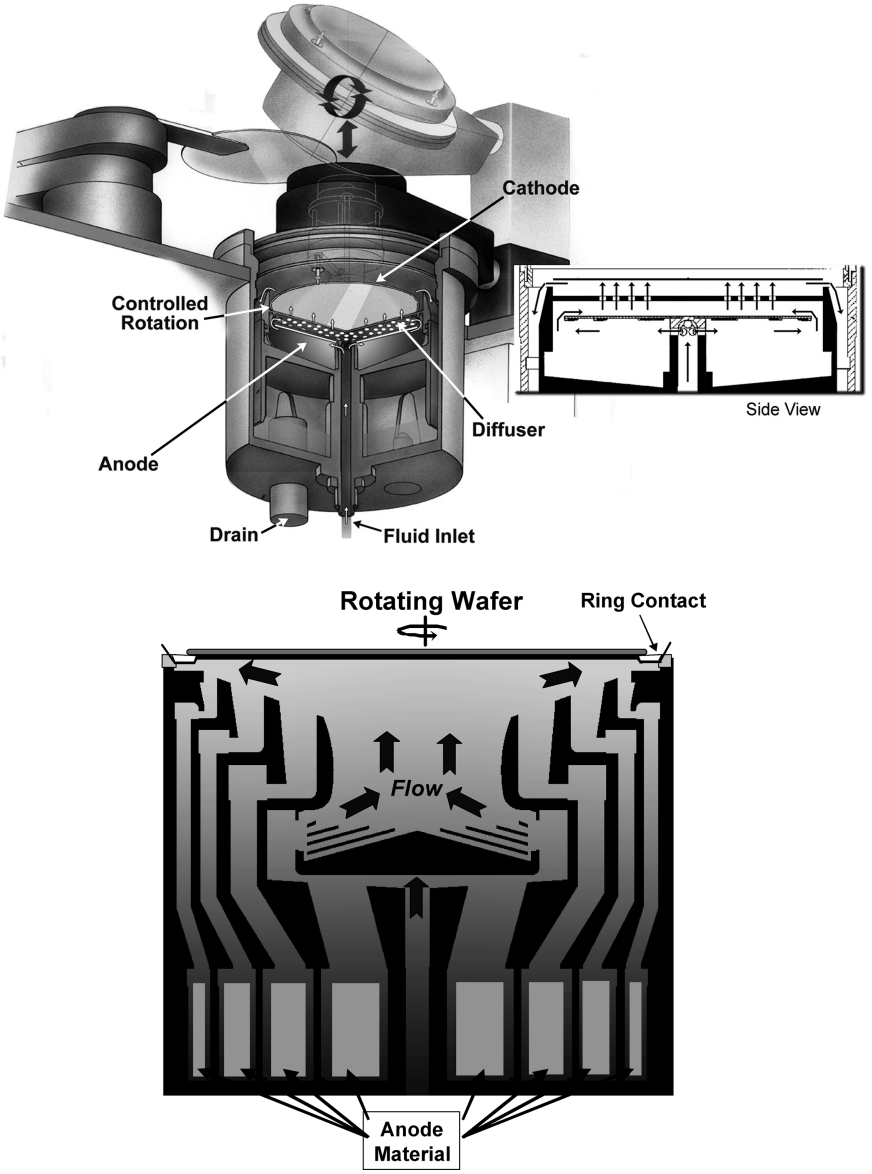

FIGURE 24.15 Two examples of common fountain plating cells used in semiconductor processing.

plating cells have the advantage of having a characteristically uniform diffusion layer thickness from center to edge when used for plating blanket films on a spinning substrate.

Since automated fountain plating systems were first introduced in the early 1990s, many improvements have been made to these electroplating cells to adapt them to the specialized needs of microelectronics plating. Most of these modifications have allowed more efficient utilization with less maintenance, lower cost of operation, or improved process performance and stability. Features such as quick-change anodes and process kits to support different wafer sizes have helped to eliminate expensive down-time associated with these maintenance activities. Incorporation of ion-selective membrane systems have increased bath life, decreased additive consumption, and improved chemical stability. Multiple electrode systems have improved current density control across the wafer and have helped automated plating systems respond to variations in incoming material. It is also becoming more common for microelectronic plating systems to incorporate automated rinsing capability as part of the plating cell, itself, which minimizes the chance of corrosion and minimizes dragout of plating chemicals.

24.7.3 Rack Platers

Semiconductor and other microelectronic substrates may also be plated in rack platers. These have already been described above, in Section 24.4, and function in much the

same way when used for microelectronic manufacturing. Substrates may be loaded automatically into racks, or fixtures, by the processing equipment or the substrate may be loaded into the rack by operators and loaded into the machine for automatic transport and processing. The racks may be transported and processed in a vertical position or in a horizontal position. Mechanical agitators and eductors provide the most common forms of solution agitation for processing microelectronic components. When using rack plating equipment, it is always critically important to make sure to rinse thoroughly to minimize carry-in of chemicals from upstream processes. These systems typically exhibit greater solution dragout than other types of wafer plating equipment.

24.7.4 Ancillary Chambers

Automated wafer processing systems will contain chambers other than electrochemical deposition (ECD) chambers to accomplish such tasks as wafer alignment (using flats or notches), prewetting, surface activation, intermediate rinses, back-side contamination cleans, final rinse and dry, thickness measurement, and anneals. In fact, they may even include chambers to strip photoresist or to etch metal seed and barrier layers after plating and photoresist stripping. Some of these chamber types are straightforward to include in a plating system, while others may require special considerations with respect to segregation of chemicals and air handling.

The configuration, or layout, of a wafer plating tool with multiple chamber types can be fairly complicated, especially if the process times can vary within a particular process chamber, as in parts with different plated thickness requirements. Multiple chambers can be used in parallel to accommodate longer processes. While more process chambers may be added to overcome bottlenecks in the process sequence, complex scheduling software is usually required to allow efficient use of all the chambers, especially when a mix of product types must be accommodated. This scheduling software may also take into account delays between process steps, which may need to be minimized in order to minimize surface oxidation between steps and maintain product quality. These scheduling algorithms may be incorporated into equipment simulators that are used to predict the equipment throughput in order to configure the tools that will best meet the expected needs with respect to product mix and fab capacity requirements [52].

24.8 SUMMARY

A wide variety of plating machines have been invented and developed to serve specific needs for electroplating parts with increased productivity and better deposit properties and at a lower manufacturing cost. There is greater use of electronic controllers and sensors to increase the level of automation in the industry. Technology exists to fully automate most plating machines. The utilization of this technology depends on its cost effectiveness and the ability of plating engineers and operators to handle advanced technology such as computers with complex control software. Plating processes continue to improve with better understanding and knowledge about the processes and the deposits produced for various applications.

ACKNOWLEDGMENTS

Figures 24.2 and 24.4 were supplied by *NAPCO*, Inc. Figures 24.6–24.10 are reprinted with permission from *The Making, Shaping and Treating of Steel*, 10th ed., AISE, 1996.

REFERENCES

1. H. J. Hawkins, *The Polishing and Plating of Metals*, Lindsay Publishing, Ormond Beach, FL (1987). Originally published in 1902.
2. M. J. Moll and L. J. Durney, *Electroplating Engineering Handbook*, 4th ed., L. J. Durney, Ed., Van Nostrand Reinhold, New York, 1984, p. 606.
3. W. H. Jackson, A. K. Graham, and R. K. Asher, *Electroplating Engineering Handbook*, 4th ed., L. J. Durney, Ed., Van Nostrand Reinhold, New York, 1984, p. 573.
4. S. E. Craig, Jr. and R. E. Harr, *Plating*, **60**, 617 (1973); **61**, 1101 (1974).
5. M. R. Kalantary, S. A. Amadi, and D. R. Gabe, *Electrochemical Engineering*, Inst. Chern. Symp. Ser. No. 112, Hemisphere, New York, 1989, pp. 199–206.
6. J. A. Lochet, company publication on vibratory plating, Vanguard Research Assoc., San Diego, CA.
7. P. A. Schopfer, company publication on vibratory plating, MECO, Bradenton, FL.
8. H. Tilton, *Electroplating Engineering Handbook*, 4th ed., L. J. Durney, Ed., Van Nostrand Reinhold, New York, 1984, p. 559.
9. H. Nakahara, *Printed Circuit Handbook*, C. F. Coombs, Ed., McGraw-Hill, New York, 1995, Ch. 20.
10. *The Making, Shaping and Treating of Steel*, 10th ed., W. Lankford Ed., Association of Iron and Steel Engineers, Pittsburgh, PA, 1996.
11. R. Winand, Belgium Patent No. 879,696 (Feb. 15, 1980).
12. E. Morgan, *Tin Plate and Modern Canmaking Technology*, Pergamon, Oxford, 1985.
13. W. E. Hoare, E. S. Hedges, and B. T. K. Barry, *The Technology of Tinplate*, Edward Arnold, London, 1965.
14. T.A. Turner, *Canmaking: The Technology of Metal Protection and Decoration*, Springer, New York, 1998.
15. R. Winard, *Oberfiache-Surf*, **25** (11) (1984).
16. A. Weymeersch, R. Winand, and L. Renard, *Plating Surf Finish.*, **68** (4), 56–59 (1981).

17. A. Weymeersch, R. Winand, and L. Renard, *Plating Surf Finish.*, **68** (5), 70 (1981).
18. D. R. Turner, *Prod. Finish.*, **66** (2) (1987).
19. D. R. Turner, *Met. Finish.*, **76** (10), 19 (1978).
20. B. W. Niebel, A. B. Draper, and R. A. Wysk, *Modern Manufacturing Process Engineering*, McGraw-Hill, New York, 1989, p. 805.
21. R. Mackiewicz, *Process/Industrial Instruments and Controls Handbook*, 4th ed., McGraw-Hill, New York, 1993, Sec. 3.32.
22. M. Baab, *Control Eng.*, **40** (4), 46 (1993).
23. A. Tvarusko, *Plating*, **58**, 983 (1971).
24. R. C. Alkire and A. Tvarusko, *J. Electrochem. Soc.*, **119**, 340 (1972).
25. A. Tvarusko, *J. Electrochem. Soc.*, **120**, 87 (1973).
26. G. F. Bidmead, *Trans. Inst. Metal Finish.*, **59**, 129 (1981).
27. J. C. Norris, in *Metal Finishing Guidebook*, M. Murphy, Ed., Elsevier, Amsterdam, 1992, pp. 301–320.
28. J. W. Dini and H. R. Johnson, *Plating Surf. Finish.*, **64** (8), 44 (1977).
29. D. A. Thompson and L. T. Romankiw, *IBM Disk Storage Tech.*, **2**, 3–5 (1980).
30. L. T. Romankiw and T. A. Palumbo, "Electrodep. Tech., Theory and Practice," *Electrochem. Soc. Proc.*, **17**, 13 (1987).
31. H. V. Reynolds, *Plating Surf. Finish.*, **82** (5), 80 (1995).
32. T. Ritzdorf, "Challenges and Opportunities for Electrochemical Processing in Microelectronics," *ECS Trans.*, **6** (8), 1 (2007).
33. M. Datta, "Electrochemical Processing Technologies in Chip Fabrication: Challenges and Opportunities," *Electrochim. Acta*, **48**, 2975–2985 (2003).
34. T. Ritzdorf, J. Klocke, B. Kim, B. Batz, R. Baskaran, D. Erickson, and E. Young, "Electrochemical Processing for Microelectronic Applications," in *Proceedings of the AIChE Annual Meeting, Symposium on Metallization Processes in Semiconductor Device Fabrication*, American Institute of Chemical Engineers, San Francisco, 2003, Paper 192d.
35. T. Ritzdorf and D. Fulton, "Electrochemical Deposition Equipment," in *New Trends in Electrochemical Technology,* Vol. *3, Microelectronic Packaging*, M. Datta, T. Osaka, J.W. Schultze (Eds.), CRC, Boca Raton, FL, 2005, pp. 495–509.
36. J. Klocke, P. McHugh, G. Wilson, K. Ritari, M. Roberts, and T. Ritzdorf, "Overcoming Terminal Effects During Electrochemical Deposition of Copper Films for 300 mm Damascene Interconnect Applications," in *Proceedings of the Advanced Metallization Conference (AMC) 2002*, B. M. Melnick, T. S. Cale, S. Zaima, and T. Ohta, Eds., Materials Research Society, Warrendale, PA, 2003, pp. 373–377.
37. S. Mehdizadeh, J. O. Dukovic, P. C. Andricacos, L. T. Romankiw, and H. Y. Cheh, "The Influence of Lithographic Patterning on Current Distribution: A Model for Microfabrication by Electrodeposition," *J. ECS*, **139** (1), 78–91 (1992).
38. S. Mehdizadeh, J. Dukovic, P. C. Andricacos, L. T. Romankiw, and H. Y. Cheh, "The Influence of Lithographic Patterning on Current Distribution in Electrodeposition: Experimental Study and Mass-Transfer Effects," *J. ECS*, **140** (12), 3497–3505 (1993).
39. B. DeBecker and A. C. West, "Workpiece, Pattern, and Feature Scale Current Distributions," *J. Electrochem. Soc.*, **143**, (2), 486–492 (1996).
40. SEMI E15, *Specifications for Tool Load Port*, Semiconductor Equipment and Materials International, San Jose, CA, 2003.
41. SEMI E19, *Standard Mechanical Interface (SMIF)*, Semiconductor Equipment and Materials International, San Jose, CA, 2002.
42. SEMI E64, *Specification for 300mm Cart to SEMI E15.1 Docking Interface Port*, Semiconductor Equipment and Materials International, San Jose, CA, 2000.
43. SEMI S8, *Safety Guidelines for Ergonomics Engineering of Semiconductor Manufacturing Equipment*, Semiconductor Equipment and Materials International, San Jose, CA, 2003.
44. SEMI S2, *Environmental, Health, and Safety Guidelines for Semiconductor Manufacturing Equipment*, Semiconductor Equipment and Materials International, San Jose, CA, 2003.
45. Directive 98/37/EC of the European Parliament and of the Council of June 22, 1998, on the approximation of the laws of the Member States relating to machinery, available: http://eur-lex.europa.eu/LexUriServ/LexUriServ.do?uri=CONSLEG:1998L0037:19980812:EN:PDF.
46. I. Kadija, J. A. Abys, V. Chinchankar, and H. K. Straschil, *Plating Surf Finish.*, **78** (7), 60 (1991).
47. J. V. Powers and L. T. Romankiw,U.S. Patent 3,652,442, (1972).
48. D. E. Rice, D. Sundstrum, M. F. McEachern, L. A. Klumb, and J. B. Talbot, *J. Electrochem. Soc.*, **135**, 2777 (1988).
49. L. T. Romankiw, J. V. Powers, and R. Acosta, "Paddle Electroplating Tool—Early Development Studies and Evolution," in *Peaks in Plating*, Semitool, Kalispell, MT, 2006.
50. G. J. Wilson and P. R. McHugh, "Unsteady Numerical Simulation of the Mass Transfer within a Reciprocating Paddle Electroplating Cell," *J. Electrochem. Soc.*, **152**, C356 (2005).
51. P. R. McHugh, G. Wilson, D. Erickson, and D. Woodruff, "Design of a Multiple-Electrode Magnetic-Alloy Plating Cell Using Numerical Modeling," *ECS Trans.* **16** (45), 283 (2009).
52. T. L. Ritzdorf, G. J. Wilson, P. R. McHugh, D. J. Woodruff, K. M. Hanson, and D. Fulton, "Design and Modeling of Equipment used in Electrochemical Processes for Microelectronics," *IBM J. Res. Dev.*, **49** (1), 65–77 (Jan. 2005).

25

MONITORING AND CONTROL

TOM RITZDORF

To obtaining quality deposits it is important to monitor and control electrochemical deposition (ECD) processes. This is also essential for an automatic plating system designed to minimize operator attention to production operations. A skilled and knowledgeable operator can maintain a reasonable plating quality with little supporting equipment. However, trends to more automation to reduce costs with higher processing speeds, application of plating to higher value products, and assurance of quality plating make it necessary to utilize many monitoring and control facilities.

Electroplating process results are dependent on process stability and control and on the chemical composition of the plating bath. This makes it important to monitor the concentration of the various species in the bath. At a minimum, it is usually important to monitor the concentration of the metal ions and the supporting electrolyte. It may also be necessary to monitor constituents that interact in trace amounts or organic additives that modify the behavior of the process.

Electroless plating, as described elsewhere, is an autocatalytic process initiated by a catalyst such as palladium and then catalyzed by the deposited metal itself [1]. Electrochemically, the system is quasi-stable, as it must be to work. This necessitates a closer control of bath chemistry than that required for electroplating solutions. Frequent electroless bath analysis and maintenance are necessary, especially when fast plating is involved, due to the speed with which the chemistry changes. Fast electroless metal deposition or poor bath control can result in spontaneous bath decomposition, causing metal particles to form and strip the solution of all metallic ions. Manual bath sampling and analysis are often not practical. Machines have been developed which automatically take samples and analyze and reconstitute the bath chemistry [2]. These will be discussed in Section 25.2.11.

This chapter has three sections: process monitoring, bath constituent concentration monitoring and replenishment, and product monitoring. The first section focuses on sensors and techniques for monitoring the plating and associated processes and how to use these to increase the automation level of plating equipment. Because the concentration monitoring and control of chemistries used in the plating processes are so important and may be handled by equipment separate from the electroplating equipment in some cases, these topics are given their own section. Finally, a short section on product monitoring and quality control is included, although the reader should understand that product monitoring should be dictated more by the product requirements than by the process used to produce it. This section is meant merely as a reference to some of the common monitoring methods in use and how they are applied to control plating processes.

25.1 PROCESS MONITORING

Plating processes, whether electrolytic or electroless, are utilized for many varied purposes. These may be for the manufacture of simple and cheap parts or for the precise manufacturing of extremely high-tech or one-of-a-kind components. In any case, decisions regarding how much effort to put in to controlling the process parameters and their impact on the process must be made based on economics, product volume, and expected results.

An electroplating line consists of a complex set of equipment, including motors, tanks, water rinses, product transport equipment, filters, heaters, electrical power supplies, process monitoring devices, process control devices, and the like. Electroplating process conditions

Modern Electroplating, Fifth Edition Edited by Mordechay Schlesinger and Milan Paunovic

to be monitored and controlled in a typical line may include:

Solution level
Solution temperature
Solution flow and agitation
Solution chemistry
- Metal concentration(s)
- pH
- Specific gravity
- Additive concentration(s)
- Impurity levels

Current at each electrochemical step
Charge passed
Cell voltages
Line speed
Blow-off air pressure
Exhaust vacuum

Methods of monitoring these parameters will be discussed in the following sections.

The designer of modern electroplating equipment has an ever-growing array of devices for monitoring and controlling almost every aspect of the process available to him or her. Plating machines can run automatically at high speeds, make adjustments, and signal an operator if help is needed. The capital investment and maintenance cost must be justified by an increased rate of production while maintaining or improving product quality. With the level of control and automation available today, completely automated equipment can be designed to handle almost any ECD task.

Semiconductor and Microelectronic Processing Equipment Equipment that is designed for semiconductor processing or for making devices such as MEMS (microelectromechanical systems) and heads for magnetic recording is usually subjected to more demanding requirements than other plating equipment. This is due to the stringent requirements for contamination control in the thin-film manufacturing technologies used to make these devices as well as the high value of the products being produced.

Semiconductor equipment is highly automated, capable of processing expensive parts with little operator intervention, and is subject to industry-specific manufacturing specifications [3–7]. These specifications are the result of many years' worth of learning regarding what materials are compatible with semiconductor manufacturing and what may lead to particle or chemical contamination, requirements from insurance companies, and what is required to interface the equipment to automated data and product handling in an automated semiconductor fabrication facility. Communication between the automated processing equipment control computer and the fab computer network is usually handled automatically and provides for the transfer and storage of large amounts of data regarding the process flow and processing of the wafers used to manufacture microelectronic devices. These data-handling requirements necessitate the incorporation of relatively powerful computers and the ability to work with host fab automation and control networks. In addition, these systems may include high-energy particulate air (HEPA) or ultralow particulate air (ULPA) filters and air ionizers to condition the environment around the wafer-handling area. Some systems may also include vision systems for verification of proper equipment operation [8, 9]. This extensive level of control requires many components. Most of the components can be implemented as simple controls or as part of a complex and automated plating system.

25.1.1 Solution Level

The liquid level or volume in the tanks used for plating is important to control for several reasons. Mechanically, enough solution must be kept in the tank to be able to operate pumps, cover any components or sensors that are meant to be immersed, and perform the plating operations themselves. Maintaining a relatively constant solution level is also important as it relates to controlling the concentrations of the constituents of the solution. In addition, it is important to be able to sense low level or absence of liquid in cases where electrical immersion heaters are used in order to prevent the possibility of fires. Liquid-level sensors are usually used to maintain solution level with replenishment of water.

The solution level in a tank can be monitored simply with a float containing a magnet that operates reed switches: one for each level in the tank to be detected. Other types of sensors that may be used to detect liquid levels include capacitive, pressure sensing, optical, and ultrasonic devices. Load cells may also be used in some cases to determine solution volume. Some of these may be used on the exterior of the plating tank (depending on materials of construction), making them less prone to attack by the typically harsh chemicals used in a plating process. There are also several types of level sensors which may be designed to provide an analog output representing the distance to the plating solution, as opposed to a simple detector that indicates that solution is present at a certain location. Plating tanks that have a high concentration of electrolyte can form salt deposits on a float causing it to become immobile. This may be avoided by directing the replenishment water at the float area. Crystallization interfering with sensor operation, reliability in harsh chemical environments, and signal-to-noise ratios under practical operating conditions are all factors that should be considered when choosing solution-level sensors. It is also important to consider the failure mode of normally open and normally closed sensors and the impact of a failure on the equipment and process.

One common exception to using automatic solution-level control is for precious metal plating tanks. Platers can be concerned about the reliability of an automatic solution-level system for a precious metal plating tank for fear of overflow and losing gold or platinum down the drain. Instead of automatic addition of water to gold and other precious metal plating tanks, an audio alarm can sound so the operator can adjust the level manually.

25.1.2 Solution Temperature

Solution temperature can be monitored with a thermocouple, thermistor, RTD (resistance temperature detector), or silicon integrated circuit device. Many sensors for plating parameters are temperature sensitive and the output signal must be compensated with an accurate temperature measurement. This is often done with an on-board silicon integrated device that senses temperature and corrects the parameter measurement [10].

25.1.3 Solution Flow

Rapid solution flow around the cathode is a common method of providing agitation to enable higher plating speeds. Large tanks for barrel or rack plating improve agitation at the cathode by moving the cathode or sparging solution or air from the bottom of the tank upward. In a strip plater that uses a line of small plating cells and reservoir tanks underneath, solution is pumped into the cells at rates sufficient to replenish the metal ion content but also, perhaps more importantly, to produce rapid agitation around the strip to enable high-speed plating. Semiconductor or microelectronic plating systems typically use some combination of solution flow, wafer rotation, and mechanical agitation systems to provide fluid agitation at the cathode surface.

For rate of flow, a rotameter, paddle wheel magnetic device, pressure differential, ultrasonic, or electromagnetic sensor can be used. It is relatively simple to buy or make a rotameter that provides output(s) indicating the actual solution flow by incorporating magnetic, optical, or capacitive sensors. There are also numerous manufacturers who produce flow sensors using some of the other technologies mentioned that are useful for plating applications. In any case, it is useful to have some understanding of the technology utilized and how the results may be impacted by viscosity, specific gravity, solution conductivity, or the presence of bubbles entrained in the solution. It is also important to note how the various flow sensors are calibrated and that the calibration may need to be repeated if the solution properties are changed.

25.1.4 Plating Current and Cell Voltage

The plating current is typically controlled during an industrial plating process because it has a direct relationship with the deposition rate and because it is not as sensitive as the cell voltage to changes in the physical system. The current at each electrochemical step can be displayed on an ammeter. It is also easily monitored by measuring the voltage drop across a resistor in series with the plating cell. That voltage can be used in an electronically controlled power supply to maintain the current at a constant value. An open circuit or power supply failure in the system can be detected by a programmable logic controller (PLC) or computer to stop a plating line and sound an alarm. Many industrial plating power supplies, or rectifiers, include automatic monitoring and control of output currents and/or voltages, along with the ability to set tolerance limits that will trigger alarms if exceeded. These alarms can be used to stop processing or to prevent additional product from being started, depending on the severity of the condition encountered.

Monitoring of electroplating cell voltages is necessary to detect cell variations such as electrical shorts or opens between the anode and cathode, contamination or polarization of the anode, or changes in solution concentrations. Shorting can occur in electropolishing cells of strip platers with close anode–cathode spacing when the strip is a copper alloy. Copper powder is produced; it collects at the cathode and eventually forms a conducting path between the anode and cathode. Methods of automatically removing the copper powder are discussed in Chapter 24. Solution changes that affect the conductivity will also impact the cell voltage, as will any extra resistance caused by corrosion of electrical components or passivation of the anode or cathode surface.

25.1.5 Timers, Ammeters, and Coulometers

Timers with ammeters were the first means of monitoring the amount of metal electroplated. In many shops they are the only instruments needed to produce an acceptable product. The first automatic control device was the ampere-hour (or ampere-minute) meter that stops plating when a preset number of coulombs has passed through the cell. Simple automatic plating machines rely on timers to advance product through processing steps. Coulometer control of plating steps is commonly included in power supplies and rectifiers designed for electroplating.

25.1.6 Sensors

A typical plating tank will include several different kinds of sensors (Fig. 25.1). It is important to choose sensors carefully with consideration given to the purpose of the sensor and its interaction with other components of the system. The impact of the chemistry (or chemistries) used on the operation of each sensor may also be an important consideration, and contact or noncontact versions of several sensing systems may be available. It is important to keep in mind that any time a device with electrical connections is added to a tank

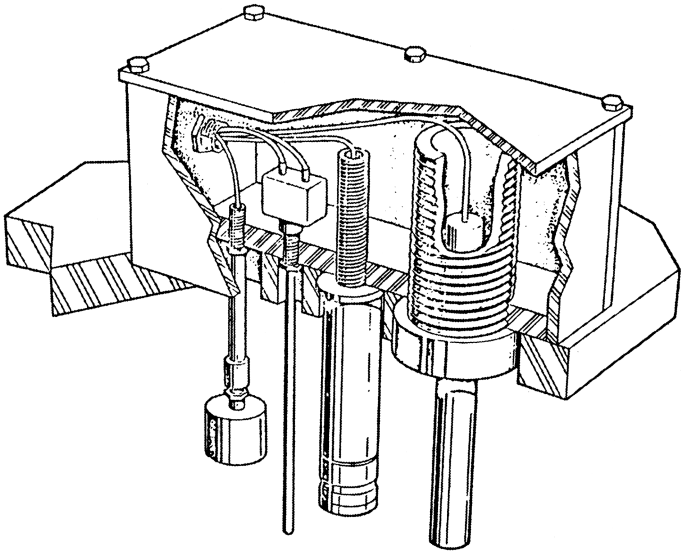

FIGURE 25.1 Typical sensor assembly on a plating tank cover. *Left to right*: Fluid level, temperature, pH, and conductivity.

containing plating chemistry there is potential for electrical interactions that may impact the process results, at a minimum upon failure of the sensor.

Advanced sensors coupled with modern control technology revolutionized automatic manufacturing [11–13]. Sensors play a vital role in providing information about plating machines and processes that is necessary for automatic monitoring and control [14]. There are three basic sensor types: on–off, analog, and digital. The on–off type can be considered a form of digital sensor without quantitative information. For many situations, an on–off sensor is sufficient. For example, when a take-up reel of strip becomes full or a payoff reel becomes empty, a simple on–off signal is adequate. Analog sensors provide quantitative information that can be read on a meter, but for automatic control it is usually necessary to convert the signal from analog to digital for electronic processing. Many sensors produce a digital signal directly. One example is a photoelectric sensor that generates pulses at a rate proportional to a plating line speed. Electronic processing then converts pulse rate to line speed which can be read on a display or fed into an electronic motor-speed controller.

An integrated system of sensors tied to an electronic controller is required to free an operator from machine watching and fine tuning critical process variables. Sensor technology has developed rapidly in recent years, and we now have a vast array of commercially available sensors, many of which are useful for plating applications. In fact the number of sensors available for some applications is so large that one must study the features of each sensor in order to make the best choice. For example, a survey showed there were 144 manufacturers of level sensors making over 20 different types [15].

There are several things to consider when choosing a sensor to monitor plating variables. The important items are accuracy, reliability, sensor life, cost, signal conditioning, and maintenance. The accuracy required depends on the process or machine function. Solution temperatures may need to be controlled to $\pm 10^{\circ}$C or to $\pm 0.2^{\circ}$C depending on the process. Cumulative variables such as plating current, plating efficiency, and line speed need to be controlled so the overall accuracy is within acceptable limits. For example, if each of these three parameters is allowed to vary as much as 1%, then the plating thickness can vary as much as $\pm 3\%$. Plating machine sensors usually must operate in a hostile environment with corrosion, fumes, and electrical noise present. For high reliability, the sensor design and choice of construction materials must be considered carefully. The sensor should hold its calibration as long as possible to minimize recalibration. The only assurance that a sensor is working properly is to either check it frequently or build in a self-checking system utilizing a sensor-within-sensor together with special electronics. These are called *smart sensors,* although sometimes there are other features included such as having the sensor directly provide a control signal to the line. Smart sensors often can be reprogrammed by an external computer. A schematic of a smart sensor and how it may interact in an automatic plating system is shown in Figure 25.2

Sensor life depends not only on how well it is designed and made but also on how it is used and maintained. A glass pH electrode, for example, once put into use must be kept wet for reliable operation. If removed from plating solution, it should be stored in water or buffer solution until returning to the bath. A float-level sensor in a plating solution can become inoperative if plating salts crystallize out on the float, causing it to stick. The problem may be avoided if water added to maintain the level is put in at the float. This removes the tendency for salts to form at the float. This is just one example of how the environment in a plating system may impact the operation of sensors that are meant to control its operation.

How much one should pay for a sensor depends on the value of the variable being sensed and the product being processed. Temperature sensors are relatively cheap and are used wherever necessary without much thought of expense. On-line plating thickness monitors are expensive, but they can save many times their cost annually by avoiding excessive gold plating or production of scrap due to underplating.

Sensor signal conditioning involves converting the electrical signal into a form that can be displayed in engineering units such as grams per liter of metal in solution. A raw signal may be conditioned using electronic hardware or computer software or a combination of the two. If only a few sensor systems are involved, hardware instead of software is usually the most cost-effective choice. Software can be developed so that a computer can convert raw sensor signals to a form useful for process control, but this tends to be more costly.

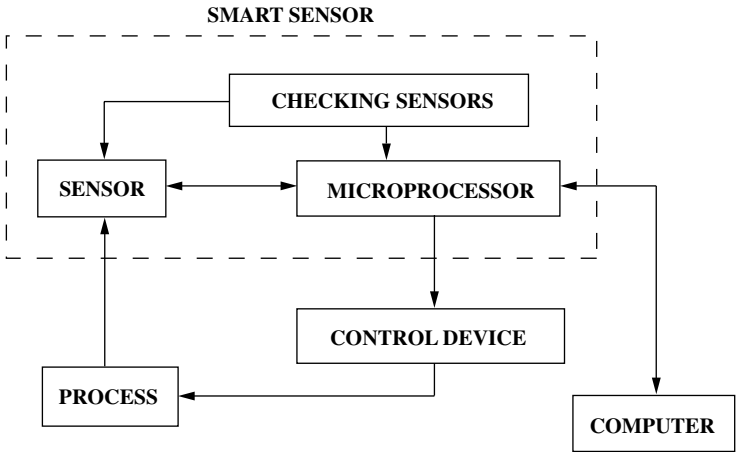

FIGURE 25.2 Smart sensor concept for monitoring with local control.

25.1.7 Line Speed

Line speed determines the dwell time of the product in each processing step in a strip plating application. In plating cells it can determine the plating thickness. Big machines that electrogalvanize steel strip monitor zinc thickness with an X-ray gauge that provides a feedback signal to a computer for line speed adjustment to maintain a specified zinc thickness [16]. Punched parts that interrupt light periodically are used to control strip speed with a photo-optical system that produces an electrical pulse as each segment moves by. An electronic pulse counter is calibrated to display line speed and provide feedback to control line speed.

25.1.8 Rinse Quality

In some cases, it makes sense to measure the quality of the rinse processes after chemical steps. This can be done by measuring the resistivity of the water that is used to rinse the parts. As chemicals are removed and the rinse water becomes less contaminated, the resistivity of the rinse water will increase. This can be especially useful when deionized water is used for the rinse operation. It is important to pay close attention to the system design, though, to ensure that contaminated rinse water is not held in the system where it will produce a high reading even after the parts are thoroughly rinsed. This can be a little tricky, since the resistivity probes normally used must be kept immersed at all times.

25.1.9 Solution Blow-Off

Solution drag-out as parts leave a processing cell can be minimized by blowing air at the part in the right direction as parts leave the tank. Large mill plating machines for electrotinning steel strip can drag out 30 gallons of solution per hour unless special measures are taken to remove as much solution as possible [16]. Standard shop floor compressors should not be used for blow-off air, since the air usually contains oil. A good roof air blower is preferred; its pressure should be monitored to ensure that adequate solution blow-off occurs.

25.1.10 Fume Exhaust

A reliable fume exhaust vacuum system is important to the health of plating shop workers and to provide a warning of faults that will lead to equipment and part corrosion. A sensor placed in the exhaust plenum detects the level of exhaust which is necessary to remove chemical fumes. One type of vacuum sensor placed in the exhaust plenum works by monitoring the cooling of a heated leg of a Wheatstone bridge. If the exhaust air stops or decreases to an unacceptable level, the sensor can trigger an alarm.

25.1.11 Programmable Logic Controllers and Computers

Sensors are the "eyes and ears" of a modern automatic monitoring and control system but PLCs and computers are the "brains" that assimilate sensor information with programmed instructions that initiate the control function.

The first automatic plating machines used timers to advance product through a line. Next a control system based on punched tape and photocells was developed that operated relays in the proper sequence to control a plating line. General Motors pioneered a wired relay logic system for machine control. Modification of that system by rewiring proved too time consuming and costly. Electronics came to the rescue when the PLC was developed in 1969. Since then PLCs have become more sophisticated with computerlike features to monitor and control many machine operations including electroplating.

While PLCs are still superior for direct machine monitoring and control, computers are better at processing data

and communicating with other plant operations. Specialty computers have been developed for direct interface with machines for monitoring and control. Fuzzy logic control is a new technique that mimics human reasoning [17].

25.1.12 Robots and Handling Systems

Robots are used in many automated plating systems. These handling and automation systems require their own monitoring and control devices. These devices may include such components as position sensors and encoders and vision systems. Automation and robotics are involved subjects which are not covered in detail here. The interested reader may find any number of references to robotic systems. When automating electrochemical processing systems with robotics, it is extremely important to remember that the environment will be corrosive due to the chemicals involved.

25.2 BATH CONSTITUENT CONCENTRATION MONITORING AND REPLENISHMENT

The composition of electroplating solutions has changed very little in recent years with the exception of high-speed plating where higher metal content and special additives are used and new solutions designed to be more compatible with health and environmental requirements. Analytical techniques have been continuously developed and improved to enable more precise or more automated control, however. Plating baths can be analyzed by evaluating their deposit properties under a specific set of conditions, by analyzing the concentrations of specific chemical species, or by analyzing the effect of a chemical species or group of species on the performance of the plating bath. Each of these methods has its own advantages and drawbacks, and oftentimes combinations of these analytical approaches are utilized as specific situations dictate.

Analysis of deposit properties may take place using a special plating apparatus or by plating a special part that is used for material property analysis, which may be destructive. This is considered a "qualification" test, and some of the testing techniques considered useful are described in the third section of this chapter. Special plating cells have been developed that can be used for plating bath analysis. Sometimes these require the qualitative judgment of an experienced technician in order to understand the relationship of the deposit produced to the chemistry in the plating bath.

Wet chemical methods of analysis have been developed to determine the composition of most plating solutions [18, 19]. Instrumentation for rapid chemical analysis of inorganic and organic species has become highly automated, providing accurate and rapid analysis. The advantage of on-line monitoring and control of plating solutions is that deviations from optimum concentration ranges can be corrected as soon as set limits are exceeded. Of course, this level of automatic monitoring comes at a cost.

Plating solution chemistry is usually monitored off-line by taking a solution sample and performing an analysis at the machine or in a chemical analysis laboratory. Solution adjustments are then made as necessary. Metal ion concentration, supporting electrolytes, additives, and pH are most often monitored. Metal ion concentrations are measured by colorimetry, polarography, or ion-selective electrodes. Automated versions of these methods have been developed for on-line analysis of many metals including nickel, copper, lead–tin, tin–silver, and gold [20–22]. On-line methods may involve extracting a sample from the bath and performing analysis or incorporating a sensor in the plating bath.

There is a fundamental question, especially when measuring bath additives, about the preference to measure the specific *concentration* of each chemical species in the bath or whether to monitor the *effect* of the chemicals that influence the performance characteristics of the plating process. While most scientists would prefer to know the exact concentration of each chemical in the system, it is often extremely difficult to quantitate the concentrations of similar organic compounds that might have a range of molecular weights, for instance. This problem becomes aggravated as the bath is used and some of the additives become oxidized and/or reduced or simply react to produce other compounds. Once you take into account complexation with metal ions, equilibrium balances, and the buildup of contaminants as parts are processed, it is sometimes much easier and more advantageous to consider the effect of these chemicals on the electrochemical activity, for instance [23]. Most electrochemical analysis methods simply measure the impact of the additives on the bath activity as being representative of the additive concentration. The impact of these decisions becomes especially important as the bath chemistry ages and impurities or additive breakdown products build up in the bath. Solution impurity buildup sometimes can be ignored, such as when drag-out removes enough solution to keep the impurity level low or when the impurity has little or no effect on the deposit or bath analysis.

25.2.1 Plating Test Cells

Test cells have been used for evaluating plating chemistry for many years [24]. These cells can be used in a development environment to understand effects of varying operating conditions on deposit properties or they can be used in a production environment to understand how a plating bath is performing compared to expected results. Also, they can provide a convenient means to separate the performance of the plating chemistry from effects produced by the equipment that is used for the process. A sample of the plating bath can be removed, tested in the test cell, then discarded or

TABLE 25.1 Electrochemical Test Cells

Hull cell	Additive concentration effects, varying CD and agitation
Rotating cylindrical Hull cell	Additive concentration effects, varying CD and agitation
Haring–Blum cell	Throwing power
Stress cells	Deposit stress as function of varying CD and thickness
Rotating disk electrode (RDE)	Polarization, limiting current density, etc.
Rotating ring disk electrode (RRDE)	Impact of electrochemical reactions on bath chemistry
Electrochemical quartz crystal microbalance (EQCM)	Deposit efficiency, absorption vs. applied potential

added back to the plating tank. Table 25.1 lists some common types of electrochemical test cells and their typical uses.

Hull Cell The Hull cell is a plating test cell that was designed to allow a quick analysis of the "health" of the plating chemistry and to allow the effect of additions to the bath to be easily scaled up to an industrial system [25–27]. An example is shown in Figure 25.3. The Hull cell is a trapezoidal plating cell that utilizes a cathode placed diagonal to the anode to cause a variation of current density across the cathode surface. The Hull cell is usually used with a magnetic stir bar on the bottom, which results in stronger agitation at the bottom of the cathode panel than at the top. This allows a panel to be plated that shows qualitatively the effects of current density and agitation variations on the deposit properties (usually deposit morphology or brightness). Small additions of additives can be made to the chemistry in the Hull cell, which usually contains 267 mL of plating bath. Once the desired performance is produced on the Hull cell panel, the additions to the plating tank can be quickly calculated since each gram added to the 267-mL Hull cell is equivalent to 0.5 oz/gal. There are many variants of Hull cells with different agitation mechanisms or temperature control capability, such as air-agitated or hanging Hull cells and Gornall cells, but they all work in generally the same way [25–27].

Rotating Cylindrical Hull Cell The rotating cylindrical Hull cell is a modification to the Hull cell concept that is especially useful for development of new chemistry and processes, as it allows for precisely controlled uniform agitation with the current density variation typical of a standard Hull cell. This cell essentially makes use of a rotating-disk electrode rotator system to control the rotation of a shaft that incorporates a cylindrical cathode. This arrangement provides uniform and controllable mass transfer across the cathode surface. The placement of the rotator with respect to the anode provides for variations in current density across the surface of the cathode [28, 29].

Haring–Blum Cell The Haring–Blum cell is a test cell that is used to measure the throwing power of a plating process. It is a 1000-mL cell that is rectangular and contains two cathodes and one anode. The cathodes are placed at different distances from the anode. Usually, one cathode is five times farther from the anode than the other. The ratio of the thickness deposited on each cathode can be used to calculate the throwing power of the system [30–32]. See Figure 25.4.

Stress Cells There are several types of stress analysis cells available. Usually, they utilize a beam-bending technique to calculate the stress of the film deposited on a cantilever cathode. This can be done by using two beams and measuring how far apart from each other they bend or by using a sort of modified Hull cell test with tabs that bend in one direction as metal is deposited on one side [33, 34].

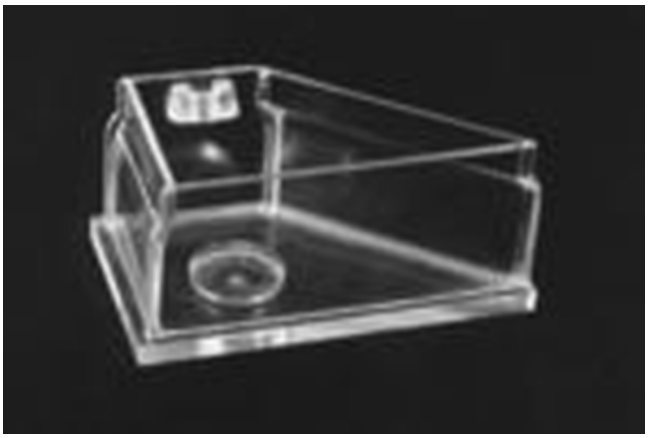

FIGURE 25.3 Hull cell.

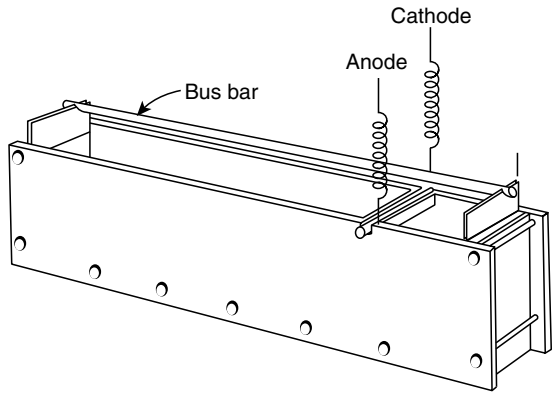

FIGURE 25.4 Haring throwing-power box.

Recently, several researchers have begun using in situ stress measurement during electroplating experiments by incorporating a laser deflection measurement system as part of an electroplating cell [35–37]. This is a powerful technique because it has the capability to measure the stress in situ as the film is being deposited. This technique provides information related to the incremental stress added at each stage of the deposition, and it can also measure changes associated with holding the sample at open-circuit potential. With the right apparatus, the impact of monolayer adsorption on the cathode surface can be seen [36].

Electrochemical Quartz Crystal Microbalance There are specialized electrochemical measurement systems called electrochemical quartz crystal microbalances, or EQCMs, that utilize a quartz crystal as a working electrode [38–40]. The quartz crystal is caused to vibrate due to the piezoelectric effect and its oscillation frequency is monitored, along with the plating current and potential as a function of time. The oscillation frequency is a function of the mass of the crystal and the deposits on it, and the instruments are typically sensitive enough to measure submonolayer adsorption of organic materials on the electrode surface or micrometer-thick deposits of metals. The Sauerbrey equation can be used to calculate the mass of a deposit on the crystal, which can be converted to thickness if the density of the deposit is known:

$$\Delta f = -\left(\frac{2f_{\mathrm{f}}^2}{Z_q}\right) m_{\mathrm{F}}$$

where Δf = frequency shift of the loaded crystal
f_{f} = fundamental frequency
Z_q = acoustic impedance of the material (8.8×10^6 kg m^{-2} s^{-1} for AT-cut quartz)
m_{F} = mass per unit area

The EQCM is a powerful tool for understanding the reactions that occur on a working electrode during a potential sweep or for understanding the cathode efficiency of a deposition. These instruments are typically used in process development or troubleshooting of electrochemical processes [41, 42].

Other Cells There are several other kinds of electrochemical cells that can provide useful information in the proper circumstances. These include cells such as jiggle cells and bent-cathode test cells [43, 44].

25.2.2 Colorimetry or Photometry

Photometric analysis techniques are fast, simple, and relatively cheap. Additionally, these techniques can be easily automated, potentially without involving extraction of a bath sample. Fiber optics has made small colorimeters practical for automatic analysis of many plating solution species [45]. A light source and absorbance detector can be placed remotely from the analysis cell via a bundle of flexible glass or plastic pipe fibers. The optimum wavelength of light to be used for a given species is best determined from a spectrographic scan over a wide range of wavelengths, A wavelength at or near a strong absorption peak is selected and a calibration curve based on Beer's law is prepared. The unknown can then be measured and its absorbance compared to the calibration curve to determine the concentration of the constituent of interest. UV/visible photometric analysis works well for the transition metals. Some examples and the wavelengths that are useful for analysis are shown in Table 25.2. For example, Cu(II) in electroless plating baths is determined at 620 nm wavelength. Cobalt(II) in hard gold baths may be analyzed by first oxidizing it with hypochlorite to Co(III). Cobalt(III) forms a pink complex with ethylenediaminetetraacetic acid (EDTA) which can be analyzed at 520 nm wavelength [46]:

$$A = \varepsilon \times l \times c \quad \text{Beer's law}$$

where A = absorbance
ε = molar absorptivity
l = path length or cell length
c = concentration

25.2.3 Electrochemical Analysis

Additives in plating baths are important to achieving the desired physical properties of many electrodeposits. Additive concentrations must be maintained within a specific range for best results. Techniques used for monitoring additive concentrations include cyclic voltametric stripping (CVS) [47–53], polarography [54], and other electrochemical methods. The method used must be able to detect the active species in the presence of degraded nonactive material and/or impurities.

Polarography Polarography using a dropping mercury electrode (DME) has made considerable progress over the past 50 years as a laboratory technique for chemical analysis of plating solutions (Table 25.3), but it was not used in the manufacturing environment until about 30 years ago, mainly because of the sensitivity of the electrode to manual handling. When manual handling is eliminated by automation, the DME can be used as a reliable and reproducible sensor in automatic analyzers and controllers in industrial applications [20, 21].

Cyclic Voltammetric Stripping *CVS* is used to determine the concentration of organic additives such as suppressors,

TABLE 25.2 Absorbed and Perceived Colors

Absorbed Wavelength (nm)	Absorbed Color	Perceived (Transmitted) Color	Metal Complexes
310	Ultra-violet	Pale yellow	$[Co(CN)_6]^{3-}$
314	Violet	Yellow	Pd-NH_3-complex
400	Violet	Green-yellow	
437	Blue	Orange	Co-NH_3-complex
450	Indigo	Yellow	
480	Blue	Orange	
500	Blue-green	Red	$[Co(NH_3)_5H_2O]^{3+}$ $[Ti(H_2O)_6]^{2+}$
512	Yellow/green	Violet/red	$CoCl_2$
530	Green	Purple	$KMnO_4$, $Cu(ED)_2{}^{2+}$
548	Yellow	Violet	Cu-$(ED)_2$-complex
570	Yellow-green	Dark blue	
600	Orange	Blue	Cu^{2+}
650–730	Red	Green	Ni^{2+}

brighteners, and levelers from the effect the additive exerts on the electrodeposition rate at a given potential. The potential of a rotating platinum electrode is cycled at a constant sweep rate in a bath sample so that a small amount of metal is deposited on the electrode and then stripped off by anodic dissolution (Fig. 25.5). The charge required to strip the metal is related to the additive concentration using predetermined calibration curves, as in Figure 25.6. By using this electrochemical approach coupled with titrations of certain bath components or other suppressors and accelerators, a reasonable correlation can be made to the additives in the electroplating bath. Computerized instruments have been developed that automatically determine additive concentrations [23]. CVS has become a very common method due to its relative simplicity and the availability of automated equipment to perform this analysis. One aspect of CVS analysis that is both an advantage and a drawback is that this technique provides a single numeric value that is used to monitor the characteristics of the plating bath. All of the information contained in the current values as the potential is dynamically scanned is lumped into a single number that is affected by all the bath constituents and contaminants at that point in time.

TABLE 25.3 Examples of Polarographic Analysis of Several Plating Baths

	Polarography Can Determine These:		
In These Baths	Major Components	Trace Metals	Organic Additives
1. Zinc Sulfate	Zinc	Copper, cadmium, arsenic	*o*-Chlorobenzaldehyde
2. Palladium	Palladium, chloride	Tin	Hydroquinone
3. Gold(I) cyanide	Gold, free cyanide	Cadmium, cobalt, copper, zinc, iron, tin, chromium	
4. Watts' nickel	Nickel, chloride, boric acid	—	Saccharin, *o*-Benzaldehyde sulfonic acid
5. Electroless copper	Copper, formaldehyde	—	Mercaptobenzothiazole
6. Copper sulfate	Copper	—	Thiourea and thiourea derivatives
7. Solder bath	Lead, Sn(II)	Sn(IV)	
8. Brass	Copper, zinc	Lead, arsenic	
9. Nickel–cobalt	Nickel, cobalt	—	

TABLE 25.4 Manufacturers of Plating Bath Analysis Systems

Company	Technique
ECI	CVS, photometry, titration
Metrohm	CVS, titration
Ancosys	CVS, photometry, HPLC, titration
Technic	CVS, polarography
ATMI/Semitool	Chronopotentiometry
Dionex	HPLC
Applikon	Titration
Ebara-Udylite	

Chronopotentiometry and Chronoamperometry These techniques have also been used to analyze the additive concentrations in plating baths [55, 56]. A version of a chronopotentiometric technique that has been commercialized is referred to as *pulsed cyclic galvanostatic analysis* (PCGA) [57]. Figure 25.7 shows an example current pulse train and a series of potential response curves that may be generated as the suppressor concentration in a copper plating bath is increased. A set of response curves such as this can be used to generate a calibration curve similar to the one in Figure 25.6, which is then used to determine the additive concentration of an unknown bath. Advantages of these techniques include that they gather more information that is related to the state of the chemical constituents and they separate the dynamic nature of the process from the steady-state bath behavior (electrochemical activity). This allows the operator to try to better differentiate between the effects of multiple components of the chemistry.

Real-Time Analyzer, or RTA™ An analysis technique based on combinations of these electrochemical techniques that utilizes a small electrode as part of a probe that can be placed in a plating tank has been developed by Technic [58–60]. This has the benefits of an electrode probe which can be placed in the plating bath and which can run multiple analysis cycles without the need for withdrawing a chemical sample from the tank. This analyzer usually uses harmonic analysis of the plating response, which has been shown to be indicative of certain components of the plating bath. The method development seems to be a bit more empirical and the operating window of these systems can be narrower than with other techniques, but it is an operator-friendly system and is simple to use.

25.2.4 Ion-Selective Electrodes

Ion-selective electrodes have been developed which can monitor the concentration of a number of anions and cations [61–64]. A list of commercially available ion-selective electrodes is given in Table 25.5. The membrane can be glass, as for a pH electrode which measures H^+ concentrations, or liquid or solid material. Some ion-selective electrodes have limited lifetimes such as the CN^- electrode. Only periodic analysis is practical with a water soak in between applications. However, this problem can be minimized with a well-designed sampling and flushing system. Care should be exercised in selecting the most appropriate ion-specific electrode or oxidation–reduction potential (ORP) electrode for a particular application. Flow-through cells using ion-selective electrodes have been used for continuous on-line monitoring of copper in electrowinning solutions [65].

Solution pH A pH electrode monitors hydrogen ion activity. Therefore it directly measures the acidity or alkalinity of a plating bath. All plating baths work best over a specific, sometimes narrow, pH range. pH sensing and control systems

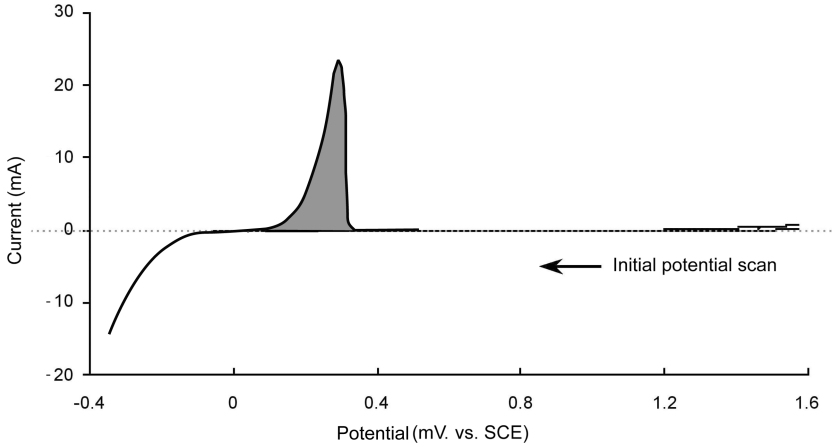

FIGURE 25.5 CVS plot from copper sulfate plating bath.

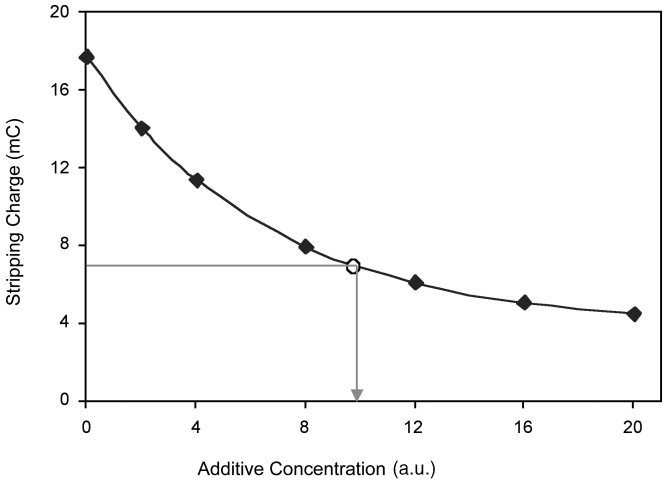

FIGURE 25.6 CVS calibration curve.

are commercially available. pH electrodes are also used to detect the concentration of certain compounds in plating baths by measuring solution before and after a reagent addition. For example, in electroless copper plating the amount of formaldehyde present can be determined by measuring the pH of a sample of solution before and after fixed amounts of H_2SO_4 and Na_2SO_3 are added. This method was used by Photocircuits and McDermid for automatic analysis and control instruments for electroless copper plating processes.

The standard glass electrode is a reliable pH electrode as long as it is kept wet. It cannot be immersed in strong alkali, fluoride or fluoborate solutions for very long before the glass is etched away. However, it can be used to measure pH in those solutions for a reasonable period of time if the electrode is rinsed and stored in distilled water after each quick pH measurement.

Of course, hydrogen ion concentration can also be measured by acid/base titration. This technique has been used in several automated bath analysis systems for plating bath analysis and control.

25.2.5 High-Performance Liquid Chromatography

High-performance liquid chromatography (HPLC) is another method that has been used to monitor the concentrations of plating bath constituents, especially organic additives. HPLC uses a pump-driven eluent stream (usually acidic) which carries the sample into a separation column containing a resin material designed to adsorb components of the bath with varying affinity. The resin material is chosen to retain the components of the sample in the column for differing amounts of time, dependent on their molecular weight and chemical interactions with the resin, which results in their separation into discrete bands before entering the detector. These bands are then detected by UV/VIS absorption, by conductivity, or possibly using an electrochemical detector. The output from this separation and detection is a chromatogram which is recorded with respect to elapsed time. As with the other techniques already discussed, the concentration of the samples can be determined by comparing their chromatogram peak heights or areas with those generated during calibration runs.

HPLC and ion chromatography techniques are most often used in off-line applications [66]. They involve relatively high capital expenditure, and the maintenance requirements tend to be intensive with these systems, which has limited their use in automatic on-line analysis [23]. These techniques provide a measurement of the concentrations of certain constituents of the plating bath, as opposed to the impact they have on the electrochemical activity. This makes the methods a more direct measurement of the chemistry, which makes it important to be able to separate the constituents and

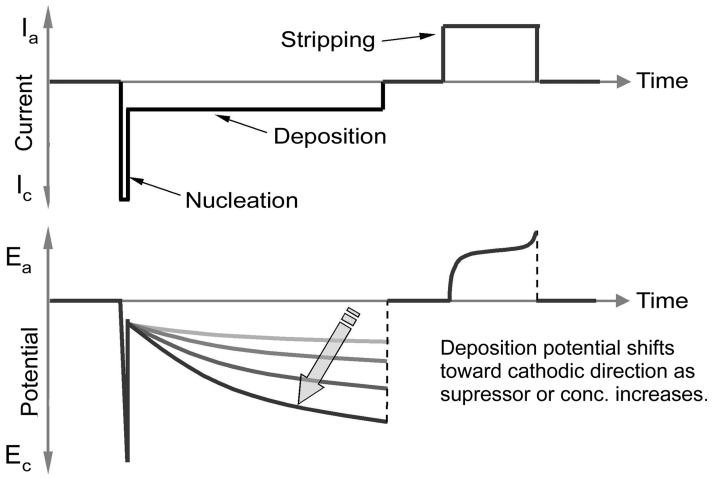

FIGURE 25.7 Current and potential plots from PCCA analysis.

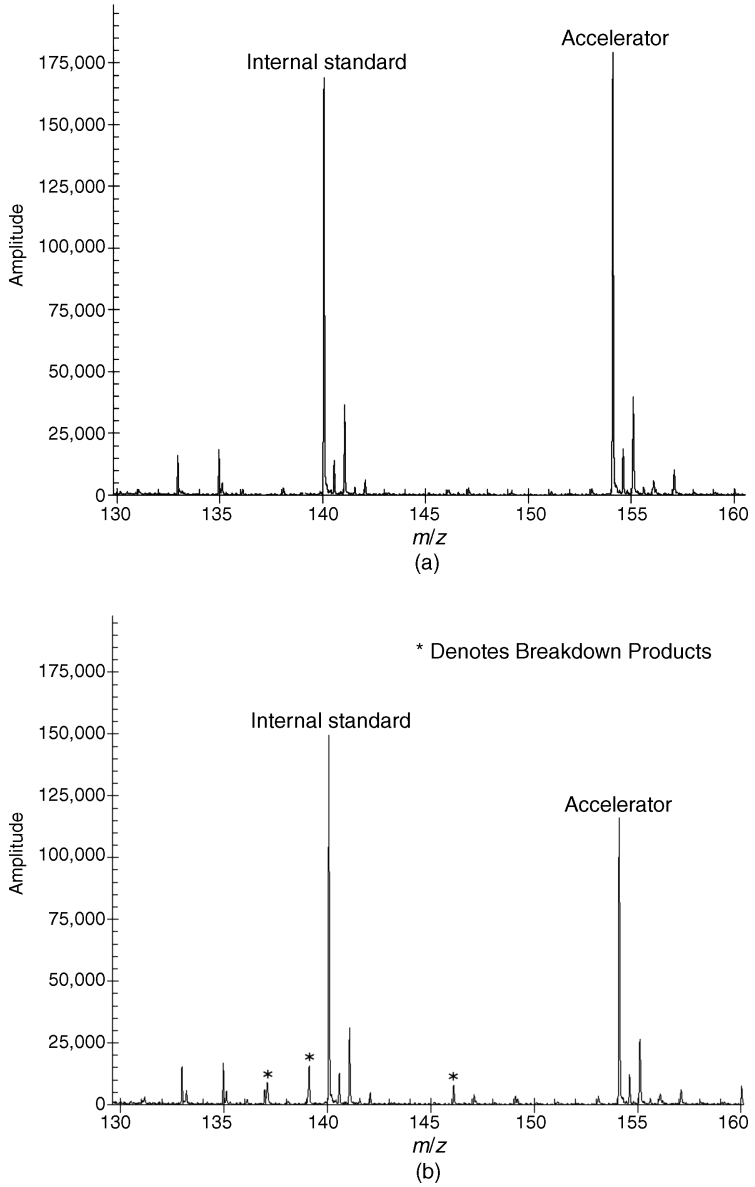

FIGURE 25.8 Mass spectroscopic analysis of fresh and used accelerator in copper plating bath.

identify the electroactive species as well as to quantitate them appropriately.

25.2.6 Mass Spectroscopy

Mass spectroscopy (MS) methods are based on separating atoms or compounds based on their mass. Mass spectrometers usually require some level of ionization, which may involve an inductively coupled plasma source (ICP-MS) or an electrospray ionization system. These systems can provide an impressive amount of information related to the chemical species present and their amounts, but they tend to be expensive and require significant data interpretation and maintenance.

A wide strip electrotinning line built by British Steel in Wales incorporates a fully automatic analytical system to monitor solutions along the line [67]. Samples are taken automatically from cleaning, pickling, and plating tanks by taking a chemical sample from each tank and conveying it to a remote analytical station. There a robot prepares the samples for analysis by an ICP mass spectrometer. Results are fed back to the control station where the operator makes the necessary adjustments.

Recently, an automated bath analysis system has been developed using mass spectroscopy (Fig. 25.8) [1, 68, 69]. This system was designed as a process control system for plating baths, but it has the additional capability of determining an entire spectrum of components in a plating bath, including

TABLE 25.5 Commercially Available Ion-Selective Electrodes

Ion	Membrane	Lower Detection Limit (*M*)	Principal Interferences
H^+	Glass	10^{-14}	None below pH 13
Na^+	Glass	10^{-6}	H^+, Ag^+
K^+	Glass	10^{-4}	H^+, Na^+, Ag^+
K^+	Liquid	10^{-4}	NH_4^+, H^+
BF_4^-	Liquid	10^{-4}	NO_3^-, Br^-, ClO_4^-, I^-
NO_3^-	Liquid	10^{-4}	I^-, Br^-
Cl^-	Liquid	10^{-4}	I^-, NO_3^-, Br^-
Ca^{2+}	Liquid	10^{-4}	Zn^{2+}, Fe^{2+}, Pb^{2+}, Cu^{2+}, I^-
Water hardness	Liquid	10^{-3}	Zn^{2+}, Fe^{2+}, Pb^{2+}, Cu^{2+}
F^-	Solid	10^{-6}	OH^- at high pH
Cl^-	Solid	5×10^{-1}	S^-, I^-, Br^-, CN^-
Br^-	Solid	5×10^{-1}	I^-, S^-, CN^-
I^-	Solid	5×10^{-1}	S^-
S^-	Solid	10^{-17}	None
CN^-	Solid	10^{-6}	S^-, I^-
Ag^+	Solid	20^{-17}	Hg^{2+}
Cd^{2+}	Solid	10^{-7}	Ag^+, Cu^{2+}, Hg^{2+}
Pb^{2+}	Solid	10^{-7}	Ag^+, Cu^{2+}, Hg^{2+}
Cu^{2+}	Solid	10^{-8}	Ag^+, Hg^{2+}

separating species that are similar but have slightly different molecular weights. This system, from Metara, provides volatilization through an electrospray system which keeps most of the constituents relatively intact for measurement purposes.

25.2.7 Atomic Absorption Spectrometry

Atomic absorption (AA) spectrometry is similar to photometry, but it utilizes an atomized sample of the liquid being analyzed and usually requires dilution of a bath sample before measurement. Atomization may be provided using a flame, an ICP source, or a graphite furnace. A narrow-wavelength spectrum source such as a hollow cathode lamp or a laser is used to excite the electrons of the atomized sample to higher energy orbitals characteristic of the metal being measured by the absorption of the light from the illumination source. The absorption is measured and used to determine the amount of that metal present

Atomic absorption analysis is fairly reliable and cheap but requires quite a bit of maintenance. Therefore, AA techniques have been used in off-line analysis in chemical laboratories but have not been used much in automated plating bath control.

25.2.8 X-Ray Fluorescence

X-ray fluorescence (XRF) analysis is discussed in Section 25.3 with respect to product monitoring, but it can also be used as a technique to monitor the metal concentrations in plating baths. It is a relatively straightforward technique as long as the fluid handling is managed and is a good way to measure the ratios of metal ion concentrations in alloy plating baths. XRF is an expensive technique, though, and care must be taken to avoid errors due to drift of the X-ray source or detector. The frequent calibration requirements and expense have prevented widespread use of XRF for solution analysis, although industrial systems for this purpose have been built [70].

25.2.9 Total Organic Carbon Analysis

Total organic carbon (TOC) analysis is sometimes used to provide a measurement of all the organic materials added to a plating bath. This usually includes additives such as grain refiners, brighteners, and surfactants as well as any other organic materials that are carried into the bath on the substrates being plated. TOC values do not include dissolved CO_2 or carbonates from inorganic sources. These are removed from the bath sample by purging prior to the TOC analysis. The TOC level is determined by oxidizing the sample using chemical, electrochemical, or photochemical means. The evolved carbon dioxide can then be measured with a CO_2 detector. TOC is a good way to evaluate the total amount of organic material introduced into the bath over its life and may be used to monitor the end of life of a plating bath due to buildup of organic additives and their breakdown products or other materials such as masking agents or photoresist components that may be leached out of the samples being processed.

Organic impurities can be removed by activated carbon treatment when necessary. However, this usually strips the bath of all organic components so additives need to be replenished afterward. Harmful impurities that are known to build up in a plating solution should be monitored routinely. Often the first sign of an excessive impurity level is off-color plating or a film roughness and morphology changes. Water for rinsing often needs to be free of organic and inorganic impurities as well [71].

25.2.10 Other Analysis Methods

Specific Gravity Specific gravity may be monitored to maintain a concentration range for sufficient solution conductivity or to detect excessive buildup of salts. A simple manually operated hydrometer can be used. A more elaborate automatic device uses a radio-frequency oscillator with a loop probe exposed to the solution. The oscillator frequency shifts in proportion to the specific gravity.

Conductivity A conductivity measurement is sometimes used to determine the presence or absence of inorganic impurities. A good strategy to minimize the amount of

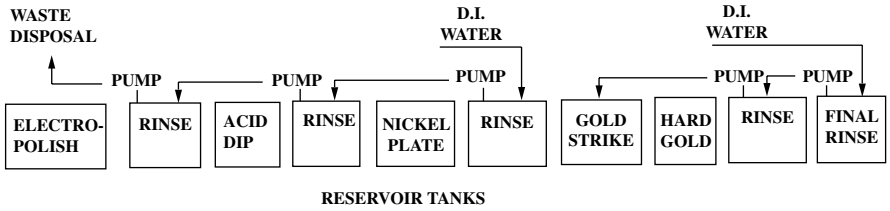

FIGURE 25.9 Water management system for a strip plater.

high-quality rinse water required and volume of wastewater produced is to use the good water first where impurities can be most harmful, for example, after nickel plating. When the rinse water conductivity reaches a set level, that water can be transferred back to the preceding rinses that do not require water of such high quality. This is illustrated in Figure 25.9 for a strip plater involving electropolishing, nickel plating, and gold plating. High-conductivity water is used only to maintain water levels in reservoir tank rinses after nickel and hard gold plating. When the conductivity in the nickel water rinse drops below a preset limit, water is pumped out of the rinse after electropolishing to waste disposal. That water is replaced by water from the rinse after acid pickling. Next water from the nickel rinse replenishes the acid rinse, and finally new water restores the rinse after nickel. The process continues until the conductivity of the nickel rinse water reaches a preset value. A similar feedback system is used in the gold plating side. The gold strike solution is operated at about 65°C (150°F) and loses water rapidly through evaporation into the exhaust. A low solution level activates a pump to transfer rinse water after hard gold to the gold strike reservoir. The final rinse water replenishes the preceding rinse. Fresh deionized (DI) water restores the level in the final rinse. In addition to conserving water, this system keeps the gold in rinses moving back to the plating solutions. A gold reclaim plating cell in the rinse tank after hard gold plating can also be used to reclaim gold.

25.2.11 Automatic Plating On-Line Monitoring and Control

Automatic electroplating may utilize on-line monitoring and control. The technology has developed rapidly with the availability of modern equipment, including sensors and electrical and electronic devices, and better mechanical designs [72–75]. Continuous-flow analysis of electroplating solutions can be fully automated [65, 76, 77]. Palladium, copper, nickel, tin, silver, iron, chromium, persulfate, peroxide, and chlorate are among substances that have been determined automatically.

Figure 25.10 illustrates how the various parts of an automatic electroplating process monitoring and control system interact. Sensors provide information about the plating process. After signal conditioning, information is sent to a PLC or a computer that is programmed to control the system. Actual conditions can be analyzed and stored and/or displayed. Deviations from the programmed limits will activate control devices such as motors, valves, and power supplies to bring the plating process back in control. If the operator must be involved, an audio alarm sounds. When there are multiple alarms, each condition may have a different audio sound so the operator can quickly recognize the type of problem or a status display will show each alarm condition. Completely automatic analysis and control systems have also been developed which do not require any operator intervention during normal operation.

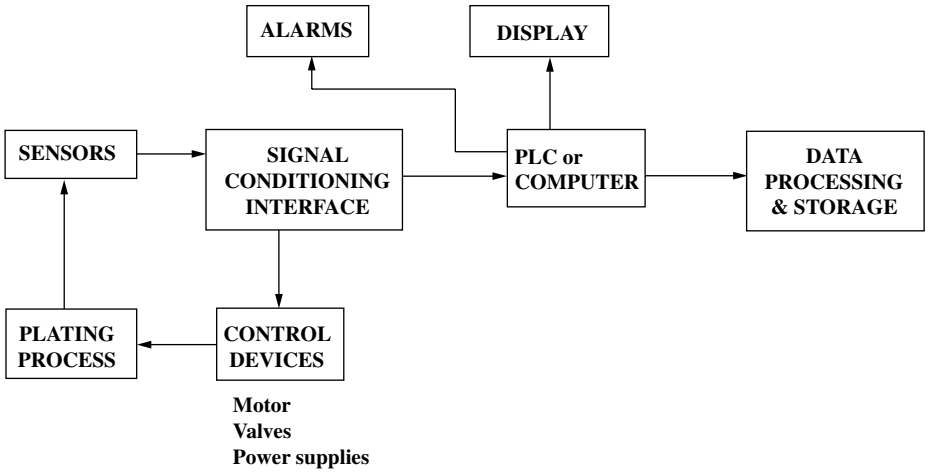

FIGURE 25.10 Schematic of an automated electroplating process monitoring and control system.

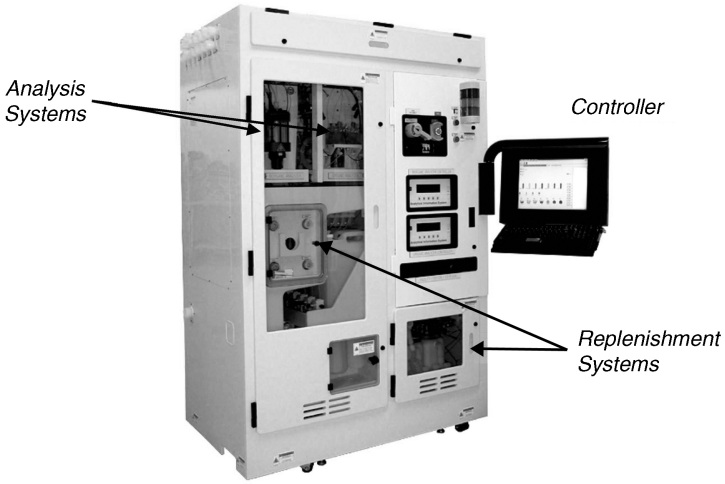

FIGURE 25.11 Automated chemical analysis and replenishment system to support semiconductor copper plating tools.

Since the mid-1990s completely automated copper analysis and replenishment systems have been used with semiconductor plating equipment for copper damascene interconnect applications (Fig. 25.11). The analysis systems usually use a titration cell for determining copper and acid concentration, titration or an ion selective electrode for ppm-level chloride determination, and titration combined with CVS or chronopotentiometry for analysis of organic additives such as suppressor, accelerator, and leveler. These systems typically make use of slipstreams that are recirculated from the plating equipment through the analyzer. The analysis system utilizes a block of valves to periodically divert a small sample from the slipstream to the analysis vessel, where it is analyzed and then sent to waste recovery.

As explained earlier, electroless plating chemistries are not very stable and require frequent bath analysis and monitoring. Electroless copper plating parameters that need monitoring and control are temperature, pH, copper concentration, formaldehyde (reducing agent), and cyanide ion. Accurate temperature monitors/controllers are readily available. The pH value is measured with a standard glass electrode. Hydroxide solution is metered in as required to maintain pH. Copper concentration can be monitored colorimetrically or by polarography. Formaldehyde may be measured by adding 0.045 *M* sulfuric acid to a bath sample to reduce the pH to about 9.5. When a 0.05 *M* sodium sulfite solution (also at pH 9.5) is added, the resulting pH is proportional to the formaldehyde content. Polarography can be used to measure both formaldehyde and cyanide bath concentrations [20].

Several on-line electroless copper plating analyzers/controllers have been developed for copper plating of printed circuit boards [2, 20, 21, 78]. They are used to monitor and control baths that deposit a thin layer of copper in through holes prior to electroplating the thicker copper. Automatic analyzers or controllers are essential when the entire copper circuit is built up by electroless plating.

In 1971 Photocircuits developed its Mark VI automatic electroless copper plating bath analyzer to monitor and control its CC-4 electroless copper plating bath. Later McDermid developed a similar automatic bath analyzer which is shown schematically in Figure 25.12 [78]. A single peristaltic pump moves a sample and the reagents through the analyzer. The pH is adjusted, then the copper ion concentration is measured spectrophotometrically. A formaldehyde reagent is added next. The resulting pH is proportional to the formaldehyde concentration. The controller activates replenishment pumps to restore the copper ion and the formaldehyde concentrations to their optimum levels.

Bell Laboratories machines utilized polarography to analyze for Cu^{2+}, HCHO, and CN^{-} [20]. With the solution still, polarographic currents are measured at -1.0 V for Cu^{2+}, -1.8 V for formaldehyde, and -0.25 V for free cyanide. This is illustrated in Figure 25.13. The machine automatically averaged 10 measurements of each component for better accuracy. The block diagram in Figure 25.14 shows how the various parts interact. The actual machine (Fig. 25.15) was built in two parts: one for wet chemistry on the left and the electronics on the right. The two units could be separated by several hundred feet if necessary. One advantage of the separation was that the wet chemistry cabinet could be hosed down occasionally. Electroless copper solution flows through the flow gauge at the left continuously. Periodically a sample is taken into the analysis cell along with some NaOH reagent. The pH is measured, and dropping mercury polarograph measurements are made. After electronic processing the results of analysis are displayed. If chemical additions are required, replenishment pumps are turned on. A complete analysis can be made every four minutes.

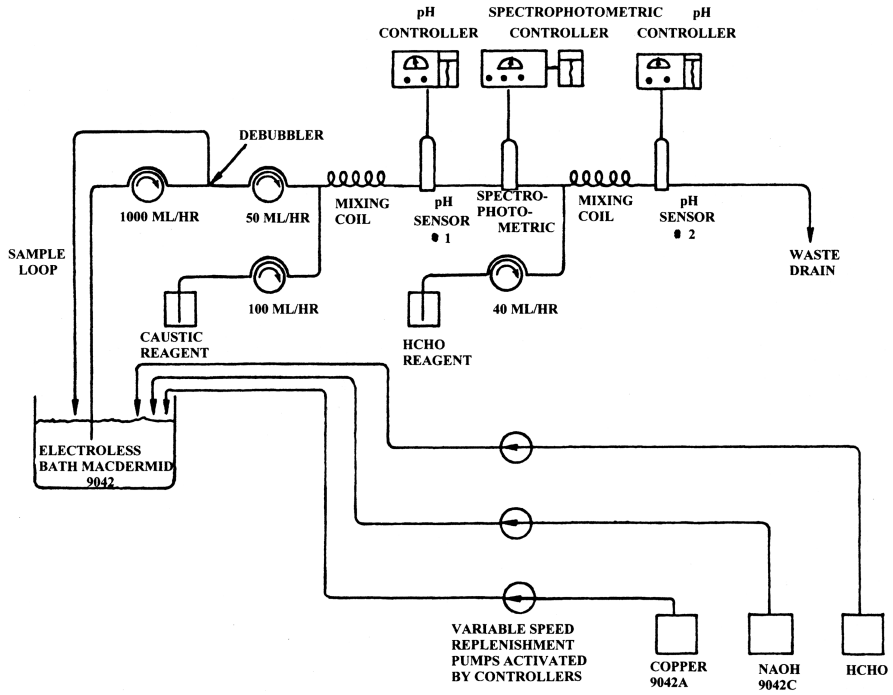

FIGURE 25.12 Schematic of McDermid electroless copper plating bath controller.

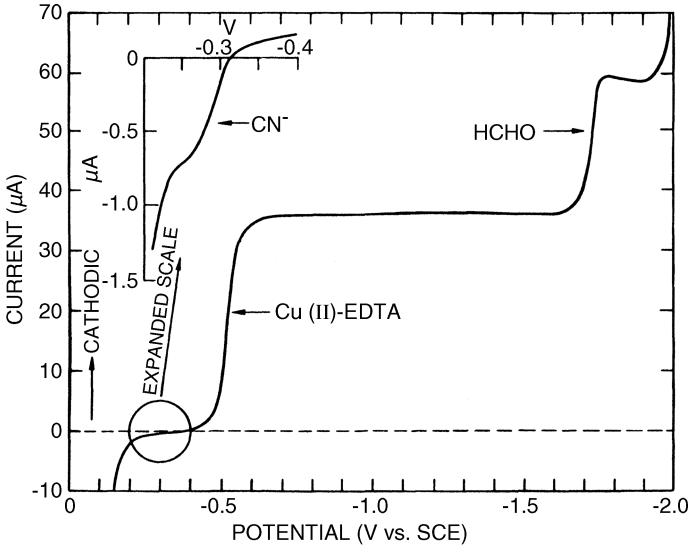

FIGURE 25.13 Polarographic analysis of electroless copper plating bath controller.

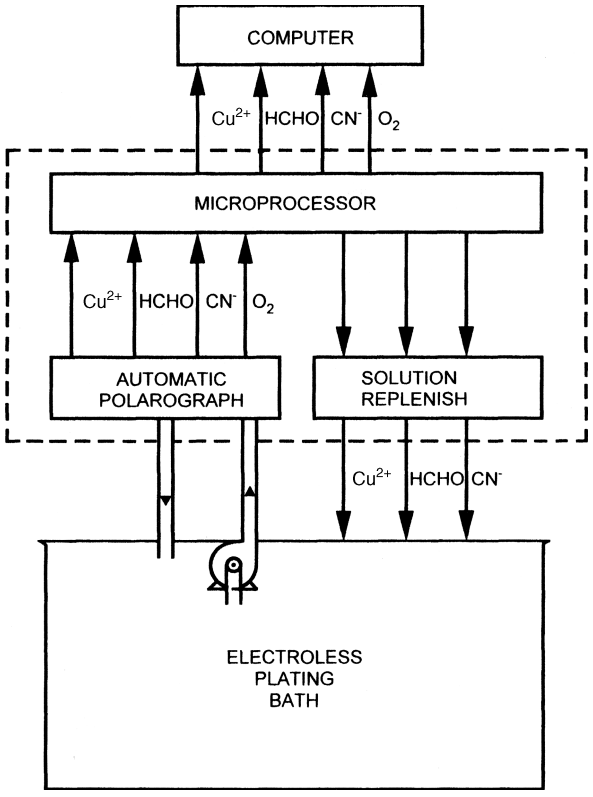

FIGURE 25.14 Electroless copper plating bath monitoring and control system.

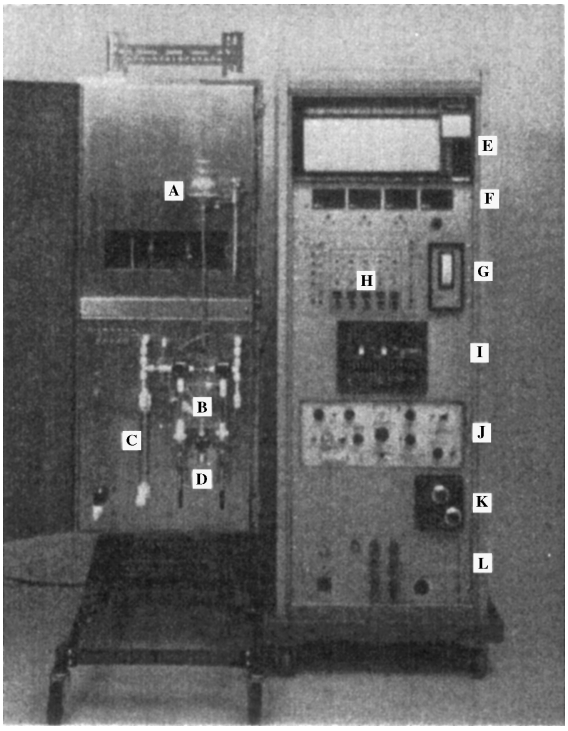

FIGURE 25.15 Electroless copper plating bath automatic analyzer and controller: (A) mercury reservoir, (B) analysis cell, (C) plating solution flowmeter, (D) motorized syringes, (E) chart recorder, (F) analysis display meters, (G) pH monitor, (H) set point controls, (I) process controller, (J) polarograph, (K) viscosity monitor, and (L) power source.

25.3 MONITORING AND CONTROL OF FINISHED PRODUCT

There are at least as many ways to measure the results of a plating process as there are products produced using plating processes. Ultimately, the monitoring of a product produced using a plating process or of the film plated should be done based on an understanding of the properties of the deposit that are important to that product. Having said that, we will review several types of measurements that are typically used for measuring the deposit quality of plated films. These are meant to be examples of common measurements and should be adjusted as necessary to ensure that a particular deposit meets the specifications demanded of it for a particular application. There is extensive literature regarding inspection of manufactured parts and quality control and inspections. These can be used to set up a statistically sound monitoring program to monitor the quality of parts being produced and to improve the product quality or reduce the variability. Typical electrodeposit properties inspected are thickness, color, brightness, hardness, magnetic properties, and alloy composition. Automatic instruments are available for off-line and on-line measurements. Off-line inspection is usually done on a statistical sample for economic reasons. The advantage of on-line inspection is that every part may be tested. If plating is out of specification, either plating conditions can be changed automatically or an operator can be alerted for a manual correction.

25.3.1 Thickness

Various wet chemical methods are available for measuring electrodeposit thickness: coulometric, dropping test, and spot test [79]. A disadvantage of these tests is that the part used generally becomes scrap.

A nondestructive thickness test is usually preferred. There are several methods available, and most have been automated as stand-alone instruments or incorporated into on-line monitoring and control plating systems [80, 81]. The methods used include beta backscatter, X-ray fluorescence, sheet resistance (eddy current or four-point probe), and magnetic field measurements. Deposited metals tested by these methods are shown in Table 25.6. Profilometry can also be used to measure deposit thickness when selective deposition is used or when part of the deposit can be etched away.

In general, there are extremely sensitive instruments that have been developed for the microelectronics industry for measuring the properties of deposits produced on semiconductor wafers or similar substrates. These instruments are commonly automated wafer handling systems that are completely computer controlled and are capable of intensive data manipulation. While these systems are far different from the typical thickness measurement tools described in the sections that follow, they are increasingly becoming important in applications involving electrochemical deposition for microelectronic applications. Some of these thickness measurement techniques are then described under Profilometry, Optical Methods, and Laser-Acoustic Methods. These are examples of some of the systems that have been developed for microelectronics applications, where the substrate is very well controlled and where extreme precision is required of the deposits on them. Other new analytical techniques are being developed at a rapid rate, specifically for the microelectronics industry.

Coulometric Method The coulometric method is based on Faraday's law: One gram equivalent weight of metal is stripped away from an anode for every 96,500 coulombs of

TABLE 25.6 Nondestructive Electroplated Deposit Thickness Tests

Method	Metals Tested
Beta backscatter	Au, Ag, Cd, Cr, Cu, Ni, Zn, alloys
X-ray fluorescence	Au, Ag, Cd, Cr, Cu, Ni, Zn
Eddy current	Cu, Zn, Cd, Ni, Cr

electricity passed through the cell. Four parameters must be controlled: surface area, current, time, and anode (deposit) dissolution efficiency. At 100% anode efficiency, the deposit thickness is calculated from the formula

$$\text{Thickness} = eit\left(\frac{10}{Ad}\right)$$

where e = electrochemical equivalent, g/A-s^{-1}
i = constant current, A
t = time, s
A = area, cm^2
d = metal density

It is necessary to use a specific electrolyte for each metal deposit and substrate [82]. The electrolyte must not chemically attack the plated film. An automated instrument can detect the endpoint by sensing a voltage change when the substrate metal is exposed. The method is capable of an accuracy of ±10% of the true value. One advantage of the method is its ability to measure combination deposits such as copper–nickel–chromium.

Dropping Test The dropping test is very simple. It is performed by dropping chemical etch solution on a particular spot at a rate of about 100 drops per minute. The operator observes the time it takes to expose the base metal. The test is calibrated using a sample with a known thickness of plated metal. For consistent results, the drop size, temperature, and etch solution must be controlled. Operator skill is an important factor in achieving reproducible results with an accuracy of ±15% [83].

Spot Test This simple test was developed as a rapid and inexpensive test for chromium deposits on nickel or stainless steel. A drop of hydrochloric acid is placed inside a ring of wax on the part to be tested. Hydrochloric acid attacks chromium with the evolution of hydrogen gas bubbles. Gassing stops when all the chromium is dissolved. The time of dissolution is proportional to the chromium thickness. The test is calibrated with a known chromium-plated thickness specimen. An accuracy of ±20% is obtained for deposits up to 1.2 μm thick [84].

Beta Backscatter The radioactive decay of certain isotopes produces beta rays, which are fast-moving electrons. When these are directed at an electrodeposit, some are slowed and change direction out of the deposit. The number of these backscattered electrons is proportional to the number of atoms per unit area and their atomic number. The backscatter is measured with a Geiger–Muller tube counter. The isotope used is chosen based on its maximum beta-ray energy and half-life. As the deposit thickness increases, the energy needed to penetrate the deposit increases. Metals with higher atomic numbers require higher energies for the same thickness. Instruments designed to measure metal deposit thickness utilize a Geiger–Muller tube electron counter and, with a built-in microprocessor, compute the thickness. The device is also capable of feedback current control of on-line plating systems [85].

X-Ray Fluorescence and X-Ray Reflectometry This method is similar to beta backscatter in that a radiation is directed at the deposit and the energy emitted is measured. The method uses X rays produced by an X-ray tube that is specific to the deposit metal. The radiation emitted from the deposit is proportional to the deposit thickness. The system may be calibrated with a known thickness and composition standard for additional accuracy. The instrument provides the thickness measurement which can be used to control the plating process.

An XRF thickness monitor is used to control the thickness of zinc plating on steel mill strip by a feedback signal to a computer that adjusts the line speed in order to maintain a specified zinc thickness [16]. Emissions are specific for each metal, so alloy compositions can be determined. Metal deposit thickness in the range of 0.25–10 μm can be measured depending on the metal. Measurement accuracy is ±10% with proper calibration [86].

Precision XRF measurement equipment has been developed for the microelectronics industry that provides much better precision than the simple instruments described above. These systems are capable of measuring with greater accuracy and potentially utilizing spot sizes as small as 50 μm. They can be used to measure thickness or composition of an alloy deposit. In some cases, XRF has been combined with X-ray reflectance (XRR) in order to provide precision thickness measurement of extremely thin metal films on flat substrates. XRR uses glancing angles close to the critical angle at which total external reflection occurs for a given film in a θ/2θ scan mode [87–89]. The value of the critical angle can be used to determine the density of the film being measured. At angles above the critical angle, the X rays penetrate the film and are reflected from the top and bottom surfaces of the film, giving rise to interference fringes which can be used to determine the film thickness based on the angular separation between the fringes. These systems are capable of measuring metal film thickness as thin as 2 nm, with accuracy on the order of 1 Å [90, 91]. XRR does not work well beyond about 200 nm, so XRF techniques are employed for thicker films. XRR techniques can also provide information related to film roughness.

Eddy Current (Sheet Resistance) Eddy current thickness gauges are electromagnetic instruments designed to measure a change in impedance of a coil that induces an eddy current into the plated metal. The phenomenon is based on the

difference between the electrical conductivity of the basis metal and the deposit that produces the change in impedance. The thickness measurement is performed with a probe which is positioned perpendicular to and sometimes in contact with the surface at the point of measurement. Thickness gauge instruments are available with a digital display, memory, and computer-prompted calibration procedure. The measurement accuracy is $\pm 10\%$ to the true thickness in the range of 5–50 μm. Factors that influence measurement accuracy are surface contours, surface roughness, and type of plating process that can influence deposit conductivity [92].

High-precision specialized sheet resistance measurement equipment based on eddy current probes or four-point electrical contact is also available for the semiconductor and microelectronics industry [89, 93]. These instruments provide a very common method of determining the thickness of metal films based on measuring the sheet resistance.

Magnetic Method The magnetic method utilizes the magnetic influence of the electrodeposit for measurement. Two types of probes are in use: (1) a mechanical device that measures the influence of the plated metal on the attractive force between a magnet and the base material and (2) an electromagnetic probe that measures the influence of the plated metal on the reluctance of a magnetic flux through the deposit and base metal. Three types of deposits can be measured with the second probe: (1) nonmagnetic deposits on ferromagnetic base metals, (2) nickel deposits on ferromagnetic base metals, and (3) nickel deposits on nonmagnetic base materials.

Both probe types require perpendicular positioning on the surface. The magnet probe works by measuring the force required to pull it from the surface. The electromagnetic probe measures the reluctance difference with and without the plated metal. The use of both probes requires a calibration, and averaging several measurements improves the accuracy. Commercial instruments utilizing the electromagnetic probe are available with microprocessors that can automate the system by averaging data, display results, store or transmit information, and provide on-line monitoring and control [94, 95].

Profilometry Profilometry is a convenient method for measuring the plated thickness of features deposited through an insulating mask such as photoresist on a flat substrate. It can also be utilized when a portion of the deposited film is etched away after the deposition. Typically, a profilometer makes use of a very small needlelike stylus that is moved across the sample as its vertical position is monitored. The height of the sample can then be plotted against the lateral dimension to provide an image of the sample surface. Once the image is leveled, it can be used to provide information such as maximum deposit thickness, average deposit thickness, or deposit roughness.

Variations of stylus profilometry have been developed using other measurement techniques. Systems for measuring semiconductor wafers and similar substrates have been developed based on optical profilometry and atomic force microscopy (AFM). Each technique has its own advantages regarding sample area or length, measurement time, and height variation that can be measured. In the end, though, each of these techniques provides a two- or three-dimensional image of the surface profile that can be used to provide thickness profiles and roughness information. The microprocessors that are used to control these systems usually have enough computing power to manipulate the information and provide statistical details or to identify features that do not fit the expected profile for quality control or yield management purposes.

Optical Methods Optical profilometers have been developed, as mentioned above. These typically use an optical lever to measure changes in step height of a sample. In addition, interferometric techniques have been used to measure height variations on flat substrates. These can be monochromatic light measurements or broad-spectrum measurements using phase shift interferometry or vertical scanning interferometry, respectively.

Optical profilers can be used to do the same job as stylus profilometers, although they more commonly produce a three-dimensional image of a surface by scanning the laser measurement point or by measuring a broad area of the sample as in interferometry. Interferometry systems are very useful for measuring large areas quickly, such as measuring the height of electroplated solder bumps on a wafer for flip-chip attachment. These systems rely on intensive computing power and calculations and are very good at identifying small numbers (ppm level) of features out of many that do not have the expected height. Examples of optical measurement systems for wafer applications are Rudolph Technology's NSX systems, Zygo's NewView interferometers, KLA-Tencor's MicroXam, and Veeco's Wyko instruments.

Laser-Acoustic Methods Laser-based optoacoustic methods have been developed recently for measuring film thickness of opaque films such as metals. There are two main techniques that have been commercialized as automated systems for measuring metal film thickness of semiconductor wafers or other flat substrates. Both techniques are capable of measuring film thickness with a high degree of precision using a small spot size and are capable of measuring the thickness of multiple films in a stack. The two techniques make use of probing and excitation lasers and mathematical models of the optical and/or acoustical properties of the film stacks in order to provide film thickness measurements. One method uses a sonar technique, and the other uses surface acoustic waves to determine the film thickness [89].

The optoacoustic technique that is known as picosecond ultrasonic laser sonar uses a very short laser pulse to thermally excite the sample surface. This launches an acoustic wave down into the film stack, which is reflected back to the surface at each material interface. As the sonic wave bounces through the film stack producing acoustic reflections, a probe laser detects the vibrations at the sample surface. A model based on the sonic velocity in each material and the expected film thickness is used to determine the actual film thickness in the stack. This method was commercialized by Rudolph Technologies as its MetaPULSE metrology tools.

The surface acoustic wave technique uses two probing lasers to produce an optical grating that launches an acoustic wave in the film stack. The time-dependent diffraction of light is then analyzed with a physical model of the acoustic wave to calculate the film thickness. This technique detects surface acoustic waves traveling in the plane of the film being measured. This technique has been commercialized by Philips Analytical and is available from Semilab AMS (Advanced Metrology Systems) in its AMS 3300 metrology system.

Both the Rudolph and Philips metrology systems rely on mathematical models of the physical system being analyzed and its acoustical properties. This makes them sensitive to variations in roughness at the film interfaces and density variations as well as defects within the small spot size being measured. On the other hand, they are high-resolution techniques that can be very useful with the proper understanding of the sample being analyzed and its relationship to the measurement configuration.

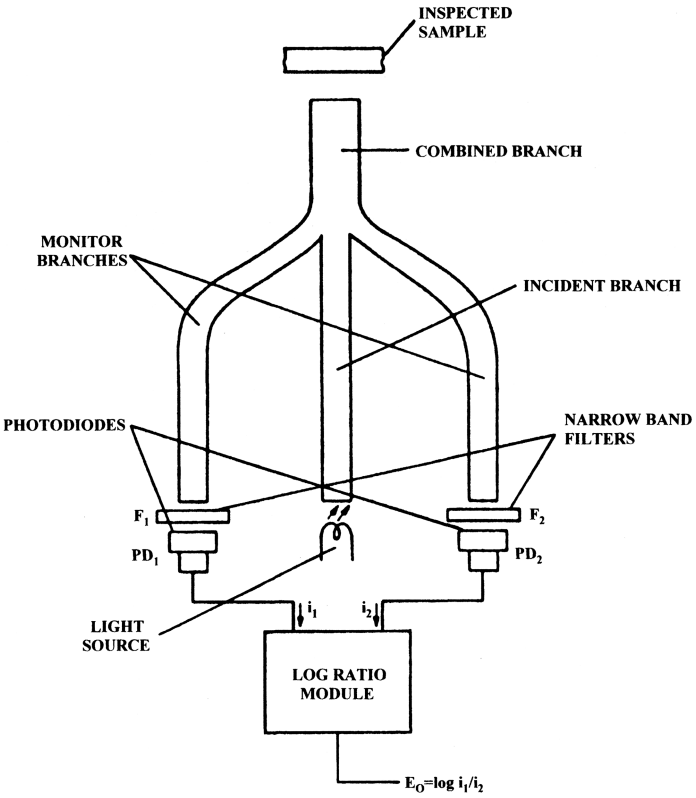

FIGURE 25.16 Schematic of an on-line gold plating color monitor.

25.3.2 Color

The color of electrodeposits has an esthetic value particularly on jewelry, home appliances, autos, and other decorative objects. Even on parts that are hidden from view when assembled into an object, an attractive appearance is considered a quality factor. Off-color plating or variable plating color often is considered a sign of a process problem. Generally, monitoring and control of color are done by visual inspection by an operator but on-line automatic inspection of color is feasible for many plating lines. An optical fiber system was developed to monitor the color of gold plating on a moving strip, shown schematically in Figure 25.16 [96]. An optical fiber bundle is positioned over a gold-plated strip. The bundle is divided into three parts. Light is directed into one arm that illuminates the moving strip. Reflected light from the gold surface passes into two separate optical fiber bundles. The light from one passes 700–800 nm through an optical filter that serves as a standard. The other light path passes 450–575 nm through the optical filter. An electronic comparator determines any deviation from the optimum color. The result can be displayed on a meter and/or fed into an automatic process control system to correct off-color plated gold.

25.3.3 Brightness

Reflectivity is a common method used to measure deposit brightness, especially in the semiconductor industry. Reflectivity measurements are simply quantitative measurements of the amount of light reflected from a given surface area. The instruments used to measure reflectivity must usually be calibrated to a reference standard, and the values reported are relative to the reference. In industrial applications, deposit brightness may be judged qualitatively by simply deciding if the deposit is bright and shiny and has the desired surface appearance.

Bright plating for decorative applications usually requires closer monitoring and control of the bath chemistry. Additives that produce brightening, usually organic, can become depleted or degraded by oxidation at the anode or from atmospheric exposure. Additive depletion is easily corrected by adding more additives, and this can be done by metering it in on the basis of plating time (coulombs) and/or elapsed time. Brightener concentration also may be controlled by

chemical analysis, plating tests (Hull cell), or CVS, as described in Section 25.2 [47, 48].

25.3.4 Roughness

Roughness of the plated surface is a measure of the quality of the plating process that is also related to the deposit brightness. A deposit that has a rough morphology will tend to be dull or matte in finish, rather than bright. Roughness can be measured quantitatively, or it can be gauged qualitatively by looking at optical or scanning electron microscopy (SEM) photomicrographs. The roughness of a deposit will typically have several dimensional scales and may be related to the grain size or the crystal structure of the deposit, as seen in Figure 25.20. In some cases, the deposit roughness may increase, become nodular, or even produce dendritic structures as the plating rate approaches the limiting current density of the system.

The deposit morphology may also be affected by other structures on the surface, such as underlying topography or masking materials such as photoresist. These effects can be used as indicators of changes in the process or chemistry or can be used to gauge how close a process is to the edges of its process window.

There has also been some work done on correlating the roughness evolution as a function of thickness for plated films. These data provide information related to the nucleation size and density and the film growth.

25.3.5 Hardness

Electroplating hardness is an important property to control in applications where minimum wear is required. There are many test methods for hardness available, but all are done off-line. Most testing is done with indentation instruments of somewhat different designs. The various types are Brinell, Rockwell, Vickers, Solersoope, Knoop, and Tukon. An indenter is used to form an indentation in the deposit using a known force, and the size of the indentation is measured to determine the hardness of the material. Care must be taken to ensure that the size of the indentation is small enough not to be affected by the film thickness or the edges of a patterned structure that is being used for measurements.

25.3.6 Film Stress

Film stress can be a very important parameter to monitor due to the possibility of creating problems with the part after plating. Excessive film stress can create problems with adhesion which lead to delamination or it can cause cracking or lead to excessive etching of the film when it is exposed to chemistry. Plating test cells for monitoring stress were discussed in Section 25.2.1. Film stress can also be measured on the part after the electroplated deposit is produced. In the semiconductor industry, global film stress is measured by evaluating the wafer bow before and after plating a film on one side. The radius of curvature, or deflection at a given distance from the center, is measured and Stoney's equation is used to determine the stress of the thin film that was added to the substrate [97]. The reaction of the relatively thick substrate to the deposited film thickness produces curvature changes, as shown in Figure 25.17.

The film stress may also be estimated from XRD measurements. These measurements are essentially a measure of the strain of individual crystals of the deposit taken from the measurement of their lattice parameter, so they may not correlate to the global film stress measured using the wafer bow or bending beam methods.

25.3.7 Grain Size

The grain size of an electrodeposited film is important in determining the mechanical properties of the material. Of course, grain size relates to the hardness of the material. It has also been shown that the grain size of electroplated copper films has a strong impact on the resistivity of these deposits [98]. There has been quite a volume of work presented on the characterization of grain size changes that occur in these films after deposition at room temperature or at elevated temperatures [99–109]. The grain size changes have been related to changes in resistivity, hardness, crystal texture, and in-film incorporation of organic additives.

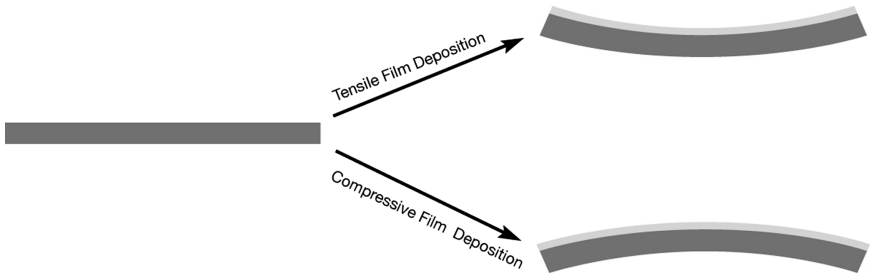

FIGURE 25.17 Effects of film stress.

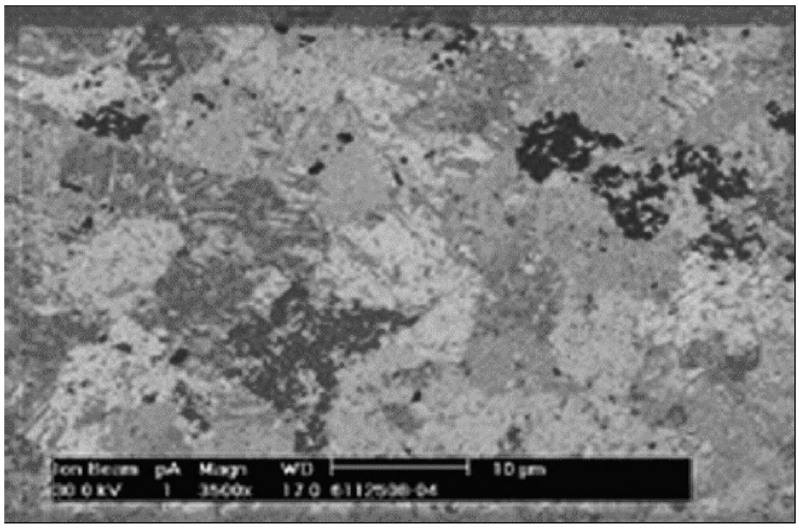

FIGURE 25.18 Grains in electrodeposited copper film.

The grain size of an electrodeposited film may be estimated from XRD data or it may be measured directly from an image that highlights the individual grains. Software may be used to identify individual grains and create grain size distribution plots, or standard methods may be used to estimate average grain sizes based on counting the number of grain boundaries intersecting a line of a given length [110]. Recently, focused ion beam (FIB), systems have been developed that utilize a focused beam of gallium ions to cut through thin films. The gallium beam may also be used to image the sample, and the channeling depth variation of the gallium ions into grains with varying orientation provides excellent contrast, as seen in Figure 25.18.

25.3.8 X-Ray Diffraction and Crystal Texture

X-ray diffraction (XRD) analysis can be useful in understanding the characteristics of a plated film. XRD analysis can provide estimates of grain size and lattice constant as well as information related to the crystallographic orientation or texture of the grains of a deposit. Theta-Two theta scans and rocking curves provide standard plots that are used for these purposes. Complete XRD pole figures may also be used to get a more complete understanding of the orientation of the crystal lattice.

The texture of plated films can be important in that it may affect the magnetic properties, the interactions with other films in a stack, or the mechanical or electrical properties of the film.

25.3.9 Recrystallization Rate

There has been an enormous amount of information published in the last decade regarding "self-annealing" or recrystallization of electrodeposited metal films, especially copper [99–108]. These publications focus on grain growth,

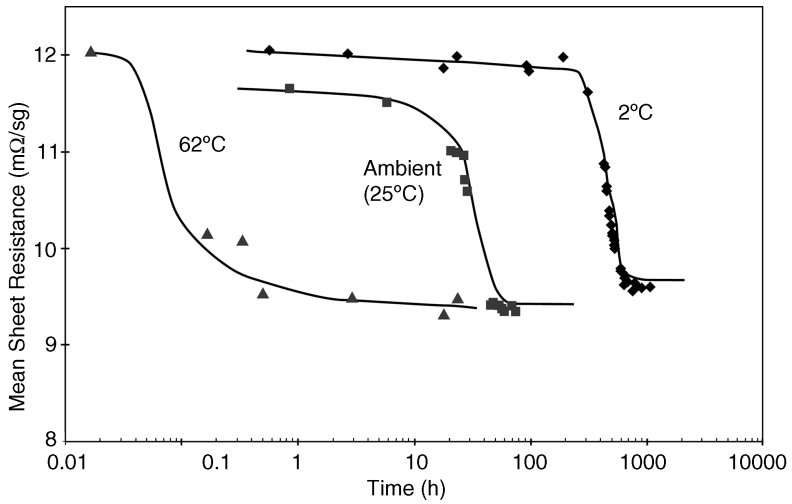

FIGURE 25.19 Effect of electroplated copper film recrystallization of sheet resistance.

reduction of resistivity, changes in film stress, and changes in crystallographic texture (see Fig. 25.19). There is also information relating to the evolution of organic contaminants that have been incorporated in the film and the coalescence of dislocations to form microvoids in the film.

Grain recrystallization and grain growth in plated films are driven by an excess of grain boundary energy. This process is accompanied by the diffusion of contaminants that have been incorporated in the film during deposition and migration of dislocations as well as stress changes in the film. These four processes are all occurring together, so the behavior can be somewhat complicated. Understanding these processes and noting differences in the extent to which they occur and their rates in plated films can be useful in understanding differences in plated grain size, dislocation density, formation of voids, incorporated contaminants, and film stress.

Some of the first work done on the "self-annealing" effect, or grain growth at room temperature, dealt with grain growth in mechanically worked sheets of copper [111–114]. The mechanical properties and XRD analysis of these metal sheets were used to characterize the effects of recrystallization and grain growth. Obviously, this effect has been known for a long time, although it has been studied most extensively in the last 10 years as electroplated copper has been used in semiconductor devices. The behavior of copper films has been shown to relate to the electromigration resistance and stress migration induced voiding that can cause reliability failures in these devices.

25.3.10 Surface Morphology

The surface morphology of plated films can be important for several reasons. The morphology can include local surface roughness as well as effects that relate to plating within masked patterns. Measurement of the morphology of plated films will depend on the application and may range from an optical inspection, or imaging with a microscope or SEM, to measurement of the surface roughness with a profilometer and calculating one of the many roughness parameters that are commonly used. There is even an example of an in-line automated reflectometer that monitors the color or the roughness of plated gold, as shown in Figure 25.16.

Roughness is an important deposit parameter that represents how the process is performing. The roughness of a plated film is determined by the plating rate, the waveform used for plating, additives in the chemistry (brighteners, levelers, grain refiners, etc.), contaminants in the chemistry, and cleanliness of the substrate before plating. If the desired deposit is bright and shiny, the roughness should be minimized. This may require the use of grain refiners and leveling agents and sometimes requires leveling of roughness that may already exist on the surface. On the other hand, sometimes a "matte" finish is desired, so a controlled amount of roughness is used to produce this surface finish. It may even be desirable to produce a rough film in order to improve mechanical adhesion or maximize surface area for some other purpose. In any case, it is important to understand the process variables that impact deposit roughness and to control them in order to minimize variations over the long term.

Morphological variations are sometimes associated with masked features on a plated part. These may be due to simple current crowding effects or they may be due to interactions of the masking with additives in the plating chemistry [115]. These effects can be seen in Figure 25.20.

25.3.11 Surface and Compositional Analysis

Of course, the composition of the electroplated deposit is usually an important parameter to measure. There are many methods available for measuring the bulk composition or surface composition of a deposit, some of which are destructive to the sample being measured. The composition may also be inferred by measuring some other property of the deposit,

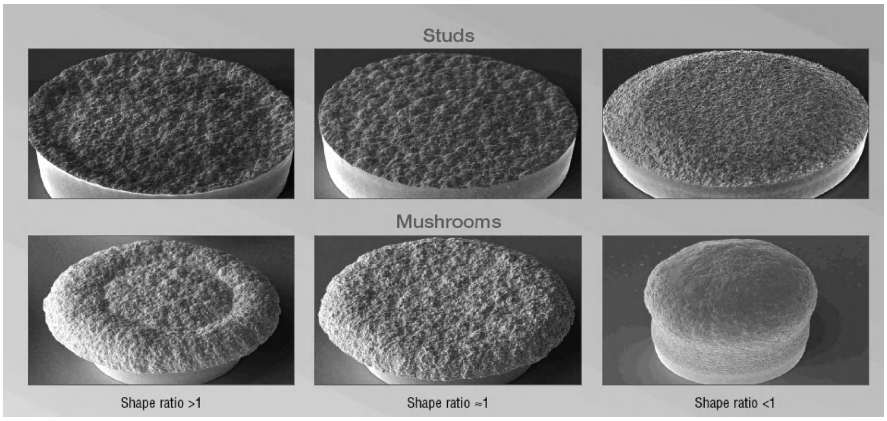

FIGURE 25.20 Morphology of through-mask electrodeposits.

such as magnetic moment, magnetostriction, or melting temperature. These methods are particularly useful for alloy deposits.

X-ray fluorescence is one of the most common methods of compositional analysis used for measuring electroplated alloy composition. It works well for measuring heavy elements like metals in quantities above 0.5% and has the additional benefit of providing thickness measurements for films less than 10 μm in thickness. XRF is a nondestructive method and can be adapted to work for many different plating applications. Equipment ranges from expensive equipment adapted for measuring films on semiconductor wafers or similar substrates, as described above, to simple hand-held instruments that are designed as portable thickness gauges [86].

Destructive methods for composition analysis usually involve dissolving the film in an acid and measuring the quantity of each metal in the solution. These methods work best for compositional analysis of alloy deposits. The most common methods in this category include AA analysis and ICP-MS.

A method somewhat similar physically to beta backscatter metrology is Rutherford backscatter spectrometry RBS. This method uses positively charged ions to bombard the sample and measures the backscattered ions. By measuring the energy loss of the backscattered electrons, the composition and thickness of thin films can be measured. This is a more involved method than beta backscatter thickness measurements that is useful for surface analysis [116].

When it is important to measure very small quantities of contaminants in plated films or to measure light elements, it is usually necessary to use some sort of surface analysis technique. The drawback is that these techniques usually measure only very near the surface of the film although they can be very sensitive. In order to measure below the surface of the film or to remove surface contamination before measuring, it may be important to use argon sputtering to remove the surface layers or to sputter through the film and make measurements in a depth profile. The most common methods used in this category include Auger electron spectroscopy (AES), electron spectroscopy for chemical analysis or X-ray photoelectron spectroscopy (ESCA or XPS), and secondary ion mass spectroscopy (SIMS).

25.3.12 Shear Testing or Pull Testing

Mechanical testing can be an important part of monitoring plated deposit performance. Shear strength testing is a method that can be used to measure the mechanical properties of a deposit or to monitor for interfacial adhesion problems. This is a common technique used for monitoring electronic components such as solder bumps or other electrical interconnect features. It is a destructive method (at least for the feature being tested) which involves shearing off a plated feature from the surface. The force required before failure is monitored, and the failure mode can be inspected to differentiate between interfacial failures, brittle bulk material failure, and ductile bulk material failure.

Wire pull testing can also be used to understand the mechanical strength of an interconnect feature with forces perpendicular to the substrate surface. In this method, a wire is bonded to the pad or feature to be tested and it is pulled straight away from the surface. Again, the force is measured and the failure mode or interface can be determined by optical inspection or compositional analysis of the failed interface. Variants of these tests can be devised to monitor the most important failure mode for a given application.

25.3.13 X-Ray Transmission Imaging

X-ray transmission imaging has been used, especially for detecting voids or similar defects, in quality control of electronic components such as plated wiring or solder bumps on boards or semiconductor wafers or chips. This technique is analogous to medical X rays in that the X rays are passed through the sample and the image shows the intensity of the X rays that pass through the sample. Voids are seen as light spots in the image. This can be an important technique for inspecting solder bumps after reflow, because it is possible that voids may be created during the reflow process, especially if the amount of organic materials incorporated into the film is high. See Figure 25.21.

Similar to medical X-ray imaging, systems are now being made that use X rays for tomographic imaging. By utilizing the relative rotation of the sample and X-ray detector, three-dimensional tomographic images may be created and used to visualize a sample. These can be useful for viewing multiple

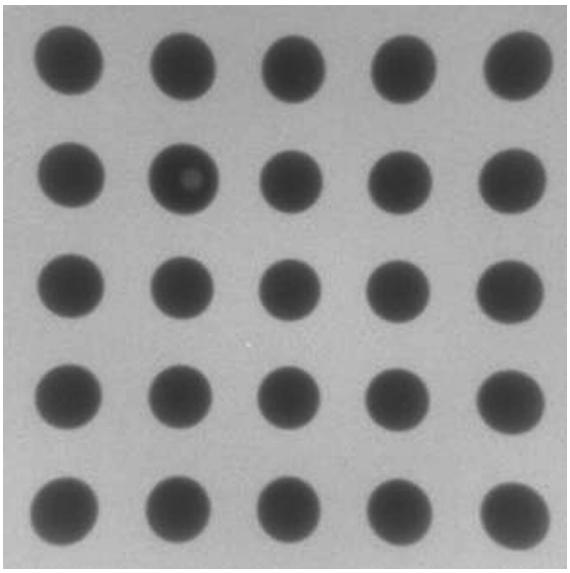

FIGURE 25.21 Transmission X-ray image of solder bumps after reflow.

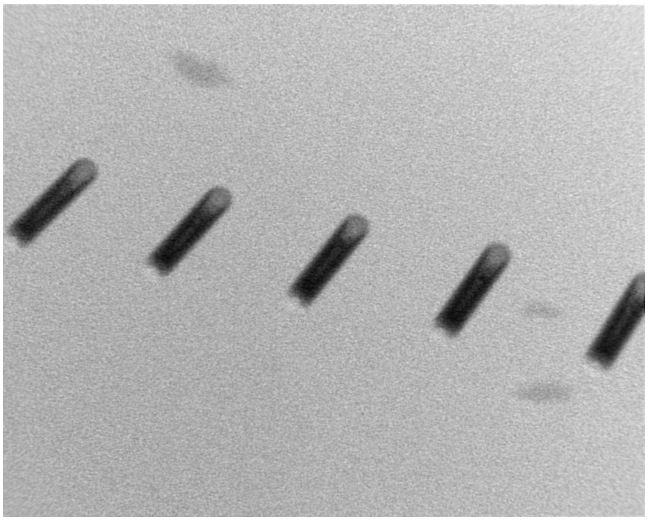

FIGURE 25.22 Transmission X-ray image of through-silicon vias.

levels of electrical interconnections on an electronic part. With improved X-ray sources and detectors, the resolution of these systems continues to be improved. See Figure 25.22.

25.4 SUMMARY

The electroplating industry has at its disposal an extensive amount of information and technology for monitoring and controlling all aspects of the plating process. Sensors have an important role in monitoring the status of each important parameter that must be controlled for successful plating. The design and engineering of individual sensor devices have improved greatly in recent years. Many incorporate a microprocessor for signal conditioning, and some now can also carry out control of certain plating conditions directly without relying on a PLC or computer. As new phenomena and technology have been converted into practical cost-saving devices for monitoring and controlling electroplating parameters and systems, the industry has adopted them. Electronic devices, computers in particular, have revolutionized the conversion of sensor signals to a useful form for monitoring and control. Cheap computers have made it easy and cost effective to automate plating systems. Further, plating information can be gathered and analyzed quickly to ensure that quality is maintained at all times. Automation of electroplating utilizing monitoring and control has resulted in lower manufacturing costs while improving quality and reproducibility of processing.

Constituent monitoring and control for solutions used for electrochemical deposition have improved dramatically as well. The emphasis has been on providing rapid analysis while reducing the chemistry usage and increasing the level of automation and control of the chemical control system. Electrochemical analysis techniques have been widely used, and other analytical techniques have been integrated into on-line analysis systems as well. The level of understanding of what is happening to the bath chemistry over time and how to control it has been continuing to improve.

Finally, the number of choices for measurement and monitoring of the finished product has continued to grow. Our ability to measure material properties with more accuracy and to ever-finer levels of resolution allows us to improve our understanding of the materials we are producing. While there has been a large number of measurement techniques discussed, there are many other techniques that were glossed over or not discussed at all. The appropriate techniques to monitor deposits for a particular application must be explored, adapted, and sometimes invented in order to ensure that the important deposit properties are being monitored to the level required to ensure product performance. The more we learn, the more we find that there is a lot more to be learned in order to completely understand our plating processes and the deposits we are creating.

REFERENCES

1. Y. Shacham-Diamand, T. Osaka, M. Datta, and T. Ohta, Eds., *Advanced Nanoscale ULSI Interconnects: Fundamentals and Applications*, Springer, New York, 2009.
2. D. R. Turner and Y. Okinaka, SUR/FIN Session M Chemical Analysis, Toronto, Canada, American Electroplaters' Society, 1981.
3. SEMI E15 Specifications for Tool Load Port, Semiconductor Equipment and Materials International, San Jose, CA, 2003.
4. SEMI E19 Standard Mechanical Interface (SMIF), Semiconductor Equipment and Materials International, San Jose, CA, 2002.
5. SEMI E64 Specification for 300mm Cart to SEMI E15.1 Docking Interface Port, Semiconductor Equipment and Materials International, San Jose, CA, 2000.
6. SEMI S8 Safety Guidelines for Ergonomics Engineering of Semiconductor Manufacturing Equipment, Semiconductor Equipment and Materials International, San Jose, CA, 2003.
7. SEMI S2 Environmental, Health, and Safety Guidelines for Semiconductor Manufacturing Equipment, Semiconductor Equipment and Materials International, San Jose, CA, 2003.
8. T. L. Ritzdorf, G. J. Wilson, P. R. McHugh, D. J. Woodruff, K. M. Hanson, and D. Fulton, "Design and Modeling of Equipment Used in Electrochemical Processes for Microelectronics," *IBM J. Res. Dev.*, **49** (1), 65–77 (Jan. 2005).
9. T. Ritzdorf and D. Fulton, "Electrochemical Deposition Equipment," in *New Trends in Electrochemical Technology*, Vol. 3, *Microelectronic Packaging*, M. Datta, T. Osaka, and J. W. Schultze, Eds., CRC, Boca Raton, FL, 2005, pp. 495–509.
10. C. Loughlin, *Sensors for Industrial Inspection*, Kluwer Academic, Boston, 1993, Sec. 8.
11. T. Seiyama, Ed. *Chemical Sensor Technology*, Elsevier, Amsterdam, 1988.

12. J. Janata, *Principles of Chemical Sensors*, Plenum, New York, 1989.
13. S. Soloman, *Sensors and Control Systems in Manufacturing*, McGraw-Hill, New York, 1994.
14. D. R. Turner, *Plating Surf. Finish.*, **73** (6), 30 (1985).
15. *Industrial and Process Control*, Oct. 15, 1985.
16. *The Making, Shaping, and Treating of Steel*, 10th Ed., American Iron and Steel Institute, Pittsburgh, PA,1996.
17. D. Drianko, H. Hellendoon, and M. Reinfrank, *An Introduction to Fuzzy Logic Control*, Springer-Verlang, New York, 1996.
18. J. Morico, in *Electroplating Engineering Handbook*, 4th ed., L. J. Durney, Ed., Van Nostrand Reinhold, New York, 1948, p. 289.
19. S. Hirsch and C. Rosenstein, *Metal Finishing Guidebook*, **93** (1A), 482 (1995).
20. Y. Okinaka, D. W. Graham, C. Wolowodiuk, and T. M. Putvinski, *Western Elect. Eng.*, **22**, 72–81 (Apr. 1978).
21. S. Newman, *Prod. Finish.*, **92** (Nov. 1980).
22. Y. Okinaka, *Plating Surf. Finish.*, **72** (10), 34 (1985).
23. T. Taylor, T. Ritzdorf, F. Lindberg, B. Carpenter, and M. LeFebvre, *Electrolyte Composition Monitoring for Copper Interconnect Applications. Electrochemical Processing in ULSI Fabrication I and Interconnect and Contact Metallization: Materials, Processes, and Reliability*, Electrochemical Society, Pennington, NJ, 1998, p. 33.
24. A. C. Tan, *Tin and Solder Plating in the Semiconductor Industry: A Technical Guide*, Chapman & Hall, Springer, New York, 1993, p. 110.
25. R. Dargis, The Hull Cell: Key to Better Electroplating, http://www.pfonline.com/articles/110502.html.
26. *Modern Electroplating*, The Electrochemical Society, New York, 1942, p. 14.
27. T. D. Mccolm and J. W. Evans, "A Modified Hull Cell and its Application to the Electrodeposition of Zinc," *J. App. Electrochemistry*, **31**, 4 (April 2001).
28. C. Madore, D. Landolt, C. Hassenpflug, and J. A. Hermann, *Plating Surf. Finish.*, **82** (8), 36 (1995).
29. P. Kern, Ch. Bonhôte, and L. T. Romankiw, *In Situ Surface pH Measurements and Rotating Cylinder Hull Cell—A Powerful Combination of Methods for Investigation of Iron Group Metal Alloys, Abstr 509*, Electrochemical Society, Pennington, NJ, 2003.
30. H. E. Haring and W. Blum, *Trans. Electrochem Soc.*, **44**, 313 (1923).
31. W. Blum, A. O. Beckman, and W. R. Meyer, *Trans. Electrochem. Soc.*, **80**, 256 (1941).
32. F.A. Lowenheim, *Electroplating: Fundamentals of Surface Finishing*, McGraw-Hill, New York, 1978, p. 148.
33. F. H. Leaman, "A New Frontier for Deposit Stress Measurements," Specialty Testing and Development, http://www.specialtytest.com/pdf/new_frontier.pdf.
34. G. Richardson and B. Stein, "Comparative Study of Three Internal Stress Measurement Methods," AESF Electroforming Symposium, San Diego, CA, October 1997.
35. O. E. Kongstein, U. Bertocci, and G. R. Stafford, "In Situ Stress Measurements During Copper Electrodeposition on (111)-Textured Au," *J. Electrochem. Soc.*, **152**, C116 (2005).
36. G. R. Stafford and C. R. Beauchamp, "In Situ Stress Measurements During Al UPD onto (111)-Textured Au from A1C13–EMImCI Ionic Liquid," *J. Electrochem. Soc.*, **155**, D408 (2008).
37. G. R. Stafford, "In situ Stress Measurements in Electrochemically Deposited Films," in *Peaks in Plating*, Semitool, Kalispell, MT, 2006.
38. R. Schumacher, "The Quartz Microbalance: A Novel Approach to the In-Situ Investigation of Interfacial Phenomena at the Solid/Liquid Junction [New Analytical Methods (40)]," *Angew. Chem. Int. Ed. Engl.*, **29**, 329 (1990).
39. S. Bruckenstein and M. Shay, "An In Situ Weighing Study of the Mechanism for the Formation of the Adsorbed Oxygen Monolayer at a Gold Electrode," *J. Electroanal. Chem. Interfacial Electrochem.*, **188**, 131 (1985).
40. D. A. Buttry and M. D. Ward, "Measurement of Interfacial Processes at Electrode Surfaces with the Electrochemical Quartz Crystal Microbalance," *Chem. Rev.* **92**, 1335 (1992).
41. H. Ashassi-Sorkhabi, A. Mirmohseni, and H. Harrafi, "Evaluation of Initial Deposition Rate of Electroless Ni–P Layers by QCM Method," *Electrochim. Acta*, **50**, (28), 5526–5532 (Sept. 30, 2005).
42. J. J. Kelly, A. C. West, "Design Tools for Copper Deposition in the Presence Additives," Electrochemical Processing in ULSI Fabrication I and Interconnect and Contact Metallization: Materials, Processes, and Reliability, Interconnect and Contact Metallization Symposium, San Diego, CA, Apr. 5, 1998, Vol. 6, Electrochemical Society Series, Pennington, NJ, 1999, pp. 23–32.
43. http://www.larrykingcorp.com/.
44. http://www.kocour.net/index.asp.
45. A. L. Harmer, *Proc. 2nd Int. Confon Optical Fiber Sensors,* Stuttgart, Sept. 17, 1984. Photo Optical Engineers Society, **468**, 174–185, Bellingham, WA.
46. V. Okinaka, *Plating Surf Finish.*, **66**, 50 (1979).
47. D. M. Tench and C. A. Ogden, *J. Electrochem. Soc.*, **125**, 194, 1218 (1978).
48. D. M. Tench and C. A. Ogden, U.S. Patent 4,132,605 (Jan. 2, 1979).
49. C. A. Ogden and D. M. Tench, *Plating Surf Finish.*, **66** (9), 30 (1979).
50. R. Haak, C. A. Ogden, and D. M. Tench, *Plating Surf Finish.*, **68**, 52 (1981).
51. R. Haak, C. A. Ogden, and D. M. Tench, *Plating Surf Finish.*, **69**, 62 (1982).
52. P. Pinches and G. Bush,*Circuits Manufacturing*, p. 36 July 1982.
53. J. R. Smith et al., *Trans. Inst. Met. Fin.*, **73** (2), 72 (1995).
54. G. J. Shugar and J. T. Ballinger, *Chemical Technicians' Ready Reference Handbook*, 4th ed., McGraw-Hill, New York, 1996.
55. L. Graham, T. Ritzdorf, and F. Lindberg, "Steady-State Chemical Analysis of Organic Suppressor Additives Used in

Copper Plating Baths," in *Interconnect and Contact Metallization for ULSI,* PV 99-31, Electrochemical Society, Pennington, NJ, 2000, pp. 143–151.

56. P. Robertson, Y. V. Tolmachev, and D. Fulton, "Galvanostatic Method for Quantification of Organic Suppressor and Accelerator Additives in Acid Copper Plating Baths," in *Morphological Evolution in Electrodeposition and Electrochemical Processing in ULSI Fabrication IV*, PV 2001-8, Electrochemical Society, Pennington, NJ, 2004, p. 309.
57. M. Datta, T. Osaka, and J. W. Schultze, *Microelectronic Packaging*, CRC Press, Boca Raton, FL, 2005.
58. A. Jaworski, K. Wikiel, and H. Wikiel, "Application of Multiblock and Hierarchical PCA and PLS Models for Analysis of AC Voltammetric Data," *Electroanalysis*, **17** (15/16), 1477–1485 (2005).
59. ECS 2003-03, pp. 396–403.
60. A. Jaworski and K. Wikiel, "Copper ECD Process Control by Means of Electroanalysis Coupled with PARAllel FACtor Analysis (PARAFAC) Multi-way Data Decomposition Chemometric Technique," in *Peaks in Plating*, Semitool, Kalispell, MT, 2006.
61. M. S. Frant, *Plating*, **58** (7), 686 (1971).
62. H. Freiser, *Ion Selective Electrodes in Analytical Chemistry*, Vols. I and 2, Plenum, New York, 1978.
63. P. L. Bailey, *Analysis with Ion-Selective Electrodes*, 2nd ed., Heyden, London, 1980.
64. ISE Guide, available: http://www.nico2000.net/Book/Guide l. html.
65. F. C. Walsh and D. R. Gabe, *J. Appl. Electrochem.*, **11**, 117 (1981).
66. K. Haak, "Ion Chromatography in the Electroplating Industry," *Plating Surf. Finish.*, **70,** 43 (Sept. 1983).
67. D. Jones and R. Herbert, *Plating Surf Finish.*, **83** (3), 22 (1996).
68. M. J. West, M. R. Anderson, Q. Wang, T. H. Bailey, A. Rosenfeld, Z. W. Sun, and K. P. Ta, in *Quantitative Monitoring of Copper Electroplating Additives and Their Breakdown Products, Electrochemical Processes in ULSI and MEMS*, H. Deligianni, T. Moffat, S. Mayer, and G. Stafford, Eds., PV 2004-17, Electrochemical Society, Pennington, NJ, 2005, pp. 41–56.
69. T. H. Bailey, Q. Wang, and M. West, *ECS Trans.*, **2** (6), Copper Electrodeposition, Advanced Metrology and Control of Copper Electrochemical Deposition I: The Decomposition Chemistry of the Accelerator SPS, 209th ECS Meeting, Vol. 2, Issue 6, May 7–May 12, 2006, Denver, Co, Electrochemical Processing in ULSI and MEMS 2, T. Moffat, H. Deligianni, J. Dukovic, T. Moffat, and J. Stickney, Eds.
70. J. M. Chalmers, Ed., *Spectroscopy in Process Analysis*, Sheffield Academic Press, Sheffield, 2000, p. 185.
71. H. Thomson et al, *Philos. Trans. R. Soc. Lond.*, **A302**, 327 (1981).
72. A. Ivaska, *Proc. Anal. Div. Chem. Soc.*, **16**, 283 (1979).
73. D. R. Turner and L. T. Romankiw, *Electrochem. Soc. Proc.*, **17**, 719 (1987).
74. J. T. Y. Yeh, *Chem. Eng.*, **93** (2), 55 (1986).
75. C. G. Smith, *Electrochem. Soc. Symp. on Chemical Sensors Proc.,* Honolulu, Electrochemical Society, Pennington, NJ, Oct. 1987, p. 39.
76. A. Aldo and J. DiLiddo, *Annu. Tech. Conf. Proc.—Am. Electroplat. Soc.,* Paper B-5 (1982).
77. J. DiLiddo and A. Conetta, *Am. Lab.*, **16** (4), 68 (1984).
78. T. A. Rau, MacDermid Electroless Copper Controller, Extended Abs., presented at Electrochem. Soc. Meet., Las Vegas, Oct. 1979, p. 445.
79. N. Sajdera, in *Metals Finishing Guidebook*, M. Murphy, Ed., Elsevier, NY, 1992, pp. 552–570.
80. "Measuring Coating Thickness," CMI International Inc., Elk Grove Village, IL, available: http://www.pfonline.com/articles/pfd0027.html.
81. L. J. Durney, *Electroplating Engineering Handbook*, 4th ed., Springer, New York, 1984, pp. 311–327.
82. American Society for Testing and Materials Standards, Vol. 02.05, B-504.
83. American Society for Testing and Materials, Vol. 02.05, B-555.
84. American Society for Testing and Materials, Vol. 02.05, B-556.
85. American Society for Testing and Materials, Vol. 02.05, B-567.
86. American Society for Testing and Materials, Vol. 02.05, B-568.
87. S. Terada, H. Murakami, and K. Nishihagi, "Thickness and Density Measurement for New Materials with Combined X-ray Technique," Technos Co., Hirakata, Osaka, Japan, available: http://www.technos-intl.com/techdoc/ASMC01TERADA.pdf.
88. http://www.icdd.com/resources/axa/VOL40/V40_164.pdf.
89. A. C. Diebold, *Handbook of Silicon Semiconductor Metrology*, Marcel Dekker, New York, 2001.
90. Jordan Valley Instruments, http://www.jordanvalley.com.
91. Technos International, http://www.technos-intl.com/index.php.
92. American Society for Testing and Materials Standards, Vol. 02.05, B-244.
93. L. Maissel and R. Glang, "Sheet Resistance," in *Handbook of Thin Film Technology*, McGraw Hill, New York, 1970, 13.5–13.13.
94. American Society for Testing and Materials Standards, Vol. 02.05, B-499.
95. American Society for Testing and Materials, Vol. 02.05, B-530.
96. F. W. Ostermayer, Jr., U.S. Patent 4,278,353 (July 14, 1981).
97. L. Maissel and R. Glang, "Stress Resistance," in *Handbook of Thin Film Technology*, McGraw Hill, New York, 1970, 12.21–12.40.
98. T. Ritzdorf, L. Graham, S. Jin, C. Mu, and D. B. Fraser, in *Proceedings of the International Interconnect Technology Conference*, IEEE, New York, 1998, p. 166.
99. S. Lagrange, S. H. Brongersma, M. Judelewicz, A. Saerens, I. Vervoort, E. Richard, R. Palmans, and K. Maex, *Microelectron. Eng.*, **50**, 449 (2000).
100. J. M. Harper, C. Cabral, Jr., P. C. Andricacos, L. Gignac, I. C. Noyan, K. P. Rodbell, and C. K. Hu, *J. Appl. Phys.*, **86**, 2516 (1999).

101. A. Furuya, Y. Oshita, and A. Ogura, *J. Vac. Sd. Technol. A*, **18**, 2854 (2000).

102. C. Lingk, M. E. Gross, and W. L. Brown, *J. Appl. Phys.* **87**, 2232 (2000).

103. S. H. Brongersma, E. Richard, I. Vervoort, H. Bender, W. Vandervorst, S. Lagrange, G. Beyer, and K. Maex, *J. Appl. Phys.*, **86**, 3642 (1999).

104. K. Ueno, T. Ritzdorf, and S. Grace, *J. Appl. Phys.* **86**, 4930 (1999).

105. C. Lingk and M. E. Gross, *J. Appl. Phys.*, **84**, 5547 (1998).

106. S. H. Brongersma, E. Richard, I. Vervoot, H. Bender, W. Vandervorst, S. Lagrange, G. Beyer, and K. Maex, *J. Appl. Phys.*, **86**, 3642 (1999).

107. C. Cabral, Jr., P. C. Andricacos, L. Gignac, I. C. Noyan, K. P. Rodbell, T. M. Shaw, R. Rosenberg, J. M. E. Harper, P. W. DeHaven, P. S. Locke, S. Malhotra, C. Uzoh, and S. J. Klepeis, in *Adv. Metallization Conf. 1998*, G. S. Sandhu, H. Koerner, M. Murakami, Y. Yasuda, and N. Kobayashi, Eds., Materials Research Society, Pittsburgh, PA, 1999, p. 81.

108. C. Lingk, M. E. Gross, W. L. Brown, W. Y.-C. Lai, J. F. Miner, T. Ritzdorf, J. Turner, K. Gibbons, E. Klawuhn, G. Wu, and F. Zhang, in *Adv. Metallization Conf. 1998*, by G. S. Sandhu, H. Koerner, M. Murakami, Y. Yasuda, and N. Kobayashi, Eds., Materials Research Society, Pittsburgh, PA, 1999, p. 89.

109. J. S. Ro, C. V. Thompson, and J. Melngailis, "Microstructure of Gold Grown by Ion Induced Deposition," *Thin Solid Films* **258**, 333 (1995).

110. P. A. Thornton and V. J. Colangelo, *Fundamentals of Engineering Materials*, Prentice Hall, Englewood Cliffs, NJ, 1985, pp. 99–101.

111. B. M. Hogan;"Microstructural Stability of Copper Electroplate;" paper presented at the AESF Conference—*SUR/FIN '84*.

112. D. S. Stoychev and M. S. Aroyo, "The Influence of Pulse Frequency on the Hardness of Bright Copper Electrodeposits," *Plating Surf. Finish.*, 26–28 (Aug. 1997).

113. I. V. Tomov, D. S. Stoychev, and I. B. Vitanova; "Recovery and Recrystallization of Electrodeposited Bright Copper Coatings at Room Temperature. II. X-Ray Investigation of Primary Recrystallization;" *J. Appl. Electrochem.* **15**, 887–894 (1985).

114. M. Cook and T. L. Richards; "The Self-Annealing of Copper;" *J. Inst. Met.* **70**, 159–173 (1994).

115. B. Kim and T. Ritzdorf, "Electrical Waveform Mediated Through-Mask Deposition of Solder Bumps for Wafer-Level Packaging," *J. Electrochem. Soc.*, **151** (5), C342–347 (2004).

116. L. C. Feldman and J. W. Mayer, *Fundamentals of Surface and Thin Film Analysis*, Prentice-Hall, Englewood Cliffs, NJ, 1986.

26

ENVIRONMENTAL ASPECTS OF ELECTRODEPOSITION

MICHA TOMKIEWICZ

26.1 BACKGROUND

Most of this book is concerned with the detailed account of electrodeposition procedures for different metals. One can write an environmental impact statement for every metal and fill a separate volume in the process. However, many of the issues are similar and can be easily extrapolated from one metal to the next. Because of the central role that the U.S. Environmental Protection Agency (EPA) plays in the regulatory environment, most of the publications that cover the environmental aspects of the technology heavily rely on EPA publications.

The corresponding chapter of the last edition [1] addressed the perspective of two complementary approaches that electrodeposition shares with other environmentally sensitive technologies: prevention through management of the discharge and development of technologies to minimize the discharge. The chapter was completed in 1998 and the book was published in 2000. The chapter relies heavily on the regulatory aspects of government involvement, which in the United States takes the form of federal regulations mainly (but not exclusively) through the EPA complemented by state and local governments. The interplay between the science, the economic impact, and the environmental consequences was mostly focused on the industrial sector. The previous edition [1, P. 241] highlighted that "the selection of materials and processes in modern manufacturing will no longer be driven solely by product performance, reliability, and cost but will be profoundly influenced by environmental and health considerations." The discussion of electrodeposition of specific metals emphasized environmental concerns such as replacement of cyanides in the electroplating process [1, pp. 115, 119], replacement of Cr(VI) [1, p 320], development of lead-free solder [1, p. 241], and environmental considerations in electroplating of nickel [1, p. 191], cobalt–nickel alloys [1, p. 578], and palladium [1, p. 546].

In this chapter I will use interchangeably the terms *electroplating industry* and *metal finishing industry*. I will focus here primarily on U.S. industry. The last 10 years have seen a major shift in this environment. This shift can be traced to many factors, for example:

- Realization that energy use, in the form of carbon footprint, is now part of environmental impact.
- Globalization of the economy that necessitates adherence to the globally most stringent regulations
- Order-of-magnitude rise in the price of energy sources and many of the commodities that serve the electroplating industry (the chapter was sent to the editors in September 2008; by December 2008, the price of oil and many of the commodities was one-third of the 2008 peak prices)
- The revolutionary increase in the efficiency and range of dissemination of information
- Improvements in analytical techniques
- Major improvement in our understanding of the ecological consequences of many anthropogenic contributions to changes in the physical environment combined with better understanding of the short- and long-term health consequences of such changes

These trends strongly suggest that an effort to accommodate a given set of regulations is necessary but is inevitably shortsighted and not productive over the long term. A considerably more productive approach is to adopt a holistic perspective that anticipates that future regulatory

Modern Electroplating, Fifth Edition Edited by Mordechay Schlesinger and Milan Paunovic

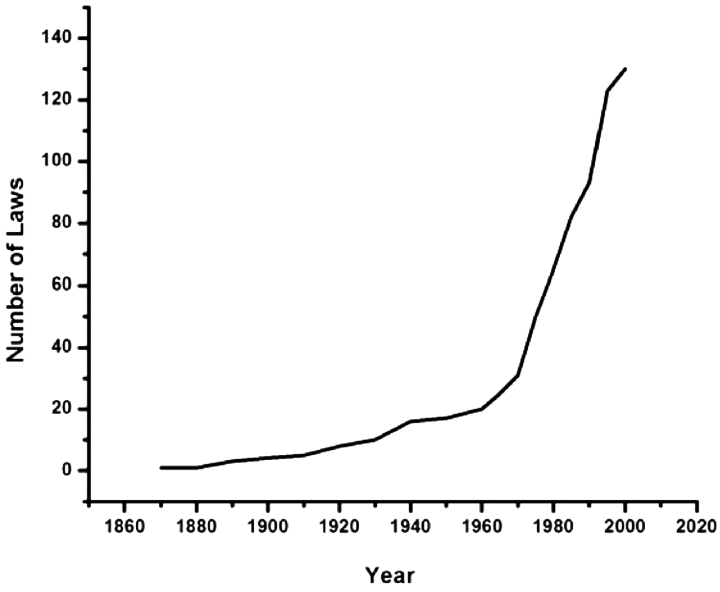

FIGURE 26.1 Time evolution of environmental regulations in the United States [2].

environment, in the home country or globally, will require "zero" perturbation of the surrounding physical environment—in more practical terms that industry will not contribute to chemical changes of the surrounding air, water, or land and that workers in the industry are entitled to a safe workplace with minimum exposure to toxic chemicals. As we will see below, this apples not only to direct discharge but also to indirect discharge such as capture and reuse of rainwater falling on the facility and taking stock of final disposal of coated items.

A demonstration of the necessity to adopt such an approach can be seen in Figure 26.1, which shows the rate of increase of the number of environmental regulations in the United States and the sharp increase in the rate following the creation of the EPA in the early 1970s.

The major driving forces behind this increase are:

- Improved analytical capabilities [inductivelly coupled plasma (ICP) can now detect the presence of most elements in the periodic table at a level of sensitivity better than 1 ppm]
- Major global effort to better understand the ecological consequences of many anthropogenic contributions to changes in the physical environment combined with better understanding of the short- and long-term health consequences of such changes
- Much better dissemination of information and public awareness of the health hazards caused by environmental contaminations.

An example is shown in Figure 26.2, which shows the timeline of acceptable childhood blood lead levels as issued by various U.S. and global agencies [3].

Another example is the recent change in regulating the release of Cr(VI) in the electroplating industry. Recent Occupational Safety and Health Administration (OSHA) regulations (August 2006) limit the Permissible exposure limits (PELs) for airborne Cr(VI) to 5 $\mu g\, m^{-3}$ after convincing epidemiological studies that indicate carcinogenicity of Cr(VI) compounds [Code of Federal Regulations (CFR) part 63, subpart N].

Future inclusion of energy in the regulatory framework is all but inevitable. The main driving force is the realization that the anthropogenic releases of greenhouse gases (GHGs) induce atmospheric chemical changes that have an effect on the radiative balance that cause climate change. The GHG that causes more than 50% of the changes is CO_2. Carbon dioxide is a necessary product of burning fossil fuels. Eighty-five percent of the global energy production originates in fossil fuels. The recent Intergovernmental Plan on Climate Change (IPCC) report [4] estimates that we have only until 2020 to reverse the sharp rise in global use of fossil fuels to limit temperature changes to "acceptable" levels (below 2°C global average and 4°C in the North and South Poles). This will require that in relatively short order energy sources throughout the world, but especially in developed countries, will need to be replaced. There is universal agreement that this will be impossible to achieve without enforcing it through the regulatory framework. It was suggested [5] that the energy intensity of most industrial processes is at least 50% higher than the theoretical minimum determined by the laws of thermodynamics. Many processes have very low energy efficiency and average energy use is much higher than the best available technology would permit. A recent EPA report [6] summarizes the energy trends in U.S. manufacturing, including a chapter on the energy audit of the surface finishing industry.

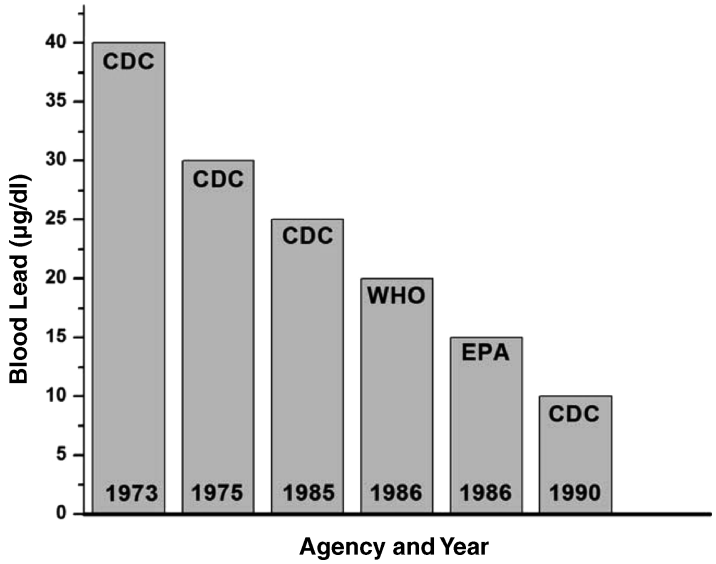

FIGURE 26.2 Regulatory changes of acceptable childhood blood lead levels in the United States [3].

The challenge to fulfill these requirements requires reevaluating every aspect of the industrial process and trying to do it in a way that will sustain the profitability of the industry and its ability to support its workers. The present focus is on two approaches: green chemistry and environmental management systems.

26.2 GREEN CHEMISTRY

The term *green chemistry* was coined by Paul Anastas, at the EPA at the time, and John Warner in their book *Green Chemistry: Theory and Practice* [7]. They were able to "distill" the essence in terms of 12 principles:

1. *Prevent waste*: Design chemical syntheses to prevent waste, leaving no waste to treat or clean up.
2. *Design safer chemicals and products*: Design chemical products to be fully effective yet have little or no toxicity.
3. *Design less hazardous chemical syntheses*: Design syntheses to use and generate substances with little or no toxicity to humans and the environment.
4. *Use renewable feedstocks*: Use raw materials and feedstocks that are renewable rather than depleting. Renewable feedstocks are often made from agricultural products or are the wastes of other processes; depleting feedstocks are made from fossil fuels (petroleum, natural gas, or coal) or are mined.
5. *Use catalysts, not stoichiometric reagents*: Minimize waste by using catalytic reactions. Catalysts are used in small amounts and can carry out a single reaction many times. They are preferable to stoichiometric reagents, which are used in excess and work only once.
6. *Avoid chemical derivatives*: Avoid using blocking or protecting groups or any temporary modifications if possible. Derivatives use additional reagents and generate waste.
7. *Maximize atom economy*: Design syntheses so that the final product contains the maximum proportion of the starting materials. There should be few, if any, wasted atoms.
8. *Use safer solvents and reaction conditions*: Avoid using solvents, separation agents, or other auxiliary chemicals. If these chemicals are necessary, use innocuous chemicals.
9. *Increase energy efficiency*: Run chemical reactions at ambient temperature and pressure whenever possible.
10. *Design chemicals and products to degrade after use*: Design chemical products to break down to innocuous substances after use so that they do not accumulate in the environment.
11. *Analyze in real time to prevent pollution*: Include in-process real-time monitoring and control during syntheses to minimize or eliminate the formation of byproducts.
12. *Minimize the potential for accidents*: Design chemicals and their forms (solid, liquid, or gas) to minimize the potential for chemical accidents, including explosions, fires, and releases to the environment.

Almost all of these principles are directly relevant to the electroplating and surface-finishing industries, but they are abstract (or academic?) and more easily interpretable in terms of basic chemical synthesis. Alternatives with different environmental impact that require choices to be made based on functionality and life-cycle assessment (LCA) are not explicitly stated. These aspects are emphasized in designing protocols for environmental management systems (EMSs).

26.3 ENVIRONMENTAL MANAGEMENT SYSTEMS

The International Organization for Standardization (ISO) promotes the development and implementation of voluntary international standards. ISO guideline 14001 refers to the international standard for environmental management systems. It requires that an organization put in place and implement a series of practices and procedures that, when taken together, result in an EMS. The EMSs are designed to put green chemistry practices on the company floor with the most important requirement to maintain full control over the flow of material and energy throughout the production process. The EPA maintains a special site (http://www.epa.gov/EMS/) designed to assist companies to implement the procedures and assist in training the personnel. A special report [8] on implementation in the metal-finishing industry was compiled with collaboration of the professional societies and includes step-by-step instructions with most of the paperwork included.

The system was summarized in terms of 13 guidelines:

1. Define the scope of your facility's EMS and assign responsibilities.
2. Create your environmental policy statement.
3. Identify your facility's environmental aspects.
4. Identify relevant legal requirements.
5. Determine your facility's significant environmental aspects.
6. Set operational controls.
7. Set and pursue your goals and action plans.
8. Set up an employee training program.
9. Create a communication strategy.
10. Set up documentation for your EMS.
11. Measure and record your performance.
12. Conduct audits and correct problems.
13. Review management.

The overall goals for the electroplating and surface-finishing industries [9] are that within five years participating metal-finishing firms that enlist in the voluntary programs pledge to become:

CLEANER by reducing hazardous emission:
- 90% reduction in organic toxic release inventory (TRI) emissions
- 50% reduction in metal emissions to air and water
- 50% reduction in hazardous sludge disposal
- Substantial reduction in sludge generation
- Reduced worker and community exposure

CHEAPER by saving money and providing economic advantages:
- 50% reduction in costs of unnecessary reporting, permitting and monitoring
- Less long-term liability

SMARTER by conserving resources:
- 98% metals utilization on products
- 50% reduction in water use
- 25% reduction in energy use

Graphic presentations of some of the results of such systems are shown in Figures 26.3–26.5 for material balance,

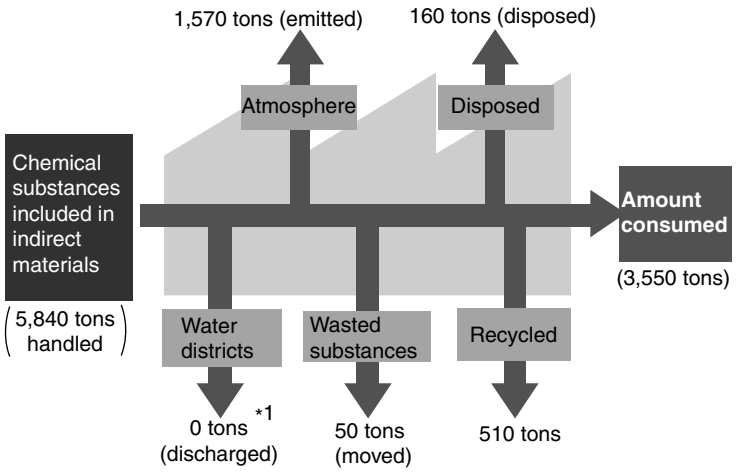

FIGURE 26.3 Material and waste balance in Toyota's environmental report [11].

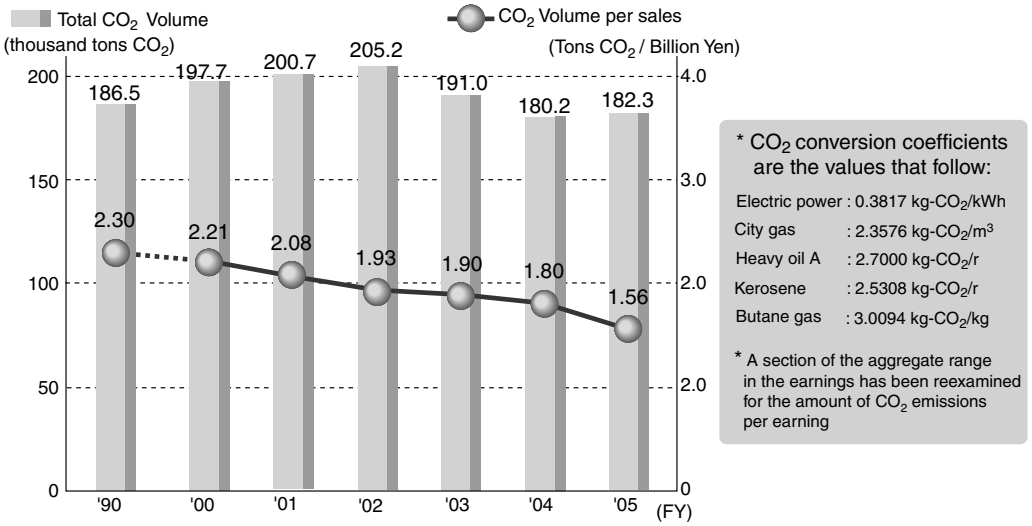

FIGURE 26.4 Carbon footprint in Toyota's environmental report [11].

carbon footprints, and volume of hazardous waste. Figure 26.5 was taken from a presentation by an owner of a small electrodeposition shop [10] that is on its way to implement EMSs in order to achieve zero-discharge operation.

Many companies are now using EMS results to issue reports that include such data as in Figures 26.3–26.5. These reports are being used not only to minimize audits by regulatory agencies but also as public relation activity that enables the companies to claim a "green" label. This is now a desired label that helps on many fronts: marketing power to people that care about the environment and are willing to use their purchasing power as a lever, export to countries with strong regulatory framework, and locating potential manufacturing sites that will help them avoid nightmares such as NIMBY (not in my backyard), NOTE (not over there either), and BANANA (build absolutely nothing anywhere never again).

A list of demonstration projects can be found on the sites of both federal and state agencies [12]. Electroplating companies are active participants and the process at Valley Chrome Plating that serves to illustrate the effort in Figure 26.5 will be described in more detail toward the end of this chapter.

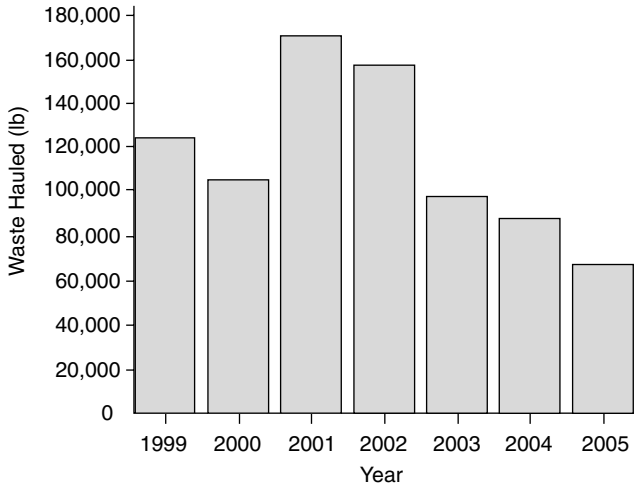

FIGURE 26.5 Hazardous waste reduction in Valley Chrome Plating [10], on its way to zero-discharge operation.

26.4 ELECTROPLATING INDUSTRY AND REGULATORY ENVIRONMENT

Metal-finishing operations are performed in two ways: (1) as a "captive" operation or department of a manufacturing company and (2) on a job-shop basis where the work is performed under contract by the owner of the product or material that is to be finished [13]. The economic census of the industry was summarized by the U.S. Census Bureau [14] (Table 26.1).

In 2002 the number of facilities with more than 20 employees was 827 and most of these facilities (730) employ between 20 and 100 employees. The total number of employees in the small facilities (below 100) was 45,000 (out of 61,000).

Roughly 7.5% of total payroll is spent on regulatory-related employees, and these employees cost on average over 20% more than other personnel. In the early 1990s, plating operations spent nearly 28% of total capital expenditures on pollution prevention and regulatory controls. Further, in 1998, total compliance operating costs for an average job shop were 6.5% of sales, or nearly $200,000 for a company with a sales volume of $3 million [13].

TABLE 26.1 Census Data on U.S. Surface-Finishing Industry

Year	Number of Companies	Number of Employees	Wages (billion US$)	Materials (billion US$)	Shipment (billion US$)	Capital Expenditures (billion US$)
2002	3050	61,093	1.26	1.71	5.5	0.18
1997	3401	74,631	1.31	1.83	6.0	0.29

Source: From [14].

The state of the industry was summarized elsewhere [6] as facing economic pressures from foreign competition that has resulted in a decline of around 11% in the number of facilities since 2000 (the report was written in 2007), 21% reduction in the number of employees, and a small profit margin. The necessity of combining environmental requirements with profitability is essential for the survival of the industry. For comparison, in 2001 China had 15,000 electroplating shops that employed nearly 500,000 workers [15]. The list of the main chemicals that are being used is given in Table 26.2 [13].

The electroplating and metal-finishing control regulations are contained in the U.S. Code of Federal Regulations (CFR) Title 40, Parts 413 and 433. All sectors of the electroplating and metal-finishing industry are covered by the metal-finishing regulations except for existing job shops and independent printed circuit board manufacturing (IPCBM) facilities which are indirect dischargers.

The principal federal laws and regulations in the United States [13] are shown in Table 26.3 (see also http://www.epa.gov).

Most countries carry and enforce their own set of regulations and incentives that are designed to protect the environment. These local legal restrictions are not the only ones that the industry needs to address. International standards for EMSs such as ISO 14001 are increasingly gaining in importance because of the global nature of many environmental issues that are reflected in present and future environmental and trade international treaties and because of the increasing global scope of the dischargers. Local industry must be aware of international and foreign regulations, because the traditional local characters of industrial products are fast changing. A simple keychain can have parts that are made in one country, assembled somewhere else, and sold all over the world. To avoid costly balkanization of the manufacturing process, shops need to accommodate the most stringent requirements. Europe [13] has recently issued the Restriction of the Use of Hazardous Substances (RoHS) Directive [16] It was announced in 2003 and became effective on July 2006. RoHS bans lead (Pb), mercury (Hg), cadmium (Cd), and hexavalent chromium (Cr^{6+}) as well as two brominated flame retardants from electronics sold in the European market. China has recently issued regulations that mimic the European RoHS Directive. In addition, in Europe the Waste from Electrical and Electronic Equipment (WEEE) Directive holds manufacturers responsible for collection and recycling of used electronics (effective 2005).

Fortunately, today the Internet offers a convenient information link that provides the opportunity for continuous monitoring of the EPA's and international regulations, publications, and proposals as well as technical help from companies that are willing and able to be subcontracted to handle the waste disposal aspects of the electroplater (http://www.nmfrc.org/bluebook).

A summary of POTW pretreatment standards in shown in Tables 26.4–26.6 [19, 20]. Since the limits are in concentrations, 40 CFR 413.14 adds, "No user introducing wastewater pollutants into a publicly owned treatment works under the provisions of this subpart shall augment the use of process wastewater or otherwise dilute the wastewater as a partial or total substitute for adequate treatment to achieve compliance with this standard." To put it differently—dilution is not a solution.

All new facilities are subject to the same new source performance standards (NSPSs) regardless of size, type of facility, or type of discharge.

TABLE 26.2 List of Main Chemicals in Use by the Electroplating Industry

Metals	Acids	Other Inorganic Compounds	Solvents and Other Organics
Aluminum	Hydrochloric	Ammonia compounds	Certain glycol ethers
Cadmium	Nitric	Chlorine	Ethyl benzene
Chromium	Phosphoric	Cyanide compounds	Formaldehyde
Copper	Sulfuric	Nitrates	Methyl ethyl ketone
Lead	—	—	Methyl isubutyl ketone
Manganese	—	—	Tetrachloroethylene
Nickel	—	—	Trichloroethylene
Silver	—	—	Toluene
Zinc and zinc compounds	—	—	Xylene

TABLE 26.3 Principal Federal Environmental Laws and Regulations in the United States

Federal Environmental Laws	Applicability
Clean Air Act (CAA) (40 CFR Parts 50–99): Establishes ambient and source emission standards and permits requirements for conventional and hazardous air pollutants. • Title V air permits and/or follows the standards for hazardous air pollutants under the National Emission Standards for Hazardous Air Pollutants (NESHAP) • State air permits	The CAA establishes a list of hazardous air pollutants (HAPs). Thirty-three substances in the Toxic Release Inventory (TRI) database for Standard Industrial Classification (SIC) code 3471 (metal finishing) are HAPs. EPA promulgates emission standards for listed source categories. These standards are known as NESHAP. Two NESHAPs affect the metal-finishing industry: • Chromium Electroplating (40 CFR 63, Subpart N) • Halogenetad Solvent Degreasing/Cleaning (40 CFR 63, Subpart T) • Aerospace Manufactering and Rework Facilities (40 CFR 63, Subpart GG)
Clean Water Act (CWA) (40 CFR Parts 100–145, 220–232, 410–471): Establishes standards and permit requirements for water pollutants, including sources that discharge directly to a water body or to a public sewer system. Also includes stormwater management requirements.	The CWA regulates the amount of chemicals that are released by direct and indirect wastewater/effluent discharges. Facilities that discharge directly into a body of water must obtain a National Pollution Discharge Elimination Systems (NPDESs) permit. Facilities that discharge to public-owned wastewater treatment (POTW) must adhere to specific pretreatment standards. These standards include concentration-based limits on the discharge of a given chemical or toxic by facility. There may be states or local conditions that require more stringent requirements than the guidelines: • Metal Finishing Effluent Guidelines (40 CFR 433) • Electroplating Effluent Guideline (40 CFR 413)
Resource Conservation Recovery Act (RCRA) (40 CFR Parts 240–299): Establishes regulations and permit requirements for hazardous waste management. Also creates standards for underground storage tanks that hold oil or hazardous substances.	RCRA classifies wastes such as solid waste sludge and requires certain methods for treatment, storage, and disposal. One of the classification under RCRA is hazardous waste. A material is considered hazardous waste if it meets the definition (40 CFR 261.20–24) or is listed as a hazardous waste (40 CFR26 1.31–33). A hazardous waste is subject to Subtitle C Generator (40 CFR 262), Transporter (40 CFR 263), and Treatment, Storage and Disposal Facility (TSDF) (40 CFR 254 and 265) requirements. Within RCRA Subtitle C, the EPA has subcategories of hazardous wastes called "F" listings. F hazardous wastes include spent solvents (F001–F005) and electroplating wastewater treatment sludge (F006).
Toxic Substances Control Act (TSCA) (40 CFR Parts 700–799)	Regulates the use, development, manufacture, distribution, and disposal of chemicals.
Comprehensive Environmental Response, Compensation and Liability Act (CERCLA or "superfund") (40 CFR Parts 300–311)	Establishes a program for cleaning up contaminated waste sites and establishes liability for clean-up costs. Provides reporting requirements for releases of hazardous substances.
Emergency Planning and Community Right-To-Know Act (EPARA) (40 CFR Parts 350–374)	Establishes a program (the TRI to inform the public about releases of hazardous and toxic chemicals. Reporting requirements apply to companies that use, process, or store specific chemicals over certain quantities.
Hazardous Materials Transportation Act (HMTA) (40 CFR Parts 100–180)	Establishes standards for the safe transportation of hazardous materials.

TABLE 26.4 Pretreatment Standards for Electroplating Categories (40 CFR 413): Facilities Discharge < 10,000 gpd

Pollutants	Daily Maximum ($mg\,L^{-1}$)	Maximum 4-Day Average ($mg\,L^{-1}$)
Cadmium	1.2	0.7
Lead	0.6	0.4
Cyanide	5.0	2.7
Total toxic organics	4.57	—

POTWs are designed to treat domestic sewage. Many industrial wastes are compatible with the treatment system but some are not. These either pass through the POTW untreated or interfere with the normal operation of the POTW. In both cases pretreatment regulations permit industry access to a central wastewater treatment system while at the same time protecting the quality of the receiving water body and the POTW.

TABLE 26.5 Pretreatment Standards for Electroplating Categories (40 CFR 413): Facilities Discharge > 10,000 gpd

Pollutants	Daily Maximum ($mg\,L^{-1}$)	Maximum 4-Day Average ($mg\,L^{-1}$)
Cadmium	1.2	0.7
Lead	0.6	0.4
Cyanide	1.9	2.7
Total toxic organics	2.13	—
Chromium	7.0	4.0
Copper	4.5	2.7
Nickel	4.1	2.6
Zinc	4.2	2.6
Silver	1.2	0.7

TABLE 26.6 Pretreatment Standards for the Metal Finishing Categories Pretreatment Standards for Existing Sources (PSESs)

Pollutants	Daily Maximum ($mg\,L^{-1}$)	Maximum 4-Day Average ($mg\,L^{-1}$)
Cadmium	0.69	0.26
Lead	0.69	0.43
Cyanide	1.2	0.65
Total toxic organics	2.13	—
Chromium	2.77	1.71
Copper	3.38	2.07
Nickel	3.98	2.38
Zinc	2.61	1.48
Silver	0.43	0.24

Websites of professional associations offer timely and specific information, particularly in terms of educational opportunities, research opportunities, and specific responses to issues that are currently under legislative consideration. Most of these sites also offer chat rooms and question-and-answer sessions that offer the opportunity for specific technical consultation. In almost all cases the chat rooms cannot guarantee the competence of the participants. Almost all of these sites are interlinked and contain links to foreign organizations and to more specialized associations. The most useful site from the environmental compliance perspective and the one that is being cited often in this chapter is the National Metal Finishing Resource Center (NMFRC) (http://www.nmfrc.org). This is an Internet-based organization that was established in 1995 by NIST (National Institute of Standards) and the EPA. It offers, among other resources, a searchable technical database containing over 7000 articles, papers, and reports covering metal-finishing process and pollution control topics.

Professional societies include the National Association of Surface Finishing (NASF) (http://www.finishing.com) and The Home Page of the Finishing Industry (http://www.namf.org). The transparency of compliance to sound environmental practices is not limited to current practices. A new field is slowly developing that might be labeled "archeology of environmental contaminations." A good example that relates to the electroplating industry is the work by Spliethoff and Hemond [17] on the history of waterborne export of toxic metals from industrial/residential watersheds.

26.5 ENVIRONMENTAL IMPACT OF ELECTROPLATING TECHNOLOGIES

A schematic of an industrial electroplating facility is shown in Figure 26.6. To be effective, EMSs require valid options in each of the three stages of operation. An example is shown in Table 26.7 for different baths for copper plating [18].

A decision has to be made as to which procedure to use. An outline of the decision-making process is illustrated on the flowchart in Figure 26.7.

Each process involves environmental consequences and costs associated with disposal. The economic aspects of waste disposal will be discussed separately. A typical flowchart is shown in Figure 26.8. However, environmental consequences are often reduced to political dimensions in which cost–benefit analysis is not always a solution. Local ordinances with zero tolerance to certain pollutants are not unknown.

Electroplaters have a number of options for cost effectively bringing a facility into compliance with water pollution control regulations. Within the three general options—modifying the process, treating the wastewater, and becoming a direct discharger—there are a wide variety of possible combinations of treatment technologies from which to choose.

Conventional wastewater treatment technologies are shown in Figure 26.9 [20]. These treatments are based on precipitating the metals as hydroxide to be concentrated as a solid waste cake that can be separately disposed. Pollutants such as cyanide are destroyed through oxidation according to the reaction

$$2CN^- + 8OH^- \rightarrow 2CO_2 + N_2 + 4H_2O + 10e^- \qquad (26.1)$$

This can be accomplished by using strong oxidants such as hypochlorite or ozone. The reaction with hypochlorite will

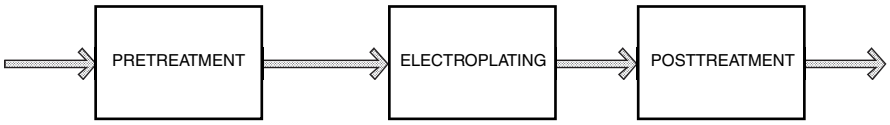

FIGURE 26.6 Schematic of industrial electroplating process [18].

TABLE 26.7 Different Baths for Cu Electrodeposition

Bath 1	Bath 2	Bath 3	Bath 4
CuCN	Copper sulfate	Copper fluoroborate	Copper pyrophosphate
NaCN (or KCN)	Sulfuric acid	Fluoroboric acid	Nitrate
NaOH (or KOH)		Boric acid	Ammonia
Rochelle salt			Orthophosphathe

take the form

$$2CN^- + 5OCl^- + H_2O \rightarrow 2CO_2 + N_2 + 5Cl^- + 2OH^- \quad (26.2)$$

Oxidized metals such as hexavalent chromium are reduced to a form suitable for the formation of an insoluble hydroxide.

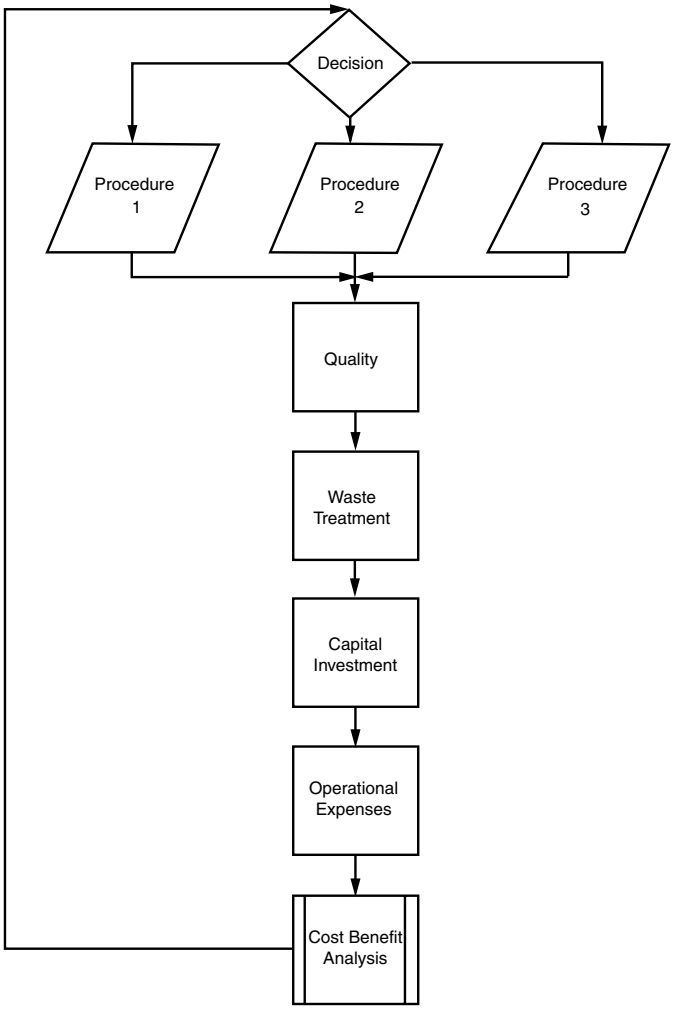

FIGURE 26.7 Flowchart of the decision-making process in choosing a cost-effective procedure for copper plating.

In cases such as in the presence of chelating agents, the solubility of the metals in alkaline environments is too high to meet the standards and special techniques are required to reduce the metal concentrations. These techniques include precipitation as sulfides and ion exchange technologies. If these alternative treatments are unsuccessful in precipitating the chelating complexes, the complexes can be dissociated by adjusting the pH to an extreme level while exchanging the complexing agents followed by neutralization of the solution.

Elimination is the ultimate reduction. Cyanide and Cr(VI) are the most urgent targets for attempts to replace them with more acceptable alternatives. This issue will be discussed in the next section.

The treatment of wastewater in electroplating processes, as mandated by national pretreatment standards, results in two streams: an effluent that must comply with regulations for acceptable pollutant discharge and residue (sludge) containing a high concentration of the substances which the wastewater regulations prohibit discharging. Most electroplating sludge contains high concentrations of toxic heavy metals and are considered hazardous. The high cost of sludge disposal demands that designers of wastewater treatment systems consider the relative volumes of the sludge generated by the different treatments. For example, insoluble sulfide precipitation can reduce the metal concentration in many waste streams to lower levels than can hydroxide precipitation. However, because this process uses ferrous sulfide as the source of the sulfide ions, ferrous ions are liberated in the reaction and converted to ferrous hydroxide, which adds considerably to the sludge volume. Efficient dewatering of the sludge can also achieve significant reduction in the volume of the sludge.

A recent example of the interplay between regulatory agencies and professional societies toward more effective recovery efforts can be found in the EPA announcement [21] to solicit response to suggested changes in the definition of solid waste to exclude certain hazardous secondary materials sent for recycling. The response of the surface finishing industries to these changes summarizes the state of recycling in the industry as follows: "Under the existing regulatory framework for hazardous secondary materials, the industry is literally throwing away valuable materials. What makes the electroplating sludge 'hazardous' in the eys of the EPA is the very metal that makes it valuable when it is recovered. In short, the sludge is only 'hazardous' if not recycled [13]." They estimate that currently 20–30% of electroplating sludge is being recycled. The small penetration is in part because of the high cost associated with managing it as hazardous waste. They further estimate that an average metal-finishing firm is throwing away over $50,000 annually in disposed metals. They further mention that the expanding demand for metals, such as nickel in China and other Asian countries, to support the manufacturing sectors

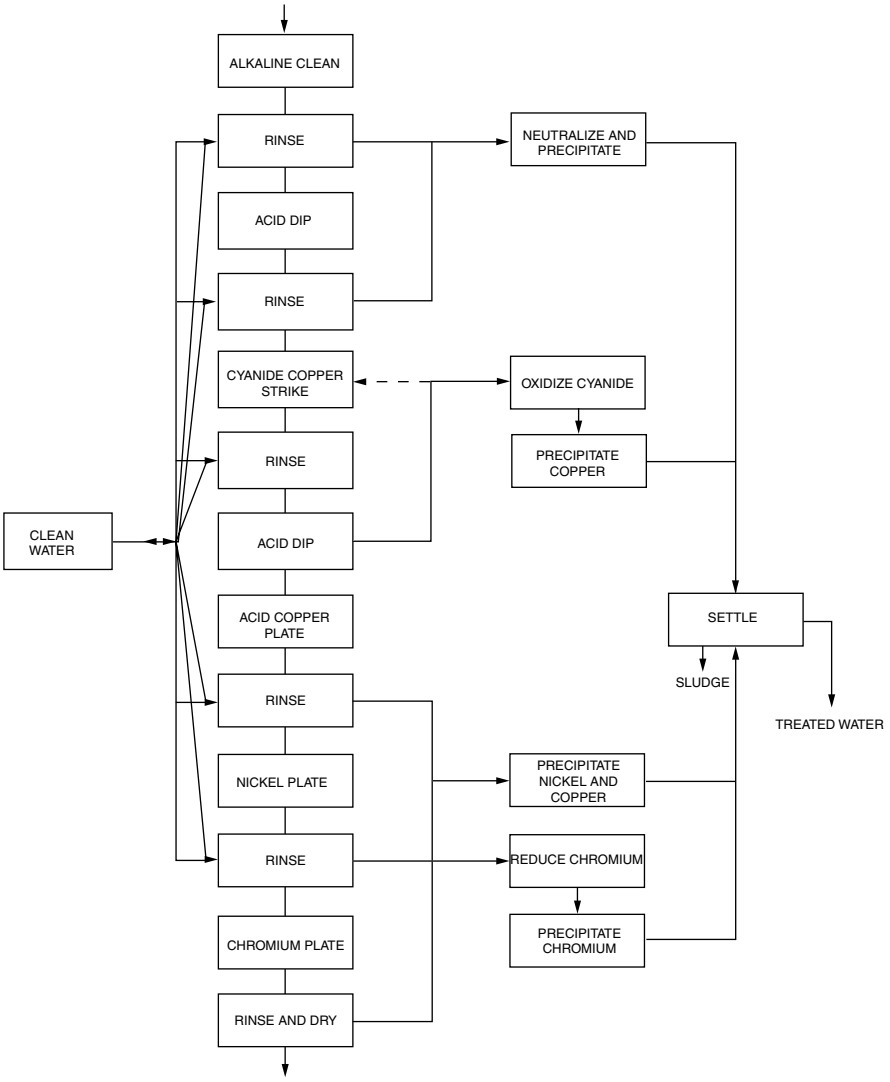

FIGURE 26.8 Schematic of conventional waste disposal procedures taken in industrial electrodeposition setting.

has decreased the worldwide supply and contributed to the price increase. This issue will be further discussed toward the end of the chapter when we comment on the economic aspects of the remediation efforts.

An efficient way to minimize disposal costs is to minimize the total volume of water that is needed for the electroplating process. Useful techniques include simple steps such as preventing leaks, installing antisiphon devices equipped with self-closing valves on water inlet lines, using multiple counterflow rinse tanks to substantially reduce rinse water volume, using spray rinse, preventing unnecessary dilutions, recycling of wastewater, and using dry cleanup when possible.

26.6 IMPACT MINIMIZATION AND ZERO DISCHARGE

The trend, where possible, to substitute modifications of the production process that result in waste minimization for waste treatment and environmental regulations is dominant in most discussions on environmental impact. The policy aspects of economic incentives will be discussed in a later section. Here we will concentrate on the technical aspects. Environmentally "acceptable" technological alternatives can often be found with varying degree of details at the EPA home page of the Waste Reduction Resource Center [22]. Today such technologies use the acronym P2 (Pollution Prevention) at an EPA website (http://www.epa.gov/p2/) with sections such as *Where you Live, Grants and Funding, Laws and Policies, Partnerships, Technical Assistance, and Tools and Publications*. The publication section contains technical papers and case studies with a reference to an alphabetical list of P2 publications [23]. Detailed applications for the electroplating industry can be found in the corresponding state sites [24].

An older publication [25] provides a comprehensive EPA review of technologies that were targeted to eliminate or

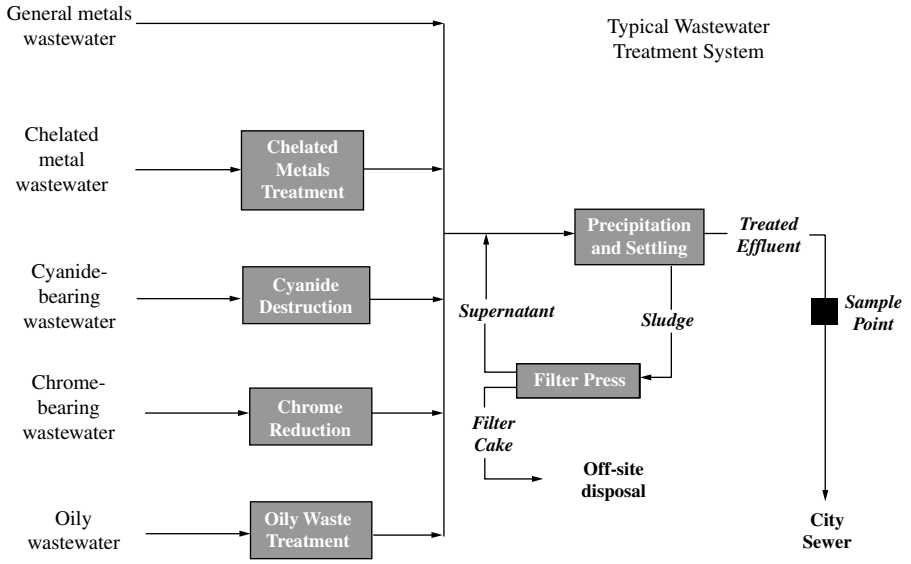

FIGURE 26.9 Schematic of wastewater system at Valley Chrome Plating [10].

significantly reduce the amount of hazardous substance, pollutant, or contaminant released to the environment. The main target for these attempts was to eliminate or reduce cyanide in the electroplating procedures. Sodium cyanide and potassium cyanide are used in electroplating bath formulations for the deposition of copper, zinc, cadmium, silver, gold, and alloys such as brass, bronze, and alballoy.

Alternative technologies that are described in detail in the report [25] include the alkaline noncyanide copper plating discussed before (Table 26.2), zinc alloy electroplating, plasma deposition, and thermal coating and work on new, environmentally friendly alloys.

Zinc alloys can be used to replace cadmium coatings in a variety of applications [26]. They offer corrosion protection and lubricity. The most promising among these are zinc–nickel and zinc–cobalt. Zinc alone can provide corrosion protection equivalent to cadmium at thicknesses above 1 mil (0.001 in.). Zinc cannot match cadmium when lubricity is desirable. An EPA report [27] describes the substitution of cadmium cyanide electroplating with zinc chloride electroplating. Product quality was defined in terms of corrosion resistance. Corrosion resistance was determined by salt-spray tests in accordance with American Society for Testing and Materials (ASTM) standard B117–90.

Zinc–nickel alloys are being introduced in Japan and Germany in the automotive industry for fuel lines and rails, fasteners, air-conditioning components, and cooling systems. Zinc–nickel coatings have also been introduced as cadmium replacements on fasteners for electrical transmission structures and on television coaxial cable connectors. Another alternative is to substitute electroplating with a dry process such as plasma deposition and thermal coating. The cost is significantly higher and severe restrictions for plating on irregularly shaped substrates exist. A nickel–tungsten–silicone–carbide coating was suggested by Takada [28] as a replacement for hard (functional) chromium. Nickel–tungsten–boron alloys were suggested as replacement for chromium. A family of these alloys is patented under the name AMLATE.

The newer technologies [22] are targeted to explore all aspects of the industry that lead to "zero discharge."

Zero-discharge processes are cyclical processes in which the water quality of the discharge is within regulatory specifications to be recycled into the public water system (Fig. 26.10). Technology to achieve zero discharge is available. Major impediments are cost and drag-in. Zero-discharge technologies are important not only in fulfilling the dream of eliminating adverse environmental consequences but in the more practical issue of establishing a baseline for the approximate price that the cleanup of pollution will cost. This "green tax" can be incorporated into the product's price structure, thus forcing manufacturers to incorporate the environmental effects into the optimization of the manufacturing processes that will maximize the profitability of the product. A good example of such a process is Valley Chrome Plating. Valley Chrome is a California plating shop that manufactures truck bumpers. Its president, Mr. Ray Lucas, is also president of NASF and a board member of STA (Surface Technology Association). In 2007 he presented his company's effort to achieve zero-discharge decorative chrome plating at a talk in New York that I was invited to attend. The company is also a certified practitioner of EMS. Mr. Lucas was kind enough to provide me with a copy of his presentation with a permission to use the material in this chapter. Three of the figures (27.5, 27.9, and 27.10) were taken from this presentation. Valley Chrome took a series of

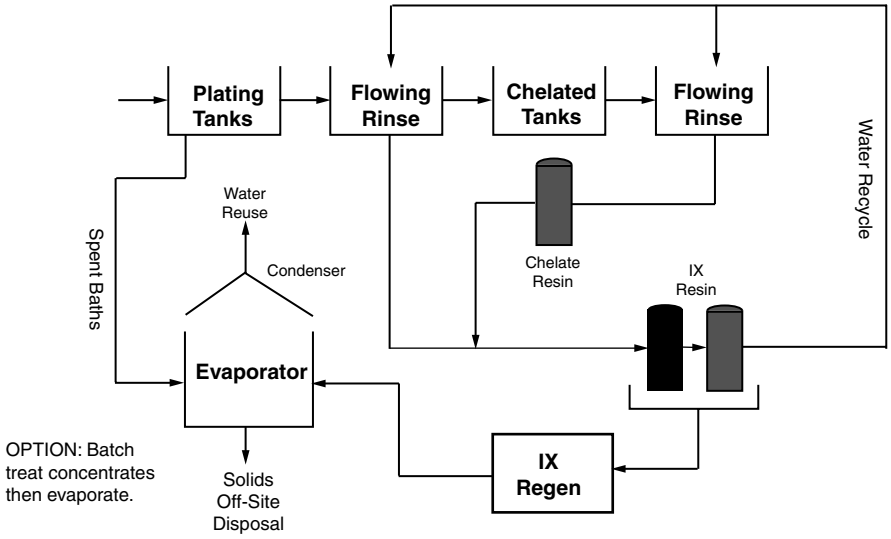

FIGURE 26.10 Zero-discharge layout at Valley Chrome Plating [10].

steps toward achieving zero discharge. These steps can be summarized in the following way:

Separate the waste stream.
- Spent concentrates
- Dragout rinsewater
- Chelated materials
- Soapy materials (includes low-volume waste, solvents,etc..)

Apply source reduction measures.
- Spill controls
- Flow controls
- Dragout controls and rinse
- Bath life extensions (acid filtration, weirs, routine maintenance, etc.)

Find a home for each waste stream.
- Spent concentrates—treat or ship
- Dragout rinsewater—recapture or treat
- Dilute rinsewater—recycle
- Chelated materials—pretreat
- Soapy materials—treat
- Solvents—offsite recycle

Develop equipment "scheme."
- Ion exchange for rinsewater recycling.
- Evaporator for treatment of concentrates.
- Shipping offsite for untreatable materials

Summary (management):
- Train.
- Retain.
- Supervise and test.
- Set training schedule in writing.
- Set expectations for employees.
- Train the employees to train.
- Do your homework and reduce liability.

26.7 APPLICATIONS OF ELECTRODEPOSITION IN METAL RECOVEY

Zero discharge is not necessarily recycling. Zero Discharge through recycling implies following the first principle of green chemistry, which requires that design processes leave no waste. For electroplating, this requires recycling. In addition, waste streams with metals are not limited to the metal-finishing industry. Examples include the tanning industry and radioactive waste removal technologies. An excellent updated overview of metal recovery technologies is available on the NMFRC site [13] and for older publications in [29–33].

Similar to electrodeposition, cathodic removal of metals may be represented by an electrowinning reaction:

$$M^{z+} + ze^- \rightarrow M \tag{26.3}$$

The soluble species may be simple hydrated cation such as $Cu^{2+}(aq)$ or a complex such as $[CuCl_4]^{3-}$ or $[Ag(S_2O_3)_2]^{3-}$. Desired cathodic reactions such as

$$Cu^{2+} + 2e^- \rightarrow Cu \tag{26.4}$$

may be accompanied by undesired solvent decomposition reactions such as hydrogen evolution and/or oxygen reduction On the anodic side oxygen evolution will dominate when inert electrodes are used:

$$2H_2O + 4e^- \rightarrow O_2 + 4H^+ \quad E = +1.23\,V \tag{26.5}$$

Standard potentials of three of the metals often found in waste streams are shown below:

$$Cu^{2+} + 2e^- \rightarrow Cu \quad E_0 = +0.34\,V$$
$$Ni^{2+} + 2e^- \rightarrow Ni \quad E_0 = -0.25\,V$$
$$Zn^{2+} + 2e^- \rightarrow Zn \quad E_0 = -0.76\,V$$

Copper is easy to electrowin because the standard potential is more positive than hydrogen. Nickel is more difficult, but raising the pH shifts the hydrogen potential to a more negative value.

Zinc electrowinning is possible only due to the high overvoltage for hydrogen evolution on a zinc cathode. This requires a very pure Zn solution because deposition of any impurities will considerably lower the overvoltage for hydrogen evolution.

An electrowinning cell design that was used by Eco-Tec for waste recovery applications is described by Brown [34]. The cell is based on Kennecott–Copper's high-efficiency air agitation (HEAA) technology with cell design optimized for recovery from waste streams. Walsh and Reade [35] describe a rotating cylinder electrode (RCE) cell for removal of metals via cathodic depositions. References for other cell designs are also mentioned there.

Clarke and Pardoe [36] describe proprietary EBONEX ceramic electrodes that are made of Magnelli phase suboxides of titanium dioxide. They find applications as cathodes in metal recovery systems from waste stream, supporting anodes in electrowinning of Zn and Cu, and as anodes for cyanide and organic waste destruction.

For effective recovery, it is often required that the metals be electrodeposited in acceptable levels of purity from waste streams that contain more than one metal. This is often done by judicial selection of the deposition potential. Armstrong et al. [37] discuss selective electrodeposition of cadmium, cobalt, and nickel in pure form from binary mixtures. Raats et al. [38] discuss Cu–Ni and Zn–Cu mixtures and Polcaro and Palmas [39] discuss deposition from a Pb–Cu mixture.

Electrowinning has traditionally been applied to metal recovery from concentrated solutions. Although attempts are being made to extend electrowinning to more dilute solutions [29], ion exchange is considered a more effective tool for metal recovery. Brown [34] describes a waste treatment system that combines the two techniques for total removal of metal contaminants.

Cation exchangers exchange metallic cations for hydrogen ions:

$$RH + CuSO_4 \rightarrow R_2Cu + H_2SO_4 \qquad (26.6)$$

Upon exhaustion, the resin must be regenerated by strong acids such as hydrochloric acid or sulfuric acids that will yield concentrated acidic copper solutions. This way, metals can be concentrated from a few parts per million to 30,000 ppm. The proper choice of regenerating acid can adjust for a desirable anion that will make the regenerated solution suitable for electrowinning and recycling. Unlike other separation processes such as evaporation and reverse osmosis that remove water from the waste, cation exchangers and electrowinning remove the metals from the waste.

Ion exchange processes have the ability to not only concentrate the pollutants but also separate and purify them by the differential affinities of the cations to the ion exchanger. Increased degree of metal separation can be achieved with application of chelating resins such as iminodiacetate chelating resins. These chelating resins can have strong enough affinity to bind metals from plating solutions that contain chelating agents such as quadrol, citrates, and ethylenediaminetetraacetic acid (EDTA). The performance of a commercial ion exchange system is described in [40].

Three case studies in which the combinations of ion exchanger and electrowinning are used for metal recycling are described in [35]. An excellent example is the one used by Hughes Aircraft in Orangeberg, South Caroliua. Copper-containing waste concentrates from various processes including electroless copper plating, nitric acid rack strip, and numerous spent acid baths are segregated and collected in batch-holding baths. The contents of these tanks are then bled into an equalization tank feeding the recovery system. After pH adjustment, it passes through filters to chelating ion exchange units (IX). The effluent from these units is monitored by a colorimeter copper analyzer which initiates regeneration at a breakthrough level of $1\,mg\,l^{-1}$. The ion exchange units are then processed in a batch-type Recowin electrowinning system where the copper is reduced from $10–20\,g\,L^{-1}$ to about $1\,g\,L^{-1}$. The spent electrowinning electrolyte is fed back through the ion exchange units to recover residual copper.

26.8 LIGHT-INDUCED PROCESSES

The possibility of using solar energy as an energy source for environmental remediation has attracted considerable interest [41–43]. Electrodeposition plays an important role in these technologies in two distinct areas: electrochemical and photoelectrochemical film deposition in the production of thin-film photovoltaic devices and in light-induced photoelectrochemical remediation.

In photoelectrochemical remediation, the pollutants might be reduced or oxidized in an electrochemical cell in which at least one of the electrodes is a photoactive semiconductor. One can use an *n*-type semiconductor that will drive photogenerated holes to the semiconductor–electrolyte interface or a *p*-type semiconductor in which photogenerated electrons will be driven to the interface. Presently most of the effort in this area is directed at photooxidation of organic pollutants [44–46].

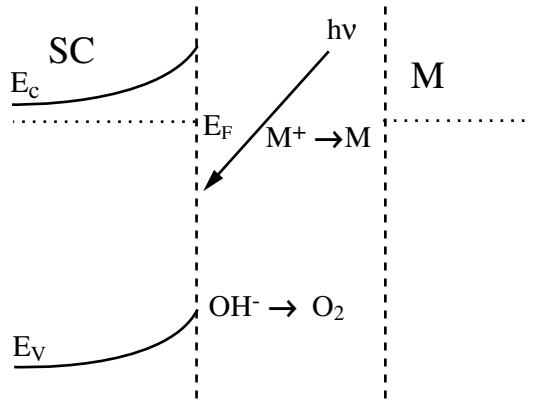

FIGURE 26.11 Energy band diagram of a photoelectrochemical system designed to photoreduce dissolved metal cations.

Within the context of environmental aspects of electrodeposition, the most interesting processes are reductive processes. The reductive processes can involve either reduction of the metal ions to metallic form similar to the reduction processes discussed before or reduction of problematic metal ions such as Cr(VI) to more treatable ions such as Cr(III).

An example of a band diagram of a photoelectrochemical system designed for metal deposition is shown in Figure 26.11. The band diagram shown in Figure 26.11 is appropriate for large crystallites that can sustain a space-charge layer and drive light-induced carriers to the semiconductor–electrolyte interface. This example shows an *n*-type semiconductor in which light-induced holes will be driven to the surface while the electrons will be driven to the counter electrode. Under normal conditions (semiconductor in depletion and no current doubling), this configuration sustains oxidation at the semiconductor–electrolyte interface and reduction at the counter electrode. The electron source can be water, as shown in Figure 26.11, or a sacrificial donor. If the equilibrium potential of the semiconductor is adjusted to match the counter electrode, the system can operate under short-bias conditions. Under these conditions, one can replace the two-electrode configuration with a semiconducting powder in which both reduction and oxidation take place on the same electrode. However, when the particle size in such powders is reduced to the nanometer scale, the particles can no longer sustain a spacecharge layer. and dopant-independent diffusion of light-induced carriers to the surface will take place. Semiconductor–electrolyte systems have been described for gold [45], silver [47], mercury [48], and platinum recycling [49]. In some cases water is the electron donor and in other cases organic solutes such as isopropyl alcohol are used as donors.

Electrochemical deposition of semiconductors is covered elsewhere in this volume. Recent work on electrochemical and photoelectrochemical film deposition of semiconducting and metal films to produce photovoltaic devices includes deposition of CdSe and CdSe/ZnSe films [50], WO_3 [51], cathodic electrodeposition of TiO_2 thin films for dye-sensitized photoelectrochemical applications [52], and photoelectrochemical characterization of electrodeposited Cu_2O [52–53] and $CuInSe_2$ [55].

26.9 ECONOMIC CONSIDERATIONS

It is not easy to arrive at figures that will clearly define the costs associated with disposal. Typical figures for the industry run at about 3% of total expenditure with a standard deviation of about 2%. However, the present economic health of the industry is such that the cost effectiveness of environmental compliance is a significant factor in the voluntary acceptance of the need for compliance. As was mentioned before, the concepts of green chemistry and EMS are fully compatible with this objective with their emphasis on recycling, material and energy control, and efficiency. The need for cost-effective compliance also became a major focal point of R&D programs to such a degree that a new acronym was proposed, P3, which stands for Profitable Pollution Prevention (Lou&Huang), to complement P2 (Pollution Prevention). A recent EPA report [56], recommends future directions for R&D efforts in the surface-finishing industry. The highest priority recommendations are targeted at various aspects of use of hexavalent chrome, wastewater treatment and recycling, and technology assistance. Medium effort should continue to search for noncyanide alternatives, characterization of air emissions from plating baths, development of risk assessment tools for the industry, and various aspects of nickel plating (electroless plating. alkaline zinc–nickel electrolyte and emissions).

Profitability, to a large extent, depends on the cost of the environmental impact, the recovery costs of recyclable materials, and savings from improved operational efficiency. Figure 26.12 shows the recent fluctuations of the price of nickel. While the high price during the end of the 1980s is attributed to the unrest in the former Soviet Union, the recent rise follows the price increased of most other commodities and is mainly due to increased demand from some of the fast-growing developing countries. The fact that a significant component of the recent price increase is driven by speculation is a sure sign that the expectation is for this trend to continue.

26.9.1 Policy

Most developed countries spend between 1 and 2% of their gross domestic product (GDP) on environmental protection, and that proportion is likely to rise. In the United States it is estimated that the 1998 effort was 2% of GDP and is expected to grow [58].

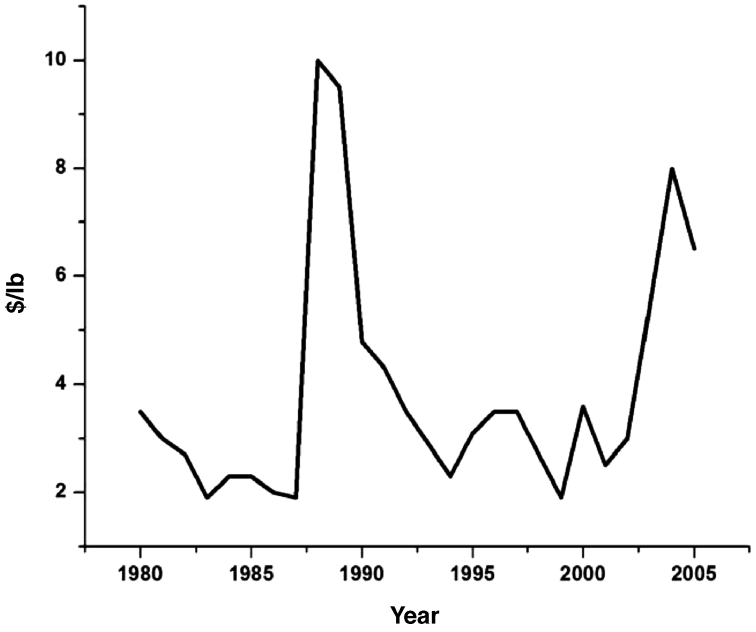

FIGURE 26.12 Changes in the price of nickel since 1980 [57].

Regulation is by far the most common tool of environmental policy. What is often referred to as "command-and-control" policy is almost universally believed not to be the most efficient policy in terms of both environmental protection and economic impact. The deficiencies of the regulations are discussed in [59]:

Encouragement of governments to do what they do worst—second-guessing companies about what is the best technology to achieve a particular goal.

- Disguised true cost
- Unequal loading of costs
- Regulations that set both a floor and a ceiling on discharge (no incentive to discharge less than the regulation allows)
- Best results with big corporations but much less effective with dispersed sources

Market-driven economic environmental instruments fall into two categories:

- *Green taxes*: that put a price on pollutants that in principle reflect the costs they impose on society. The extent to which pollution will be reduced depends on government's use of the fees. If government transfers the income into the general revenue, the effect on the pollution level will be difficult to predict.
- *Marketable permits*: that are based on absolute quantity of pollution that is to be allowed and then give or sell polluters rights to pollute up to that given level. Polluters can trade these rights with each other.

These permits make it easy to predict the total amount of pollution but very difficult to determine what the "effective" tax on polluters will be. They also make sense in environments which "share" pollution. It makes very little sense to exchange pollution permits between two aquatic reservoirs that do not mix effectively with each other, so that cleaning one pollutes the other. The whole field of environmental justice is largely based on such practices. Green taxes set a price and allow the quantity to fluctuate while permits set a fixed quantity while allowing the price to fluctuate.

A comprehensive system analysis that models the impact of nine source reduction methodologies is given in [60]. An organization theory perspective of pollution prevention in the Chinese electroplating industry is presented in [61].

The search for effective economic incentives to tackle pollution is accelerating [58]. Many countries charge a flat rate on water pollution. In many instances, green taxes are being presented as "sin taxes," which puts them in the same category as tax on cigarettes and alcohol.

26.9.2 Advocacy

The common desire of legislating the economy to operate by "automatic pilot" in order to reduce environmental impact is appealing. The cumbersome mix of regulations, jaw-boning, and green taxes is no one's favorite. The mix is different in different countries. Despite this diversity of policy tools, one must grudgingly admit that considerable progress in integrating environmental considerations into the production facilities has taken place since 1974. One relevant quantitative indicator in support of this is water use. Figure 26.13 shows the timeline of water use in the United States and the

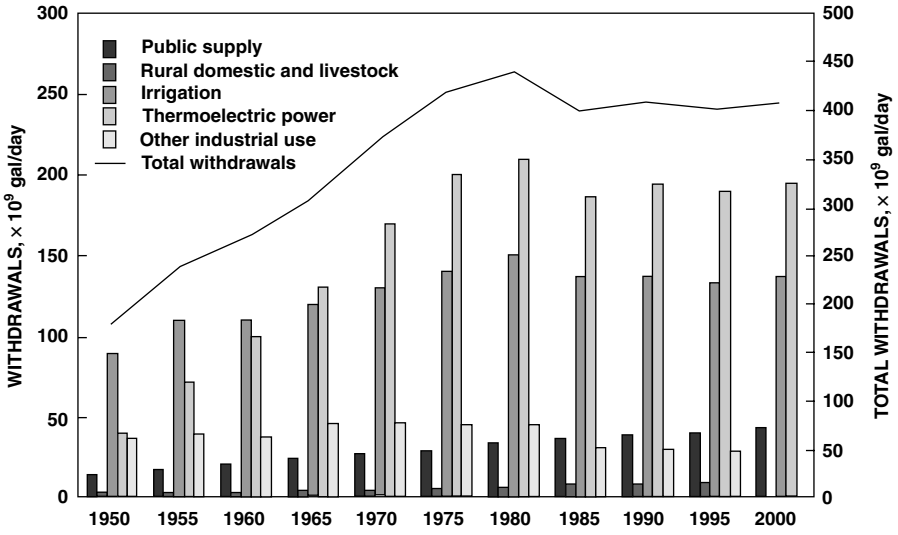

FIGURE 26.13 Timeline of U.S. water use [62].

sharp break that it takes toward the end of the 1970s. The section that is relevant to this chapter is reduced industrial use. Correlating this leveling with increase in regulatory activity, as shown in Figure 26.1, one is tempted to associate it with the increased cost of wastewater disposal.

An important aspect in which progress is limited is the incorporation of environmental considerations as an important element in the decision making. One particular aspect that limits progress in this area is the limited ability to quantify product quality and correlate it with commercial value. The two most common applications of the metal-finishing industry are functional applications: corrosion protection and ornamental applications. Some of the considerations that are involved in quantifying product quality were previously discussed in the context of adopting cyanide-free deposition procedures and substituting toxic metals such as cadmium with less toxic ones such as zinc. A typical corrosion test can follow acceptable standards and is not very difficult to perform. However, ornamental applications are almost impossible to quantify. Public education and jawboning programs, similar to the ones that are being applied in the consumer product industry ("green coating"), might be effective.

Perhaps as important as the ability of a manufacturer to perform cost–benefit analyses that incorporate environmental considerations is the ability of society to funnel research support to technologies that offer the most potential benefits. Quantification of the quality of the surface treatments in terms of more sophisticated concepts than the prevailing ones is most urgently needed. Application of chemometric principles to this issue is likely to have a major impact on research and development that will result in environmentally friendly products.

REFERENCES

1. M. Schlesinger and M. Paunovic, Eds., *Modern Electroplating*, 4th ed., Wiley, New York, 2000, Chapter 26, p. 791. (a) Y. Zhang and J. A. Abys, Chapter 6, p. 241. (b) J. W. Dini, Chapter 2, p. 115 and 119. (c) N. V. Mandich and D. L. Snyder, Chapter 7, p. 320. (d) G. A. Di Bari, Chapter 3, p. 191. (e) G. A. Di Bari, Chapter 13, p. 578. (f) J. A. Abys and C. A. Dullaghan, Chapter 12. p. 546.
2. M. Kirchhoff, available: www.stfrancis.edu/ns/diab/Greenchem/mary.PPT, 2003.
3. www.asmalldoseof.com/ppt/Tox_health_lead_school.pdf.
4. Intergovernmental Plan on Government change, available: http://www.ipcc.ch/.
5. http://www.iea.org/G8/index.asp.
6. "Energy Trends in Selected Manufacturing Sectors," available: www.epa.gov/ispd/pdf/energy/report.pdf, 2007.
7. P. Anastas and J. Warner, *Green Chemistry: Theory and Practice*, Oxford University Press, New York, 1998.
8. http://www.epa.gov/ispd/metalfinishing/ems.html#ems.
9. "National Metal Finishing Environmental R&D Plan," EPA Contract No. 68D70002 U.S. Environmental Protection Agency, Washington, DC, 2000.
10. R. Lucas,Valley Chrome Plating, presentation August 2007, New York.
11. http://www.toyota.com.
12. http://www.calepa.ca.gov/EMS/Archives/proj0600.htm.
13. "Pollution Prevention and Control Technologies for Plating Operations," available: http://www.nmfrc.org/bluebook.
14. http://www.census.gov/econ/census02/guide/INDDATE.HTM.
15. H. Fan, D. Zuo, and T. Hu, *Plating Finish.*, **23**, 16 (2001).
16. "Restriction of the use of Hazardous Substances," available: http://www.rohs.gov.uk/

17. H. M. Spliethoff and H. F. Hemond, *Env. Sci. Tech.*, **30**, 121 (1996).
18. F. A. Lowenheim, Ed. *Modern Electroplating*, Electrochemical Society, Pennington, NJ, 1974.
19. *Environmental Regulations and Technology*, EPA/625/10-85/001, U.S. Environmental Protection Agency, Washington, DC 1985.
20. http://www.roskill.co.uk.
21. *72 Fed. Reg. 14172* (Mar. 26, 2007), Docket ID No. EPA-HQ-RCRA-2002-0031, U.S. Environmental Protection Agency, Washington, DC.
22. http://wrrc.p2pays.org/industry/indsectinfo.asp?INDSECT=10.
23. http://141.156.28.142/p2_documents/p2docs_alpha.html.
24. http://www.glrppr.org/contacts/gltopichub.cfm?sectorid=47.
25. *A Guide to Cleaner Technologies and Alternative Metal Finishes*, EPA/625/R-94/007, U.S. Environmental Protection Agency, Washington, DC.
26. D. A. Schario, M. A. Klingenburg, and E. W. Brooman, Paper presented at ECS Meeting, Abstract, MA96-2309, 1996.
27. B. C. Kim, P. R. Web, J. A. Gurklis, and R. K. Smith, Eds., *Substituting Cadmium Cyanide Electoplating with Zinc Chloride Electroplating*, EPA/600/SR-94/074, U.S. Environmental Protection Agency, Washington, DC, May 1994.
28. Takada, U.S. Patent 4,892,627 (1990).
29. F. C. Walsh, in *Electrochemistry for Cleaner Environment*, J. D. Genders and N. L. Weinberg, Eds., The Electrosynthesis Company, New York, 1992, Chapter 4.
30. T. L. Hatfield, T. L. Kleven, and D. T. Pierce, *J. Appl. Electrochem.*, **26**, 567 (1996).
31. C. A. Hodges, *Science*, **268**, 1305 (1995).
32. W. J. Eilback and G. Mattock, *Chemical in Waste Water Treatment*, Wiley, New York, 1986.
33. K. E. Boumidel and R. Salhi, in *Energy and Electrochemical Processing for Cleaner Environment,* C. W. Walton and E. J. Rudd, Eds., Electrochemical Society, Pennington, NJ, 1998.
34. C. J. Brown, in *Electrochemistry for Cleaner Environment*, J. D. Genders and N. L. Weinberg, Eds., The Electrosynthesis Company, New York, 1992, Chapter 7.
35. F. C. Walsh and G. W. Reade, in *Environmental Oriented Electrochemistry*, C. A. C. Sequeira, Ed. Elsevier, New York, 1994, Chapter 1; F. C. Walsh, in *Electrochemistry for Cleaner Environment*, J. D. Genders and N. L. Weinberg, Eds., The Electrosynthesis Company, New York, 1992, Chapter 40.
36. R. Clarke and R. Pardoe, in *Electrochemistry for Cleaner Environment*, J. D. Genders and N. L. Weinberg, Eds., The Electrosynthesis Company, New York, 1992, Chapter 18.
37. R. D. Armstrong, M. Todd, J. W. Atkinson, and K. Scott, *J. Appl. Electrochem.*, **26**, 379 (1996).
38. C. M. S. Raats, H. F. Boon, and G. van der Heiden, *Chem. Ind.*, 465 (1978).
39. A. M. Polcaro and S. Palmas, in *Electrochemical Engineering and the Environment, ICHEM Symp. Ser.*, **127**, 85 (1992).
40. C. P. Jones, M. D. Neville, and A. D. Turner, in *Electrochemistry for Cleaner Environment*, J. D. Genders and N. L. Weinberg, Eds., The Electrosynthesis Company, New York, 1992, Chapter 8.
41. A. J. Nozik and R. Memming, *J. Chem. Phys.*, **100**, 13061 (1996).
42. K. Rajeshwar, *J. Appl. Electrochem.*, **25**, 1067 (1995).
43. *Proceedings of the Fifth DOE Solar Photoelectrochemistry Research Conference*, available: www.er.doe.gov/bes/chm/Publications/Contractors%20Meetings/25th_DOE_Solar_Photochemistry_crop.pdf.
44. D. F. Ollis, E. Pelizzetti, and N. Serpone; *Photocatalysis—Fundamentals and Applications*, Wiley, New York, 1989, Chapter 18.
45. N. Serpone, E. Borgarello, and M. Barbeni, *J. Photochem.*, **36**, 373 (1987).
46. D. M. Blake, in *Bibliography of Work on Heterogeneous Photocatalytic Removal of Hazardous Compounds from Water and Air*, NREL/TP-473-20300, 1995, available: http://www.nrel.gov/docs/legosti/fy96/20300.pdf.
47. K. Ito and A. Fujishima, *J. Am. Chem. Soc.*, **110**, 6267 (1988).
48. J. Domenech, M. Andres, and J. Munoz, *J. Electrochim. Acta*, **32**, 773 (1987).
49. B. Kraeutler and A. J. Bard, *J. Am. Chem. Soc*, **100**, 5985 (1978).
50. M. Boroushian, D. Karoussos, and T. Kosanovic, *Solid State Ionic*, **177**, 1855 (2006).
51. J. Georgieva, S. Armyanov, E. Valova, Ts. Tsacheva, I. Poulios, and S. Sotiropoulos, *J. Electroanal. Chem.*, **585**, 35 (2005).
52. S. Karuppuchamy, D. P. Amalnerkar, K. Yamaguchi, T. Yoshida, T. Sugiura, and H. Minoura, *Chem. Lett.*, **30**, 78 (2001).
53. R. Inguanta, C. Sunseri, and S. Piazza, *Electrochem. Solid-State Lett.*, **10**, K63 (2007).
54. P. E. de Jongh, D. Vanmaekelbergh, and J. J. Kelly, *J. Electrochem. Soc.*, **147**, 486 (2000).
55. O. Solorza-Feria and R. Rivera-Noriega, *J. Mat. Sci.*, **30**, 1573 (1995).
56. T. D. Ferguson; "National Metal Finishing Environmental R&D Plan: an Update," EPA Contract No. 68D70002, U.S. Environmental Protection Agency, Washington, DC, 2002.
57. http://minerals.usgs.gov/minerals/pubs/commodity/nickel/500798.pdf.
58. R.D. Morgenstern, R. D. Pizer, W. A. Shih, and Jhih-Shyang, available: http://yosemite1.epa.gov/ee/epa/wpi.nsf/.
59. F. Cairncross, in *Green, Inc.*, Earthscan Pub. (1995).
60. W. Glaze, Dissertation No. AAT 8919913, University of California, Los Angeles, CA. (1989).
61. K. A. Warren, Dissertation No. AAT 9630410, Stanford University, CA. (1996).
62. http://pubs.usgs.gov/circ/2004/circ1268/htdocs/figure14.html.

27

APPLICATIONS TO MAGNETIC RECORDING AND MICROELECTRONIC TECHNOLOGIES

STANKO R. BRANKOVIC, NATASA VASILJEVIC, AND NIKOLAY DIMITROV

Early applications of electrodeposition in manufacturing were mainly confined to situations where relatively thick polycrystalline metal deposits were needed. These included protective or sacrificial metal layers for corrosion protection, decorative applications, and situations where metal coatings with specific mechanical properties were needed [1]. However, development of theoretical foundations in electrochemical engineering and electrometallurgy and the sophistication of the tools used for electrodeposition have contributed to widespread electrodeposition in high-tech industry where more rigorous thickness control of the deposit is required. Nowadays, electrodeposition is recognized as a mature deposition method for the fabrication of magnetic thin-film heads [2, 3] and in microelectronics and microelectromechanical system (MEMS) technologies [4–7]. The most recent developments suggest that electrodeposition is an attractive fabrication process for many emerging fields of nanotechnology. These new applications make the future of electrodeposition research a seemingly interesting and quite exciting endeavor.

In this chapter we will review the most important electrodeposition processes used for fabrication of magnetic recording heads and in microelectronics technology. The most important parameters, criteria, and phenomena controlling the deposit morphology and properties are highlighted and discussed using the examples from the authors' own work and from the work of other prominent groups around the world.

27.1 MAGNETIC RECORDING

Nowadays electrodeposition is used for the fabrication of many important parts of magnetic recording heads, including magnetic shields and poles, Cu coils, and for connecting Cu studs, leads and pads, Au interconnects, and nonmagnetic gaps and coatings. Some of these electrodeposition processes and bath chemistries were adopted from other technologies as a common practice. However, the fabrication of the writing pole in magnetic recording heads has been the most important manufacturing step where electrodeposition has gained its fame as a cost-effective, reliable, and high-throughput operation (Fig. 27.1*a*). Over the years, the development of magnetic reader technologies, recording medias and the geometry of the magnetic recording process have posed many challenges that electrodeposition had to meet in order to stay competitive with other deposition methods. The common requirement for the alloys for magnetic pole fabrication is that they have low coercivity (softness), low magnetostriction ($\lambda \approx 0$), and relatively high magnetic moment. The electrodeposition process of these alloys has to be scalable with high-throughput manufacturing with minimum effort in process control and reproducibility. The bath chemistry has to be stable over the time and compatible with other materials and processes used in through-mask fabrication.

In the very beginning, the electrodeposited magnetic alloy for magnetic pole application was $Ni_{81}Fe_{19}$—Permalloy (inductive read heads)—with saturation magnetic flux density $B_s = 1$ T [8] (Fig. 27.2). The further development of electrodeposited soft magnetic alloys went by introduction of $Ni_{45}Fe_{55}$ with 70% higher B_s values [9] (magnetoresistive read heads) and ternary CoFeNi alloys with Co content larger than Ni and Fe and B_s ranging between 1.6 and 2.2 T [10–12] [giant magnetoresistive (GMR) read heads]. However, the recent introduction of the perpendicular magnetic recording

Modern Electroplating, Fifth Edition Edited by Mordechay Schlesinger and Milan Paunovic

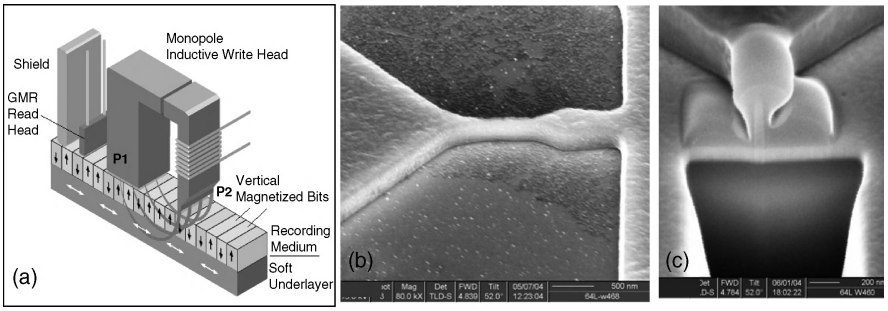

FIGURE 27.1 (*a*) Schematic of perpendicular magnetic recording head with most important parts indicated; (*b*) 2.4-T CoFe magnetic pole test structure; (c) focused on beam (FIB) cross section of ≈50-nm-wide 2.4-T CoFe magnetic pole test structure. Image (*a*) reprinted with permission from *Computer Desktop Encyclopedia* © 2006 The Computer Language Company, Inc.

geometry [13] and magnetic media with significantly larger anisotropy and coercivities requires soft magnetic alloys with the highest magnetic moment possible. Answering this challenge, academic and industrial researchers have demonstrated electrodeposited soft 2.4-T CoFe films and nanostructures with composition $Co_{30–50}Fe_{70–50}$ [14] (Fig. 27.2).

The ever-continuing drive to increase the areal density of magnetic recording inevitably brought the lithography and other processes involved in the fabrication of magnetic heads to the level of nanoscience [15, 16]. Electrodeposition, in that sense, is facing the task of delivering a controlled process and properties of soft, high-magnetic-moment alloys into photoresist features with high aspect ratio and sub-100-nm dimensions (pole width) (Fig. 27.1*b*). For future devices with >500 Gbits in.$^{-2}$ recording density it is expected that pole width will scale down to ∼40 nm in order to meet the magnetic head design requirements (Fig. 27.1*c*). At this scale, the successful electrodeposition process has to be designed by fully considering all transport limitations through the diffusion layer, the electrochemical interface stability with respect to $Fe(OH)_3$ precipitation, and the optimum conditions for additive adsorption. These criteria require that the phenomena determining the properties of soft magnetic alloys, for example, additive and $Fe(OH)_3$ incorporation, crystal structure, and effects of substrate or size effects, are examined in more detail in order to define the

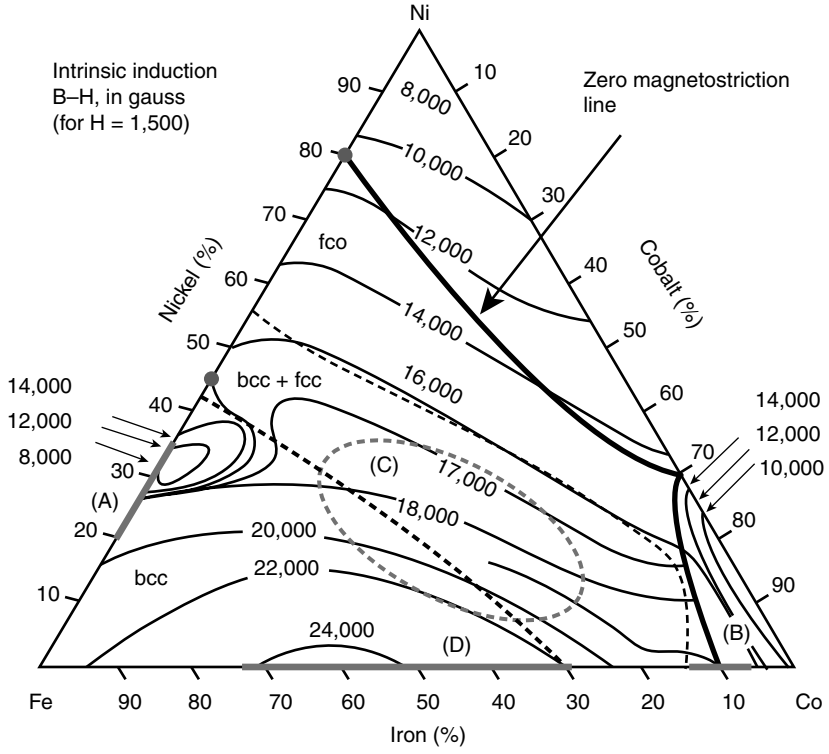

FIGURE 27.2 Ternary CoNiFe diagram indicating composition range of alloys with different saturation magnetic flux density, crystal structure, and zero magnetostriction. Reprinted with permission af Alcatel-Lucent USA Inc. [17].

parameters of the electrodeposition process for magnetic alloys and nanostructures with optimum properties and performance.

27.1.1 General Approach to Bath Design

The electrodeposited soft magnetic alloys used in magnetic recording technology represent binary NiFe and CoFe and ternary CoNiFe alloys with different atomic percentages of constituent metals. The atomic percentage of Co, Ni, and Fe in the alloy is defined by their application in the magnetic recording head. Today's magnetic head designs use electrodeposited Permalloy for magnetic shields and flux guides in read heads, while the 1.8–2.2-T CoNiFe and 2.4 T CoFe alloys are used for fabrication of write-pole structures. When designing the plating bath, one should start with consideration of the properties that the electrodeposited alloy is required to have. These properties are strong functions of the alloy composition. A commonly used diagram for this purpose for ternary CoNiFe system is presented in Figure 27.2 [2, 17]. The domains of different alloy composition with corresponding saturation magnetic flux density B_s are indicated together with the crystal structure and the $\lambda = 0$ dividing line. The common rule for bath design is that if the electrodeposited alloy is rich in one component, such as Ni in Permalloy, then the corresponding plating solution has to have the highest concentration of this ion (Ni^{2+}). However, the ratios between the metals in the alloy and their ion concentrations in solution are never the same, which makes the design of the effective bath chemistry for soft magnetic alloys a formidable task.

The steps in the electrodeposition of Co and Ni metals are presented below [18, 19], (M = Co, Ni):

$$\text{Step 1a:} \quad M^{2+} + H_2O \rightarrow M(OH)^{+}_{ads} + H^{+} \tag{27.1}$$

$$\text{Step 1b:} \quad M(OH)^{+}_{ads} + 2e^{-} \rightarrow M^{0}_{dep} + (OH)^{-} \tag{27.2}$$

$$\text{Step 2:} \quad M^{2+} + 2e^{-} \rightarrow M_{dep} \tag{27.3}$$

The deposition of Fe occurs through a slightly different reaction pathway [20]:

$$\text{Step 1:} \quad Fe^{2+} + H_2O \rightarrow Fe(OH)^{+} + H^{+} \tag{27.4}$$

$$\text{Step 2:} \quad Fe(OH)^{+} + e^{-} \leftrightarrow Fe(OH)_{ads} \tag{27.5}$$

$$\text{Step 3:} \quad Fe(OH)_{ads} + H^{+} + e^{-} \rightarrow Fe_{dep} + H_2O \tag{27.6}$$

Because the reversible potentials of considered metals are more negative than the hydrogen reversible potential, hydrogen evolution occurs in parallel:

$$2H^{+} + 2e^{-} \rightarrow H_2, \tag{27.7}$$

which leads to current efficiency being less than 1 ($\gamma < 1$). If the pH of the plating bath is low (pH < 2.5), the dominant reaction pathway for Co and Ni deposition is described by step 2. If pH > 3, a significant part of the Co and Ni deposits form in steps 1a and 1b [18, 19]. The kinetics of steps 1a and 1b is considered to be slower than the direct deposition process in step 2, which means that at lower pH the faster kinetics of Co and Ni deposition should be expected. However, the lower pH leads to lower values of current efficiency and, experimentally, lower deposition rates of Ni and Co are observed. In the case of Fe deposition, formation of adsorbed Fe hydroxide on the metal surface is a slow process [step 2, Eq. 27.5], and it is considered to be the rate-determining step in Fe deposition [20]. The increase of the solution pH increases the kinetics of this step, which results in an overall increase of the deposition rate of Fe. At the same time the pH increase in the bath increases the current efficiency of the overall metal deposition process. These two effects of pH are observed by an overall increase in deposition rate of the soft magnetic alloys and simultaneous increase of the Fe atomic percent in the deposit. The important fact that has to be mentioned here is that the hydrogen evolution reaction leads to the depletion of H^{+} ions at the electrode–solution interface and, for this reason, local increase in pH occurs. For this reason, the effects of pH on Co, Ni, and Fe deposition have to be considered in relation to the pH value at the electrode– solution interface rather than as a function of pH in the bulk solution. In general, the composition of soft magnetic alloys and their properties are complex functions of many factors: deposition conditions (current density, deposition potential), bath design (current efficiency, pH, additives, and metal ions concentrations), and diffusion layer thickness (plating cell hydrodynamics). These factors are also correlated one to another and the independent adjustment of one or several of them produces changes in ion transport and deposition kinetics with significant impact on deposit composition and properties.

One of the most peculiar phenomena that influence the plating solution design for soft magnetic alloys is anomalous codepostion. It is generally described as preferential deposition of less noble metals in the alloy from solutions containing equal concentrations of the metal ions. In the case of soft magnetic alloys, the preferential deposition of Fe occurs at the expense of Ni, resulting in NiFe and CoNiFe alloys with Fe/Ni ratio much higher than the ratio of their corresponding concentrations in the solution. The common mathematical

TABLE 27.1 Deposition Kinetics Control for Soft High Magnetic Moment Alloys

		Deposition Kinetics Control		
Magnetic Alloy	Concentration Ratio	Ni	Fe	Co
1 T $Ni_{81}Fe_{19}$	$[Fe^{2+}]/[Ni^{2+}] \ll 1$	Activation	Diffusion	—
1.7 T $Ni_{45}Fe_{55}$	$[Fe^{2+}]/[Ni^{2+}] < 1$	Activation	Mixed	—
1.8 T CoNiFe	$[Fe^{2+}]/[Ni^{2+}] < 1$, $[Fe^{2+}]/[Co^{2+}] \ll 1$	Activation/mixed	Diffusion	Activation
2.4 T $Co_{40}Fe_{60}$	$[Fe^{2+}]/[Co^{2+}] \geq 1$	—	Activation	Activation/mixed

definition of this observation is presented as

$$\frac{\text{at \% Fe}}{\text{at \% Ni}} > \frac{[Fe^{2+}]}{[Ni^{2+}]} \tag{27.8}$$

The anomalous codepostion phenomenon has been investigated by many authors [21, 22], and the generally accepted model is based on competitive adsorption between the $Fe(OH)_{ads}$[step 2, Eq. (27.5)] and the $Ni(OH)^{+}_{ads}$ intermediates. The $Fe(OH)_{ads}$ species adsorb preferentially on the electrode surface, which results in a hindered deposition rate of Ni and thus changes the incorporation symmetry expected from the ratio of the ion concentrations in the solution. The solutions with lower pH show less pronounced anomalous codepostion effect. To achieve the desired composition of the soft magnetic alloys, the design shown in Table 27.1 is followed.

The important aspect in bath design is the type of anions used. The typical choice is SO_4^{2-}, $(SO_3NH_2)^{-}$, or Cl^{-}. The last two are known to yield higher deposition rates but also higher stress level in the deposit. The sources of anions in the plating baths are also different buffer systems [23] used to moderate pH fluctuations in the bulk and to some extent ensure stability of the electrochemical interface [24]. The commonly used ones are H_3BO_3, NH_4Cl, $(NH4)_2SO_4$, and CH_3COOH [2, 3, 9–11], but other more exotic buffers systems can be found as well. A useful test in choosing the anion–metal cation combination is based on linear sweep voltammetry measurements where the solutions with the same concentrations of metal ions and pH are compared having different anions. If the choice of a particular anion (e.g., Cl^{-} vs. SO_4^{2-}) yields significantly higher current densities for the same overpotentials, then this is usually a better choice. This fact should be a guideline in deciding which anions to use in the bath unless the morphology of the deposit, stress, or other properties are significantly compromised. The typical bath and process parameters for NiFe, CoNiFe, and CoFe alloys are shown in Table 27.2.

27.1.2 Paddle Cell

The most common plating cell design used for the electrodeposition of soft magnetic alloys in the magnetic recording industry is the paddle cell [25]. Initially introduced by IBM in the 1970s, this cell design has been accepted by virtually all magnetic disk manufacturers. Today, different variants of the original design are used by magnetic recording companies and produced by plating tool manufacturers [26]. The simple schematic of the paddle cell is shown in Figure 27.3*a*. The paddle cell represents the three-electrode cell where the anode and cathode are in parallel with a 1:1 ratio of the geometric areas at a distance of ~5–10 cm (Fig. 27.3*a*). In order o minimize the primary current distribution effect in the cell, a "thief" (auxiliary) electrode is positioned around the edge of the wafer as the integral part of the wafer holder (Figs. 27.3*a*, *b*). The uniformity control is established through the adjustment of the potential difference between

TABLE 27.2 Bath and Process Design for Soft High Magnetic Moment Alloys

Alloy	Moment (T)	pH	Bath: Basic	Bath: Metals	j (mA cm^{-2})
NiFe	1	2.7–3.0	20–25 g L^{-1} H_3BO_3 0.002–0.2 g L^{-1} SDS[a] 0.1–0.8 g L^{-1} saccharin	1.8–2 g L^{-1} $FeCl_2{\cdot}4H_2O$ 100–110 g L$^{-1}{\cdot}6H_2O$	4–5
CoNiFe	1.8–2.1	2.5–3.0	20–25 g L^{-1} H_3BO_3, 15–25 g L^{-1} NH_4Cl 0.002–0.2 g L^{-1} SDS 0.1–0.8 g L^{-1} Saccharin	2–5 g L^{-1} $FeCl_2{\cdot}4H_2O$ 30–40 g L^{-1} $NiCl_2{\cdot}6H_2O$ 20–40 g L^{-1} $CoCl_2{\cdot}6H_2O$	3–3.5
CoFe	2.3–2.45	2.0–2.3	20–25 g L^{-1} H_3BO_3, 15–20 g L^{-1} $(NH_4)_2SO_4$ 0.002–0.2 g L^{-1} SDS 0.1–2 g L^{-1} Saccharin	27–31 g L^{-1} $FeSO_4{\cdot}7H_2O$ 15–20 g L^{-1} $CoSO_4{\cdot}7H_2O$	3.5–4.5

[a]SDS = sodium dodecyl sulfate.

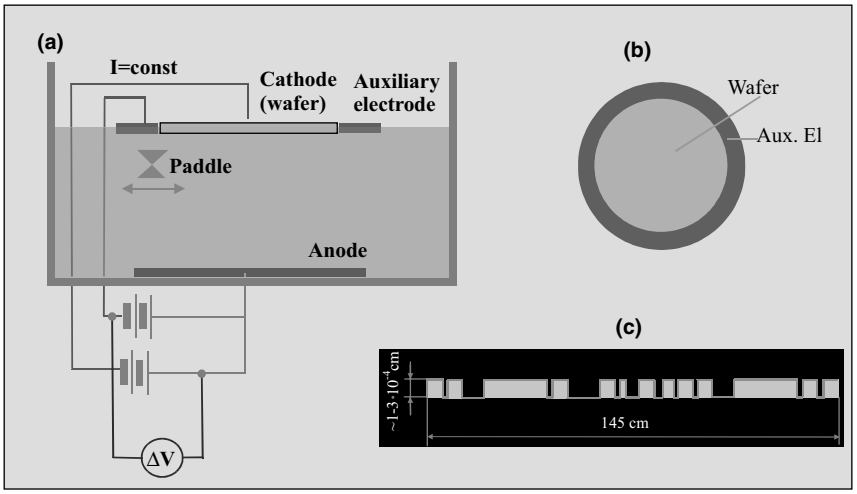

FIGURE 27.3 (*a*) Schematic of the paddle cell indicating most important parts. (*b*) Geometry of the thief auxiliary electrode. (*c*) Schematic illustrating feature size in through-mask deposition process.

the wafer and the thief electrode or by setting the level of the depositing current on the thief electrode as compared to the wafer. Other more complex models of the paddle cell include a porous layer inserted between the cathode and anode or an auxiliary electrode in the shape of a mash at some intermediate position between the wafer and the anode. If the main current path towards the metal seed is coming from the periphery of the wafer, the additional problem to maintain the uniformity and composition of the magnetic alloy occurs due to a phenomenon called "terminal effect." This phenomenon is typically expressed by lower thickness of the magnetic deposit in the center of the wafer than toward the edges, and it is more pronounced with plating seeds that have higher resistance (e.g., CoFe, CoNiFe, and Ru). The simple solution for the terminal effect problem is introduction of alternative current pathways through the grounding pads which connect the plating seed with the back of the wafer.

Agitation in the paddle cell is produced by translatory motion of the paddle, which represents the triangular rod (or two rods, Fig. 27.3*a*) with one side parallel to the surface of the wafer. The optimum distance of the paddle from the wafer surface is dependent on the overall paddle shape and speed. The important design parameter related to cell design and paddle speed is diffusion layer thickness δ. For the paddle cell described in this text, the standard procedure for its calculation is based on early work by Schwartz et al. [27]. The diffusion layer thickness can be calculated from the ratio

$$\delta = \frac{D_{\text{ion}}}{\langle k \rangle} \tag{27.9}$$

where $\langle k \rangle$ (in centimeters per second) is the average mass transfer coefficient and D_{ion} is the diffusion coefficient of the particular ion in the solution. Determination of $\langle k \rangle$ is a complex problem [26], but for practical situations encountered during the electrodeposition of magnetic alloys, a good approximation is given by the expression [27]

$$\langle k \rangle = \alpha D_{\text{ion}}^{1-\text{p}} L^{m-1} U^m \nu^{p-m}. \tag{27.10}$$

Here U is the linear velocity of the paddle (in centimeters per second) and L (in centimeters) is the characteristic mixing length defined as $L = H + h$, where H stands for the distance of the paddle surface from the wafer surface and h is the base-to-apex height of the paddle cross section (triangle). The ν is the kinematic viscosity of water ($0.01\ \text{cm}^2\ \text{s}^{-1}$). For typical frequencies of the paddle ($\omega < 0.7$ Hz) and $H/h < 1.2$, the constant α is ~0.22 [27], and the values of the constants p and m in the exponents could be taken approximately as 0.33 and 0.61 [27, 28]. The representative values of the ion diffusivities that could be used in these calculations are given in Table 27.3 [18, 29, 30].

27.1.3 Relation Between Surface Concentration of H^+ and Concentration of Fe^{3+}: Useful Criteria for Process Design and Control

Direct-Current Deposition The depletion of the hydrogen ions at the electrode–solution interface during electrodeposition of magnetic alloys leads to the local increase in pH. This effect promotes the formation of insoluble hydroxide species at the electrode–solution interface and promotes the incorporation of oxygen and nonmagnetic inclusions in Permalloy [31], CoNiFe [10] and CoFe alloys [2, 14]. The incorporation of metal hydroxides into deposit inevitably results in dilution of the saturation magnetic flux density of electrodeposited films. The most insoluble metal hydroxide when Co, Fe, and Ni are considered is $Fe(OH)_3$ ($K_{\text{p}} = 2.79 \times 10^{-39}\ \text{mol}^4\ \text{L}^{-4}$ [32]) and its incorporation in the deposit is the

TABLE 27.3 Ion Diffusion Constants

Ion	Fe^{3+}	Fe^{2+}	Ni^{2+}	Co^{2+}	H^+	OH^-
D ($cm^2\,s^{-1}$)	0.55×10^{-5}	2.56×10^{-5}	2.56×10^{-5}	2.56×10^{-5}	9.3×10^{-5}	5.5×10^{-5}

main obstacle for obtaining values of B_s equivalent to metallurgical alloys with the same composition. The presence of Fe^{3+} and $Fe(OH)_3$ in the plating solutions is mainly due to dissolved oxygen from air which oxidizes Fe^{2+} ions into Fe^{3+} ($O_2 + 4Fe^{2+} + 4H^+ \rightarrow 4Fe^{3+} + 2H_2O$). If the concentrations of Fe^{3+} and OH^- at the solution–electrode interface are such that the product of solubility for $Fe(OH)_3$ is exceeded hydroxide precipitation and incorporation into growing magnetic deposit occur [33]. The necessary condition for precipitation of the $Fe(OH)_3$ from the bulk solution for known OH^- concentration ($[OH^-]_\infty$) can be expressed in terms of bulk Fe^{3+} concentration ($[Fe^{3+}]_\infty$) as [3, 34]

$$[Fe^{3+}]^*_\infty = \frac{K_p}{10^{-42}} \times 10^{-3\cdot pH} \tag{27.11}$$

The net flux of hydrogen ions toward the electrode surface through the diffusion layer during the galvanostatic deposition can be expressed as $J_{H+} = j(1-\gamma)/F$, where j (deposition current) and γ (current efficiency) are the parameters of the deposition process and F is Faraday's constant. The concentration of the hydrogen ions at the electrode–solution interface, $[H^+]_i$, can be estimated from the simple mass balance described by *Fick's first law of diffusion*:

$$[H^+]_i = \left(10^{-pH} - \frac{(1-\gamma)j}{F}\frac{\delta}{D_{H^+}}\right) \tag{27.12}$$

Using Eqs. (27.12) and (27.11), the concentration of Fe^{3+} at the electrode–solution interface, $[Fe^{3+}]^*_i$, for which hydroxide precipitation starts can be expressed as

$$[Fe^{3+}]^*_i = \frac{K_p}{10^{-42}}\left(10^{-pH} - \frac{(1-\gamma)j}{F}\frac{\delta}{D_{H^+}}\right)^3 \tag{27.13}$$

For illustration purposes, estimates of $[Fe^{3+}]^*_i$ and $[Fe^{3+}]^*_\infty$ for parameters and solution design for electrodeposition of 2.4-T CoFe alloys are presented in the table in Figure 27.4 [35].

In order to illustrate the effect of Fe^{3+} in plating solution on the properties of electrodeposited magnetic alloys, the B_s measurements of $Co_{40-44}Fe_{60-56}$ films for different Fe^{3+} concentrations in the plating bath are shown in Figure 27.4. The magnetic moment of $Co_{40-44}Fe_{60-56}$ films starts to decrease for Fe^{3+} concentration that is very close to the calculated value of $[Fe^{3+}]^*_i$. This indicates correlation between the decrease of B_s and necessary conditions for $Fe(OH)_3$ precipitation at the electrode–solution interface [35]. These data also show that the increase of $[Fe^{3+}]$ beyond the calculated value of $[Fe^{3+}]^*_i$ results in significant reduction of B_s (~40%). The bold line in Figure 27.4 represents the analytical model that describes the decrease in B_s of $Co_{40-44}Fe_{60-56}$ films as a function of $Fe(OH)_3$ incorporation [35].

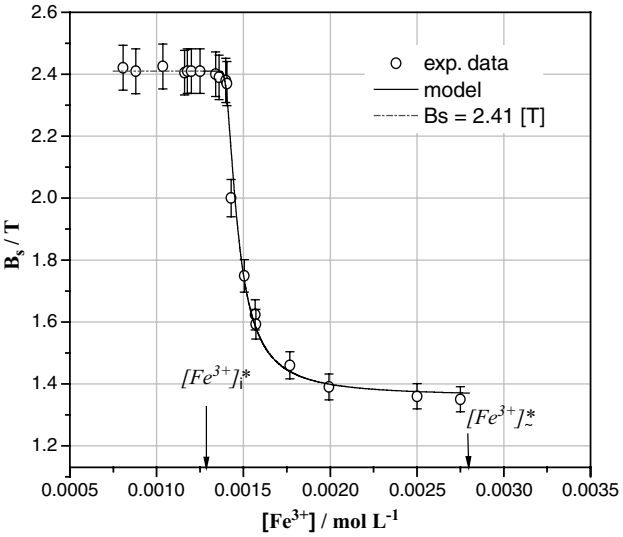

Solution and process parameters

Solution Components ($mol\cdot L^{-1}$)		Process Parameters	
$FeSO_4$	0.1	j	$3.8\ mA\cdot cm^{-2}$
$CoSO_4$	0.046	ω	300 rpm
$(NH_4)_2SO_4$	0.3	γ	~0.12
H_3BO_3	0.4	pH	2.0
T	298 K	D_{H+}/δ	$0.015\ cm\ s^{-1}$
$[Fe^{3+}]^*_i$ = $mol\cdot L^{-1}$	0.00128	$[Fe^{3+}]^*_\infty$ = $mol\cdot L^{-1}$	0.0028

FIGURE 27.4 B_s versus $[Fe^{3+}]$ dependence for electrodeposited CoFe alloys. Parameters of deposition process and solution design are given in Table 27.3. Reprinted from [35], Copyright 2008, with permission from Elsevier.

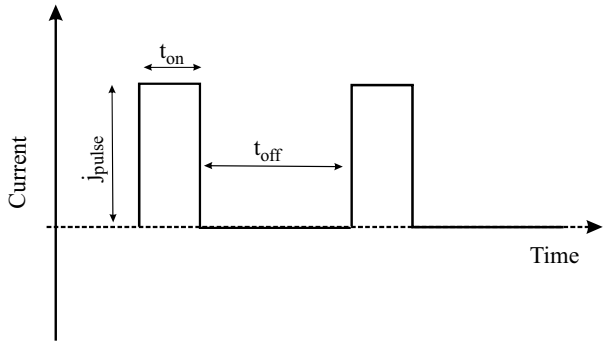

FIGURE 27.5 The pulse deposition function profile. The parameters t_{on}, t_{off}, and j_{pulse} are indicated in the figure. Reprinted from [3] with permission © 2006 IEEE.

Pulse Current Deposition The typical pulse current function that is employed in the electrodeposition process of soft magnetic alloys has the simple on–off profile shown in Figure 27.5 [3, 36]. Successful application of this pulse function is dependent on the proper determination of the pulse time t_{on}, rest time t_{off}, and magnitude of the pulse current density j_{pulse}. The useful approach to design the pulse current function is based on the criteria that ensure a stable electrode–solution interface with respect to $Fe(OH)_3$ precipitation.

The optimum duration of the pulse current stage should be such that no limitations for $[H^+]$ ion transport toward the electrode–electrolyte interface is encountered.

Mathematical treatment of H^+ diffusion through the *Nernst diffusion layer* during the galvanostatic pulse means solving Fick's second law of diffusion with appropriate initial and boundary conditions:

$$\frac{\partial[H^+]}{\partial t} = D_{H^+}\frac{\partial^2[H^+]}{\partial x^2} \tag{27.14}$$

The exact mathematical solution of Eq. (27.14) is somewhat cumbersome and is presented in the form of a *Fourier series expansion* [37]. For practical application, it is more convenient to consider approximate solutions that are dependent on the value of the term at, where a is defined as

$$a = \frac{\pi^2 D_{H^+}}{4\delta^2} \tag{27.15}$$

Evaluation of this term is dependent on an appropriate estimate of D_{H^+} and δ. For the typical paddle cell geometry and conditions met in manufacturing practice, the approximate solution of (27.14) ($a < 0.2$) can be represented as [37]

$$[H^+]_i = [H^+]_\infty - \frac{(1-\gamma)j_{pulse}\delta}{FD^{H^+}}\left[1 - \frac{8}{\pi^2}\exp\left(-\frac{\pi^2 \cdot D^{H^+}}{4\delta^2}t\right)\right] \tag{27.16}$$

The maximum duration of the pulse stage, τ, defined by formation of the conditions allowing the precipitation of Fe $(OH)_3$ at the interface is obtained by solving equation (27.16) explicitly for t. The τ defined as a function of $[Fe^{3+}]_\infty$ is then presented as [3]

$$\tau = -\frac{4\delta^2}{\pi^2 D_{H^+}} \ln\left[\frac{\pi^2}{8}\cdot\left(1 - \frac{FD_{H^+}\left[10^{-pH} - \sqrt[3]{(10^{-42}/K_p)[Fe^{3+}]_\infty}\right]}{(1-\gamma)j_{pulse}\delta}\right)\right] \tag{27.17}$$

The predictions of (27.17) are plotted in Figure 27.6*a* for different pH values of the solution and two different pulse current densities. As one can see, for a given pulse current density and sufficiently high concentration of H^+ (low pH) and low concentration of Fe^{3+} in the solution, the interfacial concentration of the H^+ ions will never reach the value required to form hydroxide precipitate, even for very long pulse times. However, this is rarely the case in practice since

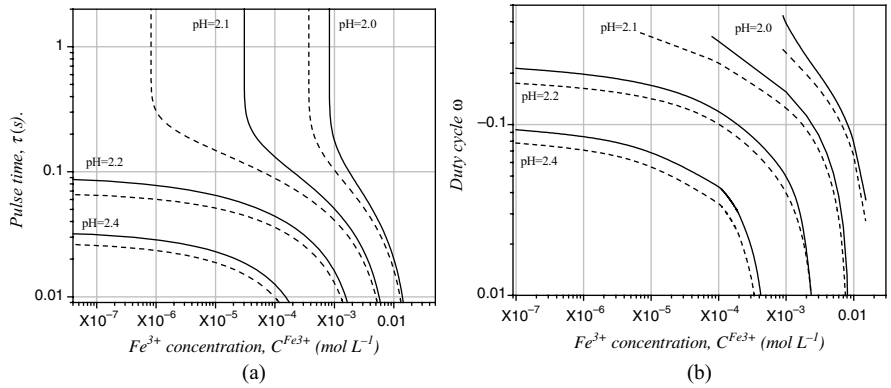

FIGURE 27.6 (*a*) Maximum duration of pulse stage τ, as a function of the Fe^{3+} concentration in solution. The dependence is presented for four different pH values of the solution and two pulse current densities, 20 mA • cm^{-2} (solid line) and 22 mA • cm^{-2} (dashed line). (*b*) Values of duty cycle ω [Eq. (27.20)] as a function of the Fe^{3+} concentration in the solution for different pH values and two pulse current densities, 20 mA • cm^{-2} (solid line) and 22 mA • cm^{-2} (dashed line). Reprinted from [3] with permission. © 2006 IEEE. The parameters used in calculation in (*a*) and (*b*) are summarized in Figure 27.4.

the aerated solutions with typical content of Fe^{2+} ions inevitably have significant presence of Fe^{3+} too. For the design of the pulse time interval t_{on}, the general rule should be to have the length of the pulse shorter than the maximum one estimated by Eq. (27.17):

$$t_{on} < \tau \tag{27.18}$$

From Figure 27.6*a* it is obvious that a small variation in pH of the solution can significantly affect the allowed duration of the pulse stage. An increase in the pH of the solution of ~5% (from 2 to 2.1) leads to a decrease of τ of more than 300%. Knowing that, in the real situation, a 5% variation in pH is considered a very possible scenario, one can anticipate the significant restriction on t_{on} as compared to the estimated value of τ. Another way of interpreting these calculations is to consider the variation of τ with an increasing pulse current density. For the same concentration of Fe^{3+} but an increase of 10% in $j_{pulse,}$ the value of τ decreases by ~40%. This is important when considering the geometrical and secondary current distribution effects on the through-mask electrodeposition process of nanoscale features [38].

The rest time of the pulse can be defined as the time necessary to recover the concentration of H^+ ions at the solution–electrode interface to some arbitrary fraction of the starting value prior to the current pulse. Assuming that the H^+ concentration is recovered to 99% of its bulk value, the rest time t_{off}, defined as a function of Fe^{3+} concentration and pH in the solution, can be written as [3]

$$t_{off} = \frac{\delta^2}{2D_{H^+}}\left[\ln\left(1 - \sqrt[3]{\frac{10^{-42}}{10^{-(3\cdot pH)}\cdot K_p}[Fe^{3+}]_\infty}\right) + 4.60\right] \tag{27.19}$$

The inspection of Eq. (27.19) indicates that for very low concentrations of Fe^{3+} in the solution, $[Fe^{3+}] \to 0$, t_{off} is almost constant, ~0.31 s. For values of Fe^{3+} closely approaching the solubility limit for a given pH of the solution, t_{off} rapidly decreases to very small impractical values.

A convenient way to discuss Eq. (27.19) in conjunction with Eq. (27.17) is by the *duty cycle* (ω), defined as

$$\omega = \frac{t_{on}}{t_{on} + t_{off}} < \frac{\tau}{\tau + t_{off}} \tag{27.20}$$

A plot of ω as a function of Fe^{3+} concentration for two different pulse current densities and different pH of solutions is shown in Figure 27.6*b*. The ω values are presented as an upper limit defined by the right side of Eq. (27.20). One can see that ω has a decreasing trend as the concentration of Fe^{3+} in the solution and pH increase. Assuming that the condition defined by (27.20) is fulfilled, the appropriate values of ω that should be used are smaller than the ones plotted in Figure 27.6*b*. The effect of the pulse current density on ω is also important, but the sensitivity of this estimate is not the same as observed for τ. This effect is particularly small as the Fe^{3+} concentration approaches the solubility limit, whereas for very low Fe^{3+} concentrations it is reflected as a ~20% increase of ω for ~10% higher j_{pulse}.

27.1.4 Additive Effect

To obtain magnetic alloys with lower coercivity, different additives have been used in the plating solutions [8–11, 14, 39]. The common action of additives is expressed through the leveling and brightening of the deposit, improvement of the crystal structure [40], smaller grain size [10, 11], and reduction of the residual stresses [41]. The last two effects are also important for obtaining ultimately soft magnetic alloys. The presence of additives in the plating solutions results in their incorporation into magnetic deposit [40, 42–45]. If the amount of the incorporated additives is small, it is generally considered as beneficial for the desired magnetic softness [11, 42]. However, the significant presence of sulfur, metal sulfides, or S-containing organic molecules and fragments in the deposit can cause a detrimental effect on magnetic alloy corrosion resistance [46, 47]. Poor alloy corrosion resistance can lead to disintegration and loss of electrodeposited magnetic nanostructures in a much shorter time than what is expected for the bulk alloys and, for these reasons, the benefits and disadvantages of additives for properties of magnetic alloys have to be considered with great attention.

Saccharin Adsorption The most common additive used for electrodeposition of soft magnetic alloys is saccharin and its derivatives. Saccharin is a condensed organic molecule with benzyl and heterocyclic rings in its structure. During the electrodeposition process, saccharin adsorbs on the metal surface, forming a condensed phase (film) [42, 48]. The saccharin molecule has a very small dipole moment and is expected to adsorb on the metal surface in the PZC region (potential of zero charge). The density and the coverage of the adsorbed phase are dependent on the potential of the electrode surface and the concentration of saccharin in the plating solution [49]. Useful information about saccharin adsorption and coverage is deduced from impedance spectroscopy [49, 50]. Examples of these measurements are shown in Figure 27.7 for CoNiFe and CoFe surfaces [42]. The apparent maximum coverage of saccharin for both surfaces is around -1.3 V. This potential is slightly more negative than the PZC for individual Fe, Co, or Ni metals [50–52] and CoFeNi and CoFe alloys [42].

Saccharin as Source of Sulfur in Deposit Sulfur incorporation into magnetic deposit coming from the saccharin occurs via either the saccharin adsorption–electroreduction process or physical incorporation of the entire saccharin molecules [44, 45]. The first mechanism represents the chemical route responsible for incorporating S-containing

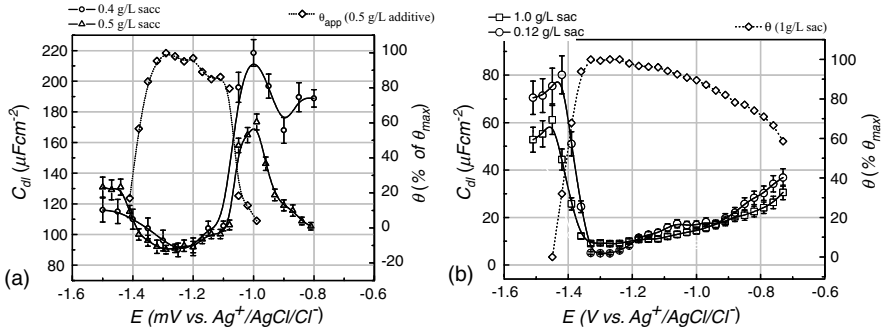

FIGURE 27.7 Double-layer capacitance versus potential dependence extracted from impedance measurements for (*a*) CoNiFe and (*b*) CoFe surface in solutions with different saccharin content. Background solution: 0.3 *M* NH_4Cl + 0.4 *M* H_3BO_3. pH in (*a*) is 2.8 and in (*b*) 2.1. Reproduced with permission from [42], Copyright 2005, The Electrochemical Society.

molecular fragments and metal sulfides in the deposit [42, 43, 53], while the second one represents the incorporation of entire molecules of saccharin having the sulfur atom as their integral part [44, 45]. In addition to these two additive-related mechanisms, the physical entrapment of sulfur-containing ions (SO_4^{2-}, SO_3^{2-}, etc.) is an additional source of sulfur in the magnetic deposit. The overall sulfur incorporation rate R_S (mol $cm^{-2}s^{-1}$) into magnetic alloys is described as the sum of the contributions coming from each of these mechanisms [45, 54, 55]:

$$R_S = R_0 + K_1\theta + K_2\theta(1-\theta) \qquad (27.21)$$

In the above expression, the first term, R_0 (mol $cm^{-2}\,s^{-1}$), represents the sulfur incorporation as part of trapped sulfates or other anions in the deposit [55], the $K_1\theta$ term (mol $cm^{-2}\,s^{-1}$) represents the sulfur incorporation via electroreduction of saccharin molecules (sulfur is a part of metal sulfides) [42, 53], and the last term, $K_2\theta(1-\theta)$ (mol $cm^{-2}\,s^{-1}$), represents the sulfur as part of the trapped saccharin molecules [54, 55]. The K_1 and K_2 terms are the saccharin electroreduction and incorporation rate constants (expressed in mol $cm^{-2}\,s^{-1}$) [45, 55]. The sulfur incorporation model is shown in Figure 27.8*a*, where the experimentally measured sulfur incorporation rate is presented as a function of saccharin coverage during the pulse deposition of 1.8-T CoNiFe alloys [42]. The fit of the data with the model [Eq. (27.21)] is shown with the dash-dot line. Where physical incorporation of saccharin molecules is the dominant source of sulfur ($K_2 \gg K_1$), the maximum incorporation rate of sulfur occurs for $\theta \approx 0.5$. Where electroreduction of saccharin and physical incorporation of saccharin molecules contribute equally to the sulfur incorporation ($K_2 \approx K_1$), the maximum incorporation rate of sulfur occurs for $\theta \approx 1$. Saccharin adsorption can be described in terms of *Langmuir formalism* [56] and sulfur incorporation rate can be presented in a more practical form as a function of its concentration in the solution, C_{sac}, [55]:

$$R_S = R_0 + K_1 \cdot \frac{bC_{sac}}{1+bC_{sac}} + K_2 \cdot \frac{bC_{sac}}{(1+bC_{sac})^2} \qquad (27.22)$$

where b is the saccharin adsorption constant. The example of sulfur incorporation rate in 2.4-T CoFe alloys as a function of saccharin concentration in the plating solution is shown in Figure 27.8*b*. The dash-dot line in the same figure represents the model fit [Eq. (27.22)] to the experimental data.

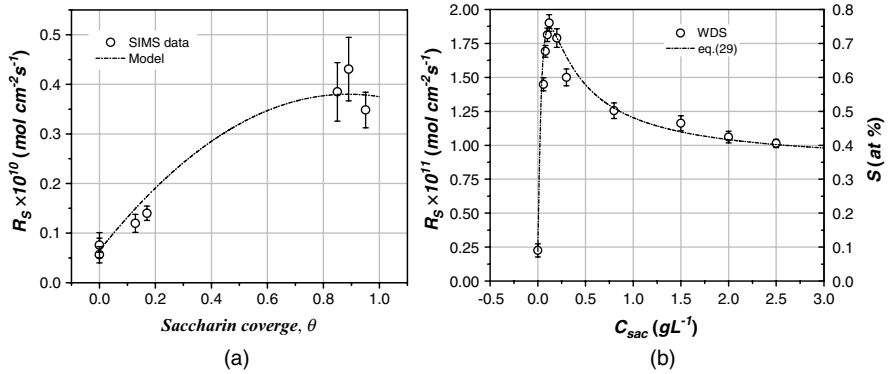

FIGURE 27.8 (*a*) R_S versus θ dependence for pulse current deposition of 1.8-T CoNiFe alloys. Data recalculated from Ref. [26]. (*b*) R_S versus C_{sac} dependence for direct-current deposition of 2.4-T CoFe alloys. On the right ordinate the corresponding at % of S in the deposit is indicated. Solution formulation and process parameters are as in Table 27.3. Reproduced with permission from [55], Copyright 2008, The Electrochemical Society.

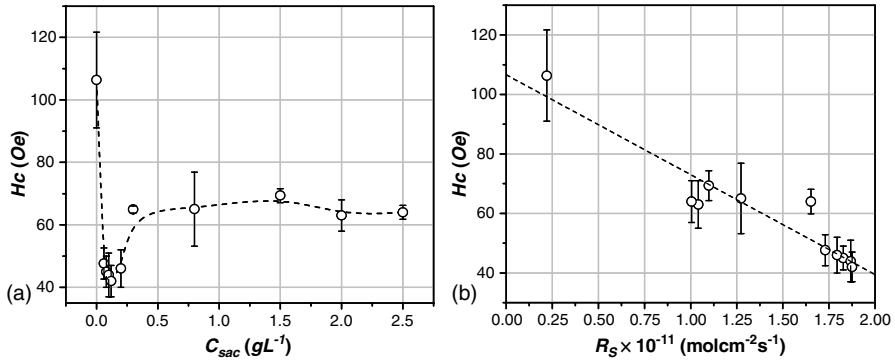

FIGURE 27.9 Coercivity versus (*a*) C_{sac} and (*b*) R_S for electrodeposited 2.4-T CoFe alloys. The substrate is polycrystalline Cu disks and the parameters of the electrodeposition process and solution dosing are presented in Figure 27.4. Reproduced with permission from [55], Copyright 2008, The Electrochemical Society.

From the model definition it is obvious that for $C_{sac} \ll (K_2 - K_1)/(K_1 b)$ sulfur incorporation into the magnetic deposit is mainly as a part of the saccharin molecule, while for $C_{sac} \gg (K_2 - K_1)/(K_1 b)$ the sulfur incorporates into deposit as a part of metal sulfides.

Coercivity versus C_{sac} and R_S One of the biggest challenges in the future development of electrodeposited soft high-magnetic-moment alloys is to further continue reducing their coercivity while simultaneously increasing their saturation magnetic flux density. These efforts inevitably will converge toward development of ultimately soft 2.4-T CoFe alloys as the most probable material for fabrication of future magnetic recording heads. The effect of saccharin concentration on the resulting coercivity of 2.4-T CoFe alloys is shown in Figure 27.9*a* [55]. This dependence is quite different than what has been reported previously for the CoNiFe and NiFe films [40, 57–59]. Rather than observing a monotone decrease of H_c (NiFe alloys [57, 59] and CoNiFe alloys [58]) or $H_c \approx$ const (CoNiFe alloy [40]) for an increasing C_{sac}, in the case of 2.4-T CoFe films, a more complex H_c-versus-C_{sac} dependence was observed. As expected, the largest values of coercivity are measured for CoFe films obtained from solution without saccharin. The small additions of this additive result in significant decreases of the deposit coercivity which has the lowest value for the CoFe films produced from solution containing 0.12-g L^{-1} of saccharin. Further increasing the saccharin concentration yields CoFe films with higher H_c values. For the CoFe films produced from solutions with $C_{sac} > 0.7$ g L^{-1}, an insignificant difference in H_c is observed ($H_c \approx$ const). This is similar to what has been reported for CoNiFe alloys for the saccharin concentration range $C_{sac} > 0.7$ g L^{-1} [40, 58]. A useful analysis of the results in Figure 27.9*a* is achieved when the H_c values are plotted as a function of the corresponding sulfur incorporation rates (Fig. 27.9*b*). From this analysis, it is obvious that higher incorporation rates of sulfur into magnetic deposit lead to alloys with lower H_c values. The important conclusion is deduced if the H_c data in Figure 27.9*a* are plotted as a function of the ratio between the sulfur incorporation rate that results from the physical incorporation of saccharin molecules,

$$R_M = K_2 \cdot \frac{bC_{sac}}{(1 + bC_{sac})^2}$$

and the sulfur incorporation rate from saccharin electroreduction,

$$R_{ER} = K_1 \cdot \frac{bC_{sac}}{1 + bC_{sac}}$$

See Figure 27.10. As one can see, as long as R_M represents the dominant contribution to the overall sulfur content in the 2.4-T CoFe alloys, $R_M/R_{ER} \gg 1$, the measured coercivity of the electrodeposited films has the lower values, between 40 and

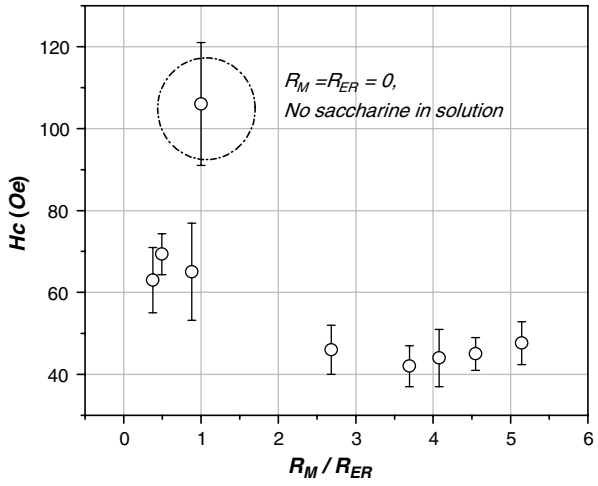

FIGURE 27.10 Coercivity versus R_M/R_{ER} ratio for electrodeposited 2.4-T CoFe alloys. Parameters of the electrodeposition process and solution design are presented in Figure 27.4. Reproduced with permission from [55], Copyright 2008, The Electrochemical Society.

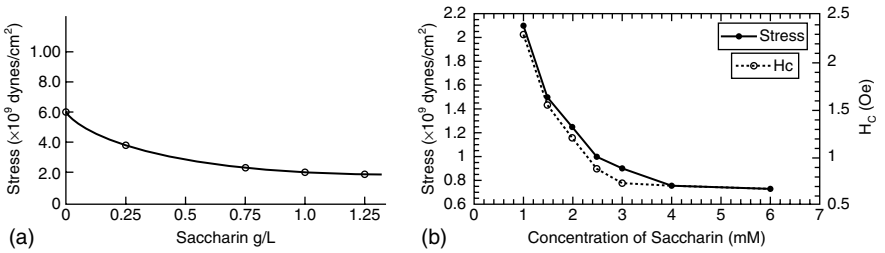

FIGURE 27.11 Residual stress as function of saccharin concentration in solution for (*a*) NiFe–Permalloy. Reproduced with permission from [59], Copyright 1970, The Electrochemical Society. (*b*) 1.8-T CoNiFe alloys. Reproduced with permission from [58], Copyright 2002, The Electrochemical Society.

50 Oe (Fig. 27.10). When R_{ER} is the predominant contribution to the sulfur content in the deposit, $R_M/R_{ER} \ll 1$, the measured coercivity of the 2.4-T CoFe films is significantly higher, above 60 Oe. The general conclusion that could be derived is that the most effective form of incorporated sulfur producing the softest 2.4-T CoFe alloys is sulfur as part of the saccharin molecule. The incorporated sulfur as part of the metal sulfides also contributes to the decrease in the CoFe alloy coercivity but less effectively. Therefore, the optimum design of the plating solutions for ultimately soft 2.4-T CoFe alloys should be such that the criterion $R_M \gg R_{ER}$ is always satisfied.

Stress versus C_{sac} The effect of stress in electrodeposited magnetic films has become very important as the critical size of magnetic recording devices and the magnetic head–media spacing in magnetic disk drives were reduced to several tens of nanometers. In general, the stress in electrodeposited soft magnetic films is dependent on many parameters. Very often, the sign of the stress in the magnetic films (compressive or tensile) is dependent on the final thickness of electrodeposited film, crystal structure, and substrate and film texture [60]. For most practical applications in magnetic recording technology the electrodeposited films of NiFe, CoNiFe, and CoFe express tensile stress which can significantly alter their magnetic properties. This is particularly important when CoFe alloys are considered since their effective magnetic anisotropy energy is a strong function of the magnetoelastic energy. One of the benefits that additives bring to the electrodeposition process of magnetic alloys is that they effectively reduce the residual stresses in the deposit and thus contribute to the overall better magnetic properties of the deposits (softness). The additives' effect is also important for postdeposition annealing of magnetic films where the final reduction of coercivity and stress of the magnetic films is achieved. An accurate description of the stress reduction process due to the additive presence in plating solutions is yet to be offered. The sulfur burring additives were found very effective as stress-relieving agents [2]. In metallurgical sense, the sulfur-related inclusions or intermetallic compounds are known to create distortion of the metal lattice and contribute to local disorder [61]. By precipitating to the grain boundaries during the deposition process as a low-surface-energy phase [62], they can act as effective intermediates and stress relievers during grain coalescence, producing the deposit with lower stress levels.

The effect of saccharin on stress in electrodeposited NiFe and CoNiFe films is shown in Figures 27.11*a*, *b*. It is the apparent similarity between these two alloy films with respect to their stress decrease with increasing concentration of saccharin in the plating solution. As discussed in the previous paragraph, sulfur incorporation into magnetic deposit via electroreduction of saccharin is the raising function of saccharin concentration which has asymptote equal to the electroreduction constant K_1. The data in Figure 27.11 suggest that stress reduction is also decreasing toward its asymptotic value for increasing saccharin content in the solution.

It could be hypothesized that stress in magnetic deposits is the inverse function of the sulfur incorporation via the electroreduction mechanism. In mathematical terms this dependence can be expressed as

$$\sigma \sim \frac{\xi}{K_1} + \frac{\xi}{K_1 b}\frac{1}{C_{sac}} \tag{27.23}$$

where ξ represents the proportionality constant while K_1 and b are as defined previously. The fit of the Eq. (27.23) to the data in Figure 27.11*b* is shown in Figure 27.12*a* [63]. The proposed σ-versus-C_{sac} dependence captures the essential features of the data presented in Figure 27.11*b* and can be used for other systems, such as NiFe (Fig. 27.11*a*), that show the same type of σ-versus-C_{sac} behavior. This analysis also suggests that electroreduction of saccharin as a route for sulfur incorporation is the most important phenomenon responsible for the stress reduction in electrodeposited NiFe and CoNiFe films. In the case of CoFe alloys (Fig. 27.12*b*), X-ray diffraction (XRD) data suggest a different σ-versus-C_{sac} trend [64]. Rather than decreasing with increasing concentration of saccharin in the plating solution, coherent strain (stress) in the electrodeposited films, deduced from body-centered-cubic (bcc) <110> 2θ peak position shift, decreases to a certain point, $C_{sac} \approx 0.3\ g\ L^{-1}$, and then starts to increase again. The correlation between the σ–C_{sac} behavior and sulfur incorporation mechanisms in CoFe alloys at this point is not straightforward and more work is necessary for an accurate description of this phenomenon.

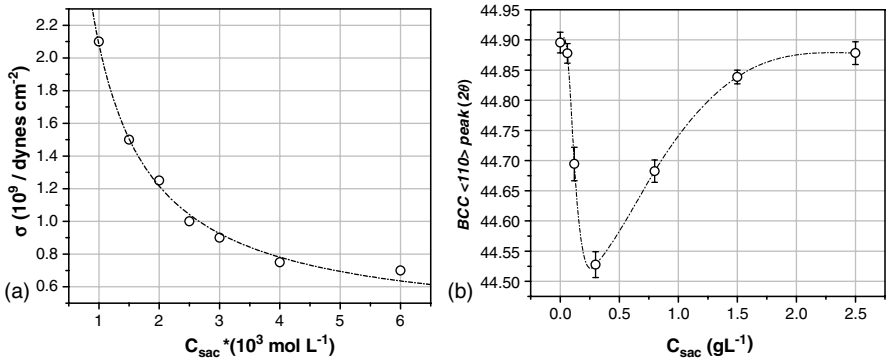

FIGURE 27.12 (*a*) Fit of Eq. (27.23) to data in Figure 27.11*b*; (*b*) bcc $\langle 110 \rangle$ 2θ peak position as function C_{sac} for electrodeposited 2.4-T CoFe alloys. Solution and process details are shown in Figure 27.4 [63].

Surface Roughness The use of additives in the electrodeposition of magnetic alloys was traditionally associated with the highly reflective appearance of the deposit surface, which gained the additives the name "brighteners." However, in magnetic recording technology, chemical mechanical polishing (CMP) is the process that directly succeeds magnetic alloy electrodeposition and the resulting smoothness of the surface of magnetic alloys is associated with the success of the CMP operation. The uncompromised need for ultimately high moment alloys like 2.4-T CoFe which are more prone to corrosion attack during the CMP process has resulted in some of the traditional processing routes involving CMP being revisited with potential advantage given to the electrodeposition of ultrasmooth surfaces and structures. Furthermore, the decrease in magnetic writing pole dimensions to sub-100-nm levels has raised expectations for the electrodeposition of magnetic nanostructures in terms of their surface quality and morphology control (Fig. 27.1). The effect of saccharin as an additive on the resulting surface roughness of electrodeposited 2.4-T CoFe alloys is illustrated in Figure 27.13*a*. The surface roughness evolution (w) is measured over the increasing length scale for 1.0-μm-thick CoFe films electrodeposited from solutions containing 0.12, 1, and 2 g L^{-1} of saccharin. The observed saturation roughness for these samples follows the $w_{\text{sat}}(0.12\,\text{g L}^{-1}) < w_{\text{sat}}\,(1\,\text{g L}^{-1}) < w_{\text{sat}}\,(2\,\text{g L}^{-1})$ trend, which is opposite from the one observed for NiFe and CoNiFe alloys [57]. The more meaning of this data is transparent if ones consider the results in Figure 27.8*b* which show that the sulfur incorporation rate follows $R_{\text{S}}\,(0.12\,\text{g L}^{-1}) > R_{\text{S}}\,(1\,\text{g L}^{-1}) > R_{\text{S}}\,(2\,\text{g L}^{-1})$ trend. In deed, the correlation between w_{sat} and R_{S} shows decreasing logarithmic dependence (see the inset in Fig. 27.13*a*). If magnetic CoFe nanostructures are considered with just ~50 nm in critical dimensions, this effect could be quite significant. For illustration purposes the surface finish between two 2.4-T CoFe top pole structures produced form solutions with different saccharine content is shown in Figures 27.13*b*, *c* [63].

The benefit that additives offer in the electrodeposition process is fully realized only if the electrode surface is in the potential range where maximum additive coverage occurs. This effect has already been demonstrated during the design of the effective pulse function (pulse current density) for the electrodeposition of 1.8-T CoNiFe [42] and 2.4-T CoFe alloys [3]. The surface coverage of the saccharin-adsorbed phase is a maximum in the potential range $E \approx -1.3$ V versus $\text{Ag}^{+}/\text{AgCl/Cl}^{-}$ (Fig. 27.7) and the optimum pulse current density used in the deposition process is the one where the electrode surface rests at the same potential during the pulse stage. To illustrate this, Figures 27.14*a–d* show the surface

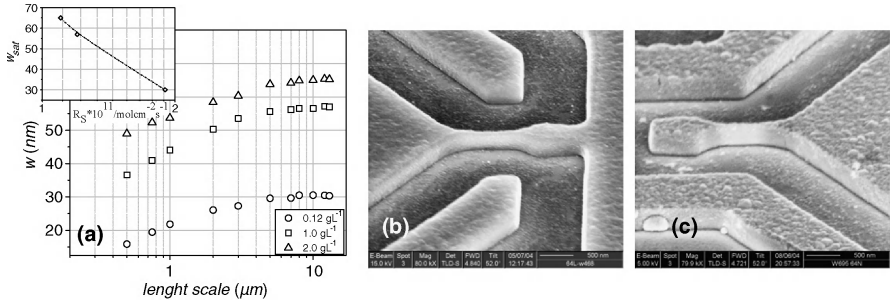

FIGURE 27.13 (*a*) 2.4-T CoFe alloy surface roughness as function of length scale for different concentrations of saccharin. Reproduced with permission from [45], Copyright 2007, The Electrochemical Society. (*b*) 2.4-T CoFe magnetic pole test structure obtained from solution containing 0.12 g L^{-1} and (*c*) 2 g L^{-1} of saccharin. Inset in (*a*) shows the saturation roughness dependence on sulfur incorporation rate. The details of the solution and electrodeposition process are given in Figure 27.4.

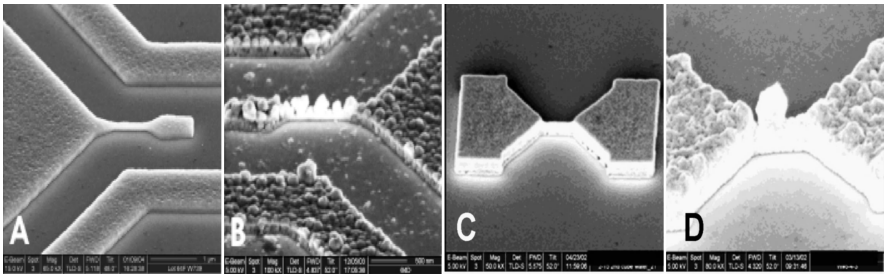

FIGURE 27.14 (*a*, *b*) Morphology of 2.4-T CoFe. Reproduced with permission from [3], © 2006 IEEE. (*c*, *d*) 1.8-T CoNiFe magnetic pole nanostructures. Reproduced with permission from [42], Copyright 2005, The Electrochemical Society.

morphology of the $Co_{37}Fe_{63}$ and CoNiFe magnetic pole test structures electrodeposited with different pulse current densities corresponding to different potentials of the electrode surface [3, 42]. The estimated saccharin coverage of the CoFe surface during the pulse stage in image (*a*) is ∼95 % ($E \approx -1.24$ V) and in image (*b*) is ∼35% ($E \approx -1.37$ V; see Fig. 27.7*b*). In image (*c*) the apparent saccharin coverage of the CoNiFe surface is ≈100% ($E \approx -1.3$ V) while in image *D* is ≈ 0 % (Fig. 27.7*a*). The saccharin concentration is the same for all images, $C_{sac} = 0.25\,g\,L^{-1}$. The surface morphology in these images differs significantly, indicating the importance of the additive coverage during the pulse stage for obtaining the optimum morphology of the magnetic pole nanostructure.

Corrosion Properties Versus R_S Sulfur incorporation represents a great problem when corrosion properties of electrodeposited alloys are evaluated [46, 47, 65, 66]. The electrodeposited alloys have corrosion potentials of several hundred milivolts more negative than the alloys produced by physical deposition with the same composition [46, 54]. This indicates significantly higher corrosion susceptibility, which is particularly pronounced when 2.4-T CoFe alloys are considered. Unlike NiFe and CoNiFe alloys, the lack of Ni in 2.4-T CoFe alloy precludes formation of stable passive film, which results in very poor corrosion resistance when compared with other soft magnetic alloys. However, the 2.4-T CoFe alloys are the most probable materials that will be used in future magnetic recording heads and their poor corrosion resistance could be an obstacle for their application.

The effect of sulfur incorporation on the corrosion properties of 2.4-T CoFe alloys is shown in Figure 27.15*a* using electrodeposited films from solutions without saccharin and from solutions containing 0.12 and 2 g L^{-1} of this additive. The noblest CoFe surface with the most positive corrosion potential, $E_c \approx -0.17$ V, is the one electrodeposited without saccharin in the solution (0.09 at % S, Fig. 27.8*b*). The surface of the CoFe sample electrodeposed from solution containing 0.12 g L^{-1} of saccharin (0.78 at % S, Fig. 27.8*b*) has the most negative corrosion potential, $E_c \approx -0.6$ V. The sample electrodeposited from the solution containing 2 g L^{-1} of saccharin (0.43 at % S, Fig. 27.8*b*) has the corrosion potential $E_c \approx -0.35$ V. The incorporation rate of sulfur and corresponding S content in the CoFe matrix for the 0.12-g L^{-1} sample is ≈2 times larger than for the 2-g L^{-1} sample and ≈8 times larger than for the 0-g L^{-1} sample, which is directly reflected in the corrosion potential of this sample indicating the poorest corrosion resistance [67]. The inset in Figure 27.15*a* shows the dependence of the 2.4-T CoFe alloy corrosion potential on the sulfur incorporation rate.

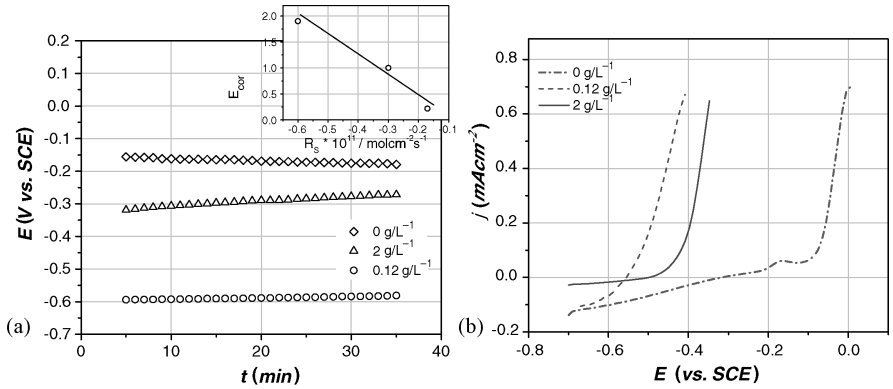

FIGURE 27.15 (*a*) Corrosion potential transients and (*b*) linear sweep voltammetry for 2.4-T CoFe alloys produced from solutions having different contents of saccharin. The inset in (*a*) shows the corrosion potential dependence on sulfur incorporation rate. The test solution is 0.5 *M* NaCl. The details of the deposition process for 2.4-T CoFe are presented in Figure 27.4. Reproduced with permission from [55], Copyright 2008, The Electrochemical Society.

The anodic linear sweep voltammetry measurements (Fig. 27.15*b*), reveal the same trend in the electrooxidation potentials of these samples.

The corrosion measurements unambiguously indicate that the samples with higher contents of sulfur and larger sulfur incorporation rates are also the ones that will corrode faster. However, the larger incorporation rates of sulfur lead to softer 2.4-T CoFe alloys (Fig. 27.9*b*). It is obvious that design of the saccharin content in the plating solution has to be done in such a way that both effects are taken into account. It is useful to evaluate the overall contribution of saccharin on both corrosion properties and coercivity of magnetic alloys through some meaningful criterion. For this purpose, using the example of CoFe alloys, the dimensionless ratio based on the achieved decrease in coercivity of the CoFe alloys with addition of saccharin in the solution and the corresponding relative increase in CoFe alloy corrosion rate is defined as [55, 68]

$$\Re = \frac{H_{c,0}}{H_c(C_{sac})}\frac{j_0}{j(C_{sac})} \tag{27.24}$$

where $H_{c,0,}$ and $H_c(C_{sac})$ stand for the coercivities of the CoFe (magnetic) films electrodeposited from solution without and with saccharin, while j_0 and $j(C_{sac})$ represent the corrosion currents (rates) of the CoFe (magnetic) films electrodeposited from solutions without and with saccharin.

The ratio $H_{c,0}/H_c(C_{sac})$ has to be obtained from magnetic measurements. Evidently, the addition of saccharin in the solution results in softer CoFe alloys and consequently the value of $H_{c,0}/H_c(C_{sac})$ is always >1. For the 2- and 0.12-g L^{-1} CoFe samples, for example, these values are 1.7 and 2.5 (Fig. 27.9*a*). The $j_0/j(C_{sac})$ ratio can be calculated using the measured corrosion potentials and taking the oxygen reduction on the CoFe (magnetic alloys) surface as the representative reduction reaction ($\alpha = 0.5$ for pH 7) [69]. For the 2- and 0.12-g L^{-1} samples the calculated current ratios are 0.08 and 0.0003. The $\Re$ values are calculated to be 0.14 (2 g L^{-1}) and 0.00075 (0.12 g L^{-1}). The values of $\Re$ being $\ll 1$ for both samples indicates that the gain achieved by decrease in coercivity of the CoFe alloys is much smaller than the corresponding increase in their corrosion rates. In the case of saccharin as an additive, $\Re$ values <1 are always observed for soft CoFe alloys. From this analysis, it is evident that the $C_{sac} = 2$ g L^{-1} solution yields CoFe films with $\Re$ value that is closer to 1 than the $C_{sac} = 0.12$ g L^{-1} solution and thus the 2 g L^{-1} saccharin concentration represents the better choice when the overall optimum in corrosion rate and magnetic softness of 2.4 T CoFe films are considered.

The poor corrosion resistance of electrodeposited soft 2.4-T CoFe alloy seriously compromises their benefit of having high magnetic moment and desirable magnetic softness. The straightforward way to improve this situation is to add a small amount of a noble metal into the alloy [3, 70, 71]. The physical concept behind adding the noble metal into the alloy is to increase the absolute value of the work function and to slightly modify the electronic structure of the alloy. As a consequence, the increase of the energy barrier for the charge transfer during the electrochemical oxidation of the metal surface is expected, yielding the lower corrosion rates. The noble metals from the Pt group would be the natural choice for alloying with 2.4-T CoFe. However, the addition of a nonmagnetic noble metal into the ferromagnetic matrix would also reduce the value of B_s. Based on the electronic structure and atomic magnetic moments calculations, the Pd and Rh were found to be the most effective choices for alloying elements [63].

As an illustration of this approach, in Figures 27.16*a*, *b*, the magnetic hysteresis loop for easy axis of pulse electrodeposited 2.4-T $Co_{37}Fe_{63}$ and 2.4-T $Co_{38}Fe_{61}Pd_1$ alloys is presented together with the corresponding corrosion potential transients for both alloys. The measured B_s values for both alloys are in the range of 2.41–2.43 T, and the only difference that could be noticed in the magnetic measurements is the slight increase of the coercivity for the $Co_{38}Fe_{61}Pd_1$ as compared to $Co_{37}Fe_{63}$ alloy (18 Oe vs. 17 Oe). The shift of corrosion potential in the anodic direction of approximately 0.15 V (Fig. 27.15*b*) is a good indication of the benefit of Pd presence in $Co_{38}Fe_{61}Pd_1$ and an increased nobility of this alloy as compared to $Co_{37}Fe_{63}$ alloy. From

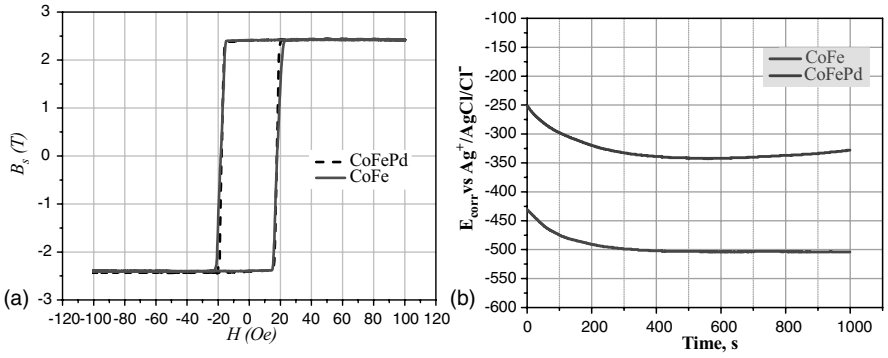

FIGURE 27.16 (*a*) *B–H* loop data for $Co_{38}Fe_{61}Pd_1$ and 2.4 T $Co_{37}Fe_{63}$ alloys. (*b*) Corrosion potential transients for $Co_{38}Fe_{61}Pd_1$ and 2.4-T $Co_{37}Fe_{63}$ alloys. Test solution is 0.5 *M* NaCl. Reprinted from [3] with permission, © 2006 IEEE.

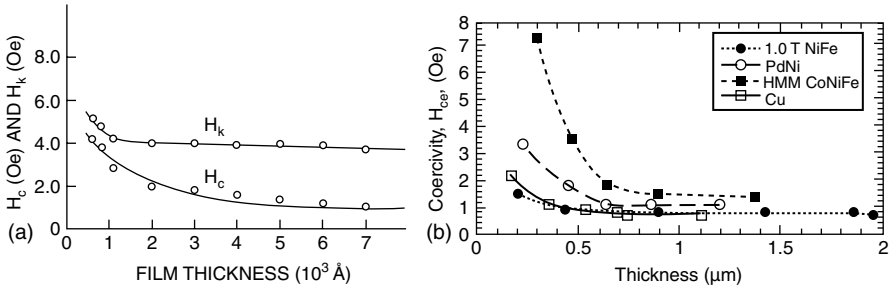

FIGURE 27.17 (*a*) H_c and H_k as function of NiFe (Permalloy) film thickness. The substrate is Au film deposited on Cr. Reproduced with permission from [59], Copyright 1970, The Electrochemical Society. (*b*) H_c as a function of 1.8-T CoNiFe film thickness deposited on different substrates. Reproduced with permission from [58], Copyright 2002, The Electrochemical Society.

these data the criterion $\Re$ can be evaluated as 12.5. The $\Re$ being $\gg 1$ strongly indicates the significantly improved overall properties of 2.4-T CoFe alloys with just ≈ 1 at % of Pd addition.

27.1.5 Substrate and Deposit Thickness Effects

There is a considerable amount of work done studying the effect of substrate and magnetic film thickness on the properties of electrodeposited NiFe and CoNiFe alloys [58, 59, 72–74]. For most practical applications the thickness range of the soft magnetic alloys is such that the coercivity shows a monotone decreases with increasing thickness of the magnetic films. This dependence can be described well within the theoretical framework developed by Neel [75],

$$H_C = At^n \tag{27.25}$$

where A is a constant and n is the exponent which has, in the original derivation, a constant value of -1.33. Although the proposed functionality has been found generally correct, in most practical studies of electrodeposited magnetic films, the value of the n exponent has been found to be very dependent on deposition conditions, magnetic film composition, and substrate. The data in the literature suggest that n could have much broader values ranging from -1.5 to -0.3 [58, 59, 72, 74]. In Figures 27.17*a*, *b* the H_c-versus-t dependence is illustrated for NiFe and CoNiFe alloys deposited on different substrates. For NiFe substrate, $n = -0.4$; for textured Cu(111), $n = -0.72$; and for PdNi substrate, $n = -1.3$ [58].

When 2.4-T CoFe alloys are considered, the same functionality described by Eq. (27.25) can be used to interpret the H_c-versus-t experimental data (Fig. 27.18*b*). However, due to the fact that electrodeposited 2.4-T CoFe alloys have bcc structure and thus significantly larger magnetic anisotropy, the effect of substrate on the resulting H_c-versus-t dependence is more pronounced.

In particular, the epitaxial misfit and the substrate texture become very important for resulting coercivity of electrodeposited 2.4-T CoFe films. The data illustrating this are shown in Figure 27.18*a* where the rocking curves around the face-centered-cubic (fcc) $\langle 111 \rangle$ direction (NiFe and Cu) or the hexagonal close-packed (hcp) $\langle 0001 \rangle$ direction (Ru) are presented. The highest degree of texture is observed for NiFe substrate (Permalloy seed) and then for Ru and Cu seeds, respectively. The lowest coercivities and corresponding highest exponent n are also observed for CoFe alloys deposited on NiFe substrate. A good texture of the starting substrate means that it is easier to achieve the parallel arrangement of the growing CoFe grains, and thus less residual stress in the deposit is developed during the CoFe growth. The rocking curves around the bcc $\langle 110 \rangle$ direction for CoFe alloys do confirm the best texture of the CoFe films

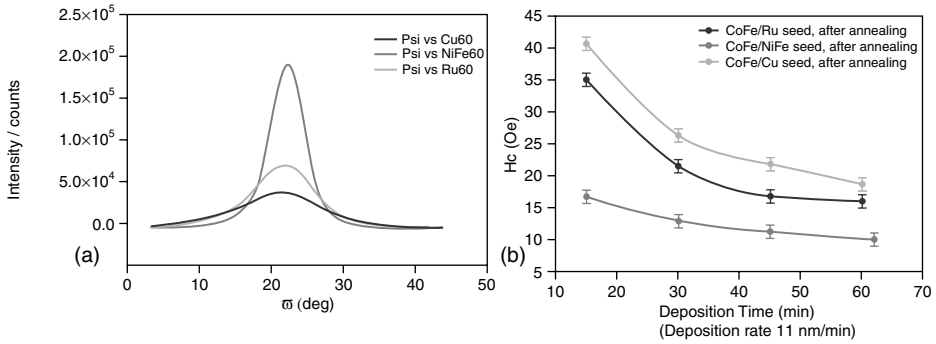

FIGURE 27.18 (*a*) Rocking curves for 60-nm-thick and highly textured Cu(111) (dark gray), NiFe(111) (gray) and Ru(0001) (light gray) seeds. (*b*) Coercivity of electrodeposited 2.4-T CoFe films on 60-nm Ru (gray), Cu (gray), and NiFe (light gray) seeds as function of CoFe film thickness.

deposited on NiFe seed. The good CoFe texture means less intrinsic stress in the deposit, which lowers the contribution of the magnetoelastic energy to the overall anisotropy energy of the CoFe films. The additional effect that contributes to the observed softness of the CoFe films on NiFe seed is magnetostatic coupling with preexisting magnetic domains in the soft magnetic seed, which could lower the propagation energy of domain walls in the CoFe films.

The good texture of Ru substrate as compared to Cu does not yield CoFe films with lower coercivity. In fact, the CoFe films deposited on Cu seed do show lower coercivity and higher values of exponent n than the ones deposited on Ru seeds. The explanation for this observation is related to epitaxial misfit between CoFe and Cu and Ru and NiFe seeds. The misfit between CoFe and NiFe is $\approx -1.2\%$, between CoFe and Cu is $\approx -3.7\%$, and between CoFe and Ru is $\approx -10\%$. The benefit of the good texture of Ru seed is overshadowed by significantly larger misfit with CoFe lattice, which results in large epitaxial strain and stress in CoFe grains and thus increased overall magnetic anisotropy of CoFe films deposited on Ru seed. The effect of epitaxial misfit is found to be dominant in the H_c-versus-t^n behavior for the CoFe films with thicknesses below 0.5 μm.

27.1.6 Nanoscale Electrode Geometry

The characterization of magnetic properties for electrodeposited alloys comprising the magnetic pole nanostructures is not possible using conventional characterization equipment and experimental techniques. However, a certain type of extrapolation is possible if the crystal structure of the magnetic material in nanostructures is known. The example of this approach is demonstrated in the following. In Figure 27.19 comparative transmission electron microscopy (TEM) images of the 2.4-T $Co_{38}Fe_{62}$ alloy thin film (*a*) and 2.4-T $Co_{38}Fe_{62}$ alloy nanostructure (*b*) are shown. Both samples are produced by pulse current electrodeposition on Ru seed. The XRD data and composition of these samples indicate a bcc crystal structure with predominant ⟨110⟩ fiber texture. The grain shape in the thin-film configuration was developed as a columnar structure with lateral dimensions of approximately 10–20 nm descending from the initial Ru seed (Fig. 27.19*a*). In the diffraction pattern of this sample all (110) diffraction peaks of the bcc ⟨110⟩ fiber texture are present indicating full freedom of the in-plane grain rotation. For this sample (thin film), characterization of the magnetic properties shows $B_s = 2.43$ T and coercivity value measured along the easy axis of ∼4 Oe. The sample representative of the magnetic pole geometry represents a several-micrometer-long strip with ∼50 nm critical dimensions. The TEM image in Figure 27.19*b* shows that the grain shape and the lateral grain size are significantly different from the thin-film sample (Fig. 27.19*a*). Starting from the Ru seed, the grain size gradually increases, which contributes to the overall hybrid type of grain structure. The 90° diffraction peak is missing, which is, in the TEM setup configuration, the $(1\bar{1}0)$ plane parallel to the incident electron beam. This means that the $(1\bar{1}0)$ plane is biased parallel to the plane we are viewing and the fiber texture is therefore not complete. Indirectly, it could be concluded that one-grain orientation is dominating, at least for the grains facing the resist walls for the magnetic pole sample geometry. Having the size of the electrode (photoresist pattern width) approaching the width of the columnar grains, the contribution of these surface grains becomes dominant to the overall crystallographic texture of the magnetic pole sample. The magnetic softness is dependent on an average grain size [76], and it is expected that the magnetic properties of the $Co_{39}Fe_{63}$ alloy in the magnetic pole geometry differ significantly from the thin film. For illustration purpose, in Figure 27.19*c*, quantitative measurements of the coercivity as a function of the grain volume are presented for 2.4-T CoFe films [2]. The small difference in the average grain volume of CoFe films yields the significant change in their coercivity. The data in Figures 27.19*a*, *b* indicate that grain volume in magnetic pole sample configuration increases more than three times and we can expect that the resulting coercivity of the $Co_{39}Fe_{63}$ alloy in the magnetic pole is much larger. According to the trend in Figure 27.19*c*, the estimate of H_c for the $Co_{39}Fe_{63}$ pole tip is ≈63 Oe.

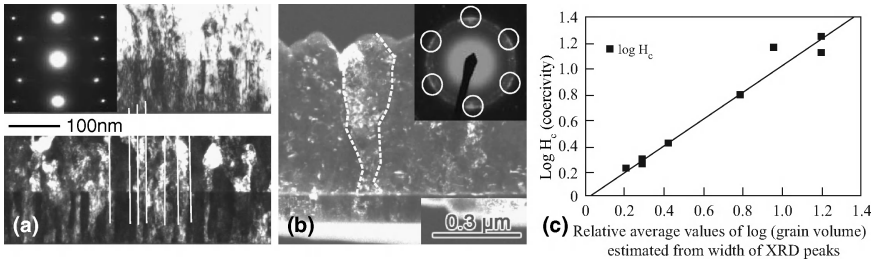

FIGURE 27.19 (*a*) TEM images of the 2.4-T $Co_{39}Fe_{63}$ alloy in thin film configuration, (*b*) in magnetic pole configuration (see Figure 27.1 for magnetic pole structures shape and other details). The insets in (*a*) and (*b*) show XRD pattern from TEM images. The lines in image (*a*) and (*b*) are drawn to guide the eye along the grain boundaries. Reprinted from [3] with permission. © 2006 IEEE. (*c*) $\log(H_c)$ vs. grain volume dependence for 2.4-T CoFe alloy. The estimate slope from this data is 1. Reproduced with permission from [2], Copyright 2001, The Electrochemical Society.

27.1.7 Conclusion

The electrodeposition of soft, high-magnetic-moment alloys has been widely used as one of the key fabrication processes in the manufacturing of magnetic recording heads for almost three decades [3]. The desire for high-magnetic-moment alloys and the need for delivering magnetic structures with dimension in the range of several tens of nanometers are new challenges that have to be addressed in the future fabrication of high-density recording devices. This complex challenge could be met by considering the conditions at the electrochemical interface for additive incorporation, iron hydroxide incorporation, and careful design of the bath chemistries and processes that would yield high-moment alloys with optimum magnetic and corrosion properties. The additional aspect of electrodeposition in the nanoconfined electrode geometry that needs to be properly evaluated is the significantly different grain structure of the deposit as compared to the thin-film sample geometry. This problem will surely deserve more attention and research efforts in the future in order to have an appropriate assessment of the possible implications for the magnetic recording process. One of the factors that will be dominant in the integration of electrodeposited 2.4-T Co–Fe alloys in the future recording heads is their corrosion resistance. To address these problem new alloys such as 2.4-T $Co_{38}Fe_{61}Pd_1$ with improved corrosion resistance has to be developed and proved as functional for the magnetic recording process. The work on other solutions for this problem undoubtedly will be one of the main research directions in the near future.

27.2 COPPER ELECTRODEPOSITION FOR MICROELECTRONICS APPLICATIONS

27.2.1 Introduction

Copper electrodeposition is a current state-of-the-art technology for chip interconnect manufacturing in the semiconductor industry [4, 77]. The pursuit of smaller and faster semiconductor devices along with the packaging complexity of integrated circuitry inevitably led to a transition from aluminum-based to copper wiring [78–80]. The main advantages of copper—low resistance, high electromigration resistance, and good scalability—were explored extensively and contributed to this major technology transition [79, 81–83]. However, integrating copper in the manufacturing process presented an enormous research and technology development challenge [79]. Development the of dual-damascene processing approach by the IBM research team integrated copper electrodeposition as a manufacturing method and marked a major breakthrough in the semiconductor industry [4, 77, 79, 80].

Integration of electrodeposition in processing requires the presence of a *barrier layer* to prevent diffusion of copper into the insulator (dielectric) precovered by a thin *seed layer* acting as a cathode for electroplating. Barrier layers such as Ta, TaN, or TiN have low resistivity and provide good adhesion to both dielectrics and copper. It is necessary for the barrier layer not only to be as thin as possible but also to continuously encapsulate all surface features [83]. The seed layer is a thin film of copper deposited by ultrahigh vacuum (UHV)–based methods, for example, physical vapor deposition (PVD) or chemical vapor deposition (CVD) [82–84]. This layer not only acts as a cathode but also serves as a nucleation layer for the electrodeposited copper. Therefore, seed layer quality (i.e., continuity, smoothness, purity) is very important in guaranteeing that seed defects do not propagate and compromise the quality and properties of electrodeposited interconnects.

The main processing steps integrating electrodeposition with other patterning and lithographic processes used in conventional through-mask and damascene processing are illustrated in Figure 27.20. The advantage of damascene processing is in the deposition on already patterned electrodes covered with barrier and seed layers. In contrast, in thought-mask plating as a first step the deposition occurs only on areas not covered with masking material. The latter one needs to be removed along with the seed layer underneath in a second step of this process. Fabrication of the hierarchical wiring structure of chips is based on the dual-damascene process illustrated in Figure 27.20*c* where simultaneous filling of two levels (trench and via) as troughs (for trench) and holes (for vias) proceeds in one metallization step. The fewer number of processing steps in the dual-damascene process in comparison with the single-damascene process and/or the processing of Al interconnects results in significantly lower cost of device fabrication.

The important advantage of the damascene process is the way to carry out electrodeposition all over the patterned surface, that is, inside and outside the features, from the bottom up and from the sides inward. However, successful manufacturing of copper interconnects requires filling of trenches and vias completely without voids or seams. Figure 27.21 shows possible evolution profiles of copper that can be obtained at different stages of electrodeposition. *Conformal plating* is characterized by uniform deposition at all points of the feature, eventually resulting in formation of seams or voids. *Subconformal* plating leads to a void formation due to the nonuniform current distribution and preferential growth on the external features. This type of growth occurs when a depletion of copper ions leads to significant concentration overpotentials inside the feature. A desirable s*uperconformal* plating, that is, complete and defect-free filling of the features, can be obtained by increasing the deposition rate on the bottom and along the sides of the feature. This phenomenon, unique for electrodeposition and leading to void-free deposits, is called *superfilling*. Local increase of the deposition rate resulting in bottom-up filling

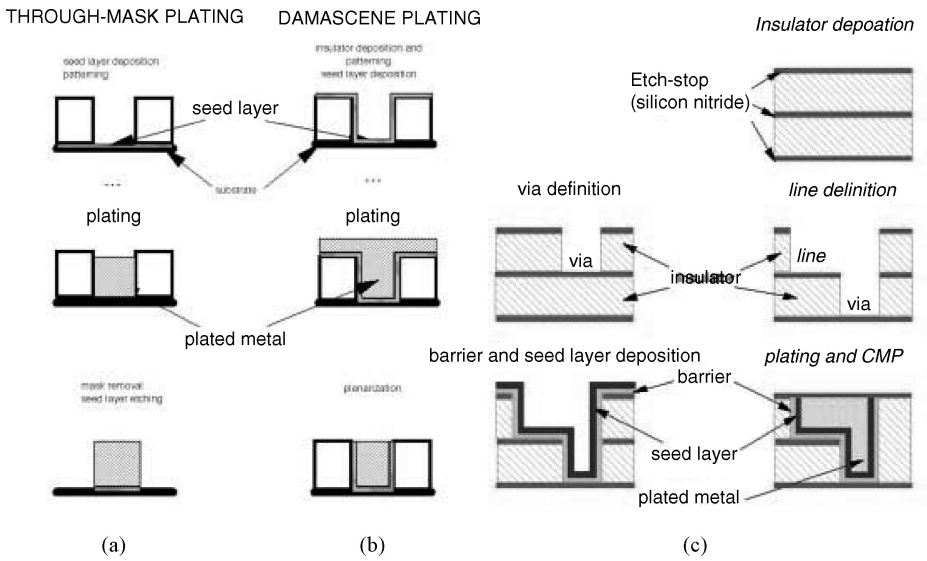

FIGURE 27.20 Fabrication processing steps integrating electrodeposition: (*a*) through-mask plating; (*b*) damascene plating; (*c*) dual-damascene plating. Reprinted from [77] by permission of IBM.

of features is dependent on the use of organic additives in the electrolyte.

27.2.2 Copper Deposition: Mechanism and Kinetics

The relationship of the deposition kinetics, morphology, and properties of the copper deposit with the concentration and nature of organic additives employed in the plating process is very complex and has been a subject of very intensive research [85–105]. It is known that additives not only influence the Cu reduction kinetics but also, owing to incorporation of their molecules and/or breakdown products, they could significantly affect the metallurgical microstructure and properties of the deposit [4, 106].

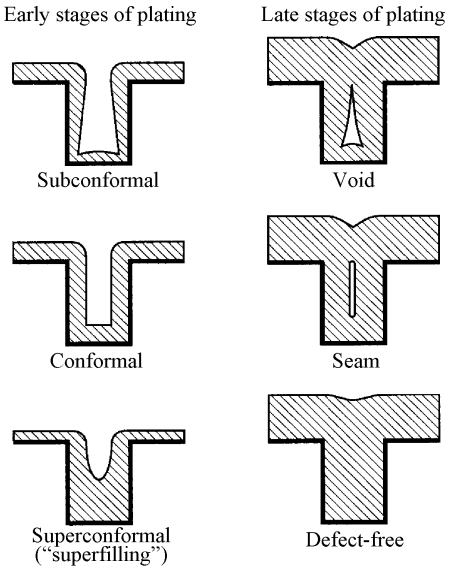

FIGURE 27.21 Different evolution profiles that can occur during electrodeposition. Reprinted from [77] by permission of IBM.

Electroplating of copper has been used for a very long time in multilevel printed wiring board (PWB) manufacturing, mostly from electrolytes based on pyrophosphate, flouroborate, and sulfate salts [84, 88]. However, the deposition requirements for copper interconnects are distinctly different from those applying to PWBs. Thus, to overcome interconnect limitations, copper plating requires modifications and extensions to suit the filling of smaller geometries. The sharply accelerated plating rate for void-free filling of submicrometer features led to the modification of existing and the development of new copper plating procedures and chemistries. Considering the cost, convenience, safety, and extensibility, the damascene process is mostly based on acid copper–sulfate baths that include halide (normally chloride) ions and organic additives. Commonly used additives fall in three general categories according to their role during deposition: suppressors, accelerators, and levelers.

Suppressors, also called *inhibitors,* are organic agents that tend to adsorb on the cathode surface, thus reducing the deposition rate. Commonly used suppressors are polyethers such as polyethylene glycol (PEG). These types of additives are known to act in combination with chloride ions (cosuppressors) by forming a current blocking adlayer on top of the copper surface.

Accelerators, often referred to as *catalysts*, are sulfur-based molecules, that is, mercapto (–SH) or disulfide (S–S) containing species, such as bis(3-sulfopropyl)disulfide [$Na_2(S(CH_2)_3SO_3)_2$] (SPS) or 3-mercapto-1-propane sulfonic acid [$NaSO_3(CH_2)_3SH$] (MPSA). In the plating process the accelerator's molecules compete with the suppressor ones for

surface adsorption sites, thereby depolarizing the interface and accelerating the deposition rate. Due to field effects accelerator concentration is different at concave and convex areas of the sample.

Levelers are a special group of *suppressive* additives used to produce a mirrorlike surface. The leveler molecules adsorb preferentially on the protruding areas of the surface, inducing local decrease in the deposition rate. The most common levelers are nitrogen-based molecule or polymers such as thiourea, benzotriazole (BTA), and Janus green B (JGB).

The deposition of copper in acidic sulfate solution has been widely studied using a variety of electroanalytical methods [94, 95, 102] and is known to proceed in two steps:

$$Cu^{2+} + e^- \rightarrow Cu^+ \quad \rightarrow \quad E^0 = -0.087\ V_{SCE}$$
$$Cu^+ + e^- \rightarrow Cu \quad \rightarrow \quad E^0 = 0.281\ V_{SCE}$$

Under standard conditions the cuprous ion is more noble than cupric ions, and the first reaction of its formation is rate determining [107–109]. The role of cuprous ions during deposition has long been acknowledged. Metallic copper, *cupric* (Cu^{2+}) and *cuprous* (Cu^+), ions can interact with each other through a reaction known as copper disprotonation, $Cu + Cu^{2+} \rightarrow 2Cu^+$. Free or uncomplexed cuprous ions are unstable in solution and readily react with the dissolved oxygen, bringing down only to trace amounts the presence of cuprous ions in sulfate solutions. However, in the plating baths cuprous ions are formed through the disprotonation reaction. Thus, they form stable complexes in the presence of complexing agents such as Cl ions (forming $CuCl_{ad}$) and SPS or MPSA [forming Cu(I) thiolate]. A list of possible reactions at the copper surface in a copper sulfate plating bath containing typical organic additives is given in Table 27.4 [94], showing five types of reactions that can be distinguished.

In typical solutions containing 0.25–0.5 M $CuSO_4$ about 0.4–0.6 m*M* of Cu ions exist at the copper surface under open-circuit conditions, which is significantly greater than the combined concentrations of all the organic additives used in the superfilling baths. Rotating-ring disc electrode studies showed that near-surface concentrations of cuprous ions, intermediates, or complexes affect the overpotential and the kinetics of Cu plating [94]. This *Cu^+ ion concentration–overpotential correlation* is such that deposition is faster at cuprous-rich than at cuprous-poor surfaces for the same applied potential. The additives regulate the presence of cuprous ions on the surface in such a way that levelers and suppressors inhibit Cu^+ formation whereas accelerating additives enhance Cu^+ formation. The differential copper deposition rate in damascene plating can be correlated to the differential formation near the electrode surface of cuprous complexes and to their polarizing or depolarizing action on cuprous ion formation.

TABLE 27.4 Reactions at the Copper-Electrolyte Interface

Reactions at the copper/electrolyte interface in copper sulfate plating baths containing Cl^-, SPS [bis(sulfopropyl)disulfide: $S(CH_2)_3SO_3H)_2$], or MPSs: $HS(CH_2)_3SO_3H$] as accelerator and a polyether suppressor molecule [$H((CH2)_xO)_yOH$]. The deprotonated MPSs thiol group is indicated as "thiolate" in the formulas [94]

Copper Disprotionation Reactions

1. $Cu + Cu^{2+} \leftrightarrow 2Cu^+$
2. $Cu + Cu^{2+} + 2Cl^- \leftrightarrow 2CuCl_{ad}$
3. $Cu + Cu^{2+} + 2MPSA \leftrightarrow 2Cu(thiolate)_{ad} + 2H^+$

Redox Reactions Involving SPS

4. $2Cu^+ + SPS + 2H^+ \leftrightarrow 2Cu^{2+} + 2MPSA$
5. $4Cu^+ + SPS \leftrightarrow 2Cu^{2+} + 2Cu(I)(thiolate)_{ad}$
6. $2Cu^{2+} + 4MPSA \leftrightarrow 2Cu(I)(thiolate)_{ad} + SPS + 4H^+$

Surface Adsorption Reactions

7. $2Cu_s + SPS \leftrightarrow 2Cu(I)(thiolate)_{ad}$
8. $nCuCl_{ad} + HO((CH_2)_xO)_yH \leftrightarrow [HO((CH_2)_xOCuCl)_n((CH_2)_xO)_{y\text{-}n}H]_{ad}$

Exchange Reactions

9. $CuCl_{ad} + MPS \leftrightarrow Cu(I)(thiolate)_{ad} + Cl^- + H^+$
10. $[HO((CH_2)_xOCuCl)_n((CH_2)_xO)_{y-n}H]_{ad} + n MPSA \leftrightarrow HO((CH_2)_xO)_yH + nCl^- + nCu(I)(thiolate)_{ad}$

Complexation Reactions

11. $Cu^+ + Cl^- \leftrightarrow CuCl_{ad}$
12. $CuCl_{ad} + Cl^- \leftrightarrow CuCl_2^-$
13. $CuCl_{ad} + MPSA \leftrightarrow CuCl(thiolate) + H^+$
14. $Cu^+ + MPSA \leftrightarrow Cu(I)(thiolate)_{ad} + H^+$
15. $Cu^+ + SPS \leftrightarrow Cu(I)(SPS) + H^+$
16. $Cu(I)(thiolate)_{ad} + MPSA \leftrightarrow Cu(I)(thiolate)_2^- + H^+$
17. $Cu(I)(thiolate)_{ad} + Cl^- \leftrightarrow Cu(thiolate)Cl$
18. $4Cu(I)(thiolate)_{ad} + Cu^{2+} \leftrightarrow Cu[Cu(I)(thiolate)]_4^{2+}$
19. $Cu(I)(thiolate)_{ad} + Cu^+ \leftrightarrow Cu(I)(thiolate)Cu(I) + H^+$

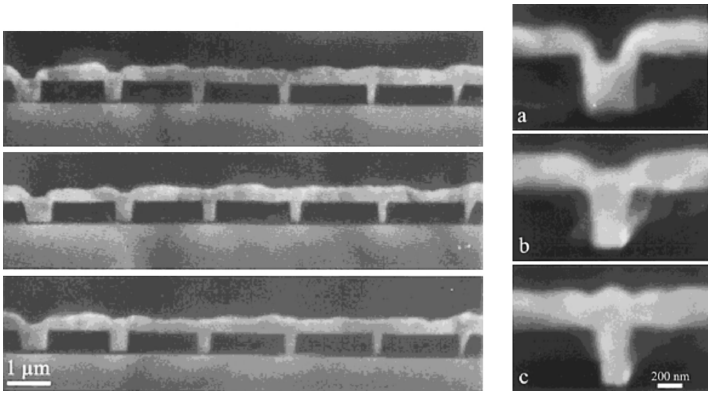

FIGURE 27.22 [103] (I) Scanning electron microscopy (SEM) images of copper deposited from Cl–PEG–MPSA electrolyte into three different trench groups with slanted sidewalls (−0.650 V for 60 s). The width at the base of each trench ranges from 560 to 120 nm corresponding to aspect ratios of 0.86 : 1 to 4.1 : 1. (II) Three SEM images of (*a*) 300-, (*b*) 250-, and (*c*) 200-nm-wide trenches revealing shape evolution during deposition from Cl–PEG–MPSA electrolyte (−0.650 V_{SSE} for 30 s). The concave growth surface and the slower deposition at the trench mouth in image (*a*) reflect the preferential filling from the trench bottom. Likewise, the inversion of curvature apparent in image (*c*). Reproduced with permission from [103], Copyright 2000, The Electrochemical Society.

27.2.3 Copper Plating Bath Chemistry

The first generation of electrolytes used in damascene Cu plating contained numerous components without much understanding of the relation between the chemistry and processing parameters on one hand and the mechanism that controls shape evolution during superfilling on the other [77, 88, 110]. The difficulty associated with understanding the superfilling was attributed to the proprietary nature of the existing knowledge. However, the simplification of additive packages in damascene processing to two (suppressor and accelerator) and three components (suppressor, accelerator, leveler) offered an enormous possibility to study and analyze the superfilling process in great detail [103, 111]. The first report of using a two-component electrolyte Cl–PEG–MPSA [103] for superconformal deposition in 500–90-nm features with quality and properties consistent with the films produced by proprietary means suggested that this system could be a model system and serve as representative of commercial electrolytes. The results illustrated in Figure 27.22 inspired further exploration of superfilling phenomena and development of new simplified bath chemistries and electrodeposition protocols.

Table 27.5 lists some of the plating solutions used in superfilling studies along with the methods used. Electrodeposition processes are usually conducted in one- or two-step protocols either galvanostatically or potentiostatically [112]. In a few cases that we will discuss later, the two-step processes involve *derivatization of copper seed layer* in accelerator solution followed by copper plating in accelerator-free solution. The derivatization procedure includes exposure of the electrode to the Cu-free solution containing only accelerator over a certain amount of time with or without potential control, during which a partial layer of catalyst chains of thiol/disulfide molecules adsorbs on the copper surface [90, 95, 97, 113]. The same process was employed in kinetic studies of copper electrodeposition with the aim of quantitatively characterizing the catalyst effect on the deposition rate. The derivatization method allowed examination of the catalyst consumption (deactivation) effect independently of the dynamics associated with the catalyst adsorption process [90, 91, 114].

Most of the Cu superfilling work has been done using SPS or MPSA as accelerator. However, investigations of the stability of MPSA in standard damascene plating baths suggest that its active role changes upon aging [93, 115]. Superfilling experiments demonstrated changes of the deposition profile with aging time of the solution related to the extent of conversion of MPSA to SPS or its derivatives. Recent UV analysis suggests that at least 12 h aging of the MPSA electrolyte results in 99% conversion to SPS [93] so the time between mixing of the electrolyte and its actual use could affect the quality of superfilling.

27.2.4 Models of Copper Superfilling

The earliest understanding of superfilling was based on traditional *transport-limited leveling models* [77, 111, 116]. The localized effect of additives on the deposition rate within the features was based on the diffusion-limited accumulation of inhibiting species onto the metal surface. This accumulation can be simply understood by low mass transfer of the inhibitor in areas such as narrow or deep features resulting in local growth rate enhancement, Fig. 27.23. Despite the required empirical modifications introduced in this model, it still failed to fully capture the experimentally observed shape changes of the growth front during feature filling [77, 111, 116]. This model could not also rationalize the overfill phenomena manifested by a transition from the originally concave surface profile

TABLE 27.5 Superfilious Bath and Process Design

Cu–Sulfate Base Solution and Additives	Deposition Conditions	Reference
0.25 $M\,L^{-1}$ $CuSO_4 \cdot 5\,H_2O$ + 1.8 $M\,L^{-1}$ H_2SO_4 1.0 m$M\,L^{-1}$ NaCl 88.2 μ$M\,L^{-1}$ PEG (Mw 3400) 10 μ$M\,L^{-1}$ MPSA	Potentiostatic deposition at $E = -0.650$ V $_{SSE}$	103
0.24 $M\,L^{-1}$ $CuSO_4 \cdot 5H_2O$ + 1.8 $M\,L^{-1}$ H_2SO_4 1.0 mM NaCl 88 μ$M\,L^{-1}$ PEG (M_w 3400) 50 μ$M\,L^{-1}$ SPS or MPSA	Two step procedure: 1. Electrode derivatization in SPS or MPS solution for 30 s in solution 1.8 M L^{-1} H_2SO_4 + 50 μM L^{-1} SPS or MPSA 2. Potentiostatic deposition in SPS-free solution at overpotential −0.25 V	90,95
0.25 $M\,L^{-1}$ $CuSO_4 \cdot 5H_2O$ 1 $M\,L^{-1}$ H_2SO_4 1 m$M\,L^{-1}$ NaCl 132 μ$M\,L^{-1}$ PEG (Mw 3400) 100 μ$M\,L^{-1}$ DPS	Two step procedure: 1. Potentiostatic deposition at −0.25 V_{SCE} for 100 s in PEG–Cl–DPS solution 2. Potentiostatic deposition at −0.25 V_{SCE} in DPS-free solution Two step procedure: 1. Electrode derivatization in DPS solution for 100 s in 100 μ$M\,L^{-1}$ DPS solution 2. Potentiostatic in DPS-free solution at −0.25 V_{SCE}	113
0.16 $M\,L^{-1}$ $CuSO_4$ + 1.8 mol L^{-1} H_2SO_4 88 μ$M\,L^{-1}$ PEG 1 m$M\,L^{-1}$ NaCl 50 μ$M\,L^{-1}$ SPS 0.1 μ$M\,L^{-1}$ PEI	Potentiostatic deposition at −0.25 V_{SCE}	100
0.16 $M\,L^{-1}$ $CuSO_4$ + 1.8 mol/L H_2SO_4 88 μ$M\,L^{-1}$ PEG 1 m$M\,L^{-1}$ NaCl 50 μ$M\,L^{-1}$ SPS 60 μmol L^{-1} DTAC	Potentiostatic deposition at −0.25 V_{SCE}	144
0.25 $M\,L^{-1}$ $CuSO_4$ + 1 M/L H_2SO_4 88 μ$M\,L^{-1}$ PEG (Mw 3400) 1 m$M\,L^{-1}$ NaCl 50 and 25 μM SPS 0.4 mM and 2 mM 1,2,3-BTA	Two step procedure: Potentiostatic deposition at −0.25 V_{SCE} 1. PEG + Cl + SPS 50 μM + BTA 0.4 mM (40 s) 2. PEG + Cl + SPS 25 μM + BTA 2 mM (140 s)	140

associated with growth in the trench to a convex one above the filled feature [117].

Electrochemical studies of a two-component system (accelerator + suppressor) resulted in the development of a *curvature-enhanced accelerator coverage* (CEAC) model [103, 118]. The model is based on a competitive adsorption interaction between *suppressors and accelerators* [95, 101, 114, 118] taking place on the electrode surface. Unlike the transport limited leveling models (TLLM), this model quantitatively describes the surface evolution during bottom-up superfilling (Fig. 27.23*b*) [95, 101, 103, 118–120]. This mechanism, proposed by the CEAC model, also provides a very good explanation for the beneficial effects of additives called brighteners on the roughness evolution [120, 121]. The generality of the CEAC model has been demonstrated for superfilling of submicrometer features with CVD copper [120] as well as with other metals of interest in the semiconductor industry, such as electrodeposited silver [122, 123] and gold [123, 124].

According to the CEAC model inhibition is provided by the interaction of PEG and Cl that rapidly adsorb on a surface and form a thin passivating layer during Cu electrode immersion. Subsequently, during deposition this layer gets disrupted or displaced by adsorption of accelerator species (SPS, MPSA), that is, catalyst short chains of disulfide/thiol molecules [95, 114]. This leads to an accelerated copper deposition rate that is simply a monotonic function of catalyst coverage. Activated in this way the deposition process is sustained under conditions for which the catalyst remains segregated on the growing surface. The deposition on a nonplanar electrode is inherently accompanied by local area change that in turn affects the local adsorbate coverage. The coverage of catalytic species increases on advancing concave sections and decreases on advancing convex sections. Since the deposition rate is proportional to the catalyst coverage, this naturally gives rise to bottom-up filling of the features and more generally to superconformal film growth.

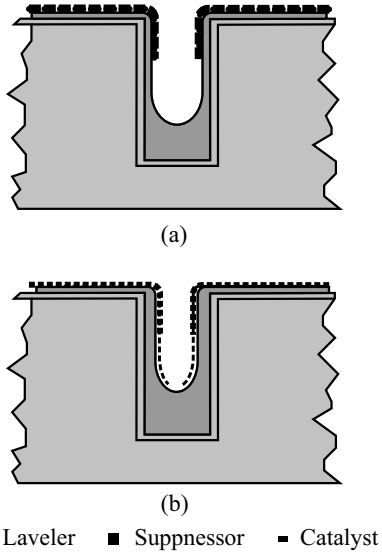

FIGURE 27.23 Schematic for superfilling mechanisms (*a*) with a strong adsorbing leveler for differential inhibition of plating in the field and at the mouth of a feature; (*b*) with a catalyst or accelerator in the bottom of the feature for achieving differential (local) acceleration. Reproduced from [94] by permission of IBM.

The CEAC model successfully predicts the evolution from an initial incubation period and near-conformal growth through superconformal "bottom-up" filling to a momentum plating of overfill bump formation [118, 119]. The combination of competitive adsorption effects is reflected in electrochemical measurements by hysteretic voltammetric response, rising current transients, and multicycle voltammetry changes. Measured on planar electrodes and used for parameterization of CEAC model algorithms, the electrochemical results clearly show potential dependence of the catalyst adsorption and its subsequent deactivation. To date three different shape-change algorithms have been used to describe the filling of submicrometer features such as trenches and vias [118, 119, 125].

27.2.5 Additive Kinetics and Effect on Cu Deposition

PEG–Cl Inhibiting Effect The addition of chloride in sulfate solutions is known to accelerate the rate of copper deposition by promoting the rate-controlling Cu^{2+}/Cu^{+} reaction [94, 102, 107–109]. Not only does the chloride adsorb on the copper surface but it also determines the structure, orientation, and dynamics of the surface [102, 126, 127]. On the other hand, the effect of PEG on the copper deposition rate is not significant by itself and the adsorption of PEG on the copper surface is weak [85–87, 92, 114, 128–130]. However, the *combination of PEG and Cl* in sulfate solution results in the formation of a barrier layer that significantly suppresses the deposition of copper at a given potential, that is, increases the overpotential required to maintain the given current density. The strong inhibiting effect of PEG and Cl on copper deposition is illustrated by η–*i* curves in Figure 27.24. These η–*i* curves can be described by generalized Bulter–Volmer (BV) equations with values of the transfer coefficient and exchange current density reported in the table in Figure 27.24. The exchange current density values suggest that copper deposition kinetics was hindered by almost two orders of magnitude in the presence of PEG–Cl additives. The insignificant changes of respective transfer coefficients suggest that the copper reduction is unaltered by the PEG–Cl layer; that is, this layer behaves as a physical barrier blocking the access of cupric ions to the electrode surface [105].

The synergic effect of PEG and Cl has been attributed to the formation of a complex layer that involves Cl^{-}, and Cu^{+} ions and PEG molecules [85–87, 91, 92, 94, 95, 105, 129, 131]. At this time, the molecular structure of this complex is unknown and various structures have been proposed [85, 128, 131, 132]. Even thought few surface-enhanced Raman

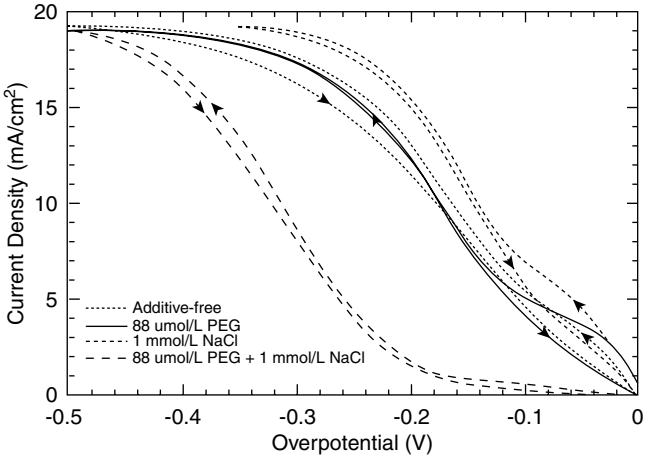

$$i = i_0\left(1-\frac{i}{i_L}\right)\left[\exp\left(\frac{-\alpha F\eta}{RT}\right)-\exp\left(\frac{(1-\alpha)F\eta}{RT}\right)\right]$$

Electrolyte composition	Transfer coefficient α	Exchange current density i_0 (mA/cm^2)
Additive–free	0.4–0.45	1.4–1.1
PEG	0.45	0.9
Cl	0.5	1.3
PEG–Cl	0.5	0.039
SPS-modified electrode in PEG–Cl	0.5–0.4	4.5–2.25

FIGURE 27.24 Inhibition of copper deposition from 0.24 mol L^{-1} $CuSO_4$ + 1.8 *M* H_2SO_4 is provided only by the simultaneous addition of Cl and PEG. The η–*i* curves were obtained at 1 mV s^{-1}. Reproduced with permission from [114], Copyright 2004, The Electrochemical Society.

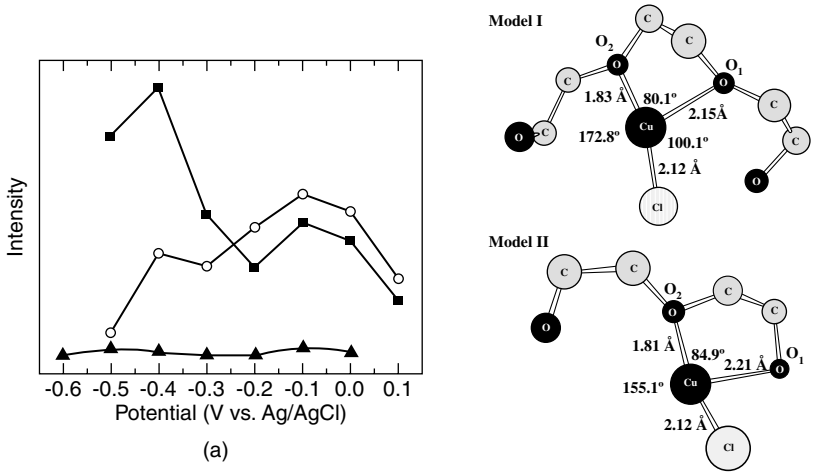

FIGURE 27.25 (*a*) SERS peak intensity as function of potential for Cu in 88 μM poly(ethylene glycol) + 2 m*M* KCl + 10 m*M* $CuSO_4$ + 0.1 *M* H_2SO4 during anodic steps for 290-cm^{-1} band (Cu–Cl square), 260-cm^{-1} band (PEG–Cu–Cl open circle), and 850-cm^{-1} band (Cu–PEG triangle). (*b*) Structural models of two PEG–Cu–Cl complexes; model I: Cu atom is associated with two ether oxygen atoms of PEG and one chloride ligand; model II: Cu atom is associated with one ether oxygen atom and one hydroxyl oxygen atom of PEG and one chloride ligand (hydrogen atoms excluded for the sake of simplicity). Reprinted with permission from [129], Copyright 2003, American Chemical Society.

spectroscopy (SERS) investigations have been conducted on this system in the past, recently [129, 133] the presence of PEG–Cl–Cu^+ has been reported. The SERS spectra reveal a strong vibration mode at 260 cm^{-1} present only in PEG + Cl + Cu solution. The low-energy band value suggests that in this complex Cu is associated with Cl^- ion because the value of the band appears close to the $Cu_{(surface)}$–Cl stretch band of 290 cm^{-1} associated with Cl^--specific adsorption. The 30 cm^{-1} red shift suggests that this new Cu−Cl bond is weaker and the possible reason for that could be the strong association of Cu with the complex (no longer metallic). Figure 27.25*a* shows a variation with the potential of SERS peak intensities corresponding to Cu−Cl (i.e., Cu−Cl stretch mode of the complex), Cu_{surf}–Cl, and Cu_{surf}–PEG. The stretch mode of PEG does not feature noticeable dependence with the potential, while Cu–Cl complex stretch modes increase with the potential (Fig. 27.25*a*). On the basis of SERS spectra, complementary modeling of a three-coordination Cu with two ether oxygen ligands from PEG and one chloride ligand is proposed, as illustrated in Figure 27.25*b*.

In contrast to Raman spectroscopy, electrochemical quartz crystal microbalance (EQCM) [86, 134] and recent in situ spectroscopic ellipsometry (SE) studies [105, 135, 136] indicate that Cu ions (neither Cu^+ nor Cu^{2+}) are not essential for the formation of PEG–Cl inhibiting layer. A recent in situ SE study [105] shows that the PEG adsorption alone is very weak and does not vary with the potential, which is consistent with Raman [129] and EQCM [86, 134] measurements.

Studies of electronic properties [105] showed that the PEG–Cl layer does not significantly affect the outer sphere electron-transfer reduction. However, a significant decrease of the interfacial capacitance is observed, which is in agreement with results of electrochemical impedance spectroscopy (EIS) that reported a capacitance reduction to almost a half value upon PEG–Cl layer formation [130].

Accelerator Effect and Superfilling Superfilling of submicrometer features cannot be achieved without accelerators and their sustained accumulation (floating) on the growing surface. As was mentioned earlier, addition of an accelerator such as SPS or MPSA in sulfate solution results in an increase of the deposition rate illustrated by the steady-state *I–E* polarization curves in Figure 27.26*a* [103]. When combined with PEG and Cl^- additives, the accelerator involves itself in an interaction yielding a net inhibition of the deposition rate relative to the additive-free solution although accelerated relative to the PEG–Cl passivated surface. Such polarization behavior clearly reflects competition between the suppressing effects of PEG and accelerating effect of MPSA on the copper plating.

The most representative signature of the additives' competitive adsorption is a significant *hysteresis in cyclic voltammetry behavior,* as shown in Figure 27.26*b* [91, 95, 103, 114, 118]. In contrast, almost reversible (little or no hysteresis) *I–E* behavior is observed in MPSA–Cl, PEG–Cl, and additive-free electrolyte (Fig. 27.25*b*) [91, 95, 103, 114, 118]. The presence of hysteresis indicates that the competing interaction of additives leads to irreversible changes in the interfacial chemistry.

The extent of accelerator effect on Cu deposition is shown in the *changes of shape and polarization behavior of the hysteresis loops* with an increase of additive concentration (Fig. 27.27*a*) [91, 95, 103, 114]. It has been shown that an increase in accelerator concentration leads to (i) an increase

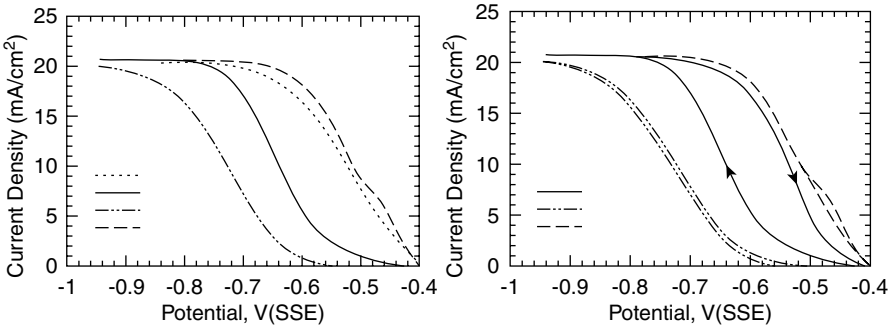

FIGURE 27.26 (*a*) Steady-state *I–E* plots for copper deposition from 0.25 *M* $CuSO_4$ + 1.8 M H_2SO_4 electrolyte (no additives) with various combinations of additives 1 m*M* Cl^-, 88.2 μ*M* PEG (3400 M_w), 0.1 μ*M* (MPSA). (*b*) Cyclic voltammetry behavior for different combinations of additives in the same system as in (*a*). Reproduced from [103], Copyright 2000, The Electrochemical Society.

in the deposition rate manifested by anodic shift of negative potential scans and (ii) a decrease in the area enclosed by the hysteresis loop. The extent of the hysteresis scales with the negative scan limit (i.e., switching potential), reflecting the potential-dependent effect of catalyst activation (Fig. 27.27). This suggests that larger overpotentials allow for larger increase of the catalyst coverage. For a given scan rate and potential scan limits the hysteresis reaches a maximum area for a certain value of SPS concentration (in Fig. 27.27*a*, case 2.59 μ*M*). After that, further addition of additives results progressively in a higher deposition rate only on the negative scans accompanied with a saturated current response in the reversed scan. The hysteretic polarization behavior can be understood as a catalytic deactivation of blocked electrode manifested by disruption of the PEG–Cl blocking layer along with thiolate/disulfate catalyst adsorption that effectively accelerates copper deposition without requiring any changes of the Cu ion reduction mechanism.

Hysteretic voltammetry changes when the concentration of SPS becomes comparable or exceeds the concentration of

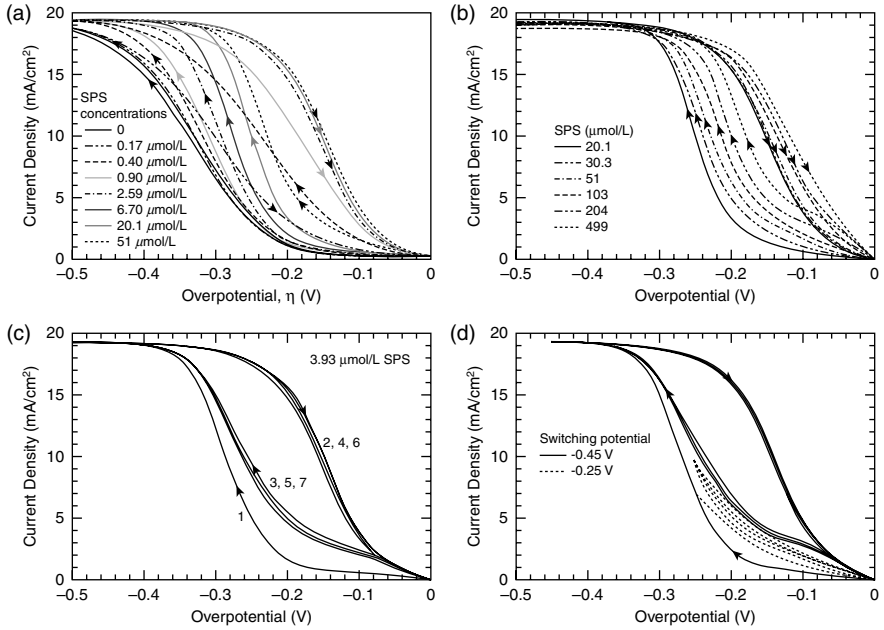

FIGURE 27.27 Hysteretic η–*i* curves obtained in 0.25 mol L^{-1} $CuSO_4$ and 1.8 mol L^{-1} H_2SO_4 + 88 μ*M* PEG + 1 m*M* NaCl solution for range of SPS concentrations. (*a*) Changes of hysterisis behavior with increase of SPS concentration. The response on the return sweep is effectively saturated beyond 2.59 μmol L^{-1} SPS. Reprinted from [95] by permission of IBM. (*b* Changes of hysteresis behavior with higher concentrations of SPS. Beyond 30 μmol L^{-1} SPS, an additional wave is evident at −0.1 V. (*c*) Multicycle voltammetry reflecting convolution of potential-dependent SPS adsorption and deactivation. The onset of significant deactivation is evident at −0.08 V. For $C_{SPS} > 2.5$ μmol L^{-1} a steady-state response is reached after one cycle. The inset numbers reflect the scan sequence. (*d*) The strong potential dependence of SPS activation is revealed by varying the switching potential. A marked increase in hysteresis is evident for $E > |-0.25|$ V. The voltammograms were collected for a fixed period of 2400 s. For η = −0.45 V, an activated state (∼e.g., I = 17 mA cm^{-2} at −0.2 V) is obtained on the return sweep after 700 s. In contrast, a maximum current of 5 mA cm^{-2} at −0.2 V is observed after 2400 s of cyclic polarization for η = −0.25 V. (*b–d*) Reproduced with permission from [114], Copyright 2004, The Electrochemical Society.

PEG in the solution. As shown in Figure 27.27*b*, for $C_{SPS} > 50\ \mu M$ additional current wave appears on the negative scans at low overpotentials. This wave could be associated with concomitant occurrence of homogenous and heterogeneous processes [94, 114] at the interface. The latter phenomenology is facilitated at high SPS concentration where strong interactions between catalyst species and surface dominate the interfacial chemistry and affect the mechanism of Cu reduction. The current increase in the positive scan at $C_{SPS} > 100\ \mu M$ is partly attributed to an area increase triggered by a roughness evolution [114, 120].

Multicycle experiments reveal changes in the voltammetry behavior with the number of cycles, particularly in the negative-going scans. The observed changes reflect a convolution of potentially dependent SPS adsorption and deactivation in the subsequent cycles, as shown in Figure 27.27*c* [95, 103, 114, 137]. Although the number of cycles depends on the SPS concentration, potential scan limits, scan rate, and so on, a stable voltammetry is usually achieved after a few cycles (at $C_{SPS} > 2.5\ \mu M$ after the first cycle). The multicycle voltammetry behavior illustrates the potential dependent extent of catalyst deactivation or consumption.

Chronoamperometric experiments (*I–t*) shown in Figure 27.28 demonstrate the polarization behavior of the PEG–Cl–SPS system that is dependent upon potential and SPS concentration. In SPS-free solution (Fig. 27.28*a*), the current transients undergo a decay associated with establishment of the boundary layer that accompanies copper deposition under mixed control [91, 114, 137]. In contrast electrolytes containing SPS exhibit *rising current transients* that eventually reach a steady-state value. The time constants of these transients are dependent on the concentration of SPS in the solution (Fig. 27.28*b*) and the overpotential for constant SPS concentration as well (Fig. 27.28*c*). This behavior is consistent with an increase of the catalyst accumulation rate at higher overpotentials.

The chronopotentiometric experiments (*E–t*) [91, 95, 137], that is, measurements of the (over)potential change at constant current, also exhibit similar rising potential transients corresponding to a decrease in the overpotential necessary to run a current that eventually reaches a steady-state value. The transition time necessary to reach a steady-state potential decreases with increases of the current density and SPS concentration, as shown in Figure 27.28*c* [91]. On the other hand, the steady-state value of the potential depends on the SPS concentration and for a given current density increases accordingly with SPS concentration. Also, the increasing current density results in a decrease of the steady-state potential, as depicted by Figure 27.28*d* [91].

Both chronoamperometric and chronopotentiometric on the one hand and multicycling voltammetry results on the other suggest SPS concentration-dependent balance between

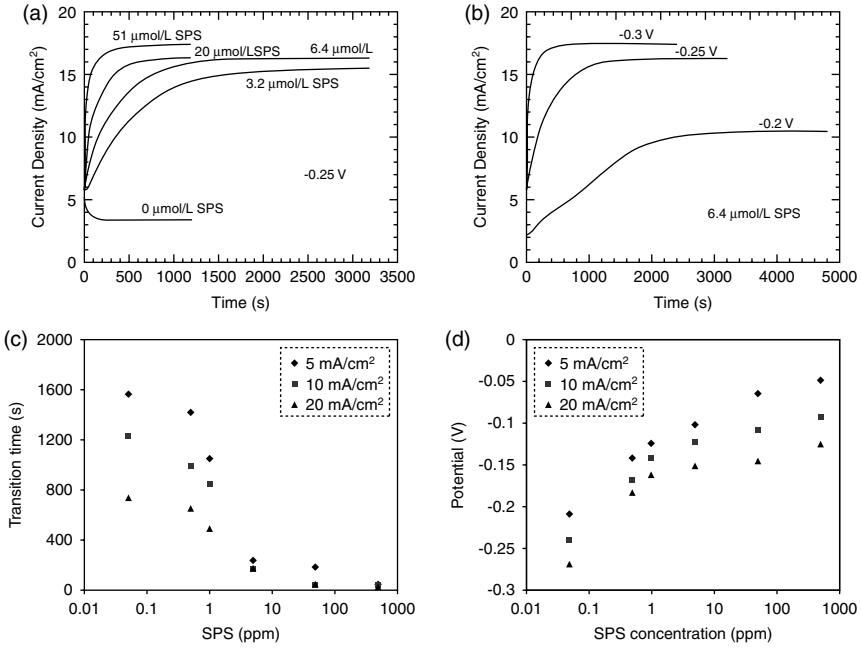

FIGURE 27.28 (*a*) Rising current transients are observed in the SPS–PEG–Cl electrolyte due to activation of PEG–Cl inhibited electrodes induced by SPS adsorption. (*b*) The apparent time constant of the rising chronoamperometric transients increases with overpotential. (*a, b*) Reproduced with permission from [114], Copyright 2004, The Electrochemical Society. (*c*) Effect of SPS concentration on transition time chronopotentiometric measurements. (*d*) Effect of SPS concentration on steady-state potential in chronopotentiometric measurements. For (*c*) and (*d*) the change of the potential less than 1 mV in a 10-min period defines a steady-state value of the potential, while the transition period is defined as the time required to reach 70% of the steady-state value. (*c,d*) Reproduced with permission from [91], Copyright 2003, The Electrochemical Society.

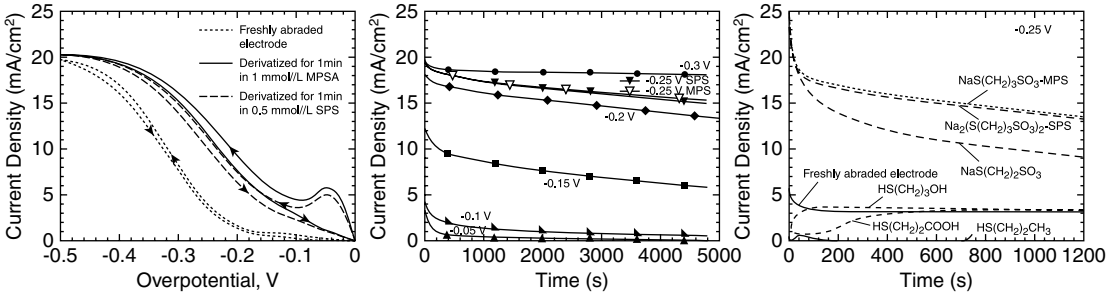

FIGURE 27.29 (*a*) The η–*i* response for copper deposition on SPS- or MPS-derivatized electrodes in a PEG–Cl electrolyte is compared with that occurring on a freshly abraded surface. (*b*) Chronoamperometry detailing the potential dependence of copper deposition on derivatized electrodes. (b) The key role of the catalyst terminal group is also evident in chronoamperometric studies. Reproduced with permission from [114], Copyright 2004, The Electrochemical Society.

the processes of adsorption and deactivation; otherwise, the steady-state values of the current or potential would be independent of the concentration of catalyst in the solution. To separate the contribution of catalyst deactivation from adsorption, *derivatized electrodes* were used to measure changes of the copper deposition rate in catalyst-free PEG–Cl solutions [91, 95, 114]. The initial coverage of catalyst on the surface here is determined by the concentration of SPS/MPS solution and the time of electrode exposure.

Cyclic voltammetry on derivatized electrode in SPS-free electrolyte shows that, depending on initial catalyst coverage, a maximum catalyst deactivation rate is observed at low overpotentials (Fig. 27.29*a*). The peak observed on the voltammetry curve reflects the onset of significant deactivation of originally highly active surface. The subsequent cycles result in additional deactivation until the electrode behavior approaches the behavior of freshly polished electrode in PEG + Cl solution. The deactivation studies using chronoamperometric measurements conducted within the range of potentials and compared to underivatized electrodes in Figure 27.28 show that convergence of respective transients occurs more rapidly at lower overpotentials too. At high overpotentials corresponding to practical plating conditions the derivatized electrodes showed significant resilience against passivation by PEG–Cl.

For instance, for the transient at −0.25 V (the overpotential most frequently used in superfilling experiments) the deactivation rate is low; that is, the catalyst effect is sustained almost an order of magnitude longer than at the low underpotential of −0.05 V (Fig. 27.29*b*). Only minor deactivation occurs for time scales of up to 100 s that are relevant for filling submicrometer features. This indicates catalyst segregation, or "floating," on the growing surface, which is one of the necessary conditions and basic principles of superfilling growth. Finally, this quantitative analysis of current transients [95] was used for the determination of deactivation (consumption) dependence on the overpotential. This dependence is of higher order than linear and it is counterintuitive since the maximum deactivation rate occurs at low deposition rates. The concurrence between maximum deactivation and stability of Cu^+ intermediates [94] suggests that the catalyst consumption might be coupled with activity of Cu^+ at the electrode surface.

Derivatized electrodes were also used to determine the important role of the sulfonate end group (Fig. 27.29*c*). Various catalyst-derivatized electrodes were examined with standard electrochemical methods. It is shown that only molecules with a sulfonate terminated group are capable of preventing the formation of passivating PEG–Cl film. In contrast, electrodes with the hydrophilic –OH and reactive –COOH end groups are rapidly consumed during metal deposition, while the hydrophobic $–CH_3$ modified electrode exhibits significantly greater inhibition than that provided by PEG–Cl (Fig. 27.29*c*).

The electrochemical measurements conducted on planar electrodes described above were used to determine key kinetic factors used in the CAEC model predictions for optimal experimental conditions in superfilling of different geometries for both trenches and vias. For more details on the CEAC mechanism, a quantitative description as well as discussion of the evolution of local catalyst coverage based on balanced adsorption and consumption of catalyst associated with the growing surface curvature for catalyst precursor concentration C_{sps} can be found in several publications [95, 101, 118, 119, 125].

The derivatization process followed by transfer to a catalyst-free solution for copper electroplating was successfully employed in superfilling of patterned electrodes in two-step electrodeposition protocols [90, 95, 97]. As an illustration, Figure 27.30*a* shows the superfilling of trenches using catalyst derivatization for 30 s in 1.8 *M* H_2SO_4 solution containing 0.5–1 μ*M* of SPS/MPSA [90, 95] followed by copper deposition at an overpotential of −0.25 V in SPS-free electrolyte: 0.24 *M* $CuSO_4$ + 1.8 *M* H_2SO_4 + 1 m*M* NaCl + 88 μ*M* PEG (M_w 3400). It is clear that the feature filling time decreases with an increase of the SPS concentration during derivatization. For the sample derivatized in 0.5 μ*M* SPS the deposition proceeded conformally followed by increased roughness during growth that led to void formation. For the

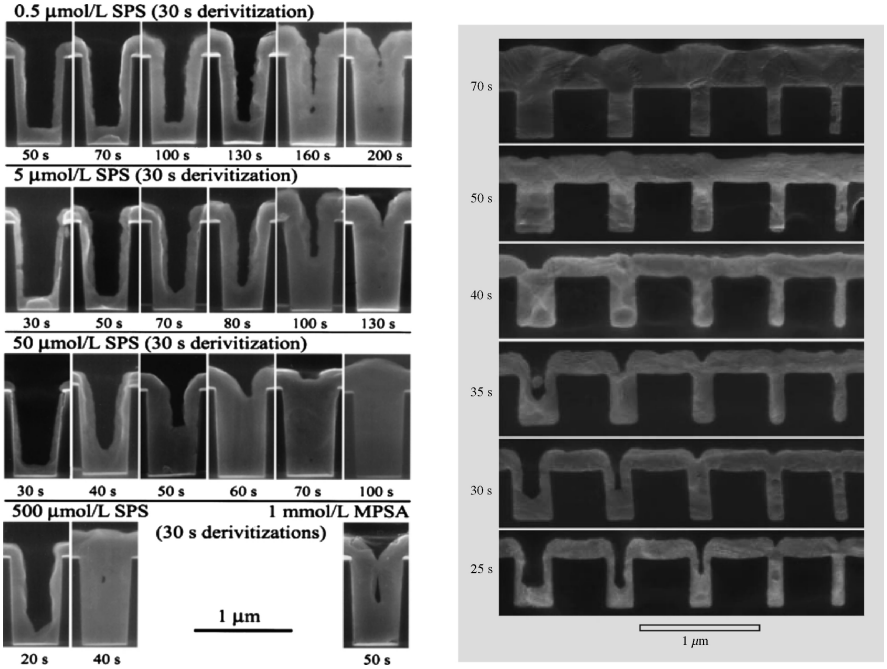

FIGURE 27.30 (*a*) Superfilling of trenches pretreated with catalyst prior to copper plating in a PEG–Cl electrolyte at overpotential −0.25 V. The conditions used for electrode derivatization are indicated. (*b*) SEM images of shape evolution accompanying trench filling. The trench widths are 350, 250, 200, 150, and 100 nm from left to right. For these processing conditions, robust superfilling was limited to an aspect ratio of less than 2. Reprinted from [95] by permission from IBM.

samples treated in 5, 50, and 500 μ*M* SPS concentrations, the initial growth is effectively conformal followed by accelerated growth manifested in the V-shaped bottom profile visible for the 70-, 40-, and 20-s durations, respectively. However, the subsequent accelerated growth is different with optimal superfilling behavior obtained only for the 50 μ*M* sample where the overfill bump formation, that is, an inversion of the growth front curvature, was also observed. An impinging of fast-growing side walls is observed for the 5 μ*M* sample while both the 500 μ*M* and 1 m*M* samples featured void formation before the growing front reached the top of the trench. The shape evolution observed during superfilling is qualitatively identical to the one obtained in a single-step procedure that took place in the same electrolyte with 6.4 μ*M* SPS and deposition overpotential of −0.25 V, as presented in Figure 27.30*a*.

Deposition of copper from PEG–Cl solution on derivatized electrodes with SPS and MPS exhibit undistinguishable behavior reflecting the key role of sulfonate end groups [95, 114]. Yet kinetic studies performed in the presence of those two additives reflect differences in their catalytic activity due to their different molecular structure [93, 115]. In situ SE registered a similar structure and characteristics of MPS and SPS adsorption on Cu. However, the displacement of the PEG/Cl layer is more effective by the thiol compound (MPSA) than by the disulfide compound (SPS). Although freshly prepared MPSA showed better catalytic activity, its aging instability toward conversion to SPS makes it less reliable for industrial use.

Morphological and Microstructural Effects in PEG–Cl–SPS/MPS Systems In addition to influencing the kinetics of copper reduction, additives are well known to determine the morphology, microstructure, and related physical properties of the deposit [78]. Copper deposition from PEG–Cl solutions does not produce bright deposits [92, 111, 138] and the atomic force microscopy (AFM) characterization showed very rough, inhomogeneous pyramidal growth. The roughness evolution measurements support the beneficial brightening effect of the catalyst present in the solution [120, 121, 139]. AFM experiments in PEG–Cl–SPS solution showed that an increase in SPS concentration results in an increase of roughness and grain size [91]. Finite-element (FE) Auger and recent secondary ion mass spectrometry (SIMS), measurements showed that SPS inhibits incorporation of PEG molecules into copper deposit [92, 139]. SIMS measurement also shows traces of SPS incorporation along with Cl in the deposit, suggesting a dominant interaction between those two additives.

Electroplated copper typically has a much higher electrical resistivity than the bulk copper owing to structural defects: grain boundaries, dislocations, vacancies, impurities, and second-phase particles. The thin films of copper which are grown from the damascene solutions [103] exhibit significant reduction of resistance at room temperature after deposition. The reduction is attributed to recrystallization and grain growth. Thin films grown with different combinations of additives (PEG–Cl, MPSA–Cl, and PEG–Cl–MPSA) exhibit

different rates of resistance change [103] with the highest and fastest resistance drop observed in the films grown in the presence of all three additives. This result indicates grain refinement and/or additive incorporation, as already confirmed by SIMS, SEM, and AFM techniques [91, 92].

Leveler Effect: PEG–Cl–SPS–LEV Systems Sustained acceleration of the deposition is beyond the feature-filling result in undesirable overfill bump formation. This phenomenon is a direct consequence of the curvature-induced enrichment of catalyst on the growing surface. It has been shown that the magnitude and extent of bump formation related to accelerator accumulation are strongly correlated to features size and density [140, 141]. The overdeposits are a source of different issues during CMP, resulting eventually in erosion and dishing [112]. Various ways have been explored to prevent and reduce this effect without affecting superconformal growth.

Different leveling strategies using organic additive levelers [100, 101, 140, 142] or electrochemical methods [112, 140, 143] focus on the deactivation of adsorbed accelerators after feature filling is complete. An ideal leveling activity in the superfilling process could be achieved by deactivation of surface rapid growth before curvature inversion and bump formation without substantially attenuating bottom-up feature filling.

The studies of three additive component systems provided enough information on the filling process to allow an extension of the CEAC model to explain the levelers' effect on superfilling [101, 142]. In general, the extended model identifies two additional processes that contribute to (SPS/MPSA) accelerator deactivation: (i) leveler adsorption from the solution and (ii) lateral interaction of adsorbed levelers during an area reduction of surface segments.

The ability and the extent of the levelers' action to deactivate accelerators have been characterized using the same electroanalytical approach and electrochemical measurements on planar electrodes that were previously employed in the characterization of accelerator effects in two-component additive systems (discussed previously). Cyclic voltammetry, chronoamperometry, and chronopotentiometry measurements are used to determine the balance between the adsorption and deactivation kinetics of levelers on copper deposition [100, 101, 142, 144]. The derivatized electrodes with fixed SPS coverage used in the deposition of copper in PEG–Cl–LEV solution allowed characterization of the leveler effects free of the kinetics of the accelerator adsorption process. Details of the CEAC extended model can be found in a number of recent publications [100, 101, 142, 144].

The effect of dodecyltrimethylammonium chloride (DTAC), a cationic surfactant identified as a prototypical leveler on the superfilling dynamics and bump formation, is examined for a range of DTAC concentrations and the pattern density is illustrated in Figure 27.31 [144]. Figure 27.31*a* shows the attenuation of the overfill bump with an increase of the DTAC concentration. For DTAC concentration of $60\,\mu\text{mol}\,\text{L}^{-1}$, the bump is eliminated while still preserving the superfill. Higher DTAC concentrations yield conformal deposition. In addition to DTCA, effective leveling following the CEAC mechanism has been achieved using polyethyleneimine (PEI) [100]. The two-step electrodeposition protocol with modulated accelerator and BTA concentrations was also shown to be effective in the prevention of bump formation without impact on the superfilling [140].

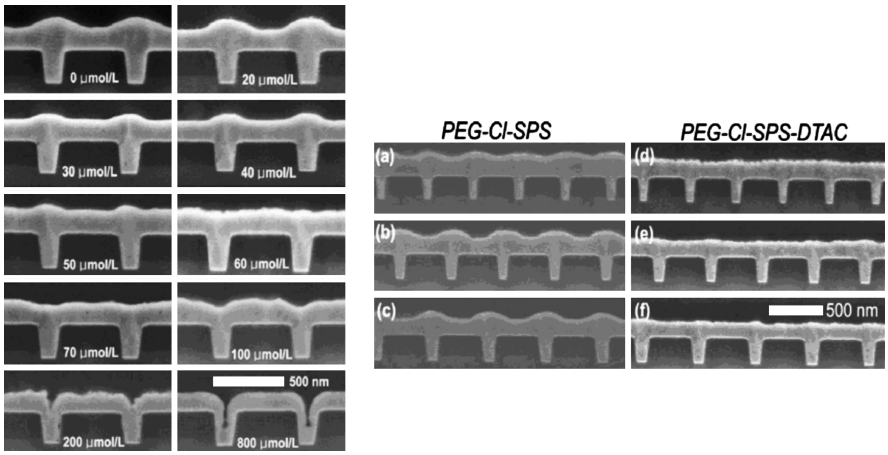

FIGURE 27.31 (*a*) Cross-sectional FE SEM images of Cu deposition on an array of trenches as function of DTAC concentration. The trenches were 120 nm in width. Deposition was carried out at $-0.250\ V_{SCE}$ saturated calomel electrode (SCE) for 30 s in the electrolyte composed of $0.16\,\text{mol}\,\text{L}^{-1}\ CuSO_4 + 1.8\,\text{mol}\,\text{L}^{-1}\ H_2SO_4 + 88\,\mu\text{mol}\,\text{L}^{-1}$ PEG $+ 1\,\text{mmol}\,\text{L}^{-1}$ NaCl $+ 50\,\mu\text{mol}\,\text{L}^{-1}$ SPS plus the indicated DTAC concentrations. (*b*) Filling of trenches with various widths: 70 nm for (*a*) and (*d*), 100 nm for (*b*) and (*e*), and 120 nm for (*c*) and (*f*) and pitches 450 nm for (*a*) and (*d*), 500 nm for (*b*) and (*e*), and 550 nm for (*c*) and (*f*) in a PEG–Cl–SPS–DTAC electrolyte. Deposition was carried out at $-0.250\ V_{SCE}$ for 30 s in electrolyte composed of $0.16\,\text{mol}\,\text{L}^{-1}\ CuSO_4 + 1.8\,\text{mol}\,\text{L}^{-1}\ H_2SO_4 + 88\,\mu\text{mol}\,\text{L}^{-1}$ PEG $+ 1\,\text{mmol}\,\text{L}^{-1}$ NaCl $+ 50\,\mu\text{mol}\,\text{L}^{-1}$ SPS $+ 60\,\mu\text{mol}\,\text{L}^{-1}$ DTAC. Reproduced with permission from [144], Copyright 2006, The Electrochemical Society.

27.3 ELECTRODEPOSITION OF COPPER ON SEEDLESS BARRIER LAYERS

The success of superconformal deposition in high-aspect-ratio structures strongly depends on the quality of the seed layer that is necessary to provide good contact and good nucleation and growth of Cu. The key requirements that the Cu seed layer must fulfill are continuous and uniform coverage with no overhangs, smooth morphology, oxide-free surface, good adhesion, and corrosion stability [82–84]. However, the continuing reduction in size and increasing aspect ratios of the damascene features (now below 70 nm) pose a significant challenge for successful PVD/CVD or atomic layer deposition (ALD) deposition of a thinner and continuous, defect-free Cu seed layer. Furthermore, with the feature size reduction, the seed–barrier layer combination is becoming a significant portion of the cross-sectional area for metallization, making the features narrower and increasing their aspect ratios. All these limitations invoked recent development and pursuit of new strategies and novel methods for Cu seedless deposition directly onto the barrier layer that would eventually lead to superconformal filling of vias and trenches.

A number of studies on planar and patterned electrodes explored Cu electrodeposition directly on commonly used Ta, TaN, TiN, and TiSiNi barrier layers [145–153]. Electrodeposition on such diffusion barrier materials generally proceeds by three-dimensional (3D) island growth, that is, Volmer–Weber growth. Here, a very high *island density N* is key for the growth of ultrathin films. For instance, for films of tenths of nanometers thickness N should be on order of $10^{11}\ \mathrm{cm}^{-2}$, as the critical thickness for the island coalescence d_{crit} is proportional to $N^{1/2}$ [154, 155]. Studies on planar electrodes using electroanalytical techniques [cyclic voltammetry (CV) and chronoamperometry] along with the structural characterization by AFM and FEG SEM have been used for analysis of the nucleation and growth dependence on the applied potential [146–151, 156, 157]. The overpotentials for the nucleation of Cu can be determined from CV and linear sweep voltammetry measurements. The current transients have been used for characterization of the nucleation (instantaneous or progressive) and growth mechanism (diffusion limited or kinetically controlled) dependence upon the deposition potential [153, 154, 156, 157]. Important parameters that control the nucleation density and growth mechanism are *solution chemistry* and *applied potential,* as illustrated in Figure 27.32. Thus, when the contact to the barrier layer is ohmic, striping measurements can be used for quantification of the deposition efficiency although the hydrogen evolution catalyzed by potential time-dependent surface should be taken into account [147–149].

The deposition of Cu on highly resistive substrates may result in nonuniform growth manifested by a thickness variation with the distance from contact owing to nonuniform current distribution. Such a phenomenon, known as a *terminal effect,* is a result of the ohmic potential drop in the electrode and was studied intensively in the past [158–161]. It was shown that the deposition of metal on a barrier layer with high resistance is often hindered by terminal effects and a number of recent models address these phenomena, suggesting optimal conditions and parameters to overcome the electrode resistance and to obtain uniform Cu film deposits [162–165].

27.3.1 Deposition of Cu on Ti and Ta-Based Barriers

The nucleation of Cu on Ta, TaN, and Ta oxide from commonly used Cu sulfate solution, even thought potentially dependent, is very poor [146, 148, 150] and generally not affected by the use of common additives such as PEG and SPS. Several other solution chemistries [148] have been explored for enhancing the Cu nucleation density on Ta and TaN. The best results have been reported for citrate-based solutions, as seen in Figure 27.32 [145, 146, 148, 150, 152, 166]. Both acidic [145, 148, 152] and basic [150] citrate solutions have shown exponential dependence of the nucleation density of Cu with the potential. Continuous and smooth deposits have been obtained using either one- or two-step deposition procedures where a potential pulse has been used to form a high density of Cu islands while the second step has involved growth at constant overpotentials under kinetic or mixed control. Also, the citrate-based copper base solution has been used for successful growth of smooth and continuous Cu films at constant current (or potentials) on an *ultrathin* (∼5-nm) *Cu seed layer* on a Ta barrier film [166].

The use of citrate-based solution has shown promising results for deposition of Cu on Ti and TiN barrier layers as well. In general, citrate baths are of interest because of their very low toxicity and the versatile functionality of the citrate ions during growth. The *solutions pH* has an important role as it correlates with the *citrate complexation ability*. The latter could be used to reduce the copper deposition rate and also to *influence the mechanism of copper nucleation* by controlling the density and shape of nuclei [151, 167] (Fig. 27.33).

The chelating citrate ligands react with copper forming different Cu–Cit complexes such as CuCit^{-}, $\mathrm{Cu_2(Cit)_2OH_3}^{-}$, and $\mathrm{Cu_2(Cit)OH}$ depending upon the $[\mathrm{Cu}^{2+}]$ and $[\mathrm{Cit}^{3-}]$ concentrations and solution pH [145, 167]. The deposition mechanism via reduction of CuCit^{-} complex has been shown to be of critical importance for the good adhesion and quality of the deposit [167]. The mechanism of CuCit^{-} reduction is complex even thought it proceeds in two steps (similar to the case of cupric ion reduction):

$$\mathrm{CuCit}^{-} + \mathrm{e}^{-} \rightarrow \mathrm{CuCit}^{2-}$$

$$\mathrm{CuCit}^{2-} + \mathrm{e}^{-} \rightarrow \mathrm{Cu\,(adatom)} + \mathrm{Cit}^{3-}$$

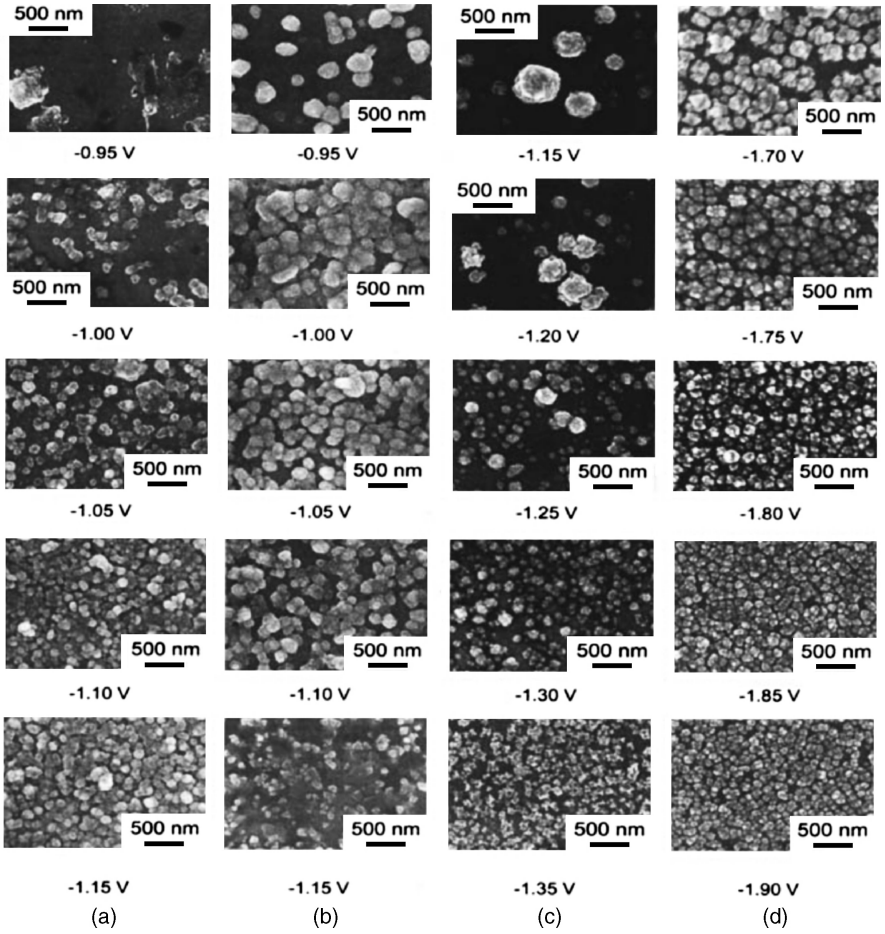

FIGURE 27.32 SEM Images of copper clusters in different solutions and growth potentials: (*a*) 50 m*M* Cu sulfate (pH 0.1); (*b*) fluoroborate solution (pH 1); (*c*) citrate (pH 3.1); (d) ethylenediaminetetracetate (EDTA) (pH 13.5). Reproduced with permission from [148], Copyright 2003, The Electrochemical Society.

This process is a combination of transport processes in the solution, adsorption, surface diffusion, and nucleation of reduced copper species [167]. As a consequence the *concentration ratio of Cu and citrate ions* is a factor that determines the morphology of deposited Cu films [145]. Cyclic voltammetry curves on both TaN and TiN are characterized by a single peak that marks an overlap of copper reduction from both Cu^{2+} and $CuCit^{-}$ ions in $[Cu^{2+}]/[Cit^{3-}] = 1$ solution (Fig. 27.34, I_1). The potentiostatic deposition at the peak potential results in 3D growth and rough

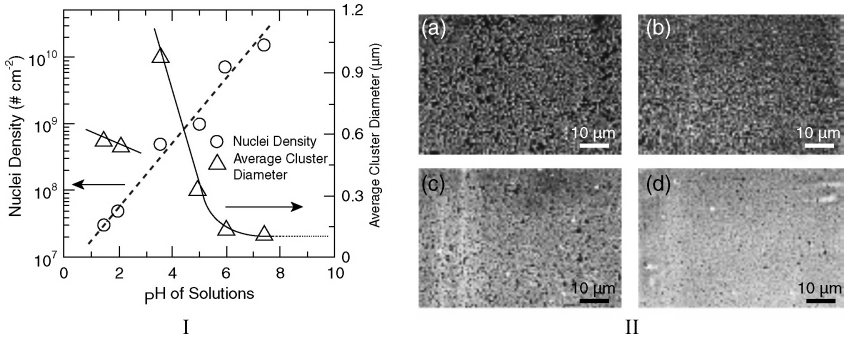

FIGURE 27.33 (I) Variation of copper nuclei density and average cluster diameter deposited on TiN in citrate solution: 0.08 M L^{-1} $CuSO_4$•5 H_2O + 0.08 M L^{-1} $(NH_4)_2HC_6H_5O_7$ of different pH. (II) SEM images of deposited copper islands: (*a*) pH 3.56 ($E = -1.55$V); (*b*) pH 5 ($E = -1.73$ V); (*c*) pH 6 ($E = -1.85$V); (*d*) pH 7.4 ($E = 2.13$ V). Reproduced with permission from [151], Copyright 2006, The Electrochemical Society.

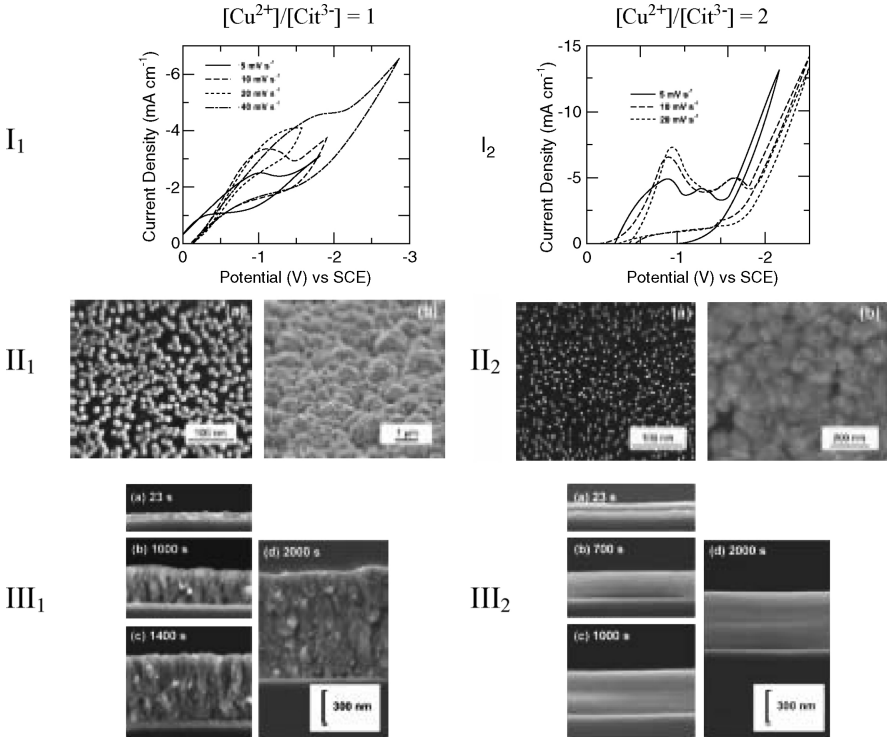

FIGURE 27.34 (I) Cyclic voltammograms of Cu–Cit bath with $[Cu^{2+}]/[Cit^{3-}] = 1, 2$ on TiN. (II) SEM images showing Cu on TiN: (II_1) after 5 and 500 s at potential -1.6 V in $[Cu^{2+}]/[Cit^{3-}] = 1$ bath; (II_2) Cu 3D clusters after 5 s at -0.95 V and Cu film grown after 500 s at potential -1.7 V in $[Cu^{2+}]/[Cit^{3-}] = 2$ bath. (III) SEM images of cross sections of copper film deposited on TaN (III_1) at -1.6 V in $[Cu^{2+}]/[Cit^{3-}] = 1$ bath; (III_2) at -1.75 V after 5 s at -0.95 V in $[Cu^{2+}]/[Cit^{3-}] = 2$ bath. Reproduced with permission from [145], Copyright 2007, The Electrochemical Society.

morphology. In contrast to that, in solution where $[Cu^{2+}]/[Cit^{3-}]$ 2, two voltammetric peaks are registered each marking the onset of $CuCit^{-}$ and Cu^{2+} reduction, respectively (Fig. 27.34, I_2). Using a two-step deposition for the case $[Cu^{2+}]/[Cit^{3-}] = 2$, smoother and lower resistivity Cu deposits are obtained on both TiN and TaN. The first deposition step here includes nucleation of Cu islands at the overpotential of $CuCit^{-}$ reduction followed by growth at higher overpotential associated with for Cu^{2+} reduction. Figure 27.34 illustrates the difference in the nucleation density and final Cu film morphology grown from the solutions $[Cu^{2+}]/[Cit^{3-}] = 1, 2$ at pH 3.56 on TiN and TaN. High nucleation density on the order of 10^8–10^{11} cm^{-2} can also be obtained for the pyrophosphate complexing solution commonly used in the electronics industry for printed circuit boards [147] on TiSiN. This finding suggests that potentiostatic growth under mixed control can also result in smooth and continuous Cu growth.

27.3.2 New Barrier Materials

Recently, new barrier layer materials have been considered to replace the commonly used Ta- and Ti-based barriers for seedless copper deposition in the damascene process [168–170]. Early work suggested a group of noble metals (i.e., Pt, Pd, Ru, Rh, Ir, Ag, Te, and Tc) [169] that could be suitable for direct Cu deposition from acidic Cu sulfate solutions. Cu seedless superfill of sub-100-nm features was demonstrated so far for Ru [169–174], Os [175], and Ir [176] (Table 27.6).

Among these candidates Ru has attracted most of the interest as a new barrier material owing to its favorable intrinsic properties such as electrical and thermal conductivity that are twice as large as those of Ta. In addition, the immiscibility of Cu and Ru would prevent possible alloying at the barrier–copper interface. A number of electrochemical [177–180] and vacuum studies [181, 182] of initial stages of Cu deposition on Ru have shown complete wetting with epitaxial and strained monolayer(s) at the initial stage followed by Stranski–Krastanov growth mode at higher thickness. Underpotential Cu monolayer (UPD) formation prior to the bulk deposition [177–180] is deemed a unique feature of Pt-based barrier layers because of its ability to serve as a wetting layer for subsequent Cu growth. UPD of Cu has been used as an analytical tool for roughness and morphology characterization of Ru (oxide-free) surface as well as an indicatior of the surface oxidation state [172, 180]. Moffat et al. [172, 173] showed in detail a very strong relationship between Ru surface pretreatment and experimental parameters of Cu deposition in standard Cu sulfate acidic solution in the presence of superfilling additives PEG, Cl, and SPS (or

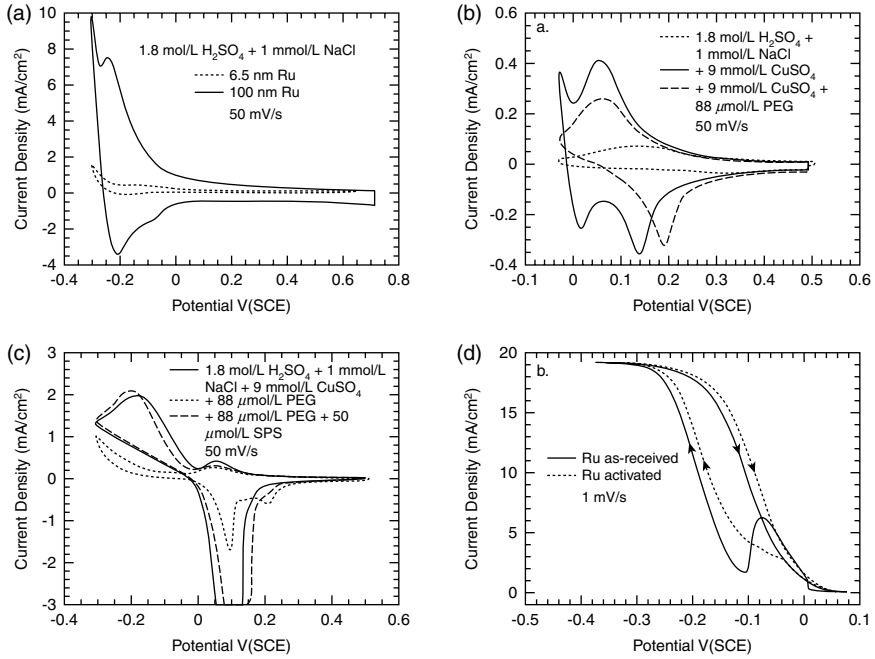

FIGURE 27.35 (*a*) Voltammetry revealing reduction of air-formed oxide on evaporated Ru films of different thickness exposed to air for more than one week. The difference in the reduction wave reflects the difference in the surface area due to roughness. (*b*) Voltammetry showing effect of PEG on Cu UPD on Ru. (*c*) Voltammetry showing effect of SPS on Cu deposition. SPS competes very effectively with PEG coadsorption during UPD on Ru-activated electrode and as a consequence the PEG-derived inhibition of bulk Cu deposition is significantly weakened. (*d*) Slow-scan voltammetry of Cu from superfilling PEG–Cl–Cu solution on activated and oxidized (as-received) Ru electrode. Hysterisis is associated with the competitive interaction of PEG and SPS and the wave observed on the oxidized Ru electrode is associated with Volmer–Weber Cu deposition. The result for activated Ru is similar to that of Cu electrode. Reproduced with permission from [172], Copyright 2006, The Electrochemical Society.

MPSA) [172, 173]. The extent of surface oxidation has significant effect on the nucleation and growth of copper. The air-grown 3D surface oxide can be reduced by polarization at -0.2 V (see Fig. 27.35*a*) in the hydrogen evolution region or by spontaneous activation in a H_2-saturated, Cu-free solution (where open circuit potential (OCP) changes from 0.69 V_{SCE} to -0.24 V_{SCE} in base solution 1.8 M H_2SO_4 + 1 mM Cl^-) [172, 173]. Subsequent anodic potential exposures result in the oxide formation that can be controlled to a monolayer level by applied potential ($<$0.5 V_{SCE}).

Electrodeposition of Cu activated by a monolayer oxide reduction electrode results in the formation of Cu UPD monolayer [177] (Fig. 27.35*b*). The presence of PEG on the activated Ru electrode influences the Cu UPD process by coadsorption of PEG–Cl, which reduces the UPD peak intensity and shifts the potential of UPD desorption to 50 mV more positive potential (Fig. 27.35*b*), thus confirming the stabilization effect of PEG on Cu–Cl UPD adlayer. The fact that the potential of Cu UPD peak formation does not change in the presence of PEG is consistent with the kinetics of this process that is controlled by the monolayer oxide reduction. The subsequent bulk deposition of Cu is inhibited by the PEG–Cl adlayer in the same manner as on the bulk Cu electrode (Fig. 27.35*c*). The presence of accelerating additive such as SPS hinders PEG–Cl blocking during Cu UPD. As a result, the bulk growth exhibits the identical electrochemical response and characteristics as on the bulk Cu electrode both in PEG–Cl–SPS solution. The high quality of Cu deposit with reliable adhesion, no terminal effects, and effective bottom-up feature filling has been observed for such activated Ru barrier layer (Figs. 27.36–27.38). Both potentiostatic (one-step) and three-step plating protocols have been employed for a successful superconformal growth. The three-potential pulse protocol (Fig. 27.38) is associated with (1) a potential step at 0.1 V_{SCE} for 30 s resulting in Cu UPD formation followed by (2) a potential step to -0.4 V_{SCE} for 1 s leading to rapid reduction of any residual oxide on the surface in combination with nucleation and coalescence of the Cu layer. The final step (3) constitutes a polarization at -0.2 V_{SCE} that has also been used for bottom-up filling of submicrometer features in a one-step procedure (Fig. 27.37).

The Cu UPD monolayer does not form on the oxidized Ru surface. The bulk deposition shown in Figure 27.35*d* proceeds following the 3D island (i.e., Volmer–Weber) growth mode. The presence of the hump on the CV is related to the nucleation of copper layer and the possible explanation is that there is no PEG–Cl adsorption on Ru [172, 183]. Thus the bulk deposition proceeds via 3D island nucleation and

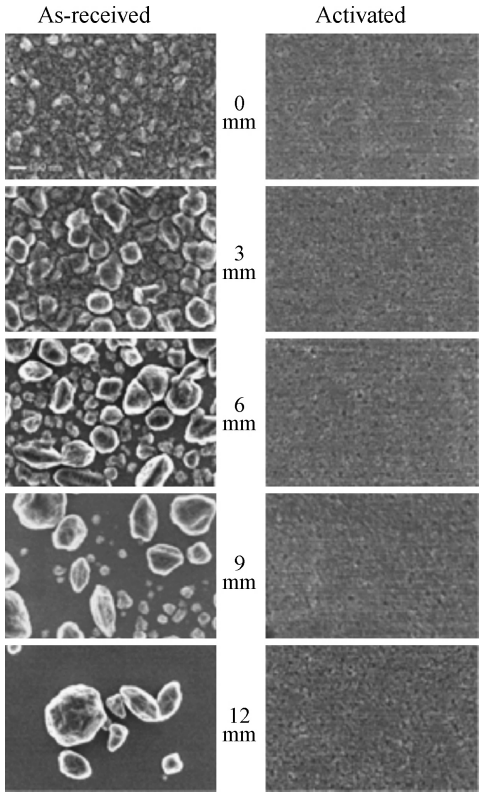

FIGURE 27.36 FEG SEM images demonstrating influence of Ru surface conditions and terminal effect on morphological evolution during Cu deposition. Cu was deposited at -0.2 V_{SCE} for 30 s in PEG–Cl–SPS electrolyte. Reproduced with permission from [172], Copyright 2006, The Electrochemical Society.

growth, that is, the Volmer–Weber growth mode (Fig. 27.35*d*). The electrochemical and optical characterizations show that on an air-oxidized Ru surface the oxide thickness influences the Cu morphology as the partial reduction of oxide can occur concomitantly with Cu deposition. In the presence of additives, Cu deposition proceeds initially by uninhibited growth that subsequently becomes quenched by PEG–Cl adsorption. Once the islands coalesce, the SPS adsorption becomes evident in the electrochemical transients. However, the resulting morphology is dramatically rougher than at the same potential for the activated Ru surface ($d_{coal} \sim 100$ monolayer). The adhesion properties of these films are very poor. A morphological heterogeneity is observed due to terminal effects on the oxide-covered surface as the potential drop significantly varies with the distance from the contact (Fig. 27.36). The oxide presence is seen as a reason for poor wetting and filling with void formation as shown in Figure 27.37.

In a separate study of nucleation and growth kinetics of Cu on air-oxidized PVD, Ru has been shown to have very rapid nucleation with nucleation density that is exponentially dependent upon the growth overpotential [171]. Although these results suggest that the concentration of additives and

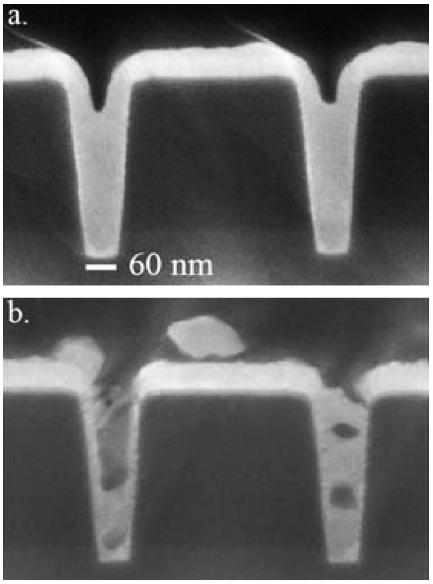

FIGURE 27.37 FEG SEM cross-sectional images illustrate the detrimental effect of Ru oxidation on trench filling with Cu deposited at -0.2 V_{SCE} for 7.6 s on (*a*) freshly deposited Ru barrier and (*b*) oxidized Ru. Reproduced with permission from [172], Copyright 2006, The Electrochemical Society.

Cu^{2+} ions in the solution do not influence the island distribution, these concentrations affect the island shape. The disc-shaped and hemispherical islands are observed in additive-free solution while irregular (flower) shaped islands (believed to result from the renucleation process) are observed in common Cu sulfate PEG–Cl–SPE solution. It

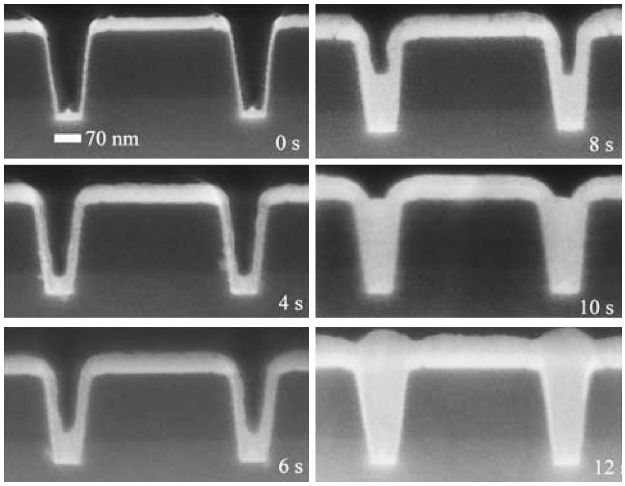

FIGURE 27.38 FEG SEM cross-sectional images of Cu superfilling using three-step pulse plating in PEG–Cl–SPS solution. The patterned PVD Ru electrode was immersed at 0.1 V for 30 s. Deposition was initiated by pulsing the potential to -0.4 V_{SCE} for 1 s and then stepping to -0.2 V_{SCE} for the duration of the experiments. Reproduced with permission from [172], Copyright 2006, The Electrochemical Society.

has been concluded, based on current transient shape and analysis of the island morphology and distribution, that Cu nucleation and growth do not follow any of the simple analytical models. Thus direct attachment, such as instantaneous or progressive nucleation followed by diffusion-limited growth of hemispherical islands, is completely ruled out. This implies that processes such as surface diffusion or mediation of intermediates play a significant role in the Cu deposition on an Ru oxide surface. The microstructure quality of a deposited Ru barrier layer and its continual coverage are essential for successful superfilling on patterned electrodes, particularly in very narrow features. Substantial porosity and roughness on side walls that can compromise the quality and performance of the final structure are observed for a PVD Ru layer. The ALD [172] and electrodeposition of Ru [174] are methods capable of producing smoother and conformal layers for which superfilling of submicrometer features was demonstrated as well.

Recently, it has been shown that Os [175] and Ir [176] can also be possible alternatives for barrier layers in Cu seedless deposition. Osmium [175] exhibits electronic, chemical and metallurgical properties similar to those of Ru. Also, the bulk electrical and thermal resistivities are lower than those of Ta. These factors along with the extremely low solubility with Cu and high (2700 K) melting temperature identify Os as a viable competitor of Ru as a diffusion barrier material. Following the work on Cu seedless deposition on Ru that showed the crucial role of surface treatment prior to deposition, a similar approach has been applied to the Os barrier layer. Samples with minimal air exposure or activated by reduction in sulfuric acid solution demonstrated superfilling in a standard Cu sulfate PEG–Cl–SPS bath by direct deposition at -0.2 V_{SCE} (Fig. 27.39*a*). Three-step pulse deposition in the same solution on Ir showed superfilling of trenches of different widths, as shown in Figure 27.39*b*. The intent of the three-step protocol was the same as the one already described in the case of Ru. It should be noted that the film conductivity of both metals Os and Ir is influenced by the terminal effect, that is, resistive iR voltage drop. However, no attempt has been made to control this effect in both cases. More studies of these systems are needed in order to determine whether the efficiency of Os and Ir is good enough for damascene interconnect applications.

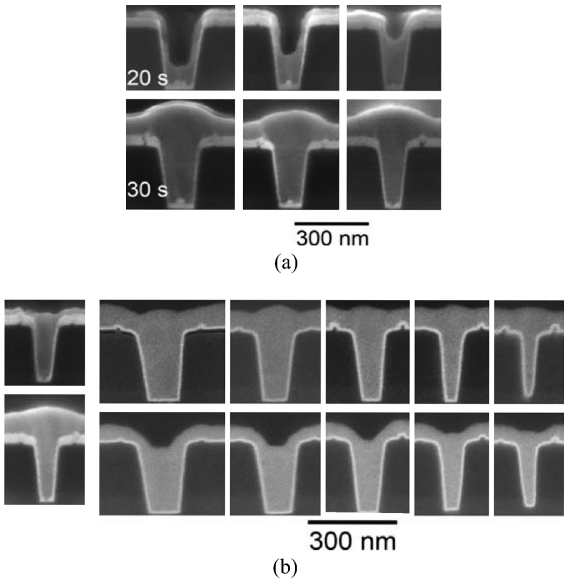

FIGURE 27.39 Cross-sectional SEM images of copper electrodeposition in trenches of various aspect ratios. (*a*) Os barrier layer: Surface was pretreated by polarization at -0.3 V_{SCE} for 30 s and the deposition proceeded at -0.2 V_{SCE}; see Table 27.6. Reproduced with permission from [175], Copyright 2006, The Electrochemical Society. (*b*) Ir barrier layer: deposition using potential step protocol; see Table 27.6. Reproduced with permission from [176], Copyright 2006, The Electrochemical Society.

27.4 DEVELOPMENT OF DEPOSITION TECHNIQUES FOR EPITAXIAL, SMOOTH, AND CONTINUOUS ULTRATHIN CU FILMS

The growth of smooth, homo- and heteroepitaxial metal layers has always been a major goal of electrodeposition [184]. Such layers are considered superior to any other kind of thin films as they strictly reproduce the crystallography and (in general) the morphology of the underlying substrate surface. In some occasions thin films are deposited on foreign substrates to achieve properties unattainable in the substrates alone [185]. Epitaxial thin films made of Au, Ag, and Cu are indispensable in the semiconductor industry as they feature reduced ohmic resistivity and electromigration that, along with their continuity [186–188], render these layers highly desirable in metal–metal junctions, barrier films, and corrosion protectors in printed circuit board fabrication and modern chip design.

Thin-film growth modes are generally classified as Frank–van der Merve or layer-by-layer 2D growth, Volmer–Weber or 3D cluster growth, and the Stranski–Krastanov (SK) mode associated with a transition from 2D to 3D growth [189]. Step-flow growth is a multilayer variant of the Frank–van der Merve mode and occurs at an appropriate step density and deposition flux. As long as a 2D mode is operating during growth (whether monolayer or multilayer), the resulting film is in the registry with the substrate structure. However, the vast majority of characterized heteroepitaxial systems display either a 3D or SK growth mode at ambient temperature regardless of the growth environment (vacuum or solution) [184]. In addition, owing to kinetic issues, 3D growth is often encountered even in overlayer/substrate systems that should, according to thermodynamic considerations, grow in a flat, 2D mode. As a result, 3D clusters that are far apart grow predominantly in the vertical direction to merge eventually at a considerable layer thickness in random fashion. This in turn gives rise to the growth of grains with

TABLE 27.6 Solutions Design for Cu Deposition on New Barrier Materials

Bath Composition	Method and Conditions	Barrier Layer	References
0.05 $M\,L^{-1}$ $CuSO_4 \cdot 5\,H_2O$ 0.5 $M\,L^{-1}$ $HOCCOOH(CH_2COOH)_2$ 0.93 M Na_2SO_4 pH 2.5–5.0	Two step procedure: • Potential pulse nucleation • Potentiostatic growth	50 nm TaN (250 μΩ-cm)	148
0.1 M $CuSO_4 \cdot 5\,H_2O$ 0.2 $M\,L^{-1}$ $HOCCOOH(CH_2COOH)_2$ 0.05 M H_3BO_3 pH 12	Potentiostatic and galvanostatic growth	Cu/Ta bilayer, Cu seed ∼ 5 nm	166
0.08 $M\,L^{-1}$ $CuSO_4 \cdot 5\,H_2O$ 0.08 $M\,L^{-1}$ $(NH_4)_2HC_6H_5O_7$ pH 3.56	Pretreated samples to remove oxide layer succeeded by deposition at −1.55 V_{SCE}	TaN, TiN	145,151
0.14 M $CuSO_4 \cdot 5\,H_2O$ 0.07 M $(NH_4)_2HC_6H_5O_7$ pH 3.5	Pretreated samples to remove oxide layers. Two step procedure: • Nucleation at −0.95 V_{SCE} (5 s) • Growth at −1.7 V_{SCE}	TaN, TiN	145
0.24 $M\,L^{-1}$ $CuSO_4 \cdot 5\,H_2O$ 1.8 $M\,L^{-1}$ H_2SO_4 1.0 mM NaCl 88 μ$M\,L^{-1}$ PEG (Mw 3400) 50 μ$M\,L^{-1}$ SPS	Activation of Ru surface by polarization at −0.2 V for 30 s in Cu-addive-free solution; then: 1. method—deposition at −0.2 V_{SCE}; method—immersion at 0.1V_{SCE} for 30 s. Pulsing the potential to −0.4 V_{SCE} for 1 s followed by stepping to −0.2 V_{SCE}	Ru	172
0.24 $M\,L^{-1}$ $CuSO_4 \cdot 5\,H_2O$ 1.8 $M\,L^{-1}$ H_2SO_4 1.0 mM NaCl 88 μ$M\,L^{-1}$ PEG (Mw 3400) 50 μ$M\,L^{-1}$ SPS	Potentiostatic deposition at −0.2 V_{SCE}	Os	175
0.24 $M\,L^{-1}$ $CuSO_4 \cdot 5\,H_2O$ 1.8 $M\,L^{-1}$ H_2SO_4 1.0 mM NaCl 88 μ$M\,L^{-1}$ PEG (Mw 3400) 50 μ$M\,L^{-1}$ SPS	1. Immersion at 0.1V_{SCE} for 30 s 2. Potential step −0.4 V_{SCE} for 1 s 3. Potential step −0.2 V_{SCE}	Ir	176

different crystallographic orientation, rendering the metal deposit polycrystalline. The mainstream effort to make these polycrystalline films more continuous, uniform, and smoother involves usage of additives considered earlier in this chapter such as PEG, SPS, and thiourea [190, 191]. However, along with their positive impact on the growth process, the additives promote the growth of polycrystalline films with relatively high concentration of defects and often contaminated by the additive molecule or by other by-products formed during the deposition process [104].

27.4.1 Defect-Mediated Growth

A major advance in electrodeposition (that is cost effective and easier to control than growth in UHV) of epitaxial metal deposits was made by Sieradzki et al. with the development of defect-mediated growth (DMG) [184]. The strategy used to manipulate the growth kinetics in DMG is based on previously published UHV deposition experiments that examined Ag/Ag(111) homoepitaxy [192]. At ambient temperature, because of kinetics, this system displays 3D growth. Rosenfeld et al. [192] found that, by depositing Ag atoms on a substrate with an artificially created high density of Ag clusters, several monolayers of layer-by-layer growth could be induced. This was accomplished by ion bombarding the surface with a low-energy Ar^+ pulse after the completion of each monolayer. DMG was developed as an electrochemical technique that serves to significantly enhance the ambient temperature nucleation of 2D islands (Fig. 27.40).

In this approach, the metal of interest is codeposited with a reversibly deposited mediator metal. The mediator is periodically deposited and stripped from the surface by appropriate cycling of the electrochemical potential while the metal of interest is steadily plated. Each cycle creates new nuclei on the surface and makes the ones developed in previous cycles bigger. A high density of 2D clusters on a growing layer is maintained by the appropriate choice of deposition flux and cycling frequency. A monolayer is completed as the growing 2D clusters eventually merge. A necessary characteristic of the mediator is that it must be

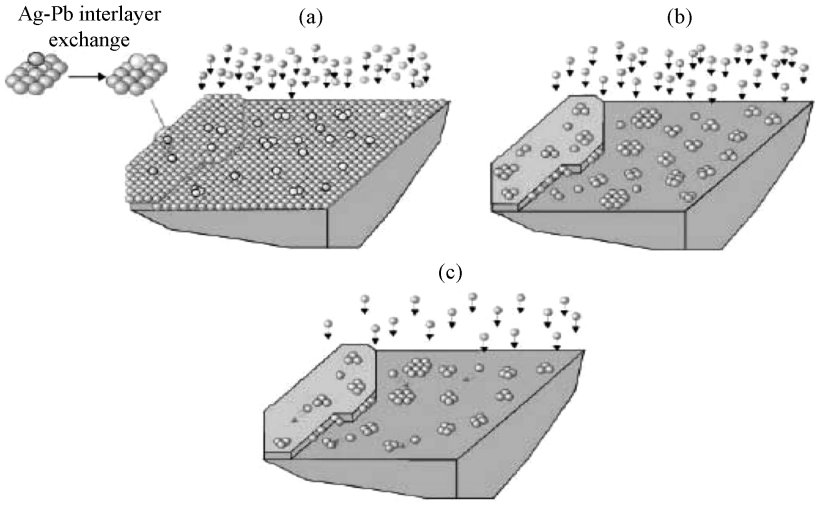

FIGURE 27.40 Schematic diagram of the proposed mechanism of Pb- and Cu-mediated deposition of Ag. The Pb, Cu, and Ag atoms are light gray, gray, and dark gray, respectively, and arrows on spheres indicate depositing metal cations in the electrolyte. (*a*) Lead mediation. A UPD Pb monolayer covers the Ag(111) surface. The deposited Ag adatoms undergo interlayer place-exchange with Pb atoms (light gray), forming 2D islands below the Pb layer. Reversing the potential the Pb layer is stripped from the surface (*c*) as Ag continues to deposit, resulting in island growth. (*b*) Copper mediation At given cathodic potential Cu adatoms are deposited on the Ag surface, froming 2D nuclei that serve as attachment sites for Ag adatoms on the surface. On the reverse portion of the cycle, Cu is selectively stripped from the surface (*c*), causing the Ag–Cu islands to decompose into 2D Ag islands that serve as growth canters as Ag continues to deposit. Reprinted from [184] by permission AAAS.

electrochemically less noble than the metal of interest. Using this approach, Sieradzki et al. [184] demonstrated the applicability of DMG for the growth of 250-monolayer (ML)–thick epitaxial Ag film on Au (111) substrates. It was also shown by Rutherford backscattering (RBS) that the as-grown Ag layer is Pb free [184]. Later Kwak et al. [193] extended the applicability of DMG to the growth of 100-ML-thick epitaxial copper film on Au (111) substrate (Fig. 27.41).

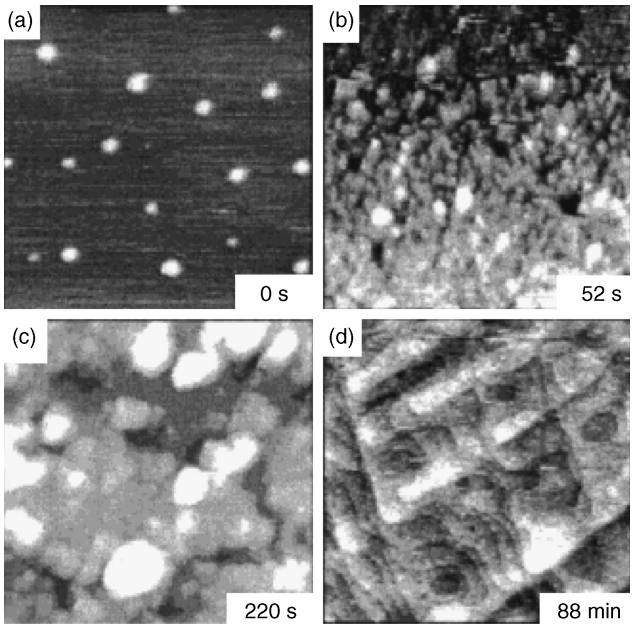

FIGURE 27.41 Temporal sequence of in situ STM images of Cu electrodeposition on Au(111) with Pb mediator: (*a*) 149 nm×149 nm image of initial stage of Cu UPD on Au(111) terrace. Growth of Cu adlayers after (*b*) two 1-s pulses to 0.050 V and (*c*) six pulses. Acquisition time of (*a–c*) was 42 s. (*d*) Thicker Cu film (∼100 MLs which was measured by stripping voltammetry) after 2000 pulses (380 nm×380 nm). At the lower right corner is shown the time at which scan started. In all images, the *y*-scan direction is downward. Reprinted with permission from [193], Copyright 2001, American Chemical Society.

Thus, the authors of [193] proved the DMG superiority to other existing deposition techniques by managing to handle deposition in a layer-by-layer mode in a heteroepitaxial system featuring atomic mismatch as large as 11% [193]. The crystallographic orientation and continuity of the ultrathin copper layer in [193] was ascertained by XRD and cyclic voltammetry of Pb UPD on bare and Cu-coated Au (111), respectively. Auger spectroscopy analysis suggested that the DMG-grown Cu layer in [193] was also Pb free. While the relaxation mechanism of the interface strain still remains unclear, the mechanism operating in the DMG method is well understood. It should be noted that results of similar quality were obtained by using Cu as mediator in the deposition of Ag on Au (111) [194]. Later, in an attempt to understand better the DMG mechanism, Wang et al. [195] demonstrated, by X-ray specular reflectivity, measurements that nearly complete mono- and bilayer Ag films could be grown in an overpotential regime by the optimized DMG protocol.

27.4.2 Surfactant-Mediated Growth

Another manifestation of the close relationship between the UHV epitaxy and electrodeposition is the development of a surfactant-mediated growth (SMG) method [196]. The protocol employed in SMG is inspired by earlier UHV work of Camarero et al. [197] demonstrating layer-by-layer growth of Cu on Pb-covered Cu(111) that occurs at 300 K. In this work [197] the Pb layer acting as "surfactant" is believed to float on the top of the depositing metal, thus facilitating the intralayer transport and promoting 2D growth [198]. In the solution version of SMG a predeposited submonolayer of Pb on the growing Ag or Cu layer was used as surfactant [196]. The Pb coverage was controlled strictly by the applied potential in the UPD range [196]. A proof-of-concept work in the late 1990s illustrated the applicability of SMG in the layer-by-layer growth of more than 200 MLs of inclusion-free Ag on Au (111) substrates. Later an SMG protocol was employed also for the epitaxial growth of more than 50 MLs of Cu on Cu (111) substrate (Fig. 27.42) [199]. Although structural characterization and elemental analysis suggest smooth and inclusion-free epitaxial films grown by DMG and SMG [184, 196], these methods are still subject to some limitations and practical inconvenience that need to be addressed. For instance, both methods are tunable over a variety of parameters, including metal concentration, scan rate, potential limits, and submonolayer coverage that are mutually dependent and thus difficult to balance. Also, the thickness control (via charge measurements) during growth is hindered by the interference of factors such as side reactions and double-layer charging that, especially in DMG, are manifested by currents comparable to (or even exceeding) the deposition current level. Finally, while very low, the possibility for incorporation of a mediator into the deposit cannot be completely ruled out at high deposition rates of the metal of interest [198].

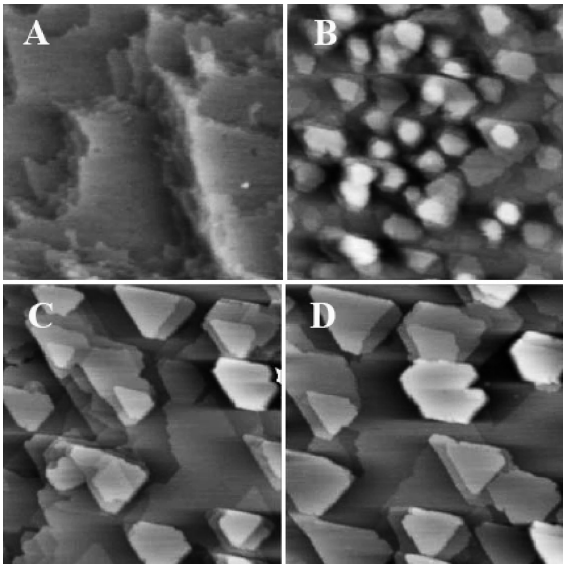

FIGURE 27.42 Time sequence of in situ STM images 255×255 nm of Pb surfactant-mediated growth of Cu on Cu (111) in $10^{-2}\,M$ $Pb(ClO_4)_2 + 10^{-4}\,M$ $Cu(ClO_4)_2 + 10^{-1}\,M$ $HClO_4$ solution. (*a*) Bare Cu (111) surface. (*b*) Copper after 3 min of deposition at $E = -0.285$ V versus $Cu/10^{-4}\,M$ Cu^{2+} that corresponds to the 1 monolayer of Pb surfactant coverage. (*c*) Cu layer after 10 min of electrodeposition. (*d*) Cu layer after 20 min of electrodeposition. Average growth rate of Cu is 2 ML min^{-1} [199].

27.4.3 Surface-Limited Redox Replacement Reaction

Early in the new century, Brankovic et al. illustrated that a predeposited, surface-limited Cu UPD adlayer can be used as a sacrificial layer to control the growth of a submonolayer amount of Pt on Au(111) by exchanging the Cu in a Pt ion solution at an open circuit (OC) (Fig. 27.43) [200, 201]. Their results suggested the growth of very small, monoatomically high nanoclusters randomly distributed over the

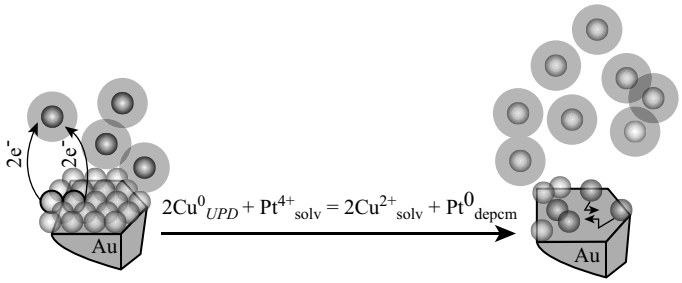

FIGURE 27.43 Schematic of replacement of Cu by Pt in charge transfer process via direct Cu^0 adatom Pt^{4+} ion interaction. Dark and light gray balls represent Pt and Cu atoms, respectively. Gray clouds around balls indicate ions. Reprinted from [200], Copyright 2001, with permission from Elsevier.

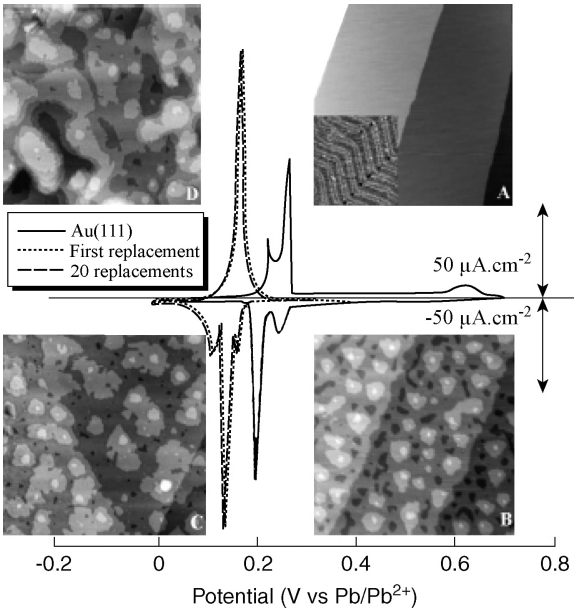

FIGURE 27.44 Cyclic voltammetry of bare and coated Ag layers Au(111) in 3×10^{-3} *M* $Pb(ClO4)_2 + 1 \times 10^{-1}$ *M* $NaClO_4$ (pH 2) at sweep rate of 10 mV s^{-1}. STM images (570 × 570 nm) illustrating (*a*) thermally reconstructed Au(111) surface _inset size 60 × 60 nm and (*b*) same surface after lifting of reconstruction. (*c*, *d*) Morphology evolution with growth of 2 and 35 Ag layers, respectively. The *Z* range is 1.5 nm for (*a*), (*b*), and (*c*) and 2.5 nm for (*d*). Reproduced with permission from [203], Copyright 2005, The Electrochemical Society.

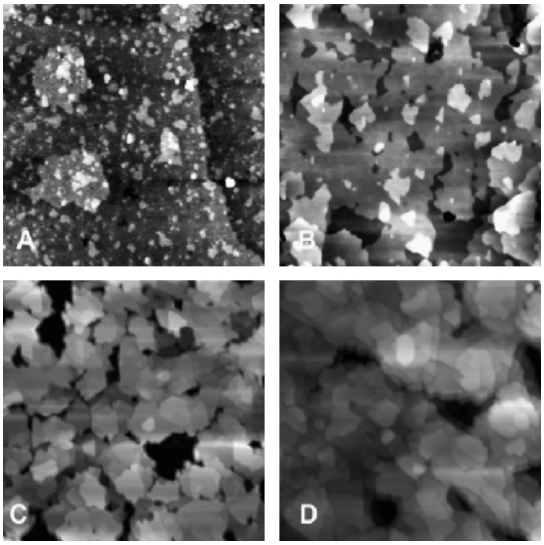

FIGURE 27.45 STM micrographs showing morphology evolution of Cu thin film deposited in "one-pot" configuration by redox replacement of Pb UPD layer on Au(111): (*a*) (Z range 3 nm), 5 MLs thick; (*b*) (Z range 3.5 nm), 15 MLs thick; (*c*) (Z range 5 nm), 50 MLs thick; and (*d*) (Z range 6.5 nm), 100 MLs thick. The scan size for all images is 250 × 250 nm. Reprinted with permission from [206], Copyright 2007, American Chemical Society.

surface [200]. Such reactions are referred to here as surface-limited redox replacement (SLRR) reactions. Despite the random distribution of these nanoparticles, the results of Brankovic et al. hinted at the possibility of forming ideal single-crystalline nanofilms of Pt by repeating this SLRR in a layer-by-layer methodology (analogically with EC-ALE [201]. In fact, Weaver et al. made first attempts to grow Pt nanofilms by repeating several times the application of SLRR [202]. Later, Stickney et al. published the first atomic-level study of multiple applications of SLRR showing that at least three displacement events are necessary for the growth of a continuous Pt layer that completely screens the underlying Au surface [204]. At the same time, Dimitrov et al. demonstrated for the first time the growth of thin Ag film of thickness exceeding 10 nm by SLRR using Pb and Tl as sacrificial metals [203, 205]. In this work the excellent quality of the deposit manifested by a steady quality of Pb UPD voltammetry and ascertained by a flat and uniform surface morphology (Fig. 27.44) demonstrated the applicability of SLRR for thin-film growth [203].

The growth of ultrathin copper films by SLRR of Pb as sacrificial metal was presented in another work of Dimitrov's group where cyclic voltammetry, in situ scanning tunneling microscopy (STM), and XRD were used to monitor the two-dimensional growth and characterize the structure of up to 100 MLs of Cu on Ag (111) and Au (111) substrates [206]. The excellent surface quality of an epitaxially grown Cu film is manifested by a distinct Pb UPD voltammetry and ascertained by in situ STM showing uniform surface morphology maintained during the entire growth process (Fig. 27.45). In an attempt to elucidate more details from the very beginning of the growth in the system in [22], Stickney et al. performed an atomic-level study of up to 10 redox replacement cycles [207]. In this work the entire study was performed

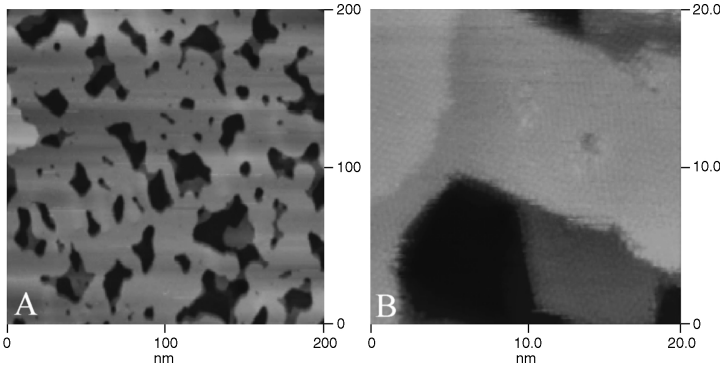

FIGURE 27.46 In situ STM images of morphology after Cu UPD and three Cu replacements (*a*) (200 × 200 nm) and (*b*) (20 × 20 nm). Reproduced with permission from [207], Copyright 2007, The Electrochemical Society.

TABLE 27.7 Experimental Conditions for Growth of Epitaxial Copper Thin Films

Method	References	Plating Solution	Polarization Conditions, Potential versus Normal Hydrogen Electrode	Characterization	Thickness
DMG	193	1 m*M* Cu(NO3)2 + 0.1 *M* HClO4 + 0.1 *M* Pb(ClO4)2	Potential cycling: 0.180 V to −0.170 V 0.5 s −0.170 V to 0.180 V 2 s	Morphology: STM and CV (Pb UPD) Structure: XRD Composition: AES	Up to 20 nm
SMG	199	0.1 m*M* $Cu(ClO_4)_2$ + 0.01 *M* $Pb(ClO_4)_2$ + 0.1 *M* $HClO_4$	Deposition at constant potential: −0.060 V for 20 min	Morphology: STM Composition: RBS	Up to 10 nm
SLRR	208	0.3 m*M* $Cu(ClO_4)_2$ + 0.010 *M* $Pb(ClO_4)_2$ + 0.010 *M* $HClO_4$.	One cycle: potential pulse to for Pb UPD layer 2 s to −0.200 V followed by 15 s at OC for the redox exchange to take place	Morphology: STM and CV (Pb UPD) Structure: XRD and High-resolution STM Composition: XPS	Up to 25 nm *By repeating the plating cycle*
SLRR	207	Solution 1: 0.1: m*M* KI + 0.1 *M* HClO4 Solution 2: 1 m*M* $CuSO_4$ + 5 m*M* H_2SO_4 Solution 3: 0.5 m*M* $Pb(ClO_4)_2$ + 0.25 m*M* KI + 0.05 M $HClO_4$	Only once 2 min OC in solution 1 to form 1 mL of iodide One cycle: In a flow cell: (i) 2 min potential pulse −0.160 V to form Pb UPD layer in solution 2 and (ii) switch to solution 3 at OC for 10 s for the redox exchange to take place	Morphology: STM and CV (I adsorption) Structure: LEED and high-resolution STM Composition: AES	Up to 2 nm *By repeating the plating cycle*

in a UHV chamber which allowed for low-energy electron diffraction, Auger spectroscopy monitoring, and STM monitoring of the deposit surface morphology and Cu layer composition. While initially rougher than anticipated, the atomic layers were found to anneal out after sufficient time. Excellent morphology in comparison with what would result from standard electrodeposition methodologies and the expected (3×3) I structure observed elsewhere [208] for Cu deposition on I-coated Au (111) was eventually registered in this study (Fig. 27.46). It should be noted that the compositional analysis carried out by either Auger spectroscopy [204, 207] or X-ray photoelectron spectroscopy (XPS) [203, 205–207] of different layers grown by SLRR suggested no presence of even traces of sacrificial metals used to assist the deposition process.

In conclusion, the techniques presented here for the growth of continuous, uniform, and epitaxial thin metal films represent significantly different methodology for copper plating to the conventional one described and summarized in the previous chapter. The quality of copper layers grown by protocols with experimental parameters summarized in Table 27.7 substantially exceeds the one of industrially plated copper. Indeed, these approaches are the only ones known to produce epitaxial copper deposits grown in a quasi-2D mode. At the same time it should be noted that techniques of this kind are substantially slower and more sensitive to impurities and/or side reagents participating in the deposition process. Overall, the methods described in this section could have limited use yet for some very specific purposes are deemed indispensable.

ACKNOWLEDGMENT

This work was supported by the University of Houston, University of Bristol, and State University of New York at Binghamton.

REFERENCES

1. C. L. Mantell, *Electrochemical Engineering*, McGraw Hill, New York, 1960.
2. E. I. Cooper, C. Bonhote, J. Heidmann, Y. Hsu, P. Kern, J. W. Lam, M. Ramasubramanian, N. Robertson, L. T. Romankiw, and H. Xu, *IBM J. Res. Dev.*, **49**, 103 (2005).
3. S. R. Brankovic, X. M. Yang, T. J. Klemmer, and M. Siegler, *IEEE Trans. Magn.*, **42**, 132 (2006).

4. P. C. Andricacos, *Electrochem. Soc. Interface*, **8**, 32 (1999).
5. M. Datta, R. V. Shenoy, C. Jahnes, P. C. Andricacos, J. Horkans, J. O. Dukovic, L. T. Romankiw, J. Roeder, H. Deligianni, H. Nye, B. Agarwala, H. M. Tong, and P. Totta, *J. Electrochem. Soc.* **142**, 3779 (1995).
6. H. Deligianni, *Electrochem. Soc. Interface*, **15**, 33 (2006).
7. W. Ehrfeld, *Electrochim. Acta*, **48**, 2857 (2003).
8. L. T. Romankiw and D. A. Thompson,U.S. Patent 4,295,173 (1981)
9. N. Robertson, H. L. Hu, and C. Tsang, *IEEE Trans. Magn.*, **33**, 2818 (1997).
10. I. Tabakovic, S. Riemer, V. Inturi, P. Jallen, and A. Thayer, *J. Electrochem. Soc.*, **147**, 219 (2000).
11. T. Osaka, M. Takai, K. Hayashi, K. Ohashi, M. Saito, and K. Yamada, *Nature*, **392**, 796 (1998).
12. X. M. Liu, G. Zangari, and M. Shamsuzzoha, *J. Electrochem. Soc.* **150**, C159 (2003).
13. S. Khizroev and D. Litvinov, *Perpendicular Magnetic Recording*, Springer-Kluwer Academic Publishers, New York, 2004.
14. T. Osaka, T. Yokoshima, D. Shiga, K. Imai, and K. Takashima, *Electrochem. Solid-State Lett.*, **6**, C53 (2003).
15. X. M. Yang, H. Gentile, A. Eckert, and S. R. Brankovic, *J. Vac. Sci. Tech. B*, **22**, 3339 (2004).
16. X. M. Yang, A. Eckert, K. Mountfield, H. Gentile, C. Seiler, S. R. Brankovic, and E. Johns, *J. Vac. Sci. Tech. B*, **21**, 3017 (2003).
17. R. M. Bozorth, *Ferromagnetism*, Van Nostrand Reinhold Co., Princeton, NJ, 1951.
18. S. Hessami and C. W. Tobias, *J. Electrochem. Soc.*, **136**, 3611 (1989).
19. J. A. Bolzan and A. J. Arvia, *Electrochim. Acta*, **7**, 589 (1962).
20. A. A. El Miligy, F. Hilbert, and W. J. Lorentz, *J. Electrochem. Soc.*, **120**, 247 (1973).
21. H. Dahms, *J. Electroanal. Chem.*, **8**, 5 (1964).
22. L. T. Romankiw, in *Electrodeposition Technology, Theory and Practice*, L. T. Romankiw and D. R. Turner, Ed., Electrochemical Society, Pennington, NJ, 1987, p. 301.
23. S. S. Zhumdahl, *Chemistry*, 3rd ed., Heath and Co., Lexinton, 1993, p. 637.
24. N. Zech and D. Landolt, *Electrochim. Acta*, **45**, 3461 (2000).
25. J. V. Powers and L. T. Romankiw, U.S. Patent 3,652,442 (1972).
26. G. J. Wilson and P. R. McHugh, *J. Electrochem. Soc.*, **152**, C356 (2005).
27. D. T. Schwartz, B. G. Higgins, P. Stroeve, and D. Borowski, *J. Electrochem. Soc.*, **134**, 1639 (1987).
28. A. A. Sonin, *J. Electrochem. Soc.*, **130**, 1501 (1983).
29. H. Schultz and M. Pritzker, *J. Electrochem. Soc.*, **145**, 2033 (1998).
30. Y. Zhuang and E. J. Podlaha, *J. Electrochem. Soc.*, **150**, C225 (2003).
31. S. Gadad and T. M. Harris, *J. Electrochem. Soc.*, **145**, 3699 (1998).
32. D. R. Lide, *CRC Handbook of Chemistry and Physics*, 86th ed., CRC Press, Boca Raton, FL, 2005, p. 8.
33. L. Pailung, *General Chemistry*, 3rd ed., W. H. Freeman, London, 1970, p. 445.
34. J. W. Mullin, *Crystallization*, 4th ed., Butterworth-Heinemann, Oxford, 2001, p. 108.
35. S. R. Brankovic, S. -E. Bae, and D. Litvinov, *Electrochim. Acta*, **53**, 5934 (2008).
36. S. R. Brankovic, K. Sendur, T. Klemmer, X. Yang, and E. C. Johns, in *Magnetic Material, Processes and Devices VII and Electrodeposition of Alloys, 202nd ECS Meeting Proceeding*, S. Krongelb, L. T. Romankiw, Y. Kitamoto, S. R. Brankovic, C. Bonhote, G. Zangari and W. Schwarzacher, Eds., Electrochemical Society, Pennington, NJ, 2003, p. 269.
37. T. R. Rosebrugh and W. L. Miller, *J. Phys. Chem.*, **14**, 816 (1910).
38. C. Wagner, *J. Electrochem. Soc.*, **98**, 116 (1951).
39. M. Schlesinger and M. Paunovic, *Modern Electroplating*, Willey, Hoboken, NJ, 2000.
40. T. Osaka, T. Sawaguchi, F. Mizutani, T. Yokoshima, M. Takai, and Y. Okinaka, *J. Electrochem. Soc.*, **146**, 3295 (1999).
41. B. N. Popov, K. -M. Yin, and R. E. White, *J. Electrochem. Soc.*, **140**, 1321 (1993).
42. S. R. Brankovic, N. Vasiljevic, T. J. Klemmer, and E. C. Johns, *J. Electrochem. Soc.*, **152**, C196 (2005).
43. J. Edwards, *Trans. Inst. Met. Finish*, **39**, 52 (1962).
44. S. R. Brankovic, F. Wiatrowski, and M. Siegler, " Sacharin Incorporation in CoFe Alloys—Consequences for Magnetic and Corrosion Properties," paper presented at ECS Meeting, Abstract 208, Quebec City, 2005, p. 475.
45. S. R. Brankovic, R. Haislmaier, and N. Vasiljevic, *Electrochem. Solid-State Lett.*, **10**, D67 (2007).
46. G. S. Frankel, V. Brusic, R. G. Schad, and J. W. Chang, *Corr. Sci.*, **35**, 63 (1993).
47. T. Osaka, M. Takai, Y. Sogawa, T. Momma, K. Ohashi, M. Saito, and K. Yamada, *J. Electrochem. Soc.*, **146**, 2092 (1999).
48. H. Kwon and A. A. Gewirth, *J. Electrochem. Soc.*, **154**, D577 (2007).
49. C. Buessherman, *Prog. Sur. Sci.*, **46**, 335 (1994).
50. B. B. Damaskin, O. A. Petri, and V. V. Batrakov, *Adsorption of Organic Compounds on Electrodes*, Plenum, New York, 1971, p. 259.
51. J. O'M. Bockris and A. K. N. Reddy, *Modern Electrochemistry*, Vol. 2, Plenum, New York, 1970, p. 791.
52. J. O'M. Bockris and D. A. J. Swinkels, *J. Electrochem. Soc.*, **111**, 736 (1964).
53. I. Tabakovic, S. Riemer, K. Tabakovic, M. Sun, and M. Kief, *J. Electrochem. Soc.*, **153**, C586 (2006).
54. S. R. Brankovic, R. Haislmaier, and N. Vasiljevic, *Electrochem. Soc. Trans.*, **3**, 71 (2007).
55. J. George, S. -E. Bae, D. Litvinov, J. Rancheler, and S. R. Brankovic, *J. Electrochem. Soc.*, **155**, D589, (2008).

56. C. H. Hamann, A. Hamnett, and W. Vielstich, *Electrochemistry*, Wiley-VCH, New York, 1998, p. 187.
57. W. Bang and K. Hong, *Electrochem. Solid-State Lett.*, **10**, J86 (2007).
58. I. Tabakovic, V. Inturi, and S. Riemer, *J. Electrochem. Soc.*, **149**, C18 (2002).
59. H. V. Venkatasetty, *J. Electrochem. Soc.*, **117**, 403 (1970).
60. L. B. Freund and S. Suresh, *Thin Film Materials: Stress, Defect Formation, and Surface Evolution*, Cambridge University Press, Cambridge, MA, 2003.
61. G. E. Dieter, *Mechanical Metallurgy*, 3rd ed., McGraw Hill, New York, 1986, p. 145.
62. J. R. Rice, *Effect of Hydrogen on Behaviour of Materials*, Metallurgical Society of AIME, Houston, TX, 1976, p. 375.
63. S. R. Brankovic, in preparation,
64. B. D. Cullity and S. R. Stock, *Elements of X-Ray Diffraction*, Prentice-Hall, Upper Saddle River, NJ, 2001.
65. L. Ricq, F. Lallemand, M. P. Gigandet, and J. Pagetti, *Surf. Coat. Technol.*, **138**, 278 (2001).
66. F. Lallemand, L. Ricq, P. Bercot, and J. Pagetti, *Electrochim. Acta*, **47**, 4149 (2002).
67. U. R. Evans, in *The Corrosion and Oxidation of Metals*, ASM-Edward Arnold, London, 1981, p. 248.
68. G. A. Prentice, *Electrochemical Engineering Principles*, Prentice-Hall, Englewood Cliffs, NJ, 1990, p. 143.
69. V. Jovancevic and J. O. M. Bockris, *J. Electrochem. Soc.*, **133**, 1797 (1986).
70. I. Tabakovic, S. Riemer, M. Sun, V. Vas'ko, J. Qui, and M. Kief, *Electrochem. Soc. Trans.*, **3**, 47 (2007).
71. Q. Huang, C. Bonhote, J. Lam, and L. T. Romankiw, *Electrochem. Soc. Trans.*, **3**, 61 (2007).
72. P. C. Andricacos and L. T. Romankiw, in *Advances in Electrochemical Science and Engineering*, Vol. 3, H. Gerischer and C. W. Tobias, Ed., VCH Publishers, Weinheim, 1994, p. 227.
73. I. W. Wolf, *J. Electrochem. Soc.*, **108**, 959 (1961).
74. X. M. Liu, G. Zangari, and L. Y. Shen, *J. Appl. Phys.*, **87**, 5410 (2000).
75. L. Neel, *J. Phys. Radium*, **17**, 250 (1956).
76. H. Hoffmann and T. Fujii, *J. Magn. Magn. Mater.*, **128**, 395 (1993).
77. P. C. Andricacos, C. Uzoh, J. O. Dukovic, J. Horkans, and H. Deligianni, *IBM J. Res. Dev.*, **42**, 567 (1998).
78. R. Rosenberg, D. C. Edelstein, C.-K. Hu and K. P. Rodbell, *Annu. Rev. Mater. Sci.*, **30**, 229 (2000).
79. R. L. Jackson, E. Broadbent, T. Cacouris, A. Harrus, M. Biberger, E. Patton, and T. Walsh, *Solid State Tech.*, **41**, 49 (1998).
80. K. K. H. Wong, S. Kaja, and P. W. DeHaven, *IBM J. Res. Dev.*, **42**, 587 (1998).
81. D. C. Edelstein, G. A. Sai-Halasz, and Y.-J. Mii, *IBM J. Res. Dev.*, **39**, 383 (1995).
82. C. Ryu, K.-W. Kwon, A. L. S. Loke, H. Lee, T. Nogami, R. A. Kavari, G. W. Ray, and S. S. Wong, *IEEE Trans. Electron Devices*, **46**, 1113 (1999).
83. B. Chin, P. Ding, B. Sun, T. Chiang, D. Angelo, I. Hashim, S. Edelstein, and F. Chen, *Solid State Tech.*, **41**, 141 (1998).
84. J. Reid, S. Mayer, E. Broadbent, E. Klawuhn, and K. Ashtiani, *Solid State Tech.*, **43**, 86 (2000).
85. D. Stoychev and C. Tsvetanov, *J. Appl. Electrochem.*, **26**, 741 (1996).
86. J. J. Kelly and A. C. West, *J. Electrochem. Soc.*, **145**, 3472 (1998).
87. J. J. Kelly and A. C. West, *J. Electrochem. Soc.*, **145**, 3477 (1998).
88. J. Reid, *Jpn. J. Appl. Phys., Part 1*, **40**, 2650 (2001).
89. A. C. West, S. Mayer, and J. Reid, *Electrochem. Solid-State Lett.*, **4**, C50 (2001).
90. T. P. Moffat, D. Wheeler, C. Witt, and D. Josell, *Electrochem. Solid State Lett.*, **5**, C110 (2002).
91. M. Tan and J. N. Harb, *J. Electrochem. Soc.*, **150**, C420 (2003).
92. M. Kang and A. Gewirth, *J. Electrochem. Soc.*, **150**, C426 (2003).
93. S.-K. Kim and J. J. Kim, *Electrochem. Solid-State Lett.*, **7**, C98 (2004).
94. P. M. Vireecken, R. A. Binstead, H. Deligianni, and P. C. Andricacos, *IBM J. Res. Dev.*, **49**, 3 (2005).
95. T. P. Moffat, D. Wheeler, M. D. Edelstein, and D. Josell, *IBM J. Res. Dev.*, **49**, 19 (2005).
96. W.-P. Dow, M.-Y. Yen, W.-B. Lin, and S.-W. Ho, *J. Electrochem. Soc.*, **152**, C769 (2005).
97. W.-P. Dow and M.-Y. Yen, *Electrochem. Solid-State Lett.*, **8**, C161 (2005).
98. M. Petri, D. M. Kolb, U. Memmert, and H. Meyer, *J. Electrochem. Soc.*, **151**, C793 (2004).
99. J.-M. Lee and A. C. West, *J. Electrochem. Soc.*, **152**, C645 (2005).
100. S.-K. Kim, D. Josell, and T. P. Moffat, *J. Electrochem. Soc.*, **153**, C616 (2006).
101. T. P. Moffat, D. Wheeler, S.-K. Kim, and D. Josell, *Electrochim. Acta*, **53**, 145 (2007).
102. W. Shao, G. Pattanaik, and G. Zangari, *J. Electrochem. Soc.*, **154**, D201 (2007).
103. T. P. Moffat, J. E. Bonevich, W. H. Huber, A. Stanishevsky, D. R. Kelly, G. R. Stafford, and D. Josell, *J. Electrochem. Soc.*, **147**, 4524 (2000).
104. W. Plieth, *Electrochim. Acta*, **37**, 2115 (1992).
105. M. L. Walker, L. J. Richter, and T. P. Moffat, *J. Electrochem. Soc.*, **152**, C403 (2005).
106. D. C. Edelstein, G. A. Sai-Halasz, and Y.-J. Mii, *IBM J. Res. Dev.*, **39**, 383 (1995).
107. O. R. Brown and H. R. Thirsk, *Electrochimica Acta*, **10**, 383 (1965).
108. J. O'M. Bockris and M. Enyo, *Trans. Faraday Soc.*, **58**, 1187 (1962).
109. E. Mattsson and J. O. M. Bockris, *Trans. Faraday Soc.*, **55**, 1586 (1959).
110. T. Taylor, T. Ritzdorf, F. Lindberg, B. Carpenter, and M. LeFebvre, *Solid State Tech.*, **41**, 47 (1998).

111. P. Taephaisitphongse, Y. Cao, and A. C. West, *J. Electrochem. Soc.*, **148**, C492 (2001).
112. M. X. Yang, D. Mao, C. Yu, J. Dukovic, and M. Xi, *Solid State Tech.*, **46**, 37 (2003).
113. S. K. Cho, S.-K. Kim, and J.-J. Kim, *J. Electrochem. Soc.*, **152**, C330 (2005).
114. T. P. Moffat, D. Wheeler, and D. Josell, *J. Electrochem. Soc.*, **151**, C262 (2004).
115. T. P. Moffat, B. Baker, D. Wheeler, and D. Josell, *Electrochem. Solid-State Lett.*, **6**, C59 (2003).
116. A. C. West, *J. Electrochem. Soc.*, **147**, 227 (2000).
117. A. C. West, S. Mayer, and J. Reid, *Electrochem. Solid-State Lett.*, **4**, C50 (2001).
118. T. P. Moffat, D. Wheeler, W. H. Huber, and D. Josell, *Electrochem. Solid-State Lett.*, **4**, C26 (2001).
119. D. Wheeler, D. Josell, and T. P. Moffat, *J. Electrochem. Soc.*, **150**, C302 (2003).
120. G. B. McFadden, S. R. Coriell, T. P. Moffat, D. Josell, D. Wheeler, W. Schwarzacher, and J. Mallett, *J. Electrochem. Soc.*, **150**, C591 (2003).
121. D. Wheeler, T. P. Moffat, G. B. McFadden, S. R. Coriell, and D. Josell, *J. Electrochem. Soc.*, **151**, C538 (2004).
122. B. C. Baker, C. Witt, D. Wheeler, D. Josell, and T. P. Moffat, *Electrochem. Solid-State Lett.*, **6**, C67 (2003).
123. D. Josell, T. P. Moffat, and D. Wheeler, *J. Electrochem. Soc.*, **154**, D208 (2007).
124. D. Josell, C. R. Beauchamp, D. R. Kelly, C. A. Witt, and T. P. Moffat, *Electrochem. Solid-State Lett.*, **8**, C54 (2005).
125. D. Josell, D. Wheeler, W. H. Huber, J. E. Bonevich, and T. P. Moffat, *J. Electrochem. Soc.*, **148**, C767 (2001).
126. O. M. Magnussen, *Chem. Rev.*, **102**, 679 (2002).
127. D. M. Soares, S. Wasle, K. G. Weil, and K. Doblhofer, *J. Electroanal. Chem.*, **532**, 353 (2002).
128. K. R. Hebert, S. Adhikari, and J. E. Houser, *J. Electrochem. Soc.*, **152**, C324 (2005).
129. Z. V. Feng, X. Li, and A. A. Gewirth, *J. Phys. Chem. B*, **107**, 9415 (2003).
130. V. D. Jovic and B. M. Jovic, *J. Serb. Chem. Soc.*, **66**, 935 (2001).
131. M. R. H. Hill and G. T. Rodger, *J. Electroanal. Chem.*, **86**, 179 (1978).
132. M. Yokoi, S. Konishi, and T. Hayashi, *Denki Kagaku oyobi Kogyo Butsuri Kagaku*, **52**, 218 (1984).
133. J. P. Healy and D. Pletcher, *J. Electroanal. Chem.*, **338**, 155 (1992).
134. K. Dolbhofer, S. Wasle, D. M. Soares, K. G. Weil, and G. Ertl, *J. Electrochem. Soc.*, **150**, C657 (2003).
135. M. L. Walker, L. J. Richter, and T. P. Moffat, *J. Electrochem. Soc.*, **153**, C557 (2006).
136. M. L. Walker, L. J. Richter, and T. P. Moffat, *J. Electrochem. Soc.*, **154**, D277 (2007).
137. J. Reid, C. Gack, and S. J. Hearne, *Electrochem. Solid-State Lett.*, **6**, C26 (2003).
138. J. J. Kelly and A. C. West, *Electrochem. Solid-State Lett.*, **2**, 561 (1999).
139. K. Kondo, T. Matsumoto, and K. Watanbe, *J. Electrochem. Soc.*, **151**, C250 (2004).
140. S.-K. Kim, S. Hwang, S. K. Cho, and J. J. Kim, *Electrochemi. Solid-State Lett.*, **9**, C25 (2006).
141. Y. H. Im, M. O. Bloomfield, S. Sen, and T. Cale, *Electrochemi. Solid-State Lett.*, **6**, C42 (2003).
142. T. P. Moffat, D. Wheeler, S.-K. Kim, and D. Josell, *J. Electrochem. Soc.*, **153**, C127 (2006).
143. S. K. Cho and J. J. Kim, *J. Electrochem. Soc.*, **153**, C822 (2006).
144. S.-K. Kim, D. Josell, and T. P. Moffat, *J. Electrochem. Soc.*, **153**, C826 (2006).
145. S. Kim and D. J. Duquette, *J. Electrochem. Soc.*, **154**, D195 (2007).
146. A. Radisic, G. Oskam, and P. C. Searson, *J. Electrochem. Soc.*, **151**, C369 (2004).
147. A. Radisic, J. G. Long, P. M. Hoffmann, and P. C. Searson, *J. Electrochem. Soc.*, **148**, C41 (2001).
148. A. Radisic, Y. Cao, P. Taephaisitphongse, A. C. West, and P. C. Searson, *J. Electrochem. Soc.*, **150**, C362 (2003).
149. G. Oskam, P. M. Vereecken, and P. C. Searson, *J. Electrochem. Soc.*, **146**, 1436 (1999).
150. M. Zheng, J. J. Kelly, and H. Deligianni, *J. Electrochem. Soc.*, **154**, D400 (2007).
151. S. Kim and D. J. Duquette, *J. Electrochem. Soc.*, **153**, C673 (2006).
152. S. Kim and D. J. Duquette, *Surf. Coat. Tech.*, **201**, 2712 (2006).
153. L. Magnagnin, A. Vicenzo, M. Bain, H. W. Toh, H. S. Gamble, and P. L. Cavallotti, *Microelectron. Eng.*, **76**, 131 (2004).
154. A. Radisic, F. M. Ross, and P. C. Searson, *J. Phys. Chem. B*, **110**, 7862 (2006).
155. A. Radisic, P. M. Vereecken, J. B. Hannon, P. C. Searson, and F. M. Ross, *Nano Lett.*, **6**, 238 (2006).
156. G. Gunawardena, G. J. Hills, I. Montenegro, and B. Scharifker, *J. Electroanal. Chem.*, **138**, 225 (1982).
157. B. Scharifker and G. Hills, *Electrochim. Acta*, **28**, 879 (1983).
158. C. W. Tobias and R. Wijsman, *J. Electrochem. Soc.*, **100**, 459 (1953).
159. R. Alkire and R. Varijan, *J. Electrochem. Soc.*, **121**, 622 (1974).
160. M. Matlosz, P.-H. Vallotton, A. C. West, and D. Landolt, *J. Electrochem. Soc.*, **139**, 752 (1992).
161. P. Desprez, M. Matlosz, J. D. Yang, and A. C. West, *J. Electrochem. Soc.*, **145**, 165 (1998).
162. M. J. Willey and A. C. West, *Electrochim. Acta*, **52**, 6484 (2007).
163. M. Takashi, *J. Electrochem. Soc.*, **147**, 1414 (2000).
164. T. O. Drews, S. Krishnan, J. C. Alameda, D. Gannon, R. D. Braatz, and R. C. Alkire, *IBM J. Res. Dev.*, **49**, 49 (2005).
165. J.-M. Lee, H. McCrabb, E. Jennings Taylor, and R. Carpio, *J. Electrochem. Soc.*, **153**, C265 (2006).

166. J. J. Kelly, M. Zheng, B. C. Baker-O'Neal, and C. Cabral Jr., *J. Electrochem. Soc.*, **154**, D406 (2007).
167. S. Kim and D. J. Duquette, *J. Electrochem. Soc.*, **153**, C417 (2006).
168. O. Chyan, T. N. Arunagiri, and T. Ponnuswamy, *J. Electrochem. Soc.*, **150**, C347 (2003).
169. M. W. Lane, C. E. Murray, F. R. McFeely, P. M. Vereecken, and R. Rosenberg, *Appl. Phys. Lett.*, **83**, 2330 (2003).
170. D. Josell, D. Wheeler, C. Witt, and T. P. Moffat, *Electrochem. Solid-State Lett.*, **6**, C143 (2003).
171. L. Guo, A. Radisic, and P. C. Searson, *J. Electrochem. Soc.*, **153**, C840 (2006).
172. T. P. Moffat, M. Walker, P. J. Chen, J. E. Bonevich, W. F. Egelhoff, L. Richter, C. Witt, T. Aaltonen, M. Ritala, M. Leskela, and D. Josell, *J. Electrochem. Soc.*, **153**, C37 (2006).
173. M. L. Walker, L. J. Richter, D. Josell, and T. P. Moffat, *J. Electrochem. Soc.*, **154**, C235 (2006).
174. Y.-S. Kim, H.-I. Kim, M. A. Dar, H.-K. Seo, G.-S. Kim, S. G. Ansari, J. J. Senkevich, and H.-S. Shin, *Electrochem. Solid-State Lett.*, **9**, C19 (2006).
175. D. Josell, C. Witt, and T. P. Moffat, *Electrochem. Solid-State Lett.*, **9**, C41 (2006).
176. D. Josell, J. E. Bonevich, T. P. Moffat, T. Aaltonen, M. Ritala, and M. Leskela, *Electrochem. Solid-State Lett.*, **9**, C48 (2006).
177. C. Nguyen Van Huong, and M. J. Gonzales-Tejera, *J. Electroanal. Chem.*, **244**, 249 (1988).
178. K. R. Zavadil, D. Ingersoll, and J. W. Rogers, *J. Electroanal. Chem.*, **318**, 223 (1991).
179. E. M. Stuve, J. W. Rodgers, Jr., D. Ingersoll, D. W. Goodman, M. L. Thoomas, and M. T. Paffett, *Chem. Phys. Lett.*, **149**, 557 (1988).
180. M. A. Quiroz, Y. Meas, E. Lamy-Pitara, and J. Barbier, *J. Electroanal. Chem.*, **157**, 165 (1983).
181. C. Gunther, J. Vrijmoeth, R. Q. Hwang, and R. J. Behm, *Phys. Rev. Lett.*, **74**, 754 (1995).
182. G. O. Potschke and R. J. Behm, *Phys. Rev. B*, **44**, 1442 (1991).
183. M. Zheng, M. Willey, and A. C. West, *Electrochem. Solid-State Lett.*, **8**, C151 (2005).
184. K. Sieradzki, S. R. Brankovic, and N. Dimitrov, *Science*, **284**, 138 (1999).
185. D. L. Smith, *Thin-Film Deposition*, McGraw-Hill, New York, 1997.
186. R. Q. Hwang and M. C. Bartelt, *Chem. Rev.*, **97**, 1063 (1997).
187. S. P. Murarka, *Metalization: Theory and Practice for VLSI*, Butterworth-Heinemann, Stoneham, 1997.
188. D. A. Neamen, *Semiconductor Physics and Devices*, Irwin, Chicago, 1996.
189. E. Bauer, *Z. Kristallographie*, **110**, 372 (1958).
190. W. U. Schmidt, R. C. Alkire, and A. A. Gewirth, *J. Electrochem. Soc.*, **143**, 3122 (1996).
191. M. H. Holzle, C. W. Apsel, T. Will, and D. M. Kolb, *J. Electrochem. Soc.*, **142**, 3741 (1995).
192. G. Rosenfeld, R. Servaty, C. Teichert, B. Poeselma, and G. Comsa, *Phys. Rev. Lett.*, **71**, 895 (1993).
193. S. Hwang, I. Oh, and J. Kwak, *J. Am. Chem. Soc.*, **123**, 7176 (2001).
194. S. R. Brankovic, PhD Thesis, Arizona State University, Tempe (1999).
195. J. X. Wang, B. M. Ocko, and R. R. Adzic, *Surf. Sci.*, **5401**, 230 (2003).
196. S. R. Brankovic, N. Dimitrov, and K. Sieradzki, *Electrochem. Solid-State Lett.*, **2**, 443 (1999).
197. J. Camarero, J. Ferron, V. Cros, L. Gomez, A. L. Vazquez de Parga, J. M. Gallego, J. E. Prieto, J. J. de Miguel, and R. Miranda, *Phys. Rev. Lett.*, **8**, 850 (1998).
198. Z. Zhang and M. G. Lagally, *Phys. Rev. Lett.*, **72**, 693 (1994).
199. N. Vasiljevic, PhD Thesis, Arizona State Univeristy, Tempe (2004).
200. S. R. Brankovic, J. X. Wang, and R. R. Adzic, *Surf. Sci.*, **474**, L173 (2001).
201. J. L. Stickney, in *Electrochemical Atomic Layer Epitaxy (EC-ALD): Nanoscale Control in the Electrodeposition of Compound Semiconductors*, Vol. 7, R. Alkire and D. M. Kolb, Eds., Wiley-VCH, New York, 2001.
202. M. F. Mrozek, Y. Xie, and M. J. Weaver, *Anal. Chem.*, **73**, 5953 (2001).
203. R. Vasilic and N. Dimitrov, *Electrochem. Solid-State Lett.*, **8**, C173 (2005).
204. Y.-G. Kim, J. Y. Kim, D. Vairavapandian, and J. L. Stickney, *J. Phys. Chem. B*, **110**, 17998 (2006).
205. R. Vasilic, L. T. Viyannalage, and N. Dimitrov, *J. Electrochem. Soc.*, **153**, C648 (2006).
206. L. T. Viyannalage, R. Vasilic, and N. Dimitrov, *J. Phys. Chem. C*, **111**, 4036 (2007).
207. J. Y. Kim, Y.-G. Kim, and J. L. Stickney, *J. Electrochem. Soc.*, **154**, D260 (2007).
208. A. Martinez-Ruiz, J. Valenzuela-Benavides, L. Morales de la Garza, and N. Batina, *Surf. Sci.*, **476**, 139 (2001).

28

MICROELECTROMECHANICAL SYSTEMS

GIOVANNI ZANGARI

28.1 INTRODUCTION

Microelectromechanical systems (MEMS) are miniaturized devices that integrate, on a single chip, sensing and actuation functions with the information storage and processing electronics required to monitor and control the system of interest [1, 2]. In this respect, MEMS extend the functionality of microelectronic circuits by providing an interface between the external environment and the electronic information processing. MEMS are capable of sensing the physical or chemical variable of interest, converting it into an electrical variable, processing the corresponding information, and finally acting on the external environment according to a set of predetermined instructions. Key attributes for MEMS are *miniaturization* and *integration*; successful MEMS devices exploit these features to provide unprecedented performance, improved reliability, and/or lower cost.

Several MEMS devices are already on the market, including accelerometers for automobile air bag systems [3], silicon diaphragms for pressure sensing [4], inkjet printer heads, and digital micromirror devices for projection displays [5]. Many more are at an advanced stage of development, and innumerable systems are being developed or designed. Most recently, microfluidic systems are being developed for biomedical and microreactor applications.

28.2 MICROFABRICATION TECHNIQUES

In order to achieve miniaturization and low cost, MEMS are made in part using batch microfabrication techniques borrowed by the integrated circuit industry. MEMS however provide new functionalities and therefore require novel designs and widely varying geometries of the various parts and utilize new materials. For these reasons, novel microfabrication techniques have been developed and a wider range of materials are being used in MEMS manufacturing which were formerly thought incompatible with microfabrication techniques. The most common microfabrication techniques for MEMS include lithography, surface and bulk micromachining, and metal deposition through high-aspect-ratio lithographic masks [6].

Lithography (Fig. 28.1) starts by spin coating a photosensitive polymer (a photoresist) onto a substrate (most commonly a silicon wafer). An opaque mask with a defined pattern of optically transparent regions is placed on top of the resist and is illuminated with near-ultraviolet (near-UV) light; the transparent regions let the light through, selectively exposing the resist and thus inducing chemical changes in the selected regions. Exposed (positive-resist) or not exposed (negative-resist) regions can thus be chemically removed by a suitable etching solution, most often an organic solvent. The patterned photoresist can later be used for spatially selective deposition or etch processes.

Surface micromachining (Fig. 28.2) is characterized by its ability to free parts of the system from the underlying layers so that the part can move. In this process, a sacrificial layer (the photoresist or silicon dioxide) is deposited and lithographically patterned. The material of choice is later grown through and on top of the sacrificial layer, which is later selectively etched away by a chemical etchant (HF in the case of SiO_2), leaving the part free to move.

Bulk micromachining (Fig. 28.3) consists in the selective etching of single-crystal silicon to produce particular shapes or functional components of the device. Controlled shapes can be obtained by utilizing etch masks (often silicon nitride, Si_3N_4) and exploiting the silicon etching process, which can be isotropic or anisotropic depending on the chemical

Modern Electroplating, Fifth Edition Edited by Mordechay Schlesinger and Milan Paunovic

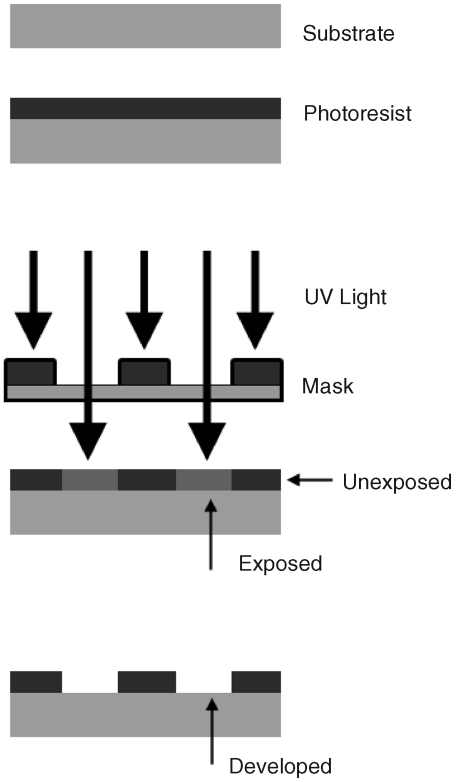

FIGURE 28.1 Photolithographic process using positive resist. (Adapted from [6].)

etchants used. In addition, reactive ion etching (RIE) using etching gases (e.g., SF_6) can be used to produce deep vertical structures in silicon.

Among the possible deposition methods available to fill high-aspect-ratio masks, electrodeposition is the most advantageous due to its ability to provide spatially selective growth at conductive or catalytic regions and conformal coverage of the areas to be filled. The diffusive material transport occurring in this deposition process in fact enables deposition into obstructed structures, at variance with

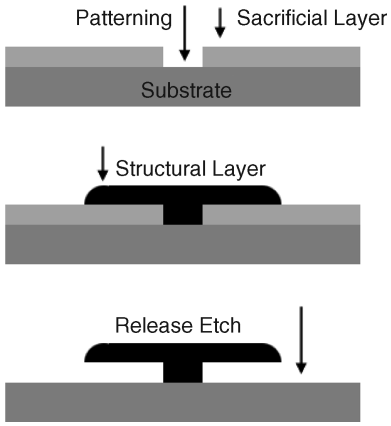

FIGURE 28.2 Surface micromachining. (Adapted from [6].)

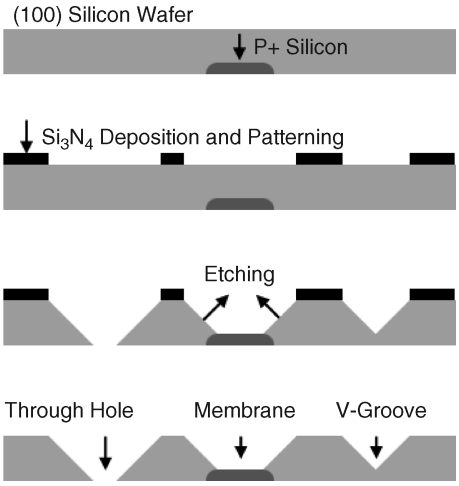

FIGURE 28.3 Bulk micromachining. The process exploits the slow etching rate of the (111) surfaces of single crystal silicon. (Adapted from [6].)

line-of-sight deposition processes such as evaporation or sputtering. Possible competitive technologies are chemical vapor deposition (CVD) and deposition from supercritical fluids [7]; these however do not exhibit the same simplicity, low capital cost, and knowledge base as electrochemical processes do.

The high-aspect-ratio (high-AR) lithographic patterns often needed in MEMS cannot be obtained via conventional photolithographic processes using visible or near-UV light, since these processes have a limited depth of focus and light is unable to penetrate through thick resists. In addition, conventional photoresists cannot be made sufficiently thick. Instead, X-ray lithography is used for the production of high AR patterns. This radiation in fact has large depth of focus and negligible diffraction effects and thus allows the use of proximity (noncontact) masks. X-ray lithography using synchrotron radiation in particular is characterized by high beam collimation and is capable of producing lithographic structures with high AR (on the order of 100) and vertical walls (Fig. 28.4). New resist formulations are also used which can be spin coated with the thickness required, can be developed across the entire thickness, and have sufficient mechanical strength to withstand possible stresses generated during the drying process, the development, and the successive plating. The most common photoresist used in these applications is polymethylmeta-acrylate (PMMA), which can be spin coated or bonded as a solid sheet to the substrate. The equipment used for the fabrication of high-quality, vertical, high-AR patterns is very expensive and cumbersome; as a consequence, many laboratories and foundries have used other means to generate X-rays or have used deep UV radiation instead. These processes do not have the same capability to achieve straight walls and high AR; ARs in deep-UV lithography are usually limited to 25. Resists used in these

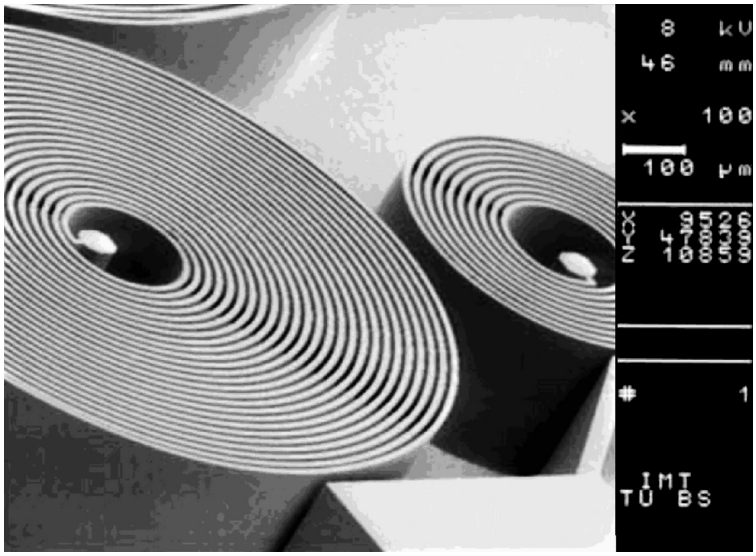

FIGURE 28.4 Typical high-aspect-ratio structure obtained with epoxy resin. (Reproduced from [8] with permission from Springer Science + Business Media.)

applications are typically Novolac resins or epoxy-based resists such as SU-8 [9].

The technology of plating through high AR patterns is conventionally called LIGA, an acronym from the German *Lithographie Galvanoformung und Abformung*, which stands for "electroplating through lithographic mask and injection molding" [10]. The technique involves the formation of a thick layer of a suitable resist, mainly PMMA, from a few micrometers up to centimeters thick, lithography with high-energy X rays, development, and plating through the mask thus obtained to fill the trenches. In the full LIGA process the metallic part is separated from the mold and used in the injection molding or hot embossing of plastic parts. In MEMS processes this last step is usually neglected and the metal part is the final component

Electrodeposition enables high-quality reproduction of lithographic features due to its selectivity. If a conductive seed layer is deposited on the Si substrate before application of the photoresist, the metal structure will grow from the conductive bottom to the top.

The MEMS components fabricated by nonconventional techniques, such as sensing and actuation parts, should be integrated with the electronic processing and data storage components, which are most commonly made by complementary metal–oxide–semiconductor (CMOS) fabrication technologies. This can be accomplished by integrating the various parts on the same chip [monolithic system on a chip (SOC)]; this helps in reducing stray capacitances and inductances and also allows fabrication of highly parallel (array) circuits. Post CMOS compatible processes are however required for SOC MEMS; these MEMS have to be fabricated at the end of line of the process at low enough temperatures to avoid damage to the CMOS circuits. The alternative approach is to fabricate the components separately and then integrate them in a package [system in a package (SIP)]; performance and miniaturization may not be optimal; however, more flexibility is allowed in the choice of the fabrication method.

28.3 CHARACTERISTIC FEATURES OF ELECTRODEPOSITION THROUGH HIGH-AR PATTERNS

Electroplating through geometrically complicated lithographic patterns, often with high ARs, presents several difficulties related to electrolyte penetration and ionic transport within the lithographically defined features.

Upon immersion of the workpiece in the bath, the electrolyte must infiltrate the narrow, deep features of the pattern; to do so, it must wet the feature walls. Unfortunately, the resist used most often, PMMA, does not wet well; in fact, the contact angle between water and PMMA at 50°C is between 70 and 80°C. Wetting can be improved by use of wetting agents; the concentration of wetting agents in the electrolytes used for plating in MEMS should therefore be higher than usual. Wetting agents, or surfactants, are organic compounds that reduce the surface energy of water by adsorbing at the liquid–solid interface. Wetting agents often used in electrodeposition include alkyl sulfate salts such as sodium lauryl sulfate or sodium dodecyl sulfate.

Electroplating of a metallic part can be a long-lasting process; when plating a transition metal such as copper or nickel at 10 mA cm^{-2}, the corresponding growth rate is about 12 µm h^{-1}. Plating of a 100-µm-thick structure would thus require more than 8 h! Plating rate can be increased by using

high metal ion concentrations and/or by decreasing the diffusion boundary layer thickness through forced electrolyte convection. The latter approach is effective on flat electrodes or on relatively shallow features at high-electrolyte-flow velocities [11], but within the patterned features convection becomes very inefficient with increasing depth, and diffusion becomes the only means by which the metal ions reach the growth front. It has been calculated that buoyancy-driven convection can enhance ion transport within the trenches; this is possible for trenches larger than 100 μm [12] or for ARs less than 1.2 for 100-μm-thick resists and for ARs less than 6 for 1-mm-thick resists (1 *M* electrolyte) [13]. Apart from these conditions, the diffusion current would be approximately given by the formula

$$J = -zFD\frac{dc}{dz} = -zFD\frac{c_B - c_S}{L}$$

where z is the valency of the metal ion, F the Faraday constant, D the ion diffusion coefficient, c_B the metal ion concentration in the electrolyte bulk (under conditions of forced convection also at the trench mouth), c_S the metal ion concentration deep in the trench, at the growth front, and L the thickness of the resist. The diffusion-limited current for a bivalent ion, assuming $D \sim 10^{-5}$ cm^2 s^{-1}, $c_B = 1\,M$, and $L = 100\,\mu$m, is about 20 mA cm^{-2}. Under conditions where diffusion effects dominate over interface kinetics, growth should occur at current densities well below this value in order to avoid growth instabilities and dendritic growth [14]. This places serious limits with regard to the range of allowable deposition rates.

Pulse plating allows the use of larger peak current densities if the duration of these pulses is shorter than the time required to deplete the reducing ion at the interface. It has been demonstrated, however, that the average current in pulse plating should be well below the limiting current in order to avoid powdery and dendritic deposits [15]; consequently, no increase in deposition rate should be possible by pulse plating. Off times to replenish the ion concentration at the trench bottoms are in fact on the order of the diffusion time $\tau = L^2/D$ (for the example above $\tau = 10$ s), and on times should be smaller than τ in order to avoid diffusion limitations [16].

Diffusion in an ideal trench would provide for a uniform current distribution deep within the trench. In practical cases, however, nonuniformities and varying transport conditions at different locations on the pattern would generate nonuniformities in the current distribution. This problem has been studied in the context of electrodeposition for microelectronics, where uniformity at the workpiece scale, at the pattern scale, and at the individual feature scale has been identified and evaluated independently [17]. At the single-feature scale [18] current distribution is initially uniform, but when the metal part is starting to fill the trench, radial diffusion and current crowding at the feature edges occur. This phenomenon may result in a localized increase of growth rate, a variation in the deposition efficiency, and in the case of alloy deposition, a local change of composition. These effects need to be minimized in order to achieve uniform, flat shapes and reproducible material properties. At the pattern scale, it was found that a higher average current density is obtained in regions having a low density of patterns to be filled [19], as schematically shown in Figure 28.5. Design rules for MEMS thus suggest that the pattern should have a uniform density of features of similar size [20]. At the workpiece scale, current crowding occurs at the edges. This problem is usually avoided by using auxiliary electrodes (current thieves) placed at optimized positions or by avoiding placing the patterns to be filled in an edge region. In general, modeling of the current distribution is required in order to achieve satisfactory quality and uniformity over the entire workpiece.

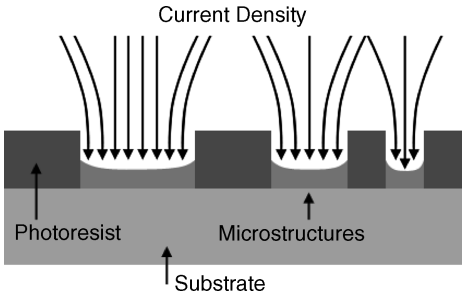

FIGURE 28.5 A high average current density is obtained in regions with a low density of patterns.

Other difficulties related to the use of thick resists include the need to closely control the dimensional changes of the resist pattern upon immersion in and extraction from the electrolyte; this may limit the range of electrolyte chemistries that may be used and the range of plating temperatures. Finally, local detachment of the resist at the trench base and the resulting underplating which may occur when using corrosive chemistries and high temperature may be exacerbated by the intrinsic stresses that may develop during or after spin coating of the resist.

28.4 ELECTRODEPOSITION OF METALS AND ALLOYS FOR MEMS

28.4.1 Gold

Gold exhibits a high corrosion resistance and environmental stability and good solderability and electrical conductivity; in addition, it is highly reflective and biocompatible. This metal is used in microelectronics and MEMS applications for electrical contacts, packaging, and assembly as it provides a low contact resistance with long lifetime. The high atomic number of gold makes this material an ideal candidate for X-ray absorber in X-ray masks used in the LIGA process. In this application, patterned films of gold about 10 μm thick with vertical walls are needed, and electroplat-

TABLE 28.1 Au Electroplating Baths

(a) Au Sulfite [23]	
Au(I) sulfite	0.15 *M*
Na_2SO_3 (total)	0.5 *M*
$Na_4P_2O_7$	0.3 *M*
pH 9.5–12.5	
(b) Au Sulfite–thiosulfite [24]	
$NaAuCl_4$	0.05 *M*
Na_2SO_3	0.42 *M*
$Na_2S_2O_3$	0.42 *M*
Na_2HPO_4	0.3 *M*
pH 6	
$T = 60°C$	
CD 5 mA cm^{-2}	

ing is the ideal method for the fabrication of these structures [21]. Biomedical applications of gold microstructures are numerous; they include, for example, electrodes in microfluidic processes, implantable electrode arrays, and implantable drug delivery systems. Most of the above applications require mechanically soft, pure gold; an exception is electrical contacts, which require high resistance to wear, usually achieved by alloying gold with small amounts of Ni, Co, As, or Sb [22].

Table 28.1 reports typical formulations for some of the gold electroplating baths described below. Conventional electrolytes for Au electroplating use potassium cyanoaurate(I), $KAu(CN)_2$, as the Au source. This complex has a very high stability constant, $K_{sc} \sim 10^{39}$, making the corresponding electrolyte very stable against decomposition. These electrolytes are preferentially operated under alkaline or slightly alkaline conditions, allow high deposition rates, and produce soft gold. One drawback of these electrolytes is the poor compatibility with the photoresist; even if the bath is used at pH values that are nominally compatible with the resist, the electrodeposition process results in an increase of pH at the electrolyte–electrode interface, which results in delamination of the resist and plating underneath the resist layer (underplating). Most importantly, however, cyanide is highly toxic and there are active efforts to completely eliminate it from plating lines.

Alternative electrolytes include baths based on the sulfite complex $[Au(SO_3)_2]^{3-}$ ($K_{sc} \sim 10^{10}$), on the thiosulfate complex $[Au(S_2O_3)_2]^{3-}$ ($K_{sc} \sim 10^{26}$), or on a mixture of both [25]. The stability of the gold sulfite complex decreases at lower pH values; however, the stability at near-neutral pH can be improved by addition of ethylene diamine. Currently, Au sulfite electrolytes at near-neutral pH are commercially available. Prolonged use however results in decomposition of the complex and in a decreasing quality of the films. The thiosulfate and particularly the mixed bath present a better stability and also better adhesion properties [26], but they do not seem to have yet found commercial applications.

Gold solutions based on sulfites or mixed sulfite/thiosulfate contain a relatively low amount of Au complex (typically 0.05 *M*) and are usually operated at 60°C and less than 10 mA cm^{-2}. Fabrication of high AR structures using gold should consequently be carefully considered due to the long duration of the corresponding process

28.4.2 Copper

Copper exhibits high conductivity and relatively high resistance to electromigration, while from the mechanical standpoint it is relatively soft. It has been used in microelectronics for the metallization of ultra large scale integrated (ULSI) circuits [27] and in the production of vias for multilevel integrated circuits and packaging [28]. Copper is also the material of choice in the manufacture of coils for the fabrication of miniaturized electromagnets for magnetic recording heads [29]. In the MEMS arena, copper is an essential material for MEMS-level wafer packaging and for the production of energizing coils in microelectromagnets and micromotors.

The technology of filling high AR submicrometer-sized (down to 32 nm) trenches for ULSI metallization has been developed and commercialized in recent years. The damascene process [27] is different from conventional through-mask plating in that a seed layer is conformally deposited over a patterned material in such a way that the plated metal covers the whole surface. Excess metal is later removed by chemical–mechanical polishing (Fig. 28.6). Essential in this process is the ability to uniformly fill the trench without void formation so as to obtain consistent resistivity and mechanical characteristics. This has been achieved by a copper chemistry [see Table 28.2, part (a)] capable of accomplishing superconformal growth, that is, the filling of the bottom of the feature faster than the side walls. This is attained by using an acidic copper sulfate electrolyte containing a series of additives that in the simplest case include an inhibitor or suppressor [often polyethylene glycol (PEG)], an accelerator [often bis(3-sulfopropyl) disulfide (SPS)], and chloride, Cl^-. PEG and Cl^- interact to quickly form an inhibiting layer at the growing surface, causing a strong decrease in the copper reduction kinetics. The inhibiting layer competes for adsorption at the electrode with the SPS, which tends to displace the PEG/Cl layer and to concentrate at concave regions with high curvature (Fig. 28.7). In these regions, SPS accelerates the copper reduction reaction and acts as a surfactant by floating on top of the growth front. The high concentration of SPS at high curvature regions results initially in faster growth at the bottom of the trenches and later, when the trench is filled, in the formation of a bump [30]. This chemistry has been extended to the process of filling through vias for multilevel

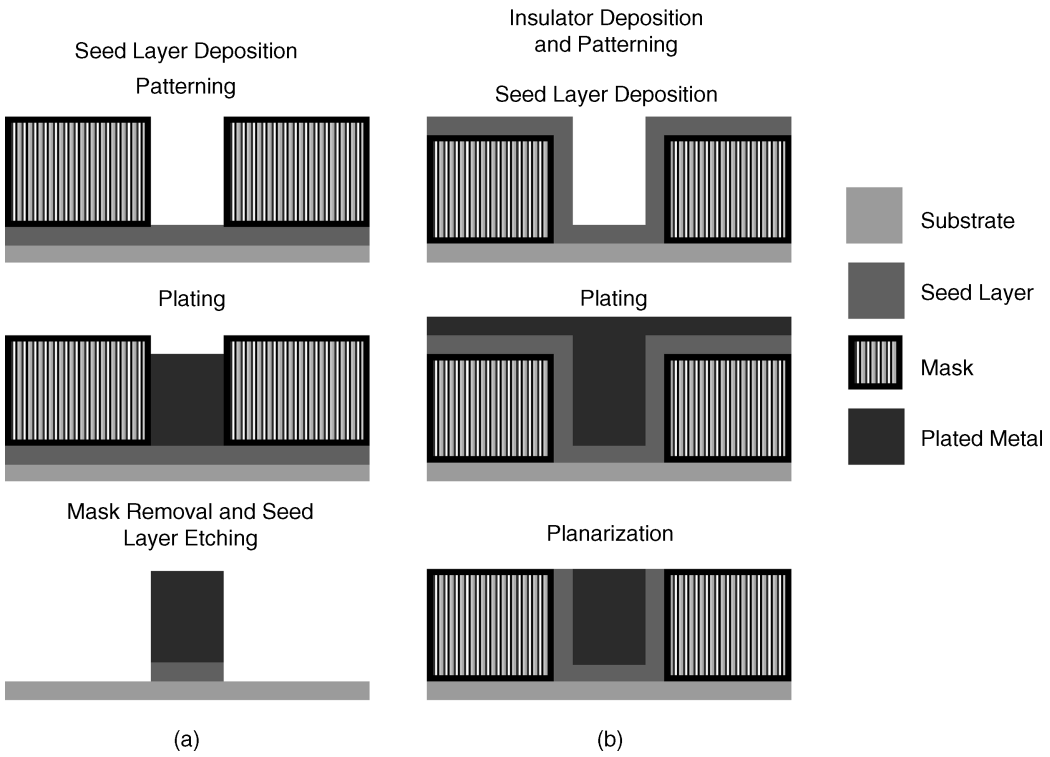

FIGURE 28.6 Comparison of process steps in conventional through-mask plating (*a*) and damascene plating (*b*).

TABLE 28.2 Copper Electroplating Baths

(a) Superconformal Copper [30]	
$CuSO_4$	0.24 *M*
H_2SO_4	1.8 *M*
NaCl	10^{-3} *M*
PEG (3400 MW)	88 μmol
SPS	0–500 μmol
(b) Pulse Reverse Fast Filling of Vias [36]	
$CuSO_4$	200 g L^{-1}
H_2SO_4	25–100 g L^{-1}
Suppressor (proprietary)	0.5–10 mg L^{-1}
Leveler (proprietary)	0–0.5 mg L^{-1}
HCl	50–150 mg L^{-1}
SPS	1–10 mg L^{-1}
Pulse reverse period	100–300 ms
Reverse/on current	1–3
Off time	100–200 ms

chip and MEMS applications, which require void-free filling over much wider trenches (up to 100 μm) and higher AR. On these length scales, nonuniformity in the distribution of the electrical potential field and in convective transport can result in a nonuniform current distribution, further complicating control of the process [31].

Filling of through-wafer interconnect vias is achieved by one of several different methods. In some designs, a conductive base for copper electroplating is provided only at the bottom of the feature, while the side walls are not conductive (Fig. 28.8) [32]. This may be achieved, for example, by sputtering a conducting layer onto the bottom side of the wafer without achieving complete coverage and closure of the via. The via is then plugged during copper electrodeposition, which initially occurs only at the pore bottom [33]. In a slightly different approach, a temporary bottom seed layer is made available by depositing this layer on a second wafer or on a polymeric substrate, then bonding the conductive surface thus obtained to the bottom side of the wafer (Fig. 28.9). A photoresist is often used as the bonding interface since its later release is easier [34]. Using one of these methods, electroplating starts from the bottom of the via and it is easier to avoid the formation of voids. During via filling, however, the effective AR of the via decreases and the primary current distribution changes. To counterbalance these changes, an optimized pulse-reverse current waveform was developed to optimize filling. This current waveform consists of a forward pulse current (growth stage) increasing with time and a reverse pulse current (dissolution stage) decreasing with time [34, 35].

In a different approach, a conformal blanket coating of a seed layer (Ti/Cu) is deposited first on top of the patterns;

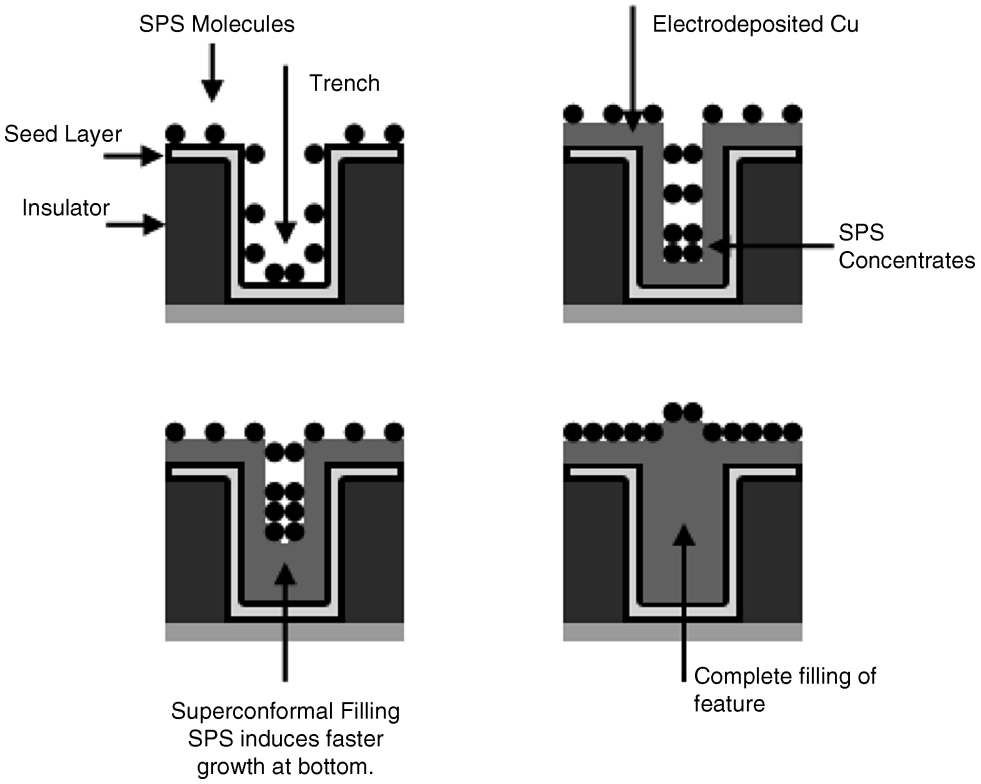

FIGURE 28.7 Schematic for superconformal filling of trenches.

deposition techniques for the seed may include CVD or electroless copper. Superconformal chemistry and/or tuning of the current waveform (pulse or pulse-reverse plating) is then used to achieve complete filling without voids [36]. See Table 28.2, part (b), for a typical chemistry and deposition conditions.

Fine tuning of the electrodeposition process in order to optimize via filling has been focused in two directions: the determination of the optimum concentration of leveler and suppressor and the optimization of the pulse-reverse waveform. It has been shown that pulse-reverse plating provides better via filling than on–off pulse plating; however, the optimum pulse-reverse waveform depends on a number of variables (bath composition, flow, plating rate, via dimensions, and geometry) such that overall process optimization becomes difficult [31].

28.4.3 Nickel and Nickel Alloys

Nickel Nickel plating is one of the most important and well-developed electrodeposition processes, used mostly for the formation of corrosion-resistant coatings. Nickel is also one of the most widely used metals in MEMS applications; its mechanical properties in fact make this material ideal for cantilevers and other parts in motion.

Nickel is usually plated from a slightly acidic electrolyte (pH 3–4) containing a nickel salt, boric acid as a buffer, wetting agents to avoid pitting due to hydrogen evolution, and stress relievers. For mechanical applications in particular, stress should be minimized, as uncontrolled stresses may lead to unexpected failures. Most commonly, nickel solutions contain nickel sulfate, but the internal stresses in nickel films obtained from these electrolytes are high, on the order of 160 MPa [37], and tensile, requiring stress-reducing agents to decrease the stress and possibly induce compressive stress. Compressive stresses are advantageous in mechanical structures under load, since they tend to inhibit crack formation and growth. The anode material in nickel plating is usually metallic nickel; chloride or halogen ions are required to activate the anode and enable its dissolution. Chloride additions in MEMS applications, however, are particularly harmful since they tend to increase the tensile stresses. These stresses can be decreased by increasing plating temperature [37], but this is not a particularly attractive option in MEMS application since higher temperatures can induce swelling of the resist and induce uncontrolled dimensional variations in the finished part. An alternative is the use of sulfur-containing compounds such as saccharin in small amounts (few millimoles/liter). These additives act as grain refiners and stress relievers, rapidly inducing compressive stresses. Grain refinement through addition of saccharin in

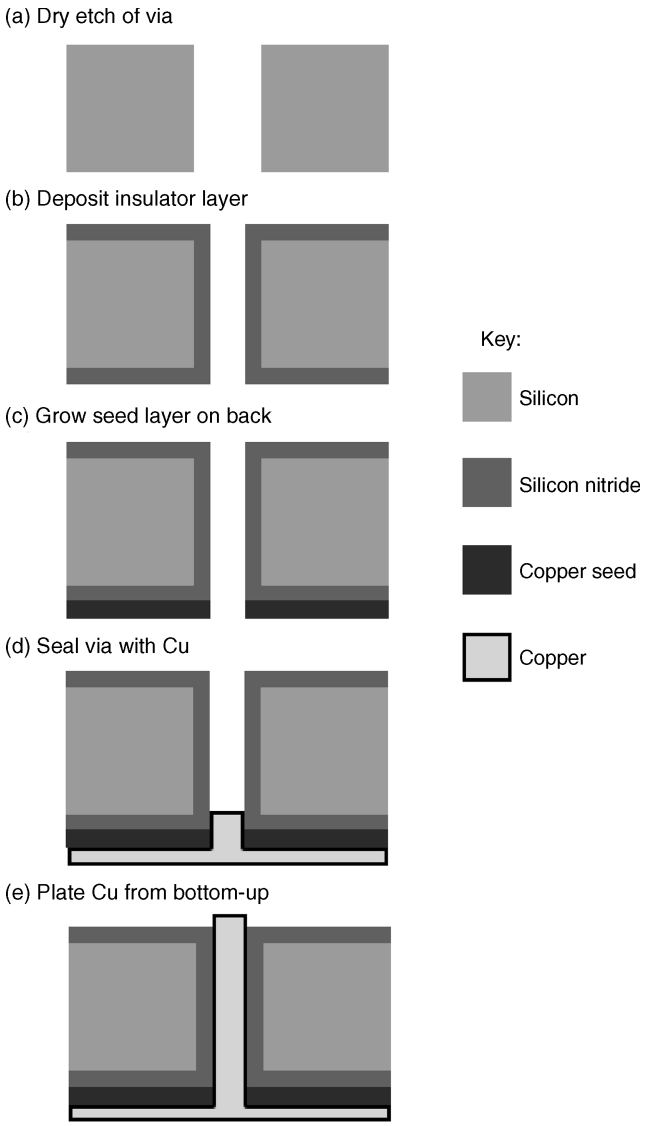

FIGURE 28.8 Via filling with electroplated copper via partial plugging of pore bottom.

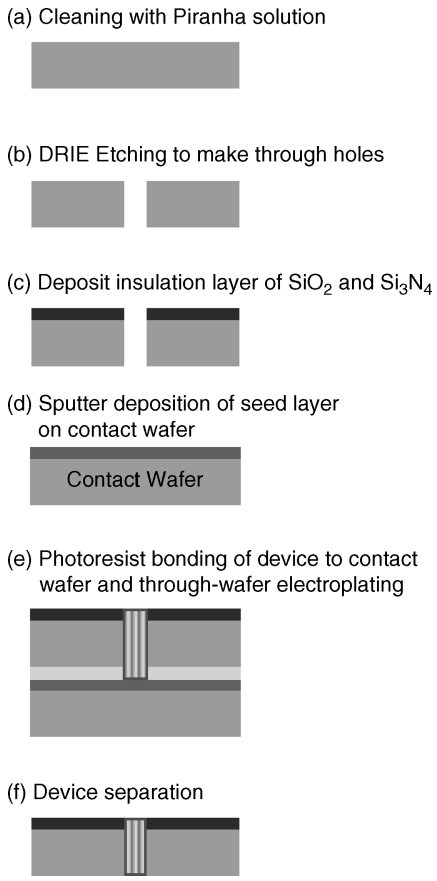

FIGURE 28.9 Via filling by electroplated copper using partial bonding:

the solution however results in the incorporation and accumulation of sulfur at the grain boundaries, which increases the susceptibility of the nickel part to corrosion.

Electrolytes based on Ni sulfamate combine low as-deposited film stress (∼60 MPa) with low sulfur content and high current efficiency of the bath [37], thus presenting very attractive properties for the production of mechanical MEMS components. See Table 28.3, part (a), for a typical electroplating bath. Nickel films grown from sulfamate solutions show tensile stress at high growth rate but compressive stress at low growth rate ($<10\,\text{mA cm}^{-2}$, $12\,\mu\text{m h}^{-1}$) [38]. Stress buildup during electrodeposition from these electrolytes is avoided by using Br^- instead of Cl^- as anode activator [39]; Br^- is in fact known to induce small internal stresses [37]. Stress does not depend on deposition temperature if chlorides are not present in the bath [40]. Nickel is usually electroplated from sulfamates at relatively high temperatures (50°C), but low (room)–temperature deposition may be preferred in MEMS applications. Table 28.3, part (b), presents a typical chemistry used in this case. Under these conditions the internal stresses and the ultimate tensile strength are higher but tend to decrease at high temperature [41]. This behavior is observed in parallel with a decrease in grain size and is attributed to inhibited growth, which was related to the formation of polyborates upon filtering. Tensile strength in conventional Ni parts grown from sulfamates is about 350 MPa, but low-temperature inhibited electrodeposition may result in yield strengths as high as 950 MPa [39, 42]; these alloys however are probably more susceptible to brittle fracture. More relevant to the operation of Ni MEMS structures is failure due to fatigue, which can occur at much lower stresses than those measured in conventional stress–-strain tests. The fatigue behavior of dog-bone Ni microstructures with cross section $200 \times 270\ \mu\text{m}^2$ is similar to that of bulk annealed Ni, with an endurance limit of 210 MPa. Crack growth in these microstructures is slower and is found to occur

through recrystallization and microvoid formation in the plastically deformed zone [43]. Controlled formation of nanosized cracks in Ni beams has been recently explored as a promising method to study deformation and fatigue processes in microsystems [44].

Pulse plating effects on nickel electrodeposition have been systematically investigated by Weil [45]. Yield strength increases with peak current density due to grain refinement and lower tensile stresses are obtained due to relaxation effects during the off time. Hydrogen was found to be periodically adsorbed and desorbed during on and off times, respectively [40].

Nickel Alloys Nickel alloys with Fe or Co potentially exhibit better mechanical properties due to the grain refinement effect and the corresponding increase in strength. Nickel–cobalt alloy electroplates containing 45–50 at % Co in particular exhibit higher yield strength and a wider range of temperature, where this strength is maintained [46]. Cobalt– nickel films from chloride solutions exhibit tensile internal stresses between 150 and 370 MPa, increasing with Co content and decreasing upon addition of saccharin. Nickel– cobalt films with low Co content and saccharin additions exhibit compressive internal stresses [47]. Table 28.3, part (c), describes an electroplating bath for Ni–Co. As-deposited Ni–Fe alloys exhibit an increase in tensile strength (up to 2000 MPa), but annealing in the temperature range 300–700°C causes embrittlement due to precipitation of sulfur at grain boundaries. Only annealing at 1000°C can restore ductility, but with lower strength [48] (Figs. 28.10*a*, *b*). Table 28.3, part (d), describes the plating formulation used in this effort. An increase in Fe content when plating from sulfamate/sulfate solutions increases the tensile stress and may reverse the stress from compressive to tensile [49].

A problem encountered in plating mutual alloys of Ni, Co, and Fe is that they exhibit anomalous codeposition; that is, the less noble metal is deposited preferentially. In order to achieve a predetermined composition, a small concentration of the less noble metal is required, particularly in Fe–Ni; this causes problems related to the diffusion-limited deposition of this metal. Pulse plating can be used to eliminate the buildup of ion concentration gradients during deposition, but this generates nanoscale gradients in composition and local dependences of the composition on the mass transfer [48]. Tailoring of mechanical properties by pulse plating appeared possible however. Pulse reverse plating of Fe–Ni could also decrease internal stresses [50].

Iron–nickel alloys with the Invar composition (Ni 36 wt %) are characterized by very low coefficient of thermal expansion and find application in precision microactuators, for example, secondary actuators for magnetic recording heads [51]. In the as-deposited state, these alloys do not exhibit the phase structure of interest, and annealing is needed

TABLE 28.3 Nickel and Nickel Alloy Electroplating Baths

(a) Sulfamate Bath [38]	
Ni sulfamate–$4H_2O$	$300\,g\,L^{-1}$
$NiCl_2$–$6H_2O$	$10\,g\,L^{-1}$
H_3BO_3	$40\,g\,L^{-1}$
Additives unspecified	
pH 3.8	
$T = 50°C$	
(b) Ni Sulfamate Low Temperature [41]	
Ni sulfamate	$1.35\,M$
Boric acid	$30\,g\,L^{-1}$
SDS	$0.2\,g\,L^{-1}$
pH 3.5	
$T = 25°C$	
(c) Ni–Co [47]	
$NiCl_2$	$0.2\,M$
$CoCl_2$	$0–0.2\,M$
NaCl	$0.7\,M$
H_3BO_3	$0.4\,M$
Saccharin	$0–0.01\,M$
pH 2–6	
CD 1–25 mA cm^{-2}	
Room temperature (24°C)	
(d) Ni–Fe [48]	
$NiSO_4$	$380\,g\,L^{-1}$
$FeSO_4$	$14\,g\,L^{-1}$
H_3BO_3	$25\,g\,L^{-1}$
NaCl	$10\,g\,L^{-1}$
Coumarin	$0.3\,g\,L^{-1}$
Saccharin	$1\,g\,L^{-1}$
SDS	$0.5\,g\,L^{-1}$
Tartaric acid	$3.75\,g\,L^{-1}$
pH 3.0	
$T = 50°C$	
CD 30 mA cm^{-2}	
Pulse plating time on/off, 3 s/3 s	
(e) Ni–W [54]	
Ni sulfamate	$80\,g\,L^{-1}$
W	$4.2–20\,g\,L^{-1}$ as citrate ($Na_2WO_4 + C_2H_8O_7$)
H_3BO_3	$30\,g\,L^{-1}$
pH near neutral	
$T = 50°C$	
(f) Ni–P	
$NiSO_4$	$0.57\,M$
$NiCl_2$	$0,17\,M$
H_3PO_3	$0.48\,M$
H_3PO_4	$0.4\,M$
pH 2 with NaOH	
CD 10 mA cm^{-2}	
$T = 50°C$ with growth rate 5 μm h^{-1}	
(g) Ni–Mn [57]	
Ni sulfamate	$1.35\,M$
Mn as $MnCl_2$	$1.0–5.0\,g\,L^{-1}$
H_3BO_3	$30\,g\,L^{-1}$
SDS	$0.2\,g\,L^{-1}$
pH 3.5–5.0	
$T = 28°C$	
CD 1–25 mA cm^{-2}	

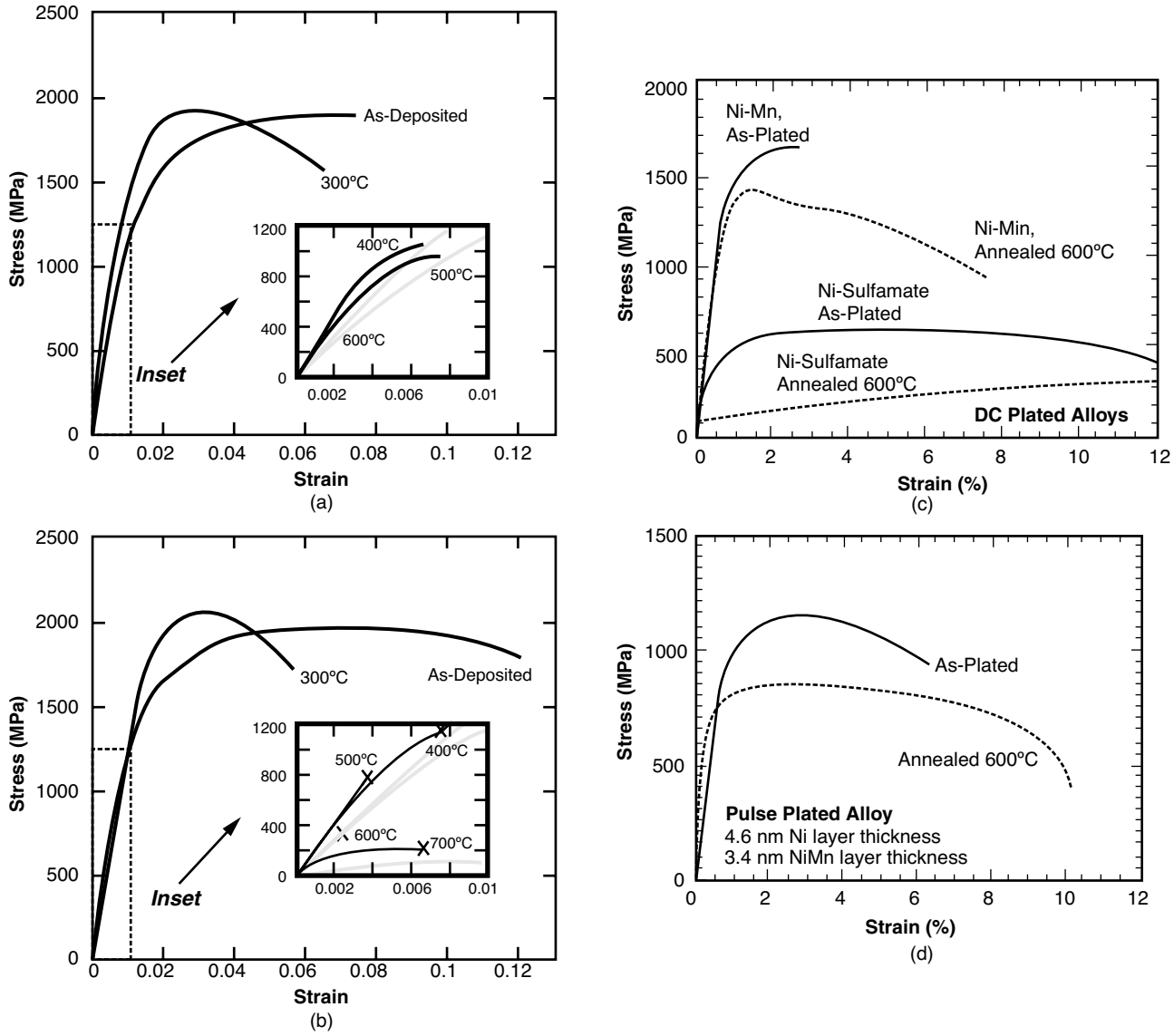

FIGURE 28.10 Tensile properties of (*a*) dc and (*b*) pulse-plated Ni–Fe Permalloy alloys and effect of thermal annealing. Comparison of as-deposited and annealed tension tests: (*c*) tensile properties of dc-electroplated Ni and Ni–Mn and effect of annealing at 600°C; (*d*) Tensile properties of Ni–Mn grown by pulse plating, before and after annealing at 600°C. [(*a, b*) Reprinted from [48] with permission of Elsevier. (*c, d*) Reprinted from [57] with permission of The Electrochemical Society.)

to achieve the transformation to the face-centered-cubic (fcc) phase. In order to avoid damage to the MEMS structure upon annealing, pulsed laser annealing was successfully demonstrated to induce this transformation without damaging the remaining structure [52].

Nickel–tungsten and Ni–Mo alloys present potentially better mechanical properties, hardness, and wear resistance than Ni, but these alloys are usually plated at high temperature and high pH [53] and can be obtained at relatively low temperatures (50°C) only by using sulfamate electrolytes [54]; a possible formulation is shown in Table 28.3, part (e). Large improvements in yield stress were obtained by the addition of 3.2 wt % W to Ni [54].

Nickel–phosphorus and Ni–B alloys can be electrodeposited from slightly acidic nickel electrolytes with the addition of phosphorous acid, H_3PO_3, or dimethylamine borane, respectively [55, 56]. Nickel–phosphorus alloys form metastable supersaturated solid solutions in the as-deposited state; the grain size decreases with increasing P content, and the alloys become amorphous for P above 9–10 wt %. Hardness of amorphous alloys is higher than that of electroplated Ni and may be tuned by gentle annealing; the alloys however are

brittle. The yield stress of Ni–P–B alloys with less than 1% each of P or B is higher than 400 MPa and may be increased by pulse plating [56]. An electrolyte used in Ni–P plating is reported in Table 28.3, part (f).

Finally, Ni–Mn alloys with up to 1 wt % Mn content plated from the electrolyte shown in Table 28.3, part (g), have shown yield strengths as high as 1000 MPa [57]. Pulse plating results in a decrease of the internal stress buildup during deposition [58], allowing the production of microfabricated structures (Fig. 28.10*b*).

28.5 MAGNETIC MEMS AND ELECTRODEPOSITION OF MAGNETIC MATERIALS

Ferromagnetic materials and components add important functionality to MEMS devices. Magnetic materials in fact could enable operation such as magnetic field sensing and generation through the use of microfabricated electromagnets (Fig. 28.11). Microinductors and microtransformers can be constructed using the same process steps. These electromagnets could also generate controlled forces for the deflection of electronic currents in electron beam columns and magnetic elements in magnetic actuation (Fig. 28.12). Magnetic actuation can be implemented by using electromagnetic interactions [61], permanent magnets [62], magnetostrictive materials, or shape memory alloys [63, 64]. These actuators present important advantages with respect to other types of actuation; for example, they allow wireless

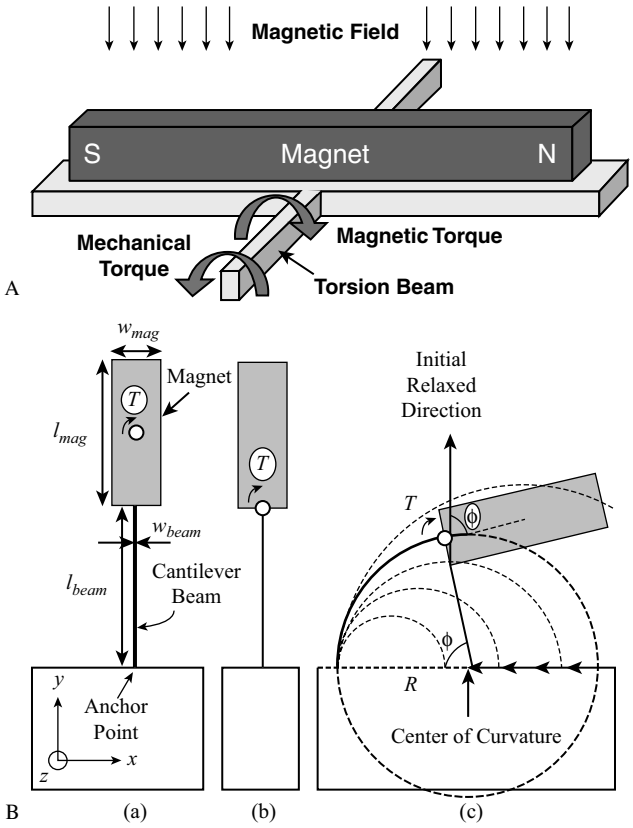

FIGURE 28.12 (*a*) magnetic actuation in uniform magnetic field, also used for operation of micromechanical magnetometer. (Reprinted from [60] with permission from Elsevier.) (*b*) Cantilever. (Reprinted from [61] with permission of IEEE.)

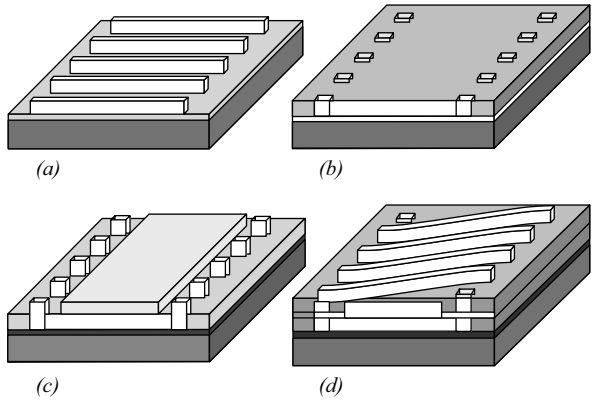

FIGURE 28.11 Process steps for fabrication of toroidal inductor: (*a*) electroplating of copper conductors; (*b*) planarization with photoresist followed by opening of via to underlying copper conductors; (*c*) electroplating of vias and magnetic core; for simplicity, the material used for the coil is the same material used for the magnetic core; (*d*) planarization and hard curing of photoresist layer followed by electroplating of top copper conductor. This design could be used to produce components for flux gate magnetic sensors, electromagnets, microinductors, and transformers. (Reprinted from [59] with permission from Elsevier.)

operation and operate at low or zero voltage, potentially enabling their use in remote and hostile environments. Moreover, they present a vastly improved performance (larger force, large throw) and better scaling behavior than piezoelectric or electrostatic counterparts [65]. Permanent magnet–based actuators can be used as bistable actuators, microfluidic valves, and switches at radio frequencies (RF) and for the actuation of micromirros for optical switches. Various experimental examples exist of these devices, including microflux gates (magnetic sensors) [59], sensors of position, velocity or acceleration, microfluidic separation of magnetic beads or nanoparticles [66], and magnetic actuation of movable mirrors [67].

28.5.1 Ferromagnetic Materials and Magnetization Processes [68]

Ferromagnetic materials possess a permanent magnetic moment and respond to an externally applied magnetic field H with a change in the magnetization M; this response is the hysteresis loop of the material (Fig. 28.13). A magnetic material is characterized by quantities such as the saturation

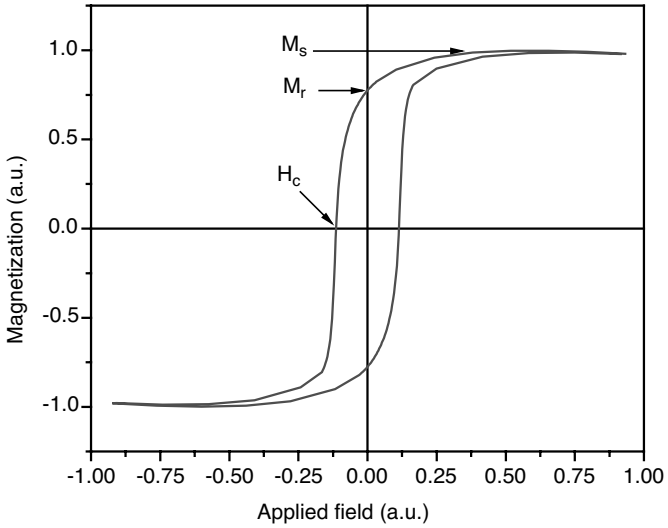

FIGURE 28.13 Typical hysteresis loop.

magnetization M_s, the remanence M_r, and the coercivity H_c; while the value of M_s is intrinsic to the material considered, M_r and H_c depend on the material microstructure. A magnetically soft material is characterized by low values of H_c (typically <10 Oe, 800 A m^{-1}) and M_r, and its magnetization is easily reversed and saturated in external magnetic fields. A magnetically hard material on the other hand is characterized by large values of M_r and H_c (typically >1 kOe, 80 kA m^{-1}), and tends to maintain its magnetization against externally applied fields (Fig. 28.14). Soft materials are able to concentrate magnetic fields and are used in transformers, inductors, electromagnets, and magnetic sensors. Hard materials are used as permanent magnets.

The response of a material to an external field depends on their relative orientation; it is said that the material exhibits a

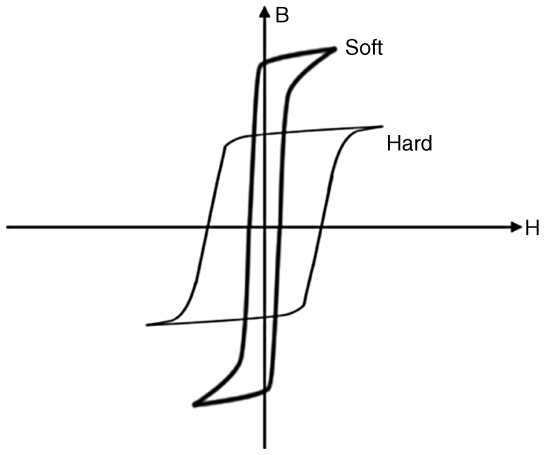

FIGURE 28.14 Typical hysteresis loops of soft and hard magnetic materials.

magnetic anisotropy; the magnetic energy density E_m of the material in the external field depends on direction and includes several contributions: the geometric shape of the material (shape anisotropy), the coupling between stress in the material and the magnetic field (magnetostriction), and the crystal structure of the material (magnetocrystalline anisotropy).

In the absence of external fields, soft materials do not exhibit any magnetization due to the formation of magnetic domains, regions where the magnetization is uniform but generally oriented in different directions, thus averaging to zero over the material volume. This configuration minimizes the energy of the material in the external magnetic field by minimizing the presence of magnetic poles; however, it introduces regions of inhomogeneous magnetization and high energy, the domain walls. The overall effect of these two opposing energy terms is that below a critical size of the crystal (between 10 and 100 nm) the multidomain state is unstable and the material is single domain.

For single-domain particles or for materials composed of weakly interacting single-domain particles, the magnetization switches by rotation of the magnetization vectors inside the material; rotation can be coherent or incoherent depending on the shape and size of the particles. Materials containing domain walls on the other hand will switch their magnetization by domain wall motion. Motion of domain walls can be hindered by nonuniformities in the material, which result in local gradients in E_m. Such regions may exhibit spatially varying internal stresses, compositional nonuniformities, nonmagnetic precipitates, and so on. Rotation of the magnetization vectors occurs easily if the magnetic energy density has little dependence on direction. Magnetization rotation will thus be difficult in parts with highly anisotropic shapes, materials with high magnetostriction, and materials with highly anisotropic crystal structures. In MEMS applications, parts with widely different geometrical shapes and aspect ratios are used; also, internal stresses in the materials cannot be easily controlled. Consequently, shape and magnetostriction effects are not reliable ways to control E_m. On the other hand, tuning magnetic anisotropy through the crystal structure is a reliable way to control the energy density. It should be stressed that a large anisotropy is not sufficient to warrant high coercivity; a suitable microstructure that hinders domain wall motion (decoupled single-domain grains or a high density of defects) is also necessary.

Soft magnets are ferromagnetic materials with a cubic or amorphous structure and with very small magnetostriction. Nickel–iron with the composition Fe ~ 20 at % is ideal in this respect since it displays a small magnetocrystalline anisotropy and near-zero magnetostriction. Mutual alloys of Fe, Co, and Ni can also be good soft magnetic materials. Among the amorphous materials, Fe or Co with the addition of P or B provide for ferromagnetic materials with very low anisotropy due to the lack of crystal anisotropy.

Hard magnetic materials include Co and its alloys with Ni, Mn, Re, P, and Pt. Intermetallic structures of Fe–Pt and Co–Pt in particular provide for very high magnetic anisotropy and thus high coercivity. High-performance, bulk permanent magnets are rare earth alloys such as Co–Sm and Nd–Fe–B. These alloys have a limited importance in electroplating for MEMS since in principle they cannot be electroplated from aqueous solutions.

28.5.2 Electrodeposition of Magnetic Materials for MEMS

Several difficulties are encountered when dealing with electroplating high-AR microstructures of magnetic materials, mostly related to the need for strict compositional control and microstructure optimization in order to achieve the magnetic properties sought for. In the case of soft materials, composition control is particularly difficult since these alloys exhibit anomalous deposition behavior and one of the depositing metal ions is present in low concentration, making the deposition rate and thus composition strongly dependent on the mass transport conditions, current distribution, and pattern geometry. In Ni–Fe, for example, small departures from the Permalloy composition may cause large changes in the magnetic properties, because of the concomitant increase in anisotropy and magnetostriction. From the microstructural standpoint, soft magnetic properties require compositional uniformity, low stresses, and the absence of precipitates of nonmagnetic matter. When plating hard materials, composition and microstructure must also be strictly controlled; in particular, the formation of cubic structures and twin defects should be avoided, as they decrease coercivity. Density of defects (to hinder domain wall motion) and composition at grain boundaries (to control magnetic coupling among the grains) should also be closely controlled. Often, nonmagnetic phases are required at these locations, and these are obtained by reduction or precipitation of oxides, hydroxides, or other nonmagnetic compounds.

Fe–Ni and Mutual Alloys of Fe–Co–Ni Mutual alloys of Fe, Co, and Ni exhibit anomalous codeposition behavior; that is, the less noble (LN) metal is deposited preferentially to the more noble (MN) one. This behavior is usually explained in terms of inhibition in the deposition of the MN metal due to competitive adsorption of intermediates of the two metals [69]. More recently, inhibition of the MN metal deposition has been observed along with an enhancement of the deposition of the LN metal in the presence of the NM one; this behavior has been tentatively modeled [70] in terms of a catalytic reaction scheme involving the formation of a heterometallic complex at the surface. Some features of the anomalous deposition process however are not completely understood yet [71]. Anomalous deposition is important at low deposition overpotentials (when the LN deposition is under kinetic limitations), but it is not as important near the diffusion limit. Anomalous effects are most important in Fe–Ni, and they become progressively less important in Fe–Co and Ni–Co.

Among the soft magnetic materials, Ni–Fe alloys are the most important. Nickel–iron (Fe $\sim$ 20%), for example, combines low magnetocrystalline anisotropy with near-zero magnetostriction to provide very low coercivities; moreover, this occurs at a Ni-rich composition which has a desirable high corrosion resistance. This is the first alloy utilized in the production of microfabricated magnetic recording heads, and it is the material of choice for the fabrication of magnetic MEMS including inductors, transformers, actuators, and micromotors. In the search for materials with higher saturation magnetization, electrodeposition processes for Ni–Fe 55% and alloys with up to 80% Fe were developed [72].

Electrolytes for Ni–Fe electrodeposition may contain either or both sulfates and chlorides of the metals, boric acid, and they are used at pH 2–3; see Table 28.4, part (a). Alloy composition is found to depend on current density (CD), with a maximum in Fe content at intermediate CD [73]. The Fe content goes through a maximum with increasing current density, this value depending on metal concentration, pH, and anion (Fig. 28.15). Addition of saccharin as stress reliever does not change this trend. It is important to operate around this maximum under conditions where the maximum is as wide as possible to provide against uncertainties in the local value of current. The maximum in Fe content is not observed (or it is pushed to very high current) if additions other than H_3BO_3 or saccharin are used. Efficiency increases with current density. Similar trends for composition versus CD have been obtained for Fe–Co and Fe–Co–Ni deposition [74]; in ternary alloys Co and Ni both act as the MN metal and their deposition is inhibited.

Nickel–iron alloys exhibit a transition from fcc to body-centered cubic (bcc) with increasing Fe content, roughly corresponding to that observed in bulk materials; polyphasic films are rougher [72].

These alloys are usually plated at CDs between 5 and 20 mA cm^{-2}; these deposition conditions have been developed for the synthesis of magnetic heads, which are at most several micrometers thick, and are not optimal for the fabrication of thick structures. By depositing at 10 mA cm^{-2}, in fact, the deposition rate is about 12 $\mu m\, h^{-1}$ and a part with 100 μm thickness would be plated in more than 8 h. A more suitable approach for MEMS applications is to use a concentrated sulfamate–chloride electrolyte [Table 28.4, part (b)]; its behavior was studied in a rotating-cylinder system in order to assess the effect of transport on the plating process [75]. Under these conditions, Fe content was found to always decrease with increasing CD, and sensitivity of alloy composition to electrolyte flow decreased at low CDs. Alloy compositions of interest could be obtained at 60 mA cm^{-2}

TABLE 28.4 Electrolytes for Electrodeposition of Soft Magnetic Materials

(a) Ni–Fe and Permalloy [73]—*see also Figure 28.15*

Solution	$NiSO_4$ (*M*)	$NiCl_2$ (*M*)	$FeSO_4$ (*M*)	$FeCl_2$ (*M*)	H_3BO_3 (*M*)	pH
1	0.50	—	0.01	—	—	3.0
2	0.50	—	0.01	—	0.40	3.0
3	—	0.50	—	0.01	—	3.0
4	—	0.50	—	0.01	0.40	3.0
5	0.50	—	0.01	—	—	2.0
6	0.50	—	0.01	—	0.40	2.0
7	—	0.50	—	0.01	—	2.0
8	—	0.50	—	0.01	0.40	2.0

(b) High-Rate Ni–Fe and Permalloy [77]

Ni sulfamate	0.2 *M*
H_3BO_3	0.4 *M*
Sodium saccharin	1.5 g L^{-1}
Sodium dodecyl sulfate	0.2 g L^{-1}
Ascorbic acid	1 g L^{-1}
$FeCl_2$	0.008–0.02 *M*

Compositions between 10 and 80 at % Fe can be obtained by varying CD in the range 20–100 mA cm^{-2} and convective mass transfer rates.

(65 μm h^{-1}). The effect of controlled convection and CD was also studied by plating Ni–Fe gears with aspect ratio 1 : 5 [76], conditions under which convection through the entire thickness of the mold is expected. In this instance, baths with a higher Ni–Fe ratio present a better uniformity, less dependence on plating conditions and stirring, and thus higher throughput [77]. From these data, it appears clear that the suitability of various processes to the fabrication of soft magnetic structures will depend on the application at hand and on the existing process constraints.

Permalloy is extensively used in magnetic MEMS; this material is used in electromagnetic amplification of a magnetic field (solenoids), for field concentration (transformer), and in electromagnetic actuation such as in valves and cantilevers. Methods for LIGA fabrication of magnetic induction machines have been developed [78] together with

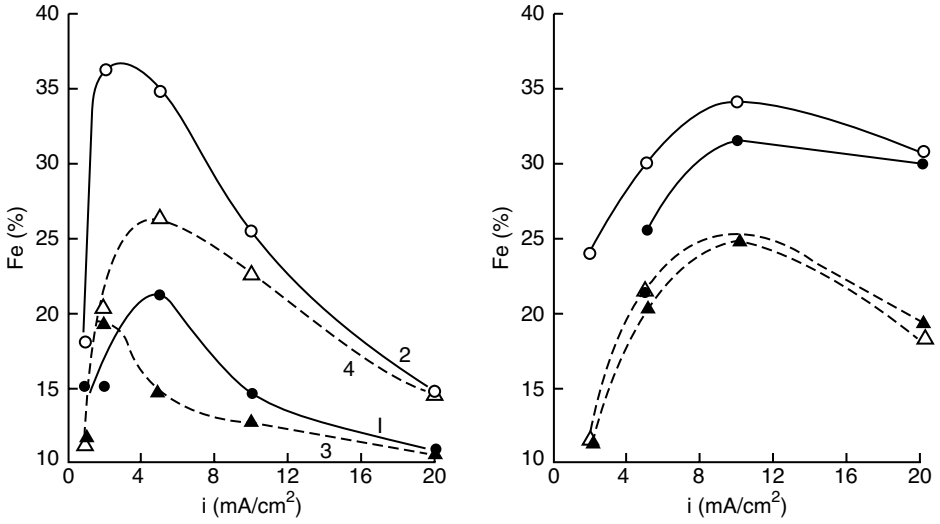

FIGURE 28.15 Dependence of Ni–Fe alloy composition as function of current density for various pH and metal concentrations. Left, pH 3; right, pH 2. The numbers in the figures correspond to those in Table 28.5, part (a). (Reproduced from [73] by permission of The Electrochemical Society.)

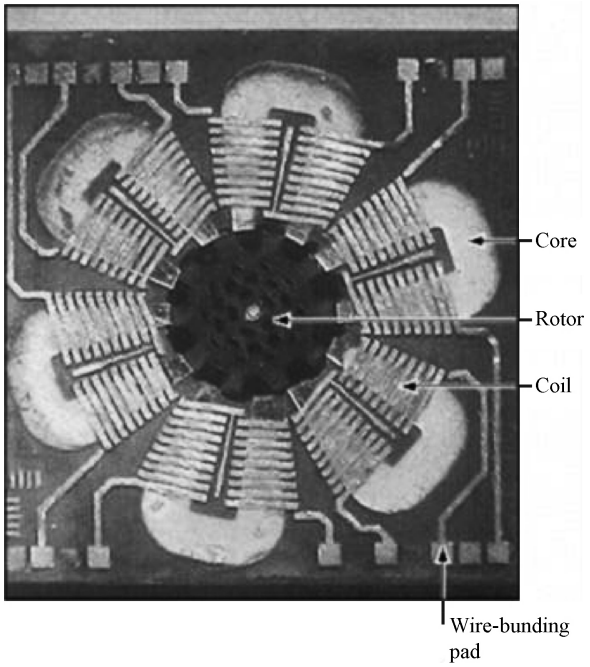

FIGURE 28.16 Top view of integrated, variable-reluctance magnetic micromotor obtained by X-ray and optical lithography followed by LIGA of Cu coils and Ni–Fe rotor and stators. The stator was electroformed separately and put in place. (Reprinted from [80] with permission of IBM.)

micromechanical magnetometers using soft materials [79] and flux gate magnetic sensors [59].

An interesting application of Permalloy electroplating consists in the fabrication of magnetic micromotors utilizing soft magnetic materials for the stator and the rotor. A particularly illuminating implementation of this process is presented in [80], which compares two designs using either optical or X-ray lithography. Plated features included about 30-μm-thick conductors and 45-μm-thick Permalloy cores (Fig. 28.16). Control of composition and thickness in Permalloy plating was achieved by using auxiliary cathodic electrodes (current thieves) and a paddle cell. The solution used for Permalloy plating was an acidic solution with pH control and automatic replenishment of Fe. Problems related to thermal mismatch and delaminating at vertical metal–polymer structures and alignment issues due to the thickness of the mask were encountered in the X-ray lithography approach.

Permanent Magnet Materials Permanent micromagnets are used in MEMS devices to generate localized magnetic fields, as biasing magnets, and to implement actuation and transduction. Despite their inherent advantages, few MEMS designs employ electroplated hard magnetic structures to implement these functions. This is due to the difficulty in developing a reliable electroplating process for the production of hard magnets. In order to deliver sufficient force under the constraint of a limited footprint on the device, the height of the magnet should be maximized, its upper limit being determined by the resist and the lithography process to 100 μm–1 mm. It is very difficult to achieve close control over the microstructure and thus obtain hard magnetic properties in such tall structures. Bulk permanent magnets, machined to the dimensions required, are instead glued to the device, with corresponding limitations in performance, reliability, and miniaturization.

Limitations of the footprint imply that most designs including actuators require a vertical motion, although there are exceptions. The electroplated permanent magnet should therefore provide for a vertical field, and this requires perpendicular magnetic anisotropy. The anisotropy should be independent of the geometry of the part shape and should preferably be of magnetocrystalline origin.

Hard magnetic materials require both a high magnetic anisotropy and a microstructure that hinders the motion of magnetic domain walls. High magnetic anisotropies are obtained in anisotropic crystal structures, the most relevant being hexagonal and tetragonal structures. Materials that satisfy these conditions are cobalt and its hexagonal alloys, in particular Co–Sm, $L1_0$ tetragonal structures such as equiatomic Fe–Pt and Co–Pt, and Nd–Fe–B. The anisotropy of the most important hard magnetic materials is given in Table 28.5. These should be compared with the maximum shape anisotropy achievable in pure metals, that of a thin film of Fe, $E_{\text{shape}} = {}^1\!/_2\ \mu_0 M_s{}^2 \sim 1.8\,\text{MJ m}^{-3}$. It is clear that the shape anisotropy can be disregarded in magnet design only when using very high anisotropy materials. When using materials that can be more easily plated, design will need to consider shape along with crystal anisotropy.

The most common materials with a high anisotropy and the potential to provide for hard magnetic properties are Co and Co alloys. Cobalt is mostly electrodeposited from acidic electrolytes containing Co salts (sulfates, chloride, sulfamates) with the addition of boric acid. An extensive study from sulfamate electrolytes [81] shows that below pH 2.5 both the hexagonal and cubic form of cobalt are observed, the latter being stabilized at low temperature, high CD, and low pH by the presence of adsorbed hydrogen. Increasing pH to 2.5–3, the films become hexagonal with a preferred orientation (PO) (11.0) + (10.0); only the PO (11.0) eventually remains at pH 3.2. Electrolytes without boric acid are

TABLE 28.5 Magnetic Anisotropy of Hard Magnetic Materials

Co	$4.1 \times 10^5\,\text{J m}^{-3}$
Co–Pt $L1_0$	$4.6\,\text{MJ m}^{-3}$
Fe–Pt $L1_0$	$6.6\,\text{MJ m}^{-3}$
Co_5Sm	$11–20\,\text{MJ m}^{-3}$
NdFeB	$5\,\text{MJ m}^{-3}$

subject to aging with progressive suppression of the (11.0) texture; this appears to be due to slow hydrolysis reactions in the plating solution, occurring over several months. The addition of $CoCl_2$ causes the formation of stable chloro complexes and eliminates this aging problem. A PO (00.1) (*c* axis perpendicular to the film plane) is obtained at high temperature and pH from sulfamate solutions [81, 82] and also using sulfates at high CD [83]. Under these conditions, colloidal hydrolized species are stable in the near-electrode region and at high pH also in the bulk, enabling precipitation and incorporation of hydroxides, mainly when growth occurs along (00.1) [84]; this results in cellular growth [82]. The (00.1) PO is further improved by addition of sulfamid [81]. These films present a coercivity around 2 kOe and have been studied for possible applications in perpendicular recording [82].

Early studies on Co alloys [85] demonstrated that the addition of elements from the VA group (P, As, Sb, Bi) and VIB group (Cr, Mo, W) of the periodic table to Co or Co–Ni films resulted in an increase of film coercivity through two effects: grain refinement and ability of the element to segregate at grain boundaries. Phosphorus was found to require the minimum additions to achieve a maximum in coercivity. Cobalt–phosphorus alloys are thus of interest as they may provide high coercivities for small P additions. Cobalt–phosphorus and Co–Ni–P films are electrodeposited from electrolytes containing the metal salt(s) (sulfate and/or chloride), boric acid, and either phosphorous acid (H_3PO_3) [86] or sodium hypophosphite as a P source. More recently, an alkaline solution based on citrate–glycine complexation of Co and sodium hypophosphite was used [87]. Cobalt–phosphorus exhibits a wide range of magnetic properties in dependence of their microstructure and P content. Under acidic conditions, the composition can be varied only to a limited extent by varying the current density [86]. ECD from alkaline electrolyes on the other hand allows tuning of the composition by using CD; in particular, P content increases with CD. Hard magnetic films are obtained only at low current densities, where the films are crystalline and contain about 10 at % P. Films grown at larger CDs are amorphous and contain $P > 10$ at % [87]. The Co–Ni–P alloys [Table 28.6, part (a)] provide hard magnetic properties when the P content is in the range 8–10 at %. These alloys exhibit a hexagonal structure and columnar growth and their coercivity originates from the precipitation of a nonmagnetic NiP phase at grain boundaries [88]. Coercivities were above 2 kOe and could be maintained up to a thickness of 10 μm [89]. Additions of Mn to these alloys have been found to promote perpendicular anisotropy; both CoMnP and CoNiMnP ($P \sim 3\%$) exhibit high remanence in the perpendicular direction; coercivity was about 1.6 kOe for Co–Mn–P, well above 2 kOe for Co–Ni–Mn–P [90, 91].

Cobalt–tungsten and Co–Mo films can be electrodeposited from both acidic and alkaline electrolytes; the magnetic properties strongly depend on the microstructure, and high coercivities are obtained when a columnar structure with magnetically separated grains is obtained. This is achieved at pH 6–6.7, where metal hydroxides tend to precipitate at grain boundaries. Cobalt–chromium alloys deposited using vacuum techniques present attractive magnetic properties; however, such properties are very difficult to reproduce by electroplating. Chromium alloys in fact can be electroplated in practice only from Cr(III) electrolytes, notoriously unstable and difficult to operate. Consequently, little effort has been dedicated to magnetic studies of electroplated Co–Cr alloys.

Platinum increases the magnetic anisotropy of Co, and it would be an ideal alloying addition to improve its hard magnetic properties. In the bulk, the solubility limit of Pt

TABLE 28.6 Electrolytes for the Electrodeposition of Hard Magnetic Materials

(a) Co–Ni–P [89]	
$CoCl_2$	0.2 *M*
$NiCl_2$	0.2 *M*
NaH_2PO_2	0.15 *M*
NaCl	0.7 *M*
H_3BO_3 0.4 M	
pH 3	
$T = 25°C$	
Hard magnetic properties are obtained at 7–10 mA cm^{-2}	
(b) Co–Pt [92–94]	
$Pt(NO_2)_2(NH_3)_2$	10 m*M*
Co sulfamate	0.1 *M*
Ammonium citrate	0.1 *M*
Glycine	0.1 *M*
NaH_2PO_2	0.1 *M*
pH 8	
T 65°C	
Hard magnetic properties are obtained at 50 mA cm^{-2}	
(c) Fe–Pt [101]	
$PtCl_4$	0.3–30 m*M*
$FeCl_2$	0.11 *M*
NaCl	0.5 *M*
pH 2.5	
Potentials to obtain various compositions are reported in Figure 28.18.	
Annealing at 650°C in Ar atmosphere to achieve hard magnetic properties	
(d) Fe–Pt [104]	
H_2PtCl_6	1 m*M*
$FeSO_4$	0.1 *M*
Na_2SO_4	0.5 *M*
pH 3	
$V = -0.78\ V_{SCE}$ to achieve equiatomic composition	
Annealing at 600–700°C in 1 bar H_2 for 10 min to achieve hard magnetic properties	

in hexagonal Co is 20 at %; at this composition the anisotropy of bulk alloys is maximum.

Various researchers have studied the electrodeposition of Co-rich, hexagonal Co–Pt alloys. Slightly alkaline electrolytes containing citrate–glycine complexes of cobalt with Pt $(NO_2)_2(NH_3)_2$ (Pt–P–salt) at pH 8 [Table 28.6, part (b)] give films whose composition is around 20–25 at % Pt, only slightly dependent on current density [92]. The films tend to grow with the hexagonal *c* axis perpendicular to the film and are hard in the as-plated condition. Coercivities can be further improved by favoring the perpendicular orientation early in the growth process using a suitable epitaxial seed layer. Maximum coercivities observed are higher than 6 kOe at 1 μm thickness using Cu(111) substrates [93], while Ru(0001) substrates provide for coercivities around 1 kOe and a 100% remanence in 10–nm-thick films [94]. In thicker films (Fig. 28.17), H_c increases to about 4 kOe but remanence decreases. The Pt content in these films is relatively high, potentially impacting the overall cost of the fabrication process; an attempt to substitute Pt in part with W was undertaken by Cavallotti, who was able to obtain Co–W–Pt films up to 20 μm thick, containing Pt ~ 8 at % and coercivity slightly below 4 kOe [95]. Growth instabilities with dendrite formation were occasionally observed. Zinc additions to the Co–Pt electrolyte switched the anisotropy axis from perpendicular to the plane of the film [95]. Gileadi used similar electrolytes to grow films up to 40 μm thick and $H_c \sim 2.8$ kOe; this work highlighted the fact that the Pt complex is unstable, as evidenced by changes in the alloy composition upon electrolyte aging [96]. Other alkaline electrolytes using various Co complexes [97, 98] did not exhibit high coercivity in the as-plated condition; H_c however could be strongly enhanced by thermal annealing [98]. Slightly acidic electrolytes have also been developed [99, 100], in some cases showing hard magnetic properties [100].

It is believed that the hardening mechanism in Co-based alloys is the formation of very fine grains, concurrent with the precipitation of nonmagnetic matter and segregation at the grain boundaries, resulting in the formation of a columnar morphology (Fig. 28.17*a*). The nature of these precipitates is determined by electrochemical equilibria at the interfacial electrolyte–substrate region. Involved in these equilibria may be metal hydroxides and possibly metal

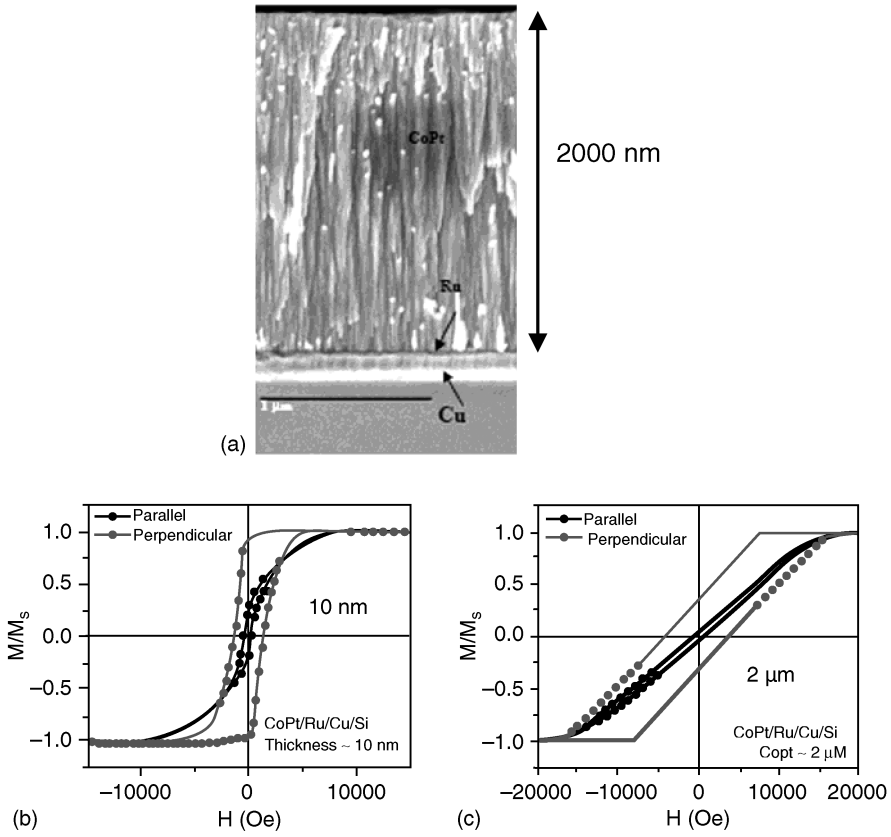

FIGURE 28.17 (*a*) Typical cellular morphology of electroplated, magnetically hard Co alloys—this is Co–Pt [94]. (*b, c*) Magnetic properties of Co-rich Co–Pt electrodeposited onto Ru(0001) with magnetic field applied parallel (dark lines) and perpendicular (lighter lines) to film plane: (*b*) 10-nm-thick film and (*c*) 2-μm-thick film.

phosphides; there is in fact some evidence that the high coercivity of electroless Co–P films is originated by the precipitation at grain boundaries of nonmagnetic Co–phosphides.

A different method has been pursued to obtain ordered equiatomic alloys of Fe–Pt and Co–Pt. In this approach, the alloys are grown under potential or current control, then annealed, preferably in a hydrogen atmosphere. Potential control was used by a group at the National Institute for Standards and Technology (NIST), who exploited an underpotential deposition phenomenon, driven by the negative free energy of alloy formation, to control the alloy composition by the potential, through a well-defined thermodynamic relationship (Fig. 28.18) [101]. A chloride-based, acidic electrolyte was used [Table 28.6, part (c)]. Equiatomic Fe–Pt alloys contained up to 30 at % oxygen, irrespective of the approach used to decrease the oxygen content. Annealing of near-equiatomic alloys electrodeposited on oriented Cu resulted in the formation of the $L1_0$ phase with the anisotropy axis oriented perpendicular to the film plane and with a coercivity of about 10 kOe [102]. A similar process, and comparable magnetic properties, could be obtained by underpotential deposition of Co–Pt, the latter containing much less oxygen [103]. In parallel, a group in Dresden used an acidic sulfate–chloride electrolyte [Table 28.6, part (d)] and current or potential control to deposit near-equiatomic Fe–Pt alloys, which were later annealed in hydrogen to reach up to 11 kOe coercivity [104]. The high oxygen content obtained when electrodepositing equiatomic alloys was decreased to 10 at % by alternating Fe-rich and Pt-rich layers using pulsed electrodeposition followed by annealing [105] (Fig. 28.19). The same authors highlighted the fact that the Co–Pt system is better behaved from the electrochemical standpoint than Fe–Pt, resulting in similar magnetic properties despite the superior magnetic properties of bulk Fe–Pt [106].

Only sporadic examples of direct integration of hard magnetic alloys within MEMS designs are available in the literature. In most cases, bulk permanent magnets are machined and glued to the device [107]. Some instances of integration of electroplated magnets in MEMS however are available. For example, permament magnet arrays of CoNiMnP have been electroplated [108] and used for vertical microactaution. In other implementations, CoPtP has been used for biasing of magnetoresistive sensors, vertical microactuators, and horizontal microswitches [109].

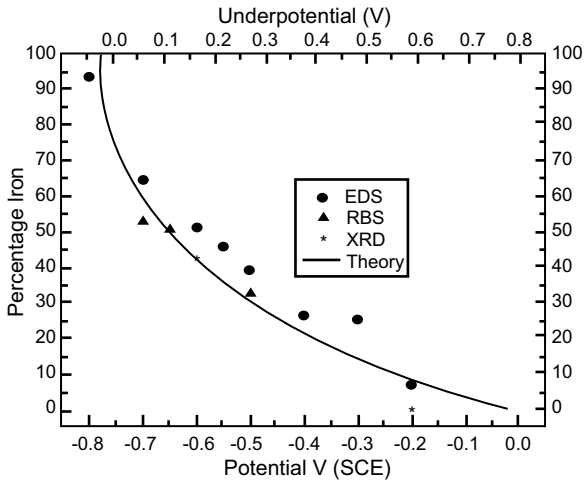

$$E_i - E_i^o = + \frac{RT}{zF} \ln \left(\frac{\alpha_i^{\text{ion}}}{X_i \exp\left(\frac{\Omega}{RT} (1\text{-}X_i)^2 \right)} \right)$$

FIGURE 28.18 Relationship between theoretical predictions and experimental data for underpotential deposition of Fe–Pt. (Reproduced from [101] by permission of The Electrochemical Society.)

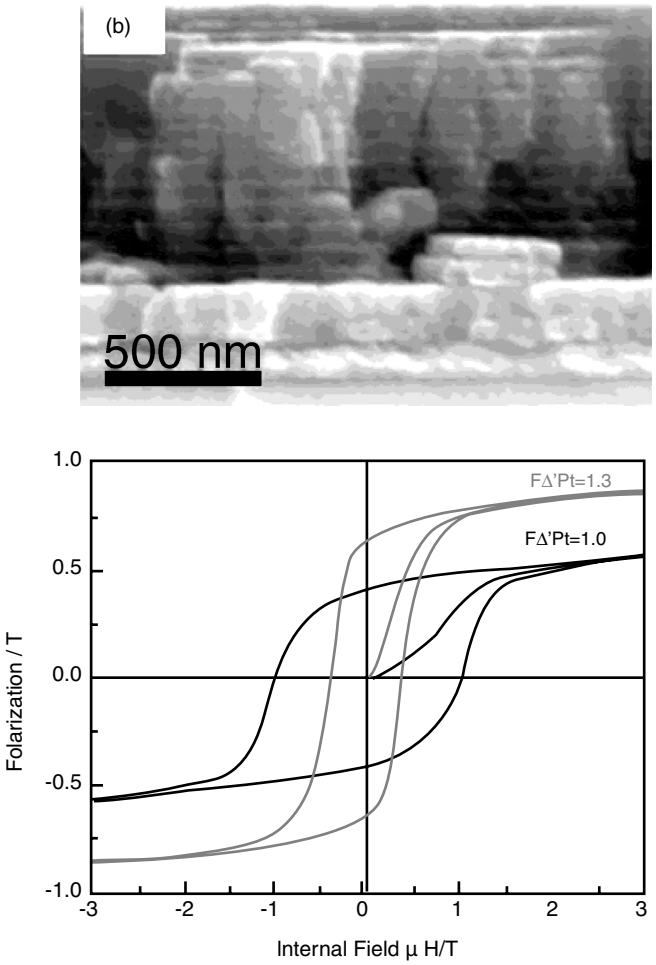

FIGURE 28.19 Morphology (before annealing) and magnetic properties (after annealing) of Fe–Pt multilayer with low oxygen content. (Reprinted from [105] with permission from Elsevier.)

ACKNOWLEDGMENT

The author would like to thank Lok-Kun Tsui at the University of Virginia for the drawing of Figures 28.1–28.3, 28.5–28.9, and 28.14.

REFERENCES

1. M. J. Madou, *Fundamentals of Microfabrication*, 2nd ed., CRC Press, Boca Raton, Fl, 2002.
2. M. Gad-el-Hak, *MEMS—Design and Fabrication*, 2nd ed., CRC Taylor & Francis, Boca Raton, FL, 2006.
3. F. Goodenough, *Electron. Design*, **39** (15), 45 (1991).
4. K. D. W. Samaun and J. B. Angell, *IEEE Trans. Biomed. Eng.*, **BM20** (2), 101–109 (1973).
5. D. M. Monk and R. O. Gale, *Microelectron. Eng.*, **27** (1–4), 489–493 (1995).
6. J. W. Judy, *Smart Mater. Struct.*, **10**, 1115–1134 (2001).
7. J. M. Blackburn et al., *Science*, **294** (5540), 141–145 (2001).
8. T. Kohlmeier, V. Seidemann, S. Buttgenbach, and H. H. Gatzen, *Microsystem Technol.* **8**, 304–307 (2002).
9. B. Loechel, *J. Micromechani. Microeng.*, **10** (2), 108–115 (2000).
10. E.W. Becker, W. Ehrfeld, P. Hagmann, A. Maner, and D. Muenchmeyer, *Microelectron. Eng.*, **4**, 35–56 (1986).
11. K. G. Jordan and C. W. Tobias, *J. Electrochem. Soc.*, **138** (7), 1933–1939 (1991).
12. K. Hayashi et al., *J. Electrochem. Soc.*, **148** (3), C145–C148 (2001).
13. R. H. Nilson and S. K. Griffiths, *J. Electrochem. Soc.*, **150** (6), C401–C412 (2003).
14. N. Ibl,in *Advances in Electrochemistry and Electrochemical Engineering*, W. Tobias, Ed., Interscience, New York, 1962, p. 49.
15. D. Landolt, "Mass Transport in Pulse Plating," in *Theory and Practice of Pulse Plating*, F. Leaman and J-C. Puippe, Eds., American Electroplaters and Surface Finishers Society, Inc., Orlando, FL, 1986.
16. A. C. West, C. C. Cheng, and B. C. Baker, *J. Electrochem. Soc.*, **145** (9), 3070–3074 (1998).
17. J. O. Dukovic, *IBM J. Res. Devel.*, **34** (5), 693–705 (1990).
18. J. O. Dukovic, *IBM J. Res. Devel.*, **37** (2), 125–141 (1993).
19. S. Mehdizadeh et al., *J. Electrochem. Soc.*, **139** (1), 78–91 (1992).
20. K. S. Drese, *J. Electrochemical Soc.*, **151** (6), D39–D45 (2004).
21. C. K. Malek et al., *J. Micromechan. Microeng.*, **6** (2), 228–235 (1996).
22. F. H. Reid and W. Goldie, Eds. *Gold Plating Technology*, Electrochemical Publications, Ayr, Scotland, 1974.
23. J. Horkans and L. T. Romankiw, *J. Electrochem. Soc.*, **124** (10), 1499–1505 (1977).
24. T. Osaka et al., *J. Electrochem. Soc.*, **144** (10), 3462–3469 (1997).
25. Y. Okinaka and M. Oshino, *Gold Bull.*, **31** (1), 3 (1998).
26. T. A. Green, *Gold Bull.*, **40** (2), 105 (2007).
27. P. C. Andricacos et al., *IBM J. Res. Devel.*, **42** (5), 567–574 (1998).
28. M. Lefebvre et al., *Circuit World*, **29** (2), 9–14 (2003).
29. L. T. Romankiw, *Electrochim. Acta*, **42** (20–22), 2985–3005 (1997).
30. T. P. Moffat, et al., *IBM J. Res. Devel.*, **49** (1), 19–36. (2005).
31. J. M. Lee and A.C. West, *J. Electrochem. Soc.*, **152** (10), C645–C651 (2005).
32. N. T. Nguyen et al., *J. Micromechan. Microeng.*, **12**, 395–399 (2002).
33. L. L. W. Leung and K. J. Chen, *IEEE Trans. Microwave Theory Techn.*, **53** (8), 2472–2480 (2005).
34. P. Dixit and J. M. Miao, *J. Electrochem. Soc.*, **153** (6), G552–G559 (2006).
35. P. Dixit, J. M. Miao, and R. Preisser, *Electrochem. Solid State Lett.*, **9** (10), G305–G308 (2006).
36. K. Kondo et al., *J. Electrochem. Soc.*, **152** (11), H173–H177 (2005).
37. J.W. Dini, *Electrodeposition*, Noyes, Norwich 1993, Chapter 9.
38. J. K. Luo et al., *J. Electrochem. Soc.*, **153** (10), D155–D161 (2006).
39. T. Fritz, H. S. Cho, K. J. Hemker, W. Mokwa, and U. Schnakenberg, *Microsyst. Tech.*, **9**, 87 (2002).
40. S. J. Hearne and J. A. Floro, *J. Appl. Phys.*, **97**, 014901 (2005).
41. J. J. Kelly, S. H. Goods, A. A. Talin, and J. T. Hachman, *J. Electrochem. Soc.*, **153** (5) C318 (2006).
42. S.H. Goods, J. J. Kelly, A. A. Talin, J. R. Michael, and R. M. Watson, *J. Electrochem. Soc.*, **153** (5) C325 (2006).
43. Y. Yang, S. Allameh, J. Lou, B. Imasogie, B. L. Boyce, and W. O. Soboyejo, *Metall. Mater. Trans.*, **A38**, 2340 (2007).
44. Y. Yang, N. Yao, B. Imasogie, and W. O. Soboyejo, *Acta Mater.*, **55**, 4305 (2007).
45. W. Kim, R. Weil, *Surf. Coat. Tech.*, **38**, 289 (1989).
46. W. H. Safranek, *The Properties of Electrodeposited Metals and Alloys*, 2nd ed., American Electroplaters and Surface Finishers Society, Inc., Orlando, FL, 1986, p. 327.
47. D. Y. Park et al., *J. Electrochem. Soc.*, **153** (12), C814 (2006).
48. T. E. Buchheit, S. H. Goods, P. G. Kotula, and P. F. Hlava, *Mater. Sci. Eng.*, **A432**, 149 (2006).
49. M. H. Byun, J. W. Cho, B. S. Han, Y. K. Kim, and Y. S. Song, *Jpn. J. Appl. Phys.*, **45** (9A) 7084 (2006).
50. Y. M. Yeh et al. *Jpn. J. Appl. Phys.*, **44** (2), 1086 (2005).
51. T. Hirano, L. S. Fan, J. Q. Gao, and W. T. Lee, *J. MEMS*, **7** (2), 149 (1998).
52. A. K. Dokania et al., *Mater. Sci. Eng.*, **A456**, 64 (2007).
53. O. Younes and E. Gileadi, *J. Electrochem. Soc.*, **149** (2), C100 (2002).
54. E. Slavcheva, W. Mokwa, and U. Schnakenberg, *Electrochim. Acta*, **50**, 5573 (2005).

55. B. P. Daly and F. J. Barry, *Int. Mat. Rev.*, **48** (5), 326 (2003).
56. D. J. Kim, M. J. Kim, J. S. Kim, and H. P. Kim, *Surf. Coat. Tech.*, **202** (12), 2519 (2008).
57. J. J. Kelly, S. H. Goods, and N. Y. C. Yang, *Electrochem. Solid State Lett.*, **6** (6), C88 (2003).
58. S. J. Hearne et al., *J. Appl. Plys.*, **99**, 053517 (2006).
59. T. M. Liakopoulos and C. H. Ahn, *Sensors Actuators*, **77**, 66 (1999).
60. H. H. Yang, N. V. Myung, J. Yee, D. -Y. Park, B. -Y. Yoo, M. Schwartz, K. Nobe, and J. W. Judy, *Sensors Actuators*, **A97–98**, 88 (2002).
61. J. W. Judy, R. S. Muller, and H. H. Zappe, *J. MEMS*, **4** (4), 162 (1995).
62. H. J. Cho and C. H. Ahn, *J. MEMS*, **11** (1), 78 (2002).
63. M. Pasquale, *Sensors Actuators*, **A106**, 142 (2003).
64. J. Enkovaara, A. Ayuela, A. T. Zayak, P. Entel, L. Nordström, M. Dube, J. Jalkanen, J. Impola, and R. M. Nieminen, *Mater. Sci. Eng.*, **A378**, 52 (2004).
65. O. Cougat, J. Delamare, and G. Reyne, *IEEE Trans. Magn.*, **39** (5), 3607 (2003).
66. L. Lagae et al., *J. Appl. Phys.*, **91** (10), 7445 (2002).
67. O. Cougat, S. Basrour, C. Divoux, P. Mounaix, and G. Reyne, *Sensors Actuators*, **A89**, 1 (2001).
68. R. C. O'Handley, *Modern Magnetic Materials—Principles and Applications*, Wiley, New York, 2000.
69. M. Matlosz, *J. Electrochem. Soc.*, **140** (8), 2272 (1993).
70. N. Zech, E. J. Podlaha, and D. Landolt, *J. Electrochem. Soc.*, **146** (8), 2892 (1999).
71. J. Vaes, J. Fransaer, and J.-P. Celis, *J. Electrochem. Soc.*, **147** (10), 3718 (2000).
72. E. I. Cooper et al., *IBM J. Res Devel.*, **49** (1), 103 (2005).
73. J. Horkans, *J. Electrochem. Soc.*, **128** (1), 45 (1981).
74. Y. Zhuang and E. J. Podlaha, *J. Electrochem. Soc.*, **147** (6), 2231 (2000).
75. S. D. Leith, S. Ramli, and D. T. Schwartz, *J. Electrochem. Soc.*, **146** (4), 1431 (1999).
76. S. D. Leith and D. T. Schwartz, *Electrochim. Acta*, **44**, 4017 (1999).
77. S. D. Leith and D. T. Schwartz, *J. MEMS*, **8** (4), 384 (1999).
78. D. P. Arnold, S. Das, F. Cros, I. Zana, M. G. Allen, and J. H. Lang, *J. MEMS*, **15** (2), 406 (2006)
79. H. H. Yang et al., *Sensors Actuators*, **A97–98**, 88 (2002).
80. E. J. O'Sullivan et al., *IBM J. Res. Devel.*, **42** (5), 681 (1998).
81. A. Vicenzo and P. L. Cavallotti, *Electrochim. Acta*, **49**, 4079 (2004).
82. T. Chen and P. L. Cavallotti, *Appl. Phys. Lett.*, **41**, 205 (1982).
83. S. Armyanov, *Electrochim. Acta*, **45**, 3323 (2000).
84. T. A. Tochitskii and V. G. Shadrov, A.V. Boltushkin, *Cryst. Res. Tech.*, **28**, 1079 (1993).
85. F. E. Luborsky, *IEEE Trans. Magn.*, **6** (3), 502 (1970).
86. Y. Fukunaka, S. Aikawa, and Z. Asaki, *J. Electrochem. Soc.*, **141** (7), 1783 (1994).
87. X. Xu and G. Zangari, *J. Electrochem. Soc.*, **155** (12), D742 (2008).
88. T. Homma, Y. Sezai, T. Osaka, Y. Maeda, and D. M. Donnet, *J. Magn. Magn. Mat.*, **173**, 314 (1997).
89. D. M. Kirkwood, G. Pattanaik, and G. Zangari, *J. Electrochem. Soc.*, **154**, D363 (2007).
90. J. Horkans, D. J. Seagle, and I.-C.H. Chang, *J. Electrochem. Soc.*, **137** (7), 2056 (1990).
91. V. Brusic, J. Horkans, and D. J. Barclay, *Adv. Electrochem. Sci. Eng.*, **1**, 249 (1990).
92. G. Pattanaik, D. M. Kirkwood, X. Xu, and G. Zangari, *Electrochim. Acta*, **52**, 2755 (2007).
93. I. Zana and G. Zangari, *Electrochem. Solid State Lett.*, **6**, C153 (2003).
94. G. Pattanaik, G. Zangari, and J. Weston, *Appl. Phys. Lett.*, **89**, 112506 (2006).
95. P. L. Cavallotti, A. Vicenzo, M. Bestetti, and S. Franz, *Surf. Coat. Tech.*, **169–170**, 76 (2003).
96. O. Berkh, Yu. Rosenberg, Y. Shacham-Diamond, and E. Gileadi, *Microelectron. Eng.*, **84**, 2444 (2007).
97. K. Hosiri, F. Wang, S. Doi, and T. Watanabe, *Mater. Trans.*, **44** (4), 653 (2003).
98. N. Fujita, S. Maeda, S. Yoshida, M. Takase, M. Nakano, and H. Fukunaga, *J. Magn. Magn. Mat.*, **272–276**, E1895 (2004).
99. T. S. Eagleton, J. Mallet, X. Cheng, J. Wang, C.-L. Chien, and P. C. Searson, *J. Electrochem. Soc.*, **152**, C27 (2005).
100. S. Franz, M. Bestetti, and P. L. Cavallotti, *J. Magn. Magn. Mat.*, **316**, E173 (2007).
101. J. J. Mallett et al., *Electrochem. Solid State Lett.*, **7** (10), C121 (2004).
102. E. B. Svedberg et al., *Appl. Phys. Lett.*, **85** (8), 1353 (2004),
103. J. J. Mallett et al., *Electrochem. Solid State Lett.*, **8** (1), C15 (2005).
104. K. Leistner, J. Thomas, H. Schloerb, M. Weisheit, L. Schultz, and S. Fahler, *Appl. Phys. Lett.*, **85** (16), 3498 (2004).
105. K. Leistner, S. Fahler, H. Schloerb, and L. Schultz, *Electrochem. Commun.,l* **8**, 916 (2006).
106. K. Z. Rozman, A. Krause, K. Leistner, S. Fahler, L. Schultz, and H. Schloerb, *J. Magn. Magn. Mat.*, **314**, 116 (2007).
107. B. Wagner, M. Kreutzer, and W. Benecke, *J. MEMS*, **2** (1), 23 (1993).
108. H. J. Cho and C. H. Ahn, *J. MEMS*, **11** (1), 78 (2002).
109. L. Vieux-Rochaz et al., *J. Micromech. Microeng.*, **16**, 219 (2006).

29

ANALYSIS OF ELECTROPLATED FILMS USING DUAL-BEAM FIB/SEM AND TEM TECHNIQUES

XIANYING MENG-BURANY

29.1 INTRODUCTION

Electroplated films are used broadly in a number of industries. Particularly, in the last few decades, electroplated copper films emerged as essential for the fabrication of interconnects in the semiconductor industry. The manufacturing process of semiconductor devices involves many steps of film plating and depositing. Mostly, integrated circuit devices are built on a silicon wafer including a large number of different components, such as transistors, capacitors, resistors, and other electronic devices. These components are connected using multiple "wires." These wires are referred to as interconnects or metallizations or simply metals in the semiconductor field. The wire must be made of a high-conductivity material (e.g., Cu and Al) and should not diffuse into its contacted parts such as Si.

Interconnects were mostly made from aluminum and tungsten up to ten years ago. Tungsten has higher resistance than aluminum and therefore is commonly used for lower level interconnects, such as plugs. Aluminum has long been the standard material for multilayer interconnects in devices; however, electromigration in aluminum is high. Aluminum metal usually is made with a small amount of Si or Cu to reduce the electromigration of the metal interconnects [1, 2]. The electrical conductivity of aluminum is only about 60% of copper. Indeed, copper has higher electrical conductivity as well as higher resistance during the electromigration process than Al–Si or Al–Cu alloys. Thus copper metallization has attracted significant interest from the integrated circuit community. However, it has been rather difficult to adapt copper to semiconductor manufacturing.

In September 1997 IBM reported that it had successfully manufactured fully integrated devices with Cu interconnects. One year later, on September 1, 1998, IBM announced that it had integrated copper technology into its productions and put the world's first copper-based microprocessor on the market. Copper chip technology is being used to enhance chip performance while reducing its size and power consumption. In the semiconductor industry the metal which is deposited first and closest to the silicon substrate is called metal 1; the following metals are called metal 2, metal 3, and so on. Figure 29.1*a* is a cross-sectional scanning electron microscopy (SEM) micrograph showing six layers of electroplated copper interconnects labeled M1 to M6. The first copper interconnect was successfully deposited on tungsten plugs with a TaN barrier layer; then the other five copper interconnects were deposited on the dielectrics. The top wire was still made from sputtered aluminum.

Typically copper interconnects are produced in etched insulating vias and trenches using one of the many copper electroplating techniques. In line with the transition of interconnect production from sputtered aluminum to electroplating copper, many new technologies have been developed and some are still being perfected—for instance, copper seeding for electroplating copper and barrier layers between the copper and tungsten plugs. Figure 29.1*b* depicts the tantalum barrier between the copper interconnect and the tungsten plug.

As is well known, the quality of integrated circuit devices is highly dependent on the quality of the copper interconnects [3–5]. In the last few years, the sizes of electroplated copper vias and trenches have been greatly reduced, down to the nanoscales. Precise and accurate failure analysis (quality control) of copper interconnects is required during manufacturing. The development of focused ion beam (FIB)

Modern Electroplating, Fifth Edition Edited by Mordechay Schlesinger and Milan Paunovic

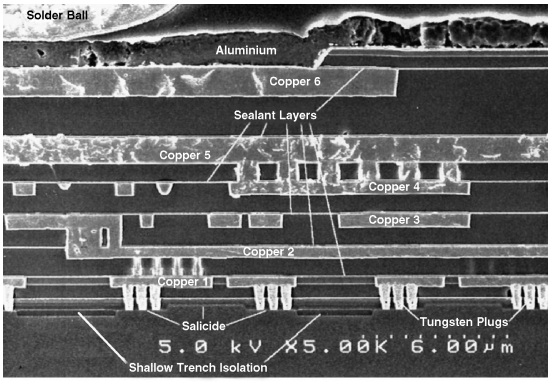

(a)

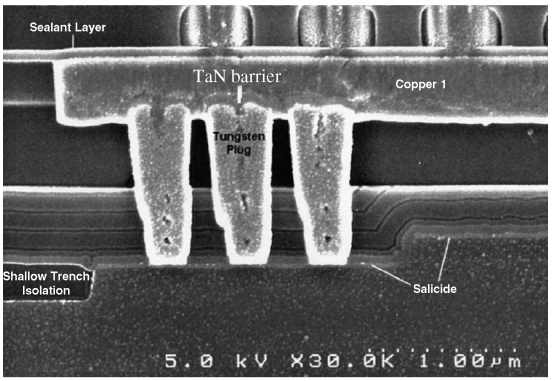

(b)

FIGURE 29.1 Cross-sectional SEM micrographs illustrating Cu interconnects built in 1997 [3]: (*a*) six layers of electroplated Cu metallization in integrated circuit device; (*b*) TaN barrier between copper 1 and W plugs.

instruments combined with SEM, so called dual-beam FIB/SEM, is driven by these requirements. Failure analysis of nanoscale electroplated copper interconnects and other metal layers using transmission electron microscopy (TEM) has also become necessary in manufacturing lines, and site-specific TEM samples must be made to perform the failure analysis. The dual-beam system offers simultaneously ion milling and observing at the specific site of interest. Therefore FIB/SEM is the most reliable tool used to prepare TEM cross-sectional samples [6, 7].

This chapter presents an introduction to the electroplating of copper on wafers; the principles of FIB, SEM, and TEM technologies; the techniques for making cross-sectional TEM samples; and an analyses of electroplated copper films and electroless deposited Ni–Zn–P and Co–P films using FIB, SEM, and TEM technologies.

29.2 INTRODUCTION TO ELECTROPLATING OF COPPER ON SILICON WAFERS

As mentioned above, copper interconnects have gradually replaced aluminum wires since 1997. Copper interconnects are deposited on printed integrated circuits on Si wafers using electroplating instead of physical vapor deposition (PVD), chemical vapor deposition (CVD), and electroless deposition. Comparing the deposition rate of these techniques, the electroplating of copper is faster than the others, as shown in Table 29.1 [8–10]. The reasons for employing electroplating copper also includes the fact that PVD of copper cannot provide defect-free filling of interconnects on silicon wafers and requires expensive equipment. The CVD of copper is unstable, and the solution employed for electroless deposition in CVD is costly since the solution requires frequent replacement. As a result the CVD of copper is considered environmentally unfriendly.

TABLE 29.1 Comparison of Deposition Rate of Copper Using Different Techniques

Technique	Deposition Rate (µm min^{-1}) of Cu
Electroplating	1.00
Electroless	0.20
CVD	0.20
PVD	0.05–1.00

29.2.1 Electroplating Copper on Silicon Wafer

The electroplating of copper onto a silicon wafer is performed at atmospheric pressure and at room temperature. The initial step of electroplating Cu onto vias and trenches patterned on the wafer is precleaning the silicon wafer by etching the surface of the wafer down to approximately 10 nm thick. Next TaN, or both TaN and Ta, barrier layers are deposited on the clean surface of the wafer (or other component) using PVD or CVD. Figure 29.1*b* shows a TaN barrier layer deposited on the W plugs before electroplating of copper takes place. The total thickness of the barrier layer is approximately 40 nm for vias smaller than 200 nm in diameter. For example, if the thickness of the TaN layer is 20 nm, then the Ta layer is also 20 nm.

For copper to be electroplated on the surface of the wafer, the surface must be coved with a conductive layer. This usually is a thin copper layer called a seed layer. The seed layer is deposited on the barrier layer using PVD, CVD, or electroless deposition. The seed layer can be deposited to a thickness of about 100 nm on the surface of the wafer. However, on the sidewalls and bottom of the vias the seed layer can be very thin or even discontinuous, which can lead to voids in the vias. Many new techniques have been developed for producing smooth and fully covered seed layers using, for instance, high-ionization PVD or combined PVD and electroless deposition. The vias seeded with PVD copper and treated with an electroless copper film are eventually well filled by the electroplated copper. There are voids in vias seeded with PVD copper only without being treated by electroless deposition of copper film [8].

After completion of the preprocesses, copper is deposited on the seed layer on the wafer using electroplating. The grain size of as-plated copper is small. Recrystallization of the small Cu grains takes place at room temperature in a few weeks. To produce stable, large, and uniform copper grains, the wafer should be annealed at 150°C for 4 min to 250°C for 2 min after completion of the electroplating. Copper interconnect wire possessing large grain structure has a relatively small amount of grain boundaries and therefore has higher conductivity [11].

The last step of the electroplating of copper on the wafer is polishing the copper plated on the surface of the wafer to flatten the wafer using chemical mechanical planarization (CMP). After the CMP polishing, the copper deposited in the vias and trenches remains in the wafer as an interconnect.

29.2.2 Reaction of Copper Plating

For the electroplating of copper the cathode in the plating cell is the wafer, which is covered by a copper seed layer. The anode is a pure copper plate or a preconditioned phosphorized copper plate. The electrolyte is copper sulfate ($CuSO_4{\cdot}5H_2O$) and some additives. When an external voltage is applied between the anode and the cathode two reactions take place. At the anode side copper dissolves into the electrolyte from the anode copper plate:

$$Cu \rightarrow Cu^{2+} + 2e$$

At the cathode side cupric ions in the electrolyte move to the cathode and consume two electrons from the external circuit:

$$Cu^{2+} + 2e \rightarrow Cu$$

Thus copper is plated on the wafer.

Figure 29.2 is a schematic of a chamber, or a plating cell, for copper electroplating. The Si wafer is placed on top of the chamber. The surface, which is covered by the seed layer on the wafer is set facing down toward the bulk copper anode, which is fixed on the bottom of the chamber. Thus the method called bottom-up filling is used for the electroplating of copper, and the deposition of copper starts from the bottom of the vias. Then the copper propagates downward to the tops of the vias because the wafer is set facing down. During electroplating, the electrolyte is pumped and made to flow upward from the bottom of the vias.

29.2.3 Solutions for Electroplating of Copper

The electrolyte used in copper electroplating consists of major chemicals in molar concentrations and of minor chemicals in parts-per-million (ppm) concentrations. The main species of the electrolyte solutions are copper sulfate ($CuSO_4{\cdot}5H_2O$). Commercial electrolytes—for example, Viaform, low-acid Viaform, and EEJA—used for the electroplating of copper interconnects are produced by chemical suppliers. Many studies are focused on electrolytes with expectations that the electrolytes should match the requirements for the filling processes of future interconnects of 35 nm in diameter. Reducing the concentration of sulfuric acid in the electrolyte to about pH 2 increases copper solubility to close to 1.4 M in the electrolytes, which is suitable for copper plating. Lowering the acid significantly improves the thickness uniformity and planarity of the electroplated copper layer, which is also of benefit in the chemical-mechanical planarization processes [11–15].

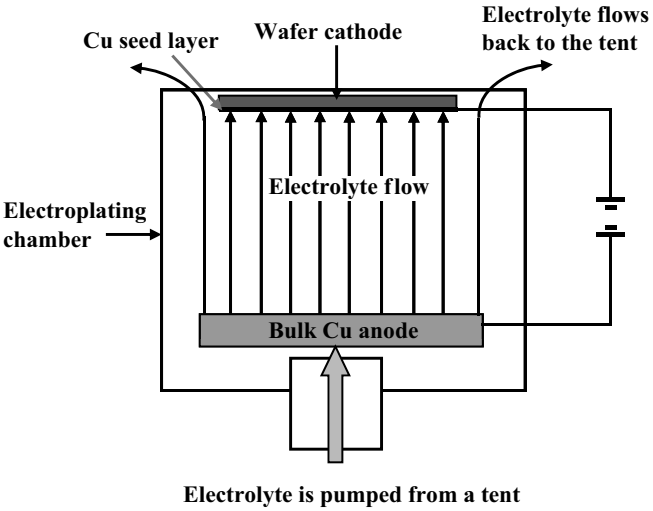

FIGURE 29.2 Schematic illustrating electroplating chamber, where cathode wafer is set at top of chamber and faces downward and bulk Cu anode is set at bottom of chamber. The electrolyte flows from the bottom to the top of the chamber.

The minor chemicals in the electrolyte used in copper electroplating are known as additives. Two types of additives (i.e., accelerator and suppressor) are selected to control the plating speed and to achieve void-free filling. The additives are organics; for instance, an organic sulfur compound is an accelerator and polyethylene glycol is a suppressor. During copper electroplating both accelerator and suppressor are preferentially being adsorbed on or constantly diffuse away from the surface of the wafer, vias, and plated layer. For defect-free filling of vias a higher deposition rate in the bottom of the vias is desired. By controlling the concentration of suppressor and accelerator at the top and bottom of the vias, the deposition rate is controlled to achieve bottom-up filling. Dordi et al. [14] reported that 250 nm vias were filled well using 7.5–12.5 ppm of accelerator and 50–80 ppm of suppressor in 150–250 L of a conventional electroplating bath. If the concentration of the accelerator was higher than 15 ppm, bottom voids are observed.

29.2.4 Instruments Used for Copper Electroplating

The electroplating cell is a cylinder-shaped chamber, as shown in Figure 29.2. The wafer, the cathode, and bulk copper plate (the anode) are immersed in the electrolyte in the chamber during plating. As mentioned earlier, the wafer is set on top of the chamber. The bulk copper anode is set on the bottom of the chamber. The electrolyte flows from a tank into the chamber from the bottom to the top. When an external voltage is applied between the anode and cathode, two reactions take place to deposit copper into vias on the wafer. The electrolyte continuously flows out from the plating cell back to the holding tank and is thus circulated. Fully automated systems for electroplating copper on wafers can be had from suppliers such as Applied Materials, Novellus, and Semitool [13].

The volume of a conventional bath of the electrolyte for copper electroplating is 150–250 L. The new generation of plating chambers feature a small-volume bath (10 L) with individual cell plumbing [16]. The small-volume bath saves plating chemicals, and the solution may be refreshed more frequently. This can minimize the residue in the plating solution and improves the stability of the plating results. It also allows multistep plating processes with different chemistries in separated plating chambers. It is easy to control the plating process of the individual cell due to each cell having its own plumbing system.

29.3 PRINCIPLES OF DUAL-BEAM FIB/SEM TECHNOLOGY

From a practical point of view, SEM is more often used in industry than TEM. This is due to the fact that its sample chamber is much larger than the TEM sample chamber. So far, the world's largest SEM chamber (LC-SEM) can scan an area of 1 m^2. The large sample chamber also allows tools to be installed into the SEM chamber, which enhances its applications. Dual-beam FIB/SEM (see Fig. 29.3) is an instrument that has both an ion column and an electron column in a conventional SEM chamber. The FIB/SEM chamber also includes a gas injection system (GIS), a sample stage, and detectors. To analyze the quality of copper films electroplated on 300-mm wafers a special loading dock was developed. The 300-mm wafer is then transferred into a large chamber by a robotic system.

Both FIB and SEM columns consist mainly of beam guns, lenses, apertures, and detectors. The beam gun consists of a beam source and its suppressor and extractor. The lenses and

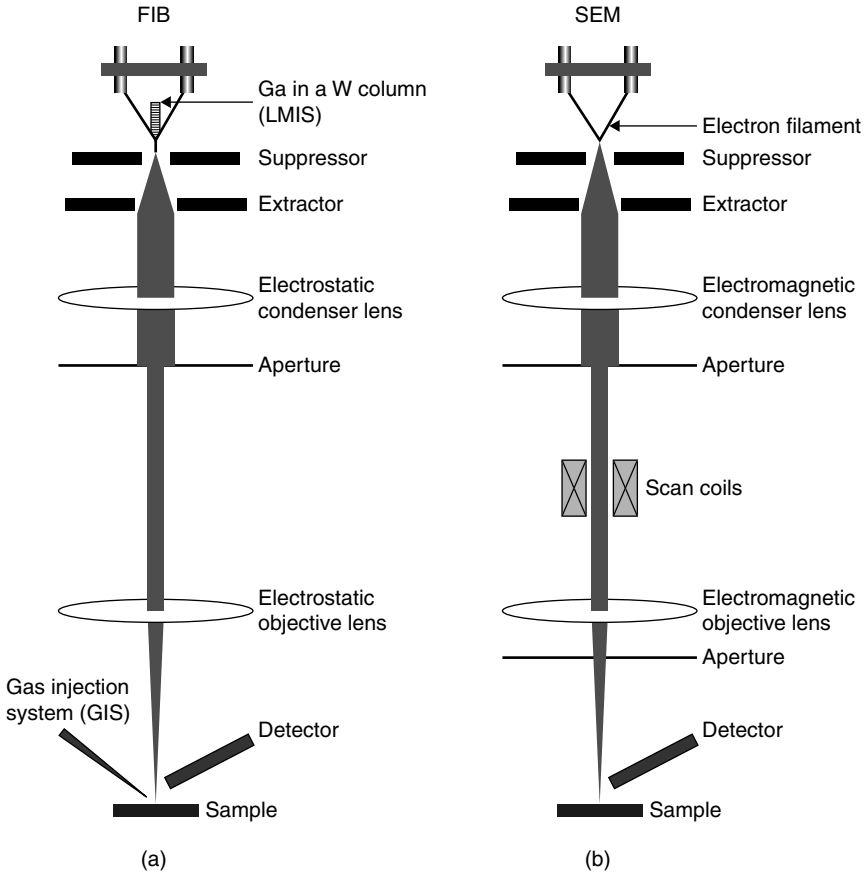

FIGURE 29.3 Schematic illustrating ray paths: (*a*) FIB ion beam; (*b*) SEM electron beam (not to scale).

the apertures are employed to focus the beams. The differences between the ion column and the electron column are the beam sources and the lenses. FIB employs a liquid metal ion source (LMIS), mostly a liquid gallium ion source. To focus the heavy gallium ions, FIB has electrostatic lenses instead of the electromagnetic lenses used in the columns in SEM and TEM to focus the electrons [17–19].

One of the advantages of the dual-beam system is that during the precise cross sectioning of a sample by the ion beam, simultaneously, the electron beam is used to inspect the ion-milling process. Another advantage is that the micrograph obtained using the FIB shows better contrast than the one acquired using the electron beam because of the channel effect of ions. The characters and applications of FIB are discussed below.

29.3.1 Liquid Gallium Ion Source

Ion beam emission from the ion gun in the ion column is analogous to the electron beam emission from the electron gun in the electron column. Figures 29.3*a*, *b* depict the ray systems, including the emission sources, extractors, and accelerators under the sources of the FIB and SEM, respectively. In contrast to an electron filament shown in Figure 29.3*b*, gallium metal in the LMIS is placed in a short column about 1 mm diameter made from tungsten wire (see Fig. 29.3*a*). Gallium is chosen to be the ion source in the FIB/SEM instrument due to the melting point of gallium, which is as low as 29.78°C, and also since gallium does not react with tungsten. Hence, the gallium source is easily made into an operation-friendly tool. Usually, the ion column is operated at 30 kV, and the gallium is heated in the tungsten wire cone. In this fashion the gallium atoms are ionized and gallium ions are emitted by the corresponding extractor and accelerator. As a result, the ion beam offers good brightness.

The lifetime of a LMIS is measured in microampere-hours, which is the emission current (in microamperes) of the source multiplied by its operating time (in hours). It should be understood that the lifetime of an ion source is strongly dependent on its operating current. For example, a gallium source provides 4800 μA-h of service when the source is operated at a current of about 1 μA. The same source will provide service for 2400 h if operated at 2 μA and only 800 h at 6 μA. Usually, the gallium source is operated at currents on the order of nanoamperes for cross sectioning and picoamperes for polishing and imaging.

During regular operation, gases inside the FIB/SEM chamber condensate and deposit on the surface of the gallium ion source, causing the ion beam to become unstable and even stop emission altogether. In such a case the ion source has to be heated to get rid of the adsorbed gases. Subsequent to heating, liquid gallium reconcentrates into its emitting region, that is, into the tungsten cone. Usually, a new gallium ion source is heated at 3.2 A for 45 s. The heating currents are decreased with the increase of the past operating hours of the source. The two plots in Figure 29.4 show the heating currents versus the operating times of two gallium ion sources which have served close to 5000 μA-h in a FIB/SEM. For comparison the third plot in Figure 29.4 is the heating current versus the operating time referring to the LMIS manufacturer [17]. After heating the ion source is ready for operation again. If the source still does not emit normally, it needs to be heated again using a higher heating current. According to the plots given in Figure 29.4 LMIS 1 and 2 served close to 5000 and 4700 μA-h, respectively.

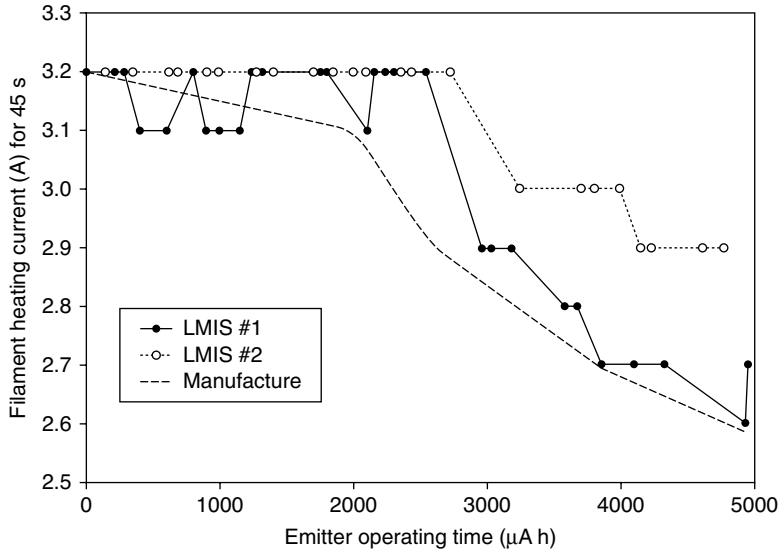

FIGURE 29.4 Plots of operating time versus filament heating current. The plots of LIMS 1 and LIMS 2 show the lifetimes of two ion sources. A plot referring to the manufacture [17] is given for comparison.

29.3.2 Geometry of Dual-Beam System and Eucentric Point of Sample Stage

Figure 29.5 illustrates the relative geometry of an ion column, an electron column, and a sample holder in an FIB/SEM chamber where the electron column is vertical, as in a conventional SEM chamber. The ion beam column is positioned 52° relative to the electron column. The sample stage can be moved in the x, y, and z orientations, rotated 360°, and tilted up to 56–60° according to FIB model used. When the sample is tilted to 52° the ion beam is perpendicular to the surface of the sample. This allows the ion beam to perform a cross section of the sample [20–26].

SEM micrographs of the cross-sectional plane can be obtained between 0° and 52° by tilting the sample stage. The true size of the vertical features on the cross-sectional plane is given as $d_{\text{true}} = d_{\text{tilt}}/\sin\theta_{\text{tilt}}$, as shown in Figure 29.5, where d_{tilt} is the size measured on the screen of the SEM and θ_{tilt} is the tilting angle. This correction is particularly important for determining the sizes of the vias on the cross-sectional SEM micrograph when the sample was tilted by a large angle, since the actual sizes of the vias are larger than the sizes seen on the micrograph.

The sample stage of FIB/SEM has a eucentric point where both the electron and the ion beams can focus upon the same selected area on the sample. This allows observing the cross-sectional process using SEM during FIB milling or polishing processes. At the eucentric point the two beams are over the stage tilt axis; therefore both the ion image and the electron image will not move as a result of tilting the sample. Moving the sample to the eucentric point in FIB/SEM is similar to that of moving the sample to the eucentric height in a TEM column. Before begining to bring the sample to the eucentric point it, is important to set the sample stage to its designed original position, the so-called home stage, and to correct the shift of the electron beam using the "zero beam shift" function in the SEM mode.

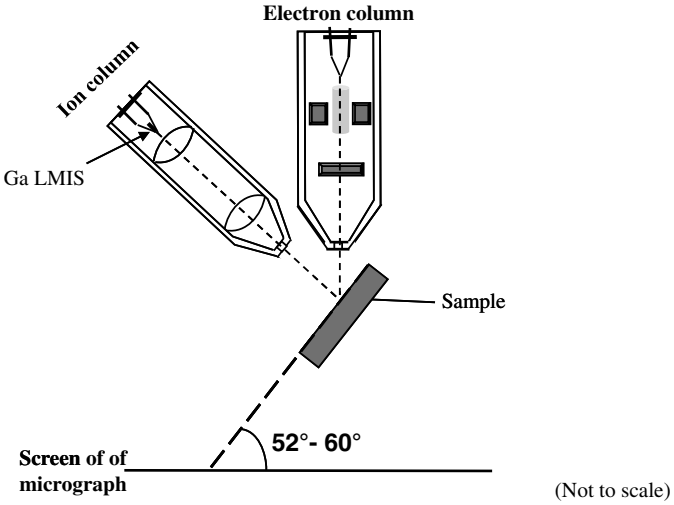

FIGURE 29.5 Schematic illustrating geometric positions of ion column, electron column, and sample stage tilted to 52° at eucentric point in FIB/SEM chamber.

The steps to bring the sample to the eucentric point are as follows. First, choose and move a sharp image of a feature in the sample to the center of the SEM screen. Second, tilt the sample by 2°–5° at a magnification of about 1000 ×. Third, bring the feature back to the center of the screen by adjusting the height of the sample using a manual height-adjusting knob (marked Z in most recent models). Fourth, increase the tilting angle, for example, up to 20°, and use the Z adjustor to bring the feature back to the center of the screen again. Then increase the tilting angle up to 52° and repeat the operation. Finally, tilt the sample to zero and to 52° and repeat the adjustment. The sample is at the eucentric point if the sample does not move away from the center of the SEM screen when tilting the sample between zero and 52°. In this position the area of interest on the sample can be observed using both the electron bean and ion beam at the same area on the SEM monitor.

29.3.3 Gas Injection System (GIS)

FIB/SEM has been developed for precisely fast milling, etching, and depositing on semiconductor wafers and fixing the devices using the GIS. The GIS-equipped FIB/SEM offers two functions: etching and depositing. Mostly, the depositing materials used in the analysis of electroplated films are platinum, tungsten, and carbon. Due to the heavy mass of the accelerated gallium ion the ion beam can damage the surface of the sample during FIB-milling cross-sectional SEM and TEM samples. When the surface structures of a sample are the investigation targets, usually a thin layer of platinum or carbon is deposited on the surface of the sample to protect it from ion beam damage.

Platinum is deposited using ion-assisted CVD of this metal from trimethyl-methylcyclopentadienyl–platinum ($C_9H_{16}Pt$) [27]. The deposition process is usually done at the eucentric point of the stage and the sample is tilted to 52°. A platinum injecting needle is inserted into its depositing position from its dock position, as shown in Figure 29.3*a*. Usually, the Pt layer can be deposited directly using an ion beam after inserting the injecting needle and heating the Pt gas. For a beam-sensitive sample, two depositing steps give better protection to the surface of the sample. First, a thin Pt layer is deposited using an electron beam with low accelerating voltage and high current, for example, 3–5 kV and 2000 nA. This thin Pt layer can protect the surface of the sample from beam damage of future ion beam deposition. Second, following electron beam deposition, a thicker Pt layer is deposited using an ion beam. Usually, a Pt strip of 2 μm in width, 2–3 μm thick, and a desirable length can be

used to cover the area of interest for making a cross-sectional TEM sample.

The Pt deposition rate is a function of the ion beam current, the ion dwelling time, the beam overlap, and the area to be deposited. A beam current in the range of 2–6 $\rho A\,\mu m^{-2}$ produces a 1-μm-thick layer on an area of $1\,\mu m^2$ in 1 min, which is the most efficient deposition rate. For instance, 2-μm-thick Pt strip in an area $2\,\mu m \times 20\,\mu m$ needs to be deposited on the surface of a sample; 160–480 pA can be chosen for the deposition carried out in 1 min. In modern FIB/SEM the software indicates the deposition time after the setup of the voltage and current of the ion beam as well as the area and the thickness that the platinum is required to be deposited.

29.3.4 Channel Effect Contrast in Ion Beam Micrographs

Similar to SEM the incident electron beam is used for imaging; the incident ion beam of FIB can also perform micrographs. When high-voltage accelerated heavy Ga^+ ions hit the sample secondary ions, electrons are emitted from the surface region of the sample. The conventional SEM detector collects the secondary electrons from the samples created by the incident electron beam. The same detector, operated at different bias, collects secondary ions from the sample created by the incident ions, as shown in Figure 29.6*a*.

The incident ions can penetrate into the sample along the crystalline planes (channels) due to their large mass and energy under a high accelerating voltage. This phenomenon

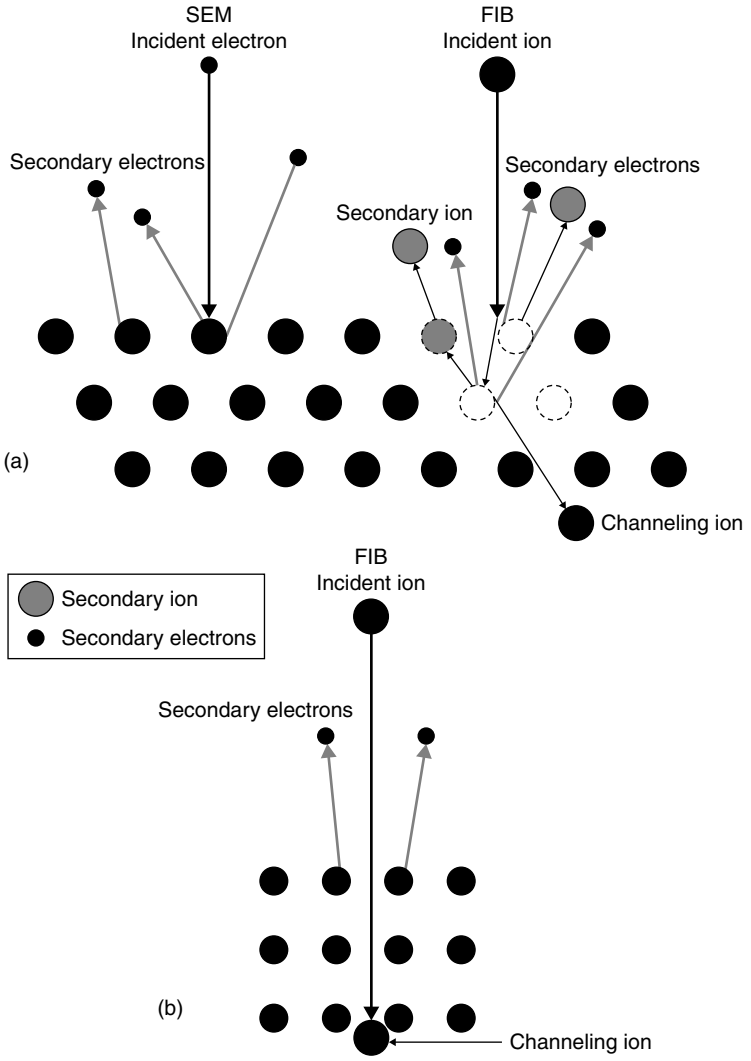

FIGURE 29.6 Schematic illustrating (*a*) interactions between incident electron beam and sample and between incident ion beam and same sample and (*b*) incident ion traveling into the channel of a crystal, which decreased the emissions of secondary ions and secondary electrons. Schematic drawing illustrating the interaction between the incident ions and (*c*) Al atoms and (*d*) Si atoms. The FIB ion image has better contrast than the SEM image due to the different sputtering yields of the two elements.

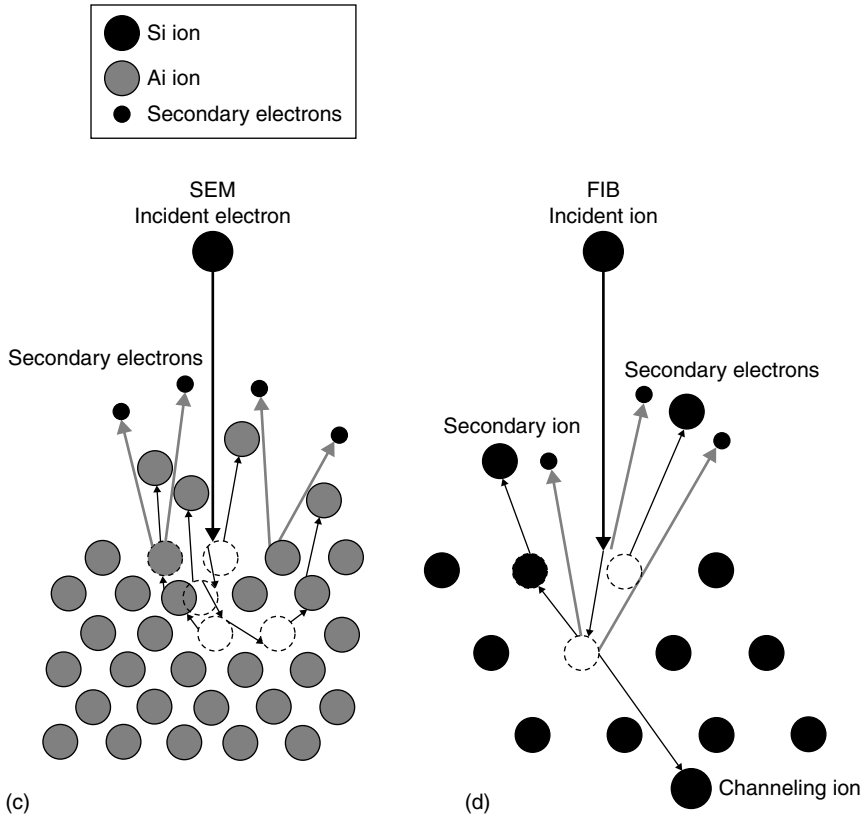

FIGURE 29.6 *(Continued)*

is termed the ion channel effect. The FIB ion micrographs have better/higher contrast than the SEM images, especially for crystalline samples, due to the ion-channeling effect. When the crystallographic axis of a grain is aligned along the incident ion beam, the ions penetrate along the crystalline plane, as shown in Figure 29.6*b*. Thus, there are less secondary ions and secondary electrons emitted by the incident ions. As a result, this grain appears darker than the others with the same composition due to its orientation and the ion channel effect [28, 29].

When high-voltage accelerated Ga^+ ions impinge upon a sample, the heavier ions also sputter the ions from the sample. The ion-sputtering yield is defined as the ratio of the number of sputtered (or ejected) ions from the sample to the number of incident ions. For instance, sputtering yields under 600 eV are 1.2 for aluminum, 0.5 for silicon, and 2.3 for copper [30]. Figures 29.6*c*, *d* schematically illustrate that more secondary ions were sputtered from one phase than from the other one because of the difference of the sputtering yield between the two phases. The sputtering yield is also a function of the crystallographic orientation of the sample versus the incident ion beam. Therefore, both the ion channel effect and the ion-sputtering yield produce higher contrast in the ion micrographs than the contrast on the electron images for the crystalline sample [31].

After a cross-sectional cut using an ion beam with high current, an ion beam with low current, for example, a few hundreds of picoamperes, is employed for fine polishing of the sample. FIB micrographs having good contrast and brightness can be obtained using ion currents of 50–350 pA depending on the model of the dual-beam instruments. An ion beam with even low current can damage the cross-sectional surface; therefore, focusing the image is always performed at an area of no interest before taking an ion micrograph at the area of interest.

The electron beams of SEM and TEM are focused using electromagnetic lenses which produce weak spherical aberration and small beam size. The focusing strength of the lens is directly related to the charge/mass ratio of a particle. In contrast with SEM and TEM, FIB uses electrostatic lenses to focus the ion beam due to the mass of ions, which is much higher than the mass of electrons. As a consequence of the aberrations of the electrostatic lenses, the resolution of an FIB ion image is lower than the resolution of an electron image. Working distance, defined as the distance between the pole piece and the sample, also strongly affects the resolution: The shorter the working distance, the higher the resolution. SEM is operated at the working distance of 5 mm and FIB at 17 mm approximately. Thus, the resolution of an FIB ion image is not as good as the resolution of an SEM image, especially at high magnification.

29.4 ANALYSIS OF ELECTROPLATED COPPER USING FIB/SEM TECHNIQUES

As delineated above, copper interconnects such as vias and trenches in integrated circuit devices have to be completely filled by copper without any voids or seams. The vias and trenches themselves are formed in the insulating or barrier layers using etching techniques before the copper deposition. Following the etching, a seed layer is plated on the bottoms and sidewalls of the vias or trenches and on the surface of the wafer producing conductive surfaces for electroplating. Electrodeposited copper will grow on the copper seed and fill the vias and trenches. The filling quality of the electroplated vias is inspected immediately after plating using FIB/SEM cross-sectional techniques to control the parameters employed for the electroplating.

29.4.1 Cross-Sectional View of Electrodeposited Cu Vias

The SEM micrograph given in Figure 29.7 depicts the morphology of the Cu seed layer deposited on a wafer. The seed layer is also deposited on the sidewalls and bottoms of vias that cannot be seen in the plane view image. The diameter of the vias is 200 nm. At present, an SEM cross-sectional view is the fastest and most convenient way to inspect the filling quality of the vias.

In general, many components are patterned on a wafer before plating the vias. To analyze the filling quality of interconnects, the locations of the vias on the wafer have to be found first according to its die photo. The cross section of the vias for SEM inspection can be done using a conventional mechanical polishing method, a cleaving method, and the FIB milling method. The device or even an entire wafer has to be cross sectioned if one is using either the conventional method or the cleaving method. The cross sectioning of vias using the FIB/SEM method can be performed at the exact sites and in small areas without breaking the wafer.

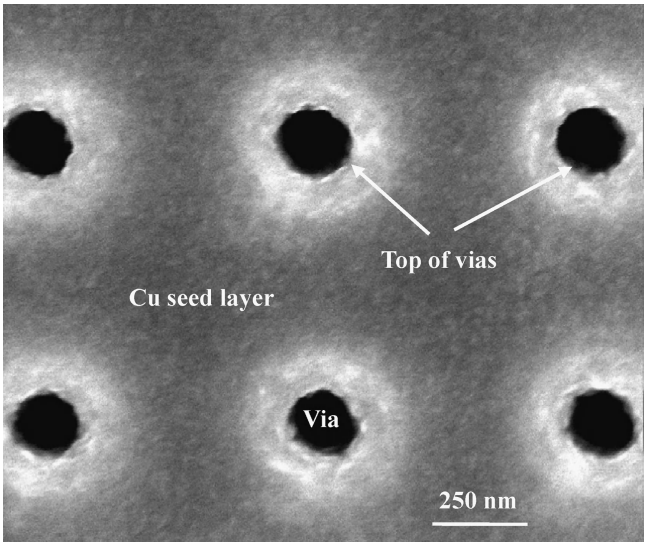

FIGURE 29.7 SEM micrograph illustrating morphology of Cu seed layer for electroplating Cu vias. The size of Cu grains is about 50 nm.

The SEM micrographs of electroplated copper interconnects given in Figures 29.1*a*, *b* were obtained from a sample cross sectioned using the conventional method. The procedure of the conventional method is similar to traditional mechanical polishing for preparing metallographic samples. However, since the size of the vias is on the order of hundreds of nanometers, a mechanical polishing tool called a tripod is employed. The tripod is equipped with three micrometers for precisely aligning the sample to control the fine polishing end at the center of the vias. Since the size of the vias is so small, for fine polishing, instead of SiC papers, diamond lapping polishing papers with a small 1-μm grid are employed. The cross-sectional surface is then etched to reveal the microstructure of the vias after the fine polishing.

Figure 29.8*a* shows a micrograph of electroplated Cu vias obtained from a sample cross sectioned using the cleavage method. Most Si wafers are oriented in the ⟨100⟩ or ⟨111⟩ crystallographic direction. Comparing the two types of wafers, the oxidation rate of silicon is largest in the ⟨111⟩ direction and smallest in the ⟨100⟩ direction. The electric traps created at the silicon surface, which increase the surface charge, are also highest in the ⟨111⟩-oriented wafers and lowest in the ⟨100⟩-oriented wafers [2]. Therefore, more wafers in the ⟨100⟩ orientation are manufactured. Interconnects are often made along the ⟨100⟩ direction and the vias are perpendicular to the surface of the wafer. It is easy to cleave the wafer along the ⟨001⟩ orientation and to perform cross sectioning of the vias. The SEM micrograph of the cleaved wafer given in Figure 29.8*a* shows clearly that the bottoms of the vias are filled with electroplated copper; the top of the vias are not filled.

Figure 29.8*b* is a cross-sectional SEM micrograph of copper interconnects plated on a 300-mm wafer. Cross sectioning of the vias is carried out using FIB without breaking the wafer. This method is commonly employed by manufacturers for quick inspection of the electroplating solution and the conditions of the plating setups. For this reason FIB/SEM is often installed inside or close to a clean room. After electroplating in the clean room, the wafers are immediately transferred to the FIB/SEM laboratory. Typically, cross sections at the center and edge of the wafer are performed quickly using FIB to check the filling quality of the vias. Usually vias located at one of 3, 6, 9, or 12 o'clock at the edge of the wafer is selected for analysis. The analysis results provide the filling quality of the electroplated vias on the entire wafer. For quick analysis, high ion beam current of nanoamperes is used for cutting, then a low ion beam current of picoamperes is used for fine polishing and imaging.

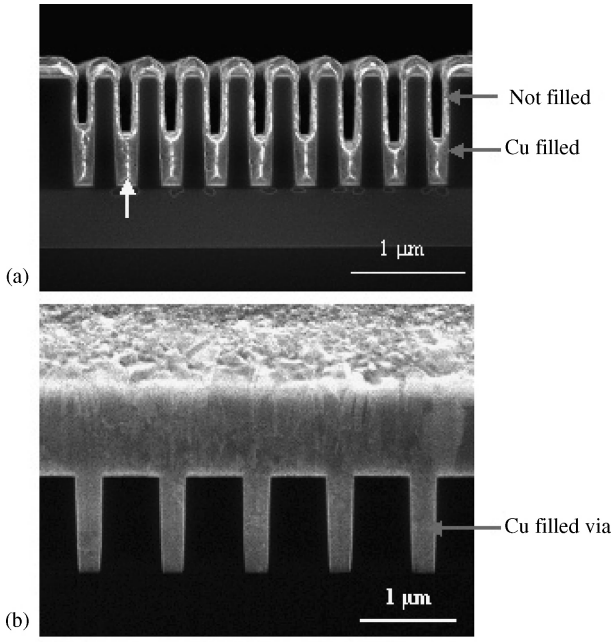

FIGURE 29.8 SEM micrographs. (*a*) Partial filled vias. The cross section is carried out using a cleave method. (*b*) Cu-filled vias. The cross section is carried out using FIB technique.

29.4.2 Secondary Ion Micrography of Electroplated Copper

Many experimental studies are focused on annealing of electroplated copper with the aim that the annealing should change the grain sizes of the copper and thus enhance the adhesion and filling qualities of the electroplated copper vias as well as to increase the Cu grain size since the conductivity of layers with larger grain is higher than the one with smaller grains. The grain size of as-plated copper is smaller than 100 nm, as shown in Figure 29.9*a*. The resistivity of the as-plated copper film is ~2.3 μΩ. The copper grains grow to larger than 1 μm over a few days when kept at room temperature. This leads the resistivity of the copper film to drop by 20–25% [32, 33]. As mentioned in Section 29.2.1, after electroplating of Cu all wafers are annealed at a temperature of 150°C for 240 s to 250°C for 120 s to cause the wafer to have similar copper grain size prior to CMP.

As mentioned above, the ion-channeling effect creates good contrast between grains possessing different orientations and between grains and their grain boundaries on FIB micrographs. Hence FIB micrography is employed to analyze the changes of the grain sizes and structures in electroplated copper after annealing. The two FIB micrographs given in Figures 29.9*a*, *b* illustrate the copper grains, the twin structure, and a void in the copper film. The grain size of as-plated copper film is about 100 nm at the bottom grown on Cu seed layer. At the top of the electroplated copper film the Cu grain size is approximately 500 nm, as shown in Figure 29.9*a*. After annealing the film at 400°C for 10 min, the size of Cu grains is greater than 1 μm, and there is a twin structure in every copper grain, as shown in Figure 29.9*b*.

29.4.3 Defect Analysis of Electroplated Films

Defect analysis is important for all of deposited films because defects can cause failure of devices. The morphology of defects can be observed using SEM and their compositions can be analyzed using X-ray energy dispersive spectrometry (EDS). The contrast between the dimensions of the defects (in nanometers) and the area of the plated films (in hundreds of millimeters) makes it impossible to find the defects on the film in a finite time. For example, on a 200-mm wafer a defect of even 100 nm is too small to be located under SEM. Therefore, practical defect analysis consists of two steps: (i) using an inspection system or inspection tool to detect detects in the deposited film and (ii) using SEM/EDS to analyze the defect. Defect analyses of electroplated copper films on wafers are used to explain the method.

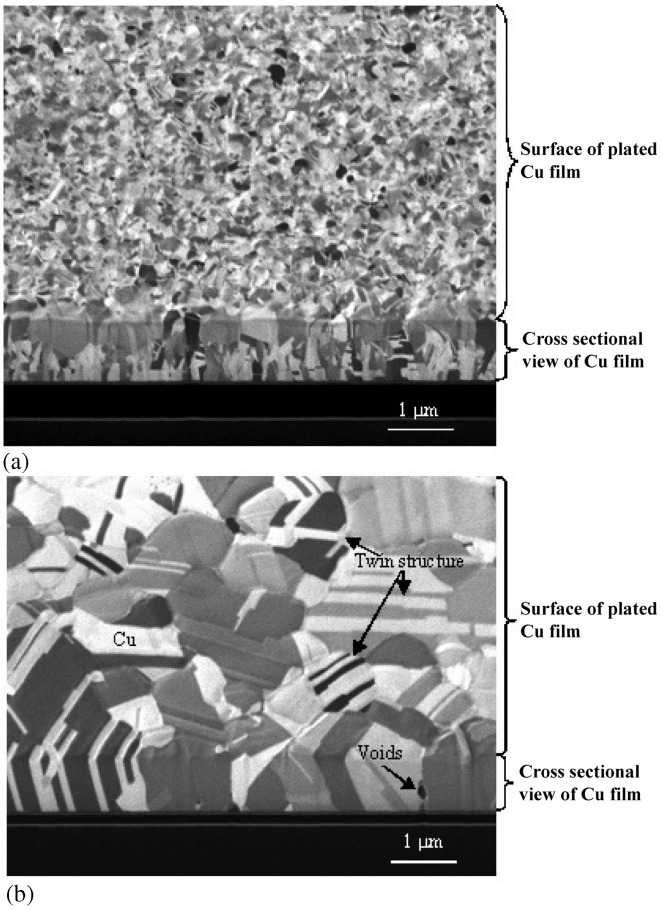

FIGURE 29.9 FIB ion micrographs illustrating microstructure of electroplated Cu film: (*a*) fine grains and column grown of as-plated Cu on wafer; (*b*) twins in Cu grains after annealing Cu film, and void at Cu grain boundary.

Record of Defect Map of Electroplated Film Using Inspection Tool The inspection tool consists of a laser system, a wafer control system, and a detector. The laser light is made to illuminate the wafer surface from above, and the light is scattered by the defects on the film deposited on the wafer. A detector collects the scattered light from a defect, including information about the location and size of the defect. The wafer is moved from one location to others by the wafer control system. The detector collects the coordinates of the location and the size of each defect which scattered the laser light. Thus, a defect map, including the coordinates and sizes of all defects in the film, is carried out and recorded [34–38]. Usually, the center of the wafer is selected as the origin of the coordinate, and the wafer is separated into four quarters having coordinates $\pm x$ and $\pm y$. Table 29.2 is an example of a partial site dialog of a defect map. Usually site dialogs list more information about each defect than given in Table 29.2. The file size of a defect map depends on the range of the defect sizes selected for the given analysis.

Since the defect analysis involves the two steps given above and use two separate instruments, at least three features, for example, three large defects or patterns, on the wafer are selected and recorded for aligning the two instruments with respect to each other. Note that each wafer has a notch at the edge of the wafer. For an unpatterned film, three alignment markers are made manually, for example, at 4, 8 and 12 o'clock on a wafer whose notch is at 6 o'clock. In each marker it is necessary to have a shape point which can be seen clearly at a magnification of 1000×. The alignment markers and the defects are recorded in one data file. Then the wafer is unloaded from the inspection tool and loaded on a FIB/SEM sample stage.

Aligning Electroplated Wafer in SEM First, the wafer on the sample stage is adjusted to the eucentric point, and then it should be aligned in the SEM to be in the same orientation as it was in the inspection tool using the three markers. In this fashion defects can be found in the SEM using the coordinates recorded by the inspection tool. For example, clicking the defect ID 80 in Table 29.2 the wafer is automatically moved to the coordinates $x = 3.2660$ mm and $y = 2.0820$ mm of the wafer. The defect 210 nm × 150 nm is observed in the SEM. The morphology and composition of the defect are analyzed using SEM and EDS. If the wafer is well aligned, most of the defects detected by the inspection tool can be found and analyzed by FIB/SEM. If the first two or three defects cannot be located on the screen of the SEM at the beginning of the analysis, the wafer has to be realigned.

When analyzing defects in a patterned wafer, a chip die origin is used as an alignment point. The alignment is carried out with relative ease. On the one hand, some defects on the patterned wafers are easy to find. On the other hand, some defects are not easy to observe due to the defects being mixed with patterned features.

Analyzing Defects of Electroplated Films Using FIB/SEM and EDS Three micrographs presented in Figures 29.10*a–c* show the defects on the surfaces of an

TABLE 29.2 Partial Defect Site Dialog

Defect ID	Coordinate x (mm)	Coordinate y (mm)	Defect Size x (nm)	Defect Size y (nm)
80	3.2660	2.0820	210	150
81	2.8220	5.3980	90	85
82	10.6430	9.8760	120	127

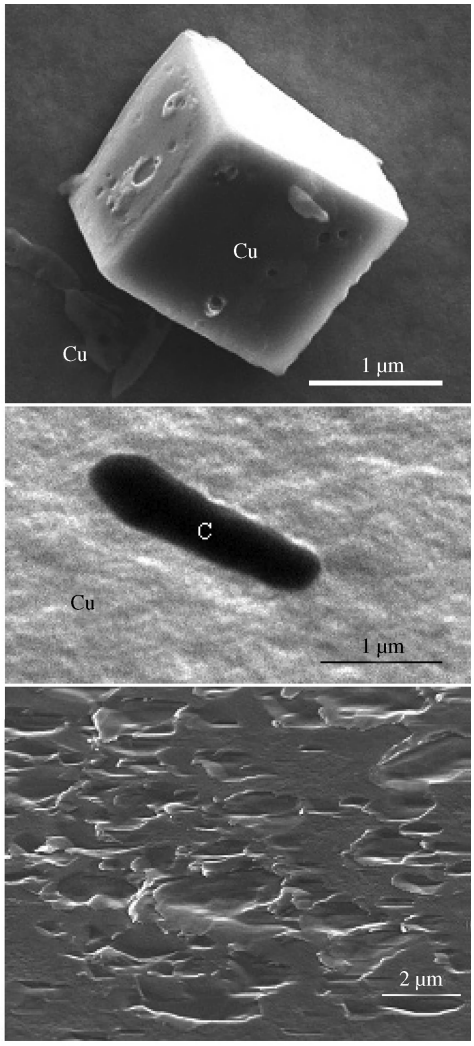

FIGURE 29.10 SEM micrographs illustrating defects on electroplated Cu films: (*a*) a large Cu crystal on surface of Cu film; (*b*) a carbon particle brought about from CMP machine; (*c*) damaged surface of electroplated Cu film.

electroplated copper films. The large cube in Figure 29.10*a* is a Cu crystal identified using EDS. A carbon particle in Figure 29.10*b* was introduced by the CMP machine. Figure 29.10*c* shows shallow damage types on the surface of a plated Cu film. These micrographs imply that the CMP and Cu plating system was not in perfect working condition.

Usually, surface damage can be ignored since the surface defects eventually will be polished away. A more troubling defect in electroplated copper film is voids clustered together which form a curved void line, as shown Figure 29.11*a*. The void line is cross sectioned using FIB and analyzed using SEM. Three voids from the void line shown in Figure 29.11*b* were selected for a cross section using FIB. The SEM micrograph of the cross-sectional view of the three voids, as shown in Figure 29.11*c*, reveals that the voids are so deep that they penetrated into the electroplated Cu film. Obviously, such a void line with a large number of voids is considered risky for the Cu interconnects because they can cause voids in the vias. Usually, organic contamination on the wafer can lead to the formation of void line defects in the copper film during electroplating. Preventing or removing the organic contamination on the wafer can minimize void line defects.

The cross-sectional SEM micrographs given in Figures 29.11*d*, *e* show particles in electroplated copper films. The particles cause cracks in the films. SEM micrographs illustrate the voids in vias; however, they cannot show the relationship between the defects and Cu grains (see Fig. 29.12*a*). Due to the ion-channeling effect the FIB ion micrographs show clearly that most of the voids in the film are formed at the Cu grain boundaries (see Fig. 29.12*b*). An FIB ion image and SEM electron image from the same area of electroplated Cu vias are given in Figures 29.12*c*, *d*. There is a void in one via. The FIB image shows the copper grains clearly.

The electroless technique is used to deposit cobalt into trenches. A large Co particle lies between two cobalt lines, as shown on an SEM view in Figure 29.13*a*. The particle can cause an electric short in the patterned device. Figure 29.13*b* shows the voids found in electroplated Cu interconnects in a device.

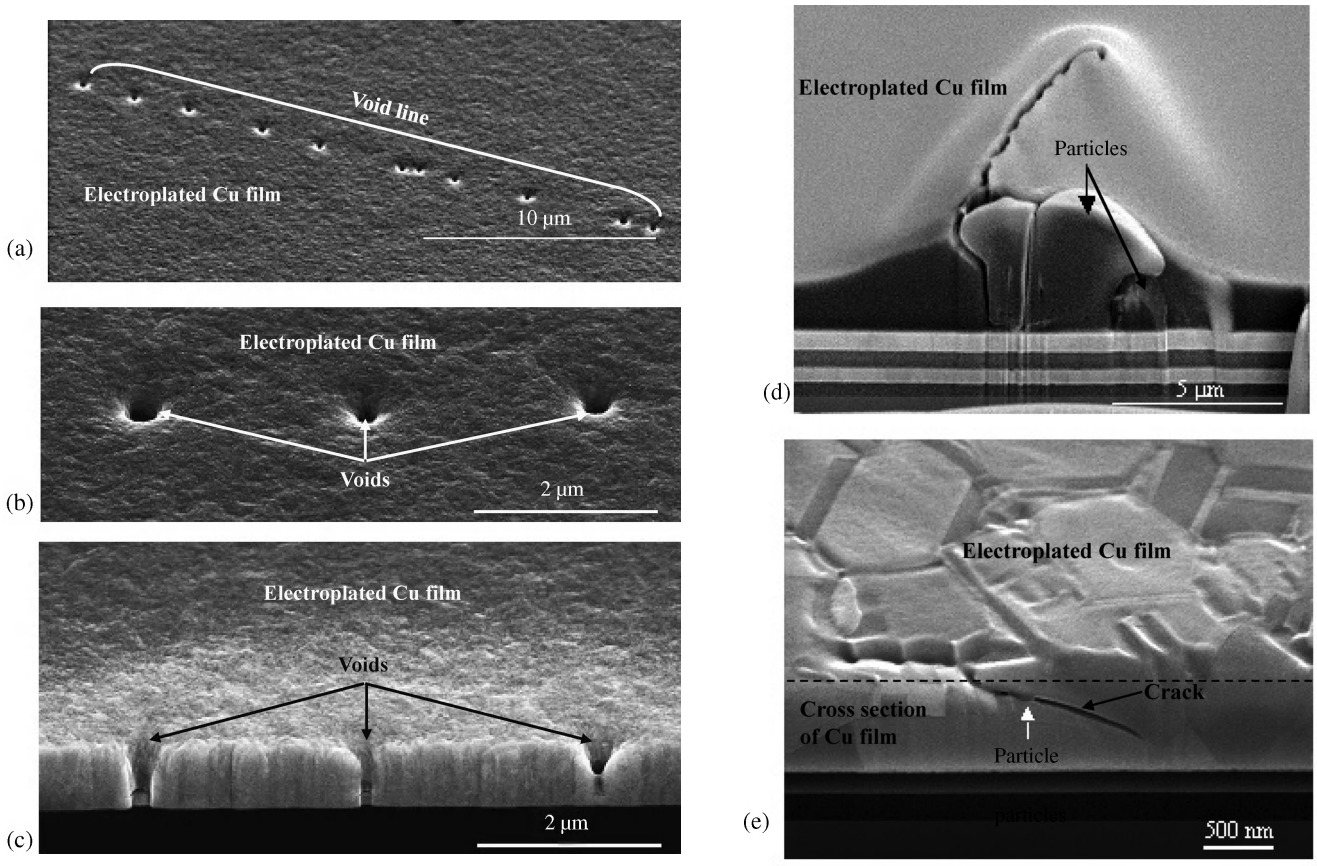

FIGURE 29.11 SEM micrographs illustrating defects on electroplated Cu film: (*a*) voids line in Cu film; (*b*) rotated wafer to bring three voids in line for ion milling; (*c*) cross-sectional view shows depths of three voids in plated Cu film. Cross-sectional SEM micrographs illustrating (*d*) a large and a (*e*) small particle causing cracks in electroplated Cu films.

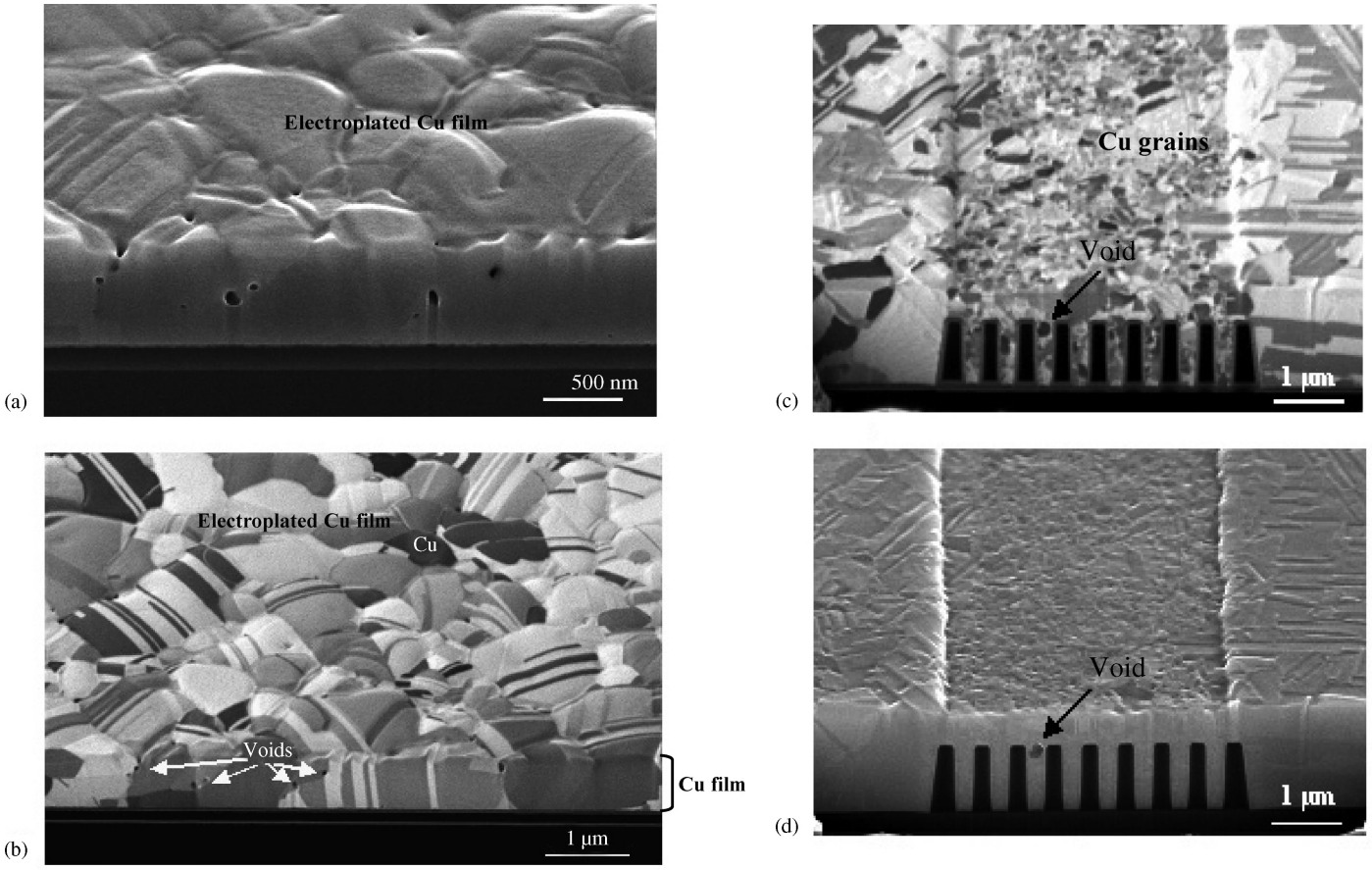

FIGURE 29.12 Cross-sectional view of (*a*) SEM and (*b*) FIB ion micrographs of electroplated Cu films. The ion image shows clearly that the voids formed at the grain boundaries of Cu. (*c*) FIB ion and (*d*) SEM cross-sectional micrographs illustrating void in electroplated Cu via.

29.5 TEM SAMPLE PREPARATION TECHNIQUES

The TEM sample must first be prepared for TEM analysis. Specifically, the goal of TEM sample preparation is to create an electron transparent region containing the area of interest. A TEM specimen of nonorganic material must be around 100 nm thick or thinner. This allows electrons accelerated by 200–300 kV to penetrate and pass the area of interest and thus produce electron micrographs. TEM sample preparation at a precisely accurate site is still a challenge due mainly to its thickness limit. Detailed TEM sample preparation techniques are given in this section.

Over the years many tools and methods have been developed to prepare TEM samples. In some cases, the TEM sample has to be made fit for test in a site-specific position for performing a precise analysis. New techniques and instruments are continually being developed to satisfy the requirements. Dimpling followed by ion milling [39, 41], a wedge technique [42], and FIB techniques [43] for making cross-sectional TEM samples are discussed in some detail in this section and illustrated by a series of micrographs and drawings.

29.5.1 Dimpling–Ion Milling Technique

Dimpling followed by ion milling works well for making a TEM sample from blanket films or large and repeated features. For instance, this method is employed to make cross-sectional TEM samples such as electroplated copper films or electroless deposited multilayer cobalt films. This method can produce samples with a relatively large thin area for TEM analysis.

To protect the surfaces of the plated film, the sample is glued between two pieces of similar materials, for example, two pieces of silicon, using a crystalbond to form a sandwich, as shows in Figure 29.14*a*. A slice is cut from the sandwich using a diamond saw, and then a disc 3 mm in diameter is cut from the slice using an ultrasonic disc cutter (see

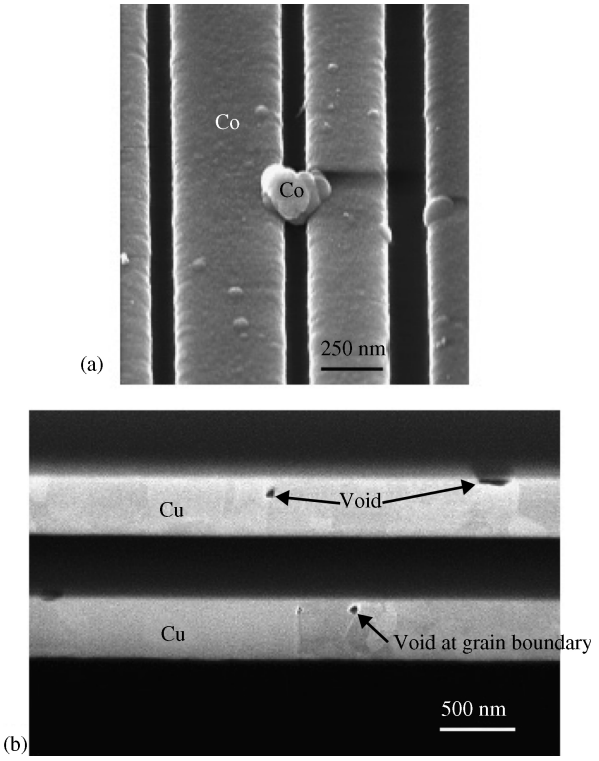

FIGURE 29.13 Cross-sectional view of SEM micrographs illustrating defects on (*a*) electroless deposited Co trenches and (*b*) electroplated Cu interconnects.

Fig. 29.14*b*). The 3-mm disc is mounted with a crystalbond onto a flattening tool for holding and flat polishing the disc. There is a glass window in the center of the flattening tool for inspecting the thickness of the 3-mm disc. After mechanically polishing both sides of the 3-mm disc down to about 400 μm thick, the disc is then dimpled down to 50 μm, as shown in Figure 29.14*c*, using a dimpler. The thickness of the 3-mm disc is frequently inspected using a micrometer during the process. At a thickness of 50 μm the dimpled area appears red in color through the transmission mode of an optical microscope, as shown in Figure 29.14*d*. Once the red color is observed, the disc is dimpled again using a 10-μm diamond slurry and is checked frequently using an optical microscope equipped with a filter. When the fringes shown in Figure 29.14*e* are observed, the disc is ready for ion milling.

The ion milling can be done using either a precision ion polishing system (PIPS) or a dual-ion-beam polisher operated at 5 kV with ion milling angles at 5°. The sample is ion milled for a few minutes until some areas appear white in color or as pinholes or as fine cracks under the optical microscope, as shown in Figures 29.14*f*, *g*. The white areas surrounding the holes or fine cracks in the sample are thin and big enough for TEM investigation.

29.5.2 Wedge Method

The wedge technique is an economical way to prepare a site-specific TEM sample. However, experience is required to use this technique to make TEM samples. In order to protect and inspect a special area of interest at the nanoscale, instead of a piece of Si, a piece of glass is glued on top of the sample to form a two-layer slide using penetrating glue, as shown in Figure 29.15*a*. This allows the direct observation of the area of interest while the sample is polished. A cross-sectional slab 1–1.5 mm thick including the area of interest in its center is cut from the two-layer slide, as shown in Figure 29.15*b*.

The cross-sectional slab is mounted on a sample stub using an adhesive such as a crystal bond with the area of interest parallel to the surface of the sample stub. A special polishing tool such as a tripod or a T-tool is employed for precision polishing. The polishing tools are equipped with two or three micrometers which can be adjusted for aligning the sample. The sample is also locked at a fixed position by the tool during the polishing. In this step, the side of interest is polished to be thinner than the other side by adjusting the micrometers to form a wedge shape. The schematic given in Figure 29.15*c* shows the wedge shape of the TEM sample after mechanical polishing.

The cross-sectional surface is polished on a glass wheel using diamond lapping papers instead of SiC abrasive papers going from coarse to fine. The sample is polished on one side to reach the area of interest. The optical micrograph of a wedge sample given in Figure 29.15*d* shows an array of the same feature due to the slope of the wedge polished on the sample. After one side of the sample is polished, the sample and the stub are immersed in acetone to separate the sample from the stub. In order to polish the second side of the sample, the polished side is glued on a TEM grid, as shown in Figure 29.15*e*, and the operation is repeated to polish the other side.

The grid of lapping paper is chosen to be approximately one-third the thickness of the sample. For instance, 15-μm lapping paper is used to polish a sample to 75 μm thick, then 6-μm lapping paper is used to polish a sample to 20 μm thick, until 1- or 0.5-μm lapping paper is used to polish a sample thinner than 10 μm. The cross-sectional sample is checked frequently under an optical microscope and is aligned for obtaining uniform thin area by adjusting the micrometers during the polishing. When the fringe is observed similar to the image in Figure 29.15*e* the sample is ready for ion milling without dimpling.

A precision ion-polishing system is employed for the ion milling. The sample is ion milled using an ion beam of 5 kV at an angle of 5° for fast milling and then using an angle of 3° for final ion polishing. When bright fringes are observed, as shown in Figure 29.15*f*, the sample is ready for analytical

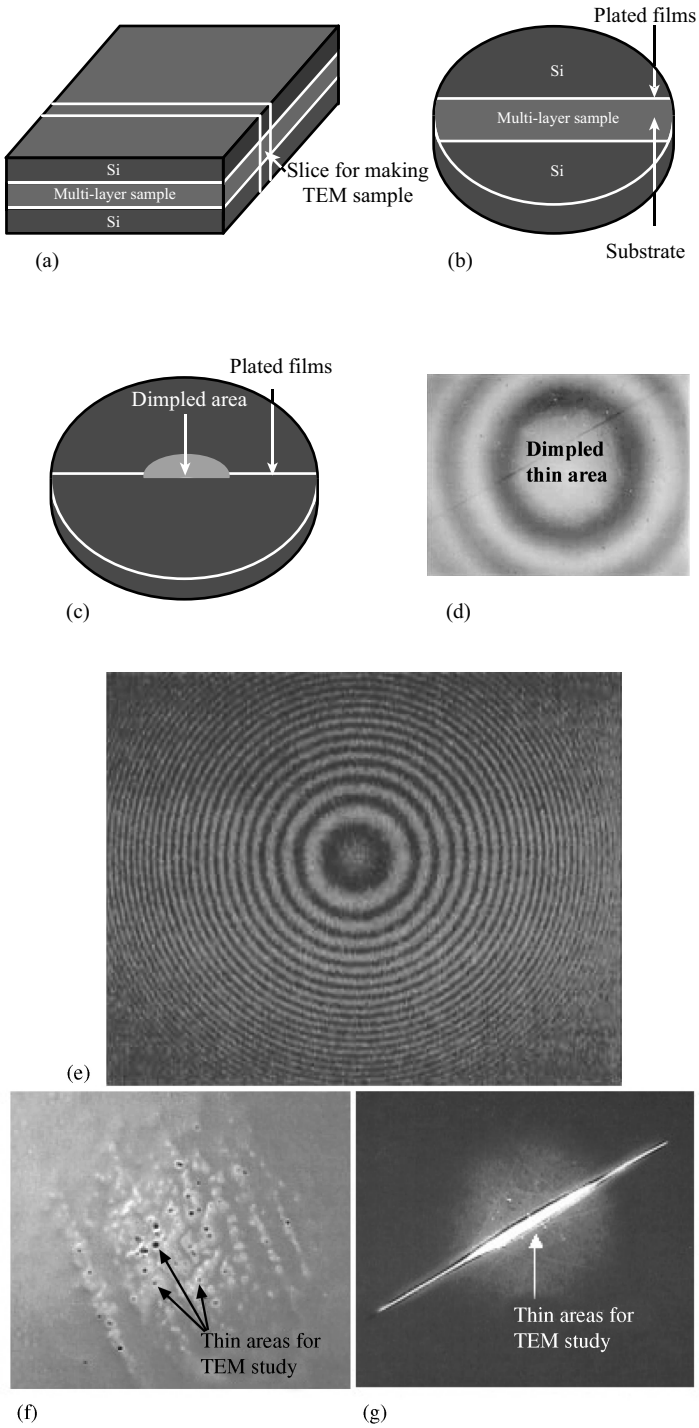

FIGURE 29.14 Dimpling—ion milling method: (*a*) make a Si-plated films–Si sandwich, then cut out a slice; (*b*) cut a disc 3 mm in diameter from the slice; (*c*) mechanical flat grading, polishing disc to thickness of about 400 μm, then dimpling; (*d*) thickness of dimpled area is around 50 μm when red color appeared; (*e*) dimple disc until fringes observed; (*f*, *g*) ion milling disc until fine holes or cracks appear, the white areas surrounding the holes or cracks are thin and big enough for TEM investigation.

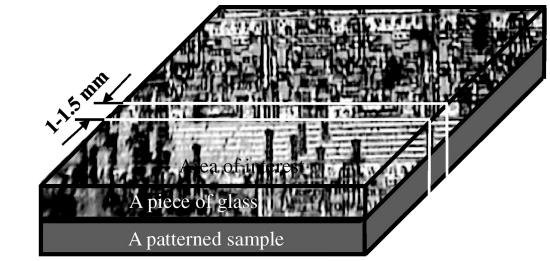

(a)

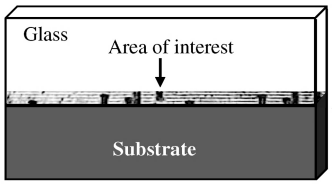

(b)

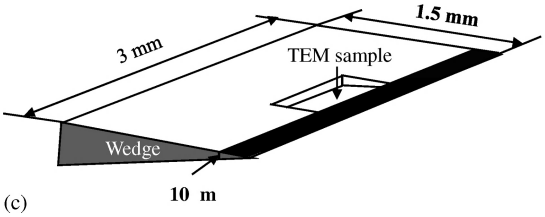

(c)

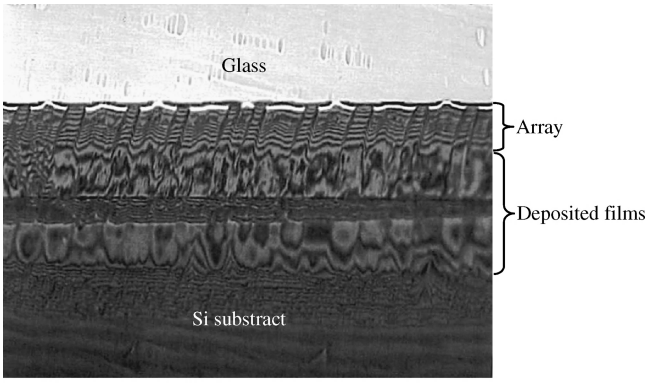

(d)

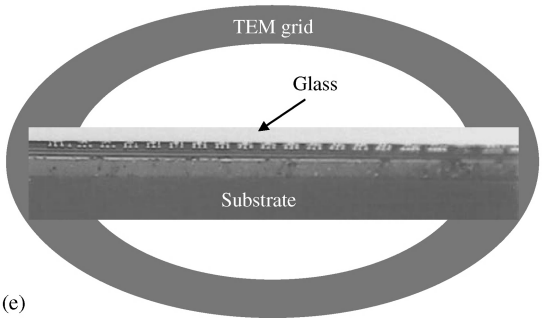

(e)

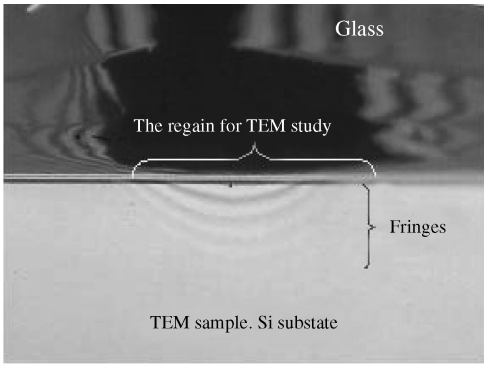

(f)

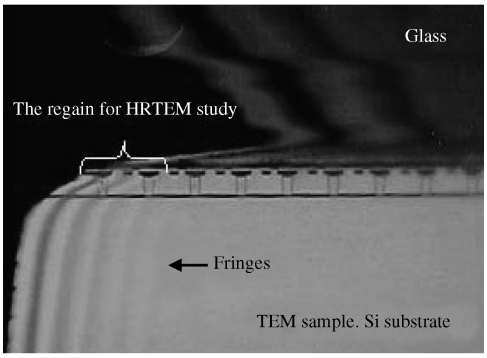

(g)

FIGURE 29.15 Wedge method of TEM sample preparation; (*a*) glue piece of glass on top of the sample and cut slice; (*b*) area of interest is kept in center of slice; (*c*) schematic diagram of wedge TEM sample; (*d*) optical micrograph illustrating array due to sample polished in an angle as a wedge; (*e*) one side of sample is polished to reach area of interest, then polished side of sample is glued on TEM grid, followed by polishing second side of sample; (*f*) optical micrographs illustrating ion-milled sample ready for TEM study; (*g*) ion-milled sample ready for high-resolution TEM study.

TEM analysis. When the fringes at the area of interest appear bright white, as shown in Figure 29.15*g*, the sample is ready for high-resolution TEM study.

29.5.3 FIB Technique

Dimpling works well for blanket films or for samples having large features or repeated patterns. However, it is difficult to use this technique to target a small special feature on a sample. In the wedge method skill is required to prepare a TEM sample. Fortunately, the FIB technique is a reliable method for making nanoscale precise cross-sectional TEM samples. Two FIB techniques are known: the H-bar method and the lift-out method. These were developed in the last decade to make site-specific, uniform, thin lamellae for TEM investigation.

The H-bar method is a conventional economical method. The name H-bar refers to the geometry of the TEM sample by which a thin lamella is held by a bulk sample at both ends as shown in the schematic diagram in Figure 29.16 This method requires pre-mechanical polishing of the sample to a thickness of approximately 30 μm with SiC abrasive papers. Then a small semicircular disc 1.5 mm in radius is cut from the sample in such a way that the area of interest occupies the 3-mm flat edge. The semicircular sample is then thinned using FIB milling and polishing.

FIB lift-out techniques can directly remove an electron-transparent lamella from a bulk specimen without pre-mechanical polishing and cutting. Lift-out techniques have two variations: the ex situ lift-out method and the in situ lift-out method. In both methods the thin TEM lamella is ion milled and polished to about 100 nm thick inside the FIB chamber. The lamella is removed from the FIB chamber and then transferred to a TEM grid using a micromanipulator—thus the name ex situ lift-out method. The in situ lift-out method is conducted entirely inside the FIB chamber and does not need additional instruments; as such it is a well-accepted technique [26–28]. The cross-sectional TEM sample preparation techniques of the two lift-out methods and the H-bar method using FIB/SEM are discussed next.

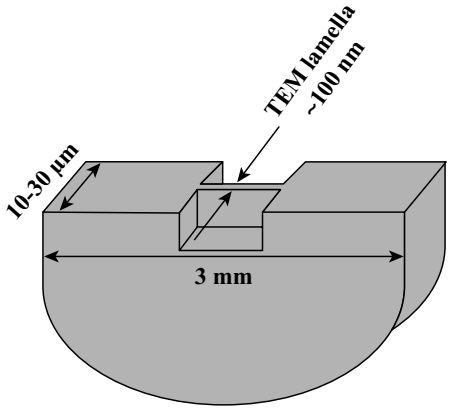

FIGURE 29.16 Schematic illustrating H geometry of TEM sample made using FIB H-bar method (not to scale).

In Situ Lift-Out Procedure The main steps of the FIB in situ lift-out method are illustrated in Figures 29.17*a–f*. The experimental parameters used in the sample preparation vary from one sample to the other. Some of the data given here are for reference only.

(a) At the eucentric point a bulk sample is tilted to 52°. A surface-protecting strip of platinum, carbon, or tungsten is deposited on the area of interest using a gas injection system, as shown in Figure 29.17*a* (hereafter we use Pt to represent all the deposited materials). In order to avoid ion beam damage during the ion deposition, the deposition of Pt is carried out in two steps using the GIS. First, a thin strip of Pt is deposited for a couple of minutes using a low-voltage (3–5 kV) and high-current (1–2 nA) electron beam. Second, an additional Pt strip 2–3 μm thick is deposited on top of the thin Pt strip using an ion beam on the order of nanoamperes operating at 30 kV.

(b) An alignment cross mark (X) is milled next to the intended milling location, as shown in Figure 29.17*b*. The mark helps to monitor the position of the sample during the milling process since the procedure takes a couple of hours. Two trenches spaced 1 μm parallel to the Pt strip at both sides of the Pt are cut out using a high ion beam current automatically or manually. In order to cut and lift out the TEM sample easily, one trench is cut bigger than the other; for example, one trench is milled to 15 μm × 5 μm × 30 μm, the other to 12 μm × 5 μm × 30 μm. After the milling, a lamella 1 μm thick is formed. At this step two sides and the bottom of the lamella connect with the original bulk sample.

(c) The sample is tilted back to 7°, which allows the ion beam to cut the connections between the lamella and the bulk sample. The lamella is partially separated from the rest of the bulk sample by milling out one edge and the bottom of the lamella, as shown in Figure 29.17*e*, or milling around the lamella at a U-shape, as shown in Figure 29.18*a*.

Two ways are commonly used to lift out the lamella from the bulk sample based on the two types of lift-out tools. One tool, an effector, is attached with a molybdenum grid called the end effector. Another one, termed AutoProbe, is attached with a tungsten or molybdenum needle. The tools for lifting the TEM lamella have been developed in the last few years; see [41–45] and the company's website (www.Omniprob.com)

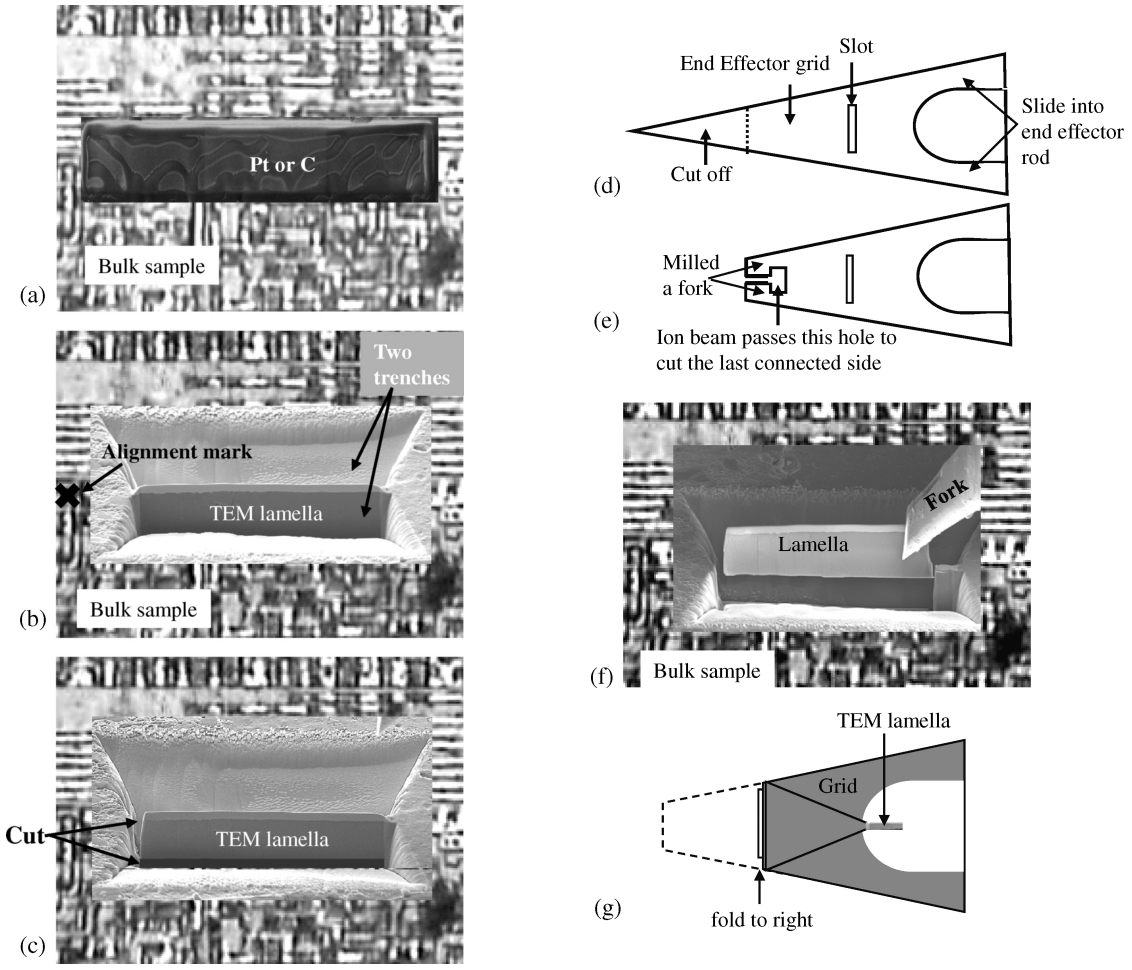

FIGURE 29.17 FIB in situ lift-out method to make TEM sample; (*a*) deposit strip of Pt or C on area of interest; (*b*) ion mill alignment mark beside area of interest, then ion mill two trenches parallel to Pt strip 1 μm apart from each other at each side of Pt strip to make TEM lamella; (*c*) cut one side and bottom of lamella to partially disconnect lamella with bulk sample; (*d*) end-effector TEM grid; (*e*) cut tip of grid and mill a fork; (*f*) move folk to hold lamella, then lift lamella out of trenches; (*g*) move grid with sample out of FIB/SEM chamber, fold TEM sample to center of grid, then polish lamella to 100 nm thick approximately.

(d) Figures 29.17*d*, *f* illustrate the way to lift out the lamella using the end effector. A schematic diagram of a TEM sample grid holder by an end effector rod is inserted into the FIB/SEM chamber, as illustrated in Figure 29.17*d*. The tip of the grid is milled out to reduce the static electric charge when connecting the grid to the lamella. A fork shape is milled at the end of the grid to hold the lamella, and a hole is milled so that the ion beam can cut out the side still connected to the bulk sample, as shown in Figure 29.17*e*. All processes for preparing the fork are done away from the lamella to avoid redeposition on it.

Then the fork-shaped grid is moved to hold the lamella followed by deposition of a small amount of Pt at the area connecting the fork and the lamella. The last side connection between the lamella and the bulk sample is cut using an ion beam through the hole made on the grid to free the lamella from the bulk sample (see Figure 29.17*e*). Finally, the lamella is gently lifted out of the trench, as shown in Figure 29.17*f,* by raising the end effector or moving down the bulk sample.

The end-effector rod holding the grid and the lamella are moved out of the FIB/SEM chamber. Under an optical microscope the grid is folded at a slot and the TEM sample is brought to the center of the grid, as shown in Figure 29.17*g*. The grid holder and the lamella together are reloaded into the FIB/SEM chamber for final polishing.

When the AutoProbe is used to lift the lamella, a tungsten needle is mounted on the probe; then the probe is inserted into the FIB/SEM chamber. The tip

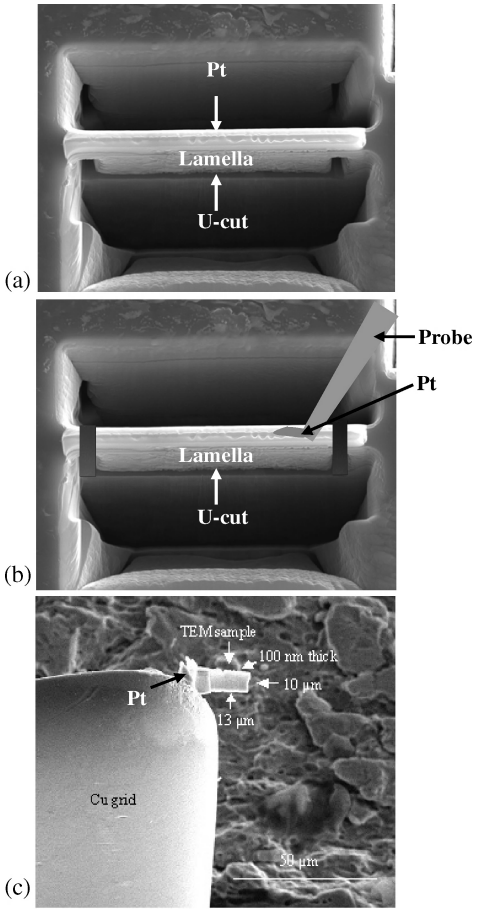

FIGURE 29.18 FIB in situ lift-out method to make TEM sample using AutoProbe tool; (*a*) deposit strip of Pt on area of interest, ion mill two trenches parallel to Pt strip 1 μm apart from each other at each side of Pt strip to make TEM lamella, then make U-cut using ion beam; (*b*) connect probe to lamella, cut off connections, lift out lamella from trench; (*c*) weld lamella on TEM grid using Pt deposition, cut off probe, then polish lamella to 100 nm thick approximately.

of the needle is ion milled away to make a fresh surface on the needle that can reduce the charging when connecting the needle to the lamella. Again, the ion milling is performed away from the lamella to avoid any redeposition to the lamella. Then the clean needle is moved and connected to the lamella. A small amount of Pt is deposited at the point connecting the needle and the lamella to hold the lamella to the needle. Next, all of the connections between the lamella and the bulk sample are cut, and the lamella is removed from the trench using the needle, as shown in Figure 29.18*b* [45, 46].

The lamella is moved and connected to a TEM grid using the needle. A small amount of Pt is deposited on the connection between the lamella and the grid, as shown in Figure 29.18*c*. Then, the needle is cut off.

(e) For fine polishing, the lamella in the FIB/SEM chamber is moved to the eucentric point, tilted to 52° again, and polished on both sides to approximately 100 nm thick using an ion beam with a current less than 350 pA. Finally, the sample is moved out of the FIB/SEM chamber and is ready for TEM analysis.

Ex Situ Lift-Out Method The first two steps of the cutting procedures of the ex situ lift-out method are similar to the in situ lift-out method, that is, depositing the Pt strip at the area of interest followed by milling two trenches at each side of the Pt strip to produce a lamella. The lamella is polished to around 100 nm thick using a low ion current. Then the thin lamella is cut free from the bulk sample, as shown in Figure 29.19*a*. The bulk sample containing the thin lamella is then removed from the FIB/SEM chamber.

Under an optical microscope a glass needle attached to a hydraulic micromanipulator is used to lift out the thin lamella from the trench performed in the bulk sample. The lamella is then removed to a TEM grid covered by carbon or Formvar film, as shown in Figure 29.19*b* [47].

Conventional H-Bar Technique The FIB H-bar technique is a convenient method used to make most TEM samples. Because the TEM lamella is held and supported by a bulk sample 3 mm in diameter, the H-bar method is particularly valuable for samples with complex structure requiring a relatively large, thin area. The main step in the H-bar method is to prepare a site-specific TEM sample, as illustrated in Figure 29.20.

(a) A slide ∼5 mm long × 1.5 mm wide × ∼3 mm thick is cut from a bulk sample. The sample is glued on a flat sample holder using resin, and the surface of interest is buried in crystalbond to avoid any damage to the area of interest. The slide is then mechanically polished on both sides to a thickness of approximately 30 μm with SiC abrasive papers, as shown in Figure 29.20*a*. The thickness of the sample to be polished varies depending on the sensitivity of the sample to the deformation during the mechanical polishing. Next, a semicircular sample with a 1.5-mm radius, as shown in Figure 29.20, is cut from the slide in such a way that the area of interest constitutes the 3-mm flat edge of the semicircular sample for future ion milling.

(b) Similar to the lift-out method, in a FIB/SEM chamber a strip of Pt 10–30 μm × 3 μm × 3 μm is deposited upon the area of interest on a surface of

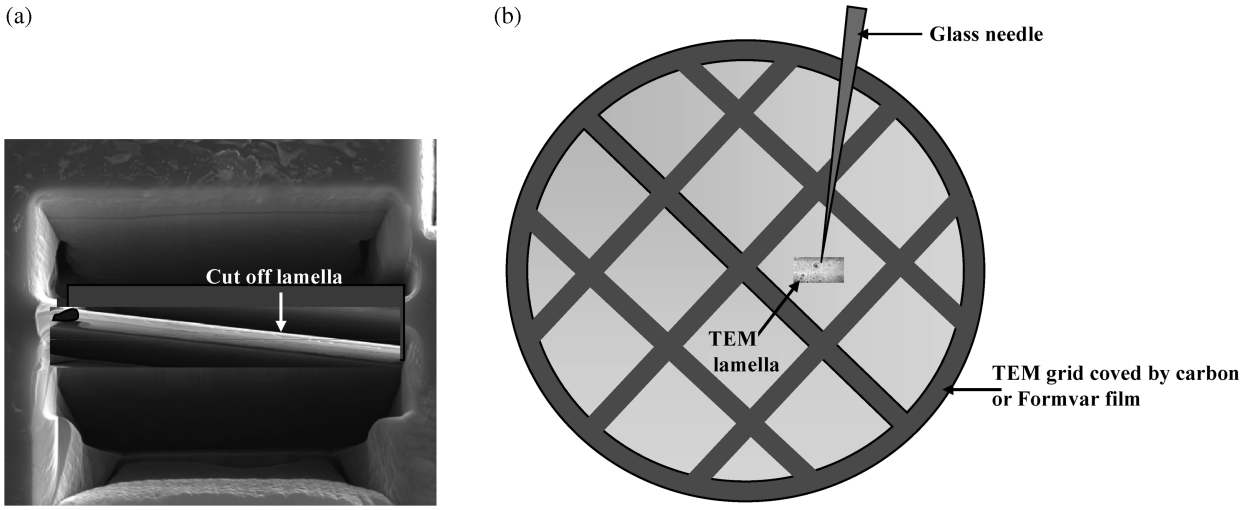

FIGURE 29.19 FIB ex situ lift-out method to make TEM sample; (*a*) lamella is polished to approximately 100 nm thick using low-current ion beam, then cutting off connection between lamella and bulk sample; (*b*) schematic diagram illustrating that after TEM sample is moved out of FIB/SEM chamber, the TEM lamella is lifted out from the trench in the bulk sample and put on a TEM grid using a glass needle under an optical microscope (not to scale).

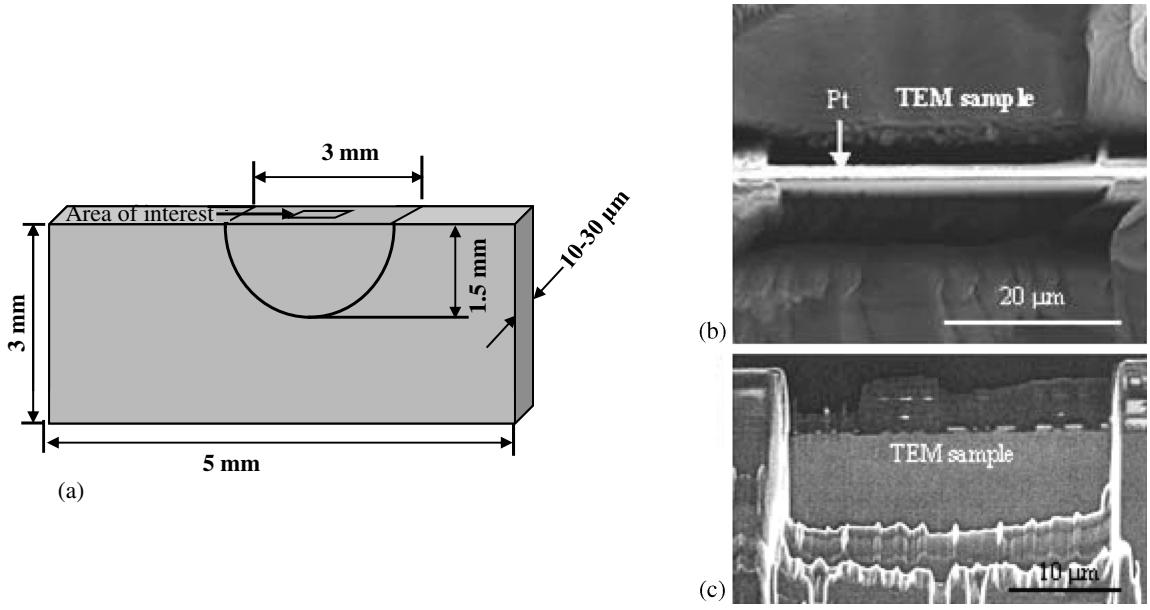

FIGURE 29.20 Schematic illustrating FIB H-bar method. A slab is mechanically ground to 10–30 μm thick. Then a semicircle shaped sample of 3 mm × 1.5 mm × 10-30 μm is cut from the slab for FIB milling. (Not to scale). SEM micrographs showing (*a*) top view and (*b*) plane view of cross sectional TEM sample.

3 mm × 30 μm and parallel to the long edge of the 3 mm to protect the sample from ion beam damage.

(c) Ion milling is first performed on one side of the sample parallel to the long side of the Pt strip starting from the edge of the semicircular sample using a high-current ion beam. The milling is continued toward the middle of the sample until the region of interest, which is protected by the Pt strip, is reached. Then, the cross-sectional face is polished using a low-current ion beam.

(d) Ion milling and polishing are then performed on the other side of the Pt strip. The cross-sectional sample is finally polished to around 100 nm thick, as shown in Figure 29.20*b*. During the final polishing, when bright color appears at the area of interest or an electron beam of 5 kV can penetrate the area of

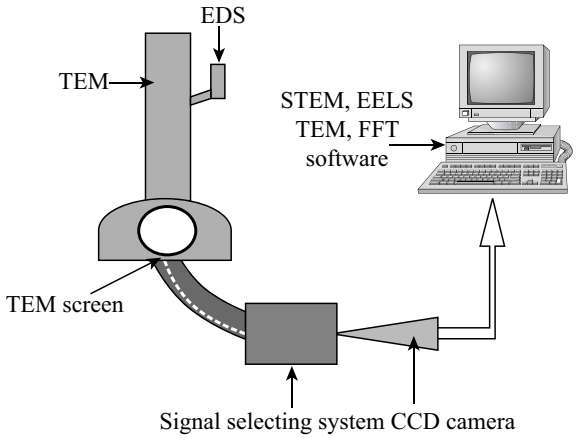

FIGURE 29.21 Schematic illustrating TEM system including TEM, STEM, EDS, EELS, CCD camera, and FFT software (not to scale).

interest, the ion polishing is stopped and the TEM sample is ready for TEM investigation.

Figure 29.20*c* is a planar view SEM micrograph of a cross-sectional TEM sample made using the H-bar technique. The thin TEM lamella is supported by the two sides 30 μm thick, as shown in Figures 29.16 and 29.20*b*, *c*. The images also show the H-shape geometry of the sample.

29.6 ANALYSIS OF ELECTROPLATED FILMS USING TEM TECHNIQUE

Following the development of thin-film electronics, nanomaterials, and the overall decrease in the dimensions of integrated circuit devices, the transmission electron microscope becomes a necessary tool in both manufacture and research. TEM also plays a very important role in the analysis of electroplated films because of its three analysis capabilities.

(i) *High-Resolution Microscopy* FIB uses electrostatic lenses to focus ions. In contrast with the FIB, TEM uses magnetic lenses to focus electrons. Since magnetic lenses have relatively low "optical" aberrations, TEM is capable of high resolution [18, 19]. A scanning transmission electron microscope (STEM) can also be attached to the TEM. A combined system-using TEM, STEM, charge-coupled device (CCD) cameras, and fast Fourier transfer (FFT) enhances markedly the resolution in TEM micrographs. A schematic drawing in Figure 29.21 shows a system consisting of TEM, STEM, a CCD camera, and FFT software.

(ii) *Electron Diffraction* In contrast to X-ray diffraction, electron diffraction can identify the structure of individual particles/grains and provide data about an area of nanodimensions. Thus, electron diffraction is used to identify phases of small sizes and quantity in a sample.

(iii) *Composition Analysis* An EDS and electron energy loss spectrometer (EELS) including parallel EELS (PEELS) equipped TEM can analyze elements starting from light element such as boron.

Some applications of TEM techniques as applied to electroplated films are introduced below.

29.6.1 TEM Analysis of Electroplated Copper films

As mentioned in Section 29.4.2, electroplated Cu is well known to exhibit grain growth or recrystallization even at room temperature over a period of time after plating. The grain sizes in the as-plated electroplated Cu film is on the order of tens of nanometers. During a period of hours to weeks copper grains can grow to 1.6 μm at room temperature. This is an advantageous phenomenon which reduces the resistivity of the electroplated copper film. FIB ion micrographs do show Cu grains in electroplated copper films (see Fig. 29.9); however, they do not have sufficient resolution to analyze fine grains. Therefore, TEM is required in the characterization of electroplated Cu films.

As-plated copper film has small polycrystalline grains throughout the film thickness observed using STEM. Some of the small grains exhibit twins or dislocations. The average grain size of the as-plated copper film is about 50 nm as determined using an image analysis program on TEM micrographs. After staying at room temperature of 21°C for three days followed by heating to 100°C for 30 min, the copper grains grow to about 1.9 μm and have high twin densities [32].

An in situ TEM technique was employed to determine the void formation mechanism in electroplated copper trenches of 180 nm. TEM samples were prepared using dimpling followed by ion milling. The authors in [48] polished the sample down to 80 μm of uniform thickness using diamond-lapping films, dimpled grinding to approximately 4 μm in thickness, then ion milled to an electron transparent thickness of less than 100 nm. In situ TEM experiments were conducted using a heating stage from room temperature to 500°C. They reported that voids formed at the triple junction of grain boundaries as well as at the interface of copper and its barrier. The electroplated copper in the trench possesses preferred crystallographic orientation. Dislocations were also observed in several grains in the electroplated copper prior to annealing. Twins were observed on the TEM micrographs of the trench and identified by electron diffraction before and after annealing.

Nanoscale twins in electroplated copper films have attracted attention in recent years due to the high electrical

conductivity and high mechanical strength required simultaneously. TEM techniques have determined that the grain sizes increase gradually from the bottom to the middle and then to the top of the vias. By controlling electroplating parameters, a high density of nanotwins exist at the bottom of vias where the bottom-to-top electroplating starts [49]. The copper grains in the middle of the vias have fewer nanotwins than the grains at the bottom. However, only a few grains have nanotwins at the top of the copper vias. The thickness of the nanotwins is about 20 nm. Change in the grain size and twin density along the copper via shows that their distribution is dependent upon the electroplating parameters.

The hardness at different locations in an electroplated copper via is related to the density of nanotwins: The higher the density of the nanotwins, the higher the hardness. The hardness at the bottom of the vias is as high, ~2.0–2.4 GPa; it decreases gradually to ~1.6 GPa at the top of the vias. The hardness of pure bulk copper is 1.0–1.2 GPa, which is much lower than the average hardness on the vias. It is considered that the twin boundary blocks the sliding of the crystal planes and so the movement of dislocation similar to what grain boundaries do. However, the electrical resistivity of the copper twin boundary is found to be one order of magnitude smaller than that of the copper grain boundary. Therefore, the contribution of the twin boundaries in increasing the electrical resistivity is less significant. The electrical conductivity of the electroplated copper in vias is about 2.2 μΩ-cm, which is close to the electrical conductivity of 1.67 μΩ-cm of pure bulk copper [50, 51].

The cross-sectional TEM sample of a via array in the above study was produced using ion-milling methods. The sample was polished to about 20 μm thick and then thinned to 50 nm by ion milling.

29.6.2 TEM Analysis of Electroless Deposited Ni–Zn–P Films

Electroless Ni–Zn–P films are simultaneously deposited on metal substrates for corrosion resistance tests and on Formvar films for microstructure analysis. A discussion of the method of making TEM Formvar film as a support substrate of electrolessly deposited film, the process of electroless deposition, and the TEM analysis of Ni–Zn–P films follows.

Making Formvar Films Formvar film coated on a glass slide is a supporting substrate for electrolessly deposited films suitable for TEM analysis. The schematic in Figure 29.22 illustrates a simple instrument used to produce the Formvar film. A glass slide is suspended inside a pipette. Four grams of polyvinyl Formvar powder is dissolved in 1 L of ethylene dichloride to make the Formvar solution. Formvar film is coated on the glass slide while the Formvar solution itself is poured into the pipette. The Formvar solution flows through the pipette to a beaker for possible recycling. The glass slide coated by the Formvar film is removed from the pipette for the film to be dried at room temperature in open air [52, 53].

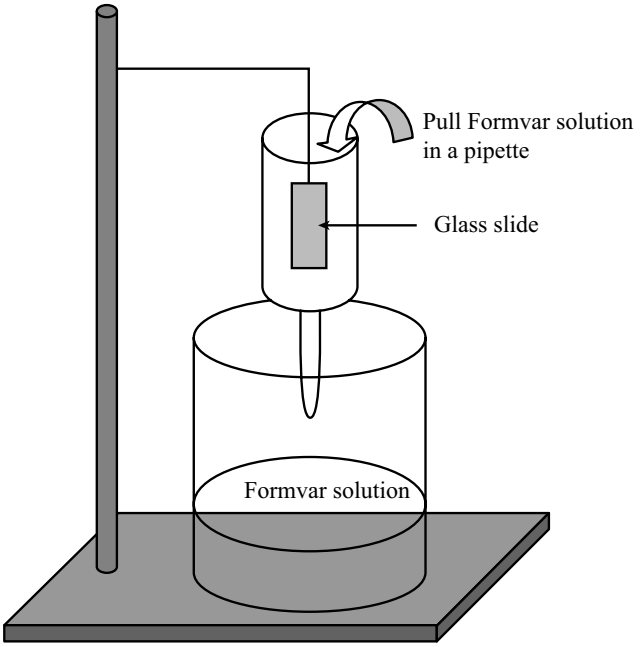

FIGURE 29.22 Schematic illustrating instrument for coating Formvar film on glass slide.

Electroless Deposition of Ni–Zn–P Films Ni–Zn–P films are deposited on the glass slide coated with the Formvar film for TEM analysis. There are three well-established simple steps to deposit the Ni–Zn–P films. First, the glass slide with the Formvar film is immersed in $SnCl_2$/HCl sensitizing solution, which consists of 0.3% HCl and 10% $SnCl_2$ in 80 mL of H_2O, for 60 s. Second, the slide is immersed into a $PdCl_2$/HCl activating bath for 1–2 min. Finally, the slide is immersed in a solution for electroless deposition of the Ni–Zn–P film. The solution for the electroless deposition consists of the following:

Hypophosphite	NaH_2PO_2	20 g L^{-1}
Nickel chloride	$NiCl_2 \cdot 6H_2O$	7.5 g L^{-1}
Ammonium chloride	NH_4Cl	12.5 g L^{-1}
Citric acid monohydrate	$H_5C_6H_5O_7 \cdot H_2O$	19.84 g L^{-1}
Zinc chloride	$ZnCl_2$	10 g L^{-1}

The pH of the electroless deposition solution is adjusted using sodium hydroxide (NaOH). At the temperature of 70–80°C the deposition rate of the film increases when the pH of the solution is increased from 6 to 12. A smooth, uniform metallic shiny Ni–Zn–P thin foil is deposited at a pH of approximately 9. Higher deposition temperature is required when the pH is lower and vice versa. However, there are difficulties in depositing the films when the pH is too high

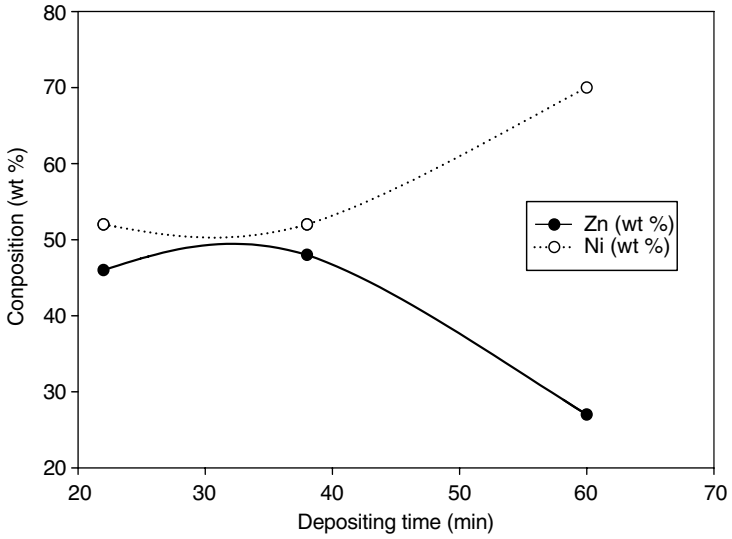

FIGURE 29.23 Plot of composition of Ni and Zn versus electroless deposition time in Ni–Zn–P films.

or too low. For pH $\geq$ 10 the deposition rate is too high so that it forms bubbles in the bath and breaks up the deposited foil. On the other hand, it takes a long time to deposit a layer at pH $\leq$ 7, and the deposit is not uniform.

Analysis of Electroless Deposited Ni–Zn–P Films The Ni–Zn–P film and its supporting Formvar film are cut/scratched thoroughly into sections about 4 mm $\times$ 4 mm. Then the glass slide is immersed in water at a slight angle until the small pieces of films separate from the glass slide and float on the surface of the water. The small pieces of deposited Ni–Zn–P films together with the Formvar film are picked up using TEM grids for TEM analysis.

The compositions of the Ni–Zn–P films are analyzed using a TEM equipped with EDS. The concentrations of Ni, Zn, and P in the electrolessly deposited films vary when the deposition conditions are changed. The highest concentration of Zn in a Ni–Zn–P film is 59 at % obtained in a bath of pH 9.5 at a temperature of 75°C and with a deposition time of 40 min. Figure 29.23 is a plot of the composition of Ni and Zn in the Ni–Zn–P thin films, which was deposited at a temperature of 78°C and pH 8.5, versus depositing time. The amount of Ni in the film increases steadily with the deposition time. The amount of Zn in the film also slightly increases with a deposition time of up to 40 min. The amount of Zn in the film reaches 50% when deposition time is approximately 40 min, then the concentration of Zn in the film reduces with the deposition time. The concentration of phosphorus is the balance percentage.

Figures 29.24*a–c* are the bright-field image, dark-field image, and electron diffraction pattern of a Ni–Zn–P film electroless deposited at pH 8.35 at 75°C. The bright-field image in Figure 29.24*a* shows the morphology of the film consisting of nanoparticles. A polycrystalline electron diffraction pattern is obtained from the film, as shown in Figure 29.24*b*. The electron diffraction rings are indexed as the diffractions from nickel with a face-centered-cubic (fcc) lattice and zinc with a hexagonal close-packed (hcp) lattice. The dark-field image in Figure 29.24*c* was obtained using diffraction rings with high intensities, that is, {111}, {200} of Ni and {101}, {102} of Zn. Thus, the dark-field image reveals that the crystalline sizes of nickel and zinc are about 30 nm.

29.6.3 TEM Analysis of Electroless Deposited Cobalt–Phosphorus Thin Film

The techniques for electroless deposition and for preparing TEM samples of Co–P magnetic films are similar to those for Ni–Zn–P films. The TEM and magnetometer analyses reveal the relationship between the microstructures and magnetic properties of the Co–P films.

Electroless Deposition of Co–P Films The Co–P films are simultaneously deposited on TEM copper grids covered by Formvar films and on the sample holder of a vibrating sample magnetometer. A commercially available Allied Kelite Disclad 601 solution may be used as the metallizing bath. The solution consists of three components: $CoCl_2{\cdot}6H_20$, which is the cobalt source; $NaH_2PO_2{\cdot}H_2O$ (sodium hypophosphite), which is the source of phosphorus; and a complexing agent [51–53]. To get high coercivity depositing parameters such as the pH and composition of the solution and the deposition temperature are varied. The microstructures of the films are investigated using bright-field imaging, dark-field imaging, and TEM electron diffraction patterns. The concentrations of phosphorus in the films are determined using a TEM equipped with an EDS.

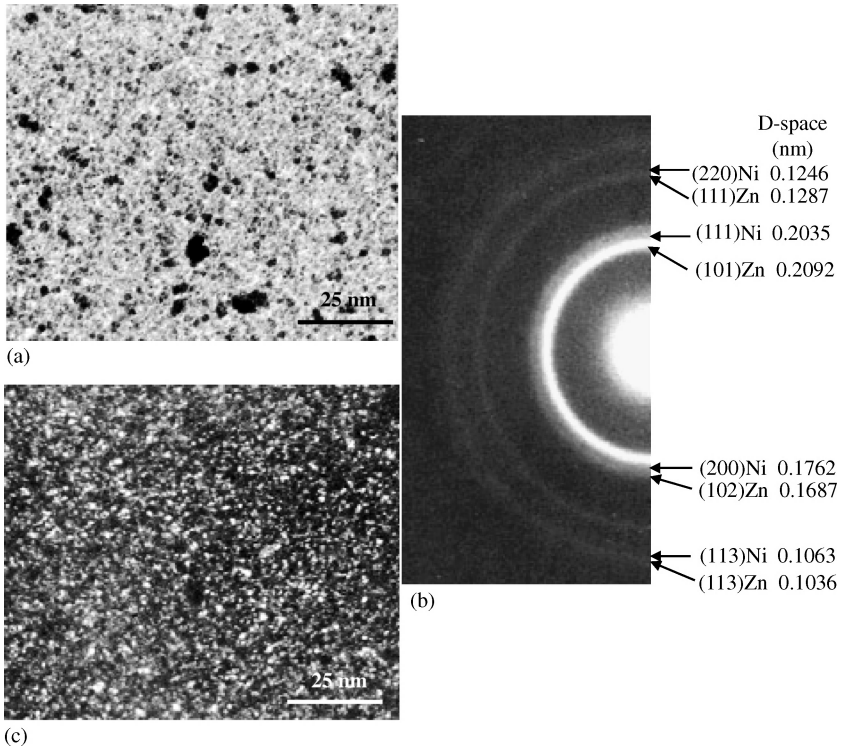

FIGURE 29.24 TEM micrographs of Ni–Zn–P film produced in solution of pH 8.35; (*a*) bright-field image; (*b*) electron diffraction pattern of film. The *d*-spaces of crystalline planes in nanometers are noted. (*c*) Dark-field image reveals the grains of Ni and Zn. (By permission of The Electrochemical Society.)

Analyses of Electroless Deposited Co–P Films The Co–P films may be plated in metallizing solutions with different pH values. The films plated in a solution of pH 9.1 have higher coercivity. The plot in Figure 29.25 reveals that when the hypo concentration in the plating solution increased from 2 to 8% by volume (v %), the phosphorous concentration in the films increased from 3 to 12 at % as analyzed using EDS. This means that the relative concentrations of cobalt in the films decreased from 97 to 88 at %. Results of magnetometer tests show that the coercivity of the Co–P films increases from 493 to 1026 Oe, then decrease to 200 Oe when the hypo concentration increased from 2 to 8 v % in the plating solution, as shown in Figure 29.26. The films with hypo concentration of 5 v% plated in the solution with pH 9.1 seem to have the maximum value of magnetic coercivity, that is, 1026 Oe [54, 55].

The grain sizes and crystalline structure of the films are analyzed using bright-field imaging, dark-field imaging, and TEM electron diffraction patterns. The relative intensities of the electron diffractions from crystalline planes identify the preferred orientation of the crystalline structure in electroless plated Co–P films. Changes in the relative intensity of electron diffraction are related to the crystallographic orientations of the crystals in the films. The preferred orientation of the cobalt crystals in electroless CoP films affects the magnetic properties of the films. In some electroless depositing conditions the cobalt crystals in electroless CoP films form the preferred orientation.

Two sets of bright-field images, dark-field images, and electron diffraction patterns of two CoP films produced at pH 9.1 for hypo concentrations of 5 and 8 v % are given in Figures 29.25*a–c* and 29.25*d–f*, respectively. Electron diffraction patterns identify the crystallographic structure of the component crystallites as hcp cobalt. Three diffraction rings of {100}, {002}, and {101} planes from crystalline Co are indexed as shown in Figures 29.25*c*, *f*. The bright-field images given in Figures 29.25*a*, *d* show the morphologies of the CoP films. The dark-field images given in Figures 29.25*b*, *e* obtained using the electron diffraction rings of {100}, {002}, and {101} crystal planes illustrate the crystalline sizes of cobalt in the films. Relative diffraction intensities of I_{100}, I_{002}, and I_{101} of {100}, {002}, and {101} crystal planes are 20 : 60 : 100 for the standard hcp cobalt [56]. The relative intensities of crystalline Co in the CoP films are measured on electron diffraction patterns using a TEM negative scanner. The electron diffraction patterns from the CoP films produced using hypo concentrations of 5 and of 8 v % are given in Figures 29.26*c*, *f*. The relative intensity ratio of I_{002} to I_{101} in the electron diffraction pattern from the CoP film produced using 5 v % hypo

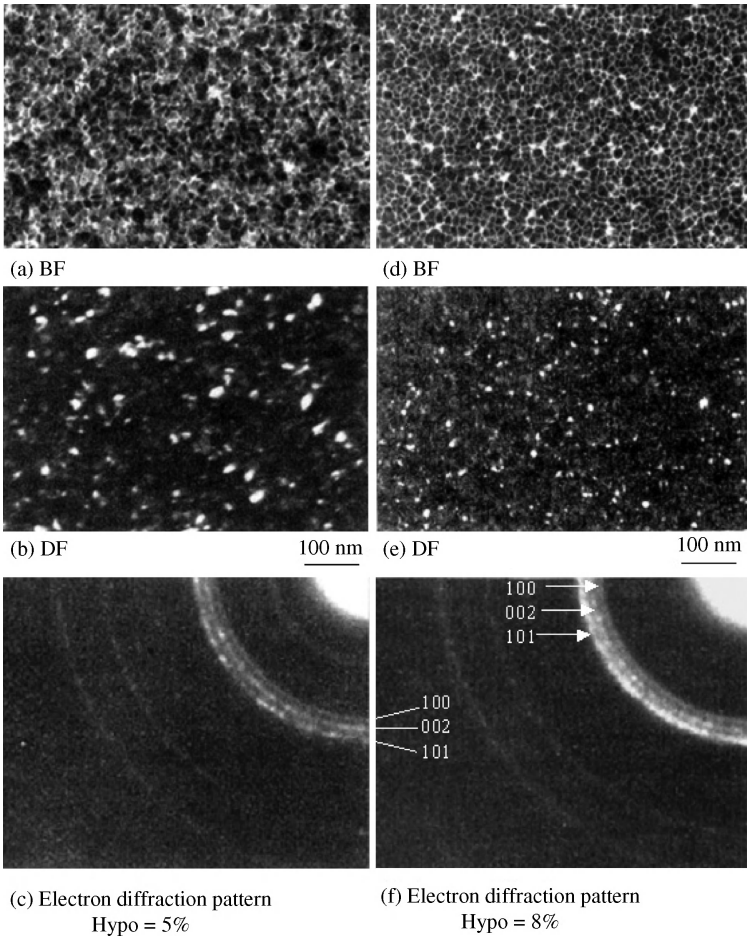

FIGURE 29.25 TEM micrographs of CoP films produced at pH 9.1 using hypo concentration of 5 v % (*a–c*) and 8 v % (*d–f*), respectively. The white particles in the dark-field image are Co. (By permission of The Electrochemical Society.)

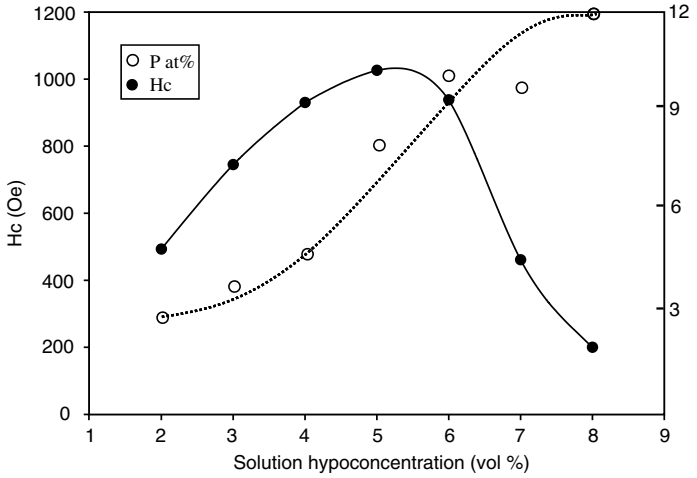

FIGURE 29.26 Plots of phosphorous concentration and coercivity of Co–P films versus hypo concentration by volume in electroplating solution.

concentration is approximately 0.6 (i.e., 60 : 100). The ratio of the intensity of the {002} and {101} diffraction rings changes with the hypo concentration of the plating solution. The relative intensity ratio of I_{002} to I_{101} in the electron diffraction pattern from the CoP film produced using hypo concentration of 8 v % is greater than 0.6, which implies that the preferred orientation of the {002} crystalline planes occurred in the Co–P film. Selecting the optimum combinations of pH and hypo concentration resulted in changes in the composition and microstructure of the films. The electrolessly deposited Co–P film has coercivity greater than 1000 Oe using a hypo concentration of 5 v % and pH 9.1, as shown in Figure 29.26.

ACKNOWLEDGMENT

The help by Caty Schippers and Daniel Wang is gratefully acknowledged.

REFERENCES

1. B. El-Kareh, *Fundamentals of Semiconductor Processing Technologies*, Kluwer Academic, Boston, 1995, p. 551.
2. T. Kikkowa, NEC Corporation, U.S. Patent 5,345,108, 09/06/1994.
3. N. Y. Fishkill, "IBM Delivers World's First Copper Chips," IBM Press room, Sept. 1, 1998.
4. P. C. Andricacos, C. Uzoh, J. O. Dukovic, J. Horkans, and H. Deligianni, *IBM J. Res. Devel.*, **42** (5), 567 (1998).
5. W. L. Masterton, E. J. Slowinski, and C. L. Stanitski, *Chemical Principles*, Saunders College Publishing, Philadelphia, PA, 1985, p. 701.
6. H. P. Fong, Y. Wu, Y. Y. Wang, and C. C. Wan, *J. Electron. Mater. Micron*, **33** (6), 515 (2002).
7. J. Mayer, L. A. Giannuzzi, T. Kamino, and J. Michael, *MRS Bull.*, **32**, 400 (May 2007).
8. U. Landau, J. J. D'Urso, and D. R. Rear, "Modeling the Deposit Thickness Distribution in Copper Electroplating of Semiconductor Wafer Interconnects," paper presented at the 195th Meeting of the Electrochemical Society, Seattle, WA, May 2–6, 1999, Abstract No 263.
9. U. Landau, Abstract No. 53, *Electrochem. Soc. Extended Abstr.*, **97-1**, 60 (1997).
10. O. Lanzi and U. Landau, *Elecrochem. Soc. Extended Abstr.*, **137**, 1139 (1990).
11. C. Lingk and M. E. Gross, *J. Appl. Phys.*, **84** (10), 5547 (1998).
12. J. Dini, "Electrodeposition of Copper," in *Modern Electroplating*, 4th ed., M. Schlesinger and M. Paunovic, Eds., Wiley, New York, 2000, p. 61.
13. J. Commander, R. Hurtubise, U. Paneccasio, X. Lin, and K. Jirage (Enthone, Inc.) U. S. Patent 7,316,772, 01/08/2008.
14. Y. Dordi and P. Hey, "Automated Chemical Managerment for Production Copper Electroplating," in *Semicond. Febtech*, 11th ed., ICG Publishing, 2000, p. 273.
15. R. L. Strong, J. D. Luttmer, D. D. Little, T. H. Teherani, and C. R. Helms, *J. Vac. Sci. Tech.*, **A5**, 3207 (1987).
16. M. X. Yang, W.-F. Yau, M. Xi, H. Lin, and J. Hsue, Semiconductor Equipment and Materials International (2003) #1-892568-78-0.
17. "Gallium Liquid Metal Ion Source Handling and Operating Instructions," FEI Company, available May 2010, www.fei.com/products/components/electron-ion-sources.
18. J. Goldstein, D. Newbury, D. Joy, C. Lyman, P. Echlin, E. Lifshin, L. Sawyer, and J. Michael, *Scanning Electron Microscopy and X-Ray Microanalysis*, 3rd Ed., Kluwer Academic/Plenum, New York, 2003, p. 21.
19. P. Hirsch, A. Howie, R. B. Nicholson, D. W. Pashley, and M. J. Whelan, *Electron Microscopy of Thin Crystals*, Robert E. Krieger Publishing, New York, 1977, p. 2.
20. B. W. Kempshall, S. M. Schwarz, B. I. Prenizer, L. A. Giannuzzi, R. B. Irwin, and F. A. Stevie, *J. Vac. Sci. Technol.*, **B19** (3), 749 (2001).
21. L. A. Giannuzzi, and F. A. Stevie, *Introduction to Focused Ion Beams: Instrumentation, Theory, Techniques and Practice*, Springer, New York, 2005, p. 173.
22. G. D. Alton and P. M. Read, *J. Appl. Phys.*, **66** (3), 1018 (Aug. 1989).
23. A. A. Tseng, *J. Micromech. Microeng.*, **14**, R15 (2004).
24. P. Gnauck, P. Hoffrogge, M. Schumann, and G. Bauhammer, *Microsc. Microanaly.*, **8** (Suppl.), 546CD (2002).
25. P. Gnauck and J. Greiser, "A New Approach to Materials Characterization Using Low Pressure and Low Voltage Field Emission Scanning Electromicroscopy," DUM-Bericht 519, Mühlheim, 2000, pp. 89–96.
26. E. Weimer and J. P. Martin, paper presented at the 13th Int. Congr. Electron Microscopy ICEM, Paris, France, 17–22 July 1994/0180(2–3), 1994, p. 67.
27. K. A. Telari, B. R. Rogers, H. Fang, L. Shen, and R. A. Weller, and D. N. Braski, *J. Vac. Sci. Technol.*, **B20.2**, 590 (2002).
28. C. A. Volkert and A. M. Minor, *MRS Bull.*, **32** 389 (2007).
29. Y. Sakai, T. Yamada, T. Suzukia, and T. Ichinokawa, *J. Anal. At. Spectrum*, **14**, 419 (1999).
30. P. Sigmund, *Phys. Rev. A*, **26**, 2497 (1982).
31. B. W. Kempshall, S. M. Schwarz, B. I. Prenizer, L. A. Giannuzzi, R. B. Irwin, and F. A. Stevie, *J. Vac. Sci. Technol.*, **B19** (3), 749 (2001).
32. L. M. Gignac, K. P. Rodbell, C. Cabral, Jr., P. C. Andricacos, P. M. Rice, R. B. Beyers, P. S. Loke, and S. J. Klepeis, *Mat. Res. Soc. Symp. Proc.*, **562**, 209 (1999).
33. C. Lingk, M. E. Gross, W. L. Brown, W. Y. C. Lai, J. F. Miner, T. Ritzdorf, J. Turner, K. Gibbons, E. Klawun, G. Wu, and F. Zhang, *Ad. Metall. Conf. Proc.*, **14**, 669 (1998).
34. A. Morina, A. Neville, *J. Phys. D: Appl. Phys.*, **40**, 5476 (2007).
35. H. Ota, M. Hachiya, Y. Ichiyasu, and T. Kurenuma, *Hitachi Rev.*, **55** (2), 78 (2006).

36. K. D. Pollard, et al., "White Ring Defect Formation in Lead-Free WLP," paper presented International Wafer Level Packaging, Conference Proceedings, San Jose, CA, Session 9, Sept. 19, 2006.
37. S. Abe, T. Sekiguchi, and H. Nakano, Dr. Eng. Minori Noguchi, *Hitachi Rev.*, **55** (2), 73 (2006).
38. T. Ishitani, H. Tsuboi, T. Yaguchi, and F. Koike, *Electron. Microsc.*, **43**, 322 (1994).
39. J. C. Bravman and R. Sinclair, *J. Electron. Microsc. Tech.* **1**, 53 (1984).
40. L. A. Gionnuzzi, J. L. Drown, S. R. Brown, R. B. Irwin, and F. A. Stevie, *Mat. Res. Soc. Proc.*, R. Anderson and S. D. Walck, Eds., **480**(19) (1997).
41. L. A. Gionnuzzi, J. L. Drown, S. R. Brown, R. B. Irwin, and F. A. Stevie, *Microsc. Res. Technique*, **41**, 285–290 (1998).
42. J. P. Benedict, S. J. Klepeis, W. G. Vandygrift, and R. M. Anderson, *EMSA Bull.*, **19**, (2) 74 (1989).
43. R. K. Nalla, A. E. Porter, C. Daraio, A. M. Minor, and V. Radmilovic, *Micron*, **36**, 672 (2005).
44. E. A. Stach, A. P. Tomsiaa, R. O. Ritchie and H. Zhang, *Thin Solid Films*, **320**, 77 (1998).
45. J. Mayer, L. A. Giannuzzi, T. Kamino, and J. Michael, *MRS Bull.*, **32**, 400 (May 2007).
46. X. Meng-Burany and A. T. Alpas, *Thin Solid Films*, **516**, 325 (2007).
47. L. G. Giannuzzi, B. W. Kempshall, S. D. Anderson, B. I. Prenitzer, and T. M. Moore, *Microelectronic Failure Analysis Desk Reference* 2002 Supplement, ASM International, Hillsboro, OR, 2002, p. 29.
48. J. H. An and P. J. Ferreira, *Mater. Res. Soc. Symp. Proc.*, **907E**, 0907-MM03-03.2 (2006).
49. L. Xu, P. Dixit, J. Miao, J. H. L. Pang, X. Zhang, K. N. Tu, and R. Preisser, *Appl. Phys. Lett.*, **90**, 033111 (2007).
50. L. Lu, Y. F. Shen, X. H. Chen, L. H. Qian, and K. Lu, *Science*, **304**, 422 (2004).
51. L. Lu, R. Schwaiger, Z. W. Shan, M. Dao, K. Lu, and S. Suresh, *Acta Mater.*, **53**, 2169 (2005).
52. M. Schlesinger, X. Meng, and D. D. Snyder, *J. Electrochem. Soc.*, **137**, (6), 1858 (1990).
53. M. Schlesinger, X. Meng, and D. D. Snyder, *J. Electrochem. Soc.*, **138**, (2), 406 (1991).
54. M. Schlesinger, X. Meng, W. T. Evans, D. A. Sounders, and W. P. Kampert, *J. Electrochem. Soc.*, **137**, (6), 1706 (June, 1990).
55. M. Schlesinger and J. Kisel, *J. Electrochem. Soc.*, **136**, 1658 (1989).
56. American Society of Testing and Materials (ASTM), X-Ray Powder Diffraction Card #5-0727.

30

IONIC LIQUID TREATMENTS FOR ENHANCED CORROSION RESISTANCE OF MAGNESIUM-BASED SUBSTRATES

ROBERT PETRO, MORDECHAY SCHLESINGER, AND GUANG-LING SONG

30.1 INTRODUCTION

Magnesium (Mg) is the eighth most abundant element on earth, possessing several advantageous properties including a high strength to weight ratio and one of the lightest metals with a density that is only two-thirds that of aluminum and one-fourth that of iron at 1.74 g cm^{-3}. Additional properties that contribute to magnesium's versatility in the automotive, electronic, and aerospace industries include a high thermal conductivity, high dimensional stability, good electromagnetic shielding characteristics, high damping characteristics, good machinability, and easy recyclability [1]. These properties make the utilization of magnesium of particular interest to the automotive and aerospace industries where the weight reduction provides a simple means to achieve higher fuel efficiencies without sacrificing structural strength.

Despite its many valuable properties, magnesium remains a very reactive element, prone to a number of undesirable properties, including poor corrosion and wear resistance, poor creep resistance, and high chemical reactivity, which have limited its wider industrial use. As such, automobiles currently possess few magnesium cast parts, averaging only a few pounds per car. Pure magnesium corrodes rapidly in humid atmospheric and/or aqueous environments where anions such as Cl^-, Br^-, I^-, and SO_x^- promote local and generalized corrosion [2–12]. Compounds like alcohols, ethers, and phenols also attack magnesium [13]. Although alloying magnesium with elements such as manganese, aluminum, zinc, zirconium, and rare earths [14, 15] can improve its properties, magnesium and its alloys continue to be extremely susceptible to galvanic corrosion, which can cause severe pitting in the metal, resulting in decreased mechanical stability and an unattractive appearance of the surface. Although uniform attack [16–18] is generally the most prevalent form of electrochemical corrosion, occurring with equal intensity over the entire surface of the metal, in the case of magnesium, especially pure magnesium, the partially protective surface film makes localized galvanic [19–24] and pitting corrosion [25–35] more common and worrisome, largely due to the difficulty in their detection and suppression. Galvanic corrosion occurs when two metals/alloys having differing compositions, and thus standard electrode potentials, are electrically coupled in the presence of an electrolyte. This coupling results in the formation of a galvanic cell, which preferentially corrodes the more reactive, or electronegative, of the two metals. Since magnesium has a highly negative standard electrode potential ($E_0 = -2.37$ V) there are few metal couples with which serious and rapid corrosion does not occur. Pitting corrosion, defined by the formation of small pits on the surface of a metal/alloy, usually stem from galvanic corrosion of a surface defect and progresses similar to crevice corrosion, where stagnant liquid in a crevice begins oxidizing the metal and/or its passive layer. Pitting is of particular concern due to quick and serious progression often going undetected until a failure occurs, and with the misleading nature of surface corrosion, due to the ability of pitting to propagate rapidly below the surface, investigations of processes to enhance corrosion resistance must take into account the total corrosion of the sample.

Perhaps one of the most effective methods to prevent corrosion is to isolate the substrate from corrosive environments by means of a corrosion-resistant, preferably metallic,

Modern Electroplating, Fifth Edition Edited by Mordechay Schlesinger and Milan Paunovic

coating. In order for a coating to provide adequate corrosion protection, the coating must be uniform, well adhered, pore free, not to mention strong, ideally self-healing, for applications where physical damage to the coating may occur. Coatings possessing pores [36] or not well adhered are prone to the formation of a galvanic couple when exposed to an electrolytic solution or moisture-filled environment. Regrettably, due to its chemical reactivity, magnesium is a difficult-to-plate metal as it forms an oxide/hydroxide layer on its surface as soon as it comes in contact with air or water. The formation of this passive oxide layer can have a detrimental effect on coating adhesion and uniformity and ultimately corrosion resistance. It is for this reason that precleaning and pretreatment processes, to introduce a surface layer that may be easily removed during the plating process and prevent oxidation, or be built upon play a critical role in the development of a good protective coating on magnesium and its alloys. The extreme reactivity of magnesium also means that care must be taken to ensure that the metal reduction pathway is the preferred electrochemical process during plating, since loose immersion layers, which inhibit good adhesion, often form readily on the surface by displacement [37]. Another challenge in the plating of magnesium is that the quality of the metal coating is dependent on the alloy substrate, in part due to intermetallic species, such as Mg_xAl_y, formed at the grain boundaries, resulting in a nonuniform surface potential across the substrate. Finally, magnesium's violent reaction with most acids and dissolution in acidic media signifies that nontraditional plating baths must be developed.

30.2 CURRENT COATING TECHNOLOGIES

Notwithstanding the difficulties in the plating of magnesium, several plating processes have been developed for magnesium and its alloys, including electro- and electroless plating methods [38]. Electroplating offers the possibility to deposit high-purity metals and the deposition of multilayers but is effective only on simple shapes as uneven distribution of the current density within the plating bath produces nonuniform coatings on complex shapes, especially holes or recessed areas. Electroless plating provides a good alternative to electroplating in that it is able to evenly coat complex shapes, with holes and recessed areas, and does not have the same limitations stemming from the uneven throwing power of the current in electroplating. An additional advantage of electroless plating is that other metals [38–40] and/or second-phase particles, such as carbides, diamonds, or polytetrafluoroethylene (PTFE), can be codeposited during the plating process to create composites to improve the hardness, abrasive properties, or lubricity of the final composite coating [41–43]. Unlike electroplating, the environmental impact of electroless plating from an aqueous solution is of serious concern due to the limited life of the deposition bath, a problem aggravated by magnesium's high reactivity and the need to replenish depleted metallic ions. The most successful example of electroless plating technology for magnesium is the process developed by PMD (UK) that is capable of six regenerations, each with a 45-min turnover time following a strict replenishment schedule [44]. However, the rigid operating conditions necessary in order to obtain optimum electroless coatings from an aqueous deposition bath, especially on magnesium, pose a significant challenge to be overcome. Nevertheless, electroless plating does have the potential to produce uniform corrosion- and wear-resistant coatings with good electrical conductivity and solderability.

Other coatings that should be mentioned include conversion coatings, gas-phase coatings, organic coatings, and anodizing. Conversion coatings provide an alternative to metallic coatings and are able to coat complex shapes by removing and replacing the native oxides via a chemical or electrochemical process to create an insulating barrier of low solubility. Conversion treatments applied to magnesium alloys generally use (di)chromate, permanganate, fluoride, phosphate, tungstate, and vanadate-containing baths [45, 46], which provide limited corrosion resistance and thus are often used as pretreatments prior to the deposition of a metallic coating [47]. The serious environmental risk associated with hexavalent chromium [Cr^{6+}] leaching from coatings has led to the development of a number of chromate-free conversion coatings, including stannate, cerium, aluminum, zirconium, niobium, zinc phosphate, and phosphate permanganate conversion coatings [48–56]. However, at this time many are in the early stages of development and not proven for industrial purposes. Another alternative is the use of gas-phase coating processes and laser surface melting/alloying/cladding to modify the surface or create coatings on magnesium; however, the line-of-sight nature of the coating process makes it difficult to uniformly coat complex shapes or inside holes or deep recesses. Additionally, the corrosion, adhesion, and wear properties of these coatings on magnesium have not yet been widely documented. Organic coatings provide an extremely versatile coating method that can be applied to many metals, provided an appropriate pretreatment can be developed for the substrate, as the adhesion and corrosion resistances of these coatings are otherwise inadequate. The coatings are best utilized to provide a purely decorative effect or to enhance the corrosion resistance and wear resistance of a prior coating system; however, multiple layers must be applied due to difficulties in obtaining perfectly uniform, pore-free coatings. Again, the adhesion and corrosion wear resistances of these coatings have not been widely documented. Currently, the most widely used commercial technology to coat magnesium and its alloys are anodizing treatments [57–59] as it is less sensitive to the type of alloy being coated. Anodizing treatments form porous ceramic-like coatings by setting the substrate as the anode within a coating bath

rather than the cathode, as in electroplating. The treatments result in good paint adhesion characteristics and excellent wear and abrasion resistance; however, the insulating, brittle, and porous coatings produced are not suitable for corrosion resistance without further sealing, not to mention load-bearing or conductive applications.

Despite the large number of coating technologies available for protecting magnesium and its alloys, there continues to be a lack of appropriate, robust protective coatings that can withstand harsh service conditions. Moreover, current coating schemes are complex and multilayered, incorporating many different technologies that must be conducted very carefully in order to achieve optimum results. It is for that reason that research has recently begun to focus on the potential of ionic liquids.

30.3 IONIC LIQUIDS

Ionic liquids (ILs) are electrically conductive liquids composed exclusively of ions. Although broadly speaking the term also includes all molten salts, such as sodium chloride (NaCl) and potassium nitrate (KNO_3), which become "ionic liquids" only at high temperatures, ionic liquids have come to be defined as salts with melting temperatures below the boiling point of water (100°C) so as to provide a distinction with classical molten salts. A further distinction within the category of ionic liquids may be made for those liquid at room temperature—room temperature ionic liquids (RTILs). Ionic liquids possess a number of interesting and advantageous characteristics, which vary depending on the individual liquid [60–62], suited to the purposes of electrochemistry. Unlike aqueous molecular electrolytes, ionic liquids have wide potential windows, some of which are in the realm of 6 V. Along with their good conductance, especially when compared to other nonaqueous solvents, ILs allow for the deposition of metals with large negative reduction potentials, such as aluminum [63, 64] or zinc [65], without the hindrance of poor current efficiencies or corrosion of the substrate or deposit. Ionic liquids are also nonvolatile, possessing high metal salt solubility and low vapor pressures, even at temperatures in excess of 300°C [66], with some being liquid down to temperatures of 175 K [67]. The nonaqueous nature of ILs provide a medium avoiding negative metal–water chemistry and are good solvents for a wide range of both inorganic and organic materials [60], while their overall stability allows for their use at a wide range of temperatures with relatively constant viscosity, which can remain similar to water, and conductivity even at elevated temperatures. Moreover, phenomena such as nucleation, surface diffusion, and crystallization associated with metal deposition can be accelerated when using ionic liquids [68].

The low melting point of ILs is a consequence of their formation from organic salts or mixtures consisting of at least one organic, generally bulky, asymmetric cationic component, such as 1-alkyl-3-methylimidazolium, 1-alkylpyridinium, and *N*-methyl-*N*-alkylpyrrolidinium, having low lattice energies [60], with the anionic component varying from simple halides to inorganic and large organics [68]. An additional feature regarding RTILs not regularly seen in higher temperature molten salts is the strong ion–ion interaction often observed [69]. The properties of specific ionic liquids are determined by, and vary depending on, the selection of the ionic constituents. For the electrodeposition of metals from ionic liquids, the size and structure of the cationic component affect physical properties of both the salt and ionic liquid, such as viscosity and conductivity, which in turn control the transport of metal ions to the electrode surface, as well as the structure of the deposit (double layer), due to adsorption of the cations on the electrode surface at the deposition potential [68]. Similarly, the anion, while also affecting the physical properties of the liquid, has a substantial effect upon stability and chemical reactivity by means of the coordination geometry around the metal ion, thereby affecting the reduction potential, reduction current, and nucleation during deposition [68].

As the anionic component of ILs is the most flexible, they are divided into two categories depending on whether the anion is discrete or complex. Discrete anion ILs are formed by the quaternization of an imidazole, pyridine, phosphine, or amine to produce the cationic component, followed by metathesis with a metal salt to exchange the desired anion [68]. This differs from the synthesis of complex anion ILs which are formed by the mixing of a quaternary ammonium halide ($NR_4^+F^-$, $NR_4^+Cl^-$) with a Lewis or Brønsted acid (electron pair acceptor or proton donor, respectively), generally with moderate heating. The complexing of the anion results in a decrease in the freezing point and delocalization of the charge forming a eutectic ionic liquid, otherwise known as a deep eutectic solvent (DES) [70]. Deep eutectic solvents are classified as ionic mixtures, not as ionic compounds such as discrete ILs, and can be split into their original components, rendering them significantly less toxic, recyclable, and occasionally biodegradable. Nevertheless, DESs share many of the tunable qualities of discrete ionic liquids, albeit there exists several differences such as a higher conductivity and wider liquid ranges without decomposition, experienced by discrete anions compared to their eutectic-based counterparts.

The equilibrium between the anion and the Lewis or Brønsted acid upon which eutectic ionic liquids are based follows the general formula $R_1R_2R_3R_4N^+$ X zY, where $R_1R_2R_3R_4N^+$ is some quaternary ammonium cation, X is generally some halide anion, Y is the Lewis or Brønsted acid, and z is the number of Y molecules which complex X. Furthermore, eutectic ionic liquids may be characterized into three types depending on the complexing agent used (Table 30.1) [68].

TABLE 30.1 Types of Eutectic ILs Based on Complexing Agent Y

Eutectic type 1	$Y = MCl_x$	M = Zn, Sn, Fe, Al, Ge, Ga
Eutectic type 2	$Y = MCl_x{\cdot}yH_2O$	M = Cr, Co, Cu, Ni, Fe
Eutectic type 3	Y = RZ	$Z = CONH_2$, COOH, OH

One should note that only certain metals (M) and alloys thereof [70] may be deposited from certain eutectic ionic liquids and type 2 eutectics, although little is known of the systems, were developed to extend the range of metals that could be included in ionic liquids [71]. Thus far, the electrochemistry, physical properties, and speciation of type 1 and 2 eutectics have been reported for a variety of metals, while studies have only begun type 3 eutectics, which use hydrogen bond donors as the complexing agents [70]. The concentration of metal ions in type 1 and 2 eutectics is interlinked with all of the physical properties of the liquid since the metal salt is the anionic component of the liquid. For example, the Lewis acidity of an $AlCl_3$–organic salt IL depends on the relative molar composition of the mixture with Lewis acidic mixtures formed from excess $AlCl_3$, Lewis basic mixture formed from excess organic salt, and neutral liquids formed with a 1 : 1 molar ratio requiring NaCl as a buffer [72]. Additionally, type 2 eutectics are extremely sensitive, although stable, to water content, and consequently temperature, due to their hydrophilic nature absorbing water from the atmosphere. A major benefit of ionic liquids for electroplating, more prevalent in eutectic-based liquids, is that all pure metals have been found to anodically dissolve in the proper ionic liquid, including Pt, Au, and Ti, which can dissolve in eutectic-based liquids, providing consumable electrodes limiting the overpotential [68]. When using eutectic ionic liquids for electroplating, the heat capacity of the liquid must be considered as lower conductivity may generate ohmic heating when significant currents are passed through the liquid [68].

The first generation of ionic liquids, formerly known as room temperature molten salts, were based on chloroaluminates in combination with organic halides, such as the type 1 eutectic aluminum chloride–1-ethyl-3-methylimidazolium chloride ($AlCl_3$–EMIC), and possessed the major disadvantage of being hygroscopic with an extreme sensitivity to moisture, requiring handling under a controlled inert gas atmosphere, in addition to being rather corrosive [72]. Second- and third-generation air- and water-stable ionic liquids, such as the type 1 zinc chloride–EMIC [73, 74] and type 3 choline chloride–ethylene glycol (ChCl:2EG) eutectic mixtures [72], do not require the special environments, generally dry nitrogen or argon, of their predecessors. Nevertheless, air/water stable ionic liquids do possess the disadvantage of not being suited for the electrodeposition of reactive metals such as aluminum, which is the primary reason for the continued use of first-generation ionic liquids (Table 30.2).

The wide potential windows and oxidation/reduction, or redox, limits of ionic liquids are dependent on the stability of the anion and cation. Most quaternary ammonium cations have relatively similar reduction potentials, with the water content within the ionic liquids able to significantly affect the breadth of potential windows. The presence of water has been found to decrease the potential window of discrete anion ILs as water molecules aggregate, making hydrogen evolution easier at the electrode surface [68]. Although eutectic ionic liquids are overall considerably less susceptible to the addition of water than discrete ionic liquids, type 1 eutectics, specifically chloroaluminate systems, retain an instability and sensitivity to water. Conversely, type 3 eutectics, although possessing significantly smaller potential windows compared to some imidazolium-based liquids with discrete anions, are significantly less sensitive to water and retain windows sufficiently wide to allow the electrodeposition of metals such as zinc and nickel with rather high current efficiencies [72]. Additionally, the hydration of water positively affects the stability and fluidity of type 2 eutectics as the water does not behave as a bulk and the potential window is limited by the reduction of the metal, as seen in the case of chromium [68], with evidence suggesting that redox potentials of metals within type 2 eutectics are related to the coordination geometry of the metal center. There have been some suggestions that the presence of small amounts of water is actually beneficial to the deposit morphology in eutectic ILs, as water in some cases may act as both a ligand and viscosity improver, including type 1 eutectics, which have

TABLE 30.2 Examples of Metals Electrodeposited from ILs [68]

Discrete anions	BF_4^- PF_6^- $(F_3CSO_2)_2N^-$	Cd, Cu, Sb, In, Sn, Pd/In, Pd, Au, Ag, Pd/Au, In/Sb Cd/Te, Pd/Ag Ag, Ge
		Li, Mg, Ti, Al, Si, Ta, La, Sm, Cu, Co, Eu, Ag, Cs, Ga, Ga/As, In/Sb, Sn, Nb/Sn
Type 1 eutectics	$AlCl_3$	Al, Fe, Co, Ni, Cu, Zn, Ga, Pd, Au, Ag, Cd, In, Sn, Sb, Te, Ti, Cr, Hg, Na, Li, Tl, La, GaAs, Pb, Bi
		Al alloys with: Ag, Fe, Mg, Mn, Ni, Cu, Co, Sr, Ti, Cr, Nb, Nd, La
	$ZnCl_2$	Zn, Sn, Zn/Sn, Zn/Fe, Zn/Pt, Zn/Co, Cd, Zn/Cd, Zn/Cu, Zn/Te, Zn/Ni, Zn/Co/Dy
Type 2 eutectics	$CrCl_3{\cdot}6H_2O$	Cr
Type 3 eutectics	Urea Ethylene glycol	Zn, Sn, Zn/Sn, Cu, Zn/Pb, Ag
		Zn, Sn, Zn/Sn

shown some tolerance to water [75, 76], though the extent has yet to be quantified. Nevertheless, for type 1 and 2 eutectics, the negative limit of the potential window is, in general, related to the reduction of the metal and thus the relative proportions of metal and quaternary ammonium salts; the more Lewis acidic the metal halide, the more negative is its reduction potential [68].

30.4 IONIC LIQUIDS AND SURFACE TREATMENTS

In the critical step of precleaning/treatment, ionic liquids have the potential to provide an environment able to remove the insulating oxide/hydroxide layer. Among the numerous methods studied, the best adhesion thus far has resulted from degreasing in a chlorinated solvent followed by an aqueous pickle, rinse, dry, and anodic etching in the ionic liquid to remove the oxide film, which is made easier by the presence of a metal that is a good oxygen scavenger, prior to deposition [68]. It should be noted that in using this scheme anodic etch potentials and times are dependent on both the substrate and the ionic liquid. Additionally, metal substrates having large negative electrode potentials such as aluminum (Al) and magnesium (Mg) require larger anodic pulses over a longer period to remove the oxide [68]. The surfaces pretreated using ionic liquids differ from aqueous pretreatments in that they must be dry before exposure to the plating solution, which may pose a problem for reactive, rapidly oxidizing metals. Another pretreatment option lies in the replacement of the oxide/hydroxide layer either as a companion for, or substitute to, further deposition. The continued research into batteries, especially lithium batteries [77, 78], has produced several new insights into the potential of ionic liquids, including their use as a surface conversion treatment on magnesium [79–81], and research into the lubrication properties of ionic liquids in wear minimization have found that the same ILs are also able to produce beneficial tribological surface layers, in part due to their dipolar structure, in aluminum–steel interfaces [82–85].

For the purposes of corrosion protection, metal thin films are most desired as they provide more robust protection than surface conversion coatings, offering wear and corrosion resistances. Among coating options aluminum and zinc thin films are perhaps the most desired as they resist both pitting and overall corrosion while remaining quite cost effective. Furthermore, both aluminum and zinc coexist more peacefully with magnesium than most other metals, as seen by their inclusion in many magnesium alloys, including AZ91D (8.3–9.7 wt % Al, 0.35–1.0 wt % Zn), AZ31 (nominally 3 wt % Al, 1 wt % Zn), AM60 (5.5–6.5 wt % Al), and ZE41 (3.5–5.0 wt % Zn), to name a few. The wide potential windows inherent within ionic liquid systems give rise to the possibility of less complicated schemes for electroless deposition, specifically allowing the possibility of electroless deposition of such metals as zinc, which traditionally required the codeposition of nickel in aqueous baths [39, 40]. The wide potential windows are also of particular use in the electrodeposition of alloys, not previously possible within aqueous media. Therefore, the possibility exists for the deposition of aluminum alloys, which had been difficult given the difference in reduction potentials between aluminum and most alloying metals. Thus far, the majority of the ionic liquids studied have been nitrogen based, with imidazolium-based cations favored due to their potential window breadth, superior fluidity, and conductivity [86, 87]. Furthermore, studies pertaining to the deposition of metallic thin films have focused on electroplating, while electroless deposition has yet to be extensively investigated. Nevertheless, the ineffectiveness of electroplating to evenly coat complex shapes, due to uneven distribution of the current density within the plating bath, remains. Hence, research into electroless methods provides valuable alternatives for industries where complex surfaces must be coated.

Given that by some estimates there exists more than 10^{18} ionic liquids [88], and that of those presently being utilized few have been characterised based on their air and water stability [87] or their toxicity [89], it is impossible to delineate the intricacies of even the most commonly used ionic liquids. For further reading, a number of excellent in-depth reviews exist focusing on the topic of ionic liquids including their properties [61, 62, 73], use in electrochemistry [64, 65, 90–93], and electrodeposition of metals [68, 72]. The goal of this chapter is to highlight the potential use of ionic liquids in the coating of magnesium and its alloys as well as review and summarize some of the recent studies conducted for that purpose. Specifically, the chapter will focus on the use of ionic liquids as surface conversion treatments and electrolytes for both electro- and electroless metal deposition.

30.5 SURFACE CONVERSION TREATMENTS

In addition to ionic liquids showing excellent potential as electrolytes for metallic deposition, on account of their high conductivity and purity, some ionic liquids may also provide excellent pretreatments for the deposition of successive layers. The tri(hexyl)tetradecyl phosphonium cation ($P^{+}_{6,6,6,14}$) has been shown to possess several desirable qualities including stability at potentials between -3.2 and $+2.6$ V (vs. Fc/Fc$+$), higher thermal stability compared to nitrogen-based ionic liquids [62], and a lack of reactivity with magnesium alloys [79, 80], making it a good, though by no means only, choice for ionic liquid treatments of magnesium [94]. The latter of these features allows for the reactivity of the ionic liquid solution to be primarily dependant on the choice of anion. In cases where no metal ions are present, the exact role of the cation is unknown; however, it is clear that the choice of

cation continues to impact the viscosity and should be selected such that it does not disadvantage the chemical processes at work. Recently, several studies have shown that an ionic liquid containing no metal salt applied to a reactive metallic substrate may result in the formation of a corrosion-resistant thin film by what amounts to a complexation of the underlying substrate.

30.5.1 Fluoride Conversion Treatment [Bis(trifluoromethanesulfonyl)amide (TFSA) Anion]

Studies by Howlett, MacFarlane, Forsyth, et al. [79–81] have demonstrated that the bis(trifluoromethanesulfonyl)amide anion [$(Tf)_2N^-$-(II) or $(CF_3SO_2)_2N^-$] can react with reactive metallic substrates, such as lithium [77, 78], to provide electrochemically desirable surface layers. Although normally stable to reduction, the TFSA anion is prone to reductive decomposition of approximately -2.0 V (vs. Fc/Fc+), particularly in the presence of water and/or O_2 [95], well before the reported cathodic limit of many ionic liquids, leading to the formation of LiF on the metallic surface along with other fluorine-containing species [77, 78, 95]. Some uncertainty in the reductive decomposition potential stems from the processes being dependent upon the electrode substrate and is influenced by the water content of the IL. [95] Combining the TFSA anion with the tri(hexyl)tetradecyl phosphonium cation provides a unique film-forming environment where one ionic component is reactive and present at high concentrations (50 mol %) without interference from superfluous solvent molecules [79]. Furthermore, treatments using the $P_{6,6,6,14}$TFSA IL are able to be conducted open to the atmosphere at room temperature due to the hydrophobic nature of the IL, which allows for only about 1% water content under experimental conditions [80]. This atmospheric stability is important as some ionic liquids, such as those containing anions such as BF_4^- and PF_6^-, although stable to reduction, are prone to slow hydrolysis by water, yielding HF, and the potential window of most imidazolium-based ILs decrease with atmospheric exposure [68]. Additionally, the $P_{6,6,6,14}$TFSA IL is not a proton donor and has an exceedingly weak tendency to act as a proton acceptor and hence can be thought of as "neutral" in acid–base terms [80].

In a study on the conversion of an AZ31 Mg alloy substrate [79], initial trials showed that the tri(hexyl)tetradecyl phosphonium cation in combination with the TFSA anion ($P_{6,6,6,14}{}^+TFSA^-$) provided superior protection, as observed by weight loss and electrochemical measurements, than either 1-ethyl-3-methyl imidazolium or *N*-methyl-*N*-propylpyrrolidinium TFSA ILs while also being significantly more viscous [80]. Exposure of the AZ31 samples to the $P_{6,6,6,14}{}^+TFSA^-$ IL produced a good deal of corrosion and pitting resistance against a Cl^--containing environment, shifting the open-circuit potential (OCP) to more noble potentials by more than 500 mV and reducing the corrosion current densities, in an aqueous 0.1 M NaCl environment, by 50 times compared to an untreated sample [79]. This improvement factor of 50 times for the corrosion resistance is by no means the best or most robust protection available; however, certain benefits exist beyond the corrosion resistance. One prominent benefit of the coating is its apparent self-healing behavior, observed by the reverse scan of the corrosion current densities with the OCP returning to almost identical values as for the initial scan. The self-healing, not observed with control samples where the high corrosion rate prevented a return scan, occurred after a breakdown in the coating, indicated by a decrease in the size of the electrochemical impedance spectroscopy (EIS) arc and negative potential shift in the OCP data. The repair was seen by a subsequent increase and regained stability in the EIS data and a return to the original trend of a steady rise in the OCP. The self-healing characteristics were observed only on those samples which possessed a good continuous coating that masked the morphology of the underlying sample, having a relatively smoother surface with occasional defects similar to those seen in electroless thin-film experiments. Overly thick, nonuniform, and highly cracked coatings underwent rapid breakdown and pitting, showing no protection relative to an untreated sample, despite very high initial corrosion resistance. This demonstrates that a critical point exists where film thickness increases and begins to be ineffective for the purpose of corrosion protection. Unfortunately, the treatment times listed vary greatly to show the extremes of no coating and overcoating alongside a well-coated sample. To that effect, the exact thickness, and thus at the critical point where the film becomes less effective, remains unknown, but it is logical to assume it is in the 100-nm-thick range comparable to other ionic liquid thin-film experiments [80, 96]. Additionally, no information is provided regarding the quality of the corrosion resistance following successive self-repair or whether self-repair requires corrosive environments and would be able to repair mechanical damage in a dry environment where oxidation of the underlying substrate may supersede the self-repairing anodic reaction to coat the sample with a reactive oxide/hydroxide layer. Nevertheless, the process does benefit from ease of preparation, as the sample requires no pretreatment outside of traditional cleaning/degreasing, with trials able to be conducted open to the atmosphere at room temperature while remaining highly reproducible, and in most cases identical, across multiple sites and samples.

The deposit structure, as revealed by X-ray photoelectron spectroscopy (XPS) and time-of-flight secondary ion mass spectrometry (ToF-SIMS) etching experiments, was bilayered, similar to those reported for lithium metal in a TFSA-based IL (Fig. 30.1) [78], where the dense and adherent film had implications for charge transfer of Li in battery applications. In the case of lithium, exposure to *N*-methyl-*N*-alkylpyrrolidinium bis(trifluoromethanesulfonyl)

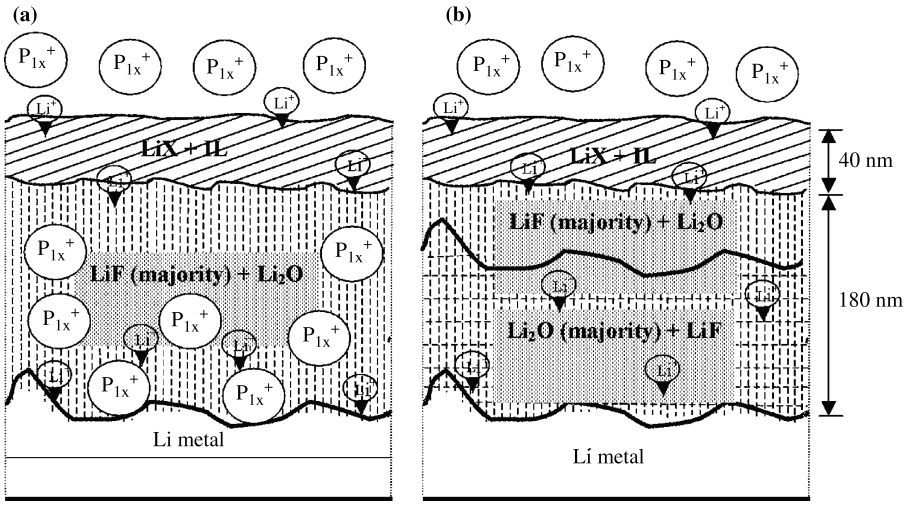

FIGURE 30.1 Simple models of the solid electrolyte interphase structure on (*a*) Li and (*b*) Li–Cu surfaces: LiX–X can be S_2O_4, F, SO_3CF_3, NSO_2CF_3, SO_3, CO_3, S, O, or OH [78].

amide [$(P_{1,x})(Tf_2N)$] resulted in a film consisting of an inner compact layer of primarily LiF and an outer more diffuse layer of various reduction products of the TFSA anion, such as LiS_2O_4, $LiSO_3CF_3$, Li_2SO_3, and Li_2S [77, 78]. For the AZ31 alloy, spectroscopic examination of the surface revealed the film was principally constructed of metal fluorides, likely MgF_2 and some AlF_3, as well as other organic species, with energy dispersive X-ray spectroscopy (EDXS) confirming the presence of F, C, P, and S elements within the film. It is the conclusion of the authors [79] that the self-healing mechanism is the result of some anodic dissolution forming an insoluble product from the available reservoir of organic species provided by the outer layer to repair damage to the inner predominantly MgF_2 surface.

The result of a subsequent series of trials investigating the interaction of 99.99% pure Mg with $P_{6,6,6,14}$TFSA IL [80] produced markedly different results in the quality of coating. Although the formation of coatings occurred, the immersion times to produce a well-adhered, continuous, corrosion-resistant film significantly differ, with the study revealing that exposure times of more than 1 h appear to be detrimental to coating quality. Macroscopic visual examination of the samples revealed that the coatings obtained following a 24-h treatment were discontinuous, showing evidence of uncoated regions, whereas the coating from 1-h treatments appeared to have more uniform coverage. High-resolution scanning electron microscopy (SEM) analysis echoed the uniformity of the surface film after a 1-h treatment, with higher magnification revealing a surface film free of cracking or major defects and containing nonperforating pin holes, or divots, about 10 nm in diameter. Additionally, the inability to collect backscattered electron diffraction pattern (EBSD) data from the sample surface indicated that either the film does not have a well-ordered crystalline structure or the film is multilayered, or ordered in a manner such that diffraction pattern collection is frustrated; given the results of other studies [77–79] a multilayered surface is likely the cause. A carefully ion milled cavity in the coated 1-h pretreated specimen revealed the presence of a well-adhered surface film at a thickness of about 87 nm and confirmed that the pin holes did not penetrate to the substrate. The EDXS spectrum collected on the film revealed the presence of organic elements P, S, O, and C within the coating; however, EDXS was not able to quantitatively detect the presence of F. The film morphology after the 2-h treatment resulted in small submicrometer-level defects, ~100 nm diameter, penetrating to the substrate; this worsened after the 24-h treatment with a significant proportion of the coating being discontinuous with large and abundant coating defects ranging from 10 nm to many micrometers in diameter. The defects also included the formation of white patches of what was thought to be hydrated $Mg(OH)_2$ products formed as a result of reaction with residual water in the IL.

The corrosion resistance of a 1-h IL-treated sample after 30 min exposure to a 0.1 *M* NaCl solution was quite good showing little if any corrosion. Signs of local corrosion did however begin to show after 4 h, with large-scale corrosion attack following around 8 h postimmersion, well later than untreated samples, which showed heavy corrosion attack after 4 h. Impedance testing, to determine the continuous time-dependent behavior of the samples within the 0.1 *M* NaCl solution, showed good agreement with macroscopic observations with the impedance of the coated sample, two to three orders of magnitude larger than the uncoated control, dropping from a relatively constant value after 8 h immersion. Potentiodynamic polarization curves collected for uncoated, 1-h, and 24-h treated samples in quiescent 0.1 *M* NaCl were taken to observe differences in the electrochemical response of the coatings. The response of the uncoated sample was a very negative ($<-1.8V_{SCE}$) corrosion, or electrochemical,

potential sustaining large current densities following the commencement of anodic polarization on the forward scan. The 1-h treated sample showed an increase in the corrosion potential to around $-1.5V_{SCE}$ with a distinct breakdown potential seen upon anodic polarization on the forward scan around $-1.45V_{SCE}$ where the current rises rapidly postbreakdown. This breakdown is also visible for the 24-h treated sample around the same potential and the corrosion potential falls between that of the 1-h and uncoated samples at around $-1.63V_{SCE}$, indicating a discontinuous coating, in line with the optical observations. Similarities in the reverse scan of the three samples suggest that following breakdown of the film on coated samples the protective properties are lost and the sample behavior returns to that of an uncoated specimen. The authors acknowledge that this behavior lies in contradiction to their work on the AZ31 alloy using the same ionic liquid [79] and that this suggests that the presence of Al in the AZ31 alloy may have impacted positively on the repassivation behavior of the alloy.

Given that the makeup of the alloy affects the quality of the coating, similar to most current treatment methods, a recent study [81] contrasted results of previous work with both AZ31 [79] and $Mg_{(99.99\%)}$ [80] with results garnered from exposing samples of ZE41 Mg alloy to the $P_{6,6,6,14}$TFSA IL, suggesting a mechanism for the formation of the thin film for this IL substrate pair. As in the cases of Mg and AZ31, the ZE41 surface showed no change in appearance following exposure to the ionic liquid; however, unlike those cases, where samples subjected to "long-term" exposure led to thick deposits, visible via SEM analysis, SEM analysis of the ZE41 substrate showed no features indicative of film formation [81]. Conversely, EIS obtained during a 24-h treatment of the ZE41 coupon revealed rapid buildup of a resistive component on the surface, during which time the OCP showed extensive noise, indicative of an ongoing electrochemical process likely occurring on the surface, both indicating likely film formation. The contradiction between the EIS and OCP data and the optical microscopy and SEM measurements can only be resolved by considering that the film on the AZ31 alloy was very thin after 24 h and the film on ZE41 may be below the detection limits of the techniques used—something that would be possible for a thin MgF_2 film.

Three possible mechanisms leading to the film formation suggested by study [81] are (1) anion adsorption onto the metal (or metal oxide) surface flowed by an electrostatic interaction with the cation to ensure charge neutrality, resulting in the formation of a double layer on the substrate; (2) chemical interaction of the anion with the metal ions formed from surface corrosion in the IL solvent; and (3) electrochemical breakdown of the anion and/or cation to form new chemical species which interacts with the surface via chemical adsorption or the formation of insoluble surface films with Mg^{2+} or other metallic ion species. It should be noted that in speaking of highly electronegative metals such as Mg, the third process would be reductive as Mg has a standard electrode potential (E_0) less than -2.7 V versus the saturated hydrogen electrode (SHE).

Of the three mechanisms for an ionic liquid interacting with a metallic surface, the third process is posited, in part, due to characterization of the AZ31 Mg alloy using XPS and ToF-SIMS indicating the presence of free fluoride [F^-] [97] and the fact that the TFSA anion is known to decompose at reductive potentials, leading to the formation of fluorine-containing species [95]. The adsorption mechanism was discounted by multinuclear solid-state nuclear magnetic resonance (NMR) spectroscopy examining the reactivity of the IL with naturally occurring oxide/hydroxide compounds found on the surface, such as Al_2O_3, MgO, ZrO_2, and $Mg(OH)_2$, determining the likelihood of film formation by means of adsorption. The subtle changes present in the $(Tf)_2N^-$ anion spectrum, as shown by ^{19}F NMR data, provided no evidence of chemical breakdown or hydrolysis of the species in the IL, removing the possibility that the phosphonium cation formed P–O–M bonds on the surface of oxides, where M is the metal ion in the oxide or hydroxide. Additionally, the paper does note that the lack of adsorption mechanism is a bit surprising given that the spectra observed for the IL adsorbed onto SiO_2 established a significant interaction with the TFSA anion [98]. Nevertheless, the observations, consistent with the optical and SEM images, indicated no preferential interaction between the TFSA-based IL and the ZE41 surface. The mechanism of chemical interaction with the metal ions forming due to surface corrosion can also be discounted as no change was observed in the morphology of the sample with no indications of corrosion.

The determination of electrochemical decomposition as the dominant mechanism in the formation of the surface film was accomplished via NMR characterization of the interphase region to identify the presence of chemical species differing from those of the pure IL—a method suggested for surface films on lithium metal [95]. The ^{19}F NMR spectrum of the interphase region formed by a 24-h immersion in the ionic liquid differed from both the pure ionic liquid and the ionic liquid adsorbed onto oxide surfaces, again supporting the report of a bilayer structure previously observed [77–79]. Furthermore, a broad peak in the NMR spectrum at -120 ppm reflects a breakdown of the TFSA anion to smaller units, possibly SO_3CF_2, CF_2, or F^- species, where the fluorine ion may form metal fluorides that then deposit onto the metal surface. Given the reductive decomposition expected from this IL substrate pair, the authors suggest a pathway from Aurbach [99] dealing with reactive lithium metal surfaces. They suggest decomposition begins with the reduction of the anion $[N(SO_2CF_3)_2^-]$ forming $SO_2CF_3^-$ and a reactive radical species, $NSO_2CF_3^-$, which further breaks down to form the CF_2^- or F^--containing species detected on the ZE41 surface.

30.5.2 Phosphate Conversion Treatment

Aside from fluorination conversion treatments, it is generally accepted that phosphate and phosphinate conversion treatments also provide good corrosion resistance. An investigation of the synthesis, physical characterization, and protective film-forming ability of six tri(hexyl)tetradecyl phosphonium cation ionic liquids using $P(O)_2(OR)_2^-$ and $P(O)_2(R)_2^-$ anion groups [96] found that most offered the ZE41 magnesium alloy some degree of protection, with the notable exception of the dibutylphosphate anion IL, which showed both greater surface corrosion and greater pitting than the untreated control after both room temperature and 50°C treatments. Based on the total corrosion (both surface and pitting corrosion) of the sample, the 10-min, 50°C treatments appeared to offer greater protection than those preformed at room temperature for 1 h. The enhanced corrosion resistance of the samples treated above room temperature is useful for the future development of procedures; however, the lack of information provided for the corrosion resistance of samples treated for 20 h at room temperature does present some ambiguity regarding the effectiveness of room temperature trials. The ionic liquids providing the best corrosion resistance were those showing no sign of impurities as detected by electrospray mass spectroscopy, namely those constructed with the diphenylphosphate, diisobutyldithiophosphinate, and bis(2-ethyl hexyl) phosphate anions. The optimum IL, out of those synthesized and tested, was formed using the diphenylphosphate (DPP) anion and produced a ~100-nm-thick film after the treatment at 50°C for 10 min. Both the surface corrosion and corrosion depth of this sample significantly decreased relative to the control, 12% at 174 μm versus 17% at >1430 μm, respectively, resulting in a considerable reduction of the roughness of the surface against an untreated sample when subject to a environment containing 0.1 *M* NaCl. Other properties of the $P_{6,6,6,14}$DPP IL, aside from providing corrosion protection, include a reductive limit at −2.5 V (vs. Fc/Fc+) somewhat less than the typical limits observed for analogous quaternary ammonium compounds [100] and an oxidative behavior characterised by two strong irreversible oxidation peaks at 1.4 and 2.0 V (vs. Fc/Fc+) on the first cycle. The suppression of the peaks in subsequent cycles is indicative of passivation of the electrode surface, likely arising from oxidation of the anion to produce an insoluble neutral species on the electrode. The passivation effect is yet another avenue to render an underlying substrate passive to material present in a subsequent deposition bath [80, 101]. Moreover, although the diisobutyldithiophosphinate anion IL was the most conductive and viscous of the ILs tested, both its surface and pitting corrosion protection lagged behind the two other impurity-free ionic liquids, reaffirming that high purity is a major factor in the creation of corrosion-resistant films.

A study on the role of mechanical versus electropolishing [102] on film formation using the $P_{6,6,6,14}$DPP IL on ZE41 Mg alloy substrate found that samples electropolished at 1 V for 20 s at room temperature in an electrolyte consisting of ethanol and orthophosphoric acid offered better corrosion resistance, as measured using EIS spectra in a 0.1 *M* NaCl aqueous solution, than those mechanically polished and finished with 0.3 μm Al_2O_3 slurry in deionized water both before and after 1 h exposure to the $P_{6,6,6,14}$DPP IL. Although the mechanically polished substrate maintained a relatively constant impedance of around 1300 Ω, the electropolished sample initially provided a much greater impedance of 2200 Ω after 15 h before decreasing to 1100 Ω, the value of the control electropolished sample. Although there exists a certain ambiguity regarding the breakdown of the electropolished coating, one might expect some surface reaction, possibly anodic, to be taking place, healing defects up until the coating is consumed, similar to the self-healing process observed on AZ31; however, this is only speculation. Optical micrographs of the samples taken after 4 h exposure to 0.1 *M* NaCl echoed the superiority of the treated electropolished surface as the surface was less corroded than the treated mechanically polished surface. Cross-sectional micrographs of the mechanically polished $P_{6,6,6,14}$DPP-treated samples showed pitting in the range of 20-μm, less than the 50-μm attack seen on the mechanically polished control, whereas no pitting was visible on the micrograph of the treated electropolished sample. Therefore, the paper [102] suggests that mechanical polishing creates a significant number of surface defect on both the metal substrate and the oxide film, potentially reducing the resistance of the surface. Conversely, while electropolishing may be superior due to a modification or replacement of the native film during the polishing process passivating the alloy surface.

A study on the mechanism of film formation for the $P_{6,6,6,14}$DPP IL ZE41 Mg alloy pair [81] revealed an increase in the resistivity of the surface film associated with increased exposure time, confirming interaction of the ionic liquid with the surface, as well as a heterogeneous surface morphology revealed by SEM after 24 h exposure to the IL, with significant thickening around but not on the grain boundary region. The heterogeneous reactivity of the ZE41 alloy, revealed by atomic force microscopy potential map studies of the metal surface [103], has been suggested to arise from the presence of zinc-rich intermetallics within the grain boundary and zirconium-rich intermetallics at the center of the grain. This arrangement heightens the reactivity in the center of the grains and results in the inhomogeneity in the reactivity and corrosion of the surface. Of the three mechanisms suggested to form protective conversion films, no electrochemical breakdown of any ionic component of the ionic liquid was observed, and no surface corrosion was visible during the exposure to the ionic liquid. As in the case of the $P_{6,6,6,14}$TFSA IL [81], the substantiation of the adsorption mechanism was carried out by means of NMR spectroscopy examining the reactivity of the IL with naturally occurring

oxide/hydroxide compounds that would be naturally found on the alloy surface. The conclusion drawn from the ^{31}P NMR data was that the phosphonium cation was principally unaffected by the presence of the inorganic surface, with strong interaction between the ionic liquid and surface occurring only where the surface contained hydroxide groups, such as $Mg(OH)_2$. To rule out any electrochemical decomposition of the ionic liquid, NMR characterization of the interphase region was conducted confirming the presence of both the cation and anion on the alloy surface, with the anion spectra being slightly shifted. The paper [81] concludes that the adsorption mechanism may be due to electrochemical reduction of the DPP anion prior to any film formation, resulting in the formation of a metal–ester bond and the slight shift in the phosphate resonance.

30.5.3 Overview

In many cases the ionic liquid treatments have been shown to result in the formation of well-adhered, continuous, relatively defect free, corrosion-resistant surface films ranging from nanometers to micrometers in thickness, provided the exposure time was kept below some characteristic time dependent on the IL–substrate pair, where defects begin to make the film discontinuous. Other factors influencing the quality of the film are analogous to known issues from other electrochemical film formation processes, including surface modifications such as surface polishing [102] the choice of ionic liquid in the IL–substrate pair, due to speciation of the Mg-based substrate as ionic liquids may not react in the same way differing alloys of the same base [79–81], and the role of the grain boundaries [103]. Advantages of these ionic treatments beyond the quality of the film include the ease of substrate preparation, the reproducibility of the results, and the ability to have the ionic liquid react with the substrate at room temperature open to the atmosphere, provided the humidity is not excessive. The investigation of similar ionic liquids, especially those using the $P_{6,6,6,14}$ cation [82] and TFSA anion [83], as lubricants for the sliding of steel on aluminum provides another source of information for potential surface conversions in a similar way to how insights have been garnered from the use of ILs as electrolytes in lithium battery experiments [77, 78]. Moreover, the documented superiority of certain ionic liquids compared to conventional hydrocarbon lubricants along with their thermal stability and dipolar bilayered crystal structure, enabling them to act in a way similar to solid lubricants like molybdenum disulfide [MoS_2] and graphite [82], will almost certainly aid in the reduction of future development costs allowing surface conversions to become industrially more appealing.

Although ionic liquid treatments do provide corrosion protection similar to other more standard treatments, the use of the treatments as pretreatments for deposition of a subsequent metallic layer has yet to be explored. In many ways, phosphonium treatments based on both the TFSA anion and the DPP anion appear to fulfill a role similar to that of conventional fluoride and phosphate–permanganate pretreatments for magnesium and its alloys, while affording superior corrosion resistance to the substrate than their aqueous treatment counterparts [38, 79, 80]. Most notably, the $P_{6,6,6,14}$TFSA IL shows significant promise as a pretreatment on the basis that it forms a relatively stable and continuous film comprised mainly of MgF_2. Traditional fluoride conditioning from an aqueous bath is known to be effective in the removal of oxides replacing them with a thin layer of MgF_2, and current methods of fluoride conditioning include the use of hydrofluoric acid (HF) and ammonium bifluoride, with the ammonium bifluoride providing for a much narrower plating window (pH 5.8–6.0 and temperature 75–77°C) than HF for acceptable adhesion [38]. Fluoride surface conversions are especially effective in the deposition of high-adherence zinc or nickel [38, 104] with fluoride being a good additive to aqueous nickel plating baths to inhibit corrosion of the substrate during plating [38, 105, 106]. As it is well known that insufficient conditioning can result in poor adhesion [38], the prospect of a guaranteed continuous layer is quite appealing as it could provide a good basis for the deposition of other layers as needed.

Overall, phosphonium ionic liquids (Fig. 30.2), especially when employing the TFSA anion, provide well-adhered, continuous surface film that does not seem prone to breakdown under normal conditions. This amounts to a promising first step in essentially making magnesium-based substrates passive to corrosion and capable of accepting the further deposition of other corrosion-resistant thin films. Other advantages of the phosphonium ionic liquids are that they provide an environment where only a single component, the anion, appears to react with magnesium-based substrates allowing for the characteristics of the film to be determined primarily on the choice of anion. Moreover, ionic liquid–based pretreatments may prove to be a less labor-intensive, more cost-effective, and environmentally friendly method of treating magnesium and its alloys. Nevertheless, surface conversion treatments in and of themselves will likely never provide the robust protection required for harsh operating conditions offered by the deposition of metallic layers.

30.6 METALLIC FILM DEPOSITION

The deposition of any metal on magnesium is complicated by the substrate's fierce reactivity and the formation of corrosive galvanic couples between it and other metals in the presence of aqueous solutions, necessitating the pursuit of nonaqueous media such as ionic liquids. Additionally, the high reactivity of aluminum (−1.67 V vs. SHE), an excellent metal for corrosion protection, requires deposition baths to be aprotic, prohibiting deposition from aqueous solutions and limiting

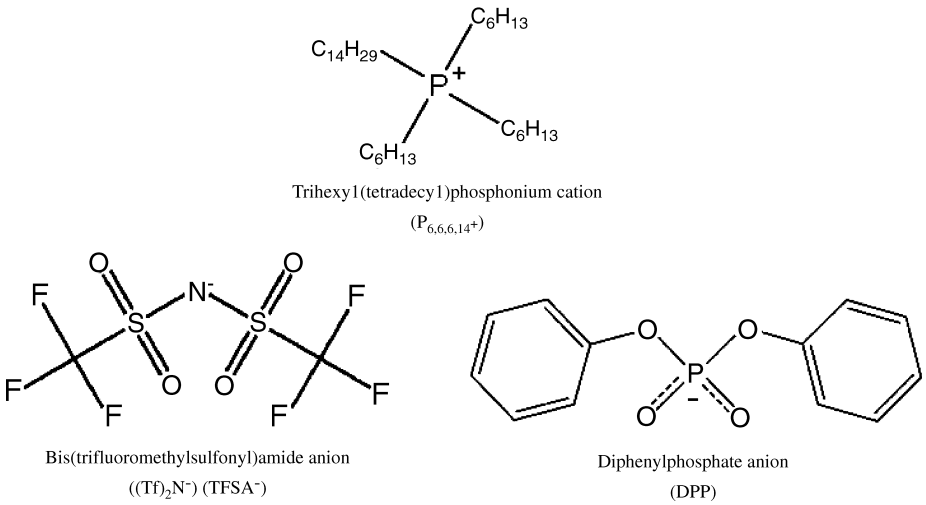

FIGURE 30.2 Ionic components of ILs used in conversion treatments [81].

deposition media to ionic liquids or organic solvents, the latter proving undesirable due to volatility concerns [72]. Other favorable qualities of aluminum coatings beyond effective corrosion protection include their light weight, ability to resist pitting, and ability to form Mg–Al intermetallic compounds between the film and substrate after proper heat treatment, which are confirmed to have good corrosion resistance [107, 108] and can aid with coating adhesion. Ionic liquids also allow for the deposition of zinc without the need of nickel codeposition or high pH for higher zinc concentration deposits required from aqueous solutions [39, 40]. Although there have yet to be any publications regarding electroless zinc from ionic liquid media, several papers exist on its electrodeposition [65, 109, 110]. Another notable benefit of both aluminum and zinc is that electroless deposition upon both substrates from aqueous solutions is well documented [111–113], allowing for the deposition of subsequent corrosion- and/or wear-resistant coatings.

The primary characteristics necessary to establish reasonable initial corrosion protection are continuous, pore-free, well-adhered coatings that disallow the formation of galvanic cells due to moisture between the magnesium-based substrate and the metallic coating. Selection of the metallic film deposition method, either electro- or electroless deposition, is dependent on the geometry and application of the substrate. While several excellent investigations and reviews exist on the use of ionic liquids in the deposition of metallic films, the focus remains on electroplating with little mention of electroless processes. Concerning magnesium-based substrates, electroplating from ionic liquids has been investigated [63, 114, 115], whereas no extensive investigation has been conducted regarding electroless deposition from ionic liquids specifically on magnesium and its alloys, albeit other substrates have received some attention [116–119]. Rather than reiterate work cited in previous electroplating books and reviews, the information presented here will focus on the aspects of the electroplating as they relate to magnesium and its alloys, taking into account the choice of bath, its reactivity with the substrate, and the quality of coatings to provide some insight for the development of electroless plating methods.

30.6.1 Electrodeposition

Although relatively new, ionic liquids have been shown to be capable of electro-depositing several metals such as aluminum, zinc, chrome, copper, iron, and nickel as well as various alloys including aluminum/chrome, zinc/tin, and copper/palladium. An excellent review by Abbott and McKenzie [68], summarizes and outlines the application of ionic liquids to the electrodeposition of metals, delineating the parameters within IL electrolytes along with providing many examples of studied systems. The appeal of ionic liquids for electroplating purposes lies largely in the fact that harsh environmentally unfriendly chemicals within deposition baths may be replaced by recyclable ionic electrolytes which often carry superior current efficiencies. For example, the Type 2 1:2-choline chloride/chrome(III) chloride hexahydrate [ChCl/$CrCl_3$ $6H_2O$] ionic liquid allows for the deposition of thick, adherent, crack-free chromium films, free of harmful CrO_3, hexavalent chromium compounds, used in traditional aqueous baths and a competing hydrogen evolution process that limits the current efficiency and leads to hydrogen embrittlement of the substrate [120].

It is only within the last few years, that studies have been published concerning the electroplating of magnesium and its alloys from ionic liquids. A set of papers by J.K. Chang, I.-W. Sun, et al. [63, 114, 121, 122] outline the electrodeposition of aluminum on the AZ91D magnesium using the first-generation type 1 eutectic ionic liquid $AlCl_3$–EMIC. The electrodeposition of aluminum can only be performed under the Lewis acidic conditions, $AlCl_3$– EMIC molar ratio

greater than 1, where the $Al_2Cl_7^-$ species, which is able to be electrochemically reduced to the metallic form [Eq. (30.1)] is in excess [123–126]:

$$4Al_2Cl_7^- + 3e^- \rightarrow 7AlCl_4^- + Al \qquad (30.1)$$

The handling of chemicals, sample preparation (grinding with 1000 grit SiC paper), synthesis of the Lewis acidic 1.5 : 1 molar ratio $AlCl_3$–EMIC ionic liquid, and deposition therein, were conducted in a glove box containing purified nitrogen atmosphere with moisture and oxygen content maintained below 1 ppm. The experiments were conducted passing a total charge of $50\,C\,cm^{-2}$, with a theoretical thickness of 17.3 μm expected, and OCP measurements of the bare AZ91D Mg alloy within the ionic liquid remained steady at around 0 V (vs Al), indicating stability of the alloy within the ionic liquid.

Surface morphologies, revealed by SEM micrographs of the coated samples, showed that deposition conducted at −0.2 V [63] possessed a crystal size in the range of around 5–10 μm with a faceted deposit layer appearing quite dense, uniformly covering the entire Mg alloy substrate regardless of underlying α (Mg solid solution) or β ($Mg_{17}Al_{12}$) substrate phases. The same sort of result was also found for current densities of −15 and $-20\,mA\,cm^{-2}$ [114] with the grain size increasing from around 5 to 10 μm with increasing current density. The similarity between deposits at −0.2 V and $-20\,mA\,cm^{-2}$ is expected as the current density, ignoring initial fluctuations from surface double-layer charging, for the −0.2-V deposition remained around $-20\,mA\,cm^{-2}$ and vice versa, essentially making one trial the inverse of the other. Similarly, SEM revealed a less compact deposit structure containing regular nodules, several small cracks, and a greater surface roughness for depositions conducted at −0.4 V [63] and $-40\,mA\,cm^{-2}$ [114]. This was attributed to the increasing current density for depositions conducted at a high deposition potential and falling deposition potential for depositions conducted with high current density away from the stable deposition potential/current density. Cross-sectional SEM analysis of the samples revealed a continuous, well-adhered, confirmed by tape tests 20-μm compact deposit, confirming good current efficiency. For current densities of $-20mA/cm^2$; while rough deposits, formed using a current density of $-40\,mA\,cm^{-2}$, were found to have uneven thicknesses.

Despite the agreement regarding the morphology of the deposit, there appears to be some ambiguity concerning purity. Both studies demonstrate the deposition of high-purity aluminum with the cathodic potential study [63] detecting no impurities in the deposited films by EDS, whereas the galvanostatic study [114] placed aluminum purity at 98 wt % with the EDS detection of impurities including carbon, oxygen, and chlorine within a 3500 s deposition at $-15\,mA\,cm^{-2}$. It is unclear whether the discrepancy is due to the method of deposition or whether the impurities are the result of the deposition time required to attain the total charge of $50\,C\,cm^{-2}$, which was under 2550 s for controlled potential samples [63], as outside contamination is unlikely within the glove box. What remains clear from all trials is that slower deposition at lower, stable, current densities produces smoother, more compact deposits resulting from a smaller grain sizes. XRD analysis of the deposits confirmed high deposit purity along with a clear face-centered-cubic (111) structure and preferred stacking orientation of the deposited aluminum (200) for the compact deposits, while analysis of the thinner and less compact deposits formed at high current densities did not fully suppress the signal from the substrate.

The detriment of the rough morphology brought about by high current densities was also readily seen in the corrosion testing of the samples. Open-circuit potentials taken in a 3.5 wt % NaCl solution revealed lower corrosion potentials associated with deposits formed using lower current densities. For the constant potential deposits, the −0.2-V deposit showed an OCP of −1.42 V, 100 mV less than the −0.4-V deposit and around 180 mV less than that measured for the bare alloy (∼−1.60 V). In the galvanostatic study, the $-15\text{-}mA\,cm^{-2}$ deposit showed an OCP of −1.40 V, 250 mV lower than the bare alloy (−1.65 V). Polarization resistances garnered from EIS data taken during OCP measurements were found to follow the same trend as the OCP data, with the deposits conducted at −15 and $-20\,mA\,cm^{-2}$ having resistances over 18 and 12 times, respectively, that of the bare alloy. The polarization curves, also measured in 3.5 wt % NaCl solution, echoed the results from the EIS and OCP data showing significant suppression of the corrosion rates, with the polarization curves revealing wide passive ranges of around 700 mV between 1.45 V and 0.75 V for constant potential and 1.40 V and 0.70 V for galvanostatic trials followed by a breakdown likely caused by pitting, a common occurrence for aluminum in a solution containing chlorides [127]. SEM analysis of a $-15\text{-}mA\,cm^{-2}$ deposit exposed to salt spray conditions for 8 hr [114] revealed no significant change in the granular structure of the aluminum coating aside from a fibrous product only observed at higher magnification, determined by EDS to be aluminum oxide.

In spite of the robustness of the resulting coatings and subsequent studies on the deposition from varying Lewis acidities [122], the atmospheric sensitivity of $AlCl_3$–EMIC baths due to their hygroscopic nature poses a limiting factor in their widespread use. Atmospherically stable ionic liquids that do not require a specialized atmosphere and are able to deposit aluminum such as 1-butyl-1-methylpyrrolidinium bis(trifluoromethylsulfonyl)amide (BMP Tf_2N), 1-ethyl-3-methylimidazolium bis(trifluoromethylsulfonyl)amide (EMI Tf_2N), and tri(hexyl)tetradecyl phosphonium bis(trifluoromethylsulfonyl)amide ($P_{6,6,6,14}Tf_2N$) are presently in development [72]; however, attempted depositions on magnesium or its alloys have yet to be undertaken and the reaction

of many ionic liquids, including $AlCl_3$–BMP-Tf_2N, with magnesium-based substrates remains unknown with initial characterization of their behavior having only just begun. Nevertheless, depositions using the atmospherically stable $AlCl_3$–BMP-Tf_2N IL have resulted in shiny, dense, adherent deposits with very fine crystallites in the nanometer range without the use of organic brighteners or pulsed plating techniques [72]. With limitations concerning the deposition of aluminum, zinc coatings, which may be deposited from atmospherically stable choline chloride–based ILs, provide an alternate means by which to protect magnesium substrates.

Work by Bakkar and Neubert [115] centered on the electrodeposition of zinc onto magnesium from five (four type 3 and one type 1) air- and water-stable choline chloride (ChCl)–based eutectic ionic liquids. Choline chloride–2 urea (ChCl:2urea), choline chloride–2 ethylene glycol (ChCl:2EG), choline chloride–2 glycerol (ChCl:2Gl), choline chloride–malonic acid (ChCl:Mal), and choline chloride–2 zinc chloride (ChCl:2$ZnCl_2$) ionic liquids were synthesized with the further addition of 0.5 *M* $ZnCl_2$ at 90°C to provide the metallic species, while electrochemical and water content measurements as well as deposition occurred at 60°C open to the air. Each specimen was ground with high-grain SiC paper and subjected to standard industrial pretreatment, including alkaline degreasing, acidic pickling, and activation, with subsequent deposition occurring on a number of alloys, including 99.99% pure Mg, AZ31, and AZ91, among others.

The result of electrochemical measurements concerning the critically important behavior of magnesium ($Mg_{99.99\%}$) within the various ionic liquid media determined the lowest corrosion rates occured in ChCl:2urea and ChCl:2Gl ILs with 3.5 and 2.7 wt % water content, respectively. Although their corrosion currents (I_{corr}) were found to be nearly identical, 0.48 and 0.49 $\mu A\,cm^{-2}$, respectively, the ChCl:2Gl IL was deemed unsuitable due to observed pitting of the magnesium surface, indicated by a sharp increase in the current density from a rise in the anodic polarization potential [115]. Additionally, comparing the corrosion currents of the $Mg_{99.99\%}$ obtained in the ChCl:2urea IL and a classic aqueous electrolyte [128] at 25°C (3711.17 $\mu A\,cm^{-2}$), the I_{corr} was found to be 7732 times lower in the ionic liquid than in the aqueous bath. Furthermore, the ionic liquid was also found to have an I_{corr} of almost 230 times less than that of low carbon steel, the most common successfully Zn-electroplated substrate, in the aqueous electrolyte, indicating excellent stability.

Electrodeposition from the ChCl:2urea + 0.5 *M* $ZnCl_2$ mixture by applying constant current densities resulted in dense, compact, adherent zinc deposits for only the rare earth–containing, aluminum-free, alloys WE43, QE22, MgGd5Sc1, and MgY4Sc1. Varying the applied current density significantly changed the morphology of the deposits with a current density of 5 $mA\,cm^{-2}$, producing dense deposited layers, while both lower (2.5 $mA\,cm^{-2}$) and higher (10 $mA\,cm^{-2}$) current densities produced porous deposits. The role of a common additive ethylenediaminetetraacetic acid (EDTA) was also explored at 10 $g\,L^{-1}$ within the 5-$mA\,cm^{-2}$ deposit on QE22 and was found to produce a finer microstructure, reducing the size of the zinc particles without altering their overall structure. No deposition appears to have been attempted from the ChCl/Mal IL, likely due to its high I_{corr} of 31.58 $\mu A\,cm^{-2}$, and depositions from the ChCl:2EG ($I_{corr} = 12.72\,\mu A\,cm^{-2}$) and ChCl:2$ZnCl_2$ ($I_{corr} = 3.86\,\mu A\,cm^{-2}$) ILs were unsuccessful, with no deposition occurring from the ChCl:2EG IL and the formation of a powdery dull surface layer comprised mainly of Mg oxide corrosion products rich in F and Cr from the chemical pretreatment was established in the ChCl:2$ZnCl_2$ IL.

Cross-sectional micrographs of the deposit on WE43 from ChCl:2urea IL + 0.5 *M* $ZnCl_2$ showed overall good adherence, with some microcracks observable at high magnification running perpendicular from the substrate up to half the total thickness of the deposit. These cracks were eliminated by means of a 2-s-on ($-5\,mA\,cm^{-2}$), 1-s-off (0.0 $mA\,cm^{-2}$) pulsed current producing a shinier, smoother, and more uniform deposit free of micro cracks in the bulk zinc layer, which was comprised of smaller grains due to an increase in the nucleation rate of the electrodeposited atoms at the expense of the growth rate. Content analysis on the deposits provided by EDX indicated the deposited zinc was largely free from impurities regardless of the type of applied current, either constant or pulsed, with a small oxygen peak attributed to atmospheric oxidation of the Zn surface along with a lesser peak for chloride, for which the mechanism leading to its presence was not determined. A comparison of the corrosion behavior of coated samples with that of their Mg alloy substrates and pure zinc, within a 0.1 *M* NaCl solution, found that samples deposited by means of a constant current possessed corrosion rates higher than the uncoated control substrates. The higher I_{corr} of the constant current occurred regardless of additives and was attributed to galvanic corrosion arising from microcracks present within those deposits. Conversely, coatings formed by pulsed current, such as that on WE43 ($I_{corr} = 1.38\,\mu A\,cm^{-2}$), were found to have corrosion current densities similar to that of zinc ($I_{corr} = 1.89\,\mu A\,cm^{-2}$); however, the corrosion protection of Mg alloys not containing Al is rather specific and not entirely practical for industrial applications.

In addition to the choice of ionic liquid, the temperature and water content of the liquid also influenced its interaction with magnesium-based substrates. Work concerning the interaction between the AZ91D Mg alloy and the 1-butyl-3-methylimidazolium bis(trifluoromethylsulfonyl)imide [C_4mim-Tf_2N] IL [129] ascertained that the slow corrosion rate increased with an increase in IL temperature and the alloy catalyzes the decomposition of the IL at lower temperatures. Furthermore, it was found that corrosion of the alloy forming

oxides and fluorides initiated the formation of a rather homogeneous interaction layer which stopped the extended corrosion process, under which alloy oxidation continues due to crevice corrosion, albeit at a much lower rate. One study by Shkurankov, El Abedin, and Endres [130] addressing the role of varying water content on the corrosion of magnesium and AZ91 alloys within the 1-butyl-3-methylimidazolium trifluoromethylsulfonate IL observed a lower corrosion potential and higher corrosion rate associated with increasing water content within the ionic liquid. Nevertheless, minimal water content alone does not guarantee the peaceful coexistence of magnesium substrates and ionic liquids as seen with ChCl:2Gl, which was shown to pit the surface of pure Mg during electrochemical testing [115]. Though a complete characterization of the behavior of magnesium in many nonaqueous environments is still missing, factors such as these are of particular importance for the further development of air and water stable ionic liquids for the coating of magnesium and its alloys and must not be overlooked.

Although ionic liquids have further increased the possibilities of electrodeposition with the deposition of alloys, as seen with the electrodeposition of zinc–tin alloys from ChCl:2urea and ChCl:2EG ILs [70], thereby limiting the advantage of alloy deposition through electroless methods on uniform surfaces, proper, even surface coverage is not attainable with electroplating on complex shapes due to the nonuniform current densities inherent in the process. Therefore, the pursuit of electroless processes remains necessary for the development of corrosion-resistant coatings suitable for industry.

30.6.2 Electroless Deposition

Electroless deposition from aqueous plating baths is perhaps most notably utilized in the electronics industry for the manufacture of printed circuit boards, where electroless silver is used to prevent degradation of exposed copper conduction tracks between manufacture and assembly of the finished device. Traditionally, aqueous electroless silver deposition utilizes $AgNO_3$ solutions in the presence of HNO_3, requiring colloidal catalysts such as palladium metal to sustain deposition beyond a few nanometers [131, 132]. In addition to the use of strong inorganic acids being of environmental concern, HNO_3 competitively etches the copper tracks during silver plating, which can result in component failures, especially as feature sizes become smaller, necessitating the development of alternative electroless deposition methods.

Two recent studies by Abbott, et al. [116, 117] describe the sustained galvanic coating of silver metal deposited on a copper substrate from a choline chloride (ChCl)–based eutectic ionic liquid without the use of catalysts. The papers focus on the use of a choline chloride–ethylene glycol type 3 eutectic ionic liquid (1ChCl:2EG) containing 10 m*M* AgCl as the room temperature plating bath and note that urea may also be used in place of ethylene glycol in the same ratio. While AgCl was the most convenient to handle, providing the most consistent results and producing adherent, bright silver finish, a range of silver salts, including $AgNO_3$, Ag_2SO_4, and $Ag(CH_3COO)$, may also be used in both ChCl-based ionic liquids, although they do not share the same qualitative appearance [116].

The silver immersion coatings occur due to the thermodynamics of Ag(I) [Ag^+] reduction and Cu(I) [Cu^+] dissolution driven by the difference in their respective redox potentials. Unlike in aqueous baths, where without a catalyst a thin silver coating quickly deactivates the copper surface, ionic liquid immersion coatings allow for thick silver deposits by allowing for the continuous diffusion of Cu^+ away from the substrate surface through pores and channels in the silver deposit. Hence, a rough surface morphology and sufficiently thick copper substrate allow for sustained silver deposition. The surface roughness was found to increase with time and temperature, thus increasing the rate of silver deposition, and estimates of deposit thickness from a 10 m*M* AgCl ChCl:2EG mixture after 5 min are placed between 500 and 900 nm, as there is a bit of a "trough" between the uncoated copper substrate and height of the silver deposit [116, 117]. The resulting silver deposits have been found to be thick, bright, and uniform, providing sufficient adhesion to prevent corrosion of the underlying Cu substrate, in addition to a decreased soldering temperature on printed circuit boards, due to its porous nature. Moreover, the electrolyte has also been found to be less sensitive to light while the absence of cyanide or strong inorganic acids make is less harmful to the environment.

Although the electroless deposition of silver is valuable to the electronics industry, due to its porosity, it is of little practical use for the formation of industrial corrosion-resistant coatings; therefore, many of the details surrounding electroless silver have been addressed here rather cursorily. It is however of note that the electroless deposition of silver from a eutectic solvent is presently being scaled up for industrial use [133], providing perhaps the first step in the widespread use of ionic liquid electrolytes. For the purpose of corrosion protection, the metallic layer must itself be continuous, corrosion resistant, as well as inexpensive for it to be industrially feasible.

A recent paper by Koura, Nagase, Sato, et al. [118] has reported the successful electroless deposition of aluminum from the first-generation, type 1 eutectic, room temperature ionic liquid $AlCl_3$–EMIC on both copper and glass substrates. The ionic liquid was synthesized by mixing a 2 : 1 molar ratio of $AlCl_3$ and EMIC followed by the treatment of the liquid with the immersion of an aluminum wire to reduce the water content by forming $Al(OH)_3$ on the wire surface and evolving H_2 [119]. Compatible reducing agents for the ionic liquid were provided by lithium hydride [LiH], lithium aluminum hydride [$LiAlH_4$], or diisobutyl aluminum

hydride (DIBAH) with focus on the use of LiH. The samples underwent standard degreasing procedures followed by catalytic activation using traditional sensitization (SnCl) and activation (PdCl) before deposition and the deposition within and synthesis of the ionic liquid were carried out in a dry argon-filled glove box, as is standard with first-generation ionic liquids. Despite some ambiguity concerning the preparation of the IL, including the temperature of the synthesis (EMIC is solid at room temperature) and the amount of wire utilized for the treatment of the $AlCl_3$–EMIC IL (the IL is deemed ready after it becomes colorless and transparent) measurements of coated samples seem to indicate good plating.

X-ray diffraction (XRD) measurements of catalytically activated glass substrates treated for 2 h at 35°C within $AlCl_3$–EMIC containing 1.0 mol L^{-1} of LiH reducing agent indicated the successful formation of an aluminum thin-film coating, with diffraction peaks of the film, and a lattice constant of 4.046 Å [118] educed thereof, in agreement with the literature (4.050 Å). Inductively coupled plasma (ICP) data indicated that the purity of the aluminum was more than 99% and SEM-EDX indicated that the pure aluminum was homogeneously distributed on the surface of the film. This conclusion is rather surprising as in electroless systems some "contamination" from the anodic reaction of the reducing agent is expected; however, the presence of Li^+ ions detected in the electrolyte after the plating would seem to corroborate the analytical evidence. The results of a depth profile carried out using glow discharge optical emission spectroscopy (GD-OES) on a copper substrate treated using $AlCl_3$–EMIC under the same parameters as the glass substrate indicated the deposit was free of impurity phases, such as C, Li, and H, that contaminated the electrolyte [118]. The lack of mention of the expectation of Sn or Pd within the deposit contributes to the ambiguity as to whether the copper substrate required catalytic treatment or whether polishing removal of the oxides was sufficient to catalyze the surface; given that the experiment was conducted in an oxygen-free environment, both are possible.

The paper [118] also investigated the impact of factors such as temperature (25, 35, and 45°C) and concentration of reducing agents (0.5, 1.0, and 2.0 mol L^{-1}) on the morphology and plating rate of the films. It was determined that thicker films were deposited with increased immersion times independent of the temperature and that particle size became larger with both longer exposure times and higher temperatures. As expected, higher temperatures resulted in increased deposition; however, this trend was only seen initially, approximately 30 min, as after 2 h the deposit was found to be 0.25 mg cm^{-2} at 45°C, while deposits at both 25 and 35°C were around 0.40 mg cm^{-2}. The paper suggests the smaller deposit is likely due to decomposition in the electrolyte at the elevated temperature in association with an increase in the reduction rate before maximum thickness was achieved. The amount and rate of deposition were also found to increase proportionally with an increase in the concentration of the reducing agent LiH; however, the source of a possible ceiling emerging in the amount of deposit of around 0.40 mg cm^{-2}, seen after 2 h for 0.5 and 1.0 mol L^{-1} concentrations of LiH, was not addressed. Additionally, it was determined that the DIBAH liquid reducing agent could be much better dispersed in the electrolyte than the solid reducing agents LiH or $LiAlH_4$ and resulted in a smoother surface film as revealed by SEM.

The formulation of a possible mechanism for the deposition of electroless aluminum is also included by analysis of the ionic liquid with Raman spectroscopy before and after deposition [118]. A growth in the peak for $AlCl_4^-$ and a decrease in the one for $Al_2Cl_7^-$ suggested that the deposition of aluminum occurred in the same way as during electroplating [Eq. (30.1)], while the reducing agent (LiH) which initiated the reaction followed [Eq. (30.1)] as Li^+ ions were detected in the electrolyte after the plating:

$$4Al_2Cl_7^- + 3e^- \rightarrow 7AlCl_4^- + Al \qquad (30.1)$$

$$LiH \rightarrow Li^+ + \tfrac{1}{2}H_2 + e^- \qquad (30.2)$$

The verification of the mechanism was accomplished by applying mixed potential theory [134] to the deposition. Polarization curves were achieved by measuring the cathodic reaction of $Al_2Cl_7^-$, from a 2 : 1 mol % $AlCl_3$–EMIC electrolyte, and the anodic reaction of LiH, from a 9 : 11 mol % $AlCl_3$–EMIC electrolyte with 1.0 mol L^{-1} LiH. The mixed potential determined was −0.130 V vs. Al(III)Al, close to the −0.125 V vs. Al(III)Al measured during the electroless plating; and the current density at the mixed potential was found to be 1.85 mA cm^{-2} [118]. Finally, the plating reaction rate derived from the mixed potential theory was 0.0101 mg cm^{-2} min^{-1}, again in good agreement with the plating rate estimated from the weight of aluminum deposit, 0.0099 mg cm^{-2} min^{-1}.

Follow-up work conducted by Shitanda, Sato, Itagaki, et al. [119] explored the effect of using a highly soluble liquid reducing agent, DIBAH, on the plating conditions, film composition, and reaction mechanism for the deposition of aluminum from a 2 : 1 $AlCl_3$–EMIC IL. The use of the liquid reducing agent not only allows for easier control of the plating bath but also had been claimed to produce smoother plated surfaces than the solid LiH reducing agent. The pretreatment regimen, synthesis of the 2:1 $AlCl_3$–EMIC ionic liquid, and use of copper and glass substrates were preserved allowing for better comparison between DIBAH and LiH reducing agents. The inclusion of the reducing agent was in the form of toluene containing DIBAH whose volume ratio was 80 : 20 at a concentration of 0.2 mol L^{-1} in solution and all preparation and deposition were carried out in a glove box containing dry nitrogen gas. Additionally, as the source of aluminum, a 2 : 1 $AlCl_3$–EMIC mixture, and reduction of aluminum within the

electrolyte [Eq. (30.1)] remained constant, only the oxidation reaction of the DIBAH reducing agent [Eq. (30.3)] is required to provide a possible deposition mechanism:

$$(CH_3)_2{-}CH{-}CH_2{-}AlH{-}CH_2{-}CH{-}(CH_3)_2 \rightarrow (CH_3)_2{-}CH{-}CH_2{-}Al^+{-}CH_2{-}CH{-}(CH_3)_2 + \tfrac{1}{2}H_2 + e^- \quad (30.3)$$

As in the prior study [118], for a 6-h treated glass substrate at 35°C, XRD results exhibited a diffraction pattern and lattice constant closely matching pure aluminum, while SEM-EDX analysis of a 3-h deposition on a glass substrate at 35°C revealed a smooth uniform aluminum deposit. Conducted under the same parameters as in the LiH study, GD-OES determined that no impurities present in the electrolyte were present within the aluminum film formed on a copper substrate after a 12-h deposition at 35°C, echoing the results of the previous study using LiH. This study does clarify both the use and detection of the sensitizing and activating agents by GD-OES, noting that although neither was detected by GD-OES, slight amounts of each were detected when the aluminum film and copper substrate were dissolved together in nitric acid and analyzed by inductively coupled plasma (ICP) emission spectroscopy.

Varying factors such as temperature (35, 55, and 65°C), concentration of the reducing agent (0.1, 0.2, and 0.3 mol L^{-1}), and relative composure of the electrolyte (66.7/33.3, 58/42, and 52/48 mol %) were investigated to determine the impact on the morphology and plating rate of the films produced from the DIBAH $AlCl_3$–EMIC IL. The amount of aluminum deposited and the grain size were found to increase with temperature and immersion time at 35 and 55°C, while at 65°C the amount of aluminum deposited was at a maximum for short depositions (~1 h), with less deposited after longer immersion times, likely due to electrolyte decomposition. SEM images also indicated smoother surface morphology for depositions at 65°C due to smaller grain sizes than those at lower temperatures; this deviation from the trend at lower temperature is attributed to an increase in the nucleation rate of aluminum indicating a critical temperature exists where the increase in grain sizes with temperature and plating times no longer holds.

Higher concentrations of the reducing agent were found to increase the amount, rate, and grain size of the deposited aluminum on an activated glass substrate from a 55°C, 2 : 1 mol ratio $AlCl_3$–EMIC IL. Comparing SEM images taken for both the LiH [118] and DIBAH [119] reducing agents, the film deposited using DIBAH was determined to be more uniform and smooth, in addition to simplifying electrolyte preparation due to its solubility and stability. The amount of aluminum deposited was maximized using the 2 : 1 mol ratio (66.7/33.3 mol %) $AlCl_3$–EMIC IL, compared to other mixtures at 55°C containing 0.2 mol L^{-1}, with the overall trend showing more deposition with an increased molar ratio of $AlCl_3$. The 58/42 mol % mixture resulted in smoother, yet thinner (almost 4 times less Al by mass) deposit allowing for the recognition of scratches on the substrate, while the 52/48 mol % mixture plated the least amount of aluminum more slowly. Given that deposition removes aluminum from the electrolyte, better plating may be achieved in devising a system in which aluminum may be replaced; however, the atmospheric instability of the IL would likely prove to be a major complication.

30.6.3 Overview

Although great strides have been made concerning electroless deposition from ionic liquid media (Fig. 30.3), there have yet to be reports of electroless deposition from ionic liquids onto magnesium-based substrates for the purpose of corrosion protection. Nevertheless, several interesting and useful details may be elicited from the electroplating of aluminum and zinc on magnesium as well as the successful electroless deposition of aluminum on both glass and copper substrates from $AlCl_3$–EMIC ILs. In conjunction, the $AlCl_3$–EMIC studies have shown that (i) magnesium substrates, particularly the AZ91D alloy, can peacefully coexist within a Lewis acidic 1.5 : 1 $AlCl_3$–EMIC IL during the electroplating process [63, 114] and (ii) electroless deposition is possible from a similarly Lewis acidic 2 : 1 $AlCl_3$–EMIC IL onto both conductive and nonconductive substrates [118, 119]. Though in a sense a bit of an oversimplification, a great deal of information is available concerning the first-generation $AlCl_3$–EMIC IL and Lewis acidic EMIC ILs, making them the most likely candidates to demonstrate a proof of concept for the electroless coating of magnesium from an ionic liquid.

Despite the high-quality aluminum deposits possible from electro- and electroless deposition, first-generation chloroaluminate ionic liquids are not favorable for widespread industrial use as their extremely reactive and hygroscopic nature remains a disadvantage, with handling and deposition mandating inert gas conditions. For this reason the development of new eutectic-based ionic liquids is of interest as they may be considerably less susceptible to the addition of water. Although the presence of small amounts of water have been found to be beneficial to deposit morphology, quantifiable results remain rather sparse [68]. Moreover, a great number of unknowns exist concerning the electroless deposition of metals from ionic liquids, as it is only recently that electroless deposition has been conducted from even first-generation ionic liquids. For example, one point that remains murky in both cited studies on electroless deposition of aluminum is the apparent plateau seen in graphs documenting the amount of deposit per area against the deposition time. The plateau seems to occur around 3 h of deposition for samples containing 66.7 mol % $AlCl_3$ and sooner for those having less. As higher concentrations of aluminum lead to more aluminum

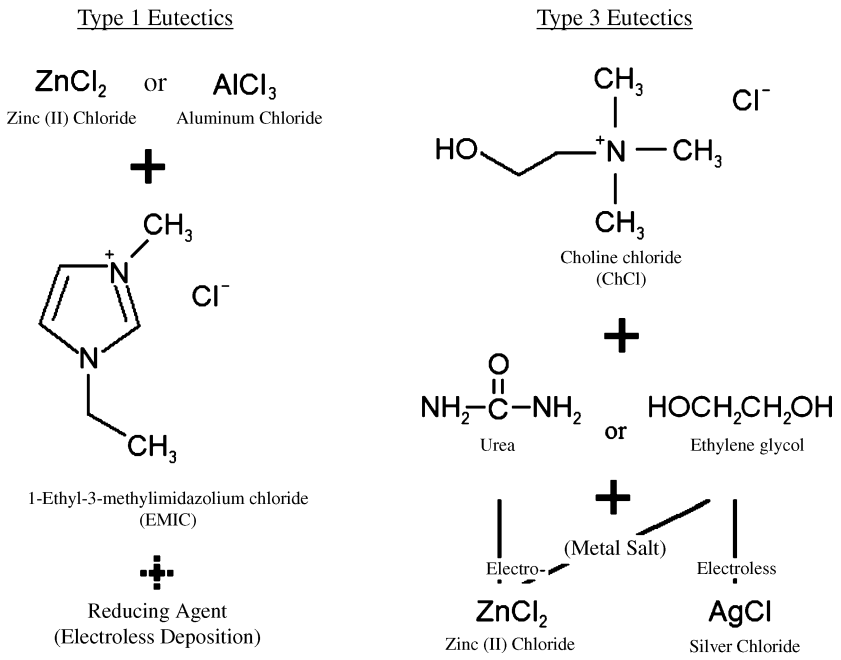

FIGURE 30.3 Schematic of current ionic components of ILs used in metallic film electro- and electroless deposition.

being deposited, it raises a question regarding the amount of aluminum able to be deposited remaining in solution and to the catalytic/autocatalytic nature of the deposition process. Additionally, from the porous deposit resulting from electroless silver, it is possible that electroless deposition on magnesium will require catalytically activated deposition using a reducing agent rather than simple immersion coatings brought on by the difference between the galvanic potentials of the ions in solution and the substrate.

Along with the development of air- and water-stable ionic liquids capable of depositing aluminum, the potential of electroless zinc deposition from air- and water-stable ionic liquid media is of great interest, especially as zinc ILs are less demanding than those for aluminum. As the development of air- and water-stable ionic liquids continues, the possibility of electrolessly depositing zinc–aluminum alloys or even highly wear- and corrosion-resistant aluminum–zinc multilayer coatings will have to be examined. Moreover, as new electrolyte baths continue to be developed, investigations into their coexistence with magnesium-based substrates will be required. Fortunately, the progress made with surface conversion treatments using ionic liquids is bringing about another avenue to passivate magnesium-based substrates to allow metallic film deposition, should it be required.

30.7 CONCLUSION

In conclusion, the well-adhered stability of the conversion treatments provides a promising avenue from which to pursue metallic film deposition, while the overall neutrality of certain ionic liquids vis-à-vis magnesium-based substrates may allow for direct deposition without the application of a pretreatment regimen. In the IL chemical conversion treatments it was observed that the fluoride-based bilayer coating on AZ31, an aluminum- and zinc-containing alloy, produced by treatment with the $P_{6,6,6,14}{}^{+}TFSA^{-}$ IL [79] allowed for some self-healing following coating breakdown, a phenomenon not observed on treatment using the same IL on pure magnesium [80]. Moreover, the inhomogeneity of the conversion processes due to interactions and potential heightened reactivity at and within grain boundaries remains of concern [81]. The role of substrate composition in successful coating was further echoed by the work of Bakkar and Neubert on the electrodeposition of zinc from several ionic liquids onto a wide array of magnesium alloys, which found that only certain IL–substrate combinations resulted in reasonable coatings; although not yet fully documented, the same has been seen to occur with electroless deposition. Therefore, composition of the substrate remains a clear factor in the production of corrosion-resistant treatments as seen in both IL chemical conversion treatments [81] and electro- [115] and likely electroless deposition.

Although a universal coating procedure is ideal, it appears as though the coating of magnesium and its alloys, as well as other materials, will remain dependent on their composition. However, the elimination of aqueous chemistry will likely allow for more generalized regimens in the plating of magnesium-based substrates, consolidating deposition to a handful of processes dependent on maintaining the content of such metals as aluminum and zinc below a critical threshold. As

previously outlined, the formation of well-adhered, continuous, and relatively defect-free corrosion-resistant conversion films from IL treatments may be useful as pretreatments, replacing aqueous pretreatments, to passivate magnesium and its alloys for the deposition of more robust metallic thin films. Although much study is required to determine the properties and interaction of such coatings with electro- and electroless deposition, concrete first steps have been made with the experiments illustrating a clear critical point where film thickness increases and begins to be ineffective for the purpose of corrosion protection.

Although the electrodeposition of metallic thin films has been documented for several years, it is only recently that the electroless deposition of aluminum from an ionic liquid onto glass and copper [118, 119] has been achieved, with none having yet been preformed on magnesium-based substrates. Presently, aluminum and zinc are favored for the metallic coating of magnesium-based substrates as they coexist well with magnesium, as observed by their inclusion in many magnesium alloys, and are well known to resist corrosion. Though there have yet to be any published studies documenting the electroless deposition of zinc from ionic liquid media, limitations pertaining to the deposition of electroplated zinc and electroless aluminum will necessitate its pursuit. The electroless deposition of metallic thin films therefore remains an important avenue for the corrosion protection of magnesium and its alloys as electroless processes, unlike electrodeposition, ensure even coatings over even more complex surfaces. The achievement of a continuous, pore-free, well-adhered coating that disallows the formation of a galvanic cell sequestering the magnesium-based substrate will also allow for a return to more traditional aqueous methods for further deposition.

Looking ahead, once the initial corrosion and reactivity problem of magnesium-based substrates is solved, further coating of the sample to reinforce wear and corrosion protection will be required. Given that enhanced wear protection may be provided by metallic thin-film multilayer deposits [135], the successful production of a pore-free, corrosion-resistant coating would also allow for a return to more well known aqueous deposition baths from which the deposition of electroless multilayers is documented [136, 137]. Furthermore, multilayer deposits of adequate thickness, a few hundred layers, have shown some self-healing characteristics as the individual thin films provide an ordered crystalline structure at a lower energy level, granting increased stability to the coating.

There remains a great deal of study necessary to expand electroless deposition processes for widespread industrial purposes, especially regarding magnesium and its alloys. The potential of modern ionic liquids as electrolytes has only begun to be recognized and offers new avenues for both electroless deposition and magnesium substrates. As coatings and coating technologies progress, the furnishing of an adequate initial deposit upon which other more wear resistant coatings may be applied is inevitable. Finally, in Appendix A we delineate a number of chemical conversion, electro- and electroless deposition, bath formulations provided in the papers reviewed.

REFERENCES

1. Y. Kojima, *Mater. Sci. Forum*, **350–351**, 3 (2000).
2. K. G. Cowan and J. A. Harrison, *Electrochim. Acta*, **24**, 301 (1979).
3. K. G. Cowan and J. A. Harrison, *Electrochim. Acta*, **25**, 899 (1980).
4. G. Song, A. Atrens, D. St John, J. Naim, and Y. Li, *Corros. Sci.*, **39**, 855 (1997).
5. T. R. Beck and G. S. Chan, *J. Electrochem. Soc.*, **130**, 1289 (1983).
6. X. Hallopeau, T. Beldjoudi, C. Fiaud, and L. Robbiola, *Corros. Rev.*, **16**, 27 (1998).
7. G. L. Song and A. Atrens, *Adv. Eng. Mater.*, **1**, 11 (1999).
8. N. Pébère, C. Riera, and F. Dabosi, *Electrochim. Acta*, **35**, 555 (1990).
9. A. Antonyraj and C. O. Augustin, *Corros. Rev.*, **16**, 127 (1998).
10. P. Germenaz, F. Nicolas, S. Rouquette, S. Lamirault, D. Ferry, and G. Picard, *Mater. Sci. Eng. A*, **120**, 329 (1989).
11. H. A. Robinson, *J. Electrochem. Soc.*, **90**, 485 (1949).
12. O. Lunder, J. E. Lein, T. Kr. Aune, and K. Nisancioglu, in *Proceedings of the 11th Scandinavian Corrosion Congress*, Stavanger, Norway, 1989, F-40.
13. I. H. Gadshov, *Metalloberflaeche*, **43** (1), 15 (1989).
14. M. Bobby Kannan, W. Dietzel, C. Blawert, A. Atrens, and P. Lyon, *Mater. Sci. Eng. A*, **480**, 529 (2008).
15. J. H. Nordlien, K. Nisancioglu, S. Ono, and N. Masuko, *J. Electrochem. Soc.*, **144**, 461 (1997).
16. K. H. W. Seah, K. B. Lim, C. H. Chew, and S. H. Teoh, *Corros. Sci.*, **34**, 1707 (1993).
17. R. J. Grossman, *IEEE Trans*, *Sonics Ultrasonics,* **SU-31**, 25 (1984).
18. T. W. Retting and M. J. Felsen, *Corrosion*, **32**, 121 (1976).
19. J. Warkus, M. Raupach, and J. Gulikers, *Mater. Corros.*, **57**, 614 (2006).
20. G. Song, B. Johannesson, S. Hapugoda, and D. St. John, *Corros. Sci.*, **46**, 955 (2004).
21. M. Verbrugge, *Corros. Sci.*, **48**, 3489 (2006).
22. J.-M. Lee, *Electrochim. Acta*, **51**, 3256 (2006).
23. J. X. Jia, A. Atrens, G. Song, and T. H. Muster, *Mater. Corros.*, **56**, 468 (2005).
24. J. X. Jia, Guangling Song, Andrej Atrens, *Corros. Sci.*, **48**, 2133 (2006).
25. S. M. Sharland, C. P. Jackson, and A. J. Diver, *Corros. Sci.*, **29**, 1149 (1989).
26. S. M. Sharland and P. W. Tasker, *Corros. Sci.*, **28**, 603 (1988).

27. J. N. Harb and R. C. Alkire, *Corros. Sci.*, **29**, 31 (1989).
28. F. Mansfeld and P. J. Stocker, *Corrosion*, **35**, 541 (1979).
29. S. Magaino, A. Kawaguchi, A. Hirata, and T. Osaka, *J. Electrochem. Soc.*, **134**, 2993 (1987).
30. A. Arora, *Corrosion*, **40**, 459 (1984).
31. R. H. Jones and M. A. Friesel, *Corrosion*, **48**, 751 (1992).
32. H. Mazille, R. Rothea, and C. Tronel, *Corros. Sci.*, **37**, 1365 (1995).
33. M. Fregonese, H. Idrissi, H. Mazille, L. Renaud, and Y. Cetre, *Corros. Sci.*, **43**, 627 (2001).
34. C. Gabrielli, S. Joiret, M. Keddam, N. Portail, P. Rousseau, and V. Vivier, *Electrochim. Acta*, **53**, 7539 (2008).
35. K. Jafarzadeh, T. Shahrabi, and M. G. Hosseini, *J. Mater. Sci. Technol.*, **24** (2), 215 (2008).
36. D. Crotty, C. Stinecker, and B. Durkin, *Products Finishing*, **60**, 44 (1996).
37. R. Ellmers and D. Maguire, *Global View Magnesium: Yesterday, Today, Tomorrow*, International Magnesium Association, 1993, p. 28.
38. J. E. Gray and B. Luan, *J. Alloys Compounds*, **336**, 88 (2002).
39. M. Schlesinger, X. Meng, and D. D. Snyder, *J. Electrochem. Soc.*, **137** (6), 1858 (1990).
40. M. Schlesinger, X. Y. Meng, and D. D. Snyder, *J. Electrochem. Soc.*, **138** (2), 406 (1991).
41. W. Paatsch, *Wire*, **42**, 320 (1992).
42. S. M. M. Vaghefi, A. Saatchi, and M. E. Hoseinabadi, *Surf. Coat. Technol.*, **168**, 259 (2003).
43. O. A. Leon, M. H. Staia, and H. E. Hintermann, *Surf. Coat. Technol.*, **120/121**, 641 (1999).
44. W. A. Fairweather, *Transactions*, **75**, 113 (1997).
45. E. F. Emley, *Principle of Magnesium Technology*, Pergamon, Oxford, 1966.
46. O. M. Briles, M. Jaworowsky, and M. A. Kryzman,U.S. Patent 6,887,320, 2005.
47. W. X. Zhang, Z. H. Jiang, G. Y. Li, Q. Jiang, and J. S. Lian, *Appl. Surf. Sci.*, **254**, 4949 (2008).
48. H. Huo, Y. Li, and F. Wang, *Corros. Sci.*, **46**, 1467 (2004).
49. M. A. Gonzalez-Nunez et al., *Corr. Sci*, **37**, 1763 (1995).
50. M. Dabala et al., *Surf. Coat. Technol.*, **172**, 227 (2003).
51. H. Umehara et al., *Surf. Coat. Technol.*, **169–170**, 66 (2003).
52. Z. C. Kwo and S. S. Teng, *Mater. Chem. Phys.*, **80**, 191 (2003).
53. A. L. Rud et al., *Corros. Sci.*, **42**, 275 (2000).
54. F. W. Eppensreiner and M. R. Jenkins, *Metal Finish*, **97**, 494 (1999).
55. P. Marcus and H. Ardelean, Patent PCT/FR 02/01843, WO 02/097164 A2, 2002, U.S. Patent 7,965, 2007.
56. H. Ardelean et al., *Corros. Sci.*, **50**, 1907 (2008).
57. Y. Zhang, C. Yan, F. Wang, H. Lou, and C. Cao, *Surf. Coat. Technol.*, **161**, 36 (2002).
58. Z. Shi, G. Song, and A. Atrens, *Corros. Sci.*, **47**, 2760 (2005).
59. H. Y. Hsiao, P. Chung, and W. T. Tsai, *Corros. Sci.*, **49**, 781 (2007).
60. T. Welton, *Chem. Rev.*, **99**, 2071 (1999).
61. P. Wasserscheid and T. Welton, *Ionic Liquids in Synthesis*, Wiley-VCH Verlag, Weinheim, Germany, 2003.
62. A. I. Bhatt, I. May, V. A. Volkovich, M. E. Hetherington, B. Lewin, R. C. Thied, and N. Ertok, *J. Chem. Soc. Dalton Trans.*, **24**, 4532 (2002).
63. J.-K. Chang, S.-Y. Chen, W.-T. Tsai, M.-J. Deng, and I.-W. Sun, *Electrochem. Commun.*, **9**, 1602 (2007).
64. Y. Zhao and T. J. Vandernoot, *Electrochim. Acta*, 42, 1639 (1997).
65. J.-F. Huang and I.-W. Sun, *Electrochim. Acta*, **49**, 3251 (2004).
66. F. Endres, *Z. Phys. Chem*., **218**, 255 (2004).
67. E. F. Borra, O. Seddiki, R. Angel, D. Eisenstein, P. Hickson, K. R. Seddon, and S. P. Worden, *Nature*, **447**, 979 (2007).
68. A. P. Abbott and K. J. McKenzie, *Phys. Chem. Chem. Phys.*, **8** (37), 4265 (2006).
69. J. S. Wilkes, *Green Chem.*, **4**(2), 73 (2002).
70. A. P. Abbott, G. Capper, K. J. McKenzie, and K. S. Ryder, *J. Electroanal. Chem.*, **599**, 288 (2007).
71. A. P. Abbott, G. Capper, D. L. Davies, and R. Rasheed, *Chem.–Eur. J.*, **10**, 3769 (2004).
72. F. Endres, D. MacFarlane, and A. Abbott, *Electrodeposition from Ionic Liquids*, Wiley-VCH,Weinheim, Germany, 2008.
73. S. Zein El Abedin and F. Endres, *ChemPhysChem*, **7**, 58 (2006).
74. Y.-F. Lin and I.-W. Sun, *Electrochim. Acta*, **44**, 2771 (1999).
75. S. Sahami and R. A. Osteryoung, *Anal. Chem.*, **55**(12), 1970 (1983).
76. A. P. Abbott, C. A. Eardley, N. S. Farley, G. A. Griffith, and A. Pratt, *J. Appl. Electrochem.*, **31**, 1345 (2001).
77. P. C. Howlett, D. R. MacFarlane, and A. F. Hollenkamp, *Electrochem. and Solid-State Lett.*, **7** (5), A97 (2004).
78. P. C. Howlett, N. Brack, A. F. Hollenkamp, M. Forsyth, and D. R. MacFarlane, *J. Electrochem. Soc.*, **153** (3), A595 (2006).
79. M. Forsyth, P. C. Howlett, S. K. Tan, D. R. MacFarlane, and N. Birbilis, *Electrochem Solid-State Lett.*, **9** (11), B52 (2006).
80. N. Birbilis, P. C. Howlett, D. R. MacFarlane, and M. Forsyth, *Surf. Coat. Technol.*, **201** (8), 4496 (2007).
81. M. Forsyth, W. C. Neil, P. C. Howlett, D. R. Macfarlane, B. R. W. Hinton, N. Rocher, Th. F. Kemp, and M. E. Smith, *Appl. Mater. Interfaces*, **1** (5), 1045–1052 (2009).
82. X. Liu, F. Zhou, Y. Liang, and W. Liu, *Wear*, **261**, 1174 (2006).
83. J. Qu, P. J. Blau, S. Dai, H. Luo, H. M. Meyer III, and J. J. Truhan, *Wear*, **267**, 1226 (2009).
84. F. Zhou, Y. Liang, and W. Liu, *Chem. Soc. Rev.*, **38**, 2590 (2009).
85. J. Qu, J. J. Truhan, S. Dai, H. Luod, and P. J. Blau, *Tribol. Lett.* **22** (3), 207 (2006).
86. H. Tokuda, K. Hayamizu, K. Ishii, M. Abu Bin Hasan Susan, and M. Watanabe, *J. Phys. Chem. B*, **109**(13), 6103 (2005).
87. J. G. Huddleston, A. E. Visser, W. M. Reichert, H. D. Willauer, G. A. Broker, and R. D. Rogers, *Green Chem.*, **3**(4), 156 (2001).

88. K. R. Seddon, "Ionic Liquids: Designer Solvents?" in *The International George Papatheodorou Symposium: Proceedings*, S. Boghosian, V. Dracopoulos, C. G. Kontoyannis and G. A. Voyiatzis, Eds., Institute of Chemical Engineering and High Temperature Chemical Processes, Patras, 1999, pp. 131.
89. J. Pernak, A. Czepukowicz, and R. Pózniak, *Ind. Eng. Chem. Res.*, **40**, 2379 (2001).
90. M. J. Earle and K. R. Seddon, *Pure Appl. Chem.*, **72**, 1391 (2000).
91. F. Endres, *ChemPhysChem*, **3**, 144 (2002).
92. J. S. Wilkes, *ACS Symp. Ser.*, **818**, 214 (2002).
93. H. Ohno (Ed.), *Electrochemical Aspects of Ionic Liquids*, Wiley, New York, 2005.
94. K. J. Fraser and D. R. MacFarlane, *Aust. J. Chem.*, **62**, 309 (2009).
95. P. C. Howlett, E. I. Izgorodina, M. Forsyth, and D. R. MacFarlane, *Z. Phys. Chem*. (Muenchen, Ger.), **220**, 1483 (2006).
96. J. Sun, P. C. Howlett, D. R. MacFarlane, J. Lin, and M. Forsyth, *Electrochim. Acta*, **54**, 254 (2008).
97. P. C. Howlett, S. K. Tan, S. Zhang, J. Efthimiadis, D. R. MacFarlane, and M. Forsyth, paper presented at the Corrosion and Protection: Australasian Corrosion Association Conference, Hobart, Australia, 2006.
98. M. Forsyth, T. F. Kemp, P. C. Howlett, J. Sun, and M. E. Smith, *J. Phys. Chem. C*, **112**, 13801 (2008).
99. D. Aurbach, I. Weissman, A. Zaban, and O. Chusid, *Electrochim. Acta*, **39**, 51 (1994).
100. J. Sun, M. Forsyth, and D. R. MacFarlane, *J. Phys. Chem. B*, **102** (44), 8858 (1998).
101. P. C. Howlett, S. Zhang, D. R. MacFarlane, and M. Forsyth, *Aust. J. Chem.*, **60** (1), 43 (2007).
102. P. C. Howlett, W. Neil, T. Khoo, J. Sun, M. Forsyth, and D. R. MacFarlane, *Isr. J. Chem.*, **48**, 313 (2008).
103. W. C. Neil, M. Forsyth, P. C. Howlett, C. R. Hutchinson, and B. R. W. Hinton, *Corros. Sci.*, **51**, 387 (2009).
104. J. K. Dennis, M. K. Y. Y. Wan, and S. J. Wake, *Transactions*, **63**, 81 (1985).
105. R. G. Golovchanskaya, L. P. Gavrilina, T. A. Smirnova, and N. T. Kudryavtsev, *Protect. Metals*, **6**, 565 (1970).
106. Z. Zhang, G. Yu, Y. Ouyang, X. He, B. Huc, J. Zhang, and Z. Wu, *Appl. Surf. Sci.*, **255**, 7773 (2009).
107. G. Song, *Adv. Eng. Mater.*, **7**, 563 (2005).
108. H. Y. Hsiao and W. T. Tsai, *J. Mater. Res.*, **20**, 2763 (2005).
109. S.-P. Gou and I.-W. Sun, *Electrochim. Acta*, **53** (5), 2538 (2008).
110. A. P. Abbott, J. C. Barron, and K. S. Ryder, *Trans. Inst. Metal Finishing*, **87** (4), 201 (2009).
111. E. Verné, C. Antonione, and L. Battezzati, *Mater. Lett.*, **23** (1–3), 59 (1995).
112. N. Backovic, M. Jancic, and L. J. Radonjic, *Thin Solid Films*, **59** (1), 1 (1979).
113. V. F. Makarov, Y. V. Prusov, I. O. Lebedeva, and V. N Flerov, *J. Appl. Chem. USSR*, **62** (9) Part 2, 1993 (1989).
114. J.-K. Chang, S.-Y. Chen, W.-T. Tsai, M.-J. Deng, and I.-W. Sun, *J. Electrochem. Soc.*, **155** (3), C112 (2008).
115. A. Bakkar and V. Neubert, *Electrochem. Commun.*, **9**, 2428 (2007).
116. A. P. Abbott, S. Nandhra, S. Postlethwaite, E. L. Smith, and K. S. Ryder, *Phys. Chem. Chem. Phys.*, **9**, 3735 (2007).
117. A. P. Abbott, J. Griffith, S. Nandhra, C. O'Connor, S. Postlethwaite, K. S. Ryder, and E. L. Smith, *Surf. Coat. Technol.*, **202**, 2033 (2008).
118. N. Koura, H. Nagase, A. Sato, S. Kumakura, K. Takeuchi, K. Ui, T. Tsuda, and C. K. Loong, *J. Electrochem. Soc.*, **155** (2), D155 (2008).
119. I. Shitanda, A. Sato, M. Itagaki, K. Watanabe, and N. Koura, *Electrochim. Acta*, **54**, 5889 (2009).
120. A. P. Abbott, G. Capper, D. L. Davies, and R. Rasheed, *Chem.–Eur. J.*, **10**, 3769 (2004).
121. J.-K. Chang, S.-Y. Chen, C.-H. Tseng, W.-T. Tsai, M.-J. Deng, and I.-W. Sun, *Electrochemistry*, **77** (8), 585 (2009).
122. J.-K. Chang, I.-W. Sun, S.-J. Pan, M.-H. Chuang, M.-J. Deng, and W.-T. Tsai, *Trans. Inst. Metal Finishing*, **86** (4), 227 (2008).
123. S. Takahashi, L. A. Curtiss, D. Gosztola, N. Koura, and M.-L. Saboungi, *Inorg. Chem.*, **34**, 2990 (1995).
124. T. J. Melton, J. Joyce, J. T. Maloy, J. A. Boon, and J. S. Wikes, *J. Electrochem. Soc.*, **137**, 3865 (1990).
125. P. Wasserscheid and T. Welton, *Ionic Liquids in Synthesis*, Wiley-VCH, Weinheim, Germany, 2002, pp. 13, 177.
126. H. A. Øye, M. Jagtoyen, T. Oksefjell, and J. S. Wilkes, *Mater. Sci. Forum*, **73** (75), 183 (1991).
127. Z. Szklarska-Smialowska, *Corros. Sci.*, **41**, 1743 (1999).
128. L. C. Archibald, in *Smithells Metals Reference Book*, 7th ed., E. A. Brandes and G. B. Brook, Eds., Butterworth–Heinemann, Oxford, 1992, Chapter 32.
129. S. Caporali, F. Ghezzi, A. Giorgetti, A. Lavacchi, A. Tolstogouzov, and U. Bardi, *Adv. Eng. Mater.*, **9** (3), 185 (2007).
130. A. Shkurankov, S. Zein El Abedin, and F. Endres, *Aust. J. Chem.*, **60**, 35 (2007).
131. C. R. Shipley, U.S. Patent 3,011,920, filed 1961.
132. S. S. Djokic, in *Electroless Deposition of Metals and Alloys in Modern Aspects of Electrochemistry*, Vol. 35, B. E. Conway and R. E. White, Eds., Springer, 2002, pp. 51–133.
133. A. P. Abbott, K. S. Ryder, U. König, *Trans. Inst. Metal Finishing*, **86** (4), (2008).
134. M. Paunovic and M. Schlesinger, *Fundamentals of Electrodeposition*, 2nd ed., Wiley, Hoboken, NJ, 2006, pp. 140–147.
135. S. H. Yao, Y. L. Su, W. H. Kao, and T. H. Liu, *Tribol. Int.*, **39** (4), 332 (2006).
136. A. Urena, M. V. Utrilla, J. Rams, P. Rodrigo, and M. Ferrer, *J. Eur. Ceramic Soc.*, **27** (13–15), 3983 (2007).
137. Y. W. Song, D. Y. Shan, and E. H. Han, *Electrochim. Acta*, **53** (5), 2135 (2008).

APPENDIX 30A

CHEMICAL CONVERSION, ELECTRO- AND ELECTROLESS DEPOSITION BATH FORMULAE

30A.1 CHEMICAL CONVERSION

Surface Conversion [76]

Ionic liquid	Tri(hexyl)tetradecyl phosphonium cation ($P^{+}_{6,6,6,14}$) Bis(trifluoromethanesulfonyl)amide anion ($TFSA^{-}$)
Operating temperature	Room temperature
Atmosphere	Open atmosphere
Substrate(s)	ZE41
Substrate pretreatment	Polishing
Post-conversion treatment	Distilled water and ethanol and nitrogen stream drying

Surface Conversion [74]

Ionic liquid	Tri(hexyl)tetradecyl phosphonium cation ($P^{+}_{6,6,6,14}$) Bis(trifluoromethanesulfonyl)amide anion ($TFSA^{-}$)
Operating temperature	Room temperature
Atmosphere	Open atmosphere
Substrate(s)	AZ31
Substrate pretreatment	SiC polishing (400, 800, 1200, and 4000 grits) Ethanol and distilled water rinse
Post-conversion treatment	Distilled water and ethanol

30A.2 ELECTRODEPOSITION OF METALLIC FILMS

Electroless Aluminum [112]

Synthesis	66.7mol% $AlCl_3$/33.3 mol% EMIC (slow addition of $AlCl_3$, mixed by stirring for 24 hrs) Treatment with Al wire (99.99%) until colorless
Synthesis temperature	Room temperature
Reducing Agent	Toluene containing DIBAH (80:20 volume ratio at a concentration of 0.2–0.3 mol L^{-1})
Operating temperature	35–60 °C
Atmosphere	Dry nitrogen gas (oxygen and water levels < 1 ppm)
Substrate(s)	Glass, Copper
Substrate pretreatment	Polish with Emery paper (#320) Methanol and acetone grease removal $SnCl_2$ (0.127 mol L^{-1}, pH 0.74, 5 min) sensitization PdCl, (1.69 mmol L^{-1} pH 0.77, 5 min) activation

Electroaluminum [64, 107]

Synthesis	60.0 mol% A1Cl_3/40.0 mol% EMIC (slow addition of $AlCl_3$, mixed by stirring for 24 hrs)
Synthesis temperature	Room temperature
Operating current	-15 mA/cm^2 to -20 mA/cm^2
Total passed.Charge	50 C/cm^2
Operating temperature	Room temperature
Atmosphere	Nitrogen atmosphere (oxygen and water levels <1 ppm)
Substrate(s)	Die-cast AZ91D Mg alloy
Substrate pretreatment	Ground with SiC papers to a grit of 1000
Post-deposition treatment	Distilled water cleaning and air drying

Electrozinc [72]

Synthesis	50.0 mol% $ZnCl_2$/50.0 mol% EMIC (mixed by stirring for 2 days)
Synthesis temperature	90 °C
Deposition potential	−0.1 V to −0.3 V
Operating temperature	40 °C
Atmosphere	Nitrogen atmosphere (oxygen and water levels < 1 ppm)
Substrate(s)	Glassy carbon, Nickel
Substrate pretreatment	Polishing
Post-deposition treatment	Dry benzene washing in glove box, deionized water rinsing outside of glove box, and vacuum drying

30A.3 ELECTROLESS METALLIC FILM DEPOSITION

Electroless Aluminum [111]

Synthesis	66.7 mol% $AlCl_3$/33.3 mol% EMIC (slow addition of A1C1$_3$, mixed by stirring for 24 hrs)
	Treatment with Al wire (99.99%) until colorless
Synthesis temperature	Room temperature
Reducing agent	0.2–0.3 mol L^{-1} LiH
Operating temperature	25–3.5°C
Atmosphere	Dry argon gas (oxygen and water levels < 1 ppm)
Substrate(s)	Glass, Copper
Substrate Pre-treatment	Polish with Emery paper (#320)
	Methanol and acetone grease removal
	$SnCl_2$ (0.127 mol L^{-1}, pH 0.74, 5 min) sensitization
	$PdCl_2$ (1.69 mmol L^{-1}. pH 0.77, 5 min) activation

Electroless Aluminum [112]

Synthesis	66.7 mol% A1C1$_3$/33.3 mol% EMIC (slow addition of A1Cl_3, mixed by stirring for 24 hrs)
	Treatment with Al wire (99.99%) until colorless
Synthesis temperature	Room-temperature
Reducing agent	Toluene containing DIBAH (80:20 volume ratio at a concentration of 0.2–0.3 mol L^{-1})
Operating temperature	35–60 °C
Atmosphere	Dry nitrogen gas (oxygen and water levels < 1 ppm)
Substrate(s)	Glass, Copper
Substrate pretreatment	Polish with Emery paper (#320)
	Methanol and acetone grease removal
	$SnCl_2$ (0.127 mol L^{-1}, pH 0.74, 5 min) sensitization
	$PdCl_2$ (1.69 mmol L^{-1}, pH 0.77, 5 min) activation

APPENDIX

This Appendix contains tables of miscellaneous information for use by electroplaters. It has been prepared by Arch B. Tripler, Jr., Battelle Memorial Institute, Columbus Laboratories, Columbus, Ohio.

Modern Electroplating, Fifth Edition Edited by Mordechay Schlesinger and Milan Paunovic

TABLE 1 Physical Constants of Selected Elements

Element	Symbol	Atomic No.	Atomic Weight 1971	Density[a] g/cm^3, 20°C	Melting Point,[a] °C	Linear Coefficient Thermal Expansion near 20°C μm/°C
Aluminum	Al	13	26.9815	2.699	660.1	0.607[e]
Antimony	Sb	51	121.75	6.62	630.5	0.22–0.27[f]
Arsenic	As	33	74.9216	5.73	(820)	0.12
Beryllium	Be	4	9.0122	1.85	1350	0.31[h]
Bismuth	Bi	83	208.980	9.78	271.3	0.34
Boron	B	5	10.81	2.3	2300 ± 300	0.21[i]
Bromine	Br	35	79.904	3.12	−7.2	—
Cadmium	Cd	48	112.40	8.65	320.9	0.757
Calcium	Ca	20	40.08	1.55	810	0.56
Carbon (graphite)	C	6	12.011	2.25	3700 ± 100	0.015–0.11[e]
Cerium	Ce	58	140.12	6.9	600 ± 50	—
Chlorine	Cl	17	35.453	—	−101.6	—
Chromium	Cr	24	51.996	7.14	1890 ± 10	0.16
Cobalt	Co	27	58.9332	8.71	1492	0.312
Copper	Cu	29	63.546	8.933	1083	0.419
Fluorine	F	9	18.9984	—	−223	—
Gallium	Ga	31	69.72	5.46	29.7	0.46
Germanium	Ge	32	72.59	5.36	958.5	—
Gold	Au	79	196.967	19.32	1063	0.361
Hydrogen	H	1	1.0079	0.08375×10^{-3}	−259.14	—
Indium	In	49	114.82	7.28	155.0	0.84
Iodine	I	53	126.9045	4.93	113.5	2.36
Indium	Ir	77	192.2	22.42	2443	0.17
Iron	Fe	26	55.847	7.86	1533	0.297
Lead	Pb	82	207.2	11.34	327.4	0.744[e]
Lithium	Li	3	6.941	0.534	186	1.42
Magnesium	Mg	12	24.305	1.74	651	0.66[j]
Manganese	Mn	25	54.9380	7.3	1260	0.56
Mercury	Hg	80	200.59	13.55	−38.87	—
Molybdenum	Mo	42	95.94	10.2	2620	0.12[e]
Nickel	Ni	28	58.71	8.8	1453	0.338[k]
Niobium (Columbium)	Nb (Cb)	41	92.9064	8.4	2500	0.18

Nitrogen	N	7	14.0067	1.1649×10^{-3}	−209.86	—
Osmium	Os	76	190.2	22.5	2700	0.12
Oxygen	O	8	15.9994	1.3318×10^{-3}	−218.4	—
Palladium	Pd	46	106.4	12.16	1552	0.30
Phosphorous (yellow)	P	15	30.9738	1.82	44.1	3.18
Platinum	Pt	78	195.09	21.37	1769	0.23
Potassium	K	19	39.098	0.87	62.3	2.1
Rhenium	Re	75	186.2	21.04	3180	0.18
Rhodium	Rh	45	102.9055	12.44	1960	0.21[e]
Selenium	Se	34	78.96	4.81	220	0.94
Silicon	Si	14	28.086	2.42	1420	0.07–0.19
Silver	Ag	47	107.868	10.49	960.8	0.50[k]
Sodium	Na	11	22.9898	0.97	97.5	1.8
Sulfur (yellow)	S	16	32.06	2.07	113–119	1.6
Tantalum	Ta	73	180.947	16.6	3005	0.17
Tellurium	Te	52	127.60	6.25	452	0.423
Thallium	Tl	81	204.37	11.86	303.5	0.71
Tin	Sn	50	118.69	7.298	231.9	0.58
Titanium	Ti	22	47.90	4.54	1820	0.22
Tungsten (Wolfram)	W	74	183.85	19.3	3380	0.11
Uranium	U	92	238.029	18.7	1130	—
Vanadium	V	23	50.941	5.87	1735	0.20
Zinc	Zn	30	65.38	7.133(25°C)	419.47	1.01[l]
Zirconium	Zr	40	91.22	6.5	1750	0.13

(*continued*)

Element	Electrical Resistivity, μΩ-cm	Electrochemical Equivalents mg/C for Valence of 1[b]	Crystal Structure[c]	Lattice Constants at 20°C kX Units[d]			
				a	*b*	*c* or Axial Angle or Temperature	Closest Approach of Atoms
Aluminum	2.655(20°C)	0.2796	fcc	4.0408	—	—	2.856
Antimony	39.0(0°C)	1.262	rh	4.4974	—	57°6.5′	2.898
Arsenic	35(0°C)	0.7765	rh[g]	4.151	—	53°49′	2.50
Beryllium	5.9(0°C)	0.09340	cph[g]	2.2810	—	3.5771	2.221
Beryllium	106.8(0°C)	2.166	rh	4.7361	—	57° 14.2′	3.105
Boron	1.8×10^{12}(0°C)	0.1120	or (?)	17.86	8.93	10.13	—
Bromine	—	0.8281	or	4.48	6.67	8.72(− 150°C)	2.27
Cadmium	6.83(0°C)	1.165	cph	2.9727	—	5.606	2.972
Calcium	3.43(0°C)	0.4154	fcc[g]	5.56	—	—	3.93
Carbon (graphite)	1375(0°C)	0.1245	hex[g]	2.4564	—	6.6906	1.42
Cerium	78(20°C)	1.452	fcc[g]	5.143	—	—	3.64
Chlorine	—	0.3674	tet	8.56	—	6.12(−185°C)	1.81
Chromium	13(28°C)	0.5389	bcc[g]	2.8787	—	—	2.493
Cobalt	6.24(20°C)	0.6108	cph[g]	2.502	—	4.061	2.501
Copper	l.673(20°C)	0.6586	fcc	3.6080	—	—	2.551
Fluorine	—	0.1969	—	—	—	—	—
Gallium	53.4(0°C)	0.7226	Ifcor	4.517	4.511	7.645	2.437
Germanium	8.9 104(0°C)	0.7523	dc	5.647	—	—	2.445
Gold	2.19(0°C)	2.041	fcc	4.0701	—	—	2.878
Hydrogen	—	0.01045	hex	3.75	—	6.12(−271°C)	—
Indium	8.37(0°C)	1.190	fct	4.585	—	4.941	3.24
Iodine	1.3×10^{15}(20°C)	1.315	or	4.777	7.251	9.773	2.70
Indium	5.3(20°C)	1.992	fcc	3.8312	—	—	2.709
Iron	9.71(20°C)	0.5788	bcc[g]	2.8606	—	—	2.476
Lead	20.65(20°C)	2.147	fcc	4.9395	—	—	3.493
Lithium	8.55(0°C)	0.07191	bcc	3.5019	—	—	3.033
Magnesium	4.46(20°C)	0.2519	cph	3.2028	—	5.1998	3.190
Manganese	185(20°C)	0.5694	cc[g]	8.894	—	—	2.24
Mercury	94.1(0°C)	2.079	rh	2.999	—	70°31.7′ (−46°C)	2.999
Molybdenum	5.17(0°C)	0.9943	bcc	3.140	—	—	2.720
Nickel	6.84(20°C)	0.6085	fcc	3.5167	—	—	2.486
Niobium (Columbium)	13.1(18°C)	0.9629	bcc	3.2941	—	—	2.853
Nitrogen	—	0.1452	hex[g]	4.03	—	6.59(−234°C)	—
Osmium	9.5(20°C)	1.971	cph	2.7298	—	4.3104	2.670
Oxygen	—	0.1658	c[g]	6.83	—	(−225°C)	—
Palladium	10.8(20°C)	1.103	fcc	3.8824	—	—	2.745
Phosphorous (yellow)	10^{17}(11°C)	0.3210	c[g]	7.17	—	(−35°C)	—
Platinum	9.83(0°C)	2.022	fcc	3.9158	—	—	2.769
Potassium	6.15(0°C)	0.4052	bcc	5.333	—	—	4.618
Rhenium	19.3(20°C)	1.930	cph	2.7553	—	4.4493	2.734
Rhodium	4.5(20°C)	1.066	fcc[g]	3.7957	—	—	2.684

Selenium	12(20°C)	0.8183	hex[g]	4.3552	—	4.9494	2.32
Silicon	10^5(0°C)	0.2911	dc	5.4173	—	—	2.346
Silver	1.59(20°C)	1.118	fcc	4.0774	—	—	2.882
Sodium	4.2(0°C)	0.2383	bcc	4.2820	—	—	3.708
Sulfur (yellow)	2×10^{23}(20°C)	0.3323	fcor[g]	10.48	12.92	24.55	2.12
Tantalum	12.4(18°C)	1.875	bcc	3.2959	—	—	2.854
Tellurium	2×10^5(19.6°C)	1.322	hex	4.4469	—	5.9149	2.86
Thallium	18(0°C)	2.118	cph[g]	3.450	—	5.514	3.401
Tin	11.5(20°C)	1.230	bct[g]	5.8194	—	3.1753	3.016
Titanium	80(0°C)	0.4964	cph[g]	2.953	—	4.729	2.91
Tungsten (Wolfram)	5.5(20°C)	1.905	bcc[g]	3.1585	—	—	2.734
Uranium	60(18°C)	2.467	or[g]	2.852	5.865	4.945	2.76
Vanadium	26(20°C)	0.5280	bcc	3.033	—	—	2.627
Zinc	5.916(20°C)[m]	0.6775	cph	2.659	—	4.935	2.659
Zirconium	41.0(0°C)	0.9454	cph[g]	3.223	—	5.123	3.16

[a] Densities and melting points taken from *Smithsonian Physical Tables,* Smithsonian Institution, Washington, D.C., 1954, 9th rev. ed.

[b] Calculated from 1967 atomic weights and value of faraday as 96,489 ± 2 C (NBS 1960, as given in *Handbook of Chemistry and Physics,* 50th ed., Chemical Rubber Company, Cleveland, Ohio, 1970, p. F78); for valences other than 1, divide value given by valence.

[c] The abbreviations used to denote crystal structure as follows:

fcc	face-centered cubic	Ifcor	one face-centered orthorhombic
rh	rhombohedral	dc	diamond cubic
bcc	body-centered cubic	cc	cubic (complex)
cph	close-packed hexagonal	c	cubic
or	orthorhombic	fcor	face-centered orthorhombic
hex	hexagonal	bct	body-centered tetragonal
tet	tetragonal	fct	face-centered tetragonal

[d] The kX unit (1000 X units), used in all crystal structure measurements, differs slightly from an angstrom (10^{-8} cm); the tabulated lattice dimensions should be multiplied by 1.00202 to put them in angstroms.

[e] From 20 to 100°C.

[f] From 20 to 60°C.

[g] Ordinary form; other modifications known or probable.

[h] From 20 to 200°C.

[i] From 20 to 750°C.

[j] At 40°C.

[k] From 0 to 100° C.

[l] For polycrystalline zinc; in single crystals, varies from 61.5 (parallel to hexagonal axis) to 15 (perpendicular to hexagonal axis).

[m] For polycrystalline zinc; in single crystals, varies from 6.16 (parallel to hexagonal axis) to 5.89 (perpendicular to hexagonal axis).

Note: Data in this table taken with permission from a similar table in *The Metals Handbook*, American Society for Metals.

TABLE 2 Electrolytic Potentials of Metals: Ions at Unit Molal Activity[a]

Metal/Ion Couple	Standard Electrode Potential, E^0 (V), 25°C	Metal/Ion Couple	Standard Electrode Potential, E^0 (V), 25°C
Li/Li^+	−3.09	Cd/Cd^{2+}	−0.403
Rb/Rb^+	−2.925	In/In^{3+}	−0.342
K/K^+	−2.925	Ti/Ti^+	−0.336
Cs/Cs^+	−2.923	Co/Co^{2+}	−0.277
As/As^+	−2.923	Ni/Ni^{2+}	−0.250
Sr/Sr^{2+}	−2.89	Mo/Mo^{3+}	ca. −0.2
Ca/Ca^{2+}	−2.87	Sn/Sn^{2+}	−0.136
Na/Na^+	−2.714	Pb/Pb^{2+}	−0.126
Mg/Mg^{2+}	−2.37	Fe/Fe^{3+}	−0.036
Pu/Pu^{3+}	−2.07	$H_a/2H^+$	0.000
Be/Be^{2+}	−1.85	Bi/Bi^{3+}	0.2
U/U^{3+}	−1.80	Sb/Sb^{3+}	0.2
Al/Al^{3+}	−1.66	As/As^{3+}	0.3
Ti/Ti^{2+}	−1.63	Cu/Cu^{2+}	0.337
Zr/Zr^{4+}	−1.53	$2Hg/Hg^{2+}$	0.789
Mn/Mn^{2+}	−1.18	Ag/Ag^+	0.7991
V/V^{2+}	ca. −1.18	Hg/Hg^{2+}	0.854
Nb/Nb^{3+}	ca. −1.1	Pd/Pd^{2+}	0.987
Zn/Zn^{2+}	−0.763	Pt/Pt^{2+}	ca. 1.2
Cr/Cr^{3+}	−0.74	Au/Au^{3+}	1.50
Ga/Ga^{3+}	−0.52	Au/Au^+	ca. 1.68
$Fe/Fe^{2\dagger}$	−0.440		

[a] The numerical values of the standard electrode potentials have been taken from *The Oxidation Stales of the Elements and Their Potentials in Aqueous Solutions,* 2nd ed.,W. M. Latimer, Prentice-Hall, Englewood Cliffs, NJ, 1952, with three exceptions. The values for trivalent bismuth, antimony, and arsenic were taken from *Theoretical and Applied Electrochemistry,* 3rd ed., M. deKay Thompson, Macmillan, New York, 1939. The sign convention used above is that of The Electrochemical Society.

TABLE 3 Standard Reference Electrodes

Half-Cell	$E_{25^\circ C}$, (V)
0.1 *N* calomel	0.334
1.0 *N* calomel	0.281
Saturated calomel	0.242
Silver–silver chloride	
Chloride ion unit activity	0.222
0.1 *N* KCl	0.288

TABLE 4 Equilibrium Constants of Interest in Electroplating[a]

$AgBr = Ag^+ + Br^-$	5.0×10^{13}
$AgCl = Ag^+ + Cl^-$	2.8×10^{-10}
$AgCN = Ag^+ + CN^-$	1.6×10^{-14}
$Ag(CN)_2^- = Ag^+ + 2CN^-$	1.8×10^{-19}
$Ag_4Fe(CN)_6 = 4Ag^+ + Fe(CN)_6^{4-}$	1.55×10^{-41}
$AgI = Ag^+ + I^-$	8.5×10^{-17}
$Ag(NH_3)_2^+ = Ag^+ + 2NH_3(aq.)$	5.9×10^{-8}
$AuCl_2^- = Au^{3+} + 4Cl^-$	5×10^{-22}
$Au(CN)_2^- = Au^+ + 2CN^-$	ca. 5×10^{-39}
$Cd(CN)_4 = Cd^{2+} + 4CN^-$	1.4×10^{-19}
$CdI_4^{2-} = Cd^{2+} + 4I^-$	ca. 5×10^{-7}
$Cd(NH_3)_4^{2+} = Cd^{2+} + 4NH_3(aq.)$	7.5×10^{-8}
$Co(NH_3)_6^{2+} = Co^{2+} + 6NH_3(aq.)$	1.25×10^{-5}
$Co(NH_3)_6^+ = Co^{3+} + 6NH_3(aq.)$	2.2×10^{-34}
$Co(NH_3)_5 \cdot H_2O^{3+} = Co^{3+} + 5NH_3(aq.) + H_2O$	1.6×10^{-35}
$CrCl_2^+ = Cr^{3+} + 2Cl^-$	1.26×10^{-2}
$HCrO_4 = H^+ + CrO_4^{2-}$	3.2×10^{-7}
$Cr_2O_7^{2-} + H_2O = 2HCrO_4^-$	2.3×10^{-2}
$Cu + Cu^{2+} = 2Cu^+$	6.3×10^{-7}
$Cu(CN)_2^- = Cu^+ + 2CN^-$	1×10^{-16}
$Cu(CN)_3^- = Cu^+ + 3CN^-$	5.6×10^{-28}[b]
$Cu(CNS) = Cu^+ + CNS^-$	4×10^{-14}
$Cu(NH_3)_2^+ = Cu^+ + 2NH_3(aq.)$	1.35×10^{-11}
$Cu(NH_3)_5^{2+} = Cu(NH_3)_4^{2+} + NH_3(aq.)$	2.8
$Cu(NH_3)_4^{2+} = Cu^{2+} + 4NH_3(aq.)$	4.7×10^{-15}
$Fe(CN)_6^{4-} = Fe^{2+} + 6CN^-$	ca. 10^{-35}
$Fe(CN)_6^{3-} = Fe^{3+} + 6CN^-$	ca. 10^{-42}
$Fe_2(C_4H_4O_6)_3(aq.) = 2Fe^{3+} + 3C_4H_4O_6^{3-}$	10^{-39}
$In^{3+} + H_2O = In(OH)^{2+} + H^+$	2×10^{-4}
$Mn(OH)_2 = Mn^{2+} + 2OH^-$	2×10^{-13}
$Ni(CN)_4^{2-} = Ni^{2+} + 4CN^-$	1×10^{-22}
$Ni(NH_3)_4^{2+} = Ni^{2+} + 4NH_3(aq.)$	1×10^{-8}
$Ni(NH_3)_6^{2+} = Ni^{2+} + 6NH_3(aq.)$	1.8×10^{-9}
$PbBr_2 = Pb^{2+} + 2Br^-$	4.6×10^{-6}
$PbBr^+ = Pb^{2+} + Br^-$	7.1×10^{-2}
$PbCl_2 = Pb^{2+} + 2Cl^-$	1.6×10^{-5}
$PbF_2 = Pb^{2+} + 2F^-$	4×10^{-8}
$PbI_2 = Pb^{2+} + 2I^-$	8.3×10^{-9}
$PbI^+ = Pb^{2+} + I^-$	3.45×10^{-2}
$PdCl_4^{2-} = Pd^{2+} + 4Cl^-$	5×10^{-13}
$PtCl_4^{2-} = Pt^{2+} + 4Cl^-$	ca. 1×10^{-16}
$PtBr_4^{2-} = Pt^{2+} + 4Br^-$	ca. 3×10^{-21}
$Sn(OH)_4 = Sn^{4+} + 4OH^-$	ca. 1×10^{-57}
$Zn(CN)_4^{2-} = Zn^{2+} + 4CN^-$	1.3×10^{-17}
$Zn(NH_3)_4^{2+} = Zn^{2+} + 4NH_3(aq.)$	3.4×10^{-10}

[a] These values have been taken from *The Oxidation States of the Elements and Their Potentials in Aqueous Solutions,* 2nd ed., W. M. Latimer, Prentice-Hall, Englewood Cliffs, NJ, 1952.

[b] From R. Ernst and C. Mann, *Trans. Electrochem. Soc.*, **61**, 363 (1952).

TABLE 5 Electrochemical Equivalents and Related Date for the Commonly Electrodeposited Metals[a]

Element	Symbol	Atomic Weight (1971)	Valence	Density, g cm^{-3} 20°C	mg C^{-1}	g A-h^{-1}	g/m^{-2} for 1 μm	A-h to Deposit 1 μm · m^2
Aluminum	Al	26.9815	3	2.7	0.0932	0.3355	2.702	8.078
Antimony	Sb	121.75	5	6.62	0.2524	0.9086	6.618	7.294
			3	—	0.4207	1.515	—	4.372
Arsenic	As	74.9216	5	5.73	0.1553	0.5591	5.729	10.26
			3	—	0.2588	0.9317	—	6.142
Bismuth	Bi	208.980	5	9.78	0.4332	1.560	9.788	6.278
			3	—	0.7220	2.599	—	3.766
Cadmium	Cd	112.40	2	8.65	0.5825	2.097	8.659	4.126
Chromium	Cr	51.996	6	7.14	0.08981	0.3234	7.146	22.11
			3	—	0.1796	0.6466	—	11.06
Cobalt	Co	58.9332	2	8.71	0.3054	1.099	8.719	7.926
Copper	Cu	63.546	2	8.93	0.3293	1.185	8.935	7.540
			1	—	0.6586	2.371	—	3.770
Gold	Au	196.967	3	19.32	0.6804	2.449	19.32	7.887
			2	—	1.021	3.676	—	5.257
			1	—	2.041	7.348	—	2.631
Hydrogen	H	1.0079	1	0.08375×10^{-3}	0.01045	0.03762	—	—
Indium	In	114.82	3	7.28	0.3967	1.428	7.278	5.092
Iron	Fe	55.847	3	7.86	0.1929	0.6944	7.867	11.32
			2	—	0.2894	1.042	—	7.540
Lead	Pb	207.2	4	11.34	0.5368	1.932	11.35	5.880
			2	—	1.074	3.866	—	2.936
Manganese	Mn	54.9380	2	7.3	0.2847	1.025	7.302	7.116
Molybdenum	Mo	95.94	6	10.2	0.1657	0.5965	10.21	17.11
Nickel	Ni	58.70	2	8.8	0.3043	1.095	8.803	8.044
Palladium	Pd	106.4	4	12.16	0.2758	0.9929	12.17	12.26
			2	—	0.5515	1.985	—	6.129
Platinum	Pt	195.09	4	21.37	0.5055	1.820	21.38	11.75
			2	—	1.011	3.640	—	5.871
Rhodium	Rh	102.905	4	12.44	0.2666	0.9598	12.44	12.95
			3	—	0.3555	1.280	—	9.730
			2	—	0.5332	1.920	—	6.481
Silver	Ag	107.868	1	10.49	1.118	4.025	10.50	2.605
Tin	Sn	118.69	4	7.3	0.3075	1.107	7.302	6.604
			2	—	0.6150	2.214	—	3.300
Zinc	Zn	65.38	2	7.14	0.3387	1.219	7.146	5.863

[a] All values are based on 100% current efficiency and absolute electrical units.

TABLE 6 Values of Hydrogen Overvoltage, Direct Method[a]

Material	CD, A cm^{-2}	Overvoltage V at $16 \pm 1°C$ in 2 *N* H_2SO_4			
		10^{-3}	10^{-2}	10^{-1}	1
Cadmium		0.98	1.13	1.22	1.25
Mercury		0.90	1.04	1.07	1.12
Tin		0.86	1.08	1.22	1.23
Bismuth		0.78	1.05	1.14	1.23
Zinc		0.72	0.75	1.06	1.23
Graphite		0.60	0.78	0.98	1.22
Aluminum		0.56	0.83	1.0	1.29
Nickel		0.56	0.75	1.05	1.21
Lead		0.52	1.09	1.18	1.26
Brass		0.50	0.65	0.91	1.25
Copper		0.48	0.58	0.8	1.25
Silver		0.47	0.76	0.88	1.09
Iron		0.40	0.56	0.82	1.29
Monel		0.28	0.38	0.62	1.07
Gold		0.24	0.39	0.59	0.80
Duriron		0.20	0.29	0.61	1.02
Palladium		0.12	0.3	0.7	1.0
Platinum		0.024	0.07	0.29	0.68
Platinum (platinized)		0.015	0.03	0.04	0.05

[a] The values listed were abstracted from the table prepared by M. Knobel, in *International Critical Tables,* Vol. 6, p. 329. E. W. Washburn, Ed., McGraw-Hill, New York, 1929. Overvoltages obtained by the direct method necessarily include the IR drop and concentration polarization.

TABLE 7 Percentage Metal In Common Plating Salts (Based on 100% Purity)

Name	Formula	Molecular	% Metal
Antimony trichloride	$SbCl_3$	228.1	53.4
Antimony oxide	Sb_2O_3	291.5	83.5
Bismuth oxide	Bi_2O_3	466.0	89.7
Cadmium cyanide	$Cd(CN)_2$	164.4	68.4
Cadmium oxide	CdO	128.4	87.5
Chromic acid	CrO_3	100.0	52.0
Cobalt ammonium sulfate	$CoSO_4 \cdot (NH_4)_2SO_4 \cdot 6H_2O$	395.2	14.9
Cobalt chloride	$CoCl_2$	129.8	45.4
Cobalt sulfate	$COSO_4$	155.0	38.0
	$CoSO_4 \cdot 7H_2O$	281.1	21.0
Copper carbonate (basic)	$2CuCO_3 \cdot Cu(OH)_2$	344.7	55.3
Copper cyanide	$CuCN$	89.6	70.9
Copper fluoborate[a]	$Cu(BF_4)_2$	237.2	26.8
Copper sulfate	$CuSO_4 \cdot 5H_2O$	249.7	25.4
Ferrous chloride	$FeCl_2$	126.8	44.0
Ferrous ammonium sulfate	$FeSO_4 \cdot (NH_4)_2SO_4 \cdot 6H_2O$	392.2	14.2
Gold chloride (ic)	$AuCl_3$	303.6	65.0
Gold chloride (ic), crystal	$AuCl_3 \cdot 2H_2O$	339.6	58.1
Gold chloride (ous)	$AuCl$	232.7	84.7
Gold cyanide	$AuCN$	223.2	88.4
Gold potassium cyanide	$KAu(CN)_2$	288.3	68.4
Gold potassium cyanide, crystal	$KAu(CN)_2 \cdot 2H_2O$	324.4	60.8
Gold sodium cyanide	$NaAu(CN)_2$	272.2	72.4
Indium cyanide	$In(CN)_3$	192.8	59.5
Lead carbonate (basic)	$2PbCO_3 \cdot Pb(OH)_2$	775.7	80.1
Lead fluoborate[a]	$Pb(BF_4)_2$	380.9	54.4
Manganous chloride	$MnCl_2 \cdot 4H_2O$	197.9	27.7
Manganous sulfate	$MnSO_4 \cdot H_2O$	169.0	32.5
Nickel ammonium sulfate	$NiSO_4 \cdot (NH_4)_2SO_4 \cdot 6H_2O$	395.1	14.9
Nickel carbonate (basic)	$2NiCO_3 \cdot 3Ni(OH)_2 \cdot 4H_2O$	587.6	49.9
Nickel chloride	$NiCl_2 \cdot 6H_2O$	237.7	24.7
Nickel sulfate	$NiSO_4 \cdot 7H_2O$	280.9	20.9
Platinum chloride, crystal (chloroplatinic acid)	$H_2PtCl_6 \cdot 6H_2O$	518.1	37.7
Potassium stannate	$K_2Sn(OH)_6$	298.9	39.7
Rhodium phosphate	$RhPO_4 \cdot 3H_2O$	251.9	40.8
Rhodium sulfate	$Rh_2(SO_4)_3 \cdot 12H_2O$	710.2	29.0
Silver chloride	$AgCl$	143.3	75.3
Silver cyanide	$AgCN$	133.9	80.6
Silver potassium cyanide	$KAg(CN)_2$	199.0	54.2
Silver sodium cyanide	$NaAg(CN)_2$	182.9	59.0
Silver nitrate	$AgNO_3$	169.9	63.5
Sodium stannate	$Na_2SnO_3 \cdot 3H_2O$	266.7	44.5
Tin chloride (ous), anhyd.	$SnCl_2$	189.6	62.6
Tin fluoborate[a]	$Sn(BF_4)_2$	292.3	40.6
Tin fluoborate[a]	$Sn(BF_4)_2 \cdot 6H_2O$	400.4	29.6
Tin sulfate	$SnSO_4$	214.8	55.3
Tungstic acid	H_2WO_4	249.9	73.6
Tungstic oxide	WO_3	231.9	79.3
Zinc carbonate	$ZnCO_3$	125.4	52.2
Zinc cyanide	$Zn(CN)_2$	117.4	55.7
Zinc fluoborate[a]	$Zn(BF_4)_2$	239.0	27.4
Zinc fluoborate[a]	$Zn(BF_4)_2 \cdot 6H_2O$	347.1	18.8
Zinc oxide	ZnO	81.4	80.3
Zinc sulfate	$ZnSO_4 \cdot 7H_2O$	287.6	22.7

[a] Does not apply to solutions as usually available.

TABLE 8 Specific Gravity–Degrees Baumé Conversion Table

Specific Gravity	Degrees Baumé	Specific Gravity	Degrees Baumé	Specific Gravity	Degrees Baumé
1.00	0.00	1.34	36.79	1.68	58.69
1.01	1.44	1.35	37.59	1.69	59.20
1.02	2.84	1.36	38.38	1.70	59.71
1.03	4.22	1.37	39.16	1.71	60.20
1.04	5.58	1.38	39.93	1.72	60.70
1.05	6.91	1.39	40.68	1.73	61.18
1.06	8.21	1.40	41.43	1.74	61.67
1.07	9.49	1.41	42.16	1.75	62.14
1.08	10.78	1.42	42.89	1.76	62.61
1.09	11.97	1.43	43.60	1.77	63.08
1.10	13.18	1.44	44.31	1.78	63.54
1.11	14.37	1.45	45.00	1.79	63.99
1.12	15.54	1.46	45.68	1.80	64.44
1.13	16.68	1.47	46.36	1.81	64.89
1.14	17.81	1.48	47.03	1.82	65.31
1.15	18.91	1.49	47.68	1.83	65.77
1.16	20.00	1.50	48.33	1.84	66.20
1.17	21.09	1.51	48.97	1.85	66.62
1.18	22.12	1.52	49.60	1.86	67.04
1.19	23.15	1.53	50.23	1.87	67.46
1.20	24.17	1.54	50.84	1.88	67.87
1.21	25.16	1.55	51.45	1.89	68.28
1.22	26.15	1.56	52.05	1.90	68.68
1.23	27.11	1.57	52.64	1.91	69.08
1.24	28.06	1.58	53.23	1.92	69.48
1.25	29.00	1.59	53.80	1.93	69.87
1.26	29.92	1.60	54.38	1.94	70.26
1.27	30.83	1.61	54.94	1.95	70.64
1.28	31.72	1.62	55.49	1.96	71.02
1.29	32.60	1.63	56.04	1.97	71.40
1.30	33.46	1.64	56.58	1.98	71.77
1.31	34.31	1.65	57.12	1.99	72.14
1.32	35.15	1.66	57.65	2.00	72.50
1.33	35.98	1.67	58.17		

TABLE 9 Specific Gravity and Degrees Baumé of Aqueous Hydrochloric Acid Solutions

Specific Gravity, 20/4°C	Degrees Baumé	% HCl	Grams per Liter	Ounces per Gallon
1.0032	0.5	1	10.03	1.34
1.0082	1.2	2	20.16	2.68
1.0181	2.6	4	40.72	5.43
1.0279	3.9	6	61.67	8.23
1.0376	5.3	8	83.01	11.08
1.0474	6.6	10	104.7	13.95
1.0574	7.9	12	126.9	16.9
1.0675	9.2	14	149.5	19.9
1.0776	10.4	16	172.4	23.0
1.0878	11.7	18	195.8	26.1
1.0980	12.9	20	219.6	29.25
1.1083	14.2	22	243.8	32.5
1.1187	15.4	24	268.5	35.8
1.1290	16.6	26	293.5	39.1
1.1392	17.7	28	319.0	42.5
1.1493	18.8	30	344.8	46.0
1.1593	19.9	32	371.0	49.5
1.1691	21.0	34	397.5	53.0
1.1789	22.0	36	424.4	56.6
1.1885	23.0	38	451.6	60.2
1.1980	24.0	40	479.2	64.0

TABLE 10 Specific Gravity and Degrees Baumé of Aqueous Sulfuric Add Solutions

Specific Gravity, 20/4°C	Degrees Baumé	% H_2SO_4	Grains per Liter	Ounces per Gallon
1.0051	0.7	1	10.05	1.4
1.0184	2.6	3	30.55	4.07
1.0317	4.5	5	51.59	6.88
1.0453	6.3	7	73.17	9.76
1.0591	8.1	9	95.32	12.7
1.0731	9.9	11	118.0	15.73
1.0874	11.7	13	141.4	18.85
1.1020	13.4	15	165.3	22.05
1.1168	15.2	17	189.9	25.3
1.1318	16.9	19	215.0	28.7
1.1471	18.6	21	240.9	32.1
1.1626	20.3	23	267.4	35.6
1.1783	21.9	25	294.6	39.3
1.1942	23.6	27	322.4	43.0
1.2104	25.2	29	351.0	46.8
1.2267	26.8	31	380.3	51.0
1.2432	28.4	33	410.3	54.7
1.2599	29.9	35	441.0	58.8
1.2769	31.4	37	472.5	62.9
1.2941	33.0	39	504.7	67.3
1.3116	34.5	41	537.8	71.6
1.3294	35.9	43	571.6	76.1
1.3476	37.4	45	606.4	80.8
1.3663	38.9	47	642.2	85.5
1.3854	40.3	49	678.8	90.5
1.4049	41.8	51	716.5	95.5
1.4248	43.2	53	755.1	100.8
1.4453	44.7	55	794.9	106.0
1.4662	46.1	57	835.7	111.5
1.4875	47.5	59	877.6	117.0
1.5091	48.9	61	920.6	122.7
1.5310	50.3	63	964.5	128.7
1.5533	51.7	65	1010	134.8
1.5760	53.0	67	1056	141.0
1.5989	54.3	69	1103	147.0
1.6221	55.6	71	1152	153.8
1.6456	56.9	73	1201	160.0
1.6692	58.1	75	1252	167.0
1.6927	59.3	77	1303	174.0
1.7158	60.5	79	1355	181.0
1.7383	61.6	81	1408	188.0
1.7594	62.6	83	1460	195.0
1.7786	63.5	85	1512	201.6
1.7951	64.2	87	1562	208.4
1.8087	64.8	89	1610	214.6
1.8195	65.3	91	1656	220.6
1.8279	65.7	93	1700	226.5
1.8337	65.9	95	1742	232.5
1.8364	66.0	97	1781	237.5
1.8342	65.9	99	1816	242.0
1.8305	65.8	100	1831	244.5

TABLE 11 Total Concentrations of Copper Sulfate Plus Sulfuric Acid in Solutions of Given Specific Gravity[a]

Specific Gravity, 25/4°C	Copper Sulfate plus Sulfuric Acid		Specific Gravity, 25/4°C	Copper Sulfate plus Sulfuric Acid	
	g L^{-1}	oz gal^{-1}		g L^{-1}	oz gal^{-1}
1.01	20	2.7	1.13	217	29.1
1.02	36	4.8	1.14	234	31.3
1.03	52	7.0	1.15	251	33.6
1.04	68	9.1	1.16	268	35.9
1.05	84	11.3	1.17	286	38.3
1.06	100	13.4	1.18	303	40.6
1.07	117	15.7	1.19	321	43.0
1.08	133	17.8	1.20	339	45.4
1.09	150	20.0	1.21	357	47.8
1.10	166	22.3	1.22	375	50.2
1.11	183	24.5	1.23	393	52.6
1.12	200	26.8			

[a] From *Principles of Electroplating and Electroforming,* W. Blum and G. B. Hogaboom, McGraw-Hill, New York, 1930, p. 410.

TABLE 12 Conversion Factors

Multiply	By	To Obtain
Amperes	1.04×10^{-5}	Faradays per second
Amperes per square foot	0.108	Amperes per square decimeter
Ampere-hours	3600	Coulombs
Ampere-hours	0.0373	Faradays
Angstrom units	3.94×10^{-9}	Inches
Angstrom units	1×10^{-8}	Centimeters
Angstrom units	10^{-1}	Nanometers
Centimeters	0.3937	Inches
Centimeters	393.7	Mils
Circular mils	7.85×10^{-7}	Square inches
Circular mils	5.07×10^{-6}	Square centimeters
Cubic centimeters	0.061	Cubic inches
Cubic feet	1728	Cubic inches
Cubic feet	7.48	Gallons
Cubic feet	29.9	Quarts (liquid, U.S.)
Cubic inches	16.39	Cubic centimeters
Drams (avoir.)	1.77	Grams
Drams (avoir.)	0.0625	Ounces (avoir.)
Drams (fluid)	3.7	Cubic centimeters
Drams (fluid)	0.125	Ounces (fluid)
Faradays	96,501.2	Coulombs (int.)
Feet	30.48	Centimeters
Gallons	4	Quarts (liquid)
Gallons	3.785	Liters
Gallons	128	Ounces (fluid)
Gallons	8	Pints (liquid)
Gallons	3.782	Kilograms water (62° F)
Gallons	8.34	Pounds (avoir.) water (62°F)
Gallons (U.S.)	0.833	Gallons (Imperial)
Gallons per minute	0.002228	Cubic feet per second
Gallons per minute	0.0631	Liters per second
Grams	0.564	Drams (avoir.)
Grams	15.43	Grains
Grams	0.03215	Ounces (troy)
Grams	0.0353	Ounces (avoir.)
Grams per liter	1000	Parts per million
Inches	2.54	Centimeters
Inches	1000	Mils
Kilograms	2.205	Pounds (avoir.)
Kilograms	2.679	Pounds (troy)
Liters	0.03532	Cubic feet
Liters	1.057	Quarts (liquid)
Micrometers	3.94×10^{-5}	Inches
Micrometers	0.001	Millimeters
Milliliters	1.0	Cubic centimeters
Mils	0.001	Inches
Mils	0.00254	Centimeters
Ounces (avoir.)	28.35	Grams
Ounces per gallon (avoir.)	7.5	Grams per liter
Ounces (troy)	31.1	Grams
Ounces (troy)	480	Grains
Ounces (troy)	20	Pennyweights
Ounces per gallon (fluid)	7.7	Milliliters per liter
Pennyweights	24	Grains
Pennyweights per gallon	0.41	Grams per liter
Pints (liquid, U.S.)	473.2	Cubic centimeters
Pints (liquid, U.S.)	16	Ounces (fluid)
Pounds (avoir.)	453.6	Grams
Pounds (avoir.)	16	Ounces (avoir.)
Pounds (avoir.)	1.215	Pounds (troy)
Pounds (troy)	373.24	Grams
Pounds (troy)	12	Ounces (troy)
Pounds per cubic foot	16.02	Grams per liter
Pounds per gallon (U.S.)	119.8	Grams per liter
Square centimeters	1.97×10^{5}	Circular mils
Square inches	10^{6}	Square mils
Square inches	1.27×10^{6}	Circular mils
Square inches	6.45	Square centimeters
Volts per inch	0.394	Volts per centimeter

TABLE 13 Temperature Conversion Table

0–38			39–76			77–212		
°C		°F	°C		°F	°C		°F
−17.8	0	32.0	3.89	39	102.2	25.0	77	170.6
−17.2	1	33.8	4.44	40	104.0	25.6	78	172.4
−16.7	2	35.6	5.00	41	105.8	26.1	79	174.2
−16.1	3	37.4	5.56	42	107.6	26.7	80	176.0
−15.6	4	39.2	6.11	43	109.4	27.2	81	177.8
−15.0	5	41.0	6.67	44	111.2	27.8	82	179.6
−14.4	6	42.8	7.22	45	113.0	28.3	83	181.4
−13.9	7	44.6	7.78	46	114.8	28.9	84	183.2
−13.3	8	46.4	8.33	47	116.6	29.4	85	185.0
−12.8	9	48.2	8.89	48	118.4	30.0	86	186.8
−12.2	10	50.0	9.44	49	120.2	30.6	87	188.6
−11.7	11	51.8	10.0	50	122.0	31.1	88	190.4
−11.1	12	53.6	10.6	51	123.8	31.7	89	192.2
−10.6	13	55.4	11.1	52	125.6	32.2	90	194.0
−10.0	14	57.2	11.7	53	127.4	32.8	91	195.8
−9.44	15	59.0	12.2	54	129.2	33.3	92	197.6
−8.89	16	60.8	12.8	55	131.0	33.9	93	199.4
−8.33	17	62.6	13.3	56	132.8	34.4	94	201.2
−7.78	18	64.4	13.9	57	134.6	35.0	95	203.0
−7.22	19	66.2	14.4	58	136.4	35.6	96	204.8
−6.67	20	68.0	15.0	59	138.2	36.1	97	206.6
−6.11	21	69.8	15.6	60	140.0	36.7	98	208.4
−5.56	22	71.6	16.1	61	141.8	37.2	99	210.2
−5.00	23	73.4	16.7	62	143.6	37.8	100	212.0
−4.44	24	75.2	17.2	63	145.4	43.0	110	230.0
−3.89	25	77.0	17.8	64	147.2	49.0	120	248.0
−3.33	26	78.8	18.3	65	149.0	54.0	130	266.0
−2.78	27	80.6	18.9	66	150.8	60.0	140	284.0
−2.22	28	82.4	19.4	67	152.6	66.0	150	302.0
−1.67	29	84.2	20.0	68	154.4	71.0	160	320.0
−1.11	30	86.0	20.6	69	156.2	77.0	170	338.0
−0.56	31	87.8	21.1	70	158.0	82.0	180	356.0
0.00	32	89.6	21.7	71	159.8	88.0	190	374.0
0.56	33	91.4	22.2	72	161.6	93.0	200	392.0
1.11	34	93.2	22.8	73	163.4	99.0	210	410.0
1.67	35	95.0	23.3	74	165.2	100.0	212	413.0
2.22	36	96.8	23.9	75	167.0			
2.78	37	98.6	24.4	76	168.8			
3.33	38	100.4						

[a] The numbers in the center of each group refer to the temperature in degrees Centigrade or Fahrenheit which it is desired to convert into the other scale. If converting from Fahrenheit to Centigrade, the equivalent will be found in the left column; if converting from Centigrade to Fahrenheit, the answer will be found in the column on the right.

INDEX

ABS (acrylonitrile, butadiene, and styrene) terpolymer, decorative nickel electrodeposition, 88–89
Accelerators. *See* Catalysts
Acid chlorides:
  palladium electrodeposition, 345–348
  zinc baths:
    composition/operating characteristics, 290
Acid cleaners, 509
Acid copper:
  addition agents, 36–39
  analytical methods, 41–42
  applications, 34–35
  current modulation techniques, 44
  diamond turning, 49–50
  electroforming, 48–49
  evolution, historical summary, 46
  high-speed electroplating, 49
  history and development, 34
  operating conditions for, 39
    agitation apparatus, 39
    anodes, 40
    current density/agitation, 39
    equipment design, 40
    filtration and purification, 39–40
    specifications, 40
    temperature condition, 39
    ultrasonic agitation, 39
  patterned electrodeposition, microelectronics, 47–48
  plating solutions impurities in, 41
  principles, 35
  printed wiring boards, 45–47
  properties and structure, 42–44
  solution constituents, 35–36
    chloride, 36
    copper and sulfuric acid, 35–36
    fluoborate, 36
  steel, zinc, plastics, and aluminum plating with, 45
  sulfate, with solution constituents, 35
Acid cyanide baths, gold electrodeposition, 119
Acid electrolytes:
  lead/lead alloys electrodepostion, 266–268
  palladium electrodeposition, 345–348
    pH level, 346
Acid electroplating, tin electrodeposition, 152–156
Acid strikes:
  palladium electrodeposition, 348
    scanning electron micrographs, 349
Acid sulfates electrolytes, palladium electrodeposition, 348
Activation energy, electroless depostion, copper compound, 442
Activity coefficient, electrode potential, 3
Adams's solution, 80
Additive-free hard gold (AFHG), 121, 122
Additives function, 151
  acid copper, 37–38
  behavior of, 151
  cyanide copper systems, 53
  electrodeposition growth mechanisms:
    consumption of, 13
    effect of, 12–13
    nucleation and, 12
  lead and lead alloys electrodeposition, 252
  magnetic recording:
    coercivity *vs.* C_{sac} and R_s, 582–583
    corrosion properties *vs.* R_s, 585–587
    saccharin adsorption, 580
    stress *vs.* C_{sac}, 583
    sulfur in deposit, 580–582
    surface roughness, 584–585

Modern Electroplating, Fifth Edition Edited by Mordechay Schlesinger and Milan Paunovic

Additives function (*Continued*)
origins, 20
palladium electrodeposition, nonadditive tetramine chloride electrolytes, 352–355
tin-lead alloys electrodeposition, 268–269
Adhesion:
nickel electroplating corrosion testing, 108
nonconductors deposition, 416–417
Adsorption:
chemisorption, 12
physisorption, 12
Advocacy groups, electrodepostion economics, environmental policy and, 569–570
Aging tests, tin–lead alloy electrodeposition, solderability test, 276–277
Agitation technique:
acid copper electrodeposition:
forms of, 39
operating conditions, 39
lead and lead alloys electrodeposition, 253
magnetic recording, paddle cell, 577
pyrophosphate copper solution, 61
tin–lead alloys electrodeposition, 272
Ag_3Sn formation, 198
Alkali cyanide, anode corrosion, 134
Alkali metal fluorosilicates:
electrolysis, 384
Alkaline baths, 451
cyanide baths, 118
formulations, 118
Alkaline cleaners, electrodepostion preparation with, 509–510
Alkaline electrolytes:
palladium electrodeposition, 340–345
buffer system, 344
counterion effects, 340
1,3-diaminopropane electrolyte, 340
ligand concentration effects, 343
limiting currents, 344
material properties, 345
quantitative hydrogen analysis, 344–345
replenishment schemes, 343
supporting electrolyte, 344
temperature and pH effects, 340–343
plumbite electrolytes, 251
pyrophosphate electrolytes, 251
Alkaline gold cyanide bath, 117
Alkaline noncyanide copper plating solutions, 58
Alkaline silver cyanide, 134
Alkaline tin, plating chemistries and processes, 155–156
Alkane sulfonic acids, 154
Alkylsulfonic acid electrolytes, tin–lead alloys electrodeposition, 267–268
Alloys, electrodeposition of:
deposition, 4
potential, 17–18
general properties, 16–17
principles, 17
ternary CoNiFe diagram, 574
All-wet process, 377, 380
Alumina, copper composites materials, 63
Aluminum compounds:
aluminum-based alloys, 442
decorative nickel electrodeposition and, 89
decorative nickel plus chromium coatings, 90
plating, acid copper electrodeposition, 45
Aluminum electrode, 427
Aluminum wires, 115
American Electroplaters and Surface Finishers (AESF) Society, 42
American Electroplaters' Society (AES), 34
American Society for Electroplated Plastics (ASEP), 89
American Society for Testing and Materials (ASTM) Standards, 355
B 117–90, corrosion resistance determination, 565
B 253, decorative nickel electrodeposition, aluminum, 89
B 254, decorative nickel electrodeposition, stainless steel, 89
B 368, nickel electroplating corrosion testing, 108
B 456
decorative nickel electrodeposition, 88–91
nickel electroplating corrosion testing, 108
B 489, ductility testing, 108
B 504, thickness quality control and testing, 107–108
B 533, adhesion testing, 108
B 571, adhesion testing, 108
B 578, microhardness testing, 109
B 604
decorative nickel electrodeposition, 89, 90
nickel electroplating corrosion testing, 108
B 627, electrolytic corrosion testing (EC test), 87
B 636, internal stress measurement, 108–109
B 727, decorative nickel electrodeposition, plastics, 89
B 764, STEP test, 88, 108
B 832, nickel electroforming, mandrels, 98
B 851, functional nickel plating, fatigue strength, 96–97
Amidosulfonate electrolytes, lead and lead alloys electrodeposition, 249–250
3-Aminopropyltriethoxy silane (APTES), organosilane layer, 377
Ammeter devices, quality control and monitoring, 529
Ammonia:
palladium–cobalt alloy, 358–360
Pd–Ni electroplating baths, 356–357
pyrophosphate copper, 59
solution analysis, 61
Ammonium ions:
bath additives, 452–454
iron electrodeposition:
ferrous sulfate bath, 310–311
nickel electroforming, 95
Amorphous compound, deposits structure and properties, 18
Andritz–Ruthner gravitel cell:
zinc/zinc alloys, continuous plating technique, 294
Anion penetration, chromium electrodeposition, 210
Annealing:
copper electrodeposition, deposit structure, 57–58
electrodeposits mechanical properties, 28
Anodes:
acid copper electrodeposition, 40
anodic process, 127
chromium electrodepostion, quality control testing, 223

iron electrodeposition, 320
lead and lead alloys electrodeposition, 252–253
pyrophosphate copper solution, 61
tin–lead alloys electrodeposition, 269–271
insoluble anodes, 270–271
metallic contaminations, 270
soluble anodes, 269–270
zinc/zinc alloys:
alkaline noncyanide zinc baths, passivation of, 289
Anodic/cathodic gas formation, 154
Anodic oxidation:
copper oxide, semiconductors electrodeposition, 398–399
electrolessdeposition, gold alloys, plating rate increases and modification of, 487–488
nickel electroforming, 98–99
Anodic partial reaction, 14, 435
Anodic polarization curves, 100, 133
Anodic process, 127
Antimony:
acid copper plating solution, impurities in, 41
chromium electrodeposition, 224
lead–antimony alloys electrodeposition, 257
tin–lead alloys electrodeposition:
anodic impurities, 274
hardness properties, 277–278
Anvil effect, electrodeposits, hardness parameter, 30
Appearance test:
gold electrodeposition, 128
Aprotic solvents:
lead and lead alloys electrodeposition, 260–261
Aquation, chromium electrodeposition, 209
Aqueous acidic solutions:
standard potentials in, 159
Aqueous cleaners, electrodeposition preparation with, 509–510
Arsenic:
acid copper plating solution, impurities in, 41
palladium–arsenic alloy, 362
semiconductor electrodeposition process, gallium arsenide (GaAs), 384–385
Ascorbic acid bath, 491
Atomic absorption (AA):
spectrometry, 539
spectrophotometry, 128
Atomic force microscopy (AFM), 16, 134, 378
Atomic layer deposition (ALD):
thin film interdiffusion, 370–371
Atomistic representation, electrodeposition kinetics, 9–11
step-edge ion-transfer mechanism, 10
terrace ion-transfer mechanism, electrodeposition kinetics, atomistic aspect of, 10–11
Au-C bilayer film, 126
Auger electron spectroscopy (AES), 485, 550
Auger elemental mapping, 172
Au(I) cyanide complex:
electrodeposition, 122
Au(III)-phosphate complex, 495
Au(I)-mercaptosuccinate, 495
Au(I) sulfite, 123
Au(I) sulfite–thiosulfate system, 494
Au(I)-thiosulfate complex, 491
Au(lll)-iodide/ascorbic acid bath, 495
Autocatalytic deposition (AD), 415. *See also* Electroless plating
definition, 416
Autocatalytic plating, 483
Autocatalytics. *See* Electroless plating
Automated electrodeposition systems, quality control and monitoring:
on-line monitoring systems, 540–543
sensor technology, 530
Automatic electroplating, 540
process monitoring and control system, 540
Auxiliary brighteners, decorative electroplating, bright nickel solutions, 84
Avogadro's number, 7
electrodeposition kinetics, Faraday's law, 7–8

Band gap engineering, multilayered structure, 21
Bandoleer plating, 521
Barrel plating, 148, 149, 514
zinc/zinc alloys electrodeposition:
acid chloride zinc baths, 289–290
alkaline noncyanide zinc baths, 288–289
alloy plating, 291–293
considerations, 290–291
cyanide zinc baths, 286–288
plating, 291–293
Barrier layer materials:
copper electrodeposition, 603
Base metal:
chromium elctrodeposition:
preparation, 226
gold electrodeposition, barrier metals, 126
Basis reproduction (BR):
copper electrodeposits, microstructure analysis, 375
zinc/zinc alloys electrodeposition, 285
Bath compositions. *See also* Specific bath solution
tin–lead alloys electrodeposition, 266–268
alkylsulfonic acid electrolytes, 267–268
pH solutions, 268
tetrafluoroboric acid electrolytes, 266–267
Bath constituent concentration monitoring, 532
atomic absorption spectrometry, 539
automatic plating on-line monitoring, 540–543
conductivity, 539–540
electrochemical analysis, 534–536
high-performance liquid chromatography (HPLC), 537–538
ion-selective electrodes, 536–537
mass spectroscopy (MS), 538–539
photometric analysis, 534
plating test cells, 532–534
specific gravity, monitoring, 539
total organic carbon analysis, 539
X-ray fluorescence (XRF), 539
BCC. *See* Body-centered-cubic lattice
Bearing alloys, tin–lead alloys electrodeposition, coating applications, 278
Bell system, 169
Benzotriazole, 493

Beryllium copper spring material, 126
Beta backscatter, quality control and monitoring, 544
Beta modification, chromium electrodeposits, 234
Binary lead-free tin alloys:
  materials properties of, 157
Binding energy:
  definition, 137
Bismuth:
  acid copper plating solutions, impurities in, 41
  lead–bismuth alloys, 257
  tin–bismuth alloys:
    electrodeposition, materials properties, 161–162
    lead-free solders using, 144
    phase diagrams for, 157–159
  tin–lead alloy electrodeposition, hardness properties, 277
Bismuth–tin binary system, 157
Black chromium deposits:
  mechanisms and structure, 228
  structural analysis, 232–234
Black nickel, functional nickel plating, 96
Black spots phenomenon, acid copper electrodeposition, diamond-turning, 50
Blistering, nickel electrodeposition, coating defects, 106–107
Body-centered cubic (bcc), 232
  deposits structure and properties, 19
  iron electrodeposition, deposit properties, 316–317
  magnetic materials electrodepostion, nickel–iron alloys, 628
Boltzmann's constant, thin films interdiffusion, 24
Bonding bumps, patterned electrodeposition, acid copper solutions, 48
Bond strengths, electrodeposit adhesion, 30
Bone glue additives, tin–lead alloy electrodeposition, 268
Boric acid:
  copper electrodeposition, fluoborate bath, 36
  iron electrodeposition, fluoborate bath, 312
  nickel plating, quality control, 103–104
Borohydride bath, 484
  characteristics, 484
  with EDTA and ethanolamine, 488
  improved, 485–487
  problems associated with, 485
Boron compounds:
  boron-nickel alloys, electroless deposition, 451–452
  cobalt alloys, electroless deposition, 501–502
  iron–boron compounds, electrodeposition with, 317
Bose–Einstein condensation:
  copper oxide, semiconductors electrodeposition, 398–399
Bragg angles, 189, 190
Bragg diffraction pattern, electrodeposition structure, 22
Brass compounds:
  mirrors, 137
  tin–lead alloy electrodeposition, interlayering process, 282–283
  zinc–copper alloys, barrel-and-rack plating, 292–293
Brass mirrors, 137
Bright acid copper electroplating, nonconductors deposition, 413–414
Bright plating solutions:
  chromium electrodeposition, 216
  nickel solution:
    decorative electroplating, 84–85
    multilayer coatings, 85–87
    semibright solution, 85
Brinell scale, chromium electrodeposition:
  hardness properties, 234–235
  wear resistance testing, 234–235
Brittleness, gold electrodeposition, 128
Bronzing, nonconductors deposition, 413
Brush plating, designer/engineering electroplating technology, 522
Buffer system, palladium electrodeposition, 344
Buffing, copper deposits, 33
Bulge test, electrodeposit mechanical properties, 28
Bulk micromachining, microfabrication techniques, 617, 618
Butler–Volmer equations, 135, 594
Butler–Volmer kinetics, gold electrodeposition, 124

Cadmium compounds:
  lead–cadmium alloys, 257–258
  semiconductor electrodeposition processes:
    cadmium selenide, 388–389
    cadmium sulfide compounds, 390–391
    cadmium telluride, 386–388
    cadmium zinc telluride, 390
    copper sulfide, 391–392
    mercury cadmium teliuride (MCT), 394
    zinc cadmium selenide, 389–390
Calcium compounds:
  iron electrodeposition, ferrous chloride bath, 311–312
  lead and lead alloy electrodeposition, molten depositions, 261
Cannizzaro reaction, electroless deposition, copper compund, 435
Carbon-14 complexes, gold electrodeposition, acid cyanide baths, 120
Carbon content:
  cyanide copper and, 51–53
  high-efficiency copper solutions, 52–53
  tin–lead alloy electrodeposition, solderability testing, 277
Carbon, diffusion coefficient, 24
Carbon disulfide, silver electrodeposition, 136
Carbon nanotubes (CNTs), 481
Carosel cell, zinc/zinc alloys, continuous plating technique, 293
Carriers:
  copper additives, 46
  decorative electroplating, bright nickel solutions, 84
Catalysts, copper electrodeposition mechanism, 590
Cathode efficiency:
  iron electrodeposition, iron–nickel–chromium alloys, 317
  nickel plating, 81
  zinc/zinc alloys, continuous plating techniques, electrolyte composition, 300
Cathode reaction mechanism:
  zinc/zinc alloys electrodeposition, cyanide-zinc baths, 287
Cathodic current efficiency, 118
Cathodic deposition, 17
Cathodic partial reaction, 14
  electroless deposition, 13–15
    copper compounds, 434, 436
  mixed-potential theory, 433

Cathodic polarization curves, 133
Cathodic process, 5
Ceramic chip capacitors:
  whiskers, 186
CFCs (chlorofluorohydrocarbons), 509
C-film, hexavalent chromium electrodeposition, 213–214
Chalcogenide semiconductors:
  semiconductors electrodeposition:
    cadmium selenide, 388–389
    cadmium sulfide, 390–391
    cadmium telluride, 386–388
    cadmium zinc telluride, 390
    copper indium diselenide, 392–394
    copper sulfide, 391
    indium selenide, 392
    indium sulfide, 385–386
    lead sulfide, 386
    mercury cadmium telluride, 394
    zinc cadmium selenide, 389–390
    zinc chalcogenides, 389
Channel-type porous chromium, properties of, 237
Chemical conditioners, nonconductors deposition, 413–414
Chemical mechanical polishing (CMP) process, 639
  electrochemical deposition process, 369
Chemical resistance, chromium electrodeposition, 237–238
Chemical sensors:
  cation-sensitive electrode, 428
  electropolymerization, 427–428
  potentiometric biosensor, for urea, 428–429
Chemical vapor deposition (CVD), 443
  electrochemical deposition process, 369
  microfabrication techniques, 618
Chemisorption, additive effect, crystal deposition, 12
Chloride compounds:
  iron electrodeposition, ferrous chloride bath, 311–317
  nickel plating:
    chloride solution, 95
    primary nickel, anodic behavior of, 100–101
    sulfate solution, 95–96
  zinc/zinc alloys:
    acid baths, 289–290
    continuous plating technique, electrolyte composition, 299
Chloride ions:
  acid copper electrodeposit and, 36
  additives effects, 373
  copper deposition, 371
  synergistic effect, 36
Chlorofluorocarbon (CFC):
  displacement method, 127
Chlorofluorohydrocarbons, 509
Choline chloride (ChCl), 134
Chromates:
  hexavalent chromium electrodeposition of, 211
Chromic acid:
  chromium electrodeposition:
    baths, operating conditions, 218–221
  hexavalent chromium electrodeposition of, 211
Chromium compounds. *See also* Hard chromium; Hexavalent chromium; Trivalent chromium
  electrodeposition of:
    anion penetration, 210
    anodes, 223–224
    aquation, 209
    basis metals, preparation, 226–227
    black chromium deposits, 228
    bulk chromium plating, 225–226
    chemical principles, 206–207
    chemical properties, 237–239
    chemical resistance, 237
    chromic acid baths, operating conditions, 218–221
    chromium-plated strip steel-tin-free steel, 238
    construction materials, 224–225
    corrosion resistance, 231
    density, 236
    deposits structure, 232–234
    deposits tests, 230–234
    ductility, 237
    electrical resistivity, 236
    expansion coefficient, 235
    fatigue strength, effect on basis metal, 236–237
    friction coefficient, 235
    hard chromium plating, 227–228
    hardness and wear resistance, 234–235
    hydrolysis, 209
    internal stress, 236
    maintenance and control process, 222–230
    melting point, 235–236
    metallic impurities, 221–222
    microcracked and microporous deposits, 231–232
    mixed catalysts and selfregulating baths, 216–218
    olation, 209
    oxidation and tarnish resistance, 237
    oxolation, 210
    plate physical properties, 234–237
    plating solutions, 214–216
    polymerization, 210
    porosity and cracking, 230–231
    porous chromium plate, 238–239
    postplating treatments, 229
    reaction rates, 210
    reflecting power, 236
    regulations, 240–241
    safety and health considerations, 225
    stripping, 230
    theory of, 207–210
    throwing power, 221
  trivalent chromium, alloy plating, 239–240
Chromium-plated strip steel-tin-free steel, electrodeposition, 238
Chromium trioxide (CrO_3), hexavalent chromium electrodeposition, 206
Cleaning procedures:
  conventional, 509–510
  for electrodeposition, 507–509
  emerging technology, 510
  measuring degree of cleanliness, 510–511
  strategies for, 511
Coalescence-induced void formation, 440
Coated-wire type electrode (CWE), chemical sensors, 428

Coating thickness:
nickel plating, 81
tin–lead alloys electrodeposition, electronic components, 281–282
Cobalt compounds:
cobalt–iron alloys, 502
electrodeposition kinetics, deposit thickness, 20
gold electrodeposition, acid cyanide baths, 119–120
iron–cobalt–nickel alloy, 316
nickel–cobalt alloys:
magnetic properties, 503
nickel–cobalt–phosphorus ternary alloy, 499
palladium-cobalt alloys, 358–360
chemistry and material properties, 359–360
current–potential curves:, 358
density, 359
phosphorus-cobalt alloys, 502
zinc–cobalt alloys, 291
barrel-and-rack plating, 291–292
continuous plating techniques, 299
Cobalt/nickel-hardened acid gold baths:
microchemical determination, 120
Cobalt–palladium multilayered film:
read–write (R/W) characteristics, 466
schematic representation, 468
surface roughness, 470
Cobalt-phosphorus alloys, magnetic properties of, 29
Cobalt salts, 119
Code of Federal Regulations (CFR), 556
Codeposition:
copper composite materials:
alumina systems, 63
characteristics of, 63
continuous fiber-reinforced composites, 64
mechanisms of, 64
properties, 63
decorative electroplating, sulfur-nickel composites, 85
gold electrodeposition, acid cyanide baths, 119–120
metal alloys, 17–18
nickel–sulfur alloys, 625
palladium compounds:
hydrogen embritttement, 335
minimization hydrogen codeposition, 338–339
semiconductor electrodeposition processes, copper indium diselenide, 393
zinc-cobalt alloys, continuous plating techniques, 299
Coefficient of thermal expansion (CTE), 122, 186
Coercive forces, magnetic properties of electrodeposits, 29
Cold chromium plating:
deposits structure, 233–234
Cold–jet CO_2 (dry ice) blasting, 510
Colloidal catalysts, electroless deposition, 417
mixed catalysts, 448
Colorimetry, solution chemistry analysis, 534
Columnar deposition, schematic cross section, 440
Columnar microstructure:
electrodeposition growth mechanisms, 12
Compact discs (CDs), 522
Complementary metal–oxide–semiconductor (CMOS) fabrication technologies, 619
Complex agents:
concentration, 465
Composite materials:
composite electroless coatings, 456–457
copper compounds:
alumina systems, 63
characteristics of, 63
continuous fiber-reinforced composites, 64
mechanism of, 64
properties, 63
heat-treated electroplated nickel alloy composites, 455–456
nickel–phosphorous coatings production, 457
zinc alloys, continuous plating techniques, 300
Composition-modulated films:
electrodeposition, 22
Conductivity measurement, 539–540
CoNiFeB soft magnetic thin film:
surface morphologies, SEM images, 466
CoNiFe ternary alloys:
phase diagram, 461
TEM bright-field images, 461
π-Conjugated system, 421
Connectors, 195
Contamination. *See* Impurities
Continuous plating, zinc/zinc alloys electrodeposition, 293–302
Conventional waste disposal procedures, schematic presentation, 564
Conversion factors, table of, 675–676
Coordination chemistry:
chromium electrodeposition, 213–214
platinum-group metals, 333
Co-planarity, palladium preplated leadframes (PPFs), 363
Copper-accelerated acetic acid salt spray (CASS), 45, 108
Copper chip technology, 637
Copper compounds. *See also* Acid copper; Alkaline noncyanide copper; Cyanide copper; Pyrophosphate copper
anodic partial reaction:
Cannizzaro reaction, 435
electrochemical oxidation, 434
kinetics, 435–436
mechanism, 435
cathodic partial reaction:
additives, effect of, 436
kinetics, 436
pH effect, 436
composites materials:
continuous fiber-reinforced composites, 64
mechanism of, 64
properties of, 63–64
current–potential curves, 434
deposition potential, 17–18
displacement deposition, 15
electroactive species, 436
electrochemical equivalent, 8
electrochemical model:
Evans diagram, 433–434
interfering reactions, 434

mixed-potential theory, 433
partial reaction, interaction, 434
electrodeposition:
accelerator effect and superfilling, 595–599
additive kinetics and effect, 594–600
aging effect of, 16
baths for, 563
carbon microanalysis, 376–377
chelating citrate ligands, 601
conformal plating, 589
crystallographic analysis, 374–375
current and overpotential, 5
current-potential relationship, 5
fabrication processing, 590
kinetics, 4–5
leveler effect, 600
mechanism and kinetics, 590–592
microelectromechanical systems, 621–623
microelectronics applications, 589
microstructure analysis, 375–376
new barrier materials, 603–606
overpotential characteristic, 6
PEG and PPG, 15–16
PEG–Cl inhibiting effect, 594–595
PEG–Cl–SPS/MPS systems, morphological and microstructural effects, 599–600
plating bath chemistry, 592
properties and structure, 42–44
scanning electron microscopy (SEM), 592
seedless barrier layers, 601–606
subconformal plating, 589
superconformal plating, 589
superfilling models, 592–594
on Ti/Ta-based barriers, 601–603
electroless copper deposition, electrochemical control system:
chronopotentiometry, 444
voltammograms, 444
electroless copper deposition, for IC fabrication, 443
diffusion barriers, 443
noncatalytic surfaces, activation of, 443
electroplating baths, 622
electroplating, on silicon wafer, 638–639
epitaxial, smooth, and continuous ultrathin films:
defect-mediated growth, 607–609
experimental conditions, 611
surface-limited redox replacement reaction, 609–611
FIB ion micrographs, electroplated Cu film, 646
FIB/SEM techniques, analysis of electroplated copper, 645–649
growth mechanism:
bulk stage, 439
electroless copper deposition, 438
thin-film stage, 439
hydrogen incorporation, 440
instruments, for electroplating, 640
iron–copper thin films:
saturation magnetic flux density, 463
X-ray diffraction patterns, 464
microporosity, 440
nanoparticles, fabrication of, 443
nanoparticles, formation of:
deposition rate of, 443
quartz crystal microbalance (QCM), 443
plating, reaction of, 639
properties:
crack-free electroless copper, 441
ductility recovery, 441
electrical resistivity, 441
electromigration resistance, 441–442
film ductility, 440–441
quality control, 637
secondary ion micrography of electroplated, 646
SEM micrographs, defects on electroplated Cu film, 647, 648
solutions for electroplating, 639
steady-state electroless copper deposition, 437
catalysis phenomena, 438
electroless copper deposition, pH effect, 437–438
induction period, 437
steady-state kinetics, 437
TEM analysis of electroplated films of, 657–658
thick-film structure, 439–440
thin-film structure, 439
using different techniques, deposition rate of, 638
vacancies in, surface mobilities of, 15
X-ray diffraction patterns, 16
Copper electrode, rest potential of, 435
Copper–gold interdiffusion, 126
Copper interconnects, 638
Copper metallization, 637
Copper-only technique. *See* Solder mask over bare copper (SMOBC) technique
Copper pillar:
with tin–silver cap, 198
Copper sulfate:
concentration of, 35
Copper trench filling:
additives effects, 371–373
by electrodeposition, 371
by electroless deposition, 377
Corrosion resistance, 477
chromium electrodeposition, 231
lead and lead alloys electrodeposition, 256
magnetc recording, 586
tin–lead alloys electrodeposition, 275
Corrosion testing:
nickel electroplating, thickness quality control, 108
Cost–benefit analyses, 570
Coumarin, decorative electroplating, semi-bright nickel, 85
Counterion effects, palladium electrodeposition, 340
Covering power (CP), chromium electrodeposition, 221
Crack-free compounds:
chromium:
decorative nickel electroplating, 87
self-regulating high speed baths, 217–218
Cracking, chromium electrodeposit testing, 230–231
Crystal-building processes, 12, 16
Crystal growth, randomization, bright deposition, 13

Crystal lattice:
  defects, 49
  metal ions, electrode potential, 1–4
Crystalline copper:
  gold, growth of, 125
Crystallographic orientation, 181
Cubic close packed lattice, deposits structure and properties, 19
Current densities (CDs):
  acid copper electrodeposition, 39
  chromium electrodeposition, bright plating solution, 221
  cyanide copper:
    high-efficiency solutions, 55
    strike and Rochelle solutions, 53
  electrode kinetics, current-potential relationship, 6–7
  electrodeposition kinetics, 4
  microelectromechanical systems (MEMS) application, 618
  nickel electroplating, 93
    coating thickness, 81
  pyrophosphate copper solution, 60
  tin-lead alloys electrodeposition, 272
Current distribution:
  nickel electroplating, 81
Current efficiency:
  electrodeposition kinetics, 8–9
  zinc/zinc alloys, 290
    continuous plating technique, 296
Current interruption cycles, cyanide copper, high-efficiency solutions, 55
Current modulation techniques:
  acid copper, 44–45
Current-potential curves:
  electroless deposition, copper compounds, Evans diagram, 14
Current–voltage curves, 351
Curvature-enhanced accelerator coverage (CEAC) model, 65
  copper electrodeposition, superfilling models, 593
Cu_6Sn_5 phase, SEM photo of, 183
Cyanide-based plating baths, 117
  zinc baths:
    acid chloride bath, 289–290
    alkaline baths, 288–289
    composition, 286–288
Cyanide baths, 489
Cyanide complexes, 119
  zinc/zinc alloys electrodeposition, barrel-and-rack plating, 286–288
Cyanide copper:
  addition agents, 53
  anodes, 57
  applications, 51
  carbonate, compared with, 52–53
  construction materials, 57
  copper cyanide solution constituents, 51
  environmental, 57
  free cyanide solution constituents, 51
  high-efficiency solutions, 55
    maintenance and control, 56–57
    operating conditions and characteristics, 55–56
  history and development, 51
  sodium/potassium formulations, comparison of, 52–53
  sodium/potassium hydroxide constituents, 52
  strike and Rochelle solutions, 53
    maintenance and control, 54–55
    operating conditions, 53–54
  structure and properties, 57–58
  tartrates and, 53
Cyanide ions:
  diffusion coefficient, electrochemical measurements, 135
Cyanide leaching, silver electrodeposition, 135
Cyanide silver plating baths, 135
Cyanide solutions:
  copper electrodeposition and, 33
  silver dissolution, process of, 135
Cyanoaurates, electroless deposition, gold alloys, plating rate increases and modification of, 483, 487
Cyano complex, 119
Cyclic pulse voltammetric stripping (CPVS), acid copper analysis, 41–42
Cyclic voltammetric stripping (CVS), 152, 534–535
  acid copper analysis, 41
  hysteresis in, 595
  pyrophosphate copper solution, 61
    impurities detection of, 61–62

Damascene copper electroplating:
  patterned electrodeposition, microelectronics, 47–48, 65
Damascene process:
  advantage of, 589
  trench filling, 372
Danglers, plating barrel design and, 514–515
Decision-making process, 562
  flowchart of, 563
Decorative electroplating:
  nickel, 84–91
    bright nickel solutions, 84
    decorative applications and market size, 91
    electrocrystallization, 84–85
    microdiscontinuous chromium, 87–88
    multilayer coatings, 85–87
    plastics, aluminum, and stainless steel electroplating, 88–89
    semibright nickel, 85
    standards and coating requirements, 89–91
    STEP test, 88
    sulfur codeposition effects, 85
Defect-mediated growth (DMG), epitaxial, smooth, and continuous ultrathin copper films, 607–609
Density measurements:
  chromium electrodeposition, 236
  lead and lead alloys electrodeposition, 256
  palladium electrodeposition, neutral electrolyte, 354
Depolarization techniques, electroless deposition, gold compounds, plating rate increases, 492
Deposit characterization, adhesion, 416–417
Deposition, on nonconductors:
  plastics, metalization of:
    electrochemical-autocatalytic methods, 415–416
    ion beam techniques, 415

photolithography, 414–415
plasma-induced deposition, 416
sputtering, 416
polyimide metalization, 414
Deposition potential:
alloy deposition, 17
Deposition preparation:
aqueous cleaning, 509
cleaning processes, approaches, 507
cleaning, strategies for, 511
conventional processes:
aqueous cleaners, 509–510
organic solvent cleaners, 509
rinsing, 510
semiaqueous cleaners, 510
for copper and alloys, 508
degree of cleanliness, measuring, 510–511
emerging technology, 510
extrinsic contaminants, 507–508
porous substrates, 507
substrate metal properties, 508
Deposition rate:
tin–lead alloys electrodeposition, 275
Deposit properties:
thickness, electrodeposition kinetics, 9
1,3-Diaminopropane electrolyte, palladium electrodeposition, 340
Diamond powders:
three-step activation procedure, 457
Diamond-turning, acid copper electrodeposition, 49–50
Dichromates, hexavalent chromium electrodeposition of, 211
Diethylenetriaminepentaacetic acid (DPTA), 161
Differential scanning calorimetry (DSC) phase transitions, 28
Diffuse reflection, electrodeposition growth mechanisms, 13
Diffusion barrier layer, 15
thin film interdiffusion, 25, 370–371
Diffusion bonding techniques, 25
Diffusion coefficient, 6, 7, 12, 23, 577
Diffusion-controlled leveling, bright deposition, 13
Diffusion process, 23
Diffusion welding, thin films interdiffusion, 25
3,5-Diiodotyrosine, 132
DIL components, tin-lead alloy composition, 280
Dimethylamineborane (DMAB) baths, 484
characterstics, 484–485
CoNiFeB ternary alloys, 464
improved, 485–488
problems associated with, 485
p-Dimethylaminobenzaldehyde (DMAB), 483, 484
Dip-and-look test:
tin-lead alloys electrodeposition, solderability test, 277
DIP components, tin-lead alloy composition, 280
Direct-current deposition, 577
Direct current (dc) plating baths, gold, 117–124
acid cyanide baths, 118–120
alkaline cyanide baths, 118
gold alloy plating, 124
neutral cyanide baths, 120–122
noncyanide baths, 122–124
Direct force, electromigration, thin films interdiffusion, 26
Discoloration, lead and lead alloys electrodeposition, 256
Dislocations:
crystal structural properties, 26
electrodeposit mechanical properties, 28
Dispersion plating, lead and lead alloys, 257
Displacement deposition, reaction of, 15
DIT bath, silver electroless deposition:
polarization, 132–133
stabilization with, 132
Divalent chromium, electrodeposition theory and, 207
Dodecyltrimethylammonium chloride (DTAC), leveler effect, 600
Drag-in impurities, tin-lead alloy electrodeposition: nickel and copper contaminants, 272–274
Drag-out control:
electrotinning manufacturing technology, 517
quality control and monitoring, solution blow-off measurements, 531
Dropping mercury electrode (DME), 534
Dual-beam FIB/SEM technology, 640–644
electroplated copper, analysis of, 645
cross-sectional view, electrodeposited Cu vias, 645–646
electroplated films, defect analysis of, 646–648
secondary ion micrography, 646
principles of, 640
channel effect contrast, 643–644
gas injection system (GIS), 642–643
geometry and eucentric point of sample stage, 642
liquid gallium ion source, 641
Ductility:
chromium electrodeposition, 237
nickel electroplating corrosion testing, 108
Dunn's experiment, 185
Dynamic equilibrium equations, in crystal lattice, electrode potential, 2–4

EBONEX ceramic electrodes, 567
Eddy current thickness gauges, quality control and monitoring, 544–545
Edge board platers, 521–522
Elasticity modulus, electrodeposit mechanical properties, 258
Electrical resistivity:
chromium electrodeposition, 236
lead and lead alloys electrodeposition, 256
tin-lead alloys electrodeposition, 277
Electric devices, conductive polymers, electropolymerization, 425–427
Electric shorts:
risk of, 170
Electroactive species, electroless deposition, copper compounds, 435
Electrochemical analysis, 534
Electrochemical atomic-layer epitaxy (ECALE):
cadmium telluride, semiconductors electrodeposition, 387–388
development, 388
growth mechanism, semiconductors electrodeposition, 389
Electrochemical-autocatalytic methods, polymer metallization, 415–416

Electrochemical cell, 4
Electrochemical deposition equivalent:
  tin-lead alloy electrodeposition, 274–275
Electrochemically grown silver deposits:
  fractality, 137
Electrochemical polymerizations, 421
Electrochemical quartz crystal microbalance, 534
  copper electrodeposition, Raman spectroscopy, 595
Electrochemical quartz crystal microgravimetry:
  semiconductors electrodeposition, 398–399
Electrochemical techniques:
  interconnected copper deposition for:
    carbon microanalysis, 376–377
    crystallographic analysis, 374–375
    electrodeposition, copper trench filling, 371–373
    electroless deposition, copper trench filling, 377
    microstructure analysis, 375–376
    physical/mechanical properties, 373–374
  interconnection, copper deposition for:
    copper trench filling, 371–377
Electrochemical test cells, 533
Electrocleaning, 510
Electrocrystallization, decorative electroplating, nickel electrodeposition, 84–85
Electrode boundary layer, 119
Electrode–electrolyte interface, 421
Electrodeposition, 447
  additives for, 461
  cell system, 462
  clusters, 138
  copper, texture and hardness, 168
  diffusion in, 24
  environmental aspects:
    advocacy, 569–570
    applications of, metal recovey, 566–567
    economic considerations, 568–570
    electroplating industry, 559–562
    environmental management systems, 558–559
    government regulatoion, 559–562
    green chemistry, 557–558
    light-induced processes, 567–568
    policy, 568–569
    research background, 555–557
    technological development, environmental impact of, 562–564
    zero discharge, 564–566
  gold, Vickers hardness of, 123
  kinetic mechanism, 4–11, 163
    atomistic aspects, 9–11
    current efficiency, 8–9
    current potential relationship, 4–6
    deposit thickness, 9
    Faraday's law, 7–8
    mass transport, electrode kinetics, 6–7
    pulse deposition techniques, 11
  materials science of:
    adhesion properties, 30
    hardness properties, 30
    internal stress, 29
    magnetic properties, 29
    mechanical properties, 28
    structural characterization, 27–28
  metallizing principles, 450
  metals:
    microhardness, 168
    purity of, 166
  nickel plating:
    adhesion, 83
    basics of, 80
    coating thickness, 81
    current and metal distribution, 81–82
    electroplating solutions, retrospective on, 79–80
    Faraday's laws, application of, 80–81
    internal stress, 82–83
    leveling and microthrowing power, 83–84
    throwing power, 82
  nucleation, 448–450
  process, 152, 159, 176
  schematic representation, 448
  soft gold, 125
  thin films, surface morphology of, 179
  tin coatings, 165
    columnar structures, 165
Electrode potential, 1
  metal ions, in crystal lattice, 1–4
Electroforming:
  acid copper electrodeposition, 48–49
  iron and iron alloys electrodeposition:
    iron–nickel alloy, 316
  nickel plating:
    anodic oxidation of sulfamate anions, 98
    applications, 99
    capabilities, 98
    electrofabrication technique, 97
    leveling agents for, 99
    mandrels, 98
    nickel-speed process, 98–99
    postelectroforming operations, 99
Electrogalvanizing strip plating machines, 517–519
Electroless Ag–W plating bath, 503
Electroless alloy:
  deposited, properties:
    magnetic properties, 503–504
    thermal stabilities, 504
Electroless cobalt–nickel–phosphorus alloys, 502
  composition of baths, 502
Electroless cobalt-phosphorus alloys, 29
Electroless copper plating bath:
  automatic analyzer and controller, 543
  monitoring and control system, 542
Electroless copper, processing steps, 418
Electroless Cu–Ni–P plating bath, 503
Electroless deposition process, 417–419
  of alloys:
    cobalt-based alloys, 501–502
    copper–nickel alloys, 502–503
    copper–selenium alloys, 502
    electroless alloy plating baths, 499
    gold–copper alloys, 502

indium-antimony alloy, 503
nickel-based alloys, 499–501
physical properties, 503–504
silver–tungsten alloys, 503
Co–P films, analyses of, 659–662
copper deposition, 433, 437, 439
glyoxylic acid, 444
hypophosphite, 444
plating conditions, 444
properties of, 440
rate of, 438, 442
gold compounds:
applications, 495–496
borohydride bath, 484–489
cyanide baths with other reducing agents, 489–491
DMAB baths, 484–489
noncyanide baths, 491–495
Ni–Zn–P film, TEM analysis of, 658–659
of palladium compounds:
alloys for, 479–480
electroless palladium plating bath, 478
hydrazine baths, 477–478
hypophosphite baths, 478
reducing agent baths, 478
reaction of, 13–14
schematic representation, 448
Electroless diffusion barrier, 15
Electroless gold, 495
plating bath, 483
Electroless In–Sb plating bath, 503
Electroless nickel-based alloys:
composition of baths, 500
Electroless nickel baths:
complexing agents, 452
Electroless nickel–boron–phosphorus films, 504
Electroless nickel deposition, 452, 454
bath compositions, 451
rate, pH effect of, 453
Electroless nickel plating, 457
corrosion resistance of, 455
dimethylaminoborane (DMAB), 453
Electroless Ni/immersion Au (ENIG), 144
Electroless Ni–P/diamond deposits, 457
Electroless Ni–Re–P plating bath, 501
Electroless Ni–W–P alloy films, 504
Electroless palladium-based ternary alloys, 479
Electroless palladium plating bath, 478
Electroless plating reaction, 31, 131, 132, 416, 516
nonconductors deposition, 413–414
of platinum, 479
acidic electroless platinum plating bath, 479
alkaline electroless platinum plating bath, 479
alloys for, 480
electroless plating bath, 479
electroless Pt–Rh alloy plating bath, 480
on specific substrates, 480–481
possesses, 447
Electroless silver deposits:
applications of, 133
SEM, 133
Electroless silver plating baths, 132
Electroless silver plating reaction, 133
Electroless silver plating solution:
partial cathodic polarization curve of, 133
substrate pretreatment, 131
Electroluminescence devices, electropolymerized polymers:
hole transporting layer, 427
light emission layer, 426–427
Electrolyte systems:
lead and lead alloys electrodeposition, 249–251
tin–lead alloys electrodeposition, 265
acid concentration, 271
alkylsulfonic acid electrolytes, 267–268
metal concentration, 271
pH solutions, 268, 269
tetrafluoroboric acid electrolytes, 266–267
types, 249–251
Electrolytic corrosion (EC) test, chromium electrodeposit testing, 231
Electromigration, 441
atomic model of, 442
thin films interdiffusion, 25–26
Electron beam–assisted deposition (EBAD), 415
polymer metallization, 415
Electron-conductive polymers, 421
Electron gases, electrodeposition kinetics, atomistic aspects of, 9–10
Electronic components:
strip plating for, 516–517
tin-lead dectrodeposition for, 280–282
Electronic devices:
electroluminescence device:
hole-transporting layer, 427
light emission layer, 426–427
electropolymerized polymers, key function of, 425–426
Electron transfer process, 160
cathodic alloy deposition, 17
Electron wind force, electromigration, thin films interdiffusion, 26
Electrooxidation, 128
Electroplated films, 169
TEM technique, analysis of, 637
Electroplated soft gold, 128
Electroplated tin deposits:
material properties of, 176
Electroplated tin–lead, 196
Electroplated tin–silver bumps, 163
Electroplating:
baths, 162
categories:
pretreatment standards for, 561, 562
copper, onto silicon wafer, 638–640
equipment, 513–514
barrel platers, 514–515
rack platers, 515–516
strip platers, 516–517
vibratory platers, 515
wire platers, 522

Electroplating (*Continued*)
methods:
bronzing, 413
graphiting, 413
metallic painting, 413
metallizing, 413
process, 148
pure tin, metallic impurities, 166
tin, future for, 199
Electroplating line, monitoring and control:
process monitoring, 527
fume exhaust, 531–532
line speed, 531
plating current and cell voltage, 529
rinse quality, 531
robots and handling systems, 532
sensors, 529–530
solution blow-off, 531
solution flow, 529
solution level, 528–529
solution temperature, 529
timers with ammeters, 529
Electropolishing, 127, 520. *See also* Anodic process
Electropolymerization, 421, 427
coatings, research and development of, 429–430
films, 421, 427
illustration of, 422
polymers, applications of, 423
Electroreductive polymerization, organic films, 421
Electrorefining, acid copper electrodeposition, 34
Electrotinning, 517
Electrotyping, iron electrodeposition, bath solutions for, 312
Electrowinning:
acid copper electrodeposition, 34
trivalent chromium, 239
zinc/zinc alloys, acid chloride baths, 289
Elongation, lead/lead alloys electrodeposition, 256
Embrittlement effect, copper electrodeposits, 43
End-of-life vehicles (ELV), 143
Energy band diagrams, light-induced electrodeposition, 568
Energy-dispersive analysis of X rays (EDAX):
cadmium telluride, semiconductors electrodeposition, 386–387
Engineering electroplating technology, 522
decoration, 522
Environmental management systems (EMSs):
green chemistry principles, 558–559
guidelines, 558
Epitaxial temperature, deposits structure and properties, 19
Epitaxy, deposits structure and properties, 19
Equilibrium state, metal-solution interphase formation, 2
Equipment requirements:
acid copper electrodeposition, 40
Erythorbic acid bath, 492–493
Etching procedure:
disadvantage of, 229
6-Ethoxy-2-mercaptobenzothiazole (EMBT), 491
Ethylene diamine, 132
Ethylenediaminetetraacetic acid (EDTA), 161, 433, 452, 477
containing solutions, 438
zinc/zinc alloys, alkaline noncyanide zinc baths, 288–289
Ethylene oxide (EO) groups:
Raman shift, 177
European Union's End-of-Life Directive, 240
Eutectic alloys:
tin-lead alloys composition, 279–280
application, 279–280
Eutectic solder:
material properties of, 142
Eutectic tin–bismuth, 161
depositing, challenges of, 161
Eutectic tin–silver, 162
Evans diagram, 434
electroless deposition, 15
Exchange-current densities:
palladium compounds:
acid chloride electrolytes, 348
hydrogen embrittlement, 335
Expansion coefficient, chromium electrodeposition, 235
Extremely thin absorber (ETA) solar cell:
zinc oxide, semiconductors electrodeposition, 397

Fabrication process, 15
Face-centered cubic (fcc):
iron electrodeposition, deposit properties, 316–317
magnetc recording, substrate and deposit thickness effects, 587–588
Faraday impedance, 135
Faraday law, 148, 434
electrodeposition kinetics, 7–8
deposit thickness, 9
nickel plating, 80–81
Faraday's constant, 3, 4
electrodeposition kinetics, overpotential, 4
palladium electrodeposition, 344
semiconductors electrodeposition process, 384–385
Fast-rate, interrupted current (FRIC), acid copper electrodeposition, 49
Fatigue strength:
chromium electrodeposition, 236–237
functional nickel plating, 96
Federal laws and regulations, 560
FePt nanoparticles, chemical synthesis of:
for high-density magnetic recording media:
FePt nanoparticles, thermal effect, 472–473
ionic liquid (IL), use of, 473–474
magnetic nanoparticles, 471–472
Ferric ions, iron electrodeposition:
chemical principle, 310
control, 318–319
Ferromagnetic materials:
electrodepostion, microelectromechanical systems, 626, 627
Ferrostan process, 152
Ferrous chloride bath, iron electrodeposition, 311–317
Ferrous ions, iron electrodeposition, chemical principle, 310
Ferrous sulfate bath, iron electrodeposition, 310–311
Fiber-reinforced plastic (FRP), iron electrodeposition, 320
FIB technology, 190
whiskers cross sectioned, images of, 191

Fick's law:
first law of diffusion, 578
second law of diffusion, 579
thin films interdiffusion, 23
Field-oriented texture (FT), zinc compound, 299
Filament tin whiskers, 169
Filtration requirements:
acid copper electrodeposition, 39–40
Finile-element (FE) Auger spectrometry, 599
Finished product, monitoring and control, 543–551
brightness, 546–547
color of electrodeposits, 546
electroplating hardness, 547
film stress, 547
grain size of electrodeposited film, 547–548
mechanical testing, 550
recrystallization rate, 548–549
roughness of the plated surface, 547
surface and compositional analysis, 549–550
surface morphology of plated films, 549
thickness, 543–546
X-ray diffraction (XRD) analysis, 548
X-ray transmission imaging, 550–551
Finishing industry, environmental hazards of electrodeposition and, 559–562
Fischer-Langbein solution, iron eiectrodeposition, ferrous chloride bath, 311–317
Flipchip wafer bumping, 142
Fluoborate:
acid copper electrodeposition, 36
impurities in, 41
advantages of, 152
ions, 152
iron electrodeposition, ferrous chloride bath, 312
nickel electroplating, functional applications, 94
solutions, copper electrodeposition and, 33
Fluoride ion, formation of, 152
Fluoroborate-based electrolytes:
lead and lead alloys electrodeposition, 257
Flux gradient vector, thin films interdiffusion, 23
Flyer plate test, 226
Foaming, 154
Focused ion beam (FIB) system, 172, 415, 637
polymer metallization, 415
SIM system:
copper electrodeposits, microstructure analysis, 375–376
Fountain cup plater, 149
Fourier transform infrared (FTIR) spectroscopy, 511
Frank–van der Merwe growth mode, 176
Free cyanide, cyanide copper plating, 51–52
Free-standing metallic whiskers, 194
Friction coefficient, 227
"Frosty" chromium plating, characteristics of, 240
Fuel cell technology, 477
Full width at half maximum (FWHM):
cadmium selenide, semiconductors electrodeposition, 389
Fume exhaust vacuum system, quality control and monitoring, 531

Functional electroplating and deposit:
nickel electroplating:
all chloride solution, 95
all sulfate solution, 95–96
applications of, 79
black nickel solution, 96
coating requirements, 93–94
deposit properties, 91–93
fatigue strength, 96–97
fluoborate solution, 94
hard nickel solution, 94–95
hydrogen embrittlement, 97
nickel-phosphorus solution, 96
sulfate-choride solution, 96

Gallium arsenide (GaAs):
electroless deposition:
metallization of, 483
offering potential advantages of, 384
ohmic contacts, 483
using hydroxylamine as reducing agent, 478
X-ray diffraction analysis, 385
iron and iron alloys electrodeposition:
iron–nickel alloy, 323
semiconductors electrodeposition process, 384–385
Gallium phosphide (GaP):
semiconductors electrodeposition process, 385
Galvanic displacement plating, 483
Galvanic exchange, 131
Gas bubble density, electroless deposition, copper compounds, ductility properties, 440–441
Gelatin, additives for, 36, 38, 42, 49, 253
General Motors Research Laboratory, 87
Giant magnetoresistance (GMR), 23, 316, 573
GIS-equipped FIB/SEM, 642
Glossmeter, 164
Gloss reflectance measurement, 175
Gold compounds, 115, 116
adhesion of, 126
anode, 118, 122
bullion price, 116
demand, in electronics industry, 116
deposition, 494
carbon, determination of, 120
mechanism of, 124–125
production, 119
purity of, 123
surface roughness of, 125
from various mixtures, polarization curves, 493–494
direct current (DC) plating baths:
acid cyanide baths, 118–120
alkaline cyanide baths, 118
cyanide-based baths, 117
gold alloy plating, 124
neutral cyanide baths, 120–122
noncyanide baths, 120–124
electrodeposition, 115
microelectromechanical systems, 620–621
electromigration resistance of, 128

Gold compounds (*Continued*)
electroplating:
baths, 620
use of, 115
gold cyanide complex, 117
gold cyanide concentration:
effect of, 121
gold films, 126
gold ions:
cyanide, 126
standard reduction potentials, 117
gold(I)–sulfite complex, 490
gold nanotubular membrane, 496
gold–palladium alloys, 124, 478
gold-plated anodes, 122
gold-plated electrodes, 118
gold–tin alloys, 124
nanotubes, 496
plating baths:
chemical formulation of, 116
plating process, 125
on aluminum alloys, 126
pulse plating, 125
reduction of, 116
salts, 489
stains, 127
substrate preparation, 125
barrier metals, 126
cleaning and surface preparation, 125–126
gold strike, 126
high-speed strip plating, 126–127
test methods:
chemical analysis, 128–129
physical properties, 128
use of, 115
wire bonding integrated circuits, 115
Gold-flashed palladium cobalt (GFPdCo), chemistry and material properties, 359–360
Gold strike:
use of, 126
Gold sulfite baths:
operating parameters of, 123
stress *vs.* plating temperature, 123
Goniometry, 511
Grain boundaries, 182
deposits structure and properties, 18
deposit structure and properties, 18–19
Grain boundary, 125
Grain refiners, 176
adsorption behavior of, 179
Grain refining:
bright deposition, 13
for bright deposition, 13
and brightening agent, 54
effect of codeposited cyano complex, 119
with insufficient, 255
tendencies of addition agents, 39
Grain structures:
of copper electrodeposits, 42–44
palladium electrodeposition, 353
Graphiting:
acid copper electrodeposition:
anodes structure and design, 40
nonconductors deposition, 413
Gravimetric analysis, 511
Gray tin, 144
Green chemistry:
principles, 557–558
Greenhouse gases (GHGs), envionmental aspects, 556
Gross domestic product (GDP):
environmental protection policy, 568
Growth mechanisms:
additives:
consumption of, 13
effect of, 12–13
brightening, 13
columnar microstructure development, 12
leveling, 13
model of, 176
nucleation, additives and, 12
overpotential dependence, 12
Guglielmi's model, copper composites materials, copper-alumina system, 63
Gullwing bend, 185

Half-cell potential, palladium electrochemistry, 334
Halide ions, hexavalent chromium electrodeposition, 212
Hall–Petch correlation, 30
Halogen chemistry:
sludge formation, 153
Halogen process, utilizing horizontal cell design, 153
Hanging Hull cells, electrodeposition, 533
Hard chromium:
applications when plating thick layers, 209
benefit from, 238
carbide coatings, 240
nitride layer, 237
plating, 227–228
plating baths frequently deficient in, 240
plating deposits, 225, 229
rapidly increasing weight loss, 238
surface, 232
Hard disk drives (HDDs):
areal density and technology development, 459–460
Hardness properties:
beneficial for wear resistance, 331
chromium electrodeposition, 234–235
commercial instrumentation and scales of, 128
conducted test of, 30
electrodeposit properties, 27
gold, electrodeposited, 20
grain size and, 547
lead and lead alloys electrodeposition, 256
to monitor, 107
palladium alloys, 355–356
palladium electrodeposition, neutral electrolyte, 354
Pd deposits, 349
precipitation of Ni_3P or Ni_3B and, 28
and PR or pulse plating, 44
tin–lead alloys electrodeposition, 277–278

Hard nickel, functional applications, 94
Haring–Blum cell, 150, 533
Haring throwing-power box, 533
HCN gas, 117
HDD areal density, 459–460
Helmholtz potential, 151
Hexa-aquo ferrate complex:
  CoNiFeB ternary alloys, 465
Hexafluorosilicate electrolytes, lead and lead alloys electrodeposition, 250
Hexagonal close-packed (hcp):
  magnetc recording, substrate and deposit thickness effects, 587–588
Hexavalent chromium:
  electrodeposition of:
    chromates and dichromates, 211
    chromic acid, 211
    polychromates, 211–214
  reflecting power, 13
High-B_s soft magnetic film:
  using electrodeposition techniques, 460–464
    Co–Fe binary alloy, 462–464
    CoNiFe ternary alloys, phase diagram of, 461
    CoNiFe thin films electrodeposition, TEM bright-field images of, 461
    $Ni_{80}Fe_{20}$ permalloy, 460–464
    two cell systems, schematic representation of, 462
High-efficiency etch-free (HEEF®):
  feature of, 216
  formulation, chromium electrodeposition, 214
High-efficiency solutions:
  advantage in, 51
  chromium electrodeposition, plating baths composition, 215–216
  cyanide copper, 55
    anodes, 57
    maintenance and control, 56–57
    operating conditions and characteristics, 55–56
High-magneticflux-density CONiFeB film, preparation of:
  film magnetic properties, enhancement of, 464–466
  soft magnetic thin film, 464
High-performance liquid chromatography (HPLC), 151, 537–538
High-speed additive-free hard gold:
  appearance and plating efficiency of, 121
High-speed electroplating:
  acid copper electrodeposition, 49
  gold electrodeposition, strip plating, 126–127
High-speed plating, 126
High-speed selective jet electrodeposition, acid copper solution, 48
High-sulfate solution:
  composition, 82
  current densities, 82
  throwing power, 82
Hole-transporting layers, electroluminescence devices, 427
Hopeite, zinc/zinc alloys, continuous plating techniques, 297
Hot-air-leveling (HAL) process:
  tin-lead alloys composition, 279–280
Hull cell, 533
Hull cell electroplating test, chromium electrodepostion, quality control, 223
Hydrazine, 480
Hydrazine bath, 477, 492
Hydrodynamically controlled Hull cell (HCHC), 151
Hydrofluoride, 478
Hydrofluoroethers, 509
Hydrogen embrittlement:
  functional nickel plating, 97
  palladium compound:
    electrokinetics, 335–337
    hydrogen overvoltage, 337–338
Hydrogen embrittlement (HE):
  electrodeposits structure and properties, 21
Hydrogen gas bubbles:
  population distribution of, 440
Hydrogen gas production, 119
Hydrogen ions, 118
Hydrogen peroxide, 491
Hydrolysis, chromium electrodeposition, 209
Hydroxylamine, 478, 480
Hypophosphite, 478
Hypophosphite bath, 492
Hypophosphite monohydrate, 478

IC fabrication, 442
IMC formation:
  cross-sectional view of, 182, 183
Impurities:
  iron electrodeposition, removal of, 319
  tin–lead alloys electrodeposition, 272–274
    anodic reactions, 274
    metallic contaminants, 273
    organic additives, 274
    tin(IV) concentration, 273–274
Incorporation, cathodic alloy deposition, 17
Independent printed circuit board manufacturing (IPCBM) facilities, 560
Indium compounds, 385
  indium–antimony alloys, 503
  indium selenide, 392
  indium sulfate, 502
  indium sulfide, 385–386
  indium tin oxide–coated glass plates, 387
  lead–indium alloys, 257–260
  palladium–indium, 361–362
  semiconductors electrodeposition, 385
Indium tin oxide (ITO) glasses, 426
Inductively coupled plasma source (ICP-MS), 538
Industrial electroplating process:
  schematic presentation, 562
Inhibitors, copper electrodeposition mechanism, 590
Inorganic/organic compounds:
  conductivity of, 422
In situ surface-enhanced Raman spectroscopy (in situ SERS), 177

Insulator:
deposits properties, 380
Ni alloys, electroless deposition, 379–380
surface modification, 378–379
Integrated circuit (IC):
electrochemical deposition process, 369
fabrication, 185
Interconnection material:
electrochemical deposition process, 370
Interdiffusion, thin films:
barrier metals, 126
diffusion barriers, 25
nickel surfaces, 24
thermal processing, 23
useful aspects of, 25
void formation, 24
Interfacial diffusion, 181
Intergovernmental Plan on Climate Change (IPCC) report, 556
Interlayers, tin–lead alloys electrodeposition, 282–283
Interlevel dielectric (ILD):
thin film interdiffusion, 370–371
Intermetallic compound (IMC), 182
Internal stress:
chromium electrodeposition, 236
electrodeposits, 29
measurement, nickel electroplating corrosion testing, 108
nickel electroplating, 82, 93
palladium film thickness, 352
International Organization for Standardization (ISO), 89, 558
Iodide–thiosulfate bath:
gold deposition, 124
3-iodotyrosine, 132
Ion beam–assisted deposition (IBAD), 415
polymer metallization, 415
Ion beam techniques, polymer metallization, 415
Ion chromatographic (IC) method, chromium electrodeposition, 222
Ionic liquid (IL), 134
interionic interactions, 474
use, iron–platinum nanoparticles preparation, 473
Ionic migration, cathodic alloy deposition, 17
Ion–ion interactions, electrode potential, 4
Ionized cluster beam (ICB), 443
Ion-selective electrodes, 536–538
Ion-sensitive field effect transistor (ISFET), 428
Ion-transfer process, 11
Iron and iron alloys:
cobalt–nickel alloy, 316
electrodeposition:
analytical technique, 319
anodes, 320
deposits characteristics, 320–323
equipment specification, 319–320
ferrous chloride bath, 311–317
ferrous sulfate bath, 310–311
impurities, 319
iron oxides, 317–318
pH levels, 319
preparation, maintenance, and control, 318–319
principles, 310
surfactants, 319
plating, bath composition and operating conditions, 313–315
Iron compounds:
nickel-iron alloy, 309
zinc–iron alloy, 310
barrel-and-rack plating, 291–292
continuous plating, 298–300
production, 317
Iron-hardened gold, 119
Iron oxides:
bath composition and operating conditions, 318
Iron–platinum nanoparticles:
growth temperature on shape and crystallinity effect, 472–473
particle size distribution curves, 474
preparation:
narrow size distribution in ionic liquids, 473–474
selected area electron deflection (SAED), 472
Iron strip production, bath solution for, 312

Janus Green B (JGB), trench filling, 371, 372
Jump frequency, thin films interdiffusion, 24

Kawasaki KC cell, zinc/zinc alloys, continuous plating technique, 293
KCN solubility product, 118
Kelvin temperature, thin films interdiffusion, 24
Kennecott Copper high-efficiency air agitation (HEAA) technology, 567
Kerr rotation angle, 471
Kirkendall void creation, thin films interdiffusion, 25
Knoop hardness, 345
electroplated soft gold, 128
Pd alloys, 359
Tukon hardness tester, measurement, 355

Langmuir formalism:
additive, magnetic recording, sulfur in deposit, 581
Large-scale integration (LSI):
electrochemical deposition process, 369
Laser-enhanced electroplating processes:
acid copper solution, 48
development of, 48
Laser processes, 127
Latent heat (LH), 137
Lattice structure, deposits structure and properties, 18
Layer growth, electrodeposition, 11–12
Lead and lead alloys:
chromium electrodepostion:
tank construction, 224–225
electrodeposition:
additives, 252
alkaline electrolytes, 251
amidosulfonate electrolytes, 249–250
anodes, 252–253
antimony-lead, 257
applications, 261–262
aprotic solvents, 260–261
bismuth–lead, 257

cadmium-lead, 257–258
cobalt–lead alloys, 260
copper–lead alloys, 259
corrosion resistance, 256–257
density, 256
dioxide compound, 260
discoloration, 256
dispersion plating, 257
electrical resistivity, 256
electrolyte agitation, 253
electrolytes, 249–251
elongation, 256
hardness properties, 256
hexafluorosilicate electrolyte, 250
indium–lead, 259–260
methanesulfonate electrolytes, 250–251
molten salts, 261
nickel–lead, 260
nodules or ''growths,'' 253–254
nonaqueous solutions, 260–261
perchlorate electrolytes, 249
plumbite electrolytes, 251
pores (voids), 254–256
pyrophosphate electrolytes, 251
silver–lead, 258
streaking or step plating, 254
temperature, 253
tensile strength, 256
tetrafluoroborate electrolyte, 250–251
thallium-lead, 257
treeing, 253
troubleshooting, 253–256
underpotential deposition, 261
zinc-lead, 258–259
functions, 224
Lead-bearing solders, 142
Lead consumption, 142
Lead dioxide compounds, electrodeposition of, 260
Lead-free solder candidates:
binary, 63Sn37Pb, 143
selection rules, 144
ternary and quaternary, 143
Lead, material properties of, 142
Levelers, copper electrodeposition mechanism, 591
Leveling:
electrodeposition growth mechanisms, 13
nickel electrodeposition, 83–84
palladium electrodeposition, neutral electrolyte, 354
theories of, 13
Levich equations, 135
L-film formation, hexavalent chromium electrodeposition, 212
Li battery system:
rechargeable, 424
$LiClO_4$–DMSO electrolyte, 424
$LiClO_4$–PC electrolyte, 424
Life-cycle analysis (LCA), green chemistry principles, 558
Ligand concentration effects, palladium electrodeposition, 343–344
LIGA technique. *See* Lithographie galvanoformung and abformung technique
Light-emitting diode (LED), 426
Light-induced processes, electrodeposition, environmental remediation using, 567–568
Limiting currents, palladium electrodeposition, 344
Liquid crystal displays (LCDs), 426
Liquid metal ion source (LMIS), 641
Lithium batteries, 423
Lithographie galvanoformung and abformung technique: microelectromechanical systems (MEMS), 619
Lithography, microfabrication techniques, 617, 618
Long-term corrosion tests, tin-lead alloys electrodeposition, 275
Low-energy electron diffraction (LEED), 485
Low-energy electron loss spectroscopy (LEELS), 174
Low-stress deposits, 123

Magnetic anisotropy, magnetic materials electrodepostion, 627
Magnetic fields, acid copper electrodeposition, 50
Magnetic materials, 29
electrodepostion:
electrolytes for, 629, 631
ferromagnetic materials, 627–628
hysteresis loop, 627, 628
magnetic anisotropy, 631
magnetization processes, 627–628
microelectromechanical systems, 626–634
mutual alloys, 628–630
permanent magnet materials, 630–634
Magnetic nanoparticles:
chemical synthesis, 471–472
Magnetic properties:
characterization of, 588
Co–P films, 659, 660
and electric, 456
electrodeposited materials, microstructure of, 29
electroless alloys, 503
film composition, 467
Magnetic recording:
additive effect, 580–587
bath design approach, 575–576
coercivity *vs.* C_{sac} and R_S, 582–583
corrosion properties *vs.* R_S, 585–587
direct-current deposition, 577–579
electrodeposition, 573
nanoscale electrode geometry, 588
paddle cell, 576–577
pulse current deposition, 579–580
saccharin adsorption, 580
schematic presentation, 574
stress *vs.* C_{sac}, 583–584
substrate and deposit thickness effects, 587–588
sulfur source, 580–582
surface roughness, 584–585
Magnetic recording systems, types, 459
Magnetism, principal structural element, 29
Magnetization processes:
electrodepostion, microelectromechanical systems, 627
Magnetostriction, electrodeposit, 29

Mandrels, nickel electroforming:
  electrofabrication with, 98
Manganese, 39
  with nickel, 92
  sulfur prevention, 92
  zinc–manganese alloys, 300, 301
Mass spectroscopy (MS), 538
Matte tin coating:
  stress measurements of, 197
Matte tin deposits:
  AFM images of, 175
  SEM photos of, 180
McDermid electroless copper plating bath controller, 542
Mechanical blast cleaning, 508
Melting point, electrodeposition, 235–236
MEMSapplications, 126
MEMS package, 126
2-Mercaptobenzoimidazole (MBI), 491
2-Mercaptobenzothiazole (MBT), 491
3-Mercapto-1-propanesulfonate (MPSA), 65
Mercaptosuccinate–L-cysteine bath, 495
Metal deposition, 135
  initial and final states, 10
Metal distribution, 150
  cathode current density, 91
  cathode polarization, 82
  current density, 81
  nickel electroplating, 81
  throwing power, 82, 150, 269
Metal finishing:
  independent printed circuit board manufacturing (IPCBM) facilities, 560
  operations, 559
  pretreatment standards for, 562
Metal–insulator–metal (MIM) switching, 426
Metal ions:
  in crystal lattice, electrode potential, 1–4
Metallic impurities:
  chromium electrodeposition, 221–222
Metallic painting, nonconductors deposition, 413
Metallization:
  cross-sectional area, 601
  Cu, 370
  electroplated Cu, 638
  GaAs microwave field-effect transistors, 483
  nonconductors deposition, 413
    plastics metalization, 414–416
    polyimide metalization, 414
  polyvinylidene fluoride (PVDF) films, 483
  resistance of, 167
Metal/oxide nanocomposites, electrodeposition, 399–400
Metal-semiconductor junction, 478
Methane sulfonic acid electrolyte, 154–155
Methanesulfonic acids (MSAs):
  antioxidants, effectiveness of, 152
  electrical conductivity, 268
  electrolyte systems, 265
Methylene chloride, 509
Microcracked chromium:
  deposits testing, 231–232
Microdiscontinuous chromium:
  decorative nickel electroplating, 87–88
Microelectromechanical systems (MEMS), 26
  electrodeposition technique:
    characteristic features, 619–620
    copper, 621–623
    Fe–Ni alloys, 628–630
    ferromagnetic materials, 627–628
    gold, 620–621
    magnetic materials, 626–634
    magnetization processes, 627–628
    nickel/nickel alloys, 623–626
    permanent magnet materials, 630–634
  high-aspect-ratio (high-AR) lithographic patterns, 618
  integration, 617
  introduction, 617
  microfabrication techniques, 617–619
  miniaturization, 617
Microelectromechanical systems (MEMSs), 64, 528
Microelectronics:
  copper plating in, 64
  Moore's law for, 65
Microelectronics and micromechanical system (MEMS) technology, 503
Microelectronic technologies:
  applications to, 573
  copper electrodeposition for:
    accelerator effect and superfilling, 595–599
    additive kinetics and effect, 594–601
    barrier materials, 603–606
    copper plating bath chemistry, 592
    copper superfilling models, 592–594
    leveler effect, 600
    mechanism and kinetics, 590–592
    PEG–Cl inhibiting effect, 594–595
    PEG–Cl–SPS/MPS systems, morphological and microstructural effects, 599–600
    on Ti and Ta-based barriers, 601–603
  technique development, 606–611
    defect-mediated growth, 606–609
    epitaxial, smooth, and continuous ultrathin Cu films, 606–611
    surface-limited redox replacement reaction, 609–611
    surfactant-mediated growth, 609
Microfabrication techniques, 617–619
Microporous deposits:
  chromium electrodeposition, 231–232
Microscopy, 511
Microthrowing power, nickel electrodeposition, 83–84
Miniaturization, 483
Mixed catalysts:
  chromium electrodeposition, bath solution with, 216–218
Mixed oxide nanocomposites, electrodeposition, 399–400
Mixed potential theory:
  electroless deposition, 14–15
Mixed-potential theory, 433
Mixed-salt gold complex, 124
Modern electroplating manufacturing technology, 514

Molten salts:
lead and lead alloys electrodeposition, 261
Molybdenum compound:
chromic acid plating baths, 240
chromic acid solutions, 240
chromium alloys, 239
hot-chloride bath, 319
nickel-based alloys, 500, 501, 503
Ni–Mo–P/ SnO2/Ti, 504
PTFE particles, 63
Monitoring procedures:
ammeter equipment, 529
automatic plating machines for, 531–532
exhaust vacuum system, 531
line speed, 531
plating current, monitoring of, 529
rinse water, monitoring, 531
robotic systems, role in, 532
sensers, for monitoring, 529–530
solution flow, monitoring of, 529
solution monitoring and control, 528–529
solution temperature, monitoring of, 529
Moore's law, microelectronics, 65
Mossbauer spectroscopy, 129
MSA-based chemistry, 154
MSA-based systems, 148
Multilayer coatings:
decorative electroplating, nickel coating, 85–87
Multilayered and composite films, 21–23
deposit analysis, 22
general properties, 21–22
nanostructures electrodeposition, 22
Multilayered coating:
zinc/zinc alloys, continuous plating technique, 298

Nanometallic whiskers, 192
Nanoparticles, palladium compound electrodeposition, 363
Nanostructural materials:
electrodeposition, 22
types, 21
National Association of Surface Finishing (NASF), 562
National Institute for Standards and Technology (NIST), 65, 206, 633
National Institute of Standards (NIST), 562
National Metal Finishing Resource Center (NMFRC), 562
Necking, electrodeposit mechanical properties, 28
NEMI's whisker testing, 187
Nernst diffusion layer, 579
Nernst diffusion layer model, 6
electrode kinetics, current-potential relationship, 6–7
Nernst equation, 2, 159, 435
electrode potential, 2–3
Nernstian response, 429
Nernstian shifts, 118
Neutral electrolytes, palladium electrodeposition, 348–355
additive tetramine electrolytes, 349–352
density, 354
deposit purity, 354
grain size, 353
hardness, 355
leveling effect, 354
solderability, 354–355
surface appearance, 353
thermal stability, 354
Neutral gold plating bath, 121
bath composition and plating conditions, 121
New source performance standards (NSPSs), 560
Nickel compounds:
anode materials, 99–103
primary nickel basket, 103
primary nickel behavior, 100–101
sulfur-containing electrolytic nickel, 102–103
titanium anode basket, 101–102
wrought nickel anode materials, 100
barrier layer, 187
composite coatings, production of, 457
composite electroless coatings, 456–457
decorative electroplating, 84–91
bright nickel solutions, 84
decorative applications and market size, 91
electrocrystallization, 84–85
microdiscontinuous chromium, 87–88
multilayer nickel coatings, 85–87
plastics, aluminum, and stainless steel electroplating, 88–89
semibright nickel, 85
standards and coating requirements, 89–91
STEP test, 88
sulfur codeposition effects, 85
electrodeposition of:
adhesion, 83
basics of, 80
coating thickness, 81
electroplating solutions, retrospective on, 79–80
Faraday's laws, application of, 79–80
internal stress, 82–83
leveling and microthrowing power, 83–84
microelectromechanical systems, 623–626
pulse plating effects, 625
throwing power, 82
electroforming with, 97–99
applications, 99
capabilities, 98
electrofabrication technique, 97
leveling agents for, 99
mandrels, 98
nickel-speed process, 98–99
postelectroforming operations, 99
electroless plating baths:
basic baths, 451–452
bath additives, 452–454
film properties:
corrosion, 455–456
electric and magnetic properties, 456
hardness, 455
structure, 454
wear resistance, 455–456
functional electroplating and deposit, 91–97
all chloride solution, 95
all sulfate solution, 95–96

Nickel compounds (*Continued*)
applications of, 79
black nickel solution, 96
coating requirements, 93–94
deposit properties, 91–93
fatigue strength, 96–97
fluoborate solution, 94
hard nickel solution, 94–95
hydrogen embrittlement, 97
nickel-phosphorus solution, 96
sulfate-choride solution, 96
iron–nickel alloys:
microelectromechanical systems, 623–626
Ni–P density:
alloy composition, effects of, 454
Ni–P films:
phosphorus, 454
thermal effect, 456
Ni–W–B plating bath, 501
phosphorus-nickel alloys, 96
pollution prevention, 109–110
quality control, 103–109
process control, 103–106
product control, 106
Nickel concentration, 120
Nickel-hardened gold, 124
Nickel–molybdenum–phosphorus alloys, 503
Nickel silver, 136
Nickel-speed process, nickel electroforming, 98–99
Nippon steel jet cell, zinc/zinc alloys, continuous plating technique, 294
Nippon steel liquid cushion cell, zinc/zinc alloys, continuous plating technique, 295
Nitrile butadiene rubber (NBR) thin film, 426
Nitrilotriacetic acid (NTA), 492
Nodulation:
acid copper additives and prevention of, 38
lead and lead alloys electrodeposition, 253–254
Nonadditive tetramine electrolytes, palladium electrodeposition, 350–352
Nonaqueous solutions:
lead and lead alloys electrodeposition, 260–261
Noncatalytic surfaces, activation:
electrochemical activation, 443
photochemical activation, 443
Nonconductive substrates, schematic representation of, 419
Nonconductors:
plating technology:
adhesion deposition characterization, 416–417
bright acid copper electroplating, 414
chemical conditioners, 413–414
electroless plating, 414
metalization, 414–416
plateable plastics, 413
recent developments, 413–414
sensitization–-catalysis, 417–419
Noncyanide baths:
with Au(III)–phosphate complex, 495
with Au(I)–mercaptosuccinate, 495
with Au(I)–sulfite complex, 490
with Au(I)–thiosulfate complex, 490–491
containing both sulfite and thiosulfate, 491–494
containing sulfite and thiocyanate, 494–495
prepared by mixing Au(lll)–iodide complex with ascorbic acid, 495
Nondestructive testing:
electroplated deposit thickness tests, 543
impurities identification, 129
nickel thickness, 108
profile measurements, 47
X-ray diffraction, 189
XRF, 550
Nonferrous metals, 136
strike, 136
Normal hydrogen electrode (NHE), 162
palladium electrodeposition, 347
NTA preparation strategy:
titanium dioxide, semiconductors electrodeposition, 395–396
Nucleation-coalescence growth mechanism, electrodeposition, 11–12

Occlusion electrosynthesis, semiconductors electrodeposition, 399
Occupational Safety and Health Administration (OSHA), 556, 583
Offset, electrodeposit mechanical properties, 28
Olation, chromium electrodeposition, 209
Ollard bonding test, electrodeposits adhesion, 30
Open-circuit potentials (OCPs), 437, 438
Optically stimulated electron emission (OSEE), 511
Optical nanoantennas, 415
Optical spectroscopic techniques, 151
Organic additives:
categories, 289
decomposition products, 62
decomposition products of, 274
gold–cobalt alloys, 124
impurities and purification, 61
nickel electroplating solutions, 104
optimum ductility, 62
oxidation of, 254
plating process, 45
pyrophosphate solutions, 62
sulfur-containing, 83, 94
unsaturated, 85
zinc deposited, 286
Organic impurities, 41, 98
carbon removes, 106
carbon treatment, 274
chromium bath, 221
iron baths, 319
lead-tin electrolytes, 270
Organic solvent cleaners, electrodeposition preparation with, 509
Original equipment manufacturers (OEMs), 187, 362
Overpotential:
current density relationship, 4
electrode kinetics, mass transport, 6–7
electrodeposition growth forms, dependence on, 12
electrodeposition kinetics, 4

Oxide films:
tin-lead alloys electrodeposition, 275–276
plug connectors, 283
Oxide semiconductors:
electrodeposition:
copper oxide, 398–399
introduction, 394–395
titanium dioxide, 395–396
tungsten trioxide, 397–398
zinc oxide, 396–397
Oxygen-free alkaline solutions:
silver cyanidation, kinetics of, 135
Oxygen gas, 118

Paddle cell, 149
agitation in, 577
magnetic recording, 576
schematic presentation, 577
Palladium compounds:
electrolee deposition:
alloys for, 479–480
electroless palladium plating bath, 478
hydrazine baths, 477–478
hypophosphite baths, 478
reducing agent baths, 478
gold–palladium alloys, 478
nucleation process, 470
palladium–ammine complex, 478
PAT8/NBR composite films, 426, 427
Patterned electrodeposition, acid copper solution, 47
$PdCl_2$–dimethylsulfoxide (DMSO) comple, 481
Pd seeds, formation of:
from $PdCl_2$ solution, 466–470
from $SnCl_2$ solution, 470–471
Perchlorate electrolytes, lead and lead alloys electrodeposition, 249
Perchloroethylene, 509
Perfluoro-octanesulfonic acid (PFOS), 240
Periodic reverse deposition waveform:
electrodeposition kinetics, 11
Periodic reverse (PR) plating:
acid copper electrodeposition, 44
Permanent magnet materials:
electrodepostion, microelectromechanical systems, 630–634
γ Phase, zinc–nickel alloys, continuous plating technique, 297
Phenolsulfonic acid (PSA), 152
acid copper additives with, 38
based chemistry, 153
Phenolsulfonic acid electrolyte/halogen electrolyte, 153–154
pH levels:
iron electrodeposition:
ferrous sulfate bath, 310–311
impurities, removal of, 319
magnetic recording, bath design approach, 575–576
palladium electrodeposition, 340–343
tin–lead alloys electrodeposition, 268
Phosphorous content:
Co–P films, 661
nickel–phosphorus, 626
pH effect of, 454
Photoelectrochemical system:
energy band diagram, 568
Photografting. *See* Photolithography
Photolithography, polymer metallization, 414–415
Physical vapor deposition (PVD), 443
deposits structure and properties, 20
electrochemical deposition process, 369
Plasma-induced deposition, polymer metallization, 416
Plastics:
decorative nickel electrodeposition, 88–89
decorative nickel plus chromium coatings, 90
deformation, electrodeposit mechanical properties, 28
acid copper electrodeposition on, 45
metallization, nonconductors deposition:
electrochemical-autocatalytic methods, 415–416
ion beam techniques, 415
photolithography, 414–415
plasma-induced deposition, 416
sputtering, 416
Plateable plastics, nonconductors deposition, 413
Plating additives, 151
Plating equipment:
types of, 148
Plating parameters, 181
Plating rate, 485–486
Plating solutions:
impurities effect in, 41
Plating stains, 127
Platinum group metals (PGMs). *See also* Gold; Platinum; Specific PGMs
geological occurrence, 327
mineral acids attack, 333
physical and chemical properties, 332–334
reaction with oxygen, 332
sources, 327
supply, demand, and uses, 327–328
Platinum nanoparticles, 480
Plexiglas substrate, 440
Plug connectors, tin–lead alloys coatings, 283
Poisson's ratio, 128
Polarization phenomena:
anodic polarization, 11
cathode polarizations, 35, 36, 82
chromium electrodeposition, 210
copper cathode, 41
copper cyanide solutions, 54
in cyanide copper, strike and Rochelle solutions operations, 54
electrodeposition process, 159
Watts solution, 101
Polarographic analysis, 484
Polarography, 129, 534
Bell Laboratories machines utilizing, 541
of electroless copper plating bath controller, 542
of several plating baths, 535
Pollution prevention:
nickel electrodeposition, 108
Poly(acrylic acid) (PAA), 429
Polyaniline, 423
cyclic voltammograms of, 423

Polycarbonate track-etched membranes (PTM), 495
Polychromates, hexavalent chromium electrodeposition of, 211–214
Polyethylene glycol (PEG):
  as suppressor, 16
Polyethylene therephthalate (PET):
  silver evaporated on, 417
Polyimide metalization, 414
Polyion complex, 429
Polymer batteries:
  electropolymerization, 422
  polymer cathode:
    Li battery, 423–424
    solid polymer electrolyte, 424–425
Polymers:
  alkaline bath formulations, 118
  benzotriazole (BTA), 591
  degradation of, 428
  electron-conductive, 421
  electropolymerization, 421
  electropolymerized, 425
  oxidation and reduction, 423
  PEGs, 66
  plastics, cleaning of, 508
  polyalkylene glycol, 38
  polyimides, 414
Polymethylmeta-acrylate (PMMA):
  microelectromechanical systems (MEMS) application, 618
Poly(*p*-phenylene benzobisoxazole) (PBO), 496
Polypropylene glycol (PPG):
  as suppressor, 16
Polypyrrole (PPy), 423
Polypyrrole and polystyrenesulfonate (PPy/PSS), 423
Polypyrrole (PPy) film, 423
  cyclic voltammograms of, 423
  electroactive composite film, 423
  electropolymerization, 421
  polyazulene, 422
Poly vinyl alcohol (PVA):
  zinc/zinc alloys, alkaline noncyanide zinc baths, 289
Poly(vinyl chloride) (PVC) membrane, 428
Polyvinylidene fluoride (PVDF) films, 483
Porosity:
  chromium electrodeposit testing, 230–231
  chromium plating, 238–239
  palladium electrodeposition, palladium–cobalt alloy, 359–360
Potassium chloride, 478
Potassium cyanide, 118
Potassium cyanoaurate, 483
Potassium hydroxide, 52
  bath composition, 134
  cyanide copper, function, 52
  dilute solution of, 61
  vs. sodium hydroxide, 52–53
Potassium silver cyanide, 135
Potassium stannate baths, 155
  bath formulations, 156
POTW pretreatment standards, 560, 561
PPhT/NBR composite film:
  EL intensity, dependence of, 426
PPy/ClO_4 film, 425
PPy/Nafion film, 424, 425, 428, 429
  composite film, 424
  cross-sectional SEM images, 425
  cyclic voltammograms of, 425
PPy/PSS composite film, 424, 428
PPy/PSS electrode, 428
Precision ion polishing system (PIPS), 650
Primary nickel:
  anodic behavior of, 100–101
  titanium anode basket and, 101–102
Printed circuit (PC), 441
Printed circuit boards (PCBs):
  acid copper electrodeposition, 47
  lead electrodeposition, 261
  tin–lead alloys composition:
    components deposits, 280–281
    eutectic alloys application, 279–280
Printed wiring board (PWB), 143
  acid copper electrodeposition:
    current modulation techniques, 44
    plating with, 45–47
  applications, 362–363
  copper electrodeposition, 590–592
  pyrophosphate copper solution, plating with, 62
Programmable logic controllers (PLCs), 520, 529, 531
Propylene carbonate (PC) electrolyte, 423
Pseudomorphism, deposits structure and properties, 19
Pt/CNT electrocatalysts, 481
Pt–Pd alloy plating bath, 480
Pulsed-current techniques:
  acid copper electrodeposition, 44
    printed wiring boards plating, 47
  application of, 44
  deposition, 579–580
Pulsed cyclic galvanostatic analysis (PCGA), 536
Pulse deposition techniques:
  electrodeposition kinetics, 11
  waveforms used in, 11
Pulse plating, 125
  nickel electrodepostion, effects, 625
  schematic concentration profile, 11
Pure gold, 128
Purification requirements:
  acid copper electrodeposition, 39–40
Push-out test, 225
PVC/(PPy/PSS)/Pt electrodes, 428
  potassium sodium ions of, 428
  potential response mechanism, 429
PWB. *See* Printed wiring board
Pyrophosphate copper:
  additives, 60
  agitation, 61
  ammonia constituents, 59
  applications, 59
  copper and pyrophosphate constituents, 59
  current density, 60–61

equipment, 61
history and development, 58–59
impurities and purification, 61–62
maintenance and control, 61–62
nitrate constituents, 59
operating conditions, 60
orthophosphate constituents, 59–60
pH levels, 60
printed wiring boards, plating with, 62
pyrophosphate-copper ratio, 60
structure and properties, 62
temperature conditions, 60
Pyrophosphate solutions, copper electrodeposition and, 33

Quality control:
nickel electrodeposition:
bright nickel plating impurities, 105
coating defects, 106
concentrations for contaminants, 105
deposits properties, controlling and testing, 107
impurities, control of, 104
pH, temperature, current density, and water quality control, 104
process control, 103, 106–109
purification techniques, 106
solution constituents of, 103
units and conversion factors for, 104
Quantitative hydrogen analysis, palladium electrodeposition, 344
nonadditive tetramine electrolytes, 349–352
Quantum wells, 21
Quantum wires, 21
Quartz crystal microbalance (QCM), 134, 443
Quaternary compound:
ammonium surfactants, 146
electrodeposit ternary, 164
lead-free alloy, 143, 144
nicotinates, 288
Ni–Sn–Cu–P alloy, 501
nitrogen atoms, 289
pyridinium compounds, 288

Rack plating, 148, 149
zinc and zinc alloys electrodeposition:
alkaline noncyanide zinc baths, 288–289
considerations, 290–291
cyanide zinc baths, 286–288
plating, 291–293
Radial cell, zinc/zinc alloys, continuous plating technique, 293
Radio frequencies (RF), magnetic materials electrodepostion, 626
Rasselstein VHC cell, zinc/zinc alloys, continuous plating technique, 294
Reaction rates, chromium electrodeposition, 210
Reactive ion etching (RIE), microfabrication techniques, 618
Real-time analyzer, 536
Recrystallization, deposits structure and properties, 19
Rectangular-pulse deposition technique:
electrodeposition kinetics, 11
Reducing agent solution, 132
Reel-to-reel plating line, 149
Reflection high-energy electron diffraction (RHEED):
cadmium selenide, semiconductors electrodeposition, 389
Relative standard electrode potential:
of Cu/Cu^{2+} electrode, 2
defined, 2–3
of M^{z+}/M electrode, 3
Replenishment schemes, palladium electrodeposition, 343–344
Residual stress, 122
magnetic recording, saccharin effect, 583
Resistance. *See also* Electrical resistivity
Restriction of Hazardous Substances (ROHS), 143
directive, 560
Reverse pulse plating, acid copper electrodeposition, 44–45
Reversible electrode potential, properties, 3
Rhenium compound, 239, 499
nickel–rhenium alloys, 500
physical constants, 666
Rinsing procedure:
electrodeposition preparation with, 510
lead electrolytes, 256
Rinsing provedure, electrodeposition preparation with, 510
Rochelle salt, 132
Rochelle solutions:
carbonate in, 52–53
cyanide copper:
anodes, 57
free cyanide, 51–52
maintenance and control, 54–55
operating conditions and characteristics, 53–54
pH control, 54
tartrates in, 53
Rotating cylinder electrode (RCE) cell, 567
Rotating cylindrical Hull cell, 533
Rotating hemispherical electrodes (RHEs), acid copper electrodeposition, striations, 50
Rotating plating barrel fixture, 514
Rutherford backscattering (RBS):
defect-mediated growth (DMG), 607–609

Saccharin, 461, 580, 581, 583
Sacrificial cathodic protection, steel, 285
Safety factors:
and health properties, 239
lead-bearing solders, 142–143
Occupational Safety and Health Administration (OSHA), 58, 556
pollution prevention, 109
workers and environment, 40
Satin bright:
AFM images of, 175
MSA chemistry, PWB/ high-speed reel-to-reel/wire applications, 154
SEM photos of, 180
tin:
chemistry, connectors, 155
coating plating, in situ stress measurement of, 189
deposits, whisker index of, 195
electroplating chemistry, HPLC monitoring of, 156
Saturated calomel electrode (SCE), 99, 100, 133, 214, 258, 434, 453

Scanning electrochemical microscopy (SECM), 28
Scanning electron micrographs, 354, 356, 361, 364
Scanning electron microscopy (SEM), 16, 27, 167, 372, 637
Scanning tunneling microscopy (STM), 27, 165, 485
Secondary ion mass spectroscopy (SIMS), 550, 599
Selenium compounds, 38
  addition agents, 53
  copper–selenium alloy, 502
  deposition of, 392
  zinc selenide, 389
Self-assembled monolayer (SAM), 15
Self-regulating high-speed bath:
  advantage, 216
  chromium electrodeposition, 216–218
  temperature of, 217
SEMATECH roadmap, 65
Semiaqueous cleaners, electrodeposition preparation with, 510
Semibright compounds, nickel:
  decorative electroplating, 85
  multilayer coatings, 85–87
  plating solutions, 80
Semibright copper plate, 41
Semiconductors:
  chalcogenide, 385
  conjugated polymers, 425
  electrodeposition process:
    cadmium selenide, 388–389
    cadmium sulfide, 390–391
    cadmium telluride, 386–388
    cadmium zinc telluride, 390
    copper indium diselenide, 392–394
    copper oxide, 398–399
    copper sulfide, 391–392
    gallium arsenide (GaAs), 384–385
    gallium phosphide (GaP), 385
    indium compounds, 385
    indium selenide, 392
    indium sulfide, 385–386
    lead sulfide, 386
    mercury cadmium telluride, 394
    mixed oxides and metal/oxide nanocomposites, 399–400
    silicon (Si), 383–384
    titanium dioxide, 395–396
    tungsten trioxide, 397–398
    zinc cadmium selenide, 389–390
    zinc chalcogenides, 389
    zinc oxide, 396–397
  pure soft gold, 483
Sensitization catalysis. *See* Electroless deposition
Sensitizers, 449
Sequential electrochemical reduction analysis (SERA), 167
Service condition numbers, decorative nickel electroplating, 90
Shear strength testing, 550
Short-term corrosion tests, tin-lead alloys electrodeposition, 275
Silicon:
  semiconductors electrodeposition process, 383–384
    cadmium selenide, 388–389
    cadmium telluride, 386–388
  wafers, 193
Silver, 131
  cyanidation, kinetics of, 135
  deposition, 135
  electrodeposition:
    additives, 136
    anodic reactions, 135–136
    bath composition, 134
    bath constituents, 134–135
    deposition, 136
    fractals, 137–138
    physical properties, 136–137
  electroless deposition, 131
    bath properties, 132
    deposition, 133–134
    metallizing baths compositions, 131–132
    polarization, 132–133
    pretreatment, 131
  electroless plating rate of, 132
  ion, electron transfer, 135
  ion solution, 131, 133
  surfaces, cyanide ions, adsorption of, 135
Silver cyanide, 135
  plating baths, composition of, 134
Single-blend additives, 47
Single crystal:
  deposits structure and properties, 18
  whiskers grown, expitaxially from, 193
Sliding wear–contact resistance, 360
Sodium borohydride electroless nickel plating solutions, composition of, 452
Sodium hydroxide, 509
  cyanide copper, function, 52
  vs. potassium hydroxide, 52–53
Sodium stannate bath:
  bath formulations, 156
Soft magnetic underlayer (SUL):
  cobalt–palladium multilayered film, 466
Solderability, 167
  failures, 167
  palladium electrodeposition, neutral electrolyte, 354–355
  tin–lead alloys electrodeposition:
    dip-and-look test, 277
    electronic components, 280–282
Soldering, 139
  history of, 139–140
  lead-bearing solders, 142–143
    environmental, health, and safety concerns, 142–143
  lead-free solder development, 140
    electronics industry, selection rules, 144
    material properties, 143
  lead, roles of, 140–142
Solder mask over bare copper (SMOBC) technique, 261
Solders:
  alloys, 139
  bump arrays, 197
  time line illustrating use of, 140
Solvent-based cleaning, 509
Solvent vapor degreaser, 125
Specific gravity, 539
  analysis methods, 539

degrees Baumé of, 673
measurements, 41
nickel electroplating facts, 103
Specular reflection, electrodeposition growth mechanisms, 13
Spiral patterns. *See* Striations
Spray method, 133
Sputtering, polymer metallization, 416
Stainless steel, 122
decorative nickel electrodeposition and, 89
decorative nickel plus chromium coatings, 90
Standard electrode potential, 2–3
properties, 3
Stannic tin, 145
anodically produced oxygen, formation of, 271
electrolyte, 269
Stannous tin, 145, 151
Steady-state mixed potential, electroless deposition, 14–15
Steel:
acid copper electrodeposition, 45
first strike bath, 136
STEP test:
decorative nickel electroplating, 88
Stransky-Krastanov growth mode, 176
Streaking, lead and lead alloys electrodeposition, 254
Stress analysis cells, 533–534
Stress-strain curve, 28
Striations, 50, 173, 233
acid copper electrodeposition, 50
Strike solutions, 53
carbonate in, 52–53
cast ball, 57
copper, 53
cyanide copper:
anodes, 57
free cyanide, 51–52
filtration of, 54
gold, 126, 540
maintenance and control, 54–55
operating conditions and characteristics, 53–54
tartrates in, 53
Stripping process, 262, 390
Strip plating for electronics, 519–522
Subdiffraction-limited (SDL) resolution, 415
Substrate-catalyzed plating, 483
Sulfamate solutions:
ammonium ions, remove, 98
nickel, 80
nickel electroforming solutions, 98
nickel films, 624
tensile stress, 83
Sulfate solutions, 5
acid copper solutions, formulations of, 35
chloride, addition of, 594
copper plating, 34
electrodeposition of copper, 5
gelatin additions, 38
specific gravity of, 41
SPS/MPSA, 595
sulfuric acid, addition of, 35
Sulfate/sulfuric acid system:
based electroplating chemistry, 153
electrolyte, 152–153
feature of, 153
Sulfite–thiosulfate:
ascorbic add bath, 491
erythorbic acid bath, 493
plating bath, 123
Sulfuric acid:
acid copper solution and, 35–36
chromium electrodeposition, 206
Sumitomo horizontal cell, zinc/zinc alloys, continuous plating technique, 295, 296
Sumitomo vertical cell, zinc/zinc alloys, continuous plating technique, 294
Superfilling mechanisms:
copper electrodeposition models, 589, 592–594
schematic presentation, 594
patterned electrodeposition, microelectronics, 48, 65
Superimposed sinusoidal deposition waveform:
electrodeposition kinetics, 11
Suppressors. *See* Inhibitors
Surface analytical techniques, 129
Surface energy (SE), 136
latent heat, relationship, 137
Surface-enhanced Raman spectroscopy (SERS), 124, 135
copper electrodeposition:
PEG–Cl inhibiting effect, 594
silver electrode, cyanide adsorbed, 135
Surface-limited redox replacement (SLRR) reaction, 609–611
Surface micromachining:
microfabrication techniques, 617, 618
Surface-mount soldering, 142
Surface Technology Association (STA), 565
Surfactant mediated growth (SMG) method, 609
Surfactants, 509
iron electrodeposition, bath solution with, 319

Tafel equation:
electrodeposition kinetics, overpotential, 4
Tafel plot, 5
Tafel slope, 124
Taguchi method:
cyanide copper plating, 51
Tarnish resistance, chromium electrodeposition, 237
Tartrates, cyanide copper, 53
Temperature:
acid copper electrodeposition, 39
diffusion welding, 25
lead and lead alloys electrodeposition, 253
palladium electrodeposition, 340–343
tin-lead alloys electrodeposition, electrolyte temperature, 271–272
TEM. *See* Transmission electron microscopy
Tensile strength:
copper electrodeposits, 42
lead and lead alloys electrodeposition, 256
nickel electrodepostion, 625
vs. inverse square root, 43

Tensile stress, 196
Ternary alloys:
  Co and Ni, 629
  CoNiFe, 460
    phase diagram, 461
  electroplate, 157
  iron–cobalt–nickel, 316
  K–Na–Pb, 261
  palladium alloy, electroless plating of, 479
  Pb–Sb–Sn, 224
  plating baths of, 502
  quaternary lead-free alloy, 143, 144
  quaternary tin alloys, 163
Terne plate, tin-lead alloys electrodeposition, coating application, 278
Test cells, 532
Tetrafluoroborate electrolytes, lead and lead alloys electrodeposition, 250–251
Tetrafluoroboric acid electrolytes, tin–lead alloy deposition, 266–267
Texture, electrodeposits structure and properties, 20
Thallium:
  grain refiner, 121
  lead–thallium, 257
  stress reducing agent, 123
  use of, 452
Thermal cycle testing:
  nickel electroplating corrosion testing, 108
Thermal stability:
  palladium electrodeposition, neutral electrolyte, 354
Thermal stress, 185
Thermodynamics:
  palladium electrochemistry, 334–335
Thin films:
  cadmium selenide (CdSe), 388–389
  Co–Fe, 462, 463
  CoNiFe, TEM bright-field images of, 461
  of copper, 599
  electrodeposition, 30
  electroluminescence (EL) device, 426–427
  interdiffusion in:
    diffusion barriers, 25
    electrodeposit diffusion, 24
    electromigration, 25–26
    general principles, 23–24
    void formation, 24–25
  MEMS fabrication, 28
  Ni–Zn–P, 659
  polycrystalline, 29
  titanium dioxide (TiO_2), 395–396
  zinc oxide, 396–397
Thiocyanate, 494
Thiosulfate, 494
Thiourea bath, 491
Three-dimensional crystallites (TDCs), 439
  coalescence, types of, 439
Throwing power:
  acid copper electrodeposition, printed wiring boards plating, 46–47
  chromium electrodeposition, 206, 221
    hexavalent *vs.* trivalent chromium, 206
  nickel electroplating, 82
Tin–bismuth plating process, aging study of, 162
Tin compound:
  alkaline media, 145
  allotropic forms of, 144
  amphoteric, 145
  anodes, purity of, 150
  anodic oxidation reactions, 147
  applications, 199
    connectors, 193–195
    leadframes, 195–196
    passive components, 196
    wafer bumping, 196–199
  corrosion behavior, in aqueous media, 145
  current–voltage behavior, 147
  cyclic voltammograms of, 147
  distilled water, 145
  electrodeposite stress, 184
  electrodeposition, 156, 161
    chemical properties, 145
    electrode reactions, 147–148
    electroplating process, 148–152
    fluoboric acid, sulfuric acid, phenolsulfonic acid (PSA), 152–156
    grain growth and roughness of, 179
    physical properties, 144–145
    practical considerations, 160–161
    redox potentials, 159
    reduction potentials, 146–147
    ternary and quaternary, 163–164
    thermodynamic treatment of, 145–146
    tin–bismuth alloy, material properties of, 161–162
    tin–bismuth/tin–copper/tin–silver, phase diagrams of, 157–159
    tin–silver alloys, material properties, 162–163
  electrolyte, anode passivation, 150
  electroplating bath, 176
  future for, 199
  grain growth, 183
  material properties and applications, 193–199
    appearance, 164–165
    ductility, 168
    hardness, 168
    purity, 166
    solderability, 167–168
    stress, 168–169
    surface morphology and texture, 165–166
  oxidation of, 151–152
  plated multilayer ceramic chip capacitor, cutaway view of, 185
  plating bath, triton X-100, Raman spectra of, 178
  reduction potentials of, 146
  scanning tunneling microscopic images of, 179, 180
  tin–bismuth alloys:
    DSC curve of, 161
    phase diagram of, 157
    plated Cu, wetting balance tests of, 163
  tin–copper alloy, 172
    phase diagram of, 158

tin–copper binary system, 158
tin(IV), tin-lead alloys electrodeposition, 273–274
tin–silver alloys, 158
tin–silver bumping process:
drawbacks of, 198
X-ray elemental mapping of, 164
tin–silver-copper (SAC) alloy, 198
tin-silver–copper (SnAgCu) family, 144
tin–silver plating process:
current density range of, 163
whisker, 172
chemical composition, 173
definition, 169–172
in electronic equipment, 169
key factors, 174–186
length of, 187, 188
properties, 172–174
physical properties, 173–174
shapes of, 172
technology breakthroughs, 170
tin dendrites, 170
tin needles, 170–171
tin pest, 171–172
whisker applications, 192–193
whisker growth mechanism, 191–192
whisker prevention, 192
whisker test conditions, observation methodology, 186–191
X-ray diffraction, 168, 169
Tin-free steel (TFS), 229, 238
Tin-lead alloys, 139
cast bars, tensile strength of, 141
electrodeposition:
additives, 268–269
agitation, 272
alkylsulfonic acid electrolytes, 267–268
alloy compositions, 265–266
anodic reactions, 274
applications, 278–283
bath compositions, 266
bearing alloys, 278
carbon content, 277
chromium plating bath anodes, 278–279
coating thickness, 281–282
contaminants, 272–274
density, 275
deposition rate, 275
electrical contact resistance, 277
electrochemical deposition equivalent, 274–275
electrolyte composition, 271
electrolyte temperature, 271–272
electronic components, 280–282
eutectic alloys, 279–280
hardness, 277–278
insoluble anodes, 270–271
interlayers, 282–283
lead–tin films, properties, 275–276
long-term corrosion tests, 275
maintenance and control, 271–274
metal concentration, 271
metallic contaminants, 273
organic additives products, 274
oxide formation, 275–276
pH solutions, 268
plug connectors, 283
short-term corrosion tests, 275
solderability test, 276, 277
soluble anodes, 269–270
terne plate, 278
tetrafluoroboric acid electrolytes, 266–267
tin(IV) concentration, 273
troubleshooting for, 270
eutectic solders, 143
soft solder compositions, 139
solders, 139, 159
electrical and thermal conductivities of, 141
phase diagram of, 141
Titanium compound:
anode, primary nickel and baskets structure, 101–102
titanium dioxide, semiconductors electrodeposition, 395–396
Total organic carbon (TOC), 539
Toyota's environmental report:
carbon footprint, 559
material and waste balance, 558
Transfer coefficients, 5
Transmission electron microscopy (TEM), 379, 588, 638
disadvantage, 27
images, 460
micrographs of CoP films produced at, 661
micrographs of Ni–Zn–P film produced in, 660
sample preparation techniques, 649
dimpling–ion milling technique, 649–651
FIB ex situ lift-out method, 656
FIB H-bar method, 656
FIB in situ lift-out method, 654–655
FIB technique, 653–657
wedge technique, 650, 652–653
system, 657
Transport-limited leveling models, copper electrodeposition, superfilling models, 592–594
Treeing, lead and lead alloys electrodeposition, 253
Trichloroethylene, 509
Trim-and-form process:
tin–lead alloys electrodeposition, electronic components, 280
Trimethylamineborane (TMAB), 462
Triton X-100
adsorption behavior of, 178
impedance measurements of, 178
Raman spectra of, 178
Trivalent chromium:
advantage of, 239
chemistry, advantage, 239
chromium alloy plating, 229–230
chromium deposits, 230
Cr–Ni/Cr–Ni–Fe alloys, 209
electroplating, 229
importance of, 205
processes, 239
wetting agent, 240

Troubleshooting, lead and lead alloys electrodeposition, 253–256
Tungsten (W), 443
  alloy deposition, 503
  cobalt–tungsten, 632
  filaments, 64
  metallized ceramics, 483
  nickel–tungsten alloys, 501
  nickel–tungsten–silicone–carbide coating, 565
  resistance, 637
  silver–tungsten, 502
  silver–tungsten alloys, 503
  wire, 64
Tungsten trioxide (WO_3), 397–398
Two-angle method, 189
Two cell systems, schematic representation, 461
Two-photon polymerization (TPP), 415
  polymer metallization, 415

ULSI interconnect fabrication process:
  electroless process for:
    background, 377–378
    insulator properties, 380
    insulator surface modification, 378–379
    Ni alloys on insulator, 379–380
ULSI interconnection devices:
  electrochemical deposition process:
    background, 369
    diffusion barrier layer, 370–371
Ultrahigh voltage (UHV)–based methods, 589
Ultra-large-scale integration (ULSI), 26, 64
  circuits, metallization, copper electrodeposition, 621
Ultrasonic agitation, 39, 46, 49, 58, 61, 63, 127, 290, 507, 516
Underpotential deposition (UPD), 486
  acid copper electrodeposition, 50–51
  lead and lead alloys, 261
Unoriented dispersion (UD), 285, 299, 375
Urea:
  biosensor, development of, 430
  sensor, type of, 429
Urease (Urs)-immobilized electrodes, 428
U.S. Code of Federal Regulations (CFR), 560
U.S. Environmental Protection Agency (EPA), 225
  creation of, 556
  driving forces, 556
  regulatory environment:
    changes, 557
    evolution of, 556
    role in, 555
U.S. Geological Survey, 364
U.S. surface-finishing industry:
  census data on, 560
UV irradiation, 418

Vickers hardness:
  electrodeposited gold, 123
  nickel plating solutions, 92
VLS process, 193
Void formation:
  lead and lead alloys electrodeposition, 254–256
  thin films interdiffusion, 24–25
Volmer–Weber growth model, 176

Wafer bumping, 196
  applications, 164
Wafer plating equipment, 149, 522–523
  ancillary chambers, 525
  fountain cells, 523–524
  paddle cells, 523
  rack platers, 524–525
Waste from Electrical and Electronic Equipment (WEEE) directive, 143, 560
Wastewater system, schematic presentation, 565
Water management system, for strip plater, 540
Water proofing, 136
Watts-type solution:
  electrodeposition growth mechanisms, additives consumption, 13
  nickel:
    anodic polarization, 101
    deposition of, 13
    plating, 80, 94
Wear-resistant:
  copper–lead alloys, 259
  corrosion, 455–456
  electroless nickel/immersion gold (ENIG), 516
  gold deposits, 128
  hardness, 234
  lead–tin–copper alloys, 260
  Pd alloys, 359
  washing machine shafts, 217
Wear tests, 128
Wet cleaning procedure, importance of, 225
Wetting agents, chromium electrodepostion, 223
Wetting balance, 167
Whisker:
  formation, 174
  growth mechanism, 174, 186
  nucleation, kinetics of, 191
  resistance, 196
  test conditions, 186–191
  test method, 187, 188
White tin, physical properties, 173
Wire plating, 265, 522
Wire pull testing, 550
Wrought carbon anodes, 100
Wrought nickel anode materials, nickel plating, 100

X-ray diffraction (XRD), 27, 29, 120, 165, 184, 189, 374
  data, CoFe alloys, 583
  measurements, cadmium telluride, semiconductors electrodeposition, 386–387
  pattern, 36
  study, 213
X-ray fluorescence (XRF), 129, 539
X-ray lithography:
  masks, 123
  microelectromechanical systems (MEMS), 618
X-ray photoelectron spectroscopy (XPS), 414, 550

Yield strength:
electrodeposition, 625
thermal effect, 96
Young's modulus, 27, 57, 128
Yttrium-aluminum-garnet (YAG) laser, 127

Zero-discharge processes, electrodeposition, environmental hazards, 564–566
Zero stress, 99
Zincate plating, alkaline noncyanide baths, 289
Zincation, 131
Zinc compounds:
acid copper electrodeposition, 45
Cockerill-Sambre belt cell, zinc/zinc alloys, continuous plating technique, 296
Cockerill-Sambre flash cell, zinc/zinc alloys, continuous plating technique, 296
deposition potential, 17–18
die castings, 226
acid copper deposits, 45
displacement deposition, 15
iron–zinc alloys:
alkaline bath parameters, 292
current efficiency, 299
electrodeposition with, 291
metallographic structures, 299, 300
metallurgical properties, 298
performance, 298
phases *vs.* thermal equilibrium, 292
surface microscope examination, 301
lead–zinc alloys, 258–259
manganese–zinc alloys, 300
nickel–zinc alloys:
parameters for, 291
phase *vs.* composition diagrams, 291
plating, 291
zinc/zinc alloys, electrodeposition:
acid chloride zinc baths, 289–290
alkaline noncyanide zinc baths, 288–289
alloy plating, 291–293
barrel-and-rack plating, 286–293
chemical properties, 285–286
continuous plating, 293–302
cyanide zinc baths, 286–288
environmental impact minimization with, 565–566
trends in, 285–286
Zintl anions, 414